Talanta

The International Journal of Pure and Applied Analytical Chemistry

Editors-in-Chief

Professor G.D. Christian, University of Washington, Department of Chemistry, 36 Bagely Hall, P.O. Box 351700, Seattle,WA 98195-1700, U.S.A.

Professor J.-M. Kauffmann, Université Libre de Bruxelles, Institut de Pharmacie, Campus de la Plaine, C.P. 205/6, Boulevard du Triomphe, B-1050 Bruxelles, Belgium

Associate Editors

Professor J.-H. Wang, Research Center for Analytical Sciences, Northeastern University, Box 332, Shenyang 110004, China

Professor J.L. Burguera, Los Andes University, IVAIQUIM, Faculty of Sciences, P.O. Box 542, 5101-A Mérida, Venezuela.

Assistant Editors

Dr R.E. Synovec, Department of Chemistry, University of Washington, Box 351700, Seattle, WA 98195-1700, U.S.A.

Professor J.-C. Vire, Université Libre de Bruxelles, Institut de Pharmacie, Campus de la Plaine, C.P. 205/6, Boulevard du Triomphe, B-1050 Bruxelles, Belgium

Talanta

R. Apak (Istanbul, Turkey)
E. Bakker (Auburn, AL, U.S.A.)
D. Barceló (Barcelona, Spain)
B. Birch (Luton, UK)
K. S. Booksh (Tempe, AZ, U.S.A.)
J.-L. Capelo-Martinez (Caparica, Portugal)
Z. Cai (Kowloon, Hong Kong)
S. Cosnier (Grenoble, France)
D. Diamond (Dublin, Ireland)
W. Frenzel (Berlin, Germany)
A.G. Gonzales (Seville, Spain)
E.H. Hansen (Lyngby, Denmark)
P. de B. Harrington (OH, U.S.A.)
A. Ho (Hsin-chu, Taiwan)
J. Kalivas (Pocatella, ID, U.S.A.)
B. Karlberg (Stockholm, Sweden)
J.-M. Lin (Beijing, China)
Y. Lin (Richland, WA, U.S.A.)
M.D. Luque de Caastro (Cordoba, Spain)
I.D. McKelvie (Victoria, Australia)
S. Motomizu (Okayama, Japan)
D. Nacapricha (Bangkwok, Thailand)
J.-M. Pingarron (Madrid, Spain)
E. Pretsch (Zürich, Switzerland)
W. Schuhmann (Bochum, Germany)
M. Shamsipur (Kermanshah, Iran)
M. Silva (Porto Alegre, Brazil)
P. Solich (Hradec Králové, Czech Republic)
K. Suzuki (Yokohama, Japan)
D.G. Themelis (Thessaloniki, Greece)
D.L. Tsalev (Sofia, Bulgaria)
Y. van der Heyden (Belgium)
B. Walzcak (Katowice, Poland)
J. Wang (Tempe, AZ, U.S.A.)
J.D. Winefordner (Gainesville, U.S.A)
Xiu-Ping Yan (Tianjin, China)
E.A.G. Zagatto (Piracicaba, SP, Brazil)

Copyright © 2008 Elsevier B.V. All rights reserved

Publication information: *Talanta* (ISSN 0039-9140). For 2008, volumes 74–76 are scheduled for publication. Subscription prices are available upon request from the Publisher or from the Regional Sales Office nearest you or from this journal's website (http://www.elsevier.com/locate/talanta). Further information is available on this journal and other Elsevier products through Elsevier's website: (http://www.elsevier.com). Subscriptions are accepted on a prepaid basis only and are entered on a calendar year basis. Issues are sent by standard mail (surface within Europe, air delivery outside Europe). Priority rates are available upon request. Claims for missing issues should be made within six months of the date of dispatch.

Orders, claims, and journal enquiries: please contact the Customer Service Department at the Regional Sales Office nearest you:
Orlando: Elsevier, Customer Service Department, 6277 Sea Harbor Drive, Orlando, FL 32887-480 USA; phone: (+1) (877) 8397126 [toll free number for US customers], or (+1) (407) 3454020 [customers outside US]; fax: (+1) (407) 3631354; e-mail: usjcs@elsevier.com
Amsterdam: Elsevier, Customer Service Department, PO Box 211, 1000 AE Amsterdam, The Netherlands; phone: (+31) (20) 4853757; fax: (+31) (20) 4853432; e-mail: nlinfo-f@elsevier.com
Tokyo: Elsevier, Customer Service Department, 4F Higashi-Azabu, 1-Chome Bldg, 1-9-15 Higashi-Azabu, Minato-ku, Tokyo 106-0044, Japan; phone: (+81) (3) 5561 5037; fax: (+81) (3) 5561 5047; e-mail: jp.info@elsevier.com
Singapore: Elsevier, Customer Service Department, 3 Killiney Road, #08-01 Winsland House I, Singapore 239519; phone: (+65) 63490222; fax: (+65) 67331510; e-mail: asiainfo@elsevier.com

USA mailing notice: *Talanta* (ISSN 0039-9140) is published monthly by Elsevier B.V. (P.O. Box 211, 1000 AE Amsterdam, The Netherlands). Annual subscription price in the USA US$ 4,085 (valid in North, Central and South America), including air speed delivery. Application to mail at periodical postage rate is paid at Rathway, NJ and additional mailing offices.
USA POSTMASTER: Send address changes to *Talanta*, Publications Expediting Inc., 200 Meacham Avenue, Elmont, NY 11003.
AIRFREIGHT AND MAILING in the USA by Publications Expediting Inc., 200 Meacham Avenue, Elmont, NY 11003.

Available online at www.sciencedirect.com
ScienceDirect
Talanta 74 (2008) 903–908
Talanta
www.elsevier.com/locate/talanta

Use of 8-sulfonamidoquinoline derivatives as chelate extraction reagents in ionic liquid extraction system

Taku Ajioka [a], Syunichi Oshima [b], Naoki Hirayama [c,d,*]

[a] *Division of Material Chemistry, Graduate School of Natural Science and Technology, Kanazawa University, Kanazawa 920-1192, Japan*
[b] *Practical Engineering Education Program, Academic Foundation Programs, Kanazawa Institute of Technology, Nonoichi, Ishikawa 921-8501, Japan*
[c] *Department of Chemistry, Faculty of Science, Kanazawa University, Kanazawa 920-1192, Japan*
[d] *Division of Material Sciences, Graduate School of Natural Science and Technology, Kanazawa University, Kanazawa 920-1192, Japan*

Received 30 June 2007; received in revised form 24 July 2007; accepted 25 July 2007
Available online 31 July 2007

Abstract

Possible use of 8-sulfonamidoquinoline derivatives as chelate extraction reagents for solvent extraction of several divalent metal cations using an ionic liquid, 1-butyl-3-methylimidazolium hexafluorophosphate ([bmim][PF_6]) as extraction phase was investigated as fundamental approach to develop novel extraction reagents for ionic liquid extraction system. The studied reagents were able to be used as extractants for the metal cations in the [bmim][PF_6] extraction system. Furthermore, their extractability in the [bmim][PF_6] system was superior to that in chloroform system. Most of the extracted species were (hydrated) neutral complexes, whereas, in use of the derivative having trifluoromethyl group, Cd^{2+} was extracted as anionic complex accompanied with anion-exchange process.
© 2007 Elsevier B.V. All rights reserved.

Keywords: Ionic liquids; Chelate extraction; Divalent metal cations; 8-Sulfonamidoquinoline derivatives; Anion-exchange

1. Introduction

Ionic liquids (strictly speaking, room temperature ionic liquids) have attracted much interest as novel solvents [1–11]. They are salts with low melting points (ca. <100 °C) and hydrolytically stable. Furthermore, several ionic liquids are water-immiscible and, therefore, can be used as solvent (extraction phase) for liquid–liquid extraction.

Use of ionic liquids as extraction phase in solvent extraction of organic materials was reported by Huddleston et al. first in 1998 [12] and that of metal cations was reported by Dai et al. first in 1999 [13], provided that studies on similar extraction systems were reported more previously [14,15]. Many researchers have studied the ionic liquid extraction system and several reviews concerning the system have been reported [16–18].

In use of ionic liquids for metal extraction, extraction of charged complexes with neutral extractants by ion-exchange processes with the ionic liquid ions, reported by Dietz and Dzielawa first in 2001 [19], has been given attention. In the extraction system, however, recovery of the extracted metals is a serious problem because of negligible volatility of the ionic liquids. On the contrary, use of anionic chelating agents such as dithizone [20], 8-hydroxyquinoline derivatives [21] and β-diketones [22,23] or neutral ligands having protonatable N-donor [24–26] as extraction reagents and back-extraction of the extracted metals into aqueous acid solution seem to be effective for the achievement of the recovery. Furthermore, in use of the anionic chelate extraction reagents, possible extracted species into the ionic liquid extraction phase are not only conventional neutral chelates but also anionic (or cationic) ones. Namely, in the ionic liquid chelate extraction system, various kinds of extraction mechanism can be constructed. However, traditional chelate extraction reagents were optimized for use of organic solvents as extraction phase and, therefore, are not always suitable for use of ionic liquids. In other words, it is necessary to

* Corresponding author at: Department of Chemistry, Faculty of Science, Kanazawa University, Kanazawa 920-1192, Japan. Fax: +81 76 264 5742.
E-mail address: hirayama@cacheibm.s.kanazawa-u.ac.jp (N. Hirayama).

0039-9140/$ – see front matter © 2007 Elsevier B.V. All rights reserved.
doi:10.1016/j.talanta.2007.07.020

develop novel extraction reagents for the ionic liquid chelate extraction system.

8-Sulfonamidoquinoline derivatives (HRsq), which are sulfonamide-type analogs of 8-hydroxyquinoline, can act as N,N$^-$-bidentate anionic chelate extraction reagents [27–37] since sulfonamide group has acidity comparable to that of phenolic-OH [38–40]. Furthermore, other sulfonamide-type ligands were researched as anionic chelate extraction reagents [41–47]. Since the HRsq derivatives are generally synthesized by reaction between 8-aminoquinoline and respective sulfonyl halides (RSO_2X, X = F, Cl or Br), it is very easy to introduce various substituents (R) onto 8-sulfonamidoquinoline structure. Namely, use of the HRsq derivatives in the ionic liquid chelate extraction system is an effective approach to develop novel chelate extraction reagents optimized for the system. Furthermore, the HRsq derivatives as well as 8-hydroxyquinoline exist as hydrophobic neutral forms at wide pH region [39]. From these viewpoints, we performed a fundamental study concerning possible use of several HRsq derivatives, such as 8-(*p*-toluenesulfonamido)quinoline [4-methyl-*N*-(8-quinolyl)benzenesulfonamide, H(C_7H_7)sq], 8-(methanesulfonamido)quinoline [8-quinolylaminosulfonylmethane, H(CH_3)sq] and 8-(trifluoromethanesulfonamido)quinoline [trifluoro(8-quinolylaminosulfonyl)methane, H(CF_3)sq] (see Fig. 1), as chelate extraction reagents for extraction of several divalent metal cations in ionic liquid chelate extraction system using 1-butyl-3-methylimidazolium hexafluorophosphate ([bmim][PF_6]).

2. Experimental

2.1. Reagents

The synthesis of H(C_7H_7)sq was performed from 8-aminoquinoline and *p*-toluenesulfonyl chloride according to the reported procedure [48]. Other ligands such as H(CH_3)sq and H(CF_3)sq were prepared in a similar manner to H(C_7H_7)sq from 8-aminoquinoline and methanesulfonyl chloride or trifluoromethanesulfonyl fluoride. The structures were identified by ^{1}H-NMR spectra and elemental analysis [39,48].

The ionic liquid [bmim][PF_6] was synthesized from 1-chlorobutane, 1-methylimidazole and hexafluorophosphoric acid according to the reported procedure [12]. Other chemicals were reagent-grade materials and were used without further purification. Distilled deionized water was used throughout.

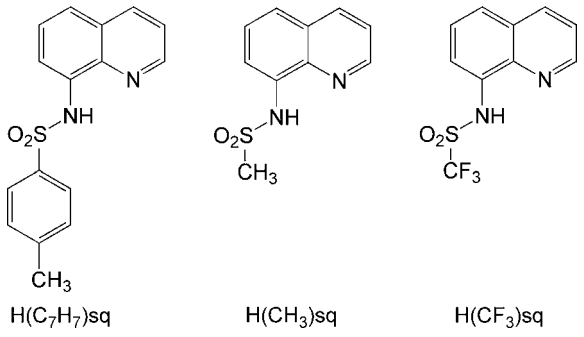


Fig. 1. Chemical structures of 8-sulfonamidoquinoline derivatives used in this study.

2.2. Apparatus

A Hitachi model Z-6100 polarized Zeeman atomic absorption spectrophotometer was used for the determination of the concentration of a metal in aqueous phase. A Horiba model F-12 pH meter equipped with a Horiba 9510-10D combined glass electrode was used to determine the pH values.

2.3. Distribution of the metals

In a centrifuge tube, an aliquot (1 cm^3) of [bmim][PF_6] containing 1×10^{-3} mol dm^{-3} of an HRsq and 5 cm^3 of an aqueous phase 1×10^{-5} to 1×10^{-4} mol dm^{-3} of M^{2+} (M = Co, Cu, Zn or Cd), 1×10^{-1} mol dm^{-3} of potassium nitrate and 1×10^{-2} mol dm^{-3} of buffer (chloroacetic acid, acetic acid or 2-(*N*-morpholino)ethanesulfonic acid) were shaken at 25 ± 1 °C for 45 min. After the two phases were separated by centrifugation, the pH and the metal concentration in the aqueous phase were determined and the measured pH was used as equilibrated pH. The metal concentration in the extraction phase was determined after back-extraction into 10-fold volume of 1 mol dm^{-3} nitric acid.

3. Results and discussion

3.1. H(C_7H_7)sq system

The extracted ratios (%*E*) of M^{2+} into [bmim][PF_6] extraction phase with H(C_7H_7)sq were plotted as a function of aqueous phase pH. The results are shown in Fig. 2 with the plots using chloroform as extraction phase. The use of [bmim][PF_6] extraction phase resulted in higher extractability for all of M^{2+} compared with the use of chloroform. In addition, Mn^{2+} was not extracted in the examined extraction conditions and extraction of Ni^{2+} needed long time for equilibration as reported previously for chloroform system [34]. The extraction selectivity order in the H[(C_7H_7)sq]–[bmim][PF_6] system was $Cu^{2+} > Zn^{2+} > Cd^{2+} \approx Co^{2+}$ ($\gg Mn^{2+}$), which was almost the same as that in use of chloroform extraction phase, $Cu^{2+} > Zn^{2+} > Co^{2+} \geq Cd^{2+}$ ($\gg Mn^{2+}$).

As reported previously [34], H(C_7H_7)sq extracts M^{2+} as neutral M[(C_7H_7)sq]$_2$ complex (probably hydrated M[(C_7H_7)sq]$_2$(H_2O)$_n$ complex) in use of an organic solvent as extraction phase. In this case, the extraction equilibrium and the extraction constant (K_{ex}) can be expressed as follows:

$$M^{2+} + 2H(C_7H_7)sq_{(e)} \Leftrightarrow M[(C_7H_7)sq]_{2(e)} + 2H^+ \quad (1)$$

$$K_{ex} = \frac{[M[(C_7H_7)sq]_2]_{(e)}[H^+]^2}{[M^{2+}][H(C_7H_7)sq]^2_{(e)}} \quad (2)$$

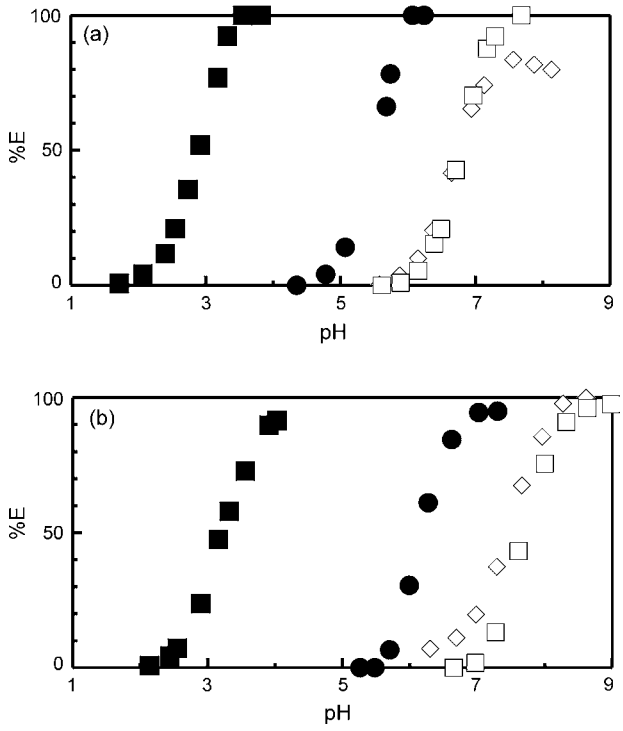


Fig. 2. Plots of the extracted ratios (%*E*) for some divalent metals as a function of the aqueous phase pH equilibrated with extraction phase in $H(C_7H_7)sq$ system. Initial $H(C_7H_7)sq$ concentration in extraction phase was 1×10^{-3} mol dm^{-3}. Extraction phase: (a) [bmim][PF_6]; (b) chloroform. Sample: (◊) Co^{2+}, (■) Cu^{2+}, (●) Zn^{2+} and (□) Cd^{2+}.

where subscript (e) denotes the extraction phase. Therefore, the distribution ratio (D) for M^{2+} can be expressed as follows:

$$D = \frac{[M[(C_7H_7)sq]_2]_{(e)}}{[M^{2+}] + [M(OH)^+] + [M(OH)_2]}$$
$$= \frac{[M[(C_7H_7)sq]_2]_{(e)}}{[M^{2+}](1 + \beta_1[OH^-] + \beta_2[OH^-]^2)}$$
$$= \frac{K_{ex}[H(C_7H_7)sq]_{(e)}^2}{[H^+]^2}(1 + \beta_1[OH^-] + \beta_2[OH^-]^2)^{-1} \quad (3)$$

where β_1 and β_2 are stability constants for hydroxo complexes of $M(OH)^+$ and $M(OH)_2$, respectively. Namely, the following approximate relationship can hold good:

$$\log D(1 + \beta_1[OH^-] + \beta_2[OH^-]^2)$$
$$= \log K_{ex} + 2\log C(H(C_7H_7)sq)_{(e)} + 2\,pH \quad (4)$$

where $C(H(C_7H_7)sq)_{(e)}$ shows the initial concentration of $H(C_7H_7)sq$ in the extraction phase. Since hydrated neutral complexes are often stabilized as extracted species in several [bmim][PF_6] extraction systems [21,22], it is expected that neutral hydrated complexes are also extracted in this system.

To confirm the extracted species and the extraction equilibria, relationship between $\log D(1 + \beta_1[OH^-] + \beta_2[OH^-]^2)$ of M^{2+} and equilibrated pH at a fixed $C(H(C_7H_7)sq)_{(e)}$ and that between the $\log D(1 + \beta_1[OH^-] + \beta_2[OH^-]^2)$ and $\log C(H(C_7H_7)sq)_{(e)}$ at fixed pH were performed. (The following β_i values for Co^{2+}, Cu^{2+}, Zn^{2+} and Cd^{2+} were used for the calculation: $\log \beta_1 = 4.35$, 6.30, 5.04 and 3.92, and $\log \beta_2 = 9.19$, 10.70, 11.09 and 7.64, respectively [49].) Fig. 3 shows these plots for Co^{2+} and Cd^{2+} as examples. In all cases, the plots showed straight lines of which slopes were close to 2. Namely, also in [bmim][PF_6] system, extraction mechanism for M^{2+} was able to be expressed as Eq. (1). In addition, the discrepancy of Co^{2+} from the line at higher pH region (pH > ca. 7) may be caused by formation of ternary complex among Co^{2+}, $(C_7H_7)sq^-$ and OH^-.

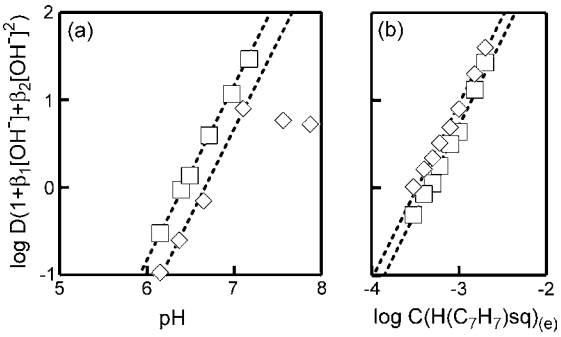


Fig. 3. Plots of the $\log D(1 + \beta_1[OH^-] + \beta_2[OH^-]^2)$ for some divalent metals as a function of the aqueous phase pH (a) and those as that of logarithmic initial concentration of $H(C_7H_7)sq$ in extraction phase (b). Initial $H(C_7H_7)sq$ concentration in extraction phase was 1×10^{-3} mol dm^{-3} on (a), and pH was 7.1 (Co^{2+}) and 7.3 (Cd^{2+}) on (b). The broken line, of which the slope is 2, was obtained by the least squares fitting. Sample: (◊) Co^{2+} and (□) Cd^{2+}.

The $\log K_{ex}$ values in the $H(C_7H_7)sq$–[bmim][PF_6] system calculated from experimental data using Eq. (4) are shown in Table 1 with those in the $H(C_7H_7)sq$–chloroform [34] and the $H(C_7H_7)sq$–toluene [33] systems. The obtained $\log K_{ex}$ values in the [bmim][PF_6] system were 0.4–2.0 log unit higher than those in the chloroform and toluene systems. This tendency was similar to that for Cu^{2+}, Ni^{2+} and Pb^{2+} in use of 4,4,4-trifluoro-1-(2-thienyl)-1,3-butanedione (thenoyltrifluoroacetone, Htta) as extraction reagent [22]. As is well known, solubility of water in [bmim][PF_6] (2.3 wt% [50]) is much higher than that in conventional organic solvent. Namely, also in this case, use of [bmim][PF_6] as extraction phase resulted in relative stabilization of the hydrated species in extraction phase compared with use of chloroform or toluene.

3.2. *H(CH₃)sq and H(CF₃)sq systems*

Fig. 4 shows plots of %*E* of M^{2+} into [bmim][PF_6] extraction phase with $H(CH_3)sq$ and those with $H(CF_3)sq$ as a function

Table 1
Determined $\log K_{ex}$ values for divalent metal cations in $H(C_7H_7)sq$ system (25 ± 1 °C)

Cation	Extraction phase		
	[bmim][PF_6]	Chloroform [34]	Toluene [33]
Co^{2+}	−7.54 ± 0.18	−7.93 ± 0.13	−8.32 ± 0.02
Cu^{2+}	0.83 ± 0.14	0.44 ± 0.04	–
Zn^{2+}	−4.35 ± 0.12	−5.54 ± 0.04	−5.65 ± 0.02
Cd^{2+}	−6.84 ± 0.03	−8.42 ± 0.02	−8.77 ± 0.02

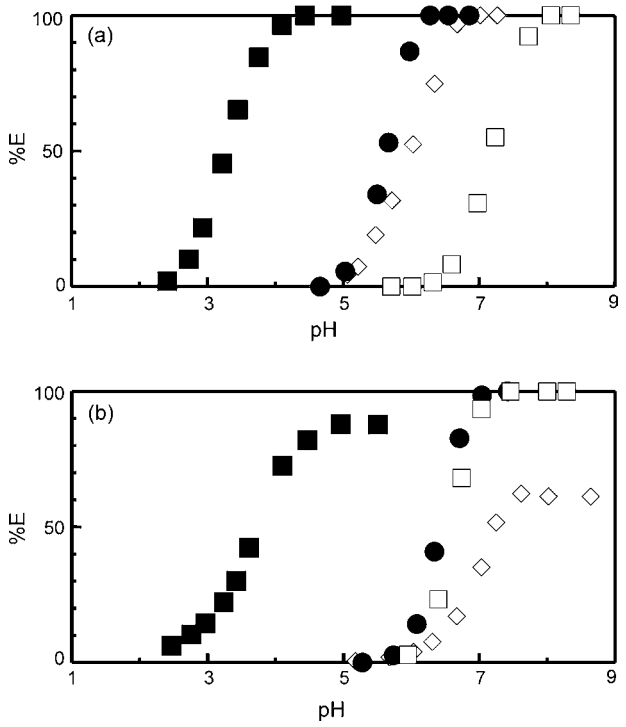


Fig. 4. Plots of the *%E* for some divalent metals as a function of the aqueous phase pH in $H(CH_3)sq$ (a) and $H(CF_3)sq$ (b) systems. Initial extractant concentration in extraction phase was 1×10^{-3} mol dm^{-3}. Extraction phase: [bmim][PF_6]. Sample: (◊) Co^{2+}, (■) Cu^{2+}, (●) Zn^{2+} and (□) Cd^{2+}.

of aqueous phase pH. In use of $H(CH_3)sq$, most metals showed similar extractability compared with that using $H(C_7H_7)sq$ except for Co^{2+}, which showed relatively high extractability. As a result, obtained extraction selectivity order was $Cu^{2+} > Zn^{2+} \geq Co^{2+} > Cd^{2+}$. On the contrary, $H(CF_3)sq$ system showed unique extraction nature. Extractability for Co^{2+}, Cu^{2+} and Zn^{2+} in $H(CF_3)sq$ system was obviously inferior to that in $H(CH_3)sq$ system, whereas that for Cd^{2+} was hardly changed. In this case, obtained extraction selectivity order was $Cu^{2+} > Zn^{2+} \approx Cd^{2+} > Co^{2+}$. In addition, the extraction selectivity in $H(CH_3)sq$–organic solvent system was reported as similar to that in $H(C_7H_7)sq$–organic solvent system [35]. Furthermore, in $H(CF_3)sq$–chloroform system, these metals were not extracted.

To determine the extracted species, relationship between $\log D(1+\beta_1[OH^-]+\beta_2[OH^-]^2)$ of M^{2+} and equilibrated pH at a fixed $C(H(CH_3)sq)_{(e)}$ or $C(H(CF_3)sq)_{(e)}$, and that between the $\log D(1+\beta_1[OH^-]+\beta_2[OH^-]^2)$ and $\log C(H(CH_3)sq)_{(e)}$ or $\log C(H(CF_3)sq)_{(e)}$ at fixed pH were performed. Fig. 5 shows these plots for Zn^{2+} and Cd^{2+} in $H(CF_3)sq$ system as examples. In almost cases, the plots showed straight lines of which slopes were close to 2, showing the extraction mechanism is same as that in $H(C_7H_7)sq$ system. On the contrary, only the exception was Cd^{2+} in $H(CF_3)sq$ system, for which both the plots showed straight lines with slopes close to 3. This result is same as that on extraction of Mn^{2+}, Co^{2+}, Zn^{2+} and Cd^{2+} into ionic liquid extraction phase with Htta [22]. Namely, in the $H(CF_3)sq$–[bmim][PF_6] system, Cd^{2+} was extracted as anionic

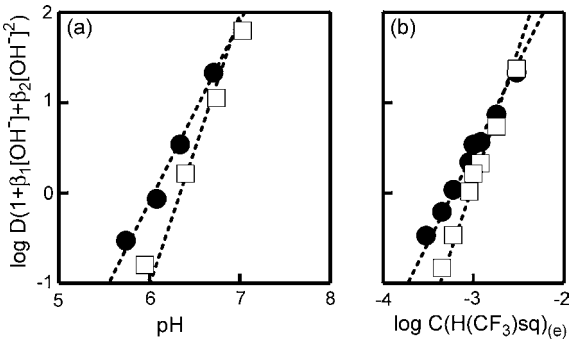


Fig. 5. Plots of the $\log D(1+\beta_1[OH^-]+\beta_2[OH^-]^2)$ for some divalent metals as a function of the aqueous phase pH (a) and those as that of logarithmic initial concentration of $H(CF_3)sq$ in extraction phase (b). Initial $H(CF_3)sq$ concentration in extraction phase was 1×10^{-3} mol dm^{-3} on (a), and pH was 6.3 (Zn^{2+}) and 6.4 (Cd^{2+}) on (b). The broken line, of which the slope is 2 (for Zn^{2+}) or 3 (for Cd^{2+}), was obtained by the least squares fitting. Sample: (●) Zn^{2+} and (□) Cd^{2+}.

1:3 complex as follows:

$$Cd^{2+} + 3H(CF_3)sq_{(e)} + {PF_6}_{(e)}^- \Leftrightarrow Cd[(CF_3)sq]_{3(e)}^- + 3H^+ + PF_6^- \quad (5)$$

$$K_{ex} = \frac{[Cd[(CF_3)sq]_3^-]_{(e)}[H^+]^3[PF_6^-]}{[Cd^{2+}][H(CF_3)sq]_{(e)}^3[PF_6^-]_{(e)}} \quad (6)$$

The solubility of [bmim][PF_6] in water was reported as 6.3×10^{-2} mol dm^{-3} [51], which is far higher than the initial metal concentration, and, therefore, not only the $[PF_6^-]_{(e)}$ value but also the $[PF_6^-]$ value can be regarded as constant in this case. Namely, the following value:

$$K_{ex}' = \frac{K_{ex}[PF_6^-]_{(e)}}{[PF_6^-]} = \frac{[Cd[(CF_3)sq]_3^-]_{(e)}[H^+]^3}{[Cd^{2+}][H(CF_3)sq]_{(e)}^3} \quad (7)$$

can be regarded as a constant.

Table 2 shows the $\log K_{ex}$ values in the $H(CH_3)sq$–[bmim][PF_6] and $H(CF_3)sq$–[bmim][PF_6] systems and the $\log K_{ex}'$ value for Cd^{2+} in the $H(CF_3)sq$–[bmim][PF_6] system calculated from experimental data.

In the $H(CH_3)sq$–[bmim][PF_6] system, why extractability for Co^{2+} was increased is unknown for the present. However, in our preparative experiment, other 8-alkylsulfonamidoquinoline

Table 2
Determined $\log K_{ex}$ and $\log K_{ex}'$ values for divalent metal cations in $H(CH_3)sq$–[bmim][PF_6] and $H(CF_3)sq$–[bmim][PF_6] systems (25 ± 1 °C)

Cation	Extraction reagent	
	$H(CH_3)sq$	$H(CF_3)sq$
$\log K_{ex}$		
Co^{2+}	−5.00 ± 0.23	−7.56 ± 0.22
Cu^{2+}	0.18 ± 0.13	−0.40 ± 0.28
Zn^{2+}	−4.63 ± 0.04	−6.19 ± 0.09
Cd^{2+}	−7.74 ± 0.19	–
$\log K_{ex}'$		
Cd^{2+}	–	−10.03 ± 0.28

systems showed similar nature to the H(CH_3)sq system, whereas other 8-arylsulfonamidoquinolione systems showed similar one to the H(C_7H_7)sq (data not shown).

In the H(CF_3)sq–[bmim][PF_6] system, the obtained log K_{ex} values for Co^{2+}, Cu^{2+} and Zn^{2+} were 0.6–2.6 log unit lower than those in the H(CH_3)sq–[bmim][PF_6] system. In general, fluorine-containing chelate extraction reagents have relatively high acidity and, therefore, have high extractability. However, in this case, existence of very bulky trifluoromethyl group close to N^--donor may result in steric hindrance on coordination of the (CF_3)sq^- to these metal cations to form M[(CF_3)sq]$_2$ complexes.

Most of anionic chelates as extracted species in previous reports contain trifluoromethyl group in extraction reagents, such as Htta [22,52] and other fluorine-containing β-diketones [23]. As well known, general hydrophobic ionic liquids have fluorine-containing anions such as PF_6^-, bis(trifluoromethanesulfonyl)imide and several monoanions having perfluoroalkyl group. Furthermore, several trialkylammonium perfluoroalkyl-β-diketonates shows nature as ionic liquids [53]. From these facts, it was considered that anionic metal chelates with fluorine-containing chelating reagents have high affinity to ionic liquids. In use of the H(CF_3)sq–[bmim][PF_6] system, formation of M[(CF_3)sq]$_3^-$ has disadvantage by the steric hindrance, whereas formed M[(CF_3)sq]$_3^-$ seems to have high stability in the [bmim][PF_6] extraction phase. Since effective ionic radius for Cd^{2+} (CN = 6) is 95 pm and larger than those for Co^{2+} (65–74.5 pm) and Zn^{2+} (74.0 pm) [54], on extraction of bulky Cd^{2+}, the ionic liquid-philic Cd[(CF_3)sq]$_3^-$ seems to be extracted preferably compared with Cd[(CF_3)sq]$_2$.

4. Conclusion

As mentioned above, possible use of several HRsq derivatives such as H(C_7H_7)sq, H(CH_3)sq and H(CF_3)sq as chelate extraction reagents for extraction of several divalent metal cations in ionic liquid chelate extraction system using [bmim][PF_6] was investigated as fundamental study. H(C_7H_7)sq and H(CH_3)sq showed suitable extractability but different extraction selectivity. The extractability of H(CF_3)sq was inferior to that of the fluorine-free derivative because of steric inhibition on the complexation. The extracted species were neutral hydrated complexes generally. However, it is interesting that, in the H(CF_3)sq system, bulky Cd^{2+} was extracted as anionic Cd[(CF_3)sq]$_3^-$. From these results, it was suggested that further investigation concerning use of various HRsq derivatives having different substituents (R) as extraction reagents in the ionic liquid system is an effective approach for optimization of the extraction selectivity in the system. Furthermore, it is expected that selection of an ionic liquid-philic group as R results in much high extractability and extraction capacity for several metals in the ionic liquid chelate extraction.

Although [bmim][PF_6] is an ionic liquid having relatively high cost-performance and its use for fundamental study, its use as extraction solvent has several disadvantages such as its relatively high solubility in water [50] and possible hydrolysis of the PF_6^- anion. From this viewpoint, application of other more stable ionic liquids, such as 1-butyl-3-methylimidazolium bis(trifluoromethanesulfonyl)imide, to these extraction systems seems to be an important research theme.

Acknowledgment

This study was financially supported in part by grant-in-aid for scientific research (no. 18550070) from the Japan Society for the Promotion of Science.

References

[1] J.S. Wilkes, M.J. Zaworotoko, J. Chem. Soc., Chem. Commun. 1992 (1992) 965.
[2] R.D. Rogers, K.R. Seddon (Eds.), Ionic Liquids: Industrial Applications for Green Chemistry, American Chemical Society, Washington, DC, 2002.
[3] R.D. Rogers, K.R. Seddon, S. Volkov (Eds.), Green Industrial Applications of Ionic Liquids, Kluwer, Dordrecht, 2003.
[4] P. Wasserscheid, T. Welton (Eds.), Ionic Liquids in Synthesis, Wiley-VCH, Weinheim, 2003.
[5] H. Ohno (Ed.), Ionic Liquids: The Front and Future of Material Development, CMC, Tokyo, 2003.
[6] R.D. Rogers, K.R. Seddon (Eds.), Ionic Liquids as Green Solvents: Progress and Prospects, American Chemical Society, Washington, DC, 2003.
[7] H. Ohno (Ed.), Electrochemical Aspects of Ionic Liquids, Wiley, New York, 2005.
[8] R.D. Rogers, K.R. Seddon (Eds.), Ionic Liquids III: Fundamentals, Progress, Challenges, and Opportunities, American Chemical Society, Washington, DC, 2005.
[9] P.J. Dyson, T.J. Geldbach, Metal Catalysed Reactions in Ionic Liquids: Catalysis by Metal Complexes, Kluwer, Dordrecht, 2006.
[10] H. Ohno (Ed.), Ionic Liquids II: Marvelous Developments and Colorful Near Future, CMC, Tokyo, 2006.
[11] S.V. Malhotra, Ionic Liquids in Organic Synthesis, American Chemical Society, Washington, DC, 2007.
[12] J.G. Huddleston, H.D. Willauer, R.P. Swatloski, A.E. Visser, R.D. Rogers, Chem. Commun. 1998 (1998) 1765.
[13] S. Dai, Y.H. Ju, C.E. Barnes, J. Chem. Soc., Dalton Trans. 1999 (1999) 1201.
[14] S. Igarashi, T. Yotsuyanagi, Proc. Symp. Solv. Extr. (1989) 51.
[15] S. Igarashi, T. Yotsuyanagi, Mikrochim. Acta 106 (1992) 37.
[16] F. Kubota, M. Goto, Solv. Extr. Res. Dev. Jpn. 13 (2006) 23.
[17] M.L. Dietz, Sep. Sci. Technol. 41 (2006) 2047.
[18] N. Hirayama, Bunseki 2006 (2006) 519.
[19] M.L. Dietz, J.A. Dzielawa, Chem. Commun. 2001 (2001) 2124.
[20] G.-T. Wei, Z. Yang, J.-C. Chen, Anal. Chim. Acta 488 (2003) 183.
[21] N. Hirayama, JAERI-Conf, 2003-021, 2004, p. 103.
[22] N. Hirayama, M. Deguchi, H. Kawasumi, T. Honjo, Talanta 65 (2005) 255.
[23] N. Hirayama, M. Deguchi, T. Honjo, Solv. Extr. Res. Dev. Jpn. 13 (2006) 83.
[24] H. Luo, S. Dai, P.V. Bonnesen, Anal. Chem. 76 (2004) 2773.
[25] H. Luo, S. Dai, P.V. Bonnesen, A.C. Buchanan III, J. Alloy Comp. 418 (2006) 195.
[26] K. Shimojo, H. Naganawa, F. Kubota, M. Goto, Chem. Lett. 35 (2006) 484.
[27] M. Takagi, T. Omori, S. Matsuo, S. Matsuno, K. Ueno, S. Ide, Chem. Lett. 1980 (1980) 387.
[28] Y.C. Hoh, C.H. Wang, J. Chem. Technol. Biotechnol. 31 (1981) 345.
[29] C.H. Wang, Y.C. Hoh, Hydrometallurgy 8 (1982) 161.
[30] S. Ide, T. Yoshida, S. Matsuno, M. Takagi, K. Ueno, Anal. Chim. Acta 149 (1983) 235.
[31] S. Ide, M. Takagi, Anal. Sci. 2 (1986) 265.
[32] K. Yoshizuka, K. Kondo, F. Nakashio, J. Chem. Eng. Jpn. 19 (1986) 396.
[33] J.M. Castresana, M.P. Elizalde, M. Aguilar, M. Cox, Chem. Scr. 27 (1987) 273.

[34] N. Hirayama, N. Sugisaka, J. Taga, S. Oshima, T. Honjo, Anal. Sci. 19 (2003) 321.
[35] A. Sakoguchi, E. Zushi, F. Nakashio, Solv. Extr. Res. Dev. Jpn. 8 (2001) 95.
[36] N. Bicak, S. Sungur, M. Gazi, N. Tan, Sep. Sci. Technol. 38 (2003) 201.
[37] A. Almela, M. Huebra, M.P. Elizalde, B. Menoyo, J. Chem. Technol. Biotechnol. 79 (2004) 299.
[38] Y. Moriguchi, T. Yoshimatsu, M. Takagi, K. Ueno, Bunseki Kagaku 31 (1982) 318.
[39] H. Nakamura, T. Yoshida, M. Todoko, K. Ueno, M. Takagi, Bull. Chem. Soc. Jpn. 57 (1984) 2839.
[40] Y. Moriguchi, T. Yoshida, M. Takagi, Bunseki Kagaku 33 (1984) 435.
[41] E. Uhlig, M. Döring, Z. Anorg. Allg. Chem. 492 (1982) 52.
[42] M. Döring, A. Heppener, E. Uhlig, B. Undeutsch, K. Gloe, P. Mühl, Z. Anorg. Allg. Chem. 556 (1988) 204.
[43] H. Kido, M. Maeda, M. Takagi, Bull. Chem. Soc. Jpn. 66 (1993) 432.
[44] N. Hirayama, J. Taga, S. Oshima, T. Honjo, Anal. Chim. Acta 466 (2002) 295.
[45] C. Squires, C.W. Baxter, J. Campbell, L.F. Lindoy, H. McNab, A. Parkin, S. Parsons, A.A. Tasker, G. Wei, D.J. White, Dalton Trans. 2006 (2006) 2026.
[46] C. Kato, N. Sugisaka, E. Hirasawa, S. Oshima, N. Hirayama, Solv. Extr. Res. Dev. Jpn. 14 (2007) 171.
[47] C. Kato, S. Oshima, N. Hirayama, J. Ion Exch., in press.
[48] J.H. Billman, R. Cherin, Anal. Chem. 34 (1962) 408.
[49] S. Kotrlý, L. Šůcha, Handbook of Chemical Equilibria in Analytical Chemistry, Ellis Horwood, Chichester, 1985.
[50] J.L. Anthony, E.J. Maginn, J.F. Brennecke, J. Phys. Chem. B 105 (2001) 10942.
[51] S. Carda-Broch, A. Berthod, D.W. Armstrong, Anal. Bioanal. Chem. 375 (2003) 191.
[52] M.P. Jensen, J. Neuefeind, J.V. Beitz, S. Skanthakumar, L. Soderholm, J. Am. Chem. Soc. 125 (2003) 15466.
[53] O.D. Gupta, B. Twamley, J.M. Shreeve, Tetrahedron Lett. 45 (2004) 1733.
[54] R.D. Shannon, Acta Cryst. A32 (1976) 751.

Available online at www.sciencedirect.com
ScienceDirect
Talanta 74 (2008) 844–850
Talanta
www.elsevier.com/locate/talanta

Determination of the spectroscopic properties and chromatographic sensitivities of substituted quinones by hexachlorate(IV) oxidation of hydroquinones☆

Guadalupe Albarran[a,b], Robert H. Schuler[b,*]

[a] *Instituto de Ciencias Nucleares, UNAM, Circuito Exterior C.U., 04510 Mexico, D.F., Mexico*
[b] *Radiation Laboratory, University of Notre Dame, Notre Dame, IN 46556, United States*

Received 7 May 2007; received in revised form 16 July 2007; accepted 17 July 2007
Available online 21 July 2007

Abstract

HPLC studies of the oxidation of substituted hydroquinones show that the corresponding quinones can, in most cases, be produced quantitatively by two electron transfer to hexachloroiridate(IV). As a consequence the chromatographic and spectroscopic properties of substituted quinones that are not readily available can be determined without the necessity of preparation of an isolatable sample. Absorption spectra and extinction coefficients of bromoquinone, chloroquinone, hydroxyquinone and carboxyquinone anion at pH 7 are reported as illustrative examples. All have intense absorption bands at ∼250 nm that are characteristic of quinones. Oxidation of carboxyhydroquinone at low pH is, however, anomalous in that a hydroxylated carboxyquinone is produced as the result of four electron transfer to hexachloroiridate.
© 2007 Elsevier B.V. All rights reserved.

Keywords: Quinone spectra; HPLC sensitivities of substituted quinones; Oxidation of hydroquinones; Hexachloroiridate(I) oxidation

1. Introduction

During the course of HPLC studies of the radiolytic oxidation of hydroxylated aromatics [1] we have had need for the spectroscopic and chromatographic properties of substituted quinones that are unstable or otherwise not readily available as references. The present study explores the application of HPLC to determine the needed information by hexachloroiridate(IV) oxidation of substituted hydroquinones. This study shows that oxidation of hydroquinone to quinone by two electron transfer to hexachloroiridate is without complications and is quantitative. This finding is in accord with electrochemical studies [2] that also show that oxidation of most hydroquinones proceeds via a two electron transfer process. As a result it is expected that in the absence of complicating secondary or side reactions the relative extinction coefficients and chromatographic sensitivities of substituted quinones can be determined by comparison of the increase in their HPLC signals with the reduction of the signals of the related hydroquinone on addition of hexachloroiridate(IV). Absolute values can then be obtained based on values for the extinction coefficients of the hydroquinones determined spectrophotometrically. Details of the present studies are given below.

2. Experimental

2.1. Sample preparation

The hydroquinones, reference quinones and potassium hexachloroiridate(IV) were from Aldrich. Chromatographic analysis showed that the available samples of bromo- and chlorohydroquinone contained ∼3% hydroquinone as an impurity. The other hydroquinones were free of any significant impurities. In most cases solutions of the hydroquinones were prepared in water acidified with formic acid (0.001–0.01 M) to minimize spurious oxidation. After addition of an appropriate amount of the hexachloroiridate, water was added to give a solution 200 μM in hydroquinone. The resultant samples were analysed immediately by HPLC. Carboxyhydroquinone (gentisic acid;

☆ Presented at 11th Latin American Congress on Chromatography and Related Techniques, Merida, Yucatan, Mexico, 26–30 June 2006.

* Corresponding author. Tel.: +1 574 631 7502; fax: +1 574 531 8968.
E-mail address: schuler.1@nd.edu (R.H. Schuler).

0039-9140/$ – see front matter © 2007 Elsevier B.V. All rights reserved.
doi:10.1016/j.talanta.2007.07.012

2,5-dihydroxybenzoic acid), that has a pK_a of ∼3, was oxidized both at pH 2 and its anionic form at pH 7 in 10 mM phosphate buffer.

2.2. Chromatography

A Waters Millennium system, equipped with a 996 diode array detector, was used to collect 3D chromatographic data from 200 to 550 nm every 100 ms. Spectra and chromatograms were extracted from these 3D records at appropriate elution times and wavelengths. Separation was isocratic on a Phenomenex 150 mm × 4.7 mm Luna C_{18} column. The eluent was an acidified water-methanol mixture (usually 85:15) at a flow rate (F) of 0.5 cm^3/min. Injection volumes (V) were 100 μl. Areas of the chromatographic peaks (A_λ), in units of absorbance seconds, were determined using the Millennium software. Where reference samples were available the chromatographic sensitivities ($S_\lambda = A_\lambda/[Q]$) were determined from the areas of the appropriate peaks and known concentrations [Q]. In cases where reference samples were not available sensitivities were determined with the decrease of the concentration of the source compound taken as the measure of the product's concentration.

In chromatographic studies the sensitivity is directly proportional to the extinction coefficient of the component of interest (E_λ), the effective optical length of the absorption cell (L) and the injection volume and inversely proportional to the eluent flow rate, i.e., $S_\lambda = E_\lambda LV/F$. For constant chromatographic conditions $S_\lambda/E_\lambda = LV/F$ is common so that where reference compounds were not readily available measurements of the sensitivities, as indicated above, provided values of their extinction coefficients. In our studies comparison of sensitivities with extinction coefficients measured spectrophotometrically gave a value of 10.25 ± 0.2 for LV/F pertinent to the values of V and F given above. This value indicates that the effective optical length of the absorption cell is 0.91 cm.

2.3. Spectrophotometry

Spectra recorded using a Hewlett-Packard 8453A diode array spectrophotometer provided a direct measure of the spectra and extinction coefficients of the hexachloroiridates, hydroquinones and available quinones. Complications in the chromatography can occur if there is any readily oxidizable material left on the column from previous analyses. While this problem is avoided in spectrophotometric studies such studies alone provide only limited information on the oxidation process because the absorptions of the chloroiridates overlap with the UV bands of most hydroquinones and quinones. Detailed examination requires application of a separation method such as HPLC.

3. Results

3.1. Spectra of the hexachloroiridates

Solutions of potassium hexachloroiridate(IV), where iridium is in its oxidized state (i.e., Ir^{4+}), were examined in the absence of aromatics both spectroscopically and chromographically. Hexachloroiridate(IV) has an intense absorption below 250 nm. It is readily reduced to hexachloroiridate(III) (i.e., Ir^{3+}) that also has an intense band at short wavelengths. In our experiments these hexachloroiridates co-elute so that measurements at short wavelengths do not provide adequate information on the relative concentrations of the two oxidation states of iridium. However, at is seen in Fig. 1, the reduced form of hexachloroiridate absorbs much less in the region above 300 nm than does its oxidized form. At 488 nm the extinction coefficient of hexachloroiridate(IV) is ∼1000 M^{-1} cm^{-1} and that of hexacholoroiridate(III) a 100-fold less.

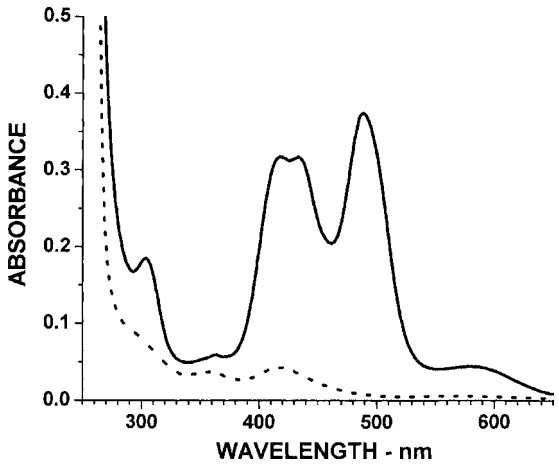


Fig. 1. Spectra recorded spectrophometrically (solid) for 400 μM hexachloroiridate(IV) and (dashed) for 400 μM hexachloroiridate(III). The latter was prepared by reducing 400 μM hexachloroiridate(IV) with hydroquinone.

3.2. Titration experiments

The relatively strong signal of hexachloroiridate(IV) at 488 nm suggests that spectrophotometric measurements at 488 nm can be used as an endpoint in what is in effect a titration of the oxidizable components in a sample, i.e., that appearance of a significant signal at ∼500 nm indicates that oxidation is complete. Such an application is illustrated in Fig. 2 where extrapolation of the absorption at 488 nm determined spectrophotometrically indicates that addition of two equivalents (400 μM) of hexachloroiridate is required to oxidize 200 μM hydroquinone. The observed discontinuity demonstrates that the oxidation of hydroquinone is relatively simple and involves transfer of two electrons to the hexachloroiridate. This result is, of course, expected since electrochemical studies have shown that oxidation of most hydroquinones is a two electron process [2]. On addition of an excess of hexachloroiridate the absorbance in Fig. 2 at 488 nm parallels that observed in the absence of hydroquinone, indicating that the titration is not complicated by oxidation of the quinone initially produced. Similar results were obtained for most of the other substituted hydroquinones examined in the present study. The oxidation mechanism is more complicated in the case of 2,5-dihydroxybenzoic acid (see below) which provides an example where electrochemical studies have indicated that oxidation of hydroquinones substituted

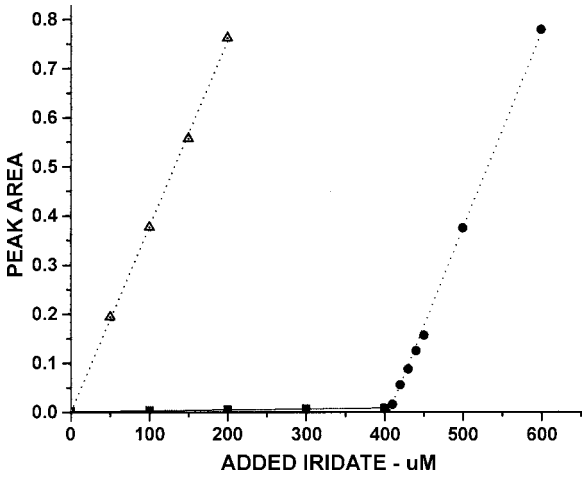


Fig. 2. Area of peak at 488 nm as a function of added hexachloroiridate(IV) for solutions initially containing (triangles) no hydroquinone and (squares and circles) 200 μM hydroquinone. In the latter case the discontinuity at 400 μM shows that oxidation is complete when two equivalents of hexachloroiridate(IV) have been added.

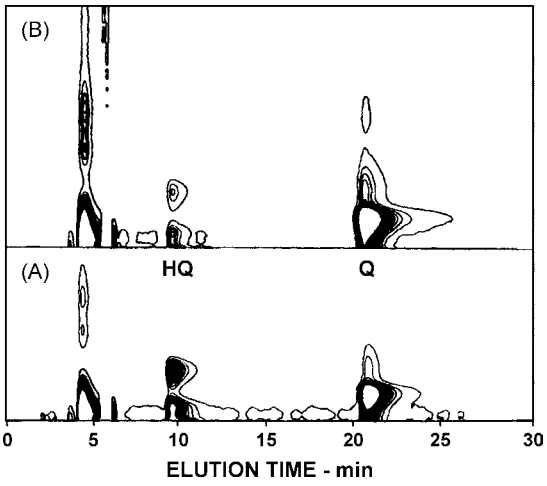


Fig. 4. Contour plots of chromatographic data for a solution initially containing 200 μM hydroquinone after addition of (A) 200 μM or (B) 400 μM hexachloroiridate(IV). The hexachloroiridates co-elute at 4.3 min, hydroquinone (HQ) at 9.3 min and quinone (Q) at 20.5 min.

with an electron withdrawing group may be more complicated and require additional oxidant [3,4].

3.3. Chromatographic studies

The three following examples, where reference samples were available, serve as tests of the approach used here.

3.3.1. Quinone

Hexachloroiridate oxidation of hydroquinone represents the simplest test in that there are no substituents to complicate the chemistry. The expected oxidation product, quinone, is readily identified in the chromatographic experiments by its strong absorption at 247 nm that is identical to that of a reference sample. As is seen in Fig. 3 an absorption band in the 250 nm region is characteristic of simply substituted quinones. All quinones show an additional band at a longer wavelength with the 295 nm band of quinone being very weak and that for hydroxyquinone at 388 nm being relatively more intense. Fig. 3 also shows that a bromine substituent has a substantially greater effect on the absorption spectrum than does a chlorine substituent.

Typical contour plots obtained in the chromatographic experiments, recorded after addition of 200 and 400 μM hexachloroiridate to 200 μM hydroquinone, are displayed in Fig. 4. These plots show that the only significant product is quinone. It is seen in Fig. 4B that only a trace of hydroquinone remains after addition of 400 μM hexachloroiridate.

The dependences of the relative area of the quinone and hydroquinone peaks on added hexachloroiridate(IV), determined from chromatograms extracted at the 290 nm hydroquinone and 247 nm quinone maxima, are given in Fig. 5. The hydroquinone consumption data, scaled by the ratio of the absolute values of the slopes (8.15), are given by the stars to indicate better their linearity and intercept with the *x*-axis. This figure shows that the consumption of hydroquinone and production of quinone are linearly dependent on the amount of hexachloroiri-

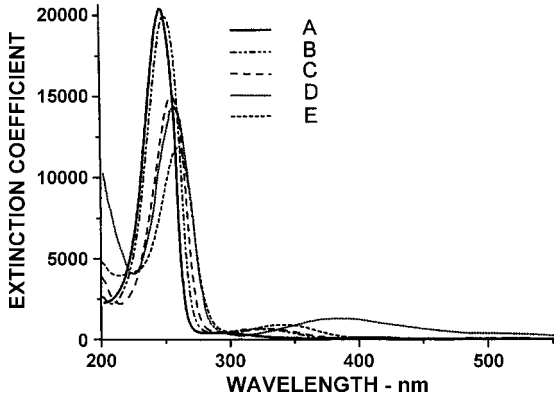


Fig. 3. Absorption spectra of chromatographically resolved (A) quinone; (B) methylquinone; (C) chloroquinone; (D) hydroxyquinone and (E) bromoquinone.

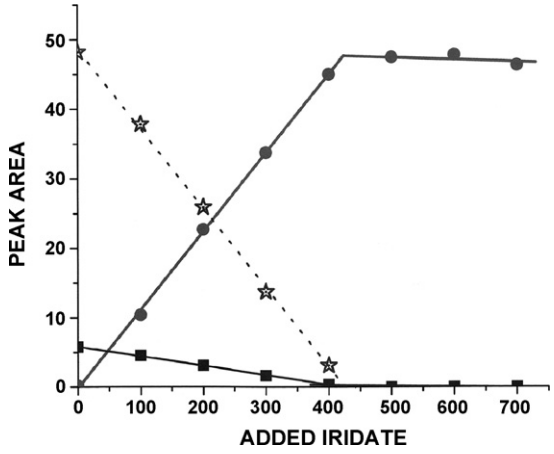


Fig. 5. Dependence on μM added hexachloroiridate(IV) of peak areas (squares) for hydroquinone at 290 nm and (circles) for quinone at 247 nm at their chromatographic maxima. The stars represent the hydroquinone data scaled by their ratio of the slopes.

Table 1
Extinction coefficients of quinones

QUINONE	Q slope	HQ slope	Ratio	λ max (nm) $Q-HQ$	ξ HQ UV	ξ Q HPLC	ξ Q UV
Benzoquinone	0.1096	−0.01345	8.15	247–290	2,530	20,620	20,600
Methyl-BQ	0.09661	−0.01375	7.02	250–290	2,845	19,990	20,170
1,4-Naphtho-Q	0.11649	−0.10919	1.06	252–243	22,150	23,480	23,320
Chloro-BQ	0.08329	−0.01846	4.51	257–295	3,320	14,970	–
Bromo-BQ	0.06846	−0.02056	3.33	262–295	3,550	11,820	–
Hydroxy-BQ	0.06567	−0.01581	4.15	258–290	3,160	13,130	–
Carboxy-hydroxy-BQ	0.04760	−0.01143	4.17	257–325	3,880	16,200	–
Carboxy-BQ anion	0.08157	−0.02127	3.83	247–318	4,085	15,670	–

date added and that oxidation is complete after addition of two equivalents of hexachloroiridate. It also shows that the quinone formed is not affected by further addition of hexachloroiridate. Multiplying the extinction coefficient of hydroquinone at 290 nm as measured spectrophotometrically (2530 M^{-1} cm^{-1}) by the ratio of the slopes (8.15) an extinction coefficient of 20,620 M^{-1} cm^{-1} is obtained for quinone at its 247 nm maximum. This value is in excellent agreement with its value of 20,600 M^{-1} cm^{-1} (cf. Table 1) determined spectrophotometrically on a reference sample during the present study and with values of 20,600 M^{-1} cm^{-1} previously reported by Land [5] and 20,842 M^{-1} cm^{-1} by Chen and Pignatello [6]. This agreement shows that the oxidation is quantitative. The low energy band of quinone at 295 nm has an extinction coefficient of 350 M^{-1} cm^{-1}.

3.3.2. Methylquinone

Hexachloroiridate oxidation of methylhydroquinone is virtually identical to that of hydroquinone. As indicated in Fig. 3 the methyl substituent has only a minor effect on the 247 nm band of quinone, shifting its maximum to 250 nm. The dependences of the concentrations of methylquinone and methylhydroquinone on added hexachloroiridate are, as expected, similar to those given in Fig. 5. Complete oxidation requires two equivalents of the iridate. In this case the ratio of the slopes for formation of methylquinone and consumption of methylhydroquinone is 7.02. Taking the spectrophotometrically measured extinction coefficient of methylhydroquinone at 290 nm as 2845 M^{-1} cm^{-1}an extinction coefficient of 19,990 M^{-1} cm^{-1} is obtained for the 250 nm absorption of methylquinone, only slightly lower than that for the unsubstituted quinone but in good agreement with the value determined spectrophotometrically on a reference sample (cf. Table 1). The low energy band of methylquinone has a maximum at 325 nm with an extinction coefficient of 560 M^{-1} cm^{-1}.

3.3.3. Naphthoquinone

A further example of the approach used here is provided by the hexachloroiridate oxidation of 1,4-dihydroxynapthalene to produce 1,4-naphthoquinone. The naphthoquinone spectrum observed in these chromatographic studies is essentially identical to that obtained spectrophotometrically. In this case quantitative studies of the hexachloroiridate oxidation were found to be somewhat complicated because the concentration of oxygen in air saturated water (0.25 mM) is comparable to that of the 1,4-dihydroxynaphthalene used. Because this dihydroxynaphthalene is readily oxidized during the preparation of solutions it was necessary to purge the water with helium before addition of the oxidant. With this precaution consumption of the dihydroxynaphthalene was found to be complete after addition of two equivalents of the hexachloroiridate. Consumption of the dihydroxynaphthalene and production of 1,4-naphthoquinone at their 243 and 252 absorption maxima were found to be linearly dependent on the concentration of added hexachloroiridate in much the same way as in the case of hydroquinone. From the ratio of the slopes of these dependences (1.06) and the relatively high extinction coefficient of 1,4-dihydroxynaphthalene at 243 nm the extinction coefficient for naphthoquinone at 252 nm was determined to be 23,480 M^{-1} cm^{-1}. This value agrees very well with the extinction coefficient of 23,320 M^{-1} cm^{-1}determined spectrophotometrically on a reference sample (cf. Table 1).

The following provide examples where reference samples were not available from the usual commercial sources.

3.3.4. Chloroquinone and bromoquinone

The chromatographic studies of the hexachloroiridate oxidation of chlorohydroquinone and bromohydroquinone showed that the principal products have spectral maxima in the 257–262 nm region (cf. Fig. 3) that identify these oxidation products as chloroquinone and bromoquinone. Small amounts (∼3%) of quinone were also produced as a result of oxidation of the hydroquinone impurity indicated in the experimental section. No other products were observed in the chromatographic studies.

The dependences of the concentrations of the haloquinones and consumption of the halohydroquinones on added hexachloroiridate(IV) are very similar to the dependences given in Fig. 5. In both cases oxidation was complete on addition of two equivalents of the iridate, indicating that the halogen substituents did not participate in the oxidation. The extinction coefficients for the haloquinones given in Table 1 were determined from the relative slopes for production of the haloquinone and consumption of the halohydroquinone and the spectrophotometrically determined extinction coefficients of the latter. It is seen in Fig. 3 that chloroquinone has a low energy band that overlaps with the similar band of methylquinone. It also has an extinction coefficient of 560 M^{-1} cm^{-1} at 325 nm. The band of bromoquinone at 345 nm (860 M^{-1} cm^{-1}) is somewhat more intense than that for chloroquinone. These haloquinones were not oxidized fur-

ther by addition of excess hexachloroiridate and appear to be stable.

3.3.5. Hydroxyquinone

The spectroscopic and chromatographic characteristics of hydroxyquinone are of special interest in that this quinone is produced as a secondary product in the radiolytic oxidation of phenol [1]. Bohuslavek and co-workers prepared hydroxyquinone by auto oxidizing 1,2,4-trihydroxybenzene and found that it has an absorption band at ~262 nm. However, they did not report any extinction coefficients [7]. Chromatographic studies carried out during the present investigation show that hydroxyquinone is readily produced as the sole product in the hexachloroiridate oxidation of 1,2,4-trihydroxybenzene. Its absorption band at 258 (cf. Fig. 3) shows it to be a quinone but is somewhat broader than that of quinone. It also has a broad and moderately intense band at 388 nm that distinguishes it from other quinones. Time resolved Raman studies [8] have shown that the intermediate semiquinone radical is fully protonated at pH 2 so the hydroxyl substituent in hydroxyquinone is not expected to be ionized at low pH.

The dependences of the production of hydroxyquinone and consumption of trihydroxybenzene on added hexachloroiridate show that oxidation is complete after addition of two equivalents of hexachloroiridate. An extinction coefficient of 13,130 M^{-1} cm^{-1} at 258 nm is obtained from the ratio of their slopes (4.15) and the extinction coefficient of 3160 M^{-1} cm^{-1} at 290 nm for 1,2,4-trihydroxybenzene determined spectrophotometrically. The hydroxyquinone band at 388 nm has an extinction coefficient of 1260 M^{-1} cm^{-1}.

During these studies it was found that hydroxyquinone is slowly reduced ($t_{1/2}$~100 min) to the starting trihydroxybenzene. This reduction has little effect on the interpretation of the data but indicates the importance of initiating analysis immediately after addition of the hexachloroiridate.

3.3.6. Oxidation of carboxyhydroquinone at pH 7

The properties of carboxyquinone are of interest because it is expected to be produced as a secondary product in the radiolysis of salicylic acid solutions [9]. Because of the anomaly described below in the oxidation of carboxyhydroquinone at pH 2, its oxidation was also studied at pH 7 where carboxyhydroquinone is in its anionic form. The only significant oxidation product observed in the chromatographic studies at the higher pH has the spectrum given in Fig. 6 with a quinone like band at 247 nm and a moderately intense band at 333 nm that distinguishes its spectrum from that of quinone. It also has a distinctly different retention time than quinone. This product is presumably carboxyquinone in its anionic form.

At pH 7 the dependences of the concentrations of carboxyhydroquinone and carboxyquinone anions on added hexachloroiridate are very similar to those illustrated in Fig. 5. Both the consumption of carboxyhydroquinone and production of the quinone anion are linearly dependent on the concentration of added hexachloroiridate. Oxidation is virtually complete on addition of two equivalents of hexachloroiridate. Based on the data given in Table 1 the extinction coefficients of the carboxyquinone anion are 15,670 and 700 M^{-1} cm^{-1} at 247 and 333 nm. The latter band is similar in intensity to the 340 nm band of bromoquinone.

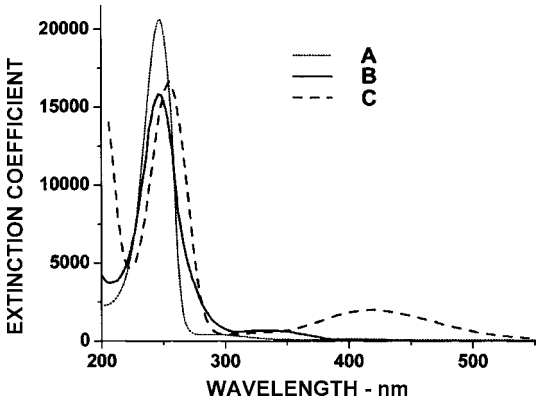


Fig. 6. Absorption spectra of (A) quinone, (B) carboxyquinone anion at pH 7 and (C) 2-carboxy-3-hydroxyquinone (at pH 2).

3.3.7. Oxidation of carboxyhydroquinone at pH 2

Oxidation of carboxyhydroquinone at pH 2, where it is mainly in its neutral form, has proven to be considerably more complicated than the examples given above. Its oxidation is anomalous in that titration experiments similar to those illustrated in Fig. 2 shows that complete oxidation of carboxyhydroquinone requires four equivalents of hexachloroiridate. This finding is in accord with the report by Papouchado and co-workers [3,4] who used cyclic voltammetry to examine the electrochemical oxidation of carboxyhydroquinone and found that transfer of four electrons was involved. They suggested that the carboxysemiquinone radical expected to be produced in the initial two electron oxidation was hydroxylated in a second two electron oxidation step. This suggestion is borne out by the results reported below.

In our studies HPLC analysis of samples immediately after addition of hexachloroiridate showed that the principal product has a spectrum that is distinctly different from that observed at pH 7 (cf. Fig. 6). It absorbs strongly at 257 nm, indicating it to be a quinone. As shown in Fig. 6 it also has a broad and relatively intense band at 418 nm. Upon addition of four equivalents of oxidant it is virtually the only significant product. The relative intensities of these bands at their maxima are in the ratio of 4.18:1. Its spectrum is essentially identical to the spectrum reported by Holmes and co-workers [10] for 2-carboxy-3-hydroxyquinone with absorption maxima at 255 and 417 nm with relative intensities of 4.2:1. Holmes and coworkers also showed that its mass spectrum exhibited an ion of mass 168, demonstrating that carboxyquinone (mass 152) had been hydroxylated. This comparison identifies the product observed in the chromatographic experiments as 2-carboxy-3-hydroxyquinone. We also have found that on standing this product decarboxylates to form hydroxyquinone, confirming that the initial product contained a hydroxyl group.

An extra product that has absorptions at 247 and 323 nm was observed to be produced as an intermediate in chromatographic studies where oxidation was incomplete. The intensities of these

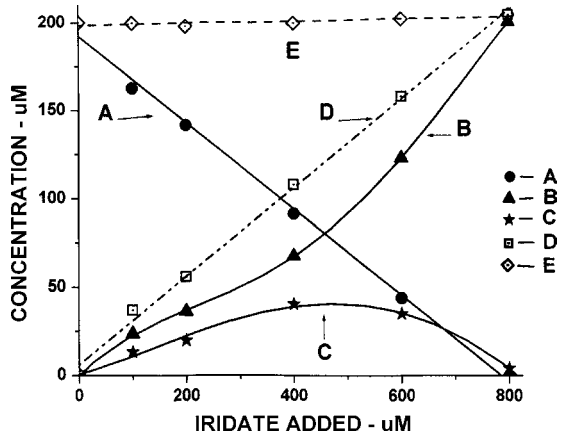


Fig. 7. Dependences of the concentrations on adding hexachloroiridate to 200 μM carboxyhydroquinone of (A) carboxyhydroquinone, (B) 2-carboxy-3-hydroxyquinone, (C) the 247 nm intermediate and (E) the total of A, B and C. Dashed curve D gives the sum of B and C. The solid lines represent optimized fits of the data to fourth order polynomials.

bands are in a ratio of 2.8:1. These maxima are similar to those reported by Holmes and co-workers for carboxyquinone. However, the similarity of these maxima to the 257 maximum of 2-carboxy-3-hydroxyquinone and the 328 nm maximum of carboxyhydroquinone suggests that this intermediate may possibly be a hydrone complex containing both of these moieties. Further studies are needed to provide positive identification of this intermediate.

Fig. 7 displays the dependences of the concentrations of (A) carboxyhydroquinone, (B) 2-carboxy-3-hydroxyquinone and (C) the 247 nm intermediate on addition of hexachloroiridate. Curve A shows that, as is also indicated by the titration experiments, oxidation is complete on addition of four equivalents of oxidant. It is seen that the dependences of B and C are very non-linear with the latter being a somewhat skewed parabola with a maximum on addition of ∼2.15 equivalents of hexachloroiridate. Curve D shows that the total of B and C is linearly dependent on the added oxidant with, however, oxidation only ∼50% complete on addition of two equivalents of hexachloroiridate. Oxidation of the intermediate and the remaining carboxyhydroquinone requires an additional two equivalents.

While the complications described above are of considerable mechanistic interest they have no effect on the comparisons involved in the determination of the extinction coefficients of 2-carboxy-3-hydroxyquinone as long as oxidation is quantitative. The relative areas of the absorption of 2-carboxy-3-hydroxyquinone and carboxyhydroquinone determined chromatographically (4.18:1) at their 257 and 325 nm peaks, multiplied by the extinction coefficient of the latter gives an extinction coefficient of 16,200 M^{-1} cm^{-1} for 2-carboxy-3-hydroxyquinone at 257 nm. It's rather strong absorption at 418 nm has an extinction coefficient of 1780 M^{-1} cm^{-1}.

In Fig. 7 the concentration of the 247 nm intermediate at its maximum, ∼38 μM, is only 19% of the total. Taking this into account, comparison of the intensities of its bands at 255 and 338 nm with that of carboxyhydroquinone at 325 nm gives values of 9800 and 3500 M^{-1} cm^{-1}, respectively, for the extinction coefficients of these bands. The ratio of these extinction coefficients (2.80) is similar to the ratio of 2.9 reported by Holmes and co-workers [10] for these bands that they assigned to carboxyquinone. Further experiments are in order to confirm the identity of this intermediate as carboxyquinone.

Because 2-carboxy-3-hydroxyquinone was known to be quite unstable [3] chromatographic data were recorded at 20 min intervals after addition of four equivalents of hexachloroiridate. Contour plots of these data show that 2-carboxy-3-hydroxyquinone is initially the only significant product but that on standing it decarboxylates with a half period ∼60 min to produce hydroxyquinone. As in the case of hydroxyquinone this decarboxylation emphasizes the importance of initiating analysis immediately after addition of the oxidant.

4. Discussion and summary

Hexachloroiridate oxidation of most hydroquinones is found, as expected, to involve transfer of two electrons to the oxidant. The mechanism of this oxidation is discussed extensively by Pelizzetti, Mentasti and Balocchi [11]. In acidic solutions the initial oxidation produces a neutral semiquinone radical. A quinone is then produced on oxidation of this semiquinone.

The spectra given in Figs. 3 and 6 show that simply substituted quinones have a strong and characteristic absorption band in the 250 nm region. Substitution tends to shift this maximum to the red with a decrease in intensity. To some extent the observed shifts and differences in intensities reflect the effect of a substituent on the electronic structure of the quinone moiety. In particular comparison of the spectra of chloro- and bromo-quinone shows the substantially greater effect of a bromine substituent than that of a chlorine substituent. All quinones studied show broad and modestly intense bands at longer wavelengths with those of hydroxyquinone at 383 nm and 2-carboxy-3-hydroxyquinone at 418 nm being the most intense.

Oxidation of carboxyhydroquinone at pH 2 is a special case and considerably more complicated than oxidation of the other hydroquinones studied. At this pH the carboxyl group apparently stabilizes the initial neutral semiquinone radical sufficiently that hydroxylation competes favorably with its ionization. As a result the second oxidation step produces the observed 2-carboxy-3-hydroxyquinone as the result of transfer of two additional electrons. The studies of Papouchado and co-workers [3,4] indicate that other electron withdrawing groups may exhibit similar complications.

The results obtained for oxidation of hydroquinone, methylhydroquinone and 1,4-dihydroxynaphthalene indicate that in the absence of complications the extinction coefficients and chromatographic sensitivities of most substituted quinones can be determined to better than a few percent. Because the extinction coefficients of the intermediate produced in the case of carboxyhydroquinone was determined under conditions of partial oxidation they are subject to substantially greater uncertainty.

In summary HPLC studies of the hexachloroiridate(IV) oxidation of hydroquinones can be used to determine the chro-

matographic sensitivities of many quinones that are unstable or otherwise not readily available without the necessity of isolating a measurable sample. We emphasize here that while the details of the oxidation mechanism are critically dependent on the relative rates of the different oxidation and ionization processes and worthy of further investigation they are of little concern in the application being discussed that only requires the oxidation to produce the quinone quantitatively.

Acknowledgements

Research described herein was supported by the Office of Basic Energy Sciences of the U.S. Department of Energy and by the Instituto de Ciencias Nucleares-UNAM. This is contribution NDRL-4721 from the Notre Dame Radiation Laboratory.

References

[1] G. Albarran, R.H. Schuler, J. Phys. Chem. A 111 (2007) 2507.
[2] D. Sazou, N. Papadopoulos, Can. J. Chem. 64 (1996) 11.
[3] L. Papouchado, G. Petrie, J.H. Sharp, R.N. Adams, J. Am. Chem. Soc. 90 (1968) 5620.
[4] L. Papouchado, G. Petrie, R.N. Adams, J. Electroanal. Chem. 38 (1972) 389.
[5] E.J. Land, J. Chem. Soc., Faraday Trans. 89 (1993) 803.
[6] R. Chen, J.J. Pignatello, Environ. Sci. Technol. 31 (1997) 2399.
[7] J. Bohuslavek, S. Chanama, R.L. Crawford, L. Xun, Biodegradation 16 (2005) 353.
[8] L. Qin, G.N.R. Tripathi, R.H. Schuler, J. Phys. Chem. 91 (1987) 1905.
[9] G. Albarran, R.H. Schuler, Radiat. Phys. Chem. 67 (2003) 279.
[10] T.J. Holmes Jr., V. John, J. Vennerstrom, K.E. Choi, J. Org. Chem. 49 (1984) 4736.
[11] E. Pelizzetti, E. Mentasi, C. Baiocchi, J. Phys. Chem. 80 (1976) 2979.

Available online at www.sciencedirect.com
ScienceDirect
Talanta 74 (2008) 1060–1065
Talanta
www.elsevier.com/locate/talanta

Short communication

Comparison of different water-miscible solvents for the preparation of plasma and urine samples in metabolic profiling studies

Muhammed Alzweiri [a,*], David G. Watson [a], Chris Robertson [b], Graeme J. Sills [c], John A. Parkinson [d]

[a] *Strathclyde Institute for Pharmaceutical and Biomedical Sciences, Strathclyde University, 27 Taylor Street, Glasgow G4 0NR, United Kingdom*
[b] *Department of Statistics and Modelling Science, University of Strathclyde, 26 Richmond Street, Glasgow G1 1XH, United Kingdom*
[c] *Epilepsy Research Unit, University Division of Cardiovascular and Medical Sciences, Western Infirmary, Glasgow G11 6NT, United Kingdom*
[d] *WestCHEM, Department of Pure and Applied Chemistry, University of Strathclyde, 295 Cathedral Street, Glasgow G1 1XL, United Kingdom*

Received 8 May 2007; received in revised form 14 July 2007; accepted 30 July 2007
Available online 14 August 2007

Abstract

The Lowry method and a capillary electrophoresis method were used to analyse protein residues in the supernatant after solvent deproteination of plasma. Acetonitrile and acetone were much more effective than methanol and ethanol at reducing the levels of proteins in plasma. The ability of different solvents to decrease levels of phospholipids in plasma samples was assessed using electrospray ionisation mass spectrometry (MS). Phospholipid signals can obscure differences between samples in general metabolite profiling (i.e. non-target compound) studies. Acetonitrile was much more effective than methanol in reducing the MS signal due to phospholipids in plasma which is a consequence of the poor solubility of phospholipids in acetonitrile. The capability of the solvents at reducing salts in urine samples was also studied by using an amperometric method. Using this approach little difference was detected between methanol, ethanol, acetonitrile and acetone in their ability to desalt urine samples.
© 2007 Elsevier B.V. All rights reserved.

Keywords: Deproteination; Phospholipids; Capillary electrophoresis; Desalting; LC–MS; Profiling studies; Metabonomics

1. Introduction

The analysis of biological samples using liquid chromatography coupled with mass spectroscopy detection (LC–MS), in particular for metabolite profiling studies, requires protein-free and/or salt-reduced preparations [1,2]. Metabonomics is an example of profiling studies concerned with finding the variability in metabolites among a collection of biological samples, followed by classification of the samples according to any revealed variability. Besides ultrafiltration and solid phase extraction, which are expensive and low-recovery deproteination procedures [3], precipitation of proteins from serum or plasma samples can be carried out by adding salts, some acids or water-miscible organic solvents [3–9]. Although all of these procedures can be used in discarding proteins prior to analysis by nuclear magnetic resonance (NMR) spectroscopy, addition of water-miscible organic solvent might be the best method prior to liquid chromatography mass spectrometry because it decreases electrolytes instead of increasing them. This should improve the MS sensitivity and avoid instrument capillary blockage. In addition, solvent deproteination has the advantage of better analyte recovery over the other methods [3,4]. In case of urine samples, some researchers prefer to reduce the salt in samples by further diluting them with water or with any water-miscible solvent [10].

In addition to removing proteins and salts from biological samples, we have found during our metabonomic studies that it is also often essential to remove phospholipids or to reduce their original concentrations because their strong signals may obscure other more important biomarkers and they tend to appear as background peaks throughout the chromatogram. In addition, they lack the reproducible responses required in MS analysis [11]. They might be consequently considered as false biomarkers by the statistical tools used for calculating the variability among biological samples as part of profiling studies. Added to this the phospholipids' ionic character can lead to further ion suppression during mass spectroscopy (MS) analysis [12].

* Corresponding author.
E-mail address: Muhammed_h_Z@yahoo.com (M. Alzweiri).

0039-9140/$ – see front matter © 2007 Elsevier B.V. All rights reserved.
doi:10.1016/j.talanta.2007.07.037

In order to assess the effect of the solvent on the biological sample composition, four semipolar solvents were used in this study, namely: methanol, ethanol, acetone and acetonitrile. A number of publications have mentioned comparing studies of analyte recovery using different semipolar solvents, but little data are reported on the evaluation of solvents for removing undesirable biological molecules before introducing samples into the LC–MS systems.

The Lowry test, a colorimetric protein-general test was used to measure all types of protein remaining in the sample liquor after discarding the majority of the proteins [13–16]. Capillary electrophoresis (CE) can be used to carry out more specific protein analysis [17–21] and in the current work was able to resolve the albumin peak as a major protein from the other proteins in the deproteinated plasma samples. However, the semipolar solvents precipitated certain amounts of salts from the urine samples; the remaining salts in the sample supernatant would be expected to govern the electrical current properties of the final preparation after subtracting the blank contribution. Integrated mode pulse amperometry was chosen to measure the amount of salt remained in the samples because it is possible to hold the integration period of the current induced by salts at a constant potential for a certain time period during the pulse [22]. Then the waveform finishes with a reductive potential in order to clean away any oxides accumulated over the gold electrode during the course of the measurements [23,24]. Additionally, the integrated mode of detection provides a compensatory mechanism for any likely aging of the electrode during the analysis period [23]. Finally, Soya lecithin, which is a common phospholipid standard material [25–28] was mixed with a constant volume of each semipolar solvent under controlled conditions, in order to measure the solubility of lecithin in each solvent. The weight difference between the undissolved lecithin before and after the experiment was utilized to measure phospholipids' solubility in each solvent. The results are also supported by a mass spectrometry infusion study.

In this work, common water-miscible solvents were compared according to their ability in removing proteins, salts and phospholipids from the plasma and urine. Protein removal from plasma samples was analysed by using the Lowry method and a capillary electrophoresis (CE) method. The urine desalting ability of the solvents was evaluated by an integrated pulse amperometry technique. Finally, gravimetric analysis and direct infusion into the mass spectrometer were used in evaluating the remaining phospholipid content in the samples.

2. Experimental

2.1. Chemicals and materials

Methanol, acetonitrile, formic acid (98%) and water of HPLC grade were purchased from VWR International Ltd. (Lutterworth, UK). Acetone, absolute ethanol and sodium hydroxide pellets were purchased from Riedel-deHaën (Germany). Hexadimethrine bromide (polybrene), ammonium formate 97%, bovine serum albumin, copper(II) sulphate hydrate, Folin-Ciocalteu's phenol reagent 2 N, potassium sodium (+)-tartarate, l-α-phosphatidyl choline (l-α-Lecithin) Type IV-S from soyabean, sodium chloride and sodium carbonate were purchased from Sigma–Aldrich (Poole, UK). Syringe filters 4 mm in diameter with 0.45 μm pore size, a PVDF membrane and a polypropylene housing having only 0.125 cm^2 surface area were purchased from Whatman International Ltd. (England). Polyvar Microscope (Leica, Germany) was used to examine the precipitate under bright field light. Pictures were taken by the colour video digital camera JVC TK-12080E (JVC, Japan).

Blank plasma samples were obtained from the blood bank at Gartnavel General Hospital (Glasgow, UK), and stored at −20 °C prior to use.

2.2. Capillary electrophoresis (CE) and Lowry test

A HP 3D CE capillary electrophoresis unit was used with Chemstation® software version 10.03 for data acquisition (Agilent Technologies, Waldbronn, Germany) equipped with a UV diode array detector. The UV detection was carried out at a wavelength of 206 nm. The cell bandwidth was 4 nm. The applied voltage was set at 12 kV, the separation was carried out under a negative polarity mode (i.e. from negative to positive), and injection was carried out hydrodynamically at 50 mbar pressure for 3 s. The column used was a bare fused silica capillary (Polymicro Technologies, Phoenix, AZ, USA) having an internal diameter of 50 μm, a total length of 33.5 cm and effective length of 25 cm. The temperature of the column was kept constant at 25 °C during the analysis period. Prior to analysis, the column was flushed for 10 min with a 0.25 M NaOH solution followed by a 10 min flush with ammonium formate buffer (25 mM, pH 3.5). Finally the column was flushed for 15 min with polybrene, a polycationic polymer (1%, w/v solution), for coating the silica surface, followed by a final flush with ammonium formate buffer (25 mM, pH 3.5) for 10 min. The Lowry test was carried out according to its original reference [29].

2.3. Sample preparation for analysis by capillary electrophoresis (CE)

Plasma (0.3 ml) was vortexed in a 1.5 ml eppendorf tube with the same volume as one of the water-miscible solvents. The samples were centrifuged for 10 min at room temperature and 7000 rpm. Following this 0.3 ml from the supernatant was mixed with 0.7 ml of distilled water. Exceptionally, the samples treated with either ethanol and methanol were further diluted 25 times with distilled water. Then they were filtered through 0.45 μm syringe filters. Standard preparations were made by dissolving bovine serum albumin in distilled water to achieve the following concentrations: 0.8, 0.16, 0.032 and 0.006 mg/ml.

2.4. Determination of phospholipid solubility

The experiment was carried out in a Clifton water bath equipped with a shaking stage. The parameters were 25 ± 1 °C and 300 St/min. Twelve 5 ml dried and screw-capped glass vials

were weighed and labelled according to the samples' ID. 100 mg of lecithin was added into each glass vial with 2 ml of a water-miscible organic solvent, the capped vials were enveloped with parafilm sheets, and then the samples were immersed in a suitable rack into the water bath.

The samples were shaken for 30 min, then removed from the water bath and their external surfaces wiped clean. Previously weighed filter caps (made in-house) were substituted with the original vial caps and the solutions were filtered with the aid of suction. Subsequently, the vials and caps were left under a fume hood overnight to guarantee drying to completion. Finally they were weighed to establish the weight of undissolved lecithin in each sample, which was then subtracted from the original weight in order to calculate the amount of phospholipid dissolved in 2 ml of solvent.

The results of the solubility experiment were supported by analysing plasma samples using direct infusion mass spectrometry (LCQ, Finnigan Mat). The analysis was carried out by using electropray ionisation in the positive mode with a capillary temperature of 250 °C, sheath gas flow 40 ml/min, zero auxiliary gas and scan range (150–2000)*m/z*. The infusion flow was 10 μl/min. The data of 32 scans was averaged for each sample. Twelve plasma samples were prepared from the same plasma stock by adding 100 μl into a 1.5 ml eppendorf tube and then the same volumes of either acetonitrile or methanol were added into the sample tube. Then the contents was vortex centrifuged for 10 min at 7000 rpm. Following this 100 μl of the supernatant was diluted to 1 ml using either acetonitrile or methanol. Finally, the samples were filtered through 0.45 μm syringe filters before infusion into the MS system. Lecithin reference solution was prepared by dissolving lecithin in methanol to a concentration of 1 μg/ml.

2.5. Comparison of salt content in the urine following addition of water-miscible organic solvents

The urine samples were collected from source and kept in the freezer at −20 °C until use. The stock urine samples were thawed then centrifuged at 2 °C for 10 min and 4000 rpm to remove suspended particles and salt agglomerates. The supernatants were taken up immediately, and then supernatants were kept on the bench for 15 min to equilibrate to room temperature. 0.5 ml of the solvents was added to 0.5 ml of each urine sample. Subsequently, each sample was vortex mixed and centrifuged for 10 min at 4000 rpm. Then 0.25 ml of the resultant solution was diluted to a total volume of 25 ml with HPLC grade water. For each solvent three samples were prepared.

Blank samples were also prepared according to the same procedure but 0.5 ml of HPLC grade water was used instead of urine. An ED 50 electrochemical detector (Dionex, UK) equipped with a titanium-body amperometry cell with a gold working electrode and Ag/AgCl reference electrode was used in integrated amperometry mode. The waveform was selected to apply a constant potential during the integration period and to end up with a reducing potential for cleaning the working electrode from the oxidised materials. To obtain the results as an area under the curve (AUC) for the detector signals, the detector was attached with a Spectra System P100 HPLC pump (Spectra-Physics) fitted with a 20 μl loop Rheodyne injector, and with a DP700 integrator (Fisons instruments). During the analysis, the pump flow rate was maintained at 1 ml/min of HPLC water. Standard solutions of sodium chloride in HPLC water with concentrations 0.2–10 mg/100 ml were prepared.

3. Results and discussion

3.1. Protein determination

In the CE analysis the experimental parameters and conditions were selected carefully to prevent adsorption of large proteins like albumin onto the surface of the fused silica capillary. In order to accomplish this, polybrene, which is a pH-independent cationic polymer, was used to coat the inner wall of the silica capillary, and the pH of the analysis buffer ensured that albumin, which has an isoelectric point of 4.9 [30], was positively charged during the analysis. Fig. 1 shows a good peak shape for both bovine serum albumin (BSA) in the standard preparation and human serum albumin (HSA) in some of the precipitated plasma test solutions. The BSA peak migrated slightly earlier than HSA due to some slight structural differences between the proteins. The humps preceding the albumin peak are interpreted as other proteins present in the plasma. The Lowry test, which is a general spectrophotometric protein test, was used to quantify total protein in the plasma samples. Although the plasma samples deproteinated by methanol and ethanol were 25 times more dilute than the samples treated by either acetone or acetonitrile, the albumin peaks were still larger in the case of both methanol and ethanol. Albumin is the main protein in the plasma [30] and it is clear from the electropherograms in Fig. 1 that acetonitrile and acetone are much stronger deproteinisers than methanol and

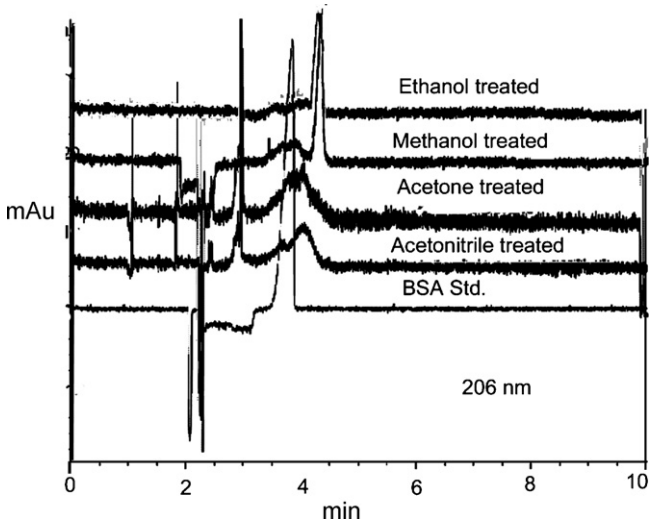


Fig. 1. Capillary electrophoresis traces showing the amount of HSA left in plasma following treatment with different water-miscible solvents in comparison with a BSA standard.

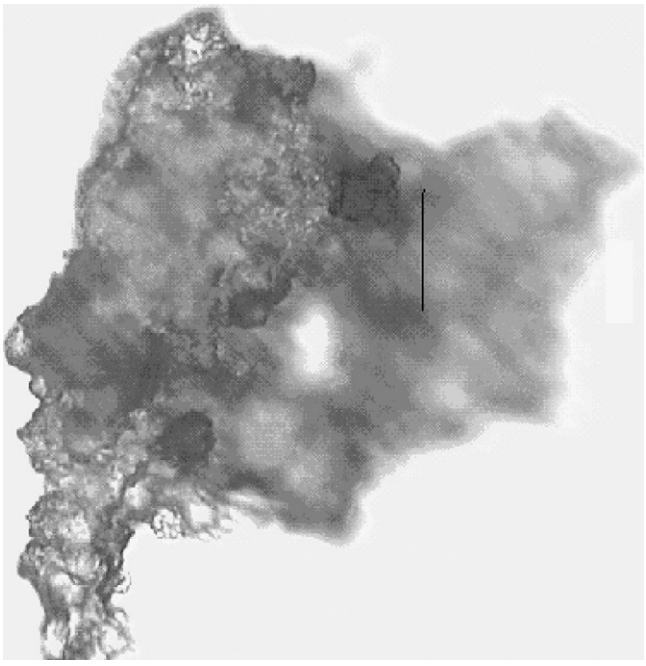


Fig. 2. Microscope picture of protein precipitated from plasma by acetonitrile (1:1). The precipitate forms an agglomerate.

ethanol. Acetonitrile and acetone have higher dielectric constant in comparison with methanol and ethanol [31] and lower viscosity. These two physical parameters control the association and dissociation forces between water and organic solvents on the one hand, and between proteins and solvent mixtures on the other. This will lead to different precipitation mechanisms for proteins according to the solvent used. Fig. 2 shows a microscopical image for a plasma sample treated with acetonitrile where the precipitation appears as a well-compacted mass, while methanol (Fig. 3) produces a precipitation like a fine suspension. The amount of albumin remaining in the sample supernatant after precipitating 1 ml of plasma with 1 ml of the solvent according to analysis by CE was 23 mg/ml for methanol and 18 mg/ml for ethanol, while the concentration was below the limit of detection (6.4 μg/ml) in the case of acetonitrile and acetone.

The Lowry test is widely used for protein analysis [32]. BSA Standard solutions showed good linearity within the range 25–200 μg/ml. According to this test the amount of protein remaining in 1 ml plasma supernatant, treated with the same volume of methanol, ethanol, acetone and acetonitrile, was calculated to be 22.5, 15.7, 2.7 and 2.25 mg/ml, respectively. The results of this test are not far from those taken from the electrophoretic analysis. This is expected because the albumin is the dominant protein in plasma [3]. In conclusion, acetone and acetonitrile are much better than methanol and ethanol for protein elimination from plasma samples.

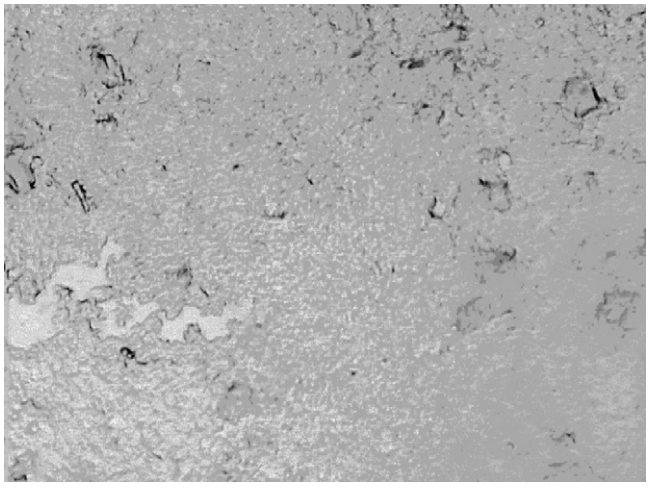


Fig. 3. Microscope picture of protein precipitated from plasma by methanol (1:1). The precipitate forms small particles.

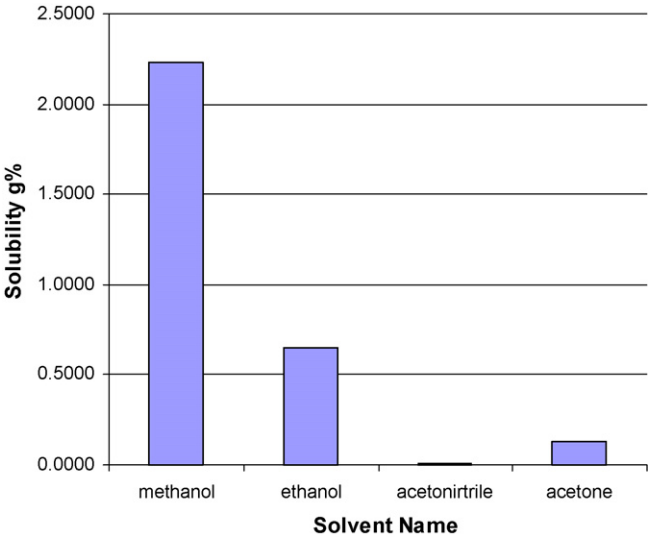


Fig. 4. Solubility of lecithin in four different water-miscible solvents.

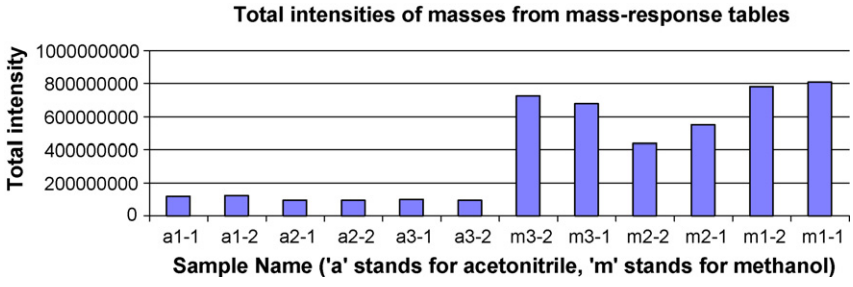


Fig. 5. Comparison of phospholipid mass spectral intensity for plasma samples treated with acetonitrile or with methanol.

3.2. Phospholipid determination

Lecithin, which is used as a standard for the analysis of phospholipids, is a complex mixture [25]. Its components lack a distinct chromophore. Thus gravimetry was chosen as a method for assessing phospholipid solubility in the water-miscible solvents. This solubility experiment was designed to make sure that the sample vials and their caps were weighed at the beginning and at the end of the experiment in order to subtract their weights upon calculation of the amount of undissolved lecithin. The amount of lecithin dissolved in methanol, ethanol, acetone or acetonitrile was calculated by taking the difference of lecithin weight remaining in the samples after carrying out the solubility study and the original weight of lecithin in each sample. The results are shown in Fig. 4. The solubility of lecithin in methanol under the described conditions was 22.3 mg/ml and in acetonitrile was 0.12 mg/ml. In order to confirm the results obtained on the solubility of phospholipids, plasma samples precipitated with either methanol or acetonitrile were infused into the mass spectrometer. The total intensity response plot for plasma samples (Fig. 5) shows that the plasma samples precipitated with methanol have much higher response for the phospholipid ions, which dominate in the total ion count (TIC) in comparison with those treated with acetonitrile. Moreover, it is shown in Fig. 6 that the vast majority of peaks in the infused plasma sample charts are related to phospholipids; lecithin standard solution showed four main peak clusters, around 500, 800, 1300 and 1600*m/z*. The peaks around 500 and 800*m/z* are for phospholipid monomers and those around 1300 and 1600*m/z* are due to hetero- and homodimers of the phospholipid molecules. The large peak clusters observed in plasma samples are located at the same mass ranges as those in the lecithin standard. Acetonitrile precipitated plasma has low responses in the region around 1300 and 1600*m/z*. This might be explained by the fact that, acetonitrile has slightly higher dielectric constant and lower viscosity than methanol. This will improve droplet dispersion in the electrospray ionization (ESI) process [31] thus reducing cluster formation.

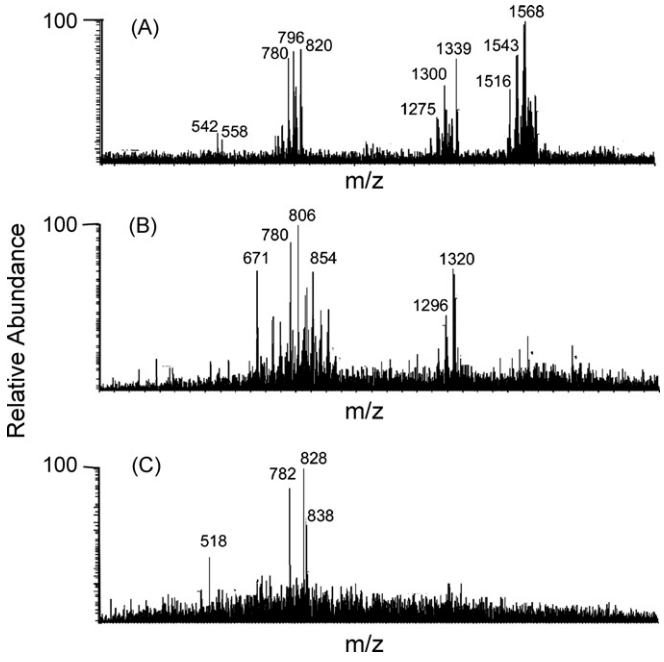


Fig. 6. Direct infusion mass spectra: (A) phospholipids in lecithin, (B) phospholipids in methanol treated plasma and (C) phospholipids in acetonitrile treated plasma.

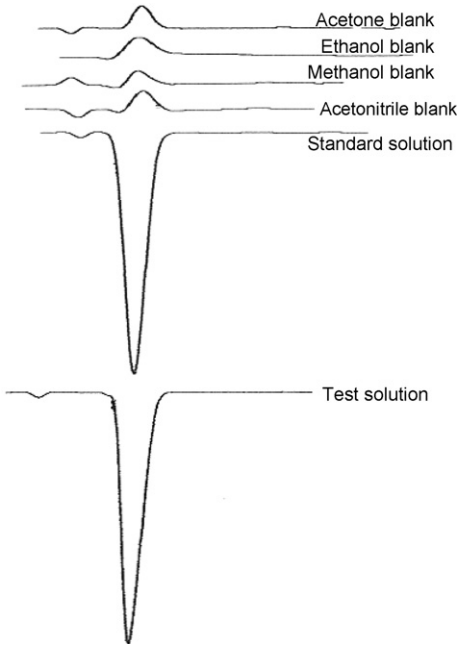


Fig. 7. Peaks obtained from urine samples treated with different organic solvents using an ED50 amperometric detector. Blank solutions have a small negative response, while the sample and the standard have clear positive peaks.

3.3. Salt determination

The ED50 detector was used to measure the amount of salt in the urine following treatment with one of the water-miscible solvents. The peak areas obtained (Fig. 7) were used to measure the salt content. Blank samples show small negative peaks participating in measurement error, which was not exceeding 5%. The linearity between the concentration of salt and the response by using ten different concentrations of sodium chloride was linear in a narrow range 1–5 mg%, so the test samples were diluted to have peak areas within this range. If the average response of acetone-desalted samples is assumed to be 100%, then acetonitrile, methanol and ethanol possessed 101.3, 79.6 and 80.9%, respectively. Thus methanol and ethanol show slightly higher desalting ability.

References

[1] H.C. Keun, Pharmacol. Ther. 109 (2006) 92.
[2] J.I. Castrillo, A. Hayes, S. Mohammed, S.J. Gaskell, S.G. Oliver, Phytochemistry 62 (2003) 929.
[3] C.A. Daykin, P.J.D. Foxall, S.C. Connor, J.C. Lindon, J.K. Nicholson, Anal. Biochem. 304 (2002) 220.
[4] S. Souverain, S. Rudaz, J.L. Veuthey, J. Chromatogr. A 61 (2004) 1058.
[5] S. Souverain, S. Rudaz, J.L. Veuthey, J. Pharm. Biomed. Anal. 35 (2004) 913.

[6] H. Jalalizadeh, E. Souri, M.B. Tehrani, A. Jahangiri, J. Chromatogr. B 854 (2007) 43.
[7] C. Georgita, F. Albu, V. David, A. Medvedovici, J. Chromatogr. B 854 (2007) 211.
[8] M. Zhou, X. Chen, D. Zhong, J. Chromatogr. B 854 (2007) 219.
[9] C. Ekhart, A. Gebretensae, H. Rosing, S. Rodenhuis, J.H. Beijnen, A.D.R. Huitema, J. Chromatogr. B 854 (2007) 345.
[10] R. Plumb, J. Granger, C. Stumpf, I.D. Wilson, J.A. Evans, E.M. Lenz, Analyst 128 (2003) 819.
[11] M. Koivusalo, P. Haimi, L. Heikinheimo, R. Kostiainen, P. Somerharju, J. Lipid Res. 42 (2001) 663.
[12] J. Hayakawa, Y. Okabayashi, J. Pharm. Biomed. Anal. 35 (2004) 583.
[13] D.H. Beezhold, D.A. Kostyal, V.J. Tomazic-Jezic, Methods 27 (2002) 46.
[14] L.F. Capitan-Vallvey, O. Duque, G. Miron-Garcia, R. Checa-Moreno, Anal. Chim. Acta 433 (2001) 155.
[15] O.H. Lowry, N.R. Rosebrough, A.L. Farr, R.J. Randall, J. Biol. Chem. 193 (1951) 265.
[16] A.L. Winters, F.R. Minchin, Anal. Biochem. 346 (2005) 43.
[17] K.D. Altria, J. Pharm. Biomed. Anal. 31 (2003) 447.
[18] J.R. Catai, H.A. Tervahauta, G.J. de Jong, G.W. Somsen, J. Chromatogr. A 185 (2005) 1083.
[19] R.W. Chiu, J.C. Jimenez, C.A. Monnig, Anal. Chim. Acta 307 (1995) 193.
[20] A. Eckhardt, I. Miksik, Z. Deyl, J. Charvatova, J. Chromatogr. A 111 (2004) 1051.
[21] V. Sanz-Nebot, F. Benavente, E. Balaguer, J. Barbosa, Electrophoresis (2003) 883–891.
[22] J. Wang, Talanta 56 (2002) 223.
[23] K. Sato, J.-Y. Jin, T. Takeuchi, T. Miwa, K. Suenami, Y. Takekoshi, S. Kanno, J. Chromatogr. A 919 (2001) 313.
[24] J.-W. Lee, I.-H. Yeo, Microchemi. J. 70 (2001) 173.
[25] M.O. Taha, H. Abdel-Halim, M. Al-Ghazawi, E. Khalil, Int. J. Pharm. 295 (2005) 135.
[26] R. Szucs, K. Verleysen, G.S.M.J.E. Duchateau, P. Sandra, B.G.M. Vandeginste, J. Chromatogr. A 738 (1996) 25.
[27] M. Sznitowska, E.A. Dabrowska, S. Janicki, Int. J. Pharm. 246 (2002) 203.
[28] H. Bunjes, M.H.J. Koch, J. Control. Rel. 107 (2005) 229.
[29] O. Lowry, N. Rosebrough, L. Farr, R. Randall, J. Biol. Chem. 193 (1951) 265–275.
[30] C.Z. Huang, W. Lu, Y.F. Li, Y.M. Huang, Anal. Chim. Acta 556 (2006) 469.
[31] L. Charles, D. Pepin, F. Gonnet, J.C. Tabet, J. Am. Soc. Mass Spectrom. 12 (2001) 1077.
[32] R. Kumar, A.K. Shukla, E. Bagga, S. Kumari, R.P. Bajpai, L.M. Bharadwaj, Anal. Biochem. 336 (2005) 132.

Available online at www.sciencedirect.com
ScienceDirect
Talanta 74 (2008) 851–859
Talanta
www.elsevier.com/locate/talanta

Development of a voltammetric procedure for assay of the antihistamine drug hydroxyzine at a glassy carbon electrode: Quantification and pharmacokinetic studies

A.M. Beltagi [a,*], O.M. Abdallah [b], M.M. Ghoneim [c]

[a] *Chemistry & Physics Department, Faculty of Education, Kafr El-Sheikh, University, 33516 Kafr El-Sheikh, Egypt*
[b] *Analytical Chemistry Department, Faculty of Pharmacy (Girls), Al-Azhar University, Nasr City, Cairo, Egypt*
[c] *Analytical Chemistry Research Unit, Chemistry Department, Faculty of Science, Tanta University, 31527 Tanta, Egypt*

Received 9 May 2007; received in revised form 17 July 2007; accepted 17 July 2007
Available online 20 July 2007

Abstract

An electrochemical study of hydroxyzine at a glassy carbon electrode was carried out in the Britton–Robinson universal buffer of pH 2–11. Hydroxyzine was oxidized in a single two-electron irreversible process controlled mainly by adsorption. A simple, sensitive and time-saving square-wave adsorptive anodic stripping voltammetric procedure has been developed for determination of hydroxyzine in its commercial tablets and human serum without prior extraction. The optimized procedural conditions were: frequency = 120 Hz, scan increment = 10 mV, pulse-amplitude = 25 mV, accumulation potential = −0.3 V, accumulation time = 90–300 s and a Britton–Robinson universal buffer of pH 4 as a supporting electrolyte. Mean recoveries of 100.5 ± 0.71 and 98.6 ± 1.12% ($n = 5$) were achieved for assay of hydroxyzine in Atarax® 10 and 25 mg dosage forms, respectively. Limit of detection of 1.5×10^{-8} mol L^{-1} (5.624 ng mL^{-1}) and limit of quantitation of 5.0×10^{-8} mol L^{-1} (18.746 ng mL^{-1}) were achieved in human serum with a mean recovery of 98.4 ± 1.22%, without prior extraction of the drug. Moreover, the described procedure was applied for evaluating the pharmacokinetic parameters of hydroxyzine in plasma of two healthy volunteers after administration of a single oral dose (Atarax®—25 mg).
© 2007 Elsevier B.V. All rights reserved.

Keywords: Hydroxyzine; Atarax® tablets; Square-wave stripping voltammetry; Glassy carbon electrode; Quantification; Pharmacokinetics

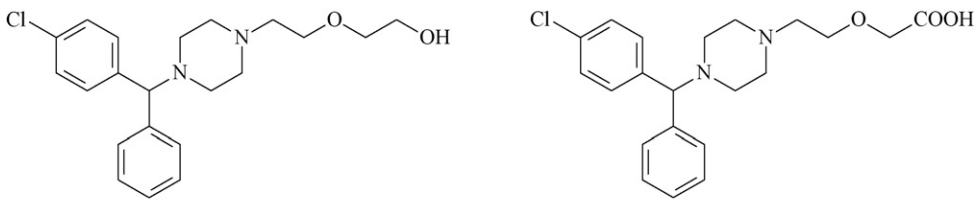
1. Introduction

Hydroxyzine hydrochloride (Scheme 1), (*RS*)-2-{2-[4-(*p*-chloro-α-phenylbenzyl)piperazin-1-yl]ethoxy}ethanol, is a piperazine antihistamine acting by diminishing the main action of histamine by competitive reversible blockade of histamine receptors sites H_1 in the tissues. It has bronchodilator activity, antihistaminic and analgesic effects with mild antianxiety action which is beneficial in the treatment of bronchial asthma. It is used also in the treatment of nervous and emotional conditions to help control anxiety and in some cases to relax patients before surgery [1–3]. Hydroxyzine can be administered orally as hydroxyzine hydrochloride or hydroxyzine embonate or as an intramuscular injection as hydroxyzine hydrochloride. When given orally, hydroxyzine is rapidly absorbed from the gastro-intestinal tract. Hydroxyzine diffuses throughout the body, but higher concentrations can be found in the skin than in the plasma. It is metabolised in liver through oxidation of the alcohol moiety to a carboxylic acid [1]. The main metabolite (45%) is the cetirizine (Scheme 1), (*RS*)-2-[4-(4-chlorobenzhydryl)piperazine-1-yl]ethoxyacetic acid, which acts also as an antihistamine. Hydroxyzine's half-life is on average 14 h for adults, but it can be as low as 5 h for small children and over 30 h for elderly people. Hydroxyzine is excreted into the urine almost wholly as metabolite [4].

Various analytical methods have been reported in literature for determination of hydroxyzine in its pharmaceutical preparations and human serum. These include high-performance liquid chromatography [5,6], thin-layer chromatography [7], micellar-liquid chromatography [8], capillary zone electrophoresis [9], potentiometry [10] and conductimetric titration [11] methods. The official USP method available for the assay of the drug in tablets employs a chromatographic system equipped with a UV-detector, where hydroxyzine can be detected at 232 nm [12].

* Corresponding author. Tel.: +20 12 3350872; fax: +20 40 3350804.
E-mail address: ambeltagi@hotmail.com (A.M. Beltagi).

0039-9140/$ – see front matter © 2007 Elsevier B.V. All rights reserved.
doi:10.1016/j.talanta.2007.07.009



Hydroxyzine Cetirizine

Scheme 1.

Most of the reported methods require sample pretreatment and extraction of the drug prior to the analysis. To date no electrochemical method is available in literature for determination of hydroxyzine.

In the present paper, a validated square-wave adsorptive anodic stripping voltammetric procedure was described for determination of hydroxyzine in pharmaceuticals and human serum without the necessity for prior drug extraction. The utility of the developed procedure in a preliminary clinical study for estimation of the pharmacokinetic parameters of hydroxyzine in plasma of healthy volunteers following an oral administration of a single oral dose of 25 mg hydroxyzine was also demonstrated.

2. Experimental

2.1. Instrumentation

The Electrochemical Analyzers Models 394 and 263A-PAR (Princeton Applied Research, Oak Ridge, TN, USA) were used for the voltammetric measurements. The electrode assembly (Model 303A-PAR) incorporated with a micro-electrolysis cell of three electrode system comprising of a glassy carbon disk electrode (G0197-PAR, 7 mm^2 surface area) as a working electrode, an $Ag/AgCl/KCl_s$ reference electrode and a platinum wire counter electrode, was used. Stirring of the solution in the micro-electrolysis cell was performed using a magnetic stirrer (305-PAR) with a star-shaped magnet to provide the convective transport during the preconcentration step. The whole measurements were automated and controlled through the programming capacity of the apparatus. The data were treated through a personal computer connected to the potentiostat and loaded with the 394 Analytical voltammetry software version 2.01—copyright© 1994 (PAR).

A Mettler balance (Toledo-AB104, Greifensee, Switzerland) was used for weighing the solid materials. A pH-meter (Crison, Barcelona, Spain) was used for the pH measurements of the supporting electrolytes. An Eppendorf centrifuge (Model 5417 C, Hamburg, Germany) was used for separation of the precipitated proteins from human serum samples prior to the assay. A micropipetter (Eppendorf—Multipette® plus) was used for transferring of the reactant solutions throughout the present experimental work. The de-ionized water used throughout the present study was supplied from a Purite-Still Plus de-ionizer connected to an AquaMatic bi-distillation water system (Hamilton Laboratory Glass Ltd., Kent, UK).

2.2. Solutions

2.2.1. Supporting electrolytes

Britton–Robinson (B–R) universal buffer of pH 2–11, acetate buffer (pH 4.5–5.5), phosphate buffer (pH 2–7.5), sodium chloride (0.1 M) and sodium nitrate (0.1 M) were prepared in de-ionized water and were used as supporting electrolytes. All chemicals used were of analytical grade and were used without further purification.

2.2.2. Solutions of bulk hydroxyzine and cetirizine hydrochlorides

Bulk hydroxyzine hydrochloride (HDXZ) and cetirizine hydrochloride were kindly supplied from Chemical Industries Development (CID), Giza, Egypt. Standard stock solutions of 5×10^{-3} mol L^{-1} bulk HDXZ and cetirizine hydrochloride were prepared in methanol (Merck) and stored in dark bottles at 4 °C. The desired solutions (1×10^{-6} to 1×10^{-4} mol L^{-1}) were prepared by appropriate dilution of the standard stock solutions with methanol.

2.2.3. Solutions of Atarax® tablets

Five Atarax® tablets (Chemical Industries Development—CID, Giza, Egypt) as labeled to containing 10 or 25 mg HDXZ per tablet were weighed and the average mass per tablet was determined. A quantity of the homogenous finely ground HDXZ was accurately weighed and transferred into a 100-mL volume calibrated flask contains 70 mL methanol (Merck). The content of the flask was sonicated for about 15 min and then made up to the volume with methanol. The solution was then filtered through a 0.45 μm milli-pore filter (Gelman, Germany) for separation of insoluble ingredients, rejecting the first portion of the filtrate. The desired concentrations were obtained by accurate dilution with methanol and were used as standard solutions. Then, the solutions were directly analyzed, according to the general analytical procedure without extraction of HDXZ prior to the analysis.

2.2.4. Solutions of human serum

Serum samples of two healthy volunteers were collected then mixed and stored frozen until assay. Samples of the human serum (each of 1 mL) were fortified with various concentrations (5×10^{-8} to 1×10^{-6} mol L^{-1}) of HDXZ in small tubes. Each of these samples was then completed to 2 mL with methanol to denature and precipitate proteins. After vortexing each of

the serum samples for 2 min, the precipitated proteins were separated by centrifugation for 3 min at 14,000 rpm. The clear supernatant layer was filtered through a 0.45 μm milli-pore filter to obtain protein-free human serum samples, which were used as standard spiked serum solutions. Then the analysis was followed up as indicated in the general analytical procedure.

2.3. Pharmacokinetic studies

Pharmacokinetics of HDXZ were studied in plasma of two healthy male volunteers following a single oral dose of Atarax® labeled to contain 25 mg HDXZ. Subjects were caffeine and alcohol free for at least 12 h before the administration of the drug and all over the counter medications were avoided for 24 h prior to the study. The two volunteers gave their written informed consent prior to anticipating in the study (at Ramadan Specialized Hospital, Tanta City, Egypt). Blood samples (1 mL each) were collected before initiation and at 0.5, 1.0, 1.5, 2, 3, 4, 6, 8, 10 and 12 h after the oral administration. The blood samples were centrifuged immediately at 3000 rpm for 15 min and then the plasma fractions were rapidly separated and stored in coded polypropylene tubes at −20 °C until the assay. Following separation of proteins by methanol, the plasma samples were analyzed using the described square-wave stripping voltammetric procedure.

2.4. Cleaning of the electrode

Before measurements, the glassy carbon electrode (GCE) was polished with aqueous slurry of 0.5 μm alumina powder on a damp silk cloth until a mirror-like finish was obtained. The electrode was then activated before recording the voltammograms by scanning the applied potential from −0.5 to 1.5 V by cyclic voltammetry for 10 cycles in a blank solution of the supporting electrolyte till a low background current was obtained. For re-generation of the electrode surface after recording each voltammogram, the CPE was transferred into a voltammetric cell contains blank electrolyte solution, then a series of cyclic scans was continued until a voltammogram corresponding to the residual current was obtained. The electrode was then ready for use in the next measurement.

2.5. General analytical procedure

Ten millilitres of the B–R universal buffer was introduced into the micro-electrolysis cell and a selected accumulation potential was then applied to the glassy carbon electrode for a selected accumulation time period, while the solution was stirred at 400 rpm. At the end of the accumulation time, the stirring was stopped and a 5 s rest period was allowed for the solution to become quiescent. The voltammogram was then recorded by scanning the potential towards the positive direction using the square-wave potential waveform. Medium exchange method [13] was used during the determination of HDXZ in the human serum to avoid blocking of the electrode surface with low molecular weight proteins which may remain after centrifugation.

To study the reproducibility, accuracy and precision of the proposed procedure for determination of HDXZ in bulk form, tablet and human serum samples, recovery experiments were carried out by means of both the calibration curve and standard addition methods. All the data were obtained at room temperature.

3. Results and discussion

3.1. Electrochemical oxidation of HDXZ

Cyclic voltammetry technique was applied as a diagnostic tool to get information about electrochemical oxidation of HDXZ at a glassy carbon electrode in the B–R universal buffer of pH (2–11). Voltammograms of HDXZ exhibited a single well-defined anodic peak over the whole pH range, which may be attributed to oxidation of the hydroxyl group of the aliphatic chain moiety of the analyte molecule. No peaks were observed in the cathodic scan; pointing to the irreversible nature of the oxidation process. The peak current intensity was much enhanced at pH values 3–5 and the peak potential shifted to less positive values with the increase of pH. The E_p versus pH plot consists of three straight portions with slope values of 65, 88 and 74 mV, respectively. The slope value = (60/α) (m/n); where α is the symmetry transfer coefficient and m and n are the number of protons and electrons involved in the electrode reaction, respectively. The symmetry transfer coefficient values were found to be 0.92, 0.68 and 0.81 (less than 1), confirming the irreversible nature of the oxidation process of HDXZ under the present experimental conditions.

The pK_a values (3.0 and 7.0), of HDXZ, obtained by the interception of the three portions of E_p versus pH graph were close to those reported in literature (2.13 and 7.13) [8]. However, HDXZ is a basic compound with two ionizable groups of pK_a value around 7 for the first protonation constant (tertiary amine group) and around 3 for the second protonation (nitrogen heterocyclic) [8].

Effect of the scan rate (ν) on the peak potential (E_p) and peak current (i_p) was examined from 25 to 300 mV s^{-1}. The peak potential was linearly shifted to more positive values with the increase of the scan rate confirming the irreversible nature of the oxidation process of HDXZ at the glassy carbon electrode [14]. A linear Randles–Seveik plot (i_p vs. ν) was obtained (correlation coefficient $r = 0.997$) indicating that adsorption of HDXZ onto the GCE is the means of mass transport [15]. This finding was confirmed by plotting $\log i_p$ versus $\log \nu$ where a straight line was obtained ($r = 0.999$) with a slope value of 0.88, however, slopes of 0.50 or 1.0 are expected for ideal reactions of solution or surface species, respectively [16]. Moreover, the interfacial adsorptive character of HDXZ onto the GCE was proved by recording cyclic voltammogram for 1×10^{-5} mol L^{-1} drug solution in a B–R universal buffer of pH 4 at a scan rate of 0.10 V s^{-1} following its preconcentration by adsorptive accumulation onto the GCE under open circuit conditions (Fig. 1, dashed scan) and then at −0.30 V for 180 s (scan 1). A substantial decrease of the anodic peak was observed in subsequent scans (scan 2).

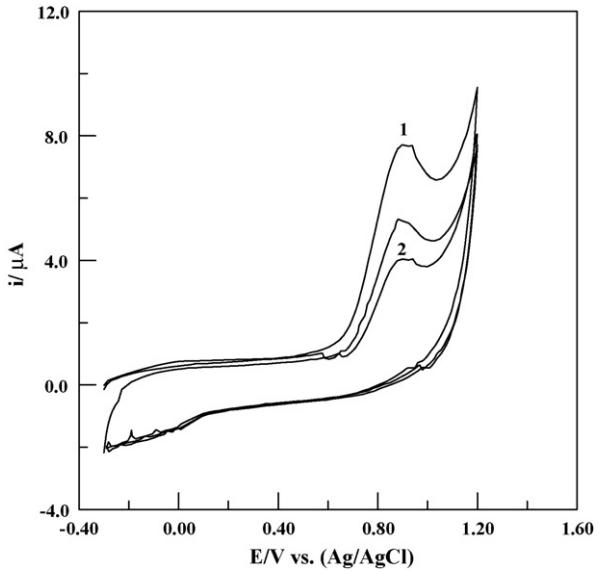


Fig. 1. Cyclic voltammograms of 1×10^{-5} mol L^{-1} HDXZ in a B–R universal buffer of pH 4 recorded following its preconcentration onto an activated GCE by adsorptive accumulation under open circuit conditions (dashed scan) and at $E_{acc} = -0.30$ V for 180 s (scans 1 and 2); scan rate = 0.10 V s^{-1}.

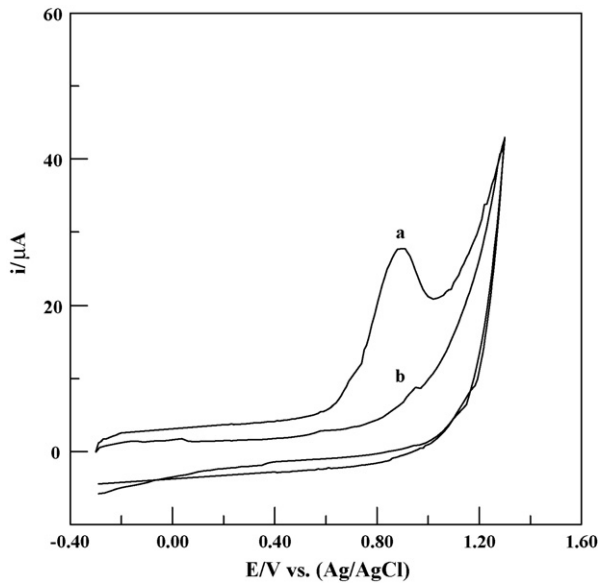


Fig. 2. Cyclic voltammograms of (a) 5×10^{-5} mol L^{-1} HDXZ and (b) 5×10^{-5} mol L^{-1} cetirizine in a B–R universal buffer of pH 4 recorded at scan rate of 0.10 V s^{-1}, following preconcentration onto an activated GCE by adsorptive accumulation at $E_{acc} = -0.30$ V for 180 s.

Accordingly, the oxidation of HDXZ at the GCE in the B–R buffer of pH 2–11 (Scheme 2) is an irreversible process controlled mainly by adsorption with some diffusion contributions and the electrochemical reaction pathway may be suggested as illustrated in Scheme 2.

The suggested electrochemical reaction pathway of HDXZ at the GCE via oxidation of its –OH group of the aliphatic chain moiety was confirmed from the electro-inactive behavior of its main metabolite "cetirizine" (Fig. 2) of a similar chemical structure in which an acetic acid (–CH_2–COOH) moiety presents instead of the ethanol (–CH_2–CH_2–OH) moiety in the aliphatic chain (Scheme 1). This behavior confirmed that the –OH group of the aliphatic chain moiety is the unique oxidizable site in HDXZ molecule.

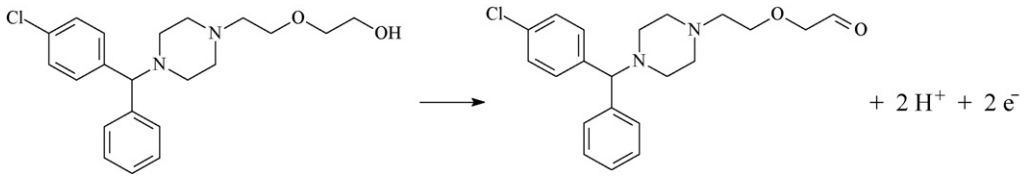
3.2. Square-wave analytical study

3.2.1. Type and pH of supporting electrolyte

In the present study, square-wave adsorptive anodic stripping (SW-AdAS) voltammograms of 5×10^{-7} mol L^{-1} HDXZ in B–R (pH 2–11), acetate (pH 3.8–6.2) or phosphate (pH 2–7.5) buffers were recorded following its preconcentration onto the GCE by adsorptive accumulation at −0.30 V (vs. Ag/AgCl/KCl_s) for 180 s. The voltammograms exhibited a single irreversible anodic peak. Sharp peak and much enhanced peak current were achieved when using the B–R universal buffer as a supporting electrolyte. The peak current increased with the increase of pH of the supporting electrolyte till it reached a much enhanced value over the pH range 3–5 (Fig. 3). At higher pH values, the peak current decreased gradually together with a poor peak definition up to pH 11. Therefore, a B–R universal buffer of pH 4 was chosen as a supporting electrolyte in the rest of the present quantitation work.

3.2.2. Instrumental parameters

The square-wave (SW) response markedly depends on the parameters of the excitement signal. In order to obtain a maximum development of a square-wave voltammetric peak current, the optimum instrumental conditions (frequency *f*, scan increment ΔE_i and pulse-amplitude ΔE_a) were studied for 5×10^{-7} mol L^{-1} HDXZ in a B–R universal buffer of pH 4 at a GCE. The frequency (*f*), in SW experiments, is an important parameter since it allows the obtain of important information about the reversibility degree and to estimate value of αn_a for an irreversible process. At a scan increment (ΔE_i) of 10 mV and a pulse-amplitude (ΔE_a) of 25 mV, square-wave voltammograms were recorded for different frequencies over the range 20–120 Hz, following preconcentration of HDXZ onto the GCE by adsorptive accumulation at 0.0 V for 180 s. The obtained linear plot of peak current (i_p) versus *f* confirmed the irreversible nature of the oxidation process. Another criterion that describes



Scheme 2.

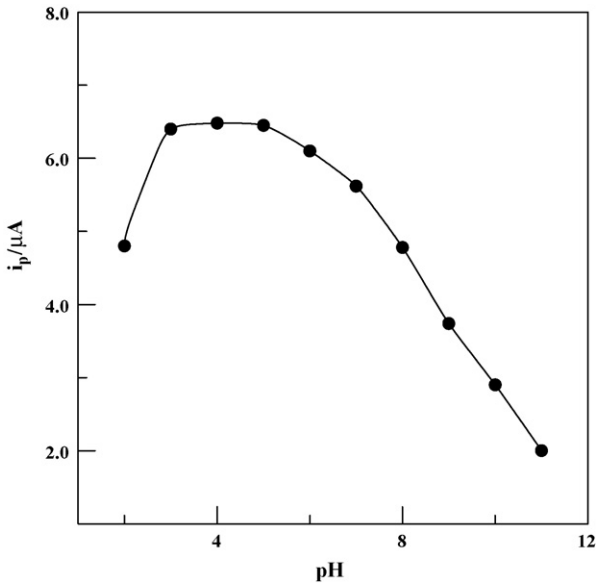


Fig. 3. Influence of pH of the B–R universal buffer on the SW-AdAS voltammetric peak current (i_p) of 5×10^{-7} mol L^{-1} HDXZ at frequency $f = 120$ Hz, scan increment $\Delta E_i = 10$ mV and pulse-amplitude $\Delta E_a = 25$ mV, following preconcentration onto the GCE by adsorptive accumulation at −0.30 V for 180 s.

the irreversibility of the system in SW voltammetry is the relationship existed between the peak potential (E_p) and logarithm of frequency, as described by Eq. (1) [17]:

$$\frac{\Delta E_p}{\Delta \log f} = \frac{2.3RT}{\alpha n_a F} \quad (1)$$

From the slope value (0.037) of the obtained linear E_p versus $\log f$ plot, αn_a was estimated (1.60) and consequently that of the symmetry transfer coefficient (α) was found to equal 0.80, since $n_a = 2$.

At a frequency of 120 Hz and a pulse-amplitude of 25 mV, the SW-AdAS voltammetric peak current intensity increased linearly with the scan increment (ΔE_i) up to 10 mV, following the relationship: i_p (μA) = 0.2341ΔE_i (mV) + 0.8689 (correlation coefficient $r = 0.995$ and number of points $n = 5$).

At a constant frequency of 120 Hz and a scan increment of 10 mV, the square-wave voltammograms were recorded over pulse-amplitude range 20–60 mV. Although the current increased linearly with the increase of pulse-amplitude, peak morphology and sharper one were obtained at 25 mV. The peak current (i_p) registered at different values of pulse-amplitude ΔE_a allows the calculation of the electrode surface coverage (Γ) by adsorbed HDXZ molecules according to Eq. (2) [18]:

$$\frac{\partial i_p}{\partial \Delta E_a} = 500 A \alpha n^2 F f \Delta E_i \Gamma \quad (2)$$

where $\partial i_p / \partial \Delta E_a$ is the slope of i_p versus ΔE_a, A is the electrode surface area (7 mm^2) and the other terms have their usual meanings. From slope value (1.12), the electrode surface coverage was obtained as 8.63×10^{-11} mol cm^{-2}. Each adsorbed HDXZ molecule therefore occupied an area of 0.52 nm^2.

Accordingly, the optimal SW-AdAS voltammetry instrumental parameters which were used over all the rest of the present investigation were: frequency $f = 120$ Hz, scan increment $\Delta E_i = 10$ mV and pulse-amplitude $\Delta E_a = 25$ mV using a B–R universal buffer of pH 4 as a supporting electrolyte.

3.2.3. Accumulation parameters

Effect of varying accumulation potential (E_{acc}) from −0.5 to +0.2 V (vs. Ag/AgCl/KCl$_s$) on the peak current intensity of the SW-AdAS voltammograms recorded for 5×10^{-7} mol L^{-1} HDXZ in a B–R buffer of pH 4 under the optimal instrumental parameters following its preconcentration onto the GCE for 180 s was also evaluated (Fig. 4). A much enhanced peak current was achieved at −0.3 V, hence, it was used throughout the present study. On the other hand, SW-AdAS voltammograms for 1×10^{-7} and 5×10^{-7} mol L^{-1} HDXZ were recorded under the optimal instrumental parameters at increased preconcentration time at −0.3 V. As shown in Fig. 5, the magnitude of the peak current depended linearly on both the analyte concentration and the accumulation time. Apparently, lower concentration of the analyte requires longer preconcentration time. This meant that, the choice of preconcentration time was dictated by the sensitivity required. In the present analytical procedure, preconcentration times of 90, 180 and 300 s were used (Table 1).

3.3. Method validation

Validation of an analytical method is the process by which it is established, by laboratory studies, that the performance characteristics of the method meet the requirements for the intended analytical applications. The elements required for method validation are: linearity range, limits of detection and quantitation, accuracy, precision, selectivity, robustness and intermediate precision [19].

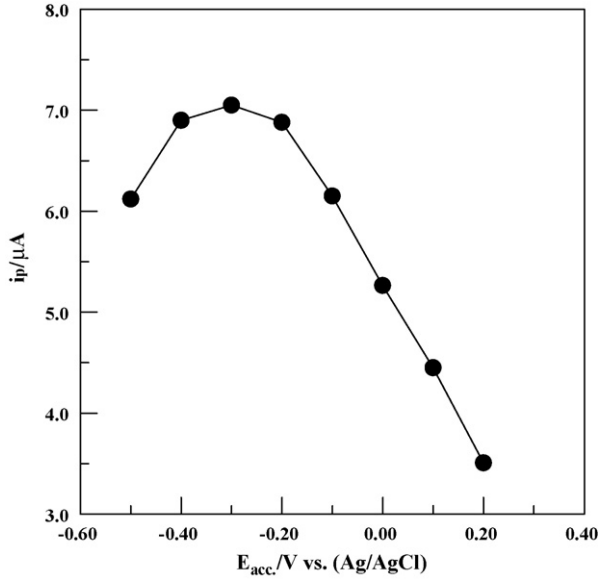


Fig. 4. Effect of accumulation potential (E_{acc}) on the SW-AdAS voltammetric peak current (i_p) of 5×10^{-7} mol L^{-1} HDXZ in a B–R universal buffer of pH 4, following preconcentration onto the GCE by adsorptive accumulation at $E_{acc} = -0.30$ V for 180 s. Other instrumental parameters are as those given in Fig. 3.

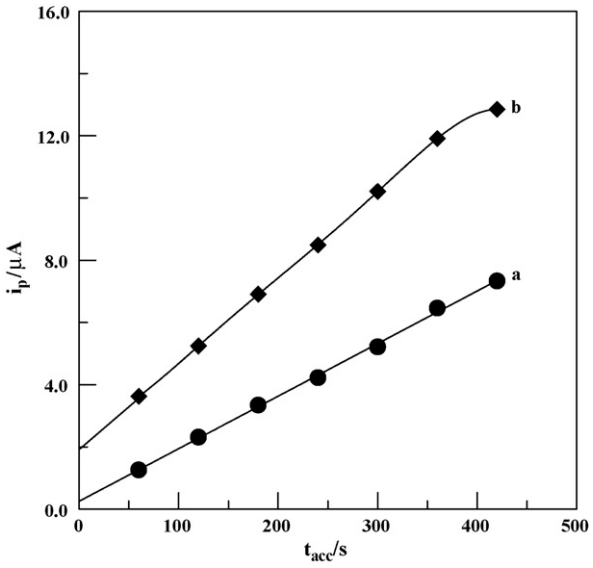


Fig. 5. Effect of the accumulation time (t_{acc}) on the SW-AdAS voltammetric peak current of (a) 1×10^{-7} mol L^{-1} and (b) 5×10^{-7} mol L^{-1} HDXZ in a B–R universal buffer of pH 4 following preconcentration onto the GCE by adsorptive accumulation at −0.30 V. Other instrumental parameters are as those given in Fig. 3.

3.3.1. Linearity

Using the optimal conditions of the described SW-AdAS voltammetric procedure, linear relations between peak current and HDXZ concentration over the ranges indicated in Table 1 were obtained referred to different accumulation times. A good linearity is evident from values of the correlation coefficients $r = 0.995$–0.998 (Table 1), thus confirmed validity of the SW-AdAS procedure for determination of HDXZ.

3.3.2. Limits of detection and quantitation

Limits of detection (LOD) and quantitation (LOQ) of HDXZ were calculated using the expression: $k \times$ S.D./b [19], where $k = 3$ for LOD and 10 for LOQ, S.D. is the standard deviation of intercept (or blank) and b is the slope of the calibration curve. The achieved LOD of 3×10^{-9} mol L^{-1} and LOQ of 1×10^{-8} mol L^{-1} following its preconcentration onto the GCE by adsorptive accumulation for 300 s confirmed the sensitivity and validity of the described SW-AdAS voltammetric procedure for assay of HDXZ (Table 1).

3.3.3. Accuracy

The accuracy of measurements by means of the described SW-AdAS voltammetric procedure was checked by calculating the recovery of a known concentration (5×10^{-7} mol L^{-1}) of HDXZ following preconcentration onto the GCE by adsorptive accumulation for 180 s. The mean percentage recovery obtained by applying the calibration curve method was 100.8% (Table 2).

Table 2
Influence of small variation in some of the optimal procedural conditions on accuracy and precision of determination of 5×10^{-7} mol L^{-1} HDXZ, following its preconcentration onto a GCE by adsorptive accumulation at −0.30 V for 180 s; $f = 120$ Hz, $\Delta E_i = 10$ mV and $\Delta E_a = 25$ mV

Variable	Conditions	% $R \pm$ S.D. ($n = 5$)
Robustness		
pH of the medium[a]		
3.5	$E_{acc} = -0.30$ V	98.8 ± 0.91
4.0		100.8 ± 0.83
4.5		99.5 ± 1.05
Accumulation potential (E_{acc})[a]		
−0.25 V	pH 4	100.3 ± 1.18
−0.30 V		100.8 ± 0.83
−0.35 V		98.6 ± 1.51
Intermediate precision		
Potentiostat 394-PAR (Lab. 1)	pH 4.0	100.8 ± 0.83
Potentiostat 263A-PAR (Lab. 2)	$E_{acc} = -0.30$ V	97.8 ± 2.03
Day (1)		100.8 ± 0.83
Day (2)		98.8 ± 1.12
Day (3)		101.1 ± 1.37

[a] Potentiostat 394-PAR.

3.3.4. Reproducibility

The high sensitivity of an analytical method is usually accompanied by very good reproducibility. This analytical performance was evaluated from five repeated measurements of electrochemical signal of 5×10^{-7} mol L^{-1} HDXZ solution following preconcentration onto the GCE by adsorptive accumulation for 180 s. The precision of the described SW-AdAS voltammetric procedure in terms of relative standard deviation was 0.83% (Table 2).

3.3.5. Stability

The stability of HDXZ in a B–R universal buffer of pH 4 was evaluated under the optimal procedural conditions by monitoring the changes in the anodic peak height of 5×10^{-7} mol L^{-1} HDXZ following its preconcentration onto the GCE for 180 s over a period of 60 min. The electroanalytical signal showed no difference in the peak current intensity which confirmed stability of HDXZ over the time period of measurements.

Table 1
Characteristics of the calibration curves of the SW-AdAS voltammetric assay of bulk HDXZ under the optimal procedural conditions following accumulation onto the GCE for different times

t_{acc} (s)	Linearity range (mol L^{-1})	Least square equation[a]		(r)	LOD (mol L^{-1})
		Intercept (μA)	Slope (μA/μmol L^{-1})		
90	1×10^{-7} to 1×10^{-5}	0.066	10.11	0.995	3.0×10^{-8}
180	5×10^{-8} to 4×10^{-6}	0.094	21.80	0.997	1.5×10^{-8}
300	1×10^{-8} to 1×10^{-6}	0.112	50.31	0.998	3.0×10^{-9}

[a] Average of three determinations.

3.3.6. Robustness

The robustness [19] of the measurements by means of the described SW-AdAS voltammetric procedure to assay of HDXZ was examined by studying the effect of small variation of some important procedural conditions (pH 4 ± 0.5) and accumulation potential E_{acc} (-0.30 ± 0.05 V). As shown in Table 2, the achieved recoveries were reliable and thus the procedure could be considered robust.

3.3.7. Intermediate precision

The intermediate precision [19] of measurements by means of the described SW-AdAS voltammetric procedure was examined by applying the procedure to assay of HDXZ using two Potentiostats, 394-PAR (Lab. 1) and 263A-PAR (Lab. 2), at different elapsed time. The results obtained due to Lab. (1) and Lab. (2) and even day to day were found reproducible (Table 2), since there was no significant difference in the recoveries of HDXZ or the standard deviations.

3.4. Interference studies

The selectivity [19] of the procedure for the assay of HDXZ was examined in the presence of the common inactive ingredients usually present in its formulations [20]: anhydrous lactose, colloidal silicon dioxide, croscarmellose sodium, FD&C Yellow No. 6, hypromellose, magnesium stearate, microcrystalline cellulose, polyethylene glycol, ploysorbate 80 and titanium dioxide. These ingredients are electro-inactive and its adsorption onto the GCE is very limited under the optimum procedural conditions. A mean recovery for 5×10^{-7} mol L^{-1} HDXZ in the presence of ingredients was found to equal $98.7 \pm 1.17\%$ ($n = 5$), which showed no significant interference from the inactive ingredients.

Moreover, the selectivity of the described procedure was examined by analysis of 5×10^{-7} mol L^{-1} HDXZ in presence of the same concentration of its electro-inactive metabolite "cetirizine". A mean percentage recovery of 98.3 ± 0.93 ($n = 5$) was achieved, which showed no significant interference from cetirizine. Accordingly, the described SW-AdAS voltammetric procedure can be considered selective for assay of HDXZ even in the presence of its metabolite "cetirizine".

3.5. Analytical application

3.5.1. Analysis of HDXZ in Atarax® tablets

The described SW-AdAS voltammetric procedure was successfully applied for the determination of HDXZ in its pharmaceutical formulations (Atarax® tablets of 10 and 25 mg HDXZ/tablet). The obtained results (Table 3) were statistically compared with those obtained by the official chromatographic method [12]. Since the calculated value of F does not exceed the theoretical value (Table 3), there was no significant difference between the described and reported methods with respect to reproducibility [21]. Also, no significant difference was noticed between the two methods regarding accuracy and precision as revealed by t-value [21], Table 3. The accuracy of the described SW-AdAS voltammetric procedure was also judged by applying the standard addition method [22]. This means that the proposed procedure should be applicable to the analysis of this and other similar formulation products containing HDXZ.

3.5.2. Assay of hydroxyzine in spiked human serum

The described SW-AdAS voltammetric procedure was also successfully applied to assay of HDXZ in spiked human serum. Medium exchange method was used following accumulation of the drug onto the GCE and before recording each voltammogram to minimize interferences resulting from macro solution constituents and to increase the efficiency of the stripping step. Variation of the peak current versus concentration of HDXZ was linear within the range 5×10^{-8} to 1×10^{-6} mol L^{-1} (Fig. 6) followed the regression equation; i_p (μA) = $45.97C$ (μM) + 0.601 ($r = 0.997$ and $n = 10$). A mean percentage recovery of HDXZ in spiked human serum was found to equal $98.4 \pm 1.22\%$. The achieved LOD and LOQ of were 1.50×10^{-8} mol L^{-1} (5.62 ng mL^{-1}) and 5.0×10^{-8} mol L^{-1} (18.75 ng mL^{-1}), respectively. These results indicated that the proposed voltammetric procedure is more sensitive and precise than most of the reported methods [5–12], since these methods offered a detection limit over the concentration range 5.42–100 ng mL^{-1} bulk HDXZ. Moreover, it was successfully applied for quantification of the drug in human serum without prior extraction of the drug which is a great advantage over most of the reported methods especially the chromatographic ones.

3.5.3. Pharmacokinetic studies

The applicability of the described SW-AdAS voltammetric procedure was proved in the pharmacokinetic of HDXZ

Table 3
Assay of HDXZ in its pharmaceutical formulations by means of the described SW-AdAS voltammetric procedure and the official chromatographic method [12]

Sample	Claimed value (mg/tablet)	Proposed voltammetric procedure (% $R \pm$ S.D.)		Official chromatographic method
		Calibration curve	Standard addition	
Atarax®	10	100.5 ± 0.71 $F = 4.77$ $t = 2.28$	98.4 ± 1.04	98.7 ± 1.55
	25	98.6 ± 1.12 $F = 1.54$ $t = 0.51$	100.5 ± 0.79	99.1 ± 1.39

Theoretical F-value = 6.39 and t-test = 2.3 at 95% confidence limit for $n_1 = n_2 = 5$.

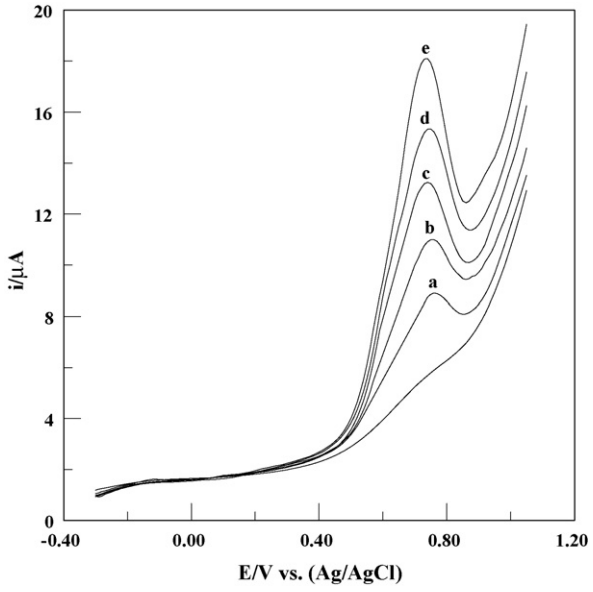


Fig. 6. SW-AdAS voltammograms for successive additions of HDXZ spiked in human serum, recorded in a B–R buffer of pH 4 following preconcentration onto the GCE by adsorptive accumulation at −0.30 V for 300 s. Each addition affected a 5×10^{-8} mol L^{-1} HDXZ and the dotted line represents the blank solution. Other instrumental parameters are as those given in Fig. 3.

in plasma of two healthy male volunteers following the administration of a single oral dose of Atarax®—25 mg. The obtained plasma concentration–time profiles of the two subjects are shown in Fig. 7. The following parameters were assessed for the period of 0–12 h: area under the plasma concentration–time curves from time zero to the last measurable sample time ($AUC_{0–12}$) and to infinity ($AUC_{0–\infty}$); maximum plasma concentration (C_{max}); time of the maximum concentration (t_{max}); terminal rate constant (K_{el}) and terminal half-life time ($t_{1/2}$). C_{max} and t_{max} were obtained directly from the concentration–time curve. The area under concentration–time curve from time zero (predose) to time of last quantifiable concentration ($AUC_{0–12}$) was calculated using the linear trapezoidal method. The terminal rate constant (K_{el}) was calculated by applying a log-linear regression analysis to at least the last three time points. The terminal half-life

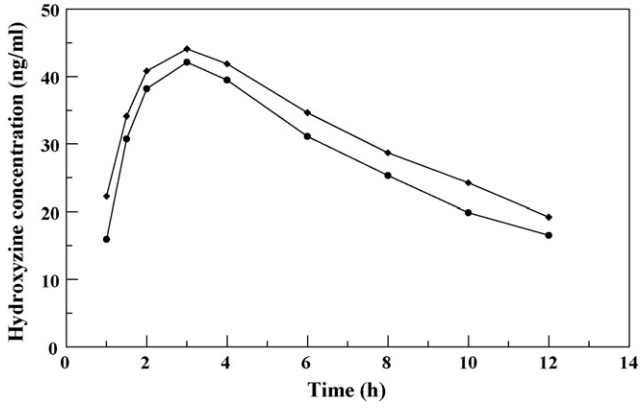


Fig. 7. Mean plasma concentration–time profiles for two male subjects following an oral administration of a single dose of Atarax®—25 mg.

Table 4
Estimated plasma pharmacokinetic parameters of two male subjects following an oral administration of a single dose (Atarax® tablet—25 mg hydroxyzine)

Parameter[a] (unit)	Estimated values[a]	
	Subject (1)	Subject (2)
C_{max} (ng mL^{-1})	42.11	44.08
t_{max} (h)	3.0	3.0
$AUC_{0–12}$ (ng h mL^{-1})	315.51	338.44
$AUC_{0–\infty}$ (ng h mL^{-1})	629.88	756.06
K_{el} (1/h)	0.048	0.042
$t_{1/2}$ (h)	14.44	16.50

[a] Average of two measurements.

time ($t_{1/2}$) was calculated as [ln $2/K_{el}$]. Area under the plasma concentration–time curves from time zero to infinity ($AUC_{0–\infty}$) was calculated as [$AUC_{0–12} + (C_{12}/K_{el})$]. The pharmacokinetic parameters obtained for the two volunteers were listed in Table 4. The obtained parameters were favorably compared with those reported in literature [23] confirming the reliability of the described procedure for the assay of HDXZ in human blood samples of medicated subjects without interferences from the biologically active (but electro-inactive) metabolite "cetirizine".

4. Conclusion

The electrochemical oxidation of hydroxyzine hydrochloride at a GCE was identified in buffered solutions and a validated SW-AdAS voltammetric procedure was described for its determination. The described procedure provides a sensitive and simple approach to the determination of hydroxyzine in pharmaceutical formulations and human blood. Its accuracy, reproducibility, simplicity and selectivity suggest its application in quality control analysis, clinical laboratories and pharmacokinetic studies.

Acknowledgements

The authors express their gratitude to the Alexander von Humboldt Foundation (Bonn, Germany) for donating the Electrochemical Analyzer (263A-PAR) and the Eppendorf centrifuge used in the present study, to M.M. Ghoneim. The authors express their gratitude also to Ramadan Specialized Hospital's staff (Tanta City, Egypt), for the very kind care of the two volunteers and for providing the great facilities in collection and treatments of plasma samples required for the pharmacokinetic studies.

References

[1] J.E.F. Reynolds, Martindale, The Extra Pharmacopoeia, 30th ed., The Pharmaceutical Press, London, 1993.
[2] S. Khalid-Khan, M. Rynn, K. Rickels, Generalised Anxiety Disorder, Martin Dunitz, UK, 2002, p. 125.
[3] S.V. Argyropoulos, J.J. Sandford, D.J. Nutt, Pharmacol. Ther. 88 (2000) 213.
[4] http://www.answers.com/topic/hydroxyzine.
[5] S.E. Roberts, M.F. Delany, J. Chromatogr. 242 (1982) 364.
[6] G.N. Menon, B.J. Norris, J. Pharm. Sci. 70 (1981) 697.

[7] H. Ackermann, F. Kretzschmann, S. Kruger, B. Lexow, Nahrung-Food 21 (1977) 603.
[8] C. Martinez-Algaba, J.M. Bermudez-Saldana, R.M. Villanueva-Camanas, S. Sagrado, M.J. Medina-Hernandez, J. Pharm. Biomed. Anal. 40 (2006) 312.
[9] M.E. Capella-Peiro, A. Bossi, J. Esteve-Romero, Anal. Biochem. 352 (2006) 41.
[10] A. Bouklouze, M. Elbouzekraoui, Y. Cherrah, M. Hassar, J.M. Kauffmann, Electroanalysis 14 (2002) 1369.
[11] R. Mikulski, B. Dembinski, Anal. Chim. Acta 272 (1993) 233.
[12] The US Pharmacopeia (USP 28), The National Formulary (NF 23), US Pharmacopeial Convention Inc., 2005, p. 982.
[13] J. Wang, B.A. Freiha, Anal. Chim. Acta 148 (1983) 79.
[14] A.M. Bond, Modern Polarographic Methods in Analytical Chemistry, Dekker (Marcel), New York, 1980, p. 195.
[15] P. Monk, Fundamentals of Electroanalytical Chemistry, Wiley, 2001, p. 162.
[16] E. Laviron, J. Electroanal. Chem. 112 (1980) 11.
[17] M. Lovric, J. Electroanal. Chem. 248 (1988) 239.
[18] M. Lovric, S.K. Lovric, R.W. Murray, Electrochim. Acta 33 (1988) 739.
[19] M. Swartz, I.S. Krull, Analytical Method Development and Validation, Dekker (Marcel), 1997, p. 62.
[20] http://www.rxlist.com/cgi/generic/hydrox.htm.
[21] G.D. Christian, Analytical Chemistry, 5th ed., John Wiley & Sons Inc., USA, 1994, p. 36.
[22] G.W. Ewing, Instrumental Methods of Chemical Analysis, 5th ed., Lippincocott-Raven, Philadelphia, PA, 1995, p. 464.
[23] F.E.R. Simons, G.L. Sussman, K.J. Simons, J. Allergy Clin. Immunol. 95 (1995) 685.

Available online at www.sciencedirect.com
ScienceDirect
Talanta 74 (2008) 998–1007
Talanta
www.elsevier.com/locate/talanta

Reflection and transmission mid-infrared spectroscopy for rapid determination of coal properties by multivariate analysis

M.T. Bona, J.M. Andrés *

Instituto de Carboquímica, CSIC, Procesos Químicos, Miguel Luesma Castán, n. 4, 50018 Zaragoza, Spain

Received 23 May 2007; received in revised form 27 July 2007; accepted 9 August 2007
Available online 22 August 2007

Abstract

In the present paper, the influence of different acquisition techniques (transmission, diffuse reflectance infrared Fourier transform and attenuated total reflectance) in the determination of nine coal properties related to combustion power plants has been studied. Raw coal samples of different origins were pooled for developing a correlation between the resultant spectra and the corresponding coal properties by multivariate analysis techniques. Thus, the existent collinearity in mid-infrared coal spectra led to the application of partial least squares regression (PLS), studying simultaneously the influence of different spectroscopic units as well as several spectral data mathematical pre-treatments. On the other hand, a principal component analysis (PCA) revealed a relationship between principal components and coal composition in both transmission and reflection techniques. Although the best accuracy and precision results were obtained for coal properties related to organic matter, the system was also able to differentiate coal samples attending to the presence of a specific mineral matter, kaolinite.
© 2007 Elsevier B.V. All rights reserved.

Keywords: Transmission; Diffuse reflectance infrared Fourier transform (DRIFT); Attenuated total reflectance (ATR); Coal analysis; Partial least squares regression (PLS); Principal component analysis (PCA)

1. Introduction

The determination of coal properties by applying a fast, accurate and real-time method is presently important to the coal industry for pricing, quality control and reduction of emissions [1]. Moreover, environmental regulations lead to a usual practice of blending different types of coals from which a continuous analysis method could provide the required information for the coal quality control process [2].

With regard to coal analysis, chemical ISO/ASTM measurements of coal parameters are well established, however they do not fulfil the needs of the coal industry due to the results can only be obtained hours or days after sampling [3–8]. Consequently, a number of techniques have been investigated the on-line analysis of coal, including capacitance measurements [9,10], microwave transmission [11], fast neutron and gamma-ray transmission [12] and nuclear magnetic resonance [13]. Although the merits of these techniques have been demonstrated, some limitations such as safety requirements or the indirect determination of some coal properties lead to consider other techniques capable of being implemented in an industrial environment.

Intending to find a solution, infrared spectroscopy provides perhaps the most valuable information about the constitution of organic materials among all the physical techniques [14,15]. Studies of coal structure, analysis and prediction of coal properties have been performed so far [16–18], verifying the viability of this optical spectroscopy technique for further applications. According to quantitative research, it is well worth remarking that the majority of papers have focused on specific spectral features such as hydroxyl [19] or aliphatic and aromatic hydrogen [20] groups, providing a restricted description of the composition, characteristics and performance in power plants. An alternative to that entails the use of the complete spectrum considered as a whole. The combination of thousands of variables and the need for rapid, reliable, accurate, and precise determinations has motivated researchers to develop and use multivariate calibration methods. Thus, multiple linear regression (MLR), principal components regression (PCR) or partial least squares (PLS) have been the object of some studies [21–26].

In this way, the aim of this work consists of studying the influence of different acquisition techniques (transmission, diffuse reflectance infrared Fourier transform and attenuated total

* Corresponding author. Fax: +34 976 73 33 18.
E-mail address: jmandres@carbon.icb.csic.es (J.M. Andrés).

0039-9140/$ – see front matter © 2007 Elsevier B.V. All rights reserved.
doi:10.1016/j.talanta.2007.08.016

reflectance) in the determination of several coal properties related to combustion power plants (% moisture, % ash, % volatile matter, % fixed carbon, heating value (kcal/kg) and % C, H, N and S). Once acquired the spectra, in order to avoid drawbacks related to such a load of spectral information, different pre-treatments (baseline correction, baseline followed by normalization, range normalization, multiplicative signal correction, first and second derivatives) have been applied. Despite the studies already reported, the novelty of this approach consists of combining a wide variety of raw coal samples and several acquisition techniques by applying multivariate analysis techniques –exploratory data and calibration analysis- to a complete mid-infrared wavelength range. This fact allows underlining the advantages and disadvantages of each technique in a more reliable way.

2. Experimental

2.1. Samples

A sample set consisted of 142 raw coals of different suppliers (Endesa Almería-12 samples; Endesa Andorra-5; Endesa Meirama-7; EVN-13; RWE Hambach-41; RWE Gazrweiler-47; Interlaboratory samples-17), covering from lignite B to anthracite, were used for the study. They were analysed for proximate analysis (moisture, ash, volatile matter, fixed carbon), heating value and elemental analysis (carbon, hydrogen, nitrogen, sulphur) following the usual ISO/ASTM standard methods [3–8]. The samples presented a particle size distribution corresponding to the specifications for pulverized coal burners [27], typically: 98% <300 μm; 95% <150 μm; 75% <75 μm. The statistical results (minimum, maximum, mean, standard deviation) of the full sample set analysis are described in a previous work [28]. A brief summary is presented in Table 1 . Likewise, the whole sample set classified according to coal rank resulted in six important clusters whose statistical results are included in Fig. 1 . The *Y*-axis represent the property value in percentage (%) and the *X*-axis shows the different clusters numbered from 1 to 6, corresponding to: 1, medium volatile bituminous-anthracite (18 samples); 2, high volatile A–B bituminous (15); 3, high volatile C bituminous (14); 4, subbituminous A–B (60); 5, subbituminous C (27); 6, lignite A–B (8). It can be observed that clusters tend to be quite homogeneous in property values even though some cases, such as ash content, present values far apart from the median. Further on, these values will be considered as potential outliers in the calibration process.

Table 1
Statistical results of full set sample analysis (142 samples)

	Minimum	Maximum	Mean	Standard deviation
Moisture (%)	0.48	37.2	11.2	7.32
Ash (%)	2.09	73.65	13.46	12.23
Volatile matter (%)	6.27	47.81	35.07	8.58
Fixed carbon (%)	10.23	78.92	40.27	12.95
Heating value (kcal/kg)	1425	7992	5153	1423
C (%)	16.18	82.24	54.95	14.16
H (%)	0.63	5.76	4.28	0.95
N (%)	0.2	2.04	0.9	0.41
S (%)	0.11	5.13	0.91	0.99

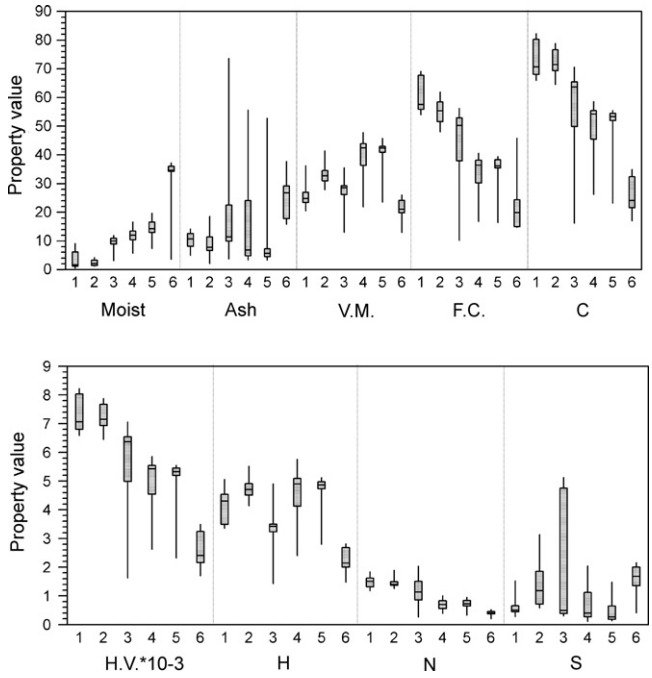


Fig. 1. Statistical results for each cluster and property value (%): 1, medium volatile bituminous-anthracite; 2, high volatile A–B bituminous; 3, high volatile C bituminous; 4, subbituminous A–B; 5, subbituminous C; 6, lignite.

2.2. Equipments and software

Transmission and DRIFT spectra were recorded on an ATI Mattson Infinity Series FTIR spectrometer equipped with a Globar source, potassium bromide beamsplitter and a DTGS detector. Two purge connectors provided separately the interferometer and sample compartment with CO_2-free dry air. The instrument was controlled and data acquired using the WinFIRST 3.5 software package by Mattson Instruments.

ATR spectra were recorded on a Bruker-Tensor 27 Series FTIR spectrometer equipped with a Globar source, potassium bromide beamsplitter and a La-DTGS detector. Interferometer and sample compartment were also provided with CO_2-free dry air. OPUS 4.0 software controlled the instrument and acquired the spectral data.

Multivariate calibration and mathematical spectral pretreatments were performed with the Unscrambler 7.5, from CAMO.

2.3. Recording of spectra

2.3.1. Transmission

Pellets for the infrared analysis were prepared by weighing 4 mg of coal and 196 mg of potassium bromide powder blended

by hand for 2–3 min [29] in an Agatha mortar. One hundred and twenty milligrams of this mixture was transferred to a Graseby Specac die and pressed into a pellet under vacuum for 10 min at a pressure of 10 tonnes. The resulting pellet was then analysed, in absorbance mode, by co-adding 16 scans over the range 400–4000 cm^{-1} at 1 cm^{-1} of digital resolution. The resolution value was the result of a previous study with a subset of 29 representative coal samples. They were acquired at 1, 2, 4, 8 and 16 cm^{-1} providing lower determination errors as the resolution increased, especially for coal properties related to organic matter compounds.

2.3.2. Diffuse reflectance infrared Fourier transform (DRIFT)

A diffuse reflectance sample cup (13 mm diameter) was used for the acquisition of the spectra. The sample cup was overfilled with the sample and the surface was flattened with a spatula. Next, it was placed into the diffuse reflectance accessory to acquire the spectrum using potassium bromide as reference material. Spectra obtained were the result of co-adding 128 scans over the range 500–4000 cm^{-1} performed at 1 cm^{-1} of digital resolution. All the spectra were acquired in absorbance mode, viz. log(1/reflectance).

A representative subset of coal samples (29) was used to study the effect that a coal sample diluted in a non-absorbing matrix causes in the calibration system. Two different situations were considered: filling the sample cup with raw coal or 5% diluted in KBr after a proper mixture. The results, in log(1/*R*) and Kubelka–Munk transformation units, showed more precise correlations with raw coal than diluted one.

2.3.3. Attenuated total reflectance (ATR)

Eighty-eight ATR spectra were collected in the range 600–4000 cm^{-1}, co-adding 16 scans by applying close contact between the surface of the coal sample and the diamond crystal (internal reflectance element, IRE). A Golden Gate-Specac ATR accessory was connected to the interferometer by means of purge bellows ensuring the way of dry air into the optic system.

The spectral differences between the three acquisition techniques are obvious in Fig. 2 , where Garzweiler 5 is represented in transmission, DRIFT and ATR mode. Variations in intensity bands and spectral deviations can be observed as it is detailed further on.

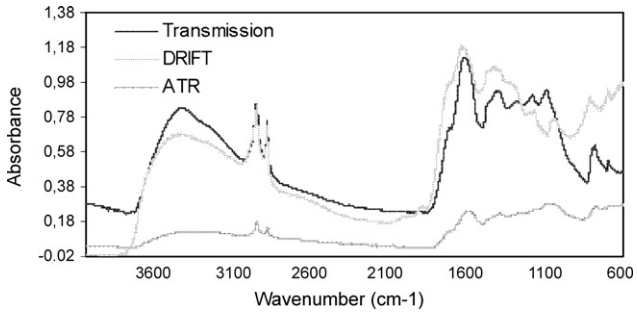


Fig. 2. Garzweiler 5 coal spectrum in transmission, DRIFT and ATR mode.

2.4. Data processing

The regression models were applied all over the corresponding wavelength range considered for each acquisition technique. Moreover, different spectral units (absorbance, transmittance or reflectance, log(1/*R*) and Kubelka–Munk transformation, respectively) were studied as well as mathematical pre-treatments for reducing extraneous effects such as differences in surface roughness, particle size or weight [30]. All spectral data were centred prior to the application of baseline offset correction, baseline followed by normalization, range normalization, multiplicative scatter correction (MSC) and first and second derivatives for each unit [31].

3. Results and discussion

3.1. Spectral profiles

Mid-infrared spectra corresponding to some of the coal samples included in the study are plotted in Fig. 3 . This figure focuses on the principal sample differences related to the main organic and inorganic coal components. Among them, it highlights those closely connected with coalification process – variations in aromatic and aliphatic hydrogen, methyl or carbonyl groups – and those related to the main mineral matter component, kaolinite [32–36].

This heterogeneity in coal composition joined to several chemical and physical acquisition effects results in a spectrum quite difficult to interpret. This is the main reason that quantitative studies require the use of multivariate data analytical methods necessary to reveal specific and useful information.

Although Fig. 3 refers to transmission coal spectra, these effects are also extensive to reflection acquisition techniques where it can be observed little wavelength and baseline drifts leading to differences in its relative spectral band intensities [37].

3.2. Reproducibility

In a quantitative analysis, random and systematic errors affect the precision and accuracy of the method [38]. In order to deter-

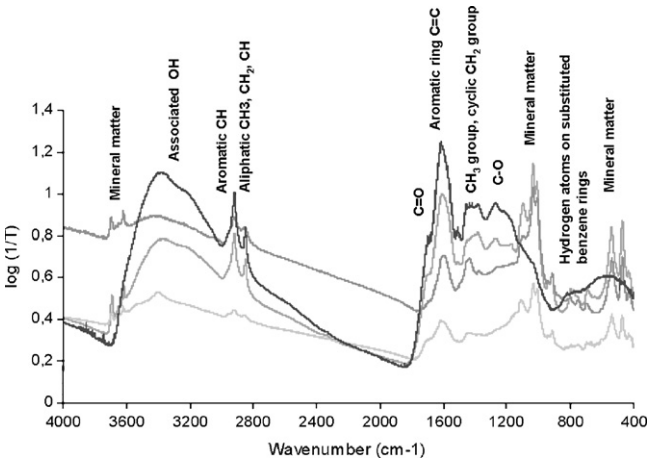


Fig. 3. Transmission MIR spectra for representative coals.

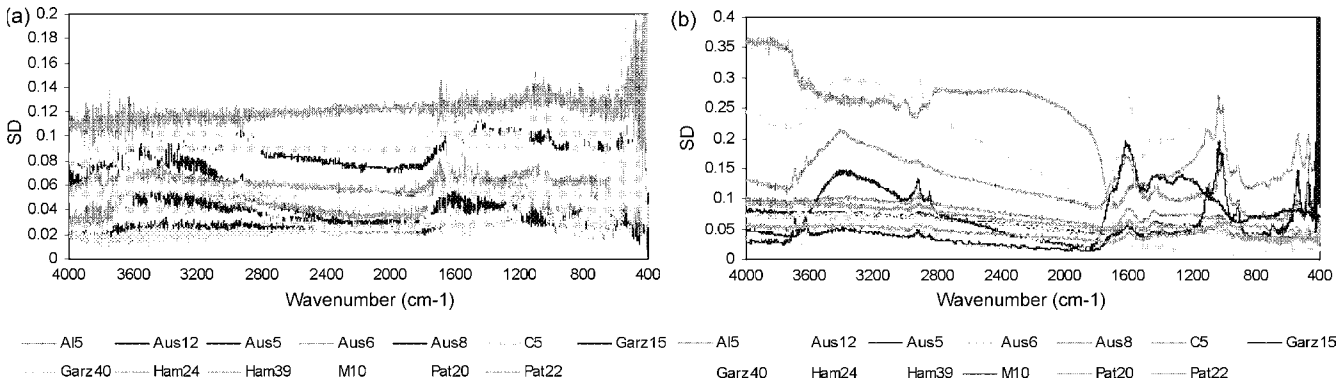


Fig. 4. Influence of sample preparation in the reproducibility study. Standard deviation for (a) reflectance diffuse mode and (b) transmission mode. The samples are classified as follows: Al5, medium volatile bituminous; Aus 12, high volatile C bituminous; Aus 5, medium volatile bituminous; Aus 6, medium volatile bituminous; Aus 8, high volatile A bituminous; C5, high volatile C bituminous; Garz 15, subbituminous B; Garz 40, subbituminous B; Ham 24, subbituminous B; Ham 39, subbituminous A; M10, lignite B; Pat 20, high volatile A bituminous; Pat 22, medium volatile bituminous.

mine those errors, it has been chosen a subgroup of 13 samples of different origins to study the reproducibility both in transmission and reflectance acquisition mode.

Thus, the influence of instrumental components (detector, movement mirror, etc.) was studied by acquiring six times the same sample once prepared in pellets or in the diffuse reflectance sample cup, as appropriate. The calculation of the standard deviation for every sample set revealed that the interference of the apparatus was negligible in both modes.

On the other hand a major influence was present in the acquisition procedure when the position of the pellet or the sample cup into the diffuse reflectance device was studied. In this section each coal sample was slightly rotated for six times to study the homogeneity of the pellet or the roughness of the surface, respectively. These variations could modify the optical pathlength resulting in different light scattering effects.

Several differences were observed between reflectance and transmission mode. Whereas standard deviations for every sample set in diffuse reflectance were nearly constant along the 500–4000 cm^{-1} interval, some coal samples in transmission mode revealed certain dependence on the spectral profile. In these transmission coal spectra, absorption bands with high intensity (mostly related to high moisture or mineral matter content) led to an increment in their standard deviation values.

Similar results were obtained when six different aliquots were acquired for the same coal sample in order to study both sample preparation and homogeneity coal composition. Fig. 4 shows the results for DRIFT and transmission mode.

3.3. Calibration models

Once acquired the spectra, a regression between wavelengths was developed in order to find any kind of linear relationship among the independent variables. This fact would support the use of multivariate calibration techniques such as partial least squares regression (PLS), which it reduces the dimensionality of the data matrix by means of linear combinations [39].

Generally, mid-infrared spectra are characterized for presenting better definition in absorption bands, in such a way that collinearity areas gets narrow (Fig. 5) if they are compared to those obtained for the same sample set in the near infrared interval [28]. Different collinearity degrees can be distinguished in the plot with correlations (R^2) covering from 0 to 1. Among them those represented diagonally were considered as ideal. Moreover, four regions can be observed: (1) intervals corresponding to 400–500 and 1100–1700 cm^{-1}, wherein the high collinearity is associated to their own absorption bandwidths; (2) weak absorption bands in the fingerprint zone (550–1100 cm^{-1}) resulting in a wider area of collinearities and highly related to C=O stretching bands (1650–1850 cm^{-1}); (3) an extensive interval between 1800 and 2700 cm^{-1} corresponding to deviations in baseline wherein it is observed a widening in collinearity as the wavenumber increases. This fact could be due to some kind of relationship between physical transmission effects and aliphatic or hydroxyl intermolecular associated groups (quelates) whose stretching vibration bands ν(O–H) extend even to 2500 cm^{-1}; (4) finally, an area covering 2700–3150 cm^{-1} assigned to aliphatic groups and vinyl, aryl bonds highly collinear to 3500–4000 cm^{-1} mainly corresponding to mineral matter hydroxyl groups also affected by baseline offset.

At the light of the results, partial least squares regression (PLS) considered as an advanced routine was applied in order to cope with collinearities and small non-linearities arising from chemical interactions in the sample [37].

On the other hand, spectral slope deviations or light scattering effects due to physical features of the sample are evident in Fig. 3, hence several mathematical pre-treatments were used to minimize these effects, improving the correlations with respect to the original spectra. Among all possible pre-treatments, the most commonly used ones to correct these spectral variations were used in this work: baseline offset, range normalization, baseline offset followed by range normalization, full multiplicative scatter correction (MSC) and first and second derivatives. All these mathematical modifications were applied to the full set of samples both in transmission and reflection techniques for absorbance ($\log(1/T)$, $\log(1/R)$), transmittance (T), reflectance (R) and Kubelka–Munk units ($f(R)$), as appropriate.

In connection with sample set, the evident variety of coal nature prevented the division of the whole set in two representative sets. The existence of several unique coals could

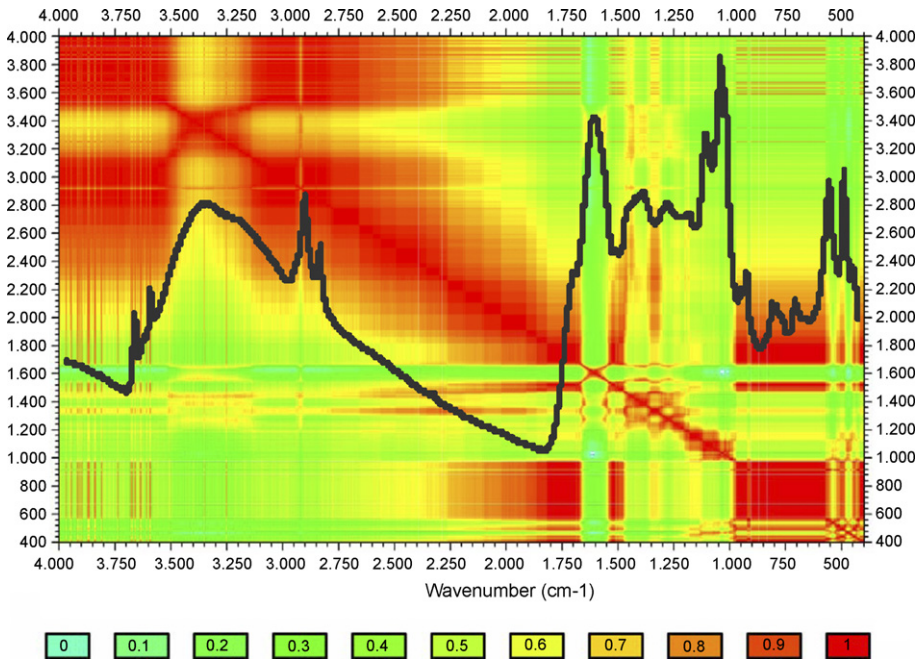


Fig. 5. Determination coefficients (R^2) for spectral-X transmission variables in MIR range. Mean coal spectrum put on top of it.

affect the results if one of them were classified in either of the two sets. In order to avoid this problem, all the assays were developed by means of a leave-one-out full cross-validation procedure. So, the root mean squared error of calibration $\mathrm{RMSEC} = \sqrt{\sum_{i=1}^{N} \hat{y}_i - y_i)^2/(N - A - 1)}$ and prediction $\mathrm{RMSECV} = \sqrt{\sum_{i=1}^{N} (\hat{y}_{\mathrm{CV},i} - y_i)^2/N}$ values obtained by this method have been considered optimistic but adequate for model comparisons. Moreover, all the error values will be plotted in percentage error around the mean to facilitate comparison purposes between coal properties results.

Even so, some coal samples were considered as outliers for each particular studied property on basis of several parameters. This is a very important step to increase the prediction ability of the estimated calibration coefficients. Thus, samples with high leverages, Hotelling-T^2 statistic, residual variance diagrams or studentized residual values over ±3 were some of the criteria to be taken into account for the selection of anomalous coal samples. For all the cases, the deletion of each outlier must be considered subjectively.

3.3.1. Transmission mode

Once established all the calibration models, combining spectroscopic units and mathematical pre-treatments, the best RMSECV (%) values for each coal property in transmission mode are presented in Table 2. With respect to spectroscopic units, there are important differences between transmittance and absorbance spectral data, regardless of what mathematical pre-treatment was applied. Although Beer–Lambert law establishes a lineal relationship between absorbance and sample concentration, in general terms it seems to be favoured the prediction ability when T units were used comparing to those obtained for $\log(1/T)$ ones. This fact may be partly due to the great influence associated to scattering effects, suggesting some kind of no linear correction when transmittance units were used.

Concerning to Pearson's coefficients (r) between calculated and measured values, properties related to organic coal matter achieved 0.98 for prediction set at the same time as nitrogen and sulphur content presented 0.94. Despite the apparently good correlations for raw coal samples, the RMSECV values for nitrogen

Table 2
Best results for prediction RMSECV (%) errors obtained for transmission mode

Property	Units	Pre-treatment	RMSECV	RMSECV (%)	r-CV	Outliers	PC	*X*-explained variance (%)	*Y*-explained variance (%)
Moisture	T	–	2.28	20.34	0.95	3	8	92.44	90.47
Ash	T	–	2.61	19.43	0.97	2	6	95.83	95.01
Volatile matter	T	Baseline/normalization	1.74	4.96	0.98	5	6	96.03	95.14
Fixed carbon	T	MSC	2.5	6.21	0.98	2	4	96.69	96.1
Heating value	$\log(1/T)$	MSC	259.07	5.03	0.98	5	4	96.66	96.14
C	T	Baseline/normalization	2.44	4.43	0.98	3	5	97.65	96.7
H	T	Baseline	0.28	6.43	0.95	1	8	92.89	90.11
N	T	MSC	0.13	14.62	0.94	7	3	88.76	87.94
S	$\log(1/T)$	MSC	0.34	37.36	0.94	2	18	96.10	87.90

and sulphur content revealed that they were not well estimated for quantitative analysis due to the low content of these properties present in the analysed coal samples. With respect to ash content, it is obvious the impossibility of predicting this property in a new coal sample at the light of the RMSECV results. Ash content refers to the remaining material after combustion process and includes mainly inorganic components such as clays, pyrite, and quartz. Despite most of them absorb along the mid-infrared region, final spectra are not representative of the ash content. The diversity of mineral phases and the variations in mineralogy that may accompany coal's rank suggest a coal cluster calibration with similar inorganic compound samples [40]. Similar results are observed for moisture which is present in coals in a number of forms including structural water, adsorbed or free water. All of them are expressed in unique ways in infrared spectra, nevertheless spectral information do not correspond to those obtained after ASTM analytical process in which only evaporated water at 105 °C in nitrogen atmosphere is measured. Finally, the best results are those obtained for coal properties related to organic coal matter (volatile matter, heating value, carbon and hydrogen content) achieving relative RMSECV (%) values around 4–5%. Those values would result in further applications focused on a semi-quantitative approximation as it shows considerably better results comparing to those obtained for commercial instruments [41].

In any case, besides the RMSECV and r obtained for each coal property to estimate the predictive ability of the model, it is necessary to study absolute residual values to check their error distribution and to verify the reproducibility levels allowed by ASTM/ISO reference methods. Thus, some properties related to organic coal matter showed absolute error values between the reproducibility tolerances of reference methods (Fig. 6a). Moreover, despite the widespread homocedasticity of the residual values, some kind of clustering would be interesting in order to improve calibration results for properties such as ash and moisture content (Fig. 6b).

Therefore, it is quite difficult to establish a direct comparison with previous studies developed with different coal sample sets; however the results obtained by using such a wide and diversity coal sample set and a complete mid-infrared spectral range suggest that the application of PLS seems to favour the prediction ability concerning both accurate and precision parameters [21,22].

3.3.2. Reflection mode

Diffuse reflectance infrared spectrometry is characterized for registering scattered radiation which contains absorption information about the sample. This information is usually accompanied by some spectral deviations caused by specular (Fresnel) reflectance. Parameters such as particle size or matrix dilution minimize this contribution; however these parameters are conditional on pulverized coal power station specifications as indicated previously, leading to differences between reflectance and transmission spectra. These differences will be translated into an increment of principal components (between 7 and 10) to explain the same percentage of variance without over-fitting.

All the RMSECV (%) errors obtained after applying PLS regression for the three spectral units (R, log(1/R) and Kubelka–Munk) are arranged in bar charts presented in Fig. 7 . The first bar represents the error obtained for the original spectral data, where no pre-treatment is applied. The successive bars are the errors for the following pre-treatments: baseline offset correction, range normalization, baseline/normalization, MSC, first and second derivatives. This is established for each property studied. Generally, relative error values quite similar to those obtained for transmission mode were observed; however in contrast to what was presented before, generally log(1/R) unit results in better error values than R or $f(R)$, maybe due to a reduction of baseline deviations associated to light scattering effects. On the other hand, Kubelka–Munk transformation, $f(R)$, presents relative RMSECV values comparable to those obtained for log(1/R) when range normalization was applied as spectral mathematical pre-treatment. This fact was really different when near infrared spectroscopy in Kubelka–Munk unit was used, leading to unfeasible calibration models [28]. These and other details are shown in Table 3 , where the best results for prediction errors are included.

3.4. Principal component analysis (PCA)

Principal component analysis is a method of data compression applied to a data matrix of samples [42,43]. New variables, principal components (PCs), are constructed by linear combinations of the original ones, capturing most of the spectral variance. In this case absorbance data matrix was decomposed both for transmission and reflection mode revealing different spectral information for the first few PCs.

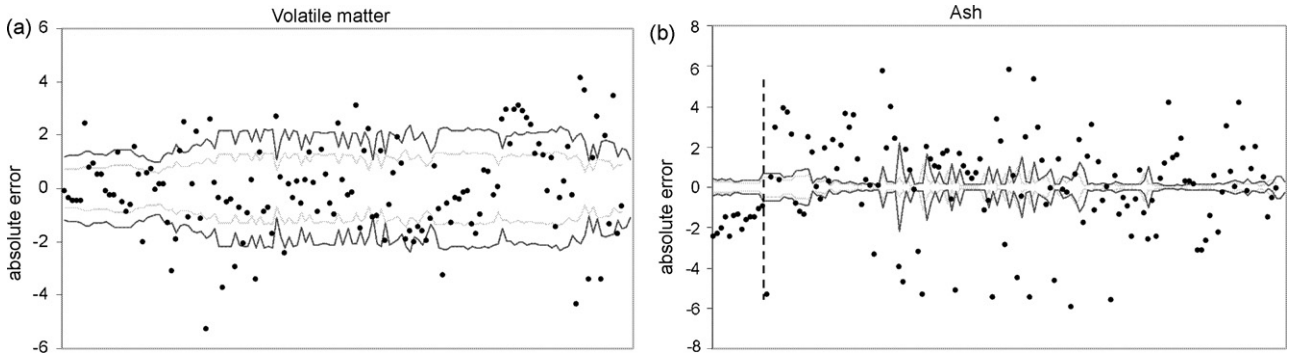


Fig. 6. Absolute residual error values for (a) volatile matter and (b) ash content.

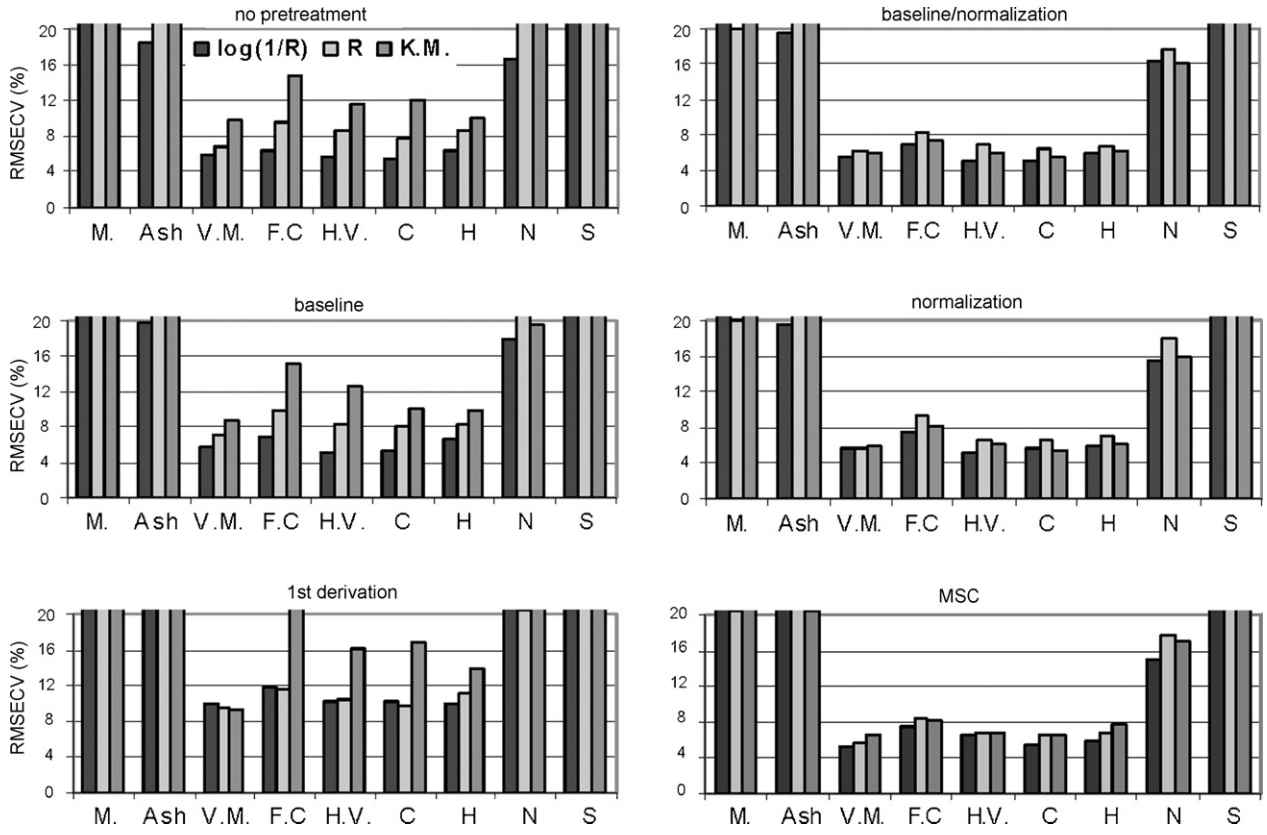


Fig. 7. RMSECV (%) obtained for each property alter applying different pre-treatments. The first bar corresponds to spectra in log(1/*R*) units, the second one in *R* units followed by Kubelka–Munk transformation.

While transmission mode computed the first four principal components to account for 99.14% of the variance, reflection mode required six PCs to account for 98.5%. PC1 versus PC2 score plots are shown in Fig. 8 , after selecting anthracite coal sample as outlier due to its high leverage value. Thus, an analysis of the score diagram combined with *X*-loading principal components plot shows a tendency of coal samples to be grouped attending to moisture content (PC1) and volatile matter (PC2) for transmission mode (Fig. 9). Simultaneously, *X*-loading PC1 presents scattering effects in reverse order than moisture content maybe due to some potassium bromide crystallization during pellet conformation. In any case, PC1 contributes with 74% of *X*-explained variance that combined with PC2 is able to differentiate between coalification ranges: cluster 1 refers to lignite; cluster 2 bituminous with ash content around 22% (blended coal); cluster 3 subbituminous coal samples; cluster 4 and 5 bituminous coal samples of different origins with variable amount of moisture. Further factors will provide more information according to inorganic components. On the other hand when PC1 versus PC2 reflectance score plot are analysed it can be observed only two important clusters, subbituminous and the rest of coal samples. The minimization of scattering effects in DRIFT accompanied with a widening absorption bands leads to a poor differentiation between clusters with the first two PCs (Fig. 10). This fact results in the need for computing more PCs than in transmission mode to explain similar spectral information. At the end, what it is observed in transmission mode it is shown in reflection for subsequent factors.

Table 3
Best results for prediction RMSECV (%) errors obtained for DRIFT mode

Property	Units	Pre-treatment	RMSECV	RMSECV (%)	r-CV	Outliers	PC	*X*-explained variance (%)	*Y*-explained variance (%)
Moisture	*R*	Baseline/normalization	2.23	19.92	0.94	4	6	90.94	88.48
Ash	Log(1/*R*)	–	2.47	18.32	0.97	4	10	97.05	94.60
Volatile matter	Log(1/*R*)	Baseline/normalization	1.95	5.57	0.97	3	7	96.12	93.90
Fixed carbon	Log(1/*R*)	–	2.58	6.41	0.98	4	10	97.65	95.55
Heating value	Log(1/*R*)	Baseline/normalization	262.13	5.09	0.98	1	8	97.64	96.48
C	Log(1/*R*)	Baseline/normalization	2.75	5	0.98	4	7	97.42	95.97
H	Log(1/*R*)	Baseline/normalization	0.25	5.89	0.96	4	7	94.38	91.66
N	Log(1/*R*)	Normalization	0.14	15.56	0.93	4	7	90.68	87.19
S	*R*	MSC	0.56	361.32	0.83	5	12	88.96	67.94

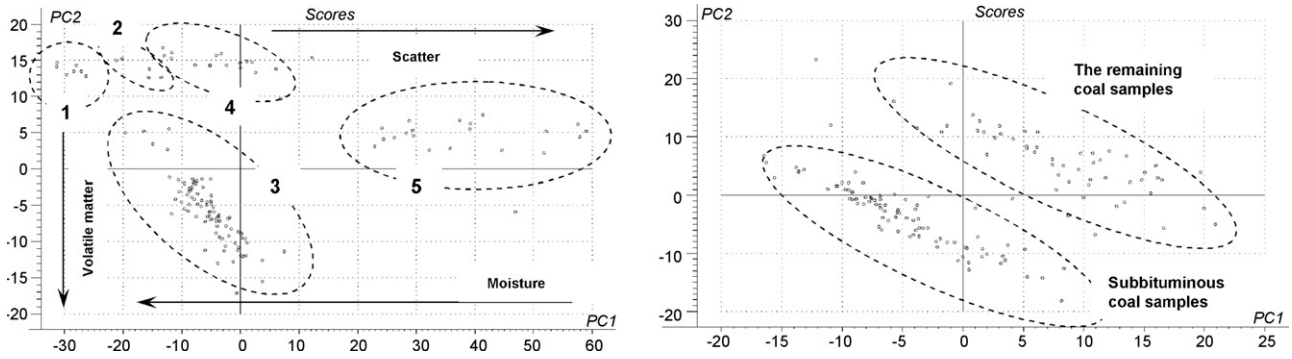


Fig. 8. PC1 vs. PC2 score plot corresponding to PCA; (left) transmittance. Cluster 1: lignite coal samples; 2: blended coal; 3: subbituminous; 4 and 5: bituminous coal samples of different origins, (right) reflectance diffuse (DRIFT).

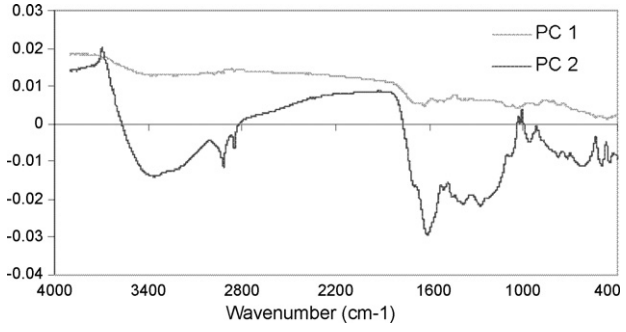


Fig. 9. PC1 and PC2 *X*-loading plot corresponding to PCA in transmission mode.

Once studied the first two principal components, there were analysed further ones. Different score plots PC3 versus PC1 and PC4 versus PC2 in transmission mode show how PC3 is directly correlated to the total ash content, whereas PC4 is able to distinguish between coal samples attending to their mineral matter compounds. Thus, coal samples with kaolinite in their composition are placed opposite to those with other aluminium-silicate phases. This behaviour is corroborated by comparing *X*-loadings PC3, PC4 plot to two infrared samples spectra (Fig. 11). Generally, positive bands in loading plot contribute to the property analysed while negative bands are discarded for the PC studied. Thus, it is observed how PC4 corresponds to kaolinite spectrum (3695, 3650, 3620, 1114, 1032, 1010, 936, 912, 790, 752, 693, 537, 468, 430 cm^{-1}), with positive bands directly comparables to Ham 7, whereas the corresponding loading of PC3 seems to be the results of the two coal spectra added. Finally, positive bands are assigned to the total mineral matter content whereas negative ones correspond to the organic part of coal samples (1600, 2850, 2915 cm^{-1} among others).

3.5. Subbituminous coal samples

A coal subset consisted of 88 subbituminous samples from Garzweiler and Hambach mines were analysed using transmission and reflection techniques, covering both diffuse reflectance (DRIFT) and attenuated total reflection (ATR) spectroscopy. At the light of the results with the full sample set, transmission mode presented better prediction ability in comparison to DRIFT; however it is a technique that requires laborious sample preparation to be implemented in an on-line system. Regarding this subject ATR is presented as a potential technique to analyse coal samples due to its simplicity. It is really suitable for powder samples provided the sample is in contact with or in close proximity to the reflecting surface. From the interaction of the evanescent wave with the sample, a spectrum can be recorded with little or no sample preparation. In this case, the spectral profile was quite similar to transmission one, despite it was observed an important reduction in absorption band intensities (Fig. 2). Moreover, scattering effects were minimized requiring exclusively some kind of range normalization or MSC spectral correction. Even so, some spectral deviations were observed as it occurred in diffuse reflectance. On the one hand, as the angle of incidence approached the critical angle, the bands tended to broaden on the long wavelength side, leading to a displacement of the minimum to longer wavelengths (lower wavenumbers); on the other hand some kind of dispersion was observed very close to and below critical angle.

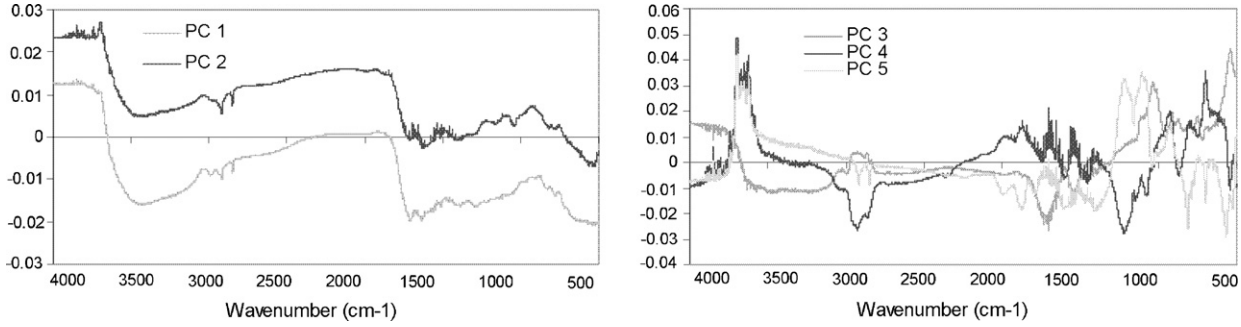


Fig. 10. *X*-loadings plot corresponding to PCA in reflectance diffuse (DRIFT) mode; (left) PC1–PC2, (right) PC3–PC5.

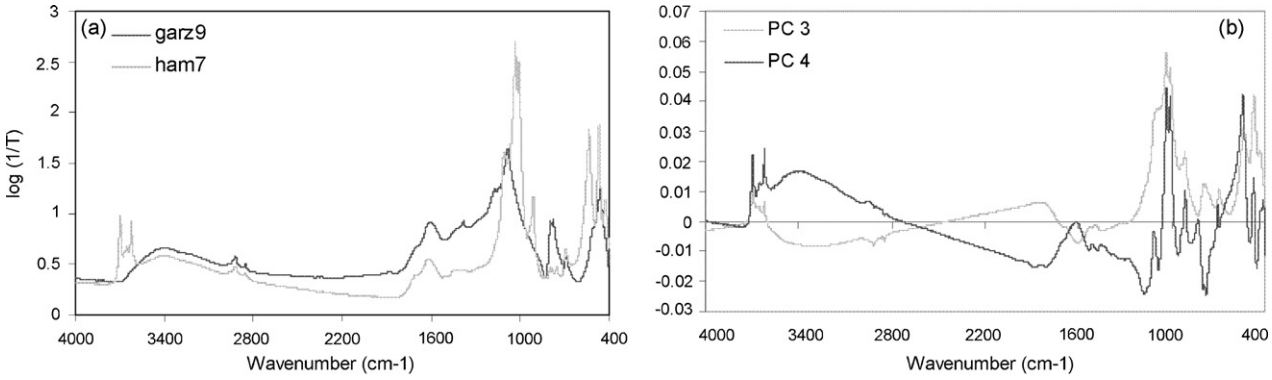


Fig. 11. (a) Loadings of PC3–PC4 corresponding to PCA for transmission mode and (b) spectra for two coal samples (Ham 7, Garz 9).

Table 4
Best results for calibration and prediction errors obtained for a coal samples subset in ATR mode

Property	Pre-treatment	RMSEC	RMSEC (%)	RMSECV	RMSECV (%)	r-CV	Outliers	PC
Moisture	MSC	0.68	5.45	0.98	7.84	0.94	3	10
Ash	Normalization	1.62	11.66	2.22	15.97	0.98	7	7
Volatile matter	Normalization	1.22	3.1	1.57	3.98	0.97	2	6
Fixed carbon	Normalization	1.04	3.04	1.47	4.3	0.97	2	8
Heating value	Normalization	118.51	2.6	165.67	3.64	0.98	5	6
C	–	1.44	2.9	1.79	3.6	0.98	2	7
H	Normalization	0.17	3.74	0.22	4.84	0.96	2	6
N	–	0.08	11.42	0.1	14.6	0.83	2	8
S	MSC	0.12	18.53	0.27	42.35	0.88	0	18

After developing PLS regression models for each coal property it could be observed comparable ATR RMSECV (%) values to those obtained for transmission mode. This fact will facilitate further on-line industrial applications. The best results are summarized in Table 4 wherein the relative error determination for properties related to organic compounds is highlighted. At the same time, the moisture calibration for more homogeneous sample set translates in a significant reduction in the RMSECV (%). The absolute residual values against repeatability and reproducibility ASTM/ISO limits reveal the goodness of volatile matter and fixed carbon determination. The rest of the properties fulfil the semi-quantitative requirements for a combustion power plant analyser.

4. Conclusions

The interest in determining coal properties in a fast and reliable way leads us to study the adequacy of transmission and reflection acquisition techniques based on Fourier transform infrared spectroscopy. The existing collinearity between spectral variables determines the use of PLS regression models. Generally, acceptable correlations were found for coal properties related to organic compounds such as fixed carbon, heating value, carbon and hydrogen content, being higher for transmission mode. Nevertheless, it is interesting to minimize sample analysis preparation for further online implementation. Thus, a subset of coal samples was calibrated both in transmission, DRIFT and ATR mode. Although it was observed slightly deviations in spectral positions, the relative error determination for ATR was quite similar to transmission mode with the advantage of requiring no sample preparation. Moreover, the determination of volatile matter and fixed carbon fulfilled the reproducibility limits of standard methods. The rest of the properties could be determined for semi-quantitative analysis, appropriate for an on-line system. Finally, a principal component analysis presented a technique able to differentiate coal samples in based on its moisture and volatile matter content. Although the system was unfeasible for ash content determination, it is important to highlight the possibility of classifying coal samples attending to their mineral matter composition and, more specifically kaolinite content from other aluminium-silicates phases.

Acknowledgements

The authors are grateful to the European Coal and Steel Community for funding this research within the framework of Project 7220-PR/118. We also thank to ENDESA, RWE Ag, EVN Ag and PPC for providing us coal samples.

References

[1] M.D. Belbot, G. Vourvopoulos, P.C. Womble, J. Paschal, Proceedings of the SPIE Conference on Penetrating Radiation Systems and Applications, vol. 3769, 2000, p. 168.
[2] A.M. Carpenter, IEA Coal Res. 81 (1995).
[3] ISO-589-1981 Hard coal-Determination of total moisture.
[4] ISO-1171-1976 Combustibles minéraux solides-Détermination des cendres.
[5] ISO-562-1974 Houille et coke-Détermination du taux de matières volatiles.
[6] ASTM D 3172-89 Standard Practice for Proximate Analysis of Coal and Coke (reapproved 1993).

[7] ISO-1928-95 Solid mineral fuels-Determination of gross calorific value by the bomb calorimetric method, and calculation of net calorific value.
[8] ASTM D 3177-89 Standard Test Methods for Total Sulfur in the Analysis Sample of Coal and Coke.
[9] N.G. Cutmore, A.F. Roczniok, B.D. Sowerby, Nucl. Geophys. 1 (4) (1987) 319.
[10] A. Klein, Aufbereitungs-Tehnik 1 (1987) 10.
[11] D.A. Hall, J.C. Spronson, W.A. Gray, J. Inst. Fuel 45 (1972) 163.
[12] B.D. Sowerby, M.J. Millen, P.T. Rafter, Nucl. Geophys. 2 (1) (1988) 55.
[13] N.G. Cutmore, B.D. Sowerby, L.J. Lynch, D.S. Webster, Fuel 65 (1986) 34.
[14] J.K. Brown, J. Chem. Soc. (1955) 744.
[15] J.G. Speight, Appl. Spectrosc. Rev. 29 (2) (1994) 117.
[16] P.A. Estep, J.J. Kovach, K. Clarence Jr., Anal. Chem. 40 (2) (1968) 358.
[17] V.A. Bell, V.R. Citro, G.D. Hodge, Clays Clay Miner. 39 (3) (1991) 290.
[18] P.C. Painter, S.M. Rimmer, R.W. Snyder, A. Davis, Appl. Spectrosc. 35 (1981) 102.
[19] P.R. Solomon, R.M. Carangelo, Fuel 61 (1982) 663.
[20] P.R. Solomon, R.M. Carangelo, Fuel 67 (1988) 949.
[21] S. Tesch, K.-H. Rentrop, M. Otto, Fresenius' J. Anal. Chem. 344 (1992) 206.
[22] C.E. Alciaturi, M.E. Escobar, R. Vallejo, Fuel 75 (4) (1996) 491.
[23] C.E. Alciaturi, T. Montero, C. De La Cruz, M.E. Escobar, Anal. Chim. Acta 340 (1997) 233.
[24] C.E. Alciaturi, M.E. Escobar, C. De La Cruz, R. Vallejo, Anal. Chim. Acta 436 (2001) 265.
[25] E.A. Cloutis, Fuel 82 (2003) 2239.
[26] M. Sobkowiak, P. Painter, Energy Fuels 9 (1995) 359.
[27] R.L. Carmichael, Proceedings of the International Symposium on Mining Technology and Science, Xuzhou, China, September 18, 1985, China Coal Industry Publishing House, Beijing, China, 1987, p. 1365.
[28] J.M. Andrés, M.T. Bona, Anal. Chim. Acta 535 (2005) 123.
[29] M.P. Fuller, I.M. Hamadeh, P.R. Griffiths, D.E. Lowenhaupt, Fuel 61 (1982) 529.
[30] T. Naes, T. Isaksson, T. Fearn, T. Davies, A User-Friendly Guide to Multivariate Calibration and Classification, NIR Publications, 2002, p. 105.
[31] P. Geladi, D. MacDougall, H. Martens, Appl. Spectrosc. 39 (3) (1985) 491.
[32] H.H. Schobert, Coal. The Energy Source of the Past and Future, American Chemical Society, Washington, DC, 1987.
[33] P.C. Painter, R.W. Snyder, M. Starsinic, M.M. Coleman, D.W. Kuehn, A. Davis, in: E.L. Fuller (Ed.), Coal and Coal Products: Analytical Characterization Techniques, vol. 205, American Chemical Society, 1982, pp. 47–76, Symposium Series.
[34] P.C. Painter, M. Sobkowiak, J. Youtchekk, Fuel 66 (1987) 973.
[35] J. Madejová, P. Komadel, Clays Clay Miner. 49 (5) (2001) 410.
[36] P.C. Painter, S.M. Rimmer, R.W. Snyder, A. Davis, Appl. Spectrosc. 35 (1) (1981) 102.
[37] P.B. Coleman, Practical Sampling Techniques for Infrared Analysis, CRC Press, 1993.
[38] J.C. Miller, J.N. Miller, Estadística para química analítica, 2nd ed., Addison-Wesley Iberoamericana, 1993.
[39] H. Wold, in: K.G. Jöreskog, H. Wold (Eds.), Systems Under Indirect Observation, Causality-Structure-Prediction, vol. 2, North Holland, Amsterdam, 1981, pp. 1–54.
[40] S.V. Vassilev, K. Kitano, C.G. Vassileva, Fuel 75 (1996) 1537.
[41] G.R. Couch, IEA Coal Research, London, IEACR/22, 1996.
[42] S. Wold, S.H. Antii, F. Lindgren, J. Öhman, Chemometr. Intell. Lab. Syst. 44 (1998) 175.
[43] J.E. Jackson, User's Guide to Principal Components, Wiley, New York, 1991.

Available online at www.sciencedirect.com
ScienceDirect
Talanta 74 (2008) 936–943
Talanta
www.elsevier.com/locate/talanta

Determination of thiolic compounds as mercury complexes by cold vapor atomic absorption spectrometry and its application to wines

Emilia Bramanti [a,*], Rosa Cavallaro [b], Massimo Onor [a], Roberto Zamboni [b], Alessandro D'Ulivo [a]

[a] *Italian National Research Council (CNR), Institute for chemical and physical processes, (IPCF) Laboratory of Instrumental Analytical Chemistry, Via G. Moruzzi 1, 56124 Pisa, Italy*
[b] *University of Pisa, Department of Chemistry and Industrial Chemistry, Via Risorgimento 35, 56126 Pisa, Italy*

Received 13 March 2007; received in revised form 25 July 2007; accepted 30 July 2007
Available online 15 August 2007

Abstract

We report on the application of a commercially available mercury analyzer, which is based on vapour generation of Hg^0 by $NaBH_4$ reduction and atomic absorption detection, to the quantification and characterization of –SH groups and its application to wine samples. The behaviour of Hg(II) and thiol–Hg(II) (RS–Hg) complexes at nanomolar level (RS = L-cysteine, DL-penicillamine, *N*-acetyl penicillamine, glutathione, cysteinylglycine, homocysteine) has been studied following their reduction with alkaline $NaBH_4$ to give Hg^0. In the absence of thiol–Hg(II) is quantitatively converted to Hg^0 by stoichiometric amount of $NaBH_4$ (reaction ratio 1/4 mole $NaBH_4$/mole Hg), while the complete reduction of Hg(II)–thiol complexes to Hg^0 requires molar excess of $NaBH_4$ up to six orders of magnitude, depending on the type of complex and on the pK_a of the thiolic group. Under an appropriate excess of reductant, Hg(II) and its thiol complexes are not distinguishable giving the same response. These properties allow the discrimination of Hg(II) from Hg(II)–thiol complexes without any preliminary separation and the quantification of thiol groups. Instrumental detection limits are as low as 2.5 pg, permitting sample dilution, therefore, minimizing the risk of possible interferences occurring with complex real matrices.

The method has been applied to quantification of thiol groups in wine samples. Comparison with results obtained by HPLC coupled to atomic fluorescence detection confirmed the promising potentialities of the method.
© 2007 Elsevier B.V. All rights reserved.

Keywords: Chemical vapor generation; Atomic absorption spectrometry; Mercury–thiol complexes; Sulfhydryl groups in wine; Tetrahydroborate

1. Introduction

Thiolic compounds are low molecular or high molecular, ubiquitous molecules widely studied in many research areas, such as geochemistry [1], biochemistry [2,3] and metabolomics [4], nanotechnology [5], medicine [6] environmental [7] and food chemistry [8–10]. They are well known to play fundamental structural and functional roles in protein chemistry, being located mainly within the active site of many enzymes and directly involved in catalysis [11].

Heavy metals have a high affinity for –SH groups and the affinity of mercury, in particular, is known to be very high in the pH range of 1–13 for low molecular weight compounds (such as gluthatione, cysteine, homocysteine) and for macromolecules (proteins, humic matter) [12]. The interaction of heavy metals and, in particular, mercury with essential thiol groups of enzymes and proteins is the basis of the mechanism of their toxic activity [13–19].

The high affinity of inorganic (Hg^{2+}) and organic mercury cations (RHg^+, where R = CH_3, phenyl, e.g.) for –SH groups

* Corresponding author. Tel.: +39 050 3152293; fax: +39 050 3152555.
E-mail address: emilia@ipcf.cnr.it (E. Bramanti).

0039-9140/$ – see front matter © 2007 Elsevier B.V. All rights reserved.
doi:10.1016/j.talanta.2007.07.041

has been used for analytical and diagnostic purposes. Hg^{2+} has been proposed for amperometric [20] and conductometric [21] titration in order to determine thiols in a concentration range of 10^{-3} to 10^{-5} mol L^{-1}; RHg^{+} has been used as biochemical molecular probe for active sulfhydryl groups [12].

A new sensitive and selective method for determination of thiol groups at nanomolar level has been developed in our laboratory [22]. It is based on the cold vapour (CV) generation technique coupled with a laboratory assembled atomic fluorescence spectrometric (AFS) detector for the characterization of Hg(II)–thiol and Hg(II)–protein complexes [22,23]. The selective reduction of inorganic Hg(II) and its thiolic complexes by varying the concentration of alkaline $NaBH_4$ combined with AFS detection of the evolved Hg^0 revealed an interesting and sensitive analytical tool for the investigation and characterization of Hg(II)–thiol complexes such as the thiolic proteins ovalbumin, hemoglobin, glyceraldehyde-3-phosphate-dehydrogenase, aldolase, pyruvate kinase, hexokinase, lactate dehydrogenase, alcohol dehydrogenase, creatine phosphokinase, lysozyme and cytochrome *C* [23].

In this paper, the cysteine–, glutathione–, penicillamine–mercury complexes, previously studied by CV-AFS, and cystein–glycine–, homocysteine– and *N*-acetyl penicillamine–mercury complexes has been investigated by flow injection cold vapor atomic absorption spectrometry (FI-CV-AAS), which integrates flow injection mercury cold vapour generation with a very sensitive atomic absorption detector. FI-CV-AAS has been adapted for the characterization of Hg(II)–thiol complexes by reduction and titration curves and it has been applied to the determination of total thiolic compounds in wines.

2. Experimental

2.1. Chemicals

Working solutions of inorganic Hg(II) in a form of $Hg(NO_3)_2$ were prepared by serial dilutions of the stock solution (1000 ± 5 μg mL^{-1}, BDH Laboratory Supplies, Poole, England) just before use. Stock solutions of thiols (L-cysteine, CYS 30119, reduced glutathione, GSH G4251, DL-penicillamine, PSH 76410, *N*-acetyl-D-penicillamine, NAP 01423, cysteinyl-glycine, Cys-Gly C0166, homocysteine, HCys H4628, ethyl-2-mercaptopropionate, Et-2-PrSH W327905 from Fluka–Sigma–Aldrich, Chemical Co., Milan, Italy), were prepared as previously reported [22,23].

Stock and working solutions of $NaBH_4$ were prepared as previously reported [22,23].

Water purified with a Milli-Q system (Millipore Filter Co., Bedford MA, USA) was used in all the operations.

2.2. Working solutions

All the working solutions containing Hg(II) and/or thiols at nanomolar level ($(5–300) \times 10^{-9}$ mol L^{-1}) are prepared just before use by proper dilutions with a solution containing 10^{-2} mol L^{-1} sodium phosphate buffer pH (7.4, 5) $\times 10^{-2}$ mol L^{-1} NaCl (indicated as PBS/NaCl). The addition of NaCl prevents the formation of insoluble mercury hydroxides through the formation of mercury–chloride complexes.

Solutions containing Hg(II) and thiol, at the desired molar ratio, lead to the formation of Hg(II)–thiol complexes. Since the reaction of inorganic Hg(II) with sulfhydryl groups is instantaneous at room temperature no incubation time is required before measurements. The solutions were analyzed within 1 h from preparation.

2.3. Hg(II)–thiol titrations

Titrations were performed for thiols by processing separate solutions each containing the same concentration of Hg(II), typically 4×10^{-8} mol L^{-1}, and increasing amounts of the thiol, typically in the range of $(0–2) \times 10^{-7}$ mol L^{-1}, in order to realize different thiol/mercury molar ratios. Solutions were prepared in PBS/NaCl in 10 mL test tubes, loaded in the autosampler and analyzed within 15 min. A total of 10 mL were enough for three replicates measurements and the entire titration required about 15 min.

2.4. Sample collection and storage

A total of 10 mL of each wine sample ($N = 8$ wine samples examined) were sampled from original glass bottles, kept tightly closed in glass test tubes in the dark at 4 °C, and analyzed within 48 h from sampling. Mercury titrations for total –SH determination were performed with wine samples diluted 50 times with PBS/NaCl. All analyses were performed in November 2006. Reduction curve were performed by analyzing a 200 mL PBS/NaCl containing 5×10^{-8} mol L^{-1} Hg(II) and 480 μL of wine.

2.5. FI-CV-AAS analyzer

The Perkin-Elmer Flow Injection Mercury System (FIMS-100) equipped with an AS-91 autosampler, was employed in the conventional configuration for mercury–thiol titrations (Fig. 1, A configuration) with an injection loop of 200 μL, the peristaltic pump operated at 40 rpm, corresponding to a measured flow rate of 3.5 mL min^{-1}. $NaBH_4$ in 0.1 mol L^{-1} NaOH was employed as reducing agent at a concentration ranging between 10^{-8} and 3×10^{-4} mol L^{-1} (see results). Sample medium and carrier was PBS/NaCl.

For reduction curves FIMS-100 configuration was modified connecting the autosampler output to the reductant line (Fig. 1, B configuration). In this configuration the autosampler delivers a sequence of 15 solutions of $NaBH_4$, 0.1 mol L^{-1} NaOH, $NaBH_4$ concentrations ranging between 3×10^{-9} mol L^{-1} and 1 mol L^{-1}. The sample loop is loaded in continuous in the "fill" position of the injection valve. In this configuration the sample solution after loop loading could be recycled, limiting the sample consumption only to the injected quantity multiplied for the number of injections. A 30 cm × 0.75 mm i.d. reduction coil has been employed [22].

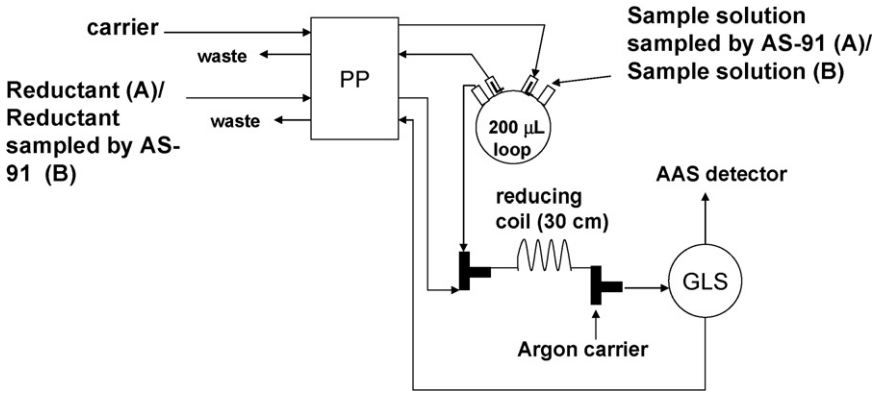


Fig. 1. Schematic representation of the FIMS-100 configuration for thiol and wine titrations (A) and for reduction curves of mercury/thiol complexes (B). GLS, gas–liquid separator; PP, peristaltic pump.

3. Results and discussion

3.1. Calibration curves of mercury in PBS/NaCl

Hg(II) calibration curves were carried out both by using conventional, acid, chemical reduction conditions (0.2% $NaBH_4$ in 0.05% NaOH; carrier = 3% (v/v) HCl) and by performing mercury reduction in alkaline medium (10^{-5} mol L^{-1} $NaBH_4$ in 0.1 mol L^{-1} NaOH; carrier = 10^{-2} mol L^{-1} phosphate buffer solution pH 7.4, 5×10^{-2} mol L^{-1} NaCl). Results show that mercury can be determined also in neutral solutions (PBS/NaCl) with a concentration of reducing agent 5000 folds more diluted than that suggested by FIMS operating manual with a detection limit of 2.5 pg, the dynamic linear range spanning from 3 pg to 30 ng (investigated range). These figures of merit were not significantly different from those obtained in HCl medium.

3.2. Determination and characterization of thiols by FI-CV-AAS

The characterization of thiol–mercury complexes originally developed for CF-CV-AFS [22] was performed by FI-CV-AAS. Three low molecular weight thiols previously investigated (CYS, GSH and PSH) and three thiols (CysGly, HCys, NAP) not previously studied were considered. The test has been performed by studying the efficiency of formation of Hg^0 in the reaction of both Hg(II) and thiols–mercury complexes ($Hg_n(RS)_m$) with $NaBH_4$ under alkaline conditions. The reaction system can be characterized by the study of the reduction curves and titration curves as reported below.

Mercury–thiol complexes, $Hg_n(SR)_m$, can be obtained in a simple way by reaction of a thiol with Hg^{2+} at room temperature. The most commonly observed complexes are $Hg(SR)_2$ and $Hg_2(SR)_2$ [20,21,24–34]. Although several authors have excluded the formation of $Hg_2(SR)_2$ compounds in the presence of chloride ion, due to the stability of $HgCl_4^{2-}$ which suppresses the reaction of excess mercury with the mercaptide [24,35], other ones did observe the formation of such complexes also in the presence of chloride ions, and particularly at basic pH [20]. In $Hg_2(SR)_2$ one mercury atom is bound firmly as mercaptide and the second one is bound more loosely [20].

The experimental curves obtained by plotting the mercury relative absorbance signal versus $NaBH_4$ concentration will be termed reduction curves; they represent the fraction of the total mercury that can be reduced to Hg^0 by a given concentration of reductant.

$Hg(SR)_2$ complexes were prepared using an excess of thiol (RSH/Hg(II) = 4) according to the equilibrium reaction:

$$Hg^{2+} + 2RSH \;=\; Hg(SR)_2 + 2H^+ \tag{1}$$

with an equilibrium constant:

$$K_F = \frac{[Hg(SR)_2][H^+]^2}{[Hg^{2+}][RSH]^2} \tag{1a}$$

Considering that the values of log K_F are around 40 (Table 1), the employment of a molar excess of thiol makes the concentration of free Hg(II) negligible with respect to total mercury concentration.

Fig. 2A shows the comparison of reduction curves of Hg(II) and of $Hg(SR)_2$ complexes (where R = GSH, CYS, NAP, CysGly, HCys, PSH) and typical titration curves of mercury with GSH (Fig. 2B).

The normalized integrated absorbance signal of $HgCl_4^{2-}$ increases with $NaBH_4$ concentration until a plateau is reached for $NaBH_4$/Hg molar ratios greater than 0.27 ± 0.02 for the reduction of 5×10^{-8} mol L^{-1} Hg(II) solutions. $NaBH_4$/Hg molar ratio has been estimated by the intersection of the linear fitting of data of the increasing part of curve a (Fig. 2A) with the plateau. This value is in agreement with the the stoichiometry of the reduction reaction of Hg(II) by $NaBH_4$ in alkaline media, as previously reported [22].

Table 2 reports C_{50} values of the six thiols studied, where C_{50} is defined as the concentration of $NaBH_4$ which gives the 50% of normalized integrated absorbance signal.

These results are in good agreement with the previous findings obtained by CF-CV-AFS [22]. It is worth noting that the magnitude of the molar excess of reductant, ranging from about 10^3–10^6, resulted to be correlated with K_a values reported in literature [36]. The plot of log C_{50} versus pK_a of –SH group of thiol is reported in Fig. 3. A linear fit of these data gave an intercept = 18.0 ± 4.4 and a slope = -2.37 ± 0.47 ($R = 0.9292$, $N = 6$).

Table 1
Summary of the stability constants of RS–Hg(II) complexes known from literature data ($K_F = \beta_1\beta_2$)

Thiol	Method	C (mol L^{-1})	T (°C)	Ion strength (mol L^{-1})	pH	Medium	log β_1	log β_2	log K_F	Ref.
PSH	ISE	10^{-3}	25	0.1	6–8	$NaClO_4$ $LiCLO_4$	38.3	6.1	44.4	[31]
	EMF	10^{-3}	25	0.1	6–8	$NaClO_4$ $LiCLO_4$	37.8	6.7	44.5	[28]
CYS	EMF	10^{-3}	25	0.1	6–8	$NaClO_4$ $LiCLO_4$	37.8	6.2	44	[28]
	GE	10^{-2}	25	0.1	>11.5	$NaNO_3$	–	–	39.4	[26]
		10^{-4} to 10^{-3}	25	0		KNO_3			43.57	[24]
	ISE	10^{-4} to 10^{-3}	12	1		KNO_3			45.4	[24]
GSH	ISE	10^{-4} to 10^{-3}	25	0	>9.5	KNO_3	–	–	41.58	[24]
		10^{-4} to 10^{-3}	12	1	>9.5	KNO_3	–	–	43.47	[24]
	GE	10^{-4}	25	0.1	>9.5	KCl	–	–	33.4	[29]

GE, glass electrode; ISE, ion selective electrode.

These results show that more acid –SH groups form more stable thiol–mercury complexes, which need higher concentration of $NaBH_4$ to be reduced to Hg^0.

From Hg(II) reduction curve it has also been observed that the stability of diluted alkaline $NaBH_4$ solutions (0.1 mol L^{-1} NaOH) is compromised if they are stored for short time in polyethylene flasks. This has been noted by comparing the reduction curves for Hg(II) obtained by using $NaBH_4$ preserved in glass (Fig. 2A, curve a) or in polyethylene flask for 16 h at room temperature (Fig. 2A, curve a′). The shift of the curve toward higher values of $NaBH_4$ concentrations indicates a significant decomposition of the reductant.

The selective reduction of Hg(II) in the presence of its thiol complexes offers the possibility to quantify thiols by the study of titration curves, which are obtained by reducing Hg(II) with $NaBH_4$ in the absence and in the presence of different amount of thiols. Fig. 2B shows, as an example, the titration curves of mercury by GSH using five different concentration of $NaBH_4$. By increasing the concentration of thiol, less Hg(II) is available for reduction and the relative absorbance signal tends to zero. At the equivalence point the Hg(II)–thiol complex will be the predominating specie while beyond the equivalence point both Hg(II)–thiol and not complexed thiol will be present. If an appropriate concentration of $NaBH_4$ is employed (for example, [$NaBH_4$] = [Hg]/4 or slightly higher) only the not complexed Hg(II) will be selectively reduced and detected. The equivalence point can be identified by the intersection of the descending branch of titration curve with the plateau obtained for thiol/Hg(II) molar ratio >number of titrable –SH groups in the solution. This type of curve can be employed for the estimation of the number of *accessible* –SH groups in a protein [23] or of total thiolic compounds in a sample (see the application).

Table 2
C_{50} values (mean ± S.D.*) obtained from reduction curves of $Hg(RS)_2$ complexes (5×10^{-8} mol L^{-1} Hg/2×10^{-7} mol L^{-1} RSH)

RSH	C_{50}*
CYS	$(7.4 \pm 0.9) \times 10^{-4}$
GSH	$(5.6 \pm 0.6) \times 10^{-5}$
HCys	$(6.0 \pm 1.3) \times 10^{-5}$
CysGly	$(1.7 \pm 0.1) \times 10^{-4}$
PSH	$(2.8 \pm 0.9) \times 10^{-3}$
NAP	$(8.9 \pm 5.0) \times 10^{-7}$

* S.D. on three independent measurements.

As previously observed, the position of the equivalent point in the titration curve is dependent on $NaBH_4$ concentration and this is a consequence of the behaviour of Hg(II)–RS complexes described by the reduction curves [22]. For four investigated thiols (GSH, Cys, CysGly, HCys) the thiol/Hg(II) ratios calculated at the end point varied between 1.14 ± 0.14 (1×10^{-8} mol L^{-1} $NaBH_4$) and 1.97 ± 0.16 (1×10^{-4} mol L^{-1} $NaBH_4$). When the reduction of thiol–mercury solutions is performed by using $NaBH_4$ concentrations for which [$NaBH_4$]/[Hg] is close to the stoichiometric reaction ratio of 0.25, then only the fraction of mercury not complexed by RSH will be reduced. Under these conditions the end point was reached for thiol/Hg(II) molar ratios close to one. This experimental finding is consistent with the formation of Hg–RS complexes of the type 1:1 or 2:2 [20]. The gradual increase of $NaBH_4$ concentration allows reduction of an increasing fraction of mercury bound to Hg–RS complexes (Fig. 2A) and the RSH/Hg(II) molar ratios obtained at the end point tended to a value of 2 which is consistent with the formation of $Hg(RS)_2$ complexes for RSH/Hg(II) molar ratios ≥2. In the limit case of using $NaBH_4$ concentration which is able to reduce completely $Hg(RS)_2$ complexes the titration curve is flat.

The reduction curves of Hg–CYS and Hg–GSH complexes were also investigated with solutions containing RSH/Hg(II) molar ratios other than four. Reduction curves obtained for [Hg(II)] = 5×10^{-8} mol L^{-1} (10 ng mL^{-1}) and molar ratios of 1/1, 2/1 and 4/1 are reported in Fig. 4.

For molar ratios ≥2, only $Hg(CYS)_2$ complexes (Fig. 4A) are obtained as demonstrated by the similarity of reduction curves (b) and (c); complete reduction is obtained at [$NaBH_4$]

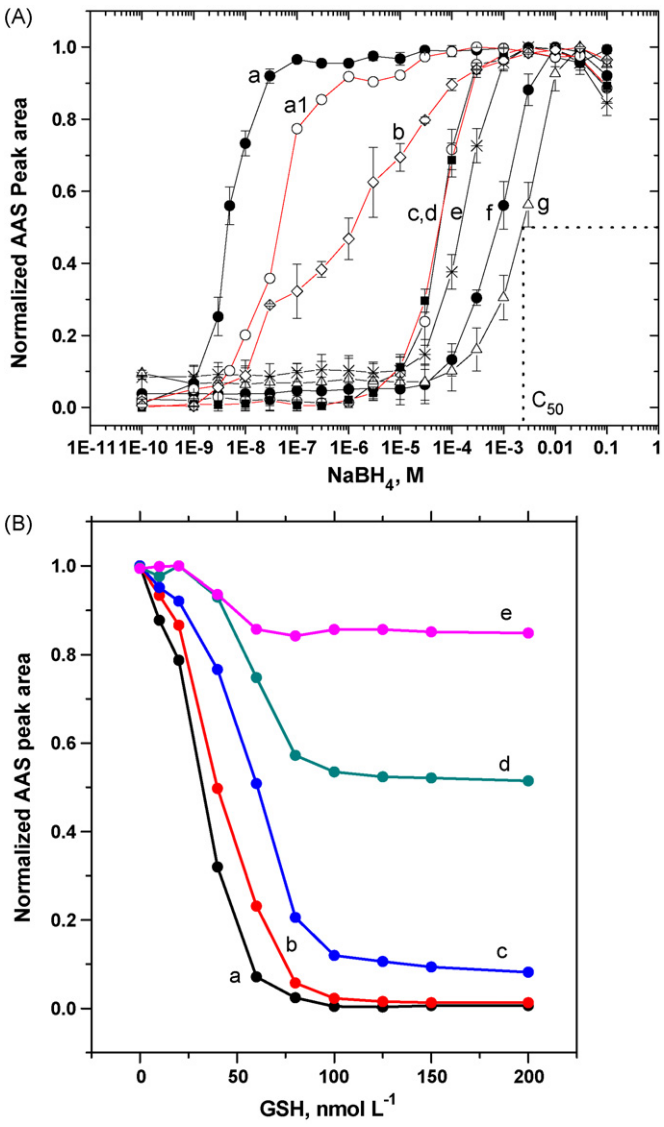


Fig. 2. (A) Reduction curves of Hg(II) and of $Hg(SR)_2$ complexes obtained with $[Hg(II)] = 5 \times 10^{-8}$ mol L^{-1} and $[RSH] = 2 \times 10^{-7}$ mol L^{-1} in PBS/NaCl: Hg(II) (a and a′, where for 'a' $NaBH_4$ stored in glass and for 'a'' $NaBH_4$ stored in polyethylene flask for 16 h at room temperature has been used), $Hg(NAP)_2$ (b), $Hg(GSH)_2$ (c), $Hg(HCys)_2$ (d), $Hg(CysGly)_2$ (e), $Hg(CYS)_2$ (f), $Hg(PSH)_2$ (g). Standard deviation of each single point takes into account the inter-day variability ($N = 3$ replicates performed in three subsequent days). (B) Titration curves of Hg(II) (4×10^{-8} mol L^{-1}) with GSH obtained by reducing the mercury–thiol solutions with five different concentration of $NaBH_4$: 1×10^{-8} mol L^{-1} (a), 1×10^{-7} mol L^{-1} (b), 1×10^{-6} mol L^{-1} (c), 6×10^{-5} mol L^{-1} (d), 3×10^{-4} mol L^{-1} (e).

$>10^{-2}$ mol L^{-1}. This is not true for GSH (Fig. 4B) which gives weaker complexes with mercury with respect to CYS. In this case the reduction curve of $Hg_n(GSH)_m$ complexes shift toward lower $NaBH_4$ concentrations, indicating a more labile complex formed by GSH at lower GSH/Hg(II) molar ratios.

Fig. 5 shows a three-dimensional plot of mercury normalized absorbance signal as a function of $NaBH_4$ concentration (log value) employed for its reduction and GSH concentration used for its titration. The 3D surface has been interpolated from data obtained by titration curves performed at different $NaBH_4$ concentrations and by reduction curves performed at different Hg(II)/GSH molar ratios.

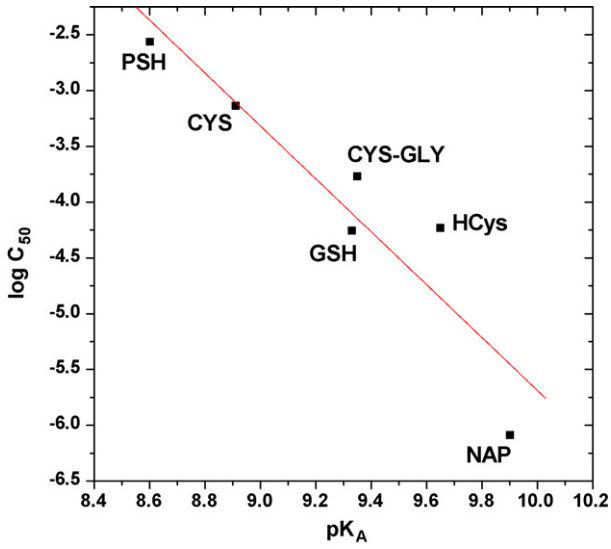


Fig. 3. Plot of the logarithm of C_{50} values vs. pK_a of the corresponding thiol –SH group. C_{50} values have been obtained for $[Hg(II)] = 5 \times 10^{-8}$ mol L^{-1} and $[RSH] = 2 \times 10^{-7}$ mol L^{-1} in PBS/NaCl.

3.3. Quantification of total thiols in wine samples

The described approach has been applied to the determination of total thiolic groups in wine samples.

Volatile sulfur products such as hydrogen sulfide (H_2S), carbonyl sulfide (COS), sulfur dioxide (SO_2), reduced thiols (RSH), sulfides (RSR), polysulfides (RS*n*R, $n = 2, 3, \ldots$) or thioesters (RCOSR′) are found in wine [37] as well as in other fermented beverages [38,39]. Polyfunctional mercaptans of higher molecular weight have been found at micromolar (GSH) and sub-micromolar concentration levels [9,10,40,41] and they are responsible for some wine aromas ([42,43] and references therein).

Fig. 6A shows as example the titration curve of 5×10^{-8} mol L^{-1} Hg(II) (5 mL) with wine diluted 1:50 obtained by plotting the normalized absorbance signal as a function of the volume (μL) of wine added. 1×10^{-7} mol L^{-1} $NaBH_4$ was used for mercury reduction, which represents a reductant concentration able to discriminate uncomplexed from complexed mercury.

The volume, V_w (expressed in L), of sample required for the titration of 5×10^{-8} mol L^{-1} Hg(II) has been extrapolated by the intersection of the descending branch of titration curve with the *x*-axis. Total RSH concentration (mol L^{-1}) in raw wine was calculated on the basis of the formation of RS–Hg complexes and the following equation:

$$[RSH] = \left[\frac{n_{Hg(II)}}{V_w}\right] \times 50 \quad (2)$$

where $n_{Hg(II)}$ indicates the moles of mercury employed and 50 is the wine dilution factor. Table 3 reports the concentration values of total RSH found in the eight wine samples examined.

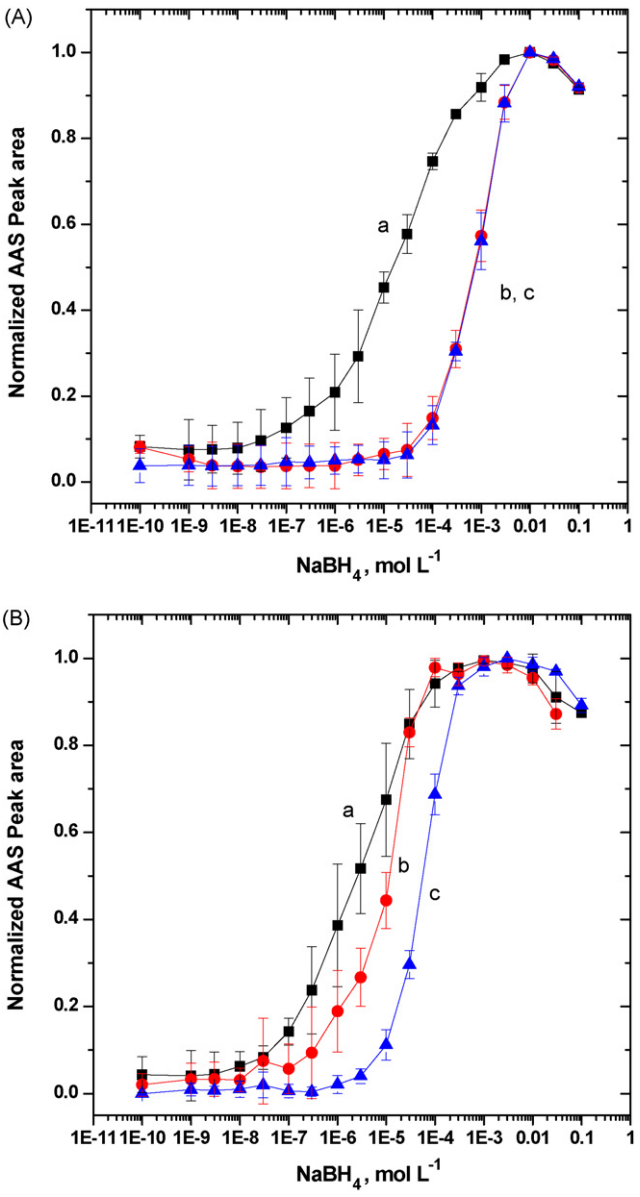


Fig. 4. Reduction curves obtained for $[Hg(II)] = 5 \times 10^{-8}$ mol L^{-1} (10 ng mL^{-1}) and RS/Hg(II) molar ratios of 1/1 (a), 2/1 (b) and 4/1 (c). (A) RS = CYS; (B) RS = GSH.

Interference problem could be originated by $S_2O_5^{2-}$, which is a common additive in wines. We found that the titration of 5×10^{-8} mol L^{-1} Hg(II) with 6.2×10^{-3} mol L^{-1} $S_2O_5^{2-}$ solution, which generates a large excess of SO_2 in solution with respect to the limit allowed of 2.5×10^{-3} mol L^{-1} did not change the mercury signal, showing that it does not interfere with RSH measurement (data not shown for brevity).

Fig. 6B shows typical reduction curves obtained for three out of eight wines. Reduction curves were not significantly different, C_{50} values being $(3.88 \pm 0.36) \times 10^{-5}$ (Rosso di Montalcino), $(5.35 \pm 0.39) \times 10^{-5}$ (Chianti rosso Nipozzano) $(2.11 \pm 0.25) \times 10^{-5}$ (Chianti Rosso Felisina).

The main drawback of the described method is the uncertainty in the knowledge of the effective reaction ratio between Hg(II) and –SH groups of the samples examined. However, data reported in the previous section show that by using a low concentration of $NaBH_4$ (nominally 10^{-8} to 10^{-7} mol L^{-1}, depending on the thiol) mercury behaves, from the stoichiometry point of view, as a monofunctional complexing agent.

Table 3
Quantification of total RSH (mean ± S.D.*) in wine samples

Vintage	Concentration of RSH (10^{-6} mol L^{-1})
Vecchia Cantina Chianti (red wine, 2005)	28.2 ± 1.9
Vecchia Cantina Chianti (white, 2005)	11.0 ± 1.0
Vinca Vermentino (white, 2005)	16.4 ± 1.9
Rosso di Montalcino Chianti (red wine, 2005)	19.0 ± 2.0
Fret Barbera d'Alba (red wine, 2004)	14.3 ± 1.6
Nero d'Avola (Sicily) (red wine, 2005)	17.2 ± 2.9
Barbera Pavia (red wine, 2005)	13.1 ± 1.0
Rosso Chianti Nipozzano Reserve (red wine, 2003)	21.7 ± 2.8

* S.D. on three independent measurements.

For this reason total RSH values found in wine samples by mercury titration method have been compared with data obtained by HPLC analysis, based on the derivatization of –SH group with the monofunctional mercurial compound *p*-hydroxymercurybenzoate (PHMB) (work in progress). Fig. 7 shows the comparison of the mercury-specific AFS chromatogram of a red and white wine (1 mL derivatized with 2×10^{-4} mol L^{-1} PHMB). All thiolic compounds elutes within 12 min, the excess of PHMB eluting as a broad peak between 16 and 30 min.

Injection of standard solutions of GSH and 3-ethylmercaptopropionate allowed identification of peaks at 10.78 and 5.62 min, respectively. Identification of the other peaks is still in progress

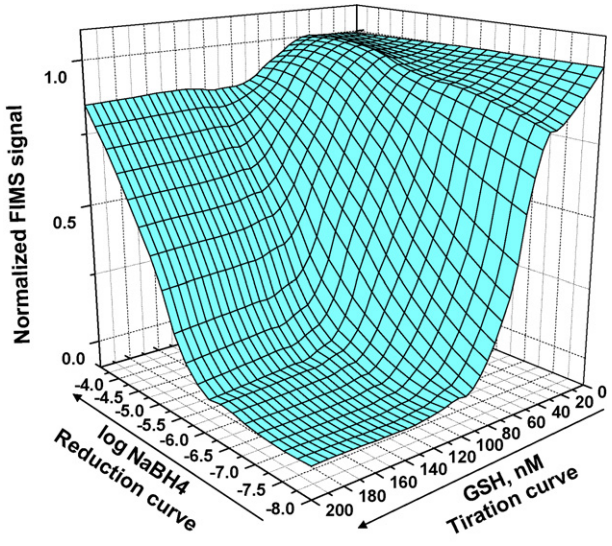


Fig. 5. 3D representation of mercury normalized integrated absorbance signal as a function of $NaBH_4$ concentration employed for its reduction (reduction curve) and GSH used for its titration (titration curve).

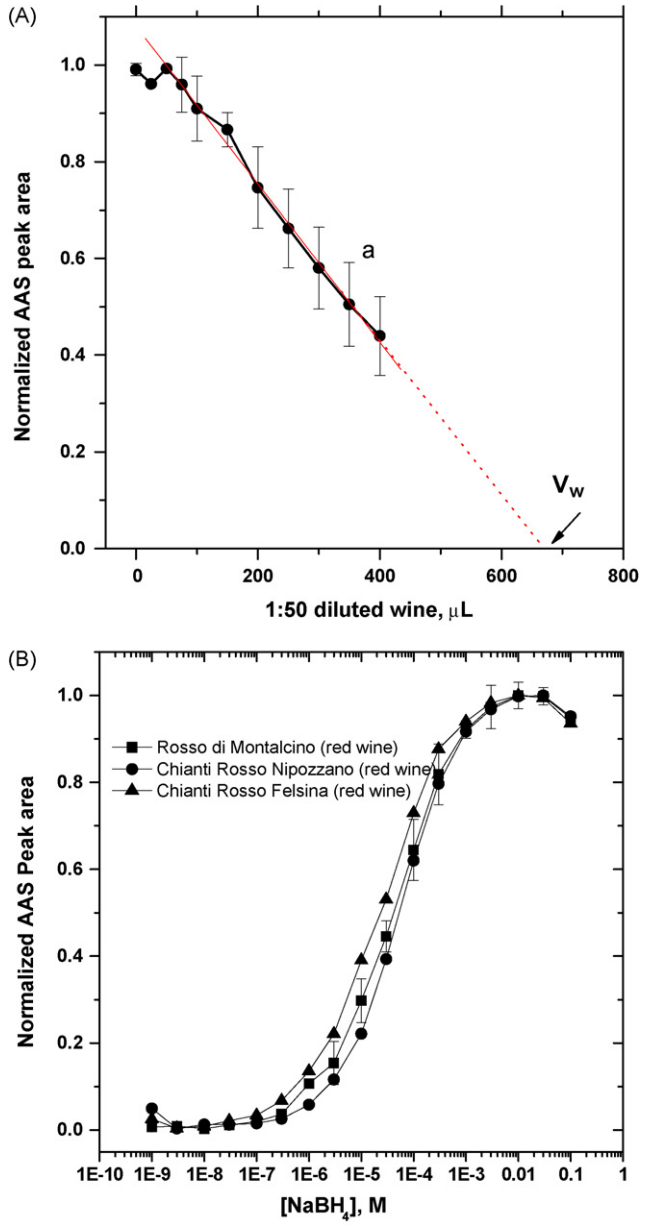


Fig. 6. (A) Titration curves of Hg(II) (5×10^{-8} mol L^{-1} in 5 mL) with wine diluted 1:50 in PBS/NaCl (a) using 1×10^{-7} mol L^{-1} $NaBH_4$ for mercury reduction. (B) Typical reduction curves of three different red wines.

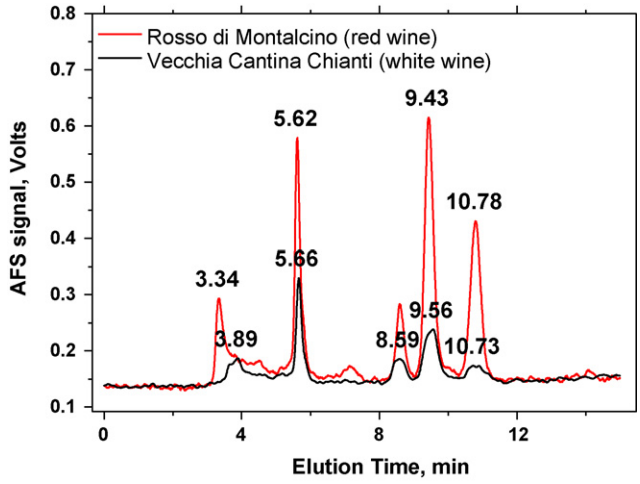


Fig. 7. Mercury-specific AF chromatogram of a red and white wine (1 mL derivatized with 2×10^{-4} mol L^{-1} PHMB). Chromatographic conditions: Hydra RPC column (Phenomenex); flow rate: 1 mL min^{-1}; 50 μL loop; isocratic elution in 97% 2×10^{-2} mol L^{-1} PBS pH 5.96, 3% MeOH. For detection conditions see ref. [45].

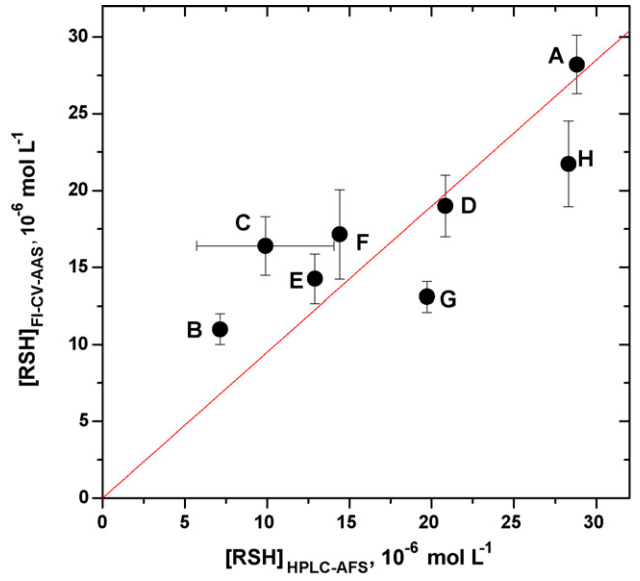


Fig. 8. Correlation plot of RSH value found by FI-CV-AAS analysis and by HPLC analysis. (A) Vecchia Cantina Chianti (red wine, 2005); (B) Vecchia Cantina Chianti (white wine, 2005); (C) Vinca Vermentino (white wine, 2005); (D) Rosso di Montalcino Chianti (red wine, 2005); (E) Fret Barbera d'Alba (red wine, 2004); (F) Nero d'Avola (Sicily) (red wine, 2005); (G) Barbera Pavia (red wine, 2005); (H) Rosso Chianti Nipozzano Reserve (red wine, 2003).

and it is beyond the aim of this paper. However, considering that all thiols complexed PHMB almost quantitatively, that Hg is quantitatively recovered in HPLC-AFS procedure [44,45] and that the analytical response is specific for mercury, a response factor can be roughly estimated on the basis of calibration curve of GS–PHMB complex [45]. Then, the sum of peak area of thiolic compounds is converted into the value of total RSH in wine samples by using the above estimated response factor. The goodness of this approximation can be verified by comparing the results obtained by FI-CV-AAS analysis and by HPLC-AFS analysis (see Fig. 8).

The fairly good correlation (slope = 0.9501 ± 0.0847, $R = 0.8185$; $N = 8$; $P = 0.095$) is compatible with the approximation introduced in calculations and supports the good potentiality of FI-CV-AAS method in thiol determination at ultratrace level.

4. Conclusion

The results presented in this work demonstrate the transferability of the method originally developed for a laboratory assembled CF-CV-AFS system in the determination and characterization of Hg(II)–thiol complexes [22], to a commercially available FI-CV-AAS mercury analyzer. The basic principles of the method [22] apply also to FI-CV-AAS and this allows the

determination of mercury-reactive –SH groups and/or the determination of total thiolic groups in the sample at nanomolar level, in a fast and simple way. Concerning the safety associated with mercury use and disposal, the concentration of Hg(II) in liquid waste is comparable to maximum allowed limit in drinking water; lower concentration can be achieved by reducing the concentration of mercury below the employed level of 10 ng mL^{-1}. The application of FI-CV-AAS method may be in principle appealing for pharmaceutical and food industry, both in the quality control of analytical processes and in the development of new thiolic drugs.

Acknowledgements

The authors would like to thank Perkin-Elmer Life and Analytical Sciences, Via Tiepolo, 24, -20052 Monza (Milano), Italy for supplying FIMS-100 and its accessories.

References

[1] M.D. Schulte, K.L. Rogers, Geochim. Cosmochim. Acta 68 (2004) 1087–1097.
[2] P.C. Jocelyn, Biochemistry of the SH Group: The Occurrence, Chemical Properties, Metabolism and Biological Function of Thiols and Disulphides, Academic Press, London, 1972.
[3] G.I. Giles, K.M. Tasker, C. Jacob, Free Rad. Biol. Med. 31 (2001) 1279–1283.
[4] F.M. Rubino, M. Pitton, G. Brambilla, A. Colombi, J. Mass Spectrom. 41 (2006) 1578–1593.
[5] I. Chakraborty, P.K. Malik, S.P. Pradip, J. Nanopart. Res. 8 (2006) 889–897.
[6] Y. Özkan, E. Özkan, B. Simsek, Int. J. Cardiol. 82 (2002) 269–277.
[7] A.K.M. Kabzinski, Talanta 46 (1998) 335–346.
[8] Y. Li, G. Wei, J. Chen, Appl. Microbiol. Biotechnol. 66 (2004) 233–242.
[9] I. Masneuf-Pomarède, C. Mansour, M.-L. Murat, T. Tominaga, D. Dubourdieu, Int. J. Food Microbiol. 108 (2006) 385–390.
[10] S.K. Park, R.B. Boulton, A.C. Noble, Food Chem. 68 (2000) 475–480.
[11] W.B. Jakoby, O.W. Griffith, Methods Enzymol. 143 (1987) 1–582.
[12] R.S. Reid, D.L. Rabenstein, Can. J. Chem. 59 (1981) 1505–1514.
[13] P.A. Rea, Proc. Natl. Acad. Sci. U. S. A. 103 (2006) 507–508.
[14] M.E. Wolfe, S. Schwarzbach, R.A. Sulaiman, Environ. Toxicol. Chem. 17 (1998) 146–160.
[15] S. Clemens, Biochimie 88 (2006) 1707–1719.
[16] F. Zahir, S.J. Rizwi, S.K. Haq, R.H. Khan, Environ. Toxicol. Pharmacol. 20 (2005) 351–360.
[17] D.W. Boening, Chemosphere 40 (2000) 1335–1351.
[18] W.L. Clevenger, B.W. Smith, J.D. Winefordner, Critical Rev. Anal. Chem. 27 (1997) 1–26.
[19] R. Puk, J.H. Weber, Appl. Organomet. Chem. 8 (1994) 293–302.
[20] I.M. Kolthoff, W. Stricks, L. Morren, Anal. Chem. 26 (1954) 366–372.
[21] L.M. Doane, J.T. Stock, Anal. Chem. 50 (1978) 1891–1895.
[22] E. Bramanti, A. D'Ulivo, L. Lampugnani, G. Raspi, R. Zamboni, J. Anal. At. Spectrom. 14 (1999) 179–185.
[23] E. Bramanti, A. D'Ulivo, L. Lampugnani, R. Zamboni, G. Raspi, Anal. Biochem. 274 (1999) 163–173.
[24] W. Stricks, I.M. Kolthoff, J. Am. Chem. Soc. 75 (1953) 5673–5681.
[25] G.R. Lenz, A.E. Martell, Biochemistry 3 (1964) 745–750.
[26] W.E. Van Der Linden, C. Beers, Anal. Chim. Acta 68 (1974) 143–154.
[27] E.J. Kuchinskas, Y. Rosen, Arch. Biochem. Biophys. 97 (1962) 370–372.
[28] M. Basinger, J. Casas, M. Jones, J. Inorg. Nucl. Chem. 43 (1981) 1419–1425.
[29] P.D. Oram, X. Fang, Q. Fernando, P. Letkeman, D. Letkeman, Chem. Res. Toxicol. 9 (1996) 709–712.
[30] D.J. Perkins, Biochem. J. 55 (1953) 649–652.
[31] J.S. Casas, M.M. Jones, J. Inorg. Nucl. Chem. 42 (1980) 99–102.
[32] M. Koul, K. Dubey, J. Inorg. Nucl. Chem. 35 (1973) 2571–2573.
[33] M. Seleim, K.A. Idriss, M.S. Saleh, H. Sedaira, Analyst 112 (1987) 1685–1688.
[34] Y. Anjaneyulu, R.P. Rao, R.Y. Swamy, Indian J. Chem. 24A (1985) 622–623.
[35] R.C. Kapoor, G. Doughty, G. Gorin, Biochim. Biophys. Acta 100 (1965) 376–383.
[36] D.A. Keire, E. Strauss, W. Guo, B. Noszal, D.L. Rabenstein, J. Org. Chem. 57 (1992) 123–127.
[37] A. Rapp, A. Guntert, J. Almy, Am. J. Enol. Vitic. 3 (1985) 219–221.
[38] B.C. Rankine, J. Sci. Food Agric. 114 (1986) 79–91.
[39] G.W.A. Fowles, J. Wine Res. 5 (1994) 103–112.
[40] R. Flamini, A. Panighel, Mass Spectrom. Rev. 25 (2006) 741–774.
[41] M. Mestres, M.P. Marti, O. Busto, J. Guasch, J. Chromatogr. A 849 (1999) 293–297.
[42] L. Mateo-Vivaracho, V. Ferreira, J. Cacho, J. Chromatogr. A 1121 (2006) 1–9.
[43] T. Tominaga, D. Dubourdieu, J. Agric. Food Chem. 54 (2006) 29–33.
[44] E. Bramanti, S. Lucchesini, A. D'Ulivo, L. Lampugnani, R. Zamboni, M.C. Spinetti, G. Raspi, J. Anal. At. Spectrom. 16 (2001) 166–171.
[45] E. Bramanti, D. Toncelli, E. Morelli, L. Lampugnani, R. Zamboni, K.E. Miller, J. Zemetra, A. D'Ulivo, J. Chromatogr. A 1133 (2006) 195–203.

Available online at www.sciencedirect.com
ScienceDirect
Talanta 74 (2008) 605–612
Talanta
www.elsevier.com/locate/talanta

Through-a-chip partial filling affinity capillary electrophoresis for estimating binding constants of ligands to receptors

Abby Brown, Christina Morales, Frank A. Gomez *

Department of Chemistry and Biochemistry, California State University, Los Angeles, 5151 State University Drive, Los Angeles, CA 90032-8202, USA

Received 25 April 2007; received in revised form 21 June 2007; accepted 21 June 2007
Available online 7 July 2007

Abstract

In this paper, we describe the development of a microfluidic/capillary electrophoresis (CE) technique employing partial filling affinity capillary electrophoresis (PFACE) to estimate binding constants of ligands to receptors using as model systems carbonic anhydrase B (CAB, EC 4.2.1.1) and vancomycin from *Streptomyces orientalis*. Using multilayer soft lithography (MSL), a microfluidic device (MD) consisting of fluid and control channels is fabricated and fitted with an external capillary column. Multiple flow channels allows for manipulation of a zone of ligand and sample containing receptor and non-interacting standards into the MD and subsequently into the capillary column. Upon electrophoresis the sample components migrate into the zone of ligand where equilibrium is established. Changes in migration time of the receptor are used in the analysis to obtain a value for the binding interaction. The manipulation of small volumes of solution on the MD minimizes the need of time-consuming pipetting steps.
© 2007 Elsevier B.V. All rights reserved.

Keywords: Affinity capillary electrophoresis; Microfluidic device; Carbonic anhydrase B; Vancomycin; Binding constants

1. Introduction

The past two decades has seen tremendous advances in the design, development and use of microelectromechanical systems (MEMS) [1–10]. Applications for microfluidic devices (MDs) have proliferated at a speed reminiscent of the use of microelectronics after the invention of the integrated circuit. MDs have been shown to have great potential in a variety of biological applications including biomolecular separations [11,12], enzymatic assays [13,14], immunhybridization reactions [15,16], and the polymerase chain reaction [17,18]. The use of nanoliter reaction volumes and parallel high-throughput sample processing are potential advantages of MDs, making them ideally suited for chemical analysis, screening applications, and other cases where reagents are limited. A major challenge associated with realizing the desired scales in MDs is to simultaneously reduce the number of pipetting steps needed to load the devices while amortizing the sample volume over several reaction or separation steps [19].

To address the issue of sample loading and manipulation a variety of valve-type techniques have been developed. The recent pioneering work of Quake et al. and his development of microvalves is a milestone in microfluidics and shows great promise in MDs [19–24]. In this technique called multilayer soft lithography (MSL) they combined soft lithography with the capability to bond multiple patterned layers of elastomer. Layered structures are constructed by binding layers of elastomer each of which is separately cast from a micromachined mold. The elastomer is made up of a two-component silicone wafer. The bottom layer (fluid or flow channels) has an excess of one of the monomers, whereas, the upper layer (control channels) has an excess of the other monomer. After the layers are cured, the upper layer is removed from its mold and placed on top of the lower layer, where a seal is formed. Reactive molecules at the interface between the two layers irreversibly bond upon curing. Where the control channels pass above the fluid channels, a valve is formed.

Capillary electrophoresis (CE) is a powerful separation technique that has gained widespread use in biological laboratories because of its versatility and ease of use. It is an excellent tool for many types of bioanalyses and is an unparalleled experimental tool for biophysical studies of interactions in biologically

* Corresponding author. Tel.: +1 323 343 2368; fax: +1 323 343 6490.
E-mail address: fgomez2@calstatela.edu (F.A. Gomez).

0039-9140/$ – see front matter © 2007 Elsevier B.V. All rights reserved.
doi:10.1016/j.talanta.2007.06.043

relevant media. Separations are based on the principles of the electrically driven flow of ions in solution. Selectivity can be manipulated by the alteration of electrolyte properties such as pH, ionic strength, and electrolyte composition, or by the incorporation of electrolyte additives. CE has great promise when used in a microfluidic format and many papers and reviews have detailed the applications thereof [25–45].

One important application of CE is affinity CE (ACE) which has been used successfully to estimate binding parameters between ligands and receptors [46–69]. Since the first papers in 1992 [49–53] demonstrating the use of ACE to measure affinity parameters between biological species, its use in probing a variety of receptor–ligand interactions has greatly expanded and includes, but is not limited to, protein–drug, protein–DNA, peptide–peptide, peptide–carbohydrate, carbohydrate–drug, and antibody–antigen. For example, Kaddis et al. has used ACE to estimate binding constants for the substrate and activator of *Rhodobacter sphaeroides* adenosine 5′-diphosphate-glucose pyrophosphorylase [46]. Li et al. used capillary isoelectric focusing (cIEF) and ACE to determine binding constants between antibodies to the prion protein [47]. Finally, Lewis et al. described the screening of antimicrobial targets using ACE [48].

ACE uses the resolving power of CE to distinguish between free and bound forms of a receptor as a function of the concentration of free ligand in the electrophoresis buffer. In a typical form of ACE a sample of receptor and standard(s) is exposed to an increasing concentration of ligand in the running buffer causing a shift in the migration time of the receptor relative to the standard(s). We recently developed a more specialized form of ACE called partial filling ACE (PFACE) [64–68]. Here, the capillary is partially filled with ligand and sample plug of receptor is introduced into the capillary and electrophoresed. During electrophoresis the zones of samples overlap within the capillary and equilibrium is established prior to the point of detection. PFACE reduces the amount of sample required for the assay and expedites the speed of analysis.

Herein, we demonstrate the use of through-a-chip PFACE to examine the interaction of CAB to arylsulfonamides and vancomycin to small peptides. In this work sample injection and electrophoresis buffer are manipulated through a microfluidic chip constructed from poly(dimethylsiloxane) (PDMS) and into a capillary column one end of which is embedded into the chip. Upon application of a voltage sample zones migrate through the capillary where equilibrium between receptor and ligand is established and is detected using an external UV–vis detector. Subsequent analysis of the change in migration time of the receptor referenced to two non-interacting standards yields a value of the binding interaction.

2. Materials and methods

2.1. Chemicals and reagents

All chemicals were analytical grade. Fig. 1 shows the structures of ligands **1**–**6** for CAB and vancomycin used in this study. CAB, dimethylformamide (DMF), horse heart myoglobin (HHM), 4-carboxybenzenesulfonamide (4-CBSA) (**6**) and *N*-acetyl-D-Ala-D-Ala (**7**) were purchased from Sigma (St. Louis, MO, USA) and were used without further purification. Carboxyfluorescein (FAM)-D-Ala-D-Ala-D-Ala (**8**) was custom synthesized by Anaspec (San Jose, CA, USA) and was used without further purification. CAB (1 mg/mL), DMF (1 mg/mL), HHM (1 mg/mL) and NADH (1 mg/mL) were each prepared by dissolving the lyophilized proteins or small molecule markers in buffer (192 mM glycine–25 mM Tris, pH 8.3). Compounds **1**–**5** (shown in Fig. 1) were gifts from S. Mallik (North Dakota State University, Fargo, ND, USA).

2.2. Apparatus

A Nikon Eclipse TE2000-U microscope (A.G. Heinze, Lake Forest, CA, USA), solenoids and fluid/air controllers (Fluidigm, San Francisco, CA, USA), Spectra 100 UV visible detector (Thermo Separation Products, Piscataway, NJ, USA) and LabVIEW 7.0 computer software (National Instruments Corporation, Austin, TX, USA) are used for fluid manipulation and electrophoresis control, detection, and data collection, respectively. The capillary tubing (Polymicro Technologies, Phoenix, AZ, USA) was of uncoated fused silica with an outer diameter of 365 μm, an internal diameter of 78 μm, a length from inlet to detector of 57.0 cm, and a length from detector to outlet of 6.5 cm.

2.3. Procedures

For CAB: using solenoid pumps with connecting tubing for sample introduction, the microfluidic device was first flushed with electrophoresis buffer (5 min) to remove any impurities that may have remained from the fabrication process. Solutions of increasing concentration of ligand **1** and a sample containing CAB (1 mg/mL), DMF (1 mg/mL) and HHM (1 mg/mL) were injected at low pressure (0.5 psi) for 10 and 2.7 s, respectively. Electrophoresis buffer was then pressure injected (0.5 psi for 10 s) into the electrophoresis channel to push the sample plug past the electrode and into the beginning of the capillary column. The electrophoresis was carried out using a Tris–Gly buffer and repeated at increasing concentrations of **1** for 8 min. For Van: similar to above except NADH was used as an internal standard.

2.4. Design and fabrication

Pneumatically actuated MDs were fabricated at the Caltech Nanofabrication lab from two patterned flexible polymer layers—the "flow layer" (containing the channels which carry reagents) and the "control layer" (containing the channels which cause pneumatic valve closure when pressurized). Each layer is fabricated from two-part-cure silicone (Dow Corning Sylgard 184) cast on a photoresist mold. The master molds are made by spin-coating photoresist onto a silicon wafer and then patterned with high-resolution transparency masks (typically 3386, 8000, or 20,000 dpi). The fluid layer mold consisted of a photoresist that can be reflowed by baking at high temperatures (Shipley SJR 5740). The mold is spin-coated with 20:1 part A:B

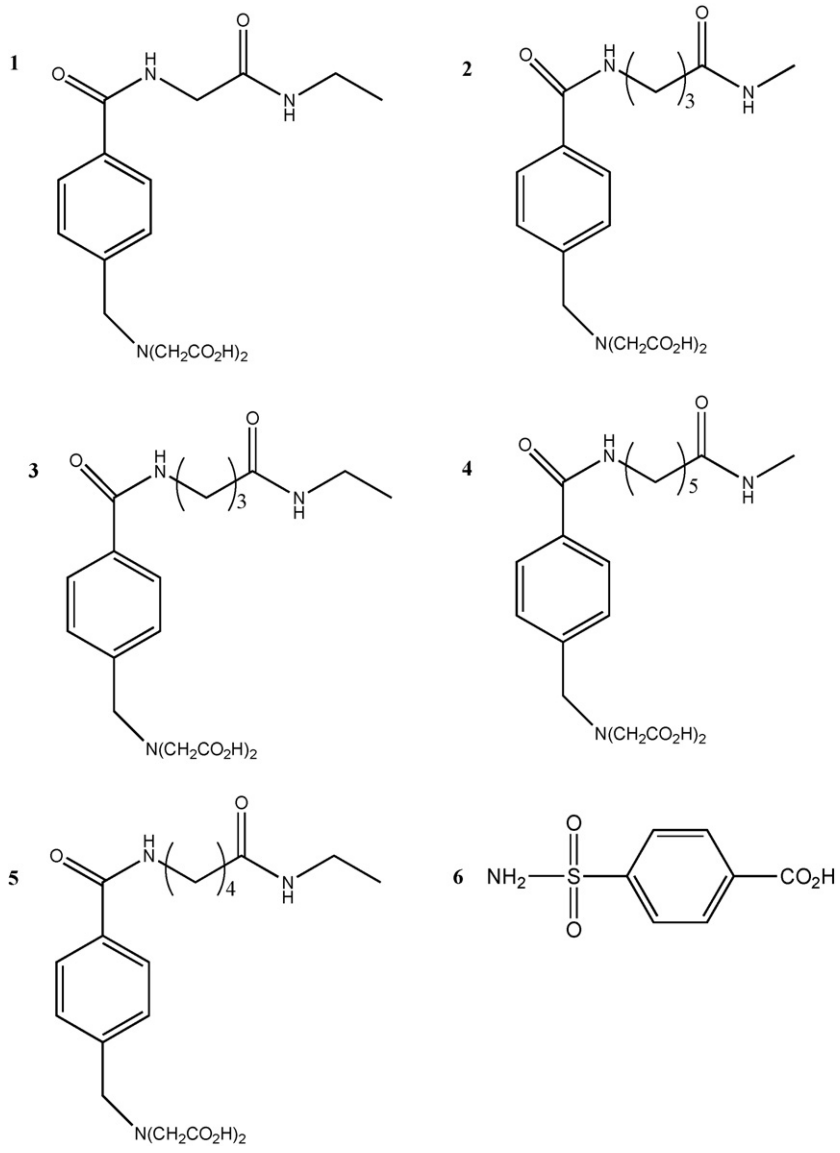


Fig. 1. Arylsulfonamide ligands **1**–**6** for carbonic anhydrase B (CAB) and vancomycin used in this study.

Sylgard at 2500 rpm for 1 min, resulting in a layer thickness of around 30 μm and channel height of approximately 13 μm. Onto this mold about 0.5 cm 5:1 part A:B Sylgard is cast to form the control layer. Each layer is cured for 30 min in an oven (80 °C). Control channel interconnect holes are punched through the thick layer (after release from the mold) by using a manual-punching machine with a hollow ram and hole plug ejector-pin system (Technical Innovations, Brazoria, TX, USA), and the layer aligned and sealed (channel-side down) onto the flow layer (still on the mold). The sample inlet, capillary and electrode holes are approximately 889 and 508 μm in diameter, respectively, which facilitates the interface between the MD and the exterior sample inlet vials and tubing, capillary and electrode. Bonding is realized by curing the devices together for an additional 45–60 min (80 °C) preventing leakage between the two layers. The resulting two-layer devices are cut from the mold and mounted onto cleaned glass microscope slides, and bonded overnight at 80 °C.

3. Results and discussion

3.1. Injection and manipulation of solution

Our first goal was to determine the feasibility of injecting two separate plugs of solution into a microfluidic channel and subsequently into a capillary column fitted at the end of the channel. It is important that the amount of sample injected into the microchip and then into the capillary column be comparable to that delivered by commercial instruments (using either hydrodynamic or electrokinetic injection). In partial filling techniques an additional factor is that the amount of ligand injected be greater than that of sample since during electrophoresis the zone of sample must migrate through the ligand zone to cause equilibrium between receptor and ligand.

Fig. 2 is a picture of the microfluidic chip used in our experiments. A schematic of the injection process is shown in Fig. 3. In Fig. 3A inlets a–c of the microfluidic chip were connected to

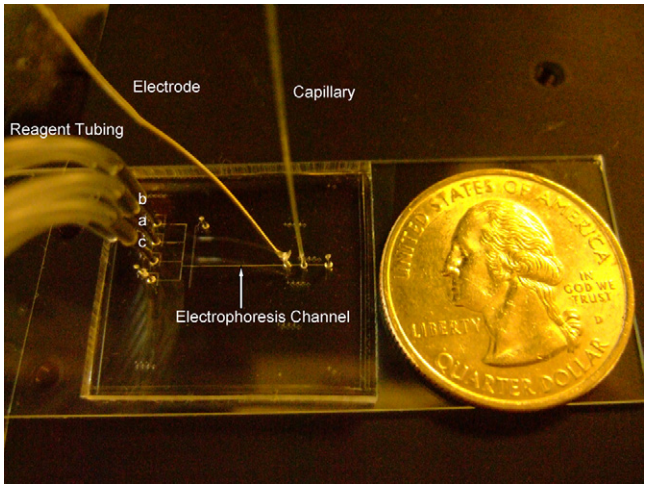


Fig. 2. Microfluidic chip used in this study.

solutions of blue and red dye, and electrophoresis buffer, respectively. A solution of red dye was first injected into the chip to illustrate the plug length of the ligand. It was determined that a pressure of 0.5 psi applied for 10 s equated to a volume of 10.4 nL. This volume of solution is comparable to that used in open-tubular CE for a typical injection of sample of ligand using partial filling techniques [64–66]. A solution of blue dye was then injected into the chip (Fig. 3C) and into the electrophoresis channel. The volume of blue dye was determined to be 2.8 nL comparable to a typical sample injection using a commercial instrument. For example, a one second injection at low pressure (0.5 psi) using a 50 μm (inner diameter) capillary and a BeckmanCoulter P/ACE CE instrument, equates to 1.2 nL of solution.

The zones of solution were subsequently manipulated into the capillary column by pressure injection of a solution of electrophoresis buffer (Fig. 3D). Fig. 3E is a picture of the two dye solutions within the microfluidic channel prior to manipulation into the capillary column (not shown). No leakage of solution around the electrode or capillary was observed on manipulating the dyes into the capillary column. This result is significant as any versatile injection scheme in a MD must be able to manipulate a solution from one point to another on the chip.

3.2. ACE experiments

In our first series of experiments, we examined the binding of an arylsulfonamide ligand (**1**) to CAB. CAB is a zinc protein of the lyase class that catalyzes the equilibration of dissolved carbon dioxide and carbonic acid. It is strongly inhibited by sulfonamide-containing molecules. We chose the CAB system for several reasons: (1) because its p*I* is 5.9, at pH 8.3, there is little propensity to adsorb onto to the walls of the capillary column, (2) we have data describing its electrophoretic behavior in other circumstances, (3) it is commercially available and inexpensive, (4) ligands for it can be easily synthesized, and (5) many ligands bind to it with values of K_b between 10^5 and 10^9 M^{-1}.

The same injection sequence was used here as that described in the dye experiments and injection volumes are comparable to those determined with the red and blue dyes respectively. Here, solutions of **1** and sample containing CAB, HHM and DMF are injected into the channel. HHM and DMF are non-interacting

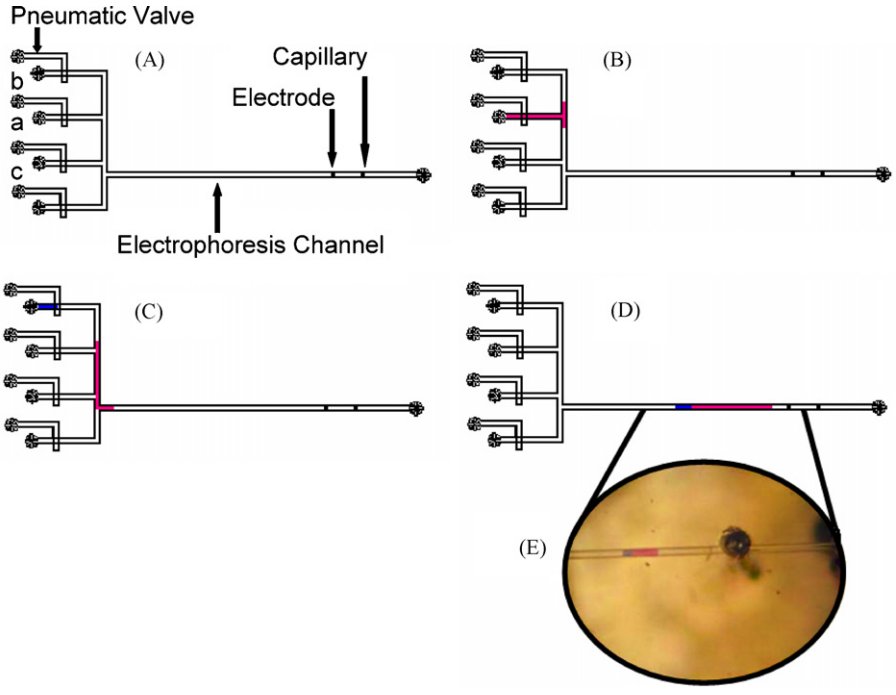


Fig. 3. Schematic illustration of the different injection and manipulation steps of solution and sample through the chip and into the capillary column. (A) Schematic of microfluidic chip depicting channels A–D; (B) plug of blue dye is introduced hydrodynamically into chip; (C) blue dye is manipulated into electrophoresis channel and a plug of red dye is injected hydrodynamically into chip; (D) electrophoresis buffer (colorless) is introduced hydrodynamically into channel thereby pushing ligand and sample towards and into the capillary column, and; (E) picture of colored dyes in channel prior to manipulation into the capillary column.

standards that do not interact with either **1** or CAB. Finally, a running electrophoresis buffer is manipulated into the channel pushing the zones of ligand and sample through the channel and into the capillary column found near the end of the channel. Upon electrophoresis, the sample flows into the zone of **1** where a dynamic equilibrium between **1** and CAB is established. Fig. 4 shows a representative set of electropherograms of CAB in a capillary partially filled with increasing concentrations (0–30 μM) of **1** in the running buffer. At the point of detection, separate peaks are observed for DMF, CAB and HHM. The complex that forms between CAB and **1** is more negatively charged then CAB and, therefore, the peak for the complex (CAB–**1**) shifts to a greater migration time on increasing the concentration of **1** in the running buffer. A small amount of inactive CAB can be seen in the series of electropherograms at the same migration time as found for uncomplexed CAB.

3.3. Analysis of binding constants

Fig. 5 is a plot of the data for **1**. In this form of analysis termed the relative migration time ratio (RMTR) (Eq. (1)), the binding constant is estimated using two non-interacting markers injected with the sample [57]. Here, t_r, t_s, and $t_{s'}$

$$\mathrm{RMTR} = \frac{t_r - t_{s'}}{t_{s'} - t_s} \quad (1)$$

are the measured migration times of CAB compound, and the two non-interacting standard peaks, respectively. In the present experiments, t_s and $t_{s'}$ are the migration times of DMF and Van, respectively. The values of $\Delta\mathrm{RMTR}_{P,L}$ obtained using Eq. (1) over a range of concentrations of **1** were then used for analysis using a standard hyperbolic equation to generate the binding isotherm (Eq. (2)).

$$y = \frac{ax}{b + x} \quad (2)$$

Here, a and b are defined as maximum $\Delta\mathrm{RMTR}_{P,L}$ and calculated $1/K_b$, respectively. Values for y and x are the change in electrophoretic mobility and concentration of **1**, respectively. The above data analyses, curve fitting functions, and statistical calculations were performed using Sigma Plot 8.0 (Jandel Scientific, Erkrath, Germany). Eq. (2) allows for the estimation of K_b on a relative time scale using two non-interacting standards and compensates for fluctuations in electroosmotic flow (EOF), background electrolyte, viscosity and electric field variations in the capillary column.

Using Eq. (2), a K_b of $4.34 \times 10^5\ \mathrm{M}^{-1}$ was obtained for the interaction between CAB and **1**. This value is comparable to our previous results using ACE ($4.70 \times 10^5\ \mathrm{M}^{-1}$) and to values obtained using other assay techniques [34,36]. A correlation coefficient (R^2) of 0.992 was obtained for the fitness of the binding isotherm plot. A series of other inhibitors of CAB (**2**–**6**, Fig. 1) were examined and the results are detailed in Table 1. These results compare favorably with those obtained using other ACE techniques [34,36,70].

We also examined the glycopeptide vancomycin (Van) from *Streptomyces orientalis*. Van is a parenteral glycopeptide antibiotic that kills bacterial cells by inhibiting peptidoglycan biosynthesis [71–77]. It functions by binding to the terminal D-Ala-D-Ala dipeptide of bacterial cell wall precursors. Historically, Van has been the drug of choice in treating infections caused by bacterial resistance to other types of antibiotics.

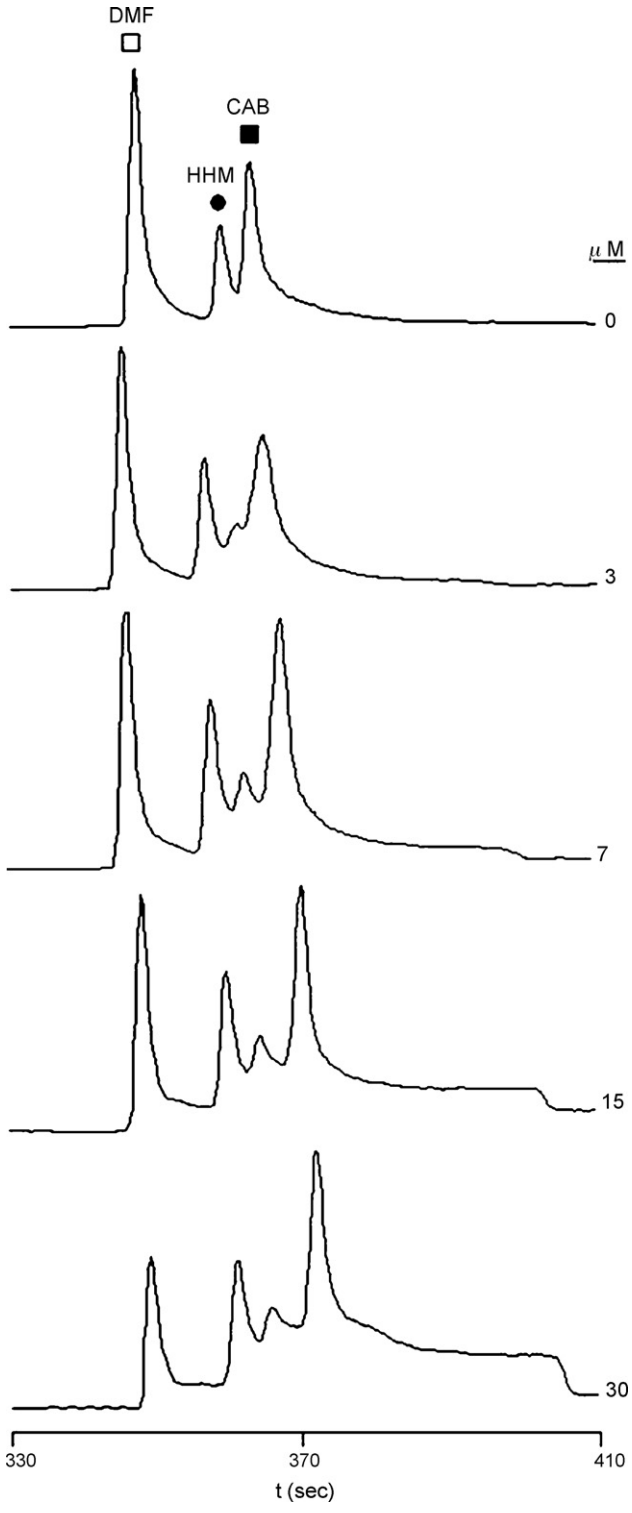


Fig. 4. A representative set of electropherograms of CAB in 192 mM glycine–25 mM Tris, pH 8.3, containing various increasing concentrations of **1**. The total analysis time in this experiment was 8.0 min at 20 kV. DMF and HHM was used as an internal standard.

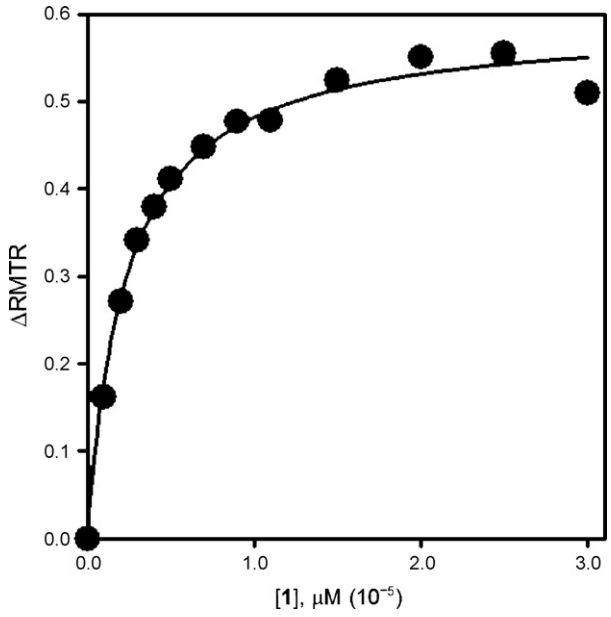


Fig. 5. Binding isotherm of the data for CAB and **1**.

Unfortunately, Van resistant enterococci (VRE) has emerged which is of major concern to the biomedical community. Van resistance is now also common in *Enterococcus faecalis*, hence, it is becoming increasingly important to develop new Van-group antibiotics, to study their physicochemical parameters, and to examine their activity against VRE.

In these experiments a similar injection scheme was utilized except that NAD was utilized as a non-interacting standard in addition to DMF. Furthermore, the injection volumes are comparable to that of the previously mentioned dye experiments. Two peptides **7** and **8** were used for these studies. In a typical experiment an increasing concentration of **7** was injected into the microfluidic channel followed by a sample containing markers and Van and then manipulated into the capillary column. Upon electrophoresis the zone of sample migrates into the plug of **7** where equilibrium is satisfied. At the point of detection the Van peak shifts to increasing migration time which is then used to obtain a value for K_b (Table 2). Fig. 6 is a representative series of electropherograms of Van exposed to increased concentrations of **7** in the electrophoresis buffer. Upon complexation to **7** the migration time for the Van peak increases the change of which

Table 1
Experimental values of binding constants K_b (10^5 M^{-1}) of CAB to ligands **1**–**6** measured by the through-a-chip PFACE technique

Ligands	K_b[a]	R^2	K_b[b]
1	4.34	0.992	4.70
2	2.99	0.943	1.93
3	2.90	0.996	3.22
4	5.85	0.984	5.88
5	5.65	0.986	3.40
6	1.33	0.992	6.90

[a] The reported binding constants are the average values from at least two experiments for each ligand.
[b] Previous estimates [71].

Table 2
Experimental values of binding constants K_b (10^3 M^{-1}) of Van to ligands **7** and **8** measured by the through-a-chip PFACE technique[a]

Ligands	K_b[a]	R^2	K_b[b]
7	3.64	0.998	3.22
8	1.04	0.992	0.992

[a] The reported binding constants are the average values from at least two experiments for each ligand.
[b] Previous estimates [71].

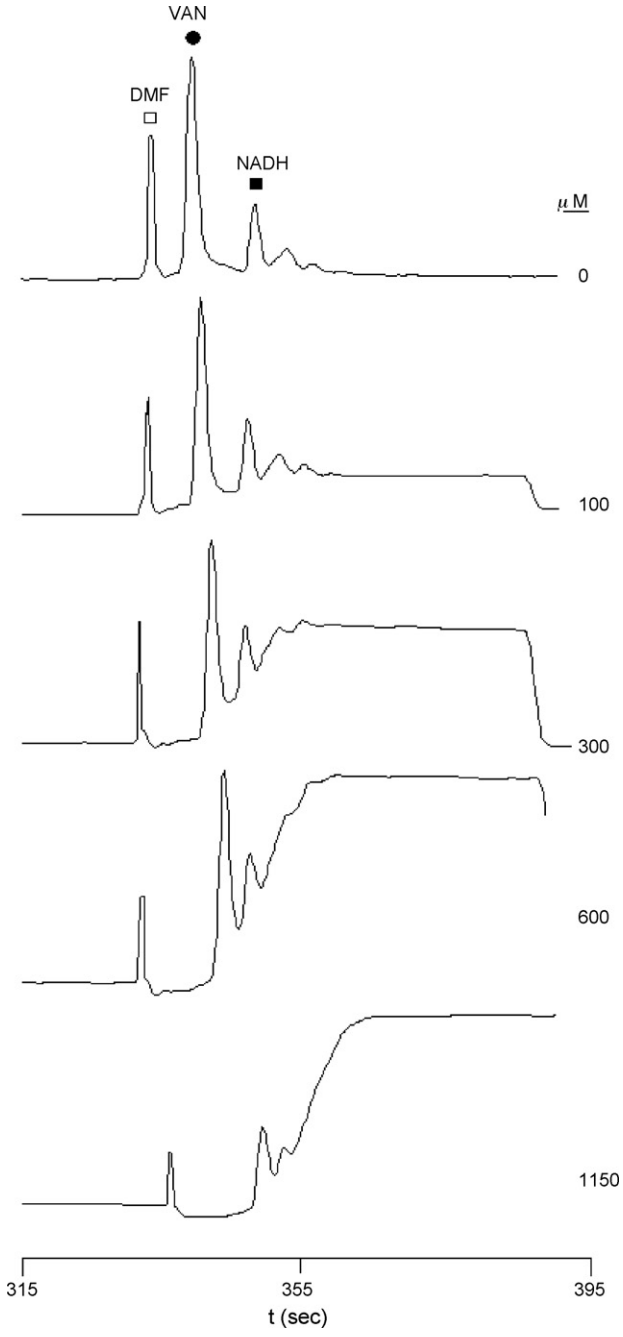


Fig. 6. A representative set of electropherograms of Van in 192 mM glycine–25 mM Tris, pH 8.3, containing various increasing concentrations of **7**. The total analysis time in this experiment was 8.0 min at 20 kV. DMF and NADH were used as internal standards.

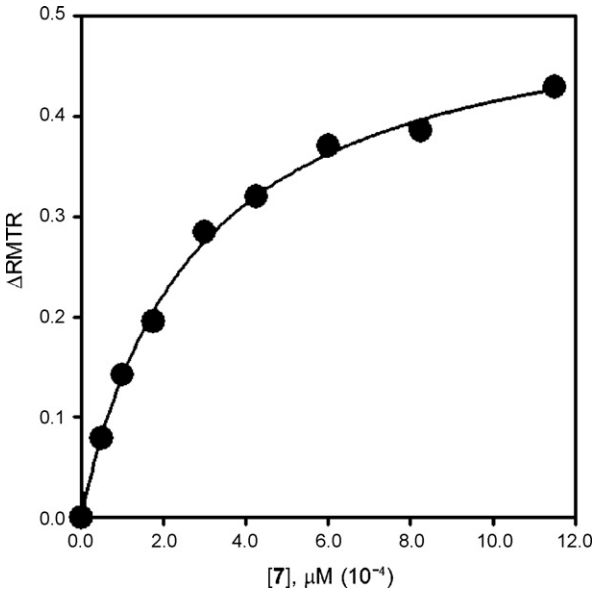


Fig. 7. Binding isotherm of the data for Van and **7**.

is used in the binding constant analysis. Fig. 7 is a plot of the data for **7**.

The work, herein, is significant for several reasons. One, unlike the majority of other microchip CE devices, the current technique does not require labeling of the receptor with a fluorescent probe. The external UV–vis detector allows for facile analysis of samples similar to that found in commercial CE systems. Two, sample injection is pressure-driven thereby eliminating sample bias caused by electrokinetic injection. Three, sample injection and rinse and wash operations are automated using an in-house computer software program. This program is robust and can be modified for injection and manipulation of fluids from multiple external vials. Four, design and fabrication of the microfluidic chip is fast and inexpensive. Multiple chips can be fabricated at any one time.

4. Conclusion

We have demonstrated that partial filling affinity capillary electrophoresis in a microfluidic format can be utilized in the estimation of binding constants between a receptor and a ligand. Using the model systems carbonic anhydrase B (CAB) and vancomycin we have shown that an MD fitted with a capillary column and coupled to an external UV–vis detector can readily be used to examine bimolecular non-covalent interactions. There are several advantages in using microchip/PFACE to study receptor–ligand interactions. One, only small quantities of receptor and ligand are required. Two, radiolabelling of the molecules or derivatization with a fluorophore is not necessary [78,79]. Three, injection of sample is easily controlled using valve and pump techniques. Four, need for expense commercial instruments is no longer required. Finally, a wide range of molecular interactions can be characterized in free solution. Further work will focus on optimizing conditions for assay, developing a high-throughput system to assay many potential drug targets, and in developing a more robust computer interface for automated drug assay.

Acknowledgments

The authors gratefully acknowledge financial support for this research by grants from the National Science Foundation (CHE-0515363 and DMR-0351848) and the National Institutes of Health (1R15AI65468-01).

References

[1] H. Lu, L.Y. Koo, W.M. Wang, D.A. Lauffenburger, L.G. Griffith, K.F. Jensen, Anal. Chem. 76 (2004) 5257.
[2] R.D. Rocklin, R.S. Ramsey, J.M. Ramsey, Anal. Chem. 72 (2000) 5244.
[3] B.M. Paegel, S.H. Yeung, R.A. Mathies, Anal. Chem. 74 (2002) 5092.
[4] J. Wang, A. Ibanez, M.P. Chatrathi, A. Escarpa, Anal. Chem. 73 (2001) 5323.
[5] B.B. Haab, R.M. Mathies, Anal. Chem. 71 (1999) 5137.
[6] N.E. Hebert, W.G. Kuhr, S.A. Brazill, Electrophoresis 23 (2002) 3750.
[7] N.R. Munce, J. Li, P.R. Herman, L. Lilge, Anal. Chem. 76 (2004) 4983.
[8] U. Backofen, F.M. Matysik, C.E. Lunte, Anal. Chem. 74 (2002) 4054.
[9] Y. Liu, J.C. Fanguy, J.M. Bledsoe, C.S. Henry, Anal. Chem. 72 (2000) 5939.
[10] J.C. McDonald, D.C. Duffy, J.R. Anderson, D.T. Chiu, H.K. Wu, O.J.A. Schueller, G.M. Whitesides, Electrophoresis 21 (2000) 27.
[11] I.M. Lazar, R.S. Ramsey, J.M. Ramsey, Anal. Chem. 73 (2001) 1733.
[12] Y. Flintschenko, W.-Y. Choi, S.M. Ngola, T.J. Shepodd, Anal. Chem. 73 (2001) 849.
[13] H.B. Mao, T.L. Yang, P.S.A. Cremer, J. Am. Chem. Soc. 124 (2002) 4432.
[14] A.G. Hadd, S.C. Jacobson, J.M. Ramsey, Anal. Chem. 71 (1999) 5206.
[15] N.H. Chiem, D. Harrison, J. Clin. Chem. 44 (1998) 591.
[16] A. Bromberg, R.A. Mathies, Anal. Chem. 75 (2003) 1188.
[17] E.T. Lagally, I. Mednitz, R.A. Mathies, Anal. Chem. 73 (2001) 565.
[18] J. Khandurina, T.E. McKnight, S.C. Jacobson, L.C. Waters, R.S. Foote, J.M. Ramsey, Anal. Chem. 72 (2000) 2995.
[19] M.A. Unger, H.-P. Chou, T. Thorsen, A. Scherer, S.R. Quake, Science 288 (2000) 113.
[20] T. Thorsen, S. Maerkl, S.R. Quake, Science 298 (2002) 580.
[21] C.L. Hansen, E. Skordalakes, J.M. Berger, S.R. Quake, Proc. Natl. Acad. Sci. U.S.A. 99 (2002) 16531.
[22] J.W. Hong, S.R. Quake, Nat. Biotechnol. 21 (2003) 1179.
[23] M.L. Adams, M.L. Johnston, A. Scherer, S.R. Quake, J. MicroMech. MicroEng. 15 (2005) 1517.
[24] J. Liu, C. Hansen, S.R. Quake, Anal. Chem. 75 (2003) 4718.
[25] G.H. Seong, R.M. Crooks, J. Am. Chem. Soc. 124 (2002) 13360.
[26] S. Hu, N.J. Dovichi, Anal. Chem. 74 (2002) 2833.
[27] D.J. Harrison, A. Manz, Z.H. Fan, H. Lido, H.M. Widmer, Anal. Chem. 64 (1992) 1926.
[28] A. Manz, D.J. Harrison, E.M.J. Verpoorte, J.C. Fettinger, A. Paulus, H. Ludi, J. Chromatogr. 593 (1992) 253.
[29] E. Verpoorte, Electrophoresis 23 (2002) 677.
[30] R. Locascio, L. Locascio, Anal. Chem. 75 (2003) 1218.
[31] A.E. Herr, J.I. Molho, K.A. Drouvalakis, J.C. Mikkelsen, P.J. Utz, J.G. Santiago, T.W. Kenny, Anal. Chem. 75 (2003) 1180.
[32] R.C. McGlennen, Clin. Chem. 47 (2001) 393.
[33] T. Vo-Dinh, B.M. Cullum, D.L. Stokes, Sens. Actuat. B. Chem. 74 (2001) 2.
[34] L.J. Kricka, J. Clin. Ligand Assay 25 (2002) 317.
[35] L.J. Jin, J. Ferrance, J.P. Landers, Biotechniques 31 (2001) 1332.
[36] C.F. Duffy, B. MacCraith, D. Diamond, R. O'Kennedy, E.A. Arriaga, Lab Chip 6 (2006) 1007.
[37] G. Xu, J. Wang, Y. Chen, L. Zhang, D. Wang, G. Chen, Lab Chip 6 (2006) 145.
[38] J.A. Vickers, M.M. Caulum, C.S. Henry, Anal. Chem. 78 (2006) 7446.
[39] J.W. Cooper, Y.L. Wang, C.S. Lee, Electrophoresis 25 (2004) 3913.

[40] P.S. Andersen, C. Jespersgaard, J. Vuust, M. Christiansen, L.A. Larsen, Hum. Mutat. 21 (2003) 455.
[41] L. Chen, J.C. Ren, Chem. High Throughput Screen. 7 (2004) 29.
[42] J.H. Ng, L.L. Ilag, J. Cell. Mol. Med. 6 (2002) 329.
[43] T. Le Bricon, Ann. Biol. Clin. Paris 60 (2002) 525.
[44] Y.L. Chen, Z.H. Lu, Prog. Biochem. Biophys. 25 (1998) 517.
[45] D.D. Cunningham, Anal. Chim. Acta 429 (2001) 1.
[46] J. Kaddis, C. Zurita, J. Moran, M. Borra, N. Polder, C.R. Meyer, F.A. Gomez, Anal. Biochem. 327 (2004) 252.
[47] G. Li, X. Zhou, Y. Wang, A. El-Shafey, N.H. Chiu, I.S. Krull, J. Chromatogr. A. 1053 (2004) 253.
[48] L.M. Lewis, L.J. Engle, W.E. Piercall, D.E. Hughes, K.J. Shaw, Bioscreen 9 (2004) 303.
[49] Y.H. Chu, G.M. Whitesides, J. Org. Chem. 57 (1992) 3524.
[50] Y.H. Chu, L.Z. Avila, H.A. Biebuyck, G.M. Whitesides, J. Med. Chem. 35 (1992) 2915.
[51] N.H.H. Heegaard, F.A. Robey, Anal. Chem. 64 (1992) 2479.
[52] Y. Baba, M. Tsuhako, M. Sawa, M. Akashi, E. Yashima, Anal. Chem. 64 (1992) 1920.
[53] J.C. Kraak, S. Busch, H. Poppe, J. Chromatogr. 608 (1992) 257.
[54] J. McKeon, L.A. Holland, Electrophoresis 25 (2004) 1243.
[55] A. Varenne, P. Gareil, S. Colliec-Jouault, R. Daniel, Anal. Biochem. 315 (2003) 152.
[56] C.F. Silverio, A. Plazas, J. Moran, F.A. Gomez, J. Liq. Chromatogr. Rel. Technol. 25 (2002) 1677.
[57] E. Mito, Y. Zhang, S. Esquivel, F.A. Gomez, Anal. Biochem. 280 (2000) 209.
[58] M. Azad, L. Hernandez, A. Plazas, M. Rudolph, F.A. Gomez, Chromatographia 57 (2003) 339.
[59] S. Kiessig, H. Bang, F. Thunecke, J. Chromatogr. A 853 (1999) 469.
[60] E. De Lorenzi, C. Galbusera, V. Bellotti, P. Mangione, G. Massolini, E. Tabolotti, A. Andreolim, G. Caccialanza, Electrophoresis 21 (2000) 3280.
[61] F. Progent, M. Taverna, I. Le Potier, F. Gopee, D. Ferrier, Electrophoresis 23 (2002) 938.
[62] Y. Ding, B. Lin, C.W. Huie, Electrophoresis 22 (2001) 2210.
[63] J. Zavaleta, D.B. Chinchilla, A. Brown, A. Ramirez, V. Calderon, T. Sogomonyan, R. Montes, F.A. Gomez, Adv. Chromatogr. 45 (2007) 125.
[64] J. Heintz, M. Hernandez, F.A. Gomez, J. Chromatogr. A 840 (1999) 261.
[65] E. Mito, F.A. Gomez, Chromatographia 50 (1999) 689.
[66] Y. Zhang, C. Kodama, C. Zurita, F.A. Gomez, J. Chromatogr. A 928 (2001) 233.
[67] A. Brown, R. Desharnais, B.C. Roy, S. Malik, F.A. Gomez, Anal. Chim. Acta 540 (2005) 403.
[68] J. Zavaleta, D.B. Chinchilla, C.F. Kaddis, K. Martinez, A. Brown, A. Gomez, A. Pao, A. Ramirez, S. Nilapwar, J.E. Ladbury, F.A. Gomez, J. Cap. Elect. Microchip Tech. 9 (2006) 101.
[69] V. Villareal, J. Kaddis, M. Azad, C. Zurita, I. Silva, L. Hernandez, M. Rudolph, J. Moran, F.A. Gomez, Anal. Bioanal. Chem. 376 (2003) 822.
[70] A. Ramirez, F.A. Gomez, J. Cap. Elect. Microchip Tech., 2007 in press.
[71] A.J.R. Heck, P.J. Bonnici, E. Breukink, D. Morris, M. Wills, Chem. Eur. J. 7 (2001) 910.
[72] D.A. Beauregard, A.J. Maguire, D.H. Williams, P.E. Reynolds, Antimicrob. Agents Chemother. 41 (1997) 2418.
[73] N.E. Allen, D.L. LeTourneau, J.N. Hobbs Jr., Antimicrob. Agents Chemother. 41 (1997) 66.
[74] G. Chiosis, I.G. Boneca, Science 293 (2001) 1484.
[75] H. Arimoto, K. Nishimura, T. Kinumi, I. Hayakawa, D. Uemura, Chem. Commun. (1999) 1361.
[76] W.C. Noble, Z. Virani, R.G.A. Cree, FEMS Microbiol. Lett. 93 (1992) 195.
[77] R. Kerns, S.D. Dong, S. Fukuzawa, J. Carbeck, J. Kohler, L. Silver, D. Kahne, J. Am. Chem. Soc. 122 (2000) 12608.
[78] X. Liu, X. Liu, A. Liang, Electrophoresis 27 (2006) 3125.
[79] E.-S. Kwak, F.A. Gomez, Chromatographia 43 (1996) 659.

Available online at www.sciencedirect.com
ScienceDirect
Talanta 74 (2008) 793–799
Talanta
www.elsevier.com/locate/talanta

Comprehensive two-dimensional gas chromatography for fingerprint pattern recognition in *cachaça* production

Z.L. Cardeal [a,*], P.P. de Souza [a], M.D.R. Gomes da Silva [b], P.J. Marriott [c]

[a] *Chemistry Department, ICEx, Federal University of Minas Gerais, Avenida Antonio Carlos 6627, 31270-901 Belo Horizonte, MG, Brazil*
[b] *REQUIMTE, Departamento de Química, Faculdade de Ciências e Tecnologia, Universidade Nova de Lisboa, 2829-516 Caparica, Portugal*
[c] *Australian Centre for Research on Separation Science, RMIT University, School of Applied Sciences, GPO Box 2476V, Melbourne 3001 Australia*

Received 18 April 2007; received in revised form 10 July 2007; accepted 10 July 2007
Available online 31 July 2007

Abstract

Cachaça samples were studied by means of comprehensive two-dimensional gas chromatography and time-of-flight mass spectrometry (GC × GC/TOFMS) during the fermentation process and after ageing in different wood materials. The analyses of the aroma compounds were performed after headspace-solid phase microextraction method (HS-SPME) using an 85 μm polyacrylate (PA) fibre. Fingerprint monitoring of the distillation process allowed the easy determination of the turning points of the process and high-resolution comparison of *cabeça* (head), *coração* (core) and *cauda* (tail) fractions. The ageing process in different wood materials was well characterised through fingerprint similarity observations; in the absence of a suitable metric for expressing the overall similarity, here we use a visual and retention time comparison to identify co-incident peaks and those that differ between samples. For quality control purposes, a simple observation of the contour plots obtained can thus allow the identification of the type of wood used in the ageing process, and the process of ageing, without further statistical treatment or peak identifications. In this manner, peaks, which discriminated most between the different mixtures studied were readily found, i.e. unique compounds were identified in each stage of the distillation process. Approximate first dimension linear retention indices (LRI) for these identified compounds were calculated in a bi-dimensional polar/non-polar column set in the GC × GC experiment and were used in conjunction with mass spectral library searching for tentative identification. Along the progression of the distillation process, 70 compounds appear to visually discriminate between samples and their retention indices are indicated, presenting good correlation with literature data.
© 2007 Elsevier B.V. All rights reserved.

Keywords: Comprehensive two-dimensional gas chromatography; *Cachaça*; Volatile organic compounds; SPME; GC × GC/TOFMS; Fingerprinting

1. Introduction

The Brazilian sugarcane spirit, popularized as *cachaça*, is liquor distilled directly from the juice of unrefined sugarcane. *Cachaça* was first produced by the early Portuguese settlers of Brazil, around 1540. The absence of description of *cachaça* requires a brief introduction to this beverage. Workers at local sugar mills discovered that the sugarcane juice (*garapa*), cooked and left standing, would ferment and turn into a mild alcoholic beverage. The product, named *cagaça*, was consumed by slaves as a cheap substitute for the natives' *cauim*. Soon after, distillation technology was introduced to the crude ferment, and thus the beverage known as *cachaça* was produced [1]. The process of production of sugarcane spirit starts with cut of the cane (except the green cane which produces methanol) and the extraction of the quite clean cane juice. The first phase of the fermentation is called "handmade", when a starter for *cachaça* production is prepared as a mixture of crushed corn, lemons, rice, and starch as sources of supplementary substrates forming a paste and left for spontaneous fermentation at room temperature for 12–24 h. Then sugarcane juice is added to the paste until it is submerged and left to rest for more than 24 h [2]. For distillation the fermented juice is transferred to the still to be heated up and distil over the alcohol in a single stage process to increase the alcohol content. At the beginning the distillate has very high ethanol content, about 75 g L^{-1}, and it contains methanol (among other low mass compounds such as aldehydes and ethers). Near the end, the distillate almost has no ethanol. In order to obtain a high quality product, only the fractions that present an ethanol amount between 38 and 68 g L^{-1} are col-

* Corresponding author. Fax: +55 31 34995700.
E-mail address: zenilda@ufmg.br (Z.L. Cardeal).

0039-9140/$ – see front matter © 2007 Elsevier B.V. All rights reserved.
doi:10.1016/j.talanta.2007.07.021

lected. These fractions are called *coração* ("core"). The fraction collection criterion performed according to the ethanol content is not reliable because slight modifications on the *cachaça* production process can produce major differences to the ethanol amount [2]. After distillation, the sugarcane brandy can be bottled or aged for 6–18 months, or longer depending on the wood type used as barrel material. There are many types of woods and the most common are amburana (A*mburana cearencis*), jequitibá (*Cariniana estrellensis* and *Cariniana legalis*), ipê (*Tabebuia* genus), balsam wood (*Myrocarpus frondosus avium and Prunus cerasus*), and Brazilian and foreign oak (*Quercus* genus) [3].

A quick method that could show differences among *cachaça* samples aged in different types of woods would be very useful for industrial applications, in order to assure spirit quality and to avoid fraud such as the addition of taints, flavours or other wood types, different from the one reported by the producer. Brazil is a leading producer and consumer of spirits, with a yearly production amounting to 1.3 billion L of *cachaça*. Two hundred million litres [1] of *cachaça* are produced from thousands of small mills spread all over the country, with Minas Gerais state reputedly the best source. There is a widespread interest in establishing quality standards for the beverage, as frequently declared by academic and industrial sectors, government, and producer associations. The physicochemical and organoleptic characteristics of *cachaça* depend on several factors concerning the fermentation conditions and ageing, among others [2,4]. This beverage can be described as a complex mixture of flavour compounds in an ethanol–water matrix such as higher aliphatic and aromatic alcohols, ethyl esters, aldehydes, a series of aromatic compounds and terpenes [5–7]. The solid-phase microextraction (SPME) sampling method has been previously applied to chromatogram comparison analysis and has an important role in order to perform quality control analysis as well in adulteration determination in the food industry. Vinaixa et al. [8] analysed rancidity in potato crisps using SPME and the results obtained were statistically analysed by means of linear discriminant analysis (LDA) as a pre-processing step in order to have access to validated vectors to then input them into a neural network. SPME was also used in hop oil studies [9], using principal component analysis (PCA) as a statistical tool in order to determine and verify hop varieties. In spirit beverages, such as wine, an elegant headspace-MS fingerprint analysis was performed [10] in order to classify wines by variety, origin and age. In the referred study, the VOC were extracted by SPME and directly studied by mass spectrometry. The mass spectrometric data obtained were analysed, and the differences among the wines according to the mass fragment patterns obtained were statistically determined. Nevertheless, no peak assignments were possible since the sample was not submitted to a chromatographic separation.

The determination of VOC in spirit beverages is most frequently performed by gas chromatographic methods using an isolation and pre-concentration technique. Liquid–liquid extraction requires, in general, the use of a range of organic solvents in multi-step experiments for each sample [11–13]. Moreover, part of the solvent must be partly removed before the GC run, in order to concentrate the final extract, risking the evaporative loss of some of the more volatile components. This frequently masks important characteristic compounds presenting very low boiling points, such as low molecular mass alcohols, ethers and carbonyl compounds. Solid phase extraction (SPE), although less time consuming, presents similar drawbacks as liquid extraction, since solvent is needed for the elution of the compounds from the stationary phase [13]. In a previous study, a headspace solid-phase microextraction (SPME) method was developed for the determination of secondary compounds from Brazilian *cachaça*, by GC–FID and GC/MS [6]. This study demonstrates the good performance of SPME to analyse VOC in *cachaça*, but limited resolution is observable from the chromatograms suggesting that a more powerful separation technique should be used for adequate characterization of the chemical composition of the headspace. Greater resolution also assists in rapidly identifying the components that differentiate samples, and so aids the concept of fingerprint comparison. Comprehensive two-dimensional gas chromatography (GC × GC) with either non-selective flame ionization (FID) or selective time-of-flight mass spectrometric (TOFMS) detection seems to be an ideal methodology for this purpose. GC × GC involves the use of two columns with different separation characteristics serially coupled through a suitable interface that allows peaks from the primary column to be transferred onto the second column for an additional separation. The focusing obtained through this modulation process reduces the peak width, and thus the peak height and sensitivity increase [14–18].

In this work the *cachaça* sample was produced by an artisan methodology in a mill, located in Minas Gerais state, Brazil. This State is responsible for an average *cachaça* production of around 100,000 L per year. The headspace of *cachaça* samples was studied, with samples taken during the distillation process. The *cachaça* samples were analysed by means of HS-SPME-GC × GC/TOFMS, with a longitudinally modulated cryogenic system (LMCS) [15,19] used as an interface for GC × GC analysis as described previously for flavour analyses [20–22].

2. Experimental

2.1. Cachaça samples

All the *cachaça* samples were obtained from a Minas Gerais state mill in Belo Horizonte, Brazil. The production follows the traditional (artisan) methodology for the production of *cachaça*.

2.2. Sample preparation and SPME procedure

The manual SPME holder and the 85 μm polyacrylate (PA) fibre were purchased from Supelco (Bellefonte, PA, USA). Prior to use, the fibres were conditioned following the manufacturer's instructions. The fibre was exposed to sample headspace for a suitable adsorption time of 25 min at 60 °C and introduced into the GC injector to allow thermal desorption of the analytes at the temperature of 240 °C for 3 min period, for a splitless time of 30 s according to previous work [6].

For the SPME procedure an aliquot of 4.00 mL of spirit samples was used. This aliquot was diluted in water in a volumetric flask of 50.00 mL with the addition of 2.5 g of sodium

chloride [6]. An aliquot of 10.0 mL was introduced into 22 mL Pyrex vials, and the vials were immediately sealed with aluminium caps containing Teflon septa. For the blank sample, the same procedure was performed without *cachaça* addition to the volumetric flask.

For retention indices determination, samples were spiked with 3 μL of a 10 mg L^{-1} hydrocarbon (C9–C22) stock solution in hexane.

2.3. Equipment

The GC × GC/TOFMS system consisted of a HP 6890 (Agilent Technologies, Burwood, Australia) gas chromatograph and a Pegasus III time-of-flight mass spectrometer (LECO, St. Joseph, MI, USA). To implement the modulation process, a longitudinally modulated cryogenic system (LMCS; Chromatography Concepts, Doncaster, Australia) was used, and was operated at a modulation period of 6 s with a cryotrap temperature of −20 °C. The TOFMS was operated at a storage rate of 100 Hz, using a mass range of 45–415 u and a multi-channel plate voltage of 1700 V. Data were processed using LECO Corp. ChromaTOF^{TM} software.

The column sets used for GC × GC experiments comprised a BPX5 (5% phenyl-dimethyl polysilphenylene-siloxane phase) primary column; 30 m × 0.25 mm i.d. × 0.25 μm film thickness (d_f), directly coupled to a BPX20 (polyethyleneglycol phase) second column of 1.5 m × 0.1 mm i.d. × 0.1 μm d_f. Both columns were from SGE International (Ringwood, Australia). The oven temperature program began at 35 °C, held for 5 min and was then raised to 210 °C at 3 °C min^{-1}, then to 240 °C at 40 °C min^{-1} and held for 10 min at this temperature. Helium was used at a flow rate at 1.3 mL min^{-1}. The transfer line column for the GC × GC/TOFMS system was a 0.50 m deactivated fused silica column with 0.1 mm i.d. (0.21 m inside the transfer line and 0.29 m inside the oven) from SGE International.

Initial comparison of the 2D GC × GC chromatogram results was undertaken by overlaying the respective plots to identify components that are either common to the two samples being compared, or are unique to either of the samples. The unique compounds can then be simply further identified by mass spectral library searching of the target component. Retention index calculation supports tentative identification of the compound.

3. Results and discussion

A distillation process of one *cachaça* batch was followed by means of GC × GC/TOFMS. During this process, three samples from different stages of the distillation were taken, *cabeça* (head), *coração* (core) and *cauda* (tail). In common distillation procedure practice, the *cabeça* (5–10% of the total distillate) and *cauda* (10–15% of the total distillate) fractions are discarded. In general, the first has ethanol as the major constituent and other volatile and semi-volatile alcohols, aldehydes, esters and oxygenated compounds that are associated with toxic effects [23]. The major contributors to the later fraction, with higher water content, are heavier alcohols, which do not allow its use for *cachaça* production. Fig. 1A–C shows a sequence of three contour plots that reflects the progression of the distillation process. In general, only the compounds that visually differ from sample to sample, and thus are unique for each sample, are indicated in each contour plot, unless they are identified for subsequent discussion below; they are also identified in Table 1 . Here, the identification was made by comparing the obtained spectra with the Adams and NIST 98 mass spectra database libraries. The

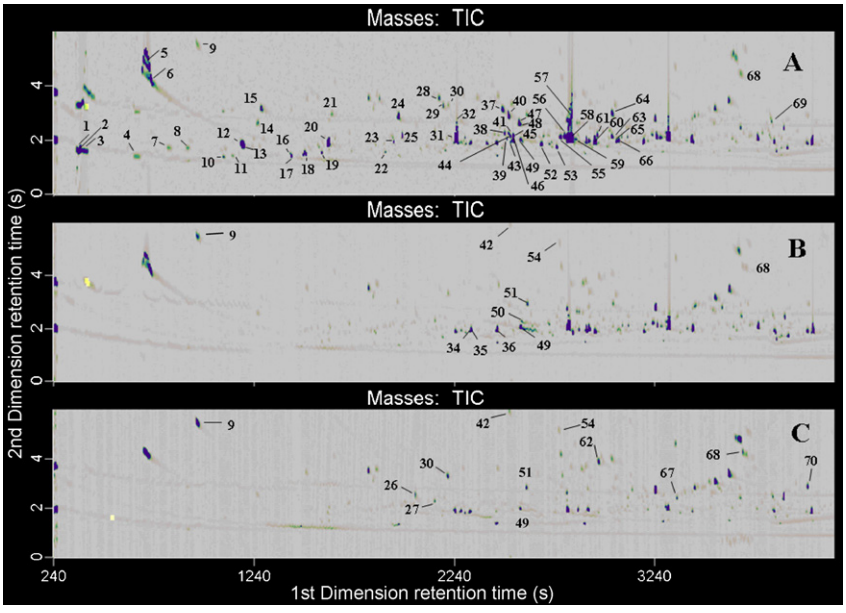


Fig. 1. GC × GC/TOFMS contour plots of SPME headspace extracts of the distillation process during *cachaça* distillation. (A) Contour plot obtained for the first fraction (*cabeça* "head") with high content of ethanol (not shown; mass scanning starts after elution of ethanol) and the more volatile and semi-volatile compounds. (B) *coração* "core" fraction depleted of more volatile compounds and richer in the semi-volatile compounds. (C) *cauda* "tail" fraction corresponding to the end of the distillation with enhanced water content and less volatile compounds. Peak numbering and assignment (tentative) as presented in Table 1. For sampling and chromatographic conditions see text.

Table 1
Tentative identification peaks identified in Fig. 1 based on comparison of their mass spectra to reference databases (MS) and retention indices (RI) [25,26], after HS-SPME-GC × GC/TOFMS analysis

Peak no.	^1t_R	^2t_R	Compound	*m/z* Pattern fragmentation	Literature RI	Calculated RI
1	408	1.65	2-Methyl-propan-1-ol		647	670
2	414	1.61	Ethyl acetate		628	670
3	630	1.71	Ethyl propanoate		717	726
4	648	1.42	1,2-Diethoxyethane		734	738
5	684	5.05	3-Methylbutan-1-ol		741	749
6	720	4.6	2-Methylbutan-1-ol		736	759
7	816	1.75	Isobutyl acetate		776	783
8	912	1.73	Ethyl butanoate		804	810
9	960	5.54	2-Hydroxyethyl propanoate		813	824
10	1086	1.4	1,1-Diethoxy-2-methyl-propane		865	859
11	1098	1.70	Ethyl-3-methylbutanoate		858	861
12	1182	1.87	3-Methylbutanol acetate		876	885
13	1194	1.81	2-Methylbutyl acetate		880	888
14	1260	2.66	Cyclooctatetraene		889	907
15	1278	3.17	Heptan-2-ol		896	912
16	1428	1.43	1,1-Diethoxy-3-methyl-butane		959	953
17	1428	1.42	1,1-Diethoxy-2-methyl-butane		939[a]	953
18	1488	1.48	1-(1-Ethoxyethoxy) pentane		1004[a]	970
19	1578	1.56	1,1-Diethoxypentane		1004[a]	995
20	1614	1.93	Ethyl hexanoate		998	1005
21	1626	2.98	Octan-2-ol		995	1009
22	1896	1.59	1,1-Diethoxyhexane		1003[a]	1092
23	1938	1.95	Ethyl heptanoate		1099	1106
24	1962	2.87	Nonan-2-ol		1100	1113
25	1974	2.10	Nonanal		1104	1118
26	2070	1.72	2-Phenylethanol		1107	1140
27	2142	2.38	Tetramethyl substituted benzene	M^+ 134 (36), 119 (100), 103 (8), 91 (37), 77 (22), 65 (13), 51 (17)	–	1171
28	2166	3.55	Benzene C4-substituted	M^+ 134 (89); 119 (68), 91 (100), 65 (72), 51 (25)	–	1179
29	2184	3.27	Nonan-1-ol		1169	1185
30	2208	3.32	Diethyl butanedioate		1179	1192
31	2244	2.06	Ethyl octanoate		1197	1204
32	2274	2.72	Decan-2-ol		1198	1215
33	2286	2.30	2-(4-Methyl-1-cyclohex-3-enyl) propan-2-ol		1195	1219
34	2316	1.91	3-Butylcycloheptan-1-one		1370[a]	1229
35	2222	1.83	Trimethyl 1,2,3,4-tetrahydro-naphthalene		–	1231
36	2322	1.950	Trimethyl 1,2,3,4-tetrahydro-naphthalene		–	1277
37	2478	3.15	Decan-1-ol		1270	1286
38	2490	2.26	n.i.	M^+ 166 (13); 56 (61), 67 (77), 81 (100), 98 (72), 137 (33)	–	1289
39	2502	2.05	Ethyl non-3-enoate (isomer)		1290[a]	1294
40	2508	2.94	Undec-10-en-1-ol (isomer)		1285[a]	1296
41	2514	2.25	n.i.	M^+ 166 (13); 56 (61), 67 (77), 81 (100), 98 (72), 137 (32)		1298
42	2520	0.01	4-Ethyl-2-methoxy-phenol		1287	1299
43	2520	2.01	Propyl octanoate		1277	1300
44	2520	2.150	Ethyl non-3-enoate (isomer)		1272[a]	1300
45	2532	2.27	Ethyl nonanoate		1296	1304
46	2544	2.15	Undecan-2-one		1294	1306
47	2561	2.95	Undecen-2-ol (isomer)		1295[a]	1314
48	2562	2.83	Undecan-2-ol		1311	1315
49	2574	2.02	Tetramethyl, 2,3-dihydro-1H-indene		–	1319
50	2604	2.93	Anisole derivative	M^+ 180 (14); 165 (89), 137 (100), 109 (57), 91 (48), 77 (60), 65 (36)	–	1330
51	2676	1.85	2-Methylpropyl octanoate		1348	1355
52	2748	1.76	1,1-Diethoxynonane		1401[a]	1381
53	2766	5.250	2-Methoxy-4-propyl-phenol		1369	1386
54	2772	2.12	(E)-Ethyl dec-4-enoate		1382	1389
55	2790	2.15	Ethyl dec-9-enoate (isomer)		1389	1396
56	2820	3.01	n.i.	97 (100); 45 (25)	–	1407
57	2826	2.00	Ethyl decanoate		1396	1409
58	2844	2.04	Decyl-acetate		1408	1416

Table 1 (*Continued*)

Peak no.	^1t_R	^2t_R	Compound	*m/z* Pattern fragmentation	Literature RI	Calculated RI
59	2934	1.9	3-Methylbutyl octanoate		1446	1453
60	2952	2.18	Ethyl dec-2-enoate (isomer)		1389[a]	1458
61	2964	3.95	n.i.	M^+ 192 (3); 91 (100), 105 (55), 133 (52), 177 (66), 159 (83)	–	1461
62	3012	2.12	Ethyl undecenoate (isomer)		1471[a]	1481
63	3024	3.03	n.i.	55 (60); 67 (64); 79 (100); 93 (31); 107 (23)		1486
64	3048	3.31	Propyl decanoate		1493	1495
65	3060	2.00	Ethyl undecanoate		1479	1500
66	3348	2.46	n.i.	M^+ 218 (7); 115 (41), 128 (44), 142 (28), 157 (100), 172 (35), 189 (11) 203 (8)	–	1621
67	3666	4.48	(E)-Ethyl-tetradecanoate (isomer)		–	1770
68	3822	2.71	C15-Ethyl ester	M^+ 270 (2); 55 (40), 73 (22), 88 (100), 101 (51), 115 (6), 157 (10)	–	1852
69	3822	2.71	C15-Ethyl ester	M^+ 270 (2); 55 (40), 73 (22), 88 (100), 101 (51), 115 (6), 157 (10)	–	1852
70	4002	2.91	Phtalate (blank impurity)		–	1991

Retention times on the ^{1}D (^1t_R) and ^{2}D (^2t_R) columns are presented. The calculated retention indices were obtained based on retention times across the dual column set. n.i. denotes non-identified peak; in this case the characteristic mass fragment ions are presented.

[a] Estimated index value according to reference [27].

respective retention indices were calculated according to van den Dool and Kratz equation [24] and the literature retention indices [25–27] are also listed when they were available in the literature.

The *cabeça* fraction shows, as expected, a major contribution from the most volatile compounds. Ethanol, not appearing in the contour plots shown, since the mass scanning was started after its elution, is the major contributor in all the fractions. Hence, ethanol is of little interest in a comparative sense. Only in the first fraction can one observe the presence of isobutanol, ethyl acetate and ethyl propanoate. 3-methyl-butan-1-ol (5) and 2-methyl-butan-1-ol (6) are far reduced in the *cauda* fraction when compared to the first fraction. While 2-hydroxy-ethylpropanoate (9) increased in concentration from the first to the latest sample, the compounds 7 and 8 and 10–25 (see Table 1) almost disappeared in the same sequence. This demonstrates that the early stages of the distillation process eliminates from the mother liquor the most volatile components, some of them being recognizably strong negative contributors to the organoleptic characteristics of the *cachaça* aroma [23], such as the case of the ether compounds with ethoxy moieties (normally associated with tannin degradation products [28]), or the low molecular mass alcohols; both these classes are normally associated with 'green' flavoured notes. On the other hand, the distillation process also eliminates other compounds that may be important for positive organoleptic characteristics of *cachaça*, such as the esters, normally associated with fruity and pleasant attributes. Comparing the contour plots, one can observe the evolution of the distillation process through the collected fractions, where the first fraction (Fig. 1A) is richer in the most volatile compounds and the latter (Fig. 1C) in the less volatile components.

The *coração* fraction (Fig. 1B), which is the origin of the final *cachaça* selected as the beverage product, is richer in the semi-volatile compounds, being mostly sesquiterpenes and esters, generally considered as essential flavour contributors for many natural products. Since the aim of this work is the differentiation between samples through visual discrimination, a detailed description of the volatile compound composition is not given. This objective is the main subject of ongoing work. Nevertheless by using GC × GC more compounds were found and separated compared to a previous 1D GC method [6] used after *cachaça* samples have been submitted to the same extraction procedure. The *coração* sample, when compared with the final product (upper contour plot, Fig. 2), reveals a significant resemblance in compound constitution or overall pattern. This final product is constituted by all collected fractions from the middle of the distillation process, which is the reason why it presents more peaks in the semi-volatile zone than the presented *coração* sample. The core sample presented in Fig. 1B constitutes only one discrete aliquot of one fraction, among all the others that are collected in the middle of the distillation process. Nevertheless, in both contour plots the more volatile compounds and the heavier compounds are almost absent.

The control of the distillation process, i.e. the identification of the turning points of the *cachaça* distillation, is a sensible task to employ, in order to allow criteria such as elimination of toxic compounds, but at the same time, avoiding the elimination of important flavour-impact constituents, assuring however that the ethanol content should be held between 38 and 68% (g 100 mL^{-1}). In the *cachaça* industry the selection and reassembling of the different distillation stages is time controlled, based on basic criteria. This demands significant experience from the operator in order to be able to differentiate and recognize, empirically, each distillation fraction, and to preserve or assure the quality of the final product. This methodology is far from accurate, and lacks objective knowledge about the effective composition of each distillate, and likely depends largely upon olfactory and gustatory sampling.

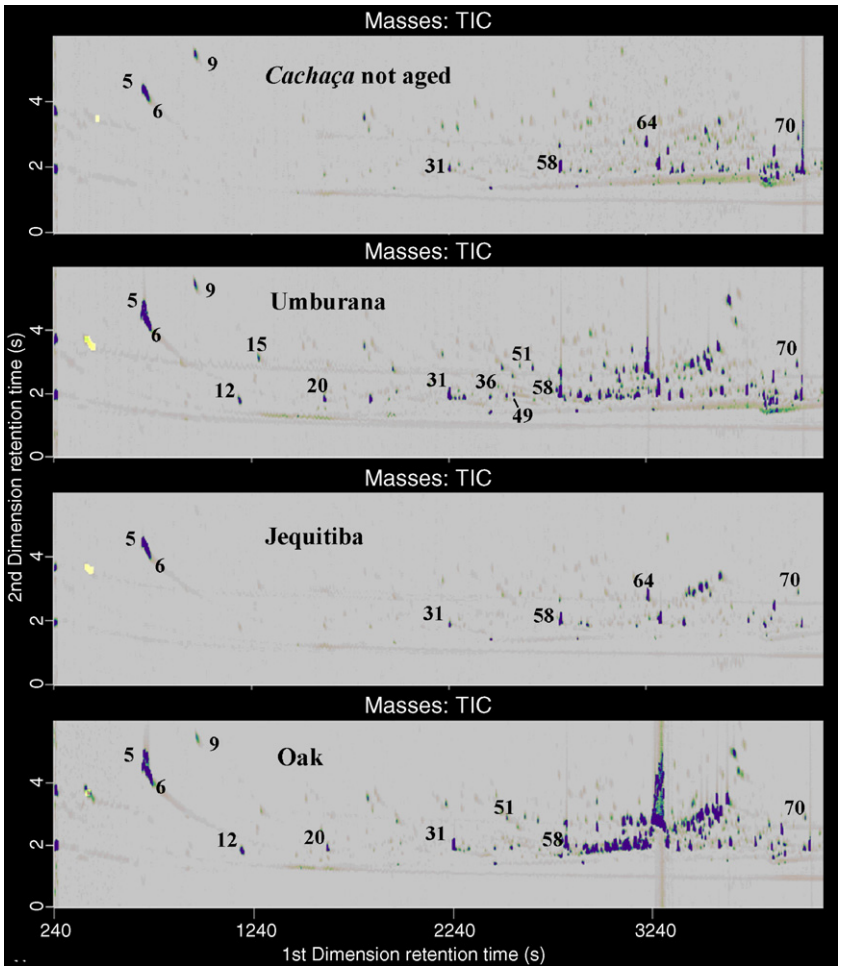


Fig. 2. GC × GC/TOFMS contour plots of SPME headspace extracts showing a *cachaça* sample aged in three different wood materials. The uppermost contour plot shows the original *cachaça* (not aged) corresponding to the "core" fraction. The three lower contour plots result after an ageing period in three different wood barrel materials. For sampling and chromatographic conditions see text.

Using the GC × GC system one would be able to clearly identify the different turning points of the distillation process, by simple visualization and comparison of the contour plots. This methodology can be applied for industrial use in a very simple way by simple monitoring of the distillation process, and, for instance, would permit easy identification of the key compounds that should not be present in the final product in order to reject a particular fraction. Each fraction can be monitored by GC × GC analysis, which in an optimized fast run, can give an accurate profiling or pattern of the aroma composition of a particular fraction; in other words, an easily recognizable fingerprint that represents the distillate composition upon which decision regarding collection or discarding is made according to the parameters considered acceptable by the producer. Once identified, the key compounds that clearly distinguish different distillates and comprise the desirable individual organoleptic qualities of those fractions can be collected and reassembled into *cachaça*.

Another important application of the fingerprint approach is the comparison between different contour plots obtained from the same *cachaça* submitted to three different ageing processes in three different wood matrices. Fig. 2 shows a sequence of four contour plots, representing in the first contour plot, the original *cachaça*, and in the three other contour plots, the result of ageing in three different types of wood. Among the three wood types studied, the Jequitiba contour plot shows a more considerable depletion of compounds than the other wood types when compared to the original *cachaça*. This is consistent with the fact that in contrast with the other two wood materials, Jequitiba is characterized by decreasing the acidity, softening its taste, and maintaining the colour of the beverage. On the other hand, Umburana and Oak promote colour and strong taste changes. All of them contribute to decline in both the alcohol content and the volume. It is also not surprising that each wood type generates a different flavour note to the original product, which should be chemically identifiable and should be reflected and clearly visualized in the contour plots. Apparently the contribution of each wood to the *cachaça* headspace composition, originating from the reaction/extraction events between distillate and the wood during the storage period, varies significantly, thereby producing distinguishable contour plots. The higher number of peaks in oak aged *cachaça* could be associated with the fact that this sam-

ple was aged for a longer period of time (30 months) compared to the 12-month maturation in the case of other wood types. It may also depend on the barrel (and wood) age. This suggests the proposed methodology can be used to fingerprint many chemical profiles that arise from environmental/chemical and ageing parameters during beverage production.

An evident application of the patterns generated by GC × GC, and the information comprising the patterns (e.g., peak area or even mass spectrometric data) is the possible selection of variables (peaks) for multivariate analysis, such as principal component analysis (PCA). An application may be, for example, characterising the effects of distinct types of wood, the same wood from different origins, or even ageing time. For PCA studies, where objects (the samples) are characterized in a two-dimensional space by means of linear combinations of the independent variables (principal components), GC × GC offers a more suitable or reliable approach to generating a database of the chemical composition of each sample [29]. Two different and independent separation mechanisms, on two analytical columns with different polarity, separate compounds of a mixture in two-dimensional space. The orthogonality of the system achieves reduced co-elution, and improves the quality of the selection of variables for object characterization in multivariate studies. The advantage is clear, since instead of a time consuming trial to determine which variables should be considered for the PCA study [30], the selection may now become as simple as comparison or inspecting of the contour plots. The total validation process can be performed in a quicker manner. While this approach has not implicitly mentioned identification of the compounds in each sample and just relies on the peak distribution in 2D space, identification is still a necessary objective, since it will give a chemical significance to the sample differences. Again, for GC × GC data with MS detection, the spectra obtained should be pure or nearly pure compound spectra, through reduction of co-elution that lessens ambiguities and doubtful identifications.

4. Conclusions

Comprehensive two-dimensional GC allows facile comparison between samples arising from monitoring of *cachaça* production. It is suited to following the progression of the distillation process reducing the dependence on statistical methods in order to identify the turning points of the distillation process. Wood storage materials and the ageing period can be also monitored, making this method suited for product quality analysis. This can be extended to applications such as inspection for fraudulent practices and product substitution, having ramifications on high value added products or those purportedly made with more expensive processes. Fingerprinting offers a way to obtain an essentially complete sample characterization, since sampling, extraction and analysis takes approximately 1–2 h per sample (if on site laboratory facilities are available), suggesting that even inexperienced operators might be able to perform the quality control/assurance task. Ability to visually recognize patterns should be the only requisite needed for industrial production monitoring, quality control and certification.

Acknowledgements

The authors would like to acknowledge and thank Mr. Paul Morrison for his technical assistance, SGE International for provision of capillary columns, and support from Agilent Technologies for gas chromatography facilities. LECO Corp. is thanked for maintenance of the TOFMS system; M.D.R. Gomes da Silva acknowledges the Scholarship from Fundação Calouste de Gulbenkian, Portugal and the support of the project POCI/AGR/55432/2004; and Z.L. Cardeal was supported by CAPES (Ministério da Educação, Brazil) to spend time as sabbatical visiting scholars in the ACROSS laboratory at RMIT University.

References

[1] A.G.H. Lea, J.R. Piggott, Fermented Beverage Production, cap 15, second ed., Kluwer Academic/Plenum Publisher, New York, 2003, pp. 335–346.
[2] M.A. Vicente, L.G. Fietto, I. de Miranda Castro, A.N. Gonçalves dos Santos, M.X. Coutrim, R.L. Brandão, Int. J. Food Microbiol. 108 (2006) 51.
[3] P.P. de Souza, H.G.L. Siebald, D.V. Augusti, W.B. Neto, V.M. Amorim, R.R. Catharino, M.N. Eberlin, R. Augusti, J. Agric. Food Chem. 55 (2007) 2094.
[4] R.F. Nascimento, J.C. Marques, B.S. Lima Neto, D. De Keukeleire, D.W. Franco, J. Chromatogr. A 782 (1997) 13.
[5] R.F. Nascimento, D.R. Cardoso, B.S.L. Neto, D. Franco, Chromatographia 48 (1998) 757.
[6] E.A. Nonato, F. Carazza, F.C. Silva, C.R. Carvalho, Z.L. Cardeal, J. Agric. Food Chem. 49 (2001) 3533.
[7] M.D.C.A. De Souza, P. Vasquez, N.L. Del Mastro, T.E. Acree, E.H. Lavin, J. Agric. Food Chem. 54 (2006) 485.
[8] M. Vinaixa, A. Vergara, C. Duran, E. Llobet, C. Badia, J. Brezmes, X. Vilanova, X. Correig, Sens. Actuators B-Chem. 106 (2005) 67.
[9] M. Kovacevic, M. Kac, J. Chromatogr. A 918 (2001) 159.
[10] M.P. Marti, O. Busto, J. Guasch, J. Chromatogr. A 1057 (2004) 211.
[11] J. Villén, F.J. Señoráns, G. Reglero, M. Herraiz, J. Agric. Food Chem. 43 (1995) 717.
[12] R. Eisert, K. Levsen, J. Chromatogr. A 733 (1996) 143.
[13] P.L. Buldinia, L. Ricci, J.L. Sharma, J. Chromatogr. A 975 (2002) 47.
[14] W. Bertsch, J. High Resol. Chromatogr. 23 (2000) 167.
[15] P.J. Marriott, R. Shellie, Trends Anal. Chem. 21 (2002) 573.
[16] J. Dallüge, J. Beens, U.A.Th. Brinkman, J. Chromatogr. A 1000 (2003) 69.
[17] T. Górecki, J. Harynuk, O. Panić, J. Sep. Sci. 27 (2004) 359.
[18] M. Adahchour, J. Beens, R.J.J. Vreuls, U.A.Th. Brinkman, Trends Anal. Chem. 25 (2006) 540.
[19] P.J. Marriott, R.M. Kinghorn, Anal. Chem. 69 (1997) 2582.
[20] X. Di, R.A. Shellie, P.J. Marriott, C.W. Huie, J. Sep. Sci. 27 (2004) 451.
[21] D. Ryan, P. Watkins, J. Smith, M. Allen, P. Marriott, J. Sep. Sci. 28 (2005) 1075.
[22] G. Eyres, J.-P. Dufour, G. Hallifax, S. Sotheeswaran, P.J. Marriott, J. Sep. Sci. 28 (2005) 1061.
[23] W. Wardencki, P. Sowiński, J. Curylo, J. Chromatogr. A 984 (2003) 89.
[24] H. Van Den Dool, P.D. Kratz, J. Chromatogr. 11 (1963) 463.
[25] R.P. Adams, Identification of Essential Oil Components by Gas Chromatography/Quadrupole Mass Spectrometry, Allured Publishing Corp., Ilinois, USA, 2001.
[26] http://webbook.nist.gov/chemistry, NIST Standard Reference Database Number 69, June 2005 Release, accessed April 2007.
[27] Mass Spectra Library NIST version 2.0, 2005.
[28] J.R. Mosedale, J.-L. Puech, Trends Food Sci. Technol. 9 (1998) 95.
[29] J.L. Hope, B.J. Prazen, E.J. Nilsson, M.E. Lidstrom, R.E. Synovec, Talanta 65 (2005) 380.
[30] M.D.R. Gomes da Silva, H.J. Chaves da Neves, J. High Resol. Chromatogr. 20 (1997) 275.

Available online at www.sciencedirect.com
ScienceDirect
Talanta 74 (2008) 1075–1078
Talanta
www.elsevier.com/locate/talanta

Short communication

Quantitative determination of glyphosate in human serum by ^{1}H NMR spectroscopy

Bernard Cartigny [a], Nathalie Azaroual [b], Michel Imbenotte [c,*], Daniel Mathieu [d], Erika Parmentier [d], Gaston Vermeersch [b], Michel Lhermitte [a,c]

[a] *Laboratoire de Toxicologie et Génopathies, Hôpital Calmette, 59045 Lille Cedex, France*
[b] *Laboratoire de Physique, d'Application RMN, UMR CNRS 8009, Université de Lille 2, France*
[c] *Laboratoire de Toxicologie, Université de Lille 2, France*
[d] *Urgences Respiratoires et Réanimation Médicale, 59 Lille, France*

Received 5 April 2007; received in revised form 26 July 2007; accepted 30 July 2007
Available online 3 August 2007

Abstract

The determination and quantification of glyphosate in serum using ^{1}H NMR spectroscopy is reported. This method permitted serum samples to be analysed without derivatization or any other sample pre-treatment, using 3-trimethylsilyl 2,2′,3,3′-tetradeuteropropionic acid (TSP-d_4) as a qualitative and quantitative standard. Characterization of the herbicide *N*-(phosphonomethyl)glycine was performed by analysing chemical shifts and coupling constant patterns. Quantification was performed by relative integration of CH_2-P protons to the TSP-d_4 resonance peak. The method was tested for repeatability ($n = 5$) and yielded coefficients of variation of 1% and 3%, respectively: detection and quantification limits were also determined and were 0.03 and 0.1 mmol/L, respectively. The method was applied to the quantification of glyphosate in a case of acute poisoning.
© 2007 Published by Elsevier B.V.

Keywords: Glyphosate; Serum; Nuclear magnetic resonance

1. Introduction

Glyphosate, *N*-(phosphonomethyl)glycine, CAS registry number [1071-83-6], is a broad spectrum herbicide and is currently the most widely used herbicide in the world, and has progressively replaced other more toxic herbicides like paraquat or atrazine. The number of trade names of glyphosate-containing herbicides has considerably increased in the last 10 years with more than 50 commercial preparations currently available. The associated cation is often isopropylammonium, such as in Roundup®, but can also be sodium, ammonium, trimethylsulfonium and polyoxyethyleneammonium in other formulations. Depending on the different uses of the herbicide, percentages of glyphosate also vary in the trade formulations.

Among commercial formulations, Garryo® is a herbicide containing 360 g/L of glyphosate associated with isopropylammonium. Its use is recommended for agricultural purposes as well as for gardens, public parks and sidewalks in urban settings.

Glyphosate exposure in humans is generally cutaneous and observed most commonly among agricultural workers during spraying work. Oral ingestions are generally due to the result of an attempted suicide, though some are accidental. Exceptional cases of accidental inhalation [1] and parental self-poisoning [2] have also been reported.

Glyphosate itself is generally not considered to be very toxic for mammals when used normally, hence its availability from a wide range of commercial outlets most often in the form of glyphosate-containing herbicides for use in private gardens. They can irritate the skin and eyes and lead to more or less acute dermatitis with sensitisation among highly exposed workers [3], while accidental contact with the skin may cause chemical burns [4], but when glyphosate is deliberately ingested to attempt suicide, sequelae or death can occur. Many deaths have

* Corresponding author. Tel.: +33 3 20 964917.
E-mail address: michel.imbenotte@univ-lille2.fr (M. Imbenotte).

0039-9140/$ – see front matter © 2007 Published by Elsevier B.V.
doi:10.1016/j.talanta.2007.07.029

been reported following suicidal ingestion and glyphosate toxicity may be refractory even to the most intensive of medical treatment [5].

More recent studies have pointed out not only the toxicity of glyphosate itself, but also that of the formulation as a whole, since the surfactants present in commercial mixtures contribute to their overall toxicity [2,6]. In a recent Japanese study, mortality due to glyphosate herbicide was less than 10%, whereas that from paraquat poisoning was more than 70% [7]. The poison control centre for northern France listed 133 phone calls for herbicide poisoning in 2005, during which period only one accidental death of a 91-year-old man and one suicide attempt of a 68-year-old man were directly related to glyphosate. The only study presently published on the link between glyphosate exposure and human cancers was inconclusive [8].

Glyphosate can be measured by several conventional analytical methods such as GC/MS, HPLC with UV or MS detection and amino acid analysers. A revue of conventional methods to determine glyphosate has been published by Stalikas and Konidari [9], but most of these methods require a derivitization step, that potentially generate by-products, but also prevent the simultaneous determination of glyphosate and the associated ions such as isopropylammonium.

NMR spectroscopy has previously been used in our laboratory for the diagnosis of acute poisonings with herbicides [10,11] without the need of a separation and/or derivatization step. In this study, we tested the applicability of proton NMR spectroscopy for the determination of glyphosate in serum samples in a case of poisoning by Garryo®.

2. Experimental

2.1. Reagents

D_2O and internal standard: 3-trimethylsilyl 2,2′,3,3′-tetradeuteropropionic acid (TSP-d_4), were purchased from Eurisotop (Saint Aubin, France). Standard glyphosate and succinic acid were obtained from Sigma–Aldrich (St. Quentin Fallavier, France).

2.2. Proton NMR spectroscopy

Five hundred megahertz ^{1}H NMR spectra were recorded using a Bruker Avance 500 spectrometer. 128 scans of 64 K data points were acquired with a spectral width of 8012 Hz (16 ppm), acquisition time of 4.09 s, recycle delay of 2 s and flip angle of 30°. Solvent suppression was achieved using the presaturation sequence. All NMR measurements were performed at ambient probe temperature (295 K).

Data processing was carried out with Topspin 1.3 program from Bruker. The FIDs were Fourier transformed (0.3 Hz broadening) and the spectra were phased and the baseline corrected.

Five hundred microlitres of serum was introduced into a 5 mm NMR tube. A capillary tube containing a titrated solution of TSP-d_4 in D_2O was subsequently inserted into the NMR tube. TSP-d_4 is a molecule known to bind with proteins in biological samples and therefore could not provide a reliable internal quantification if it was mixed in the serum [12], hence its isolation from the biological sample in the capillary tube. D_2O served as the field frequency lock and all spectra were referenced to the signal from TSP-d_4 at $\delta = 0.00$ ppm.

TSP-d_4 was also used as a quantitative reference, given its proton content and relative peak area, and was separately quantified by analysing the capillary tube in a succinic acid solution of known concentration. The TSP-d_4 solution in the capillary tube was thus calibrated to 1.95 mmol/L for proton content.

Calibration data for glyphosate were obtained from spiked control serum samples. From a stock solution, successive dilutions were performed to prepare 0.05, 0.1, 0.5, 1.0, 2.0, 5.0, 10.0, 15.0 and 20.0 mmol/L concentrations. Calibration data were subjected to linear regression analysis and the significance of correlation coefficients was checked using Student's t-test. Intra-day and day-to-day analysis ($n = 5$) precisions were obtained from spiked control serum at 1 and 10 mmol/L of added standard glyphosate. Detection and quantification limits were linked to the ability of integrating the signal without interference of overlapping signals from other chemical species. The detection limit was thus determined as equivalent to 3-fold the noise signal and the quantification limit estimated as being 10-fold the noise signal.

2.3. Case history

A 25-year-old man, having intentionally ingested two glasses of Garryo®, was admitted to an intensive care department. On admission, he was drunk, presented vomiting and diarrhoea and complained of stomach pain. He was intubated and ventilated. Renal failure occurred and rhabdomyolysis took place. Recuperation was slow, but he was eventually discharged after 2 months.

2.4. Collecting serum samples

Numerous serum samples were collected from the patient from the time of admission to day 21. On the day after admission, hemodialysis was performed in order to eliminate a significant amount of the ingested glyphosate. Sera were centrifuged when necessary to obtain a clear medium and these were stored at −20 °C until proton NMR spectroscopy analysis.

3. Results and discussion

3.1. Qualitative proton NMR analysis: characterization of glyphosate

TSP-d_4 provides a reference for proton chemical shift ($\delta = 0.00$ ppm). Spectra recorded with and without TSP-d_4 revealed no disturbing signal around 0 ppm (Fig. 1a and b). As shown in Fig. 1a, when analysing control sera by ^{1}H NMR spectroscopy with water suppression sequences, some large resonances appeared. For instance, CH_2 and CH_3 groups from

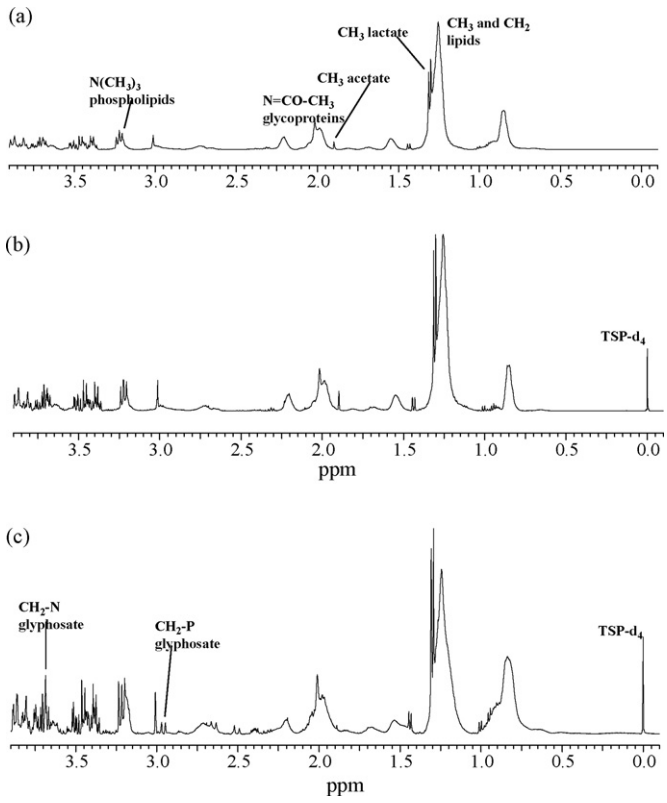


Fig. 1. Partial ^{1}H NMR spectrum (a) from control serum without capillary, (b) from control serum with capillary and (c) from serum spiked with glyphosate.

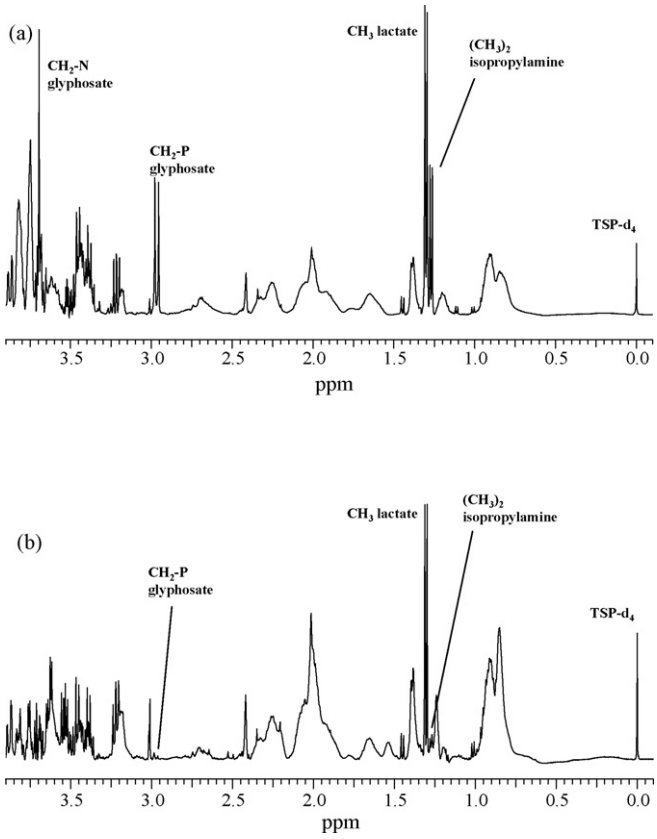


Fig. 2. Partial ^{1}H NMR spectrum from patient's serum. Note the lack of interfering signal in the region around 0 ppm: (a) serum on day 2, before hemodialysis (CH_2-P glyphosate: 5.06 mmol/L) and (b) serum on day 4 (CH_2-P glyphosate: 0.12 mmol/L).

lipids can be observed between 0.5 and 1.5 ppm, as well as N–CO–CH_3 groups from glycoproteins around 2.0 ppm, and $N(CH_3)_3$ groups from phospholipids about 3.2 ppm [13].

The thin resonances coming from small molecules such as lactate, acetate, but also glyphosate, were superimposed on the larger ones. Typical spectra of spiked control serum with glyphosate are presented in Fig. 1c. Glyphosate is characterised by two signals using ^{1}H NMR spectroscopy: a doublet at 2.96 ppm assigned to the CH_2-P group and a singlet at 3.69 ppm corresponding to the CH_2-N group. These ppm values are somewhat different from those of previously published work because chemical shift values in biological media depend on pH, temperature and ionic strength. The CH_2-P group doublet is quite easy to identify as the coupling constant ^2J between proton and phosphorus nucleide is 12.8 Hz. Compared to 300 MHz, spectral resolution was improved with 500 MHz spectrometer.

Fig. 2 shows a spectrum from the poisoned patient on the second day after admission, before hemodialysis was performed. The glyphosate signals can be easily identified, especially the doublet of CH_2-P group. Compared to the spectrum of the spiked control serum (data not shown), some other resonances appear which can be assigned to the isopropylammonium: a doublet at 1.27 ppm ($^3J = 6.6$ Hz) can be related to the two methyl groups of this cation; moreover, an heptuplet at about 3.44 ppm can be observed in the spectrum which is due to the methane group, though this heptuplet is not generally seen in serum analyses because of interfering signals.

3.2. Quantitative proton NMR analysis

For the protons of CH_2-P group of glyphosate, longitudinal relaxation T_1 was found to be 2.65 s. For the spiked control serum samples, the relative peak area of the CH_2-P group was found to be a linear function of concentration with a very significant correlation coefficient $r = 0.999$ (Student's $t = 1039.5$ and $P = 2 \times 10^{-9}$) from 0.05 to 20 mmol/L. No disturbance from the biological fluid was observed because of the high specificity of

Table 1
Quantitative measurement of glyphosate and isopropylammonium in patient's serum at days 2 and 4

	CH_2-P glyphosate (mmol/L)	CH_2-N glyphosate (mmol/L)	$(CH_3)_2$ isopropyl ammonium (mmol/L)
Serum day 2	5.06 (0.06)	5.11 (0.06)	1.59 (0.02)
Serum day 4	0.12 (0.01)	–	0.21 (0.01)

Mean concentrations are given (standard deviations).

NMR parameters. This specificity was previously found to be useful to detect glyphosate poisonings using a 300 MHz NMR spectrometer [14]. The variation coefficients for intra-day and day-to-day analyses were 1.0% and 3.0% for 1 mmol/L concentration and 0.6% and 2.0% for 10 mmol/L concentration. Because of the more powerful magnetic field, the quantification limit in this study was found to be 0.1 mmol/L and the detection limit was around 0.03 mmol/L, compared to a detection limit of 0.2 mmol/L that was determined in previous work with a 300 MHz spectrometer [14]. The inherent, relatively low sensitivity of ^{1}H NMR spectroscopy is improved by increasing the magnetic field from 7.05 to 11.75 T. Moreover, its simplicity and specificity can lead to new applications in clinical toxicology.

After this validation step, quantitative measurements were performed on the patient's serum samples. Compared to a control sample, signals of both glyphosate and isopropylamine could be easily identified on the ^{1}H NMR spectrum from the poisoned patient. Because of interfering signals from sera, of these two chemical species, only the CH_2-P signal of glyphosate and the doublet of isopropylamine can be used for quantification in most cases of poisoning. The CH_2-N singlet of glyphosate and the heptuplet of isopropylamine give signals in a part of the spectrum where important interfering signals may occur such as sugars coming from perfusions. These signals are sometimes difficult to identify and integrate, especially when concentrations are low. Owing to 500 MHz spectrometer capacities and for massive poisonings, further quantitative data can be collected.

Quantitative results are given in Table 1. Serum concentrations of glyphosate ranged from 0.12 to 5.06 mmol/L. The highest glyphosate concentration was measured on the day after admission. The hemodialysis proved to be efficient as it reduced the glyphosate concentration from 5.06 mmol/L on the second day, to 0.12 mmol/L on the fourth day. Daily sera samples were analysed by ^{1}H NMR spectroscopy from day 1 to day 12. From day 6 onwards, no signal belonging either to glyphosate or to isopropylamine was detected. Of the utility of quantifying isopropylamine has not previously been published. Nevertheless, we have shown here that it can provide useful information on the trade formulation of the ingested herbicide. Detection of isopropylamine is easier than that of herbicide itself because of its doublet at 1.26 ppm corresponding to six protons. Moreover, very few herbicides are associated to isopropylammonium ion and this cation can be easily identified, even if the herbicide signal is relatively low.

Acknowledgements

The 500 MHz NMR facilities were jointly funded by the region Nord-Pas de Calais (France), the Ministère de la Jeunesse, de l'Education Nationale et de la Recherche (MJENR, France), and the Fonds Européens de Développement Régional (FEDER).

The authors are grateful to Mr. Mike Howsam for his expert advice in the revision of the English manuscript.

References

[1] M. Ishiguro, S. Mikasa, M. Otani, Chudoku Kenkyu 17 (2004) 51.
[2] J.Y. Wu, S.S. Chang, C.P. Tseng, J.F. Deng, C.C. Lee, Am. J. Emerg. Med. 24 (2006) 504.
[3] H. Penagos, C. Ruepert, T. Partanen, C. Wesseling, Dermatitis 15 (2004) 137.
[4] P. Amerio, A. Motta, P. Toto, S.M. Pour, R. Pajand, C. Feliciani, A. Tulli, J. Toxicol. Clin. Toxicol. 42 (2004) 317.
[5] J. Stella, M. Ryan, Emerg. Med. Aust. 16 (2004) 235.
[6] S.M. Bradberry, A.T. Proudfoot, J.A. Vale, Toxicol. Rev. 23 (2004) 159.
[7] H. Nagami, Y. Nishigaki, S. Matsushima, T. Matsushita, S. Asanuma, N. Yajima, M. Usuda, M. Mirosawa, Int. J. Occup. Environ. Health 11 (2005) 180.
[8] A.J. De Roos, A. Blair, J.A. Rusieki, J.A. Hoppin, M. Svec, M. Dosemeci, D.P. Sandler, M.C. Alavanja, Environ. Health Perspect. 113 (2005) 49.
[9] C.D. Stalikas, C.N. Konidari, J. Chromatogr. A 907 (2001) 1.
[10] M. Imbenotte, N. Azaroual, D. Mathieu, B. Cartigny, G. Vermeersch, M. Lhermitte, J. Anal. Toxicol. 23 (1999) 586.
[11] B. Cartigny, M. Imbenotte, N. Azaoual, D. Mathieu, G. Vermeersch, M. Lhermitte, Ann. Toxicol. Ann. 15 (2003) 221.
[12] K.P.R. Gartland, F.R. Bonner, J.K. Nicholson, Mol. Pharmacol. 35 (1989) 242.
[13] M. Liu, J.K. Nicholson, J.C. Lindon, Anal. Chem. 68 (1996) 3370.
[14] B. Cartigny, N. Azaroual, M. Imbenotte, D. Mathieu, G. Vermeersch, J.P. Goullé, M. Lhermitte, Forensic Sci. Int. 143 (2004) 141.

Available online at www.sciencedirect.com
ScienceDirect
Talanta 74 (2008) 683–689
Talanta
www.elsevier.com/locate/talanta

Fast and simultaneous detection of heavy metals using a simple and reliable microchip-electrochemistry route: An alternative approach to food analysis

Orawon Chailapakul [a,*], Sarawadee Korsrisakul [a], Weena Siangproh [b], Kate Grudpan [c]

[a] *Sensor Research Unit, Department of Chemistry, Faculty of Science, Chulalongkorn University, Phyathai, Bangkok 10330, Thailand*
[b] *Department of Chemistry, Faculty of Science, Srinakharinwirot University, Sukhumvit 23, Wattana, Bangkok 10110, Thailand*
[c] *Department of Chemistry, Faculty of Science, Chiang Mai University, Chiang Mai 50200, Thailand*

Received 11 April 2007; received in revised form 25 June 2007; accepted 26 June 2007
Available online 1 July 2007

Abstract

This paper reports, for the first, the fast and simultaneous detection of prominent heavy metals, including: lead, cadmium and copper using microchip CE with electrochemical detection. The direct amperometric detection mode for microchip CE was successfully applied to these heavy metal ions. The influences of separation voltage, detection potential, as well as the concentration and pH value of the running buffer on the response of the detector were carefully assayed and optimized. The results clearly show that reliable analysis for lead, cadmium, and copper by the degree of electrophoretic separation occurs in less than 3 min using a MES buffer (pH 7.0, 25 mM) and L-histidine, with 1.2 kV separation voltage and −0.8 V detection potential. The detection limits for Pb^{2+}, Cd^{2+}, and Cu^{2+} were 1.74, 0.73 and 0.13 μM (S/N = 3). The %R.S.D. of each peak current was <6% and migration times <2% for prolonged operation. To demonstrate the potential and future role of microchip CE, analytical possibilities and a new route in the raw sample analysis were presented. The results obtained allow the proposed microchip CE-ED acts as an alternative approach for metal analysis in foods.
© 2007 Elsevier B.V. All rights reserved.

Keywords: Microchip CE; Electrochemical detection; Heavy metals; Microanalysis

1. Introduction

The traditional format of capillary electrophoresis is quickly being replaced by microdevice platforms in modern analytical chemistry, offering improvements in cost, resolution, speed, quantitation and automation. This aspect of miniaturization is well matched with the ultimate goal of rapid screening and simultaneous detection of a large number of samples [1,2]. The miniaturization of an integrated system improves the advantages inherent to capillary electrophoresis.

Heavy metals are particularly worrisome contaminants in foods and the environment. In general, they are not biodegradable and they have long biological half-lives. Heavy metals have potential for accumulation in humans from various plants and other natural sources, posing serious health hazards for conditions such as renal failure, symptoms of chronic toxicity, and liver damage. According to the World Health Organization (World Health Organization, 1995), lead, cadmium, chromium, and other heavy metals must be controlled in food sources in order to assure public safety.

Lead and cadmium are among the most abundant heavy metals on earth, and are particularly toxic. Excessive concentrations of these metals in food is associated with the etiology of a number of diseases, especially with cardiovascular, renal, neurological, and bone diseases [3,4]. In addition, they are also implicated in causing carcinogenesis, mutagenesis, and teratogenesis [5]. Copper, another important metal, is an essential trace element for the human body and contributes to important intracellular metabolic events [6]. A copper imbalance can result in a severe human ailment, from either an excess or deficiency of this key element [7]. A major reason to monitor levels of toxic metals in foods follows from the fact that contamination of the general environment has increased. The sources of this environmental pollution are quite varied, ranging from industrial

* Corresponding author. Tel.: +662 218 7615.
E-mail address: corawon@chula.ac.th (O. Chailapakul).

0039-9140/$ – see front matter © 2007 Elsevier B.V. All rights reserved.
doi:10.1016/j.talanta.2007.06.034

and traffic emissions to the use of purification mud and agricultural expedients. In order to study the toxicity of heavy metals in food, a simple, sensitive and accurate detection method is required.

Many analytical methods have been developed for determination of individual metals in food products, including: titration [8], colorimetric analysis [9,10], UV–vis spectroscopy [11–13], and either flame or graphite furnace atomic absorption spectrometry (AAS) [14–17]. In addition to these techniques, methods for multi-elemental determination have been developed; these are ion chromatography (IC) [18–20] and inductively coupled plasma combined with either atomic emission spectrometry (ICP–AES) [21,22] or mass spectrometry (ICP–MS) [23–25]. Although these methodologies are rapid and sensitive for the determination of trace amounts of metals, they require complicated instrumentation with high capital and operational costs. Furthermore, these methods are not easily implemented into fully portable analytical tools for screening, detecting, identifying, and quantifying metal ions.

Capillary electrophoresis (CE) has been widely applied to the separation and determination of different metal species, and has proved to be a fast, high-resolution separation technique [26–31]. The detection methods typically used in combination with CE separation technique are ultraviolet light (UV), fluorescence or laser-induced fluorescence (LIF) detection. The lack of a strong chromophore from metal ions has certainly been one of the major limitations in the analysis of most metals by these methods. In addition, these detection modes suffer from lack of sensitivity when a miniaturized device is used. Electrochemical detection (ED) offers high sensitivity and selectivity for metals that are readily oxidized or reduced. This technique is readily suitable and compatible with microfabrication technology that has been successfully employed in microchip CE.

Separation of metal ions by microchip CE has attracted significant attention, offering a number of advantages including speed of analysis, portability, flexibility, and compatibility with integrated analytical systems, allowing development of "micro-total-analysis systems (μTAS)" [1,32–38]. There are a few published examples of metal ion separation performed on a microchip CE. The detection methods are largely focused on the utilization of complexing agents, such as fluorescent metal complexation [39]. Although excellent separation of metal ions was obtained, the designs of microchip sensors were not compact or portable, but tedious and expensive. Unlike other researchers, Li et al. [40] reported the use of microchip CE with indirect amperometric detection of heavy metals. Their results demonstrated good separation and detection, unfortunately, the configuration of microchip and detector was still complicated. Alternatively, we have focused on the simple, direct quantitation of metals by electrochemical reaction, which will enable the incorporation of a portable, simple, and inexpensive detector.

This work addresses the need for developing an inexpensive and field portable analytical device for metal ions which would permit the rapid screening and detection of contaminated food or waste materials on site. The detection of metal ions was accomplished using a microchip CE/amperometric detection system, in which screen-printed carbon electrode is placed at the end of channel. This approach simplifies the fabrication of the working electrode and also provides a convenient and sensitive method for the determination of metal ions by amperometry. Furthermore, by simply changing the electrode, we can easily remove or clean the detection electrode, which is prone to contamination. In this manner, we propose an attractive portable device for screening and analyzing a complex system containing different metal species, such as food. The optimization, characterization, and attractive performance characteristics of a microchip CE, and its successful application to complex samples (such as vegetable juices) are reported in the following sections.

2. Experimental

2.1. Chemicals

Lead(II) nitrate was obtained from Aldrich (Germany). Cadmium(II) sulfate was obtained from Baker Analyzed (USA). Copper(II) sulphate was obtained from BDH (England). Standard stock solutions of all analytes were freshly prepared each day. The running buffer solution (BGE) for separation was prepared from 2-morpholinoethanesulfonic acid (MES), (s)-2-amiono-3-(4-imidazyl) propionic acid (L-histidine) which were obtained from Fluka (USA). Sodium hydroxide and Hydrochloric acid were purchased from Merck (Germany), and were used for pH adjustment of the electrolytic buffer solution. All reagents were used without further purification. Pure deionized water (Millipore, USA) was used to prepare all aqueous solutions. The sample solutions were prepared by diluting corresponding stock solutions in running buffer. All solutions for electrophoresis experiments were filtered through a 0.45 μm membrane filter (Altech) before use.

2.2. Apparatus

Borofloat glass chips with simple-cross single-separation channels (16 mm × 95 mm × 2.2 mm) were obtained from Micralyne (model MC-BF4-001, Canada). The microchip has a four-way injection cross that are connected to the three reservoirs and the channel. The original waste reservoir was cut off, leaving the channel outlet at the end of the chip, facilitating the end-column electrochemical detection. The chip had a 90 mm long separation channel (from injection cross to the channel outlet) and a 10 mm long injection channel (between the sample and buffer reservoir). All channels were etched to a depth of 20 μm and a width at the top of the channel of 50 μm.

The integrated CE-ED microchip system was described previously [36]. The CE microchip was placed in a laboratory-built Plexiglas holder for housing the separation chip and electrochemical detector, allowing convenient replacement. The holder consisted of a sample, running buffer, and unused reservoirs. Short pipette tips were cut and inserted into the fluidic ports of the various reservoirs on the glass chip for providing solution contact between the channel on the chip and the corresponding reservoir on the chip holder. Platinum wires were inserted into the compartments to provide the electrical contacts to a high-

voltage power supply. A home-made high voltage power supply, with an adjustable voltage range between 0 and +4000 V, was used for controlling the injection and separation. The amperometric detector, placed in the waste reservoir, at the separation channel outlet, consisted of an Ag/AgCl wire reference electrode, a platinum wire counter electrode, and a screen-printed carbon working electrode.

2.3. End-column amperometric detection

Amperometric detection was performed with a computer controlled electrochemical analyzer (Autolab potentiostat, PG-30, Methrom) using the "amperometric *i–t* curve" mode. The electropherograms were recorded at a fixed detection potential, −0.8 V versus Ag/AgCl wire. The screen-printed carbon working electrode was placed opposite the outlet of the separation channel through a plastic screw. The distance between the electrode surface and the channel outlet was controlled by a plastic screw and a thin-layer spacer. The electrochemical detection compartment was filled with 25 mM MES/L-histidine buffer solution (pH 7.0). All experiments were done at room temperature, sample injection were performed after the baseline current had stabilized.

2.4. Electrophoresis procedures

Before electrophoresis, the channels of each glass chip were treated by rinsing with deionized water, 0.1 M NaOH, and again with deionized water for 10 min each. The reservoirs were cleaned and the reservoir for sample solution was filled with sample solution, while all other reservoirs were filled with running buffer. Each of the corresponding pipette tips on the micro-channel chip was filled with their respective solution. Injection was carried out by applying the desired potential, 1200 V, between the sample reservoir and the grounded detection reservoir for 3 s, while all other reservoirs were allowed to float. Separation was performed by switching the high-voltage contacts and applying the corresponding separation voltages to the running buffer reservoir with the detection reservoir grounded. As soon as the voltage was switched to perform electrophoresis separation, the electrochemical analyzer was actuated to record signals.

2.5. Sample preparation

Sample solutions were blended for 300 s with a homogenizer. Two millilitre of sample solution was placed in capped centrifuge tubes and then centrifuged for 10 min at 3500 rpm. 0.5 mL of supernatant was then transferred to a centrifuge tube fitted with a filter membrane (0.45 μm Nylon membranes) and centrifuged for 5 min. The filtrate was placed in capped tubes. 0.5 mL of filtrate-sample solution was spiked with 50–100 μL of 2 mM mixed metal ion stock solution (lead(II), cadmium(II), and copper(II) ions) and further diluted with 25 mM MES and L-histidine buffer (pH 7.0) to give final concentrations of 100, 200, 400, 600, 800, and 1000 μM, respectively. Finally, the solutions were analyzed by microchip CE-ED.

3. Results and discussion

In general, the first step in using microchip CE for the determination of metal ions is the selection of the background electrolyte co-ion and subsequently, the optimization of the resolution and detection sensitivity of system. In this work, since electrochemical detection is used; the background electrolyte has a large effect on the signal sensitivity. To obtain a high signal-to-noise ratio, the conductivity of the background electrolyte co-ion, which is directly related to the electrophoretic mobility, should differ from those of analytes as much as possible. It is well known that carrier electrolytes with low-mobility co-ions are preferred for the analysis of small ions. 2-(*N*-Morpholino)ethanesulfonic acid (MES) + histidine is a typical carrier electrolyte with a low-mobility co-ion used for the separation of small ions because both compounds have relatively low mobilities. Moreover, their pK_a values are almost identical, which make them excellent components of buffer system. In the following parts, the influence of some experimental parameters such as the buffer pH, buffer concentration, the separation voltage and the detection potential on the separation efficiency and detection sensitivity are reported in detail.

3.1. Influence of the buffer pH

The running buffer pH is the first important parameter for optimization in microchip CE, the same as in conventional CE. Running buffer pH has effect on EOF rate, degree of ionization, mobility, and separation efficiency of analytes. Thus, the pH values of running buffer were examined in the pH range 6.0–8.5. All buffers contained 20 mM MES and 20 mM L-histidine. Table 1 shows the currents obtained and resolution of three metal ions (Cd(II), Pb(II), and Cu(II)). It can be seen that as buffer pH changed from 6.5 to 7.5, the three metal ions could be well separated. The highest current signal was obtained at buffer pH 7.0. Since the background noise increased relative to the signal intensity and took longer to stabilize between samples, a buffer pH of 7.0 was selected as the optimal pH for all subsequent work.

3.2. Influence of the buffer concentration

Buffer concentration is another important parameter that affects the separation efficiency and detection sensitivity. Electropherograms of 1.0 mM lead, cadmium and copper were performed in varying concentrations of pH 7.0 running buffer.

Table 1
Current and Resolution of three metal ions standards

pH of BGE	Current (nA)			Resolution	
	Pb(II)	Cd(II)	Cu(II)	$R_{Pb,Cd}$	$R_{Cd,Cu}$
6	7.35	7.35	1.87	–	7.75
6.5	1.98	14.81	7.88	2.58	2.51
7	13.49	25.71	17.09	1.91	3.33
7.5	13.25	18.48	10.99	2.18	2.31
8	14.69	20.42	13.69	1.45	1.18
8.5	11.38	11.89	10.35	1.79	1.05

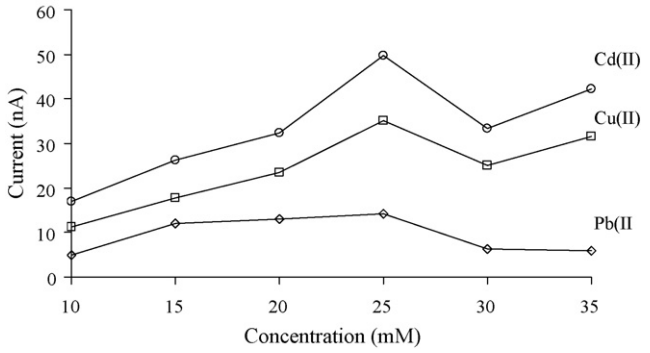


Fig. 1. The effects of the buffer concentration on peak currents. Experimental parameters: sample, 1.0 mM lead, cadmium and copper cations; running buffer, MES and L-His pH 7.0; separation voltage, 1000 V; detection potential, −0.8 V; sampling time, 3 s; working electrode, screen-printed carbon electrode.

We found that the peak current of the three cations increased with increasing buffer concentrations from 10 to 25 mM, and then decreased with further increase of the buffer concentration as shown in Fig. 1. This phenomenon can be attributed to two reasons: (1) higher concentrations of running buffer result in high ionic strength, which will decrease the difference of conductivity between the sample zone and running buffer zone and result in low signal, and (2), higher concentrations of the running buffer makes for electrostacking, which results in relatively higher concentration of the sample zone and then a relatively high signal is obtained. A running buffer concentration of 25 mM was chosen for optimal detection sensitivity.

3.3. Influence of detection potential

Since the detection potential strongly affects the sensitivity and detection limits of microchip CE with an electrochemical system, the optimal detection potential was determined by investigating a hydrodynamic voltammogram. Fig. 2 shows the results which must draw a balance between low applied potentials and enough sensitivity for all the metal ions involved at screen-printed carbon electrode. We observed that the amperometric signal of heavy metals ions increased with the increase of detection potential from −0.70 to −0.85 V. However, the baseline current and the corresponding noise level become large at higher reduction potential. The sensitivity of the signal for the three ions with the change of detection potential was also different. In order to perform the simultaneous determination of lead, cadmium, and copper, the detection potential which most influences the measurement process was optimized. From the results, it can be seen that cadmium and copper have a similar change rate of the signal, while the relative peak current of lead has a lower change rate with changing the detection potential. This suppression of the lead signal could be explained by intermetallic effect of cupper [41]. There is the formation of intermetallic/solid between Cu–Pb. The phenomenon may result in low signal of Pb^{2+}, also resulting in possible calibration problem. To compromise between the sensitivity and signal-to-noise characteristics of three metals, especially Pb^{2+}, a detection potential of −0.8 V was chosen since it offered the most favorable results.

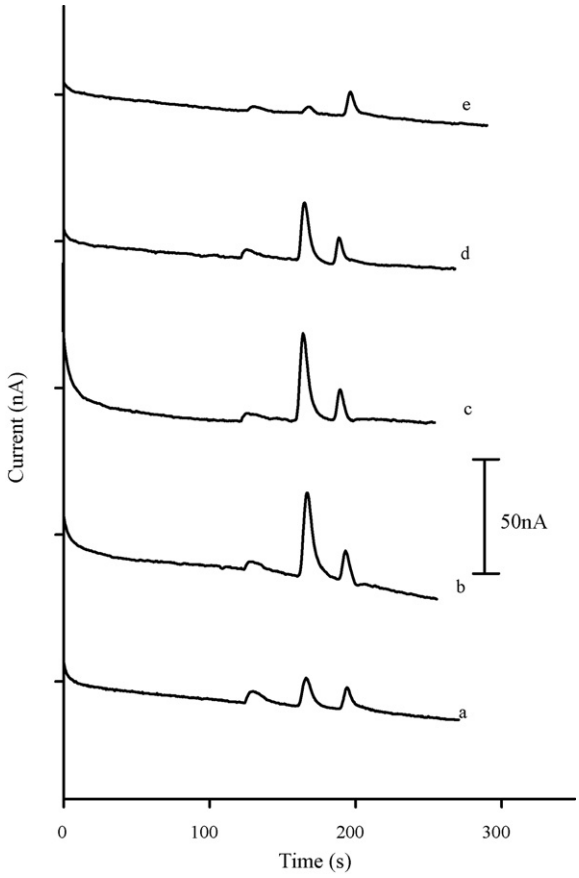


Fig. 2. Electropherograms of 1.0 mM lead, cadmium and copper cations at different detection potentials, −0.90 V (a), −0.85 V (b), −0.80 V (c), −0.75 V (d), −0.70 V (e). Experimental parameters: running buffer, 25 mM MES and L-His pH 7.0; separation voltage, 1000 V; sampling time, 3 s; working electrode, screen-printed carbon electrode.

3.4. Influence of separation voltage

The separation voltage affects the electric field strength, which in turn affects the EOF and the migration velocity of charged particles, which determine the migration times of the analytes. Moreover, higher separation voltages may result in higher Joule heating. The effect of separation voltage on the migration time of the analytes is shown in Fig. 3A. As expected, increasing the voltage gives shorter migration times but also increases the background noise, resulting in a higher detection limit. The migration times were dramatically decreased for all three metal ions, from 120 to 90 s for lead, 150 to 110 s for cadmium, and 175 to 140 s for copper. Although the resolution of analytes can be improved to some extent, too low a separation voltage will increase the analytical time considerably, which in turn causes severe peak broadening (Fig. 3B). Based on experiments, 1200 V was chosen as the optimum voltage to strike a good compromise.

3.5. Effect of oxygen

The effect of oxygen using batch system by screen-printed carbon electrode compared to that by glassy carbon electrode

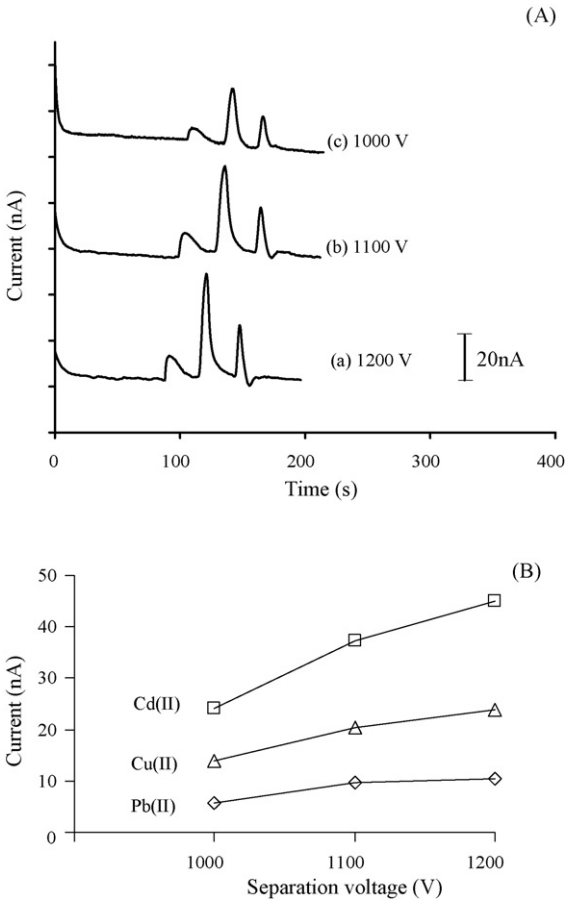


Fig. 3. Electropherograms of 1.0 mM lead, cadmium and copper cations at different separation voltages. The relationship between the peak currents and the separation voltage (A), 1200 V (a), 1100 V (b), 1000 V (c). The relationship between the peak current and the separation time (B). Other parameters same as in Fig. 2.

was studied. It was found that there was a little effect of oxygen on the background signal using screen-printed carbon electrode whereas the high effect of oxygen on the background signal using glassy carbon was obtained. It indicates that screen-printed carbon electrode is less sensitive to oxygen. We also investigated the effect of oxygen of three metals using normal and degas solutions. It was found that the peak current decreased around 11% for $Cd^{2+}$and 21% for Pb^{2+}, respectively. For Cu^{2+}, very small change of the peak current was obtained (data not shown). For the microchip separation system, the experiment was performed in a very small system. Therefore, the effect of oxygen on the determination of these metals can be negligible. From this point, it should be an advantage of this proposed method that it does not need to perform the experiment under the oxygen-free condition.

3.6. Linear range and detection limits

According to the previous studies on pH value and concentration of the running buffer, as well as the separation voltage and the detection potential; optimized conditions of 1200 V separation voltage, −0.8 V detection potential, with 25 mM (pH 7.0) of MES + L-histidine as running buffer were obtained. Under

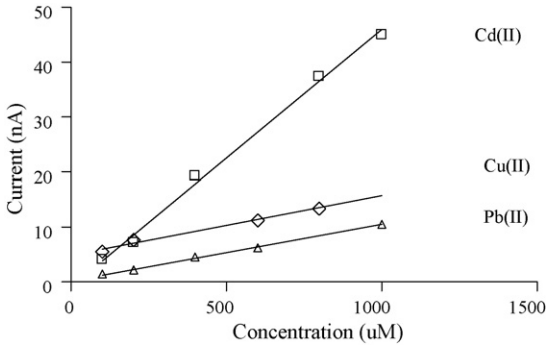


Fig. 4. The relationship between the peak currents and the concentrations. Experimental parameters: running buffer, 25 mM MES and L-His pH 7.0; separation voltage, 1200 V; detection potential, −0.8 V; sampling time, 3 s; working electrode, screen-printed carbon electrode.

the selected conditions, a series of the standard mixture solutions of lead, cadmium, and copper with a concentration range of 100–1000 μM was tested to determine the linearity for all analytes at the screen-printed carbon electrode in this system. The data are shown in Fig. 4. The results of regression analysis on calibration curves are 0.9977, 0.9902, and 0.9958 for lead, cadmium, and copper, respectively. The detection limits were evaluated on the basis of a minimum signal-to-noise ratio of 3. The calibration curves exhibit excellent linear behavior over the concentration range of about micromolar orders of magnitude, with detection limits ranging from 0.13 to 1.74 μM for all the metal ions (data shown in Table 2).

A standard mixture solution of lead, cadmium, and copper (1 mM each) was analyzed ten times to determine the reproducibility of the peak current and migration time for all analytes under the optimal conditions in this experiment. The relative standard deviations (R.S.D.s) of peak current and migration time are 4.20% and 1.47% for lead, 5.27% and 1.40% for cadmium, 3.92% and 1.20% for copper, respectively. It is indicated that the proposed system exhibited an excellent performance on both separation and detection for prolonged operation.

3.7. Sample analysis

The analytical potential of screen-printed carbon electrodes in constant EC detection coupled with microchip CE for the separation of lead, cadmium, and copper in juice samples were investigated. By applying the optimum conditions described above, the injection of three metal ions were analyzed by standard addition method. We studied the metal ions of three different juice samples obtained from a local market. The results are

Table 2
The reproducibility of peak current, retention time and limit of detection of metals

Metal ions	%R.S.D. of peak current	%R.S.D. of retention time	LOD (μM)
Cu(II)	3.92	1.20	0.13
Cd(II)	5.27	1.40	0.73
Pb(II)	4.20	1.47	1.74

Table 3
Determination of Pb(II), Cd(II), and Cu(II) in different samples by means of microchip CE-ED using screen-printed carbon electrode

Sample	Amount added (μM)			Amount found (μM)			%Recovery ($n=3$)			%R.S.D. ($n=3$)		
	Pb	Cd	Cu	Pb	Cd	Cu	Pb	Cd	Cu	Pb	Cd	Cu
Green vegetable juice	1000	750	750	1032	791.85	784.35	103.20	105.58	104.58	2.93	2.10	2.11
	750	500	500	757.95	477.15	459.65	101.06	95.43	91.93	2.37	2.39	2.67
	500	250	250	486.95	269.75	250.08	97.39	107.90	100.03	3.40	2.13	3.75
Tomato juice	1000	800	800	1012.8	775.44	781.84	101.28	96.93	97.73	2.65	0.90	2.68
	800	600	400	791.12	603.06	389.80	98.89	100.51	97.45	4.25	1.63	4.76
	400	200	200	399.92	200.50	191.18	99.98	100.25	95.59	6.48	6.07	6.23
Pine apple juice	800	800	800	819.12	803.84	810.96	102.39	100.48	101.37	3.56	2.87	2.28
	600	600	600	586.26	639.66	621.66	97.71	106.61	103.61	1.57	2.71	2.25
	400	200	500	396.56	214.62	490.05	99.14	107.31	98.01	2.13	1.87	2.57

shown in Table 3. Recoveries ranged from 91.93 to 107.90 with ten replicate each, giving %R.S.D.s of 0.90–6.48. The results show that the proposed methods can be efficiently used for the determination of metal ions in practical samples. Such the high speed of analysis and efficiency of proposed method, it should be possible to separate and detect other metals in different kinds of food by simply varying the detection potential.

4. Conclusions

This work presents the first application of microchip CE-ED in direct mode for the simultaneous determination of lead, cadmium, and copper in vegetable juices. It has been demonstrated that microchip CE-ED is characterized by its simplicity, quickness, higher resolution and sensitivity, excellent reproducibility, low expense of operation and minor amounts of samples and reagent. The reproducibility of quantitative analysis by this method is satisfactory. Electrochemical detection coupled with microchip CE enables selective and sensitive detection of the electroactive constituents and simplification of the electropherograms. We conclude that microchip CE-ED is a powerful technique for the study of heavy metal ions and has become an alternate, competitive and supplementary method for HPLC, because of its special attributes. In particular, microchip CE-ED provides an attractive approach for a portable analytical device for rapid screening and the analysis of complex systems simultaneously containing metals and heavy metals. Such a microchip CE-ED system may have wide applications, particularly in food analysis.

Acknowledgements

The authors would like to acknowledge the support from the National Research Council of Thailand (NRCT) through the improvement of food safety and food quality for new world economy project, the Thailand Research Fund (Research Team Promotion Grant), and Graduate Thesis Grant, Chulalongkorn University.

References

[1] J. Khandurina, A. Guttman, Curr. Opin. Chem. Biol. 7 (2003) 595.
[2] J. Khandurina, A. Guttman, Curr. Opin. Chem. Biol. 6 (2002) 359.
[3] K. Steenland, P. Boffetta, Am. J. Ind. Med. 38 (2000) 295.
[4] WHO, Lead Environmental Health Criteria, WHO, Geneva, 1995.
[5] C.H. Pitot, P.Y. Dragan, Chemical Carcinogenesis, McGraw Hill, New York, 1996.
[6] B. Hultberg, A. Andersson, A. Isaksson, Clin. Chim. Acta 262 (1997) 39.
[7] W. Cerpa, L. Varela-Nallar, A.E. Reyes, A.N. Minniti, N.C. Inestrosa, Mol. Aspects Med. Trace Elem. Human Health 26 (2005) 405.
[8] K.V. Raju, G.D. Sudhakar, T.B. Patrudu, Asian J. Chem. 19 (2007) 683.
[9] A. Abbaspour, M.A. Mehrgardi, A. Noori, M.A. Kamyabi, A. Khalafi-Nezhad, M.N. Soltani Rad, Sens. Actuator B-Chem. 113 (2006) 857.
[10] J. Yun, H. Choi, Talanta 52 (2000) 893.
[11] J.-P. Cornard, A. Caudron, J.-C. Merlin, Polyhedron 25 (2006) 2215.
[12] N. Tounsi, L. Dupont, A. Mohamadou, M. Aplincourt, R. Plantier-Royon, F. Massicot, D. Harakat, C. Portella, J. Inorg. Biochem. 99 (2005) 2423.
[13] A. Torreggiani, M. Tamba, A. Trinchero, S. Bonora, J. Mol. Struct. 744–745 (2005) 759.
[14] N. Panichev, K. Mandiwana, M. Kataeva, S. Siebert, Spectroc. Acta Pt. B-Atom. Spectr. 60 (2005) 699.
[15] J. Falandysz, A. Jdrusiak, K. Lipka, K. Kannan, M. Kawano, M. Gucia, A. Brzostowski, M. Dadej, Chemosphere 54 (2004) 461.
[16] C.J. de Castro Maciel, G.M. Miranda, D.P. de Oliveira, M.E.P.B. de Siqueira, J.N. Silveira, E.M.A. Leite, J.B.B. da Silva, Anal. Chim. Acta 491 (2003) 231.
[17] M.V. Aguilar, C.J. Mateos, M.C. Martinez Para, J. Trace Elem. Med. Biol. 16 (2002) 221.
[18] W. Zeng, Y. Chen, H. Cui, F. Wu, Y. Zhu, J.S. Fritz, J. Chromatogr. A 1118 (2006) 68.
[19] M.J. Shaw, P.R. Haddad, Environ. Int. 30 (2004) 403.
[20] C. Sarzanini, M.C. Bruzzoniti, Trac-Trends Anal. Chem. 20 (2001) 304.
[21] M. Turkmen, C. Ciminli, Food Chem. 103 (2007) 670.
[22] M.D. Ioannidou, G.A. Zachariadis, A.N. Anthemidis, J.A. Stratis, Talanta 65 (2005) 92.
[23] Y. Sahan, F. Basoglu, S. Gucer, Food Chem. 105 (2007) 395.
[24] J.-P. Goulle, L. Mahieu, J. Castermant, N. Neveu, L. Bonneau, G. Laine, D. Bouige, C. Lacroix, Forensic Sci. Int. 153 (2005) 39.
[25] E. Urdova, L. Vavrukova, M. Suchanek, P. Baldrian, J. Gabriel, Talanta 62 (2004) 483.
[26] A.V.C. Simionato, M.D. Cantu, E. Carrilho, Microchem. J. 82 (2006) 214.
[27] S. Suarez-Luque, I. Mato, J.F. Huidobro, J. Simal-Lozano, Talanta 68 (2006) 1143.
[28] F. Qu, J.-M. Lin, Z. Chen, J. Chromatogr. A 1022 (2004) 217.
[29] E. Naujalis, A. Padarauskas, J. Chromatogr. A 977 (2002) 135.
[30] Z. Chen, R. Naidu, J. Chromatogr. A 966 (2002) 245.
[31] J.E. Harris, N. Desai, K.E. Seaver, R.T. Watson, N.A.P. Kane-Maguire, J.F. Wheeler, J. Chromatogr. A 919 (2001) 427.
[32] J.H. Ng, L.L. Ilag, in M.R. El-Gewely (Editor), Elsevier, 2003.
[33] J.-H. Kim, C.J. Kang, D. Jeon, Y.-S. Kim, Microelectron. Eng. 78–79 (2005) 563.

[34] R.S. Keynton, T.J. Roussel, M.M. Crain, D.J. Jackson, D.B. Franco, J.F. Naber, K.M. Walsh, R.P. Baldwin, Anal. Chim. Acta 507 (2004) 95.
[35] A.J. Gawron, R.S. Martin, S.M. Lunte, Eur. J. Pharm. Sci. 14 (2001) 1.
[36] J. Wang, M.P. Chatrathi, B. Tian, Anal. Chim. Acta 416 (2000) 9.
[37] M.U. Kopp, H.J. Crabtree, A. Manz, Curr. Opin. Chem. Biol. 1 (1997) 410.
[38] J.E. Prest, S.J. Baldock, P.R. Fielden, N.J. Goddard, K. Kalimeri, B.J. Treves Brown, M. Zgraggen, J. Chromatogr. A 1047 (2004) 289.
[39] G.E. Collins, Q. Lu, Sens. Actuator B-Chem. 76 (2001) 244.
[40] X.-A. Li, D.-M. Zhou, J.-J. Xu, H.-Y. Chen, Talanta 71 (2007) 1130.
[41] K.C. Honeychurch, D.M. Hawkins, J.P. Hart, D.C. Cowell, Talanta 57 (2002) 565.

Available online at www.sciencedirect.com
ScienceDirect
Talanta 74 (2008) 512–517
Talanta
www.elsevier.com/locate/talanta

A general approach to the screening and confirmation of tryptamines and phenethylamines by mass spectral fragmentation

Bo-Hong Chen [a], Ju-Tsung Liu [b], Wen-Xiong Chen [a], Hung-Ming Chen [a], Cheng-Huang Lin [a,*]

[a] *Department of Chemistry, National Taiwan Normal University, 88 Sec. 4, Tingchow Road, Taipei, Taiwan*
[b] *Forensic Science Center, Military Police Command, Department of Defense, Taipei, Taiwan*

Received 6 March 2007; received in revised form 12 June 2007; accepted 13 June 2007
Available online 19 June 2007

Abstract

Certain characteristic fragmentations of tryptamines (indoleethylamine) and phenethylamines are described. Based on the GC–EI/MS, LC–ESI/MS and MALDI/TOFMS, the mass fragmentations of 13 standard compounds, including α-methyltryptamine (AMT), *N*,*N*-dimethyltryptamine (DMT), 5-methoxy-α-methyltryptamine (5-MeO-AMT), *N*,*N*-diethyltryptamine (DET), *N*,*N*-dipropyltryptamine (DPT), *N*,*N*-dibutyltryptamine (DBT), *N*,*N*-diisopropyltryptamine (DIPT), 5-methoxy-*N*,*N*-dimethyltryptamine (5-MeO-DMT), 5-methoxy-*N*,*N*-diisopropyltryptamine (5-MeO-DIPT), methamphetamine (MAMP), 3,4-methylenedioxyamphetamine (3,4-MDA), 3,4-methylenedioxymethamphetamine (3,4-MDMA) and 2-methylamino-1-(3,4-methylenedioxyphenyl)butane (MBDB), were compared. As a result, the parent ions of these analytes were hard to be obtained by GC/MS whereas the protonated molecular ions can be observed clearly by means of ESI/MS and MALDI/TOFMS. Furthermore, two major characteristic fragmentations, namely and α-cleavage ($[M+H]^+ \rightarrow$ [3-vinylindole]$^+$) and β-cleavage ($[M+H]^+ \rightarrow [CH_2N^+R_{N1}R_{N2}]$), are produced when the ESI and MALDI modes are used, respectively. In the case of ESI/MS, the fragment obtained from α-cleavage is the major process. In contrast to this, in the case of MALDI/TOFMS, the major fragment is produced via β-cleavage. The ionization efficiency and fragments formed from either α- or β-cleavages are closely related to the degree of alkylation of the side chain nitrogen in both cases.
© 2007 Elsevier B.V. All rights reserved.

Keywords: Tryptamine; Phenethylamine; GC/MS; ESI/MS; MALDI/TOFMS

1. Introduction

Tryptamine alkaloids are normally used by humans for their psychotropic effects. The degree of alkylation of the side chain nitrogen in a tryptamine has a significant effect on its psychoactivity. Substitutions to the tryptamine molecule give rise to a group of compounds, and as a result, a number of tryptamine-like illegal drugs are produced in underground labs and sold on the streets. The first encounter of α-methyltryptamine (AMT) and 5-methoxy-*N*,*N*-dipropyltryptamine (5-MeO-DIPT) occurred in 1999; with the street names of "Foxy" and "Spirals", respectively. There have been increasing reports on the availability, distribution, and use of these compounds that have highly attention by the U.S. Department of Justice [1–4]. By February 2003, the Drug Enforcement Administration reported law enforcement seizures and reports of abuse in 12 states and placed AMT and 5-MeO-DIPT into Schedule I of the Controlled Substances Act [5]. MDMA (3,4-methylenedioxy-*N*-methylamphetamine) is a semi-synthetic entactogen of the phenethylamine family, most commonly known today by the street name "ecstasy". In fact, lots of tryptamine and phenethylamine compounds have been described by Ann and Alexander Shulgin under the title TiHKAL (Tryptamines I Have Known and Loved) and PiHKAL (Phenethylamines I Have Known and Loved), respectively [6,7]. However, from the point of view of screening and confirmation of tryptamine and phenethylamine derivatives on the illicit market by mass spectral methods, more detailed information on the characteristic mass fragments produced under different types of ionization methods is needed. Currently, GC–EI/MS [8–13] and LC–ESI/MS [14–19] are the most popular and well-developed methods for their identification. However, thousands of samples are frequently involved in routine testing and, as a result, a rapid and soft-ionization method which is also reliable and complementary to GC–MS or LC–MS for use in forensic analysis would be highly desirable. Matrix-assisted laser desorption ionization time-of-flight mass spectrometry (MALDI/TOFMS)

* Corresponding author. Tel.: +886 2 8931 6955; fax: +886 2 2932 4249.
E-mail address: chenglin@ntnu.edu.tw (C.-H. Lin).

0039-9140/$ – see front matter © 2007 Elsevier B.V. All rights reserved.
doi:10.1016/j.talanta.2007.06.012

is one such soft-ionization method, and has become a very popular and powerful tool in many fields. We previously reported on the rapid screening of clandestine tablets [20], suspect urine samples [21], and nerve agent degradation products [22]. In this study, we report on a method for the screening and confirmation of synthetic tryptamines and phenethylamines based on MALDI/TOFMS. Results obtained from GC–EI/MS and LC–ESI/MS were also compared.

2. Experimental

2.1. Apparatus

The linear type of time-of-flight mass spectrometer (TOFMS), a modified Wiley-McLaren design (R.M. Jordan Co., Grass Valley, CA), the laser source, and the data acquisition system used were similar to that described previously [20–22] and are abbreviated herein. A gas chromatograph (GC 6890 Hewlett–Packard, Avondale, PA, USA) equipped with a mass spectrometer (Hewlett–Packard 5973 mass selective detector) was used for the detection. A capillary column (30 m × 0.25 μm i.d.) with an HP-5MS (cross-linked 5% PH ME siloxane) bonded stationary phase film, 0.25 μm in thickness (Agilent Technologies, USA) was used. The inlet temperature was maintained at 250 °C. The column oven was held at 70 °C for 1 min, then programmed from 70 to 200 °C at 15 °C/min, held for 2 min, and then programmed from 200 to 260 °C at 20 °C/min, finally, held for 8.84 min (carrier gas: helium, flow rate: 1 mL/min). The mass spectrometry conditions were as follows: ionization energy, 70 eV; ion source temperature, 230 °C. Data were collected using the Hewlett–Packard Chem-Station software. A LC/MS system (Finnigan LCQ Classic LC/MS/MS) consisting of an electrospray ionization (ESI) probe operated in the positive ion mode and an Xcalibur data system was used. Infusion into the mass spectrometer was performed by a built-in syringe pump at a flow rate of 0.01 mL/min. Scan mode used was full scan; the capillary temperature and spray voltage were set to 150 °C and 4.5 kV, respectively. The tube lens offset was set at −5 V; sheath gas and auxiliary gas flow rates were 60 and 10 (arb), respectively.

2.2. Reagents

α-Cyano-4-hydroxycinnamic acid (CHCA) and 2,5-dihydroxybenzoic acid (2,5-DHB) were purchased from Sigma–Aldrich (St. Louis, MO, USA). α-Methyltryptamine (AMT), *N*,*N*-dimethyltryptamine (DMT), 5-methoxy-α-methyltryptamine (5-MeO-AMT), *N*,*N*-diethyltryptamine (DET), *N*,*N*-dipropyltryptamine (DPT), *N*,*N*-dibutyltryptamine (DBT), *N*,*N*-diisopropyltryptamine (DIPT), 5-methoxy-*N*,*N*-dimethyltryptamine (5-MeO-DMT), and 5-methoxy-*N*,*N*-diisopropyltryptamine (5-MeO-DIPT), methamphetamine, 3,4-methylenedioxyamphetamine (3,4-MDA), 3,4-methylenedioxymethamphetamine (3,4-MDMA) and 2-methylamino-1-(3,4-methylenedioxyphenyl)butane (MBDB) were generously donated by the Military Police Command, Forensic Science Center, Taiwan. The procedures for their synthesis have been described previously by Ann and Alexander Shulgin in their published book titled TiHKAL and PiHKAL, respectively [6,7]. Following the synthesis steps, the final products were identified by NMR, IR and verified by GC–MS. LSD (lysergic acid diethylamide) was acquired from Radian International (Austin, TX, USA). All the other chemicals were of analytical grade and were obtained from commercial sources.

2.3. Sample preparation

2.3.1. Matrices

Ten milligrams of CHCA was dissolved in a 1.0 mL aliquot of a water/acetonitrile (v/v, 50/50) solution that contained of 0.1% trifluoroacetic acid. In the case of 2,5-DHB, 10.0 mg of 2,5-DHB was dissolved in a 1.0 mL aliquot of water/acetonitrile (v/v, 50/50) which also contained 0.1% trifluoroacetic acid.

2.3.2. Standards

Solutions for each of the analogues were prepared by dissolving the appropriate amount in methanol to obtain a final concentration. A drop of the aqueous (1.0 μL) matrix compound solution was mixed with the analyte solution (0.01 mg/1 mL methanol) and dried, resulting in a solid deposit of analyte-doped matrix crystals that was used in the TOFMS for analysis. Preparation of analytes for GC/MS and LC/MS were same as described above, but without any matrix.

3. Results and discussion

Table 1 shows the abbreviations used for the nine substituted tryptamines (tabulated by structure) used in this study. Fig. 1 shows a general schematic outline for the α-cleavage and β-cleavage of tryptamine and phenethylamine. This scheme shows that, in the case of tryptamine, if a tryptamine acquires a proton that will form a $[M+H]^+$ ion. The α-cleavage would progress at the C_α–N bond, and as a result, a cation (indole-containing group) and small neutral amine ($NHR_{N1}R_{N2}$) are be formed. However, the proton also could be donated itself to the C_β atom (the β carbon), leading to C_α–C_β bond breakage (i.e. β-cleavage). As a result, an iminium ion ($CH_2{=}N^+R_{N1}R_{N2}$) and a neutral indole-containing fragment are formed. In the case of phenethylamine, similar consequence can be found. Fig. 2 shows the EI/MS, ESI/MS and MALDI/TOFMS spectra of *N*,*N*-dimethyltryptamine (DMT); corresponding to spectra A, B and C, respectively. As shown in mass spectrum 2A (based on the EI mode), the peak at $m/z = 58$ is the major fragment. This suggested that this is a stable fragment ion that forms after electron impact. However, it is obvious that, the EI mode is not the most useful rapid screening tool if it is only dependent on the major peak at $m/z = 58$. In contrast to this, stable protonated ions form after ESI (spectrum 2B) or MALDI (spectrum 2C). The protonated parent ion $[M+H]^+$, can be clearly observed in both cases at $m/z = 189$. We found that in the case of ESI/MS, α-cleavage is the major process that would produce a fragment at $m/z = 144$, indicating the loss of a neutral fragment, $189 - 144 = 45$ ($NH(CH_3)_2$). Meanwhile, the β-cleavage process also occurs, in which a peak at $m/z = 58$ ($H_2C{=}N^+(CH_3)_2$) was observed, indicat-

Table 1
Substituted tryptamines (tabulated by structure) used in this study

Abbreviation	R_5	R_{N1}	R_{N2}	Full name	M_w
AMT		H	H	α-Methyltryptamine	174.24
DMT		CH_3	CH_3	*N*,*N*-Dimethyltryptamine	188.13
5-MeO-AMT	OCH_3	H	H	5-Methoxy-α-methyltryptamine	204.27
DET		CH_2CH_3	CH_2CH_3	*N*,*N*-Diethyltryptamine	216.16
DPT		$CH_2CH_2CH_3$	$CH_2CH_2CH_3$	*N*,*N*-Dipropyltryptamine	244.19
DBT		$CH_2CH_2CH_2CH_3$	$CH_2CH_2CH_2CH_3$	*N*,*N*-Dibutyltryptamine	272.22
5-MeO-DMT	OCH_3	CH_3	CH_3	5-Methoxy-*N*,*N*-dimethyltryptamine	218.29
DIPT		$CH(CH_3)_2$	$CH(CH_3)_2$	*N*,*N*-Diisopropyltryptamine	244.19
5-MeO-DIPT	OCH_3	$CH(CH_3)_2$	$CH(CH_3)_2$	5-Methoxy-*N*,*N*-diisopropyltryptamine	274.40

ing the loss of a larger neutral fragment, $189 - 58 = 131$. This is always the minor process under the ESI/MS method, although some minor peaks can also be observed (at $m/z = 65$, 74, 87, etc.). The ion intensity order of tryptamines, is as follows: $[M+H]^+ \gg$ fragment formed by the α-cleavage process > fragment formed by the β-cleavage process. This means that during the electrospray process a neutral molecule of ($HNR_{N1}R_{N2}$) is more stable than an iminium ion ($H_2C{=}N^+R_{N1}R_{N2}$), especially in the case of a tertiary amine. In order to realize the competition of α- and β-cleavage, tandem MS (a process almost conducted in the gas phase for the $[M+H]^+$ ion, at $m/z = 189$, occurs, as shown in the inset of spectrum 2B. We found that only three conspicuous peaks were produced (at $m/z = 189$, 144 and 58), corresponding to the $[M+H]^+$ ion, and fragments from α- and β-cleavage, respectively. The ratio of the peaks (at $m/z = 144$ and 58) could be changed, depending

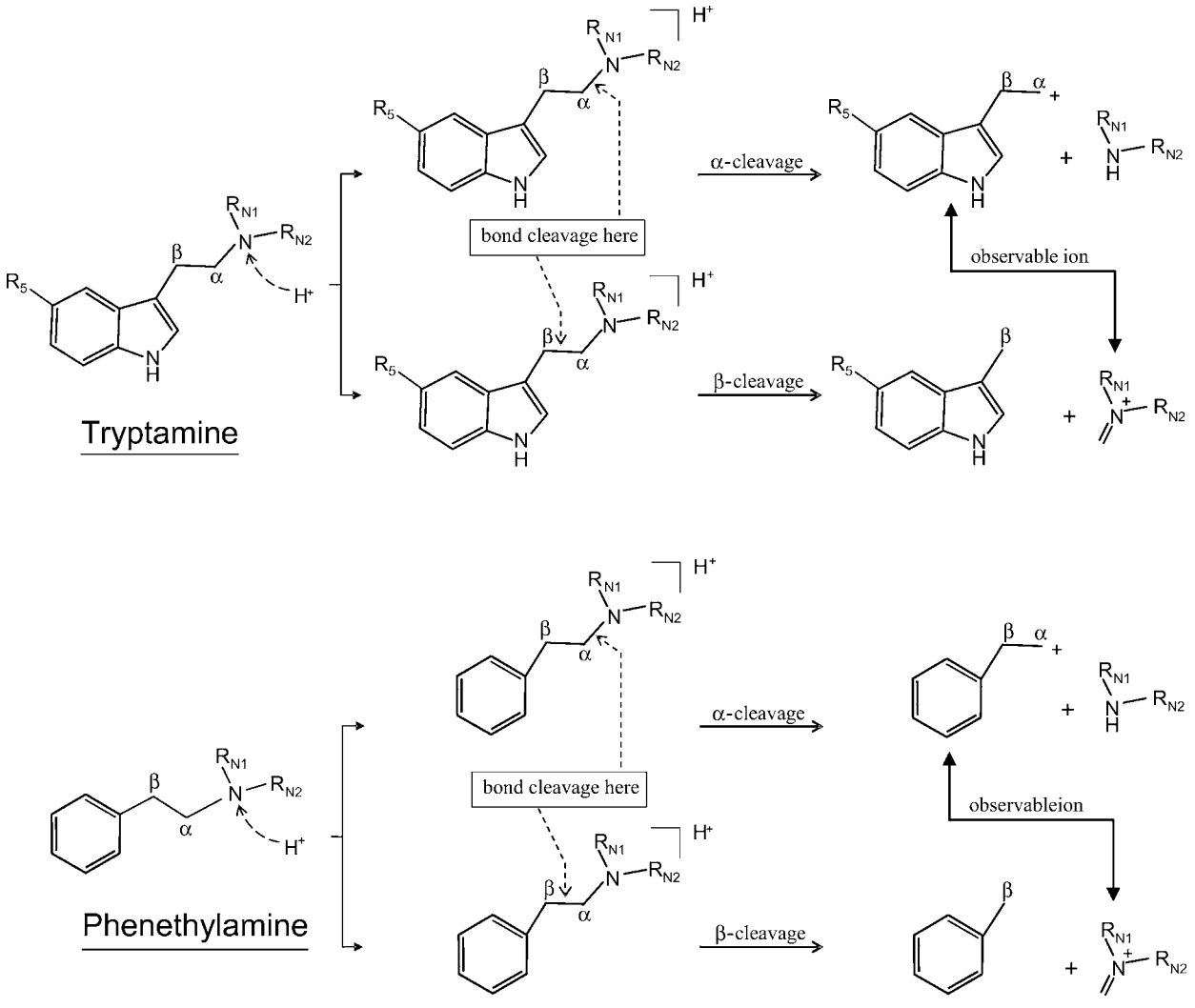


Fig. 1. A general schematic outline for α-cleavage and β-cleavage of tryptamine and phenethylamine.

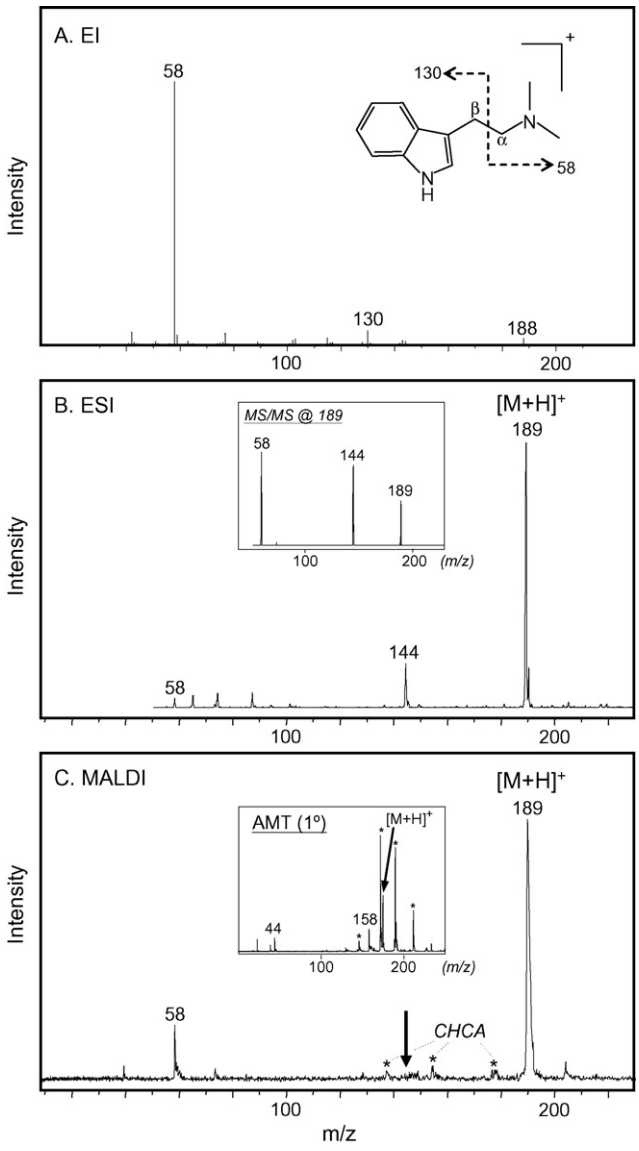


Fig. 2. The EI/MS, ESI/MS and MALDI/TOFMS spectra of *N,N*-dimethyltryptamine (corresponding to spectra A, B and C; each 100 μg/1 mL methanol), respectively. The mass conditions are shown in the text; the major fragments of CHCA are indicated as "*". Inset of spectrum (2B) shows a tandem MS for the $[DMT+H]^+$ ion (at $m/z = 189$); inset of spectrum (2C) shows a MALDI-TOFMS for AMT (a primary amine) at a higher concentration (1 mg/1 mL methanol), respectively.

on the conditions used, such as the voltage (positive or negative), temperature for electrospray process. It should be clearly pointed out that if it is limited to a gas phase (where tandem MS is performed), α- or β-cleavage could occur depending on the mass conditions. It should be noted that, three characteristic peaks ($[M+H]^+$, the peaks from α-cleavage, and β-cleavage processes) are very unique and constitute useful information for investigators who are interested in identifying tryptamines in actual forensic cases. The ionization efficiency is proportional to the degree of alkylation of the side chain nitrogen. However, to the primary amines, including AMT and 5-MeO-AMT, only the α-cleavage process was observed, since if the β-cleavage process also produced, a peak at $m/z = 44$ should be observed (data not shown). However, this is out of the detection range of the instrument (Finnigan LCQ Classic). On the other hand, in the case of MALDI/TOFMS, we found that the β-cleavage is the only the consequence to tertiary tryptamines, irrespective of matrix (such as 2,5-DHB) used or if a different laser power/wavelength is used (data not shown). Fig. 2C shows the mass spectrum of DMT obtained by MALDI/TOFMS (matrix, CHCA; laser source Nd:YAG, 355 nm); the major fragments of CHCA are indicated as "*". The ion intensity order of tertiary tryptamines is as follows: $[M+H]^+ \geqq$ the fragment from the β-cleavage process. If α-cleavage occurs, a peak at $m/z = 144$ should be observed; however, this peak is missing, as indicated by an "arrow". In order to recognize this, we examined AMT (a primary amine) at a higher concentration and found that both fragments from α-cleavage (a peak at $m/z = 158$) and β-cleavage (a peak at $m/z = 44$) were produced, as shown in the inset of

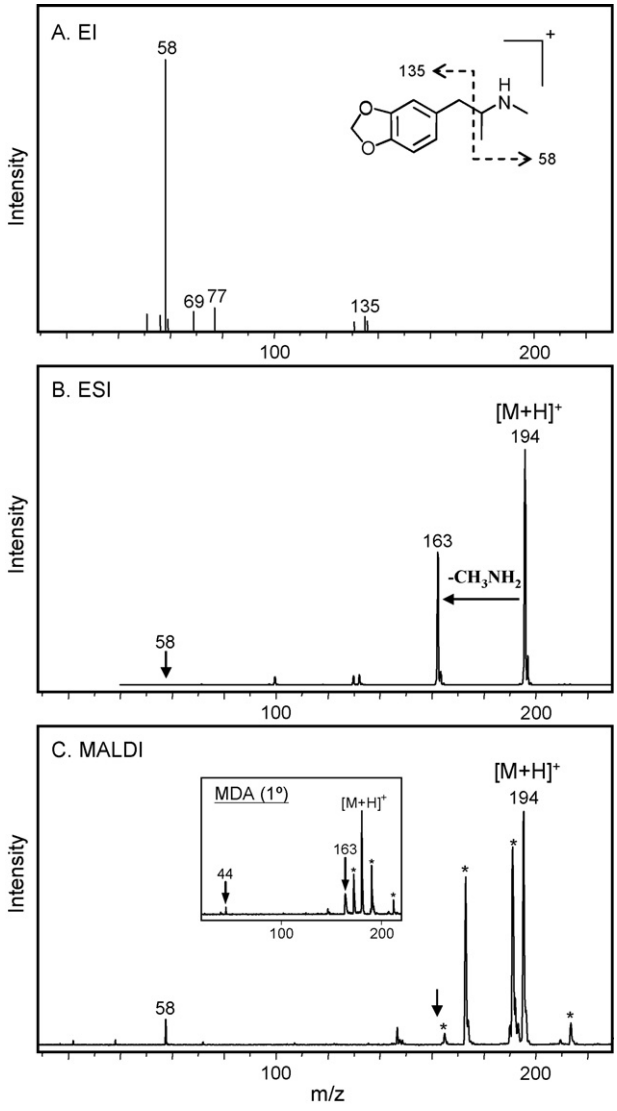


Fig. 3. The EI/MS, ESI/MS and MALDI/TOFMS spectra of 3,4-MDMA (corresponding to spectra A, B and C; each 100 μg/mL), respectively. The mass conditions are shown in the text; the major fragments of CHCA are indicated as "*". Inset of spectrum (3C) shows a MALDI-TOFMS for 3,4-MDA (a primary amine) at a higher concentration (1 mg/1 mL methanol).

spectrum 2C; the major fragments of CHCA are indicated as "*". Similar mass pattern was found for 5-MeO-AMT. Thus, we conclude that, in a tertiary tryptamine, the alkyl group of the side chain nitrogen plays an important role in the β-cleavage process, and is proportional to the degree of alkylation. In contrast to this, in a primary tryptamine, both α-cleavage and β-cleavage could be observed, even though the fragments are insignificant. Fig. 3 shows the EI/MS, ESI/MS and MALDI/TOFMS spectra of 3,4-MDMA (a phenethylamine; secondary amine); corresponding to spectra A, B and C, respectively. As shown in mass spectrum 3A (based on the EI mode), the peak at $m/z = 58$ is the major fragment, suggesting again that this is a stable fragment ion that forms after electron impact. As can be seen from the spectra 3B (ESI/MS) and 3C (MALDI-MS), the protonated molecular ion $[M + H]^+$, can be clearly observed in both cases at $m/z = 194$. In the case of ESI/MS, α-cleavage is the major process that would produce a fragment at $m/z = 163$. Meanwhile, the β-cleavage process also occurs, in which a peak at $m/z = 58$ ($H_2C{=}N^+(CH_3)_2$) was observed. The ion intensity order of 3,4-MDMA, is as follows: $[M + H]^+$ > fragment formed by the α-cleavage process ≫ fragment formed by the β-cleavage process. The ionization efficiency is also proportional to the degree of alkylation of the side chain nitrogen. In the case of MALDI/TOFMS, we found that the β-cleavage is the only consequence to 3,4-MDMA, as shown in Fig. 3C (matrix, CHCA; laser source Nd:YAG, 355 nm); the major fragments of CHCA are indicated as "*". The ion intensity order of 3,4-MDMA is as follows: $[M + H]^+$ > the fragment from the β-cleavage process. If α-cleavage occurs, a peak at $m/z = 163$ should be observed; however, this peak is missing, as indicated by an "arrow". In order to recognize this, we examined 3,4-MDA (a primary amine) at a higher concentration and found that both fragments from α-cleavage (a peak at $m/z = 163$) and β-cleavage (a peak at $m/z = 44$) were produced, as shown in the inset of spectrum 2C; the major fragments of CHCA are indicated as "*". Fig. 4

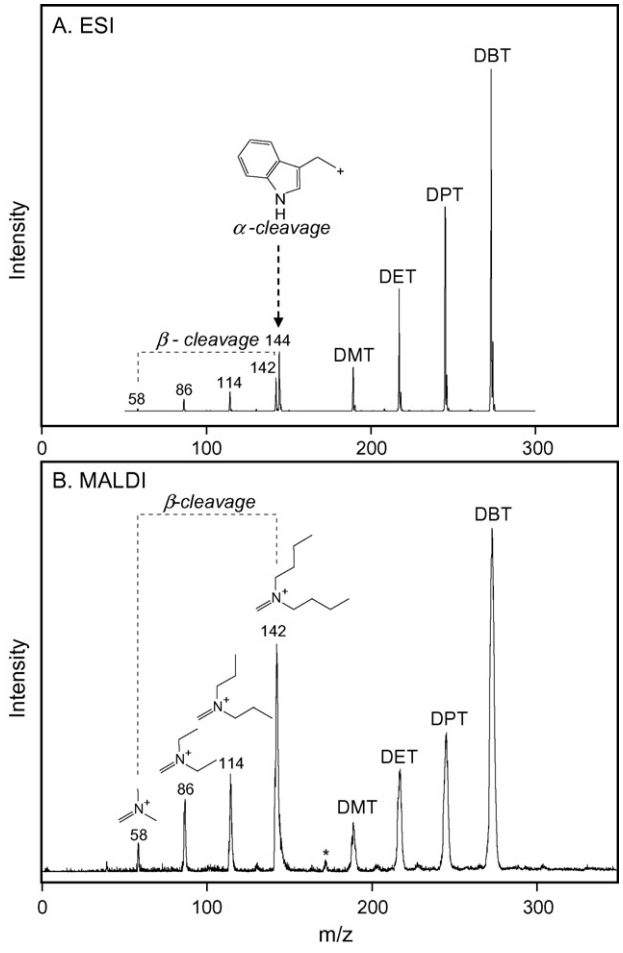


Fig. 4. The mass spectra of a mixture, including DMT, DET, DPT and DBT obtained by ESI/MS (spectrum A) and MALDI/TOFMS (spectrum B), respectively; concentration level: each 10 μg/1 mL methanol.

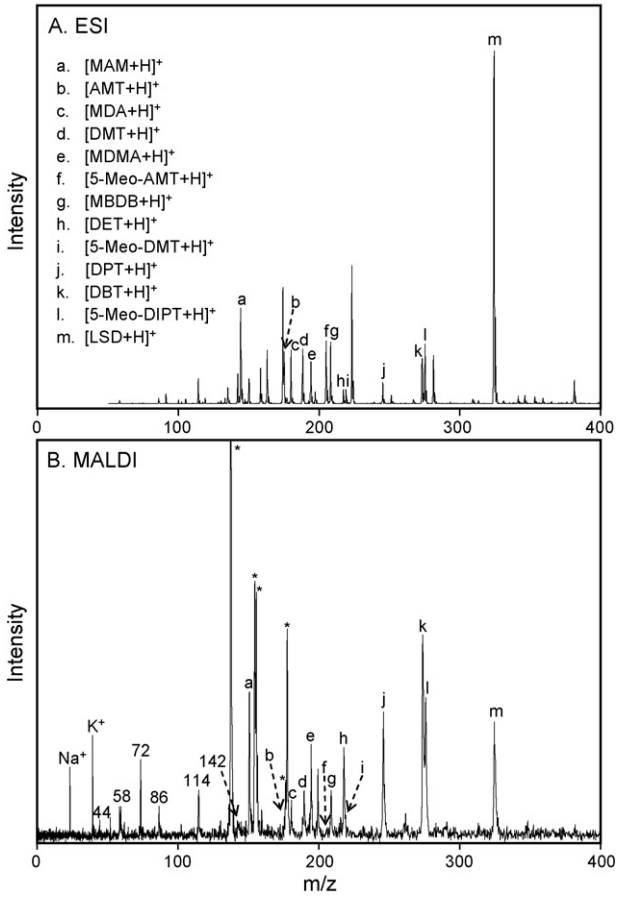


Fig. 5. Mass spectra of a mixture, including 13 types of illicit drugs obtained by ESI/MS (spectrum A) and MALDI/TOFMS (spectrum B), respectively; the major fragments of 2,5-DHB are indicated as "*". concentration level: (A) each 1 μg/1 mL methanol and (B) primary tryptamine, each 20 μg/1 mL methanol; secondary tryptamine, each 20 μg/1 mL methanol; tertiary tryptamines: each 1 μg/1 mL methanol. *Abbreviations*—(a) MAMP: methamphetamine; (b) AMT: alphamethyltryptamine; (c) MDA: 3,4-methylenedioxyamphetamine; (d) DMT: *N*,*N*-dimethyltryptamine; (e) MDMA: 3,4-methylenedioxymethamphetamine; (f) 5-MeO-AMT: 5-methoxy-alphamethyltryptamine; (g) MBDB: 2-methylamino-1-(3,4-methylenedioxyphenyl)butane; (h) DET: *N*,*N*-diethyltryptamine; (i) 5-MeO-DMT: 5-methoxy-dimethyltryptamine; (j) DPT: *N*,*N*-dipropyltryptamine; (k) DBT: *N*,*N*-dibutyltryptamine; (l) 5-MeO-DIPT: 5-methoxy-*N*,*N*-diisopropyltryptamine; (m) LSD: lysergic acid diethylamide.

shows the mass spectra of a mixture, including DMT, DET, DPT and DBT by ESI/MS and MALDI/TOFMS, respectively, corresponding to mass spectra 4A and 4B. This shows that the degree of alkylation greatly affects the ionization efficiency, in which the ion intensities of $[M+H]^+$ and the fragment from β-cleavage would be altered in both cases. The two characteristic peaks ($[M+H]^+$ and the fragment from β-cleavage) are very unique, providing useful information when MALDI is applied to this problem. We conclude that, limited to the nine tryptamine standards, the effect of alkylation on ionization efficiency is as follows: di-methyl- < di-ethyl- < di-propyl- (∼ diiso-propyl-, data not shown) < di-butyl-. Furthermore, this phenomenon is more obvious in the case of the MALDI/TOFMS than ESI/MS. In the other words, for a tertiary amine, MALDI/TOFMS would be a very sensitive method for its detection. However, if a mixture of primary and tertiary amines, is examined by means of MALDI/TOFMS, the fragments of the primary amines would be severely suppressed by the tertiary amines, causing a problem if a primary amine is the analyte. This is the reason for why a certain peptide or protein, if it is a primary amine, would be suppressed in a complicated sample, such as a urine or blood sample, when MALDI/TOFMS is used. Fig. 5 shows the mass spectra of a mixture, including 13 types of tryptamine and phenethylamine standards. We found that they provide similar characterisation, i.e. both α- and β-cleavage can be found. With this characteristic fragments, the analytes can be recognized from a complicated mixture. In the case of ESI/MS (mass spectrum 5A), all of the protonated molecular ions $[M+H]^+$, can be identified. Most of the fragments from the α-cleavage process can also be identified. In the case of MALDI/TOFMS (mass spectrum 5B), the concentration levels of primary, secondary and tertiary tryptamine are 20, 20 and 1 μg/mL, respectively. However, as mentioned above the protonated molecular ions of primary amines are suppressed, even with a 20-fold increase in the concentration level compared to tertiary amines. Finally, we also found that the methoxy-group of 5-MeO-AMT, 5-MeO-DMT and 5-MeO-DIPT does not affect ionization efficiency (data not shown).

4. Conclusion

If a direct sample injection is possible based on LC–ESI/MS, this would be an ideal method for the rapid screening of tryptamines and phenethylamines. Meanwhile, such studies also can be performed by means of MALDI/TOFMS since the sample substrate used in MALDI can be easily inserted and changed. However, the unbalance ionization efficiency of different degrees of alkylation should keep in mind and attention should be paid to this.

Acknowledgement

This work was supported by grants from the National Science Council of Taiwan under Contracts of No. 95-2745-M-003-001.

References

[1] U.S. Drug Enforcement Administration, Microgram Bull. 36 (2) (2003) 31.
[2] U.S. Drug Enforcement Administration, Microgram Bull. 36 (5) (2003) 90.
[3] U.S. Drug Enforcement Administration, Microgram Bull. 36 (8) (2003) 173.
[4] U.S. Drug Enforcement Administration, Microgram Bull. 37 (1) (2004) 1.
[5] Drug Enforcement Administration (DEA), Department of Justice, Schedules of controlled substances: temporary placement of alpha-methyltryptamine and 5-methoxy-*N*,*N*-diisopropyltryptamine into Schedule I, Final rule. Fed. Regist. 68 (65) (2003) 16427.
[6] A. Shulgin, A. Shulgin, THINKAL (Tryptamines I Have Known and Loved): The Continuation, Transform Press, Berkeley, 1997.
[7] A. Shulgin, A. Shulgin, PHINKAL (Phenethylamines I Have Known and Loved): The continuation, Transform Press, Berkeley, 1991.
[8] T. Ishida, K. Kudo, A. Kiyoshima, H. Inoue, A. Tsuji, N. Ikeda, J. Chromatogr. B 823 (2005) 47.
[9] J.M. Wilson, F. McGreorge, S. Smolinske, R. Meatherall, Forensic Sci. Int. 148 (2005) 31.
[10] S.D. Brandt, S. Freeman, P. McGagh, N. Abdul-Halim, J.F. Alder, J. Pharm. Biomed. Anal. 36 (2004) 675.
[11] R. Kikura-Hanajiri, M. Hayashi, K. Saisho, Y. Goda, J. Chromatogr. B 825 (2005) 29.
[12] S.D. Brandt, D. Mansell, S. Freeman, I.A. Fleet, J.F. Alder, J. Pharm. Biomed. Anal. 41 (2006) 872.
[13] S.P. Vorce, J.H. Sklerov, J. Anal. Toxicol. 28 (2004) 407.
[14] S.D. Brandt, S. Freeman, I.A. Fleet, P. McGagh, J.F. Alder, Analyst 130 (2005) 330.
[15] S. Laks, A. Pelander, E. Vuori, E. Ali-Tolppa, E. Sippola, I. Ojanpera, Anal. Chem. 76 (2004) 7375.
[16] E. Tanaka, T. Kamata, M. Katagi, H. Tsuchihashi, K. Honda, Forensic Sci. Int. 163 (2006) 152.
[17] A. Numan, N.D. Danielson, Anal. Chim. Acta 460 (2002) 49.
[18] W.F. Smyth, V.N. Ramachandran, E. O'Kane, D. Coulter, Anal. Bioanal. Chem. 378 (2004) 1305.
[19] S. Mclean, R.C. Robinson, C. Shaw, W.F. Smyth, Rapid Commun. Mass Spectrom. 16 (2002) 346.
[20] A.-K. Su, J.-T. Liu, C.-H. Lin, Talanta 67 (2005) 718.
[21] A.-K. Su, J.-T. Liu, C.-H. Lin, Anal. Chim. Acta 546 (2005) 193.
[22] Y.-R. Shu, A.-K. Su, J.-T. Liu, C.-H. Lin, Anal. Chem. 78 (2006) 4697.

Available online at www.sciencedirect.com
ScienceDirect
Talanta 74 (2008) 1056–1059
Talanta
www.elsevier.com/locate/talanta

Short communication

Nanoporous niobium oxide for label-free detection of DNA hybridization events

Jinsub Choi [a,*], Jae Hoon Lim [a], Sangchul Rho [b], Deokjin Jahng [b], Jaeyoung Lee [c], Kyung Ja Kim [a]

[a] *Nanomaterials Application Division, Korea Institute of Ceramic Engineering and Technology (KICET), Seoul 153-801, South Korea*
[b] *Department of Environmental and Biotechnology Engineering, Myongji University, Yongin, Gyunggi-do 449-728, South Korea*
[c] *Department of Environmental Science and Engineering, Gwangju Institute of Science and Technology, Gwangju 500-712, South Korea*

Received 30 April 2007; received in revised form 2 July 2007; accepted 2 July 2007
Available online 17 July 2007

Abstract

We found that DNA probes can be immobilized on anodically prepared porous niobium oxide without a chemical modification of both the DNA probes and the substrate. By using the porous niobium oxide with a positive surface charge, DNA hybridization events are detected on the basis of the blue-shift of a maximum absorption peak in UV–vis-NIR spectroscopy. The blue-shift is ascribed to the change of surface charge upon single- or double-stranded DNA. The method does not require a label and shows high sensitivity with the detection limit of the concentration of 1 nM.
© 2007 Elsevier B.V. All rights reserved.

Keywords: Anodization; Niobium oxide; Porous oxide; Biosensor; Surface charge

1. Introduction

Biosensors that accurately recognize DNA hybridization events are of significant interest due to their potential applications in clinics [1–3]. Even though there have been tremendous investigations for the improvement of sensitivity, selectivity and reproducibility at the practically useful level, many advanced methods still rely on fluorescent and electrochemical principles that require a label such as dyes and intercalators [4]. Since dyes generally are unstable against light and most of intercalators are harmful to be practically used, label-free biomolecular recognition methods have attracted attention as the next generation method to obtain reliable and reproducible biosensing signals. For example, electrochemical reaction in nanoporous electrode [5,6], enzyme catalyzed precipitation [7], impedance [8,9], quartz crystal micro-balance [10,11] and photoluminescence in microcavity resonator of porous silicon [12] have been proposed for the label-free confirmation of DNA hybridization.

More recently, photoelectrochemistry has been introduced to quantitatively analyze the hybridization events with ultra-sensitivity [13,14] but the mechanism has not yet been clearly understood. Rajh et al. reported that the charge pair separation is extended when hybridization events occur on photoactive metal oxide, leading to distinguishable electron paramagnetic resonance (EPR) signal between single- and double-stranded oligonucleotides [15–17].

In this communication, label-free detection of DNA hybridization events by using semiconductive porous niobium oxide that strongly absorbs DNA probes without a chemical modification of the probes or the substrate will be described. We demonstrate that the absorption peak in UV–vis-NIR spectra is shifted by means of hybridization events and it is ascribed to a change of electron trapped in surface state (ETS) upon single- and double-stranded DNA.

2. Experimental

2.1. Preparation of anodic porous oxides

The preparation of porous niobium oxide, porous alumina oxide and porous titanium oxide by electrochemical anodization was described elsewhere in detail [18,19]. In brief, Nb foil with a purity of 99.9% and a thickness of 0.25 mm (goodfellow,

* Corresponding author. Tel.: +82 2 3282 2457; fax: +82 2 3282 7769.
E-mail address: jinsub@kicet.re.kr (J. Choi).

0039-9140/$ – see front matter © 2007 Elsevier B.V. All rights reserved.
doi:10.1016/j.talanta.2007.07.007

UK) was cleaned by ultrasonication in acetone for 5 min, washed with ethanol and dried with a stream of N_2 gas. Anodization was carried out at a constant voltage of 2.5 V in the mixture of 1 wt.% HF + 1 M H_3PO_4 at room temperature for 1 h, using a potentiostat/galvanostat (AutoLab PGSTAT12, Eco Chemie) interfaced to a computer. The cell was a three-electrode system consisting of a Pt mesh acting as the counter electrode, Ag/AgCl/3 M KCl as the reference electrode and an Nb foil with a size of 1 cm^2 as the working electrode. During the anodization, the stirring rate of the electrolyte was kept constant (∼180 rpm). As a result, porous niobium oxide with an average pore diameter of 10 nm, a length of 120 nm and a pore density of $4.6 \times 10^{15}/m^2$ was prepared as shown in Fig. 1. Note that the pore length is the same as the niobium oxide thickness.

For anodic aluminum oxide, anodization was carried out in 0.3 M oxalic acid for 48 h under the two-electrode system consisting of a Pt mesh and a high purity aluminum foil. Afterwards, the first formed oxide was selectively removed by chromic acid containing solution and the aluminum was re-anodized under the same condition as the first anodization for 1 h. The highly ordered porous alumina with a pore diameter of around 100 nm and a thickness of around 2 μm was prepared.

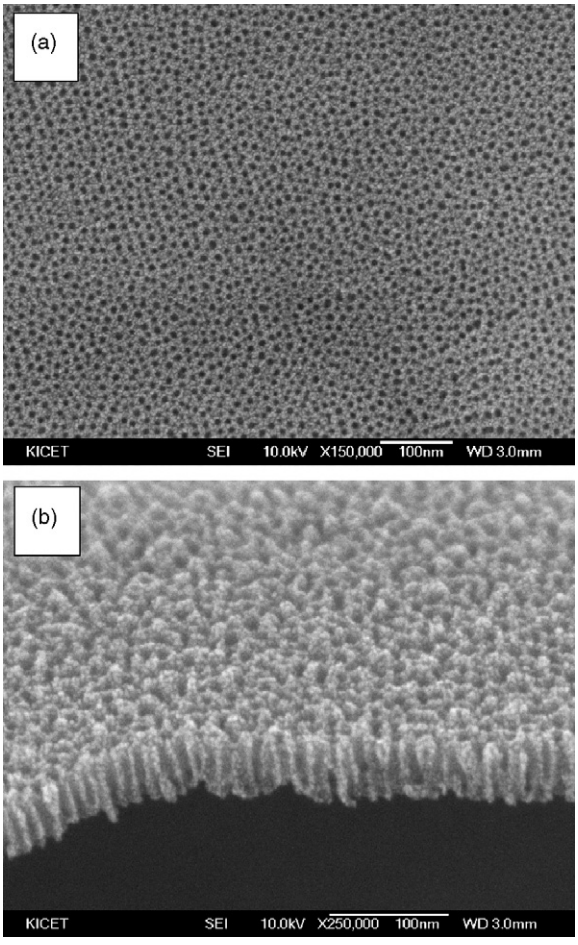


Fig. 1. FE-SEM (field emission scanning electron microscopy) images of porous niobium oxide that is prepared by anodization of niobium foils in 1 wt.% HF + 1 M H_3PO_4 at 2.5 V (vs. Ag/AgCl, 3 M KCl) for 1 h: (a) top view and (b) cross-sectional view.

For the preparation of porous titanium oxide, the experimental was carried out with the recipe suggested by Grimes's group [20]. The final thickness was adjusted to the same thickness of the porous niobium oxide.

2.2. Immobilization of oligonucleotides on niobium oxide

Tris–EDTA (TE) buffer (100× concentrate, 1.0 M Tris–HCl, 0.1 M EDTA, pH 8.0), 23 mer oligonucelotides (5′-TTT GTT ACT GTG GTA GAT ACT AC-3′, 100) and its complementary oligonucelotides were purchased from Bioneer Corp. (Korea). The above all reagents were free of DNase and RNase. The oligonucleotides were diluted with autoclaved water to make the concentration of 100 μM and kept in the refrigerator (−20 °C) when not used.

The anodically prepared niobium oxide was immersed in the 5 ml of TE buffer under the vacuum of 0.1 MPa in three times to completely wet the wall of pores with TE buffer.

Afterwards, a 20 μl-droplet of 23 mer probe oligonucelotides was dropped on the wet niobium oxide and then it was dried under the vacuum at 30 °C for 1 h.

2.3. Hybridization

After 20× SSC buffer (87.65 g sodium chloride, 44.1 g sodium citrate, adjusted to pH 7.0 with NaOH) was received from Bioneer Corp., it was diluted with autoclaved water by 10 times. For hybridization, 3 ml of SSC buffer containing complementary oligonucelotides (20 μl of 100 μM) was dropped on the niobium oxide where the probe oligonucelotides are immobilized, followed by drying in refrigerator for overnight.

2.4. Optical measurements

The immobilization of DNA on the nanostructures was examined by using a microarray scanner (GeneTACTM LS IV scanner, USA) and the absorption shift was characterized by using a UV–vis-NIR spectrophotometer (JASCO V550, USA).

3. Results and discussion

Fig. 1 shows anodically grown porous niobium oxide with a thickness of 120 nm. Because of the fast dissolution of the formed porous oxide in aqueous electrolyte containing HF, the maximum thickness is limited to less than a few hundred of nanometers. As already discussed in the previous work [18], the addition of H_3PO_4 strongly suppresses the chemical dissolution and results in producing a thicker porous structure. The roles of HF and H_3PO_4 on the pore formation were described in the reference [18] in detail.

Similar to protein immobilization on nanoporous niobium oxide [21], we found that the oligonucleotides are firmly absorbed to the surface of niobium oxide and the immobilization is stable even after strong washing with TE buffer (see Fig. 2(a) and (c)). For the comparison, the immobilization of the probe DNA on anodically grown titanium oxide that has a diameter and thickness similar to the niobium oxide is examined as shown in

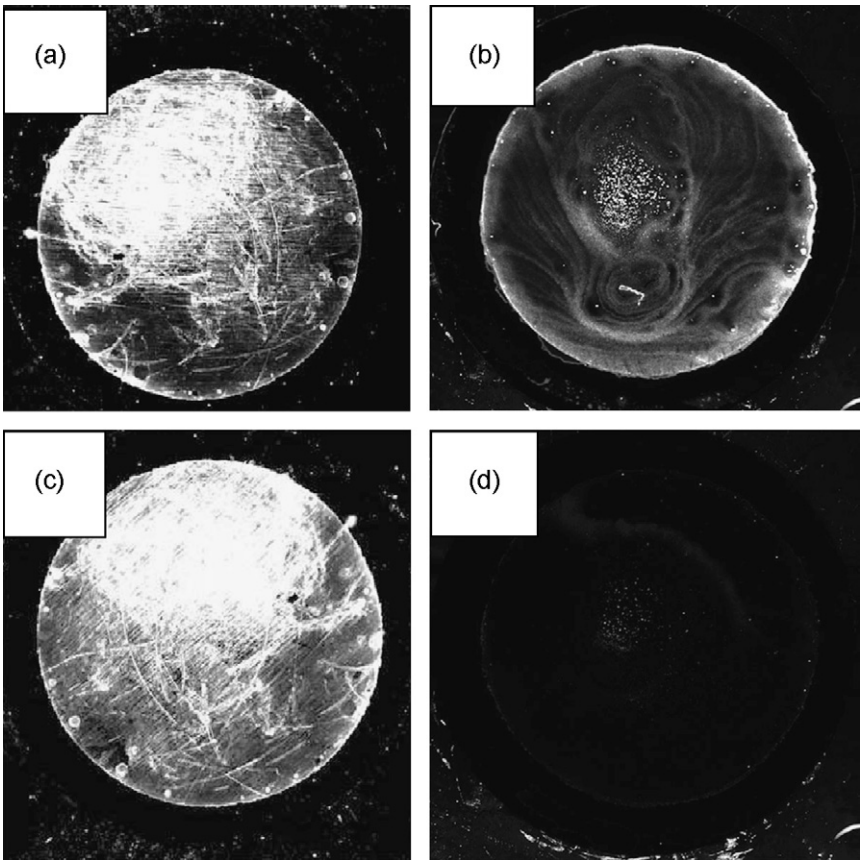


Fig. 2. Microarray scanner scanning image: immobilization of probe DNA modified with 6-carboxytetramethylrhodamine (Tamar) dye on (a) anodic porous niobium oxide and (b) anodic porous titanium oxide, respectively. The microarray images after strong washing of the samples of (a) and (b) with TE buffer are shown in (c) and (d), respectively. The bright area is caused by Tamar dye, meaning that the DNA is immobilized. The images demonstrate that the probe DNA immobilized on porous niobium oxide is strongly adsorbed even after strong washing with TE buffer whereas the immobilization of the probe DNA on porous titanium oxide is not very strong.

Fig. 2(b) and (d). In this case, we found that the probe DNA is removed after a strong washing with TE buffer, suggesting the immobilization of DNA on porous niobium oxide is stable more than that on porous titanium oxide. It is ascribed to that the surface of niobium oxide is positively charged whereas that of titanium oxide is negatively charged in the pH 8 buffer solution [22].

For the label-free detection of hybridization events, a shift of absorption peak is evaluated. UV–vis-NIR absorption spectra that were measured in each step as schemed in Fig. 3(a) are depicted in Fig. 3(b). In sample (1) of Fig. 3(b), distinguishable absorption peaks are observed at the wavelength of 320 and 460 nm, respectively. Since the niobium oxide is semiconductive metal oxide with the bandgap of 3.4–5.3 eV which depends on the preparation methods, the threshold of absorption with the maximum peak of 320 nm can be ascribed to its bandgap (BG). On the other hand, the maximum peak at the wavelength of 460 nm can be assigned to ETS, keeping in mind that a similar absorption peak at the wavelength of 600 nm, caused by ETS, is reported on UV–vis-NIR absorption spectra of TiO_2 nanoparticles. Compared to the broad absorption peaks in case of TiO_2 nanoparticles, the sharp absorption peaks are observed in this work, which might be due to nanoporous structures with a narrow distribution of pore size.

For the comparison of absorption peaks in a porous insulator, UV–vis-NIR absorption spectrum of anodized porous alumina with the bandgap of 7–9.5 eV was measured as illustrated in sample (7) of Fig. 3(b) [20]. Absorption maximum from ETS is not observed in the case of the porous alumina due to the wide bandgap.

After the single-stranded oligonucleotide is immobilized on the niobium oxide, the maximum absorption peak is red-shifted from 460 to 480 nm, corresponding to the energy of 0.1 eV (sample (2) of Fig. 3(b)). Considering that there is the same shift in absorption peak after the niobium oxide is treated by TE buffer that does not contain oligonucleotides (sample (5) of Fig. 3(b)), the shift in sample (2) of Fig. 3(b) can be attributed to a modification of the surface of niobium oxide by TE buffer. This is in good agreement with the observation by Rajh et al. that surface-modified TiO_2 shows a red shift in UV–vis absorption spectra as compared to unmodified nanocrystallites [15]. They explained that the optical shift is as a result of the change of dipole moment of the Ti–ligand complex at the surface. For the absorption peaks caused by BG (at the wavelength of 320 nm), there is no significant difference before and after modification of surface with the TE buffer, indicating that bandgap itself is not changed by immobilization of probe DNA. A noticeable finding is that after the hybridization event occurs in SSC

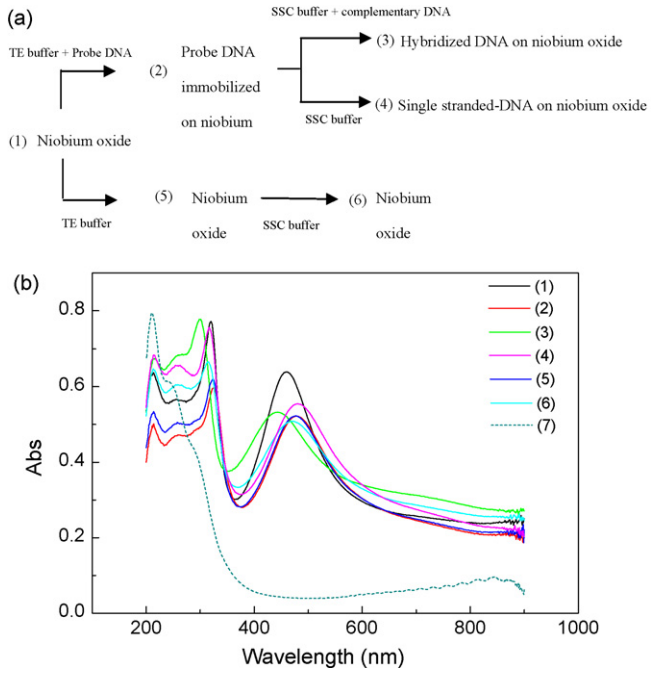


Fig. 3. (a) Experimental procedures and (b) their corresponding UV–vis-NIR absorption spectra: anodized porous niobium oxide (1), immobilization of probe oligonucleotides on the niobium oxide (2), hybridization on the niobium oxide (3), SSC buffer treatment of probe oligonucleotides immobilized on the niobium oxide (4), TE buffer treatment of niobium oxide (5), SSC buffer treatment of the niobium oxide after TE buffer treatment (6), and porous alumina (7).

buffer, the absorption peak is blue-shifted from 480 to 442 nm as shown in sample (3) of Fig. 3(b). We found that SSC buffer does not affect on the blue-shift in the absorption spectra as shown in samples (4) and (6) of Fig. 3(b). These results demonstrate that the shift in sample (3) of Fig. 3(b) is originated not from surface modification by SSC buffer but from hybridization events. Since photogenerated holes are scavenged in double-stranded DNA [15], the hole and the electron localized in surface cannot be readily recombined in double-stranded DNA compared to the single-stranded DNA, leading to the change of absorption spectra. Based on this method, we could measure hybridization events with the detection limit of concentration of around 1 nM, which is more than 10 times sensitive, compared to the conventional electrochemical DNA sensors. Studies on further improving the detection limit are under the investigation.

4. Conclusions

In conclusions, we demonstrated that semiconductive porous niobium oxide can be used for a label-free confirmation of DNA hybridization events based on the change of surface charge upon single- or double-stranded DNA. As a result, the blue-shift in absorption peak is observed when hybridization events occur. Even though detail mechanism is under the investigation, it is noteworthy that DNA hybridization is recognized with high sensitivity by surface charge changing.

As indicated in the introduction, DNA biosensors based on label-free detection techniques have been studied for the applications in clinics. However, improvement in sensitivity and reproducibility at a low cost is still required for the previous reported label-free detection methods. The concept reported in this article might give us a cost-effective and reliable DNA detection method. We surely expect that the method can be further applied to the detection of proteins such as hormones in terms of the similar principles.

Acknowledgments

Support from MOCIE (Ministry of Commerce, Industry and Energy) of Korea and KICET is gratefully acknowledged. The authors thank Dr. J.H. Chang for assistance with the measurement of UV–vis-NIR spectroscopy and Dr. S.C. Lee for stimulating discussions.

References

[1] E. Katz, I. Willner, J. Wang, Electroanalysis 16 (2004) 19.
[2] G.H. Wu, R.H. Datar, K.M. Hansen, T. Thundat, R.J. Cote, A. Majumdar, Nat. Biotechnol. 19 (2001) 856.
[3] L. He, M.D. Musick, S.R. Nicewarner, F.G. Salinas, S.J. Benkovic, M.J. Natan, C.D. Keating, J. Am. Chem. Soc. 122 (2000) 9071.
[4] K. Kerman, M. Kobayashi, E. Tamiya, Meas. Sci. Technol. 15 (2004) R1.
[5] J. Liua, Q. Huo, Appl. Phys. Lett. 87 (2005) 133902.
[6] I. Vlassiouk, P. Takmakov, S. Smirnov, Langmuir 21 (2005) 4776.
[7] H.C. Yoon, H.S. Yang, Y.T. Kim, Analyst (Cambridge, U.K.) 127 (2002) 1082.
[8] T.C. Hang, A. Guiseppi-Elie, Biosens. Bioelectron. 19 (2004) 1537.
[9] M. Archer, M. Christopherse, P.M. Fauchet, Biomed. Microdevices 6 (2004) 203.
[10] X.C. Zhou, L.Q. Huang, S.F.Y. Li, Biosens. Bioelectron. 16 (2001) 85.
[11] X.D. Su, R. Robelek, Y.J. Wu, G.Y. Wang, W. Knoll, Anal. Chem. 76 (2004) 489.
[12] S. Chan, Y. Li, L.J. Rothberg, B.L. Miller, P.M. Fauchet, Mater. Sci. Eng. C 15 (2001) 277.
[13] Z. Cao, N.C. Tansil, Nucleic Acids Res. 33 (2005) e123.
[14] H. Tokudome, Y. Yamada, S. Sonezaki, H. Ishikawa, M. Bekki, K. Kanehira, M. Miyauchia, Appl. Phys. Lett. 87 (2005) 213901.
[15] T. Rajh, Z. Saponjic, J.Q. Liu, N.M. Dimitrijevic, N.F. Scherer, M. Vega-Arroyo, P. Zapol, L.A. Curtiss, M.C. Thurnauer, Nano Lett. 4 (2004) 1017.
[16] N.M. Dimitrijevic, Z.V. Saponjic, B.M. Bartels, M.C. Thurnauer, D.M. Tiede, T. Rajh, J. Phys. Chem. B 107 (2003) 7368.
[17] N.M. Dimitrijevic, Z.V. Saponjic, B.M. Rabatic, T. Rajh, J. Am. Chem. Soc. 127 (2005) 1344.
[18] J. Choi, J.H. Lim, K.J. Kim, S.C. Lee, J.H. Chang, M.A. Cho, Electrochim. Acta 51 (2006) 5502.
[19] K. Nielsch, J. Choi, K. Schwirn, R.B. Wehrspohn, U. Gösele, Nano Lett. 2 (2002) 677.
[20] D. Gong, C.A. Grimes, O.K. Varghese, W. Hu, R.S. Singh, Z. Chen, E.C. Dickey, J. Mater. Res. 16 (2001) 3331.
[21] X. Xu, B.Z. Tian, J.L. Kong, S. Zhang, B.H. Liu, D.Y. Zhao, Adv. Mater. 15 (2003) 1932.
[22] S. Liu, A. Chen, Langmuir 21 (2005) 8409.

Available online at www.sciencedirect.com
ScienceDirect
Talanta 74 (2008) 441–442
Talanta
www.elsevier.com/locate/talanta

Editorial

A half-century of *Talanta*

The year 2008 marks the fiftieth anniversary of the publication of *Talanta*. The journal was started at the request of Professor Ronald Belcher, University of Birmingham, England, being initially published by Pergamon Press, Ltd., with publishing offices in London. Volume 1, issues 1–2, pages 1–196, July, 1958 appeared in August 1958. Fritz Feigl wrote the foreword for the first issue, stating, "Existing journals are not sufficient to ensure the rapid publication which is demanded both by authors and readers. It is therefore highly opportune that TALANTA, this new international journal of analytical chemistry in its broadest sense, is being introduced."

As "An International Journal of Analytical Chemistry", manuscripts were accepted in English, German, and French, a policy that remained for nearly 30 years. The first paper was "A critical evaluation of gravimetric methods for the determination of the platinum metals," a review by F.E. Beamish of the University of Toronto, received 21 January, 1958, and abstracts were published in English, German, and French. Research papers in the first volume included contributions from analytical pioneers E.H. Swift, H. Flaschka, H. Diehl, F. Feigl, C.N. Reilley, R. Přibil, R. Belcher, and T.S. West. Quite a remarkable start.

The symbol for the journal was a Greek balance taken from one of the Hope Vases. The name *Talanta* derives from the Greek word ταλαυτα, used by Homer to mean "a pair of scales". Such a balance was used for measuring talants, or gold coins.

The first Editor-in-Chief was Professor Cecil L. Wilson of Queen's University in Belfast, Ireland, who retained that role until his retirement in 1965, having firmly established the journal in the analytical community. Dr. Maurice (Mo) Williams served a short stint as Editor-in-Chief in 1965 until being appointed Journals Manager at Pergamon. Professor Robert A. Chalmers at the University of Aberdeen, Scotland was then appointed Editor-in-Chief in January 1966, remaining for 23 years till the end of 1988. Bob Chalmers was a powerful force in furthering the journal during his many years at the helm. He sadly passed away in September 2006, and his remarkable life and contributions to the journal are chronicled in an obituary by his colleague, Professor Mary Masson (*Talanta*, 72 (2007) 863).

Professors Gary D. Christian (University of Washington, Seattle) and David Littlejohn (University of Strathclyde, Scotland) assumed the roles of joint Editors-in-Chief in January 1989. David Littlejohn handled manuscripts from Europe, the Middle East, and Africa, while Gary Christian handled those from the rest of the world. At that time, the Editorial Board decided that henceforth only papers written in English would be considered for publication. The new editors were ably assisted by secretaries Sheila Parker in Seattle (who served for 18 years till her retirement in 2006) and Alison Berrie in Strathclyde. In January 1991, Professor Elo Hansen at the Technical University of Denmark, Copenhagen, replaced David Littlejohn as joint Editor-in-Chief until January 1995 when Professor Jean-Michel Kauffmann from the Université Libre de Bruxelles was appointed in that role, along with his colleague Professor Jean-Claude Viré as Assistant Editor. When Gary Christian assumed administrative responsibilities as Divisional Dean of Sciences at the University of Washington in 1993, he obtained needed help with the appointment of his colleague, Professor Robert A. Synovec, as Assistant Editor. The teams from Brussels and Seattle continue in their roles today, and so 2008 marks the beginning of the twentieth year for Gary Christian as joint Editor-in-Chief for the journal.

A major change for the journal occurred in 1991 when the flamboyant publisher Robert Maxwell sold Pergamon Press to Elsevier Science, Ltd. The first issue copyrighted by Elsevier Science was 41(2) in February 1994. It remained a Pergamon publication, with the Pergamon logo, and publishing continued in Oxford, England until January 1996, when the Elsevier tree logo appeared on 43(1). At that time, publishing headquarters moved from Oxford to Amsterdam; the publishing operation is carried out largely in Shannon, Ireland.

Manuscript submissions grew substantially over the years, and additional editorial help was needed. Professor Jianhua Wang from Northeastern University in Shenyang, China was appointed Associate Editor in 2005 and now handles all papers from China. Professor José Luis Burguera at Los Andes University, Merida, Venezuela was appointed Associate Editor in 2006 to take on manuscripts from South America, the Middle East, and Africa, ably assisted by his wife, Professor Marcela Burguera.

Other major changes occurred with the arrival of the electronic age. In 2002 Elsevier implemented their electronic submission system, Elsubmit, for improving the publication process. While manuscripts could still be submitted as hardcopy or by email, accepted manuscripts were submitted to the publisher

0039-9140/$ – see front matter © 2007 Elsevier B.V. All rights reserved.
doi:10.1016/j.talanta.2007.09.011

on a computer disk so they could be processed electronically. A further improvement came in 2005 with implementation of the web-based Elsevier Electronic System (EES). Manuscripts must now be submitted via EES, and all correspondence, reviews, revisions, and manuscript processing are handled through this system. It speeds the entire process and minimizes errors.

Professor James D. Winefordner at the University of Florida in Gainesville was a leading force in shaping the journal. He served for 21 years as Chairman of the Editorial Board, from 1984 until 2005. (See Tribute to James D. Winefordner, *Talanta*, 69 (2006) 533.) Jim's advice and leadership helped the journal to flourish and become one the leading journals in analytical chemistry. Over 1900 papers are now submitted each year, with acceptance rates of about 40%. *Talanta's* impact factor and immediacy index place it among the top journals in general analytical chemistry.

The success of the journal is due to the efforts of conscientious referees and editorial advisory board members, the submission of superior papers by researchers, and the readership. Our thanks to all!

We editors and the publishers are proud to celebrate 50 years of achievement, and look forward to continuing to serve the analytical sciences community.

G. Christian*
University of Washington, Department of Chemistry, Seattle, WA 98195-1700, United States

* Fax: +1 206 685 3478.
E-mail address: christian@chem.washington.edu

Available online 19 September 2007

Available online at www.sciencedirect.com
ScienceDirect
Talanta 74 (2008) 642–647
Talanta
www.elsevier.com/locate/talanta

Validation of an isotope dilution, ICP-MS method based on internal mass bias correction for the determination of trace concentrations of Hg in sediment cores

E. Ciceri [a], S. Recchia [a,*], C. Dossi [a], L. Yang [b], R.E. Sturgeon [b]

[a] *Department of Chemical and Environmental Sciences, University of Insubria, Via Valleggio 11, 22100 Como, Italy*
[b] *Chemical Metrology, Institute for National Measurement Standards, National Research Council Canada, Ottawa, Ontario K1A 0R6, Canada*

Received 9 February 2007; received in revised form 14 June 2007; accepted 25 June 2007
Available online 1 July 2007

Abstract

The development and validation of a method for the determination of mercury in sediments using a sector field inductively coupled plasma mass spectrometer (SF-ICP-MS) for detection is described. The utilization of isotope dilution (ID) calibration is shown to solve analytical problems related to matrix composition. Mass bias is corrected using an internal mass bias correction technique, validated against the traditional standard bracketing method. The overall analytical protocol is validated against NRCC PACS-2 marine sediment CRM. The estimated limit of detection is 12 ng/g. The proposed procedure was applied to the analysis of a real sediment core sampled to a depth of 160 m in Lake Como, where Hg concentrations ranged from 66 to 750 ng/g.
© 2007 Elsevier B.V. All rights reserved.

Keywords: ICP-MS; Hg determination; Sediments core; Trace determination

1. Introduction

In the past few decades mercury has become recognized as a hazardous heavy metal due to its neurotoxicity as well as unique properties with respect to migration and accumulation phenomena in trophic food chains. As a consequence, many studies have been devoted to the development of sensitive and accurate methods for the determination of Hg in biological and water samples [1–9]. Limits of detection (LODs) ranging from 0.024 to 14 ng/mL have been reported for the determination of Hg in water [10–14], with superior performance being achieved when cold vapor generation (CVG) is coupled to ICP-MS for detection [12,13]. In this respect, Yang et al.[14] achieved a LOD of 0.024 ng/L in water when CVG was coupled to a sector field ICP-MS and isotope dilution was used for calibration.

The determination of Hg concentrations in sediment cores is a problem of great environmental significance [15,16]. The vertical distribution of mercury, as well as those of other metals in sediments can, in fact, be regarded as an historical record of environmental changes. Various studies have shown that Hg concentration profiles in lake sediments can be effectively used to assess paleo contamination events [17–24] with the pre-industrial concentration usually considered as the background [25–28].

Such measurements pose a difficult analytical problem, mainly as a consequence of the complexity of the sediment matrix, where mercury is normally present as an ultra-trace constituent. For example, flame and electrothermal atomic absorption spectrometry (ET-AAS) are not used for this purpose because the detection limits with these techniques are too poor to address endogenous levels of the analyte. Occasionally, these techniques have been coupled with pre-concentration steps, such as amalgamation of mercury with gold, but this process may increase external contamination without yielding any improvement in the achievable LODs [1]. Cold vapor atomic absorption spectrometry (CV-AAS) and cold vapor atomic fluorescence spectrometry (CV-AFS) techniques achieve LODs on the order of 0.01 ng/mL. However, for reliable results, oxidation of organic matter is necessary for release of mercury from the matrix, followed by the quantitative production of a single labile mercury species [Hg(II)] and its quantitative reduction to Hg^0. As a consequence, the efficiency of cold vapor generation

* Corresponding author. Tel.: +39 0312386450; fax: +39 0312386449.
E-mail address: sandro.recchia@uninsubria.it (S. Recchia).

0039-9140/$ – see front matter © 2007 Elsevier B.V. All rights reserved.
doi:10.1016/j.talanta.2007.06.029

can be significantly influenced by the matrix composition [4,29,30].

Due to high sensitivity, ICP-MS techniques can, in principle, bypass the necessity of a pre-concentration step, thereby avoiding all problems associated with it. In fact, considering the reported background levels for Hg in cores of lake sediments, the utilization of any pre-concentration strategy is not mandatory with this technique.

The sensitivity for mercury may be significantly decreased by the presence of large amounts of concomitant elements such as iron, which is always present in such samples following mineralization. Quantitation of Hg is therefore more difficult using external calibration as the sample composition must be well-known and proper matrix corrections introduced. Although single and multiple additions methods can generally circumvent this problem, the low concentrations of Hg in lake sediment benefit significantly from application of robust isotope dilution (ID) calibration approaches. In this respect, sector field ICP-MS (SF-ICP-MS) is preferable to quadrupole-based instruments (q-ICP-MS) because the resulting flat-topped peak shape obtained in low resolution mode enables a more precise isotope intensity measurement to be achieved [31]. It should be noted that, as in the case for other calibration strategies, isotope dilution cannot compensate for random contamination which may occur during sample workup; intensive blank monitoring is thus always necessary [32]. However, once the correct addition of the spike solution has fully equilibrated with the sample, it is not necessary to quantitatively handle the sample in subsequent operations because the spike isotope (^{201}Hg) and the other isotopes (^{200}Hg and ^{202}Hg) respond to all effects in the same manner.

In this study, we have developed an analytical protocol for determination of Hg in sediments by ID SF-ICP-MS. Particular attention was paid to the applicability of a recently proposed technique for mass bias correction [8]. This technique, which is called *internal mass bias correction*, offers significant advantages over traditional bracketing or internal standard techniques because: (i) better precision is achieved since no machine time is spent recording external standard intensities or signals from other added isotopes, (ii) improved accuracy is possible as the technique is independent of any potential drift in mass-bias and (iii) this technique yields significantly higher productivity.

Validation of the entire analytical protocol was achieved by analysis of NRCC PACS-2 marine sediment CRM. In order to demonstrate the applicability of the proposed procedure to real samples, the mercury concentration profile in a sediment core sampled in Lake Como was determined and interpreted on the basis of atmospheric and anthropogenic emissions of mercury in the Northern Lombardy region of Italy.

2. Experimental

2.1. Instrumentation

A ThermoFinnigan Element2 SF ICP-MS instrument was used for the determination of mercury. Optimization of the instrument was performed as recommended by the manufacturer; operating conditions are summarized in Table 1.

Table 1
Operating conditions for ThermoFinnigan Element2 SF ICP-MS

Plasma power (RF) (W)	1150
Plasma Ar gas flow rate (L/min)	15.0
Auxiliary Ar gas flow rate (L/min)	1.05
Ar carrier gas flow rate (L/min)	1.15
Sampler cone (nickel) (mm)	1.00
Skimmer cone (nickel) (mm)	0.88
Lens voltage (V)	
Focus	−830
x-Deflection	−0.95
y-Deflection	1.60
Shape	105
Resolution	300
Points per peak	1
Dwell time (ms)	50
Passes	40
Mass window (%)	5
Runs	5
Dead time (ns)	16
Total time (min)	5

Several mercury isotopes, i.e., ^{200}Hg, ^{201}Hg and ^{202}Hg, were monitored. The dwell time and total time of analysis were adjusted to optimize the precision of the isotope ratio measurement using a 10 ng/mL standard solution of Hg. Dead time was determined using the approach of Nelms et al.[33] (method 2) wherein the ^{238}U/^{235}U ratio was measured in standard solutions at concentrations of 0.5, 1.0, 2.0 and 4.0 ng/mL. It must be recalled that, with this method, it is not necessary to know the isotope ratio of the standard. A dead time of 16 ns was derived from a plot of the measured ^{238}U/^{235}U ratios versus concentration of U.

2.2. Reagents and solutions

Samples and standard solutions were prepared and handled in a class-10 or class-100 clean room environment. High purity de-ionized water (DIW) was obtained from a NanoPure mixed bed ion exchange system fed with reverse osmosis domestic feed water. Nitric acid and hydrochloric acid were purified in-house prior to use by sub-boiling distillation of reagent grade feedstock in a quartz still.

A 0.2 mol/L BrCl solution was prepared in a fume hood by dissolving 27 g of KBr (Fisher Scientific, Nepean, Canada) in 2.5 L HCl then slowly adding 38 g of $KBrO_3$ while stirring.

Glass volumetric flasks (100 and 25 mL) with glass stoppers were used for preparation of samples and standards. After cleaning with dilute nitric acid and rinsing in high purity DIW, they were stored with 1% BrCl and rinsed with DIW immediately before use.

Standard solutions of uranium used for the determination of the dead time were prepared from a 10 ng/mL standard solution. A 10 ng/mL standard solution of Hg(II) containing 0.002 mol/L BrCl was prepared from a 14 mg/L stock solution. This diluted solution was used for optimization of the SF-ICP-MS and for mass bias correction.

"Natural abundance" high purity Hg metal was purchased from Johnson Matthey & Co. Ltd. (London, UK). A 1000 μg/g stock solution was prepared in 5% HCl. A working standard (1 μg/g) used for ^{201}Hg reverse ID was prepared by serial dilution of the stock in 2% HCl.

Enriched ^{201}Hg isotope (isotopic enrichment > 98.11 at.%) was purchased from Oak Ridge National Laboratory (Oak Ridge, TN, USA) as the metal. A 300 μg/g stock solution, prepared in 5% HCl, was serially diluted to prepare the working spike solution. Accurate concentration of the enriched spike was determined by reverse isotope dilution against the gravimetrically prepared natural abundance Hg standard.

2.3. Sediment core

During November 2002, a 130-cm long core was collected in Lake Como at a depth of about 160 m. The sediment core was dated based on measurements of ^{137}Cs, providing calculated sedimentation rates of approximately 0.22 cm/year to a depth of 3.5 cm (1986 Chernobyl reactor accident) and 0.3 cm/year in the range 3.5–10.5 cm depth (1963 nuclear test in the atmosphere) [34].

This core was conserved in a refrigerated room; 130 samples were prepared at approximately 1 cm intervals and dried at 40 °C for several days. The samples were collected from the interior of the core to avoid contamination from the external coring, and stored in pre-cleaned plastic vessels. Before analysis, the dried sediment samples were powdered in an agate mortar. All data are reported on a dry weight basis. Dry weight was established by treating a separate specimen of each sample at 70 °C until constant weight is achieved.

2.4. Sample preparation and ID calibration

All sample preparation was undertaken in a class 100 clean room or in class 10 fume cupboards as warranted. Approximately 0.25 g test portions of each sample of sediment (only 0.125 g for PACS-2) were weighed into individual pre-cleaned Teflon digestion vessels. After the addition of suitable amounts of ^{201}Hg-enriched isotope standard, 5 mL of nitric acid were added. The amount of enriched spike solution added was determined from an earlier estimate (roughly quantified by external calibration using three different segments of the real sediment core) of the concentration of mercury in the samples such as to provide for an approximately unit ratio in the measured intensities of the two isotopes in question. Two sample blanks were also prepared concurrently but with the addition of only 10% of the amount of enriched isotope standards used for the sample.

Samples and blanks were then digested in a CEM MDS-2100 microwave oven using the heating program outlined in Table 2.

After cooling, 0.5 mL volumes of the digestion solution along with 0.2 mol/L BrCl were transferred to pre-cleaned 25 mL volumetric flasks and diluted to 25 mL with DIW prior to analysis.

Six reverse spike isotope dilution calibration samples were prepared to quantify the concentration of the diluted enriched ^{201}Hg spike (Hg estimated concentration 0.2538 μg/g). A 0.1 g aliquot of enriched spike and 0.12 g of the 1 μg/g natural abundance Hg standard solution were accurately weighed into a pre-cleaned glass volumetric flask. The resulting solutions were then diluted to 25 mL with 0.002 mol/L BrCl [9] to oxidize all forms of mercury to soluble Hg(II) species and to minimize memory effects in the spray chamber. Accordingly, the mercury signal could be reduced to its baseline level in a few minutes by washing with a solution of 0.002 mol/L BrCl; this approach was used as a washing step following the introduction of each sample and standard.

Table 2
Heating program for microwave assisted digestion of sediment

Time (min)	Pressure (psi)	Power (%)
5	20	60
5	40	60
15	80	70
20	120	70
25	120	70

The ^{202}Hg/^{201}Hg and ^{200}Hg/^{201}Hg reference spike isotope pairs were used for analysis.

The total concentration of mercury in the sediment samples was determined by ID calibration coupled with blank correction in accordance with the following "double ID" equation, which simultaneously permits quantitation of the enriched spike:

$$C_x = C_z \frac{m_y}{m_x} \frac{m_z}{m'_y} \frac{A_y - B_y R_m}{B_{xz} R_m - A_{xz}} \frac{B_{xz} R'_m - A_{xz}}{A_y - B_y R'_m} - C_b \quad (1)$$

where C_x is the final blank corrected analyte concentration in the sample (μg/g), C_z the concentration of mercury in the primary standard (μg/g), m_y the mass of spike solution used to prepare the sample and spike mixture (g), m_x the test mass of sample used (g), m_z the mass of primary standard used (g), m'_y the mass of spike used to prepared the of spike and primary assay standard mixture (g), A_y the abundance of reference isotope in the spike, B_y the abundance of the spike isotope in the spike, A_{xz} the abundance of reference isotope in the sample or primary assay standard, B_{xz} the abundance of spike isotope in the sample or primary assay standard, R_m the measured reference/spike isotope ratio in the mixed solution of sample and spike, R'_m the measured reference/spike isotope ratio in the mixed solution of spike and primary assay standard and C_b is the blank concentration normalized to a sample weight (μg/g).

3. Results and discussion

3.1. Matrix effects and ID calibration

Mercury in sediments must be regarded as a micro-component in this complex matrix. Taking into account that iron is one of the most abundant of matrix elements in these cores, the dependence of the signal for Hg on the presence of Fe was initially examined to establish whether an ID calibration protocol was necessary. Fig. 1 shows the raw intensities for blank and standard solutions containing 3 ng/mL of Hg in the presence and absence of 10 μg/mL of Fe. An Fe concentration of 10 μg/mL was chosen based on the evidence that real sedi-

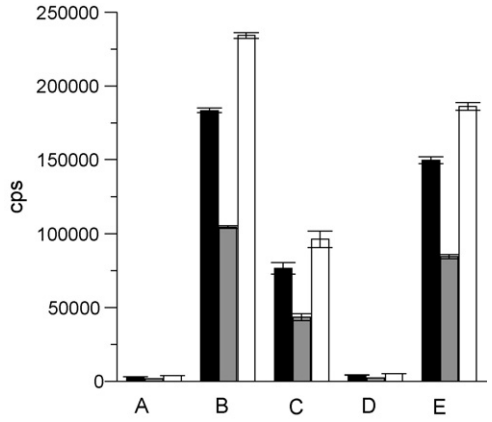


Fig. 1. ^{200}Hg (black), ^{201}Hg (grey) and ^{202}Hg (white) raw-signal intensities arising from sequentially introduced solutions: A, blank solution; B, Hg(II) std. solution (3 ng/mL); C, Hg(II) std. solution (3 ng/mL) in the presence of Fe(III) (10 μg/mL); D, blank solution; E, Hg(II) std. solution (3 ng/mL).

ments coming from Lake Como usually contain 20–50 mg/g of iron [35], which means a final Fe concentration in digested solutions between 20 and 50 μg/mL, whereas Hg in such solutions (as shown later in this study) is usually below 1 ng/mL. In this situation, which probably represents one of the most favorable cases (i.e., with very low Fe concentrations and very high Hg), it can be clearly seen that about a 65% loss of signal intensity occurs in the presence of iron and that a memory effect is also visible when introducing the subsequent iron-free Hg standard. Although a ubiquitous contaminant, Fe is not typically known as an element that is difficult to remove from sample introduction systems. Memory effects could be tentatively explained assuming that its very high concentration does not allow a rapid restoration of the initial conditions. In any case, this effect was accepted at face value and not investigated further; it simply provided additional evidence of the need for ID calibration as opposed to external calibration for the determination of Hg. The Hg isotopic ratios, calculated directly from the raw data reported in Fig. 1, are completely independent of the presence or absence of iron (see Table 3) because the relative sensitivity of the various Hg isotopes is a mass-independent parameter, as expected. This was also verified (see the bottom of Table 3) for solutions having a lower Hg concentration and an Fe concentration of 50 μg/mL, which simulates the maximum expected Fe content in our samples.

Although effects of matrix composition on mass discrimination cannot be ruled out, the data in Table 3 indicates that these effects are of minor importance, since their impact on the precision attainable with a single-collector mass spectrometer is fully acceptable. This evidence suggests that an ID calibration method can be successfully developed, despite the suppressive interference effect from iron being particularly severe.

3.2. Mass bias correction

With ID, good precision and accuracy in the measurement of the selected isotope pairs plays a fundamental role in the quality of the final result. Poor accuracy is obtained if mass bias (or mass discrimination) effects are not adequately corrected.

Table 3
Effect of presence of Fe in solution on calculated isotope ratios

	^{200}Hg/^{201}Hg	^{202}Hg/^{201}Hg
Hg(II) 3 ng/mL	1.7502	2.2560
S.D.	0.00089	0.0016
R.S.D. (%)	0.051	0.072
Hg(II) 3ng/mL + Fe(III) 10 μg/mL	1.7504	2.2547
S.D.	0.0011	0.0017
R.S.D. (%)	0.063	0.079
Hg(II) 3 ng/mL after	1.7500	2.2513
S.D.	0.0012	0.0014
R.S.D. (%)	0.070	0.065
Hg(II) 0.5 ng/mL + Fe(III) 50 μg/mL	1.7505	2.2544
S.D.	0.0030	0.0032
R.S.D. (%)	0.17	0.14
Hg(II) 0.5 ng/mL after	1.7504	2.2538
S.D.	0.0014	0.0015
R.S.D. (%)	0.080	0.066

S.D. and R.S.D.s refer to 10 replicates.

Mass bias causes a systematic deviation of the measured isotope ratio from the true value due to the differential transmission of the instrument of different isotopes of the same element [36], with the heavier ones being better transmitted than the lighter. In order to correct for this effect, an external calibration is normally used. With this method, the mass bias factor (f) is determined from the true ratio (R^{true}) divided by the experimentally determined ratio (R^{obs}) measured using a stable natural abundance standard solution:

$$f = \frac{R^{\text{true}}}{R^{\text{obs}}} \tag{2}$$

The isotope ratios measured for the samples are then corrected using the following equation:

$$R^{\text{corr}}_{\text{sample}} = fR^{\text{obs}}_{\text{sample}} \tag{3}$$

Hg concentrations are thus calculated with Eq. (1), using these mass bias corrected ratios instead of uncorrected ones. Considering that the differential transmission of masses potentially drifts over the duration of experiment, and that the quality of the data obtained with ID calibration is primarily dependent on the accuracy of the measurement of isotope ratios, the mass bias factor must be periodically determined during the measurement of samples [9,14]. As a consequence, a standard bracketing sequence is usually adopted, leading to low throughput due to frequent repetition of standard measurements.

Rodrìguez-Gonzàlez et al. [8] have recently proposed an alternative method for mass bias correction based on internal standardization. This method utilizes measurement of both the ^{202}Hg/^{201}Hg and the ^{200}Hg/^{201}Hg ratios which are influenced by mass bias in a converse way. Assuming that mass discrimination effects are constant over the narrow mass range from m/z 200 to 202, the concentration of mercury can be directly obtained using the average of the two measured concentrations, calcu-

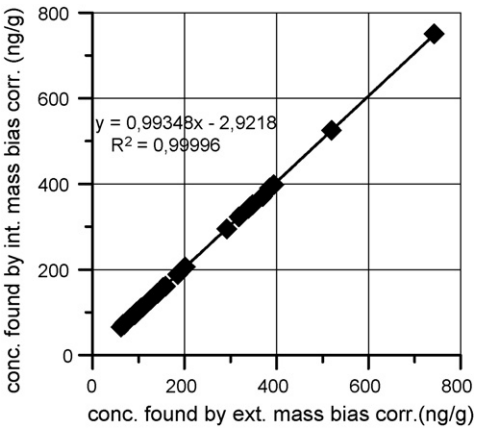


Fig. 2. Comparison of data obtained with external mass bias correction using $^{202}Hg/^{201}Hg$ and internal mass bias correction using the average of $^{202}Hg/^{201}Hg$ and $^{200}Hg/^{201}Hg$.

lated with Eq. (1), applied to the two isotopes pairs. It should be noted that in this case, R^{obs} rather than R^{corr} are used in Eq. (1).

Both procedures were used and compared in this study. Fig. 2 shows a comparison of the data obtained based on external mass bias correction using the $^{202}Hg/^{201}Hg$ and internal mass bias correction using the average of $^{202}Hg/^{201}Hg$ and $^{200}Hg/^{201}Hg$. The slope of the regression line is close to unity, the intercept is approximately zero and the r^2 factor is 0.9999. Results obtained using internal calibration are not statistically different from those obtained using the traditional protocol based on external calibration. Moreover, any drift in the mass bias is better compensated for with the internal calibration protocol since the two ratios are measured almost simultaneously.

3.3. Validation of the method

For method validation, four replicate measurements of NRCC CRM PACS-2 marine sediment CRM were compared with the certified value. A calculated mean ($n = 4$) value of 3.07 ± 0.22 ($2s_m$) mg/kg compares well with the certified value of 3.04 ± 0.20. Neither spectral nor matrix interference effects were found to affect the accuracy of the analytical data using the developed protocol.

The reproducibility of the analytical procedure was estimated from results for three real samples; for each sample, three independent measurements in three different sample measurement sessions were obtained using the same experimental conditions from the digestion to the analysis. The concentrations and relative standard deviations found in these samples are summarized in Table 4.

Table 4
Analytical results for three samples

Sample	Concentration (mg/kg)	S.D.($2s_m$)	R.S.D. (%)
2_115 ($n = 3$)	0.1084	0.0050	4.6
2_9 ($n = 3$)	0.3823	0.0018	0.3
2_35 ($n = 3$)	0.1061	0.00080	0.8

As can be seen, the R.S.D.s are always less than or equal to about 4%, from which it may be concluded that the reproducibility of this procedure is adequate for the analysis of low concentrations of mercury, such as those found in core sediments from Lake Como (see later). The variability of the reported uncertainties could be ascribed, as mentioned earlier, to differences in signal suppression caused by the presence of different quantities of iron.

The procedural limit of detection (LOD) was estimated based on three times the standard deviation of the mean concentration of mercury determined in eight replicated blank measurements following the same analytical protocol used for the analysis of samples. A value of 12 ng/g was obtained.

3.4. Hg profile for the Lake Como core

The validated procedure developed in this study was applied to the determination of the mercury concentration profile in a sediment core sampled in Lake Como. Mercury concentrations in the core ranged from 66 to 750 ng/g and are reported in Fig. 3. In the deepest part of the core, the average mercury concentration is found to be about 120 ng/g. The concentrations found in these strata are similar to the pre-industrial (before 1850) ones in European and American lake sediments [37]. This contamination can be dated back, assuming an approximately constant sedimentation rate to the beginning of the 19th century. The increase in mercury after the 'industrial revolution' has already been reported by many research groups around the world [38,39] in lake sediments [40–42], peat bogs [21] and ice samples from the Artic, Antarctica and Alpine glaciers [43,44]. Prior to the introduction of the regulatory controls for mercury emissions, inorganic Hg and organomercurials were used in a wide variety of industrial applications: as catalysts; in the chlor-alkali industry; in the pulp and paper industry; in

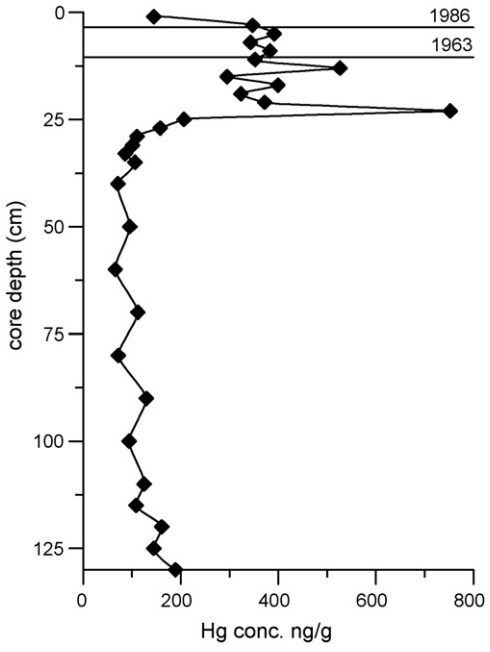


Fig. 3. Mercury concentration profile in the sediment core of Lake Como.

batteries, paints and pharmaceuticals [45]. As many of these uses of Hg and organomercurials were banned in Europe, the USA and other countries, industries were prompted to develop alternative methods that do not rely on use of Hg. This practice has resulted in an overall decrease in the direct discharge of Hg to the aquatic environment. Since the introduction of regulatory controls, other sources of anthropogenic mercury emission have substantially changed raking among the remaining source categories. Currently, coal burning and waste incineration (of municipal refuse, medical waste and sewage sludge) have been identified as the primary anthropogenic sources of atmospheric Hg in the industrialized world [46,47].

Such a decrease in the mercury concentrations is also found in the investigated core sample. In fact, the concentration of Hg decreases in the very last strata; reaching a value of 140 ng/g in the upper part of the core. This concentration is similar to the levels found in the pre-industrial region of the same core and could be an indication of the positive effect of recently started sewage treatment plants, together with the introduction of more stringent legal regulation on the use and the discharge of mercury [12].

4. Conclusions

The main goal of this study was to investigate the suitability of an ID protocol for the development of a robust method for the determination of mercury in sediment cores. Application of many other analytical techniques can be ruled out for these samples because of the combined effects of the complex matrix, its variation between layers and the very low Hg levels. The results obtained in this study prove that the proposed method is appropriate for the trace analysis of mercury in sediments; applicability to other complex environmental matrices such as peat bogs, biological samples and fish tissues is clear. Utilization of a cold vapor enrichment step is not necessary, since the estimated LOD is sufficiently low for such samples.

The data obtained characterizing the Lake Como sediment core suggest that mercury was principally released into the environment after the 'industrial revolution' in the early 19th century and continued until the last 20–30 years.

References

[1] G.S. Walker, M.J.G. Ridd, J. Brunskill, Rapid Commun. Mass Spectrom. 10 (1996) 96.
[2] F.X. Han, W.D. Patterson, Y. Xia, B.B.M. Sridhar, Y. Su, Water Air Soil Pollut. 170 (161) (2006).
[3] R.G. Smith, Anal. Chem. 65 (1993) 2485.
[4] J. Murphy, P. Jones, S.J. Hill, Spectrochim, Acta B 51 (1996) 1867.
[5] J. Yoshinaga, M. Morita, J. Anal. Atom. Spectrom. 12 (1997) 417.
[6] D.R. Evans, H. Hintelmann, P.J. Dillon, J. Anal. Atom. Spectrom. 16 (2001) 1064.
[7] J.L. Manzoori, M.H. Sorouraddin, H.A.M. Shabani, J. Anal. Atom. Spectrom. 13 (1998) 305.
[8] P. Rodríguez-González, J. Ruiz Encinar, G.I.J. Alonso, A. Sanz-Medel, J. Anal. Atom. Spectrom. 17 (2002) 824.
[9] L. Yang, R.E. Sturgeon, J. Anal. Atom. Spectrom. 18 (2003) 1452.
[10] J. Allibone, E. Fatemian, P.J. Walker, J. Anal. Atom. Spectrom. 14 (1999) 235.
[11] B. San Vicente de la Riva, J.M. Costa-Fernández, W.J. Jin, R. Pereiro, A. Sanz-Medel, Anal. Chem. Acta 455 (2002) 179.
[12] J.L. Mann, S.E. Long, C.A. Shuman, R.W. Kelly, Water Air Soil Pollut. 163 (2005) 19.
[13] J.L. Mann, S.E. Long, R.W. Kelly, J. Anal. Atom. Spectrom. 16 (2003) 1293.
[14] L. Yang, S. Willie, R.E. Sturgeon, J. Anal. Atom. Spectrom. 20 (2005) 1226.
[15] S.M. Klein, L.A. Jacobs, Water Air Soil Pollut. 80 (1995) 1035.
[16] R.D. Evans, Arch. Environ. Contam. Toxicol. 15 (1986) 505.
[17] H. Yang, N.L. Rose, Sci.Total Environ. 304 (2003) 391.
[18] I. Renberg, Hydrobiologia 143 (1986) 379.
[19] M. Verta, K. Tolonen, H. Simola, Sci. Total Environ. 87/88 (1989) 1.
[20] A.C. Heyvaert, J. Reuter, D.G. Slotton, C.R. Goldman, Environ. Sci. Technol. 34 (2000) 3588.
[21] P.P. Madsen, Nature 293 (1981) 127.
[22] A.L.W. Kemp, J.D.H. Williams, R.L. Thomas, M.L. Gregory, Water Air Soil Pollut. 10 (1978) 381.
[23] M.H. Hermanson, Water Air Soil Pollut. 101 (1998) 309.
[24] P.F. Schuster, D.P. Krabbenhoft, D.L. Naftz, D.L. Cecil, M.L. Olson, J.F. Dewild, D.D. Susong, J.R. Green, M.L. Abbott, Environ. Sci. Technol. 36 (2002) 2303.
[25] M. Lucotte, A. Mucci, C. Hillaire-Marcel, P. Pichet, A. Grondin, Water Air Soil Pollut. 80 (1995) 467.
[26] D.R. Engstrom, E.B. Swain, Environ. Sci. Technol. 31 (1997) 960.
[27] W.L. Lockhart, P. Wilkinson, B.N. Billeck, R.A. Danell, R.V. Hunt, G.J. Brunskill, J.V. Delaronde, St. Louis, Biogeochemistry 40 (1998) 163.
[28] W.F. Fitzgerald, Water Air Soil Pollut. 80 (1995) 245.
[29] D.L. Nunes, E. Pereira de Santos, J.S. Barin, S.R. Mortari, V.L. Dressler, E. Marlon de Moraes Flores, Spectrochim. Acta B 60 (2005) 731.
[30] I. Rokkjer, B. Hoyer, N. Jensen, Talanta 40 (1993) 729.
[31] L. Yang, Z. Mester, R.E. Sturgeon, J. Anal. Atom. Spectrom. 18 (2003) 1365.
[32] L. Yang, R.E. Sturgeon, J. Anal. Atom. Spectrom. 20 (2005) 724.
[33] S.M. Nelms, C.R. Quétel, T. Prohaske, J. Vogl, P.D.P. Taylor, J. Anal. Atom. Spectrom. 16 (2001) 333.
[34] PhD Dissertation Thesis, Daniela Fanetti University of Insubria, Italy, 2005.
[35] G. Parise, G. Paleologo, G. Premazzi, P. Pulici, A. Riva, T. Ruaro, Eur. Appl. Res. Rept.-Environ. Res. Sect. 1 (1981) 385.
[36] I.S. Begley, B.L. Sharp, J. Anal. Atom. Spectrom. 12 (1997) 395.
[37] L. Håkansson, Water Res. 14 (1980) 975.
[38] H.R. Von Gunten, M. Sturm, R.N. Moser, Environ. Sci. Technol. 31 (1997) 2193.
[39] J.O. Nriagu, J.M. Pacyna, Nature 333 (1988) 134.
[40] C.P. Gubala, D.H. Landers, M. Monetti, M. Heit, T. Wade, B. Lasorsa, S. Allen-Gil, Sci. Total Environ. 160/161 (1995) 347.
[41] W.R. Schell, M.J. Tobin, C.D. Massey, Sci. Total Environ. 87/88 (1989) 19.
[42] M. Wessels, A. Lenhard, F. Giovanoli, A. Bollhöfer, Aquat. Sci. 57 (1995) 291.
[43] C.F. Boutron, U. Görlach, J.P. Candelone, M.A. Bolshov, R.J. Delmas, Nature 353 (1991) 153.
[44] C.F. Boutron, J.P. Candelone, S. Hong, Geochim. Cosmochim. Acta 58 (1994) 3217.
[45] P.J. Craig, Organomercury Compounds in the Environment, in: P.J. Craig (Ed.), Organometallic Compounds in the Environment, Longman, Essex, 1986, pp. 65–110.
[46] E.G. Pacyna, J.M. Pacyna, Water Air Soil Pollut. 137 (2002) 149.
[47] D.B. Porcella, C. Ramel, A. Jernelov, Water Air Soil Pollut. 97 (1997) 205.

Available online at www.sciencedirect.com
ScienceDirect
Talanta 74 (2008) 922–929
Talanta
www.elsevier.com/locate/talanta

The use of microspectrofluorimetry for the characterization of lake pigments

Ana Claro [a,b], Maria J. Melo [a,b,*], Stephan Schäfer [b], J. Sérgio Seixas de Melo [c], Fernando Pina [a], Klaas Jan van den Berg [d,**], Aviva Burnstock [e]

[a] *REQUIMTE-CQFB and Faculty of Sciences and Technology of the New University Lisbon, Campus da Caparica, Portugal*
[b] *Department of Conservation and Restoration, New University Lisbon, Campus da Caparica, Portugal*
[c] *Department of Chemistry, University of Coimbra, Coimbra, Portugal*
[d] *ICN-Instituut Collectie Nederland, Netherlands Institute for Cultural Heritage, P.O. Box 76709, Amsterdam, Netherlands*
[e] *Department of Conservation and Technology, Courtauld Institute of Art, Somerset House, London WC2R ORN, United Kingdom*

Received 8 December 2006; received in revised form 30 March 2007; accepted 30 July 2007
Available online 11 August 2007

Abstract

In this paper, the potential of confocal microfluorescence spectroscopy is explored for the characterization of selected red lake pigments and paints based on alizarin, purpurin and eosin (weak, medium and strong emitters). The anthraquinone pigments have been used since ancient times by artists, and eosin lakes were used by impressionist painters. Reconstructions of artists paints based on 19th century recipes are examined. The paints were made using the lake pigments bound in a range of binding media including gum arabic, collagen, a vinyl emulsion and linseed oil. The acquisition of the spectra is rapid, with high spatial resolution and the data reliable and reproducible. Together with full emission spectra, it was possible to acquire well-resolved excitation spectra for purpurin, alizarin and eosin based colors. The present investigation suggests that micro-emission fluorescence can also be used as a semi-quantitative method for madder lake pigments, enabling the determination of purpurin lake ratio in a mixture of purpurin and alizarin, which is important for provenance studies. The data obtained with microfluorescence emission with those acquired with fiber-optic fluorimetry are compared. The spatial resolution used, 8 μm, is appropriate for the analysis of individual pigments particles or aggregates in a paint film. Micro-emission molecular fluorescence proved to be a promising analytical tool to identify the presence of selected red lake pigments combined with a range of binding media.
© 2007 Elsevier B.V. All rights reserved.

Keywords: Red lake pigments; Microfluorescence spectroscopy; *In situ* dye analysis

1. Introduction

Anthraquinones and their hydroxy derivatives have been used as red dyes since pre-historic times [1] (Fig. 1), and there are written accounts of their use in ancient Egypt [2]. These red chromophores were extracted from the roots of a variety of plant from the Rubiaceae family (madder family) [1a,3], being alizarin and purpurin the major occurring species in *Rubia tinctoria* L. (Fig. 1). Purpurin and alizarin have been classified among the organic dyes most resistant to light-induced fading [4]. Recent identification of these dyes in more than 1000-years-old archaeological textiles has confirmed this [3]. The red extracts were also prepared to use as a pigment for painting, by precipitating the extract in solution with aluminum salts, such as alum. The pigments were known as "lakes". Madder lake, a mixture of alizarin and purpurin lakes, was widely used in manuscript illuminations [5] and paintings, and is still in use as an artists' material. More recently, these molecules (as chromophores) have found new and high-tech applications, namely in solar energy conversion and development of new imaging materials [6].

During the last decades of the 20th century, there has been a comprehensive body of published work on the physical-chemistry and chemical properties of hydroxy, amino and acylamino derivatives, including significant contributions to the field by Salem and Zewail [7], Gillispie and Marasinghe [8]

* Corresponding author at: Department of Conservation and Restoration, New University Lisbon, Campus da Caparica, Portugal. Tel.: +351 21 294 83 22; fax: +351 21 294 83 22.
** Corresponding author. Tel.: +31 20 3054710; fax: +31 20 3054700.
E-mail addresses: mjm@dq.fct.unl.pt (M.J. Melo), Klaas.Jan.vd.Berg@icn.nl (K.J. van den Berg).

0039-9140/$ – see front matter © 2007 Elsevier B.V. All rights reserved.
doi:10.1016/j.talanta.2007.07.036

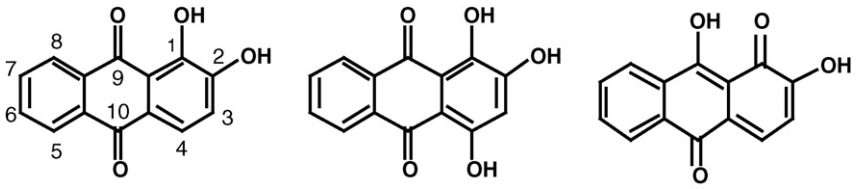


Fig. 1. Alizarin (1,2-dihydroxy anthraquinone), purpurin (1,2,4-tri-hydroxy anthraquinone) and the 1,10 keto tautomer of alizarin, T. Both, alizarin and purpurin are 9,10 quinones.

and Smith and Barbara [9]. The acidochromic effects in the excited state properties, for purpurin and alizarin, have been recently studied by Favaro and Milliani [10]. From these studies it has been concluded that the substitution pattern of hydroxy anthraquinones determines their excited state properties, where efficient radiationless processes, such as excited state proton transfer (ESPT) and excited state intra- and intermolecular proton transfer (ESIPT) play a determinant role in the overall stability of the molecules; it was shown that the excited-state surface can be sensitively controlled by substituents, allowing the formation of a 1,10 keto tautomer, T*, which ratio (compared to the excited 9,10) can be varied at least two orders of magnitude (Fig. 1); the ESIPT process can be extremely rapid (<300 fs) and was believed to involve proton tunneling [9b]. ESPT and ESIPT with excited state tautomer formation can be considered to induce a photoprotective mechanism for the molecule, enabling a very fast and effective dissipation of the excess energy of the excited state. Light is absorbed; an excited state tautomer is formed (involving an adiabatic proton transfer), and will decay with recovery of the initial ground state molecule. Such photoprotection mechanisms, where energy is absorbed and released by radiationless processes involving H bond breaking and formation in the excited state, are widely used for UV screeners.

Moreover, the hydroxy derivatives are multi acid–base equilibria systems, *interconvertible* by pH inputs (Scheme 1) [10]. Therefore, in the ground state the system is easily characterized through the acid–base equilibrium constants, pK_a, but in the excited state the acid–base equilibria are found to compete with intra- and intermolecular proton transfer (ESIPT) [8–10].

The formation of an excited 1,10 keto tautomer, T*, (Fig. 1) was observed in α-hydroxyanthraquinones which lack the 1,4-substitution pattern, and the dyes are all weak emitters [8,9]. On the other hand, in the presence of a 1,4-substitution pattern, the fluorescence quantum yield was found to be moderate to high

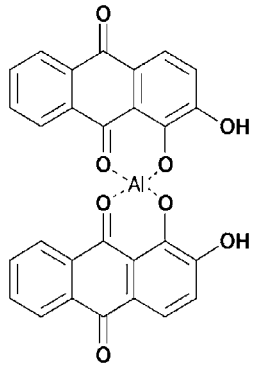
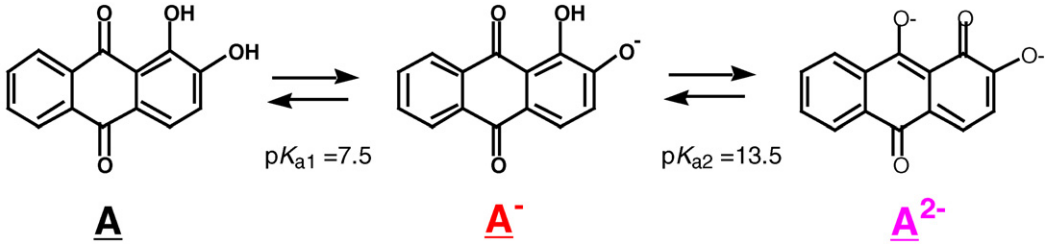


Fig. 2. Molecular structure for an Al^{3+}:alizarin 1:2 complex.

[8a]. The above results are consistent with purpurin acting as a moderate emitter (no ESIPT) and alizarin a very weak one (EISPT present) [8–10]. The fact that ESIPT is suppressed in the case of the 1,4-hydroxy substitution is an intriguing result, and a possible explanation was already proposed by Gillispie in 1984, based on the existence of six-membered *pseudo*-ring created by the intramolecular hydrogen bonds: "In the 1,4-substituted compounds there are two such rings which can interact conjugatively through their common outer ring of the anthraquinone skeleton. Probably this leads to a stabilization of the 9,10-keto form in the S_1 (first excited singlet state) sufficiently strong to make ESPT energetically unfavourable" [8a].

While there is significant data from studies of anthraquinone derivatives in solution, less is known about the excited state properties of red lakes (Fig. 2) in the solid state [11]. This is important as these complexes are used for textiles, manuscript illuminations, paintings and other objects that make up cultural heritage. Identification of these materials in art objects, and characterization of their deterioration are of great importance to historians and conservators. However, the fugacity of these materials and the difficulty in obtaining samples for



Scheme 1.

analysis may explain why they have received relatively little attention in the literature. Other important red lake pigments are eosin and other fluorescent lakes, that were synthesized in the 19th century, and were used as a pigment for paintings, for example by post-impressionist painter Vincent van Gogh. Eosin lakes are particularly unstable and fade on exposure to light sometimes within a few years (sometimes during the artists' lifetime) [12]. Changes in pigments, whether used pure or mixed with other pigments can alter the appearance of a painting significantly. The identification and state of degradation of lake pigments, in paintings is of fundamental interest since it provides critical information about the artists' aesthetic perspective, conceptions and choices, and how the work has changed with time. Therefore, it is desirable to develop methods that can characterize these materials non-invasively or from small samples that are infrequently available from works of art.

In this paper, the potential of confocal microfluorescence spectroscopy for the characterization of selected red lake pigments and paints based on alizarin, purpurin and eosin is examined. Analytical techniques based on fluorescence detection were selected to take advantage of the opportunity for high sensitivity and selectivity, combined with good spatial resolution [13]. Using fluorescence microscopy in confocal configuration an excitation area of 0.2–0.3 μm can be defined for visible radiation with the advantage of similar resolution in three-dimensions [13a]. Fluorescent molecules can also be used to probe and characterize their environment, which is one of the reasons for their popularity in biochemical and pharmaceutical applications and in medicine, for monitoring of species of clinical relevance. Although analytical techniques based on fluorescence detection are widely used, this paper is the first to investigate the potential for emission fluorescence microspectroscopy for the study of red lakes, with the possibility of acquisition of emission and excitation spectra. In the present study, spectra obtained with microfluorescence emission are compared with those acquired using fiber-optic fluorimetry, a set-up currently used in a variety of applications namely, in transportable spectrofluorimeters. Reconstructions of artists' paints made with red lake pigments bound in linseed oil, based on 19th century recipes were examined. Additional test paints were made using the same lake pigments bound in a range of binding media including gum arabic, collagen, PVAc (a vinyl emulsion). Samples were prepared on different supports, including paper and melinex, glass slides and sapphire cells.

A recently commercialized microSPEX spectrofluoremeter (Spex® FluoroMap) was used, that offers the possibility to acquire complete steady-state fluorescence spectra *in situ*, from samples placed directly on a programmable $x-y-z$ microscope stage. Fluorescence from the sample is directed back up into the microscope. It is also possible to view the fluorescence directly, through a binocular eyepiece and a digital camera. Beam splitting, that enables the separation of emission and excitation light, is achieved using dichroic filters [14]. The optimal conditions for the acquisition of the steady-state spectra will be discussed.

2. Experimental

2.1. Materials

For the historic reconstructions distilled water, reagent grade chemicals, Madder ground root from Kremer and Eosin, Meister Lucius and Brüning, ICN-reference collection, inv. no. 4328 were used. Linseed oil was obtained from organic linseeds, and prepared as described elsewhere [12].

2.2. Preparation of the samples

The set of samples prepared to test the technique can be divided in two categories, model samples and historic reconstructions; in the first category, purpurin and alizarin lakes were bound in each of the following media: gum arabic, parchment glue (collagen) and PVAc emulsion. Lakes made using known ratios of alizarin and purpurin were also set; this is important, because in madder lakes, obtained from natural sources, the ratio between purpurin and alizarin is dependent on the species and methods of preparation. Historic reconstructions were made following 19th century English and French recipes [15], for the red lake pigments, which were then made into linseed oil paints, similar to paints that were found in paintings by Van Gogh [12]. A complete description of the procedures used can be found in the "Supplementary information".

2.3. Absorption spectroscopy and fluorescence emission measurements

UV–vis absorption spectra were recorded on a Shimadzu UV-2501PC or Cary 100 Bio spectrophotmeter and fluorescence spectra were acquired using a Jovin-Yvon Spex Fluorog 3-2.2 spectrofluorometer. For the measurements with the optic-fiber a SPEX Model F-3000 fiber-optic adaptor was used, and the signal optimized as recommended by the manufacturer. Measurements with the microSPEX (Spex® FluoroMap with Manual Microscope Stage) were obtained with a set-up described elsewhere [14], where the Spex Fluorog 3-2.2 is hyphened to a Olympus BX51M confocal microscope, with spatial resolution controlled with multiple-pinhole turret (pinholes 1–10 corresponding to 2–60 μm spot with a 50× objective). For steady-state fluorescence spectra, a continuous 450 W xenon lamp, providing an intense, broad spectrum from the UV to near-IR, is directed into a double-grating monochromator. Monochromatic light from the monochromator is fed across a spectrofluorometer-microscope interface into a multiple-pinhole turret of the Olympus BX51 confocal microscope. The incident excitation beam is directed onto the sample, resting on a programmable $x-y-z$ microscope stage. Fluorescence from the sample is directed back up into the microscope. To view the sample's fluorescence directly, a binocular eyepiece and a digital camera are available. Beam-splitting is obtained with dichroic filters; standard dichroic filters, 1-in. diameter (25 mm), of 478 nm, 510, 500 (Glen Spectra) and 570 nm were used at 45°; they reflect the short wavelengths (excitation) and transmit the long wavelengths (emission). The

optimization of the signal, through mirror alignment in the optic pathway of the microscope, was performed daily, for all the pinhole apertures, following the manufacturer instructions.

Fluorescence spectra, in homogeneous media, were corrected for the wavelength response of the system; for all the solid state measurements uncorrected spectra are presented. The absorption and emission measurements, in homogeneous media, were performed with 5×10^{-5} M for alizarin/purpurin and with 2×10^{-6} M solutions for the respective lakes. The fluorescence quantum yield for the lakes were determined using purpurin as standard ($\phi_f = 0.004$ in MeOH:H_2O (75:25, v:v); the fluorescence quantum yield of purpurin was obtained by comparison with a fluorescein standard solution ($\phi_f = 0.79$ in 0.1 M NaOH) [16]. The ϕ_f value for the purpurin compares well with previously published values, using quinine sulphate as standard [10].

In heterogenous media, for the microSPEX, spectra were acquired after focusing, and for the optic fiber by gentle contact through a black o-ring.

Spectroscopic or equivalent grade solvents and Millipore filtered water were used for all the spectroscopic studies.

The pH of the solutions was measured with a Metrohm 713 pH meter or a MetLab pHM240. Calibration was performed with a set of Metrohm buffers of pH 4.00 and 7.00. Adjustment of the desired pH values was accomplished by addition of $HClO_4$ or NaOH.

Moreover, when studying the fluorescence emission of purpurin and alizarin, the greatest care had to be taken to avoid contamination by metal ions that are able to form fluorescent complexes with the anthraquinone hydroxy derivatives. Low concentration of metal ions, such as 10^{-6} M may induce a significant contribution in the global fluorescence emission in solution where purpurin concentration is typically $\approx 10^{-6}$ to 10^{-7} M. Hence, it is advisable to not use toilet paper or analogous for the cleaning of the pH electrode or other glassware as it contains a large amount of Al^{3+} ions. In alternative, use filter paper. Also, when studying alizarin lake care should be taken to avoid contamination with purpurin lake, as the excitation and emission spectra are quite similar, since the purpurin lake emission quantum yield is 40 times that of alizarin lake (see below).

3. Results and discussion

The results obtained with the historic reconstructions, the paint samples made to resemble 19th century paints, and other model samples will be presented and discussed.

3.1. Aqueous, homogeneous media

As there are no comparable published results from studies of the photophysics of the aluminum complexes in solution, a brief study was carried out for purpurin and alizarin in the presence of aluminum ion, Al^{3+}. The alizarin lake is an aluminum two-ligand complex, in which the Al atom co-ordinates two dye molecules through the 1-hydroxy oxygen and the adjacent carbonyl oxygen (Fig. 2), forming a six-membered chelate ring structure [17]. Excitation and emission spectra were obtained to be used as reference guides to the understanding of the solid-state behaviour of the paint models (Fig. 3). Fluorescence quantum yields, for the Al^{3+} chelates, were also obtained and are reported in Table 1, where they can be compared to fluorescence quantum yields of the neutral forms of the respective free chromophores in solution. As expected for fluorogenic ligands where the metal chelates are much more fluorescent than the free ligands themselves [18], the aluminum complexation enables more than a 10-fold increase in the ϕ_f values; the ϕ_f of the alizarin aluminum complex compares with the emission quantum yield of neutral form of purpurin, and the purpurin lake displays the strongest emission, and may be considered a moderate to strong emitter. Moreover, the spectra represented in Fig. 3A show a reasonably good mirror-image relationship between the excitation and emission spectra for the purpurin complex, with small Stokes' shift, which can reflect the absence of ESIPT processes.

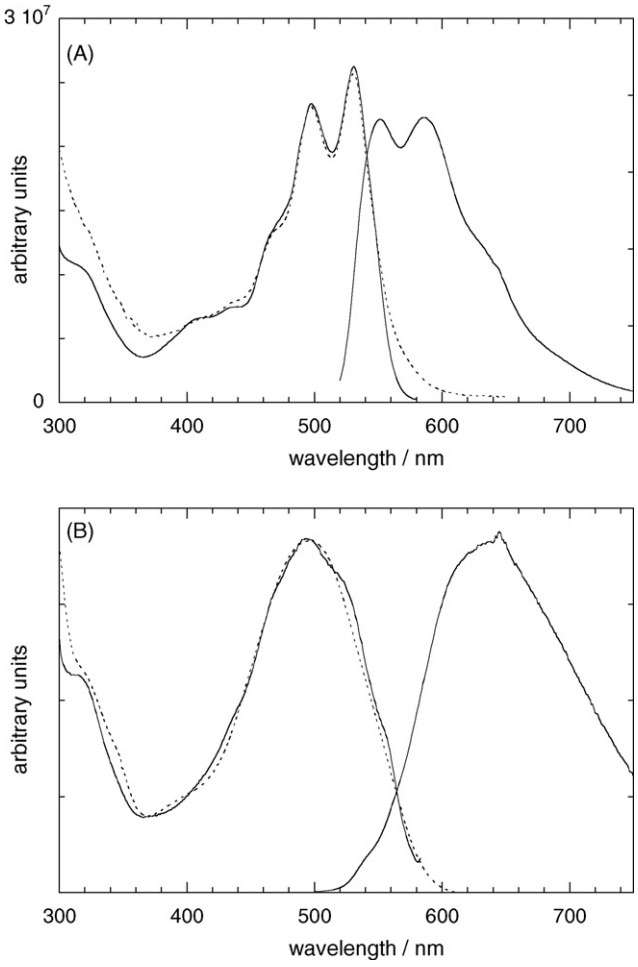


Fig. 3. Corrected emission and excitation spectra ($\lambda_{em} = 590$ nm and $\lambda_{exc} = 503$ nm; abs at the λ_{exc} for both solutions ≈ 0.018), full line, for purpurin (A) and alizarin (B) aluminum complex, in the presence of a 1:100 excess of Al^{3+}, in a methanol/water solution (75:25%) at pH 3.4. Dotted line, absorption spectra.

Table 1
Spectral and photophysical data obtained in solution, MeOH:H_2O (75:25, v/v) @ 293 K, for the neutral forms of alizarin and purpurin and for 1:100 ratio aluminum complexes (pH 3.7)

Alizarin	Purpurin	Alizarin + Al^{3+}	Purpurin + Al^{3+}
$\lambda_{max}^{abs} = 430$ nm (530; 570)[a]	$\lambda_{max}^{abs} = 480$ nm (510; 545)[a]	$\lambda_{max}^{abs} = 500$ nm	$\lambda_{max}^{abs} = 531$ nm
$\varepsilon_{max} = 5830\ M^{-1}\ cm^{-1}$	$\varepsilon_{max} = 7770\ M^{-1}\ cm^{-1}$	$\varepsilon_{max} = 7440\ M^{-1}\ cm^{-1}$	$\varepsilon_{max} = 9540\ M^{-1}\ cm^{-1}$
$\lambda_{max}^{fluo} = 578$ nm	$\lambda_{max}^{fluo} = 582$ nm	$\lambda_{max}^{fluo} = 640$ nm	$\lambda_{max}^{fluo} = 595$ nm
$\phi_f = 5.1 \times 10^{-4}$[b]	$\phi_f = 0.004$	$\phi_f = 0.006$	$\phi_f = 0.29$

[a] Absorption maxima for the A^- and A^{2-} forms of the chromophore.
[b] Value obtained from Ref. [10].

3.2. Solid, heterogeneous media

3.2.1. Model samples

The purpurin and alizarin lake model samples were used to test the reproducibility of the microfluorescence data; the model samples used were the 1 cm square paintings of purpurin and alizarin lakes and their mixtures, in a PVAc emulsion, applied in a Whatmann filter paper, with four replicates for each composition; for each of the prepared paintings 6–9 emission and excitation spectra were acquired, in different days, in different points, and the data was shown to be completely reproducible. Other supports, including melinex sheets, glass slides and sapphire cells, were also used and do not influence the shape of the emission/excitation spectra obtained. To test the potential of the technique as semi-quantitative, mixtures of purpurin and alizarin lakes of known concentration were prepared and the respective spectra acquired (Fig. 4); each concentration point results from a mean value of 36 spectra, obtained in four different experiments (9×4). Taking into account the intrinsic heterogeneity of the solid media, the correlation coefficient of the curve representing the concentration of purpurin in the mixture as a function of the emission intensity can be considered very good, $R^2 = 0.96$ (inset Fig. 4). Also, the emission spectra for the solid state are satisfactory resolved, comparing well with the spectra acquired in solution (Fig. 3A). From Fig. 4 it can be observed that the spectra decrease in intensity with the increase of alizarin proportion in the mixture. This is an expected behaviour due to the relative fluorescence yields of the two compounds (see Table 1). Even if it is difficult to see the emission spectra of the alizarin lake with the scale axes of Fig. 4, there is also a blue-shift of the overall spectra since the maximum emission of alizarin is also blue-shifted relative to purpurin. Due to this shift and also to the difference between the fluorescence quantum yields of the two lakes, it was possible to collect the purpurin lake emission directly from the raw data, without any further spectral deconvolution.

Also, the emission spectra acquired for both lakes using parchment glue and arabic gum as binding media compares well to what obtained using PVAc as the binder.

The emission from the model samples was also collected with a fiber-optic adaptor (without microscope) and the results obtained, for four different experiments, are represented in Fig. 5. In this case, for each sample, only one emission spectrum was acquired as the area covered by the fiber-optic, 0.5 cm, takes into account the heterogeneity of the sample. Again, a similar trend in the emission spectra was observed. The linear fitting for the concentration of purpurin in the mixture as a function of the emission intensity was very good, $R^2 = 0.98$ (inset Fig. 5), enabling a semi-quantitative analysis to be carried out.

However, the spectra envelope was less resolved than that obtained with the microSPEX. This could be explained by the

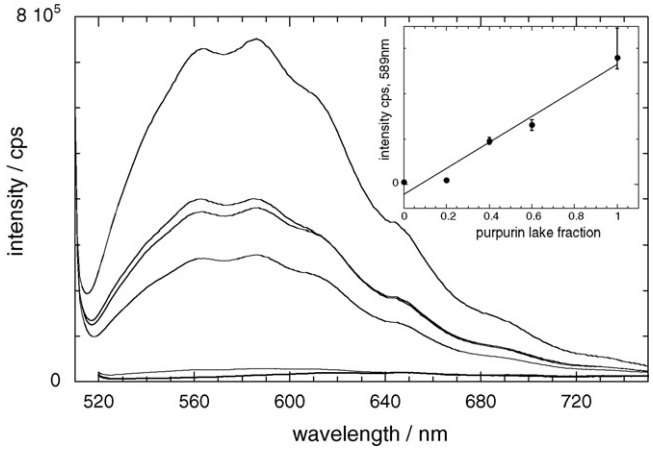


Fig. 4. Micro-emission spectra (not corrected) obtained for mixtures of purpurin and alizarin lakes in a PVA medium, applied in Whatmann filter paper; mixtures, weight:weight, of purpurin:alizarin, 0:100, 20:80, 40:60, 60:40 and 100:0 with $\lambda_{exc} = 490$ nm and dichroic filter of 500 nm. In the inset, the resulting calibration curve with $R^2 = 0.98$ is shown ($y = 8212.5x - 61557$); the calculated uncertainties correspond to a confidence level of 95%.

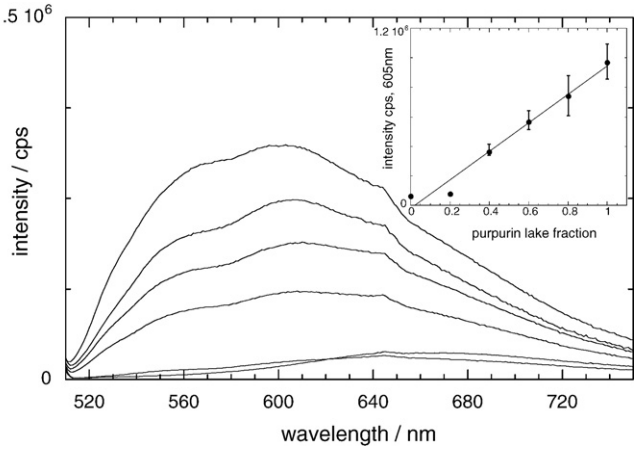


Fig. 5. Emission spectra (not corrected) obtained for mixtures of purpurin and alizarin lakes in a PVA medium, applied in Whatmann filter paper, through fiber-optic; mixtures, weight:weight, of purpurin:alizarin, 0:100, 20:80, 40:60, 60:40, 80:20 and 100:0 with $\lambda_{exc} = 490$ nm and dichroic filter of 500 nm. In the inset, the resulting calibration curve with $R^2 = 0.98$ is shown ($y = 9634x - 19537$); the calculated uncertainties correspond to a confidence level of 95%.

relatively higher light intensity output of the fiber-optic compared with the microscope, and also that, the light reflected from the sample is more efficiently collected. Therefore, it is possible that interference due to reflection affected the emission spectra obtained with fiber-optic system.

Another disadvantage of using fiber-optic is that it is not possible to acquire excitation spectra of the samples, as it will be the case with the microSPEX; this will be described in the forthcoming discussion.

In the insets of Figs. 4 and 5, the results and associated uncertainties are given considering a confidence level of 95%. The detection limits found are ≈11% for both cases, MicroSPEX and fiber-optic (calculated as three times the standard deviation of the sample where the amount of purpurin was 0%-blank signal [19]). This reveals that below this percentage of purpurin in the alizarin:purpurin mixture there is a significant degree of uncertainty in the measurements.

3.2.2. Historical reconstructions

3.2.2.1. Kopp's Al^{3+} lakes. Fig. 6 shows the emission and excitation spectra from the historic reconstructions for *Kopp's Purpurin* lake, where lead white was applied as an underlayer and the lake is applied in oil media. The emission spectra were obtained using 510 and 570 nm dichroic filters, and it was concluded that the 570 nm cannot be used for this red lakes as part of the emission is cut-off, with consequent loss of information that can induce to a misinterpretation of the experimental results. On the other hand, it was possible to obtain good excitation spectra with the 570 nm dichroic filter. The excitation spectra reproduce the absorption spectra of the sample, enabling a better identification of the chromophore. This is an important advantage in the field of cultural heritage, since in ancient samples, complex aged mixtures can display also a complex emission spectra, and having access to a well resolved excitation spectra will facilitate the characterization of the chromophores present.

All the spectra represented in Fig. 6 were obtained with high spatial resolution (8 μm spot) using pinhole 5. The same conditions were used to collect the emission for the same sample in a resin, as a model for cross sections of painting samples. The results acquired were analogous to those presented in Fig. 5.

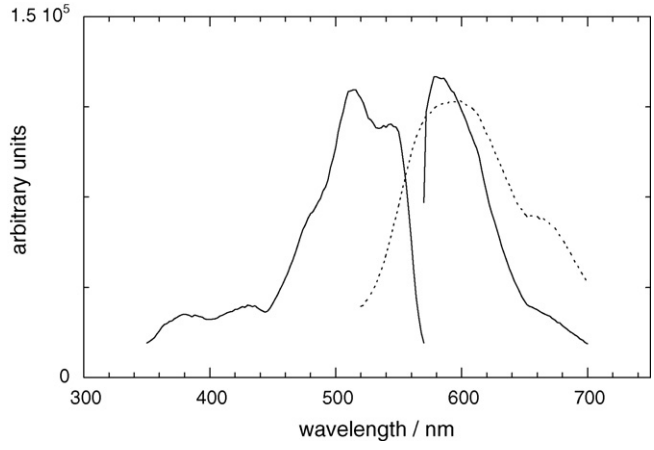


Fig. 6. Kopp's purpurin lake emission (570 – full line – and 510 nm – dotted line – dichroics) and excitation (570 nm dichroic) spectra (8 μm spot).

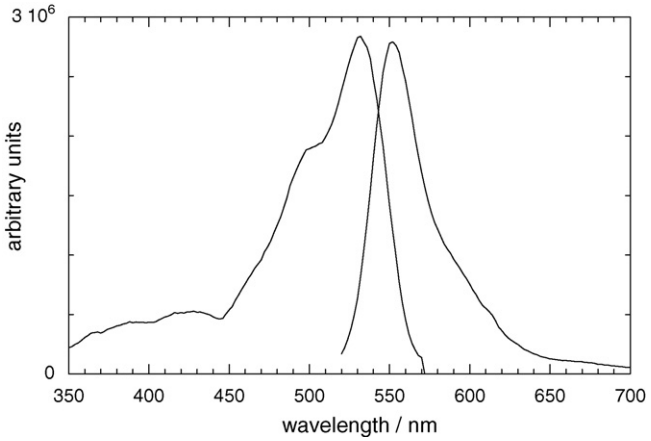


Fig. 7. Eosin lake emission and excitation (570 nm dichroic) spectra with an 8 μm spot.

3.2.2.2. Eosin Al^{3+} lakes. The emission and excitation spectra for the eosin lakes were obtained, as for *Kopp's Purpurin* lake, from a cross section, in 8 μm and 4 μm spots, and representative emission and excitation spectra are given in Fig. 7. Here, again, it was possible to acquire an excitation spectrum with the 570 nm dichroic filter. Besides, as expected, being eosin a strong fluorophore, the emission intensity is *circa* one order of magnitude higher than that obtained for *Kopp's* lake.

3.2.2.3. GEO© fluorescent colors. The spatial resolution of the technique was tested in a complete cross-section, were a paint sample with a chalk ($CaCO_3$) preparation and a white lead ($PbCO_3{\cdot}Pb(OH)_2$) *imprimatura* was used for a fluorescent vinyl commercial paint, GEO©, inset Fig. 8. Again remarkably good excitation and emission spectra were acquired with a high spatial resolution of 8 μm.

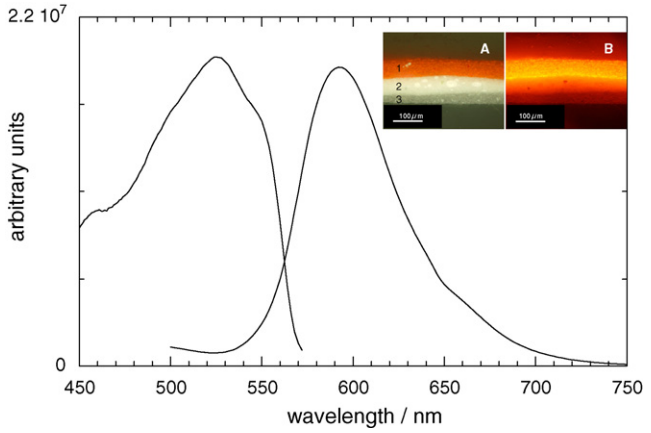


Fig. 8. In the inset, GEO fluorescent vinyl paint (1) over a chalk preparation (3) and white lead *imprimatura* (2), in a ester resin cross section: (A) image acquired with visible light and (B) exciting with green light (filter set 14—BP510-560 FT580 LP590). The emission and excitation spectra were obtained under excitation with an 8 μm spot, using the 570 nm dichroic filter.

4. Conclusions

Micro-emission molecular fluorescence proved to be a promising analytical tool to identify the presence of selected red lake pigments combined with a range of binding media. Red lakes that displayed characteristic emission spectra included purpurin and eosin-based pigments although the potential for identification of lake pigments other than those examined in the present study may apply to a wider range of artists' materials. The radiation used is of low intensity and non-destructive to the molecules. Analysis may be carried out *in situ*, without sampling, or on prepared paint cross-sections that offers the opportunity to look at materials in discrete layers of a painting. The acquisition of spectra is rapid, with high spatial resolution and the data reliable and reproducible. Together with full emission spectra, it was possible to acquire well-resolved excitation spectra, which is a great advantage when studying complex aged samples. The present investigation suggests that micro-emission fluorescence can also be used as a semi-quantitative method for madder lakes, enabling the determination of purpurin lake fraction in a mixture of purpurin and alizarin.

The analytical method developed here for the identification of red lakes prepared as aluminum complexes with purpurin and eosin defines the optimal conditions for the acquisition of the steady-state emission fluorescence spectra using a 500 nm or 510 nm dichroic filter, with excitation at 490 nm for the red anthraquinone lakes. For eosin type lakes the 570 nm dichroic filter was used, and excitation was performed at the absorption maxima. All steady-state excitation spectra were acquired with the 570 nm dichroic. The experimental set-up employed a pinhole 5 (8 μm) to define the area analyzed in cross sections. This spatial resolution is appropriate for the analysis of individual pigments particles or aggregates in a paint film. Generally, it offers an optimized signal to noise ratio and good spatial resolution for artists' paints. For the eosin type compounds it was possible to acquire spectra with smaller pinholes apertures (4 μm). When spatial resolution was not an important requirement a pinhole 8 (30 μm) was selected. Another method to be explored might be to gather data from selected areas, thus providing the opportunity to characterize materials in paint that contains mixtures of pigments in different layers.

Although the molecular structures of lakes are difficult to determine by fluorescence emission alone, combined with data from other analytical techniques, information about the environment [20] of the colorant and its state of degradation can be obtained. Work is currently in progress on the analysis of red lakes in cross sections, aiming to extend the application of the technique for a wider range of lake pigments in different states of degradation, in samples from painted works of art. Exploring the in-depth profiling, future work will investigate the application of this non-destructive technique for analysis of red lakes on actual works of art, even when varnished.

With regard to the comparison of the method with the currently available transportable fiber-optic spectrofluorimeters, the more significant advantages of micro-emission molecular fluorescence are: (i) the possibility to acquire both emission and excitation spectra, (ii) high spatial resolution and also (iii) in-depth profiling; this last feature was not explored in this work. Moreover, this work shows that the quality of the spectral information, namely the spectral resolution and the signal to noise ratio, is very high when compared to those obtained with the fiber-optic spectrofluorimeters, as was shown in this work. It is important to stress the fact that, an excitation spectrum reproduces the chromophore absorption spectrum, a relevant parameter for the characterization of a dye or a pigment. The simultaneous acquisition of emission and excitation (absorption) spectra together with the high spectral resolution will facilitate a more accurate identification of dye molecules and lakes.

Acknowledgments

This work was supported by the Portuguese Science Foundation and FEDER, through the Associate Laboratory for Green Chemistry and the projects POCI/QUI/55672/2004 "The Molecules of Color in Art: a Photochemical Study" and POCTI/EAT/33782/2000 "An interdisciplinary approach to the study of color in Portuguese manuscript illuminations".

Appendix A. Supplementary data"Supplementary

Supplementary data associated with this article can be found, in the online version, at doi:10.1016/j.talanta.2007.07.036.

References

[1] (a) D. Cardon, Le monde des Teintures naturelles, 2nd ed., Belin, Paris, 2003;
(b) J. Wouters, N. Rosario-Chirinos, JAIC 31 (1992) 237.
[2] Halleux, R. (Ed.), Les Alchimistes Grecs: Papyrus de Leyde (1st ed., 1981), Papyrus de Stockholm, Recettes, Les Belles Lettres, Paris, 2002.
[3] (a) D. Cardon, Teintures précieuses de la Méditerranée: Poupre ∼ Kermès ∼ Pastel, Musée des Beaux-Arts de Carcassonne, Centre de Documentació I Museu Tèxtil de Terrassa, Carcassonne, 1999;
(b) E.W. Fitzhugh (Ed.), Artists' Pigments, A Handbook of their History and Characteristics, vol. 3, National Gallery of Art, Washington, 1997;
(c) B. Szostek, J. Orska-Gawrys, I. Surowiec, M. Trojanowicz, J. Chromatogr. A 1012 (2003) 179;
(d) X. Zhang, R.A. Laursen, Anal. Chem. 77 (2005) 2022.
[4] D.K. Palit, H. Pal, T. Mukherjee, J.P. Mittal, J. Chem. Soc. Faraday Trans. 86 (1990) 3861.
[5] (a) C. Cennini, Il Libro dell' Arte, In: F. Frezzato (Ed.), Neri Pozza Editore, Vicenza, 2003;
(b) F. Brunello (Ed.), De Arte Illuminandi e altri trattati sulla miniatura medievale, Neri Pozza Editore, Vicenza, 1992;
(c) S. Blondheim, JQR 19 (1928) 97.
[6] (a) R. Huber, J. Moser, M. Gratzel, J. Wachtweitl, J. Phys. Chem. B 106 (2002) 6494;
(b) J. Kim, J. Kang, D. Han, C. Lee, K. Ahn, Chem. Mater. 10 (1998) 2332.
[7] M.S. El Ezaby, T.M. Salem, A.H. Zewail, R. Issa, J. Chem. Soc. B 7 (1970) 1293.
[8] (a) M.H. Van Benthem, G.D. Gillispie, J. Phys. Chem. 88 (1984) 2954;
(b) P.A.B. Marasinghe, G.D. Gillispie, Chem. Phys. 136 (1989) 249.
[9] (a) T.P. Smith, K.A. Zaklika, K. Thakur, G.C. Walker, K. Tominaga, P.F. Barbara, J. Phys. Chem. 95 (1991) 10465;
(b) R.A. Denny, B. Bagchi, P.F. Barbara, J. Chem. Phys. 115 (2001) 6058.
[10] C. Miliani, A. Romani, G. Favaro, J. Phys. Org. Chem. 13 (2000) 141.

[11] (a) E.R. de la Rie, Stud. Conserv. 27 (1982) 1;
(b) A. Favaro, C. Miliani, G. Romani, M.J. Vagnini, Chem. Perkin Soc. Trans. 2 (13) (2002) 192;
(c) T. Del Giacco, L. Latterini, F. Elisei, Photochem. Photobiol. Sci. 2 (2003) 681–687.
[12] A. Burnstock, I. Lanfear, K.J. van den Berg, L. Carlyle, M. Clarke, E. Hendriks, J. Kirby, Preprints of the 14th Triennial Meeting of the ICOM Committee for Conservation, vol. 1, The Hague, 2005, p. 459.
[13] (a) B. Valeur, Molecular Fluorescence: An Introduction—Principles and Applications, Wiley-VCH, Weinheim, 2002;
(b) C. Clementi, C. Miliani, A. Romani, G. Favaro, Spectrochim. Acta A 64 (2006) 906;
(c) E. Destandau, V. Alain, É. Bardez, Anal. Bional. Chem. 378 (2004) 402;
(d) J. Seixas de Melo, A.P. Moura, M.J. Melo, J. Phys. Chem. A. 108 (2004) 6975.
[14] http://www.biosciencetechnology.com/ShowPR.aspx?PUBCODE=090&ACCT=9000003025&ISSUE=0307&RELTYPE=PR&ProdCode=00005878&PRODLETT=A.
[15] J. Kirby, in: M. Clarke, J.H. Townsend, A. Stijnman (Eds.), Postprints of the Conference Approaching the Art of the Past: Sources and Reconstructions, Archetype, London, 2005, pp. 69–77.
[16] R.E. Kellogg, R.G. Bennett, J. Chem. Phys. 41 (1964) 3042.
[17] A.E. Martell, R.M. Smith, R.J. Moteikatis, NIST Critical Stability Constants of Metal Complexes Database NIST Standard Reference Databases, version 6.0, NIST, Gaithersburg, MD, 2001, p. 20899.
[18] E. Bardez, V. Alain, E. Destandau, A. Fedorov, J.M.G. Martinho, J. Phys. Chem. A 105 (2001) 10613.
[19] D.C. Harris, Quantitative Chemical Analysis, 6th ed., W.H. Freeman and Company, New York, 2003.
[20] (a) A.P. de Silva, P. Tecilla, J. Mater. Chem. 15 (2005) 2637;
(b) D.C. Magri, J.F. Callan, A.P. de Silva, D.B. Fox, N.D. McClenaghan, K.R.A.S. Sandanayake, J. Fluorescence 15 (2005) 769;
(c) S. Uchiyama, Y. Matsumura, A.P. de Silva, K. Iwai, Anal. Chem. 76 (2004) 1793;
(d) Y.-L. Wei, J.-Q. Li, C. Dong, S.-M. Shuang, D.-S. Liu, C.W. Huie, Talanta 70 (2006) 37.

Available online at www.sciencedirect.com
ScienceDirect
Talanta 74 (2008) 547–554
Talanta
www.elsevier.com/locate/talanta

Three-way principal component analysis of the volatile fraction by HS-SPME/GC of aceto balsamico tradizionale of modena

Marina Cocchi [a,*], Caterina Durante [a], Margherita Grandi [a], Daniela Manzini [b], Andrea Marchetti [a]

[a] *Dipartimento di Chimica, Università di Modena e Reggio Emilia, via Campi 183, 41100 Modena, Italy*
[b] *Centro Interdipartimentale Grandi Strumenti, Università degli Studi di Modena e Reggio Emilia, via Campi 213/a, 41100 Modena, Italy*

Received 13 July 2006; received in revised form 1 June 2007; accepted 15 June 2007
Available online 19 June 2007

Abstract

The present research is aimed at monitoring the evolution of the volatile organic compounds of different samples of aceto balsamico tradizionale of modena (ABTM) during ageing. The flavouring compounds, headspace fraction, of the vinegars of four *batterie* were sampled by solid phase microextraction technique (SPME), and successively analysed by gas chromatography. Obtaining a data set characterized by different sources of variability such as, different producers, samples of different age and chromatographic profile. The gas chromatographic signals were processed by a three-way data analysis method (Tucker3), which allows an easy visualisation of the data by furnishing a distinct set of graphs for each source of variability.

The obtained results indicate that the samples can be separated according to their age highlighting the chemical constituents, which play a major role for their differentiation.

The present study represents an example of how the application of Tucker3 models, on gas chromatographic signals may help to follow the transformation processes of food products.
© 2007 Elsevier B.V. All rights reserved.

Keywords: ABTM; Vinegar; HS-SPME; Tucker; Multi-way data analysis; VOC

1. Introduction

Aceto balsamico tradizionale of modena (ABTM), is one of the most representative Italian artisan gastronomic food and, despite its limited production, it is known and commercialized all around the world. In 2000, this product obtained the protected denomination of origin (PDO) certification from the European Commission, because of its typical and unique production procedures and the well-defined geographical area of production [1]. ABTM is traditional balsamic vinegar, which is obtained by alcoholic fermentation and acetic bio-oxidation of condensed cooked grape musts. The fermented cooked must is aged for a long time (at least 12 years), in a set of barrels (batteria) composed by a variable number (from 5 to 10) of wooden casks of different volumes. During the ageing process the liquid in each barrel is kept constant by transferring a certain amount of vinegar from one barrel to another in a decreasing progression with a procedure known as "topping up" [2]. In the first year the vinegar is mainly transformed by a microbial activity and successively by enzymatic and chemical reactions.

Due to this production method, which implies a wide transformation of the raw materials, the characterization of ABTM of different ages, coming from the several barrels of a batteria, could be extremely interesting and useful for the authentication of the product and for the comprehension of the phenomena that take place during the ageing period. Investigations about samples coming from different batterie may be helpful to discriminate products of various ages and to differentiate the marketable one, which is at least 12 years old, from the younger ones. In fact, studies about ABTM, usually take into account only the old product and only few works [2–5] have dealt with different aged samples.

The volatile organic compounds, which concur to the olfactory characteristics, have a fundamental importance for the final

* Corresponding author. Tel.: +39 059 2055029; fax: +39 059 373543.
E-mail address: cocchi.marina@unimore.it (M. Cocchi).

0039-9140/$ – see front matter © 2007 Elsevier B.V. All rights reserved.
doi:10.1016/j.talanta.2007.06.016

evaluation of the product and, probably, they may play a considerable role in differentiating vinegars on a time base scale, i.e. vinegars of different age. Therefore, one of the aims of the present research is to monitor the evolution of the volatile organic compounds of ABTM samples during ageing. Besides all the analytical techniques used for the flavour composition characterization, the gas chromatography (GC) equipped with head space solid phase microextraction technique [6,7] (HS-SPME) may represent an innovative breakthrough and an a hyphenated approach when linked with chemometric signals processing tools [8].

In the present work, a three-way data set has been analysed, as the ABTM ageing process is affected by different sources of variability, such as the different ageing of vinegar samples, the different batterie and the chromatographic profile. Traditional bilinear chemometrics methods, such as principal component analysis (PCA), may allow extracting useful information from higher order data sets, i.e. data characterized by more than two sources of variability, by using unfolding procedures but, on the other hand, unfolding may be often unfavorable and. it has been recently demonstrated that the use of an *N*-way approach can significantly improve the visualization and interpretation of multi-way data [9,10]. In this particular case, the advantage offered by three-way analysis is due to the possibility of not overwhelming the intra-batteria variability with the inter-batterie variability, as a results it will be possible to depict both the similar evolution of vinegar samples with ageing inside each series of barrels and the distinctive features among batterie due to the traditional conduction procedure.

Tucker3 method is one of the most popular *N*-way methods [9,11], and it can be fairly considered as a natural extension of bilinear PCA. Multi-way methods have been successfully applied to the analysis of different kinds of instrumental data, mainly spectroscopic ones [12–15]. On the other hand, very few applications on gas chromatograms have been reported [13,15] and therefore it is also of interest to test the performance of these methods on this experimental data set.

The data have been organized as a three-way array: samples × HS-SPME/GC-FID signal points × batterie. Owing to this set-up it should be possible: (i) to stress out how the changes of the volatile organic fraction (different composition and/or concentration) is reflected in the ageing process; (ii) to obtain an overview of the relationships between the volatile fraction and the vinegars age and finally and (iii) to assess similarities and dissimilarities among the investigated batterie.

Furthermore, a comparative analysis of the results obtained by Tucker3 analysis with PCA unfolding has been accomplished.

2. Materials and methods

2.1. Sampling

Four different batterie were analyzed, namely batterie "O", "R", "Sa" and "Sd". Each batteria is composed by six barrels. The first barrel (1) contains the oldest vinegar product (the marketable ABTM) and the last barrel (6) the youngest one.

Among the investigated cask series, batteria "O" is the oldest one, being started 50 years ago, while batteria "Sd", which was started about 7 years ago, is the youngest one. Finally, batterie "R" and "Sa" were started 10 and 18 years ago, respectively.

From each barrel, of different size, different wood and different product ageing, a test sample of 100 mL was obtained following the described procedure; five aliquots of 100 mL of product were taken at different depth and homogenized to obtain a barrel representative sample (500 mL). Successively, an aliquot of 100 mL (test sample) was taken while the rest of the vinegar (400 mL) was re-introduced in the barrel.

All the samples were stored in polystyrene boxes at 4 °C in order to prevent any matrix modification such as fermentation or other chemical modifications. Before analysis, samples were kept at room temperature with continuous mixing to return the product to its initial condition.

2.2. Head space solid phase microextraction (HS-SPME) analysis

The volatile organic composition was monitored by sampling the headspace of the vinegar by using the solid phase microextraction technique (HS-SPME). The experimental set up and analytical procedure has already discussed in a previous work [8]. An aliquot of 1.00 mL of each sample was transferred by a calibrated syringe in a 10 mL flask equipped with a screw-top quick fit adaptor and a Teflon-coated silicone septum. The flask was held in a warm water bath at 40.0 °C for 1 h to allow equilibrium between the sample and headspace, prior to SPME sampling. The fibre was then inserted into the sample container through the septum and exposed to the headspace for 15 min. Finally, it was desorbed in the GC injector for 4 min by splitless injection mode.

The analysis of all the samples was twice replicated, with the exception of the samples of batteria "O", because of their extremely low amount.

2.3. Gas chromatography (GC)

Samples were analyzed with a Varian 3400 Gas Chromatograph provided with flame ionization detector (FID) and a non-polar fused silica capillary column (CPSil 5MS; length 60 m; internal diameter 0.25 mm; film thickness 1 μm) was used. Helium was used as carrier gas (column head pressure was 28 PSI; linear velocity was 25 cm s^{-1} at 200 °C).

The injector temperature was 240 °C and the split valve was closed for 4 min during sample injection and then opened for the rest of the chromatographic run. The injector was equipped with a special deactivated SPME glass insert (0.75 mm internal diameter). The GC oven starting temperature was 55 °C (5 min); then it was increased at 4 °C min^{-1} to 150 °C, and at 8 °C min^{-1} to 250 °C and finally at 10 °C min^{-1} to 270 °C (5 min). The FID temperature was set at 280 °C.

The chromatograms were acquired at constant sampling rate, $\nu = 20$ Hz, for a total time of 59 min and 15 s, by using the software Chromeleon© Version 4.12 (distributed by SOFTRON GmbH).

In order to rationalize the chemical transformation occurring during the ageing process of ABTM, gas chromatography–mass spectrometry (HS-SPME/GC–MS) analysis was performed on some representative ABTM samples, using the same experimental condition optimized in a previous work [8], allowing the identification of some of the main chromatographic peaks. The GC–MS system used was formed by a 3400 Varian GC coupled to a Finnigan SSQ710AMS capable of electron impact ionization. The identification of unknown compounds was based on matches to the NIST and GP libraries, supplied by Finnigan.

2.4. Data analysis

Because of high dimensionality of collected HS-SPME/GC-FID signals, data analysis was performed on the reduced chromatograms, obtained after a sub-sampling of 1/8 of the collected points, since the chromatographic profile was unaltered, i.e. after sub-sampling peak width at half height, typically measuring 0.06 min, was not altered.

Furthermore, the first 3 min and the last 10 min were cut because there were no peaks at all, resulting in an HS-SPME/GC-FID signal vector of 7018 points.

The main issue with this data set is to capture the interrelationships among objects (samples), variables (HS-SPME/GC-FID signal points) and the variation occurring along the series. Thus, taking into account the different samples age together with the different features and age of the ABTM batterie, the structure of the data set is characterized by three different sources of variability. Multi-way models lead to an easier identification of the effects present in each of the three modes and allow a simultaneous analysis of the different sources of variation.

Therefore, the data set was organized as a three-way array, in which the three modes are constituted by the samples, the HS-SPME/GC-FID signal points and the batterie, with dimensionality 6 samples × 7018 HS-SPME/GC-FID signal points × 7 batterie (4 batterie plus 3 replicate batterie).

Centering across the first mode (samples) was applied as data pretreatment to remove the constant difference among the samples.

As far as scaling is concerned, working with unscaled data seems preferable since in this case there is the risk of dramatically up weighting components present in very small amount and showing little variation (such as spectral background or baseline). However, given the presence of major and minor constituents, it is desirable to give to the different volatile compounds a comparable influence in the data analysis. In order to do this, the data set was scaled within the second mode (HS-SPME/GC-FID signal points) by using a block scaling procedure called "block-adjusted non-scaled data" [4,16]. In practice, this pretreatment requires to subdivide the HS-SPME/GC-FID signals in different regions (blocks) whose values will be scaled in order to attain the same block-variance after pretreatment. The subdivision in blocks is shown in Fig. 1a, where a representative HS-SPME/GC-FID signal is reported. The vertical line represents the subdivision in two blocks/regions. The variables

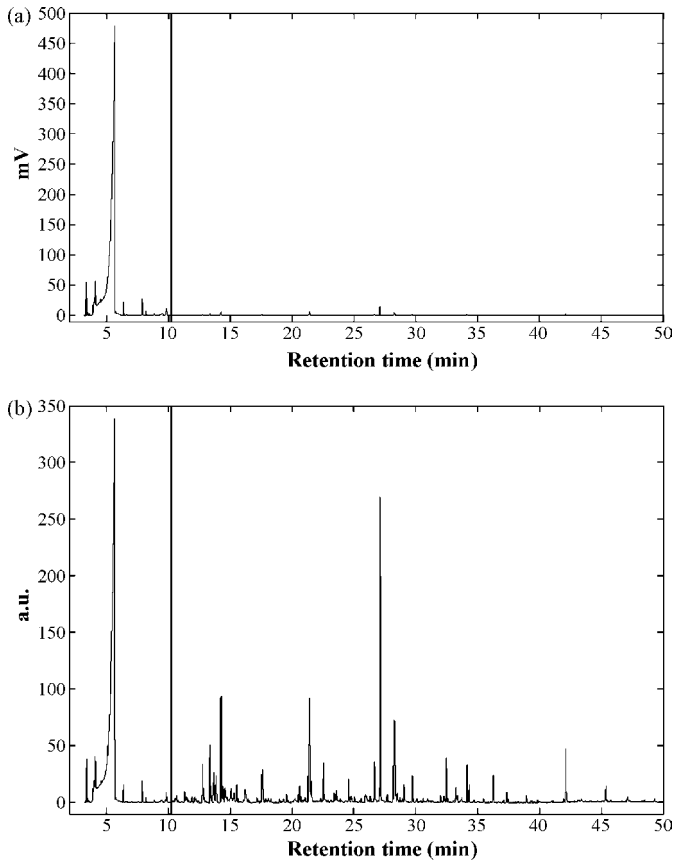


Fig. 1. (a) Representative chromatogram of an ABTM sample. The vertical line divides the signal in the two regions selected for performing the block-scaling pretreatment; (b) the corresponding 'blockscaled' signal.

belonging to the same block are equally weighted and the corresponding pretreated signal is reported in Fig. 1b. Thus, this pretreatment allows minor constituents that could play a fundamental role in the ageing process, to contribute to the model without altering the relative scale of variables belonging to the same block.

Finally, explained variation and 'core array analysis' were used to estimate the number of significant factors (F) and the Tucker3 models were calculated under no constrains.

2.5. Tucker3 model

Tucker3 is a decomposition method and it can be fairly considered as a generalization of singular value decomposition (SVD) to higher order array.

In this section a short introduction is given, referring the reader to the literature [9,17,18] for a detailed description of the properties and characteristics of this multi-way technique.

Briefly a three-way array X, of dimension $I \times J \times K$, is decomposed into triplets of loadings vectors. Each triplet is called component or factor (F) or latent variable (LV).

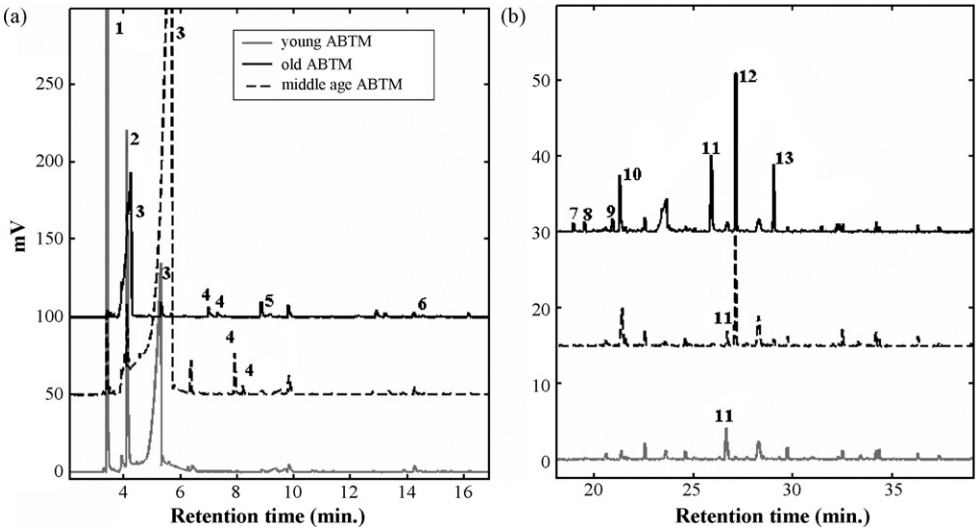


Fig. 2. Different zoom of representative chromatographic regions, the identified chemical species follow: (a) (1) ethanol; (2) ethyl acetate; (3) acetic acid; (4) 2,3-butanediol; (5) furfural; (6) 5-methyl furfural; (b) (7 and 8) isomers of 2,3-butanedioldiacetate; (9) 1,3-propanedioldiacetate; (10) 2-phenyl-ethanol; (11) 5-hydroxymethyl furfural; (12) 2-phenyl-acetate; (13) 5-acetoxymethyl furfural.

The decomposition can be mathematically expressed by the following equation:

$$x_{ijk} = \sum_{p=1}^{P}\sum_{q=1}^{Q}\sum_{r=1}^{R} t_{ip} w^{j}_{jq} w^{k}_{kr} g_{pqr} + e_{ijk}$$

where t_{ip}, w^{j}_{jq} w^{k}_{kr} are the elements of the first mode score matrix T ($I \times P$), and of the second, W^J ($J \times Q$), and the third modes, W^K ($K \times R$), weights, respectively. e_{ijk} is a residual term containing all the unexplained variation.

P, Q and R are the number of factors extracted for each mode; g_{pqr} is the element of the core array G of order $P \times Q \times R$.

The core array G is composed of singular values; it represents the value by which the single component product is weighted. Therefore, the value and the sign of each core element, give information about the entity of the interaction among the components of the different modes. The squared elements of the core array are proportional to the variation explained by the combination of the factors corresponding to their indices, i.e. if g_{112} is the largest core element, special attention in interpreting the model has to be given to the interaction between Factor 1 of mode 1, Factor 1 of mode 2 and Factor 2 of mode 3.

2.6. Unfolding PCA

In the case of unfolding PCA the data array has been unfolded to a bi-dimensional data matrix: IK (barrels and batterie, on rows) $\times J$ (GC signal points, on columns) of dimension 42×7018. Prior to PCA the same variables block scaling procedure, as for the Tucker3 model, was applied as data pretreatment.

2.7. Software

Tucker3 results have been obtained by using the N-way Toolbox [19] for MATLAB©. PCA unfolding has been carried out by using the PLS-toolbox 3.5 (distributed by Eigenvector Research Inc., Wenatchee, WA).

3. Results and discussion

In this work, the main organic compounds, which concur to the volatile fraction, were identified through the reference mass spectra libraries; furthermore, the identification was supported by comparing the retention times with those reported in a previous work [8].

The behavior of the volatile fraction in the several vinegar samples is extremely interesting as it reflects the three main phases that can be identified during the ageing process, corresponding to fermentation, maturation and ageing.

Fig. 2 reports overlaid representative chromatograms of a young, a middle age and an old ABTM sample coming from the same batteria. For a better graphical visualization of the chromatograms, two distinct plots a and b, covering the 2–17 and 18–40 min regions, respectively, have been done. A different shift degree on the Y-axis among the three chromatograms (young, middle age and old) has been used in Fig. 2a and b, moreover a zoom of the Y-axis is applied in Fig. 2b. The main chromatographic peaks visible in Fig. 2a and b, have been identified as ethanol (no. 1, Rt $\approx$ 3.4 min), ethyl acetate (no. 2, Rt $\approx$ 4.17 min) and acetic acid (no. 3, Rt $\approx$ 5 min), which is the major product of acetic bio-oxidation. Although these organic compounds are the principal species detected in traditional balsamic vinegars, many other molecules concur to the organoleptic properties and to the characterization of this product, such as the two isomers of 2,3-butanediol (no. 4, Rt $\approx$ 5–8 min), furfural (no. 5, Rt $\approx$ 8.8–9.2 min) and 5-methylfurfural (no. 6, Rt $\approx$ 14–14.5 min). In the retention times interval from 18 to 20.5 min are present low intensity peaks, corresponding to the two isomers of 2,3-butanediol diacetate (nos. 7 and 8). Furthermore, the compounds **1**–**3** propanediol diacetate (no. 9, Rt $\approx$ 20.5 min), 2-phenyl-ethanol (no. 10, Rt $\approx$ 21.3 min),

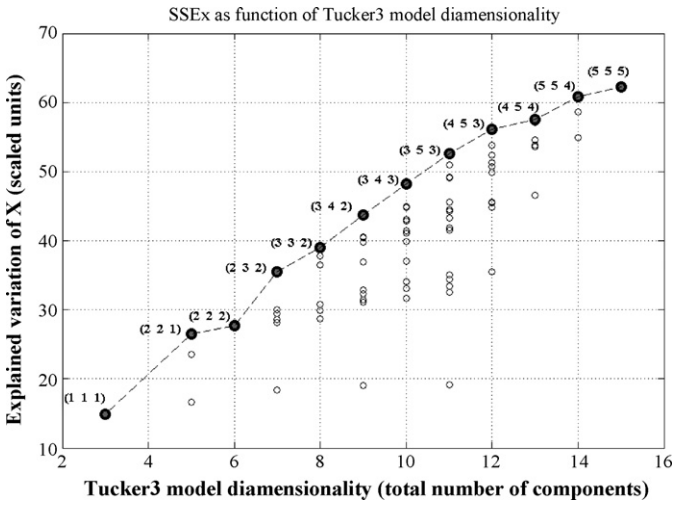


Fig. 3. Variance explained (%) by the different Tucker3 models expressed with respect to scaled data, the labels report the dimensionality of the Tucker3 model with respect to each mode, while on the *x*-axis the global model dimensionality is reported. For the sake of clarity, labels are reported only for the models on the edge.

5-hydroxymethyl-furfural (no. 11, Rt ≈ 25.9 min), 2 phenylacetate (no. 12, Rt ≈ 27.1 min) and 5-acetoxymethyl-furfural (no. 13, Rt ≈ 29 min) were also detected in the vinegars.

In order to assess the degree of variability of the different organic compounds during vinegar ageing and the similarity/dissimilarity among batterie a Tucker3 analysis was employed on data arranged as a three-way array of 6 samples × 7018 HS-SPME/GC signal points × 7 batterie dimensions.

In order to choose the best complexity of the Tucker3 model, i.e. the number of factors for each mode, the tuck test routine [9,19] was applied. The results are shown in Fig. 3, and according to the best compromise between good fit and a low number of factors, a [2 3 2] Tucker3-model, explaining 54% of total variance with respect to raw data, have been chosen. Although the [3 3 2] Tucker3-model explains more variance than the [2 3 2] model, the analysis of the core array elements of both the models pointed out that the third factor (F3) in mode 1 is not necessary (results not shown). Table 1 reports the main core array elements of the chosen model. For the sake of clarity, the squared elements of the core array are proportional to the variation explained by the combination of the factors corresponding to their indices. For example the (1 1 1) is the largest core element, which alone represents the 25% of the explained variance of the core array. This means that the interaction between Factor 1 (F1) of the first, second and third modes, is the most important one and it has to be mainly taken into account in the interpretation of the model.

Table 1
Largest core entries for the [2 3 2] Tucker model

Index of the core elements	Explained core variance (%)	Value of the core elements
[1 1 1]	25	2111
[2 2 1]	19	1825
[1 3 2]	18	1779

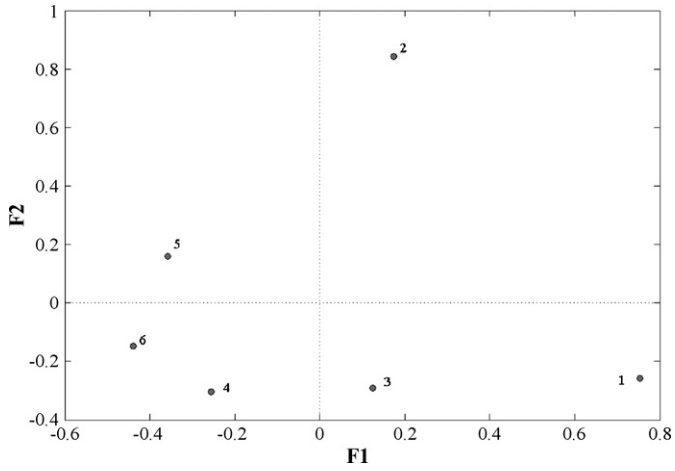


Fig. 4. Scores plot of mode 1 (samples) for the first two factors (results of Tucker3 applied on block scaled HS-SPME/GC-FID signals).

A careful analysis of the first two factors (F1 versus F2) scores plot of mode 1 (Fig. 4) shows that the first factor (F1) describes quite well the evolution of the ageing process of the several batterie, differentiating the degree of ageing of the vinegar samples. In fact, vinegar samples are well ordered on the basis of their age on the first factor, decreasing their scores values from the oldest sample to the youngest one.

Fig. 5 reports the second mode (HS-SPME/GC-FID signals) loadings plot of the first three factors.

Taking into account the highest absolute loadings values, the differentiation of the vinegar samples is strongly influenced by four main chromatographic regions corresponding to the following retention times—(i) Rt: 3–6 min; (ii) Rt: 12–15 min; (iii) Rt: 20–23 min; and (iv) Rt: 25–30 min.

The interpretation is based on loadings plots combined with the information in the core array elements. The first important core element (1 1 1) indicates interaction among Factor 1 (F1) of all the three modes. Considering the positive value of this interaction term, it could be said that the volatile compounds belonging to the chromatographic regions with highest loading

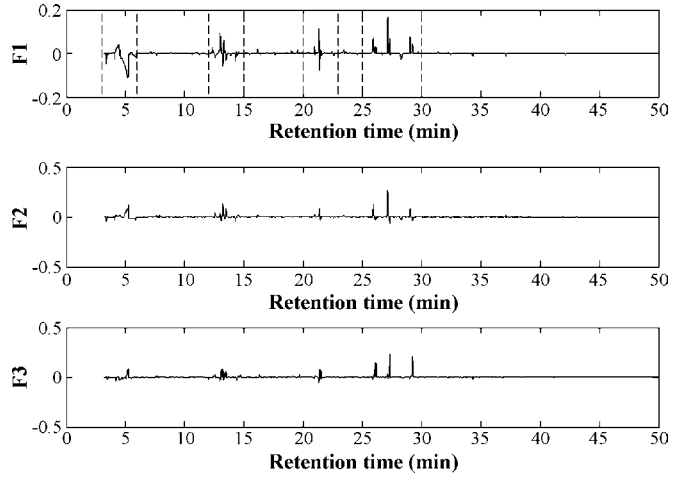


Fig. 5. Loadings plot of mode 3 (batterie) for the first two factors (results of Tucker3 applied on blockscaled HS-SPME/GC-FID signals).

values (referred to F1) are generally present in lower concentration in the younger samples (negative F1 scores values) and increase from middle to oldest samples, respectively.

In general, the compounds which concur to the volatile fraction of the product go through a variation when passing from the young to the middle age samples, while they have a tendency to concentrate during ageing, because of the loss of water.

Now, owing to the constancy of the overall instrumental conditions, i.e. chromatographic elution and detection, together with the experimental set up, namely the sample and flask volumes, temperature, conditioning, sampling time and SPME fibre, some further considerations might be carried out from a deeper evaluation of the chromatographic profiles reported in Fig. 1 and the Tucker loadings plots (Figs. 4 and 5).

In particular, the young samples are characterized by remarkable amount of ethanol and acetic acid (negative F1 loading value), which decreases with age and is no more present in old vinegars (positive F1 value). This behavior probably depends on the fermentation and bio-oxidation processes, which take place only in the young barrels. Initially, yeasts ferment sugars to alcohols, especially ethanol, which is successively oxidized to acetic acids by acetic acid bacteria. During ageing, the amount of acetic acid diminishes, probably because of a slow evaporation of this species.

The behavior of ethyl acetate, that is one of the species detected in young samples is similar to ethanol (they have both a negative loadings value in the respective modes). The ethyl acetate may be obtained from condensation reaction of ethanol and acetic acid. It is rather abundant during the first phase of maturation and is extremely reduced with time.

In the second chromatographic zone, Rt: 12–15 min, it has not been possible to assert the identity of the peaks on the basis of the libraries matches.

As far as 5-methyl-furfural is concerned (Rt: 14–14.5 min), its amount is relatively consistent (modest contribution to loadings of mode 2) in all samples in spite of the occurrence of the evaporation process, confirming also for this species the presence of a transformation/conversion process [20–22].

From a comparison between the F1 Tucker scores mode (samples mode) and the third zone of Fig. 4a, 2-phenyl-ethanol undergoes a concentration process during ageing.

Finally, phenyl-acetate, 5-hydroxymethyl-furfural (5HMF), and 5-acetoxymethyl-furfural is other significant molecule. The two compounds belonging to furfural family, 5HMF and 5-acetoxymethyl-furfural are produced during the cooking of the grape must to obtain the starting raw materials for ABTM, namely condensed cooked must [20]. 5HMF is present in all the samples (Fig. 2), but its concentration is definitely higher in old samples, mainly because of water evaporation, as well as 5-acetoxymethyl-furfural, that is mainly produced during ageing (both contribute with a positive loadings in F1 of mode 2). Finally, phenyl-acetate is present in low concentration in young samples and its amount significantly increases in middle age and old samples.

In addition, it is interesting to observe the third mode (batterie) loadings plot (Fig. 6): the batterie "Sa" and "O" lie on the extreme positions along the first and second factors, respectively. The second (2 2 1) and third (1 3 2) important core array elements seem to particularly highlight the peculiarity of the two oldest batterie.

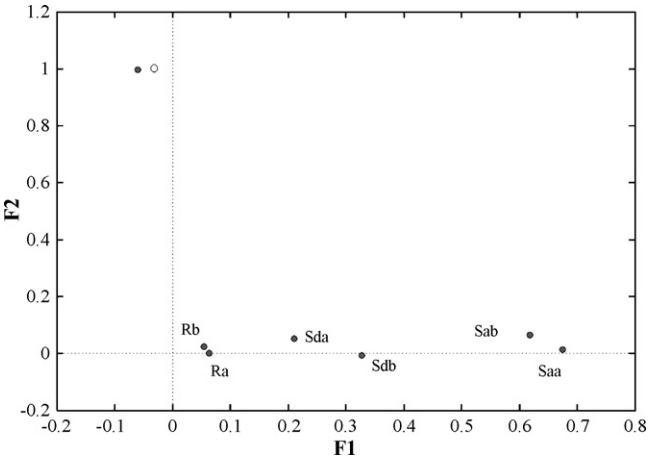


Fig. 6. Loadings plot of mode 2 (GC-signals) for the first two factors (results of Tucker3 applied on blockscaled HS-SPME/GC-FID signals).

As regards the interaction described by the (2 2 1) core array element, batteria Sa is quite peculiar, mainly because of sample 2, which has the highest amount of 2-phenyl-acetate and acetic acid and this determines its extreme position on high F2 values in mode 2 loadings plot.

The (1 3 2) core array element highlights the peculiar features of "O" batteria (the oldest one). The fact that Factor 2 of "batteria mode" interacts with Factor 1 of "barrel mode" can be interpreted as the ageing inside the barrel depends on whether the product starts to age in the oldest batteria "O" or in the younger ones. Considering Factor 3 of "retention time mode" are mainly influential the higher contents of phenyl-acetate, 5-hydroxymethyl-furfural (5HMF), and 5-acetoxymethyl-furfural species in oldest "O" samples with respect to the other batterie.

Although batteria "O" is the oldest ones, its position does not follow the ageing order along F1 in Fig. 6. This behavior could be due to a shift on retention times values for its samples with respect to the corresponding samples of the other batterie, as shown in Fig. 7, where a zoom of the chromatographic regions

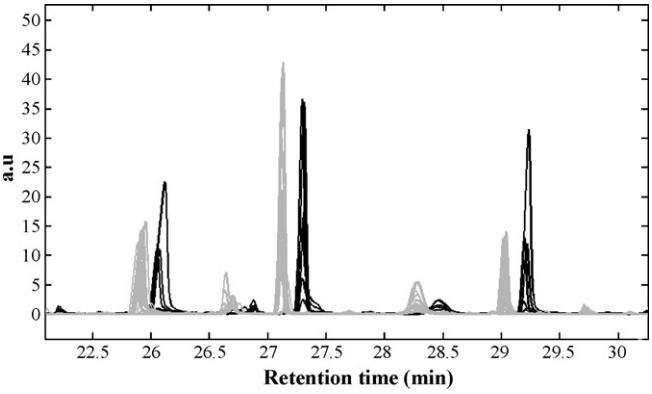


Fig. 7. The chromatograms of the oldest samples (1) of each batteria are reported overlaid. The black solid line refers to the chromatogram of batteria "O" oldest sample.

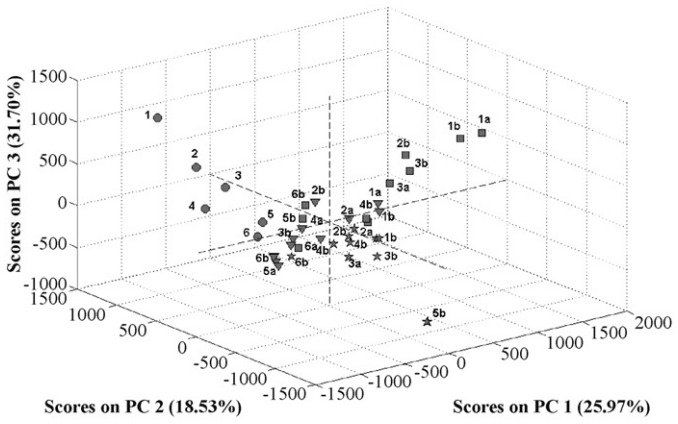


Fig. 8. Scores plot for the first three principal components (results of PCA-unfolding analysis applied on blockscaled data). The % of explained variance by each component is reported on parenthesis and it is expressed with respect to raw data. Labels from 1 to 6 refer to casks, replicates are labelled with 'a' and 'b' letters. Symbols: circles, batteria "O"; stars, batteria "R"; squares, batteria "Sa" and triangles, batteria "Sb".

between 25 and 31 min of the raw HS-SPME/GC-FID signals (grey lines) of all the batterie, together with the batteria "O" (black lines) is reported. "O" batteria's samples are actually shifted with respect to the other ones and the shift problem is more evident among the Factor 3 loadings value.

In order to deal with the shift issue an attempt to use PARAFAC2 method has been done, but neither using the "retention times × samples × batterie" nor the "retention times × batterie × samples" arrangement we did get any better result. To consider the eventual performance of different alignment algorithms as preprocessing step will be dealt in a future work.

However, it has to be noticed how Tucker3 model has been able to hold the major information on the first two factor and living out the shifting problem mainly in Factor 3.

In order to highlight the advantages offered by a three-way approach, the Tucker3 results have been compared with standard two-dimensional PCA analysis. PCA has been performed by unfolding the 6 vinegar samples × 7018 HS-SPME/GC-FID signal points × 7 batterie data array to a bi-dimensional matrix with all the vinegar samples on the rows (42 samples resulting from 6 samples × 7 batterie) and the HS-SPME/GC-FID signal points on the columns.

The same pretreatment of the three-way case has been applied in order to obtain a more fair comparison among bi- and three-dimensional tools. A three principal components model, explaining 68% of the total data variance, seemed appropriate taking into account the screen plot (not shown) and the information that can be gathered by the corresponding scores plots.

Fig. 8 reports component 1 (PC1) versus component 2 (PC2) versus component 3 (PC3) PCA score plot. The samples have been labelled in the same way as for the three-dimensional case, i.e. the label 1 refers to the oldest samples and the label 6 to the youngest ones. The replicates are labelled with a and b letters. The several batterie are represented with different symbols, as reported in the legend of Fig. 8. Even if a good discrimination is observed for batteria "O", with all of its vinegar samples totally located on the right side of Fig. 8, an higher degree of overlap among the others batteries is evident. Furthermore, it is rather difficult to extrapolate any kind of information as far as the ageing process of ABTM samples is concerned due to overlapping among the different barrels. In fact, due to the batterie peculiarities, it is reasonable that 'young' samples coming from old batterie are somehow similar to 'old' samples that belong to young batterie. Concluding, PCA analysis mainly highlights the inter-batterie differences and not the intra-batteria ones, giving limited information about the ABTM ageing process.

As far as PCA loadings plot is concerned, the most influential chromatographic peaks are substantially the same with respect to Tucker3 mode 2 loading plot and thus PCA loadings plots have not been reported.

Summarizing, adopting unfolding strategy does not give any information as far as ABTM ageing process is concerned since the patterns in the scores plot are less recognizable, thus there is an obvious advantage by using methods, which takes into account the true tri-dimensional structure of the data set.

4. Conclusions

This work is focused on the analyses of the volatile compounds of ABTM samples of different age, coming from different batterie. Tucker3 model was applied for the analyses of the whole signal data, performing a block scaling pretreatment to emphasise the importance of minor constituents. The batterie showed an analogous trend in the evolution of the volatile organic compounds observable in the first mode scores plot, where samples are grouped according to vinegar age. It was possible to observe that the compounds which concur to the volatile fraction of the product are extremely transformed from the young to the middle age samples, besides they have a tendency to concentrate during ageing, because of the natural loss of water.

Generally, the separation of vinegar samples of different age is due both to the different amount of acetic acid, ethyl acetate and ethanol (that are the principal products of the alcoholic fermentation and bio-oxidation processes) and of furfurals and other minor compounds.

Moreover, it was observed that the three-way method is more efficient for the study of these types of data than unfolding PCA, as it offers an easier visualisation of the data structure, in particular capturing the trends which are common to the different batterie in the samples mode plot and the variability due to the different batterie in the third mode loadings plot.

References

[1] Council Regulation (EC) No. 813/2000 of 17 April, 2000, Official J. L 100, 20/04/2000, pp. 0005–0006.
[2] M. Cocchi, P. Lambertini, D. Manzini, A. Marchetti, A. Ulrici, J. Agric. Food Chem. 50 (2002) 5255.
[3] M. Cocchi, G.C. Franchini, M. Manfredini, D. Manzini, A. Marchetti, A. Ulrici, J. Agric. Food Chem. 52 (2004) 4047.
[4] M. Cocchi, C. Durante, M. Grandi, P. Lambertini, D. Mancini, A. Marchetti, Talanta 69 (2006) 1166.

[5] F. Masino, F. Chinnici, G.C. Franchini, A. Ulrici, A. Antonelli, Food Chem. 92 (2005) 673.
[6] C.L. Arthur, J. Pawliszyn, Anal. Chem. 62 (1990) 2145.
[7] O. Pinho, I.M.P.L.V.O. Ferreira, Anal. Chem. 74 (2002) 5199.
[8] M. Cocchi, C. Durante, G. Foca, D. Manzini, A. Marchetti, A. Ulrici, Chemom. Intell. Lab. Syst. 71 (2004) 129.
[9] A. Smilde, R. Bro, P. Geladi, Multi-way Analysis, Applications in the Chemical Science, Wiley, England, 2004.
[10] V. Pravdova, C. Boucon, S. De Jong, B. Walczak, D.L. Massart, Anal. Chim. Acta 462 (2002) 133.
[11] R. Bro, C.A. Andersson, H.A.L. Kiers, J. Chemom. 13 (1999) 295.
[12] R. Bro, Chemom. Intell. Lab. Syst. 46 (1999) 133.
[13] D. Bylund, R. Danielsson, G. Malmquist, K.E. Markides, J. Chromatogr. A 961 (2002) 237.
[14] F. Guimet, J. Ferrè, R. Boquè, R. Xavier, Anal. Chim. Acta 515 (2004) 75.
[15] A.E. Sinha, J.L. Hope, B.J. Prazen, C.G. Fraga, E.J. Nilsson, R.E. Synovec, J. Chromatogr. A 1056 (2004) 145.
[16] S. Wold, E. Johansson, M. Cocchi, in: H. Kubinyi (Ed.), 3D QSAR in Drug Design: Theory, Methods and Applications, ESCOM Science Publishers, Leiden, 1993, p. 523.
[17] L. Munck, L. Nørgaard, S.B. Engelsen, R. Bro, C.A. Andersson, Chemom. Intell. Lab. Syst. 44 (1998) 31.
[18] R. Henrion, Chemom. Intell. Lab. Syst. 25 (1994) 1.
[19] C.A. Andersson, R. Bro, The *N*-way toolbox for Matlab can be downloaded from http://www.models.kvl.dk/source/nwaytoolbox/, 1998.
[20] M. Cocchi, G. Ferrari, D. Manzini, A. Marchetti, S. Sighinolfi, J. Food Eng. 79 (2007) 1438.
[21] T. Modig, G. Liden, M.J. Taherzadeh, Biochem. J. 363 (2002) 769.
[22] M.J. Taherzadeh, L. Gustafsson, C. Niklasson, G. Liden, Appl. Microbiol. Biotechnol. 53 (2000) 701.

Available online at www.sciencedirect.com
ScienceDirect
Talanta 74 (2008) 711–716
Talanta
www.elsevier.com/locate/talanta

Analysis of elements in wine using near infrared spectroscopy and partial least squares regression

D. Cozzolino [a,b,*], M.J. Kwiatkowski [a,b,1], R.G. Dambergs [a,b,1], W.U. Cynkar [a,b,1], L.J. Janik [a,b,1], G. Skouroumounis [a,b,1], M. Gishen [a,b,1,2]

[a] *The Australian Wine Research Institute, Waite Road, Urrbrae, PO Box 197, Adelaide, SA 5064, Australia*
[b] *The Cooperative Research Centre for Viticulture, PO Box 154, Glen Osmond, SA 5064, Australia*

Received 10 May 2007; received in revised form 29 June 2007; accepted 29 June 2007
Available online 7 July 2007

Abstract

The use of visible (VIS) and near infrared spectroscopy (NIRS) to measure the concentration of elements in Australian wines was investigated. Both white ($n = 32$) and red ($n = 94$) wine samples representing a wide range of varieties and regions were analysed by inductively coupled plasma mass spectrometry (ICP-MS) for the concentrations of calcium (Ca), potassium (K), magnesium (Mg), phosphorus (P), sodium (Na), sulphur (S), iron (Fe), boron (B) and manganese (Mn). Samples were scanned in transmittance mode (1 mm path length) in a monochromator instrument (400–2500 nm). The spectra were pre-treated by second derivative and standard normal variate (SNV) prior to developing calibration models using partial least squares (PLS) regression method with cross-validation. The highest coefficients of determination in cross-validation (R^2_{val}) and the lowest errors of cross-validation (SECV) were obtained for Ca (0.90 and 9.80 mg L^{-1}), Fe (0.86 and 0.65 mg L^{-1}) and for K (0.89 and 147.6 mg L^{-1}). Intermediate R^2_{val} (<0.80) and SECV were obtained for the other minerals analysed. The results showed that some macro- and microelements present in wine might be measured by VIS–NIRS spectroscopy.
© 2007 Elsevier B.V. All rights reserved.

Keywords: Elements; Wine; Near infrared spectroscopy; Partial least squares

1. Introduction

Element analysis in wine is undertaken to determine legal limits for export purposes, to monitor trace contaminants, to monitor the content of certain metal salts (e.g. calcium and potassium), for authenticity purposes and as an indication of potential changes in colour and oxidation, and its health benefits [1–7]. Among spectroscopic techniques, near infrared (NIR) spectroscopy (NIRS) has been used as a method to predict the quality of different foods and agricultural products due to the speed of analysis, minimal sample preparation and low cost [8–10]. The NIR spectrum of an organic material can give a global signature of composition based basically on the assessment of the organic chemical structures containing O–H, N–H and C–H bonds which, with the application of chemometric techniques (e.g. principal component analysis and partial least squares regression), can be used to elucidate particular compositional characteristics in the food matrix not easily detected by targeted chemical analysis [8–10]. NIRS has been used to determine macro- and microelements in a wide range of agricultural products and foods. However, the determination of inorganic compounds is more challenging compared to organic compounds owing to the lack of a direct relation between the element involved and the spectra obtained [11–17]. NIRS could be used for determining mineral concentration, due to the association between minerals and organic functional groups in the food matrix and the effect on O–H bonding [11–17]. The estimation of mineral elements by NIRS is therefore generally dependent on the presence of those elements in mixtures of organic or hydrated compounds and salts (cations and anions) [11,15,17].

In agricultural products NIRS has been used to measure mineral content in plants and meat samples [11,15,17,18]. Despite

* Corresponding author at: The Australian Wine Research Institute, Waite Road, Urrbrae, PO Box 197, Adelaide, SA 5064, Australia.
Fax: +61 8 8303 6601.
E-mail addresses: Daniel.Cozzolino@awri.com.au (D. Cozzolino), mark.gishen@internode.on.net (M. Gishen).
[1] Fax: +61 8 8303 6601.
[2] Current address: Gishen Consulting, PO Box, Hahndorf, SA 5425, Australia.

0039-9140/$ – see front matter © 2007 Elsevier B.V. All rights reserved.
doi:10.1016/j.talanta.2007.06.045

the reports of many satisfactory calibrations for mineral elements for a particular material, it is difficult to apply the results from one food to another because the form of the organic molecule/mineral compounds can vary seasonally and/or among species, type of food and processing methods [18]. This may lead to unstable calibrations, inconsistent results and difficulty to expanding calibrations beyond a well-characterised population [11–18]. Therefore, the development of universal calibrations for minerals is difficult [18]. For example, phosphorus occurs in plants mainly as ionic organic molecules of phytate, phospholipids and nucleic acids, and the proportion of total P in these forms varies among food, plant species and seasonally [11–18]. Thus, in order to develop a NIRS calibration model for minerals in wines, it would be necessary to include a wide range of varieties.

The use of VIS–NIR spectroscopy in the Australian wine industry has mainly been restricted to the measurement of the concentration of total anthocyanins (colour), total soluble solids and pH in red grapes [19], methanol in spirits [20] and phenolics in red wines [21]. Only one reference describing the use of NIRS to determine elements in wine was found in the literature [1]. These authors attempted to determine six elements (K, Na, Mg, Ca, Fe and Cu) using 24 white wine samples. As far as we know, this is the first report on the use of NIRS to determine elements in a wide range of red and white wine varieties.

The purposes of this study were to establish the relationships between elements in wine and NIRS, to evaluate the potential of this method as a quantitative analytical technique and to evaluate the use of a normalization technique (logarithmic transformation) in order to develop the calibration models.

2. Materials and methods

2.1. Wine samples and elemental analysis

A total of 126 available commercial wine samples were used in this study, comprising of 94 red wine samples including Cabernet Sauvignon ($n = 30$), Shiraz ($n = 40$) and Merlot ($n = 24$) and 32 white wine samples including Chardonnay ($n = 10$), Riesling ($n = 15$), Sauvignon Blanc ($n = 5$) and Verdelho ($n = 2$). The wines were analysed for calcium (Ca), potassium (K), magnesium (Mg), manganese (Mn), boron (B), sodium (Na) and sulphur (S) using inductively coupled plasma atomic emission spectrometry (ICP-MS), performed by the Waite Analytical Services, School of Agriculture and Wine, University of Adelaide. Samples were digested with nitric acid and hydrochloric acid [22]. All analyses were done in duplicate.

2.2. Spectroscopic measurements

Wine bottles were opened for testing and scanned on the same day in transmission mode (400–2500 nm) using a scanning monochromator FOSS NIRSystems6500 (FOSS NIRSystems, Silver Springs, MD, USA). Spectral data collection was made using Vision software (version 1.0, FOSS NIRSystems, Silver Spring, USA). Samples were scanned in a rectangular cuvette with a 1 mm path length (FOSS NIRSystems, part number 7063-1) and temperature equilibrated at 33 °C for 2 min in the instrument before scanning [23,24].

2.3. Data analysis and interpretation

Spectra were exported from the Vision software in NSAS format for chemometric analysis in The Unscrambler software (version 9.5, CAMO ASA, Norway). Principal component analysis (PCA) was performed before partial least squares regression (PLS) models were developed. PCA was used to examine any relevant and interpretable structure in the data as well as outlier detection [25]. Calibration models between elements and VIS–NIR spectra were developed using PLS regressions with full cross-validation. The optimum number of terms in the PLS calibration models was determined as indicated by the lowest number of factors that gave the closest to minimum value of the PRESS (prediction residual error sum of squares) function in cross-validation, in order to avoid overfitting of the models [25,26]. The second derivative of the spectral data was used as a mathematical treatment to correct for baseline effects and to separate overlapping peaks and it was performed using Savitzky-Golay transformation and smoothing (five smoothing points and second polynomial order filtering) [25]. In smoothing, X-values (wavelengths) are averaged over one segment symmetrically surrounding a data point. Thus the raw value on this point is replaced by the average over the segment, thus creating a smoothing effect [25]. Standard normal variate (SNV) is a row-oriented transformation which centres and scales individual spectra. Each value in a row of data is transformed according to the formula [new value = (old value − mean (old row)]/standard deviation (old row), thus the practical result of SNV is that it removes scatter effects from spectral data [27]. The spectra in the region between 1800 and 2000 nm were off scale, and therefore were not used to build the calibration models.

Of the overall set of 126 samples, 63 samples were used for cross-validation as the training or calibration set (red wines $n = 47$; white wines $n = 16$), and 63 as the validation set for testing the model (red wines $n = 47$; white wines $n = 16$). Selection of both training and validation sets was performed using the algorithms available in the WinISI (v. 1.50) software package [28]. Samples used in the NIRS analysis were selected to represent the whole spectral and chemical variability in the target population in the calibration and validation groups. This enabled PCA to be performed on the registered spectra. The Mahalanobis distance (H) was used as a criterion for selecting those samples in the population as being more variable on the basis of spectra features [28]. The ISI algorithm CENTER was used to establish population boundaries with a maximum standardized H distance of 3.0. Then, the algorithm SELECT was used for efficient selection, by choosing samples with a minimum standardized H distance of 0.6 from their nearest neighbours [28].

Statistics calculated for the calibrations included coefficients of determination in cross-validation (R^2_{val}) and the standard error of cross-validation (SECV). The prediction accuracy of the models was tested on the validation set using the standard error of prediction (SEP), bias, slope and the coefficient of correlation (r) [25,26]. The residual predictive deviation (RPD = S.D./SECV),

defined as the ratio between the standard deviation of the population (S.D.) and the SECV for the NIR predictions, is a useful statistic that is often applied to evaluate how well a calibration model can predict chemical data [29,30]. If the SECV is large compared with the range of compositions (as S.D.), a relatively small RPD value results, and the NIR calibration model is considered not robust. The higher the value of the RPD the greater the probability of the model to predict the chemical composition accurately in samples outside the calibration set. An RPD value greater than three (range 3.1–4.9) is considered fair and recommended for screening purposes, an RPD value greater than 5 (range 5–6.4) is considered good for quality control [29,30]. Only optimal models are presented and discussed in this paper.

3. Results and discussion

3.1. Sample composition

The mean, range, standard deviation (S.D.) and coefficient of variation (CV) for the elements measured in both the calibration and validation sets are shown in Table 1. The samples analysed showed a wide range in elemental composition as shown by the range and CV. High CV was observed for Na (58.9%), Fe (51%) and Mn (41.7%) and possibly due to the different varieties and regions used. The ranges in values observed are in accordance with typical values expected in Australian wines [31,32]. Therefore, the variability in elemental composition in both calibration and validation sets was considered suitable for developing NIR calibrations for these elements.

Table 1
Mean, standard deviation, minimum, maximum and coefficient of variation of elements measured in both red and white wines using the reference method (ICP-MS)

mg L^{-1}	Mean	S.D.	Min.	Max.	CV
Calibration set ($n = 63$)					
Ca	59.13	15.08	24.0	107.0	25.4
Mg	121.56	28.91	69.0	210.0	23.8
Na	41.3	24.2	4.6	117.0	58.9
K	874.43	248.5	300.0	1360.1	29.3
P	207.6	65.9	87.0	500.0	31.7
S	160.6	38.9	82.0	260.1	24.2
Fe	1.64	0.85	0.19	4.0	51.5
Mn	1.63	0.68	0.50	3.5	41.7
B	6.59	2.5	1.8	11.1	37.9
Validation set ($n = 63$)					
Ca	60.22	13.57	33.0	93.0	22.5
Mg	123.19	34.52	63.0	220.0	28.0
Na	40.46	22.03	11.0	114.1	54.4
K	878.23	281.10	290.0	1600	32.0
P	213.1	57.54	35.1	390.1	27.0
S	151.02	31.92	97.0	240.1	21.1
Fe	1.52	0.83	0.41	4.3	54.6
Mn	1.60	0.88	0.30	4.1	55.0
B	6.39	2.52	3.0	15.1	39.4

S.D.: standard deviation; Min.: minimum; Max.: maximum; CV: coefficient of variation.

Table 2
Visible and near infrared partial least squares (PLS) calibration statistics for elemental concentration in the calibration set of wine samples

	n	R^2_{val}	SECV (mg L^{-1})	PLS factors	RPD
Ca	54	0.90	9.80	8	1.5
Mg	50	0.73	19.2	3	1.5
Na	35	0.77	8.7	1	2.7
K	55	0.89	147.6	3	1.7
P	42	0.79	33.7	3	2.0
S	45	0.70	32.10	3	1.2
Fe	47	0.86	0.65	8	1.3
Mn	43	0.78	0.44	2	1.5
B	53	0.81	2.26	7	1.1

n: number of samples after outlier removal; SECV: standard error in cross-validation; R^2_{val}: coefficient of determination in cross-validation; RPD: residual predictive deviation.

3.2. Calibration models

Statistics for the PLS calibration models developed for Ca, Mg, Na, K, P, S, Fe, B and Mn in wines using VIS and NIR wavelength regions are shown in Table 2. The highest coefficients of determination in cross-validation (R^2_{val}) and the lowest errors of cross-validation (SECV) were obtained for Ca (0.90 and 9.80 mg L^{-1}), Fe (0.86 and 0.65 mg L^{-1}) and K (0.89 and 147.6 mg L^{-1}). Intermediate R^2_{val} and SECV were obtained for the other minerals in the wine samples analysed. The results showed that some macro- and microelements present in wine might be measured by VIS–NIR spectroscopy. The RPD obtained for the calibration models developed were lower than 3, similar to those obtained by other authors using Sauvignon Blanc [1], indicating that the PLS calibrations developed could be used only as indicative of the mineral content in wine. However, a more qualitative interpretation of the RPD is given by other authors [34], where a RPD value lower than 1.5 were considered insufficient for most applications while NIRS calibration models with values greater than 2 were considered excellent [33,34]. Calibration models with values higher than 1.5 and lower than 2 were judged useful contingent on accuracy requirements of the desired application [29,30]. In this study, calibration models for Ca, Mg, K, P and Mn were considered accurate for qualitative analysis. The SECV and R^2 values generally indicate how well the equations will perform within the same population. However, with minerals in wine, the R^2 may not be a good indicator because of the small range of values. Other authors argue that mineral equations based on NIRS should be evaluated by coefficient of variation, rather than the R^2, as the range in concentration could render R^2 values misleading [18]. Additionally the interpretation of the R^2 is dependent of the distribution of analytical values. Clark et al. [10,11] proposed the use of the CV (SEP/mean) as a tool in evaluating NIRS calibration equations for minerals, although, the size and interpretation of the CV depends partly on the source of data used [33,34]. For example, CV values higher than 5% may accrue from the determination of the reproducibility of functionality parameters but in general CV values lower than 20% are considered adequate to predict elements [10,11].

Table 3
Visible and near infrared validation statistics for the prediction of elements in wine samples

	n	R	SEP (mg L^{-1})	Bias	Slope	CV prediction
Ca	56	0.66	11.9	−0.87	0.76	19
Mg	54	0.69	18.29	2.08	0.40	14.8
Na	40	0.50	9.88	−0.89	0.50	24.4
K	54	0.79	152.0	6.6	0.69	17.3
P	50	0.63	39.5	−18.8	0.49	18.5
S	50	0.30	27.5	6.3	0.23	18.2
Fe	42	0.60	0.55	0.10	0.49	36.2
Mn	45	0.43	0.58	0.19	0.38	36.3
B	45	0.61	1.65	0.98	0.42	25.8

R: coefficient of correlation; n: number of samples in the validation set; SEP: standard error of prediction; CV: coefficient of variation.

Table 4
Visible and near infrared partial least squares (PLS) calibration statistics for elements in the set of wine samples after logarithmic transformation

	n	R^2_{val}	log SECV (mg L^{-1})	PLS factors
Ca	54	0.90	0.17	6
Mg	55	0.71	0.19	2
Na	40	0.55	0.46	1
K	57	0.81	0.22	2
P	52	0.40	0.22	1
S	50	0.78	0.14	2
Fe	50	0.72	0.55	3

n: number of samples; SECV: standard error in cross-validation; R^2_{val}: coefficient of determination in cross-validation; RPD: residual predictive deviation.

Table 3 shows the validation statistics (SEP, R, slope and bias) for the elements measured in wine. Good predictions were obtained for K (SEP = 152 mg L^{-1}), Ca (SEP = 11.9 mg L^{-1}), Fe (SEP = 0.55 mg L^{-1}), Mg (SEP = 18.3 mg L^{-1}), P (SEP = 39.5 mg L^{-1}) and B (SEP = 1.65 mg L^{-1}) while poor prediction was achieved for the other elements measured in wine. Although the calibrations developed are not accurate enough to provide a reliable analytical method, they can be used for a large-scale screening. The CV calculated indicates that the best calibrations were for Mg and K, intermediate for Ca and P, and not reliable for Fe, Mn, B and Na, in the set of wines analysed.

3.3. Logarithmic transformation

It was observed that the distribution of composition for Na, Fe, Mn and B was skewed with a long upper end tail and shortened lower end (see Fig. 1). Therefore logarithmic transformation of the mineral compositional data was attempted when the NIRS calibrations were developed for two main reasons. Firstly, this transformation had the effect of reducing the skewness by compressing the upper end (tail) and stretching the lower end of the distribution. Secondly, it reduced the within group variability, resulting mainly because of the fact that a wide range of samples of different varieties were used. The PLS calibration models developed using the logarithmic transformation in the wine element analysed using VIS and NIR wavelength regions are shown in Table 4. The use of the logarithmic transformation did not improve the performance of the PLS calibrations for the elements measured in the set of wine samples analysed.

3.4. PLS loadings

Loadings from the PLS calibration often resemble spectra in that they express the correlations between each wavelength

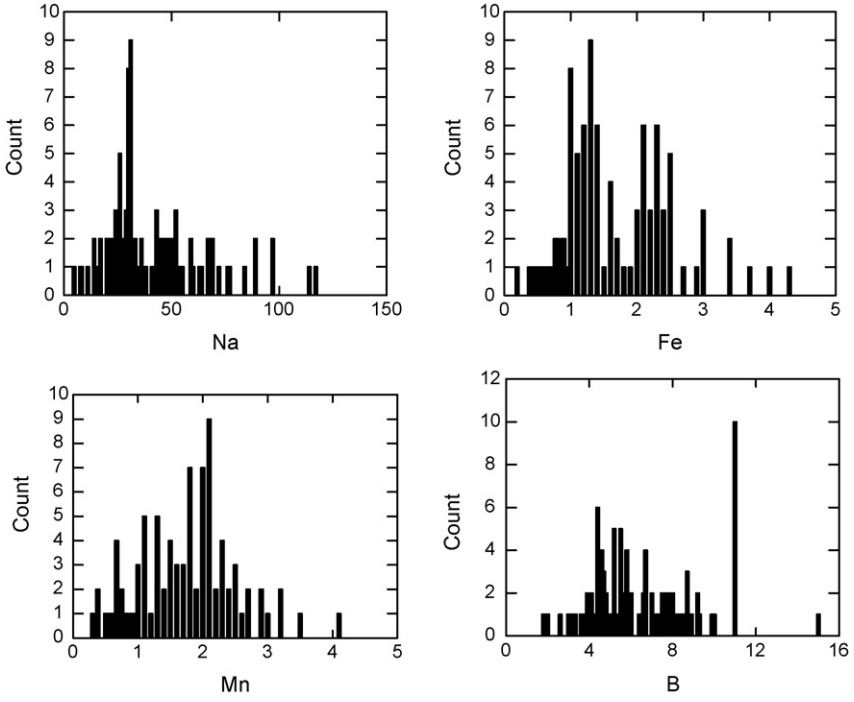


Fig. 1. Compositional distribution for Mn, Fe, Na and B in the set of wines analysed.

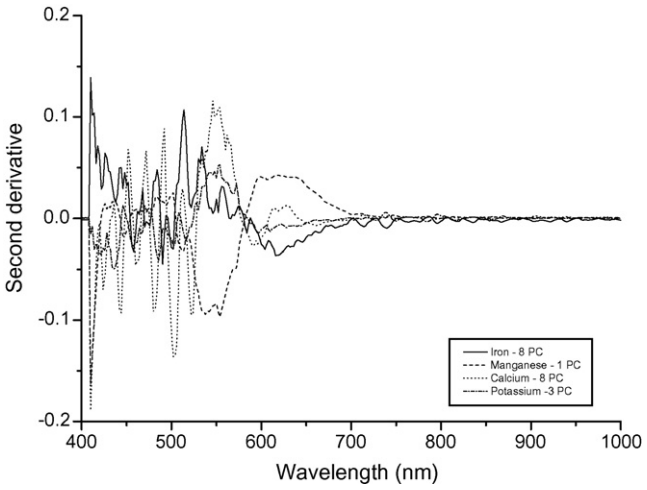


Fig. 2. Partial least squares loadings for optimal calibration models in the visible and short near infrared wavelengths (400–1000 nm).

point and may contain troughs and peaks, which can be attributed to overtone bands related to corresponding components in the matrix. However, this method could not be used directly because there was no absorption peak of inorganic components in the NIR region. The PLS loadings in the VIS region (Fig. 2) show that those wavelengths associated with changes in aging or oxidation, and pigments (around 550 nm) in both red and white wine samples have a positive influence in particular for K and Fe. Loadings in the NIR region show that the wavelengths at 1400 nm, between 1600 and 1700 nm related with O–H and C–H tones (e.g. sugars, water and ethanol) and between 2100 and 2200 nm related with C–H combinations tones had a large influence on the different calibration models developed, in particular for Ca and Fe, although no distinct NIR region dominated (Fig. 3). Inverse loadings were observed between the calibration for Ca and K, compared with Fe, mainly in the NIR region between 2100 and 2200 nm (C–H combination tones). For the other elements the loadings were spread along the NIR region, being difficult to assign to any particular bond.

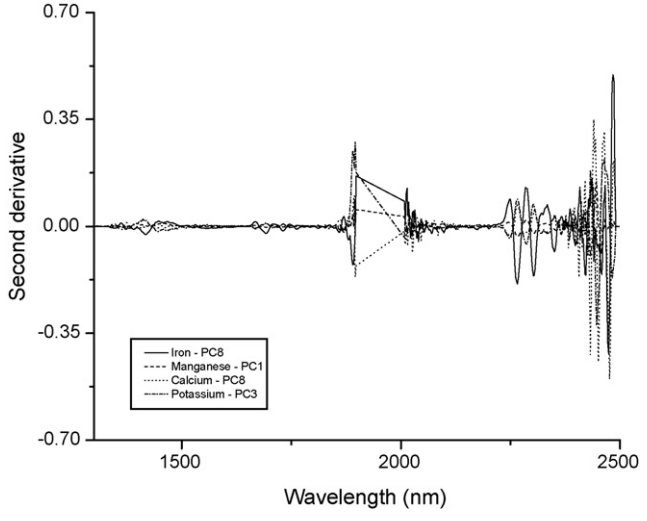


Fig. 3. Partial least squares loadings for optimal near infrared calibration models for elements in wine (1400–2500 nm).

It must be taken in consideration, however, that it is often difficult to assign wavelengths to specific molecular absorptions in the NIR region. This is especially true in the case of dissolved metal ions in solution, where the NIR absorption spectra are most likely affected by changes in the hydrogen bonding around the metal cations and associated organic compounds. If the element being measured is bonded within organic compounds the distortion of the spectrum may be detectable by certain wavelengths suggesting that NIRS could predict some elements. Additionally, some minerals (e.g. Ca and P) do not have absorption in the NIR region but could be indirectly detected through their linkage with diverse organic complexes such as chelates and pigments [10,11,18,33,34].

4. Conclusions

This study has shown that some relationships exist between NIR spectra and the concentration of some elements in wine. A simple measurement technique for a range of practically relevant elements in wine using NIR spectroscopy was proposed. At this stage the VIS and NIR calibrations are not suitable for quantitative routine use in an analytical laboratory, and further development with larger data sets will be required for the calibrations to become stable.

Acknowledgments

The author's thank Dr. M. Herderich and Dr. E.J. Waters of The Australian Wine Research Institute for their comments and suggestions on the manuscript. We thank Mrs. Teresa Fowles from the Waite Analytical Services, School of Agriculture and Wine, University of Adelaide for wine element analysis. This project is supported by Australia's grapegrowers and winemakers through their investment body the Grape and Wine Research and Development Corporation, with matching funds from the Australian Government, and by the Commonwealth Cooperative Research Centres Program. The work was conducted by The Australian Wine Research Institute and formed part of the research portfolio of the Cooperative Research Centre for Viticulture (CRCV).

References

[1] L. Sauvage, D. Frank, J. Stearne, M.B. Milikan, Anal. Chim. Acta 458 (2002) 223.
[2] M.J. Baxter, H.M. Crews, M.J. Dennis, I. Goodall, D. Anderson, Food Chem. 60 (1996) 443.
[3] M.M. Castiñeira, I. Feldmann, N. Jakubowski, J.T. Andersson, J. Agric. Food Chem. 52 (2004) 2962.
[4] S. Frias, J.E. Conde, J.J. Rodriguez-Bencomo, F. Garcia-Montelongo, J.P. Perez-Trujillo, Talanta 59 (2003) 335.
[5] J. Cacho, J.E. Castells, A. Esteban, B. Laguna, N. Sagristá, Am. J. Enol. Vitic. 46 (1995) 380.
[6] J. Danilewicz, Am. J. Enol. Vitic. 54 (2003) 2.
[7] R.I. Mellican, J. Li, H. Mehansho, S.S. Nielsen, J. Agric. Food Chem. 51 (2003) 2304.
[8] B.G. Osborne, T. Fearn, P.H. Hindle, Practical NIR Spectroscopy with Applications in Food and Beverage Analysis, Longman Scientific and Technical, Essex, UK, 1993, p. 227.

[9] E.R. Deaville, P.C. Flinn, in: D.I. Givens, E. Owen, R.F.E. Axford, H.M. Omedi (Eds.), Forage Evaluation in Ruminant Nutrition, CABI Publishing, Reading, UK, 2000, p. 301.
[10] D.H. Clark, E.E. Cary, H.F. Mayland, Agron. J. 81 (1989) 91.
[11] D.H. Clark, H.F. Mayland, R.C. Lamb, Agron. J. 79 (1987) 485.
[12] D. Cozzolino, A. Morón, Anim. Feed Sci. Technol. 111 (2004) 161.
[13] C. Petisco, B. Garcia-Criado, B.R. Vazquez de Aldana, I. Zabalgogeazcoa, S. Mediavilla, B. Garcia-Ciudad, Anal. Bional. Chem. 378 (2005) 458.
[14] I. Gonzalez-Martin, C. Gonzalez-Perez, J. Hernadez-Mendez, N. Alvarez-Garcia, Anal. Chim. Acta 468 (2002) 293.
[15] J.S. Shenk, M.O. Westerhaus, M.R. Hoover, J. Dairy Sci. 62 (1979) 807.
[16] B.R. Vazquez de Aldana, A. Garcia-Ciudad, B. Garcia-Criado, M.E. Perez-Corona, Commun. Soil Sci. Plant Anal. 26 (1995) 1383.
[17] A. Ruana-Ramos, A. Garcia-Ciudad, B. Garcia-Criado, Anim. Feed Sci. Technol. 77 (1999) 331.
[18] C.A. Roberts, J. Stuth, P.C. Flin, in: C.A. Roberts, J.J. Workman, J.B. Reeves (Eds.), Near Infrared Spectroscopy in Agriculture, ASA, CSSA, SSSA, Madison, WI, USA, 2004, p. 231.
[19] D. Cozzolino, W.U. Cynkar, R.G. Dambergs, M. Gishen, J. Near Infrared Spectrosc. 14 (2006) 279.
[20] R.G. Dambergs, A. Kambouris, I.L. Francis, M. Gishen, J. Agric. Food Chem. 50 (2002) 3079.
[21] D. Cozzolino, M. Kwiatkowski, M. Parker, M. Gishen, R.G. Dambergs, W. Cynkar, M. Herderich, Anal. Chim. Acta 513 (2003) 73.
[22] M.C. Almeida, M.T.S.D. Vasconcelos, M. Barbaste, B. Medina, Anal. Bioanal. Chem. 374 (2002) 314.
[23] D. Cozzolino, H.E. Smyth, M. Gishen, J. Agric. Food Chem. 51 (2003) 7703.
[24] D. Cozzolino, L. Liu, W.U. Cynkar, R.G. Dambergs, L. Janik, M. Gishen, C.B. Colby, Anal. Chim. Acta 588 (2007) 224.
[25] T. Naes, T. Isaksson, T. Fearn, T. Davies, A User-friendly Guide to Multivariate Calibration and Classification, NIR Publications, Chichester, UK, 2002, p. 420.
[26] M.J. Adams, Chemometrics in Analytical Spectroscopy, RSC, Analytical Spectroscopy Monographs, The Royal Society of Chemistry, Cambridge, UK, 1995, p. 216.
[27] R.J. Barnes, M.S. Dhanoa, S.J. Lister, Appl. Spectrosc. 43 (1989) 772.
[28] J.S. Shenk, M.O. Westerhaus, Analysis of Agriculture and Food Products by Near Infrared Reflectance Spectroscopy, Infrasoft International [ISI], MD, USA, 1993.
[29] T. Fearn, NIR News 13 (2002) 12.
[30] P.C. Williams, in: P.C. Williams, K.H. Norris (Eds.), Implementation of Near-infrared Technology, American Association of Cereal Chemist, St. Paul, MN, USA, 2001, p. 145.
[31] P. Godden, M. Gishen, Austr. N.Z. Wine Ind. J. 20 (2005) 21.
[32] B. Rankine, Making Good Wine: A Manual of Winemaking Practice for Australian and New Zealand, The Macmillan Company of Australia, 1998, p. 374.
[33] B.W. Dunn, G.D. Batten, S. Ciavarella, Aust. J. Exp. Agric. 42 (2002) 607.
[34] C.W. Chang, D.A. Laird, M.J. Mausbach, C.R. Hurburgh, Soil Sci. Soc. Am. 65 (2001) 480.

Available online at www.sciencedirect.com
ScienceDirect
Talanta 74 (2008) 703–710
Talanta
www.elsevier.com/locate/talanta

Determination of oxygenated polycyclic aromatic hydrocarbons in atmospheric aerosol samples by liquid chromatography–tandem mass spectrometry

Olivier Delhomme [a,b], Maurice Millet [b,*], Pierre Herckes [a]

[a] *Department of Chemistry and Biochemistry, Arizona State University, AZ 85287-1604, Tempe, USA*
[b] *Laboratoire de Physico-Chimie de l'Atmosphère, Centre de Géochimie de la Surface (UMR 7517 CNRS - Université Louis Pasteur), 1 rue Blessig, 67084 Strasbourg, France*

Received 25 April 2007; received in revised form 27 June 2007; accepted 28 June 2007
Available online 3 July 2007

Abstract

In this paper, the development of an analytical method using liquid chromatography–tandem mass spectrometry (LC–MS–MS) with atmospheric pressure chemical ionization (APCI) for the determination of 17 oxygenated polycyclic aromatic hydrocarbons (OPAH) is described. These OPAH include ketones, pyrones and diketones.

The APCI interface parameters have been optimized for maximum sensitivity.

Positive ion mode was proved to be most sensitive for ketones and pyrones while negative ion mode gave better detection limits for target diketones.

The detection limits of the method ranged from less than 1.20 $\mu g\,L^{-1}$ for several OPAH solutions (between 0.10 and 0.70 $\mu g\,L^{-1}$ for positive mode and between of 0.19 and 1.20 $\mu g\,L^{-1}$ for negative mode).

The analytical method was applied particulate matter ($PM_{2.5}$) samples collected over 24–48 h periods between March 2005 and June 2005 in Tempe (Arizona, USA). Before analysis aerosol samples were solvent extracted and concentrated to a final volume of 1 mL of methanol. OPAH concentrations observed for this urban site ranged from 0.22 to 3.60 $ng\,m^{-3}$.
© 2007 Elsevier B.V. All rights reserved.

Keywords: Oxygenated polycyclic aromatic hydrocarbon; Liquid chromatography coupled to mass spectrometry; Liquid chromatography with fluorescence detection; Atmospheric pressure chemical ionization interface; Particulate matter

1. Introduction

Oxygenated polycyclic aromatic hydrocarbons (OPAH) are an important class of semivolatile organic compounds. Atmospheric OPAH can be formed through incomplete combustion of organic matter such as fossil fuels or biomass and are directly emitted as primary aerosol components. OPAH can also be of secondary origin as formed by photo-oxidation of polyaromatic hydrocarbons (PAH) [1]. Both primary and secondary sources influence the OPAH abundance and profiles in ambient air.

Studies performed on diesel exhaust particles (DEP) and extracts as well as on concentrated air particulates led to the conclusion that organic compounds, adsorbed on particulate matter play an important role about the generation of adverse health effects [2–7]. OPAH are of particular interest in this regard as many of them are known or suspected to be toxic, carcinogenic, mutagenic, or allergenic. In addition to open air OPAH can be formed in the human metabolism of PAH or inhaled directly with fuel combustion aerosols and cigarette smoke [8,9]. Moreover OPAH can be considered more toxic than the parent PAH, because they have been identified as having a direct mutagenic potency whilst PAH requires a prior enzymatic activation [10]. Surprisingly little information is available on OPAH concentrations in the atmosphere, despite the obvious interest in their concentration levels [11].

Several analytical techniques have been proposed for the determination of OPAH. These include the determination of OPAH using the reversed-phase high performance liquid chromatography with fluorescence detection (HPLC–FD) [12,13].

* Corresponding author.
E-mail address: millet@illite.u-strasbg.fr (M. Millet).

0039-9140/$ – see front matter © 2007 Elsevier B.V. All rights reserved.
doi:10.1016/j.talanta.2007.06.037

However, many OPAH especially diketones cannot be directly detected in this way, and require an online reduction to the corresponding hydroxy-PAH. This latter method was tested within the framework of the current study.

For some OPAH, gas chromatography coupled to mass spectrometry (GC–MS) can be an useful analytical method [14]. However, for thermally labile substances or compounds with low vapour pressure and high polarity this method is usually applicable only after derivatization [14].

HPLC coupled to mass spectrometry (LC–MS) was applied to a variety of OPAH. It did not need derivatization and solved other limitations of GC–MS and HPLC fluorescence techniques. Most published LC–MS methods used single mass experiments with in-source fragmentation [11,15,16]. Tandem mass spectrometry (MS–MS) seemed to have the peculiarity of producing selective fragmentation patterns, which holds valuable structural information, for every substance. In addition, specific mass losses can be used for identification and quantification leading to an increase of selectivity [17].

An LC–APCI–MS–MS method for the determination of selected OPAH in aerosol samples was developed, optimized and applied to high-volume air particulate samples collected between March 2005 and June 2005 in Tempe (Arizona, USA). The target OPAH include benzanthrone, chromone, xanthone, benz[*b*]fluoren-11-one, perinaphthenone, anthraquinone, benz[*a*]anthracen-7,12-dione, 1,4-naphthoquinone, 1,4-benzoquinone, acenaphthenequinone, phenanthrenequinone, 2-methylanthraquinone, pyrene-4,5-dione, aceanthrenequinone, 2-ethylanthraquinone, 1,4-chrysenedione and 5,12-naphthacenequinone.

2. Experimental

2.1. Chemicals and solutions

Dichloromethane and methanol of Optima grade quality were purchased from Fisher Scientific (Pittsburgh, PA, USA). High-purity water was obtained from a Milli-Q water system from Millipore (Billerica, MA, USA).

The OPAH (anthraquinone, benzanthrone, benz[*a*]anthracen-7,12-dione, 1,4-naphthoquinone, chromone, xanthone and benz[*b*]fluoren-11-one) were supplied by Aldrich (L'Isle d'Abeau, France) and (1,4-benzoquinone, perinaphthenone, acenaphthenequinone, phenanthrenequinone, 2-methylanthraquinone, pyrene-4,5-dione, aceanthrenequinone, 2-ethylanthraquinone, 1,4-chrysenedione and 5,12-naphthacenequinone) were purchased from Acros Organics (Noisy le Grand, France).

1,4-Benzoquinone-d_4 and Benzophenone-2,3,4,5,6-d_5 were purchased from Aldrich and were used as internal standards.

Stock solutions of each OPAH at $1\,g\,L^{-1}$ and calibration standard solutions were prepared in methanol.

2.2. Aerosol samples

Twenty three aerosol samples were collected between March 2005 and June 2005 at the meteorological station on the campus of the Arizona State University (ASU) in Tempe (Arizona, USA). The site was chosen in order to be representative of urban conditions.

Fine particulate matter ($PM_{2.5}$) samples were collected on quartz fiber filters (QM-A, Whatman, Florham Park, NJ) using a high-volume air sampler (Thermo Andersen, Smyrna, GA) which was operated between 24 and 48 h at a flow rate of $1.13\,m^3\,min^{-1}$ using a $PM_{2.5}$ impactor stage (TE231, Tisch Environmental, Cleves, OH) to remove particulate matter larger than 2.5 μm in diameter. Before use, all filters were pre-fired at 600 °C for at least 12 h in a muffle furnace to remove organic contaminants. After sampling the filters were stored in a freezer at −18 °C until analysis.

2.3. Extraction

Two 1/8 sections of the high-volume quartz fiber filters were used for OPAH analysis. To verify the homogeneity of the samples two filters were each cut into eight pieces and the OPAH concentrations on each individual piece were determined. Coefficients of variations varied between 1 and 6%.

The two 1/8 sections of the filter were spiked with a known concentration ($0.1\,mg\,L^{-1}$) of the two deuterated internal standards (1,4-benzoquinone-d_4 for the diketones and benzophenone-2,3,4,5,6-d_5 for the ketones and pyrones), for the determination of recovery of this extraction. Results were adjusted based on these results. These two sections are cut into small pieces with solvent cleaned blades and put together in a jar with 20 mL of dichloromethane (DCM). The jar was then subjected to ultrasonic agitation for 20 min at ambient temperature. The DCM extract is transferred in another jar and the sample composite was then extracted two more times with 20 mL DCM under sonication [18].

These three DCM extracts were combined and evaporated to near dryness under purified nitrogen and the solvent was exchanged with 1 mL of methanol. The final extract volume to be analyzed was 1 mL.

2.4. LC–APCI–MS–MS

The LC–MS–MS experiments were performed using a Varian (Palo Alto, CA, USA) series 1200 triple quadrupole mass spectrometer equipped with an atmospheric pressure chemical ionization (APCI) source and a Varian Prostar HPLC system (quaternary pump, column thermostat and auto sampler).

The LC separation was performed using a C_{18} reverse phase column (Supelco 100-5 C_{18} PAH, 250 × 3 mm i.d., Supelco Park, Bellefonte, PA, USA), with water (solvent A)/methanol (solvent B) eluent as the mobile phase at a flow rate of $0.85\,mL\,min^{-1}$. The column oven temperature was set to 25 °C and the injection volume was 20 μL.

For the ketones and pyrones the separation started with 60% of B for 2.5 min followed by a linear increase of B to 100% in 3.5 min. Mobile phase B was held at 100% for 2.5 min and then reduced within 2.5 min to the initial conditions. Finally, the column was equilibrated for 5 min between each analytical run.

For the diketones the elution gradient started with 30% B for 3 min followed by a linear increase of B to 75% in 12 min. Mobile

Table 1
Optimum values of different parameters for APCI interface

Parameters	Optimum value	
	Diketones	Ketones and pyrones
Ionization mode	Negative	Positive
Drying gas temperature (°C)	300	250
Drying gas flow (L min^{-1})	2.5	2.5
Drying gas pressure (psi)	20	18
Auxiliary gas temperature (°C)	450	450
Auxiliary gas flow (L min^{-1})	2	2
Auxiliary gas pressure (psi)	17	17
Nebulizer gas flow (L min^{-1})	2	2
Capillary voltage (V)	40	100
Corona current (μA)	−5	7.5

phase B was kept at 75% for 13 min, then B increased to 100% in 2 min and then reduced within 4 min to the initial conditions. Finally, the column was equilibrated for 6 min between each analytical run.

The mass spectrometer was connected to the HPLC system via an APCI interface. The parameters for the APCI interface have been optimized and are detailed in Table 1.

For all species under consideration a scan of standard solutions by Q1 (first ionization) produced dominant pseudo molecular ions: $[M+H]^+$ for the ketones and pyrones, $[M]^-$ for the diketones. These pseudo molecular ions were chosen as precursor ions to undergo fragmentation. Argon was introduced into collision cell Q2 with a pressure of 2 mTorr to collide with precursor ions and fragmentation was achieved. All diketones showed fragment ions due to double CO elimination $[M-28-28]^-$ and all ketones and pyrones produced fragment ions due to CO + H elimination $[M+H-29]^+$. The collision energy was adjusted for each OPAH to yield highest sensitivity. The precursor ions, selected fragments and collision energies are listed in Table 2.

2.5. HPLC-fluorescence

The HPLC analysis with fluorescence detection was performed using a Kontron (Serlabo Technologie, Avignon, France) HPLC system consisting of two Kontron 420 pumps, a M 491 Kontron mixing chamber, a 482 Kontron controller, a Kontron 465 automatic injector, a Jasco (Bouguenais, France) FP-1520 scanning fluorescence detector, two 402 Kontron thermostat controller and a 3493 Kontron degassing system.

The analytical column oven temperature was set to 25 °C, the injection volume was 20 μL and the mobile phase was methanol containing 10 mM zinc chloride, 5 mM sodium acetate and 5 mM acetic acid [13] at a flow rate of 1 mL min^{-1}.

A reversed phase chromatographic column (Macherey-Nagel EC 250/8/4 Nucleosil 100-5 C_{18} PAH, 250 × 4 mm i.d., MN, Hoerth, France) inline with a guard column (CC 8/4 100-5 C_{18} PAH, MN, Hoerth, France) were used.

The on-line post-column reduction of the OPAH to the corresponding hydroxy-PAH was performed using a 20 mm × 4.6 mm i.d. metal column densely packed with a zinc catalyst (Interchim, Montluçon, France).

The excitation (λ_{ex}) and emission (λ_{em}) wavelengths used for the detection of different compounds were determined with a spectrofluorometer and were 280/350 for the hydroxyquinone, 250/325 for the 1,4-dihydroxynaphthalene and 230/310 for the 9 hydroxyxanthene.

3. Results and discussion

3.1. Optimization of the LC–MS–MS method

The MS system could alternately be equipped either with electron spray ionization (ESI) or APCI. In order to achieve highest method sensitivity both sources were evaluated for all targets OPAH.

Table 2
Precursor ions and selected fragments of OPAH used for the detection in MS–MS with APCI interface

Compounds	Precursor ion (m/z)	Selected fragment	Mass loss (Da)	Other product ions (m/z)	Collision energy (V)
Ketones and pyrones					
Chromone	147	118	29	147,91	8
Perinaphthenone	181	152	29	181,169	20
Xanthone	197	168	29	197,141	10
Benzanthrone	231	202	29	231,200	24
Benz[*b*]fluoren-11-one	231	202	29	231	22
Diketones					
1,4-Benzoquinone	108	52	56	108,80	20
1,4-Naphthoquinone	158	102	56	158,130	14
Acenaphthenequinone	182	126	56	182,154	18
Phenanthrenequinone	208	152	56	208,180	30
Pyrene-4,5-dione	232	176	56	232,204	26
Aceanthrenequinone	232	176	56	232,204	18
Anthraquinone	208	152	56	208,180	10
2-Methylanthraquinone	222	166	56	222,194	14
2-Ethylanthraquinone	236	180	56	236,208	14
1,4-Chrysenedione	258	202	56	258,230	20
5,12-Naphthacenequinone	258	202	56	258,230	18
Benz[*a*]anthracene-7,12-dione	258	202	56	258,230	18

Table 3
Limit of detection and limit of quantification for the LC–APCI–MS–MS method with negative or positive ionization

Compounds	Retention times (min)	Limit of detection ($\mu g\,L^{-1}$)		Limit of quantification ($\mu g\,L^{-1}$)		R^2
		APCI (−)	APCI (+)	APCI (−)	APCI (+)	
Ketones and pyrones						
Chromone	2.38	2.45	0.15	8.16	0.5	0.9997
Perinaphthenone	4.67	0.60	0.10	2.0	0.34	0.9996
Xanthone	6.90	250.00	0.70	832.50	2.33	0.9988
Benzanthrone	8.03	1.86	0.17	6.20	0.57	0.9991
Benz[*b*]fluoren-11-one	8.40	16.00	0.50	53.28	1.67	0.9844
Diketones						
1,4-Benzoquinone	1.96	1.20	ND	4.0	ND	0.9978
1,4-Naphthoquinone	11.09	0.40	ND	1.34	ND	0.9995
Acenaphthenequinone	11.20	0.31	1.28	1.04	4.26	0.9859
Phenanthrenequinone	14.13	1.15	6.60	3.83	22.00	0.9995
Pyrene-4,5-dione	16.13	0.44	ND	1.47	ND	0.9951
Aceanthrenequinone	16.76	0.87	2.25	2.90	7.50	0.9992
Anthraquinone	18.10	0.92	ND	3.06	ND	0.9979
2-Methylanthraquinone	20.88	0.23	4.46	0.77	14.85	0.9977
2-Ethylanthraquinone	23.97	0.19	1.45	0.63	4.83	0.9994
1,4-Chrysenedione	24.90	0.32	3.45	1.07	11.49	0.9983
5,12-Naphthacenequinone	25.50	0.28	1.92	0.93	6.40	0.9996
Benz[*a*]anthracene-7,12-dione	30.20	0.20	7.00	0.67	23.30	0.9937

ND: not detected; R^2 = correlation coefficient.

ESI with negative or positive ionization provided poor results. Most tested compounds were not detected (benzanthrone, chromone, xanthone, phenanthrenequinone, 2-methylanthraquinone, pyrene-4,5-dione, aceanthrenequinone, 2-ethylanthraquinone and 1,4-chrysenedione). For the remaining ones, the limit of detection (LOD) was very high: 0.4 $mg\,L^{-1}$ for 1,4-naphthoquinone, 0.35 $mg\,L^{-1}$ for perinaphthenone and 0.20 $mg\,L^{-1}$ for acenaphthenequinone.

The APCI source was evaluated in both modes of ionization (positive and negative) and the results are presented in Table 3 (detection limits obtained under optimized APCI interface conditions).

By operating in negative mode, APCI provided LOD ranging from 0.19 to 1.20 $\mu g\,L^{-1}$ for diketones, and from 0.60 $\mu g\,L^{-1}$ to 250 $\mu g\,L^{-1}$ for ketones and pyrones.

By contrast, LOD between 0.10 and 0.70 $\mu g\,L^{-1}$ were obtained for ketones and pyrones with APCI in the positive ionization mode. For the diketones, some of them were not detected and the others presented LOD ranging from 1.28 to 7.00 $\mu g\,L^{-1}$ (Table 3).

To detect as many compounds as possible at high sensitivity, two separate runs with the two different ionization modes were applied, i.e. APCI (+) for ketones and pyrones, and APCI (−) for diketones.

Some experiments were performed to optimize ionization parameters (data summarized in Table 1).

The drying gas flow in APCI is lower than in ESI mode (generally 4 $L\,min^{-1}$) but it is still critical for the dissociation of ion/solvent clusters before the sampling orifice. For both ionization modes the optimal gas flow is species dependent. The increase of drying gas flow from 1.5 to 2.5 $L\,min^{-1}$ provided good results, while extension to 4 $L\,min^{-1}$ did not add further marked improvements for mass response. On the other hand, higher flows increased the signal to noise ratio. Therefore, a value of 2.5 $L\,min^{-1}$ was chosen as a best compromise.

The nebulizer gas flow and the auxiliary gas flow, have both been increased from 1.5 to 1.9 $L\,min^{-1}$, have a too low rate and consequently induce an unstable baseline. While the values higher than 2.2 $L\,min^{-1}$ show a substantial decrease in response. Therefore, the nebulizer gas flow and the auxiliary gas flow were set to 2 $L\,min^{-1}$ for the two ionization modes.

The temperature of the auxiliary gas induced a small influence on the detector response compared to that of the drying gas. To render the interior of the ion source as dry as possible, a high value of auxiliary gas temperature is necessary, but no significant changes were observed above 450 °C. Thus, in both ionization modes the auxiliary gas temperature was fixed at 450 °C.

A strong influence of the drying gas temperature on the eluent evaporation and spray formation was observed. By increasing the temperature from 150 to 300 °C, the response initially was improved, however above 250 °C for positive mode and 300 °C for negative mode no significant increase is observed anymore. Therefore, the drying gas temperature was set slightly lower than the auxiliary gas, 250 °C for the ketones and pyrones in positive ionization mode and 300 °C for the diketones in negative ionization mode.

3.2. HPLC with fluorescence detection

Liquid chromatography with fluorescence detection after online reduction of the OPAH to the corresponding hydroxy-PAH was tested [10]. Generally the OPAH exhibited only very weak fluorescence signals as opposed to hydroxy-PAH. However, the fluorescence of hydroxy-PAH is lower than PAH fluorescence [19].

Table 4
Relative standard deviation (RSD) of LC–MS–MS determination of OPAH in standard solutions and aerosol samples

Compounds	Within-series imprecision R.S.D. (%)		Between-day imprecision R.S.D. (%)	
	Standard solutions	Aerosol sample	Standard solutions	Aerosol sample
Chromone	2.6	<LOQ	2.9	<LOQ
Perinaphthenone	4.2	4.6	4.0	7.2
Xanthone	3.2	<LOQ	3.7	<LOQ
Benzanthrone	2.5	1.8	3.5	3.0
Benz[*b*]fluoren-11-one	1.4	2.9	5.2	4.2
1,4-Benzoquinone	1.9	<LOQ	4.1	<LOQ
1,4-Naphthoquinone	2.1	<LOQ	2.8	<LOQ
Acenaphthenequinone	2.9	<LOQ	3.7	<LOQ
Phenanthrenequinone	3.5	3.9	6.8	3.8
Pyrene-4,5-dione	2.7	3.1	5.9	5.0
Aceanthrenequinone	2.6	<LOQ	2.0	<LOQ
Anthraquinone	2.9	2.3	5.5	6.2
2-Methylanthraquinone	2.3	3.5	6.2	2.9
Benz[*a*]anthracene-7,12-dione	3.7	3.3	4.7	6.6

Abbreviation: R.S.D. = relative standard deviation; LOQ = limit of quantification.

The first choice to use fluorescence detection was to obtain a very specific, sensitive and simple alternative to LC–MS–MS. However, the sensitivity of this method was not satisfactorily for the detection of low concentrations. For example, the limit of detection (LOD) for 1,4-dihydroxynaphthalene was 0.07 and 0.05 mg L^{-1} for the 9-hydroxyxanthene. In comparison using LC–MS–MS, LOD of 0.40 and 0.70 μg L^{-1} respectively, were achieved resulting in an improvement by several orders of magnitude. The efficiency of OPAH reduction ranged from 11 to 23% for the three compounds studied.

3.3. Calibration and uncertainties

The LC–MS–MS method was externally calibrated for the quantification of the 17 target OPAH in atmospheric samples. For this, standard solutions ranging from 0.005 to 0.5 mg L^{-1} were used. A good linearity was observed for the responses, with correlation coefficients (data summarized in Table 3) varying between 0.9844 for benz[*b*]fluoren-11-one and 0.9997 for chromone.

Within-series uncertainties were determined analyzing successively five times one standard with concentration of 0.05 mg L^{-1}. An authentic aerosol sample was also analyzed using the same approach. Results are presented in Table 4.

For the calculation of between-day uncertainty the standard solution of 0.05 mg L^{-1} and the aerosol sample were analyzed at three different dates (Table 4). The relative standard deviations (R.S.D.) were slightly higher for the between-day imprecision but the differences were small. Moreover daily variations of the LC–MS–MS were detected by processing regularly calibration standards during analysis of real samples.

To evaluate the method accuracy, matrix effects were investigated. For this purpose, a sample was divided into four aliquots. Two aliquots were processed at the optimum conditions, and the concentrations of OPAH in the aerosol sample were determined. The remaining two parts were spiked with a solution containing the target OPAH (0.05 mg L^{-1}) and were treated like the two other aliquots as described above (section extraction, page 5). Results for compounds present in the real sample are summarized in Table 5.

The concentrations of OPAH, in the four parallel experiments were almost the same and the slight differences observed were not significant taking into account the uncertainty of the method.

Table 5
Matrix effect for LC–MS–MS determination of OPAH

Compounds	Aerosol sample		Spike standard	
	Concentration AV (mg L^{-1})	R.S.D. (%)	Concentration AV (mg L^{-1})	R.S.D. (%)
Chromone	0.059	3.3	0.107	2.3
Perinaphthenone	0.241	0.8	0.293	7.4
Xanthone	0.062	3.6	0.113	5.2
1,4-Benzoquinone	0.171	1.8	0.217	5.5
1,4-Naphthoquinone	0.245	1.1	0.298	4.0
Phenanthrenequinone	0.332	1.5	0.384	1.3
Pyrene-4,5-dione	0.178	2.9	0.225	4.9
Anthraquinone	0.259	1.2	0.308	2.8
2-Methylanthraquinone	0.413	1.4	0.461	3.6
Benz[*a*]anthracene-7,12-dione	0.196	0.9	0.248	6.1

Abbreviation: R.S.D. = relative standard deviation; AV = average value.

The internal standards were used for the determination of recovery of the extraction. It was important to evaluate that the matrix constituents that are not separated from the internal standards do not affect the ionization process and thus decrease the sensitivity. For this purpose the overall method recoveries were calculated based on the recoveries of the internal standards in all analyzed samples. The recoveries were very reproducible and varied between 94.6% ± 0.5 for the diketones (1,4-benzoquinone-d_4) and 95.3% ± 0.6 for the ketones (benzophenone-2,3,4,5,6-d_5). This indicates that no matrix effect should be expected when analyzing aerosol samples.

The limit of detection (LOD) and the quantification limit (LOQ) defined as the lowest standard concentrations differing significantly from zero (S/N = 3 and S/N = 10 respectively), are summarized in Table 3.

3.4. Application to aerosol samples

The optimized method was applied to the analysis of OPAH in 23 aerosol samples.

Fine particulate matter ($PM_{2.5}$) samples were collected regularly between March and June 2005 in Tempe (Arizona, USA). The results are presented in Table 6. The concentration of OPAH varied between 0.22 and 3.60 ng m^{-3}.

The samples obtained during this campaign were analyzed to show the applicability of the method to ambient aerosol. The number of observations was insufficient to investigate the environmental behaviour of OPAH, which would go beyond the scope of this work, however some interesting preliminary results were obtained.

Among the 17 OPAH targeted, only 2-ethylanthraquinone, 1,4-chrysenedione and 5,12-naphthacenequinone were not detected.

Phenanthrenequinone, pyrene-4,5-dione, anthraquinone and 2-methylanthraquinone were the prevalent OPAH since they were present in all samples.

Phenanthrenequinone was the predominant OPAH (1.90 ng m^{-3}) followed by anthraquinone (1.63 ng m^{-3}). A previous study suggested that select OPAH (especially anthraquinone) can be considered markers of particulates emitted by automobile exhausts [20].

Concentrations of OPAH measured in this study and those previously reported in the literature, for the same compounds, in urban environments are presented in Table 7.

Our results were similar to those reported for Munich (Germany) [21], however, these last ones were annual averages while our study occurred only in spring. Allen et al. [22] reported OPAH concentrations in Boston (USA) during summer similar to those found in our study but the number of identical compounds was insufficient allow for further interpretation and conclusions. Oda et al. reported [20] OPAH concentrations in a tunnel to Japan higher than those found in our study except for 1,4-naphthoquinone and acenaphthenequinone. The similar concentrations for these two compounds could indicate that their primary source was not automobile exhaust. Cho et al. [23] and Maria del Rosario Sienra [14] published, in California (USA) and Santiago (Chile), concentrations which were lower than those reported in our study. Seasons of sampling were similar with Tempe, but the spring in Tempe was characterized by high UV radiation and O_3 concentrations which can promote photo-degradation and oxidation of PAHs leading to the formation of OPAH. The lack of meteorological data during the sampling in California and Santiago does not allow for further discussions.

Many studies observed that OPAH concentrations fluctuate significantly within a year, with higher concentrations in the cold

Table 6
Total concentrations of OPAH from atmospheric samples collected between March and May 2005 in Tempe

Compounds	Concentration (ng m^{-3})			
	FOQ	Minimum	Maximum	Mean
Ketones and Pyrones				
Chromone	9	<LOQ	0.80	0.41
Perinaphthenone	12	0.65	2.40	1.26
Xanthone	13	<LOQ	0.38	0.25
Benzanthrone	9	0.26	2.2	1.25
Benz[*b*]fluoren-11-one	8	0.30	1.06	0.85
Diketones				
1,4-Benzoquinone	10	0.36	0.89	0.63
1,4-Naphthoquinone	15	<LOQ	1.93	1.03
Acenaphthenequinone	11	0.35	1.32	0.77
Phenanthrenequinone	23	0.80	3.60	1.90
Pyrene-4,5-dione	23	0.34	1.67	0.82
Aceanthrenequinone	9	1.20	1.90	1.50
Anthraquinone	23	0.62	2.40	1.63
2-Methylanthraquinone	23	0.24	2.68	1.31
2-Ethylanthraquinone	ND			
1,4-Chrysenedione	ND			
5,12-Naphthacenequinone	ND			
Benz[*a*]anthracene-7,12-dione	16	0.22	0.46	0.35

ND: not detected; LOQ: limit of quantification; FOQ: frequency of quantification.

Table 7
Average concentrations of OPAH in particulate matter quantified worldwide

Compounds	Concentration (ng m^{-3})	Particle matter from	Reference
Perinaphthenone	0.18	Augsburg, Germany	[24]
	1.59	Munich, Germany	[21]
	1.26	Tempe, USA	This work
Xanthone	0.03	Santiago, Chile	[14]
	3.30	Kurashiki City, Japan	[20]
	0.25	Tempe, USA	This work
Benzanthrone	1.18	Boston, USA	[22]
	1.25	Tempe, USA	This work
Benz[*b*]fluoren-11-one	0.15	Augsburg, Germany	[24]
	0.82	Munich, Germany	[21]
	0.85	Boston, USA	[22]
	0.85	Tempe, USA	This work
1,4-Naphthoquinone	0.14	Californie, USA	[23]
	0.85	Kurashiki City, Japan	[20]
	1.03	Tempe, USA	This work
Acenaphthenequinone	1.15	Kurashiki City, Japan	[20]
	0.77	Tempe, USA	This work
Phenanthrenequinone	0.44	California, USA	[23]
	0.43	Boston, USA	[22]
	1.90	Tempe, USA	This work
Anthraquinone	0.11	California, USA	[23]
	0.47	Augsburg, Germany	[24]
	0.56	Santiago, Chile	[14]
	0.96	Munich, Germany	[21]
	42.20	Kurashiki City, Japan	[20]
	1.63	Tempe, USA	This work
2-Methylanthraquinone	0.49	Santiago, Chile	[14]
	6.00	Kurashiki City, Japan	[20]
	1.31	Tempe, USA	This work
Benz[*a*]anthracene-7,12-dione	0.04	Augsburg, Germany	[24]
	0.41	Munich, Germany	[21]
	0.47	Santiago, Chile	[14]
	0.35	Tempe, USA	This work

season [14,17,24–26]. Fig. 1 shows that total OPAH concentrations were decreasing concurrently with increasing temperature. This could indicate that the presence of OPAH in the sample could also come from chemical reactions in the atmosphere.

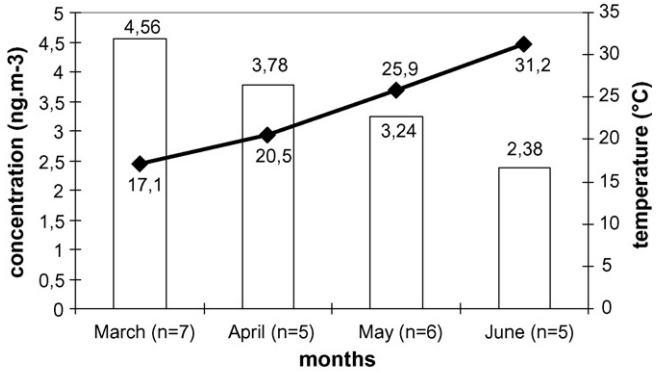


Fig. 1. Sum of all OPAH concentrations (ng m^{-3}) in aerosol samples by month.

We could not draw any main information about the primary or secondary nature of ambient OPAH.

Given the lengthy sampling times, there could be a possibility of oxidation of precursors during sampling and hence a positive artefact formation [27]. However, among the 14 OPAH quantified to the aerosol sample in this study, 9 compounds have high volatilities precursor species and are in the gas phase. For the benzanthrone, phenanthrenequinone and pyrene-4,5-dione their precursors were at about 95% in the gas phase during hot sampling period. Therefore, they will not be retained by the filters and could not be oxidized post sampling. Finally, only two compounds (benz[*a*]anthracene-7,12-dione and benz[*b*]fluoren-11-one) quantified in our study could have been possibility formed by the oxidation of particulate PAH precursors collected on the filter. This is different from studies reporting volatile PAH collected on sorbents, as these could be oxidized during sampling.

Future work should address the variability of OPAH concentrations over a wider range of meteorological conditions (temperature, photochemical activity) and ideally include simultaneous measurements of OPAH with their potential PAH precursor species.

4. Conclusions

Two LC methods for the determination of OPAH in atmospheric samples were developed, based upon fluorescence or mass spectrometric detection. The MS-atmospheric pressure chemical ionization was found more effective than MS-electron spray ionization as well as fluorescence detection. Due to the presence of the major fragment ion $[M-28–28]-$ or $[M+H–29]+$, a reliable identification and quantification was possible.

Limits of detection varied from $0.10\,\mu g\,L^{-1}$ (perinaphthenone) to $1.20\,\mu g\,L^{-1}$ (1,4-benzoquinone). These values correspond of uncertainty to 0.06 and $0.74\,pg\,m^{-3}$ for $1630\,m^3$ of air sampled, in our experimental conditions.

After further optimization the method was applied to the determination of OPAH at very low concentrations levels in atmospheric aerosol samples collected in Tempe (AZ). OPAH concentrations varied between 0.22 and $3.60\,ng\,m^{-3}$. Among the 17 OPAH targeted, only 2-ethylanthraquinone, 1,4-chrysenedione and 5,12-naphthacenequinone were not detected. The phenanthrenequinone was the predominant OPAH ($1.90\,ng\,m^{-3}$) followed by anthraquinone ($1.63\,ng\,m^{-3}$).

The evaluation of occurrence, distribution and fate of OPAH needs further investigation with longer sampling campaigns and a wider variety of sampling sites.

Acknowledgements

Olivier Delhomme wishes to thank all the members of the environmental chemistry group in the Department of Chemistry and Biochemistry at ASU, in particular James Jones and Kristi Husman for the collection of aerosol samples.

References

[1] J.T. Barbas, M.E.S. Sigman, R. Dabestani, Environ. Sci. Technol. 30 (1996) 1776.
[2] J.Y.C. Ma, J.K.H. Ma, J. Enviroment. Sci. Health C20 (2002) 111.
[3] T.S. Hiura, M.P. Kaszubowski, N. Li, A.E. Nel, J. Immunol. 163 (1999) 5582.
[4] A.E. Nel, D. Diaz-Sanchez, N. Li, Curr. Opin. Pulm. Med. 7 (2001) 20.
[5] D. Diaz-Sanchez, A. Tsien, J. Fleming, A. Saxon, Clin. Immunol. 90 (1999) 313.
[6] F. Tao, B. Gonzalez-Flecha, L. Kobzik, Free Rad. Bio. Med. 35 (2003) 327.
[7] N. Li, M. Hao, R.F. Phalen, W.C. Hinds, A.E. Nel, Clin. Immunol. 109 (2003) 250.
[8] B.J. Finlayson-Pitts, J.N. Pitts, Chemistry of the Upper and Lower Atmosphere, Academic press, London, 2000.
[9] P.M. Kim, U. Deboni, P.G. Wells, Free Rad. Bio. Med. 23 (1997) 579.
[10] C.A. Menzie, B.B. Potocki, J. Santodonato, Environ. Sci. Technol. 26 (1992) 1278.
[11] T. Letzel, U. Pöschl, R. Wissiack, E. Rosenberg, M. Grasserbauer, R. Niessner, Anal. Chem. 73 (2001) 1634.
[12] K.W. Davidson, J.A. Sadowski, Methods Enzymol. 282 (1997) 408.
[13] Z.H. Gao, R.G. Ackman, Food Res. Int. 28 (1995) 61.
[14] M. Maria del Rosario Sienra, Atmos. Environ. 40 (2006) 2374.
[15] R. Koeber, J.M. Bayona, R. Niessner, Int. J. Environ. Anal. Chem. 66 (1997) 313.
[16] T. Letzel, E. Rosenberg, R. Wissiak, M. Grasserbauer, R. Niesser, J. Chromatogr. A 855 (1999) 501.
[17] J. Lintelmann, K. Fischer, E. Karg, A. Schröppel, Anal. Bioanal. Chem. 381 (2005) 508.
[18] S.G. Brown, P. Herckes, L. Ashbaugh, M.P. Hannigan, S.M. Kreidenweis, J.L. Collet Jr., Atmos. Environ. 36 (2002) 5807.
[19] L.A. Citta, R.J. Hurtubise, Microchem. J. 34 (1986) 56.
[20] J. Oda, S. Nomura, A. Yasuhara, T. Shibamoto, Atmos. Environ. 35 (2001) 4819.
[21] J. Schnelle-Kreis, I. Gebefügi, G. Welzl, T. Jaensch, A. Kettrup, Atmos. Environ. 35 (Suppl. No. 1) (2001) S71.
[22] J.O. Allen, N.M. Dookeran, K. Taghizadeh, A.L. Lafleur, K.A. Smith, A.F. Sarofim, Environ. Sci. Technol. 31 (1997) 2064.
[23] A.K. Cho, E. Di Stefano, Y. You, C.E. Rodriguez, D.A. Schmitz, Y. Kumagai, A.H. Miguel, A. Eiguren-Fernandez, T. Kobayashi, E. Avol, J.R. Froines, Aerosol Sci. Technol. 38 (S1) (2004) 68.
[24] J. Schnelle-Kreis, M. Sklorz, A. Peters, J. Cyrys, R. Zimmermann, Atmos. Environ. 39 (2005) 7702.
[25] C. Schauer, R. Niessner, U. Pöschl, Environ. Sci. Technol. 37 (2003) 2861.
[26] A.M. Caricchia, S. Chiavarini, M. Pezza, Atmos. Environ. 33 (1999) 3731.
[27] Y. Liu, M. Sklorz, J. Schnelle-Kreis, J. Orasche, T. Ferge, A. Kettrup, R. Zimmermann, Chemosphere 62 (2006) 1889.

Available online at www.sciencedirect.com
ScienceDirect
Talanta 74 (2008) 478–488
Talanta
www.elsevier.com/locate/talanta

Capillary zone electrophoretic determination of cytochrome *c* in mitochondrial extracts and cytosolic fractions: Application to a digitalis intoxication study

Leonardo del Valle-Mondragón, Margarita Ramírez-Ortega, Gabriela Zarco-Olvera, Alicia Sánchez-Mendoza, Gustavo Pastelín-Hernández, Fermín Alejandro Tenorio-López *

Departamento de Farmacología, Instituto Nacional de Cardiología "Ignacio Chávez", Juan Badiano No. 1, Sección XVI, 14080 Tlalpan, Mexico D.F., Mexico

Received 7 May 2007; received in revised form 6 June 2007; accepted 7 June 2007
Available online 17 June 2007

Abstract

We describe a capillary zone electrophoretic procedure with photodiode-array detection for the determination of the apoptogenic protein cytochrome *c* in cytosolic fractions and mitochondrial extracts from guinea pig hearts. Optimal separation was achieved with a 100 mM phosphates electrolyte solution at pH 2.05. The applied voltage was 25 kV and the capillary temperature was kept constant at 25 ± 0.5 °C. The method was linear over the concentration range of 0.2–600 pM. All determination coefficients were higher or equal to 0.9989. Limits of detection and quantitation were 0.06 pM (S/N = 3) and 0.21 pM (S/N = 10), respectively. The present method offers a time-saving way to determine cytochrome *c* since it can be completed in 12 min, compared to a time scale of days for Western blotting methods, or hours for ELISA-based methods. The procedure is illustrated by experiments that quantify cytochrome *c* released under control conditions and in a digitalis intoxication experimental animal model, in which cytochrome *c* content was successfully determined and was found to be (mean ± standard deviation): control cytosol (0.48 ± 0.01 pM), digitalis-intoxicated cytosol (0.85 ± 0.01 pM), control mitochondria (1.11 ± 0.1 pM) and digitalis-intoxicated mitochondria (0.75 ± 0.02 pM). Recovery results ranged from 98.4 to 110.2%. Hence, the proposed analytical method could be useful to elucidate the digitalis intoxication mechanism as well as the role of cytochrome *c* in mediating apoptosis.
© 2007 Elsevier B.V. All rights reserved.

Keywords: Cytochrome *c*; Capillary zone electrophoresis; Apoptosis; Mitochondria; Digitalis intoxication

1. Introduction

Mitochondrial damage is a key event in the pathogenesis of ischemic cell injury promoting cell death by apoptosis, especially in events that involve oxidative stress, hypoxia/ischemia and drug-induced cytotoxicity [1–3]. Recent findings suggest that most proapoptotic stimuli require a mitochondrial-dependent step, involving outer membrane permeabilization controlled by pro- and antiapoptotic members of the Bcl-2 family. This leads to intracytosolic release of mitochondria intermembrane proteins, such as cytochrome *c*, which can trigger caspase activation [4–6]. Cytochrome *c* release from mitochondria is considered a critical, early event in the induction of the caspase cascade that ultimately leads to programmed cell death [7–9].

Cytochrome *c* (Fig. 1) is a small heme protein (molecular weight about 12,000 Da) found loosely associated to the inner membrane of mitochondria. It is a soluble protein, unlike other cytochromes, and is an essential component of the electron transfer chain. It is capable of undergoing oxidation and reduction, but does not bind oxygen. The isoelectric point (p*I*) of cytochrome *c* from the equine heart is 10.2 [10,11]. Since, in mammalian cells, cytochrome *c* is involved in apoptosis, it is important to quantify this analyte with accurate and reliable procedures, to be able to study its cellular compartmentalization, as well its release kinetics under several conditions. This knowledge might contribute to elucidate several important questions, such as how

* Corresponding author. Tel.: +52 55 5573 2911x1317; fax: +52 55 5573 0926.
E-mail addresses: fatl@att.net.mx, ft24@hotmail.com (F.A. Tenorio-López).

0039-9140/$ – see front matter © 2007 Elsevier B.V. All rights reserved.
doi:10.1016/j.talanta.2007.06.010

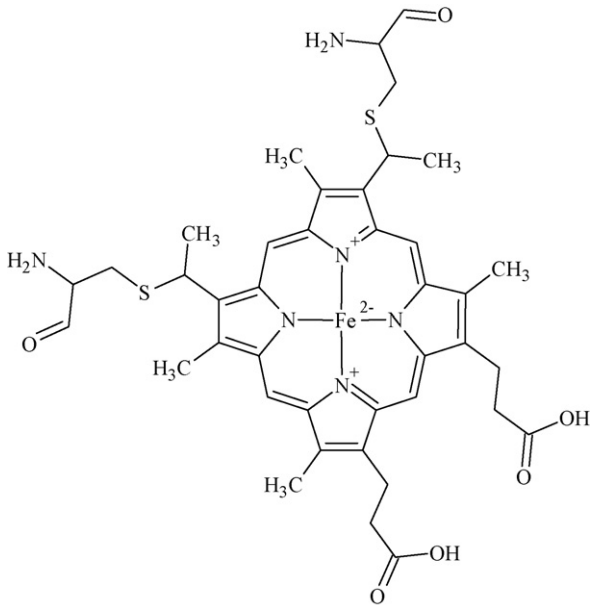


Fig. 1. Molecular structure of cytochrome *c* heme moiety.

widespread is the cytochrome *c*-dependent pathway of cell death [12]. Recently, it has been reported that in mammalian mitochondria the enzyme $p66^{Shc}$ can oxidize cytochrome *c* to generate reactive oxygen species (ROS), which act as signaling molecules for apoptosis [13].

On the other hand, heart failure (HF) is associated with high mortality and morbidity. Pharmacological treatment, as it stands today, is a combination of preventive and symptomatic strategies. The mainstay life-saving drugs are angiotensin-converting enzyme inhibitors and beta blockers. Additional benefits are obtained when angiotensin-receptor blockers or aldosterone antagonists are added. Digitalis and/or diuretics are useful for symptom reduction [14]. However, it has been reported that in the HeLa tumor cell line, digitalis compounds at concentrations greater than 10 nM induce cell death in a concentration- and exposure period-dependent fashion. These results correlated with an increased cytochrome *c* release from the mitochondria into the cytosol [15].

Regarding quantitative analysis of cytochrome *c*, or closely related compounds, by liquid chromatography-assorted techniques, several methods for its determination have been published. Lui et al. reported a method that comprised Mono-Q fast protein liquid chromatography (FPLC) and C18 reversed-phase (RP) high-performance liquid chromatography (HPLC) with a water/acetonitrile gradient in 0.1% trifluoroacetic acid [16], employed for the quantitative analysis of cytochrome *c* oxidase, a multisubunit membrane complex, from bovine heart. Another study by Picklo et al. employed C4 RP-HPLC using ultraviolet (UV) detection at 393 nm for the quantitative analysis of cytochrome *c* content in mitochondria from rat brain, obtaining a quantitation limit of 10 ng (0.8 pmol) [17]. Batthyány et al. used cation-exchange HPLC for the analysis of mono-, di- and tri-nitrated cytochrome *c* species, using a sulfopropyl-TSK column, separating the nitrated products by means of a linear gradient of ammonium acetate (pH 9.0) from 10 to 400 mM over the course of 50 min [18]. On the other hand, Chen et al. employed a Prodigy ODS column using a 50 mM ammonium formate buffer at pH 5.5 as the mobile phase. UV detection was performed at 393 and 287 nm for 8-nitroguanosine and 8-aminoguanine, and at 376 and 287 nm for 8-nitroxanthine and 8-aminoxanthine. This system was used to investigate the possible metabolic fate of these nitrated DNA adducts, by examining if they can be reduced to their corresponding amino analogues by biological reducing agents in the presence of hemin or hemoproteins, including hemoglobin and cytochrome *c* [19]. Other analytical approaches include Western blotting (WB) and ELISA-based methods. WB-based methods are the most commonly used for examining cytochrome *c* release from mitochondria. However, WB is a semiquantitative method that cannot give precise information about the amount and kinetics of release under different conditions. It is also a lengthy and inconvenient procedure for processing multiple samples; hence, the results cannot be obtained within the time frame of the actual experiments, as is sometimes desirable [20].

Nowadays, capillary electrophoresis (CE) is an analytical separation technique capable of a high-resolution separation of a diverse range of chemical compounds since it provides considerably higher separation efficiencies (plate number) than HPLC. Other advantages of CE are its low sample consumption, compatibility with autosampling, permits easy cleaning of the capillary, as well as different modes of electrophoretic separation that can be applied with the same CE equipment [21,22], being UV absorbance and laser-induced fluorescence (LIF) the most common detection devices used in CE. Recently, several studies designed for the separation and quantitation of cytochrome *c* by CE have been published. Meagher et al. analyzed a mixture of lysozyme, cytochrome *c*, ribonuclease A and myoglobin employing fused-silica capillaries coated with a tri(ethylene glycol)-terminated alkyltrichlorosilane, a protein-resistant self-assembled monolayer coating that has shown to be flexible for a range of applications, potentially including capillary electrophoresis-mass spectrometry (CE-MS) [23]. In another study, performed by Mohan and Lee, a microdyalisis junction was employed as the interface for on-line coupling of capillary isoelectric focusing with transient isotachophoresis-zone electrophoresis in a two-dimensional separation system. This system allowed for the separation of cytochrome *c*, ribonuclease A and carbonic anhidrase II. The maximal peak capacity was estimated to be around approximately 1600 [24]. Verzola et al. employed capillary zone electrophoresis (CZE) to monitor folding/unfolding transitions of proteins, such as cytochrome *c* [25]. Zhang et al. used silanized fused-silica capillaries by in situ copolymerization of vinylbenzyl chloride and ethylene glycol dimethacrylate in the presence of propanol and formamide as porogens. Under these conditions, a tryptic digest of cytochrome *c* was analyzed in about 5 min at 55 °C and 75 kV m^{-1} with hydro-organic mobile phases containing acetonitrile in a 50 mM phosphates buffer at pH 2.5 [26]. Other approaches to improve sensitivity and resolution include off-line and on-line capillary zone electrophoresis-electrospray ionization time-of-flight mass spectrometry (CZE-ESI-TOF-

MS) and transient isotachophoresis (ITP) focusing for the on-line analysis of peptides by CZE-MS, requiring spectrometry instrumentation that is not readily available, as well as a gold-coated CE-ESI interface prepared through gold vapor deposition [27,28]. A recent study by Armenta et al. employed a butyl methacrylate-*co*-ethylene dimethacrylate (BuMA-*co*-EDMA) monolith synthesized via a two-step procedure (permanent coating with poly(vinyl)alcohol to prevent protein/wall interactions followed by a 1 cm long BuMA-*co*-EDMA synthesized using photoinitiated polymerization for on-line preconcentration of proteins followed by CE separation of protein mixtures (cytochrome *c*, lysozyme and trypsinogen A) using on-column UV detection at 214 nm [29]. MacDonald and Lucy used a surfactant/polymer wall coating consisting of the doubly chained cationic surfactant dimethyldioctadecylammonium bromide (DODAB) and polyoxyethylene (POE) 40 stearate. Basic proteins such as cytochrome *c*, lysozyme, ribonuclease A and α-lactalbumin are separated using a 0.1 mM DODAB/0.1% POE 40 stearate coating with a 50 mM sodium phosphate at pH 3.0 as electrolyte solution, with UV detection at 214 nm [30]. In another study by Schoenherr et al., an integrated on-column microreactor was developed for the rapid digestion of protein fractions into peptides, which are then separated in a second dimension before being introduced into a MS/MS analysis for bottom-up analysis [31]. Busnel et al. employed narrow pH cuts of carrier ampholytes for the analysis of protein tryptic digests. Under these conditions, three proteins of different molecular masses (cytochrome *c*, β-lactoglobulin and human transferrin) were detected. The feasibility of the coupling of carrier ampholyte-based CE with ESI-MS was demonstrated through the study of cytochrome *c* tryptic digest [32].

It is noteworthy that, according to our latest literature survey, no CZE-photodiode-array (PDA) detection methods have been reported that describe the quantitative determination of cytochrome *c* in biological samples under a digitalis intoxication study. Hence, it was desirable to establish a simple, fast and robust analysis of cytochrome *c* release in mitochondrial extracts and cytosolic fractions from guinea pig hearts by CZE-PDA, and to apply it on digitalis intoxication studies, that may contribute to elucidate the digitalis intoxication mechanism. In addition, due to the critical role of cytochrome *c* release in mediating apoptosis, prevention of cytochrome *c* release becomes an attractive therapeutic target, and, to this end, a quantitative measurement of cytochrome *c* release from mitochondria in either biomedical or clinical studies, with reliable and accurate results, is required.

In the present study, we assessed CZE determination of cytochrome *c* in mitochondrial extracts and cytosolic fractions using PDA detection. Various separation parameters, such as the pH and concentration of the background electrolyte, the applied voltage, the injection time, the temperature, as well as PDA conditions, were optimized. The applicability of the optimized CZE-PDA system was tested by the determination of cytochrome *c* in mitochondrial extracts and cytosolic fractions from guinea pig hearts under control and digitalis-intoxicated conditions.

2. Experimental

2.1. Chemicals

Dimethylsulfoxide (DMSO), sodium hydroxide, sodium hydrogenphosphate heptahydrate, sodium dihydrogenphosphate monohydrate, sodium chloride and phosphoric acid were purchased from Merck KGaA (Darmstadt, Germany). Cytochrome *c* from equine heart, HEPES, boric acid, sodium tetraborate decahydrate, EDTA, ouabain, Tris–HCl, IGEPAL CO-630 and Nagarse (serine endopeptidases isolated from *Bacillus subtilis*) were obtained from Sigma Chemical Co. (St. Louis, MO, USA). Sucrose was obtained from Mallinckrodt Baker (Xalostoc, Estado de Mexico, Mexico). Complete (protease inhibitor cocktail tablets) was from Roche Diagnostics GmbH (Mannheim, Germany). All other chemicals were of analytical grade and were used without further purification. Cytochrome *c* stock solution (40 μM) was prepared in HSE buffer and was stable to storage at −70 °C, as indicated by absorbance measurements at 410 nm obtained upon thawing. HSE buffer composition was as follows (in mM): 250 sucrose, 10 HEPES, 1 EDTA and 10 Tris–HCl, at pH 7.4. Working standard solutions were prepared daily by dilution of the stock standard solutions with HSE buffer. Deionized water (≥18.2 MΩ cm) used throughout the study was obtained with a Simplicity System (Millipore SAS, Molsheim, France).

2.2. Apparatus

All experiments were performed with a Beckman Coulter (Fullerton, CA, USA) P/ACE^{TM} MDQ Capillary Electrophoresis System equipped with PDA and controlled by means of the P/ACE MDQ Capillary Electrophoresis System software, version 7.0 (Beckman Coulter Inc., Fullerton, CA, USA). The 57 cm (50 cm to the detector) × 75 μm i.d. fused-silica capillary from Polymicro Technologies (Phoenix, AZ, USA) was maintained at 25 °C in a cartridge with a 100 μm × 800 μm detection window. The use of a PDA allowed us to confirm the identity of the peaks, not only by their migration time, but also by the overlay of the UV–vis spectra of the samples with a cytochrome *c* standard solution. PDA was set at an acquisition range from 190 to 600 nm (bandwidth 6 nm) at a spectral acquisition rate of 1.25 scans s^{-1} (peak width 0.2 min). A Corning pH/ion analyzer 350 (Corning Inc., Corning, NY, USA) with Hanna HI 1230B combined pH/ORP electrodes (Hanna Instruments, Woonsocket, RI, USA), calibrated with Sigma (St. Louis) reference standard buffers (pH 4.00 ± 0.01, 7.00 ± 0.01 and 10.00 ± 0.01, respectively), was employed for the pH measurements.

2.3. Capillary conditioning and electrophoretic separation conditions

The capillary was treated prior to its first use by flushing 1 M NaOH for 60 min, deionized water for 60 min and finally with the background electrolyte (BGE) for 20 min, to ensure a clean capillary surface. Daily, before the first sample injection,

the capillary was flushed with 1 M NaOH for 2 min, followed by deionized water for 2 min and finally with the BGE for 4 min. Samples were introduced from the anodic end of the capillary by hydrodynamic injection for 10 s at 0.5 psi. PDA was set at an acquisition range from 190 to 600 nm (bandwidth 6 nm) at a spectral acquisition rate of 1.25 scans s^{-1} (peak width 0.2 min). As BGEs, several solutions were prepared as follows: a 100 mM phosphates buffer at pH 2.05 was prepared by mixing equal volumes of a 55.73 mM H_3PO_4 solution and a 44.27 mM $NaH_2PO_4{\cdot}H_2O$ solution, and then the volume of the mixture was adjusted to 100 mL with deionized water; a 100 mM tetraborate buffer at pH 9.08 was prepared by mixing equal volumes of a 68.57 mM H_3BO_3 solution and a 31.43 mM $Na_2B_4O_7{\cdot}10H_2O$ solution. Then, the volume of the mixture was adjusted to 100 mL with deionized water; a 50 mM HEPES at pH 7.0 was prepared by accurately weighing 1.3080 g of HEPES and adjusting the volume to 100 mL with deionized water. Before use, BGEs based on tetraborates and HEPES were adjusted accurately to the desired pH value with either 0.1 M HCl or 0.1 M NaOH, whereas BGE based on phosphates was adjusted to the desired pH value with the addition of 0.1 M H_3PO_4. All BGEs were degassed by sonication (T490DH instrument, Elma, Singen, Germany), and filtered through 0.22 μm mixed cellulose ester filters (Millipore, Billerica, MA, USA). Unless otherwise stated, no more than 100 μL of 0.1 M HCl, 0.1 M NaOH or 0.1 M H_3PO_4 were required for pH adjustment. All operations were performed at 25 ± 0.5 °C. To avoid BGE and sample evaporation, BGE and sample reservoirs were capped. The migration times corresponding to the electroosmotic flow (EOF) were determined conventionally by injecting DMSO as the EOF marker. Between runs, a rinse cycle by flushing the capillary with 1 M NaOH for 2 min followed by deionized water for 2 min, and then with BGE for 4 min, was employed. Data acquisition was achieved with a ThinkCentre (IBM Corporation, White Plains, NY, USA) workstation.

2.4. Animals

For this study, male guinea pigs (600–750 g), maintained at the animal facility of the Instituto Nacional de Cardiología "Ignacio Chávez" were used. They were housed under standard conditions of temperature and light (12-h light:12-h dark cycle) and fed standard diet (Guinea Pig LabDiet 5025, PMI Nutrition International, Richmond, IN, USA) and tap water ad libitum. All animal procedures were conducted in accordance with our Federal Regulations for Animal Experimentation and Care (Ministry of Agriculture, SAGARPA, NOM-062-ZOO-1999, Mexico), which follows the Guidelines for Care and Use of Laboratory Animals, and were approved by the Institutional Animal Care and Use Committee. During the experiments, all efforts were made to minimize animal suffering.

2.5. In vivo digitalis intoxication model

The design of the digitalis intoxication experiments was based on the study performed by Ramirez-Ortega et al. [33], modifying the injection route as follows: an intraperitoneal administration with ouabain at a dose of 121 μg kg^{-1} of body weight was performed. Ouabain was dissolved in ethanol and adjusted to an 8.0 mL volume with isotonic saline solution to be infused intraperitoneally to guinea pigs. The control group only received 8 mL of isotonic saline solution. A rest period of 18 h was allowed before recording an electrocardiogram (ECG) to assure the presence of digitalis intoxication and killing the animals with a lethal dose of sodium pentobarbital.

2.6. Isolation of heart mitochondria and cytosol fractions for cytochrome c determination and sample preparation for the CZE-PDA analysis

Mitochondria from guinea pig hearts were isolated by the method of Bhattacharya et al. [34]. Hearts from guinea pigs from either control or ouabain-treated groups were quickly removed and minced on ice, and resuspended in 10 mL of ice-cold HSE buffer supplemented with a mixture of protease inhibitors (Complete, Roche Diagnostic Co.). Fragments were rinsed four times, and 10 mL of the HSE buffer plus Nagarse (0.4 mg g^{-1} of heart) were added. After 5 min on ice, tissues were centrifuged at 9047 × *g* for 10 min at 4 °C (Sorvall RC-28S, rotor SS34, DuPont, Newtown, CT, USA). Pellets were homogenized (five times) in 10 mL of HSE buffer with a Potter–Elvehjem homogenizer and centrifuged at 1370 × *g* for 10 min at 4 °C. Pellets were discarded and supernatants were then centrifuged at 1,1169 × *g* for 10 min at 4 °C. Mitochondrial pellets were resuspended in buffer HSE (250 μL) and the supernatant was centrifuged at 100,000 × *g* for 90 min at 4 °C to obtain cytosol used for cytochrome *c* determination. Protein concentrations were determined by the Lowry et al. method [35]. Mitochondrial fraction (one mg; control and ouabain-treated, respectively) was resuspended in 1 mL of HSE buffer with 0.5% IGEPAL and Complete added for cytochrome *c* extraction; mitochondria in solution were left on ice for 15 min and centrifuged at 100,000 × *g* (Sorvall- Ultra Pro 80, rotor T880, DuPont, Newtown, CT, USA) for 60 min at 4 °C. The supernatants were used for cytochrome *c* determination. Prior to their use, samples were filtered through 0.45 μm mixed cellulose ester syringe filters (Nihon Millipore Kogyo K.K., Tokyo, Japan); 100 μL of these supernatants were employed for the CZE-PDA analysis.

2.7. Statistical analysis

Data analysis was carried out using SPSS 12.0.1 for Windows software (SPSS Inc., Chicago, IL, USA) with one-way analysis of variance (ANOVA) followed by Student's *t*-test for independent samples. All results were expressed as mean ± standard deviation of 14 independent determinations. A value of $p < 0.05$ was considered as statistically significant.

3. Results and discussion

3.1. Optimization of the test electrophoretic procedure

To optimize the CZE-PDA separation of cytochrome *c* from other compounds present in the analyzed matrix, the effect

of several variables was systematically explored: pH of the BGE (2.05, 7.00 and 9.08, respectively), concentration of the BGE (20–100 mM), applied voltage (5–30 kV), injection time (3–11 s), temperature (15–30 °C), as well as PDA conditions.

3.1.1. Effect of pH

It has been repeatedly demonstrated that the inner wall of the fused-silica capillary is a potential site for interactions among the separated analytes [36]. In the particular case of proteins, the solute–wall interactions generally spoil the results because of non-specific attachment of the separated analytes to the capillary wall (stacking) [37]. This results not only in sample loss, but in poor reproducibility and decreased efficiency as well. In CE, proteins can adsorb to the capillary wall causing alterations of the EOF and band broadening. Especially with bare-fused silica capillaries, the adsorption of proteins to the capillary wall can lead to a very poor migration time and low plate number. In order to minimize such effects, the separation of protein mixtures are run at extreme pH values, by which either the dissociation of the silanol groups of the capillary wall is minimized (at acid pH) or the dissociation of the free amino groups of the proteinous solutes is decreased (at high pH values) [38]. On the other hand, pH regulation is an important purpose of the BGE in order to keep the migration velocity of the analytes and the velocity of the EOF constant. In this way, a stable and reproducible migration behavior of the sample components can be obtained [39]. In CZE, the whole system is filled with a BGE, whose main purposes are to transport the electric current if a voltage is applied over the system, to provide an electric field strength and to facilitate the separation of the analytes. Optimization of the CE system started with selecting the BGE for the analysis of cytochrome *c* content on mitochondrial extracts and cytosolic fractions. For this purpose, the following buffer solutions were selected as BGEs: a 100 mM phosphates buffer at pH 2.05 (which may favor positive mobility since the net charge of the cytochrome *c* molecule is positive at pH 2.05) [10,11], a 50 mM HEPES at pH 7.00 (selected due to low-conductivity buffering properties) [40] and finally, a 100 mM borate buffer at pH 9.08 (selected because borate can chelate with the analytes to form more soluble complex anions) [41]. Under the experimental conditions, a 195 pM standard solution of cytochrome *c* prepared in HSE buffer showed an adequate behavior with all selected BGEs. However, to explore whether each BGE showed adequate performance when real samples were analyzed, it was decided to analyze mitochondrial extracts and cytosolic fractions from both control and digitalis-intoxicated animals, and samples were either unspiked or spiked with a 195 nM cytochrome *c* standard solution prepared in HSE buffer. Then, performance parameters such as resolution, peak area and plate number were calculated for unspiked or spiked samples. It was found that by increasing pH, resolution decreased (Fig. 2A). In order to achieve an adequate separation, the peak area and the plate number were calculated. It was observed that the best resolution (Fig. 2A), plate number (Fig. 2B) and peak area (Fig. 2C) were obtained when employing as BGE a 100 mM phosphates buffer at pH 2.05. Although a more convenient migration time (Fig. 2D) was obtained at pH 7.00 than that obtained at pH 2.05, based on results obtained with respect to resolution, plate number and peak area, respectively, it was decided to employ a 100 mM phosphates buffer (pH 2.05) for further experiments. In addition, it was observed that with

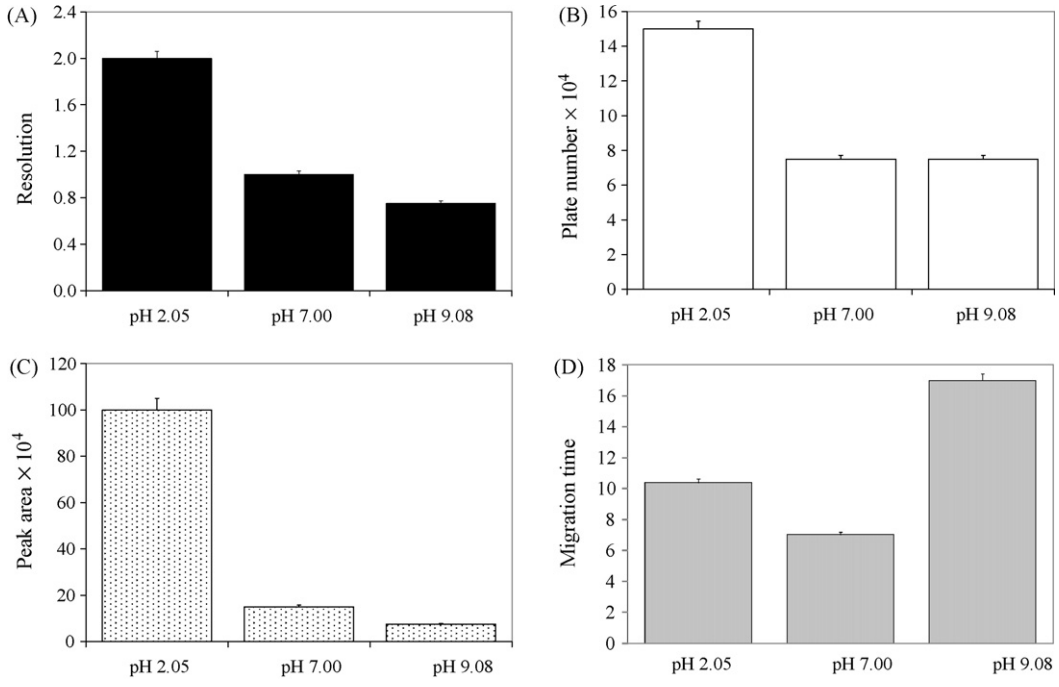


Fig. 2. Influence of the background electrolyte (BGE) pH on resolution (A), plate number (B), peak area (C) and migration time (D) of cytosolic fractions and mitochondrial extracts. Mean and standard deviation of 10 experiments are depicted. Experimental conditions: fused-silica capillary 75 μm i.d. × 50 cm effective length; BGEs: 100 mM phosphates buffer (pH 2.05), 50 mM HEPES (pH 7.00) and 100 mM borates buffer (pH 9.08). Separation voltage, 25 kV; hydrodynamic injection at 0.5 psi for 10 s; temperature, 25 ± 0.5 °C; 195 pM cytochrome *c* standard solution was prepared in HSE buffer.

BGEs based on 50 mM HEPES at pH 7.00 or on 100 mM borates buffer at pH 9.08, cytochrome *c* and its coexisting interferences could not be separated well in these electrolyte solutions. Moreover, at higher pH values, the analyte could be more susceptible to oxidation. However, although it was initially hypothesized that cytochrome *c* may display a positive mobility, calculation of its effective electrophoretic mobility (μ, expressed as $m^2\,V^{-1}\,s^{-1}$), showed that cytochrome *c* μ was opposite to the EOF ($\mu = -101.84\,m^2\,V^{-1}\,s^{-1}$). EOF effective electrophoretic mobility (μ_{EOF}) was calculated as $95\,m^2\,V^{-1}\,s^{-1}$. μ and μ_{EOF} were calculated using the following equations [42,43]:

$$\mu = \frac{L_t \times L_d}{V}\left(\frac{1}{t_m} - \frac{1}{t_o}\right) \times 10^9$$

$$\mu_{EOF} = \frac{L_t \times L_d}{V \times t_o} \times 10^9$$

where μ and μ_{EOF} are expressed in $m^2\,V^{-1}\,s^{-1}$, L_t and L_d the total capillary length and length to the detector window in meters, V the applied voltage in volts and t_m and t_o are the migration times for the analyte and the EOF in seconds.

3.1.2. Effect of BGE concentration

The concentration of the BGE plays an important role in separation resolution in electrophoresis. If a constant voltage is applied over the capillary, the electric current will increase at higher BGE concentrations and this can cause extra peak broadening due to a strong increase in Joule heat. Provided the generated Joule heat is not too high to affect peak efficiency, a higher buffer concentration can produce better peak shapes at high analytic concentrations and will also lead to improved peak reproducibility [39]. Our previous experiments showed that the most adequate pH analyzed to studied biological samples was 2.05. Therefore, the next step was to study the influence of BGE concentration, in the range of 20–100 mM, on the separation of cytochrome *c*. At BGE concentrations above 100 mM, unacceptably high currents were observed (data not shown). As the BGE concentration increased, both resolution (Fig. 3A) and plate number (Fig. 3B) increased, achieving a resolution of 2.0 and plate number of approximately 150,000 when 100 mM phosphates buffer at pH 2.05 was employed. The increase of the plate number observed for the positively charged cytochrome *c* is probably due to a reduced interaction with the capillary wall and not to stacking, which is more apparent when the difference of conductivity between the BGE and the injection zone is very large.

3.1.3. Effect of the applied voltage

The ideal separation in CZE is usually obtained by using a voltage as high as possible in order to obtain the best separation, in the shortest time, with the best efficiency. However, high voltages lead to difficult heat dissipation during the electrophoretic separation due to Joule heat, which is known to affect the EOF, diffusion of analytes, and therefore, the efficiency and reproducibility of the separation. For this reason, it is important to control this phenomenon. To choose the most appropriate voltage in the electrophoretic separation, the effect of the voltage applied from 5 to 30 kV (steps of 5 kV) was investigated. A voltage of 25 kV yielded the best compromise in terms of lower migration times and higher areas and resolutions. Voltages higher than 25 kV permit bubble formation within the capillary and current courts are observed.

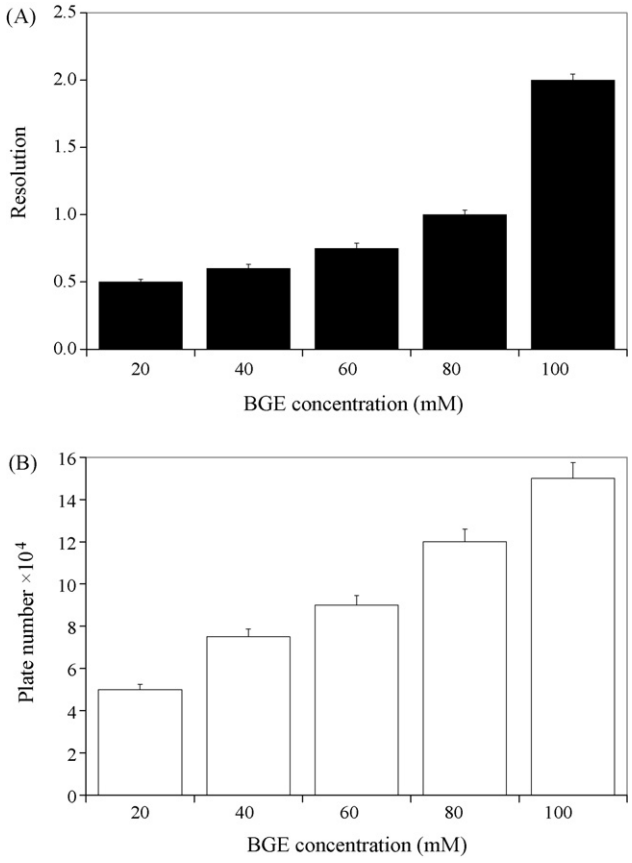


Fig. 3. Effect of BGE concentration on resolution (A) and plate number (B) of cytosolic fractions and mitochondrial extracts. Mean and standard deviation of 10 experiments are depicted. BGE: phosphates buffer, pH 2.05. Other experimental conditions as indicated in Fig. 2.

3.1.4. Optimization of the injection time

In order to decrease the limit of detection, the injection time was varied between 3 and 11 s (steps of 2 s). As expected, when the injection time increased, the peak area of all compounds also increased, but for injection times lower than 10 s, a loss of resolution between peaks was observed. For this reason, a 10 s injection time was chosen as optimal value, while the separation efficiency remained largely unchanged. In all cases, the injection pressure was kept constant at 0.5 psi.

3.1.5. Effect of temperature

Changes in capillary temperature can cause variations in efficiency, viscosity, migration times, injection volumes and detector response. Temperature variations and corresponding changes in viscosity have been determined to be detrimental to obtain reproducible results. The effect of temperature on the separation was investigated in the range 15–30 ± 0.5 °C (15, 20, 25 and 30 ± 0.5 °C). As temperature increases, the viscosity of

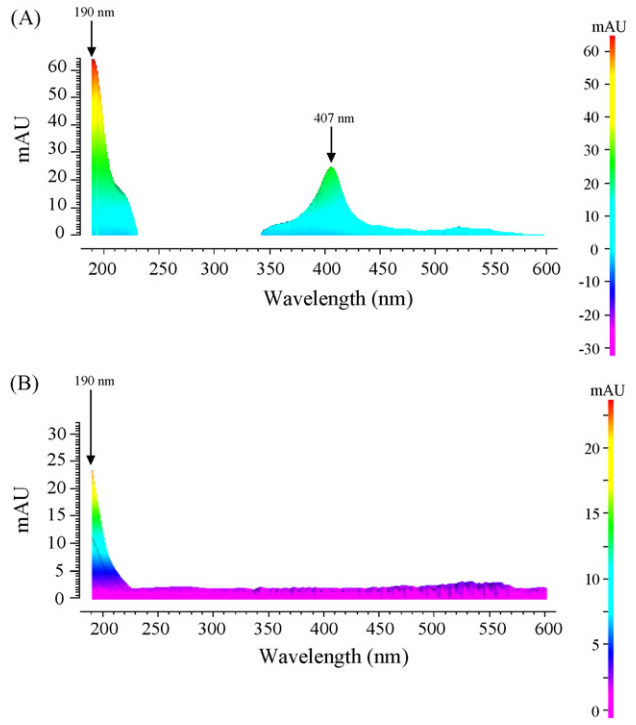


Fig. 4. UV–vis spectrum for a 195 pM cytochrome *c* standard solution prepared in HSE buffer (A). UV–vis spectrum for an extracted sample employed for the quantitative analysis of cytochrome *c* in mitochondrial extracts and cytosolic fractions (B). Experimental conditions: fused-silica capillary 75 μm i.d. × 50 cm effective length; running buffer 100 mM phosphates buffer (pH 2.05); PDA was set at an acquisition range from 190 to 600 nm (bandwidth 6 nm) at a spectral acquisition rate of 1.25 scans s^{-1} (peak width 0.2 min). Other experimental conditions as indicated in Fig. 2.

the buffer decreases, so the resistance of the buffer decreases. The decrease in the migration times of cytochrome *c* results in poor resolution, which might be caused by the direct effect of temperature on the rate of EOF, that might be increased, and buffer depletion occurs more rapidly. More directly, changes in viscosity alter the injected amount when using hydrodynamic injection. Therefore, the selected temperature was 25 ± 0.5 °C because it resulted in the best resolution.

3.1.6. Selection of optimal wavelength

Although it has been reported previously that because cytochrome *c* contains a protein-bound proto-heme moiety that could provide a useful detection chromophore [44], it has been observed that the maximal absorption shifts from 410 nm (the γ-Soret band) at neutral pH to 393 nm when acidified with 0.1% trifluoroacetic acid [17]. Maximal absorption at 393 nm had an absorbance about 50% greater than that at 410 nm at neutral pH. Other CE approaches reports that cytochrome *c*, with UV detection, is detected at 214 nm [29,30]. However, data collection from 190 to 600 nm shows that in a 100 mM phosphates buffer at pH 2.05, a cytochrome *c* standard solution was best detected at 190 nm (Fig. 4A). A similar absorption spectrum was obtained when cytochrome *c* standard solution was prepared in deionized water at pH 2.05. A similar analysis of extracted samples for the quantitative analysis of cytochrome *c* in mitochondrial extracts and cytosolic fractions, revealed that cytochrome *c* was best detected at 190 nm (Fig. 4B). Therefore, this wavelength was selected for the quantitative analysis of cytochrome *c* in mitochondrial extracts and cytosolic fractions.

The above results revealed that optimal separation conditions were: 100 mM phosphates buffer, pH 2.05, applied voltage 25 kV, hydrodynamic injection mode at 0.5 psi for 10 s, capillary cartridge temperature maintained at 25 ± 0.5 °C and PDA operating at 190 nm (bandwidth 6 nm). Fig. 5 shows the electropherograms obtained for cytosolic fractions and mitochondrial extracts from control and digitalis-intoxicated animals, which where employed for the quantitative determination of cytochrome *c* release under the proposed experimental conditions.

3.2. Validation of the electrophoretic procedure

Method validation protocol encompassed stability, linearity, precision, specificity, limit of detection, limit of quantitation, recovery and robustness.

3.2.1. Stability of the solutions

The stability of the standard and test solutions of cytochrome *c* was determined by comparing the response factors (concentration/average peak areas) of triplicate solutions stored at 4 °C, in darkness, with those of freshly prepared triplicate solutions. A concentration difference greater than 2% was found between the freshly prepared standard solution and the solutions prepared 7 days before. For this reason, it is advisable to employ freshly prepared cytochrome *c* solutions.

The stability of unspiked and spiked mitochondrial extracts and cytosolic fractions was evaluated by comparing the relative peak areas obtained at different time intervals with those of freshly prepared fractions. It was found that the fractions were stable for at least 2 h. For this reason, it is recommended that CZE-PDA analysis be carried out immediately after the preparation of such extracts and fractions.

3.2.2. Linearity

Linearity is the ability to show that the results are directly proportional to the analyte concentrations in samples within a given range. The sample matrix can affect the area and migration rate of cytochrome *c* when real samples are analyzed in the CZE system, causing deviations from those of pure standards. Therefore, the quantitation of cytochrome *c* was performed by applying a standard addition technique for cytosolic fractions and mitochondrial extracts. However, according to our experience, the conventional quantitation based on a calibration curve created by prepared standard solutions can be applied as well. To assess the linearity of the proposed CZE-PDA method, six independent calibration plots, analyzed per triplicate, were constructed over the calibration range of 0.2–600 pM. The curves were prepared on 5 different days, and linear regression was evaluated. Analytical figures of merit are shown in Table 1.

3.2.3. Precision

The precision of a method is determined by the extent to which the test results of multiple injections of standards agree.

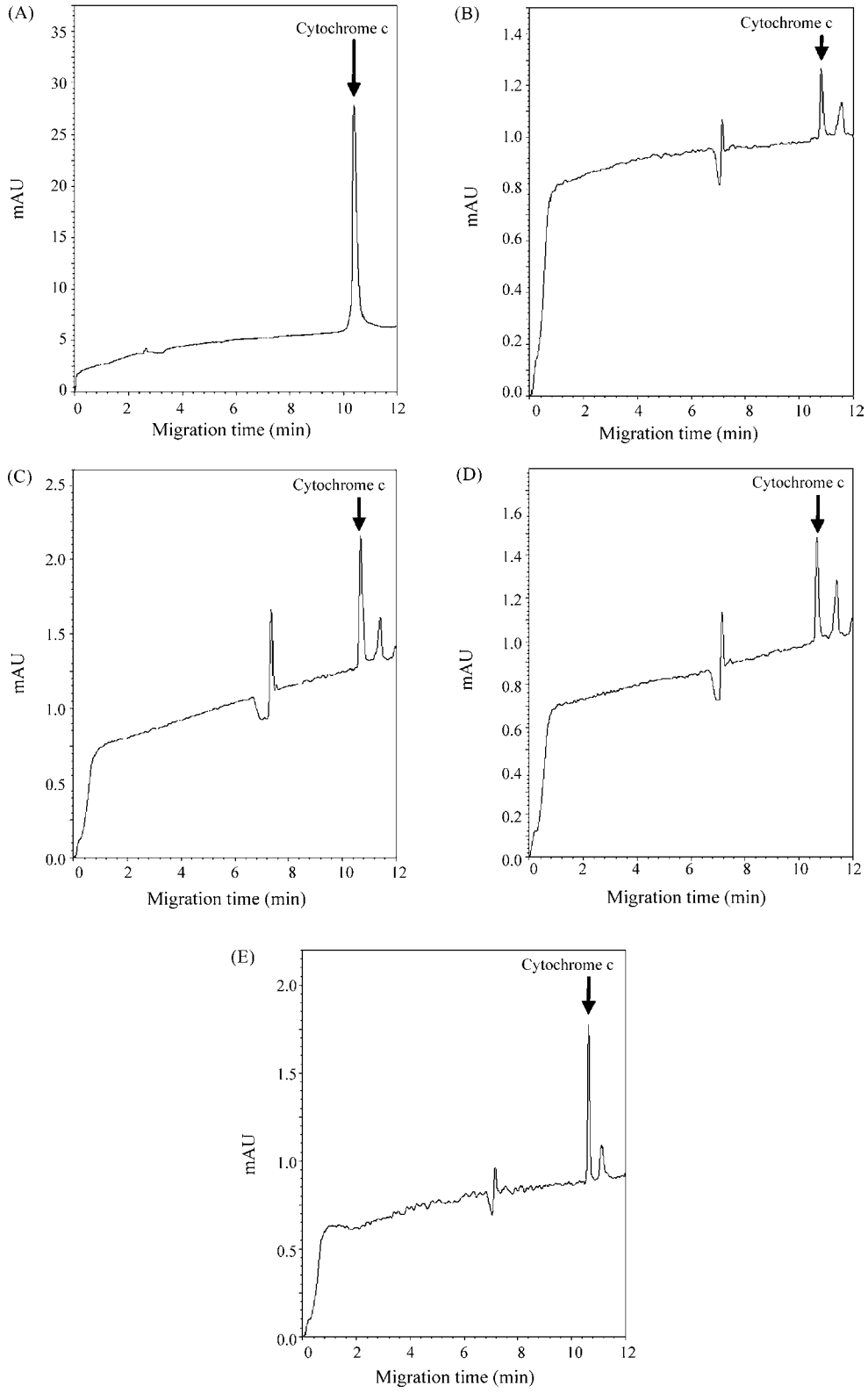


Fig. 5. Electropherograms obtained from a 195 pM cytochrome *c* standard solution prepared in HSE buffer (A), cytosol from control animals (B), mitochondrial extract from control animals (C), cytosol from digitalis-intoxicated animals (D) and mitochondrial extract from digitalis-intoxicated animals (E). Other experimental conditions as indicated in Fig. 2.

Table 1
Linearity and sensitivity

Analyte	t_m (min) R.S.D. ($n = 14$)	Linear range (pM)	Linear regression $y = (mx + b)$	Coefficient of determination (R^2)	Area R.S.D. ($n = 14$)[a]	LOD (pM)[b]	LOQ (pM)[c]
Cytochrome *c*	10.40 (0.1%)	0.2–600	$y = (1.6149 \times 10^5)x + 3.4579 \times 10^4$	0.9989	2.7681×10^5 (2.26%)	0.06	0.21

CZE conditions: BGE, 100 mM phosphates buffer (pH 2.05); hydrodynamic injection at 0.5 psi for 10 s; PDA detection at 190 nm (bandwidth 6 nm); *x*, analyte concentration (pM); *y*, peak area.
[a] Calculated from peak areas for 195 pM of cytochrome *c* prepared in HSE buffer.
[b] LOD is calculated based on S/N = 3.
[c] LOQ is calculated based on S/N = 10.

The precision of the proposed method is expressed in terms of relative standard deviation (R.S.D.). In order to test the precision of the overall process, five different samples of cytosolic fractions and mitochondrial extracts spiked with cytochrome *c* were carried sequentially. The precision of the migration times and relative peak area were good with a R.S.D. between 0.20 and 0.24% for migration times and between 1.98 and 2.86% for relative peak areas.

3.2.4. Specificity

Specificity can also be determined by measurement of peak homogeneity. Because the different techniques available in a PDA are not equal for the detection of possible impurities or interferences in an electrophoretic peak, the use of several techniques is recommended [45]. In this work the techniques used to validate the peak purity of cytochrome *c* present in the cytosol fractions and mitochondrial extracts were [46]: (a) normalization and comparison of spectra from different peak sections and (b) absorbance at two wavelengths (190 and 407 nm, respectively). Both techniques provided a high level of purity of the peaks corresponding to the studied compound in the samples.

3.2.5. Limits of detection (LOD) and quantitation (LOQ)

The limit of detection (LOD), defined as the lowest concentration of an analyte that the analytical procedure can reliably differentiate from background noise, was evaluated based on a signal-to-noise ratio (S/N) of 3 (S/N = 3) [47]. The limit of quantitation (LOQ), is defined as the level at, or above, in which the measurement precision is satisfactory for quantitative analysis. In our case, the LOQ was evaluated based on a S/N = 10 [47]. Results are shown in Table 1.

3.2.6. Recovery

Recovery is reported as the extraction efficiency of an analytical process, reported in percentage. It should be emphasized that the lack of suitable internal standards requires finding alternative ways to evaluate the recovery of cytochrome *c*. In order to test the accuracy of the proposed method, several aliquots of cytochrome *c* standard solutions were added into the mitochondrial extracts and the cytosolic fractions. As can be observed in Table 2, good results were obtained. Recoveries of an added amount were calculated by using the calibration curves, taking into account the endogenous cytochrome *c* concentration.

3.2.7. Robustness

Robustness is an important feature in the development of analytical methods since it evaluates the influence of small changes in the operating conditions of the analytical procedure on measured or calculated responses. Since variables such as BGE pH, as well as its concentration, proved to be crucial in early stages of method development, it was decided to explore whether deliberate changes in these parameters could affect the CZE-PDA

Table 2
Analytical results and recovery of cytochrome *c* in cytosol fractions and mitochondrial extracts from control and digitalis-intoxicated guinea pig hearts

Sample	Cytochrome *c* content (pM)[a]	R.S.D. (%, $n = 14$)	Added (pM)	Total found (pM)[a]	Recovery (%)[b]
Control cytosol	0.49 ± 0.05	2.04	1	1.51 ± 0.1	102.0 ± 1.4
			195	196.0 ± 0.4	100.3 ± 0.7
			400	400.5 ± 0.2	100.0 ± 1.5
Digitalis-intoxicated cytosol	0.85 ± 0.03*	1.18	1	1.9 ± 0.2	105.0 ± 0.6
			195	194.0 ± 0.5	99.5 ± 1.1
			400	401.0 ± 0.9	100.0 ± 0.5
Control mitochondria	1.1 ± 0.02	0.90	1	2.2 ± 0.3	110.0 ± 0.2
			195	197.3 ± 0.6	100.6 ± 0.5
			400	401.5 ± 1.2	100.1 ± 1.7
Digitalis-intoxicated mitochondria	0.75 ± 0.04*	2.67	1	1.8 ± 0.1	105.0 ± 1.3
			195	209.3 ± 0.5	106.9 ± 0.8
			400	401.0 ± 0.2	100.1 ± 1.6

CZE conditions: BGE, 100 mM phosphates buffer (pH 2.05); hydrodynamic injection at 0.5 psi for 10 s; PDA detection at 190 nm (bandwidth 6 nm).
[a] Results are expressed as mean ± standard deviation of 14 independent measurements.
[b] Recovery = (total found − found in the sample)/added (%). Results are expressed as mean ± standard deviation of 14 independent measurements.
* $p < 0.05$ vs. control group, one-way ANOVA followed by Student's *t*-test.

separation. Results showed that selectivity was good enough for all the responses in the buffer pH range from 2.00 to 2.15. Phosphate concentration is restricted from 95 to 100 mM in order to have a resolution greater or equal to 2.0. It means that the method is robust within this range.

3.3. Applications

3.3.1. Digitalis intoxication study

In order to test the applicability of the method, a digitalis intoxication study was performed during 18 h and samples from cytosolic fractions and mitochondrial extracts from control and digitalis intoxicated animals were analyzed with the developed CZE-PDA method. Under the optimized conditions, cytochrome *c* and other unknown compounds, were all successfully separated. Cytochrome *c* produced a single peak and was sufficiently resolved from other unknown endogenous compounds to permit accurate determination. The concentration of cytochrome *c* (expressed as mean ± standard deviation) found in these samples, using the proposed method, as well as results from recovery experiments, are shown in Table 2. It has been repeatedly demonstrated that mitochondria-mediated apoptosis is initiated by the release of cytochrome *c* to the cytosol. This event is followed by ATP-dependent formation of the apoptosome complex composed of cytochrome *c*, and the apoptotic protease-activating factor-1 (Apaf-1) which triggers its oligomerization, after which pro-caspase-9 is recruited and undergoes activation [48]. A previous in vitro study by Ramirez-Ortega et al. showed that digitalis induced the release of cytochrome *c* in the HeLa cell line, a highly sensitive cell line to the toxic effect of digitalis. In that study, either 70 nM ouabain or 230 nM digoxin-induced cytochrome *c* release from mitochondria [15] was detected by WB. An in vivo study in guinea pig hearts by Ramirez-Ortega et al. [33], showed that, following digitalis intoxication, cytochrome *c* is released from the mitochondria into the cytosol, which was confirmed by WB and by a spectrophotometric assay. On the other hand, Raghavendra et al. studied a polyphenolic cardiac glycoside (oleandrin) isolated from the leaves of *Nerium oleander* that has been used to treat congestive heart failure. It was demonstrated that in a mitochondrial extract from 100 ng mL^{-1} oleandrin-treated cells (U-937 cells isolated from histiocytic lymphoma), the amount of cytochrome *c* released from the mitochondria with increasing time of oleandrin treatment corresponded with its release into the cytoplasm [49]. In the present study, it can be observed that cytochrome *c* is released from the mitochondria into the cytosol, which is in agreement with previous observations [15,33,49]. Analysis of cytochrome *c* release through spectrophotometric assays is based on recording the difference between oxidized and reduced cytochromes by dual wavelength double beam spectrophotometry and, although rapid and simple, information regarding LOD and LOQ is unknown [50].

4. Conclusion

The determination of cytochrome *c* in a complex biological sample is an analytical challenge. Therefore, a simple, rapid and sensitive capillary electrophoretic method has been developed for the quantitative analysis of cytochrome *c* in both cytosolic fractions and mitochondrial extracts from guinea pig hearts. Although this analyte has been previously analyzed by HPLC with PDA using 393 nm detection, this is the first report, to our best knowledge, that deals with the determination of cytochrome *c* in cytosolic fractions and mitochondrial extracts obtained from guinea pig hearts following a digitalis intoxication in an in vivo model. Compared to previous HPLC methods [17,19], this method obtains comparable LOD (0.06 pM) and LOQ (0.21 pM) for this analyte. However, in the previously reported methods, a non-linear response between peak area and amount of cytochrome *c* below 0.8 pmol has been observed. The proposed CZE-PDA method has been validated and the reliability of the electrophoretic procedure for its desired application was demonstrated by means of the experimental results regarding linearity, accuracy, specificity, sensitivity and precision. Major advantages of the present CE method are the use of PDA detection and that no sample pre-treatment other than filtration, as well as a capillary coating, are required prior to the CZE-PDA analysis. Compared to previous CE methods with UV absorbance detection at 214 nm [29,30], the proposed CZE-PDA provides similar results regarding analysis time and recovery. In addition, this method may be useful to elucidate the role of apoptosis in myocardial diseases, in particular in cases of digitalis intoxication, which is a fact that has attracted considerable attention as a potentially reversible cause of cardiac functional deterioration.

Acknowledgements

The authors are grateful to Fundación Río Arronte for the donation of a Beckman Coulter P/ACE™ MDQ Capillary Electrophoresis System and to Dr. Ingrid Mascher for her English Language editorial review. This work was partially supported by a CONACYT (Mexico) grant 44173-M (A. Sánchez-Mendoza).

References

[1] D. Arnoult, P. Parone, J.C. Martinou, B. Antonsson, J. Estaquier, J.C. Ameisen, J. Cell Biol. 159 (2002) 923.
[2] R. Markuniene, A. Jekabsone, V. Borutaite, FEBS Lett. 521 (2002) 53.
[3] E.J. Griffiths, A.P. Halestrup, J. Mol. Cell. Cardiol. 25 (1993) 1461.
[4] L.C. Trost, J.J. Le Masters, J. Pharmacol. Exp. Ther. 278 (1996) 1000.
[5] A.F. Schinderr, E.C. Olson, N.C. Spitzer, M. Montal, J. Neurosci. 16 (1996) 6125.
[6] N. Zamzami, G. Kroemer, Nat. Rev. Mol. Cell. Biol. 2 (2001) 67.
[7] M. Ehrlichova, M. Koc, J. Truksa, Z. Naldova, R. Vaclavikova, J. Kovarr, Anticancer Res. 25 (2005) 4215.
[8] H.I. Lin, Y.J. Lee, B.F. Chen, M.C. Tsai, J.L. Lu, C.J. Chou, G.M. Jow, Cancer Lett. 230 (2005) 248.
[9] G. Petrosillo, F.M. Ruggiero, M. Pistolese, G. Paradies, J. Biol. Chem. 279 (2004) 53103.
[10] E.O. Lee, J.R. Lee, K.H. Kim, N.I. Baek, S.J. Lee, B.H. Lee, K.D. Cho, K.S. Kahn, S.H. Kim, Biol. Pharm. Bull. 29 (2006) 1.
[11] D. Mohan, C.S. Lee, J. Chromatogr. A 979 (2002) 271.
[12] I. Bertini, G. Cavallaro, A. Rosato, Chem. Rev. 106 (2006) 90.
[13] M. Giorgio, E. Migliaccio, F. Orsini, D. Paolucci, M. Moroni, C. Contursi, G. Pelliccia, L. Luzi, S. Manucci, M. Marcaccio, P. Pinton, R. Rizzuto, P. Bernardi, F. Paolucci, P.G. Pelicci, Cell 122 (2005) 221.

[14] R. Adorisio, L. De Luca, J. Rossi, M. Gheorghiade, Heart Fail. Rev. 11 (2006) 109.
[15] M. Ramirez-Ortega, V. Maldonado-Lagunas, J. Melendez-Zajgla, J.F. Carrillo-Hernandez, G. Pastelin-Hernandez, O. Picazo-Picazo, G. Ceballos-Reyes, Eur. J. Pharmacol. 534 (2006) 71.
[16] Y.C. Lui, L.H. Sowdal, N.C. Robinson, Arch. Biochem. Biophys. 324 (1995) 135.
[17] M.J. Picklo, J. Zhang, V.Q. Nguyen, D.G. Graham, T.J. Montine, Anal. Biochem. 276 (1999) 166.
[18] C. Batthyány, J.M. Souza, R. Durán, A. Cassina, C. Cerveñansky, R. Radi, Biochemistry 44 (2005) 8038.
[19] H.J. Chen, C.M. Chang, Y.M. Chen, Free Radic. Biol. Med. 34 (2003) 254.
[20] E.D. Crouser, M.E. Gadd, M.W. Julian, J.E. Huff, K.M. Boeckemeier, K.A. Robbins, D.R. Pfeiffer, Anal. Biochem. 317 (2003) 67.
[21] L. Ding, X.X. Zhang, W.B. Chang, W. Lin, M. Yang, Chromatographia 61 (2005) 85.
[22] R. Ramautar, G.W. Somsen, G.J. de Jong, Anal. Bioanal. Chem. 387 (2007) 293.
[23] R.J. Meagher, J. Seong, P.E. Laibinis, A.E. Barron, Electrophoresis 25 (2004) 405.
[24] D. Mohan, C.S. Lee, Electrophoresis 23 (2002) 3160.
[25] B. Verzola, F. Fogolari, P.G. Righetti, Electrophoresis 22 (2001) 3728.
[26] S. Zhang, J. Zhang, C. Horvath, J. Chromatogr. A 914 (2001) 189.
[27] M.E. McComb, A.N. Krutchinsky, W. Ens, K.G. Standing, H. Perreault, J. Chromatogr. A 800 (1998) 1.
[28] M. Larsson, E.S. Lutz, Electrophoresis 21 (2000) 2859.
[29] J.M. Armenta, B. Bu, C.D. Thulin, M.L. Lee, J. Chromatogr. A 1148 (2007) 115.
[30] A.M. MacDonald, C.A. Lucy, J. Chromatogr. A 1130 (2006) 265.
[31] R.M. Schoenherr, M. Ye, M. Vanatta, N.J. Dovichi, Anal. Chem. 79 (2007) 2230.
[32] J.M. Busnel, S. Descroix, T. Le Saux, S. Terabe, M.C. Hennion, G. Peltre, Electrophoresis 27 (2006) 1481.
[33] M. Ramirez-Ortega, G. Zarco, V. Maldonado, J.F. Carrillo, P. Ramos, G. Ceballos, J. Melendez-Zajgla, N. Garcia, C. Zazueta, J. Chanona, J. Suarez, G. Pastelin, Eur. J. Pharmacol. 566 (2007) 34.
[34] S.K. Bhattacharya, J.H. Thakar, P.L. Johnson, D.R. Shanklin, Anal. Biochem. 192 (1991) 344.
[35] O.H. Lowry, N.J. Rosebrough, A.L. Farr, R.J. Randall, J. Biol. Chem. 193 (1951) 265.
[36] S.F.Y. Li, Capillary Electrophoresis, second ed., Elsevier, Amsterdam, 1993, p. 21.
[37] E. Szökö, Electrophoresis 18 (1997) 74.
[38] R.G. Nielsen, E.C. Rickard, J. Chromatogr. 516 (1990) 99.
[39] J.L. Beckers, P. Bocek, Electrophoresis 24 (2003) 518.
[40] M. Horká, K. Šlais, Electrophoresis 21 (2000) 2814.
[41] S. Hoffstetter-Kuhn, A. Paulus, E. Gassmann, H. Michael, Anal. Chem. 63 (1991) 1541.
[42] A. Jouyban, A. Batish, S.J. Rumbelow, B.J. Clark, Analyst 126 (2001) 1958.
[43] M. Wang, F. Qu, X. Shan, J. Lin, J. Chromatogr. A 989 (2003) 285.
[44] A. Tzagoloff, Mitochondria, Plenum Press, New York, 1983, p. 61.
[45] H. Farbe, A. Lebris, M.D. Blanchin, J. Chromatogr. A 697 (1995) 81.
[46] L. Huberm, Applications of Diode-Array Experience, vol. 12, Hewlett-Packard Publication, 1989, p. 5953.
[47] D. Brynn Hibbert, Analyst 131 (2006) 1273.
[48] Y. Tsujimoto, T. Nakagawa, S. Shimizu, Biochim. Biophys. Acta 1757 (2006) 1297.
[49] P.B. Raghavendra, S. Sreenivasan, G.T. Ramesh, S.K. Manna, Apoptosis 12 (2007) 307.
[50] F. Appaix, M.N. Minatchy, C. Riva-Lavieille, J. Olivares, B. Antonsson, V.A. Saks, Biochim. Biophys. Acta 1457 (2000) 175.

Available online at www.sciencedirect.com
ScienceDirect
Talanta 74 (2008) 1043–1049
Talanta
www.elsevier.com/locate/talanta

Short communication

Graphite–silicone rubber composite electrode: Preparation and possibilities of analytical application

Aline Carlos de Oliveira [a], Sidney Xavier dos Santos [b], Éder Tadeu Gomes Cavalheiro [b,*]

[a] *Departamento de Química, Universidade Federal de São Carlos, C.P. 676, 13565-905 São Carlos, SP, Brazil*
[b] *Departamento de Química e Física Molecular, Instituto de Química de São Carlos, Universidade de São Paulo, Av Trabalhador São Carlense 400, C.P. 676, 13560-970 São Carlos, SP, Brazil*

Received 2 April 2007; received in revised form 19 June 2007; accepted 22 June 2007
Available online 1 July 2007

Abstract

Composite electrodes were prepared using graphite powder and silicone rubber in different compositions. The use of such hydrophopic materials interned to diminish the swallowing observed in other cases when the electrodes are used in aqueous solutions for a long time. The composite was characterized for the response reproducibility, ohmic resistance, thermal behavior and active area. The voltammetric response in relation to analytes with known voltammetric behavior was also evaluated, always in comparison with the glassy carbon. The 70% (graphite, w/w) composite electrode was used in the quantitative determination of hydroquinone (HQ) in a DPV procedure in which a detection limit of 5.1×10^{-8} mol L^{-1} was observed. HQ was determined in a photographic developer sample with errors lower then 1% in relation to the label value.
© 2007 Elsevier B.V. All rights reserved.

Keywords: Composite electrode material; Graphite; Silicone rubber; Ferricyanide; Hydroquinone

1. Introduction

Since the earlier 1960s many different procedures to prepare solid carbon-based electrodes for electroanalytical use have been proposed [1]. This search looks for working electrodes to be used in voltammetric and amperometric measurements in the anodic potential range in which mercury is not applicable.

Among these solid electrode materials one can highlight the composites in which the carbon is dispersed in polymeric matrices. The polymer phase of the composite defines the viscosity of the paste before curing. At this point, the material is soft and can be molded into different shapes and sizes [2]. Solid composite electrodes present several advantages in relation to other materials such as easiness of surface renewing, rigidity, easiness of fabrication, possibility of using in non-aqueous solvents, using in flow procedures and possibility of bulk modification.

According to Tallman and Petersen [3], a composite electrode can be defined as "a material consisting of at least one conductor phase commingled with at least one insulator phase, the typical case being a material containing one conducting and one insulating phase". In that review, the authors also provided a classification and a discussion on the preparation and applications of such devices in several determinations.

The low cost of carbon-based composites makes them ideal for mass produced sensors, especially when compared to other materials such as gold and platinum.

Perhaps the most popular composite electrode material is the carbon paste, first proposed by Adams [1] and widely used in several analytical applications after modification including the incorporation of enzymes [4–6]. In this case the graphite conductor phase is agglutinated by an inert mineral oil insulating phase. The resulting paste is usually limited to use in aqueous media although some special carbon paste formulations can also be used in mixed solutions containing polar organic solvent (e.g. methanol).

On the other hand solid composites based on graphite-polymer matrix present good results in voltammetric techniques

* Corresponding author. Fax: +55 1633738054.
E-mail address: cavalheiro@iqsc.usp.br (É.T.G. Cavalheiro).

0039-9140/$ – see front matter © 2007 Elsevier B.V. All rights reserved.
doi:10.1016/j.talanta.2007.06.033

as well as in the preparation of detectors for amperometric and chromatographic procedures [3], even in non-aqueous media. Examples of graphite composites with styrene–acrylonitrile copolymer [7], polyolefin [8], poly(vinylchloride) [9], poly(tetrafluorethylene) [10,11], wax [12], PVC, Nylon-6, Nylon-11, polyethylene [13,14], epoxy [15], sol–gel [16], Kel-F [17] and castor oil-based polyurethane [18] have been described for applications with different techniques in the detection and quantification of different analytes.

Pungor and Szepesváry first described the preparation and use of the graphite–silicone rubber composite electrode (GSR) [19,20]. The authors had presented a short review on the development of many types of carbon-based electrodes and had considered the use of GSR in voltammetry. The magnitude of residual current was investigated, the relation between the electroactive species concentration and the peak current, as well as its reproducibility. The electrochemical behavior of some organic and inorganic compounds was also studied.

Then the Hungarian group presented some works on the voltammetric use of these composites as working electrodes [19–25]. However, surprisingly, the use of this interesting composite material was interrupted and only potentiometric studies [26–34] where further presented. May be that the cathodic range limitations of the electrode led it to be neglected.

In the present work, the possibilities of using a composite prepared from graphite and commercial silicone rubber is described as an electrode material, with advantage of possible use in to organic solvents, mechanical resistance and easy surface renewing.

Here we retake the GSR as an electrode material regarding aspects not well clarified in the past such as its best composition, surface microscopy, the useful potential window in different media and the determination of hydroquinone (HQ) in photographic developer sample as a test to demonstrate the quantitative capabilities of the composite electrode. Although the cathodic limitations some advantages in relation to sensitivity and useful potential window in acidic and neutral medium has been observed.

2. Experimental

2.1. Reagents and solutions

All reagents were of analytical grade and used as received. Solutions were prepared with water distilled twice in quartz stiller.

A 5.0 mmol L^{-1} potassium ferrycianide (Mallynckrodt) in 0.50 mol L^{-1} KCl (Mallynckrodt) and 5.0 mmol L^{-1} HQ (Vetec) in 0.10 mol L^{-1} acetate buffer pH 4.0 solutions were used as a probe in the initial studies.

The useful potential window investigations were performed in 0.10 mol L^{-1} H_2SO_4, 0.10 mol L^{-1} acetate buffer pH 4.0, 0.10 mol L^{-1} phosphate buffer pH 7.0, 0.10 mol L^{-1} ammonium buffer pH 10 and 0.10 mol L^{-1} NaOH solutions.

The Kodak D-76 photographic developer (Kodak, Brazil), was purchased from a local store and analyzed using the proposed composite electrode.

2.2. Apparatus

Voltammetric experiments were performed using a BAS-CV50W potentiostat. A three-electrode cell (20 mL full capacity) was used with the composite (graphite 30–70% graphite, w/w) as working, saturated calomel (SCE) as a reference and platinum wire as auxiliary electrodes. All the measurements were performed at room temperature.

Scanning electron microscopy was performed in a Zeiss DSM 940-A microscope, operated at 20 kV, in different magnitudes.

Ohmic resistance of the composite electrodes was estimated with a HP-3478A multimeter (Hewlett-Packard) by immersing the electrode in a mercury pool contact.

The thermogravimetric analysis of the composites was realized in a TGA-951 module connected to TA-2000 thermoanalyzer, both from TA Instruments.

HPLC chromatograms were recorded in a Schimadzu HPLC system equipped with a LC-10ADVp pump, SPD-M10AVP UV–vis detector (at 280 nm) and a C18 HP column (200 mm length, 4.6 mm internal diameter) under a 1.0 mL min^{-1} flow of a methanol:water 75:25 (v/v) mobile phase.

2.3. Preparation of the composite and working electrodes

The GSR was prepared by mixing graphite powder (1–2 μm, Aldrich, USA) and commercial silicone rubber (Siltrade). Suitable amount of graphite and silicone were weighted in order to obtain 30–70% graphite w/w in the composite. The final mixture was then homogenized in a glass mortar for 10 min.

The electrode assembling was made by the insertion of the composite, in the desired compositions, in glass tubes (3 mm internal diameter). The composite inside the tube was pressed at *ca.* 5 kgf for 24 h until the cure. The electric contact was established connecting a copper wire to the composite with the help of a EPO-TEK 410 E silver epoxy (Epoxy Technology, USA), and let to cure for 24 h.

2.4. Procedures

Voltammetric measurements were performed without deaeration. Cyclic voltammetric curves were obtained between −0.15 and +0.65 V (ferricyanide) and −0.5 and +1.1 V (HQ), at different scan rates at both the glassy carbon (GC) and the composite electrodes for comparison.

Differential pulse voltammograms for 5.0×10^{-5} mol L^{-1} HQ in acetate buffer pH 4, were obtained between −0.2 and +0.6 V at different scan rates (5, 10, 25, 50 and 100 mV s^{-1}) and different pulse amplitudes (10, 25, 50 and 100 mV) in order to evaluate the best experimental conditions at the 70% (graphite, w/w) composite.

Chronocoulometric determinations were performed using 5.0 mmol L^{-1} $Fe(CN)_6^{3-}$ in 0.5 mol L^{-1} KCl ($D_0 = 7.7 \times 10^{-6}$ cm^2 s^{-1} [35]), with step from 400 to 0 mV during 1 s in order to estimate the active area of the composite electrodes using the Cottrell equation [36].

Thermogravimetric measurements were performed using *ca.* 10 mg sample mass, 10 °C min^{-1} heating rate and platinum sam-

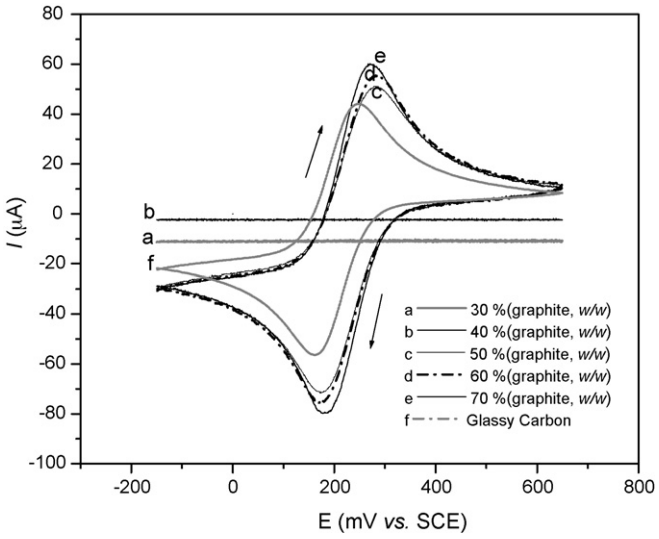


Fig. 1. Cyclic voltammetric response of the composite electrodes (a) 30%, (b) 40%, (c) 50%, (d) 60%, (e) 70% and (f) glassy carbon at 5.0 mmol L^{-1} $K_3[Fe(CN)_6]$ in 0.5 mol L^{-1} KCl solution. Scan rate 50 mV s^{-1} and potential from −0.15 to +0.65 V.

ple holder. The furnace atmosphere was first saturated with nitrogen flowing at 100 mL min^{-1} and the sample heated up to 700 °C. Then the atmosphere was changed to dry air at the same flow rate and the sample heated up to 900 °C.

In the voltammetric determination of HQ a sample of the photographic developer was dissolved in acetate buffer pH 4 in order to be close to 1.0×10^{-4} mol L^{-1}, considering the label information. Then an aliquot of this solution was transferred to the voltammetric cell and three differential pulse voltammograms (DPV) were recorded. After that three additions of 100 μL of a standard 2.00×10^{-2} mol L^{-1} HQ solution in acetate buffer pH 4 were performed. After each addition three DPV voltammograms were recorded and the mean peak current determined.

For the chromatographic comparative method an approximately 40.0 ppm HQ sample solution in acetate buffer pH 4 was prepared according to the label value. Aliquots of this solutions were dissolved in the same buffer after adding an appropriate amount of a 1000 ppm stock HQ solution in acetate buffer pH 4 in order to have 0, 1.82×10^{-4}, 3.63×10^{-4} and 5.46×10^{-4} mol L^{-1} (correspondent to 0, 20, 40 and 60 ppm, respectively) of standard added. Then three chromatograms were recorded for each one of such solutions and the mean peak areas calculated.

Table 1
Ohmic resistance estimated for the composite electrodes by a mercury pool contact compared with that of GC electrode

Electrode composition (%)	Resistance (Ω)
30	290,000
40	78,000
50	75
60	11
70	6
GC	4

3. Results and discussion

3.1. Evaluation of the graphite content in the composite and electrode response

The composite electrodes with different compositions (30–70% graphite, w/w) were evaluated in relation to the cyclic voltammetric curves of 5 mmol L^{-1} $Fe(CN)_6^{3-}$ in 0.5 mol L^{-1} KCl solutions and compared with the GC electrode. Typical results are presented in Fig. 1. Compositions of 30 and 40% (graphite, w/w) presented very high resistance and no response could be observed. Currents higher than GC were obtained using the electrodes with 50, 60 and 70% graphite, which presented increasing peak currents as the graphite content increased. Similar background currents were observed in all the cases.

The estimated ohmic resistances of the electrodes are summarized in Table 1. The resistance is very high at 30 and 40% (graphite, w/w) decreasing suddenly from 50% up to 70%, in agreement with cyclic voltammetric data.

According to the data presented in Table 2, the anodic peak currents at 70% (graphite, w/w) composite are higher than those observed at the other compositions and it presents much more reproducible currents between successive renewing of the surface. It was also observed that the peak currents reproducibility of the electrodes is dependent on the surface treatment when they are just rubbed with 600-grit sand paper or polished in 600-grit sand paper followed by γ-Al_2O_3 suspension. The second

Table 2
Reproducibility of the composite electrodes response after polishing with 600-grit sand paper followed by 1 μm γ-Al_2O_3 and currents measured for 5.0 mmol L^{-1} $Fe(CN)_6^{3-}$ in 0.5 mol L^{-1} KCl solution

Graphite content (%, w/w)	Parameter (μA)					Mean ± S.D.[a] (μA)
Anodic peak current (μA)						
50	7.175	6.735	6.945	6.730	6.914	6.899 ± 0.183
60	7.288	7.247	7.517	7.010	7.622	7.325 ± 0.245
70	7.766	7.828	7.863	7.745	8.040	7.848 ± 0.117
Anodic peak potential (mV)						
50	278	281	284	278	276	279 ± 3
60	278	281	280	294	286	284 ± 6
70	274	267	272	276	286	275 ± 7

[a] Standard deviation.

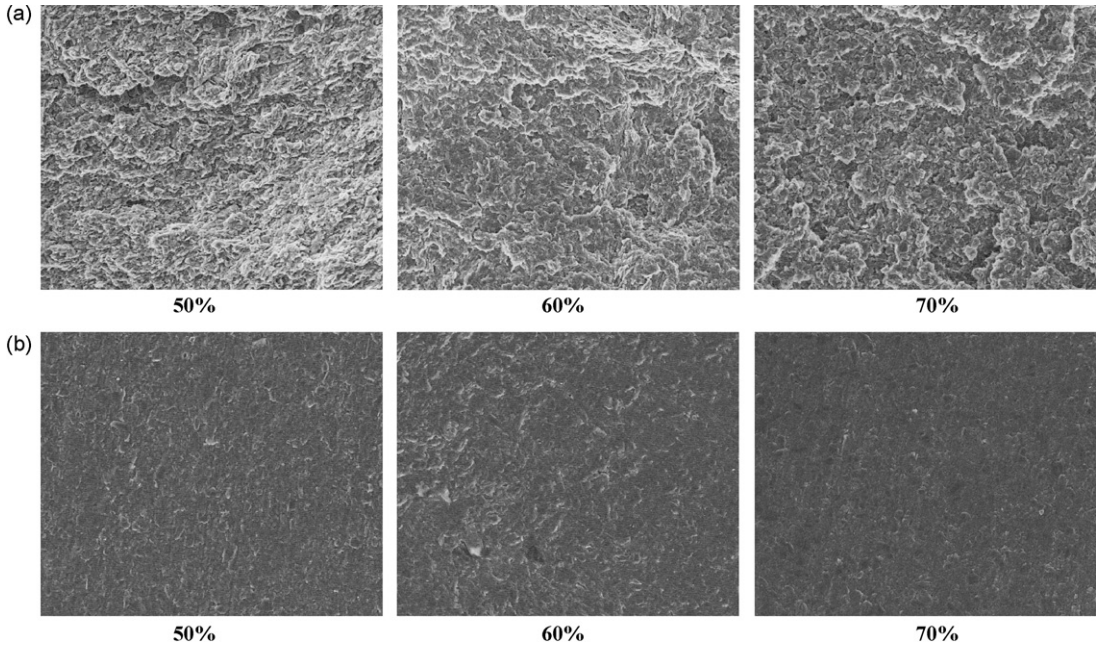


Fig. 2. Scanning electron micrographs (20 kV) for GSR 50, 60 and 70% (graphite, w/w) composites before treatment (a) and after polishing in 600-grit sand paper followed by 1 μm γ-Al_2O_3 (b). Magnification 500×.

treatment resulted in lower dispersion in the peak current values for successive voltammetric ferrycianide runs. The anodic peak potential presented a similar behavior.

The 70% (graphite, w/w) composite was the less sensitive to this effect. Thus this composition was chosen for further studies.

The anodic peak data were presented here just as an example. The same behavior was observed for the cathodic peak current and potentials.

Micrographies of the 50–70% (graphite, w/w) composites surfaces, before and after polishing in 600-grit sand paper followed by γ-Al_2O_3 suspension are presented in Fig. 2. According to this figure, before treatment (Fig. 2a), the composites presents similar surfaces with almost the same roughness. After polishing (Fig. 2b) again similar scaled surfaces are observed. The 70% (graphite, w/w) composite presented the smoother surface when compared with the 50 and 60% ones.

Trijueque et al. [37,38] described a composition of 62% as that which presents the best electroanalytical properties for graphite–epoxy electrodes based on the second threshold percolation theory. Our previous findings with the graphite–polyurethane composite pointed out to a 60% (graphite, w/w) as the best composition in that case [18]. In the case of the graphite–BS composite it was possible to prepare the 70% (graphite, w/w) without crumbling and low ohmic resistance. This higher composition permitted to obtain a more conductive material with higher peak currents, probably due to the better contact between the graphite particles in the composite.

Table 3
Useful potential window for the composites in different supporting electrolytes, limited to a background current of <2 μA

Supporting electrolytes	Potential window (mV vs. SCE)
0.10 mol L^{-1} H_2SO_4	−500 to +1400
0.10 mol L^{-1} acetate buffer pH 4.0	−500 to +1400
0.10 mol L^{-1} phophate buffer pH 7.0	−300 to +1300
0.10 mol L^{-1} ammonium buffer pH 10.0	−300 to +900
0.10 mol L^{-1} NaOH	−300 to +800

3.2. Useful potential window in different supporting electrolytes

Fig. 3 shows the potential windows in which the 70% (graphite, w/w) composite electrodes can be used presenting background currents <2 μA, in relation to the SCE. These experiments were performed in different supporting electrolytes such as 0.10 mol L^{-1} H_2SO_4, 0.10 mol L^{-1} acetate buffer pH 4, 0.10 mol L^{-1} phosphate buffer pH 7, 0.10 mol L^{-1} ammonium buffer pH 10 and 0.10 mol L^{-1} NaOH solutions.

The narrowest window was found when the GSR is used in basic medium in which the electrode is limited in both anodic and cathodic ranges. Pungor had described this before [19], pointing out to the limitation of this electrode material in the cathodic range. However it still an alternative to mercury considering the anodic range in neutral or acidic medium. Table 3 resumes the results for the potential window in which the electrodes presented background currents <2 μA.

The limitations can be related to the presence of functional groups in the polymers that can be oxidized or reduced in basic medium causing increase in the background current. These redox processes seems to be pH dependent.

3.3. Chronocoulometry

The active areas of the prepared electrodes were estimated from the Cottrell equation [36] using chronocoulometric

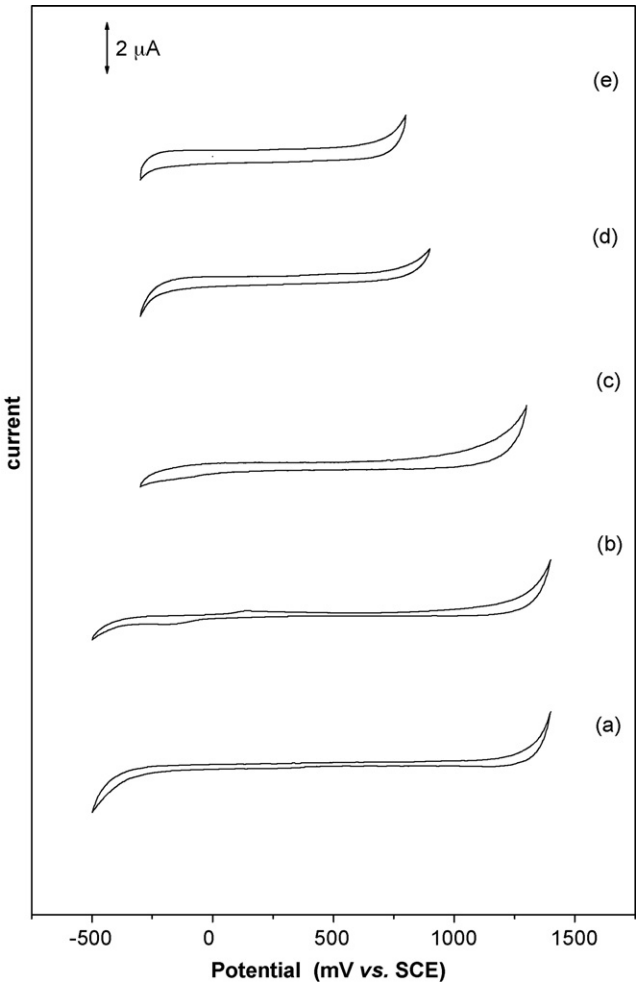


Fig. 3. Cyclic voltammograms obtained with the 70% (graphite, w/w) composite electrode in different solutions: (a) 0.10 mol L^{-1} H_2SO_4; (b) 0.10 mol L^{-1} acetate buffer pH 4; (c) 0.10 mol L^{-1} phosphate buffer pH 7; (d) 0.10 mol L^{-1} ammonium buffer pH 10; (e) 0.10 mol L^{-1} NaOH. Scan rate 25 mV s^{-1}, potentials vs. SCE.

data and the current density from cyclic voltammograms of 5.0 mmol L^{-1} $Fe(CN)_6{}^{3-}$ in 0.5 mol L^{-1} KCl. These results are presented in Table 4. The areas of the 60 and 70% (graphite, w/w) are higher than that for the GC electrode, while in the 50% (graphite, w/w) composition, a lower active area was observed. This is probably due to the presence of higher resin content resulting in a less conducting material being part of the conductive area occupied by the insulating polymeric phase, despite the SEM images suggest that the composites presented similar aspect.

Table 4
Areas determined by chronocoulometry of 5.0 mmol L^{-1} $Fe(CN)_6{}^{3-}$ in 0.5 mol L^{-1} KCl (other conditions as in the text)

Electrode	Area (cm^2)	Current density[a] ($\mu A\,cm^{-2}$)
Composite 50%	0.214	32.25
Composite 60%	0.237	30.93
Composite 70%	0.238	32.98
GC	0.227	33.26

Anodic peak currents from cyclic voltammetry were used for the current density estimative.
[a] Obtained at a 50 mV s^{-1} scan rate.

3.4. Thermal analysis

Thermogravimetric data were used in order to determine the actual graphite content in each composite (curves not shown). The unmodified SR and the composites were heated under nitrogen up to 700 °C, in order to decompose the further polymer and thus the atmosphere was changed to air letting the carbon to burn.

The pure polymer decomposes in a single step between 338 and 600 °C, resulting in a 11.1% residue in the sample holder at 850 °C, which was taken in account during the calculations of the graphite content in the composites.

The composites presented a mass loss correspondent to that observed in the unmodified polymer in the same temperature range. An intense carbon burn can be observed at 700 °C, when the furnace atmosphere is changed to air. Details of the thermal decompositions, such as mass losses and temperature ranges are described in Table 5.

The graphite contents were close to the expected, showing that the graphite is well dispersed in the material. If a non-homogeneous material was obtained the graphite content will be different along the composite rod.

3.5. Determination of hydroquinone

HQ was chosen as a probe in order to evaluate the analytical potentialities of the GSR 70% (graphite, w/w) composite electrode, since it presents a well-known voltammetric behavior. We had chosen differential pulse voltammetry (DPV) for quantitative measurements since it presents better resolution in relation to the non-faradayc currents.

Typical DPV voltammograms of HQ at GC electrode and GSR 70% (graphite, w/w) composite electrode are presented in Fig. 4. It is possible to observe that higher anodic peak currents can be reached with the composite under the same experimental conditions as well as a better peak definition. In these experiments a 10 mV s^{-1} scan rate, 50 mV pulse amplitude, were used after an optimization study.

Under the optimized conditions a linear response between the anodic peak current as a function of the HQ concentration was observed in the range investigated 1.99×10^{-7}–8.3×10^{-6} mol L^{-1}, according to

$$I_{pa}\,(\mu A) = 0.134\,(\mu A) + 0.059[HQ]\,(10^7\ mol^{-1}\ L\ \mu A),$$
$$R = 0.999, \quad n = 10 \qquad (1)$$

In this range a limit of detection of 5.1×10^{-8} mol L^{-1} can be found (3× blanck standard deviation/angular coefficient) [39]. Using a 60% (graphite, w/w) graphite–polyurethane (PU) composite a 9.8×10^{-7} mol L^{-1} detection limit was previously found, using similar conditions [40].

The electrode was submitted to 10 successive determinations of HQ using a 5.0×10^{-5} mol L^{-1} in acetate buffer pH 4.0 solution in order to evaluate the repeatability of the measurements.

Table 5
Mass loss, temperature range and determined graphite contents for GSR composites, using thermogravimetry

Sample (% graphite, w/w)	ΔTemperature (°C)	Mass loss or residue (%)	Graphite content (%)
30	Polymer decomposition (300–571)	62.35	29.88
	Graphite burning (638–857)	29.84	
	Residue (871)	8.054	
40	Polymer decomposition (300–567)	53.06	40.28
	Graphite burning (624–838)	38.11	
	Residue (882)	8.295	
50	Polymer decomposition (300–567)	43.91	50.54
	Graphite burning (619–867)	48.23	
	Residue (900)	8.333	
60	Polymer decomposition (300–577)	28.66	66.9
	Graphite burning (629–862)	63.96	
	Residue (900)	8.000	
70	Polymer decomposition (300–586)	23.23	73.46
	Graphite burning (633–871)	76.46	
	Residue (900)	4.742	
Silicon rubber	Polymer decomposition (338–600)	98.90	–
	Residue (900)	11.10	

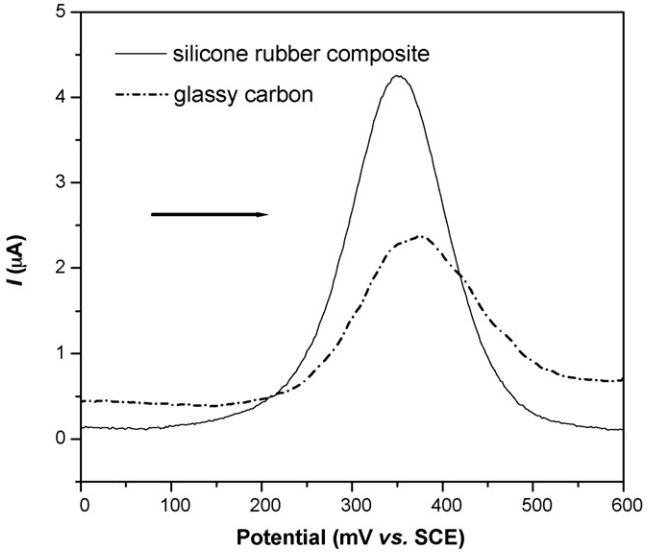


Fig. 4. Pulse voltammograms of 2.0×10^{-4} mol L^{-1} hydroquinone in 0.1 mol L^{-1} acetate buffer pH 4.0 at both 70% (graphite, w/w) composite and GC electrodes. Scan rate 10 mV s^{-1}, pulse amplitude 50 mV.

Table 6
Determination of hydroquinone in Kodak D-76 photographic developers using GSR in DPV

Hydroquinone (mg g^{-1})				
Labeled value	Found: DPV	Relative errors[a] (%)	Found: HPLC	Relative errors[b] (%)
50	50.4	1	51	−1
50	49.7	−1	51	−2

[a] $E_1 = [(\text{DPV} - \text{labeled})/\text{labeled}] \times 100\%$.
[b] $E_2 = [(\text{DPV} - \text{HPLC})/\text{HPLC}] \times 100\%$.

The electrode surface was renewed after each determination resulting in a mean peak current of 1.78 ± 0.08 μA ($n = 10$).

The results obtained in such determinations are represented in Table 6. The voltammetric procedure permitted to determine the HQ in the photographic developer with a lower standard deviation. The results from the voltammetric and chromatographic method agree within 95% confidence level according to the Student's *t*-test.

4. Conclusion

According to the results presented in this work the GSR electrodes presented interesting features for analytical use, in both cyclic and pulse voltammetric experiments. These electrodes presented relatively easy preparation, low cost, sensitivity, resistance to some organic solvents [41,42] and good mechanical resistance. The best voltammetric response was obtained with the 70% (graphite, w/w) composite, which was not previously described in the literature. This composition presented the best surface renewing and appropriated electric resistance to be used in the preparation of voltammetric sensor devices.

When compared with the glassy carbon and PU composite 60% (graphite, w/w), the 70% (graphite, w/w) composite presented higher sensitivity for hydroquinone. The potential window was limited in the cathodic branch. However in neutral or acidic media the composite can be used in a wild anodic potential range. The introduction of chemical modifiers should allow to the determination of several analytes and will be a research subject in the future.

Acknowledgements

The authors are indebted to FAPESP for the research support (grant 05/04297-1) and to CNPq for SXS fellowship.

References

[1] R.N. Adams, Anal. Chem. 30 (1958) 1576.
[2] F. Céspedes, E. Martínez-Fàbregas, S. Alegret, Trends Anal. Chem. 15 (1996) 296.
[3] D.E. Tallman, S.L. Petersen, Electroanalysis 2 (1990) 499.
[4] I. Svancara, K. Vytras, J. Barek, J. Zima, Crit. Rev. Anal. Chem. 31 (2001) 311.
[5] A.-E. Radi, Curr. Pharm. Anal. 2 (2006) 1.
[6] K. Vytras, K. Kalcher, I. Svancara, K. Schachl, E. Khaled, J. Jezkova, J. Konvalina, R. Metelka, Proc. Electrochem. Soc. 18 (2001) 277.
[7] J.Y. Jin, F. Xu, T. Miwa, Electroanalysis 12 (2000) 610.
[8] V. Haddadi-Asl, M.S. Rabbani, Iran. Polym. J. 7 (1998) 185.
[9] F. Albertús, A. Llerena, J. Alpízar, V. Cerdá, M. Luque, A. Rios, M. Valcárcel, Anal. Chim. Acta 355 (1997) 23.
[10] C. Fernández, A.J. Reviejo, J.M. Pingarrón, Anal. Chim. Acta 305 (1995) 192.
[11] L.N. Klatt, D.R. Connell, R.E. Adams, I.L. Honigberg, J.C. Price, Anal. Chem. 47 (1975) 2470.
[12] J. Wang, N. Naser, Anal. Chim. Acta 316 (1995) 253.
[13] V. Haddadi-Asl, M. Kazacos, M.S. Kazacos, J. Appl. Polym. Sci. 57 (1995) 1455.
[14] T.R.I. Cataldi, D. Centonze, Anal. Chim. Acta 326 (1996) 107.
[15] J. Navarro-Laboulais, J. Trijueque, F. Vicente, H. Scholl, J. Electroanal. Chem. 397 (1994) 159.
[16] G. Gum, M. Tsionsky, O. Lev, Anal. Chim. Acta 294 (1994) 261.
[17] E. Weisshaar, D.E. Tallman, Anal. Chem. 55 (1983) 1146.
[18] R.K. Mendes, S. Claro-Neto, E.T.G. Cavalheiro, Talanta 57 (2002) 909.
[19] E. Pungor, É. Szepesváry, Anal. Chim. Acta 43 (1968) 289.
[20] E. Pungor, É. Szepesváry, J. Havas, Anal. Lett. 1 (1968) 213.
[21] E. Pungor, Z. Feher, G. Nagy, Magy. Kem. Foly. 77 (1971) 298.
[22] E. Pungor, G. Nagy, Z. Feher, Magy. Kem. Foly. 77 (1971) 294.
[23] Z. Feher, G. Nagy, K. Toth, E. Pungor, Analyst 99 (1974) 699.
[24] E. Pungor, Z. Feher, G. Nagy, Pure Appl. Chem. 44 (1975) 595.
[25] Z. Niegreisz, G. Horvai, K. Toth, E. Pungor, Symp. Biol. Hung. 31 (1986) 83.
[26] E.R. Szepesváry, E. Pungor, Magy. Kem. Foly. 77 (1971) 502.
[27] E. Szepesváry, E. Pungor, Anal. Chim. Acta 54 (1971) 199.
[28] E.R. Szepesváry, E. Pungor, Anal. Lett. 3 (1970) 603.
[29] E. Siska, Hung. Sci. Inst. 33 (1975) 13.
[30] F. Mohamed, E. Pungor, G. Nagy, Anal. Chim. Acta 82 (1976) 285.
[31] T.J. Pastor, V.J. Vajgand, Z. Simonovic, É. Szepesváry, Anal. Chim. Acta 98 (1978) 233.
[32] T.J. Pastor, M.M. Pastor, Z. Simonovic, E. Szepesváry, Talanta 29 (1982) 521.
[33] M. Mascini, G. Marrazza, Anal. Chim. Acta 231 (1990) 231.
[34] E. Lindner, Z. Niegreisz, K. Toth, E. Pungor, M. Erdosy, P.B. Richard, Magy. Kem. Foly. 97 (1991) 345.
[35] M. Stackelberg, M. Pilgram, V. Toome, Z. Electrochem. 57 (1953) 342.
[36] W.R. Heineman, P.T. Kissinger, Large-amplitude controlled potential techniques, in: P.T. Kissinger, W.R. Heineman (Eds.), Laboratory Techniques in Electroanalytical Chemistry, 2nd ed., Marcel Dekker, New York, 1996 (Chapter 3).
[37] J. Navarro-Laboulais, J. Trijueque, F. Vicente, H. Scholl, J. Electroanal. Chem. 379 (1994) 159.
[38] J. Trijueque, J.J. García-Jareño, J. Navarro-Laboulais, A. Sanmantías, F. Vicente, Electrochim. Acta 45 (1999) 789.
[39] J. Miller, J. Miller, Statistic for Analytical Chemistry, 3rd ed., Ellis Horwood PTR Prentice Hall, New York, 1993, p. 115.
[40] R.K. Mendes, P. Cervini, E.T.G. Cavalheiro, Talanta 68 (2006) 708.
[41] E. Pungor, Z. Feher, G. Nagy, Lucr. Conf. Nat. Chim. Anal. 1 (1971) 215.
[42] S. Budavari (Ed.), The Merck Index, 12th ed., Merck & Co., Whitehouse Station, 1996.

Available online at www.sciencedirect.com
ScienceDirect
Talanta 74 (2008) 717–723
Talanta
www.elsevier.com/locate/talanta

Quantitative imaging of zinc, copper and lead in three distinct regions of the human brain by laser ablation inductively coupled plasma mass spectrometry

J. Dobrowolska [a,c], M. Dehnhardt [b], A. Matusch [b], M. Zoriy [a], N. Palomero-Gallagher [b], P. Koscielniak [c], K. Zilles [b], J.S. Becker [a,*]

[a] *Central Division of Analytical Chemistry, Research Centre Jülich, 52425 Jülich, Germany*
[b] *Institute of Medicine, Research Centre Jülich, 52425 Jülich, Germany*
[c] *Jagiellonian University, Faculty of Chemistry, Laboratory for Forensic Chemistry, Cracow, Poland*

Received 23 May 2007; received in revised form 29 June 2007; accepted 29 June 2007
Available online 25 July 2007

Abstract

Laser ablation inductively coupled plasma mass spectrometry (LA-ICP-MS) was used to determine the distribution of the trace elements zinc, copper and lead in insular, central and hippocampal areas of thin tissue sections (thickness 20 μm) through an entire human brain hemisphere. For the investigation of the tissue samples, a commercial laser ablation system was coupled to a double-focusing sector field ICP-MS. The regions of interest of healthy brain tissue (thickness 20 μm) were scanned (raster area ~200 mm^2) with a focused laser beam (wavelength 266 nm, diameter of laser crater 200 μm and laser power density 3×10^9 W cm^{-2}). The ion intensities of $^{64}Zn^+$, $^{63}Cu^+$ and $^{208}Pb^+$ were measured by LA-ICP-MS within the ablated area. For quantification purposes, matrix-matched laboratory standards were prepared by means of dosing of each analyte to the pieces of brain tissue. The mass spectrometric analysis yielded inhomogeneous and largely reciprocal distributions of Zn and Cu in the selected areas of investigated brain samples. The highest concentrations of Zn and Cu with the most distinct distribution pattern were found in the hippocampus (up to 15 μg g^{-1}). In contrast to zinc and copper, for lead, a more homogeneous distribution throughout all regions examined was found at a low concentration (in the ng g^{-1} range) level within the analytical range of LA-ICP-MS.
© 2007 Elsevier B.V. All rights reserved.

Keywords: Brain tissue; Imaging mass spectrometry; LA-ICP-MS; Quantification; Trace elements

1. Introduction

Trace elements play a functional role in signaling, metabolism and homeostasis of the cell [1–3]. Of many tissue types, nervous tissue is particularly sensitive to alterations in the concentration of essential trace elements and to the accumulation of toxic trace elements [4]. Pathological diseases of the brain may be closely related to very basic alterations such as alternations of trace element concentration and distribution [3,5,6]. Knowledge of these may contribute to the investigation of diseases such as Parkinson's disease [7,8], Huntington's disease [9], Alzheimer's disease [3,5,6] or epilepsy [10].

Investigating element distribution in thin tissue slices requires sensitive analytical techniques [11]. Several analytical techniques (histochemical staining techniques e.g. autometallography [12], cation-sensitive fluorescent dyes [13]) for imaging of element distributions in tissue sections are not sensitive enough to detect the elements at trace and ultratrace level and difficult to quantify. Moreover, these methods are not multi-elemental. Other methods, such as scanning electron microprobes (SEM) with energy dispersive X-ray analysis (EDX) [14], microproton-induced X-ray emission spectrometry [15] and neutron activation followed by autoradiography [16] have limited sensitivity particularly to heavy trace elements. Secondary ion mass spectrometry (SIMS) could also be applied for the analysis of element distribution. However, this suffers from huge matrix effects and high molecular ion formation rates such that no quantitative data are obtained [17]. All techniques using

* Corresponding author. Tel.: +49 2461 612698; fax: +49 2461 612560.
E-mail address: s.becker@fz-juelich.de (J.S. Becker).

0039-9140/$ – see front matter © 2007 Elsevier B.V. All rights reserved.
doi:10.1016/j.talanta.2007.06.051

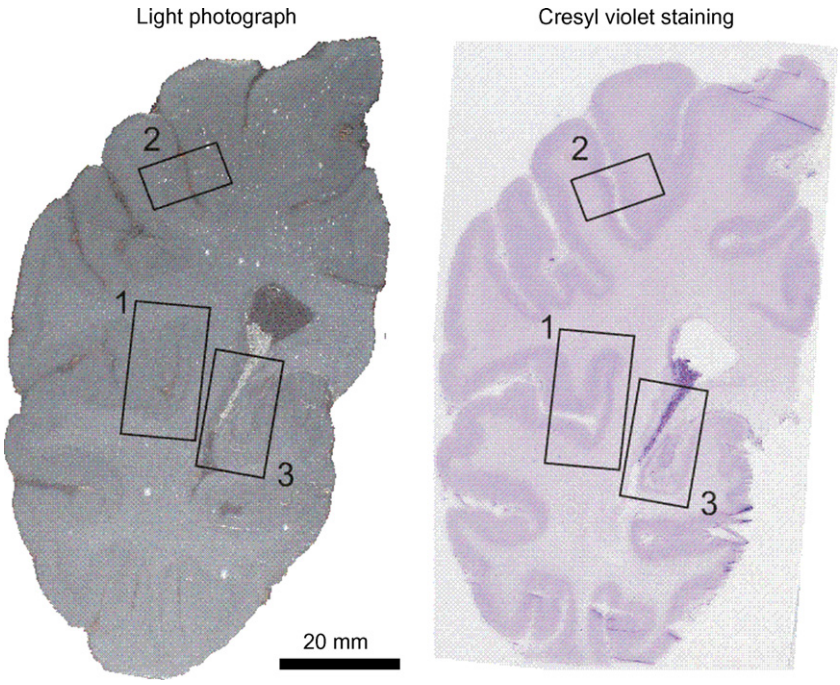


Fig. 1. Light photograph (left) of the slice of a left brain hemisphere before laser ablation and cresyl violet staining (right) of the adjacent slice as histological control ("neurological" orientation, left side left). The rectangular regions which were cut out for laser ablation are drawn in: (1) posterior insular region, (2) region around the central sulcus and (3) hippocampus region.

a particle beam to scan the sample are limited by a small field of view (in the order of 1 mm^2) and a low depth of analysis (few micrometers). Only the dedicated configuration of scanning transmission ion microscopy or tomography (STIM or STIM-T) was able to analyse 30 μm thick samples [18] but is in a more early phase of development and the field of view did not exceed 400 μm × 400 μm.

In the last few years, laser ablation inductively coupled plasma mass spectrometry (LA-ICP-MS) has been established as a powerful and sensitive surface analytical method with multi-elemental capability for the direct determination of elements in biological samples [19–21]. This surface analytical method permits two-dimensional mapping of element distributions within thin sections of biological tissues on a mesoscopic scale [6].

Recently, analytical methods using LA-ICP-MS with a cooled ablation chamber for the two-dimensional mapping of trace elements such as Cu, Zn, U, Th and other elements in thin tissue sections, together with appropriate calibration techniques for proper quantification were developed in our laboratory [11,22–26]. The differential and layered distribution of Zn and Cu in human hippocampus was shown [11]. The present study aimed to assess the consistence of this first result obtained from a single sample in a more systematic approach and to address its biological validity. The reproducibility of element mapping was tested on adjacent sections and several other representative brain regions (insula, central cortex and hippocampus) from the same brain were analyzed in one series of measurements. In addition to Zn and Cu the distribution of Pb as a toxic element was determined in this tissue.

2. Experimental

2.1. LA-ICP-MS instrumentation

A double-focusing sector field ICP-MS (ELEMENT, Thermo Fisher Scientific, Bremen, Germany) coupled to a laser ablation system LSX 200 (CETAC LSX 200, Cetac Technologies, Omaha, NE, USA) was used to determine the distribution of Zn, Cu and Pb within thin sections of the brain. Laser ablation of brain tissue was performed using a Nd:YAG laser (wavelength: 266 nm, repetition frequency: 20 Hz, spot diameter: 200 μm, laser power density: 3×10^9 W cm^{-2}). The ablated material was transported into the inductively coupled plasma (ICP) using argon as the carrier gas. The ICP torch was shielded with a grounded platinum electrode (GuardElectrode, Thermo Fisher Scientific). The experimental parameters of LA-ICP-MS were optimized with respect to the maximum ion intensity of $^{64}Zn^+$ using homogenized brain tissue cut into 20 μm sections. Maximum ion intensity was observed at a carrier gas flow rate of 1.85 L min^{-1} for the transport of ablated material into the ICP-MS. The optimized experimental parameters for LA-ICP-MS measurements are summarized in Table 1.

2.2. Sample and sample preparation

Human brain samples were obtained during autopsy from a healthy, 75-year-old female with no known neurological or psychiatric disorders (post-mortem time 3 h), as part of the body donor program of the C&O Vogt Institute for Brain Research at Heinrich Heine University Düsseldorf. Serial 20 μm

Table 1
Optimized experimental parameters of LA-ICP-MS

ICP-MS	ELEMENT, Thermo Electron
Rf power (W)	1250
Auxiliary gas flow rate (L min^{-1})	1.25
Carrier gas flow rate (L min^{-1})	1.2
Mass resolution (m/Δm)	300
Number of runs	8000–12,000[a]
Number of passes	2
Laser ablation system	CETAC, LSX 200
Wavelength of Nd-YAG laser (nm)	266
Laser power density (W/cm^2)	3.5×10^9
Laser pulse duration (ns)	5
Scan speed (μm s^{-1})	30
Repetition frequency (Hz)	20

[a] Depending on sample size.

sections were cut in a cryostat (Leica, CM3500) at −20 °C and thaw-mounted on glass slides. Regions of interest (insular, central and hippocampal, Fig. 1, left) were selected from cryosections of the whole hemisphere, cut out, dried and stored at −20 °C. Adjacent sections were processed to visualize the cell bodies by cresyl violet staining (Fig. 1, right). Cresyl violet staining followed standard protocols [27]. In brief, slices were fixed in 4% of para-formaldehyde, washed in PBS and stained for 1 h in cresyl acetate solution. Following differentiation in steps of increasing alcohol concentration slices were coverslipped with a polymeric resine (DPX, Fluka, Seelze, Germany). Photomicrographs were obtained from a KS-400 camera imaging system (Karl Zeiss, Oberkochen, Germany).

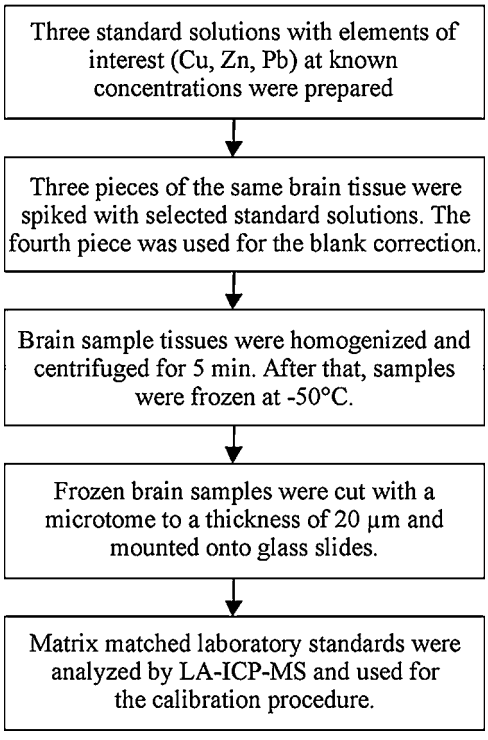


Fig. 2. Workflow of the preparation of matrix-matched standards for quantification of analytical data in LA-ICP-MS.

2.3. Preparation of matrix-matched laboratory standards and quantification procedure

For the quantification of analytical data, a calibration procedure using matrix-matched laboratory standards was applied as previously described [11]. A schematic of the workflow is given in Fig. 2. Three dilutions containing a mixture of elements of interest (Cu, Zn, Pb) were prepared from a mixture of standard stock solutions. Known volumes of these solutions were added to three pieces (each ∼1 g) of the same brain from which sections originated to yield final tissue concentrations of 5, 10, 15 μg g^{-1} of Cu, Zn and 0.1, 0.5, 1 μg g^{-1} of Pb, respectively. A fourth piece (not spiked) was used as "blank" sample. After that, all brain samples were homogenized, centrifuged for 5 min and frozen at −50 °C. Frozen matrix-matched laboratory standards were cut into 20 μm thick sections and placed on glass slides. Glass slices with brain tissue and glass slices with prepared laboratory standards were placed together in the laser ablation chamber. First, matrix-matched standards were scanned (three lines for each standard). Then the region of interest in brain sample tissue was scanned line by line with focused laser beam. Ions intensities ($^{64}Zn^+$, $^{63}Cu^+$ and $^{208}Pb^+$) were measured by LA-ICP-MS. The calibration of analytical data was performed using the standard addition mode.

3. Results and discussion

3.1. Quantification of analytical data

Matrix-matched laboratory standards used for the quantification procedure were measured together with the tissue samples. Calibration curves for Cu, Zn and Pb, measured by LA-ICP-MS are shown in Fig. 3. The correlation coefficient of calibration curves obtained from laboratory standards was 0.997, 0.994 and 0.993 for Cu, Zn and Pb, respectively.

LA-ICP-MS was applied to produce images of Cu, Zn, and Pb distribution in three regions of human brain. Fig. 4 shows a raw image of $^{64}Zn^+$ ion intensities in the insula in a scale covering a high range of concentrations in order to visualize positive outliers amongst the data points. Concentration maps of Cu, Zn and Pb in insular, central and hippocampal regions are presented in Figs. 5–7. For anatomical orientation, photomicrographs of congruent regions on adjacent sections treated with the cell body stain cresyl violet are shown. The concentrations determined by LA-ICP-MS refer to the wet sample. Generally, the cortex with higher Cu and Zn concentration is sharply separated from white matter. Layered cortical distribution patterns of Zn and Cu parallel to the brain surface are visible as well as borders orthogonal to the surface separating areas of different layer architecture. Apparently zinc is more abundant in the outermost cortical layer (layer I) and in subregions of the fascia dentata and CA3.

Artifacts on the edges of some sections result from folding and buckling of the 20 μm tissue flap on the slide (left edge of Fig. 5). Lead was in the ng g^{-1} concentration range and homogeneously distributed throughout grey and white matter.

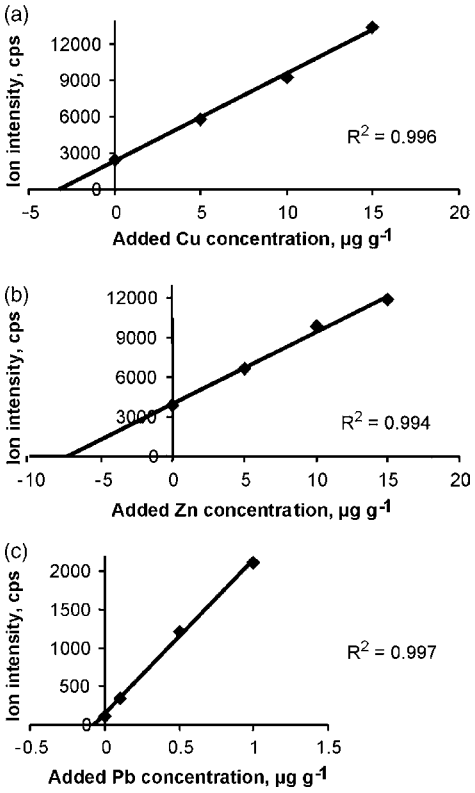


Fig. 3. Calibration curves for added copper (a), zinc (b) and lead (c), from matrix-matched standards measured by LA-ICP-MS.

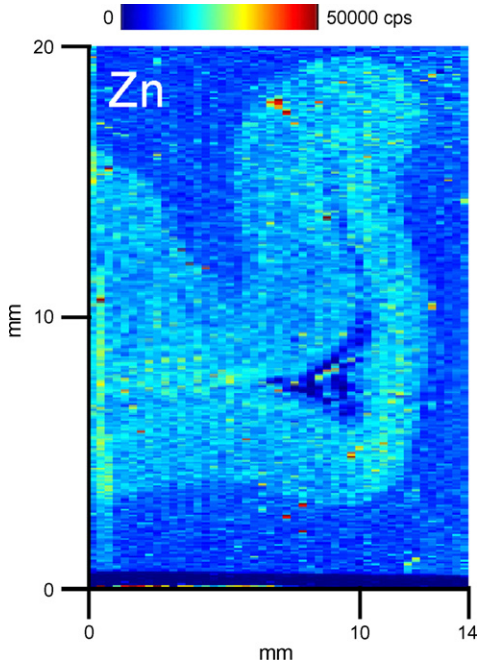


Fig. 4. Raw image of Zn distribution measured by LA-ICP-MS in the insular region. The scale covers a high range of ion intensities in order to visualize positive outliers (compare with Fig. 5).

3.2. Limits of detection and performance of LA-ICP-MS measurement

The detection limits (LODs) for zinc, copper and lead were calculated according to LOD = 3 × σ/S, where σ is the standard deviation of the blank ion intensity (n = 10) and S is the sensitivity. The LODs of LA-ICP-MS determined on thin sections of brain tissue were found to be 0.5 µg g^{-1} for zinc, 0.1 µg g^{-1} for copper and 10 ng g^{-1} for lead. Thus, all concentrations measured were within the analytical range of the configuration of LA-ICP-MS used in this study. Mean concentrations averaged over rectangular areas are given in Tables 2 and 3. As these rectangles cover layers of very different element concentration standard deviations are not meaningful and not given. Uncertainties are given in the calibration curves (Fig. 3). The measured average concentrations from different brain areas for Zn (cortex 2.5–11.2 µg g^{-1}, white matter 1.6–2.0 µg g^{-1}) and Cu (cortex 1.5–6.2 µg g^{-1}, white matter 0.9–1.3 µg g^{-1}) are in accordance with other authors. Using atomic absorption

Table 2
Mean element concentrations in the grey matter of the examined insular regions

Region	Mean concentration/µg g^{-1}	
	Zn	Cu
OP 1	2.5	1.7
Retroinsular cortex	2.8	2.2
Insular cortex proper	3.1	2.6
Temporal operculum	2.6	1.8

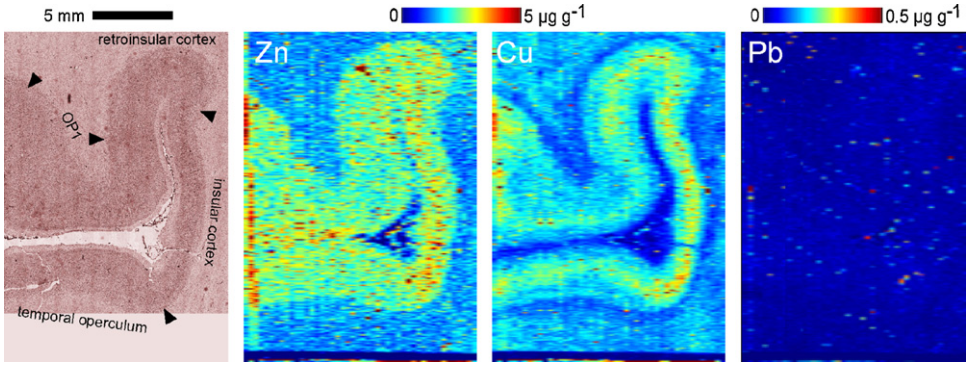


Fig. 5. Distribution of Zn, Cu and Pb in the posterior insular region measured by LA-ICP-MS. In a light photomicrograph (left) of an adjacent section stained by cresyl violet cortical regions are indicated. (OP 1: opercular area 1). Arrowheads show borders between areas of different layering pattern determined by optical inspection.

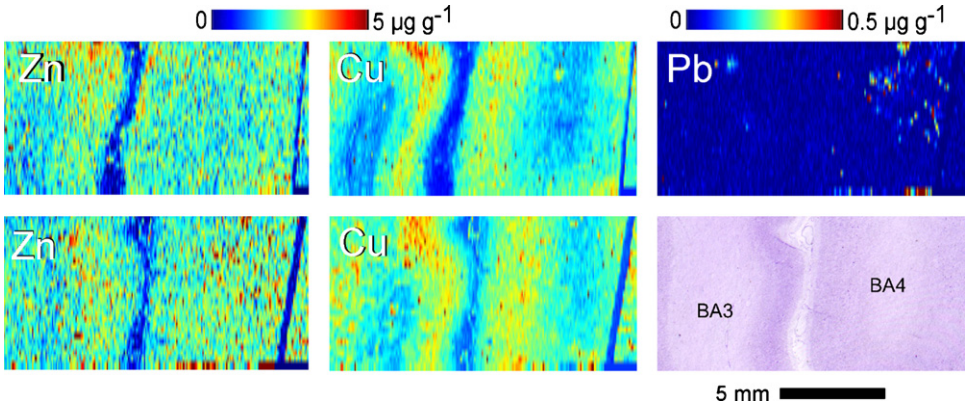


Fig. 6. Distribution of Zn, Cu and Pb in a region around the central sulcus measured by LA-ICP-MS. The lower right image is a light photomicrograph of an adjacent section stained by cresyl violet. Parts of somatosensory cortex (area BA3, left) and motor cortex (area BA4, right) are included in the field of view. As described for the insular cortex, Zn and Cu laminar distribution patterns also differ considerably in the cortex surrounding the central sulcus. Additionally, BA3 and BA4 present a differential Cu laminar distribution pattern, though they do not differ significantly in their Zn content. In order to control the reproducibility of the method a congruent area was scanned (lower row) in a neighboring section 80 μm distant from the first.

Table 3
Mean element concentrations in the grey matter of the examined regions within the central sulcus

Region	Mean concentration/μg g^{-1}	
	Zn	Cu
BA3	2.9	2.6
BA4	3.0	2.8

spectroscopy, Yoshinaga and Shimizu [28] measured Cu concentrations (AAS) of 11.2 μg g^{-1} in white matter and 29.1 μg g^{-1} in grey matter (dry weight, water content of white matter: 70%, grey matter: 79%) [29]. Another AAS study found 26.5 μg g^{-1} Cu and 51.2 μg g^{-1} Zn (dry weight) in frontal cortex [30]. In a recent ICP-MS study of homogenates, wet weight concentrations of 12.9 μg g^{-1} were reported for Zn both in the frontal brain and cerebellum and concentrations of 3.8 and 6.0 μg g^{-1} for Cu in the frontal brain and cerebellum, respectively. Pb was detected in the cerebellum in a concentration of 0.03 μg g^{-1} [31]. To our knowledge no study of Pb imaging on a mesoscopic scale in brain tissue has yet been published.

In comparison to our previous work [11], the method of imaging LA-ICP-MS could be transferred successfully to different instrumental settings using the CETAC LSX 200 ablation system with 200 μm spot diameter (present study) instead of the Ablascop (Bioptic) with 50 μm spot diameter. Both laser wavelengths 213 nm (Ablascop) and 266 nm (CETAC) enabled efficient ablation of brain tissue. By visual inspection of the elemental maps resulting from these two setups, the same structures can be recognized. In contrast, the sensitivity was increased as the entire material was ablated from the glass support without interline residuals. In addition, the measurements were performed at low resolution (m/Δm – 300 instead of 4400). We could reproduce the pattern of element distribution for Zn and Cu by the measurement of a congruent region from a neighboring section 80 μm distant from the first.

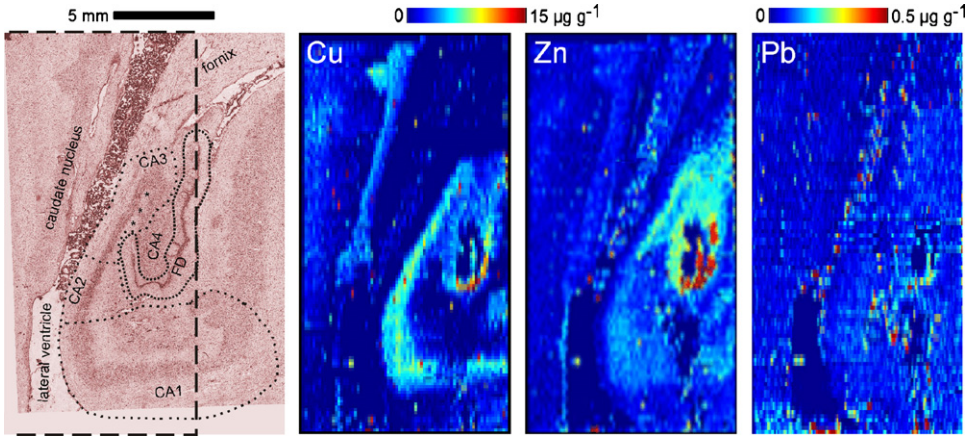


Fig. 7. Distribution of Zn, Cu and Pb in the hippocampus region measured by LA-ICP-MS. In a light photomicrograph (left) of an adjacent section stained by cresyl violet cortical regions are labeled: (FC: fascia dentata circumscribed by a densly dotted line; CA1–4: cornu ammonis, part 1–4 circumscribed by loosely dotted lines, respectively; asterisks: stratum lucidum of CA3). Borders between these areas were determined by optical inspection. The dashed box open to the left indicates the overlap of the LA-ICP-MS images with this photomicrograph.

3.3. Element distribution in different cortical areas

A part of the insular cortex including a part of the parietal and temporal operculum is depicted in Fig. 5. The Cu distribution shows a clear laminar pattern, which in combination with the thickness of the cortex allows a discrimination of different areas. The lowest Cu concentration was found in the frontal opercular area OP 1 [32] and in the temporal operculum. A medium Cu concentration was found in the retroinsular cortex and the highest Cu concentration in the proper insular cortex (Table 2). Overall, Cu is most concentrated in a band in the middle of the cortex cross section. Zn displays the same regional pattern as Cu regarding regional concentrations. Thus, the retroinsular cortex contains slightly higher Zn concentrations than OP 1 or the temporal operculum, but slightly lower values than those measured in the insular cortex proper (Table 2). In contrast to Cu, Zn is more homogeneously distributed throughout all cortical layers. Mean concentrations of Pb in the cortex are extremely low and not distinguishable from mean concentration in the white matter.

A region around the central sulcus with partitions of area BA3, which is a part of the somatosensory cortex [33], and area BA4, which is a part of the motor cortex, face to face, is shown in Fig. 6. The laminar distribution of Cu is more differentiated in BA3 than in BA4. Whereas BA3 shows a clear Cu enrichment in layers II–Va, BA4 presents a homogeneous distribution of Cu throughout all layers. BA3 contains mean (averaged over all cortical layers) Cu concentrations comparable to BA4 (Table 3). As described above for the insular cortex, also in BA3 and BA4 the laminar distribution of Zn is more homogeneous than that of Cu. BA3 and BA4 contain comparable mean (averaged over all cortical layers) Zn concentrations (Table 3). Pb concentrations in areas BA3 and BA4 were low and indistinguishable from those in the surrounding white matter. Measurement of Zn and Cu in two neighboring sections yielded identical laminar and regional distribution patterns, further supporting the reliability of the method presented in this study.

In contrast to our previous study [11], the coronal section analyzed here crosses the hippocampus at a more posterior position (Fig. 7). Therefore, the diameter of this structure is smaller and the layering pattern reaches the limit of spatial resolution. Our previous findings were fully reproduced. Compared to the other regions examined, Zn, Cu and Pb occurred at higher concentrations in the hippocampus, which could reflect a different pattern of cell types in this area. A summary of the results for copper and zinc distribution within various regions and layers of the hippocampus is given in Table 4. Copper and zinc are localized differentially. An overlay of a photomicrograph of a cresyl violet stained adjacent section onto element maps is shown in Fig. 8. Highest hippocampal Cu concentrations were found in the inner molecular and granular layers of the dentate gyrus. Along the pyramidal layer of the cornu ammonis, Cu concentration is clearly higher in CA1–3 than in CA4. The stratum radiatum and lacunosum moleculare of CA1–3 contain little Cu. In the alveus, which constitutes a white matter layer adjacent to the ventricle, no Cu was detected. Zn concentration is highest in the inner molecular and granular layers of the dentate gyrus including the stratum multiforme and is high in a zone of CA3 including the stratum pyramidale and the stratum lucidum. CA2 and 1 contain very little Zn.

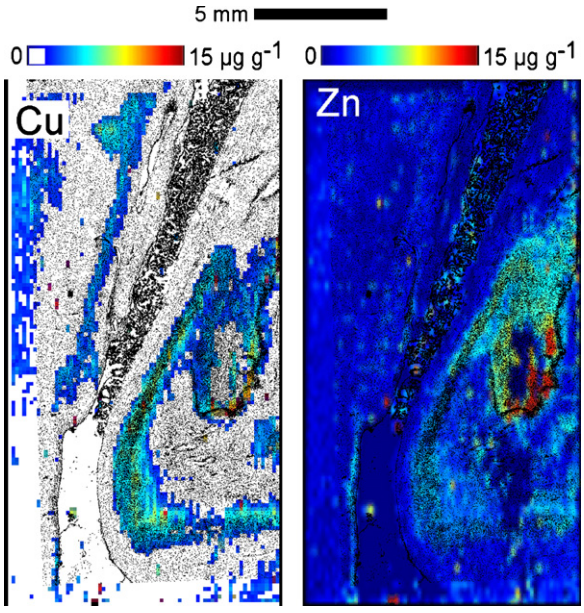


Fig. 8. Overlay of pseudo-color coded metal concentration maps and cresyl violet stain of an adjacent section (black). The presence of Zn in the inner zone of the fascia dentata and in zones of CA3 exceeding the stratum pyramidale is discernable.

Table 4
Element concentrations measured in selected regions (CA1–4, FD) and layers (pyramidal, lucidum) of the hippocampus

Region	Mean concentration/µg g^{-1}	
	Zn	Cu
CA1	2.6	1.5
Pyramidal layer CA1	4.4	5.2
CA2	3.1	1.7
Pyramidal layer CA2	3.6	4.9
CA3	4.0	1.5
Pyramidal layer CA3	6.5	3.6
Lucidum layer CA3	5.7	2.8
CA4	1.7	0.7
FD	11.5	6.2

CA: cornu ammonis; str. luc.: stratum lucidum; FD: molecular and granular layers of fascia dentata.

4. Conclusions

The recently developed analytical LA-ICP-MS method for two-dimensional imaging of trace elements in thin tissue sections in combination with matrix-matched calibration was transferred to different instrumental settings with higher sensitivity and proved valid throughout several regions of the human brain. The method was sensitive to detect layered structures and distinct areas in the distribution of Cu and Zn. The distribution of Pb was imaged and found to be homogenous (<0.2 µg g^{-1}) in the four regions examined. LA-ICP-MS method provides a pow-

erful tool for further understanding the role of various elements like Cu, Zn and Pb in brain function.

References

[1] R.J. Cousins, J.P. Liuzzi, L.A. Lichten, J. Biol. Chem. 281 (2006) 24085.
[2] E.M. Rees, D.J. Thiele, Curr. Opin. Microbiol. 7 (2004) 175.
[3] R.W. Hutchinson, A.G. Cox, C.W. McLeod, P.S. Marshall, A. Harper, E.L. Dawson, D.R. Howlett, Anal. Biochem. 346 (2005) 225.
[4] L.M. Bahiga, N.A. Kotb, E.A. El-Dessoukey, Z. Ernahrungswiss 17 (1978) 84.
[5] K. Hierholzer, R. Schmitt (Eds.), Pathophysiologie des Menschen, VCH, 1991.
[6] Y. Gelinas, J. Lafond, J.P. Schmit, Biol. Trace Elem. Res. 59 (1997) 63.
[7] V.N. Uversky, J. Li, A.L. Fink, J. Biol. Chem. 276 (2001) 44284.
[8] S. Coon, A. Stark, E. Peterson, A. Gloi, G. Kortsha, J. Pounds, D. Chettle, J. Gorell, Environ. Health Perspect. 114 (2006) 1872.
[9] J.H. Fox, J.A. Kama, G. Lieberman, R. Chopra, K. Dorsey, V. Chopra, I. Volitakis, R.A. Cherny, A.I. Bush, S. Hersch, PLoS ONE 2 (2007) e334.
[10] H.H. Sandstead, C.J. Frederickson, J.G. Penland, J. Nutr. 130 (2000) 496S.
[11] J.S. Becker, M.V. Zoriy, C. Pickhardt, N. Palomero-Gallagher, K. Zilles, Anal. Chem. 77 (2005) 3208.
[12] G. Danscher, M. Stoltenberg, M. Bruhn, C. Sondergaard, D. Jensen, J. Histochem. Cytochem. 52 (2004) 1619.
[13] Y. Li, C.J. Hough, S.W. Suh, J.M. Sarvey, C.J. Frederickson, J. Neurophysiol. 86 (2001) 2597.
[14] V. Mizuhira, H. Hasegawa, Brain Res. Bull. 43 (1997) 53.
[15] J. Mesjasz-Przybylowicz, W.J. Przybylowicz, Nuclear Instrum. Methods Phys. Res. Section B-Beam Interact. Mater. Atoms 189 (2002) 470.
[16] A. Takeda, H. Tamano, S. Enomoto, N. Oku, Cancer Res. 61 (2001) 5065.
[17] S. Chandra, Appl. Surf. Sci. 203 (2003) 679.
[18] T. Butz, C. Meinecke, M. Morawski, T. Reinert, M. Schwertner, D. Spemann, Appl. Surf. Sci. 252 (2005) 43.
[19] J.S. Becker, H.J. Dietze, Int. J. Mass Spectrom. 197 (2000) 1.
[20] S.F. Durrant, N.I. Ward, J. Anal. Atom Spectrom. 20 (2005) 821.
[21] N.S. Mokgalaka, J.L. Gardea-Torresdey, Appl. Spectrosc. Rev. 41 (2006) 131.
[22] C. Pickhardt, J.S. Becker, H.J. Dietze, Fresen J. Anal. Chem. 368 (2000) 173.
[23] J.S. Becker, M.V. Zoriy, C. Pickhardt, K. Zilles, J. Anal. Atom. Spectrom. 20 (2005) 912.
[24] M.V. Zoriy, M. Dehnhardt, G. Reifenberger, K. Zilles, J.S. Becker, Int. J. Mass Spectrom. 257 (2006) 27.
[25] J.S. Becker, S.F. Boulyga, C. Pickhardt, E. Damoc, M. Przybylski, Int. J. Mass Spectrom. 228 (2003) 985.
[26] C. Pickhardt, A.V. Izmer, M.V. Zoriy, D. Schaumloffel, J.S. Becker, Int. J. Mass Spectrom. 248 (2006) 136.
[27] M. Powers, G. Clark, Stain Technol. 30 (1955) 83.
[28] T. Yoshinaga, N. Shimizu, Acta Histochem. 30 (1968) 90.
[29] H. Neeb, K. Zilles, N.J. Shah, Neuroimage 29 (2006) 910.
[30] R.J. Uitti, A.H. Rajput, B. Rozdilsky, M. Bickis, T. Wollin, W.K. Yuen, Can J. Neurol. Sci. 16 (1989) 310.
[31] R. Rahil-Khazen, B.J. Bolann, R.J. Ulvik, Biometals 15 (2002) 87.
[32] S.B. Eickhoff, A. Schleicher, K. Zilles, K. Amunts, Cereb. Cortex 16 (2006) 254.
[33] S. Geyer, A. Schleicher, K. Zilles, Neuroimage 10 (1999) 63.

Available online at www.sciencedirect.com
ScienceDirect
Talanta 74 (2008) 1014–1019
Talanta
www.elsevier.com/locate/talanta

Sub-monolayer assemblies of octanethiol and octadecylthiol at gold electrodes for the direct analysis of 4,4′-oxydianiline in wastewaters and shoe-dyeing samples

C.S.H. Domínguez, C. Quintana, J. Vicente, P. Hernández, L. Hernández *

Dpto. Química Analítica y Análisis Instrumental, Facultad de Ciencias, Universidad Autónoma de Madrid, Cantoblanco, 28049-Madrid, Spain

Received 8 March 2007; received in revised form 2 August 2007; accepted 9 August 2007
Available online 15 August 2007

Abstract

Self-assembled monolayers (SAMs) of di-*n*-octadecyldisulphide (C_{18}) and *n*-octanethiol (C_8) were prepared on gold electrodes. From the studies carried out by cyclic voltammetry and square wave voltammetry, it was observed that the electrochemical behaviour of 4,4′-oxydianiline on these electrodes is affected by the length chain of the alkanethiol. After the optimization of all the variables involved in the electrochemical response of 4,4′-oxydianiline by square wave voltammetry employing the modified electrodes, it is possible the determination of 4,4′-oxydianiline with a detection limit of 0.04 μg/mL (C_{18}) and 0.06 μg/mL (C_8) and determination limits of 0.12 and 0.22 μg/mL, respectively. The calculated Er $(\%)_{n=10}$ and R.S.D.$(\%)_{n=10}$ values were minor than 2.2% and 3.7%. The proposed methods were successfully applied to the analysis of oxydianiline in wastewater and shoe-dyeing samples.
© 2007 Elsevier B.V. All rights reserved.

Keywords: 4,4′-Oxydianiline; Square wave voltammetry; SAM's of alkanethiols; Wastewater; Shoe-dyeing

1. Introduction

It is known that the use of aromatic amines in the manufacturing of polyimides or dyes is very widespread. Among these compounds the 4,4′-oxydianiline (ODA) is widely used in the production of polyimides and poly(ester)imides resins employed in a great variety of high temperature resistant products [1,2]. On the other hand, ODA is also used as a raw material in the treatment and dyeing processes in leather manufacturing as well as an intermediate in the manufacturing of epoxy resins. Therefore, this compound may be released in waste streams from its production and uses. In the atmosphere, it is expected to degree rapidly. Occupational exposure (through inhalation of dust or through eye and skin contact) is most likely to occur during its manufacturing. Although no data are available to evaluate the carcinogenicity of ODA in humans [2,3] it is reasonably anticipated to be a human carcinogen based on sufficient evidence of carcinogenicity in experimental animals [1,3,4].

Among the analytical applications of ODA, it has been used as qualitative reagent in the analysis of aliphatic and aromatic aldehydes to get coloured azomethines. In addition to this, several analytical procedures involving LC-UV [5,6], LC/MS [7,8], LC-MS/MS [9,10] or CG usually with MS detection [11,12], have been described to quantify 4,4′-oxidianiline in samples containing different aromatic amines. On the other hand, alternative detection techniques are also reported, for instance, Dados et al. [13] developed a GC/ECD procedure involving the analytes bromation.

Although most of ODA analysis were carried out in textile or dye samples [5,6,8,9,12,13], 4,4′-oxidianiline has also been determined in water samples after the optimization of a SPME method for sample preparation [7]. On the other hand, due to the fact that primary aromatic amines are substances that can be transferred from food packaging materials into foodstuffs [14], several analyses of 4,4′-oxydianiline in aqueous food simulant have been reported [10,11]. In addition to this, impurities of ODA in the production of *p*-aminophenol, have been determined

* Corresponding author. Tel.: +34 914974149; fax: +34 914974931.
E-mail address: lucas.hernandez@uam.es (L. Hernández).

0039-9140/$ – see front matter © 2007 Elsevier B.V. All rights reserved.
doi:10.1016/j.talanta.2007.08.006

by You et al. [15] by HPLC with electrochemical detection (EC). Electrochemical measurements are unusual instrumental techniques for 4,4′-oxydianiline determination. In relation to this, as far as we know, there is no studies about neither electrochemical behavior of 4,4′-oxydianiline nor its electrochemical quantification. In this work, the modification of Au electrodes with self-assembled organic monolayers of alkanethiols is proposed to the electrochemical determination of ODA. The discovery of spontaneous assemblies of organic thiols on gold surfaces has been a great advance in disciplines ranging form biomedicine [16], sensors [17] or electronics [18]. The use of functionalised aromatic and aliphatic organo thiols for a great variety of analytical applications is widespread as it is shown by the high number of papers reported on the subject [17,19]. On the other hand, non-functionalised alkanethiols self-assembled monolayers have served as model organic surfaces in fundamental studies of molecular adsorption, wetting and lubrication [20–22]. For many applications, alkanethiols terminated with functional groups, such as NH_2, CH_2OH and COOH are more appropriate. This paper is focused on the self-assembly CH_3-terminated alkanethiols in order both, to test the influence of their molecular packing structure in the electrochemical signal of ODA and to build preferential entrance channels for analyte to reach the electrode surface avoiding the arrival of possible interferences with higher molecular size as well as to facilite apolar interactions between the terminal CH_3 of the alkanethiol chains with the analyte.

2. Experimental

2.1. Reagents

Pure standard of 4,4′-oxydianiline (>99%) was purchased from Sigma–Aldrich Chemical Co. (USA). Working stock solution was prepared in methanol at a concentration level of 500 μg/mL and used for further dilution in supporting electrolyte. The standard solution was kept at 4 °C and protected from light.

Di-*n*-octadecyldisulphide (C_{18}) and octanethiol (C_8) were obtained from Lancaster Synthesis (England) and Aldrich Chemical Co. (USA), respectively. All the alkanethiol solutions were prepared in tetrahydrofuran from Scharlab (Spain). All reagents used were of analytical reagent grade and ultrapure water was purified with a Millipore MilliQ System (Waters). All solutions were prepared just prior to use.

2.2. Apparatus

The electrochemical measurements were carried out using a Bionalytical System (BAS) Epsilon Potentiostat workstation. A conventional three electrode cell was used. In all experiments, a large-area coiled platinum wire was employed as a counter electrode. All potentials are reported against a Ag/AgCl/KCl 3 M reference electrode. For pH adjustment, a pH-meter Methrom C831 was employed as well as a circulation ultrathermostat Frigiterm-10 (P-Selecta, Spain) for control of temperature during the modification of the electrodes.

2.3. Procedure

2.3.1. Electrode activation

In order to desorb the alkanethiol monolayer from the electrode and to prepare the electrode for a new experiment, the activation and regeneration of the electrode surface was carried out by successive and multiple cyclic voltammetric scans in 0.5 M H_2SO_4 solution between 0.0 an 1.5 V at 100 mV/s. When required, piranha solution (H_2O_2/H_2SO_4:20/80(v/v)) was used to clean the electrode surface before the activation procedure described before.

2.3.2. Formation of SAM's of alkanethiols: modification of the electrode surface

The self assembled monolayer of C_{18} or C_8 onto the Au electrode surface was obtained immersing the bare electrode in the modifier solution at a specific concentration under temperature and speed magnetic stirring control during a fixed time. Next, the electrode was taken out from the solution and rinsed with ultrapure water before the electrochemical measurement.

2.3.3. Electrochemical measurement

Once the modified electrode was prepared, it was employed as working electrode in an electrochemical cell containing 10.0 mL of ODA in supporting electrolyte at the appropriate pH and at 13 °C. The temperature control during the modification was needed in order to get reproducible results.

The measurement was realised after an accumulation time at 0.0 V. When the measurement was realised without accumulation no signal was obtained.

3. Results and discussion

All the experiments leading to the optimization of the variables affecting both, the modification of the electrode surface and the analysis of 4,4′-oxydianiline by square wave anodic stripping voltammetry were realized with solutions of ODA 1.0 μg/mL. As initial conditions, an accumulation time of 20 s at 0.0 V, a square wave amplitude of 20 mV, a frequency value of 200 Hz and a step of 1 mV were chosen. Each variable was modified to study its best value, maintaining the rest of them fixed at the initial values.

3.1. Formation of SAM's of alkanethiols: modification of the electrode surface

The aim of this work is to control the access of the analyte to the electroactive surface by the building of restricted entrance channels to the electrode surface. The amount of modifier and the organization of the adsorbed monolayer allow some molecules to reach the Au surface or not, acting as a physical barrier making the analyte oxidation more difficult.

The control of the amount of molecules adsorbed on the electrode surface must be done by the study of the influence of the modifier concentration, the modification time and the effect of the temperature in the self-assembly process.

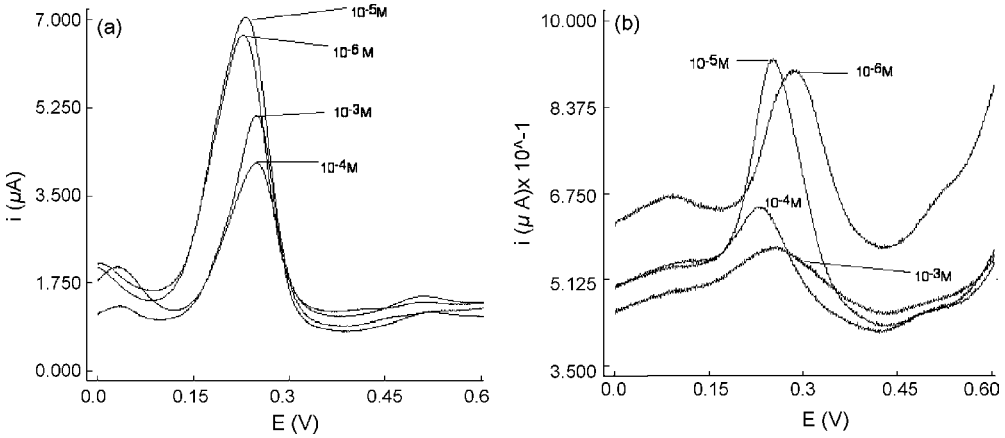


Fig. 1. Influence of C_{18} (a) and C_8 (b) concentration. Modification time = 5 min. ODA 1 μg/mL in acetate buffer 0.5 M pH 5.0; t_{ac} = 20 s, ΔE = 1 mV, a = 20 mV; f = 200 Hz.

The influence of the concentration of solutions of C_{18} and C_8 was studied in the 10^{-3} to 10^{-6} M range. To this end, the clean electrode was immersed into solutions of each alkanethiol for 5 min under constant stirring. Next, the resulting electrode, once rinsed with ultrapure water, was set in a voltammetric cell containing 1.0 μg/mL ODA in supporting electrolyte. After an accumulation process at a potential of 0.0 V for 20 s, the corresponding square wave voltammograms were recorded. The results obtained in each case are shown in Fig. 1.

In both cases, 10^{-5} M was shown as the best alkanethiol concentration to create entrance channels for ODA to reach the electrode surface (the highest current intensity with the lowest peak width). Under the same conditions, higher intensity currents were obtained when working with C_{18}, indicating that more electroactive surface was available after the modification than with C_8. As it was expected, the arrival of the analyte to the electrode surface was greatly impeded when high modifier concentrations (up to 10^{-4} M) were employed as inferred from the strong decrease in the current intensity. This decrease was more important with C_8 SAM's. In this case, the signal was almost lost indicating strong access restriction to the electroactive surface. In addition to this, a slight shift to more positive values was observed in the E_p values which can be of great interest in interference studies. These results are in good agreement with published papers about the organization of monolayers of alkanethiols of different chain length on Au surface [22].

3.2. Modification time

The amount of alkanethiol adsorbed onto the Au electrode was in relation with the time during the electrode was into the alkanethiol solution. Very similar results were obtained for both alkanethiols. The intensity current increased with the modification time up to 10 min (Fig. 2). Longer modification times lead to an obstacle to the analyte oxidation. On the other hand, an influence of the chain length was observed. When C_8 was used, E_p turned to be more positive while I_p decreased indicating that the oxidation was getting more difficult and the mass transport was affected.

3.2.1. Parameters affecting electrochemical response

Square wave voltammetry was chosen as redissolution electrochemical technique. All variables affecting the accumulation and redissolution steps have been optimized.

3.2.1.1. Accumulation parameters. The pH of the supporting electrolyte (0.5 M phosphate, acetate and borate buffers) was modified in the 2–11 range. An increase in the peak current

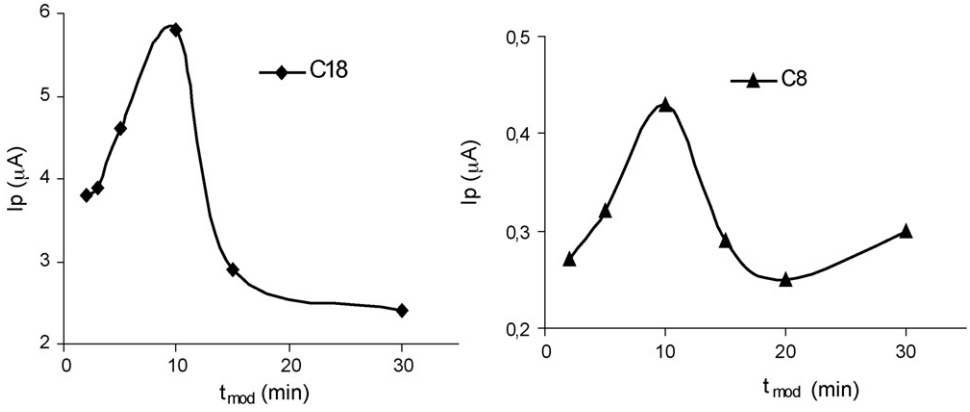


Fig. 2. Influence of the modification time in the peak current. Alkanethiols 10^{-5} M. [ODA] = 1 μg/mL. 0.5 M acetate buffer pH 5. Accumulation time = 20 s. ΔE = 1 mV, a = 20 mV, f = 200 Hz.

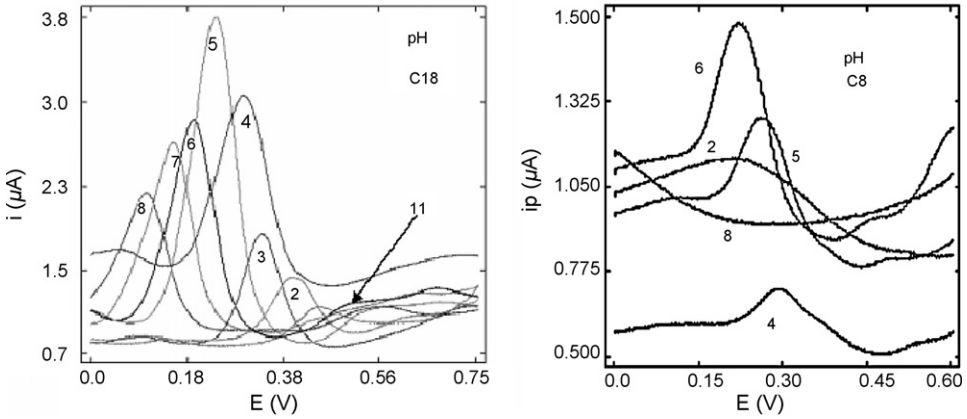


Fig. 3. Variation of the peak current with pH modification. Modification time = 5 min. $C_{18} = 10^{-5}$ M, ODA 1 μg/mL; $t_{ac} = 20$ s, scan increment = 1 mV, $a = 20$ mV; $f = 200$ Hz.

was observed until pH 5 and pH 6 for C_{18} and C_8, respectively. For higher pH values, the analytical signal decreased and even disappeared at pH 8 at C_{18} electrode (Fig. 3). This loss of signal was observed at lower pH values if C_8 was employed. Again, the modification with the shortest alkanethiol leads to more difficult electrochemical process.

The results obtained as a function of accumulation time are shown in Fig. 4. In both cases, the electrochemical signal due to the analyte oxidation process increased with the increment of the accumulation time for an applied potential of 0.0 V. For t_{ac} lower than 90 s (when C_{18} is used as modifier) fast increases of I_p were observed coupled with well defined peaks. Longer accumulation times resulted in a signal stabilization as a consequence of an equilibrium between analyte concentration in solution and on the electrode surface. Higher accumulation time were needed to reach this equilibrium situation when the modification of the electrode surface was performed with C_8 electrode. In this case, the increase of I_p was observed during the first 180 s of accumulation. From these results, t_{ac} of 90 s and 180 s, respectively, were chosen for the rest of the studies.

3.2.1.2. Instrumental parameters. In order to optimize the square wave response of 4,4′-oxydianiline on the Au modified electrode, the instrumental parameters affecting this electrochemical technique were studied. These studies also allowed to obtain insight into the mechanisms governing the analyte oxidation. An accumulation time of 20 s at 0.0 V, a frequency of square wave (f) of 200 Hz, a scan increment of 1 mV and amplitude of square wave (a) of 20 mV were used as initial conditions. Then, the f was scanned from 20 to 500 Hz, obtaining scanning rates from 20 to 500 mV s^{-1}, and the square wave voltammograms were recorded. According to the results of these experiments and in order to get the best sensitivity without a high increment of peak weight, f values of 300 and 200 Hz were chosen (for C_{18} and C_8, respectively) for further experiments.

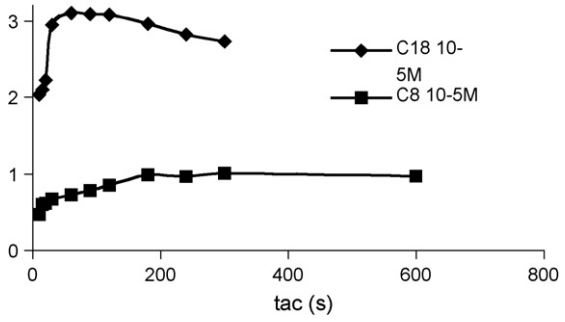


Fig. 4. Influence of the accumulation time in the peak current. Modification time = 5 min. ODA 1 μg/mL in acetic acid 0.5 M pH 5.0; $t_{ac} = 20$ s, scan increment = 1 mV, $a = 20$ mV; $f = 200$ Hz.

The effect of the difference in the chain length of both alkanethiols was shown from the analysis of the data. When the electrode was modified with C_{18}, a linear relation between I_p and $f^{1/2}$ (I_p (mA) = $-1.97 + 0.44f^{1/2}$ Hz) was observed. On the other hand, no significant variation in the E_p value was detected. Both results lead to conclude that the electrochemical process was reversible and controlled mainly by diffusion [23]. However, when C_8 was used, I_p fitted with log f according to I_p (μA) = $-0.33 + 0.29 \log f$ (Hz) and E_p turned more positive by increasing frequency values. From the slope of the relation I_p/log f, a n value of 0.9 was calculated. These results agreed with a quasi-reversible system with an adsorptive oxidation process.

Both, the peak height and peak width were affected by the variation of the scan increment. The results obtained at the C_{18} electrode showed that when this parameter was modified in the 1–10 mV range (corresponding to 20–2000 mV/s scan speeds) an increase of I_p from 0.35 to 1.01 μA was observed. The linear relation $I_p/v^{1/2}$ I_p (μA) = $0.037 + 0.031v^{1/2}$ mV indicated a diffusion controlled process, which is in agreement with the results obtained from the study of the frequency. Also the peak width became higher when scan increment increased, a value of 2 mV was chosen for further experiments in order to get a good agreement between selectivity and sensitivity.

Different results were obtained with the C_8 electrode. In this case, I_p fitted with log v according to I_p (μA) = 179.51 + 0.024 log v (mV) which it is indicative of an adsorptive phenomenon.

An increment in the analytical signal as well as an increment in the peak width was produced when the pulse amplitude was increased in both alkanethiols. In order to reach a compromise

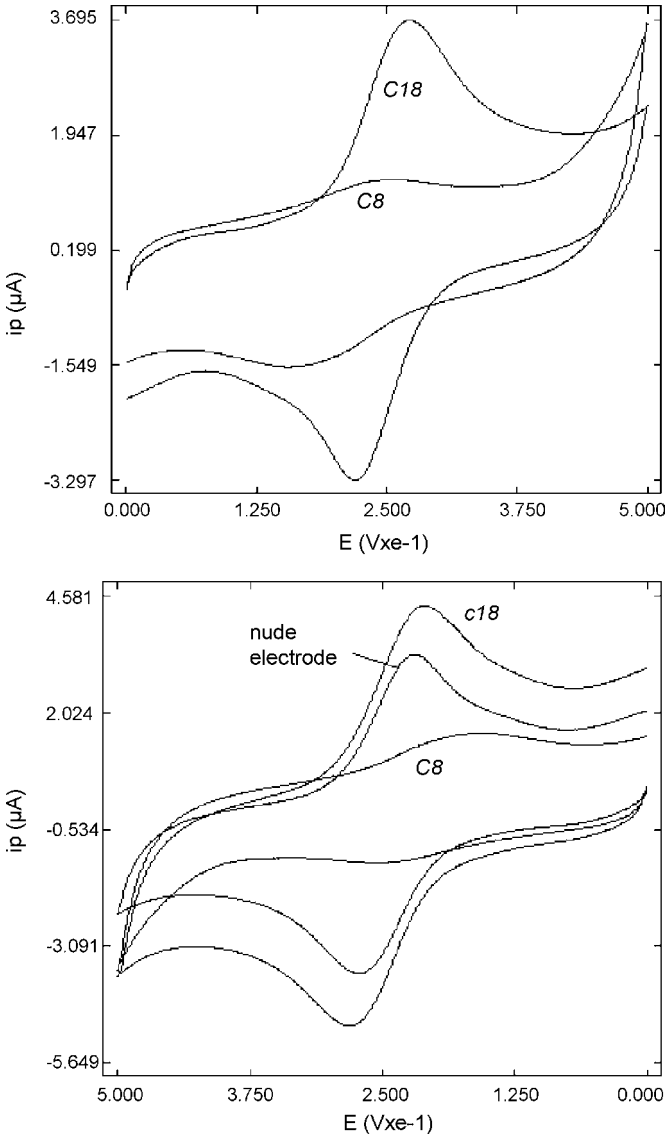


Fig. 5. Cyclic voltammograms of ODA 1 μg/mL in acetate buffer 0.5 M pH 5. $V_b = 100$ mV/s.

between sensitivity and selectivity, a pulse amplitude of 30 and 20 mV were chosen as the optimal ones.

If cyclic voltammograms were recorded (Fig. 5), we may observe the difference in the electrochemical response of ODA as a result of the modifier chosen to build the monolayers. The impediment created to ODA to reach the electrode surface by the use of C_8 gave undefined waves with $\Delta E_{a\text{-}c}$ of 125 mV in contrast with the results obtained in the same conditions both with C_{18} or with the naked Au electrode (ca. 70 mV).

3.3. Analytical figures of merit

The analytical performances of the stripping methods developed for oxydianiline determination were evaluated. From the stripping voltammograms recorded for increasing amounts of ODA using the parameters described above with a C_{18} modified Au electrode, it was observed that the peak current increased with the analyte concentration in the range of 0.05–1.50 μg/mL (I_p (μA) = −0.20 + 3.83 μg/mL, $r = 0.98$). The high sensitivity of the method was inferred from the LOD (3σ) (0.04 μg/mL) and LOQ (10σ) (0.12 μg/mL) values. On the other hand, the R.S.D. and Er values of 2.2% and 0.8%, respectively ($n = 10$ at the 0.8 μg/mL level) indicated the accuracy and reproducibility of the proposed method.

It was proceeded in the same way when octanethiol was assembled to the Au surface. So, stripping voltammograms were recorded for increasing amounts of ODA in the optimal conditions found for its determination. The linear response was found in the 0.10–1.00 μg/mL range according to I_p (μA) = 0.069 + 1.01C μg/mL; $r = 0.996$ with an Er (%) = 0.05 and R.S.D. of 3.71% ($n = 10$ at 0.8 μg/mL level). The minimum detectable amount was 0.06 while a concentration of 0.22 was calculated as determination limit.

3.3.1. Analytical application

Under the selected conditions, the proposed methods were applied to analysis of 4,4′-oxydianiline in wastewater (from a north Spain paper industry) and shoe-dyeing (T2000, from Tekno, Spain). In both cases, a dilution in the supporting electrolyte was the only pretreatment carried out before the electrochemical measurements.

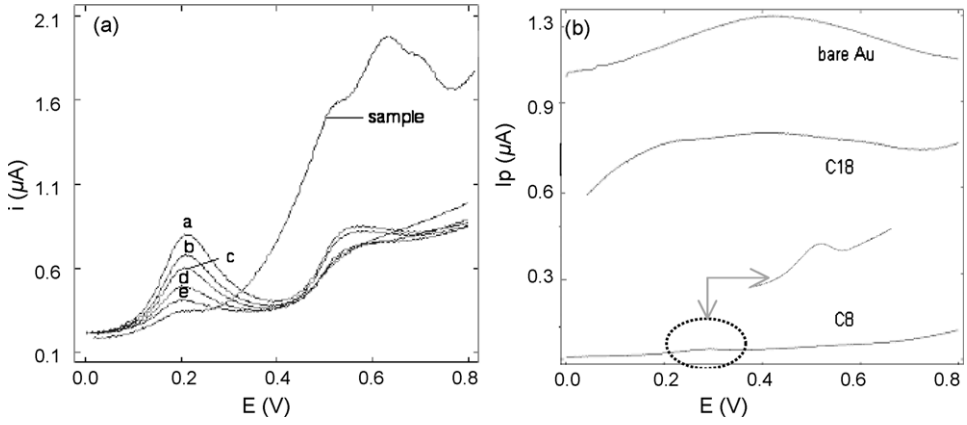


Fig. 6. Square wave voltammograms obtained from a (a) wastewater and (b) shoe-dyeing samples analysed with the proposed method. Standard additions at (a) 2.5 μg/mL, (b) 1.5 μg/mL, (c) 0.5 μg/mL, (d) 0.3 μg/mL, (e) 0.1 μg/mL level.

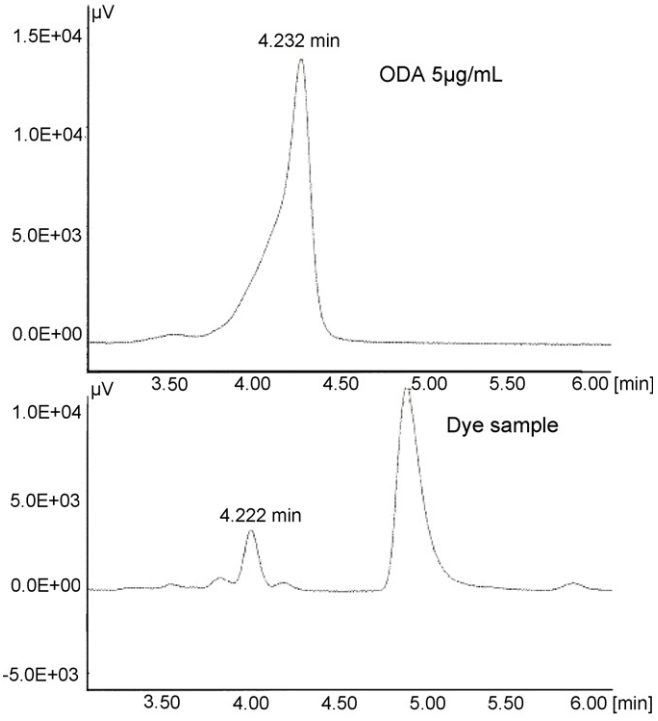


Fig. 7. HPLC determination of oxydianiline UV detection at 250 nm, C_{18} column and acetonitrile-phosphate of pH 5 (30:70).

The square wave voltammograms obtained from waste water sample (2.0 mL diluted to 50.0 mL final volume with acetic acid 0.5 M pH 5) are shown in Fig. 6a. As we can observe, it was possible to detect the characteristic signal of ODA only with the modification with di-*n*-octadecyldisulphide, just the opposite than the results obtained for the analysis of shoe-dyeing (Fig. 6b). In this case, the decrease in the background produced in the Au modified with octanethiol, allowed the clear identification of the ODA oxidation signal. In both cases, the quantitation of ODA was carried out with the standard addition method. For the analysis of wastewater samples the Au electrode modified with C_{18} was used and for the analysis of shoe-dyeing, an electrode modified with C_8 was used. From the linear relations found, I_p (μA) = 1.94 + 0.97C (μg/mL); r = 0.992 and I_p (μA) = 0.13 + 0.038C (μg/mL); r = 0.993, respectively) a concentrations of 2.01 μg/mL (R.S.D.$_{n=3}$ = 4.5%) and 3.40 μg/mL (R.S.D.$_{n=3}$ = 5.2%) of 4,4′-oxydianiline were calculated for waste water and shoe-dyeing, respectively.

Validation was performed by comparing the proposed procedure with HPLC and UV detection at 254 nm (method developed in reference 4). In Fig. 7 are included the chromatogram obtained for a 4,4′-oxydianiline standard and a dye sample.

HPLC procedure allows to obtain a linear response with a correlation coefficient of R^2 = 0.9908. Comparison between electrochemical and HPLC procedures shows a difference of values of 1.2%.

4. Conclusions

It is possible to perform the electrochemical determination of oxydianiline with Au electrodes modified with SAMs of both *n*-octadecyldisulphide and octanethiol at ng/mL level. The electrochemical behavior of the analyte is influenced by the alkanethiol length chain. In Au modified with SAMs of di-*n*-octadecyldisulphide, ODA oxidation showed an electrochemical reversible behavior controlled mainly by diffusion. However, this electrochemical behavior turned to a quasi-reversible system controlled by adsorption if a shorter length alkanethiol (*n*-octanethiol) was used to modify the electrode surface. The determination of ODA can be successfully carried out in real samples with the proposed methods without any separation step before the electrochemical measurements.

Acknowledgement

Authors thank to MEC (CTQ 2004-04142) for financial support.

References

[1] NCI 1980 Bioassay of 4,4′-oxidianiline for possible carcinogenicity (CAS no. 101-80-4), Technical Report Series No 205. DHHD(NIH) Publication No. 80–1761, National Institutes of Health, Bethesda, MD, 131 pp.
[2] IARC 1987, Overall Evaluations of Carcinogenicity, IARC Monographs on the Evaluation of Carcinogenic Risk of Chemical to Humans, Supplement 7, International Agency for Research on Cancer, Lyon, France, 440 pp.
[3] IARC 1982, Some Industrial Chemicals and Dyestuff, IARC Monographs on The Evaluation of Carcinogenic Risk of Chemical to Humans, Supplement 7, International Agency for Research on Cancer, Lyon, France, 416 pp.
[4] IARC 1978, Some N-Nitroso Compounds, IARC Monographs on the Evaluation of Cancerogenic Risk of Chemical to Humans, vol. 17, International Agency for Research on Cancer, Lyon, France, 365 pp.
[5] B. Jeretin, M. Durjava, Zbornik Referatov s Posvetovanja Slovenski Kemijski Dnevi, Maribor, Slovenia, Sept. 28–29 (2000) (Pt 1) p. 366.
[6] M.C. Garrigos, F. Reche, M.L. Marin, A. Jimenez, J. Chromatogr. A 976 (2002) 309.
[7] W.Y. Chang, Y.H. Sung, S.D. Huang, Anal. Chim. Acta 495 (2003) 109.
[8] U. Hauri, B. Lutolf, U. Schlegel, C. Hohl, Mitteilungen aus Lebensmitteluntersuchung und Hygiene 96 (5) (2005) 321.
[9] P. Sutthivaiyakit, S. Achatz, J. Lintelmann, T. Aungpradit, R. Chanwirat, S. Chumanee, A. Kettrup, Anal. Bioanal. Chem. 381 (1) (2005) 268.
[10] S.K. Mortensen, X.T. Trier, A. Foverskov, J.H. Petersen, J. Chromatogr. A 1091 (1–2) (2005) 40.
[11] C. Brede, I. Skjevrak, H. Herikstad, J. Chromatogr. A 983 (2003) 35.
[12] F. Cioni, G. Bartolucci, G. Pieraccini, S. Meloni, G. Moneti, Rapid commun. mass Sp. 13 (18) (1999) 1833.
[13] A.E. Dados, C.D. Stalikas, G.A. Plidis, Chromatographia 59 (5/6) (2004) 335.
[14] C. Lambert, M. Larroque, J.C. Lebrun, J.F. Gerard, Food Addit. Contam. 14 (1997) 199.
[15] J. You, C. Gao, X. Sun, L. Zhou, Fenxi Huaxue 23 (9) (1995) 1059.
[16] D.G. Castner, B.D. Ratner, Surf. Sci. 500 (2002) 28.
[17] S. Campuzano, B. Serra, M. Pedrero, F.J. Manuel de Villena, J.M. Pingarrón, Anal. Chim. Acta 494 (2003) 187.
[18] J.M. Tour, Molecular Electronic: Commercial Insighis, Chemistry, Devices, Architecture and Programming, World Scientific, River Edge, New Jersey, 2003.
[19] N. Wanichacheva, E.R. Soto, C.R. Lambert, W.G. McGimpsey, Anal. Chem. 78 (2006) 7132.
[20] G.E. Poirier, M.J. Tarlov, H.E. Rushmeir, Langmuir 10 (9) (1994) 3383.
[21] Q. Jin, J.A. Rodriguez, C.Z. Li, Y. Darici, N.J. Tao, Surf. Sci. 425 (1999) 101.
[22] F. Schoreiber, Prog. Surf. Sci. 65 (2000) 151.
[23] F. Scholz, Electrochemical Methods, Springer, Germany, 2002, p. 115.

Available online at www.sciencedirect.com
ScienceDirect
Talanta 74 (2008) 766–772
Talanta
www.elsevier.com/locate/talanta

Electrochemical pesticide sensitivity test using acetylcholinesterase biosensor based on colloidal gold nanoparticle modified sol–gel interface

Dan Du [a,*], Shizhen Chen [a], Jie Cai [b], Aidong Zhang [a,*]

[a] *Key Laboratory of Pesticide & Chemical Biology of Ministry of Education, College of Chemistry, Central China Normal University, Wuhan 430079, PR China*
[b] *The Technology Center of Wuhan Iron & Steel Company, Wuhan 430080, PR China*

Received 17 March 2007; received in revised form 6 July 2007; accepted 9 July 2007
Available online 24 July 2007

Abstract

Based on the change in electrochemical behavior of enzymatic activity induced by pesticide, a novel electrochemical method for investigation of pesticide sensitivity using acetylcholinesterase (AChE) biosensor was developed. The sol–gel-derived silicate network assembling gold nanoparticles (AuNPs-SiSG) provided a biocompatible microenvironment around the enzyme molecule to stabilize its biological activity and prevented them from leaking out of the interface. The composite was characterized using atomic force microscopy and proved to be chemically clean, porous and homogeneous. AuNPs promoted a conductive pathway for electron transfer and improved electrochemical reactions at a lower potential. Typical pesticides such as monocrotophos, methyl parathion and carbaryl were selected for pesticide sensitivity tests. Due to the inhibitions of pesticides, the electrochemical responses of substrate on AChE-sensors decreased greatly. The inhibition curves showed good correspondence with the results by UV spectrophotometry assay. The proposed electrochemical pesticide sensitivity test exhibited high sensitivity, desirable accuracy, low cost and simplified procedures. This method could be developed as a conventional method to select efficient enzyme inhibitors and investigate toxic compounds against to enzyme.
© 2007 Elsevier B.V. All rights reserved.

Keywords: Acetylcholinesterase; Biosensor; Electrochemical test; Gold nanoparticles; Pesticide sensitivity

1. Introduction

Pesticides (herbicides, fungicides, insecticides) are widely used in agriculture and industry due to their high insecticidal activity [1,2]. Many of them are highly toxic and their accumulation in living organisms can be a cause of serious diseases [3,4]. With exploration of many new pesticides, considerable current interest in food safety is not only to determine the trace content but also to select high efficient and low environmental existent pesticides [5]. Thus there is an essential need to develop a method for simple pesticide sensitivity test to select the most effective one.

The toxic actions of pesticides are based on their abilities to irreversibly modify the catalytic serine residue in acetylcholinesterases (AChE); subsequent inhibition of the AChE effectively prevents nerve transmission by blocking breakdown of the transmitter choline [6]. Traditional methods such as UV spectrophotometry and colorimetry are usually used to determine enzymatic activity based on pesticide inhibition [7,8]. However, these methods include complicated pretreatment procedure, professional operators and expensive instruments, which limit their applications for on-site screening of these compounds. In order to simplify the test procedure, decrease the test cost and enhance the test sensitivity, a novel electrochemical method for pesticide sensitivity test based on AChE biosensor was proposed.

In recent years, the use of AChE and thiocholine in biosensor technology has gained enormous attention, in particular with respect to pesticide detection. It has proven possible to use a screen-printed biosensor for the detection of pesticides in water miscible organic solvents based on the use of *p*-aminophenyl acetate as AChE substrate [9]. Solna et al. reported that the screen-printed four-electrode system could be used as an

* Corresponding author. Tel.: +86 27 67867953.
E-mail address: dudan@mail.ccnu.edu.cn (D. Du).

0039-9140/$ – see front matter © 2007 Elsevier B.V. All rights reserved.
doi:10.1016/j.talanta.2007.07.014

amperometric biosensor for determination of phenols and pesticides using immobilized AChE [10]. Electropolymerization of phenylenediamine monomers has been reported to produce thin nonconducting permselective polymers for immobilization of AChE with rapid response times [11].

When AChE was immobilized on working electrode surface, its interaction with substrate of acetylthiocholine obtained an electro-active product of thiocholine, which produced an irreversible oxidation peak. The inhibition of pesticide on AChE was monitored by measuring the oxidation current of thiocholine. Due to the notable change in electrochemical signal of AChE, a simple method for determination of pesticides and comparison of pesticide sensitivity was established.

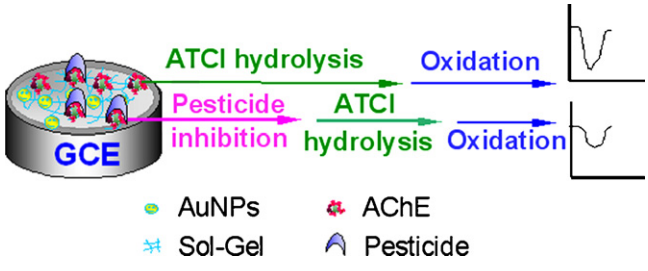
For fabrication of biosensor, immobilization of enzyme to solid electrode surface is a crucial step [12,13]. Sol–gel technology provides an attractive way for the immobilization of biological entitles including full cell, enzyme, protein and antibody or antigen due to the inert low-temperature process [14]. The class of sol–gel silicate matrix possesses attractive features including chemical inertness, physical rigidity, tenable porosity and thermal stability [15], which led to an intensive research in the fabrication of biosensors [16–18]. Recently, nanoparticles, particularly the gold nanoparticles (AuNPs) have received considerable attention in analytical electrochemistry since they have been appeared as highly conductive (fast electron transfer) nanomaterials and are of tremendous current interest [19]. Willner's group has extensively studied the electrochemical and optical applications of AuNPs and the ability to promote the electron transfer [20–22].

This work assembled AuNPs nanoparticles on a sol–gel-derived silicate network for immobilization of AChE, leading to a stable AChE biosensor for investigation of pesticide sensitivity (Scheme 1). Typical pesticides such as monocrotophos, methyl parathion and carbaryl were selected to verify this proposed method. The developed electrochemical method combining the advantages of electrochemical technique with AuNPs was sensitive and accurate for studying the sensitivity of different pesticide. The results obtained were in good agreement with those with UV method.

2. Materials and methods

2.1. Reagents

Acetylthiocholine chloride (ATCl), acetylcholinesterase (Type C3389, 500 U/mg from electric eel) was purchased from Sigma–Aldrich (St. Louis, USA) and used as received. Tetrathoxysilane (TEOS) was obtained from international laboratory (USA). Monocrotophos, carbaryl, methyl parathion and Gold (III) chloride hydrate (3.9 g/mL) were purchased from Treechem Co. (Shanghai, China). The solution of 17 nm-diameter AuNPs was prepared according to reference [23] and stored in a brown bottle at 4 °C. Chitosan (95% deacetylation), phosphate buffer solution (PBS, pH 7.0) and other reagents used were of analytical reagent grade. All the chemicals were of analytical grade and aqueous solutions were prepared with double distilled water.



Scheme 1. Principle of electrochemical pesticide sensitity test based on AChE biosensor.

2.2. Instruments

Electrochemical measurements were performed on a Bioanalytical System (BAS, cv-50w, USA) with a conventional three-electrode system comprising platinum wire as auxiliary electrode, saturated calomel electrode (SCE) as reference and AChE combined to silica sol–gel (SiSG) assembling AuNPs composite modified glass carbon electrode (AChE–AuNPs-SiSG/GCE) as working electrode. The static water contact angle was measured at 25 °C by a contact angle system OCA 20 (Dataphysics, Germany).

UV spectra were recorded using a UV-2501 spectrophotometer (Shimadzu, Kyoto, Japan). Atomic force microscopy (AFM) experiments were performed on SPA-300 HV atomic force microscopy with a SPI 3800 controller (Seiko, Japan). It was carried out in liquid (PBS solution) using tapping mode. The SI-DF-3 cantilevers (Seiko Instruments Inc.) were used (spring constant was about 3 N/m, resonance frequency ranging from 90 to 150 kHz).

2.3. Preparation of silica sol–gel assembling AuNPs composite

A homogenous silica sol–gel assembling AuNPs composite was prepared by mixing 20 μL of TEOS, 60 μL of ethanol, 150 μL of AuNPs, 600 μL of 0.5 mg/mL chitosan solutions (final concentration 0.3%). This mixture was stirred for 1 h until a clear sol–gel composite was formed and its pH was adjusted to 4.0–6.0 using 170 μL 0.1 M NaOH solution. The obtained sol–gel composite can be stored for several months at 4 °C.

2.4. Preparation of the biosensor

GCE was polished to mirror finish using the BAS-polishing kit with 0.3 and 0.05 μm Al_2O_3 paste. After sonicated with ethanol and water, the electrode was applied a potential of +1.75 V under string in pH 5.0 PBS for 300 s and then the electrode was scanned from +0.3 to +1.25 V and +0.3 to −1.3 V until a steady-state current–voltage curve was obtained [24]. After this treatment, a homogeneous aqueous film can be observed on the activated electrode surface [25]. The electrode then allowed the conjugation of the SiSG film with high stability.

Three microliters of the above AuNPs-SiSG composite was coated on a pretreated GCE and allowed for reaction at 20 °C for 4 h. The obtained electrode was then coated with 4.0 μL AChE solutions, which was incubated at 25 °C for 30 min. After evaporation of water, the modified electrode was washed with PBS to remove the unbound AChE. The obtained AChE–AuNPs-SiSG/GCE was stored at 4 °C when not in use.

2.5. Measurement procedure

For measurements of pesticides, the obtained AChE–AuNPs-SiSG/GCE was first immersed in the PBS solution containing different concentrations of standard pesticides for 10 min, and then transferred to the electrochemical cell of 1.0 mL pH 7.0 PBS containing 1.0 mM ATCl to study the electrochemical response by cyclic voltammetry (CV). The inhibition of pesticide was calculated as follows:

$$\text{Inhibition } (\%) = \frac{i_{\text{P,control}} - i_{\text{P,exp}}}{i_{\text{P,control}}} \times 100$$

where $i_{\text{P,control}}$ is the peak current of ATCl on the AChE–AuNPs-SiSG/GCE and $i_{\text{P,exp}}$ is the peak current of ATCl on the AChE–AuNPs-SiSG/GCE with pesticide inhibition.

3. Results and discussion

3.1. Surface hydrophilicity

The hydrophilicity of the electrode surface after pretreatment was characterized by measuring the contact angles of untreated GCE and treated GCE. Their contact angles were 64.6° and 20.8°, respectively (Fig. 1). The treated GCE showed lower contact angle compared with the untreated electrode, indicating the better hydrophilic surface for film adhesion. According to the results of Kepley and Bard [26], the activation of GCE involved the formation of a new phase, which contained a significant amount of microcrystallinity and graphite oxide, thus increased the surface hydrophilicity [27].

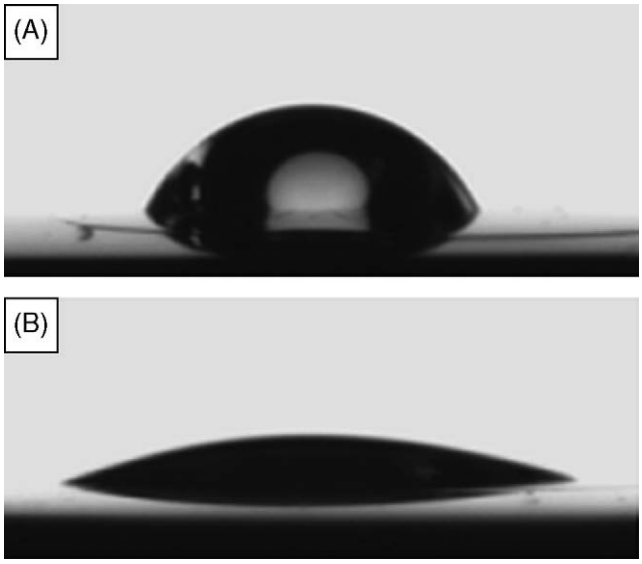


Fig. 1. Contact angle graphs: (A) untreated GCE and (B) treated GCE.

3.2. AFM characterization

AFM measurement is an effective method to provide surface topography and phase images. As seen from Fig. 2, the AuNPs-SiSG composite displayed a porous and netlike structure with uniform distribution (Fig. 2A). This structure provided a significant increase of effective electrode surface for immobilization of biomolecules. After AChE was immobilized on the AuNPs-SiSG composite, some bright particles of AChE were observed clearly (Fig. 2B). The AuNP embedded in SiSG film provided an environment similar to that of biomolecules in native system and efficiently prevented the leakage from electrode.

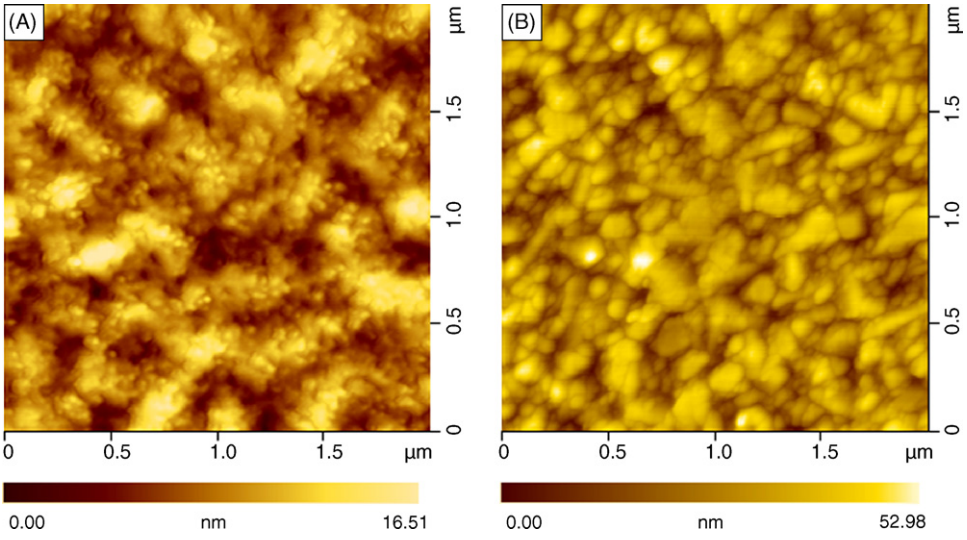


Fig. 2. AFM images: (A) AuNPs-SiSG surface and (B) AChE–AuNPs-SiSG surface.

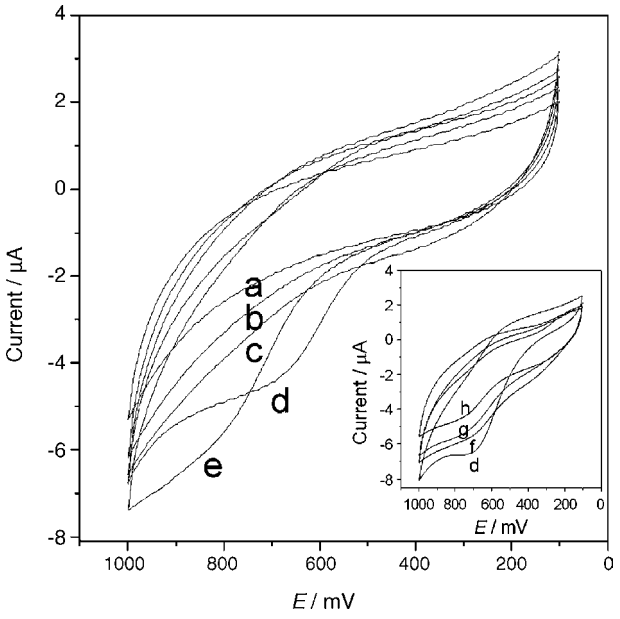


Fig. 3. Cyclic voltammograms: (a) GCE; (b) AChE–AuNPs-SiSG/GCE in pH 7.0 PBS; (c) AuNPs–SiSG/GCE; (d) AChE–AuNPs-SiSG/GC; (e) AChE–SiSG/GCE in pH 7.0 PBS containing 1.0 mM ATCl. (Inset) Cyclic voltammograms of AChE–AuNPs-SiSG/GCE in pH 7.0 PBS containing 1.0 mM ATCl after inhibition with 10 μg/ml pesticides for 10 min, (f) methyl parathion, (g) carbaryl and (h) monocrotophos.

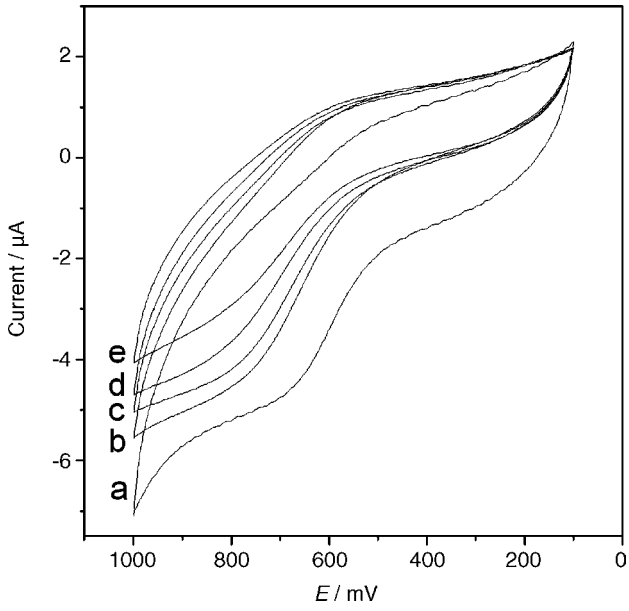


Fig. 4. Cyclic voltammograms of AChE–AuNPs-SiSG/GCE in pH 7.0 PBS containing 1.0 mM ATCl after inhibition with monocrotophos of different concentrations for 10 min: (a) 0 μg/mL, (b) 1 μg/mL, (c) 5 μg/mL, (d) 10 μg/mL and (e) 15 μg/mL.

3.3. Cyclic voltammetric behavior of AChE–AuNPs-SiSG/GCE

Fig. 3 showed the cyclic voltammograms of different electrodes in absence and presence of ATCl in pH 7.0 PBS. No peak was observed at GCE (curve a) and AChE–AuNPs-SiSG/GCE (curve b) in pH 7.0 PBS. When 1.0 mM ATCl was added into PBS, the cyclic voltammograms of AChE–AuNPs-SiSG/GCE showed an irreversible oxidation peak at 689 mV (curve d), while no detectable signal was observed at AuNPs-SiSG/GCE without immobilization of AChE (curve c). Obviously this peak came from the oxidation of thiocholine, hydrolysis product of ATCl, catalyzed by immobilized AChE. The produced current by thiocholine was used as a quantitative measurement of the enzymatic activity, which reflected the biological effect of pesticide involved in the inhibition action. Furthermore, this peak current was much higher and the peak potential shifted negatively compared to that on the silica sol–gel modified electrode without AuNPs (AChE-SiSG/GCE) (curves e and d). This phenomena was due to the presence of AuNPs in the sol–gel film, which possessed inherent conductive properties and catalytic behavior, thus AuNPs-SiSG provided a conductive pathway to electron transfer and promote electron transfer reactions at a lower potential. If AuNPs were directly coated on the electrode surface instead of entrapment in cross-linked sol–gel, much higher background current was observed. Thus AuNPs-SiSG showed excellent conductivity and then AChE–AuNPs-SiSG/GCE was used in the following experiments. Furthermore, the effect of AuNPs content between 0 and 30% (V_{Au}/V) on response was studied in our previous work. The anodic current gradually increased with increasing amount of AuNPs and reached a maximum at 15% (V_{Au}/V) (Fig. S1). Further increase of the AuNPs led to the decrease of peak current. This phenomenon was possibly attributed to the increase of the resistance and double layer capacitance of the modified electrode. So 15% (V_{Au}/V) AuNPs was used for preparation of the biosensor.

As shown from inset of Fig. 3, the produced currents of 1.0 mM ATCl on AChE–AuNPs-SiSG/GCE decreased drastically (curve f: methyl parathion; curve g: carbaryl; curve h: monocrotophos) comparing with the control (curve d) after AChE–AuNPs-SiSG/GCE was immersed in standard solutions of three pesticides for 10 min, respectively. This was because pesticides exhibited fairly high acute toxicity and involved in the irreversible inhibition action to AChE, thus reduced the activity of enzyme to its substrate. However, their inhibition rates were related to their interaction between pesticide and enzyme. Due to the notable change in voltammetric signal of the AChE–AuNPs-SiSG/GCE, the simple electrochemical method for determination of pesticides and investigation of pesticide sensitivity was established.

3.4. Effect of monocrotophos on activity of immobilized AChE

Since the substrate concentration can affect the degree of inhibition, the absolute quantity of ATCl was first optimized. With the increasing concentration of ATCl the amperometric response increased linearly in the range of 10.0–1000 μM and then tended to a plateau value (Fig. S2), showing a typical Michaelis–Menten process. Thus 0.1 mM ATCl was selected for obtaining the maximum response.

Pure biological reagent monocrotophos was firstly selected to evaluate the effect on activity of immobilized AChE. As shown in Fig. 4, upon AChE–AuNPs-SiSG/GCE was immersed

in the standard solution of monocrotophos at a known concentration for 10 min, a notable change in voltammetric signal on AChE–AuNPs-SiSG/GCE was observed. The presence of monocrotophos resulted in a decrease of the peak current, indicating a decrease of the activity of immobilized AChE. This was because monocrotophos as one of the organophosphate pesticide exhibited fairly high acute toxicity and involved in the irreversible inhibition action on AChE, thus reduced enzymatic activity to its substrate. At high concentrations, the inhibition of monocrotophos trended to a maximum value, indicating the binding interaction with active target groups in enzyme could reach saturation, at which the maximum inhibition occurred.

3.5. Electrochemical pesticide sensitivity test

Based on the results obtained above, this work further explored pesticide sensitivity to AChE. Three pesticides, monocrotophos, carbaryl and methyl parathion, were used for this purpose. The treatment by pesticides resulted in the change in cyclic voltammetric response of ATCl at AChE–AuNPs-SiSG/GCE. Fig. 5 showed the inhibition curves of these three pesticides.

With an increase of immersing time in different pesticide solution, the peak currents of ATCl on AChE–AuNPs-SiSG/GCE decreased greatly. Although they played increased inhibition to AChE with increased time, the increase rate of monocrotophos (curve a) was much faster than those of carbaryl and methyl parathion (curves b and c). For monocrotophos, when the immersing time was longer than 10 min the peak current of ATCl on AChE–AuNPs-SiSG/GCE trended to a stable value, indicating the binding interaction with active target groups in enzyme reached saturation. However the inhibitions of carbaryl or methyl parathion trended to stable after 12 min and 18 min, respectively. Although the maximum values of inhibitions of three pesticides were not 100%, which was likely to attribute to the binding equilibrium between pesticide and binding sites in enzyme, the maximum inhibition of monocrotophos was about 90%. This value was much higher than those of carbaryl (~80%) and methyl parathion (~70%). The inhibition of these three pesticides was in the order of monocrotophos > carbaryl > methyl parathion. This conclusion is in agreement with model prediction [28] based on the reported V_{max}/K_m values for these compounds [29]. The inhibition rate was related to their interaction between pesticide and enzyme. Consequently, the pesticides changed the electrochemical response of substrate, from which a novel method for pesticide sensitivity test by voltammetric measurements could be evaluated.

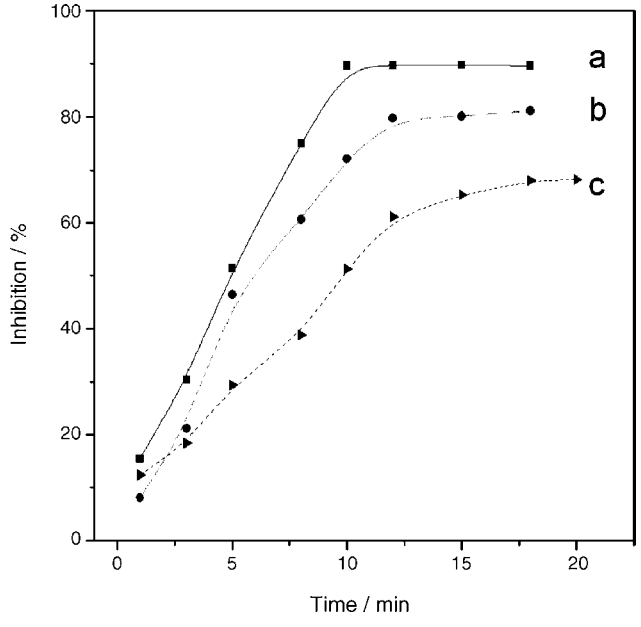


Fig. 5. Dependence of inhibition curves of three pesticides on inhibition time: (a) monocrotophos, (b) carbaryl and (c) methyl parathion.

3.6. Comparison of proposed electrochemical pesticide sensitivity with UV assay

As shown in Fig. 6, the proposed electrochemical pesticide sensitivity test and UV assay gave increasing inhibitions of these three pesticides with the increasing concentrations. These curves trended to the maximum values at high pesticide concentrations, indicating the binding interaction with active target groups in tumor cells could reach saturation when the pesticide concentration increased, at which the maximum incubation occurred. These curves were similar to the shape of Michaelis–Menten relationship. Obviously, the maximum values of inhibition of these three pesticides obtained with two assay methods were in good accordance. The slight difference might be attributed to the different conditions and assay procedures. Thus, the proposed electrochemical method was credible for pesticide sensitivity test.

3.7. Precision, reproducibility and stability of AChE–AuNPs-SiSG/GCE

The inter-assay precision was estimated by determining the response of 1.0 mM ATCl at six different electrodes, which were immersed in 0.1 μg/mL and 5.0 μg/mL monocrotophos for 10 min, respectively. The coefficients of variation were calculated to be 2.3% and 1.7%, respectively, indicating acceptable fabrication reproducibility. The intra-assay precision of the sensors was evaluated by assaying one enzyme electrode for six replicate determinations, and the R.S.D. was 0.8% at the ATCl concentration of 1.0 mM.

After AChE–AuNPs-SiSG/GCE was stored in a refrigerator at 4 °C for 3 weeks, no obvious decrease of ATCl was observed. After a 30-day storage period, the sensor retained 90% of its initial current response. This indicated that silica sol–gel provided a biocompatible microenvironment around the enzyme to stabilize its biological activity to a large extent. The large quantities of hydroxyl groups in the sol–gel hybrid material were able to form strong hydrogen bonds. These hydrogen bonds and the intermolecular interactions between enzyme molecule and specific sites of the silica sol–gel prevented the immobilized enzyme from leaking out of the film.

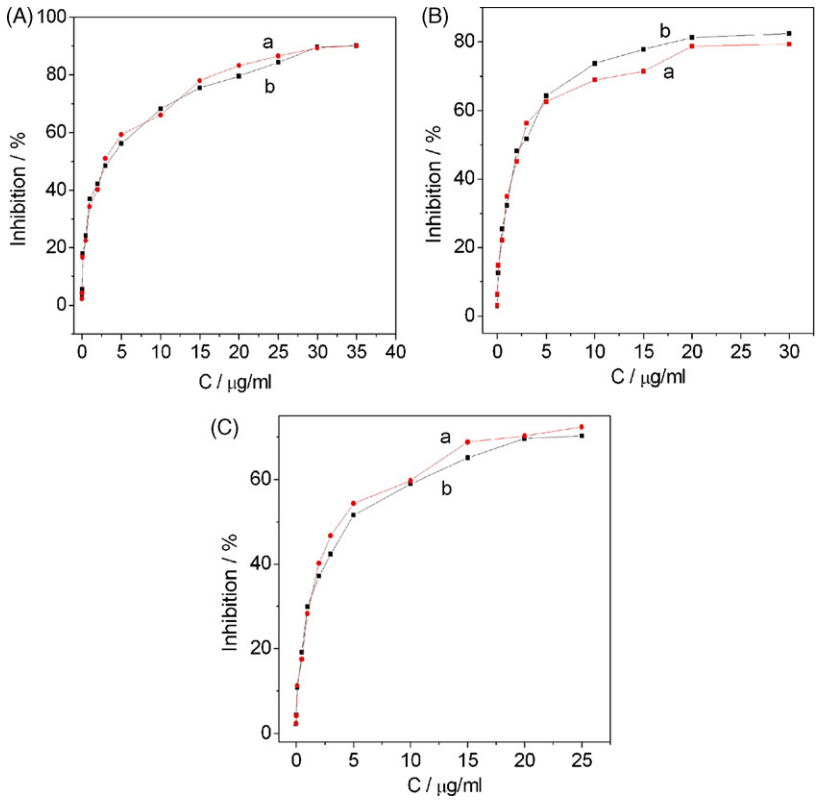


Fig. 6. (A) Inhibition curves of monocrotophos with different methods: (a) proposed electrochemical method and (b) UV assay. (B) Inhibition curves of carbaryl with different methods: (a) proposed electrochemical method and (b) UV assay. (C) Inhibition curves of methyl parathion with different methods: (a) proposed electrochemical method and (b) UV assay.

4. Conclusions

This work proposed an electrochemical pesticide sensitivity test combining with nanoparticles. The large quantities of hydroxyl groups in the sol–gel hybrid material formed strong hydrogen bonds, which interacted with the immobilized enzyme and prevented them from leaking out of the film. The assembled AuNPs nanoparticles on a sol–gel-derived silicate network exhibits superior character of conductibility and favors the interface enzymatic hydrolysis reaction to form electroactive substance, amplificating the sensitivity and amperometric response of the biosensor. The proposed method shows good accuracy with other conventional assays, which has potential application in the selection of enzyme inhibitors and investigation of toxic compounds against to enzyme. To sum up, the proposed electrochemical approach for pesticide sensitivity test with AChE biosensor is a sensitive, accurate and low-cost technique. We are currently facing the challenges of semi-automated procedures, which could be achieved through further improvement in miniaturization of electrochemical system.

Acknowledgements

The authors are gratefully acknowledging the financial support of the Natural Science Foundation of Hubei Province (No. 2006ABA183) and the National Natural Science Foundation of China (No. 20672043).

Appendix A. Supplementary data

Supplementary data associated with this article can be found, in the online version, at doi:10.1016/j.talanta.2007.07.014.

References

[1] F. Arduini, F. Ricci, C.S. Tuta, D. Moscone, A. Amine, G. Palleschi, Anal. Chim. Acta 580 (2006) 155–162.
[2] B.X. Li, Y.Z. He, C.L. Xu, Talanta 72 (2007) 223–230.
[3] J.R. Garbin, D.M.B.P. Milori, M.L. Simoes, W.T.L. da Silva, L.M. Neto, Chemosphere 66 (2007) 1692–1698.
[4] M. Khanmohammadia, M.A. Karimi, K. Ghasemi, M. Jabbari, A.B. Garmarudi, Talanta 72 (2007) 620–625.
[5] K. Fytianos, N. Raikos, G. Theodoridis, Z. Velinova, H. Tsoukali, Chemosphere 65 (2006) 2090–2095.
[6] M.H. Shi, J.J. Xu, S. Zhang, B.H. Liu, J.L. Kong, Talanta 68 (2006) 1089–1095.
[7] S.S. Soares, H. Martins, R.O. Duarte, J.J.G. Moura, J. Coucelo, C. Gutierrez-Merino, M. Aureliano, J. Inorg. Biochem. 101 (2007) 80–88.
[8] W. Kielan, J. Suzanowicz, M. Siewinski, Y. Saleh, A. Janocha, A. Skalski, R. Tarnawa, Gastric Cancer 7 (2004) 17–23.
[9] S. Andreescu, T. Nogue, V. Magearu, J.L. Marty, Talanta 57 (2002) 169–176.
[10] R. Solna, S. Sapelnikova, P. Skladal, M. Winther-Nielsen, C. Carlsson, J. Emneus, T. Ruzgas, Talanta 65 (2005) 349–357.
[11] H. Yang, T.D. Chung, Y.T. Kim, C.A. Choi, C.H. Jun, H.C. Kim, Biosens. Bioelectron. 17 (2002) 251–259.
[12] E. Casero, M. Darder, F. Pariente, E. Lorenzo, J. Martin-Benito, L. Vazquez, Nano Lett. 2 (2006) 577–582.
[13] C.A. Marquette, M. Cretich, L.J. Blum, M. Chiari, Talanta 71 (2007) 1312–1318.

[14] D. Du, F. Yan, S.L. Liu, H.X. Ju, J. Immunol. Methods 283 (2003) 67–75.
[15] Y. Wang, Z. Tang, M.A. Correa-Duarte, L.M. Liz-Marzan, N.A. Kotov, J. Am. Chem. Soc. 125 (2003) 2830–2831.
[16] Y.Z. Xian, F. Liu, L.F. Feng, F.H. Wu, L.W. Wang, L.T. Jin, Electrochem. Commun. 9 (2007) 773–780.
[17] B.K. Jena, C.R. Raj, Anal. Chem. 78 (2006) 6332–6339.
[18] G.H. Wang, L.M. Zhang, J. Phys. Chem. B 110 (2006) 24864–24868.
[19] M.C. Daniel, D. Astruc, Chem. Rev. 104 (2004) 293–346.
[20] I. Willner, V. Pavlov, Y. Xiao, Nano Lett. 5 (2005) 649–653.
[21] I. Willner, R. Baron, B. Willner, Adv. Mater. 18 (2006) 1109–1120.
[22] Y. Xiao, V. Pavlov, B. Shlyahovsky, I. Willner, Chem. Eur. J. 11 (2005) 2698–2704.
[23] Y. Xiao, H.X. Ju, H.Y. Chen, Anal. Chim. Acta 391 (1999) 73–82.
[24] D. Du, H.X. Ju, X.J. Zhang, J. Chen, J. Cai, H.Y. Chen, Biochemistry 44 (2005) 11539–11545.
[25] D. Du, X. Huang, J. Cai, A.D. Zhang, J.W. Ding, S.Z. Chen, Anal. Bioanal. Chem. 387 (2007) 1059–1065.
[26] L.J. Kepley, A.J. Bard, Anal. Chem. 60 (1988) 1459–1467.
[27] Z. Dai, F. Yan, J. Chen, H.X. Ju, Anal. Chem. 75 (2003) 5429–5434.
[28] M.J. Eddowes, Theoretical methods for analysing biosensor performance, in: A.E.G. Cass (Ed.), Biosensors: A Practical Approach, IRL Press, Oxford University Press, Oxford, 1990, pp. 211–263.
[29] J.R. Mason, F. Briganti, J.R. Wild, in: J.R. Wild, S.D. Varfolomeyev, A. Scozzafava (Eds.), Perspectives in Bioremediation: Technologies for Environmental Improvement, Kluwer Academic Publishers, Dordrecht, The Netherlands, 1997, pp. 107–118.

Available online at www.sciencedirect.com
ScienceDirect
Talanta 74 (2008) 443–457
Talanta
www.elsevier.com/locate/talanta

Review

New perspectives in the use of semipermeable membrane devices as passive samplers

Francesc A. Esteve-Turrillas, Vicent Yusà, Agustín Pastor*, Miguel de la Guardia

Analytical Chemistry Department, University of Valencia, Edifici Jeroni Muñoz, 50th Dr. Moliner, 46100 Burjassot, Valencia, Spain

Received 8 March 2007; received in revised form 4 June 2007; accepted 15 June 2007
Available online 22 June 2007

Abstract

This review shows the state of the art, from 2000 to nowadays, of the use of semipermeable membrane devices (SPMDs) for monitoring persistent organic pollutants in both, air and aquatic environments. Since their first use in 1990, SPMDs have been employed for many environmental purposes, like air and water pollution monitoring. We have focussed the study in three subjects: (i) novel compounds accumulated by SPMDs, (ii) modifications of SPMDs to improve their specific uptake properties and (iii) alternatives in sample pre-treatment for the determination of pollutants accumulated in SPMDs.
© 2007 Elsevier B.V. All rights reserved.

Keywords: SPMD; Semipermeable membrane devices; Triolein; Passive sampler; Water; Air

Contents

1. Introduction 444
2. Scientometric evaluation of the literature on SPMDs 444
3. Evolution of passive samplers based on SPMDs 445
   3.1. Generic configuration 445
   3.2. Solvent-free low density polyethylene 446
   3.3. Solvent-containing passive samplers 446
   3.4. Ionic liquid-containing semipermeable membrane devices 446
   3.5. Triolein-containing cellulose acetate low density polyethylene devices 448
4. Applicability of SPMDs 448
   4.1. Water samples 448
   4.2. Air sampling 448
5. SPMD handling 449
6. Analytical procedures for sample processing 449
   6.1. External cleaning 449
   6.2. Pollutant extraction procedures 449

Abbreviations: ASE, accelerated solvent extraction; BTEX, benzene, toluene, ethyl benzene and xylene; CA, cellulose acetate; *o*-CPh, *o*-chlorophenol; *p*-CDB, *p*-dichlorobenzene; ECD, electron capture detector; FD, fluorescence detector; FID, flame ionization detector; GC, gas chromatography; GFF, glass fibre filter; GPC, gel permeation chromatography; HCB, hexachlorobenzene; HPLC, high-performance liquid chromatography; IL-SPMD, ionic liquid-containing semipermeable membrane devices; K_{ow}, octanol–water coefficient; LDPE, low-density polyethylene; MAE, microwave-assisted extraction; MC, musk compounds; MS, mass spectrometry; MS–MS, tandem mass spectrometry; OCP, organochlorinated pollutants; PAH, polycyclic aromatic hydrocarbon; PBDE, polybrominated diphenyl ethers; PCB, polychlorinated biphenyl; PCDD, polychlorinated dibenzo-*p*-dioxin; PCDF, polychlorinated dibenzo-*p*-furan; PCN, polychlorinated naphthalenes; POP, persistent organic pollutant; PRC, performance reference compounds; PUF, polyurethane foam; QA, quality assurance; QC, quality control; SEC, size exclusion chromatography; SPMD, semipermeable membrane devices; TCAPE, triolein-containing cellulose acetate low density polyethylene; TECAM, triolein-embedded cellulose acetate membrane; TOF, time of flight; TRIMPS, trimethylpentane-containing passive sampler; UAE, ultrasound assisted extraction; UV, ultraviolet

* Corresponding author. Tel.: +34 96 354 44 54; fax: +34 96 354 48 38.
E-mail address: agustin.pastor@uv.es (A. Pastor).

0039-9140/$ – see front matter © 2007 Elsevier B.V. All rights reserved.
doi:10.1016/j.talanta.2007.06.019

6.2.1. Dialysis 449
6.2.2. Accelerated solvent extraction 450
6.2.3. Microwave-assisted extraction 450
6.2.4. Ultrasonic extraction 451
6.2.5. Head-space direct determination 451
6.3. Clean-up of extracts 452
6.3.1. Gel permeation chromatography 452
6.3.2. Adsorption columns 452
6.4. Methods for pollutant determination 452
6.4.1. Bioassays 453
6.4.2. Chromatography 453
7. Estimation of air/water pollutant concentrations 453
8. Biofouling effect 454
9. Comparison of SPMDs with standard samplers 454
9.1. SPMD against biomonitoring 454
9.2. SPMD against active samplers 455
10. Future trends 456
Acknowledgements 456
References 456

1. Introduction

Semipermeable membrane devices (SPMDs), introduced by Huckins et al. [1], consist of an additive free lay-flat tube, made of low-density polyethylene (LDPE), filled with triolein, spreading it into the tube surface and then heat-sealed at each end. The low interfacial tension causes an intimate contact between the triolein and the LDPE.

Passive sampling of pollutants by using SPMDs has been widely used for screening and source identifications of a variety of non-polar and moderately polar organic contaminants from aqueous and air environments.

SPMDs mimic the absorption of compounds through cell membranes and also can be used to evaluate the bioconcentration factor in aquatic animals. Organic pollutants present in water can be dissolved or adsorbed to particles, such as humic acids or sediments; being the adsorbed compounds less available to animals. So, SPMDs are often used as an indicator of the bioavailability of hydrophobic contaminants in the environment [2].

SPMDs have been successfully tested as passive samplers for several kinds of persistent organic pollutant (POPs), such as polycyclic aromatic hydrocarbons (PAHs), polychlorinated biphenyls (PCBs), polychlorinated dibenzo-*p*-dioxins (PCDDs), polychlorinated dibenzo-*p*-furans (PCDFs) and several organochlorinated pesticides (OCPs). The sampling rate of different series of chemicals depends on their physical–chemical properties, being the octanol–water coefficient (K_{ow}) the most important. However, other environmental variables also affect the contaminant uptake, including temperature, turbulence, flow rate and biofouling [3].

The use of SPMDs have several advantages compared to other sampling methods: (i) can be deployed for extended time periods to integrate long-term data; (ii) only bioavailable compounds are sampled; (iii) are easy to use and less expensive than active samplers; and (iv) are more reproducible than live biota samplers, avoiding drawbacks related to migration, mortality, metabolism or selective depuration of contaminants. As well as a passive sampler, the use of SPMDs provides selective analyte isolation and especially pre-concentration [4]. So, the selectivity and sensitivity of pollutants determination methods can be considerably improved.

2. Scientometric evaluation of the literature on SPMDs

An extensive review of SPMDs used for monitoring pollutants in various media has been published by Petty et al. in 2000 showing a summary of considerations for their effective and efficient uses [3]. Later Lu et al. in 2002 reviewed conventional applications of SPMDs in aquatic environments that emphasizes in their use in chemical monitoring and in their comparison to biomonitoring organisms [5]. Additionally, in a revision of Stuer-Lauridsen for passive accumulation devices a special attention has been made for the use of SPMD samplers [6]. Finally, two books are commercially available related to the use of SPMDs as samplers of organic chemicals in the environment [7,8].

The scientific references found in the literature related to different applications of SPMDs have been growing significantly in the latest years (see Fig. 1). From this figure, it can be seen that after a period of time of 5 years, till 1995 in which the number of published studies remain practically constant the literature about this topic increases at a rate of 13.6 papers per year till 2000. From this date till 2006, a two times increased speed of 28.6 papers $year^{-1}$ was reached, indicating that nowadays SPMDs are well accepted by the scientific community and start to be applied to solve as much as possible environmental control processes.

The classification of published papers by the journals of publication is shown in Fig. 2. Most of them have been published in environmental journals (Environmental Sciences with a 49% and Environmental Engineering with 17% of total published studies) while a minority has been published in basic or applied analytical journals (only a 13%) [9].

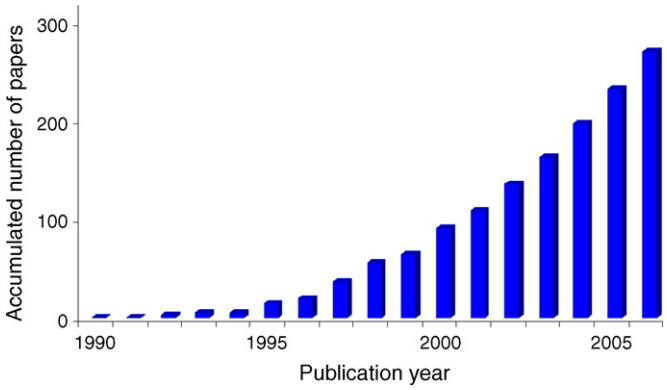


Fig. 1. Evolution of the accumulated number of published papers on the use of SPMDs. *Note*: references compiled in ISI Web of Knowledge for the period 1945–2006 [9].

The aforementioned results show that most of the studies carried out involving SPMDs are field studies, and only a few research groups have been worked on new applications or methodological improvements of the use of these devices.

Three are the main reasons for the tremendous increase of the literature about SPMDs in the new century: (i) the considerable modifications in the SPMD standard devices, (ii) the search for alternatives to long and tedious dialysis procedures classically used for sample processing after retention of analytes in SPMDs and (iii) the studies on novel compounds to be sampled with SPMDs.

3. Evolution of passive samplers based on SPMDs

As indicated before, the initial configuration of SPMDs proposed by Huckins included a LDPE tube filled with triolein, but this generic configuration has been replaced, in some cases by the use of solvent free low density polyethylene samplers or LDPE tube filled with isooctane, ion liquid or triolein containing cellulose acetate.

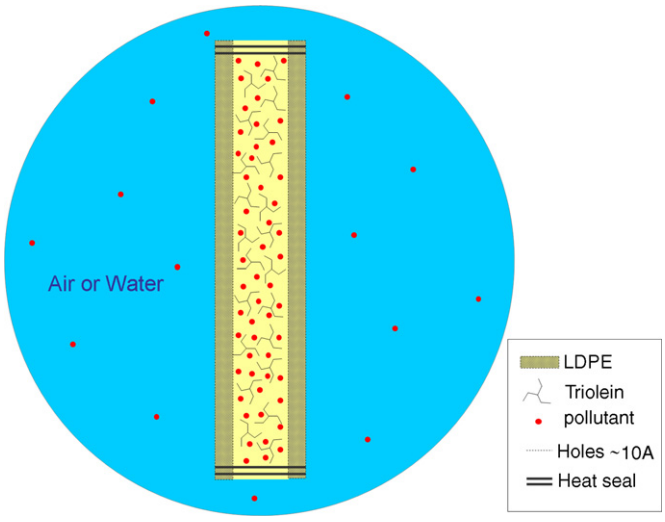


Fig. 3. Scheme of a generic SPMD device.

3.1. Generic configuration

LDPE tubing, 70–90 μm wall thickness is described as non-porous material, but random thermal motions of the polymer chains form transient cavities with maximum diameters of approximately 10 Å. Because of the small size and dynamic character of these cavities, hydrophobic solutes are essentially dissolved by the polymer. This solute size limitation excludes large molecules as well as those that are adsorbed on colloids or humic acids. Only truly dissolved (bioavailable) and non-ionised contaminants diffuse through the LDPE membrane and can be separated by the sampler. A scheme of a conventional SPMD is shown in Fig. 3.

The advantages in the use of triolein (1,2,3-tris-*cis*-9-octadecenoyl glycerol), a major non-polar lipid found in aquatic organisms, in front of other lipids are: (i) the easy availability as a high purity synthetic product, (ii) the low melting point (close to 0 °C) and (iii) the large capacity to dis-

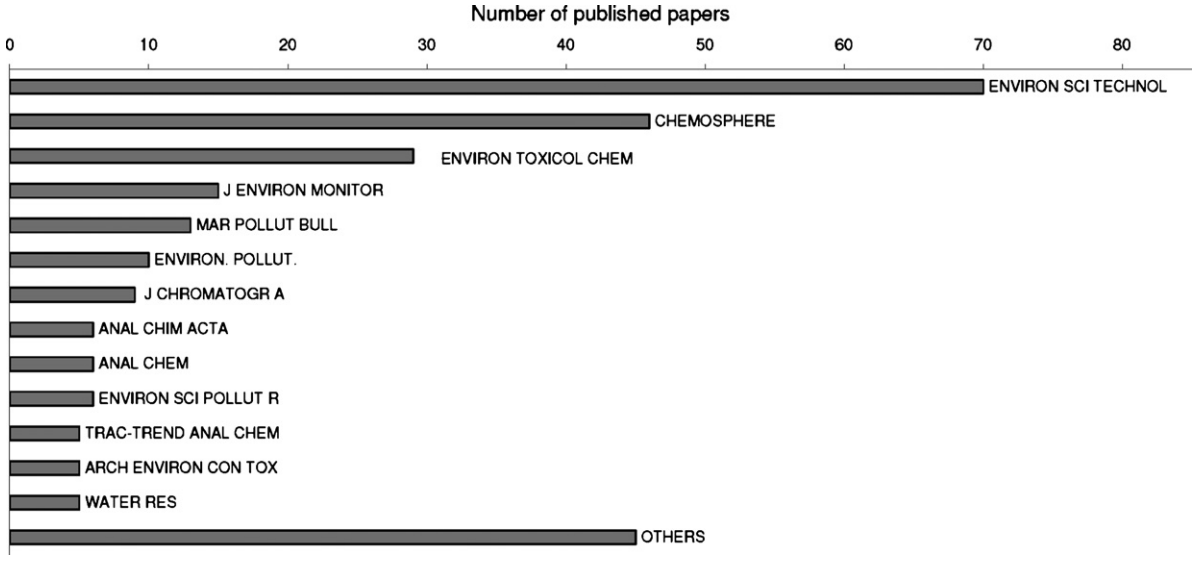


Fig. 2. Classification of published papers on SPMDs by journal of publication. *Note*: references compiled as indicated in Fig. 1.

solve non-polar compounds. Furthermore, there is a close correlation between triolein–water partition coefficients and octanol–water ones, being the latter easy-known for whatever compound.

Usually, the commercially available SPMD consists of a piece of 106 cm long and 2.54 cm wide that contain 1 mL pure triolein inside [3]. The device weights approximately 4.5 g, is about 20% triolein and the surface area–triolein volume ratio is about 460 cm^2/mL. However, some studies have been carried out with mini-SPMD of 10 cm long, filled with 0.1 mL triolein [10,11] or 30 cm long, filled with 0.3 mL triolein [12]. Any SPMD length is considered to be a "standard" SPMD if the surface area–triolein volume ratio is maintained at 460 cm^2/mL.

3.2. Solvent-free low density polyethylene

"Is triolein indispensable in the use of SPMD?" It is one of the most frequently questions about the use of SPMD. Thus, some authors have studied the pollutant uptake behaviour using only LDPE strips without triolein [12–16]. In these studies LDPE layflat tubing is cut twice along the side edges in order to obtain a single layered strip, being it used in the same way than generic SPMDs.

Difficulties in the spike of LDPE were solved by Booij et al., which incorporated deuterated PAHs and PCBs on the polymer by soaking it in aqueous/methanolic solutions [13].

The effect of temperature on PAH sampling rates in air has been evaluated using both SPMDs and LDPE strips under controlled flow conditions [12]. No significant differences were observed on sampling rates, but LDPE samplers reached equilibrium faster because of their smaller sorption capacity. Moreover, LDPE water partition coefficients were larger at low temperatures, while for SPMD remained invariable.

A comparison of PAHs uptake in LDPE strips, SPMDs and pink salmon eggs was also performed in aqueous environments, being observed that accumulations of PAHs were highly similar in strips than those observed in SPMDs [16].

The uptake of 12 priority PAHs was evaluated for LDPE strips at two different thicknesses (100 and 200 μm), but with the same cross-section area [15]. In this study, when equilibrium is approached, the PAH amount accumulated and the time required to reach it, is proportional to LDPE thickness. So, authors suggest the use of an unique sampler composed with two LDPE strips, in the thinner one the smaller PAHs reach equilibrium and in the thicker one the larger PAHs are in the linear uptake, being both behaviours considered by standard SPMD models.

Finally, it must be emphasized the importance of the absence of triolein in LDPE samplers, because it considerably decreases the cost of each device.

3.3. Solvent-containing passive samplers

A simple modification of SPMDs was introduced by Leonard et al. [17], by using 2,2,4-trimethylpentane (isooctane) instead of triolein. These devices were so called trimethylpentane-containing passive samplers (TRIMPS). The change of the lipid provides two great advantages as passive sampler: (i) the absence of periphytic growth or biofouling, that can affect the sampling rates of absorbed pollutants; and (ii) the simplification of the sample processing, being not required any clean-up step after the dialysis of retained analytes. However, the use of TRIMPS could release trimethylpentane to the surrounding water. The release of solvents is only influenced by the deployment time and not by the river flow or water temperature [17]. The kinetics of uptake for non-polar pesticides (log K_{ow} >3.5) is linearly proportional to the ratio of chemical activity of the pesticide between water and trimethylpentane [18]. Thus, TRIMPS have been successfully applied for the sampling of endosulfan, chlorpyrifos-ethyl, profenofos and sulprofos [17] and of tributylphosphate, endosulfan sulfate and chlorpyrifos-ethyl [19] in river waters.

A study of accumulation of PAH and petroleum biomarker compounds (22 steranes and 31 hopanes) in SPMD, LDPE strips and TRIMPS samplers, performed by Luellen et al., shows that the LDPE sampling rates are 30% higher than the other two designs [20]. In spite of it, the three passive samplers tested are effective for discriminate petroleum sources.

A binary solvent mixture of 1-dodecanol and isooctane (3:2) was used by Hyne et al., being effective in the measurement of polar pesticides from waters [18].

Other devices tested have been LDPE membrane bags of 7.5 cm length filled with 100 μL dimethyl sulfoxide. These devices, employed by Roger et al., were used for toxicity assays of toxic industrial chemicals in air. When the deployment time is reached, SPMD is cut and dimethyl sulfoxide analyzed directly through rapid toxicity assays [21].

3.4. Ionic liquid-containing semipermeable membrane devices

Ionic liquids are organic salts, which are liquids at ambient temperatures. Their exclusive properties such as nonvolatility, nonflammability, and excellent chemical and thermal stability have made them an environmentally attractive alternative to conventional organic solvents. One of the most special properties for ionic liquids is their high polarity, thus the replacing of triolein for an ionic liquid in SPMD samplers was recently suggested for Zhao et al. [22].

Eighteen centimetres long segments layflat LDPE tubing were filled with 0.5 mL ionic liquid, forming a ionic liquid-containing semipermeable membrane devices (IL-SPMD). The ionic liquid employed was 1-butyl-3-methylimidazolium hexafluorophosphate ([C4MIM][PF6]) and the effective length was 15 cm.

IL-SPMDs were used for monitoring five PAHs in water. PAHs in the ionic liquid were directly analyzed by HPLC, without the dialysis plus clean-up procedures. A comparative study was carried out in the Yellow River in China; both IL-SPMDs and conventional triolein containing SPMDs were deployed for 5 days in several sites and PAH residues were measured. Ionic liquid devices provided lower amounts of PAHs, these differences are explained by authors because of the sample processing in the case of IL-SPMDs only concerns the ionic liquid measurement and involves the whole LDPE membrane with triolein in classical devices.

Table 1
Deployment conditions of SPMDs for sampling novel compounds

Type	Compounds	Matrix and location	Deployment time (days)	Concentration found	References
Degradation of alkylphenol ethoxylate surfactants	Nonylphenol, octylphenol, nonylphenol monoethoxylate, nonylphenol diethoxylate	Sewage plant, Great Lakes (USA)	–	–	[26]
Organotin	tributyltin, dibutyltin, monobutyltin	Seawater—Oslo fjord (Norway)	15–30	0.4–10 ng/L	[27,28]
Polycyclic Musk	Galaxolide, tonalide, celestolide, phantolide, traseolide, musk xylene, musk ketone	Sewage Moldau river (Czech Republic)	–	–	[29–31]
Triclosan	triclosan (T), methyl triclosan (mT)	Water—Greifensee lake (Switzerland) Water—Air Basin river (UK)	21–42	70–1300 ng/L (T) 1–11 ng/L (mT)	[32–34]
Petroleum biomarkers	Sterane, hopane	Water	29	–	[10]
UV filters	Benzophenone-3, 4-methylbenzylidene camphor, ethylhexyl methoxy cinnamate, octocrylene, butyl methoxydibenzoylmethane	Water—Zurich lake (Switzerland), Water–Greifensee lake (Switzerland)	24–48	1–35 ng/L	[35,36]
Nitrated PAH	1-Nitronafthalene, 2-nitronaphtalene, 2-nitrofluorene, 9-nitroanthracene, 3-nitrofluoranthene, 1-nitropirene	Air—(Austria, Czech Republic, Poland, Slovakia and Sweden)	21	0.001–4 ng/day	[37]
Toxic industrial chemicals	Diketene, Phosphorusoxychloride, acrolein, trichloroacetyl chloride, methanesulfonyl chloride, stilbene, 1-octanethiol, sulfuryl chloride, formaldehyde, allylamine, methyl chloroformate, chloroacetone, methyl chlorsilane, diisopropylfluorophosphate, Methylhydrazine, acetone cyanohydrin, 1,2-dibromoethane	Contaminated air	1	–	[21]
Polychlorinated naphthalenes (PCN)	Tri-PCN, Tetra-PCN, Penta-PCN, Hexa-PCN	Air	2–450	0.17–32.5 pg/m^3	[38]
	PCN-54, PCN-67, PCN-73, PCN-75	Sewage treatment plant—Carraixet (Spain)	20	–	[39]
BTEX	Benzene, toluene, ethylbenzene, xylenes	Vehicle compartments (VC) (Spain)	1	0.6–160 μg/m^3 (VC)	[40]
		Petrol station air (PSA) (Spain)		0.04–58 mg/m^3 (PSA)	
Herbicides	Diuron, simazine, atrazine, hexazinone, fluometuron	Great Barrier Reef (Australia)	8–11	0.06–2.5 ng/L	[41]
Pesticides	Atrazine, chlorpyrifos, chlorothalonil	Estuarine ecosystems (FL, USA)	4	2.7–48 ng/L	[42]
Pyrethroid insecticides	Allethrin, prallethrin, tetramethrin, bifenthrin, phenothrin, λ-cyhalothrin, permethrin, cyfluthrin, cypermethrin, flucythrinate, esfenvalerate, fluvalinate, deltamethrin, piperonyl butoxide	Contaminated indoor air (Spain)	2	–	[43]
Pesticides	Propamocarb, propoxur, carbosulfan, diazinon, pirimicarb, ethiofencarb, chlorpyrifos-methyl, metribuzin, metalaxyl, terbutryn, malathion, chlorpyrifos, fenthion, pendimethalin, allethrin, oxadiazon, buprofezin, oxyfluorfen, diclofop-methyl, propargite, carbofuran, bifenthrin, tetramethrin, fenoxycarb, phenothrin, λ-cyhalothrin, permethrin, flucythrinate, fluvalinate, esfenvalerate	Irrigation water, Albufera Lake (Spain)	30	4–1450 ng/SPMD	[44]
Polar pesticides	Diuron, atrazine, metolachlor, fipronil, molinate	Irrigation water, Murrumbidgee (Australia)	22	0.0001–32.9 μg/L	[18]

3.5. Triolein-containing cellulose acetate low density polyethylene devices

Xu et al. have studied the use of triolein-embedded cellulose acetate membrane (TECAM) as passive sampling devices; they were produced by embedding triolein drops in the matrix of cellulose acetate polymers [23]. Results from both laboratory and field experiments indicate that TECAM can quickly and efficiently accumulate hydrophobic OCPs from water. The uptake rate of 16 PAHs in aquatic environments shows that these pollutants required shorter times to achieve equilibrium in TECAMs than in SPMDs [24].

A combination between SPMD and TECAM is proposed by Liao et al. The device consists of a thin film of neutral lipid triolein, enclosed in thin-walled tubing made of composite cellulose acetate membrane (CA) supported by linear LDPE. The whole device, so-called TCAPE, is formed with a LDPE support (25 μm thickness), an external slide of CA (10 μm thickness) and filled with 0.5 mL triolein. TCAPE keep the standard surface area–triolein volume ratio of 450 cm^2/mL. In a comparative study, TCAPE accumulates hydrophobic OCPs in water more quickly and efficiently than standard SPMDs; where in only 20 h the uptake equilibrium is reached [25].

4. Applicability of SPMDs

4.1. Water samples

Uptake of compounds from the environment depends upon their chemical and physical properties, such as molecular weight, water solubility, K_{ow} and of course also upon media conditions (temperature, flow rate and biofouling). In general, any neutral and hydrophobic compound with a log K_{ow} higher than three can be significantly concentrated by SPMDs, although compounds with log K_{ow} values bigger than one could be also retained. Ionic species and very polar organic compounds are not concentrated in SPMDs. Petty et al. show, in their review in 2000, a list of environmental contaminants that have been effectively sampled in different environments by SPMDs, such as; PAHs, polychlorinated biphenyls (PCBs), organochlorinated pollutants (OCPs), polychlorinated dibenzo-*p*-dioxin (PCDDs), polychlorinated dibenzo-*p*-furan (PCDFs), alkylated phenols, organophosphate and pyrethroid insecticides, neutral organometallic compounds, polybrominated diphenyl ethers (PBDEs) and some heterocyclic aromatic compounds [3]. Nowadays, a large number of compounds, summarized in Table 1, have been added to this list.

Novel compounds have been sampled in different sites, such as: butyltin derivates in seawater [27,28]; petroleum biomarkers in water [10]; polycyclic musk xylene, musk ketone and their amino metabolites in water from river and from sewage plants [29–31]; triclosan [32–34] and UV filters [35,36] in lake waters; or polychlorinated naphthalenes (PCNs) in sewage plants [39].

Uptake of pesticide compounds using SPMD has been widely used in several studies, mainly for chlorinated pesticides. Recently, a few categories of other pesticides have been studied such as: the pesticides atrazine, chlorpyrifos, chlorothalonil in estuarine ecosystems [42]; the herbicides diuron, simazine, atrazine, hexazinone and flumeturon in seawater [41], or the polar pesticides diuron, atrazine, metolachlor, fipronil, and molinate in irrigation waters [18].

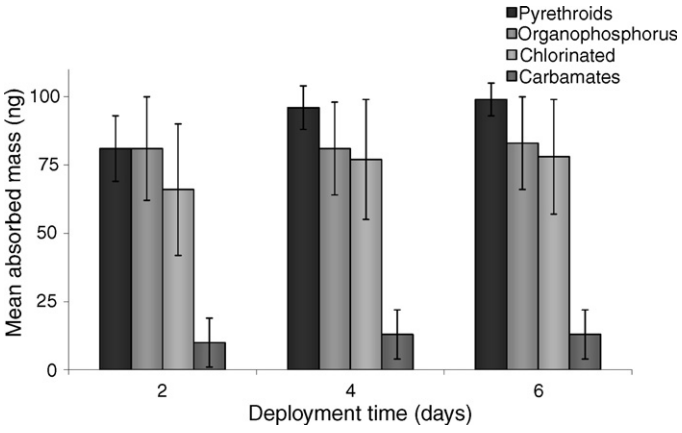


Fig. 4. Recovery of different pesticide families from 2 L water spiked with 100 ng of each studied compound by using SPMDs after different deployment times, from 2 to 6 days.

The uptake of pesticides from water was evaluated by Esteve-Turrillas et al. using 37 neutral pesticides with different properties, with log K_{ow} ranging from 0.08 to 8.00 and water solubility from 5 μg/L to 7 g/L [44]. This study classifies the SPMD pesticide uptake by families, such as chlorinated, organophosphorus, pyrethroid, carbamates and others. Fig. 4 shows a bar graphic with the mean uptake of pesticides, using SPMD, from spiked water after 2, 4 and 6 deployment days. The graphic shows that pyrethroid compounds are the most easily retained, due mainly to their high log K_{ow} values followed by organophosphorus and chlorinated compounds. Carbamates were weakly absorbed.

4.2. Air sampling

SPMDs were developed in a first attempt for water sampling of organic pollutants. In fact, most of the published papers are focussed in water field studies. Even solid matrices have been also sampled by using SPMDs, for the determination of organochlorined pollutants in contaminated lake soils or in indoor household compost [45,46]

In 1993, Petty et al. proposed the use of SPMDs for air sampling purposes [3]. However, only few papers have studied the uptake of pollutants, mainly for PCBs, PAHs and OCPs sampling [47,48]. Nowadays, there is an increasing interest on the use of SPMDs for air sampling of novel compounds and the comparison with other well-established samplers.

New compounds sampled in air are PBDEs [49,50], pyrethroid insecticides and pyperonyl butoxide [43], nitrated PAHs [37], toxic industrial chemicals [21], PCNs [38], or benzene, toluene, ethylbenzene and xylenes (BTEX) [40].

Several comparative studies were performed for the use of SPMD in front of active samplers [51,52], passive samplers [38] or biological samplers, such as semiaquatic plants [53] or pine needles [54].

The effect of different wind-speeds on the calibration of SPMD uptakes of PAHs and PCBs from air, using performance compounds reference was evaluated by Soderstrom and Bergqvist [55].

SPMDs have been also used to sample the air houses with an extensive burning of domestic wood. Strandberg et al. found PAHs and PCBs in these sites, being the PAHs levels comparables to urban contaminated sites, while PCBs levels were slightly lower [56].

5. SPMD handling

Different protective apparatus are usually employed during the sampling with SPMDs, being preferred the use of stainless steel surfaces in front of plastic components, to minimize the possible release of organic compounds. Hardware employed must maximize the effective area of the sampler. For the sampling of photosensible compounds, SPMD must to shade from sun with a special cover. In addition, hardware employed must to be moored and hidden in order to avoid losses and any kind of vandalism or sabotage.

The deployment time for sampling with SPMDs can varied from days to months depending on the expected concentration levels and the kind of contaminants. Deployment times of 10–30 days are typically employed for POPs uptake in water sampling, but in the case of air the deployment time is of the order of 24 h.

SPMD uptake of all types of chemicals can be intensively affected by environmental variables, such as temperature, flow-rate, water composition, level of biofouling and others.

It would be important to fill a detailed documentation for each SPMD sampling that includes as much data as possible, including field conditions, visual evaluation of biofouling and an estimation of flow-rates.

Differences in absorbed amounts of PCBs and PAHs generally cannot be attributed to changes in temperature, except when very large geographic scales or summer/winter comparisons are involved [12]. Although in other studies it has been reported that uptake rates of PAHs, PCDDs, PCDFs and PCBs decreased slowly with temperature [57,58].

In a laboratory study, Cicenaite et al. estimated the temperature influence on the SPMD-air coefficient partition for naphthalene, *o*-chlorophenol and *p*-dichlorobenzene. Temperatures tested were −16, −4, 22 and 40 °C, being the time required to reach equilibrium inversely proportional to air temperature [59].

The water flow velocity has a considerably influence on the sampling rate, with values ranging from 4 to 200 L day^{-1} for chlorobenzenes, PCBs and PAHs performed in water at several velocities, as it has been shown by Booij et al. [12]. Others studies have confirm this behaviour, showing the significant differences in the release kinetic of PAHs at different flow rates [60].

Sampling rates for PAHs were evaluated under different water conditions, concluding that salinity does not affects the uptake, but there is a slight effect in the solubility of these compounds in salted water [57].

In a recent study, the behaviour of SPMDs was assessed for the uptake of neutral pesticides from waters as a function of water temperature (10, 18 and 25 °C), ion strength (0, 0.1, 1 and 5 g/L of NaCl), pH (4, 7 and 9 with HCl and NaOH), presence of solvents (0.1, 0.5 and 1 mL acetone) and presence of organic matter (1 g/L of both glucose and starch). Authors concluded that there is no big variation in the pesticide uptake from water at different salinity, pH or organic matter composition, but temperature has a strong influence on the absorption rates, increasing at high temperatures [44].

6. Analytical procedures for sample processing

Extraction of analytes retained in SPMDs is commonly made by dialysis with organic solvents, with the exception of specific applications such as PAHs sampling using IL-SPMDs, where ionic liquid is directly measured by HPLC [22].

Although SPMDs are generally easier to be analyzed than other environmental matrices, such as sediments, tissues, etc., analysis of contaminants retained in SPMDs can be affected by the presence of polyethylene waxes, oleic acid and methyl oleate evolved from the sampling device [7].

6.1. External cleaning

A general recommendation, by Petty et al., for a right external cleaning of a SPMD after deployment in water involves: removal of the superficial biofouling and debris using hexane, brushing and immersion in dilute acid; and rinsing of the SPMD surface with water, acetone and isopropanol [3]. When SPMDs are used as air samplers, the surface is not affected by biofouling and thus the external cleaning can be avoided or carried out rinsing with water and organic solvents.

6.2. Pollutant extraction procedures

Dialysis and modern extraction alternatives, based on accelerated solvent extraction (ASE), microwave-assisted extraction (MAE) and ultrasound assisted extraction (UAE) have been employed to extract pollutants retained on SPMDs, additionally than the direct determination of volatile compounds through head space gas chromatography.

6.2.1. Dialysis

A general view of the dialysis procedures used in the literature, for POPs extraction is summarised in Table 2. Hexane is employed as solvent is most of cases. As it can be seen, standard methods are time-consuming, from 24 to 72 h, and require the use of high volumes of solvent, from 100 to 900 mL. The main drawbacks of dialysis procedures are high extraction times and excessive solvent consumption that increase considerably the cost of analysis. Because of that nowadays a high effort has been do in the use of environmentally friendly procedures that minimizes solvent consumption and waste generation, based on the use of ASE, MAE, USE or head-space (HS) direct volatilization of the analytes (see Table 3). On the other hand, Fig. 5 shows

Table 2
Dialysis procedures employed in the literature for the recovery of pollutants retained in SPMDs

Sample	Contaminant	Solvent	Volume (mL)	Time (h)	References
Air	PCBs	Hexane	250	48	[61]
Air	PAHs	Hexane	300	48	[62]
Air	Naph, *o*-CPh, *p*-CDB	Hexane	100	24	[59]
Air/water	PCBs, HCBs	Hexane-DCM (80:20)	120	48	[63]
Sewage	PCBs, PAHs, OCPs,	Cyclohexane	100	48	[64]
Water	PAHs	Hexane	150	48	[57]
Water	PCDDs, PCDFs	Hexane	900	48	[65]
Water	PCBs, OCPs	Hexane	250	48	[66]
Water	PAHs	Cyclopentane	–	24	[67]
Water	PCDDs, PCDFs, PCBs	Hexane	400	48	[45]
Water	PAHs	Hexane	150	48	[4]
Water	PAHs, OCPs, PCBs	Hexane	750	72	[68]

Abbreviations: *o*-CPh, *o*-chlorophenol; *p*-CDB, *p*-dichlorobenzene; HCB, hexachlorobenzene; Naph, naphthalene; OCP, organochlorinated pollutants; PAH, polycyclic aromatic hydrocarbon; PCB, polychlorinated biphenyl; PCDD, polychlorinated dibenzo-*p*-dioxin; PCDF, polychlorinated dibenzo-*p*-furan.

a flow chart that can help us to select the appropriate extraction procedure depending on the analyte selected.

6.2.2. Accelerated solvent extraction

This technique, also known as pressurized fluid extraction or pressurized liquid extraction uses an organic solvent or a combination of solvents at high pressure and temperature. The extraction under these conditions provides increased solubility, better desorption and enhanced diffusion of POPs from the matrix. Thus the extraction time can be considerably reduced.

In 2004, Wenzel et al. suggest the first reported procedure as a good alternative to dialysis extraction of POPs for SPMDs. The so-called "rapid dialysis procedure" employs an accelerated solvent device to extract OCPs, PCBs and PAHS [11]. The procedure is suitable for two SPMD sizes: 10 and 91 cm length, using for both 33 mL cells, but it is necessary the use of an stainless steel mesh that ensures the optimal, reproducible fixing of the SPMD in the cell and to avoid contact with the inner walls of the cell.

The effect of several instrumental parameters such as: extraction pressure, temperature and time, solvent composition, and number of cycles were evaluated on spiked SPMDs. The optimal parameters were an adjusted extraction pressure of 3.45 MPa, a temperature of 50 °C, extraction time of 10 min, *n*-hexane/acetone 9:1 as solvent and four extraction cycles. The average recovery values found varied from 88 to 100% for OCPs, to about 100% for all the PCBs studied and from 89 to 123% for PAHs [11].

6.2.3. Microwave-assisted extraction

MAE has attracted growing interest, as it allows rapid extraction of solutes from solid matrices by employing microwave

Table 3
Comparison of extraction conditions used in recent publications for the recovery of preconcentrated POPs in SPMDs

Parameter	Dialysis	MAE	ASE	Sonication	Head space
Studied compounds	POPs	PCBs, PAHs, OCPs, PBDEs, PCNs, pesticides	OCPs, PCBs, PAHs	MCs, PCBs, PBDEs, OCPs	BTEX
Samples	Air/water	Air/water	Air	Water	Air
Solvents	Hexane/cyclohexane	Hexane:water (10:1, v/v); Hexane:acetone (1:1, v/v); Toluene	Hexane:acetone (10:1, v/v)	Hexane	None
Solvent consumption	100–900 mL	60–120 mL	140 mL	300 mL	None
Sample processing time	6–48 h	5–60 min	40 min	60 min	20 min
Clean-up required	Yes	Yes	Yes	Yes	No
Automation	No	Yes	Yes	No	Yes
Serial extraction	Yes	12 reactors	36 reactors	Yes	32 vials
Main advantages	Easy	Rapid	Rapid	Rapid	Rapid
	No instrumentation required; few triolein coextraction	Low solvent consumption	Low solvent consumption	Easy; no instrumentation required	Direct; no sample treatment; no solvent consumption
Main drawbacks	Very slow	Analyte unstability; risk of SPMD collapse; high matrix coextraction	Analyte unstability; a internal mesh is required; high matrix coextraction	High sample manipulation; easy contamination; high matrix coextraction	Only for very volatile compounds; SPMD collapse
Investment	Low	Low; moderate	High	Low	Moderate
Equipments used	–	Domestic oven; Milestone ETHOS SEL	Dionex ASE 200; Dionex ASE 300	Ultrasonic water bath	Thermo AS2000
References	[3,7]	[39,43,44,69]	[11]	[31]	[40]

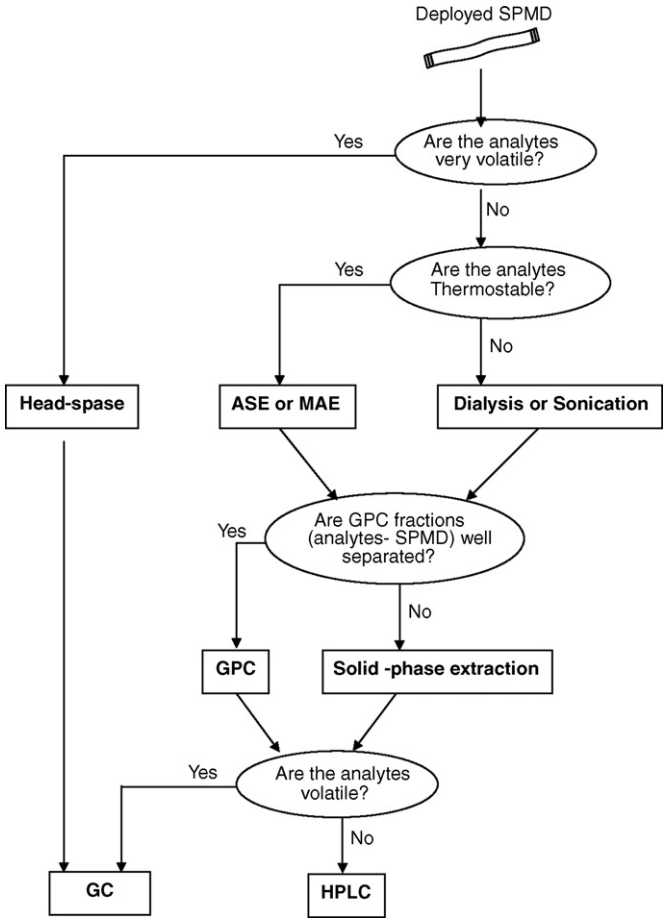


Fig. 5. Flowchart to select an appropriate analytical procedure for POPs determination in SPMDs.

energy as a source of heat, with extraction efficiency values comparable to that of classical techniques. The partitioning of analytes from the sample matrix to the extractant solvent depends upon the temperature and the nature of the solvent. As compared with classical heating systems, microwave radiation provides a fast and selective heating of polar compounds, leading to a very short extraction time.

Yusà et al. proposed the use of MAE for the extraction of POPs from SPMDs. First studies were carried out using domestic microwave ovens, were the only modifiable parameters were the maximum power exit and the extraction time. OCPs, PCBs and PAHs were extracted by using several mixtures of solvents, as hexane–acetone (1:1, v/v), hexane–water (10:1, v/v), toluene–water (10:1, v/v) and isooctane–acetonitrile, (1:1, v/v), being found that hexane–water provided the highest recoveries for all compounds tested, being the results comparables with those found by the dialysis procedure. The solvent volume employed was 33 mL, enough to cover up the whole SPMD inside the reactor. Finally, three cycles of 3 min each one and a total volume of 90 mL hexane were required for MAE [69].

Experiments carried out by using a laboratory Milestone ETHOS SEL microwave oven, which allows a better manage of the process with the accurate control of the extraction temperature, evidenced that polyhalogenated compounds PBDEs and PCNs can be extracted from SPMDs using a hexane–acetone mixture (1:1, v/v) [39]. The effects of time, volume of solvent and temperature on the yield of the extraction of PBDEs and PCNs were evaluated using a full factorial design. The optimized extraction conditions were 60 mL of solvent, a temperature of 85 °C and two extraction cycles of 1 min each one (with a total time of 5 min). Recoveries obtained varied between 72 and 91% for PBDEs and between 96 and 103% for PCNs.

Esteve-Turrillas et al. used MAE for the extraction of pyrethroid insecticides from SPMDs [43]. The maximum temperature resisted by SPMDs, depends on the solvent employed. High polarity solvents; such as acetonitrile or ethyl acetate, permit treatments at 100 °C in front of the low temperatures (till 70 °C) resisted in the presence of apolar solvents as hexane or toluene. Mixtures of toluene and hexane with acetone allow extraction temperatures of 90 °C. Treatments with high temperatures than those indicated dissolve and collapse the polyethylene membrane and do not allow the compound determination due to the high amount of plastic residues coextracted. The best recoveries were obtained for toluene with values ranging from 69 ± 3 to $113 \pm 4\%$ and for hexane:acetone with recovery data from 61 ± 8 to $103 \pm 7\%$.

6.2.4. Ultrasonic extraction

Sonication is a simple extraction technique, in which the sample is immersed in an appropriate solvent inside a vessel and placed in an ultrasound water bath. The efficiency of extraction depends on the polarity of the solvent, the homogeneity of the matrix and the sonication time.

Šetková et al. suggest the use of an ultrasound bath for the extraction of OCPs, PCBs, PBDEs and musk compounds (MCs) retained in SPMDs [31]. The sampler was lengthwise cut using sharp scissors and then extracted three times with 100 mL hexane for 20 min each. A total volume of 300 mL hexane and 1 h was needed for the extraction of each SPMD. The corresponding extract dissolves the whole amount of triolein inside the SPMD and, because of that a clean-up step based in GPC was applied by authors to remove interferent compounds. Recoveries of all the target compounds varied in the range of 89 to 103%.

6.2.5. Head-space direct determination

HS is widely applied in the analysis of volatile organic compounds such as flavour, fragrance and many POPs in both environmental and food samples. Esteve-Turrillas et al. introduced the use of HS for the direct determination of BTEX compounds from SPMDs, 10 cm long filled with 0.1 μL triolein [40]. Oven temperature and extraction time are the main parameters that affect the extraction by head space. After an optimization of these parameters, using a central composite design, a temperature of 150 °C and an extraction time of 20 min were considered as the optimum. In this study, calibration curves were prepared with spiked SPMDs.

The great advantages provided by HS in front of all considered previous extraction alternatives, include the absence of sample handling, the reduction of interferences and the possibilities of a full automation of the method. A total processing time of 20 min for each sample allows a sample throughput of 72

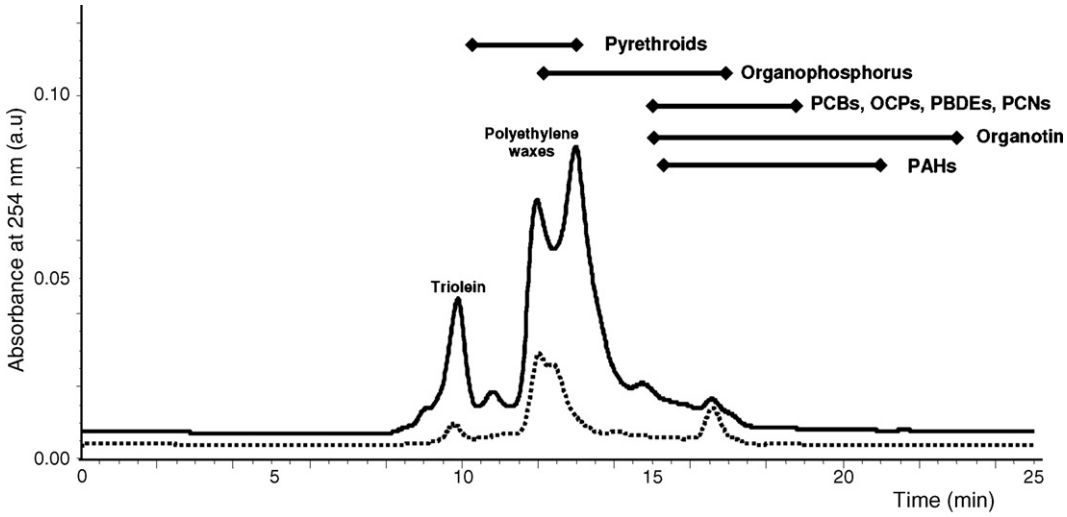


Fig. 6. GPC chromatogram elution windows (Waters Envirogel^{TM} 19 mm × 150 mm and 19 mm × 300 mm) of different families of POPs compared with these obtained for undeployed SPMD devices extracted by both, dialysis (· · · ·), two cycles with 125 mL hexane for 24 h, and MAE (—), three cycles with 33 mL hexane:water (10:1, v/v) for 3 min. Elution windows were obtained from literature data [27,39,69,72].

samples per day, being the fastest methodology developed for the determination of volatile compounds retained in SPMDs.

6.3. Clean-up of extracts

Compounds coextracted with analytes from SPMDs, are basically triolein, polyethylene oligomers and triolein impurities, as oleic acid and ethyl oleate. The main source of methyl oleate is 95% triolein that contains about 40 mg/mL of it and most is extracted by dialysis; while oleic acid source is a methyl oleate hydrolysation on the exterior side of SPMD which diffuses back [7,70]. If SPMDs are manufactured with 99% triolein instead 95%, the problems related to methyl oleate and oleic acid interferences may be prevented.

After the extraction of analytes retained in SPMDs, it is mandatory to remove the aforementioned compounds in order to avoid capillary column degradation and to reduce the background noise on the baseline. Elemental sulphur is also a potential interference, above all when bioassays are employed for toxicity evaluation. Gel permeation chromatography and adsorption columns were employed to do a correct clean-up of extracts.

6.3.1. Gel permeation chromatography

This method, sometimes referred as size exclusion chromatography (SEC), is particularly suitable for the clean-up of fatty samples, such as oil, egg or fish muscle. The different compounds injected are separated based on their size. So, when it is used for the treatment of SPMD extracts, the separation takes place principally between the big molecules as polyethylene waxes or triolein, and the small molecules of the analytes.

Most studies used S-X3 BioBeads (200–400 mesh) in a range of column sizes and solvents [31,48,71]; and currently also two Waters Envirogel^{TM} GPC columns (19 mm × 150 mm and 19 mm × 300 mm) coupled in series using dichloromethane as mobile phase [27,39,69] for the clean-up of SPMD extracts. Fig. 6 shows the elution windows for several compounds and the Envirogel GPC chromatogram of a SPMD extracted by dialysis with two cycles with 125 mL hexane for 24 h, and MAE using three cycles with 33 mL hexane:water (10:1, v/v) for 3 min.

GPC not only removes the interfering materials, but also can fractionate the analytes. Some compounds can not be separated from SPMD matrix using GPC (see Fig. 6), and because of that a clean-up based on adsorption columns must be performed. Finally, the great advantages of GPC in front conventional methodologies are that it can be fully automated and it is easily applicable to the isolation of unknown contaminants.

6.3.2. Adsorption columns

Alumina, silica and florisil columns in different mesh sizes, levels of activity and column size, either separately or in combination, have been widely used to reduce matrix interferences from different samples. There are many studies that involve the use of these adsorbents, above all in the cases where the GPC elution window of the analytes overlaps with the SPMD matrix, e.g. the use of C_{18}-alumina cartridges for the clean-up of pyrethroid insecticide residues extracted from SPMDs [43].

Chromatographic fractionations on silica gel, florisil, or alumina can separate methyl oleate from some analytes, but methyl oleate has approximately the same polarity as PAHs and some pesticides. Thus, complete separations cannot always be achieved [70].

In some cases a combination of GPC with adsorption columns were proposed, e.g. S-X3 BioBeads and florisil were employed for PCBs determination [61] and also for musk compounds determination [29].

6.4. Methods for pollutant determination

Bioassays and chromatography procedures are the main systems used for the determination of POPs retained in SPMDs.

6.4.1. Bioassays

In order to avoid instrumental methods of analysis, complex mixtures of chemicals concentrated by SPMDs can be assessed using bioindicator experiments. These methodologies are faster than instrumental methods, but do not provide information about identification and concentration of pollutants. The pre-concentrated extracts obtained from SPMDs can subsequently be combined with a variety of bioassay procedures to assess both, the level and the biological effects of water contaminants [73].

Selection of suitable bioassays is an important factor in the use of SPMDs for toxicity and genotoxicity screening of POPs. An extensive study was performed by Sabaliunas et al., using bioassays such as Microtox, Mutatox, Daphnia pulex immobilization assay and the sister chromatid exchange genotoxicity test [74]. Microtox seems to be a compatible assay with SPMDs, while the suitability of the other assays is questionable, due to insufficient sensitivity and complexity. Additionally, Gilli et al. evaluate the toxicity of drinking waters by using bioassays Microtox and Ames mutagenicity test, being also highlighted the usefulness of Microtox toxicity test [75].

Sometimes, dialyzed extracts were highly toxic in Microtox but the toxicity was significantly reduced after clean-up procedures. This toxicity is well correlated with the abundance of hydrophobic elemental sulphur, which may be reduced to sulphides in the bacterial cell, being this compound very toxic in various bioassays [74].

Chec et al. propose a procedure based on direct addition of tester bacteria cultures into SPMDs [76]. A bacterial (*Vibrio harveyi*) culture was added directly inside a deployed SPMD, which was then re-sealed and deployed. After that, SPMDs were incubated for an indicated time and then luminescence of the internal liquid was measured. The developed procedure provides more sensitive and more rapid results than those based on testing the extracts.

6.4.2. Chromatography

The extract obtained after SPMDs treatment can be analyzed by several chromatographic methodologies, depending on the type of analyte and the concentration reached. Gas chromatography (GC) separation and detection with FID or ECD has been the common method of choice for routine analysis. GC coupled to mass spectrometry (MS) is a more reliable technique for the quantization of analytes, because of its improved selectivity, good sensitivity and the availability of deuterated or ^{13}C labelled compounds. Moreover, the numerous operation modes, as negative chemical ionization (NCI), that enhances the specificity of MS, make it an extremely flexible tool for the analysis of different compounds. Thus, in some studies the concentration of OCPs in SPMDs has been determined by GC–MS–NCI [66].

Tandem mass (MS–MS) acquisition, performed by ion trap or triple quadrupole MS, allows exceptional selective determinations and lower detection limits than MS. Therefore, MS–MS has been used for the determination of several contaminants as OCPS, PCBs, PBDEs, PCNs or some pesticides retained on SPMDs [39,43,69].

The use of time of flight (TOF) detectors provides the highest sensitivity, which is really useful in the identification of unknown compounds found in SPMDs. As example, TOF-MS has been employed for the determination of high-molecular-weight PAHs in SPMDs exposed in air and water near to a chemical plant in the Czech Republic [77].

High-performance liquid chromatography (HPLC) can be also used for the quantification of different compounds from SPMDs. UV detectors rarely provides enough sensitivity and selectivity, thus more selective detectors are employed, as fluorescence (FD) or MS ones. PAHs were retained in SPMDs and determined by using HPLC-FD [69,78,79] and also using HPLC-MS [77].

7. Estimation of air/water pollutant concentrations

Data obtained for the concentration of analytes in SPMDs must be treated to establish the corresponding concentration in the media of deployment and to do it mathematical models must be assayed.

The uptake of chemicals into passive samplers is initially linear over time, then moves into a curvilinear stage, and finally can approach equilibrium (see Fig. 7). There are mathematical models for both, lineal and equilibrium behaviours. In these models it is always assumed that air/water concentrations are constant. The different compounds studied exhibit a wide range of physical and chemical properties and because of that, for a selected deployment time, the SPMD can be used as equilibrium sampler for some chemicals and as kinetic sampler for others [7].

Mathematical models used to estimate water or air concentrations from amounts found in SPMDs have been discussed by some authors [15,80]. The equilibrium partitioning is described by Eq. (1), where C_{Media} is the POP concentration in the deployed media (air or water), C_{SPMD} is the POP amount found in SPMD and $K_{SPMD/Media}$ the SPMD-media distribution factor.

$$C_{Media} = \frac{C_{SPMD}}{K_{SPMD/Media}} \quad (1)$$

The linear absorption of a POP is explained by Eq. (2), where N_{SPMD} is the POP amount found in SPMD, R_s is the sampling rate of a selected compound and t is the deployment time of

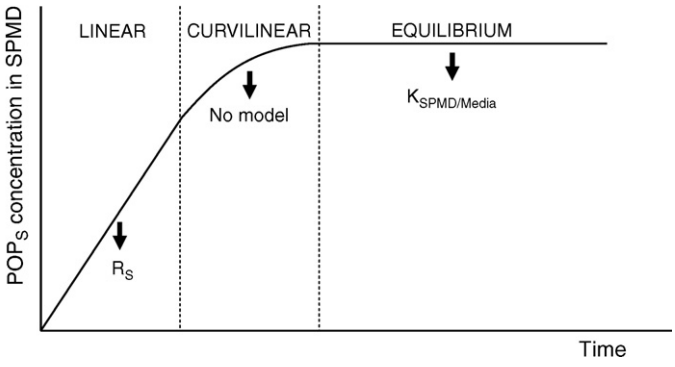


Fig. 7. Model of variation of POPs concentration in SPMDs as a function of time.

SPMD.

$$C_{\text{Media}} = \frac{N_{\text{SPMD}}}{R_S t} \quad (2)$$

Some studies calculate R_s values for the most studied POPS, such as PAHS or PCBs under different conditions, as temperature, deployment time, etc. [7].

The use of SPMDs in laboratory studies generally provides good precision between replicates. However, in real media, it is difficult to control parameters as biofouling, turbulence and temperature [81]. The uptake and release of organic contaminants are governed by the same molecular processes. So, it has been suggested that any change in the uptake rate of contaminants to SPMDs should be reflected by a change in the dissipation rate from SPMDs. Spikes of SPMDs with permeability reference compounds (PRCs), usually deuterated or ^{13}C compounds, are widely used as a quality control tool for the sampling step [82]. The function of PRCs is similar to that of internal standards and they are added to the SPMDs to correct for any changes in uptake rates as a result of unknown environmental factors.

8. Biofouling effect

The external surface of LDPE membranes submersed in water eventually become colonised by bacteria and various flora and fauna that may form a biofilm. The composition and thickness of this biofilm depend on the aquatic system and they can be very variable. Biofouling affects the resistance to mass transfer by both reasons: (i) increasing the thickness of the barrier and (ii) blocking any water-filled pores in the LDPE membranes [73]. Thus a decreasing in samples rates can be produced in devices with big amounts of biofouling.

Two methodologies have been used to quantify the biofouling effect on sampling rates [83]. The first approach involves biofouling of LDPE membrane in the field, followed by measuring the contaminant uptake rates in the laboratory by using biofouled and non-biofouled SPMDs. The second method is based on the assumption that biofouling has a similar effect on uptake and release of compounds, then PRCs were spiked into the triolein prior to exposure and differences in release rates of PCRs were related to differences in biofouling [84].

Richardson et al. used LDPE membranes previously biofouled at a clean site in coastal waters for periods of 1–4 weeks. Later, triolein was added to the SPMDs and they were exposed to a range of OCP and PAH concentrations in waters under laboratory conditions. Some unfouled devices were also exposed as control samples. Results evidenced that the uptake of contaminants by SPMDs was severely reduced until a 50% using biofouled devices in comparison to unfouled ones. Authors concluded that using PRC inside SPMDs allows a realistic evaluation of POPs concentration in aquatic environments [85].

A number of attempts have been made to reduce the biofouling colonisation of the SPMDs. Thus, Huckins et al. suggested that the addition of organic solvents and small amounts of pesticides may help to reduce biofouling [1]. Some solvent-filled membrane devices (e.g. TRIPMS) are protected from biofouling by slow release of solvent from the sampler during exposure [73]. Moreover, Luellen et al. do not observed biofouling on SPMDs that were wiped and dipped in a solution of copper sulphate and an herbicide every 2 days [20].

9. Comparison of SPMDs with standard samplers

Biomonitoring and active samplers are the standard methods used to determine short and long term exposition of air and water to toxic substances. In our opinion SPMDs are compatible with the aforementioned systems and offers complementary information.

9.1. SPMD against biomonitoring

SPMDs were designed to mimic the parts of animals that cause bioconcentration. Thus, contaminants which are less available to animals would also be less available to these samplers. SPMDs do not need to be fed, they do not eat each other or die from disease, predators, lack of oxygen in the water, or from the contaminants that we are trying to measure. So, the great advantage of SPMDs is that they can be used in almost any environment. Additionally, analyte recovery and enrichment procedures for SPMDs usually require less effort than those for tissue and sediment matrices, due to the perfect knowledge of the components of the sampler. Another advantage is that we can use samplers to back-calculate a water-borne contaminant concentration, by using mathematical models, which were usually unable to do with fish or mussel [2]. Evidently, SPMD is not a perfect model for the uptake of pollutants to fish or mussel, because organisms can depurate some contaminants and pick up contaminants through their diet.

Both mussels and SPMDs have proven to be rugged and effective in concentrating trace levels of non-polar organic contaminants from water, providing time-integrated contaminant information. SPMD takes the water-soluble fraction of pollutants, which is probably the most important route of exposure for organisms; while the residues found in mussels represent both the water-soluble and particle-bound fraction. So both techniques give important information about the bioavailability of POPs to marine organisms [86].

The blue mussel *Mytilus edulis* and the green mussel *Perna viridis* have been used for multitude of comparative uptake studies instead SPMDs (see Table 4). Several studies show that mussels are more efficient to sequester PAHs from water than SPMDs [87,91,97]. This behaviour is also observed for PCBs and OCPs compounds [92,98]. In a study carried out with blue mussels, the bioaccumulation of PBDEs was calculated as 10 times higher than for PCBs [89]. Additionally, a good correlation was found between SPMDs and mussels for the uptake of organotin compounds in a study carried out in water of the Norwegian fjord [28].

Other studies have been made employing others mussel species, and as an example *Mytilus trossulus* has been compared with SPMDs for the uptake of PAHs, being these devices more efficient to sequester small PAHs than mussels [95]. The lake mussels *Anodonta piscinalis* was also employed for the

Table 4
Published papers in recent years related to comparative studies between SPMDs and biosamplers in several environments

Biosampler	Compounds evaluated	Deployment site	SPMD deployment time (days)	References
Blue mussel (*Mytilus edulis*)	PAHs, PCBs, OCPs, Organotin, PBDEs	Fjord water (Norway); North Sea water (Netherlands); North Sea water (Norway); Aluminium reduction plant (Sweden); Dorchester and Duxbury Bays (MA, USA); Corio Bay (Australia)	28–95	[28,86–94]
Blue mussel (*Mytilus trossulus*)	PAHs	Beach sediment (Alaska, USA)	30	[95]
Green mussel (*Perna viridis*)	PAHs, OCPs	Spiked seawater; Coastal waters (Hong Kong, China)	20–30	[96–98]
Lake mussel (*Anodonta piscinalis*)	OCPs, Pesticides	Water laboratory studies; Lake water (Finland)	20	[99,100]
Mussel (*Elliptio complanata*)	Surfactants	Great Lakes (USA)	–	[26]
Brown trout (*Salmo trutta*)	PCBs	Contaminated groundwater	28	[101]
Rainbow trout (*Oncorhychus mykiss*)	PAHs, OCPs	Water laboratory studies	21–28	[102,103]
Carp (*Cyprinus carpio*)	PAHs	Water	–	[104]
Rudd, Tench, Crucian carp, Eel	Musk compounds	–	–	[29]
Fish	PAHs	–	–	[105]
Pink salmon egg	PAHs	Water	–	[16]
Pacific oyster (*Crassostrea gigas*)	PAHs	Water laboratory studies	20	[106]
Oligochaetes (*Lumbriculus variegatus*)	PAHS, PCBs	Lake Höytiäinen sediment (Finland)	–	[107]
Oligochaetes (*Lumbriculus variegatus*)	PAHs	Lake Höytiäinen sediment (Finland)	28	[108]
Pine needles	PAHs	Air (China)	90	[54]

evaluation of pesticide uptake in a laboratory study, being the uptake rates four to six times higher in SPMDs than in mussels [99].

The accumulation of pollutants in fish muscle has been also compared with SPMDs. Several fishes and shellfishes, such as trout, carp or oyster, have been studied. The rate constants for the uptake of PAHs, PCBs and OCPs by SPMDs and fishes were very similar, with Rs values for SPMDs ranging from 1 to 2.5 times those of the fish [101,102]. Pink salmon eggs were also compared for the uptake of pollutants from aqueous environments, where accumulations of PAH were highly similar to those in SPMDs [105]. In the case of oysters, the concentration factors for PAHs were, from 4 to 20 times lower than those of the same compounds in SPMDs. An exception is the case of PAH compounds with log K_{ow} greater than 5.5, where levels in oysters were higher than in SPMDs [106].

Other organisms have been employed to compare the uptake from sediments instead SPMDs, such as oligochaetes for PCBs and PAHs [107,108].

Pine needles were employed to compare the uptake of PAHs from air instead SPMD sampling [54]. Total concentrations found for these compounds were similar for both samplers, however pine needles preferably accumulate small and high volatile PAHs, while SPMD collect high molecular weight ones.

9.2. SPMD against active samplers

Persistent organic pollutants are conventionally monitored in the atmosphere using high volume air samplers, also called active samplers. These systems incorporate a pump together with a filter or a sorbent, such as polyurethane foam (PUF) or Tenax. The main drawbacks of active samplers are their expensive preparation, maintenance and operation, where power supply is often required. So, SPMDs provide clear advantages to be used for POPs determination in atmosphere.

The main disadvantages of SPMD in front of active sampling are that (i) they only sample the bioavailable fraction, not the total amount, (ii) the absorption of hydrophobic compounds by triolein is seriously reduced in waters with high levels of organic matter and the (iii) risk of theft, vandalism or possible loss of devices. The cost of SPMDs has been considered by some authors as a significant inconvenience, but this problem can be overcome by the use of alternatives to triolein filling.

Some researchers have employed both SPMDs and an active sampler on the same site, to compare the uptake behaviour of each one. Parallel studies have been carried out with PUF as active sampler of air for the uptake of several compounds as PAHs, PCBs, OCPs, PCNs [38,54,109,110], while other samplers such as XAD-2 resin for air or Tenax-TA and polyethylene tube dialysis for sediments have been used to evaluate the PAH uptake [108,111,112].

Conventional techniques for water sampling, as bailing, low-flow and bailing/filtering, have been compared with the use of SPMD for monitoring PAHs [4]. PAH concentrations in the groundwater evaluated with SPMDs were similar to values obtained by the conventional techniques. Furthermore, a high sensitivity was observed for SPMD sampling, allowing the detection of some PAHs not detected by conventional approaches.

Wastewater has been sampled both by liquid–liquid extraction with hexane and by SPMD passive devices for the determination of PCBs and OCPs [113]. The wastewater concentrations estimated from SPMDs were slightly lower than those obtained by liquid–liquid active sampling, but the sampling with SPMDs was able to evaluate the global contamination of hydrophobic compounds at trace concen-

tration. Authors remark that data obtained for both, active and passive samplers are complementary and both must be employed for the evaluation of the POP contamination of waters.

10. Future trends

Research focussed on the development and search for applications of SPMDs in sampling air and water is increasing. Future trends could be in the following areas: (i) novel pollutants, mainly non-polar compounds with low octanol–water coefficient; (ii) increasing of environmentally friendly methodologies for the extraction of pollutants retained in SPMDs, based principally in the reduction of analysis times and minimization of solvent consumption and waste generation; (iii) improvement of calibration models and sampling rates evaluation of studied compounds; (iv) comparative studies to evaluate the sampling of SPMDs in front alternative samplers; and (v) new applications of SPMDs, specially as air sampling or occupational exposure measurements.

So, it can be expected a growth of studies on SPMDs in the next years and especially concerning the development of screening methodologies for as much as possible classes of pollutants in both, water and air.

Acknowledgements

The authors acknowledge the financial support of the Ministerio de Educación y Ciencia (Project CTQ2005-05604, FEDER), Direcció General d'Investigació i Transferència Tecnològica de la Generalitat Valenciana (Project ACOMP/2007/131) and Universitat de Valencia (Convocatòria d'Accions Especials, Project UV-AE-20070213). F.A.E.T. also thanks the grant "*V Segles*" provided by the *Universitat de València* to carry out this study.

References

[1] J.N. Huckins, M.W. Tubergen, J.A. Lebo, R.W. Gale, T.R. Schwartz, J. Assoc. Off. Anal. Chem. 73 (1990) 290.
[2] A. Kot, B. Zabiegala, J. Namiesnik, Trends Anal. Chem. 19 (2000) 446.
[3] J.D. Petty, C.E. Orazio, J.N. Huckins, R.W. Gale, J.A. Lebo, J.C. Meadows, K.R. Echols, W.L. Cranor, J. Chromatogr. A 879 (2000) 83.
[4] K.E. Gustavson, J.M. Harkin, Environ. Sci. Technol. 34 (2000) 4445.
[5] Y.B. Lu, Z.J. Wang, J.N. Huckins, Aquat. Toxicol. 60 (2002) 139.
[6] F. Stuer-Lauridsen, Environ. Pollut. 136 (2005) 503.
[7] J.N. Huckins, J.D. Petty, H.F. Prest, R.C. Clark, D.A. Alvarez, C.E. Orazio, J.A. Lebo, W.L. Cranor, B.T. Jonson, A Guide For The Use Of Semipermeable Membrane Devices (SPMDs) as Samplers of Waterborne Hydrophobic Organic Contaminants, American Petroleum Institute (2002) Publication Number 4690.
[8] J.N. Huckins, J.D. Petty, K. Booij, Monitors of Organic Chemicals in the Environment Semipermeable Membrane Devices, Springer, 2006.
[9] Isi Web Of Knowledge, The Thompson Corporation, http://isiwebofknowledge.com. 2000.
[10] D.R. Luellen, D. Shea, Chemosphere 53 (2003) 705.
[11] K.D. Wenzel, B. Vrana, A. Hubert, G. Schuurmann, Anal. Chem. 76 (2004) 5503.
[12] K. Booij, H.E. Hofmans, C.V. Fischer, E.M. Van Weerlee, Environ. Sci. Technol. 37 (2003) 361.
[13] K. Booij, F. Smedes, E.M. Van Weerlee, Chemosphere 46 (2002) 1157.
[14] L. Wennrich, B. Vrana, P. Popp, W. Lorenz, J. Environ. Monit. 5 (2003) 813.
[15] M.E. Bartkow, D.W. Hawker, K.E. Kennedy, J.F. Muller, Environ. Sci. Technol. 38 (2004) 2701.
[16] M.G. Carls, L.G. Holland, J.W. Short, R.A. Heintz, S.D. Rice, Environ. Toxicol. Chem. 23 (2004) 1416.
[17] A.W. Leonard, R.V. Hyne, F. Pablo, Environ. Toxicol. Chem. 21 (2002) 2591.
[18] R.V. Hyne, M. Aistrope, Development of a passive sampler device for polar pesticides, Rural Industries Research And Development Corporation No 06/009, July 2006.
[19] R.V. Hyne, F. Pablo, M. Aistrope, A.W. Leonard, N. Ahmad, Environ. Toxicol. Chem. 23 (2004) 2090.
[20] D.R. Luellen, D. Shea, Environ. Sci. Technol. 36 (2002) 1791.
[21] K.R. Rogers, S.L. Harper, G. Robertson, Anal. Chim. Acta 543 (2005) 229.
[22] W.Y. Zhao, M. Han, S.U. Dai, J.A. Xu, Wang, Chemosphere 62 (2006) 1623.
[23] Y.P. Xu, Z.J. Wang Zj, R.H. Ke, S.U. Khan, Environ. Sci. Technol. 39 (2005) 1152.
[24] R.H. Ke, Y.P. Xu, Z.J. Wang, S.U. Khan, Environ. Sci. Technol. 40 (2006) 3906.
[25] L.B. Liao, X.M. Xiao, Chemosphere 64 (2006) 1592.
[26] E.R. Bennett, C.D. Metcalfe, Environ. Toxicol. Chem. 19 (2000) 784.
[27] N. Folsvik, E.M. Brevik, J.A. Berge, J. Environ. Monit. 2 (2000) 281.
[28] N. Folsvik, E.M. Brevik, J.A. Berge, J. Environ. Monit. 4 (2002) 280.
[29] R. Gatermann, S. Biselli, H. Huhnerfuss, G.G. Rimkus, M. Hecker, L. Karbe, Arch. Environ. Contam. Toxicol. 42 (2002) 437.
[30] R. Gatermann, S. Biselli, H. Huhnerfuss, G.G. Rimkus, S. Franke, M. Hecker, R. Kallenborn, L. Karbe, W.A. Konig, Arch. Environ. Contam. Toxicol. 42 (2002) 447.
[31] L. Setkova, J. Hajslova, P.A. Bergqvist, V. Kocourek, R. Kazda, P. Suchan, J. Chromatogr. A 1092 (2005) 170.
[32] A. Lindstrom, L.J. Buerge, T. Poiger, P.A. Bergqvist, M.D. Muller, H.R. Buser, Environ. Sci. Technol. 36 (2002) 2322.
[33] D. Sabaliunas, S.F. Webb, A. Hauk, M. Jacob, W.S. Eckhoff, Water Res. 37 (2003) 3145.
[34] M.E. Balmer, T. Poiger, C. Droz, K. Romanin, P.A. Bergqvist, M.D. Muller, H.R. Buser, Environ. Sci. Technol. 38 (2004) 390.
[35] T. Poiger, H.R. Buser, M.E. Balmer, P.A. Bergqvist, M.D. Müller, Chemosphere 55 (2004) 951.
[36] M.E. Balmer, H.R. Buser, M.D. Muller, T. Poiger, Environ. Sci. Technol. 39 (2005) 953.
[37] H. Soderstrom, J. Hajslova, V. Kocourek, B. Siegmund, A. Kocan, W. Obiedzinski, M. Tysklind, P.A. Bergqvist, Atmos. Environ. 39 (2005) 1627.
[38] M. Shoeib, T. Harner, Environ. Sci. Technol. 36 (2002) 4142.
[39] V. Yusà, A. Pastor, M. de la Guardia, Anal. Chim. Acta 565 (2006) 103.
[40] F.A. Esteve-Turrillas, A. Pastor, M. de la Guardia, Anal. Chim. Acta 593 (2007) 108.
[41] M. Shaw, J.F. Muller, Mar. Pollut. Bull. 51 (2005) 876.
[42] G.I. Scott, M.H. Fulton, E.F. Wirth, G.T. Chandler, P.B. Key, J.W. Daugomah, D. Bearden, K.W. Chung, E.D. Strozier, M. DeLorenzo, S. Sivertsen, A. Dias, M. Sanders, J.M. Macauley, L.R. Goodman, M.W. LaCroix, G.W. Thayer, J. Kucklick, J. Agric. Food Chem. 50 (2002) 4400.
[43] F.A. Esteve-Turrillas, A. Pastor, M. de la Guardia, Anal. Chim. Acta 560 (2006) 118.
[44] F.A. Esteve-Turrillas, A. Pastor, M. de la Guardia, Anal. Bioanal. Chem. 387 (2007) 2153.
[45] A.L. Rantalainen, J. Paasivirta, S. Herve, Chemosphere 36 (1998) 1415.
[46] B. Strandberg, N. Wagman, P.A. Bergqvist, P. Haglund, C. Rappe, Environ. Sci. Technol. 31 (1997) 2960.
[47] W.A. Ockenden, H.F. Prest, G.O. Thomas, A. Sweetman, K.C. Jones, Environ. Sci. Technol. 32 (1998) 1538.
[48] R. Lohmann, B.P. Corrigan, M. Howsam, K.C. Jones, W.A. Ockenden, Environ. Sci. Technol. 35 (2001) 2576.
[49] F.M. Jaward, N.J. Farrar, T. Harner, A.J. Sweetman, K.C. Jones, Environ. Sci. Technol. 38 (2004) 34.

[50] T.M. Jaward, G. Zhang, J.J. Nam, A.J. Sweetman, J.P. Obbard, Y. Kobara, K.C. Jones, Environ. Sci. Technol. 39 (2005) 8638.
[51] T. Gouin, T. Harner, P. Blanchard, D. Mackay, Environ. Sci. Technol. 39 (2005) 9115.
[52] D.T. Waite, N.R. Droneck, L. Tuduri, J.F. Sproull, D.F. Chau, D.V. Quiring, Bull. Environ. Contam. Toxicol. 74 (2005) 1011.
[53] H.S. Soderstrom, P.A. Bergqvist, Environ. Sci. Technol. 37 (2003) 47.
[54] G. Liu, G. Zhang, J. Li, X. Li, X. Peng, S. Qi, Atmos. Environ. 40 (2006) 3134.
[55] H.S. Soderstrom, P.A. Bergqvist, Environ. Sci. Technol. 38 (2004) 4828.
[56] B. Strandberg, P. Gustafson, H. Soderstrom, L. Barregard, P.A. Bergqvist, G. Sallsten, J. Environ. Monit. 8 (2006) 257.
[57] J.N. Huckins, J.D. Petty, C.E. Orazio, J.A. Lebo, R.C. Clark, V.L. Gibson, W.R. Gala, K.R. Echols, Environ. Sci. Technol. 33 (1999) 3918.
[58] A.L. Rantalainen, W. Cretney, M.G. Ikonomou, Chemosphere 40 (2000) 147.
[59] A. Cicenaite, J.N. Huckins, D.A. Alvarez, W.L. Cranor, R.W. Gale, V. Kauneliene, P.A. Bergqvist, Atmos. Environ. 41 (2007) 2844.
[60] B. Vrana, G. Schüürman, Environ. Sci. Technol. 36 (2002) 290.
[61] J.D. Petty, J.N. Huckins, J.L. Zajicek, Chemosphere 27 (1993) 1609.
[62] A.L. Rantalainen, T. Hyötyläinen, M. Saramo, I. Niskanem, Toxicol. Environ. Chem. 68 (1999) 335.
[63] K. Booij, B.L. van Drooge, Chemosphere 44 (2001) 91.
[64] Y. Wang, Z. Wang, M. Ma, Z. Mo, Chemosphere 43 (2001) 339.
[65] J. Lebo, R. Gale, J.D. Petty, D. Tillit, J.N. Huckins, J. Meadows, C. Orazio, K. Echols, D. Schroeder, Environ. Sci. Technol. 29 (1995) 2886.
[66] G.S. Ellis, J.N. Huckins, C.E. Rostad, C.J. Schmitt, J.D. Petty, P. MacCarthy, Environ. Toxicol. Chem. 14 (1995) 1875.
[67] J. Lebo, J. Zajicek, C. Orazio, J.D. Petty, J.N. Huckins, Polycycl. Aromat. Compd. 8 (1996) 53.
[68] B. Vrana, A. Paschke, P. Popp, G. Schüürman, Environ. Sci Pollut. Res. 8 (2001) 27.
[69] V. Yusà, A. Pastor, M. de la Guardia, Anal. Chim. Acta 540 (2005) 355.
[70] J.A. Lebo, F.V. Almeida, W.L. Cranor, J.D. Petty, J.N. Huckins, A. Rastall, D.A. Alvarez, B.B. Mogensen, B.T. Johnson, Chemosphere 54 (2004) 1217.
[71] J. Louch, G. Allen, C. Erickson, G. Wilson, D. Schmedding, Environ. Sci. Technol. 37 (2003) 1202.
[72] F.A. Esteve-Turrillas, A. Pastor, M. de la Guardia, Anal. Chim. Acta 553 (2005) 50.
[73] B. Vrana, G.A. Mills, L.J. Allan, E. Dominiak, K. Svensson, J. Knutsson, G. Morrison, R. Greenwood, Trends Anal. Chem. 24 (2005) 845.
[74] D. Sabaliunas, J.R. Lazutka, I. Sabaliuniene, Environ. Pollut. 109 (2000) 251.
[75] G. Gilli, T. Schilirò, C. Pignata, D. Traversi, E. Carraro, C. Baiocchi, R. Aigotti, D. Giacosa, E. Fea, Chemosphere 61 (2005) 1691.
[76] E. Chęć, B. Podgórska, G. Węgrzyn, Mutat. Res. Genet. Toxicol. Environ. 611 (2006) 17.
[77] J. Caslavsky, P. Kotlarikova, Polycycl. Aromat. Compd. 23 (2003) 327.
[78] V. Koci, T. Ocelka, M. Mlejnek, R. Grabic, Cent. Eur. J. Chem. 2 (2004) 91.
[79] K.S. Williamson, J.D. Petty, J.N. Huckins, J.A. Lebo, E.A. Kaiser, Chemosphere 49 (2002) 703.
[80] J.N. Huckins, G.K. Manuweera, J.D. Petty, D. Mackay, J.A. Lebo, Environ. Sci. Technol. 27 (1993) 2489.
[81] L. Chimuka, E. Cukrowska, R.E. Majors, LC GC Eur. 19 (2006) 402.
[82] K. Booij, H.M. Sleiderink, F. Smedes, Environ. Toxicol. Chem. 17 (1998) 1236.
[83] K. Booij, R. van Bommel, A. Mets, R. Dekker, Chemosphere 65 (2006) 2485.
[84] J.N. Huckins, J.D. Petty, J.A. Lebo, F.V. Almeida, K. Booij, D.A. Alvarez, W.L. Cranor, R.C. Clark, B.B. Mogensen, Environ. Sci. Technol. 36 (2002) 85.
[85] B.J. Richardson, P.K.S. Lam, G.J. Zheng, K.E. Mcclellan, S.B. De Luca-Abbott, Mar. Pollut. Bull. 44 (2002) 1372.
[86] T.I.R. Utvik, S. Johnsen, Environ. Sci. Technol. 33 (1999) 1963.
[87] G. Durell, T.R. Utvik, S. Johnsen, T. Frost, J. Neff, Mar. Environ. Res. 62 (2006) 194.
[88] O.A. Voie, A. Johnsen, H.K. Rossland, Chemosphere 46 (2002)1367.
[89] K. Booij, B.N. Zegers, J.P. Boon, Chemosphere 46 (2002) 683.
[90] A. Granmo, R. Ekelund, M. Berggren, E. Brorstrom-Lunden, P.A. Bergqvist, Environ. Sci. Technol. 34 (2000) 3323.
[91] J. Axelman, K. Naes, C. Naf, D. Broman, Environ. Toxicol. Chem. 18 (1999) 2454.
[92] C.S. Hofelt, D. Shea, Environ. Sci. Technol. 31 (1997) 154.
[93] C.S. Peven, A.D. Uhler, F.J. Querzoli, Environ. Toxicol. Chem. 15 (1996) 144.
[94] H.F. Prest, B.J. Richardson, L.A. Jacobson, J. Vedder, M. Martin, Mar. Pollut. Bull. 30 (1995) 543.
[95] P.D. Boehm, D.S. Page, J.S. Brown, J.M. Neff, A.E. Bence, Mar. Pollut. Bull. 50 (2005) 740.
[96] B.J. Richardson, E.S.C. Tse, S.B. De Luca-Abbott, M. Martin, P.K.S. Lam, Mar. Pollut. Bull. 51 (2005) 975.
[97] B.J. Richardson, G.J. Zheng, E.S.C. Tse, S.B. De Luca-Abbott, S.Y.M. Siu, P.K.S. Lam, Environ. Pollut. 122 (2003) 223.
[98] B.J. Richardson, G.J. Zheng, E.S.C. Tse, P.K.S. Lam, Chemosphere 45 (2001) 1201.
[99] D. Sabaliunas, J. Lazutka, I. Sabaliuniene, A. Sodergren, Environ. Toxicol. Chem. 17 (1998) 1815.
[100] S. Herve, H.F. Prest, P. Heinonen, T. Hyotylainen, J. Koistinen, J. Paasivirta, Environ. Sci. Pollut. R. 2 (1995) 24.
[101] J.C. Meadows, K.R. Echols, J.N. Huckins, F.A. Borsuk, R.F. Carline, D.E. Tillitt, Environ. Sci. Technol. 32 (1998) 1847.
[102] Y.B. Lu, Z.J. Wang, Water Res. 37 (2003) 2419.
[103] J.J. Whyte, N.A. Karrow, H.J. Boermans, D.G. Dixon, N.C. Bols, Polycycl. Aromat. Compd. 18 (2000) 71.
[104] J. Xu, P. Wang, X. Zhong, S. Dai, H. Sun, Y. Hao, Bull. Environ. Contam. Toxicol. 77 (2006) 211.
[105] T. Baussant, S. Sanni, G. Jonsson, A. Skadsheim, J.F. Borseth, Environ. Toxicol. Chem. 20 (2001) 1175.
[106] J.N. Huckins, H.F. Prest, J.D. Petty, J.A. Lebo, M.M. Hodgins, R.C. Clark, D.A. Alvarez, W.R. Gala, A. Steen, R. Gale, C.G.I. Ingersoll, Environ. Toxicol. Chem. 23 (2004) 1617.
[107] M.T. Leppanen, J.V.K. Kukkonen, Aquat. Toxicol. 49 (2000) 227.
[108] M.T. Leppanen, J.V.K. Kukkonen, Environ. Pollut. 140 (2006) 150.
[109] T. Harner, M. Shoeib, M. Diamond, G. Stern, B. Rosenberg, Environ. Sci. Technol. 38 (2004) 4474.
[110] B.L. Van Drooge, J.O. Grimalt, K. Booij, L. Camarero, J. Catalan, Atmos. Environ. 39 (2005) 5195.
[111] J.D. Macrae, K.J. Hall, Environ. Sci. Technol. 32 (1998) 3809.
[112] M.E. Bartkow, J.N. Huckins, J.F. Muller, Atmos. Environ. 38 (2004)5983.
[113] A. Katsoyiannis, C. Samara, Chemosphere 67 (2007) 1375.

Available online at www.sciencedirect.com
ScienceDirect
Talanta 74 (2008) 1020–1025
Talanta
www.elsevier.com/locate/talanta

Chemically functionalized silica gel with alizarin violet and its application for selective solid-phase extraction of lead from environmental samples

Jing Fan [a,*], Chunlai Wu [a,c], Haizhu Xu [b], Jianji Wang [a], Chuanyun Peng [a]

[a] *School of Chemistry and Environmental Science, Henan Key Laboratory for Environmental Pollution Control, Henan Normal University, Xinxiang, Henan 453007, PR China*
[b] *Henan Yubei Administrative Office of the National Natural Conservation Area for Birds and Wetland, Xinxiang, Henan 453000, PR China*
[c] *Department of Environmental and Chemical Engineering, Luoyang Institute of Science and Technology, Luoyang, Henan 471023, PR China*

Received 11 June 2007; received in revised form 7 August 2007; accepted 9 August 2007
Available online 14 August 2007

Abstract

A new material for solid-phase extraction of Pb(II) was prepared using chemically functionalized silica gel with alizarin violet. This material is stable in 6 mol L^{-1} of HCl, 6 mol L^{-1} of H_2SO_4, common organic solvents and pH 1.0–9.0 aqueous solutions. The influences of analytical parameters including pH of the aqueous solution, amount of the functionalized silica gel, stirring time and flow rates of sample solutions on the quantitative recoveries of Pb(II) were investigated. At the optimum conditions, Pb(II) can be adsorbed with almost 100.0% retention, the adsorption equilibration for Pb(II) was achieved within 15 min, and the adsorption capacity of the sorbent for Pb(II) is 3.45 mg g^{-1} of dry functionalized silica gel. For Pb(II) solution of 10 ng mL^{-1}, the pre-concentration factor is as high as 500, and the recovery is higher than 92%. The new solid-phase extractant has been used for the pre-concentration of low level of Pb(II) in water and soil samples with high recoveries. The standard reference water sample (GSBZ 50009-88(2)) was introduced for accuracy and precision of analytical data.
© 2007 Elsevier B.V. All rights reserved.

Keywords: Silica gel; Alizarin violet; Solid-phase extraction; Separation/pre-concentration; Pb(II)

1. Introduction

Lead is a harmful element for human beings and animals. It can cause body metabolize obstacle especially for nerve system. Since lead and their compounds are widely used as chemical materials in modern society, they are widespread in natural waters and soils. Because of low concentration of Pb(II) and complex matrix interferences in water and soil samples, direct determination of Pb(II) is usually insufficient, although atomic absorption spectrometry [1–3] and inductively coupled plasma atomic emission spectrometry [4–6] were often used. Therefore, a separation/pre-concentration step is required.

The traditional separation and pre-concentration methods for metal ions include liquid–liquid extraction, coprecipitation, ion exchange and others. These methods often require large amount of high purity organic solvents, some of which are harmful to health and cause environmental problems. Nowadays, several methods have been used for pretreatment of the samples solid-phase extraction (SPE) [7–12] is one of them. Its advantage [13] includes: (i) higher enrichment factors; (ii) safety with respect to hazardous samples; (iii) minimal costs due to low consumption of reagents. So, SPE has been widely used for the isolation and enrichment of target analytes, and for the clean up of samples (eliminate of matrix interferences) in pharmaceutical, clinical, environmental and food chemistry [14].

The choice of sorbent is a key point in SPE, because it can control the analytical parameters such as selectivity, affinity and capacity [15,16]. Preparation of new material for selective solid-phase extraction of analytes is an important trend of solid-phase extraction [13]. Reagents can be modified on organic or inorganic support as solid-phase extractants. Silica gel presents the advantages of no swelling, fast kinetics, mechanical, thermal and chemical stability under various conditions [17]. Therefore, it is a widely used support for various solid-phase extractants.

* Corresponding author.
E-mail address: fanjing@henannu.edu.cn (J. Fan).

0039-9140/$ – see front matter © 2007 Elsevier B.V. All rights reserved.
doi:10.1016/j.talanta.2007.08.003

Recently, some chelating reagents have been modified on silica gel as solid-phase extractants for separation/pre-concentration of some metal ions.

Safavi et al. [18] used glycerol-modified silica gel to enrich Co(II) in aqueous solutions before determination. Nadzhafova et al. [19] enriched Al(III) using silica gel modified with lumogallion before spectroscopic determination. Chang et al. [20] used Fe(III)-imprinted functionalized silica gel for solid-phase extraction of Fe(III) and Kumar et al. [21,22] used aniline formaldehyde condensate coated silica gel, separately, for pre-concentration of Cr(VI) and Cu(II) in aqueous solutions. Wu et al. [23] used polyamidoamine-modified silica gel to enrich and separate Pd(II) prior to flame atomic absorption spectrometry determination. Zougagh et al. [24] used the column packed with methylthiosalicylate-modified silica gel for pre-concentration of Pb(II) in water.

So far as we know, several sorbents have been used for solid-phase extraction of Pb(II) [11,25–28]. They are produced by immobilization of complexing or chelating reagents on different solid surface through physical loading or chemical bonding. Generally speaking, chemical bonding is more stable than physical loading. Alizarin violet is a normal chelating reagent, it can form complexing with Pb. In the present work, alizarin violet was chemically functionalized on silica gel as a new sorbent for selective solid-phase extraction of Pb(II). The utility of the new sorbent for separation and pre-concentration of low level of Pb(II) was evaluated. The results showed that the new sorbent can selectively extract Pb(II) in the presence of common coexisting metal ions. This new solid-phase extractant has been used for separation and pre-concentration of trace amount of lead from different samples.

2. Experimental

2.1. Reagents and apparatus

Analytical reagent grade chemicals were employed for preparation of all solutions. Doubly distilled water was used for the experiment. Standard solutions of 1.000 mg mL^{-1} of Cd(II), Ni(II), Co(II), Mn(II), Hg(II), Zn(II), Cu(II) and Pb(II) were prepared by dissolving the corresponding metal salts in 0.03 mol L^{-1} of nitric acid, hydrochloric acid or sulfuric acid.

The reagents used in detecting metal ions were as follows: 5.0×10^{-3} mol L^{-1} of 4-(2-pyridylazo)resorcinol (PAR); 5.0×10^{-3} mol L^{-1} of 1-(2-pyridylazo)-2-naphthol (PAN). The following buffer solutions (0.2 mol L^{-1}) were used for pH adjustment: pH 1.0–2.0 (HCl–KCl); pH 3.0–6.0 (NaAc–HAc); pH 6.0–8.0 (KH_2PO_4–Na_2HPO_4); pH 6.0–9.0 (KH_2PO_4–NaOH). 110 to 125 μm diameter particles of silica gel (Qingdao Haiyang Chemical Factory, Qingdao, China), aminopropyltriethoxysilane (Sigma Chemical Co., St. Louis, MO, USA), alizarin violet (ShangHai SSS Reagent Co. Ltd., Shanghai, China) and *N*,*N*′-dicyclohexylcarbodiimide (Shanghai Medpep Co. Ltd., Shanghai, China). A glass tube of Ø3 mm × 20 mm was washed with 6 mol L^{-1} HCl, 95% ethanol and doubly distilled water, and then used as a chromatographic column.

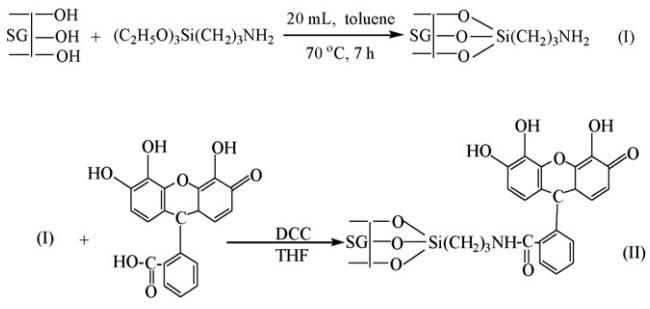
A 722 spectrophotometer (Xiamen XingSha Instrument Co. Ltd., Xiamen, China) and a WFX-120 atomic absorption spectrometer (Rayleigh Analytical Instrument Corp., Beijing, China) were used for the determination of absorbance at a given wavelength. For the spectrophotometer, the determination wavelength is 510 nm and the pH of the solution was adjusted to 10.0; for the atomic absorption spectrometer, the determination wavelength is 283.2 nm, the slit is 0.4 nm and the flow rate of air and acetylene is 6.5 and 1.5 L min^{-1}, respectively. A pHS-3C digital pH meter (Dongxing Instrument Factory, Hangzhou, China) was used for the pH measurements.

2.2. Preparation of the alizarin violet functionalized silica gel

In order to remove any adsorbed metal ions and increase the content of –OH, silica gel (SG) was activated by dipping in 6 mol L^{-1} of hydrochloric acid for 2 days, then filtered and washed repeatedly with distilled water until no detectable Cl^- can be found in the filtrate. Such treated silica gel was dried in an oven at 110 °C to remove any adsorbed water on the surface. The process for the preparation of alizarin violet functionalized silica gel was shown in Scheme 1. Step (I) was performed according to the method described in literature [29]. Ten grams of dried silica gel was mixed with 10 mL of aminopropyltriethoxysilane in anhydrous toluene incubated in a sealed flask at 70 °C, the reaction was completed within 7 h, and the product aminopropyl silica gel (APSG) was filtered, washed with acetone and dried under vacuum. The dried aminopropyl silica gel was added in a flask, then added 50 mL of tetrahydrofuran (THF) and 8.3 g of *N*,*N*′-dicyclohexylcarbodiimide and 13 g of alizarin violet, stirred at room temperature for 24 h, the resulting solid phase was filtered, washed with ethanol and water until the filtrate showed no characteristic color of alizarin violet. The solid was then dried at 80 °C for 6 h to obtain the alizarin violet functionalized silica gel. The amount of alizarin violet loaded on silica gel is got by the different amount of the alizarin violet functionalized silica gel and the aminopropyl silica gel is 0.15 g.

2.3. Batch experiments

Alizarin violet functionalized silica gel was stirred in a solution with suitable amount of metal ion for a fixed period of



Scheme 1. Preparation of alizarin violet functionalized silica gel.

time at room temperature. The supernatants were taken for the unextracted metal ions measurements by spectrophotometry. This method was used to study the effects of pH and stirring time on the retention of metal ions on the alizarin violet functionalized silica gel, and to determinate the maximum adsorption capacity of Pb(II) on the functionalized silica gel.

2.4. Column experiments

For the column experiment, alizarin violet functionalized silica gel was packed in a glass column, a solution containing metal ions was adjusted to pH 6.0 and passed through the column at a certain flow rate. Metal ion retained on the column was eluted with 0.3 mol L^{-1} of HCl at a lower flow rate and its concentration was determined by spectrophotometry or atomic absorption spectrometry.

2.5. Formulas

The adsorption capacity, extraction percentage, distribution ratio and selectivity coefficient were calculated, respectively, by the following equations:

$$Q = \frac{(C_0 - C_e)V}{W} \quad (1)$$

$$E\,(\%) = \frac{C_0 - C_e}{C_0} \times 100 \quad (2)$$

$$D = \frac{Q}{C_e} \quad (3)$$

$$\alpha_{Pb/M} = \frac{D_{Pb}}{D_M} \quad (4)$$

where Q represents the adsorption capacity (mg g^{-1}), C_0 and C_e the concentrations of metal ions before and after preconcentration (μg mL^{-1}), W the mass of the functionalized silica gel (g) V the volume of metal ion solution (L), E (%) the extraction percentage, D the distribution ratio (mL g^{-1}) and $\alpha_{Pb/M}$ denotes the selectivity coefficient of Pb(II) with respect to other common coexisting metals, indicating the selectivity factor of the functionalized silica gel.

3. Results and discussion

3.1. Analysis of the IR spectrum of the functionalized silica gel

IR absorption bands found for the silica gel at 3448, 1636 and 1081 cm^{-1} is assigned to the stretching vibration for –OH, bending vibration for –OH and absorption band for –Si–O–, respectively. The bands at 971, 807 and 472 cm^{-1} are assigned to the absorption bands for the background of the silica gel. Comparison of the IR spectrum between the silica gel and the functionalized silica gel reveals a new band at 1616 cm^{-1}, which is the bending vibration for –C–N–O.

3.2. The stability of the functionalized silica gel

0.2 g of the functionalized silica gel was added in some organic solvents (ethanol, acetone and chloroform), 6.0 mol L^{-1} of HCl, 6.0 mol L^{-1} of H_2SO_4 and aqueous solutions with pH 1.0–9.0, respectively. The systems were stirred for 30 min, and the supernatants were found to be colorless. The solid was filtered, washed with water, and then added into 20 mL of solution containing 80 μg of Pb(II). The mixture was stirred for 30 min, the Pb(II) in the supernatant was determined by spectrophotometry. The adsorption of Pb(II) is almost 100%, the functionalized silica gel is thus fairly stable in these media. Such a behavior strongly supports the fact that alizarin violet is chemically functionalized on the silica gel.

3.3. Effect of pH on the adsorption of metal ions

The pH value is one of the important factors controlling the extraction of metal ions from aqueous solutions. In order to obtain optimum extraction condition, the adsorption of metal ions on the functionalized silica gel was examined with different solutions pH by the batch mode experiments. For this purpose, 0.2 g of the functionalized silica gel was added into 20 mL of solution containing 80 μg of Pb(II) at different pHs. The mixture was stirred for 30 min, and then the unextracted metal ions in the supernatants were determined by spectrophotometry. It was found that the retention of Pb(II) varies significantly with change in the pH. At low pHs, the retention of Pb(II) is low, few of Pb(II) can be absorbed on the functionalized silica gel. With the increase of pH, the retention of Pb(II) was also increased, Pb(II) in solution can be easily absorbed on the functionalized silica gel. The possible mechanism for this is suggested below: at low pHs, few of Pb(II) can chelate with the functionalized silica gel because of the protonation of alizarin violet; with the increase of pH, the protonation of the alizarin violet functionalized silica gel become weak, which enhances the chelation and absorption of Pb(II). At pH > 6.5, the retention of Pb(II) decreased because of the hydrolyze of Pb(II). Therefore, pH 6.0 was chosen for the separation and pre-concentration of Pb(II) in the following studies.

3.4. Absorption of metal ions on the silica gel and the functionalized silica gel

In order to compare the absorption of metal ions on the silica gel and the functionalized silica gel, 0.2 g of the silica gel and the functionalized silica gel was added into 20 mL of solution containing 80 μg of metal ions at pH 6.0. The system was stirred for 30 min, and the unextracted metal ions in the supernatant were determined by spectrophotometry. From the experimental data we can know that no selective absorption of metal ions has been observed for the silica gel.

At the chosen pH, we calculated the distribution ratio and selectivity coefficient of Pb(II) by Eqs. (3) and (4) from the concentration data for single metal ions in the supernatant determined in the batch mode experiments. As can be seen from

Table 1
The distribution ratio of Pb(II) and selectivity coefficient with respect to other metal ions

	Metal ion							
	Zn(II)	Cd(II)	Ni(II)	Mn(II)	Co(II)	Cu(II)	Hg(II)	Pb(II)
D	3.06	4.43	0.41	4.19	0.86	39.1	41.8	6566.7
$\alpha_{Pb/M}$	2145.9	1482	16,016	1567.2	7635	167.9	157.0	–

Table 1, the values of distribution ratio of Pb(II) between the functionalized silica gel and water is as large as 6566.7, which is several hundreds of times higher than that for the common coexisting metals. This result indicates that the functionalized silica gel has excellent selectivity for Pb(II), and could be used to enrich Pb(II) selectively in the presence of Co(II), Cd(II), Mn(II), Hg(II), Cu(II) and Zn(II).

3.5. Effect of the amount of the functionalized silica gel

The effect of the amount of the functionalized silica gel on absorption of Pb(II) was examined by a batch mode experiment. For this purpose, 20 mL of solution containing 80 μg of Pb(II) at pH 6.0 was stirred for 30 min with different amount of the functionalized silica gel added, and then the Pb(II) concentration in the supernatants was determined by spectrophotometry. 0.2 g of the functionalized silica gel was sufficiency for 100% retention of Pb(II). Therefore, not less than 0.2 g of the functionalized silica gel was used in the following experiment.

3.6. Effect of stirring time

The stirring time taken for the adsorption of the metal ion by the functionalized silica gel and the attainment of the equilibrium conditions are of considerable importance. Effect of stirring time on the retention of Pb(II) was studied by the batch experiments. Fifteen minutes of the stirring time is necessary for the adsorption equilibrium of Pb(II). This confirmed the fact that modification of silica gel surface with organic chelate reagent results in metal ion extractants, which need only a few minutes to complete extraction processes [30]. This is one of the advantages of using silica gel support for immobilization of chelating compounds.

3.7. Adsorption capacity of Pb(II) on the functionalized silica gel

The adsorption capacity of the functionalized silica gel is an important parameter for determining how much functionalized silica gel is required to quantitatively adsorb a specific amount of metal ion from solution [22]. For investigation of the adsorption capacity of Pb(II) at pH 6.0, the same volumes of Pb(II) solutions with different concentrations was stirred with 0.5 g of the functionalized silica gel for 30 min, then the concentration of Pb(II) in solutions were determined. Concentration change in the adsorption of Pb(II) by the functionalized silica gel was measured. The adsorption capacity of Pb(II), as calculated by Eq. (1), is found to be 3.45 mg g^{-1} of dry functionalized silica gel at the optimum conditions. This is satisfactory for the trace analysis of Pb(II).

3.8. Effect of flow rate on retention of Pb(II)

In the column experiment, 0.5 g of the functionalized silica gel was conditioned with an appropriate solution and packed in a glass column, and then 20 mL of solution containing 80 μg of Pb(II) was passed through the column. The flow rate of solution is an important factor affecting the retention of Pb(II), it is necessary to choose an appropriate flow rate that ensures a higher lead uptake. Hence, the influence of flow rate on species retention was studied in the range from 0.2 to 3 mL min^{-1}. Hundred percent of Pb(II) was adsorbed by the functionalized silica gel when the flow rate is less than 2 mL min^{-1}. However, when the flow rate is up to 3 mL min^{-1}, the retention of Pb(II) is only 52.7%. It is known that when the flow rate is too fast, Pb(II) cannot be adsorbed sufficiently by the functionalized silica gel in the column. Therefore, we choose 1.5 mL min^{-1} as sample flow rate in the following experiments.

3.9. Elution curve for Pb(II)

Twenty milliliters of solution containing 20 μg of Pb(II) at pH 6.0 was passed through the column with a flow rate of 1.5 mL min^{-1}. Pb(II) retained in the column was eluted by 0.3 mol L^{-1} of HCl with a flow rate of 0.5 mL min^{-1}. Four milliliters of the eluent was collected in two aliquots, the concentration of Pb(II) in the eluent was determined and the total recovery of 100% of Pb(II) was obtained. Hence, a flow rate of 0.5 mL min^{-1} and 4.0 mL of the eluent were selected for the following studies.

3.10. The breakthrough capacity of the column

A solution containing 5 μg mL^{-1} of Pb(II) was allowed to pass through the column which packed 0.5 g of the functionalized silica gel at the optimum conditions, the sample flow rate is 1.5 mL min^{-1}, and the percentage of Pb(II) in the effluent was determined. From the variation of Pb(II) percentage in the effluents with the solution volumes passed through the column, the breakthrough volume and the volume needed to reach the saturation for the Pb(II) can be determined. It is found that the breakthrough volume of the column is generally reached after passing 10 mL of the solution containing 5 μg mL^{-1} of Pb(II). The breakthrough capacity of the functionalized silica gel column for Pb(II) was calcu-

Table 2
Effect of the common ion on the recovery of Pb(II)

Metal ion	Permit ratio	Metal ion	Permit ratio
Ca(II)	1420	K^+	2340
Al(III)	30	Mg(II)	1560
As(III)	60	V(V)	130
Co(II)	50	Ag(I)	50
Cd(II)	35	Ni(II)	50
Cu(II)	7	Hg(II)	6
Bi(III)	120	Mo(VI)	200
Sr(II)	165	Mn(II)	50
NH_4^+	350	Zn(II)	50
Cl^-	2240	Br^-	2210
F^-	1950	CO_3^{2-}	1050
SCN^-	200	SO_4^{2-}	100

lated to be 4.83×10^{-4} mmol g^{-1} of dry functionalized silica gel.

3.11. Pre-concentration and recoveries of Pb(II)

The pre-concentration and recovery of Pb(II) were performed by the column method. Solutions containing 20 μg of Pb(II) but in different volumes were made up and passed through the column. The Pb(II) retained in the column was eluted and its content was determined. It is found that the recovery of 92.7% and the pre-concentration factor of 500 were obtained even when the concentration of Pb(II) is as low as 10 ng mL^{-1}. Therefore, it is possible to enrich low level of Pb(II) from aqueous solutions by the functionalized silica gel.

3.12. Effect of common coexisting ions on the recovery of Pb(II)

To assess the possibility of analytical applications for the proposed procedure, the effects of some foreign ions, which interfere with the determination of Pb(II) and often accompany with Pb(II) in various real samples were examined under the optimum conditions. For this purpose, different amount of each ions were mixed with 20 μg of Pb(II) in 20 mL of solution at pH 6.0. These mixtures were passed through the column, then the Pb(II) retained in the column was eluted with 4 mL of HCl, and the concentration of Pb(II) in the eluent was determined. The permit ratios of ions were given in Table 2 as the relative error is less than 5%. It is clear that ions which often coexisted with Pb(II) in various real samples did not interfere with the recoveries and the determination of Pb(II). This suggests that the new solid-phase extractant has good selectivity for recovery of Pb(II).

Table 4
The results for reference standard water sample ($n = 3$)

Element	Pb(II) (μg mL^{-1})
GSBZ 50009-88(2)	
Certified value	1.20 ± 0.07
Our value	1.19

3.13. Analysis of environmental water and soil samples

Water samples used in the present work include lake water, the yellow river water, snow water and tap water in campus of Henan Normal University. The samples were filtered to eliminate the solid impurity. The Pb(II) in the water samples was determined directly by atomic absorption spectrometry. However, no Pb(II) in the waters could be detected because of the low concentration of this metal. Thus, 500 mL of each water sample was adjusted to pH 6.0 and passed through the column. Four milliliters of eluent was collected and the concentration of Pb(II) in the eluent was determined by atomic absorption spectrometry, the results were listed in Table 3 .

Soil samples used in the present work include riverbank soil and bed sullage of wastewater treatment factory. The samples was dipped in 5 mol L^{-1} of HNO_3 for 24 h, then filtrated and evaporated near to 4 mL. After 2 mL of 1.0 mol L^{-1} $HClO_4$ was added, the system was further evaporated until emitting white smog to remove HNO_3. The solution was adjusted to pH 6.0 by using 2.0 mol L^{-1} of NaOH and diluted to 100 mL with water. The reagent blank was treated in the same way. Finally, the Pb(II) in the soil samples was determined by atomic absorption spectrometry before and after column pre-concentration. The results were summarized in Table 5. The high recoveries of Pb(II) confirmed the validity of this new solid-phase extractant. It is also noted from Table 5 that even the samples have complex matrix, Pb(II) is still enriched and separated selectively by the functionalized silica gel.

Standard solution of Pb(II) (GSBZ 50009-88(2)) was analyzed by the column method. Twenty milliliters of the standard solution was adjusted to pH 6.0 and passed through the column. Four milliliters of eluent was collected and the concentration of Pb(II) in the eluent was determined by atomic absorption spectrometry, the result was listed in Table 4. From that we can know, the result has good agreement to the standard date, this confirmed the utility of the functionalized silica gel column.

3.14. The regenerability of the functionalized silica gel

The self made chromatographic column can be reused for 50 times and the recovery of Pb(II) is higher than 95%. The

Table 3
The determination of Pb(II) before and after column pre-concentration by the atomic absorption spectrometry ($n = 3$)

Sample	Lake water	River water	Snow water	Tap water	Riverbank soil	Bed sullage
Before column pre-concentration	–	–	–	–	–	29.6 μg g^{-1}
After column pre-concentration	21 ng mL^{-1}	32 ng mL^{-1}	–	–	–	29.5 μg g^{-1}
Added (ng)	100	100	100	100	100	100
Recovery	99.4	99.6	100	100	100.3	101.2

Table 5
Comparison of the alizarin violet functionalized silica gel with other reported sorbents for Pb(II) absorption

Solid-phase extractant	Capacity ($mg\,g^{-1}$)	Pre-concentration factor	Equilibrating time (min)	Metal ions investigate	Reference
Dowex Optipore V-493	8.6	50	–	Cu(II), Mn(II), Cr(III), Ni(II)	[7]
Aminothioamidoanthraquinone modified silica gel	116	–	5	Cu(II), Ni(II), Co(II), Cd(II)	[25]
Thioureasulfonamide resin		60	30	Cd(II)	[26]
4-(4-Methoxybenzylidenimine) thiophenole modified alumina	0.27	240	–	Co(II), Ni(II), Zn(II), Cd(II)	[31]
Ambersorb-572	35.2	75	–	Mn(II), Co(II), Fe(III), Al(III)	[32]
Alizarin violet functionalized silica gel	3.45	500	15	Cd(II), Ni(II), Co(II), Mn(II), Zn(II), Cu(II)	This work

experimental can still be reproduced after the functionalized silica gel is kept in a desiccator for 5 months, demonstrating the regenerability and stability of the functionalized silica gel.

3.15. Comparison with alternative sorbents

Table 5 shows the adsorption of Pb(II) by other sorbents reported in the literature. It is clear that although these sorbents can be used for the effective adsorption of Pb(II), there is a scope for further improvement. The functionalized silica gel described in this work showed high pre-concentration factor, good regenerability and high selectivity.

4. Conclusions

A new material for solid-phase extraction of Pb(II), alizarin violet functionalized silica gel has been prepared and properly characterized. This solid-phase extractant has the following advantages: (i) it can be used for selective separation and pre-concentration of Pb(II) in the presence of common coexisting metal ions; (ii) it can be used to eliminate the interference of complex matrix; (iii) the separation/pre-concentration produced is simple, rapid and low cost; (iv) it has high pre-concentration factor and can be reused for many times.

Acknowledgements

The work was supported financially by the Science and Technology Department of Henan Province (no. 072102320007) and Henan Key Laboratory for Environmental Pollution Control.

References

[1] A.F. Barbosa, M.G. Segatelli, A.C. Pereira, A.S. Santos, L.T. Kubota, P.O. Luccas, C.R. Tarley, Talanta 71 (2007) 1512.
[2] S.Q. Memon, S.M. Hasany, M.I. Bhanger, M.Y. Khuhawar, J. Colloid Interf. Sci. 291 (2005) 84.
[3] M.N. Amin, S. Kaneco, Y. Nakano, Microchem. J. 86 (2007) 89.
[4] Y.Y. Xu, J.F. Zhou, G.X. Wang, J.F. Zhou, G.H. Tao, Anal. Chim. Acta 584 (2007) 204.
[5] F. Zheng, B. Hu, Talanta 72 (2007) 372.
[6] L. Hakim, A. Sabarudin, M. Oshima, S. Motomizu, Anal. Chim. Acta 588 (2007) 73.
[7] E. Melek, M. Tuzen, M. Soylak, Anal. Chim. Acta 578 (2006) 213.
[8] M.M. Ariffin, E.I. Miller, P.A. Cormack, R.A. Anderson, Anal. Chem. 79 (2007) 256.
[9] C. Isaacson, T.K. Mohr, J.A. Field, Environ. Sci. Technol. 40 (2006) 7305.
[10] G.P. Rao, K. Seshaiah, Y.K. Rao, M.C. Wang, J. Agric. Food. Chem. 54 (2006) 2868.
[11] Z. Wan, Z.R. Xu, J.H. Wang, Analyst 131 (2006) 141.
[12] J. Fang, Y. Jiang, X.P. Yan, Z.M. Ni, Environ. Sci. Technol. 39 (2005) 288.
[13] C.F. Poole, Trends Anal. Chem. 22 (2003) 362.
[14] J. Haginaka, Trends Anal. Chem. 24 (2005) 407.
[15] J.R. Dean, Extraction Methods for Environmental Analysis, Wiley, New York, USA, 1998, 40pp.
[16] N. Masqué, R.M. Marcé, F. Borrull, Trends Anal. Chem. 17 (1998) 384.
[17] P.K. Jal, S. Patel, B.K. Mishra, Talanta 62 (2004) 1005.
[18] A. Safavi, N. Iranpoor, N. Saghir, S. Momeni, Anal. Chim. Acta 569 (2006) 139.
[19] O.Y. Nadzhafova, O.A. Zaporozhets, I.V. Rachinsk, Talanta 67 (2005) 767.
[20] X.J. Chang, N. Jiang, H. Zheng, Q. He, Z. Hu, Y.H. Zhai, Y.M. Cui, Talanta 71 (2007) 38.
[21] P.A. Kumar, M. Rayb, S. Chakraborty, J. Hazard. Mater. 143 (2007) 24.
[22] G.P. Kumar, P.A. Kumar, S. Chakraborty, M. Ray, Sep. Purif. Technol. 57 (2007) 47.
[23] X.Z. Wu, P. Liu, Q.S. Pu, Q.Y. Sun, Z.X. Su, Talanta 62 (2004) 918.
[24] M. Zougagh, A.G. Torres, E.V. Alonso, J.M. Pavón, Talanta 62 (2004) 503.
[25] W. Ngeontae, W. Aeungmaitrepirom, T. Tuntulani, Talanta 71 (2007) 1075.
[26] B.F. Senkal, M. Incei, E. Yavuz, M. Yaman, Talanta 72 (2007) 962.
[27] J.H. Wang, E.H. Hansen, J. Anal. At. Spectrom. 17 (2002) 1278.
[28] Y. Wang, M.L. Chen, J.H. Wang, Appl. Spectrosc. Rev. 42 (2007) 103.
[29] M.M. Hassanien, K.S. Sherbini, Talanta 68 (2006) 1550.
[30] M.A. Akl, I.M. Kenawy, R.R. Lasheen, Microchem. J. 78 (2004) 143.
[31] M. Ghaedi, M. Montazerozohor, M. Soylak, J. Hazard. Mater. 142 (2007) 368.
[32] S. Baytak, A.R. Türker, J. Hazard. Mater. 129 (2006) 130.

Available online at www.sciencedirect.com
ScienceDirect
Talanta 74 (2008) 896–902
Talanta
www.elsevier.com/locate/talanta

Determination of pharmacologically active compounds in root extracts of *Cassia alata* L. by use of high performance liquid chromatography

Vivian E. Fernand [a], David T. Dinh [b], Samuel J. Washington [a], Sayo O. Fakayode [c], Jack N. Losso [d], Rick O. van Ravenswaay [e], Isiah M. Warner [a,*]

[a] *Department of Chemistry, Louisiana State University, Baton Rouge, LA 70803, USA*
[b] *College of Basic Sciences, Louisiana State University, Baton Rouge, LA 70803, USA*
[c] *Department of Chemistry, Winston-Salem State University, Winston-Salem, NC 27110, USA*
[d] *Department of Food Science, Louisiana State University, Baton Rouge, LA 70803, USA*
[e] *Center for Agricultural Research in Suriname, University of Suriname, Suriname*

Received 8 June 2007; received in revised form 23 July 2007; accepted 24 July 2007
Available online 8 August 2007

Abstract

A simple high performance liquid chromatography (HPLC) method was developed and validated for the determination of six phenolic compounds, five anthraquinones (rhein, aloe-emodin, emodin, chrysophanol and physcion) and a flavonoid (kaempferol), in root extracts from *Cassia alata* L. Solid-phase extraction, using C_{18} cartridges, was used to remove interfering substances from the root extracts. The extracts were analyzed on a C_{18} column using an isocratic mobile phase which consisted of acetonitrile, methanol, and 10 mM aqueous ammonium acetate (25:55:20, v/v). Identification of the analytes was performed by use of standards and on-line mass spectrometric detection using atmospheric pressure chemical ionization. The concentration of the phenolic compounds in the root extracts was determined using HPLC with ultraviolet detection at 260 nm. The limits of detection obtained for the anlytes were in the range of 0.23–4.61 ppm. The overall R.S.D. precision values (intra- and inter-day) for the retention times and peak-areas were lower than 0.16 and 2.10%, respectively. In addition, the recovery of the developed method for the analysis of these phenolic compounds was determined, and ranged from 81.2 ± 4.3 to $106 \pm 2\%$.
© 2007 Elsevier B.V. All rights reserved.

Keywords: Anthraquinones; Kaempferol; Phenolic compounds; LC–MS; Solid-phase extraction; Recovery

1. Introduction

Ringworm cassia or golden candle (*Cassia alata* Linn, Leguminosae), a wild-growing shrub often cultivated as an ornamental plant, is indigenous to South America, but now widely distributed in the tropics [1–5]. This worldwide important herbal medicine has been recognized for centuries in traditional medicine for its role as a laxative as well as in the treatment of a variety of skin and respiratory diseases [1,2,5–7]. In Suriname, root extracts from *C. alata* are used for the treatment of uterus disorders [1]. Pharmacological investigations performed so far on *C. alata* have shown that this herb has several biological activities, such as antimicrobial [8,9], antifungal [2,10,11], purgative [4], anti-inflammatory [11,12], analgesic [1,11,13], antitumor [14], and hypoglycemic [11] activities.

C. alata is one of the most important species of the genus *Cassia* which is rich in anthraquinones and polyphenols [13,15]. The leaves of *C. alata* have been qualitatively analyzed for the presence of primarily five pharmacologically active anthraquinones: rhein, aloe-emodin, chrysophanol, emodin, and physcion [16], as well as the flavonoid kaempferol [17]. Rhein and chrysophanol are known to be present in the roots [2], in addition to two other quinone pigments [18]. These anthraquinone derivatives are well known to exhibit a variety of biological activities [19], such as antimicrobial [2], antifungal [20], antitumor [21], antioxidant [22], cytotoxic [23], and hypoglycemic [24] activities. The flavonoid kaempferol has been reported to have anticancer properties [25,26]. It is clear that there is a correlation between

* Corresponding author. Tel.: +1 225 578 3945; fax: +1 225 578 3971.
E-mail address: iwarner@lsu.edu (I.M. Warner).

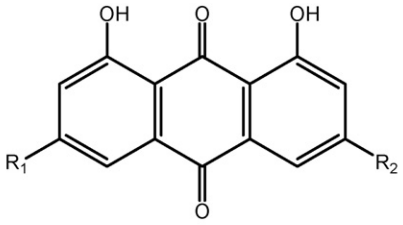
0039-9140/$ – see front matter © 2007 Elsevier B.V. All rights reserved.
doi:10.1016/j.talanta.2007.07.033

the ethno-pharmacological properties ascribed to this herbal medicine and the biological activities of these phenolic compounds. Therefore, it is of great importance to determine the amount of these bioactive constituents in *C. alata*. However, to our knowledge there are no reports in the literature on the determination of these phenolic compounds in the roots of *C. alata*. This leads to the necessity of developing an analytical method for the simultaneous analysis and identification of these bioactive compounds in the roots of *C. alata*.

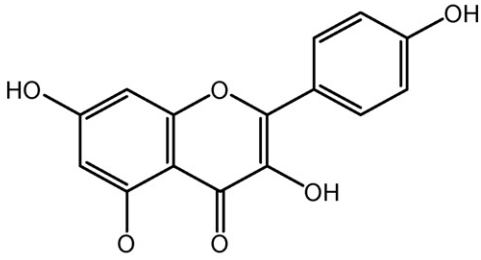
Previously, *C. alata* extracts were analyzed for the presence of kaempferol-3-*O*-gentiobioside in various parts of the plant (leaves, flowers, rachis, stem and seed) using high performance liquid chromatography (HPLC) [27]. Several analytical methods such as thin-layer chromatography [28], micellar electrokinetic capillary chromatography [29], capillary zone electrophoresis [30], capillary electrophoresis–mass spectrometry (CE–MS) [31], gas chromatography [32], and gas chromatography–mass spectrometry (GC–MS) [33] have been used for the determination of anthraquinones in various medicinal plants and natural products. In addition, analytical methods involving the use of HPLC [32–36] and liquid chromatography–mass spectrometry (LC–MS) [37–40] have also been used for anthraquinone analysis in several natural products.

Although CE, GC, and HPLC methods can afford sufficient sensitivity for the analysis of anthraquinones in natural products, they all lack accurate peak identification in comparison with CE–MS, GC–MS, and LC–MS methods. Generally, the use of LC–MS is advantageous over the use of CE–MS and GC–MS because it affords high separation efficiency and accurate identification of analytes over a wide range of molecular structures, chemical reactivities, polarities, and volatilities. Hence, separation of analytes as well as mass identification and confirmation of analytes can be achieved simultaneously in one experimental run using LC–MS. For example, LC–MS using electrospray ionization (ESI) [37,38] and atmospheric pressure chemical ionization (APCI) [39,40] has been used for accurate identification of anthraquinones in plant extracts. In comparison with APCI-MS detection, the use of ESI-MS detection for anthraquinone identification is less effective, because the latter requires mobile phase additives other than the buffer to enhance analyte ionization [37,38]. Moreover, aside from eluent additives, the efficiency of the mass detection of anthraquinones using an ESI interface depends on the pK_a value of the analyte [38].

The aim of this study was to develop an HPLC-UV detection method for quantitative analysis of rhein (**1**), kaempferol (**2**), aloe-emodin (**3**), emodin (**4**), chrysophanol (**5**), and physcion (**6**) in root extracts of *C. alata*. The structures of these analytes are shown in Fig. 1. The root extracts were purified by use of solid-phase extraction and separation of the phenolic compounds was performed by use of reversed-phase HPLC using isocratic elution. In addition, on-line mass spectrometric detection using an APCI probe in the negative ionization mode was used to confirm the presence of these phenolics in the root extract. To the best of our knowledge, this study represents the first investigation of the simultaneous analysis and identification of these six phenolic compounds in root extracts of *C. alata* using LC-UV–APCI-MS.



Compound	R_1	R_2	MW
Rhein (**1**)	H	COOH	284
Aloe-emodin (**3**)	H	CH_2OH	270
Emodin (**4**)	OH	CH_3	270
Chrysophanol (**5**)	H	CH_3	254
Physcion (**6**)	OCH_3	CH_3	284



Kaempferol (**2**), MW= 286

Fig. 1. Chemical structures of six phenolic compounds in *C. alata* root extract.

2. Experimental

2.1. Chemicals and materials

Rhein, kaempferol, aloe-emodin, emodin, and chrysophanol standards were purchased from Sigma–Aldrich (St. Louis, MO, USA), while the physcion standard was purchased from Micro Source Discovery System (Gaylordsville, CT, USA). Ammonium acetate (NH_4Ac) buffer was purchased from Fluka (Amsterdam, the Netherlands). HPLC grade acetonitrile, ethanol, methanol, water, and Whatman no. 1 filter paper were obtained from Fisher Scientific (Houston, TX, USA). Doubly distilled deionized water, used throughout the study, was obtained by use of an Elga Genetic Ultra-Pure water polishing system from US Filter (Lowell, MA, USA). Maxi-clean RP solid-phase extraction (SPE) C_{18} cartridges and 0.45 μm filters were purchased from Altech (Deerfield, IL, USA). *C. alata* root samples were collected by the Center of Agricultural Research in Suriname, and identified at the National Herbarium of the University of Suriname, Paramaribo, Suriname (Reference number: Jansen Jacobs 5027).

2.2. Preparation of standard solutions

Standard stock solutions of compounds **2**–**6** were prepared in ethanol at a concentration of 0.5 mg/mL, while rhein (**1**) was prepared at 0.25 mg/mL. Standard mixture solutions were prepared in ethanol at various concentration levels in the range of 5–250 ppm. All solutions were filtered prior to analysis through a 0.45 μm syringe filter and injected four times into the HPLC. The calibration curve for each compound was constructed by plotting the peak area as a function of the standard analyte concentration.

2.3. Sample preparation

The *C. alata* root samples were oven dried at 40 °C for 5 days. The dried roots were ground by use of a Wiley Mill grinder (Standard Model No. 3) to particle sizes of 6 mm or smaller. Ten grams of ground roots were extracted with 100 mL ethanol on an orbital shaker for 12 h at room temperature. The extraction procedure was repeated two times, after which the two extracts were combined and filtered using Whatman no. 1 filter paper. The extraction solvent was removed by use of rotary evaporation and the residue was reconstituted in 10 mL ethanol and diluted with water (1:1, v/v).

Solid-phase extraction (SPE) was used to remove unwanted interfering phytochemicals from the root extract. The SPE procedure was performed on an Altech extraction manifold system. SPE C_{18} cartridges (4 mL; 600 mg) were first conditioned with 4 mL methanol, followed with 4 mL water. Following the conditioning step, 4 mL of the diluted root extract was loaded onto the cartridge. After sample loading, the interfering compounds were removed with 2 mL of 10% aqueous ethanol. Finally, the fraction containing compounds **1**–**6** were eluted with 2 mL of hot ethanol (60 °C). The vacuum pressure was kept at 10 mmHg during the pre-conditioning step and was held constant at 2 mmHg during the loading and eluting steps. Four replicate SPE extracts were collected. Each eluate was diluted to 5 mL with ethanol. The diluted SPE root extract, the eluate, was then filtered through a 0.45 μm syringe filter and injected into the HPLC. Each diluted SPE root extract was injected into the HPLC five times, and the average peak area was reported and used for analyte quantification.

2.4. HPLC analysis

Separation and quantitative analyses of compounds **1**–**6** were performed on a Shimadzu HPLC system (Kyoto, Japan) consisting of an SCL-10A system controller, two LC-10AD pumps, a DGU-14A degasser, a SIL-10AD auto injector and an SPD-10AV UV-VIS detector (λ = 260 nm). Separation of the analytes was performed at 40 °C on a Phenomenex Luna C_{18} (2) column, 100 Å pore size, 5 μm particle size, 250 × 4.6 mm i.d. column containing a guard column (Phenomenex, Torrance, CA, USA). The analytes were eluted isocratically at a flow rate of 0.4 mL/min using an acetonitrile/methanol/buffer (25:55:20, v/v), where the buffer is 10 mM ammonium acetate (NH_4Ac) at pH 6.8. The injection volume was 10 μL.

2.5. LC–APCI-MS analysis

Analyte identification was performed by use of a Shimadzu LCMS-2010 system (Kyoto, Japan). Operating conditions for the HPLC were as described in the previous section. The mass spectrometer used for the identification of the analytes consists of a Q-array-octapole-quadrupole mass analyzer with an APCI interface used in the negative ionization mode and coupled to the Phenomenex Luna C_{18} (2) column described above. The APCI probe was operated at a temperature of 400 °C, while the CDL and block temperatures were operated at 200 °C. The detector voltage was 1.5 kV and the probe was operated in the negative ionization mode with a voltage of −4.0 kV. The nebulizing gas was nitrogen at a flow rate of 2.5 L/min. The optimum operating conditions for the LC–APCI-MS were determined for the separation and identification of compounds **1**–**6** in the scan mode with minimum fragmentation of the analytes. The scan rate of the mass analyzer was at 1 s/scan within the mass range of *m*/*z* 100–1000.

2.6. Method validation

Precision (reproducibility) of the method was obtained by calculating the relative standard deviation (R.S.D.) from repeated injections of the standard mixture solutions at 15, 45, and 75 ppm for all analytes, except for kaempferol (**2**) that was determined at 30, 90, and 150 ppm. The intra-day precision was determined by six replicate injections, while the inter-day precision was determined by six injections for 6 days, for both the retention times and peak-areas [41].

A recovery study was performed to validate the accuracy of the developed method. Hence, root samples (10 g) were spiked with standard stock solutions of the analytes in triplicate at two different concentrations. The spiked root samples were extracted with 100 mL ethanol following the procedure for sample preparation as described in Section 2.3. Finally, the spiked samples were analyzed using the same experimental and instrumental conditions as previously described for the analysis of the unspiked roots. The recovery was determined by comparing the amount of analyte added to the root sample and the amount of analyte detected during HPLC analysis [42].

3. Results and discussion

3.1. HPLC optimization

Several preliminary studies were conducted to develop an HPLC method for the separation of compounds **1**–**6** in the *C. alata* root extract. The LC separation conditions of the analytes were optimized by systematically adjusting the methanol and acetonitrile content in the mobile phase with the addition of different buffers, such as trifluoroacetic acid, formic acid, and ammonium acetate to obtain better resolution of the phenolic compounds. The retention times of the analytes decreased with an increase in the amount of methanol in the eluent. This observation was in agreement with a previous report by Ding et al. [35]. An increase in the amount of acetonitrile in the eluent also

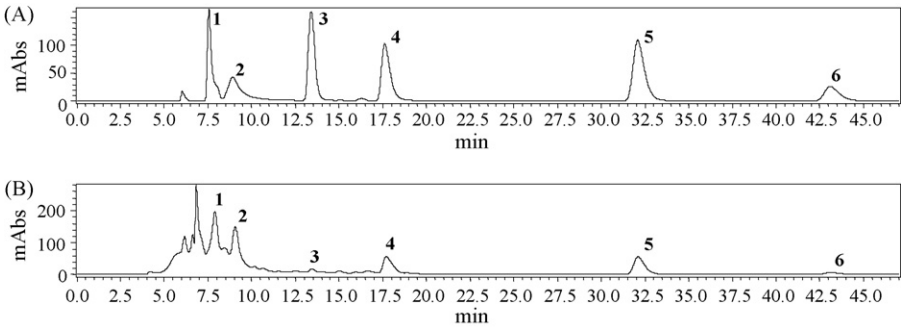


Fig. 2. (A) HPLC chromatogram of the phenolic standard mixture (30 ppm), λ = 260 nm. Rhein (**1**, 7.57 min); kaempferol (**2**, 8.92 min); aloe-emodin (**3**, 13.41 min); emodin (**4**, 17.63 min); chrysophanol (**5**, 32.06 min); physcion (**6**, 43.07 min). (B) HPLC chromatogram of *C. alata* root extract, λ = 260 nm. Rhein (**1**, 7.91 min); kaempferol (**2**, 9.05 min); aloe-emodin (**3**, 13.43 min); emodin (**4**, 17.69 min); chrysophanol (**5**, 32.04 min); physcion (**6**, 43.01 min).

resulted in a decrease in retention time of compounds **1**–**6**. The addition of 10 mM NH_4Ac buffer to the mobile phase resulted in the best peak resolution of compounds **1**–**6**. Addition of NH_4Ac buffer to the mobile phase not only improved the resolution, but also resulted in complete deprotonation of compounds **1**–**6** $[M-H]^-$.

The pH of the mobile phase was also optimized to obtain better resolution of compounds **1**–**6**. Separation at pH 4.8 using NH_4Ac buffer resulted in co-elution of rhein (**1**) and kaempferol (**2**). Therefore, resolution of only compounds **3**–**6** could be obtained. At pH 8.8 (adjusted with NH_4OH) compounds **1**–**3** co-eluted. Complete separation of compounds **1**–**6** were only achieved at pH 6.8 using NH_4Ac buffer. The flow rate of the eluent was also optimized at 0.4 mL/min for best resolution and MS detection. The use of flow rates greater than 0.4 mL/min resulted in overloading of the mass spectrometer detector.

Optimal separation of the analytes was obtained within 45 min for standard mixtures as well as the *C. alata* root extract by use of an isocratic mobile phase of ACN/MeOH/NH_4Ac buffer at pH 6.8 (25:55:20, v/v). We optimized the retention times of the analytes using a gradient elution system containing ACN/MeOH/NH_4Ac buffer at pH 6.8 (25:55:20, v/v) for solvent A and ACN/MeOH/NH_4Ac buffer at pH 6.8 (25:65:10, v/v) for solvent B, allowing successful separation of all analytes within 30.0 min. However, we did not use the gradient elution system for quantification of the analytes because it was not reproducible.

The phenolic compounds **1**–**6** were identified in the *C. alata* root extract by spiking the extracts with the respective standards. Prior to this procedure, all standards were run separately to determine the retention time of each analyte. The chromatographic separation of compounds **1**–**6** is shown in Fig. 2A for the standard mixture at 30 ppm as an example, and in Fig. 2B for the root extract (without spiking). In addition to the analyte peaks obtained in Fig. 2B, an unidentified first eluting peak (at 6.83 min) was also observed. We have isolated this unknown using flash column chromatography, followed by purification using preparative HPLC. However, after performing spectroscopic studies (UV, IR, MS, and NMR), we concluded that this unknown peak is an impurity composed of a mixture of compounds. No further analysis of this peak was attempted.

3.2. LC–MS analysis

Simultaneous separation and identification of phenolic compounds **1**–**6** in the *C. alata* root extracts were performed by use of LC–APCI-MS detection. Identification of the peaks was achieved by comparison of the retention times, UV spectra, as well as MS data of the separated compounds with the respective standards. The total ion chromatograms (TIC) of analytes **1**–**6** in the standard mixture and root extract were recorded in the scan mode, and are shown in Fig. 3A and B, respectively. As seen in Fig. 3B, the peak intensities for aloe-emodin (**3**) and physcion (**6**) are very low, as a result of their low concentration ('vide infra') in the root extract as determined by HPLC in this study.

The mass spectra of the phenolic compounds **1**–**6** in the root extract are presented in Fig. 4. The presence of each analyte in the root extract was confirmed by its respective $[M-H]^-$ *m*/*z*. In addition to the ions at $[M-H]^-$ of compounds **1**–**6**, the

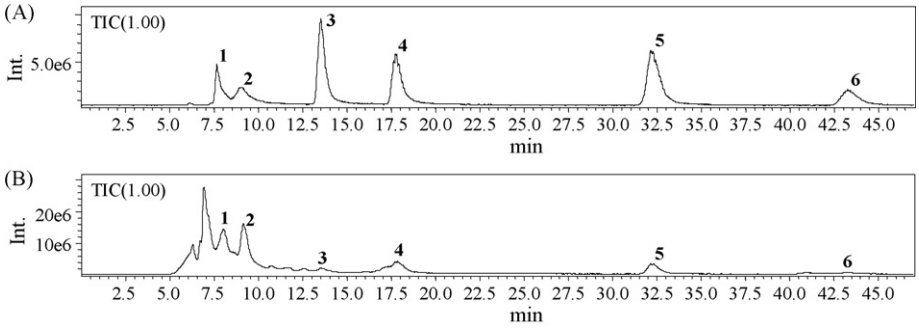


Fig. 3. Total ion chromatograms of (A) standard mixture (30 ppm); (B) *C. alata* root extract.

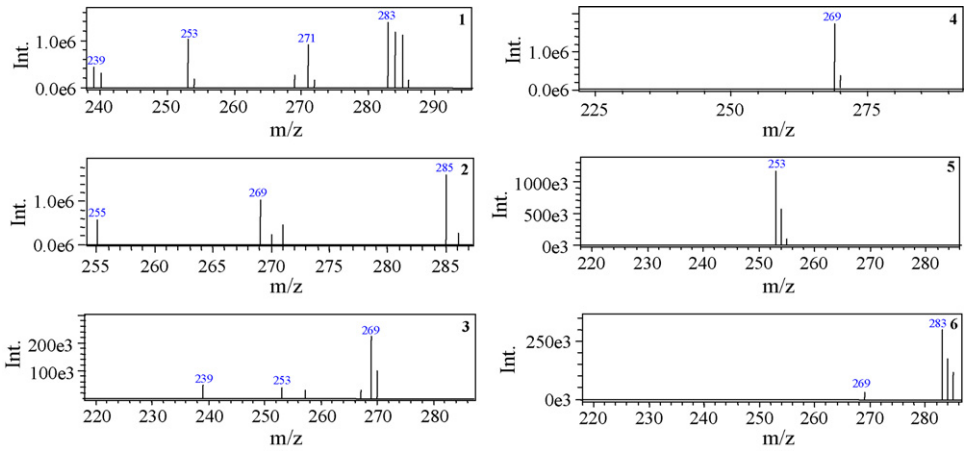


Fig. 4. Mass spectra of rhein (**1**); kaempferol (**2**); aloe-emodin (**3**); emodin (**4**); chrysophanol (**5**); physcion (**6**) from the *C. alata* root extract.

ion at *m/z* 239 was registered in the mass spectrum of rhein (**1**) and aloe-emodin (**3**) due to fragmentation of molecular ions of the analyte resulting in $[M-COOH]^-$ and $[M-CH_2OH]^-$, respectively. The ions at *m/z* 253 and 271 were also recorded in the mass spectrum of rhein (**1**) which are assumed to be a fragment derived from the molecular ion resulting in $[M-CH_2OH]^-$ and an adduct formation between the ion at *m/z* 239 and methanol ($[M-COOH+MeOH]^-$), respectively. The ion at *m/z* 253 obtained in the mass spectrum of aloe-emodin (**3**) was due to the loss of a hydroxyl group, resulting in $[M-OH]^-$. The ions at *m/z* 255 and 269 observed in the mass spectrum of kaempferol (**2**) are possibly due to fragmentation of the molecular ion resulting in $[M-CH_2OH]^-$ and $[M-OH]^-$, respectively. Finally, the ion at *m/z* 269 recorded in the mass spectrum of physcion (**6**) is due to the loss of a methyl group leading to $[M-CH_3]^-$.

3.3. Calibration curves

In this study, as well as in previous reports [38,39], the analysis of anthraquinones using on-line mass spectrometric detection was found to be less sensitive than on-line UV detection. Therefore, HPLC-UV was chosen for the determination of compounds **1**–**6**. The investigated compounds in the root extract were quantified by integration of the peak-areas at 260 nm using an external calibration method.

Calibration curves were constructed for each analyte by using a series of standard mixture solutions. Least-squares linear regression was used to determine the calibration parameters for each of the six standards. A summary of the calibration studies for the six analytes is presented in Table 1. The linearity of all calibration curves was determined by calculating the correlation coefficients, which varied from 0.9971 for kaempferol to 0.9999 for emodin and physcion.

The limit of detection (LOD), defined as the lowest detectable concentration of an analyte, was calculated using the formula $LOD = (b + 3\sigma_b)/a$, where a is the slope of the calibration curve; b is the intercept; and σ_b is the standard deviation associated with the intercept. The LOD for the analytes were in the range of 0.23–4.61 ppm. In addition, the limit of quantification (LOQ), defined as the lowest measurable analyte concentration was determined according to the formula $LOQ = (b + 10\sigma_b)/a$, where all parameters are as defined for the LOD. The LOQ is reported in Table 1 as the lower limit from the linear range.

3.4. Method validation and quantification

The method was validated by determining the intra- and inter-day precision. The relative standard deviation (R.S.D.) values for the retention times and peak-areas for the intra-day precision were 0.07–0.15 and 0.27–1.63% ($n = 6$), respectively. The R.S.D. values obtained for the inter-day precision study for the retention times and peak-areas were 0.07–0.16% and 0.39–2.10 ($n = 6$), respectively (Table 2).

In order to determine the accuracy of the method, the mean recovery of the phenolic compounds **1**–**6** was calculated at two concentration levels as reported in Table 3 for each analyte. The overall mean recovery ranged between $81.2 \pm 4.3\%$ for aloe-emodin and $106 \pm 2\%$ for emodin ($n = 3$).

Table 1
Calibration parameters of HPLC analysis for phenolic compounds **1**–**6**

Compound	*a*	*b*	*r*	Linear range (ppm)	LOD (ppm)
Rhein (**1**)	145,321	69934	0.9985	13.1–115	4.61
Kaempferol (**2**)	60,862	−26171	0.9971	5.27–230	0.98
Aloe-emodin (**3**)	160,496	−43698	0.9998	3.06–145	0.54
Emodin (**4**)	98,680	−29660	0.9999	2.18–115	0.23
Chrysophanol (**5**)	170,751	46224	0.9998	6.04–115	2.19
Physcion (**6**)	142,579	−43473	0.9999	3.26–105	0.55

Note: The relationship between peak area and analyte concentration is expressed as linear regression lines ($y = ax + b$), where y is the peak area measured by UV detector, x is the concentration (ppm) of the analytes, and a and b are the respective slope and intercept of the calibration curve. The correlation coefficient is r.

Table 2
Relative standard deviation values for intra- and inter-day precision for compounds **1–6**

Compound	Intra-day precision ($n=6$)		Inter-day precision ($n=6$)	
	Retention time (R.S.D., %)	Peak area (R.S.D., %)	Retention time (R.S.D., %)	Peak area (R.S.D., %)
Rhein (**1**)	0.08	1.25	0.07	1.33
Kaempferol (**2**)	0.07	1.63	0.07	2.10
Aloe-emodin (**3**)	0.08	0.32	0.08	0.45
Emodin (**4**)	0.09	0.28	0.11	0.46
Chrysophanol (**5**)	0.12	0.27	0.13	0.46
Physcion (**6**)	0.15	0.31	0.16	0.39

Table 3
Concentrations and recoveries of phenolic compounds **1–6** in the root extract of *C. alata*

Compound	Root concentration (ppm)	Spiked concentration (ppm)	Total concentration detected (ppm)	Recovery (%) (mean ± S.D.)
Rhein (**1**)	68.4 ± 1.6	45.4	121 ± 1	106 ± 1
		90.8	151 ± 10	90.4 ± 6.1
Kaempferol (**2**)	122 ± 7	65.0	192 ± 2	103 ± 1
		130	257 ± 1	102 ± 1
Aloe-emodin(**3**)	4.02 ± 0.37	3.30	6.43 ± 0.27	87.7 ± 3.7
		6.61	8.64 ± 0.46	81.2 ± 4.3
Emodin (**4**)	26.5 ± 5.0	13.8	42.7 ± 0.9	106 ± 2
		27.6	52.5 ± 2.9	97.0 ± 5.3
Chrysophanol (**5**)	21.6 ± 6.5	11.3	30.1 ± 0.6	91.4 ± 1.8
		22.5	37.1 ± 1.5	84.1 ± 3.4
Physcion (**6**)	4.45 ± 0.71	2.62	7.37 ± 0.12	104 ± 2
		5.24	8.78 ± 0.20	90.6 ± 2.0

The concentration of each investigated compound in the root extract was determined by substituting its peak area for y in the equation listed in Table 1. The concentrations of compounds **1–6** detected in the root extract are given in Table 3. Among the six analytes determined in the root extracts, the concentrations of rhein (68.4 ± 1.6 ppm) and kaempferol (122 ± 7 ppm) were found to be highest.

4. Conclusions

A simple and reliable LC-UV–APCI-MS method has been developed for the simultaneous analysis and identification of six pharmacologically active compounds in root extracts of *C. alata*. The extracts were purified by SPE and separated on a C_{18}-HPLC column using isocratic elution. The investigated phenolic compounds in the root extract were identified by their UV spectra and MS data. The compounds were ionized using an APCI interface and their molecular masses as well as their fragmentation patterns were determined. Finally, HPLC-UV was used to determine the amount of these phenolic compounds in the root extract.

This valuable information concerning the concentration of these pharmacologically active compounds in the root extract of *C. alata* could aid in determining their active component(s), which can be of great importance for pharmaceutical industry. However, further studies involving complete characterization and bioassay analysis of these phenolic compounds in the root extract of *C. alata* are necessary. There is ongoing research in this direction in our laboratory which will be reported in a future manuscript.

Acknowledgements

We acknowledge the National Science Foundation (CHE0616824) and the National Institutes for Health (R1GM39844) for financial support. We also acknowledge the helpful discussions of Dr. Xiaodong Huang and Dr. Ginger Powe.

References

[1] H. Heyde, Medicijn Planten in Suriname, Medicinal Plants in Suriname, third ed., Uitg. Stichting Gezondheidsplanten Informatie, Paramaribo, 1990, p. 120.
[2] L.L. Co, Common Medicinal Plants of the Cordillera Region, Bustamante Press, Quezon City, 1989, p. 11.
[3] S.V. Agarkar, D.R. Jadge, Asian J. Chem. 11 (1999) 295.
[4] P.P. Rai, Curr. Sci. 47 (1978) 271.
[5] F.R. Irvine, Woody plants of Ghana with special reference to their uses, Oxford University Press, London, 1961, p. 178.
[6] K.R. Kirtikar, B.D. Basu, Indian Medicinal Plants, vol. 2, Periodical Experts, New Delhi, 1975, p. 870.
[7] L.S. de Padua, G.C. Lugod, J.V. Pancho, Handbook on Phillippines Medicinal Plants, vol. 2, third ed., University of the Phillipines, Los Baños, 1980, p. 37.
[8] D. Ibrahim, H. Osman, J. Ethnopharmacol. 45 (1995) 151.
[9] M.N. Somchit, I. Reezal, I. Elysha Nur, A.R. Mutalib, J. Ethnopharmacol. 84 (2003) 1.
[10] S. Damodaran, S. Venkataraman, J. Ethnopharmacol. 42 (1994) 19.

[11] I.M. Villaseñor, A.P. Canlas, M.P. Pascua, M.N. Sabando, L.A.P. Soliven, Phytother. Res. 16 (2002) S93.
[12] H. Moriyama, T. Iizuka, M. Nagai, H. Miyataka, T. Satoh, Yakugaku Zasshi 123 (2003) 607.
[13] S. Palanichamy, S. Nagarajan, J. Ethnopharmacol. 29 (1990) 73.
[14] M. Belkin, B. Fitzgerald Dorothea, W. Cogan, J. Natl. Cancer Inst. 13 (1952) 139.
[15] S.M. Yagi, S. El Tigani, S.E. Adam, Phytother. Res. 12 (1998) 324.
[16] R. Smith, S. Ali, N.Z. J. Sci. 22 (1979) 123.
[17] J.V.L. Rao, P.S.R. Sastry, R.Y.K. Rao, M. Vimaladevi, Curr. Sci. India 44 (1975) 736.
[18] R.D. Tiwari, O.P. Yadava, Planta Med. 19 (1971) 299.
[19] R.H. Thomson, Naturally Occurring Quinones III: Recent Advances, third ed., Chapman and Hall Ltd., University Press, Cambridge, 1987, pp. 345–526.
[20] S.K. Agarwal, S.S. Singh, S. Verma, S. Kumar, J. Ethnopharmacol. 72 (2000) 43.
[21] J. Koyama, I. Morita, K. Tagahara, M. Ogata, T. Mukainaka, H. Tokuda, H. Nishino, Cancer Lett. 170 (2001) 15.
[22] G. Yen, P. Duh, D. Chuang, Food Chem. 70 (2000) 437.
[23] H. Wang, T. Chen, P. Yang, T. Ueng, DMD 29 (2001) 1229.
[24] S.B. Choi, B.S. Ko, S.K. Park, J.S. Jang, S. Park, Life Sci. 78 (2006) 934.
[25] Y. Nakamura, C. Chang, T. Mori, K. Sato, K. Ohtsuki, B.L. Upham, J.E. Trosko, Carcinogenesis 26 (2005) 665.
[26] J.K. Campbell, J.L. King, M. Harmston, M. Lila, J.W. Erdman Jr., J. Food Sci. 71 (2006) S358.
[27] H. Moriyama, T. Iizuka, M. Nagai, Y. Murata, Fitoterapia 74 (2003) 425.
[28] N.P. Singh, A.P. Gupta, A.K. Sinha, P.S. Ahuja, J. Chromatogr. A 1077 (2005) 202.
[29] T.F. Jiang, Z.H. Lv, Y.H. Wang, J. Sep. Sci. 28 (2005) 2225.
[30] K. Tian, Y. Wang, Y. Chen, X. Chen, Z. Hu, Talanta 72 (2007) 587.
[31] M. Puchalska, M. Orlińska, M.A. Ackacha, K. Poleć-Pawlak, M. Jarosz, J. Mass Spectrom. 38 (2003) 1252.
[32] L.G. Harruff, M.A. Vazquez, Tappi 64 (1981) 109.
[33] M.A. ElSohly, W. Gul, T.P. Murphy, Int. Immunopharmcol. 4 (2004) 1739.
[34] J. Steinert, H. Khalaf, M. Rimpler, J. Chromatogr. A 723 (1996) 206.
[35] M. Ding, S. Ma, D. Liu, Anal. Sci. 19 (2003) 1163.
[36] G.C.H. Derksen, G.P. Lelyveld, T.A. van Beek, A. Capelle, Æ. de Groot, Phytochem. Anal. 15 (2004) 397.
[37] M.M. Nindi, B.V. Kgarebe, J.L. Wolfender, B.M. Abegaz, Phytochem. Anal. 10 (1999) 69.
[38] G.C.H. Derksen, H.A.G. Niederländer, T.A. van Beek, J. Chromatogr. A 978 (2002) 119.
[39] S.O. Mueller, M. Schmitt, W. Dekant, H. Stopper, J. Schlatter, P. Schreier, W.K. Lutz, Food Chem. Toxicol. 37 (1999) 481.
[40] W. Li, C. Chan, H. Lueng, J. Pharm. Pharmacol. 52 (2000) 723.
[41] J.M. Miller, Chromatography: Concepts, Contrasts, second ed., John Wiley & Sons, Inc., 2005, pp. 24–29.
[42] D.A. Skoog, F.J. Holler, T.A. Nieman, Principles of Instrumental Analysis, fifth ed., Thomson Learning, United States, 1998, pp. 11–15.

Available online at www.sciencedirect.com
ScienceDirect
Talanta 74 (2008) 699–702
Talanta
www.elsevier.com/locate/talanta

Direct determination of iron and manganese in wine using the reference element technique and fast sequential multi-element flame atomic absorption spectrometry

Sérgio L.C. Ferreira [a,*], Anderson S. Souza [a], Geovani C. Brandao [a], Hadla S. Ferreira [a], Walter N.L. dos Santos [b], M. Fernanda Pimentel [c], Maria Goreti R. Vale [d]

[a] *Universidade Federal da Bahia, Instituto de Química, Núcleo de Excelência em Química Analítica da Bahia, Campus Universitário de Ondina, Salvador 40170-290, BA, Brazil*
[b] *Universidade do Estado da Bahia, Rua Silveira Martins 2555, Cabula, CEP 41.195.001, Salvador, BA, Brazil*
[c] *Universidade Federal de Pernambuco, Departamento de Engenharia Química, Recife 50740-521, PE, Brazil*
[d] *Instituto de Química, Universidade Federal do Rio Grande do Sul, Av. Bento Gonçalves 9500, Porto Alegre 91501-970, RS, Brazil*

Received 1 June 2007; received in revised form 25 June 2007; accepted 27 June 2007
Available online 3 July 2007

Abstract

A procedure is proposed for the direct determination of manganese and iron in wine employing fast sequential flame atomic absorption spectrometry and the reference element technique to correct for matrix effects. Cobalt, silver, nickel and indium have been tested as reference elements. The results demonstrated that cobalt and indium at a concentration of 2 and 10 mg L^{-1} were efficient for quantification of manganese and iron, respectively. Under these conditions, manganese and iron could be determined with quantification limits of 27 and 40 μg L^{-1}, respectively. The proposed method was applied to the determination of manganese and iron in 16 wine samples. The content of manganese varied from 0.78 to 2.89 mg L^{-1} and that of iron from 0.88 to 9.22 mg L^{-1}. The analytical results were compared with those obtained by inductively coupled plasma optical emission spectrometry after complete mineralization using acid digestion. The statistical comparison by a *t*-test (95% confidence level) showed no significant difference between the results.
© 2007 Elsevier B.V. All rights reserved.

Keywords: Wine; Reference element technique; Iron determination; Manganese determination; Matrix effects; Fast sequential flame atomic absorption spectrometry

1. Introduction

The mineral content of wine depends on several factors including absorption of metals from the soil, contamination by atmospheric emissions, the type of grape, herbicidal treatment and the wine-making process. The metal content has a great influence on the quality of a wine, and several studies have been performed involving this subject [1–5]. Cacho et al. [6] studied the influence of iron, copper, and manganese on wine oxidation, measuring the evolution of different compounds sensitive to this process, such as anthocyanins, tannins, total phenol content and acetaldehyde. They concluded that the oxidation depends directly on the concentration of these cations in the wine. They also found that manganese and iron play an important role in chemical processes with acetaldehyde: manganese favors its formation and iron catalyzes acetaldehyde combination with phenolic compounds. Benitez et al. [7] concluded that iron, copper, manganese and zinc modify the stability, color, and clarity of wines. Zinc and iron might affect the organoleptic characteristics of a wine.

The direct determination of metals in wine employing spectroanalytical techniques such as inductively coupled plasma optical emission spectrometry (ICPOES), inductively coupled plasma mass spectrometry (ICP-MS) and flame atomic absorption spectrometry (FAAS) is difficult, because wine is a complex matrix that contains ethanol, sugars and other organic compounds [1]. The methods proposed for the determination of metals in wine by these techniques therefore typically include some sample preparation. This might consist of elimination of the alcohol, acid digestion, evaporation to dryness and disso-

* Corresponding author.
E-mail address: slcf@ufba.br (S.L.C. Ferreira).

0039-9140/$ – see front matter © 2007 Elsevier B.V. All rights reserved.
doi:10.1016/j.talanta.2007.06.038

Table 1
Wavelength and concentration used and linear regression equations obtained for the determination of manganese and iron in the absence (standard calibration technique) and in the presence of four different elements used as RE

Reference element	Wavelength (nm)	RE concentration (mg L^{-1})	Linear regression equation (Mn)	Linear regression equation (Fe)
Cobalt	240.7	2.0	$A = 0.1311C_{Mn} + 0.1462$ ($R = 0.9995$)	$A = 0.0633C_{Fe} + 0.0623$ ($R = 0.9961$)
Indium	303.9	10.0	$A = 0.1610C_{Mn} + 0.0992$ ($R = 0.9480$)	$A = 0.0774C_{Fe} + 0.0531$ ($R = 0.9994$)
Nickel	232.0	2.0	$A = 0.1456C_{Mn} + 0.1175$ ($R = 0.9952$)	$A = 0.0759C_{Fe} + 0.0617$ ($R = 0.9929$)
Silver	328.1	2.0	$A = 0.1484C_{Mn} + 0.0959$ ($R = 0.9868$)	$A = 0.0703C_{Fe} + 0.0498$ ($R = 0.9959$)
Results using the standard calibration technique			$A = 0.1363C_{Mn} + 0.0128$ ($R = 0.9991$)	$A = 0.0744C_{Fe} + 0.0081$ ($R = 0.9962$)

R: correlation coefficient.

lution of the residue in nitric acid [8,9], mineralization in a digestion block using concentrated acids [10,11], microwave-assisted acid digestion [12–14], UV irradiation-assisted digestion [15], dilution of the wine sample and use of the analyte addition technique [16] and also the reference element technique employing ICPOES or ICP-MS [17,18].

The reference element technique is used to overcome matrix effects that might influence the analytical signal in the quantification step. It requires simultaneous or fast sequential measurement of the analyte(s) and the reference element and it has therefore been widely used in ICPOES and ICP-MS [19,20]. The use of the reference element technique in FAAS has become feasible with the introduction of a fast sequential (FS) multi-element system for this technique [21]. It has been used by several authors for FS multi-element FAAS [21–24]. da Silva et al. [25] used this system and nickel as reference element for the determination of iron in hydrated ethanol with FSFAAS.

The present paper proposes the use of the reference element technique for correction of matrix effects in the direct determination of manganese and iron in wine employing FSFAAS.

2. Experimental

2.1. Instrumentation

A Varian model SpectrAA 220 FS flame atomic absorption spectrometer (Mulgrave, Vistoria, Australia), equipped with a deuterium background corrector and automatic switching of hollow-cathode lamps was used. The iron and manganese hollow-cathode lamps were operated with a current of 5.0 mA for both elements. The analytical wavelengths at 248.3 and 279.5 nm were used with a spectral bandwidth of 0.1 nm for both metals. An air–acetylene flame was used with an acetylene flow rate of 2.0 L min^{-1}, an airflow rate of 13.5 L min^{-1} and a burner height of 13.5 mm.

2.2. Reagents

All reagents were of analytical grade unless otherwise stated. Ultrapure water was obtained from an EASYpure RF purification system (Barnstedt, Dubuque, IA, USA). Nitric and hydrochloric acid were of Suprapur® quality (Merck, Darmstadt, Germany). Nitric and hydrochloric acid solutions were prepared from the concentrated acids by dilution with water.

Laboratory glassware was kept overnight in 10% (v/v) nitric acid solution. Before use the glassware was rinsed with deionized water and dried in a dust-free environment.

Calibration solutions were prepared from 1000 mg L^{-1} manganese and iron stock solutions (Merck) by appropriate dilution with a 1% (v/v) nitric acid solution.

The concentration of the reference element solutions was 2.0 mg L^{-1} for silver, nickel, cobalt and 10.0 mg L^{-1} for indium.

2.3. Procedure for total digestion of wine

A volume of 10.0 mL of wine was introduced into a 125-mL Erlenmeyer flask, and 3.0 mL of concentrated nitric acid and 5.0 mL of 30% (v/v) hydrogen peroxide were added. The samples were heated and evaporated to dryness on a hot plate; the residue was dissolved in 0.5 mol L^{-1} nitric acid, transferred to a 25-mL volumetric flask and diluted to volume with 0.5 mol L^{-1} nitric acid solution. Manganese and iron were determined in the diluted solutions by ICPOES. All samples were analyzed in triplicate.

2.4. Direct determination using FSFAAS and the reference element technique

For the direct determination 10.0 mL of wine and 2.5 mL each of a 20.0 μg mL^{-1} cobalt and 100 μg mL^{-1} indium standard solution, respectively, were introduced into a 25-mL volumetric flask and diluted to volume using 1.0 mol L^{-1} nitric acid solution. The final concentration of cobalt and indium in this solution was 2 and 10 μg mL^{-1}, respectively.

3. Results and discussion

3.1. Selection of the reference element for the determination of manganese and iron

The reference elements (RE) tested were cobalt, indium, nickel and silver. The lines and concentrations used for quan-

Table 2
Evaluation of the precision of the method ($N = 11$)

Analyte	Concentration added (mg L^{-1})	RSD using RE (%)	RSD without RE (%)
Iron (RE: In)	0.5	0.52	1.9
	2.5	0.88	2.5
Manganese (RE: Co)	0.2	0.91	1.4
	1.0	1.14	1.9

Table 3
Determination of iron and manganese in wine using FSFAAS without and with RE and using ICPOES after acid digestion

Sample	Wine	Fe without RE ($mg\,L^{-1}$)	Fe with RE ($mg\,L^{-1}$)	Fe ICPOES ($mg\,L^{-1}$)	Deviation without RE (%)	Deviation with RE (%)	Mn without RE ($mg\,L^{-1}$)	Mn with RE ($mg\,L^{-1}$)	Mn ICPOES ($mg\,L^{-1}$)	Deviation without RE (%)	Deviation with RE (%)
1	Dry table red	2.69 ± 0.10	3.04 ± 0.10	3.08 ± 0.28	−12.7	−1.3	2.12 ± 0.15	2.21 ± 0.12	2.30 ± 0.03	−7.8	−3.9
2	Dry table red	1.27 ± 0.11	1.56 ± 0.07	1.61 ± 0.08	−21.1	−3.1	2.52 ± 0.24	2.58 ± 0.22	2.61 ± 0.07	−3.4	−1.1
3	Dry table red	6.25 ± 0.29	7.45 ± 0.07	7.59 ± 0.13	−17.7	−1.8	2.62 ± 0.10	2.89 ± 0.07	2.83 ± 0.05	−7.4	2.1
4	Dry table red	1.82 ± 0.39	2.55 ± 0.23	2.62 ± 0.18	−30.5	−2.7	2.00 ± 0.08	2.28 ± 0.05	2.38 ± 0.04	−16.0	−4.2
5	Dry red	8.54 ± 0.63	9.22 ± 0.33	9.30 ± 0.12	−8.2	−0.9	1.27 ± 0.11	1.44 ± 0.11	1.47 ± 0.11	−13.6	−2.0
6	Dry red	2.48 ± 0.39	3.02 ± 0.18	3.11 ± 0.22	−20.2	−2.9	1.18 ± 0.19	1.35 ± 0.07	1.40 ± 0.11	−15.7	3.6
7	Sweet red	1.76 ± 0.25	2.45 ± 0.20	2.56 ± 0.22	−31.3	−4.3	0.63 ± 0.23	0.78 ± 0.19	0.80 ± 0.03	−21.3	−2.5
8	Sweet red	1.28 ± 0.12	1.92 ± 0.11	1.86 ± 0.16	−31.2	3.2	1.66 ± 0.10	1.86 ± 0.08	1.87 ± 0.10	−11.2	−0.5
9	Sweet red	3.73 ± 0.53	5.20 ± 0.34	5.01 ± 0.03	−25.5	3.8	2.06 ± 0.21	2.27 ± 0.15	2.36 ± 0.03	−12.7	−3.8
10	White table	1.31 ± 0.15	2.15 ± 0.12	2.22 ± 0.14	−41.0	−3.2	2.23 ± 0.10	2.59 ± 0.06	2.51 ± 0.03	−11.2	3.2
11	White table	5.62 ± 0.23	6.25 ± 0.07	6.11 ± 0.16	−8.0	2.3	2.11 ± 0.09	2.40 ± 0.04	2.45 ± 0.04	−13.9	−2.0
12	White table	0.70 ± 0.12	1.00 ± 0.07	0.96 ± 0.09	−27.1	4.2	1.57 ± 0.15	1.85 ± 0.11	1.98 ± 0.05	−20.7	−6.6
13	Dry white	1.68 ± 0.08	2.02 ± 0.06	2.00 ± 0.10	−16.0	1.0	1.34 ± 0.04	1.61 ± 0.01	1.62 ± 0.11	−17.3	−0.1
14	Dry white	1.22 ± 0.23	1.54 ± 0.08	1.60 ± 0.08	−23.8	−3.8	0.82 ± 0.13	1.03 ± 0.07	1.06 ± 0.06	−22.6	−2.8
15	Sweet white	2.72 ± 0.48	3.74 ± 0.39	3.82 ± 0.19	−28.8	−2.1	1.91 ± 0.24	2.14 ± 0.23	2.23 ± 0.06	−14.3	−4.0
16	Sweet white	0.74 ± 0.26	0.88 ± 0.17	0.85 ± 0.17	−12.9	3.5	1.21 ± 0.14	1.44 ± 0.08	1.39 ± 0.05	−12.9	3.6

Also shown is the relative deviation of the FSFAAS values compared with the ICPOES results.

tification were the same as proposed by Projahn et al. [21]. Analytical curves were established by spiking a wine sample with increasing concentrations of manganese and iron. All the results found are summarized in Table 1. The analytical signals obtained in this experiment were corrected employing the RE technique for all the four RE tested. The corrections were done using the expression:

$$(AS_C) = (AS) \times \frac{(AS^{\circ}_{RE})}{(AS_{RE})} \quad (1)$$

where (AS) is the analytical signal obtained during the quantification of the analyte, (AS°_{RE}) the average of the analytical signals obtained for the RE in the calibration solutions and blank, (AS_{RE}) the analytical signal obtained for the RE in the sample solution and (AS_C) is the corrected analytical signal. The relative standard deviation for the analytical signals obtained for the RE was 2.0% for indium (RE used for iron) and 3.0% for cobalt (RE used for manganese).

The slope of the analytical curve for manganese $(0.1363 \pm 0.0042)C_{Mn(mg\,L^{-1})}$ obtained by the standard calibration technique expressed as confidence interval [26] is quite comparable with the slope $(0.1311 \pm 0.0033)C_{Mn(mg\,L^{-1})}$ of the analytical curve obtained with the RE technique using cobalt as reference element. Similarities are also observed for the slopes of the analytical curves established for iron employing the standard calibration technique $(0.0744 \pm 0.0063)C_{Fe(mg\,L^{-1})}$ and the RE technique using indium as reference element $(0.0774 \pm 0.0080)C_{Fe(mg\,L^{-1})}$. These results demonstrate that the RE technique (using cobalt as reference element for manganese and indium for iron) is perfectly efficient for correcting the matrix effect observed in the determination of these elements in wine using FSFAAS. All the experiments involving silver as reference element were performed in nitric acid media. Hydrochloric acid cannot be used because of precipitation of silver(I) ion as the chloride.

3.2. Analytical characteristics of the method

The precision expressed as relative standard deviation (RSD) was evaluated for the quantification of manganese and iron in solutions of 10.0 mL of wine, additions of manganese and iron, RE, and dilution with 1.0 mol L^{-1} nitric acid solution to a final volume of 25.0 mL. The RE used was cobalt for manganese and indium for iron. The results in Table 2 demonstrate that the precision of the method improved considerably when the RE technique was applied for both metals.

The limits of detection ($3\sigma/S$) and quantification ($10\sigma/S$) were 12 and 40 μg L^{-1} for iron, and 8 and 27 μg L^{-1} for manganese, respectively, calculated according to IUPAC recommendations, where σ is the standard deviation of the blank ($n = 10$) and S is the slope of the analytical curve [27].

3.3. Application of the method

The proposed method has been applied for the determination of manganese and iron in 16 wine samples (including white wine, red wine, dry wine, table wine and sweet wine) bought

in supermarkets in Salvador City, Brazil. The manganese content varied from 0.78 to 2.89 mg L^{-1} and that of iron from 0.88 to 9.22 mg L^{-1}. The analytical results were compared with the results obtained by the analysis of these samples after complete mineralization using acid digestion and determination with ICPOES. All results are summarized in Table 3. The linear regression method was used for comparing the results obtained by the proposed method using the RE technique and the ICPOES method for both metals. The equations found expressed as confidence intervals were:

$$\text{Fe}: \quad [\text{RET}] = 0.9973 \pm 0.0101[\text{ICPOES}] - 0.0103 \pm 0.0416, \quad r = 0.9993,$$

$$\text{Mn}: \quad [\text{RET}] = 0.9961 \pm 0.0268[\text{ICPOES}] - 0.0254 \pm 0.0546, \quad r = 0.9950$$

These results demonstrate that the calculated slopes and intercepts do not differ significantly from the "ideal" values of 1 and 0, respectively, and that there is no evidence for a systematic difference between the two methods for both metals.

The *t*-test (95% confidence level) showed no significant difference between these results. The accuracy of the method was also evaluated by determination of the relative deviation (%), considering the results obtained with acid digestion and determination using ICPOES as the more probable result. This deviation was calculated using the expression:

$$\text{deviation } (\%) = \left\{ \frac{\text{Rf} - \text{Rf}_{\text{ad}}}{\text{Rf}_{\text{ad}}} \right\} \times 100 \quad (2)$$

where Rf is the results found with and without application of the RE technique and Rf_{ad} are the results found with acid digestion and determination by ICPOES. The deviations for manganese were between −3.2% and −22.6% using the standard calibration technique, and between −0.1% and −3.9% using cobalt as RE, respectively. For iron, the deviations varied between −8% and −41% using the standard calibration technique, and between −4.3% and +3.8% using indium as RE. It is interesting to note that in the absence of an RE all results exhibit a negative bias, i.e. a systematic deviation, whereas in the presence of an RE the deviations are much more randomly distributed and even exhibit positive values.

The manganese and iron contents found for the 16 samples are in agreement with data reported in the literature [2].

4. Conclusion

The determination of metals in wine is of great interest because it allows establishing criteria for the evaluation of the identity and authenticity of the samples. The results demonstrate that the RE technique provides reliable results with the advantage that no further manipulation of the sample is needed. The technique might well be applied for the determination of other trace elements in wine after careful selection of an appropriate RE.

Acknowledgements

The authors are grateful to Fundação de Amparo a Pesquisa do Estado da Bahia (FAPESB), Conselho Nacional de Desenvolvimento Científico e Tecnológico (CNPq) and Coordenação de Aperfeiçoamento de Pessoal de Nível Superior (CAPES) for providing grants and fellowships and for financial support.

References

[1] K. Pyrzynska, Crit. Rev. Anal. Chem. 34 (2004) 69.
[2] M. Aceto, O. Abolino, M.C. Bruzzoniti, E. Mentasti, C. Sarzanin, M. Malandrino, Food Addit. Contam. 19 (2002) 126.
[3] A.L. Waterhouse, V.F. Laurie, Am. J. Enol. Viticult. 57 (2006) 306.
[4] P.L. Teissedre, M. Krosniak, K. Portet, F. Gasc, A.L. Waterhouse, J.J. Serrano, J.C. Cabanis, G. Cros, Food Addit. Contam. 15 (1998) 585.
[5] A. Santalad, R. Burakham, S. Srijaranai, K. Grudpan, Microchem. J. 86 (2007) 209.
[6] J. Cacho, J.E. Castells, A. Esteban, B. Laguna, N. Sagrista, Am. J. Enol. Viticult. 46 (1995) 380.
[7] P. Benitez, R. Castro, C.G. Barroso, Anal. Chim. Acta 458 (2002) 197.
[8] V.A. Lemos, M. de La Guardia, S.L.C. Ferreira, Talanta 58 (2002) 475.
[9] R. Lara, S. Cerutti, J.A. Salonia, R.A. Olsina, L.D. Martinez, Food Chem. Toxicol. 43 (2005) 293.
[10] F.F. Lopez, C. Cabrera, M.L. Lorenzo, M.C. Lopez, Sci. Total Environ. 220 (1998) 1.
[11] C. Mena, C. Cabrera, M.L. Lorenzo, M.C. Lopez, Sci. Total Environ. 181 (1996) 201.
[12] E. Tatár, V.G. Mihucz, I. Virág, L. Rácz, G. Záray, Microchem. J. 85 (2007) 132.
[13] V.G. Mihucz, C.J. Done, E. Tatár, I. Virág, G. Záray, E.G. Baiulescu, Talanta 70 (2006) 984.
[14] Kh.Z. Brainina, N.Yu. Stozhko, G.M. Belysheva, O.V. Inzhevatova, L.I. Kolyadina, C. Cremisini, M. Galletti, Anal. Chim. Acta 514 (2004) 227.
[15] C.M. Almeida, M.T.S.D. Vasconcelos, Anal. Chim. Acta 463 (2002) 165.
[16] I. Karadjova, B. Izgi, S. Gucer, Spectrochim. Acta B 57 (2002) 581.
[17] M.M. Castiñeira, R. Brandt, A. von Bohlen, N. Jakubowski, Fresen. J. Anal. Chem. 370 (2001) 553.
[18] M. Iglesias, E. Besalú, E. Ântico, J. Agric. Food Chem. 55 (2007) 219.
[19] A.C. Davis, C.P. Calloway, B.T. Jones, Microchem. J. 84 (2006) 31.
[20] R.M. de Souza, A.L.S. Meliande, C.L.P. da Silveira, R.Q. Aucélio, Microchem. J. 82 (2006) 137.
[21] H.D. Projahn, U. Steeg, J. Sanders, E. Vanclay, Anal. Bioanal. Chem. 378 (2004) 1083.
[22] P. Niedzielski, Anal. Chim. Acta 551 (2005) 199.
[23] F.A.C. Amorim, S.L.C. Ferreira, Talanta 65 (2005) 960.
[24] E.G.P. da Silva, A.C.N. Santos, A.C.S. Costa, D.M.N. Fortunato, N.M. José, M.G.A. Korn, W.N.L. dos Santos, S.L.C. Ferreira, Microchem. J. 82 (2006) 159.
[25] J.E. da Silva, F.A. da Silva, M.F. Pimentel, R.S. Honorato, V.L. da Silva, M.C.B.S.M. Montenegro, A.N. Araújo, Talanta 70 (2006) 522.
[26] D.L. Massart, B.G.M. Vandeginste, L.M.C. Buydens, S. de Jong, P.J. Lewi, J. Smeyers-Verbeke, Handbook of Chemometrics and Qualimetrics: Part A, Elsevier, Amsterdam, 1977.
[27] IUPAC, Analytical Chemistry Division, Spectrochim. Acta B 33 (1978) 242.

Available online at www.sciencedirect.com
ScienceDirect
Talanta 74 (2008) 655–660
Talanta
www.elsevier.com/locate/talanta

Isolation, purification and determination of 4-*n*-nonylphenol and 4-*tert*-octylphenol in aqueous and biological samples

Renata Gadzała-Kopciuch *, Anna Filipiak, Bogusław Buszewski

Department of Environmental Chemistry and Bioanalytics, Faculty of Chemistry, Nicolaus Copernicus University, 7 Gagarin St, 87-100 Toruń, Poland

Received 9 January 2007; received in revised form 18 June 2007; accepted 25 June 2007
Available online 1 July 2007

Abstract

The aim of the present study was to attempt to describe the procedure of isolation, purification, enrichment and determination of 4-*n*-nonylphenol (4-*n*-NP) and 4-*tert*-octylphenol (4-*t*-OP) in water and biological samples (fish tissue). There were five procedures of solid phase extraction (SPE) tested using different sorbents for the isolation of analytes from water samples. Moreover, we isolated these chemicals from biological matrices with the aid of various extraction methods. The purpose of it was to perform an optimisation of ultrasonic bath, accelerated solvent extraction (ASE) and solid phase extraction process of alkylphenols from biological samples, through the choice of selective sorbents (octadecyl, octadecyl end-capped and amine) and search solvents (methylene chloride, methanol, hexane). Reversed-phase HPLC with diode array detection was used for the determination of 4-*n*-NP and 4-*t*-OP in water and fish tissue samples. Sensitivity was evaluated by determining the limit of detection (LOD = 0.06 and 0.04 ng μL^{-1}) and limit of quantification (LOQ = 0.18 and 0.16 ng μL^{-1}) of 4-NP and 4-*t*-OP, respectively. A series of standard solutions for 4-*n*-NP and 4-*t*-OP provided the basis for plotting an analytical curve and obtaining a linear dependence in the range of approximately 1–25 ng μL^{-1}. The best efficiencies obtained for 4-*n*-NP and 4-*t*-OP in water samples were 76.65% (±1.49) and 83.08% (±3.73), respectively. In the case of fish tissue, different situation was observed because the obtained values were considerably lower, being 68.32% for 4-*t*-OP using hexane (program 1) as solvent and 72.35% (program 2) for 4-*n*-NP using acetonitrile.
© 2007 Elsevier B.V. All rights reserved.

Keywords: Alkylphenols; Endocrine disruptor; Solid phase extraction; HPLC analysis

1. Introduction

In recent years, the release of various organic chemicals into the environment has attracted great attention of scientists because of the toxicity and widespread use of these compounds [1]. One such organic chemical are alkylphenol ethoxylates (APE), which are structured from two groups attached to an aromatic ring located in *para* position, that is from a nonpolar hydrocarbonate chain and from polar ethoxy units. APE are non-ionic surfactants which have been widely used for over 40 years in domestic and industrial applications, primarily in the manufacture of plastics, elastomers, agricultural chemicals, paper, and pulp [2,3]. Therefore, they are widespread in ecosystems like soil, and mainly surface natural water, and sediment. APEs are biodegraded by removal of ethoxy groups to alkylphenols (AP), which are more toxic than their parent compounds [4,5].

Alkylphenols, especially nonylphenols (NP) and octylphenols (OP) have been reported to bio-accumulate in the lipids of water organisms [6–8]. These xenobiotics are also called *endocrine disrupting compounds* (EDCs) because they disturb endocrine functions by binding to hormone receptors (17-β-estrogen) inducing synthesis of vitellogenin (Vtg) and zona radiata protein (Zrp) [9,10].

Endocrine disrupting chemicals cause modifications of sexual development and reproductive function in wildlife [11–14]. That is why some European countries have restricted or banned the use of nonylphenols surfactants [15]. Various reports suggest that these substances also induce various effects in the human body, for example lower sperm counts, undescended testicles, early puberty, and thyroid dysfunction [16].

Because of high toxicity of alkylphenols, mainly nonylphenols, it is necessary to control the level of these compounds in our environment. That is why there is a necessity for the selection

* Corresponding author. Tel.: +48 56 611 47 53; fax: +48 56 611 48 37.
E-mail address: rgadz@chem.uni.torun.pl (R. Gadzała-Kopciuch).

0039-9140/$ – see front matter © 2007 Elsevier B.V. All rights reserved.
doi:10.1016/j.talanta.2007.06.028

of appropriate methods for sampling preparation and analysis of these analytes in water and organisms [17–19], which are living in this ecosystem (e.g.: fish, crabs, etc.). A high level of chromatography development and the possibility of combining it with other analytical methods (e.g.: mass spectrometry, infrared spectrometry, atomic spectrometry, etc.) allows to choose a sensitive and selective method for analyte determination. One of the main techniques for analysis of environmental pollutants is liquid [19–24] and/or gas chromatography coupled to mass spectrometry [25–28].

The main task of this study was focused on the selection of the dedicated sorbent for solid phase extraction (SPE) and the adaptation of the methodology for the determination of 4-*n* nonylphenol and 4-*tert*-octylphenol in aquatic samples by HPLC. Also, we attempted to optimize the technique of preparing biological samples using a simple automated extraction method for the determination of alkylphenolic compounds in fish tissue. These compounds appear at a very low level of concentration, hence it is necessary to find selective methods of isolation and enhancement of these analytes from different environmental matrices, and sensitive techniques for quantitative determination. It is recognized that fish tissue represents a very complex matrix and the isolation of its analytes is challenging to chemists who work with sample preparation and determination of compounds.

2. Experimental

2.1. Materials

Both 4-*n*-nonylphenol (Lancaster, Morecambe, England) and 4-*tert*-octylphenol (Sigma–Aldrich Chemie, Steinheim, Germany) were used in ethanol in a standard manner. Solvents for HPLC (LabScan, Dublin, Ireland) and redistilled water (Mili-Q, Milipore, El Passo, TX, USA) were employed for conditioning of extractive column, analytes elution and chromatographic analysis (mobile phases). Sodium sulphate anhydrous (POCh, Gliwice, Poland) was used as a drying agent.

2.2. Equipment

Chromatographic measurements were taken using an HP1100 liquid chromatograph (Agilent Technologies, Waldbronn, Germany) equipped with a diode array detector and an autosampler. Separations were performed on a Supelcosil LC-C18-DB column (Supelco Inc., Bellefonte, PA, USA) (250 mm × 4.6 mm i.d., d_p = 5 μm particle size). SPE of water samples was performed using a vacuum set (J.T. Baker, Groß-Gerau, Germany). SPE columns were filled with graphitized carbon black (Carbograph – Alltech, Poznań, Poland); other cartridges like octadecyl (Bakerbond C18, Speedisk C18 column – J.T. Baker; LiChrolut C18 – Merck, Darmstadt, Germany) and polymeric SDB1 (J.T. Baker) were used for preparation of aqueous samples. In addition, diol (Supelco) and aminopropyl silica (J.T. Baker) columns were used for extracts of biological samples (fish tissue). Fish extracts were obtained using accelerated solvent extraction ASE-200 (Dionex, San Diego, CA, USA).

2.3. Analysis

All samples were analysed by HPLC. Chromatography was performed using a Supelcosil LC-C18-DB column and mobile phase consisting of acetonitrile, water and methanol (43/14/43%, v/v/v). The flow rate was 1 mL min^{-1} in all chromatographic analyses. The volumes of samples were 20 and 100 μL for extracts from aqueous and biological matrices, respectively. Identification of analytes was done at wavelength λ = 277 nm.

2.4. Extraction of water samples

Five procedures of solid phase extraction were tested using different sorbents to isolation of 4-*n*-NP and 4-*t*-OP in water samples. The physico-chemical characteristics of applied sorbents (graphitized carbon, octadecyl base on the silica gel and polymeric) are listed in Table 1. For carbonic sorbent, only one procedure of solid phase extraction [21] was tested. The analytes were eluted with 3 × 2.5 mL of methylene chloride/methanol (80:20%, v/v) acidified with 50 mM L^{-1} of formic acid; for octadecyl C18 sorbent two procedures were chosen – in the first method the analytes were eluted with two 2 mL portions of methanol [22], whereas in the second method elution it was carried out with two aliquots of 2.5 mL cyclohexane [21]. Two procedures were also employed for polymeric sorbent. In the first method 4-*n*-NP and 4-*t*-OP were eluted with 12 mL of methylene chloride, 12 mL of methanol and 12 mL of acetone [27]

Table 1
Characteristics of SPE packing used for 4-NP and 4-*tert*-OP isolation from water samples

Column	Manufacturer	Specific surface area (m^2/g)	Particle size (μm)	Pore size (Å)	Modifier	Carbon content (%)
Octadecyl sorbents						
Bakerbond C_{18}	J.T. Baker	330	40	56	Tri[a]	17.8
Speedisk column C_{18}	J.T. Baker	345	40	60	Tri + EC[a]	16.5
LiChrolut C18	Merck	600	40–63	60	Tri + EC[a]	–
Polymer sorbent						
SDB1	J.T. Baker	940	43–125	–	Copolymer PS-DVB	–
Carbon sorbent						
Carbograph^{TM}	Alltech Associates, Inc.	100	38–125	–	–	–

[a] Silane used for modification – trifunctional silane (Tri) and secondary silanization (end-capping EC).

Table 2
ASE operating conditions

	Program 1	Program 2
Extraction solvent	Methanol, acetonitrile, methylene chloride, hexane	Methanol, acetonitrile
Pressure (psi)	1000	1700
Temperature (°C)	100	120
Static time (min)	10	5
Static cycles	3	3
Flush (%)	90	90
Purge (s)	200	200
Cell size (mL)	33	

whereas in the second procedure two aliquots of 2.5 mL ethyl acetate were used for elution of analytes from water [21]. Water samples spiked with a known concentration of alkylphenol were analysed.

2.5. Biological samples

Rainbow trout (*Oncorhynchus mykiss*) without innards and head was bought at the local commercial food market. The skin was stripped off and the muscle was homogenized and stored deep-frozen until analysis.

Frozen fish was thawed and spiked with standards of 4-*n*-nonylphenol and 4-*tert*-octylphenol and was placed for 24 h in a refrigerator. Then homogenized fish tissue was mixed with draining agent (Na_2SO_4) (2:1) and it was performed following the procedure described by Datta et al. [23]. The mixture of sample was packed into a stainless steel cell for accelerated solvent extraction using the following conditions described in Table 2. Extracts were roto-evaporated to dryness and reconstituted completed with to 1 mL methylene chloride. Concentrated fish extracts were diluted with 7 mL in hexane. Two cleanup cartridge systems were tested: diol (Supelco) and aminopropyl silica (J.T. Baker). Each of the diol cartridges were conditioned with 3 mL of acetone, methylene chloride, hexane and methylene chloride/hexane (9:1, v/v). The fish extract was divided into three equal portions (2 mL) and loaded onto three conditioned cartridges. Then, 1 mL rinse of hexane was added. The cartridge was eluted with 6 mL of hexane/2-propanol (9:1, v/v). Eluants from the three cartridges were polled and evaporated to dryness with a gentle stream of nitrogen and reconstituted with methanol to a final volume of 1 mL. A somewhat different methodology was carried out with aminopropyl silica cartridge. They were each cleaned and conditioned with 3 mL of acetone, methylene chloride and hexane. Similar to the previous one, fish extract was divided into three equal portions and loaded onto three conditioned cartridges. 1 mL of hexane and additional 3 mL of hexane were used to wash the cartridge. The analytes were eluted with 7 mL hexane/2-propanol (9:1, v/v). The following procedure is just like the previous one.

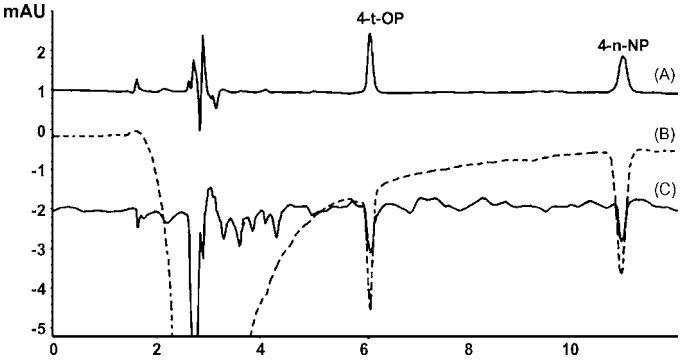


Fig. 1. Chromatogram of standard mixture 4-*n*-NP (1.245 ng μL^{-1}) and 4-*t*-OP (1.288 ng μL^{-1}) (A) and recovered 4-*n*-NP and 4-*t*-OP from spiked extracts of fish tissue (B) and water (C) (extraction conditions – Table 2).

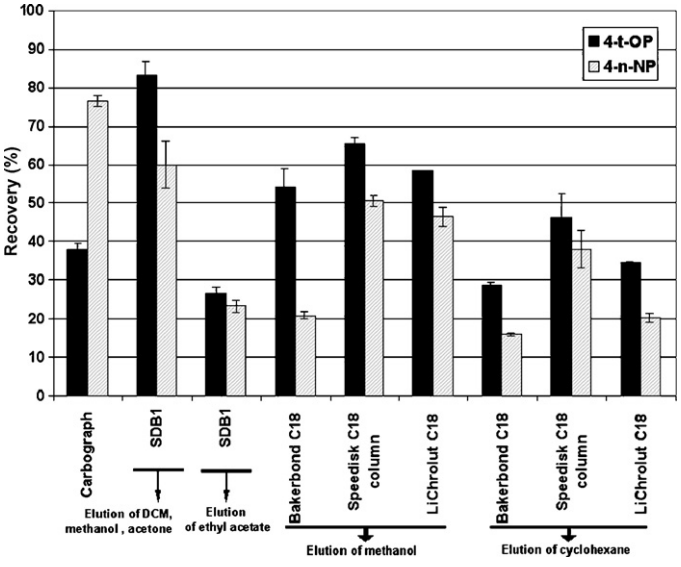


Fig. 2. Recovery of 4-*n*-NP and 4-*t*-OP using different SPE procedures.

Table 3
Parameters of calibration of the 4-*n*-NP and 4-*t*-OP determined by HPLC

Parameters	Abbreviation	Value	
		4-*n*-NP	4-*t*-OP
Concentration range (ng μL^{-1})	c_{st}	1.245–24.9	1.288–25.76
Equation of regression line (for peak area)		$y = 48.452x - 7.5715$	$y = 46.276x - 3.5525$
Correlation coefficient	R^2	0.9984	0.9989
Limit of detection (ng μL^{-1})	LOD	0.06	0.04
Limit of quantification (ng μL^{-1})	LOQ	0.18	0.16

$n = 5$.

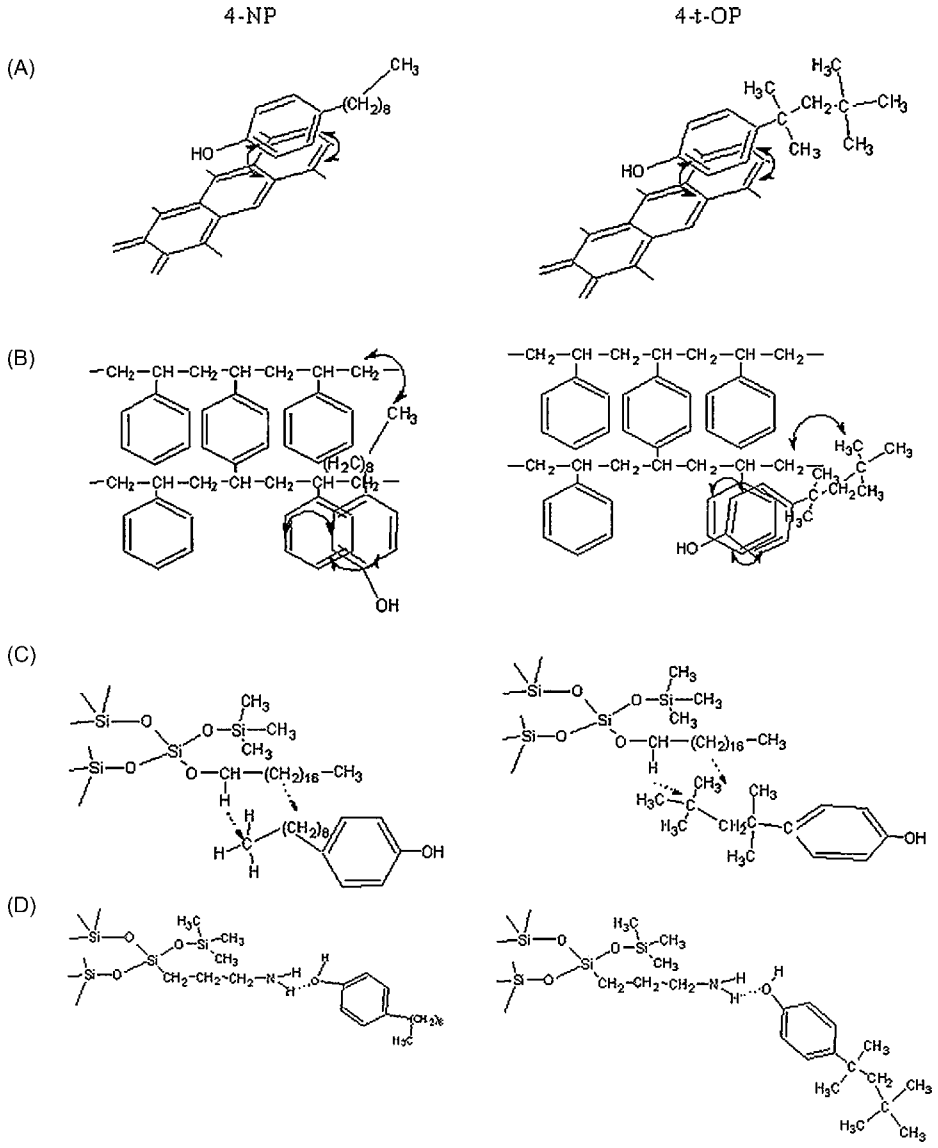


Fig. 3. Scheme illustrating the sorption mechanism of 4-*n*-NP and 4-*t*–OP on the modified surface: graphitized carbon (A), copolymer styrene-divinylbenzene (B), octadecyl (C) and aminopropyl (D) sorbents.

3. Results and discussion

With elution on a reversed-phase column, alkylphenolic compounds were separated depending on alkyl chain length (Fig. 1). Quantitative analysis of 4-*n*-NP and 4-*t*-OP in environmental samples was preceded by fixing the limit of quantification ($LOQ_{4\text{-}n\text{-}NP} = 0.18\ ng\ \mu L^{-1}$ and $LOQ_{4\text{-}t\text{-}OP} = 0.16\ ng\ \mu L^{-1}$) and the limit of detection ($LOD_{4\text{-}n\text{-}NP} = 0.06\ ng\ \mu L^{-1}$, $LOQ_{4\text{-}t\text{-}OP} = 0.04\ ng\ \mu L^{-1}$). The results obtained show that liquid chromatography with UV–Vis detection at a wavelength $\lambda = 277$ nm may be applied for determining this analyte at low concentrations. Linear range was 1.245–24.9 ng μL for 4-*n*-nonylphenol and 1.288–25.76 ng μL for 4-*t*-OP (Table 3).

3.1. Water samples

In order to compare the effectiveness of isolating 4-*n*-NP and 4-*t*-OP from aqueous samples, five methods of solid phase extraction were tested using three different sorbents. Analyzing the obtained results (Fig. 2), one can notice that higher recovery rate (*R*) for 4-*n*-NP is obtained for the first used method SPE with cartridges filled with graphitized carbon black ($R = 76.65 \pm 1.49\%$, coinciding with a previous work [21], where the highest recovery was achieved for carbon packings. Lower values for polymeric sorbent SDB (Table 1) were obtained using the first method (elution with methylene chloride, methanol and acetone) because the recovery is equaled to $59.97 \pm 6.01\%$. The lowest recovery ($R = 16.27 \pm 1.54\%$) of 4-*n*-NP was for Bakerbond C18 sorbent using the second method (elution with cyclohexane). Entirely different results were obtained for 4-*t*-OP. The best procedure SPE of preparation of aqueous sample spiked with 4-*t*-OP was the method with polymeric sorbent (elution with methylene chloride, methanol and acetone). The recovery of 4-*t*-OP was very high $R = 83.08 \pm 3.73\%$. Considerably lower values were received for cartridges filled with graphitized

carbon black (Carbograph) because recovery was equaled to $R = 38.11 \pm 1.50\%$. Therefore, the worst procedure for 4-*t*-OP is method with polymeric sorbent with elution with ethyl acetate. In this case the obtained recovery was: $26.85 \pm 1.36\%$ (Fig. 2.).

It has been shown that carbonic sorbent is very sensitive and effective, but only for 4-nonylphenol. Cross-linked aromatic rings enabled electron-donor interactions between the sorbents and the π bonds of the substance isolated, which additionally intensified the analyte-sorbent interactions (Fig. 3A and B). The aromatic rings of the matrix network permit electron-donor interactions between the sorbent (SDB1) and π bonds of 4-*t*-OP, which may further increase analyte interactions (increasing the energy absorption) (Fig. 3B). In conclusion this typing sorbent is recommended for isolation of 4-*t*-OP, but only in the case when elution is with methylene chloride, methanol and acetone (Fig. 2). The procedure with elution with ethyl acetate is not so effective, neither for 4-*n*-NP nor 4-*t*-OP. From the group of octadecyl C18 sorbents, the highest recoveries for both 4-*n*-NP and 4-*t*-OP were obtained for Speedisk C18 column, independently on the used procedure. The mechanism of isolation of an analyte by a polar surface (Fig. 3D) involves the sorption of the functional groups of the solute in the polar sites of the packing material versus the solubility of the solute in the mobile phase of the column.

3.2. Biological samples

In order to isolate 4-*n*-NP and 4-*t*-OP from biological material like fish tissue of rainbow trout, two programs (Table 2) of accelerated solvent extraction (ASE) was used. Four solvents were tested for the extraction: methanol, methylene chloride, acetonitrile and hexane [29]. Received extracts were cleaned using diol (Supelco) and aminopropyl SPE (J.T. Baker) cartridges. Surprising results were obtained and they are shown in Fig. 4.

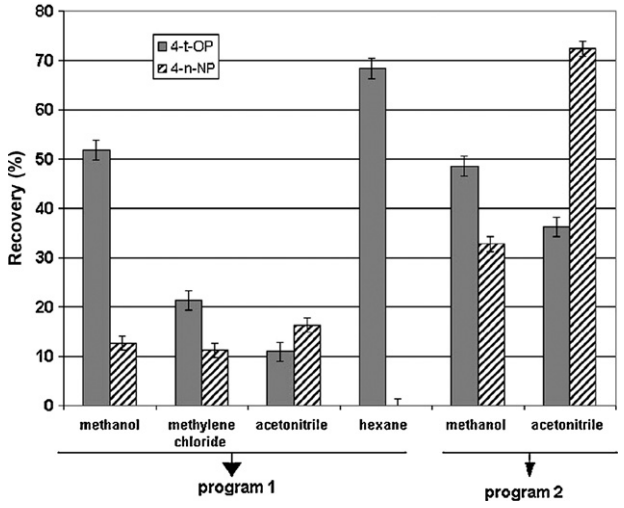


Fig. 4. Comparison of recovery for 4-*n*-NP and 4-*t*-OP obtained using two extraction programs of ASE (Table 2) and purification of extract of fish tissue on aminopropyl silica cartridge.

Analysing this data, it can be observed that a better method for 4-*n*-NP and 4-*t*-OP (compared with propyldiol sorbent) isolation from fish tissue is accelerated solvent extraction coupled with purification of extract on aminopropyl silica sorbent (Table 1, Fig. 3). In the case of ASE method coupled with purification process realized on aminopropyl phases, the highest recovery for 4-*t*-OP was obtained using hexane solvent ($R = 68.32\%$) and extraction condition (program 1, see Table 2). When methanol was used as a solvent, the recovery for 4-*t*-OP was a little lower ($R = 51.89\%$). In the case of using methanol and methylene chloride, values are very similar (methanol: 12.67%; methylene chloride: 11.24%). The satisfactory value for 4-*n*-NP was obtained by using second program of ASE (Table 2) and acetonitrile as a solvent ($R = 72.35\%$).

A somewhat different situation was encountered, when ASE coupled with purification on propyldiol sorbent was used. However, the highest unsatisfactory, recovery for 4-*t*-OP was received applying ethanol ($R = 29.19\%$). However, using hexane as a solvent, this value for 4-*t*-OP was low, because it is equal to 4.35%. On the other hand, when methylene chloride and acetonitrile were applied, there was no peak for 4-*t*-OP on chromatograms. For 4-*n*-NP, a peak was obtained only in the case when methylene chloride was applied, whereas for methanol, acetonitrile and hexane, a peak for this compound cannot be identified.

4. Conclusions

Sample pre-treatment is a very important step in the analysis of APs in water and especially in biological tissues. A preferable technique should require minimum amounts of solvents and be time-efficient. This article describes different procedures of SPE used to prepare aqueous samples. The comparison of recoveries of SPE techniques shows that Carbograph is the best sorbent for 4-*n*-NP preconcentration ($R = 76.65 \pm 1.49\%$), while SDB1 (styrene-divinylbenzene) with elution of DCM, methanol and acetone respectively, is the best choice for 4-*t*-OP enrichment ($R = 83.08 \pm 3.73\%$).

To the isolation of analytes (4-*n*-NP and 4-*t*-OP) from biological sample (fish tissue), rapid and simple ASE method coupled with SPE cleanup was used. Four solvents were tested in ASE, i.e. methanol, acetonitrile, methylene chloride and hexane, and two sorbents in SPE (aminopropyl silica and propyldiol). The best sorbent (used in SPE) for isolation of alkylphenols from fish tissue is aminopropyl silica (APS) because analytes bind to APS, allowing facile cleanup of fish lipids and enabling polar solvents mixture eluting the analytes. In this case, the values obtained from recoveries were considerably lower than from water samples, being $R = 68.32\%$ for 4-*t*-OP using hexane (procedure 1, see Table 2), and $R = 72.35\%$ for 4-*n*-NP using acetonitrile and second program of extraction (see Table 2).

Acknowledgement

This research was financially supported by grant (project No. R05 037 03) from the Ministry of Science and Higher Education (Warsaw, Poland).

References

[1] C. Yaqi, J. Guibin, L. Jingfu, Z. Qingxiang, Anal. Chem. 75 (2003) 2517.
[2] J.A. Brotons, M.F. Olea-Serrano, M. Villalobos, V. Pedraza, N. Olea, Environ. Health Perspect. 103 (1995) 608.
[3] A.C. Nimrod, W.H. Benson, Crit. Rev. Toxicol. 26 (1996) 335.
[4] R.J. Maguire, Water Qual. Res. J. Can. 34 (1999) 37.
[5] M.A. Manzano, J.A. Perales, Wat. Res. 33 (1999) 2593.
[6] M.R. Servos, Water Qual. Res. J. Can. 34 (1999) 123.
[7] A.M.R. Ferreira-Leach, E.M. Hill, Marine Environ. Res. 51 (2001) 75.
[8] M. Ahel, J. McEvoy, W. Giger, Environ. Pollut. 79 (1993) 243.
[9] T. Christiansen, B. Korsgaard, Å. Jespersen, J. Exp. Biol. 201 (1998) 179.
[10] A. Arukwe, S.W. Kullman, K. Berg, A. Goksøyr, D.E. Hinton, Comp. Biochem. Physiol. 132 (2002) 315.
[11] M. Aoki, M. Kurasaki, T. Saito, S. Seki, T. Hosokawa, Y. Takahashi, H. Fujita, T. Iwakuma, Life Sci. 74 (2004) 2301.
[12] R. Thbaut, L. Debrauwer, D. Rao, J.P. Cravedi, Marine Environ. Res. 46 (1998) 521.
[13] S. Jobling, J.P. Sumpter, Aquat. Toxicol. 27 (1993) 361.
[14] B. Berecka, R. Gadzała-Kopciuch, J. Bartoszewicz, B. Buszewski, Anal. Chem. (Warsaw) 48 (2003) 413.
[15] A. di Corcia, R. Cavallo, C. Crescenzi, M. Nazzari, Environ. Sci. Technol. 34 (2000) 3914.
[16] T. Benijts, W. Lambert, A. de Leenheer, Anal. Chem. 76 (2004) 704.
[17] T. Tsuda, A. Takino, M. Kojima, H. Harada, K. Muraki, J. Chromatogr. B 723 (1999) 273.
[18] M. Zhao, F. van der Wielen, P. de Voogt, J. Chromatogr. A 837 (1999) 129.
[19] T. Tsuda, A. Takino, M. Kojima, H. Harada, K. Muraki, M. Tsuji, Chemosphere 41 (2000) 757.
[20] J.M. Dominic, F.W. Graham, J. Bacteriol. 180 (17) (1998) 4332.
[21] R. Gadzała-Kopciuch, B. Berecka, T. Ligor, B. Buszewski, J. Liq, Chromatogr. Related Technol. 27 (19) (2004) 2997.
[22] M. Petrovic, A. Diaz, F. Ventura, D. Barceló, Anal. Chem. 73 (2001) 5886.
[23] S. Datta, J.E. Loyo-Rosales, C.P. Rice, J. Agric. Food Chem. 50 (2002) 1350.
[24] K. Inoue, Analyst 125 (2000) 1959.
[25] K. Inoue, M. Kawaguchi, F. Okada, N. Takai, Y. Yoshimura, M. Horie, S. Izumi, T. Makino, H. Nakazawa, Anal. Chim. Acta 486 (2003) 41.
[26] A. Diaz, L. Vazquez, F. Ventura, M.T. Galceran, Anal. Chim. Acta 506 (2004) 71.
[27] J. Loyo-Rosales, I. Schmitz-Afonso, C.P. Rice, A. Torrents, Anal. Chem. 75 (2003) 4811.
[28] B.L.L. Tan, M.A. Mohd, Talanta 61 (2003) 385.
[29] B. Buszewski, Encyclopedia of Separation Sciences, Academic Press, London, 2000.

Available online at www.sciencedirect.com
ScienceDirect
Talanta 74 (2008) 930–935
Talanta
www.elsevier.com/locate/talanta

Comparing the effect of sub-critical water extraction with conventional extraction methods on the chemical composition of *Lavandula stoechas*

E. Sultan Giray [a,*], Saliha Kırıcı [b], D. Alpaslan Kaya [b,c], Murat Türk [a], Özgür Sönmez [a,d], Memet İnan [b]

[a] *Department of Chemistry, Faculty of Science and Arts, Çukurova University, 01330 Adana, Turkey*
[b] *Department of Field Crops, Faculty of Agriculture, Çukurova University, 01330 Adana, Turkey*
[c] *Department of Field Crops, Faculty of Agriculture, Mustafa Kemal University, 31020 Hatay, Turkey*
[d] *Department of Chemistry, Faculty of Science and Arts, Mersin University, 33030 Mersin, Turkey*

Received 31 January 2007; received in revised form 18 July 2007; accepted 30 July 2007
Available online 15 August 2007

Abstract

The volatile extract composition of *Lavandula stoechas* flowers obtained by hydrodistillation (HD), subcrtical water extraction (SbCWE) and organic solvent extraction under ultrasonic irradiation (USE) were estimated by gas chromatography–mass spectrometry (GC–MS). One hundred and twenty four components were detected in SbCWE extracts while 94 and 65 signals were gained from HD and USE extracts, respectively. Most of the constituents were identified. The major compounds in all three extracts were fenchon, camphor, myrtenyl acetate, myrtenol and 1,8-cineol, but they differ in quantitatively. The total monoterpene hydrocarbons are higher in HD and USE extracts than those of SbCWE extract. However, SbCWE extract had higher concentration of light oxygenated compounds which contributes to the fragrance of the oil in a major extension. Heavy-oxygenated compounds was also in higher abundance in SbCWE extract (9.90%) than those of HD and USE extracts (3.19 and 4.78%, respectively). Effect of temperature on the extraction yield of SbCWE was investigated and while oil yield was increasing with an increase in temperature, a decrease in the extraction ability of sub-critical water toward the more polar compounds such as, 1,8-cineol, camphor and fenchon, was observed. Kinetic studies shown that SbCWE is clearly quicker than conventional alternatives. Most of components of volatile compounds were extracted at 15 min.
© 2007 Elsevier B.V. All rights reserved.

Keywords: Sub-critical water extraction; Essential oil; *Lavandula stoechas*

1. Introduction

Lavandula genus is an important member of Labiatae (Lamiaceae) family. *Lavandula* species are widely distributed in the Mediterranean region and cultivated in France, Spain and Italy. In Turkey, mainly two species, *Lavandula stoechas* and *Lavandula angustifolia* and their subspecies and hybrid forms grow wildly or are cultivated. *Lavandula* species are great commercial value due to their intense and pleasant aroma. Both the plant material and its essential oil are mainly demanded in perfumery, cosmetic, and food industries. The medicinal importance of the plant is well documented and the drugs prepared from this plant are registered in many Pharmacopeia [1]. The plant is used as expectorant, antispasmodic, carminative, a good stimulan, deobstruent, resoluent and wound healing. The essential oil obtained from its flowering twigs has been used as a remedy against colic and chest affections, to relieve nervous headache, bliousness and for cleansing wounds [2].

With better understanding of natural products, researchers have become interested in studying the active natural products as medicine**,** food additives or as natural pesticides [3]. The pharmaceutical studies of natural products are one of the most interesting and active research areas. Since pharmacologically active compounds in herbal plants usually are in low concentration, a great deal of research has been done to develop more effective and selective extraction methods for recovery of these compounds from the raw materials**.** The conventional methods used to prepare essential oils are steam distillation and solvent extraction. Steam distillation is also most used methods to prepare essential oils on a commercial basis. However, there are few

* Corresponding author. Tel.: +90 322 338 74 11; fax: +90 322 338 60 70.
E-mail address: esgiray@cu.edu.tr (E.S. Giray).

0039-9140/$ – see front matter © 2007 Elsevier B.V. All rights reserved.
doi:10.1016/j.talanta.2007.07.040

adjustable parameters to control the selectivity of these methods. Therefore, developing alternative extraction methods and with better selectivity and efficiency are highly desirable. Recently, more efficient extraction methods, such as supercritical fluid extraction (SCFE) have been used for the isolation of organic compounds from various natural products [4,5]. Because SCFE has several distinct properties, it is regarded as a promising alternative technique to conventional solvent extraction method. Most widely used supercritical fluid is (SCF) CO_2 because of its preferred critical properties, low toxicity and chemical inertness [6]. It has also an advantage with its low critical constants over other SCF. This technique has recently been used for the isolation of essential oils from plants [7–9]. However, CO_2 is not enable to dissolve some moderately polar compounds such as alcohols, esters, aldehydes and ketons.

In recent years, a continuo and static sub-critical water extraction technique has been used for extraction of solid materials. Sub-critical water extraction uses water as an extractant at temperatures between 100 and 374 °C and at a pressure high enough to maintain the liquid state. It has been reported that sub-critical water for the extraction of essential oils is a powerful alternative, because it enables a rapid extraction and the use of low working temperatures [6,10–16]. This avoids the loss and degradation of volatile and termolable compounds. It is also simple and has a favourable environmental impact.

The main objectives of this study was to develop an approach for the SbCW extraction of medicinal essential oils and to compare the proposed method with others based on the use of hydrodistillation, organic solvent extraction under ultrasonic irradiation. It was also aimed to introduce an alternative; faster and cheaper method in the pharmaceutical and food field.

2. Experimental

2.1. Plant materials

L. stoechas was harvested at flowering stage (March 2004) from an experimental field of Cukurova University, Adana. Flower's spikes were separated from the branch and dried at room temperature.

2.2. Sub-critical water extraction (SbCWE)

Sub-critical water extraction was performed in a laboratory built apparatuses. The water was sonicated to remove dissolved oxygen then was used in an HPLC pump programmed for a constant flow of 1 mL min^{-1}. The extractor heated in a temperature programmable oven. A 2 m long pre-heated coil was used to equilibrate the water to the desired temperature. A 14 mL extraction cell equipped with 10 μm frit at the inlet and outlet, was connected to a 1 m cooling loop out side of the oven. Extraction cell contained sea sand at both ends. SbCWE was carried out using 2 g of *L. stoechas* flower's spikes at temperatures 100, 125 and 150 °C, a pressure of 60 bar and 30 min extraction time. After SbCWE, a liquid–liquid extraction step was performed by using 5 mL dichloromethane (DCM). Extract and DCM placed in a separation funnel and about 1 g NaCl was added to facilitate the breaking the emulsion. Extraction was carried out in triplicate.

2.3. Ultrasound-assisted extraction (USE)

Ultrasound-assisted extraction was performed in an ultrasound cleaning bath (Lab-Line Instruments Inc. 9314-1 model, 310 380 200 mm internal dimensions) at the fixed-frequency of 35 kHz. The temperature of the sonicated bath was 25 °C. The 50 mL sample flask was charged with 2 g *L. stoechas* flower's spikes and 30 mL of *tert*-butylmethyl ether. Sonication was held for 18 h. Extraction was carried out in triplicate.

2.4. Hydrodistillation (HD)

Hundred grams of *L. stoechas* flower's spikes were submitted for 3 h to water distillation using a Clevenger type apparatus. A liquid–liquid extraction step was performed as described for SbCWE.

2.5. GC–MS analysis

Qualification and quantification were carried out by using a Finnigan-Trace GC–MS equipped with an auto sampler. One microlitre of sample volume was injected using split method with 50 split ratio. Chromatographic separations were accomplished with a Zebron ZB-5 capillary column (5% phenyl–95% dimethylpolysiloxane, 0.25 mm i.d. × 60 m, film thickness 0.25 μm) with injections in the split mode with 50 split ratio. Analysis was carried out using helium as the carrier gas, flow rate 1.0 mL/min. The column temperature was programmed from 50 to 240 °C at 3 °C/min. The sample size was 2 mL. The injection port temperature was 250 °C. The ionization voltage applied was 70 eV, mass range *m/z* 41–400 a.m.u. The separated components were identified tentatively by matching with GC–MS results of National Institute of Standards and Technology (NIST) mass spectral library data because their reference reagent were not available. The quantitative determination was carried out based on peak area integration.

3. Results and discussion

3.1. Chemical composition of the SbCWE, HD and USE extracts

A comparison of the composition of the extracts is reported in Table 1, from which two main facts can be inferred: (a) the identified components of EO is similar in all of the extracts; (b) substantially higher amounts of oxygenated compounds are present in the SbCW extract while monocyclic terpenes were almost absent in the extract. The other variable was the extraction yield, expressed in mass ratio of the extract to the starting dried material.

[*Y* % = g of extract/g of dried material × 100]. The yield of essential oil is highest in the sub-critical water extract. The overall yield of essential oil of *L. stoechas* obtained by HD,

Table 1
Essential oil constituents of Lavandula stoechas determined by GC-MS*

Component	Type	Area %		
		SbCWE	HD	USE
α-Pinen	M	t	2.94	0.41
Camphene	M	t	2.08	0.62
Limonen	M	t	2.52	0.31
1,8-Cineol	LOC	4.38	7.67	3.06
Epoxy linalool	LOC	1.25	0.78	0.31
Fenchon	LOC	26.93	32.03	34.23
Linalool	LOC			
β-Pinen	M	0.96	1.64	–
Camphor	LOC	29.64	14.71	41.09
p-Mentha-1,5-dien-8-ol	LOC	0.53	0.25	0.31
Isoborneol	LOC	0.52	0.25	–
4-Terpineol	LOC	0.70	0.55	
p-Cymen-8-ol	LOC	1.42	0.61	0.65
α-Terpineol	LOC	1.05	0.62	
Myrtenol	LOC	3.82	1.95	0.84
Verbenone	LOC	1.18	0.10	0.64
trans-Carveol	LOC	0.87	0.17	0.78
Carvon	LOC	1.08	1.24	0.26
Bornyl acetate	LOC	0.31	1.68	1.97
Myrtenyl acetate	LOC	1.66	11.70	4.97
Terpendiol	LOC	0.72	0.13	–
α-Campholenic acid	LOC	t		0.63
Myrtensaeure	LOC	1.53	t	t
(+) Cycloisosativene	S	0.23	0.62	0.25
2(E)-4-Methyl-3-penteylidene-Butadienal	LOC	0.77	–	–
Sesquisabinenhydrate	HOC	0.16	1.68	0.48
δ-Cadinol	HOC	0.14	1.17	0.24
δ-Cadinene	S	–	0.58	0.14
3-Caren-10-al	LOC	3.16	0.20	0.30
α-Cetone	HOC	0.51	0.20	
$C_{15}H_{22}O$	HOC	t	0.65	
Nopyl acetate	LOC	1.55	0.49	0.21
Caryophyllene oxide	HOC	0.21	0.56	0.16
Viridiflorol	HOC	0.16	2.32	1.17
Epiglobulol	HOC	0.13	0.12	0.62
$C_{15}H_{22}O$	HOC	0.31	0.97	0.17
$C_{17}H_{24}O$	HOC	0.85	0.19	0.14
Izovelleral	HOC	0.54	–	–

USE and SbCWE techniques was 1.61 ± 0.03; 3.92 ± 0.03 and 4.19 ± 0.05 g/100 g dried flower, respectively.

Fig. 1 shows GC–MS chromatograms of essential oils of *L. stoechas* flowers extracted by HD, SbCWE and USE methods. Generally fenchon and camphor were found as major compounds and associated with 1,8-cineol, myrtenol and myrtenylacetate in all extracts. Unidentified compounds were present with very low contents. Although, the main components were similar, the results of GC–MS analysis indicated that, chemical composition of the extracts of this three extraction methods differ qualitatively and quantitatively. For SbCWE extract, 124 GC signals were determined with the major components as camphor (29.64%), fenchon (26.93%), 1,8-cineol (4.38%), myrtenol (3.82%) and 3-caren-10-al (3.16%). Fenchone and camphor were also found the major volatile components in $SCCO_2$ extracts of Turkish Lavender flowers [17]. The essential oil constituent of HD extract gave 94 GC signals with the major constituents as fenchon (32.03%), camphor (14.71%), myrtenyl acetate (11.70%) and 1,8-cineol (7.67%). GC–MS analysis of USE extract revealed only 65 component with most dominant constituent Camphor (41.09%). In USE extract, the relative amount of fenchon 34.23%, of myrtenyl acetate 4.97% and of 1,8-cineol 3.06%. The fenchone/camphor ratios of SbCWE, HD and USE extracts were 0.90; 2.17 and 0.83, respectively. Other compounds such as bornyl acetate, carvon, linalool oxide, verbenone, nopyl acetate and viridifloral were present almost in all extracts. It is well known that a good Lavender contains high portion of linalyl acetate and linalool and a low portion of camphor [ref]. However, the dominant components of lavender species especially Lavandula Stoaches L. from Turkey, Corsica, Crete, Spain, Cyprus, Morocco and France are camphor and fenchone or cineol and myrtenyl acetate and the levels of linalyl acetate and linalool are very low or absent [17–20]. It is also well known that the fragrance composition of plants varies with the species, cultivation environment, weather condition, region, harvesting season and extraction method.

The quality and price of some essential oils are based on the percentage content of some components contained in the essential oil, so separation and measurement of these components is very important. Terpenic hydrocarbons are unstable to heat and light and they degrade to produce the compounds with undesirable off-flavours when exposed to light or heat for long a time. Furthermore, terpene hydrocarbons do not contribute much to the flavour or fragrance of the oil, even at higher concentrations [21]. The removal of limonene and other monoterpene hydrocarbons is necessary to stabilize and concentrate the flavour product to enable its use in the food and perfumery industries. However, the oxygenated compounds such as aldehydes, esters and alcohols determine the characteristic flavour and odour of essential oils so valuable for their application in a number of industries.

To clarify the efficiency of the extraction techniques on the chemical composition of the Lavandula stoaches volatile extracts, the identified compounds were classified into four main groups; monoterpenes (M), sequiterpenes (S), low molecular weight oxygenated compounds (LOC) and heavy molecular weight oxygenated compounds (HOC). The flavour compound of Lavandula consists mainly of light oxygenated compounds such as camphor, fenchnon or linalool and linanyl acetate according to the location of grow. As seen from Fig. 2 , monoterpenes constitute the second predominant group of the HD extract (10.51%) and of the USE extract (1.67%) but the same group constitutes only 0.42% in the SbCWE extract. This difference may be due to the fact that these compounds are highly volatile and not completely trapped in the depressurizing step of the SbCWE. Low molecular oxygenated compounds constitute the major class in the all three extracts but USE extract possessed highest in the relative abundance of this class (92.93%) than those of SbCWE and HD extracts (85.59 and 84.04%, respectively). Heavy molecular weight oxygenated compounds was in higher abundance in SbCWE extract (9.90%) than those of HD and USE extracts (3.19 and 4.78%, respectively). Cycloisosativene was the only sesquiterpene identified in the SbCWE while cycloisosativene and δ-cadinene were the only sesquiterpenes identified in HD and USE extracts. In this study, SbCWE was found a compound class selective extraction method, because of lower concentration of monoterpenes

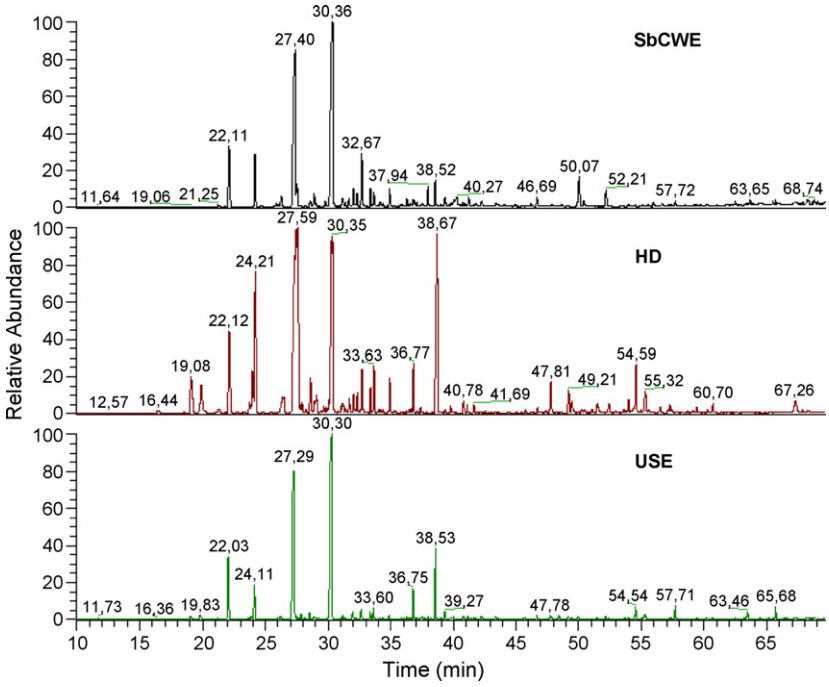


Fig. 1. GC–MS chromatograms of essential oils of *Lavandula stoechas* flowers extracted by SbCWE, HD, and USE methods.

and the higher amount of oxygenated compounds in essential oil from Lavandula stoaches L. from Turkey.

4. Extraction at individual temperatures

The optimal sub-critical water extraction conditions were decided upon by using various pressure and temperatures. The pressures studied were 40, 60, 70 and 90 atm. It was observed that there were no significant differences in the yield of extraction. Hence a pressure of 60 (±6) atm was selected for further experiments because of being an intermediate value. Therefore, we considered the interest of evaluating the ability of the sub-critical water at the different temperatures toward the specific extraction of different compounds. Dried *Lavandula* flowers were extracted at 100, 125 and 150 °C to compare the effect of temperature on the yield of EO and the chemical composition of the extract. The yields of essential oils of *Lavandula stoaches* flowers were 1.61 ± 0.03; 1.69 ± 0.03 and 1.67 ± 0.03% at 100, 125 and 150 °C, respectively. The yields are given as weight percentage on the basis of 100 g dried flowers. They are the means of the three experiments and the relative standard deviation was in a range 2–4%. Although, fenchon and camphor were recovered as major components at all three experiments, GC–MS analysis of essential oils of extract at 150 °C resulted only 52 signals but 122 and 128 signals were received from 125 and 100 °C extracts, respectively. These results showed that only half of the all components obtained at higher temperature. A burning smell of extract appeared during the extraction at 150 °C and the colour of extract was darker than those of 100 and 125 °C extracts. Therefore, 100 °C was chosen for the further kinetic studies (Fig. 3)

In Table 2, most abundant constitutes of the three different temperature extracts were presented. As seen from table, light-

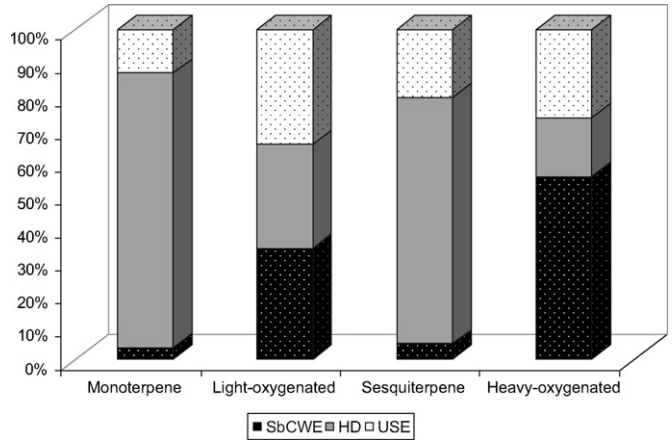


Fig. 2. Effect of HD, SbCWE and USE techniques on the main chemical classes of the *Lavadula Stoaches* flowers extracts.

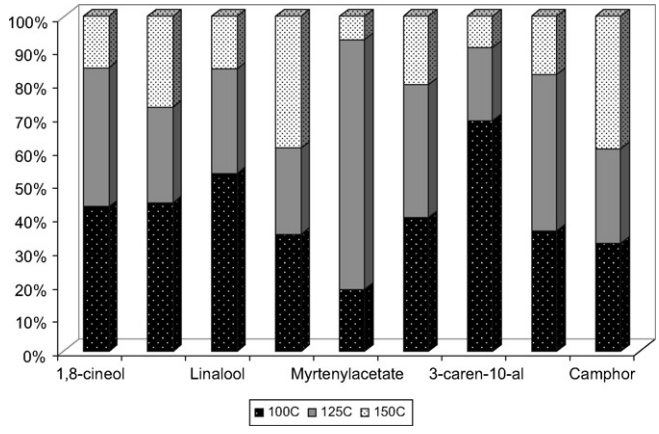


Fig. 3. Effect of the temperature on the most abundant constituents of *Lavadula Stoaches* flowers extracts.

Table 2
Essential oil composition of Lavandula stoaches extracts obtained by sub-critical water at different temperatures

	Area %		
	100 °C	125 °C	150 °C
Essential oil content (%)	1.61	1.69	1.68
1,8-Cineol	4.16	4.01	1.48
Epoxy linalool	1.19	0.76	0.73
Linalool	1.01	0.59	
Fenchone	25.58	18.99	28.98
Fenchyl alcohol	1.00	0.67	0.51
Camphor	28.15	24.66	34.62
$\tilde{p}$-Cymen$\widetilde{8}$ol	1.35	1.39	1.77
α-Terpineol	0.84	0.99	–
Myrtenol	3.63	4.75	1.76
Verbenone		0.95	1.03
Fenchyl acetate	1.00	1.50	0.62
Carvon	1.03	1.03	0.53
3-Caren-10-al	3.00	0.95	0.40
Bornyl acetate	0.29	1.08	0.50
Myrtenyl acetate	1.57	6.36	0.6
Myrtensauere	1.45	0.73	1.76
Nopyl acetate	1.47	0.46	0.21
Dehydroaromadenrene	–	1.62	–
Viridifloral	0.15	2.58	–

oxygenated compounds constitute the major class in all extracts but the extract of at 100 °C possessed higher concentration of this class than those of at 125 and 150 °C. The number of components common at all temperatures is 37. Some of the components (39) observed only at 100 °C and some available (27 and 8) at only 125 and 150 °C, respectively. As seen from Table 2, solubility of major constituents did not show a smooth change by an increase in temperature. Relative abundances of fenchone, camphor, *p*-cymen-8-ol and myrtensaeure were found highest at 150 °C. Solubility of myrtenol, myrtenylacetate, fenchylacetate, bornylacetate, 3-caren-10-al, carvon, dehydroaromadendrene, viridifloral and sesquisabinenhydrate was highest at 125 °C while 1,8-cineol, linalool oxide, linalool, fenchyl alcohol, carvon, myrtensaure and nopylacetate reached maximum relative amount at 100 °C. The result indicated that high oxygenated compounds and sesquiterpenes were extracted mostly at 125 °C while light oxygenated compounds were extracted mostly at 100 °C. Fig. 2 shows, as a bar diagram, the composition of the oxygenated compounds of the extracts obtained at the three different individual temperatures tested. As can be seen, when temperature increased from 100 to 150 °C, a decrease in the extraction ability of sub-critical water toward the more polar compounds such as, 1,8-cineol, linalool and linalooloxide, was observed. On the contrary, Miller and Hawthorne reported that the solubility of some Essential oils such as d-limonen, carvon, euguneol, 1,8-cineol and nerol increased with increasing temperature [22].

5. Effect of the static extraction time on the overall extraction kinetics

The influence of the static extraction time both the extraction kinetics and composition (quality) of the oil was studied by performing extraction with sub-critical water at 100 °C with static extraction times of 0, 5, 10, 15, 20, 25 and 30 min followed by 20 min of dynamic extraction. The influence of extraction time on the extraction kinetics for main common components (camphor, fenchon, 1,8-cineol, myrtenol, myrtenylacetate and 3-caren-10-al) is shown in Table 3 and in Fig. 4, as bar diagram. As seen from both of them, extraction for most abundant two components, fenchon and camphor was mostly completed at 15 min. Other major components, 1,8-cineol, myrtenol and myrtenyl acetate were reached the relative maximum amount at 20 min of the extraction. The behaviour of the compounds allowed them to be divided into the following three groups:

(1) compounds in which the extraction kinetics reaching the maximum at first 5 min of the extraction, such as myrtenyl acetate, verbenone, carvon and myrtenol;
(2) compounds with no correlation between static extraction time and kinetics of extraction, but the extraction completed at 15 or 20 min such as camphor, fenchon, 1,8-cineol, 3-caren-10-al, nopyl acetate and linalool oxide;
(3) compounds in which the extraction kinetic did not change by time such as carvon, verbenone, bornyl acetate, myrtenol and bornyl acetate.

Table 3
Comparison of the chemical composition of *Lavadula Stoachas* flowers extracts obtained at different static extraction time at 100 °C with sub-critical water

	5 min	10 min	15 min	20 min	25 min	30 min
Components						
1,8-Cineol	3.5	2.7	5.8	0.4	3.5	4.2
Epoxy Linalool	2.0	0.8	2.3	1.4	2.1	1.2
Linalool	1.1	0.3	0.2	0.2	0.5	1.0
Fenchone	22.8	25.2	33.4	20.5	32.5	25.6
Camphor	28.9	26.0	26.1	32.6	28.3	28.2
Myrtenol	2.5	1.9	2.1	1.4	1.3	3.6
1-Verbenone	1.3	1.0	0.7	1.1	1.0	0.3
Carvon	0.9	0.9	0.6	0.8	0.5	1.0
3-Caren-10-al	3.1	4.3	2.7	5.3	2.0	3.0
Bornyl acetate	0.5	0.4	0.5	0.4	0.6	0.4
Myrtenyl acetate	1.3	0.7	0.7	0.7	0.4	1.6
Myrtensauere	1.4	1.1	0.7	0.6	1.5	1.0

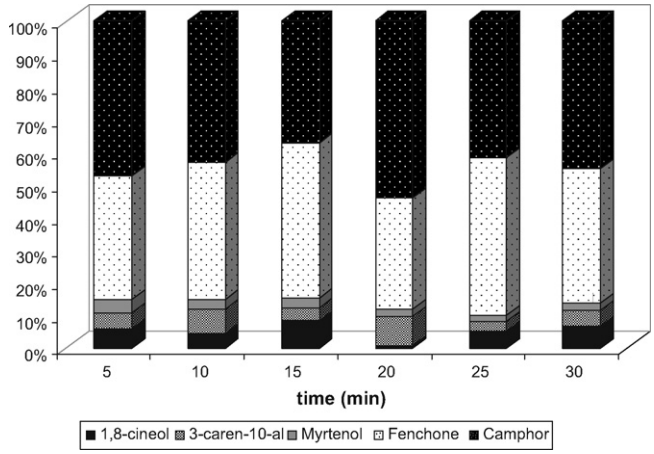


Fig. 4. Effect of the extraction time on the most abundant constituents of *Lavadula Stoaches* flowers extracts.

6. Conclusions

(1) Essential oil of SbCW extract was poor for cyclic monoterpenes, however, oxygenated compounds were found in higher amounts. The quality of the oil can be linked to the amount of oxygenated compounds present in it. According to these facts, sub-critical water can be suggested as a good extractant for the extraction of essential oils from *L. stoechas*.
(2) Sub-critical water extraction is clearly quicker than conventional alternatives. Total extraction time of 55 min (consisting of 30 min of static extraction plus 20 min of dynamic extraction) was used during SbCWE whereas 3 h is required in hydrodistillation and 18 h for organic solvent extraction.
(3) SbCWE is also a very clean method which avoids both the use of large amounts of organic solvent and generation of toxic residue. The aroma of the essential oil produced by this method was also found to be more concentrated and powerful than that of the HD and USE.
(4) According to the GC–MS results, optimum extraction temperature for SbCWE of *L. stoechas* decided as 100 °C.

References

[1] A.C. Goren, G. Topcu, G. Bilsel, M. Bilsel, Z. Aydogmus, J.M. Pezzuto, Z. Naturforsch. 57 (2002) 797.
[2] I. Gulcin, I.G. Sat, S. Baydemir, M. Elmastaş, O.I. Kufrevioglu, Food Chem. 87 (2004) 393.
[3] Q. Lang, C.M. Wai, Talanta 53 (2001) 771.
[4] A. Kubatova, A.J.M. Lagadec, D.J. Miller, S.B. Hawthorne, Flav. Fragr. J. 16 (2001) 64.
[5] M. Moldao-Martins, A. Palavra, M.D. Beirao da Costa, M.G. Bernardo-Gil, J. Supercrit. Fluids 18 (2000) 25.
[6] V. Fernandez-Perez, M.M. Jimenez-Carmona, M.D. Luque de Castro, Analyst 125 (2000) 481.
[7] E. Reverchon, F. Senatore, J. Agric. Food Chem. 42 (1994) 154.
[8] S.B. Hawthorne, D.J. Miller, Anal. Chem. 70 (1998) 472.
[9] S.B. Hawthorne, M.L. Riekkola, K. Serenius, Y. Holm, R. Hiltunen, K. Hartonen, J. Chromatogr. A 634 (1993) 297.
[10] R.S. Jimenez-Carmona, J.L. Ubera, M.D. Luque de Castro, J. Chromatogr. A 855 (1999) 625.
[11] R.S. Ayala, M.D. Luque de Castro, Food Chem. 75 (2001) 109.
[12] A. Kubatova, D.J. Miller, S.B. Hawthorne, J. Chromatogr. A 923 (2001) 187.
[13] L. Gamiz-Gracia, M.D. Luque de Castro, Talanta 51 (2000) 1179.
[14] A. Basile, M.M. Jimenez-Carmona, A.A. Clifford, J. Agric. Food Chem. 46 (1998) 5205.
[15] A.A. Clifford, A. Basile, S.H.R. Al-Saidi, Fresenius J. Anal. Chem. 364 (1999) 635.
[16] N. Ada, S. Dinçer, E. Bolat, J. Supercrit. Fluids 7 (1994) 93.
[17] D. Ristorcelli, F. Tomi, J. Casanova, Flav. Fragr. J. 13 (1998) 154.
[18] N.S. Kim, D.S. Lee, J. Chromtogr. A 982 (2002) 31.
[19] M. Skoula, C. Abidi, E. Kokkalou, Biochem. Syst. Ecol. 24 (1996) 255.
[20] M.Z. Ozel, F. Gogus, A.C. Lewis, Food Chem. 82 (2003) 381.
[21] M. Kondo, N. Akgun, M. Goto, A. Kodama, T. Hirose, J. Supercrit. Fluids 23 (2002) 21.
[22] D.J. Miller, S.B. Hawthorne, J. Chem. Eng. Data 45 (2000) 315.

Available online at www.sciencedirect.com
ScienceDirect
Talanta 74 (2008) 1032–1037
Talanta
www.elsevier.com/locate/talanta

A novel sensor based on the porous plastic probe for determination of dissolved oxygen in seawater

Liangqia Guo, Qinyan Ni, Jiaqian Li, Lan Zhang, Xucong Lin, Zenghong Xie, Guonan Chen *

Ministry of Education Key Laboratory of Analysis and Detection Technology for Food Safety (Fuzhou University), Fuzhou, Fujian 350002, China

Received 29 May 2007; received in revised form 12 August 2007; accepted 13 August 2007
Available online 22 August 2007

Abstract

A new sensor based on the porous plastic probe has been developed for the detection of dissolved oxygen. This probe was prepared by co-polymerization of monomer, cross-linking reagent, porogent and luminescent ruthenium(II)diimine complex. The porous plastic probe exhibits good response to dissolved oxygen and resistance to indicator leaching out due to its high hydrophobicity. The preparation and characteristics of the probe were investigated in detail. This porous plastic probe serves as analyte-sensitive function as well as optical wave-guide, which make it easy to assemble the fiber-optical chemical sensor (FOCS). The developed sensor has been applied to the determination of dissolved oxygen in seawater with satisfactory results compared with the standard method.
© 2007 Elsevier B.V. All rights reserved.

Keywords: Porous plastic optical fiber; Dissolved oxygen; Fiber-optical chemical sensor; Co-polymerization

1. Introduction

The determination of dissolved oxygen is of great importance in environmental, biomedical and industrial analysis. Considerable efforts have been devoted to the development of optic oxygen sensors. These sensors have great advantages over electrochemical devices, such as no oxygen consumption in the sensing process, no requirement for reference electrode, inertness against sample flow rate or stirring speed, and immunity to exterior electromagnetic field interference [1].

Usually, the optical film of an optical sensor consists of an analyte-sensitive dye and a support matrix. Besides being inert, suitable matrices must be able to disperse or dissolve the dye, be permeable to oxygen and hydrophobic to isolate other ions. Among the published literatures, sol–gel-based films or nanoparticles [2–9] have been proven to be promising matrices for oxygen sensing, due to their high oxygen permeability, optical transparence, and good mechanical and chemical stability. Although the sol–gel technique has been used increasingly in the fabrication of chemical and biochemical sensors, the success of manufacturing a sol–gel film depends heavily on the rates of hydrolysis and the condensation process, both of which are greatly affected by a number of parameters including precursor type, water/precursor mole ratio, catalyst type, pH, relative humidity and temperature [2]. It is difficult to control the sol–gel process and to obtain reproducible sol–gel films. In addition, the sol–gel films are generally very brittle and easy to break upon mechanical shock [1]. Other matrices which have been addressed such as polydimethylsiloxane polymer [10], siliceous zeolite [11], mesoporous silica [12], silicone rubber [13,14], silica gel [1], polystyrene [15–18], polyvinylchloride (PVC) and ethyl cellulose (EC) [19], cellulose acetate butyrate (CAB) and poly methyl methacrylate (PMMA) [20]. In addition, a composite matrix [21–23] or co-polymer [24] has also been used.

Optical dissolved oxygen sensors are generally fabricated by spreading the dissolved sensing material on planar surfaces, dip-coating on fibers or by spin-coating technique. The film sensing membranes help oxygen diffuse from the surrounding medium into the films and result in relatively fast response times. However the thin films suffer from two drawbacks in practical application. Firstly, the sensitive dyes or indicators in the thin membranes are apt to leaching out. Secondly, the sensing mem-

* Corresponding author. Tel.: +86 591 87893315; fax: +86 591 83713866.
E-mail address: gnchen@fzu.edu.cn (G. Chen).

0039-9140/$ – see front matter © 2007 Elsevier B.V. All rights reserved.
doi:10.1016/j.talanta.2007.08.014

brane cannot withstand abrasive in aqueous environments and are apt to brush off from the probe over a long period of time.

Porous fiber-optic sensors are developed due to their high sensitivity and convenience for loading of reagent-phase. Glass is one of the general matrices of porous fiber-optic sensor. Zhou et al. [25] used a porous glass fiber-optic sensor for the high-sensitivity measurement of humidity. But it was very difficult to prepare and treat this kind of porous glass optical fiber, the lifetime of the probe is limited due to its crisp mechanism property, and the indicators adsorbed physically onto the porous glass matrix are easily leaked out. To overcome these problems, we developed a novel porous plastic probe [26] by co-polymerization technique. This porous plastic probe serves as analyte-sensitive function as well as optical wave-guide, so it is easy to couple with the common optic fiber. Moreover, the probe exhibits good gas permeability, optical transparence, physical and mechanical properties. In this work, we fabricated a porous plastic probe for dissolved oxygen. The fluorescent ruthenium diimine complex tris(4,7-diphenyl-1,10-phenanthroline) ruthenium(II)chloride [3,7,23,27,28], $[Ru(dpp)_3]Cl_2$, was chosen as the sensing reagent because of its highly emissive metal-to-ligand charge transfer state, long lifetime, high luminescence quantum yield and large stokes shift. Furthermore, the strong absorption in the blue–green region of the spectrum is more compatible with high-brightness blue light-emitting diodes. The fabrication and characterization of the porous plastic probe were investigated in this paper, and a fiber-optical chemical sensor was developed for determination of dissolved oxygen in seawater.

2. Experimental

2.1. Chemicals

Tris(4,7-diphenyl-l,l0-phenanthroline)ruthenium(II)Chloride ($[Ru(dpp)_3]Cl_2$) used as an oxygen sensitive indicator was synthesized as described in Ref. [29]. Diethylene glycol dimethacrylate (DGDM), isobutyl methacrylate (IBM) and 2,2,3,3-tetrafluoropropyl methacrylate (TFPM) were all obtained from Sigma. Before polymerization, IBM and TFPM were washed with 0.5 mol L^{-1} NaOH in order to remove the inhibitor, followed by washing in double-distilled water to pH 7.0, then dried with $MgSO_4$. Azobis (isobutyronitrile) (AIBN) was recrystallized from ethanol before use.

2.2. Fabrication of the porous plastic probe

IBM and TFPM were chosen as the monomers, DGDM as the cross-linking reagent, $Ru(dpp)_3Cl_2$ as the indicator, toluene as the porogent and AIBN as the initiator. Monomer, cross-linking reagent, porogent, indicator and initiator were mixed equably at a proper ratio, and then the mixture was injected into a 10 cm length glass capillary (200 μm in diameter). The glass capillary was then sealed by an adhesive. When the adhesive was solidified, the glass capillary was immersed in water at about 60 °C for 24 h to complete the polymerization. After polymerization, the uniform optical transparent plastic polymer was pulled out of the capillary. And then it was put in ethanol to remove the porogent and superfluous indicator. Finally the porous plastic polymer was polished and coupled with the general optical fiber to assemble the fiber-optic chemical sensor.

2.3. Instrumental setup

The instrumental setup is shown in Fig. 1A. Fluorescence intensities were collected by USB-2000 fluorescence spectrometer (Ocean Optic Inc., USA), the 470 nm excitation light from the light source LS-450 (Ocean Optic Inc., USA) was directed into one bundle of the bifurcated optic fiber QBIF600-UV-VIS (Ocean Optic Inc., USA) and reach the common end of the bifurcated fiber, with which the porous plastic probe was connected. The 610 nm light emitted from the probe was transmitted to the other bundle of the bifurcated optic fiber, which was connected with USB-2000 fluorescence spectrometer. Data acquisition and signal processing were performed using a portable computer with the OOIBase32 software (Ocean Optic Inc., USA). The probe was equipped in a flow cell (see Fig. 1B). The samples with different dissolved oxygen concentration were carried and regulated by a flow injecting apparatus model IFIS-C (Xian Remex analysis instrument Co. Ltd., China,). All measurements were performed under air-conditioned environment having a constant temperature of 25 ± 1 °C. The dissolved oxygen samples were calibrated by a Dissolved Oxygen Meter Model 850A (Orion, USA). Parts of the tests for the porous plastic probe were car-

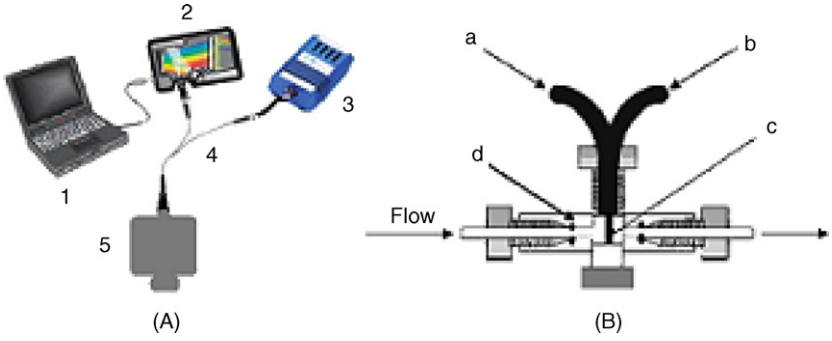


Fig. 1. Diagram of the instrumental setup (A) and design of the flow cell (B). (1) Personal computer; (2) fluorescence spectrometer (USB2000 FLG); (3) excitation source (LS/450); (4) bifurcated fiber-optic probe; (5) flow cell; (a) excitation optical fiber; (b) emission optical fiber; (c) porous plastic probe; (d) O-ring.

ried out on a fluorescence spectrophotometer model 970 CRT (Shanghai analytical instrument factory, China).

3. Results and discussion

3.1. The principle of novel porous plastic probe

The porous plastic probes were fabricated by a co-polymerization technique. This procedure involved the monomer and cross-linking reagent, which can be polymerized at the presence of the porogent. Usually the porogents are inert solvents, which could not be chemically bound to the polymer network and be readily removable from the polymer to leave an interconnected porous structure. The amount of cross-linking reagent would affect the cross-linking degree of the polymer. The configuration of micro-pores could be controlled by the porogent. The indicator could be immobilized on the polymer fiber by chemical or physical method during polymerization. The polymer can be then assembled to be a fiber-optic chemical sensor by coupling with the optic-fiber based on the wave-guide technique.

The principle involved in the preparation of the porous plastic optical fiber probe for dissolved oxygen is shown in Fig. 2. This polymer fiber was of high dissolved oxygen permeability and water impermeability. Therefore, in aqueous solution dissolved oxygen would easily diffuse into the probe to react with the fluorescent indicator, while other ions would be prohibited outside of the probe. After dissolved oxygen diffuses into the fiber probe, the fluorescence of $[Ru(dpp)_3]^{2+}$ was then quenched. The quenched fluorescent intensity of the indicator was related to the concentration of dissolved oxygen in solution.

3.2. Optimization of porous plastic probe

The composition of the probe would influence the physical properties as well as the sensitivity of probe for dissolved oxygen. Several monomers such as styrene, methyl methacrylate, IBM, and TFPM were tested. It was found that when IBM and TFPM were selected as monomers, the porous plastic probe for dissolved oxygen obtained the best sensitivity. The result indicates that the fluorinate polymer is a good host for oxygen sensor due to their chemical inertness, high oxygen permeability and photo-stability [8,21–23]. The ratio of IBM and TFPM also influenced the sensitivity of the probe for dissolved oxygen. When the ratio of IBM and TFPM reached 1:1% (v/v), the I_{N_2}/I_{air} value of the probe for dissolved oxygen was the highest.

The proportion of porogent and cross-linking reagent would affect the distribution of micro-pores and the optical property [26], and further affect the physical properties of the probe and the response sensitivity for dissolved oxygen. The optimal amount of DGDM was 0.05 ml in the experiment. The porogent could change the porosity in the porous plastic fiber. Since the pores could be acted as an O_2 channel to quench $[Ru(dpp)_3]^{2+}$ entrapped in the polymer matrix, the increase in porosity led to an increase in the bimolecular quenching rate constant, and then resulted in enhanced sensitivity of the probe for dissolved oxygen. On the other hand, the optical diffusion increased and this would result in the block of the optical transmittance. Moreover, the excessive of porogent would decrease the porosity on the contrary and resulted in a decrease in the bimolecular quenching rate constant and sensitivity of the probe for dissolved oxygen. Toluene was tested as the porogent in the experiment, and the results showed that the optimal composition of the probe is TFPM: 25%, IBM: 25%, DGDM: 25%, toluene: 25% (v/v). A typical scanning electron microscope (SEM) image (JSM-35CF) is shown in Fig. 3. SEM verified that the porogent could not be chemically bound to the polymer network during polymerization due to its inertness and be removable from the polymer to leave an interconnected porous structure.

In contrast to the probe sensitivity, the response time was related to the diffusion and reaction equilibrium, and it is expected to depend largely upon the rate of diffusion into the encapsulating medium [30]. The diameter of the porous plastic fiber would affect the response time for dissolved oxygen. Several diameter scales of porous plastic fiber samples from 1000 to 200 μm were prepared. The result showed that the time to achieve 95% of the full response t_{95} varied from 17 to 1.5 min when the diameter of porous plastic fiber was minished from 1000 to 200 μm. Moreover, the porous plastic probe with 200 μm in diameter exhibited better mechanical strength and flexibility.

3.3. Probe characteristics

The fluorescence spectroscopy of $[Ru(dpp)_3]^{2+}$ is dominated by metal-to-ligand charge transfer (MLCT) process which involves the promotion of an electron from a metal d orbital to a ligand π^* orbital. The fluorescence spectra of $[Ru(dpp)_3]^{2+}$

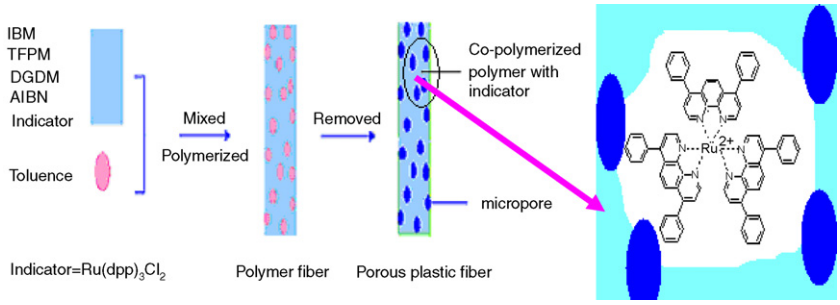


Fig. 2. The principle involved in preparation of the porous plastic optical fiber probe for dissolved oxygen.

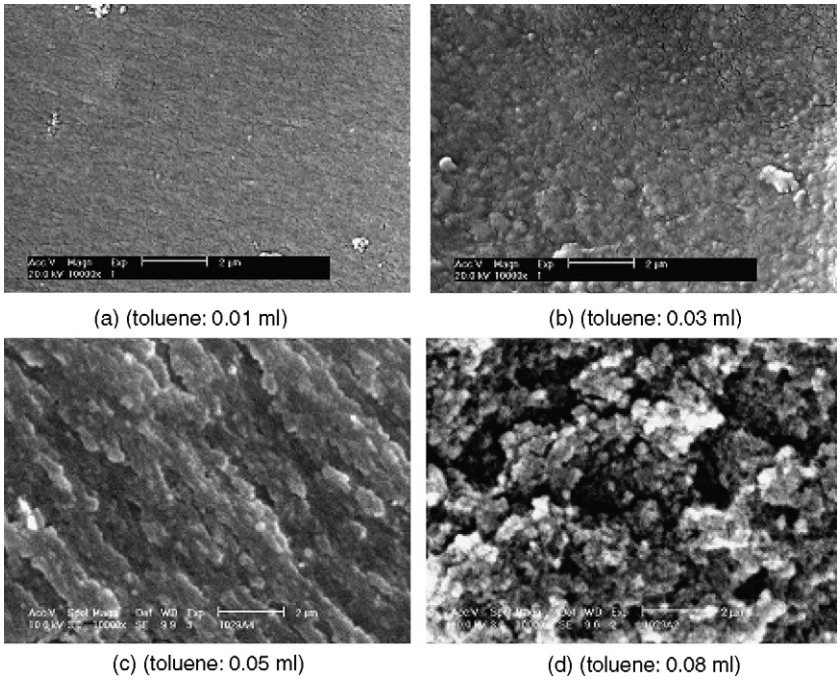


Fig. 3. SEM image of porous plastic optic fiber sample with different amount of the porogent. TFPM: 0.05 ml; IBM: 0.05 ml; DGDM: 0.05 ml; $[Ru(dpp)_3]Cl_2$: 1.0×10^{-4} mmol. (a) Toluene: 0.01 ml, (b) toluene: 0.03 ml, (c) toluene: 0.05 ml, and (d) toluene: 0.08 ml

encapsulated in porous plastic probe is shown in Fig. 4. The I_{N_2}/I_{air} value of the probe for dissolved oxygen was 4.00.

Fig. 5 showed the typical dynamic response of the probe on exposure to N_2- and air-saturated water. The stable and reproducible signals could be obtained. T_{95} were about 1.5 min on going from N_2- to air-saturated water and 3.0 min on going from air- to N_2- saturated water. The obvious difference of such two equilibrium times would be explained by the faster diffusion rate of O_2 than that of N_2 in porous plastic fiber probe.

In the simplest hypothesis of a luminophore in a homogeneous micro- environment, luminophore quenching follows the Stern–Volmer relationship:

$$\frac{I_0}{I} = 1 + K_{SV}[O_2]$$

where I_0 and I represent the steady-state luminescence intensities in the absence and presence of O_2, respectively, K_{SV} is the Stern–Volmer quenching constant, and $[O_2]$ is the O_2 concentration. The fluorescence spectra obtained from the porous plastic probe at different dissolved oxygen concentrations are shown in Fig. 6. It can be seen that the fluorescence of $Ru(dpp)_3Cl_2$ immobilized in porous plastic probe was quenched by dissolved oxygen. The intensity of fluorescence decreased with the increased oxygen concentration. Typical Stern–Volmer plot (Fig. 6) was fairly linear up to about 14 mg L^{-1} of dissolved oxygen and the approximate Stern–Volmer constant K_{sv} obtained from the linear part of the graph was 0.5523 L mg^{-1}. The limit of detection of the sensing probe was 0.1 mg L^{-1}, which was defined at a signal-to-noise ratio of S/N = 3.

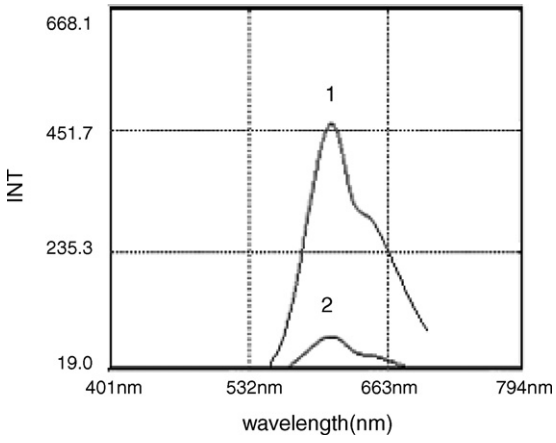


Fig. 4. Fluorescence spectra of porous plastic optic fiber probe in N_2-saturated water and air-saturated water. (1) N_2-saturated water and (2) air-saturated water.

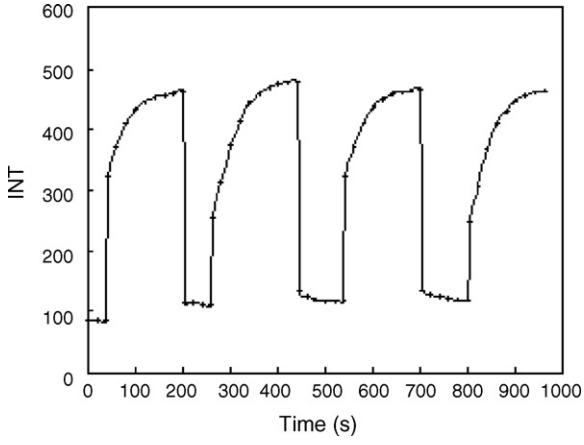


Fig. 5. Response time, reproducibility and relative intensity change of porous plastic fiber probe on exposure to N_2- and air-saturated water.

Table 1
Determination of dissolved oxygen in seawater samples by the proposed and standard method

Sample no.	Proposed method[a] (mg L^{-1})	Iodimetry[b] (mg L^{-1})	Relative error (%)	Average error (%)
1	7.97 ± 0.28	7.61 ± 0.14	4.73	3.15
2	8.40 ± 0.20	8.22 ± 0.08	2.19	
3	8.35 ± 0.24	8.21 ± 0.10	1.70	
4	8.43 ± 0.25	8.50 ± 0.08	−0.07	
5	8.67 ± 0.21	8.30 ± 0.09	4.46	
6	8.43 ± 0.23	8.85 ± 0.11	−4.46	
7	8.58 ± 0.19	8.20 ± 0.12	4.63	

[a] $n = 6$.
[b] $n = 3$.

The leakage of $[Ru(dpp)_3]^{2+}$ immobilized in the probe was also investigated. Because of the high hydrophobic property of the probe, the I_{N_2}/I_{air} value was constant after the probe was stored in water for a month. The porous plastic fiber probe was found independent of the salinity over the range from 5 to 40‰, this might also be attributed to the high hydrophobicity of the probe, which prevented the penetration of ions into the matrix and made it possible to on-line application in aggressive seawater.

3.4. Application for real seawater samples

The developed sensor system has been used for detection of dissolved oxygen in real seawater samples. The seawater samples were obtained from Xiamen area of Fujian, China. The salinity of the seawater sample in this area was measured and found to be 3.5043%, which mainly consists of NaCl (3.0065%) and $MgSO_4$ (0.4978%). The samples were filtered through a 0.45 μm pore size membrane filter before being pumped into the flow cell. These seawater samples were also analyzed by the national standard method of China iodimetry for comparison with the proposed method. The results are shown in Table 1. It can be seen from Table 1 that there is no obvious difference between the proposed method and the standard method. The average error is lower than 4%.

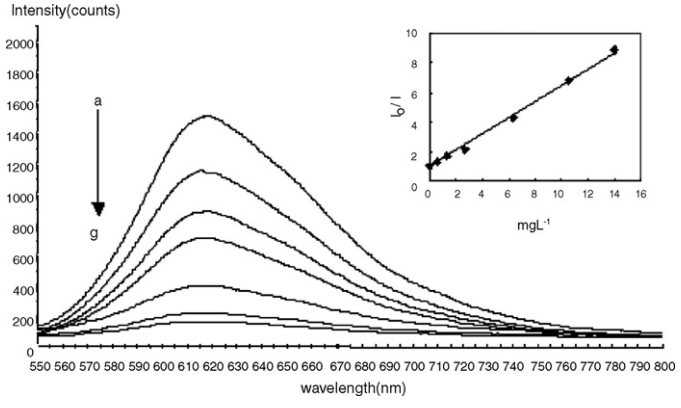


Fig. 6. Fluorescence spectrum of $Ru(dpp)_3Cl_2$ in porous plastic fiber under different concentration of dissolved oxygen. (a) 0 mg L^{-1}; (b) 0.56 mg L^{-1}; (c) 1.36 mg L^{-1}; (d) 2.71 mg L^{-1}; (e) 6.36 mg L^{-1}; (f) 10.0 mg L^{-1}; (g) 14.0 mg L^{-1} dissolved oxygen. Conditions: $\lambda_{ex} = 470$ nm; $\lambda_{em} = 610$ nm; silt = 5 nm (ex), 10 nm (em) inset: Stern–Volmer plot.

4. Conclusion

A novel fiber-optical chemical sensor was developed for determination of dissolved oxygen in seawater based on the porous plastic probe, which serves as analyte-sensitive function as well as optical wave-guide. The porous plastic probe exhibited good response to dissolved oxygen except the relatively long response time. And the probe was prepared by cross-linking co-polymerization, which made the probe high hydrophobicity. This is very important for the sensor to resist the indicator leaching out and ion interference. The porous plastic probe shows promise as a relatively inexpensive, easily constructed sensor for the optical detection of dissolved oxygen in aqueous environment.

Acknowledgements

The project was financially supported by 863 project (2002AA639140), NSFC (50503006 and 20575011) and Nature Science Foundation (D0310010, E0310014 and D0410010) of Fujian Province of China.

References

[1] M.M.F. Choi, D. Xiao, Anal. Chim. Acta 387 (1999) 197–205.
[2] C. McDonagh, B.D. MacCraith, A.K. McEvoy, Anal. Chem. 70 (1998) 45–50.
[3] C. McDonagh, C. Kolle, A.K. McEvoy, D.L. Dowling, A.A. Cafolla, S.J. Cullen, B.D. MacCraith, Sens. Actuat. B 74 (2001) 124–130.
[4] X. Chen, Z.M. Zhong, L. Zhao, Y.Q. Jiang, X.R. Wang, K. Wong, Sens. Actuat. B 87 (2002) 233–238.
[5] R.T. Bailey, F.R. Cruickshank, G. Deans, R.N. Gillanders, M.C. Tedford, Anal. Chim. Acta 487 (2003) 101–108.
[6] P.A.S. Jorge, P. Caldas, C.C. Rosa, A.G. Oliva, J.L. Santos, Sens. Actuat. B 103 (2004) 290–299.
[7] Y.L. Koo, Y. Cao, R. Kopelman, S.M. Koo, M. Brasuel, A. Martin, M.A. Philbert, Anal. Chem. 76 (2004) 2498–2505.
[8] R.M. Bukowski, R. Ciriminna, M. Pagliaro, F.V. Bright, Anal. Chem. 77 (2005) 2670–2672.
[9] Y. Cao, Y.L. Koo, S.M. Koo, R. Kopelman, Photochem. Photobiol. 81 (2005) 1489–1498.
[10] R.D. Bowman, K.A. Kneas, J.N. Demas, A. Periasamy, J. Microsc. 211 (2003) 112–120.
[11] P. Payra, P.K. Dutta, Micropor. Mesopor. Mater. 64 (2003) 109–118.
[12] B.H. Han, I. Manners, M.A. Winnik, Chem. Mater. 17 (2005) 3160–3171.
[13] L. Klimant, O.S. Wolfbeis, Anal. Chem. 67 (1995) 3160–3166.
[14] B.J. Basu, A. Thirumurugan, A.R. Dinesh, C. Anandan, K.S. Rajam, Sens. Actuat. B 104 (2005) 15–22.

[15] D.B. Papkovsky, G.V. Ponomarev, W. Trettnak, P. O'Leary, Anal. Chem. 67 (1995) 4112–4117.
[16] D.B. Papkovsky, A.N. Ovchinnikov, V.I. Ogurtsov, G.V. Ponomarev, T. Korpela, Sens. Actuat. B 51 (1998) 137–145.
[17] A.J. Palma, J. Lopez-Gonzalez, L.J. Asensio, M.D. Fernandez-Ramos, L.F. Capitan-Vallvey, Sens. Actuat. B 121 (2007) 629–638.
[18] J.F. Fernandez-Sanchez, T. Roth, R. Cannas, Md.K. Nazeeruddin, S. Spichiger, M. Graetzel, U.E. Spichiger-Keller, Talanta 71 (2007) 242–250.
[19] P. Douglas, K. Eaton, Sens. Actuat. B 82 (2002) 200–208.
[20] A. Mills, A. Lepre, Anal. Chem. 69 (1997) 4653–4659.
[21] X. Lu, I. Manners, M.A. Winnik, Macromolecules 34 (2001) 1917–1927.
[22] R.N. Gillanders, M.C. Tedford, P.J. Crilly, R.T. Bailey, J. Photochem. Photobiol. A: Chem. 163 (2004) 193–199.
[23] R.N. Gillanders, M.C. Tedford, P.J. Crilly, R.T. Bailey, Anal. Chim. Acta 545 (2005) 189–194.
[24] R.N. Gillanders, M.C. Tedford, P.J. Crilly, R.T. Bailey, Anal. Chim. Acta 502 (2004) 1–6.
[25] Q. Zhou, M.R. Shahriari, D. Kritz, Anal. Chem. 60 (1988) 2317–2320.
[26] Z.H. Xie, L.Q. Guo, X.H. Zheng, X.C. Lin, G.N. Chen, Sens. Actuat. B 104 (2005) 173–178.
[27] K.B. Guice, M.E. Caldorera, M.J. McShane, J. Biomed. Opt. 10 (2005) 64031–64041.
[28] L. Lin, L.L. Xiao, S. Huang, L. Zhao, J.S. Cui, X.H. Wang, X. Chen, Biosens. Bioelectron. 21 (2006) 1703–1709.
[29] R.J. Watts, G.A. Crosby, J. Am. Chem. Soc. 93 (1971) 3184–3188.
[30] A. Mills, Q. Chang, Analyst 117 (1992) 1461–1466.

Available online at www.sciencedirect.com
ScienceDirect
Talanta 74 (2008) 977–985
Talanta
www.elsevier.com/locate/talanta

Synthesis of cross-linked chitosan functionalized with threonine moiety and its application to on-line collection/concentration and determination of Mo, V and Cu

Lukman Hakim, Akhmad Sabarudin, Koji Oshita, Mitsuko Oshima, Shoji Motomizu *

Department of Chemistry, Faculty of Science, Okayama University, 3-1-1 Tsushimanaka, Okayama 700-8530, Japan

Received 2 July 2007; received in revised form 3 August 2007; accepted 3 August 2007
Available online 19 August 2007

Abstract

A novel chitosan-based resin functionalized with threonine moiety was synthesized, and applied to the collection/concentration of Mo, V and Cu in environmental water samples, followed by their determination using inductively coupled plasma-atomic emission spectrometer (ICP-AES). The synthesized resin, cross-linked chitosan-threonine (CCTS-Thr), showed good adsorption behavior toward trace amounts of Mo, V and Cu in a wide pH range. The adsorbed elements can be easily eluted using 2 mol L^{-1} of nitric acid, and their recoveries were found to be 90–100%. The CCTS-Thr was packed in a mini-column, which was then installed in a computer-controlled auto-pretreatment system (Auto-Pret System) for on-line trace elements collection and determination by ICP-AES. Experimental parameters related to the improvement of sensitivity and reproducibility were optimized. The limits of detection (LODs) for target metals were found to be in sub-ppb level. The proposed method with CCTS-Thr resin was successfully applied to the determination of Mo, V and Cu in environmental water samples. The recovery test showed that common matrices which exist in environmental water samples did not interfere with the determination.
© 2007 Published by Elsevier B.V.

Keywords: Resin; Chitosan; Threonine moiety; Molybdenum; Vanadium; Copper; On-line pretreatment; Computer control; Inductively coupled plasma-atomic emission spectrometry

1. Introduction

Molybdenum has been recognized as an essential trace element for many species including human. It is a component of many enzymes and also participates in a large number of enzymatic reactions. A deficiency of molybdenum in human diet adversely affects growth and may lead to neurogical disorders and even death [1]. On the other hand, the intake of high concentration of Mo results in severe gastrointestinal irritation and death due to cardiac failure [2]. Its excess may also cause bone deformation, teeth vulnerable to caries and disturbances in the metabolism of fats and proteins. Similar to molybdenum, vanadium is also a metal of interest in medical field due to its importance as an essential trace element which possesses specific physiological function. Both elements share left/right-sided cell receptors and are considered to be essential for human health. However, vanadium also has been recognized as a potentially dangerous pollutant in the class of lead, cadmium and mercury [3]. Although both molybdenum and vanadium naturally exists as trace elements in earth crust, human activities intense the discharge of both metals to environmental. World production of molybdenum ores is more than 100,000 t/year, and the worldwide usage of Mo in many industry sectors increases the chance of molybdenum intrusion into aquatic system and water supply. Oil and coal combustion for energy production increase the content of vanadium in environment [4]. Due to their dual effect toward living organism, both metals determination is receiving attention in pollution and nutritional studies.

The sensitivity of inductively coupled plasma-atomic emission spectrometer (ICP-AES) enables the measurement of molybdenum and vanadium in ppb level, but separation techniques are often necessaries prior to measurements because of

* Corresponding author. Tel.: +81 86 251 7846; fax: +81 86 251 7846.
E-mail address: motomizu@cc.okayama-u.ac.jp (S. Motomizu).

0039-9140/$ – see front matter © 2007 Published by Elsevier B.V.
doi:10.1016/j.talanta.2007.08.012

serious interferences from matrix condition of samples [2,5]. Moreover, the concentration of molybdenum and vanadium in relative clean water falls in sub-ppb level, thus caused the direct measurement even more difficult to be done and adequate preconcentration step become necessary prior to measurement.

In recent years, the importance of separation and concentration techniques involving solid phase extraction in trace analysis has risen substantially. The pretreatment of aqueous solutions by the sorption technique not only can increase analyte concentrations to detectable levels, but also can eliminate matrix effects [6]. Several preconcentration methods of Mo and V, separately or simultaneously, based on solid phase extraction have been reported [3–5,7–17]. The utilization of commercially available amberlite XAD-7 resin [7] and polyurethane foam [11], however, required reduction of molybdenum and complexation with thiocyanate to be included before column pretreatment. Such method may raise disposal problem because organic waste will be generated continuously. Quercetin immobilized on silica gel was used to selectively preconcentrate Mo [10], but the column capacity toward Mo was found to be low. Resin suspension–injection method in which cellulose nitrate resin was used to preconcentrate Mo provide low detection limit [12], but the method required tedious sample pretreatment before the column-adsorption can be carried out, and it also suggested the continuous replacement of the resin since the resin was consumed during each measurement.

Although the sample pretreatment with solid phase extraction method has a potential to improve the sensitivity of trace metals analysis, the operation of the pretreatment procedures may become tedious and time consuming if it is carried out in a manual batch-wise procedure where stringent control of the laboratory environment is required to avoid sample contamination, especially if the determination of trace levels of analytes is attempted. Such drawback can be overcome by utilizing an automated on-line preconcentration procedure, where less contamination and less reagent consumption can be achieved [3,18–22].

Chitosan, an *N*-deacetylated product of chitin which can be obtained in large quantity from crustacean shells, is a promising natural polymer for resin base material because of their unique properties, such as high chelating ability compared to other natural polymers obtained from seafood wastes, easy derivatization and biodegradability [23]. The reactive amino groups in chitosan provide easiness in introducing various moieties for wider applications in solid phase extraction. Compared to other synthetic polymers, chitosan possesses higher hydrophilicity which provides faster adsorption rate in aqueous medium.

Several researchers have reported the synthesis of cross-linked chitosans to improve the chemical durability of chitosan against acid mediums along with their application [24–28]. Cross-linked chitosans itself have been derivatized with several functional groups and applied to solid phase extraction techniques. Those are serine [29] and 3,4-dihydroxybenzoic acid [30] moieties for U collection, leucine moiety for Mo collection [31], dithiocarbamate [32] and iminodi(methylphosponic acid) [33] moieties for the collection of trace elements, *N*-methyl-D-glucamine moiety for B collection [34], 3,4-diaminobenzoic acid moiety for the collection of As and Se [35], and ethylenediamine moiety for Ag collection [36].

In this work, cross-linked chitosan (CCTS) was chemically modified with threonine moiety through the extension arm of chloromethyloxirane. The synthesized resin was packed in a mini-column, and the mini-column was installed on a laboratory-assembled automated pretreatment system coupled with ICP-AES (Auto-Pret AES System). The system was then utilized to carry out automated procedures for the collection and determination of Mo, V and Cu. Experimental variables, which are related to the improvement of sensitivity and reproducibility, also have been optimized. The proposed method provides effective automated on-line preconcentration and determination with numerous advantages such as high sensitivity, good reproducibility, fast analysis, less reagent consumption and less waste.

2. Experimental

2.1. Instruments

The adsorption behavior of 55 elements on CCTS-Thr resin was examined using inductively coupled plasma mass-spectrometer (ICP-MS) SPQ8000H System of Seiko Instruments (Chiba, Japan). Infrared spectra (4000–400 cm^{-1}) of the synthesized resin were recorded by using Jasco FT/IR-4100 Jasco International Co. Ltd. (Tokyo, Japan). A modular digital syringe pump Cavro (San Jose, CA, USA) with volume capacity of 10 mL, a six-port selection valve and a six-port switching valve of Hamilton (Reno, NV, USA) were used as a part of Automated Pretreatment System. This system was coupled with ICP-AES Vista-pro Seiko Instruments (Chiba, Japan) to measure the concentration of target analytes. The operating condition for ICP-AES is shown in Table 1.

2.2. Reagents

Chitosan, flake type with 80% deacetylation degree, was purchased from Tokyo Kasei Co. Ltd. (Tokyo, Japan). DL-threonine (min. 95%) was purchased from Wako Pure Chemical (Osaka, Japan). All other reagents used for the synthesis of CCTS-Thr resin were of analytical reagent grade.

Multi-element standard solutions were prepared from several kinds of single element standard solution for atomic absorption (1000 $\mu g\,mL^{-1}$) purchased from Wako Pure Chemicals. Two multi-element stock solutions for ICP-MS, XSTC-13 and XSTC-1 provided by Spex CertiPrep Inc. (Metuchen, NJ, USA) were mixed with the single element solutions to give a multi-element standard solution containing 63 elements. The XSTC-13 contains 10 $\mu g\,mL^{-1}$ of 31 elements: Th, Ag, Al, As, Ba, Be, Bi, Ca, Cd, Co, Cr, Cs, Cu, Fe, Ga, In, K, Li, Mg, Mn, Na, Ni, Pb, Rb, Se, Sr, TL, V, Zn, U and Hg, and the XSTC-1 contains 10 $\mu g\,mL^{-1}$ of 16 elements: Ce, Dy, Er, Eu, Gd, Ho, La, Lu, Nd, Pr, Sm, Sc, Tb, Tm, Yb and Y. The mixed solution was diluted with 1 M nitric acid before column pretreatment to give a solution containing 10 $ng\,mL^{-1}$ of each element. Accurate dilution of the standard solutions was carried out by weight.

Table 1
Operating conditions of ICP-AES

Spectrometer	Vista-pro
Plasma conditions	
RF power	40 MHz, 1.2 kW
Plasma gas flow rate (L min^{-1})	Ar 15.0
Auxiliary gas flow rate (L min^{-1})	Ar 1.50
Nebulizer gas flow rate (L min^{-1})	Ar 0.75
Spray chamber	Glass cyclonic spray chamber
Nebulizer	K-style concentric glass nebulizer
Torch	One-piece low flow extended torch in the axial view mode
Data acquision	
Measurement mode	Time scan mode

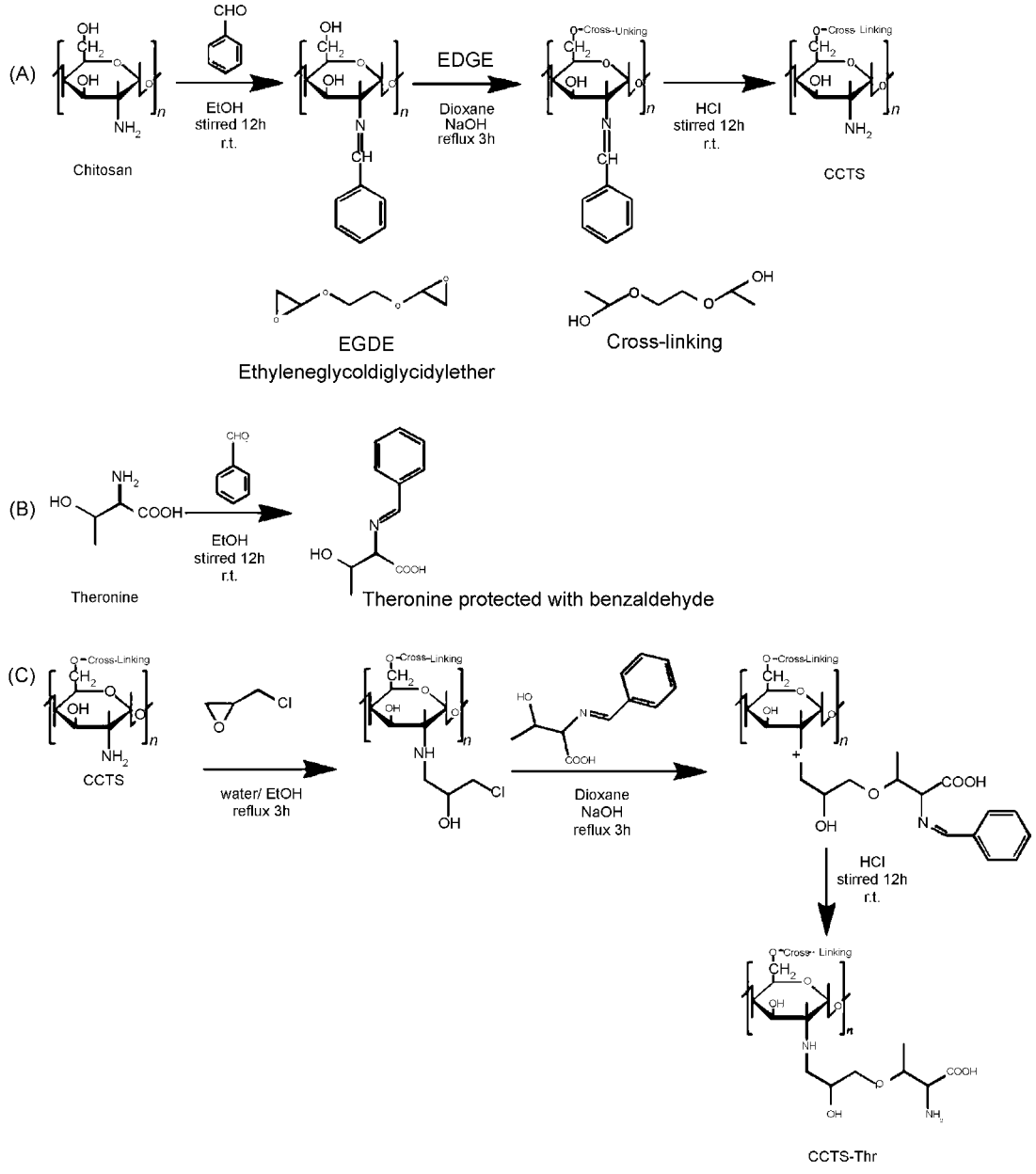


Fig. 1. Synthesis scheme of (A) CCTS, (B) protected-threonine and (C) CCTS-Thr; CCTS: cross-linked chitosan; CCTS-Thr: cross-linked chitosan functionalized with threonine moiety.

Ultrapure grade nitric acid (60%, density 1.38 g mL^{-1}) Kanto Chemicals (Tokyo, Japan) was diluted with ultrapure water to give 0.5–3 M nitric acid. Acetic acid (minimum 96%) and ammonia water (29%), which were used for preparing ammonium acetate buffers, were electronic industrial reagent grade Kanto Chemicals. Ultrapure water (18.3 MΩ cm^{-1} resistance) prepared by Elix 3/Milli-Q Element system Nihon Millipore (Tokyo, Japan) was used for diluting standard solution.

2.3. Synthesis of CCTS-Thr

The cross-linked chitosan derivatized with threonine (CCTS-Thr) was synthesized in two major steps: synthesis of cross-linked chitosan and introduction of threonine moiety.

Chitosan dissolves in acidic medium which is considered to be a serious disadvantage from the view-point of metal analysis. Therefore, in order to improve the mechanical and chemical durability of chitosan, a cross-link structure of chitosan was synthesized with ethyleneglycoldiglycidylether (EGDE) as the cross-linker. Among two reactive groups in chitosan, hydroxyl group was used as a terminal for the cross-link structure, while the reactive amino group was kept for further derivatization. The detail of synthesis procedure of EGDE cross-linked chitosan had been reported by other co-workers [24].

In the second step, the cross-linked chitosan was chemically modified by introducing threonine moiety with the aid of chloromethyloxirane extension arm. The cross-linked chitosan (5 g) was refluxed with chloromethyloxirane (10 g) in a mixture of water (50 mL) and ethanol (50 mL) for 3 h to couple cross-linked chitosan with chloromethyloxirane. The product was then filtered and washed three times with ethanol followed by water to remove the remaining chloromethyloxirane. Separately, amino group in threonine was protected as a Schiff base by reacting threonine (10 g) with benzaldehyde (30 g) in ethanol (30 mL). The protected-threonine was obtained by filtration, and the product was washed with ethanol. The protected-threonine was coupled with CCTS by refluxing the mixture in dioxane (100 mL) for 3 h. The product was filtered and washed each three times with ethanol followed by water. The product was then suspended in 1 M HCl (500 mL), and the suspension was stirred at room temperature for 12 h to cleave the Schiff base and recover the amino group of threonine. The CCTS-Thr was then filtered, and washed each three times with ethanol, followed by water. Before it was packed in a column for further application, the obtained CCTS-Thr was suspended in 100 mL of 2 M HNO_3 and stirred for 6 h to remove metals which were possibly adsorbed during synthesis process. The synthesis scheme of CCTS-Thr is shown in Fig. 1.

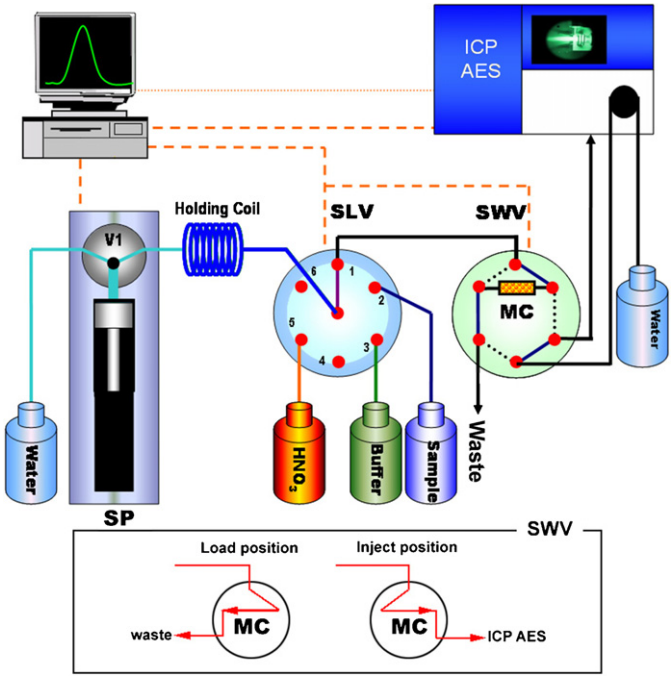


Fig. 2. Laboratory-assembled automated-pretreatment system (Auto-Pret AES System) manifold for on-line preconcentration and determination of Mo, V and Cu. SP: syringe pump; V1: syringe valve; SLV: six-port selection valve; SWV: six-way switching valve; MC: mini-column.

2.4. On-line metal collection and determination procedure

The manifold of Auto-Pret AES system is shown in Fig. 2. The system was composed of a syringe pump (SP) with volume capacity of 10 mL, a six-port selection valve (SLV), and a six-way switching valve (SWV). CCTS-Thr resin was packed in a PTFE column (i.d. 2 mm × 4 cm), and the column was installed on SWV in the position as shown in Fig. 2. PTFE tubing with 0.8 mm inner diameter was used for all connecting lines, except for holding coil where PTFE tubing with 1.6 mm inner diameter was used. The on-line pretreatment procedure was carried out in four major steps: *column conditioning*, *preconcentration*, *washing* and *elution*.

Column conditioning step: Two milliliters of 0.5 M ammonium acetate buffer solution (pH 5) was aspirated at flow rate of 400 μL s^{-1} into the holding coil through port 3 of SLV. While the SWV was kept in the load position, the solution in the holding coil was injected at flow rate of 40 μL s^{-1} into the column in order to adjust the pH of the resin.

Preconcentration step: Five milliliters of sample was aspirated at flow rate of 400 μL s^{-1} into the holding coil through port 2 of SLV. The aspirated sample was then injected into the column at flow rate of 30 μL s^{-1} for the adsorption of target analytes on the resin and the removal of the matrices.

The *washing step* was carried out by aspirating 1 mL of ultrapure water at flow rate of 400 μL s^{-1} into the syringe pump, and then the water was injected into the column at flow rate of 40 μL s^{-1}. This process will force the sample remained in the line to pass through the column, and at the same time remove matrices and un-adsorbed metal ions.

Finally, in the *elution step*, 0.5 mL of 3 M nitric acid was aspirated into the holding coil at flow rate of 400 μL s^{-1} from port 5 of SLV, and. The position of syringe pump was set to 2.5 mL by aspirating ultrapure water into the syringe pump. This step was made to ensure that the next injection would completely drive the eluent passing through the column and reach ICP-AES. After the eluent preparation had been done, the position of SWV was turned to inject-position, and the eluent was flowed into the

column at flow rate of 25 μL s^{-1}, and the effluent zone moved into the ICP-AES for measurement.

The entire sequence described above was automatically controlled by a home-made software developed by the authors using Microsoft Visual Basic 6.

2.5. Adsorption behavior study

The adsorption behavior of 55 elements on CCTS-Thr resin was investigated by using the same procedure as for on-line metals determination described in Section 2.4, with a few exceptions as follows: the injected sample volume in *preconcentration step* was 2.5 mL, the eluent in *elution step* was 2.5 mL of 2 M HNO_3, and the effluent was collected in polypropylene test-tubes instead of being flowed into ICP-AES. The collected eluent was then measured using ICP-MS. The buffer solutions used in *column conditioning step* were prepared by mixing ammonium acetate (NH_4OAc) with acetic acid (HOAc), ammonia, and nitric acid as follows: 0.5 M NH_4OAc + HOAc (pH 4–6), 0.5 M $NH_4OAc + NH_3$ (pH 7–9) and 0.5 M $NH_4OAc + HNO_3$ (pH 1–3).

2.6. Adsorption capacity study

Adsorption capacity of CCTS-Thr toward Mo, V and Cu was investigated for each individual species. Stock solution of Mo, V and Cu was prepared separately by dissolving $(NH_4)_6Mo_7O_{24}{\cdot}4H_2O$, NH_4VO_3 and $CuSO_4{\cdot}5H_2O$, respectively, with 0.5 M ammonium acetate solution. Then into each stock solution, 0.1 g (dry weight) of CCTS-Thr was added and the mixture was stirred for 24 h. The adsorption capacity of CCTS-Thr toward each metal ion was calculated from the difference of initial concentration and final concentration of the metal ions in the solution.

2.7. Samples

River water samples were collected from Zasu and Asahi river which flow through Okayama city, Japan. Tap water was collected from a tap water faucet located in Faculty of Science of Okayama University, in which the water was discarded 30 min before sampling. These samples were acidified to about pH 1 by adding concentrated nitric acid, followed by filtration with 0.45 μm membrane filter before storage.

3. Results and discussion

3.1. Characteristics of CCTS-Thr resin

The products obtained from each synthesis step were characterized by measuring their IR spectra. The alteration of CCTS to CCTS-threonine was marked by the appearance of peak in 1739 cm^{-1}, which corresponds to carbonyl vibration of carboxylic acid group from threonine moiety. The intensity of this peak, however, is weaker compared to peak in 1637 cm^{-1} which represents carbonyl group from chitin monomer which may exist in chitosan as a result from incomplete deacetylation process. Peak shifting from 1526 to 1559 cm^{-1} confirms the difference of N-H scissoring of primary amine in chitosan and the primary amine in threonine moiety. This is also supported by the shifting of N-H wagging peak from 897 to 827 cm^{-1}.

3.2. Adsorption behavior of trace elements on CCTS-Thr

The result of CCTS-Thr adsorption behavior study is summarized in Fig. 3, expressed as the recovery of each 10 μg L^{-1} of 55 elements at pH 1–9 using the procedure described in Section 2.5. Almost all of the adsorbed metal ions can be quantitatively recovered with 2 M HNO_3 as the eluent. The synthesized resin shows good adsorption capability toward Mo (pH 2–6), V (pH 6–9), Cu (pH 2–9) and Ga (pH 3–9). Among these metal ions, Mo, V and Cu have a potential to harm human and environment because of their toxicity at certain concentration level.

The base material of CCTS-Thr resin, that is CCTS, has ability to adsorb Mo, V, Cu and Ga. However, compared to its base material, the adsorption of CCTS-Thr toward Mo is superior in term of pH range, recovery value, and adsorption capacity. In the case of V and Cu, CCTS cannot quantitatively adsorb and desorb V (recovery was less than 80%), and it can only adsorb Cu at pH ≥5 [24]. The derivatization of CCTS with threonine moiety had improved the adsorption capability toward V into wider pH range with higher recovery value. An improvement in Cu adsorption was also observed where Cu could be quantitatively adsorbed and desorbed at pH ≥4.

3.3. CCTS-Thr adsorption capacity

It was reported that the introduction of cross-linked structure might reduce chitosan adsorption capacity toward Mo by 2–2.6 times because the metals accessibility to the sorption sites changes due to the modification of polymer structure [23]. Although the reduction of chitosan adsorption capacity toward Mo also might be attributed to the saturation of amine sites for cross-link structure terminal, our observation shows that even the CCTS whose EGDE cross-link terminal does not involve amine sites also has a lower adsorption capacity compared to the chitosan itself. However, in the present study, the threonine functional group was introduced to the chitosan through the extension arm of chloromethyloxirane, thus providing better access for the metal ions to the functional group. Based on the result obtained using batch-wise procedure, the adsorption capacity of CCTS-Thr toward Mo was found to be 3.47 mmol g^{-1}. Compared to CCTS-leucine [31] and epichlorohydrin-CCTS [27], the adsorption capacity of CCTS-Thr toward Mo is superior because the amino group in threonine moiety, which can act as a functional group to adsorb Mo(VI), is not saturated. In CCTS-leucine, the amino group was used to couple leucine with CCTS, thus its adsorption capacity toward Mo became lower. The adsorption capacity of CCTS-Thr toward V and Cu was found to be 0.92 and 0.62 mmol g^{-1}, respectively. The capacity of this resin for adsorbing Cu is superior to CCTS-leucine, and nearly equal to CCTS-serine [29].

A combination between chelating and ion-exchange mechanism was expected to be active since Mo(VI) and V(V) as their oxoanion can be adsorbed on the resin through anion exchange mechanism and hydrogen bonding, while Cu(II) can be adsorbed through chelating mechanism. Several chelating groups which were attached on the adjacent chitosan-monomer may also coordinate with the Cu ions. Thermodynamic data suggest that Mo should have an oxidation state of Mo(VI) in oxygenated waters [2], and Mo principally occurs as molybdate (MoO_4^{2-}) ions [37]. Vanadate ion at pH 4–8 exists as $H_2VO_4^-$ species, if its concentration is lower than $10^{-3.5}$ M [38]. The adsorption mechanism of Mo(VI), V(V) and Cu(II) is shown in Fig. 4:

3.4. Optimization of the auto-pretreatment system

3.4.1. Effect of sample pH and sample flow rate

In solid phase extraction studies, the influence of pH is one of the important factors for quantitative collection and elution of the analytes. Moreover, element such as molybdenum and vanadium exists as oxoanion with several forms whose existence are depend on pH of the medium.

The influence of pH to the collection and recovery of 55 elements was investigated at the ranges of 1–9 as described in Section 2.5 and the results are shown in Fig. 3. The resin shows good selectivity toward Mo in low pH, especially at pH 3 where only Mo can be quantitatively adsorbed. This pH can be selected to analyze the content of Mo(VI) selectively in environmental water sample. On the other hand, simultaneous adsorption of Mo(VI), V(V) and Cu(II) can be carried out in pH 5, and thus this pH can be selected if simultaneous analysis of Mo(VI), V(V) and Cu(II) contents in sample is attempted. In this work, pH 5 was selected for simultaneous enrichment of Mo(VI), V(V) and Cu(II), followed by their determination using ICP-AES.

Sample flow rate determines the contact time of sample solutions with the resin in the column. In general, longer contact time will result in better adsorption efficiency of the analytes on the resin. However, a compromise between the sample flow rate and the sample throughput should be considered. In the present study, the effect of the sample flow rate on the collection of metals was examined in the ranges of 20–40 $\mu L\,s^{-1}$. It was observed that the variation of sample flow rates did not give significant effect to the adsorption of Mo, V and Cu because the adsorption rate was considerably fast due to the hydrophilicity of chitosan. However, increasing flow rate to be more than 50 $\mu L\,s^{-1}$ caused leaking in the system due to the pressure inside chitosan column. In this study, the flow rate of 30 $\mu L\,s^{-1}$ was chosen as the compromise of sensitivity and analysis time.

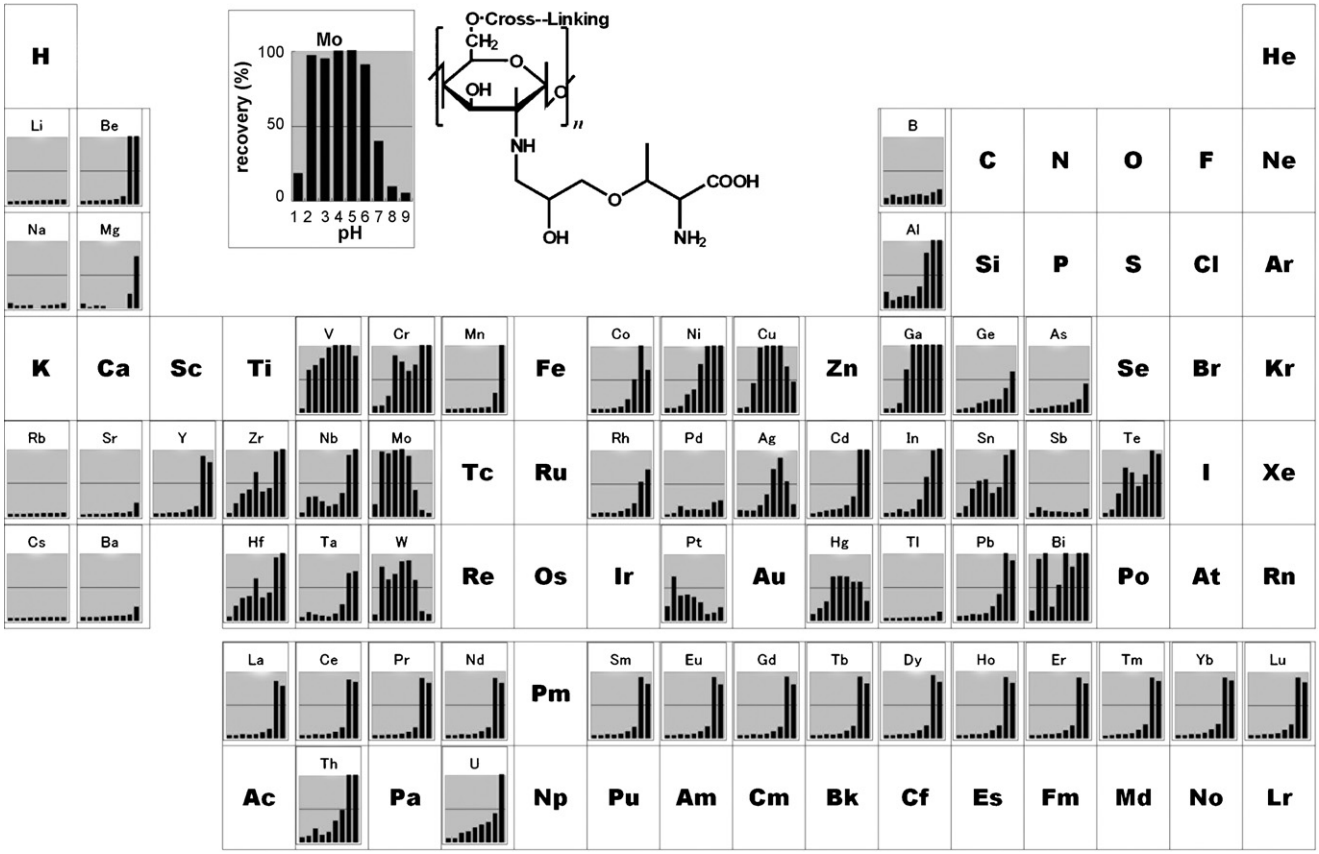


Fig. 3. Adsorption behavior of CCTS-Thr resin toward various elements. Samples: 2.5 mL of solution containing 10 $\mu g\,L^{-1}$ various elements; eluent: 2.5 mL of 2 M HNO_3.

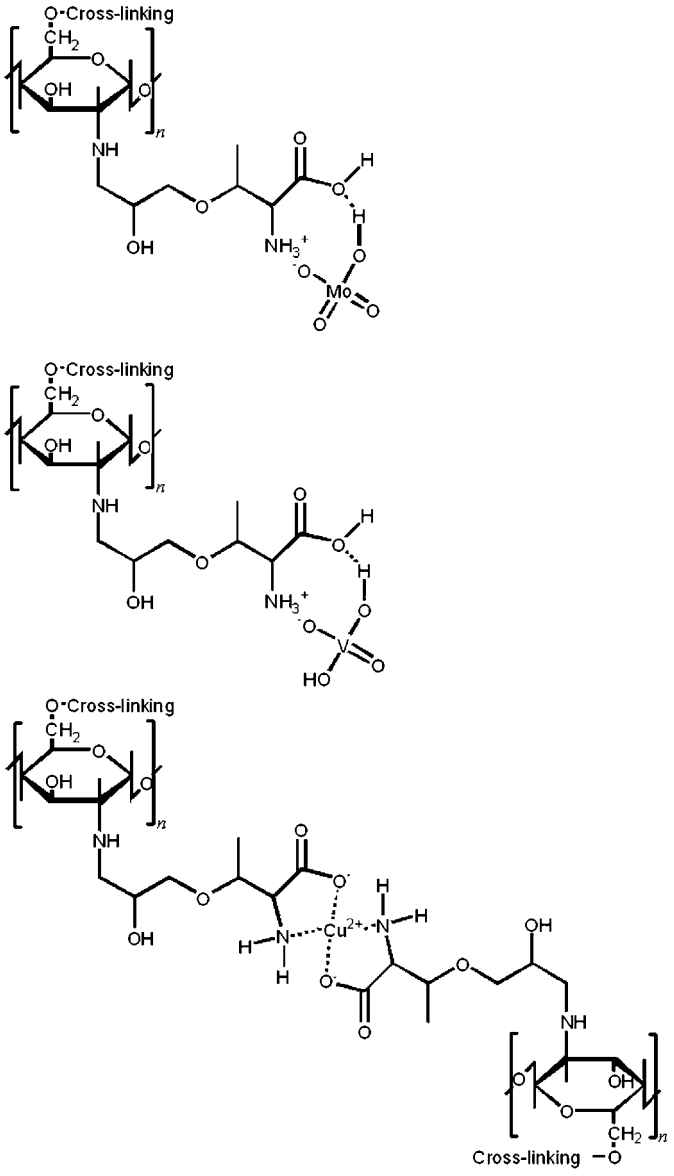


Fig. 4. Proposed adsorption mechanisms of Mo, V and Cu adsorption on CCTS-Thr.

3.4.2. *Effect of concentration, volume and flow rates of eluent*

Nitric acid, whose spectrum is similar to water in ICP-AES system, was used as the eluent in this study. Its concentration and flow rates were optimized to improve the sensitivity of the system.

The concentration of nitric acid affects the effectiveness of the desorption process, and also affects the desorption rate. Since in an on-line preconcentration system the desorbed analytes are concentrated in the tip of eluent zone, rapid elution would allow analytes to be desorbed and concentrated in a narrow zone, and thus improve the sensitivity of the system. In contrast, less rapid elution would cause the analytes to be distributed in a wider zone, which leads to lower sensitivity. The effect of nitric acid concentration was studied in the range of 0.5–3 M. It was found that 0.5 M was not effective to elute the adsorbed elements and gave the lowest sensitivity among the concentrations studied. Quantitative recovery of the adsorbed elements can be carried out by using 2 M of nitric acid. However, considering the elution rate which affected the distribution of the desorbed analytes in the eluent zone, 3 M nitric acid was found to give the best sensitivity, and therefore, it was used for further experiments.

Table 2
Optimized conditions for Auto-Pret AES System

Parameter	Range examined	Selected conditions
pH of sample	1–9	5
Sample loading flow rate ($\mu L\,s^{-1}$)	20–40	30
Eluent (HNO_3) concentration (M)	0.5–3	3
Eluent (HNO_3) volume (mL)	0.5–1.75	0.5
Eluent (HNO_3) flow rate ($\mu L\,s^{-1}$)	20–40	25

The effect of eluent (3 M HNO_3) volume was examined by varying its value from 0.25 to 1.5 mL to ascertain the complete elution of the analytes, and at the same time to provide the highest sensitivity. It was found that the highest peak height was obtained when 0.5 mL of eluent was used, thus this volume was used in the further experiment.

The flow rate of eluent determines the contact time of the eluent with the resin, and longer contact time is supposed to give better desorption efficiency. The effect of eluent flow rate was examined by varying the flow rate between 20 and 40 $\mu L\,s^{-1}$. It was found that the flow rate larger than 30 $\mu L\,s^{-1}$ cause a significant decrease in the peak height because of insufficient contact time. Based on such result, the eluent flow rate of 25 $\mu L\,s^{-1}$ was selected as the optimal condition.

In solid phase extraction, target analytes are trapped at the front-end of column where the sample solution began to flow in. If the elution is carried out in the same direction with sample flow, a dispersion of analytes in eluent zone may occur since the effluent will pass along the column. This situation can be avoided by reversing the eluent flow, where eluent will first pass through the column, and at the end of column the adsorbed analytes will be desorbed and directly enter the connection lines to ICP-AES. Therefore, the reversed eluent flow was used in further experiments by installing the mini-column on the switching valve as shown in Fig. 2.

The optimized parameters of the auto-pretreatment system were summarized in Table 2, and an example of flow signal of Mo in sub-ppb level is shown in Fig. 5.

Table 3
Analytical figures of the proposed method

Elements	Emission wavelength (nm)	R^2[a]	SEF[b]	LOD[c] ($\mu g\,L^{-1}$)
Mo(VI)	202.0	0.998	13	0.09
V(V)	292.4	0.996	26	0.09
Cu(II)	324.7	0.997	35	0.05

[a] Linearity of the calibration graph.
[b] Sensitivity enhancement factor.
[c] Limits of detection: correspond to the three times of signal-to-noise ratio (S/N = 3).

Table 4
Analytical results of environmental water samples

Samples	Mo			V			Cu		
	Added ($\mu g\,L^{-1}$)	Found ($\mu g\,L^{-1}$)	Recovery (%)	Added ($\mu g\,L^{-1}$)	Found ($\mu g\,L^{-1}$)	Recovery (%)	Added ($\mu g\,L^{-1}$)	Found ($\mu g\,L^{-1}$)	Recovery (%)
[1]River water A	0	0.25 ± 0.02		0	0.78 ± 0.02		0	1.41 ± 0.04	
	0.2	0.46 ± 0.01	105	0.3	1.08 ± 0.04	100	1	2.40 ± 0.05	99
[2]River water B	0	0.39 ± 0.02		0	0.70 ± 0.05		0	1.36 ± 0.05	
	0.2	0.59 ± 0.02	100	0.3	1.01 ± 0.01	103	1	2.39 ± 0.04	103
[3]Tap water	0	0.27 ± 0.02		0	0.49 ± 0.02		0	1.37 ± 0.06	
	0.2	0.47 ± 0.03	100	0.3	0.80 ± 0.06	103	1	2.40 ± 0.25	103

[*1]River water A was sampled at Asahi river, Okayama city, Japan. [*2]River water B was sampled at Zasu river, Okayama city, Japan. [*3]Tap water was taken from tap water faucet in faculty of science, Okayama University. Five milliliters of the sample was used, and experimental conditions were the same as in Table 2.

3.5. Analytical figures of merit

The performance of the proposed method was evaluated by examining the sensitivity enhancement factor and the detection limits obtained by using the Auto-Pret AES System. The correlation coefficient of the linear equations for the calibration graph of trace elements, which were constructed at sub-ppb levels, showed good linearity for the examined elements ($R^2 \geq 0.99$).

The sensitivity enhancement factors were calculated from the slope ratio of linear equation obtained under the optimal conditions by the Auto-Pret AES System to those obtained by directly injecting the samples into ICP-AES. The sensitivity enhancement factor was found to be 13, 26 and 35 for Mo, V and Cu, respectively. Elution in an on-line system creates a segment of concentrated analytes in the tip of eluent zone. The concentration of the analytes in such segment is greatly affected by retention strength of resin toward the analytes. Strong retention causes adsorbed analytes cannot be instantly collected and the analytes will be distributed in wider zone, thus caused lower sensitivity. This explains why the sensitivity enhancement factor of Mo is inferior to V and Cu.

Limits of detection (LODs) for the examined analytes are defined as the concentration corresponding to the three times of the signal-to-noise ratio. LODs were found to be 0.09, 0.09 and 0.05 $\mu g\,L^{-1}$ for Mo, V and Cu, respectively. Lower detection limits can be expected when larger volume of sample is used. These values are summarized in Table 3. From these results, the proposed method provides a significant improvement in sensitivity and enables the measurement of Mo, V and Cu to be carried out in sub-ppb levels.

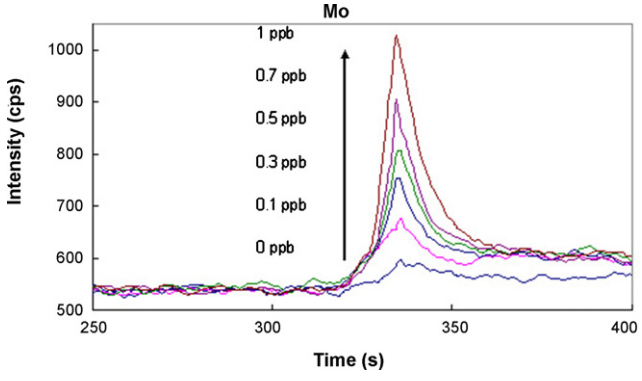


Fig. 5. Example of flow signals of Mo determination. Sample volume: 5 mL; other conditions are the same as summarized in Table 2.

3.6. Application to real environmental water samples

The method was applied to the determination of Mo, V and Cu in river water and tap water samples. The results obtained by the proposed method using 5 mL of the sample solutions, are shown in Table 4. Since it was found that V(IV) is stable only at pH 2 and gradually oxidized at higher pH [39], and since all water samples used in this work were initially acidified by using concentrated HNO_3 which has property of oxidizing acid, it can be assumed that V(IV) which exists in low concentration was oxidized to V(V), and thus the determination result reflected the concentration of total V. The concentration of metal ions was found to be higher than the LODs of measurement, and good reproducibility was obtained. The results from recovery tests, which were carried out by spiking a recorded-amount of analytes, indicated that the existence of matrices in environmental water samples did not interfere with the determination.

4. Conclusion

A novel chitosan resin functionalized with threonine moiety was synthesized and its potential to be applied in solid phase extraction method was examined. The synthesized resin showed good adsorption capability toward Mo, V and Cu. Simultaneous adsorption of those metals can be carried out in pH 5, while selective adsorption of Mo can be carried out in pH 3.

The utilization of the synthesized resin along with the Auto-Pret AES System provides fast analysis, good sensitivity, and excellent detection limit. The method was successfully applied to the determination of Mo, V and Cu in river water and tap water samples. The recovery test showed excellent recovery values, and indicated that common matrices which exist in environmental water samples do not interfere with the determination.

References

[1] Z. Marczenko, R. Lobinski, Pure Appl. Chem. (1991) 63.
[2] A.K. Das, R. Chakraborty, M.L. Cervera, M. Guardia, Talanta 71 (2007) 987.
[3] R.G. Wuilloud, J.A. Salonia, J.A. Gásquez, R.A. Olsina, L.D. Martinez, Anal. Chim. Acta (2000) 420.
[4] Z. Fang, B. Hu, Z. Jiang, Part B Spectrochim. Acta (2005) 60.
[5] H. Filik, K.I. Berker, N. Balkis, R. Apak, Anal. Chim. Acta (2004) 518.
[6] D. Bilba, D. Bejan, L. Tovan, Croat. Chem. Acta 71 (1998) 155.
[7] A. Tunçeli, A.R. Tűrker, Microchim. Acta (2004) 144.
[8] A.M. Diaz, M.I.P. Reguera, E.L. Veganzones, M.L.F. Cordova, L.F.C. Vallvey, Talanta 43 (1996) 185.
[9] V.L.A. Monte, A.J. Curtius, J. Anal. At. Spectrom. 5 (1990) 21.
[10] L.C. Azeredo, M.A.A. Azeredo, R.N. Castro, M.F.C. Saldanha, D.V. Perez, Part B Spectrochim. Acta (2002) 57.
[11] S.L.C. Ferreira, H.C. Santos, R.C. Campos, Talanta (2003) 61.
[12] I. Nukatsuka, Y. Shimizu, K. Ohzeki, Anal. Sci. (2004) 20.
[13] Q. Li, X. Zhao, X. Guan, G. Liu, Anal. Chim. Acta (2006) 562.
[14] H.C.D. Santos, M.G.A. Corn, S.L.C. Ferreira, Anal. Chim. Acta (2001) 426.
[15] Y. Wu, Z. Jiang, B. Hu, Talanta (2005) 67.
[16] C. Ekinci, Ü. Kőklű, Part B Spectrochim. Acta (2000) 55.
[17] C.Y. Huang, N.M. Lee, S.Y. Lin, C.Y. Liu, Anal. Chim. Acta (2002) 466.
[18] C. Hang, B. Hu, Z. Jiang, N. Zhang, Talanta 71 (2007) 1239.
[19] A. Ali, Y. Ye, G. Xu, X. Yin, T. Zhang, Microchem. J. 63 (1999) 365.
[20] V.A. Lemos, J.S. Santos, L.S. Nunes, M.B. Carvalho, P.X. Baliza, R.T. Yamaki, Anal. Chim. Acta 494 (2003) 87.
[21] X.Z. Wu, P. Liu, Q.S. Pu, Q.Y. Sun, Z.X. Su, Talanta 62 (2004) 918.
[22] M.S. Jimenez, R. Velarte, J.R. Castillo, Spectrochim. Acta, Part B 57 (2002) 391.
[23] A.J. Varma, S.V. Deshpande, J.F. Kennedy, Carbohydr. Polym. 55 (2004) 77.
[24] K. Oshita, Y. Gao, M. Oshima, S. Motomizu, Anal. Sci. 17 (2001) 317.
[25] K. Oshita, M. Oshima, Y. Gao, K. Lee, S. Motomizu, Anal. Sci. 18 (2002) 1121.
[26] E. Guibal, L. Dambies, C. Milot, J. Roussy, Polym. Int. 48 (1999) 671.
[27] S.H. Qian, A.F. Xue, M. Xiao, H. Chen, J. Appl. Polym. Sci. 101 (2006) 432.
[28] A.R. Kulkarni, V.I. Hukkeri, H. Sung, H. Liang, Macromol. Biosci. 5 (2005) 925.
[29] K. Oshita, M. Oshima, Y. Gao, K. Lee, S. Motomizu, Anal. Chim. Acta 480 (2002) 239.
[30] A. Sabarudin, M. Oshima, T. Takayanagi, L. Hakim, K. Oshita, Y.H. Gao, S. Motomizu, Anal. Chim. Acta 581 (2007) 214.
[31] K. Oshita, J. Xu, Y. Gao, K. Lee, M. Oshima, S. Motomizu, Bull. Chem. Soc. Jpn. 76 (2003) 1555.
[32] T. Ninomiya, K. Oshita, M. Oshima, S. Motomizu, Bunseki Kagaku 52 (2003) 811.
[33] S. Yamakawa, K. Oshita, A. Sabarudin, M. Oshima, S. Motomizu, Bunseki Kagaku 53 (2004) 1039.
[34] A. Sabarudin, K. Oshita, M. Oshima, S. Motomizu, Talanta 66 (2005) 136.
[35] A. Sabarudin, K. Oshita, M. Oshima, S. Motomizu, Anal. Chim. Acta 542 (2005) 207.
[36] R.K. Katarina, T. Takayanagi, M. Oshima, S. Motomizu, Anal. Chim. Acta 558 (2006) 246.
[37] K. Pyrzynska, Anal. Chim. Acta 590 (2007) 40.
[38] M.T. Pope, Heteropoly and Isopoly Oxometalates, Springer Verlag, 1983, p. 35.
[39] K. Pyrzynska, T. Wierzbicki, Talanta 64 (2004) 823.

Available online at www.sciencedirect.com
ScienceDirect
Talanta 74 (2008) 909–914
Talanta
www.elsevier.com/locate/talanta

Fabrication of bulk-modified carbon paste electrode containing α-$PW_{12}O_{40}^{3-}$ polyanion supported on modified silica gel: Preparation, electrochemistry and electrocatalysis

Hassan Hamidi [a], Esmaeil Shams [b,*], Bahram Yadollahi [a], Farhad Kabiri Esfahani [a]

[a] *Institute for Advanced Studies in Basic Sciences, Zanjan 45195-1159, Iran*
[b] *Chemistry Department, University of Isfahan, Isfahan 81746-73441, Iran*

Received 10 May 2007; received in revised form 26 July 2007; accepted 27 July 2007
Available online 2 August 2007

Abstract

α-$PW_{12}O_{40}^{3-}$ (PW_{12}) supported on the surface of silica gel derivatized by 3-aminopropyl(triethoxy)silane (devoted briefly as $SiNH_3PW_{12}$) was synthesized and used as bulk modifier to fabricate a renewable three-dimensional chemically modified electrode. The electrochemical behavior of the modified electrode was characterized by cyclic voltammetry. There is an ionic bonding character between PW_{12} and the surface amino groups of modified silica, which greatly improves the stability of $SiNH_3PW_{12}$-modified carbon paste electrode due to insolubility of silica gel in water. The $SiNH_3PW_{12}$ bulk-modified carbon paste electrode not only maintains the electrochemical activity of PW_{12}, but also exhibits remarkable advantages of renewability, as well as simple preparation and inexpensive material. The modified electrode offers an excellent and stable electrocatalytic response for the reduction of IO_3^- and hydrogen peroxide. The $SiNH_3PW_{12}$-CPE is successfully applied as an electrochemical detector to monitor IO_3^- in flow injection analysis (FIA). The catalytic peak current was found to be linear with the IO_3^- concentration in the range 5×10^{-6} to 1×10^{-3} mol L^{-1}. The detection limit of the proposed method was found to be 3.1×10^{-6} mol L^{-1} for IO_3^- determination.
© 2007 Elsevier B.V. All rights reserved.

Keywords: PW_{12}; Silica gel; Carbon paste electrode; Electrocatalysis; IO_3^-; H_2O_2

1. Introduction

Due to their numerous possibilities of composition and to their very rich redox chemistry, polyoxometalates (POMs) show unusual properties in several domains, including catalysis and medicine [1,2]. The importance of polyoxometalates (POMs) in the manufacture of chemically modified electrodes has been recognized in the recent years owing to their excellent electrochemical, electrocatalytic properties and thermal stability [3–6]. Attaching redox-active POMs onto electrodes simplifies their electrochemical studies and facilitates their applications in many fields. A number of strategies have been developed to prepare chemically modified electrodes (CMEs) with a variety of POMs. Several groups have immobilized POMs using various techniques, such as electrochemical deposition [7–9], adsorption [10–13], immobilization in polymeric matrices [14,15] and fabrication of multilayer ultra-thin films by alternative deposition of heteropolyanions with bipolar cationic compounds based on electrostatic interaction [4–6]. A serious drawback in the application of these thin film-modified electrodes is their poor long-term stability; moreover, electrode surfaces cannot be renewed in the case of leakage, contamination and passivation [3,16]. In addition, POMs attached to the surface of electrodes often does not display the same electrochemical properties and therefore has a different electrocatalytic activity [17,18]. It seems desirable to develop and exploit a new, simple and reliable procedure for preparing POM-modified electrodes. Recently, an interest has focused on the design and preparation of novel POM-based hybrid materials, as well as application of them in the three-dimensional bulk-modified electrodes.

Carbon paste (CP) is one of the convenient conductive matrixes to prepare the chemically modified electrodes (CMEs) by simple mixing of graphite/binder paste and modifier [19]. These kinds of electrodes are inexpensive and possess many advantages such as low background current, wide range of used potential, easy fabrication and rapid renewal [20]. The draw-

* Corresponding author. Tel.: +98 311 7932702; fax: +98 311 6689732.
E-mail address: e_shams@chem.ui.ac.ir (E. Shams).

0039-9140/$ – see front matter © 2007 Elsevier B.V. All rights reserved.
doi:10.1016/j.talanta.2007.07.026

back of modified carbon paste electrodes is that the modifier in these sensors are in loose association or physical contact with the electrode, thus the sensor may easily degrade over time from depletion of modifier, especially when modifier has a high degree of solubility. In general, the modifiers used with carbon paste electrodes should be insoluble in the analytic solution, or they should at least strongly adsorb to the paste components in order to avoid dissolution of the modifiers from the electrode surface during the measurement. Therefore, the traditional POMs cannot be directly used as a bulk modifier of CPE owing to their good solubility. However, if the modifiers are first immobilized onto insoluble substrates (*i.e.*, high surface area silica supports) before being embedded in the carbon graphite matrix, the chemical functionality of the sensor is retained despite diffusion, abrasive wear, or degree of solubility of the modifiers. Wang et al. have designed and synthesized a kind of insoluble inorganic–organic hybrid material containing 12-molybdophosphate: $(C_{21}H_{38}N)_3PMo_{12}O_{40}\cdot H_2O$, which is insoluble in water, and fabricated a three-dimensional bulk-modified CPE employing the hybrid material by direct mixing [21]. Chemically modified electrodes involving silica-based materials have recently attracted much attention in the field of electroanalysis. Among them, organically modified silicates (ORMOSILs) hold considerable promise in the development of new devices for analytical and electroanalytical applications due to their good mechanical and chemical stability, and the ease with which they can be prepared and modified [22–24]. Indeed, ORMOSILs combine the rigid three-dimensional structure of inorganic lattice with the intrinsic chemical properties of organic moieties. There are some reports on the immobilization of POMs on the silica via amine moieties and their applications as catalyst and/or electrocatalyst [25–29].

As a continuation of our work in the application of modified silica in the fabrication of chemically modified carbon paste electrodes for analytical applications [30–32], in the present work we have made use PW_{12} that is supported on organofunctionalized amorphous silica with 3-aminopropyl(triethoxy)silane in the preparation of carbon paste electrodes. It is found that the PW_{12} supported on the organofunctionalized amorphous silica ($SiNH_3PW_{12}$) has very low solubility in aqueous solutions and retains its electrochemical properties and electrocatalytic activities. These properties are very advantageous to expand POM-based materials' application in chemically bulk-modified electrode. The electrochemistry of this sensor is studied and it is found that the ($SiNH_3PW_{12}$) modified carbon paste electrode shows good electrocatalytic activities toward reduction of hydrogen peroxide and IO_3^-. Such a system can provide a novel electrochemical sensor for the reductive determination of IO_3^-. Since there is no leaching of the electrode because of the low solubility of PW_{12} supported on ORMOSIL in aqueous solution, a single electrode surface can be used for multiple analytical determinations over several days. Another advantage of proposed sensor is that the $SiNH_3PW_{12}$-modified CPE can easily be renewed in a repeatable manner by squeezing a little carbon paste out the tube and a fresh surface is exposed whenever needed. Although, the modified electrode showed electrocatalytic activities towards both hydrogen peroxide and iodate, but the sensitivity of the electrode to the reduction of iodate was much better. Therefore, the performance of the $SiNH_3PW_{12}$-modified CPE was optimized for the purpose of evaluating its potential as an analytical sensor for IO_3^- detection. Being a preliminary attempt, this modified electrode was utilized in flow injection analysis (FIA) as an amperometric detector. The result was satisfactory.

2. Experimental

2.1. Apparatus and procedure

All electrochemical experiments were conducted with a computer-controlled potentiostat, the Autolab electrochemical analyzer model PGSTAT30 (Eco Chemie, Utrecht, The Netherlands). Electrochemical measurements were carried out under nitrogen atmosphere in a conventional one-compartment cell with an Ag/AgCl (3M KCl) reference electrode, a platinum auxiliary electrode and a carbon paste or modified carbon paste electrode. All redox peak potentials were measured and reported versus the Ag/AgCl, KCl (3M) reference electrode.

A Metrohm 713 pH meter was used to determine the pH of solutions.

Flow injection analysis (FIA) was performed with a peristaltic pump model minipuls3 (Gilson, France) with silicon tubing and a Rheodyne injection system model EV 700-100 with Teflon tubing (i.d.: 0.5 mm). A home-made wall-jet cell was employed as the electrochemical detector with the potential monitored by a Metrohm 791 VA detector. The mobile phase was 1 mol L^{-1} sulfuric acid solution which its pH was adjusted to 1 by sodium hydroxide solution. This was deaerated and delivered at a constant flow rate of 0.6 mL min^{-1}. The injection volume was 75 μL.

2.2. Preparation of silica gel-modified PW_{12}

The modified silica gel was prepared according to the methodology already described in the literature [33,34]. This methodology contains two main steps.

In the first step, silica gel derivatized by 3-aminopropyl (triethoxy)silane was prepared according to the following procedure

100 g of silica gel (K-60) was mixed with 300 mL solution of 6 mol L^{-1} hydrochloric acid and was refluxed for 24 h. The resulting mixture was filtered, washed with large amount of water and dried in 130 °C overnight. Ten grams of hydrated silica gel was added to absolute ethanol solution of 3-aminopropyl(triethoxy)silane (200 mL, 150 mmol L^{-1}) and stirred at room temperature for 24 h. The resulting material ($Si–RNH_2$) was washed by decantation with ethanol, and then dried in 95 °C. For protonation of amino groups, 5 g of resulting solid particles were mixed with 200 mL of 3 M $HClO_4$ for 24 h and then washed with large amount of water for elimination of adsorbed protons on surface of silica and then dried in 90 °C over night.

In the second step, a 2.0 g quantity of $Na_2WO_4\cdot 2H_2O$ was dissolved in 2 mL water, was followed by addition of 0.8 mL

H_3PO_4 (85%) and 2 mL HCl (37%). The resultant suspension was stirred for 12 h. Then 12 mL water was added to the suspension and resulting clear solution that containing the PW_{12} complex was precipitated by adding 5 g of resulting material in the first step (Si–RNH_3^+). The resulting mixture was stirred at room temperature for 2 days. Finally, the mixture was filtered and washed with 1 M HNO_3 thoroughly (so that PW_{12} residual molecules which might be adsorbed on silica gel matrix can be eliminated), and then dried in air.

2.3. Fabrication of the modified carbon paste electrodes

Carbon paste electrode modified with silica was prepared by adding 0.25 g paraffin oil and 0.1 g silica gel to 0.65 g carbon powder. $SiNH_3PW_{12}$-modified carbon paste electrodes were prepared by substituting corresponding amounts of the carbon powder (5, 10, 15 and 20% weight-to-weight ratio of the modifier relative to the carbon powder) by $SiNH_3PW_{12}$ and then adding the paraffin oil (0.25 g) and thoroughly hand-mixing in a mortar and pestle. A portion of the pastes were packed into the end of an insulin syringe (i.d.: 2 mm) and arranged with a copper wire serving as an external electric contact. The surface was smoothed on a piece of weighing paper. When necessary, a new surface was obtained by pushing an excess of paste out of the tube, removing this excess, and polishing again mechanically the electrode surface.

3. Results and discussion

3.1. Electrochemical behavior of the $SiNH_3PW_{12}$-modified CPE

The PW_{12} anion, which has Keggin structure, is unstable in neutral and basic aqueous solution and undergoes a series of hydrolysis processes [3]. Therefore, electrochemical studies of $SiNH_3PW_{12}$-modified CPE were carried out in acidic aqueous solutions.

Fig. 1 shows the cyclic voltammograms in 1 M H_2SO_4 aqueous solution (that its pH was adjusted to 1 by concentrated sodium hydroxide solution) at a bare CPE (Fig. 1a) and a $SiNH_3PW_{12}$-CPE (Fig. 1b). It can be seen from Fig. 1 that in the potential range 0.2 to −0.4 V (versus Ag/AgCl), there is no redox peak at the bare CPE, while the voltammograms of $SiNH_3PW_{12}$-CPE exhibit two characteristic consecutive redox processes which are similar with these processes in solution at bare CPE electrode (Fig. 1c).

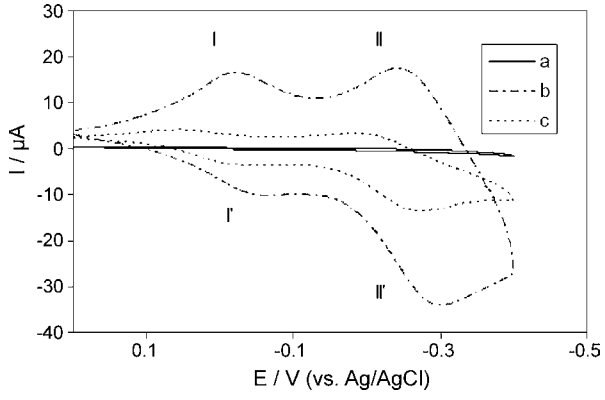


Fig. 1. Cyclic voltammograms of bare CPE (a) and $SiNH_3PW_{12}$-CPE (b) in the 1 M $Na_2SO_4 + H_2SO_4$ with pH 1 and (c) for bare CPE in the 1 mM PW_{12} and 1 M $Na_2SO_4 + H_2SO_4$ with pH 1 solution. Scan rate: 50 mV s^{-1}.

The mean peak potentials $E_{1/2} = (E_{pa} + E_{pc})/2$ were −0.029 V (I) and −0.279 V (II), respectively. The peak potential separations were 20 mV (I) and 55 mV (II), respectively, instead of the value of zero expected for a reversible surface process, which might be due to non-ideal behavior [19]. Comparing the voltammograms of $SiNH_3PW_{12}$-CPE with PW_{12} in solution (Fig. 1c) showed that the immobilization of negatively charged PW_{12} on positively charged-modified silica, led to a negative shift of the peak potentials and an increase of the separation of the peak potentials which are in agreement with the previously reported results [3].

The above experimental results showed that PW_{12} can be supported on the surface of 3-aminopropylated silica based on electrostatic interaction and keep its electrochemical properties in solution.

3.2. Effect of carbon paste composition on the voltammetric response of $SiNH_3PW_{12}$-modified CPE

The effect of the carbon paste composition on the voltammetric response of the electrode modified with $SiNH_3PW_{12}$ was evaluated by cyclic voltammetry. Electrodes with different percent of modifier were prepared and examined for their voltammetric signals under identical conditions. The amount of $SiNH_3PW_{12}$ in carbon paste has a marked influence on the response of the electrode and the peak currents increase with increasing the percent of the $SiNH_3PW_{12}$ in carbon paste electrode. However, at concentration higher than 10% of $SiNH_3PW_{12}$ the paste is too rigid and its treatment is very hard. Hence an electrode containing 10% $SiNH_3PW_{12}$ was employed for all subsequent experiments.

3.3. Effect of scan rate on the electrochemical behavior of the $SiNH_3PW_{12}$-modified CPE

Fig. 2A presents cyclic voltammograms obtained at different scan rates for a $SiNH_3PW_{12}$-CPE immersed in 1 M H_2SO_4 (pH 1) and Fig. 2B is the corresponding dependence of peak currents on scan rate. When the scan rate was varied from 10 to 200 mV s^{-1}, the cathodic peak currents were almost the same as the corresponding anodic peak currents. At scan rates lower than 60 mV s^{-1}, the peak currents were proportional to the scan rate, suggesting that the redox process is surface-confined; however, at scan rates higher than 60 mV s^{-1}, the peak currents were proportional to the square root of the scan rates which indicates that the redox process is diffusion controlled. It is known that, the electrochemical reduction of polyoxometalates is accompanied by proton transfer, and at high scan rates the rate of polyoxometalate reduction is controlled by the rate of mass transfer of proton [35].

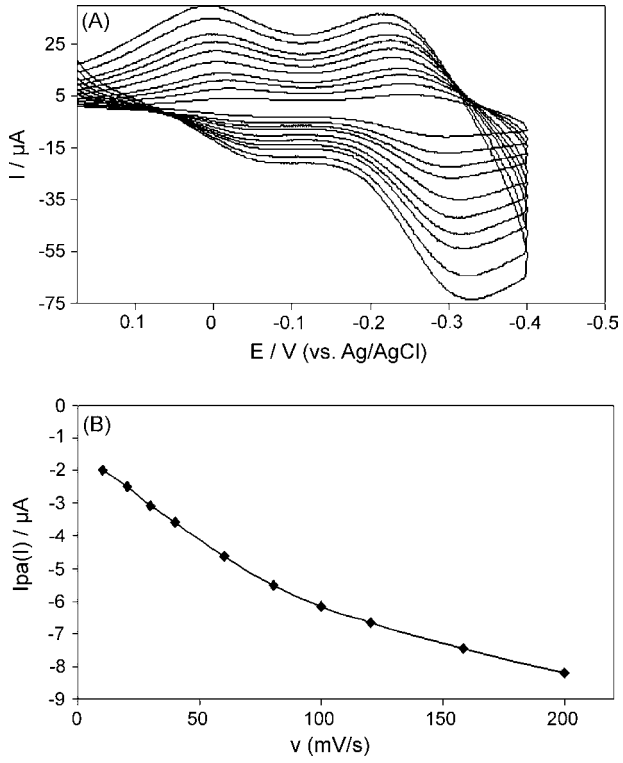


Fig. 2. (A) Cyclic voltammograms for $SiNH_3PW_{12}$-CPE in $Na_2SO_4 + H_2SO_4$ with pH 1 solution with different scan rates (from inner to outer: 10–40, 60, 80, 100, 120, 160, 200 mV s^{-1}). (B) The dependence of cathodic peak (*I*) current on scan rates.

3.4. Electrocatalytic activity of the $SiNH_3PW_{12}$-modified CPE

3.4.1. Electrocatalytic effect of the $SiNH_3PW_{12}$-modified CPE on reduction of IO_3^-

In experiments, we found that the carbon paste electrode modified with $SiNH_3PW_{12}$ has a catalytic effect on the reduction of IO_3^-. As is known the electroreduction of IO_3^- requires a large overpotential, no obvious response is observed in the range of 0.2 to −0.4 V on an unmodified carbon paste electrode in 1 M H_2SO_4 solution (pH 1) containing 1×10^{-3} M IO_3^-, as shown in Fig. 3a. The catalytic reduction of IO_3^- by PW_{12} supported on the surface of aminopropylated silica gel in carbon paste electrode can be seen clearly in Fig. 3. From Fig. 3 (voltammograms b–d) it can be seen that adding IO_3^- to the cell produces a dramatic change in the cyclic voltammograms with an increase in cathodic currents and a concomitant decrease in anodic currents. The catalytic current increases with the concentration of IO_3^-. The catalytic waves appear on the both waves of PW_{12}. The IO_3^- is reduced by both reduced species in the presence of protons to yield I^-. It can also be seen that the second reduced species has a larger catalytic activity toward IO_3^- than the first reduced species. Therefore, the electrochemical behavior of a $SiNH_3PW_{12}$-CPE towards IO_3^- could be regarded as an EC′ catalytic mechanism.

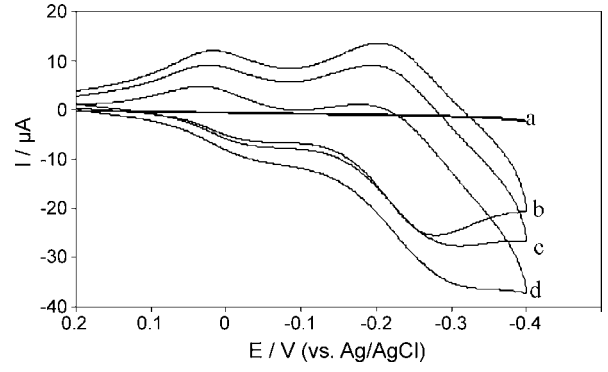


Fig. 3. Cyclic voltammograms of bare CPE (a) in 1 mM IO_3^- and $SiNH_3PW_{12}$ (b–d) in solution of 1 M $Na_2SO_4 + H_2SO_4$ with pH 1 containing IO_3^- concentrations of 0.0 (b), 0.5 mM (c), and 1 mM (d). Scan rate: 50 mV s^{-1}.

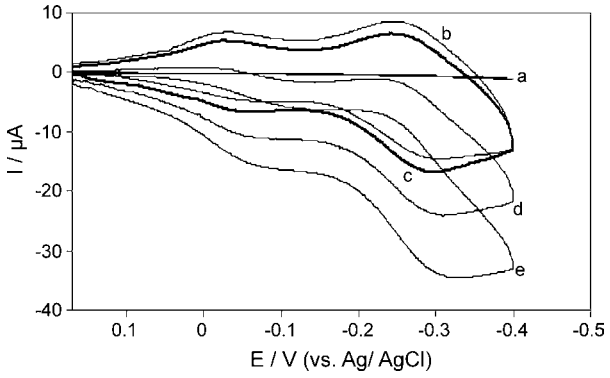


Fig. 4. Cyclic voltammograms of bare CPE (a) in 15 mM H_2O_2 and $SiNH_3PW_{12}$ (b–e) in solution of 1 M $Na_2SO_4 + H_2SO_4$ with pH 1 containing H_2O_2 concentrations of 0.0 (b), 1 mM (c), 5 mM (d), and 15 mM (e). Scan rate: 50 mV s^{-1}.

3.4.2. Electrocatalytic effect of the $SiNH_3PW_{12}$-modified CPE on reduction of hydrogen peroxide

The direct electroreduction of hydrogen peroxide requires a large overpotential at most bare electrode surfaces. In the present work, we found that the $SiNH_3PW_{12}$-modified CPE showed catalytic activity toward the reduction of hydrogen peroxide. Fig. 4 shows the electrocatalytic reduction of hydrogen peroxide on a $SiNH_3PW_{12}$-modified CPE. With the addition of hydrogen peroxide, the two reduction peak currents increase whereas the corresponding oxidation peak currents decrease, suggesting that hydrogen peroxide is reduced by both reduced species of polyoxometalate. It has been noted that the second reduced species has a larger catalytic activity toward hydrogen peroxide than the first reduced species. Hence the catalytic activity of PW_{12} toward hydrogen peroxide increases with the extent that PW_{12} is reduced.

3.5. FIA application

On the basis of the voltammetric results described above, it appears that amperometric detection of IO_3^- and hydrogen peroxide by the $SiNH_3PW_{12}$-modified CPE is possible. Flow injection analysis is performed to verify whether or not the electrocatalytic reduction of hydrogen peroxide and IO_3^- by the $SiNH_3PW_{12}$-modified CPE can be conducted under flow conditions and to evaluate its potential as an electrochemical detector for hydrogen peroxide and IO_3^- determination. Our preliminary

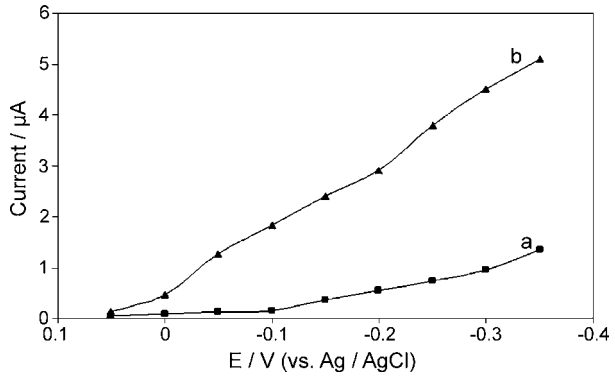


Fig. 5. Plot of FIA response to IO_3^- vs. applied potential on (a) bare CPE and (b) $SiNH_3PW_{12}$-CPE. Carrier: 1 M $Na_2SO_4 + H_2SO_4$ with pH 1.0. Volume of sample injection loop 75 μL and flow rate: 0.6 mL min^{-1}.

experiments showed that the sensitivity and reproducibility of the $SiNH_3PW_{12}$-modified CPE for the determination of IO_3^- is much better than its sensitivity and reproducibility for hydrogen peroxide. Therefore, the method was optimized for the determination of IO_3^-.

In order to obtain the best sensitivity and selectivity of the electrochemical detection for IO_3^- the effect of applied potential on the amperometric signal of IO_3^- was studied. Applied potential has remarkable effect on both catalytic and uncatalytic currents. As it is shown in Fig. 5, in the potential range of +100 to −100 mV the IO_3^- reduction current on modified CPE increased with changing the applied potentials while the current on the unmodified carbon paste electrode is small and independent of applied potential. In the potential range of −100 to −250 mV, peak currents on both modified and unmodified CPEs increased with changing the applied potential. An applied potential of −100 mV was used for the optimized analytical procedure.

The effects of flow rate and volume of sample loop of FIA system were also studied. The best results were obtained for 0.6 mL/min of flow rate and 75 μL for volume of sample injection loop.

Fig. 6 shows the amperometric FIA responses of various concentrations of IO_3^-. The results showed that the electrode response was linear for IO_3^- within the concentration range 5×10^{-6}–1×10^{-3} mol L^{-1}, with a sensitivity of 0.4312 nA

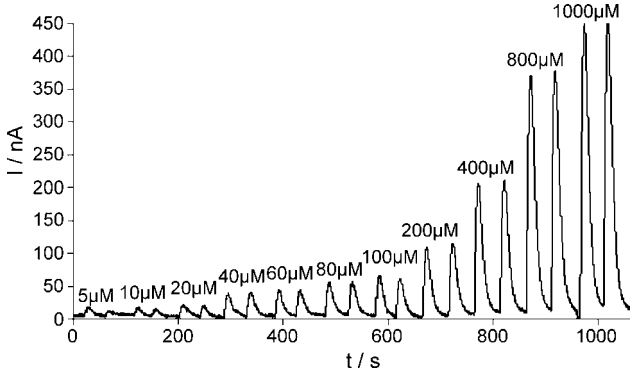


Fig. 6. FIA response of various concentrations of IO_3^- at $SiNH_3PW_{12}$-CPE. Carrier: 1 M $Na_2SO_4 + H_2SO_4$ with pH 1.0. Applied potential: −100 mV (vs. Ag/AgCl). Volume of sample injection loop 75 μL and flow rate: 0.6 mL min^{-1}.

$(\mu mol\,L^{-1})^{-1}$ and correlation coefficient of $r = 0.999$. The detection limit (3 s) was found to be 3.1×10^{-6} mol L^{-1}. The reproducibility was estimated by making repetitive injection (eighteen times) of 1×10^{-3} mol L^{-1} IO_3^- under the same conditions every 40 s. The relative standard deviation of the peak current is found to be 2.2%. Therefore, the response at the $SiNH_3PW_{12}$-modified CPE is very stable and reproducible.

3.6. Repeatability of surface-renewal and long-term stability

Compared with polyoxometalates (POMs)-modified film electrodes fabricated by conventional methods, the $SiNH_3PW_{12}$-modified CPE have certain advantages. The main attraction of using the modified electrode is that the electrode surface can be renewed after every use. The bulk-modified electrode can be renewed by squeezing a little carbon paste out the tube and a fresh surface is exposed whenever needed. This is especially useful for electrocatalytic studies since the catalytic activity is known to decrease when the electrode is fouled. Indeed, 10 successive renewing of a $SiNH_3PW_{12}$-modified CPE resulted in an R.S.D. of 3.6%. Another advantage of the proposed-modified electrode is that the resulting carbon paste electrode is of a good long-term stability. Such stabilization action was tested by measuring the decrease in voltammetric currents during potential cycling of the modified carbon paste electrode. For example, when in the potential range 0.2 to −0.4 V and in 1 M H_2SO_4 with (pH adjusted to 1.0) solutions the modified electrode was subjected to 70 potential cycles, no significant change (<10%) in the voltammetric currents was observed. When the electrode was stored in the atmosphere, the current response remained almost unchanged for 1 month. The high stability of the $SiNH_3PW_{12}$-modified CPE could be related to the strong electrostatic interaction between derivatized silica gel and PW_{12} and insolubility of silica gel in water.

4. Conclusions

A new chemically modified carbon paste electrode has been developed using $PW_{12}O_{40}^{3-}$ supported on silica gel derivatized by aminopropyl(triethoxy)silane. The electrochemistry of the modified electrode was studied using cyclic voltammetry. The $SiNH_3PW_{12}$-modified CPE shows activity toward the reduction of IO_3^- and hydrogen peroxide. The proposed sensor was used as amperometric detector in the FIA determination of IO_3^-. Compared with the iodate sensors reported previously [36–41], the $SiNH_3PW_{12}$-modified carbon paste electrode exhibits better or comparable sensitivity, and detection limit. The electrode offers attractive properties compared to the pervious studies such as reproducibility, simplicity of electrode preparation, high stability and a distinct advantage of polishing in the event of surface fouling. Also there is no leaching of the electrode because of the low solubility of $SiNH_3PW_{12}$ in aqueous solution and hence a single electrode surface can be used for multiple analytical determinations. Although the new concept has been presented in the context of PW_{12}-modified CPE, it could be readily extended

to the construction of other three-dimensional POMs-modified CPEs and the measurement of other environmentally important compounds.

Acknowledgements

The authors acknowledge the Institute for Advanced Studies in Basic Science (IASBS) and Center of Excellence of Catalyst of Department of Chemistry of University of Isfahan for financial support. We are also grateful to Dr. B. Haghighi for providing FIA system and his helpful suggestions.

References

[1] J. Wang, Ch. Hu, M. Jian, J. Zhang, G. Li, J. Catal. 240 (2006) 23.
[2] M.T. Pope, A. Muller (Eds.), Polyoxometalates: From Platonic Solids to Antiretroviral Activity, Kluwer, Dordrecht, 1994.
[3] M. Sadakane, E. Steckhan, Chem. Rev. 98 (1998) 219, and references therein.
[4] Sh. Gao, R. Cao, X. Li, Thin Solid Films 500 (2006) 283.
[5] G. Yang, J. Gong, R. Yang, H. Guo, Y. Wang, B. Liu, Sh. Dong, Electrochem. Commun. 8 (2006) 790.
[6] N. Fay, E. Dempsey, T. McCormac, J. Electroanal. Chem. 574 (2005) 359.
[7] B. Keita, E. Abdeljalil, L. Nadjo, R. Contant, R. Belgiche, Electrochem. Commun. 3 (2001) 56.
[8] Z.Y. Tang, S.Q. Liu, E.K. Wang, S.J. Dong, E.B. Wang, Langmuir 16 (2000) 5806.
[9] B. Keita, R. Contant, E. Abdeljalil, F. Girard, L. Nadjo, Electrochem. Commun. 2 (2000) 295.
[10] B. Wang, S. Dong, Electrochim. Acta 41 (1996) 895.
[11] S. Dong, Z. Jin, J. Chem. Soc. Chem. Commun. (1987) 1871.
[12] A. Kuhn, F.C. Anson, Langmuir 12 (1996) 5481.
[13] X. Xi, S. Dong, Electrochim. Acta 40 (1995) 2785.
[14] Sh.-M. Chen, Y.-H. Fa, J. Electroanal. Chem. 567 (2004) 9.
[15] X. Zou, Y. Shen, Z. Peng, L. Zhang, L. Bi, Y. Wang, S. Dong, J. Electroanal. Chem. 566 (2004) 63.
[16] W. Song, Y. Liu, N. Lu, H. Xu, C. Sun, Electrochim. Acta 45 (2000) 1639.
[17] W. Song, X. Chen, Y. Jiang, Y. Liu, C. Sun, X. Wang, Anal. Chim. Acta 394 (1999) 73.
[18] L. Li, W. Li, C. Sun, L. Li, Electroanalysis 14 (2002) 368.
[19] J. Wang, Analytical Electrochemistry, 2nd ed., Wiley, New York, 2000.
[20] T.H. Degefa, B.S. Chandravanshi, H. Alemu, Electroanalysis 11 (1999) 1305.
[21] X.-L. Wang, E.B. Wang, Y. Lan, Ch. Hu, Electroanalysis 14 (2002) 1116.
[22] A. Walcarius, Electroanalysis 13 (2001) 701.
[23] W.J. Hunks, A. Ozin, J. Mater. Chem. 15 (2005) 3716.
[24] J. Liu, L. Cheng, B. Liu, S. Dong, Langmuir 16 (2000) 7471.
[25] W. Li, L. Li, Z. Wang, A. Cui, C. Sun, J. Zhao, Mater. Lett. 49 (2001) 228.
[26] L. Li, C. Liu, A. Geng, C. Jiang, Y. Guo, C. Hu, Mater. Res. Bull. 41 (2006) 319.
[27] A. Lapkin, B. Bozkaya, T. Mays, L. Borello, K. Edler, B. Crittenden, Catal. Today 81 (2003) 611.
[28] A. Tarlani, M. Abedini, A. Nemati, M. Khabaz, M.M. Amini, J. Colloid Interf. Sci. 303 (2006) 32.
[29] B.J.S. Johnson, A. Stein, Inorg. Chem. 40 (2001) 801.
[30] E. Shams, R. Torabi, Sens. Actuator B 117 (2006) 86.
[31] E. Shams, F. Alibeygi, R. Torabi, Electroanalysis 18 (2006) 773.
[32] R. Torabi, E. Shams, M.A. Zolfigol, Sh. Afshar, Anal. Lett. 39 (2006) 2643.
[33] M. Filowitz, R.K.C. Ho, W.G. Klemperer, W. Shum, Inorg. Chem. 18 (1979) 93.
[34] S. Paul, J.H. Clark, Greem Chem. 5 (2003) 635.
[35] A. Mahmoud, B. Keita, L. Nadjo, O. Oung, R. Contant, S. Brown, Y. de Kouchkovsky, J. Electroanal. Chem. 463 (1999) 129.
[36] Y. Li, W. Bu, L. Wu, C. Sun, Sens. Actuator B 107 (2005) 921.
[37] L. Tian, L. Liu, L. Chen, N. Lu, H. Xu, Sens. Actuator B 105 (2005) 484.
[38] D. Sun, L. Zhu, H.P. Huang, J. Electroanal. Chem. 597 (2006) 39.
[39] A. Salimi, H. Mamkhezri, S. Mohebbi, Electrochem. Commun. 8 (2006) 688.
[40] X. Lin, C. Jiang, Anal. Sci. 22 (2006) 697.
[41] A. Salimi, A. Noorbakhsh, M. Ghadermarzi, Sens. Actuator B 123 (2007) 530.

Available online at www.sciencedirect.com
ScienceDirect
Talanta 74 (2008) 986–991
Talanta
www.elsevier.com/locate/talanta

Rapid and sensitive determination of polycyclic aromatic hydrocarbons in atmospheric particulates using fast high-performance liquid chromatography with on-line enrichment system

Yuki Hashi [a,b], Tian-Ran Wang [a], Wei Du [b], Jin-Ming Lin [a,*]

[a] *State Key Laboratory of Environmental Chemistry and Ecotoxicology, Research Center for Eco-Environmental Sciences, Chinese Academy of Sciences, Beijing 10085, China*

[b] *Shimadzu International Trading (Shanghai) Co. Limited, Beijing 100020, China*

Received 1 June 2007; received in revised form 6 August 2007; accepted 7 August 2007
Available online 19 August 2007

Abstract

A method using on-line enrichment and fast high-performance liquid chromatography (HPLC) with fluorescence detection has been developed and validated for the determination of polycyclic aromatic hydrocarbons (PAHs) in atmospheric particulate samples. The evaporation step for sample preparation can be eliminated since this system allows the injection of 1000 μL of sample solution. PAH recoveries were between 87% and 120% for spiked atmospheric particulate samples. The limit of detection was 0.02–0.23 ng/mL (signal/noise ratio = 3.3). There was good linear correlation between HPLC peak area and PAH concentration, with a linear range of 0.4–40 ng/mL and correlation coefficients >0.997. Furthermore, compared to conventional approaches that include an evaporation step, the method proposed is acceptable for detecting PAHs in atmospheric particulate samples.
© 2007 Elsevier B.V. All rights reserved.

Keywords: On-line enrichment; High-performance liquid chromatography; Atmospheric particulates; Polycyclic aromatic hydrocarbons

1. Introduction

As atmospheric particulates contain many hazardous heavy metals, acidic oxides, organic substances and bacterial viruses which affect the atmospheric environment and are harmful to human health. Therefore, research on atmospheric particulates is an important field in environmental science [1]. Polycyclic aromatic hydrocarbons (PAHs) are widely distributed in the environment, and some kinds of PAHs have organic pollutant characteristic of carcinogenic, teratogenic or mutagenic. They may react with O_3 and NO_x in the atmosphere and generate more harmful compounds with stronger carcinogenic activity and mutagenicity [2,3]. In recent years, research on PAHs in atmospheric particulates in China has mainly focused on the particle type, particle size distribution, concentrations, seasonal changes, sources and influences. Because PAHs are unstable and volatile, the sample pretreatment of atmospheric particulates is a key point in the analysis of PAHs [4,5]. Currently, sample pretreatment of PAHs in atmospheric particulates includes extraction and enrichment steps. Soxhlet extraction and ultrasonic extraction are typical methods used [6]. For the concentration or enrichment of samples, evaporator or solid-phase extraction (SPE) is generally adopted. Owing to the high consumption of organic solvents, as well as PAH instability and volatility, these traditional methods may involve partial sample losses, resulting in greater error and longer analysis times. Moreover, consistent operation may be difficult to maintain with off-line manual pretreatment. This may also lead to poor repeatability of the experimental results [7,8]. In order to dissolve these problems, Asakawa et al. [9–12] developed an on-line dilution technique to realize on-line enrichment. Our group has also been using this technique to determine bisphenol A and 4-octylphenol in serum [13]. This system allows large volume injections for on-line enrichment using an on-line dilution function. The concentration column can also work as a sample clean-up, therefore, this system also allows direct injection without any sample preparations. In this study, we investigated the feasibility to combine

* Corresponding author. Present address: Department of Chemistry, Tsinghua University, Beijing 100084, China. Tel.: +86 10 62792343; fax: +86 10 62792343.
E-mail address: jmlin@mail.tsinghua.edu.cn (J.-M. Lin).

0039-9140/$ – see front matter © 2007 Elsevier B.V. All rights reserved.
doi:10.1016/j.talanta.2007.08.011

this on-line enrichment system to a fast HPLC system to minimize the analysis time. Use of a packing material of 2.2 μm particle size in the chromatographic column allows minimization of the analysis time without a high column back pressure. Here we describe the usefulness of the enrichment function of this system using on-line dilution and a fast HPLC system with fluorescence detection.

2. Experimental

2.1. Chemicals

All chemicals used were of analytical reagent or chromatographic grade. Acetonitrile was obtained from Tedia Company Inc. (USA). All water was freshly deionized using a Milli-Q water purification system with a 0.22 μm filter. PAH standards (anthracene, fluoranthene, chrysene, benzo[*b*]fluoranthene, benzo[*k*]fluoranthene, benzo[*a*]pyrene, dibenzo[*a*,*h*]anthracene and benzo[*g*,*h*,*i*]perylene) were purchased from Accustandard Company (USA).

2.2. Apparatus

The system used in the present study consisted of three LC-20AD pumps, a DGU-20A3 degassing unit, a SIL-20AC auto-sampler, a CTO-20AC column oven including FCV-12AH flow-channel selection valves and an RF-10Axl fluorescence detector with semi-microflow cell (Shimadzu Corporation, Kyoto, Japan). System control and data acquisition were performed using LC-Solution version 1.21 workstation software. A Shim-Pack VP-GODS (4.6 mm i.d. × 10 mm; Shimadzu Corporation) guard column and a Shim-Pack XR-ODS (3 mm i.d. × 150 mm, 2.2 μm; Shimadzu Corporation) analytical column were used. A HV-700F sampling apparatus (Shibata Corporation, Japan) including quartz fiber filter (Dylec Co. Ltd., Japan, Tissu quartz 2500 QAT-UP, 25.5 cm × 20.5 cm, 0.3 μm) was used for collection of atmospheric particulate samples.

2.3. Sample preparation and treatment

2.3.1. Preparation of standard mixture compounds

Samples of 40 mg of the eight PAH standards were weighed and dissolved in 100 mL of acetonitrile. The stock solutions were diluted with acetonitrile to yield working standard solutions of 400, 200, 100, 40, 20, 10, 4, 2, 1 and 0.4 ng/mL. These solutions are sealed and stored below −40 °C.

2.3.2. Sample collection

Atmospheric particulate samples were collected on the quartz fiber filter of the sampling apparatus (700 L/min, 24 h collection). The sampling site was located on top of the Comprehensive Building of the Research Center for Eco-Environmental Sciences, Chinese Academy of Sciences. The sampling was carried out in September 2006, and the filters were kept in the plastic bag with a zipper and stored below −40 °C.

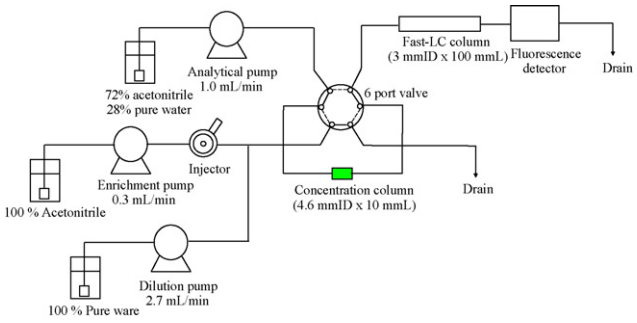


Fig. 1. Flow diagram of the on-line enrichment system.

2.3.3. Pretreatment of atmospheric particulate samples

Before analysis, a 1 cm^2 was cut from the sample filter and soaked with ultrasonic extraction in approximately 30 mL of acetonitrile for 10 min. The extraction was repeated three times and the extracts were combined and the volume was adjusted to exactly 100 mL with acetonitrile. After filtration through a 0.45 μm membrane filter, 1000 μL of sample was directly injected into the HPLC with the on-line enrichment system. For conventional sample pretreatment, 20 mL of the extract was transferred to a 50 mL sample tube and evaporated to 1 mL under a stream of nitrogen. Then 20 μL of this solution was injected into a conventional HPLC system.

2.4. Flow diagram of the on-line enrichment system

A flow diagram of the on-line enrichment system is previously reported [14] and shown in Fig. 1. Unlike conventional on-line enrichment approaches, this system includes a dilution function for large-volume injection. The dilution line is installed after the sample injection device to dilute the sample with a suitable dilution solvent for better enrichment. The diluted sample is then effectively trapped by the concentration column, regardless of the sample load amount and the sample solvent. As a concentration column, a general guard column of ODS type which has the particle size of 5 μm and the column dimension of 4.6 mm inner diameter and 10 mm column length can be utilized. In this case, 100% acetonitrile was used as the sample solvent. Therefore, for large-volume injection, since a large amount of acetonitrile is also transferred to the concentration column, the target PAH compounds are easily eluted with the organic solvent and are not retained in the column. When a dilution line is used, before the sample reaches the concentration column, the organic solution of the sample is diluted by pure water, and then the target PAH compounds can be retained on the concentration column. On the other hand, hydrophilic compounds were eluted from the concentration column; therefore, a clean-up of the sample can be carried out at the same time. After the target PAH compounds are trapped, the 6-port valve is switched to transfer the sample to the analytical column linked to a fluorescence detector.

2.5. Chromatographic conditions

Acetonitrile at 0.3 mL/min was used as the enrichment pump solvent, with pure water at 2.7 mL/min as the dilution

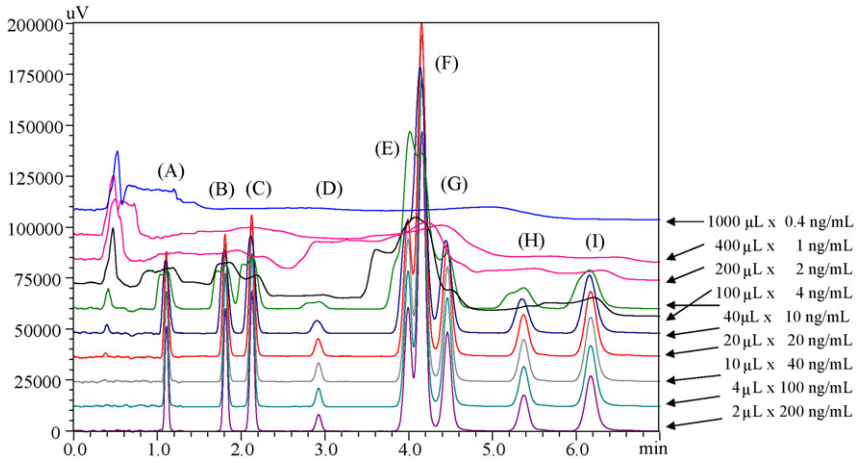


Fig. 2. Chromatograms for the same amount of PAHs in different injection volume without on-line enrichment. The PAH elution is (A) naphthalene, (B) anthracene, (C) fluoranthene, (D) chrysene, (E) benzo[*b*]fluoranthene, (F) benzo[*k*]fluoranthene, (G) benzo[*a*]pyrene, (H) dibenzo[*a*,*h*]anthracene and (I) benzo[*g*,*h*,*i*]perylene.

solvent. Therefore, the sample was diluted 10-fold in pure water. To analyze the target PAH compounds, a solvent mixture of acetonitrile (72%) and pure water (28%) at 1.0 mL/min was used as the optimized mobile phase. Since benzo[*b*]fluoranthene and benzo[*k*]fluoranthene are structural isomers, mobile phase composition needs to be optimized to separate these two compounds. The column temperature was set at 35 °C. An excitation wavelength of 220 nm was selected for naphthalene, and 250 nm for anthracene, fluoranthene and chrysene, and 293 nm for benzo[*b*]fluoranthene, benzo[*k*]fluoranthene, benzo[*a*]pyrene, dibenzo[*a*,*h*]anthracene and benzo[*g*,*h*,*i*]perylene. Emission was monitored at 330 nm for naphthalene and 450 nm for other PAHs.

3. Results and discussion

3.1. Determination of PAHs using large-volume injection

Ten concentrations (0.4, 1, 2, 4, 10, 20, 40, 100, 200 and 400 ng/mL) of the PAHs were prepared and volumes equivalent to an absolute amount of 0.4 ng of each PAH were injected (1000, 400, 200, 100, 40, 20, 10, 4, 2 and 1 µL, respectively). Chromatograms obtained for the fast HPLC system without on-line enrichment are shown in Fig. 2. The PAHs could be separated within 7 min by fast HPLC with a packing material of 2.2 µm. Even though the same absolute amount of each PAH compound was injected, serious distortions of the peak shape were observed for large-volume injection without on-line enrichment system. On the other hand, when the on-line enrichment system with a dilution function was used, no distortion of PAH peak shape was observed, even for an injection volume of 1000 µL (Fig. 3). Since the sample solvent was diluted 10-fold with pure water, the target PAH compounds can be effectively trapped and concentrated on the concentration column. Fig. 4 shows a comparison of the trap efficiency of the on-line enrichment system. When the dilution line was removed from the on-line enrichment system, the trap efficiency drastically decreased for large-injection volumes. On the other hand, the on-line enrichment system achieved trap efficiency of almost 100% over the whole range of injection volumes. These results indicate that the conven-

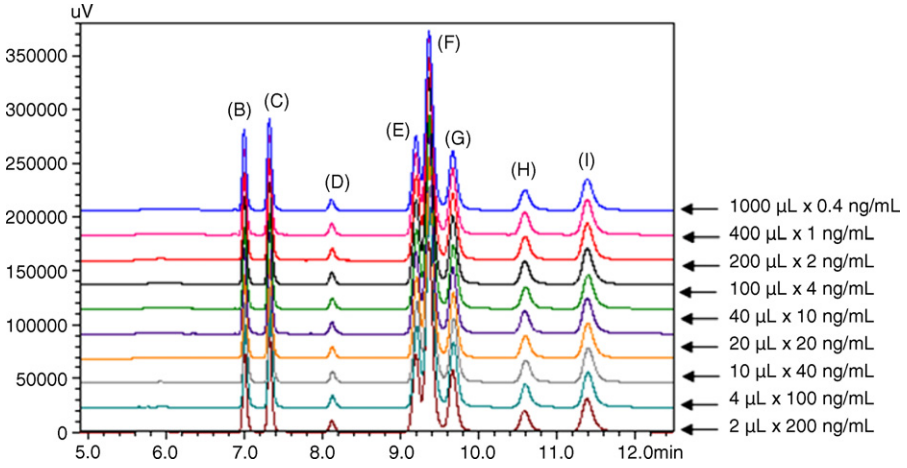


Fig. 3. Chromatograms for the same amount of PAHs in different injection volume using the on-line enrichment system. The PAH elution is (B) anthracene, (C) fluoranthene, (D) chrysene, (E) benzo[*b*]fluoranthene, (F) benzo[*k*]fluoranthene, (G) benzo[*a*]pyrene, (H) dibenzo[*a*,*h*]anthracene and (I) benzo[*g*,*h*,*i*]perylene. Since on-line sample enrichment was carried out until 5 min, chromatogram between 0 and 5 min was eliminated.

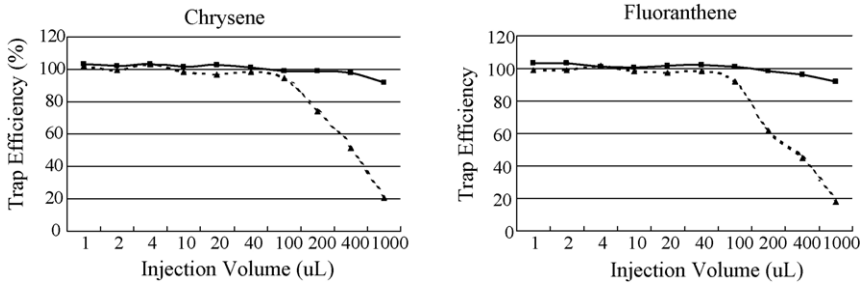


Fig. 4. Comparison of the trap efficiency of the on-line enrichment system for chrysene and fluoranthene. Solid line: with dilution function; dotted line: without dilution function.

tional on-line enrichment HPLC system which does not have the dilution line is difficult to inject large-volume sample into the column, and that the sample must be concentrated or enriched before injection. If the sample solvent can be transferred to water rich conditions such as 90% water/10% acetonitrile, the conventional on-line enrichment system can be also accepted for large-volume injection (Fig. 5 lower chromatogram). However, sample solvent transferring procedure must be included in sample pretreatment step. On the other hand, using on-line enrichment with a dilution function, large volumes of PAH samples with 100% acetonitirile sample solvent can be separated and analyzed effectively (Fig. 5 upper chromatogram). This is the most advantage for use of dilution function. Moreover, the fast HPLC system with packing material of 2.2 μm particle size is compatible with the on-line enrichment system. Therefore, analysis including on-line sample enrichment can be completed within 15 min. These results demonstrated that the system proposed can simplify the complicated pretreatment process for sample enrichment and can reduce the sample losses involved in the manual process.

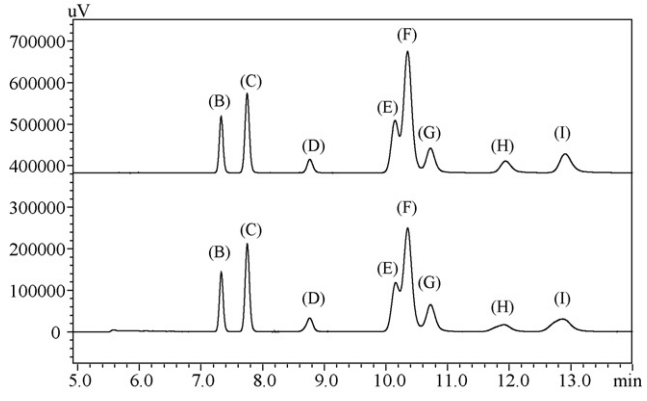


Fig. 5. Chromatogram comparison obtained by different on-line enrichment systems with different sample solvents. Upper chromatogram: on-line enrichment HPLC system with dilution line (1000 μL injection, sample solvent: 100% acetonitrile). Lower chromatogram: conventional on-line enrichment HPLC system without dilution line (1000 μL injection, sample solvent: 90% water/10% acetonitrile). The PAH elution is (B) anthracene, (C) fluoranthene, (D) chrysene, (E) benzo[*b*]fluoranthene, (F) benzo[*k*]fluoranthene, (G) benzo[*a*]pyrene, (H) dibenzo[*a*,*h*]anthracene and (I) benzo[*g*,*h*,*i*]perylene (each 1 ng/mL). Since on-line sample enrichment was carried out until 5 min, chromatogram between 0 and 5 min was eliminated.

3.2. Validation of the on-line enrichment system

The accuracy of the method was evaluated by using 0.4, 2, 10 and 40 ng/mL of PAH standard mixtures. One thousand microlitres of each PAH standard mixture was injected five times, repeatedly. As an evaluation of the accuracy, the averaged concentrations obtained by each standard mixture were normalized (Table 1). Although over 100% of normalization results were observed at lowest concentration of PAH standards, the accuracy of the method was confirmed. The reproducibility of intra-day and inter-day was also evaluated by using 1 ng/mL of PAH standard mixtures. The averaged concentrations were shown in Table 2. No difference concentration results of intra-day and inter-day were obtained. The linear relationship of peak area with the concentration of PAH in the range of 0.4–40 ng/mL is shown in Table 3. The sample

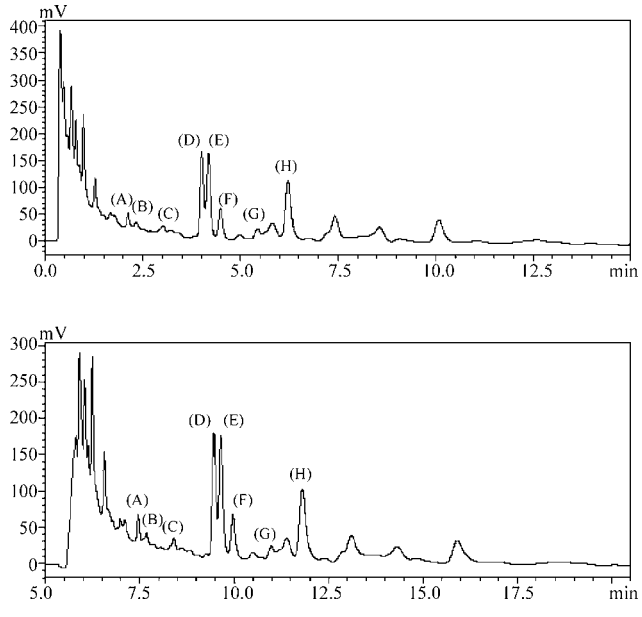


Fig. 6. Chromatogram of atmospheric particulates. Upper chromatogram: conventional sample pretreatment with normal HPLC system (20 μL injection). Lower chromatogram: on-line enrichment HPLC system (1000 μL injection). The PAH elution is (A) anthracene, (B) fluoranthene, (C) chrysene, (D) benzo[*b*]fluoranthene, (E) benzo[*k*]fluoranthene, (F) benzo[*a*]pyrene, (G) dibenzo[*a*,*h*]anthracene and (H) benzo[*g*,*h*,*i*]perylene. Since on-line sample enrichment was carried out until 5 min, chromatogram between 0 and 5 min was eliminated.

Table 1
Accuracy for the PAHs (1000 μL injection, $n = 5$)

	0.4 ng/mL	2 ng/mL	10 ng/mL	40 ng/mL
Anthracene	104.7% (2.77%)	100.5% (1.06%)	99.2% (0.26%)	100.0% (0.13%)
Fluoranthene	101.8% (2.35%)	100.1% (0.23%)	99.2% (0.26%)	100.0% (0.07%)
Chrysene	104.7% (4.34%)	99.7% (2.58%)	99.0% (0.50%)	100.1% (0.36%)
Benzo[*b*]fluoranthene	103.5% (1.95%)	98.7% (0.47%)	99.5% (0.24%)	100.0% (1.54%)
Benzo[*k*]fluoranthene	105.6% (1.77%)	100.8% (0.43%)	98.9% (0.26%)	100.1% (0.64%)
Benzo[*a*]pyrene	105.3% (1.29%)	102.4% (3.13%)	96.8% (1.75%)	100.4% (0.86%)
Dibenzo[*a*,*h*]anthracene	105.7% (1.18%)	96.7% (1.14%)	97.7% (0.23%)	100.1% (0.34%)
Benzo[*g*,*h*,*i*]perylene	104.9% (2.23%)	98.6% (2.51%)	96.1% (0.63%)	100.2% (0.53%)

R.S.D. values are shown in the bracket.

Table 2
Reproducibility of intra-day and inter-day (1000 μL injection, $n = 5$, unit: ng/mL)

	Intra-day		Inter-day	
	1st	2nd	1 day	2 day
Anthracene	1.16	1.09	1.11	1.16
Fluoranthene	1.13	1.09	1.09	1.13
Chrysene	1.01	0.97	0.99	1.01
Benzo[*b*]fluoranthene	1.01	0.98	0.98	1.01
Benzo[*k*]fluoranthene	1.13	1.09	1.09	1.13
Benzo[*a*]pyrene	1.09	1.01	1.08	1.09
Dibenzo[*a*,*h*]anthracene	1.17	1.12	1.12	1.17
Benzo[*g*,*h*,*i*]perylene	1.13	0.98	1.08	1.13

concentration and the peak area of the PAHs showed an excellent linear relationship. Regression coefficients were all greater than 0.997. The limit of detection (LOD) for the method was determined as 3.3 of signal/noise ratio and yielded values of 0.02–0.23 ng/mL.

3.3. Recovery and repeatability of the method

Sample recovery was determined by adding three different concentrations (1, 10 and 20 ng/mL) to atmospheric particulate samples. Acceptable recovery results of 87–120% were obtained for the PAHs since recovery range between 70% and 130% is described in U.S. Environmental Protection Agency (EPA) method TO13 (PAHs in ambient air). The repeatability of the method was also determined from five repeated injections of a solution of all the standard samples. The relative standard deviation for the retention time and peak areas was less than 0.03% and 1.75% ($n = 5$), respectively. The recovery and repeatability results are shown in Tables 4 and 5, respectively.

Table 4
Recovery results (1000 μL injection, $n = 5$)

Compound	Recovery (%)		
	1 ng/mL	10 ng/mL	20 ng/mL
Anthracene	116	103	98
Fluoranthene	119	100	97
Chrysene	120	119	102
Benzo[*b*]fluoranthene	118	93	87
Benzo[*k*]fluoranthene	114	100	93
Benzo[*a*]pyrene	112	96	91
Dibenzo[*a*,*h*]anthracene	120	107	101
Benzo[*g*,*h*,*i*]perylene	101	96	92

Table 5
Result of repeatability (1 ng/mL, 1000 μL injection, $n = 5$)

Compound	R.S.D. (%)	
	Retention time	Peak area
Anthracene	0.02	1.68
Fluoranthene	0.02	1.71
Chrysene	0.02	1.7
Benzo[*b*]fluoranthene	0.03	1.16
Benzo[*k*]fluoranthene	0.03	1.64
Benzo[*a*]pyrene	0.03	1.63
Dibenzo[*a*,*h*]anthracene	0.03	1.56
Benzo[*g*,*h*,*i*]perylene	0.03	1.28

Table 3
Linearity and LOD for the PAHs (0.4–40 ng/mL, 1000 μL injection)

Compound	Regression equation	Regression coefficient (r^2)	LOD (ng/mL)
Anthracene	$y = 1.372e^{-5} \times -0.542$	0.9971	0.05
Fluoranthene	$y = 1.444e^{-5} \times -0.571$	0.9974	0.05
Chrysene	$y = 4.716e^{-5} \times -1.705$	0.9988	0.23
Benzo[*b*]fluoranthene	$y = 6.145e^{-6} \times -0.566$	0.9976	0.04
Benzo[*k*]fluoranthene	$y = 2.583e^{-6} \times -1.415$	0.9982	0.02
Benzo[*a*]pyrene	$y = 6.494e^{-6} \times -1.174$	0.9983	0.04
Dibenzo[*a*,*h*]anthracene	$y = 1.255e^{-5} \times -1.332$	0.9975	0.09
Benzo[*g*,*h*,*i*]perylene	$y = 1.190e^{-5} \times -1.118$	0.9979	0.12

Table 6
Concentration of PAHs in atmospheric particulates analyzed on a normal HPLC system and the on-line enrichment HPLC system

	Concentration (ng/m^3)									
	Sample 1		Sample 2		Sample 3		Sample 4		Sample 5	
	A	B	A	B	A	B	A	B	A	B
Anthracene	0.019	0.070	–	0.036	–	0.054	–	0.033	0.009	0.043
Fluoranthene	0.039	0.105	0.076	0.078	0.073	0.122	0.045	0.061	0.060	0.078
Chrysene	0.068	0.061	0.108	0.086	0.092	0.086	0.053	0.049	0.060	0.081
Benzo[*b*]fluoranthene	0.424	0.447	0.733	0.677	0.620	0.561	0.326	0.352	0.501	0.579
Benzo[*k*]fluoranthene	0.178	0.197	0.281	0.267	0.246	0.225	0.138	0.151	0.204	0.241
Benzo[*a*]pyrene	0.180	0.189	0.295	0.273	0.290	0.258	0.184	0.194	0.220	0.252
Dibenzo[*a*,*h*]anthracene	0.105	0.075	0.156	0.126	0.142	0.112	0.081	0.078	0.111	0.115
Benzo[*g*,*h*,*i*]perylene	0.562	0.543	0.787	0.706	0.764	0.667	0.402	0.425	0.664	0.749

A: conventional sample pretreatment with normal HPLC system (20 μL injection), B: on-line enrichment HPLC system (1000 μL injection).

3.4. Actual PAH concentrations in atmospheric particulate samples

Five atmospheric particulate samples were collected in the Research Center for Eco-Environmental Sciences, Chinese Academy of Sciences, Beijing. Acetonitrile was used as the extraction solvent, with on-line enrichment and a fast HPLC system for separation and fluorescence detection of eight PAHs. Samples were injected in triplicate, with 1000 μL for each injection. In order to evaluate the on-line enrichment method, measurement of conventional sample pretreatment method with a normal HPLC system, which is composed of one pump, one auto-injector (20 μL injection), ODS separation column, column oven and fluorescence detector, was also tried. Chromatograms are shown in Fig. 6. Since sample concentration and clean-up process were needed in on-line enrichment system, the chromatogram during sample pretreatment (up to 5 min) does not have any peaks. So, except this period, the chromatograms were quite similar for determination of PAHs in atmospheric particulates. The PAH results for the normal HPLC system (A) and the on-line enrichment HPLC system (B) are shown in Table 6. Most of the results are similar, except for anthracene and fluoranthene. Since conventional sample pretreatment involves an evaporation step using a nitrogen stream, PAHs with lower boiling points may be lost. Therefore, on-line enrichment, which does not involve sample evaporation, can avoid sample losses, leading to a more accurate result. In addition, it may take 5 min to concentrate a sample to determine PAHs in atmospheric particulates, whereas conventional sample pretreatment may take 30 min. Therefore, the method proposed is suitable for rapid on-line PAH detection in atmospheric particulates.

4. Conclusions

A method of on-line enrichment and HPLC with fluorescence detection has been developed and validated for the determination of eight PAHs in atmospheric particulates. The on-line enrichment system with a large volume direct injection of atmospheric particulate sample was compatible with a fast HPLC system and minimizes the analysis time. Even for an injection volume of 1000 μL, this system can still effectively separate and analyze eight PAHs. The peak shape of the PAHs is excellent. This method simplifies the complicated process of sample pretreatment, saves sample treatment time and reduces waste and solvent pollution. The method has been validated in terms of recovery, repeatability and linearity and allows rapid PAH determination in atmospheric particulate samples.

Acknowledgements

This work was supported by the National Natural Science Foundation of China (No. 20437020) and Major Research Program of Chinese Academy of Sciences (KZCX3-SW-432).

References

[1] M. Wang, Chin. J. Clim. Environ. Res. 6 (2001) 119.
[2] N. Tang, R. Taga, T. Hattori, K. Tamura, A. Torobam, R. Kizu, K. Hayakawa, Anal. Sci. 20 (2004) 119.
[3] Y. Hung, Y. Di, J. Shi, Chin. J. Res. Environ. Sci. 14 (2001) 4.
[4] L. Zhu, X. Shen, Y. Liu, Chin. J. Environ. Sci. 22 (2001) 86.
[5] M.J. Wornat, E.B. Ledesma, A.K. Sandrowitz, M.J. Roth, S.M. Dawsey, Y.-L. Qiao, W. Chen, J. Environ. Sci. Technol. 35 (2001) 1943.
[6] A. Anastasia, T. Eleni, S. Constantini, Environ. Sci. Pollut. Res. 3 (2002) 140 (special issue).
[7] N. Barnabe, P. Laurier, J. Environ. Sci. Technol. 37 (2003) 2094.
[8] C.L. Gigliotti, J. Dachs, E.D. Nelson, A.P. Brunciak, S. Einsenreich, J. Environ. Sci. Technol. 37 (2003) 3547.
[9] E. Yamamoto, K. Murata, Y. Ishihama, N. Asakawa, Anal. Sci. 19 (2001) 1155.
[10] S. Kawano, H. Murakia, E. Yamamoto, N. Asakawa, J. Chromatogr. B 792 (2003) 49.
[11] E. Yamamoto, T. Sakaguchi, T. Kajima, N. Mano, N. Asakawa, J. Chromatogr. B 807 (2004) 327.
[12] S. Kawano, M. Takahashi, T. Hine, E. Yamamoto, N. Asakawa, Rapid Commun. Mass Spectrom. 19 (2005) 2827.
[13] M. Liu, Y. Hashi, F. Pan, J. Yao, G. Song, J.-M. Lin, J. Chromatogr. A 1133 (2006) 142.
[14] S.S. Sonu, J. Manish, S. Hiten, G. Sapna, T. Purav, S. Ruchy, B.L. Braj, J. Chromatogr. B 813 (2004) 247.

Available online at www.sciencedirect.com
ScienceDirect
Talanta 74 (2008) 773–778
Talanta
www.elsevier.com/locate/talanta

Development of a differential pulse voltammetric method for the determination of Silymarin/Vitamin E acetate mixture in pharmaceuticals

Ekram M. Hassan *, Essam F. Khamis, Eman I. El-Kimary, Magda A. Barary

Faculty of Pharmacy, Department of Pharmaceutical Analytical Chemistry, University of Alexandria, El-Messalah, Alexandria 21521, Egypt

Received 7 November 2006; received in revised form 8 July 2007; accepted 9 July 2007
Available online 14 July 2007

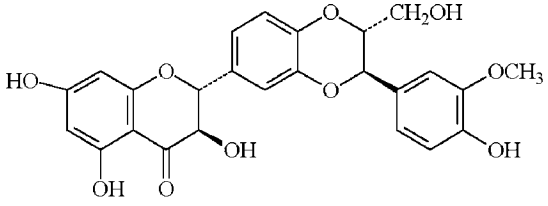
Abstract

Differential pulse voltammetric method was developed for determination of Silymarin (SMR)/Vitamin E acetate (VEA) mixture in pharmaceuticals. SMR and VE gave well-resolved diffusion-controlled anodic peaks at +756 and +444 mV, respectively (versus Ag/AgCl) in Britton–Robinson buffer at pH 2.8. The solution conditions and instrumental parameters were optimized for their quantitative determination. The linear response was obtained in the range 0.1–4.0 mg L^{-1} with a detection limit of 0.03 mg L^{-1} for SMR and 0.05–4.0 mg L^{-1} with a detection limit of 0.01 mg L^{-1} for VEA.
© 2007 Published by Elsevier B.V.

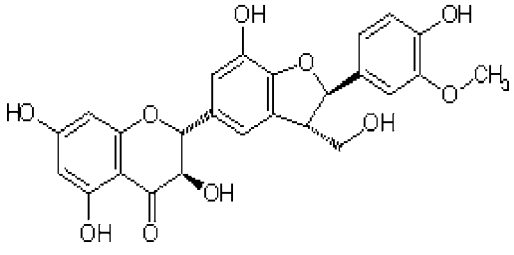
Keywords: Silymarin/Vitamin E acetate mixture; Differential pulse anodic voltammetry; Pharmaceuticals

1. Introduction

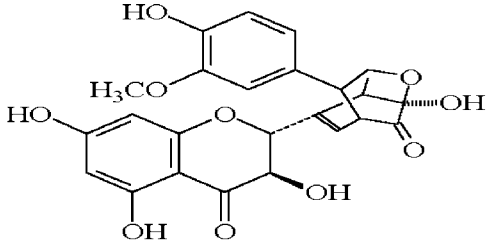
Silymarin (SMR) is the extract of Silybum marianum (Gaertner) plant. It has been used in liver diseases for a better and preventive recovery. The antihepatotoxic or liver protective constituent of Silybum marianum is SMR. It is a mixture consisting chiefly of silybin, silydianin and silychristin [1,2]. SMR is a free radical scavenger, which has been used for the treatment of hepatic disorders. It has been found to be effective in preventing hepatic damage following Amanita poisoning [3]. The structural formula of silybin, silychristin and silydianin [4,5] are given below:



Silybin



Silychristin



Silydianin

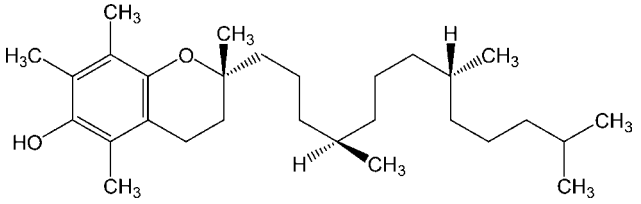
SMR is a non-official drug. The literature revealed that SMR has been determined in biological fluids almost exclusively

* Corresponding author. Tel.: +20 3 4871317; fax: +20 3 4873273.
E-mail address: ekram_mahm@yahoo.com (E.M. Hassan).

0039-9140/$ – see front matter © 2007 Published by Elsevier B.V.
doi:10.1016/j.talanta.2007.07.006

based on HPLC [6,7]. In pharmaceuticals several analytical procedures have been reported for the determination of SMR including spectrophotometry [8], HPLC [9], colorimetry [10] and TLC [11]. Analysis of the active components of SMR has been performed using capillary zone electrophoresis [12] and HPLC [12,13]. To our knowledge no electro-analytical methods, for the determination of SMR in pharmaceuticals, have been reported in the literature to date.

Vitamin E acetate (VEA) DL-α-tocopheryl acetate is a synthetic preparation of a naturally occurring lipid D-α-tocopherol. It acts mainly as an antioxidant, protecting other lipids principally in cell membranes from oxidative and free radical damage [14]. The structural formula of α-tocopherol is given below:



Different methods have been reported for the determination of VE in pharmaceuticals including differential pulse voltammetry at an ultramicroelectrode [15], anodic oscillography at wax impregnated graphite electrode [16] HPLC [17], GC [18], spectophotometry [19,20], electrokinetic chromatography [21] and colorimetry [22–24] or in biological fluids including HPLC [25,26] and enhanced chemiluminescence [27]. An extended bibliography can be found in the analytical profile [28]. VE and its capsules are official in the USP, while α-tocopheryl acetate and its powder form are official in the BP. In USP [29] and BP [30] VE is assayed using GC. The objective of this work is to investigate the voltammetric behavior of SMR at a glassy carbon electrode using differential pulse mode and to develop an electrochemical methodology for its quantitative determination in pharmaceuticals. The proposed method has been applied for the analysis of SMR/VE mixture in capsules where no attempt has been made for the analysis of this mixture before.

2. Experimental

2.1. Apparatus

Voltammetric measurements were performed using Metrohm AG 9101 Herisau consisting of Metrohm 693 VA processor and Metrohm 694 VA potentiostat. The three-electrode system consisted of a glassy carbon working electrode (disk diameter 2.0 ± 0.1 mm), Ag/AgCl (3 M KCl) reference electrode and a Pt auxiliary electrode (3.0 ± 0.05 mm).

All pH measurements were made using a Cyberscan pH meter model 510 calibrated with standard buffers at pH 4, 7 and 10.

2.2. Materials and reagents

- Authentic samples of Silymarin (SMR) and Vitamin E acetate (VEA) were kindly supplied by (El-Amria Co.) and its purity has been checked before use by comparing the calculated *A* (1%, 1 cm) values for solutions measured in methanol with the reported values [2].
- Levatech® capsules (Pharma-Green) labeled to contain 140 mg SMR/capsule, Legalex® tablets (Alexandria Co.) labeled to contain 70 mg SMR/tablet, Silymarin® packets (SEDICO) labeled to contain 140 mg SMR/packet and Seralon-E® capsules (Tiba pharmaceuticals) labeled to contain 140 mg SMR and 100 mg VEA/capsule.
- Solution of Vitamin E (VE) was prepared from VEA by saponification of 25 mg of VEA with 25 mL of 2 M methanolic KOH in a conical flask. The mixture was refluxed for 30 min. The saponified solution was extracted with three successive portions of ethyl ether (3× 15 mL). The extract was evaporated under nitrogen and the residue was dissolved in methanol, quantitatively transferred to 25 mL volumetric flask and diluted to volume with methanol [16]. The resulted solution, equivalent to 1.00×10^3 mg L^{-1} VEA, was stored protected from light at 4 °C. The reproducibility of the method was checked by preparation of VE solution several times, where comparable peak currents were obtained for the same concentration.
- Concentrated solution of SMR (1.00×10^3 mg L^{-1}) in methanol was prepared. More diluted stock solutions of both SMR and VE were prepared daily by accurate dilution with methanol just before use
- Britton–Robinson (BR) buffer (0.08 M in each have acetic, *O*-phosphoric and boric acids) adjusted to the required pH with 0.5 M sodium hydroxide solution.
- All solvents and chemicals used were of analytical grade.

2.3. Construction of calibration curves

Different aliquots from the stock solutions of SMR and VE (0.1–1.0 mL) within the concentration ranges stated in Table 1 were transferred into two sets of 10 mL volumetric flasks. Dilution was made to volume with BR buffer pH 2.8 and the contents of each flask were transferred into the measuring vessel. Before each measurement the glassy carbon electrode was polished for about 30 s with aqueous slurry of alumina on a smooth polishing cloth and gently dried with tissue paper. The differential pulse

Table 1
Regression and statistical parameters for the determination of SMR and VE using the proposed method

Parameters	Analyte	
	SMR	VE
Concentration range (mg L^{-1})	0.10–4.00	0.05–4.00
Slope	0.36	0.67
Intercept	2.04×10^{-3}	1.25×10^{-2}
Correlation coefficient	0.99999	0.99989
S_b	1.04×10^{-3}	5.58×10^{-3}
S_a	1.95×10^{-3}	1.04×10^{-2}
$S_{y/x}$	3.28×10^{-3}	1.83×10^{-2}
LOD (mg L^{-1})	3.00×10^{-2}	1.36×10^{-2}
LOQ (mg L^{-1})	9.00×10^{-2}	4.55×10^{-2}

S_b is the standard deviation of slope, S_a the standard deviation of intercept and $S_{y/x}$ is the standard deviation of residuals.

scan from +200 to +1000 mV was conducted using the optimized parameters for both SMR and VE: pulse amplitude = +90 mV, time interval for voltage step = 0.1 s, measurement time = 20 ms, pulse time = 40 ms, scan rate = 120 mV/s. Peak current was measured at +756 and +444 mV for SMR and VE, respectively.

2.4. Applications

2.4.1. Analysis of SMR pharmaceutical preparations

An accurately weighed portion of the mixed contents of 10 Levatech® capsules or of the ground 10 Legalex® tablets after decoating or of the mixed contents of 5 Silymarin® packets equivalent to 25 mg SMR was transferred into a 25 mL volumetric flask using about 15 mL methanol. The mixture was shaken for 30 min completed to volume with methanol, and filtered. The procedure was completed on the filtrate as previously mentioned in Section 2.3.

2.4.2. Analysis of SMR/VE mixture in their pharmaceutical preparation

2.4.2.1. Determination of SMR content. An accurately weighed portion of the mixed contents of 10 Seralon-E® capsules equivalent to 35 mg SMR and 25 mg VEA was transferred into a 25 mL volumetric flask using about 15 mL methanol, shaken for 30 min, completed to volume with methanol and filtered. The procedure was completed on the filtrate as previously mentioned in Section 2.3.

2.4.2.2. Determination of VEA content. Another portion of the mixed contents of the 10 capsules equivalent to 35 mg SMR and 25 mg VEA was transferred into a conical flask and a solution of VE was prepared as mentioned in Section 2.2. The procedure was completed on VE solution as previously mentioned in Section 2.3.

3. Results and discussion

3.1. The electrode reaction

SMR exhibited a well-defined differential pulse anodic peak in the pH range 2.4–10 in the potential range of 584–770 mV, while the anodic peak of VE was exhibited in a narrow pH range of 2.4–4.5 in the potential range of 348–444 mV. Maximum peak current for both drugs was obtained using BR buffer pH 2.8 which has been successfully used for their determination by measuring the peak current at peak potential of +756 and +444 mV for SMR and VE, respectively (Fig. 1).

To study the reversibility of the oxidation process, the technique reported by Birke et al. [31] was used. The differential pulse voltammogram was recorded with a positive going potential pulse (+100 mV) then with a negative going potential pulse (−100 mV). It was found that both SMR and VE oxidation processes correspond to the quasi-reversible criteria:

$$E_p^c - E_p^a < |\Delta E|$$

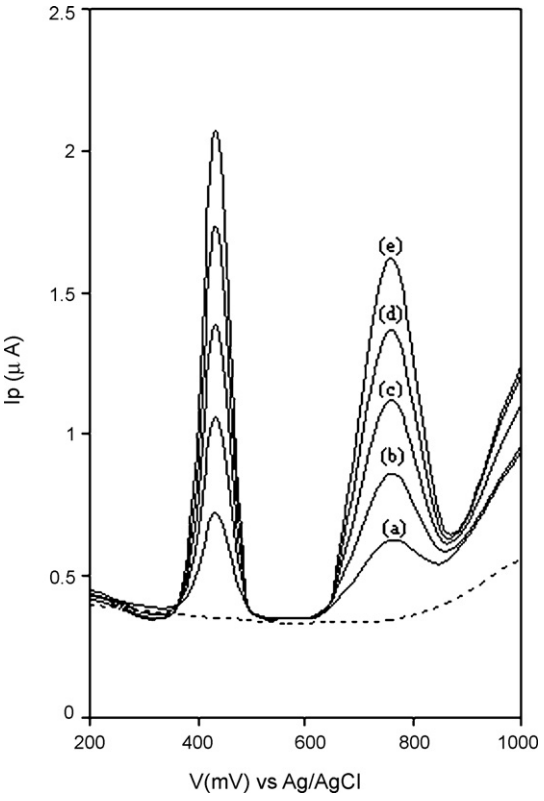


Fig. 1. Differential pulse voltammogram of (a) 0.5 mg L^{-1} VE and 0.7 mg L^{-1} SMR, (b) 1 mg L^{-1} VE and 1.4 mg L^{-1} SMR, (c) 1.5 mg L^{-1} VE and 2.1 mg L^{-1} SMR, (d) 2 mg L^{-1} VE and 2.8 mg L^{-1} SMR, (e) 2.5 mg L^{-1} VE and 3.5 mg L^{-1} SMR and Britton–Robinson buffer pH 2.8 (- - -) using pulse amplitude +90 mV and scan rate 120 mV/s.

where E_p^c is the cathodically scanned potential, E_p^a the anodically scanned potential and ΔE is the pulse amplitude.

$$\frac{I_p^a}{I_p^c} < 1$$

where I_p^a is the current measured at anodically scanned potential and I_p^c is the current measured at cathodically scanned potential.These values were $E_p^c - E_p^a = 12$ mV for both SMR and VE ($\Delta E = 100$ mV) and $I_p^a/I_p^c = 0.53$ for SMR and 0.46 for VE (both < 1).

The E_p values for both drugs varied upon changing the pH indicating the proton involvement in the electrode processes. A linear plot of peak current (I_p) versus the square root of the scan rate ($\nu^{1/2}$) was obtained for both drugs indicating that diffusion is the means of mass transport [32]. Correlation coefficient of the linear plot was 0.99434 for SMR and 0.99819 for VE.

The anodic peaks exhibited by the two drugs are attributed to the phenolic OH groups found in their structures. One OH group in each structure is oxidized to quinone group with the involvement of one electron and one proton.

3.2. Development and optimization of the method

In order to quantify the diffusion current resulted from the electro-oxidation of SMR and VE at the glassy carbon electrode; differential pulse and square wave techniques have been tried.

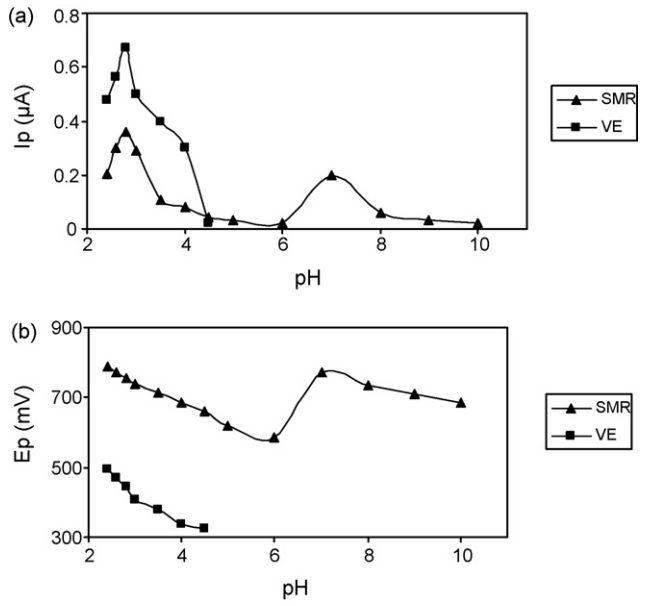


Fig. 2. Effect of pH on (a) peak current and (b) peak potential of SMR and VE (1 mg L^{-1} each) in Britton–Robinson buffer using pulse amplitude +90 mV and scan rate 120 mV/s.

Both techniques gave comparable results, but due to its simplicity and higher sensitivity differential pulse technique have been chosen, as it requires less parameters adjustment.

Various supporting electrolytes, such as, phosphate buffer, Britton–Robinson buffer and citrate/HCl buffer were investigated. The best results with respect to signal enhancement accompanied by sharper response for both drugs were obtained with Britton–Robinson buffer at pH 2.8.

The effect of pH of BR buffer on peak current (I_p) and peak potential (E_p) was studied over the pH range 2.4–10. The peak current shows maximum value for both drugs at pH 2.8 (Fig. 2a) which was used for their determination. SMR shows smaller peak at pH 7. I_p of VE reaches nearly zero at pH 4.5 where the peak disappeared thereafter.

The peak potential moved to less positive values with increasing pH (2.4–4.5) for VE (Fig. 2b). The relation is linear with a slope = -75.77 mV $pH^{-1} = (60/\alpha)$ (m/n) (α = transfer coefficient, m and n = number of protons and electrons involved in the reaction, respectively). The transfer coefficient was found to be 0.792 (<1) indicating the incomplete reversibility of the oxidation reaction. Regarding SMR, E_p first decreased from pH 2.4 to 6 then increased to reach maximum at pH 7 and finally decreased in alkaline pH (Fig. 2b). This shows that the mechanism is different under different pH conditions. The relation is linear in the pH range 2.4–4 with a slope = -69.55 mV $pH^{-1} = (60/\alpha)$ (m/n). The transfer coefficient for VE was found to be 0.863 (<1) again indicating the incomplete reversibility of the oxidation reaction.

The magnitude of the peak currents of both drugs increased with increasing the pulse amplitude from +20 to +90 mV then remained nearly constant till +100 mV (Fig. 3). +90 mV was chosen as the most suitable pulse amplitude to give the highest peak height.

Peak currents of both drugs increased gradually with increasing the scan rate of the sweep from 10 to 120 mV/s (the upper instrumental limit) (Fig. 4). Scan rate of 120 mV/s was chosen to obtain maximum sensitivity. The peak potential of both drugs was variable with the scan rate confirming the incomplete reversibility of the oxidation processes at the glassy carbon electrode [33].

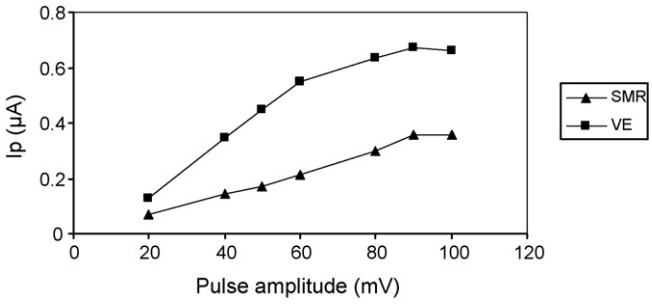


Fig. 3. Effect of pulse amplitude on the peak current of SMR and VE (1 mg L^{-1} each) in Britton–Robinson buffer pH 2.8 using scan rate 120 mV/s.

3.3. Validation

3.3.1. Linearity

The quantitative determination of SMR and VE was carried out based on the linear dependence of the peak current (μA) on the concentration (mg L^{-1}). Table 1 summarizes the characteristics for the calibration plot as well as the standard deviation of the intercept (S_a), slope (S_b) and residuals ($S_{y/x}$).

3.3.2. Limits of detection and quantification

In accordance to IUPAC [34], the limit of detection, LOD = 3S/b and the limit of quantification, LOQ = 10S/b, where S is the standard deviation of replicate blank responses (under the same conditions as for sample analysis) and b is the slope of the regression equation. The LOD and LOQ mentioned in Table 1 are calculated using these formulae.

3.3.3. Precision and accuracy

In order to assess precision, as percentage relative standard deviation (R.S.D.%), and accuracy, as percentage relative error (Er%), of the proposed method, solutions containing three different concentrations of SMR (for its determination alone) or synthetic mixtures with different ratios of SMR and VE (for the determination of SMR/VE mixture) were prepared and analyzed in three replicates. The data for this investigation are summarized in Table 2.

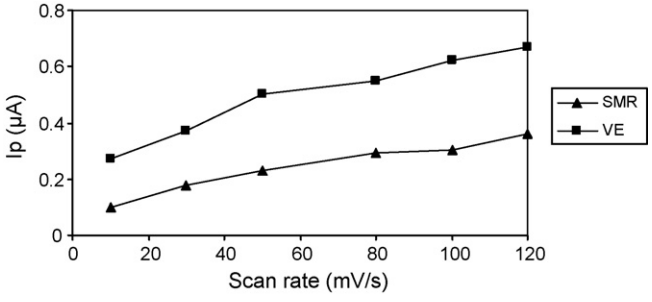


Fig. 4. Effect of scan rate on the peak current of SMR and VE (1 mg L^{-1} each) in Britton–Robinson buffer pH 2.8 using pulse amplitude +90 mV.

Table 2
Evaluation of precision and accuracy of the proposed method

(a) Precision and accuracy for the determination of SMR

Nominal value of SMR ($mg\,L^{-1}$)	Mean % recovery ± S.D.[a]	R.S.D.%[b]	Er%[c]
0.10	99.1 ± 1.5	1.5	0.9
2.00	99.2 ± 0.8	0.8	0.8
4.00	99.5 ± 0.4	0.5	0.5

(b) Precision and accuracy for the determination of SMR/VE mixture

SMR:VE	Nominal value ($mg\,L^{-1}$)		Mean % recovery ± S.D.[a]	
	SMR	VE	SMR	VE
9:5	0.18	0.10	99.9 ± 0.9	100.4 ± 0.9
7:5	1.40	1.00	100.2 ± 0.9	99.3 ± 0.4
5:5	2.00	2.00	99.5 ± 0.5	99.6 ± 0.7
Mean R.S.D.%[b]			0.8	0.7
Mean Er%[c]			0.2	0.3

[a] Mean ± standard deviation of three determinations.
[b] Percentage relative standard deviation.
[c] Percentage relative error.

Table 3
Statistical comparisons for the determination of SMR in its pharmaceutical preparations using the proposed method and the reference one

	Levatech® capsules		Legalex® tablets		Silymarin® packets	
	Proposed method	Reference method[b]	Proposed method	Reference method[b]	Proposed method	Reference method[b]
Found ($mg\,L^{-1}$)[a]	1.99	1.97	1.98	1.95	2.03	2.00
	2.00	1.98	1.97	1.97	2.01	2.00
	1.98	1.98	1.94	1.97	1.99	1.98
	1.98	1.98	1,98	1.96	2.02	2.01
	1.99	1.98	1.98	1.95	2.00	2.01
Mean found ± S.D. ($mg\,L^{-1}$)	$1.99 \pm 8.37 \times 10^{-3}$	$1.98 \pm 4.04 \times 10^{-3}$	$1.97 \pm 1.70 \times 10^{-2}$	1.96 ± 0.01	$2.01 \pm 1.60 \times 10^{-2}$	$2.00 \pm 1.20 \times 10^{-2}$
Mean % recovery ± S.D.	99.35 ± 0.51	98.94 ± 0.21	98.59 ± 0.81	98.06 ± 0.49	100.57 ± 0.80	99.95 ± 0.65
t[c]	1.67		1.25		1.39	
F[c]	5.98		2.82		1.14	

[a] Samples are prepared to contain $2.00\,mg\,L^{-1}$.
[b] A (1%, 1 cm) in methanol.
[c] Theoretical values of F and t are 6.39 and 2.31, respectively, at 95% confidence limit.

3.3.4. Selectivity

The selectivity of the proposed method was checked by analyzing synthetic mixtures containing different ratios of both drugs, where good percentage recoveries were obtained indicating that they did not interfere with each other (Table 2). In addition, the application of the proposed method for the determination of the two drugs in dosage forms; without interference from the excipients clearly demonstrate the selectivity of the method (Tables 3 and 4).

3.4. Applications

3.4.1. Analysis of SMR pharmaceutical preparations

The proposed technique was applied to SMR tablets, capsules and packets. The results obtained were compared with A_{max}

Table 4
Analysis of SMR/VE mixture in pharmaceutical preparation using the proposed method

Parameter	Seralon-E® capsules	
	SMR	VEA
Found ($mg\,L^{-1}$)[a]	2.83	2.02
	2.83	2.01
	2.80	2.03
	2.79	2.00
	2.79	2.01
Mean found ± S.D. ($mg\,L^{-1}$)	$2.81 \pm 2.05 \times 10^{-2}$	$2.01 \pm 1.14 \times 10^{-2}$
Mean % recovery ± S.D.	100.32 ± 0.729	100.65 ± 0.66

[a] Samples are prepared to contain $2.00\,mg\,L^{-1}$ VEA and $2.80\,mg\,L^{-1}$ SMR.

method (by calculating A (1%, 1 cm) in methanol and comparing it with the reference values [2]) which has been applied directly on the extract in case of capsules and tablets and after a clean up procedure (involving washing the weighed portion of the packets with water, centrifugation for 10 min before extracting the residue with methanol) in case of packets. Statistical analysis of the results was done using the Student's t-test and variance ratio F-test (Table 3). The calculated values did not exceed the theoretical ones (95% confidence limits for four degrees of freedom), which indicate that there is no significant variation between the proposed method and the reference one. Common capsule, tablet or packet excipients did not interfere with the analysis.

3.4.2. Analysis of SMR/VE mixture in their pharmaceutical preparation

Seralon-E® capsules were analyzed with the proposed method. The precision and accuracy of the proposed method were satisfactory for the label claims (Table 4). The R.S.D.% and Er% for the assay results showed high reproducibility and accuracy of the proposed method. Common capsule excipients did not interfere with the analysis.

4. Conclusion

The developed electro-analytical method presented in this work represents a rapid and simple technique for the quantitative determination of SMR alone or SMR/VE mixture in bulk or in pharmaceutical preparations. The method is easy to adopt and the lowest concentration level possible for VE determination is better than its existing voltammetric methods [13,14]. In general, electro-analytical methods have the advantage of being considerable timesavers besides to the overall low cost of analysis compared with chromatographic methods.

References

[1] L. Farkas, M. Gabor, F. Kally, Some effects of flavonoids on mammalian cell systems, in: Flavonoids and Bioflavonoids, Elsevier, New York, 1985.
[2] S. Budavari, The Merck Index, 13th ed., Merck & Co., Inc., Whitehouse Station, NJ, 2001.
[3] S.C. Sweetman, Martindale, The complete Drug Reference, 34th ed., The Pharmaceutical Press, London, 2005.
[4] V.A. Kurkin, G.G. Zapesochraya, A.V. Volotsueva, E.V. Avdeera, K.S. Pimenov, Chem. Nat. Comp. 37 (2001) 315.
[5] J.I. Lee, B.H. Hsu, D. Wu, J.S. Barrett, J. Chromatogr. A 1116 (2006) 57.
[6] P. Kosina, J. Bartek, Chem. Listy 94 (2000) 1115.
[7] E.M. Martinelli, P. Morazzoni, S. Livio, E. Uberti, J. Liq. Chromatogr. 14 (1991) 1285.
[8] N. Rahman, N.A. Khan, S.N.H. Azmi, Pharmazie 59 (2004) 112.
[9] A. Rajasekaran, M. Kumar, B. Jayakar, East. Pharm. 40 (1997) 131.
[10] S.S. Zarapkar, N.S. Kanyawar, S.H. Rane, Indian Drugs 37 (2000) 133.
[11] M.C. Guinea-Lopez, A. Pizarro-Sanz, Ann. R. Acad. Farm. 53 (1987) 413.
[12] F. Kvasnicka, B. Biba, R. Sevcik, M. Voldrich, J. Kratka, J. Chromatogr. A 990 (2003) 239.
[13] P. Wang, R.Z. Cong, J.D. Wang, L.F. Zhang, Sepu. 16 (1998) 510.
[14] C. Dollery, Therapeutic Drugs, 2nd ed., Churchill Livingstone, 1999.
[15] M. Coatarea, A. Darchen, D. Hauchard, Sens. Actuator B 76 (2001) 539.
[16] Z. Xi, L. Xiao, Y. Yu, Fenxi. Huaxue 19 (1991) 423.
[17] R. Yomauchi, H. Noro, M. Shimoyamada, K. Kato, Lipids 37 (2002) 515.
[18] D.C. Liebler, J.A. Burr, L. Philips, A.J.L. Ham, Anal. Biochem. 236 (1996) 27.
[19] Pranjothy, C.B. Patil, Indian Drugs 37 (2000) 236.
[20] A.F. El-Walily, F. El-Anwar, S. Zamel, Anal. Chim. Acta 248 (1991) 583.
[21] O. Naess, T. Tilander, S. Pederson-Bjergaard, K.E. Rasmussen, Electrophoresis 19 (1998) 2912.
[22] P. Prieto, M. Pineda, M. Aquiler, Anal. Biochem. 269 (1999) 337.
[23] E. Tutem, R. Apak, E. Gunayd, K. Sozgen, Talanta 44 (1997) 249.
[24] C.S.P. Sastry, N.R.P. Singh, M.N. Reddy, R.V.R. Reddy, Indian Drugs 23 (1986) 633.
[25] J.C. Alvarez, P. De-Mazancourt, J. Chromatogr. B: Biomed. Appl. 755 (2001) 129.
[26] C. Lauridsen, S.W. Leonard, D.A. Griffin, D.C. Liebler, T.D. McClure, M.G. Traber, Anal. Biochem. 289 (2001) 89.
[27] T.P. Whitehead, G.H.G. Thorpe, S.R.S. Maxwell, Anal. Chim. Acta 266 (1992) 265.
[28] K. Florey, Analytical Profiles of Drug Substances, Academic Press, Inc., New York, 1974.
[29] The United States Pharmacopeia and The National Formulary 23–28th revision, United States Pharmacopeial Convention, Inc., Whashington, 2005.
[30] The British Pharmacopoeia, HMSO, London, 2003.
[31] R.L. Birke, M.H. Kim, M. Strassfeld, Anal. Chem. 53 (1981) 852.
[32] P. Monk, Fundamentals of Electroanalytical Chemistry, Wiley and Sons, New York, 2001.
[33] A.M. Bond, Modern Polarographic Methods in Analytical Chemistry, Marcel Dekker Inc., 1980.
[34] J.N. Miller, Analyst 116 (1991) 3.

Available online at www.sciencedirect.com
ScienceDirect
Talanta 74 (2008) 821–830
Talanta
www.elsevier.com/locate/talanta

5-Methyl-2-[3-(4-phenylthiazol-2-yl)triazenyl]benzenesulfonic acid as a chromogenic reagent of *N*-cetylpyridinium chloride Synthesis, mechanism and analytical application

Xiao-Ling He [a,*], Yong-Qiu Wang [a], Ke-Qing Ling [b,*]

[a] *Department of Chemistry, Huaibei Coal Industry Teacher's College, Huaibei, Anhui 235000, China*
[b] *Department of Chemistry, Case Western Reserve University, Cleveland, OH 44106, USA*

Received 8 June 2007; received in revised form 16 July 2007; accepted 16 July 2007
Available online 1 August 2007

Abstract

Despite that triazene reagents have been widely used for spectrophotometric determinations of cationic surfactants, the mechanism underlying such applications has yet to be studied. We report the synthesis of a new triazene reagent 5-methyl-2-[3-(4-phenylthiazol-2-yl)triazenyl]benzenesulfonic acid (MPTTBSA) and its interaction with *N*-cetylpyridinium chloride (CPC). The reagent was synthesized by coupling 4-methyl-2-sulfobenzenediazonium salt with 2-amino-4-phenylthiazole. Spectral evidence suggests that the neutral reagent (H_2R) exists in a triazenium sulfonate zwitterion form. Two ionizations were detected at weak acidic (H_2R/HR^-, pK_{a1} 2.71 ± 0.20) and alkaline pH (HR^-/R^{2-}, pK_{a2} ca. 13.5), respectively. In the presence of 3.5 equivalents of CPC, a 2.71 unit decrease in pK_{a1} and a 3.0 unit decrease in pK_{a2} were observed. While the optical properties of H_2R are essentially unaffected, CPC causes a 53 nm red shift and a 31 nm red shift in maximum absorption wavelengths (λ_{max}), and a 24% increase and a 29% increase in extinction coefficients (ε) of HR^- and R^{2-}, respectively. These data suggest that CPC forms ion associates with HR^- and R^{2-}, but its interaction with H_2R is weak. Associations of CPC with HR^- and R^{2-} both follow a 3:1 stoichiometry, and the apparent stability constants of the two associates were estimated as 6.02×10^{18} and 2.42×10^{22} M^{-3}, respectively. Consistent with their high stability constants, the two ion associates did not show any changes in optical properties under submicellar and micellar conditions. The strict 3:1 association stoichiometry was interpreted in terms of electrostatic-induced, topology-defined π-stacking and hydrophobic interactions, which not only change the optical properties of the reagent anions, but also provide the driving force to shift the two ionization equilibria to the right and cause the decreases in pK_a. Compared to the first ionization, perturbation of the second ionization by CPC provides a color reaction that is more sensitive and has a better color contrast, which was used to develop a new protocol for spectrophotometric determination of CPC. This is the first mechanistic study on the interaction between a triazene reagent and a cationic surfactant.
© 2007 Elsevier B.V. All rights reserved.

Keywords: 5-Methyl-2-[3-(4-phenylthiazol-2-yl)triazenyl]benzenesulfonic acid; Ionization; *N*-Cetylpyridinium chloride; Ion associates; Mechanism; Spectrophotometry

1. Introduction

Surfactants are amphiphilic compounds consisting of a long-chain hydrocarbon "tail" and a polar "head" [1]. The electronic feature of the polar head defines a surfactant as cationic if positively charged; nonionic if neutral; or anionic if negatively charged. In aqueous solutions, surfactant molecules can aggregate into organized molecular assemblies known as micelles if the concentration of the surfactant exceeds a certain value. Critical micelle concentration (CMC) refers to the very concentration at which micelles begin to form. Cationic surfactants, usually of quaternary ammonium nature, are widely used as antimicrobial, emulsifying, anticorrosion and softening agents in pharmaceutical preparations, cosmetic formulations and disinfectants, and as softeners and anti-static agents in paper and fabric industries [1,2]. Oral intake of cationic surfactants can be lethal, and the symptoms of cationic surfactant ingestion include corrosive burns of the mouth and throat, nausea, vomiting, diarrhea, dermal necrosis, lung complications and hypotension [1,2]. Thus, it is important to develop novel methods to estimate the content of cationic surfactants in biological, industrial and environmental

* Corresponding authors.
E-mail addresses: hbhxl111@hotmail.com (X.-L. He), kxl56@case.edu (K.-Q. Ling).

0039-9140/$ – see front matter © 2007 Elsevier B.V. All rights reserved.
doi:10.1016/j.talanta.2007.07.024

samples. Numerous instrumental methods have been reported for the determination of cationic surfactants, including titrimetry [3], capillary electrophoresis (CE) [4], spectrophotometry [5], fluoremetry [6] and liquid chromatography–mass spectrometry (LC–MS) [7]. Recently, a chemiluminescence method was reported, which offers a versatile tool for determination of various surfactants [8]. More recently, a fluorescence quenching technique was developed specifically for quantification of cationic surfactants [9]. Compared to other methods, chromogenic reagent-based spectrophotometry has the advantages of sensitivity, selectivity, low cost, simplicity and convenience. Moreover, chromogenic reagents can also be used as "naked-eye" chemosensors without the need of instrumentation if a sharp color reaction can be achieved.

Aromatic triazenes represent a class of relatively new chromogenic reagents, and have received considerable attention due to their highly sensitive color reactions with a number of metal ions [10]. In the past decade, there has been an increasing volume of reports dealing with spectrophotometric determinations of surfactants, especially cationic surfactants, using triazene reagents [11]. Unfortunately, the mechanism underlying such applications has not yet been addressed, and research in this area remains more or less of trial and error nature. Understanding the mechanism of interactions of surfactants with triazene reagents may not only lead to rational design of new reagents for spectrophotometric determination of cationic surfactants, but may also provide useful information about how surfactants sensitize the color reactions of triazene reagents with metal ions, the latter has been the key to achieving high sensitivities and large color contrasts of these color reactions [10,12].

Reported herein is our effort to unravel the mechanism of interactions of a new triazene reagent, namely 5-methyl-2-[3-(4-phenylthiazol-2-yl)triazenyl]benzenesulfonic acid (MPTTBSA), with a typical cationic surfactant *N*-cetylpyridinium chloride (CPC). After fully characterizing the dissociation chemistry of the reagent, we were able to observe interactions of CPC with all the three acid–base species of the reagent. Our experimental data provided unambiguous evidence that CPC forms ion associates with the reagent anions, but not with the neutral reagent. The association stoichiometries and stability constants of these ion associates were then measured, and the fates of these associates under submicellar and micellar concentrations of CPC were studied. Computer-aided molecular modeling was employed to help understand the unique features of these ion associates. The significant changes in acid–base and optical properties of the reagent caused by CPC allowed us to develop a new protocol for spectrophotometric determination of CPC. To our knowledge, this is the first mechanistic study on the interaction between a triazene reagent and a cationic surfactant.

2. Experimental

2.1. Apparatus and reagents

^{1}H NMR spectrum was obtained on a Varian Inova 400 instrument (at 399.75 MHz), with chemical shifts being referenced to the solvent peak. Elemental analysis was performed on a Perkin-Elmer analyzer. UV–visible spectra were obtained using a TU-1901 double beam spectrophotometer (Beijing General Instrument Company Ltd.). pH was measured with a pHS-3D pH meter which was equipped with a combination glass electrode (Chengdu Analytical Instrument Company). 2-Amino-4-phenylthiazole was synthesized according to a literature method [13]. All the commercially available reagents are of A.R. grade. All the aqueous solutions were prepared using double distilled deionized water. All the spectrophotometric titrations and analytical measurements were conducted at room temperature.

Stock solutions of MPTTBSA (1.00×10^{-4} M) and *N*-cetylpyridinium chloride (CPC, 1.00×10^{-4} or 5.00×10^{-3} M) were prepared in alcohol and water, respectively. Universal buffer for pH 1.8–11.9 was made of 0.4 M of phosphoric acid, 0.4 M of acetic acid and 0.4 M of boric acid, and was adjusted to an operating pH using 0.2 M of NaOH as monitored with a pH meter. Alkaline buffer for pH > 11.9, consisting of 1.0 M of aqueous NaOH, was adjusted to a desired pH with 0.5 M of aqueous HCl as monitored by a pH meter. Strong acid buffer (pH < 1.8) was prepared by mixing appropriate volumes of 98% H_2SO_4 and water to a desired pH as monitored with a pH meter.

2.2. Synthesis of 5-methyl-2-[3-(4-phenylthiazol-2-yl)triazenyl]benzenesulfonic acid (MPTTBSA)

To a 5% aqueous NaOH solution (5 mL) was added anhydrous 2-amino-4-methylbenzenesulfonic acid (0.035 g, 5 mmol). The mixture was warmed under stirring until all the solid materials had been dissolved. After cooling down to room temperature, a solution of $NaNO_2$ (0.365 g, 5 mmol) in 3 mL of water was added and the mixture was cooled in an ice–salt bath to 0–5 °C. To the resulting mixture was added dropwise 7 mL of 3.5N aqueous HCl under vigorous stirring, while the temperature was maintained below 5 °C. The mixture was further stirred for 15 min to ensure completion of the diazotization. The resulting 4-methyl-2-sulfobenzenediazonium solution was slowly added to a solution of 2-amino-4-phenylthiazole (0.88 g, 5 mmol) in 10 mL of ethanol under stirring at 0–5 °C, and the mixture was maintained at pH 3–5 by adding 20% of cold aqueous Na_2CO_3. After the addition was complete, the mixture was allowed to stand overnight at room temperature. Filtration of the mixture, followed by washing of the solid with water and ethanol afforded 1.66 g of crude product (4.43 mmol, 88.6% yield), which was further purified by crystallization in 3:1 (v/v) ethanol–water to give pure MPTTBSA as an orange powder: mp 230 °C dec; ^{1}H NMR (DMSO-d_6) δ 2.27 (s, 3H, CH_3), 7.12 (dd, 1H, J = 2.0, 8.0 Hz), 7.20 (d, 1H, J = 8.0 Hz), 7.32–7.44 (3H, ArH), 7.41 (s, 1H), 7.62 (d, 1H, J = 2.0 Hz), 8.06 (br, 2H, NH), 8.16 (dd, 2H, J = 1.6, 8.4 Hz); Anal. calcd. for $C_{16}H_{14}N_4O_3S_2$: C, 51.32; H, 3.77; N, 14.96; found: C, 51.73; H, 3.78; N, 14.58.

2.3. Spectrophotometric pH titration

For experiments without CPC, to a 10 mL calibrated tube were added 5 mL of a buffer solution with a given pH (strong

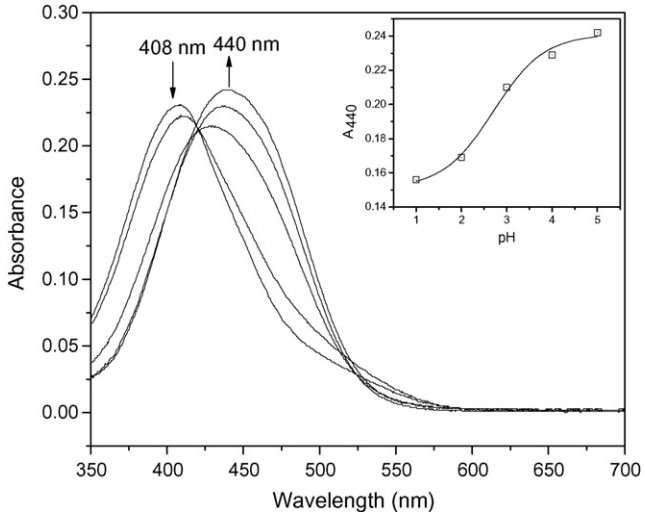


Fig. 1. Spectrophotometric pH titration of MPTTBSA (1.0×10^{-5} M) in acidic buffers, and the corresponding pH–A_{440} plot (inset). The pH values were 1.0, 2.0, 3.0, 4.0 and 5.0, respectively, along the arrow direction.

acidic, universal or alkaline) and 1 mL of a stock solution of MPTTBSA (1.00×10^{-4} M). The solution was brought to mark with water, mixed thoroughly, and then subjected to UV–vis scanning on a spectrophometer at room temperature using 1 cm cuvettes with water as reference (Figs. 1 and 2).

For experiments with CPC, to a 10 mL calibrated tube were added 5 mL of a buffer solution with a given pH, 3.5 mL of a stock solution of CPC (1.00×10^{-4} M) and 1 mL of a stock solution of MPTTBSA (1.00×10^{-4} M). The solution was mixed, brought to mark with water, mixed again and then was allowed to stand at room temperature for 5 min before being subjected to UV–vis scanning with water as reference (Figs. 5 and 7).

2.4. Spectrophotometric titration of MPTTBSA with CPC

To a 10 mL calibrated tube were added sequentially 5 mL of a buffer solution (pH 5.0 or 12.8), 1 mL of a stock solution

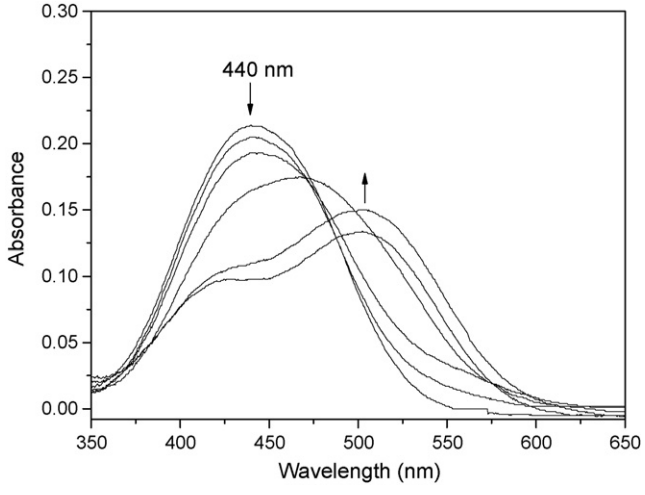


Fig. 2. Spectrophotometric pH titration of MPTTBSA (1.0×10^{-5} M) in alkaline buffers. The pH values were 11.0, 12.4, 12.8, 13.2, 13.6 and 13.8, respectively, along the arrow direction.

of MPTTBSA (1.00×10^{-4} M) and an appropriate volume of a stock solution of CPC (1.00×10^{-4} M or 5.00×10^{-3} M). The solution was brought to mark with water, mixed thoroughly, allowed to stand at room temperature for 5 min, and then subjected to UV–vis scanning or single wavelength measurement at 493 or 556 nm using 1 cm cuvettes with water as reference (Figs. 9, 10, 12 and 13).

2.5. Optimized protocol for determination of CPC in synthetic water samples

To a 10 mL calibrated tube were added 1 mL of a synthetic water sample and an appropriate amount of CPC. The solution was mixed thoroughly, and then 1 mL of 1 mg/mL aqueous Na_2EDTA and 5 mL of pH 12.8 alkaline buffer were added. The solution was mixed again, and then 1.5 mL of a stock solution of MPTTBSA (1.00×10^{-4} M) was added. After further mixing, the solution was allowed to stand at room temperature for 5 min, and then was subjected to spectrophotometric measurement at 556 nm using 1 cm cuvette with the same buffer solution containing only the same concentration of MPTTBSA as reference. The results are listed in Table 3.

3. Results

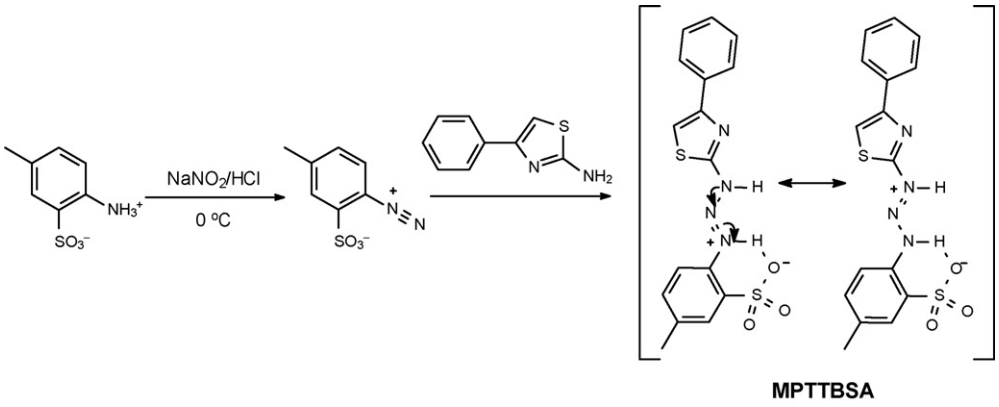
3.1. Synthesis

The new reagent was synthesized in excellent yield by coupling 2-amino-4-phenylthiozole with 4-methyl-2-sulfobenzenediazonium salt under weak acidic conditions; the latter was generated *in situ* by treating 2-amino-5-methylbenzenesulfonic acid with $NaNO_2$ under strong acidic conditions (Scheme 1). The crude product was purified simply by crystallization in aqueous alcohol, and the pure product was characterized by elemental analysis and NMR.

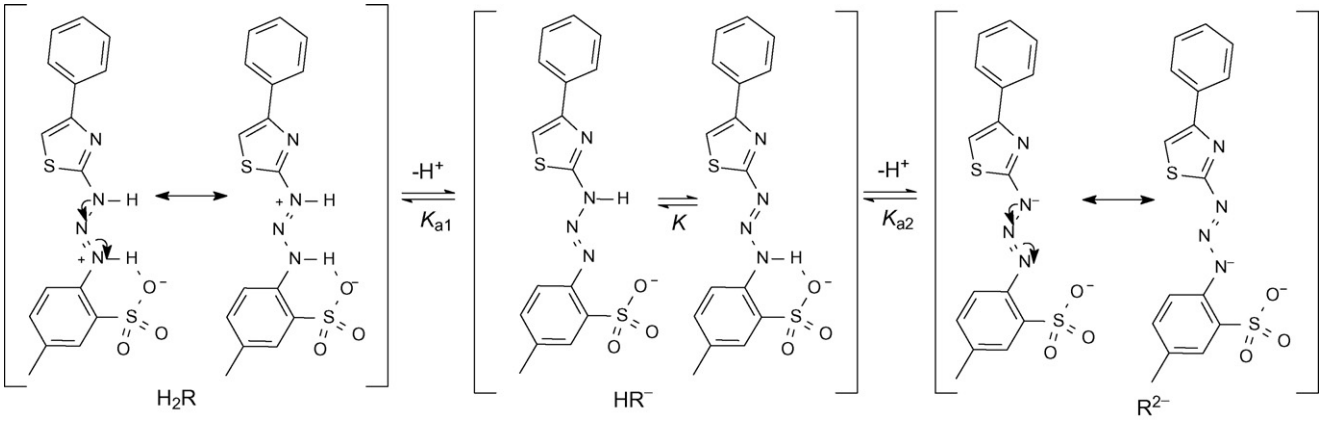
Several structural features of MPTTBSA should be noted. First, given that sulfonic acid is a strong acid (the pK_a of benzenesulfonic acid is −6.5), and that triazene is a weak base (similar to an amidine), the neutral form of MPTTBSA should exist as a zwitterionic triazenium sulfonate rather than the anticipated triazenylbenzenesulfonic acid form (Scheme 1). Second, one of the two NH protons in MPTTBSA can be shared between the sulfonate oxygen and the triazene nitrogen through intramolecular hydrogen bonding, forming a stable six-member ring structure (Scheme 1). Third, the zwitterionic form of MPTTBSA can be stabilized by resonance mainly between two quasi-equivalent resonance structures (Scheme 1), thereby making the two NH protons indistinguishable by NMR. Indeed, in addition to other well-resolved signals of aromatic protons, there is a singlet at 8.06 ppm consisting of two exchangeable protons in low field region on the ^{1}H NMR spectrum of MPTTBSA in DMSO-d_6.

3.2. Ionizations of MPTTBSA

Despite the zwitterionic nature, MPTTBSA still is a diacid. The two ionization equilibria and structures of the three



Scheme 1. Synthesis of the new reagent MPTTBSA.



Scheme 2. Ionization equilibria of MPTTBSA (H_2R).

acid–base species (H_2R, HR^- and R^{2-}) are shown in Scheme 2. Note that the HR^- form of MPTTBSA can exist in two triazene tautomers, but only one of them can be stabilized by intramolecular hydrogen bonding, forming a six-member ring structure as in the case of H_2R (Scheme 2). Moreover, as in the case of H_2R, R^{2-} can also be stabilized by resonance mainly between two quasi-equivalent resonance structures (Scheme 2). Spectrophotometric pH titration revealed that the first ionization of MPTTBSA occurs in weak acidic pH as evidenced by the isosbestic conversion of an absorption band at 408 nm to another band at 440 nm when pH goes from 1.0 to 5.0 (Fig. 1). Nonlinear least squares fit of the pH–A_{440} plot according to the Henderson-Hasselbalch equation yielded an acid dissociation constant (pK_{a1}) of 2.71 ± 0.20. This number is far larger than that of a typical arylsulfonic acid, and agrees well with the anticipated pK_a of a triazenium salt. This result further confirms the zwitterionic nature of MPTTBSA. Thus, the 408 nm species was identified as the conjugate acid form (H_2R), and the 440 nm species was assigned to the conjugate base form (HR^-) of MPTTBSA. The extinction coefficients (ε) of these two species are listed in Table 1. It should be noted that the measured λ_{max} and ε of HR^- represent average values of the equilibrium mixture of its two tautomers (Scheme 2). The optical properties of the two individual tautomers and the equilibrium constant (K) of the tautomerism remain unknown.

Spectrophotometric pH titration of MPTTBSA was extended to higher pH (Fig. 2). From pH 5.0 through pH 11.0, no new absorption bands were observed. Starting from pH 11.0, however, an isosbestic conversion of the 440 nm band to a shoulder in the range of 500–550 nm was evident (Fig. 2), indicative of the occurrence of the second ionization. Unfortunately, despite our best efforts, the pH titration spectra would invariably lose

Table 1
Acid–base and optical properties of MPTTBSA

Properties	Without CPC	With CPC	Difference
pK_{a1}	2.71 ± 0.20	0.00 ± 0.01	−2.71
pK_{a2}	~13.5	10.50 ± 0.02	−3.0
H_2R			
λ_{max} (nm)	408	406	−2
ε ($cm^{-1}\,M^{-1}$)	2.31×10^4	2.28×10^4	-3×10^2
HR^-			
λ_{max} (nm)	440	493	53
ε ($cm^{-1}\,M^{-1}$)	2.42×10^4	3.00×10^4	5.8×10^3
R^{2-}			
λ_{max} (nm)	~525	556	31
ε ($cm^{-1}\,M^{-1}$)	~2.49×10^4	3.21×10^4	7.2×10^3

All the parameters were measured at room temperature using 1.0×10^{-5} M of MPTTBSA with or without 3.5×10^{-5} M of CPC.

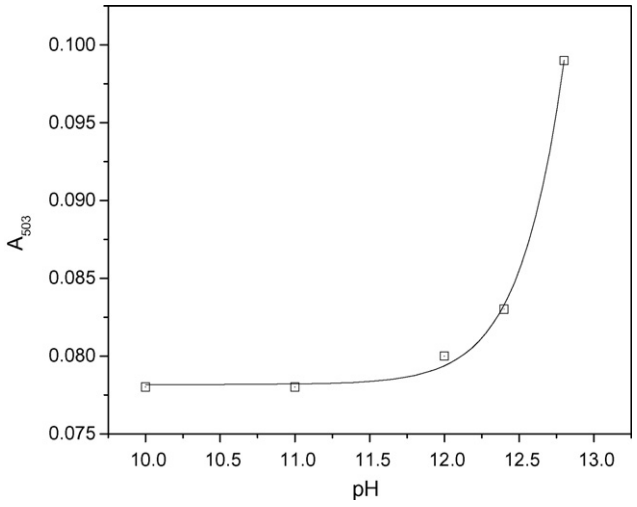


Fig. 3. pH–A_{503} plot obtained from an independent spectrophotometric pH titration of MPTTBSA (1.0×10^{-5} M) in the range of pH 10.0–12.8.

isosbesticity starting from pH 13.0, suggesting that the reagent becomes significantly unstable at and above this pH. Thus, all the spectra taken at pH ≥ 13 cannot be used in calculating the ionization constant. However, an independent spectrophotometric titration in the range of pH 10.0–12.8 provided enough data for a nonlinear least squares fit (Fig. 3), and the ionization constant (pK_{a2}) was estimated as 13.5.

The drastic decomposition of MPTTBSA at high pH made it impossible for us to directly observe real spectrum of the triazenide anion R^{2-}. Nonetheless, we were able to extrapolate the optical parameters of R^{2-} by computer-aided simulations (Fig. 4). First, the three UV–vis spectra at pH 11.0, 12.4 and 12.8 were selected, where only $HR^- \rightarrow R^{2-} + H^+$ occurred as judged by their isosbestic nature. Since no ionization was evident at pH 11.0, spectrum at this pH should represent pure HR^- (S_{HR}), and spectra at 12.4 and 12.8 represent mixtures of HR^- and R^{2-} (S_{HR+R}). Then, the spectra of R^{2-} (S_R) could be extracted simply by linear combination using Origin 7.5 according to equation $S_R = S_{HR+R} - nS_{HR}$, where n (0–100%) represents the fraction of HR^-, and could be adjusted appropriately until the resulting difference spectrum (S_R) became symmetrical (Fig. 4). The estimated λ_{max} and ε for R^{2-} are listed in Table 1.

3.3. Effect of CPC on the ionizations of MPTTBSA

To study the effects of CPC on the ionizations of MPTTBSA, the above spectrophotometric titrations of MPTTBSA were repeated in the presence of 3.5 equivalents of CPC. As shown below, the concentration of CPC used (3.5×10^{-5} M) is well below its CMC. Therefore, only CPC monomer was involved in the following experiments. No spectral change was observed in the range of pH 1.0–7.5, suggesting that the two ionizations must occur outside this pH range. By lowering the buffer pH, the first ionization was found at pH < 1.0 as revealed by an isosbestic conversion of the 493 nm band to a new band at 408 nm (Fig. 5). A nonlinear least squares fit of the pH–A_{493} plot obtained from an independent spectrophotometric titration to the Henderson-Hasselbalch equation gave a pK_{a1} value of 0.00 ± 0.01 (Fig. 6). On the other hand, an isosbestic conversion of the 493 nm peak to a new peak at 556 nm was observed at basic and alkaline pH (Fig. 7), indicating that the second ionization occurred. The pK_{a2} was calculated as 10.50 ± 0.02 by a nonlinear least squares fit of the pH–A_{556} plot obtained from an independent titration (Fig. 8). The optical properties of the three acid–base species of MPTTBSA in the presence of CPC are listed in Table 1. Also noted is that the R^{2-} form of MPTTBSA was significantly stabilized by CPC: the reagent did not show any decomposition even at pH 13.6. Stabilization of triazenes by surfactants has been observed previously [14].

Data in Table 1 reveal interesting aspects of interactions between CPC and MPTTBSA. First, CPC caused a 2.71 unit decrease in pK_{a1} and a 3.0 unit decrease in pK_{a2} of MPTTBSA, indicating significant interactions between CPC and MPTTBSA. Second, while a 53 nm red shift and a 31 nm red shift were observed for HR^- and R^{2-} in the presence of CPC, only a 2 nm blue shift was seen for H_2R. Third, the presence of CPC also increased the extinction coefficients of HR^- and

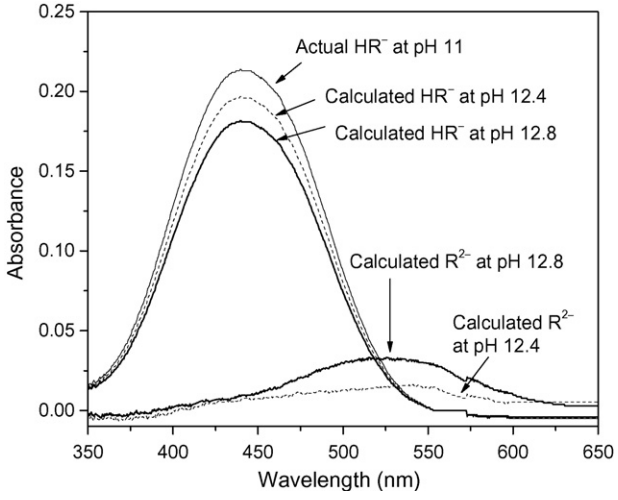


Fig. 4. Extrapolation of optical properties of R^{2-} from experimental pH titration spectra.

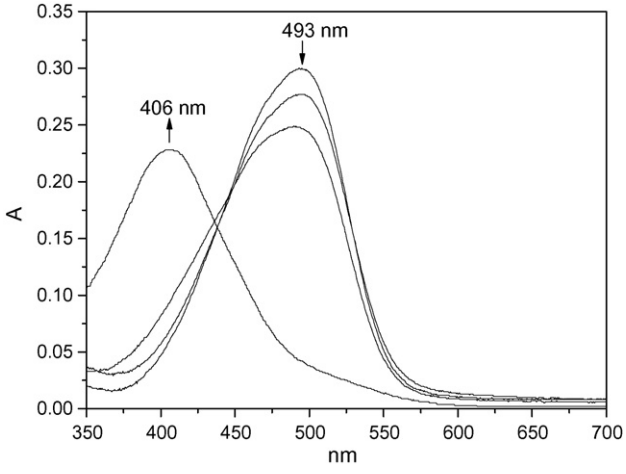


Fig. 5. UV–vis spectra of MPTTBSA (1.0×10^{-5} M) in acidic media in the presence of 3.5×10^{-5} M of CPC. The pH values were 1.0, 0.6, 0.3 and −0.8, respectively, along the arrow direction.

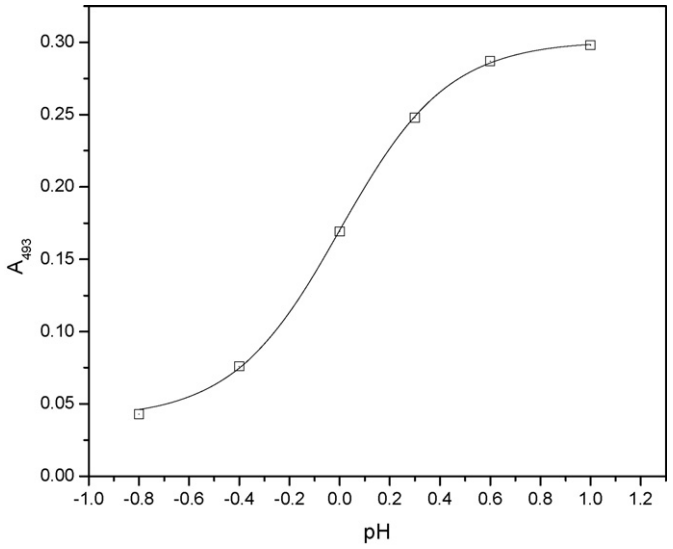


Fig. 6. pH–A_{493} plot obtained from an independent spectrophotometric pH titration of MPTTBSA (1.0×10^{-5} M) in the range of pH −0.8 to 1.0.

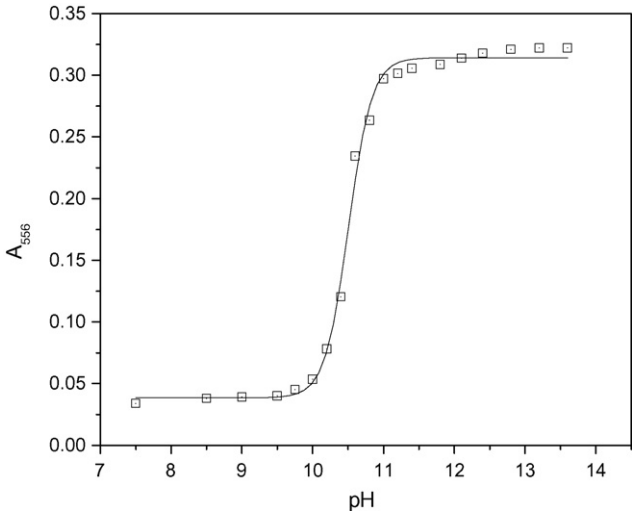


Fig. 8. pH–A_{556} plot obtained from an independent spectrophotometric pH titration of MPTTBSA (1.0×10^{-5} M) in the presence of 3.5×10^{-5} M of CPC.

R^{2-} by a factor of 24 and 29%, respectively, whereas only a slight decrease (1.3%) in the extinction coefficient of H_2R was observed. These data provide unambiguous evidence that CPC strongly interacts with HR^- and R^{2-}, but only weakly with H_2R. Given that H_2R is neutral, HR^- and R^{2-} are negatively charged, and CPC is positively charged, one may immediately reach the conclusion that CPC forms ion associates with HR^- and R^{2-}. Thus, the 493 and 556 nm bands actually represent the CPC-HR^- and CPC-R^{2-} ion associates, respectively.

3.4. Stoichiometries and stability constants of CPC-MPTTBSA ion associates

The stoichiometries of the two ion associates (CPC-HR^- and CPC-R^{2-}) were determined as 3:1 in both cases by analyzing the molar ratio plots obtained by spectrophotometric titrations of MPTTBSA with CPC at pH 5.0 (Fig. 9) and 12.8 (Fig. 10), respectively. At pH 5.0, H_2R fully dissociates into HR^- without significant dissociation of $(CPC)_3HR^-$. Thus, the apparent stability constant of $(CPC)_3HR^-$ was estimated as $6.02 \times 10^{18}\ M^{-3}$ from the difference between theoretical and experimental A_{493} values at the 3:1 stoichiometric point according to the following equation:

$$3CPC + HR^- \rightleftharpoons (CPC)_3HR^-$$

For $(CPC)_3R^{2-}$, however, the molar ratio plot could be constructed only at pH 12.8 due to the poor stability of free R^{2-}. At this pH, $(CPC)_3HR^-$ fully dissociates into $(CPC)_3R^{2-}$ while HR^- only partially dissociates to R^{2-}. Thus, the apparent stability constant of $(CPC)_3R^{2-}$ was estimated as $2.42 \times 10^{22}\ M^{-3}$ similarly as in the case of $(CPC)_3HR^-$, but the following two

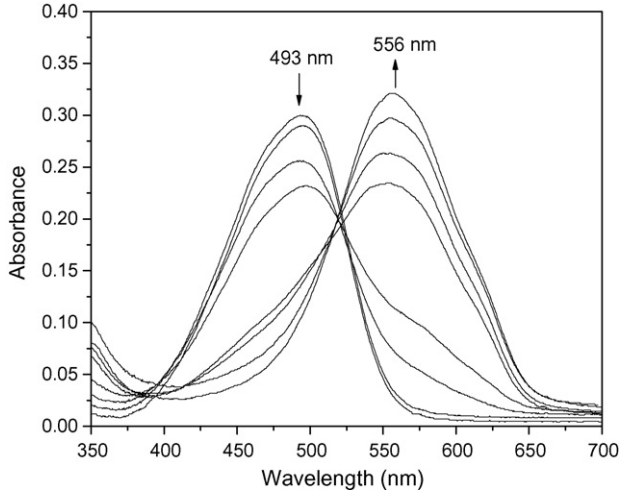


Fig. 7. Spectrophotometric pH titration of MPTTBSA (1.0×10^{-5} M) at pH ≥ 7.5 in the presence of 3.5×10^{-5} M of CPC. The pH values were 7.5, 8.5, 10.2, 10.4, 10.6, 10.8, 11.0 and 12.6, respectively, along the arrow direction. The spectrum at pH 13.6 was identical with that at pH 12.6.

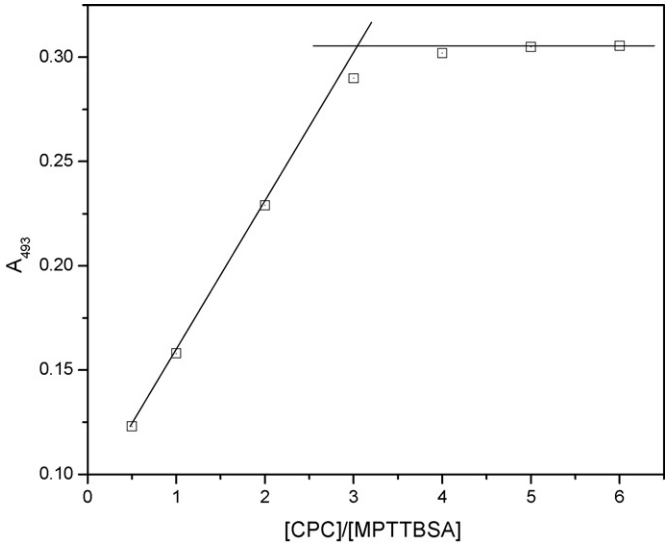


Fig. 9. Molar ratio plot obtained by a spectrophotometric titration of MPTTBSA (1.0×10^{-5} M) with CPC at pH 5.0.

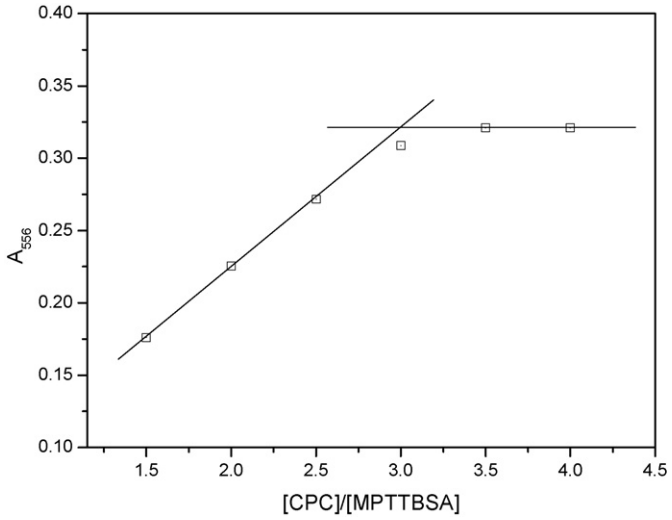


Fig. 10. Molar ratio plot obtained by a spectrophotometric titration of MPTTBSA (1.0×10^{-5} M) with CPC at pH 12.8.

equilibria had to be taken into account simultaneously:

$$HR^- \rightleftharpoons R^{2-} + H^+$$

$$3CPC + R^{2-} \rightleftharpoons (CPC)_3R^{2-}$$

3.5. Effect of CPC micelle formation on the optical properties of MPTTBSA-CPC ion associates

The behaviors of MPTTBSA with CPC under submicellar and micellar conditions were examined to see whether micelle formation has any impact on the optical properties of the ion associates. The CMC of CPC at pH 12.8 was measured as 2.54×10^{-4} M using the maximum bubble pressure method (Fig. 11) [15]. It was found that MPTTBSA caused a concentration-dependent decrease in CMC of CPC, which dropped to 2.36×10^{-4} M at 1.0×10^{-5} M of MPTTBSA, and

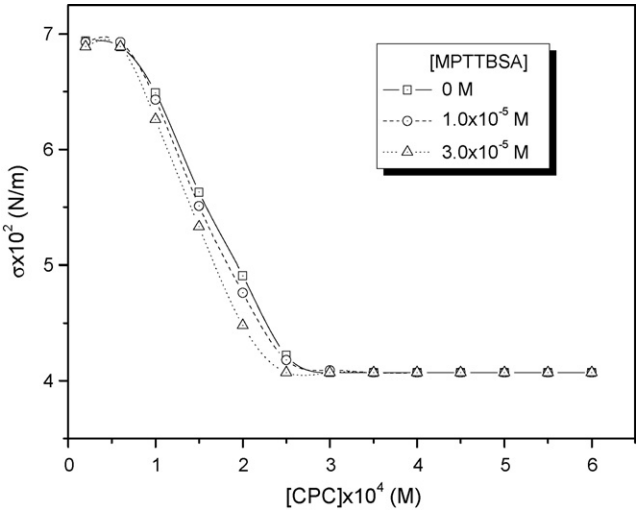


Fig. 11. Surface tension curves of CPC obtained by maximum bubble pressure method at pH 12.8 in the absence and presence of MPTTBSA.

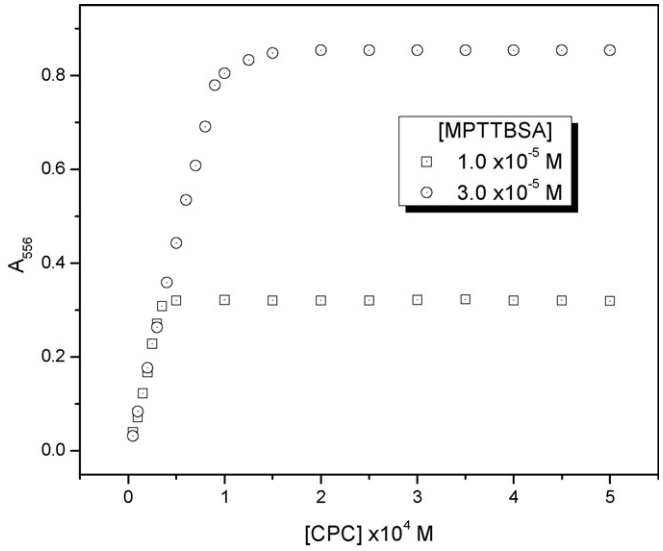


Fig. 12. A_{556}–[CPC] plots obtained by spectrophotometric titration of MPTTBSA with CPC at pH 12.8.

to 2.21×10^{-4} M at 3.0×10^{-5} M of MPTTBSA (Fig. 11). Similar phenomenon has also been observed in other dye-ionic surfactant systems [16]. On the other hand, the formation of CPC micelles appeared to have no effect on the optical properties of $(CPC)_3R^{2-}$: the absorbance at 556 nm for $(CPC)_3R^{2-}$ maximized when the concentration of CPC reached ca. three times that of MPTTBSA, and then remained constant even if the concentration of CPC far exceeded its CMC (Fig. 12). The ion associate $(CPC)_3HR^-$ also behaves similarly: the CMC of CPC at pH 5.0 was measured as 1.60×10^{-4} M, which decreased to 1.40×10^{-4} M in the presence of 1.0×10^{-5} M of MPTTBSA; whereas the A_{493} of MPTTBSA (1.0×10^{-5} M) reached maximum at ca. 3.0×10^{-5} M of CPC, and then stayed constant at up to 5×10^{-4} M of CPC (not shown).

3.6. Analytical application

The perturbation of ionizations of MPTTBSA by CPC can be utilized to develop useful protocols for spectrophotometric determination of CPC. Theoretically, high sensitivity and large color contrast can be achieved if the pH is controlled in between the pK_a values of an ionization in the presence and absence of CPC to ensure complete dissociation of the MPTTBSA-CPC complex without significant dissociation of free reagent. Based on this notion, perturbation of the first ionization by CPC would be expected to furnish a color reaction from yellow (λ_{max} 408 nm, H_2R) to red (λ_{max} 493 nm, $(CPC)_3HR^-$), whereas perturbation of the second ionization by CPC would offer a color reaction from yellow (λ_{max} 440 nm, HR^-) to blue (λ_{max} 556 nm, $(CPC)_3R^{2-}$).

We decided to focus on the second color reaction due to the large color contrast between HR^- and $(CPC)_3R^{2-}$ ($\Delta\lambda$ 116 nm), and the high extinction coefficient of $(CPC)_3R^{2-}$ (Table 1). As predicted, at optimized pH (12.8), a clean isosbestic conversion of the peak at 440 nm for HR^- to the peak at 556 nm for $(CPC)_3R^{2-}$ was observed when a solution of

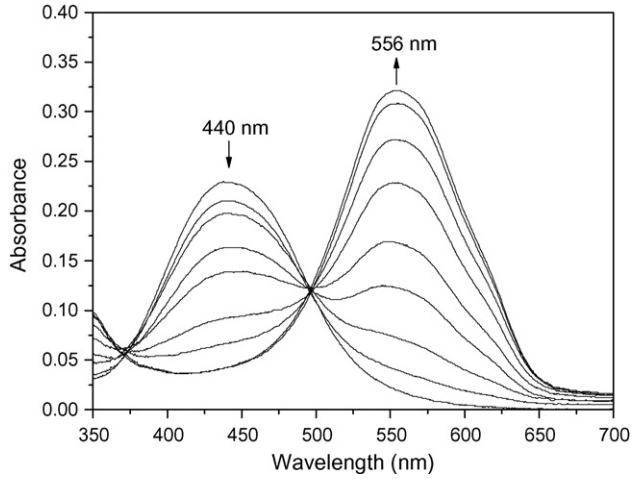


Fig. 13. Spectrophotometric titration of MPTTBSA (1.0×10^{-5} M) with CPC at pH 12.8. The CPC added were 0, 5.0×10^{-7}, 5.0×10^{-6}, 1.0×10^{-5}, 1.5×10^{-5}, 2.0×10^{-5}, 2.5×10^{-5}, 3.0×10^{-5} and 3.5×10^{-5} M, respectively, along the arrow direction. The spectra in the presence of higher concentrations of CPC were identical with that at 3.5×10^{-5} M of CPC.

MPTTBSA was titrated with CPC (Fig. 13). During the titration, the color of the solution gradually changed from yellow to green and finally to blue. Optimization of other reaction conditions ended up with an assay protocol, which involves reaction of MPTTBSA (1.5×10^{-5} M) with CPC in 0.5 M of pH 12.8 NaOH buffer at room temperature for 5 min (the association complex was stable at least for 2 h), followed by spectrophotometric measurement at 556 nm against reagent blank. Under such conditions, an excellent linear relationship was observed between A_{556} and concentration of CPC in the range of 0–114 μg/10 mL of CPC (Fig. 14). The regression equation is $A_{556} = 0.00378C - 0.00085$ (C, μg/10 mL CPC), and the correlation coefficient is 0.99994. The sensitivity (apparent ε at 556 nm in terms of CPC) was 1.07×10^4 cm^{-1} M^{-1}, and the Sandell's sensitivity was 3.36×10^{-2} μg/cm^2.

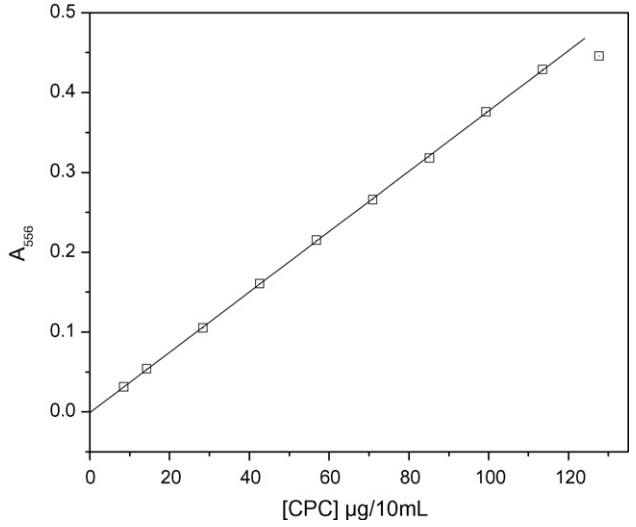


Fig. 14. Calibration plot constructed for the reaction of MPTTBSA (1.5×10^{-5} M) with varying concentrations of CPC in pH 12.8 NaOH buffer. The A_{556} was measured against reagent blank without CPC.

Table 2
Effects of foreign species on CPC measurements[a]

Foreign species	Tolerance limit (μg/10 mL)[b]
K^+, Na^+, NH_4^+, Li^+, CO_3^{2-}, Cl^-, SO_3^{2-}, SO_4^{2-}, PO_3^{3-}, NO_2^-, NO_3^-	5000[c]
Tartrate, thiourea, $Na_4P_2O_7$, EDTA	5000[c]
F^-, acetate, I^-	3000
Triton X-100	650
Zn^{2+}, Al^{3+}, Ca^{2+}	400
Ba^{2+}, Pb^{2+}, Mn^{2+}, Hg^{2+}	200
Fe^{3+}, Mg^{2+}	150
Sodium dodecylbenzenesulfonate (SDBS)	120
Sodium dodecylsulfate (SDS)	100
Co^{2+}, Pd^{2+}, Cr^{3+}	50
Cd^{2+}, Cu^{2+}	30
Ni^{2+}	10 (60)[d]
Ag^+	3 (30)[d]

[a] All the measurements were conducted with a 10 mL water sample containing 99 μg (3.5×10^{-5} M) of CPC following the optimized protocol.
[b] Tolerance limit is the amount of foreign species that causes an error of ±5%.
[c] The upper limits were not determined.
[d] Tolerance limits in the presence of 1.0 mg/10 mL EDTA as masking agent.

Table 2 summarizes the effects of foreign species on determination of CPC (99 μg) in 10 mL of water samples. Whereas the interferences from Ni^{2+} and Ag^+ can be masked by EDTA, the method is free from interferences of most foreign species tested. Of particular interest is that while there was a report on spectrophotometric determinations of several anionic surfactants based on their ternary associations with CPC and a triazene reagent, namely 1-pyridine-3-(4-phenylazophenyl)-triazene [11d], surprisingly high tolerance limits of SDBS and SDS were observed in our case (Table 2), suggesting that either ternary associations of these anionic surfactants with CPC and MPTTBSA do not occur under our reaction conditions, or the ternary associates do form, but possess similar optical properties as those of CPC-MPTTBSA binary associate. Structural difference between MPTTBSA and 1-pyridine-3-(4-phenylazophenyl)-triazene (MPTTBSA bears an extra anionic sulfonate group) must play a key role in their different association behaviors.

The new protocol was applied to spectrophotometric determination of CPC in synthetic water samples prepared according to the national standard of ground water quality, containing Hg^{2+}, Co^{2+}, Ni^{2+} and Cr^{3+} (2 μg/10 mL each); Mn^{2+}, Cu^{2+} and Fe^{3+} (5 μg/10 mL each); Zn^{2+}, Pb^{2+} and Cd^{2+} (10 μg/10 mL each); and Mg^{2+} and Ca^{2+} (500 μg/10 mL each), respectively [12a]. A 1.0 mL aliquot was taken and a certain amount of CPC was added. The amount of CPC was then determined according to the optimized protocol (Table 3), showing excellent recovery values and very small relative standard deviations (R.S.D.).

The new method provides an alternative to other reported methods for determination of CPC [3–8]. The apparent advantages are accuracy, sensitivity, selectivity, simplicity, convenience, and especially the omission of toxic organic solvents, which is environmentally important. Moreover, with comparable sensitivity and selectivity, our method has a wider linear range compared to some of the reported spectrophotometric methods [5,11]. Also, the sharp color change (yellow to blue) in our

Table 3
Determination of CPC in synthetic water samples

Sample #	CPC (μg)		Recovery (%)	R.S.D. (%)
	Theoretical	Experimental[a]		
1	15.00	14.98	99.9	1.00
2	30.00	30.05	100.2	0.49

[a] Mean of five replicate measurements.

method, which is not often seen in other reported spectrophotometric methods, suggests that MPTTBSA may potentially be used as a colormetric probe for fast detection of CPC without the use of instrumentation.

4. Mechanistic discussion

Interactions of surfactants with organic dyes have been studied intensely [16]. Usually, surfactant-dye associates would form even below CMC, but the stoichiometries and/or optical properties of the association complexes would change significantly under micellar conditions, suggesting widespread rearrangements of the association complexes [16]. It is thus surprising that CPC associates with MPTTBSA anions strictly according to a 3:1 stoichiometry, and the resulting ion associates do not show any changes in optical properties even in the presence of large excess of MPTTBSA, and at CPC concentrations far below or far above its CMC. These unique behaviors indicate that the binding affinities between MPTTBSA anions and CPC are extremely high such that rearrangements of these ion associates under micellar conditions become thermodynamically unfavorable. Indeed, both ion associates have exceptionally high apparent stability constants (ca. 10^{19} for $(CPC)_3HR^-$ and ca. 10^{22} for $(CPC)_3R^{2-}$), which are comparable with or even higher than those of some of the most stable metal chelates (e.g., the stability constant of Cu(EDTA) is ca. 10^{19}).

It is intriguing to conceive possible assembly modes of CPC-MPTTBSA ion associates to account for their unique properties. Shown in Fig. 15 is an energy-minimized (MM2) all head-to-head binding model proposed for the apparent 3:1 ion associate between CPC and MPTTBSA monoanion HR^-. Interestingly, any other not all head-to-head arrangements would end up with higher energies, and the 1:1, 2:1, and 4:1 CPC-MPTTBSA all head-to-head binding models were also less stable. Thus, the 3:1 association stoichiometry must represent the best compromise between maximum favorable interactions of CPC with the reagent, and minimum topological crowdness around the reagent molecule. Given that no significant interaction was evident between CPC and H_2R, electrostatic interaction between the pyridinium cation in CPC and the sulfonate anion in MPTTBSA anions must play a determinant role in initiating the whole association process [16]. Once triggered, association can then be reinforced by other favorable interactions such as π-stacking between the pyridine ring of CPC and the aromatic rings of MPTTBSA, as well as hydrophobic interactions between the hydrocarbon tail of CPC and the triazene moiety and aromatic rings of MPTTBSA (Fig. 15). The more than three orders of magnitude difference in apparent stability constants

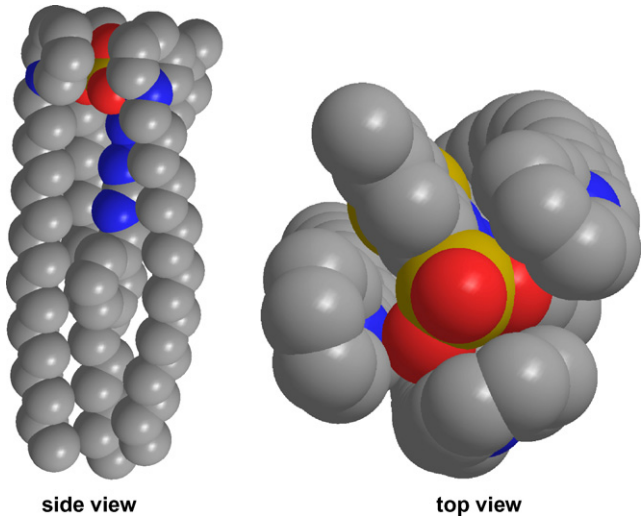


Fig. 15. Energy-minimized model proposed for the apparent 3:1 ion associate of CPC with MPTTBSA monoanion.

of $(CPC)_3HR^-$ and $(CPC)_3R^{2-}$ suggests that formation of the second anion on the triazenate of R^{2-} further enhances binding affinity, but to a lesser extent than does the sulfonate anion if one considers the large apparent stability constant of $(CPC)_3HR^-$. This is reasonable because the negative charge of the triazenate anion is actually dispersed in the whole aromatic system of MPTTBSA by resonance, whereas the negative charge of sulfonate anion can only delocalize among the three oxygen atoms of the sulfonate group [16]. Thus, a localized anion appears to be the most important factor in future design of tight binding chromogenic reagents for cationic surfactants.

Once the nature of interactions between CPC and MPTTBSA is clear, it is easy to understand the impact of such interactions on the properties of reagent. The π-stacking between the pyridine ring of CPC and the aromatic rings of MPTTBSA results in electron delocalization, which appears to be what causes the red shifts in λ_{max} and increases in ε of the two MPTTBSA anions [16]. Under micellar conditions, the extremely tight binding ion associates would simply insert as a whole into the CPC homomicelles such that the microenvironment of reagent would be essentially unchanged. This explains the lack of effect of micelle formation on the optical properties of the reagent-CPC associates. On the other hand, since neutral reagent does not interact significantly with CPC, stabilization of HR^- upon formation of $(CPC)_3HR^-$ must constitute the major driving force to facilitate the first ionization, whereas the switch of charge property of HR^- from an anion to a dication upon association with three CPC cations, which helps kick out the triazene NH proton, appears to be the major driving force to facilitate the second ionization.

5. Conclusion

We have presented a mechanistic study on the interactions of a new triazene reagent MPTTBSA with the cationic surfactant CPC. Experimental data clearly demonstrate that CPC cations selectively associate with the two reagent anions, result-

ing in widespread changes in acid–base and optical properties of the reagent. The fully characterized ionization chemistries of MPTTBSA with and without CPC allowed us to develop a new protocol for spectrophotometric determination of CPC in a rational way as opposed to the normal way of trial and error. This strategy should be useful in future development of spectrophotometric methods for quantitative analysis of surfactants. Furthermore, our results also highlight the key role of a sulfonate group on the reagent molecule in triggering the stoichiometric and high affinity ion associations, which should be useful in future design of surfactant-sensitive triazene reagents. Finally, since cationic surfactants have been used extensively in reactions of trizenes with various metal ions to improve sensitivity, information generated in this study could also help understand the mechanisms of how surfactants sensitize such color reactions. Interactions of MPTTBSA with other cationic surfactants and interactions of anionic surfactants with MPTTBSA and cationic surfactants are currently under investigation.

Acknowledgement

XLH thanks Mrs. Ya-Lin Wang, College of Environmental Science and Engineering, Shanghai Jiao Tong University, for assistance in elemental analysis.

References

[1] For recent reviews, see:
(a) J. Hibbs, R.J. Farn (Eds.), Chemistry and Technology of Surfactants, Blackwell Publishing Ltd., Oxford, 2006;
(b) T.P. Knepper, J.L. Berna, T.P. Knepper, D. Barcelo, P. De Voogt (Eds.), Comprehensive Analytical Chemistry, Elsevier Science B.V., Amsterdam, 2003, p. 1.

[2] For a review specifically on cationic surfactants, see:
J. Cross, E.J. Singer, Cationic Surfactants—Analytical and Biological Evaluation, Surfactant Science Series, vol. 53, Marcel Dekker, New York, 1994, p. 3.

[3] K. Heinig, C. Vogt, G. Werner, J. Chromatogr. A 781 (1997) 17.

[4] (a) J.M.H. Martynez, E.F.S. Alfonso, C.M. Femandez, J. Chromatogr. A 895 (2000) 227;
(b) K. Heinig, C. Vogt, Electrophoresis 20 (1999) 3311.

[5] (a) M. Kamaya, J. Takahashi, K. Nagashima, Microchim. Acta 144 (2004) 35;
(b) K. Agrawal, G. Agnihotri, K. Shrivas, G.L. Mundhara, K.S. Patel, P. Hoffmann, Microchim. Acta 147 (2004) 273.

[6] C.A. Lucy, J.S.W. Tsang, Talanta 50 (2000) 1283.

[7] F. Bruno, R. Curini, A. Di Corcia, I. Fochi, M. Nazzari, R. Samperi, Environ. Sci. Technol. 36 (2002) 4156.

[8] Z. Cao, C. Lau, J. Lu, Analyst 129 (2004) 1262.

[9] J. Liu, X. Wang, L. Wang, Microchim. Acta 151 (2005) 123.

[10] For a recent review, see:
Z. Li, Q. Zhang, J. Pan, Rev. Anal. Chem. 22 (2003) 191;
Z. Li, Q. Zhang, J. Pan, Chem. Abstr. 140 (2004) 433275.

[11] For recent reports, see:
(a) Y.L. Feng, Z.M. Chen, D.Z. Kuang, J.S. Xu, R.Y. Zeng, Fenxi Shiyanshi 24 (2005) 75;
Y.L. Feng, Z.M. Chen, D.Z. Kuang, J.S. Xu, R.Y. Zeng, Chem. Abstr. 143 (2005) 165651;
(b) Y.L. Feng, Z.M. Chen, D.Z. Kuang, J.S. Xu, Fenxi Shiyanshi 23 (2004) 88;
Y.L. Feng, Z.M. Chen, D.Z. Kuang, J.S. Xu, Chem. Abstr. 142 (2005) 341288;
(c) Y.L. Feng, D.Z. Kuang, Huaxue Shiji 25 (2003) 353;
Y.L. Feng, D.Z. Kuang, Chem. Abstr. 140 (2004) 292086;
(d) Y.L. Feng, D.Z. Kuang, J.S. Xu, J.Q. Wang, M.Q. Liu, Fenxi Huaxue 30 (2002) 189;
Y.L. Feng, D.Z. Kuang, J.S. Xu, J.Q. Wang, M.Q. Liu, Chem. Abstr. 136 (2002) 403499.

[12] For recent examples, see:
(a) X.L. He, Y.Q. Wang, K.Q. Ling, Talanta 72 (2007) 747;
(b) S. Chatterjee, A. Pillai, V.K. Gupta, Talanta 57 (2002) 461.

[13] R.M. Dodson, L.C. King, J. Am. Chem. Soc. 67 (1945) 2242.

[14] C. Ebert, L. Lassiani, P. Linda, M. Lovrecich, C. Nisi, F. Rubessa, J. Pharm. Sci. 73 (1984) 1691.

[15] R.Y.Z. Hu, A.T.A. Wang, J.P. Hartnett, Exp. Therm. Fluid Sci. 4 (1991) 723.

[16] M.E. Diaz Garcia, A. Sanz-Medel, Talanta 33 (1986) 255 (and references cited therein).

Available online at www.sciencedirect.com
ScienceDirect
Talanta 74 (2008) 694–698
Talanta
www.elsevier.com/locate/talanta

Capillary zone electrophoresis method for the determination of famotidine and related impurities in pharmaceuticals

N. Helali [a], N.T. Tran [b], L. Monser [a,*], M. Taverna [b]

[a] *Institut National des Sciences Appliquées et de Technologie, Laboratoire de Chimie Analytique et Electrochimie 04UR12-01, Centre Urbain Nord, B.P. No. 676, 1080 Tunis Cedex, Tunisia*

[b] *Univ Paris-Sud, Laboratoire des Protéines et Nanotechnologies en sciences séparatives, JE 2495-IFR 141, Chatenay-Malabry, Cedex F-92296, France*

Received 21 April 2007; received in revised form 25 June 2007; accepted 27 June 2007
Available online 1 July 2007

Abstract

A simple and rapid capillary zone electrophoresis (CZE) method with UV detection has been developed for the determination of famotidine and its potential impurities in pharmaceutical formulations. The electrophoretic separation of these compounds was performed using a fused silica capillary and 37.5 mmol L^{-1} phosphate buffer pH 3.5 as the electrolyte. Under the optimised conditions, six impurities could be resolved from the famotidine peak in less than 7 min. The calibration curves obtained for the seven compounds were linear over the concentration range investigated (from 1.5 to 78.5 μg mL^{-1}). The intra- and inter-day relative standard deviations for the migration times and corrected peak areas were less than 2% and 5%, respectively. The detection limits were found to be 0.09 μg mL^{-1} for famotidine, and from 0.1 to 0.62 μg mL^{-1} depending on the impurities. The method has been successfully applied to the determination of famotidine in commercial dosage forms.
© 2007 Elsevier B.V. All rights reserved.

Keywords: Capillary electrophoresis; Famotidine; Pharmaceuticals

1. Introduction

Famotidine (FMT) N^2-(aminosulphonyl)-3-[[[2-[(diaminomethylene)amino]thiazol-4-yl] methyl] thio]propanamidine is an H_2 receptor antagonist used in the treatment of gastric and duodenal ulcers. It inhibits gastric acid secretion by blocking the H_2 receptors located on parietal cells [1]. A range of synthetic and degradative impurities of FMT has been identified and semi-quantitatively determined using thin layer chromatography [2,3]. The structures of FMT and its potential impurities are shown in Fig. 1.

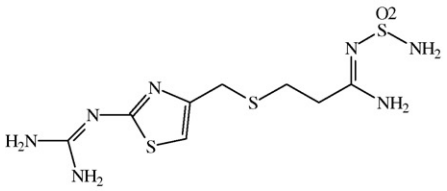
Several analytical techniques such as, spectrophotometry [4–8], potentiometry [9], flow injection analysis [10,11] and more extensively high performance liquid chromatography (HPLC) [12–19] have been reported for the individual and simultaneous determination of FMT and other antihistaminic analogues. However, among the most extensively used HPLC methods, only few of them describe the simultaneous determination of FMT and of all related compounds [20–28]. Furthermore, these methods require mobile phase with high proportions of organic solvents, and elution gradient and relatively time consuming.

Capillary electrophoresis (CE) has become a useful tool in many fields because of its advantages over other separation techniques such as simplicity, speed, high resolution and low solvent consumption. Many reviews have been dedicated to CE for drug analysis and purity control of pharmaceuticals [29–32]. Several capillary electrophoresis methods have been developed for the determination of FMT and other antihistaminic products [33–35], but none of them have yet reported the separation of FMT and its six potential impurities, such that the degradation products and also impurities that could be formed in the final product such the chloromethyl derivative (FPI), and 3-[[[2-[(diaminomethylene)amino]thiazol]4-yl]methyl)thio]-*N*-cyanopropionamidine (CYN).

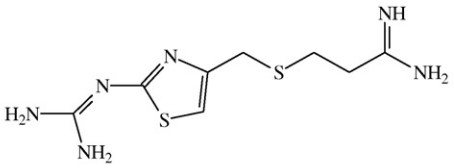
In this study, a simple and rapid capillary zone electrophoresis (CZE) method is developed for the separation of FMT and its related impurities. The effects of the nature, pH and ionic strength of buffer, as well as common electrophoretic parameters were evaluated. The performances of the method were evaluated

* Corresponding author.
E-mail address: lotfi.monser@insat.rnu.tn (L. Monser).

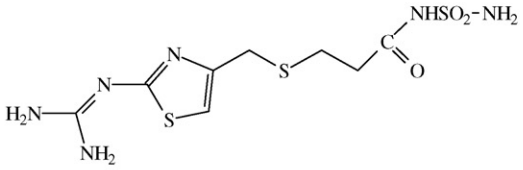
0039-9140/$ – see front matter © 2007 Elsevier B.V. All rights reserved.
doi:10.1016/j.talanta.2007.06.036



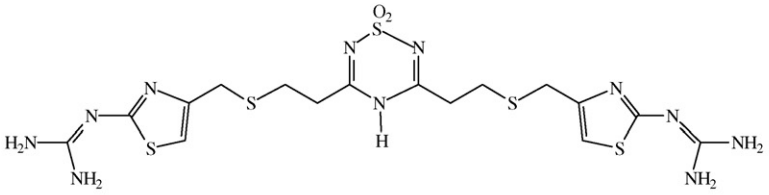
FMT



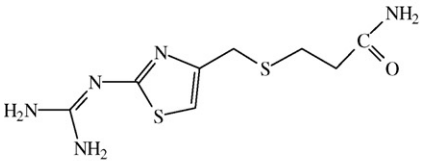
3-[[[2-[(diaminomethylene)amino]thiazol-4-yl]methyl]thio]propanamidine
(Impurity A)



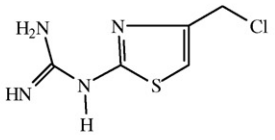
N-(aminosulfonyl)-3-[[[2-[(diaminomethylene)amino]thiazol-4-yl]methyl]thio-Propanamide
(Impurity C)



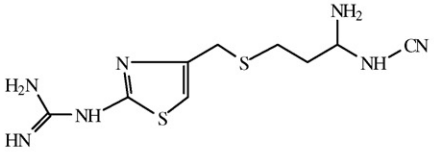
3,5-bis-[2-[[[[(diaminomethylene)amino]thiazol-4-yl]methyl]thio]ethyl]-4H-1,2,4,6-thiatriazine 1,1-dioxyde
(*Impurity B)*



3-[[[2-[(diaminomethylene)amino]thiazol-4-yl]methyl]thio]-propanamide
(Impurity D)



Chloromethyl derivative
(Impurity FPI)



3-[[[2-[(diaminomethylene)amino]thiazol]4-yl]methyl)thio]-N-cyano propionamidine
(Impurity CYN)

Fig. 1. Chemical structures of FMT and its related impurities.

and its potential for the determination of famotidine in tablets was investigated.

2. Experimental

2.1. Capillary electrophoresis

A P/ACE 2000 system and a P/ACE MDQ system (Beckman Coulter Instrument, Fullerton, CA, USA) equipped with a UV-detector were used for the optimisation and the validation of the CZE method, respectively. CZE separation was performed using a 37 or 40.2 cm (30 cm effective length) × 50 μm i.d. fused silica capillary when using P/ACE 2000 or the P/ACE MDQ, respectively. Samples were hydrodynamically injected into the capillary for 10 s at 0.5 psi. The separation was performed using a 37.5 mmol L^{-1} sodium phosphate buffer at pH 3.5 and under a voltage of +20 kV. The capillary was maintained at 25 °C. The detection was monitored at 214 nm and data from PACE MDQ instrument were collected and analysed using Gold software.

The capillary was pre-conditioned prior to its first use by flushing with water for 10 min, 1 mol L^{-1} NaOH for 20 min, water for 10 min, 1 mol L^{-1} HCl for 20 min, water for 10 min and running buffer for 30 min. Between runs, the capillary was washed with water for 3 min and running buffer for 3 min.

2.2. Chemicals and reagents

FMT was purchased from the pharmaceutical company Ibn Al Baytar (Tunis Carthage, Tunisia). FMT related impurities were obtained from *ERCROS INDUSTRIAL*, S.A, Fyse (Madrid, Spain) and Pepdine tablets were supplied by MSD-Chibret (Paris, France). Ultra pure Water was drawn from a Milli-Q Water purification system (Millipore, France). Phosphoric acid, acetic acid, formic acid and sodium hydroxide were from Prolabo (Paris, France). Ammonium hydroxide was from Sigma (Paris, France).

Running buffers were prepared by mixing different volumes of 1 mol L^{-1} sodium hydroxide or ammonium hydroxide and 1 mol L^{-1} of corresponding acid.

2.3. Sample preparation

2.3.1. Standard solutions

Stock solutions (500 μg L^{-1}) of each compound were prepared by dissolving reference compound in water. A mixture of FMT and its six impurities was prepared daily by mixing the stock solutions in water. The mixture containing 36 μg mL^{-1} impurity A, 27 μg mL^{-1} impurity FPI, 78.5 μg mL^{-1} impurity B, 37 μg mL^{-1} impurity D, 40 μg mL^{-1} impurity CYN and 48 μg mL^{-1} FMT and impurity C was used for the method development and validation studies. The analysed samples were spiked with 10 μg mL^{-1} and 20 μg mL^{-1} of famotidine in an attempt to study the accuracy of the method. The limits of detection were determined by serial dilution of standard solutions.

2.3.2. Tablet preparation

Ten FMT tablets Pepdine (MSD-Chibret, Paris, France) were finely powdered and weighed. An accurately weighed quantity of the mixed powder containing an equivalent of 40 mg of FMT was dissolved in 100 mL of water. The solution was then sonicated for 10 min, filtered through a nylon membrane of 0.2 μm (Millipore) and diluted with water to yield FMT solution with a final concentration of 100 μg mL^{-1}.

3. Results and discussion

Several parameters were investigated to determine the optimal separation conditions. These parameters included the nature, pH and concentration of the running buffer, applied voltage, temperature and capillary length.

3.1. Method development

3.1.1. Effect of buffer

From the molecular structures of FMT and its related substances (positively charged at acidic pH), it was anticipated that these compounds could be separated by CZE using low buffer pHs. In order to find the suitable buffer pH, the effect of pH on migration times and on resolution was investigated over the range of 2.5–4.5, using 50 mmol L^{-1} phosphate buffer. As shown in Fig. 2, the migration times of the seven studied compounds decreased with increasing buffer pH. Since the buffer pH affect both positive charge of the analytes and the magnitude of electroosmotic flow (EOF), the observed increase of apparent mobilities with increasing the buffer pH was attributed to a predominant effect of pH on EOF. A pH value of 3.5 was selected because it yields an optimum resolution within an acceptable analysis time.

In an attempt to shorten the analysis time and to improve resolution of the proposed method, several buffers including ammonium formate and sodium acetate were used at a similar ionic strength (50 mmol L^{-1}) and at a pH 3.5. Since phosphate buffer provided the best results with regards to current intensity

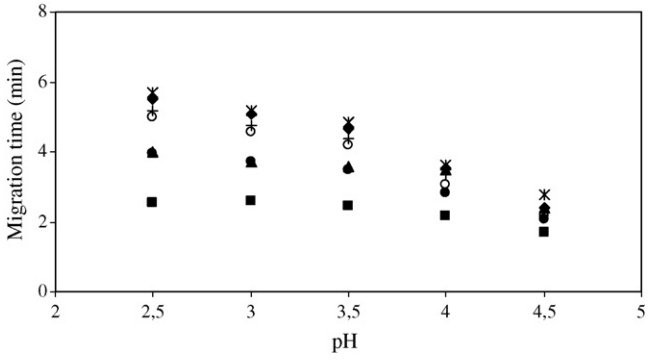


Fig. 2. Effect of the pH of sodium phosphate buffer on the migration of the seven compounds. Separation conditions: 50 mmol L^{-1} sodium phosphate buffer, applied voltage 20 kV (detector at cathodic side), fused silica capillary (37 cm × 50 μm i.d.), detection wavelength 214 nm, operating temperature 25 °C. (♦) FMT, (■) impurity A, (▲) impurity B, (⋆) impurity C, (◯) impurity D, (●) impurity FPI, (+) impurity CYN.

(≈56–58 μA), peak symmetry, and analysis time, it was selected for further studies.

The effect of the ionic strength of phosphate buffer on the separation of these compounds was studied over the range 25–75 mmol L^{-1} at constant pH of 3.5. The obtained results showed that the migration time of solutes was slightly effected below 50 mmol L^{-1}, however, above 50 mmol L^{-1} an increase in the migration times of all solutes were observed. Therefore, an ionic strength of 37.5 mmol L^{-1} was selected as optimum, because it resulted in the best compromise between peak symmetry, resolution and analysis time.

3.1.2. Other electrophoretic parameters

In order to shorten the separation time and further improve the efficiency, the effect of applied voltage was tested. However, higher applied voltages caused higher currents and joule heating. To prevent this problem, an applied voltage of 20 kV was selected.

To further shorten the analysis time, the effect of temperature and capillary length were tested. However, higher temperatures or shorter capillary lengths deteriorate the resolution. Then, the selected temperature and capillary length were 25 °C and 37 cm total length (30 cm effective length), respectively. Fig. 3 presents the best separation of FMT and its six related impurities by the optimised CZE.

3.2. Method performances

The performance of the CZE method for the potential determination of FMT as drug product was evaluated under the optimum electrophoretic conditions described above. Satisfactory separation of famotidine and its related impurities was achieved within 7 min.

Calibration graphs were investigated by injecting a mixture of FMT and its related impurities at five different concentration levels. The ranges of studied concentrations are specified in Table 1. Calibration curves of corrected peak areas versus concentration of all studied compounds showed high regression coefficients that varied from 0.9978 to 1 (Table 1).

The limit of detection (LOD) was estimated by injecting a mixture of the seven compounds at various concentrations. The LOD was determined for a signal to noise ratio equal to three. It was estimated at: 0.09 μg mL^{-1} for FMT, 0.14 μg mL^{-1} for impurities A and D, 0.62 μg mL^{-1} for impurity B, 0.18 μg mL^{-1} for impurity C, 0.1 μg mL^{-1} for impurity FPI and 0.15 μg mL^{-1} for impurity CYN. The percentage of impurities with respect to famotidine concentration was varied between 0.1% and 0.6% (m/m). Figs. 4 and 5 demonstrates the sensitivity of the proposed method that afford to detect low concentration of impurities in famotidine real samples.

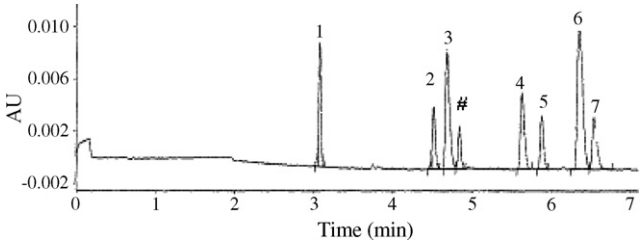


Fig. 3. Typical electropherogram of FMT and its six impurities. Peaks: (1) impurity A; (2) impurity FPI; (3) impurity B; (#) unknown impurity; (4) impurity D; (5) impurity CYN; (6) FMT; (7) impurity C. 37.5 mmol L^{-1} sodium phosphate buffer at pH 3.5. Other conditions: see Fig. 2.

Table 1
Linear regression data for the calibration curves of FMT and its related impurities

Compounds	Concentration range (μg mL^{-1})	Equation of the line	R^2
Impurity A	2.3–36.8	$Y = 132.81x - 69.609$	0.9978
Impurity FPI	1.6–27	$Y = 86.388x - 28.022$	0.9982
Impurity B	9.8–78.5	$Y = 22.175x - 75.697$	0.9988
Impurity D	2.3–37	$Y = 78.576x - 0.0618$	0.9998
Impurity CYN	2.5–40	$Y = 42.226x + 3.2917$	1.0000
FMT	1.5–48	$Y = 141.134x - 21.602$	0.9992
Impurity C	3–48	$Y = 43.734x + 4.75$	0.9997

The stability of the electrophoretic method was evaluated by studying the variation of the peak area and the migration time for all analytes (Table 2). The intra-day precision of migration times and corrected peak areas for FMT and its related impurities was studied with five successive injections of the mixture. The relative standard deviations (RSD) of the corrected peak area of all analytes were varied between 0.98% and 1.84% and that for migration times were less than 0.5%. The inter-day precision was evaluated over 3 days by performing five replicate injections

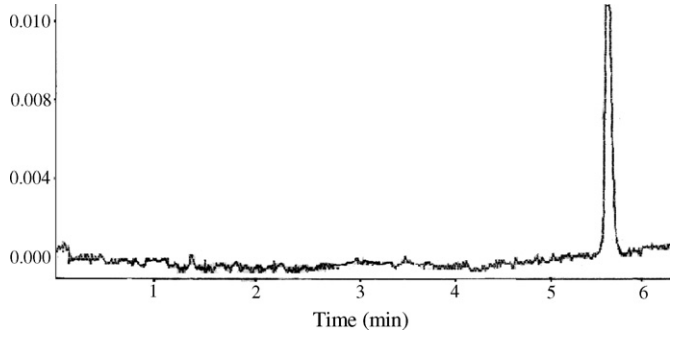


Fig. 4. Electropherogram of pepdine sample analysed under similar conditions to that in Fig. 3.

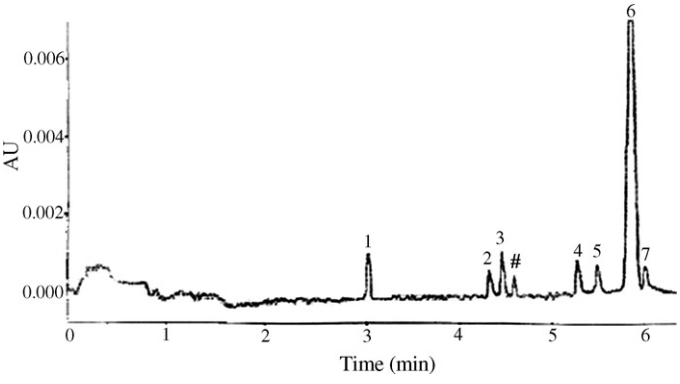


Fig. 5. Electropherogram of pepdine sample spiked with trace levels of FMT impurities (0.5% (m/m) impurities/famotidine ratio). Peak identification and conditions are similar to Fig. 3.

Table 2
Intra-day and inter-day precision of the optimised CZE method

Compounds	Migration times (mean)	RSD (%)			
		Intra-day precision		Inter-day precision	
		Migration times ($n=5$)	Corrected peak area ($n=5$)	Migration times ($n=5$)	Corrected peak area ($n=5$)
Impurity A	3.13	0.34	1.30	0.91	4.52
Impurity FPI	4.61	0.41	1.70	0.37	4.32
Impurity B	4.79	0.45	0.98	0.47	4.06
Impurity D	5.67	0.35	1.75	1.49	4.80
Impurity CYN	5.98	0.33	1.84	0.39	4.42
FMT	6.40	0.33	1.32	1.64	4.11
Impurity C	6.54	0.44	1.64	1.79	4.98

each day. Satisfactory results were obtained for migration times and corrected peak areas with RSD values of less than 1.8% and 5%, respectively. Thus, acceptable results with respect to precision (RSD < 5%) were obtained for all analytes.

3.3. Application to the determination of FMT in a tablet formulation

The applicability of the proposed method for the determination of FMT was investigated by analysing commercial pepdine tablets. Results obtained showed that the amount of FMT found correspond to the drug label (claim: 40 mg; found: 40.2 mg). The results are in good agreement with the label claim, which shows that the method can be used for the determination of FMT in tablets. Furthermore, in an attempt to estimate the recovery percent, three different concentrations of FMT standard (5, 10 and 20 mg mL^{-1}) were added to pepdine tablets and each sample was injected three times. The recoveries were varied between 98% and 101%.

The method was further evaluated by comparing the results obtained by the proposed method with those obtained with previously published method [28]. Results obtained with CE method (40.4 mg) were in close agreement with published method (39.6 mg) and compare reasonably with the label claimed.

4. Conclusion

A capillary zone electrophoresis method was developed for the separation of FMT and its six impurities in drug products. The analysis of these compounds was achieved within 7 min using 37.5 mmol L^{-1} sodium phosphate buffer at pH 3.5. The method showed acceptable performances with respect to linearity, intra- and inter-day precision for migration times and corrected peak areas and LODs. It is a potential method for the quality control of FMT as drug substance and for the determination of FMT in tablet formulation.

References

[1] Goodman, Gilman, The Pharmacological Basis of Therapeutics, 9th ed., McGraw-Hill, New York, 1996, pp. 904–907.
[2] European Pharmacopeia, 5th ed., Council of Europe, Strasbourg, 2007, pp. 1705–1706.
[3] The United States Pharmacopeia, 29th ed., United States Pharmacopeial Convention, Rockville, MD, 2006, pp. 881–883.
[4] A. Abu Zuhi, R. Shubietah, G. Badah, J. Pharm. Biomed. Anal. 21 (1999) 459–465.
[5] K. Kelani, A. Azziz, M. Hegazy, L. Abdel Fattah, Spectrosc. Lett. 35 (2002) 543–563.
[6] A. Amin, S. Shama, I. Ahmed, E. Gouda, Anal. Lett. 35 (2002) 1851–1862.
[7] S. Nassr, M. Brunet, P. Lavoie, J. Brazier, J. Liq. Chromatogr. 24 (2001) 265–281.
[8] N. Rahman, M. Kasihif, Il Farmaco 58 (2003) 1045–1050.
[9] M. Ayed, A. Shalaby, H. Abdellatef, H. Elsaid, J. Pharm. Biomed. Anal. 29 (2002) 247–254.
[10] N. Helali, N. Adhoum, L. Monser, J. Flow Injection Anal. 22 (2005) 129–133.
[11] M. Walash, M. Sharaf-El Din, M. Metwally, M. Shabana, Chin. Chem. Soc. 52 (2005) 71.
[12] J. Novakovic, J. Chromatogr. A 864 (1999) 193–198.
[13] H. Chih, H. Hsi-Min, H. Shu-Ying, S. Ching-Yih, C. Ber-Lin, Drug Dev. Ind. Pharm. 25 (1999) 379–385.
[14] H. Maurer, J. Chromatogr. 531 (1990) 369–405.
[15] B. Carkir, A. Tosun, M. Sahin, Pharm. Sci. 3 (1997) 493–496.
[16] L. Zhong, K. Yeh, J. Pharm. Biomed. Anal. 16 (1998) 1051–1057.
[17] M. Campanero, I. Bueno, M. Arangoa, M. Escolar, E. Quetglas, A. Lopez-Ocariz, J. Azanza, J. Chromatogr. B 763 (2001) 21–33.
[18] T. Dowling, R. Frye, J. Chromatogr. B 732 (1999) 239–243.
[19] A. Zoest, S. Wanwimoluk, C. Hung, J. Chromatogr. B 572 (1991) 227–238.
[20] B. Kamath, K. Shivram, B. Newalkar, A. Shah, J. Liq. Chromatogr. 16 (1993) 1007–1014.
[21] S. Singh, S. Kumar, N. Sharda, A. Chakraborti, J. Pharm. Sci. 91 (2002) 253–257.
[22] Z. Degim, I. Agabeyoglu, Il Farmaco 57 (2002) 729–735.
[23] M. Suleiman, H. Muti, M. Abdel-Hamid, M. Hassan, Y. El-Sayed, N. Najib, Anal. Lett. 22 (1989) 1499–1512.
[24] G. Junnarkar, S. Stavchansky, Anal. Lett. 255 (1992) 1907–1913.
[25] S. Biffar, D. Mazzo, J. Chromatogr. 363 (1986) 243–249.
[26] S. Hussain, S. Khalid, V. Nagaraju, R. Nageswara-Rao, J. Chromatogr. A 743 (1996) 328–334.
[27] X.-Z. Qin, Ip. Dominic, K. Chang, P. Dradransky, M. Brooks, T. Sakuma, J. Pharm. Biomed. Anal. 12 (1993) 221–233.
[28] N. Helali, F. Darghouth, L. Monser, Chromatographia 60 (2004) 455–460.
[29] H. Nishi, Electrophoresis 20 (1999) 3237–3258.
[30] K. Altria, A. Marsh, C. Sanger-van de Griend, Electrophoresis 27 (2006) 2263–2282.
[31] K. Altria, J. Chromatogr. A 856 (1999) 443–463.
[32] K. Altria, D. Elder, J. Chromatogr. A 1023 (2004) 1–14.
[33] T. Perez-Ruiz, C. Martinez-Lozano, V. Tomas, E. Bravo, R. Galera, J. Pharm. Biomed. Anal. 30 (2002) 1055–1061.
[34] S.M. Wu, Y.H. Ho, H.L. Wu, S.H. Chen, H.S. Ko, Electrophoresis 22 (2001) 2717–2722.
[35] S.M. Wu, Y.H. Ho, H.L. Wu, S.H. Chen, H.S. Ko, Electrophoresis 22 (2001) 2758–2762.

Available online at www.sciencedirect.com
ScienceDirect
Talanta 74 (2008) 871–878
Talanta
www.elsevier.com/locate/talanta

Discrimination of Venezuelan spirituous beverages by a trace element-radial basis neural network approach

Edwin A. Hernández-Caraballo [a,b,*], Rita M. Ávila de Hernández [b,c], Francklin Rivas-Echeverría [b], Tarcisio Capote-Luna [a]

[a] *Departamento de Química y Suelos, Programa de Ingeniería Agronómica, Decanato de Agronomía, Núcleo "Héctor Ochoa Zuleta", Universidad Centroccidental Lisandro Alvarado, Cabudare 3023, Venezuela*
[b] *Laboratorio de Sistemas Inteligentes, Escuela de Ingeniería de Sistemas, Facultad de Ingeniería, Universidad de Los Andes, Mérida 5101, Venezuela*
[c] *Departamento de Procesos Agroindustriales, Programa de Ingeniería Agroindustrial, Decanato de Agronomía, Núcleo Obelisco, Universidad Centroccidental Lisandro Alvarado, Barquisimeto 3002, Venezuela*

Received 17 April 2007; received in revised form 20 July 2007; accepted 23 July 2007
Available online 26 July 2007

Abstract

Radial basis neural networks (RBNNs) were developed and evaluated for discrimination of specimens of 'aguardiente de Cocuy', a spirituous beverage produced in the northwestern region of Venezuela. The beverage is distilled from the must of *Agave cocui* Trelease in an artisanship fashion with little quality control. Forty specimens, with known concentrations of copper, iron, and zinc, were used in this study. The specimens were previously collected in various locations around Sucre Municipality (Falcón State) and Urdaneta Municipality (Lara State). The normalized concentrations of these elements served as indirect descriptors of origin (input data). They were presented to the neural networks through 1–3 input nodes in seven different combinations. In addition, two categories (two collection sites) and four categories (two collection sites + two manufacturing conditions) were designated as output data, in order to assess the impact of such selection on the discrimination performance. The overall performance of the four-category RBNNs was as follows (the input data is indicated in parentheses): (Cu–Fe) > (Cu–Zn) > (Cu) > (Zn) > (Fe–Zn) > (Cu–Fe–Zn) > (Fe). In this case, the highest percentage of correct hits was 82.5%. For the two-category RBNNs, the performance decreased as indicated below: (Cu) > (Cu–Fe) > (Cu–Zn) > (Fe–Zn) > (Zn) ≈ (Cu–Fe–Zn) > (Fe).

The reduction in the number of categories led to an increase in the discrimination performance of all the RBNNs, the best of which was 90.0%. The possibility of discriminating specimens of 'aguardiente de Cocuy' with such an accuracy, based on a single-element determination, is particularly attractive as it would result in a reduction of analysis' costs and laboratory's response time.
© 2007 Published by Elsevier B.V.

Keywords: Spirituous beverages; Cocuy; Radial basis neural networks; Copper; Iron; Zinc

1. Introduction

Alcoholic beverages, along with tea and coffee, are certainly among the most consumed liquid commodities worldwide. Tradition, social status, globalization, even local beliefs, among others, tilt preferences towards one or the other. Regardless the preferences of the consumers, it is of crucial importance to maintain high quality standards along the production/sales chain as, aside from the enormous impact this will have on the physical and chemical characteristics of the final product and, consequently, on regional and even national economies, it will ultimately affect consumers.

Indirect estimation of authenticity, geographic origin, etc., has been performed by means of the determination of organic and inorganic species. On this regards, the use of the latter offers two attractive features [1–3]. First, their concentrations show more stability than their organic counterpart does, as the latter may be subject to decomposition due to environmental and storage factors. Second, they can be correlated with either environmental characteristics (soil and water chemical

* Corresponding author at: Departamento de Química y Suelos, Programa de Ingeniería Agronómica, Decanato de Agronomía, Núcleo "Héctor Ochoa Zuleta", Universidad Centroccidental Lisandro Alvarado, Cabudare 3023, Venezuela. Tel.: +58 251 2592476.
E-mail address: ehernandez@ucla.edu.ve (E.A. Hernández-Caraballo).

0039-9140/$ – see front matter © 2007 Published by Elsevier B.V.
doi:10.1016/j.talanta.2007.07.017

composition, fertilization practices, etc.) or production practices proper of the regions where the raw material is grown or transformed into the final product. Therefore, a significant body of work has been published on the application of inorganic information for classification of alcoholic beverages [2–14]. Due to the intrinsic multivariate nature of the data which can be easily collected with modern spectrometers, conventional chemometric methods (principal component analysis, discriminant analysis, soft-independent modeling of class analogy, etc.) [2–4,7–11,13,14], or increasingly more often artificial neural networks [2,3,5,6,9], are employed for discrimination tasks. When it comes to ANNs, the backpropagation algorithm is the usual choice for training feed-forward neural networks [3,5,6,9]. However popular such algorithm is, it leads to a time-consuming development process. This is the result of the number of variables that must be optimized before achieving maximum performance, e.g., number of hidden neurons, learning rate, momentum factor, and transfer functions. The latter have propelled neural network's users in either one of two directions: (i) using NNs trained with more efficient variations of the backpropagation training rule; or (ii) using other types of NNs. Radial basis neural networks (RBNNs) are among the tools available to those who have chosen the second option. These are particularly attractive because only the width of the transfer function has to be optimized, thus making the overall development process much faster [15–17]. Additionally, the size of the databases may be smaller, as RBNNs are not susceptible to overtraining, i.e., the incapacity to classify unknown samples due to the memorization of the characteristics of the training set. The latter may play a vital role in those cases were sample collection may be difficult. In spite of this, only a few applications in the classification of food commodities can be found in the literature, in none of which inorganic species has been used as descriptors so far [18–22].

In the present work, we make use of radial basis neural networks for discrimination of forty specimens of 'aguardiente de Cocuy' (Cocuy firewater), a spirituous beverage produced in the northwestern region of Venezuela. Production of this beverage has been made for centuries in an artisanship fashion under rugged conditions. Despite being highly demanded by knowledgeable consumers, it has been a relatively low profitable activity with a high ecologic impact. In an attempt to correct such situation, while improving the lifestyle of the producers, Venezuela's National Congress recently declared Cocuy a "Natural, Cultural, and Ancestral Heritage" [23]. Nevertheless, little information on its chemical characteristics is available [3,24–29], and only a few attempts have been made for its discrimination among the various localities in which it is produced [3,25,28,29]. With this in mind, Cu, Fe, and Zn concentrations, previously determined in those specimens of 'aguardiente de Cocuy' [24], will be use as indirect indication of their collection sites (Sucre and Urdaneta Municipalities) and of the conditions under which they were manufactured (presence/absence of sugar). Fourteen radial basis neural networks will be developed and evaluated for modeling the relationships between these variables for predicting purposes.

2. Experimental

2.1. Samples

Forty specimens were collected in acid-washed glass bottles from different producers scattered around Sucre Municipality (Falcón State) and Urdaneta Municipality (Lara State). The manufacturing conditions may or may not include the addition of sugar, an aspect also taken into account in the classification process. Table 1 indicates the number of specimens belonging to each of these categories, as well as the average concentrations and concentration intervals of copper, iron, and zinc.

2.2. Radial basis neural network

A RBNN with two active layers, a hidden layer with 39 neurons (number of training patterns) and an output layer with one neuron (category), was employed. The input layer consisted of 1, 2 or 3 nodes, depending on the number of descriptors used in each case (normalized concentrations of Cu, Fe, and Zn). A radial basis function (RBF) was implemented in the hidden layer (also known as the radial basis layer) [30]:

$$\mathrm{RBF} = \exp\left(-\frac{(\|c_i - p_i\| b)^2}{\sigma_\iota}\right) \quad (1)$$

whereby c_i, σ_i are the centroid and width of the i-th radial basis function, respectively; p_i the i-th value of the input vector, and b is the bias. The software estimates the bias for the hidden layer according to (0.8326/SPREAD) [30], whereby the SPREAD value is a non-zero real number. The RBF determines the closeness of an input vector to the training vector, and generates a vector of probabilities as output. The output, or competitive, layer determines the maximum of this probability vector, assigning a one to the largest element of the probability vector and a zero to the rest of them, thus indicating the belonging of such a vector to a given category.

2.3. Procedure

The data matrix consisted of 40 input vectors (number of specimens). The input data was normalized according to Eq. (2):

$$(X_{ij})_{\mathrm{N}} = \frac{(X_{ij})}{(X_j)_{\max}} \quad (2)$$

whereby $(X_{\mathrm{ij}})_{\mathrm{N}}$ and (X_{ij}) correspond to the i-th normalized and raw concentrations of the j-th element; and $(X_{\mathrm{ij}})_{\max}$ is the maximum concentration of the j-th element. The output was simply coded with a number from 1 to 4, depending upon the categories involved in each case.

Training and validation were conducted by means of the so-called "leave-one-out" procedure, by which $\mathrm{N}-1$ patterns are employed in the training session, whereas the remaining one is left out for validation purposes. The process is repeated until all patterns have been iteratively presented to the neural networks. The performance of the radial basis neural network models was

Table 1
Average concentrations and concentration intervals for zinc, copper, and iron in 'aguardiente de Cocuy' samples from Sucre Municipality (Falcón state) and Urdaneta Municipality (Lara state), discriminated according to their provenance and the presence/absence of sugar during their manufacture

Element	Sucre Municipality (Falcón state)[a,b]			Urdaneta Municipality (Lara state)[a,b]		
	Global ($N=22$)	Without sugar ($N=12$)	With sugar ($N=10$)	Global ($N=18$)	Without sugar ($N=12$)	With sugar ($N=6$)
Zinc	0.50 ± 0.43a (0.03–1.00)	0.12 ± 0.05b (0.03–0.17)	0.97 ± 0.04b (0.89–1.00)	0.20 ± 0.19a (0.02–0.65)	0.23 ± 0.21 (0.02–0.65)	0.13 ± 0.02 (0.03–0.38)
Copper	29.54 ± 20.33c (6.11–85.69)	28.03 ± 27.99 (6.12–85.69)	31.36 ± 0.67 (30.64–33.13)	14.94 ± 12.50c (4.48–58.46)	14.63 ± 14.69 (4.49–58.46)	15.58 ± 0.07 (7.82–26.12)
Iron	(0.18–0.51)	0.32 ± 0.07d (0.27–0.51)	0.26 ± 0.06d (0.18–0.36)	0.35 ± 0.15 (0.12–0.59)	0.36 ± 0.13 (0.20–0.55)	0.33 ± 0.01 (0.12–0.59)

[a] Reported values correspond to the average concentration ± standard deviation (mg L^{-1}). The minimum and maximum values of the concentration intervals are presented in parenthesis.
[b] Equal letters indicate statistically significant differences at $p = 0.05$.

assessed by calculating the estimation and prediction percentage accuracy, i.e., the percentage of correct classifications with the training and testing data sets, respectively.

3. Results and discussions

3.1. Evaluation of Cu, Fe, and Zn concentrations in 'aguardiente de Cocuy' samples

The results presented in Table 1 have been previously discussed in detail elsewhere [3]. However, a few aspects are worthy of been highlighted. The most attractive features are the elevated dispersion of the data, and the high concentrations of copper, a recurrent fact in the few investigations conducted on this beverage [24–26,29]. Such high concentrations result from the leaching of this element from the copper coils employed as part of the homemade stills. Copper concentrations are an average of *ca*. six times higher than the maximum permissible concentration (MPC: 4 mg L^{-1}) in the Venezuelan Norm corresponding to 'Cocuy Pecayero' [31], a similar beverage elaborated in the region of Pecaya (Falcón State, Venezuela). Iron concentrations are approximately one order of magnitude lower that the MPC established in the same Norm (2 mg L^{-1}) [31]. No legislation exists on zinc's MPC either for Cocuy or for any other alcoholic beverage in Venezuela. In a previous article [3], it was deemed that iron and zinc could also be leached from the copper coil. However, a comparison of the concentrations of these elements with those present in other alcoholic beverages suggests that the possibility of these elements arising from the raw material should not be discarded.

3.2. Discrimination of 'aguardiente de cocuy' specimens on a conventional basis

Principal component analysis (PCA) is one of the tools most frequently employed for a first analysis of the data's internal structure. However, it was deemed unnecessary to resort to such tool in our study due to the small number of variables available. Instead, a simpler approach was applied, which consisted of a scatter plot of the specimens in a three-dimensional space defined by the normalized concentrations of the analytes (see Fig. 1).

Various interesting features can be observed in Fig. 1. First, there are two "apparent" groups, the larger one consisting of specimens belonging to both Falcón and Lara States, whereas the smaller one comprises only specimens from Falcón State (Sucre Municipality). Even more, the smaller group is completely homogeneous, corresponding to such specimens for which sugar was added during their manufacture. Second, sugar's addition seems to contribute to the separation of the specimens collected within Falcón State. Observe that each group occupies different regions in the space, albeit the group to which no sugar was added shows a higher dispersion. The same is not true for those specimens gathered in Lara State. The latter is not surprising as the concentrations of zinc and iron in the specimens sampled in Falcón State were statistically different (see Table 1).

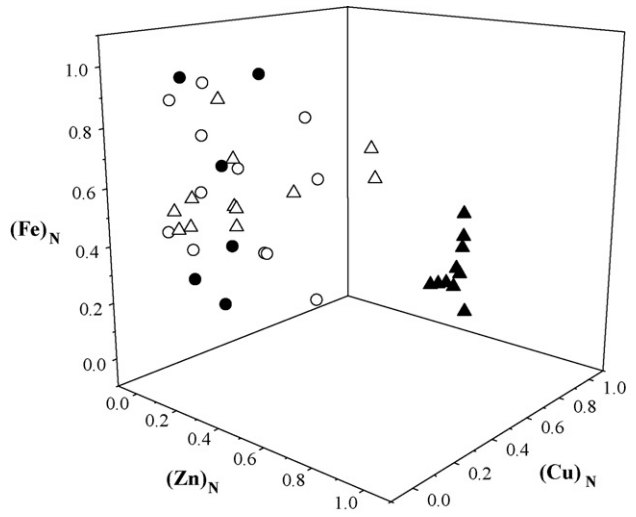


Fig. 1. Three-dimensional scatter plot of 'aguardiente de Cocuy' specimens represented in the space defined by Cu, Fe, and Zn normalized concentrations. (△▲) Sucre Municipality (Falcón state); (◯●) Urdaneta Municipality (Lara state). The white and black symbols indicate the absence and presence of sugar during the manufacturing process.

A cluster analysis was also conducted on the data summarized in Table 1. The resulting dendogram, shown in Fig. 2, was obtained by Ward's method for cluster amalgamation and Pearson's distance for linkage. Unlike the preceding figure, the dendogram can be studied quantitatively, thus adding a deeper dimension to the analysis. Two groups can be clearly distinguished at a similarity level of −213.34 (discontinuous line). Nevertheless, such groups, and particularly Group 1, are very heterogeneous. On this regards, 94.4% of the specimens (17/18) gathered in Urdaneta Municipality lie within Group 1; however, 40.9% of the specimens (9/13) within the same group were collected in Sucre Municipality. Quite contrarily, 92.9% of Group 2's specimens (13/14) belong to Sucre Municipality.

Four groups (labeled a–d) can be observed at a similarity level of 17.80 (dotted lines). In this case, the groups at the left side of the dendogram are more heterogeneous than those on the right side are. Effectively, 56.2% of the specimens in Group (a) were collected in Urdaneta Municipality, whereas the remaining 45.8% were gathered in Sucre Municipality. Group (b) is predominantly constituted by specimens from Urdaneta Municipality (80%), while the opposite is true for Group (c), which is conformed by 75% of specimens from Sucre Municipality. Finally, Group (d) is formed exclusively by specimens from Sucre Municipality. The latter Group, in fact, is the one forming a separate cluster in Fig. 1.

It is clear from the analysis of Figs. 1 and 2, that the application of conventional chemometric techniques may not discriminate the specimens under study, at least with the data gathered so far (copper, iron, and zinc's concentrations). In fact, a previous study in which linear and quadratic discriminant analysis were employed for discrimination purposes, the percentage of correct classifications was barely 50 and 72.5%, respectively [24]. Therefore, tools with higher discriminating power are required for classification of these specimens. There are various mathematic contraptions available, artificial neural networks being but one of them. In the section that follows, radial basis neural networks will be evaluated in the discrimination of these alcoholic beverages. Formerly, a neural network trained with the more popular backpropagation algorithm was used with the same purpose [3], the performance of which will be presented for comparison purposes.

3.3. Discrimination of 'aguardiente de Cocuy' specimens using artificial neural networks

Fourteen radial basis neural networks were developed and evaluated, each one comprising a different combination of inputs (normalized concentrations) and outputs (categories). Unlike the approach followed in a previous article [3], it was deemed interesting to assess the impact of the input's and output's characteristics on the performance of the RBNNs. On this regards, the input's nodes were varied from 1 to 3 (number of normalized concentrations introduced in each case); whereas the output neuron was set to either four categories (Municipality where the

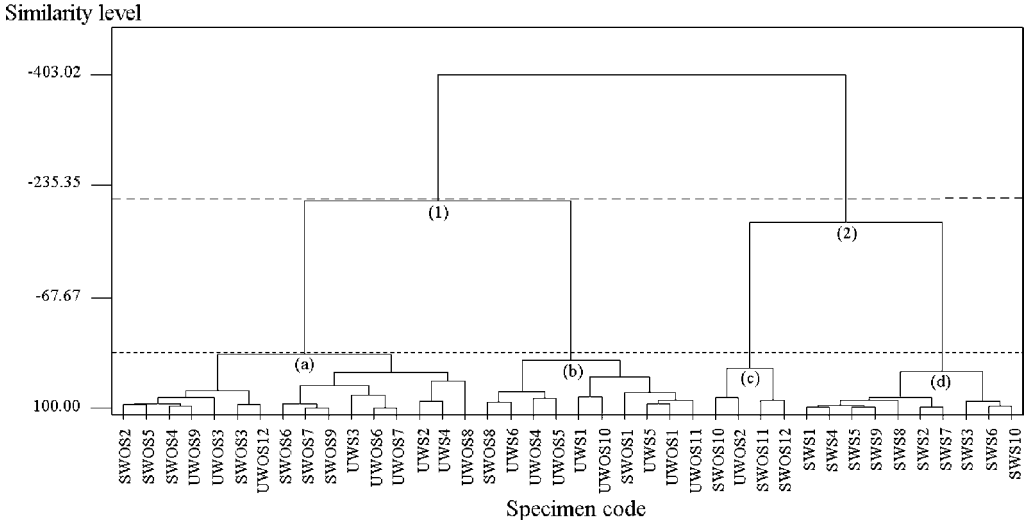


Fig. 2. Dendogram of 'aguardiente de Cocuy' specimens using Cu, Fe, and Zn normalized concentrations as variables.

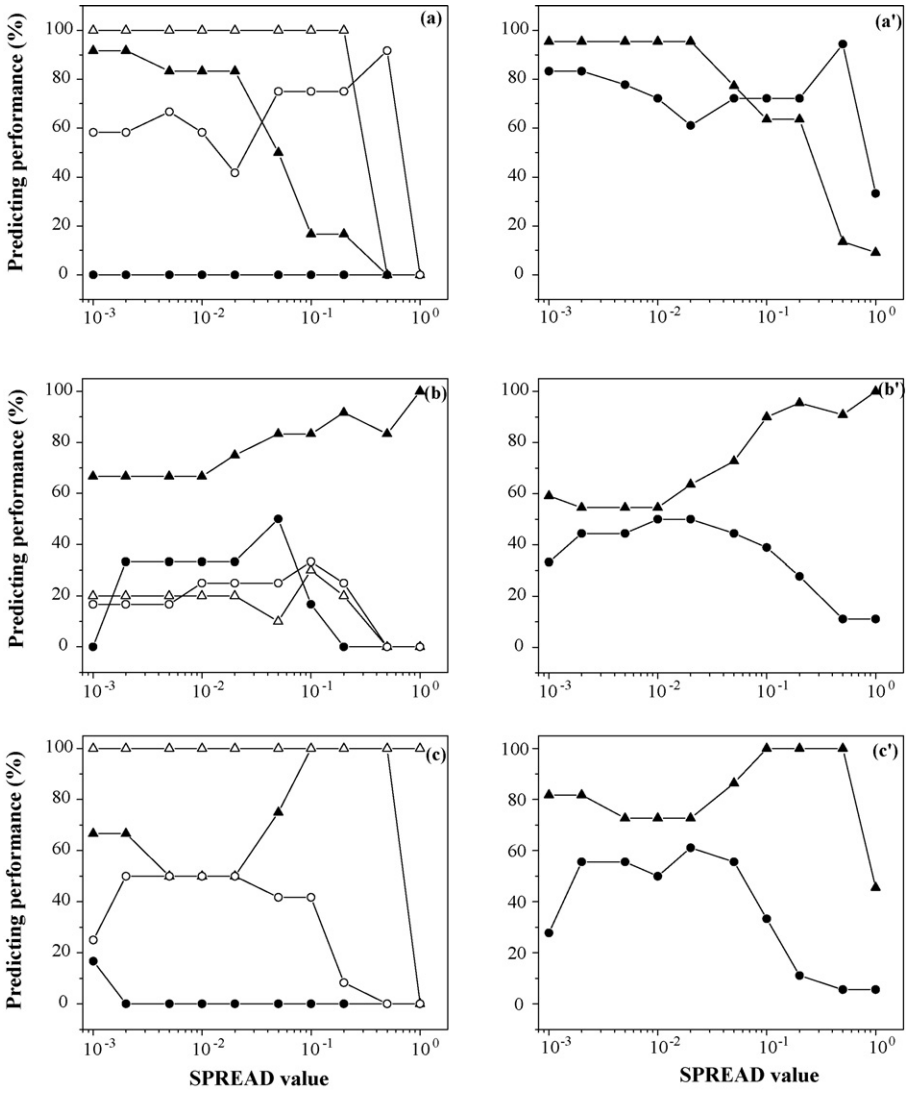


Fig. 3. Variation of the predicting performance of (a and a′) Cu, (b and b′) Fe, and (c and c′) Zn single-input radial basis neural networks as a function of the SPREAD value. (a,b, and c) Four-category output: (▲) Sucre without sugar; (△) Sucre with sugar; (●) Urdaneta without sugar; (◯) Urdaneta with sugar. (a′,b′, and c′) Two-category output: (▲) Sucre municipality, and (●) Urdaneta municipality.

specimens were collected + presence/absence of sugar) or two categories (Municipality where the specimens were collected).

Figs. 3–5 show the variation of the predicting performance (number of correct hits with the validation set) of the resulting 14 RBNNs, as a function of the SPREAD value. Clearly, each neural network presents a particular trend, yet some aspects are worthy of a detailed discussion. In general, the specimens collected in Sucre Municipality were assigned with a higher degree of accuracy than those collected in Urdaneta Municipality. In addition, the classification performance tended to be more stable, and even improved in some cases, over a wider SPREAD range in the case of the specimens sampled in the former place. The latter observation, however, holds true only for the two-category neural networks, but not when the number of categories was increased to four. In these cases, the predicting performance tended to be even erratic sometimes, which suggests that the indirect descriptors of origin (normalized concentrations) are more strongly related to the collection site (Municipality) than to the variations in the manufacturing process (presence/absence of sugar).The highest predictive classification performances of the RBNNs are recorded in Tables 2 and 3. The classification capacity of the RBNNs could be arranged in the following order of decreasing overall performance, depending upon the number of categories selected as outputs:

- Four categories:
  (Cu–Fe) > (Cu–Zn) > (Cu) > (Zn) > (Fe–Zn) > (Cu–Fe–Zn) > (Fe)
- Two categories:
  (Cu) > (Cu–Fe) > (Cu–Zn) > (Fe–Zn) > (Zn) ≈ (Cu–Fe–Zn) >(Fe)

where the input vector (normalized concentration) is indicated in parentheses for each RBNN.

The predicting performance of the two-category RBNNs was 5–22.5% higher than the performance of the corresponding four-category counterparts. It is interesting to notice that those RBNNs for which the normalized concentration of copper was

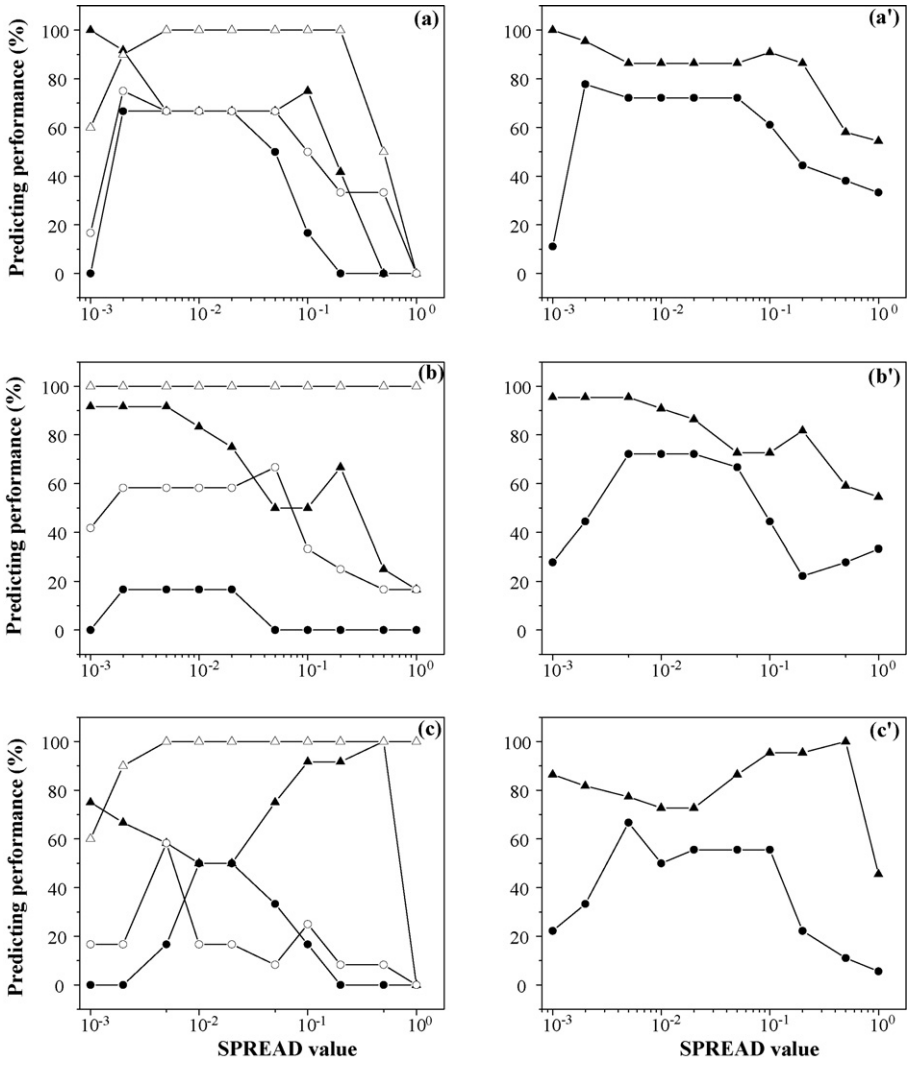


Fig. 4. Variation of the predicting performance of (a and a′) Cu–Fe, (b and b′) Cu–Zn, and (c and c′) Zn–Fe two-input radial basis neural networks as a function of the SPREAD value. (a,b, and c) Four-category output: (▲) Sucre without sugar; (△) Sucre with sugar; (●) Urdaneta without sugar; (◯) Urdaneta with sugar. (a′,b′, and c′) Two-category output: (▲) Sucre municipality, and (●) Urdaneta municipality.

used as input, either alone or in combination with one more element (binary combinations), were the ones showing the best performances. In fact, the two-category (Cu)–RBNN showed the best overall performance of all the networks evaluated (90% correct hits). An opposite trend was observed with zinc's and iron's normalized concentrations which, either individually or paired with each other, are the worst descriptors. Surprisingly enough, the three-input RBNN was among the networks with

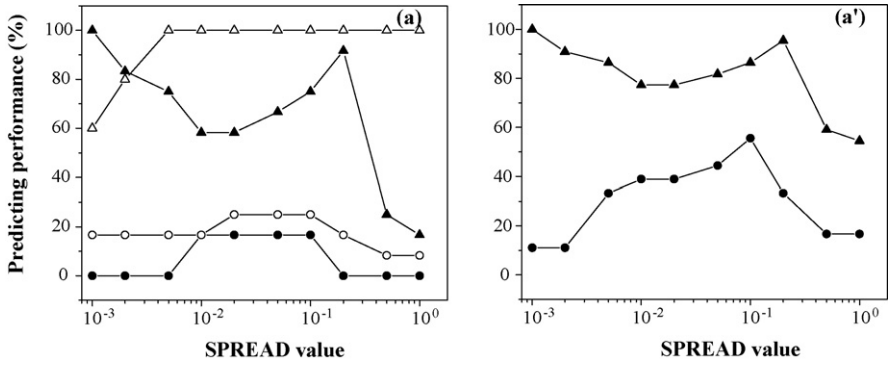


Fig. 5. Variation of the predicting performance of Cu–Fe–Zn three-input radial basis neural networks as a function of the SPREAD value. (a) Four-category output: (▲) Sucre without sugar; (△) Sucre with sugar; (●) Urdaneta without sugar; (◯) Urdaneta with sugar. (a′) Two-category output: (▲) Sucre municipality, and (●) Urdaneta municipality.

Table 2
Discrimination performance of artificial neural networks with one, two, and three input nodes, based on the four-category output[a]

Category[b]	One-input neural networks			Two-input neural networks			Three-input neural networks	
	Cu[c] (0.001)	Fe[c] (0.1)	Zn[c] (0.1)	Cu–Fe[c] (0.002)	Cu–Zn[c] (0.002/0.005)	Fe–Zn[c] (0.005)	RBNN[c] (0.1)	BPNN[d]
SWOS	91.7	83.3	100	91.7	91.7	58.3	75.0	100
SWS	100	30.0	100	90.0	100	100	100	100
UWOS	0.0	16.7	0.0	66.7	16.7	16.7	16.7	83.3
UWS	58.3	33.3	41.7	75.0	58.3	58.3	25.0	100
Overall	70.0	45.0	67.5	82.5	72.5	62.5	57.5	97.1

[a] Discrimination performance (%) achieved with the prediction set only.
[b] The code indicates the provenance of the sample and whether sugar was added during their manufacture. SWOS: Sucre without sugar; SWS: Sucre with sugar; UWOS: Urdaneta without sugar; UWS: Urdaneta with sugar.
[c] Radial basis neural networks. The input vector is indicated in each case, as well as the optimum SPREAD value (in parentheses).
[d] Backpropagation neural network (results taken from Ref. [3]).

Table 3
Discrimination performance of radial basis neural networks with one, two, and three input nodes, based on the two-category output[a]

Category[b]	One-input neural networks			Two-input neural networks			Three-input neural networks	
	Cu[c] (0.001)	Fe[c] (0.1)	Zn[c] (0.05)	Cu–Fe[c] (0.002)	Cu–Zn[c] (0.005)	Fe–Zn[c] (0.1)	RBNN[c] (0.1)	BPNN[d]
Sucre	95.5	90.9	86.4	95.5	95.5	95.5	86.4	100
Urdaneta	83.3	38.9	55.6	77.8	72.2	55.6	55.6	93.8
Overall	90.0	67.5	72.5	87.5	85.5	77.5	72.5	97.1

[a] Discrimination performance (%) achieved with the prediction set only.
[b] The code indicates the provenance of the sample and whether sugar was added during their manufacture. SWOS: Sucre without sugar; SWS: Sucre with sugar; UWOS: Urdaneta without sugar; UWS: Urdaneta with sugar.
[c] Radial basis neural networks. The input vector is indicated in each case, as well as the optimum SPREAD value (in parentheses).
[d] Backpropagation neural network (unpublished results estimated from formerly collected data).

the lowest predicting performances, even though a significant improvement was recorded when the number of categories was reduced from four to only two.

The fact that excellent results were achieved in our case with a single-element neural network such as the two-category (Cu)–RBNN, is particularly interesting for two reasons. In the first place, the predicting performance is comparable to those reported in other publications in which the number of descriptors (elements' concentrations) has been significantly higher [4–14]. In the second place, it is worth highlighting the fact that conducting a discrimination of specimens of 'aguardiente de Cocuy' on the basis of a single-element measurement redounds in an significant reduction of analysis' costs and response times, which is favorable to both producers and laboratory analysts involved in the manufacturing/quality assurance processes of such a spirituous beverage.

An aspect deserving further discussion is related to the difference in performance of the RBNNs, when compared to that shown by a backpropagation neural network (BPNN) developed in a previous article [3], the predicting percentage of which is also presented in Tables 2 and 3. The fact that the BPNN shows a consistently higher performance, indistinctly of the number of categories designated as outputs, may lead to the false conclusion of its superior discriminating power. However, it was serendipitously found that the training/validation approach played an important role on this matter. Effectively, the first sessions were conducted using the conventional practice of randomly splitting the data into training and prediction sets (a validation set is not required in this case). Under these circumstances, three RBNNs showed overall predicting performances equal to or higher than those reported for the BPNN: Cu–Fe–RBNN (97.1%), Cu–Fe–Zn–RBNN (97.1%), and Cu–Zn–RBNN (100%). However, the validity of the split-data set approach was subjected to some critiquing, which led us to adopt the "leave-one-out" method for the development and evaluation of the neural networks. The latter approach resulted in predicting performances that were slightly lower, an observation also made by other workers [6], but which may be better reflections of the true discriminating powers of the neural networks. Therefore, the results presented in Tables 2 and 3 are an artifact, a product of the training/validation method, and by no means should they be taken as evidence of the BPNN "superior" performance.

4. Conclusions

Radial basis neural networks are fast and effective tools for discrimination purposes. The most attractive feature of RBNNs is that they can be developed in a fraction of the time required to train their backpropagation counterpart. Of the fourteen networks developed and evaluated in the present work, the Cu–RBNN showed the highest predicting performance. Such neural network was able to predict, with an overall accuracy of 90%, the municipalities where the forty specimens of the Venezuelan spirituous beverage known as 'aguardiente de Cocuy' were sampled. The fact that a single-element RBNN could render such results is particularly appealing, because the latter translates into reduced analysis costs and shorter labora-

tory response times, which benefits both laboratory analysts and beverage producers.

Acknowledgement

The authors publicly thank the anonymous reviewer who suggested the change in the training/validation approach, for which it allowed us to see an aspect of working with artificial neural networks that would have passed unperceived otherwise.

References

[1] K.A. Anderson, B.W. Smith, J. Agric. Food Chem. 50 (2002) 2068.
[2] S. Frías, J.E. Conde, J.J. Rodríguez-Bencomo, F. García-Montelongo, J.P. Pérez-Trujillo, Talanta 59 (2003) 335.
[3] E.A. Hernández-Caraballo, R.M. Ávila-Gómez, T. Capote, F. Rivas, A.G. Pérez, Talanta 60 (2003) 1259.
[4] D. Bellido-Milla, J.M. Moreno-Perez, M.P. Hernández-Artiga, Spectrochim, Acta Part B 55 (2000) 855.
[5] A. Alcázar, F. Pablos, Ma. Jesús Martín, A. Gustavo, González, Talanta 57 (2002) 45.
[6] A.M. Cameán, I. Moreno, M. López-Artíguez, M. Repetto, A.G. González, Talanta 54 (2001) 53.
[7] Z. Murányi, Z. Kovács, Microchem. J. 67 (2000) 91.
[8] S. Rebolo, R.M. Peña, M.J. Latorre, S. García, A.M. Botana, C. Herrero, Anal. Chim. Acta 417 (2000) 211.
[9] S. Pérez-Magariño, M. Ortega-Heras, M.L. González-San José, Anal. Chim. Acta 458 (2002) 187.
[10] M. Barbaste, B. Medina, L. Sarabia, M.C. Ortiz, J.P. Pérez-Trujillo, Anal. Chim. Acta 472 (2002) 161.
[11] A. Jos, I. Moreno, A.G. González, G. Repetto, A.M. Cameán, Talanta 63 (2004) 377.
[12] S. Pérez-Magariño, M. Ortega-Heras, M.L. González-San José, Z. Boger, Talanta 62 (2004) 983.
[13] J.M. Jurado, A. Alcázar, F. Pablos, M.J. Martín, A.G. González, Talanta 66 (2005) 1350.
[14] A.P. Fernandes, M.C. Santos, S.G. Lemos, M.M.C. Ferreira, A.R.A. Nogueira, J.A. Nóbrega, Spectrochim, Acta Part B 60 (2005) 717.
[15] N.K. Bose, P. Liang, Multilayer networks, in: Neural Network Fundamentals with Graphs, Algorithms and Applications, McGraw-Hill, Inc., USA, 1996, Chapter 5, pp. 204–209.
[16] P.H. Fidêncio, I. Ruisánchez, R.J. Poppi, Analyst 126 (2001) 2194.
[17] P.H. Fidêncio, R.J. Poppi, J.C. de Andrade, Anal. Chim. Acta 453 (2002) 125.
[18] F.R. Jack, G.M. Steele, Food Qual. Prefer. 13 (2002) 163.
[19] R. Dutta, E.L. Hines, J.W. Gardner, D.D. Udrea, P. Boilot, Meas. Sci. Tecnol. 14 (2003) 190.
[20] J. Lozano, J.P. Santos, I. Sayago, J. Gutierrez, M.C. Horrillo, Proc. IEEE 24–27 (2004) 345–348.
[21] V. Dixit, J.C. Tewari, B.K. Cho, J.M.K. Irudayaraj, Appl. Spectrosc. 59 (2005) 1553.
[22] P. Ciosek, T. Sobanski, E. Augustymak, W. Wróblewski, Meas. Sci. Tecnol. 17 (2006) 6.
[23] Gaceta Oficial de la República Bolivariana de Venezuela, Acuerdo con motivo de declarar al AGAVE COCUI y sus productos y derivados artesanales, Patrimonio Natural, Ancestral y Cultural de la Nación, 38.325, pp. 343.060–343.061, 2005 (In Spanish).
[24] T. Capote, L.M. Marcó, J. Alvarado, E.D. Greaves, Spectrochim. Acta Part B 54 (1999) 1463.
[25] E.M. Garrido de Dávila, Cocuy from Urdaneta Municipality: Manufacture and Physical-Chemical Characteristics, Universidad Centroccidental Lisandro Alvarado, Barquisimeto, Venezuela, 2001, (In Spanish, unpublished results).
[26] G.J.L. Ventura, Characterization of the artisan manufacturing process of Cocuy Pecayero, Undergraduate work, Universidad Nacional Experimental Francisco de Miranda, Punto Fijo, Venezuela, 2001 (In Spanish, unpublished results).
[27] Y. Petit de Peña, B. Paredes, W. Rondón, M. Burguera, J.L. Burguera, C. Rondón, P. Carrero, T. Capote, Talanta 64 (2004) 1351.
[28] T. Capote, L.M. Marcó, E. Garrido, E. Hernández, E. Greaves, Memories of the V Venezuelan Chemistry Congress, April 1–5, Maracaibo, Venezuela, 2001, pp. 765–767 (In Spanish, with English Abstract).
[29] T.J. Capote Luna, Applications of Total Reflection X-ray Fluorescence to the Analysis of Alcoholic Beverages, PhD. Thesis, Universidad Simón Bolívar, Caracas, Venezuela, 2004 (In Spanish, unpublished results).
[30] H. Demuth, M. Beale, Neural Network Toolbox for use with MATLAB, User's Guide Version 4, pp 7-1–7-20 2000.
[31] Comisión Venezolana de Normas Industriales, Cocuy Pecayero, Norma Venezolana 3662:2001, FONDONORMA, Venezuela, 2001 (In Spanish).

Available online at www.sciencedirect.com
ScienceDirect
Talanta 74 (2008) 1008–1013
Talanta
www.elsevier.com/locate/talanta

Potentiometric determination of aqueous dissociation constants of flavonols sparingly soluble in water

José M. Herrero-Martínez, Carme Repollés, Elisabeth Bosch, Martí Rosés, Clara Ràfols *

Departament de Química Analítica, Universitat de Barcelona, Martí i Franqués, 08028 Barcelona, Spain

Received 20 March 2007; received in revised form 30 July 2007; accepted 9 August 2007
Available online 15 August 2007

Abstract

Two different approaches were evaluated and used to estimate the aqueous pK_a values of some flavonols sparingly soluble in water (morin, fisetin and quercetin) from their pK_a values in methanol/water mixtures obtained by potentiometry. Both approaches lead to similar results, although one of them requires only one pK_a value at one unique methanol/water mixture, whereas the other (the classical Yasuda–Shedlovsky plot) requires several pK_a data at different methanol/water mixtures. Thus, the first approach is recommended because it is faster and simpler. The automated potentiometric method is strongly recommended for pK_a determination of these types of compounds because of its simplicity and speed of operation.
© 2007 Elsevier B.V. All rights reserved.

Keywords: Flavonols; Dissociation constant; Potentiometry; Methanol/water mixtures

1. Introduction

The acidic dissociation constant, pK_a, is an important parameter in ADMET (absorption, distribution, metabolism, excretion, toxicity) research because it helps to explain chemical phenomena such as absorption, distribution and elimination of substances. Potentiometry [1], spectrophotometry [2] and capillary electrophoresis (CE) [3,4] are well-established current methods for pK_a determination of compounds of pharmaceutical or biological interest. Potentiometry and spectrophotometry require purity and stability of the sample. Potentiometry is a more general method because it does not require the presence of a chromophore, although the compound must be soluble enough in water. When the compounds are sparingly soluble in water, the pK_a determination is commonly done in organic/water mixtures and the obtained pK_a value extrapolated to the aqueous one. Methanol/water mixtures [5–8] are often used because they have a lower polarity than pure water, but keeping a similar environment. CE methods do not require high purity of solute since CE is a separation technique. The pK_a of compounds insoluble in water can be determined by dissolving the sample in an organic solvent (e.g. methanol), which is directly injected into the aqueous buffer inside the capillary. However, it is an open question whether the pK_a value obtained is in pure water or in an aqueous solvent that may contain a small but unknown amount of organic solvent from the sampling solvent. The disadvantage of CE methods as compared with automated potentiometric titration methods is that they are not yet fully automated and since they require the preparation of several buffers the total time spent in the determination of several consecutive pK_a values can be quite high.

The aqueous pK_a determination of most compounds with a pK_a value between 4 and 10 is usually straightforward, but when the compound has very low or very high pK_a or it shows several and close pK_a values the determination of pK_a may be much more complex. This is the case of flavonoids. These compounds are polyphenols and because of their strong antioxidant activity they play an important role in human diet [9,10]. They show a variety of pharmacological activities, including anticancer, antiinflamatory, antibacterial, anti-allergic, and antiviral activity and reduce the risk of coronary heart disease [9]. There are also reports of flavonoids inhibiting the activities of an array enzymes, including lipoxygenase, cyclooxygenase and DADH-oxidase. The inhibition of the enzymes by flavonoids could be due to a reaction of the flavonoid with free radical generated at the active site of the enzymes [11]. The role of flavonoids is

* Corresponding author. Tel.: +34 934034874; fax: +34 934021233.
E-mail address: crafols@ub.edu (C. Ràfols).

0039-9140/$ – see front matter © 2007 Elsevier B.V. All rights reserved.
doi:10.1016/j.talanta.2007.08.007

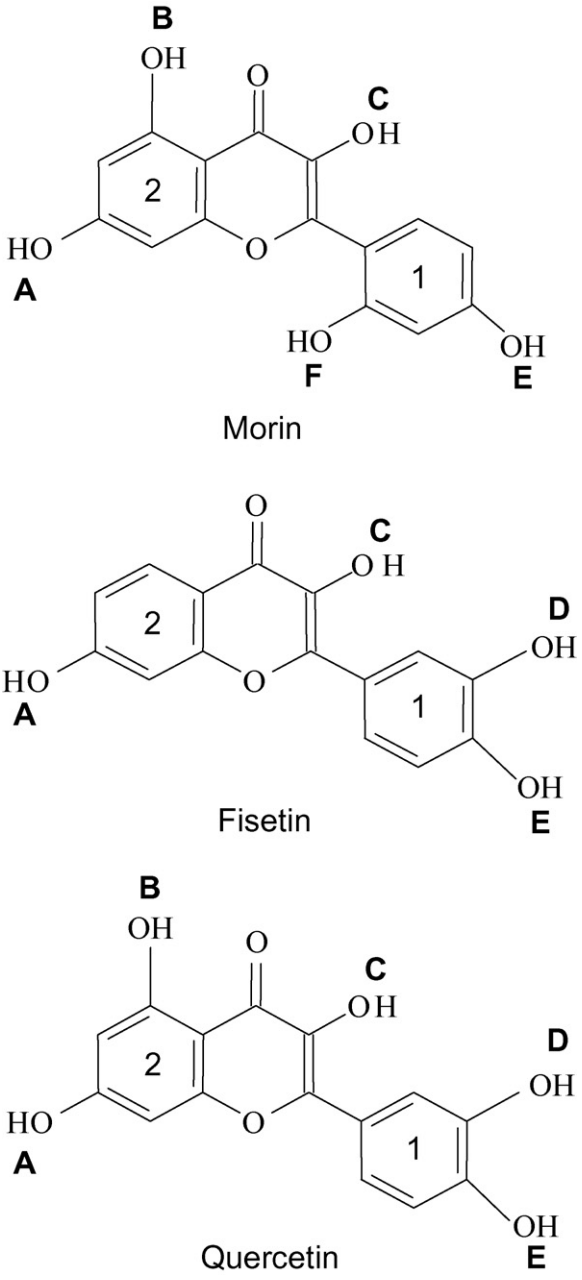


Fig. 1. Molecular structures of the studied flavonols.

related to their chemical structure, for instance their antioxidant efficiency is related to their hydrogen radical donating abilities and to the number of hydroxyl groups in the molecule [11–14]. The hydroxyl moiety deprotonation has influence in the intrinsic antioxidant potential of the flavonoid, deprotonation generally enhances the antioxidant action of the flavonoid [14], thus the knowledge of their physicochemical parameters, such as pK_a, is important to predict their antioxidant capacity. In addition, the pK_a values determine the precise species present in a biological medium and their knowledge is fundamental in bioclinical and pharmacological research studies.

Flavonols are one class of flavonoids and the basic structure of these compounds are given in Fig. 1. They present several ionisable hydroxyl groups with pK_a values higher than 7 and relatively close one to each other. Moreover, most of them are sparingly soluble in water and, consequently, accurate aqueous pK_a determination is not an easy task. There are a few pK_a values of these compounds reported in the literature, but they show a great disparity. In fact, some of them are determined in mixtures of water with an organic solvent [4,15–24].

The aim of this work is the pK_a determination of flavonols by potentiometry in order to establish and test procedures for the accurate determination of dissociation constants of compounds with several high pK_a values and sparingly soluble in water. Two procedures are used to estimate the aqueous pK_a values from the pK_a values determined in methanol/water mixtures. Yasuda–Shedlovsky equation relates the pK_a values determined in methanol/water systems, ${}^{s}_{s}\mathrm{p}K_a$, with the reverse of the dielectric permittivity of the binary solvent. This extrapolation method involves the determination of ${}^{s}_{s}\mathrm{p}K_a$ in at least three or four methanol/water mixtures with a percentage of methanol lower than 60% in weight [5,6,25]. The other estimation equation used, is the linear correlation we proposed [8,26]. This equation allows the estimation of aqueous pK_a values, ${}^{w}_{w}\mathrm{p}K_a$, from the ${}^{s}_{s}\mathrm{p}K_a$ values in only one methanol/water mixture and works for any percentage of methanol. The extrapolated values are compared with those obtained by CE in a previous work [4], as well as with a few ones that can be directly obtained in water.

2. Experimental

2.1. Reagents and chemicals

Methanol (Merck for chromatography) and water purified by Milli-Q plus system from Millipore were used to prepare the solvent mixture. Hydrochloric acid (p.a. 25%, w/w) and potassium chloride (AR grade) were purchased from Merck and potassium hydroxide (1 M titrisol) from Carlo Erba.

Quercetin dihydrate were purchased from Fluka (Buchs, Switzerland), fisetin from Sigma (St Louis, MO, USA) and morin from Riedel de Haën (Seelze, Germany).

2.2. Apparatus and procedure

All titrations were carried out by means of an automatic titrator PCA 101 instrument (Sirius Analytical Instruments, East Sussex, England) equipped with a Sirius 010604 combined electrode. The electrode system was standardized according to the specifications of literature [5]. About 0.01 or 0.005 g of flavonol dissolved in 15 ml of water or methanol/water mixture (methanol content between 5 and 60% in weight) were preacidified to pH 1.8 with 0.5 M standardized aqueous HCl and titrated with 0.5 M standardized aqueous KOH until pH 12.2. In the case of morin and for aqueous determination, the solution was first basified (pH ≅ 12.2) and titrated with HCl. All titrations were performed in solutions of constant ionic strength (0.15 M KCl) under nitrogen atmosphere at $25 \pm 0.1\,^{\circ}$C.

2.3. Computation

The ${}^{s}_{s}pK_a$ values were obtained using the pK_a LOGP™ software (v5.2, Sirius), where ${}^{s}_{s}pK_a$ refers to the pK_a value in the particular pH scale of the working methanol/water mixture. PCA 101 instrument works at a constant ionic strength, and then the pK_a values obtained were in the molar concentration scale. To obtain the thermodynamic values the activity coefficients of each species must be considered. Debye–Hückel equation was used to compute the activity coefficients:

$$\log \gamma = -\frac{Az^2\sqrt{I}}{1 + a_0 B\sqrt{I}} \quad (1)$$

where γ is the activity coefficient of the involved species, z the ion charge of the ion and I is the ionic strength of the solution. A and B parameters are functions of temperature and dielectric constant of the medium. For aqueous solution at 25 °C, $A = 0.51$ and $B = 0.33$. The a_0 value depends strictly on the solvated radius of the ions but, since this is unknown, the Bates–Guggenheim convention is usually applied [27]. This convention assigns $a_0 = 4.56$ Å for aqueous solutions, and thus $a_0B = 1.5$. A and a_0B parameters for each methanol/water mixture can be calculated from the empirical equations previously reported:

$$A = 0.51 + 0.14w + 2.01w^2 - 3.18w^3 + 2.39w^4 \quad (2)$$

$$a_0B = 1.50 + 0.19w + 0.74w^2 - 1.04w^3 + 0.67w^4 \quad (3)$$

where w is the weight fraction in methanol [8].

The software of PCA 101 includes the Yasuda–Shedlovsky extrapolation equation to estimate aqueous pK_a values (${}^{w}_{w}pK_a$) from those in methanol/water. It relates ${}^{s}_{s}pK_a$ to the reverse of the dielectric permittivity of the binary solvent by means of the equation:

$${}^{s}_{s}pK_a + \log[H_2O] = \frac{a_\varepsilon}{\varepsilon} + b_\varepsilon \quad (4)$$

where ε is the dielectric permittivity, and a_ε and b_ε are the empirical fitting constants [5,6,7,25,28].

In earlier papers [8,26,29,30] we proposed linear equations such as Eq. (5) for neutral and cationic acids to correlate their pK_a values in methanol/water mixtures (${}^{s}_{s}pK_a$) to the aqueous pK_a (${}^{w}_{w}pK_a$):

$${}^{s}_{s}pK_a = a_w {}^{w}_{w}pK_a + b_w \quad (5)$$

where a_w and b_w are related with the solvent composition. Twenty-eight phenols with literature pK_a data in 6–53 different methanol/water mixtures were analyzed in order to relate a_w and b_w to solvent composition. The following equation were obtained:

$$a_w = \frac{1 - 0.305w - 0.195w^2}{1 - 0.542w + 0.002w^2} \quad (6)$$

$$b_w = \frac{-0.573w + 1.227w^2}{1 + 0.498w - 1.311w^2} \quad (7)$$

where w is the weight fraction of methanol in the binary solvent.

3. Results and discussion

The flavonol compounds shown in Fig. 1 differ in the number and position of the hydroxyl groups attached to the rings, but all of them have more than three ionizable hydroxyl groups. The first pK_a value is higher than 7 except for morin, and the others are relatively close together [4]. Moreover, they are sparingly soluble in water and their pK_a values cannot be directly determined in aqueous solution by potentiometry. Then, several titrations have been carried out at different methanol/water mixtures for the studied flavonols using the automatic PCA101 titrator. The Sirius methodology measures at the physiological ionic strength ($I \cong 0.15$ M) and the pK_a values obtained are referred to this working ionic strength (pK_a ($I = 0.15$ M)). The thermodynamic ones (pK_a ($I = 0$ M)) are obtained from these values and the values of the activity coefficients. Table 1 shows the ${}^{s}_{s}pK_a$ values obtained experimentally at different methanol/water mixtures ${}^{s}_{s}pK_a$ ($I = 0.15$ M) and their corresponding thermodynamic ones (${}^{s}_{s}pK_a$ ($I = 0$ M)). The solvent mixtures with lowest methanol content were 10%, 25% or 40% (in weight) depending on the solubility of the studied flavonol. Morin is the most soluble one and quercetin the most insoluble. We have been able to determine three pK_a values for morin and quercetin and two for fisetin. The third pK_a of fisetin is higher than 12 [15,31] and thus it could not be determined by potentiometry. As expected, the ${}^{s}_{s}pK_a$ ($I = 0.15$ M) of flavonols, like all polyphenols, increases when the percentage of methanol increases [26], except for ${}^{s}_{s}pK_{a1}$ ($I = 0.15$ M) which remains practically constant in all the range of methanol percentages studied. Table 1 also reports the ${}^{w}_{w}pK_a$ ($I = 0$ M) estimated from each methanol/water mixture using Eq. (5). The mean ${}^{w}_{w}pK_a$ ($I = 0$ M) values and its standard deviations are also given. In all cases the standard deviations are lower than 0.11. This fact shows the good agreement in the ${}^{w}_{w}pK_a$ ($I = 0$ M) values estimated from single ${}^{s}_{s}pK_a$ ($I = 0.15$ M) determination at any methanol/water composition.

${}^{w}_{w}pK_a$ ($I = 0.15$ M) values have also been estimated by means of Eq. (4). Fig. 2, shows a straight line in all cases according to the Yasuda–Shedlovsky plots.

Table 2 summarizes the values extrapolated to aqueous solution and corrected to zero ionic strength using Eqs. (4) and (1). Table 2 also shows the ${}^{w}_{w}pK_a$ ($I = 0$ M) estimated by Eq. (5) and those obtained by capillary electrophoresis (CE) [4]. Morin is slightly soluble in neutral and basic aqueous solutions (anionic morin forms), but it is sparingly soluble in acidic aqueous solution (neutral form). Then, potentiometric titrations could be carried out directly in water adding KOH in excess and using HCl as a titrant. The titration curves showed a jump close pH 5 attributed to the poor solubility of the neutral morin and the aqueous pK_{a1} could not be directly determined in water. The ${}^{w}_{w}pK_{a2}$ ($I = 0.15$ M) and ${}^{w}_{w}pK_{a3}$ ($I = 0.15$ M) values obtained were 7.73 ± 0.02 and 9.53 ± 0.04, respectively. The thermodynamic ones were obtained applying activity coefficient correction and they are also presented in Table 2.

For morin, the extrapolations by means of Eq. (4) have been carried out from only 10% in weight of methanol and the ${}^{w}_{w}pK_a$ ($I = 0$ M) values estimated by this equation are in very good agreement with those obtained by Eq. (5). Moreover, the

Table 1
${}^{s}_{s}pK_a$ ($I = 0.15$ M) and ${}^{s}_{s}pK_a$ ($I = 0$ M) of flavonoids at several methanol/water mixtures and pK_a in water (${}^{w}_{w}pK_a$ ($I = 0$ M))

MeOH (wt.%)	${}^{s}_{s}pK_{a1}$ ($I =$ 0.15 M)	${}^{s}_{s}pK_{a2}$ ($I =$ 0.15 M)	${}^{s}_{s}pK_{a3}$ ($I =$ 0.15 M)	${}^{s}_{s}pK_{a1}$ ($I =$ 0 M)	${}^{s}_{s}pK_{a2}$ ($I =$ 0 M)	${}^{s}_{s}pK_{a3}$ ($I =$ 0 M)	${}^{w}_{w}pK_{a1}$ ($I =$ 0 M)	${}^{w}_{w}pK_{a2}$ ($I =$ 0 M)	${}^{w}_{w}pK_{a3}$ ($I =$ 0 M)
Morin									
10.7	4.843 ± 0.014	7.818 ± 0.010	9.556 ± 0.010	5.11	8.35	10.36	5.03	8.20	10.16
16.1	4.709 ± 0.023	7.876 ± 0.016	9.786 ± 0.016	4.99	8.44	10.63	4.87	8.20	10.31
21.1	4.845 ± 0.016	7.919 ± 0.011	9.752 ± 0.012	5.15	8.52	10.65	4.98	8.20	10.24
21.4	4.787 ± 0.021	7.970 ± 0.016	9.825 ± 0.016	5.08	8.56	10.71	4.91	8.24	10.29
31.1	5.024 ± 0.011	8.136 ± 0.009	9.923 ± 0.010	5.36	8.80	10.93	5.08	8.32	10.31
31.9	4.877 ± 0.018	8.055 ± 0.011	9.938 ± 0.012	5.21	8.71	10.93	4.93	8.22	10.29
40.5	5.163 ± 0.021	8.252 ± 0.019	9.905 ± 0.019	5.53	8.99	11.01	5.14	8.34	10.21
41.5	4.895 ± 0.020	8.224 ± 0.015	10.158 ± 0.016	5.27	8.96	11.27	4.89	8.30	10.43
44.9	5.155 ± 0.009	8.322 ± 0.007	10.161 ± 0.008	5.54	9.10	11.32	5.10	8.37	10.41
49.8	5.181 ± 0.010	8.388 ± 0.008	10.241 ± 0.010	5.59	9.20	11.46	5.09	8.39	10.45
52.9	5.100 ± 0.039	8.423 ± 0.027	10.280 ± 0.029	5.51	9.24	11.50	4.97	8.37	10.43
61.0	5.095 ± 0.032	8.484 ± 0.025	10.366 ± 0.032	5.55	9.40	11.73	4.90	8.37	10.49
Mean							4.99 ± 0.09	8.29 ± 0.08	10.33 ± 0.11
Fisetin									
26.6	7.664 ± 0.022	9.169 ± 0.023		7.98	9.74		7.60	9.32	
31.9	7.683 ± 0.019	9.290 ± 0.017		8.01	9.95		7.56	9.37	
37.2	7.734 ± 0.012	9.344 ± 0.012		8.08	10.04		7.55	9.37	
42.5	7.836 ± 0.018	9.402 ± 0.018		8.20	10.13		7.58	9.37	
51.0	7.929 ± 0.007	9.437 ± 0.007		8.34	10.25		7.58	9.33	
52.9	7.891 ± 0.009	9.423 ± 0.010		8.30	10.24		7.51	9.28	
56.4	8.049 ± 0.013	9.577 ± 0.018		8.48	10.44		7.63	9.40	
58.1	8.030 ± 0.021	9.544 ± 0.021		8.46	10.41		7.58	9.34	
58.2	8.005 ± 0.013	9.514 ± 0.015		8.44	10.38		7.55	9.31	
58.2	8.015 ± 0.010	9.509 ± 0.011		8.45	10.37		7.56	9.31	
63.6	8.067 ± 0.031	9.643 ± 0.035		8.53	10.56		7.54	9.38	
Mean							7.57 ± 0.03	9.34 ± 0.04	
Quercetin									
31.9	7.734 ± 0.013	9.242 ± 0.013	–	8.06	9.90	–	7.61	9.33	–
37.1	7.728 ± 0.013	9.231 ± 0.013	–	8.08	9.93	–	7.54	9.26	–
39.1	7.870 ± 0.004	9.346 ± 0.004	11.197 ± 0.013	8.24	10.08	12.29	7.66	9.37	11.42
39.4	7.857 ± 0.005	9.299 ± 0.005	11.246 ± 0.011	8.22	10.03	12.34	7.65	9.32	11.46
40.6	7.813 ± 0.006	9.320 ± 0.007	11.262 ± 0.019	8.18	10.06	12.37	7.59	9.33	11.47
43.6	7.929 ± 0.003	9.382 ± 0.003	11.361 ± 0.014	8.31	10.15	12.50	7.67	9.36	11.53
44.0	7.861 ± 0.006	9.329 ± 0.006	11.242 ± 0.015	8.25	10.10	12.39	7.60	9.30	11.42
47.9	7.968 ± 0.015	9.464 ± 0.015	11.548 ± 0.098	8.37	10.26	12.74	7.65	9.39	11.66
49.0	7.925 ± 0.003	9.406 ± 0.003	11.429 ± 0.010	8.33	10.21	12.64	7.60	9.32	11.54
49.9	7.873 ± 0.013	9.369 ± 0.013	11.399 ± 0.013	8.28	10.18	12.62	7.54	9.28	11.51
52.2	8.022 ± 0.005	9.479 ± 0.005	11.533 ± 0.041	8.44	10.32	12.79	7.65	9.36	11.62
52.5	8.030 ± 0.004	9.514 ± 0.004	11.489 ± 0.026	8.45	10.35	12.74	7.66	9.39	11.57
54.5	7.964 ± 0.013	9.542 ± 0.013	11.649 ± 0.013	8.39	10.39	12.93	7.57	9.39	11.70
59.1	8.091 ± 0.005	9.575 ± 0.005	11.708 ± 0.042	8.54	10.47	13.05	7.63	9.38	11.72
59.7	8.069 ± 0.010	9.588 ± 0.024	11.643 ± 0.072	8.52	10.49	13.00	7.60	9.39	11.66
60.6	8.020 ± 0.007	9.519 ± 0.008	11.626 ± 0.032	8.47	10.43	12.99	7.55	9.39	11.63
Mean							7.59 ± 0.06	9.33 ± 0.04	11.56 ± 0.10

estimated ${}^{w}_{w}pK_{a2}$ ($I = 0$ M) and ${}^{w}_{w}pK_{a3}$ ($I = 0$ M) values agree with those directly obtained in water, but they are slightly lower than the ones obtained by CE. The differences found with the two techniques could be attributed to the difficulties in determining pK_a values very close together or to the presence of some residual methanol from the sampling solvent in the CE determination. For ${}^{w}_{w}pK_{a1}$ ($I = 0$ M), which differs by more than 3 units from the ${}^{w}_{w}pK_{a2}$ ($I = 0$ M), the values estimated by potentiometry are consistent with the ones obtained by CE. This value is lower than the ones obtained for fisetin and quercetin. In general, the most acidic group of flavonols corresponds to the OH group in position A [4], but morin is an exception, the first ionization corresponds to the OH group in position F [4,32]. This fact can be attributed to the anion stabilization by formation of an intramolecular hydrogen bond [24].

For fisetin and quercetin there is a small difference between the ${}^{w}_{w}pK_a$ ($I = 0$ M) values estimated by Eqs. (4) and (5). The ${}^{w}_{w}pK_a$ ($I = 0$ M) values estimated by Eq. (4) are slightly higher than the ones estimated by Eq. (5) (except for ${}^{w}_{w}pK_{a3}$ ($I = 0$ M) of quercetin). This fact was already observed by Avdeef et al. [5]

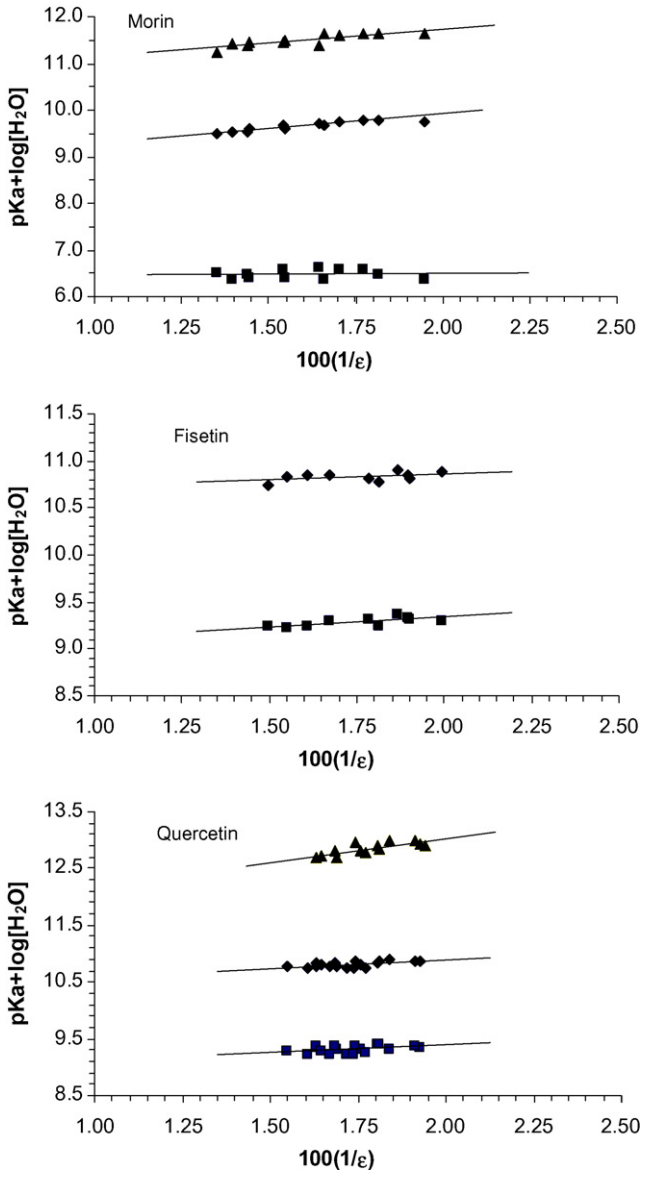


Fig. 2. The Yasuda–Shedlovsky plots of the studied flavonols. (■) Plot for pK_{a1}; (♦) plot for pK_{a2}; (▲) plot for pK_{a3}.

Table 2
${}^{w}_{w}pK_a$ ($I = 0$ M) values of studied flavonols

	${}^{w}_{w}pK_a$ determined in water	Estimated ${}^{w}_{w}pK_a$		CE[a] ${}^{w}_{w}pK_a$ values
		From Eq. (4).	From Eq. (5).	
Morin				
pK_{a1}		4.99 ± 0.00	4.97 ± 0.09	5.06
pK_{a2}	8.25	8.23 ± 0.03	8.29 ± 0.08	8.64
pK_{a3}	10.30	10.34 ± 0.04	10.33 ± 0.11	10.62
Fisetin				
pK_{a1}		7.70 ± 0.03	7.57 ± 0.03	7.36
pK_{a2}		9.54 ± 0.04	9.34 ± 0.04	9.71
Quercetin				
pK_{a1}		7.71 ± 0.06	7.59 ± 0.06	7.19
pK_{a2}		9.44 ± 0.04	9.33 ± 0.04	9.36
pK_{a3}		11.46 ± 0.07	11.56 ± 0.10	11.56

[a] From Ref. [4].

for neutral acids. When Yasuda–Shedlovsky extrapolation was carried out from the methanol rich region (>30% in weight), which is the case of fisetin and quercetin, the extrapolated pK_a values are slightly higher that the ones directly obtained in pure water. Anyway, the values obtained from potentiometric data are consistent and lead to reliable ${}^{w}_{w}pK_a$ ($I = 0$ M) values.

For fisetin the ${}^{w}_{w}pK_{a1}$ ($I = 0$ M) estimated by potentiometry is slightly higher and the ${}^{w}_{w}pK_{a2}$ ($I = 0$ M) slightly lower than the ones obtained by CE. For quercetin the ${}^{w}_{w}pK_{a1}$ ($I = 0$ M) estimated by potentiometry is also slightly higher than the one obtained by CE whereas the ${}^{w}_{w}pK_{a2}$ ($I = 0$ M) and ${}^{w}_{w}pK_{a3}$ ($I = 0$ M) are similar with the CE ones. In general the pK_a values estimated by Eq. (5) are closer to the pK_a values obtained by CE than those estimated by Eq. (4).

4. Conclusions

The aqueous pK_a values (${}^{w}_{w}pK_a$ ($I = 0$ M)) of three flavonols sparingly soluble in water and with several ionizables hydroxyl groups have been estimated by potentiometry. Because of their poor solubility in water, they have been titrated in methanol/water mixtures and two equations (Eqs. (4) and (5)) have been used to estimate the aqueous values. For morin, which is the most soluble studied flavonol, the aqueous pK_a values obtained by the two equations are practically the same and equal to the ones obtained by titration in pure water. For fisetin and quercetin, the estimations were done from a high percentage of methanol, and the aqueous pK_a values obtained by the two equations are slightly different, but not by more than in 0.15 units. Eq. (5) allows a very good estimation of ${}^{w}_{w}pK_a$ ($I = 0$ M) from only one experimental ${}^{s}_{s}pK_a$ ($I = 0.15$ M) value, determined in any methanol/water mixture, whereas Eq. (4) requires at least three (in fact five or six) independent titrations in different methanol/water mixtures. Thus, we recommend the use of Eq. (5).

These compounds present two or three pK_a values higher than 7 and very close one to each other, then the determination of these pK_a values is a difficult task by any technique (i.e. potentiometry or CE). The differences in ${}^{w}_{w}pK_a$ ($I = 0$ M) values obtained by potentiometric method with respect to the ones obtained previously by CE [4] (not more than 0.4 units) are in an acceptable agreement, given the difficulty of obtaining these pK_a values. Since the pK_a values are very close, about 15 buffers with close pH were necessary to obtain accurate determinations by CE method. pK_a determination by potentiometry can be done by a direct and automated acid–base titration, previous appropriate calibration, and thus is much faster than the CE determination.

Acknowledgements

We thank financial support from the Spanish Government (Project CTQ2004-00965/BQU).

References

[1] A. Albert, E.P. Serjeant, Potentiometry and Potentiometric Titrations, John Wiley and Sons, New York, 1984.

[2] A. Albert, E.P. Serjeant, The determination of Ionization Constant, Chapman and Hall, London, 1971.
[3] Y. Ishihama, Y. Oda, N. Asakawa, J. Pharm. Sci. 83 (1994) 1500.
[4] J.M. Herrero-Martínez, M. Sanmartin, M. Rośes, E. Bosch, C. Ràfols, Electrophoresis 26 (2005) 1886.
[5] A. Avdeef, J.E.A. Comer, S.J. Thomson, Anal. Chem. 65 (1993) 42.
[6] A. Avdeef, K.J. Box, J.E. Comer, M. Gilges, M. Hadley, C. Hibbert, W. Patterson, K.Y. Tam, J. Pharm. Biomed. Anal. 20 (1999) 631.
[7] K. Takacs-Novak, K.J. Box, A. Avdeef, Int. J. Pharm. 151 (1997) 235.
[8] R. Ruiz, M. Rośes, C. Ràfols, E. Bosch, Anal. Chim. Acta 550 (2005) 210.
[9] C.A. Rice-Evans, L. Parker, Flavonoids in Health and Diseases, Marcel Dekker, New York, 1998.
[10] L. Magnani, E.M. Gaydou, J.C. Hubaud, Anal. Chim. Acta 411 (2000) 209.
[11] G. Cao, E. Sofic, R.L. Prior, Free Radic. Biol. Med. 22 (1997) 749.
[12] W. Bors, W. Heller, C. Michel, M. Saran, in: Packer Lester, Alexander N. Glazer (Eds.), Flavonoids as antioxidants: Determination of Radical-scavenging Efficiencies. Methods in Enzymology, Academic Press, 1990, pp. 343–355.
[13] C.A. Rice-Evans, N.J. Miller, G. Paganga, Free Radic. Biol. Med. 20 (1996) 933.
[14] K. Lemanska, H. Szymusiak, B. Tyrakowska, R. Zielinski, A.E.M.F. Soffers, I.M.C.M. Rietjens, Free Radic. Biol. Med. 31 (2001) 869.
[15] S.V. Jovanovic, S. Steenken, M. Tosic, B. Marjanovic, M.G. Simic, J. Am. Chem. Soc. 116 (1994) 4846.
[16] Y. Fan, Y. Zheng, Anal. Chim. Acta 281 (1993) 353.
[17] A. Niazi, A. Yazdanipour, J. Ghasemi, M. Kubista, Collect. Czech. Chem. Commun. 71 (2006) 1.
[18] B. Bujonek, Pol. J. Chem. 67 (1993) 1339.
[19] S.R. Jagasis, B.C. Haldar, J. Indian Chem. Soc. 40 (1963) 287.
[20] V. Kuntic, N. Pejic, S. Micic, D. Malesev, Z. Vujic, Pharmazie 58 (2003) 439.
[21] N. Sauerwald, M. Schwenk, J. Polster, E. Bengsch, Z. Naturforsch. B: Chem. Sci. 53 (1998) 315.
[22] H. Liu, G. Yang, D. Wang, S. Sun, J. Ma, Chin. J. Chem. 19 (2001) 675.
[23] M. Thompson, C.R. Williams, G.E.P. Elliot, Anal. Chim. Acta 85 (1976) 375.
[24] E.N. Muzafarov, B.N. Ivanov, A.N. Mal'yan, E.K. Zolotareva, Biochem. Physiol. Pflanz. 181 (1986) 381.
[25] M. Yasuda, Bull. Chem. Soc. Jpn. 32 (1959) 429.
[26] F. Rived, I. Canals, E. Bosch, M. Róses, Anal. Chim. Acta 439 (2001) 315.
[27] R.G. Bates, Determination of pH: Theory and Practice, 2nd ed., Wiley, New York, 1973.
[28] T. Shedlovsky, Electrolytes, Pergamon Press, New York, 1962.
[29] R. Ruiz, C. Ràfols, M. Rośes, E. Bosch, J. Pharm. Sci. 92 (2003) 1473.
[30] M. Rosés, F. Rived, E. Bosch, J. Chromatogr. A 867 (2000) 45–56.
[31] Sparc, http://ibmlc2.chem.uga.edu/sparc/.
[32] P.K. Agrawal, H. Schneider, Tetrahedron Lett. 24 (1983) 177.

Available online at www.sciencedirect.com
ScienceDirect
Talanta 74 (2008) 760–765
Talanta
www.elsevier.com/locate/talanta

A simple electrochemical method for the determination of hydroxyl free radicals without separation process

Yu-Lin Hu [a], Yu Lu [a], Guo-Jun Zhou [b,*], Xing-Hua Xia [a,*]

[a] *Key Laboratory of Analytical Chemistry for Life Science, School of Chemistry and Chemical Engineering, Nanjing University, Nanjing 210093, China*
[b] *Technology Center, China Tobacco Zhejiang Industrial Corporation, 77 South Zhongshan Road, Hanzhou 310008, China*

Received 30 March 2007; received in revised form 5 July 2007; accepted 5 July 2007
Available online 17 July 2007

Abstract

Generally speaking, measurement of hydroxylated radical products of salicylic acid requires a fussy separation process. In this study, we describe a simple method to electrochemically detect hydroxyl radicals (•OH) using 4-hydroxybenzoic acid (4-HBA) as the •OH trap. The •OH is generated by the Fenton reaction from iron (II) sulfate and hydrogen peroxide in a phosphate buffer solution. Experimental results show that our method can detect the •OH with high sensitivity without any separation process. The differential pulse voltammetric responses show a linear dependence on the concentration of •OH in a range of 2.0×10^{-6} and 1.0×10^{-3} M with a determination limit down to 5.0×10^{-7} M. As a demonstration, the kinetics of the Fenton reaction was mapped by measuring the reaction product of hydroxyl radical trapped by 4-HBA. The result is in good agreement with that reported previously. All the results show that the present approach could provide a simple, inexpensive and promising method for biomedicine and iatrology.
© 2007 Elsevier B.V. All rights reserved.

Keywords: Electrochemical analysis; Hydroxyl radicals; 3,4-DHBA; 4-HBA; Fenton reaction

1. Introduction

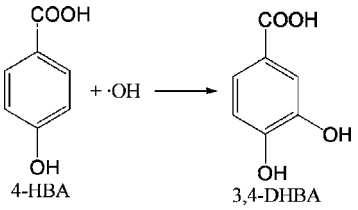
It has been recognized that free radicals, particularly the most reactive hydroxyl radical (•OH), have been implicated in the pathophysiology of many diseases via breaking the homeostasis in vivo [1]. The •OH, which can be usually generated via the Fenton reaction in vivo plays a major role in maintaining the homeostasis at cellular level in normal [2]. When the •OH is generated in excess with the cellular antioxidant defense being deficient, some free radical chain reactions may take place by its interaction with proteins, lipids and nucleic acids. These may cause cellular damage and induce many diseases, such as ischemia/reperfusion injury [3], hepatitis [4,5], Parkinson's and Alzheimer's disease [6–8], rheumatoid arthritis [9,10], brain ischemia [11], stroke [12], and carcinogenesis [13–16]. Obviously, fast and selective determination of •OH is of importance in biomedicine and iatrology. However, the •OH is a very active species and its half-life time is as short as 10^{-10} s [17]. Therefore, its steady-state concentration is very low, which makes the accurate and sensitive determination of such short-lived species in vivo very difficult [1].

Hydroxylated radical products of salicylate or its related compounds have been often utilized as a marker for the generation of •OH. During the past decades, many techniques have been developed and applied to detect •OH or its adducts, such as electron spin resonance (ESR) [18–21], chemiluminescence [22,23], high performance liquid chromatography with electrochemical determination (HPLC-ED) [24–27], gas chromatography mass spectrum (GC–MS) [28–30], capillary electrophoresis (CE) [24,31], fluorescence [32], micellar electrokinetic capillary chromatography (MECC) coupled with UV (MECC-UV) [33], UV–vis spectrometry [34] and resonance scattering (RS) [35]. These methods require almost the same process. Firstly, various reagents were used to trap the •OH to form stable adducts. Then, the reagent and corresponding adducts (usually are not one component) were separated with the HPLC or CE. Finally, the adducts were detected to figure out the quantification of the •OH. The whole process is very fussy, long-period and high-cost.

* Corresponding author. Tel.: +86 25 83597436; fax: +86 25 83597436.
E-mail addresses: guojunzhou@yahoo.com (G.-J. Zhou), xhxia@nju.edu.cn (X.-H. Xia).

0039-9140/$ – see front matter © 2007 Elsevier B.V. All rights reserved.
doi:10.1016/j.talanta.2007.07.008

In the present paper, a simple and highly sensitive electrochemical method for •OH determination has been proposed. We used 4-hydroxybenzoic acid (4-HBA) to trap the •OH because it has high trapping efficiency and the resulting adduct is only the 3,4-dihydroxybenzoic acid (3,4-DHBA) (see reaction (1)) [36]. Furthermore, the oxidation of 4-HBA to 3,4-DHBA can be a reliable and accurate indicator for the existence of •OH [37]. Prominent difference in electrochemistry of 4-HBA and 3,4-DHBA on a carbon disk electrode in 20 mM KH_2PO_4–K_2HPO_4 buffer solution (PBS, pH 7.4) allows us to directly detect •OH generated from the Fenton reaction without a prior separation process. As a demonstration, the kinetics of this Fenton reaction was monitored. The present method could provide a simple, inexpensive and promising method for biomedicine, iatrology.



(1)

2. Experiments

2.1. Chemicals

4-HBA and 3,4-DHBA were of chemical grade and purchased from Shanghai Chemical Reagent Factory (Shanghai, China). All the other reagents were of analytical grade. Solutions were prepared with deionized water (18.2 MΩ, PureLab Classic Corp., USA).

2.2. Instrumentation

Electrochemical measurements were performed on a CHI 630 electrochemical workstation (CH Instrument, USA). The electrochemical cell consisted of a three-electrode configuration with a carbon disk electrode, laboratory-built with pencil lead (Ø 300 μm, Staedtler, German), as the working electrode; a platinum wire and a saturated Ag/AgCl electrode were used as the counter electrode and the reference electrode, respectively. All potentials in this paper refer to this saturated Ag/AgCl electrode.

2.3. Preparation of the carbon disk electrode

A 300 μm-diameter carbon disk electrode was made from pencil lead (Staedtler, German). A 15 mm long pencil lead was inserted into a 3 cm long glass capillary (inner diameter: 0.56 mm, outer diameter: 1.48 mm) until approximately 2–3 mm was left behind. The lead was then sealed in the glass capillary with epoxy glue. Carbon powder was used to make electric contact between the pencil lead in the glass capillary and a copper wire [38]. Prior to use, the carbon disk electrode was polished with emery paper followed by sonication in deionized water for 1 min.

2.4. Fenton reaction kinetics

Hydroxyl radical was produced via the Fenton reaction in the presence of 1.0 mM Fe^{2+}, 2.0 mM H_2O_2, 1.0 mM EDTA, 2.0 mM 4-HBA and 20 mM PBS (pH 7.4) in a final volume of 20 ml. Solutions of H_2O_2 and Fe^{2+} were prepared freshly before use with deionized water and weak acidic solution (pH 4); the iron salt was previously mixed with the EDTA before adding into the Fenton reaction system. With the Fenton reaction evolution, the product (3,4-DHBA) was electrochemical detected with cyclic voltammetric technique every ca. 5 min.

3. Results and discussion

3.1. The electrochemical behaviors of 4-HBA and 3,4-DHBA at carbon disk electrode

As we know, hexacoordinated ferrous EDTA can be oxidized by H_2O_2 to form •OH radial by the Fenton reaction according to reaction (2). Because of the different molecular structure between the trap reagent (4-HBA) and the trap product (3,4-DHBA), they have different electrochemical characteristics. Cyclic voltammograms (CVs) of the 3,4-DHBA and 4-HBA at a carbon disk electrode in a PBS (pH 7.4) solution are shown in Fig. 1. The carbon disk electrode did not show any electrochemical response in the studied potential window besides the double layer charging current (curve 3). Upon addition of 4-HBA, a complex current–potential profiles were observed (curve 2). A relative large oxidation current peak appeared at ca. 0.83 V. The total reaction of 4-HBA is shown in reaction (3). The reaction mechanism corresponding to each pair of peaks is not yet clear. However, the electrochemistry of 3,4-DHBA on the carbon disk electrode showed a clear pair of redox peaks located at ca. 0.27 V (curve 1). This couple of peaks corresponds to the electrochemical transformation between 3,4-DHBA and its oxidizing state (see reaction (4)). It is clear that the electrochemical response of 3,4-DHBA on the carbon disk electrode is hardly affected by the

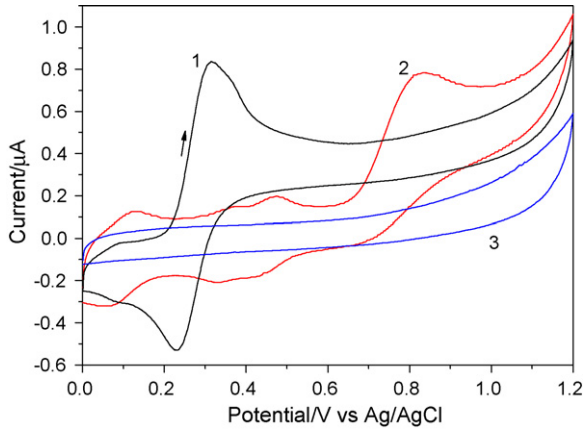


Fig. 1. Cyclic voltammograms of a carbon disk electrode in a solution of 20 mM phosphate buffer solution (pH 7.4) containing 2 mM 3,4-DHBA (curve 1) or 2 mM 4-HBA (curve 2) at a scan rate of 50 mV/s. For comparison, a CV (curve 3) of the carbon disk electrode in the phosphate buffer solution (pH 7.4) under the same conditions is also displayed.

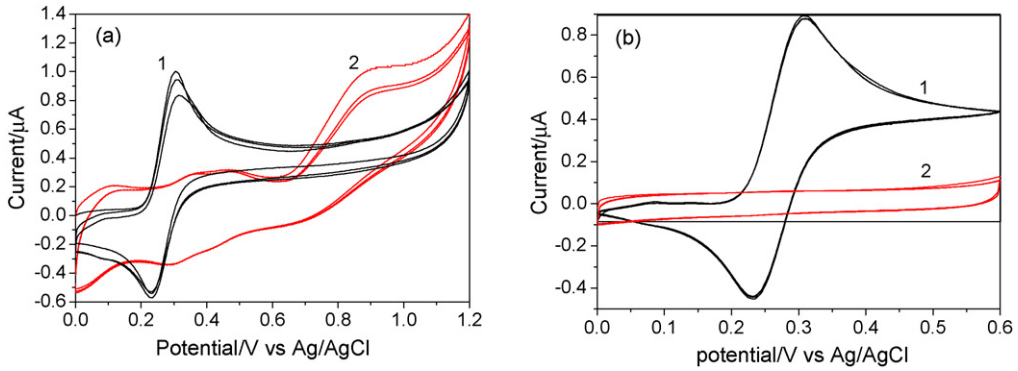
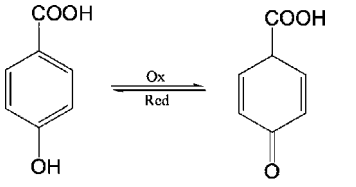


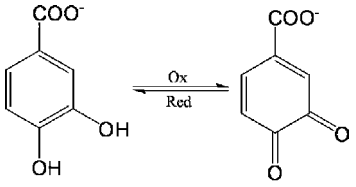
Fig. 2. Cyclic voltammograms of a carbon disk electrode in a solution of 20 mM PBS (pH 7.4) containing 2 mM 3,4-DHBA (curves 1) or 2 mM 4-HBA (curves 2) at a scan rate of 50 mV/s. Potential scan range: (a) 0.0 to 1.2 V and (b) 0.0 to 0.6 V.

electrochemical reaction of 4-HBA. Therefore, directly electrochemical analysis of 3,4-DHBA can be achieved in the presence of its reactant of 4-HBA. This method is simple and does not require any separation processes as usually used in literature [39]:

$$[\mathrm{Fe(II)–EDTA}]^{2-} + \mathrm{H_2O_2} \rightarrow [\mathrm{Fe(III)–EDTA}]^{-} + \mathrm{OH^-} + {}^{\bullet}\mathrm{OH} \quad (2)$$



(3)



(4)

3.2. The influence of upper limit-potential on the analysis of 3,4-DHBA

When a carbon disk electrode was continuously scanned in a potential window of 0.0–1.2 V in a solution of PBS (pH 7.4) containing 3,4-DHBA, the peak currents at ca. 0.27 V decreased continuously (Fig. 2a, curves 1). The oxidation peak current in the third potential scan considerably decreased to 87% of the current in the first scan. This decrease could be due to the electrode fouling possibly caused by the electrooxidized product at relative positive potentials or the change of properties of the carbon disk electrode at high positive potentials. This fouling effect was also observed for the electrooxidation of 4-HBA at the carbon disk electrode (Fig. 2a, curves 2). It has been reported that carbon disk electrode can be activated at high potentials. Activation of carbon disk electrodes results in the formation of microcrystallinity and various oxygenated functional groups on the electrode surface. The conductivity and activity of the electrode were functions of the state of reduction of the oxidized layer and the redox potential in solution [40]. These microcrystallinity and oxygenated functional groups are stable in this potential window, decreasing the surface sites available for the present electrochemical reactions (3) and (4). This electrode fouling effect can be almost completely eliminated by using lower upper-limit potential. As shown in Fig. 2b, curves 1, the decrease in peak currents for reaction (4) is negligible. The decrease in the anodic peak current for the first and second potential scans is only 1%. The peak current retains constant after the second potential scan. In addition, the slightly interference from the 4-HBA can be eliminated (compare the curves 1 and the curves 2 in Fig. 2b). In the case of 4-HBA, a featureless CV was observed (Fig. 2b, curves 2). Therefore, this potential window of 0.0–0.6 V is essential for achieving determination of the 3,4-DHBA with high sensitivity and selectivity.

3.3. The influence of pH on the analysis of 3,4-DHBA

Solution pH is another important factor influencing the electrochemistry of 3,4-DHBA at the carbon disk electrode. As shown in Fig. 3, the solution pH changes not only the reaction mechanism, but also the peak currents. At solution pH higher than 6.5, there appeared only one pair of redox peaks in the CVs

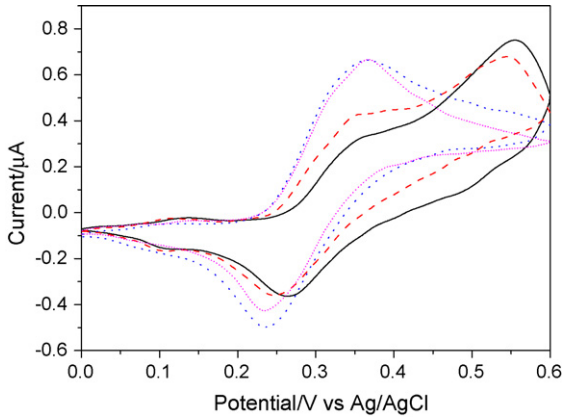


Fig. 3. Cyclic voltammograms of a carbon disk electrode in a solution of 20 mM PBS with different pH (6.0 (solid curve), 6.2 (dash curve), 6.5 (dotted curve), 6.7 (short dotted curve)) containing 2 mM 3,4-DHBA at a scan rate of 50 mV/s.

of 3,4-DHBA at carbon disk electrode (Fig. 3). It was found that the peak currents of the anodic and cathodic peaks changed slightly with the change of solution pH. However, as the solution pH was lower than 6.5, another pair of redox peaks appeared at ca. 0.52 V beside the original couple of redox peaks at ca. 0.27 V. In this case, the currents for the new pair of peaks increased with the decrease of solution pH, while the currents for the original pair of peaks decreased with the increase of solution pH. In addition, the anodic peak of new redox pair is much larger than its cathodic one. With the lowering of the solution pH, the cathodic peak became much clearer. This indicates that the solution pH changes the reaction mechanism of 3,4-DHBA at the carbon disk electrode. The pK_{a1} and pK_{a2} of 3,4-DHBA are 4.48 and 8.67, respectively [41]. As the solution pH is lower than 6.5, 3,4-DHBA will gradually form its acidic structure, reducing the reaction concentration of 3,4-DHBA and thus the peak currents at ca. 0. 27 V. The new pair peaks at ca. 0.52 V should correspond to the electrochemistry of the acidic structure of 3,4-DHBA. These results demonstrate that the sensitive analysis of 3,4-DHBA by using a carbon disk electrode can be achieved as the solution pH is higher than 6.5. Since the finally destination of the present work is directed to the study of biological systems, the solution pH of 7.4 was chosen in the following measurements.

In addition, the dependence of the redox peak potentials of 3,4-DHBA on the solution pH was investigated. It was found that the electrochemical reaction of 3,4-DHBA at a carbon disk electrode occurs with the participation of 2 protons.

3.4. The influence of the potential scan rate

The influence of scan rate on the response of 3,4-DHBA on a carbon disk electrode in a PBS (pH 7.4) was also investigated. Fig. 4 shows the cyclic voltammograms of 2 mM 3,4-DHBA at the carbon disk electrode in PBS (pH 7.4) at different scan rates. The anodic and cathodic peak currents increased linearly with the square root of scan rate (5–500 mV/s) (see insets in Fig. 4). This linear relationship indicates that the corresponding electrochemical reaction is a solution diffusion-limited process. In addition, it was found that the anodic and cathodic peak potentials shifted to more positive and more negative values with the increase of scan rate, respectively, indicating that the electrochemical reaction is a quasi-reversible process. According to the shifts of peak potentials with scan rate, the electron transfer rate constant was calculated to be 2.8 m/s in terms of the Nicholson equation [42] by assuming the diffusion constant of 3,4-DHBA be 1.0×10^{-9} m^2/s.

3.5. Determination of hydroxyl radicals

Since hydroxyl radical can be effectively trapped by 4-HBA, forming 3,4-DHBA. Therefore, by analysis of 3,4-DHBA, indirectly electrochemical determination of the hydroxyl radical can be achieved by using the carbon disk electrode. After optimization of the experimental factors based on the above investigations, electrochemical determination of hydroxyl radicals was performed. A series of standard solutions of 3,4-DHBA with concentration range from 1×10^{-8} to 1×10^{-3} M in 20 mM phosphate buffer solution (pH 7.4) was analyzed by the differential pulse voltammetric technique in the potential window from 0.0 to 0.6 V at scan rate of 80 mV/s. As shown by the inset in Fig. 5, a well anodic peak due to the oxidation of 3,4-DHBA on carbon disk electrode appeared. The peak current shows a linear dependence on the 3,4-DHBA concentration in the range of 2.0×10^{-6} to 1.0×10^{-3} M and the determination limit was as low as 5.0×10^{-7} M.

3.6. Study of the Fenton reaction kinetics

Since the present method shows high sensitivity and selectivity toward the analysis of hydroxyl radical, the kinetics of the Fenton reaction can be monitored. Before studying the kinetics

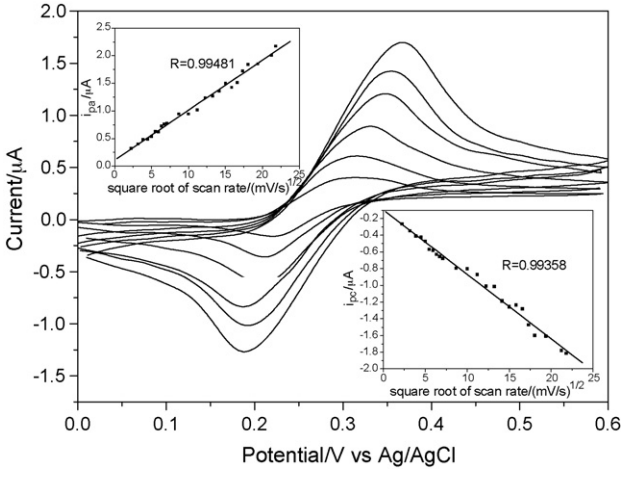


Fig. 4. Cyclic voltammograms of a carbon disk electrode in 20 mM PBS (pH 7.4) containing 2 mM 3,4-DHBA at different scan rate. From inner to outer CVs, the scan rates were 5–500 mV/s. The right-bottom inset and the upper left inset are the plot of the cathodic and anodic peak currents as a function of the square root of scan rate in the range of 5–500 mV/s.

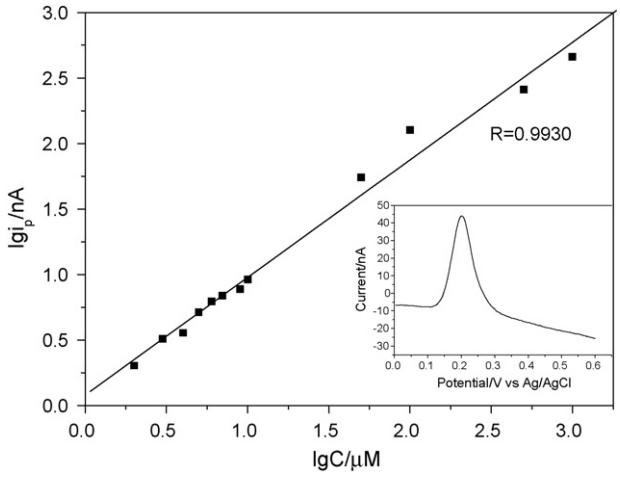


Fig. 5. The linear response of the anodic current on the concentration of 3,4-DHBA in the range of 2×10^{-6} to 1×10^{-3} M. Inset shows the differential pulse voltammogram of 50 μM 3,4-DHBA in a 20 mM phosphate buffer solution (pH 7.4) at the carbon disk electrode at a scan rate of 80 mV/s.

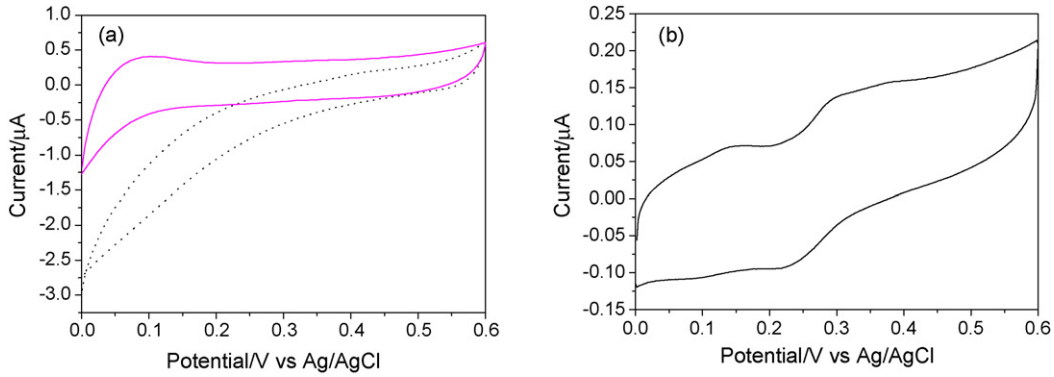


Fig. 6. (a) Cyclic voltammograms of a carbon disk electrode in a 20 mM PBS (pH 7.4) containing 2 mM Fe^{2+} + EDTA (solid curve), 2 mM H_2O_2 (dotted curve) at scan rate of 50 mV/s. (b) Cyclic voltammogram of the carbon disk electrode in the 20 mM PBS (pH 7.4) containing $^{\bullet}$OH trapped by 4-HBA for 31 min at a scan rate of 50 mV/s.

of the Fenton reaction, the electrochemistry of the carbon disk electrode in 2 mM Fe^{2+} + EDTA, H_2O_2, or the $^{\bullet}$OH trapped by 4-HBA was performed at a scan rate of 50 mV/s. As shown in Fig. 6a, the solution of Fe^{2+} + EDTA showed featureless CV (Fig. 6a, solid curve). The electrochemistry of hydrogen peroxide showed a reduction current at potentials negative to 0.47 V (Fig. 6a, dotted curve). The observed cathodic current is due to the reduction of hydrogen peroxide at the carbon disk electrode. Then the carbon disk electrode was inserted in the Fenton reaction system. A CV of this system at a reaction time of 31 min is shown in Fig. 6b. As expected, a small pair of redox peaks corresponding to the electrochemical reaction of 3,4-DHBA appeared, which overlapped on the wave for the reduction of hydrogen peroxide. Because the Fenton reaction system is very complex and the reaction reagents are excessive, the characteristics of CVs are the integration of the electrochemical responses of 3,4-DHBA and the reaction reagents. Nevertheless, the anodic and cathodic peak currents of the trapped 3,4-DHBA could be distinguished, which increased with the reaction time. This result demonstrates that the hydroxyl radical can be effectively trapped by 4-HBA to form the product of 3,4-DHBA which can be in turn electrochemically detected without interference from the reaction system.

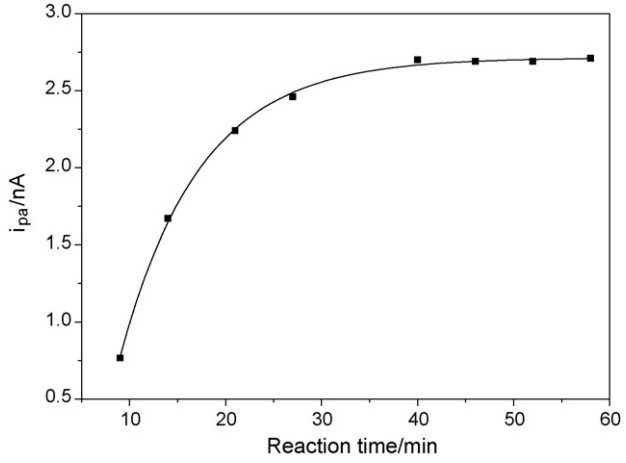


Fig. 7. The anodic current (at 0.27 V) corresponding to the trapped hydroxyl radical from the Fenton reaction as a function of reaction time. Data were obtained from Fig. 6.

Fig. 7 shows the dependence of the anodic peak current (subtracted by the background and the reduction current for hydrogen peroxide) at ca. 0.27 V on the reaction time. The peak current increases with the reaction time exponentially. Since the peak current is directly proportional to the formation rate of hydroxyl radical in the Fenton reaction, the kinetics of this reaction can be followed. This result demonstrates that the formation of hydroxyl radical from the Fenton reaction is formed rapidly within the first 20 min, and then reaches a plateau which indicates the dynamic equilibrium of the Fenton reaction. This result of the Fenton reaction kinetics is in good agreement with that reported previously [43].

4. Conclusions

In summary, we for the first time report the electrochemical determination of hydroxyl radicals on a carbon disk electrode without any separation processes. The proposed method with a relatively high sensitivity and selectivity is simple and easy to operate. The linear ranges of 3,4-DHBA was between 2.0×10^{-6} and 1.0×10^{-3} M, and the determination limit was 5.0×10^{-7} M. In addition, the feasibility of the present method was proofed by indirectly measuring the reaction product of $^{\bullet}$OH generated from the Fenton reaction. It is clear that the present method is a convenient and sensitive approach to indirectly determine the $^{\bullet}$OH in complex systems. The application of the present method in the biomedicine and iatrology is undergoing.

Acknowledgements

This work was supported by grants from the Tobacco Zhejiang Industrial Corporation, the National Natural Science Foundation of China (NSFC, No. 20535010) and the National Science Fund for Creative Research Groups (20521503).

References

[1] F.C. Cheng, J.F. Jen, T.H. Tsai, J. Chromatogr. B 781 (2002) 481.
[2] B.B. Li, P.L. Gutirrez, N.V. Blough, Anal. Chem. 69 (1997) 4295.
[3] S. Cuzzocrea, R.J. Reiter, Eur. J. Pharmacol. 426 (2001) 1.

[4] P. Biemond, A.J. Swaak, H.G. van Eijk, J.F. Koster, Free Radical Biol. Med. 4 (1988) 185.
[5] H. Yamamoto, T. Watanabe, H. Mizuno, K. Endo, T. Hosokawa, A. Kazusaka, R. Gooneratne, S. Fujita, Free Radical Biol. Med. 30 (2001) 547.
[6] S. Turnbull, B.J. Tabner, D.R. Brown, D. Allsop, Biochemistry 42 (2003) 7675.
[7] B.J. Tabner, S. Turnbull, O.M.A. El-Agnaf, D. Allsop, Free Radical Biol. Med. 32 (2002) 1076.
[8] C. Schöneich, D. Pogocki, G.L. Hug, K. Bobrowski, J. Am. Chem. Soc. 125 (2003) 13700.
[9] D.P. Naughton, J. Knappitt, K. Fairburn, K. Gaffney, D.R. Blake, M. Grootveld, FEBS Lett. 361 (1995) 167.
[10] C.L. Hawkins, M.J. Davies, Free Radical Biol. Med. 24 (1998) 1396.
[11] T. Yamamoto, S. Yuki, T. Watanabe, M. Mitsuka, K.I. Saito, K. Kogure, Brain Res. 762 (1997) 240.
[12] H. Negishi, K. Ikeda, Y. Nara, Y. Yamori, Neurosci. Lett. 306 (2001) 206.
[13] K. Ito, S. Inoue, Y. Hiraku, S. Kawanishi, Mutat. Res.-Genet. Toxocol. Environ. 585 (2005) 60.
[14] J.H. Kang, Toxicol. Lett. 145 (2003) 181.
[15] H.J.J. Moonen, J.J. Briede, J.M.S. van Maanen, J.C.S. Kleinjans, T.M.C.M. de Kok, Mol. Carcinog. 35 (2002) 196.
[16] A.M. Mohamadin, J. Inorg. Biochem. 84 (2001) 97.
[17] B. Halliwell, J.M.C. Gutterridge, Free Radicals in Biology and Medicine, 2nd ed., Clarendon Press, Oxford, 1989, p. 30.
[18] S. Kataoka, H. Yasui, M. Hiromura, H. Sakurai, Life Sci. 77 (2005) 2814.
[19] H.H. Shi, X.R. Wang, Y. Luo, Y. Su, Aquat. Toxicol. 74 (2005) 365.
[20] A. Nakajima, M. Tahara, Y. Yoshimura, H. Nakazawa, J. Photochem. Photobiol. A 174 (2005) 89.
[21] H.H. Shi, Y.X. Sui, X.R. Wang, Y. Luo, L.L. Ji, Comp. Biochem. Phys. C 140 (2005) 115.
[22] C.W. Lau, X.J. Qin, J.Y. Liang, J.Z. Lu, Anal. Chim. Acta 514 (2004) 45.
[23] B.A. Southworth, B.M. Voelker, Environ. Sci. Technol. 37 (2003) 1130.
[24] S.Y. Ai, Q.J. Wang, H. Li, L.T. Jin, J. Electroanal. Chem. 578 (2005) 223.
[25] F. Blandini, E. Martignoni, R. Ricotti, F. di Jeso, G. Nappi, J. Chromatogr. B 732 (1999) 213.
[26] T.H. Tsai, F.C. Cheng, L.C. Hung, C.F. Chen, J. Chromatogr. B 734 (1999) 277.
[27] L. Diez, M.H. Livertoux, A.A. Stark, M.W. Rousseau, P. Leroy, J. Chromatogr. B 763 (2001) 185.
[28] B. Pal, P.A. Ariya, Environ. Sci. Technol. 38 (2004) 5555.
[29] S.M. Aschmann, J. Arey, R. Atkinson, Environ. Sci. Technol. 36 (2002) 625.
[30] X.P. Luo, D.C. Lehotay, Clin. Biochem. 30 (1997) 41.
[31] Y.H. Cao, Q.C. Chu, J.N. Ye, Anal. Bioanal. Chem. 376 (2003) 691.
[32] C. Tai, X.X. Gu, H. Zou, Q.H. Guo, Talanta 58 (2002) 661.
[33] S.A.J. Coolen, F.A. Huf, J.C. Reijenga, J. Chromatogr. B 717 (1998) 119.
[34] C. George, D. Rousse, E. Perraudin, R. Strekowski, Phys. Chem. Chem. Phys. 5 (2003) 1562.
[35] A.H. Liang, S.M. Zhou, Z.L. Jiang, Talanta 70 (2006) 444.
[36] L. Ste-Marie, D. Boismenu, L. Vachon, J. Montgomery, Anal. Biochem. 241 (1996) 67.
[37] M. Liu, S.M. Liu, L.P. Steven, M. Minoru, K.J. Liu, Mol. Cell. Biochem. 234/235 (2002) 379.
[38] F.Y. He, A.L. Liu, J.H. Yuan, K.T.C. Wendell, C. Emanuel, X.H. Xia, Anal. Bioanal. Chem. 382 (2005) 192.
[39] E. Kilinc, Talanta 65 (2005) 876.
[40] L.J. Kepley, A.J. Bard, Anal. Chem. 60 (1988) 1459.
[41] Lange's Handbook of Chemistry: section 8, "Electrolyte, Electromotive Force and Chemical Equlibrium", 15th edition, edited by A.J. Dean, McGraw Hill, 1999, p. 8.41.
[42] R.S. Nicholson, Anal. Chem. 37 (1965) 1351.
[43] X.F. Yang, X.Q. Guo, Analyst 126 (2001) 1800.

Available online at www.sciencedirect.com
ScienceDirect
Talanta 74 (2008) 815–820
Talanta
www.elsevier.com/locate/talanta

Sensitive detection of trifluoperazine using a poly-ABSA/SWNTs film-modified glassy carbon electrode

Guiying Jin, Fei Huang, Wei Li, Shaoning Yu, Song Zhang, Jilie Kong *

Department of Chemistry and Institutes of Biomedical Sciences, Fudan University, Shanghai 200433, PR China

Received 25 April 2007; received in revised form 10 July 2007; accepted 15 July 2007
Available online 31 July 2007

Abstract

A poly-ABSA/SWNTs composite-modified electrode was fabricated by electropolymerizing aminobenzene sulphonic acid (ABSA) on the surface of glassy carbon electrode (GCE) modified with single-wall carbon nanotubes (SWNTs). SWNTs provide a 3D porous and conductive network for the polymer immobilization. The nanocomposite film was characterized by scanning electron microscope (SEM) and electrochemical impedance spectroscopy (EIS). The results indicated that this composite-modified electrode had strong electrocatalytic activity toward the oxidation of trifluoperazine (TFP). TFP could effectively accumulate on the modified electrode and generate a sensitive anodic peak at 0.72 V (versus SCE) in pH 6.1 phosphate buffer solution. Under the selected conditions, the anodic peak current of TFP was linear with its concentration within the range from 1.0×10^{-7} to 1.0×10^{-5} mol L^{-1} and 1.0×10^{-5} to 1.0×10^{-4} mol L^{-1}, and the detection limit was 1.0×10^{-9} mol L^{-1} (S/N = 3). This method was successfully applied to the detection of trifluoperazine in drug samples and the recovery was satisfactory. In comparison with the SWNTs/GCE or poly-ABSA/GCE prepared in the similar way, this composite-modified electrode exhibited better catalytic activity.
© 2007 Published by Elsevier B.V.

Keywords: Aminobenzene sulphonic acid; Carbon nanotube; Trifluoperazine; Electropolymerization; Electrocatalysis

1. Introduction

Trifluoperazine (TFP, Scheme 1) is a derivative of phenothiazine. It has been widely used in the treatment of psychotic patients for the neuroleptic and antidepressive action [1]. For such function and application, TFP has become the object of intense research currently and it is essential to develop rapid and simple methods for its detection. Generally, the detection of TFP is performed with spectrophotometry [2], capillary zone electrophoresis [3], titrimetry [4], fluorometry [5], high-performance liquid chromatography [6], etc. Nevertheless, there are few reports about TFP studied by electrochemical methods for its low redox activity under normal conditions [7].

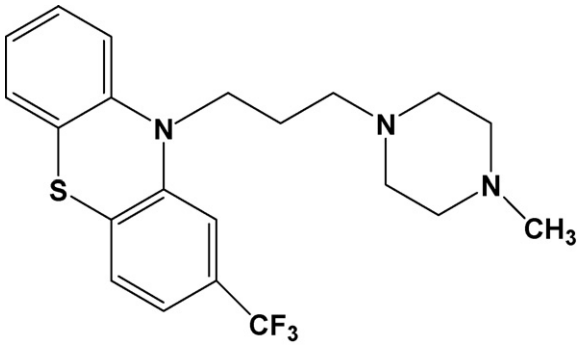
Carbon nanotubes (CNTs) have attracted enormous interest over the past years, mainly due to their exceptional electrical, chemical and mechanical properties, which make them as an attractive candidate for diverse applications such as in nanoelectronics and sensors [8–11]. The carbon nanotubes modified electrodes can enhance the electron transfer between electroactive species and electrodes. So far, there are many reports on the electrochemical studies of CNTs [12–18]. Single-wall carbon nanotubes (SWNTs) are a well-defined system in terms of electronic properties, and exhibit quantum dots and wires at very low temperatures [19].

Polymer-modified electrodes have received great attention in recent years, as polymer films have good stability, reproducibility, more active sites, homogeneity in electrochemical deposition and strong adherence to electrode surface [20,21]. Electropolymerization is a good approach to immobilize polymers to prepare modified electrode as adjusting the electrochemical parameters can control film thickness, permeation and charge transport characteristics. Glassy carbon electrodes (GCEs) have been widely used compared with metal electrodes due to its biocompatibility with tissue, having low residual current over a wide potential range and minimal propensity to show a deteriorated response as a result of electrode fouling [22–24].

In this work, a novel nanocomposite material, which combined SWNTs and polymer, was fabricated for analytical applications. This nanocomposite was prepared by electropolymerizing ABSA on a SWNTs functionlizing glassy

* Corresponding author. Tel.: +86 21 65642138; fax: +86 21 65641740.
E-mail address: jlkong@fudan.edu.cn (J. Kong).

0039-9140/$ – see front matter © 2007 Published by Elsevier B.V.
doi:10.1016/j.talanta.2007.07.023



Scheme 1. The chemical structure of trifluoperazine.

carbon electrode (poly-ABSA/SWNTs/GCE). Compared with the SWNTs or poly-ABSA film modified electrode, the poly-ABSA/SWNTs/GCE could remarkably improve the electrochemical response of TFP.

2. Experimental

2.1. Chemicals

Aminobenzene sulphonic acid was purchased from Sanaisi Reagent Factory (Shanghai China). SWNTs were purchased from Shenzhen Nanotech Port Co. Ltd. (Shenzhen, China). The as-received SWNTs were treated under sonication in 1:3 concentrated nitric–sulfuric acids at ca. 50 °C. Trifluoperazine hydrochloride ($C_{21}H_{24}F_3N_3S^{\bullet}2HCl$) was purchased from Sigma. The stock solutions (0.01 mol L^{-1}) were prepared with twice distilled water and stored at +4 °C in darkness. The drug tablets came from Yixin Chemical Limited Company (Shanghai, China). Prior to determination, they were ground into powder, dissolved in water, filtered into a container and then diluted to certain volume. All other chemicals were of analytical grade and used without further purification. Phosphate buffer solutions (PBS) were prepared by 0.1 mol L^{-1} NaH_2PO_4–Na_2HPO_4, and adjusted the pH with 0.1 mol L^{-1} H_3PO_4 and 0.1 mol L^{-1} NaOH. All aqueous solutions were prepared with double distilled, de-ionized water.

2.2. Apparatus

Electrochemical measurements were carried out on CHI 660 A electrochemical workstation (CH Instruments, Chenhua Co., Shanghai, China). A conventional three-electrode system was employed with a bare GCE or modified GCE (2.5 mm in diameter) as the working electrode, a saturated calomel electrode (SCE) as the reference electrode, and a platinum electrode as the counter electrode. All the potentials given in this paper were referred to the SCE. A magnetic stirrer was used for the convective transport when necessary. Scanning electron microscopy (SEM) images were obtained on a Philips XL30 Microscope (Japan). UV–vis absorption spectroscopy was performed using 8453-model spectrophotometer (Agilent, USA). Solution pH was measured with a Mettler–Toledo 320-s pH meter (Shanghai, China).

2.3. Preparation of the modified electrodes

The bare GCE was polished successively with 0.3 and 0.05 μm Al_2O_3 slurry on emery paper before modification. Then it was rinsed with double distilled water and sonicated in 1:1 nitric acid, acetone and double distilled water for 10 min, respectively. A 0.1 mg mL^{-1} suspension of SWNTs was first obtained by dispersing 1.0 mg SWNTs in 10.0 mL *N*,*N*-dimethylformamide (DMF). A droplet (5 μl) suspension of the acid treated SWNTs (0.1 mg mL^{-1}) was dropped onto the surface of clean GCE. Then the solvent was evaporated under an infrared lamp forming the SWNTs-modified GCE, denoted as the SWNTs/GCE.

The ABSA was electropolymerized on the electrodes by cyclic sweeping from −1.5 to +2.5 V for 10 circles in pH 7.0 PBS containing 0.01 mol L^{-1} ABSA on an SWNTs/GCE. The same procedure was used for electropolymerization on a bare GCE for comparison. These electrodes were rinsed by water and stored in PBS before use.

3. Results and discussion

3.1. Electropolymerization of ABSA at the SWNTs/GCE surface

Voltammograms of 0.01 mol L^{-1} ABSA in pH 7.0 PBS at the SWNTs/GCE were shown in Fig. 1. Anodic peak and cathodic peak were observed with peak potential value at +1.5, 0.2 and −0.7 V, respectively. Then larger peaks were observed upon continuous scanning, reflecting the continuous growth of the film. These facts indicated that ABSA was deposited on the surface of SWNTs/GCE by electropolymerization mode. A uniform adherent blue polymer film was formed on the electrode surface. The experimental results showed polymer could not effectively promote electron transfer when the sweep segments were lower than 16 or more than 30. Generally, 20 sweep segments were chosen in modification process. The electrochemical behavior of ABSA at SWNTs/GCE may be as follows [25,26]: ABSA was oxidized

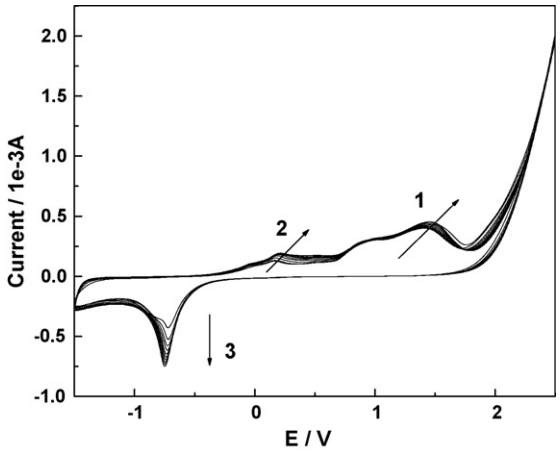


Fig. 1. Repetitive cyclic voltammograms of 0.01 mol L^{-1} ABSA in pH 7.0 PBS solution; terminal potential: +2.5 V; initial potential: −1.5 V; sensitivity: 1.0×10^{-4} A V^{-1}; scan rate: 100 mV s^{-1}.

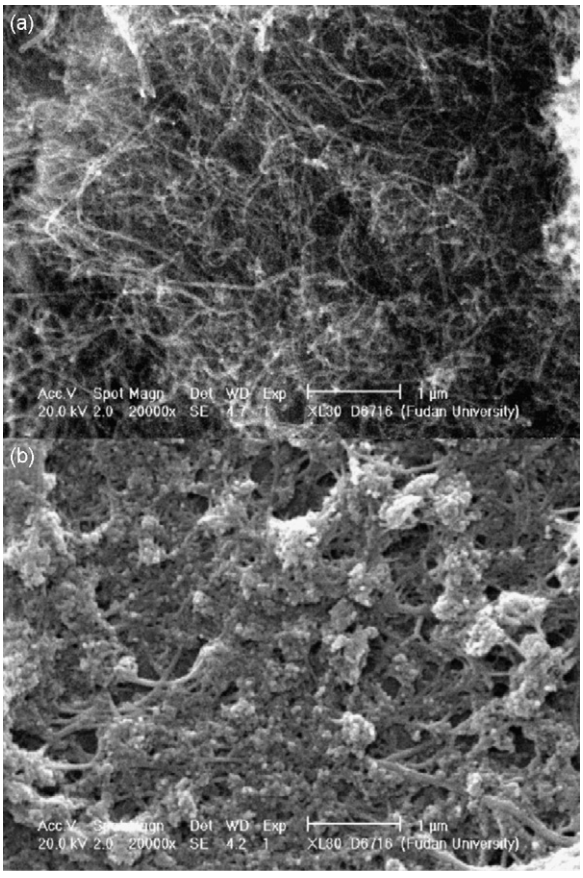


Fig. 2. SEM images of the glassy carbon electrodes coated with (a) SWNTs, (b) poly-ABSA/SWNTs.

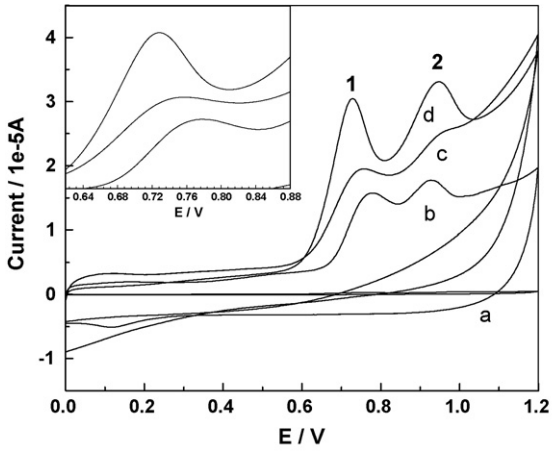


Fig. 3. Cyclic voltammograms of 1.0×10^{-5} mol L^{-1} TFP in pH 6.1 PBS with different electrode coated with (a) the bare, (b) the SWNTs, (c) the poly-ABSA and (d) the poly-ABSA/SWNTs. Inset displays the anodic peak 1 at different electrodes for a clear comparison.

to free radical (peak 1) at first; the free radical combined together rapidly to hydrazobenzene sulfonic acid; then hydrazobenzene sulfonic acid was oxidized to azobenzene sulfonic acid (peak 2), and azobenzene sulfonic acid reduced to hydrazobenzene sulfonic acid (peak 3).

The typical SEM images of the SWNTs/GCE and the poly-ABSA/SWNTs/GCE were shown in Fig. 2a and b, respectively. It could be seen that SWNT bundles were well dispersed on the surface of GCE, with a diameter in the range of 40–60 nm, and with a length of up to several micrometers. After ABSA polymerized in and on the SWNTs matrix, the diameter of SWNTs increased. The nanocomposite film was uniformly cast on the electrode surface forming a homogenous, porous and three-dimensional film structure.

3.2. Cyclic voltammogram of TFP at modified electrode

As shown in Fig. 3, cyclic voltammogram of TFP was presented at the poly-ABSA/SWNTs/GCE in comparison with that at the correspondingly prepared SWNTs/GCE, poly-ABSA/GCE, and a bare GCE. The electrode process was irreversible. At the bare GEC (curve a), TFP exhibited a poor electrochemical response. At the SWNTS/GCE (curve b), two well-formed anodic peaks of TFP appeared at about 0.78 V and 0.93 V, respectively. The large oxidation current may be attributed to the enlarged effective surface area of the electrode by the SWNTs modification. TFP presented much larger oxidation currents at poly-ABSA/GCE (curve c). The reason may be as follows: ABSA has electron-rich N atom and high electron density of sulphonic group. Hence, the poly-ABSA film is negatively charged, which can greatly attract TFP cation. However, at the poly-ABSA/SWNTs/GCE, TFP exhibited more sensitive electrochemical response with anodic peaks at 0.72 V and 0.94 V, respectively (curve d). The peak current was increased greatly and the anodic peak 1 potential shifted negatively 37 mV and 64 mV compared with polymer and SWNTs-modified electrode, respectively. It was ascribed to a composite effect of the SWNTs and polymer, so TFP can be effectively accumulated on the modified electrode surface.

The electrochemical behavior of TFP at modified electrode was similar to the reference reported [27]. The reaction mechanism may be described as follows: TFP can lose two electrons in oxidation process. If two electrons were lost together in one step, there was only one anodic peak. But under the condition with poly-ABSA/SWNTs film, the two electrons were lost in two steps, thus two peaks appeared. Additionally, the anodic peak shift observed in peak 1 was not observed in peak 2. The reason may be attributed to the formation of relative stable product in the first step. As the anodic peak at 0.72 V was more sensitive, it was chosen as the analytical signal.

3.3. Effect of scan rate

The effect of the scan rate (υ) on TFP peak current was investigated. As shown in Fig. 4, the potential scan window was from 0 to +1.0 V and the anodic peak at about 0.72 V was chosen as analytical signal. The anodic peak current grew continuously with scan rate increasing. It was found that anodic peak current was proportional to the scan rate over the range of 50–500 mV s^{-1}. The linear regression equation was i_p (10 μA) = 2.1192 + 0.0099υ (mV s^{-1}), with a correlation coefficient of 0.998. Therefore, the contribution of adsorption played a more important role in the electrode process. In addition, the

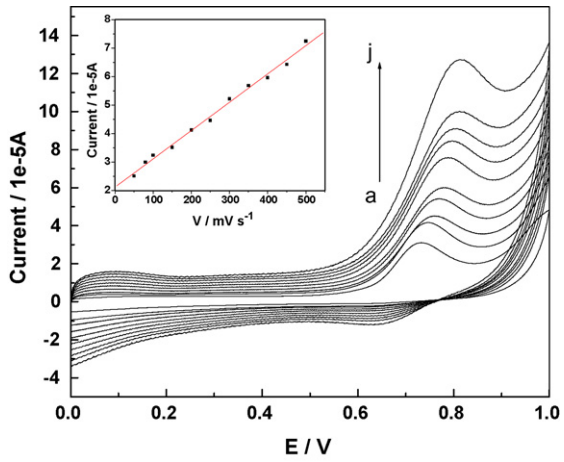


Fig. 4. Cyclic voltammograms at the poly-ABSA/SWNTs/GCE in the presence of 1.0×10^{-5} mol L^{-1} TFP in pH 6.1 PBS at scan rate of (a–j): 50, 80, 100, 150, 200, 250, 300, 350, 400, 450 and 500 mV s^{-1}. Inset: plot of the anodic current vs. the scan rate.

peak potential and the logarithm of scan rate showed a linear relationship, following the equation:

$$E_p = 0.584 + 0.0386 \ln \upsilon \, (E_p(V, r = 0.0994)$$

According to the equation [28]:

$$I_p = n^2 F^2 \upsilon A \Gamma_0^* / 4RT = nFQ\upsilon / 4RT$$

thus n was calculated to be 1.1, meaning two electrons were lost in two steps. It was in accordance with TFP oxidation mechanism as described in Section 3.2.

The adsorbed amount of TFP on the modified electrode should be related to the feature of the nanocomposite film. With the SWNTs porous 3D structure, electropolymerized ABSA film can provide high active surface and catalytic activities. As TFP exists as a cation at neutral pH, electrostatic attraction between the TFP cations and the negative sulphonic groups at the modified electrode promoted the electron transfer. So the TFP can be sensitively detected.

3.4. Optimization of the analytical conditions

The surface adsorption and catalytic activity of the poly-ABSA/SWNTs/GCE provided the applicability for determination of TFP. For higher sensitivity and better potential resolution, the differential pulse voltammetry (DPV) technique was used. Because of the surface adsorption of TFP, the effect of surface accumulation time was investigated when accumulation potential was changed from −0.5 to 0.6 V. The results showed the peak current of TFP increased with extending time of the accumulation in the first 60 s, and then became constant afterward. The optimized accumulation time was selected as 80 s.

In addition, the effect of solution pH on the response of TFP was investigated over the range of 3–10. Anodic peak current increased with the increase of solution pH until it reached 6.1 and then decreased. The mechanism of pH effect may be as follows: the negative sulfonic group on electrode surface is increased with increase of pH, so more TFP cations were attracted to electrode surface. The TFP anodic peak current increased with the pH over the range of 3–6.1. Then the protonated degree of TFP decreased with the increase of pH. In basic surrounding, TFP turned into neutral molecule and it became difficult for the TFP to accumulate on the composite film modified electrode. Thus, pH 6.1 was chosen as the optimum pH value.

3.5. Electrochemical impedance characterization of modified electrode

The EIS experiments were carried out in 5.0×10^{-3} mol L^{-1} $K_3[Fe(CN)_6]/K_4[Fe(CN)_6]$ solution. Fig. 5 shows the type complex plane diagram (Z'' versus Z', Nyquist plot) of the EIS obtained at the bare electrode (a), SWNTs (b), poly-ABSA (c), and poly-ABSA/SWNTs-modified electrode (d). Curve b was a line, indicating SWNTs prominent electricity. Curve c and d included a semicircle part and a linear part, the semicircle part at higher frequencies corresponds to the electron-transfer limited process, and the linear part at lower frequencies corresponds to the diffusion process. The electron-transfer resistance, R_{et}, equals to 4.5 and 1.3 kΩ, respectively. The resistance became larger at higher frequencies while slope became smaller at lower frequencies after modification polymer. The reason should be as follows: poly-ABSA contains negatively charged sulphonic group, so larger repulsion effect is between the negatively charged $[Fe(CN)_6]^{3-/4-}$ and the negatively charged polymer film [29].

EIS can give information on the impedance changes of the electrode surface with different immersion time. The poly-ABSA/SWNTs/GCE was dipped into PBS containing 2.0×10^{-3} mol L^{-1} TFP, and then was washed with double distilled water, then put into 5.0×10^{-3} mol L^{-1} $[Fe(CN)_6]^{3-/4-}$ to perform the EIS experiments. The immersion time of the modi-

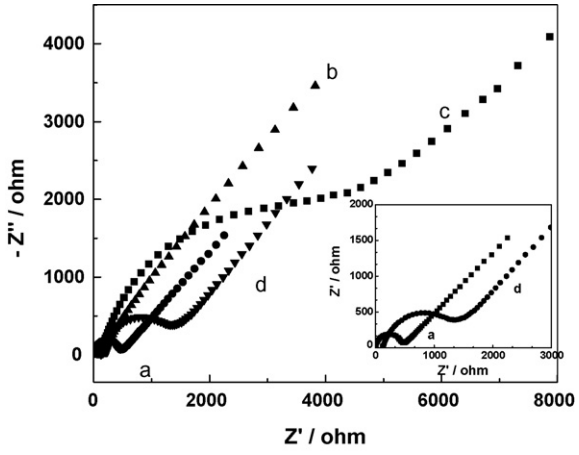


Fig. 5. The Nyquist diagram (Z'' vs. Z') for the EIS measurements in 5.0×10^{-3} mol L^{-1} $[Fe(CN)_6]^{3-/4-}$ by applying an ac voltage with 5 mV amplitude in a frequency range from 0.05 to 100 kHz. (a) the bare, (b) the SWNTs, (c) the poly-ABSA and (d) the poly-ABSA/SWNTs-modified electrode. Inset displays Nyquist plots of bare (curve a) and poly-ABSA/SWNTs modified (curve d) electrodes for a clear comparison.

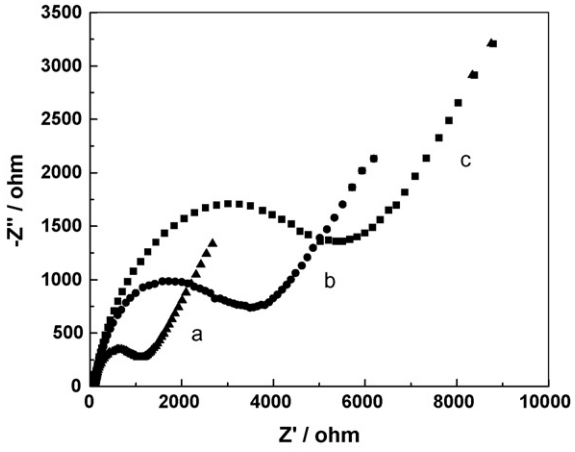


Fig. 6. The Nyquist diagram (Z'' vs. Z') for the EIS measurements under different adsorption time. (a) 0 h (b) 24 h and (c) 48 h. Other conditions as in Fig. 5.

fied electrode in the TFP solution had great effect on the surface state and the electron-transfer impedance.

Fig. 6 shows the complex plane diagram of EIS after the modified electrode soaked in TFP solution at various time, which indicated that the adsorption had an important effect on electron transfer impedance. It can be seen that the diameter of the semicircle increased to higher frequencies with the increase of adsorption time. That is to say, the longer that the modified electrode soaked in TFP solution, the larger the interfacial electron-transfer resistance was. The reason can still be due to repulsion between the probe ions and the polymer film [30]. When the soaking time in the TFP solution was over 48 h, there was no dramatically change of the interfacial electron-transfer resistance, which meant the adsorption of TFP reached a saturated state.

3.6. Calibration curve and interference

The DPV curves of the nanocomposite film modified electrode in the presence of TFP in the PBS were shown in Fig. 7.

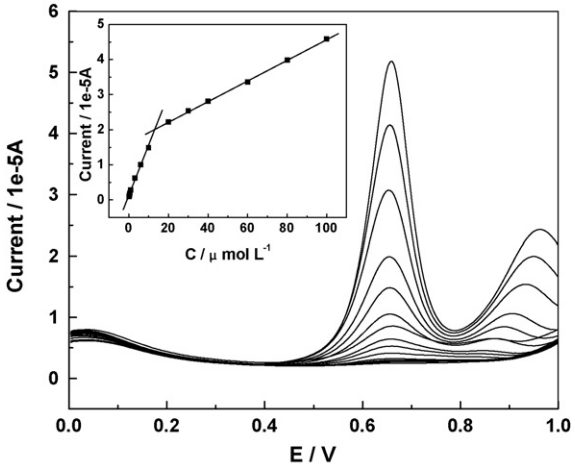


Fig. 7. DPV recordings of TFP at poly-ABSA/SWNTs modified electrode in pH 6.1 PBS. TFP concentration (a–p): 0.003, 0.006, 0.01, 0.02, 0.03, 0.06, 0.1, 0.3, 0.6, 1, 3, 6, 10, 30, 60 and 100 μmol L^{-1}.

Table 1
Determination results of trifluoperazine in drug tablets ($n = 6$)

Sample	Labeled (mg/mL)	Found (mg/mL)	R.S.D. (%)	Recovery (%)	UV method (mg/mL)
1	0.20	0.192	3.5	96.0	0.198
2	0.20	0.201	2.7	100.5	0.205
3	0.20	0.204	3.1	100.2	0.207
4	0.20	0.196	2.6	98.0	0.203
5	0.20	0.207	3.8	103.5	0.208

The i_{pa} of TFP at 0.64 V was proportional to the concentration over two intervals, *viz.*, 1.0×10^{-7} to 1.0×10^{-5} mol L^{-1} and 1.0×10^{-5} to 1.0×10^{-4} mol L^{-1}. The linear regression equation was i_p (μA) = 14.7116 + 0.3142C(μmol L^{-1}) and i_p (μA) = 16.3880 + 0.2929C (μmol L^{-1}), with the correlation coefficient 0.998 and 0.999, respectively. The detection limit (S/N = 3) was 1.0×10^{-9} mol L^{-1}. The relative standard deviation of 10 successive scans was 3.2% for 1.0×10^{-5} mol L^{-1} trifluoperazine, indicating excellent reproducibility of modified electrode.

The influence of foreign compounds was tested. It was found that the poly-ABSA/SWNTs/GCE could also electrocatalyze the oxidization of some other compounds. Dopamine, adrenalin and ascorbic acid gave anodic peak at 0.16, 0.18 and −0.01 V, respectively. These compounds have no interference with the TFP determination. Furthermore, 100-fold antipyrine, norfloxacin, propranolol, clozapine, hippuric acid, citric acid, cysteine, glucose, 50-fold imipramine and clomipramine had no obvious effect on the determination. 200-fold metal ions such as Cu^{2+}, Fe^{3+}, Pb^{2+}, Zn^{2+}, Ca^{2+} had no interference too. However, fluphenazine and phenylephrine interfered severely.

In addition, the stability of the modified electrode has been investigated. The peak current was daily testing in the pH 6.1 PBS containing 1.0×10^{-5} mol L^{-1} TFP. No apparent decrease in the current response was found over 5 days, and ∼28% decrease after 7 days and kept almost constant afterward.

3.7. Analytical applications

Under the optimum conditions, the poly-ABSA/SWNTs/GCE modified electrode was applied to the determination of TFP in tablets. The pretreatment and determination procedure were the same as described in Section 2.1. The analytical results were shown in Table 1, the recovery was 96–103.5%. It was in accordance with the result by the China Pharmacopoeia method (the UV absorbance of TFP at 256 nm in 1:20 HCl solution was chosen as the quantitative criterion) [31], showing that the proposed methods could be efficiently used for routine analysis.

4. Conclusions

The ABSA has been polymerized on the surface of SWNTs functionalizing glassy carbon electrode with the electrochemical method to fabricate an electrochemical biosensor, poly-ABSA/SWNTs/GCE. The prepared electrode was active for both the surface adsorption and electrocatalyze the oxida-

tion of TFP. The nanocomposite film can effectively attract TFP cations through negative poly-ABSA film and SWNT porous 3D structure. This electrode was sensitive, reproducible, stable, and can be used as an amperometric biosensor for routine analysis of total TFP in real samples.

Acknowledgements

The authors gratefully acknowledge the financial support from the National Nature Science Foundation of China (Grant No: 20335040, 20525519, 20605005 and 90606014).

References

[1] S. Holroyd, R.L. Seward, Clin. Pharmacol. Ther. 66 (1999) 323.
[2] K. Basavaiah, G. Krishnamurthy, Talanta 46 (1998) 665.
[3] R.Y. Wang, X.N. Lu, H.J. Xin, M.J. Wu, Chromatographa 51 (2000) 29.
[4] K. Basavaiah, G. Krishnamurthy, Talanta 47 (1998) 59.
[5] T. Perezruiz, C. Martinezlozano, V. Tomas, C.S. Decardona, Talanta 40 (1993) 1361.
[6] E.M. Abdel-Moety, K.A. Al-Rashood, A. Rauf, N.A. Khattab, J. Pharm. Biomed. Anal. 14 (1996) 1639.
[7] E. Bioship, W. Hussein, Analyst 109 (1984) 73.
[8] M.F. Chalin, C. Buche, Enzyme Technology, Cambridge University Press, Cambridge, UK, 1990.
[9] F.A. Armstrong, H.A. Heering, J. Hirst, Chem. Soc. Rev. 26 (1997)169.
[10] J.F. Rusling, A.E.F. Nassar, J. Am. Chem. Soc. 115 (1993) 11891.
[11] J. Yang, N.F. Hu, Bioelectrochem. Bioenerg. 48 (1999) 117.
[12] P.J. Britto, K.S.V. Santhanam, P.M. Ajayan, Bioelectrochem. Bioenerg. 41 (1996) 121.
[13] H. Yao, N. Li, J.Z. Xu, J.J. Zhu, Talanta 71 (2007) 550.
[14] C.Y. Liu, A.J. Bard, F. Wudl, Solid State Lett. 2 (1999) 577.
[15] X. Chu, D.X. Duan, G.L. Shen, R.Q. Yu, Talanta 71 (2007) 2040.
[16] P.J. Britto, K.S.V. Santhanam, V. Alonso, A. Rubio, P.M. Ajayan, Adv. Mater. 11 (1999) 154.
[17] F.H. Wu, G.C. Zhao, X.W. Wei, Electrochem. Commun. 4 (2002) 690.
[18] Y.J. Zou, L.X. Sun, F. Xu, Talanta 72 (2007) 437.
[19] S.J. Tans, M.H. Devoret, H. Dai, A. Thess, R.E. Smalley, L.J. Geerligs, C. Dekker, Nature 386 (1997) 474.
[20] Y. Ohnuki, T. Ohsaka, H. Matsuda, N. Oyama, J. Electroanal. Chem. 158 (1983) 55.
[21] Y.F. Sha, L. Qian, Y. Ma, H.X. Bai, X.R. Yang, Talanta 70 (2006) 556.
[22] R.F. Lane, C.D. Blaha, Langmuir 6 (1990) 56.
[23] A.G. Ewing, M.A. Dayton, R.M. Wightman, Anal. Chem. 53 (1981) 1842.
[24] J.S. Mattson, T.T. Jones, Anal. Chem. 48 (1976) 2164.
[25] G.Y. Jin, Y.Z. Zhang, W.X. Cheng, Sens. Actuator B: Chem. 107 (2005) 528.
[26] F. Xu, M.N. Gao, L. Wang, G.Y. Shi, W. Zhang, L.T. Jin, J. Jin, Talanta 55 (2001) 329.
[27] J. Karpinska, B. Starczewska, H. Puzanowska-Tarasiewcz, Anal. Sci. 12 (1996) 161.
[28] A.J. Bard, L.R. Faulkner, Electrochemical Methods: Fundamentals and Applications, 1st ed., John Wiley & Sons, New York, 1980, p. 595.
[29] G. Wang, J.J. Xu, H.Y. Chen, Electrochem. Commun. 4 (2002) 506.
[30] G.C. Zhao, L. Zhang, X.W. Wei, Z.S. Yang, Electrochem. Commun. 5 (2003) 825.
[31] Pharmacopoeia of People's Republic of China, The pharmacopoeia committee of PR China (Part II), Chemical Industry Press, Beijing, 2005, p. 461.

Available online at www.sciencedirect.com
ScienceDirect
Talanta 74 (2008) 867–870
Talanta
www.elsevier.com/locate/talanta

Determination of trace chlorine dioxide based on the plasmon resonance scattering of silver nanoparticles

Cai Yan Kang [a,b], Dan Li Xi [a,*], Yuan-Yuan Chen [b], Zhi Liang Jiang [b,c,**]

[a] College of Environmental Science and Engineering, Donghua University, Shanghai 200051, China
[b] School of Environment and Resource, Guangxi Normal University, Guilin 541004, China
[c] Department of Material and Chemical Engineering, Guilin University of Technology, Guilin 541004, China

Received 10 April 2007; received in revised form 18 July 2007; accepted 19 July 2007
Available online 6 August 2007

Abstract

A plasmon resonance scattering (PRS) method for chlorine dioxide is reported based on the oxidization of silver nanoparticles (NPs) by it, in pH 9.1 ammonia–ammonium nitrate buffer solutions. Silver NPs exhibit strong PRS signals at 470 nm, and can be oxidized by ClO_2, which results in PRS quenching at 470 nm. It was found that the PRS quenching intensity is proportional to the concentration of chlorine dioxide over the range of 0.0011–0.185 μg/mL, with a detection limit (3σ) of 0.00050 μg/mL and the correlation coefficient of 0.9995. The method is simple, rapid and cost effective. It was applied to the determination of chlorine dioxide in drinking water, with satisfactory results.
© 2007 Elsevier B.V. All rights reserved.

Keywords: Chlorine dioxide; Silver nanoparticle; Plasmon resonance scattering quenching

1. Introduction

Chlorine is the most widely used chemical disinfectant for treatment of drinking water. However, the water chlorination results in the formation of trihalomethanes (THMs) [1], which are possible carcinogens. Therefore the use of chlorine dioxide as alternative disinfectant has become increasingly attractive. Because there are some health effects [2] associated with chlorine dioxide and its inorganic byproducts like chlorite and chlorate ions, accurate methods for determination of these species are required.

Several methods have been reported for the determination of ClO_2, including electrochemistry [3], spectrophotometry [4–8], flow injection analysis (FIA) [9], high-pressure liquid chromatography (HPLC) [10] and gas chromatography–mass spectrometry [11]. Electroanalytical-based procedures are often unattractive to routine analysis because they require regular cleaning and regeneration of the electrodes. A voltammetric method was proposed to determine 2 μg L^{-1} ClO_2 [3], however, the operation was time-consuming. *N*,*N*-Diethyl-*p*-phenylenediamine (DPD) method has conventionally been used to monitor chlorine dioxide residuals, but reagent is toxic and harmful to operator's health, and the repeatability and selectivity are poor [4]. Using a purge trap preconcentration system, a FIA procedure was presented for the analysis of 0.005–1.5 mg L^{-1} ClO_2 with a detection limit of 0.005 mg L^{-1} [9]. HPLC is an analytical technique with high separation efficiency. A post-column assay was proposed for the determination of ClO_2 as low as 1 mg L^{-1}, with good accuracy [10] and a highly sensitive GC–MS method was reported for the determination of 1.0 ng L^{-1} ClO_2, but the operation is complex and the cost was expensive [11]. Therefore it is very necessary to establish a simple, rapid, sensitive, selective method for the determination of ClO_2.

Resonance scattering (RS) was a new, sensitive and simple spectral analytical technique, and was applied to determination of trace substances, with satisfactory results [12–15]. Recently, it has been reported that some metal NPs such as nanosilver exhibited novel optical and electronic properties, and were utilized to nanoanalytical chemistry [16–18]. For example, the PRS of silver NPs were used to detect trace organic substance such as sudan red [19]. Up to date, there is no report about a PRS method for ClO_2, using silver NPs.

* Corresponding author.
** Corresponding author at: School of Environment and Resource, Guangxi Normal University, Guilin 541004, China.
E-mail address: zljiang@mailbox.gxnu.edu.cn (Z.L. Jiang).

0039-9140/$ – see front matter © 2007 Elsevier B.V. All rights reserved.
doi:10.1016/j.talanta.2007.07.032

2. Experimental

2.1. Reagent

ClO_2 standard solution: a stock solution containing about 40 μg/mL ClO_2 was prepared with a laboratory scale generator by the reaction between sodium chlorite and sulfuric acid [20]. Trace Cl_2 was adsorbed and removed through saturated $NaClO_2$ solution. Pure ClO_2 solution was thereby obtained. Its concentration was standardized by iodiometry or by spectrophotometry [21] and its molar absorptivity was 1250 L/mol cm. The standard solution was stored in refrigerator (4 °C). The working solution of ClO_2 was obtained by diluting the standard solution.

A silver NPs (*a* 1.00×10^{-4} mol/L, calculated by concentration of Ag) was prepared according to reference [22]. A pH 8.3–11.0 buffer solution of NH_4NO_3–$NH_3 \cdot H_2O$ was used. All of the reagents were of analytical grade and all of the water used throughout was distilled doubly.

2.2. Apparatus

The PRS spectrum was obtained by means of synchronous scanning of the emission wavelength λ_{em} and excited wavelength λ_{ex} ($\lambda_{ex} - \lambda_{em} = \Delta\lambda = 0$). The plasmon absorption was measured with a model TU-1901 double beams UV–vis spectrophotometer (Beijing Purkinje General Instrument Limited Company, China). A model H-600 transmission electron microscope (Electronic Stock Limited Company) was used to measure the TEM images of silver NPs. A model of NaNo-ZS90 particle sizer and Zeta potentiometric analyzer were used to record the particle size distribution and its density distribution in solution. The average particle size was also given by the NaNo-ZS90 particle sizer. A model 79-1 magnetic heat agitator (Zhongda Instrumental Plant, Jiangsu, China) was used for the preparation of silver colloid. A model L8-60M ultracentrifuge (Beckman Instruments, Inc., USA) was used to separate silver NPs and solution. A model WFX-110 atomic absorption spectrophotometer (AAS) (Bijing Ruili Analytical Instrument Company, China) was used.

2.3. Procedure

A 0.50 mL of pH 9.1 NH_4NO_3–$NH_3 \cdot H_2O$ buffer solution, 0.30 mL of silver nanoparticle solution and certain volume of chlorine dioxide solution were added successively into a 10-mL marked tube. The mixed solution was then diluted to 5 mL with doubly distilled water and mixed thoroughly. Then the spectrum and the PRS intensity at 470 nm *I* were recorded. The reagent blank (I_0) was measured and the value of $\Delta I = I_0 - I$ was calculated.

3. Results and discussion

3.1. Characterization of silver NPs reaction

TEM, laser scattering, AAS and the colored reagents were used to study the silver NPs reaction. TEM images of sil-

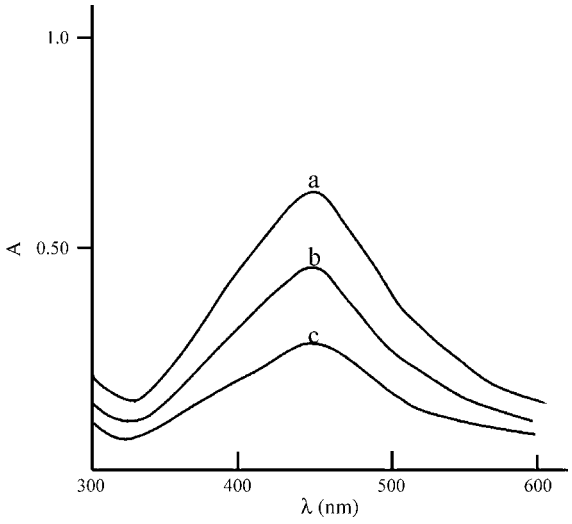


Fig. 1. Plasmon absorption spectra of silver-nanoparticle system. (a) 1.4×10^{-4} mol/L Ag; (b) *a*-1.0 μg/mL ClO_2; (c) *a*-2.0 μg/mL ClO_2.

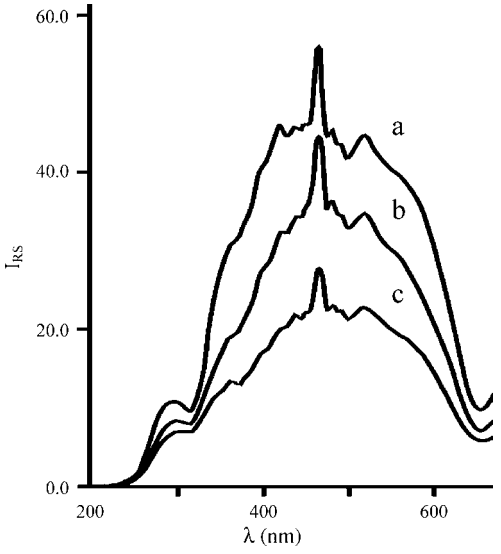


Fig. 2. PRS spectra of silver NPs system. (a) 6.0×10^{-6} mol/L Ag; (b) *a*-0.216 μg/mL ClO_2; (c) *a*-0.503 μg/mL ClO_2.

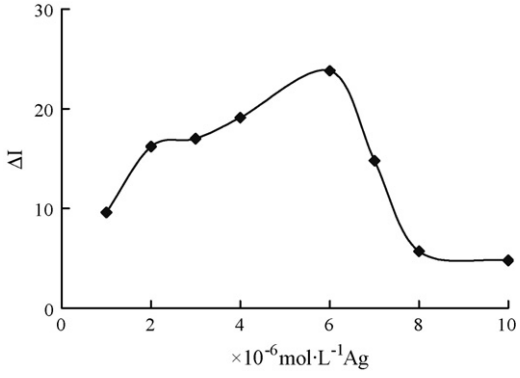


Fig. 3. Effect of silver nanoparticle concentration pH 9.1–0.414 μg/mL ClO_2. Low sensitivity, ordinate scale 7.

Table 1
Influence of foreign substance (FS) (0.083 μg/mL ClO_2)

FS	Tolerance (μg/mL)	Relative error (%)	FS	Tolerance (μg/mL)	Relative error (%)
Cu^{2+}	3.2	+4.6	ClO_3^-	2200	−3.8
K^+	348	−5.0	Hg^{2+}	8.0	+4.2
Na^+	170	−4.2	Mn^{2+}	0.3	+1.2
Cd^{2+}	4.2	+5.6	Br^-	140	+3.8
Zn^{2+}	3.21	+2.6	IO_3^-	0.40	+3.8
Ni^{2+}	3.1	−2.4	IO_4^-	4.6	+4.6
Co^{2+}	3.1	+4.3	Ac^-	300	−2.4
Al^{3+}	17.6	+4.6	ClO_2^-	3.6	+2.1
Pb^{2+}	5.31	−5.0	Urea	50	+2.8
$C_2O_4^{2-}$	10.0	+4.9	ClO^-	20	+5.0
Mg^{2+}	8.0	+2.2	Tartrate	100	+5.4

Table 2
Comparison of several methods for ClO_2

Methods[a]	Linear range (μg/mL)	Detection limit (μg/mL)	Comments	Reference
RhB Spect	0–1.5	0.040	Cl_2, ClO_2^- do not interfere	[8]
CPR Spect	0.13–1.9	0.12	Cl_2, ClO_2^- do not interfere	[6]
DPD Spect	0.60–40	0.30	Cl_2, ClO_2^- do not interfere	[4]
LG Spect	0–0.5	0.03	Cl_2, ClO_2^- do not interfere	[5]
4-AA FI	0.005–1.5	0.005	ClO_2^-, ClO^- do not interfere	[9]
4-AA HPLC	1–20	0.2	ClO_2^-, ClO^- do not interfere	[10]
Ag PRS	0.0011–0.185	0.0005	Cl_2, ClO_2^- do not interfere	This method

[a] Spect represents spectrophotometry; RhB represents rhodamine B; CPR represents chlophonel red; DPD represents *N*,*N*-diethyl-*p*-phenylenediamine; LG represents lissamine green; 4-AA represents 4-aminoantipyrine.

ver NPs showed that the number of silver NPs obviously reduced after adding ClO_2. This demonstrated that the silver NPs were oxidized to Ag^+ by ClO_2. Laser scattering showed that the average size of silver NPs was about 54.1 nm. After ClO_2 was added into the silver NPs, the size increased to 98.8 nm. This is because that smaller size silver NPs have stronger reaction activity, and can react preferentially with ClO_2.

To demonstrate the product was Ag^+, the mixture of the ClO_2–silver NPs was separated at 30,000 rpm for 10 min on the centrifuge, and the atomic absorption value of the top pellucid liquid was measured, under the conditions of 328.1 nm, 2 mA lamp current, 0.4 nm spectral pass band, air/acetylene flow rate of 6.5 L min^{-1}/1.5 L min^{-1}. Results showed that the value increased with increasing ClO_2. This identified that the product was Ag^+. Phenanthroline and bromopyrogallol red were good colored reagents for Ag^+ [23]. The mixed solution of the top pellucid liquid-phenanthroline–bromopyrogallol red was in blue color. This was also indicated that there are silver ions in the top pellucid liquid.

3.2. Plasmon absorption and resonance scattering spectra

The silver NPs were stable in yellow color. Fig. 1 indicates that the adsorption band of the silver NPs over the range of 360–520 nm, characterized at 460 nm, should be ascribed to the plasmon absorption of silver NPs according to references [19,24]. The absorption peak at 460 nm reduced with increasing chlorine dioxide, while the color turned from light yellow to colorless. It could be concluded that chlorine dioxide oxidizes silver NPs to Ag^+. The light scattering signals being in the region of absorption band should be ascribed to the resonance scattering [25–27]. Fig. 2 shows that silver NPs exhibited a PRS peak 470 nm. A wavelength of 470 nm was chosen for use.

3.3. Effect of pH value

NH_4NO_3–$NH_3{\cdot}H_2O$ is one of the favorable masking agents for free chlorine, which can efficiently eliminate the effect of free chlorine on the determination of chlorine dioxide [5,8], so NH_4NO_3–$NH_3{\cdot}H_2O$ buffer solution was used to adjust pH value.

Table 3
Results for the determination of ClO_2 in water

Sample no.	Found (μg/mL)	Means value (μg/mL)	R.S.D. (%)	Reference [14] (μg/mL)
1	0.0308, 0.0324, 0.0312, 0.0320, 0.0316	0.0316 ± 0.0006	2.0	0.0319
2	0.0453, 0.0442, 0.0465, 0.0457, 0.0446	0.0453 ± 0.0009	2.1	0.0455
3	0.0618, 0.0621, 0.0633, 0.0618, 0.0610	0.0620 ± 0.0008	1.3	0.0614
4	0.0812, 0.0830, 0.0824, 0.0845, 0.0860	0.0834 ± 0.0019	2.2	0.0826
5	0.111, 0.120, 0.119, 0.113, 0.116	0.116 ± 0.0038	3.3	0.120

The effect of the pH value on ΔI was examined in the range of 8.3–11.0. The result showed that when pH value is in the range of 8.89–10.4, ΔI value is comparatively bigger. Thus, a pH value 9.1 was chosen for the system and the volume of NH_4NO_3–$NH_3{\cdot}H_2O$ buffer solution was 0.50 mL.

3.4. Effect of silver nanoparticle concentration

As is shown in Fig. 3, when silver nanoparticle concentration is 6.0×10^{-6} mol/L, the ΔI value reached its maximum. Therefore, a concentration of 6.0×10^{-6} mol/L silver NPs was selected.

3.5. Stability of the system

According to the procedure, the effect of the reaction time on the ΔI value was tested. The results show shat after the reaction carry out for 15 min, the ΔI value reached its maximum and was stable at least 60 min.

3.6. Effect of coexistence substances

The effects of coexistence substances on the PRS were examined according to the procedure. When chlorine dioxide concentration was 0.083 μg/mL, the tolerance and relative error are shown in Table 1. It can been seen from Table 1 that most of the ions normally present in water do not interfere with the determination, the tolerance of ClO^-, $ClO_2{}^-$ and $ClO_3{}^-$ are also comparatively bigger, which demonstrate the method as good selectivity.

3.7. Calibration graph

Under optimal experimental conditions, the relationship curve between the ΔI value and ClO_2 concentration (C) was plotted. The result indicated that the linear range was 0.0011–0.185 μg/mL, the regression equation was $\Delta I = 262.2C + 1.22$, with a detection limit of 0.00050 μg/mL. The selectivity and sensitivity of the proposed methods and this new method were presented in Table 2. It can be seen that the selectivity and sensitivity of this new method is better than that of the other methods and is one of the better analytical methods for determination of chlorine dioxide.

3.8. Samples analysis

A suitable volume of water sample was added to the 10-mL tube. The ClO_2 content of the samples was determined as the procedure and the results are given in Table 3. It can be seen that they are good agreement with results obtained using RhB spectrophotometry [8].

4. Conclusion

A simple, sensitive and selective PRS quenching method was proposed to detect 0.0011–0.185 μg/mL chlorine dioxide, based on ClO_2 oxidation of silver NPs to silver ions and the PRS quenching effect of silver NPs. This ClO_2 PRS quenching method was applied to analysis of ClO_2 in real sample, with satisfactory results.

References

[1] T.A. Bellar, J.J. Lichtenberg, R.C. Kroner, J. Am. Water Works Assoc. 66 (1974) 703.
[2] Drinking Water and Health: Disinfectants and Disinfectant By-products, vol. 7, National Academy Press, Washington, DC, 1987, p. 207.
[3] F. Quentel, C. Elleouet, C. Madec, Anal. Chim. Acta 295 (1994) 85.
[4] G. Fordon, W.J. Cooper, R.G. Rice, G.E. Pacey, Disinfectant Residual Measurement Methods, 2nd ed., American Water Works Association, Denver, CO, 1992, p. 142.
[5] B. Chiswell, K.R. O'Halloran, Analyst 116 (1991) 657.
[6] D.L. Sweetin, E. Sullivan, G. Gordor, Talanta 43 (1996) 103.
[7] Z.L. Jiang, B.M. Zhang, A.H. Liang, Talanta 66 (2005) 783.
[8] X. Zang, Analyst 120 (1995) 1199.
[9] T. Watanabe, T. Ishii, Y. Yoshimura, H. Nakazawa, Anal. Chim. Acta 341 (1997) 257.
[10] T. Watanabe, T. Idehara, Y. Yoshimura, J. Chomatogr. A 796 (1998) 397.
[11] H.S. Shin, D.G. Jung, J. Chromatogr. A 1123 (2006) 92.
[12] C.Z. Huang, Y.F. Li, Talanta 70 (2006) 609.
[13] A.H. Liang, S.M. Zhou, Z.L. Jiang, Tlanta 70 (2006) 444.
[14] H. Zhong, J.J. Xu, H.Y. Chen, Talanta 67 (2005) 749.
[15] C.Y. Kang, D.L. Xi, S.M. Zhou, Z.L. Jiang, Talanta 68 (2006) 974.
[16] Y. Liang, J.L. Gong, Y. Huang, Y. Zheng, J.H. Jiang, G.L. Shen, R.Q. Yu, Talanta 72 (2007) 443.
[17] Y.C. Cao, R. Jin, C.S. Thaxton, C.A. Mirkin, Talanta 67 (2005) 449.
[18] K. Aslan, P. Holley, L. Davies, J.R. Lakowicz, C.D. Geddes, J. Am. Chem. Soc. 127 (2005) 12115.
[19] L.P. Wu, Y.F. Li, C.Z. Huang, Q. Zhang, Anal. Chem. 78 (2006) 5570.
[20] X.D. Liu, Chin. J. Anal. Chem. 30 (2002) 50.
[21] R.G. Kieffer, G. Gordon, Inorg. Chem. 7 (1968) 235.
[22] F.X. Zhong, Z.L. Jiang, F. Li, T.S. Li, Spectros. Spectr. Anal. 20 (2000) 724.
[23] S.X. Chai, C. Huang, Precious Metal Analysis, 1st ed., Metallurgical Industry Publishing House, Beijing, 1984, p. 195.
[24] L. Tokareva, E.J. Hutter, J. Am. Chem. Soc. 126 (2004) 15784.
[25] M. Hou, S.J. Sun, Z.L. Jiang, Talanta 72 (2007) 463.
[26] Z.L. Jiang, W.X. Huang, A.H. Liang, B. Chen, Talanta 73 (2007) 938.
[27] H.Y. Wang, Y.F. Li, C.Z. Huang, Talanta 72 (2007) 1698.

Available online at www.sciencedirect.com
ScienceDirect
Talanta 74 (2008) 879–886
Talanta
www.elsevier.com/locate/talanta

Glucose biosensors based on platinum nanoparticles-deposited carbon nanotubes in sol–gel chitosan/silica hybrid

Xinhuang Kang [a,b], Zhibin Mai [a], Xiaoyong Zou [a,*], Peixiang Cai [a], Jinyuan Mo [a]

[a] School of Chemistry and Chemical Engineering, Sun Yat-Sen University, Guangzhou 510275, PR China
[b] College of Science, Guangdong Ocean University, Zhanjiang 524088, PR China

Received 31 May 2007; received in revised form 22 July 2007; accepted 23 July 2007
Available online 31 July 2007

Abstract

A new strategy for fabricating a sensitivity-enhanced glucose biosensor was presented, based on multi-walled carbon nanotubes (CNT), Pt nanoparticles (PtNP) and sol–gel of chitosan (CS)/silica organic–inorganic hybrid composite. PtNP-CS solution was synthesized through the reduction of $PtCl_6^{2-}$ by $NaBH_4$ at room temperature. Benefited from the amino groups of CS, a stable PtNP gel was obtained, and a CNT–PtNP–CS solution was prepared by dispersing CNT functionalized with carboxylic groups in PtNP–CS solution. The CS/silica hybrid sol–gel was produced by mixing methyltrimethoxysilane (MTOS) with the CNT–PtNP–CS solution. Then, with the immobilization of glucose oxidase (GOD) into the sol–gel, the glucose biosensor of GOD–CNT–PtNP–CS–MTOS–GCE was fabricated. The properties of resulting glucose biosensor were measured by electrochemical impedance spectroscopy (EIS) and cyclic voltammetry (CV). In phosphate buffer solutions (PBS, pH 6.8), nearly interference free determination of glucose was realized at low applied potential of 0.1 V, with a wide linear range of 1.2×10^{-6} to 6.0×10^{-3} M, low detection limit of 3.0×10^{-7} M, high sensitivity of 2.08 μA mM^{-1}, and a fast response time (within 5 s). The results showed that the biosensor provided the high synergistic electrocatalytic action, and exhibited good reproducibility, long-term stability. Subsequently, the novel biosensor was applied for the determination of glucose in human serum sample, and good recovery was obtained (in the range of 95–104%).
© 2007 Elsevier B.V. All rights reserved.

Keywords: Glucose; Biosensors; Carbon nanotubes; Platinum nanoparticles; Sol–gel; Chitosan

1. Introduction

Since Clark and Lyons [1] reported their enzyme electrode for measuring glucose, great attention has been devoted to glucose biosensors [2–6]. It is important to develop the methods with high sensitivity, good reproducibility, fast response, and easy fabrication for the determination of glucose in both clinical diagnostics and food industry analysis. In recent years, nanomaterials, such as carbon nanotubes (CNT) and metal nanoparticles, have been widely applied to biosensors. CNT have good performances of high surface-to-volume ratios and fast electron-transfer kinetic for a wide range of electroactive species in the construction of biosensor [7–12]. Metal nanoparticles can display following unique advantages over macroelectrodes when used for electroanalysis: enhancement of mass transport, catalysis, high effective surface area and control over electrode microenviroment [13]. For example, Pt and Au nanoparticles are very effective as a matrix of enzyme sensors by taking advantage of the biocompatibility and huge surface [14,15]. Most work has been carried out using transition metal nanoparticles for biosensors, such as platinum [3], copper [4], silver [16] palladium [17], and gold [18]. Recently, there are some interesting researches on integrating nanoparticles with CNT to fabricate biosensors and easily to gain synergistic action with the hybrid of nanomaterials. The methods of nanohybridization are completed by solvent DMF [19], polymers, such as CS [20–22], Nafion [23–26], and an appropriate surfactant dihexadecyl hydrogen phosphate (DHP) [27]. The used techniques included sol–gel [3] process, metal nanoparticles self-assembly [28–31] and electrodeposition on the surface of CNT from metal salt solutions [32–35].

The immobilization of enzymes is a key step for the fabrication of biosensors. The common methods for immobilizing enzymes on electrodes include entrapment techniques [3], elec-

* Corresponding author. Fax: +86 20 84112455.
E-mail address: ceszxy@mail.sysu.edu.cn (X. Zou).

0039-9140/$ – see front matter © 2007 Elsevier B.V. All rights reserved.
doi:10.1016/j.talanta.2007.07.019

trochemical copolymerization [36], covalent or cross-linking [24], and adsorption [32]. Lately, sol–gel-derived materials have been applied for the immobilization of biomolecules to improve the performance of the biosensor [2,3,9,37,38]. The biosensor fabricated by this method possesses several advantages, such as high stability, wide potential window, and easy fabrication at room temperature and encapsulation for electrocatalysts and biocatalysts. Furthermore, porous and open frameworks of sol–gel ensure that the analytes can effectively and fast access to the active functionalities immobilized at the interface between electrode and solution, which results in a high sensitivity to the electrochemical response, as most electron transfer processes are diffusion-controlled. However, the silica sol–gel, which is common used, is brittle and low biocompatible. In order to overcome these obstacles, silica-based organic–inorganic hybrids are adopted as attractive composite materials for the fabrication of biosensors [39]. Some polymers are hybridized into a silica sol–gel matrix, such as polyhydroxyle (PVA–g–PVP) [2], CS [9,40], poly(vinyl alcohol)(PVA) [41], which can effectively avoid the brittleness of pure inorganic sol–gel and the swelling of some pure polymers.

In this work, a new glucose biosensor was developed, based on the signal-enhanced effect of CNT, PtNP and sol–gel of CS/silica organic–inorganic hybrid composite film. The properties of resulting glucose biosensor were characterized by EIS and CV. The resulting biosensor exhibited several advantages, such as high sensitivity at a low potential, good stability, and easy fabrication at room temperature and encapsulation for nanomaterials and biocatalysts. Furthermore, the biosensor was applied for the determination of glucose in human serum sample.

2. Experimental

2.1. Materials and apparatus

CNT (∼95% purity) were purchased from Shenzhen Nanotech Port Co. (China). Glucose oxidase (EC1.1.3.4, 195,000 unit g^{-1}) was obtained from Sigma. CS (90% deacetylated, MW $\sim 1 \times 10^6$) was bought from Shanghai Biochemical (China). Methyltrimethoxysilane (MTOS) was purchased from Aldrich. D-Glucose and H_2PtCl_6 were obtained from Guangzhou Chemical reagent company (China). PBS (20 mM KH_2PO_4 + 20 mM K_2HPO_4 + 0.1 M KCl, pH 6.8) was used as supporting electrolyte. A stock solution of D-glucose (0.1 M) was allowed to mutarotate at room temperature for 24 h before use.

The electrochemical experiments were performed with CHI660A electrochemical workstation (China). All experiments were carried out by three-electrode system with a glassy carbon electrode (GCE, $\Phi = 3$ mm) as the working electrode, a platinum wire as the auxiliary electrode, and an Ag/AgCl/3.0 M KCl as the reference electrode. JEM-2010 transmission electron microscope (TEM; Japan) was operated for the TEM experiment at an accelerating voltage of 200 kV. JSM-6330F scan electron microscopy (SEM; Japan) was applied for the SEM experiment. X-Ray diffraction (XRD) data of the sample was recorded on a Rigaku D/max 2200vpc diffractometer (Japan) using Cu Kα1 radiation ($\lambda = 0.154056$ nm) with a Ni filter.

2.2. Preparation of the modified electrodes

PtNP–CS solution was prepared according to the literature [20,42]. Briefly, CS solution was mixed with H_2PtCl_6, and then the reduction of $PtCl_6^{2-}$ by $NaBH_4$ yielded a clear black colored solution, which was designated as 100% PtNP stock solution. The other stock solutions were prepared by dispersing 2.0 mg CNT functionalized with carboxylic groups in 1.0 mL 0.2% CS solution or PtNP–CS solution. The sol–gel of CNT–PtNP–CS–MTOS was prepared by mixing 10 μL MTOS, 20 μL ethanol, and 1.0 mL CNT–PtNP–CS solution in a 2.0 mL PVC tube [9]. The mixture was sonicated for 10 min, and then stored at room temperature for 3 h. 10.4 mg GOD was dissolved in 1.0 mL PBS as a stock solution (2 U μL^{-1}), and stored at 4 °C. Fifty microliter CNT–PtNP–CS–MTOS sol–gel and 50 μL GOD solution were mixed in a 0.5 mL PVC tube. GOD–CNT–PtNP–CS–MTOS–GCE biosensor was fabricated after 8 μL of the mixture was dropped on the surface of GCE and dried at 4 °C in a refrigerator for 24 h. All the enzyme modified electrodes were stored at 4 °C in the dry state.

3. Results and discussion

3.1. Physical characterization of PtNP–CS and PtNP–CNT–CS–MTOS

TEM image (Fig. 1A) showed PtNP was well dispersed in the CS solution. The size of particles was observed around 3–4 nm, which illustrated that amino groups played an important role in the stabilization of PtNP in CS solution. No aggregation of the nanoparticles was noticed after 2 months. When CNT functionalized with carboxylic groups and MTOS were added and sonicated, the nanohybrid and sol–gel were formed. Fig. 1B depicted PtNP and CNT were dispersed in sol–gel. XRD spectrum of PtNP–CS composite was illustrated in Fig. 1C. The diffraction pattern clearly indicated there were three major peaks at 39.6°, 46.1° and 67.2°, which can be assigned to (1 1 1), (2 0 0), and (2 2 0) planes of the face-centered cubic lattice of Pt(0), respectively. Based on Scherrer formula [43], $L = 0.9\,\lambda_{Ka1}/B_{(2\theta)}\cos\theta_B$, where L is the average size of particles, λ_{ka1} the X-ray wavelength, $B_{(2\theta)}$ the peak broadening, and θ_B is the angle of the peak maximum. From the experimental result, L value of 4.1 nm was calculated, which is in good agreement with the result from the TEM image.

Robust and uniform CS membranes were easily formed at room temperature by evaporating water from CS solution, due to hydrogen bonds between hydroxy and amino groups. CS was hybridized with MTOS to improve the permeability of CS and to utilize the advantages of organic–inorganic hybrid materials. The hybrid film has good performance for the biosensor, when the ratio of MTOS and CS was 1:1 [9]. The SEM images showed that the CS–MTOS hybrid film was porous and open framework (Fig. 1D), and it was uniformity with GOD (Fig. 1E).

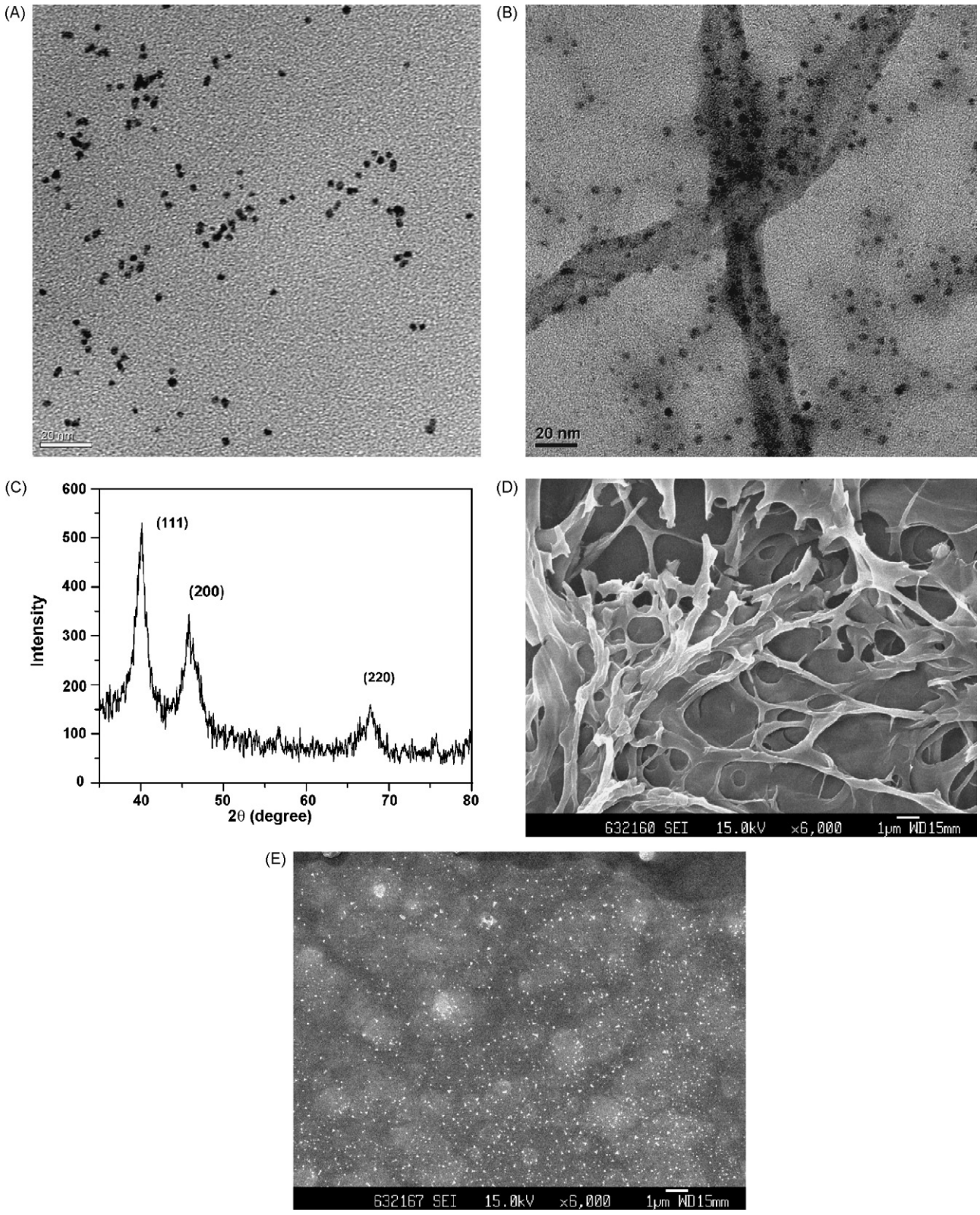


Fig. 1. TEM images of PtNP–CS solution (A) and CNT–PtNP–CS–MTOS sol–gel (B); XRD pattern of PtNP–CS composite (C); SEM images of the hybrid film of MTOS–CS (D) and GOD–MTOS–CS (E).

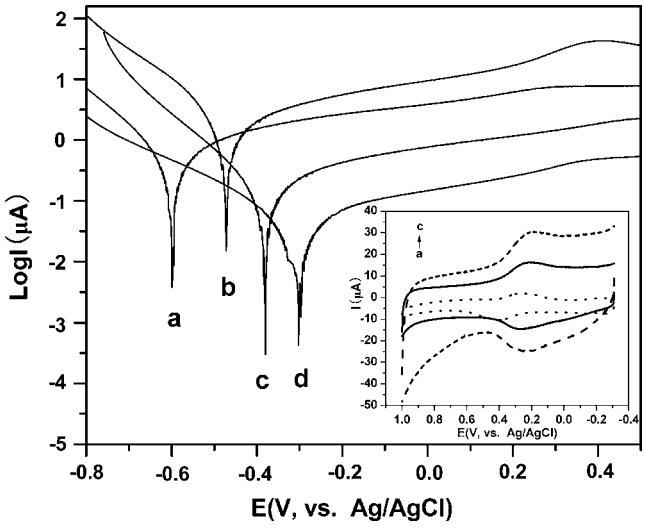


Fig. 2. (A) Polarization curves for unmodified and modified GCEs: (a–d) CNT–CS–MTOS–GCE, CNT–PtNP–CS–MTOS–GCE, PtNP–CS–MTOS–GCE, GCE in 0.5 M H_2SO_4 at 10 mV s^{-1}. Inset: CVs in 0.5 M H_2SO_4 at 50 mV s^{-1}: (a–c) PtNP–CS–MTOS–GCE, CNT–CS–MTOS–GCE, CNT–PtNP–CS–MTOS–GCE.

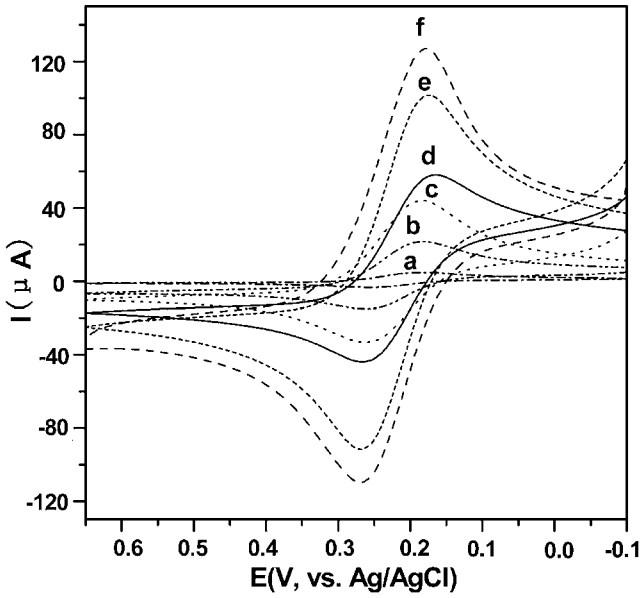


Fig. 3. CVs of unmodified and modified GCEs in 20 mM $[Fe(CN)_6]^{4-}$ with 0.2 M KCl at 20 mV s^{-1}: (a–f) CS–GCE, CS–MTOS–GCE, PtNP–CS–MTOS–GCE, CNT–CS–MTOS–GCE, GCE, CNT–PtNP–CS–MTOS–GCE.

3.2. Electrochemical characterization of the modified electrodes

Linear sweep voltammetry (LSV) was conducted for four different types of electrodes: bare GCE, CNT–CS–MTOS–GCE, PtNP–CS–MTOS–GCE and CNT–PtNP–CS–MTOS–GCE. The CNT–CS–MTOS–GCE provoked a negative shift of corrosion potential (E_{corr}) from −0.31 V of the bare GCE (Fig. 2d) to −0.60 V (Fig. 2a), due to the specific electrochemical properties of CNT. The E_{corr} of the PtNP–CS–MTOS–GCE (Fig. 2c) shifted from −0.31 V of the bare GCE to −0.38 V. The E_{corr} of the CNT–PtNP–CS–MTOS–GCE (Fig. 2b) shifted in the opposite direction from −0.60 to −0.47 V, which was ascribed to the more noble electrochemical characteristics of platinum. The variety of less negative values of potentials clearly showed that PtNP hybrid in sol–gel revealed higher stability of the CNT–PtNP–CS–MTOS–GCE. The CV (Fig. 2 inset c) indicated a high electrocatalytic activity for the oxygen reduction between −0.20 and + 0.40 V, which was in accordance with the literature [20]. Smaller currents to O_2 reduction were observed (Fig. 2 inset a and b) for the PtNP–CS–MTOS–GCE and CNT–CS–MTOS–GCE, respectively.

Fig. 3 showed the CVs of bare GCE and the modified electrodes in 20 mM $[Fe(CN)_6]^{4-}$ with 0.2 M KCl at 20 mV s^{-1}. Quasi-reversible one-electron redox behavior of ferricyanide ion was observed on the bare GCE (Fig. 3e) with a peak separation (ΔE_p) of 70 mV. After the electrode was modified with CS, the lower peak current (I_p) and larger ΔE_p were observed (Fig. 3a), due to the CS membrane hindering the diffusion of ferricyanide ion towards the GCE surface. For CS–MTOS–GCE (Fig. 3b), I_p increased in comparison with that of the CS–GCE, because of the sol–gel hybrid with porous and open frameworks. It was illustrated in Fig. 3c that larger I_p and smaller ΔE_p were observed for PtNP–CS–MTOS–GCE compared with CS–MTOS–GCE, which indicated that PtNP played a role in the increase of the electroactive surface area. Fig. 3d showed the voltammetric response of ferricyanide ion on the CNT–CS–MTOS–GCE because CNT have a very high catalytic active surface and aspect ratio. For CNT–PtNP–CS–MTOS–GCE (Fig. 3f), I_p was the highest among the electrodes. The results confirmed that the CNT–PtNP–CS–MTOS composite film, which was effectively immobilized on the GCE surface, can provide the necessary conduction pathways, and promote the electron transfer of analyte between the interface of solution and electrode. It also indicated the largest electroactive surface area, according to the Randles–Sevcik equation ($I_p = 2.69 \times 10^5 AD^{1/2} n^{3/2} \nu^{1/2} C$) [44]. The average value of the electroactive surface area for CNT–PtNP–CS–MTOS–GCE (1.0 mg/mL CNT in 100% PtNP sol–gel) was $(7.67 \pm 0.20) \times 10^{-2}$ cm^2 ($n = 6$), compared with $(7.07 \pm 0.10) \times 10^{-2}$ cm^2 ($n = 6$) for bare GCE.

EIS can provide information on the impedance changes of the electrode surface during the modification process. The electron-transfer resistance (R_{ct}) at the electrode surface is equal to the semicircle diameter. Fig. 4 presented the Nyquist plots of the impedance spectroscopy of the bare GCE and modified electrodes. The R_{ct} of CS film (Fig. 4g, 1050 Ω) was much larger than that of bare GCE (Fig. 4b, 180 Ω), which indicated that a film of CS was formed on the electrode surface, and could block the electron transfer of $[Fe(CN)_6]^{3-/4-}$ in some degree. For the porous film of MTOS–CS (Fig. 4f), R_{ct} decreased to 800 Ω compared with that of the CS film, because the electron transfer became easy between the solution and the electrode. After the films of PtNP–CS–MTOS and CNT–CS–MTOS were formed, R_{ct} decreased to about 520 and 400 Ω, respectively (Fig. 4e and d). When the film of CNT–PtNP–CS–MTOS was formed, R_{ct} was the lowest around 150 Ω (Fig. 4a), which was in accordance with the fact that the film of sol–gel integrated PtNP with CNT enhanced the synergistic electrocatalytic activity. The results

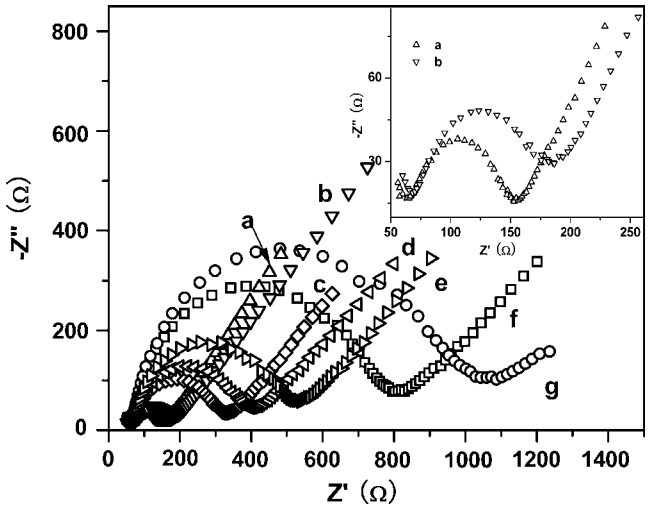


Fig. 4. Nyquist plots of EIS for: (a–g) CNT–PtNP–CS–MTOS–GCE, GCE, GOD–CNT–PtNP–CS–MTOS–GCE, CNT–CS–MTOS–GCE, PtNP–CS–MTOS–GCE, MTOS–CS–GCE, CS–GCE, inset: magnified of (a and b). Supporting electrolyte was 10 mM $[Fe(CN)_6]^{3-/4-}$ with 0.1 M KCl. The applied potential was 0.16 V.

were in agreement with CV (Fig. 3). However, R_{ct} increased to 340 Ω (Fig. 4c) by immobilizing the GOD onto the CS–MTOS.

3.3. Electrochemical performance of the glucose biosensor

CVs were shown in Fig. 5 for bare GCE and modified with CNT–PtNP–CS–MTOS in PBS without and with 0.1 mM H_2O_2. For the GCE modified with CNT–PtNP–CS–MTOS, the current signal to H_2O_2 (Fig. 5d) is higher than that of the bare GCE (Fig. 5b). The excellent electrocatalytic activity of the electrode to H_2O_2 made it attractive for the fabrication of biosensor, as H_2O_2 is a product of a number of oxidase-based enzyme reactions. Glucose oxidase was selected as a model enzyme. Many glucose biosensors are based on GOD, which catalyzes the oxidation of glucose to gluconolactone and hydrogen peroxide:

$$\text{Glucose} + O_2 \rightarrow H_2O_2 + \text{Gluconolactone}$$

The GOD–NT–tNP–CS–MTOS–GCE was formed by immobilizing GOD on the electrode surface through sol–gel of CS/silica organic–inorganic hybrid with CNT and PtNP.

The effect of pH and the amount of enzyme loaded in the composite on the response current of the biosensor was investigated (Fig. 6A). Maximum response current was obtained at pH 6.8, when 12 unit GOD was applied for the determination of 0.5 mM glucose at 0.4 V. Fig. 6B depicted that the current signals increased with the varying content of CNT from 0.2 to 1.0 mg mL^{-1}, due to the increase of electroactive material in the composite. No changes of the response current were

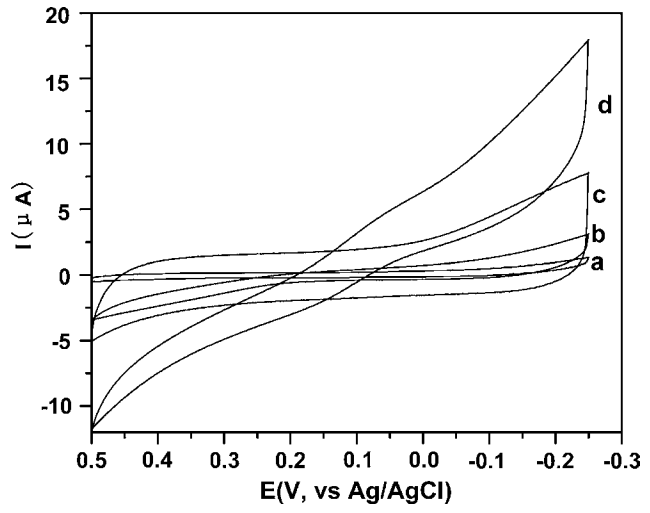


Fig. 5. CVs of GCE (a, b) and CNT-PtNP-CS-MTOS-GCE (c, d) in PBS at 50 mV s^{-1} in the absence (a, c) and presence (b, d) of 0.1 mM H_2O_2.

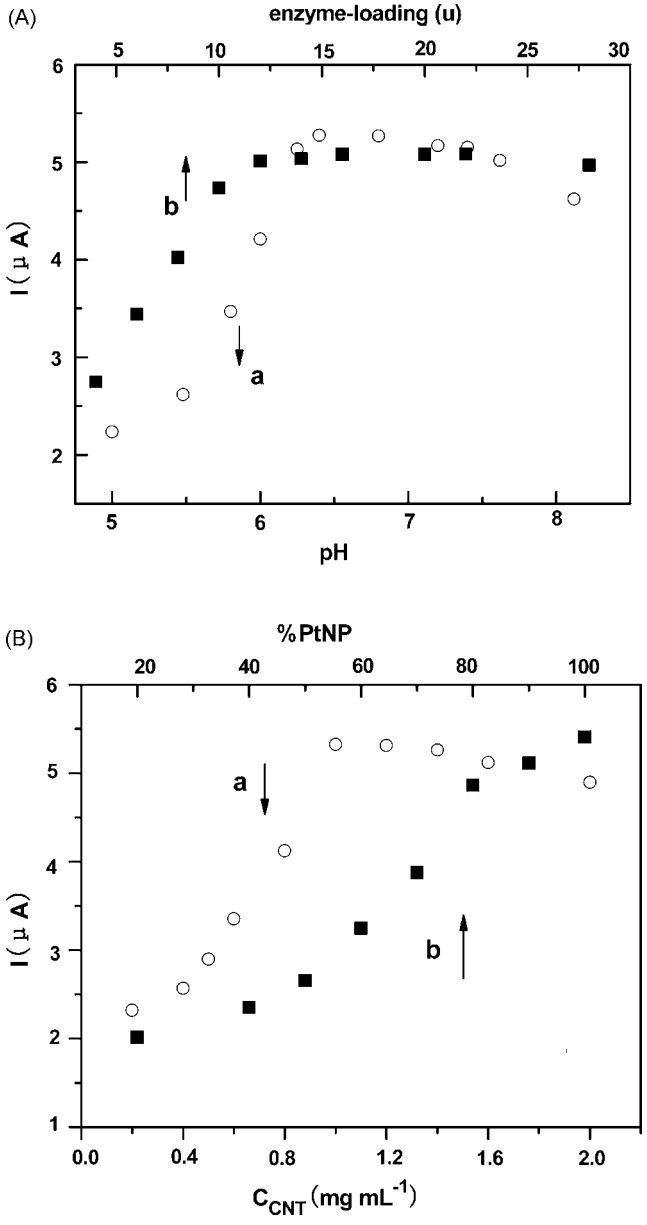


Fig. 6. (A) Effect of pH (a) and enzyme loading (b); (B) effect of CNT (a) and %PtNP concentration (b) for GOD–CNT–PtNP–MTOS–CS–GCE on current response of 0.5 mM glucose at 0.4 V.

noticed when the loading amount of CNT exceeded 1 mg mL^{-1}, which may be attributed to the poor dispersant of CNT in sol–gel and the leakage of CNT from the film of the modified electrode. With fixed CNT content of 1 mg mL^{-1}, the current response obviously increased by varying PtNP–CS from 20% to 100%. Consequently, the CNT content of 1 mg mL^{-1} and 100% PtNP–CS in the stock solution were selected to modify the electrodes.

The electrocatalytic activity of GOD–CNT–PtNP–MTOS–CS–GCE to glucose was also investigated. Fig. 7A showed the response currents to 0.2 mM glucose at various applied potential from 0.0 to 0.6 V. At 0.2 V, the observed response current was insignificant. However, the cathodic response current increased at 0.0 and 0.1 V. While varying the applied potential from 0.3 to 0.6 V, the anodic response currents increased, in addition, the response time was very fast (within 5 s). The results can be attributed to the fast diffusion of glucose in the hybrid film, the fast electrons transfer for the integration of PtNP with CNT, and the fast chemical reaction equilibrium. Fig. 7A indicated that the fabricated biosensor has a flexible operating potential range for the monitoring of the oxidation/reduction of H_2O_2 that is a product of the oxidase-based GOD reaction. And by choos-

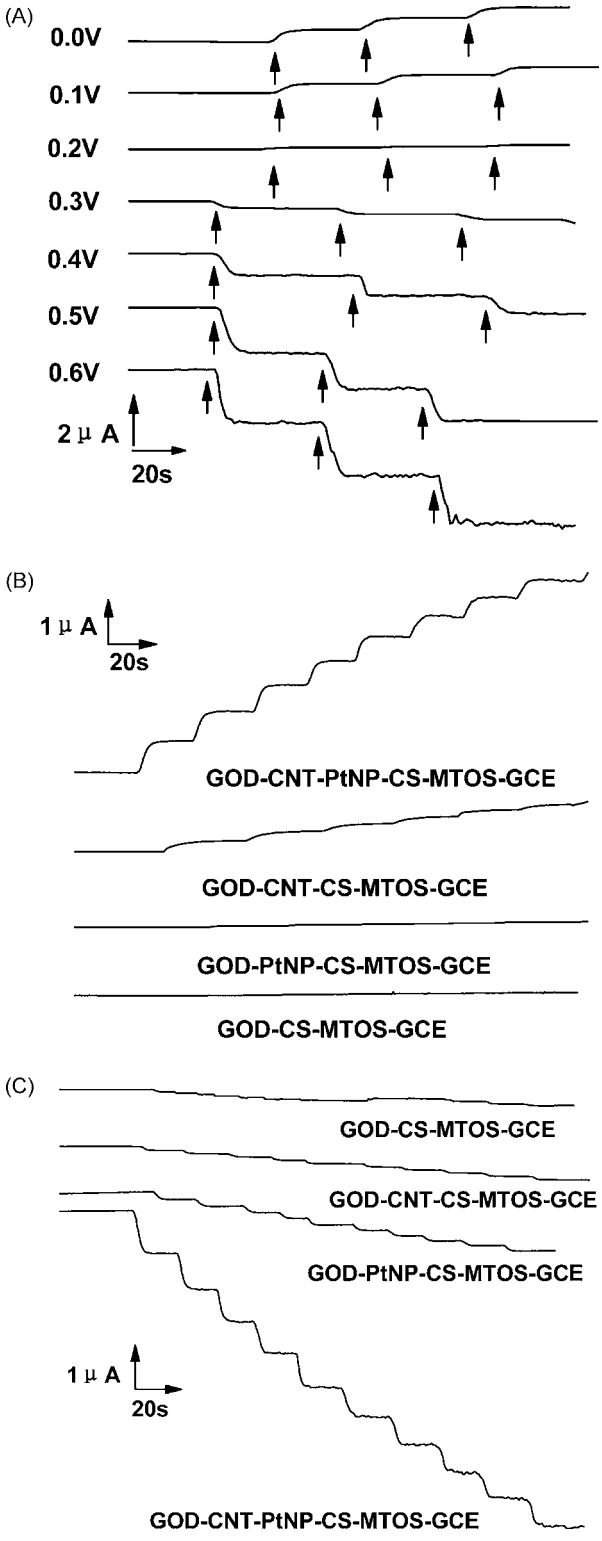


Fig. 7. Current response of GOD–CNT–PtNP–CS–MTOS–GCE at various applied potential (A) and different modified electrodes to 0.2 mM glucose in PBS at 0.1 V (B), 0.4 V (C).

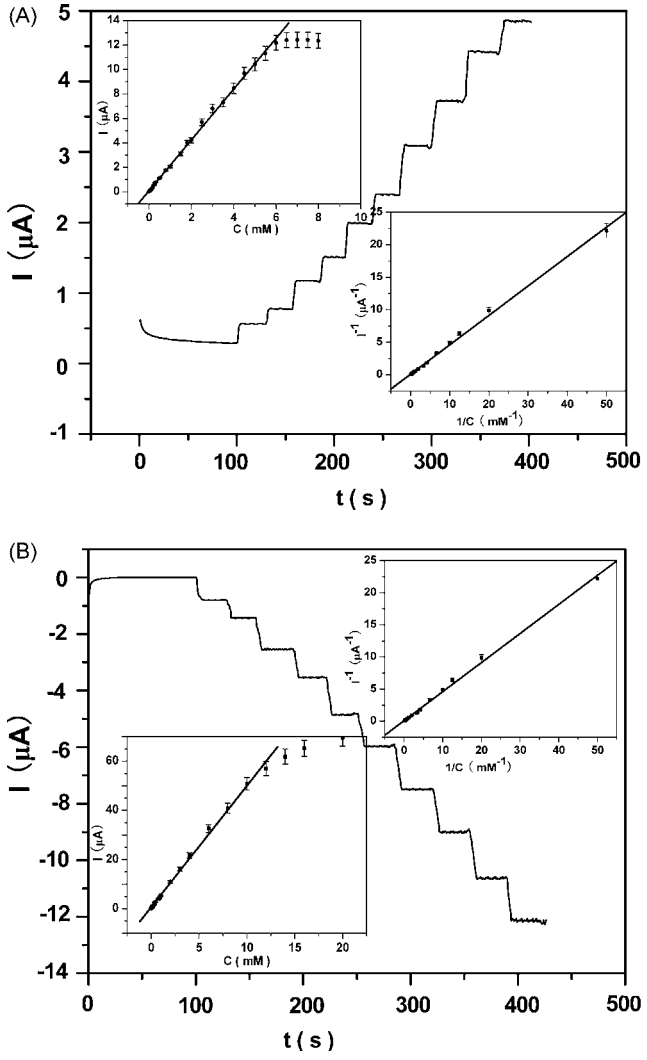


Fig. 8. Current response of GOD–CNT–PtNP–CS–MTOS–GCE to various concentrations of glucose at 0.1 V (A) and 0.4 V (B); Calibration curves and Lineweaver–Burk plots of the biosensor at 0.1 V (A inset left, right) and 0.4 V (B inset right, left).

Table 1
Summary on the performance of various CNT–PtNP-based glucose biosensors

Fabrication of biosensors	Sensitivity ($\mu A\,mM^{-1}$)	Linear range (mM)	Response Time (s)	Applied potential (V)	K_m^{app} (mM)
GOD/PtNP/CNT/Carbon paste [3]	–	0.1–35	<10	0.6	–
	0.28	1–25	<15	0.1	–
GOD/PtNP–CNT–Nafion/GCE [24]	2.11	0.0005–5	3	0.55	–
GOD/Nafion/PtNP/CNT/GCE [26]	0.64	0.02–4	<5	0.5	–
Nafion/GOD/PtNP/ACNT [30]	–	0.01–7	<5	0.3	9.28
(Pt-DENs/GOD)$_4$/CNT/Pt electode [31]	0.96	0.005–0.65	<5	0.0	–
Nafion/GOD/PtNP/CNT/Graphite [32]	14.5	0.1–13.5	<5	0.6	10.11
GOD–CNT–PtNP–CS–MTOS/GCE	2.08	0.0012–6	<5	0.1	5.8
(This work)	4.94	0.002–12	<5	0.4	7.9

Table 2
Determination of glucose in blood serums ($n = 6$)

Sample	Hospital (mM)	Biosensor (mM)	Relative error (%)	R.S.D. (%)	Added (mM)	Recovery (%)
1	5.5	5.4	−1.8	2.8	0.5	104
2	5.0	5.2	+4.0	3.2	0.5	98
3	5.2	5.0	−4.0	2.6	0.5	95
4	6.0	6.2	−3.3	2.8	0.5	102
5	4.2	4.5	+7.1	4.4	0.5	96
6	4.1	4.2	+2.4	3.0	0.5	104

ing the appropriate operating potential, commonly encountered electroactive interferences can be selectively avoided. At the applied potential of 0.1 and 0.4 V, the response current to glucose of the four types of modified electrodes were illustrated in Fig. 7B and C, respectively. The observed response current can be ignored for the GOD–CS–MTOS–GCE, and small response currents were noticed for GOD–PtNP–CS–MTOS–GCE and GOD–CNT–CS–MTOS–GCE. However, the response current for GOD–CNT–PtNP–CS–MTOS–GCE was the largest, which may be caused by the synergistic electrocatalytic action with the combination of PtNP and CNT.

Fig. 8 illustrated current-time plots for the biosensor on successive step changes of glucose concentration at the applied potential of 0.1 V (A) and 0.4 V (B), respectively. The calibration curves for the biosensor under the optimized experimental conditions were shown in Fig. 8A (left inset) and Fig. 8B (right inset). At 0.1 V, the biosensor displayed a linear range (1.2×10^{-6} to 6.0×10^{-3} M glucose) with a correlation coefficient of 0.9989, a sensitivity of 2.08 $\mu A\,mM^{-1}$, and the detection limit of 3.0×10^{-7} M at a S/N ratio of 3. At 0.4 V, it had a linear range from 2.0×10^{-6} to 1.2×10^{-2} M of glucose with a correlation coefficient of 0.9982, a sensitivity of 4.94 $\mu A\,mM^{-1}$, and the detection limit of 4.0×10^{-7} M when S/N is 3. The apparent Michaelis–Menten constant (K_m^{app}) was 5.8 mM (0.1 V) and 7.9 mM (0.4 V), respectively, according to the Lineweaver–Burk equation [45] from Fig. 8A (right inset) and Fig. 8B (left inset). These values were compared with those of the reported results of CNT–PtNP–based glucose biosensors (Table 1). The results confirmed that the biosensor had the good performances of high sensitivity, wide linear range, fast response, low applied potential, and small K_m^{app}, due to the enhancement of electroactive surface area and the synergistic electrocatalytic activity by combining PtNP with CNT, together with the use of biocompatible sol–gel of CS/silica organic–inorganic hybrid with porous and open framework.

The fabrication reproducibility of six GOD–CNT–PtNP–CS–MTOS modified electrodes was investigated by detecting 0.3 mM glucose at 0.4 and 0.1 V. The R.S.D.s were 5.2% and 5.5%, respectively. The storage stability of the biosensor was examined over 30-day-period for the response to 0.3 mM glucose at 0.1 V. After 30 days of storage at 4 °C, the response current was still retained above 80% of the initial response, which indicated the biosensor had a good reproducibility and stability. The interferences, such as ascorbic acid, uric acid, and lactic acid, are common problems in the electrochemical determination of glucose in physiological samples. At 0.4 V, the biosensor response was significantly affected by the acids at 0.1 mM level, the response signals of the acids were nearly eliminated at the potential of 0.1 V. At 0.1 V, the ratio of I_{G+I} to I_G was 1.007, 1.002 and 1.001 of ascorbic acid, uric acid, and lactic acid, respectively, where I_G is the response current to 0.5 mM glucose and I_{G+I} is the response to 0.5 mM glucose in the presence of interferences at 0.1 mM content.

The application of the biosensor was assessed by the determination of glucose concentration in human serum. 0.2 mL serum was added into 5.0 mL PBS, and the response current was obtained at 0.1 V. The results (Table 2) were in agreement with those detected by the hospital (human serum samples and spectrometric results were supplied by the first hospital attached to Sun Yat-Sen University).

4. Conclusions

In this paper, a new composite biosensor was constructed by integrating PtNP with CNT in the sol–gel of CS/silica organic–inorganic hybrid. CS with amino and hydroxy groups

can stabilize PtNP, disperse CNT, and form organic–inorganic hybrid sol–gel with MTOS. Consequently, the synergistic electrocatalytic action can be easily obtained by the integration of PtNP with CNT. With the immobilization of GOD, the glucose biosensor has the characteristics of high sensitivity, good reproducibility and stability, together with low applied potential, fast response, and free interferences. Other enzyme may be immobilized to construct useful biosensors for the detection of other target analytes. It is also possible to fabricate microbiosensors with this technique for the on-line spot detection.

Acknowledgements

This work was supported by the NNSF of China (No. 20475068, 20575082), the Natural Science Foundation of Guangdong Province (No. 031577, 7003714) and the Scientific Technology Project of Guangdong Province (No. 2005B30101003).

References

[1] L.C. Clark, J.C. Lyons, Ann. N. Y. Acad. Sci. 102 (1962) 29–45.
[2] B. Wang, B. Li, Q. Deng, S. Dong, Anal. Chem. 70 (1998) 3170–3174.
[3] M.H. Yang, Y.H. Yang, Y.L. Liu, G.L. Shen, R.Q. Yu, Biosens. Bioelectron. 21 (2006) 1125–1131.
[4] Q. Xu, Y. Zhao, J.Z. Xu, J.J. Zhu, Sens. Actuators B 114 (2006) 379–386.
[5] M. Zhao, A. Smith, W. Gorski, Anal. Chem. 76 (2004) 5045–5050.
[6] P.A. Fiorito, C.M.A. Brett, S.I.C. de Torresi, Talanta 69 (2006) 403–408.
[7] P.P. Joshi, S.A. Merchant, Y. Wang, D.W. Schmidtke, Anal. Chem. 77 (2005) 3183–3188.
[8] A. Merkoci, M. Pumera, X. Llopis, B. Perez, M. del Valle, S. Alegret, Tre. Anal. Chem. 24 (2005) 826–838.
[9] X.C. Tan, M.J. Li, P.X. Cai, L.J. Luo, X.Y. Zou, Anal. Biochem. 337 (2005) 111–120.
[10] J. Wang, M. Musameh, Y. Lin, J. Am. Chem. Soc. 125 (2003) 2408–2409.
[11] Q. Zhao, Z.H. Gan, Q.K. Zhuang, Electroanalysis 14 (2002) 1609–1613.
[12] L. Qian, X. Yang, Talanta 68 (2006) 721–727.
[13] C.M. Welch, R.G. Compton, Anal. Bioanal. Chem. 384 (2006) 601–619.
[14] Y. Ikariyama, S. Yamauchi, T. Yukiashi, H. Ushioda, Anal. Lett. 20 (1987) 1791–1801.
[15] S. Zhang, N. Wang, H. Yu, Y. Niu, C. Sun, Bioelectrochemistry 67 (2005) 15–22.
[16] X. Ren, X. Meng, D. Chen, F. Tang, J. Jiao, Biosens. Bioelectron. 21 (2005) 433–437.
[17] S. Lim, J. Wei, J. Lin, Q. Li, J. You, Biosens. Bioelectron. 20 (2005) 2341–2346.
[18] M.C. Daniel, D. Astruc, Chem. Rev. 104 (2004) 293–346.
[19] J. Li, Q. Yu, T. Peng, Anal. Sci. 21 (2005) 377–381.
[20] M. Yang, Y. Yang, H. Yang, G. Shen, R. Yu, Biomater. 27 (2006) 246–255.
[21] S. Qu, J. Wang, J. Kong, P. Yang, G. Chen, Talanta 71 (2007) 1096–1102.
[22] X.H. Kang, Z.B. Mai, X.Y. Zou, P.X. Cai, J.Y. Mo, J. Nanosci. Nanothech. 7 (2007) 1618–1619.
[23] K.B. Male, S. Hrapovic, Y. Liu, D. Wang, J.H.T. Luong, Anal. Chem. Acta 516 (2004) 35–41.
[24] S. Hrapovic, Y. Liu, K.B. Male, J.H.T. Luong, Anal. Chem. 76 (2004) 1083–1088.
[25] N. Zhu, Z. Chang, P. He, Y. Fang, Anal. Chim. Acta 545 (2005) 21–26.
[26] Y.C. Tsai, H.Y. Chien, J. Nanosci. Nanothech. 7 (2007) 1611–1617.
[27] Y. Wu, S. Hu, Colloids Surf. B: Biointerface 41 (2005) 299–304.
[28] M. Zhang, L. Su, L. Mao, Carbon 44 (2006) 276–283.
[29] X. Chu, D. Duan, G. Shen, R. Yu, Talanta 71 (2007) 2040–2047.
[30] K. Zhao, S. Zhuang, Z. Chang, H. Songm, L. Dai, P. He, Y. Fang, Electroanalysis 19 (2007) 1069–1074.
[31] L. Xu, Y. Zhu, L. Tang, X. Yang, C. Li, Electroanalysis 19 (2007) 717–722.
[32] H. Tang, J. Chen, S. Yao, L. Nie, G. Deng, Y. Kuang, Anal. Biochem. 331 (2004) 89–97.
[33] J. Ye, H. Cui, Y. Wen, W. Zhang, G. Xu, F. Sheu, Microchim. Acta 152 (2006) 267–275.
[34] L. Rong, C. Yang, Q. Qian, X. Xia, Talanta 72 (2007) 819–824.
[35] X.H. Kang, Z.B. Mai, X.Y. Zou, P.X. Cai, J.Y. Mo, Anal. Biochem. 363 (2007) 143–150.
[36] X. Luo, J. Xu, Q. Zhang, G. Yang, H. Chen, Biosens. Bioelectron. 21 (2005) 190–196.
[37] I. Gill, A. Ballesteros, Trend Biotech. 18 (2000) 282–296.
[38] T.M. Park, E.I. Iwuoha, M.R. Smyth, R. Freaney, A.J. McShane, Talanta 44 (1997) 973–978.
[39] A. Walcarius, D. Mandler, J.A. Cox, M. Collinson, O. Lev, J. Mater. Chem. 15 (2005) 3663–3689.
[40] X. Tan, Y. Tian, P. Cai, X. Zou, Anal. Bioanal. Chem. 381 (2005) 500–507.
[41] B. Wang, J. Zhang, G. Cheng, S. Dong, Anal. Chim. Acta 407 (2000) 111–118.
[42] H. Huang, Q. Yuan, X. Yang, Colloids Surf. B 39 (2004) 31–37.
[43] V. Radmilovic, H.A. Gasteiger, P.N. Ross, J. Catal. 154 (1995) 98–106.
[44] A.J. Bard, L.R. Faulkner, Electrochemical Methods Fundaments and Applied, John Willey and Sons Press, New York, 2000.
[45] R.A. Kamin, G.S. Willson, Anal. Chem. 52 (1980) 1198–1205.

Available online at www.sciencedirect.com
ScienceDirect
Talanta 74 (2008) 753–759
Talanta
www.elsevier.com/locate/talanta

Vapour phase Fourier transform infrared spectrometric determination of L-cysteine and L-cystine

K. Kargosha *, S.H. Ahmadi, M. Zeeb, S.R. Moeinossadat

Chemistry and Chemical Engineering Research Center of Iran, P.O. Box 14335-186, Iran

Received 21 February 2007; received in revised form 4 July 2007; accepted 5 July 2007
Available online 10 July 2007

Abstract

A novel and selective procedure for the determination of L-cysteine and L-cystine based on vapour-generation Fourier transform infrared spectrometry is described. Potassium iodate solution was injected into a glass vessel containing L-cysteine and/or L-cystine. The evolved CO was swept by a stream of nitrogen to an infrared gas cell. The vapour phase FTIR spectra were continuously recorded, as a function of time, between 2240 and 2000 cm^{-1}, which includes the CO absorption band. The maximum absorbance at 2170 cm^{-1} was selected as a measurement criterion. The calibration curve was linear over the range 6–300 mg L^{-1}. The method provided a limit of detection of 2 mg L^{-1} of L-cysteine, a throughput of 12 samples h^{-1} and an R.S.D. of 1.76% for five independent analyses of a 75 mg L^{-1} L-cysteine solution. For the measurement of L-cysteine and L-cystine separately, after measuring total concentration of L-cysteine and L-cystine, L-cysteine was masked with *p*-benzoquinone at a pH of 3 and individual L-cystine was determined. The amount of L-cysteine was obtained by difference. The method was applied to the determination of L-cysteine and L-cystine in pharmaceutical and urine samples. Results obtained for real samples compared well with those obtained by a reference spectrometric method.
© 2007 Elsevier B.V. All rights reserved.

Keywords: FTIR spectrometry; Vapour phase; L-Cysteine; L-Cystine

1. Introduction

L-cysteine (CSH) and L-cystine (CSSC) are important compounds in a wide range of samples such as biological tissues, body fluids, food products and medicines. L-Cysteine is a sulfur amino acid and contains a sulfhydryl group. When L-cysteine is exposed to air, it is oxidized to form L-cystine, which is a dimer of two L-cysteine molecules joined by a weak disulfide bond. Hepatic cystinuria and some other diseases are characterized by high concentration of L-cysteine and L-cystine in urine (usually > 400 mg L^{-1}).

The analysis of L-cysteine and L-cystine is essential and often difficult, although they can be determined by electrophoretic [1–5], chromatographic [6–11], electrochemical [12–14] and spectrometric [15–20] methods. However, some of these methods are insensitive, tedious, time consuming or expensive. The analysis of mixture of L-cysteine and L-cystine has been rarely performed by non-chromatographic techniques. In addition, there are some interferences in electrochemical and spectrometric methods. For example, ethylenediaminetetraacetic acid (EDTA), metal ions, surfactants, and *N*-acetyl cysteine or other sulfhydryl thiols are the main interferences in electrochemical methods [12,13]. Most of chromatographic methods [7,9,11] are combined with pre- or post-column derivatization. These methods are time consuming and use expensive reagents and equipment.

FTIR spectroscopy is very useful for carrying out determinations in gaseous or vapour samples owing to the high transparency of gases, the low background values and the possibilities offered by the use of multiple-pass cells, which can provide good sensitivity [21]. By using oxidation of L-cysteine and/or L-cysteine with potassium iodate and generation of CO gas, we have developed a simple vapour phase FTIR analytical method for the determination of L-cysteine and L-cystine in aqueous solutions. The system employed for vapour generation is a simple Pyrex glass reactor, into which liquid samples are introduced and potassium iodate solution is directly injected through a septum; the generated vapour is transported by an inert carrier gas flow and the correspond-

* Corresponding author. Fax: +98 21 44580762.
E-mail addresses: K.Kargosha@ccerci.ac.ir, K_Kargosha@yahoo.com (K. Kargosha).

0039-9140/$ – see front matter © 2007 Elsevier B.V. All rights reserved.
doi:10.1016/j.talanta.2007.07.003

ing transient signals are measured in the gas cell of an FTIR instrument.

The aforementioned methodology was employed for the determination of L-cysteine and L-cystine in pharmaceutical and urine samples, without interference from other amino acids.

2. Experimental

2.1. Apparatus and reagents

A vector 22 FTIR spectrometer from Bruker (Ettlingen, Germany) equipped with a DTGS mid-range detector, a KBr Ge/Sb_2S_3-coated beamsplitter and a Globar source was employed for spectral measurements; spectra were obtained by accumulating 20 scans at a resolution of 4 cm^{-1}, using a laboratory-made gas cell made of PTFE with a length of 10 cm and an internal diameter of 0.9 cm, equipped with ZnSe windows. Version 4 of Opus software, developed by Bruker, was employed to control the instrument, for data acquisition and also for processing the analytical results.

The manifold employed for vapour-generation FTIR measurements (Fig. 1) was a single-channel manifold with a nitrogen carrier flow, which included a laboratory-made removable glass sample vessel of 20 mL internal volume with a gas inlet, a gas outlet and a septum.

Sample vessel (reactor) was introduced inside a hot water-bath, the temperature of which was controlled by means of a thermocouple and operated using laboratory-made electrically controlled heater. To avoid the presence of water drops inside the measurement cell, at the exit of the glass reactor a small stainless steel u-form tube was introduced inside an ice-bath to act as a water trap in which the excess water vapour condensed before passing through the gas cell. Other tubes employed in the manifold were made of PTFE.

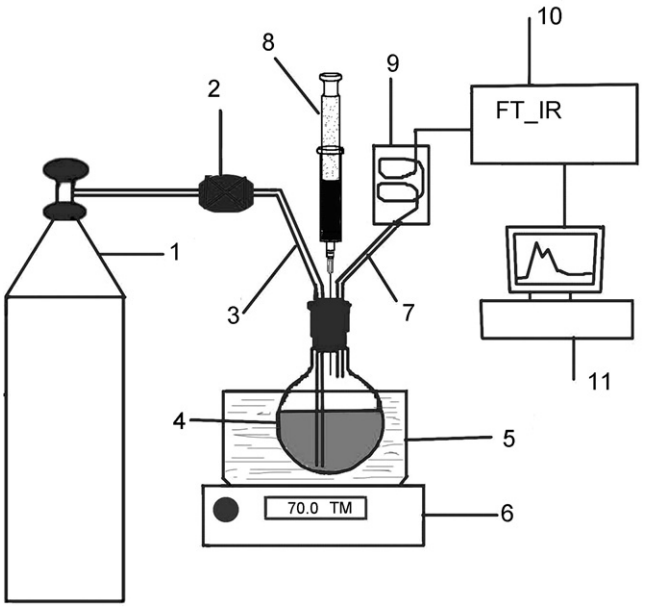


Fig. 1. Manifold employed for vapour generation and FTIR determination of L-cysteine and L-cystine: (1) nitrogen gas, (2) flow meter, (3) tube for entrance of nitrogen gas, (4) reactor, (5) water-bath, (6) heater, (7) tube for exit of nitrogen gas, (8) syringe for injection of oxidant, (9) water trap, (10) FTIR and (11) computer.

A trio 1000 GC–MS instrument from Fisons (Manchester, England) was employed for separating and detecting the generated gases. The column used for this separation was a Pro Plot-Q from Chrompack.

All chemicals used were of analytical-reagent grade. L-Cysteine, L-cystine, potassium iodate, sodium metaperiodate, *p*-benzoquinone, citric acid monohydrate, tri-sodium citrate dihydrate and 37% (v/v) hydrochloric acid were obtained from Merck. A 1500 mg L^{-1} stock CSH solution was daily prepared by dissolving 0.15 g of L-cysteine in de-ionized water and diluting to 100 mL with citric acid buffer solution. A 1500 mg L^{-1} stock CSSC solution was daily prepared by dissolving 0.15 g L-cystine in 2 mL 37% (v/v) HCL and diluting to 100 mL with citric acid buffer solution. Working solutions of both analytes were prepared from stock solution by appropriate dilution. Citric acid buffer was obtained by dissolving 1.7963 g citric acid monohydrate and 0.4265 g tri-sodium citrate dihydrate in de-ionized water and diluting to 1 L. Nitrogen of 99.95% purity was employed as the carrier gas and de-ionized water was used throughout.

2.2. Vapour phase FTIR analysis

A 2 mL volume of 4% (m/v) potassium iodate solution was injected into a glass vessel containing 10 mL of (6–300 mg L^{-1}) L-cysteine and/or L-cystine solution. Prior to any measurement, an N_2 carrier flow was passed through the empty vessel and the corresponding background was obtained. A new vessel containing the sample or standard solution was placed in a water-bath at 70 °C; N_2 flow was passed through the vessel; the potassium iodate solution was injected and the CO generated was transported to the gas cell of the FTIR spectrometer using a nitrogen carrier flow of 4.4 mL min^{-1}, without the need for an equilibrium time before measurement. FTIR spectra were obtained from 20 accumulated scans at a resolution of 4 cm^{-1} between 2240 and 2000 cm^{-1} which includes the CO absorption band. The maximum absorbance at 2170 cm^{-1}, corrected by a baseline established between 2240 and 2000 cm^{-1}, was selected as a measurement criterion.

2.3. Reference spectrometric method

A spectrometric method based on the reaction of CSH with sodium arsenate and the absorbance measurement at 335 nm was applied as the reference method [15]. The reference method is specific for CSH and in mixtures of CSH and CSSC both amino acids can be determined separately by analysing two samples, one without and one with KCN. The colour is developed at room temperature for 2 h.

3. Results and discussion

The oxidation of CSH and CSSC in aqueous solutions with potassium permanganate, potassium iodate, potassium

iodide, sodium metaperiodate, sodium bismuthate and *N*-bromosuccinimide was evaluated. Appreciable amount of carbon monoxide was produced only when potassium iodate or sodium metaperiodate was used as oxidizing agent. Beside CO, CO_2 was also generated by using these two oxidants. These gases were detected by injecting the evolved gases into a GC–MS spectrometer (see Fig. 2). The vapour phase FTIR spectrum of the gaseous species produced in sample vessel containing CSH, CSSC and either of these two oxidants are shown in Fig. 3.

Figs. 2 and 3 reveal that the main gaseous species produced in the oxidation of CSH or CSSC by potassium iodate or sodium metaperiodate are CO and CO_2. Fig. 3(A) shows that the height of the CO absorbance signal is about twice of the CO_2 signal in using potassium iodate as oxidant. Sodium metaperiodate is a stronger oxidant and can oxidize other amino acids (serine and theronine) and organic compounds with formation of CO_2. These amino acids and organic compounds are usually present in pharmaceutical and urine samples. On the other hand by selecting CO instead of CO_2 as the final analyte, more precise results were obtained. However, potassium iodate was selected as optimum oxidant.

Vapour phase FTIR spectra of eight L-cysteine standard solutions with different concentrations (6–300 mg L^{-1}) present well defined and intense bands in the range 2240–2000 cm^{-1} (see Fig. 4). The resulting difference spectra show that the relative changes in absorbance appear to be linearly spaced.

The oxidation of CSH and CSSC with potassium iodate solution, the generation of CO and the introduction of the evolved gas from reactor into the gas cell of the FTIR spectrometer are the most important steps of the proposed method. Different chemical and physical variables affect these steps. These variables must be optimized to introduce the highest and most reproducible amount of CO into the gas cell. Since the behaviour of CSH and CSSC toward these variables was found to be the same, only CSH samples were used through the rest of the work.

3.1. Effect of potassium iodate concentration on CO generation

The concentration and volume of the oxidant necessary for the complete generation of CO from CSH was evaluated. Experiments were carried out in a monoparametric mode and the results demonstrated that, consistent data can be achieved by using excess amount of oxidant (4%, m/v) and 2 mL volume of KIO_3.

3.2. Effect of reactor temperature

The oxidation reaction between L-cysteine or L-cystine and potassium iodate leading to the release of CO is very efficient but not very rapid and the effect of temperature is a decisive factor; it also affects the kinetics of the reaction and the rate of CO releasing out of the solution. As can be seen in Fig. 5, the absorbance of the transient peaks increases, as the reactor temperature increases. However, from an experimental point of view

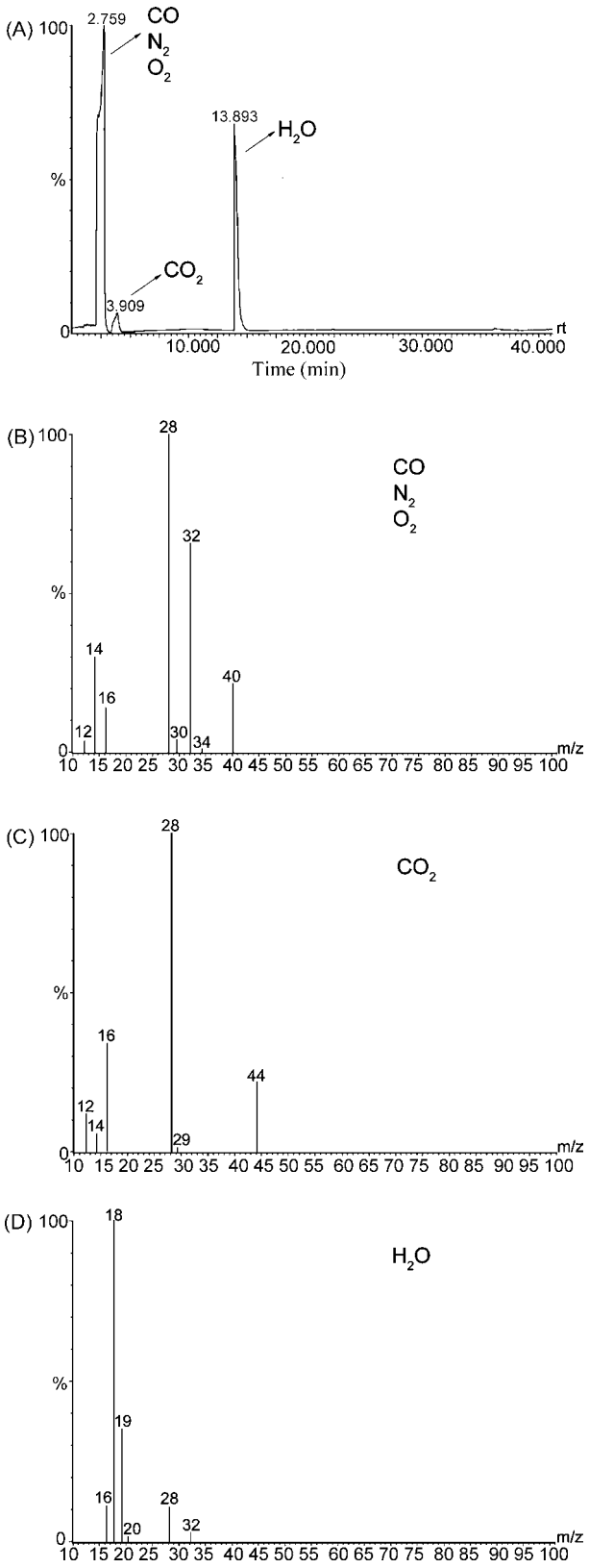


Fig. 2. (A) vapour phase GC–MS of the gaseous spices produced in the oxidation L-cysteine or L-cystine by potassium iodate. (B)–(D) are mass spectra of each chromatogram component.

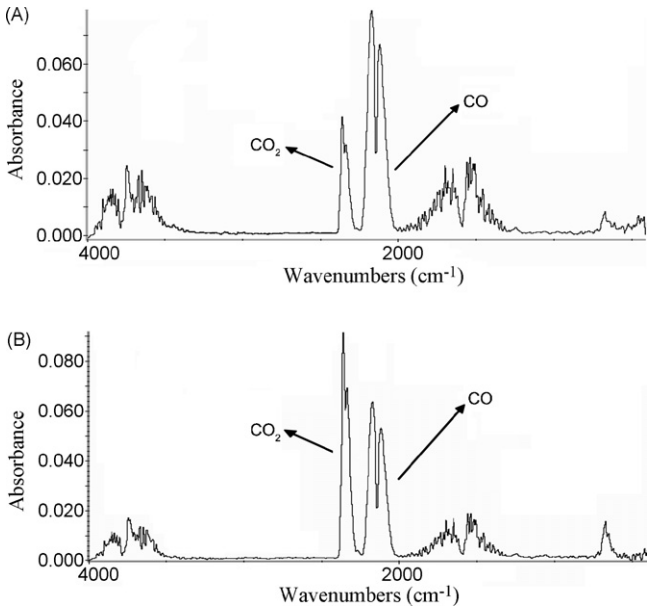


Fig. 3. Vapour phase FTIR spectrum of the gaseous spices produced in the oxidation of L-cysteine or L-cystine by (A) potassium iodate and (B) sodium metaperiodate.

extremely fast measurement of CO creates problems. Therefore, a temperature of 70 °C was selected in order to decrease water vapour transfer to a minimum and to obtain a compromise between speed, sensitivity, simplicity and reproducibility of the analytical signals.

3.3. Effect of reactor volume

An increase in the reactor volume, which increases the CO dispersion by increasing the total volume of the system, has very small influence on the analytical signals obtained from the absorbance of the transient peaks. A reactor volume of 20 mL (the most readily available glass vial) is recommended for the determination of CSH and CSSC.

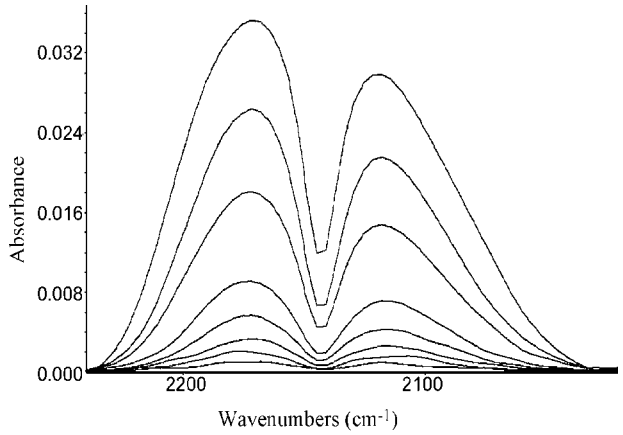


Fig. 4. Eight vapour phase co-added FTIR spectra obtained for eight standard solutions of L-cysteine with different concentrations (6, 15, 30, 45, 75, 150, 225 and 300 mg L^{-1}). Spectra were obtained from 20 accumulated scans at a resolution of 4 cm^{-1}.

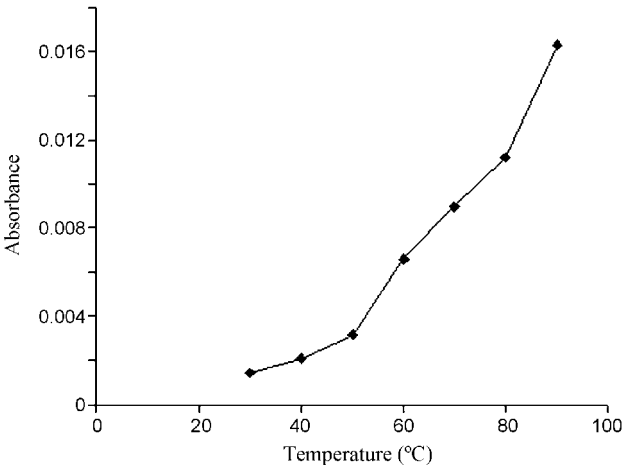


Fig. 5. Effect of the reactor temperature on vapour phase FTIR determination of L-cysteine. Experimental condition: 10 mL of 75 mg L^{-1} L-cysteine, 20 mL reactor volume, 4.4 mL min^{-1} N_2 flow rate, pH of 3 and 2 mL of 4% (m/v) potassium iodate were employed.

3.4. Effect of N_2 carrier flow rate

The flow rate of the carrier gas (N_2) is a critical parameter in vapour phase FTIR spectrometric analyses [22–25], which affects the analytical sensitivity and the sampling frequency. This parameter controls the volatility of the analytes and the speed of vapour introduction into the measurement cell. As can be seen in Fig. 6, an increase in the carrier flow rate causes a decrease in sensitivity, but increases the sampling frequency. Hence a nitrogen flow rate of 4.4 mL min^{-1}, which allows a 12 h^{-1} sampling frequency, was selected in order to achieve a compromise between analytical sensitivity and sample throughput.

3.5. Effect of a fixed reaction time

The possible sensitivity improvement was evaluated by carring out a series of additional experiments under the condition

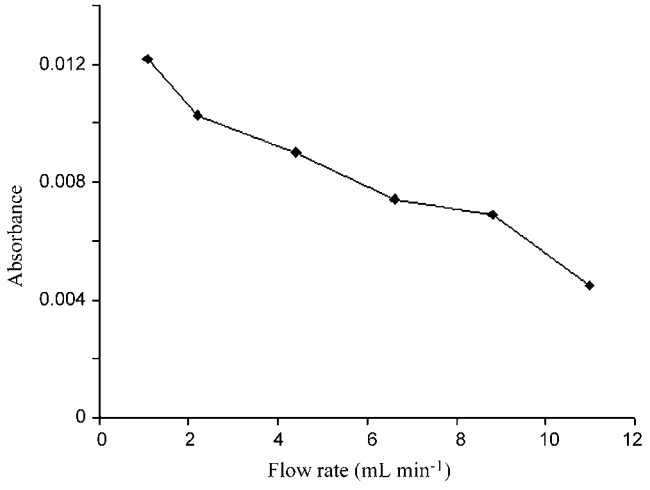


Fig. 6. Effect of N_2 carrier flow rate on vapour phase FTIR determination of L-cysteine. Experimental condition: 10 mL of 75 mg L^{-1} L-cysteine, 20 mL reactor volume, reactor temperature of 70 °C, pH of 3 and 2 mL of 4% (m/v) potassium iodate were employed.

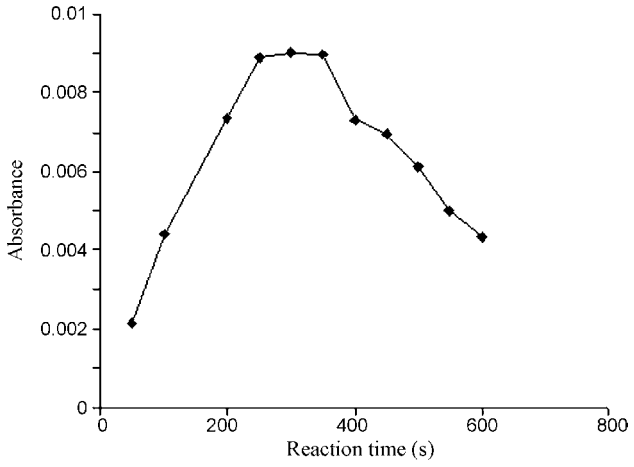


Fig. 7. Effect of equilibrium time on vapour phase FTIR determination of L-cysteine. Experimental condition: 10 mL of 75 mg L^{-1} L-cysteine, reactor temperature of 70 °C, 20 mL reactor volume, 4.4 mL min^{-1} N_2 flow rate, pH of 3 and 2 mL of 4% (m/v) potassium iodate were employed.

of stop flow mode. In this mode of experiments, the stream of N_2 carrier gas is stopped for a period of time to allow the oxidation reaction and CO release to reach an equilibrium. In fact in this mode, the oxidant is injected and after a fixed reaction time the evolved CO is introduced into the measurement cell by the stream of carrier gas. Times between 50 and 600 s were tried as fixed reaction times before the measurement. Fig. 7 reveals that an increase in fixed reaction time up to 300 s leads to an increase in the analytical signal and then to a decrease. Maximum obtainable sensitivity in 300 s fixed reaction time shows no improvement compared to sensitivity obtained by continuous flow mode (see Figs. 6 and 7).

3.6. Effect of pH and individual determination of L-cysteine and L-cystine

The pH affects the chemical behaviour of KIO_3 as an oxidant. The possibility of using potassium iodate as a selective oxidant to form more CO from CSH or CSSC by changing the pH was studied. To evaluate this possibility, nine samples (containing 75 mg L^{-1} CSH) with different pH values were tested. This study was assessed in the pH rang of 0.5–4.5. The pH of each solution was adjusted to a fixed value using appropriate buffer. As shown in Table 1, the signal increased as pH increased up to 3.5 and then decreased. However the pH of 3 (using citric acid buffer) was selected as most convenient pH because of two reasons: (1) the best reproducibility was obtained at this pH (see Table 1) and (2) the optimum pH for individual determination of CSH and CSSC was found to be 3.

The resolution of L-cysteine and L-cystine mixtures is based on the fact that at pH 3 the *p*-benzoquinone (PBQ) reacts with the thiol group of L-cysteine and mask it to prevent its oxidation with KIO_3 [18]. At this pH amino groups of CSH and CSSC are protonated and do not react with PBQ [13]. L-Cystine is a dimer of two L-cysteine molecules joined by a weak disulfide bond which cannot react with PBQ at the pH 3. The effect of pH on masking the L-cysteine with PBQ and the determination of L-cystine was investigated. Study was performed by analysing samples with variable pH which contain 75 mg L^{-1} of each amino acid. Based on the results obtained in this study the pH of 3 was selected as an optimum pH value. This pH was established by using citric acid buffer. However, in mixtures of CSH and CSSC both amino acids can be determined separately by analysing two samples, one without and one with PBQ. L-Cystine is determined alone by analysing the sample with PBQ and the concentration of L-cysteine plus L-cystine is determined by analysing the sample without PBQ.

Table 1
Effect of pH on vapour phase FTIR determination of L-cysteine

pH	Absorbance $\pm$ ($s_{n-1} \times 10^{-4}$)
0.5	0.00123 ± 2.51
1	0.00239 ± 2.96
1.5	0.00381 ± 2.11
2	0.00634 ± 2.98
2.5	0.00893 ± 2.53
3	0.00898 ± 1.49
3.5	0.00932 ± 2.12
4	0.00912 ± 2.39
4.5	0.00873 ± 3.21

Experimental condition: 10 mL of 75 mg L^{-1} L-cysteine, reactor temperature of 70 °C, 20 mL reactor volume, 4.4 mL min^{-1} N_2 flow rate and 2 mL of 4% (m/v) potassium iodate were employed. The standard deviation values correspond to three independent measurements.

3.7. Effect of interfering compounds

An interference study, aimed at the determination of L-cysteine and/or L-cystine in pharmaceutical preparations and urine samples, was performed. Samples containing fixed concentrations of L-cysteine (100 mg L^{-1}) or L-cystine and various concentrations of the interfering compounds were subjected to the proposed method. The tolerance limit was defined as interfering compound and L-cysteine concentrations ratio causing a relative error of ≤5. The results are shown in Table 2.

Table 2
Effect of various interfering compounds on the determination of 100 mg L^{-1} L-cysteine or L-cystine using optimum conditions reported under vapour phase FTIR analysis

Substance	Tolerance ratio[a] ([substance]/[cysteine or cystine])
Amino acids: Ile, Lys, Phe, Thr, Val, Arg, His, Gly, Ala, Pro, Ser, Tyr, Leu, Trp, Asp, Asn, Glu, Nty, Acy	250
Citric, maleic, malic, tartaric, lactic, benzylic and mendelic acid	220
Glycerol and ethylene glycerol	200
Glocose and fructose	170
Provic and glycolic acid	160
Albomine, bilirubin, insulin, urea and uric acid	150
Ascorbic acid	50
N-Acetyl cysteine	20

[a] Maximum concentration ratio of interfering compounds to cysteine causing a relative error of ≤5%.

Table 3
The declared content of Amino plasmal 10% solution ($g\,L^{-1}$)

Isoleucine	5.10
Leucine	8.90
Lysine hydrochloride	7.00
Methionine	3.80
Phenylalanine	4.10
Theronine	4.10
Tryptophan	1.80
Valine	4.80
Arginine	9.20
Histidine	5.20
Glycine	7.90
Alanine	13.70
Proline	8.90
Aspartic acid	1.30
Asparagine·H_2O	3.72
Acetylcysteine	0.68
Glutamic acid	4.60
Ornithine hydrochloride	3.20
Serine	2.40
Tyrosine	0.30
N-Acetyltyrosine	1.23

4. Applications

4.1. Spiked pharmaceutical product

Three samples of a two times diluted commercial pharmaceutical product, Amino plasmal 10% (purchased from B. Braun Melsungen AG Company, Germany), were spiked with different amounts of CSH and CSSC. Amino plasmal was diluted with citric acid buffer. The recovery study was performed by analysing these spiked samples with the proposed method. The composition of Amino plasmal is shown in Table 3. The results of this recovery study are shown in Table 4. The mean recoveries for L-cysteine and L-cystine were 101.57 and 101.43, respectively.

4.2. Urine samples

The accuracy of the proposed method was evaluated by the determination of L-cysteine and L-cystine in five different human urine samples. The urine samples were diluted by mixing it with the same volume of citric acid buffer solution. The values obtained for urine samples were compared with those found by a reference spectrometric method [15]. The results are summarized in Table 5.

4.3. Analytical figures of merit

The main analytical characteristics of the method were established from typical calibration lines, obtained under the optimum experimental conditions and from the analysis of real samples.

A typical expression for a calibration obtained from 6 to 300 $mg\,L^{-1}$ of L-cysteine is $y = 0.0001643 + 0.0001169x$ with $r = 0.9997$ where y is the absorbance of the transient peak and x is the concentration of L-cysteine ($mg\,L^{-1}$). A limit of detection of 2 $mg\,L^{-1}$ of L-cysteine was obtained by using the criterion, $LOD = ks_{bl}/m$, where k is a factor (=2), s_{bl} the standard deviation of the blank measurements and m is the calibration slope. The R.S.D. for five independent analyses of a standard sample with a concentration of 75 $mg\,L^{-1}$ L-cysteine was 1.76%. The Same calibration curve and analytical figures of merit can be obtained in the determination of L-cystine.

The precision of L-cysteine and L-cystine determination in real samples can be established from the relative standard deviation (R.S.D.) of three independent analysis. As can be seen from the data in Table 5 an average of R.S.D. <4% was obtained. The sampling frequency of the method is 12 h^{-1}, including the time required for the installation of glass sample vial in manifold.

Table 4
Recoveries obtained for L-cysteine and L-cystine in pharmaceutical samples by vapour phase FTIR spectrometry

Pharmaceutical sample	L-Cysteine			L-Cystine		
	Added ($mg\,L^{-1}$)	Found ($mg\,L^{-1}$)	Recovery (%)	Added ($mg\,L^{-1}$)	Found ($mg\,L^{-1}$)	Recovery (%)
1	60	60.60	101.00	60	60.86	101.43
2	75	76.16	101.55	75	76.09	101.45
3	150	153.23	102.15	150	152.11	101.40
Mean			101.57			101.43

Table 5
Results obtained for the determination of L-cysteine and L-cystine in urine samples by vapour phase FTIR spectrometry and by a reference method [15]

Urine sample	L-Cysteine ($mg\,L^{-1}$)		L-Cystine ($mg\,L^{-1}$)	
	Proposed method $\pm s_{n-1}$	Reference method $\pm s_{n-1}$	Proposed method $\pm s_{n-1}$	Reference method $\pm s_{n-1}$
1	52.03 ± 1.55	49.18 ± 1.42	21.14 ± 0.62	20.19 ± 0.89
2	66.20 ± 2.06	64.01 ± 2.50	38.22 ± 1.19	36.36 ± 1.33
3	45.12 ± 1.16	42.12 ± 1.91	16.11 ± 0.49	14.02 ± 0.47
4	60.02 ± 1.61	59.46 ± 2.12	40.51 ± 1.27	38.12 ± 1.10
5	53.22 ± 1.31	50.11 ± 1.70	25.13 ± 0.94	23.16 ± 0.79

The standard deviation values correspond to three independent measurements.

5. Conclusion

From the experimental results we conclude that both L-cysteine and L-cystine can be oxidized by KIO_3 to form carbon monoxide. At pH 3 thiol group of L-cysteine can be masked with PBQ and individual L-cystine can be oxidized to form CO. This is confirmed by recording the FTIR spectra of all gaseous species produced by this oxidation reaction. In addition, these results indicate that the proposed method can be useful for the determination of L-cysteine and L-cystine in pharmaceutical and urine samples and it provides excellent reproducibility and appropriate sensitivity.

References

[1] R.M. Latorre, S.H. Cassou, J. Saurina, J. Chromatogr. A 934 (2001) 105.
[2] K. Arlt, S. Brandt, J. Kehr, J. Chromatogr. A 926 (2001) 319.
[3] M. Ummadi, B.C. Weimer, J. Chromatogr. A 964 (2002) 243.
[4] Z. Shen, Z. Sun, L. Wu, K. Wu, S. Sun, Z. Huang, J. Chromatogr. A 979 (2002) 227.
[5] R.M. Latorre, J. Saurina, S.H. Cassou, J. Chromatogr. A 976 (2002) 55.
[6] P. Chaimbault, K. Petritis, C. Elfakir, M. Dreux, J. Chromatogr. A 855 (1999) 191.
[7] E. Bald, R. Glowacki, J. Drzewoski, J. Chromatogr. A 913 (2001) 319.
[8] H. Yu, Y.S. Ding, S.F. Mou, P. Jandik, J. Cheng, J. Chromatogr. A 966 (2002) 89.
[9] A. Namera, M. Yashiki, M. Nishida, T. Kojima, J. Chromatogr. B 776 (2002) 49.
[10] J. Xu, Y. Wang, Y. Xian, L. Jin, K. Tanaka, Talanta 60 (2003) 1123.
[11] K. Amarnath, V. Amarnath, K. Amarnath, H.L. Valentine, W.M. Valentine, Talanta 60 (2003) 1229.
[12] F.G. Banica, J.C. Moreira, A.G. Fogg, Analyst 119 (1994) 309.
[13] G. Hignett, S. Threlfell, A.J. Wain, N.S. Lawrence, S.J. Wilkins, J. Davis, R.G. Compton, M.F. Cardosi, Analyst 126 (2001) 353.
[14] N. Spataru, B.V. Sarada, E. Popa, D.A. Tryk, A. Fujishima, Anal. Chem. 73 (2001) 514.
[15] J. Chrastil, Analyst 115 (1990) 1383.
[16] T.P. Ruiz, C.M. Lozano, V. Tomas, J. Carpena, Analyst 117 (1992) 1025.
[17] M.C. Icardo, L.L. Zamora, M. Calatayud, Analyst 123 (1998) 1685.
[18] D.A.M. Zaia, K.C.L. Ribas, C.T.B.V. Zaia, Talanta 50 (1999) 1003.
[19] L. Nie, H. Ma, M. Sun, X. Li, M. Su, S. Liang, Talanta 59 (2003) 959.
[20] F. Tanaka, N. Mase, C.F. Barbas, Chem. Commun. (2004) 1762.
[21] P.L. Hanst, Fresenius, J. Anal. Chem. 324 (1986) 579.
[22] A.P. Ponce, J.M. Garrigues, S. Garrigues, M. de la Guardia, Analyst 123 (1998) 1817.
[23] K. Kargosha, M. Khanmohammadi, M. Ghadiri, Analyst 126 (2001) 1432.
[24] M. Gallignani, M. Valero, C. Ayala, M. del Rosario Brunetto, A. Sanchez, J.L. Burguera, M. Burguera, Talanta 64 (2004) 1290.
[25] N.M.M. Coelho, S. Garrigues, M. de la Guardia, Talanta 68 (2006) 836.

Available online at www.sciencedirect.com
ScienceDirect
Talanta 74 (2008) 860–866
Talanta
www.elsevier.com/locate/talanta

Poly(4-amino-1-1′-azobenzene-3, 4′-disulfonic acid) coated electrode for selective detection of dopamine from its interferences

S. Ashok Kumar, Chun-Fang Tang, Shen-Ming Chen *

Department of Chemical Engineering and Biotechnology, National Taipei University of Technology, No. 1, Section 3, Chung-Hsiao East Road, Taipei 106, Taiwan, ROC

Received 20 June 2007; received in revised form 17 July 2007; accepted 18 July 2007
Available online 24 July 2007

Abstract

Here, we described a new method for electrochemically selective detection of dopamine (DA). In this report, for the first time, electrochemical polymerization of 4-amino-1-1′-azobenzene-3,4′-disulfonic acid (acid yellow 9 dye (AY)) was carried out onto the surface of glassy carbon (GC) electrode and indium tin oxide coated electrode (ITO) from acidic solution containing AY monomers. A polymerized film of acid yellow on the surface of a glassy carbon electrode was characterized by cyclic voltammetry (CV). The redox response of the poly(AY) film on the GC electrode showed a couple of redox peak in 0.1 M sulfuric acid solution and the pH dependent peak potential was −58 mV/pH which was close to the Nernst behavior. The poly(AY) film-coated GC electrode (GC/PAY) exhibited excellent electrocatalytic activity towards the oxidations of dopamine (DA) in 0.1 M phosphate buffer solution (PBS, pH 7.0) and increased the anodic peak current three time higher than bare GC electrode. GC/PAY did not reduce the considerable overpotential for oxidation of DA when compare to bare GC electrode. However, in contrast to other polymer modified electrode, due to the strong negatively charged back bone of poly(AY) highly repelled the important interference of DA, such as ascorbic acid (AA), uric acid (UA) and reduced form of nicotinamide adenine dinucleotide (NADH) in 0.1 M PBS (pH 7.0) and did not showed any response for oxidation of these interferences. This behavior makes the GC/PAY for selective detection of DA in the presence of higher concentrations AA, UA and NADH. Using differential pulse voltammetry the calibration curves for DA were obtained over the range of 1–100 μM with good selectivity and sensitivity. The proposed method provides a simple method for selective detection of DA from its interferences.
© 2007 Elsevier B.V. All rights reserved.

Keywords: Poly(acid yellow 9); Modified electrodes; Electrocatalysis; Determination of dopamine; Electroactive polymer; Ascorbic acid; Uric acid; NADH; Sensor

1. Introduction

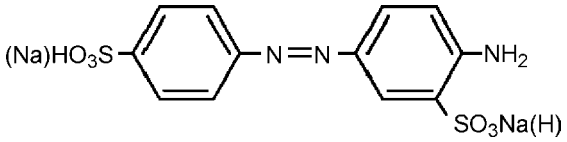
Neurotransmitters (Dopamine) are the chemicals which account for the transmission of signals from one neuron to the next across synapses. They are also found at the axon endings of motor neurons, where they stimulate the muscle fibers to contract. DA exists in the mammalian brain in the presence of several neurotransmitter amines including AA and UA. Recently, the identification and determination of DA with electrochemical procedures have attracted much attention. However, it is difficult to determine DA by direct oxidation at bare electrodes because of the high overpotential [1] and the fouling effect by its oxidation products [2]. Moreover, the oxidation waves of AA, UA, NADH and DA are at nearly the same potential and overlapped, which results in poor selectivity and reproducibility. The ability to determine AA or DA selectively in the presence of each other has been a major goal of electroanalytical research [3]. Various methods, mainly based on the chemical modification of traditional electrode materials, have been developed to resolve the problem [4–7].

The poor reproducibility of direct electrochemical oxidation of DA has led to interest in the use of mediators and modified electrodes to catalyze the electrochemical oxidation of DA. For example, electrode surfaces modified with immobilized organic monolayers [8,9], polymers films [10–14], carbon nanotube [15], surfactant [16] and quinone [17] have been used.

Electropolymerization is a good approach to immobilize polymers to prepare polymer modified electrodes (PMEs) as adjusting the electrochemical parameters can control film thick-

* Corresponding author. Tel.: +886 2 27017147; fax: +886 2 27025238.
E-mail addresses: sakumar80@gmail.com (S.A. Kumar), smchen78@ms15.hinet.net (S.-M. Chen).

0039-9140/$ – see front matter © 2007 Elsevier B.V. All rights reserved.
doi:10.1016/j.talanta.2007.07.015



Scheme 1. Chemical structural formula of acid yellow 9.

ness, permeation and charge transport characteristics. PMEs have many advantages in the detection of bio-molecules because of its selectivity, sensitivity and homogeneity in electrochemical deposition, strong adherence to electrode surface and chemical stability of the film [18,19]. Various PMEs were studied towards the electrocatalytic oxidation of DA, UA and AA [20]. GC electrode modified with poly(*N*,*N*-dimethylaniline) could simultaneously detect AA and DA which coexisted in a homogeneous solution [21]. There were other reports using glutamic acid [22], aminobenzoic acid [23] and *p*-nitrobenzenazo resorcinol [24] as an electropolymerized layer to modify GC electrode for the detection of DA.

To the best of our knowledge, the electropolymerization of 4-amino-1-1′-azobenzene-3,4′-disulfonic acid (acid yellow 9) (Scheme 1) has not been reported previously. Hence in this paper, for the first time we report the electrochemical polymerization of AY and its electrochemical properties. Poly(AY) coated electrode was found to be good sensor for selective determination of DA without its interference. Scanning electron microscope (SEM) was used for surface characterization of poly(AY) coated electrode.

2. Experimental

All chemicals and reagents used in this work were of analytical grade and used as received without further purification. These were 4-amino-1-1′-azobenzene-3,4′-disulfonic acid (AY, dye content about 95%), reduced form of β-nicotinamide adenine dinucleotide (purity 98%), dopamine hydrochloride (purity 98%) and uric acid (purity 99%) were purchased from Sigma–Aldrich (St. Louis, MO, USA). Sulfuric acid (H_2SO_4, purity 95%) and sodium hydroxide (NaOH, purity 93%) were purchased from Wako pure chemicals (Osaka, Japan). Ascorbic acid (purity 99%), sodium acetate (CH_3COONa) and sodium dihydrogen phosphate (NaH_2PO_4) were received from E-Merck (Darmstadt, Germany).

Supporting electrolytes used for electrochemical experiments were 0.1 M H_2SO_4 (pH 0.98), 0.1 M H_2SO_4 + 0.1 M NaOH (for pH 2.0–3.0), 0.2 M CH_3COOH + 0.2 M CH_3COONa (for pH 4.0–5.0) and 0.1 M NaH_2PO_4 + 0.1 M NaOH (for pH 6.0–12.0). The required values of pH solutions were obtained with the described solutions by mixing and the pH of the medium was measured using a Suntex Model SP-701 pH meter (Jiangsu, China). The aqueous solutions were prepared by using doubly distilled deionized water, and before each experiment the solutions were deoxygenated by purging with pre-purified nitrogen gas.

Electrochemical measurements were performed with CH Instruments (TX, USA) Model-400 potentiostat with conventional three-electrode cell. A BAS glassy carbon and platinum wire are used as the working electrode and counter electrode, respectively. All the cell potentials were measured with respect to an Ag/AgCl (KCl (sat)) reference electrode. Hitachi scientific instruments (London, UK) Model S-3000H Scanning Electron Microscope was used for surface image measurements. All experiments were carried out at room temperature.

2.1. Electrode modification

Prior to the film deposition, the GC electrode was mechanically polished with alumina powder (Al_2O_3, 0.05 μm) up to a mirror finish and ultrasonicated in distilled water for 5 min. ITO substrates were cleaned by using detergent, diluted hydrochloric acid and then finally rinsed with distilled water. Then GC electrode was electrochemically activated by using 20 times cycling potential sweeps in the range of −0.5 to 2.0 V in 0.1 M H_2SO_4 solution at a scan rate of 100 mV/s. The modified electrode was fabricated in 0.5 mM AY under the same conditions as those in the electrode activation procedure. The as-prepared blue colored polymer films were smooth and strongly adherent to the substrates. Subsequently, the modified electrode was rinsed thoroughly with distilled water and then it was dried in air for 30 min at room temperature.

3. Results and discussion

3.1. Fabrication of poly(AY) film coated electrode and its electrochemical properties

Fig. 1A shows the cyclic voltammograms (CVs) of AY polymer growth onto a GC electrode by scanning over the range of −0.5 to 2.0 V at 100 mV/s for 20 cycles. During the electro-polymerization process, an anodic peak (P_{a1}) at 1.10 V corresponding to the oxidation of NH_2– group of AY monomers was observed. Consequently, oxidized species results two new cathodic peaks (P_{c1} = +0.54 V, P_{c2} = −0.24 V) and one

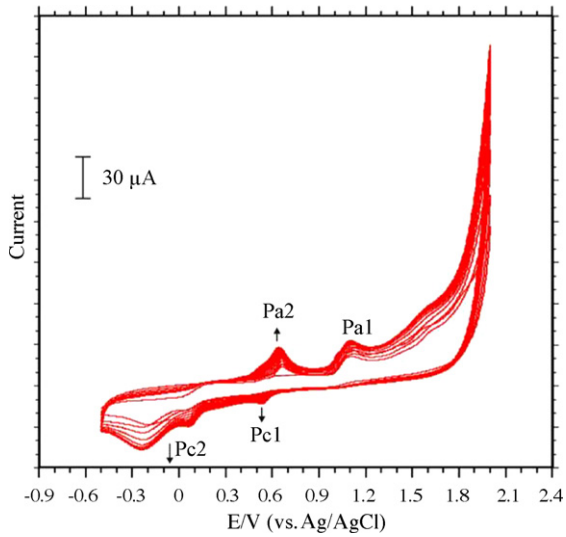


Fig. 1. CVs of the poly(AY) film growth on GC electrode from electrolyte 0.1 M H_2SO_4 solution containing 0.5 mM AY monomers. Scan rate = 0.1 V/s.

new anodic peak (P_{a2} = +0.66 V) with incessant scans and the peak currents also increased continuously. Anodic peak (P_{a2}) is the counter part of cathodic peak at +0.54 V (P_{c1}) and trended to be stable after 20 cycles. Then larger peaks were observed upon continuous scanning, reflecting the continuous growth of the polymer film. These facts indicated that poly(AY) films were deposited on the surface of GC electrode by electropolymerization. A uniform adherent blue polymer film was formed on the GC electrode surface. The electrochemical behavior of poly(AY) at the GC electrode was in good agreement with previous findings referring to the electrochemical responses of a few azo compounds at solid electrode [25,26]. The electrochemical polymerization mechanism of AY monomers was similar to the references reported [14,27,28]. The reaction mechanism may be described as follows AY was first oxidized to free radical (P_{a1}); the free radical combined together rapidly to hydrazobenzene sulfonic acid; then hydrazobenzene sulfonic acid was oxidized to azobenzene sulfonic acid (P_{a2}), and azobenzene sulfonic acid reduced to hydrazobenzene sulfonic acid (P_{c1}) [28]. After polymerization started, cathodic peak (P_{c2}) centered at −0.24 V was developed. It may due to the insertion of anions (for example SO_4^{2-}) accompanied by the hydrogenation of polymer site [28] and similar kinds of observations were reported for some azo compounds [25,26].

Fig. 2 exhibits the typical voltammogram of the GC/PAY electrode in the range of 20–500 mV/s at various sweep rates in 0.1 M H_2SO_4 solution. A pair of redox peaks (I_{pa} and I_{pc}) was obtained in each of the cyclic voltammogram at formal potential ($E^{0\prime} = (E_{pc} + E_{pa})/2) + 0.31$ V. And the anodic peak currents (I_{pa}) were linearly dependent of scan rate with the linear equation: I_p (μA) = $-0.09x - 0.7$ ($r^2 = 0.999$), and the ratio of anodic peak current to cathodic peak current (I_{pa}/I_{pc}) was almost equal to unity (Fig. 2B). The separation of peak potentials ($\Delta E_p = E_{pa} - E_{pc}$) was 40 mV at low scan rate (5–10 mV/s).

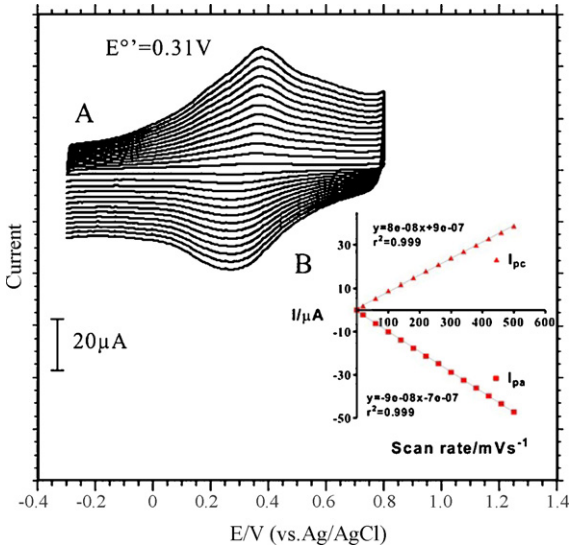


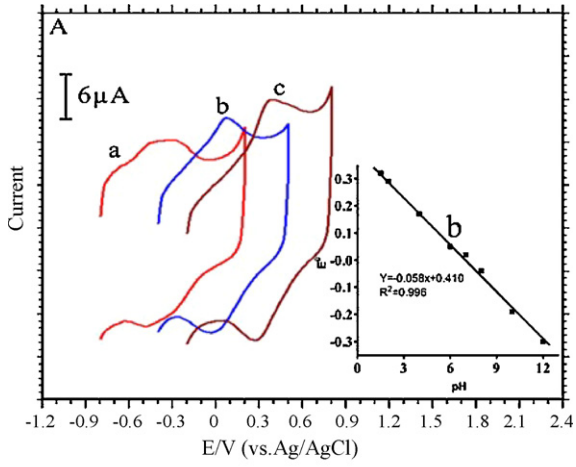
Fig. 2. (A) CVs of GC/PAY modified electrode in 0.1 M H_2SO_4 (pH 0.98) at different scan rates. The scan rates from inner to outer are 0.02, 0.06, 0.1, 0.14, 0.18, 0.22, 0.26, 0.30, 0.34, 0.38, 0.42, 0.46, 0.50 V/s, respectively. (B) Plot of I_{pa} and I_{pc} vs. scan rate.

With increasing scan rate, ΔE_p would not be changed. The above results suggest that the electrode reaction was an electrochemical response of the GC/PAY anticipated for a surface-confined redox process [29]. Therefore, the peak current could be correlative with scan rate by the equation:

$$I_p = n^2 F^2 \frac{A\Gamma\nu}{4RT} \quad (1)$$

where Γ represents the surface coverage concentration (mol/cm^2), ν is the scan rate, A (0.0707 cm^2) the electrode surface area and I_p is the peak current [30]. The slope of anodic peak current against scan rate is −0.09. ΔE_p (= 40 mV) is close to $2.3RT/nF$ (or $59/n$ mV at 25 °C), which identifies that the number of electrons involved in the reaction was two. Thus, the calculated surface concentration of poly(AY) is 4.8×10^{-10} mol/cm^2, which further confirms the immobilized state of the poly(AY).

The effect of pH value of the supporting electrolyte solution on the electrochemical behavior of poly(AY) film modified electrode was also investigated. With increasing pH from 1 to 12, a pair of redox peaks was observed in each of the CVs, and both the anodic and the cathodic peaks potential shifted negatively (Fig. 3A). The anodic peak potential (E_{pa}) linearly depended on pH value varying from 1 to 12. The slope of the $E^{0\prime}$ versus pH was −58 mV/pH, indicating that the total numbers of



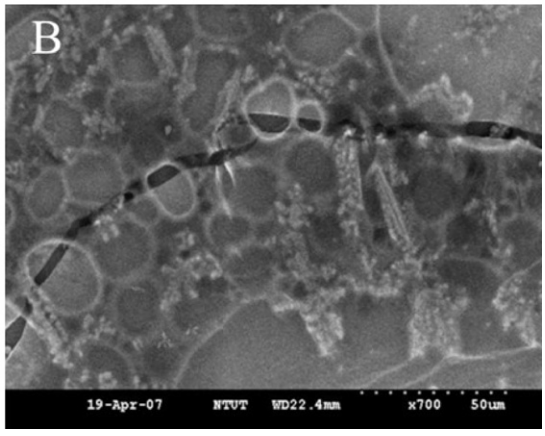
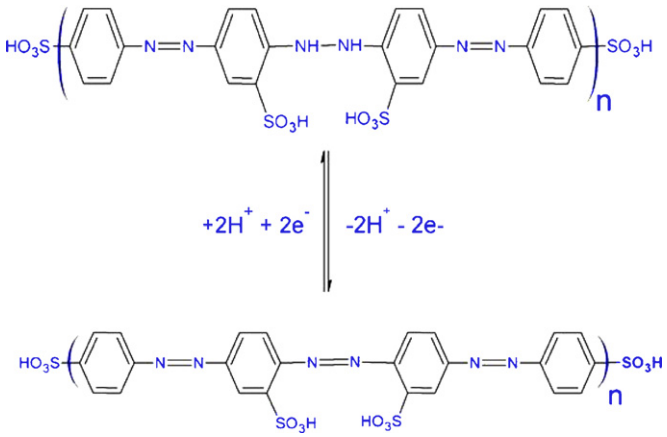


Fig. 3. (A) (a) CVs of GC/PAY modified electrode in different pH values (a) 12.0 (b) 7.0 (c) 2.0, Scan rate 0.1 V/s. (b) $E^{0\prime}$ as a function of pH. (B) SEM image of poly(AY) film.



Scheme 2. Redox reactions of poly(AY) coated GC electrodes.

electrons and the protons taking part in the charge transfer was the same, i.e., poly(AY) redox reaction occurs by transfer of the same number (two) of electrons and protons (Fig. 3Ab). Collectively, the electrode reaction of the GC/PAY can be presented as in Scheme 2 [14,26–28]. SEM images of the poly(AY) film coated ITO electrode is shown in Fig. 3B. It is confirmed that the poly(AY) thin film on the electrode surface. This study further confirmed that the thin polymer film almost uniformly covered the electrode surface.

3.2. Electrocatalytic oxidation of DA at GC/PAY modified electrode

Fig. 4A shows the CVs of DA in pH 7.0 PBS at a bare GC electrode and a GC/PAY electrode. At a bare GC electrode, a pair of ill-defined redox peak was observed with the oxidation peak potential at 0.23 V and the reduction peak potential at 0.17 V (curve c). Under the same conditions, the GC/PAY modified electrode gave a highly enhanced peak current and a more reversible electron transfer process to DA. A well-defined and stable redox wave of DA was observed with the anodic and cathodic peak potentials at 0.220 and 0.197 V, respectively (curve b). The separation of peak potentials at the GC/PAY film modified electrode, ΔE_p was 23 mV, which was on accordance with a near Nernst reversible behavior and identified that the number of electrons involved in the reaction was about equal to two. Intensive increase in peak current was also observed owing to the improvement in the reversibility of electron transfer process and the larger real surface area of the poly(AY) film. This suggests an efficient oxidation reaction toward DA at the GC/PAY modified electrode. The effect of scan rate on the anodic peak current (I_{pa}) of DA was studied by cyclic voltammetry. With the scan rate increasing, the I_{pa} increased. A good linearity between the scan rate and I_{pa} was obtained within the range of 10–100 mV/s, suggesting a surface-confined process on the modified electrode surface. The linear equation was I_{pa} (μA) = $-0.1x - 0.7$ ($r = 0.998$).

Effect of pH on the formal potential ($E^{0\prime}$) and peak currents were examined by cyclic voltammetry in the presence of 50 μM DA in aqueous buffer solution with the increasing pH from 2.0 to 12, both the E_{pa} and E_{pc} shifted negatively and were dependent linearly on pH with the slopes of -55 and -57 mV/pH, respectively, indicating that the proportion of the electrons and protons involved in the redox of DA was 1:1 and the oxidation of DA at the GC/PAY modified electrode had been inferred to be a double-electron transfer reaction [26].

It could also be observed that both the oxidation and reduction peak current obtained a maximum at pH 7, which could be partly explained on the basis of the dissociation ability of –SO_3Na (H) group of poly(AY) film in different pH environments. When the solution pH was equal to 7, the –SO_3Na group of poly(AY) film could dissociate favorably into a negative charge group –SO_3^-. Under this condition, the –NH_2 group of DA molecules (pK_a: 8.9) [26] could obtain a proton and form the positive ion of DA. Therefore, the negative charge group –SO_3^- on the surface of poly(AY) modified electrode had a well affinity to the DA positive ions and could catalyze and promote the oxidation of DA

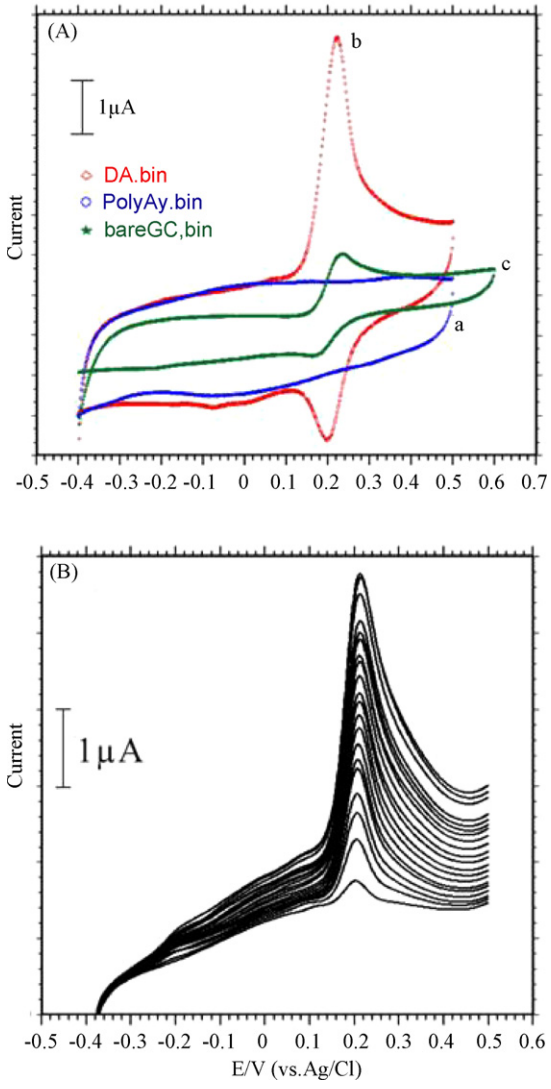


Fig. 4. (A) CVs of GC/PAY modified electrodes in pH 7.0 PBS: DA = (a) 0.0 μM, (b) 100 μM and (c) bare GC electrode with 100 μM DA; scan rate 10 mV/s. (B) Linear sweep voltammograms of GC/PAY modified electrode in pH 7.0 PBS with increasing DA concentration in the range 6–120 μM. Scan rate = 10 mV/s.

in the neutral buffer solution (pH 7). While pH was below 7, the $–SO_3Na$ group of poly(AY) film could form $–SO_3H$ and exclude the DA positive ions. However, when pH value was beyond 7, decreased DA peak currents seemed to be contradicted to the above-mentioned dissociation presumption. Actually, to interpret the effect of pH on the electrocatalytic oxidation of DA, it should not be overlooked that poly(AY) film at electrode acted as a mediator of electron transfer for DA's oxidation, whose electron transfer process could be affected by pH. Indeed, the anodic peak current of poly(AY) film reaction at GC electrode was observed to decrease gradually with increasing pH from 7 to 12. It was identified that with increasing pH the rate of electron transfer of the poly(AY) film could also decrease gradually, which was disadvantageous to the electrocatalytic reaction of DA at the poly(AY)-coated electrode. Thus, pH was a dual-conditioner to the oxidation of DA at the poly(AY)-coated GC electrode. On other hand, increasing pH of electrolyte solution from 2 to 7 could promote the formation of the $–SO_3^-$ radical on poly(AY) film resulting in that the poly(AY) modified electrode had a well affinity to the DA positive ions and enhanced the oxidation of DA. Hence, the pH 7 was an optimum protocol for the electrocatalytic oxidation of DA at the poly(AY) modified GC electrode. According to the above discussions, the course of DA's oxidation at the poly(AY) modified GC electrode could be described as in Eqs. (2) and (3) [14,26].

$$[\text{poly(AY)}]_{\text{red}} \leftrightarrow [\text{poly(AY)}]_{\text{ox}} + 2H^+ + 2e^- \quad (2)$$

$$[\text{poly(AY)}]_{\text{ox}} + [\text{DA}] \rightarrow [\text{poly(AY)}]_{\text{red}} \quad (3)$$

3.3. Dopamine detection using linear sweep voltammetry (LSV)

Next, we investigated the application of the poly(AY)-coated GC electrode for the determination of DA in aqueous solutions. First, the electrochemical characterization of GC electrode coated with poly(AY) films was performed in pH 7.0 phosphate buffer; pH 7.0 was selected since it has been found to be the optimum pH value for DA oxidation using poly(AY) coated GC electrode. Fig. 4B shows the voltammetric responses of the GC/PAY-modified electrode to the addition of DA into a pH 7.0 phosphate buffer solution. Distinct voltammetric peaks were obtained for concentrations as low as 6 μM DA. The peak current values showed a strong linear correlation with DA concentration, I_p (μA) = 0.032x + 2.051, displaying an r^2 value of 0.998. The calibration curve exhibited a linear range up to 120 μM, with a limit of detection (based on 3σ) for DA of 0.5 μM. The high sensitivity of the electrode for DA was found to be 0.2 μA/μM. Note that this detection limit and sensitivity are good comparable to existing methodologies [10–15].

3.4. Anti-sensing properties towards AA, UA and NADH

AA, UA and NADH are the most important interferences in biological samples. Moreover, at bare electrodes, the oxidation of AA, UA and NADH occurred at a potential close to that of DA [13,16,17]. Therefore, it is very important to measure the DA without interferences. In contrast to other polymer modified electrodes reported elsewhere [12–14], poly(AY) coated electrode did not shown any electrocatalytic activities towards AA or UA or NADH. Even in the presence of very high concentrations of these interferences in the pH 7 phosphate buffer solutions, the poly(AY) coated GC electrode neglected these species.

As we seen in Fig. 5, the voltammetric response for the successive additions of 10 mM AA, 10 mM UA and 15 mM NADH at GC/PAY modified electrode were recorded, it was observed that these interferences not shown any response at this modified electrode. Which could be partly explained on the basis of the dissociation ability of $–SO_3Na$ (H) group of poly(AY) film in different pH environments, in pH 7.0 phosphate buffer solution SO_3^- groups are negatively charged and these makes polymer backbone to repel the negatively charged species away from the surface of the electrode. In contrast, poly(*p*-amino benzene sulfonic acid) modified GC electrodes separated the anodic oxidation peak of AA from DA and it has been used for simultaneous separation of both analytes since each of *p*-amino benzene sulfonic acid has a SO_3^- group [14]. But in the case of AY molecules, each of the monomers has two SO_3^- groups. Hence, it may make them polymer more negatively charged. Since AA, UA and NADH are negatively charged at pH 7 [1–6] hence it is reasonable that anti-sensing behavior of poly(AY) coated GC towards AA, UA and NADH. These results clearly indicated that AA, UA and NADH are no longer interferences in the steady-state current during the detection of DA at poly(AY) coated GC electrode in this propped method.

3.5. Determination of DA by differential pulse voltammetry (DPV)

DPV was used for the determination of DA at the poly(AY) film-coated GC electrode because of its higher current sensitivity and better resolution than cyclic voltammetry. Same conditions

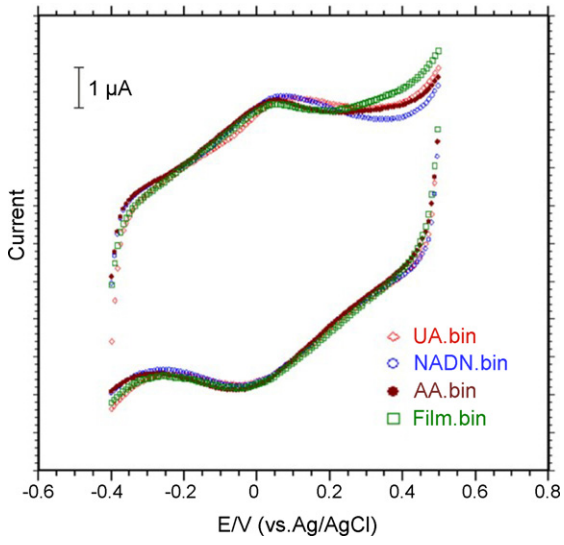


Fig. 5. Typical CVs obtained with a GC/PAY modified electrode in 0.1 M PBS (pH 7.0) with successive additions of (Brown line) 10 mM ascorbic acid, (red line) 10 mM uric acid and (Blue line) 15 mM NADH solutions. Scan rate = 0.1 V/s.

Table 1
The comparison of analytical data's obtained by LSV and DPV

Technique	Analyte	Concentration ranges (μM)	Regression equations	r^2	Detection limits (μM)
LSV	Dopamine	6–120	I_p (μA) = 0.032x + 2.051	0.998	0.5
DPV	Dopamine	1–100	I_p (μA) = 0.796x + 12.86	0.954	0.1

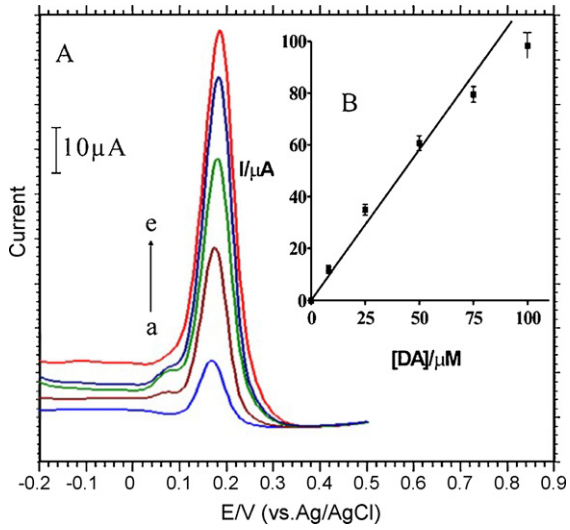


Fig. 6. (A) DPV graphs of (a) 10, (b) 25, (c) 50, (d) 75, (e) 100 μM DA in pH 7.0 PBS at the poly(AY)-modified GC electrode. (B) Plot of I_{pa} vs. DA concentrations.

are used as described in Section 3.3. The determination of DA was performed at the poly(AY) coated GC electrode. The results are shown in Fig. 6. From Fig. 6A, it can be seen that the peak current of DA is positively proportional to its concentration increasing from 1 to 100 μM. The peak current values showed a strong linear correlation with DA concentration, I_p (μA) = 0.796x + 12.86, displaying an r^2 value of 0.954. The calibration curve exhibited a linear range up to 100 μM, with a limit of detection (based on 3σ) for DA of 0.1 μM. No changes in the peak currents and potentials of DA oxidation when AA, UA and NADH can be found and their higher concentrations in same buffers solutions. No interference can be observed for the determination of DA by the coexisting other three species (AA, UA and NADH). All the results identifies that it is possible to selective detection of DA from its interferences in samples at the poly(AY) modified GC electrode. The calibration parameters for the determination of DA by LSV and DPV are listed in Table 1.

3.6. Reproducibility and stability of the GC/PAY electrode

In order to study the reproducibility of the sensor and reliability of fabrication procedure, five GC electrodes modified with poly(AY) were prepared independently. CVs of sensors were recorded in buffer solution. The relative standard deviation (R.S.D.) value of measured anodic peak currents was 3.5%. Furthermore, the five electrodes showed acceptable reproducibility with R.S.D. of about 4.2% for the current determination of 100 μM DA. For poly(AY) modified GC electrode, the R.S.D. determined by nine successive assays of a 100 μM DA was 3.8%. Good reproducibility and stability of the sensor can be attributed to the irreversible deposition and the strong adherent of poly(AY) onto GC electrodes.

The linear range and detection limit of this proposed method is compared with other existing methods in Table 2. One can understand from the data's presented in Table 2, our proposed method has wide linear range and good detection limit than earlier reports [11,17,24,31–33] and also our proposed method is a good alternative to the results in Refs. [12–14,23,26]. In addition, important advantages of poly(AY)/GC coated electrode over existing methods is its anti-sensing properties towards AA, UA and NADH. This behavior made poly(AY)/GC electrode is an unique than the earlier methods. The proposed method provides a possibility for selective detection of DA in the presence of interferences such as AA, UA and NADH in biological samples.

Table 2
Electrochemical methods for determination of DA

Electrode substrate	Modifier	pH	Linear range (μM)	Limit of detection (μM)	References
GCE	Poly(*p*-aminobenzene sulfonic acid)	7.0	0.1–100	0.02	[14]
GCE	Poly(phenosafranine)	7.1	50–500	0.02	[13]
GCE	Poly(2-picolinic acid)	7.0	0.25–10	0.03	[12]
GCE	Poly(cresol red)	7.0	10–100	1.5	[11]
CPE	Tetrabromo-*p*-benzoquinone	7.0	10–100	NA	[17]
GCE	Poly(eriochrome black T)	4.0	0.1–200	0.02	[26]
GCE	Poly(*p*-nitrobenzenazo resorcinol)	4.0	5–25	0.3	[24]
GCE	Poly(*p*-aminobenzoic acid)	5.0	0.05–20	0.02	[23]
GCE	Poly-chromotrope 2B	5.0	2–80	0.3	[31]
GCE	PPyox/SWNTs	4.0	1–50	0.38	[32]
GCE	PAT-Aunano-ME	7.0	10–50	–	[33]
GCE	Poly(acid yellow 9)	7.0	1–100	0.1	Proposed method

Abbreviations: GCE-glassy carbon electrode; ITO-indium tin oxide coated glass electrode; NA-not available; PPyox/SWNTs-overoxidized polypyrrole/single-walled carbon nanotubes; PAT-Aunano-ME-embedded gold nanoparticles/poly(4-aminothiophenol).

4. Conclusions

The poly(AY) film coated GC electrode exhibits highly electrocatalytic activity to the oxidations of DA in physiological condition. The modified electrode displays higher selectivity in voltammetric measurements of DA from its interferences (AA, UA and NADH) in their mixture solution. In contrast to other reported polymer modified electrodes, poly(AY) coated electrode have anti-sensing properties to AA, UA and NADH. This behavior make poly(AY) coated electrode as unique for selective detection of DA in neutral pH with the good sensitivity, excellent detection limit and wide linear range.

A conclusion can be drawn from the above results that our proposed method is efficient for the selective detection of DA by LSV and DPV. Finally, the proposed method provides a possibility for selective detection of DA in real samples too.

Acknowledgements

This project work was financially supported by the Ministry of Education and the National Science Council of Taiwan, ROC.

References

[1] R.N. Adams, Anal. Chem. 48 (1976) 1126A.
[2] M.A. Kutnink, W.C. Hawkes, E.E. Schaus, S.T. Omaye, Anal. Biochem. 166 (1987) 424.
[3] J.A. Stamford, J.B. Justice Jr., Anal. Chem. 68 (1996) 359a.
[4] S.A. Wring, J.P. Hart, B.J. Birch, Anal. Chim. Acta 229 (1990) 63.
[5] M.E.G. Lyons, W. Breen, J. Cassidy, J. Chem. Soc., Faraday Trans. 87 (1991) 115.
[6] J.M. Leal, P.L. Domingo, B. Garcia, S. Ibeas, J. Chem. Soc., Faraday Trans. 89 (1993) 3571.
[7] H. Mao, P.G. Pickup, J. Electroanal. Chem. 265 (1989) 127.
[8] L. Zhang, X. Lin, Y. Sun, Analyst 126 (2001) 1760.
[9] A. Fragoso, E. Almirall, R. Cao, L. Echegoyen, R. González-Jontec, Chem. Commun. (2004) 2230.
[10] H. Olivia, B.V. Sarada, D. Shin, T.N. Rao, A. Fujishima, Analyst 127 (2002) 1572.
[11] W. Chen, X. Lin, L. Huang, H. Luo, Microchim. Acta 151 (2005) 101.
[12] H. Zhao, Y. Zhang, Z. Yuan, Analyst 126 (2001) 358.
[13] T. Selvaraju, R. Ramaraj, Electrochem. Commun. 5 (2003) 667.
[14] G. Jin, Y. Zhang, W. Cheng, Sens. Actuat. B 107 (2005) 528.
[15] Z. Wang, J. Liu, Q. Liang, Y. Wang, G. Luo, Analyst 127 (2002) 653.
[16] S.M. Chen, W.Y. Chzo, J. Electroanal. Chem. 587 (2006) 226.
[17] H.R. Zare, N. Nasirizadeh, M. Mazloum Ardakani, J. Electroanal. Chem. 577 (2005) 25.
[18] S. Cosnier, Anal. Bioanal. Chem. 377 (2003) 507.
[19] L. Xu, W. Chen, A. Mulchandani, Y. Yan, Angew. Chem. Int. Ed. 44 (2005) 6009.
[20] G. Milczarek, A. Ciszewski, Electroanalysis 16 (2004) 1977.
[21] P.R. Roy, T. Okajima, T. Ohsaka, Bioelectrochemistry 59 (2003) 11.
[22] A.M. Yu, H.Y. Chen, Anal. Chim. Acta 344 (1997) 181.
[23] F. Xu, M.N. Gao, L. Wang, G. Shi, W. Zhang, L. Jin, J. Jin, Talanta 55 (2001) 329.
[24] X. Lin, Y. Zhang, W. Chen, P. Wu, Sens. Actuat. B 122 (2007) 309.
[25] A. Eriksson, L. Nyholm, Electrochim. Acta 44 (1999) 4029.
[26] H. Yao, Y. Sun, X. Lin, Y. Tang, L. Huang, Electrochim. Acta 52 (2007) 6165.
[27] S.A. Kumar, S.M. Chen, Sens. Actuat. B 123 (2007) 964.
[28] J. Yue, A.J. Epstein, J. Am. Chem. Soc. 112 (1990) 2800.
[29] A.P. Brown, F.C. Anson, Anal. Chem. 49 (1977) 1589.
[30] M. Sharp, M. Petersson, K. Edstrom, J. Electroanal. Chem. 95 (1979) 123.
[31] X. Lin, Q. Zhuang, J. Chen, S. Zhang, Y. Zheng, Sens. Actuat. B 125 (2007) 240.
[32] Y. Li, P. Wang, L. Wang, X. Lin, Biosens. Bioelectron. 22 (2007) 3120.
[33] A.I. Gopalan, K.-P. Lee, K.M. Manesh, P. Santhosh, J.H. Kim, J.S. Kang, Talanta 71 (2007) 1774.

Available online at www.sciencedirect.com
ScienceDirect
Talanta 74 (2008) 613–618
Talanta
www.elsevier.com/locate/talanta

An optical fiber biosensor for chlorpyrifos using a single sol–gel film containing acetylcholinesterase and bromothymol blue

Bambang Kuswandi *, Chulaifah Indah Fikriyah, Agus Abdul Gani

Chemo and Biosensors Group, School of Pharmacy, University of Jember, Jember 68121, Indonesia

Received 24 April 2007; received in revised form 22 June 2007; accepted 22 June 2007
Available online 7 July 2007

Abstract

An optical fiber biosensor consisting of acetylcholinesterase (AChE) and bromothymol blue (BTB) doped sol–gel film was employed to detect organophosphate pesticide chlorpyrifos. The main advantage of this optical biosensor is the use of a single sol–gel film with immobilized AChE and BTB. The compatibility of this mixture (AChE and BTB) with the sol–gel matrix has prevented leaching of the film. The immobilization of the enzyme and indicator was simple without chemical modification. The biosensing element on single sol–gel film has been placed inside the flow-cell for flow system. In the presence of a constant AChE, a color change of the BTB and the measured reflected signal at wavelength 622 nm could be related to the pesticide concentration in the sample solutions. The performance of optical biosensor in the flow system has been optimized, including chemical and physical parameters. The response time of the biosensor is 8 min. A linear calibration curve of chlorpyrifos against the percentage inhibition of AChE was obtained from 0.05 to 2.0 mg/L of chlorpyrifos (18–80% inhibition, $R^2 = 0.9869$, $n = 6$). The detection limit for chlorpyrifos was 0.04 mg/L. The results of the analysis of 0.5–1.5 mg/L of chlorpyrifos using this optical biosensor agreed well with chromatographic method.
© 2007 Elsevier B.V. All rights reserved.

Keywords: Optical fiber biosensor; Acethylcholinesterase; Sol–gel; Chlorpyrifos

1. Introduction

A wide variety of pollutants from industrial, agricultural and other human activities can contaminate aquatic environments. Among environmental pollutants, pesticides are of relevant concern, due to their toxicity and the prevalence of their use. In particular, organophosphate pesticides are widely used for agricultural and other domestic purposes. Even, these pesticides have relatively low persistence in the environment; however they have high acute toxicity to human health and ecosystems [1]. Chlorpyrifos is one of the most frequently used organophosphate pesticides in agriculture as commonly insecticide used to control insect and arthropod pests on agricultural and vegetable crops (e.g. grains, nuts, cottons and fruits). Due to agricultural and point source discharges, chlorpyrifos is most responsible for aquatic life toxicity [2]. Therefore, detection of chlorpyrifos is importance, which has enforced different regulatory agencies for chlorpyrifos detection. For example, under joint decision by the Ministers of Health and Agriculture Republic of Indonesia, No. 881/Menkes/SKB VIII/1996 and No. 771/Kpts/Tp. 270/8/1996, the maximum limit permitted for chlorpyrifos as pesticide residue is 0.05 mg/L [3]. Thus, it has strictly limited the discharges, emissions and losses of chlorpyrifos.

A wide variety of analytical methods have been reported in the literature for pesticide determination. Standard analytical methods, such as liquid chromatography (LC) [4], high performance liquid chromatography (HPLC) [5], and gas chromatography (GC) [6], have been commonly used for an efficient determination of chlorpyrifos and its metabolites [7]. However, these methods are time-consuming; require labor-intensive preparation of samples and skilled personnel.

An alternative to chromatographic methods, the enzyme-based biosensors have been described in literature [8–15]. For instance, different kinds of cholinesterases as biosensing elements have been employed to measure the loss of enzyme activity after inhibited reaction by analyte. The detection of organophosphate compounds with acetylcholinesterase-based biosensors have been proposed using potentiometric [13], amperometric [14] and optical transducers (spectrometric or fluorometric) [9–15].

* Corresponding author.
E-mail address: b_kuswandi@farmasi.unej.ac.id (B. Kuswandi).

0039-9140/$ – see front matter © 2007 Elsevier B.V. All rights reserved.
doi:10.1016/j.talanta.2007.06.042

Optical transducers in particular, have many interests in recent years [9]. Since, many new materials can be used in optical biosensors such as zeolite, conducting polymers, sol–gel, etc. [8,9]. Sol–gel for instance, there are many advantages, such as its optical clarity, the ability to entrap biomolecules (e.g. enzymes, DNA, antibody), thermal and chemical stability, simplicity of preparation and flexibility in controlling pore size and geometry [10]. Many works have reported the use of sol–gel and enzymes as optical biosensors for the determination of pesticides [10,11,16–18]. For optical biosensor based on sol–gel using pH indicator as transducer, the immobilization of indicator is an essential part of the biosensor fabrication process. A number of pH indicators have been incorporated into sol–gel film and in most cases, covalent binding is required to prevent leaching and loss of the pH indicator from the film [11,16]. In addition, a simple approach has been proposed by Ahmad and co-workers [18] using a chromoionophore (ETH5294) doped sol–gel film interfaced with another sol–gel film immobilized with acetylcholinesterase (AChE). However, this optical biosensor has been used double sol–gel layers for biosensing element, which in turn can lengthening sensor response time (12 min), reducing detection limit (0.5 mg/L) and reproducibility (<16%) for organophosphate pesticides (dichlorvos), since the measurements were also performed in batch mode.

In this work, we have entrapped a bromothymol blue (BTB) and AChE in a single sol–gel film with simple procedure without further chemical modification. The optical fiber biosensor proposed has faster response time (8 min), lower detection limit (0.04 mg/L) and better reproducibility (<1.5%) for organophosphate pesticide (chlorpyrifos) compared to previous work [18]. The suitability of this biosensor in the flow system for detection of chlorpyrifos has also described, which allow its utilization as alarm warning system in the pesticides monitoring. We also describe the validation of the biosensor results by comparison with a chromatographic method.

2. Experimental

2.1. Reagents

Acetylcholinesterase (E.C. 3.1.1.7) from electric eel (Type V I-S, 480 U/mg solid, AChE) and acetylcholine chloride (ACh) were purchased from Sigma Chemicals, chlorpyrifos was purchased from Riedel-de Haen, tetraethoxysilane (TEOS), a precusor of sol–gel, 2-pyrimidine aldoxime methiodide (2-PAM) and bromothymol blue were purchased from Merck. All other chemicals were of analytical grade and used as received without further purification. All solutions were prepared with double distilled or deionized water.

2.2. Enzyme and pH indicator immobilization

The sol–gel was prepared as described before with minor modification [10,18]. The acid-catalyzed sol solution was prepared by mixing 4.5 mL of tetraethoxysilane (TEOS), 1.4 mL of double distilled and deionized water and 0.10 mL of 0.1 M HCl in a glass vial. The mixture was then stirred (5 h) until a clear solution was formed and left overnight at room temperature before used. A solution of 1.5 mg/mL BTB was prepared by dissolving the BTB in absolute ethanol as a solvent. For the preparation in sol–gel film, 3 μL of BTB solution, 3 μL of sol solution and 10 μL of Tris–HCl buffer 0.1 M (pH 8) were mixed together. Then 30 μL 100 U/mL enzyme solutions in 0.1 M Tris–HCl buffer (pH 8) was added to the mixture of sol solution before spin coated with speed of 300 rpm for 10 s. The mixture was then put in designed circular mold (1 cm in i.d. and 1 mm depth) left for 5 days at a refrigerator (4 °C) where the film formed. The final biosensor film was taken from the mold and stored in a sealed container and kept in a refrigerator (4 °C) until used. Here, the addition of Tris–HCl buffer in sol–gel process is needed in order to reserve enzyme activity in the sol–gel matrix.

2.3. Optical fiber biosensors construction

The construction of the optical fiber biosensor has been carried out by carefully placed a single sol–gel film doped with AChE and BTB into the specially designed flow-cell [12,19]. In this biosensor design, it allows reducing the effect of other incident light levels on the flow-cell and optical system. Furthermore, the single film used was possible in this biosensor construction, due to the fact that AChE did not inhibited by BTB, either in sol–gel or in solution [20]. Thus, this single film makes the biosensor really simple and eases to be constructed in such optical fiber biosensor design.

In order to monitor a color change of the film as a function of the biosensor response, the flow-cell was then directly faced and geometrically adapted to the circular end of a fiber optic bundle probe. The flow-cell device incorporated two stainless-steel needles (1 mm o.d., 20 mm length), positioned at 120° opposite each other, to serve as inlet/outlet for solution flow. To provide a reflective surface backing, the circular bottom end of the flow-cell was also fitted with a with PTFE disk (at 2 mm distance from the probe tip). The internal flow-cell has a measuring volume of approximately 20 μL.

2.4. Flow manifold and measurement procedure

The flow-cell set-up described above was integrated with flow injection analysis (FIA) system, with the flow manifold configuration as shown in Fig. 1. The FIA system comprises three injection valves (Omnifit 1106) and four channels peristaltic pump equipped with Tygon tubing (1.0 mm i.d). Teflon® tubing was used between all components in the FIA system (FIA 5010, Tecator). The determination of chlorpyrifos is based on inhibition of AChE in the presence of the substrate (ACh). In the absence of chlorpyrifos, acetylcholine is bio-catalytically hydrolyzed to yield acetic acid and choline. The release acid originates a pH decrease that is sensed by the BTB, the color of which varies from green to yellow leading to an increase in the reflected signal intensity (at 622 nm) measured by optical fiber. In the presence of increasing amount of pesticide and a constant ACh concentration, the activity of the enzyme AChE decreases so that a smaller pH change occurs and a change in the reflected signal intensity of the sensor is measured using

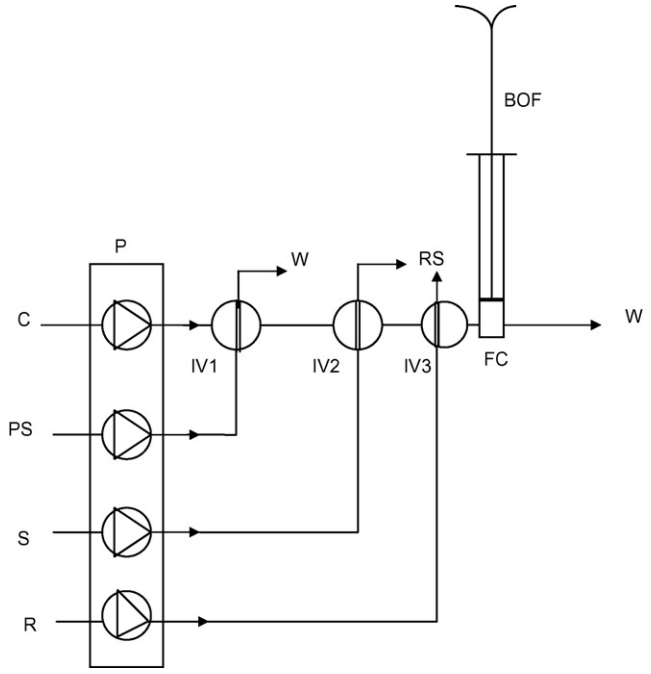


Fig. 1. Flow manifold used for measurement of enzymatic determination of chlorpyrifos. C, carrier (pH 7.5, 7.5 mM Tris buffer); PS, sample (pesticides solution); S, substrate (acetylcholine solution); R, reactivation solution; P, peristaltic pump; IV, injection valve; RS, reservoir; FC, flow-cell; BOF, bifurcated optical fiber; W, waste.

an optical fiber spectroscopy (USB2000 spectrometer) as that described previously [12,19].

Initially, a carrier stream of a Tris buffer was pumped through the FIA system in order to obtain a baseline signal. Three injection valves were connected in series; the substrate (ACh) solution was injected manually through injection valve 2 to determine the initial activity of enzyme (i.e., absence of inhibition (E_0)). The sample solution of chlorpyrifos was injected, using valve 1, into the carrier stream. After inhibition, the residual enzyme activity was revealed by substrate (ACh) injection and the percentage inhibition (E_c) was calculated according to the following expression:

$$\text{inhibition}\,(\%I) = \left[\frac{(E_0 - E_c)}{E_0}\right] \times 100 \quad (1)$$

where E_0 and E_c are the peak height reflected signal intensity for substrate and substrate plus inhibitor, respectively. After the inhibition measurement, the reactivation solution (2-PAM) had to be introduced via injection valve 3 in order to remove chlorpyrifos from the immobilised enzyme effectively and recover its activity. The whole cycle measurement was repeated for other concentrations of chlorpyrifos. Furthermore, the sol–gel film had to be carefully washed with water after each set of measurement in order to avoid the precipitation of the salts present in the buffering solution that could also be block the flow system.

2.5. Determination with chromatographic methods

To compare the results of analysis with standard methods for chlorpyrifos determination, gas chromatography using mass spectrometry detection (GC–MS) method was chosen [21]. Water samples for analysis were first spiked with different concentrations of chlorpyrifos from 0.5 to 1.5 mg/L. For GC–MS analysis, the samples were first extracted with solid-phase extraction SPE column (Bakerbond spe^{TM}). Each column contained 6 mL disposable extraction cartridges packed with 200 mg styrene divinylbenzene copolymer. To extract and concentrate all samples, an Autotrace SPE workstation and TurboVap LV evaporator were used. Water samples of 500 mL, in which 5 mL of methanol had been added, were passed over the conditioned sorbent. Afterwards, the sorbent was dried under nitrogen for 20 min. Elution was performed by soaking and eluting the cartridge with 5 mL of ethyl acetate. The eluted was then dried and the final volume was precisely adjusted to 0.5 mL of isooctane.

A GC 8000 series capillary gas chromatograph coupled to a MD800 mass spectrometer (Fisons Instruments) was used for chlorpyrifos analysis. Chromatographic separations were conducted on a DB-5 MS fused-silica capillary column, 30 m × 0.25 mm i.d. × 0.25 μm film thicknesses, with helium as a carrier gas, at a flow rate of 1.5 mL/min. Injections of 1 μL volume of sample were performed on a splitless injector using an AS 800 autosampler (CE Instruments). The mass spectrometer operated in the EI mode. The injector temperature was set at 270 °C, whilst the interface and ion source temperatures were maintained at 270 and 200 °C, respectively. The identification and quantification of chlorpyriphos were carried out by monitoring *m/z* 314 and 316 with the instrument. The linear plot (peak area versus concentration) was constructed.

3. Results and discussion

3.1. Optimization of experimental parameters

In order to determine the optimum operating parameters (chemical and physical) for this method a series of preliminary investigations were performed and Table 1 shows the range over which each of the parameter was investigated and its optimum value. Within the chemical parameters, the most importance ones was found to be those directly involved in the enzymatic process, i.e. the buffer, pH and substrate (ACh) concentration. For the enzymatic reaction, Tris buffer was used as the buffer at a concentration of 7.5 mM, where both the blank and the inhibition signals were optimum. Above this concentration the reaction

Table 1
Optimisation of experimental parameters

Experimental conditions	Value range	Optimal value
[ACh] (mM)	2.5–100	40
pH	6.0–8.0	7.5
Buffer concentration (mM)	1.0–10.0	7.5
Substrate injection volume (mL)	1.0–5.0	2.0
Pesticide injection volume (mL)	1.0–5.0	1.5
Flow rate (mL/min)	0.1–5.0	0.2
Inhibition time (min)	1.0–10.0	7.0
Reactivation solution (mL)	1.0–10.0	1.0

rate decreases along with inhibition degree, and below this concentration the reproducibility of response is slightly poor. A pH 7.5 was found to be optimum for the enzymatic process. Here, both ionic strength (buffer concentration) and pH are importance in determining the biosensor response, due to the fact that the biosensing process is based on the net of pH change before and after inhibition of the enzyme with pesticides. Furthermore, though low concentrations of ACh produced measurable blank signal and inhibition degree, it resulted in a low level of the blank signal. Thus, a concentration of 40 mM of ACh was chosen as a compromise.

In general the FIA parameters were important in the optimisation of the inhibition process, in particular, flow-rate, reagents and sample injections, and time of inhibition. A low flow-rate of 0.2 mL/min was chosen as it allowed the blank signal to develop to a greater extent with relatively low concentration of ACh. The injection volume of substrate (ACh) was found to be optimum at 2.0 mL, as the smaller volume caused a decrease in the blank signal, which in turn, the degree of inhibition was decreased as well. The optimum time of inhibition was selected at 7 min, as compromise between the sensitivity, sample throughput and lifetime of the enzyme. The sample injection volume was optimised in the range of 1.0–5.0 mL, and 1.5 mL was selected as a trade of between sensitivity and sampling rate. The reactivation (1 mM 2-PAM,) injection volume was also optimised in the range of 1.0–5.0 mL, and 1.0 mL was selected as desired volume for reactivation of the inhibited AChE.

3.2. The response of optical biosensor toward chlorpyrifos

The biosensor resulting from immobilisation of AChE and BTB on sol–gel film has been tested towards chlorpyrifos as organophosphate pesticides. In uninhibited scheme or blank solution, the biosensor measures a pH change generated by the release of acetic acid during the enzymatic reaction according to the Eq. (2). While in inhibited scheme, the biosensor also measures a pH change where enzyme AChE is inhibited by pesticides. As a whole measurement, actually the biosensor measures a net of pH change before and after inhibition of the enzyme AChE. The inhibition of AChE is normally attributed to the acylation of the serine–OH in the active site of the enzyme by this compound [22]. The reaction with AChE is analogous to the enzyme–substrate reaction, whereby a Michaelis enzyme–pesticide complex is first formed, followed by the transfer of the pesticide acyl groups to the serine–OH of enzyme, and the concomitant release of the side product (HB). Therefore, the enzymatic inhibition by chlorpyrifos is carried out according to the Eq. (3):

$$\text{acethylcholine} + H_2O \xrightarrow{\text{AChE}} \text{acetic acid} + \text{choline} \qquad (2)$$

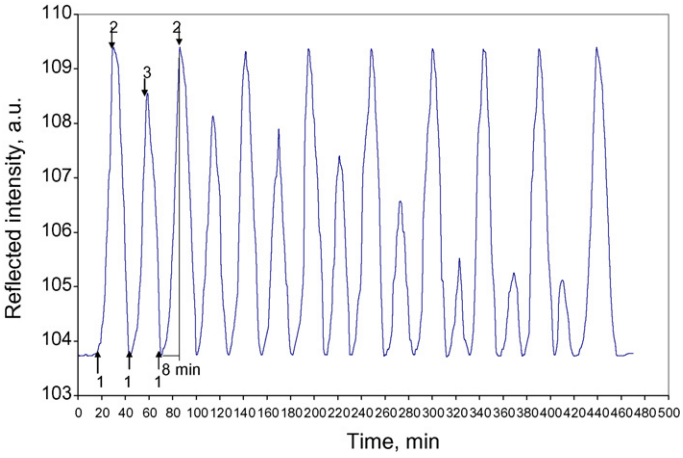
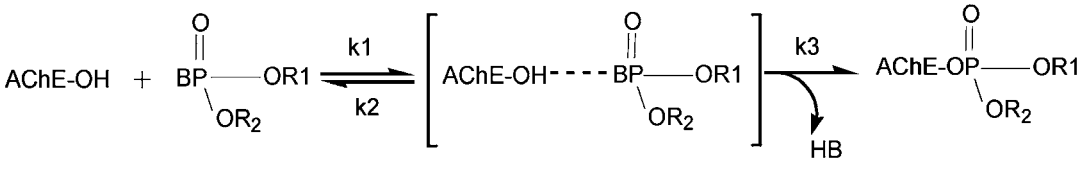


Fig. 2. The response of the biosensor towards various concentrations of chlorpyrifos (0–4 mg/L). The response time was 8 min. The arrows indicate the injection point of substrate (ACh) [1], chlorpyrifos [2] and reactivation solution, 2-PAM [3]. From the left to the right, first peak is for uninhibited biosensor response (blank response), second peak for chlorpyrifos 0.05 mg/L, third inhibited peak for 0.1 mg/L, fourth inhibited peak for 0.2 mg/L, fifth inhibited peak for 0.5 mg/L, sixth inhibited peak for 1.0 mg/L; seventh inhibited peak for 2.0 mg/L, eighth inhibited peak for 3.0 mg/L and ninth inhibited peak for 5.0 mg/L of chlorpyrifos concentration respectively.

where $k_{(1–3)}$ are rate constants. The rate-limiting step is the formation of the AChE-organophosphate complex. However, the rate of hydrolysis of phorphorylated AChEs was very slow. Consequently, when the enzymes are reacted again with the natural substrate (ACh), a lower pH change would be detected since the enzyme not fully reactivated (remains inhibited). In order to activate the enzyme again, the reactivation/regeneration solution is needed, where in this case 2-PAM (1 mM) was used [11]. The difference in the pH change before and after the pesticide inhibition provides information on the amount of the pesticide, which in turn can be utilized for chlorpyrifos determination.

The response of the biosensor towards various concentrations of chlorpyrifos is given in Fig. 2, for which the response time of the optical biosensor is 8 min. This lower response time compared to previous work [18] would be due to a single sol–gel film and flow system used, which in turn can increase response time. Here, the time limiting step is controlled by the diffusion of analyte within the film in a flow mode, while in a batch mode, it controlled by the convective mass extraction from the film of the aqueous solution that goes on until the required amount of analyte is reached [23].

Based on Fig. 2 the calibration curves for chlorpyrifos could be constructed. The percentage inhibition increase linearly with increasing chlorpyrifos concentration in the range of 0.05–2.0 mg/L ($\%I = 0.0333$ [chlorpyrifos] + 18.028) equal



(3)

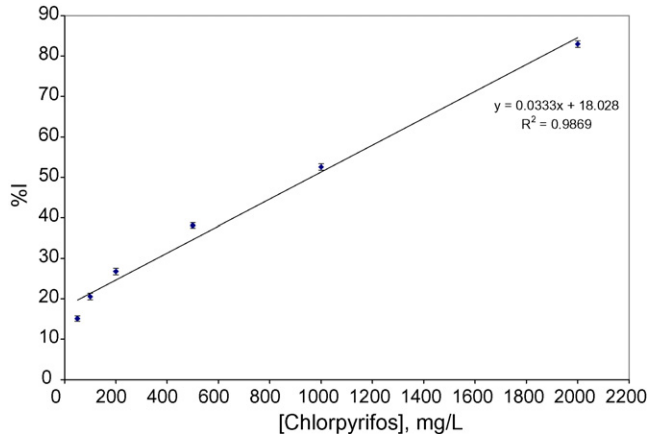


Fig. 3. The percentage inhibition increase linearly with increasing chlorpyrifos concentration in the range 0.05–2.0 mg/L (each data point is an average of three replicates).

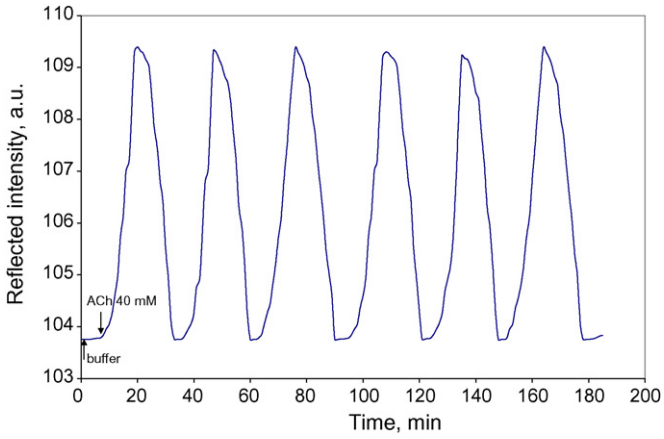


Fig. 4. The responses of the biosensor toward substrate, acethylcholine [40 mM ACh].

to 18–80% inhibition ($r^2 = 0.9869$, $n = 6$) where each point was the average of three injections (Fig. 3). For higher chlorpyrifos concentrations, flat response of the biosensor was reached. The reactivation of the immobilized AChE was achieved by injection with the reactivation solutions (2-PAM). The detection limit (3ε) of the biosensor for chlorpyrifos was 0.04 mg/L. This value was 10-fold lower than previously work reported [18], and could allow the detection of chlorpyrifos within the maximum residue concentration permitted by Indonesian Government (0.05 mg/L) [3].

3.3. Reactivation and reproducibility

It is desirable for inhibited enzyme-based optical biosensor that its enzyme activity be recovered easily and efficiently. Thus, it will allow a more economical use of the sensor and facilities its easier handling [19]. However, like in this case, results have shown that the AChE that has been exposed to chlorpyrifos, a spontaneous recovery of AChE activity was not achieved, even with a repetitive treatment of substrate (ACh) solution. This can be due to the strong ester linkage between the dimethyl phosphate group and the serine moiety of enzyme. Significant reactivation of the enzyme-based biosensor signal was attained after the biosensor has been treated with 1 mM 2-PAM as shown in Fig. 2. The reactivation effect of 2-PAM is due to its strong nucleophilic character. Thus, it makes reactive toward the electrophilic phosphorous atom of the phosphorylated AChE. By doing so, it displaces the AChE from its attachment to the phosphorus, then yielding the free and active form of AChE again [11,12].

The reproducibility of the biosensor has been evaluated toward substrate (ACh) as a blank signal, pesticides (inhibited AChE) as inhibition measurements, and the reactivation/regeneration process. The biosensor was injected with substrate only, for the blank signal reproducibility, while for inhibition, the biosensor was alternately reacted with 1 mg/L chlorpyrifos and then regenerated using 1 mM 2-PAM. The results have been shown that the reproducibility of biosensor towards substrate as a blank signal was good (R.S.D. < 1.5% for $n = 6$) as given in Fig. 4. While for inhibition and reactivation steps were fairly reproducible (R.S.D. inhibition = 1.5% for $n = 3$ and R.S.D. reactivation = 1.2% for $n = 3$) as given in Fig. 5. The stability of the biosensor was good and even after repetitive use for a week, in the presence of chlorpyrifos, the biosensor retained 80% of its original activity. In fact, the biosensor produces reproducible and stable responses up to 2 months, as long as, the sol–gel film of AChE–BTB keep in 4 °C. After this time the biosensor behaviour gradually deteriorates. This is due to the fact that the biosensor response reduced within 25–30% compared to its original signal.

3.4. Comparison with chromatographic methods

The validation of optical biosensor was performed by using gas chromatography coupled to mass spectrometry (GC–MS) as the reference method. Samples spiked with chlorpyrifos at five different concentrations: 0.5, 0.75, 1.0, 1.25 and 1.5 mg/L were analyzed by both methods. The variability of the method was studied by injecting three replicate of each chlorpyrifos

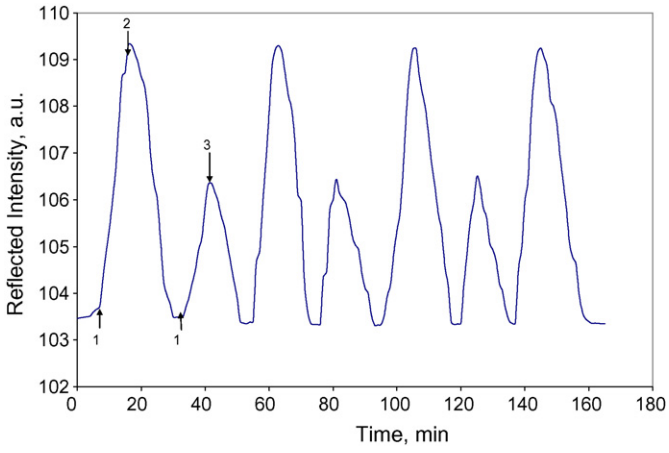


Fig. 5. The responses of the biosensor toward substrate [40 mM ACh] (1), inhibition [chlorpyrifos, 1 mg/L] (2) and reactivation solution [1 mM 2-PAM] (3).

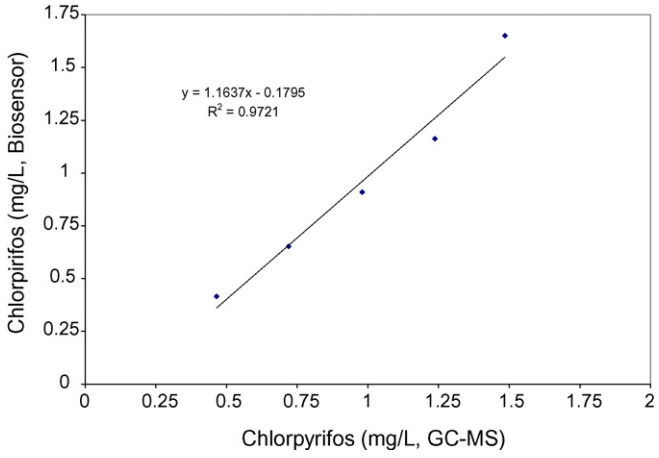


Fig. 6. A correlation of the concentrations of chlorpyrifos determined by the biosensor directly with that determined by GC–MS after solid-phase extraction procedure.

concentration. The linear regression analysis provided the calibration equation ($y = 1.1637x - 0.1795$) as shown in Fig. 6. The correlation data indicates a good agreement between methods ($r^2 = 0.9721$) and no significant discrepancies were found when comparing the biosensors and GC–MS methods, as shown by the slope of the linear regression analysis (1.16). However, the deviation from ideal value (1.0) might be due to the different on the recovery factor as a result of the random errors that could be occurred in both methods.

4. Conclusions

This work shows the utilization of optical fiber biosensor based on single sol–gel film containing of AChE–BTB in flow system for detection of widely used chlorpyrifos based on enzyme inhibition scheme. The main advantage of this optical biosensor is the use of a single sol–gel film with AChE and BTB, which in turn, resulting fast response time, low detection limit and good reproducibility. Furthermore, the immobilization of the biosensing element on sol–gel film was simple without any chemical modification. The biosensor developed can be used for the screening of chlorpyrifos in water samples. The comparison of the biosensor measurements with classical chromatographic method (GC–MS) demonstrated the suitability of biosensor for rapid analysis of pesticides, as compared with the long extraction pre-treatment methods required by the conventional method.

The fully automation of the optical fiber biosensor sensor in the flow system, could be achieved by using microfluidics incorporated in a platform of reduced size. This approach would provide very low reagents and sample used, which in turn, can achieved lower detection limit of pesticides, simple, fast analysis and real-time monitoring, which is currently been developed in our group.

Acknowledgements

The authors thank the DP3M Higher Education Republic of Indonesia for consumable expenditures via Hibah Bersaing XIII and the International Foundation for Science, Stockholm, Sweden and Organization for the Prohibition of Chemical Weapons (OPCW), The Hague, Netherlands, for donation of the fiber optic spectroscopy (Ocean Optic, USB 2000) through a grant to BK.

References

[1] USEPA, Preliminary Cumulative Risk Assessment of the Organophosphorus Pesticides, USEPA, Washington, DC, 2001.
[2] K.E. Banks, D.H. Hunter, D.J. Wachal, Environ. Int. 31 (2005) 351.
[3] Join decision by the Ministers of Health and Agriculture Republic of Indonesia, No. 881/Menkes/SKB VIII/1996, No. 771/Kpts/Tp. 270/8/1996 concerning maximum limit of pesticide residues available on the Ministry of Agricultural website, http://www.deptan.go.id.
[4] S. Lacorte, D. Barceló, J. Chromatogr. A 712 (1995) 103.
[5] M.L. Reyzer, J.S. Brodbelt, Anal. Chim. Acta 436 (2001) 11.
[6] P. Pugliese, J.C. Molto, P. Damiani, R. Marin, L. Cossignani, J. Manes, J. Chromatogr. A 1050 (2004) 185.
[7] D. Simon, S. Helliwell, K. Robards, Anal. Chim. Acta 360 (1998) 1.
[8] B. Kuswandi, M. Mascini, Curr. Enzyme Inhib. 1 (2005) 11.
[9] B. Kuswandi, R. Andres, R. Narayanaswamy, Analyst 126 (2001) 1469.
[10] R.A. Doong, H.C. Tsai, Anal. Chim. Acta 434 (2001) 239.
[11] R.T. Andres, R. Narayanaswamy, Talanta 44 (1997) 1335.
[12] B. Kuswandi, N.W. Swandari, Sens. Trans. 76 (2007) 978.
[13] C. Ristori, C. DelCarlo, M. Martini, A. Barbaro, A. Ancarani, Anal. Chim. Acta 325 (1996) 151.
[14] G. Jeanty, C. Ghommidh, J.L. Marty, Anal. Chim. Acta 436 (2001) 119.
[15] A.L. Simonian, T.A. Good, S.S. Wang, J.R. Wild, Anal. Chim. Acta 534 (2005) 69.
[16] M.P. Xavier, B. Vallejo, M.D. Marazuela, M.C. Moreno-Bondi, F. Baldini, A. Falai, Biosens. Bioelectron. 14 (2000) 895.
[17] V.G. Andreou, Y.D. Clonis, Biosens. Bioelectron. 17 (2002) 61.
[18] F.C.M. Wong, M. Ahmad, L.Y. Heng, L.B. Peng, Talanta 69 (2006) 888.
[19] B. Kuswandi, Anal. Bioanal. Chem. 376 (2003) 1104.
[20] A.A. Gani, C.I. Fikriyah, B. Kuswandi, Proceedings of the ICPBAR International Conference, 2006, p. 207.
[21] J. Quintana, I. Marti, F. Ventura, J. Chromatogr. A 938 (2001) 3.
[22] R. O'Brien, in: C. Wilkinson (Ed.), Insecticides Biochemistry and Physiology, John Wiley and Sons Ltd, London, 1976, pp. 271–296.
[23] B. Kuswandi, Nuriman, H.H. Dam, D.N. Reinhoud, W. Verboom, Anal. Chim. Acta 591 (2007) 208.

Available online at www.sciencedirect.com
ScienceDirect
Talanta 74 (2008) 458–469
Talanta
www.elsevier.com/locate/talanta

Review

Quantitative liquid chromatography/mass spectrometry for the analysis of microdialysates

Katrien Lanckmans, Sophie Sarre, Ilse Smolders, Yvette Michotte*

Research Group Experimental Pharmacology, Department of Pharmaceutical Chemistry, Drug Analysis and Drug Information, Vrije Universiteit Brussel, Laarbeeklaan 103, 1090 Brussels, Belgium

Received 19 April 2007; received in revised form 16 July 2007; accepted 30 July 2007
Available online 2 August 2007

Abstract

Microdialysis (MD) is an *in vivo* sampling technique used to investigate biochemical events in the extracellular fluid of animal and human tissues. MD produces protein- and cell-free, aqueous samples which can be analyzed without further sample clean-up. Liquid chromatography coupled to tandem mass spectrometry (LC–MS/MS) is a sensitive and selective analysis technique which is suitable to quantify low concentrated target analytes in microdialysates. This paper reviews the LC–MS/MS methods which are described for the quantification of endogenous molecules, such as neurotransmitters and peptides, and of exogenous molecules, such as drugs, in microdialysates.

Since miniaturization of the LC–MS/MS methods is the key to obtain maximal sensitivity of the analytical technique, this feature is discussed in the paper. In addition, critical issues related to the quantification of low concentrated molecules in microdialysates are described such as the presence of matrix effects, the low MD efficiency and the sticking of, for instance, neuropeptides.
© 2007 Elsevier B.V. All rights reserved.

Keywords: Microdialysis; LC–MS/MS; Quantification; Matrix effects

Contents

1. Introduction 459
2. Endogenous compounds 459
   2.1. Neurotransmitters 459
      2.1.1. Introduction 459
      2.1.2. Acetylcholine 460
      2.1.3. Biogenic amines 461
      2.1.4. Amino acids 461
      2.1.5. Other neuromediators 462
   2.2. Neuropeptides 462
      2.2.1. LC–MS/MS analysis of neuropeptides in MD samples 463
      2.2.2. Validation of the LC–MS/MS method 463
      2.2.3. Enhanced microdialysis efficiency for peptides 464
      2.2.4. Sticking of peptides 464
      2.2.5. Stability of peptides in dialysates 464
3. Exogenous compounds 464
4. Matrix effects 464
5. Concluding remarks 467
   Acknowledgements 467
   References 467

* Corresponding author. Tel.: +32 2 477 47 48; fax: +32 2 477 41 13.
E-mail address: ymichot@vub.ac.be (Y. Michotte).

0039-9140/$ – see front matter © 2007 Elsevier B.V. All rights reserved.
doi:10.1016/j.talanta.2007.07.027

1. Introduction

Microdialysis (MD) is an *in vivo* sampling technique used to investigate biochemical events in the extracellular fluid of animal and human tissues, including the brain. The technique enables the collection of small, hydrophilic endogenous compounds – such as neurotransmitters and peptides – and exogenous compounds – such as drugs – and allows the simultaneous local administration of exogenous substances. MD sampling provides several advantages, such as direct *in vivo* sampling in anaesthetized or freely moving animals and continuous sampling from specific target tissues without fluid loss. The MD technique is based on the principle of kinetic dialysis. The basic tool for MD sampling is a tubular semipermeable dialysis membrane, commonly known as a MD probe, which is implanted in the tissue of interest. The inlet of the MD probe is connected to a MD pump which provides a constant pulse-free flow-rate (between 0.5 and 10 μL/min) of the perfusion fluid, which is a physiological salt solution. Low volume microdialysates (1–40 μL) are collected at the end of the probe outlet. The MD probe membrane is characterized by a certain cut-off value between 5 and 35 kDa. Indeed, the pore size of the semipermeable membrane should be large enough to allow free diffusion of solute molecules, but small enough to restrict the passage of proteins and macromolecules. Due to the absence of enzymes and proteins, respectively, the stability of some compounds in microdialysates, such as peptides, is expected to be improved. Moreover, for drugs only the pharmacologically active free fraction is present in the dialysates. Dialysate concentrations are only reflections of the true extracellular concentrations. To obtain an exact quantification of the analyte of interest, the probe must be calibrated. This is achieved by determining the recovery of the probe for the substance of interest. The relative recovery is defined as the ratio between the concentration of a substance in the dialysate and the concentration of the same substance in the solution outside the probe, usually expressed as a percentage. There are several factors influencing the relative recovery of the probe, such as the membrane (length, diameter, material), the diffusion coefficient of the analyte, the time factor, temperature, composition of the perfusion fluid, perfusion flow-rate and the properties of the substances [1].

The protein- and cell-free microdialysates can be analyzed by liquid chromatography (LC) without further sample clean-up. However, they are still complex mixtures of small molecules and peptides. Besides the need of a selective analytical technique, sensitivity of the method is a critical issue since compounds, such as neurotransmitters and neuropeptides are present in low concentrations (nM–pM range) in the extracellular space. Moreover, MD probe recovery is often low (<20%). Furthermore, the administration of highly protein-bound or potent drugs results in low amounts of drug and metabolites in the dialysates. Finally, but not less important, is the MD temporal resolution. Since the sample volume is time and flow dependent, the temporal resolution of the sampling is inversely related to the dialysate volume. Enhanced MD temporal resolution is especially a requisite in behavioral or pharmacokinetic studies of drugs with a short half-life. This presents a considerable challenge for simultaneous detection and accurate quantification of the low amount of analytes, recovered in the low volume samples.

Several analytical methodologies such as LC, capillary electrophoresis (CE), mass spectrometry (MS), radioimmunoassay (RIA), electrochemistry (ECD), fluorescence detection, biosensors, or combinations of some of these methods have been used to measure analyte concentrations in the microdialysates [2]. The last decade, there was a boost in the use of the LC–MS technique because of superior sensitivity and selectivity. Quantitative MS detection can be performed with single quadrupoles and ion traps. However, a triple quadrupole MS, operated in the selected reaction monitoring (SRM) mode provides an additional dimension of selectivity since specific product ions, resulting from the dissociation of the precursor ion, are monitored. As a result, the signal-to-noise ratio of the ion chromatographic peak of an analyte is significantly higher than that obtained in the selected ion monitoring mode. In addition, LC–MS/MS analytical systems have minimal baseline drift and can be equilibrated very rapidly [3].

Downscaling of the LC dimensions enhances mass sensitivity [4–7] and miniaturization of the ESI process, also called micro- or nanospray, further improves the method limit of detection (LOD) due to enhanced ionization efficiency [6,8–10]. Therefore, miniaturization of the LC–MS process is the key to achieve maximal sensitivity, which is a requisite to quantify low concentrated compounds in biological fluids.

This review focuses on the LC–MS/MS methods developed for the quantification of endogenous (such as acetylcholine, biogenic amines, amino acids and other neuromediators and neuropeptides) and exogenous compounds (drugs and other substances) in MD samples.

2. Endogenous compounds

2.1. Neurotransmitters

2.1.1. Introduction

Detection of extracellular levels of neurotransmitters remains an analytical and technical challenge due to the low levels of neurotransmitters collected (fmol amounts) and the small MD sample size (<40 μL). GC–MS assays are inadequate due to low sensitivity, low selectivity and time consuming sample preparation [3]. The most popular methods for detection of classical neurotransmitters were ECD, fluorescence, ultraviolet and MS, routinely coupled to LC separation. However, only LC–MS detection provides a direct and sensitive measurement and the analyte can be identified by both its retention time and molecular weight. Ikarashi and Maruyama [11] have successfully used LC–MS/MS for the determination of neurotransmitters. This study showed that the obtained specificity of the LC–MS/MS analysis is very high and, in contrast to ECD, trace analysis can be performed and sample throughput is significantly higher. Recently, Zhang and Beyer reviewed the applications of *in vivo* MD–LC–MS to measure levels of acetylcholine (Ach), dopamine (DA), noradrenaline (NAD) and γ-aminobutyric acid (GABA) [3]. In our paper, we extended this to all neurotransmitters, monitored with LC–MS/MS in *in vivo*

MD samples, including Ach, the biogenic amines (DA, NAD, serotonin (5HT)), amino acids (GABA and glutamate (Glu)) and other neuromediators (such as purine and pyrimidine bases, (deoxy)ribonucleosides, anandamide, prostaglandins).

2.1.2. Acetylcholine

Within the central nervous system, Ach has been implicated in the control of temperature, blood pressure, motor coordination, learning, memory and sleep [12]. Therefore, the measurement of Ach in the brain is important for the study of, e.g., Alzheimer's disease and Parkinson's disease. The concentrations of Ach and its metabolite choline in the extracellular fluid range from 0.1 to 6 nM and from 0.6 to 5 μM, respectively [13]. Enzymatic hydrolysis of Ach in the synaptic cleft is fast and hence the extracellular concentration of Ach in the brain is low. Therefore, highly sensitive and selective analytical methods are required. LC coupled to ECD and ESI-MS/MS detection has most commonly been used for the analysis of Ach in MD samples [14]. Most LC–ECD methods used an Ach esterase inhibitor, such as physostigmine or neostigmine, in the perfusion medium to enhance basal Ach levels. However these compounds can affect neuronal activity and the pharmacology of the neuronal circuits under investigation [14,15–17]. Therefore, improved LC–ECD methods were developed, where no Ach esterase inhibitor was included in the perfusate [18,19].

To date, the best sensitivity for Ach assays has been achieved with LC–ESI-MS/MS. Table 1 summarizes most important features of the published methods where MD was coupled to LC–ESI-MS/MS for the quantification of Ach in brain. For a discussion of the papers published before 2006, we refer to the review of Zhang and Beyer [3].

The detection limits of the LC–ESI-MS/MS methods (0.01–0.1 nM) are more than an order of magnitude lower than what was previously achieved with ECD (0.3–1 nM) [20]. Moreover, LC–MS/MS detection allows the analysis of basal Ach levels without inclusion of an esterase inhibitor in the perfusion medium, which was not always possible with ECD. Given these advantages, LC–MS/MS is the method of choice for the routine analysis of Ach in microdialysates.

Because Ach is a polar compound, its retention on standard reversed phase LC columns is generally poor. Therefore, Zhu et al. [21] and Hows et al. [22] used ion-pair reagents and concentrated buffers in their mobile phases. However, these additives may suppress the ESI process and therefore, deteriorate method sensitivity. To avoid this, Uutela et al. [13] developed a hydrophilic interaction chromatography (HILIC) method, in which a diol column was used, not only for the separation of Ach, choline and the IS, but also for the separation of the analytes from inorganic salts and endogenous compounds within a chromatographic run time of 10 min. In the analysis of the MD samples, the salts were washed to waste by gradient after the elution of Ach and choline using column switching.

Recently, Zhang et al. described a validated LC–MS/MS method for the simultaneous monitoring of Ach, choline and *iso*-Ach in rat brain microdialysates [24]. The MS conditions were optimized to achieve high sensitivity, enabling the detec-

Table 1
Overview of LC–MS/MS methods for the quantification of acetylcholine in microdialysis samples

Compounds	LC	MS	MD	IS	LOD	Reference
Ach	C18 (150 mm × 2.1 mm) ammonium acetate, heptafluorobutyric acid and methanol; pH 3.2	ESI-ion trap	2 μL/min, 25 min samples	β-methyl-Ach	28 pM	[21]
Ach and neostigmine	C18/SCX (150 mm × 2.1 mm) ammonium acetate, ammonium formate and acetonitrile; pH 4.0	ESI-triple quad	1.2 μL/min, 20 min samples collected in vials containing acetic acid	No	0.1 nM	[22]
Ach and choline	HILIC diol (125 mm × 4 mm) ammonium formate and acetonitrile; pH 3.3	ESI-triple quad	2.5 μL/min, pooled samples	β-methyl-Ach	20 pM (Ach), 1 nM (choline)	[13]
Ach and two selective D_3 receptor antagonists: SB-277011A (a) and SB-414796A (b)	C18/SCX (150 mm × 2.1 mm) ammonium acetate, ammonium formate and acetonitrile; pH 4.0	ESI-triple quad	1.5 μL/min, 20 min samples collected in glass vials containing oxalic acid	No	0.1 nM (Ach), 1.0 nM (a and b)	[23]
Ach	Capillary columns with integrated ESI emitters (5 cm × 50 μm) ammonium acetate, ammonium formate and methanol; pH 4.0	ESI-ion trap	0.6 μL/min, 2.4 min intervals, on-line coupling	No	40 pM (8 amol)	[25]
Ach, choline and *iso*-Ach	SCX (150 mm × 2.1 mm) ammonium acetate, ammonium formate and acetonitrile; pH 4.0	ESI-triple quad	1 μL/min, 20 min samples	β-methyl-Ach	10 pM (Ach), 0.1 nM (choline), 30 pM (*iso*-Ach)	[24]

tion of basal Ach. Since Ach and *iso*-Ach are isobar molecules and since they are both present in extracellular brain fluid, their baseline separation is essential for accurate quantification. An unknown chemical interference peak for Ach was also observed in many microdialysates from rat brains. Therefore, baseline separation of Ach and this chemical interference was essential in accurately determining small drug-related changes in Ach levels. The use of β-methyl-Ach as internal standard (IS) also appeared to be important for accurate analysis of Ach.

Although higher sensitivity is achieved with MS/MS detection, the MD temporal resolution using off-line sampling was limited (sampling times of 20 min). Shackman et al. reported the on-line coupling of MD with capillary LC, utilizing capillary chromatography columns with integrated ESI emitters [25]. With on-line injection, it was possible to acquire chromatograms every 2.4 min allowing improved temporal resolution for monitoring Ach *in vivo* with the convenience and utility of not collecting fractions.

2.1.3. Biogenic amines

In vivo MD is currently one of the main techniques used for continuous monitoring of biogenic amines in the extracellular fluid of the brain. The analytical technique that is used for the analysis of DA, 5HT and NAD is LC–ECD [26–30]. Using microbore LC–ECD, LOD's of about 40 pM were described by Sarre et al. [31,32]. Hows et al. [33] described for the first time the combination of *in vivo* MD with LC–MS/MS detection for the simultaneous measurement of DA, NAD, 5HT and cocaine in biological samples.

Biogenic amines are polar molecules, especially NAD, and consequently their retention on RP–LC columns is poor. Therefore, ion-exchange [34] and ion-pair [35] chromatography was performed in combination with ECD. However, ion-pair reagents and buffers are not volatile and therefore not compatible with MS detection. Hows et al. [33] used formic acid, a volatile ion-pairing agent, to minimize ion suppression and to maintain the pH of the eluent. Two RP columns were found suitable to separate the biogenic amines and cocaine, namely Discovery HS C18 and Synergi Hydro-RP. The Discovery phase could only be used with eluents containing a small percentage of organic modifier. The Synergy stationary phase could be used with aqueous eluents because of a polar embedded group. A rapid gradient profile was designed to separate analytes with a range of polarities within 4 minutes, which is much faster than the previously developed LC–ECD methods.

Detection was performed in the positive ESI mode and using a triple quadrupole MS. The detection limits for DA, NAD and 5HT were 200, 1000 and 900 pM, respectively. The detection of basal levels of NAD was unfortunately not possible with the developed LC–MS/MS method, since the protonated molecular ion of NAD was not the predominant ion, because this molecular ion was unstable and rapidly dissociated in the ESI source. Monitoring the protonated molecular ion would result in reduced sensitivity [3]. Therefore, the simultaneous separation and detection of all three biogenic amines in brain MD samples using LC–MS/MS remains a technical challenge.

The superior selectivity of the MS/MS method over ECD detection for the monitoring of biogenic amines was also shown by Hows et al. [33]. They found that the basal levels of DA in MD samples, determined by LC–MS/MS, were much lower than obtained with their own LC–ECD method. However, these lower concentrations were consistent with concentrations of DA in dialysates, published by others. They showed that the LC peak detected with ECD could not be attributed solely to DA and was most probably an artifact.

2.1.4. Amino acids

The amino acid neurotransmitters include aspartate and Glu as the major excitatory neurotransmitters, whereas GABA and glycine are important inhibitory transmitters. So far, the coupling of *in vivo* MD sampling to LC–MS/MS detection for these amino acid neurotransmitters has not yet been published. In 1999, Ma et al. published a LC–APCI-MS method for the simultaneous determination of GABA and Glu in rat brain homogenates [36]. After extraction (on an ion-exchange column) and evaporation, the dried residue was dissolved in water and analyzed by LC–API-MS. The separation of GABA and Glu was carried out on an Inertsil ODS-2 packed column (150 mm × 4.6 mm, i.d.) and with a mobile phase composed of acetonitrile (ACN), ammonium acetate and water. In the APCI-MS system, the quasi-molecular ions of both amino acids were observed as base peaks at *m/z* 104 for GABA and *m/z* 148 for Glu. The limits of detection for GABA and Glu were 24 and 34 μM, respectively. This detection limits are insufficient to detect basal GABA and Glu concentrations in microdialysates. Consequently, the LC–APCI-MS assay needs further optimization to enhance method sensitivity. Possible solutions are the miniaturization of the LC column and the use of a tandem MS detector in order to analyze GABA and Glu in the MRM mode. These manipulations were performed by Song et al., who developed a capillary-ESI-MS/MS method for the determination of GABA in physiological fluid samples, using GABA-d_2 as IS [37]. Prior to separation on a capillary LC column (25 μm ID), the samples were derivatized with 7-fluoro-4-nitrobenzoxadiazole (NBD-F) followed by a clean-up and preconcentration step on an extraction column. Since GABA is very hydrophilic, it has a low affinity for the reversed phase (RP) column. Precolumn derivatization of GABA using NBD-F increases its hydrophobicity and molecular size and hereby strengthens the retention of GABA on the LC column. Moreover, the resultant NBD-GABA could be effectively ionized in the ESI source, producing the molecular ion *m/z* 267, which was CID fragmented into the predominant product ion with *m/z* 249, by loss of H_2O. The selectivity of the SRM transition could be argued since the neutral loss was not structurally characteristic. The LOD for GABA was 48 nM, which is 500 times lower than the previously published LC–MS method by Ma et al. [36]. In this study, only plasma and CSF samples were analyzed. However, this method could potentially be used for the determination of extracellular levels of GABA in the brain, using *in vivo* MD.

Recently, Berna and Ackermann published a validated LC–MS/MS method for the selective measurement of D- and L-serine in rat brain microdialysates [38]. Resolution of the ser-

ine enantiomers was accomplished with chemical derivatization using Marfey's reagent followed by RP chromatography. The LOQ for D- and L-serine was 10.3 ng/mL. Basal hippocampal levels of D-serine were found to be approximately 200 ng/mL and of L-serine about 2 μg/mL.

2.1.5. Other neuromediators

2.1.5.1. Purine and pyrimidine bases, nucleosides and deoxynucleosides. The measurement of endogenous purine and pyrimidine bases, nucleosides and deoxynucleosides may provide information related to their possible transmitter or neuromodulator function in the brain. The characterization of nucleoside, nucleotide and modified nucleotides by LC–MS has been reviewed by Esmans et al. [39]. LC–MS has been widely used to determine nucleosides in biological samples [40–44]. However, the determination of these endogenous compounds in MD samples is so far only described by Dobolyi et al. [45] and Zhu et al. [46]. The first group reported a gradient chromatographic system with a cooled RP column for the detection of these compounds in very low concentrations in microsamples, such as microdialysates and micropunches. The narrowbore RP column was cooled, first to improve the separation by increasing the affinity for the stationary phase of the most hydrophilic compounds with low retention times and second to decrease band-broadening and thereby increasing the detectability of the hydrophobic compounds with high retention times. ESI-MS/MS allowed the identification of certain of theses compounds at extreme low concentrations. The LOD's lie in the range of 0.1–1 pmol/50 μL for all measured compounds. They reported for the first time the interstitial concentrations of many (deoxy)nucleosides and pyrimidine bases in the brain, such as uridine, 2′ deoxyuridine, uracil, cytidine, 2′ deoxycytidine, thymidine, thymine, 2′ deoxyadenosine and 2′ deoxyguanosine.

Zhu et al. [46] determined brain basal nucleosides (inosine, guanosine and adenosine) in microdialysates from the striatum and cortex of the rats using a narrowbore LC (cyano column) coupled to ESI-MS/MS (ion trap) detection. The detection limit for inosine and guanosine was 15 nM, while for adenosine the LOD was 6 nM.

2.1.5.2. Anandamide. Anandamide is an endocannabinoid and is the endogenous eicosanoid derivative (arachidonoylethanolamide). Anandamide plays an important role in various stages of human reproduction. Properties of cannabinoids that might be of therapeutic use include analgesia, muscle relaxation, immunosuppression, anti-inflammation, anti-allergic effects, sedation, improvement of mood, stimulation of appetite, anti-emesis, lowering of intraocular pressure, bronchodilatation, neuroprotection and antineoplastic effects [47]. *In vivo* monitoring of anandamide is therefore relevant. Walker et al. [48] developed an *in vivo* MD method coupled to an LC–APCI-MS assay to study the release of endogenous anandamide in the periaqueductal gray (PAG). The LC–MS assay was modified from that of Koga et al., who demonstrated that anandamide can be measured by APCI-LC/MS [49]. Walker et al. included 30% β-cyclodextrin in the perfusion buffer and a 15-fold increase in the *in vitro* recovery of anandamide was observed. MD samples, collected during 15 or 30 min, were chromatographed on a C18 column (50 mm × 4.6 mm) with a mobile phase consisting of 85% methanol/1 mM ammonium acetate/0.05% acetic acid. Ionization occurred in the APCI mode and a single quadrupole was operated in selected ion monitoring mode (*m/z* 348.3). The basal level of anandamide found in dialysis samples was 186 ± 18 pM, which is similar to those of other neurotransmitters or -modulators, involved in pain and found in the PAG, such as Met-enkephalin. After electrical or painful stimulation, elevated anandamide levels were observed. The data supported the existence of an endogenous cannabinergic circuitry in the dorsal and lateral PAG that is triggered by pain and promotes analgesia through the release of anandamide.

2.1.5.3. Prostaglandins. Prostaglandins are important mediators in inflammation, pain and fever. Especially PGE_2 is involved in spinal nociceptive processing. In contrast, PGD_2 may be involved in anti-inflammatory processes. In vivo MD sampling of prostaglandins is mostly coupled to immunoassays. However, immunological assays do not allow for the determination of more than one compound in one sample and cross-reactivity among prostaglandins may occur. GC–MS detection is more sensitive than immunoassays, but requires time-consuming sample derivatization and long run times. This motivated Schmidt et al. to develop an LC–MS/MS assay to determine PGE_2 and PGD_2 in *in vivo* MD samples of the dorsal horn [50]. First, PGE_2 and PGD_2 were extracted using liquid-liquid extraction with ethyl acetate to prevent the MS from salt impurities and to develop a robust high throughput method. Using a linear gradient, a short run time (6 min) was achieved on a Synergi Hydro-RP column (150 mm × 2.0 mm). The mobile phase contained acetonitrile (ACN) as organic modifier, since methanol was not able to separate PGE_2 from PGD_2. However, in the second part of the gradient methanol was selected because of its better sensitivity for prostaglandins as compared to ACN. Since formic acid leads to decreased signal intensities in the negative ion mode, formic acid was omitted from the mobile phase, but was present in the sample solvent, to obtain better signal-to-noise ratios. To obtain maximal sensitivity, the same product ion (*m/z* 271) was monitored for both prostaglandins. $[^2H_4]$-PGD_2 was used as IS because the isotopic purity of $[^2H_4]$-PGE_2 was only 99.0%. The lower limit of quantification for PGE_2 was 71 pM and for PGD_2 was 142 pM. Analysis of spinal cord microdialysates of rats showed similar concentrations of PGE_2 as published previously with immunoassays. However concentrations of PGD_2 were below LOD, so more sensitive LC–MS/MS assays need to be developed to show whether PGD_2 is involved in spinal nociceptive processing.

2.2. Neuropeptides

Neuropeptides are present in brain tissue as well as in cerebrospinal fluid. Their coexistence with one or more classic neurotransmitters suggests that they are involved in modulatory processes and probably in many other types of functions. It

seems that neuropeptides are of particular importance when the nervous system is challenged (e.g., by stress, injury, drug abuse, epilepsy) [51]. Since they do not participate in fast synaptic transmission, their pharmacotherapeutical application could be less prone to side effects as compared to drugs which act on the classical fast-acting neurotransmitters. Despite the significance of these compounds, they are rarely monitored *in vivo*. Instead, peptide function is most often studied by analyzing tissues for peptides or mRNA, injection or reverse dialysis of peptides into select brain regions, and by use of pharmacological agents. The presence or the release of neuropeptides into the extracellular space can be monitored by the *in vivo* MD technique.

2.2.1. LC–MS/MS analysis of neuropeptides in MD samples

Due to the very dilute nature of MD samples and the low concentrations (ranging from sub pico- to femtomolar levels) of endogenous neuropeptides in the brain, ultrasensitive detectors are required, such as RIA and MS. MD in combination with RIA has been the common method for studying *in vivo* release of neuropeptides in the rat brain [52,53]. Although RIA provides high sensitivity, the molecular specificity is limited. Cross-reactivity among peptides with similar sequences is common. Therefore, miniaturized LC–MS detection is the method of choice for the analysis of individual neuropeptides in brain dialysates.

So far, only a limited number of endogenously released neuropeptides have been monitored using *in vivo* MD and LC–MS [52]. The combination of brain dialysis with micro-electrospray-tandem MS for the analysis of neuropeptides was first described by Andren and Caprioli for [Met]^5-enkephalin (Met-enk) [54] and neurotensin (NT) [54,55]. The key features of this pioneering work, were that MD samples from the globus pallidus/ventral pallidum (Met-enk and NT) or from hypothalamus (NT) were collected every 30 min with a perfusion flow-rate of 436 nL/min. Consequently, 10 μL of the dialysis samples were preconcentrated and desalted on a nano-flow solid-phase extraction (SPE) column containing C18 RP resin particles, packed in the tip of a 50 μm i.d. fused silica capillary micro-ESI needle. With this device, peptides were concentrated and adsorbed to the column, which was rinsed to desalt the sample using a mobile phase containing 2% methanol and 0.25% acetic acid. The peptides of interest were subsequently eluted with a solvent containing 50% methanol and 0.25% acetic acid and introduced into the triple quadrupole MS. Basal levels of both neuropeptides were close to the LOD of the method, which was estimated at 4 pM. Release of the peptides was stimulated following a 1 μL local bolus injection of artificial CSF containing 100 mM KCl. In addition, the release of Met-enk increased 2.6 times after systemic administration of morphine.

Haskins et al. improved the sensitivity of this pioneering method for the simultaneous monitoring of endogenous Met-enk, Leu-enk and unknown neuropeptides [56]. Using capillary LC columns with an i.d. of 25 μm and integrated ESI emitters, interfaced to a quadrupole ion trap MS, LOD's of 2 pM for 1.8 μL injections were obtained with 30 min temporal resolution. The sensitivity of the system was sufficient to achieve at least 3.3 min temporal resolution, however, this would require faster on-line analysis or off-line collection and analysis of fractions. Another striking feature is the use of a pulse of N_2 gas to remove salt droplets from the ESI emitter before the emitter was positioned at the entrance of the MS. Unknown peptides could also be identified at low pM concentrations using time-segmented scans and MS^2. These authors applied this method in another paper for discovery and neurochemical screening of peptides in brain extracellular fluid [57]. They observed a surprising amount of chemical noise considering the low background expected for MS^2 detection. This noise can be decreased by applying MS^3. Indeed, with each stage of MS, both chemical noise and signal decrease; however, chemical noise decreases faster. To obtain higher S/N, Baseski et al. used MS^3 for the determination of enkephalines in the rat brain striatum [58]. Although for standard solutions, the LOD's were similar, greater background discrimination was observed when analyzing actual dialysate samples. The MS^3 method also proved to be significantly more reproducible (RSD was 5% in stead of 20% at 60 pM). The temporal resolution was also improved to 15 min by optimizing the gradient. Unfortunately, homemade columns with integrated ESI emitters had to be produced daily to alleviate tip breakage and prevent clogging.

Nyitrai et al. used LC–ESI-MS to measure increases in the extracellular level of somatostatin in the hippocampus of the rat after local administration of a $GABA_B$ receptor antagonist (CGP-36742) [59]. The estimated detection limit was 0.3–0.6 nM.

2.2.2. Validation of the LC–MS/MS method

Limited validation of the above-mentioned methods was carried out because the aim of these papers was to investigate the feasibility of miniaturized LC–MS/MS to detect or monitor extremely low amounts of neuropeptides in MD samples. However, more attention should be paid to method validation. In 2005, Wilson et al. [60] published a validated MD method coupled to capillary column switching LC–TOF-MS for the determination of bradykinin and arg-bradykinin in rat muscle tissue. The LOD for both analytes was approximately 100 pM, using an injection volume of 500 μL. The presence of salts in the dialysis samples could disturb the ion-pairing between the analytes and the formate ions in the loading mobile phase. However, no breakthrough was observed on the loading column when injection volumes were below 800 μL. (Tyr^8)-bradykinin was used as IS in order to obtain good quantitative precision. Unfortunately, method accuracy was not investigated. Sinnaeve et al. indicated that miniaturized LC–MS methods tend to present somewhat larger variability in terms of precision and deviation in terms of accuracy [61]. Therefore, they preferred the use of capillary LC–ESI-MS to nano methods for the quantification of enkephalines in cerebrospinal fluid. Oosterkamp et al. introduced an IS because the reproducibility of their method for endothelin analysis was unsatisfactory. The introduction of the IS reduced the RSD from >50% to below 25% [62].

Recently, we published a paper in which we described that a stable isotope labeled (SIL-) IS should be used instead of a structural analogue for the accurate and precise determination of the neuropeptide angiotensin IV (Ang IV) in rat brain MD samples [63]. The SIL-Ang IV IS not only corrected for matrix

effects but also for degradation of Ang IV in the samples. The additional benefit of using the SIL- analogue was that linearity could be improved.

2.2.3. Enhanced microdialysis efficiency for peptides

Overall, basal concentrations of neuropeptides were close to (or below) the detection limits of the above-described miniaturized methods. Not only the low extracellular concentrations of the peptides are responsible for the difficulty to monitor them in microdialysis samples, but also the low MD efficiency for peptides hampers detectability. Therefore, optimizing microdiaysis recovery is just as important as enhancing method sensitivity. Peptides have a different behavior towards each probe membrane type. Therefore, the optimal membrane type should be identified for the peptide of interest [53,64–69]. Lowering the perfusion flow-rate is the most straightforward and the most applied approach to increase recovery. However, a lower flow-rate is detrimental for the sample collection time and thus for the MD temporal resolution. In this paper we summarize shortly possible strategies to improve MD recovery of peptides. For further details on the principles of the different techniques, we refer to the cited papers. Ao et al. described the 12-fold enhanced recovery of cytokines due to the inclusion of antibody-coated microspheres in the perfusion fluid which increase the analyte diffusive driving force across the dialysis membrane [70]. Duo et al. reviewed their studies where cyclodextrines and antibodies were used as agents to improve recovery, next to the antibody-immobilized bead MD sampling enhancement and the non-antibody based enhancement compounds [71]. Pettersson et al. published a promising study of solid supported enhanced MD for peptides [72]. Due to an increased flux, a selective uptake of hydrophilic peptides across the membrane and enrichment on the solid particles, an (up to ten times) improved relative recovery was obtained. It is important to note that all these recovery-enhancement and sticking-reducing manipulations were not tested in combination with miniaturized LC–ESI-MS detection.

2.2.4. Sticking of peptides

Peptides can have the tendency to stick to pipette tips, test and storage tubes, tubing connections, injection syringes or to chromatographic columns. Adsorption phenomena have to be considered when developing quantitative procedures [73].

Maidment et al. made an attempt to reduce sticking of cholecystokinin and NT by acidification of MD samples, but this proved inadequate for NT [65]. The addition of bovine serum albumine (BSA) to the perfusion medium is efficient to reduce sticking of several peptides in the MD tubing or onto the membrane [64–66,69,74–79]. MD sampling has the benefit to produce protein-free samples. Adding BSA to the samples to minimize sticking counteracts one of the most important merits of MD. Mertes et al. observed that interstitial neuropeptide Y sampling required the addition of BSA to the perfusion medium to avoid adhesion of the peptide to the probe [76]. However, it also diminished the MD efficiency by limiting mass transfer of NPY towards the interstitium. We conclude that the use of BSA to minimize non-specific adsorption of the analyte to MD material should be well considered, certainly in combination with miniaturized LC–ESI-MS detection.

Carry-over is a phenomenon often associated with LC–MS analysis of peptides. Carry-over effects should be minimized by for instance, using separate injection syringes for each manual injection and by flushing the injection loop with ACN followed by water and by performing blank injections prior to sample injections [60]. We performed several injections of ACN/water/FA (50:50:0.1, v/v/v) until carry-over of Ang IV was below the LOD of the method [63].

2.2.5. Stability of peptides in dialysates

Some papers describe precautions, such as removing aliquots under laminar flow hood, filter-sterilization of samples, flushing tubings and syringes with ethanol and even the addition of peptidase inhibitors to the perfusion fluid to minimize the presence of peptidases, produced by bacteria and capable of degrading the already low levels of peptides *in vivo* samples [64,65,77,80]. We previously showed that the use of a SIL-IS corrected for degradation of Ang IV in microdialysates [63].

3. Exogenous compounds

MD has been demonstrated to be applicable in many different organs for studying the tissue specific pharmacokinetics of a large variety of drugs [81]. The use of MD in pharmacokinetic studies is limited by the sensitivity of the analytical method. The last decade, MS/MS became a popular alternative to UV, fluorescence and ECD detection because of superior sensitivity and selectivity. Table 2 summarizes all LC–MS methods developed for quantification of exogenous compounds in MD samples of different tissues. Linear ranges covered mostly three orders of magnitude. Limits of detection were mainly situated in the low to medium nM range. Most applications were performed at narrowbore, and some at conventional LC dimensions because of good method precision and accuracy results. However, microbore and capillary LC columns were also used. The key factor to obtain maximal sensitivity is downscaling the LC dimensions and miniaturizing the ESI process. We made a comparison between microbore, capillary and nano LC–MS/MS methods for the quantification of oxcarbazepine, its active metabolite (10-11-dihydro-10-hydroxycarbamazepine) and the IS for probe calibration (2-methyl-5H-dibenz(*b*,*f*)azepine-5-carboxamide). Indeed, the limits of detection improved 5 and 50 times when downscaling from microbore to capillary and nano-LC–MS/MS, respectively [82].

4. Matrix effects

A drawback of the use of ESI is its sensitivity to matrix effects. Co-eluting matrix compounds can cause ion suppression and sometimes even ionization enhancement. The consequences are accuracy and precision problems and reduced sensitivity. Although MD samples are protein-free aqueous solutions, they contain a large amount of salts and other small molecules. These non-volatile compounds can cause ion suppression of the analytes of interest and can clog the MS source. Different strategies

Table 2
Overview of exogenous compounds, quantified with LC–MS in microdialysis samples

Analyte	MD	LC	MS	Linear range	LOD	IS	Reference
Acyclovir and its prodrugs: valacyclovir and val-valacyclovir	Rabbit eye anterior chamber	C8, 2.1 mm	ESI-single quad	n.d.	n.d.	No	[83]
6-Aminobutylphthalide	Rat brain striatum, 4 mm	C18, 3.0 mm	ESI-triple quad	2–200 ng/mL	2 ng/mL	No	[84]
Amphetamine	Rat brain medial prefrontal cortex, 4 mm	C18, 2.1 mm	ESI-ion trap	5–100 ng/mL	1 ng/mL	No	[85]
Amphetamine	Rat brain medial prefrontal cortex, 4 mm	C18, 2.1 mm	ESI-single quad	10–1000 ng/mL	2 ng/mL	No	[86]
Celecoxib	Rat dorsal horn of spinal cord	C18, 2.0 mm	ESI-triple quad	0.5–20 ng/mL	0.5 ng/mL*	Yes	[87]
Cetirizine enantiomers	Guinea pig: jugular vein (10 mm) and brain (3 mm)	Chiral α_1-acid glycoprotein column, 4.0 mm	ESI-triple quad	0.25–50 ng/mL	0.25 ng/mL	Yes	[88]
CI-1007	Rat brain striatum, 4 mm	C18, 300 μm	ESI-ion trap	0.1–1 ng/mL	0.1 ng/mL	No	[89]
Cocaine and its metabolite benzoylecgonine	Rat brain medial prefrontal cortex, 4 mm	C18, 3.0 mm	ESI-single quad	Cocaine: 3–300 ng/mL, benzoylecgonine: 0.1–10 μg/mL	Cocaine: 1.5 ng/mL, benzoylecgonine: 10 ng/mL	No	[90]
Cocaine	Rat brain nucleus accumbens, 2 mm	C18, 2 mm	ESI-triple quad	0.03–300 ng/mL	1 pg/mL (API3000), 0.1 pg/mL (API4000)	No	[33]
Cocaine	Rat jugular vein (10 mm), bile duct (7 cm) and brain striatum (3 mm)	C18, 3.0 mm	ESI-triple quad	0.05–100 μg/mL	10 ng/mL	No	[91]
Contrast agents	Rat carotid vein, 10 mm	C18, 2.0 mm	ESI-single quad	n.d.	n.d.	No	[92]
CS-866 and its active metabolite RNH-6270	In vitro MD, 10 mm	No LC	ESI-triple quad	0.1–10 μg/mL	n.d.	Yes for RNH-6270 (d6)	[93]
Diclofenac	Human subcutaneous adipose tissue, 16 mm	RP, 3.0 mm	ESI-triple quad	1–1050 ng/mL	1 ng/mL	Yes	[94]
Ertapenem	Human medial vastus muscle and subcutaneous layer of the thigh, 30 mm	RP, 2.0 mm	ESI-triple quad	0.1–50 μg/mL	40 pg/mL	Yes	[95,96]
HIV protease inhibitors Indinavir Saquinavir Nelfinavir Amprenavir	Rat liver	C18, 2.1 mm	APCI-single quad	5–2000 ng/mL	3–5 ng/mL	Yes	[97]
5-HT2a receptor antagonist (MDL 100,907) and active metabolite (MDL 105,725)	Rat brain medial prefrontal cortex, 2 mm	C8, 1 mm	ESI-triple quad	n.d.	n.d.	Yes	[98]
Ketoprofen	Rat dermal tissue,	Polymeric SPE, 2.1 mm	ESI-triple quad	25–5000 ng/mL	3 ng/mL	Yes	[99]
Melatonin	Rat jugular vein, 10 mm	C18, 3.2 mm	APCI-triple quad	0.5–500 ng/mL	0.5 ng/mL	No	[100]
Methotrexate	Dog stifle joint space, 4 mm	C18, 1 mm	ESI-triple quad	0.45–450 ng/mL	n.d.	Yes	[101]
8-Methoxypsoralen	Human subcutaneous dorsal forearm	C18, 2.0 mm	ESI-triple quad	0.25–50 ng/mL	0.1 ng/mL	No	[102]
Morphine	Rat femoral and jugular veins (10 mm); brain hippocampus	C18, 2.0 mm	ESI-triple quad	n.d.	0.5 ng/mL	Yes	[103]

Table 2 (*Continued*)

Analyte	MD	LC	MS	Linear range	LOD	IS	Reference
Morphine and its 3- and 6-glucuronide metabolites	Sheep fetuses: brain and vein	HILIC, 4.6 mm	ESI-triple quad	0.5–500 ng/mL	0.2–0.5 ng/mL	No	[104]
N-acetyl-aspartyl-glutamate (NAAG) and its peptidase inhibitor 2-PMPA (2-(phosphonomethyl)pentanedioic acid)	Rat brain caudatus putamen, 4 mm	C18, 4.6 mm	ESI-triple quad	0.6–1500 ng/mL	0.6 ng/mL	No	[105]
Neuropeptide FF antagonist dansylated tripeptide amide	Rat brain striatum, 4 mm	C18, 300 μm	ESI-quad ion trap	n.d.	n.d.	Yes	[106,107,108]
Oxcarbazepine, its active metabolite (10,11-dihydro-10-hydroxycarbamazepine) and IS for probe calibration 2-methyl-5H-dibenz(*b*,*f*)azepine-5-carboxamide	Rat brain hippocampus, 3 mm	C18, 1 mm	ESI-triple quad	1–1000 ng/mL	40, 60 and 30 pg/mL	No	[109]
Opioidmimetics	Rat brain striatum, 3 mm	C8, 2.0 mm	ESI-triple quad	10–100 ng/mL	1–5 ng/mL	No	[110]
R-84760	Rat jugular vein, 10 mm	No LC separation, only sheath liquid 50 μL/min	ESI-triple quad	5–500 ng/mL	5 ng/mL	Yes (d8)	[111]
Ropivacaine and metabolite (pipecoloxylidide)	Human plasma, 20 mm	C18, 0.2 mm	ESI-triple quad	0.027–27 ng/mL	27 pg/mL*	Yes	[112]
Scopolamine	Human subcutaneous adipose tissue	C18, 2 mm	ESI-triple quad	0.05–10 ng/mL	0.02 ng/mL	No	[113]
Scopolamine	Human abdominal subcutaneous tissue	C18, 2 mm	ESI-triple quad	0.05–10 ng/mL	0.05 ng/mL*	No	[114]
Sinomenine	Rat skin, 30 mm	C18, 2.1 mm	ESI-single quad	2–10000 ng/mL	0.5 ng/mL	No	[115]
Tetrahydroisoquinoline derivatives	Rat brain frontal cortex, 3 mm	Phenyl, 250 μm	ESI-ion trap	5–500 ng/mL	2–3 ng/mL	No	[116]
1-Benzyl-1,2,3,4-tetrahydroisoquinoline	Rat brain frontal cortex, 3 mm	Phenyl, 250 μm	ESI-ion trap	1–200 ng/mL	0.2 ng/mL	No	[117]
Topiramate	Rat brain nucleus accumbens, 3 mm	C8, 4.6 mm	Thermospray-triple quad	0.03–1 μg/mL	34 ng/mL	Yes (d12)	[118]
Tryptanthrin	Pig foreleg dermis, 5 cm	C18, 2 mm	ESI-single quad	12.5–400 ng/mL	5 ng/mL	Yes (d8)	[119]
Vesnarinone and its metabolites OPC-8230, OPC-18136 and OPC-18137	Human dialysate	C18, 4.6 mm	ESI-triple quad	Vesnarinone: 2–10 ng/mL; metabolites: 0.5–25 ng/mL	Vesnarinone: 2 ng/mL; metabolites: 0.5 ng/mL*	Yes	[120]

The microdialysis (MD) parameters (tissue and probe length), the LC parameters (stationary phase and column i.d.), the type of MS detector, the method linear range and limit of detection (LOD) are summarized. The use of an internal standard (IS) is indicated (yes or no). If the linear range and/or LOD was not determined, it was indicated by n.d. If instead of the LOD, only the LOQ was stated, it was indicated by asterisk (*).

can be applied to prevent salts from entering the ion source. A first possibility is the use of a divert valve that guides the LC eluent to waste during the first minutes of a chromatographic run [88,89,100,103,116,117,119]. Secondly, some papers described the use of water or water/ethanol as perfusion medium instead of Ringer's solution to reduce the salt content in the ion source and to avoid the need of sample clean-up [111,118]. However, the perfusion of a hypotonic solution is not physiological and is therefore not a first choice solution. Gao et al. added an ice-cold 2 M K_3PO_4 solution to the liver dialysis samples to salt the HIV protease inhibitors out and afterwards an ether extraction was performed [97]. Igarashi et al. added methanol to the dialysates to extract opioidmimetics from the matrix [110]. Sekar et al. performed a solid phase extraction (SPE) for the analysis of vesnarinone and its metabolites in human urine and dialysate fluid [120]. Pickl et al. coupled a short polymeric SPE column on-line with the MS detector to desalt the microdialysates for the analysis of ketoprofen with run times of only 1.5 min [99]. On-line desalting and sample stacking on the RP analytical column by using water as mobile phase during the first minutes of the chromatographic run is another frequently used desalting step [106,107,116,117]. Finally, different groups applied the column switching technique, which is an elegant solution for desalting dialysis samples [82,99,104,110,112]. The additional benefit is the simultaneous preconcentration of the samples. The injection volumes on miniaturized LC columns are limited and to enhance the concentration sensitivity, preconcentration of the samples can be performed. We previously showed that column switching is a prerequisite for the analysis of oxcarbazepine and its active metabolite in rat brain dialysates with miniaturized LC–MS/MS to minimize salt effects or matrix effects from other dialysate matrix compounds. Moreover, to obtain accurate results, Ringer's solution and not water should be used as a solvent for the calibration standards since not all salts could be washed away using column switching when the injection volume exceeded 1 μL [82].

Some papers described the addition of BSA to the perfusion medium to minimize the sticking of the drugs onto the walls of the MD tubings [88,94]. As a result, the samples contained BSA which can hamper the LC–MS/MS assay performance and therefore, protein precipitation with methanol or ACN, followed by centrifugation, is an essential sample clean-up step.

Not only matrix components are responsible for ion suppression, but also the mobile phase solvents can deteriorate sensitivity. For example, Fuh et al. added trifluoroacetic acid as an ion-pairing agent to the mobile phase for the analysis of amphetamine with LC–MS/MS [86]. Amphetamine is a basic compound with a primary amine group and the interaction between the protonated amphetamine molecule and the silanol groups in LC packing material can cause severe peak tailing effects. Using a basic mobile phase could minimize this effect, however, it reduces the sensitivity of ESI-MS detection. Therefore, they chose to use TFA as the mobile phase additive and to minimize ion suppression effects, post-column addition of propionic acid was successfully utilized.

5. Concluding remarks

While for exogenous compounds and for some endogenous neurotransmitters, such as Ach, LC–MS/MS has become well-established, routine analysis of neuropeptides in dialysates using miniaturized LC–ESI-MS/MS is still challenging for the analytical chemist. Miniaturized LC–ESI-MS/MS methods have an unsurpassed sensitivity and selectivity, but are known to be less robust and precise. So far, little attention has been paid to the validation of the methods to monitor endogenous compounds in dialysis samples. Since ESI-MS is sensitive to matrix effects, investigation of the presence and eventually elimination of dialysate matrix effects should be a standard part of method development, especially if low analyte concentrations need to be quantified because matrix effects deteriorate method sensitivity. The use of an (SIL-) IS should be considered since it can correct for these matrix effects, solving possible accuracy and precision problems.

Acknowledgements

This work was supported by the Research Fund (OZR) from the Vrije Universiteit Brussel and also by the Fund for Scientific Research Flanders (FWO-Vlaanderen). We also thank the Koningin Elisabeth Stichting for financial support. I. Smolders is a postdoctoral fellow of the FWO-Vlaanderen.

References

[1] H. Benveniste, J. Neurochem. 52 (1989) 1667–1679.
[2] M.I. Davies, J.D. Cooper, S.S. Desmond, C.E. Lunte, S.M. Lunte, Adv. Drug Deliv. Rev. 45 (2000) 169.
[3] M.Y. Zhang, C.E. Beyer, J. Pharm. Biomed. Anal. 40 (2006) 492.
[4] J.P. Chervet, M. Ursem, J.P. Salzmann, Anal. Chem. 68 (2004) 1507.
[5] C. Legido-Quigley, N.W. Smith, D. Mallet, J. Chromatogr. A 976 (2002) 11.
[6] H.D. Meiring, E. Van der Heeft, G.J. Ten Hove, A.P.J.M. De Jong, J. Sep. Sci. 25 (2002) 557.
[7] S. Roy, A. Rieutord, J.Y. Zhou, A. Baillet, P. Prognon, P. Chaminade, Biomed. Chromatogr. 17 (2003) 297.
[8] S.J. Gaskell, J. Mass Spectrom. 32 (1997) 677.
[9] J. Abian, A.J. Oosterkamp, E. Gelpi, J. Mass Spectrom. 34 (1999) 244.
[10] M. Kranendijk, J.C.M. Waterval, G.W. Somsen, G.J. De Jong, J. Sep. Sci. 28 (2005) 1796.
[11] Y. Ikarashi, Y. Maruyama, J. Chromatogr. 587 (1991) 306.
[12] I. Wessler, C.J. Kirkpatrick, K. Racke, Pharmacol. Ther. 77 (1998) 59.
[13] P. Uutela, R. Reinilä, P. Piepponen, R.A. Ketola, R. Kostiainen, Rapid Commun. Mass Spectrom. 19 (2005) 2950.
[14] T.H. Tsai, J. Chromatogr. B: Biomed. Sci. Appl. 747 (2000) 111.
[15] P. De Boer, B.H. Westerink, A.S. Horn, Neurosci. Lett. 116 (1990) 357.
[16] E. Acquas, H.C. Fibiger, J. Neurochem. 70 (1998) 1088.
[17] P. Izurieta-Sanchez, N. Jonkers, S. Sarre, G. Ebinger, Y. Michotte, Brain Res. 856 (2000) 250.
[18] T. Huang, L. Yang, J. Gitzen, P.T. Kissinger, M. Veeke, A. Heller, J. Chormatogr. B 670 (1995) 323.
[19] T. Kato, J.K. Liu, K. Yamamoto, P.G. Osborne, O. Niwa, J. Chromatogr. B 682 (1996) 162.
[20] A. Gobert, B. Di Cara, L. Cistarelli, M.J. Millan, J. Pharmacol. Exp. Ther. 305 (2003) 338.
[21] Y. Zhu, S.H. Wong, M. Cregor, J.F. Gitzen, L.A. Coury, P.T. Kissinger, Rapid Commun. Mass Spectrom. 14 (2000) 1695.

[22] M.E.P. Hows, A.J. Organ, S. Murray, L.A. Dawson, R. Foxton, C. Heidbreder, Z.A. Hughes, L. Lacroix, A.J. Shah, J. Neurosci. Methods 121 (2002) 33.
[23] L.P. Lacroix, K. Ceolin, A. Zocchi, G. Varnier, M. Garzotti, O. Curcuruto, C.A. Heidbreder, J. Neurosci. Methods 157 (2006) 25.
[24] M.Y. Zhang, Z.A. Hughes, E.H. Kerns, Q. Lin, C.E. Beyer, J. Pharm. Biomed. Anal. 44 (2007) 586.
[25] H.M. Shackman, M. Shou, N.A. Cellar, C.J. Watson, R.T. Kennedy, J. Neurosci. Methods 159 (2007) 86.
[26] B.H.C. Westerink, G. Damsma, H. Rollema, J.B. De Vries, A.S. Horn, Life Sci. 41 (1987) 1763.
[27] T. Sharp, T. Zetterström, H.G. Series, A. Carlsson, D.G. Grahame-Smith, U. Ungerstedt, Life Sci. 41 (1987) 869.
[28] S. Sarre, Y. Michotte, P. Herregodts, D. Deleu, N. De Klippel, G. Ebinger, J. Chromatogr. 575 (1992) 207.
[29] S. Sarre, C.A. Marvin, G. Ebinger, Y. Michotte, J. Chromatogr. 582 (1992) 29.
[30] F. Cheng, J. Kuo, J. Chromatogr. B: Biomed. Appl. 665 (1995) 1.
[31] S. Sarre, D. Vandeneede, G. Ebinger, Y. Michotte, J. Neurochem. 70 (1998) 1730.
[32] S. Sarre, H. Yuan, N. Jonkers, A. Van Hemelrijck, G. Ebinger, Y. Michotte, J. Neurochem. 90 (2004) 29.
[33] M.E.P. Hows, L. Lacroix, C. Heidbreder, A.J. Organ, A.J. Shah, J. Neurosci. Methods 138 (2004) 123.
[34] C.A. Heidbreder, L. Lacroix, A. Atkins, A.J. Organ, S. Murray, A. West, A.J. Shah, J. Neurosci. Methods 112 (2001) 135.
[35] C.S. Chaurasia, C.E. Chen, A. Ashby, J. Pharm. Biomed. Anal. 19 (1999) 413.
[36] D. Ma, J. Zhang, K. Sugahara, T. Ageta, K. Nakayama, H. Kodama, J. Chromatogr. B 726 (1999) 285.
[37] Y. Song, M. Shenwu, D.M. Dhossche, Y.M. Liu, J. Chromatogr. B: Anal. Technol. Biomed. Life Sci. 814 (2005) 295.
[38] M.J. Berna, B.L. Ackermann, J. Chromatogr. B 846 (2007) 359.
[39] E.L. Esmans, D. Broes, I. Hoes, F. Lemière, K. Vanhoutte, J. Chromatogr. A 794 (1998) 109.
[40] J.F. Banks Jr., S. Shen, C.M. Whitehouse, J.B. Fenn, Anal. Chem. 66 (1994) 406.
[41] J.V. Weber, K. Sampino, R. Dunphy, D.J. Burinsky, T. Williams, M.G. Motto, J. Pharm. Sci. 83 (1994) 525.
[42] M. Abdel-Hamid, L. Novotny, H. Hamza, J. Pharm. Biomed. Anal. 22 (2000) 745.
[43] N. Takeda, H. Yoshizumi, T. Niwa, J. Chromatogr. B 746 (2000) 51.
[44] R. Tuytten, F. Lemière, W. Van Dongen, E.L. Esmans, H. Slegers, Rapid Commun. Mass Spectrom. 16 (2002) 1205.
[45] A. Dobolyi, A. Reichart, T. Szikra, N. Szilágyi, A.K. Kékesi, T. Karancsi, P. Slégel, M. Palkovits, G. Juhász, Neurochem. Int. 32 (1998) 247.
[46] Y. Zhu, P.S.H. Wong, Q. Zhou, H. Sotoyama, P.T. Kissinger, J. Pharm. Biomed. Anal. 26 (2001) 967.
[47] K. Smita, V. Sushil Kumar, J.S. Premendran, Fundam. Clin. Pharmacol. 21 (2007) 1.
[48] J.M. Walker, S.M. Huang, N.M. Strangman, K. Tsou, M.C. Sañudo-Peña, Proc. Natl. Acad. Sci. U.S.A. 96 (1999) 12198.
[49] D. Koga, T. Santa, T. Fukushima, H. Homma, K. Imai, J. Chromatogr. B: Biomed. Sci. Appl. 690 (1997) 7.
[50] R. Schmidt, O. Coste, G. Geisslinger, J. Chromatogr. B 826 (2005) 188.
[51] T. Hokfelt, T. Bartfai, F. Bloom, Lancet Neurol. 2 (2003) 463.
[52] R.T. Kennedy, in: B.H.C. Westerink, T.I.F.H. Cremers (Eds.), Handbook of Microdialysis: Methods, Applications and Clinical Aspects, Academic Press/Elsevier, Oxford, 2007, pp. 279–295.
[53] J. Silberring, R. Ekman, Mass Spectrometry and Hyphenated Techniques in Neuropeptide Research, John Wiley and Sons, New York, 2002, pp. 23–28.
[54] M.R. Emmett, P.E. Andren, R.M. Caprioli, J. Neurosci. Methods 62 (1995) 141.
[55] P.E. Andren, R.M. Caprioli, Brain Res. 845 (1999) 123.
[56] W.E. Haskins, Z. Wang, C.J. Watson, R.R. Rostand, S.R. Witowski, D.H. Powell, R.T. Kennedy, Anal. Chem. 73 (2001) 5005.
[57] W.E. Haskins, C.J. Watson, N.A. Cellar, D.H. Powell, R.T. Kennedy, Anal. Chem. 76 (2004) 5523.
[58] H.M. Baseski, C.J. Watson, N.A. Cellar, J.G. Shackman, R.T. Kennedy, J. Mass Spectrom. 40 (2005) 146.
[59] G. Nyitrai, K.A. Kékesi, Z. Emri, É. Szárics, G. Juhász, J. Kardos, Eur. J. Pharmacol. 478 (2003) 111.
[60] S.R. Wilson, F. Boix, A. Holm, P. Molander, E. Lundanes, T. Greibokk, J. Sep. Sci. 28 (2005) 1751.
[61] B.A. Sinnaeve, M.L. Storme, J.F. Van Boxlaer, J. Sep. Sci. 28 (2005) 1779.
[62] A.J. Oosterkamp, E. Gelpi, J. Abian, J. Mass Spectrometry 33 (1998) 976.
[63] K. Lanckmans, S. Sarre, I. Smolders, Y. Michotte, Rapid Commun. Mass Spectrom. 21 (2007) 1187.
[64] N.T. Maidment, D.R. Brumbaugh, V.D. Rudolph, E. Erdelyi, C.J. Evans, Neuroscience 33 (1989) 549.
[65] N.T. Maidment, B.J. Siddall, V.R. Rudolph, E. Erdelyi, C.J. Evans, Neuroscience 45 (1991) 81.
[66] N.T. Maidment, C.J. Evans, in: T.E. Robinson, J.B. Justice (Eds.), Microdialysis in Neuroscience, Elsevier Science Publishers B.V., Oxford, 1991, pp. 275–303 (Chapter 12).
[67] J.M. Radke, C. Spyraki, K. Thermos, Neuroscience 54 (1993) 493.
[68] H. Takahashi, Y. Shintani, T. Okauchi, M. Ishikawa, H. Bando, T. Azekawa, Y. Morita, S. Saito, J. Neurosci. Methods 52 (1994) 33.
[69] M.M. Ernberg, P.J. Alstergren, J. Neurosci. Methods 132 (2004) 185.
[70] X. Ao, T.J. Sellati, J.A. Stenken, Anal. Chem. 76 (2004) 3777.
[71] J. Duo, H. Fletcher, J.A. Stenken, Biosens. Bioelectron. 22 (2006) 449.
[72] A. Pettersson, A. Amirkhani, B. Arvidsson, K. Markides, J. Bergquist, Anal. Chem. 76 (2004) 1678.
[73] H. John, M. Walden, S. Schäfer, S. Genz, W.G. Forssmann, Anal. Bioanal. Chem. 378 (2004) 883.
[74] E. Merlo Pich, G.F. Koob, M. Heilig, F. Menzaghi, W. Vale, F. Weiss, Neuroscience 55 (1993) 695.
[75] P.M. Mertes, B. Beck, Y. Jaboin, A. Stricker, J.P. Carteaux, G. Pinelli, K. El-Abassi, J.P. Villemot, C. Burlet, M. Boulange, Regul. Pept. 49 (1993) 81.
[76] P.M. Mertes, K. El-Abassi, Y. Jaboin, C. Michel, B. Beck, G. Pinelli, J.P. Carteaux, J.P. Villemot, C. Burlet, J. Mol. Cell Cardiol. 28 (1996) 1995.
[77] K.H. Blakeman, Z. Wiesenfeld-Hallin, P. Alster, Exp. Brain Res. 139 (2001) 354.
[78] W.J. Trickler, D.W. Miller, J. Pharm. Sci. 92 (2003) 1419.
[79] M. Orlowska-Majdak, Acta Neurobiol. Exp. 64 (2004) 177.
[80] K.M. Kendrick, Methods Enzymol. 168 (1989) 182.
[81] N. Plock, C. Kloft, Eur. J. Pharm. Sci. 25 (2005) 1.
[82] K. Lanckmans, A. Van Eeckhaut, S. Sarre, I. Smolders, Y. Michotte, J. Chromatogr. A 1131 (2006) 166.
[83] C. Dias, Y. Nashed, H. Atluri, A. Mitra, Curr. Eye Res. 25 (2002) 243.
[84] J.P. Qiao, Z. Abliz, F.M. Chu, P.L. Hou, L.Y. Zhao, M. Xia, Y. Chang, Z.R. Guo, J. Chromatogr. B 805 (2004) 93.
[85] M.R. Fuh, C.H. Haung, S.L. Lin, W.H.T. Pan, J. Chromatogr. A 1031 (2004) 197.
[86] M.R. Fuh, C.H. Haung, T.Y. Wu, S.L. Lin, W.H.T. Pan, Rapid Commun. Mass Spectrom. 18 (2004) 1711.
[87] L. Bräutigam, G. Vetter, I. Tegeder, G. Heinkele, G. Geisslinger, J. Chromatogr. B 761 (2001) 203.
[88] A. Gupta, B. Jansson, P. Chatelain, R. Massingham, M. Hammarlund-Udeneas, Rapid Commun. Mass Spectrom. 19 (2005) 1749.
[89] R.N. Iyer, M.D. Davis, P.L. Juneau, A.B. Giordani, J. Pharm. Pharmacol. 50 (1998) 1147.
[90] M.R. Fuh, Y.L. Tai, W.H.T. Pan, J. Chromatogr. B 752 (2001) 107.
[91] Y.F. Chen, C.H. Chang, S.C. Wang, T.H. Tsai, Biomed. Chromatogr. 19 (2005) 402.
[92] P. Michelsen, G. Pettersson, Rapid Commun. Mass Spectrom. 8 (1994) 517.
[93] N. Kobayashi, I. Fujimori, M. Watanabe, T. Ikeda, Anal. Biochem. 287 (2000) 272.
[94] B.X. Mayer, K. Namiranian, P. Dehghanyar, R. Stroh, H. Mascher, M. Müller, J. Pharm. Biomed. Anal. 33 (2003) 745.

[95] O. Burkhardt, M. Brunner, S. Schmidt, M. Grant, Y. Tang, H. Derendorf, J. Antimicrob. Chemother. 58 (2006) 632.
[96] T. Koal, M. Deters, K. Resch, V. Kaever, Clin. Chim. Acta 364 (2006) 239.
[97] W. Gao, T. Kishida, K. Kimura, M. Kageyama, M. Sumi, Y. Yosikawa, N. Shibata, K. Takada, Biomed. Chromatogr. 16 (2002) 267.
[98] D.O. Scott, T.G. Heath, J. Pharm. Biomed. Anal. 17 (1998) 17.
[99] K.E. Pickl, C. Magnes, M. Bodelenz, T.R. Pieber, F.M. Sinner, J. Chromatogr. B: Anal. Technol. Biomed. Life Sci. 850 (2007) 432.
[100] P.S.H. Wong, K. Yoshioka, F. Xie, P.T. Kissinger, Rapid Commun. Mass Spectrom. 13 (1999) 407.
[101] M. Qian, W. West, J.T. Wu, B. Lu, D.D. Christ, Pharm. Res. 40 (2003) 605.
[102] L. Bräutigam, M. Seegel, I. Tegeder, H. Schmidt, S. Meier, M. Podda, R. Kaufmann, M. Grundmann-Kollmann, G. Geisslinger, J. Chromatogr. B 798 (2003) 223.
[103] E.L. Heinzen, G.M. Pollack, Brain Res. 1023 (2004) 175.
[104] J. Bengtsson, B. Jansson, M. Hammarlund-Udenaes, Rapid Commun. Mass Spectrom. 19 (2005) 2116.
[105] J. Nagel, I. Belozertseva, S. Greco, V. Kashkin, A. Malyshkin, A. Jirgensons, E. Shekunova, B. Eilbacher, A. Bespalov, W. Danysz, Neuropharmacology 51 (2006) 1163.
[106] L. Prokai, A.D. Zharikova, T. Janáky, K. Prokai-Tatrai, Rapid Commun. Mass Spectrom. 14 (2000) 2412.
[107] L. Prokai, A. Zharikova, T. Janáky, X. Li, A.C. Braddy, P. Perjési, L. Matveeva, D.H. Powell, K. Prokai-Tatrai, J. Mass Spectrom. 36 (2001) 1211.
[108] C.S. Tamvakopoulos, L.F. Colwell, K. Barakat, J. Fenyk-Melody, P.R. Griffin, R. Nargund, B. Palucki, I. Sebhat, X. Shen, R.A. Stearns, Rapid Commun. Mass Spectrom. 14 (2000) 1729.
[109] K. Lanckmans, R. Clinckers, A. Van Eeckhaut, S. Sarre, I. Smolders, Y. Michotte, J. Chromatogr. B: Anal. Technol. Biomed. Life Sci. 831 (2006) 205.
[110] K. Igarashi, Y. Murabayashi, K. Hotta, Y. Kitamura, F. Kasuya, K. Shiotani, L. Tingyou, A. Miyazaki, Y. Tsuda, Y. Okada, S. Fukushima, J. Chromatogr. B 806 (2004) 53.
[111] N. Kobayashi, M. Kazui, T. Ikeda, J. Pharm. Biomed. Anal. 21 (2000) 1233.
[112] S.K. Bergström, K.E. Markides, J. Chromatogr. B 775 (2002) 79.
[113] R. Oertel, K. Richter, U. Ebert, W. Kirch, J. Chromatogr. B: Biomed. Sci. Appl. 750 (2001) 121.
[114] P.M. Stetina, B. Madai, V. Kulemann, W. Kirch, C. Joukhadar, Int. J. Pharmacol. Ther. 43 (2005) 134.
[115] H. Zheng, L.F. Shi, J.H. Hu, Biomed. Chromatogr. 21 (2007) 101.
[116] Y. Song, J. Xu, A. Hamme, Y.M. Liu, J. Chromatogr. A 1103 (2006) 229.
[117] Y. Song, Y. Feng, M.H. Leblanc, N. Castagloni Jr., Y.M. Liu, Neurosci. Lett. 395 (2006) 63.
[118] J.A. Masucci, M.E. Ortegon, W.J. Jones, R.P. Shank, G.W. Caldwell, J. Mass Spectrom. 33 (1998) 85.
[119] C. Oberthur, C. Heinemann, P. Elsner, E. Benfeldt, M. Hamburger, Planta Med. 69 (2003) 385.
[120] K.S. Sekar, S.L. Bramer, J. Pharm. Biomed. Anal. 33 (2003) 711.

Available online at www.sciencedirect.com
ScienceDirect
Talanta 74 (2008) 1079–1083
Talanta
www.elsevier.com/locate/talanta

Short communication

Discrimination of allied species within the genus *Turbinaria* (Fucales, Phaeophyceae) using HRMAS NMR spectroscopy

K. Le Lann [a], N. Kervarec [b], C.E. Payri [c,d], E. Deslandes [a], V. Stiger-Pouvreau [a,*]

[a] *Laboratoire d'Ecophysiologie et de Biotechnologie des Halophytes et des Algues Marines (LEBHAM EA 3877), Institut Universitaire Européen de la Mer, Université de Bretagne Occidentale, Place Nicolas Copernic, 29280 Plouzané, France*
[b] *Résonance Magnétique Nucléaire-Résonance Paramagnétique Électronique, 6 avenue, Victor-Le-Gorgeu-CS93837, 29238 Brest Cedex 3, France*
[c] *UMR 7138/UR R148 "Systématique, Adaptation, Evolution", Institut de Recherche pour le Développement, B.P. A5 98848, Nouméa Cedex, Nouvelle-Calédonie, France*
[d] *Université de la Polynésie Française, Tahiti, France*

Received 23 May 2007; received in revised form 31 July 2007; accepted 9 August 2007
Available online 23 August 2007

Abstract

A novel chemotaxonomical method based on 1D ^{1}H HRMAS NMR spectroscopy is being tested for taxonomical purposes. This powerful technique allowed us to discriminate between specimens belonging to two sister species of *Turbinaria*, which are difficult to tell apart using only morphological characters. Based on spectra analysis, the results allowed us to successfully group the specimens according to their species. Thus, the efficiency of HRMAS NMR spectroscopy for the discrimination of algal species and for the pre-screening of potential chemomarkers is demonstrated.
© 2007 Elsevier B.V. All rights reserved.

Keywords: HRMAS NMR spectroscopy; *Turbinaria* species; Phaeophyceae; Chemotaxonomy; Species discrimination

1. Introduction

Turbinaria is a widespread tropical genus within the Phaeophyceae. It is relatively species-poor; with so far only 17 species having been described and assigned to the genus [1]. However, the web site AlgaeBase lists 54 species names, of which 22 are actually flagged as current [2]. In the Indo-Pacific region, *Turbinaria ornata*, *Turbinaria conoides* and *Turbinaria decurrens* are currently recorded. While *T. ornata* is the most common and widespread species extending its distribution from the African east coast to the central Pacific Ocean including Hawaii and French Polynesia, *T. conoides* is not recorded from the French Polynesian area or Hawaiian waters, and *T. decurrens* is restricted to the western part of the tropical Pacific Ocean. Taxonomically speaking, *T. decurrens* is the most easily distinguishable from morphological features, while both *T. conoides* and *T. ornata* display great morphological variations which can generate identification ambiguities, especially when looking at the shapes of the leaf blades [3].

Despite the limited number of *Turbinaria* species, this genus is morphologically complex. Several authors recognized a wide variety of forms [1] (for review). This plasticity is correlated with habitat in response to environmental conditions [1,4,5]. Various studies on *T. ornata* have shown the effect of hydrodynamism on the thallus morphology, the buoyancy and the phenological plasticity [6–9]. Despite this high phenological variability, the morphological species concept remains the basis for algal taxonomy [10], including the genus *Turbinaria* [1] for which the shape of the leaf is one of the major taxonomical criteria to tell the species apart [1,3,11,12]. Because of the complex morphological variations, this criterion may be a source of confusion in identifications, and morphological classifications need to be improved by molecular studies [12]. However these tools depend on the nature of the biological material, i.e. buds or reproductive organs for DNA extraction, and the availability of good genetic markers; these studies can be long, difficult and expensive, especially since *T. ornata* and *T. conoides* are two closely related sister species [12]. In this context, high-resolution magic angle spinning (HRMAS) NMR spectroscopy, a recent

* Corresponding author. Tel.: +33 2 98 49 88 06; fax: +33 2 98 49 87 72.
E-mail addresses: Valerie.Stiger@univ-brest.fr, stiger@univ-brest.fr (V. Stiger-Pouvreau).

0039-9140/$ – see front matter © 2007 Elsevier B.V. All rights reserved.
doi:10.1016/j.talanta.2007.08.021

non-invasive technique, has been considered as a promising analytical method to discriminate between the species concerned. It was shown, for instance, to be a reliable tool to differentiate strains of bacteria [13,14], to analyse food materials [15–20] or to diagnose the spread of prostate cancer [21]. This method is a fast, non-destructive technique, which does not require any preliminary extraction and requires only a little sample preparation. Moreover, HRMAS allows obtaining high-resolution spectra from intact samples, comparable to those achievable with liquid extracts [22]. At this time, with HRMAS, it is possible to analyse minute amounts of intact plant material using 1D and 2D spectra of *in vivo* low molecular mass compounds, as well as spectra of structural polymers [23]. The HRMAS technique is also well suited to the monitoring of the accumulation or disappearance of various classes of metabolites. Some studies indicated that this method could discriminate food material samples according to their geographical origin [17–20].

In this study, the usefulness of HRMAS as an analytical tool to discriminate closely related macroalgal species of the genus *Turbinaria* is demonstrated for the first time.

2. Materials and methods

2.1. Sampling sites and species

Specimens of *T. conoides*, *T. decurrens* and *T. ornata* were collected during the austral winter, from two different regions of the South Pacific, namely the Solomon Island (SI) and New Caledonia (NC), as shown in Table 1. Some samples were not named because morphological ambiguities could not allow us to differentiate *T. ornata* from *T. conoides* and they were then labelled as *Turbinaria* sp. (Table 1).

Field–collected samples were separated into two batches: one was freeze-dried and sent to the first author for chemotaxonomical analysis (this study) and the second was used for a molecular and taxonomical studies [12]. *T. decurrens* was considered as the outgroup of our analysis, since this species is easily distinguishable from the two closely related species, *T. conoides* and *T. ornata*.

2.2. NMR spectroscopy

The method developed in this study is based on the use of HRMAS NMR spectroscopy.

All HRMAS spectra were acquired on a Bruker DRX 500 spectrometer equipped with an indirect HRMAS $^{1}H/^{31}P$ probehead with gradient *Z* at 25 °C. A typical proton ^{1}H HRMAS spectrum consisted of 64 scans, and was performed with presaturation of the water peak. Each spectrum was phased and baseline-corrected using a polynomial function.

2.3. HRMAS sample preparation

For the HRMAS spectra, peduncles of leaves were randomly selected on the sampled thalli belonging to each region (SI and NC). About 5 mg of each peduncle was put in a vial with zirconium oxide, and set into a 4 mm MAS rotor. Approximately 30 μL of D_2O was added into the rotor with the leaf sample for ^{2}H field locking (depending on the quantity of the freeze-dried leaf sample). The sample was placed in a rotor spinning around an axis, which is oriented at the so-called magic angle of 54°7 with respect to the magnetic field $\mathbf{B}_0$. Good homogenization was obtained at a spinning rate of 5000 Hz. This results in a high-resolution NMR spectrum approaching that obtained using liquid samples, making spectra analysis possible.

In this study, three HRMAS spectra, corresponding to three independently prepared rotors, were recorded for each sample. Thus 6 spectra for *T. decurrens*, 9 for *T. ornata*, 15 for *T. conoides* and 9 for *Turbinaria* sp. were obtained.

Peduncles of leaves were chosen because: (1) leaves are useful for morphological taxonomy [12] and (2) the shape of peduncles allows a very good fit within the HRMAS rotor. In this way, spectra resolutions were improved.

Table 1
List of species, sampling data and herbarium accession numbers of *Turbinaria* species used in this present study

Species	Locality	Accession number	Date	Collector
Turbinaria decurrens	Solomon, Malaïta island, Anuta Paina	IRD—S.852-740	July 18, 2004	Payri
T. decurrens	Solomon, Malaïta island, Lau Lagoon	IRD—S.848-685	July 16, 2004	Payri
Turbinaria conoides	Solomon, Nggela Island, NW	IRD—S.842-566	July 12, 2004	Payri
T. conoides	Solomon, Malaïta island, Lau Lagoon	IRD—S.850-702	July 17, 2004	Payri
T. conoides	New Caledonia, Séche Croissant	KLL—Tc.1	April 5, 2006	Payri
T. conoides	New Caledonia, Séche Croissant	KLL—Tc.2	April 5, 2006	Payri
T. conoides	New Caledonia, Séche Croissant	KLL—Tc.3	April 5, 2006	Payri
Turbinaria ornata	Solomon, Malaïta island, Anuta Paina	IRD—S.852-741	July 18, 2004	Payri
T. ornata	New Caledonia, Séche Croissant	KLL—To.1	April 5, 2006	Payri
T. ornata	New Caledonia, Séche Croissant	KLL—To.2	April 5, 2006	Payri
T. ornata	New Caledonia, Séche Croissant	KLL—To.3	April 5, 2006	Payri
Turbinaria sp.	New Caledonia, Nouville	KLL—T.sp.1	April 4, 2006	Payri
Turbinaria sp.	New Caledonia, Nouville	KLL—T.sp.2	April 4, 2006	Payri
Turbinaria sp.	New Caledonia, Nouville	KLL—T.sp.3	April 4, 2006	Payri
Turbinaria sp.	New Caledonia, Nouville	KLL—T.sp.4	April 4, 2006	Payri
Turbinaria sp.	New Caledonia, Nouville	KLL—T.sp.5	April 4, 2006	Payri
Turbinaria sp.	New Caledonia, Nouville	KLL—T.sp.6	April 4, 2006	Payri

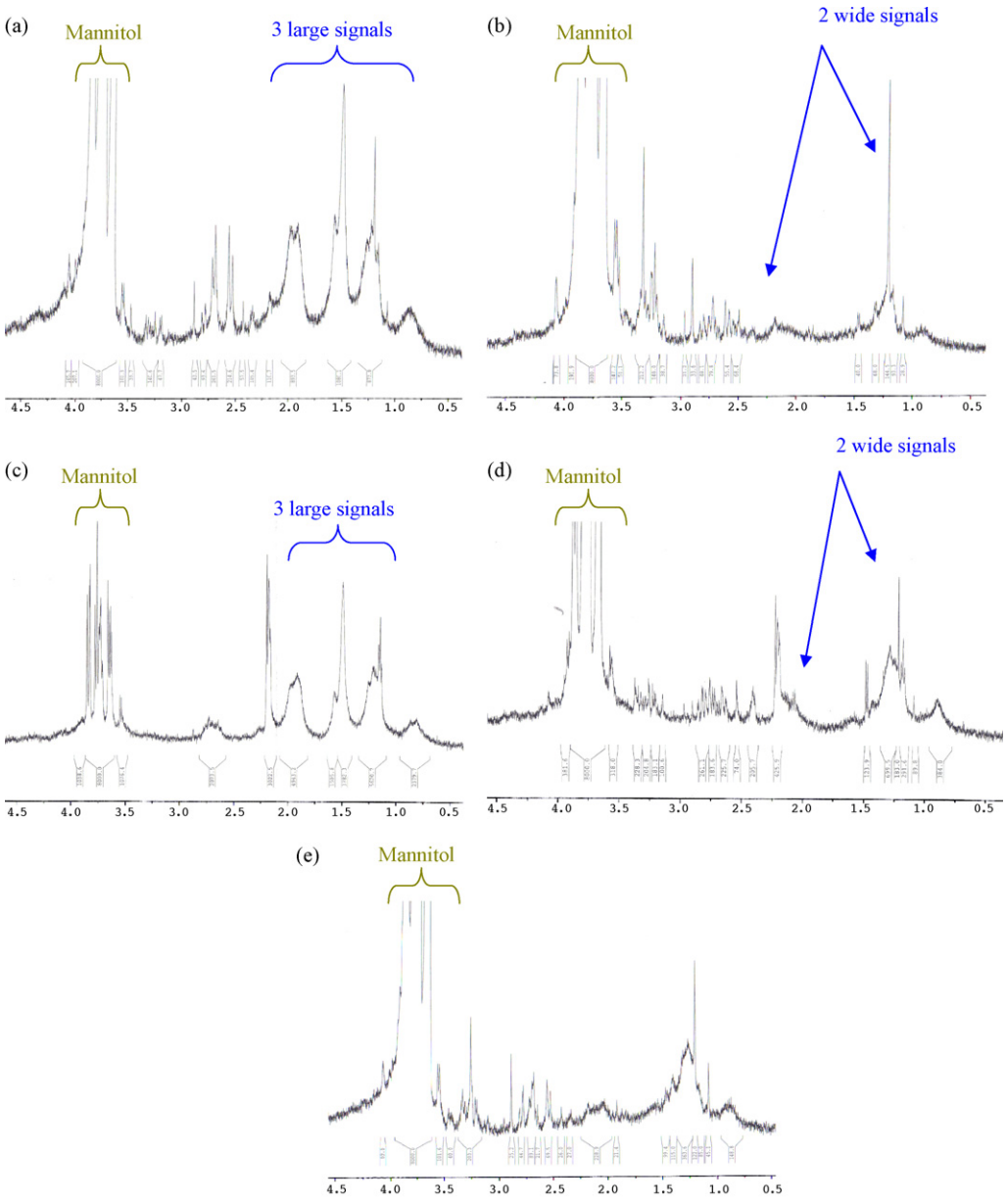


Fig. 1. Proton of HRMAS NMR spectra of (a) *Turbinaria conoides* from Salomon Islands, (b) *Turbinaria ornata* from Solomon Islands, (c) *T. conoides* from New Caledonia, (d) *T. ornata* from New Caledonia and (e) *Turbinaria decurrens* from Solomon Islands.

2.4. Statistical analysis

HRMAS data were subjected to statistical analysis. Statsoft Statistica release 6.0 for Windows was used to perform tests. The statistical procedure used in this study was based on a principal components analysis (PCA) to illustrate *Turbinaria* species' HRMAS discrimination. PCA test was performed with the following three species: *T. decurrens*, *T. ornata* and *T. conoides* to highlight the powerfulness of the HRMAS method. Variables used to perform the PCA were the signals of each HRMAS spectrum (three for each sample) between 0 and 4.00 ppm, since some chemical shifts appeared to differ between species samples in this specific spectral region.

3. Results and discussion

The comparison of the ^{1}H HRMAS NMR spectra (four of them are shown in Fig. 1) revealed one main difference between *T. ornata* and *T. conoides* spectra, whatever the geographic region: spectra of *T. ornata* show two wide signals, while spectra of *T. conoides* has three large signals between 0.8 and 3 ppm. The spectra of *T. decurrens* are similar to those of *T. ornata*. These different signals between *T. conoides* and *T. ornata* spectra were observed in the characteristic domain of saturated and unsaturated fatty acids, as already demonstrated in other materials [17,18,20]. The different profiles of fatty acids in *Turbinaria* appear to relate to the species, and not to the geographical origin. For two *Sargassum* species, some significant variations in

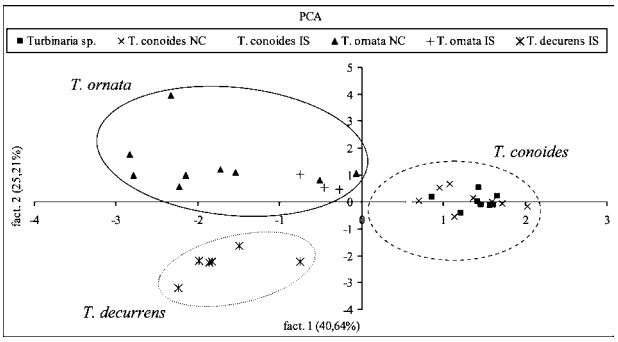


Fig. 2. Principal component analysis (PCA): projection of 36 spectral observations issued from the three species, *T. conoides*, *T. ornata* and *T. decurrens* on the Factor 1 vs. Factor 2 planes. NC: New Caledonia; SI: Solomon Islands.

the fatty acid contents were observed from specimens coming from the Yellow Sea (China) and from the Japan Sea [24]. However, geographical variations of metabolites composition of marine algae were non-significant and could be minimised [25,26]. However, seasonal variations in algal metabolites content still exist [27], and it is the reason why our material was sampled during the same season (austral winter). Nevertheless, the same experiment should be carried out during the austral summer to test for any seasonality in the fatty acid contents in these species.

Fig. 2 shows a biplot of the normalized scores in the Factor 1–Factor 2 areas. From this plot, one can see that it seems reasonable to attempt a clustering of these objects in the terms of these PCAs. All principal components or factors had an eigenvalue greater than 1, and explained 100% of the total variance. The sample projection on all the factor axes allowed us to choose Factors 1 and 2, which represented 65.85% of the total variance. The clustering technique is based on the sample similarity expressed according to the presence of signal. The *T. ornata* group is located on the negative side of the Factor 1-axis and on the positive side of the Factor 2-axis, whereas the *T. conoides* group is located on the positive side of the two factors axes. The outgroup consisting of *T. decurrens* has dispersed scores on the negative side of the two factors axes. Statistical tests applied to the HRMAS NMR data discriminate without ambiguity the different samples, especially the two sister species *T. ornata* and *T. conoides*.

Furthermore, this method was validated by processing all HRMAS spectra without knowing their species rank. The species assignment for the specimens was 100% correct. *Turbinaria* sp. samples of NC were located with the *T. conoides* group. The specificity of these samples was later confirmed using morphological and molecular studies [3]. The dispersion of scores in PCA could be explained by the heterogeneity of samples within a same group, as demonstrated in [19]. Despite the small number of samples studied, HRMAS NMR spectra combined with statistical analysis allowed us to discriminate between *T. ornata* and *T. conoides*. We obtained 100% correct reclassification although these species are considered like "sister species" [12]. This score was better than other HRMAS studies [16–20]. However, the latter studies focussed on geographical variations, whereas the present study looked at interspecific variations.

While a few studies have used the HRMAS technique for taxonomical purposes, none had approached chemotaxonomy. Most of the authors have used this technique for a geographical discrimination and/or classification for cheese [17,19,20] or for dried beef [18]. This technique was also applied to bacteria for separating mutant from non-mutant strains [14] and to diagnose for the spread of cancer [21]. All of these studies, included our own experimental analysis on a genus of brown algae, highlight the powerfulness of HRMAS to discriminate between samples at the specific level.

However, our results should be confirmed by the analysis of a larger set of specimens sampled from various geographical regions (e.g. Fiji Islands, Micronesia, Samoa, Australia). The characterisation of the non-polar chemomarkers of *T. ornata* and *T. conoides* is currently in progress with NMR and GC analyses.

4. Conclusion

HRMAS NMR appears to be a quick and reliable method for discrimination and taxonomic studies, providing results analogous to those of standard analysis protocols in the case of the brown algal genus *Turbinaria*. The main advantage of HRMAS is the rapidity in obtaining the results (about 10 min for each analysis), even in the absence of reproductive organs or enough buds, which are the limiting factors in DNA extraction of macroalgae. The limited pre-treatment of the samples and the sensitivity of the method make the HRMAS technique an efficient taxonomical tool to discriminate between species. Even if the HRMAS method cannot be substituted to either morphological or molecular phylogenetic analyses, its first taxonomical use within the genus *Turbinaria* is a promising start for other studies.

Acknowledgments

This study is part of the Ph.D. project carried out by the first author at IUEM (UBO), within the Laboratory of Ecophysiology and Biotechnology of Halophytes and Marine algae (LEBHAM), in collaboration with the Common NMR Service of the University of Occidental Brittany (Université de Bretagne Occidentale). This research was supported in part by the Coral Reef Initiative Programme for South Pacific (CRISP) and by the French Ministère de l'Education Nationale, de l'Enseignement supérieur et de la Recherche. This is contribution No. 1045 of the IUEM, European Institute for Marine Studies (Brest, France). Additional thanks are due to Dr. A. N'Yeurt for revising the English of the manuscript and to two anonymous reviewers for their helpful suggestions.

References

[1] M.J. Wynne, Phycol. Res. 50 (2002) 283.

[2] M.D. Guiry, G.M. Guiry, AlgaeBase version 4.2, 2007. http://www.algaebase.org.
[3] A. Rohfritsch, PH.D. Thesis, Sciences de l'environnement marin, Université de Polynésie Française, 2006, p. 242.
[4] L.N. De Senerpont Domis, N. Lisette, P. Fama, A.J. Bartlett, W.F. Prud'homme Van Reine, C.A. Espinosa, C.G. Trono, J. Phycol. 39 (2003) 1019.
[5] M. Koehl, Proceedings of the Third International Plant Biomechanics Conference, Thieme Verlag, Stuttgart, 2000, pp. 295–308.
[6] C.E. Payri, Bot. Mar. 27 (1984) 327.
[7] V. Stiger, C.E. Payri, Bot. Mar. 42 (1999) 295.
[8] H.L. Stewart, J. Marine Syst. 49 (2004) 157.
[9] H.L. Stewart, Mar. Biol. 149 (2006) 721.
[10] R. Wattier, C.A. Maggs, Adv. Bot. Res. 35 (2001) 171.
[11] R.W.M. Taylor, J. Linn. Soc. 58 (1963) 475.
[12] A. Rohfritsch, C.E. Payri, V. Stiger, F. Bonhomme, Biochem. Syst. Ecol. 35 (2007) 91.
[13] W. Li, Analyst 131 (2006) 777.
[14] S. Gudlavalleti, C.M. Szymanski, H.C. Jarrell, D.S. Stephens, Carbohydr. Res. 341 (2006) 557.
[15] A.M. Gil, I.F. Duarte, I. Delgadillo, I.J. Colquhoun, F. Casuscelli, E. Humpfer, M. Spraul, J. Agric. Food Chem. 48 (2000) 1524.
[16] A.P. Sobolev, A. Segre, R. Lamanna, Magn. Reson. Chem. 41 (2003) 237.
[17] L. Shintu, F. Ziarelli, S. Caldarelli, Magn. Reson. Chem. 42 (2004) 396.
[18] L. Shintu, S. Caldarelli, B.M. Franke, Meat Sci. 76 (2007) 700.
[19] L. Shintu, S. Caldarelli, J. Agric. Food Chem. 53 (2005) 4026.
[20] L. Shintu, S. Caldarelli, J. Agric. Food Chem. 54 (2006) 4148.
[21] L.L. Cheng, M.A. Burns, J.L. Taylor, W. He, E.F. Halpern, W.S. McDougal, C.-L. Wu, Cancer Res. 65 (2005) 3030.
[22] L.L. Cheng, C.-L. Wu, M.R. Smith, R.G. Gonzalez, FEBS Lett. 494 (2001) 112.
[23] M. Defernez, I.J. Colquhoun, Phytochemistry 62 (2003) 1009.
[24] V.E. Vaskovsky, S.V. Khotimchenko, B. Xia, L. Hefang, Phytochemistry 42 (1996) 1347.
[25] A. Praud, R. Valls, L. Piovetti, B. Banaigs, J.-Y. Benaïm, Phytochemistry 40 (1995) 495.
[26] R. Valls, L. Piovetti, Biochem. Syst. Ecol. 23 (1996) 723.
[27] G.V. Joshi, C.A. Gowda, Ind. J. Mar. Sci. 4 (1975) 165.

Available online at www.sciencedirect.com
ScienceDirect
Talanta 74 (2008) 498–504
Talanta
www.elsevier.com/locate/talanta

Analysis of phthalates via HPLC-UV in environmental water samples after concentration by solid-phase extraction using ionic liquid mixed hemimicelles

Jidong Li [a,b], Yaqi Cai [a,*], Yali Shi [a], Shifen Mou [a], Guibin Jiang [a]

[a] *State Key Laboratory of Environmental Chemistry and Ecotoxicology, Research Center for Eco-Environmental Sciences, Chinese Academy of Sciences, Beijing 100085, China*
[b] *General Research Institute for Non-ferrous Metals, Beijing 100088, China*

Received 16 April 2007; received in revised form 11 June 2007; accepted 11 June 2007
Available online 17 June 2007

Abstract

Ionic liquid mixed hemimicelles-based solid-phase extraction for the preconcentration of five phthalates in environmental water sample was investigated in this paper. A comparative study on the use of room temperature ionic liquids (RTILs) 1-hexyl-3-methylimidazolium bromide ([C_6mim]Br) and 1-dodecyl-3-methylimidazolium bromide ([C_{12}mim]Br)-coated silica as sorbents was presented. Owing to having bigger adsorption amounts for analytes [C_{12}mim], Br-coated silica was selected as SPE material and the five analytes di-ethyl-phthalate (DEP), di-*n*-propyl-phthalate (DnPP), di-*n*-butyl-phthalate (DnBP), di-cyclohexyl-phthalate (DcHP) and di-(2-ethylhexyl)-phthalate (DEHP) can be quantitatively extracted under optimal conditions. The analytes retained on the cartridge were desorbed completely with 3 mL methanol (pH 2). Predominant factors influencing the extraction efficiency, such as RTILs concentration, pH value, ionic strength and breakthrough volume were discussed. The proposed method had been applied to determining the five phthalates in four environmental water samples and concentration factor of 600 was achieved easily. Detection limits obtained ranged between 0.12 and 0.17 μg/L. The accuracy of this method was evaluated by recovery measurement on spiked samples, and good recovery results (85–107%) with relative standard deviation (R.S.D.) of below 6% were achieved.
© 2007 Elsevier B.V. All rights reserved.

Keywords: Ionic liquid; Mixed hemimicelles; Solid-phase extraction; Phthalates; HPLC-UV

1. Introduction

Phthalic acid esters (phthalates, PAEs) are widely used as polymer additives in the manufacture of plastics (primarily polyvinyl chloride), rubber and styrene to make them flexible. Globally, over 18 billion pounds of PAEs are used each year. They can be leached from the above-mentioned products and find a way to various environmental matrices such as environmental water, soil and plants [1–3]. Nowadays, due to its massive use and persistent character, PAEs are considered as ubiquitous environmental pollutants. A number of researches proved that PAEs exerted a pernicious impact on human health; furthermore, some PAEs can cause endocrine system disorders [4,5], produce carcinogenic effects and afflict the development of reproductive system [6].

The very low concentration level of PAEs and the complex matrix of many environmental samples make sample preconcentration necessary for a reliable determination of these compounds. Several analytical methods have been developed for determining PAEs by gas chromatography (GC) [7,8], high performance liquid chromatography (HPLC) [9,10] using different preconcentration techniques such as liquid–liquid extraction (LLE) [11], solid-phase microextraction (SPME) [12,13] and solid-phase extraction (SPE) [14–17] in several types of matrices. Among above-mentioned sample pretreatment procedures, solid-phase extraction based on different types of sorbents such as C_8 [15], organic polymers [16] was widely used.

Recently, a new SPE method based on hemimicelles and admicelles (mixed hemimicelles) has been proposed for the preconcentration of a variety of organic pollutants from complex

* Corresponding author at: Research Center for Eco-Environmental Sciences, Chinese Academy of Sciences, P.O. Box 2871, Beijing 100085, China. Tel.: +86 10 62849182; fax: +86 10 62849239.
E-mail address: Caiyaqi@rcees.ac.cn (Y. Cai).

0039-9140/$ – see front matter © 2007 Elsevier B.V. All rights reserved.
doi:10.1016/j.talanta.2007.06.008

environmental matrices [9,18–20]. The sorbents used are produced by adsorbing ionic surfactants (such as sodium dodecyl sulfate or cetyltrimethylammonium bromide) on the metal oxides (such as alumina or silica) surface. Mixed hemimicelles used in SPE have many advantages, such as high extraction efficiency, high breakthrough volume, easy elution of analytes and high flow rate for sample loading; furthermore, this kind of SPE technique requires no clean-up steps and the sorbents is easy to regenerate, and is thus able to meet the needs of rapid analysis.

Room temperature ionic liquids (RTILs) are ionic compounds that are liquids at ambient temperature and consist of ionic species [21]. RTILs belong to a relatively new class of solvents which are amphiphilic molecules with a hydrophilic polar headgroup (ionic in nature) and a hydrophobic hydrocarbon chain (the tail). In recent years, RTILs have attracted great attentions due to their unique chemical and physical properties such as nonvolatile (environmentally benign), excellent solvation qualities, non-flammable and high thermal stability [22,23]. As a result, RTILs are widely used in liquid–liquid extraction [24,25], synthesis [26,27], separation [28,29] and electrochemistry [30,31]. Some research groups have also studied the aggregation and micelles formation of ionic liquids in aqueous solution [32]. As RTILs can dissolve many kinds of organic, organometallic and inorganic compounds [33,34], their applications in analytical chemistry have also received attentions recently [35–39]. He et al. determined the testosterone and epitestosterone in human urine using cloud extraction method based on aqueous two-phase systems consisting of ionic liquid 1-butyl-3-methylimidazolium chloride, coupled with HPLC/spectrophotometry detection, the detection limit of 1 ng/mL was obtained [38]. Generally, cloud extraction method was a simple, rapid and effective sample pretreatment technique; however, some limitations still existed, such as the RTILs-rich phase was dense and it was not easy to be injected into HPLC for analysis; high concentration of ionic liquid in sampling solution may produce large interferential peaks.

In this paper, we investigated the applications of RTILs [C_6mim] Br and [C_{12}mim] Br mixed hemimicelles for the preconcentration of five phthalates DEP, DnPP, DnBP, DcHP and DEHP in environmental water sample. Mixed hemimicelles were prepared by adsorbing [C_6mim] Br and [C_{12}mim] Br on silica surface and predominant experimental factors affecting the extraction efficiency were studied. To the best of our knowledge, this was the first time that RTILs mixed hemimicelles-based SPE was applied for the pretreatment of PAEs in environmental water samples.

2. Experimental

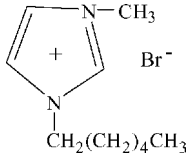
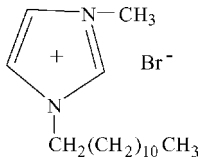
2.1. Chemicals and materials

All reagents were of analytical grade and used as supplied. Five PAEs were obtained from Beijing Chemicals Corporation (Beijing, China). A stock solution containing 200 mg/L each phthalate was prepared in methanol and stored under dark conditions at 4 °C. The RTILs [C_6mim] Br and [C_{12}mim] Br were supplied by Kemo Reagent Corporation (Hangzhou, China) and their structures were listed in Table 1. Silica was purchased from Sigma Corporation (Steinheim, Germany) and the physical properties were as follows: surface area (300 m^2/g); point of zero charge (PZC, 2.9); particle diameter range (70–150 μm), mean pore size (150 Å) and density (1.15 cm^3/g). HPLC-grade acetonitrile and methanol were supplied by Merck Corporation (Germany). Water (18.3 MΩ) used in all experiments was prepared using a compact ultrapure water system from Barnstead Corporation (Iowa, USA).

2.2. Sample collection and preservation

Effluent wastewater sample was collected from the Gaobeidian sewage treatment plant (Chaoyang District), the largest sewage treatment plants in Beijing. It is located in the east of Beijing and it receives about the same level of domestic and industrial wastewater. River water samples were taken from the Xiaoqing River (Haidian District, Beijing) and Jingmi Canal (Haidian District) in November 2006. Tap water sample was taken from our lab in Haidian District. All water samples were collected randomly. Samples were collected into pre-cleaned, light-preserved glass bottles and 5000 mL each sample was filtered immediately through 0.22 μm nylon membranes in order to remove suspended solids. We realized that these filters maybe contain a considerable amount of phthalate such as DnBP, so their cleaning with acetone was carried out prior filtration. The

Table 1
Chemical structure of RTILs [C_6mim] Br and [C_{12}mim] Br

Name	Molecular formula	Structure	Abbreviation
1-Hexyl-3-methylimidazolium bromide	$C_{10}H_{19}N_2Br$		[C_6mim] Br
1-Dodecyl-3-methylimidazolium bromide	$C_{16}H_{31}N_2Br$		[C_{12}mim] Br

filtered samples were adjusted to pH 2 with 1 M HNO_3 and stored at dark conditions at 4 °C until analysis.

2.3. SPE based on mixed hemimicelles

An extraction cartridge was prepared by using a SPE plastic tube (6 mL, polypropylene) and 0.5 g silica was packed into it. To prepare mixed hemimicelles column, 25 mL solution containing 25 mg [C_{12}mim] Br was passed through the cartridge column, then the water samples was adjusted to pH 6.5 and passed through the column. Sample loading was performed by using a DOA-PlOU-BN vacuum pump (Michigan, USA) at a flow rate of 5 mL/min. Target analytes were eluted with 3.0 mL methanol (pH 2) and dried with a stream of nitrogen at 60 °C, followed by dissolved in 0.5 mL methanol. The methanol solution was vibrated in an ultrasonic bath for 5 min in order to insure that the phthalates can be dissolved into methanol completely. Finally, a 20 μL of the solution was injected into the HPLC system for analysis.

2.4. HPLC analysis

The five phthalates were separated and quantified by using a liquid chromatography–spectrophotometry system (P680 HPLC Pump with a PDA100 Photodiode Array Detector, Dionex, USA) with an automatic sample injector (ASI-100, Dionex, USA). The analytical column was a 250 mm Diamonsil-C_{18} column (4 μm particle diameter and 4.6 mm i.d.) supplied by Dikma Technologies Corporation (Beijing, China). The mobile phase consisted of acetonitrile and water (acetonitrile: water, 75:25, v/v) and the flow-rate was set at 1 mL/min. Spectrophotometry detection of analytes was performed at 226 nm wavelengths.

2.5. Adsorption studies

The adsorption studies were carried out in batch mode and all experiments were carried out at 25 ± 1 °C in a water bath. Both the adsorption isotherms of [C_6mim]Br and [C_{12}mim]Br on silica were obtained by adding 0.5 g silica to 25 mL aqueous solution containing [C_6mim]Br or [C_{12}mim]Br (0–50 mg), and the initial pH of solutions was adjusted to 6.5. After vigorous stirring of the solutions for 5 min, partial solution of every glass vial was centrifuged at 4000 rpm for 10 min. The concentration of [C_6mim] Br and [C_{12}mim] Br in the supernatants was determined by ESI-MS (ABI, USA) at *m/z* 251 and 167 through different factors of diluting, respectively. The analysis was carried out in the "ESI (+) mode" and the operational parameters used were as follows: Declustering potential, −30 V; entrance potential, −2.8 V; collision cell entrance potential, −11 V; collision energy, −13 V; collision cell exit potential, −4.5 V; source temperature, 300 °C and maximal accumulation time, 50 ms. The zeta-potentials of solutions (after centrifuged) were determined with an zetasizer 2000 apparatus (Malvern, United Kingdom).

The effects of RTILs concentration, pH value and ionic strength on the adsorption were studied by mixing 25 mL aqueous solution containing 1.0 mg/L of DEP, DnPP and DnBP each with 0.5 g silica. Adsorption studies did not involve DcHP and DEHP owing to their low solubility in water. Both the added amounts of [C_6mim] Br and [C_{12}mim] Br were varied in the range of 0–50 mg. The solution was vigorously stirred for 5 min, and then it was centrifuged at 4000 rpm for 10 min. The concentration of PAEs in the supernatants was determined by LC–spectrophotometry.

3. Results and discussion

3.1. Adsorption isotherms of RTILs on silica particles

The adsorption isotherms of RTILs on silica were useful for understanding the theory of extraction process and optimizing the SPE conditions. As can be seen from Fig. 1 that, before a certain loading point reached (approximately 0.6 and 0.4 mg/g for [C_{12}mim] Br and [C_6mim] Br, respectively), nearly no RTILs were left in the aqueous phase. With the increase of RTILs concentration, both the adsorption amounts of RTILs on silica increased gradually. Maximum adsorption approximately 8 and 14 mg/g for [C_6mim] Br and [C_{12}mim] Br were obtained respectively when the concentration of [C_6mim] Br and [C_{12}mim] Br was about 65 and 80 mg/L, respectively. The amounts of RTILs adsorbed onto silica were clearly a function of the alkyl

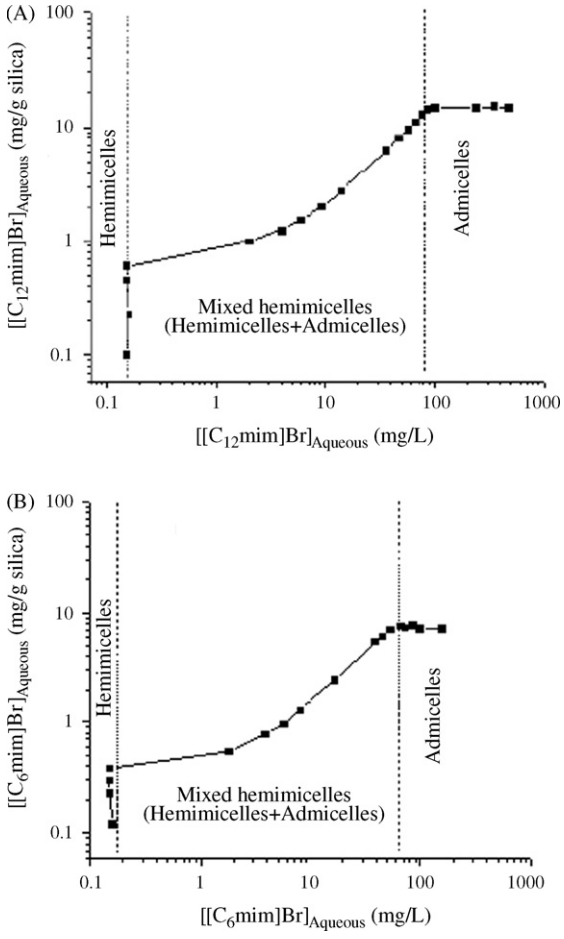


Fig. 1. Adsorption isotherms of RTILs on silica at pH 6.5: (A) [C_{12}mim] Br and (B) [C_6mim] Br.

chain length. These adsorption isotherms did not fit conventional adsorption models (e.g. Langmuir) very well, which was probably because adsorbing RTILs onto silica surface was not a simple surface phenomenon but a multistep process involving different kinds of interactions. Generally, ionic surfactant adsorption isotherms on metal oxides can be divided into three regions [40,41]. In the first region the adsorbed ionic surfactant molecules spread themselves on the surface to form single-layer coverage (hemimicelles), probably through coulombic attractive interactions between charged metal oxides surface and the oppositely charged surfactants head group. The second region involves hydrophobic and electrostatic interactions, which result in the formation of bilayers (admicelles). The process of solubilizing analytes in hemimicelles and admicelles (mixed hemimicelles) is termed as "adsolubilization". Both the above-mentioned regions were suitable for SPE method. At the end of isotherm region the overall surface of metal oxide is compensated and surfactants begin to form micelles in solution, which may result in the solubilization of analytes into micelles in bulk solution again and this isotherm span is unsuitable for SPE.

3.2. Effect of RTILs concentration on the zeta-potential of silica particles

Zeta-potential measurements can provide very useful information on adsorption phenomena since changes in the zeta-potential reflect the adsorption on surface directly. In order to study the process of self-aggregated micelles formed on metal oxide surface, many research groups investigated the zeta-potential curves of ionic surfactants adsorbed onto various metal oxides surfaces [42–44]. Fig. 2 showed that the zeta-potential of silica particles was a function of RTILs concentration. It can be observed that both the zeta-potentials of silica increased from negative to zero and converted to positive with increasing RTILs concentration. The zeta-potential changes can be interpreted as follows. At first the silica particles had a negative zeta-potential for the reason that the solution pH was higher than the silica PZC (about 3.0). At low RTILs concentrations (<5 mg added amount) a zeta-potential plateau of two systems about −13 MV was observed, which indicated that the RTILs adsorption amounts were not detectable. With the increase of RTILs concentration, the RTILs molecules began to adsorb on negatively charged silica surface obviously through electrostatic attraction interactions, and the self-assembled surface micelles were formed gradually. The formed micelles screened the partial negative charges of silica surface, which resulted in a less negative zeta-potential. With the sign reversing after passing through a zero zeta-potential, the zeta-potential became positive with further RTILs adsorption, and attained a maximum of 9.8 and 7.2 MV when the added amounts of [C_{12}mim] Br and [C_6mim] Br were about 25 and 20 mg, respectively. The zeta-potential values did not change with a further increase in RTILs concentration, indicating the silica surface was saturated by RTILs adsorption. After compensation of the surface charge, the zeta-potential became almost independent of the RTILs concentration.

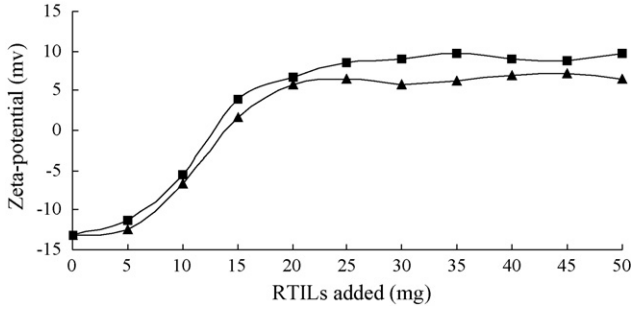


Fig. 2. The zeta-potential of silica particles as a function of RTILs concentration at pH 6.5: (■) [C_{12}mim] Br; (▲) [C_6mim] Br.

3.3. Sorbent selection

Fig. 3 depicted the adsorption percentages of adsorbed PAEs as a function of the RTILs amount added. In the absence of RTILs, the PAEs hardly adsorbed onto the silica surface. In contrast, with increases in RTILs concentration, both the PAEs adsorption amounts of micelles systems increased remarkably. The increase in adsorption amounts can be explained by the gradual formation of mixed hemimicelles (hemimicelles and admicelles) on silica surface, and then the analytes were extracted gradually. Maximum adsorption percentages were obtained when the added amounts were in the range of 15–30 mg for [C_{12}mim] Br and 10–20 mg for [C_6mim] Br, respectively. Both the DnBP maximum adsorption percentages were above 90%; the main difference was the maximum adsorption percentages of DEP and DnPP, which were about 70 and 85% for [C_{12}mim]Br-coated silica system while 60 and 80% for

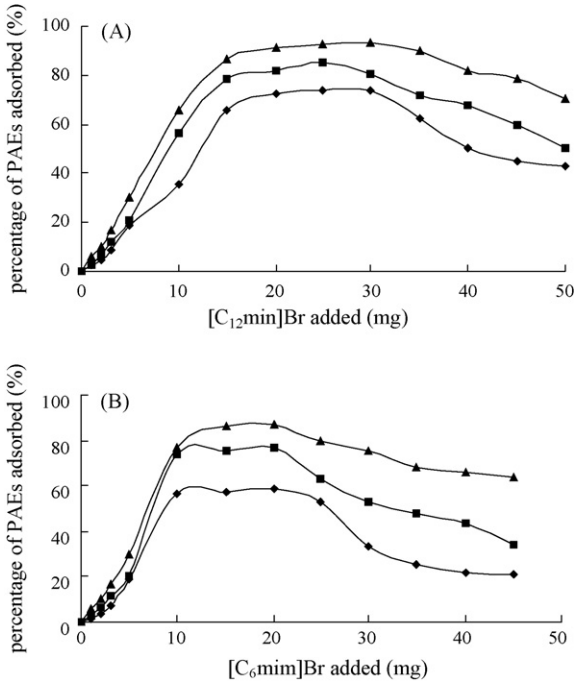


Fig. 3. Effect of the added amounts of (A) [C_{12}mim] Br and (B) [C_6mim] Br on the PAEs adsorption percentages at pH 6.5: (▲) DnBP; (■) DnPP; (♦) DEP.

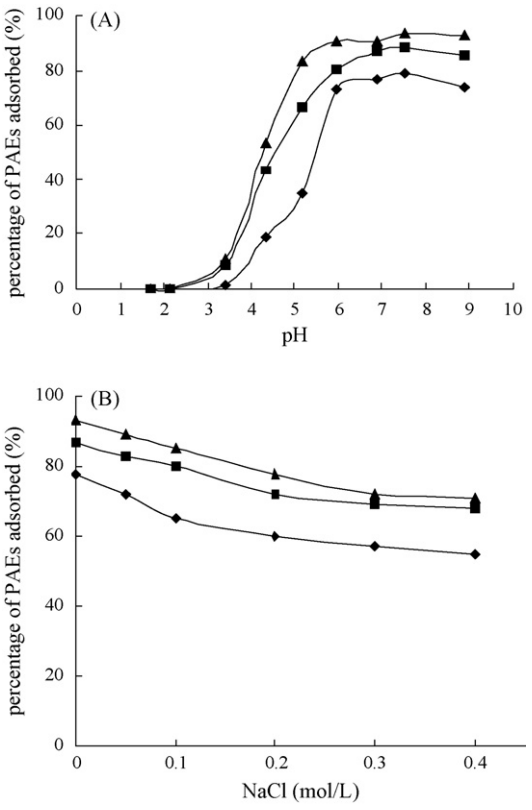


Fig. 4. Effect of (A) pH and (B) ionic strength on the extraction percentages: (▲) DnBP; (■) DnPP; (♦) DEP.

[C_6mim]Br-coated silica system, respectively. The experimental results also indicated clearly that the adsorption amounts had a positive relationship with the RTILs alkyl chain length. After a maximum adsorption plateau, the adsorption amounts began to decrease when the added amounts exceeded 30 mg for [C_{12}mim] Br and 20 mg for [C_6mim] Br, which can be explained that with more ionic liquids added the RTILs molecules began to form micelles in the bulk aqueous solution; furthermore, the micelles made the PAEs redistribute into the solution again. Given these findings, the [C_{12}mim] Br adsorption system had higher adsorption amount than [C_6mim] Br and was more suitable for SPE method; therefore, 25 mg [C_{12}mim] Br was adopted in the following studies.

3.4. Effect of pH

pH is one of the prime factors influencing the adsorption behavior of a mixed hemimicelles system. In present study the effect of pH was examined by varying pH between 1.5 and 9.0. As shown in Fig. 4(A), the [C_{12}mim] Br-coated silica system exhibited no obvious adsorption for three PAEs when pH was between 1.5 and 3.5. With the increase of pH, the PAEs adsorption amounts increased dramatically before reaching a maximum above pH 6.0. This can be attributed to the fact that the silica surface was positive charged when the pH was below its PZC (2.9) and the $[C_{12}mim]^+$ was hardly adsorbed to the silica surface. With increases in pH value, the silica surface gradually became negative charged such that there was a strong electrostatic attraction interaction between RTILs molecules and the negatively charged silica surface, which was sufficient to produce a great adsorption affinity for PAEs. Therefore, pH 6.5 was selected for the following studies.

3.5. Effect of ionic strength

NaCl concentration ranged between 0.05 and 0.4 M/L. It can be seen from Fig. 4(B) that the adsorption amounts of three PAEs decreased with increasing ionic strength. The experimental results suggest that the role of electrostatic interactions in the adsorption process was significant and the competition of sodium ions for the silica substrate was existed obviously. As we known that in the first adsorption region the adsorbed RTILs ions spread themselves on the silica surface to form a single-layer coverage through coulombic attraction interactions. As a result, the effect of salt concentration was to suppress the thickness of electrical adsorption layer at the silica/solution interface, which led to the decrease of mixed hemimicelles formed on the silica surface.

3.6. Breakthrough volume and desorption

The breakthrough volume for PAEs was determined using a series of different volume aqueous solution (100–500 mL) spiked with 1 μg of each the PAEs at pH 6.5. Insufficient recovery was considered to occur when the recovery was below 90%. With the increase of solution volume, insufficient recoveries occurred when aqueous solution volume was above 300 mL; for instance, the recovery of 78, 82, 85, 86 and 89% for DEP, DnPP, DnBP, DcHP and DEHP were obtained respectively when the passing volume was 400 mL. The sample loading rate experiments (1–10 mL/min) were carried out by passing 300 mL aqueous solution spiked with 1 μg of each the PAEs. The sample loading rate was considered too fast when the recoveries of PAEs in eluate were below 90%. The experimental results indicated that good recoveries were obtained when loading rate was between 1 and 5 mL/min; when loading rate increased to 8 mL/min, insufficient recoveries of 76, 83, 85, 85 and 84% for

Table 2
Analytical parameters of the proposed method

Analytes	Linearity range (μg/L)	Correlation coefficient (r^2)	LOD (μg/L)	Preconcentration factor	R.S.D. (%) ($n=6$)
DEP	0.6–50	0.9912	0.17	600	5.9
DnPP	0.6–50	0.9910	0.15	600	4.8
DnBP	0.6–50	0.9924	0.13	600	5.2
DcHP	0.6–50	0.9921	0.14	600	4.9
DEHP	0.6–50	0.9918	0.12	600	4.1

Table 3
Determination and recoveries of PAEs in real water samples

Samples	Added (μg/L)					Founded[a] (μg/L)					Recovery[b] (%)				
	DEP	DnPP	DnBP	DcHP	DEHP	DEP	DnPP	DnBP	DcHP	DEHP	DEP	DnPP	DnBP	DcHP	DEHP
Tap water	0	0	0	0	0	n.d.[c]	n.d.[c]	n.d.[c]	n.d.[c]	n.d.[c]					
	1.0	1.0	1.0	1.0	1.0	0.85	0.93	1.05	0.92	0.90	85 ± 3	93 ± 4	105 ± 6	92 ± 4	90 ± 5
Jingmi Canal	0	0	0	0	0	0.82	n.d.[c]	0.52	n.d.[c]	0.53					
	1.0	1.0	1.0	1.0	1.0	1.78	0.87	1.46	1.02	1.49	96 ± 5	87 ± 3	94 ± 5	102 ± 5	96 ± 4
Xiaoqing River	0	0	0	0	0	1.15	n.d.[c]	0.51	0.46	1.36					
	1.0	1.0	1.0	1.0	1.0	2.10	0.96	1.56	1.53	2.26	95 ± 4	96 ± 5	105 ± 5	107 ± 6	90 ± 3
Gaobeidian effluent	0	0	0	0	0	n.d.[c]	n.d.[c]	0.67	0.49	0.52					
	1.0	1.0	1.0	1.0	1.0	0.93	0.87	1.58	1.36	1.47	93 ± 4	87 ± 5	91 ± 4	87 ± 3	95 ± 5

[a] Mean of three determinations.
[b] S.D. for three determinations.
[c] Not detected.

DEP, DnPP, DnBP, DcHP and DEHP were obtained, respectively. Therefore, 300 mL solution volume and 5 mL/min flow rate was selected for the next studies.

Desorption of PAEs from the [C_{12}mim] Br-coated silica mixed hemimicelles column was studied with different organic solvent such as acetonitrile, methanol and methanol (pH 2, adjusted with 1 M HNO_3). Quantitative recoveries (above 90%) of PAEs were obtained using 3 mL methanol (pH 2). When using 3 mL acetonitrile, the recoveries were 76, 70, 83, 82 and 79% for DEP, DnPP, DnBP, DcHP and DEHP were achieved, respectively, and a higher volume acetonitrile (8 mL) was required for desorbing the PAEs completely. When using 3 mL methanol, the recoveries were 81, 76, 85, 82 and 88% for DEP, DnPP, DnBP, DcHP and DEHP, respectively. Thus, 3 mL methanol (pH 2) was recommended for desorption. By drying the desorption solution with a nitrogen flow and redissolving the analytes in 0.5 mL methanol, the preconcentration factor of 600 for each PAEs was obtained.

3.7. Analytical performance

Quantitative parameters of the proposed method such as linear range, correlation coefficients, limits of detection (LODs) and relative standard deviation (R.S.D.), were evaluated by enriching 300 mL standard solutions (Table 2). Calibration curves were run using 300 mL deionized water spiked with 0.6–50 ng/mL each the PAEs. According to the overall SPE procedure and HPLC analysis method above-mentioned, the calibration curves were established. Each analyte exhibited good linearity with correlation coefficient (r^2) > 0.99 in the studied range. The limits of detection, calculated on the basis of signal-to-noise ratio of 3 (S/N = 3) [45] ranged between 0.12 and 0.17 μg/L. The precision of analytical method was investigated using six replicate experiments with 300 mL standard solution containing each the PAEs 1.0 μg/L, and the relative standard deviation (R.S.D.) of below 6.0% was obtained.

3.8. Analysis of real water samples

In order to validate the method, the method was applied to four real environmental water samples with the results shown in

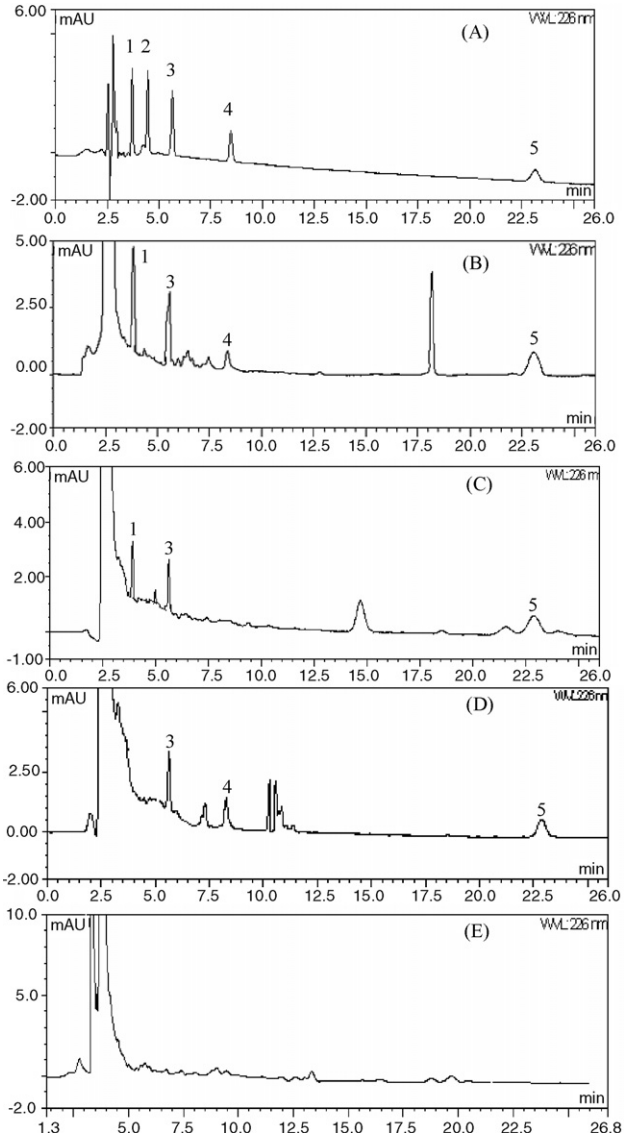


Fig. 5. Solid-phase extraction/LC–spectrophotometry chromatograms: (A) standard solution containing 0.3 mg/L of each the PAEs; (B) Xiaoqing River water sample; (C) Jingmi Canal; (D) Gaobeidian effluent; (E) tap water. (1) DEP; (2) DnPP; (3) DnBP; (4) DcHP; (5) DEHP.

Table 3. No PAEs were found in the tap water; for the case of other three water samples, different PAE contents were found. The accuracy of the method was evaluated by a recovery test carried out with PAEs-spiked water samples. Recoveries ranged between 85 and 108% for the five PAEs. The chromatograms of all the water samples were shown in Fig. 5.

4. Conclusions

A novel SPE method based on [C_{12}mim] Br-coated silica mixed hemimicelles was developed for the analysis of five PAEs in four environmental water samples. The method was effective for the preconcentration of trace PAEs in environmental water prior to HPLC analysis. The strong hydrophobic interactions between the mixed hemimicelles and PAEs resulted in the high retention of analytes; however, the retained PAEs can be desorbed easily with 3 mL methanol (pH 2) and no carryover was observed in the next analysis. Good recovery and precision were obtained, which indicated that [C_{12}mim] Br-coated silica mixed hemimicelles SPE method has high analytical potential for the preconcentration of other trace organic pollutants from water samples.

Acknowledgments

We gratefully acknowledge the support of this work by National Basic Research Program of China (2003CB415001), the National Natural Science Foundation of China (20577058, 20475060) and Major Research Program of Chinese Academy of Sciences (KZCX3-SW-432).

References

[1] A.C. Staple, D.R. Peterson, T.H. Parkerton, W.J. Adams, Chemosphere 35 (1997) 667.
[2] M. Castillo, A. Oubina, D. Barcelo, Environ. Sci. Technol. 32 (1998) 225.
[3] H.M. Koch, B. Rossbach, H. Drexler, J. Angerer, Environ. Res. 93 (2003) 177.
[4] C.R. Tyler, S. Jobling, J.P. Sumpter, Crit. Rev. Toxicol. (1998) 319.
[5] I. Coĺon, D. Caro, J. Carlos, C.J. Bourdony, O. Rosario, Environ. Health Perspect. 108 (2000) 895.
[6] S.H. Swan, K.M. Main, F. Liu, S.L. Stewart, R.L. Kruse, A.M. Calafat, C.S. Mao, J.B. Redmon, Ch.L. Ternard, S. Sulivan, J.L. Teague, Environ. Health Perspect. 113 (2005) 1056.
[7] Y.L. Feng, J.P. Zhua, S. Robert, Anal. Chim. Acta 538 (2005) 41.
[8] E. Cortazar, O. Zuloaga, J. Sanz, J.C. Raposo, N. Etxebarria, L.A. Ferńandez, J. Chromatogr. A 978 (2002) 165.
[9] F. Jośe López-Jimenez, S. Rubio, D. Pérez-Bendito, Anal. Chim. Acta 551 (2005) 142.
[10] D. DeOrsi, L. Gagliardi, R. Porra, S. Berri, P. Chimenti, A. Granese, I. Carpani, D. Tonelli, Anal. Chim. Acta 555 (2006) 238.
[11] C.S. Giam, M.K. Wong, J. Food Protect. 50 (1987) 769.
[12] K. Luks-Betlej, P. Popp, B. Janoszka, H. Paschke, J. Chromatogr. A 938 (2001) 93.
[13] G. Prokupkova, K. Holadova, J. Poustka, J. Hajslova, Anal. Chim. Acta 457 (2002) 211.
[14] H. Katsumata, A. Beguma, S. Kaneco, T. Suzuki, K. Ohta, Anal. Chim. Acta 502 (2004) 167.
[15] M.L. Davi, M. Liboni, M.G. Malfatti, Int. J. Environ. Anal. Chem. 74 (1999) 155.
[16] S. Jonsson, H. Bońen, J. Chromatogr. A 963 (2002) 393.
[17] Y.Q. Cai, G.B. Jiang, J.F. Liu, Q.X. Zhou, Anal. Chim. Acta 494 (2003) 149.
[18] F. Merino, S. Rubio, D. Pérez-Bendito, Anal. Chem. 76 (2004) 3878.
[19] M. Cantero, S. Rubio, D. Pérez-Bendito, J. Chromatogr. A 1067 (2005) 161.
[20] T. Saitoh, S. Matsushima, M. Hiraide, J. Chromatogr. A 1069 (2002) 271.
[21] S.M. Mwonggela, A. Numan, N.L. Gill, R.A. Agbaria, I.M. Warner, Anal. Chem. 75 (2003) 6089.
[22] E.G. Yanes, S.R. Gratz, M.J. Baldwin, S.E. Robinson, A.M. Stalcul, Anal. Chem. 73 (2001) 3838.
[23] J.L. Anderson, J. Ding, T. Welton, D.W. Armstrong, J. Am. Chem. Soc. 124 (2002) 14247.
[24] M.S. Selvan, M.D. Mckinley, R.H. Dubois, J.L. Atwood, J. Chem. Eng. Data 45 (2000) 841.
[25] J. Liu, J. Peng, Y. Chi, G. Jiang, Talanta 65 (2005) 705.
[26] R. Sridhar, P.T. Perumal, Tetrahedron 61 (2005) 2465.
[27] N.E. Leadbeater, H.M. Torenius, J. Org. Chem. 67 (2002) 3145.
[28] L.A. Blanchard, D. Hancut, E.J. Beckman, J.F. Brennecke, Nature 399 (1999) 28.
[29] A.E. Visser, R.D. Rogers, J. Solid State Chem. 171 (2003) 109.
[30] P.Y. Chen, C.L. Hussey, Electrochim. Acta 50 (2005) 2533.
[31] E.V. Dickinson, M.E. Willaims, S.M. Hendrickson, H. Masui, R.W. Murray, J. Am. Chem. Soc. 121 (1999) 613.
[32] Z. Miskolczy, K. Sebok-Nagy, L. Biczok, S. Gokturk, Chem. Phys. Lett. 400 (2004) 296.
[33] P. Wasserscheid, W. Keim, Angew. Chem. Int. Ed. 39 (2000) 3772.
[34] T. Welton, Chem. Rev. 99 (1999) 2071.
[35] D.W. Armstrong, L. He, Y.S. Liu, Anal. Chem. 71 (1999) 3873.
[36] D.W. Armstrong, L. Zhang, L. He, M.L. Gross, Anal. Chem. 73 (2001) 3679.
[37] D. Giovanelli, M.C. Buzzeo, N.S. Lawrence, C. Hardacre, K.R. Seddon, R.G. Compton, Talanta 62 (2004) 904.
[38] C.H. She, H. Li, H.W. Liu, K.A. Li, F. Liu, J. Chromatogr. A 1082 (2005) 143.
[39] S.H. Li, C.Y. He, H.W. Liu, K.A. Li, F. Liu, J. Chromatogr. B 826 (2005) 58.
[40] K. Nagashima, F.D. Blum, J. Colloid Interf. Sci. 214 (1999) 8.
[41] A. Fan, P. Somasundaran, N.J. Turro, Langmuir 506 (1997) 13.
[42] V.K. Paruchuri, A.V. Nguyen, J.D. Miller, Colloids Surf. A 250 (2004) 519.
[43] C.E. McNamee, M. Matsumoto, P.G. Hartley, M. Nakahara, Colloids Surf. A 193 (2001) 175.
[44] N.K. Dimov, V.L. Kolev, P.A. Kralchevsky, L.G. Lyutov, G. Broze, A. Mehretea, J. Colloid Interf. Sci. 256 (2002) 23.
[45] I. Taverniers, M.D. Loose, E. Van Bocstaele, Trends Anal. Chem. 23 (2004) 535.

Available online at www.sciencedirect.com
ScienceDirect
Talanta 74 (2008) 958–964
Talanta
www.elsevier.com/locate/talanta

Atmospheric ozone measurement with an inexpensive and fully automated porous tube collector-colorimeter

Jianzhong Li [1], Qingyang Li, Jason V. Dyke, Purnendu K. Dasgupta *

Department of Chemistry, Texas Tech University, Lubbock, TX 79409-1061, United States

Received 29 May 2007; received in revised form 1 August 2007; accepted 1 August 2007
Available online 9 August 2007

Abstract

The bleaching action of ozone on indigo and related compounds is well known. We describe sensitive automated instrumentation for measuring ambient ozone. Air is sampled around a porous polypropylene tube filled with a solution of indigotrisulfonate. Light transmission through the tube is measured. Light transmission increases as O_3 diffuses through the membrane and bleaches the indigo. Evaporation of the solution, a function of the RH and the air temperature, can, however cause major errors. We solve this problem by adding an O_3-inert dye that absorbs at a different wavelength. Here we provide a new algorithm for this correction and show that this very inexpensive instrument package (controlled by a BASIC Stamp Microcontroller with an on-board data logger, total parts cost US$ 300) provides data highly comparable to commercial ozone monitors over an extended period. The instrument displays an LOD of 1.2 ppbv and a linear span up to 300 ppbv for a sampling time of 1 min. For a sampling time of 5 min, the respective values are 0.24 ppbv and 100 ppbv O_3.
© 2007 Elsevier B.V. All rights reserved.

Keywords: Ozone; Bleaching; Colorimetry; Ambient air

1. Introduction

Ozone is one of the criteria pollutants in ambient atmosphere as designated by the US Environmental Protection Agency (USEPA). Ozone exposure has many effects on human health [1]. In most countries, the upper permissible limit of ozone in ambient air is around 100 parts per billion by volume (ppbv).

There are many methods available for measuring atmospheric ozone concentrations; these are based either on ozone's physical properties or on its considerable chemical reactivity. Ozone absorbs strongly in the ultraviolet and fortuitously the absorption maximum is located close to the principal emission line (254 nm) of a low pressure Hg-lamp. Most commercial ozone analyzers thus rely on measuring optical absorption at 254 nm over an extended path length. There are other compounds in ambient air that absorb at 254 nm; to compensate for such absorption, the sampled air stream is put through a "scrubber" that selectively and catalytically destroys ozone and used as the reference. UV-absorption based ozone monitors do not require frequent calibration as the light path is fixed and the relevant extinction coefficient is already known; they can provide continuous data output over an extended period. It is not without shortcomings; selective removal of ozone to provide a reference stream is not fully successful in the presence of significant concentrations of aromatic compounds [2].

Ozone is such a strong oxidant that not only it can oxidize many compounds; the product of the oxidation is often a species in the excited state, which then produces chemiluminescence (CL). Ethylene–O_3 and NO–O_3 CL reactions have been commonly used for measurement [3–5]. Many dyes and related compounds react in solution or even in the solid phase with O_3 to produce intense CL [6]; one recently introduced method uses alkaline chromotropic acid and responds to ozone particularly fast (10–90% rise time 80 ms) and with high sensitivity (limit of detection, (LOD) 40 parts per trillion by volume (pptv)) [6]. Indigo and indigo derivatives also react with ozone with 1:1 stoichiometry and produces CL [7]. It is also simul-

* Corresponding author. Present address: Department of Chemistry and Biochemistry, The University of Texas at Arlington, Arlington, TX 76019-0065, United States.
E-mail address: Dasgupta@uta.edu (P.K. Dasgupta).
[1] Present address: 1 Bridgelake Circle, #F, Cockeysville, MD 21030, United States.

0039-9140/$ – see front matter © 2007 Elsevier B.V. All rights reserved.
doi:10.1016/j.talanta.2007.08.002

taneously bleached; the decolorization is the standard method for measuring ozone residuals in water in disinfection applications [8]. The CL that occurs during the indigo O_3 reaction is relatively weak and is also very fast; as such photometric measurement of bleaching is not affected by the CL. Ozone oxidizes nitrite to nitrate. Filters coated with nitrite have been used as dosimeters, as the amount of nitrate formed on the dosimeter is proportional to the ozone exposure [9,10]. Like many other oxidants, ozone oxidizes iodide to iodine which forms a deep blue color with starch. Yimit et al. described a starch-iodide coated optical fiber based disposable sensor that responds to ozone (and other oxidants) by evanescent interaction [11].

1.1. The tubular gas collector-colorimeter

Color-forming or selective bleaching reactions are particularly attractive for monitoring purposes. We developed a unique amorphous fluropolymer (Teflon AF) tube based gas sensor [12,13] which took advantage of both the very low refractive index of Teflon AF (an aqueous solution filled tube of which behaves as an optical fiber/liquid core waveguide (LCW)) and its high gas permeability. The tube is filled with a suitable solution while monochromatic light from a light emitting diode (LED) is launched into the liquid via an optical fiber and detected at the other end with an optical fiber coupled photodiode (PD). As a gas, for example, ambient air, is sampled around the tube, analytes permeate through the tube wall and cause a color change (formation or bleaching) and this is monitored over the significant path length (15–30 cm) of the tube. Subsequently an improved approach was developed with porous hydrophobic membrane tubes made from polypropylene (PP), or polytetrafluoroethylene (PTFE). While these tubes do not behave as effective liquid-filled optical fibers, because of the air trapped in the tube walls, the effective refractive index is low and light transmission is much better than solid wall polymer tubes, although not nearly as good as Teflon AF. More modest lengths, e.g., 5 cm of these tubes can be used in gas sensing applications, with sufficient light throughput at the other end. What is lost in a reduced pathlength, however, is more than made up in improved mass transport; analyte gas transport to the solution through free pore space is much more facile than permeation through Teflon AF [14]. Several applications were described. The rapid bleaching of indigotrisulfonate by ozone was a reaction with which we were very familiar [15]; therefore, we chose this reaction for the measurement of ozone.

1.2. Change in light transmission of a porous tube over time and compensation

Light transmission of a porous hydrophobic polymer tube decreases over a period of time as the interior aqueous liquid increasingly penetrates into the pores and changes the effective refractive index. Fig. S1 in electronic supporting information indicates that this decrease can be significant and compensation is necessary. In the first exposition of the tubular gas collector-colorimeter [14] this compensation was achieved by alternately measuring the light throughput from a second LED at a different wavelength (a near infrared LED at 850 nm was used, ITS has no absorption at this wavelength).

1.3. Effects of humidity and the approach to compensation

While transfer of the analyte gas of interest in to the collection liquid contained in the porous membrane is facile, the transfer of evaporated liquid vapor through the pores of the tube into the flowing sample gas is also obviously facile. Especially for bleaching based methods (or more accurately, any method that has a finite reagent blank) this can cause problems when the rate of evaporation occurring during sampling is different from that during calibration. The rate of evaporation is dependent on both sample temperature and humidity. Obviously both will vary over time in any ambient air sampling situation, thus contributing to a variable bias. Ozone bleaches the dye, whereas evaporation contributes to the dye getting more concentrated in the lumen of the fiber. It may thus seem at first sight that this will lead to a negative bias in ozone determination. In reality, quantitation by any such instrumentation is not absolute but is calibration-based. Ozone generation and calibration are nearly always carried out with dry gas. As such, nearly maximal evaporation is already occurring during calibration and as such when lesser evaporation occurs during sampling, the bias is actually positive. Monitoring transmission loss of the tube as described in the foregoing section cannot compensate for this and there can be large errors in the measurement of ozone (or other gases).

We report here on a successful solution to these problems and the development of a robust, inexpensive, self-contained, fully automated ozone monitor based on the porous tube gas collector-colorimeter principle. While we focus here on an ITS-bleaching based ozone monitor, the principles are equally applicable for any selective bleaching or chromogenic reaction induced by a gaseous analyte.

2. Principles of compensation for evaporation

There are two separate and independent issues that must be solved. One is to compensate for the slow but definite change in light transmission characteristics of the tube over a period of time (Fig. S1). The second is to compensate for evaporation loss during a measurement cycle, which must be able to accommodate the variation in such loss from cycle to cycle. Our chosen strategy was to incorporate an ozone-inert dye in the ITS reagent, the concentration of which can be followed *independently* from that of ITS. This means that the absorption of such a dye must occur in at least one window where ITS has no absorption. Additional considerations are that the dye should be highly hydrophilic and not adsorb to the membrane walls. It would also be preferred that like ITS, the dye be nontoxic. We made a preliminary survey of food coloring, and quickly established that FD&C yellow No. 5 (hereinafter abbreviated as FY5) meets the above criteria. FY5 has a λ_{max} of 430 nm. The LED used to interrogate FY5 absorption has an emission wavelength of 460 nm, at which the absorptivity of the dye is still >80% of its maximum. The absorbance spectra of FY5, ITS, and the

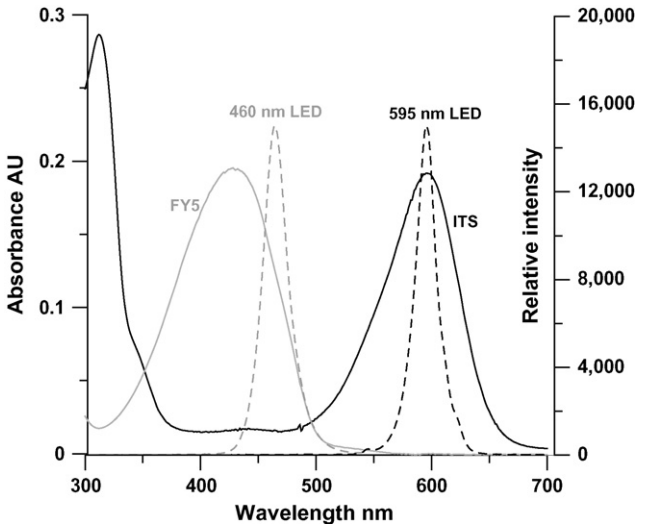


Fig. 1. Absorbance spectra of ITS and food yellow (left ordinate) and emission spectra of bicolor LEDs (right ordinate).

emission spectra of the 460 nm/595 nm LED used are shown in Fig. 1.

In the following, we do not take into account this finite absorption of ITS at the wavelength at which FY5 is monitored. Initially and every time the reagent is changed, the sampling fan is turned off, the tube is first washed with water and the two light intensities registered on the photodiode, as the two individual LEDs are individually turned on, I^0_{460} and I^0_{595} are recorded. (For simplicity we assume here the dark signal of the photodiode is zero. In reality the dark signal is always measured at the beginning of a measurement cycle and is always subtracted from all the other readings.) As the absorbing solution is filled in the tube, the intensities I_{460} and I_{595} are recorded. Specifically, since the reagent is unchanging, the initial absorbance of the yellow dye, A^0_{FY5}, is constant and is given by

$$A^0_{\mathrm{FY5}} = -\log\left[\frac{I_{460}}{I^0_{460}}\right] \tag{1}$$

The value of A^0_{FY5} is stored in memory. Note that A^0_{FY5} is a constant and it is the absorbance of FY5 at the start of any measurement cycle (a similar argument will be true for ITS as well; but it is better to choose FY5 as no photostability issues are involved). The ratio of I^0_{595} and I^0_{460}, K, is also stored in memory.

$$K = \left[\frac{I^0_{595}}{I^0_{460}}\right] \tag{2}$$

At the beginning of any measurement cycle with the fresh reagent in the tube the respective light intensities, $I^{t=0}_{460}$ and $I^{t=0}_{595}$ are measured, but the corresponding I^0 values (i.e., values corresponding to a water-filled tube) are not measured. The duration of a measurement cycle is short (~5 min) and it is assumed that $I^{0,t}$ do not change within that measurement period ($t=0$ to $t=$ end). However, $I^{0,t}$ values may be different from the original I^0 values because of changes in light transmission of the tube. The value of $I^{0,t}_{460}$ is computed from the constancy of A^0_{FY5}:

$$I^{0,t}_{460} = I^{t=0}_{460} 10\hat{A}^0_{\mathrm{FY5}} \tag{3}$$

Since both LEDs are consistently driven by highly repeatable current pulses the ratio K in Eq. (2) is also expected to be a constant throughout. Therefore, $I^{0,t}_{595}$ is computed from

$$I^{0,t}_{595} = K I^{0,t}_{460} \tag{4}$$

Eq. (4) holds good when there is no spectral crosstalk between the two measured species, experiments show that the small amount of spectral interference that exists (ITS has a small but finite absorbance at 460 nm and the product of ITS bleaching also has a similar absorbance at 460 nm) is minimized when the FY5 and ITS starting absorbance values at their respective wavelengths are the same. Eqs. (3) and (4) are thus used in this way to compensate for the change in light transmission of the tube over time.

At the end of the measurement cycle ($t=$ end) the signals $I^{t=\mathrm{end}}_{460}$ and $I^{t=\mathrm{end}}_{595}$ are recorded. The absorbance of FY5, $A^{t=\mathrm{end}}_{\mathrm{FY5}}$ is given by:

$$A^{t=\mathrm{end}}_{\mathrm{FY5}} = -\log\left[\frac{I^{t=\mathrm{end}}_{460}}{I^{0,t}_{460}}\right] \tag{5}$$

The evaporative concentration factor E is thus given by

$$E = \left[\frac{A^{t=\mathrm{end}}_{\mathrm{FY5}}}{A^0_{\mathrm{FY5}}}\right] \tag{6}$$

The absorbance of ITS at the beginning and end of the measurement cycle, $A^{t=0}_{\mathrm{ITS}}$ and $A^{t=\mathrm{end}}_{\mathrm{ITS}}$, are respectively computed from

$$A^{t=0}_{\mathrm{ITS}} = -\log\left[\frac{I^{t=0}_{595}}{I^{0,t}_{595}}\right] \tag{7}$$

and

$$A^{t=\mathrm{end}}_{\mathrm{ITS}} = -\log\left[\frac{I^{t=\mathrm{end}}_{595}}{I^{0,t}_{595}}\right] \tag{8}$$

In the absence of any ozone bleaching, the absorbance due to ITS would have been $EA^{t=0}_{\mathrm{ITS}}$. Therefore, the decrease in absorbance from this, ΔA_{ITS} is the quantity directly relatable to the ozone concentration, regardless of the extent of evaporation:

$$\Delta A_{\mathrm{ITS}} = EA^{t=0}_{\mathrm{ITS}} - A^{t=\mathrm{end}}_{\mathrm{ITS}} \tag{9}$$

Both instrument calibration and the interpretation of ambient air data are conducted in terms of Eq. (9). The equations are not limited to specifically the end of the measurement cycle but also apply to any time τ within a measurement cycle. From cycle to cycle or within each cycle different values of τ may be used, in such a case the average ozone concentration from $t=0$ to $t=\tau$ would be related to $\Delta A_{\mathrm{ITS}}/\tau$.

3. Experimental

3.1. The instrument

The general configuration of the instrument is very similar to that originally described [14]. The ozone sensor is schematically shown in Fig. 2. A 25 mm diameter fan F (http://www.eagletechcomputers.com/20lapcoolfan.html) provides 17 L/min airflow at 4 V through tube ST made of a 30 cm^3 disposable plastic syringe barrel. The collector tube, a porous membrane tube M 5 cm in length (Accurel PP Q3/2, 600 μm i.d., 200 μm wall, pore size 0.2 μm, http://www.membrana.com) is suspended within the 21 mm i.d. syringe barrel using tees (http://www.ark-plas.com). Acrylic optical fibers, 0.5 mm in diameter (http://www.edmundoptics.com) were inserted inside the membrane tube within the tees. Initially we used a large bore Teflon tube instead of a syringe barrel; however, there was no discernible degradation of ozone on the much less expensive polyolefin syringe barrels at the high sampling rates used in this work. The syringe barrels were henceforth adopted. The input optical fiber was connected to a bicolor LED L (N500TBY4D, http://www.lc-led.com) that had separate blue (460 nm) and amber (595 nm) emitters in a clear enclosure. The 3-pin device has a common cathode and separate anodes for each emitter. The output optical fiber was connected to a photodiode-operational amplifier combination (OPT 301, http://www.ti.com) operated at a gain of $\sim 5 \times 10^8$ V/A. The liquid input arm of the tee is connected to a gravity-fed reagent bottle RB, protected from ambient O_3 with activated carbon as a vent trap (VT); it is also wrapped in Al foil to prevent photobleaching. The liquid output tube is connected to a waste bottle WB via a solenoid valve SV. All components except the bottles were enclosed inside a black plastic enclosure to shield from ambient light. A view inside the box is shown in Fig. S2.

A microcontroller (BASIC Stamp II) was used to control the LEDs and the solenoid valve. The microcontroller also converted the analog signal from the photodiode into digital form using a 12 bit A/D converter (MCP3204). The microcontroller also performed all the mathematical manipulations involved in processing the signal (*vide infra*), converted the raw data into an ozone concentration based on a preset calibration curve, and displayed the ozone concentration on a panel meter using separate electronics. Ozone concentration data and time data were stored on two 1 MB EEPROMs (AT24C1024-10PI2.7-ND, http://www.digi-key.com) chips, large enough to store 45 days of data. To record the time at which the data was acquired, a real-time clock (DS1307N-ND, Digi-Key) was built into the BASIC Stamp II system. The data could be directly also sent to a personal computer in real-time via the serial port. Since the memory chip is removable, a BASIC Stamp based memory reader was also developed. After the data had been collected, the EEPROM chip was removed and inserted into the corresponding socket of the memory reader and the data could be read and recorded by a computer via a serial port. Details of microcontroller and illustrative program codes are given in supporting information.

The gas collector-colorimeter monitor can operate either in continuous flow and stopped flow modes [14]. The latter was exclusively used in this work. Reagent refill is governed by SV and could be programmed in two ways: (a) reagent is refilled when some preset detector signal has been reached (bleaching has depleted the dye to a point needing replacement) or (b) at some preset constant interval. Although reagent consumption is minimized in (a), we used (b) for simplicity. Every 5 min, the valve was turned on for 12 s, sufficient to refill the collector. The reagent consumption rate, which includes evaporative losses (the relative humidity of the sampled air was typically 30%, at an average temperature of 30 °C) was ∼25 μL/min, 500 mL reagent lasting for ∼2 weeks. The height of the reservoir bottom was 21 cm above the membrane.

3.2. Procedure

When the instrument is first started or whenever reagent refill is needed, the porous tube is first washed out with water and I^0_{460} and I^0_{595} are recorded. The reagent bottle is then connected and fresh ITS-FY5 reagent is allowed to refill the tube. During all porous tube refill intervals (12 s, ca. 70 μL reagent flows through), both LEDs and the sampling fan are turned off. After the 12 s refill period, the solenoid valve is closed and the LEDs are turned on while the sampling fan remains off for another 12 s. During this time the LEDs are turned on and off alternatively to measure the initial transmitted light intensities $I^{t=0}_{460}$ and $I^{t=0}_{595}$.

3.3. Comparative measurements

A 3.2 cm (5/4 in.) diameter PVC pipe, 1.2 m (4 ft) long and lined with a polyester (Mylar) sheet was used as the sampling manifold, the open end protruding out of the laboratory window. A fan connected to the laboratory end of the PVC pipe aspirated sample air from the outside at a sampling rate of ∼100 L/min so that O_3 was sampled with minimal residence time. The open syringe end of the porous tube gas collector and a commercial photometric ozone monitor (Model 202, http://www.twobtech.com) tapped directly into opposing sides of the PVC conduit, the latter through a 1/4 in. Teflon tube, with sampling rates of 17 L/min and 2 L/min, respectively.

3.4. Reagents

A ITS stock solution (1 mM) was prepared by dissolving 61.67 mg potassium indigotrisulfonate (http://www.sial.com) in 100 mL water and refrigerated in a well sealed brown glass bottle. The stock solution is stable for at least 3 months. FD&C Yellow No. 5 (Tartrazine, an azo dye, see for structure http://en.wikipedia.org/wiki/Tartrazine) was bought from local grocery store as McCormick brand yellow food coloring in a 29 mL package. The working solution was composed of 5 mL of the ITS stock solution (1 mM), 56 μL of the yellow dye solution and 1 mL of syrupy H_3PO_4, diluted to 1 L with water. At these respective concentrations, the observed starting absorbance at 460 nm and 595 nm with the LED light source

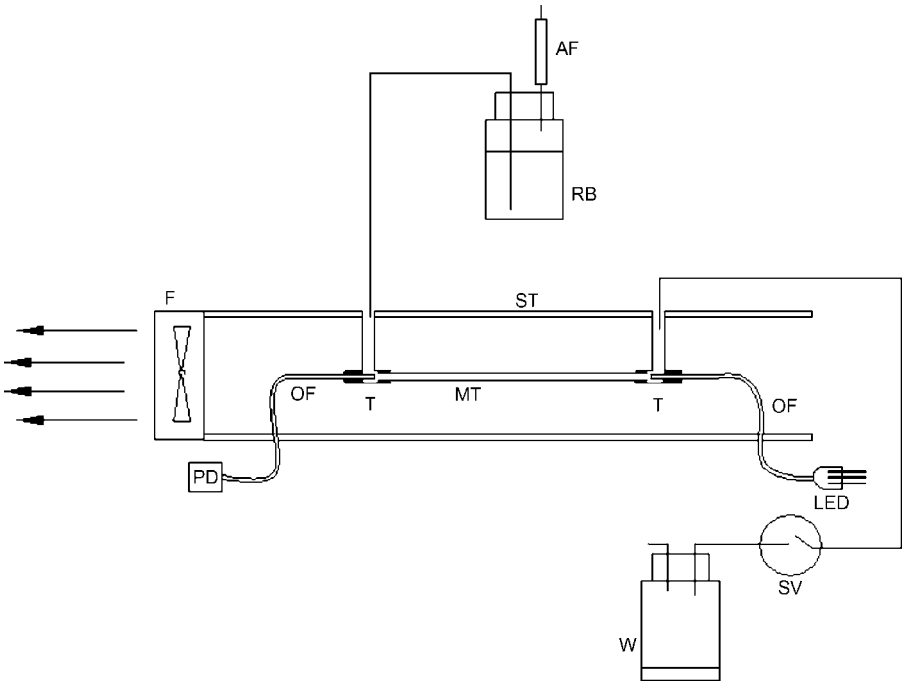


Fig. 2. Porous tube gas collector-colorimeter ozone analyzer schematic. ST: 30 mL plastic syringe barrel; MT: Accurel PP Q3/2 membrane tubing; T: membrane tubing support Tees; OF: optical fiber; F: 25 mm diameter fan; RB: reagent bottle; AF: reagent bottle air filter; LED: bicolor light emitting diode (460 nm/595 nm); PD: OPT301 photo diode; SV: solenoid valve; W: waste bottle.

used are the same. Opaque tubing was used to carry to reagent into the porous tubing.

4. Results and discussion

4.1. Porous tube diameter

It was previously derived [14] that the observed change in absorbance, ΔA in our generic experimental system due to color formation or bleaching (without any consideration of evaporative losses, etc.) would be related by Beers' law to the optical path length (tube length) L and the optical absorptivity ε of the product formed or reagent bleached as:

$$\Delta A = \frac{4k\varepsilon LC_g t}{d} \tag{10}$$

where the mass transfer constant k is dependent on the diffusion coefficient of the gas of concentration C_g and membrane characteristics, the exposure time is t and the porous tube inner diameter is d. It is obvious that the system will have greater sensitivity as the conduit diameter is reduced, however at very small diameters light throughput may control the detector S/N. Of membranes and light sources available to us, we found the 5 cm length of a 0.6 mm i.d., 0.2 mm wall to provide the best results, this tube is ~3× smaller in diameter and ~1.5× thinner than the membrane used in previous efforts [14], which used a membrane tube otherwise identical in pore size (0.2 μm), fractional porosity (70%) and matrix polymer (polypropylene).

Fig. 3 shows the remarkable gain in sensitivity and response time merely as a result of these dimensional reductions. While the sensitivity is improved by using a smaller diameter tube, the increase in the surface to volume ratio increases the relative evaporation loss as well. This makes the need to compensate for evaporation more acute, an issue not even taken into consideration in previous efforts. The internal volume of a 5 cm × 0.6 mm i.d. porous tube is ~14 μL. In our described configuration, sampling ambient air of ~30% RH and a temperature of 23 °C, 8.5 μL liquid evaporates during a 5 min measurement cycle. As the evaporated liquid is replaced by fresh reagent automatically by gravity, there is actually 1.6× as much reagent present in

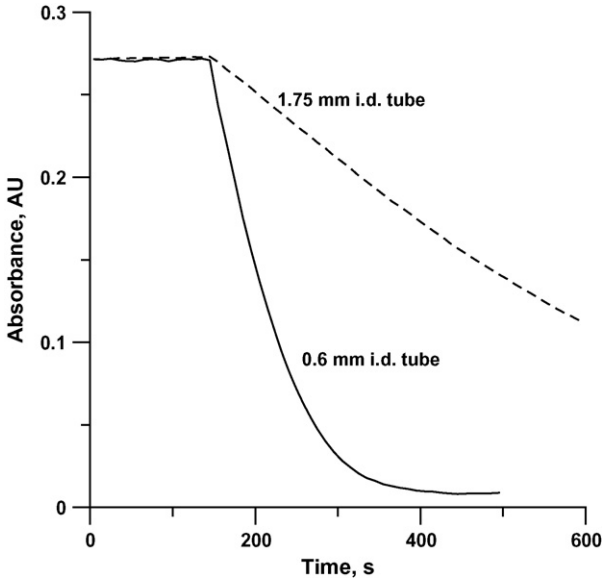


Fig. 3. Bleaching of 4 μM ITS by 127 ppb O_3 in 1.75 mm i.d. and 0.6 mm i.d. porous polypropylene tubes.

the tube relative to that before evaporation occurred. The need for compensation is therefore acute. Fig. 4 shows two cycles of sampling O_3-free air at 20% RH over 5 min periods. The water evaporation causes the observed continuous absorbance increase during sampling. This is completely compensated for by using a reference wavelength and a reference dye.

4.2. Performance

Calibration curves are shown in Fig. 5 for different sampling intervals. It can be seen that the sensitivity (slope) and the linear dynamic range both depend upon the sampling interval. Longer sampling times have higher sensitivities but a lower linear span. As absorbance is essentially continuously monitored and corresponding ΔA calculations are made, a mode of an adjustable sampling interval, where refill occurs after a preset ΔA value is reached can be easily carried out but was not implemented in this work. The sensitivity and dynamic range are also related to the ITS concentration used. Lower ITS concentrations provide better light throughput and as in any negative signal high blank method, the limit of detection improves as the baseline is reduced. However, upper measurable concentration is sacrificed. With 5 μM ITS and a sampling time of 1 min, the absorbance change was linear up to O_3 concentration of 300 ppbv and an LOD (S/N = 3) of 1.2 ppbv O_3. With a 5 min sampling period, the absorbance change was linear up to 100 ppbv O_3, and the LOD was 0.24 ppbv. For measurements in Lubbock, TX, we chose the latter mode. The microcontroller was set to refill the porous tube with new reagent every 5 min and the data logger recorded data every min.

Fig. 5 also clearly indicates that the response becomes nonlinear considerably before all the ITS the tube is bleached. This is much more pronounced than in a larger diameter tube and arises from the fact that both the mass transfer of ozone through the porous tube and the ITS-O_3 reaction are much faster than liquid phase diffusion. The ITS near the wall is bleached rapidly by O_3 and for further reaction to occur, either the excess ozone in the outer layer must diffuse to the interior or the ITS in the core must diffuse out. It is for this reason also that the linear dynamic range is dependent on the ITS concentration.

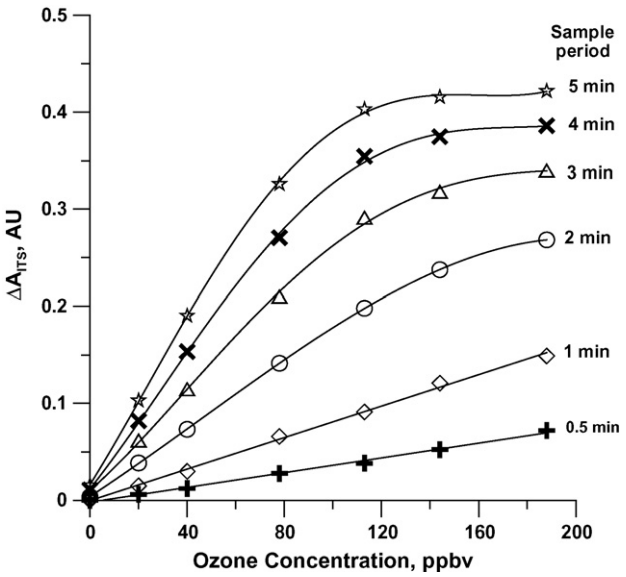


Fig. 5. Calibration curve for determination O_3. ITS concentration: 5 μM, FY5 concentration: 0.0056% (v/v), sampling periods as indicated in the figure.

4.3. Instrument intercomparison

The results for a 20-day intercomparison in Lubbock, TX (latitude 33°35′N, longitude 101°50′W, altitude 988 m MSL) with a commercial UV photometric ozone monitor is shown in Fig. 6. By and large excellent agreement is observed.

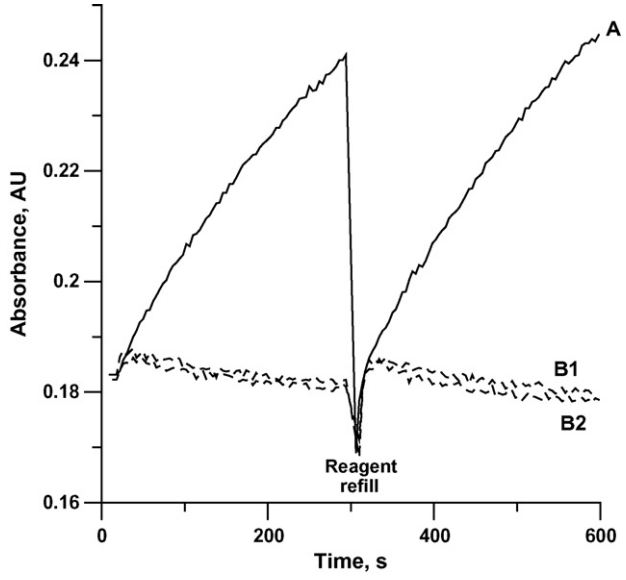


Fig. 4. Water evaporation and compensation results. (A) 2.0 μM ITS without evaporation compensation; (B1) Evaporation compensation with 0.003% FY5 and (B2) Evaporation compensation with 0.008% FY5.

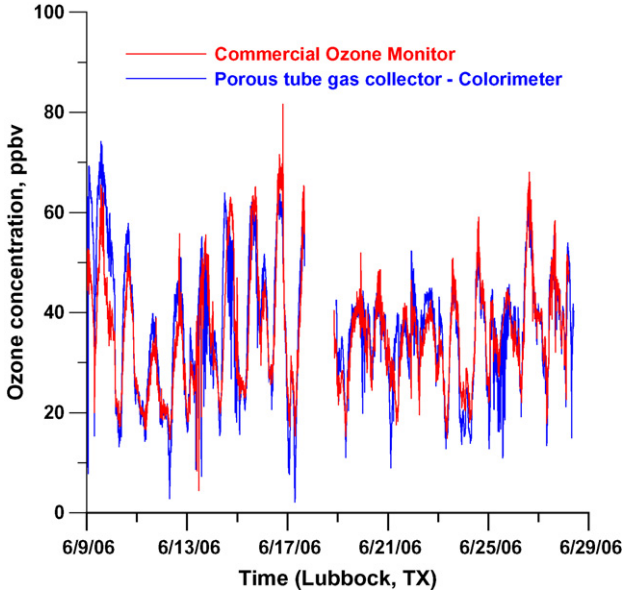


Fig. 6. Intercomparison measurements, Lubbock, TX. Present instrument vs. commercial UV-photometric monitor.

This inexpensive, fully automatic and integrated O_3 monitor has excellent performance in measuring atmospheric O_3 concentration. Perhaps more importantly, this is a generically applicable concept for the measurement of a gas whenever a selective, reasonably rapid color reaction and a spectrally independently addressable inert dye is available for evaporation compensation. The concept is also readily amenable to miniaturization.

Appendix A. Supplementary data

Supplementary data associated with this article can be found, in the online version, at doi:10.1016/j.talanta.2007.08.002.

References

[1] The United States Environmental Protection Agency, Ground-level Ozone, http://www.epa.gov/air/ozonepollution/.
[2] C. Eipel, P. Jeroschewski, I. Steinke, Anal. Chim. Acta 491 (2003) 145–153.
[3] A.M. Mihalatos, A.C. Calokerinos, Anal. Chim. Acta 303 (1995) 127–135.
[4] J.P. Lodge Jr., Methods of Air Sampling and Analysis, third ed., 1988, pp. 407–411.
[5] J.R. Pearson, Rev. Sci. Instrum. 61 (1990) 907–916.
[6] T. Takayanagi, X.L. Su, P.K. Dasgupta, K. Martinelango, G. Li, R.S. Al-Horr, R.W. Shaw, Anal. Chem. 75 (2003) 5916–5925.
[7] K. Takeuchi, S. Kutsuna, T. Ibusuki, Anal. Chim. Acta 230 (1990) 183–187.
[8] American Public Health Association, Standard Methods for the Examination of Water and Wastewater Online, 2006, Method 4500-O3 Ozone (Residual), Approved 1997, http://www.standardmethods.org/Store/ProductView.cfm?ProductID=196.
[9] M. Helaleh, S. Ngudiwaluyo, T. Korenaga, K. Tanaka, Talanta 58 (2002) 649–659.
[10] A.C. Franklin, L.G. Salmon, J.M. Wolfson, C.S. Christoforou, J. Air Waste (MA) 54 (2004) 1312–1320.
[11] A. Yimit, K. Itoh, M. Murabayshi, Electrochemistry 70 (2002) 798–801.
[12] P.K. Dasgupta, Z. Genfa, S.K. Poruthoor, S. Caldwell, S. Dong, S.Y. Liu, Anal. Chem. 70 (1998) 4661–4669.
[13] P.K. Dasgupta, S.Y. Liu, US Patent 6,011,882 (2000).
[14] K. Toda, K.I. Yoshinka, S.I. Ohira, J. Li, P.K. Dasgupta, Anal. Chem. 75 (2003) 4050–4056.
[15] J.L. Darby, D.P.Y. Chang, P.S. Coggin, H.K. Chung, P.K. Dasgupta, Process Contr. Qual. 6 (1996) 229–243.

Available online at www.sciencedirect.com
ScienceDirect
Talanta 74 (2008) 788–792
Talanta
www.elsevier.com/locate/talanta

Determination of formaldehyde in foodstuffs by flow injection spectrophotometry using phloroglucinol as chromogenic agent

Ziwei Li [a,1], Hongbing Ma [b], Huihui Lu [a], Guanhong Tao [a,*]

[a] *College of Chemistry and Chemical Engineering, Soochow University, District of Industrial Park, Suzhou, Jiangsu 215123, China*
[b] *School of Life Science, Soochow University, Suzhou, Jiangsu 215007, China*

Received 10 April 2007; received in revised form 10 July 2007; accepted 10 July 2007
Available online 21 July 2007

Abstract

A spectrophotometric method for the determination of formaldehyde in foodstuffs was described by using phloroglucinol as the chromogenic agent. The reaction between formaldehyde and phloroglucinol could occur rapidly at room temperature under mild conditions. The spectrophotometric measurements were conducted at 474 nm of an unstable intermediate orange product of the reaction, which greatly increased the sample throughput. Flow injection technique was used to control the merging and reaction timing of the reagents and sample. A detection limit (3σ) of 0.023 μg ml^{-1} was achieved. The relative standard deviation was 0.29% for the determination of 7 μg ml^{-1} formaldehyde ($n = 11$). The proposed method was applied to the analyses of formaldehyde in several preserved foodstuffs and the results were in good agreement with those obtained by a standard method.
© 2007 Elsevier B.V. All rights reserved.

Keywords: Formaldehyde; Phloroglucinol; Spectrophotometry; Flow injection analysis; Foodstuffs

1. Introduction

Formaldehyde is widely present in the environment [1]. It originates from both natural sources, e.g. forest fires and direct human sources, such as automotive combustion and industrial uses. Formaldehyde is a potential mutagen and carcinogen in laboratory animal tests for its serious toxicological properties [1]. Thus, formaldehyde is forbidden to be used as a food additive in China [2]. However, it is often used illegally in the food processing industry because addition of formaldehyde can prolong the storage life for some foodstuffs and give a face-lift by changing their color and smell. Therefore, the determination of formaldehyde in preserved foodstuffs is of prime importance.

A lot of methods for the determination of formaldehyde have been reported, which include spectrophotometry [3–8], high-performance liquid chromatography [9], gas chromatography [10,11], fluorimetry [12,13], polarography [14], and potable formaldehyde sensors-based spectrometric [15,16] and electrochemical [17,18] principles. Among these methods, spectrophotometry is the most widely used one due to its inexpensive instrumentation, simple operation, and fairly good sensitivity. Various chromogenic agents, such as chromotropic acid [3], pararosaniline [4], 4-amino-3-pentene-2-one (Fluoral-P) [5], acetylacetone [6], 4-amino-5-hydrazine-3-mercapto-1,2,4-triazole (AHMT) [7], 3-methyl-2-benzothiazolone hydrazone (MBTH) [8] have been used. The chromotropic acid method [3] and pararosaniline method [4] are the two old and classical methods for the detection of formaldehyde, but provide poor limits of detection and the product of pararosaniline is sticky, which causes difficulty for handling samples. Fluoral-P [5], which is originally used as a fluorescent reagent, can also be used for formaldehyde spectrophotometric measurements. However it suffers from low sensitivity, unstable chromogenic product and needs for acetonitrile as a solvent. AHMT method [7] and MBTH method [8] are getting popular due to their higher sensitivity compared to other methods. Yet, the two methods need two-step reactions and require a relative long reaction time (>20 min) for the final color development. In addition, the chromogenic agents are fairly expensive.

* Corresponding author. Fax: +86 512 65880089.
E-mail address: taogh@suda.edu.cn (G. Tao).
[1] On leave from Department of Biochemistry and Environmental Science, Yili Normal College, Yining, Xinjiang 835000, China.

0039-9140/$ – see front matter © 2007 Elsevier B.V. All rights reserved.
doi:10.1016/j.talanta.2007.07.011

A simple and rapid method for the spectrophotometric determination of formaldehyde was reported using 1,3,5-trihydroxybenzene (phloroglucinol) as the chromogenic agent [19,20]. Formaldehyde could react with phloroglucinol in an alkaline solution [19] or an acidic medium [20] to produce colored species, which allowed the measurement of trace amounts of formaldehyde. Although the color developing reaction could be carried at room temperature with pH above 9, the authors noticed the colored species was not stable. Such a phenomenon was also observed in our lab. Gayathri and Balasubramanian [20] used a strong acidic medium (9 mol l^{-1} H_2SO_4) to carry out the chromogenic reaction between formaldehyde and phloroglucinol. Because the reaction was slow, the heat generated during the addition of concentrated H_2SO_4 was utilized to expedite the color development process. Moreover, the chromogenic species was not stable; the yellow color faded gradually immediately after reaching its maximum in a short time. Thus the operational conditions were rather harsh and hard to control repeatedly. These defects hindered the method from routine measurements of formaldehyde.

In the present paper, attempts were made to develop a rapid, sensitive and practical spectrophotometric method for the determination of formaldehyde in foodstuffs by using phloroglucinol as the chromogenic agent. Flow injection technique [21] was employed to reproducibly and precisely control the merging and reaction timing of the reagents and sample. Mild conditions were used for the reaction of color development. An intermediate orange product of the reaction was used, which could take place rapidly at room temperature, with an objective to establish a fast, simple and inexpensive method.

2. Experimental

2.1. Instrumentation

An SP-2000 spectrophotometer (Spectrum Instruments, Shanghai, China) with an 18-μl flow cell was used as the detector. The spectrophotometer was controlled and the absorbance output was recorded by a PC through its serial port. A FIAS-400 (Perkin-Elmer) flow injection system was used, which was equipped with one injection valve and two peristaltic pumps. The rotation speed of the two pumps, their stop-and-go intervals and the actuation of the valve were programmed on and controlled through an IEEE port by the same computer as used for controlling the spectrophotometer.

2.2. Reagents and standards

All chemicals used were of analytical-reagent grade. All solutions were prepared with sub-boiling distilled deionized water.

A formaldehyde stock solution was prepared according to a standard method [6]. 2.8 ml of commercially available formaldehyde aqueous solution (36–38%), Sinopharm Group, Shanghai) was diluted to 1 l of deionized water containing 0.5 ml concentrated sulfuric acid. Its precise concentration was determined using iodometric method. Working standard solutions were prepared daily by appropriate dilution of the stock solution and addition of KOH to a concentration of 0.4 mol l^{-1}. A phloroglucinol solution was prepared by dissolving 0.20 g of phloroglucinol (Merck) in 100 ml deionized water, and stored in a brown bottle.

2.3. Operating procedures

The FIA manifold is schematically shown in Fig. 1. The flow rates for the reagents and sample are illustrated in the figure. After the sample loop (400 μl) was filled with a sample in the loading step, which lasted 30 s, the injection valve was switched to the injection position to introduce the sample into the carrier stream. The injected sample was merged with the chromogenic agent. Reactions took place in the reaction coil while the mixture of the sample and reagent being transported towards the detector. When the reacting mixture entered the flow cell, i.e., 15 s after the injection valve was switched, both pumps were stopped (the so-called stopped-flow technique [21]). The stopped-flow step lasted 57 s to prolong the reaction time so as to enhance the sensitivity of measurement. The program returned to the loading step and a new analytical cycle was initiated. The sample residing in the flow cell was washed to waste and the analytical signal reached the baseline during the new loading step. In total, 102 s were required to complete an analytical run. The detection wavelength was set at 474 nm.

2.4. Sample preparation

Samples, including bean curd stick, pickled jerryfish, dry mushroom, and vermicelli, were ground. Five to 25 g of the ground sample were put into a distillation flask. Eighty millilitres deionized water, 10 ml phosphoric acid (10%), 10 g sodium sulfate and 2.5 ml paraffin liquid were added. Water vapor, generated from boiling the water in a flask, was introduced continuously into the distillation flask to distill the sample. The vapor out of the distillation flask was condensed and collected into a 250-ml round bottom flask, which was immersed into an ice-water bath. One millilitre of 1% KOH was added as

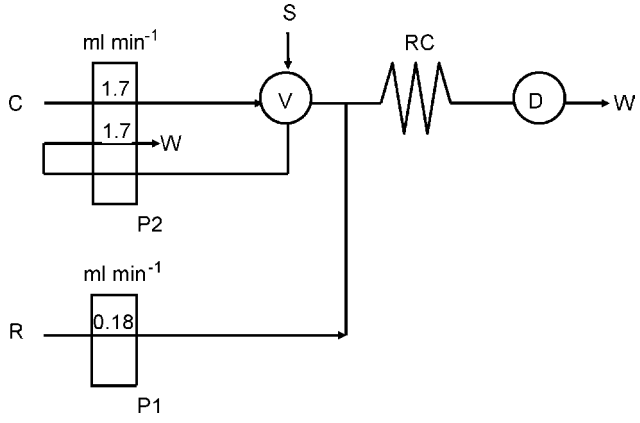


Fig. 1. Schematic diagram of FIA manifold for the determination of formaldehyde using spectrophotometric method. P1 and P2, peristaltic pumps; RC, knotted reaction coil (90 cm long, 0.7 cm i.d.); V, injector valve with a 400-ml sample loop; D, detector (λ = 474 nm); C, carrier (0.4 mol l^{-1} KOH); R, 0.2% phloroglucinol; S, standard or sample solutions; W, waste.

the absorption solution. The distillation process was stopped when ca. 80 ml of distillate were collected. The collected solution was diluted to an appropriate concentration for analysis using 0.4 mol l^{-1} KOH. Blank tests were carried out at the meantime. The sample preparation procedure lasted about 2–3 h depending upon the sample amount to be treated. Using distillation, formaldehyde can be extracted sufficiently and particularly matrix interferences can be eliminated effectively. Thus it is the most commonly used method for preparing food samples.

2.5. The standard acetylacetone method [6]

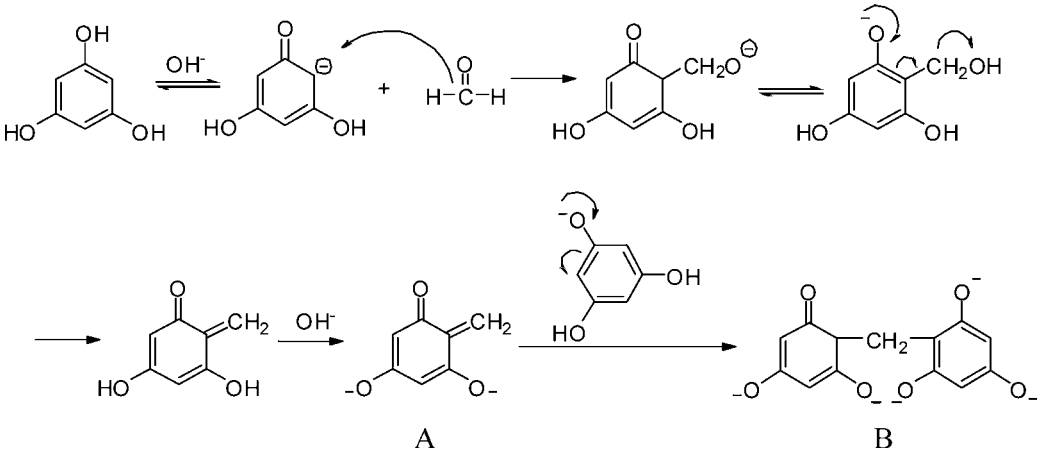
A standard method using acetylacetone as chromogenic agent was used to evaluate the accuracy of the proposed method. The method is described briefly below. The samples were treated as described in the section of samples preparation. Then 1 ml acetylacetone solution was added to the 5 ml distillate. The mixture was soaked in a water bath at 100 °C for 5 min. After cooling down to room temperature, it was measured at 435 nm against the blank of acetylacetone solution.

3. Results and discussion

3.1. The nature of chromogenic species

In the present paper, the determination of trace amounts of formaldehyde was based on the reaction between phloroglucinol and formaldehyde. The absorption spectrum indicated that an orange product with a maximum absorbance at 474 nm was formed. Thus the detection wavelength was set at 474 nm in this study. It was observed that the color development process took place immediately after the reagents and sample were mixed, as shown in Fig. 2. However, the orange color faded gradually and the solution became colorless. Because the colored product was not stable for any period of time, it was very difficult to utilize this chromogenic reaction for quantitative analysis of formaldehyde if conventional manual operation was used. However, the absorbance of the product could reach to the maximum rapidly at room temperature. This could be exploited to develop a fast analytical method by measuring the absorbance of the transient product if the measurements could be conducted at a preset timing repeatedly with satisfactory precision. In this work, the FIA technique was used to reproducibly control the timing of the reactions and measurements.

In this work, no attempt was made to study the mechanism of the chromogenic reaction and identify the color-forming species in detail. Yet, a possible reaction mechanism was proposed as shown below.



The intermediate product A might be the species responding for the transient orange color due to the conjugation of four double bonds and p electrons of two oxygen atoms. The final product B does not have great conjugation thus no color was observed. This proposal was confirmed by the following manual experiments. When extremely excessive formaldehyde reacted with phloroglucinol, the orange color did not fade. This might be because the last reaction of the whole reaction process could not continue when phloroglucinol was present insufficiently. Yet, when phloroglucinol was added excessively, the orange color faded gradually. This could be explained by that

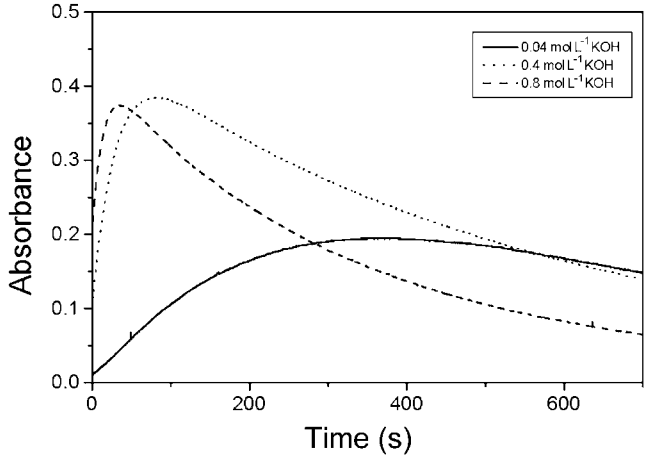


Fig. 2. Absorbance vs. stopped-flow time measuring at 474 nm, monitoring the color development of the intermediate orange product from 10.0 μg ml^{-1} CH_2O. Shortly after the sample and reagents entered the flow cell of the spectrophotometer, the FIA pumps were stopped to record the absorbance changes. Different concentrations of KOH were tested as the reaction media. Other conditions are the same as shown in Fig. 1.

the last reaction could continue when phloroglucinol was present excessively.

3.2. Optimization of FIA manifold parameters

A simple FIA manifold was used in the present study. The parameters of the FIA manifold were optimized with the objective of achieving maximum sensitivity with the current spectrophotometric method so that it could be applied to the analysis of formaldehyde in foodstuffs. In order to enhance the mixing of reagents and sample, and decrease the sample dispersion, a knotted reaction coil was used. It was made of 90 cm long PTFE tubing with 0.7 mm i.d. The knotted reactor could also eliminate effectively the Schlieren effect due to the sufficient mixing of sample and reagents before they entered the flow cell [22].

The stopped-flow technique was employed in this study to ensure the adequate reaction time and save the reagents. It could effectively decrease the dispersion, increase the sensitivity and reduce the consumption of reagents [21]. With the stopped-flow technique, it was critical to set the time for stopping pumps and the length of the stopped-flow period. Different time points from the injection of sample to the stopping of pumps were tested in this study. It was observed that the least dispersed sample plug entered the flow cell 15 s after the sample was injected. Thus at this moment the pumps stopped immediately. Various stopped-flow periods were also investigated. The absorbance reached the maximum when the pumps were stopped for 57 s. Thus a stopped-flow period of 57 s was chosen.

The flow rates of the carrier stream and reagents usually exert an important influence on the sensitivity in the conventional FIA systems. However, their influence became less significant in the present study because the stopped-flow technique was used. After optimization, flow rates of 1.7 and 0.18 ml min^{-1} were chosen for the carrier and the chromogenic agent, respectively. The flow-rate ratios of the carrier and phloroglucinol solution were set relatively high so as to reduce the dilution of sample when the carrier stream merged with the reagent, and a low flow rate of the chromogenic agent could save the reagent and produce less wastes.

The effect of sample volume on the sensitivity was examined by varying it from 100 to 500 μl. The absorbance increased sharply with increasing volumes from 100 to 400 μl, whereas only a slight increase in the peak height was observed from 400 to 500 μl. Because signal tailing could become more serious and thus a longer washing period was required if larger sample volumes were used, a sample volume of 400 μl was employed in this study.

The optimized values of the FIA manifold parameters are given in Fig. 1 and its caption.

3.3. Optimization of reaction conditions

KOH was chosen as the reaction medium in this study. Its concentration played an important role on the system's performance. As shown in Fig. 1, with lower KOH concentrations (0.04 mol l^{-1} in the figure), the reaction between phloroglucinol and formaldehyde took place slowly and the chromogenic product disappeared gradually. With higher KOH concentrations (0.4 and 0.8 mol l^{-1}), the absorbance reached maximum rapidly and so did the orange color fade. Yet, higher peak heights, i.e., better sensitivities could be achieved with higher KOH concentrations. However, KOH concentrations higher than 1.0 mol l^{-1} could cause the unstability of phloroglucinol and formaldehyde, and more importantly resulted in the difficulty to control the timing of the stopped flow due to the rapid reaction. Moreover, Schlieren effect became serious if high concentration KOH was used [22]. Therefore, 0.4 mol l^{-1} KOH was used in the present study.

The effect of phloroglucinol concentrations on the sensitivity of the method was studied over the range of 0.025–0.3%. The peak heights increased gradually with increase in phloroglucinol concentration. The response remained almost constant beyond 0.1%. Yet, higher concentrations of phloroglucinol could enhance the reaction rate of color development, thus shorten the time period of stopped flow. Therefore, 0.2% phloroglucinol was chosen for the further study.

In order to study the effect of reaction temperature, reaction coils were immersed in a temperature-controllable water bath. For the temperatures tested, i.e., 15, 17, 20, 25, 30, and 35 °C, there was no significant difference between the temperatures above 17 °C. Thus, room temperature was used for the convenience of operation.

3.4. Interference studies

The effects of potential interferences in the determination of formaldehyde by the proposed system were studied. The results shown in Table 1 indicate the general freedom from interferences.

3.5. Analytical performance and its use for practical assays

The system was calibrated with a series of formaldehyde standards having concentrations up to 10 μg ml^{-1}. Calibration graphs obeyed the equation $H = 0.00497 + 0.0400C_{CH_2O}$ ($r = 0.9998$), where H is peak-height absorbance and C_{CH_2O} is the formaldehyde concentration in μg ml^{-1}. The detection limit was 0.023 μg ml^{-1}, based on 3σ of a blank solution ($n = 11$). The relative standard deviation of the signals at a level of 7 μg ml^{-1} CH_2O was 0.29% ($n = 11$). The sample throughput was 36 h^{-1}, i.e., about 12 samples/h measured in triplicate. A typical record-

Table 1
Effect of potential interferents on the recovery of formaldehyde measurements (7.00 μg ml^{-1})

Interferents	Concentration (mg l^{-1})	Recovery (%)
Phenol	5600	98
CH_3COO^-, NH_4^+, NO_2^-	3500	98, 103, 100
Ethanol	1400	96
SO_4^{2-}	700	98
Methanol, acetaldehyde	35	99, 102
Acetone, furfuraldehyde, glucose	7000	96, 103, 99

All results are averages of three measurements with 1–2% R.S.D.

Table 2
Analytical results of some preserved foodstuffs and recovery tests by proposed method[a]

No.	Sample	Measured concentration ($\mu g\,g^{-1}$)		Recovery (%)	
		Present method	AHMT method	Present method	AHMT method
1	Bean curd stick	264 ± 1.1	271 ± 3.8	94.5	91.4
2	Preserved jerryfish	58.8 ± 0.23	58.1 ± 0.46	99.3	96.6
3	Dry mushroom	340 ± 1.5	334 ± 4.0	98.5	101
4	Vermicelli 1	20.1 ± 0.083	20.3 ± 0.30	98.1	99.0
5	Vermicelli 2	3.20 ± 0.014	3.09 ± 0.068	95.6	96.8

[a] The measurements were run in triplicate. For the recovery tests, 5–10 $\mu g\,l^{-1}$ formaldehyde was spiked after the distillates of foodstuff samples were diluted appropriately.

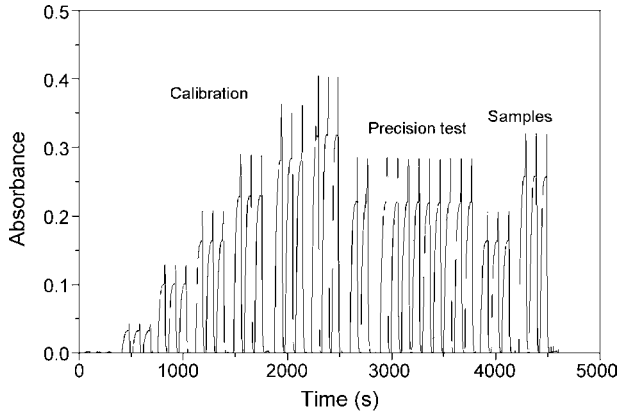


Fig. 3. Recorded tracings for a series of formaldehyde standard solutions, precision test ($\mu g\,ml^{-1}$) and analyses of two samples using optimized conditions. The concentrations of standard were 0, 1.00, 3.00, 5.00, 7.00, 9.00, and 10.0 $\mu g\,ml^{-1}$, respectively.

ing of the analyses of a standard series and samples is shown in Fig. 3.

The practical feasibility of the proposed system was tested on several foodstuff samples. The results are shown in Table 2 and recoveries of the spiked samples are generally satisfactory. The accuracy of the proposed system was evaluated by analyzing the samples with a national standard method. The results were in good agreement with those obtained with the standard method.

4. Conclusion

The developed FIA spectrophotometric method was applied successfully on the determination of formaldehyde in foodstuffs. By using phloroglucinol as the chromogenic agent, the color development reaction could be conducted easily at room temperature. The FIA system used made it possible to quantitatively analyze formaldehyde by measuring the unstable intermediate orange product of the reaction between formaldehyde and phloroglucinol. This could not only automate the analytical procedure and improve the system precision but also decrease the consumption of reagents and samples greatly. Therefore, comparing with other reported spectrophotometric methods, the proposed method was characterized by low cost, high analytical frequency and simple system configuration. These made the system promising to be used in routine analysis applications.

Acknowledgements

The National Natural Science Foundation of China is thanked for financial support (Project Nos. 20345006 and 20575043). The authors are grateful to Professor Jianping Zhou and Mr. Chengrong Lu for their valuable suggestions on the reaction mechanism.

References

[1] R.G. Liteplo, R. Beauchamp, M.E. Meek, R. Chénier, Concise International Chemical Assessment Document 40, World Health Organization, Geneva, 2002.
[2] National Hygienic Standards for the Usage of Food Additives, GB 2760-1996, Standardization Administration of China, 1996.
[3] E. Sawicki, T.R. Hauser, S. McPherson, Anal. Chem. 34 (1962) 1460.
[4] L. Gamiz-Gracia, M.D. Luque de Castro, Analyst 124 (1999) 1119.
[5] H. Tsuchiya, S. Ohtani, K. Yamada, M. Akagiri, N. Takagi, M. Sato, Analyst 119 (1994) 1413.
[6] Standard Method for Indoor Air Quality Measurement, GB/T 18883-2002, Chinese Standardization Administration of China, 2002.
[7] M.S. Qoesenberry, Y.C. Lee, Anal. Biochem. 234 (1996) 50.
[8] E.A. Pereira, P.K. Dasgupta, Int. Environ. J. Anal. Chem. 66 (1997) 201.
[9] M.K.L. Bicking, W.M. Cooke, F.K. Kawahara, J.E. Longbottom, J. Chromatogr. 455 (1988) 310.
[10] D. Pierotti, J. Atmos. Chem. 10 (1990) 373.
[11] L. Nondek, R.E. Milofsky, J.W. Birks, Chromatographia 32 (1991) 33.
[12] Q. Li, M. Oshima, S. Motomizu, Talanta 72 (2007) 1675.
[13] F. Santos de Oliveira, E.T. Sousa, J.B. de Andrade, Talanta 73 (2007) 561.
[14] Z.-Q. Zhang, H. Zhang, G.-F. He, Talanta 57 (2002) 317.
[15] C. Zhao, M. Li, K. Jiao, J. Anal. Chem. 61 (2006) 1204.
[16] K. Toda, K. Yoshioka, K. Mori, S. Hirata, Anal. Chim. Acta 531 (2005) 41.
[17] K. Kawamura, K. Kerman, M. Fujihara, N. Nagatani, T. Hashiba, E. Tamiya, Sens. Actuators B 105 (2005) 495.
[18] L. Campanella, M. Battilotti, R. Dragone, I. Mevola, Int. J. Environ. Pollut. 27 (2006) 313.
[19] K.N. Ramachandran, V.K. Gupta, Chem. Anal. 38 (1993) 513.
[20] N. Gayathri, N. Balasubramanian, Anal. Lett. 33 (14) (2000) 3037.
[21] J. Ruzicka, E.H. Hansen, Flow Injection Analysis, 2nd ed., John Wiley & Sons, New York, 1988.
[22] Z. Fang, Flow Injection Separation and Preconcentration, VCH, Weinheim, 1993, p. 39.

Available online at www.sciencedirect.com
ScienceDirect
Talanta 74 (2008) 915–921
Talanta
www.elsevier.com/locate/talanta

Simultaneous determination of arsenic, antimony, bismuth and mercury in geological materials by vapor generation-four-channel non-dispersive atomic fluorescence spectrometry

Zhongxi Li *, Xiaoming Yang, Yuean Guo, Haitao Li, Yuhuan Feng

The Research Center of Analytical Technique & Instrument, Northwest Geological Research Institute, No. 25 Xiying Road, Xi'an 710054, PR China

Received 7 June 2007; received in revised form 26 July 2007; accepted 27 July 2007
Available online 3 August 2007

Abstract

Chemical vapor generation (CVG) coupled with non-dispersive atomic fluorescence spectrometry (NDAFS) has been widely used for determination of vapor-forming elements, but most of such works have been focused on single element analysis, and reports dealing with more than three elements simultaneous determination by CVG-NDAFS are rare. In this work, a sensitive and robust analytical procedure for the simultaneous determination of arsenic, antimony, bismuth and mercury in geological materials using vapor generation-four-channel non-dispersive atomic fluorescence spectrometry has been developed. The conditions of instrumentation and vapor generation of arsenic, antimony, bismuth and mercury were optimized. The optimized concentrations of KBH_4 and HCl required for analytes generation were 1.3% (m/v) and 20% (v/v), respectively. The interferences of coexisting ions and mutual hydride interferences were investigated carefully. One thousand milligrams per litre of Fe^{3+}; 500 mg l^{-1} of Pb^{2+}, Zn^{2+}, Mn^{2+}; 50 mg l^{-1} Cu^{2+}, Ni^{2+}, Cr^{6+}, Co^{2+}; 10 mg l^{-1} Ag^{+} and 5 mg l^{-1} Au^{3+} does not interfere with the determination of As, Sb, Bi and Hg. Associating a dilution of 1:250 (m/v) in the procedure of sample pretreatment, the tolerant concentrations of As, Sb, Bi and Hg in real geological materials are 2500, 1000, 250 and 5000 ppm, respectively. Under optimal conditions, the detection limits for As, Sb, Bi and Hg were determined to be 0.068, 0.047, 0.037 and 0.008 ng ml^{-1}, respectively. The precisions for seven replicate determinations at the 5 ng ml^{-1} of As, Sb, Bi and 1 ng ml^{-1} of Hg were 0.47, 0.60, 0.97 and 0.93% (R.S.D.), respectively. Sample digestion was carried out on 500 mg sample with 3 ml HNO_3 and 10 ml HCl, followed by addition of thiourea solution for the quantitative reduction of As(V), Sb(V) to As(III), Sb(III). The proposed method was successfully applied to the simultaneous determination of As, Sb, Bi and Hg in a series of certified geological reference materials using simple aqueous standard calibration technique. The results obtained are in good agreement with the certified values.
© 2007 Elsevier B.V. All rights reserved.

Keywords: Vapor generation; Four-channel non-dispersive atomic fluorescence spectrometer; Arsenic, antimony, bismuth and mercury; Simultaneous determination; Geological materials

1. Introduction

It is well-known that some elements like As, Sb, Bi and Hg are used in mineral exploration as pathfinders for epithermal precious metal and base metal deposits. In addition, the determination of As, Sb, Bi and Hg in environmental systems are gaining increasing importance, mainly because of the toxic characteristics of these elements. At the Geological Survey of PR China, the use of chemical vapor generation-double-channel atomic fluorescence spectrometry is recommended to determine these elements in geological samples (including rocks, soils and sediments) with the analysis of over three hundred thousand samples per annum this restriction to single or double-element analysis results in near one million determinations. While this technique has served well in analysis for As, Sb, Bi and Hg, it has shortcoming of single or

* Corresponding author. Fax: +86 29 88138203.
E-mail address: lizhongxi8@163.com (Z. Li).

0039-9140/$ – see front matter © 2007 Elsevier B.V. All rights reserved.
doi:10.1016/j.talanta.2007.07.028

double-element analysis. There is a need for methods for the simultaneous determination of these elements in a variety of matrices, which are simple, rapid, accurate and low detection limits.

Chemical vapor generation (CVG) presently can be considered as one of the most popular sample introduction technique for the determination of trace and ultra-trace amounts of As, Sb, Bi, Se, Te, Ge, Sn, Pb, Hg, Cd and Zn in combination with various atomic spectrometry such as atomic absorption spectrometry (AAS), atomic fluorescence spectrometry (AFS), inductively coupled plasma atomic emission spectrometry (ICP-AES) and inductively coupled plasma mass spectrometry (ICP-MS) [1–4]. However, chemical vapor generation methods were mainly developed and applied for single element measurements. The first successful hyphenated technique for simultaneous multi-element determinations of vapor-forming elements was performed in combination with ICP-AES in 1978 [5]. For the same technique, several multi-element applications were described in the following years [6–10]. However, the higher detection limits its use in the analysis of real samples. More recently, ICP-MS [11–13] has been used instead of ICP-AES for its high sensitivity and excellent detection. But it is not easy to apply the method for the determination of trace As and Se because of the serious interferences from polyatomic ions, e.g., $^{75}ArCl^+$ interferes with the isotope of $^{75}As^+$ and $^{80}ArAr^+$ overlap the isotope of $^{80}Se^+$; of course, with the introduction of commercial simultaneous multi-element graphite furnace atomic absorption spectrometry (MEGFAAS) instrumentation, further work appeared in this field applying in situ trapping GFAAS [14–16]. In addition, hydride generation microwave-induced plasma optical emission (HG-MIP-OES) [17] and hydride generation inductively coupled plasma time-of-flight mass spectrometry (HG-CP-TOFMS) [18,19] were also used for the simultaneous multi-element determination of vapor-forming elements. However, either ICP-MS, multi-element GFAAS, MIP-OES or ICP-TOFMS, the higher purchase price of instruments is not always bearable by most of the common laboratories.

CVG-NDAFS might be preferred to other analytical techniques for determination of vapor-forming elements because of its high sensitivity, wide linear dynamic range, speed of analysis, ease of use and low cost of instrumentation; at the same time, the possibility of multi-element simultaneous determination is the main advantage of atomic florescence spectrometry. However, a literature survey revealed that most of previous works concentrated on single or double-element analysis because of the lack of suitable multi-channel NDAFS [20–26].

In the last few years, our research group has dedicated to design the chemical vapor generation-multi-channel non-dispersed atomic fluorescence spectrometer (CVG-MC-NDAFS) [27] and studied the analytical methods for simultaneous multi-element determination of vapor-forming elements using this instrument [28]. In this work, a sensitive VG-four-channel NDAFS method was developed for simultaneous determination of As, Sb, Bi and Hg in geological materials. Optimization of the VG system for the simultaneous determination of these elements was studied carefully. The interferences caused by transition metals and mutual hydrides were studied in detail. The developed method was successfully applied to the simultaneous determination of trace amount of As, Sb, Bi and Hg in geological samples.

2. Experimental

2.1. Instrumentation

A self-designed four-channel non-dispersive atomic fluorescence spectrometer fitted with a programmable intermittent reactor was employed throughout this work. Details about the construction of the instrument can be found in Ref. [28]. The As, Sb, Bi and Hg hollow cathode lamps with a period of 30 μs for the modulated pulse that were specially designed for AFS were used as the radiation sources so that high lamp currents could be applied for generating a high intensity of radiation. The lamps were operated in a four-modulated mode to discriminate the fluorescence signals of the four elements. As, Sb, Bi and Hg lamps were operated at 50, 60, 60 and 20 mA, respectively. A model R7154 "solar blind" photomultiplier was used as the detector in the non-dispersive detection system; a voltage of 300 V was used in this work. A schematic diagram of the intermittent reactor is described in Ref. [29]. The working program of the intermittent reactor is described in Table 1. An electrically heated quartz furnace [30] was used as the atomizer into which the volatile species and the hydrogen evolved from the reactor were swept by an argon flow. The gas mixture was self-ignited at the outlet of the furnace, and a hydrogen–argon–air-entrained flame was maintained without the addition of any auxiliary hydrogen. Peak area was used for evaluating the results throughout the work.

2.2. Reagents

For the preparation of all solutions, high purity water (18.2 MΩ cm) from a Milli-Q system (Millipore, Milford, MA, USA) was used. Chemicals used for digestions were: nitric acid (65%, highest available purity, Xi'an Chemical Reagent Co., China), hydrochloric acid (32%, highest available purity, Xi'an Chemical Reagent Co., China). For the HG system coupled to AFS, 5% (v/v) HCl as carrier solution was prepared from hydrochloric acid. 1.3% (m/v) KBH_4 was prepared daily by dissolving appropriate amounts of powdered KBH_4 (analytical-reagent grade, Tianjin Institute of Chemical Reagents, China) in 0.2% (m/v) KOH (analytical-reagent grade, Beijing Chemical Reagent Co., China). Single-element stock solutions of 1.0 g l^{-1} of As, Sb, Bi and Hg, commercial standard solutions (National standard material center of China) were used. Working standard solutions of As, Sb, Bi and Hg were prepared by stepwise dilution of the stock solutions just before use. As(V) and Sb(V) were reduced to As(III) and Sb(III) with 0.5% (m/v) thiourea (analytical reagent grade, Xi'an Chemical Reagent Co., China). Two percent (m/v) tartaric acid was prepared by dissolving appropriate amounts of powdered tartaric acid (analytical reagent grade, Xi'an Chemical Reagent Co.,

Table 1
Working program for the intermittent flow reactor

Step	Flow rate (ml min^{-1})	Time (s)	Function
1	Sample: 6, reductant (1.3% (m/v) KBH_4): 6	8	Insertion of sampling tube into sample solution
2	Sample: 0, reductant (1.3% (m/v) KBH_4): 0	3	Change over of sampling tube into carrier solution
3	Carrier (0.5 mol l^{-1} HCl):7.2, reductant (1.3% (m/v) KBH_4): 7.2	14	Readout
4	Carrier (0.5 mol l^{-1} HCl):0, reductant (1.3% (m/v) KBH_4): 0	3	Return to step 1

China) to prevent the hydrolyzation of Sb in sample preparation step.

2.3. Procedure

The test solutions containing 10 ng ml^{-1} of As, Sb, Bi and 2 ng ml^{-1} of Hg were used for optimization studies of: carrier gas flow rate; shield gas flow rate; HCl concentration; and KBH_4 concentration.

The mutual interferences of As, Sb, Bi and Hg by VG-AFS method were carefully investigated. For study the interference from As, various concentrations of As were added into several standard solutions of 10 ng ml^{-1} of Sb, Bi and 2 ng ml^{-1} of Hg; and the solutions were determined by HG-AFS and signal intensities of Sb, Bi and Hg were obtained. In the same way, the interferences from Sb, Bi and Hg were also investigated.

Transition metal interferences in the determination of As, Sb, Bi and Hg by VG-AFS method were also investigated; and according the characteristic of geological samples, Fe, Cu, Pb, Zn, Co, Ni, Cr, Mn, Au and Ag were selected as the interfering ions. The procedure involved spiking a standard solution of 10 ng ml^{-1} of As, Sb, Bi and 2 ng ml^{-1} of Hg in 20% (v/v) HCl and the presence of 0.5% (m/v) thiourea with various concentrations of Fe, Cu, Pb, Zn, Co, Ni, Cr, Mn, Au and Ag. These solutions were determined and the signal intensities of As, Sb, Bi and Hg were obtained. The recoveries were calculated by comparison with the As, Sb, Bi and Hg standard without the interfering ions.

2.4. Sample pretreatment

Aliquots 500 mg of powdered geological samples such as rocks, soils and sediments were weighted into a 50 ml glass beaker. Three millilitres of nitric acid was first added to the powders and gently shaken to mix the contents, followed by addition of 10 ml of hydrochloric acid. Then covered with glass and gently heated on a hot plate for about 90 min. After cooling for about 15 min, 5 ml of 2% (m/v) tartaric acid was added to prevent the hydrolyzation of Sb in the step of dilution and the solution was transferred to a 25 ml volumetric flask; and then diluted to volume with water. After 2 h, 2 ml of the clear supernatant was transferred to a 10 ml volumetric flask, to which 2 ml of 50% (v/v) HCl and 1 ml of 5% (v/v) thiourea were added and diluted to volume with water. After 30 min, the sample was reacted with KBH_4 to generate the gaseous species, which were carried into the AFS instrument for determination.

3. Results and discussion

3.1. Optimization of AFS instrument parameters

Pure argon was used as the carrier gas and the influence of the carrier gas flow rate on the signal response of the four vapor-forming elements was studied and the results are shown in Fig. 1. It can be clearly seen that the signal intensity of Sb decreased with increasing carrier gas flow rate. There was a maximum of the signal intensities at the flow rate of carrier gas (250–350 ml min^{-1} for As, 300–400 ml min^{-1} for Bi and 200–350 ml min^{-1} for Hg). At lower flow rates, the signal intensities increased with the flow rate of the carrier gas. However, at higher flow rates, the dilution of the evolved volatile species and short residue of the analyte species in the atomizer would be dominant, leading to the decrease of the signal densities. Therefore, an argon flow rate of 300 ml min^{-1} was used as carrier gas.

In this work, an argon shield gas was employed to prevent extraneous air from entering the flame in order to increase the fluorescence efficiency. The relationship between the flow rate of shield gas and the normalized intensities of As, Sb, Bi and Hg is shown in Fig. 2. It can be clearly seen that there is a maximum of the signal intensities for As at 800–850 ml min^{-1}, for Sb at 800 ml min^{-1}, for Bi at 1000 ml min^{-1} and for Hg at 850–1000 ml min^{-1}. Considering the sensitivities of As, Sb, Bi and Hg, an argon flow rate of 800 ml min^{-1} shield gas was used as a compromise.

Observation height is the distance from the quartz furnace outlet to the point where the atomic fluorescence signal is mea-

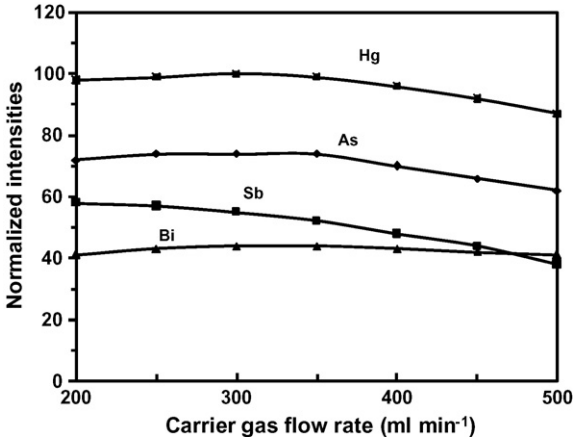


Fig. 1. The effect of carrier gas (Ar) flow rate on the normalized intensities of As, Sb, Bi and Hg. Ten nanograms per millilitre of As, Sb, Bi and 2 ng ml^{-1} of Hg; shield gas flow rate: 800 ml min^{-1}.

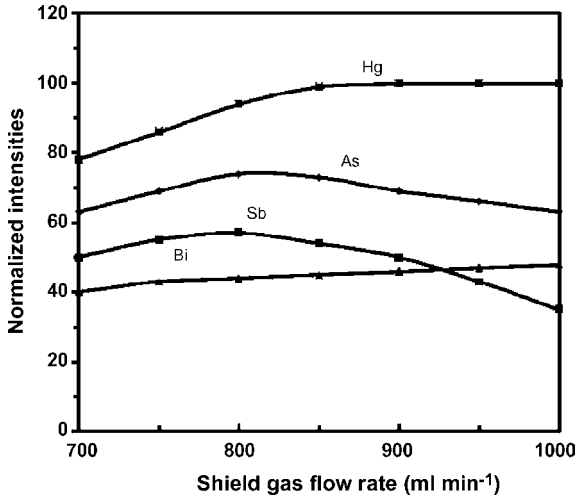


Fig. 2. The effect of shield gas (Ar) flow rate on the normalized intensities of As, Sb, Bi and Hg. Ten nanograms per millilitre of As, Sb, Bi and 2 ng ml^{-1} of Hg; carrier gas flow rate: 300 ml min^{-1}.

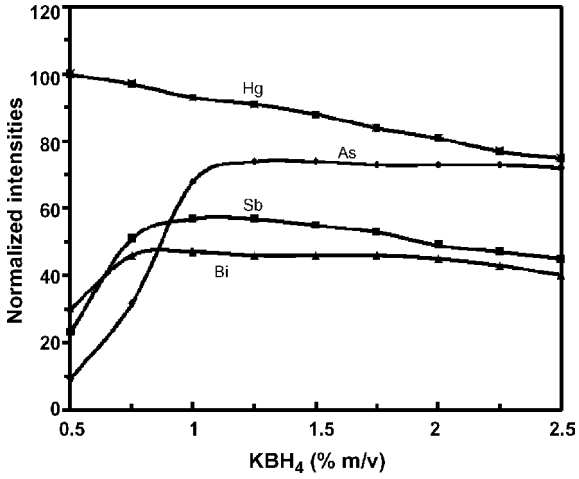


Fig. 3. The effect of KBH_4 concentrations on the normalized intensities of As, Sb, Bi and Hg. Ten nanograms per millilitre of As, Sb, Bi and 2 ng ml^{-1} of Hg in 20% (v/v) HCl solution containing 0.5% (m/v) thiourea.

sured. The effect of varying observation height on the signal for As, Sb, Bi and Hg was studied. The signal of As reduced with an increase in the observation height from 5 to 10 mm; and the fluorescence signal of Sb remarkably increased with the observation height increase from 5 to 8 mm; and the fluorescence signal intensities of Hg and Bi almost leveled off between the observation height from 5 to 10 mm. However, the noise of the background signal also increased with a decrease in observation height for the bad scattering from the furnace top and the flame root. For further experiments, an observation height of 7 mm was used as a compromise.

3.2. Optimization of chemical variables

In the CVG-AFS system employed, KBH_4 is used not only as the reductant, but also as the hydrogen supply to sustain the argon–hydrogen flame. The concentration of KBH_4 had a large impact on the vapor generation process and the argon–hydrogen flame. Optimization of KBH_4 concentration was carried out between 0.5 and 2.5% (m/v). Fig. 3 illustrates the effect of the concentration of KBH_4 on the signal intensities of As, Sb, Bi and Hg. Generation of AsH_3 could be carried out with KBH_4 concentrations ranging from 0.5 to 2.5%, but the sensitivity decreased rapidly when KBH_4 concentrations were below 1.25%. The fluorescence intensity remained constant when the KBH_4 concentration was increased from 1.25 to 2.5%. Generation of SbH_3 could be carried out with KBH_4 concentrations ranging from 0.5 to 2.5%, but the sensitivity decreased rapidly when KBH_4 concentrations were below 1.0%. The fluorescence intensity remained constant when the KBH_4 concentration was increased from 1.0 to 1.5%. At higher KBH_4 concentrations (2.0%), the fluorescence intensity slowly dropped. Generation of BiH_3 could be carried out with KBH_4 concentrations ranging from 0.5 to 2.5%, but the sensitivity decreased rapidly when KBH_4 concentrations were below 0.75%. At higher KBH_4 concentrations (1.0%), the fluorescence intensity slowly dropped. Lower concentrations of KBH_4 could be fitted for generation of Hg vapor. The signal intensity of Hg decreased with increasing KBH_4 from 0.5 to 2.5%. It is well known that some additional drawbacks such as causing very noisy background, taking more water vapor to atomization and bringing higher standard deviation, hamper the performance of the CVG-AFS system when the concentrations of KBH_4 are too high. 1.3% KBH_4 was chosen for further experiments because it provided the optimum signal to noise ratios for As, Sb, Bi and Hg.

The generation efficiency of the volatile species greatly depends upon the acidity at which the reaction is performed. Using 1.3% KBH_4 as reductant and the flow rate of sample being designed to be approximately equality that of the potassium tetrahydroborate flow rate, the effect of various HCl concentrations on signal intensities was investigated within the range of 5–30% and the results are shown in Fig. 4. As shown in Fig. 4, an HCl concentration of 15–30% yielded a response plateau wherein the best results were obtained for As and Sb; and the observed Bi and Hg signal intensities were virtually unaltered

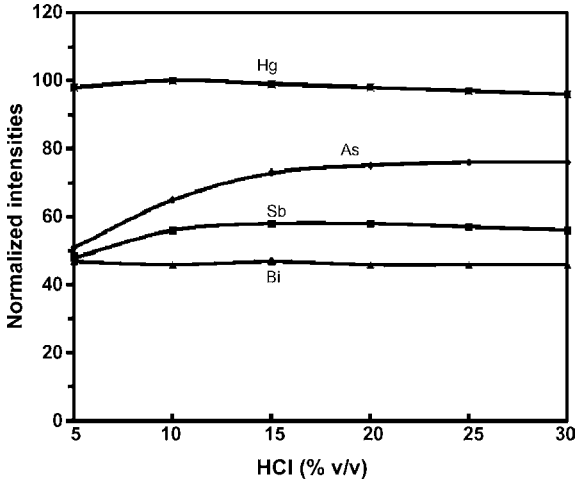


Fig. 4. The effect of HCl concentrations on the normalized intensities of As, Sb, Bi and Hg. Ten nanograms per millilitre of As, Sb, Bi and 2 ng ml^{-1} of Hg in 0.5% (m/v) thiourea; 1.3% (m/v) KBH_4 in 0.2% (m/v) KOH as reductant.

in the acid range studied. However, the reagent background was increased with the increase of HCl concentration. Therefore, a concentration of 20% HCl, which was near the lower edge of the optimization plateau, was chosen as the final working value.

3.3. Pre-reduction

The importance of selecting suitable pre-reduction procedures to quantitatively convert As^{5+} and Sb^{5+} to As^{3+} and Sb^{3+} should not be disregarded. The most commonly used reducing agents are iodide, L-cysteine and thiourea. However, Chen et al. [31] reported that the performance of L-cysteine for As^{5+} pre-reduction was hardly satisfying. Otherwise, the use of thiourea is not only as reducing agent to reduce As^{5+} and Sb^{5+} but also as masking reagent to eliminate the interferences from transition metal. Using 30 min as reducing time, a series of thiourea solutions of different concentrations (0–1.0%, m/v) was tested in order to investigate: (1) the appropriate amount of thiourea necessary for the quantitative pre-reduction of As^{5+} and Sb^{5+} to As^{3+} and Sb^{3+}; (2) the effect of thiourea concentration on the determination of Bi and Hg. The results are illustrated in Fig. 5.

As shown in Fig. 5, at least 0.3 and 0.2% of thiourea were needed to achieve complete reduction of As and Sb in the standard solution, respectively. The presence of thiourea could slightly suppress the signal of Hg. The signal of Bi remained constant when the concentrations of the thiourea were in the range of 0–1.0%. However, the solutions of digested samples contain large numbers of oxidizing ions such as NO_3^+, NO_2^+ and Fe^{3+}. Considering the pre-reduction procedures of As and Sb, difference between the standard solutions and the real sample solutions, three geological standard reference materials were used and further experiments were carried out by applying thiourea to analyte solutions of digested samples. These experiments revealed that higher concentration of thiourea (0.5%, m/v) was needed for complete pre-reduction of As and Sb under oxidising conditions. Therefore, a concentration of 0.5% thiourea was chosen as for the pre-reduction throughout this work.

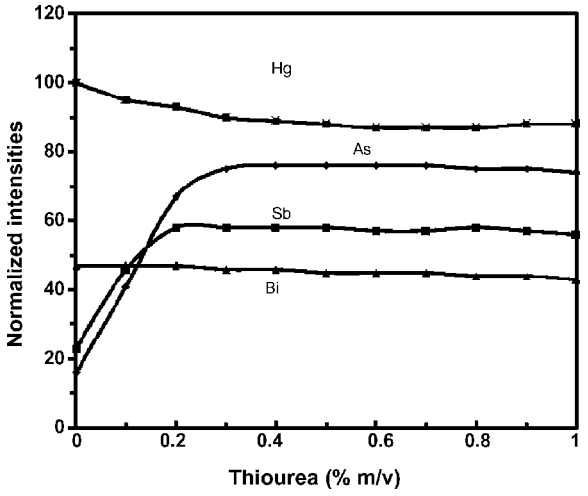


Fig. 5. The effect of thiourea concentrations on the normalized intensities of As, Sb, Bi and Hg. Ten nanograms per millilitre of As, Sb, Bi and 2 ng ml^{-1} of Hg; 30 min reducing time; 1.3% (m/v) KBH_4 in 0.2% (m/v) KOH as reductant.

3.4. Interferences studies

The potential interfering effects of 10 metals at various concentration levels were thus investigated in the presence of 0.5% thiourea. The results show that 1000 mg l^{-1} of Fe^{3+}; 500 mg l^{-1} of Pb^{2+}, Zn^{2+}, Mn^{2+}; 50 mg l^{-1} Cu^{2+}, Ni^{2+}, Cr^{6+}, Co^{2+}; 10 mg l^{-1} Ag^+ and 5 mg l^{-1} Au^{3+} does not interfere with the determination of As, Sb, Bi and Hg under the optimal chemical conditions within the error range of ±5%. The contents of the aforementioned metals in the majority geological samples are well within the tolerant concentration range by using the present samples preparation protocol.

Mutual vapor-forming element interference is a well-known phenomenon in vapor generation coupled techniques [32–34]. In this work, the mutual interferences in the determination of As, Sb, Bi and Hg by vapor generation atomic fluorescence spectrometry were studied. The interference work is defined as an effect causing a positive or negative change in the analyte signal within the error range of ±5%. The mutual interferences can be summarized as follows: (1) no interferences were evident in the measurement of Sb, Bi and Hg in the presence of 0–10 μg ml^{-1} of As. However, further increase in the concentration of As, the intensities of Sb, Bi and Hg were depressed slightly; (2) Sb caused a dramatic decrease of the As signal, the sensitivity of As was depressed badly when the concentration of Sb up to 4 μg ml^{-1}; and it is interesting that the interfering degree is less severe for Sb from As compared with As from Sb. However, there was no interference on Bi and Hg from Sb at levels up to 10 μg ml^{-1}; (3) the interferences from Bi were the most serious, increasing concentrations of Bi up to 1 μg ml^{-1} led to a suppression of the signals of As and Sb (about 10%); and with further increase in the concentration of Bi, the intensities of As and Sb became essentially constant. However, the intensity of Hg continuously decreased when the concentration of Bi was up to 4 μg ml^{-1}; (4) no interferences were evident in the measurement of As, Sb and Bi in the presence of 0–10 μg ml^{-1} of Hg.

Associating a dilution of 1:250 (m/v) in the procedure of sample pretreatment, the tolerant concentrations of As, Sb, Bi and Hg in real geological materials are 2500, 1000, 250 and 5000 ppm, respectively. It is well known that the contents of As, Sb, Bi and Hg in the majority geological samples are under their tolerant concentrations. Thereby, the mutual interferences are not of concern for the analysis of geological materials by VG-AFS. If the interferers were high in mineralized samples, then it is probable that As, Sb, Bi and Hg would also be determined and dilution could be used to negate interference.

3.5. Analytical characteristics

The analytical characteristics of the developed method are summarized in Table 2. It should be noted that the analytical characteristics (including calibration functions, detection limits and precision) for simultaneous determination of As, Sb, Bi and Hg were in good agreement with those for individual determination of the four elements under the same operation conditions, indicating that the proposed method for simultaneous determi-

Table 2
Detection limits, precision and calibration functions for determination of As, Sb, Bi and Hg using the proposed method

Measurement method	Element	Calibration functions[a]	Correlation coefficient	R.S.D. (%)[b]	LOD[c] (ng ml^{-1})
Simultaneous determination	As	I_f[d] = 13.2 + 184.9C_{As}[e]	0.9985	0.47	0.068
	Sb	$I_f = -6.9 + 143.5C_{Sb}$	0.9982	0.60	0.047
	Bi	$I_f = 0.9 + 110.7C_{Bi}$	0.9992	0.97	0.037
	Hg	$I_f = 77.2 + 1387.4C_{Hg}$	0.9996	0.93	0.008
Single element determination	As	$I_f = 11.7 + 187.3C_{As}$	0.9990	0.61	0.062
	Sb	$I_f = -4.3 + 145.6C_{Sb}$	0.9984	0.72	0.042
	Bi	$I_f = -1.3 + 109.3C_{Bi}$	0.9991	0.89	0.041
	Hg	$I_f = 66.2 + 1363.9C_{Hg}$	0.9993	0.91	0.006

[a] Five sets of calibration curves (As, Sb and Bi concentrations range from 0.5 to 20 ng ml^{-1}, Hg concentrations range from 0.1 to 4 ng ml^{-1}).
[b] Relative standard deviation for 5 ng ml^{-1} As, Sb, Bi and 1 ng ml^{-1} of Hg ($n = 7$).
[c] $3\sigma_{n-1}$ of 11 runs of the blank.
[d] Signal intensity.
[e] Concentration (ng ml^{-1}).

Table 3
The results for the determination of As, Sb, Bi and Hg in the certified reference materials

CRMs	Element	Certified value (μg g^{-1})	Found value (μg g^{-1})
GBW07104 (rock)	As	2.1 ± 0.4	2.0 ± 0.1
	Sb	0.12 ± 0.04	0.12 ± 0.01
	Bi	0.081 ± 0.016	0.08 ± 0.01
	Hg	0.0041 ± 0.0012	0.005 ± 0.002
GBW07106 (rock)	As	9.1 ± 1.2	8.8 ± 0.3
	Sb	0.60 ± 0.11	0.57 ± 0.03
	Bi	0.18 ± 0.03	0.17 ± 0.01
	Hg	0.008 ± 0.002	0.009 ± 0.002
GBW07304 (marine sediment)	As	19.7 ± 1.7	20.8 ± 1.0
	Sb	1.84 ± 0.18	1.84 ± 0.05
	Bi	0.60 ± 0.10	0.64 ± 0.04
	Hg	0.044 ± 0.008	0.047 ± 0.005
GBW07310 (marine sediment)	As	25 ± 3	24.8 ± 0.9
	Sb	6.3 ± 0.6	6.42 ± 0.26
	Bi	0.38 ± 0.04	0.36 ± 0.02
	Hg	0.28 ± 0.03	0.29 ± 0.02
GBW07404 (soil)	As	58 ± 6	56.3 ± 2.7
	Sb	6.3 ± 1.1	6.64 ± 0.39
	Bi	1.04 ± 0.13	0.98 ± 0.06
	Hg	0.59 ± 0.05	0.60 ± 0.03
GBW07408 (soil)	As	12.7 ± 1.1	12.8 ± 0.8
	Sb	1.0 ± 0.2	1.06 ± 0.07
	Bi	0.30 ± 0.04	0.29 ± 0.01
	Hg	0.017 ± 0.003	0.018 ± 0.003

nation of As, Sb, Bi and Hg is reliable. From Table 2, it can be clearly seen that the analytical characteristics of the present method are at the same levels as compared with those of the single element determination. Compared with the established atomic fluorescence spectrometric methods, the main advantage of the present method is that the analytical speed is enhanced at least three times for the simultaneous determination of As, Sb, Bi and Hg.

In order to demonstrate the accuracy of the present method, we applied it to the simultaneous determination of As, Sb, Bi and Hg in the following geological certified reference materials (Institute of Geophysical and Geochemical Exploration, Langfang, China): two certified rock reference materials (GBW07104 and GBW07106), two certified marine sediment reference materials (GBW07304 and GBW07310) and two certified soil reference materials (GBW07404 and GBW07408). The results for the simultaneous determination of As, Sb, Bi and Hg in these certified reference materials (CRMs) are shown in Table 3. All mean values and standard deviations are the results of three independent digestions of the certified reference materials followed by the simultaneous determination of As, Sb, Bi and Hg by VG-four-channel atomic fluorescence spectrometry. As can be clearly seen from Table 3, the results for those elements in the various samples agreed well with the certified values. Even though the certified concentrations of As, Sb, Bi and Hg in GBW07104 are very low.

4. Conclusions

This work demonstrated the feasibility for simultaneous determination of trace As, Sb, Bi and Hg in geological samples by VG-four-channel NDAFS. The developed method is simple, fast and sensitive and is promising for routine analysis of trace As, Sb, Bi and Hg in geological materials.

References

[1] J. Dedina, D.L. Tsalev, Hydride Generation Atomic Absorption Spectrometry, John Wiley, Chichester, 1995.
[2] D.L. Tsalev, J. Anal. Atom. Spectrom. 14 (1999) 147.
[3] P. Pohl, Trends Anal. Chem. 24 (2004) 81.
[4] M.L. Chen, A.M. Zou, Y.L. Yu, R.H. He, Talanta 73 (2007) 599.
[5] M. Thompson, B. pahlavanpour, S.J. Walton, G.F. Kirkbright, Analyst 103 (1978) 568.
[6] L. Zhang, X.Q. Shan, Z.M. Ni, Fresenius J. Anal. Chem. 332 (1988) 764.
[7] P. Pohl, W. Zyrnicki, Anal. Chim. Acta 468 (2002) 71.
[8] P. Pohl, A. Lesniewicz, W. Zyrnicki, Int. J. Environ. Anal. Chem. 83 (2003) 963.
[9] I. Rojas, M. Murillo, N. CarriÓn, J. Chirinos, Anal. Bioanal. Chem. 376 (2003) 110.
[10] H. matusiewicz, M. Ślachciński, Microchem. J. 86 (2007) 102.
[11] Z.F. Zhang, S.Y. Chen, H.M. Yu, M. Sun, W.Q. Liu, Anal. Chim. Acta 513 (2004) 417.
[12] A.S. Ribeiro, M.A. Vieira, A.J. Curtius, Spectrochim. Acta B 59 (2004) 243.
[13] M.A. Vieira, A.S. Ribeiro, L.F. Dias, A.J. Curtius, Spectrochim. Acta B 60 (2005) 643.
[14] R.E. Sturgeon, S.N. Willie, G.I. Sproule, P.T. Robinson, S.S. Berman, Spectrochim. Acta B 44 (1989) 667.
[15] J. Moreda-Piñeiro, C. Moscoso-Pérez, M. Piñeiro-Iglesias, P. López-Mahía, S. Muniategui-Lorenzo, E. Fernández-Fernández, D. Prada-Rodríguez, Talanta 71 (2007) 1834.
[16] L. Zhang, Y. Morita, K. Yoshikawa, A. Isozaki, Anal. Sci. 23 (2007) 365.
[17] H. Matusiewicz, M. Ślachciñski, Microchem. J. 82 (2006) 78.
[18] N.H. Bings, Z. Stefánka, S.R. mallada, Anal. Chim. Acta 479 (2003) 203.
[19] L. Abrankó, Z. Stefánka, P. Fodor, Anal. Chim. Acta 493 (2003) 13.
[20] C.B. Zheng, Y. Li, Y.H. He, Q.M.X.D. Hou, J. Anal. At. Spectrom. 20 (2005) 764.
[21] J.H. Wang, Y.L. Yu, Z.D.Z.L. Fang, J. Anal. At. Spectrom. 19 (2004) 1559.
[22] Y.L. Yu, Z. Du, J.H. Wang, J. Anal. At. Spectrom. 22 (2007) 650.
[23] Y.L. Yu, Z. Du, M.L. Chen, J.H. Wang, J. Anal. At. Spectrom. 22 (2007) 800.
[24] Y.M. Yin, J. Liang, L.M. Yang, Q.Q. Wang, J. Anal. At. Spectrom. 22 (2007) 330.
[25] Z.X. Li, J. Anal. At. Spectrom. 21 (2006) 435.
[26] X.H. Li, Y.Y. Su, K.L. Xu, X.D. Hou, Y. Lv, Talanta 72 (2007) 1728.
[27] Y.A. Guo, Z.X. Li, Y.H. Feng, ZL patent 03 2 62710.0. (2003).
[28] Z.X. Li, Y.A. Guo, Talanta 65 (2005) 1318.
[29] X.W. Guo, X.M. Guo, Spectrosc. Spectral Anal. (China) 15 (1995) 97.
[30] J.M. Zhang, Q. Zhang, J.T. Ning, T.L. Huo, Rock Min. Anal. (China) 1 (1998) 22.
[31] B. Chen, M. Krachler, Z.I. Gonzalez, W. Shotyk, J. Anal. At. Spectrom. 20 (2005) 95.
[32] P. Grinberg, I. Takase, R.C. de Campos, J. Anal. At. Spectrom. 14 (1999) 827.
[33] M.A. Quijano, A.M. Gutiérrez, M.C.P. Conde, C. Camara, J. Anal. At. Spectrom. 10 (1995) 871.
[34] K. Petrick, V. Krivan, Fresenius J. Anal. Chem. 327 (1987) 338.

Available online at www.sciencedirect.com
ScienceDirect
Talanta 74 (2008) 944–950
Talanta
www.elsevier.com/locate/talanta

Studies of the interaction between Aloe-emodin and DNA and preparation of DNA biosensor for detection of PML-RARα fusion gene in acute promyelocytic leukemia

Xin Hua Lin [a,*], Hong Yan Wan [a,*], Ya Feng Zhang [b], Jing Hua Chen [a]

[a] *Department of Pharmaceutical Analysis, Faculty of Pharmacy, Fujian Medical University, Fuzhou 350004, PR China*
[b] *Xi'an Institute for Drug Control, Xi'an 710054, PR China*

Received 19 March 2007; received in revised form 29 July 2007; accepted 30 July 2007
Available online 14 August 2007

Abstract

The interaction of Aloe-emodin (AE) with salmon sperm DNA in 0.1 M Tris–HCl buffer (pH 4.4) and at the DNA-modified glassy carbon electrode (GCE) was systemically studied with voltammetry and ultraviolet–visible (UV–vis) spectroscopy. AE had excellent electrochemical activity on the GCE with a couple of redox peaks. We propose that AE can intercalate into DNA strands forming a nonelectroactive complex, which results in the decrease of the reduction peak current of AE. The Langmuir adsorption constants of AE at ss- and dsDNA/GCE were $(2.1 \pm 0.4) \times 10^5$ and $(2.7 \pm 0.2) \times 10^5$ M^{-1}, respectively. The difference between AE at ss- and dsDNA has been used for the preparation of a sequence-specific DNA electrochemical biosensor for detection of PML-RARα fusion gene in acute promyelocytic leukemia (APL) with a detection limit of 6.7×10^{-8} M and a linear range from 1.5×10^{-8} to 1.5×10^{-7} M. The selectivity of ssDNA-modified electrode was also described.
© 2007 Elsevier B.V. All rights reserved.

Keywords: Aloe-emodin; Salmon sperm DNA; Interaction; Voltammetry; APL; DNA electrochemical biosensor

1. Introduction

DNA biosensors based on nucleic acid hybridization are currently under intense investigation owing to their increasing importance in the diagnosis of disease with low cost and low power requirements [1–3]. These sensors can be prepared by immobilizing single-stranded DNA probes on the surface of different electrodes. These devices can be used to detect sequence-specific hybridization events directly [4] or by DNA intercalators (anticancer agents [5,6], organic dyes [7,8], and metal complexes [9,10], etc.), which form complexes with the nitrogenous bases of DNA.

The interaction of DNA with small molecules represents a fundamental issue in life science and has been the subject of several investigations [11,12]. The small molecules which noncovalently interact with DNA, are stabilized in binding to DNA through a series of weak interactions, such as the π-stacking interactions associated with intercalation of aromatic heterocyclic groups between the base pairs, hydrogen-bonding, and van der Waals interactions of functionalities bound along the groove of the DNA helix. It would be valuable to understand quantitatively the contributions from these different modes to stabilization of the bound complex at a DNA site [13]. Aloe-emodin (1,8-dihydroy-3-[hydroxymethyl]-anthraquione), a bioactive anthraquinone from the root and rhizome of *Rheum palmatum* L. (Polygonaceae) [14], has been found to have antitumor, genotoxicity, antioxidation, and antibacterial effects [15–18]. The interaction of anthraquinone derivatives with DNA was reported. McKnight et al. [19] studied the DNA binding characteristics of a series of homologous 2, 6-disubstituted anthraquinone threading intercalators. They found that the binding constant decreased with the increase of the side chain length. Bi et al. [20] investigated the anthraquinones such as emodin, rhein, aloe-emodin, and aloin binding properties with serum albumin (BSA or HSA) by fluorescence quenching and absorption spectroscopic techniques. It has been revealed that there were relatively strong binding affinity for the four anthraquinones with HSA and BSA. To our knowledge, there are no reports on detailed investigation of the

* Corresponding authors. Tel.: +86 591 22862016; fax: +86 591 22862016.
E-mail addresses: xinhua63@163.com (X.H. Lin), whypolaris@126.com (H.Y. Wan).

0039-9140/$ – see front matter © 2007 Elsevier B.V. All rights reserved.
doi:10.1016/j.talanta.2007.07.038

interaction mechanism of AE with ss- and dsDNA by voltammetry.

Acute promyelocytic leukemia (APL) accounts for about 5–15% of all acute myeloid leukemias and is characterized by the chromosomal translocation t(15;17), which fuses the retinoic acid receptor (RAR) α gene to the promyelocytic leukemia (PML) gene[21,22]. The PML-RARα fusion gene plays an important role in leukemogenesis through antagonizing retinoic acid signalling and the regulatory pathways mediated by PML. The availability of genotype-specific therapy for PML/RARα acute promyelocytic leukemia requires a precise diagnosis of the disease and DNA biosensors can provide a rapid, precise, and sensitive means for disease diagnosis.

In this paper, we investigated the interactions of AE with DNA in solutions and at ss- and dsDNA-modified GCE. The intercalative binding of AE with DNA forms a nonelectroactive supramolecular complex. In addition, based on the peak current change in electrochemical measurements, a sequence-specific DNA electrochemical sensor for detection of PML-RARα fusion gene in APL was prepared. It was developed by immobilizing covalently single-stranded PML-RARα DNA fragments to a modified GCE. The surface hybridization of the immobilized single-stranded PML-RARα gene fragment with its complementary DNA fragment was evidenced using AE as a novel electrochemical indicator with a detection limit of 6.7×10^{-8} M and the selectivity of ssDNA-modified electrode was also described. This will bring further insight about the interaction mechanism between AE and DNA, and is helpful for further research to design novel antitumor drugs and diagnosis disease.

2. Experimental

2.1. Apparatus

Cyclic voltammograms (CVs) and differential pulse voltammograms (DPVs) were recorded on an electrochemical workstation 660B (CH Instrument, China). A conventional three-electrode system was used throughout the experiments. A GCE (3 mm diameter) was used as the working electrode, a twisted platinum wire as auxiliary electrode, and an Ag/AgCl (with saturated KCl) electrode as the reference electrode. UV–vis absorbance spectra were measured with a UV-2501PC spectrophotometer (SHIMADZU, Japan) using a quartz cell having 1.0 cm optical pathway.

2.2. Reagents

The 18-base synthetic oligonucleotides were purchased from Shanghai Chemical Reagents Company (China); their base sequences are as follows:

- immobilized probe(18-base sequence S_1)-5′-NH3 TCT CAA TGG CTG CCT CCC-3′;
- target (18-base sequence S_2)-5′-GGG AGG CAG CCA TTG AGA-3′;
- single-base mismatch (18-base sequence S_3)-5′-GGG AAG CAG CCA TTG AGA-3′;
- non-complementary (18-base sequence S_4)-5′-ACG TGG TCC CCA GCT CTC-3′.

All oligonucleotides stock solutions (100 μg/mL) were prepared with TE solution (10 mM Tris–HCl, 1.0 mM EDTA, and pH 8.00) and kept frozen. More dilute solutions were prepared with 20 mM acetate buffer (pH 4.80). Salmon sperm DNA was obtained from Aldrich and used as received. Real samples were kindly donated by Fujian institute of hematology, the affiliated union hospital of Fujian medical university. Stock solutions of salmon sperm DNA (1.0 mg/mL) were prepared by dissolving nucleic acids in a 0.1 M Tris–HCl buffer (pH 7.0) and stored at 4 °C. Denatured ssDNA was produced by heating a dsDNA solution in a water bath at 100 °C for 5 min, immediately followed by rapid cooling in an ice bath. Aloe-emodin was purchased from National Institute for the control of pharmaceutical and biological products (China). It was dissolved in ethanol and stored in the dark. *N*-hydroxysulfosuccinimide and *N*-(3-dimethylamion)propyl-*N*′-ethyl carbodiimidehydrochloride were obtained from Sigma. The stock solution of 5 mM DEC and 8 mM NHS was prepared in 50 mM phosphate buffer solutions (PBS, pH 7.40). All the buffer solutions contained 20 mM NaCl. Other chemicals were of analytical reagent grade. All solutions were prepared with double-distilled water (DDW).

2.3. Electrochemical study on the interaction between AE and DNA

2.3.1. Interaction of AE with different concentration of dsDNA

Twenty microliters of 1.0×10^{-3} M AE solution was transferred into 10 mL volumetric flask containing 100, 200 or 400 μL salmon sperm dsDNA stock solution. Each mixture was diluted to the mark using 0.1 M Tris–HCl buffer (pH 4.4). The test solution was subsequently placed in the cell and deaerated with highly pure nitrogen for 3 min prior to measurements. After that, the electrode was placed into the test solution and for CV and DPV scans after adequately stirred for 180 s at open circuit.

2.3.2. Interaction of AE with ss- or dsDNA in solution

Two-hundred microliters of salmon sperm ss- or dsDNA stock solution was transferred into 10 mL volumetric flask and then it was mixed with 20 μL of 1.0×10^{-3} M AE solution. Each mixture was diluted to the mark using Tris–HCl buffer (pH 4.4). The following procedure was the same as above.

2.3.3. Binding constants of AE to ss- or dsDNA-modified electrode

The GCE was mechanically polished with 0.05 μM Al_2O_3 slurry, and then washed ultrasonically in water followed by ethanol for a few minutes. Afterwards, the electrode was oxidized at 0.5 V for 1 min in 50 mM PBS (pH 7.40), followed by

thorough rinse with DDW. Salmon sperm ssDNA (1.0 mg/mL and 10 μL) was pipetted onto the GCE surface. After air-drying, the electrode was rinsed with distilled water. The dsDNA-modified GCE was prepared by dropping salmon sperm dsDNA instead of ssDNA on the GCE surface. The modified electrode was immersed in 2.0×10^{-6} M AE solution for 6 min and then was transfered to blank Tris–HCl buffer (pH 4.4) which had been deaerated with highly pure nitrogen for 3 min for DPV scans.

2.4. UV–vis absorbance spectroscopic studies of the interaction between AE and ss- or dsDNA

Volumes of 1.0 mL Tris–HCl buffer and 100 μL AE solution were transferred into a 5 mL volumetric flask. 200 μL of salmon sperm ss- or dsDNA DNA stock solution was also added. The above solutions were then mixed, diluted to the volume with Tris–HCl buffer (pH 4.4) and mixed thoroughly. Then UV–vis absorbance spectra was measured after leaving the mixture at room temperature for 90 min. Pure AE solution was prepared in a similar manner without DNA.

2.5. Preparation of the electrochemical DNA biosensor

The electrochemical DNA biosensor developed was based on the covalent immobilization of ssDNA on the modified electrode. Modification of the electrode was achieved by dropping 20 μL solution containing 5 mM DEC and 8 mM NHS in 50 mM PBS. After the solution was air-dried, the fabricated electrode was rinsed with DDW for several times. Subsequently, 10 μL ssDNA solution (S_1) was dropped on the modified GCE surface and air-dried to dryness. Then the electrode was rinsed with DDW to eliminate the DNA adsorbed.

2.6. Electrochemical detection of the target-specific DNA hybridization

To achieve the DNA interaction, the S_1-immobilized electrode was immersed in pH 7.0 Tris–HCl buffer containing complementary S_2, single-base mismatch S_3 and non-complementary S_4, respectively. The hybridization was allowed for 30 min at 45 °C. Afterwards, the electrode was dried at room temperature and then thoroughly rinsed with the same Tris–HCl buffer and DDW successively to eliminate the adsorbed S_2, S_3, and S_4.

For DPV detection of the DNA hybridization, AE was used as a hybridization indicator. To accumulate AE on the electrode surface, S_1-immobilized GCE and the modified electrodes obtained after hybridization with complementary S_2, single-base mismatch S_3 or non-complementary S_4 were immersed in Tris–HCl buffer (pH 4.4) containing 2.0×10^{-6} M AE for 6 min at room temperature. Then, the electrodes were rinsed with the PBS and DDW successively. After this modified electrode was transferred into the blank Tris–HCl buffer which had been deaerated with highly pure nitrogen for 3 min, DPV were collected from −0.1 to −0.8 V with amplitude of 10 mV at 50 mV/s scan rate.

2.7. Hybridization detection in real samples

cDNA was obtained by applying a reverse transcription method from total RNA which was extracted using mini DNA-free total RNA extraction kit from venous blood as described previously [23]. The hybridization detection of real samples was transduced by means of DPV. The procedure of hybridization detection of the real samples consisted of the following steps. GCE pretreatment, probe immobilization, and hybridization with DNA fragments obtained from venous blood by using the same electrode surface, indicator binding, and voltammetric transduction of the electrode surface.

3. Results and discussion

3.1. Interaction of AE with dsDNA in solution

As shown in Fig. 1 (curve a), upon the addition of 2.0×10^{-6} M AE to Tris–HCl buffer, a couple of reversible redox peaks appeared with anodic and cathodic peak potentials at about −429 and −456 mV, respectively. Note that the anodic peak was smaller compared to the cathodic peak. As the pH value was increased, the anodic peak disappeared, while the cathodic peak increased. Therefore, the cathodic peak was chosen as the focus for the following investigation. The reduction peak current obtained for AE showed linear dependence on the scan rate, suggesting the adsorption of AE on the electrode surface. The linear equation was: $y = 0.0153x + 2.0582$; $r = 0.9998$. The pH value plays an important role in the electrochemical behavior of AE and AE–DNA complex. With the pH value of the solution increasing, the peak potential shifted to more negative values and the peak currents changed significantly. In the pH range from 3.0 to 7.4, the relation between peak potential and pH was directly investigated and the linear regression equations, $E^{\circ\prime}$ (mV) = −50.26 and pH 247.4 ($r = 0.9966$) for AE and $E^{\circ\prime}$ (mV) = −47.60 and pH 264.8 ($r = 0.9943$) for AE–DNA complex, were obtained. This showed that the uptake of electrons was accompanied by an equal number of protons [24,25], indepen-

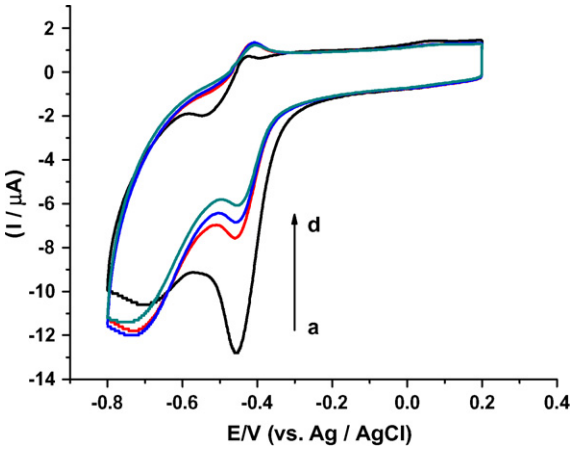


Fig. 1. CVs for 2.0×10^{-6} M AE in the absence (curve a) and presence of 3.1×10^{-5} M (curve b), 6.2×10^{-5} M (curve c), and 1.2×10^{-4} M dsDNA (curve d). Scan rate: 100 mV/s; scan range: 0.2 V to −0.8 V; rest time: 2 s.

dent of the presence of DNA. For a reversible adsorption peak [26], the value of peak separation (ΔE_p) is 58/n mV at 25 °C. For the couple of redox peaks of AE and AE–DNA complex, ΔE_p were 27 and 32 mV, respectively. Thus, the estimated numbers of electrons transferred during the electrode reaction were 2 in both cases. So it can be concluded that, no matter whether DNA is present or not, the electrode reaction processes are both two-electron transfer with two-proton uptake.

Cyclic voltammograms of AE in the absence and presence of DNA were shown in Fig. 1. As can be seen, the decrease of peak current was also observed with increasing of DNA. The reduction peak current (I_{pc}) of AE decreased and the peak potentials did not change. The binding equilibrium time during which AE was in contact with DNA had a great influence on both the stability of the peak and the decrease in peak current. With increased the soaking time of the electrode in AE–DNA complex solution, the peak current decreased and then trended to a steady value. So a time of 6 min was the optimal waiting time.

The phenomena mentioned above were further studied by DPV. The decrease of peak current was also observed with increasing of DNA. As far as ΔI_{pc} was concerned, it was found to be in linear proportion to the concentration of DNA in the range of 1.86×10^{-5} to 1.12×10^{-4} M with a regression equation $\Delta I_{pc} = 0.0079 C_{DNA} + 2.0 \times 10^{-6}$, and a correlation coefficient $r = 0.9992$.

The possible reason for the decrease of the peak current after addition of DNA to AE solution is that the presence of DNA may alter the electrochemical kinetics of AE. The values of the major electrochemical kinetic parameters of AE in the absence and the presence of dsDNA can indicate whether the presence of DNA influences the electrochemical kinetics of AE. The electron transfer coefficient α and the standard rate constant k_s can be determined via the theory of Laviron [27]. A graph of $E_{pc} = f(\log v)$ yields a straight line with a slope equal to $-2.3RT/\alpha nF$ for the cathodic peak, where v stands for the scan rate, n the number of electrons, and R, T, and F have their normal meanings. Plotting E_{pc} versus log v produces a linear range, so α has been estimated to be 0.24 for the AE redox reaction in the absence of dsDNA. k_s can be calculated according to the following equation (valid when $n\Delta E_p > 200$ mV):

$$\log k_s = \alpha \log(1-\alpha) + (1-\alpha)\log\alpha - \log\frac{RT}{nFv} - \frac{\alpha(1-\alpha)nF\Delta E_p}{2.3RT} \quad (1)$$

from which k_s has been determined to be 12.40 s^{-1} (at a scan rate of 100 mV/s). Similarly, α and k_s for the AE redox reactions in the presence of dsDNA have been calculated to be 0.20 and 10.35 s^{-1}, respectively. Obviously, the presence of dsDNA does not significantly alter the kinetics of the AE redox reactions at the GCE surface. From the results above it can be assumed that there is a binding and complexation between AE and DNA. Because of the interaction between AE and DNA, an electrochemically inactive complex forms according to the Ref. [28], the AE–DNA complex, which cannot be oxidized at the electrode surface.

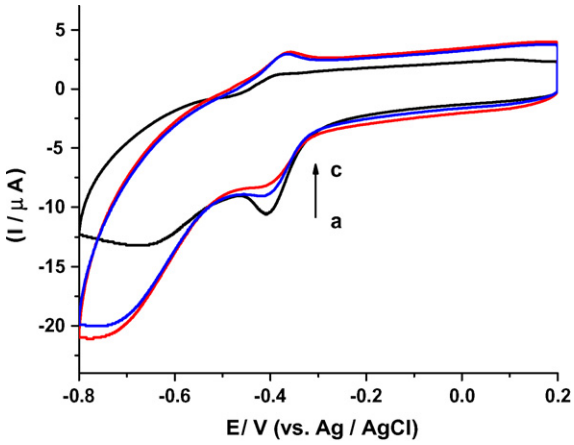


Fig. 2. CVs for 2.0×10^{-6} M AE in the absence (curve a), presence of 6.2×10^{-5} M ssDNA (curve b), and 6.2×10^{-5} M dsDNA (curve c). Other conditions as Fig. 1.

3.2. Interaction of AE with dsDNA or ssDNA in solution

The different electrochemical behaviors of AE with the addition of dsDNA or ssDNA in the buffer solution also demonstrate the interaction between AE and DNA. As shown in Fig. 2, although the peak current of AE decreases in both cases, the peak current decreases more sharply at dsDNA-modified electrode.

The UV–vis absorption spectrum also provides potent evidence for the possible intercalation of AE into DNA. As shown in Fig. 3, although a slight shift in the AE adsorption peak from 407 to 414 nm is observed after the addition of dsDNA, the absorption peak decreases significantly. In contrast with dsDNA, the absorption peak of denatured ssDNA decreases slightly. These phenomena suggest the possible intercalation of AE into dsDNA strands [29–31]. The studies described above indicated that upon binding to DNA the planar anthraquinone ring of AE could slide into adjacent base pairs [32], resulting in that they were in an environment in which it was unable to H bond with the solvent water molecules. In contrast, the random coil-like, disordered ssDNA does not provide a favorable environment for AE intercalation.

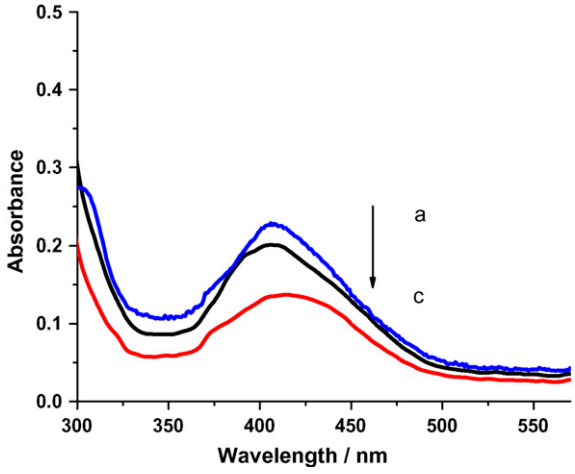


Fig. 3. UV–vis absorption spectrum for 2.0×10^{-5} M AE in the absence (curve a) and presence of 40.0 μg mL^{-1} M ssDNA (curve b) and dsDNA (curve c).

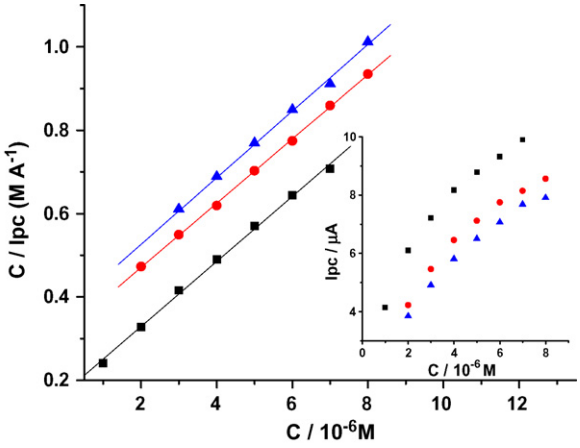


Fig. 4. Plots of C/I_{pc} vs. AE concentration at bare GCE (■), salmon sperm dsDNA/GCE (●) and salmon sperm ssDNA/GCE (▲). Inset: relations between cathodic peak currents and AE concentration. The scan rate, pulse amplitude, and pulse period were 20 mV/s, 50 mV, and 60 ms, respectively.

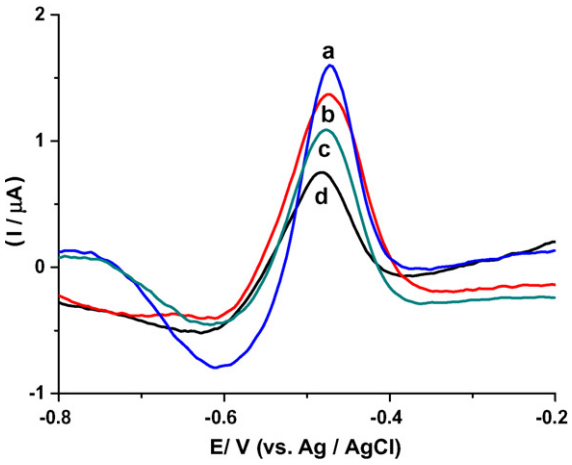


Fig. 5. DPVs of AE accumulated on the bare GCE (curve a), ssDNA modified GCE (curve d) and after hybridization with non-complementary sequence (curve c), and complementary sequence (curve b) in a 0.1 M Tris–HCl buffer (pH 4.40) with 20 mM NaCl. Other conditions as Fig. 4.

3.3. Binding constants of AE to dsDNA/GCE and ssDNA/GCE

The cyclic voltammograms of AE at different concentrations at bare GCE, ss- or dsDNA/GCE electrodes showed that the peak current increased with increasing AE concentration, as expected shape of Langmuir adsorption [33] (Fig. 4). Thus, the adsorption thermodynamics is given in the following equation:

$$\frac{C}{I_p} = \frac{1}{KI_{p,max}} + \frac{C}{I_{p,max}} \quad (2)$$

where I_p, $I_{p,max}$, C, and K are the peak current, maximum peak current, AE concentration, and the adsorption or binding constant of AE at bare GCE, ss- or dsDNA/GCE surface. From the slope and intercept of C/I_p versus C the maximum peak current, $I_{p,max}$, and the adsorption constant, K, can be obtained.

Fig. 4 shows the plots of C/I_p versus C at three electrodes. From the linear regression equation, the adsorption constants of AE at bare glass carbon electrode and the binding constant of AE to ssDNA/GCE and dsDNA/GCE at pH 4.4 were calculated to be $(4.5 \pm 0.2) \times 10^5$, $(2.1 \pm 0.4) \times 10^5$ and $(2.7 \pm 0.2) \times 10^5$ M^{-1}, respectively. The adsorption constant of AE at bare electrode is much larger than the binding constant of AE to ssDNA/GCE and dsDNA/GCE, which indicated that an intense adsorption process of AE on the electrode surface. Although the amount of adsorbed ssDNA is more than that of adsorbed dsDNA, the dsDNA/GCE shows a larger peak current of AE and a larger binding constant. Under the same conditions, the larger binding constant of AE to dsDNA/GCE than to ssDNA/GCE indicates that AE can be used as a novel electroactive indicator for detection of DNA hybridization.

3.4. Electrochemical detection of the target-specific DNA hybridization

Since AE could intercalate into the bases of dsDNA, the DNA biosensor using AE as electrochemical hybridization label was developed. The selectivity of the electrochemical DNA sensor developed was studied using DPV. Fig. 5 shows the DPV curves obtained in blank Tris–HCl buffer after background subtraction. The bare GCE shows the biggest current peak, which could be due to the specific adsorption of AE at the bare GCE electrode surface (curve a). As the GCEs were modified with ssDNA (curve d) and after hybridization with non-complementary sequence (curve c), complementary sequence (curve b), the current peak for the reduction of AE decreased, indicating that the concentration of AE decreased on the surface of the modified GCEs due to the interaction between AE and DNA. The peak currents of AE decreased in the order of bare GCE, complementary sequence, single-base mismatch sequence and ssDNA-modified electrode and the relative standard deviation is 3.20, 6.43, 8.35, and 8.11%, respectively. These results showed that ssDNA was immobilized on the GCE, and complementary sequence was hybridized with the probe ssDNA. When the ssDNA-modified GCE interacted with the complementary sequence in solution, the peak current for the AE increased significantly. This increase in current clearly showed that the ssDNA modified on the GCE had successfully hybridized with its complementary sequence. The greater peak currents indicated that more AE molecules were concentrated or bound to dsDNA helix than to ssDNA helix. The effective discrimination against single-base mismatch was also studied. In the presence of oligonucleotide containing a single-base mismatch, significant decreased voltammetric signal was obtained compared to the complementary sequence. This difference indicates that the complete hybridization was not accomplished due to the base mismatch. In addition, as expected, there was no significant current difference for the ssDNA-modified GCE and its hybridization with non-complementary sequence, since no successful hybridization occured due to the sequence mismatch between the modified ssDNA and the non-complementary sequence. This means that the surface properties of the ssDNA-modified GCE was not changed after its interaction with non-complementary sequence.

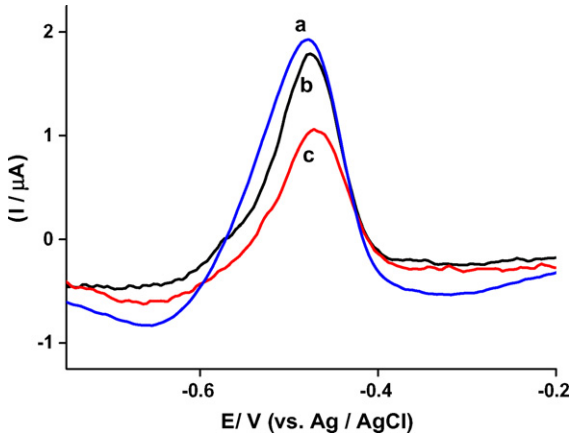


Fig. 6. DPVs responses using the reduction signal of AE for APL probe modified GCE (curve b), APL probe modified GCE after hybridization with negative real sample (curve a), and APL probe modified GCE after hybridization with positive real sample (curve c). Other conditions as Fig. 4.

The sensitivity of the electrochemical hybridization assay was investigated by varying the target oligonucleotide concentration according to the procedure described. The different current value obtained in the DPV response of AE after hybridization of probe with target was recorded with three repetitive measurements. The current response at about −471 mV increased in proportion to the amount of the target sequence used. The average current response showed excellent correlation with the amount of the complementary oligonucleotides applied over the range from 1.5×10^{-8} to 1.5×10^{-7} M. The regression equation was $y = 0.4068x + 3.2729$ (x is the amount of the target DNA (mol) and y is the DPV peak current of AE (μA)) and the regression coefficient of the linear curve were 0.9958. A detection limit of 6.7×10^{-8} M of the target DNA can be estimated using 3σ (where σ is the standard deviation of the blank solution $n = 8$).

Fig. 6 represents the AE signals obtained, when the probe for PML/RARα was immobilized and hybridized with real samples in the hybridization step. A series of three repetitive measurements resulted in reproducible results. The AE signals obtained from the probe modified GCE gave a mean average signal of 2.43 μA with a relative standard deviation (R.S.D.) value of 6.2%. The AE signals obtained from the hybridization of the probe with the positive and negative real samples gave mean average signals of 1.47 μA with a R.S.D. value of 8.9% and 2.60 μA with a R.S.D. value of 7.7%, respectively. The AE signals of the PML/RARα probe modified GCE was higher than that of PML/RARα probe modified GCE after hybridization with positive real sample. The obvious decrease in the magnitude of the AE signals were obtained with positive real samples. The decrease in the voltammetric signals showed that the hybridization at the GCE surface occurred and AE could not interact with the bound guanine base of the hybrid. The decrease in the reduction signal of AE was attributed to the steric inhibition of the reducible groups of AE because of the formation of hybrid at the GCE surface. If the blood sample, from which DNA was extracted, were negative, the negative real sample would not contain a target sequence complementary to the specific PML/RARα probe. The interaction between these negative real samples and the immobilized probe did not lead to the hybridization, so the magnitude of the AE signal was nearly as high as the probe signal (Fig. 6).

4. Conclusions

The interaction between AE and salmon sperm DNA was studied using cyclic voltammetry and differential pulse voltammetry. All the experimental results indicate that the binding mode of AE–DNA is intercalative. In addition, the calculated electrochemical parameters transfer coefficient α and standard electron transfer rate constant k_s reveal that the interaction of AE with DNA forms a nonelectroactive supramolecular complex. The Langmuir adsorption constants of AE at a bare GCE, ssDNA/GCE and dsDNA/GCE were also calculated. The difference in binding constants of AE to ss- and dsDNA suggests that AE can be used as an electrochemical indicator for preparation of DNA hybridization biosensor with a detection limit of 6.7×10^{-8} M, which has been evidenced by the hybridization recognition of immobilized single-stranded PML-RARα fusion gene fragment to its complementary DNA fragment. The utility of AE as an electrochemical hybridization indicator for detection of PML-RARα fusion gene in acute promyelocytic leukemia can provide a simple, rapid detection and might have a promising future in transducing DNA hybridization. The electrochemical DNA sensor developed might have the potential application in diagnosis of diseases.

Acknowledgments

The authors gratefully acknowledge the financial support of the National High Technology and Development of China (863 Project: 2006AA02Z4Z1), the National Natural Science Foundation of China (20675015), the Foundation of Fujian Provincial Technology International Cooperation (2006I0016) and the Foundation of Fujian Education Department (2005K051) and the Foundation of Fujian Health Department (2005123).

References

[1] X.M. Li, H.O. Ju, C.F. Ding, S.S. Zhang, Anal. Chim. Acta 582 (2007) 158.
[2] C.S. Riccardi, K. Dahmouche, C.V. Santilli, P.I. Costa, H. Yamanaka, Talanta 70 (2006) 637.
[3] J. Yang, T. Yang, Y. Feng, K. Jiao, Anal. Biochem. 365 (2007) 24.
[4] E. Komarova, M. Aldissi, A. Bogomolova, Biosens. Bioelectron. 21 (2005) 182.
[5] C. Carrasco, A. Joubert, C. Tardy, N. Maestre, M. Cacho, M.F. Brana, C. Bailly, Biochemistry 42 (2003) 11751.
[6] A. Erdem, M. Ozsoz, Anal. Chim. Acta 437 (2001) 107.
[7] X.H. Lin, P. Wu, W. Chen, Y.F. Zhang, X.H. Xia, Talanta 72 (2007) 468.
[8] B. Meric, K. Kerman, D. Ozkan, P. Kara, S. Erensoy, U.S. Akarca, M. Mascini, M. Ozsoz, Talanta 56 (2002) 837.
[9] K. Maruyama, Y. Mishima, K. Minagawa, J. Motonaka, Anal. Chem. 74 (2002) 3698.
[10] S.S. Zhang, S.Y. Niu, B. Qu, G.F. Jie, H. Xu, C.F. Ding, J. Inorg. Biochem. 99 (2005) 2340.
[11] X. Zhou, S. Zheng, D. Li, X. He, B. Lin, Talanta 72 (2007) 561.

[12] Y.Q. Li, Y.J. Guo, X.F. Li, J.H. Pan, Talanta 71 (2007) 123.
[13] A.M. Pyle, J.P. Rehmann, R. Meshoyrer, C.V. Kumar, N.J. Turro, J.K. Barton, J. Am. Chem. Soc. 111 (1989) 3051.
[14] F. Yang, T. Zhang, G. Tian, H. Cao, Q. Liu, Y. Ito, J. Chromatogr. A 858 (1999) 103.
[15] K.E. Malterud, T.L. Farbrot, A.E. Huse, R.B. Sund, Pharmacology 47 (1993) 77.
[16] H.Z. Lee, S.L. Hsu, M.C. Liu, C.H. Wu, Eur. J. Pharmacol. 43 (2001) 1287.
[17] S.O. Muller, H. Stopper, Biochim. Biophys. Acta 1428 (1999) 406.
[18] H.H. Wang, J.G. Chung, C.C. Ho, L.T. Wu, S.H. Chang, Planta Med. 64 (1998) 176.
[19] R.E. McKnight, J.G. Zhang, D.W. Dixon, Bioorg. Med. Chem. Lett. 14 (2004) 401.
[20] S. Bi, D. Song, Y. Kan, D. Xu, Y. Tian, X. Zhou, H. Zhang, Spectrochim. Acta A 62 (2005) 203.
[21] A. Laurenzana, F. Pettersson, W.H. Miller Jr, Drug Discov. Today 3 (2006) 499.
[22] E. Paietta, O. Goloubeva, D. Neuberg, J.M. Bennett, R. Gallagher, J. Racevskis, G. Dewald, P.H. Wiernik, M.S. Tallman, Eastern Cooperative Oncology Group, Cytometry B Clin. Cytom. 59 (2004) 1.
[23] R. He, B. Liu, C. Yang, R.C. Yang, G. Tobelem, Z.C. Han, Cancer Gene Ther. 10 (2003) 879.
[24] J. Chen, J. Zhang, Q. Zhuang, S. Zhang, X. Lin, Talanta 72 (2007) 1805.
[25] L. Tan, S. Yao, Q. Xie, Talanta 71 (2007) 827.
[26] A.J. Bard, L.R. Faulkner, Electrochemical Methods Fundamentals and Applications, Wiley, New York, 1980, pp. 166.
[27] E. Laviron, J. Electroanal. Chem. 101 (1979) 19.
[28] X. Zheng, A. Chen, T. Hoshi, J.I. Anzai, G. Li, Anal. Bioanal. Chem. 386 (2006) 1913.
[29] E.C. Long, J.K. Barton, Acc. Chem. Res. 23 (1990) 271.
[30] Y.F. Long, C.Z. Huang, Talanta 71 (2007) 1939.
[31] Z. Sun, Z. Ma, W. Zhang, X. Wang, C. Fan, G. Li, Anal. Bioanal. Chem. 379 (2004) 283.
[32] H. Zhou, Z.Y. Sun, T. Hoshi, Y. Kashiwagi, J.I. Anzai, G. Li, Biophys. Chem. 114 (2005) 21.
[33] H.X. Ju, Y.K. Ye, Y.L. Zhu, Electrochim. Acta 50 (2005) 1361.

Available online at www.sciencedirect.com
ScienceDirect
Talanta 74 (2008) 965–970
Talanta
www.elsevier.com/locate/talanta

Amperometric sensor for hydrogen peroxide based on electric wire composed of horseradish peroxidase and toluidine blue-multiwalled carbon nanotubes nanocomposite

Ying Liu, Jianping Lei, Huangxian Ju *

MOE Key Laboratory of Analytical Chemistry for Life Science, School of Chemistry and Chemical Engineering, Nanjing University, Nanjing 210093, PR China

Received 9 May 2007; received in revised form 1 August 2007; accepted 3 August 2007
Available online 7 August 2007

Abstract

A kind of nanocomposites with good dispersion in water was prepared through noncovalent adsorption of toluidine blue (Tb) on multiwalled carbon nanotubes (MWCNT) for electric communication between horseradish peroxidase (HRP) and electrode. The nanocomposites could be conveniently cast on electrode surface. With the aid of chitosan, HRP was then immobilized on the nanostructure to form a reagentless amperometric sensor for hydrogen peroxide. UV–vis spectroscopy and electrochemical impedance spectroscopy were used to characterize the adsorption of Tb on MWCNT. The presence of both Tb as mediator of electron transfer and MWCNT as conductor enhanced greatly the enzymatic response to the reduction of hydrogen peroxide. The novel biosensor exhibited fast response towards hydrogen peroxide with a detection limit of 1.7×10^{-6} M and the linear range extended up to 4×10^{-4} M without the interference of ascorbic acid and uric acid. The Michaelis–Menten constant (K'_m) of the immobilized HRP was evaluated to be 0.16 mM.
© 2007 Elsevier B.V. All rights reserved.

Keywords: Amperometric sensor; Carbon nanotubes; Toluidine blue; Nanocomposites modified electrode; Hydrogen peroxide

1. Introduction

In recent years carbon nanotubes (CNTs) have been extensively used for electrochemical study and preparation of electrochemical sensors due to their electrical conductivity, unique structural and catalytic properties. However, a major barrier for the preparation of CNTs-based biosensors is the insolubility of CNTs in most solvents. Although the challenge of solubilizing CNTs has been addressed by several methods, including temporarily dispersing in some organic solvent [1,2], oxidation treatment [3] and polymer wrapping or grafting [4–7], these methods possibly impair the chemical properties of CNTs or decrease their conductivity. Therefore, the new strategy for improving the solubility of CNTs and keeping their pristine mechanical and electronic properties has attracted considerable attention. The CNTs exhibit a special sidewall curvature and possess a π-conjugative structure with a highly hydrophobic surface, which allow them to interact with some aromatic compounds [8] such as anthracene derivatives [9], methylene blue (MB) [10], and thionine [11] through π–π electronic and hydrophobic interactions. By use of these interactions, this work prepared a kind of nanocomposites through noncovalent adsorption of toluidine blue (Tb) on multiwalled carbon nanotubes (MWCNT). The nanocomposites showed good dispersion in water, and could thus be conveniently cast on an electrode surface for preparation of biosensors.

The integration of redox mediators and CNTs has been used for development of electrochemical sensors [12–18]. Gorski proposed two β-nicotinamide adenine dinucleotide (NADH) amperometric sensors by covalently attaching Azure dye [12] and Tb [13] as redox mediators to polysaccharide chains of chitosan, which were then mixed with CNTs and cast on electrode to provide remarkable synergistic augmentation of sensor responses. Other amperometric sensors for NADH have been prepared with thionine adsorbed CNTs [14], which also show the synergistic augmentation and sensitive response to nitrite [15], and poly(Tb)/MWCNT composite formed on a glassy carbon electrode through electropolymerization [16]. One amperomet-

* Corresponding author. Tel.: +86 25 83593593; fax: +86 25 83593593.
E-mail address: hxju@nju.edu.cn (H.X. Ju).

0039-9140/$ – see front matter © 2007 Elsevier B.V. All rights reserved.
doi:10.1016/j.talanta.2007.08.001

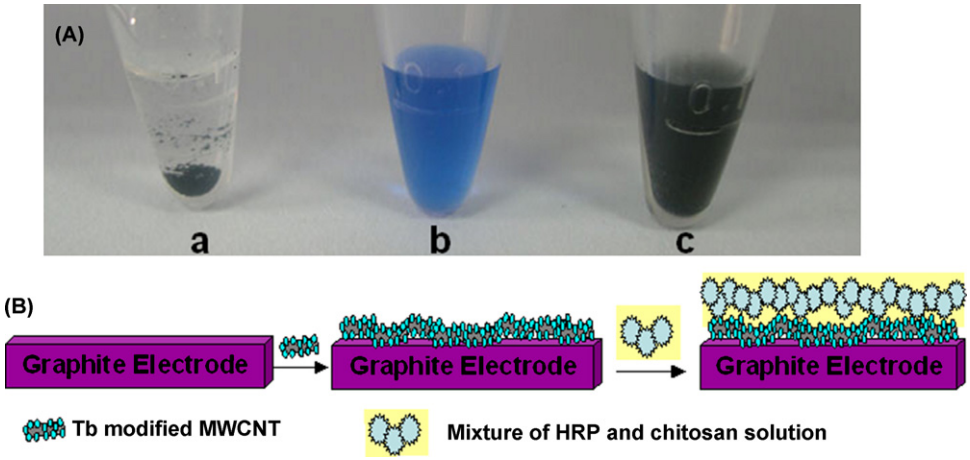


Fig. 1. (A) Photos of (a) pristine MWCNT, (b) 0.5 mM Tb solution and (c) Tb–MWCNT solution containing 2 mg mL^{-1} MWCNT, and (B) fabrication process of the sensor.

ric sensor for hydrogen peroxide based on the electrocatalytic reduction by thionine immobilized covalently on MWCNTs has been reported [17]. Chen and co-workers [18] prepared a sensor for hydrogen peroxide by using tetrahydrofuran to disperse MWCNTs and then incorporating horseradish peroxidase (HRP) and electron transfer mediator MB in the matrix. Obviously the presence of tetrahydrofuran would decrease the activity of the immobilized enzyme, and the hydrophobic surface of CNTs was also a disadvantage to the enzymatic reaction. This work conveniently used the Tb adsorbed noncovalently on MWCNT as a mediator for electric communication between HRP and its substrate to prepare a hydrogen peroxide biosensor by using chitosan to immobilize HRP on the film of Tb–MWCNT nanocomposites. The chitosan provided good biocompatibility for maintaining the activity of the immobilized HRP. The constructed sensor showed good stability and reproducibility. The synergistic effects of Tb as a mediator for electron transfer and MWCNT as an excellent conductor on the enzymatic reaction between HRP and hydrogen peroxide produced a sensitive reagentless biosensor for hydrogen peroxide.

2. Experiments

2.1. Chemicals and instruments

Horseradish peroxidase (HRP) (240 U mg^{-1}) was purchased from Huamei Bioengineering Company (China). Stock solution of 2 mg mL^{-1} HRP was prepared by directly dissolving HRP in 0.2 M phosphate buffer solution (PBS) (pH 7.0) and stored at 4 °C. Toluidine blue and chitosan (85%) were purchased from Sigma. One weight precent chitosan solution was prepared by dissolving chitosan flakes in 0.1 M HCl and adjusting the pH to 5.0 with NaOH solution. Multiwalled carbon nanotubes (average diameter of about 20 nm) were purchased from Nanoport Co. Ltd. (Shenzhen, China) and used as received without any pretreatment. Other reagents were commercially available and all of analytical reagent grade. Aqueous solutions were prepared with doubly distilled water, 0.2 M PBS (pH 7.0) was always employed as supporting electrolyte and deaerated by bubbling nitrogen prior to the experiments.

Amperometric, cyclic voltammetric and electrochemical impedance spectroscopic experiments were performed on a CHI 660B Electrochemical Workstation (CH Instruments Inc., USA). All experiments were carried out using a conventional three-electrode system with a modified graphite electrode as working, a platinum foil as auxiliary, and a saturated calomel electrode as reference electrodes. Ultraviolet–vis absorption (UV–vis) spectra were recorded with a Lambda 35 UV–vis spectrometer (Perkin-Elmer instruments, USA).

2.2. Preparation of soluble nanocomposites

Two milligrams of pristine MWCNT was added into 1 mL 0.5 mM Tb solution. After the mixture was sonicated for 1 h at room temperature, the resulting suspension was filtered with a millipore porous filter (0.45 μm, Millipore). The sediment was then washed with distilled water to remove nonadsorbed Tb. The obtained Tb–MWCNT nanocomposites could be dispersed in 1 mL doubly distilled water to obtain a stable nanocomposites suspension, as shown in Fig. 1A.

2.3. Preparation of HRP/Tb–MWCNT-modified electrode

After the home-made graphite electrode (inner-diameter: 3.0 mm; outer-diameter: 4.6 mm) was abraded with fine silicon carbide paper, it was successively polished with 0.3 and 0.05 μm alumina slurry, and sonicated in water and absolute ethanol. Three microlitters of Tb–MWCNT suspension was spread onto the electrode surface and allowed to dry in air. After washed with water to remove any loosely adsorbed species, the Tb–MWCNT-modified electrode was further modified by dropping 3 μL mixture of 2 mg mL^{-1} HRP solution and 1 wt% chitosan solution. The resulting HRP/Tb–MWCNT-modified electrode was washed with doubly distilled water and stored at 4 °C in air. The fabrication process of the modified electrode was shown in Fig. 1B. For comparison, the HRP/Tb or HRP/MWCNT-

modified graphite electrode was prepared by coating TB or MWCNT and then the mixture of HRP and chitosan on electrode surface.

3. Results and discussion

3.1. Characteristics of Tb–MWCNT

Tb can be easily attached onto MWCNT through the strong π–π stocking force between two conjugated frames. Fig. 1A compares the dispersion of pristine MWCNT, Tb, and Tb–MWCNT nanocomposites. It is difficult to disperse the pristine MWCNT in water because of its hydrophobic surface (photo a, Fig. 1A). Tb is a kind of purple dye and can be easily dissolved in water (photo b, Fig. 1A). Its adsorption on MWCNT greatly improved the dispersion of MWCNT in water due to the hydrophilicity of the adsorbed Tb molecules. The resulting Tb–MWCNT nanocomposites can be easily dispersed in water (photo c, Fig. 1A). The suspension of the nanocomposites is stable for at least 2 weeks, which highly facilitates the application of MWCNT in development of biosensors.

The UV–vis spectrum of Tb showed two characteristic absorption peaks of Tb around 288 and 633 nm and one absorption peak ascribed to the absorption of Tb dimer at 598 nm [19] (curve a, Fig. 2). The suspension of oxidized MWCNT in water did not cause any special absorbance except a broad absorption peak at 250 nm (curve c, Fig. 2) [10], which was the typical UV absorption of MWCNT. The two characteristic absorption peaks of Tb could be observed in Tb–MWCNT nanocomposite suspension (curve b, Fig. 2), indicating the presence of Tb molecules on MWCNT. However, the absorption wavelength of one characteristic peak shifted from 288 to 275 nm, and the absorption peak at 598 nm disappeared (curve b, Fig. 2). In comparison with

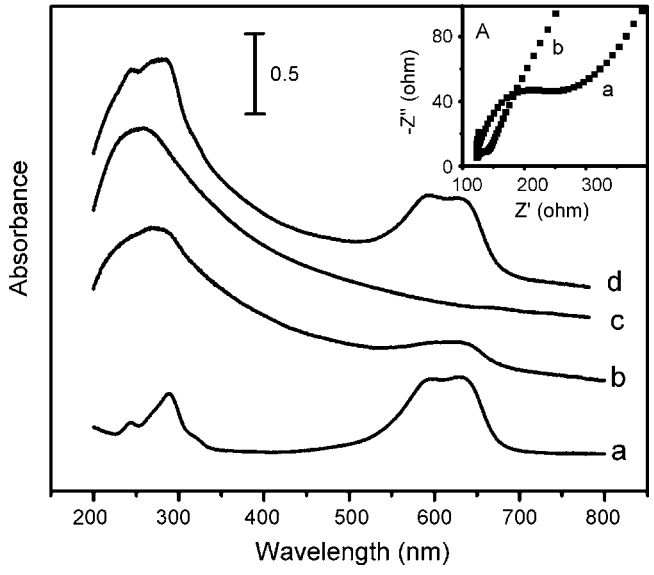


Fig. 2. UV spectra of (a) Tb, (b) Tb–MWCNT nanocomposites, (c) oxidized MWCNT, and (d) the arithmetical addition of the UV spectra of Tb and oxidized MWCNT. Inset: Nyquist diagrams of (a) Tb-modified and (b) Tb–MWCNT nanocomposites-modified electrodes in 1.0 M KCl containing 10 mM $[Fe(CN)_6]^{3-/4-}$.

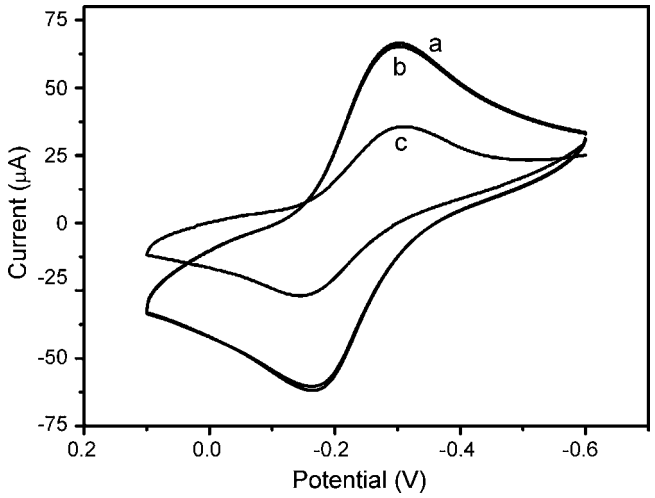


Fig. 3. Cyclic voltammograms of Tb–MWCNT nanocomposites-modified electrode at the first (a) and the 20th (b) scanning circles, and HRP/Tb–MWCNT-modified electrode (c) in 0.2 M PBS (pH 7.0) saturated with nitrogen at 100 mV s^{-1}.

the arithmetic addition of the UV spectra of toluidine blue and the oxidized MWCNT (curve d, Fig. 2), the blue shift resulted from the interactions between Tb and MWCNT and the steric barrier for the free conformation of Tb on MWCNT [20], and the disappearance of Tb dimer [11] was due to the formation of Tb–MWCNT nanocomposites.

The Tb–MWCNT nanocomposites-modified electrode was stable (Fig. 3) and showed low electron transfer impedance, R_{et}, due to the presence of MWCNT (inset, Fig. 2). The cyclic voltammogram of the modified electrode showed a couple of redox peaks at −0.300 and −0.165 V (curve a, Fig. 3), which were ascribed to the reduction and oxidation of the adsorbed TB. After continuously scanning for 20 cycles in PBS the cyclic voltammogram remained the same behavior (curve b, Fig. 3). The R_{et} value of $[Fe(CN)_6]^{3-/4-}$ at Tb–MWCNT-modified electrode was about 24 Ω, while it was 204 Ω at Tb-modified electrode. The MWCNT in the nanocomposites membrane was excellent conductor for electron transfer between the enzymatic system and electrode.

3.2. Electrocatalytic reduction of H_2O_2 on HRP/Tb–MWCNT-modified electrode

Chitosan displays excellent biocompatibility, nontoxicity, and high mechanical strength, and has thus been used as immobilization matrix for protein and biomolecule [21]. After the mixture of chitosan and HRP was coated on Tb–MWCNT-modified electrode, the cyclic voltammetric peak currents of Tb–MWCNT decreased and the separation of peak to peak hardly changed (curve c, Fig. 3). The decrease in the peak currents resulted from the block of the chitosan–HRP membrane to the diffusion of proton needed in the redox process of Tb. The same peak-to-peak separation indicated the presence of HRP–chitosan membrane did not affect the electron transfer rate.

At a bare graphite electrode the reduction of H_2O_2 showed great overpotential (Fig. 4A). In the potential window studied

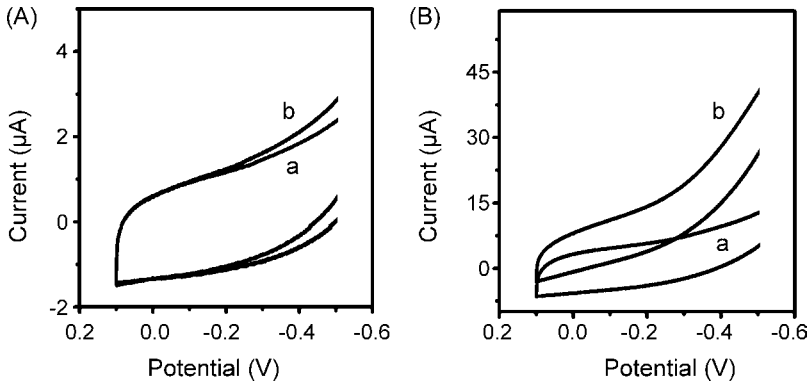


Fig. 4. Cyclic voltammograms of (A) bare and (B) HRP/MWCNT-modified electrodes in (a) 0.2 M PBS (pH 7.0) saturated with nitrogen and (b) 10 mM H_2O_2 at 100 mV s^{-1}.

the response of H_2O_2 was very low. Upon addition of 10 mM H_2O_2 an increase of 0.24 μA was detected at −0.4 V, while the value was about 17.3 μA at HRP/MWCNT-modified electrode (Fig. 4B).

The HRP/Tb-modified electrode exhibited only a pair of redox peak at of Tb (curve a, Fig. 5A). Upon addition of 10 mM H_2O_2, the reduction peak current increased greatly (from 18.6 to 42.9 μA) with slightly negative shift of peak potential and the oxidation peak current decreased (curve b, Fig. 5A), indicating an obvious electrocatalytic process of Tb to the enzymatic reduction of H_2O_2 by the immobilized HRP. The Tb acted as an electron transfer mediator. At HRP/Tb–MWCNT-modified electrode the electrocatalytic process was further enhanced (Fig. 5B). The increase in reduction peak current was about 64.4 μA (from 27.1 to 91.5 μA), which was about 2.65 times the electrocatalytic response at HRP/Tb-modified electrode. The electrocatalytic mechanism could be followed that reported previously [22].

From the CVs of $[Fe(CN)_6]^{3-}$ at HRP/Tb and HRP/Tb–MWCNT-modified electrodes, the presence of MWCNT increased the apparent surface of electrode for 1.6 times. Thus, the change of 2.65 times in the electrocatalytic response was attributed to the enlarged electrode surface, the good conductivity of MWCNT and the synergy of MWCNT and Tb in the Tb–MWCNT nanocomposites. The nanocomposites acted as the electric wire between the enzymatic system and electrode.

3.3. Applied potential and optimal pH for amperometric detection of H_2O_2

The amperometric response of the HRP/Tb–MWCNT-modified electrode to 20 μM hydrogen peroxide was investigated over the potential range of −0.1 to −0.6 V. The response increased sharply from −0.1 to −0.3 V and reached its peak value at −0.4 V, similar to the trend of cyclic voltammetric response. Thus, −0.4 V was selected as the applied potential for detection of H_2O_2.

The activity of immobilized HRP was related to the pH of detection solution. At the applied potential of −0.4 V the amperometric response increased quickly from pH 4.5 to 6.5, and decreased from pH 7.0 to 9.5, which was in agreement with that for the HRP immobilized on electrode surface through gold nanoparticles and sol–gel [23]. Thus, the presence of Tb–MWCNT nanocomposite did not change the optimal pH value for the enzymatic reaction.

3.4. Performance of the amperometric sensor

Amperometric measurements were performed in a stirred 0.2 M PBS (pH 7.0) at an applied potential of −0.4 V. Fig. 6 shows the typical current–time responses at both HRP/Tb and HRP/Tb–MWCNT-modified electrodes for successive addition of H_2O_2. At HRP/Tb–MWCNT-modified electrode a sharp increase of current was observed after each addition of H_2O_2,

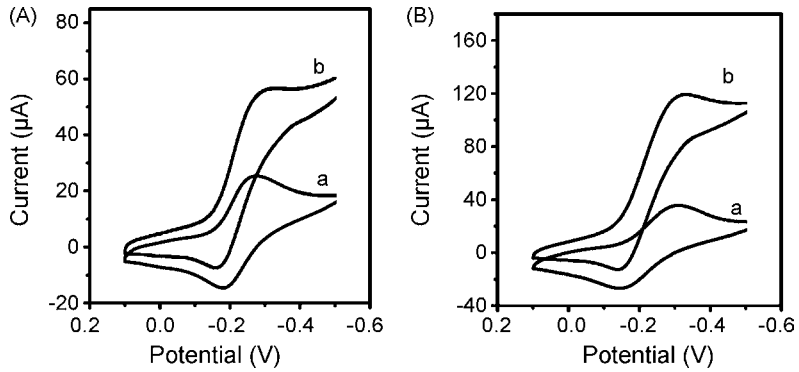


Fig. 5. Cyclic voltammograms of (A) HRP/Tb and (B) HRP/Tb–MWCNT-modified electrodes in (a) 0.2 M PBS (pH 7.0) saturated with nitrogen and (b) 10 mM H_2O_2 at 100 mV s^{-1}.

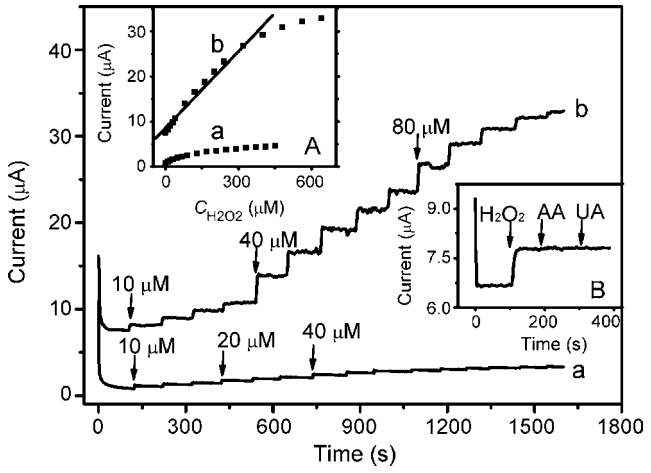


Fig. 6. Amperometric responses of (a) HRP/Tb and (b) HRP/Tb–MWCNT-modified electrodes at an applied potential of −0.4 V to successive addition of H_2O_2 in a stirred 0.2 M PBS (pH 7.0) saturated with nitrogen. Inset (A) calibration curves at (a) HRP/Tb and (b) HRP/Tb–MWCNT-modified electrodes, and (B) amperometric response of 10 μM H_2O_2, 10 μM AA, and 10 μM UA at an applied potential of −0.4 V in a stirred 0.2 M PBS (pH 7.0) saturated with nitrogen.

and the response reached 95% of the steady state value within 8 s. The HRP/Tb showed relatively low amperometric response. The linear calibration range of H_2O_2 at HRP/Tb–MWCNT-modified electrode extended up to 0.4 mM ($R = 0.990$, $n = 11$) (curve b, inset A in Fig. 6), a little higher than 0.34 mM at thionine–MWCNT-modified electrode [17] and much higher than 73.0 μM based on the direct electrochemical behavior of HRP entrapped in a zirconia enhanced grafted collagen trihelix scaffold [24] and 19 μM based on the immobilization of HRP on electropolymerized polyaniline films doped with CNTs [25]. The sensitivity of HRP/Tb–MWCNT-modified electrode was about 56.8 μA mM^{-1}, better than those of 49.0 μA mM^{-1} based on the direct electrochemistry of HRP immobilized on SWCNT-modified electrode [26] and 2.45 μA mM^{-1} at HRP and MB–SiO_2 nanocomposite coimmobilized gelatine matrix-modified electrode [27]. In comparison, the linear calibration range of the HRP/Tb-modified electrode was only up to 0.07 mM with the sensitivity of about 21.1 μA mM^{-1} (curve a, inset A in Fig. 6). Furthermore, the detection limit of HRP/Tb–MWCNT-modified electrode was estimated to be 1.7×10^{-6} M at a signal-to-noise ratio of 3, lower than those of 4.0×10^{-6} M reported in Ref. [27], 1.03×10^{-5} M at HRP cross-linked MWCNT/chitosan film [28], and 3.4×10^{-6} M based on the direct electrochemistry of hemoglobin [29].

The calibration curve of the sensor for H_2O_2 exhibited a typical characteristic of Michaelis–Menten kinetics at high concentrations. The apparent Michaelis–Menten constant (K'_m) was evaluated to be 0.16 mM derived from the Lineweaver–Burk equation. The value was similar to that of 0.12 mM at MB/HRP/CNT-modified electrode [18] and much smaller than the reported 23.85 mM based on the direct electrochemistry of HRP in sol–gel derived ceramic–CNT nanocomposite film [30], and 0.9 mM for HRP coimmobilized in MB–SiO_2 nanocomposite mixed gelatine matrix [27]. This result indicated that the immobilized HRP had higher biological affinity to H_2O_2.

The effects of common interfering species on the biosensor response were examined. After the injection of 10 μM H_2O_2, the amperometric response at the applied potential of −0.4 V increased greatly. The injection of the same concentration of ascorbic acid (AA) or uric acid (UA) did not cause interference to the amperometric response of H_2O_2 (inset B in Fig. 6).

To prove the precision and practicability of the proposed method, the reproducibility and storage stability of the biosensor were also examined. The relative standard deviation (R.S.D.) of the biosensor response to 10 mM H_2O_2 was 2.8% for eight successive measurements. When stored at 4 °C in air and measured everyday, it retained about 80% of its original sensitivity after 3 weeks. Both the reproducibility and the stability were better than those of 4.5% R.S.D. for eight repetitive measurements and retaining 80% of original sensitivity after 2 weeks at the electrode modified with MWCNT as a coimmobilization matrix to incorporate HRP and electron transfer mediator MB [18].

4. Conclusions

A simple method is proposed to prepare a kind of nanocomposites of MWCNT and electron transfer mediator with good dispersion in water. The nanocomposites can be conveniently used for preparation of amperometric biosensor by immobilizing enzyme on the surface of nanocomposites membrane with chitosan. The presence of MWCNT as a good conductor in the HRP/Tb–MWCNT system decreases the electron transfer impedance. The chitosan can maintain the enzymatic activity of the immobilized HRP. The synergy of MWCNT and Tb in the Tb–MWCNT nanocomposites enhances the electrocatalytic action of Tb to the enzymatic reduction of H_2O_2 by HRP and the electric communication between HRP and electrode, resulting in a sensitive amperometric sensor for H_2O_2. The proposed sensor shows good performance.

Acknowledgements

This work was supported by the National Science Fund for Distinguished Young Scholars (20325518) and Creative Research Groups (20521503), the Key Program (20535010) and Special Program (20745003) from the National Natural Science Foundation of China, and the Science Foundation of Jiangsu (BK 2007570).

References

[1] F.H. Wu, G.C. Zhao, X.W. Wei, Electrochem. Commun. 4 (2002) 690.
[2] X.X. Yan, D.W. Pang, Z.X. Lu, J.Q. Lu, H. Tong, J. Electroanal. Chem. 569 (2004) 47.
[3] W. Zhao, C. Song, P.E. Pehrsson, J. Am. Chem. Soc. 124 (2002) 12418.
[4] J. Wang, M. Musameh, Y.H. Lin, J. Am. Chem. Soc. 125 (2003) 2408.
[5] M.G. Zhang, A. Smith, W. Gorski, Anal. Chem. 76 (2004) 5045.
[6] H.T. Zhao, H.X. Ju, Anal. Biochem. 350 (2006) 138.
[7] P. Santhosh, K.M. Manesh, A. Gopalan, K.P. Lee, Anal. Chim. Acta 575 (2006) 32.
[8] X. Lu, Z.F. Chen, Chem. Rev. 105 (2005) 3643.

[9] J. Zhang, J.K. Lee, Y. Wu, R.W. Murray, Nano Lett. 3 (2003) 403.
[10] Y.M. Yan, M.N. Zhang, K.P. Gong, L. Su, Z.X. Guo, L.Q. Mao, Chem. Mater. 17 (2005) 3457.
[11] Q.W. Li, J. Zhang, H. Yan, M.S. He, Z.F. Liu, Carbon 42 (2004) 287.
[12] M.G. Zhang, W. Gorski, Anal. Chem. 77 (2005) 3960.
[13] M.G. Zhang, W. Gorski, J. Am. Chem. Soc. 127 (2005) 2058.
[14] N.S. Lawrence, J. Wang, Electrochem. Commun. 8 (2006) 71.
[15] K. Zhao, H.Y. Song, S.Q. Zhuang, L.M. Dai, P.G. He, Y.Z. Fang, Electrochem. Commun. 9 (2007) 65.
[16] J.X. Zeng, W.Z. Wei, L. Wu, X.Y. Liu, K. Liu, Y. Li, J. Electroanal. Chem. 595 (2006) 152.
[17] D.R. Shobha Jeykumari, S. Ramaprabhu, S. Sriman Narayanan, Carbon 45 (2007) 1340.
[18] J.Z. Xu, J.J. Zhu, Q. Wu, Z. Hu, H.Y. Chen, Electroanalysis 15 (2003) 219.
[19] T. Sagara, K. Niki, Langmuir 9 (1993) 831.
[20] F.Y. Cheng, A. Adronov, Chem. Eur. J. 12 (2006) 5053.
[21] K.J. Feng, Y.H. Yang, Z.J. Wang, J.H. Jiang, G.L. Shen, R.Q. Yu, Talanta 70 (2006) 561.
[22] K. Aoki, H. Kaneko, J. Electroanal. Chem. 247 (1988) 17.
[23] J.B. Jia, B.Q. Wang, A.G. Wu, G.J. Cheng, Z. Li, S.J. Dong, Anal. Chem. 74 (2002) 2217.
[24] S.Z. Zong, Y. Cao, Y.M. Zhou, H.X. Ju, Langmuir 22 (2006) 8915.
[25] X.L. Luo, A.J. Killard, A. Morrin, M.R. Smyth, Anal. Chim. Acta 575 (2006) 39.
[26] X. Yu, D. Chattopadhyay, I. Galeska, F. Papadimitrakopoulos, J.F. Rusling, Electrochem. Commun. 5 (2003) 408.
[27] H. Yao, N. Li, S. Xu, J.Z. Xu, J.J. Zhu, H.Y. Chen, Biosens. Bioelectron. 21 (2005) 372.
[28] L. Qian, X.R. Yang, Talanta 68 (2006) 721.
[29] Y. Wang, W.P. Qian, Y. Tan, S.H. Ding, H.Q. Zhang, Talanta 72 (2007) 1134.
[30] H.J. Chen, S.J. Dong, Biosens. Bioelectron. 22 (2007) 1811.

Available online at www.sciencedirect.com
ScienceDirect
Talanta 74 (2008) 625–631
Talanta
www.elsevier.com/locate/talanta

Determination of trace glucose and forecast of human diseases by affinity adsorption solid substrate-room temperature phosphorimetry based on triticum vulgaris lectin labeled with dendrimers-porphyrin dual luminescence molecule

Jia-Ming Liu [a,*], Zhen-Bo Liu [b], Guo-Hui Zhu [c], Xue-Lin Li [a], Xiao-Mei Huang [c], Fei-Ming Li [a], Xiu-Mei Shi [a], Li-Qing Zeng [a]

[a] *Department of Chemistry and Environmental Science, Zhangzhou Normal College, Zhangzhou 363000, PR China*
[b] *Department of Orthopedics and Traumatology, Fujian College of Traditional Chinese Medicine, Fuzhou, 363000, PR China*
[c] *Department of Food and Biological Engineering, Hangzhou Institute of Technology, Zhangzhou, 363000, PR China*

Received 4 August 2006; received in revised form 3 December 2006; accepted 23 June 2007
Available online 5 July 2007

Abstract

In this paper, 3.5-generation polyamidoamine dendrimers (3.5G-D)-porphyrin (P) dual luminescence molecule (3.5G-D-P) was developed as a new phosphorescence-labeling reagent. Meanwhile, the room temperature phosphorescence (RTP) characteristics of 3.5G-D-P and its product of labeling triticum vulgaris lectin (WGA) on the surface of polyamide membrane (PAM) were studied. Results showed that in the presence of heavy atom perturber LiAc, 3.5G-D and P of 3.5G-D-P molecule could emit strong and stable RTP on the PAM. And the Tween-80 would spike thoroughly the phosphorescence signal of 3.5G-D and P; moreover, specific affinity absorption (AA) reaction between the products (Tween-80-3.5G-D-P-WGA) of WGA labeled with Tween-80-3.5G-D-P and glucose (G) was carried out. The products of the AA reaction could keep good RTP characteristics of 3.5G-D and P dual luminescence molecule, and the ΔI_p was linear correlation to the content of G. According to the facts above, a new method of affinity adsorption solid substrate-room temperature phosphorimetry (AA-SS-RTP) for the determination of trace G was established, basing on WGA labeled with Tween-80-3.5G-D-P dual luminescence molecule. The detection limit of this method was 0.13 fg spot^{-1} (1.7×10^{-12} mol l^{-1}, 3.5G-D) and 0.14 fg spot^{-1} (2.2×10^{-12} mol l^{-1}, P). Determination of G in human serum using excitation/emission wavelength of either 3.5G-D or P, the result was coincided with enzyme-linked immunosorbent assay (ELISA). Not only the sensitivity and accuracy of this method were higher, but also the flexibility of AA-SS-RTP was obviously improved and the applicability was wider.
© 2007 Elsevier B.V. All rights reserved.

Keywords: Glucose; Dendrimers-porphyrin; Label; Triticum vulgaris lectin; Affinity adsorption solid substrate-room temperature phosphorimetry

1. Introduction

As protein and nucleic acid, glucose (G) is also a very important biological macro molecule [1] which is the carrier of information with high density and the continuation of gene information. G joins in many processes of physiology and pathology, and many occurrences and cures of diseases are something of it [2]. In recent years, the researches on G function have made great progress; meanwhile, it has brought forward a new challenge for the determination of G analysis [3]. There are many methods on the determination of G at home and abroad. Such as surface-enhanced Raman spectroscopy (detection limit: 4.6×10^{-4} mol) [4], flow-injection analysis (detection limit: 1.0×10^{-6} mol l^{-1}) [5], iodide ion selective electrode (linear range is 75–650 mg glucose/100 ml) [6], rapid enzymatic chemiluminescent assay (detection limit: 4.0×10^{-6} mol l^{-1}) [7], nafion modified electrode assay (detection limit: 3.0×10^{-5} mol) [8], novel reverse photoinduced electron transfer (LD: 5×10^{-5} mol l^{-1}) [9], etc. But these methods could not meet the requirement of determination of the low content of G in biological samples with the disadvantages of low sensitivity. Obviously, searching for a method with high sensitivity and precision for the determination of G has an important academic research value and application prospects, meanwhile,

* Corresponding author. Tel.: +86 596 2591352.
E-mail address: zzsyliujiaming@163.com (J.-M. Liu).

0039-9140/$ – see front matter © 2007 Elsevier B.V. All rights reserved.
doi:10.1016/j.talanta.2007.06.040

it has significance in prediction, prevention and cure of human diseases.

There have some reports about the determination of trace alpha fetoprotein (detection limit: 6.7 fg spot^{-1}, corresponding concentration: 17 ng l^{-1}) [10] by solid substrate-room temperature phosphorimetry (SS-RTP), indicating that SS-RTP has high sensitivity and wide application prospects. And searching for a phosphorescence-labeling reagent with high quantum efficiency is one of the basic ways to further improve the sensitivity of SS-RTP. Fluorescence labeling reagents, such as antibody-FITC, antibody-dendrimers-FITC and dendrimers-FITC conjugate compounds, have been developed at abroad [11]. When antigen was added to the fluorescence labeling reagents mentioned above, much stronger fluorescence signal was obtained than that of antibody-FITC, which was named as a strategic method of signal magnification.

We suppose to use 3.5-generation polyamidoamine dendrimers (3.5G-D) to react with porphyrin (P) to form 3.5G-D-P labeling reagent. In the disturbance of heavy atom, the rigid construction of 3.5G-D-P molecule was used to make 3.5G-D-P emit room temperature phosphorescence (RTP) of 3.5G-D and P. Meanwhile, a new dual luminescence molecule 3.5G-D-P was developed as phosphorescence labeling reagent, which would broaden the analytical application of dendrimers in SS-RTP.

It was found in the research that in the presence of heavy atom perturber LiAc, 3.5G-D and P of 3.5G-D-P molecule could emit strong and stable RTP signal on the surface of polyamide membrane (PAM). Tween-80 could spike thoroughly the phosphorescence signal of 3.5G-D and P (When the system added Tween-80, the ΔI_p improved once (P) or twice (3.5G-D) more than that without it). Specific affinity adsorption (AA) reaction between the products (Tween-80-3.5G-D-P-WGA) of triticum vulgaris lectin (WGA) labeled with Tween-80-3.5G-D-P and G was carried out. The products of the reaction could keep good characteristics of RTP of 3.5G-D and P dual luminescence molecule, and the ΔI_p was linear correlation to the content of G. According to the facts above, a new method of affinity adsorption solid substrate-room temperature phosphorimetry (AA-SS-RTP) for the determination of trace G was established, basing on WGA labeled with Tween-80-3.5G-D-P dual luminescence molecule. The detection limits of the method were 0.14 fg spot^{-1} with 3.5G-D and 0.17 fg spot^{-1} with P for sandwich method, respectively, and the sensitivity was obviously high. Determination of G in human serum using excitation/emission wavelength of either 3.5G-D or P, the result was coincided with enzyme-linked immunosorbent assay (ELISA), the flexibility of AA-SS-RTP was obviously improved and the applicability was wider. Moreover, the determination of trace G by AA-SS-RTP based on dendrimer-porphyrin dual luminescence molecule labeling WGA has not yet been reported.

2. Experimental

2.1. Apparatus and reagents

Phosphorescent measurements were carried out on a LS-55 luminescence spectrophotometer with a front-surface attachment (Perkin Element Corporation of America). The instrument's main parameters are as follows: delay time 0.1 ms, gate time 2.0 ms, cycle time 20 ms, flash count 1, Ex Slit 10 nm, Em Slit 10 nm, scan speed 1500 nm min^{-1}. A KQ-250B ultrasonic washing machine (Ultrasonic Machine Company Limited of Kunshan), an AE240 electronic analytical balance (Mettler-Toledo Instruments Company Limited), and a 0.5 μl flat head micro-injector (Medical Laser Instrument Plant) were used.

G (*N*-Acetyl-D-glucosamine), BSA (bovine serum albumin), WGA (triticum vulgaris lectin) are all from Sigma Corporation and stored at 0–4 °C. 700.0 ng ml^{-1} WGA, 10 mg ml^{-1} BSA, 1.0×10^{-3} mol l^{-1} 3.5G-D, 1.0×10^{-3} mol l^{-1} porphyrin (P), 3.5G-D-P (synthesized by ourselves), 1% Tween-80, Na_2CO_3–$NaHCO_3$ buffer solution, Tris (hydroxymethyl aminomethane), HCl, NaCl, Tween-20, LiAc, HAc, etc. All reagents were A.R. grade except that G and BSA were of biological reagents. The used water was distilled three times.

Preparation of 0.067 mol l^{-1} KH_2PO_4–Na_2HPO_4 buffer solution: 192 ml of 0.067 mol l^{-1} KH_2PO_4 and 808 ml of 0.067 mol l^{-1} Na_2HPO_4 were mixed together. The pH value was 7.40 at 20 °C.

Preparation of 0.1 mol l^{-1} Na_2CO_3–$NaHCO_3$ buffer solution: 200 ml of 0.1 mol l^{-1} Na_2CO_3 and 800 ml of 0.1 mol l^{-1} $NaHCO_3$ were mixed together. The pH values were 9.40 at 20 °C and 9.12 at 37 °C.

Preparation of 0.05 mol l^{-1} Tris–HCl buffer solution: 250 ml of 0.2 mol l^{-1} Tris and 400 ml of 0.1 mol l^{-1} HCl containing 150 mmol l^{-1} NaCl were mixed together, and then the mixture was diluted to 1000 ml with water. The pH value was 7.40 at 25 °C.

Preparation of washing buffer solution (Tris–HCl–0.10% Tween-20): 1.00 ml of Tween-20, 250 ml of Tris solution (0.20 mol l^{-1}) and 400 ml of HCl solution (0.10 mol l^{-1}) containing 150 mmol l^{-1} NaCl were mixed together, and then the mixture was diluted to 1000 ml with water.

Preparation of solution contained BSA: BSA was diluted to 10.00 mg ml^{-1} with 0.10 mol l^{-1} Na_2CO_3–$NaHCO_3$ buffer solution and then stored at 4 °C for the following experiments.

Polyamide membrane (PAM), acetyl cellulose membrane (ACM), and nitrocellulose membrane (NCM) were purchased from Luqiaosijia biochemical plastic plant. The paper sheets were pre-cut into wafers ($\Phi = 1.5$ cm).

2.2. Experimental method

2.2.1. Labeling of WGA

0.4 μl of WGA with different concentrations (w/v, diluted with KH_2PO_4–Na_2HPO_4 buffer solution of pH 7.4) and volumes were suspended onto the indentation ($\Phi = 4$ mm) of PAM wafers by a 0.5 μl flat head micro-injector. Took PAM out, then 1.00 ml 1.0% (v/v) Tween-80 and 1.00 ml 1.0×10^{-3} mol l^{-1} 3.5G-D-P as the labeling reagents were added and stored at 37 °C for 2 h. Took it out and washed it by washing buffer solution, ultrasonic oscillation wash for three times in series to get rid of the remaining labeling reagent on PAM, then it was sipped up by filter paper for preparation. The optimal concentration and volume of label-

ing WGA were selected according to AA reaction with different concentrations of G and the phosphorescence measurements.

2.3. Affinity adsorption reaction and the measurement of RTP

The type of AA reaction used in this paper is sandwich method. To the indentation ($\Phi = 4$ mm) of PAM wafers, a 0.4 μl drop of WGA was suspended onto the indentation of membrane by a 0.50 μl micro-injector, then stored at 4 °C overnight. The substrate wafer was immersed into 10 mg ml^{-1} BSA solution for 0.5 h. 0.40 μl of different concentrations of G solution (diluted gradually with Na_2CO_3–$NaHCO_3$ buffer solution of pH 9.12) were suspended at the center of each sheet ($\Phi = 4$ mm) by a 0.50 μl micro-injector, after set at 37 °C for 2 h, washed for three times, sipped up by filter paper. Then a 0.4 μl drop of labeled WGA (Tween-80-3.5G-D-P-WGA) was suspended onto the indentation of membrane; after set at 37 °C for 2 h, washed for three times again, sipped up by filter paper; the substrate wafer was then immersed in LiAc solution for 10 s, then dried at 90 ± 1 °C for 2 min. Scanned its phosphorescence spectrum. At the same time, blank experiment was also conducted. The blank reagent phosphorescence intensity (Tween-80-3.5G-D-P-WGA, I_{p1}) and sample phosphorescence intensity (Tween-80-3.5G-D-P-WGA-G-WGA, I_{p2}) were recorded. Each sample was measured six times. Then ΔI_p (=I_{p2}–I_{p1}) were calculated.

3. Results and discussion

3.1. RTP Spectrum

3.1.1. Phosphorescence labeling reagent

The phosphorescence spectra for Tween-80-P, Tween-80-3.5G-D and Tween-80-3.5G-D-P were scanned according to the method mentioned above (Figs. 1 and 2, Tables 1 and 2). Results showed that both P ($\lambda_{ex}^{max}/\lambda_{ex}^{max}$ = 511.0/680.9, I_p = 34.3) and 3.5G-D ($\lambda_{ex}{}^{max}/\lambda_{em}{}^{max}$ = 475.4/645.1, I_p = 42.9) could emit strong and stable RTP on PAM, respectively. The phosphorescence intensity of P ($\lambda_{ex}^{max}/\lambda_{ex}^{max}$ = 511.30/680.8, I_p = 43.7, ΔI_p = 9.4) and 3.5G-D ($\lambda_{ex}^{max}/\lambda_{ex}^{max}$ = 477.0/644.4 °C, I_p = 57.9 ΔI_p = 15.1) increased in the presence of Tween-80. Obviously, Tween-80 could both increase the phosphorescence intensity of P and 3.5G-D. For 1.0 ml 3.5G-D-P, it also could emit RTP of P ($\lambda_{ex}^{max}/\lambda_{ex}^{max}$ = 550.4/711.5, I_p = 34.4) and 3.5G-D ($\lambda_{ex}^{max}/\lambda_{ex}^{max}$ = 510.4/675.4, I_p = 52.6) (Curve 4.4′), and the λ_{ex}^{max} of P and 3.5G-D was Einstein shifted by 29 and 30 nm, respectively. The RTP of P and 3.5G-D also increased in the presence of Tween-80 (Curve 5.5′), which indicated that Tween-80-3.5G-D-P preserved the good RTP characteristics of P and 3.5G-D with little change of the $\lambda_{ex}^{max}/\lambda_{ex}^{max}$.

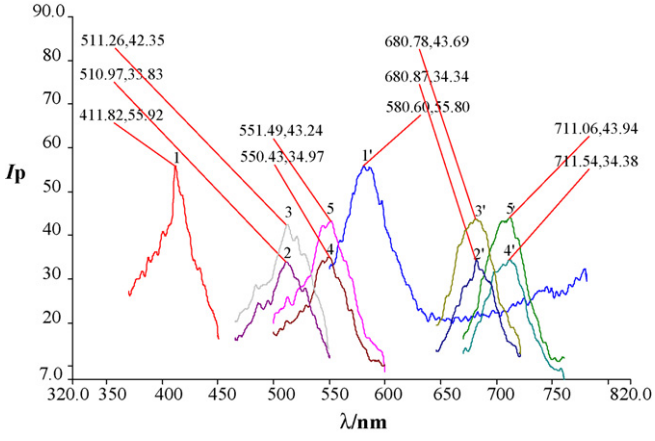


Fig. 1. The phosphorescence spectra for Tween-80-3.5G-D-P-WGA(P).

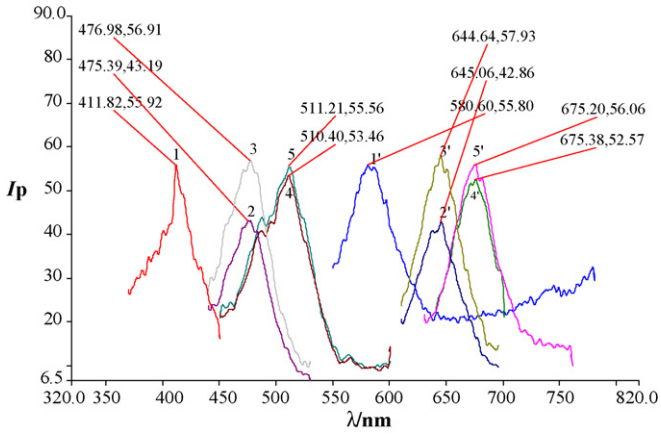


Fig. 2. The phosphorescence spectra for Tween-80-3.5G-D-P-WGA(3.5G-D).

Table 1
RTP characteristics of Tween-80-3.5G-D-P-WGA system (P)

System	λ_{ex} (nm)	λ_{em} (nm)	I_p	Note
1.1′ PAM	411.8	580.6	55.8	
2.2′ 1.0 ml P	511.0	680.9	34.3	P
3.3′ 2.2 + 1.0 ml Tween-80	551.3	680.8	43.7	P
4.4′ 1.0 ml 3.5G-D-P	550.4	711.5	34.4	P
5.5′ 4.4′ + 1.0 ml Tween-80	551.5	711.1	43.9	P

3.1.2. The product of the AA reaction

The phosphorescence spectra for the WGA-G-WGA-P-3.5G-D-Tween-80 system were scanned using sandwich method (Fig. 3 Fig. 4 Table 3). Results showed that when WGA labeled with Tween-80-3.5G-D-P, the $\lambda_{ex}^{max}/\lambda_{ex}^{max}$ of P and 3.5G-D were 550.2/710.1 and 509.1/675.5, respectively, and the I_p were 54.1 and 62.7, respectively. The I_p of P and 3.5G-D increased sharply in the presence of 700.0 pg G (the ΔI_p were 277.3 and 332.1, respectively), while the value of $\lambda_{ex}^{max}/\lambda_{ex}^{max}$ was almost the same, indicating that the product of the AA reaction (WGA-G-WGA-

Table 2
RTP characteristics of Tween-80-3.5G-D-P-WGA system (3.5G-D)

System	λ_{ex} (nm)	λ_{em} (nm)	I_p	Note
1.1′ PAM	411.8	580.6	55.8	
2.2′ 1.0 ml 3.5G-D	475.4	645.1	42.9	3.5G-D
3.3′ 2.2′ + 1.0 ml Tween-80	477.0	644.6	57.9	3.5G-D
4.4′ 1.0 ml 3.5G-D-P	510.4	675.4	52.6	3.5G-D
5.5′ 3.3′ + 1.0 ml Tween-80	511.2	675.2	56.1	3.5G-D

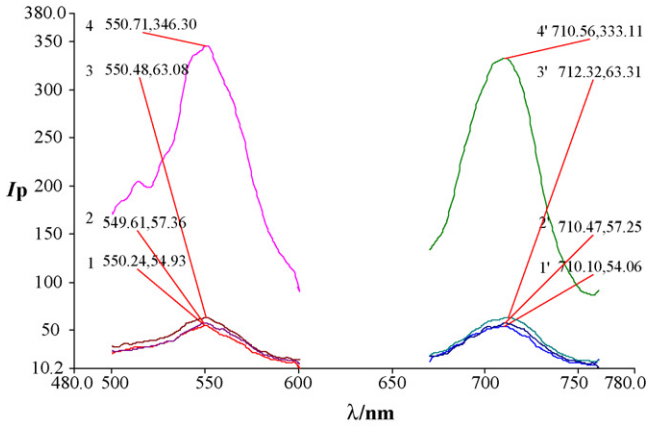


Fig. 3. The phosphorescence spectra by WGA-G-WGA-P-3.5G-D-Tween-80 method (P).

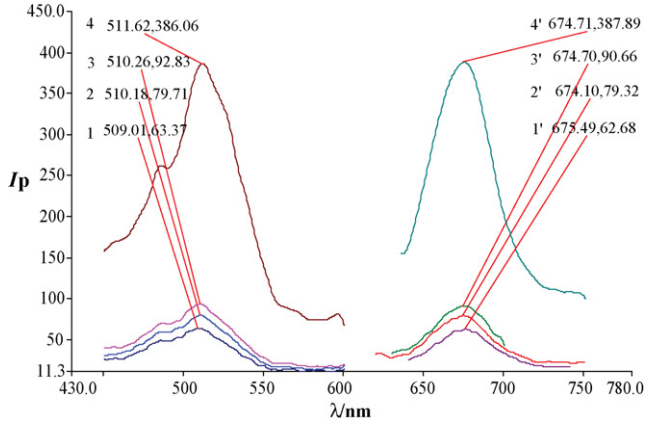


Fig. 4. The phosphorescence spectra by WGA-G-WGA-P-3.5G-D-Tween-80 method (3.5G-D).

P-3.5G-D-Tween-80) preserved the good RTP characteristics of P and 3.5G-D. So 510/675 or 550/711 nm was chosen as the working wavelength for the determination of trace G.

3.2. Optimum measurement conditions

3.2.1. Concentration and volume of reagent

For the system containing 60.0 fg G spot^{-1}, the effects of concentration and volume of reagents on ΔI_p were studied according to the experiment method mentioned above. Results showed that when 1.00 ml 1.0×10^{-3} mol l^{-1} P, 1.00 ml 1.0×10^{-3} mol l^{-1} 3.5G-D, 0.50 ml 1.0×10^{-3} mol l^{-1} 3.5G-D-P, 1.0 ml 1.0% Tween-80, 1.00 ml 700 ng ml^{-1} WGA were used, the ΔI_p of the system reached maximum and remained stable (Table 4).

3.2.2. Selection of solid substrate

For the system containing 60.0 fg G spot^{-1}, the effects of different solid substrates such as ACM, NCM and PAM on ΔI_p were studied according to the experiment method mentioned above. Results showed that ACM and NCM were not adaptable, as they would dissolve into the solution of the system. When PAM was used, the ΔI_p of 3.5G-D and P were 75.2 and 58.3, respectively. Furthermore the membrane has one bright side, which is easy to recognize and suspend, the soaking and drying of heavy atom perturbers carry on easily, and it can preserve good rigidity after washed for many times. So PAM is chosen in this experiment.

3.2.3. Selection of sensitizer

For the system containing 60.0 fg G spot^{-1}, the effects of different sensitizers such as Tween-80, sodium lauryl sulfonate, poly sodium acrylate, cetyl pyridinium bromide on ΔI_p were studied according to the experiment method mentioned above, respectively. Results showed that ΔI_p of P were 58.4, 42.4, 36.2, 30.1 and ΔI_p of 3.5G-D were 75.2, 57.0, 47.7, 43.2, respectively, so Tween-80 was chosen as the sensitizer. When Tween-80 was added, ΔI_p was once (P) or twice (3.5G-D) more than that without it. It might be that Tween-80 and 3.5G-D-P reacted to form the sensitized-micelle inclusion complex, which made the rigidity of 3.5G-D-P increase.

3.2.4. Ion perturbation

As we know, in the presence of heavy atom, fluorescence will obviously quench while phosphorescence is selectively enhanced. In the phosphorescence analysis, heavy atom effect is always used to enhance the solid substrate room temperature phosphorescence intensity and improve the fine structure of spectrum. Consequently, for the system containing 60.0 fg G spot^{-1}, the effects of ions such as 1.00 mol l^{-1} Mg^{2+}, Ca^{2+}, Li^{+} and Sr^{2+} on ΔI_p were examined according to the experiment method mentioned above, respectively. Results showed that ΔI_p of P were 31.3, 43.5, 58.4, 38.4 and ΔI_p of 3.5G-D were 42.7, 61.2, 75.2, 53.7, respectively, so Li^{+} was selected as ion perturber. Meanwhile, the effects of concentration of Li^{+} on ΔI_p were also examined. Results showed that when concentration of Li^{+} were 0.10, 0.50, 1.0, 1.5, 2.0 and

Table 3
RTP characteristics of WGA-G-WGA-P-3.5G-D-Tween-80 system (P and 3.5G-D)

System	λ_{ex}^{max} (nm)	λ_{ex}^{max} (nm)	I_p	ΔI_p	Note
1.1′ 3.5G-D-P + 700 ng WGA	550.2	710.1	54.1		P
	509.0	675.5	62.7		3.5G-D
2.2′ Tween-80-3.5G-D-P	549.6	710.5	57.2		P
+700 ng WGA	510.2	674.1	79.3		3.5G-D
3.3′ WGA + 1.0 pg G + WGA-P-3.5G-D-Tween-80	550.5	712.3	63.3		P
	510.3	674.7	90.7		3.5G-D
4.4′ WGA + 700 pg G + WGA-P-3.5G-D-Tween-80	550.7	710.6	333.1	277.3	P
	511.6	674.7	387.9	332.1	3.5G-D

Table 4
Optimization of the concentration and volume of reagents

Reagent	Concentrations or volumes	ΔI_p	Optimum
1.0×10^{-3} mol l^{-1}P (ml)	0.50, 0.10, 1.00, 2.00, 3.00	18.0, 37.9, 58.4, 58.2, 58.2 (P)	1.00 ml
1.0×10^{-3} mol l^{-1}3.5G-D (ml)	0.50, 0.10, 1.00, 2.00, 3.00	30.9, 44.5, 75.2, 75.1, 75.2 (3.5G-D)	1.00 ml
1.00 ml P($\times 10^{-3}$ mol l^{-1})	0.10, 0.50, 1.0, 1.5, 2.0	18.1, 38.0, 58.3, 58.3, 58.3 (P)	1.0×10^{-3} mol l^{-1}
1.00 ml 3.5G-D($\times 10^{-3}$ mol l^{-1})	0.10, 0.50, 1.0, 1.5, 2.0	30.9, 44.5, 75.2, 75.0, 75.1 (3.5G-D)	1.0×10^{-3} mol l^{-1}
1.0% Tween-80 (ml)	0.10, 0.50, 1.00, 2.00, 3.00	18.0, 38.0, 58.3, 58.2, 58.3 (P) 31.0, 44.6, 75.1, 70.7, 70.7 (3.5G-D)	1.00 ml
1.00 ml Tween −80 (%)	0.10, 0.50, 1.0, 1.50, 2.0	18.1, 38.0, 58.3, 58.2, 58.3 (P) 31.0, 44.5, 75.2, 75.2, 75.2 (3.5G-D)	1.0%
0.50 ml 3.5G-D-P (mol l^{-1})	0.050, 0.10, 0.50, 1.00, 2.00	18.0, 38.0, 58.3, 58.4, 58.4 (P) 30.9, 44.5, 75.2, 75.2, 75.2 (3.5G-D)	1.0×10^{-3} mol l^{-1}
1.0×10^{-3} mol l^{-1} 3.5G-D-P(ml)	0.05, 0.10, 0.50, 1.00, 1.50	18.0, 38.0, 58.3, 58.4, 58.4 (P) 30.9, 44.5, 75.2, 75.2, 75.2 (3.5G-D)	0.50 ml
700 ng ml^{-1} WGA (ml)	0.10, 0.50, 1.00, 1.50, 2.00	17.9, 38.0, 58.3, 58.4, 58.3 (P) 30.9, 44.5, 75.2, 75.2, 75.2 (3.5G-D)	1.00 ml
1.00 ml WGA (ng ml^{-1})	500.0, 600.0, 700.0, 800.0, 900.0	17.9, 38.0, 58.4, 58.3, 58.3 (P) 30.9, 44.5, 75.2, 75.2, 70.7 (3.5G-D)	700 ng ml^{-1}

Table 5
Analytical parameters

Method	Analytical range fg spot^{-1} (pg ml^{-1})	Regression equation fg spot^{-1}(pg ml^{-1})	Correlation coefficient (r)	Detection limit fg spot^{-1}(mol l^{-1})	R.S.D. (%)	Note
WGA-G-WGA-P-3.5G-D-Tween-80	4.0−320(10−800)	$\Delta I_p = 8.1430 + 0.8594\ m_G$	0.9994	0.14(2.2×10^{-12})	2.1−3.2	P
		$\Delta I_p = 15.653 + 0.9299 m_G$	0.9991	0.13(1.7×10^{-12})	1.6−2.9	3.5G-D

2.5, the ΔI_p of P of the system were 43.5, 58.3, 58.4, 58.3, 58.3 and 58.3, and the ΔI_p of 3.5G-D were 60.2, 75.1, 75.3, 75.2, 75.2 and 75.2, respectively. So 1.00 mol l^{-1} Li^+ was the optimal. For 3.5G-D-P, the heavy atom effects of Li^+ were obviously higher than that of perturbers commonly used such as Mg^{2+}, Ca^{2+} and Sr^{2+}. Meanwhile, the heavy atom effect of Li^+ was the highest and the phosphorescence intensity reached the maximum. This indicated the heavy atom effects of light element ions.

3.2.5. Time and temperature for desiccating

For the system containing 60.0 fg G spot^{-1}, the effects of desiccating temperature and time on ΔI_p were examined according to the experiment method mentioned above. Results showed that when the desiccating temperatures were 60, 70, 80, 90 and 95 °C, the ΔI_p of the P system were 42.3, 47.7, 51.0, 59.0 and 53.2; and the ΔI_p of the 3.5G-D system were 62.3, 65.6, 67.3, 75.2 and 66.5, respectively. When the desiccating time were 0.5, 1.0, 1.5, 2.0 and 2.5 min, the ΔI_p of the P system were 16.4, 30.2, 48.3, 57.9 and 50.4; and the ΔI_p of the 3.5G-D system were 20.4, 38.6, 52.5, 75.2 and 67.5, respectively. When the desiccating temperature and time were 90 °C and 2 min, respectively, the ΔI_p reached maximum and remained stable.

3.2.6. Oxygen and humidity

For the system containing 60.0 fg G spot^{-1}, the effects of oxygen and humidity on ΔI_p were examined according to the experiment method mentioned above. Results showed that when desiccated N_2 was passed for 5, 10 and 15 min, the ΔI_p of P and 3.5G-D were 58.3, 58.4, 58.3 and 75.3, 75.1, 75.2, respectively. When desiccated N_2 was not passed, the ΔI_p of P and 3.5G-D were 58.2, 58.3, 58.1 and 75.2, 75.3, 75.1, respectively. Results

Table 6
Effects of coexistent materials

Coexistent materials	This method		Ref. [9] method		
	The allowed concentration (multiple)	Relative error (%)	The allowed concentration (multiple)		Relative error (%)
	90	1.3	5	No interference	–
Saccharose	500	2.8	20	No interference	–
Serum protein	450	3.7	20	No interference	–
Glutamic acid	500	1.2	20	No interference	–
Uric acid	450	2.4	20	No interference	–
Ascorbic acid	13	3.2	1	Critical interference	
Fructose					

Table 7
Phosphorescence lifetime of AA products

Method	Measurement wavelengths $\lambda_{ex}^{max}/\lambda_{ex}^{max}$ (nm)	Regression equation of the phosphorescence delay curve (ms, $n=5$)	Correlation coefficient (r)	Phosphorescence lifetime (τ) ms	Note
WGA-G-WG	550/710	$\ln I_p = 5.2849 - 0.01014t$	−0.9738	98.6	P
A-P-3.5G-D-Tween-80	510/675	$\ln I_p = 5.1199 - 0.00949t$	−0.9288	105.4	3.5G–D

showed that the system was remained stable whether desiccated N_2 was passed or not.

3.2.7. Stability of RTP emission

Under the optimal conditions above, when the time were 10, 20, 30, 40, 50, 60 and 70 min, the ΔI_p of the P system were 58.4, 58.4, 58.4, 58.4, 58.4, 60.3 and 62.0; and the ΔI_p of the 3.5G-D system were 75.2, 75.2, 75.2, 75.2, 75.2, 77.4, 79.2, respectively. It showed that the ΔI_p of the system almost stayed invariable and had good repeatability within 50 min.

3.3. Working curve, detection limit and precision

WGA labeled with Tween-80-3.5G-D-P was used to determine G by sandwich method according to the optimal conditions above. Results showed that the ΔI_p was linear correlation to the content of G. The working curve, correlation coefficient, the detection limit (calculated by 3Sb/k, Sb is the standard deviation of blank reagent; k is the slope of regression equation. $n=11$), R.S.D. (relative standard deviation) (%) were listed in Table 5. It showed that this method was of high sensitivity, wide linear range and good repeatability for determination of G.

3.4. Interference test

For the system containing 60.00 fg G spot^{-1}, the allowed concentration multiple of coexistent materials ($E_r = \pm 5\%$) were listed in Table 6 according to the experiment method mentioned above. The multiple of coexistent materials were higher than that mentioned in Ref. [9], which indicated this method had high selectivity.

3.5. Phosphorescence lifetime of immunoassay

For the sample containing 60.00 fg G spot^{-1}, phosphorescence lifetime (τ) can be calculated by phosphorescence delay method according to the experiment method mentioned in Ref. [12]. The regression equation of lnI_p–t, correlation coefficient (r) and the phosphorescence lifetime (τ) were listed in Table 7, respectively.

3.6. Analysis of samples

1.00 ml of the serums from nine persons (A, B, C, D, E, F, G, H and I who were hollow), were diluted with Na_2CO_3–$NaHCO_3$ buffer solution (pH 9.12) to 500.00 ml, then 1.00 ml of this solution was diluted to 100.00 ml, the contents of G in human serum were determined according to experimentation method. Meanwhile, a standard addition recovery experiment was also conducted. This method was compared with the determination results using glucose kit (Zhongsheng Beijing Biology Technique Co. ltd.) and HITACHI series auto-Biochemistry analyzer in the Zhangzhou Hospital of Chinese Medicine. The results were listed in Table 8.

Table 8
The analytical results of glucose in human serum ($n=8$)

Sample	This method obtained (mg ml^{-1})	Measurement wavelengths $\lambda_{ex}^{max}/\lambda_{ex}^{max}$ (nm)	R.S.D. (%)	Added (mg ml^{-1})	Recove (mg ml^{-1})	Percent recovery (%)	ELISA (mg ml^{-1})
Serum A	0.743	510/675	3.2	1.00	0.983	98.3	0.730
	0.746	550/711	3.6	1.00	1.02	102	0.728
Serum B	1.024	510/675	4.7	1.00	1.01	101	1.044
	0.997	550/711	4.1	1.00	0.99	99.0	1.012
Serum C	0.935	510/675	3.2	1.00	0.98	98.0	0.942
	0.941	550/711	2.9	1.00	1.00	100	0.953
Serum D	0.495	510/675	2.9	1.00	1.01	101	0.482
	0.486	550/711	3.7	1.00	0.979	97.9	0.475
Serum E	0.453	510/675	4.1	1.00	0.987	98.7	0.443
	0.469	550/711	3.9	1.00	1.00	100	0.456
Serum F	0.398	510/675	3.5	1.00	1.03	103	0.412
	0.406	550/711	3.0	1.00	1.01	101	0.415
Serum G	1.472	510/675	3.5	1.00	1.01	101	1.488
	1.465	550/711	2.9	1.00	0.998	99.8	1.478
Serum H	1.607	510/675	4.5	1.00	0.992	99.2	1.594
	1.592	550/711	4.3	1.00	0.998	99.8	1.583
Serum I	1.508	510/675	4.1	1.00	1.01	101	1.515
	1.514	550/711	4.0	1.00	0.994	99.4	1.529

From Table 8, we can see that the recovery of G in serum of the persons (A, B, C, D, E, F, G, H and I) is 97.9–103% and the R.S.D. is 2.9–4.7%, which showed that this method was of good precision and high accuracy. The level of G in serum of healthy human who is hollow is 0.702–1.098 (mg ml^{-1}); the level of G in serum of hypoglycemic suffer is lower than 0.504 (mg ml^{-1}); the level of G in serum of diabetic is equal to or higher than 1.26 mg ml^{-1}. So we can diagnose that A, B, C are of healthy human, D, E, F are of hypoglycemic suffer, and G, H, I are of diabetic suffer. The forecast was coincided with the results of clinical detection and diagnosis in the Zhangzhou Hospital of Chinese Medicine.

4. Conclusion

With the perturbation of Li^+, Tween-80-3.5G-D-P could emit RTP of P and 3.5G-D on PAM. Compared with the RTP of single P and 3.5G-D, the values of I_p were improved and $\lambda_{ex}{}^{max}$ were einstein shift by 29, 30 nm, respectively. The reason might be that –OH in P reacted with $-OCH_3$ in 3.5G-D to eliminate CH_3OH to form the new compound 3.5G-D-P [13]. When WGA labeled with Tween-80-3.5G-D-P, –OH in P reacted with –COOH in WGA to eliminate H_2O. The product of the reaction was 3.5G-D-P-WGA which could slightly enhance the I_p of 3.5G-D and P. The AA reaction between WGA-3.5G-D-P-Tween-80 and G could be carried out. The reason might be $-NH_2$ in WGA reacted with –OH in G to eliminate H_2O, and the product of the reaction was WGA-G-WGA-P-3.5G-D-Tween-80, which could sharply enhance the RTP signals of 3.5G-D and P. The $\lambda_{ex}^{max}/\lambda_{ex}^{max}$ of the products by labeling reaction and AA reaction was unchanged, so we could use $\lambda_{ex}^{max}/\lambda_{ex}^{max}$ of 3.5G-D-P, 3.5G-D or P to determine trace G. The mechanism for the determination of G using AA-SS-RTP by WGA labeled with Tween-80-3.5G-D-P needs further discussion.

WGA was labeled with Tween-80-3.5G-D-P, which was used as a new phosphorescence labeling reagent. Specific AA reaction between the labeling product (WGA-3.5G-D-P) and G was carried out. The product of AA reaction could preserve good characteristics of RTP of 3.5G-D and P. Using excitation/emission wavelength of either 3.5G-D or P to determine the content of G in human serum; the result was coincided with ELISA. The method greatly improved the applicability and flexibility of AA-SS-RTP. This not only develops a new application of dendrimers and lectin, but also promotes the research development of SS-RTP, dendrimers and lectin.

Acknowledgement

This work was supported by Fujian Province Natural Science Foundation (Grant No. C 0510028, D 0510027)

References

[1] S.Z. Zhang, Chem. Life 19 (1999) 103.
[2] Y.G. Tang, Chemistry in Life: Important Chemical Problems in Life Process, Hu'nan Science & Technology Press, Changsha, 1997, 24.
[3] L. Zhang, N. Li, F.L. Zhao, K.A. Li, Chin. J. Anal. Chem. 33 (2005) 1023.
[4] Z.S. Wu, G.Zh. Zhou, J.H. Jiang, G.L. Shen, R.Q. Yu, Talanta 70 (2006) 533–539.
[5] E. Turkusic, J. Kalcher, E. Kahrovic, N.W. Beyene, H. Moderegger, E. Sofic, S. Begic, K. Kalcher, Talanta 65 (2005) 559.
[6] G. Somer, G. Ekmekci, Talanta 65 (2005) 87.
[7] P. Panoutsou, A. Economou, Talanta 67 (2005) 603.
[8] I.L.D. Mattos, M.C.D.C. Areias, Talanta 66 (2005) 1281.
[9] S.H.L. Wei, G.H. Deng, Chin. J. Anal. Chem. 29 (2001) 425.
[10] S.R. Hu, J.M. Liu, T.L. Yang, H.Z. Liu, J.L. Huang, Q.W. Lin, G.H. Zhu, X.M. Huang, Microchim. Acta 152 (2005) 53.
[11] K.K. Ong, A.L. Jenkins, R. Cheng, D.A. Tomalia, H.D. Durst, J.L. Jensen, P.A. Emanuel, C.R. Swim, R. Yin, Anal. Chim. Acta 444 (2001) 143.
[12] Y.S. Wei, W.J. Jin, Y. Yang, C.S. Liu, Chin. J. Anal. Chem. 26 (1998) 515.
[13] N.J. Duan, J.H. Zhong, H. Chen, J. Hubei Univ. (Nat. Sci.) 19 (1997) 69.

Available online at www.sciencedirect.com
ScienceDirect
Talanta 74 (2008) 887–895
Talanta
www.elsevier.com/locate/talanta

Quantification of pegylated liposomal doxorubicin and doxorubicinol in rat plasma by liquid chromatography/electrospray tandem mass spectroscopy: Application to preclinical pharmacokinetic studies

Yanhong Liu [a], Yuhui Yang [b,*], Xiangtao Liu [a], Tao Jiang [a]

[a] *Key Laboratory of Animal Virology of Ministry of Agriculture, State Key Laboratory of Veterinary Etiological Biology, Lanzhou Veterinary Research Institute, Chinese Academy of Agricultural Sciences, Lanzhou 730046, PR China*
[b] *Chrom-Matrix Inc., 2455 George Washington Way, Suite M271, Richland, WA 99354, United States*

Received 1 June 2007; received in revised form 22 July 2007; accepted 24 July 2007
Available online 31 July 2007

Abstract

A high-performance liquid chromatography–tandem mass spectrometric method (LC/MS/MS) has been developed and validated for the determination of pegylated liposomal doxorubicin and its metabolite doxorubicinol in rat plasma. One hundred microliters plasma samples were treated with Triton X-100 to immediately disperse the liposome. Then the samples were extracted by a single methanol:acetone protein precipitation step in the presence of additional 50 μL of 70% (w/v) zinc sulfate, and subsequently analyzed by LC/MS/MS using positive turbo-ion spray ionization mode operating the instrument in the multiple-reaction-monitoring (MRM) mode. The related compound daunorubicin was used as internal standard. The validated concentration ranges were from 20 to 8000 ng/mL for doxorubicin and from 0.05 to 20.0 ng/mL for doxorubicinol. An effective LC–MS/MS method was developed to quantify trace amount of doxorubicinol with little interference from doxorubicin. The autosampler carryover was minimized from 285 to 10.5% by increasing the washing times of the valves when the used pentafluorophenylpropyl HPLC column had no contribution to the carryover. The relative matrix effect from six unique lots was absent for both compounds. Results obtained from the GLP validation study demonstrated good accuracy (85–110%) and precision (CV less than 14%) across the calibration ranges for both compounds. This method was applied to study the pharmacokinetic profiles of doxorubicin and doxorubicinol in rats after a single dose administration of Stealth®-49 liposomal doxorubicin HCl. The mean AUC value for doxorubicinol was found to be only 0.011% of that of doxorubicin.
© 2007 Elsevier B.V. All rights reserved.

Keywords: Doxorubicin; Doxorubicinol; Liposome; LC–MS/MS; Carryover

1. Introduction

Doxorubicin is an anthracycline glycoside antibiotic originally produced by *Streptomyces peucetius* var. *caesius*. The drug displays a broad spectrum of anti-tumor activity, including activity against acute leukemia, Hodgkin's and Non-Hodgkin's lymphomas, breast cancer, lung cancers and sarcomas [1]. It is one of the most important anticancer agents in use [1]. However, the clinical use of doxorubicin is hampered by dose-dependent myelosuppression, a significant incidence of irreversible cardiotoxicity, and the occurrence of intrinsic or acquired drug resistance [2]. There is a growing body of evidence to suggest that its metabolite, doxorubicinol, is cytotoxic and may be responsible for some of the major adverse effects, especially on the heart [3]. In order to alleviate acute toxicities and chronic cardiomyopathy associated with administration of conventional doxorubicin injection, while maintaining or improving its antitumor effect, PEGylated liposomal (Stealth®) doxorubicin with a prolonged duration of circulation in the plasma and increased microvascular permeability of the tumors has been developed and approved as clinical products in the US (Doxil®, Johnson & Johnson, Mountain View, CA, USA) and in Europe (Caelyx®, Schering-Plough). A similar product, Doxorubicin Liposome, has also been successfully developed in China as the clinical product by Shanghai Fudan-Zhangjiang BioPharmaceutical Co. Ltd.

To date, a number of publications have been reported for the quantification of pegylated liposomal doxorubicin in order

* Corresponding author. Tel.: +1 2146369175; fax: +1 9726925198.
E-mail address: yyang@chrom-matrix.com (Y. Yang).

0039-9140/$ – see front matter © 2007 Elsevier B.V. All rights reserved.
doi:10.1016/j.talanta.2007.07.022

to establish and optimize its pharmacokinetics and biodistribution profiles [4–9]. Nevertheless, little information regarding the pharmacokinetics and toxicokinetics of the active doxorubicin metabolite, doxorubicinol, has been obtained. The present study reveals that when the pegylated liposomal doxorubicin HCl is administrated by intravenous infusion, the concentration of doxorubicinol is actually from a few thousand up to twenty thousand times less than its parent. Because of insufficient selectivity and sensitivity, doxorubicinol concentrations in the biological samples administrated with the liposomal doxorubicin cannot be determined by the conventional LC-fluorescence methods [4–7] and LC-UV method [8]. A liquid chromatography/electrospray tandem mass spectrometry had also been developed by Arnold et al. [9] for quantification of pegylation liposomal doxorubicin and metabolites in rat plasma and tissue samples. Because of insufficient selectivity, doxorubicinol as well as the other metabolites in the biological samples could not be quantitatively measured by the method [9]. On the other hand, the concentration–time profiles of doxorubicinol in the biological samples administrated with non-liposomal doxorubicin (such as Adriamycin, an earlier version of free doxorubicin formulation) have been reported [10–13]. The information provided by these studies are valuable for a reference purpose, but cannot be used for the prediction of toxicity of liposomal doxorubicin because liposomal drugs should be regarded as new entities different from free drugs [14,15]. It is well known that the pegylated liposomal encapsulation dramatically changes drug pharmacokinetics and profoundly leads to a marked change in toxicity profile compared to non-liposomal doxorubicin [5,6,14,15].

This report develops a fast, sensitive, selective and robust LC/MS/MS method for the simultaneous analysis of pegylated liposomal doxorubicin and doxorubicinol in rat plasma. The method has been fully validated according to US FDA bioanalytical validation guidelines [16] and then applied to determine the concentration–time profiles of doxorubicin and doxorubicinol in rats to which an intravenous bolus injection of 5 mg/kg Stealth®-49 liposomal doxorubicin HCl is given. The data for reproducibility, accuracy, matrix effects and stability is presented. An optimized LC/MS/MS method is developed to minimize the carryover effect and quantify trace amount of doxorubicinol with little interference from doxorubicin.

2. Experimental

2.1. Chemicals

Daunorubicin hydrochloride, doxorubicin hydrochloride and doxorubicinol hydrochloride were ≥98% pure and were from Chrom-Matrix Inc. (Richland, WA, USA). Triton X-100 and 5-sulfosalicyclic acid were purchased from Sigma–Aldrich (St. Louis, MI, USA). Methanol, acetone and acetonitrile were of chromatographic or optima grade and originated from Fisher Scientific (Bridgewater, NJ, USA). Water was purified and deionized by the Milli-Q-UF system (Millipore, Milford, MA, USA). Rat plasma was from Bioreclamation (Hicksville, NY, USA). Stealth®-49 liposomal doxorubicin HCl injection vials were obtained from Alza Pharmaceuticals (Palo Alto, CA, USA). The product appeared as a sterile, translucent, red liposomal dispersion in a 10-mL glass vial. It contained 2 mg/mL doxorubicin HCl.

2.2. Preparation of stock solutions, spiking solutions, calibration and quality control standards

2.2.1. Preparation of stock solutions and spiking solutions

The accurate amounts of drugs were weighted on a calibrated Mettler Toledo MX5 balance with a repeatability of 0.9 μg. Stock solutions of doxorubicin (0.8 mg/mL), doxorubicinol (0.8 mg/mL) and daunorubicin (0.8 mg/mL) were prepared by dissolving the accurate amount of drug in methanol:water (1:1, v/v) and stored in glass bottles protected against light at −40 °C. After weighted, the amount of doxorubicin, doxorubicinol, and danorubicin were corrected for free of hydrochloride and impurities. The daunorubicin stock solution (0.80 mg/mL) was diluted 4000-fold by the use of methanol:water (1:1, v/v) to make the internal standard at a concentration of 0.20 μg/mL. The internal standard was stored in a glass bottle protected against light at −40 °C prior to use.

The stock solutions of both doxorubicin and doxorubicinol were made in duplicates. It was found that the difference between the two doxorubicin stocks was 2.3% and the difference between the two doxorubicinol stoks was 1.5%. The stocks were found to be stable at least for 4 months.

One of the two set stocks was used to make nine calibration standard spiking solutions by a serial dilution. The other set of

Table 1
Summary of accuracy and precision

Analyte (QC)	Concentration (ng/mL)	Accuracy derivation (%)	Intra-assay CV (%) ($n = 6$)	Inter-assay CV (%) ($n = 18$)
Doxorubicinol (LLOQ)	0.0500	94.4	14.7	NA
Doxorubicinol (low)	0.150	103	7.8	10.2
Doxorubicinol (mid)	1.00	97.2	5.4	8.8
Doxorubicinol (high)	16.0	104	4.4	7.6
Doxorubicinol (dilution)	300	104	8.8	NA
Doxorubicin (LLOQ)	20.0	96.5	3.2	NA
Doxorubicin (low)	60.0	103	3.5	5.8
Doxorubicin (mid)	400	105	2.1	3.8
Doxorubicin (high)	6400	97.8	5.4	6.6
Doxorubicin (dilution)	1,200,000	95.3	11.2	NA

stock solutions were used to make five quality control standard spiking solutions.

2.2.2. Preparation of calibration standards

Nine calibration standards were freshly made daily. Ten microliters of a doxorubicin spiking solution and 10.0 μL of a doxorubicinol spiking solution were spiked into 980 μL rat plasma by using Gilson Microman® positive displacement pipettes to make a calibration standard. The dilution factor from the spiking solution to the corresponding calibration standard was 100. For the calibration standard curve, the final concentrations of doxorubicin and doxorubicinol in rat plasma were as follows: 20.0, 42.0, 90.0, 190, 400, 850, 1800, 3800, 8000 ng/mL for doxorubicin, and 0.0500, 0.100, 0.200, 0.500, 1.00, 2.00, 4.50, 9.50, 20.0 ng/mL for doxorubicinol. A similar protocol for preparing the calibration standards had been listed as Tables 1 and 2 in a previous publication in more detail [17]. The standard curve values were fixed according to the regression design.

2.2.3. Preparation of quality control standards

Two hundred microliters of a doxorubicin spiking solution and 200 μL of a doxorubicinol spiking solution were spiked into 19.6 mL rat plasma by using Gilson Microman® positive displacement pipettes to make a quality control standard at a volume of 20.0 mL. The final concentrations of doxorubicinol and doxorubicin in rat plasma are listed in Table 1.

The QC samples were stored in Sarstedt 0.5 mL polypropylene tubes with an O-ring sealed cap protected against light at −70 °C prior to use.

2.3. Liquid–liquid extraction

Extraction was executed in a yellow-light room.

Removed approximately 50 mL of rat plasma from storage and allowed it to equilibrate to room temperature for making calibration standards, dilution QCs and blanks. In addition, the QC standards (two 0.5 mL polypropylene tubes at each concentration level) were also removed from storage to equilibrate to room temperature.

After equilibration, 100 μL of blank plasma, QC standards as well as freshly made calibration standards were taken into 1.5-mL Eppendorf microcentrifuge polypropylene tubes.

Fifty microliters of the Diluted QC was mixed with 950 μL of rat plasma by using Gilson Microman® positive displacement pipettes to make 20-fold dilution. Then 100 μL of the diluted sample was taken into a 1.5-mL Eppendorf microcentrifuge polypropylene tube.

Ten microliters of the internal standard, daunorubicin at a concentration of 200 ng/mL was added in all the calibration and quality control standards by using an Eppendorf repeater. Ten microliters of blank solvent (methanol:water, 1:1, v/v) was added into the blank plasma to make one matrix blank. Ten microliters of the internal standard was added was added into 100 μL of the blank plasma to make one control blank.

For a typical validation batch, the sample sequence started from one matrix blank, the first calibration standard set, one control blank, six LLOQ QC, six Low QC, six Mid QC, six High QC, six Diluted QC, the second matrix blank, the second set of calibration standard and the second control blank.

Added 10 μL 3.0% (v/v) Triton X-100 into every sample vial. The mixture was vortexed for 10 s and 10 μL 65% (w/v) 5-sulfosalicylic acid dehydrate was added [5,8]. Vortexed for 30 s. Centrifuged at 15,000 rpm for 3 min. It was not necessary to decant isolate the supernatant from the sediment. Added 15 μL 3.0 M sodium acetate to buffer the pH of the supernatant. Added 50 μL of 70% (w/v) zinc sulfate into each vial. Vortexed for 30 s. Adding 1.0 mL of methanol:acetone (1:1, v/v) into each vial. Vortexed for another 5 min. Centrifuged at 15,000 rpm for 3 min. Transferred 900 μL of the supernatant from each vial into a blank 2-mL 96-well plate for evaporation to dryness at 45 °C. Finally, the dried samples were reconstituted with 90 μL of acetontrile:water:formic acid (30:70:0.1) for LC/MS/MS bioanalysis.

2.4. LC/MS/MS bioanalysis

The instruments used were a Perkin-Elmer Series LC-200 HPLC system, a CTC high-throughput autosampler and a Sciex API 4000 triple quadrupole mass spectrometer with a turbo-ionspray interface and the positive mode. The Analyst software (Version 1.4.1) was used to operate the integrated system.

An Innovation™ PFPP (silica-based pentafluorophenyl-propyl bonded phase) 3 μm 10 cm × 2.1 mm HPLC column from Chrom-Matrix Inc. (Richland, WA, USA) was used for the LC/MS/MS bioanalysis. Mobile phase A: DI water containing 0.1% formic acid; mobile phase B: acetonitrile containing 0.1% formic acid. Flow rate: 400 μL/min; injection volume: 80 μL. Needle rinse solution 1: methanol:water (50:50, v/v); needle rinse solution 2: acetonitrile:water (80:20, v/v). Before and after

Table 2
Relative matrix effect from six unique plasma spiked with Low-QC standards

	Lot 1	Lot 2	Lot 3	Lot 4	Lot 5	Lot 6
Doxorubicinol						
Mean concentration found (ng/mL)	0.154	0.145	0.158	0.160	0.141	0.138
CV (%) ($n=6$)	7.2	8.4	6.4	4.2	7.8	5.5
Accuracy derivation (%)	2.7	−3.3	5.3	6.7	−6.0	−8.0
Doxorubicin						
Mean concentration found (ng/mL)	60.4	58.2	57.4	61.8	63.8	65.2
CV (%) ($n=6$)	3.1	3.8	2.8	3.5	2.5	5.1
Accuracy derivation (%)	0.7	−3.0	−4.3	3.0	6.3	8.7

injections, the needle was washed by the needle rinse solutions twice, respectively. After each injection, the valve was washed by both of the needle rinse solutions four times, respectively. The 8-min HPLC gradient program was described below: In the first half minute, an isocratic run by 70% (v/v) mobile phase A and 30% mobile phase B (v/v); from 0.5 to 7.5 min, a linear gradient from 70% (v/v) mobile phase A to 55% (v/v) mobile phase A; from 7.5 to 7.7 min, an isocratic run at 55% (v/v) mobile phase A; from 7.7 to 7.8 min, a linear gradient from 55% (v/v) mobile phase A to 70% (v/v) mobile phase A; from 7.8 to 8.0 min, an isocratic run by 70% (v/v) mobile phase A and 30% mobile phase B (v/v).

Doxorubicinol, doxorubicin and daunorubicin were determined by MRM scan mode. Dwell times were 150 ms for all the compounds. MRM transitions were 546 → 363 (doxorubicinol), 544 → 361 (doxorubicin) and 528 → 321 (daunorubicin). The declustering potential (DP) values for doxorubicinol were 62 (doxorubicinol), 100 (doxorubicin) and 50 (daunorubicin). The collision energy (CE) values were 35 (doxorubicinol), 50 (doxorubicin) and 26 (daunorubicin). The collision exit potential (CXP) values were 10 (doxorubicinol), 15 (doxorubicin) and 26 (daunorubicin). Source temperature was set at 400 °C and the ion spray voltage was set at 4500 V. The mass spectrometric sensitivities were maximized for both doxorubicinol and daunorubicin under the current conditions. On the other hand, the used DP, CE and CXP values for doxorubicin were far from the best values in order to de-tune the MRM signal of doxorubicin and such a step effectively prevented the saturation of the mass spectrometer.

2.5. Method validation

The validation was done according to US FDA guidance for industry on bioanalytical method validation [16].

Three days of calibration curves, with six replicates of quality controls at each concentration level were performed to determine intraassay and interassay *variance* and accuracy. After the LC–MS/MS bioanalysis, the third batch was stored at 4 °C for a re-injection to establish a 48-h extraction stability.

In the third batch, the true recovery and absolute matrix effect were evaluated in both Low-QC and High-QC levels. Six extracted matrix blank were dried and then spiked with 90 μL of acetontrile:water:formic acid (30:70:0.1) containing Low-QC or High-QC concentration levels of doxorubicin and doxorubicinol. In addition, six replicate of 90 μL of acetontrile:water:formic acid (30:70:0.1) containing Low-QC or High-QC concentration levels of doxorubicinol and doxorubicin were added at the end of the running sequence. The absolute matrix effect and the true recovery were calculated by the comparison of the integration area.

The fourth batch was used to evaluate the relative matrix effect from six unique matrix lots, at the Low-QC level.

Finally, the stability of the biological samples at 4 °C, the matrix freeze/thaw (F/T) stability and a 3-month −70 °C storage stability were evaluated.

MRM chromatograms were automatically integrated using Analyst software and then the data were transferred into Watson LIMS (Innaphase, Version 6.4.0.02) to compute the least-square linear regression.

2.6. Administration of Stealth®-49 liposomal doxorubicin HCl to rats

The experimental animals were male Sprague–Dawley rats (225–249 g). The animals were housed, cared for, and used following an approved protocol in compliance with the guidelines of International Guiding Principles for Animals Research (WHO Chronicle, 39: 51–56, 1985; A CIOMS Ethical Code for Animal Experimentation). Animals were housed separately in a metabolic cage and kept on a 12-h light:12-h dark cycle for a minimum of 3 days before being used in experiments. Food and water were available *ad libitum*.

Under general anesthesia, a catheter was introduced into the rat jugular vein, positioned subcutaneously with the tip in the interscapular region. The rat was allowed to recover for 24 h, and the blood catheter was flushed with KCl 0.9% solution and K_3EDTA to avoid the possibility of clot obstruction. On the day of the experiment, Stealth®-49 liposomal doxorubicin HCl at a dose of 5 mg/kg was administrated intravenously within 4 min to five rats. Blood samples (150 μL) were serially collected prior to the injection (as the time zero), after 15, 30 min and 1, 2, 4, 8, 12, 18, 24, 36, 48, 60, 72, 84 and 96 h after the injection. Immediately after blood sampling, the tubes were centrifuged and the plasma supernatant was stored within 30 min at −70 °C prior to a dry-ice shipment.

2.7. Pharmacokinetics

The collected plasma was treated by Triton X-100 to disperse the liposome, followed by the internal standard spiking and then a protein precipitation step described above. When the preclinical samples were analyzed, only three replicates of quality control standards at each concentration level were used in each LC/MS/MS run, and the preclinical samples were set between quality control standards. The validated LC/MS/MS bioanalytical method was used to investigate the time courses of doxorubicin and doxorubicinol.

The plasma concentration data were fitted using Kinetica™ Version 4.0 pharmacokinetic software (Innaphase Corporation, PA, USA), to calculate the area under the concentration–time curve (AUC), half-life of the terminal phase of the plasma concentration decay curve ($T_{1/2}$), maximum concentration (C_{max}), plasma clearance (CLp) and volume of distribution at steady state (V_{dss}).

3. Results and discussion

3.1. Use of free doxorubicin for preparation of standard curves

For the determination of pegylated liposomal doxorubicin in plasma, free doxorubicin is used to prepare the calibration standards and quality control standards.

The use of pegylated liposomal doxorubicin as both of the standards would make the assay complicated. The concentration of clinical formulation of pegylated liposomal doxorubicin, Doxil®, remains unknown and the value varies by ±10% [18]. An additional HPLC method development and validation is necessary to measure the concentrations of Doxil® in specific lots prior to their uses for the preparation of the standards. Furthermore, a part of free doxorubicin would progressively release from Doxil® into plasma and rapidly redistribute into tissues. Thus, the separation of liposome-associated doxorubicin from protein-bond and free doxorubicin is required [19], and two sets of calibration standards and quality standards had to be used.

The present study is to just measure total doxorubicin in the plasma and not drug specificically entrapped in the liposome. This, however, may not be a preclinical and clinically important factor in the determination of pegylated liposomal pharmacokinetics since the pharmacokinetics of total and pegylated liposomal doxorubicin have been reported to be similar [8,20].

Triton X-100 is used to immediately disperse the liposome and release doxorubicin [8]. Chin et al. found that the relative recovery of doxorubicin from the pegylated liposomal doxorubin was almost identical (>96%) to that of free doxorubicin from plasma, suggesting that complete dispersion of the liposomal formation formulation occurred [8]. It also makes the uses of free doxorubicin calibration standards and quality control standards logical.

Methanol:acetone:zinc sulfate is used for the extraction of doxorubicin and doxorubicinol [17]. The use of zinc sulfate makes the protein precipitation thoroughly and enhances the detection sensitivity of doxorubicinol at low concentration [17]. When methanol is used as the sole solvent for extraction, a lot of inorganic salts including zinc sulfate move into the supernatant to contaminate the mass spectrometric sources. The addition of acetone into methanol successfully prevents water and water-soluable salt into the supernatant, making the reconstituted samples definitely cleaner [17].

3.2. LC/MS/MS method

The technical challenge for studying the pharmacokinetics profile of pegylated liposomal doxorubicin drug is how to accurately determine the concentrations of its metabolites, particularly doxorubicinol. The concentration of doxorubicin can be readily determined by all the published methods [4–9,14,19,20]. On the other hand, it is necessary to develop and optimized a novel LC/MS/MS method for determining the concentration of doxorubicinol after intravenous infusion administration of Stealth® liposomal doxorubicin.

The MRM chromatogram of doxorubicinol from a preclinical sample is shown as Fig. 1. The corresponding MRM chromatogram of doxorubicin is shown in Fig. 2.

The concentration of doxorubicinol is 6.75 ng/mL when the concentration of its parent, doxorubicin, is 74.3 μg/mL. The concentration ratio is 1:11,007. It is very difficult to use conventional HPLC-fluorescence and HPLC-UV detection for the determination of doxorubicinol due to inherently low instrument selectivity.

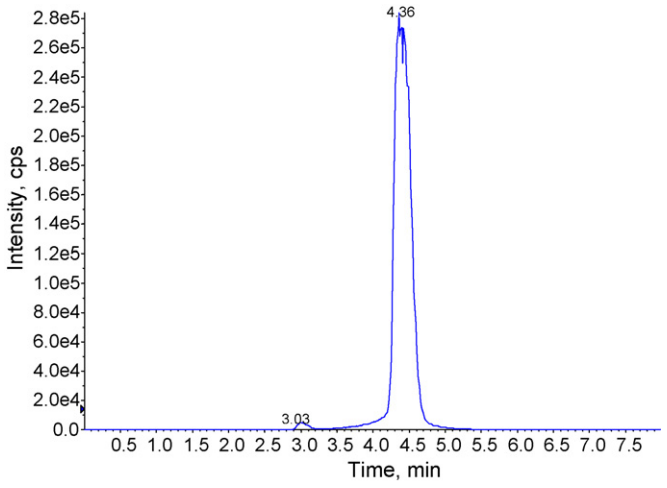


Fig. 1. MRM chromatogram of doxorubicinol in the extracted plasma at the 4-h time point after a male Sprague–Dawley rat was i.v. administrated with a single dosage of Stealth®-49 (5 mg/kg). The plasma sample was diluted ten times prior to the extraction.

The problem is solved here by an optimized LC–MS/MS method. Although the peak assigned to doxorubicin also exists in the MRM chromatogram of doxorubicinol (Fig. 1), its integration area in the doxorubicinol MRM channel is only 6.3% of the integration area from its own MRM channel (Fig. 2) due to high selectivity of MRM mode. As a result, the small peak assigned to doxorubicinol is observed when it is usually hidden into the huge background of doxorubicin when a conventional detection method is applied. It is noted that when the peak assigned to doxorubicin starts from 2.4 min in its own MRM channel (Fig. 2), the corresponding peak starts from 2.8 min in the MRM chromatogram of doxorubicinol (Fig. 1).

The other key to the success is to optimize the HPLC methodology. A lot of HPLC columns in both reversed phase and hydrophilic interaction modes have been tried with insufficient isolation between doxorubicinol and doxorubicin. Finally, the PFPP HPLC column used herein is found to offer acceptable results. In Fig. 1, a baseline isolation between doxorubicinol

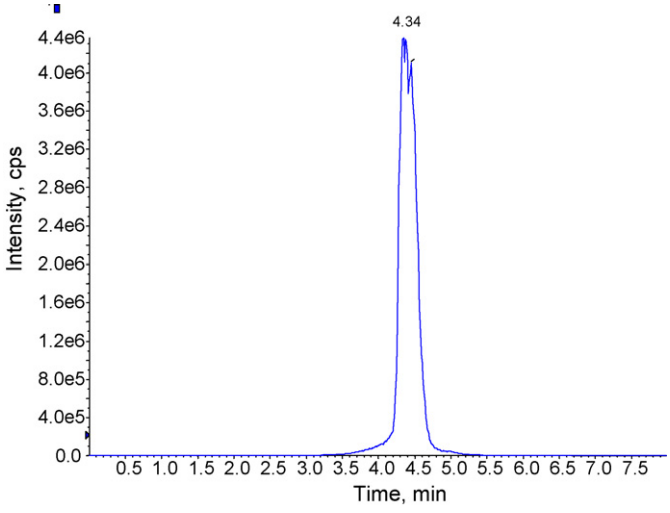


Fig. 2. MRM chromatogram of doxorubicin from the same sample above.

and doxorubicin is not reached. Although a longer column may offer better isolation, the current method has been able to reliably detect doxorubicinol in the preclinical samples. There is a compromise between the data quality and the production efficiency.

The selectivity of this method is also demonstrated by the absence of substantial endogenous interference (Figs. 1 and 2).

The MRM chromatogram of daunorubicin is shown in Fig. 3. Because of the longer retention time of daunorubicin, the running time for each injection has to be set for eight minutes. Nevertheless, the analytical time is still considerably shorter than the conventional HPLC-fluorescence and HPLC-UV methods [4–8]. The merit is important because a lot of samples could be analyzed without the concern about their extraction stability.

3.3. Carryover assessment

In the previous LC/MS/MS studies, carryover had not been mentioned [9,13]. However, the carryover is one of the important issues in bioanalysis [16]. In some cases, followed a sample injection, one or a couple of blank samples have to be injected for minimization of the carryover. Such a step would make high-throughput LC/MS/MS assay into a time-consuming process.

In the default Analyst® method, the syringe is pre-cleaned by two needle rinse solvents once, respectively, prior to the injection. After the injection, both of the syringe and the valve are cleaned by each solvent once. Zero blank is used to evaluate the carryover effect from the highest calibration standard. The LC/MS/MS MRM chromatogram of doxorubicin in the zero blank is shown in Fig. 4. The LC/MS/MS MRM chromatogram of the lowest calibration standard is shown in Fig. 5.

It is found that the carryover from the highest calibration standard for doxorubicin is equal to 285% of the integration area of the calibration standard one. In addition, 20 ng of doxorubicinol (the highest calibration standard) has a carryover equal to 0.25 ng of doxorubicinol. It is clearly unacceptable!

Generally speaking, the carryover in the LC–MS/MS has two sources. One is from the LC/MS/MS system and the other from the used HPLC column. The carryover from the LC/MS/MS system should be first eliminated or minimized. To identify the carryover from the system, no HPLC column is connected. Eighty microliters of the lowest calibration standard and then the highest calibration standard are injected into the mass spectrometer. After that, 80 μL of a blank sample (acetontrile:water:formic acid 30:70:0.1) is injected to record the carryover from the highest calibration standard. The integration area of doxorubicin from the blank is about three times than the value from the lowest calibration standard, implying that the carryover is from the system.

Most of the systematic carryovers can be readily solved by an empirical selection of autosampler rinse solutions and the optimization of rinse times in the LC/MS/MS method. In this present study, the needle is rinsed by the two needle rinse solutions three times, respectively, before and after the injection of

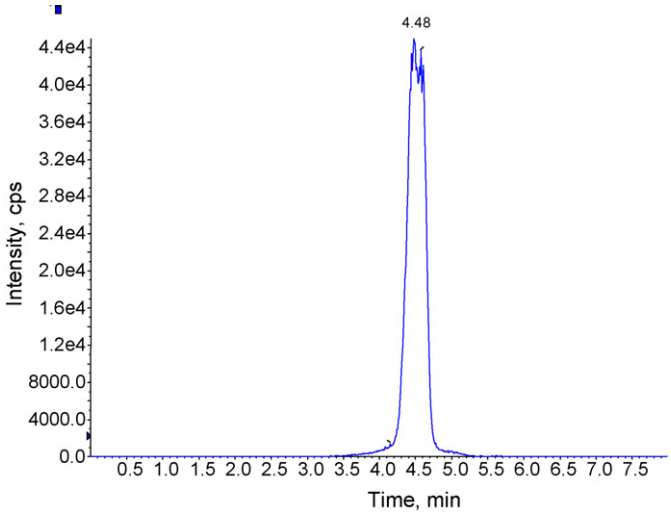


Fig. 4. MRM chromatogram of doxorubicin of the zero blank. After the highest calibration standard was injected, a zero blank was injected to make the carryover assessment. The syringe was pre-cleaned by two needle rinse solvents once, respectively, prior to the injection. After the injection, both of the syringe and the valve were cleaned by each solvent once.

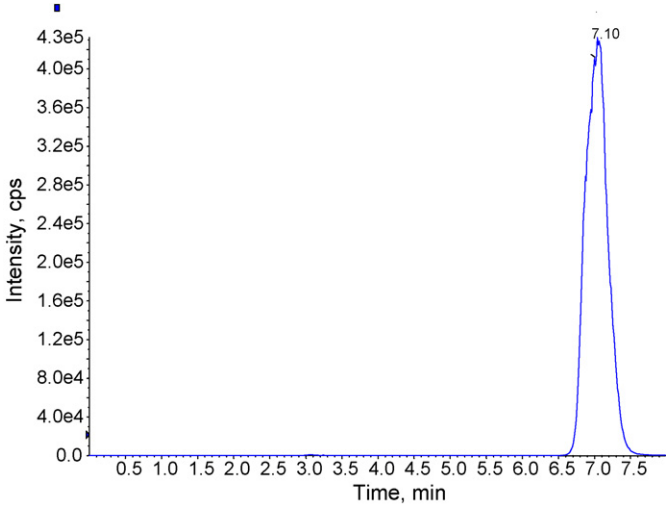


Fig. 3. MRM chromatogram of daunorubicin.

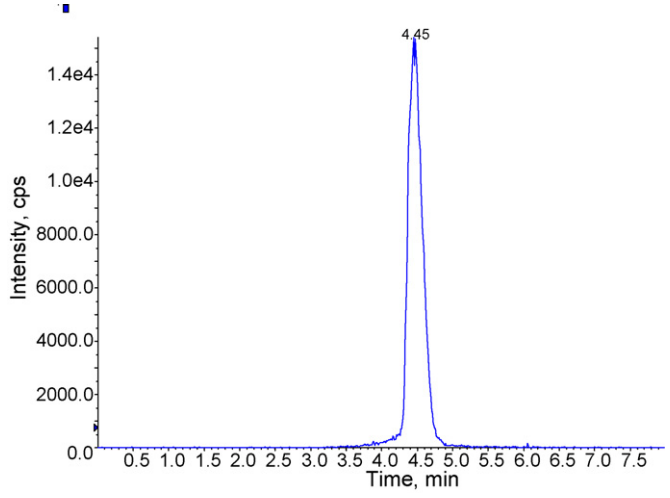


Fig. 5. MRM chromatogram of doxorubicin at a concentration of 20 ng/mL.

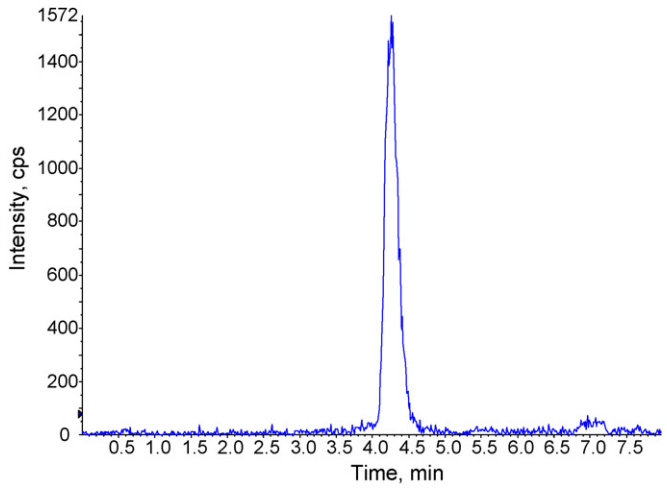


Fig. 6. MRM chromatogram of doxorubicin of the zero blank. In the optimized LC/MS/MS method, the syringe was rinsed by the two needle rinse solutions three times, respectively, before and after the injection of a sample. The valve from the leap technologies were washed four times after an injection by the two sets of the rinse solutions, respectively.

a sample. More importantly, the valve from the leap technologies are washed four times after an injection by the two sets of the rinse solutions, respectively, since the valve from Leap Technologies is the major source for the carryover.

With the use of the optimized aytosampler washing protocol, the LC/MS/MS MRM chromatogram of doxorubicin in the zero blank (after the injection of the highest calibration standard) is shown in Fig. 6.

In comparison between Figs. 5 and 6, the carryover becomes 10.5% for doxorubicin by the generic protocol mentioned above. In addition, the carryover for both doxorubicinol and daunorubicin becomes zero.

It must be mentioned when the PFPP HPLC column contributes little for the carryover because the carryover values between the flow injection (without column connection) and the LC/MS/MS MRM chromatogram are just identical. In addition, since the system cleanup and the LC/MS/MS run happen simultaneously, nothing is delayed for the sample assay.

To the best experience of the authors, the carryover from HPLC columns are more challenging in practical applications. Conventional RP-HPLC phases usually have significant carryover effect. On the other hand, HPLC columns with hydrophilic interaction chromatographic modes and mixed-modes such as pentafluorophenylpropyl (PFPP) bonded phase have nearly zero carryover.

According to US FDA bioanalytical validation guidance [16], the carryover value is required to be less than 20%. Although the carryover can be further reduced, the present method has met the acceptance criteria.

3.4. Precision and accuracy

Over the range of 20–8000 ng/mL for doxorubicin, the calibration curves are better fitted with quadratic model using $1/x$. The least-squares linear regression constants (r^2) are always equal to higher than 0.995 for doxorubicin. Over the range of 0.05–20.0 ng/mL for doxorubicinol, the calibration curves are fitted with linear models using $1/x^2$ weighting factors. The least-squares linear regression constants (r^2) are always equal to higher than 0.992 for doxorubicinol. Concentrations of quality control standards are calculated from each curve. The accuracy is obtained by comparing the averaged calculated concentrations to their nominal values (% of nominal) and the precision by the percent coefficient of variation (%CV). The results from a 3-day precision and accuracy batches are listed in Table 1. The current US FDA regulatory requirements expect that the lower limit of quantitation (LLOQ) standard back-calculated concentrations must be within ±20% of theoretical nominal concentrations and all other standards' back-calculated concentrations must be within ±15% of their nominal theoretical concentrations. The results in Table 1 completely meet with the acceptance criteria.

3.5. Extraction recovery, matrix effect and process efficiency

Absolute matrix effect, true recovery during the extraction procedure and apparent recoveries are almost identical to those reported in a previous study [17].

3.6. Specificity

Six unique lots of rat plasma spiked with Low-QC standards are compared, and the data are listed in Table 2. Relative matrix effect is not observed.

3.7. Freeze–thaw stability, refrigerated stability and extraction stability

The three-cycle freeze–thaw stability, the 14-h refrigerated stability (4 °C) and the 48-h extraction stability (4 °C) have been successfully established. The data are shown in Table 3.

It is noted that the concentration of doxorubicin drops 13.8% after the three frezee/thaw cycles.

3.8. Freezer stability

A 3-month stability at −70 °C is evaluated on rat plasma Low-QC and High-QC quality control standards. The results are also shown in Table 3. Both of the compounds are considered stable at −70 °C for 3 months. Nevertheless, the concentration of doxorubicinol drops to 85.5%, very close to the bottom line.

3.9. Application

The validated LC/MS/MS method is used for the simultaneous determination of doxorubicin and doxorubicinol in rat plasma after the intravenous administration of 5 mg/kg Stealth®-49 liposomal doxorubicin HCl to rats.

Fig. 7 illustrates the liposomal doxorubicin concentration–time profile in the plasma. Data are represented as the means of five rats. Analysis of plasma collected before the start of the infusion does not reveal the presence of

Table 3
Stability of doxorubicinol and doxorubicinol in rat plasma

Analyte (QC)	Concentration (ng/mL)	Accuracy derivation (%)	CV (%) ($n=6$)
Three freez–thaw cycles			
Doxorubicinol (low)	0.150	94.2	7.7
Doxorubicinol (high)	16.0	96.0	4.9
Doxorubicin (low)	60.0	95.3	2.8
Doxorubicin (high)	6400	86.2	3.3
Forty-eight-hour extraction stability			
Doxorubicinol (low)	0.150	99.3	6.8
Doxorubicinol (high)	16.0	102	4.4
Doxorubicin (low)	60.0	95.7	2.6
Doxorubicin (high)	6400	94.3	6.4
Refrigerated stability in matrix			
Doxorubicinol (low)	0.150	94.2	4.5
Doxorubicinol (high)	16.0	95.4	2.8
Doxorubicin (low)	60.0	96.1	1.8
Doxorubicin (high)	6400	91.0	2.4
Three-month storage stability			
Doxorubicinol (low)	0.150	88.4	11.2
Doxorubicinol (high)	16.0	85.5	7.2
Doxorubicin (low)	60.0	95.6	7.6
Doxorubicin (high)	6400	94.4	8.5

doxorubicin and doxorubicinol. Most of the preclinical samples have to be diluted 50-fold prior to the analysis. Thus, only a smaller amount of plasma (50 μL) is taken at each time point and it enables many sampling points.

The data fit well with an one-compartment model characterized by a prolonged monophasic elimination profile (Fig. 7). The pharmacokinetics parameters (mean ± standard derivation, $n=5$) are summarized as follows: $AUC_{0–96h}$ $1886 \pm 123\ \mu g\,h\,mL^{-1}$; C_{max} $115 \pm 9.5\ \mu g\,mL^{-1}$; $T_{1/2}$ 20.4 ± 1.9 h; V_{dss} 13.7 ± 0.73 mL; CL_p $0.52 \pm 0.04\ mL\,h^{-1}$.

The pharmacokinetics of doxorubicin is profoundly influenced by administration as a pegylated, liposomal formulations [20]. In comparison with conventional doxorubicin infusion solutions, smaller liposomes (70–100 nm) with a polyethylene glycol-coated lipid phase can evade detection and destruction by the immune system, which produces a prolonged duration of circulation in the plasma and increases tumor exposure [4–9,14].

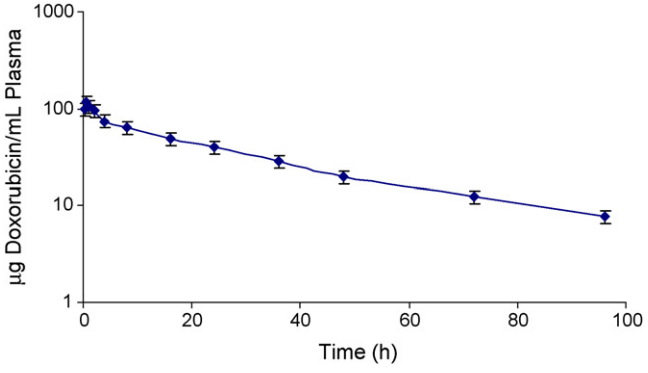


Fig. 7. Plasma doxorubicin concentration–time profile after an intravenous bolus injection of Stealth®-49 at a single dose of 5 mg/kg to rats. Data are represented as means ($n=5$ rats).

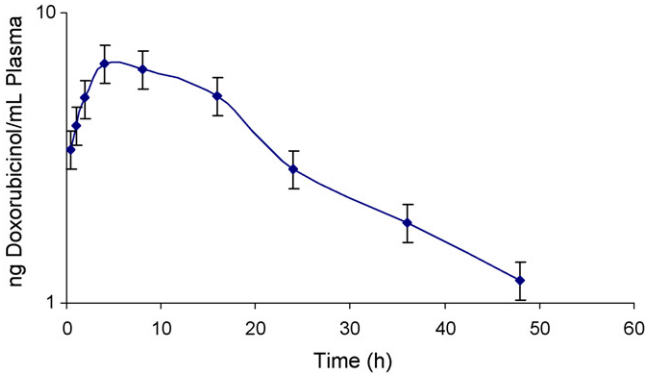


Fig. 8. Plasma doxorubicinol concentration–time profile after an intravenous bolus injection of Stealth®-49 at a single dose of 5 mg/kg to rats. Data are represented as means ($n=5$ rats).

When two of the previous PK studies for liposomal doxorubicin report that doxorubicinol is below the detection [8,9], doxorubicinol is able to be quantitatively analyzed by the present method. Fig. 8 is the corresponding doxorubicinol concentration–time profile for doxorubicinol.

The $AUC_{0–96h}$ value for doxorubicinol is $0.204 \pm 0.094\ \mu g\,h\,mL^{-1}$ and its $T_{1/2}$ value is 25.2 ± 7.8 h. The C_{max} of doxorubicinol is $6.7 \pm 2.1\ ng\,mL^{-1}$ and it occurs between 4 and 8 h. The mean $AUC_{0–96h}$ value for doxorubicinol is 0.011% of that of doxorubicin. Compared to the results from the previous studies for the free doxorubicin formulation [11–13], the concentration of doxorubicinol is much less when Stealth®-49 liposomal doxorubicin is administrated. This indicates a much lower conversion of doxorubicin to doxorubicinol when doxorubicin is administrated in pegylated liposomal form. Doxorubicinol is cytotoxic and may be responsible for some of the major adverse effects, especially on the heart [3]. The data in the present study may be able to be referred as one of the scientific evidences to explain the significantly reduced cardiotoxicity of pegylated liposomal doxorubicin in both preclinical and clinical studies [14,15]. The significant decrease of doxorubicinol concentration in the plasma and the reduced cardiotoxicity allow a larger cumulative dose than that acceptable for free doxorubicin [14].

4. Conclusion

A sensitive, selective, fast and reliable LC/MS/MS method has been successfully developed and validated for the simultaneous quantification of pegylated liposomal doxorubicin and doxorubicinol. The optimization of autosampler washing process minimizes the carryover effect and the optimized LC/MS/MS methodology greatly gets rid of the interference from doxorubicin in the quantification of doxorubicinol. This method has been applied to study the pharmacokinetic profiles of doxorubicin and doxorubicinol in rats after a single dose administration of Stealth®-49 liposomal doxorubicin HCl. The mean $AUC_{0–96h}$ value for doxorubicinol is found to be only 0.011% of that of doxorubicin. The data is in good agreement with the significantly less cardiotoxicity of pegylated

liposomal doxorubicin shown in the preclinical and clinical studies.

Acknowledgements

This study was supported by The Special Funds for Major State Basic Research Projects of China (2005CB523201) and Gansu Spark Program (5HS-066-A-91-013-02). The content of the work reflects the personal view of the author and not necessarily the view of the organization.

References

[1] V.T. DeVita, S.A. Rosenberg, S. Hellamn, Cancer: Principles and Practice of Oncology, Lippincott, Willams & Wilkins, Philadelphia, 2005.
[2] J. Robert, Drugs 45 (1993) 20.
[3] R.B. Weiss, Semin. Oncol. 19 (1992) 670.
[4] J.C. Wang, X.Y. Liu, W.L. Lu, A. Chang, Q. Zhang, B.C. Goh, H.S. Lee, Eur. J. Pharm. Biopharm. 62 (2006) 44.
[5] J.X. Cui, C.L. Li, W.M. Guo, Y.H. Li, C.X. Wang, L. Zhang, L. Zhang, Y.L. Hao, Y.L. Wang, J. Controll. Release 118 (2007) 204.
[6] D.C. Bibby, J.E. Talmadge, M.K. Dalal, S.G. Kurz, K.M. Chytil, S.E. Baryy, D.G. Shand, M. Steiert, Int. J. Pharm. 293 (2005) 281.
[7] R.B. Desai, M.S. Schwartz, B.K. Matuszewski, J. Chromatogr. Sci. 42 (2004) 317.
[8] D.L. Chin, B.L. Lum, B.I. Sikic, J. Chromatogr. B 779 (2002) 259.
[9] R.D. Arnold, J.E. Slack, R.M. Straubinger, J. Chromatogr. B 808 (2004) 141.
[10] C.M. Gilbert, R.P. McGeary, L.J. Filippich, R.L.G. Norris, B.G. Charles, J. Chromatogr. B 826 (2005) 273.
[11] P. de Bruijn, J. Verweij, W.J. Loos, H.J. Kolker, A.S.T. Planting, K. Nooter, G. Stoter, A. Sparreboom, Anal. Biochem. 266 (1992) 216.
[12] Q. Zhou, B. Chowbay, J. Pharm. Biomed. Anal. 30 (2002) 1063.
[13] R. DiFrancesco, J.J. Griggs, J. Donnelly, R. DiCenzo, J. Chromatogr. B 852 (2007) 545.
[14] A. Grabizn, H. Shmeeda, Y. Barenholz, Clin. Pharmacokinet. 42 (2003) 419.
[15] M.R. Ranson, S. Cheeseman, S. White, J. Margison, Crit. Rev. Oncol./Hematol. 37 (2001) 115.
[16] Department of Health and Human Services, Food and Drug Administration, Guidance for Industry on Bioanalytical Method Validation, Fed. Regist. 2001, 66 (100), 28526 (Docket No. 98D-1195) (available at http://www.fda.gov/cder/guidance/4252fnl.pdf).
[17] Y.H. Yang, Talanta 71 (2007) 596.
[18] Anon, Alza Pharmaceuticals, Product Information, 2000.
[19] S. Druckmann, A. Gabizon, Y. Barenholz, Biochim. Biophys. Acat Biomembr. 980 (1989) 381.
[20] A. Gabizon, R. Catane, B. Uziely, B. Kaufman, T. Safra, R. Cohen, F. Martin, A. Huang, Y. Barenholz, Cancer Res. 54 (1994) 987.

Available online at www.sciencedirect.com
ScienceDirect
Talanta 74 (2008) 1026–1031
Talanta
www.elsevier.com/locate/talanta

A reproducible method for determination of nitrocellulose in soil

Denise K. MacMillan [a,*], Chelsea R. Majerus [b], Randy D. Laubscher [c], John P. Shannon [c]

[a] *Engineer Research and Development Center, Environmental Laboratory, 3909 Halls Ferry Road, Vicksburg, MS 39180, USA*
[b] *University of Nebraska at Omaha, S 60th and Dodge, Omaha, NE 68132, USA*
[c] *SpecPro, Incorporated, 3909 Halls Ferry Road, Vicksburg, MS 39180, USA*

Received 16 March 2007; received in revised form 8 August 2007; accepted 9 August 2007
Available online 19 August 2007

Abstract

A reproducible analytical method for determination of nitrocellulose in soil is described. The new method provides the precision and accuracy needed for quantitation of nitrocellulose in soils to enable worker safety on contaminated sites. The method utilizes water and ethanol washes to remove co-contaminants, acetone extraction of nitrocellulose, and base hydrolysis of the extract to reduce nitrate groups. The hydrolysate is then neutralized and analyzed by ion chromatography for determination of free nitrate and nitrite. A variety of bases for hydrolysis and acids for neutralization were evaluated, with 5N sodium hydroxide and carbon dioxide giving the most complete hydrolysis and interference-free neutralization, respectively. The concentration of nitrocellulose in the soil is calculated from the concentrations of nitrate and nitrite and the weight percentage of nitrogen content in nitrocellulose. The laboratory detection limit for the analysis is 10 mg/kg. The method acceptance range for recovery of nitrocellulose from control samples is 78–105%.
© 2007 Published by Elsevier B.V.

Keywords: Nitrocellulose; Propellants; Base hydrolysis; Ion chromatography

1. Introduction

Nitrocellulose (NC) is used by the military as a component of solid propellants and blasting materials, and also commercially in inks and lacquers. Also known as guncotton, pyroxilin, or pyrocellulose, NC is a polymer of cellulose with three hydroxyl positions available for nitration per monosaccharide unit (Fig. 1). The degree of nitrate incorporation is expressed as a percentage according to weight of nitrogen; a fully nitrated cellulose polymer contains 14.14% nitrogen. The level of nitration influences the chemical properties of NC and, accordingly, its uses. For example, NC with 12.5–13.3% nitrogen content is used as gun propellant and NC with lower nitrogen content is used in varnishes and films [1].

Though NC is not toxic, it may be a safety hazard when exposed to an ignition source, and is a concern to the military as a potential environmental contaminant at ammunition packing and manufacturing sites as well at weapons firing points. Building demolition on formerly used ammunition facilities is especially dangerous due to the presence of nitrocellulose in the surrounding soil. Analytical methods for determination of NC in soil have not yielded reproducible, accurate quantitation [2], and thus have not provided sufficient data quality for decision-making and ensuring worker safety. Some methods measure NC through quantitation of nitrate and nitrite formed during base hydrolysis, which has long been known to degrade NC [3]. Su recently utilized alkaline hydrolysis combined with sonolysis to digest nitrocellulose-containing propellants as a step in a treatment technology [4]. An automated analytical method [5] developed by the United States Army Toxic and Hazardous Materials Agency (USATHAMA) is used by some commercial laboratories for determination of NC in soil. The reported detection limit of 60 mg/kg provides sufficiently sensitivity, but the method requires a 12 h extraction prior to hydrolysis, uses a flow injection analyzer which may not be standard equipment in commercial analytical laboratories, and is difficult to implement accurately and reproducibly [2].

Methods for detection of nitrocellulose in matrices other than soil have been developed. Methods such as thin layer chromatography for detection of nanogram quantities of NC on hand

* Corresponding author. Present address: U. S. Environmental Protection Agency, 109 TW Alexander Drive, Mail Drop D305-02, RTP, NC 27511 USA. Tel.: +1 919 541 4128.
E-mail address: macmillan.denise@epa.gov (D.K. MacMillan).

0039-9140/$ – see front matter © 2007 Published by Elsevier B.V.
doi:10.1016/j.talanta.2007.08.013

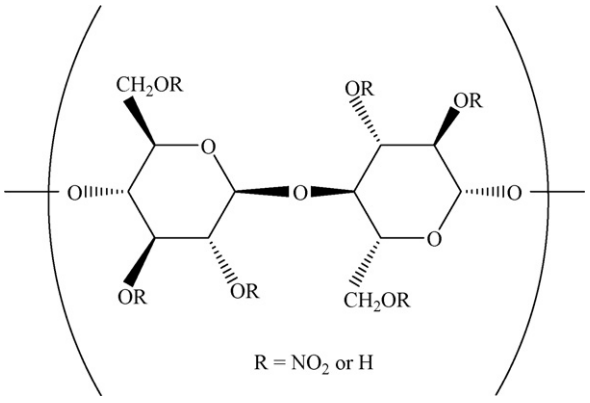


Fig. 1. Chemical structure of nitrocellulose.

swabs and to qualitatively differentiate NC used as a propellant from NC used in ink are described by Yinon and Zitrin [6]. Pyrolysis/gas chromatography/mass spectrometry has been used for qualitative identification of nitrocellulose residues after hydrolysis of wastewater containing nitrocellulose fines [7]. Electrochemical detection coupled with size-exclusion chromatography was identified for detection of trace NC in paints, lacquers, wood-filler, explosives, and other materials [8].

The goal of this work was to develop an analytical method for NC in soil that is fast, uses instrumentation that is commonly available to environmental analytical laboratories, and yields data with sufficient precision and accuracy, such as are observed for EPA method 300.1 [9] for determination of inorganic anions, to enable appropriate site decisions. The method described here is amenable to use by typical environmental analytical laboratories since it uses familiar techniques and instrumentation likely to be available already. The method is initiated with two solvent rinses to eliminate interfering co-contaminants prior to NC extraction with acetone and base hydrolysis. The concentrations of nitrate and nitrite released upon hydrolysis are determined by ion chromatography and are used, along with an estimate of the percentage of NC nitrogen content, to calculate the concentration of NC in the soil. Sensitivity, accuracy, and precision for this method are achieved through reduction of chromatographic interferences and incorporation of an optimized hydrolysis step.

2. Experimental

All chemicals, reagents, and solvents were obtained from Fisher Scientific (Pittsburgh, PA) unless otherwise noted. Standard solutions were prepared from NC (12% nitrogen) (Aldrich, St Louis, MO) that was dried to constant weight in a vacuum desiccator in the dark. Dried NC (4.166 g) was dissolved in acetone (Burdick and Jackson, Muskegon, MI) to give a final concentration of 4.17 g/L NC. Nitrocellulose control samples were prepared by spiking 10 g Ottawa sand with 1.0 mL NC standard solution for a final NC concentration of 417 mg/kg (nitrogen equivalent concentration for NC with 12% nitrogen content is 50 mg/kg) or nitrogen as nitrate/nitrite concentration of 20 mg/L in the hydrolysate. Clean sand is frequently used as a soil surrogate for control samples for environmental analytical methods. The sand was rinsed with acetone and allowed to dry prior to addition of the standard solution. The spiking solvent was also allowed to evaporate from the control samples prior to proceeding. Soil samples, which were collected near a light anti-tank weapon (LAW) firing point on Canadian Force Base Gagetown, New Brunswick, Canada, were the kind gift of Mr. Alan Hewitt (Cold Regions Research and Development Laboratory, Hanover, NH). Samples were collected at points 0–1, 1–2, 2–5, 5–10, 10–20, 30–40, and 40–50 m behind the firing point. Background samples were collected from outside the training zone. The soils were air dried, passed through a #10 sieve (<2 mm), and the fines ground in a puck mill (LabTech Essa Pty. Ltd., Bassendean, WA, Australia) for five 1 min intervals prior to preparation for analysis. For control and soil samples, 10 g sand or soil were stirred at 30 rpm on a rotary stirrer with 10 mL reagent grade water for 10 min. For samples expected to have high concentrations of NC present, 0.5–2.0 g sample sizes were used to minimize dilution of the final extract. The stirred samples were centrifuged by using a swinging bucket rotor at moderate speed for 10 min or until the supernatants were clear, after which the supernatants were decanted and discarded. The water rinse step was repeated once. A 10 mL aliquot of ethanol (VWR International, Inc., West Chester, PA) was added to each sample after the water rinses. Samples were stirred for 10 min on a rotary stirrer at 30 rpm, centrifuged at moderate speed for another 10 min or until the supernatants were clear. The ethanol layer was decanted and discarded. Acetone (15 mL) was then added to each sample, and the samples were again stirred and centrifuged as described previously for the water and ethanol washes. Once the supernatant was clear, it was decanted and reserved in a clean 50 mL polypropylene centrifuge tube. The acetone extraction was repeated and the extracts combined. The extract was evaporated to dryness under a gentle stream of forced air. The dried extracts were combined with base, and the vials were placed in a boiling water bath. Optimal hydrolysis time was determined to be 10 min. Bases evaluated for optimal hydrolysis were sodium hydroxide (NaOH), calcium hydroxide ($Ca(OH)_2$), and ammonium hydroxide (NH_4OH). After cooling, the hydrolyzed samples were diluted with 20 mL reagent water and adjusted to pH 8 by addition of acid. Several acids were evaluated for neutralization including phosphoric acid, acetic acid, hydrochloric acid, and sulphuric acid. Dionex (Sunnyvale, CA) OnGuard ion exchange clean-up cartridges were used in some instances to reduce pH and interferences prior to analysis. Optimal chromatography with minimal interferences was obtained by neutralization with a flow (approximately 2 L/min) of industrial grade (98.5%) compressed carbon dioxide (Linweld, Lincoln, NE) after which the sample was diluted to a final volume of 25 mL with reagent water. The hydrolysates were analyzed for nitrate and nitrite according to EPA method 300.1 [9] by using a Dionex DX-120 ion chromatograph equipped with a Dionex AS14 Ionpak column and a conductivity detector. The mobile phase was 0.5 M carbonate: 0.5 M bicarbonate and the flow rate was 1.8 mL/min. Appropriate quality controls specified in the EPA method were met. Potassium nitrate and sodium nitrite were used as standards and were obtained from Mallinckrodt Laboratory Chemicals (Phillipsburg, NJ).

The nitrocellulose concentration was calculated from the sum of the concentrations of nitrate and nitrite and the percentage of NC nitrogen content. For purchased NC, the percent nitrogen provided by the vendor was used for the calculation. For real-world samples, the nitrogen percentage of the NC propellant from the particular ordnance used at the collection site, if known, could be incorporated into the calculation.

To evaluate whether co-contaminant explosives in samples containing NC would create interferences, three sand samples were spiked with 100 mg/kg each of the 14 explosives included in the EPA SW-846 Method 8330 [10] target analyte list (HMX (octahydro-1,3,5,7-tetranitro-1,3,5,7-tetrazocine), RDX (hexahydro-1,3,5-trinitro-1,3,5-triazine), 1,3,5-trinitrobenzene, 1,3-dinitrobenzene, tetryl (methyl-2,4,6-trinitrophenylnitramine), nitrobenzene, 2,4,6-trinitrotoluene, 4-amino-2,6-dinitrotoluene, 2-amino-4,6-dinitrotoluene, 2,4-dinitrotoluene, 2,6-dinitrotoluene, 2-nitrotoluene, 3-nitrotoluene, and 4-nitrotoluene). Explosives standards were purchased from Supelco (St. Louis, MO). A second three sample set was prepared from sand spiked with each of the 14 explosives at a concentration of 100 mg/kg plus NC at a concentration of 417 mg/kg (nitrogen equivalent concentration of 20 mg/L in the extract). Both sample sets were rinsed with water and ethanol, extracted with acetone, and hydrolyzed with 5N NaOH as described above. A third set of three samples was prepared from sand and the Method 8330 target analyte mixture components, each with individual concentrations of 100 mg/kg. For each experiment, 10 g sand samples were used. To evaluate nitrate and nitrite generation from the Method 8330 analytes alone, the samples in the third set were not treated with the water and ethanol rinses prior to acetone extraction and base hydrolysis. Rinsates were analyzed by modified EPA Method 8330 [10] reverse phase high performance liquid chromatography (HPLC) for determination of explosives by using Spectra-Physics (Mountain View, CA) components (Model SP8800 pump, Model 8880 Autosampler and Spectra Focus detector) equipped with a Phenomenex (Torrance, CA) C18 Ultracarb 5μ ODS (20), 250 mm × 4.6 mm column. The mobile phase was 55:45 (v/v, %) methanol:water with a flow rate of 0.8 mL/min. A 200 μL injection volume was used. The detector was monitored at 254 and 280 nm. Quality control guidelines specified in the Method 8330 were followed and met. Laboratory reporting limits for the explosives were 1.0 mg/kg or below for all analytes with the exception of HMX which had a reporting limit of 2.2 mg/kg.

Interferences from nitroglycerin and nitroguanidine were evaluated in separate preparations. For one evaluation, nitroguanidine was added to a real-world sample for a final spike concentration of 5 mg/kg. The sample was extracted according to the solid phase extraction procedure described in Method 8330 and analyzed by HPLC using a Thermo Scientific (Waltham, MA) Surveyor system with UV 6000 detector monitored at 280 nm, the column described above, and 60:40 (v/v, %) methanol:water mobile phase. The sample was also subjected in triplicate to the nitrocellulose method described here, with rinsates collected and analyzed by HPLC for nitroguanidine. A second sample with a high concentration of nitroglycerin present was prepared for nitrocellulose determination. Residual nitroglycerin was determined in the rinsates by HPLC.

An inter-laboratory study was performed to validate the method. Columbia Analytical Services, Inc (Redding, CA) and CT Laboratories (Baraboo, WI) each received seven firing point samples with NC concentrations ranging from approximately 2000–20,000 mg/kg for determination by the method described here.

3. Results

Hydrolysis times and bases were evaluated to identify the conditions for complete hydrolysis. Nitrocellulose was extracted from soil, and then hydrolyzed for 1 h with saturated calcium hydroxide solution. Calcium, base, and other interferences were removed with ion exchange cartridges. Recoveries of NC after 1 h were less than 20% of expected due to incomplete hydrolysis. Increased digestion efficiency would be expected with longer hydrolysis times, but a digestion of more than 1 h exceeded the goal of a fast method. Hydrolysis with weak NaOH for up to 1 h was also incomplete, as standard recoveries were only 12–41% of expected. Hydrolysis with ammonium hydroxide, which would not require subsequent neutralization since the base would boil off as ammonia and water, gave nitrocellulose recoveries that were in the range of 16–36%. Optimal results for hydrolysis were obtained by using a 10 min boil with 5N NaOH which yielded NC recoveries above 75%. Shorter boil times of 1 or 3 min gave unacceptable recoveries below 50%, likely due to incomplete hydrolysis. Su observed similar results with lower base concentrations and hydrolysis temperatures [4]. Longer boil times also resulted in low nitrate and nitrite recovery, likely due to loss of nitrogen as nitrogen oxides or other gaseous species.

Several acids were evaluated for neutralization of the hydrolysate and generation of interference-free ion chromatograms. Phosphoric acid neutralization gave broad, abundant phosphate peaks in the ion chromatograms. Samples required dilution over a range from 1:10 to 1:100, depending on the sample, to prevent co-elution of phosphate and nitrate. Samples were applied to cation exchange columns to remove base and other interferences, but sufficient co-contamination was not removed to warrant continued use. Sulphuric acid neutralization generated sulphate ions in the sample, but since sulphate elutes minutes later than nitrate and nitrite with this column/mobile phase combination, was less likely to interfere with nitrate detection. Use of sulphuric acid did add an unidentified broad peak in the same retention time region as nitrite and nitrate, however.

Carbon dioxide proved to be most effective for neutralization of the hydrolysate, and yielded chromatograms that were free of interferences. When used with the 10 min hydrolysis with 5N NaOH, average recovery of nitrocellulose was 91.6%. The control chart range calculated according to 3 standard deviations around the mean was 78–105% (Fig. 2). The relative standard deviation was 4.7%. This range compares favorably to the acceptable range of recovery of 75–115% for laboratory fortified blanks specified in EPA method 300.1 [9].

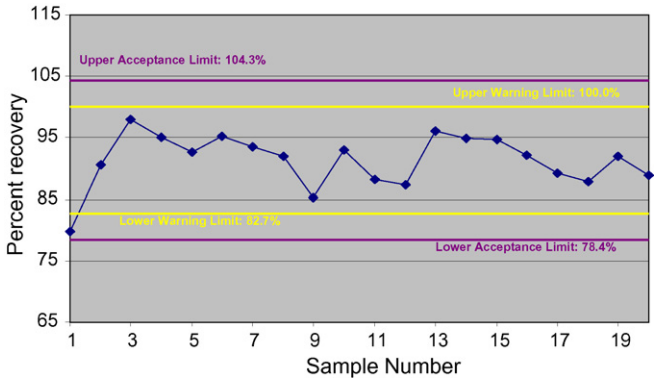


Fig. 2. Control chart of nitrocellulose recovery.

Laboratory detection limit studies were performed according to the method described in the Federal Register [11]. A set of seven sand samples was spiked with 20 mg/kg dried nitrocellulose and subjected to all steps in the method. From the data, 10 mg/kg was calculated to be the method detection limit (MDL). The value is six times lower than the MDL reported for the USATHAMA method [5]. The laboratory reporting limit for NC was set at 20 mg/kg. This value is consistent with guidance for establishing the minimum reporting level for an analyte indicated in EPA method 300.1 [9] and was used for the concentration of the low calibration standard for measurement of NC in soil samples. Results that are bracketed by the method detection limit and the laboratory reporting limit are considered to be estimated concentrations.

As shown in Table 1, total nitrogen recovery from the samples spiked with the Method 8330 target analytes alone was less than the ion chromatography laboratory detection limit. The average total nitrogen equivalent concentration produced upon hydrolysis of the Method 8330 analytes without the water and ethanol rinses was 17 ± 1 mg/L. The samples spiked with NC and the Method 8330 target analytes and subjected to all the steps in the analytical method gave an average nitrogen equivalent concentration of 20 ± 4 mg/L, an amount which is approximately equal to the amount of NC as nitrogen spiked into the samples.

Similarly, a real-world soil sample containing 6700 mg/kg nitroglycerin and 110 ± 9.0 g/kg nitrocellulose was examined in triplicate for residual nitroglycerin after the water rinse steps and the ethanol rinse step from the nitrocellulose method. The nitroglycerin concentration for this sample was the highest observed for the real-world samples in this study, and thus presented an excellent test of removal of potential interference. Nitroglycerin was determined by high performance liquid chromatography as described in SW-846 Method 8330. Nitrocellulose was determined by the method described here. The reported concentration is the average of the determinations by the three laboratories that participated in the inter-laboratory validation of the method. Nitroglycerin is present with NC in double-base propellants to increase energy content. Analysis of the rinsed samples for nitroglycerin gave 10.4 ± 1.4 mg/kg residual nitroglycerin, and indicated that, on average, 99.8% of the nitroglycerin originally present in the sample had been removed by the initial solvent washes. Base hydrolysis of the residual nitroglycerin would provide an insignificant contribution to the already substantial nitrocellulose concentration present in this sample.

Method 8330 analysis showed that approximately 91% (4.5 ± 0.14 mg/kg) of the nitroguanidine spike was removed with the water rinse and approximately 14% (0.86 ± 0.10 mg/kg) was recovered in the ethanol rinse. Nitroguanidine was not detected in the acetone extract. For the samples without the spike, nitroguanidine was detected in the water rinse at 0.041 ± 0.004 mg/kg, and in the ethanol rinse at 0.16 ± 0.01 mg/kg. When the soil sample was analyzed by HPLC after solid phase extraction, only 0.015 mg/kg nitroguanidine was detected, likely due to the differences between extraction methods. Nitroglycerin was observed in the ethanol rinse at 44 ± 4.5 mg/kg but not in the water rinse above 7.5 mg/kg for the soil sample alone. When spiked with nitroguanidine, the water rinse from the soil sample yielded 148 ± 27 mg/kg nitroglycerin and the ethanol rinse yielded 88 ± 10 mg/kg nitroglycerin. The nitroguanidine spiked soil gave a nitrocellulose concentration of 289 ± 67 mg/kg as compared to 366 ± 67 mg/kg nitrocellulose in the soil alone.

The nitrocellulose method was validated through an inter-laboratory study with two commercial environmental analytical laboratories. Concentrations of nitrocellulose obtained by the commercial laboratories were in good agreement with the values obtained in-house, as shown in Table 2 . Relative standard deviations between results for the seven firing point samples were less than 20% for all samples with the exception of sample FP-7 which showed irreproducible results. The source of the variation in the results from the different laboratories for this sample could not be determined. Duplicate analysis of sample FP-7 in-house gave a relative standard deviation of 29%.

Table 1
Study of contribution of explosives co-contaminants to nitrate/nitrite concentrations

Sample	Nitrate as N (mg/L extract)	Nitrite as N (mg/L extract)	Total N (mg/L extract)	%NC recovery	Nitrate/nitrite ratio
Method 8330 analytes[a]	nd	nd	–	–	–
NC/Method 8330 analytes[b]	5.8 ± 1.5	14 ± 4	20 ± 4	101 ± 19	0.41
Method 8330 analytes, hydrolysis only[c]	14 ± 1	2.2 ± 0.3	17 ± 1	–	6.36

nd: Not detected.
[a] 10 g sand spiked with Method 8330 analytes and subjected to water and ethanol rinses and base hydrolysis according to the NC analytical method.
[b] 10 g sand spiked with NC and Method 8330 analytes and subjected to water and ethanol rinses and base hydrolysis according to the NC analytical method.
[c] 10 g sand spiked with Method 8330 analytes and subjected to base hydrolysis without prior solvent rinses.

Table 2
Inter-laboratory study of NC concentration in selected firing point samples

Sample	ERDC NC concentration (mg/kg)[a]	Laboratory 2 NC concentration (mg/kg)[a]	Laboratory 3 NC concentration (mg/kg)[a]	Average NC concentration (mg/kg)[a]	%R.S.D.
FP-1	19,200	23,300	18,800	20,400	12
FP-2	81,300	87,600	86,700	85,200	4.0
FP-3	103,000	107,000	122,000	110,000	9.0
FP-4	71,700	96,500	81,800	83,300	15
FP-5	30,800	43,900	38,600	37,800	17
FP-6	19,800	21,600	21,100	20,800	4.3
FP-7	2,530	2,040	4,260	2,940	40

ERDC: Engineer Research and Development Center; FP: firing point; R.S.D.: relative standard deviation. *Note*: All concentrations are rounded to 3 significant figures.
[a] NC concentration as mg/kg nitrogen as nitrate/nitrite.

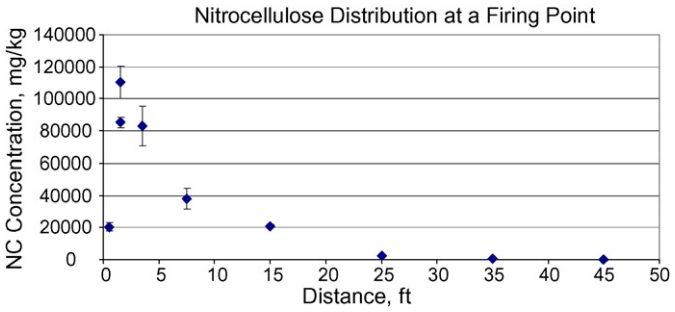


Fig. 3. Relationship between NC concentrations and distance behind LAW rocket firing point.

The relationship between NC concentrations observed in a set of firing point samples and the distance of the sample collection point behind the LAW rocket firing point is shown in Fig. 3 . LAW rockets are open-ended shoulder-fired weapons which produce a back-blast danger zone 30 m behind the firing position and a caution zone 60 m behind the danger area [12]. Samples collected within 1 m of the firing point have lower NC content than those up to 15 m away. NC concentrations approach background levels further than 25 m from the source point. The NC distribution is consistent with the observed decrease in nitroglycerin concentrations with increasing distance detected behind firing points where single-base propellants were used [13], and with the danger and caution zones specified by the military.

4. Discussion

Nitrocellulose is likely to occur in the environment with other ordnance-related compounds and other species which may interfere with a precise and accurate determination of NC concentration. The rinse steps in the analytical method are designed to eliminate ordnance-related co-contaminants as well as inorganic and organic nitrates in the soil that may be susceptible to base hydrolysis to form free nitrates. Inorganic nitrates form weak outer-sphere complexes with soil and leach into water readily; thus a water wash is expected to effectively displace free nitrates and other potentially interfering anions. In addition to leaching, some organic nitrates such as those from agricultural sources or waste materials are reduced to free nitrates in water [14]. Of organic nitrates such as explosives and ordnance-related materials, nitroglycerin and nitroguanidine show the highest water solubility: 0.15 g/100 mL [6] and 0.44 g/100 mL [15], respectively. NC is slightly less soluble in ethanol (0.6 g/100 mL) than in methanol (1 g/100 mL), and insoluble in water [6]. Previous methods used only methanol for extraction [5]. Nitroglycerin, expected to be a co-contaminant with NC originating from double-base propellants, is nearly ten times more soluble in ethanol [6] than in methanol [15].

The effectiveness of the rinse steps for reducing interferences is demonstrated by the elimination of the Method 8330 target analytes from the sand samples, as indicated in Table 1. The average recovery of NC in the samples that also included the Method 8330 analytes approximated the amount of the NC spike with a relative standard deviation of less than 20%. Nitrogen as nitrate plus nitrite in the samples containing only the Method 8330 analytes was below detectable levels when the samples were subjected to water and ethanol rinse steps, acetone extraction, and base hydrolysis. Extracts of samples spiked with the Method 8330 analytes but not rinsed with water and ethanol prior to extraction with acetone and hydrolysis yielded an average total nitrogen equivalent concentration of 17 ± 1 mg/L. Had the co-contaminants not been eliminated by the rinse steps, the average total nitrogen concentration in the NC plus Method 8330 analyte extracts would be expected to be approximately 37 mg/L based on the summed contribution of 20 mg/L N from NC and approximately 17 mg/L N from the Method 8330 analytes. In addition to this experiment, Method 8330 analysis of a real-world sample known to contain both nitroglycerin and NC showed nearly complete elimination (99.8%) of nitroglycerin after the sample was subjected to the water and ethanol rinses of the current method. Similarly, chromatographic analysis of a real-world sample with added nitroguanidine showed that the rinse steps quantitatively (105%) removed nitroguanidine from the sample prior to the acetone extraction step. These data are evidence that the water and ethanol rinses prior to acetone extraction of NC from soil are effective for removal of potential interferences including nitrated co-contaminants such as explosive compounds and munitions constituents such as nitroglycerin and nitroguanidine.

Interestingly, the nitrate/nitrite ratios for the NC plus Method 8330 analyte sample extracts and the Method 8330 analyte sample extracts (Table 1) are significantly different. Typically, for NC samples analyzed by this method, the observed nitrate/nitrite ratio for the extract was less than 1. As show in Table 1, nitrate/nitrite ratio is greater than 1 for the Method 8330 analyte only samples. Since the hydrolysis conditions were identical

for both sample sets, the difference may reflect mechanistic differences in hydrolysis of the ONO_2 moieties present on NC and the NO_2 moieties present on the Method 8330 analytes.

Two commercial environmental analytical laboratories performed the method and obtained good agreement for results for samples obtained from a LAW rocket firing point with the exception of one sample with low levels of NC. The result obtained by one laboratory for the low level sample was nearly twice the concentration obtained by the other commercial laboratory and this laboratory. The inter-laboratory reproducibility for the firing point samples is otherwise within the acceptable range for reproducibility between duplicate samples for Method 300.1 for determination of nitrate and nitrite.

5. Conclusion

An analytical method for determination of nitrocellulose in soil has been demonstrated with standards and with soils from a LAW rocket firing point. The method incorporates solvent rinses which effectively reduce the presence of co-contaminants, base hydrolysis to free nitrate and nitrite, and conductivity detection. The method was performed by two commercial laboratories in addition to the development laboratory with satisfactory reproducibility. The laboratory detection limit for the method was calculated to be 10 mg/kg. Acceptable recovery performance for spiked samples was shown to be 78–105% with relative standard deviation equalling 4.7%.

Acknowledgements

The use of trade, product, or firm names in this paper is for descriptive purposes only and does not imply endorsement by the U.S. Government. Unless otherwise noted the work described here was conducted under the U.S. Army Environmental Quality and Installations Program, Engineer Research and Development Center. Permission was granted by the Chief of Engineers to publish this information.

References

[1] J. Akhavan, The Chemistry of Explosives, second ed., Royal Society of Chemistry, Cambridge, UK, 2004, p. 32.

[2] ESTCP, Environmental Security Technology Certification Program, Cost and Performance Report CU-0130, Applied Innovative Technologies for Characterization of Explosives-Contaminated DoD Building Foundations and Underlying Soils, February 2004, http://www.estcp.org/documents/techdocs/cu-0130.pdf.

[3] W.O. Kenyon, H.L. Gray, Am. Chem. Soc. J. 58 (8) (1936) 1422.

[4] T.-L. Su, Alkaline Hydrolysis of Nitrocellulose and Nitrocellulose Containing Rocket Propellants and Biodegradability of Post-Hydrolysis Products, UMI Number 9736478, UMI Company, Ann Arbor, MI, 1997.

[5] J.J. Barkley, D.H. Rosenblatt, Automated nitrocellulose analysis, U.S. Army Medical Bioengineering Research and Development Laboratory, Technical Report 7807, ADA067081, 1978.

[6] J. Yinon, S. Zitrin, Modern Methods and Applications in Analysis of Explosives, John Wiley and Sons Ltd., West Sussex, UK, 1993, pp. 8, 13–14, 35–36.

[7] D. Cropek, B. Dankowski, Sonolysis of Nitrocellulose Fines, 2000, ERDC/CERL TR-00-14, Engineering Research and Development Center, Construction Engineering Research Laboratory, Champaign, IL. http://www.cecer.army.mil/TechReports/cropek_sonolysis_NCfines/cropek_sonolysis_NCfines.pdf.

[8] J.B.F. Lloyd, Anal. Chem. 56 (1984) 1907.

[9] U.S. EPA, United States Environmental Protection Agency, Method 300.1: Determination of Inorganic Anions in Drinking Water by Ion Chromatography, U.S. Environmental Protection Agency National Exposure Research Laboratory, Cincinnati, OH, 1999. http://www.epa.gov/safewater/methods/pdfs/met300.pdf.

[10] U. S. EPA, United States Environmental Protection Agency, Method 8330 Nitroaromatics and Nitramines by High Performance Liquid Chromatography (HPLC), in Test Methods for Evaluating Solid Wastes Physical Chemical Methods (SW-846), 1994, http://www.epa.gov/epaoswer/hazwaste/test/pdfs/8330.pdf.

[11] Federal Register, Guidelines Establishing Test Procedures for the Analysis of Pollutants, 40 cfr part 136, 1999, http://www.access.gpo.gov/nara/cfr/waisidx_99/40cfr136_99.html.

[12] Marine Corps University, Introduction to Countermechanized and Mechanized Weapons, The Basic School, US Marine Corps, B2113 Student Handout, 2002, http://www.usna.edu/USMCInfo/Documents/Pubs/b2113.pdf.

[13] T.F. Jenkins, S. Thiboutot, G. Ampleman, A.D. Hewitt, M.E. Walsh, T.A. Ranney, C.A. Ramsey, C.L. Grant, C.M. Collins, S. Brochu, S.R. Bigl, J.C. Pennington, Identity and Distribution of Residues of Energetic Compounds at Military Live-Fire Training Ranges, 2005, ERDC TR-05-10, Engineer Research and Development Center, Cold Regions Research and Engineering Laboratory, Hanover, NH. http://www.crrel.usace.army.mil/techpub/CRREL_Reports/reports/ERDC-TR-05-10.pdf.

[14] D.L. Sparks, Environmental Soil Chemistry, Academic Press, San Diego, CA, 1995, pp. 133–186 (Chapter 5).

[15] M.J. O'Neill (Ed.), The Merck Index, 13th ed., Merck and Co. Inc., Whitehouse Station, NJ, 2001, p. 1135.

Available online at www.sciencedirect.com
ScienceDirect
Talanta 74 (2008) 586–592
Talanta
www.elsevier.com/locate/talanta

Simultaneous on-line pre-concentration and determination of trace metals in environmental samples by flow injection combined with inductively coupled plasma mass spectrometry using silica gel modified with niobium(V) oxide

Heloisa França Maltez, Mariana Antunes Vieira, Anderson Schwingel Ribeiro, Adilson José Curtius, Eduardo Carasek *

Departamento de Química, Universidade Federal de Santa Catarina, 88040-900 Florianópolis, Brazil

Received 14 March 2007; received in revised form 3 May 2007; accepted 16 June 2007
Available online 28 June 2007

Abstract

This work presents the development of an on-line pre-concentration system for simultaneous determination of Cd, Cu, Ni, V, Zn, Co and Pb in aqueous environmental samples and detection by inductively coupled plasma mass spectrometry. The system is based on cationic retention of the analytes onto a mini-column filled with silica gel modified with niobium(V) oxide. The effects of chemicals and flow variables have been investigated. The optimized operating conditions, selected as a compromise between sensitivity and analytical frequency were: sample pH 7.0, sample flow rate of 6.0 mL min^{-1}, eluent flow rate of 2.0 mL min^{-1}, and eluent (HNO_3) concentration of 2.5 mol L^{-1}. The relative standard deviation ($n = 7$), enrichment factor and linear working range were 0.8–4.5%, 23.3–37.2 and 0.05–25.0 μg L^{-1}, respectively. Limits of detection were between 0.01 and 0.03 μg L^{-1}. The accuracy of the proposed method was checked with certified materials (NASS-4, NASS-5, CASS-4 and SRM 1643e). Values obtained were in accordance with those reported for the certified materials. Recovery was found to be in the range of 90–110% for a suit of water samples with variable matrices (seawater, tap water and ground water) collected in Florianopolis, Brazil.
© 2007 Elsevier B.V. All rights reserved.

Keywords: Inductively coupled plasma mass spectrometry; Simultaneous pre-concentration; Silica gel modified with niobium(V) oxide

1. Introduction

One of the most significant environmental problems is the growing discharge of metals from different industries into the soil, water and air. As is the case for most of these metals, even in trace amounts their toxicity potential cannot be overemphasized. It therefore becomes imperative that adequate assessment of the effect of these metals on the environment be carried out. Due to the low concentration levels of these metals in the environment, the use of new analytical methods and techniques with very high sensitivity and selectivity is required for their investigations. Techniques such as flame atomic absorption spectrometry (FAAS) [1–3], graphite furnace atomic absorption spectrometry (GFAAS) [4,5], inductively coupled plasma mass spectrometry (ICP-MS) [6], and inductively coupled plasma optic emission spectrometry (ICP-OES) [7] have been used for this purpose. ICP-MS is obviously the most appropriate technique due to its high sensitivity, generation of a simple spectrum, and the ability of multi-elemental analysis and rapid data generation, besides the ability to measure isotopic ratio of the elements [8,9]. However, the ICP-MS suffers some limitations related to instrumental drift caused by solid deposition on the orifice [10], signal suppression, instability in the plasma due to the high energy necessary to dissociate organic compounds, isobaric polyatomic interferences and clogging of the sample introduction system because of samples with high-dissolved salts [11–13].

To overcome these difficulties, researchers have described various procedures for sample pre-treatment. These include liquid–liquid extraction (LLE) [14], solid phase extraction (SPE) [15], and cloud point extraction (CPE) [16]. The SPE method is particularly attractive, especially when coupled to a flow injection system on-line to ICP-MS. This combination and the

* Corresponding author. Fax: +55 48 37216845.
E-mail address: carasek@qmc.ufsc.br (E. Carasek).

0039-9140/$ – see front matter © 2007 Elsevier B.V. All rights reserved.
doi:10.1016/j.talanta.2007.06.025

availability of different types of sorbents are some of the important advantages of this technique [17], not only providing an improvement in the detection limits but also reducing the interference from matrix [18].

Among the SPE sorbents used for pre-concentration, metal-oxide systems have been investigated in the past few years [19–21]. Activated alumina [22,23] and, more recently, nano-sized alumina [6] have been used as a good sorbent material. The adsorption characteristics of titanium dioxide also have been investigated with success as a sorbent material for pre-concentration of metals [24]. The adsorption properties for metallic ions of silica gel chemically modified with zirconium(IV) have also been investigated using batch [25,26] and on-line systems [27,28]. Another recent metal-oxide sorbent explored with good results is the niobium(V) oxide grafted on silica gel surface (Nb_2O_5–SiO_2) [29]. This material was used for pre-concentrating trace level Cd, Cu, Co and Zn in water and fuel alcohol, using an off-line [30] and an on-line [31,32] flow injection system for detection by FAAS.

The purpose of this work is to assess the feasibility of using Nb_2O_5–SiO_2 as an adsorbent in an on-line system coupled directly to ICP-MS for simultaneous determination of Cd, Cu, Zn, Co, and Pb from seawater and underground water samples. In this work not only the Nb_2O_5–SiO_2 adsorbent was coupled to ICP-MS but also Ni, V and Pb were studied for the first time on this adsorbent.

2. Materials and methods

2.1. Instrumentation

All measurements were carried out with an ELAN 6000 Inductively Coupled Plasma Mass Spectrometer (Perkin-Elmer-Sciex, Thornhill, Ont., Canada), equipped with a pneumatic system, a peristaltic pump and a FIAS 400 flow injection system (Perkin-Elmer). The instrument performance was assessed daily prior to its usage. Argon 99.996% (White Martins, SP, Brazil) was used. The instrumental parameters and the program used for the flow system are shown in Tables 1 and 2, respectively.

Table 1
Operational parameters for Elan 6000 ICP-MS

RF power	1000 W
Sampler and skimmer cones	Pt
Signal measurement	Peak area
Resolution	0.7 amu (at 10% peak height)
Readings per replicate	240
Replicate	3
Auto lens	On
Gas flow rates	
Principal	15.0 L min^{-1}
Intermediate	1.0 L min^{-1}
Nebulizer	0.98 L min^{-1}
Dead time	35 ns
Dwell time	25 ms

2.2. Chemicals

Deionized water from a Milli-Q water purification system (Millipore) was used to prepare all solutions. All chemicals were of analytical grade. Nitric acid (65% w/v) obtained from Merck® was double distilled below its boiling point in a quartz distillation apparatus (Kürner Analysentechnik, Rosenheim, Germany).

The laboratory glassware was initially kept for 24 h in 2% (v/v) Extran solution (Merck®, Darmstadt, Germany) and then washed with distilled water. They were later transferred into a 20% (v/v) nitric acid solution (Vetec, Rio de Janeiro, Brazil) and kept for another 48 h followed by ultrasonication bath for 1 h. Finally, the glassware was washed with deionized water and dried in a dust free environment.

Potassium acid phthalate–hydrochloric acid buffer solution was prepared by mixing 0.1 mol L^{-1} potassium acid phthalate (Carlo Erba, Milan, Italy) and 0.1 mol L^{-1} hydrochloric acid (Merck®) to obtain pH 2. In order to obtain pH 4.0, 5.0, and 6.0, various volumes of 0.1 mol L^{-1} sodium hydroxide (Vetec, Rio de Janeiro, Brazil) were mixed with 0.1 mol L^{-1} potassium acid phthalate solution.

Sörensen buffer solution (pH 7) was prepared by mixing 0.067 mol L^{-1} Na_2HPO_4 and 0.084 mol L^{-1} KH_2PO_4 solutions (Vetec, Rio de Janeiro, Brazil).

Tris(hydroxymethyl)aminomethane (Mallinckrodt, Paris, France) buffer solution was prepared by dissolving 1.2 g of the chemical in water and adjusting the pH to 8 and 9 using a 0.1 mol L^{-1} nitric acid solution to a final volume of 100 mL.

A mixed working standard solution of Cd, Cu, Ni, V, Co, and Pb (3.0 μg L^{-1}) was prepared by diluting their respective stock solution (SPEX, Edison, NJ, USA). The pH of the solution was adjusted to 6 by adding 5 mL of $C_8H_5O_4K$–NaOH buffer solution to a final volume of 50 mL. This solution was used to optimize the chemical and flow variables. In preliminary studies

Table 2
FIAS 400 program used for pre-concentration and elution steps

	Time (s)	Pump 1 (mL min^{-1})	Pump 2 (mL min^{-1})	Valve	Step
Pre-sample	3	0	0	2	–
1	15	0	0	2	Regeneration
2	5	0	6.0	2	Pre-sample
3	5	0	0	1	Valve rotation
4	60	0	6.0	1	Pre-concentration
5	10	6.0	0	1	Clean-up
6	30	0	0	2	Elution

0.5 mol L^{-1} nitric acid solution was used as eluent and sorbent regenerator.

The concentrations of the standards used for the calibration, prepared using stock solution of each metal, ranged between 0.01 and 100 μg L^{-1}.

The samples were collected, filtered through 0.45 μm cellulose membrane (Millipore) and acidified with HNO_3 close pH 2. Thus, the samples were stocked in PTFE flasks under refrigeration at 4 °C until the analysis. The tap water and seawater samples were collected and analyzed in the same day. For analyses an aliquot of the sample had its pH adjusted and it was submitted for the proposed pre-concentration procedure.

The details about the syntheses and characterization of the silica gel modified with niobium(V) oxide can be found in the works published previously [29,30].

2.3. Flow pre-concentration system

To check the working conditions, chemicals and flow variables were optimized by a univariate method. The diagram of the flow system is shown schematically in Fig. 1. The flow system was made up of two peristaltic pumps fitted with Tygon® and PTFE tubes, a rotator valve and a mini-column made of PTFE (43 mm length and 3 mm internal diameter) filled with 100 mg of Nb_2O_5–SiO_2 sorbent material. The mini-column was sealed at both ends with glass wool to prevent material losses. During the pre-concentration and elution steps, entrance of air into the flow system was prevented because potential bubbles formation could affect the sorption efficiency.

In the sample-loading step, the valve was switched to position 1 allowing the sample to flow through the mini-column while the peristaltic pump of the ICP-MS pumped 2.0 mL min^{-1} of eluent to the nebulizer. Before the elution step, water was pumped through the mini-column to eliminate residues from the sample matrix. In the elution step the valve was switched for position 2 and the eluent was pumped through the mini-column in a reverse flow relative to the pre-concentration step. Thus, the eluate was taken directly to the nebulizer system (N) of the ICP-MS. Transient signals were measured as peak area by using instrument software.

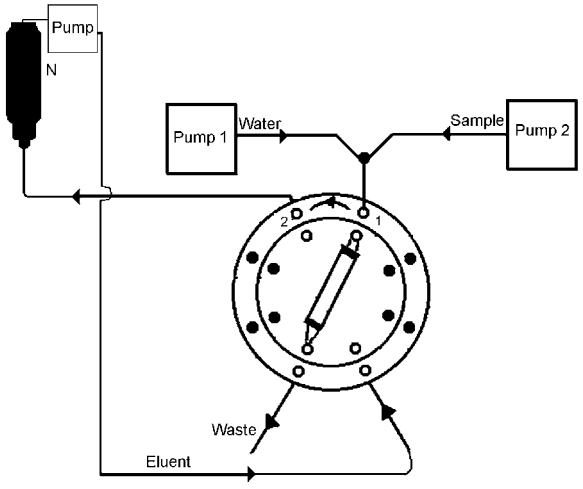


Fig. 1. Diagram of the flow system (N: nebulizer; 1: pre-concentration position; 2: elution position).

2.4. Procedure for sample quantification

The analytes ^{114}Cd, ^{63}Cu, ^{58}Ni, ^{51}V, ^{66}Zn, ^{59}Co and ^{208}Pb were quantified using calibration graphs in which the concentration of the working solutions ranged between 0.05 and 25 μg L^{-1}. The working solutions were subjected to the optimized pre-concentration procedure.

The enrichment factor was calculated using a calibration graph without a prior pre-concentration procedure. In this case, the range of concentration for the working solution was between 10 and 100 μg L^{-1} in a 2.5 mol L^{-1} nitric acid solution.

The proposed procedure was applied to the analysis of tap water, underground water collected in a quality control well from fuel station, and seawater from Florianópolis, SC, Brazil. The samples were filtered and the pH of an aliquot adjusted prior to the pre-concentration step.

The accuracy of the method was demonstrated determining the concentration of the analytes in the following certified materials: seawater NASS-4, NASS-5, CASS-4 National Research Council of Canada-NRCC (Ottawa, Canada) and fresh water SRM 1643e National Institute of Standards & Technology (Gaithersburg, USA).

3. Results and discussion

The determination of trace elements in aqueous environmental samples is difficult not only due to the low analyte concentrations present but also due to the complexity of the samples. An additional problem associated with trace element determinations in seawater is the high salinity (approximately 35 g L^{-1}) of the sample matrix, which can cause a variety of spectral and non-spectral interference in the ICP-MS. Thus, the proposed procedure describes the simultaneous separation and pre-concentration of the target analytes from the matrix before quantification by ICP-MS. Therefore, several problems related to interferences species were decreased or eliminated.

The univariate method was used to determine the best experimental condition for the chemicals and flow variables. For this purpose each parameter was optimized individually. The initial conditions used were based on literature [30–32] that explored the adsorption of ions on the silica gel modified with niobium(V) oxide. The following parameters were initially used: the pre-concentration was carried out with 6 mL of a solution contained 3.0 μg L^{-1} of Cd, Cu, Ni, V, Zn, Co and Pb buffered at pH 6.0 and a flow rate of 6.0 mL min^{-1}; the elution step was carried out using HNO_3 0.5 mol L^{-1} and a flow rate of 2.0 mL min^{-1}. The elution flow rate of 2.0 mL min^{-1} was fixed for all experiments due to the better performance of the ICP nebulizer system. All analyses were performed in triplicate.

3.1. Influence of sample pH

The sample pH is a critical condition that affects directly the sorption of the ions on the Nb_2O_5–SiO_2 surface, which works

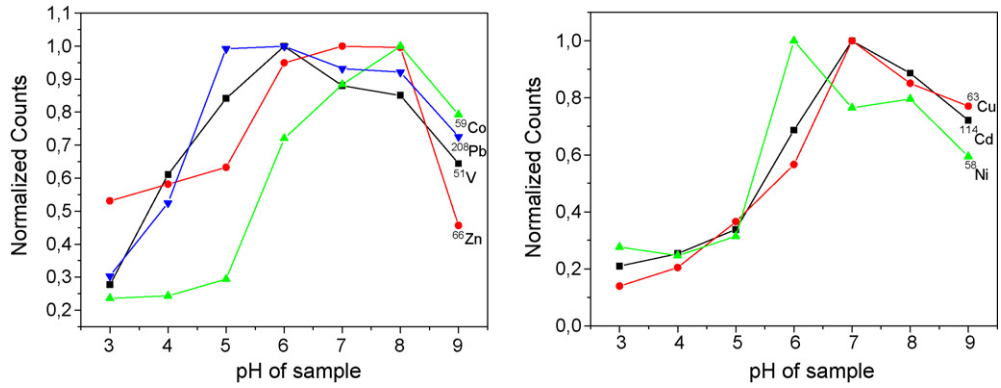


Fig. 2. Effect of sample pH on the retention of analytes on the Nb_2O_5–SiO_2. Sample volume of 6.0 mL; concentration of the eluent of 0.5 mol L^{-1}; sample flow rate of 6.0 mL min^{-1}; concentration of each analyte of 3.0 μg L^{-1}.

as a cationic exchanger. The study of the pH influence on the retention of the analytes was carried out between pH 3 and 9 using an appropriate buffer. The influence of the sample pH on the pre-concentration of the analytes ^{114}Cd, ^{63}Cu, ^{58}Ni, ^{51}V, ^{66}Zn, ^{59}Co and ^{208}Pb is shown in Fig. 2. The lower capacity of adsorption for all analytes below pH 5 can be attributed to competition between the metals and the hydrogen ions for the active sites on Nb_2O_5–SiO_2 surface, except for Pb ions that exhibited maximum adsorption at pH 5. However, high signal intensities were obtained for Cd, Cu, Ni, V, Co and Zn at pH between 6 and 8. As a compromise between sensitivity and sample pH for the adsorption of the analytes on the Nb_2O_5–SiO_2 surface, pH 7 was chosen in subsequent studies.

3.2. Influence of the eluent concentration

The effect of the eluent concentration for simultaneous elution of the analytes from the mini-column was studied. The eluent concentration ranged between 0.25 and 2.5 mol L^{-1}. To avoid the possible damage of the mini-column and the Tygon® tube lower concentrations of HNO_3 were used. It is pertinent therefore to emphasize that the efficiency of the sorption directly relates to the activation of the mini-column. From the results shown in Fig. 3, Zn displayed maximum desorption with 0.25 mol L^{-1} HNO_3 concentration while the other metals gave significant analytical signal on increasing the eluent concentration.

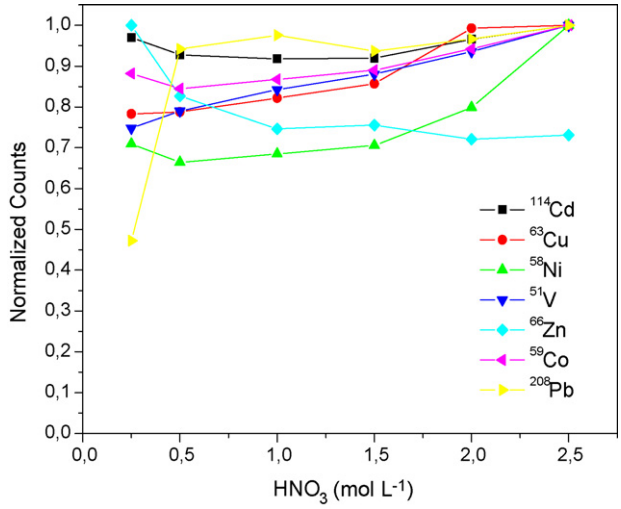


Fig. 3. Effect of eluent concentration on the simultaneous desorption of analytes from the mini-column. Sample volume 6.0 mL; sample flow rate of 6.0 mL min^{-1}; sample pH 7; analytes concentration of 3.0 μg L^{-1} each.

3.3. Effect of sample flow rate

The sample flow rate is a very important operational parameter for the pre-concentration efficiency and it determines the sample volume to be used. In general, for on-line systems the sample flow rate is limited by its pressure and/or sorption efficiency.

Fig. 4 illustrates the effect of different sample flow rates (0.7–7.0 mL min^{-1}) on the simultaneous retention of the analytes. The sample flow rate of 6.0 mL min^{-1} was chosen due to the maximum signal reached.

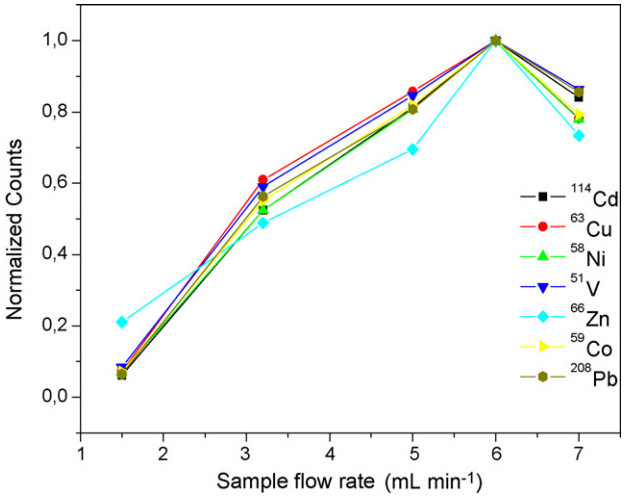


Fig. 4. Influence of the sample flow rate on the simultaneous retention of analytes on the Nb_2O_5–SiO_2 surface. Sample volume 6.0 mL; sample flow rate of 6.0 mL min^{-1}; sample pH 7; eluent concentration of 2.5 mol L^{-1}; 3.0 μg L^{-1} of each analyte.

Table 3
Analytical parameters of merit for the pre-concentration system studied and for direct measures (no pre-concentration procedure)

Isotope	With pre-concentration					No pre-concentration		
	R	Slope (L μg^{-1})	LOD ($\mu g\,L^{-1}$)	EF	R.S.D. (%)	*R*	Slope (L μg^{-1})	LOD ($\mu g\,L^{-1}$)
^{114}Cd	0.9997	182660	0.02	28.9	0.8	0.9962	6320	0.9
^{63}Cu	0.9999	160434	0.01	23.3	1.0	0.9975	6886	0.4
^{58}Ni	0.9999	177899	0.02	27.3	3.6	0.9961	6516	0.5
^{51}V	0.9997	233930	0.03	23.6	4.5	0.9967	9912	0.8
^{66}Zn	0.9993	45462	0.02	24.0	2.2	0.9955	1894	0.3
^{59}Co	0.9996	358326	0.03	28.5	3.2	0.9967	12573	0.5
^{208}Pb	0.9966	488680	0.01	37.2	4.1	0.9954	13137	0.4

3.4. Sample load time and washing time

The effect of time on the rate of adsorption was investigated and the results are illustrated in Fig. 5. It could be seen that the analytical signal increased linearly with the time at a constant sample flow rate. However, an increase in load time reduces the analytical frequency and uses larger volumes of sample. In addition, it is less cost-effective since it will require the use of larger quantities of chemicals. Taking this into consideration, a pre-concentration time of 60 s was chosen in this study.

The proposed flow injection system not only results in a pre-concentration of the analytes but also in their separation from the matrix sample. Therefore, many of the interference problems as indicated in the literature is reduced or eliminated. However, residues from the matrix sample, such as Cl^-, Ca^{2+}, Na^+ and Mg^{2+} that are not adsorbed on the Nb_2O_5–SiO_2 material, could be present in the dead volume of the mini-column and possibly pose a potential source of error. These residues can be eliminated washing the mini-column with deionized water before the elution step. The complete removal of the matrix residues from the mini-column was therefore investigated with washing time between 5 and 35 s. A washing time of 10 s using flow rate at 6.0 mL min^{-1} was later selected.

3.5. Capacity of the mini-column

The capacity of the mini-column packed with 100 mg of Nb_2O_5–SiO_2 using the optimized conditions was studied by measuring the maximum quantity of the ions Cd, Cu, Ni, V, Co, Zn and Pb sorbed on the Nb_2O_5–SiO_2 surface. The pre-concentration procedure was carried out with 6.0 mL of the working solution (sample load time of 60 s), and the analytes concentrations ranging between 0.1 and 125.0 $\mu g\,L^{-1}$. The maximum retention for Cd, Cu, Ni, Co, and Zn on the mini-column

Table 4
Comparison between the concentrations of the ions found using the proposed method and the certified reference materials

Analyte	Sample			
	SRM 1643e ($\mu g\,L^{-1} \pm$ S.D.)	CASS-4 ($\mu g\,L^{-1} \pm$ S.D.)	NASS-4 ($\mu g\,L^{-1} \pm$ S.D.)	NASS-5 ($\mu g\,L^{-1} \pm$ S.D.)
Cd				
Certified	6.568 ± 0.073	0.026 ± 0.003	0.016 ± 0.003	0.023 ± 0.003
Obtained	6.492 ± 0.065	<LOD	<LOD	<LOD
Cu				
Certified	22.76 ± 0.31	0.592 ± 0.055	0.228 ± 0.011	0.297 ± 0.046
Obtained	23.02 ± 0.25	0.612 ± 0.048	0.235 ± 0.009	0.305 ± 0.051
Ni				
Certified	62.41 ± 0.69	0.314 ± 0.030	0.228 ± 0.009	0.253 ± 0.028
Obtained	62.97 ± 0.55	0.320 ± 0.020	0.232 ± 0.011	0.261 ± 0.020
V				
Certified	37.86 ± 0.59	1.18 ± 0.16	not certified	1.2[a]
Obtained	37.21 ± 0.70	1.06 ± 0.20	0.95 ± 0.15	0.98 ± 0.22
Zn				
Certified	78.5 ± 2.2	0.381 ± 0.057	0.115 ± 0.018	0.102 ± 0.039
Obtained	79.3 ± 1.9	0.405 ± 0.035	0.122 ± 0.019	0.113 ± 0.025
Co				
Certified	27.06 ± 0.32	0.026 ± 0.003	0.009 ± 0.001	0.011 ± 0.003
Obtained	26.92 ± 0.27	<LOD	<LOD	<LOD
Pb				
Certified	19.63 ± 0.21	0.0098 ± 0.0036	0.105 ± 0.016	0.008 ± 0.005
Obtained	19.50 ± 0.30	<LOD	0.099 ± 0.013	<LOD

[a] Information value only ($n = 3$, confidence level 95%).

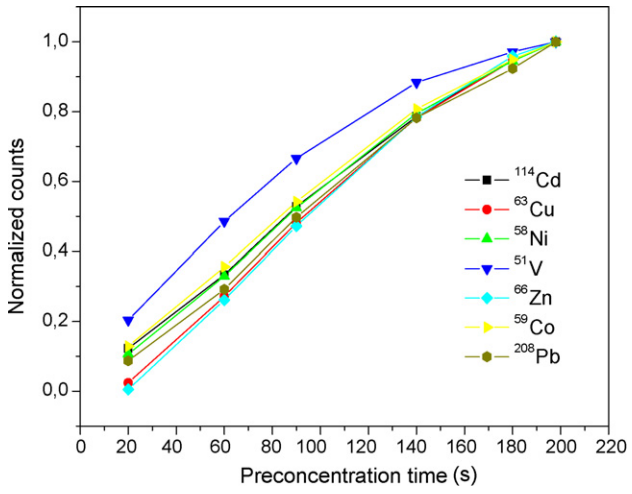


Fig. 5. Effect of the sample load time on the simultaneous retention of each analytes at 3.0 μg L^{-1}. Mini-column contained 100 mg of Nb_2O_5–SiO_2; sample flow rate at 6.0 mL min^{-1}; sample pH 7; eluent concentration of 2.5 mol L^{-1}.

was with a 100 μg L^{-1} solution and 110 μg L^{-1} for V. The saturation of the mini-column for the Pb was not reached, probably due to the higher affinity of this ion for the active sites or other special properties that it has in relation to the other ions.

3.6. Analytical performance

The results of the analytical performance for the simultaneous pre-concentration and for direct measures of Cd, Cu, Ni, V, Co, Zn and Pb are presented in Table 3. The precision of the pre-concentration procedure was determined with a 6.0 mL of the working solution at 3.0 μg L^{-1} for the optimized pre-concentration system. The relative standard deviation for the pre-concentration procedure of seven consecutive measurements of 3.0 μg L^{-1} of each ion studied was lower than 4.5%. Calibration graphs with and without pre-concentration were used to calculate the sensitivity, linear working range and the enrichment factor (EF). The EF for the proposed method was calculated as the ratio of the slopes of the calibration graphs with and without pre-concentration. The linear working range studied

Table 5
Recovery studies for the different types of water samples

Analyte	Sample			
	Ground water (μg L^{-1} ± S.D.)	Tap water (μg L^{-1} ± S.D.)	Seawater 1 (μg L^{-1} ± S.D.)	Seawater 2 (μg L^{-1} ± S.D.)
Cd				
Contents	0.25 ± 0.030	ND	ND	0.07 ± 0.01
Added	0.30	0.30	0.30	0.30
Found	0.57 ± 0.025	0.301 ± 0.003	0.309 ± 0.007	0.39 ± 0.02
Recovery	104%	100%	103%	105%
Cu				
Contents	0.58 ± 0.045	5.0 ± 0.10	0.92 ± 0.09	1.52 ± 0.12
Added	0.30	0.30	0.30	0.30
Found	0.89 ± 0.033	5.5 ± 0.20	1.29	1.85 ± 0.16
Recovery	101%	104%	106%	102%
Ni				
Contents	0.63 ± 0.009	ND	0.09 ± 0.01	0.135 ± 0.015
Added	0.30	0.30	0.30	0.30
Found	0.92 ± 0.008	0.28 ± 0.01	0.36 ± 0.04	0.431 ± 0.011
Recovery	99%	93%	92%	93%
V				
Contents	0.60 ± 0.015	ND	ND	0.063 ± 0.009
Added	0.30	0.30	0.30	0.30
Found	0.91 ± 0.020	0.29 ± 0.02	0.28	0.354 ± 0.007
Recovery	101%	97%	93%	97%
Zn				
Contents	18.9 ± 0.51	15.0 ± 0.11	9.1 ± 0.2	5.33 ± 0.13
Added	0.30	0.30	0.30	0.30
Found	20.1 ± 0.40	15.7 ± 0.21	9.45 ± 0.15	5.65
Recovery	105%	103%	100%	100%
Co				
Contents	0.101 ± 0.007	ND	0.11 ± 0.05	0.08 ± 0.01
Added	0.30	0.30	0.30	0.30
Found	0.393 ± 0.010	0.28 ± 0.03	0.40 ± 0.03	0.37 ± 0.02
Recovery	98%	93%	97%	97%
Pb				
Contents	0.089 ± 0.009	ND	0.05 ± 0.01	ND
Added	0.30	0.30	0.30	0.30
Found	0.383 ± 0.011	0.29 ± 0.03	0.32	0.28 ± 0.03
Recovery	98%	97%	91%	93%

ND: not detectable.

for the system with pre-concentration procedure was between 0.05 and 25.0 $\mu g\,L^{-1}$ and for direct measures was between 20 and 100 $\mu g\,L^{-1}$. The limit of detection (LOD) was calculated as $3\sigma/S$, where S is the slope of the calibration curve and σ is the standard deviation of 11 consecutive measurements of the blank solution. This procedural blank integrates acid blank (because the samples were acidified to pH 2 as a preservation to prevent losses due to wall adsorption), buffer, column blank, and instrument blank. A comparison between the results obtained using the proposed pre-concentration procedure and direct measures, shown in Table 3, demonstrated the importance of the pre-concentration system in spite of the high sensitivity of the ICP-MS technique.

The accuracy of the proposed method was investigated analyzing some standard reference material. The results are presented in Table 4. The values of studied ions found in the standard reference materials are in accordance with the certified data.

Water samples collected from quality control wells in fuel station (ground water), tap water and seawater in Florianópolis, SC, Brazil were spiked with the metals of interest and subjected to the same pre-concentration procedure to determine the recovery of the resin. The results of this study can be seen in Table 5. Recoveries were found to range between 90 and 110%, indicating that matrix effects were negligible.

4. Conclusions

The new method developed resulted in an efficient analytical performance of an on-line pre-concentration system for simultaneous determination of Cd, Cu, Ni, V, Zn, Co and Pb in aqueous environmental samples. The Nb_2O_5–SiO_2 sorbent was chemically stable throughout the analyses (several months). The instrumentation and method described in this study proved to be a convenient and high tool for pre-concentration and separation of the analytes studied in a simple analytical cycle. Furthermore, the method presents simplicity, fast analytical frequency and low consumption of analytes and reagents.

Acknowledgment

The authors thank Conselho Nacional de Desenvolvimento Cientifico e Tecnológico (CNPq) for financial support.

References

[1] M.H.A. Melo, S.L.C. Ferreira, R.E. Santelli, Microchem. J. 65 (2000) 59.
[2] S.L.C. Ferreira, J.R. Ferreira, A.F. Dantas, V.A. Lemos, N.M.L. Araújo, A.C.S. Costa, Talanta 50 (2000) 1253.
[3] V.A. Lemos, W.N.L. Santos, J.S. Santos, M.B. Carvalho, Anal. Chim. Acta 481 (2003) 283.
[4] J. Chwastowska, W. Skwara, E. Sterlińska, L. Pszonicki, Talanta 66 (2005) 1345.
[5] J. Chwastowska, W. Skwara, E. Sterlińska, L. Pszonicki, Talanta 64 (2004) 224.
[6] J. Yin, Z. Jiang, G. Chang, B. Hu, Anal. Chim. Acta 540 (2005) 333.
[7] J. Sysalovaa, J. Szakova, Environ. Res. 101 (2006) 287.
[8] D. Beauchemin, Anal. Chem. 74 (2002) 2873.
[9] K.E. Jarvis, A.L. Gray, R.S. Houk, Handbook of Inductively Coupled Plasma Mass Spectrometry, Chapman and Hall, New York, 1992.
[10] R.S. Houk, Anal. Chem. 58 (1986) 97.
[11] C. Duyck, N. Miekeley, C.L.P. da Silveira, P. Szatmari, Spectrochim. Acta B 57 (2002) 1979.
[12] D. Karunasagar, J. Arunachalam, Anal. Chim. Acta 441 (2001) 291.
[13] V.L. Dressler, D. Pozebon, A.J. Curtius, Anal. Chim. Acta 438 (2001) 235.
[14] E. Carasek, Talanta 51 (2000) 173.
[15] E.L. da Silva, E.M. Ganzarolli, E. Carasek, Talanta 62 (2004) 727.
[16] E.K. Paleologos, D.L. Giokas, M.I. Karayannis, Anal. Chem. 24 (2005) 426.
[17] E.H. Hansen, J. Wang, Anal. Chim. Acta 467 (2002) 3.
[18] K. Benkhedda, H.G. Infante, F.C. Adams, Anal. Chim. Acta 506 (2004) 137.
[19] S. Li, N. Deng, F. Zheng, Y. Huang, Talanta 60 (2003) 1097.
[20] N. Nagata, L.T. Kubota, M.I.M.S. Bueno, P.G. Peralta-Zamora, J. Colloid Interf. Sci. 200 (1998) 121.
[21] Y. Gushikem, S.S. Rosatto, J. Brazil Chem. Soc. 12 (2001) 695.
[22] M.L. Cervera, M.C. Arnal, M. de la Guardia, Anal. Bioanal. Chem. 375 (2003) 820.
[23] A.M.H. Shabani, S. Dadfarnia, K. Dehghan, Talanta 59 (2003) 719.
[24] J.C. Yu, X.J. Wu, Z. Chen, Anal. Chim. Acta 436 (2001) 59.
[25] E. Matoso, L.T. Kubota, S. Cadore, Talanta 60 (2003) 1105.
[26] N. Nagata, L.T. Kubota, M.I.M.S. Bueno, P.G.P. Zamora, J. Colloid Interf. Sci. 200 (1998) 121.
[27] E. Vassileva, N. Furuta, Fresenius J. Anal. Chem. 370 (2001) 52.
[28] H.F. Maltez, E. Carasek, Talanta 65 (2005) 537.
[29] Y. Gushikem, S. Denofre, Y. Kawano, J. Chem. Soc., Faraday Trans. 89 (1993) 1057.
[30] D. Budziak, E.L. da Silva, S.D. Campos, E. Carasek, Microchim. Acta 141 (2003) 169.
[31] R.L. Dutra, H.F. Maltez, E. Carasek, Talanta 69 (2006) 488.
[32] E.L. da Silva, D. Budziak, E. Carasek, Anal. Lett. 37 (2004) 1909.

Available online at www.sciencedirect.com
ScienceDirect
Talanta 74 (2008) 800–805
Talanta
www.elsevier.com/locate/talanta

Single drop micro-extraction with *O*,*O*-diethyl dithiophosphate for the determination of lead by electrothermal atomic absorption spectrometry

Heloísa França Maltez [a], Daniel L.G. Borges [a,*], Eduardo Carasek [a], Bernhard Welz [a,b], Adilson J. Curtius [a]

[a] *Departamento de Química, Universidade Federal de Santa Catarina, Campus Universitário Trindade, 88040-900 Florianópolis, SC, Brazil*
[b] *Grupo de Pesquisa em Química Analítica, Instituto de Química, Universidade Federal da Bahia, 40170-290 Salvador, BA, Brazil*

Received 2 March 2007; received in revised form 11 July 2007; accepted 13 July 2007
Available online 21 July 2007

Abstract

Lead was extracted as the *O*,*O*-diethyldithiophosphate (DDTP) complex from aqueous solution into a drop of $CHCl_3$ immersed in the solution. Unlike previously reported procedures using single drop micro-extraction (SDME) for the extraction of inorganic analytes, the complexation reaction was conducted in the aqueous phase, as the ammonium salt of DDTP is soluble in water. The concentration of DDTP was optimized as 0.01% (m/v). Experimental parameters such as extraction time (7 min) and organic drop volume (3 μL) were optimized and selected as a compromise between sensitivity and stability of the organic drop in the aqueous solution. The sensitivity with electrothermal atomic absorption spectrometry (ET AAS) was low, probably due to infiltration of the organic drop into the totally pyrolytic graphite platform. To overcome this problem, tungsten (400 μg) was thermally deposited onto the platform surface. A short pyrolysis stage at 700 °C was included to reduce background absorption. Under these conditions, five certified reference materials with different characteristics were analyzed using calibration against aqueous standards submitted to the SDME procedure, resulting in good agreement between certified and found concentration values at a 95% confidence level. Two real water samples have also been analyzed, with recoveries ranging from 85 to 92% after enrichment with Pb. An enhancement factor of 52 allowed a detection limit of 0.2 μg L^{-1} or 0.04 μg g^{-1}, demonstrating the high detection capability of the proposed procedure, with a relative standard deviation typically below 4%.
© 2007 Elsevier B.V. All rights reserved.

Keywords: Single drop micro-extraction; Diethyl dithiophosphate; Lead determination; Electrothermal atomic absorption spectrometry; Chloroform; Tungsten-treated platform

1. Introduction

In the past few decades, the intensification of anthropogenic activities has become responsible for a great charge of polluting substances that were released to the environment, contaminating soil, air and water. One of the most widespread inorganic contaminants is lead, due to its extensive use in industry, such as in the manufacture of batteries, alloys, X-ray protection devices, etc. [1,2], although its use as anti-knocking additive to gasoline has been banned in many countries at the beginning of the 1990s. Lead can be harmful to practically all organs and systems in the human body, although it affects particularly the nervous system [3]. Due to these adverse effects, monitoring of lead concentration in all kind of samples has been a subject of extensive research in analytical chemistry [4–6].

Despite the obvious advances in the field of instrumental analysis in the past few decades, many of the instruments are still limited concerning sensitivity and tolerance to concomitants [7]. The growing interest in the study of the effects of trace elements in the environment has lead to more rigid regulations all around the world regarding what should be expected as 'normal' or 'acceptable' concentration of trace elements in samples of the most diverse nature. However, in order to fit the rigid requirements for trace analysis, particularly concerning sensitivity, a pre-concentration step is frequently necessary to achieve the lowest possible limits of detection (LOD). Several extraction

* Corresponding author. Fax: +55 48 3721 6850.
E-mail address: daniel@qmc.ufsc.br (D.L.G. Borges).

0039-9140/$ – see front matter © 2007 Elsevier B.V. All rights reserved.
doi:10.1016/j.talanta.2007.07.010

and pre-concentration procedures have been described in the literature, such as conventional liquid–liquid extraction (LLE) [8], solid-phase extraction [9] and more recently a particular form of LLE, known as cloud point extraction [10].

Liquid–liquid extraction has been used for decades, but it has some disadvantages such as the requirement for relatively large amounts of organic solvents with toxic properties [11]. Improvements in the traditional LLE routine resulted in the development of novel extraction techniques, such as liquid–liquid microextraction [12,13] and single-drop micro-extraction (SDME) [14,15]. Both techniques are based on the same principles as the traditional LLE, but with advantages that include significant reduction in the amount of organic solvent used, simplicity, cost-effectiveness and higher analytical frequency.

SDME is a well-established extraction procedure for the determination of organic compounds using chromatographic techniques [16]. In SDME, the extracting phase is a microvolume drop of a water-immiscible solvent, which is held at the tip of a capillary syringe that is immersed into the aqueous sample solution [16]. SDME has also been applied recently to the extraction of inorganic compounds, as was demonstrated by Xia et al. [17] and Li et al. [18], who developed methods to determine trace elements in biological samples using electrothermal vaporization inductively coupled plasma mass spectrometry. Another possible configuration used for SDME extraction consists on leaving the drop in the headspace, as was applied in combination with hydride generation and electrothermal atomic absorption spectrometry (ET AAS) for the determination of selenium [19,20], methylmercury [21] and arsine [22]. Electrothermal AAS has also been employed with SDME for the determination of antimony using Rh as permanent modifier and *N*-benzoyl-*N*-phenylhydroxylamine as chelating agent [23] and for the determination of cadmium using Ir as permanent modifier and dithizone as the chelating agent [24]. The number of publications involving SDME for the quantification of inorganic analytes, however, is still restricted to a few examples, although the technique has demonstrated to have a great potential for applications in this field of research.

In this work, the determination of Pb by ET AAS will be demonstrated after its extraction as the *O*,*O*-dietyhyl dithiophosphate complex into a drop of $CHCl_3$ using the SDME procedure.

2. Experimental

2.1. Instrumentation

All measurements were carried out in an AAnalyst 100 atomic absorption spectrometer with deuterium-arc background correction, equipped with an HGA 800 graphite tube atomizer (Perkin Elmer, Norwalk, CT, USA). A Pb hollow cathode lamp (Perkin Elmer, part no. N305-0157), operated at 10 mA, was used. All measurements were carried out at 283.3 nm, with a spectral bandwidth of 0.7 nm. Longitudinally heated pyrolytic graphite-coated graphite tubes with pyrolytic graphite L'vov platforms (Perkin Elmer, part no. B0 109322) were used throughout this work. Argon 99.996% (White Martins, São Paulo, SP, Brazil) was used as purge and protective gas. Integrated absorbance (peak area) was used exclusively for signal evaluation. The temperature program used to determine Pb by ET AAS is shown in Table 1. Prior to the analysis, L'vov platforms were treated with tungsten, using 10 injections of 40 μL each of a 1000 mg L^{-1} W and applying the temperature program previously described [25] after each injection, resulting in a total deposited mass of 400 μg W.

Table 1
Temperature program for the determination of Pb using SDME-ET AAS

Step	Temperature (°C)	Ramp (s)	Hold (s)	Ar flow rate (mL min^{-1})
Drying	70	10	5	250
Pyrolysis	700	10	10	250
Atomization	1700	0	4	0
Cleanout	2000	1	3	250

Samples were digested using a MLS 1200 Mega microwave oven (Milestone, Sorisole, Italy).

2.2. Reagents, solutions and samples

All reagents used were at least of analytical grade. Water was deionized to a resistivity of 18 MΩ cm in a Milli-Q system (Millipore, Bedford, MA, USA). Nitric acid (Merck, Darmstadt, Germany) was doubly distilled in a sub-boiling quartz distillation apparatus (Kürner Analysentechnik, Rosenheim, Germany). Hydrofluoric acid (Fluka, Buchs, Switzerland) was doubly distilled at sub-boiling temperature in a PTFE still (Kürner Analysentechnik). Hydrogen peroxide (Suprapur®, Merck) was used without purification. A lead stock solution (1000 mg L^{-1} Pb) was prepared dissolving high-purity $Pb(NO_3)_2$ (SPEX, Eddison, NJ, USA). Working solutions were prepared daily in 1% (v/v) HNO_3 by proper dilution of the stock solution. Ammonium *O*,*O*-diethyl dithiophosphate (DDTP) was supplied by Aldrich (Milwaukee, WI, USA) and used after purification in a silica gel C18 column (Merck). Chloroform (Tedia, Fairfield, OH, USA) was used as supplied.

The following certified reference materials (CRM) were used in this work: NIST SRM 1640 (Trace Elements in Natural Water), NIST SRM 1643e (Trace Elements in Water) and NIST SRM 1575 (Pine Needles), from the National Institute of Standards & Technology (Gaithersburg, MA, USA); SOIL-7 (Soil) from the International Atomic Energy Agency (Vienna, Austria), and STSD-2 (Stream Sediment) from CANMET (Ottawa, Ontario, Canada).

2.3. Procedure

2.3.1. Sample treatment

Solid CRM (NIST 1575, SOIL-7 and STSD-2) were digested prior to analysis by SDME-ET AAS. Aliquots containing approximately 250 mg of NIST 1575 were weighed in PTFE flasks and 3 mL concentrated HNO_3 and 1 mL concentrated H_2O_2 were added. For SOIL-7 and STSD-2, aliquots containing approximately 100 mg were weighed and 3 mL HNO_3 and 1 mL HF were added. All samples were submitted to the follow-

ing microwave program: 2 min at 250 W, 2 min at 0 W, 6 min at 250 W, 5 min at 400 W and 5 min at 650 W, followed by 5 min of ventilation. Deionized water was added up to the final volume of 50 mL. Real water samples were collected from an artesian well and from Peri Lagoon, in the city of Florianópolis, SC, Brazil. The samples were collected and stored in poly(propylene) bottles under refrigeration until use. These samples have been directly submitted to the SDME procedure described below.

2.3.2. SDME procedure

The SDME apparatus consists of a 10-μL micro-syringe (Hamilton, NV, USA), a magnetic bar stirrer (Microquímica, São Paulo, SP, Brazil) and a 5-mL capacity vial with a PTFE septum. A 3-μL volume of $CHCl_3$ was taken up with the syringe and the vial containing the sample (2 mL) was placed with a magnetic bar on the magnetic stirrer. The syringe needle was then introduced into the vial by perforating the PTFE septum. The needle was immersed into the sample solution and the micro-drop was exposed. An important characteristic of this procedure is that DDTP has been added to the sample solution at the optimized concentration of 0.01% (m/v), unlike other SDME procedures described in the literature in which the chelating agent is dissolved in the organic drop. The micro-drop was left for 7 min under constant stirring, and after that it was aspirated back into the micro-syringe and inserted manually into the graphite furnace. The temperature program in Table 1 followed each injection. Calibration was performed using aqueous calibration solutions submitted to the same SDME procedure described above.

3. Results and discussion

3.1. Pyrolysis and atomization curves

One of the desirable properties of a solvent to be used in SDME is a high density (higher than the density of water), which will improve the stability of the micro-drop once it is submerse. Organochloride solvents, such as $CHCl_3$, can usually fulfill this requirement. Chloroform is also inexpensive and less toxic than other typical solvents. The first experiments for optimization of the ET AAS parameters were carried out without using a modifier; however, later it was found that $CHCl_3$ was infiltrating into the graphite platform pores, resulting in poor atomization efficiency. In fact, under these conditions, a Pb signal could only be detected at atomization temperatures higher than 2000 °C and considerable memory effect was observed, calling for some surface modification. Tungsten has been shown to be an appropriate coating, as its carbide-forming properties were useful to reduce the porosity of the platform surface, hence preventing penetration of $CHCl_3$ and enhancing the atomization efficiency. In order to optimize pyrolysis and atomization temperatures, a 5-mL aliquot of $CHCl_3$ was added to an aqueous solution containing 5 μg L^{-1} Pb and 0.1% (m/v) DDTP, and conventional LLE (manual shaking and centrifugation) was used. The organic extract was manually injected into the graphite furnace in 5-μL aliquots, resulting in the curves shown in Fig. 1. In a first attempt using a treated tube, the pyrolysis stage was eliminated from the temperature program, as apparently only the removal of $CHCl_3$ was necessary. However, in the absence of a pyrolysis stage or at pyrolysis temperatures below 500 °C, elevated background was observed, possibly due to an excess of DDTP extracted by $CHCl_3$ that was vaporized at the atomization stage. This caused a significant signal suppression, which resulted in the low integrated absorbance values for low pyrolysis temperatures shown in Fig. 1. To overcome this effect, a pyrolysis temperature of 700 °C was selected, requiring a holding time of only 5 s in order to efficiently eliminate the background signal. The atomization temperature has similarly been optimized, as shown in Fig. 1, and an atomization temperature of 1700 °C was selected for further studies.

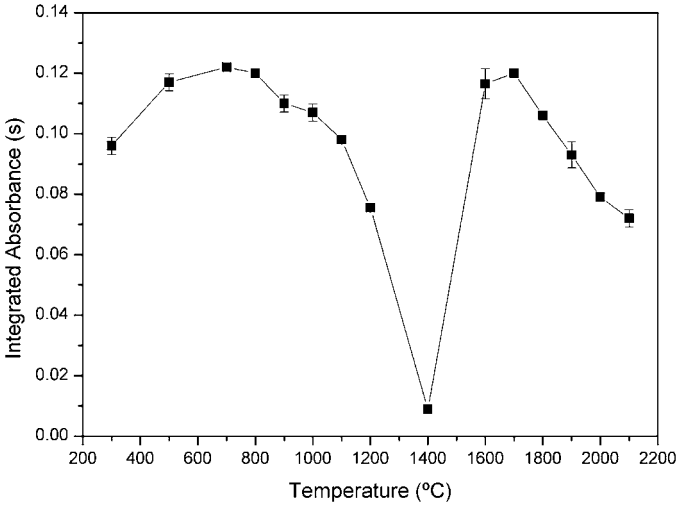


Fig. 1. Pyrolysis and atomization curves for Pb using a platform treated with 400 μg W. Lead has been extracted as the DDTP complex into $CHCl_3$ after conventional liquid–liquid extraction. *Conditions*: Pb concentration: 5 μg L^{-1} (aqueous solution); 0.1% (v/v) HNO_3; 0.01% (m/v) DDTP.

3.2. SDME conditions

3.2.1. DDTP concentration

Several factors were responsible for the choice of DDTP as the chelating agent, such as its solubility in water, its high stability in acidic media and its high formation constant for Pb complexation. Due to its solubility, DDTP could be added to the aqueous phase (sample or calibration solutions), allowing the complex to be generated before extraction, which considerably facilitated the procedure. Other SDME procedures use solubilization of the chelating agent in the organic drop [17,18], which has a few inconveniences, particularly related to the choice and handling of the organic solvent and to volatilization. The influence of DDTP concentration on the integrated absorbance signal has been evaluated in the range 0–0.01% (m/v), as shown in Fig. 2. As complexation occurs in acidic media, 0.1% (v/v) HNO_3 was added to the aqueous solution. The sensitivity increased rapidly with increasing DDTP concentrations from 0 to 0.001% (m/v), as a result of the high extraction efficiency of the Pb–DDTP complex to the organic micro-drop. For DDTP concentrations above 0.001% (m/v), the sensitivity remained essentially unchanged, as excess DDTP did not

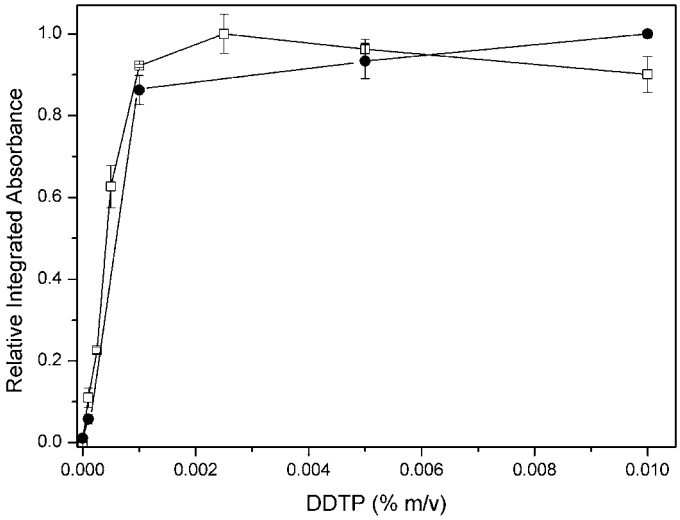


Fig. 2. Effect of DDTP concentration on the analytical signal for Pb using SDME-ET AAS and extraction from aqueous solution containing 5 μg L^{-1} Pb (-□-), and extraction from multi-element solution containing 29 elements at 25 μg L^{-1} in addition to Pb (-●-). *Conditions*: 0.1% (v/v) HNO_3; 7 min extraction time; micro-drop volume of 3 μL; platform treated with 400 μg W.

improve extraction efficiency or mass transfer. As this particular study has been carried out using a synthetic solution containing only Pb, a second study was conducted with a multi-element solution in order to assure that DDTP is in sufficient excess and that parallel complexation with concomitant ions in solution will not decrease the extraction efficiency for the procedure. For this study a multi-element calibration standard, containing 29 concomitant ions, all at a concentration of 25 μg L^{-1}, was used. As seen in Fig. 2, the profile of the curve obtained with a multi-element solution was very similar to that obtained with Pb only, indicating that a DDTP concentration of 0.01% (m/v) is sufficient to maintain the maximum achievable extraction efficiency, even in the presence of concomitant ions. The difference in this case was typically less than 4%.

3.2.2. Micro-drop volume and stirring speed

The volume of the micro-drop is an essential parameter to determine the extraction efficiency. Three different volumes have been evaluated (1, 2 and 3 μL), and there was a 2-fold increase in sensitivity for a 3-μL micro-drop when compared to a 1-μL micro-drop, which is according to expectations. The surface area increases with an increase in the drop volume, resulting in a more efficient mass transfer from the bulk aqueous solution to the organic drop. However, the micro-drop becomes unstable and can be easily released from the tip of the syringe needle when volumes larger than 3 μL are used, so that this volume was adopted throughout.

Stirring speed is also an important factor as it defines the diffusion of the analyte to the organic micro-drop, which means that stirring in fact reduces the time required for the mass transfer to reach equilibrium. However, a steep increase in the stirring speed could cause release of the micro-drop from the tip of the syringe needle, promoting the formation of an air bubble inside the micro-drop. Increasing stirring speed also results in a reduction of the micro-drop volume, as it disturbs the water film that is formed on the surface of the drop, hence stimulating the release of small volumes of the drop that might be solubilized in the aqueous phase. As a compromise between drop stability and higher diffusion of the analyte, a low magnetic stirring speed (usually lower than 400 rpm [23,24]) was selected.

3.2.3. Extraction time

Mass transfer is a time-dependent process and the transfer rate is reduced when the system approaches equilibrium. However, reaching equilibrium is not necessary, as long as the extraction conditions are reproducible. In this sense, the extraction time has been optimized by varying the exposure time of the micro-drop to the aqueous solution from 0 to 10 min. It can be seen in Fig. 3 that the integrated absorbance signal increased significantly with an increase in extraction time. The profile of the curve obtained in Fig. 3 indicates that equilibrium has not actually been reached, but 10 min was the maximum exposure time possible, as for longer periods the drop became unstable and was released from the syringe tip. As a compromise between extraction efficiency and analytical frequency, an extraction time of 7 min was adopted throughout this work.

3.2.4. Ionic strength

The addition of an ionic substance, such as NaCl, to the extraction medium might also affect the extraction process. In theory, an increase in the ionic strength could decrease the solubility of hydrophobic species such as the Pb–DDTP complex in the aqueous medium, hence improving the extraction efficiency. In order to evaluate this effect, NaCl, in concentrations ranging from 0 to 2.0 mol L^{-1}, was added to the aqueous solution containing Pb before submission to the SDME procedure. The results have shown that there was a very distinct increase in sensitivity for a NaCl concentration of up to 0.01 mol L^{-1}, possibly caused by an increased mass transfer from the bulk of the aqueous phase to the organic micro-drop. The addition of

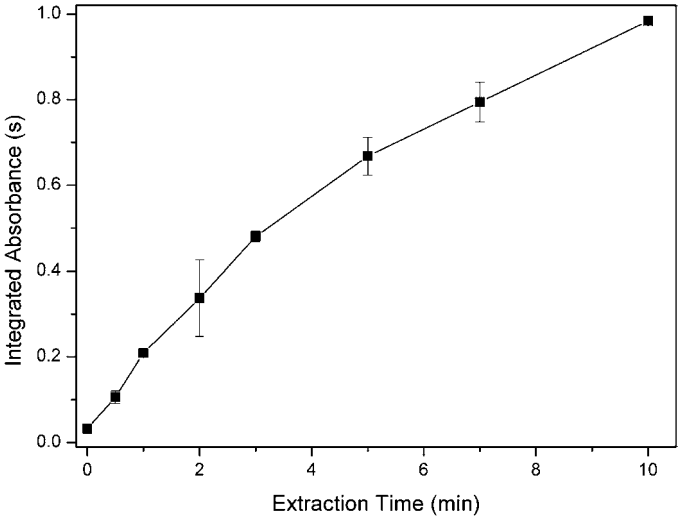


Fig. 3. Effect of extraction time on analytical signal obtained for 5 μg L^{-1} Pb using SDME-ET AAS. *Conditions*: 0.1% (v/v) HNO_3; 0.01% (m/v) DDTP; micro-drop volume of 3 μL; platform treated with 400 μg W.

larger concentrations of NaCl, however, resulted in a considerable decrease in the integrated signal; a reduction of about 30% in the analytical signal was observed for a NaCl concentration of 0.5 mol L^{-1}. One possible explanation for this effect could be changes in the physical properties of the water film formed on the micro-drop, which affects the diffusion process of the analyte [26]. Another possibility would be the formation of charged chloride complexes in the aqueous phase, which would decrease the extraction efficiency due to the hydrophilic properties of such complexes. Co-extracted chloride could also cause interference, when in excess.

3.3. Figures of merit and analytical results

Under optimized conditions, the analytical figures of merit, shown in Table 2, were obtained for the SDME procedure. The limit of detection (LOD), calculated as three times the standard deviation of 10 blank readings divided by the slope of the calibration curve submitted to SDME, demonstrates a good detection capability for the method, particularly considering that an aliquot of only 3-μL of the organic extract is analyzed. The enhancement factor was calculated as the ratio between the LOD obtained for the SDME procedure and the LOD obtained for calibration solutions in $CHCl_3$ without pre-concentration (determined as 10.3 μg L^{-1}). The 52-fold improvement in LOD demonstrates that mass transfer and diffusion are fairly high, even carrying out the procedure in non-equilibrium conditions. Comparison with previously published data [18] using a similar SDME procedure with ETV-ICP-MS detection, as shown in Table 2, demonstrates that even using a typically less sensitive technique, such as ET AAS, the detection limit obtained is more than a factor of 2 better, demonstrating the efficiency of the proposed procedure particularly in improving the precision. The extraction efficiency for the SDME-ETV-ICP-MS procedure using 8-hydroxiquinoline as chelating agent, however, is higher, which is mostly due to the fact that the determination was carried out at equilibrium conditions. Although the use of ETV-ICP-MS is certainly interesting due to the multi-element capability of ICP-MS, the ET AAS procedure appears to be an interesting alternative not only due to the comparable sensitivity, but also due to the considerably higher analytical frequency and far lower gas consumption, which implies in a more cost-effective procedure. In the work of Li et al. [18], each extraction requires 15 min, which means that at each four SDME replicates the plasma has to be left on for 1 h. Nevertheless, both procedures lead to good analytical results.

Table 2
Analytical figures of merit for the proposed SDME-ET AAS procedure and comparison with the results from Li et al. [18](n.a. = not available)

Parameter	Li et al. [18]	This work
Calibration range (μg L^{-1})	0.01–50	1.0–15.0
R	>0.99	0.9996
Slope (L s μg^{-1})	n.a.	0.0484
LOD (μg L^{-1})	0.55	0.2
LOD (μg g^{-1})	n.a.	0.04
EF	190	52
RSD (%)	12	4[a]

[a] Obtained from a 5 μg L^{-1} solution; $n = 7$.

Table 3
Results obtained for the determination of Pb in CRM using SDME-ET AAS with a tungsten-coated graphite tube ($n = 3$; t-Student applied for 95% confidence level;$t = 0.1874$ for the group of results)

Sample	Certified	Found
NIST 1643e	19.63 ± 0.21[a]	20.82 ± 0.10[a]
NIST 1640	27.89 ± 0.14[a]	29.49 ± 3.20[a]
NIST 1575	10.08 ± 0.50[b]	12.0 ± 0.2[b]
SOIL-7	60 (55–71)[b]	50.7 ± 6.5[b]
STSD-2	66[b,c]	68.5 ± 4.5[b]

[a] μg L^{-1}.
[b] μg g^{-1}.
[c] Informed value.

To verify the accuracy of the proposed procedure, five CRM with different characteristics have been analyzed using the SDME procedure. As shown by the results in Table 3, good agreement between certified and found values was obtained at a 95% confidence level, indicating that calibration carried out using aqueous standard solutions submitted to the SDME procedure results in good accuracy. To assure the homogeneity and statistical validity of the method, a paired t-test was applied to the group of results; the determined "t" value was 0.187, which is below the reference t-value for a 95% confidence interval ($t = 2.78$). The SDME procedure has also been applied to an artesian well water and to a lagoon water sample. Although the natural concentrations were found to be below the limit of quantification (0.6 μg L^{-1}), recoveries from 85 to 92% were obtained after the addition of 3.0 μg L^{-1} Pb, showing the good accuracy of the method for the analysis of real samples. In addition, the results have shown that matrix effects and/or changes in the mass transfer due to the presence of substances used in the preparation of samples or in the extraction procedure (e.g., HNO_3 and HF) are inexistent or negligible. Good precision was obtained, with a typical relative standard deviation of 4%.

4. Conclusion

The combination of SDME with ET AAS resulted in a relatively simple and fast method to determine Pb in liquid and digested samples, with good enhancement factor and low LOD. The use of DDTP as the chelating agent facilitated the procedure to a great extent, allowing the complex to be formed in the aqueous phase. This same procedure is probably applicable to other samples and analytes that form complexes with DDTP.

Acknowledgements

The authors are thankful to Conselho Nacional de Desenvolvimento Científico e Tecnológico (CNPq) and Fundação de Amparo à Pesquisa do Estado da Bahia (FAPESB) for financial support. B.W. has a research scholarship from FAPESB and other co-authors have scholarships from CNPq.

References

[1] A.N. Anthemidis, S.J.V. Koussoroplis, Talanta 71 (2007) 1728.
[2] M.R.M.P. De Aguiar, A.C. Novaes, A.W.S. Guarino, Quim. Nova 25 (2002) 1145.
[3] M.G. Korn, J.B. de Andrade, D.S. de Jesus, V.A. Lemos, M.L.S.F. Bandeira, W.N.L. dos Santos, M.A. Bezerra, F.A.C. Amorim, A.S. Souza, S.L.C. Ferreira, Talanta 69 (2006) 16.
[4] M.O. Luconi, R.A. Olsina, L.P. Fernández, M.F. Silva, J. Hazard. Mater. 128 (2006) 240.
[5] M. Tuzen, E. Melek, M. Soylak, J. Hazard. Mater. 136 (2006) 597.
[6] M. Yaman, Y. Dilgin, S. Gucer, Anal. Chim. Acta 410 (2000) 119.
[7] A. Ceccarini, I. Cecchini, R. Fuoco, Microchem. J. 79 (2005) 21.
[8] Y.K. Agrawal, K.R. Sharma, Talanta 67 (2005) 112.
[9] C.R.T. Tarley, S.L.C. Ferreira, M.A.Z. Arruda, Microchem. J. 77 (2004) 163.
[10] G.L. Donati, C.C. Nascentes, A.R.A. Nogueira, M.A.Z. Arruda, J.A. Nóbrega, Microchem. J. 82 (2006) 189.
[11] W. Wardencki, J. Curylo, J. Namieśnik, J. Biochem. Biophys. Methods 70 (2007) 275.
[12] E. Carasek, Talanta 51 (2000) 173.
[13] E. Carasek, J.W. Tonjes, M. Scharf, Talanta 56 (2002) 185.
[14] E. Zhao, L. Han, S. Jiang, Q. Wang, Z. Zhou, J. Chromatogr. A 1114 (2006) 269.
[15] V. Colombini, C. Bancon-Montigny, L. Yang, P. Maxwell, R.E. Sturgeon, Z. Mester, Talanta 63 (2004) 555.
[16] L. Xu, C. Basheer, H.K. Lee, J. Chromatogr. A 184 (2006) 1152.
[17] L.B. Xia, B. Hu, Z.C. Jiang, Y.L. Wu, Y. Liang, Anal. Chem. 76 (2004) 2910.
[18] L. Li, B. Hu, L.B. Xia, Z.C. Jiang, Talanta 70 (2006) 468.
[19] S. Fragueiro, I. Lavilla, C. Bendicho, Talanta 68 (2006) 1096.
[20] R. Figueroa, M. Garcia, I. Lavilla, C. Bendicho, Spectrochim. Acta Part B 60 (2005) 1556.
[21] S. Gil, S. Fragueiro, I. Lavilla, C. Bendicho, Spectrochim. Acta Part B 60 (2005) 145.
[22] S. Fragueiro, I. Lavilla, C. Bendicho, Spectrochim. Acta Part B 59 (2004) 851.
[23] Z. Fan, Anal. Chim. Acta 585 (2007) 300.
[24] Z. Fan, W. Zhou, Spectrochim. Acta Part B 61 (2006) 870.
[25] D.L.G. Borges, A.F. Silva, B. Welz, A.J. Curtius, U. Heitmann, J. Anal. Atom. Spectrom. 21 (2006) 763.
[26] E. Psillakis, N. Kalogerakis, Trends Anal. Chem. 21 (2002) 53.

Available online at www.sciencedirect.com
ScienceDirect
Talanta 74 (2008) 736–740
Talanta
www.elsevier.com/locate/talanta

Rapid leaching of Cr(VI) in soil with Na_3PO_4 in the determination of hexavalent chromium by electrothermal atomic absorption spectrometry

Khakhathi L. Mandiwana *

Department of Chemistry, Tshwane University of Technology, Private Bag X31, Rosslyn 0200, South Africa

Received 7 May 2007; received in revised form 29 June 2007; accepted 3 July 2007
Available online 7 July 2007

Abstract

A method has been developed that leaches Cr(VI) selectively from soil samples. Hexavalent chromium was leached completely from soil with 0.01 mol L^{-1} Na_3PO_4. This was achieved by boiling the soil–reagent solution mixture for a period of 5 min. The leached Cr(VI) was then quantified by electrothermal atomic absorption spectrometry (ET-AAS) after filtration of the sample solutions through Hydrophilic Millipore PVDF 0.45 μm filter.

Statistical evaluations indicated that the new developed method is reliable since neither its comparison with the established method nor the comparison of the sum of the concentrations of chromium species to that of the total concentration of chromium show any difference at 95% level of confidence. The spiking of soil samples with Cr(III) standards before pretreatment show that Cr(III) was not oxidized to Cr(VI) during leaching as the Cr(VI) content never increased. The detection limit established was 0.07 μg g^{-1}, which is an improvement to that of the US EPA method 3060A by a factor of more than 500.

The maximum concentrations of Cr(VI) found in soil samples collected around the new chromium mine was 8.0 μg g^{-1} and falls within acceptable level of 15 μg g^{-1} in accordance with the Italian Guidelines.
© 2007 Elsevier B.V. All rights reserved.

Keywords: Hexavalent chromium; Soil; Leaching; Electrothermal atomic absorption spectrometry

1. Introduction

Chromium is the metallic element that exists primarily in the mineral chromite, which is present in soils, waters, rocks, fauna and gases. It occurs mainly as a result of human activities through the production of waste water in metal smelting, electroplating, tanning, metallurgy and mining. After processing, chromium occurs in several chemical species and it is not biodegradable in the environment [1].

The increase in demand of the industrial uses of chromium and its unregulated application has led to the contamination of soil, sediment, surface and ground waters thereby posing serious health problems to humans and animals [2]. Soil conditions like electron donor availability, soil texture, competing ions, adsorption capabilities, pH, moisture content, temperature, and the presence of vegetation are the principal factors that govern the mobility of chromium in soil [3–7].

Chromium exists mainly in the III and VI oxidation states in soil. Hexavalent chromium, Cr(VI), is an oxyanion commonly occurring as relatively water-soluble chromate, CrO_4^{2-} or dichromate, $Cr_2O_7^{2-}$. In temperate region soil, where negatively charged clay minerals predominate, Cr(VI) anions are repelled by the negative charge of soil particles. Due to these charge repulsions, hexavalent chromium is quite mobile in soil [8]. Cr(VI) is a strong oxidizer and this makes it toxic to biological systems [9–13]. Hexavalent chromium's toxicity is enhanced by its ability to diffuse through cell membranes and oxidize biological molecules.

Trivalent chromium, Cr(III), is relatively non-reactive and less toxic due to its slow ligand exchange kinetics but long-term exposures are known to cause allergic skin reactions and cancer [14]. Cr(III) occurs as a cation in soils, forming relatively insoluble oxide and hydroxide compounds [15]. With its large positive charge, Cr(III) is attracted to negatively charged soil particles, and has been found to associate with the smallest size fractions in soils [16]. Thus, Cr(III) is less mobile in soils than Cr(VI).

* Tel.: +27 12 382 0706; fax: +27 12 382 0820.
E-mail address: MandiwanaKL@tut.ac.za.

0039-9140/$ – see front matter © 2007 Elsevier B.V. All rights reserved.
doi:10.1016/j.talanta.2007.07.002

Although most researches have been focused on the extraction and detection of chromium species in liquid samples such as natural and waste waters [17–19], there are limited publications on the extraction of Cr(VI) from soils [20,21] and that requires additional efforts [22]. The most recommended method for determining Cr(VI) in solid matrices is the US EPA method 3060A. This method is based on the reaction of diphenylcarbazide (DPC) with Cr(VI) followed by spectrophotometric detection. However, under the strong alkaline conditions of this method, humic compounds including species that absorb at 540 nm (analytical wavelength for measuring the absorbance of the DPC-Cr colored complex) are released from soil. Such species interferes with the correct determination of Cr(VI), moreover, spectrophotometric techniques suffer from poor detection limits. This makes the US EPA method 3060A unsuitable for determining Cr(VI) species at ultra-lower levels.

In this present research, a method has been developed to leach Cr(VI) selectively from soil with sodium phosphate reagent solution, followed by detection of the analyte by ET-AAS.

2. Experimental

2.1. Apparatus

A Perkin–Elmer Analyst 600 atomic absorption spectrometer that equipped with Zeeman-effect background correction system was used for all measurements. The chromium hollow cathode lamp (25 mA) was operated at 357.9 nm while the spectral band pass was set at 0.7 nm. Transversely heated graphite tubes (THGA) with integrated L'vov platforms (Perkin–Elmer, part N B050–4033) were used as atomizers with Ar as the sheath gas throughout.

2.2. Reagents and standard solutions

Standard stock solutions containing 1000 mg L^{-1} Cr(VI) as K_2CrO_4 (Merck) was used for the preparation of working standards for chromium. Ultra-pure water (resistivity, 18.2 MΩ cm), obtained from a Milli-Q water purification system (Millipore Corp., USA), was used for all dilutions and sample preparations. Ultra-pure HNO_3 (Merck), HF (Merck) and HCl (Merck) were used to digest samples for the total chromium determination. Hydrophilic PVDF 0.45 μm filters (Millipore Millex, USA) were employed for the filtration of all solutions. Certified Reference Material: CRM 027–050 (sandy loam soil from a moderately contaminated site located in the Western United States) was applied as quality control sample for the evaluation of analytical results of total Cr determination.

2.3. Samples and sample preparation

2.3.1. Samples

Samples of top sandy loam soil were taken at the site of a new chromium mine, Thorncliff, South Africa. The soil samples that represent 20 cm of the upper soil layer were collected into plastic bags. They were then air-dried and ground to a particle size less than 75 μm in a tungsten carbide milling vessel.

2.3.2. Determination of water-soluble fraction of Cr(VI)

A nominal mass of 0.25 g sub-sample of soil was transferred into a plastic tube in which 25.0 mL deionized water was added. The content of the tube was shaken periodically for 24 h. The sample solution was then filtered through Hydrophilic Millipore PVDF 0.45 μm filter [prior determination of Cr(VI) by ET-AAS] to remove Cr(III) species that may be trapped in the colloidal suspension.

2.3.3. Leaching of Cr(VI) with Na_3PO_4

Approximately 0.25 g of soil was transferred into a 100 mL glass beaker. Twenty-five milliliters of 0.01 mol L^{-1} Na_3PO_4 were added and the contents of the beaker were boiled on a hot-plate for 5 min. After cooling, the sample was filtered through Whatman No. 540 filter paper and diluted to a final volume of 25.0 mL with deionized water. The sample solution was filtered through Hydrophilic Millipore PVDF 0.45 μm filter prior determination of Cr(VI) by ET-AAS.

2.3.4. Determination of Cr(III) in soil

The precipitate that was collected on Whatman No. 540 filter paper after the filtration was transferred into Teflon digestion vessel (CEM type) and 5.0 mL conc. HNO_3, 3.0 mL conc. HF and 1.0 mL conc. HCl were added. The vessel was capped and the sample was digested in microwave at a pressure of 120 psi for 20 min. After cooling, the cap was removed and the open vessel was heated on a hot-plate to evaporate the excess acid. The content was dissolved in 5.0 mL of 1% (v/v) HNO_3 and diluted to 25.0 mL with deionized water. The resulting solution was then analyzed by ET-AAS.

2.3.5. Determination of total amount of chromium

Approximately 0.25 g of soil was accurately weighed in a Teflon digestion vessel (CEM type) and 5.0 mL conc. HNO_3, 3.0 mL conc. HF and 1.0 mL conc. HCl were added. The vessel was capped and the sample was digested at a pressure of 120 psi for 20 min. After cooling, the cap was removed and the open vessel was heated on a hot-plate to evaporate the excess acid. The content was dissolved in 5.0 mL of 1% (v/v) HNO_3 and diluted to 25.0 mL with deionized water. The resulting solution was then analyzed by ET-AAS.

3. Results and discussions

3.1. Chromium determination by ET-AAS

The ET-AAS determination of chromium was achieved using the optimized temperature program summarized in Table 1.

Table 1
Temperature program for the determination of Cr

Step	Temperature (°C)	Ramp (s)	Hold (s)	Ar (mL min^{-1})
1	110	1	10	250
2	250	5	20	250
3	1300	10	30	250
4	2400	0	5	0

The integrated absorption signals obtained did not differ in their appearance time thereby signifying that the presence of the matrix did not interfere with the correct determination of Cr.

The calibration curve of chromium standards was linear up to 70 $\mu g\,L^{-1}$ and is described by the following equation: $Y = 0.0061x + 0.0043$, where x is the analyte concentration ($\mu g\,L^{-1}$) and Y is the integrated absorbance, with correlation coefficients, $R^2 = 0.9940$ ($n = 5$), respectively.

The limit of detection (LOD) for Cr(VI) determination has been established using blank solutions of Na_3PO_4. The LOD, calculated according to the equation: $LOD = X_{bl} + 3s_{bl}$ ($n = 25$), was found to be 0.7 $\mu g\,L^{-1}$ for a 10 μL sample aliquot. With respect to the soil samples, assuming that 0.25 g of soil after digestion has been adjusted to a volume of 25.0 mL, the LOD for Cr(VI) determination was estimated to be 0.07 $\mu g\,g^{-1}$. The accuracy and trueness for the Cr determination was verified by the analysis of CRM 027–050 with good agreement between certified ($26.9 \pm 0.90\ \mu g\,g^{-1}$) and found ($26.5 \pm 0.75\ \mu g\,g^{-1}$) values.

3.2. Optimization of the leaching of Cr(VI) from soil

Several concentrations of Na_3PO_4 ranging from 1×10^{-4} to 0.1 $mol\,L^{-1}$ were used to leach Cr(VI) from soil to obtain the most appropriate concentration of the reagent solution that can transfer the analyte completely into solution. Precautions were made so as not to use extremely concentrated Na_3PO_4 solution, thus minimizing the effects of the matrix in the graphite tube.

A plot of [Cr(VI)] against $-\log [PO_4^{3-}]$ (Fig. 1) shows that the leaching of Cr(VI) compounds from soil is connected with the presence of PO_4^{3-} ions as the level of Cr(VI) extracted increases as the concentration of the extracting reagent solution increases. Cr(VI) was extracted completely from soil with 0.01 $mol\,L^{-1}$ Na_3PO_4. The multiple extraction of Cr(VI) by fresh portions of 0.01 $mol\,L^{-1}$ Na_3PO_4 indicated that 98% of the analyte was extracted by a single leaching. The efficiency of the leaching of Cr(VI) from soil was further optimized by boiling

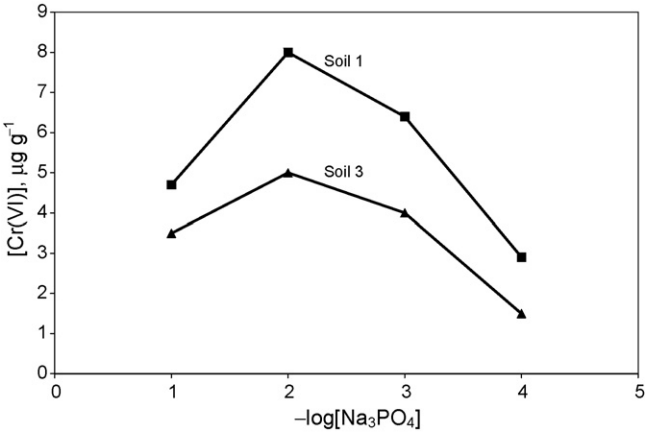


Fig. 1. Optimization of Na_3PO_4 concentration during the leaching of Cr(VI) from soil samples in 5 min.

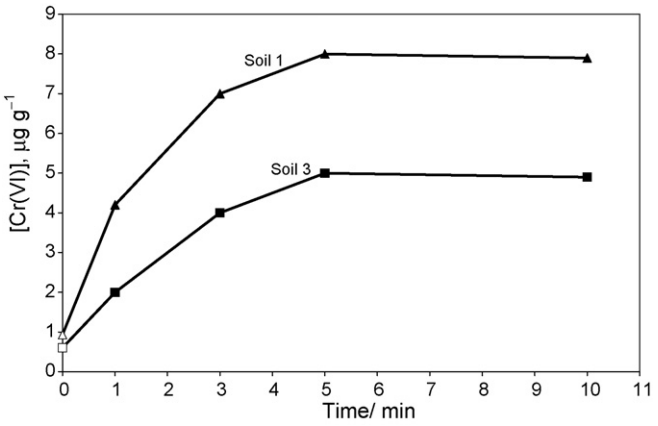


Fig. 2. Extraction of Cr(VI) from soil with 0.01 $mol\,L^{-1}$ Na_3PO_4 as a function of time: (▲) Soil 1; (■) Soil 3; (△) water-soluble fraction in Soil 1; (□) water-soluble fraction in Soil 3.

the mixture at different time intervals. The results of this investigation presented in Fig. 2, show that 0.01 $mol\,L^{-1}$ Na_3PO_4 leaches all Cr(VI) species within 5 min. The leaching of Cr(VI) in soil with 0.01 $mol\,L^{-1}$ Na_3PO_4 at room temperature for 48 h did not result in quantifiable increase of the concentration of Cr(VI).

Atomization profiles of chromium, which were obtained during the determination of Cr(VI) in the water-soluble fraction, in standard solution of Cr(VI) and in soil treated with Na_3PO_4 have the same the appearance time (Fig. 3). This suggests that the presence of relatively high Na_3PO_4 matrix has no influence on the release of Cr during atomization, owing to the high pyrolysis temperature that eliminated the majority of the matrix prior to atomization.

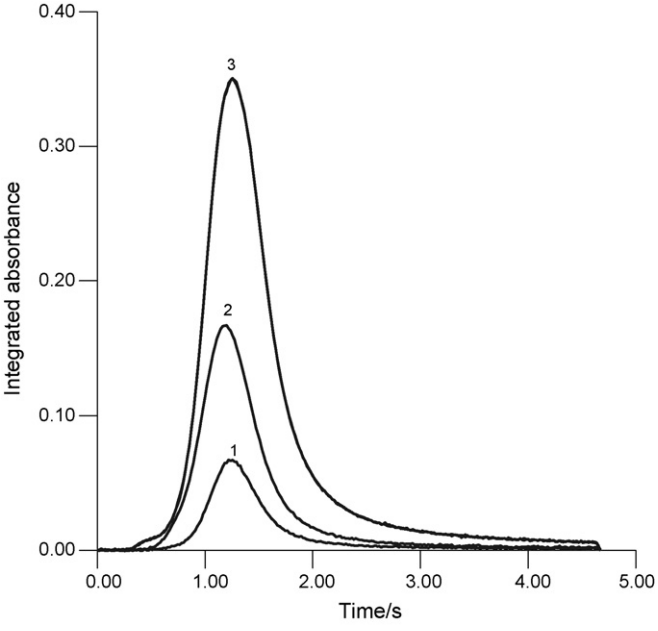


Fig. 3. Absorbance-time signals of Cr(VI): (1) water-soluble fraction in Soil 3; (2) Cr(VI) standard solution, 22 $\mu g\,g^{-1}$; (3) total Cr(VI) concentration in Soil 3.

Table 2
Results of Cr(III), Cr(VI) and total Cr determination in soil samples ($n = 6$)

Sample	Water-soluble [Cr(VI)] ($\mu g\,g^{-1}$)	[Cr(VI)] ($\mu g\,g^{-1}$)	[Cr(III)] ($\mu g\,g^{-1}$)	{[Cr(VI)] + [Cr(III)]}[a] ($\mu g\,g^{-1}$)	{Total [Cr]}[b] ($\mu g\,g^{-1}$)
Soil 1	0.90 ± 0.05	8.0 ± 0.5	1005 ± 15	1013	1015 ± 50
Soil 2	0.75 ± 0.03	5.8 ± 0.3	1068 ± 20	1074	1075 ± 45
Soil 3	0.80 ± 0.04	5.5 ± 0.4	1117 ± 30	1123	1125 ± 30
Soil 4	0.70 ± 0.02	5.1 ± 0.2	1062 ± 20	1067	1070 ± 50
Soil 5	0.80 ± 0.04	6.5 ± 0.4	1341 ± 40	1348	1350 ± 60

[a] Sum of [Cr(VI)] and [Cr(III)] in each sample.
[b] Total chromium concentration determined by an independent method.

3.3. Mechanism for the separation of Cr(VI) from Cr(III) in soil

The leaching of samples with Na_3PO_4 transform insoluble Cr(VI) compounds, like $BaCrO_4$, to soluble form according to the equation

$$3BaCrO_4(s) + 2Na_3PO_4(aq) \rightarrow 3Na_2CrO_4(aq) + Ba_3(PO_4)_2(s)$$

The procedure removes all common metals, including Cr(III) as insoluble phosphates, oxides or hydroxides [23]. After filtration, the solution contains only CrO_4^{2-} anions that were originally present in the sample in the form of insoluble salts of Cr(VI).

Though chromium exists in the form of different oxidation states ranging from 0 to +6, the oxidation states that naturally coexist in solids including soil are +3 and +6 [24]. Therefore, after the treatment of samples with 0.01 mol L^{-1} Na_3PO_4, all Cr(VI) species goes into solution and the remaining chromium species in the precipitates is only Cr(III) such that the digestion of the precipitates with acids lead to the determination of the total concentration of Cr(III) in soil samples. Cr(III) is not expected to have been oxidized to Cr(VI) during leaching due to unfavourable high pH (∼12) and moreover the concentration of the probable oxidizing agent, MnO_2, was very low to have an impact, viz. 3.0 $\mu g\,g^{-1}$ [25].

3.4. Validation of the method

The developed method was validated by comparison with an established method and by comparison of the sum of Cr species with total Cr concentration in the sample since solid certified reference materials with certified values of Cr(VI) are still lacking. A comparison of the concentration of the sum of chromium species with the total chromium concentration indicated that there is no difference between them at 95% level of confidence (Table 2). Similarly, no difference was established in the results of the determination of Cr(VI) by the new method and established method [19] based on the leaching of samples with Na_2CO_3 (Fig. 4).

Soil samples were also spiked with 100–500 $\mu g\,g^{-1}$ of Cr(III) standard solutions, to evaluate any potential conversion to Cr(VI) during leaching. The results of the investigation showed that there were no increase in Cr(VI) concentration and the mean % recovery of Cr(III) was 97 ± 3, thereby confirming that the leaching procedure is quantitative. The leaching of soil with Na_3PO_4 results in strong alkaline solution (pH ∼ 12), which preserved Cr(VI) for period of at least 6 months without noticeable changes in oxidation state. It could, therefore, be concluded that 0.01 mol L^{-1} Na_3PO_4 leaches Cr(VI) completely from soil samples.

3.5. Results of Cr(VI) determination in soil

The proposed procedure was applied in the determination of Cr(VI) in soil by water (Table 2). The results show that not all Cr(VI) complexes are soluble in water since the level of Cr(VI) leached was always present in relatively small amount (0.90 ± 0.05 $\mu g\,g^{-1}$) (Fig. 3). The amount of Cr(VI) leached by 0.01 mol L^{-1} Na_3PO_4 represents the total concentration of Cr(VI) in a given soil sample. The concentration of Cr(VI) found in soil samples collected from the site of the new chromium mine, Thorncliff, South Africa, were within maximum acceptable levels of 15 $\mu g\,g^{-1}$ in accordance with the Italian Guidelines [26]. Unfortunately, maximum allowable concentrations (MAC) for Cr(VI) in soils are still not well established and differ from one country to the other. The levels of Cr(VI) found in soil collected from the new chromium mine could be attributed to the lower period the mine had been operating. The total concentration of Cr in soil samples were relatively higher as compared to that of Cr(VI), the highest being 1400 $\mu g\,g^{-1}$.

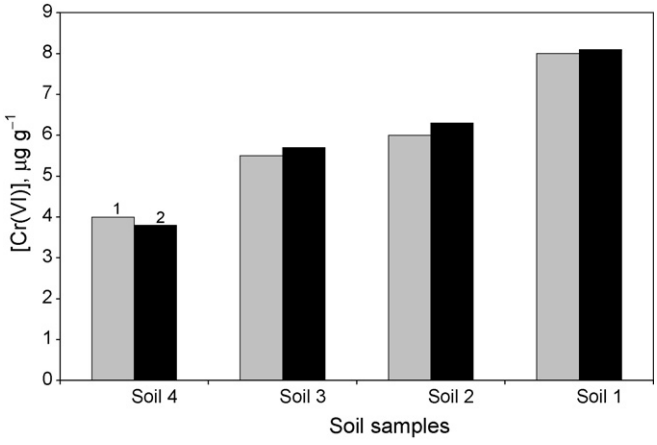


Fig. 4. Validation of Cr(VI) leaching by comparing the leaching efficiency of Na_3PO_4 with that of Na_2CO_3: (1) 0.01 mol L^{-1} Na_3PO_4 (5 min); (2) 0.1 mol L^{-1} Na_2CO_3 (10 min).

4. Conclusions

From the results of the investigation, it can be concluded that Cr(VI) could be leached selectively and completely in soil samples by 0.01 mol L^{-1} Na_3PO_4. The new method was validated by statistical evaluation which indicated that the sum of concentrations of chromium species is the same as the total concentration of total chromium at 95% level of confidence. The comparison of results of Cr(VI) in soil samples by the new method and the established method that utilizes Na_2CO_3 also show no difference between the two methods. The main advantage of using Na_3PO_4 over Na_2CO_3 is the shorter time required to leach Cr(VI) completely from soil. The developed method offers much lower detection limit (0.07 μg g^{-1}) than the recommended US EPA method 3060A (50 μg g^{-1}). The soil samples collected around the new chromium mine were found to contain Cr(VI) concentrations that were within maximum acceptable levels.

Acknowledgement

This study was supported by the National Research Foundation of South Africa.

References

[1] V. Gómez, M.P. Callao, Trends Anal. Chem. 25 (2006) 1006.
[2] M.D. Szulczewski, P.A. Helmke, W.F. Bleam, Environ. Sci. Technol. 31 (1997) 2954.
[3] J.M. Zachara, C.C. Ainsworth, C.E. Cowan, C.T. Resch, Soil Sci. Soc. Am. J. 53 (1989) 418.
[4] A.T. Hanson, B.D. Dwyer, Z.A. Samani, D. York, J. Environ. Eng. 119 (1993) 825.
[5] B.R. James, J. Environ. Qual. 23 (1994) 227.
[6] R. Milacic, J. Stupar, Environ. Sci. Technol. 29 (1995) 506.
[7] J.M. Chen, O.J. Hao, Water Environ. Res. 68 (1996) 1156.
[8] S.E. Fendorf, R.J. Zasoski, Environ. Sci. Technol. 26 (1992) 79.
[9] L. Ebdon, L. Pitts, R. Cornelis, H. Crews, O.F.X. Donard, Ph. Quevauviller (Eds.), Trace Element Speciation, for Environment, Food and Health, The Royal Society of Chemistry, Cambridge, 2001.
[10] J.W. Hamilton, K.E. Wetterham, in: H.G. Seiler, H. Sigel, A. Sigel (Eds.), Handbook on Toxicity of Inorganic Compounds, Marcel Dekker, New York, 1988, p. 239.
[11] Agency for Toxic Substances Disease Registry (ATSDR), Toxicological Profile for Chromium, US Department of Health and Human Services, Public Health Service, Atlanta, GA, 2000.
[12] M.J. Marqués, A. Salvador, A. Morales-Rubio, M. de la Guardia, Fresenius J. Anal. Chem. 367 (2000) 601.
[13] S. Melaku, R. Cornelis, F. Vanhaecke, R. Dams, L. Moens, Microchim. Acta 150 (2005) 225.
[14] R. Eisler, Chromium hazards to fish, wildlife, and invertebrates: a synoptic review, Biological Report 85 1.6, Contaminated Hazard Reviews Report 6, US Department of the Interior, Fish and Wildlife Service, Laurel, MD, 1986.
[15] T. Wittbrodt, C.D. Palmer, Environ. Sci. Technol. 29 (1995) 255.
[16] F.C. Richard, A.C. Bourg, Water Res. 25 (1991) 807.
[17] N.K. Hamadi, X.D. Chen, M.M. Farid, M.G.Q. Lu, Chem. Eng. 84 (2001) 95.
[18] Y. Martínez-Bravo, A.F. Roig-Navarro, F.J. López, F. Hernández, J. Chromatogr. A 926 (2001) 265.
[19] N. Panichev, K. Mandiwana, G. Foukaridis, Anal. Chim. Acta 491 (2003) 81–89.
[20] N. Köleli, Chemosphere 57 (2004) 1473.
[21] G. Hu, R.L. Deming, Anal. Chim. Acta 535 (2005) 237.
[22] M.J. Marqués, A. Salvador, A. Morales-Rubio, M. de la Guardia, Fresenius J. Anal. Chem. 362 (1998) 239.
[23] G. Svehla (Ed.), Vogel's Qualitative Inorganic Analysis, 7th ed., Longman Singapore Publishers Ltd., 1996.
[24] J. Kotaś, Z. Stasicka, Environ. Pollut. 107 (2000) 263.
[25] A.D. Apte, V. Tare, P. Bose, J. Hazard. Mater. 128 (2006) 164.
[26] Decreto Ministeriale n. 471, Gazzetta Ufficiale Supplemento Ordinario N. 293, 1999.

Available online at www.sciencedirect.com
ScienceDirect
Talanta 74 (2008) 779–787
Talanta
www.elsevier.com/locate/talanta

Investigating chemical constraints to the measurement of phosphorus in soils using diffusive gradients in thin films (DGT) and resin methods

Sean Mason [a,*], Rebecca Hamon [b], Hao Zhang [c], Jenny Anderson [b]

[a] School of Earth and Environmental Sciences, University of Adelaide, Australia
[b] CSIRO Land and Water, PMB 2, Glen Osmond, SA 5064, Australia
[c] Department of Environmental Sciences, IENS, Lancaster University, Lancaster LAI 4YQ, UK

Received 13 April 2007; received in revised form 9 July 2007; accepted 9 July 2007
Available online 14 July 2007

Abstract

The effect of potential chemical constraints on the performance of two relatively new soil P testing methods, anion exchange membrane (AEM) and diffusive gradients in thin films (DGT), were evaluated. Exposures to ranges of anion (Cl^-, NO_3^-, SO_4^{2-} and HCO_3^-) concentrations relevant to agricultural soils had minimal effect on P recoveries using DGT. It has also been shown previously that DGT P recoveries are unaffected by varying pH (3–9). In contrast, increasing NO_3^- and SO_4^{2-} concentrations in solution reduced the recovery of P using the resin method (anion exchange membrane, AEM) by 24% at 50 mg L^{-1} NO_3^- and by 47% at 12 mg L^{-1} SO_4^{2-} when the P concentration of the test solution was 2 mg L^{-1}. Phosphorus sorption by the resin decreased with increasing Cl^- concentrations until there was a 100% decrease at 300 mg L^{-1} Cl^- when the P concentration of the test solution was 2 mg L^{-1} and a 92% reduction at 700 mg L^{-1} Cl^- when the P concentration of the test solution was 0.2 mg L^{-1}. There was also a small but significant effect of carbonate species on P sorption to the resin at carbonate concentrations that can occur in agricultural soils. Changing the pH of the solution had minimal effects on the resin P measurements in solutions above pH 4, but below pH 4, resin P measurements decreased dramatically. A poor coefficient of determination for the regression fit between DGT and resin measurements on eight agricultural soils suggested that these two methods are measuring different amounts of P for different soils. Resin P measurements increased significantly, but non-uniformly across soils, when the soil:water ratio was decreased but this did not result in an improved relationship with DGT P. There was a minimal effect on measured P using either Cl^- or HCO_3^- as counter ions on the resin.
© 2007 Elsevier B.V. All rights reserved.

Keywords: Phosphorus extraction; Soil testing; Diffusive gradients in thin films; Anion exchange membranes

1. Introduction

Assessment of available P through soil testing methods is important for efficient fertilizer application. Phosphorus is frequently the most expensive major nutrient used in broadacre cropping [1]. An accurate and reliable soil test would reduce the cost associated with unnecessary fertilizer application and also reduce the risks of environmental pollution as a result of excessive fertilizer application [2].

The ideal soil test should measure the form of P that is available to the plant, reflecting diffusional supply from the soil solution and its replenishment from the soil solid phase. The soil test should also give reliable information on available P irrespective of soil type. Due to their simplicity, extraction methods are still commonly used as soil tests for assessment of available P. Numerous authors have highlighted the problems associated with using extraction methods. Extraction solutions typically contain a competing ion that displaces the exchangeable forms of P from the soil. It has been reported that these competing ions in some cases can displace non-labile and relatively stable forms of P from the soil consequently over

Abbreviations: DGT, diffusive gradients in thin films; AEM, anionic exchange membrane; DI, deionised; ICPMS, inductively coupled plasma mass spectrometer; MBL, mixed binding layer; WHC, water holding capacity; DIFS, DGT induced fluxes in sediments

* Corresponding author. Tel.: +61 8 8303 8107; fax: +61 8 8303 6717.
E-mail address: sean.mason@adelaide.edu.au (S. Mason).

0039-9140/$ – see front matter © 2007 Elsevier B.V. All rights reserved.
doi:10.1016/j.talanta.2007.07.005

predicting availability [3]. These solutions may also fail to extract available P if they are used on soil types for which they are inappropriate [3]. Before the increased prominence of the resin method, Menon et al. [3] concluded that the search for a method capable of predicting plant responses under a wide variety of soil conditions had so far been unsuccessful.

The increasingly popular method which uses anion exchange membranes (AEM), known as the "resin P" test, has been shown in some studies to be an improvement over extraction methods as a soil test for predicting plant yield [1,4–9]. The diffusive gradients in thin films (DGT) method was also found in a recent study to be an improvement over the extraction methods for assessing plant available P [4]. These methods are likely to be improvements on the extraction methods as they potentially mimic plant P uptake by creating a well-defined sink for P. These tests lower the concentration of P in the solution phase, promoting resupply from the soil solid phase. For the resin P method, an AEM is placed in a 1:30, soil to water ratio while the DGT method, which uses a ferrihydrite binding gel as the sink, is placed in situ directly on the soil at >80% WHC. The DGT measurement incorporates both the diffusional supply of P from soil solution and the resupply from the soil solid phase.

Some limitations to the resin method have been evaluated during the method development phase of the soil test. In one of the earliest studies, using resin beads in nylon bags, Sibbesen [10] found that the amount of P extracted was dependent on the anionic counterion associated with the resin. In a calcareous soil he found that resin beads in the HCO_3^- form extracted more HPO_4^{2-} than resin beads in the Cl^- form. Another study by Sibbesen and Rubaek [11] also reported similar observations using a sandy loam with a pH of 4.6. Sibbesen [10] therefore recommended that resins should be used in bicarbonate form. However, when Sibbesen [10] compared resin P values with the uptake of P by ryegrass there was little difference between the relationship when the resin was in HCO_3^- form ($r^2 = 0.9$) versus the Cl^- form ($r^2 = 0.88$). In contrast, Bache and Ireland [12] and Sherrod et al. [13] found little difference between using HCO_3^- or Cl^- as the counter ions on the resin to assess P in a calcareous soil. One proposed advantage of using HCO_3^- form is that the HCO_3^- displaced by the nutrient ions may mimic HCO_3^- produced by the rhizosphere due to the excretion of CO_2 by plant roots and microorganisms [14]. Numerous authors have used the bicarbonate form as it also maintains low Ca concentrations in solution and has been reported to enhance P extraction from the soil [5,15,16]. Arguments for using the Cl^- form are that HCO_3^- can increase the supernatant pH, it also complicates the acid desorption step through CO_2 evolution and the membranes must be converted to HCO_3^- each time for re-use [17]. However, based on the observations of Sibbesen [10], Sherrod et al. [13] stated that the best resin counter ion for P testing depends on the inherent soil properties.

In recent studies, the use of an AEM has been preferred over the use of resin beads [7,8,15,18] due to the procedural disadvantages of using either resin beads mixed with soil [19] or resin beads in nylon bags [10,20,21]. The AEM is not specific for binding P [22] and experiments have been performed using the AEM to measure N and S concentrations in soils [16,23]. Sherrod et al. [13] stated that despite the use of resins for more than 40 years, resin use among researchers is not uniform and interpretive differences between methods are poorly understood. Reported capacities of the AEM for P are lacking, possibly due to these numerous variations with the resin method. Studies on the potential competitive effects of common environmental anions on the assessment of P by resins have also been limited. In one of the few studies looking at the effect of potential competitive anions on the measurement of P by resins, Cooperband and Logan [24] reported NO_3–N concentrations of 50 and 100 mg L^{-1} reduced AEM P sorption by 50 and 75%, respectively. They also reported that SO_4–S concentrations of 500 and 1000 mg L^{-1} reduced AEM P sorption by 98%. Turrion et al. [25] assessed the influence of NO_3^- and SO_4^{2-} on the extraction of P using AEM in HCO_3^- form. They found that as both NO_3^- and SO_4^{2-} concentrations increased, the AEM P extraction decreased to approximately 60% at 50 mg L^{-1} N and at 30 mg L^{-1} S. Also when the P concentration in the solution increased, the extraction of P decreased in the presence of these anions, possibly indicating that capacity had been reached. In both studies the concentrations of anions used were not put into an agricultural context and the possible effects of Cl^- and CO_3^- concentrations in solution were not examined.

The aims of this study were to investigate the potential effects of the anions (NO_3^-, SO_4^{2-}, Cl^- and HCO_3^-) on the sorption of P to the AEM (resin method) and ferrihydrite binding layer (DGT method), to compare resin P and DGT measurements obtained on agricultural soils, and to assess the performance of the resin test using an AEM with two different counter ions (HCO_3^- and Cl^-).

2. Experimental

2.1. General protocols

2.1.1. Diffusive gradients in thin films

The theory underlying the diffusive gradients in thin films technique has been discussed extensively [26]. Recently the DGT method has been modified to allow simultaneous measurement of both selected anions and cations with the development of a mixed binding layer (MBL) containing ferrihydrite as the sorbent for P and Chelex resin as the sorbent for transition metal cations. Detailed information regarding the preparation and initial testing of the MBL is given in ref. [27]. The MBL was the binding layer used in the current study. DGT assemblies also contained a 0.8 mm diffusive gel plus a protective filter membrane and were deployed for 24 h in all experiments. After deployment the DGT devices were removed and rinsed with ultra pure H_2O (Milli Q). The MBL was retrieved and placed in 1 mL of 1 M HCl. The resulting mass of P (M) in the eluant solution was measured using an inductive coupled plasma mass spectrometer (ICP-MS) and converted to DGT measured concentration (C_{DGT}) or effective concentration (C_E) [27], after adjustment for the elution efficiency of 92%. The DGT concen-

tration, C_{DGT}, can be calculated using Eq. (1)

$$C_{DGT} = \frac{M\,\Delta g}{DAt} \quad (1)$$

where Δg is the thickness (cm) of the diffusive layer, D ($cm^{-2}\,s^{-1}$) the diffusion coefficient of the analyte in the diffusive layer at the temperature of deployment, A (cm^2) the area of the exposure window and t (s) is the time of deployment.

2.1.2. Resin method

Anion exchange membranes were obtained from BDH and cut into strips (62.6 mm × 25 mm). The AEM strips were pretreated as described by Saggar et al. [15], but substituting Cl^- for HCO_3^- by immersing them in a solution of 0.1 M HCl and 0.1 M NaCl [28]. To determine resin P, one strip was immersed in experimental solutions and the solutions shaken for 17 h [15]. The AEM strips were removed and rinsed with deionised water and the P was extracted from the strip by placing it in a solution of 0.1 M NaCl/HCl for at least 2 h. Ammonium molybdate reactive P concentrations were determined employing a modified version of the Murphy and Riley method [29] using a segmented flow analyser. Prior to each analysis the colour reagent containing 2.4 g L^{-1} ammonium molybdate, 4 g L^{-1} ascorbic acid, 0.2 g L^{-1} potassium antimony tartarate and 1 M H_2SO_4 was prepared. The colour reagent and sample were allowed to react for 2 min and 15 s before passing through a spectrometer where P absorbance was measured at 880 nm. Calibration standards were prepared using the same matrix as the resin P eluant solution.

2.2. P capacity and effect of pH

To determine the capacity of the AEM strips for P, the strips were placed in 30 mL solutions covering a range of P concentrations up to 105 mg L^{-1}. Experimental procedure was performed as explained in Section 2.1.2. The capacity of DGT using the MBL has been previously assessed [27].

For direct comparison between the two methods, the effect of pH on P binding to the AEM strips was investigated by placing strips in solutions with pH ranging from 3 to 9. Two concentrations (0.2 and 2 mg L^{-1}) of P were used at each pH to represent concentrations relevant to a P responsive and a non-responsive soil [1]. Experimental procedure was performed as explained in Section 2.1.2.

The influence of pH on DGT measurement of P using the MBL was investigated previously [27].

2.3. Competition experiments

2.3.1. DGT

To investigate the competitive effect of other anions binding onto the MBL, three DGT assemblies were deployed in 3 L (500 mL for HCO_3^-) solutions composed of a range of concentrations of the competing anions of interest. Phosphorus concentrations in the solutions were kept constant at 0.2 mg L^{-1}. Concentrations of the other anions in solution were as follows: SO_4^{2-} (as Na_2SO_4) ranged from 0 to 0.6 g L^{-1}, NO_3^- (as $NaNO_3$) from 0 to 1.2 g L^{-1}, Cl^- (as NaCl) from 0 to 1.5 g L^{-1} and HCO_3^- (as $NaHCO_3$) from 0 to 93 g L^{-1}. Due to the large amounts of added $NaHCO_3$ required, solution volumes for DGT deployment were reduced to 500 mL. For standard DGT deployment the soil moisture content is typically increased to 80–100% of the soil water holding capacity (WHC), and the WHC of soils is generally in the range of 150–500 mL kg^{-1}, hence soil to water ratios for DGT deployment are very roughly 3:1. These concentrations of anions were selected to cover the range of concentrations likely to be found in 3:1 (soil:water) extracts of agricultural soils (see Section 3).

2.3.2. Resin method

For a direct comparison with the performance of DGT, AEM strips were deployed in 50 mL solutions containing increasing concentrations of SO_4^{2-}, NO_3^-, Cl^- and HCO_3^-. For each concentration of SO_4^{2-}, NO_3^-, Cl^- and HCO_3^-, two concentrations of P were used, one at 0.2 mg L^{-1} typical of a P responsive soil and the other at 2 mg L^{-1} reflective of a P non-responsive soil [1]. Anion concentrations in the solutions ranged from 0 to 12 mg L^{-1} SO_4^{2-}, 0 to 40 mg L^{-1} NO_3^-, 0 to 0.7 g L^{-1} Cl^- and 0 to 2.2 g L^{-1} HCO_3^-. These concentrations are reflective of the possible range of concentrations found in solution in 1:30 (soil:water) extracts of agricultural soils (see Section 3) which is a common soil to water ratio used in the determination of P by the resin method [1,7].

2.4. Application of DGT and resin method on agricultural soils

Results obtained by the DGT and resin methods were compared for eight Australian agricultural soils. Selected soil chemical properties are given in Table 1. Soil preparation for DGT deployment consisted of incubating air-dried, sieved (<2 mm) soil at 50% water holding capacity (WHC) for 2 days and then the moisture content was increased to 80% WHC the day prior to DGT deployment. DGT devices were deployed on the soil for 24 h and a diffusive gel thickness of 0.8 mm was used. DGT measured concentrations (C_{DGT}) were converted to C_E (effective concentration) using 2D DIFS [30]. A detailed explanation of the concept and the calculation of C_E has been published previously [31].

For the resin method 1 g of air-dried, sieved soil was used per 30 mL of DI water. The procedure for the measurement of P was the same as described above. Measurements were also performed in these soils at different soil (g) to water (mL) ratios (0.1:30, 0.3:30 and 0.6:30). One AEM strip in Cl^- form was placed in each solution and samples were run in duplicate for each soil.

2.5. Effect of AEM counter ions

The performance of the AEM prepared as either the Cl^- or HCO_3^- form [7] was investigated using six different Australian agricultural soils (see Table 1) using 1 g of soil per 30 mL of DI water. Solution pH was measured after the removal of each AEM strip and compared to original pH values of the soils in order

Table 1
Selected soil properties of the eight Australian soils used in this study

Site	Location	Soil classification	pH (H_2O)	EC (1:5) (μs cm^{-1})	P (total) (mg kg^{-1})	Cl^- (mg kg^{-1})	IC (1:5) (mg kg^{-1})	DOC (1:5) (mg kg^{-1})	TOC (%)
Mt. Damper	SA	Grey calcareous	8.0	203	93	4	8	20	0.6
Birchip	Vic.	Calcarosol	8.8	204	242	32	16	26	1.3
Horsham	Vic.	Vertosol	8.3	279	185	10	16	19	1.2
Kalkee	Vic.	Vertosol	8.5	265	196	27	23	23	1.3
Lower Norton	Vic.	Red-brown earth	7.9	210	181	14	11	65	1.5
Mildura	Vic.	Calcarosol	8.0	129	121	12	7	44	0.7
Gillingarra	WA	Podosol	5.5	108	270	11	0.4	40	2.5
Meckering	WA	Chromosol	5.9	122	160	22	0.8	47	1.1
		Minimum	5.5	108	93	4	0.4	19	0.6
		Maximum	8.8	279	270	32	23	65	2.5

to evaluate the influence of AEM in either counter ion form on solution pH.

3. Results and discussion

3.1. Capacity of AEM strips

The accumulated P on the AEM strip increased linearly with the concentration of P in solution up to a concentration of 4.8 mg L^{-1}. It corresponds to 126 μg P sorbed per AEM strip (with specific dimension of 62.6 mm × 25 mm) (Fig. 1), which equals 8 μg cm^{-2}. Beyond a P concentration of 4.8 mg L^{-1}, the amount of sorbed P deviated from linearity, indicating that the capacity of AEM had been reached. The capacity corresponds to a P value in soil of 144 mg kg^{-1} taking the soil to water ratio of 1:30 into account. Previous studies, using even heavily P fertilised soils, have observed the majority of the P measured by resin method to be well below this value [4,8]. Hence, the capacity of the AEM for P would be unlikely to be a limitation for measuring P in P responsive and non-responsive soils. The capacity of the DGT device using a MBL was found to be lower at 12 μg P per device or 5 μg cm^{-2} [27]. However, in DGT technology the flux of P onto the binding layer is restricted due to the placement of the diffusive layer and deployment times for DGT can also be reduced to overcome capacity issues. At MBL capacity the maximum C_{DGT} value obtainable for a 24 h deployment at 25 °C is approximately 850 μg L^{-1} which is considerably larger than the C_{DGT} values (24–166 μg L^{-1}) obtained for the eight soils used in this study. This suggests there will be no capacity issues for the assessment of P on agricultural soils using DGT.

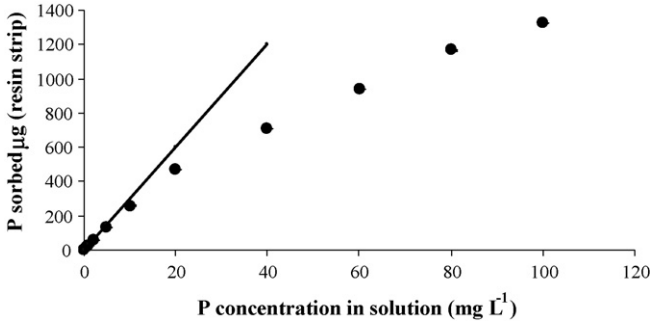


Fig. 1. Measured mass of P on the resin strip with increasing solution P concentration. Solid line represents the linear relationship from the first four solution concentrations. Error bars (not noticeable) represent ±1 standard error (two replicates).

3.2. Effect of pH

Phosphorus deficiencies are common in acidic soils due to the very high sorption capacity of Al and Fe hydrous oxides for P at low pH [32]. This highlights the importance of a soil test that functions well under acidic conditions. DGT performance for measuring P has shown to be unaffected by pH within the range 3–9 [27]. The binding of P onto the AEM strip was also found to be unaffected significantly by pH within the range of 4–9 (Fig. 2). Below pH 4 the resin P concentrations decreased significantly. However, this is unlikely to be a limitation to the use of the resin method for determining P for agronomic purposes as very acidic soils (pH < 5) are not optimal for plant growth, due primarily to aluminium/manganese toxicity, and therefore are either not used for growing crops, or are limed to increase pH before use [27].

3.3. Selection of anion concentrations for competition experiments

Potential sources of chloride deposition in soils include rainwater, fertilizer applications (KCl), irrigation waters, sea spray, dust and air pollution [33]. A review from Eynard et al. [34]

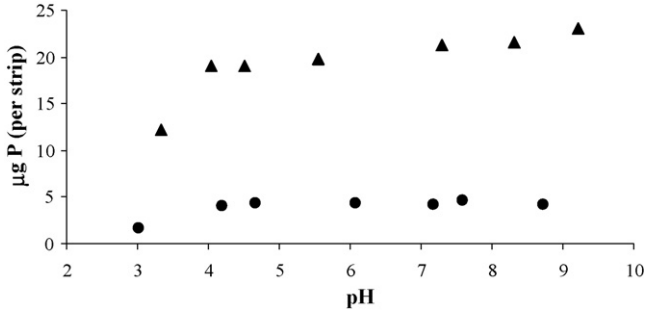


Fig. 2. Effect of pH on the recovery of resin P values: (▲) represents a typical P concentration of a P non-responsive soil and (●) represents a P responsive soil concentration.

reported that salt-affected soils where plant growth is limited by an excess of salts have electrical conductivities >4 dS m^{-1}, which equates to >2200 mg kg^{-1} [35]. Bower and Wilcox [36] reported that the yields of many crops are restricted at total dissolved solids (TDS) concentrations of 250–500 mg L^{-1} in a 1–5 soil to water extract, equivalent to 1250–2500 mg kg^{-1} in soil. They also reported that only a few salt tolerant plants yield satisfactorily at TDS concentrations of 2500–5000 mg kg^{-1}. It appears there is potential for severely decreased crop yields at Cl^- concentrations anywhere from 1250 to 5000 mg kg^{-1}. Therefore, to cover the most extreme case, the DGT method was tested at chloride solution concentrations up to 15,000 mg L^{-1} (i.e. 5000 mg Cl^- kg^{-1} at 3:1 soil to water ratio) and the resin method was tested beyond the most extreme case (167 mg L^{-1} including dilution factor) up to 700 mg L^{-1}.

Nitrogen fertilizers are applied each year at rates, dependant on the type of soil and crop grown at each locality, that range from less than 20 to >100 kg N ha^{-1} (100 kg N ha^{-1} is approximately 80 mg N kg^{-1} or 350 mg NO_3^- kg^{-1}), e.g. ref. [37]. There is typically minimal nitrate adsorption by soils, but significant nitrate losses through leaching and crop uptake can occur [38,39]. The NO_3–N concentration (in 1:30, soil:water) analysed in 21 Australian agricultural soils ranged from <2 to 68.4 mg kg^{-1}, which equates to a maximum soluble NO_3^- concentration of approximately 300 mg kg^{-1}. We therefore assumed a 'worst case' scenario of 400 mg NO_3^- kg^{-1} soil. This corresponds to a concentration of 1200 mg L^{-1} NO_3^- for testing the performance of DGT and approximately 40 mg L^{-1} NO_3^- for testing the performance of the resin method.

Literature on the range of concentrations of SO_4^{2-} likely to be found in agricultural soils is limited. Soluble S (1:5, soil:water) concentration in 21 Australian agricultural soils ranged from 1.7 to 62.9 mg kg^{-1}. Assuming that the entire soluble S was in the form of SO_4^{2-}, this equates to a maximum SO_4^{2-} concentration of approximately 180 mg kg^{-1}. These concentrations are significantly lower than those found in acid sulfate soils [40], but such soils are unlikely to be agriculturally productive. We therefore assumed a maximum SO_4^{2-} concentration of 200 mg kg^{-1}, equivalent to solution concentrations of 600 mg L^{-1} SO_4^{2-} for DGT testing and approximately 12 mg L^{-1} SO_4^{2-} for the resin method.

The concentration of carbonate in soils used for agricultural purposes is variable, but can be very high. For example, soils from Southern Australia used for grain growing are renowned for having very high concentrations of calcium carbonate, with percentages ranging up to 90% [1]. Studies have been performed on the chemical characteristics of P from these soils but the actual amount of soluble HCO_3^- in solution in these highly calcareous soils has not been measured. We used concentrations up to 1 g of HCO_3^-, as soluble $NaHCO_3$, per 30 mL of DI water to test the resin method. This assumes a soil composed of 100% carbonate with the majority of the carbonate free in solution, which is clearly a significant overestimate in comparison to soils where carbonate solubility is generally controlled by sparingly soluble Ca or Mg. Corresponding HCO_3^- concentrations used for DGT testing were up to 93 g L^{-1}. In this case, the solubility product was exceeded for the highest concentrations.

3.4. Effect of anion competition on DGT P

The concentration of P in solution as assessed by DGT (C_{DGT}) agreed well with the concentration of P that was measured directly in solution (200–220 μg L^{-1}). Furthermore, there was minimal effect of increasing concentrations of NO_3^- (Fig. 3a), SO_4^{2-} (Fig. 3b) or Cl^- (Fig. 3c) on the amount of P bound to the MBL. Increasing bicarbonate concentrations in solution had a marked effect on the amount of P that was bound to the MBL, which decreased to 0.7 μg P at HCO_3^- concentration of 93 g L^{-1} (Fig. 3d). However, this was in a system containing only Na as the cation and, as discussed above, the solubility of carbonate is much lower in calcareous soils where Ca and Mg control carbonate solubility. Soluble carbonate concentrations obtainable in a closed system at four different pH levels (charge balanced using Cl^-), where solubility is controlled by Ca or Mg, were modelled using GEOCHEM [41]. The maximum concentrations of soluble carbonate in solution were 1800, 350, 100 and 20 mg L^{-1} at pH 6, 7, 8 and 9, respectively, using calcium as the associated cation. At these concentrations, the maximum reduction in P measured using DGT at the highest concentration of carbonate species (pH 6) was only 7% (Table 2). Using Mg as the associated cation increased the maximum possible concentrations of soluble carbonate species in comparison to Ca. However, even for this extreme example DGT-measured P only decreased by 18% (Table 2). Tyler and Olsson [42] obtained HCO_3^- concentrations of approximately 1 mM (63 mg L^{-1}) in soil solution after 15 g kg^{-1} of $CaCO_3$ had been applied to the soil. For these conditions there is little effect of HCO_3 on DGT P measurements.

Collectively these results show that there is unlikely to be any competitive or interfering effects of anions on measurements of P using DGT in the majority of agricultural soils.

3.5. Effect of anion competition on resin P

The same anion concentrations in soils (adjusted for the 1:30 soil to water ratio) as used for DGT tests were used to assess the performance of the resin method for measuring P.

Table 2
Concentration of total soluble inorganic carbon (IC) species calculated by GEOCHEM for a closed system at different pH values with charge balanced using Cl^- for Ca and Mg as the associated cation with the corresponding decrease in P sorption that would be anticipated (refer to Figs. 3d and 4d) for both the DGT and resin methods

pH	Percentage reduction in P sorption		
	IC (mg L^{-1})	DGT	Resin
Ca			
6	1707	7	61
7	266	0.9	11
8	68	0.4	2.6
9	21	0	0.8
Mg			
6	3901	18	88
7	1505	6.5	58
8	356	1.3	15
9	105	0.4	4.1

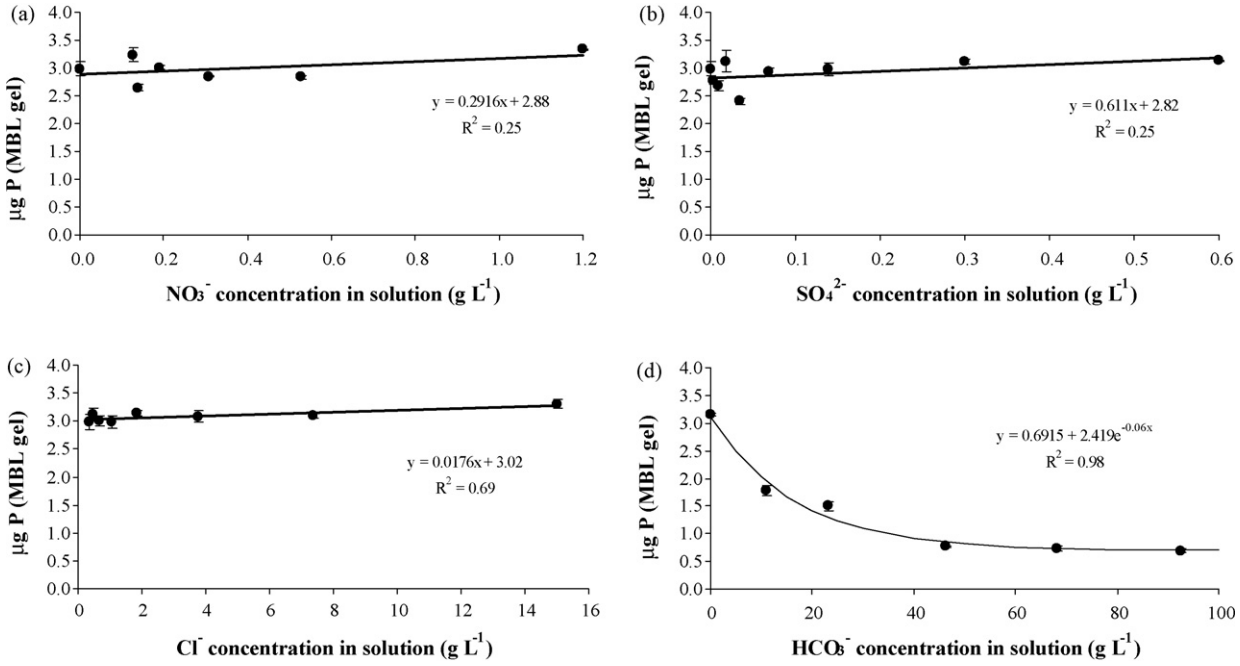


Fig. 3. DGT measurements (µg P on the MBL gel) with increasing anion solution concentrations: (a) nitrate, (b) sulfate, (c) chloride and (d) bicarbonate. Error bars represent ±1 standard error (three replicates).

Phosphorus sorption onto the AEM was slightly affected by increasing NO_3^- concentrations up to 40 mg L^{-1} (Fig. 4a). At the highest NO_3^- concentration P sorption was reduced by 24% at 2 mg L^{-1} P and by 6% at 0.2 mg L^{-1} P. Increasing the sulfate concentrations decreased the P sorption onto the AEM by 47% at 12 mg L^{-1} SO_4^{2-} for a P concentration of 2 mg L^{-1} (Fig. 4b). This value decreased to 27% for the corresponding P concentration at 0.2 mg L^{-1}. Increasing the Cl^- and HCO_3^- concentration in solution had a large impact on P sorption due to the higher concentrations of Cl^- and HCO_3^- used compared to SO_4^{2-} and NO_3^- (Fig. 4c and d). Phosphorus sorption was reduced by 100% at a concentration of 300 mg L^{-1} Cl^- at a P concentration of 2 mg L^{-1}. At a P concentration of 0.2 mg L^{-1} P sorption was reduced by 85 and 92% at Cl^- concentrations of 300 mg L^{-1} and 700 mg L^{-1}, respectively. At the Cl^- concentration of 40 mg L^{-1} which corresponds to a concentration of

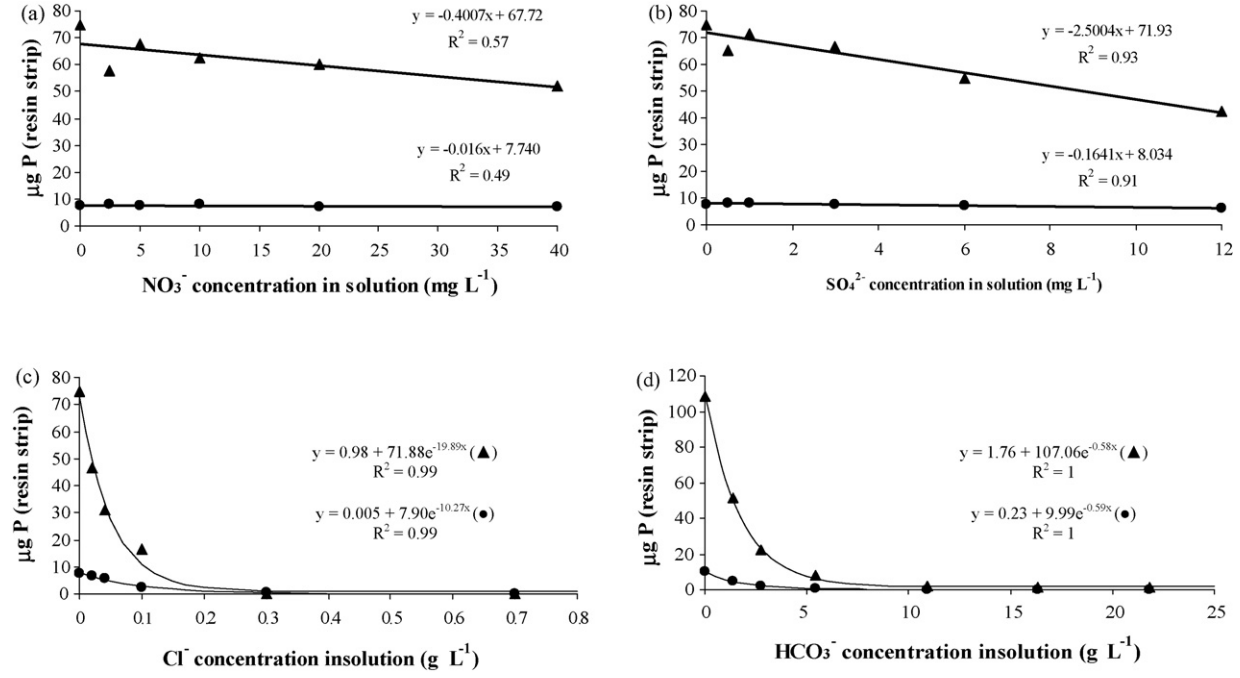


Fig. 4. Resin P values with increasing anion solution concentrations: (a) nitrate, (b) sulfate, (c) chloride and (d) bicarbonate: (▲) represents P concentration typical of a P non-responsive soil and (●) represents a P responsive soil concentration.

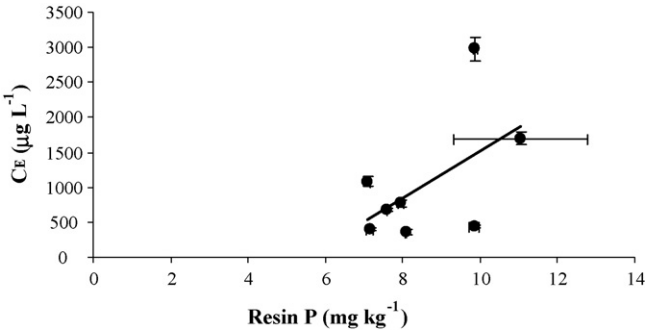


Fig. 5. Relationship between DGT measurements (C_E) and resin P measurements (1:30 soil to water ratio) on eight Australian agricultural soils. Error bars represent ±1 standard error (two replicates resin, four replicates DGT).

1200 mg kg^{-1} (30× dilution) in a soil, where no visible reduction in yield is observed [36], P sorption was reduced by 62% at a P concentration of 2 mg L^{-1} and by 27% at a P concentration of 0.2 mg L^{-1}. The performance of the resin P method may be markedly affected at possible realistic concentrations of soluble carbonate species in solution, as modelled using GEOCHEM (Table 2 and Fig. 4d). A cumulative effect of various anions in solution, on the measurement of P using the resin method cannot be ruled out.

3.6. DGT and resin performance on soil

Comparison of DGT and resin P measurements on eight agricultural soils revealed some major discrepancies between the two methods (Fig. 5). The poor coefficient of determination for the regression fit ($r^2 = 0.31$, not significant $p < 0.05$) suggests the pool of P measured by DGT is different from the pool measured by the resin method. The poor relationship could also be due to varying competition effects between the two methods.

As discussed above, increasing anion concentrations in solution can have a marked impact on P sorption onto the AEM due to competition. Therefore, the possible competitive impact of anions in the soils on the resin method was explored by changing the soil:water ratio to 'dilute' out any interfering anion. Resin P measurements increased significantly with an increased proportion of water (decreasing soil to water ratios) (Table 3). For the eight soils the increases in resin P values were not uniform. Maximum concentrations of Cl^- and SO_4^{2-} and inorganic carbon concentrations were 1.1 and 2.1 and 3.8 mg kg^{-1}, respectively (30× dilution based on results from Table 1 and Section 3.3). Some studies have shown that resin P measurements decrease when there is proportionally less water [17,18], but McLaughlin et al. [17] found that increasing the amount of soil from 1 to 10 g using 100 mL of water had no effect on resin P results using resin beads in nylon bags. However, that study also increased the amount of resin in proportion to the increase in soil, which may have overcome any interference or competitive effect.

The possible competitive effect of DOC on P sorption by the resin has not been investigated, and this could also be a contributing factor. Alternatively the increase in resin P measurements with decreasing soil:water ratio (increasing dilution) could simply reflect P resupply from the soil solid phase that occurs at higher dilutions as the soil buffers the solution P concentrations. Schoenau and Huang [18] similarly observed an increase in water extractable P with widening soil to water ratios. They suggested that when the soil to water ratio is high only the most soluble Ca–P precipitates dissolve and enter the solution. At lower soil to water ratios further dissolution occurs as the most soluble forms dissolve completely and less soluble forms begin to enter the solution [18]. Measurements by DGT devices (2) placed in soil solutions containing the soil:water ratios used for the resin P experiment also increased with decreasing amounts of soil used per 30 mL of DI water; however, increases were not as large as resin P measurements (Table 3). This supports the theory of solution replenishment as a major cause for increased P at lower soil to water ratios as the DGT method was shown to have only minor competitive effects (Fig. 3) by anions under most deployment conditions. The dependence of the resin P method on the soil to water ratio is likely to be dependent on the P buffering capacity of the individual soil. Therefore, there is considerable doubt over which soil to water ratio will most accurately reflect plant available P. In contrast, DGT devices are placed on the soil in situ at water contents, which more closely reflect the environment of the rhizosphere.

There was no improvement in the correlation between DGT and resin P measurements in mixtures with different resin P soil to water ratios. Coefficients of determinations for the regression fit (r^2) using 0.6, 0.3 and 0.1 g soil per 30 mL of DI water were 0.41, 0.3 and 0.52, respectively. These low values are surprising, given that the resin method is a more accurate measurement of plant available P compared to extraction methods [1,4,8] and DGT has been shown to provide a good prediction of both plant P [4] and plant metal availability [31]. As the current study suggests that they are assessing different amounts of P, a comparison of DGT and resin P measurements with plant responsiveness is required in order to be able to assess which

Table 3
Resin P values (mg kg^{-1}) and DGT measurements (µg kg^{-1}) obtained for solutions containing varying amounts of the eight soils per 30 mL of DI water

Soil	Amount soil (g) per 30 mL H_2O			
	0.1	0.3	0.6	1
Resin P (mg kg^{-1})				
Birchip	24.5	18.0	13.7	10.9
Gillingarra	17.7	10.7	8.7	7.9
Horsham	13.1	9.8	8.9	8.1
Kalkee	12.4	11.2	8.0	7.2
Lower Norton	15.0	10.0	10.2	9.8
Meckering	19.8	12.5	11.2	9.9
Mildura	13.6	9.4	8.0	7.6
Mt. Damper	16.2	11.3	9.3	7.1
DGT P (µg kg^{-1})				
Birchip	14.7	10.9	7.4	4.8
Gillingarra	5.4	5.8	4.3	3.9
Horsham	6.7	4.5	3.2	2.2
Kalkee	5.2	3.7	2.3	1.8
Lower Norton	6.2	5.8	4.3	3.7
Meckering	6.2	5	5.7	5.4
Mildura	10.7	4.6	4	3.2
Mt. Damper	4.5	3.5	3.1	2.9

of the two methods is the more reliable test for plant available soil P.

3.7. AEM counter ion

Previous studies have suggested that the resin counter ion can affect the amounts of P sorbed onto the resin. Since Sibbesen [10], most studies have used the resin/AEM in bicarbonate form. We investigated the effect of two counter ions on the AEM for sorption of P from six agricultural soils with varying pH (5.4–8.5). Previously work has shown (1) significantly increased sorption of P to resin in nylon bags when HCO_3^- rather than Cl^- is used as a counter ion [10,11] and (2) more consistent pH values obtained for the HCO_3^- form with changing soil to water ratios, attributed to the buffering capability of HCO_3^- [10]. However, in the current study the overall recovery of P from the AEM in HCO_3^- form was not significantly different to the AEM in Cl^- form. When the resin P values using each counter ion were compared a slope of 1.11 and a coefficient of determination for the regression fit of 0.83 (excluding outlier with large standard error), revealed that there was little apparent bias with P sorption using either counter ion form of AEM.

The AEM in Cl^- form has little influence on the solution pH compared to the HCO_3^- form. When pH values obtained from the 1:30 soil:water solutions after AEM removal were compared against the original pH values of the soils, linear relationships resulted in slopes of 1.19 ($r^2 = 0.86$) for AEM in Cl^- form and 1.88 ($r^2 = 0.69$) for AEM in HCO_3^- form (data not shown).

4. Conclusion

Comparison of the DGT and resin methods for measuring P in solutions of different compositions identified potential problems with use of the resin method with an AEM. DGT performance has previously been shown to be independent of pH (3–9) and was unaffected by anions (SO_4^{2-}, NO_3^- and Cl^-) present in solution at concentrations relevant to agricultural soils. Bicarbonate did affect DGT performance, but only at unrealistically high concentrations of soluble carbonate. Resin P performed well at all pH values down to pH 4, below which, measured values were appreciably lowered. Elevated SO_4^{2-} and NO_3^- had a limited effect on the P sorption at concentrations relevant to agricultural soils. Increasing Cl^- concentrations however had a marked effect on sorption of P onto the AEM. Increasing HCO_3^- concentrations also reduced P sorption onto the AEM strip significantly at concentrations that could exist in agricultural soils. Resin P measurements increased when the soil:water ratio was decreased. The increases in resin P values were not uniform for the eight agricultural soils used in this experiment, which indicates that the increase is due to the inherent soil properties. DGT measurements also increased with decreasing soil:water ratios, suggesting the increase is in response to the replenishment of P from solid phases to solution and not due to diluting out any anionic interferences. There were major discrepancies observed between DGT and resin measurements using eight agricultural soils, which suggest that they are measuring different pools of available P. Further studies will need to be performed comparing DGT P and resin P against plant responsiveness to assess whether either of these two methods accurately reflect plant available P.

Acknowledgements

This work was supported in part by the Grains Research and Development Corporation project number CSO00007. SM gratefully acknowledges provision of a Ph.D. faculty scholarship from the University of Adelaide. We would like to thank Jason Kirby and Claire Wright (CSIRO Land and Water) for their assistance with the ICP-MS analyses. We would also like to thank Bill Bowden (Department of Agriculture, WA) for his assistance in collecting soils.

References

[1] T.M. McBeath, R.D. Armstrong, E. Lombi, M.J. McLaughlin, R.E. Holloway, Aust. J. Soil Res. 43 (2005) 203.
[2] D.M. Nash, D.J. Halliwell, Aust. J. Soil Res. 37 (1999) 403.
[3] R.G. Menon, S.H. Chien, L.L. Hammond, Commun. Soil Sci. Plant Anal. 21 (1990) 1131.
[4] N.W. Menzies, B. Kusumo, P.W. Moody, Plant Soil 269 (2005) 1.
[5] B. van Raij, J.A. Quaggio, N.M. da Silva, Commun. Soil Sci. Plant Anal. 17 (1986) 547.
[6] V. Kumar, R.J. Gilkes, M.D.A. Bolland, Fert. Res. 33 (1992) 35.
[7] S. Saggar, M.J. Hedley, R.E. White, P.E.H. Gregg, K.W. Perrot, I.S. Cornforth, Fert. Res. 33 (1992) 135.
[8] S. Saggar, M.J. Hedley, R.E. White, K.W. Perrot, P.E.H. Gregg, I.S. Cornforth, A.G. Sinclair, Nut. Cycl. Agr. 55 (1999) 35.
[9] C.A. Bissani, M.J. Tedesco, F.A. de, O. Camargo, G.L. Miola, C. Gianello, Commun. Soil Sci. Plant Anal. 33 (2002) 1119.
[10] E. Sibbesen, Plant Soil 50 (1978) 305.
[11] E. Sibbesen, G.H. Rubaek, Commun. Soil Sci. Plant Anal. 25 (1994) 1671.
[12] B.W. Bache, C. Ireland, J. Soil Sci. 31 (1980) 297.
[13] S.K. Sherrod, J. Belnap, M.E. Miller, Commun. Soil Sci. Plant Anal. 34 (2003) 1981.
[14] P. Qian, J.J. Schoenau, Can. J. Soil Sci. 82 (2002) 9.
[15] S. Saggar, M.J. Hedley, R.E. White, Fert. Res. 24 (1990) 173.
[16] P. Qian, J.J. Schoenau, W.Z. Huang, Commun. Soil Sci. Plant Anal. 23 (1992) 1791.
[17] M.J. McLaughlin, P.A. Lancaster, P.G. Sale, N.C. Uren, K.I. Peverill, Aust. J. Soil Sci. 32 (1994) 229.
[18] J.J. Schoenau, W.Z. Huang, Commun. Soil Sci. Plant Anal. 22 (1991) 465.
[19] F. Amer, D.R. Bouldin, C.A. Black, F.R. Duke, Plant Soil 6 (1955) 391.
[20] D. Binkley, Soil Sci. Soc. Am. J. 48 (1984) 1181.
[21] D.J. Gibson, Plant Soil 96 (1986) 445.
[22] S.E.A.T.M. Van der Zee, L.G.T. Fokking, W.H. van Riemsdijk, Soil Sci. Soc. Am. J. 51 (1987) 599.
[23] S.A. Collins, D.W. Allinson, Commun. Soil Sci. Plant Anal. 30 (1999) 2267.
[24] L.R. Cooperband, T.J. Logan, Soil Sci. Soc. Am. J. 58 (1994) 105.
[25] M.-B. Turrion, J.-F. Gallardo, M.-I. Gonzalez, Commun. Soil Sci. Plant Anal. 30 (1999) 1137.
[26] H. Zhang, W. Davison, Anal. Chem. 67 (1995) 3391.
[27] S.D. Mason, R.E. Hamon, A.L. Nolan, H. Zhang, W. Davison, Anal. Chem. 77 (2005) 6339.
[28] R.E. Hamon, M.J. McLaughlin, Aust. J. Soil Res. 40 (2002) 1383.
[29] J. Murphy, J.P. Riley, Anal. Chim. Acta 27 (1962) 31.
[30] L. Sochaczewski, W. Tych, W. Davison, H. Zhang, Env. Modell. Software 22 (2007) 14–23.
[31] H. Zhang, F.-J. Zhao, B. Sun, W. Davison, S.P. McGrath, Env. Sci. Technol. 35 (2001) 2602.
[32] R.J. Haynes, M.S. Mokolobate, Nutr. Cycl. Agroesyst. 59 (2001) 47.

[33] P.J. White, M.R. Broadley, Ann. Bot. 88 (2001) 967.
[34] A. Eynard, R. Lal, K. Wiebe, J. Sustain. Agr. 27 (2005) 5.
[35] N. Hunt, B. Gilkes, Farm Monitoring Handbook, The University of Western Australia, 1992.
[36] C.A. Bower, L.V. Wilcox, in: C.A. Black (Ed.), Methods of Soil Analysis, American Society of Agronomy Inc., Madison, Wisconsin, 1965, p. 933.
[37] V. Rasiah, J.D. Armour, Aust. J. Soil Res. 39 (2001) 329.
[38] A.S. Black, S.A. Waring, Aust. J. Soil Res. 17 (1979) 271.
[39] G.C. Anderson, I.R.P. Fillery, F.X. Dunun, P.J. Dolling, S. Asseng, Aust. J. Agric. Res. 49 (1998) 345.
[40] A.E. McElnea, C.R. Ahern, N.W. Menzies, Aust. J. Soil Res. 40 (2002) 1115.
[41] D.R. Parker, W.A. Norvell, R.L. Chaney, in: R.H. Loeppert, S. Goldberg (Eds.), Chemical Equilibrium and Reaction Models, Soil Science Society of America, Madison, Wisconsin, 1995, p. 253.
[42] G. Tyler, T. Olsson, Eur. J. Soil Sci. 52 (2001) 151.

Available online at www.sciencedirect.com
ScienceDirect
Talanta 74 (2008) 690–693
Talanta
www.elsevier.com/locate/talanta

Isotopic analysis of lead present in the cinnabar of Roman wall paintings from the Xth Regio "(Venetia et Histria)" by ICP-MS

G.A. Mazzocchin [a,*], P. Baraldi [b], C. Barbante [c,d]

[a] *Dip. Chimica Fisica, Università Ca' Foscari di Venezia, Calle Larga S. Marta 2137, 30123 Venezia, Italy*
[b] *Dip. Di Chimica, Università di Modena e Reggio Emilia, Via G. Campi 183, 41100 Modena, Italy*
[c] *Dip. Di Scienze Ambientali, Università Ca' Foscari di Venezia, Calle Larga S. Marta 2137, 30123 Venezia, Italy*
[d] *Istituto per la Dinamica dei Processi Ambientali, IDPA-CNR, calle Larga S. Marta 2137, 30123 Venezia, Italy*

Received 13 July 2006; received in revised form 26 June 2007; accepted 26 June 2007
Available online 25 July 2007

Abstract

The analysis of Roman wall paintings coming from Verona, Vicenza, Padova, Pordenone and Trieste evidentiated the presence of cinnabar.

In this work, the isotopic composition ^{206}Pb, ^{207}Pb and ^{208}Pb of trace of lead present in cinnabar is reported, via ICP-MS measurements. The isotopic ratio values are compared with the values obtained from samples coming from Roman wall paintings of Pompeii and from the mines of Almaden (Spain) Monte Amiata (Grosseto Italy) and Idria (Slovenia).

All the isotopic data can be represented by a "field" ranging from Huelva, to Almeria Spanish provinces. This trend could be due to the mixing of cinnabar products treated in Rome.
© 2007 Elsevier B.V. All rights reserved.

Keywords: Cinnabar; Roman painting; Lead isotope analysis

1. Introduction

From studies carried out on fragments of wall paintings taken from cities of the Xth Regio of the Roman Italy (Verona, Vicenza, Padova, Pordenone and Trieste) the presence of cinnabar (HgS) has been verified [1–3].

This pigment was the most expensive of all those used in the Roman epoch; Augusti [4] reports that a pound of cinnabar could cost up to 300 assi, while another relatively costly pigment such as Egyptian Blue could cost 100 assi. The presence of cinnabar, therefore, characterises "Domus" and public buildings of high quality and regard and characterise the proprietor as a person with great economic possibilities and an elevated social standing. The determination of the provenance of this pigment is of great interest and can yield information on trade routes that existed during the construction period of these buildings and on the taste of the person who commissioned the work and the principal artist.

The lead isotopic composition of the cinnabar samples from the Villas of Verona (S. Cosimo and Vicolo Agnello), Vicenza (S. Biagio), Montegrotto, Padova (Terme Neroniane), Pordenone (Torre) and Trieste (Crosada) was determined and compared with samples from Pompeii (Insula del Centenario and Casa del Bracciale d'Oro) and from samples coming from mines of Almaden (Spain) Mount Amiata (Grosseto, Italy) and Idria (Slovenia).

The choice of measuring the isotopes of lead, present as an impurity in the mercury minerals was made because of the relative precision of these measurements; measurements on the stable isotopes of sulphur have been also made [5].

In 1982, Frizot [6] reviewed the study of pigments from ancient pictures and in 1990 Barbet [7], Guineau [8] and Delamare [9] investigated the use of the pigments and colorants in France during the Roman period. Barbet [7] observed that this pigment was becoming less available over the centuries up to the Low Roman Empire, when it seemed that most of the pigment

* Corresponding author. Tel.: +39 041 2348530.
E-mail address: gian.antonio.mazzocchin@unive.it (G.A. Mazzocchin).

0039-9140/$ – see front matter © 2007 Elsevier B.V. All rights reserved.
doi:10.1016/j.talanta.2007.06.048

came from the Balkan Peninsula instead of Spain. Our work slots into this research line and would contribute to the general knowledge of Roman painting.

2. Experimental

2.1. Instrumentation, reagents and standards

Sample analysis was carried out on an Agilent 7500i ICP-MS (Agilent Technologies, Yokogawa Analytical Systems, Tokyo, Japan), with a quartz double pass spray chamber, thermostatted to 2 °C, and fitted with a V-groove low flow (<500 μl min^{-1}) nebulizer (Agilent Technologies). High purity de-ionised water (18 MΩ cm^{-1} resistivity) (Purelab Ultra, Elga, High Wycombe, UK) and high purity acids (Suprapur grade, Merck, Darmstadt, Germany) were used for sample digestion. A sample of SRM 981 Common Lead Isotopic Standard (NIST, Gaithersburg, MD, USA) was dissolved in cold nitric acid and was serially diluted to give a final concentration of 50 μg l^{-1} (total Pb), and was used as a mass bias correction solution for isotope ratio analysis.

2.2. Sample preparation

A 15–30 mg sample of cinnabar was dissolved in an acid cleaned glass beaker, heated on a hotplate after the addition of 3 ml of hydrochloric acid and 2 ml of nitric acid. Once dissolved, the sample was allowed to cool and was made up to 50 ml with ultra pure water in a polypropylene vessel.

Aliquots of the principal solution were serially diluted to obtain solutions with an appropriate lead content for ICP measurements (<100 μg/ml) to prevent the detector going into analogue mode. The samples were kept refrigerated at 4 °C until analysis.

All samples were analyzed using the isotope analysis acquisition parameters for isotope ratio analysis. The instrumental operating conditions for isotope ratio analysis were the following: the number of scans is pre-set to 1000 in the ICP-MS software [10], so only three parameters can be optimised, the points per peak, the integration time per measurement and the number of replicates. The integration times were set to give similar count rates for the three isotopes studied (^{206}Pb, ^{207}Pb and ^{208}Pb) to obtain a similar measurement precision for each isotope. The ^{204}Pb isotope was not available for measurement as mercury has an isotope at *m/z* 204 which swamped the lead signal (Fig. 1). Three points per peak were chosen as this gives the best precision for quadrupole instruments [10] and five replicates were chosen to give a total analysis time of 190 s. Samples were diluted so that all the isotopes were acquired in pulse counting mode, as this ensures that the same integration time is used throughout the measurement, after each sample the Common Lead Isotopic Standard was run to correct for any drift in mass bias.

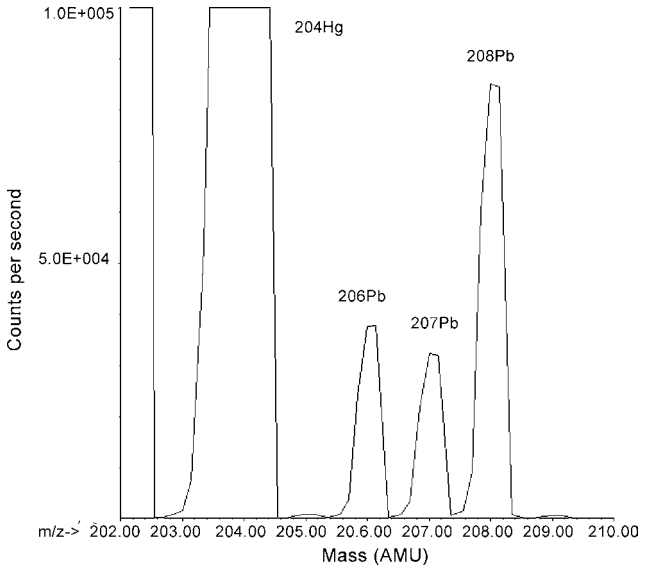


Fig. 1. Mass scan between *m/z* 202 and 210 of a solution of cinnabar showing the isotopes of lead and the large signal for mercury at *m/z* 204.

The natural cinnabar samples coming from China, Monte Amiata (Italy) and Almaden (Spain) were Kremer pigmente GmbHαCo, Airchstetten.

The Idria cinnabar sample was kindly supported by Dr. Uros Erzen of Idria Mercury Mine (Idria, Slovenia).

Table 1
Lead isotope data for the cinnabar samples analyzed

Sample	Provenance sample	$^{206/207}$Pb	$^{208/207}$Pb	$^{208/206}$Pb	$^{207/206}$Pb
A	Verona (San Cosimo)	1.168 ± 0.001	2.446 ± 0.004	2.093 ± 0.005	0.856 ± 0.001
B	Verona (Vicolo Agnello)	1.202 ± 0.001	2.475 ± 0.005	2.059 ± 0.004	0.832 ± 0.002
C	Vicenza (S. Biagio)	1.199 ± 0.002	2.484 ± 0.003	2.071 ± 0.003	0.834 ± 0.001
D	Montegrotto Terme (PD)	1.189 ± 0.002	2.478 ± 0.004	2.085 ± 0.003	0.841 ± 0.001
E	Pordenone (Torre)	1.182 ± 0.005	2.450 ± 0.006	2.073 ± 0.005	0.846 ± 0.001
F	Trieste (Crosada)	1.188 ± 0.006	2.472 ± 0.006	2.081 ± 0.004	0.842 ± 0.003
G	Pompeii (Insula Cent)	1.182 ± 0.005	2.458 ± 0.007	2.079 ± 0.003	0.846 ± 0.003
H	Pompeii (Casa BO)	1.179 ± 0.006	2.455 ± 0.003	2.082 ± 0.003	0.848 ± 0.003
I	Almaden 1 (Spain)	1.168 ± 0.001	2.442 ± 0.006	2.091 ± 0.003	0.856 ± 0.001
L	Almaden 2 (Spain)	1.169 ± 0.003	2.447 ± 0.008	2.093 ± 0.002	0.855 ± 0.002
M	Monte Amiata (Italy)	1.172 ± 0.003	2.444 ± 0.006	2.086 ± 0.004	0.853 ± 0.002
N	Idria (Slovenia)	1.167 ± 0.002	2.455 ± 0.005	2.104 ± 0.003	0.857 ± 0.002
O	China	1.194 ± 0.002	2.442 ± 0.005	2.045 ± 0.002	0.837 ± 0.002

Reported data are obtained after five replicates on the some sample aliquot.

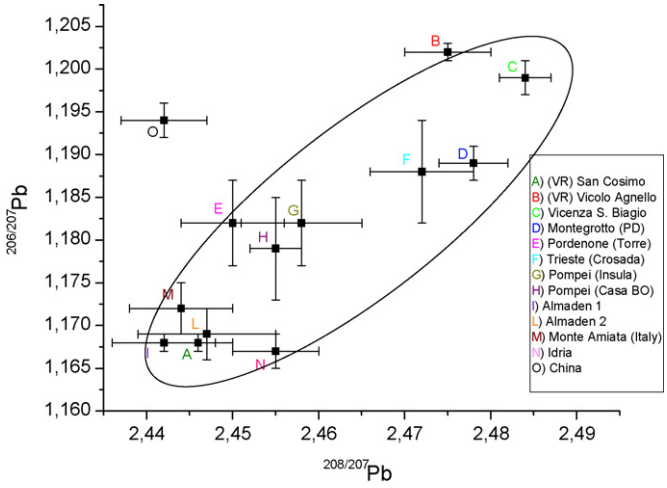


Fig. 2. Plot of the lead isotopic data ($^{206/207}$Pb vs. $^{208/207}$Pb) for the cinnabar samples.

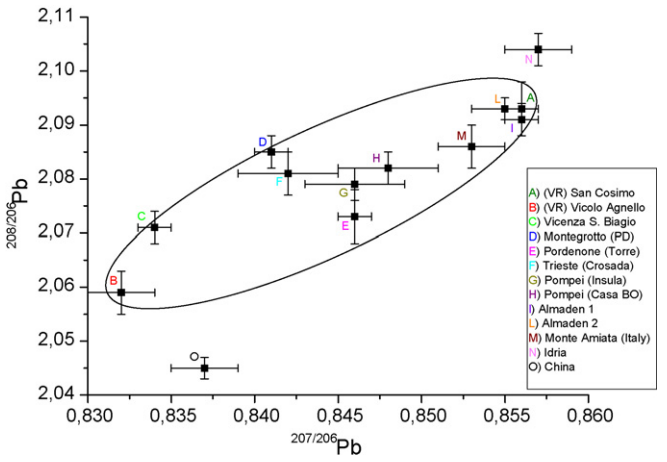


Fig. 3. Plot of the lead isotopic data ($^{208/206}$Pb vs. $^{207/206}$Pb) for the cinnabar samples.

3. Results and discussion

Table 1 report the lead isotopic ratios together with the standard deviation of the five different measurements performed on the samples coming from the cities of the North-East of Italy, Pompeii and from HgS samples coming from mines of Almaden (Spain), Monte Amiata (Italy) Idria (Slovenia) and China.

The reported isotopic ratios are: $^{206/207}$Pb, $^{208/207}$Pb$^{208/206}$Pb and $^{207/206}$Pb.

Isotope ratios are used to make plots with two complementary variables where we put all the isotopic abundance experimental data to identify a field of values representative of a lead ore region.

To this purpose, Rosman et al. [11] used the $^{206/207}$Pb vs. $^{208/207}$Pb plot to define lead ores in Aegean, British, German, Greek and Spanish regions.

Stos-Gale et al. [12,13] and Rohl [14] used the $^{208/206}$Pb vs. $^{207/206}$Pb plot for ores of western Mediterranean, Aegean, Britain and Ireland.

In Fig. 2, our experimental data of the ratio $^{206/207}$Pb vs. $^{208/207}$Pb are reported. The data lie in an elliptic area confined by a line.

In Fig. 3, the experimental data of the ratio $^{208/206}$Pb vs. $^{207/206}$Pb are reported; also in this case, an area is identified and the data distribution is similar to that of Fig. 2.

In Fig. 4 the plot of Rosman [11], which includes also the data of Rohl and Stos-Gale [12–14] $^{206/207}$Pb vs. $^{208/207}$Pb is shown together with the area of our data. As it can be seen, the area extends from the region of Rio Tinto (Huelva–Spain) to the Spanish regions of Cabo de Garta and Mazarron (Almeria), in agreement with historical records that report intensive mining of south Spanish regions by the Romans.

The distribution of the experimental isotopic data along a narrow ellipse can be explained by tacking into account that the raw material, coming from the silver or cinnabar mines, was triturated treated and washed in Rome, as the product was under a monopoly system. It cannot be excluded hence that in the some cases the pigment supplied to the painters was a mixture of cinnabars coming from different Spanish mines, whose isotope ratios were intermediate between the values of the pure components.

In some case the cinnabar seems to arise from a precise region; the samples of Verona (S. Cosimo) seems to originate from the region of Rio Tinto while the samples of Verona (Vicolo Agnello) and Vicenza (S. Biagio) seem to arise from mines of South-East of Spain (Cabo de Garta–Mazarron).

The samples of Montegrotto (PD), Pordenone (Torre) and Trieste (Crosada) on the contrary, seems to be mixtures of Spanish cinnabars.

The mines used by Romans were Spanish as Theaphrastus asserted 200 years before Vitruvius [4], hence the "fields" of Britain and Europe in Fig. 4 can be disregarded.

In addition it can be observed that the samples of Pompeii lie near to the sample of Pordenone and hence we can think that existed a single cinnabar source for Pompeii, Rome and provinces; all the cinnabar used in Italy comes from a single processing centre.

From Fig. 4 it can be seen also that the area of isotopic ratios of Lavrion (Greece) is close but out of our field. Also the data

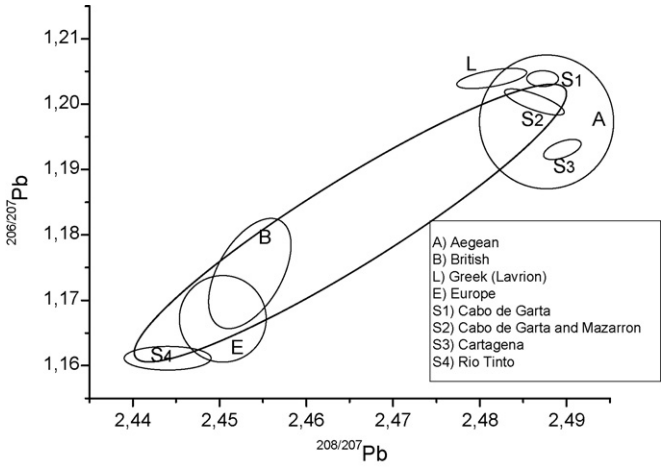


Fig. 4. "Field" of experimental data superimposed to the Rosman plot.

of Idria (see also Fig. 2) are nearby but out of the field of our data suggesting that probably these mines were not used during the Roman Empire up to the IIIrd century A.D., when were built the "Domus" object of this paper.

The cinnabar of Monte Amiata (Tuscany) shows isotopic ratios close to those of Almaden (Spain); this circumstance is not surprising as lead isotope data of the mines of Grosseto (Tuscany, Italy) are similar to those of Cartagena (Murcia) [12].

The datum referring to a cinnabar sample coming from China is reported only for comparison and is far away from all the literature data and experimental ones, as expected.

The precision of the data obtained with a quadrupole ICP-MS instrument is not very high, as could be obtained via a double-focusing mass spectrometer, however, the precision seems sufficient to individuate reliably fields of isotope ratios, as demonstrated also by the results of repeated distinct measurements carried out on Almaden and Pompeii samples.

The ascertained presence of small iron contents in some cinnabar samples (as in Verona, Vicolo Agnello) suggests that sometime the painters adulterated the expensive cinnabar with hematite.

Finally we report that in the "Domus" of Vicenza and Pordenone the cinnabar was spread out on an ochre coloured undercoat, as discussed by Barbet [7], but this was not verified at Verona, Montegrotto and Trieste. The use of undercoat could be connected to the fear of a reaction between cinnabar and the quick lime that, according to the artisans of that era, could make the cinnabar to go black.

Acknowledgements

The authors thank Dr. Warren Cairns (IDPA-CNR, Venice, Italy) for the useful scientific discussions and laboratory assistance. ELGA LabWater is gratefully acknowledged for providing the PURELAB Option-R and Ultra Analytic, which produced the ultra pure water used in these experiments.

References

[1] G.A. Mazzocchin, F. Agnoli, S. Mazzocchin, I. Colpo, Talanta 61 (2003) 565–572.
[2] G.A. Mazzocchin, F. Agnoli, M. Salvadori, Talanta 64 (2004) 723–741.
[3] G.A. Mazzocchin, D. Rudello, E. Murgia, Ann. Chim. 97 (2007) 807–822.
[4] S. Augusti, I colori pompeiani Ed. De Luca., Roma, 1967.
[5] D. Damiani, E. Gliozzo, I. Memmi Turbanti, J.E. Spangenberg, Archaeometry 25 (2003) 341–354.
[6] M. Frizot, Revue d'Archeometrie 6 (1982) 47–59.
[7] A. Barbet, Pigments et Colorants de l'Antiquité et du Moyen Age, Colloque International du CNRS, Paris, 1990, pp. 255–271.
[8] V. Guichard, B. Guineau, Pigments et Colorants de l'Antiquité et du Moyen Age, Colloque International du CNRS, Paris, 1990, pp. 245–254.
[9] F. Delamare, L. Delamare, B. Guineau, G.S. Odin, Pigments et Colorants de l'Antiquité et du Moyen Age, Colloque International du CNRS, Paris, 1990, pp. 103–116.
[10] J. Ruiz Encinar, J.I. Garcia Alonso, A. Sanz-Medel, S. Main, P. Turner, J. Anal. At. Spectrom. 16 (2001) 315–321.
[11] K.J.R. Rosman, W. Chisholm, S. Hong, J.P. Candelone, C.F. Boutron, Environ. Sci. Technol. 31 (12) (1997) 3413–3416.
[12] Z.A. Stos-Gale, N.H. Gal, J. Houghton, R. Speakmane, Archaeometry 37 (1995) 407–415.
[13] Z.A. Stos-Gale, N.H. Gal, N. Annetts, Archaeometry 38 (1996) 381–390.
[14] B.M. Rohl, Archaeometry 38 (1996) 165–180.

Available online at www.sciencedirect.com
ScienceDirect
Talanta 74 (2008) 992–997
Talanta
www.elsevier.com/locate/talanta

Rapid aryl hydrocarbon receptor based polymerase chain reaction screening assay for polychlorinated dibenzo-*p*-dioxins and furans in soil and sediment

Daniel R. McAlister [a,*], Michael J. Fern [a], Randy L. Allen [b]

[a] *Eichrom Technologies, LLC 8205 S Cass Avenue, Suite 106, Darien, IL 60561, United States*
[b] *Hybrizyme Corporation, 2801 Blue Ridge Road, Suite G-70, Raleigh, NC 27607, United States*

Received 27 April 2007; received in revised form 7 August 2007; accepted 8 August 2007
Available online 14 August 2007

Abstract

A method for the estimation of polychlorinated dibenzo-*p*-dioxin and furan (PCCD/F) toxicity equivalent quotient (TEQ) of soil and sediment matrices is described. The method includes extraction, isolation of the PCDD/Fs from interfering compounds, such as polychlorinated biphenyls (PCBs) and polycyclic aromatic hydrocarbons (PAHs), and measurement of PCDD/F using the PROCEPT® aryl hydrocarbon (AhR) receptor based polymerase chain reaction (PCR) assay. The values obtained using the PROCEPT® assay correlate well with reference TEQ values generated from gas chromatography–high resolution mass spectrometry (GC-HRMS), with a linearity coefficient (R^2) of 0.94. Applied in a screening mode at 50 pg/g PCDD/F TEQ, the PROCEPT® assay yielded five false positive results (2.6%) and no false negative results for 196 analyses of spiked soils and environmental samples obtained from US EPA Superfund sites.
© 2007 Elsevier B.V. All rights reserved.

Keywords: Persistant organic pollutants; Dioxin; Ah-receptor; PCR

1. Introduction

Polychlorinated dibenzo-*p*-dioxins and furans (PCDD/F) are a class of persistent organic pollutants, which are highly resistant to vertebrate metabolism and can accumulate in high concentrations in top predator species. Most of the toxic and biological effects of PCDD/Fs have been attributed to interaction with the aryl-hydrocarbon receptor (AhR), a cytosolic receptor protein found in most vertebrate tissues [1]. The world health organization (WHO) has assessed the relative toxicity of 17 PCDD/F congeners (a PCDD/F compound containing a specific number and pattern of chlorine substituents) based on the ability of the congener to bind to the AhR, elicit AhR-mediated biochemical and toxic responses and be persistent and accumulate in the food chain [1]. These seventeen PCDD/F congeners have been assigned toxicity equivalent factors (TEFs) relative to the most toxic congener, 2,3,7,8-tetrachlorodibenzo-*p*-dioxin (Table 1), in order to provide consistent recommendations to national regulatory authorities for the establishment of monitoring levels. In 1998, the United States Agency for Toxic Substances and Disease Registry set a guideline screening concentration for PCDD/F in residential soils near contaminated sites of 50 pg/g (50 ppt) [2].

The standard method for the determination of PCDD/Fs is to measure the concentration of each of the 17 WHO PCDD/F congeners by gas chromatography–high resolution mass spectrometry (GC-HRMS) [3]. A toxicity equivalent quotient (TEQ) is then calculated from the sum of the concentration of each congener multiplied by its TEF value. The GC-HRMS method requires extensive sample preparation and a significant investment in capital equipment (>$500k). Therefore, a rapid screening method capable of measuring PCDD/F TEQs below 50 pg/g using less expensive laboratory equipment could facilitate the more efficient and more thorough screening of residential soils.

This paper details a rapid *in vitro* AhR based PCR assay (PROCEPT®) for the measurement of PCDD/F and a chromatographic method for the isolation of PCDD/F from components of soil and sediment and other aryl hydrocarbon compounds. The assay utilizes the affinity of the aryl hydrocarbon receptor

* Corresponding author. Tel.: +1 630 963 0320; fax: +1 630 963 0381.
E-mail address: dmcalister@pgrf.com (D.R. McAlister).

0039-9140/$ – see front matter © 2007 Elsevier B.V. All rights reserved.
doi:10.1016/j.talanta.2007.08.005

Table 1
AhR-PCR assay response factors vs. WHO TEF values for PCDD/F

Compound	WHO 2005 TEF	AhR-PCR assay response factor
2,3,7,8 TCDD	1	1
1,2,3,7,8 PCDD	1	0.6
1,2,3,4,7,8 HxCDD	0.1	0.4
1,2,3,6,7,8 HxCDD	0.1	0.1
1,2,3,7,8,9 HxCDD	0.1	0.5
1,2,3,4,6,7,8 HpCDD	0.01	0.01
1,2,3,4,6,7,8,9 OCDD	0.0003	0.000003
2,3,7,8 TCDF	0.1	0.06
1,2,3,7,8 PCDF	0.03	0.1
2,3,4,7,8 PCDF	0.3	0.3
1,2,3,4,7,8 HxCDF	0.1	0.4
1,2,3,6,7,8 HxCDF	0.1	0.2
1,2,3,7,8,9 HxCDF	0.1	0.3
2,3,4,6,7,8 HxCDF	0.1	0.1
1,2,3,4,6,7,8 HpCDF	0.01	0.05
1,2,3,4,7,8,9 HpCDF	0.01	0.02
1,2,3,4,6,7,8,9 OCDF	0.0003	0.0005
PCB-77 (3,3′,4,4′)	0.0001	0.00003
PCB-81 (3,4,4′,5)	0.0003	0.00005
PCB-105 (2,3,3′,4,4′)	0.00003	$<3 \times 10^{-7}$
PCB-114(2,3,4,4′,5)	0.00003	0.00001
PCB-118(2,3′,4,4′,5)	0.00003	$<3 \times 10^{-7}$
PCB-123 (2′,3,4,4′,5)	0.00003	0.000009
PCB-126 (3,3′,4,4′,5)	0.1	0.01
PCB-156(2,3,3′,4,4′,5)	0.00003	0.00003
PCB-157(2,3,3′,4,4′,5′)	0.00003	0.00004
PCB-167(2,3′,4,4′,5,5′)	0.00003	0.000001
PCB-169(3,3′,4,4′,5,5′)	0.03	0.001
PCB-189(2,3,3′,4,4′,5,5′)	0.00003	$<3 \times 10^{-7}$
Indeno(1,2,3 -cd)pyrene	N/A	0.8
Benzo(k)fluoranthene	N/A	0.5
Benzo(b)fluoranthene	N/A	0.6
Dibenzo(a,h)anthracene	N/A	0.3
Benzo(a)pyrene	N/A	0.1
Benzo(a)anthracene	N/A	0.05
Chrysene	N/A	0.04
Benzo(g,h,i)perylene	N/A	0.004

Data reproduced from McAlister et al. [11].

for PCDD/F compounds, forming complexes composed of PCDD/F, the AhR, an aryl hydrocarbon nuclear translocator protein (ARNT) and a specific DNA response element (DRE) [4–8]. This complex is then bound to a plastic strip coated with a polyclonal antibody specific for the c-terminus of the ARNT. Excess AhR, ARNT and DNA are washed away and the amount of DNA is amplified and measured using real-time polymerase chain reaction (PCR). The degree of interaction of individual PCDD/F congeners with the AhR is proportional to the TEF established by the WHO (Table 1), therefore, the amount of DNA measured by the PCR is proportional to the PCDD/F TEQ of the sample. However, the PROCEPT® assay does not provide information on the amount of each individual PCDD/F congener.

Several other classes of aryl hydrocarbon compounds also interact with the AhR [9], including polycyclic aromatic hydrocarbons (PAHs), polychlorinated biphenyls (PCBs) and brominated and mixed brominated/chlorinated dibenzo-*p*-dioxins and furans (Table 1). Therefore, in order to measure PCDD/Fs using the AhR-PCR assay, a sample preparation method capable of separating PCDD/Fs from other AhR active compounds is necessary. The method employed in this study is similar to the GC-HRMS sample preparation method [3], but simplified by removing the graphitized carbon column and modified to provide additional decontamination from PAH and PCB compounds [9,10].

The PROCEPT® assay is based on a 96-well format, allowing for the measurement in duplicate of TEQ values for up to 38 unique samples including a 7-point calibration curve, assay blank, method blank and recovery standard. Measuring up to 38 samples simultaneously in 4–5 h offers a significant time savings over GC-HRMS (>24 h). However, further improvement in analysis time will require reduction in the time needed for extraction and sample clean-up.

Capital expenditures for the equipment needed to perform the assay (real-time PCR, 96-well plate shaker and 96-well plate washer) are approximately $40–50k, approximately one-tenth of the cost of a GC-HRMS instrument.

2. Experimental

2.1. Materials

Sodium sulfate and Florisil (Sigma–Aldrich) were washed with 1:1 hexane:methylene chloride using an accelerated solvent extraction apparatus (ASE100, Dionex) to remove organic impurities and then heated at 140 °C for 24 h and cooled in a dessicator. The 44% sulfuric acid silica, 10% silver nitrate silica, 2% potassium hydroxide silica, washed silica, toluene (99.9%, HPLC grade), methylene chloride (HPLC, >99.9%), hexanes (HPLC, >98.5%), acetone (histological, >99.5%) and heptane (HPLC, >99%) were used as received from Sigma–Aldrich. Brilliant QPCR mastermix (Stratagene) and the PROCEPT® AhR-PCR assay (Eichrom Technologies) were stored according to manufacturer's instructions until use. Standard solutions of 2,3,7,8-tetrachlorodibenzo-*p*-dioxin in isooctane, and all other PCDD/F standards, were obtained from Cambridge Isotopes.

2.2. Preparation of soil samples

Spiked soils were prepared by drying playground sand and potting soil at 110 °C for 48 h and cooling in a dessicator. The potting soil was then pulverized using a mortar and pestle and sifted to remove large particles. An aliquot of the dried soil or sand was then weighed into a glass round bottom flask and hexane was added to a level ~3 cm above the soil level. A mixture of tetra-octa chlorinated dibenzo-*p*-dioxins was added to achieve the desired PCDD/F TEQ. The mixture was then equilibrated on a rotary evaporator at room temperature for 2 h (100 rpm), and the hexane was slowly removed under vacuum. Additional "real world" samples were obtained through the United States Environmental Protection Agency Superfund Innovative Technology Evaluation (SITE) Program.

2.3. Soil extraction

PCDD/Fs were extracted from the soils by accelerated solvent extraction (ASE) using a mixture of 70:30 toluene:acetone at 100 °C and 1500 psi using a Dionex ASE100. Five grams of soil was added to a 33 mL stainless steel extraction cell (Dionex) equipped with a glass fiber filter (Dionex) and filled ~1/3 with diatomaceous earth dispersion agent (Dionex). Diatomaceous earth was then added on top of the soil to fill the remaining space in the cell and the cell was sealed by hand tightening. Each soil was then extracted for two static cycles of five minutes and flushed with 30% of the cell volume between cycles. A sixty second nitrogen flush completed the extraction procedure and the extract was collected in a 200 mL glass bottle. Other extraction methods and solvent systems including Soxhlet extraction or ultrasonic extraction can be used provided sufficient recovery of PCDD/F can be demonstrated.

2.4. Extract purification

Following extraction, 2 mL of dodecane was added to the soil extracts, and the extracts were concentrated to ~10 mL at 50 °C using a stream of dry air. The extracts were then transferred to 40 mL glass vials with two 5 mL portions of hexane, and the removal of toluene and acetone was completed using a stream of dry air. Ten milliliters of hexane and 5 g of 44% sulfuric acid silica gel were added to the concentrated extracts. The 40 mL vials were then sealed and gently agitated overnight to begin the removal of PAH compounds and other organics extracted from the soil matrix.

Immediately prior to use, multi-layer silica columns (from top to bottom in a 50 mL glass column, 17 mm i.d.: glass wool, 1 g washed silica, 2.5 g 10% silver nitrate silica, 1 g 2% potassium hydroxide silica, 1 g washed silica, 10 g 44% sulfuric acid silica, 2.5 g dried sodium sulfate) and Florisil columns (from top to bottom in a 25 mL glass column, 14 mm i.d.: glass wool, 2 g Florisil, 1.5 g dried sodium sulfate) were prepared. The silica and Florisil columns were prewashed with 30 mL and 10 mL of hexane, respectively.

For each extract, a silica column was placed in series above a Florisil column in a fume hood. The extract/44% sulfuric acid silica mixture was then slurried and added to the silica column to complete the PAH compound removal. The transfer of the extract from the vial to the column was completed using three 5 mL portions of hexane. Once the level of fluid reached the top of silica column bed, 45 mL of hexane was added to complete the elution of PCDD/F on the silica column. The entire PCDD/F eluate from the silica column was collected and passed through the Florisil column, which retains the PCDD/F compounds, but not the PCBs. Once the solvent level reached the top of the Florisil column bed, rinses of 10 mL 2% methylene chloride in hexane and 10 mL of 5% methylene chloride in hexane were performed to complete the separation of PCBs from the PCDD/F. The PCDD/F fraction was then eluted from the column using 15 mL of 50% methylene chloride in hexane and collected in a 20 mL glass test tube. The PCDD/F fraction was then concentrated at room temperature using a stream of dry air, transferred to a 1.5 mL glass vial with methylene chloride, evaporated and dissolved in 0.2–1.5 mL of heptane. A final batch contact with 50–100 mg of 10% silver nitrate silica was then performed in the 1.5 mL glass vial to remove any traces of PAH compounds remaining in the extract.

2.5. PROCEPT® AhR-PCR assay

The PROCEPT® AhR-PCR was performed according to the manufacturer's instructions. All solution dispensing and measuring was performed using delivery pipets and plastic barrier pipet tips. Plastic wells were prepared by washing on a plate washer (BioTek ELx50) using the manufacturer supplied wash solution, adding 50 mL of the thawed antibody solution (stored at −20 °C) to each well, equilibrating on a plate shaker (Heidolph Titramax 1000) for 60–90 min and washing on the plate washer to remove excess antibody. While the plastic wells were equilibrating, 5 μL of each purified soil extract, standard, assay blank, method blank or recovery standard were added to a 96-well plate of glass vials containing 25 μL of the manufacturer supplied buffer solution. Samples, standards, assay blanks (heptane), method blanks (blank soil processed through the entire method) and recovery standards (known soil or PCDD/F standard mix processed through the entire method) were analyzed in duplicate (Fig. 1). Twenty-five microliters of solution containing the AhR, ARNT and DRE (stored at −80 °C and thawed immediately prior to use) were then added to each glass vial, and the plate of glass vials was equilibrated on the plate shaker for 60 min. Following equilibration, 30 μL of solution from the glass vials was added to prepared plastic wells and equilibrated for 30 min on the plate shaker to bind the AhR/ARNT/DRE/PCDD/F complexes. Excess AhR, ARNT, and DRE were removed by washing on the plate washer.

2.6. Polymerase chain reaction

PCR reagents were prepared according to the manufacturer's instructions by adding 40% DNase free water, 50% 2× PCR

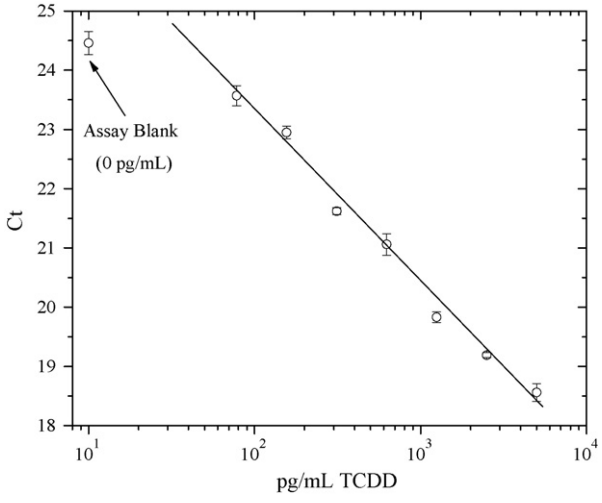


Fig. 1. Calibration curve for AhR-PCR assay (Threshold cycle, Ct vs. pg/mL 2,3,7,8-TCDD). Error bars determined from duplicate analyses.

mastermix ($MgCl_2$, Taq polymerase, DNA bases, buffer, ROX reference dye) and 10% primer/probe solution. Forty microliters of PCR reagent were added to each plastic well. The plastic wells were sealed using optically clear adhesive film (Applied Biosystems) and placed in the real-time PCR instrument (Stratagene M×3000P). The PCR protocol included 2 min at 50 °C, 10 min at 95 °C and then 40 cycles of 15 s at 95 °C and 60 s at 60 °C.

The output from the PCR instrument for each sample is a threshold cycle (Ct). The Ct is the number of real-time PCR temperature cycles at which the fluorescence measurement exceeds a threshold level. By comparing the Ct value for an unknown sample to a calibration curve of known standards (Fig. 1), the TEQ value for a sample extract can be calculated ($TEQ_{extract}$). The value of $TEQ_{extract}$ can then be used to determine the TEQ of the soil sample (TEQ_{sample}) using the following equation:

$$TEQ_{sample} = \frac{(TEQ_{extract} - MB)(V)(RF)}{W}$$

where $TEQ_{extract}$ is the value exported by the PCR instrument (pg/mL) by comparing the Ct for the unknown sample to a calibration curve of known standards (Fig. 1). The MB is the method blank, V is the volume in milliliters of heptane in which the purified sample extract has been dissolved, RF is the recovery factor (ratio of the known TEQ of the recovery standard/measured value) and W is the dry weight of the soil sample in grams.

3. Results and discussion

3.1. Method blank

Method blank results were generated by processing soils certified to be free of PCDD/F, PCB and PAH contamination. Method blank samples were analyzed after employing a final batch contact of the purified extract with 50–100 mg of 10% silver nitrate silica, with a final contact with 0.3 mL of concentrated sulfuric acid and with no further treatment following the elution of the PCDD/F fraction from the Florisil column.

The results for the method blanks (Table 2) show the importance of the final batch contact with silver nitrate silica or sulfuric acid. The final batch contact reduces the background response from impurities (likely PAH) in the solvents, column materials and glassware used to process the samples. Silver nitrate silica gel was chosen over sulfuric acid for subsequent analyses of soil samples due to observed faster kinetics, more efficient removal of PAHs found to have high response on the AhR-PCR assay and concerns of the long term stability of extracts stored over concentrated sulfuric acid.

Table 2
Method blank for AhR-PCR assay vs. method of post-Florisil column treatment

Batch contact	Method blank (pg/mL)[a]	Standard deviation
None	18	6
H_2SO_4	1.1	0.9
10% $AgNO_3$ silica	0.4	0.3

[a] Six replicates, 5 g blank soil, 200 μL final extract volume.

PCDD/F compounds also have a small affinity for the 10% silver nitrate silica. However, no significant decrease in the response of PCDD/F standards was observed as long as the ratio of the volume of heptane used to dissolve the standard (microliters) to the mass of 10% silver nitrate silica (mg) was higher than 6.

The detection limit of the assay was estimated using three standard deviations of the assay blank. For a 5 g sample, dissolved in 200 μL of solvent, the calculated detection limit of the AhR-PCR assay is 1 pg/g (1 ppt). Actual achievable method detection limits will depend on the size of the sample, the volume of the final purified sample extract, and the amount of non-PCDD/F compounds in the sample which have a response on the AhR-PCR assay.

3.2. PAH/PCB removal

Soil samples spiked with high levels of PAH mixtures and individual PCB standards were processed to verify the removal of these compounds from the PCDD/F fraction by the sample preparation method. The amount of PAH or PCB remaining in the PCDD/F fraction following the extract purification was determined by response on the AhR-PCR assay (Table 3). The removal of PAH compounds was also verified using UV–vis spectrometry on the purified extracts. Greater than 99.999% of PAH compounds and greater than 99.8% of PCB-126 and 99.98% of PCB-169 were removed by the chromatographic sample preparation method.

Table 3
Decontamination of PAH and PCB from PCDD/F fraction

Sample	Average AhR-PCR response				
	Number of replicates	Concentration (pg/g)	Following clean-up (pg/g)	Standard deviation	% Contaminant removed
PAH mix A[a]	5	1.E+09	2.9	2.9	>99.999%
PAH mix B[b]	5	2.E+09	3.2	0.9	>99.999%
PCB-126[c]	5	1.E+06	17	7	99.8%
PCB-169[c]	5	1.E+06	3.6	0.9	99.98%
Method blank	5	N/A	3.4	0.9	N/A

[a] 1000 μg/g of 3-methylcholanthrene, 7H-dibenzo(c,g)carbazole, Benzo[j]fluoranthene, dibenzo[a,e]pyrene, dibenzo[a,h]acridine, dibenzo[a,j]acridine, dibenzo[a,h]pyrene and dibenzo[a,i]pyrene.

[b] 2000 ug/g of acenaphthene, acenaphthylene, anthracene, benz[a]anthracene, benzo[a]pyrene, benzo[b]fluoranthene, benzo[g,h,i]perylene, benzo[k]fluoranthene, chrysene, dibenz[a,h]anthracene, fluoranthene, fluorene, indeno[1,2,3-c,d]pyrene, naphthalene, phenanthrene and pyrene.

[c] % Contaminant removed for PCB-126 and PCB-169 calculated using the response factor for these anlaytes on the AhR-PCR assay.

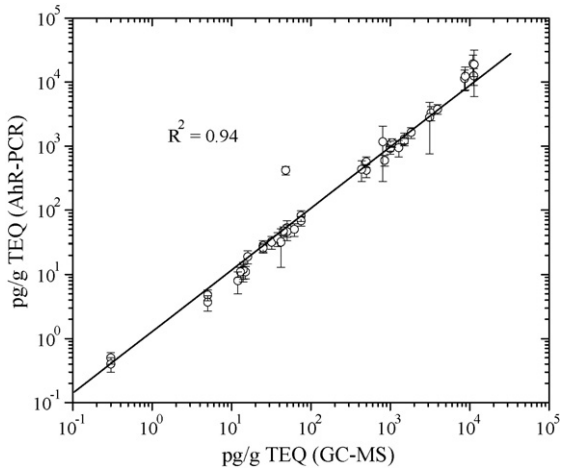


Fig. 2. Correlation of Procept AhR-PCR assay and GC-HRMS analysis of PCDD/F in soil and sediment. Error bars determined from 4–6 replicates processed through the entire method (extraction, purification and measurement).

Selected purified soil extracts were analyzed by GC-MS (Battelle Laboratories, Columbus, OH) to determine what types of compounds remain in the PCDD/F fraction following the extract purification. The GC-MS data revealed alkanes, alkenes, phthalates, silicones and benzophenone. At the levels observed in the GC-MS, none of these compounds was found to have significant response on the Procept assay or induce an antagonistic effect on the measurement of PCDD/F compounds.

3.3. Correlation with GC-HRMS

The AhR-PCR assay TEQ values were found to directly correlate with TEQ values obtained by GC-HRMS (Fig. 2) with a correlation coefficient (R^2) of 0.94. This data includes 84 determinations of spiked soils and 112 determinations of environmental samples obtained from US EPA Superfund sites. The range TEQ of values obtained with the PROCEPT® AhR-PCR assay was 71–168% of the corresponding GC-HRMS result, with a mean value of 99% and a median value of 96%. The average relative standard deviation of the TEQ measured for 4–6 replicates of soil samples processed through extraction, clean-up and measurement on the PROCEPT® assay (196 total measurements) was 24%. The relative standard deviation of the PROCEPT® measurement itself for duplicate measurements of the same purified extract was 11%.

3.4. Screening at 50 pg/g

In Table 4, the same data plotted in Fig. 2 is evaluated in a screening mode at an action level of 50 pg/g. The AhR-PCR assay correctly identified samples below 50 pg/g and samples above 50 pg/g, yielding no false negative values and five false positive values for the analysis of 112 environmental samples and 84 spiked samples. The five false positive results were observed for environmental samples obtained from US EPA Superfund sites. The false positive results are all well above the limit of detection and are likely due to compounds other than the 17 WHO PCDD/F congeners which have a response on the PROCEPT® AhR-PCR assay, but are not removed during the sample preparation method. Attempts to identify these compounds by GC-MS have been unsuccessful. However, compounds which could cause a high bias in the PROCEPT® measurement include compounds of similar structure to PCDD/F such as, polybrominated dibenzo-*p*-dioxins and furans, mixed chlorinated/brominated dibenzo-*p*-dioxins and furans, polychlorinated xanthenes (analogue of dibenzo-*p*-dioxin with one bridging oxygen replaced with a methylene group), polychlorinated thiophenes (sulfur analogue of furans) and PCDD/F congeners other than the 17 assigned TEF values by the WHO. A complete list of all cross-reactive compounds studied on the PROCEPT® assay can be found in reference [9].

Table 4
Screening results at 50 pg/g (50 ppt)

Result	Environmental samples	Spiked samples	Total
False positive	5 (4.5%)	0 (0.0%)	5 (2.6%)
False negative	0 (0.0%)	0 (0.0%)	0 (0.0%)
Total samples	112	84	196

4. Conclusions

The PROCEPT® rapid dioxin assay, an aryl-hydrocarbon based polymerase chain reaction assay, has been evaluated for the measurement of polychlorinated dibenzo-*p*-dioxin and furan toxicity equivalent quotients (TEQ) of soil and sediment samples. TEQ values obtained using the PROCEPT® assay correlate well with TEQ values obtained using the standard gas chromatography–high resolution mass spectrometry method ($R^2 = 0.94$). Evaluation of the PROCEPT® assay in a screening mode at 50 pg/g (ppt), yielded 0% false negative results and 2.6% false positive results for 196 TEQ determinations. False positive results are consistent for certain environmental samples and likely arise from the presence of dioxin-like compounds which are not removed during chromatographic purification of soil extracts.

Acknowledgements

The authors wish to thank Steven Billets of the US EPA SITE program and Amy Dindal of Battelle for their assistance, providing soil samples, GC-HRMS analysis and helpful discussions.

References

[1] M. Van den Berg, L.S. Birnbaum, M. Denison, M. De Vito, W. Farland, M. Feeley, H. Fiedler, H. Hakansson, A. Hanberg, L. Haws, M. Rose, S. Safe, D. Schrenk, C. Tohyama, A. Tritscher, J. Tuomisto, M. Tysklind, N. Walker, R.E. Peterson, Toxicol. Sci. 93 (2) (2006) 223–241.
[2] Fed. Reg. 71 (2006) 78441.
[3] United States Environmental Protection Agency Method 8290, Polychlorinated Dibenzodioxins and Polychlorinated Furans by High Resolution Gas Chromatography–High Resolution Mass Spectrometry. Method 1613. Tetra—through Octa—Chlorinated Dioxins and Furans by Isotope Dilution HRGC/HRMS.
[4] R.L. Allen, J.J. Willey, Organohalogen Compd. 58 (2002) 341–343.

[5] Y.Z. Gu, J.B. Hogenesch, C.A. Bradfield, Annu. Rev. Pharmacol. Toxicol. 40 (2000) 519–561.
[6] S. Heid, R. Pollenz, H. Swanson, Mol. Pharmacol. 57 (1) (2000) 82–92.
[7] C.A. Foy, H.C. Parkes, Clin. Chem. 47 (6) (2000) 990–1000.
[8] M. Korkalainen, J. Tuomisto, R. Pohjanvirta, Biochem. Biophys. Res. Commun. 285 (2001) 1121–1129.
[9] D.R. McAlister, M.J. Fern, Organohalogen Compd. 69 (2007) 1226–1229.
[10] Dioxins and Furans in Soils and Sediment, Eichrom Technologies, LLC. Method DFS01. www.eichrom.com/dioxins.
[11] D.R. McAlister, M.J. Fern, R.L. Allen, K. Sakata, B. Le Bizec, P. Marchand, Organohalogen Compnd. 68 (2006) 940–943.

Available online at www.sciencedirect.com
ScienceDirect
Talanta 74 (2008) 675–682
Talanta
www.elsevier.com/locate/talanta

Determination of piceid by photochemically induced fluorescence and second-derivative Response surface methodology for the optimization of a liquid–liquid extraction procedure for its analysis in wine samples

Isabel Durán Merás *, Teresa Galeano Díaz, Diego Airado Rodríguez

Department of Analytical Chemistry, University of Extremadura, 06071 Badajoz, Spain

Received 21 February 2007; received in revised form 25 June 2007; accepted 25 June 2007
Available online 25 July 2007

Abstract

trans-Piceid itself is weakly fluorescent, but the fluorescence signal ($\lambda_{exc/em}$ = 260/361 nm) is greatly enhanced by UV-irradiation of its hydroethanolic solutions. Employing the photoinduced emission signal at 361 nm or the amplitude of the second-derivative-photoinduced emission spectrum, between 353 and 361 nm, a linear relation is found in the assayed range 5.7–31.4 ng mL^{-1} of *trans*-piceid and limits of detection of 1.7 and 2.1 ng mL^{-1}, respectively, are obtained. A previous liquid–liquid extraction is necessary for the determination of piceid in wine. Experimental design (Central Composite Design) together with the Response Surface Methodology have been used to find optimum conditions for the extraction procedure. For this purpose, the difference between the photoinduced-fluorescence signal ($\lambda_{exc/em}$ = 260/361 nm) of the aqueous phase, before and after being extracted, has been considered as Response Function. A tartrate buffer (pH 5.0) concentration of 0.15 mol L^{-1} and a phase ratio of 1 are determined as optimum conditions. The amplitude of the second-derivative-emission spectrum, corresponding to the evaporated and re-dissolved organic phase, between 353 and 361 nm has been employed as analytical signal. Standard addition method has been applied to the analysis of piceid in different wine samples under optimum conditions. Results of wine analysis have been satisfactorily validated by HPLC.
© 2007 Elsevier B.V. All rights reserved.

Keywords: Piceid; Wine; Photochemically-induced fluorescence; Second-derivative; Response surface methodology; Liquid–liquid extraction

1. Introduction

Piceid (3,4′,5-trihydroxystilbene-3-β-mono-D-glucoside) is a glucoside of the stilbene-like resveratrol. These are phenolic compounds present in many families of plants, but grapes and related products, e.g. wine, are considered the most important dietary sources of these substances [1].

The determination of phenolic compounds in wine is very important because most of them play an important role in several sensorial characteristics such as colour, flavour, astringency and hardness of wine [2,3]. Some others, like piceid, have been intensively studied in the past decade due to their biological or pharmaceutical importance, as discussed below.

Resveratrol and piceid occur as *trans*- and *cis*-isomers. The chemical structure of *trans*-piceid is shown in Fig. 1. Due to the generally high ratio of *trans*- to *cis*-isomers found in wines, it has been suggested that the *cis*-isomers could arise from light exposure of must or wine during the wine-making process or possibly from light exposure of wine bottles during storage [4].

Piceid has received such attention as resveratrol because, in grape products, the concentration of the glucoside is usually significantly higher than the aglycone [4]. The relative distribution between the glycosylated and aglycone forms in wines is dependent on a number of factors such as fermentation and ecological conditions [5]. On the other hand, resveratrol in all

* Corresponding author. Tel.: +34 924289375; fax: +34 924289375.
E-mail address: iduran@unex.es (I.D. Merás).

0039-9140/$ – see front matter © 2007 Elsevier B.V. All rights reserved.
doi:10.1016/j.talanta.2007.06.049

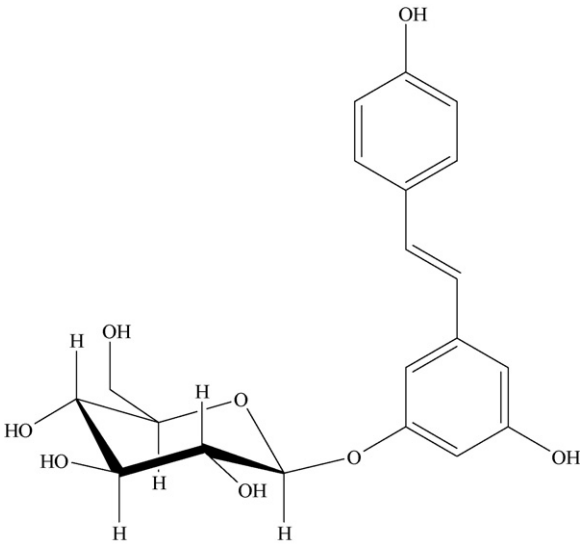


Fig. 1. Chemical structure of *trans*-piceid.

its forms is found in much higher concentration in red grape varieties compared with white grape varieties.

Piceid is the major polyphenol found in the root of *Polygonum cuspidatum*. The powder of this root is used in China and Japan as a treatment for atherosclerosis and for other therapeutic purposes [6,7]. The evidence for piceid in red wines was established by the use of a piceid standard extracted from *P. cuspidatum* [4]. Piceid isomers have properties similar to those of resveratrol in inhibiting platelet aggregation [8–10] and inhibiting oxidation of human low-density-lipoproteins [11]. On the other hand, in a less active manner than *trans*-resveratrol, *trans*-piceid reduces the elevations of lipid levels [12] and inhibits eicosanoid synthesis [7].

However, the human digestive tract is known to have glycosidase activity [13], so it is possible that the glucoside of resveratrol could release the aglycone on ingestion.

Liquid chromatography (LC) has been widely exploited for the analysis of piceid in several food samples, but no spectroscopic methods have been published so far. Thus, in the last years, reverse phase high performance liquid chromatography (RP-HPLC) by acidic solvent gradient elution, has been the most commonly used procedure for the determination of piceid in wine, either with diode array detection (DAD) [14–17], fluorimetric detection [18], DAD–fluorimetric detection [19], DAD–fluorimetric–electrochemical detection [20] or with mass spectrometry (MS) [20] and DAD-MS [21,22]. The detection based on electrochemistry, luminiscence and MS offer higher sensitivity than DAD. Capillary zone electrophoresis (CZE), with DAD [23] has been also employed for the analysis of this compound.

Regarding to the sample preparation, extraction with organic solvent, commonly ethyl acetate, followed by solvent evaporation and re-dissolution of the residue is widely employed [20,22], although an additional stage of cation-exchange chromatography has been also employed [14] previously to the injection in the chromatographic system. Solid phase extraction is other common treatment previous to the chromatographic [21] or electrophoretic [23] analysis. Nevertheless some methods are reported, in which wine samples are filtered through cellulose filters and directly injected into the chromatographic system [15,17,18].

Piceid itself is weakly fluorescent but it has been demonstrated that intense UV irradiation of piceid contained in the grape skins gives rise to the formation of the *cis*-isomer, which very quickly disappears in favour of a compound highly fluorescent in the ultraviolet range [24]. For the first time we have exploited the photochemical behaviour of piceid with an analytical purpose. The photoinduced-spectrofluorimetric study of piceid has been carried out and a sensitive, new, simple and inexpensive extractive-fluorimetric method, employing the amplitude of the second-derivative-emission spectra as analytical signal has been proposed for the analysis of piceid in wine samples previous liquid–liquid extraction.

In the development of the extractive procedure, experimental design (Central Composite Design) and the Response Surface Methodology (RSM) have been used to elucidate the manner in which the assayed variables affect the response function (RF) [25,26]. The use of these tools has the advantage of reaching the optimum values of the variables with the smallest number of experiments and in the shortest time possible.

2. Experimental

2.1. Chemicals

For all experiments, analytical reagent grade chemicals and solvents were used. Ultrapure water was obtained from a Millipore Milli-Q System.

trans-Piceid was purchased from Aldrich Chem. Co. and used as received. Standard ethanolic stock solutions containing 50.0 μg mL^{-1} were prepared in colored volumetric flasks by weighting and suitable dilution of the commercial product. This solution was stored at 4 °C avoiding the exposure to direct light. Fresh solutions of lower concentrations were prepared by appropriate dilution of the stock solution with absolute ethanol and water.

Buffer solution sodium hydrogen tartrate/disodium tartrate 0.26 mol L^{-1} was prepared by dissolving the suitable amount of disodium tartrate dihydrate with water and adjusting the pH of the resulting solution to 5.0 with hydrochloric acid.

2.2. Wine samples

Several samples of young red wines, barrel-aged red wines and white wines were provided by "*Viñaoliva*, Cooperative Society" (Almendralejo, Badajoz, Extremadura, Spain) and three different pools were made with the whole samples. All of them were previously filtered through a 0.45 μm cellulose acetate filter. Samples were kept at 4 °C avoiding exposure to direct light.

2.3. Instrumentation and software

Fluorescence spectral measurements were performed using a Varian Cary Elipse fluorescence spectrophotometer, equipped

with two Czerny-Turner monochromators and a xenon flash lamp, and connected to a PC microcomputer via an IEEE 488 (GPIB) serial interface. The Cary Elipse software was used for data acquisition. Fluorescence measurements were recorded in a 10-mm quartz cell at 20 ± 0.1 °C, by use of a thermostatically controlled cell holder and a Selecta Model 382 thermostatically controlled water-bath.

An Osram 200-W mercury lamp with an Oriel model 8500 power supply was used for the UV-irradiation of resveratrol solutions.

A Milton Roy Spectronic 3000 diode-array spectrophotometer, provided with the Milton Roy Rapid Scan software package V2.2, was used for acquisition and treatment of spectrophotometric data. Photometric measurements were recorded in a 10-mm quartz cell at 20 °C, by use of a thermostatic cell holder and a Selecta thermostatic bath.

The software package THE UNSCRAMBLER® 6.11_b CAMO ASA [27], running under Windows XP, was used for the application of chemometrics.

2.4. Procedures for the photochemically induced fluorimetric determination of total piceid

2.4.1. Calibration graph of total piceid

In a quartz cell, 5.0 mL of ultrapure water, different volumes of an ethanolic diluted stock *trans*-piceid solution containing between 57 and 320 ng of analyte, and ethanol up to 2% were added. The resulting solution was irradiated for 180 s, under a high pressure mercury lamp. Ethanol and water were added to the irradiated solution up to 10 mL (40%, v/v ethanol). The corresponding emission spectra (λ_{exc} = 260 nm) were registered and the fluorescence intensity at 361 nm was employed as analytical signal.

2.4.2. Recommended procedure for determining total piceid in wine

Aliquots of 0.10 mL of red wine or 0.50 mL of white wine, were diluted to 5.0 mL with ultrapure water and absolute ethanol, in a final percentage 2/98 ethanol/water (v/v). The resulting solutions were irradiated for 180 s under a high pressure mercury lamp, in a quartz cell with magnetic stirring. The irradiated solutions were transferred to a separatory funnel, and 5.0 mL of buffer solution (sodium hydrogen tartrate/disodium tartrate 0.26 mol L^{-1}, pH 5.0), were added. These aqueous phases were extracted with 10.0 mL of ethyl acetate by shaking for 150 s. The organic phases were evaporated to dryness at room temperature in a rota-evaporator. The residues were re-dissolved in 4.0 mL of absolute ethanol and ultrapure water was added up to 10.0 mL. Aliquots of 3.0 mL of the resulting solutions were transferred to the measure cell and a standard addition was carried out by adding successively small volumes of *trans*-piceid standard solution irradiated for 180 s in the same conditions as the diluted wine sample. The corresponding emission spectra (λ_{exc} = 260 nm) were registered. These spectra were smoothed by the moving average method with a segment of seven data points. Their second derivatives were calculated by Savitzky-Golay algorithm ($\Delta\lambda$ = 5 nm) and they were smoothed again in the same conditions as the spectra. The amplitude between 353 and 361 nm was employed as analytical signal. The analysis of every wine sample was carried out by triplicate.

3. Results and discussion

3.1. Determination of piceid by means of photochemically induced fluorescence

The ultraviolet absorption spectra of *trans*-piceid in aqueous, ethanolic or any hydroethanolic media are characterized by a single wide band around 312 nm with a band width of 15 nm, and two little maxima centered to 306 and 318 nm, respectively (Fig. 2A).

In order to establish the basic chemico-physical characteristics of *trans*-piceid, the influence of acidity on the absorbent properties of *trans*-piceid in aqueous medium was studied. The pH of the solution was varied by the addition of small volumes, in order of microlitres, of diluted solutions of hydrochloric acid or sodium hydroxide, in presence of 0.10 mol L^{-1} of potassium chloride to keep the ionic strength. A bathochromic shift to 343 nm and a narrowing of the absorption band was observed in basic medium. The absorbance at 343 nm keeps minimum

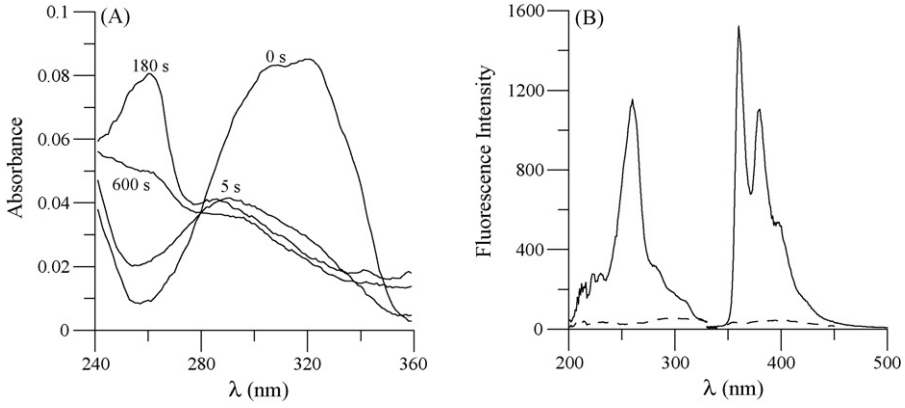


Fig. 2. (A) Absorption spectra corresponding to 1.14 μg mL^{-1} of *trans*-piceid in hydroethanolic medium containing 40% (v/v) of ethanol, irradiated for different times and without being irradiated. (B) Excitation (left) and emission (right) fluorescence spectra corresponding to a 1.2 μg mL^{-1} hydroethanolic (40%, v/v ethanol) solution of *trans*-piceid, non-irradiated (- - -) ($\lambda_{exc/em}$ = 318/380 nm) and irradiated for 180 s under a high pressure mercury lamp (—) ($\lambda_{exc/em}$ = 260/380 nm).

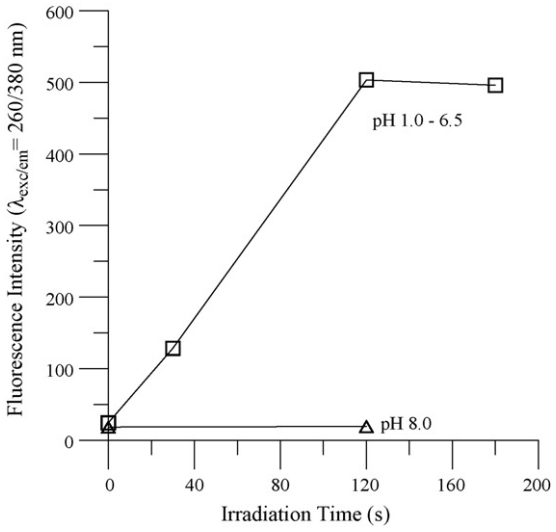


Fig. 3. Influence of irradiation time on the fluorescence intensity ($\lambda_{exc/em}$ = 260/380 nm) of 0.60 μg mL^{-1} *trans*-piceid in ethanol:water 40:60 (v/v) medium in presence of sodium chloride 0.1 mol L^{-1} in neutral, acid and basic media.

to pH 7.5 and increases in the 7.5–11.0 pH interval, remaining constant and independent of the acidity for higher pH values. Based on this experience, pK_a = 9.3 was calculated by Wilson and Lester method [28] for *trans*-piceid, in accordance with the reported value of 9.4 [29].

When *trans*-piceid aqueous, ethanolic or hydroethanolic solutions are UV-irradiated, the band corresponding to *trans*-piceid, disappears, and a new maximum centered to 290 nm, corresponding to *cis*-piceid [24,30], appears immediately, as shown in Fig. 2A. For irradiation times higher than 60 s another maximum centered to 260 nm (Fig. 2A) can be observed in solutions containing between 40% and 60% (v/v) of ethanol, corresponding to the highly fluorescent photoproducts discussed below, while the absorptivity at 290 is kept. This new maximum is negligible in purely ethanolic solutions and very weak in hydroethanolic media containing more than 60% (v/v) ethanol. The highest intensity of this maximum is reached for irradiation times around 180 s but decreases for higher irradiation times and turns negligible for irradiation times higher than 600 s, probably due to the UV-destruction of the highly fluorescent photoproducts.

A similar photochemical study was carried out by fluorescence. Hydroethanolic solutions of *trans*-piceid are slightly fluorescent and present excitation and emission maxima centered to 230 and 300, and 395 nm, respectively (Fig. 2B). Intense UV-irradiation of *trans*-piceid solutions, transforms *trans*-piceid into a highly fluorescent compounds, with a sharp excitation maximum (λ_{em} = 361 or 380 nm) at 260 nm and two emission maxima (λ_{exc} = 260 nm) centered to 361 and 380 nm, respectively (Fig. 2B). It was found that the intensity of the photoinduced signal and the optimum irradiation time are highly influenced by the solvent, but not the identity of the photoproducts because no changes were observed in the shape of spectra recorded in different media. Water, organic solvents of different polarities like methanol, ethanol, acetonitrile, dimethylsulfoxide, *N*,*N*-dimethylformamide, 1,4-dioxane, cyclohexane and hexane and some hydro-organic mixtures were assayed. The photoreaction rate is higher in any purely organic media than in hydro-organic ones, but the fluorescence quantum yield of the photoproducts is higher in hydroethanolic media.

Absorption and fluorescence spectra have been on-line obtained, after chromatographic separation for *trans*-piceid and its photoproducts [32], and the shape of these spectra are completely in agreement with the reported data [24,30].

Finally, the photoreaction was studied in different hydroethanolic media, and it was found that the ethanol percentage influenced in different ways to the kinetic of the photochemical process and to the quantum yield fluorescence of the generated photoproducts. The ethanol percentage in the medium for the photochemical reaction and for the fluorescence measure was varied between 0 and 100%. The best results were obtained by irradiating for 180 s hydroethanolic solutions of *trans*-piceid containing 2% (v/v) ethanol followed by a subsequent addition of ethanol up to 40% (v/v) before the fluorescence measurement.

With regard to the influence of the acidity, several solutions containing 0.60 μg mL^{-1} of *trans*-piceid in ethanol:water 40:60 (v/v), were prepared in presence of sodium chloride 0.10 mol L^{-1} at different pH values, fixed by the addition of aqueous hydrochloric acid or sodium hydroxide. The influence

Table 1
Analytical and statistical parameters for the determination of total piceid

	Photoinduced-fluorescent method ($\lambda_{exc/em}$ = 260/361 nm)	Second-derivative-photoinduced-fluorescent method $^2D_{353–361}$ (λ_{exc} = 260 nm)
Assayed concentration range (ng mL^{-1})	5.7–31	5.7–31
Intercept (a) ± s_a	18 ± 2	−0.17 ± 0.06
Slope (b) ± s_b (mL ng^{-1})	6.7 ± 0.1	0.18 ± 0.01
Determination coefficient (r^2)	0.9967	0.9947
Analytical sensitivity (γ^{-1}) (ng mL^{-1})	0.68	0.86
LOD[a] (ng mL^{-1})	0.85	1.3
LOD[b] (ng mL^{-1})	1.7	2.1
% RSD[c] (14.3 ng mL^{-1})	2.3	5.9

[a] Long and Winefordner method (k = 3) [33].
[b] Clayton et al. method ($\alpha = \beta$ = 0.05) [34].
[c] Relative standard deviation (n = 11).

Table 2
Optimization of the extractive procedure (experiments resulting of a central composite design)

Experiment	Design position	[Buffer] (mol L^{-1})	Shaking time (s)	Phase ratio
1	Low A[a]	0.026	155	2.5
2	High A[a]	0.19	155	2.5
3	Low B[a]	0.11	12	2.5
4	High B[a]	0.11	298	2.5
5	Low C[a]	0.11	155	0.99
6	High C[a]	0.11	155	4.0
7	Cube 1	0.06	70	1.6
8	Cube 2	0.16	70	1.6
9	Cube 3	0.06	240	1.6
10	Cube 4	0.16	240	1.6
11	Cube 5	0.06	70	3.4
12	Cube 6	0.16	70	3.4
13	Cube 7	0.06	240	3.4
14	Cube 8	0.16	240	3.4
15	Central a	0.11	155	2.5
16	Central b	0.11	155	2.5
17	Central c	0.11	155	2.5

[a] Experiments in a star point in the model.

of the irradiation time was carried out in all of them, and it was found (Fig. 3) that the greatest enhancement of the fluorescent signal is obtained in acid and neutral media.

The use of an irradiation time of 180 s makes the photochemically induced-fluorescent determination of *trans*-piceid in presence of its aglycone possible, because the fluorescence of the aglycone photoproducts becomes negligible for irradiation times longer than 60 s, probably because they are destroyed [31].

Finally the influence of the irradiation time was also carried out in presence of other typical polyphenols found in wines, concretely 4-hydroxy-3-methoxybenzoic acid, quercetin, caffeic acid, gallic acid, (−)-epicatechin and (+)-catechin and substantial changes in the photochemical process were not observed.

Under optimum conditions, satisfactory linear relation between fluorescence intensity and *trans*-piceid concentration was found in the assayed concentration range 5.7–31 ng mL^{-1}. Analytical figures of merit for the determination of *trans*-piceid are summarized in Table 1.

3.2. Application: analysis of piceid in wine samples

A previous liquid–liquid extraction of diluted wine samples is necessary to analyse piceid by means of photoinduced-fluorescence, in order to reduce the background signal. Firstly, the behaviour of the analyte with regard to the extraction in different organic solvents, was studied by molecular absorption, and it was found that the better extraction recoveries were obtained by extracting not the *trans*-piceid but its photoproducts, with ethyl acetate. However the quantum fluorescence yield of the photoproducts in ethyl acetate is minor than the obtained in the optimum hydroethanolic medium (40%, v/v ethanol) and it would be necessary to evaporate the organic extracts to dryness and re-dissolve the residue with the optimum hydroethanolic mixture.

It was proven that the dihydroxy-stilbene-glucoside neutral species is the predominant in acid and neutral media. Thus, the pH of the aqueous phase was fixed at 5.0 by the addition of hydrogen sodium tartrate/disodium tartrate buffer.

Anyway the extraction recovery was much lower than 100% and the implied physical–chemical variables, such as shaking time, phase ratio and buffer concentration in aqueous phase were optimized chemometrically by means of the Response Surface Methodology (RSM) to get the better recovery value.

3.3. Optimization of the extraction procedure by the RSM

For the optimization of buffer concentration, shaking time and phase ratio (aqueous/organic) an experimental design, central composite design, was used with the aim of calculating simultaneously the effect of the change in each one of these variables and also their possible interactions. Five levels were fixed for each variable. Three central samples were also included, giving rise to a total of 17 experiments (Table 2). This design is rotatable and therefore the precision in the calculation of the response is uniform over the whole experimental field.

The aqueous samples were constituted by standard solutions containing 57 ng mL^{-1} of *trans*-piceid in a final volume of 10.0 mL (2% ethanol), in presence of different amounts of buffer, irradiated for 180 s previously to the addition of the buffer solution, because a decrease in the photoinduced signal was observed when irradiating in presence of buffer.

The fluorescence emission spectra ($\lambda_{exc} = 260$ nm) of the aqueous phases were recorded before and after extracting them as marked by the design, and the difference between the fluorescence intensity of aqueous phase at 361 nm before and after the extraction was employed as RF.

$$RF = \text{F.I.}(\lambda_{exc/em}\, 260/361)_{\text{before extracting}} - \text{F.I.}(\lambda_{exc/em}\, 260/361)_{\text{after extracting}}$$

The optimization of the model was made with THE UNSCRAMBLER® software package [27], and the results were interpreted with the RSM. In the corresponding analysis of variance (ANOVA) a second-grade quadratic model is assumed.

From this ANOVA, the results of which are summarized in Table 3, it was deduced which of the considered effects contribute significantly to the model for a 95% confidence level. In this case, buffer concentration and phase ratio were significant variables but not the shaking time or the interactions between them. Fig. 4 shows the response surfaces estimated by the model, for each pair of variables. In these diagrams, it can be noticed that appreciable variations in the response function occurs when the two specified factors, buffer concentration or phase ratio are varied. In these surfaces, the maximum value of RF is located at the following values of the variables: 0.16 mol L^{-1} of buffer, phase ratio of 0.7, considered optimum conditions. The predicted value of phase ratio was out of the assayed points in the experimental design, nevertheless it was proven that the extraction percentage obtained with a phase ratio of 1 is similar to the obtained with a phase ratio of 0.7. Because of this, an optimum phase ratio of 1 was finally selected. The shaking time was fixed at an arbitrary value of 150 s.

The extraction recovery under these conditions was calculated as the ratio between the slopes of the calibration curve and a calibration curve constructed extracting standards, and it resulted to be 61%.

3.4. Determination of piceid in wine samples

Despite extracting wine samples, an important background signal from the matrix was observed in the optimum conditions to obtain the fluorescent spectra of the photoproducts. Nevertheless this contribution was reduced to a great extent by obtaining derivative signals, fundamentally the second-derivative-emission spectra. It was also examined the linearity between different signals measured on the second-derivative-emission spectra and the original *trans*-piceid concentration, and it was found a linear relationship employing the amplitude of the second-derivative-emission spectra between 353 and 361 nm as analytical signal. The analytical and statistical parameters for

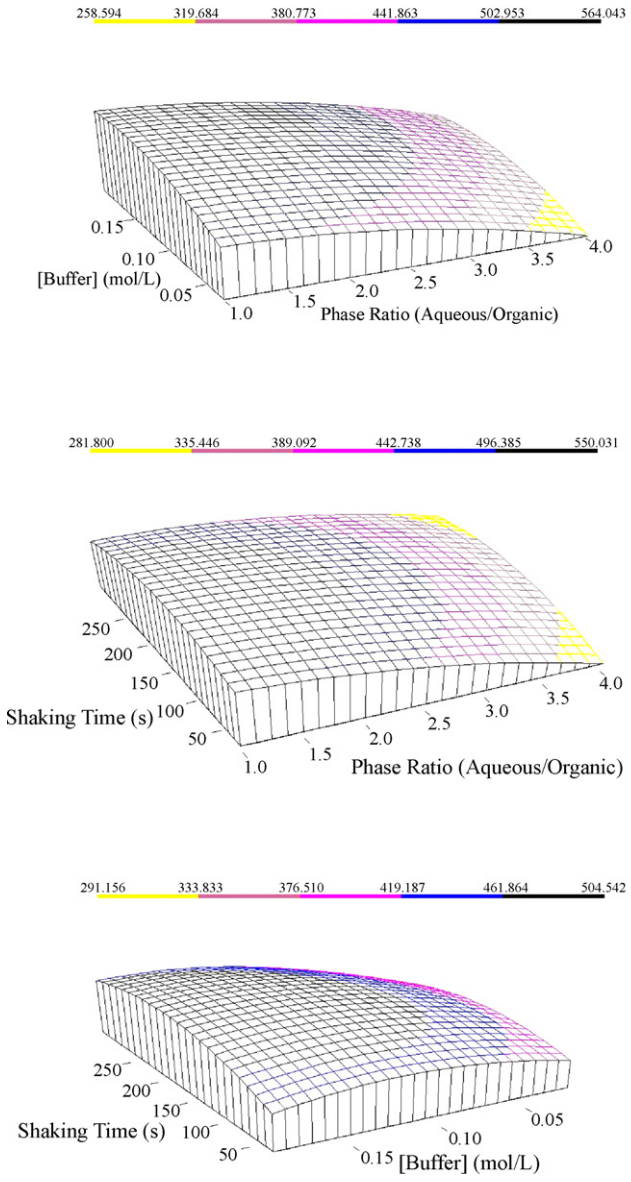


Fig. 4. Estimated response surfaces for each pair of variables.

Table 3
Optimization of the extractive procedure (results from the ANOVA of effects contributing to the model (by RSM))

Effect	Sum of squares	d.f.[a]	Mean square	*F*-ratio	*p*-value[b]
A ([Buffer])	11750	1	11750	6.614	0.0422
B (Shaking time)	362.705	1	362.705	0.204	0.6673
C (Phase ratio)	47950	1	47950	26.981	0.0020
AB	1128	1	1128	0.635	0.4561
AC	17.645	1	17.645	0.009929	0.9239
BC	167.952	1	167.952	0.09451	0.7689
AA	2359	1	2359	1.327	0.2931
BB	4562	1	4562	2.567	0.1602
CC	2055	1	2055	1.156	0.3235
Total error	10660	6	1777		
Total (corrected)	77260	15	5150		

[a] Degrees of freedom.
[b] Effect is declared significant if *p*-value <0.05.

Table 4
Piceid concentration found by the extractive-derivative-photoinduced-fluorescence method and by HPLC [32] in the validation stage

Method	[Piceid] ($\mu g\,mL^{-1}$)		
	Young red wine	Barrel-aged red wine	White wine
Extractive-derivative-photoinduced-fluorescence[a]	0.75 ± 0.11	0.84 ± 0.14	0.17 ± 0.03
HPLC[b]	0.72 ± 0.05	0.76 ± 0.08	0.20 ± 0.01

[a] Standard addition (three additions by triplicate).
[b] Average ± standard deviation ($n = 3$).

the determination of *trans*-piceid in these conditions are summarized in Table 1.

The optimized extractive-photoinduced-fluorescence-derivative method was applied to the analysis of total piceid in wine samples. Young and barrel-aged red wine and white wine pools were analyzed in order to representing the commonest interferences in any future wine analysis. The standard addition method was applied in any case on the diluted wine samples by adding them increasing volumes of a *trans*-piceid ethanolic stock solution before irradiating, and the correspondent plots analytical signal *vs* added concentration of *trans*-piceid, were constructed. The slopes comparison test was applied between these plots and the constructed by extracting irradiated standards of *trans*-piceid without wine, and it was found that there was matrix effect, and the standard addition method is necessary in order to eliminate it.

Lastly, in order to improve the simplicity and speed of the method it was proven that the standard addition can be carried out on the final hydroethanolic reconstituted solution, by adding successively small volumes of a *trans*-piceid standard solution irradiated in the same conditions as the diluted wine samples, instead of on separated diluted wine solutions before extracting. We have found that these two calibration plots, taking into account the recovery percentage in the extraction, have similar slopes, which involves that the matrix effect does not occur in the extraction nor in the photoreaction stage, but in the fluorescence measure. This means that a single extraction is necessary per wine sample, and the results are not altered.

The concentrations of piceid in wines, calculated taking into account the 61% extraction recovery, are summarized in Table 4 in comparison with those calculated by a HPLC method with isocratic elution (C18 column; mobile phase: acetonitrile/acetic acid (10%, v/v)/water, 19/33/48, v/v/v, $0.8\,mL\,min^{-1}$) and photochemical pre-column derivatization and fluorescence detection ($\lambda_{exc/em}$ 260/364 nm), developed by the authors [32], in the validation stage.

4. Conclusions

It has been demonstrated that a very weakly fluorescent analyte has been photochemically converted into highly fluorescent products. Based on literature data [35], it is possible that phenanthrene derivatives to be originated as a result of the UV-irradiation of piceid solutions. The complete structural elucidation for these photoproducts is a new challenge for the future research work of this group. It has been proposed a new, simple, fast and inexpensive method for the determination of piceid in wine by second-derivative-photochemically induced fluorescence coupled with liquid–liquid extraction. The optimization of the variables involved in the extraction procedure by using chemometric tools (Central Composite Design and Response Surface Methodology) gives good results. The accuracy of the proposed method has been validated by comparison with a chromatographic method developed by the authors and it has been applied successfully to different wine samples. Limits of detection (according to Clayton criteria [34]) five times lower than the better reported [18] (S/N = 3) have been achieved. Better precision (% RSD) values than ours have been previously reported [14] when precision is evaluated at higher concentration levels ($\mu g\,mL^{-1}$). Although a previous clean-up stage is needed, the solvent used is rapidly eliminated, which implies a fast analysis, so the spent time in the whole procedure, is comparable to the expended time in the fastest reported HPLC methods, when sample preparation is not necessary [15,17,19].

Acknowledgements

The authors acknowledge to *Ministerio de Educación y Ciencia* (Project: CTQ2005-02389) for financial support. Diego Airado Rodríguez is grateful to the *Consejería de Infraestructura y Desarrollo Tecnológico de la Junta de Extremadura* for a fellowship (DOE 22/06/04). Dra. Dolores López Soto (*Viñaoliva S.C.*) is also acknowledged for providing wine samples.

References

[1] R.M. Lamuela Raventós, A.L. Waterhouse, Methods Enzimol. 299 (1999) 184.
[2] J.L. Robichaud, A.C. Noble, J. Sci. Food Agric. 53 (1990) 343.
[3] G. Mazza, Crit. Rev. Food Sci. Nutr. 35 (1995) 341.
[4] R.M. Lamuela Raventós, A.I. Romero Pérez, A.L. Waterhouse, M.C. de la Torre Boronat, J. Agric. Food Chem. 43 (1995) 281.
[5] J.F. Moreno-Labanda, R. Mallavia, L. Pérez-Fons, V. Lizama, D. Saura, V. Micol, J. Agric. Food Chem. 52 (2004) 5396.
[6] Y. Kimura, H. Ohminami, H. Okuda, K. Baba, M. Kozawa, S. Arichi, Planta Med. 49 (1983) 51.
[7] Y. Kimura, H. Okuda, S. Arichi, Biochim. Biophys. Acta 834 (1985) 275.
[8] M.I. Chung, C.M. Teng, K.L. Cheng, F.N. Ko, C.N. Lin, Planta Med. 58 (1992) 274.
[9] F. Orsini, F. Pelizzoni, L. Verotta, T. Aburjai, C.B. Rogers, J. Nat. Prod. 60 (1997) 1082.
[10] C. Shan, S. Yang, H. He, S. Shao, P. Zhang, Acta Pharmacol. Sin. 11 (1990) 527.
[11] J.M. Mérillon, B. Fauconneau, P. Waffo, L. Barrier, A. Decendit, F. Huguet, Proceedings of the 18th International Conference on Polyphenols; Polyphenols Communications 96, Bordeaux (France), 1996.
[12] H. Arichi, Y. Kimura, H. Okuda, K. Baba, M. Kozawa, S. Arichi, Chem. Pharm. Bull. 30 (1982) 1766.
[13] A.M. Hackett, The metabolism of flavonoid compounds in mammals, in: V. Cody, E. Middleton Jr., J.B. Harborne (Eds.), Plant Flavonoids in Biology and Medicine, Liss, New York, 1986, pp. 177–194.
[14] M.T. Ribeiro de Lima, P. Waffo-Téguo, P.L. Teissedre, A. Pujolas, J. Vercauteren, J.C. Cabanis, J.M. Mérillon, J. Agric. Food Chem. 47 (1999) 2666.
[15] J. Burns, T. Yokota, H. Ashihara, M.E.J. Jean, A. Crozier, J. Agric. Food Chem. 50 (2002) 3337.

[16] X. Vitrac, A. Bornet, R. Vanderline, J. Valls, T. Richard, J.C. Delaunay, J.M. Mérillon, P.L. Teissédre, J. Agric. Food Chem. 53 (2005) 5664.
[17] M. Abert Vian, V. Tomao, S. Gallet, P.O. Coulomb, J.M. Lacombe, J. Chromatogr. A 1085 (2005) 224.
[18] X. Vitrac, J.P. Monti, J. Vercauteren, G. Deffieux, J.M. Mérillon, Anal. Chim. Acta 458 (2002) 103.
[19] P. Jeandet, A.C. Breuil, M. Adrian, L.A. Weston, S. Debord, P. Meunier, G. Maume, R. Bessis, Anal. Chem. 69 (1997) 5172.
[20] M.N. Bravo, S. Silva, A.V. Coelho, L. Vilas Boas, M.R. Bronze, Anal. Chim. Acta 563 (2006) 84.
[21] C. Domínguez, D.A. Guillén, C.G. Barroso, J. Chromatorgr. A 918 (2001) 303.
[22] M.A. Pozo-Bayón, M.T. Hernández, P.J. Martín-Álvarez, M.C. Polo, J. Agric. Food Chem. 51 (2003) 2089.
[23] V. Brandolini, A. Maietti, P. Tedeschi, E. Durini, S. Vertuani, S. Manfredini, J. Agric. Food Chem. 50 (2002) 7407.
[24] J.P. Roggero, J. Food Comp. Anal. 13 (2000) 93.
[25] G.E.P. Box, K.B. Wilson, J. R. Stat. Soc. B 13 (1951) 1.
[26] D.C. Montgomery, Design and Analysis of Experiments, second ed., Wiley, New York, 1984.
[27] Unscrambler v. 6.11b, CAMO A/S Olav Tryggvasonsgt, N-7011, Trondheim, Norway.
[28] R.F. Wilson, G.W. Lester, Talanta 10 (1963) 319.
[29] J. Cao, G.H. Chen, Y.S. Du, F.F. Hou, Y.L. Tian, J. Liquid Chromatogr. Rel. Technol. 29 (2006) 1457.
[30] J.P. Roggero, C. García-Parrilla, Sci. Aliments 15 (1995) 411.
[31] T. Galeano Díaz, I. Durán Merás, D. Airado Rodríguez, Anal. Bioanal. Chem. 387 (2007) 1999.
[32] T. Galeano, I. Duran-Merás, D. Airado, J. Sep. Sci., in press.
[33] G.L. Long, J.D. Winefordner, Anal. Chem. 55 (1983) 712.
[34] C.A. Clayton, J.W. Hines, P.D. Elkins, Anal. Chem. 59 (1987) 2506.
[35] Y.-H. Chen, Y.-L. Cheng, C.-H. Lin, J. Chromatogr. A 943 (2002) 287.

Available online at www.sciencedirect.com
ScienceDirect
Talanta 74 (2008) 578–585
Talanta
www.elsevier.com/locate/talanta

Highly sensitive and selective catalytic determination of formaldehyde and acetaldehyde

Ashraf A. Mohamed [a,b,*], Ahmed T. Mubarak [a], Zakaria M.H. Marestani [a], Khaled F. Fawy [a]

[a] *Department of Chemistry, Faculty of Science, King Khalid University, Abha 9033, Saudi Arabia*
[b] *Department of Chemistry, Faculty of Science, Ain Shams University, Abbassia, Cairo 11566, Egypt*

Received 11 March 2007; received in revised form 1 May 2007; accepted 16 June 2007
Available online 22 June 2007

Abstract

A highly sensitive, simple and selective kinetic method was developed for the determination of ultra-trace levels of formaldehyde and acetaldehyde based on their catalytic effect on the oxidation of *N*,*N*-diethyl-*p*-phenylenediamine (DPD) with hydrogen peroxide. The reaction was monitored spectrophotometrically by tracing the formation of the red-colored oxidized product of DPD at 510 nm, within 30 s of mixing the reagents. The optimum reaction conditions were: 20 mmol L^{-1} DPD, 250 mmol L^{-1} H_2O_2, 150 mmol L^{-1} phosphate, 150 mmol L^{-1} citrate and pH 6.60 ± 0.05 at 25 °C. Following the recommended procedure, formaldehyde and acetaldehyde could be determined with linear calibration graphs up to 0.50 and 1.4 μg mL^{-1} and detection limits, based on the $3S_b$-criterion, of 0.015 and 0.035 μg mL^{-1}, respectively. In addition, analytical data for other 10 aldehydes were also presented. The high sensitivity and selectivity of the proposed method allowed its successful application to rain water, mainstream smoke (MSS) and disposed tips of smoked cigarettes (DTSC). A sample aliquot was directly analyzed for its total water-soluble aldehyde content. A second sample aliquot was heated at 80 °C for 10 min to expel acetaldehyde and the aliquot was analyzed for its content of other water-soluble aldehydes (expressed as formaldehyde equivalent), and acetaldehyde was determined by difference. The analytical results were in excellent agreements with those obtained following the standard HPLC method based on pre-column derivatization with 2,4-dinitrophenylhydrazine. Moreover, published catalytic-spectrophotometric methods for the determination of aldehydes were reviewed.
© 2007 Elsevier B.V. All rights reserved.

Keywords: Catalytic determination of acetaldehyde and formaldehyde; *N*,*N*-Diethyl-*p*-phenylenediamine-H_2O_2 redox reaction; Rain water; Mainstream smoke and disposed cigarette tips

1. Introduction

Formaldehyde and acetaldehyde are ubiquitous components of the environment that have been identified in food, beverages, vehicle exhaust and in wastes from various industries, especially those based on open burning and incineration of gas, fuel oil and coal [1]. Nevertheless, tobacco smoke represents a significant source of exposure to formaldehyde and acetaldehyde for a majority of the general population. Analysis of mainstream smoke (MSS) is one of the most challenging tasks for an analytical chemist as MSS is an extremely complex mixture that contains trace concentrations of about 4000 organic and inorganic chemical constituents [2,3].

Therefore, sensitive determination of formaldehyde and acetaldehyde is receiving increased interests in environmental and biochemical studies due to their relatively high adverse effects. Low concentrations of formaldehyde and/or acetaldehyde can cause irritation of the eyes, nose, throat and skin. However, higher levels are carcinogenic to human and animals [4–8]. Therefore, the National Institute for Occupational Safety and Health (NIOSH) considered formaldehyde as immediately dangerous to life and health at 24 mg m^{-3} (20 μg mL^{-1}), and recommended an exposure limit of 90 μg m^{-3} (0.016 μg mL^{-1}) HCHO [8]. Moreover, the International Program on Chemical Safety (INCHEM) adopted a 90 μg m^{-3} (0.05 μg mL^{-1}) concentration as the odor threshold for acetaldehyde [6].

A number of instrumental procedures have been utilized for the determination of formaldehyde and acetaldehyde in different samples based on spectrophotometric [8], spectrofluorimetric [9–11], chemilumenscence [12,13], HPLC [8,14,15] and GC techniques [2,7,8]. However, the reaction

* Corresponding author. Tel.: +20 104998054; fax: +20 24831836.
E-mail address: aamohamd@hotmail.com (A.A. Mohamed).

0039-9140/$ – see front matter © 2007 Elsevier B.V. All rights reserved.
doi:10.1016/j.talanta.2007.06.020

with chromotropic acid in concentrated sulfuric acid medium was adopted as a standard spectrophotometric method for the determination of 0.02–4.00 μg mL^{-1} HCHO [8]. Moreover, the HPLC method based on pre-column derivatization with 2,4-dinitrophenylhydrazine was adopted as an other standard for the determination of 0.012–2.00 and 18.00–372.00 μg mL^{-1} HCHO and CH_3CHO, respectively [8]. On the other hand, catalytic spectrophotometric methods offer low-cost, simple and highly sensitive alternatives for the determination of trace levels of environmental pollutants [16–18], but formaldehyde and acetaldehyde received relatively little attention. To date, few papers reported the kinetic determination of formaldehyde based on its reaction with a dye [19,20], or its catalytic effect on the oxidation of a substrate with a suitable oxidant [21–33] and only one paper reported the determination of 0.20–10.0 μg mL^{-1} acetaldehyde based on its inhibitory effect on the malachite green-sulfite reaction [34]. However, the limited sensitivity and/or selectivity are common disadvantages [21–34].

On the other hand, *N*,*N*-diethyl-*p*-phenylenediamine (DPD) was adopted as a reagent for the conventional determination of Cr(VI) [35], Mn(III, IV) [36], sulphide [37] and chlorine [7,38,39]. Also, it was applied to the catalytic determination of H_2O_2 [40,41], Co(II) [42], Fe(III) and phosphate [43] and V(V) [44] ions based on their effects on the DPD reactions with peroxidase [40,41], H_2O_2 [42,43] and ClO_3^- ions [44], respectively.

The current paper describes an original method for the low-cost, highly sensitive and selective catalytic determination of trace levels of formaldehyde and/or acetaldehyde. The method was successfully applied to rain water, mainstream smoke (MSS) and disposed tips of smoked cigarette (DTSC). Moreover, published kinetic-spectrophotometric methods for the determination of formaldehyde were reviewed (Table 1) revealing that the proposed method is one of the highest sensitivity methods among the available literature for catalytic spectrophotometric determination of formaldehyde and acetaldehyde.

Table 1
Comparison of dynamic ranges and detection limits of kinetic spectrophotometric methods for formaldehyde determination

Reaction system	Dynamic range (detection limit) (μg mL^{-1})	References
Ethyl green-SO_3^{2-}	1.00–20.00[a]	[19]
Pararosaniline + SO_3^{2-}	0.05–0.25	[20]
Bordeaux R + ClO_3^-	0.02–0.50[a]	[21]
Rhodamine 6G + ClO_3^-	0.02–1.80[a]	[22]
Butyl rhodamine B + ClO_3^-	0.02–0.27[a]	[23]
Sulfonazo III + BrO_3^-	0.005–2.80[a]	[24]
Gallocyanin + BrO_3^-	0.50–7.00[a]	[25]
Methyl orange + BrO_3^-	0.00–0.16[a]	[26]
Ethyl orange + BrO_3^-	0.10–1.50[a]	[27]
Methylene blue + BrO_3^-	0.48–5.60[a]	[28]
Crystal violet + BrO_3^-	0.018–1.40[a]	[29]
2,5-Diaminotoluene + H_2O_2	(110.0)	[30]
4-Aminodiphenylamine + H_2O_2	(50.0)	[30]
1,4-Phenylenediamine + H_2O_2	50.0–500.0	[31]
	3.0–300.0	[32]
	0.05–0.25[b]	[33]
N,*N*′-Dimethyl-*p*-phenylenediamine + H_2O_2	50.0–500.0	[31]
N,*N*-Diethyl-*p*-phenylenediamine + H_2O_2	0.00–0.500 (0.015)	This work

[a] Methods based on decolorization of a dye.
[b] Measurements were made in a 10.0 cm cell.

2. Experimental

2.1. Apparatus and reagents

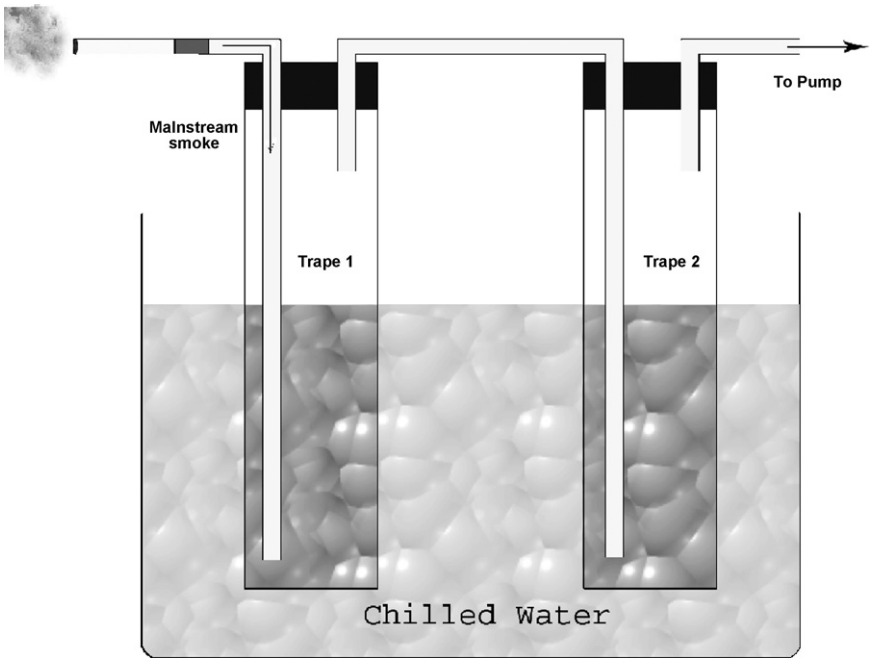
Absorbance measurements were made on a Shimadzu UV-1601 PC spectrophotometer (Kyoto, Japan), equipped with a Shimadzu CPS 240A thermostated multi-cell positioner with a temperature stability of ±0.1 °C, using 10 mm matched cells. Eppendorf vary-pipettes (10–100 and 100–1000 μL) were used to deliver accurate volumes. pH measurements, with an accuracy of ±0.01, were made on a calibrated Hanna pH-mV meter model 211. A thermostated water bath, GFL 1003 type (Burgwedel, Germany), with an accuracy of ±0.1 °C, was also used. Ultra-pure water was daily prepared using a Barnstead Nanopure diamond water purification system (Dubuque, IA, USA), and was used throughout. All glassware and storage bottles were soaked in 10% HNO_3 overnight and thoroughly rinsed with water prior to use.

Unless otherwise stated, all chemicals were of analytical reagents grade and were purchased from Merck (Darmstadt, Germany), Aldrich (Milwaukee, WI, USA) or Fluka (Buchs, Switzerland).

Stock standard aqueous solutions of 1000 μg mL^{-1} formaldehyde, 1000 μg mL^{-1} acetaldehyde and 3.75 mol L^{-1} H_2O_2 were prepared [7,8]. A working buffer mixture was prepared by dissolving 75 mmol of each of citric acid and Na_2HPO_4 in about 80 mL of water, adjusting the pH to 6.60 ± 0.05 with dil. NaOH/HCl and diluting to the mark in a 100 mL measuring flask. A 50 mL reagent-masking agent working solution was daily prepared containing 100 mmol L^{-1} DPD and 0.17 mmol L^{-1} *N*,*N*,*N*′,*N*′-tetramethylethylenediamine sulfate (Fluka, Switzerland), wrapped with an aluminum foil and kept at 4 °C when not in use.

2.2. Treatment of rain water for the determination of water-soluble aldehydes

A collected rain water sample was filtered through a 0.45 μm membrane filter and promptly analyzed to avoid losses of acetaldehyde. A sample aliquot was analyzed following the recommended procedure. An other aliquot (100 mL) was heated in a water bath at 80 °C with occasional shaking for 10 min to expel acetaldehyde, cooled under running tap water, completed to the mark in a 100 mL volumetric flask, analyzed following the recommended procedure and the concentration of the remaining water soluble aldehydes was calculated and expressed as a formaldehyde equivalent; whereas the acetaldehyde concentration was determined by difference. For validation, a third aliquot was analyzed following the standard HPLC method based on the pre-column derivatization with 2,4-dinitrophenylhydrazine [8].



Scheme 1.

2.3. Collection and treatment of MSS and DTSC for the determination of water-soluble aldehydes

A simple homemade smoking apparatus was constructed as shown in Scheme 1 and was used to collect MSS and DTSC. Each trap tube (25 mm × 200 mm, 70 mL capacity) contained about 35 mL of chilled water. Just after smoking five cigarettes, the two trap solutions containing the water soluble fraction of aldehydes in MSS were combined, filtered through a 0.45 μm membrane filter, diluted to 500 mL in a volumetric flask and sample aliquots were promptly analyzed (to avoid losses of acetaldehyde) as described in Section 2.2.

Five tips of smoked cigarettes were freshly collected, added to a 100 mL chilled water in a 150 mL stoppered quick-fit conical flask and placed in an ultrasonic bath at 10 ± 5 °C for 5 min. Then, the tips were squeezed several times with a glass rod and the solution was filtered through a 0.45 μm membrane filter. The filtrates and washings were combined in a 500 mL measuring flask and sample aliquots were analyzed as described in Section 2.2.

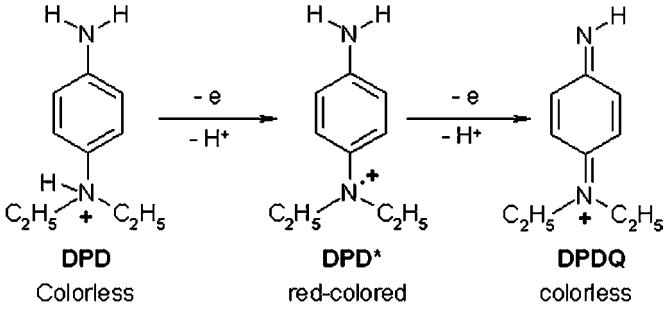
2.4. Recommended procedure

The working solutions, unknown sample solutions, and ultrapure water were kept at 25 °C in the thermostated water-bath for 10 min to attain the equilibrium temperature. Transfer ≤1600 μL of a sample aliquot to one of the thermostated spectrophotometric cells and dilute with water to 1600 μL. Add 600 μL of the working buffer mixture, 600 μL of the working DPD reagent-masking solution and 200 μL of the working H_2O_2 solution. Mix well using a disposable Eppendorf tip and record the absorbance (A)–time (t) graph at 510 nm against water as a reference, allowing a lag time of 5 s. The rate can be calculated from the slope of the initial linear part of the A–t graph, within 30 s of pressing the start button of the spectrophotometer. The acetaldehyde concentration and the formaldehyde equivalent of an unknown sample were determined from the calibration equations, similarly prepared with the working standard acetaldehyde or formaldehyde solutions.

3. Results and discussion

3.1. Preliminary considerations

In the presence of H_2O_2, *N*,*N*-diethyl-*p*-phenylenediamine (DPD) is first oxidized to a red-colored semiquinonoid cationic radical, DPD* (Wurster's dye) that is further oxidized in the presence of an excess oxidant to a colorless quinonediimine derivative DPDQ (Scheme 2) [45], where DPD* showed strong absorption maxima at 510 and 552 nm in the visible region of the spectrum (Fig. 1), with the former peak exhibiting a slightly higher sensitivity. Preliminary experiments showed that, the positions of the two bands did not change with varying pH or reagent's concentrations. Therefore, the studied DPD–H_2O_2



Scheme 2.

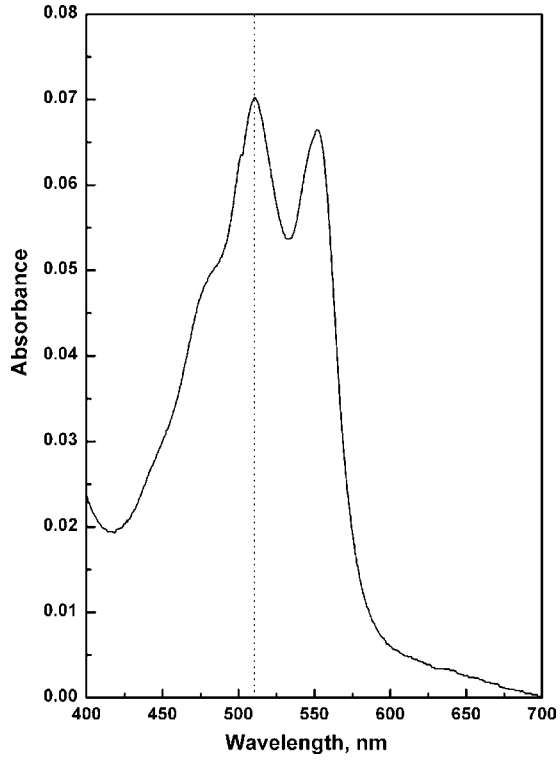


Fig. 1. Absorption spectra for the oxidation of 20 mmol L^{-1} DPD with 250 mmol L^{-1} H_2O_2 in the presence of 0.50 μg mL^{-1} HCHO, following the recommended procedure, after 2 min of mixing the reagents.

reaction was monitored spectrophotometrically by tracing the oxidized product at 510 nm. Trace levels of formaldehyde and/or acetaldehyde exerted a pronounced catalytic effect on the DPD–H_2O_2 reaction; however, formaldehyde was used for optimization of the reaction variables due to the greater stability of its solutions compared to those of acetaldehyde.

3.2. Effects of pH and buffer concentration

The effect of pH was studied in the range of 5.50–7.70. The initial reaction rates, in the presence (k_c) or absence (k_u) of 0.30 μg mL^{-1} formaldehyde or 0.70 μg mL^{-1} acetaldehyde, increased gradually with pH. However, the sensitivity ($k_c - k_u$) attained an almost constant value at pH ≥ 6.45 (Fig. 2a). Therefore, a pH of 6.60 ± 0.05 was adopted in the recommended procedure to give a low blank value. A mixed phosphate–citrate buffer was used because of its remarkable masking effects towards transition metal ions and as it gave very good sensitivity ($k_c - k_u$).

The effects of 0–350 mmol L^{-1} concentrations of each of citrate and phosphate buffers on the reaction rates were studied at pH 6.60 ± 0.05. The reaction rates k_c and k_u gradually decreased with citrate concentrations up to 150 mmol L^{-1} citrate; whereas the sensitivity ($k_c - k_u$) remained almost constant at concentrations ≥50 mmol L^{-1} citrate (Fig. 2b). Therefore, 150 mmol L^{-1} citrate was adopted in the recommended procedure to provide a low blank value. On the other hand, the reaction rates and the sensitivity gradually increased with phosphate concentrations up to 150 mmol L^{-1} phosphate (Fig. 2c). Therefore, a 150 mmol L^{-1} phosphate concentration was adopted in the recommended procedure to provide a moderate blank value and a high sensitivity. The dependence of the sensitivity values ($k_c - k_u$) on phosphate concentrations indicates a typical activating effect of phosphate ions.

3.3. Effect of DPD concentration

The reaction rates and the sensitivity gradually increased with DPD concentration up to 20 mmol L^{-1}; thereafter, the sensitivity attained an equilibrium value (Fig. 2d). Therefore, a concentration of 20 mmol L^{-1} DPD was adopted in the recommended procedure to provide a high sensitivity and a low reagent blank.

3.4. Effect of H_2O_2 concentration

The rates k_c and k_u gradually increased with H_2O_2 concentration; however, the sensitivity ($k_c - k_u$) increased very slowly at concentrations of 200–500 mmol L^{-1} H_2O_2 (Fig. 2e). Therefore, an H_2O_2 concentration of 250 mmol L^{-1} was adopted in the recommended procedure to provide a high sensitivity and a low reagent blank.

3.5. Effect of temperature

The reaction rates and the sensitivity gradually increased with temperature (Fig. 2f); however, a temperature of 25 °C was adopted in the recommended procedure because of its convenience for operation and its relatively low blank value. The activation energies were calculated from linear regression analysis of *Arrhenius* plots. The activation energy for the uncatalyzed reaction was 14.58 kcal mol^{-1}, whereas that for the reaction catalyzed by 0.300 μg mL^{-1} HCHO was 11.42 kcal mol^{-1}, showing efficient catalysis.

3.6. Effects of the order of addition and standing time

A reversed order of addition in which H_2O_2 was added before the buffer mixture or DPD solutions gave lower rate values, probably because of a partial oxidation of HCHO with the high local concentration of H_2O_2. Moreover, k_c slightly decreased with increasing the standing time before addition of H_2O_2. Namely, a standing time of 1, 5 and 10 min resulted in 2, 10 and 15% reduction in the nominal rate value, respectively, with a proportional increase in the initial absorbance readings. This may be attributed to partial consumptions of DPD and/or HCHO in side reactions other than the catalyzed oxidation process. Therefore, any undue delay between additions of reagents was avoided.

3.7. Effects of interfering species

Effects of the possible interfering species, which may accompany HCHO and CH_3CHO in natural-water, waste-water or tobacco smokes were investigated in the determination of 0.100 μg mL^{-1} HCHO or 0.300 μg mL^{-1} CH_3CHO, following the recommended procedure. Table 2 shows the maximum tolerable concentrations of 94 foreign species

where, a species was considered as a serious interferent when it gave a determination error of more than 5%. Except for Cu(II) ions, all the tested species were tolerated to a great extent without any pre-treatment. The use of the mixed citrate–phosphate buffer conferred enhanced selectivity for the proposed method. But, strong masking agents such as ethylenediaminetetraacetic acid (EDTA), diethylenetriaminepentaacetic acid (DTPA), 8-hydroxyquinoline (oxine), 1,10-phenanthroline, diethyldithiocarbamate, thioacetamide, or α-benzoinoxime could not successfully eliminate the overall positive interferences of Cu(II) and Fe(III) ions. All of these masking agents succeeded with Cu(II) but greatly enhanced the catalytic effect of Fe(III). However, 20 μg mL^{-1} *N*,*N*,*N*′,*N*′-tetramethylethylenediamine sulfate successfully eliminated the serious interference of 0.10 μg mL^{-1} Cu(II) and 0.10 μg mL^{-1} Fe(III) ions as shown in Table 2.

Despite of its simplicity and high sensitivity, the most interesting feature of the implemented method is its selectivity, especially towards ketones, alcohols, organic acids and transition metal ions that are known to react with DPD, catalyze its oxidation process [35–44] and/or interfere in the determination of aldehydes.

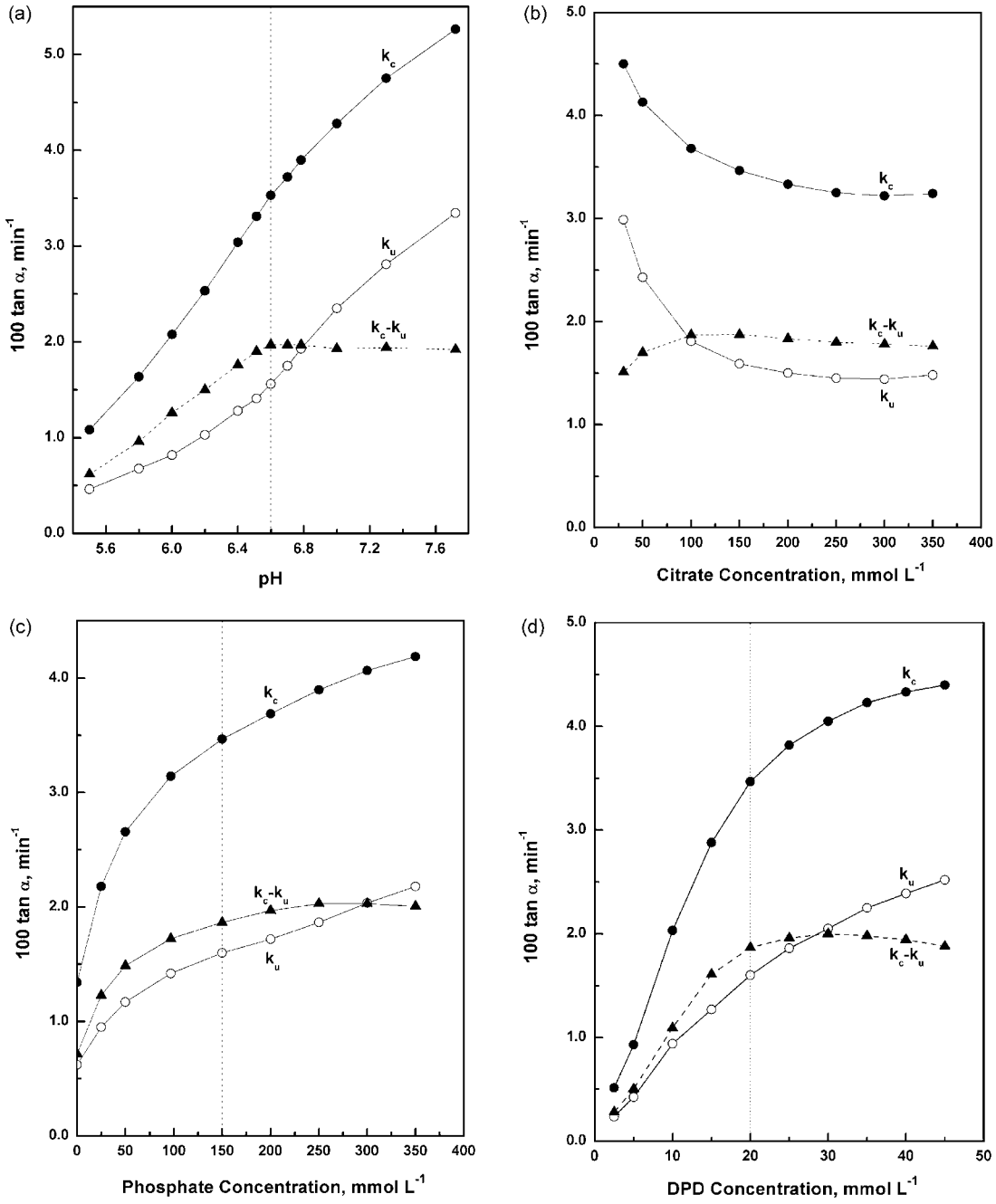


Fig. 2. Effects of reaction variables. Except for the abscissa variable, conditions were those given in the recommended procedure, in the presence (k_c) or absence (k_u) of 0.30 μg mL^{-1} HCHO or 0.70 μg mL^{-1} CH_3CHO.

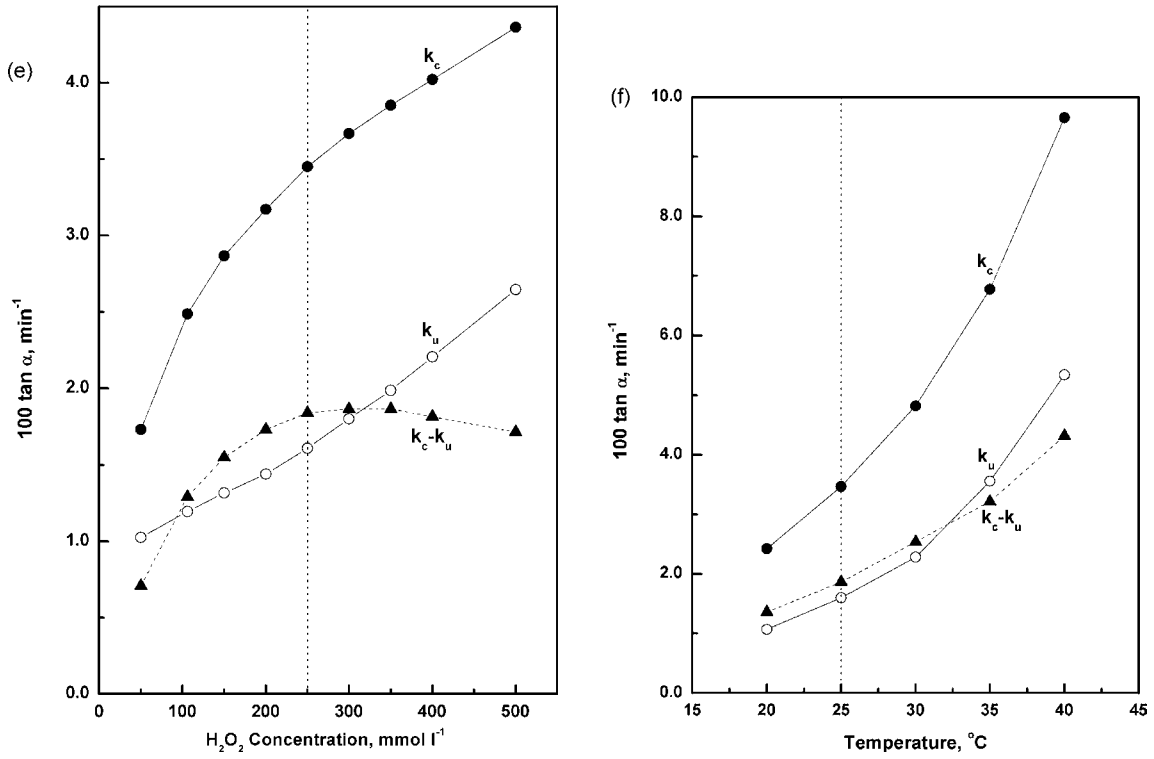


Fig. 2. (*Continued*).

Table 2
Tolerance levels of foreign species in the determination of 0.10 μg mL^{-1} formaldehyde or 0.30 μg mL^{-1} acetaldehyde[a]

Tolerance level (μg mL^{-1})	Foreign species[b]
≥1000	Acetone, 2-butanone, ethanol, methanol, *n*-propanol, glycerol, acetate, formate, propionate, tartrate, glucose, HCO_3^-, Cl^-, $B_4O_7^{2-}$, SO_4^{2-}, Li^+, Na^+, K^+, NH_4^+
≥100	Nicotine, phenol, resorcinol, salicylate, benzoate, urea, chloralhydrate, 8-hydroxyquinoline, *t*-butanol, acetophenone, benzophenone, diethyldithiocarbamate
≥20	*N*,*N*,*N*′,*N*′-Tetramethylethylenediamine, phenanthroline, oxalate, α-benzoinoxime, sulfamate, thioacetamide, catechol, F^-, Br^-, ClO_4^-, NO_3^-, Be(II), Ca(II), Mg(II), Pb(II), Zn(II), Al(III), La(III), Ce(III), As(V)
3	DTPA, ethylenediamine, SCN^-, Tl^+, Hg(II), Cd(II), Mn(II), Ni(II), As(III), Bi(III)
1	NO_2^-, Ag^+, Sn(IV), Ti(IV), Zr(IV), Hf(IV), Th(IV), Nb(V), Ta(V), Mo(VI), W(VI), U(VI)
0.2	EDTA, I^-, S^{2-}, Sn(II), Cr(III), V(IV)
0.1	SO_3^{2-}, $S_2O_5^{2-}$, Co(II), Cu(II)[c], Fe(II), Fe(III), Rh(III), Re(IV)
0.02	Pd(II), Pt(II), Ru(III), Au(III), V(V)
0.01	Cr(VI), Mn(VII)
0.001	Cu(II)

[a] Reaction conditions were those given in the recommended procedure.
[b] The pH of solutions of interfering species exhibiting buffering actions was adjusted to 6.60 ± 0.10 before studying their effects. Ethanol was used to dissolve water-insoluble species.
[c] In the presence of 20 μg mL^{-1} *N*,*N*,*N*′,*N*′-tetramethylethylenediamine as a masking agent.

3.8. Calibration graphs and detection limits

The oxidation of DPD with H_2O_2 is a slow process that was found to be catalyzed by trace level concentrations of aliphatic aldehydes; especially formaldehyde and acetaldehyde. Following the optimum conditions of the recommended procedure, linear calibration graphs ($r^2 \geq 0.995$) were obtained for formaldehyde, acetaldehyde and other seven water-soluble aliphatic aldehydes in addition to three water-sparingly soluble aromatic aldehydes (Table 3). The 12 calibration graphs can be described

Table 3
Analytical characteristics for the determination of aldehydes following the proposed method[a]

Aldehyde	Linear range (μg mL^{-1})	Slope (*X*)	Detection limit (μg mL^{-1})
Formaldehyde	0.00–0.50	6.22	0.015
Acetaldehyde	0.00–1.40	2.70	0.035
Propionaldehyde	0.00–1.20	2.44	0.040
Acroline	0.00–2.70	1.57	0.06
Glyceraldehyde	1.00–18.00	0.40	2.50
n-butraldehyde	0.00–1.45	1.60	0.06
Iso-butraldehyde	0.05–1.30	1.85	0.055
Crotonaldehyde	0.05–1.15	2.61	0.04
Glyoxal	0.00–2.60	0.78	0.13
Benzaldehyde[b]	0.20–9.50	0.29	0.35
Salicylaldehyde[b]	4.00–27.00	0.08	1.25
Cinnamaldehyde[b]	1.00–25.00	0.11	1.00

[a] The linear regression's equation of calibration graphs have the general formula: 100 tan α (min^{-1}) = 1.60 + slope [aldehyde conc., μg mL^{-1}].
[b] Ethanol was used to prepare the stock solutions.

Table 4
Determination of acetaldehyde and formaldehyde in complex environmental samples

Sample		Added[a]		Acetaldehyde found[b] ± S.D. ($n=5$)			Formaldehyde found[b] ± S.D. ($n=5$)		
No.	Type	CH_3CHO	HCHO	Proposed method	*R*%	Standard method[c]	Proposed method	*R*%	Standard method[c]
1	Rain water[d]	–	–	–	–	–	0.425 ± 0.011	–	0.430 ± 0.015
		0.500	0.250	0.490 ± 0.015	98	0.485 ± 0.017	0.673 ± 0.014	99.5	0.670 ± 0.016
2	Tips of smoked	–	–	63.1 ± 1.9	–	63.5 ± 2.1	38.7 ± 1.4[e]		
	L&M lights cigarettes	100.0	50.0	164.2 ± 3.4	101.1	–	87.9 ± 2.1[e]	98.4	
3	Tips of smoked	–	–	110.7 ± 2.8	–	109.2 ± 3.5	32.9 ± 1.2[e]		
	Rothmans cigarettes	100.0	50.0	208.9 ± 4.5	98.2	–	83.1 ± 2.2[e]	100.4	
4	MSS from L&M	–	–	840.2 ± 22.1	–	845.2 ± 26.1	26.8 ± 0.9[e]		
	Lights cigarettes	500.0	50.0	1340.0 ± 30.6	100.0	–	76.5 ± 2.0[e]	99.4	
5	MSS from	–	–	1030.9 ± 25.4	–	1026.9 ± 32.1	31.6 ± 1.1[e]		
	Rothmans cigarettes	500.0	50.0	1518.6 ± 29.5	97.5	–	82.4 ± 2.3[e]	101.6	

S.D., standard deviation; *R*%, recovery%.
[a] Added to sample solution just after collection and before any further treatment.
[b] Expressed in $\mu g\,mL^{-1}$ (for rain water) or μg cigarette^{-1} (for MSS and DTSC) samples.
[c] Standard HPLC method based on pre-column derivatization with 2,4-dinitrophenylhydrazine, Ref. [8].
[d] Collected on 30 January 2007 on the roof of King Khalid University, Abha, KSA.
[e] Formaldehyde equivalent.

by a linear regression equation having the general formula:

$$100 \tan\alpha\,(\text{min}^{-1}) = 1.60 + X\ [\text{aldehyde}]$$

where X is the slope and square brackets represent the aldehyde concentration in $\mu g\,mL^{-1}$. The detection limits were calculated as three times the standard deviation of the blank divided by the slope of the respective calibration graph ($3S_b$-criterion [46]).

The precision of the method was assessed according to the IUPAC recommendations [46] by analyzing 0.05, 0.10, 0.30 and 0.50 $\mu g\,mL^{-1}$ HCHO and 0.10, 0.30, 0.70, 1.0 and 1.40 $\mu g\,mL^{-1}$ CH_3CHO in aqueous solutions that gave quantitative recoveries of ≥99.1%, where the within-run (inter-day) R.S.D.'s were ≤1.8% ($n=5$) and the between-run (intra-day) R.S.D.'s were ≤2.3% ($n=5$) and the Student's t-test values were ≤2.1, showing that the t-test could not detect any systematic error and revealed the high accuracy and precision of the proposed method (the tabulated t-value for the 95% confidence level and $n=5$ is 2.78 [46]).

3.9. Separation of acetaldehyde from formaldehyde

Carbonyls are among the 15 classes of organic compounds identified in MSS [2,3]. However, in real samples of air, rain water and mainstream smoke (MSS), acetaldehyde and formaldehyde are the two most abundant aldehydes while other aldehydes may have low contributions, if any [1–3]. To analyze the extremely complex matrix of MSS for acetaldehyde and formaldehyde it was necessary to separate acetaldehyde based on its high volatility. Thus, when test tubes containing 10 mL aqueous solutions of 0.10, 0.70 and 1.40 $\mu g\,mL^{-1}$ CH_3CHO were heated on a water-bath for 10 min at 35, 50, 65 and 80 °C, cooled under running tap water, completed to the mark in 10 mL volumetric flasks, and analyzed following the recommended procedure, it gave recoveries of 83, 48, 9 and 0%, respectively. However, similar treatments of aqueous solutions of 0.05, 0.25 and 0.50 $\mu g\,mL^{-1}$ HCHO gave average recoveries of ≥97.4% over the entire temperature range studied; an observation that was attributed to the high stability of aqueous formaldehyde solutions. Therefore, in the recommended procedure, MSS was collected in chilled water while avoiding any undue delay between sampling and analysis to minimize the possible losses of acetaldehyde by volatilization. Moreover, two aqueous sample aliquots were analyzed; the first aliquot gave the total water soluble aldehyde content, while the second aliquot was heated in a water bath at 80 °C with occasional shaking for 10 min to quantitatively expel acetaldehyde and the concentration of the remaining water soluble aldehyde fraction was expressed as a formaldehyde equivalent; whereas the acetaldehyde concentration was determined by difference. (The formaldehyde equivalent is calculated as the net rate value divided by the slope of the calibration graph for HCHO; i.e., formaldehyde equivalent = [(rate value − 1.60)/6.22].)

3.10. Application of the proposed method to complex environmental samples

The sensitivity and selectivity of the developed method prompted us to directly analyze complex environmental samples of rain water, MSS and DTSC without any pre-concentration or laborious separation steps and the data are given in Table 4. It is worthy to mention that, these data could not be correlated with those obtained following the standard chromotropic acid method adopted by NIOSH [8] as the latter method would gave very high results due the strong interference of NO_x and/or NO_2^- ions; therefore, the analytical results were validated by comparison with the standard HPLC method [8]. The obtained analytical results gave quantitative recoveries (97.5–101.6%) and were in excellent agreements with those obtained with the standard HPLC method showing the validity and reliability of the proposed method to analyze complex environmental sample.

4. Conclusion

A simple, low-cost highly sensitive and selective method is proposed for the determination of trace levels of formaldehyde and acetaldehyde based on their catalytic effect on the H_2O_2 oxidation of *N*,*N*-diethyl-*p*-phenylenediamine in a mixed phosphate-citrate buffer medium. The advantageous sensitivity and selectivity make the proposed method a favorable competitive to the NIOSH standard spectrophotometric method [8] and the previously published kinetic spectrophotometric methods for the determination of formaldehyde and acetaldehyde.

Acknowledgements

This work was supported by a grant in aid (No. AT 22-80) from King Abdulaziz City for Science and Technology. This is gratefully acknowledged.

References

[1] R.E. Kirk Othmer, Kirk Othmer Encyclopedia of Chemical Technology, 5th ed., John Wiley, New York, 2004.
[2] X. Lu, J. Cai, H. Kong, M. Wu, R. Hua, M. Zhao, J. Liu, G. Xu, Anal. Chem. 75 (2003) 4441.
[3] A. Rodgman, C.R. Green, Beitr. Tabakforsch. Int. 20 (2003) 481.
[4] ATSDR, Agency for Toxic Substances and Disease Registry: U.S. Department of health and human services, Toxicological profile for formaldehyde, Atlanta, Georgia, 1999.
[5] H. Lovschall, M. Eiskjaer, D. Arenholt-Bindslev, Toxicol. In Vitro 16 (2002) 63.
[6] International Program on Chemical Safety: http://www.inchem.org/documents/ehc/ehc/ehc167.htm.
[7] E. Greenberg, L.S. Clesceri, A.D. Eaton (Eds.), Standard Methods for the Examination of Water and Waste-water, 20th ed., American Public Health Association, Washington, DC, 2000.
[8] National Institute for Occupational Safety and Health, NIOSH Manual of Analytical Methods, 4th ed., Department of Health and Human Services, NIOSH, Cincinnati, OH, USA, 1994.
[9] P. Sritharathikhun, M. Oshima, S. Motomizu, Talanta 67 (2005) 1014.
[10] K. Motyka, P. Mikuska, Anal. Chim. Acta 518 (2004) 51.
[11] H.L.C. Pinheiro, M.V. de-Andrade, P.A. de-Paula-Pereira, J.B. de-Andrade, Microchem. J. 78 (2004) 15.
[12] B.X. Li, M.L. Liu, Z.J. Zhang, C.L. Xu, Anal. Sci. 19 (2003) 1643.
[13] Z.H. Song, S.A. Hou, Int. J. Environ. Anal. Chem. 83 (2003) 807.
[14] G. Burini, R. Coli, Anal. Chim. Acta 511 (2004) 155.
[15] J.F. Liu, J.F. Peng, Y.G. Chi, G.B. Jiang, Talanta 65 (2005) 705.
[16] D. Perez-Bendito, M. Silva, Kinetic Methods in Analytical Chemistry, Ellis Horwood, Chichester, 1988.
[17] A.A. Mohamed, A.T. Mubarak, Z.M.H. Marstani, K.F. Fawy, Talanta 70 (2006) 460.
[18] A.T. Mubarak, A.A. Mohamed, K.F. Fawy, A.S. Al-Shihry, Microchim. Acta 157 (2007) 99.
[19] S.L. Feng, J. Fan, A.J. Wang, X.G. Chen, Z.D. Hu, Anal. Lett. 37 (2004) 2545.
[20] M. Pedrero-Munoz, F.J. Manuel-de-Villena-Rueda, L.M. Polo-Diez, Anal. Quim. 86 (1990) 49.
[21] L.Q. Tian, A.M. Zhang, Fenxi-Ceshi Xuebao 22 (2003) 107.
[22] L.Q. Tian, A.M. Zhang, L.Q. Tian, J.Y. Zhai, Fenxi-Shiyanshi 23 (2004) 63.
[23] A.M. Zhang, L.Q. Tian, Fenxi-Kexue Xuebao 20 (2004) 519.
[24] A.A. Ensafi, E. Honarmand, Anal. Sci. 21 (2005) 545.
[25] Z.Q. Zhang, H.T. Yan, X.F. Yue, Microchim. Acta 146 (2004) 259.
[26] X.Q. Lai, G.T. Luo, J. Xue, Fenxi Kexue Xuebao 22 (2005) 87.
[27] J. Fan, A.J. Wang, S.L. Feng, F.L. Cui, Fenxi-Shiyanshi 23 (2004) 13.
[28] X.Q. Zhan, M.J. Lei, Lihua-Jianyan, Huaxue-Fence 38 (2002) 433.
[29] S.H. Wang, L.Y. Du, A.M. Zhang, Fenxi-Huaxue 28 (2000) 628.
[30] N.C. Santiris, N.P. Evmiridis, Quim. Anal. 15 (1996) 301.
[31] B.W. Bailey, J.M. Rankin, Anal. Chem. 43 (1971) 782.
[32] N.P. Evmiridis, N.C. Sadiris, M.I. Karayannis, Analyst 115 (1990) 1103.
[33] T. Perez-Ruiz, C. Martinez-Lozano, V. Tomas, F.J. Carrion, Int. J. Environ. Anal. Chem. 53 (1993) 195.
[34] A. Afkhami, H. Parham, M. Rezaei, Anal. Lett. 33 (2000) 527.
[35] M.H. Zhang, Q.R. Zhang, Z. Fang, Z.C. Lei, Talanta 48 (1999) 369.
[36] D. Johnson, B. Chiswell, Talanta 40 (1993) 533.
[37] M.O. Babiker, J.A.W. Dalziel, Anal. Proc. 20 (1983) 609.
[38] British Standards, BS 6068, Section 2.26, 1986, p. 10.
[39] B.J. Johnson, D.W. Emerson, L.M. Song, J. Floyd, B. Tadepalli, Analyst 124 (1999) 1853.
[40] H. Bader, V. Sturzenegger, J. Hoigne, Water Res. 22 (1988) 1109.
[41] M. Fukushima, K. Tatsumi, Talanta 47 (1998) 899.
[42] A. Malahoff, I.Ya. Kolotyrkina, L.K. Shpigun, Analyst 121 (1996) 1037.
[43] R.P. Igov, T.G. Pecev, G.Z. Miletic, J. Serb. Chem. Soc. 51 (1986) 277.
[44] V. Jaromir, F. Jaroslav, Sb. Vys. Sk. Chem. Technol. Praze, Anal. Chem. 5 (1969) 25.
[45] L. Michaelis, M.P. Schubert, S. Granick, J. Am. Chem. Soc. 61 (1939) 1981.
[46] J. Inczedy, T. Lengyel, A.M. Ure, IUPAC Compendium of Analytical Nomenclature: Definitive Rules, Blackwell Science Inc., 1998.

Available online at www.sciencedirect.com
ScienceDirect
Talanta 74 (2008) 632–641
Talanta
www.elsevier.com/locate/talanta

Determination of vinegar acidity by attenuated total reflectance infrared measurements through the use of second-order absorbance-pH matrices and parallel factor analysis

J. Moros [a], F.A. Iñón [b], S. Garrigues [a,*], M. de la Guardia [a]

[a] *Department of Analytical Chemistry, Universitat de València, Edifici Jeroni Muñoz, 50th Dr. Moliner, 46100 Burjassot, Valencia, Spain*
[b] *Research and Development, JENCK S.A., Av. Álvarez Thomas 228 Buenos Aires (CCP1427), Argentina*

Received 17 January 2007; received in revised form 14 June 2007; accepted 25 June 2007
Available online 15 August 2007

Abstract

Univariate (zero-order), multivariate (first-order) and multiway (second-order) calibrations were assayed for the determination of vinegar acidity using a mechanized procedure based upon vibrational spectroscopy and the emerging multicommutation methodology. The second-order methodology relies on the use of a flow system based on multicommutation and binary sampling. The flow network comprises a set of three-way solenoid valves, computer-controlled to provide facilities to handle the sample and to generate a time-dependent pH gradient using two carrier solutions. The procedure is based on the volumetric fraction variation approach that maintains the same volume of sample solution and dynamically varies its pH. The analysis of second-order absorbance-pH matrices was performed using parallel factor analysis (PARAFAC). Results were compared with first-order absorbance data analyzed with linear calibration and partial least squares regression (PLS) and they were employed for a discussion of the relative advantages of the applied chemometric tools. As excellent accuracy is obtained without the need of any sample pre-treatment, the procedure can be fully mechanized (i.e., by means of an auto-sampler device).

Accuracy of the different strategies assayed was assessed by comparing the results achieved with those obtained by titration reference procedure.
© 2007 Elsevier B.V. All rights reserved.

Keywords: Infrared; Multicommutation; Second-order calibration; Parallel factor analysis (PARAFAC); Partial least square (PLS); Vinegars; Acetic acid

1. Introduction

The Codex Alimentarius (1987) Commission of FAO/WHO joint commission defined vinegar as a liquid fit for human consumption, produced from a suitable raw material of agricultural origin, containing starch, sugars or starch and sugars, by the process of double fermentation, alcoholic and acetous, that can constrains a specified amount of acetic acid.

The United States Food and Drug Administration (FDA) require that any product called "vinegar" contain at least 4% acidity. The Codex standard proposed a minimum of 6% for wine vinegar and 5% for others because the percent of acetic acid present in the product varies according to what they are made from. Vinegars also contain other components, such as esters, and possibly small amounts of sugars, thus the determination of acidity cannot distinguish between true vinegar and a product made by dilution of synthetic acetic acid [1].

In this paper we have explored the possibilities of attenuated total reflectance Fourier transform infrared (ATR-FT-IR) spectroscopy for the quality control of commercially available vinegars. As vibration of the C=O of esters and carboxylic acid are overlapped [2], the use of different chemometric techniques was evaluated.

Different methodologies have been published for the determination of acetic acid in vinegars, such spectrophotometry using a fiber-optic sensor with a dye-modified chitosan/poly(vinyl alcohol) [3], capillary electrophoresis and ion-exclusion chromatography with conductimetric detection [4], liquid chromatography and gas chromatography [5], titration system with spectrophotometric detection at 480 nm [6] and by the use of a disposable voltammetric cell using three pencil leads as working, reference, and counter electrodes [7].

* Corresponding author. Tel.: +34 96 354 3158; fax: +34 96 354 4838.
E-mail address: salvador.garrigues@uv.es (S. Garrigues).

0039-9140/$ – see front matter © 2007 Elsevier B.V. All rights reserved.
doi:10.1016/j.talanta.2007.06.046

However, in spite of the general use of IR techniques in the food industry in recent decades; no reference about the acetic acid determination using any vibrational procedure was found in the literature.

In the present work, a multicommutation-ATR-FT-IR procedure based on the generation of a pH gradient, obtained by mixing dynamically sodium hydroxide and hydrochloric acid solutions, was developed for acetic acid determination in commercial vinegar samples. This procedure presents many advantages as low-reagent consumption and the ability to handle various reagent solutions employing a multiple pumping channel. Moreover two important characteristics related to the chemometric analysis of second-order bilinear spectroscopic data methodologies were achieved in our method: (i) better robustness to the presence of unsuspected constituents in the analysis of complex multi-component samples (achieved through to the so-called second-order advantage which is inherent to second-order data) [8] and (ii) better figures of merit such as prediction errors (more accurate results), precision, sensitivity among others [9], as compared with first-order treatments.

2. Experimental

2.1. Apparatus and reagents

A Bruker Tensor 27 (Bremen, Germany) FT-IR spectrometer equipped with a temperature-stabilized deuterated tryglycine sulfate (DGTS) detector, was employed for spectral measurements, using the in-compartment ATR accessory DuraSamplIR II equipped with a 9 reflection diamond DuraDisk plate (Smiths Detection, Inc., Warrington, England). For instrument control and data acquisition the OPUS program version 4.1 from Bruker was employed. Spectra treatment and data manipulation have been carried out using Omnic 2.1 and OmnicMacros 2.1 software from Nicolet (Madison, WI, USA).

For the multicommutation-ATR-FT-IR measurements, the microvolume liquid cell with clamp (Smiths Detection, Inc., Warrington, England) was attached to the DuraDisk. A Gilson P-2 Minipuls peristaltic pump (Villiers-le-Bel, France) was employed for sample and standards introduction in the measurement cell.

Reaction coils and flow lines were made of polytetrafluoroethylene (PTFE) tubing (i.d. = 0.5 mm). Four NResearch 161T031 three-way solenoid isolation valves (Stow, MA, USA) and a 486 microcomputer equipped with a PCL 711S Advantech electronic interface, were also employed for the multicommutation experiments.

A in lab-software written in QUICKBASIC 4.5 was developed to control solenoid valves program.

Glacial acetic acid (≥99.5%) purchased from Fluka (Barcelona, Spain) was used to prepare standard solutions.

Reagent grade hydrochloric acid 37% and potassium hydroxide pellets were supplied by Scharlau (Barcelona, Spain) and were used to prepare solutions employed as carrier and pH gradient generation in multicommutation.

Potassium hydrogen phthalate primary standard grade for sodium hydroxide solution normalization was purchased from Carlo-Erba (Milan, Italy) and 2% phenolphthalein (Riedel-de Haën) solution in ethanol was used as indicator in the reference titration method.

2.2. Samples and standards

Ten commercial vinegar samples were obtained from the Spanish market, covering an important range of available types of vinegars, such as wine vinegar, sherry vinegar, apple cider vinegar or balsamic vinegar. Table 1 shows a brief description of each sample.

All the evaluated models were based on the use of five synthetic external acetic acid standards in water as calibration set, covering a concentration range from 2.34 to 9.47% (w/v).

2.3. Reference procedure

Commercial vinegar samples were analyzed by titration to determine the total acidity content following the AOAC reference method [10]. In this experiment a NaOH solution normalized with potassium hydrogen phthalate primary standard

Table 1
General description of samples employed in this study

Sample number	Type	Additional components	Acidity (%, w/v)	
			Declared[a]	Titration[b]
1	Wine vinegar	–	6	6.05 ± 0.03
2	Apple cider vinegar	–	5	5.009 ± 0.017
3	Aging wine vinegar	–	8	8.005 ± 0.017
4	Modena balsamic vinegar	Concentrated grape must and natural grape must caramel	6	–
5	White wine vinegar	–	6	6.001 ± 0.017
6	Red wine vinegar	–	6	6.050 ± 0.017
7	Wine vinegar	Garlic	6	6.07 ± 0.03
8	Apple cider vinegar	–	5	4.980 ± 0.017
9	Sherry wine vinegar	–	7	7.100 ± 0.017
10	Wine vinegar	Tarragon	6	6.001 ± 0.017

[a] Total acidity content declared by the manufacturer.
[b] Total acidity content determined by AOAC official method. Data correspond to the average of three independent analysis ± its standard deviation except in the case of Modena balsamic vinegar which cannot be analyzed by the reference procedure.

(ACS), was gradually added to a 5 mL of the vinegar solution. The complete neutralization was observed by the phenolphthalein added indicator color change. Samples were analyzed by triplicate and the average of the three analyses was used as reference value. The mean standard error (pooled standard deviation divided by the average acidity content) was 0.32%.

Apart from the tedious, slow and operator dependent results, one of the main drawbacks of the simple titration technique is that colored samples cannot be directly analyzed. For example sample number 4 need to be decolorized first, if not it will mask the color change of the indicator.

In spite of the fact that in natural vinegar samples we were dealing with mixtures of acids rather than a single one, the general procedure is to quote values in terms of one of the acids (usually the one which predominates). So acidity value was calculated according to:

$$\text{acidity content}\,(\%) = \frac{\text{mass of acetic acid}}{\text{volume of solution}} \times 100$$

2.4. Direct analysis procedure by ATR-FT-IR

Original samples and standards were placed in the same temperature controlled room where the spectrometer was located before to carry out the analysis. The sample compartment temperature was monitored and it remained stable at $26 \pm 1\,^{\circ}C$ during the acquisition of ATR spectra of all analyzed samples.

Any previous chemical treatment on the sample was carried out on-line before filling the ATR cell. Standards and samples were poured directly into the ATR cell and the FT-IR spectra were taken as described below. As all samples were free from appreciable solid material, the effect of the acquisition time and the possible deposition of substances on the ATR cell were not considered necessary to evaluate. This assumption was made based upon previous results reported by our laboratory in a much more complicated matrix, such as natural juices [11], in which no effect on spectra was obtained in the time elapsed for spectra acquisition. In this sense, ensuring a compromise between rapidity, precision and a good signal-to-noise (S/N) ratio to carry out the quantitative analysis of samples using multireflection ATR the following conditions were chosen: sample spectra were scanned between 3800 and 700 cm^{-1} (that corresponds to 1608 digitalized variables), by averaging 32 scans per spectrum with a nominal resolution of 4 cm^{-1}. The acquisition of each averaged spectrum requires 26.4 s.

The background and blank spectra were collected filling the ATR cell with Millipore Q-purified water (Bedford, MA, USA) and using the same instrumental conditions than those employed in the case of samples. Background spectrum was scanned at eight samples interval, while blank spectrum was collected after the measurement of each sample, for assessing that cross-contamination of IR spectra was avoided after cleaning the ATR crystal. It is worthy to note that background spectrum is need to compute FT-IR spectra, while the spectrum of a blank solution is used here only for assessing the absence of cross-contamination.

Both, sample and blank spectra were collected in the absorbance mode. The spectra of the three replicates (subsamples) of each sample were taken by refilling the ATR cell each time.

2.5. Proposed procedure based on multicommutation-ATR-FT-IR

The manifold scheme depicted in Fig. 1 was set up and the experimental steps detailed below were used for developing a multicommutation based on-line procedure able to provide three-way data. These data were obtained by generating in situ a time-dependent pH gradient and by acquiring its FT-IR spectrum at a given sample time interval. A second-order multivariate calibration strategy was followed for data analysis.

The flow network comprises a set of four three-way solenoid valves computer-controlled to provide solutions handling by using a multiple pumping channel. Previously to run the multicommutation measurements ATR-background spectrum was established using a NaOH carrier solution pumped through the flow system.

By means of the configuration indicated in Fig. 1, when the control software started the "analyze program", solenoid valves, V_1, V_2 and V_4 were switched on (energized), thus

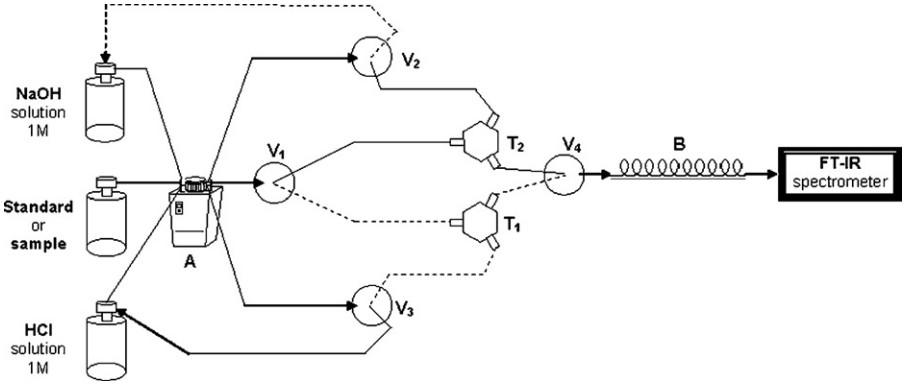


Fig. 1. Manifold employed for the multicommutation ATR-FT-IR determination of vinegar acidity through second-order multivariate calibration. V_1, V_2, V_3, and V_4, three-way solenoid valves; B, mixing coil 22 cm length; A, peristaltic pump; T_1 and T_2, joint points. Solid lines inside the valves symbol indicate the flow pathway when valves are switched on, while dashed lines indicate the flow pathway when valves are switched off.

standard/sample and NaOH solutions flowed to the FT-IR spectrometer after mixing them at the confluence point T_2, while V_3 remained switched off (not energized) and HCl solution was flowed to its storage vessel by a recirculation system.

Following the valves timing course strategy, the solenoid valve V_3 was switched on for a variable time fraction at the same time that V_1, V_2, V_4 were switched off. By this way, standards/sample and hydrochloric acid solutions were merged together through the confluence point T_1.

In this sense, during the displacement towards the spectrometer, the composition of the global solution mixed into the reaction coil B after valve V_4 was linearly varied from 100% of the solution flowing by T_2 (sample/standard plus NaOH) to a 0% (100% of the solution flowing by T_1) in 1 min and then returns to the 100% after another 1 min time interval. Thus, this strategy generates a "V" gradient shape with a 2 min period.

It must be taken into consideration that, in each channel, the dilution factor between the sample and the NaOH solution (or HCl solution) was the same and was controlled through the selection of the i.d. diameter of the lines and the chosen peristaltic tubes and the length of the PTFE tubes connected to V_2 and V_3 valves.

Using the aforementioned strategy, each standard/sample solution was measured at different pH values over time, and thus, different spectra were obtained for each pH value.

Although actual pH values are unknown parameters, it is possible to plot the time spectra series (Fig. 2) recorded for each sample as a function of the spectrum-index number, which in fact depends on the pH of the studied solution.

In this sense, for pH-gradient reproducibility it is essential to ensure time reproducibility, thus justifying the use of multicommutation.

In each case three sample aliquots (replicates) were analyzed by means of the multicommutation system and the corresponding time dependent profile was continuously recorded in the spectral range between 3800 and 700 cm^{-1} by averaging 6 scans per spectrum with a nominal resolution of 8 cm^{-1}. Under these conditions the acquisition of each averaged spectrum requires 3.64 s and the total spectral series was recorded during 2.55 min.

The duration of the pH gradient was selected in order to be able to complete the analysis in about 3 min. It may be argued that this process can be improved by increasing the acquisition time; however, in such case the sample through put will decrease.

Taking into account the time for collecting each averaged spectrum, for each sample/standard solution 43 ATR-FT-IR spectra were obtained for each sample with a 3.6 s time interval.

2.6. Data analysis

Data obtained from OPUS were converted to jcamp-dx file format and analyzed using OmnicMacros 2.1 and TurboQuant Analyst 6.0 software developed by Thermo Nicolet Corp. (Madison, WI, USA) for building the PLS calibration models and, on the other hand, exported in text format and analyzed using Matlab® from The Mathworks Inc. (South Natick, MA, USA) for second-order treatment.

For the evaluation of the different ATR-FT-IR methodologies assayed, several quality indicators were considered. Among them, the mean difference (d_{x-y}) between ATR-FT-IR predicted values ($\hat{C}_i$) and titration reference data (C_i), the standard deviation of mean differences (s_{x-y}), the quality coefficient (QC) value, which gives some indication of the percentage error to be expected for the estimated concentration (see Eq. (1)), and the pooled standard error of prediction for validation samples (s_{reg}) were calculated [12].

$$QC = \sqrt{\frac{\sum_{i=1}^{n}(\hat{C}_i - C_i)^2}{n-1}} \quad (1)$$

where $\hat{C}_i$ is the average predicted value for the three replicates measured for every n samples in the validation set.

Moreover, several figures of model's fit to the data and predictive power, such as Root Mean Square Error of Calibration (RMSEC), and Root Mean Square Error of Prediction (RMSEP)

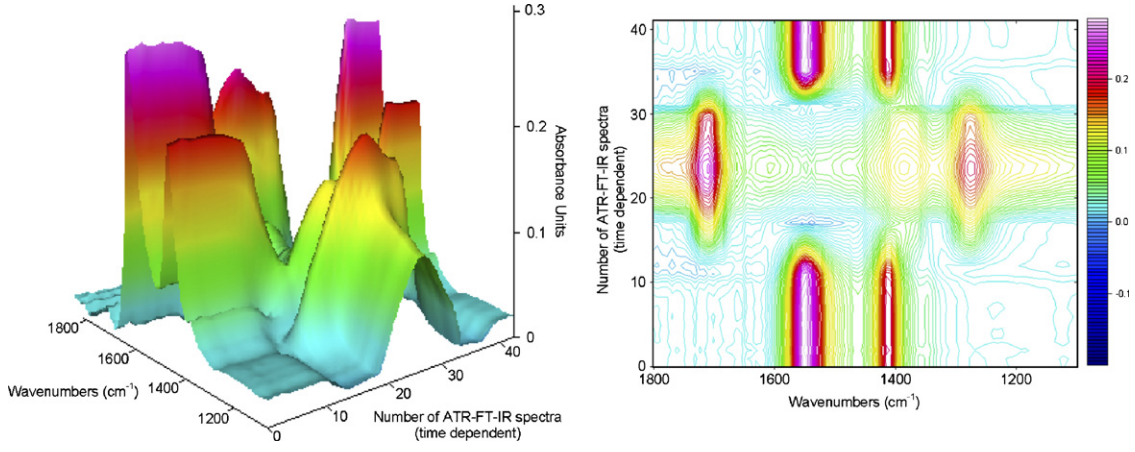


Fig. 2. Typical time dependent spectra series recordings obtained through multicommutation based ATR-FT-IR for an acetic acid in water standard solution of 6.56% (w/v) in the wavenumber range between 1800 and 1000 cm^{-1}. (For more details see the text.)

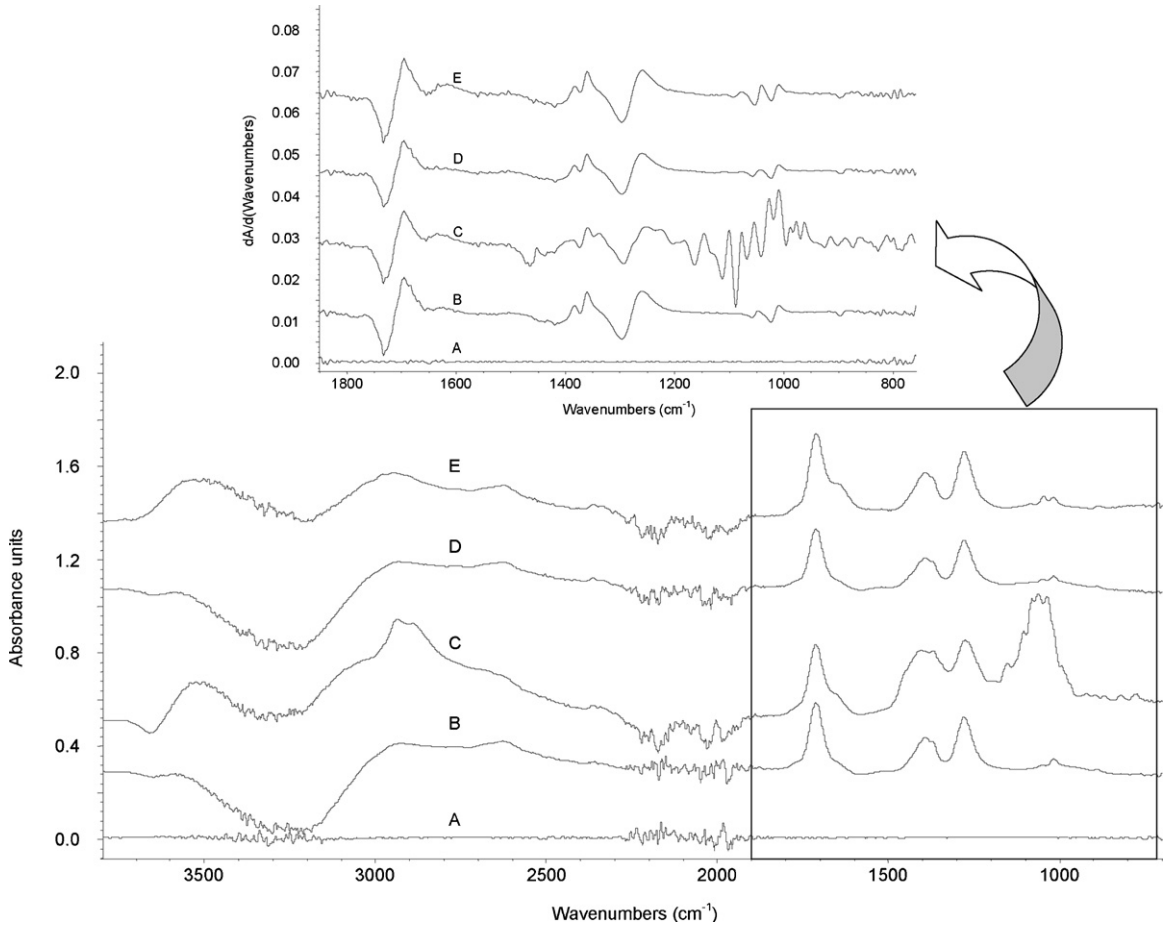


Fig. 3. ATR-FT-IR spectra for some evaluated vinegar samples: Modena balsamic vinegar (C), Red wine vinegar (D) and Sherry wine vinegar (E), compared with a pure acetic acid standard 6.56% (w/v) (B) and a reference blank of Millipore Q-purified water (A), in the wavenumber range from 3800 to 700 cm^{-1}. The inset corresponds to the first derivative spectra in the wavenumber range from 1850 to 750 cm^{-1}. Instrumental conditions: 32 scans averaged per spectrum with a nominal resolution of 4 cm^{-1}. Note: spectra were shift on the *y*-axis to clearly show their bands.

were also used [13]. In all the cases, the scope was to estimate the average deviation of the model from the reference data.

It is beyond the scope of this work to provide any theoretical background in parallel factor analysis (PARAFAC). The interested reader can address the Bro's review [14] for particular details. In fact, second-order calculations were done using MATLAB 6.0.

Appropriate routines for applying PARAFAC, developed by Bro, are available on internet [15], and were implemented through a useful MATLAB graphical interface for easy data manipulation and graphics presentation. This interface also implements other second-order methods, such as, multi-way partial least squares (N-PLS), self-weighted alternating trilinear decomposition (SWATLD) and bilinear least-squares (BLLS), but for this work only PARAFAC, which is one of the methods exploiting the second-order advantage, was considered. Many comparisons between these methods have been published, and in general PARAFAC, performance seems at least equals or better than the other ones [16].

The selection of restricted spectral regions was considered in order to decrease computation time. The number of factors was selected following *core consistency diagnostic* (CORCONDIA) [17] and calibration curves were obtained using the pseudo-univariate calibration graphs strategy [14].

3. Results and discussion

3.1. ATR-FT-IR vinegar spectrum

Fig. 3 shows the ATR-FT-IR spectra for some evaluated vinegars compared with a pure acetic acid standard in water together with a reference blank of Millipore Q-purified water, in the wavenumber range from 3800 to 700 cm^{-1}.

On comparing the ATR spectra of acetic acid standard and raw vinegar samples it can be observed the presence of the main absorption bands of acetic acid, located at 1711 cm^{-1}, assigned to the C=O group, and two bands near 1290 and 1410 cm^{-1} both involving interacting C–O stretch and C–O–H in-plane bending (stretch-open and stretch-bend) [2], which all could be considered suitable for the acidity content determination using a univariate approach.

As it can be appreciate the region between 2317 and 1841 cm^{-1} was not considered, as it was observed that variations in this region can be ascribed to the lack of transparency of the diamond cell.

Table 2
Prediction capabilities of univariate models for the determination of vinegar total acidity by ATR-FT-IR using both, zero-order absorbance and first-order derivative measurements

Parameters	Univariate calibration models				
	Absorbance		First derivative		
	Model A	Model B	Model C	Model D	Model E
Peak area (cm^{-1})	1303–1252	1745–1676	1712–1664	1279–1236	1374–1352
Baseline correction (cm^{-1})	1333	1500	1550	1150	1374
R^2	0.9992	0.9994	0.9994	0.996	0.9990
RMSEC (%, w/v)	0.093	0.081	0.084	0.20	0.10
RMSEP (%, w/v)	0.6	0.4	1.3	1.6	0.5
RRMSEP (%)	10	7	21	26	8
d_{x-y} (%, w/v)	−0.4	0.12	−1.1	−0.6	−0.4
s_{x-y} (%, w/v)	0.5	0.4	0.7	1.5	0.3
QC (%)	11	7	21	28	9
s_{trip} (%, w/v)	0.004	0.009	0.08	0.06	0.09

Note: RMSEC is the Root Mean Square Error of Calibration; RMSEP is the Root Mean Square Error of Prediction and RRMSEP is the RMSEP divided by the mean value of acetic acid concentration in the validation dataset. s_{trip} is the standard deviation of 3 replicates. d_{x-y} and s_{x-y} are the mean difference and the standard deviation of mean differences between predicted and actual acetic acid concentration (%, w/v), respectively. QC is the quality coefficient.

3.2. Univariate (zero-order) approach

In order to choose the best analytical performance of the ATR-FT-IR determination of total acidity in vinegars, the aforementioned bands with the appropriate baseline correction criteria were evaluated using both, zero- and first-order derivative spectra (see inset in Fig. 3). These univariate models were named from A to E. Table 2 summarizes their prediction capabilities.

In terms of sensitivity (results not shown), it is clear that peak area measurements provide at least one order magnitude of better sensitivity than peak height values. So, only the use of peak area absorbance measurement mode was considered.

Moreover, data in Table 3 report the % w/v of acetic acid in all vinegar samples tested using different univariate calibration models built from the direct ATR-FT-IR analysis compared with values obtained by the reference titration procedure.

As it can be appreciate in Table 2, in spite of built models, which show good calibration figures that seem to be suitable for carrying out the determination of acetic acid, data summarized in Table 3 evidence the lack of accuracy for some samples analyzed, possibly due to the signal contributions from other compounds present in the sample.

3.3. Multivariate (first-order) approach

It is well known that in spectrometric analysis the application of first-order multivariate calibration techniques for the analysis of mixture components with strong overlapping spectra is required. In this sense, taking into account the poor results obtained using univariate calibration models, it was assayed the use of a multivariate calibration technique, the partial least squares (PLS) approach, for the treatment of direct measurements based ATR-FT-IR data of vinegar samples. An interesting characteristic of this approach is that calibration can be performed by ignoring the concentrations of all other components except the analyte of interest, in this case the acetic acid concentration.

To build PLS calibration models it was decided to use synthetic standards instead of natural samples. Although this

Table 3
Data of total acidity of vinegar samples obtained by titration and by means direct ATR-FT-IR, using both, zero-order absorbance and first-order derivative measurements

Sample	Titration	ATR-FT-IR acidity (%, w/v)				
		Absorbance		First derivative		
		Model A	Model B	Model C	Model D	Model E
1	6.05 ± 0.03	5.647 ± 0.004	5.728 ± 0.006	5.61 ± 0.10	5.726 ± 0.018	5.49 ± 0.10
2	5.009 ± 0.017	4.5516 ± 0.0016	4.733 ± 0.004	4.72 ± 0.08	4.65 ± 0.04	4.30 ± 0.10
3	8.005 ± 0.017	7.7814 ± 0.0015	8.318 ± 0.004	6.130 ± 0.009	7.921 ± 0.013	7.58 ± 0.03
4	6[a]	4.320 ± 0.009	6.099 ± 0.017	5.45 ± 0.15	1.06 ± 0.04	6.36 ± 0.04
5	6.001 ± 0.017	5.592 ± 0.003	5.681 ± 0.005	5.44 ± 0.10	5.76 ± 0.03	5.48 ± 0.04
6	6.050 ± 0.017	5.607 ± 0.002	5.660 ± 0.017	5.67 ± 0.04	5.791 ± 0.018	5.42 ± 0.12
7	6.07 ± 0.03	6.068 ± 0.003	6.550 ± 0.004	4.36 ± 0.08	6.10 ± 0.13	5.97 ± 0.11
8	4.980 ± 0.017	4.891 ± 0.004	5.434 ± 0.005	3.427 ± 0.014	4.97 ± 0.09	4.74 ± 0.11
9	7.100 ± 0.017	7.11 ± 0.004	7.687 ± 0.011	5.28 ± 0.08	7.50 ± 0.04	6.30 ± 0.09
10	6.001 ± 0.017	6.077 ± 0.004	6.573 ± 0.014	4.26 ± 0.07	6.07 ± 0.06	5.86 ± 0.05

Note: concentration values are the average of three independent analyses ± the corresponding standard deviation.
[a] Declared value.

Table 4
Prediction capabilities of PLS-ATR-FT-IR for the determination of vinegar total acidity

Parameters	Partial least squares models	
	Model F	Model G
Spectral region (cm^{-1})	1811–1174	1510–1120
Baseline correction type	Linear removed	Linear removed
PLS factors extracted	1	1
R^2	0.9998	0.9997
RMSEC (%, w/v)	0.062	0.062
RMSEP (%, w/v)	0.41	0.25
RRMSEP (%)	7	4
d_{x-y} (%, w/v)	−0.10	−0.11
s_{x-y} (%, w/v)	0.4	0.2
QC (%)	7	4.5
s_{trip} (%, w/v)	0.004	0.002

Note: number of factors was selected looking for the best prediction capabilities of the model for the validation set considering a leave-one-out cross-validation. See Table 2 for details about the meaning of the different parameters evaluated.

Table 5
Data of total acidity of vinegar samples obtained by titration and PLS-ATR-FT-IR

Sample	Titration	PLS-ATR-FT-IR acidity (%, w/v)	
		Model F	Model G
1	6.05 ± 0.03	5.723 ± 0.004	5.673 ± 0.003
2	5.009 ± 0.017	4.8305 ± 0.0018	4.707 ± 0.002
3	8.005 ± 0.017	7.691 ± 0.005	7.8908 ± 0.0004
4	6[a]	7.046 ± 0.005	6.1017 ± 0.0010
5	6.001 ± 0.017	5.647 ± 0.002	5.605 ± 0.002
6	6.050 ± 0.017	5.667 ± 0.005	5.631 ± 0.004
7	6.07 ± 0.03	5.8931 ± 0.0008	6.1204 ± 0.0019
8	4.980 ± 0.017	4.897 ± 0.003	5.0645 ± 0.0010
9	7.100 ± 0.017	7.005 ± 0.007	7.225 ± 0.003
10	6.001 ± 0.017	5.894 ± 0.003	6.119 ± 0.003

Note: see Table 3.
[a] Declared value.

decision may arise some disagreement, we are focused in developing a methodology that can be applied without a time consuming calibration procedure. In many of our previous contributions we success in using a reduced calibration set of real samples, selected after a hierarchical cluster analysis, for predicting unknown samples composition [11]. In this contribution we want to go one step further and use a reduced synthetic calibration set for predicting the composition of natural samples. We are aware of the fact that this is a very difficult test for many multivariate models, but we are convinced that it can be considered a very beneficial and important characteristic for routine analysis of end-products.

As PLS is sensitive to the presence of unmodeled interferents, as may happen when dealing with natural samples of complex composition, such as vinegars, the use of synthetic standards should carefully evaluated, for example through the previous selection of different spectral regions.

Although, several spectral regions were tested and different models were built and compared in terms of RMSEP, only the most significant results are summarized below.

Table 4 shows and compares analytical figures of merit of two different PLS-ATR-FT-IR models, named F and G, built to determine acetic acid in vinegars. Mean centering spectra data pre-treatment was employed to eliminate common spectral information in all the cases prior the model development.

The spectral ranges between 1811–1174 cm^{-1} (model F) and between 1510–1120 cm^{-1} (model G), that are equivalent to 331 and 203 variables, respectively, were used for building multivariate calibration models. "Linear removed" baseline correction criterion was employed in both cases. The leave one out cross-validation procedure was used to obtain the best number of latent variables using the predicted residual error sum of squares (PRESS). Based on the aforementioned criterion, for both models 1 PLS factor was enough to explain more than the 98% of the variance in the spectral data. The prediction capability of PLS-ATR-FT-IR models assayed provided RMSEP values slightly better than those found through univariate calibration, but they cannot be considered adequate taking into consideration the level of the analyte in samples under study.

The mean difference (d_{x-y}) of the total acidity and the standard deviation of mean differences (s_{x-y}) data found, were of the same order for the two spectral regions considered. The repeatability of the determination, established from the mean standard deviation of triplicate analysis of the validation set samples was also approximately the same for both, univariate and PLS calibration models (first-order derivative based models not considered). Nevertheless, only the quality coefficient (QC), an estimator for the error of a new result, is better for model G than for model F and univariate models.

The aforementioned data clearly show that the possible presence of different active ingredients in some commercial vinegar samples strongly affect the prediction capability of PLS models at least when a single set of external standards was used to built the calibration. The use of real samples in the calibration set may help to overcome this problem, as it was shown for other complex matrix samples in our previous contributions [11].

Table 5 summarizes data on the acidity content of samples determined by using PLS-ATR-FT-IR models and from the experimental errors found, it can be concluded that ATR-FT-IR data must be processed on using a most powerful methodology suitable to solve the problem of unexpected interferents and thus second-order data treatment [14] was assayed.

3.4. Proposed methodology

In spite of the aforementioned PLS characteristic, all first-order methods, including PLS, are sensitive to the presence of unmodeled components. A good alternative to this problem is to move to second-order data [14], which are particularly suitable for the quantitative analysis of complex multi-component samples (as some "especial" vinegar sample).

The development of the proposed methodology can be divided in two aspects. The first one regarding on the experimental set up, that can produce pH gradients in a flow system with minimum intervention of the analyst. The second related

to the chemometric treatment of the second-order (three-way) data.

For the former aspect, we were inspired by the work presented by Marsili et al. [18] for the determination of antimicrobials in orange juices, in which a sample, previously basified, was introduced in a flow injection system with UV-detection in which an HCl solution was used as carrier.

When using a FT-IR spectrometer as detector, the pH gradient must to be much longer (less sharp) than that required for UV measurements because the time required for acquiring and averaging the obtained spectra is much longer for IR than in the case of UV. For this reason a multicommutation systems was chosen.

On the other hand, with the proposed system, a minimum sample handling is required. Actually, in our case, any samples contain suspended solids. So, samples were directly introduced in the system through the "standard/sample" channel indicated in Fig. 1. A specific procedure was included in the software to self prime the whole flow system. Additional details were already given in Section 2.

Regarding to the chemometric treatment, PARAFAC was chosen as the multiway method to resolve the multi-component mixtures. This iterative algorithm is widely employed as it is considered to be less sensitive to instrumental noise and model deviations, joint to the uniqueness and optimality of its results. The most important prerequisite for the successful application of PARAFAC model in analytical chemistry is, however, that the data arrays should follow the so-called trilinear model [19].

In this case, decomposition of a three-way data array built with response matrices measured for a number of samples is often unique, allowing spectral profiles as well as relative concentrations of individual sample components to be extracted directly (the aforementioned second-order advantage, fully exploited by this algorithm).

In order to reduce the long time required to calculate the models (disadvantage of iterative algorithms), only the spectra between 1800 and 1230 cm^{-1} was considered. This region was chosen taking into account that it comprises the most significant carbonyl absorption bands.

PARAFAC is a decomposition procedure in which a three dimensions (3D) array (comprised by the stacked spectrum of all the calibration samples plus that of the sample to be analyzed) is deconvoluted into three loading matrices (one related to the spectra profile, the other to the time profile – pH variation – and the third to the relative concentration of individual component).

One of the first requirements in order to apply PARAFAC is to determine the optimum number of factors required to deconvolute the 3D array in each vinegar sample. These factors have chemical meaning, that is, can be related to the chemical species that produces the spectral features changes picked up by the 3D data. This analysis can be carried out evaluating the value of the core consistency test of each model [17]. For all the samples the consistency value obtained for the array composed by the 15-calibration plus each sample at time was calculated as a function of the component number. In all the cases the core consistency drops to a negligible value when using three (3) spectral components to model the array, suggesting that 2 is an optimum choice [17]. The spectral profile of each component is quite related to the vinegar spectrum at acid and basic pH (data not shown), that is, the spectrum of acetic acid and that of acetate, respectively.

Table 6
Prediction capabilities of PARAFAC-ATR-FT-IR for the determination of vinegar total acidity

Parameters	PARAFAC
Spectral region (cm^{-1})	1547–1238
Baseline correction type	–
PLS factors extracted	2
RMSEC (%, w/v)	0.150
RMSEP (%, w/v)	0.180
RRMSEP (%)	3.0
d_{x-y} (%, w/v)	0.093
s_{x-y} (%, w/v)	0.15
QC (%)	2.99
s_{trip} (%, w/v)	0.09
s_{reg} (%, w/v)	0.05

Note: see Table 2 for details about the meaning of the different parameters evaluated. s_{reg} is the standard error of prediction.

Absolute analyte concentrations were obtained after proper calibration by employing the calibration set described in Section 2. The procedure involves decomposing the 3D array (formed by joining the spectra of calibration samples and one of the training unknown samples) and it implies that the array decomposition should be repeated for each newly analyzed sample.

Prediction capabilities for PARAFAC for the analysis of multi-component mixtures from the use of single component aqueous standards are listed in Table 6. As it can be seen, in spite that this methodology shows a slightly worse RMSEC value (0.15%, w/v) than that obtained for the best previously univariate (model B) and partial least squares (model G) approaches assayed, the quantitative capabilities of the PARAFAC methodology seem to be better compare to zero- and first-order calibration strategies as given by the RRMSEP or QC values. The RRMSEP was 3%, 4% and 7% for acidity by PARAFAC, partial least squares (model G) and univariate (model B) calibrations, respectively.

Regarding to the precision of the models, established from the pooled standard deviation between replicates, it can be appreciate that PARAFAC shows a s_{trip} value a little bit higher than those provided by either univariate or PLS approaches. This fact may be ascribed to the complexity of the experimental set up, involving the generation of pH gradients, and the possibility of time shifts in the spectra acquisition. Nevertheless this difference can be considered negligible as the standard error of prediction (s_{reg}) of the determination based on PARAFAC, which also permits the study of the precision of the model, was 0.05 (%, w/v).

On the other hand, Table 7 shows the total acidity content values achieved for samples under study by using PARAFAC. As it can be seen there is an excellent agreement between the reference method and the proposed methodology, even for difficult samples such as the Modena vinegar.

3.5. Critical comparison

To compare the performance of the different ATR-FT-IR methodologies assayed, it was used the elliptic joint confi-

Table 7
Data of total acidity of vinegar samples obtained by titration and PARAFAC-ATR-FT-IR

Sample	Titration	PARAFAC-ATR-FT-IR acidity (%, w/v)
1	6.05 ± 0.03	6.35 ± 0.09
2	5.009 ± 0.017	5.19 ± 0.07
3	8.005 ± 0.017	8.07 ± 0.02
4	6[a]	5.87 ± 0.13
5	6.001 ± 0.017	6.30 ± 0.06
6	6.050 ± 0.017	5.94 ± 0.12
7	6.07 ± 0.03	6.10 ± 0.10
8	4.980 ± 0.017	5.07 ± 0.10
9	7.100 ± 0.017	7.26 ± 0.12
10	6.001 ± 0.017	6.03 ± 0.01

Note: see Table 3. Mean value ± s_{trip}.
[a] Declared value.

dent region (EJCR) [20] for the slope and the intercept of the regression line between data found by FT-IR and reference titration results for samples analyzed. Fig. 4 shows the ideal point (1, 0) with the line equation for the proposed methodology, [slope = 0.99 (std. error 0.05), intercept = 0.1 (std. error 0.3)]; PLS-model G, [slope = 1.03 (std. error 0.10), intercept = −0.3 (std. error 0.6)] and univariate model B [slope = 1.131 (std. error 0.16), intercept = −0.7 (std. error 1.0)]. As it can be seen, the proposed methodology performs better than the others, as it yields a narrower ellipsis comprising in it the ideal point.

Although the size of the ellipsis can be related with the precision of the method, it may be argued that it is influenced by the quality of the regression and not only to the precision in the quantification of each sample. Therefore the pooled standard deviation for the triplicate measurement of all the samples was compared. In this case it can be seen that all methods have similar precision and they are also similar to that of the reference method. Nevertheless, only that based on the proposed methodology provide an excellent accuracy when employing synthetic standards of acetic acid as calibration set. This is also confirmed by the better values obtained in PARAFAC-ATR-FT-IR than for other models for indicators such as d_{x-y}, s_{x-y} and QC.

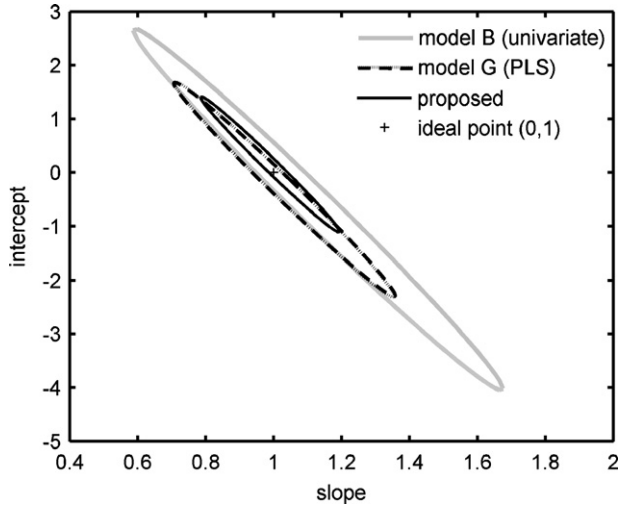


Fig. 4. Elliptic joint confidence test for the slope and intercept obtained from the regression between the concentration data and the reference titration data predicted for the best of each zero-, first- and second-order models built for the total acidity determination by ATR-FT-IR in 10 commercially available vinegar samples.

4. Conclusions

In this work different strategies were evaluated for the determination of the vinegar acidity by means of the use of ATR-FT-IR and chemometric treatment. The main objective of the present work was to keep as far as simple the calibration procedure, by means of the use of a reduced set of synthetic external standard solutions of acetic acid in water, rather than to use natural samples. Although this aspect is a test that many predictive models (mainly those based on standard linear regression and first-order multivariate data) may fail, it can be considered a very beneficial and important characteristic for end-products in routine analysis. In spite of excellent calibration results can be obtained through the use of univariate and first-order multivariate treatment of the FT-IR spectra, prediction results for real samples are not acceptable. Nevertheless, the automated system described herein supplies three-way data which provide accurate results comparable to those obtained by reference methods. As it is supported by the evidence shown above, we greatly succeeded to fulfil this objective.

It was shown that multicommutation methods coupled to three-way chemometric analytical methods can be used for the development of robust sensors for the analysis of acidity in vinegar samples.

Acknowledgements

The authors acknowledge the financial support of the Ministerio de Educación y Ciencia (Project CTQ2005-05604, FEDER) and Direcció General d'Investigació i Transferència Tecnològica de la Generalitat Valenciana (Project ACOMP/2007/131) and Universitat de València (Convocatòria d'Accions Especials, Project UV-AE-20070213).

References

[1] http://www.codexalimentarius.net/.
[2] D. Lin-Vien, N.B. Colthup, W.G. Fateley, J.G. Grasselli, Infrared and Raman Characteristic Frequencies of Organic Molecules, Academic Press, London, England, 1991.
[3] Y. Kurauchi, T. Ogata, N. Egashira, K. Ohga, Anal. Sci. 12 (1996) 55.
[4] R. Castro, M.V.G. Moreno, R. Natera, F. Garcia-Rowe, M.J. Hernandez, C.G. Barroso, Chromatographia 56 (2002) 57.
[5] M. Cocchi, P. Lambertini, D. Manzini, A. Marchetti, A. Ulrici, J. Agric. Food Chem. 50 (2002) 5255.
[6] N. Lenghor, J. Jakmunee, M. Vilen, R. Sara, G.D. Christian, K. Grudpan, Talanta 58 (2002) 1139.
[7] N. Kitamura, A. Kotani, F. Kusu, Bunseki Kagaku 53 (2004) 1097.
[8] K.S. Booksh, B.R. Kowalski, Anal. Chem. 66 (1994) 782A.
[9] A.C. Olivieri, N.M. Faber, J. Ferré, R. Bosqué, J.H. Kalivas, H. Mark, Pure Appl. Chem. 78 (2006) 633.
[10] Association of Official Analytical Chemists—AOAC, Official Methods of Analysis of the Association of Official Analytical Chemists. AOAC Official Method 930.35, vol. 1, 16th ed., AOAC, 1995.
[11] J. Moros, F.A. Iñón, S. Garrigues, M. de la Guardia, Anal. Chim. Acta 538 (2005) 181.

[12] D.L. Massart, B.G.M. Vandeginste, L.M.C. Buydens, S. de Jong, P.J. Lewi, J. Verbeke, Handbook of Chemometrics and Qualimetrics (Part A and B), Elsevier Science B.V., Amsterdam, 1997.
[13] F.A. Iñón, S. Garrigues, M. de la Guardia, Anal. Chim. Acta 513 (2004) 401.
[14] R. Bro, Chemom. Intell. Lab. Syst. 38 (1997) 149.
[15] http://www.models.kvl.dk/source/.
[16] P.C. Damiani, A.J. Nepote, M. Bearzotti, A.C. Olivieri, Anal. Chem. 76 (2004) 2798.
[17] R. Bro, H.A.L. Kiers, J. Chemom. 17 (2003) 274.
[18] N.R. Marsili, A. Lista, B.S. Fernandez Band, H.C. Goicoechea, A.C. Olivieri, J. Agric. Food Chem. 52 (2004) 2479.
[19] R. Bro, J. Chemom. 10 (1996) 47.
[20] A.G. González, M.A. Herrador, A.G. Asuero, Talanta 48 (1999) 729.

Available online at www.sciencedirect.com
ScienceDirect
Talanta 74 (2008) 533–538
Talanta
www.elsevier.com/locate/talanta

Optimization of conditions for the determination of boron by a ruthenium(II) complex having diol moiety: A mechanistic study

Eiko Nakano [a], Satoshi Iwatsuki [b], Masahiko Inamo [c], Hideo D. Takagi [d], Koji Ishihara [a,e,*]

[a] *Department of Chemistry, School of Science and Engineering, Waseda University, Okubo, Shinjuku-ku, Tokyo 169-8555, Japan*
[b] *Advanced Research Institute for Science and Engineering, Waseda University, Okubo, Shinjuku-ku, Tokyo 169-8555, Japan*
[c] *Department of Chemistry, Aichi University of Education, Kariya 448-8542, Japan*
[d] *Inorganic Chemistry Division, Research Center for Materials Science, Nagoya University, Furo-cho, Chikusa, Nagoya 464-8602, Japan*
[e] *Materials Research Laboratory for Bioscience and Photonics, Graduate School of Science and Engineering, Waseda University, Okubo, Shinjuku-ku, Tokyo 169-8555, Japan*

Received 14 May 2007; received in revised form 13 June 2007; accepted 13 June 2007
Available online 22 June 2007

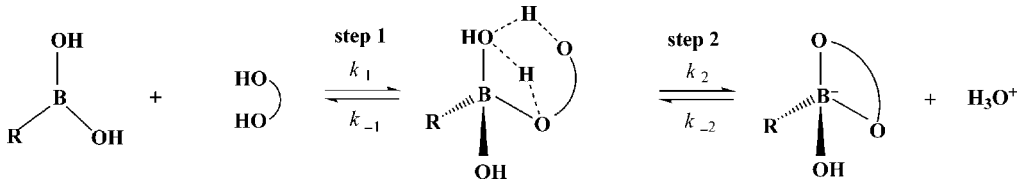
Abstract

Two ruthenium(II) complexes, $[Ru(bpy)_2(dhbpy\text{-}H_{-1})]^+$ and $[Ru(bpy)_2(dhphen)]^{2+}$ (bpy = 2,2′-bipyridine, dhbpy = 3,3′-dihydroxy-2,2′-bipyridine, dhphen = 5,6-dihydroxy-1,10-phenanthroline) were examined for use as a colorimetric reagent for the determination of boron. The reactions of boric acid with these two complexes were thermodynamically and kinetically studied in detail in order to specify the reactive species and to set up optimum condition for the determination of boron. The detailed analysis of the kinetic data for the reaction of the latter water-soluble complex showed that both boric acid and borate ion were reactive in an alkaline solution. The thermodynamically and kinetically optimum pH for the determination of boron was ca. 9 at 25 °C. A spectrofluorimetric determination of boron with the latter complex was attempted at 600 nm with excitation at 360 nm, and at pH 8.9 using CHES (*N*-cyclohexyl-2-aminoethanesulfonic acid) buffer. It was found that a trace amount of boron as low as ca. 2×10^{-5} M (∼1 ppm) could be detectable.
© 2007 Elsevier B.V. All rights reserved.

Keywords: Boric acid; Determination; Complexation; Kinetics

1. Introduction

The complexation of boronic acids $[RB(OH)_2]$ with bidentate ligands (H_2L), e.g., dicarboxylic acids, α-hydroxycarboxylic acids, 1,2-benzenediols, and polyols, proceeds through the two steps as shown in Eq. (1) [1]. In step 1, changes in coordination number from 3 to 4 and in structure from sp^2 to sp^3 occur, and in step 2, ligand substitution on the tetrahedral intermediate occurs to form the chelate complex. We have reported some kinetic studies on the complexations of boric and boronic acids [1–8] including the reaction mechanisms of boric acid with chromotropic acid [2] and H-resorcinol [3] which are used as reagents for the spectrophotometric determination of boron.



(1)

It has been known that the reactivities of bidentate ligands having considerable acidity decrease as the deprotonation of the ligand promotes: $H_2L > HL^- > L^{2-}$ [9,10]. We recently confirmed this order and concluded that at least one proton is necessary for the OH^- of boronic acid in the tetrahedral inter-

* Corresponding author. Tel.: +81 3 5286 3241; fax: +81 3 5286 3241.
E-mail address: ishi3719@waseda.jp (K. Ishihara).

0039-9140/$ – see front matter © 2007 Elsevier B.V. All rights reserved.
doi:10.1016/j.talanta.2007.06.021

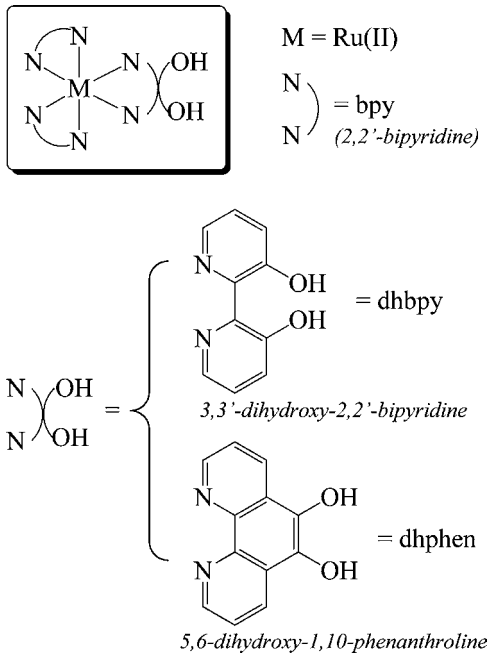


Fig. 1. The structures and abbreviations of the Ru(II) complexes having diol moieties.

mediates (Eq. (1)) to be eliminated smoothly as water forming the final product [1], which indicates that lower pH is favorable, whereas Eq. (1) indicates that higher pH is favorable for complexation because the released proton is neutralized. On the other hand, it is believed that tetrahedral boronate ion in base form reacts much faster than trigonal boronic acid in acid form [11,12]. Recently, we demonstrated based on the detailed kinetic analyses that boronic acid is always a reactive species irrespective of the pH of the solution and the reactivity of the boronate ion is comparable with or less than that of boronic acid even in alkaline solution [8]. In this situation, to optimize the determination condition is indispensable.

We propose here a new strategy for effective boron determination by using a metal complex as detector, because the organic reagents for colorimetric analyses mentioned above have some defects, e.g., slow reaction rate. Recently, a spectrofluorimetric determination of sugars using a Ru(II)–bipyridine complex and boronic acid in aqueous solution was reported [13]. This suggests the possibility of the determination of boron by analogous Ru(II) complexes.

In this study, in order to set up the optimum condition for the determination of boron by the ruthenium(II) complexes having diol moiety (Fig. 1), we performed kinetic and equilibrium investigations for the reaction of boric acid with the ruthenium(II) complexes, and estimated the efficiency of the ruthenium(II) complex reagent for the determination of boron.

2. Experimental

2.1. Reagents

Boric acid was purified as described previously [2]. Sodium hydroxide solution (N/10 and 5N, Kanto Chemical Co. Inc.) was used as received. Sodium perchlorate was purified according to the literature [14]. Doubly distilled water was used for preparation of all aqueous solutions. CHES (*N*-cyclohexyl-2-aminoethanesulfonic acid, Dojindo) was used without further purification.

2.2. Measurements

The ionic strength was adjusted to 0.10 M with sodium perchlorate and sodium hydroxide. For spectral measurements, spectrophotometers (UV2450 and 2550, Shimadzu, Kyoto) and a spectrofluorometer (FP-750, JASCO, Tokyo) were used. The reaction of boric acid with $[Ru(bpy)_2(dhphen)]^{2+}$ was followed at 240 nm or 250 nm by using a stopped-flow spectrophotometer (USP-600, UNISOKU Scientific Instruments, Osaka). The temperature of the solutions was kept constant within ±0.1 °C.

Kinetic measurements were performed under the pseudo first-order conditions of the large excess concentration of boric acid (C_B) compared to that of the Ru complex (C_{Ru}). Under the present experimental conditions ($C_{Ru} \ll C_B < 0.025$ M, pH 7.8–9.5), boric acids exist solely as monomers, $B(OH)_3$ and $B(OH)_4^-$ [15], and the pH of the solution is kept constant due to self-buffering. All the absorbance changes with time were single exponential, for which the conditional pseudo first-order rate constants, k_{obs}, were determined by applying a non-linear least-squares fitting.

In the emission measurements (in the range 540–700 nm, $\lambda_{exc} = 360$ nm) for the boron determination, CHES buffer was used, since the concentration of boric acid was too low to keep constant the pH of the solution. The Ru(II) complex seemed to be light-sensitive in an alkaline solution, so the following procedure was adopted: 0.8 mL of a 0.1 M NaOH solution was added to 3 mL of sample solutions ($C_{Ru} = 4.5 \times 10^{-5}$ M, $C_B = 0$–1.5×10^{-4} M, $C_{NaClO_4} = 0.10$ M, $C_{CHES} = 0.10$ M) just before the measurement, and after waiting for temperature equilibrium (ca. 5 min), spectrofluorimetric measurements were started.

2.3. Synthesis of $[Ru(bpy)_2(dhbpy\text{-}H_{-1})]PF_6 \cdot NaPF_6$

The $[Ru(bpy)_2(dhbpy\text{-}H_{-1})]^+$ complex was prepared based on the reported procedure [16], and purified by column chromatography with acetonitrile/water/saturated aqueous KNO_3 [100/10/<0.5 (v/v/v)] as eluent. The elemental analysis was consistent with the formula, $[Ru(bpy)_2(dhbpy\text{-}H_{-1})]PF_6 \cdot NaPF_6$. The ^1H NMR and absorption data of the isolated complex were consistent with those of the reported complexes, $[Ru(bpy)_2(dhbpy\text{-}H_{-1})]BPh_4$ and $[Ru(bpy)_2(dhbpy\text{-}H_{-1})]PF_6$ [16].

2.4. Synthesis of $[Ru(bpy)_2(dhphen)](PF_6)_2$

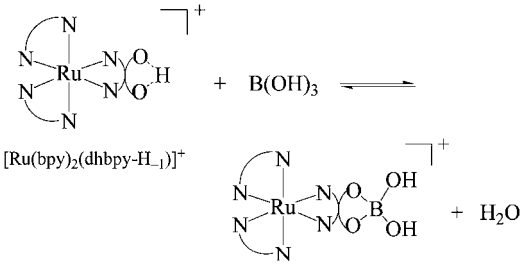
Two preparation methods have been reported for this complex; one is by Shukla and Das [17], and the other is by Murtaza et al. [13]. The latter method was adopted because the complex obtained by the former method was rather unstable. The compound was purified not by column chromatography but

by recrystallization; the complex was dissolved in a minimum amount of acetone, and ether was added slowly to crystallize. The elemental analysis and ^{1}H NMR data of the isolated complex were consistent with those reported [17].

3. Results and discussion

3.1. Reaction of $[Ru(bpy)_2(dhbpy\text{-}H_{-1})]^+$ with boric acid in acetonitrile

Though the reaction of $[Ru(bpy)_2(dhbpy\text{-}H_{-1})]^+$ with boric acid (Eq. (2)) did not substantially proceed in water, they proceeded in organic solvents. This is partially because the original Ru(II) complex is already deprotonated, so its reactivity toward boric acid is substantially decreased as mentioned above. Further, the reverse reaction in Eq. (2) is much more effective compared to the forward reaction in aqueous solution due to water production, whereas in organic media having considerably high dielectric constants such as acetonitrile, the reaction proceeds smoothly to produce water molecule.

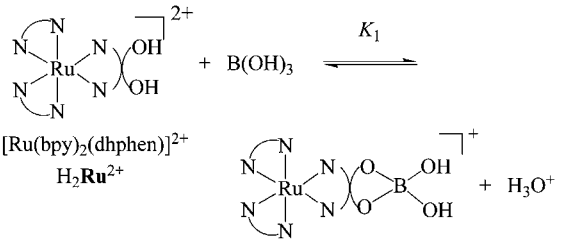


(2)

The UV–vis spectral change with time for the present reaction in acetonitrile is shown in Fig. S1. We also found that emission property changes when the concentration of boric acid increases, as shown in Fig. 2. These results indicate that this Ru(II) complex can be used for the determination of boron. However, it was found that this reaction system has some drawbacks: (i) only a trace amount of the complex dissolves in water, (ii) the rate of the reaction between the complex and boric acid is very slow, (iii) the reaction in acetonitrile is sensitive to the trace water in the reaction medium, (iv) the diol moiety in the complex does not form a five- or six-membered ring during the complex formation with boric acid, and (v) the reaction mechanism is very complicated (see an attempt to analyze the reaction and Figs. S1–S4 in Supporting data). To remove these drawbacks, it is necessary to prepare a Ru(II) complex with (a) a higher formal charge for enhancing water-solubility and (b) a ligand having fully protonated diol moiety.

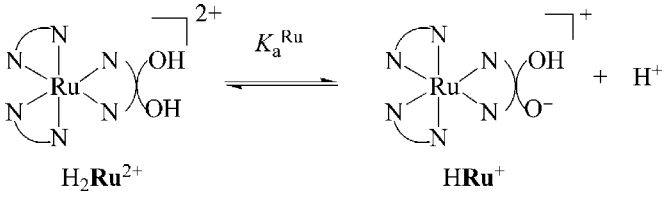
3.2. Reaction of $[Ru(bpy)_2(dhphen)]^{2+}$ with boric acid in water

The synthesized complex, $[Ru(bpy)_2(dhphen)]^{2+}$ (H_2**Ru**$^{2+}$), with higher formal charge (2+) than that of the above-mentioned complex (1+), was water-soluble and the reaction with boric acid (Eq. (3)) proceeded promptly in water as expected.



(3)

At first, the acid dissociation constant (K_a^{Ru}) of the complex (Eq. (4)) was determined spectrophotometrically at 25 °C and I = 0.10 M. Fig. 3 shows the UV–vis spectra of $[Ru(bpy)_2(dhphen)]^{2+}$ at various pHs. From simultaneous analysis of the data at 300–600 nm in Fig. 3 using SPECFIT program [18], K_a^{Ru} was determined to be $pK_a^{Ru} = 8.79 \pm 0.05$.



(4)

Considering the acid dissociation constants of both the $[Ru(bpy)_2(dhphen)]^{2+}$ complex ($pK_a^{Ru} = 8.79$ at 25 °C) and boric acid ($pK_a^B = 8.98$ at 25 °C [19]), the whole reaction has four possible reaction paths under the present conditions (pH 6–11), as shown in Scheme 1.

3.3. Determination of the equilibrium constant K_1

The equilibrium constant (K_1) for Eq. (3) (the first path in Scheme 1) was determined by spectrophotometry at 25 °C and I = 0.10 M. Change in UV–vis spectra with pH which was

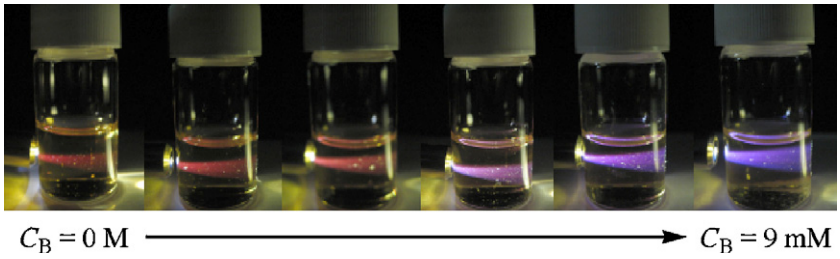


Fig. 2. Change in emission property of $[Ru(bpy)_2(dhbpy\text{-}H_{-1})]^+$ with increasing C_B. $C_{Ru} = 5 \times 10^{-5}$ M.

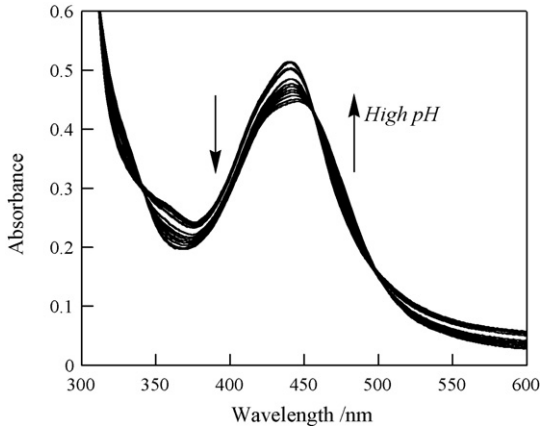


Fig. 3. UV–vis spectra of $[Ru(bpy)_2(dhphen)]^{2+}$ in aqueous solution at various pHs. $C_{Ru} = 5 \times 10^{-5}$ M, pH = 3.93–10.45, $I = 0.10$ M, and $T = 25\,^{\circ}C$.

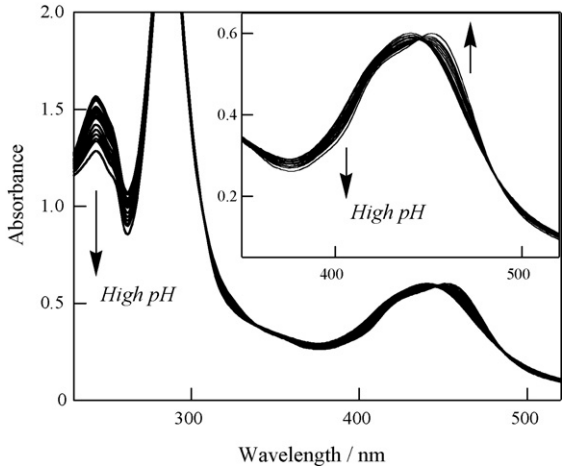


Fig. 4. UV–vis spectra of the reaction mixture of $[Ru(bpy)_2(dhphen)]^{2+}$ and boric acid at various pHs. $C_{Ru} = 4.70 \times 10^{-5}$ M, $C_B = 1.26 \times 10^{-3}$ M, pH = 5.70–9.68, $I = 0.10$ M, and $T = 25\,^{\circ}C$.

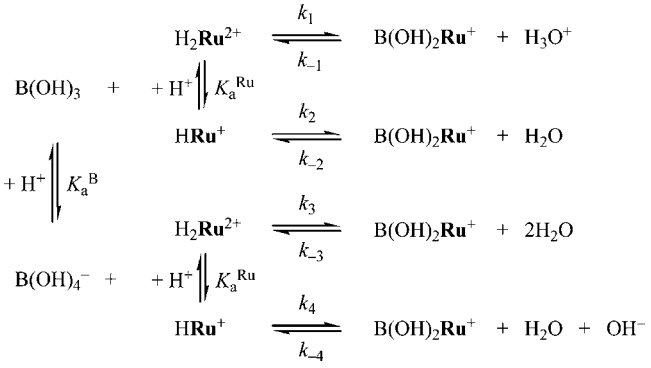
measured under the conditions of the large excess concentration of boric acid compared to that of the Ru(II) complex ($C_B \gg C_{Ru}$) is shown in Fig. 4. Only the absorption spectra in the range of pH < 10 were analyzed, because the Ru(II) complex, $[Ru(bpy)_2(dhphen)]^{2+}$, gradually decomposed at pH > ca. 10. From simultaneous analysis of the data at 300–600 nm in Fig. 4 using SPECFIT program [18], K_1 was determined to be $\log K_1 = -5.13 \pm 0.05$. Change in the emission spectra with pH (Fig. S5) was also measured, however, the K_1 value could not be determined, because the intensity is not linearly related to the concentration of the species under the present conditions [20].

3.4. Conditional formation constant K'

The present reaction system (Scheme 1) is abbreviated as Eq. (5),

$$B' + \mathbf{Ru}' \overset{K'}{\rightleftharpoons} B(OH)_2\mathbf{Ru}^+ \tag{5}$$

where K' is the conditional formation constant depending on the pH of the solution, and B′ and **Ru**′ denote ($B(OH)_3$ and $B(OH)_4^-$) and ($H_2\mathbf{Ru}^{2+}$ and $H\mathbf{Ru}^+$), respectively, since only one reaction product ($B(OH)_2\mathbf{Ru}^+$) was detected by ^{11}B NMR spectra under the present reaction conditions. As mentioned above, the reactivity of boronic acid towards bidentate ligands decreases as: $H_2L > HL^- > L^{2-}$, which is opposite to those of metal ions,



Scheme 1.

and the reactivity of tetrahedral boronate ion is comparable with or less than that of boronic acid, and trigonal boronic acid is always a reactive species irrespective of the pH of the solution. Therefore, it is convenient for optimizing the determination condition of boron to express the reaction of boric acid with the Ru(II) complex by Eq. (3). The K' is given by Eq. (6),

$$K' = \frac{[B(OH)_2\mathbf{Ru}^+]}{[B'][\mathbf{Ru}']} = \frac{K_1}{K^*[H^+]} \tag{6}$$

where $[B'] = [B(OH)_3] + [B(OH)_4^-] = [B(OH)_3](1 + K_a^B[H^+]^{-1})$, $[\mathbf{Ru}'] = [H_2\mathbf{Ru}^{2+}] + [H\mathbf{Ru}^+] = [H_2\mathbf{Ru}^{2+}](1 + K_a^{Ru}[H^+]^{-1})$, and $K^* = (K_a^B[H^+]^{-1} + 1)(K_a^{Ru}[H^+]^{-1} + 1)$. Differentiation of Eq. (6) with respect to $[H^+]$ indicates that K' will reach to a maximum at $pH = (pK_a^{Ru} + pK_a^B)/2 = 8.89$ (Fig. 5), which is thermodynamically optimum pH. In Fig. 5, K' approaches to zero at lower pH (<6) as well as at higher pH (>12), that is, no reaction occurs, in which pH ranges the reaction mainly proceeds through k_1 path and k_4 path, respectively, if occurs. In the pH range, 6 < pH < 12, the reaction proceeds through k_2 and/or k_3 in addition to k_1, as will be mentioned later.

3.5. Reaction kinetics

Kinetic study was carried out for the present reaction system (Eq. (5)) in order to specify the reaction routes in Scheme 1. Formation rate of the product ($B(OH)_2\mathbf{Ru}^+$) was first-order with respect to the total concentration of the uncomplexed ligand ($[\mathbf{Ru}'] = [H_2\mathbf{Ru}^{2+}] + [H\mathbf{Ru}^+]$), under the conditions, $C_B \gg C_{Ru}$, and is given by Eq. (7),

$$\frac{d[B(OH)_2\mathbf{Ru}^+]}{dt} = k_{obs}[\mathbf{Ru}'] \tag{7}$$

where k_{obs} is the conditional pseudo first-order rate constant depending on C_B. As shown in Fig. 6, the k_{obs} is linearly dependent on C_B at a given pH, so is expressed by Eq. (8) at a given pH,

$$k_{obs} = k_f C_B + k_d \tag{8}$$

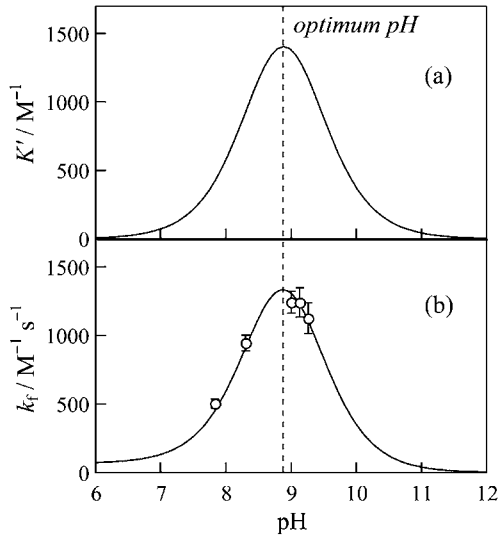


Fig. 5. Dependences of K' at 25 °C (a) and k_f at 10 °C (b) on pH for the reaction of $B(OH)_3$ with $[Ru(bpy)_2(dhphen)]^{2+}$ at $I = 0.10$ M. The plots in (b) were obtained from the slopes in Fig. 6.

where k_f and k_d are the rate constants for the forward and reverse reactions in Eq. (5), respectively. The slopes of the straight lines in Fig. 6 increase with increasing pH up to ca. 9, then decrease. The conditional formation constants can be calculated kinetically as $K' = k_f/k_d$ at a given pH, and the K' values are consistent with those determined by spectrophotometric measurements within the experimental errors (e.g., K' = ca. 1500 at pH 9).

From the precise kinetic assessment (see the detailed kinetic analyses and Fig. S6 in Supporting data), Eq. (9) was finally obtained for the present system.

$$k_{obs} = \frac{k_1 + (k_2 K_a^{Ru} + k_3 K_a^{B})[H^+]^{-1}}{K^*} C_B + k'_d \quad (9)$$

where k'_d denotes the rate constant for the reverse reaction assuming to be constant, as the pH effect on the intercepts in Fig. 6 was not observed experimentally. It is obvious from Eq. (9) that k_2 and k_3 are indistinguishable kinetically, so the upper limits for k_2 and k_3 were calculated by assuming that only one of the two paths contributes to the reaction. By applying a non-linear least-squares fitting of Fig. 6 to the experimental data, the rate constants in Eq. (9) (k_1 and the upper limits for k_2 and k_3 at 10 °C) were determined to be $k_1 = 67 \pm 17\ M^{-1}\ s^{-1}$, k_2 (upper limit) $= (4.3 \pm 0.1) \times 10^3\ M^{-1}\ s^{-1}$ and k_3 (upper limit) $= (6.6 \pm 0.1) \times 10^3\ M^{-1}\ s^{-1}$, respectively. It is worth noting that the trigonal $B(OH)_3$ is a reactive species also in the present system. The k_f [$=\{k_1 + (k_2 K_a^{Ru} + k_3 K_a^{B})[H^+]^{-1}\} K^{*-1}$, cf. Eqs. (8) and (9)] can be calculated at various pHs by using the rate constants determined above, which are plotted against pH in Fig. 5. It can be seen from Fig. 5 that k_f reaches to a maximum value at almost the same pH (ca. 9) as in the case of K'. This is because $k_1 \ll (k_2 K_a^{Ru} + k_3 K_a^{B})[H^+]^{-1}$ under the present conditions (at pH 8–10), so k_f reaches to a maximum at pH $= (pK_a^{Ru} + pK_a^{B})/2$ as in the case of K' (Eq. (5)). This means that tetrahedral $B(OH)_4^-$ would be substantially reactive in the present system, as apparent from Fig. 5, considering the general reactivities of H_2L and HL^- ($H_2L > HL^-$), though we do not know the real reactivity of $B(OH)_4^-$ due to "proton ambiguity". This is in contrast to the previous results for the reactions with H_2L [8], and would mainly come from the effective electrostatic interaction between the ligand having the Ru(II) complex detector (H_2**Ru**$^{2+}$) and boronate ion [$B(OH)_4^-$] in the present system. Thus, pH 8.9 is kinetically optimal.

3.6. Sensing of boron using $[Ru(bpy)_2(dhphen)]^{2+}$ complex as a detector

As mentioned above, pH 8.9 is kinetically and thermodynamically optimal (Fig. 5). So, the spectrofluorimetric boron determination was examined by measuring the emission spectra of the solutions containing $[Ru(bpy)_2(dhphen)]^{2+}$ complex and boric acid at pH 8.9 using CHES buffer (Fig. 7). The plot of the emission intensity at 600 nm against C_B (Fig. S7) clearly indicates that a trace of boron as low as 2.1×10^{-5} M (1.3 ppm) can be detected with the emission spectrum of the metal complexes.

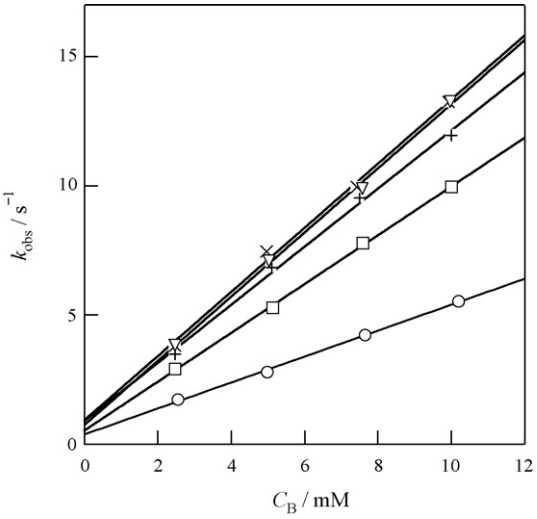


Fig. 6. Dependence of k_{obs} on C_B for the reaction of $B(OH)_3$ with $[Ru(bpy)_2(dhphen)]^{2+}$ at $I = 0.10$ M and $T = 10$ °C. pH = 7.83 (◯), 8.30 (□), 8.64 (△), 9.00 (▽), 9.13 (×), 9.26 (+).

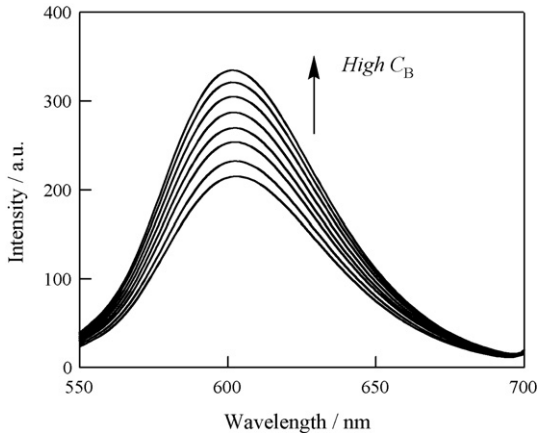


Fig. 7. Emission spectra of the reaction mixtures of $[Ru(bpy)_2(dhphen)]^{2+}$ and boric acid at pH = 8.9. $C_{Ru} = 4.5 \times 10^{-5}$ M, C_B = 0–1.5×10^{-4} M, $I = 0.10$ M, and $T = 25$ °C.

Thus, an MLCT probe such as $[Ru(bpy)_2(dhphen)]^{2+}$ complex can be used for optical sensing of boron in aqueous solution. It is also of note that the determination reaction is completed within a few seconds, which constitutes an alternative method of boron determination.

4. Conclusions

It was found that the change in the emission property of the $[Ru(bpy)_2(dhphen)]^{2+}$ due to complexation with boric acid can be successfully utilized for the determination of boron. Both the thermodynamically and kinetically optimum pHs were equal to $(pK_a^{Ru} + pK_a^{B})/2 = 8.9$. It was found for the present system that both boric acid and borate ion were reactive even in an alkaline solution of pH 9.

Acknowledgement

We wish to express our thanks for financial supports from 21COE "Practical Nano-Chemistry" project from MEXT, Japan and from Waseda University Grant for Special Research Projects (Grant 2005B-133).

Appendix A. Supplementary data

Supplementary data associated with this article can be found, in the online version, at doi:10.1016/j.talanta.2007.06.021.

References

[1] H. Ito, Y. Kono, A. Machida, Y. Mitsumoto, K. Omori, N. Nakamura, K. Ishihara, Inorg. Chim. Acta 344 (2003) 28.
[2] K. Ishihara, Y. Mouri, S. Funahashi, M. Tanaka, Inorg. Chem. 30 (1991) 2356.
[3] N. Takao, A. Suto, Y. Kondo, K. Ishihara, Inorg. Chim. Acta 290 (1999) 222.
[4] K. Ishihara, A. Nagasawa, K. Umenoto, H. Ito, K. Saito, Inorg. Chem. 33 (1994) 3811.
[5] Y. Kono, K. Ishihara, A. Nagasawa, K. Umemoto, K. Saito, Inorg. Chim. Acta 262 (1997) 91.
[6] Y. Yamamoto, T. Matsumura, N. Takao, H. Yamagishi, M. Takahashi, S. Iwatsuki, K. Ishihara, Inorg. Chim. Acta 358 (2005) 3355.
[7] T. Matsumura, S. Iwatsuki, K. Ishihara, Inorg. Chem. Commun. 8 (2005) 713.
[8] S. Iwatsuki, S. Nakajima, M. Inamo, H.D. Takagi, K. Ishihara, Inorg. Chem. 46 (2007) 354.
[9] S. Friedman, R. Pizer, J. Am. Chem. Soc. 97 (1975) 6059.
[10] G. Lorber, R. Pizer, Inorg. Chem. 15 (1976) 978.
[11] L. Babcock, R. Pizer, Inorg. Chem. 19 (1980) 56.
[12] R. Pizer, C.A. Tihal, Inorg. Chem. 31 (1992) 3243.
[13] Z. Murtaza, L. Tolosa, P. Harms, J.R. Lakowiez, J. Fluores. 12 (2002) 187.
[14] S. Funahashi, K. Haraguchi, M. Tanaka, Inorg. Chem. 16 (1977) 1349.
[15] F.A. Cotton, G. Wilkinson, Advanced Inorganic Chemistry, fifth ed., Wiley-Interscience, New York, 1988, p. 169.
[16] A.M.W. Cargill Thompson, J.C. Jeffery, D.J. Liard, M.D. Ward, J. Chem. Soc., Dalton Trans. (1996) 879.
[17] A.D. Shukla, A. Das, Polyhedron 19 (2000) 2605.
[18] R.A. Binstead, B. Jung, A.D. Zuberbühler, SPECFIT/32™ Global Analysis System, ver. 3.0 for 32-bit Windows systems, Spectrum Software Associates, Marlborough, U.S.A (2000).
[19] N. Ingri, Acta Chem. Scand. 16 (1962) 439.
[20] Under the present conditions ($C_{Ru} \sim 5 \times 10^{-5}$ M), the absorbance at excitation wavelength ($\lambda_{exc} = 360$ nm) of the Ru(II) complex, A_{exc}, is larger than 0.1, to which the single term approximation of MacLaurin series, $I \propto I_0(1 - 10^{A_{exc}}) \approx A_{exc} I_0 \cdot \ln 10 (\propto C)$, is not applicable [21].
[21] J. Polster, H. Lachmann, Spectrometric Titrations, VCH, Weinheim, 1989, p. 346.

Available online at www.sciencedirect.com
ScienceDirect
Talanta 74 (2008) 539–546
Talanta
www.elsevier.com/locate/talanta

Determination of natural olive fruit fly pheromone in insect samples by enzyme linked immunoassays

Afroditi Neokosmidi [a,b], Valentine Ragoussis [b,*], Christos Zikos [a], Maria Paravatou-Petsotas [a], Evangelia Livaniou [a], Nikitas Ragoussis [c], Gregory Evangelatos [a]

[a] *NCSR "Demokritos", RRP Institute, Immunopeptide Chemistry Laboratory, Aghia Paraskevi, 153 10 Athens, Greece*
[b] *University of Athens, Department of Chemistry, Laboratory of Organic Chemistry, Panepistimiopolis Zographou, 157 71 Athens, Greece*
[c] *VIORYL S.A. Research Department 28th Km Athens-Lamia Nat. Road, 190 14 Afidnes, Greece*

Received 12 March 2007; received in revised form 27 May 2007; accepted 15 June 2007
Available online 19 June 2007

Abstract

The olive fruit fly pheromone avidin–biotin ELISA immunoassay, based on the use of polyclonal G antibodies derived from rabbits (reported previously) and a newer assay, based on the use of polyclonal Y antibodies isolated from the eggs of laying hens (reported in this paper), were applied successfully for the analysis of natural pheromone in virgin adult female olive fruit flies. According to the results obtained, the pheromone content in the glands of adult female olive fruit flies increases from the third to the ninth day of their age. During the calling period, the female olive fruit flies seem to emit ∼1.1 μg pheromone/insect/day at least.

The immunoassay, based on the Y antibodies, is slightly more sensitive (detection limit 40 ng/mL) than the assay based on polyclonal anti-pheromone rabbit antiserum (detection limit 80 ng/mL). As revealed by thorough cross-reactivity studies, including 14 structurally similar to the olive fruit fly pheromone molecules, the newer immunoassay is less selective than the previous one and seems to cross react with few molecules bearing the spiroketal moiety.
© 2007 Elsevier B.V. All rights reserved.

Keywords: Olive fruit fly; *Bactrocera oleae* (Gmelin); Pheromones; Anti-pheromone polyclonal G and Y antibodies; ELISA; Avidin–biotin system

1. Introduction

The olive fruit fly *Bactrocera oleae* (Gmelin) (Dipt. Tephritidae) is the major pest of olives in the Mediterranean area. Control of the insect population is mainly achieved through the application of chemical insecticides, the over-use of which may cause serious problems in the environment and the public health. During the last years, considerable effort has been paid towards the development of suitable techniques for the biological control of the olive fruit fly. Among those, the most promising results have been obtained by the mass-trapping [1] and mating disruption techniques [2], which are both based on the use of the synthetic insect's pheromone, the racemic 1,7-dioxaspiro[5.5]undecane **1**. However, a prerequisite for the wide application of the above alternative techniques is the ability to measure rapidly and accurately the amount of pheromone present in the traps, the environment and insect samples by a simple, rapid, sensitive and cost effective analytical method.

We have recently developed a competitive avidin–biotin ELISA immunoassay for the olive fruit fly pheromone, based on the use of polyclonal G antibodies raised in rabbits [3], against (±)-β-[3-(1,7-dioxaspiro[5.5]undecane)]propionic acid **2** (hapten I) conjugated to the carrier protein keyhole limpet hemocyanin (KLH) [4], and the conjugation to a biotin moiety of (±)-δ-[3-(1,7-dioxaspiro[5.5]undecane)]butylamine **3** (hapten II), for indirect immobilization onto ELISA micro wells pre-coated with the glycoprotein avidin (Fig. 1).

During the last years, development of Y antibodies (immunoglobulins Y, IgY) in laying hens has been considered advantageous compared to the widely used immunization of mammals, for a series of practical reasons, e.g. because hens are rather tolerant animals under laboratory conditions, collection of their eggs is a simple procedure not requiring skilled personnel and Y antibodies can be easily obtained from the yolk

* Corresponding author.
E-mail address: ragousi@chem.uoa.gr (V. Ragoussis).

0039-9140/$ – see front matter © 2007 Elsevier B.V. All rights reserved.
doi:10.1016/j.talanta.2007.06.015

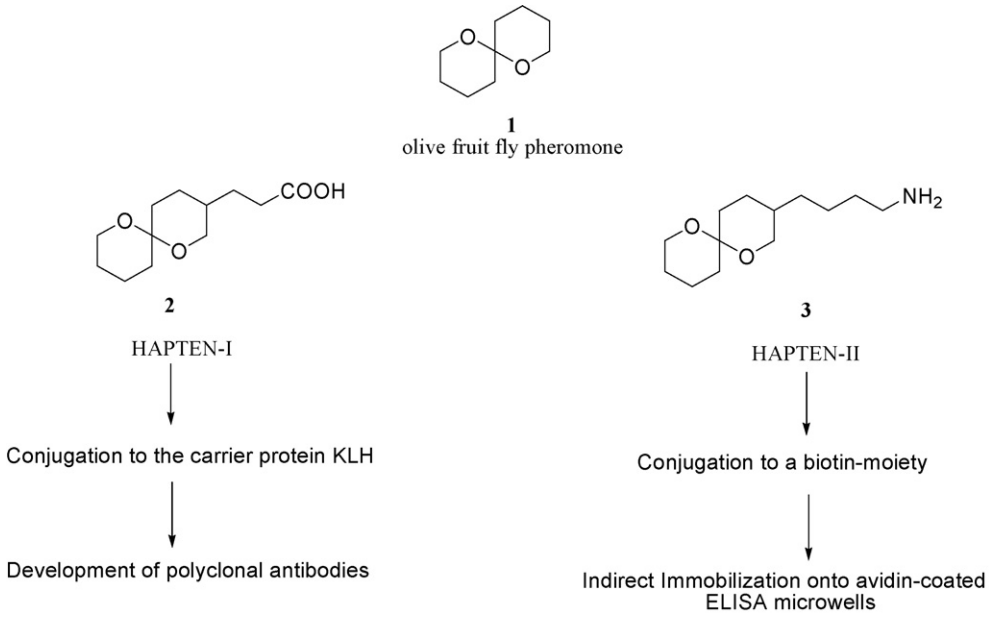


Fig. 1. The olive fruit fly pheromone **1**, the pheromone-hapten I **2**, the pheromone-hapten II **3** and their schematic use in the development of the ELISA immunoassays for the olive fruit fly pheromone.

of immune eggs at large quantity—batches showing uniform characteristics [5,6]. This latter advantage is of special interest, if formulation of the antibodies as an immunoassay kit-reagent has been envisaged.

In this work we present: (a) a new approach to the previously reported immunoassay, based on the use of polyclonal Y antibodies derived from the eggs of laying hens, (b) cross-reactivity studies of both immunoassays with 14 structurally similar to the olive fruit fly pheromone molecules and (c) representative results on the determination of natural olive fruit fly pheromone in insect samples (virgin female adult olive fruit flies).

2. Experimental

2.1. Reagents and instrumentation

All chemical reagents and solvents were of analytical grade and were used as supplied. Avidin and the goat anti-rabbit IgG-HRP were products of Sigma–Aldrich. The sulfo-NHS-LC-biotin was a product of Pierce and the rabbit anti-chicken IgG-HRP was a product of Chemicon. The (±)1,7-dioxaspiro[5.5]undecane, of analytical grade, was a gift from Vioryl S.A. (Athens, Greece). GC analyses were performed with SUPELCO SPB-1 fused silica capillary column (30 m × 0.32 mm i.d.), (carrier gas helium 1 mL/min; injector temperature 220 °C; oven temperature 50 °C, 10 min isothermal and then raised at 2 °C/min up to 200 °C) on a Varian 3600 device. An incubator (Precision, AEG), an ELISA-washer (Multiwash II, Tricontinent) and an ELISA-reader (MR 5000, Dynatech) were used in the ELISA experiments, which were performed on 96-well microtiter-plates from Corning. SDS-PAGE analyses were made on a SERVA Blue Vertical 101 Mini Slab Gel system.

2.2. Immunization and isolation of hen Y antibodies from the egg yolk

Three-month old laying hens (Leghorn hybrids) were used for raising polyclonal antibodies. Routinely, the conjugate of hapten-I to KLH, dissolved in saline (quantity of conjugate corresponding to 200 μg KLH/0.5 mL) was thoroughly emulsified with an equal volume of Freund's complete adjuvant. The emulsion was subcutaneously injected on the neck of the hen. The first boost was given 2 weeks after the first immunization, while the following ones were given every 4 weeks in the same manner. The egg collection was started after the first boost. Eighty five eggs were collected in total, which were divided into groups.

Isolation of Y antibodies from the egg yolk was performed by using a combination of the so-called acidic water dilution [7] and PEG-precipitation [8] methods. More specifically: acidified water (pH 5.2) was added to the egg yolk mixture in a ratio of 1:3 (v/v). After thorough mixing, the mixture was stored at 4 °C overnight. On the following day, the mixture was centrifuged (2–6 °C, 9500 × *g*, 30 min), the lipid residue was removed and the supernatant was obtained. After adding PEG-6000 (3.5%), the supernatant was centrifuged (2–6 °C, 8500 × *g*, 10 min) and the new supernatant was carefully obtained, after filtration through pharmaceutical gauze. After adding PEG-6000 (8.5%), the supernatant was centrifuged (2–6 °C, 8500 × *g*, 10 min), the new supernatant was discarded and the residue was re-dissolved in a small volume of deionized water and PEG-6000 (12%) was added. Then, the mixture was centrifuged (2–6 °C, 8500 × *g*, 10 min) and the new residue, containing the immunoglobulins Y, was obtained. The IgYs were dialyzed against water (4 °C, 72 h, MW cut off: 50 kDa) and, finally, they were lyophilized.

2.3. SDS-PAGE analysis of the isolated Y antibodies

All samples (20 μL each) were treated for 3 min at 100 °C in SDS-loading buffer (0.05 M Tris–HCl pH 6.8, 0.1 M DTT, 2% SDS, 0.1% bromophenol blue, 10% glycerol) and were further subjected to SDS-PAGE on 12% polyacrylamide gel slabs, under reducing conditions [9]. The protein bands were visualized with Coomassie Brilliant Blue R-250. The purity of the isolated Y antibodies was found higher than 90%.

2.4. Titer determination of the isolated Y antibodies

The titer curve for the anti-pheromone IgY was determined by the procedure already described for the antipheromone antiserum [3], using an anti-pheromone IgY solution [0.25–0.032 μg/mL in dilution buffer, i.e. 0.05% (v/v) Tween 20 in pH 7.4 PBS, which contained 0.2% (w/v) BSA]. The titer of the hen Y antibodies was found to be 0.125 μg/mL.

2.5. Cross-reactivity studies

Fourteen molecules with a spiroketal skeleton, presenting close structural similarities with the structure of the olive fruit fly pheromone, were tested as putative cross-reacting molecules with both, the rabbit antiserum and the hen Y antibodies. With the rabbit antiserum, the cross-reactivity was determined in a ELISA system, as it had been previously described for some simple organic molecules [3]. Exactly the same protocol was followed for the determination of the cross-reactivity with the hen Y antibodies. For both immunoassays the selectivity was expressed as cross-reactivity percentage for each interfering compound.

2.6. Determination of the olive fruit fly pheromone in insect samples

During this study, a protocol for the analysis of the natural pheromone on virgin adult female olive fruit flies was developed. The insects were a generous gift of the Chemical Ecology and Natural Products Laboratory of the Institute of Biology of NCSR "Demokritos", from their rearing facilities. The pheromone content in insect glands or whole abdomens was determined: (a) in relation to the age of the insect (1–10 days) and (b) in relation to the time of the day. For the first study, insects were collected every day at 10:00 h in the morning and the samples for the analysis were prepared within the next hour. For the second study, the 6-day old females were chosen, because at this age their glands contain enough pheromone for the calling action. So the first series of insects were collected at 9:30 h in the morning and the second series at 16:00 h, after the calling period of the female olive fruit flies.

2.6.1. Sample preparation

Whole abdomens or glands or heads of the insect were removed from virgin female olive flies and were homogenized in the presence of phosphate buffer pH 7.4, containing an appropriate quantity of organic solvent (DMF, 0.5%) and centrifuged (1500 × *g*). The supernatants were collected, diluted to an appropriate volume of phosphate buffer pH 7.4 containing DMF 0.5% (10 insects/2.5 mL) and used as a sample in the ELISA assay.

For the analysis of a sample by conventional gas chromatography, 1 mL of the above sample was extracted with hexane (4 × 1 mL). The organic phase was dried over anhydrous sodium sulfate, the adequate quantity of the internal standard (methyl decanoate 99.9%; 100 μL of a solution of 1.5 mg in 10 mL of hexane) was added and the volume was made up to 5 mL with hexane. One microliter of the solution was injected in the gas chromatograph and the quantity of the pheromone was found by the ratio of the peak areas of the pheromone and the internal standard, reported to a suitable calibration curve.

2.6.2. Immunoassay protocol and standard curves

The immunoassay, using the rabbit antiserum, followed the already described protocol in the competitive immunoassay for the synthetic olive fruit fly pheromone [3] and the same protocol was used for the immunoassay with the hen Y antibodies.

The intra-assay precision of the immunoassay, obtained with the Y antibodies, was determined by measuring three unknown insect samples, 10 times each, in duplicate in the same displacement curve. The corresponding coefficients of variation (∼5%) were calculated according to a well-established mathematical formula [13]. The inter-assay precision was determined by measuring three different unknown insect samples, in seven displacement curves on 7 successive weeks. The corresponding coefficients of variation (5–25%) were calculated as %mean/standard deviation, according to a well-established method [13].

3. Results and discussion

3.1. Isolation of hen Y antibodies and immunoassay design

In the present work, laying hens were immunized against the conjugate of a synthetic derivative of pheromone, hapten I **2**, to the carrier protein keyhole limpet hemocyanin [3]. The Y antibodies were isolated at large quantities (∼0.13 g/yolk) and in highly pure form, from the immune egg yolk by following an in-house protocol, in which acidified water [7] and polyethylene glycol [8] are used in combination. The purity of the isolated Y antibodies was evaluated by SDS-PAGE electrophoresis [9] and found higher than 90%.

The same assay design was followed with either rabbit antiserum or hen Y antibodies. More specifically, the synthetic derivative of pheromone bearing a free $–NH_2$ group (hapten II 3) was suitably biotinylated and then indirectly immobilized onto ELISA microwells, which had been precoated with avidin [10,11]. This adduct, consisting an "immobilized pheromone", was left subsequently to compete with pheromone in standard solutions for the binding sites of the anti-pheromone Y antibodies. Efficient biotinylated pheromone derivative was obtained, when biotinylation was performed using an active ester of biotin, bearing a long chain spacer arm [12], presumably because in this

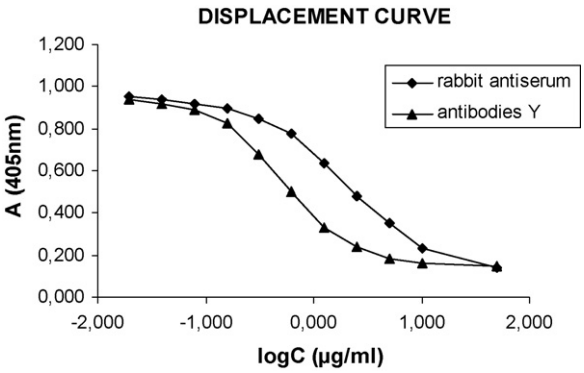


Fig. 2. Typical displacement curve of the immunoassay for the olive fruit fly pheromone using hen polyclonal Y antibodies, in comparison with the displacement curve of the immunoassay based on rabbit polyclonal antiserum (polyclonal G antibodies) [3].

derivative the pheromone moiety was kept in enough distance apart from the biotin moiety and, thus, it was more accessible to the anti-pheromone antibody for binding [12].

3.2. Displacement curve and validation of the method

A typical displacement curve of the immunoassay obtained with the Y antibodies using standard solutions of pure synthetic olive fruit fly pheromone, is shown in Fig. 2, in comparison with the displacement curve of the immunoassay with rabbit antiserum [3]. The optimal conditions, used in the ELISA protocol and the most important features of the above ELISA standard curves, are summarized in Table 1. The working range of both curves is similar, but the ELISA displacement curve using the hen Y antibodies has a slightly lower detection limit (40 ng/mL) than the ELISA curve, using the rabbit antiserum (80 ng/mL).

The accuracy of both immunoassays was evaluated by linearity or endogenous recovery studies (recovery of endogenous pheromone in serially diluted unknown insect samples) and was found to be 81–129%. In the same time exogenous recovery studies (recovery of exogenous synthetic pheromone added to unknown insect samples) were done in parallel with conventional analysis of the same samples by GC. Three aliquots of an insect sample, containing less than the minimum detectable by the immunoassay amount of pheromone, were spiked with a solution of synthetic pheromone, so that the expected amount of pheromone was known. These three aliquots were analyzed by both immunoassays and also by the conventional gas chromatography. The results are summarized in Table 2. The recovery values obtained, ranged between 105 and 120% for the immunoassay using rabbit antiserum and 102–114% for the immunoassay using hen Y antibodies, show a good accuracy of both immunoassays. The comparison of the results of both immunoassays with those of the conventional analysis by GC, has been proved quite satisfactory.

3.3. Cross-reactivity studies

The cross-reactivity of both immunoassays with 14 different synthetic molecules, all presenting high structural similarity with the natural olive fruit fly pheromone, was investigated. The results, expressed as cross-reactivity percentage, are summarized in Table 3 .

The hen Y antibodies cross react with compounds **13**, **14**, **15** and **16**. This lower specificity of the hen Y antibodies, however,

Table 1
Features of the ELISA displacement curve, using rabbit antiserum (rabbit G antibodies) and hen Y antibodies

	Rabbit antiserum $\overline{X} \pm$ S.D. (CV%)	Y antibodies $\overline{X} \pm$ S.D. (CV%)
A_{st0} (A_{ref})	1.015 ± 0.059 (5.8%)	1.055 ± 0.052 (4.9%)
A_{st1} (A_{min})	0.213 ± 0.024 (11.5%)	0.166 ± 0.010 (6.3%)
A_{st2}	0.279 ± 0.027 (9.8%)	0.188 ± 0.013 (7.1%)
A_{st3}	0.392 ± 0.045 (11.4%)	0.236 ± 0.019 (8.0%)
A_{st4}	0.553 ± 0.055 (10.0%)	0.324 ± 0.034 (10.6%)
A_{st5}	0.713 ± 0.059 (8.3%)	0.458 ± 0.056 (12.3%)
A_{st6}	0.846 ± 0.047 (5.5%)	0.638 ± 0.066 (10.3%)
A_{st7}	0.919 ± 0.036 (3.9%)	0.802 ± 0.082 (10.2%)
A_{st8} (A_{max}, rabbit antiserum)	0.956 ± 0.025 (2.6%)	0.905 ± 0.075 (8.3%)
A_{st9} (A_{max}, Y antibodies)	–	0.961 ± 0.080 (8.4%)
A_{blank}	0.097 ± 0.005 (5.4%)	0.107 ± 0.016 (14.6%)
IC_{50}[a] (μg/mL)	1.237 ± 0.139 (11.3%)	0.429 ± 0.040 (9.2%)
Working range	80 ng/mL–10 μg/mL	40 ng/mL–10 μg/mL
Detection limit[b]	80 ng/mL	40 ng/mL
r^2	0.9927 ± 0.003 (CV: 0.3%)	0.9927 ± 0.003 (CV: 0.3%)
Slope	−0.4625 ± 0.030 (CV: 6.6%)	−0.4850 ± 0.050 (CV: 10.4%)

A: optical absorbance, i.e. the signal measured in an enzyme immunoassay in which a chromatogenic substrate is used, st0: zero standard solution, i.e. the standard solution which contains no pheromone; A_{st0}: the absorbance value (=reference absorbance, A_{ref}) measured in the wells containing st0. st1: the standard solution which contains the highest concentration of pheromone; A_{st1}: the absorbance value measured in the wells containing st1. A_{st1} is the minimum absorbance value (A_{min}), since the immunoassay described is competitive. These data were obtained by measuring the Absorbance values of each pheromone standard solution (or the blank tubes), run in triplicate in seven displacement curves on seven successive weeks, and then calculating the corresponding coefficient of variation (%mean/standard deviation).

[a] The concentration of the analyte (free pheromone), at which half of the maximal signal intensity (optical absorbance) is obtained.

[b] The concentration of the analyte (free pheromone), which causes 5% reduction in A_{max}.

Table 2
Recovery of exogenous synthetic pheromone added to unknown insect samples

Pheromone concentration (μg/mL)	Measured pheromone concentration (μg/mL)					
	Rabbit antiserum	Recovery (%)	Hen Y antibodies	Recovery (%)	GC	Recovery (%)
1.90	2.00	105	1.95	102	1.83	96
0.80	0.92	115	0.88	110	0.74	93
0.50	0.60	120	0.57	114	0.46	92

is not expected to affect data reliability during analysis of insect or environmental samples, because in olive orchards, where most of the samples of interest will be collected, natural sources of the above cross-reacting spiroketals do not exist.

The rabbit antiserum specificity is remarkable. Only one synthetic compound, the 1-oxaspiro[5.5]undecane **8**, cross reacts at 17.5% only. There is no other interference from the structurally similar compounds tested, either from those of natural origin [14], or from the synthetic ones.

3.3.1. Determination of the olive fruit fly pheromone in insect samples

Both immunoassays were used for the determination of the olive fruit fly pheromone in the insect samples, so that the data obtained could be "cross-checked". They were both considered sensitive enough to allow measurement of the pheromone present in intact insects; moreover, the immunoassay based on polyclonal G antibodies from rabbits showed the additional advantage of being exceptionally specific for the pheromone molecule.

The objective of the measurements was to determine (a) the content in pheromone of the glands of female olive fruit flies, in relation to their age and (b) the quantity of the pheromone emitted in one day, by an adult female in the beginning of the calling period.

Virgin female olive fruit flies of different age, from 1 to 10 days, were collected the same time of the day and the content of their abdomens or their gland in natural pheromone was measured. The pheromone in the glands of female olive fruit flies appears from the first day of their life and increases from the third to the sixth day and then a maximum concentration was found the ninth day of their age (Fig. 3). This is in agreement with previously reported [15] data. However, the absolute pheromone concentration values, previously reported, are quite lower than those measured by the present immunoassay methods. The observed differences may be attributed to the preparation of the GC samples, which may have resulted in some losses of volatiles during the concentration of the extract and to the lack of sensitivity of the GC analysis used at that time.

The fact that the pheromone content in the female glands started to appear in significant quantity the third day of their life and that virgin males started to respond to pheromone exposure at the same age, with a maximum of response after their fifth day of age [16], led us to determine the emitted quantity of pheromone from virgin females at the same age period. We can reasonably assume that from the sixth day there is enough pheromone in female glands for the calling action and at the same time males show the maximum response to the emitted pheromone.

For that reason several insects were collected the morning of the sixth day at 9:30 and a number of insects were collected the afternoon at 16:00, after the calling period. Their glands were separated and homogenized and their content in pheromone was measured by both immunoassays. The glands of the insects collected in the afternoon were found to contain lower quantity of pheromone (Table 4). It is reasonable to assume that this difference in the pheromone content, which averages 1.1 μg/insect, represents the pheromone emitted by the insects during the calling period of their sixth day of age. The following days, as the pheromone content in the female glands is higher and the response of males to the pheromone is stronger, the emitted pheromone should be higher.

Two other points of interest, according to our experimental data, are that (a) the quantity of pheromone present in the whole abdomens of the insects is higher than the quantity in their glands and (b) in the rest of the body of the insect the quantity of pheromone is negligible (Table 4).

Finally, a series of gland extracts were analyzed in parallel with the two immunoassays, for comparison of the obtained results. The samples were chosen randomly and in most (9 out of 10) cases, very close pheromone concentration values were obtained. The measured concentrations of the pheromone using the hen Y antibodies, are in general slightly lower (70–90%) than the results obtained using the rabbit antiserum. The results are summarized in Table 5.

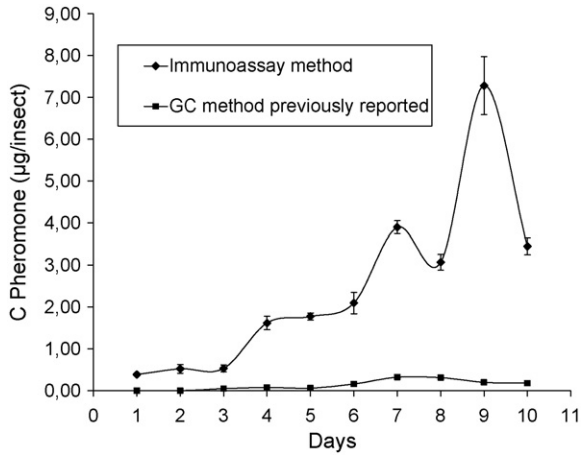


Fig. 3. Amount of pheromone measured in homogenates of 1–10-day-old virgin female insects. Corresponding amounts measured with GC, which were previously reported in the literature [15] are also shown.

Table 3
Cross-reactivity of both immunoassays and the structure of the tested molecules

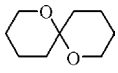
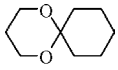
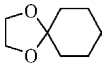
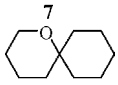
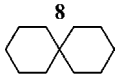
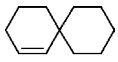
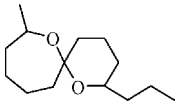
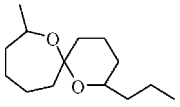
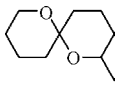
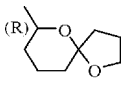
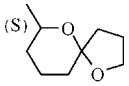
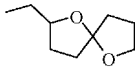
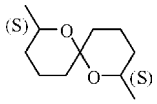
Name	Structure	Distribution in insects [15]	Cross-reactivity (%)	
			Rabbit antiserum	IgY
1,7-Dioxaspiro[5.5]undecane, olean	**1** 	*Bactrocera* (*Dacus*) *oleae*, *Bactrocera cacuminata*, *Bactrocera umbrosa*, *Bactrocera distincta*, *Partamona cupira*	100	100
1,5-Dioxaspiro[5.5]undecane	**4** 	Synthetic compound	<5	n.d.
1,5-Dioxaspiro[5.4]decane	**5** 	Synthetic compound	<5	n.d.
1,4-Dioxaspiro[4.5]decane	**6** 	Synthetic compound	<5	<1
1,6-Dioxaspiro[4.4]nonane	**7** 	Synthetic compound	n.d.	<1
1-Oxaspiro-[5.5]undecane	**8** 	Synthetic compound	17.5	n.d.
Spiro[5.5]undecane	**9** 	Synthetic compound	n.d.	n.d.
Spiro[5.5]undec-1-ene	**10** 	Synthetic compound	n.d.	n.d.
8-Methyl-2-propyl-1,7-dioxaspiro[5.6]dodecane type A	**11** 	Synthetic compound	n.d.	n.d.
8-Methyl-2-propyl-1,7-dioxaspiro[5.6]dodecane type B	**12** 	Synthetic compound	n.d.	n.d.
2-Methyl-1,7-dioxaspiro [5.5]undecane	**13** 	*Epeolus cruciger*, *Melipona bicolor*, *Agapanthia villosoviridescsens*	<5	14
(*R*)-7-Methyl-1,6-dioxaspiro[4.5]decane	**14** 	Wasps of Vespula sp., *Conophthorus* sp.	<5	>100
(*S*)-7-Methyl-1,6-dioxaspiro[4.5]decane	**15**	Wasps of *Vespula* sp., *Conophthorus* sp.	n.d.	37

Table 3 (*Continued*)

Name	Structure	Distribution in insects [15]	Cross-reactivity (%)	
			Rabbit antiserum	IgY
2-Ethyl-1,6-dioxaspiro [4.4]nonane, chalcogran	 **16**	*Pityogenes chalcographus*, *Pityogenes quadridens.*	<5	70
(*S*,*S*)-2,8-Dimethyl-1,7-dioxaspiro[5.5]undecane	 **17**	*Bactrocera* sp., *Andrena* sp.	n.d.	<1

n.d.: non detectable.

Table 4
Pheromone amount in 6-day old female olive fruit flies determined by both immunoassays

Unknown sample	Pheromone (μg)/insect	
	Rabbit antiserum (G antibodies)	Hen Y antibodies
Extract of abdomens obtained from 39 insects (collection time: 9:30)	2.19 ± 0.17	2.05 ± 0.26
Extract of glands obtained from 30 insects (collection time: 9:30)	1.54 ± 0.06	1.43 ± 0.11
Extract of glands obtained from 11 insects (collection time: 16:00)	0.38 ± 0.03	0.33 ± 0.06
Extract of heads obtained from 39 insects (collection time: 9:30)	n.d.	n.d.

n.d.: non detectable

Table 5
Analysis of the same insect samples with both immunoassays

Sample no.	Measured pheromone concentration (μg/insect)		
	Rabbit antiserum (G antibodies)	Hen Y antibodies	%
1	0.892	0.838	94
2	1.314	0.904	69
3	0.581	0.637	110
4	0.908	0.830	91
5	0.604	0.431	71
6	1.031	0.803	78
7	0.336	0.241	72
8	0.934	0.681	73
9	0.429	0.352	82
10	1.838	0.976	53

4. Conclusions

In conclusion, in the present work a variation of the immunoassay for the olive fruit fly pheromone was developed, based on polyclonal anti-pheromone Y antibodies, which were raised in laying hens and isolated from the immune egg yolk at large quantity—batches showing uniform characteristics. These antibodies could be eventually formulated as the specific binding reagent of an *in vitro* immunoassay kit for the olive fruit fly pheromone. The new immunoassay is slightly more sensitive (detection limit 40 ng/mL) than the previously reported one, which was based on a polyclonal rabbit anti-pheromone antiserum (detection limit 80 ng/mL). Although more sensitive, the new immunoassay is not as highly specific as the first one, giving cross-reactivity with few molecules bearing the spiroketal moiety. Both immunoassays were used successfully for the determination of natural pheromone in virgin adult female olive fruit flies. According to the results obtained, the pheromone content in the glands of adult female olive fruit flies increases from the third to the ninth day of their life. During the calling period the female olive fruit flies seem to emit ∼1.1 μg pheromone/insect/day at least.

Acknowledgements

The authors wish to thank Professor W. Franke for a generous gift of the synthetic spiroketals **11**, **12**, **14**, **15**, **16** and **17**, and Dr. B. Mazomenos for the generous offer of the synthetic compounds **4**, **5**, **6**, **7**, **8**, **9**, **10** and of alive olive fruit flies from the rearing facilities of his laboratory in NCSR "Demokritos".

Appendix A. Supplementary data

Supplementary data associated with this article can be found, in the online version, at doi:10.1016/j.talanta.2007.06.015.

References

[1] T. Broumas, G. Haniotakis, C. Liaropoulos, T. Tomazou, N. Ragoussis, J. Appl. Entom. 126 (2000) 217.
[2] R.T. Carde, in: R.L. Ridgway, R.M. Silverstein, M.N. Insoe (Eds.), Behaviour—Modifying Chemicals for Insect Management, Marcel Dekker Inc., New York, 1990, p. 47.
[3] A. Neokosmidi, V. Ragoussis, C. Zikos, M. Paravatou-Petsotas, E. Livaniou, N. Ragoussis, G. Evangelatos, J. Agr. Food Chem. 52 (2004) 4368.
[4] R. Jennemann, C. Gnewunch, S. Boisslet, B.L. Bauer, H. Wiegandt, J. Biochem. 115 (1994) 1047.
[5] G.W. Warr, K.E. Magor, D.A. Higgins, Immunol. Today 16 (1995) 392.
[6] R. Schade, in: I. Behn, M. Erhard, A. Hlinak, C. Staak (Eds.), Chicken Egg Yolk Antibodies, Production and Application, IgY–Technology, Springer–Verlag, Berlin, 2000, p. 1.
[7] E.M. Akita, S. Nakai, J. Immunol. Methods 160 (1993) 207.

[8] A. Polson, M.B. Vonwechmar, M.H.V. Vanregenmortel, Immunol. Comm. 9 (1980) 475.
[9] B.D. Hames, in: B.D. Hames, D. Rickwood (Eds.), Gel Electrophoresis of Proteins: A Practical Approach, second ed., Oxford University Press, New York, 1990, p. 1.
[10] M.N. Green, in: M. Wilchek, E.A. Bayer (Eds.), Methods in Enzymology: Avidin-Biotin Technology, Academic Press Inc., San Diego, California, 1990, p. 51.
[11] E.A. Bayer, M. Wilchek, E.P. Diamandis, TK. Christopoulos (Eds.), Immunoassay, Academic Press, London, 1996, p. 237.
[12] C.J. Strasburger, F. Kohen in:, M. Wilchek, E.A. Bayer (Eds.), Methods in Enzymology: Avidin-Biotin Technology, Academic Press Inc., San Diego, California, 1990, p. 481.
[13] T. Chard, in: R.H. Burdon, P.H. van Knippenberg (Eds.), An Introduction to Radioimmunoassay and Related Techniques, third ed., Elsevier, Amsterdam, 1987, p. 194.
[14] W. Francke, W. Kitching, Curr. Org. Chem. 5 (2001) 233.
[15] B. Mazomenos, J. Insect Physiol. 30 (1984) 765.
[16] G.E. Haniotakis, I.S. Pittara, Environ. Entomol. 23 (1994) 726.

Available online at www.sciencedirect.com
ScienceDirect
Talanta 74 (2008) 570–577
Talanta
www.elsevier.com/locate/talanta

Multivariate optimisation and validation of a capillary electrophoresis method for the analysis of resveratrol in a nutraceutical

Serena Orlandini, Iacopo Giannini, Sergio Pinzauti, Sandra Furlanetto *

Department of Pharmaceutical Sciences, University of Florence, Via U. Schiff 6, 50019 Sesto Fiorentino, Florence, Italy

Received 17 April 2007; received in revised form 12 June 2007; accepted 15 June 2007
Available online 28 June 2007

Abstract

A rapid and simple method based on capillary electrophoresis was developed for the quality control of nutraceuticals containing resveratrol. Setting the UV detector at 280 nm, the optimisation involved the separation of 11 effervescent tablet components, including the active compounds vitamin C, vitamin B_2, flavanones and hydroxycinnamic acids. Flufenamic acid was employed as internal standard. The effects of background electrolyte concentration, acetonitrile percentage and voltage were investigated by means of response surface methodology, considering as responses the critical resolution values and analysis time. The optimum conditions were found by Derringer desirability function. The background electrolyte consisted of 23 mM borate buffer, adjusted to pH 10.0 with 1 M sodium hydroxide, containing 7% (v/v) acetonitrile. Temperature and voltage were set at 25 °C and 26 kV, respectively. Applying these conditions, the analysis time was below 7 min. The performances of the method were tested in terms of selectivity, robustness, linearity and range, accuracy and precision and system suitability, following ICH guidelines.
© 2007 Elsevier B.V. All rights reserved.

Keywords: CZE; Experimental design; Nutraceuticals; Resveratrol; Validation

1. Introduction

Resveratrol (RES, (*E*)-5-[2-(4-hydroxyphenyl)ethenyl]-1,3-benzenediol) is a phytoalexin present in a range of plant sources including species of *Arachis*, *Pinum*, *Polygonum*, *Veratrum*, and *Vitis*. It is thought to be one of the compounds responsible for the cardioprotective action of wine and is promoted as an antioxidant for the prevention of atherosclerosis. It also has mixed agonist/antagonist activity at oestrogen receptors and some anti-inflammatory and antiproliferative activity, and is under investigation in the prevention and treatment of malignancy [1].

Due to these properties, resveratrol is used in commercial preparations, as dietary supplements and herbal products, which are nowadays considered "nutraceuticals". This term has been recently described as any substance that is a food or a part of a food and provides medical or health benefits [2,3].

Effervescent tablets containing RES extracted from *Polygonum cuspidatum* have appeared lately on the Italian market with the trade name Resvis XR® (Biofutura Pharma, Milan, Italy). In this preparation other active compounds, including L-ascorbic acid, vitamin B_2, zinc lactate trihydrate, red orange extract containing the antioxidants anthocyanins (kuromanin hydrochloride), hydroxycinnamic acids (caffeic, coumaric, ferulic and sinapic acids) and flavanones (hesperidin, narirutin) are associated with RES. For such a complex mixture, having available a rapid and reliable analytical method for determining resveratrol is necessary for quality control of the formulation.

Capillary electrophoresis has been gaining increasing importance in quality control laboratories, especially for small-molecule pharmaceuticals [4], for its speed, efficiency, ultra-small sample volume, and reduced consumption of solvent [5–7]. The use of CZE [8–14], CZE-ITP [15], MEKC [10,16–20], and non-aqueous CE [21] has been investigated for the determination of RES in wines. CZE has also been employed for the determination of RES in plant matrices [22,23], in particular in *P. cuspidatum* [12,24,25] and propolis extract [26]. To the best of our knowledge, there is only one CZE method reported for the analysis of RES in health food (capsules) [12].

The aim of this study was to set up, using a multivariate strategy [27,28], a rapid, simple and selective CZE method for the analysis of RES contained in effervescent tablets of Resvis XR®,

* Corresponding author. Tel.: +39 055 4573717; fax: +39 055 4573779.
E-mail address: sandra.furlanetto@unifi.it (S. Furlanetto).

0039-9140/$ – see front matter © 2007 Elsevier B.V. All rights reserved.
doi:10.1016/j.talanta.2007.06.024

obtaining the complete separation of the other active components/excipients detectable at the selected wavelength of analysis. The method was validated according to ICH guidelines [29].

2. Experimental

2.1. Chemicals

All chemicals and reagents used were of analytical-reagent grade with no further purification. Sodium borate was from BDH Laboratory Supplies (Poole, UK). Methanol, acetone, acetonitrile (all HPLC grade) and the reference standards of resveratrol (RES), hesperidin (HES), L-ascorbic acid (ASC), vitamin B_2 (sodium riboflavin 5′-monophosphate, RIB), caffeic acid (CAF), *p*-coumaric acid (COU), ferulic acid (FER), sinapic acid (SIN), kuromanin hydrochloride (KUR) were purchased from Sigma–Aldrich (St. Louis, MO, USA). Narirutin (NAR) was obtained from LabService Analytica (Bologna, Italy). Effervescent tablet excipients (citric acid anhydrous, sodium hydrogen carbonate, sodium carbonate, sorbitol, E162 red beet powder, orange flavour, acesulfame K (ACE), aspartame, polysorbate 20, simethicone dry (emulsion 30%)) were obtained from Biofutura Pharma. Resvis XR® effervescent tablets (Biofutura Pharma), labelled to contain 2.5 mg of RES, were purchased locally in pharmacies. Flufenamic acid (FLU), employed as internal standard, was from Sigma–Aldrich. Ultrapure water used throughout the study was provided by a Simplicity 185 system (Millipore, Billerica, MA, USA) after an electrodeionisation treatment using an Elix system (Millipore).

2.2. Solutions and sample preparation

Standard stock solutions of HES, NAR, CAF, COU, FER, SIN, FLU (each 1 mg mL^{-1}), ASC (10 mg mL^{-1}), ACE (5 mg mL^{-1}) and RES (0.5 mg mL^{-1}) were prepared in methanol. A standard stock solution of RIB (1 mg mL^{-1}) was prepared in water. All solutions were stored at 4 °C and used within 1 week. Standard working solutions were obtained daily adding the appropriate amount of each of the stock solutions directly in a vial and filling up to 500 μL with water.

In the optimisation phase, the test concentration values were: HES, NAR, RIB, CAF, COU, FER, SIN, 0.04 mg mL^{-1}; FLU, 0.05 mg mL^{-1}; ASC, 1.95 mg mL^{-1}, ACE, 0.2 mg mL^{-1}. These concentration values were chosen as they were equal or higher than the values corresponding to a test concentration of RES of 0.05 mg mL^{-1}, obtained when diluting 1 tablet in 50 mL of solvent.

The background electrolytes were prepared by mixing an adequate volume of 0.1 M sodium borate, adjusting pH with 1 M sodium hydroxide, adding the proper amount of acetonitrile and filling up to the volume with water.

With regard to sample preparation, 20 effervescent tablets were crushed, the powder was homogenised and an amount of sample corresponding to the mean mass (about 4 g, corresponding to 2.5 mg resveratrol) was transferred for the analysis to a 50 mL beaker. The content was diluted with 25 mL of a methanol/water 60:40 (v/v) mixture, shaken vigorously, sonicated for 10 min and shaken again. One millilitre of the mixture was then centrifuged; 250 μL of the surnatant were diluted in a vial up to 500 μL by adding 25 μL of FLU stock solution, 10 μL acetone (EOF marker) and 215 μL water.

2.3. Equipment and capillary electrophoretic conditions

An ultrasonic bath (300 UltraSonik, Ney Company, Bloomfield, USA) and a centrifuge (5415D, Eppendorf, Hamburg, Germany) were employed to sonicate and centrifuge solutions, respectively. A Metrohm 691 pH Meter (Metrohm, Herisau, Switzerland) was used to measure pH values.

An Agilent Technologies ^{3D}CE system (Agilent Technologies, Waldbronn, Germany), equipped with an on-column UV–visible diode-array detector and an air thermostating system, was employed for all separations. The system was controlled by ^{3D}CE ChemStation software (Rev.A.09.01, Agilent Technologies). The fused-silica capillaries (inner diameter 50 μm, outer diameter 375 μm) were purchased from Composite Metal Services (Ilkley, UK) and had a total and effective length of 48.5 and 40.0 cm, respectively. The detection window was built-in by burning off the polyimide coating on the capillary. Detection wavelength was 280 nm. Hydrodynamic injection of sample was performed at 50 mbar for 5 s and was followed by a buffer plug injection (50 mbar for 5 s). The capillary temperature was maintained at 25 °C and the voltage was set to 26 kV. The standard run buffer consisted of an aqueous solution of 23 mM sodium borate adjusted to pH 10.0 with 1 M sodium hydroxide, containing 7% (v/v) acetonitrile. Applying these conditions, a current of 50 μA was typically generated. The capillary was treated prior to its first use by flushing with 1 M NaOH for 5 min, 0.1 M NaOH for 5 min and water for 5 min. Between two runs, a rinse-cycle, 1 M NaOH, 0.1 M NaOH, and water each for 1 min and run buffer for 4 min was applied.

2.4. Calibration curves

Regression curves for RES were obtained by plotting the corrected area of RES divided by the corrected area of FLU *versus* the concentration of RES. The corrected area was calculated dividing the integrated peak area by migration time in order to take into account the different mobilities of the solutes and thus their different residence times in the detection window. The regression curve was evaluated both in aqueous solution and in the nutraceutical formulation across the 50–150% range of the test concentration (0.05 mg mL^{-1}). In both the cases, five different concentrations were prepared and each solution was analysed twice. With regard to the commercial preparation, separate weightings of synthetic mixtures of the effervescent tablets components were used.

2.5. Calculations and software

Resolution values were measured according to the formula

$$R = \frac{2(t_2 - t_1)}{w_2 + w_1}$$

where t_1, t_2 are the migration times and w_1, w_2 are the corresponding widths at the bases of the peaks of adjacent peak pairs, respectively [30].

The NEMROD-W software package was used to generate experimental designs and to perform statistical analysis of the data [31].

3. Results and discussion

The effervescent tablet components which showed a detectable peak at the test concentration and at the selected wavelength (280 nm) included, in addition to resveratrol, two flavanones (HES and NAR), L-ascorbic acid, vitamin B_2, four hydroxycinnamic acids (CAF, COU, FER, SIN) and the excipient acesulfame K. Their structures are reported in Fig. 1. Considering also the internal standard flufenamic acid, the separation involved a total of 11 compounds.

Due to the phenolic/acidic nature of most of the compounds, a 20 mM borate alkaline buffer system was initially examined with pH values ranging between 8.5 and 10.5 with steps of 0.5. A significant effect on the number of resolved peaks was evidenced and the higher selectivity was obtained in the range 9.5–10.5. However, also in this narrow interval, inversions of the migration order of hydroxycinnamic acids and acesulfame K peaks were observed. Promising results were obtained at pH 10.0, and this pH value was chosen for the subsequent measurements. The choice of fixing pH value in this preliminary step was due to the need to keep the migration order of the compounds constant for the next phase of the study, involving response surface methodology [28]. In fact, to apply this multivariate strategy it is basic to be able to univocally measure the response resolution. From then on the migration order of the compounds was the following: HES, NAR, RES, FLU, ASC, RIB, SIN, FER, ACE, COU, CAF.

In any case, in the plain pH 10.0 aqueous buffer selected some peaks were still not fully separated. Thus, in order to achieve the complete separation of the compounds in a low analysis time, addition of an organic solvent to the buffer was found to be suitable and the best results were obtained adding acetonitrile to the BGE. The concentration of this organic modifier, together with buffer concentration and voltage, were deeply investigated by response surface methodology [28].

3.1. Response surface methodology

The purpose of response surface methodology is to obtain a predictive model for each response which adequately represents changes in the response within the zone of interest, depending on the input variables. Thus, RSM makes it possible to obtain a map of the response in the form of a surface and to predict the considered responses over the whole of the domain. Moreover, the models obtained can be used for optimisation in the problem of treating multiple responses [28].

In this study, the considered factors were buffer concentration, percentage of acetonitrile and voltage. The factors were studied in the following experimental range: X_1, buffer concentration (BGE conc.), 7–23 mM; X_2, percentage of acetonitrile (%ACN), 0–16% (v/v); X_3, voltage (V), 18–30 kV. This domain was chosen on the basis of preliminary knowledge of the system, taking mainly into account analysis speed. The considered responses were the analysis time (to be minimised), corresponding to the migration time of caffeic acid, and the critical resolution values between peak pairs (to be maximised), i.e. between hesperidin and narirutin (R_1), resveratrol and flufenamic acid (R_3), and ferulic acid and acesulfame K (R_8). The other resolutions pointed out no particular issue, thus they were not taken into consideration.

A quadratic model describing the relationship between the factors and the response was postulated and a central composite design (CCD) was employed to estimate its coefficients. In general, this design for k factors consists of 2^k experiments corresponding to a full factorial design for the estimate of first-degree and interaction terms, $2k$ star points for the estimate of the square terms, and n experiments at the centre of the domain to estimate the experimental variance [28]. Thus, for three factors a total of 18 experiments were required, including four centre points. The experimental plan is shown in Table 1, with the measured responses.

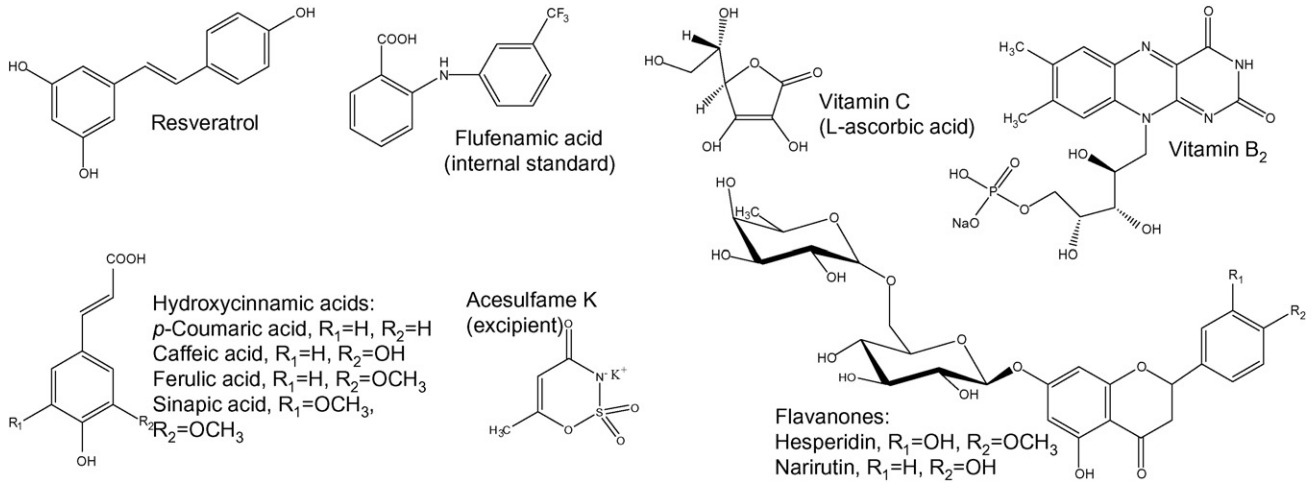


Fig. 1. The molecular structures of the compounds.

Table 1
Central composite design experimental plan and responses

Experiment number	BGE conc. (mM)	%ACN (%v/v)	V (kV)	R_1	R_3	R_8	t (min)
1	10	3	20	1.04	3.95	1.21	8.68
2	20	3	20	1.36	1.03	2.14	8.02
3	10	13	20	1.02	1.96	0.87	7.18
4	20	13	20	1.45	2.98	2.26	10.17
5	10	3	28	0.70	2.86	1.15	4.04
6	20	3	28	1.23	0.82	2.57	5.18
7	10	13	28	1.23	1.87	0.54	4.75
8	20	13	28	1.51	3.00	4.04	6.52
9	7	8	24	0.99	0.01	0.01	4.58
10	23	8	24	1.54	2.47	4.26	7.84
11	15	0	24	1.07	1.91	0.01	5.25
12	15	16	24	1.40	0.78	2.47	7.62
13	15	8	18	1.38	0.01	1.36	8.63
14	15	8	30	1.00	0.77	1.05	4.72
15	15	8	24	1.45	0.54	0.89	6.41
16	15	8	24	1.19	0.01	1.37	5.94
17	15	8	24	1.24	0.23	0.91	6.32
18	15	8	24	1.14	0.01	1.43	5.90

The four calculated regression models, one for each considered response, were evaluated by means of analysis of variance (ANOVA) [27,28,32]. Each of them resulted valid and significant apart from the model for R_3, which was significant but not valid. For this latter model the residuals were examined and it was determined that the lack of fit was mainly due to experiment 9, where an almost complete overlap of RES and FLU made it difficult to determine exactly the real resolution value. The same overlap occurred in experiment 13, and for these two experiments an arbitrary resolution value of 0.01 had been initially introduced as response in order to fulfil the software requirements. At this point, as a consequence of the obtained results on the validity of the model, we decided to directly discard these two experiments. The statistical properties of the new matrix were evaluated by means of quality criteria [28] in order to determine the consequences of the modification of a standard design on the estimation of the coefficients, from the point of view of prediction. In particular, variance inflaction factors provided an overall measure of the co-linearity of the variables, the determinant and the trace of the dispersion matrix provided the precision and the independence of the estimation of the coefficients, respectively [28]. The quality criteria were found satisfactory, thus a new model was calculated and subjected to a new statistical treatment. This model was both significant and valid for all the responses and was retained.

In order to reach a compromise among the responses which could better satisfy the objectives, the Derringer desirability function was used, thus converting a multi-response problem into a single-response one [33]. Before discussing desirability function, it is worthwhile analysing the single response surfaces in order to obtain the description of the system. The single response surfaces were not directly utilised to find the optimal conditions but were important to obtain information about the system from an electrophoretic point of view.

In RSM, rather than estimating the effect of each variable examining the single coefficients, the response surfaces are directly investigated [28]. The response surfaces obtained by plotting buffer concentration *versus* acetonitrile percentage, setting voltage at the centre of its experimental range, are reported in Fig. 2. In order to maximise R_1 it was necessary to set both the factors at high level (Fig. 2a). For R_3 positive quadratic effects were evidenced for the two considered factors (Fig. 2b). Moreover, a positive interaction between BGE conc. and %ACN was found, which led to a maximisation of the response when both factors were set at high or low level. Observing the graph, the best results could be obtained for R_3 by setting low levels of both the factors. High levels of these factors maximised R_8 (Fig. 2c), but these conditions led to high values of analysis time as well (Fig. 2d).

Examination of the response surfaces drawn plotting buffer concentration *versus* voltage (Fig. 3), setting %ACN at the centre of the experimental domain, showed that voltage had no important effect on R_1 (Fig. 3a) or R_3 (Fig. 3b) in the studied domain. High levels of voltage and buffer concentration led to maximise R_8 (Fig. 3c), and high levels of voltage were required for minimising analysis time, as expected (Fig. 3d).

To find the optimum conditions, considering each calculated model, in any point of the domain predicted response values can be transformed into an appropriate desirability function representing the satisfaction *versus* the response. The partial desirabilities d_i of the responses are drawn with $d_i = 0$, $d_i = 1$, $0 < d_i < 1$ for undesirable, desirable and acceptable values of the response i, respectively.

In this case, for the resolution values a target value of 1.5 was defined, corresponding to a baseline resolution, and no value below this one was accepted. The fully desired analysis time was set below 7, partially accepting values between 7 and 8. The overall desirability D was then calculated within the experimental domain by $D = \sqrt[4]{d_1 d_2 d_3 d_4}$, where the partial desirability functions d_1, d_2, d_3 and d_4 corresponded to the responses R_1, R_3, R_8 and analysis time, respectively. According to this formula, when an undesirable value is obtained for one response, the overall desirable value is 0. On the contrary, when each requirement gets completely satisfied, the overall desirability value is 1. Finally, when $0 < D < 1$, an acceptable compromise between the different responses has been found [34]. The graphical representation of D is depicted in Fig. 4, where D is shown for two factors at a time, setting the other at its optimised value. The zone where the requirements were satisfied was quite small and corresponded to high levels of borate concentration, medium-high values of both acetonitrile percentage and voltage. The selected experimental conditions corresponded to: X_1, buffer concentration, 23 mM; X_2, percentage of acetonitrile, 7% (v/v); X_3, voltage, 26 kV.

Applying these conditions, complete separation of the compounds was obtained in less than 7 min, and a typical electropherogram of the mixture is reproduced in Fig. 5. The predictivity of each considered model was verified by evaluating if the measured values for the responses fell within the confidence intervals, centred on the predicted values and defined considering the standard deviation from CCD replicates and a probability

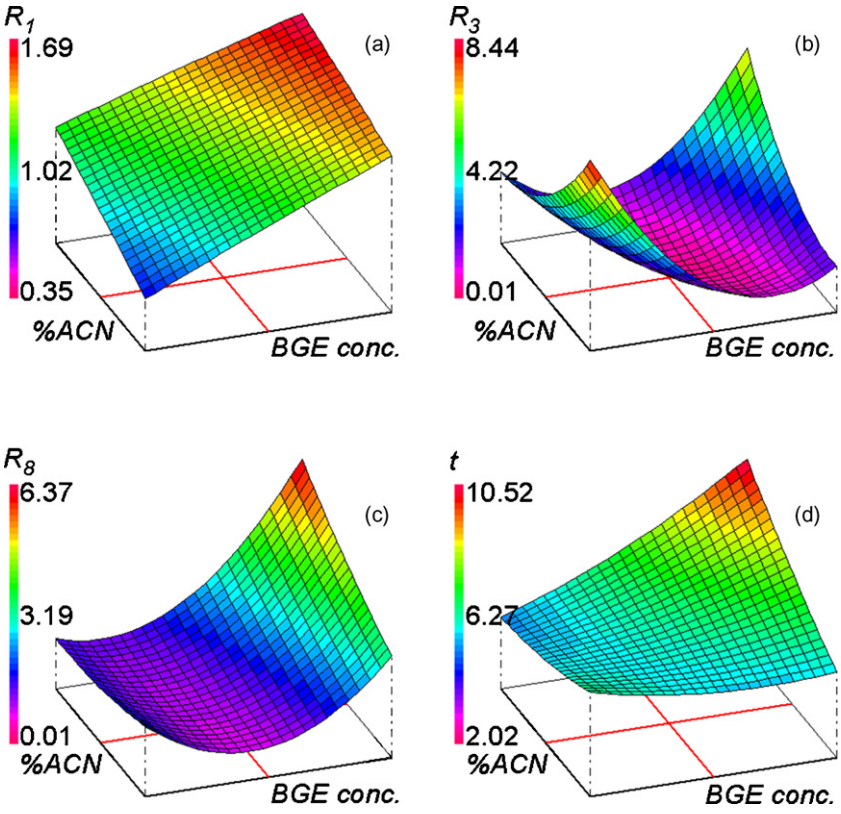


Fig. 2. Response surfaces obtained plotting buffer concentration *vs.* acetonitrile percentage and setting voltage at 24 kV: (a) response HES/NAR resolution (R_1); (b) response RES/FLU resolution (R_3); (c) response FER/ACE resolution (R_8); (d) response analysis time (t).

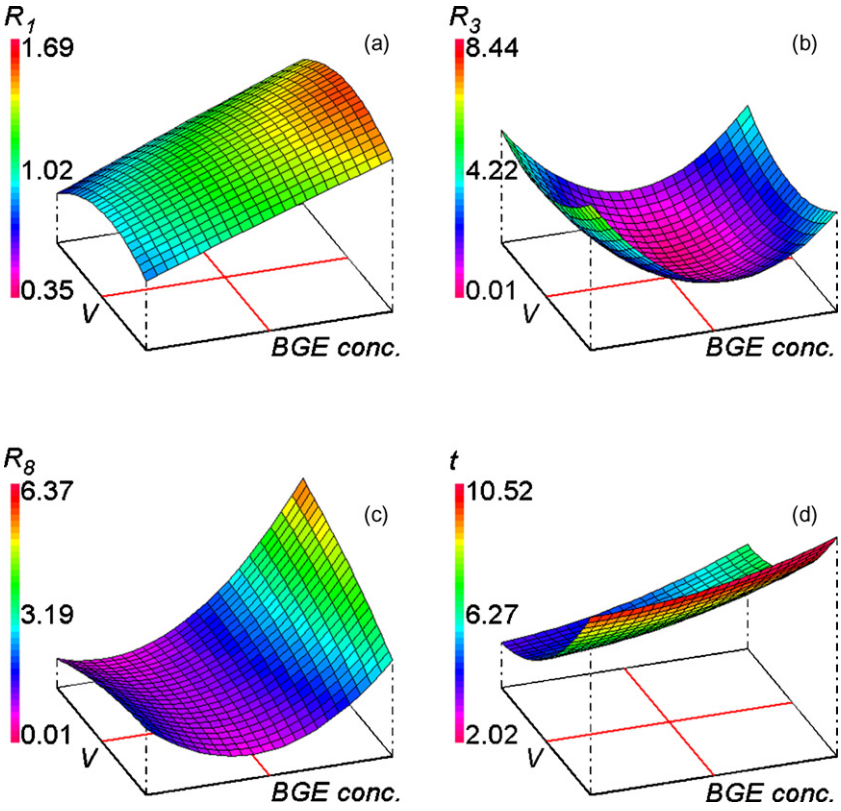


Fig. 3. Response surfaces obtained plotting buffer concentration *vs.* voltage and setting acetonitrile percentage at 8% (v/v): (a) response HES/NAR resolution (R_1); (b) response RES/FLU resolution (R_3); (c) response FER/ACE resolution (R_8); (d) response analysis time (t).

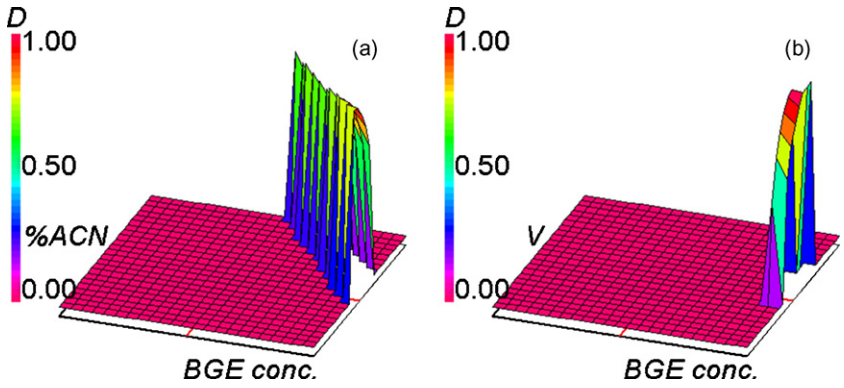


Fig. 4. Desirability function graph obtained plotting: (a) buffer concentration *vs.* acetonitrile percentage, setting voltage at 26 kV; (b) buffer concentration *vs.* voltage, setting acetonitrile percentage at 7% (v/v).

level of 95%. The experimental values found were included in the confidence limits, thus a good agreement between predicted and observed responses was verified.

3.2. Validation

The developed CE method was validated with respect to all the parameters described in ICH guidelines [29] applying the optimised conditions. Unless otherwise stated, the analyses were run at the test concentrations reported in Section 2. Validation was performed both in aqueous solution and in nutraceutical product.

3.2.1. Selectivity

Interference by the other active compounds and the excipients in the analysis of resveratrol in Resvis XR® was verified. The active compounds were evaluated at the test concentration values reported in Section 2, while the excipients were added at the concentration expected when diluting one tablet in 50 mL of solvent, corresponding to the test concentration of RES (0.05 mg mL^{-1}). No excipient showed a detectable peak, with the exception of ACE. At 280 nm the absence of any co-eluting peak indicated a good selectivity (Fig. 5), as confirmed by the measured critical resolution values ($n=4$, $\alpha/2=0.025$): R_1, 1.68 ± 0.13; R_3, 2.78 ± 0.53; R_8, 4.19 ± 0.22. The identity of the peaks was confirmed by separate spiking with each of the standards.

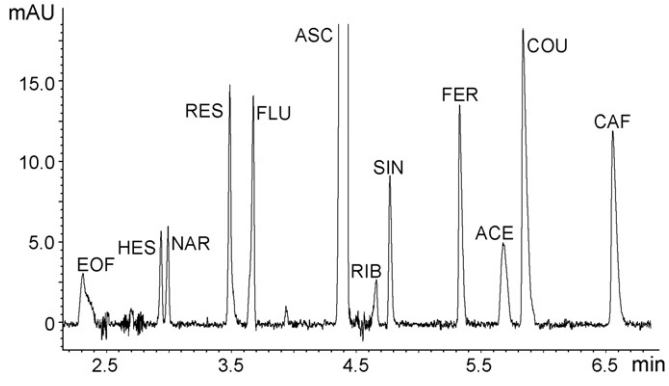


Fig. 5. The typical electropherogram referring to optimised experimental conditions: BGE, 23 mM borate buffer, 7% (v/v) ACN; 26 kV; 25 °C. Hydrodynamic injection: 50 mbar, 5 s. Detection wavelength: 280 nm.

3.2.2. Robustness

Robustness testing was performed using a multivariate approach [35–37]. The considered responses were R_1, R_3 and R_8, in order to evaluate the effect of the factors on selectivity. The factors were X_1, buffer concentration (BGE conc.), X_2, pH, X_3, acetonitrile percentage (%ACN), X_4, temperature (T) and X_5, voltage (V). These variables were studied in a small experimental range, defined symmetrically around the optimised values described in the procedure: BGE conc., 22–24 mM; pH, 9.9–10.1; %ACN, 6–8% (v/v); T, 24–26 °C; V, 25–27 kV. An eight-run Plackett-Burman matrix [28] was chosen and the corresponding experimental plan, together with the measured responses, is shown in Table 2. Graphic analysis of effects [38] was used to identify the critical factors, after introducing the experimental variance ($n=4$) for each response. A bar graph was constructed where each bar corresponds to an effect and the bar's length is proportional to the absolute value of the effect. In Fig. 6, the significant effects were evidenced as those exceeding the reference lines, which were calculated on the basis of the experimental error. The response R_3 was significantly dependent on buffer concentration, while R_1 and R_8 were influenced by pH. In particular, the effect of pH on R_8 had the highest absolute value, and through an effective examination of the responses corresponding to the higher pH value tested (pH 10.1) it was evident that a significant decrease of R_8 always occurred. The effect of pH on selectivity was already pointed out in the optimisation

Table 2
Robustness testing: Plackett-Burman experimental plan and responses

BGE conc. (mM)	pH	%ACN (%v/v)	T (°C)	V (kV)	R_1	R_3	R_8
24	10.1	8	24	27	2.41	6.98	0.43
22	10.1	8	26	25	2.02	2.38	0.90
22	9.9	8	26	27	1.75	5.13	4.31
24	9.9	6	26	27	1.77	4.63	3.95
22	10.1	6	24	27	2.16	2.62	0.82
24	9.9	8	24	25	1.89	5.66	5.00
24	10.1	6	26	25	2.13	6.81	0.50
22	9.9	6	24	25	1.60	5.05	4.84

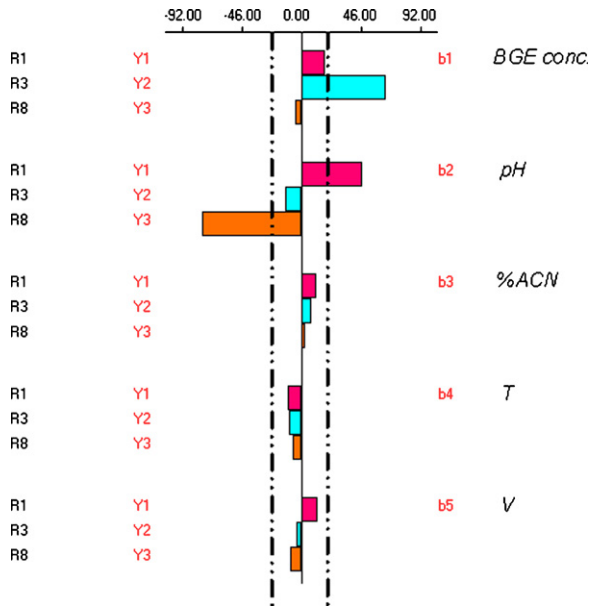


Fig. 6. Robustness testing: graphic analysis of effects.

step, when fixing pH value before performing response surface study. Thus, these results bore out that in order to maintain a good selectivity particular attention has to be given to the preparation of the background electrolyte, especially to pH.

3.2.3. Linearity and range

The linearity of an analytical procedure is its ability (within a given range) to obtain test results which are directly proportional to the concentration of analyte in the sample [29]. The specified range of linearity depends on the intended application of the procedure and for assay procedures a minimum range from 80 to 120% of the test concentration should be considered [29]. In this case linearity was verified in the five-level range 0.025–0.075 mg mL^{-1} (50–150% of the test concentration), repeating each experiment twice. In aqueous solution, the calibration equation was $y = 19.843x - 0.1193$ ($R^2 = 0.9982$, $R^2_{CV} = 0.9970$) and for the nutraceutical product the equation was $y = 17.786x - 0.1701$ ($R^2 = 0.9971$, $R^2_{CV} = 0.9954$), where y is the corrected peak area and x is the concentration of RES in mg mL^{-1}.

3.2.4. System precision

Within-day precision and between-day precision of analysis time, referring to the last migrating peak (CAF), and corrected peak area of RES were evaluated by analysing the test mixture six times each day over a 3-day period. For analysis time, the obtained within-day R.S.D. values were 1.6, 1.4 and 0.5%, and between days the R.S.D. value was 3.1%. For corrected peak area, R.S.D. values were 1.1, 0.8 and 2.0% for within-day and 4.8% for between-day.

3.2.5. Accuracy and precision

According to ICH guidelines [29], accuracy and precision were evaluated at three concentration levels (low, 0.03 mg mL^{-1}; central, 0.05 mg mL^{-1}; high, 0.07 mg mL^{-1}), each with three replicates, covering the linearity range. Accuracy was measured as percent recovery by the assay of known added amount of analyte in the sample together with the confidence interval ($n = 3$, $\alpha/2 = 0.05$) and precision was simultaneously measured as R.S.D. of the recovery values found. For aqueous solution, the obtained results were: 100.9 ± 3.1%, R.S.D. = 1.2% (low level); 97.9 ± 5.5%, R.S.D. = 2.3% (medium level); 101.0 ± 1.2%, R.S.D. = 0.5% (high level). For nutraceutical formulation, at the same concentration levels the measured values were, respectively, 103.3 ± 6.3%, R.S.D. = 2.4%; 101.0 ± 5.4%, R.S.D. = 2.2%; 101.8 ± 3.7%, R.S.D. = 1.4%.

3.2.6. System suitability

System suitability parameters are used in order to check the behaviour of the analytical system [39], constituted by equipment, electronics, analytical operations and samples [29]. In this study resolution R_3 was chosen as performance parameter [35,39] and the interval $2.20 < R_3 < 3.05$ defined the requirements that this system must meet prior to analysis. This range was chosen as a consequence of system precision, which is an important parameter for system suitability tests as it provides valuable information about the variability of the analytical system [35]. The lower and higher limits of the interval corresponded to the extreme values observed during system precision study over 3 days.

3.3. Application of the method

The proposed method was successfully applied to the determination of resveratrol in its formulation, consisting of effervescent tablets (Resvis XR®) containing 2.5 mg of RES. For the assay of the real sample, a calibration curve for the nutraceutical matrix, obtained by separate weightings of synthetic mixtures, was used. The recoveries obtained agreed with the declared compositions. Percentage recovery of 102.6 ± 2.5 with a R.S.D. value of 1.5%, based on four replicate measurements ($\alpha/2 = 0.025$), was achieved. With some practical adjustments, the application of the developed method could be extended to the determination of other active compounds contained in the tablets. In this case it would be necessary to select the proper test concentration for the different compounds, taking simultaneously into account the need to obtain a signal for the analyte which could be used for quantitative aims and to maintain a good resolution between the two adjacent peaks. If needed, a possible way to reach this purpose could be a variation in injection time, leading to higher or lower peaks.

4. Conclusions

In this work, a capillary electrophoresis method for quality control of nutraceuticals containing resveratrol has been developed. The method was optimised by using response surface methodology which made it possible to achieve good resolution and low analysis time (7 min) also in the presence of a complex sample matrix. The method was validated following ICH guidelines and its performances made it suitable for routine analysis of resveratrol formulation.

References

[1] S.C. Sweetman (Ed.), Martindale, The Complete Drug Reference, vol. I, Part 2, 35th ed., Pharmaceutical Press, London, 2007, p. 2155.
[2] S. DeFelice, Nat. Biotechnol. 16 (1998) 728.
[3] B. Chankvetadze, A. Cifuentes, J. Pharm. Biomed. Anal. 41 (2006) 1485.
[4] K. Altria, A. Marsh, C. Sanger-van de Griend, Electrophoresis 41 (2006) 2263.
[5] S.F.Y. Li, Capillary Electrophoresis, Elsevier, Amsterdam, 1992.
[6] B. Chankvetadze, Capillary Electrophoresis in Chiral Analysis, John Wiley & Sons Ltd., Chichester, 1997.
[7] C.F. Poole, The Essence of Chromatography, Elsevier, Amsterdam, 2003.
[8] L. Arce, M.T. Tena, A. Rios, M. Valcárcel, Anal. Chim. Acta. 359 (1998) 27.
[9] J.J.B. Nevado, A.M.C. Salcedo, G.C. Penalvo, Analyst 124 (1999) 61.
[10] X. Gu, Q. Chu, M. O'Dwyer, M. Zeece, J. Chromatogr. A 881 (2000) 471.
[11] Z. Dobiasova, J. Pazourek, J. Havel, Electrophoresis 23 (2002) 263.
[12] L.Y. Gao, Q.C. Chu, J.N. Ye, Food Chem. 78 (2002) 255.
[13] Y.Y. Peng, Q.C. Chu, F.H. Liu, J.N. Ye, J. Agric. Food Chem. 52 (2004) 153.
[14] M. Spanilá, J. Pazourek, M. Farková, J. Havel, J. Chromatogr. A 1084 (2005) 180.
[15] R. Hamoudová, M. Urbánek, M. Pospíšilová, M. Polášek, J. Chromatogr. A 1032 (2004) 281.
[16] B.C. Prasongsidh, G.R. Skurray, Food Chem. 62 (1998) 355.
[17] Q.Y. Chu, M. O'Dwyer, M.G. Zeece, J. Agric. Food Chem. 46 (1998) 509.
[18] X.L. Gu, L. Creasy, A. Kester, M. Zeece, J. Agric. Food Chem. 47 (1999) 3223.
[19] V. Brandolini, A. Maietti, P. Tedeschi, E. Durini, S. Vertuani, S. Manfredini, J. Agric Food Chem. 50 (2002) 7407.
[20] E.G. Fan, K. Zhang, C.Y. Yao, C. Yan, Y.H. Bai, S. Jiang, Chromatographia 62 (2005) 289.
[21] Z. Demianová, H. Sirén, R. Kuldvee, M.L. Riekkola, Electrophoresis 24 (2003) 4264.
[22] M. Vaher, M. Koel, J. Chromatogr. A 990 (2003) 225.
[23] S. Ehala, M. Vaher, M. Kaljurand, J. Agric. Food Chem. 53 (2005) 6484.
[24] Q.C. Chu, Y.Y. Peng, J.N. Ye, Electroanalysis 16 (2004) 1434.
[25] Y.Y. Peng, Q.C. Chu, J.N. Ye, Am. Lab. 36 (2004) 40.
[26] N. Volpi, Electrophoresis 25 (2004) 1872.
[27] D.L. Massart, B.G.M. Vandeginste, L.M.C. Buydens, S. de Jong, P.J. Lewi, J. Smeyers-Verbeke, Handbook of Chemometrics and Qualimetrics: Part A, Elsevier, Amsterdam, 1997.
[28] G. Lewis, D. Mathieu, R. Phan-Tan-Luu, Pharmaceutical Experimental Design, Marcel Dekker, New York, 1999.
[29] ICH Harmonised Tripartite Guideline, Q2(R1), Validation of Analytical Procedures: Text and Methodology, 2005.
[30] The United States Pharmacopeia, 29th Revision, The United States Pharmacopeial Convention, Rockville, MD, 2006, p. 2647.
[31] D. Mathieu, J. Nony, R. Phan-Tan-Luu, Nemrod-W, LPRAI sarl, Marseille.
[32] R. Carlson, Design and Optimisation in Organic Synthesis, Elsevier, Amsterdam, 1992.
[33] G. Derringer, R. Suich, J. Qual. Technol. 12 (1980) 214.
[34] G. Pages, C. Delaurent, R. Phan-Tan-Luu, M. Sergent, Chemom. Intell. Lab. Sys. 86 (2007) 159.
[35] J. Ermer, J.H.McB. Miller (Eds.), Method Validation in Pharmaceutical Analysis—A Guide to Best Practice, Wiley-VCH, Weinheim, 2004.
[36] Y. Vander Heyden, A. Nijhuis, J. Smeyers-Verbeke, B.G.M. Vandeginste, D.L. Massart, J. Pharm. Biomed. Anal. 24 (2001) 723.
[37] S. Furlanetto, S. Orlandini, P. Mura, M. Sergent, S. Pinzauti, Anal. Bioanal. Chem. 377 (2003) 937.
[38] D. Mathieu, R. Phan-Tan-Luu, M. Sergent, Criblage et Étude des Facteurs, LPRAI, Marseille, 1996.
[39] European Pharmacopoeia, vol. 1, fifth ed., Council of Europe, Strasbourg, 2004, p. 78.

Available online at www.sciencedirect.com
ScienceDirect
Talanta 74 (2008) 593–598
Talanta
www.elsevier.com/locate/talanta

On-line preconcentration and speciation analysis of inorganic vanadium in urine using L-methionine immobilised on controlled pore glass

Pablo H. Pacheco [a,b], Roberto A. Olsina [a,c], Patricia Smichowski [c,d], Luis D. Martinez [a,c,*]

[a] *Department of Analytical Chemistry, Faculty of Chemistry, Biochemistry and Pharmacy, National University of San Luis, Chacabuco and Pedernera, 5700 San Luis, Argentina*
[b] *Fondo para la investigación científica y tecnológica (FONCYT), Avda. Córdoba 831, Piso 6 (C1054AAH), Ciudad de Buenos Aires, Argentina*
[c] *Consejo Nacional de Investigaciones Científicas y Técnicas (CONICET), Rivadavia 1917, CP C1033 AAJ, Ciudad de Buenos Aires, Argentina*
[d] *Comisión Nacional de Energía Atómica, Unidad de Actividad Química, Av. Gral. Paz 1499, B1650KNA-San Martín, Argentina*

Received 31 May 2007; received in revised form 8 June 2007; accepted 16 June 2007
Available online 22 June 2007

Abstract

A study was undertaken to ascertain the analytical capabilities of combined ICP–OES with ultrasonic nebulization to perform on-line preconcentration and speciation of inorganic V species in urine samples using a micro-column packed with L-methionine immobilized on controlled pore glass (CPG) as solid phase extractant. At pH 5.0, L-methionine is selective only towards V(V) while, total vanadium was quantitatively adsorbed by the solid phase at pH 9.0 [as V(V)] due to V(IV) oxidation in alkali media. Vanadium species retained by L-methionine were quantitatively eluted from the column with 10% HCl. Effects of acidity, sample flow rate, concentration of eluent and interfering ions on the recovery of the analytes have been systematically investigated. The detection limit (3σ) of V is 0.008 ng mL^{-1} for USN–ICP–OES with an enhancement factor of 900 (10 for USN and 90 for L-methionine), and the relative standard deviation (R.S.D.) is better than 2%. The proposed method has been applied to the determination of inorganic V(V) and V(IV) in urine.
© 2007 Elsevier B.V. All rights reserved.

Keywords: L-Methionine; Vanadium; Speciation; USN–ICP–OES; Urine

1. Introduction

Vanadium is widely distributed in the earth's crust but in low abundance [1]. Environmental pollution caused by vanadium is almost entirely due to industrial activities, such as the production of steel, pigments, photographic materials and insecticides. Vanadium is also released on oil combustion [2].

Vanadium at trace amounts is beneficial to normal cell growth, being one of the so-called essential elements. Its role in physiological systems includes an insulin-like effect, an inhibitory effect on some enzymes and cholesterol synthesis, a catalytic effect in the oxidation of various amines and normalisation of sugar levels [3–7]. At higher concentrations it was shown to be a toxic element and the toxicity of its species is well documented [8]. It can exist in many oxidation states from −1 to +5 and in a number of oxoanionic and oxycationic forms. V(V)is more toxic than V(IV) [9]. In this context, not only total vanadium determination is important, speciation analysis of V acquires relevance too.

Vanadium is absorbed from a variety of foods with a relatively low efficiency, but in sufficient quantities to be absorbed at detectable levels in many body tissues [10]. For a comprehensive exposure study, knowledge of V levels in urine is required to ascertain any relationship to exposure, been V used as a biomarker. Quantification of trace levels of vanadium in biological fluids is a difficult analytical task, due not only to the very low analyte concentrations that need to be addressed, but also by the relatively complexity of the matrix. Yang et al. reported a maximum concentration of vanadium in urine of 1.5 μg L^{-1} [11].

Inductively coupled plasma optical emission spectrometry (ICP–OES) [12] or electrothermal atomic absorption spectrometry (ETAAS) [13,14] have been extensively used for the determination of traces of V, but the low levels of V in urine are not compatible with the detection limits of these techniques.

* Corresponding author. Fax: +54 2652 430224.
E-mail address: ldm@unsl.edu.ar (L.D. Martinez).

0039-9140/$ – see front matter © 2007 Elsevier B.V. All rights reserved.
doi:10.1016/j.talanta.2007.06.018

Preconcentration is an effective means for extending the detection limits of ICP–OES technique. In addition, the on-line preconcentration mode using microcolumns for V determination presents several advantages over batch or off-line procedures improving the detection power and precision and allows a higher sampling throughput.

Unfortunately, major interferences, mainly spectral, (arising from the sample matrix) hampers accurate determination of V in matrices as urine when using ICP–OES. As a result, separation of the analyte from the matrix prior to ICP–OES determination is often needed to ensure accurate results.

For this purpose several packing materials have been used in on-line systems for the preconcentration and separation of V, such as immobilized yeast cell [1], quinine modified resin [15], thenoyltrifluoroacetone immobilized on microcrystalline naphthalene [16] and Amberlite XAD-7 resin [17].

The use of new substrates such as aminoacids and polyaminoacids chains for metal retention, separation and/or speciation has been successfully used [18–24]. However, to the best of our knowledge these systems have not been employed for V preconcentration and/or speciation.

The aim of this study is to take advantage of the high selectivity and retention capacity of L-methionine immobilized on CPG, for V(V) determination using ultrasonic nebulization-inductively coupled plasma optical emission spectrometry (USN–ICP–OES) for detection. Speciation of V(IV) and V(V) in the on-line system was reached by only adjusting the pH of the samples solution. The retention and elution conditions for of V(V) and V(IV) have been studied and the optimized experimental conditions were established. The proposed method was applied to inorganic vanadium speciation in urine.

2. Experimental

2.1. Reagents

Unless otherwise stated, the chemicals used were of analytical grade, and therefore no further purification was required.

Vanadium(IV) stock standard solution, 1000 mg mL^{-1} was prepared by dissolving 4.9680 g of vanadyl sulphate (Merck, Darmstadt, Germany) in 1000 mL of ultrapure water containing 1 mL of concentrated nitric acid.

Vanadium(V) stock standard solution, 1000 mg mL^{-1} was prepared by dissolving 2.2966 g of ammonium metavanadate (99.99%, Merck) in 1000 mL of ultrapure water.

Ultrapure water (18 MΩ cm^{-1}) was obtained from a EASY pure RF Barnstedt, Iowa, USA. Nitric acid 65% was obtained from Flucka (Sigma–Aldrich, Steinheim, Germany).

L-methionine was obtained from Fluka (A. G. Switzerland). Controlled pore glass (CPG, pore diameter 240 Å, mesh size 240–400), 8-aminopropiltriethoxysilane and glutaraldehyde were supplied by Sigma (St. Louis, USA).

2.2. Instrumentation

Measurements were performed with a sequential ICP spectrometer Baird ICP 2070 (Bedford, MA, USA.). The 1 m Czerny–Turner monochromator had a holographic grating with 1800 grooves/mm. The FI system used is shown in Fig. 1. An ultrasonic nebulizer, U 5000 AT [CETAC Technologies (Omaha, NE, USA)], with desolvation system was used. The ICP and ultrasonic nebulizer operating conditions are listed in Table 1. A Minipulse 3 peristaltic pump, Gilson (Villiers-Le-Bell, France) was used. Sample injection was achieved using a Rheodyne (Cotati, CA, USA) Model 50, four-way rotary valve. Tygontype

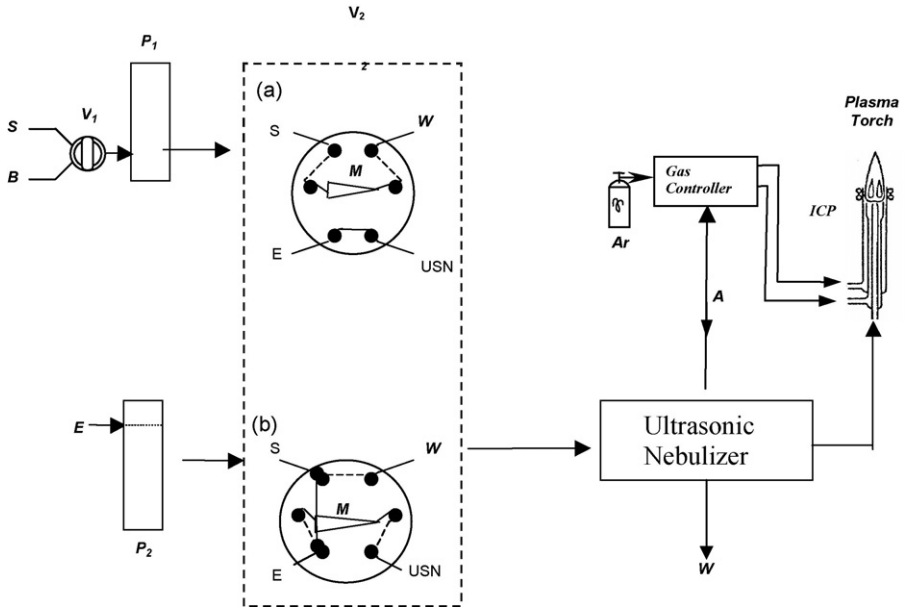


Fig. 1. Schematic diagram of the instrumental setup. S: sample (flow rate: 10 mL min^{-1}); B: buffer; E: eluent (flow rate: 1.0 mL min^{-1}); A: Ar (flow rate: 0.7 L min^{-1}); W: waste; P_1, P_2: peristaltic pumps; C: minicolumn packed with L-methionine-CPG; V: injection valve. Valve positions: (a) sample loading and (b) injection.

Table 1
USN–ICP instrumental parameters

ICP conditions	
RF generator power (kW)	1.0
Frequency of RF generator (MHz)	40.68
Plasma gas flow rate (L min^{-1})	8.5
Auxiliary gas flow rate (L min^{-1})	1
Observation height above load coil (mm)	15
Analytical line: V (nm)	310.2
USN conditions	
Heater temperature (°C)	140
Condenser temperature (°C)	4
Carrier gas flow (L min^{-1})	1

pump tubing (Ismatec, Cole Parmer, Vernon Hills, IL, USA.) was employed to propel the sample, reagents and eluent. The V 310.2 nm spectral line was used.

2.3. Column preparation

The conical minicolumn was prepared by placing 60 mg of L-methionine-CPG into a conical tip using the dry packing method. To avoid loss of filling when the sample solution passed through the conical minicolumn, a small amount of quartz wool was placed at both ends of conical minicolumn. The column was then connected to a peristaltic pump with PTFE tubing to form the preconcentration system.

2.4. Immobilisation procedure

A 0.2 g portion of L-methionine was suspended in 15 mL 0.1 mol L^{-1} phosphate buffer at pH 7.0. Silanization of the CPG using 8-aminopropyltriethoxysilane and the use of the bifunctional property of glutaraldehyde to prepare the glutaraldehyde-treated CPG was the same used previously [25]. The glutaraldehyde-treated CPG was filtered and washed with ultrapure water. To the baker containing the methionine solution, 1.0 g of the treated glass was added and N_2 was flushed for 15 min. The mixture was kept at 4 °C for 24 h under a N_2 atmosphere and then air-dried filtered.

2.5. Sampling of urine

Urine samples were collected from adult male and female individuals aged 20–30 years living in San Luis (Argentina), without having eaten breakfast. Urine samples were filtered through a 0.45 μm pore size membrane and stored in plastic containers without adding preservatives. The samples were analysed immediately to avoid possible species transformation or interconversion.

2.6. Preliminary studies

The evaluation of V retention and filling flow rates were studied off-line. About 25 mL of aqueous solution containing V(IV) or V(V) buffered to different pHs were loaded on the column filled with L-methionine immobilised on CPG at a flow rate of 2 mL min^{-1}. Finally, the retained metalloid was eluted with 5 mL of HCl 10% (v/v).

Vanadium concentrations were determined by USN–ICP–OES. Recoveries were calculated against the theoretical concentration.

2.7. Procedure for preconcentration and speciation of vanadium

The manifold for flow injection system for preconcentration, separation and subsequent determination of V is shown in Fig. 1. Before loading, the column was conditioned for preconcentration at the correct pH [5.0 for V(V), 9.0 for total V], valve V_1 in position B. A desired volume of sample was then loaded on the conical-minicolumn (M) at flow rate of 10 mL min^{-1} with valve V_1 in position S and valve V_2 in load position (a). Finally, valve V_2 was switched to the injection position (b) and the vanadium retained was eluted with 10% (v/v) hydrochloric acid solution. After that, it was introduced directly into the USN unit and subsequently to ICP torch. The operation conditions were established and the determination was carried out.

3. Results and discussion

3.1. Parameters affecting vanadium retention

The effect of pH on vanadium retention in the micro-column was evaluated at different pH values varying between 1.0 and 11.0 and the results are shown in Fig. 2. Vanadium(V) was completely retained in the column in the pH range 5.0–9.0, whereas vanadium(IV) was quantitatively retained at pH 9.0, when the oxidation due to alkaline media was complete. These results indicate that the speciation of vanadium can be achieved with the following procedures: (i) An aliquot of the sample, adjusted to pH 5.0, is passed through the micro-column to separate V(V) from V(IV). (ii) Another aliquot adjusted to pH 9.0 is passed through the micro-column to retain both vanadium species [as V(V)] and the concentration of vanadium(IV) was calculated by subtracting the vanadium(V) concentration from the total concentration.

The sorption capacity of CPG, including silanization and glutaraldehyde-treatement, for V(V) retention without L-methionine was tested and no retention was observed, con-

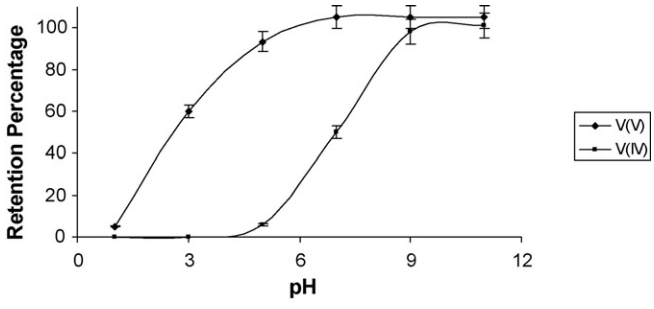


Fig. 2. Dependence of vanadium (IV and V) retention on pH of loading solutions. Volume of sample: 10 mL; V(IV) and V(V) concentration: 0.5 mg L^{-1}; HCl concentration: 10.0% (v/v).

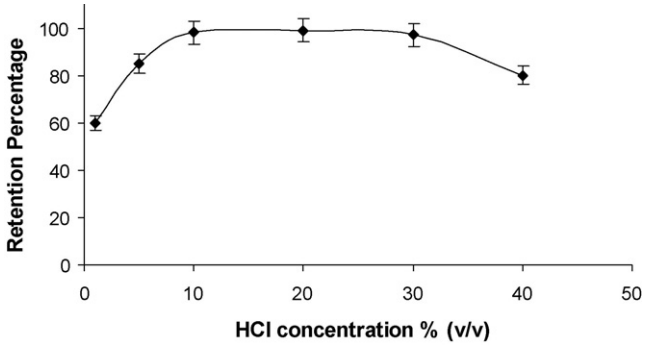


Fig. 3. Influence of HCl concentration on V(V) signal during elution step. Preconcentration of 10 mL of V(V) solutions; vanadium concentration was 50 μg L^{-1}; hydrochloric acid concentration was 5.0, 10.0, 15.0, 20.0 and 30.0% (v/v).

cluding that only L-methionine was responsible for vanadium retention.

Different HCl concentrations were tested and no significant difference in V retention was observed between HCl 10% (v/v) and HCl 30% (v/v) (Fig. 3). We decide to use a 10% HCl to diminished reactive consumption. Higher concentrations of HCl were no tested to avoid a permanent damage to the column.

As the FI manifold has a time-based control, the influence of the contact time sample/filling on the sorption kinetics was investigated. The retention capacity of L-methionine resulted of 1×10^{-2} mmol g^{-1}. The flow rates and preconcentration times were varied in order to keep constant the total mass of analyte loaded onto the column. No significant differences were observed in the concentration efficiency for sample flow rates ranging between 1 and 15 mL min^{-1} where the retention was maximal. Therefore, a sample loading flow rate of 10 mL min^{-1} was selected because higher sampling flow rate could generate inappropriate back pressure and damage the minicolumn.

The effect of the flow rate of eluent was studied and the highest USN–ICP–OES signal was achieved at 1.00 mL min^{-1}.

3.2. Study of possible interferences

The effects of potential interference species (at the concentration levels at which they may occur in the studied sample) were tested. As(III), Cr(III), Cr(VI), Cu(II), Fe(III), Ni(II), Se(IV) and Al(III) were tolerated up to at least 1000 μg L^{-1}. Other concomitant elements such as alkali and alkaline elements were not retained on the immobilised L-methionine under the working conditions. On the other hand, anions such as Cl^-, CO_3^{2-} and SO_4^{2-} were tolerated up to at least concentrations of 2500 μg L^{-1}. These characteristics of the system are important because it avoids that possible components of urine could interfere in the determination of inorganic V species.

To avoid the spectral interference of Al in 309.311 nm V line the 310.2 nm spectral line of V was selected.

3.3. Separation of vanadium(IV) and vanadium(V)

In order to assess the selectivity of the proposed method for V(IV) and V(V), it was applied to various synthetic samples and using different concentration relationships between the two oxidation states. In Table 2, it can be observed that the two species of V are completely separated and quantitatively recovered. The method was thus shown to have an acceptable accuracy under different conditions, with recoveries varying between 97.3 and 101.2% for V(IV) and between 98.0 and 102.5% for V(V).

Changes in the redox equilibrium state may occur between V(V) and V(IV) in the presence of O_2 air, and thus the contents of V species in aqueous solutions may be changed. Total vanadium extraction is reach at pH 9 due to V(IV) oxidation to V(V) occurs in alkali solutions, in the presence of air [26].

3.4. Analytical performance

The overall time required for the preconcentration of 20 mL of sample (2 min, at a flow rate of 10 mL min^{-1}), elution (0.5 min, at a flow rate of 1 mL min^{-1}), and washing and conditioning (0.4 min) was about 2.9 min; hence, throughput was approximately 20 samples h^{-1}. The calibration graph using the preconcentration system for V was linear with a correlation coefficient of 0.9989 from concentrations close to the detection limit up to at least 1000 μg L^{-1}. The detection limits (DL) were calculated as the amount of V required to yield a net peak that was equal to three times the standard deviation of the background signal (3σ). As the preconcentration of V is regarded, the detection limit of ICP–OES depends, among others, on the sample volume loaded onto the column. It resulted to be 0.008 ng mL^{-1} when 20 mL of sample were passed through the column. The reliability of the overall procedure is proven by the good repeatability of measurements as shown in Table 2. At these low V concentrations relative standard deviations (R.S.D.s) turned out to be better than 2%, and total enhancement factor was of 900

Table 2
Evaluation of the separation of V(IV) and V(V) species

V(V):V(IV) ratio	Vanadium(IV)			Vanadium(V)		
	Added (μg L^{-1})	Found (μg L^{-1})	Recovery (%)	Added (μg L^{-1})	Found (μg L^{-1})	Recovery (%)
0.025	50	49.50	99.0	1.25	1.27	101.60
0.125	40	40.20	100.5	5	5.10	102.00
0.5	20	20.30	101.5	10	9.98	99.80
2	10	9.75	97.5	20	19.65	98.25
8	5	5.10	102.0	40	40.15	100.37
40	1.25	1.22	97.6	50	49.55	99.10

Table 3
Procedures for preconcentration and determination of vanadium

Detection limit (ng mL^{-1})	Enrichment/enhancement factor	Sample volume (mL)	Technique	Speciation analysis	References
0.008	900	20	USN–ICP–OES	Yes	This work
0.019	225	10	USN–ICP–OES	Yes	[17]
0.019	180	10	USN–ICP–OES	Yes	[12]
0.060	45	10	ICP-OES	No	[1]
0.060	50	5	ETV-ICP–OES	Yes	[16]
0.072	62.5	50	ETV-ICP–OES	Yes	[15]
0.016	250	50	ICP–OES	No	[28]
0.086	74	3.5	ETV-ICP–OES	Yes	[29]

Table 4
Recovery study (95% confidence interval, $n = 6$)

Aliquot	Base value (μg L^{-1})	V(V) added (μg L^{-1})	V(IV) added (μg L^{-1})	V found (μg L^{-1})	Recovery (%)[a]
1[b]	0.25	0.00	0.00	0.25 ± 0.05	–
2[b]	0.25	0.50	0.00	0.76 ± 0.10	102.0
3[b]	0.25	1.00	0.00	1.27 ± 0.08	102.0
4[b]	0.25	1.50	0.00	1.74 ± 0.07	99.3
5[c]	1.18	0.00	0.00	1.18 ± 0.05	–
6[c]	1.18	0.25	0.25	1.66 ± 0.20	96.0
7[c]	1.18	0.50	0.50	2.19 ± 0.10	101.0
8[c]	1.18	1.00	1.00	3.17 ± 0.17	99.5

[a] 100 [(found-base)/added].
[b] Recuperation for V(V).
[c] Recuperation for total V [as V(V)].

(90 for the preconcentration system, and 10 for the USN). A comparison between the analytical performance of *this method* and other methods used for preconcentration and speciation of V is given in Table 3. L-methionine-CPG improves limit of detection, due mostly to a higher enhancement factor for the determination of V in urine samples at the expected values.

3.5. Validation study

Unfortunately, there are no standard reference materials with a certified content of individual species of V. In this case, a recovery study can be considered as a validation alternative. Urine samples were spiked with 0.5, 1.0 and 1.5 ng mL^{-1} of V(V) to calculate V(V) recovery, and with 0.25, 0.50 and 1.00 ng L^{-1} of V(V) and V(IV) to calculate total V. Although this practice should be avoided, in general, because it disregards the nature of the chemical species in which the element is present, is an alternative to estimate at least the accuracy. Urine was divided in portions of 20 mL each. The proposed method was applied to six portions (three for total V and three for V(V)) and the mean V concentration of each was taken as a base value. Then, increasing quantities of V(IV) and V(V) were added to the other aliquots and the same procedure was followed. As shown in Table 4 the recovery values were between 99.3% and 102.0% for V(V) and 99.0–101.5% for total V. The results were compared with the *t*-test and no significant differences were observed at 95% confidence level. The recovery studies for the other samples showed similar performance.

3.6. Application to real samples

The method was applied to inorganic vanadium determination in urine. The concentrations found were in the range 0.21–0.38 μg L^{-1} of V(V), and 1.14–1.21 μg L^{-1} of V(IV). These results were obtained by the standard addition method, and are shown in Table 3 and the relation of V(IV)/V(V) is in good agreement with those obtained by Caruso et al. [27].

4. Conclusion

This study supports that L-methionine immobilised on CPG is an appropriate substrate for vanadium retention, allowing its preconcentration and speciation. The coupled system provides an accurate and precise means for determining both V(IV) and V(V) inorganic species at ng L^{-1} levels with quantities recoveries. The method is simple, no masking agents are necessary, no oxidation/reduction is required, and only by adjusting the pH both species are preconcentrated in complex matrix as human urine. The analytical performance of the method shows a high enrichment factor of 900 and the detection power afforded by this analytical approach is adequate to comply with the levels of analyte usually expected in urine. To the best of our knowledge this is the first time that L- methionine is employed for vanadium separation and speciation in urine.

Acknowledgements

This work was supported by Consejo Nacional de Investigaciones Científicas y Técnicas (CONICET), Agencia Nacional

de Promoción Científica y Tecnológica (FONCYT) (PICTBID), Universidad Nacional de San Luis (Argentina) and Comisión Nacional de Energía Atómica (CNEA).

References

[1] S. Moyano, G. Polla, P. Smichowski, J.A. Gasqueza, L.D. Martinez, J. Anal. At. Spectrom. 21 (2006) 422.
[2] C. Wann, S. Jiang, Anal. Chim. Acta 257 (1997) 211.
[3] D.C. Crans, M. Shaia Gottlieb, J. Tawara, R.L. Bunch, L.A. Theisen, Anal. Biochem. 88 (1990) 53.
[4] C.M. Krejsa, J.M. Esselstyn, S.G. Nadler, T.J. Kavanagh, J.A. Ledbette, G.L. Schieven, J. Biol. Chem. 272 (1997) 11541.
[5] E. Tsiani, I.G. Fantus, Trends Endocrinol. Metab. 8 (1997) 41.
[6] S. Jandhyala, G.J. Hom, Life Sci. 33 (1983) 1325.
[7] K. Kofuji, C.J. Qian, Y. Murata, S. Kawashima, J. Inorg. Biochem. 99 (2005) 1329.
[8] M. Tomlison, J. Wang, J. Caruso, J. Anal. At. Spectrom. 9 (1994) 957.
[9] M. Taylor, J. van Staden, Analyst 119 (1994) 1263.
[10] B. Patel, G. Henderson, S. Haswell, R. Grzeskowiak, Analyst 115 (1990) 1063.
[11] Lu Yang, Ralph E. Sturgeon, Dennis Prince, Stephan Gabos, J. Anal. At. Spectrom. 17 (2002) 1300.
[12] R.G. Wuilloud, J.A. Salonia, R.A. Olsina, L.D. Martinez, Spectrochim. Acta Part B 55 (2000) 671.
[13] Y. Saavedra, P. Fernandez, A. Gonzalez, Anal. Bioanal. Chem. 379 (2004) 72.
[14] H. Günter, J. Kart, V. Wolfgang, Anal. Chim. Acta 386 (1999) 145.
[15] Yiwei Wu, Zucheng Jiang, Bin Hu, Talanta 67 (2005) 854.
[16] Fan Zhefeng, Hu Bin, Jiang Zucheng, Spectrochim. Acta Part B 60 (2005) 65.
[17] R.G. Wuilloud, J.A. Salonia, J.A. Gásquez, R.A. Olsina, L.D. Martinez, Anal. Chim. Acta 420 (2000) 73.
[18] H.A. Jurbergs, J.A. Holcombe, Anal. Chem. 69 (1997) 1893.
[19] M. Howard, H.A. Jurbergs, J.A. Holcombe, J. Anal. At. Spectrom. 14 (1999) 1209.
[20] E. Gutierrez, et al., Environ. Sci. Technol. 33 (1999) 1664.
[21] T.C. Miller, J.A. Holcombe, J. Hazard. Mater. 83 (2001) 219.
[22] M. Howard, H.A. Jurbergs, J.A. Holcombe, Anal. Chem. 70 (1998) 1604.
[23] L. Malachowski, J.A. Holcombe, Anal. Chim. Acta 495 (2003) 151.
[24] P.H. Pacheco, R.A. Gil, P. Smichowski, G. Polla, L.D. Martinez, J. Anal. At. Spectrom. 22 (2007) 305.
[25] H.A.M. Elmahadi, G.M. Greenway, J. Anal. At. Spectrom. 6 (1991) 643.
[26] P.C. Cole, G.H. Eckert, K.L. Williams, Anal. Chim. Acta 61 (1983) 153.
[27] M.J. Tomlinson, J. Wang, J.A. Caruso, J. Anal. At. Spectrom. 9 (1994) 957.
[28] G.M. Wuilloud, J.C.A. de Wuilloud, R.G. Wuilloud, M.F. Silva, R.A. Olsina, L.D. Martinez, Talanta 58 (2002) 619.
[29] L. Li, B. Hu, Talanta 72 (2007) 472.

Available online at www.sciencedirect.com
ScienceDirect
Talanta 74 (2008) 747–752
Talanta
www.elsevier.com/locate/talanta

First-order derivative resolution of overlapped PAH peaks with common mass spectra in gas chromatography–mass spectrometry

Guillermo Quintás [a,*], Bernhard Lendl [a], Agustín Pastor [b], Miguel de la Guardia [b]

[a] *Institute for Chemical Technologies and Analytics, Vienna University of Technology, Getreidemarkt 9-164, A-1060 Vienna, Austria*
[b] *Department of Analytical Chemistry, Universitat de València, Edifici Jeroni Muñoz, 50th Dr. Moliner, 46100 Burjassot, Spain*

Received 13 April 2007; received in revised form 26 June 2007; accepted 26 June 2007
Available online 25 July 2007

Abstract

First-order derivative of 15 points smoothed chromatograms of mixtures of benzo(*b*)fluoranthene (BbF) and benzo(*k*)fluoranthene (BkF) for the *m*/*z* 252 ion obtained using two microscans has been proposed as a simple alternative to the resolution of overlapped chromatographic peaks of these two compounds which have identical mass spectra. The procedure provides limits of detection of 12 and 29 ng g^{-1} for BbF and BkF, respectively and offers the possibility to use the 250 and 248 ions to confirm the identity of these analytes.
© 2007 Elsevier B.V. All rights reserved.

Keywords: First derivative; Gas chromatography–mass spectrometry; Polycyclic aromatic hydrocarbons

1. Introduction

Chemometrics has been widely applied for exploring chromatograms using, for example, the deconvolution of the high performance liquid chromatography-diode array detection (HPLC–DAD) chromatograms using orthogonal polynomials [1] or the deconvolution of coeluting HPLC–DAD peaks based on purity ratios [2]. Multivariate data analysis has also been applied to HPLC–DAD evolving factor analysis and heuristic latent projections [3]. Deconvolution approaches based upon determining purity curves and multiple linear regression have been applied to resolve overlapping HPLC–DAD tailing peaks [4], and to gas chromatography with mass spectrometry detection (GC–MS) [5–8]. The application of wavelet transform algorithms (WT) in hyphenated chromatographic techniques has been proven to be useful for a variety of tasks such as denoising, baseline correction as well as for the determination of component number in overlapping chromatograms [9].

The capacity of partial least squares (PLS-1 and PLS-2) as well as principal component regression (PCR) has been proved for resolving overlapped peaks in chromatography [10]. More recently, the use of multivariate curve resolution-alternating least squares (MCR-ALS) has been proposed for data treatment of LC–MS and GC–MS data [11–14].

It is remarkable that, in spite of the relatively high number of chemometric methods employed for the resolution of overlapped peaks in HPLC and GC, and the increase of the number of methods based on MS detection, most of the proposed procedures cannot be applied to the resolution of analytes with identical mass spectra and thus, the use of multivariate curve resolution techniques can be applied for resolution of compounds with similar spectra, but not for those with common spectra.

Polycyclic aromatic hydrocarbons (PAHs) are ubiquitous semivolatile organic pollutants formed by the incomplete combustion of organic matter and generated whenever fossil fuels or vegetation are burned. Concern with the occurrence of these compounds in the environment is well justified, as it is the development of analytical methods for their determination because some of them are known to be mutagenic or carcinogenic [15,16].

The toxicity of PAHs has justified their inclusion in food and environmental legislation worldwide. The European Union requires continuous air-quality monitoring with long-term assessment of benzo(*a*)pyrene (BaP), used as a marker for carcinogenic risk of PAHs in ambient air, and other relevant PAHs that include benzo(*b*)fluoranthene (BbF) and benzo(*k*)fluoranthene (BkF) [17].

* Corresponding author. Fax: +43 1 58801 151 99.
E-mail address: guiquin@alumni.uv.es (G. Quintás).

0039-9140/$ – see front matter © 2007 Elsevier B.V. All rights reserved.
doi:10.1016/j.talanta.2007.06.050

The chromatographic detection of PAHs is usually carried out by liquid chromatography with fluorescence detection (HPLC–FLD) [18] or by gas chromatography with mass spectrometric detection (GC–MS) [19–21]. The former has a high sensitivity but presents an important disadvantage: the lack of unambiguous confirmation of the identity of the analytes. GC–MS avoids this disadvantage but provides limits of detection significantly higher than those provided by HPLC–FLD. Moreover, with GC–MS it is not always possible to achieve a complete chromatographic separation of the PAHs and, in some cases coeluting components have identical or closely similar mass spectral characteristics, as in the case of BbF and BkF. In these situations it is not possible to improve the separation of the analytes neither by measuring a characteristic ion, nor by carrying out a second or higher order fragmentation of the molecule.

On the other hand, derivative techniques have been widely applied in spectrometry in order to correct spectral interferences, but its use is not frequent in chromatography to resolve coeluting peaks [10,22].

The objective of this work is the development of a simple and fast mathematical procedure for the quantitative resolution of the elution profiles of coeluting analytes (BbF and BkF) in GC–MS, using the first derivative of the chromatographic peaks. On the other hand, the developed procedure will include criteria for the confirmation of the analytes identity according to the ratio of three characteristic ions of each analyte.

2. Experimental

2.1. Apparatus and reagents

Chromatographic analyses were performed on a Trace GC–ion trap MS spectrometer (Thermo-Finnigan, San Jose, CA, USA). Separation was carried out on a BPX5 capillary column (SGE Scientific, Ringoes, NJ, USA), 30 m × 0.25 mm i.d., 0.25 μm film thickness. High purity helium (99.999%) was employed as a carrier gas. For data manipulation Xcalibur 1.3 (Thermo-Finnigan, San Jose, CA, USA) and Omnic 6.1 (Thermo-Finnigan, San Jose, CA, USA) software were used.

The GC temperature program was: initial 110 °C, hold 1 min, rate 5 °C min^{-1} to 300 °C, hold 5 min. The mass spectrometer was operated in the electron impact mode (EI) using 70 eV ionization voltage. The ion source temperature was 220 °C and the GC–MS interface was set to 250 °C. The analyses were performed by SIM detection mode using the *m/z* ions 248, 250 and 252 (±0.5). Mass calibration and lens tuning was made in EI mode using the autotune program included in the Xcalibur 1.3 software also using perfluorotributylbutylamine (PFTBA).

Analytical standards of benzo(*b*)fluoranthene (BbF) and benzo(*k*)fluoranthene (BkF), used in this study were supplied by Dr. Ehrenstorfen GmbH (Augsburg, Germany). Standard solutions were prepared by dilution in hexane and stored in capped amber vials at −20 °C.

2.2. Chromatographic determination

Using the aforementioned instrumental conditions, samples and standards were dissolved in toluene and 1 μl injected in the splitless mode.

Confirmation criteria for the detection of PAHs should include the following: (a) retention time for two monitored ions for a given analyte should maximize simultaneously ±1 s, with signal-to-noise ratio ≥3 for each diagnostic ion and (b) the ratio between the two monitored ions should be within 15% of the documented value.

Raw GC–MS data was smoothed using the Savitsky–Golay function with a smoothing interval of 15 points, and after that, the first derivatives of the chromatograms (FDC) were calculated. Then, an external calibration line using BbF and BkF standards in the concentration range from 150 to 900 ng g^{-1} was established using the smoothed FDC corresponding to the 252 *m/z* ion. To determine the concentrations of BbF and BkF in samples, FDC peak areas corresponding to elution of BbF and Bk, were measured and interpolated in the calibration line. The ratio between ions was calculated by interpolation of the FDC corresponding to 248 and 250 *m/z* ions in the 252 *m/z* ion regression line.

3. Results and discussion

3.1. GC–MS chromatograms of BbF and BkF

Fig. 1 shows the structures as well as the mass spectra of BbF and BkF, measured in the SIM conditions described previously. It must be noted that both analytes have identical mass spectra and so the resolution of their overlapping is not feasible neither by measuring a characteristic ion, nor by the application of tandem mass spectrometry (MS/MS).

An alternative could be the modification of the experimental conditions in order to obtain the chromatographic separation of the two components, but it is not feasible in this case because of the high similarity between both studied PAHs.

The detection of PAHs was carried out in selected ion monitoring (SIM) mode because the use of this measurement mode can improve the detection limits for PAHs dramatically from those achieved by full scan GC–MS. Three selected characteristic ions (*m/z* values: 248, 250 and 252) were measured, because too many SIM events would take too long leading to improper sampling and poor peak shapes.

One of the main instrumental parameters that affect the signal in GC–MS in the SIM mode is the number of microscans. A mass spectrum is obtained by running the scan function defined by the user a number of times specified by the number of microscans; the signals which compose the mass spectrum are the result of averaging those obtained from each microscan [25]. The number of microscans depends on the type of experiment that you are performing. A scan with a high number of microscans provides a high signal averaging but takes a long time to be acquired, thus reducing the number of data points during the elution of the analyte in GC–MS.

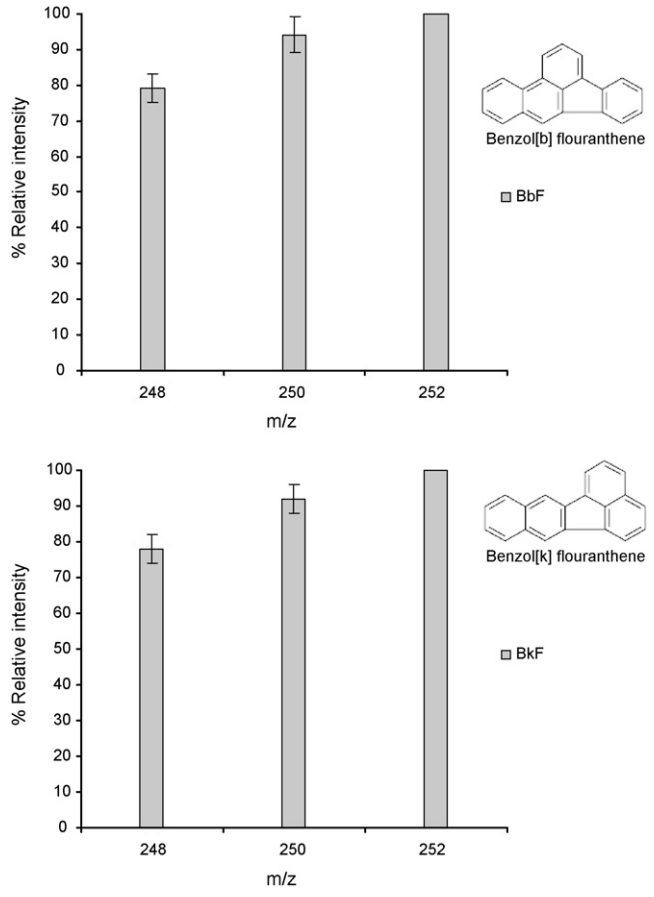


Fig. 1. Relative intensities of the characteristic ions of BbF and BkF using the selected GC–MS instrumental conditions. Values are the average ± S.D. of three injections of BbF and BkF in the range 100–750 ng g^{-1}.

Fig. 2 shows GC–MS chromatograms at *m/z* 252 using a five points Boxcar smoothing function, of a solution containing 0.71 and 0.66 μg g^{-1} of BbF and BkF, respectively, using increasing number of microscans.

It can be seen that although a complete resolution between peaks is never achieved, the resolution is affected by the number of microscans and to obtain two peaks, a low number of microscans must be selected. Furthermore, a high number of data points per peak are needed to improve the repeatability and accuracy of further measurements using the first derivative of the chromatographic peaks. Additionally, the noise level of the chromatogram is strongly related to the number of microscans and so, the increase of this value increases systematically the signal to noise ratio. So, in order to ensure a compromise between sensitivity and resolution, a number of two microscans was employed in further measurements.

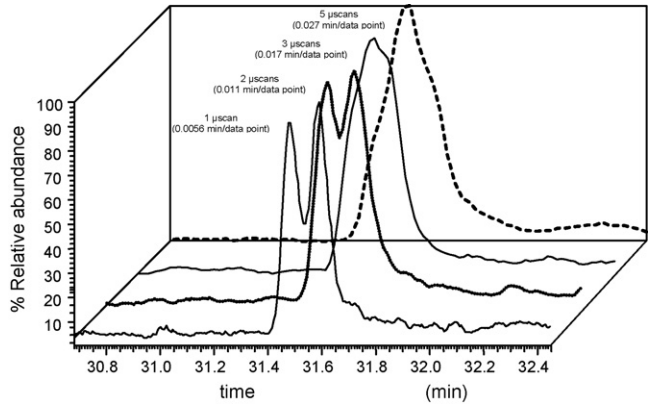


Fig. 2. Effect of the number of microscans on the resolution of both, the BbF and BkF peaks. *Note*: experimental conditions as indicated in the text.

3.2. Derivative signals of GC–MS chromatograms

The differentiation of the chromatographic signal in the time domain can be used to improve the resolution of overlapping peaks [22]. The use of derivative chromatograms can reveal overlapping peaks due to the presence of interfering coeluting compounds, thus increasing the possibilities for the resolution of difficult samples. Fig. 3 shows the zero order, the first- and the second-order derivatives of chromatograms at 252 *m/z* obtained for BbF and BkF pure standard solutions and mixtures. From this figure it is clear that the integration of the raw chromatograms leads to inaccurate results. Moreover, the confirmation criteria for the determination of PAHs include that the ratio between the monitored ions should be within 15% of the documented value, and so, using the raw spectra, the peak purity of both compounds cannot be adequately ensured.

On the other hand, the sensitivity of the procedure when using the first- or second-order derivatives is reduced as compared to that found when using the zero-order data.

Fig. 3 shows that the overlapped peaks can be resolved using the first derivative of the chromatograms obtained from smoothed zero-order ones. The FDC regions selected for the determination of BbF and BkF are shown in Fig. 3 and correspond to the inflection points of the ascending and descending parts of the peaks, to determine BbF and BkF, respectively. On the other hand, the use of a second derivative of the signal is not recommended because it reduces drastically the sensitivity of the procedure.

Another additional advantage of the use of the first derivative of the GC–MS data is that chromatographic baselines are removed, avoiding the baseline drifting due to the bleeding of the column in late eluting peaks.

3.3. Selection of data pre-treatment to improve calibration

Data treatment of first derivative GC–MS signals can be troublesome at low concentrations because of the high noise level. To overcome, or at least to reduce, this drawback, different smoothing functions (Savitsky–Golay, Gaussian and Boxcar) of the zero-order raw data using different smoothing intervals ranging from 9 to 15 points were tested and results compared to those obtained without the use of any smoothing function. The importance of the selection of an appropriate smoothing is clearly shown in Fig. 4. As an example, in this figure it is depicted the effect of different smoothing intervals using a Savitsky–Golay smoothing on the FDC of a standard solution containing 400 ng g^{-1} BbF and 770 ng g^{-1} BkF. When the number of smoothing points increases, both the signal intensity

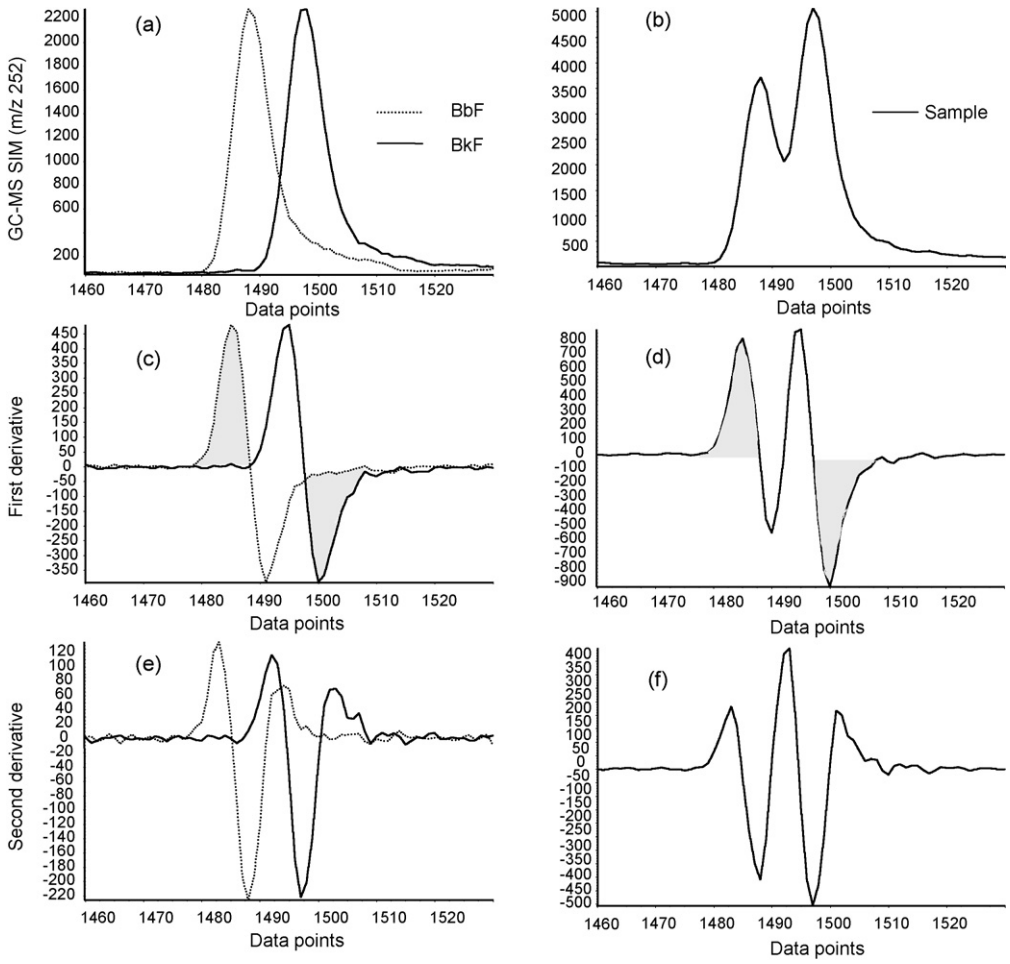


Fig. 3. Zero-order (1, 2), first-order (3, 4) and second-order (5, 6) derivative chromatograms of both, pure BbF and BkF standards (1, 3, 5) and a mixture of the aforementioned compounds (2, 4, 6) obtained using two microscans. *Note*: for the rest of conditions see the text. The grey areas in the first derivatives chromatograms are the selected peaks used for the quantification of BbF and BkF.

and the noise decrease. The selection of the most appropriate smoothing was based on the linearity of the regression curves achieved as well as on the noise level of the FDC.

Calibration results using different smoothing conditions are summarized in Table 1. Peak area results are less influenced by little variations in the FDC showing better linearity and lower limits of detection than those provided by peak height measurements. A 15-points Savitsky–Golay smoothing was selected as yielding one of the highest signal to noise ratios providing also a good linearity of the calibrations.

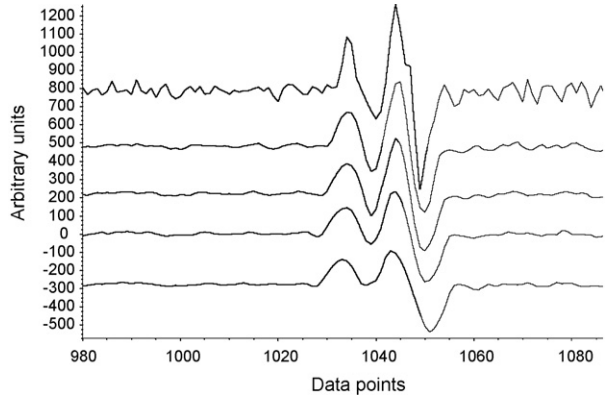


Fig. 4. Effect of increasing smooth interval ranges on the first derivative chromatogram (*m/z* 252) of a solution containing 400 ng g^{-1} BbF and 770 ng g^{-1} BkF. *From top to bottom*: No smooth of the raw GC–MS data; 9 points smooth; 11 points smooth; 13 points smooth; 15 points smooth.

3.4. Sample analysis

A set of 11 mixtures of BbF and BkF were prepared and analyzed as described before in order to validate the method and to test the applicability of the procedure in real sample analysis. BbF and BkF concentrations ranged between 0 and 0.88 and from 0 to 0.73 μg g^{-1}, respectively, with BbF/BkF ratios from 0.5 to 3.1. Concentrations obtained using the selected conditions are shown in Table 2. Results were accurate in the BbF/BkF ratio interval studied. Additionally a high repeatability was found with relative standard deviations lower than 15% for both PAHs that would be improved using an internal standard.

Results of BbF and BkF concentrations obtained using the 252 *m/z* ion by FDC were represented in front of the real ones, and adjusted to a linear regression curve. The BbF regression line had an intercept value of (0.01 ± 0.02) and a slope

Table 1
Analytical features of the first derivative GC–MS (*m/z* 252) determination of BbF and BkF using different measurement criteria and smoothing of the raw data.

Analyte	Smooth	$A=(a\pm s_a)+(b\pm s_b)$ [BbF] ($\mu g\,g^{-1}$)	R^2	LOD	LOQ	$H=(a\pm s_a)+(b\pm s_b)$ [BbF] ($\mu g\,g^{-1}$)	R^2	LOD	LOQ	Noise
BbF	None	$(129\pm138)+(2337\pm332)C$	0.9418	183	604	$(8\pm12)+(817\pm30)C$	0.9960	151	498	30
	S–G[a] 9 points	$(32\pm30)+(2444\pm72)C$	0.9974	43	142	$(2\pm6)+(-612\pm14)C$	0.9984	43	142	15
	S–G 11 points	$(19\pm18)+(2359\pm42)C$	0.9990	41	135	$(1\pm9)+(532\pm21)C$	0.9953	31	102	14
	S–G 13 points	$(-24\pm21)+(2414\pm51)C$	0.9987	35	116	$(2\pm3)+(457\pm6)C$	0.9994	67	221	13
	S–G 15 points	$(-5\pm12)+(2405\pm29)C$	0.9995	12	40	$(1\pm4)+(371\pm8)C$	0.9990	21	69	11
	Gaussian 5 points	$(-30\pm49)+(2406\pm17)C$	0.9929	36	119	$(4\pm7)+(674\pm18)C$	0.9979	49	162	19
	Gaussian 7 points	$(14\pm28)+(2186\pm66)C$	0.9972	23	76	$(3\pm3)+(578\pm7)C$	0.9996	43	142	15
	Boxcar 5 points	$(15\pm15)+(2205\pm36)C$	0.9992	24	79	$(3\pm9)+(501\pm22)C$	0.9939	39	129	14
	Boxcar 7 points	$(-5\pm9)+(1955\pm21)C$	0.9996	25	83	$(4\pm6)+(355\pm14)C$	0.9952	25	83	14

Analyte	Smooth	$A=(a\pm s_a)+(b\pm s_b)$ [BkF] ($\mu g\,g^{-1}$)	R^2	LOD	LOQ	$H=(a\pm s_a)+(b\pm s_b)$ [BkF] ($\mu g\,g^{-1}$)	R^2	LOD	LOQ
BkF	None	$(-13\pm123)+(-2361\pm266)C$	0.9628	129	426	$(-42\pm57)+(-759\pm124)C$	0.9235	222	733
	S–G[a] 9 points	$(-49\pm46)+(-2138\pm100)C$	0.9935	126	416	$(-6\pm6)+(-502\pm13)C$	0.9980	82	271
	S–G 11 points	$(-4\pm9)+(-2091\pm20)C$	0.9997	27	89	$(-15\pm14)+(-411\pm31)C$	0.9930	33	109
	S–G 13 points	$(-23\pm26)+(-1932\pm56)C$	0.9985	49	162	$(-4\pm4)+(-386\pm8)C$	0.9986	44	145
	S–G 15 points	$(-8\pm11)+(-1851\pm23)C$	0.9995	29	96	$(-7\pm7)+(-362\pm15)C$	0.9967	49	162
	Gaussian 5 points	$(-9\pm10)+(-2205\pm23)C$	0.9997	55	182	$(-4\pm8)+(-541\pm17)C$	0.9969	61	201
	Gaussian 7 points	$(-20\pm18)+(-2335\pm50)C$	0.9991	58	191	$(-6\pm6)+(-462\pm13)C$	0.9987	31	102
	Boxcar 5 points	$(-17\pm16)+(-1900\pm35)C$	0.9990	32	106	$(-19\pm18)+(-394\pm38)C$	0.9814	113	373
	Boxcar 7 points	$(-10\pm17)+(-1666\pm37)C$	0.9985	33	109	$(-10\pm10)+(-318\pm21)C$	0.9914	81	267

Calibration line calculated from the measurement of six standards of BbF and BkF with concentrations ranging between 150 and 900 ng g^{-1}. A = peak area, H = peak height. Noise measured in the analytes elution window as R.M.S. (root mean square) in a blank injection. LOD = $3S_b/b$ and LOQ = $(10S_b/b)$ are expressed as ng g^{-1}, being s_b the S.D. of six measurements of a 150 ng g^{-1} solution and b the sensitivity expressed as the slope of the calibration line.

[a] S–G: Savitsky–Golay smoothing function.

Table 2
First derivative GC–MS determination of BbF and BkF in samples

Analyte	Sample	*m/z* 248		*m/z* 250		*m/z* 252		Real conc. ($\mu g\,g^{-1}$)	([BbF]/[BkF]) $_{real}$	([BbF]/[BkF])$_{calc}$
		Analyte[a] ($\mu g\,g^{-1}$)	Relative intensity	Analyte ($\mu g\,g^{-1}$)	Relative intensity	Analyte ($\mu g\,g^{-1}$)	Relative intensity			
BbF	1	0.137 ± 0.003	78	0.164 ± 0.003	93	0.18 ± 0.03	100	0.16	0.80	0.90
	2	0.163 ± 0.004	83	0.2043 ± 0.0007	97	0.21 ± 0.03	100	0.23	0.52	0.50
	3	0.17 ± 0.01	78	0.199 ± 0.001	92	0.22 ± 0.03	100	0.24	0.33	0.28
	4	0.674 ± 0.005	75	0.806 ± 0.005	90	0.90 ± 0.02	100	0.88	2.32	2.59
	5	0.297 ± 0.009	79	0.36 ± 0.02	96	0.376 ± 0.005	100	0.40	0.65	0.59
	6	0.572 ± 0.011	82	0.686 ± 0.005	99	0.70 ± 0.04	100	0.72	3.13	3.06
	7	0.47 ± 0.02	86	0.524 ± 0.007	96	0.55 ± 0.03	100	0.58	1.35	1.31
	8	0.49 ± 0.03	75	0.61 ± 0.03	93	0.655 ± 0.001	100	0.69	1.08	1.08
	9	0.107 ± 0.003	75	0.13 ± 0.02	92	0.143 ± 0.004	100	0.15	1.07	1.10
	10	0.079 ± 0.004	77	0.10 ± 0.02	98	0.103 ± 0.013	100	0.08	–	–
	11	0.003 ± 0.004	100	0.002 ± 0.003	100	−0.001 ± 0.003	100	0	0.00	−0.02
BkF	1	0.154 ± 0.003	76	0.173 ± 0.008	86	0.20 ± 0.02	100	0.20		
	2	0.304 ± 0.004	72	0.38 ± 0.04	91	0.423 ± 0.006	100	0.44		
	3	0.582 ± 0.015	74	0.695 ± 0.002	88	0.79 ± 0.02	100	0.73		
	4	0.286 ± 0.006	82	0.334 ± 0.003	96	0.348 ± 0.006	100	0.38		
	5	0.533 ± 0.002	83	0.57 ± 0.02	88	0.64 ± 0.03	100	0.62		
	6	0.17 ± 0.01	77	0.201 ± 0.003	88	0.229 ± 0.003	100	0.23		
	7	0.32 ± 0.02	77	0.360 ± 0.005	86	0.42 ± 0.02	100	0.43		
	8	0.46 ± 0.01	76	0.54 ± 0.05	89	0.609 ± 0.004	100	0.64		
	9	0.104 ± 0.008	80	0.12 ± 0.03	96	0.13 ± 0.02	100	0.14		
	10	−0.004 ± 0.005	100	−0.004 ± 0.002	100	−0.0003 ± 0.0005	100	0		
	11	0.003 ± 0.001	56	0.036 ± 0.007	77	0.05 ± 0.02	100	0.06		

In every case, area values were interpolated in a linear regression curve calculated from the injection of six standards of BbF and BkF using the *m/z* 252. The relative intensities of the different ions can be employed for the confirmation of the identity of the analytes.

[a] Mean concentration obtained for three independent replicates. GC–MS data were smoothed (15 points) for the calculation of the concentrations of both PAHs.

Table 3
Evaluation of the accuracy of both peak height and area measurement for the determination of BbF and BkF in zero-order GC–MS chromatograms

Measurement mode	Regression line ($[PAH]_{calc} = (a \pm s_a) + (b \pm s_b)\ [PAH]_{real}$					
	Height			Area		
	Intercept	Slope	R^2	Intercept	Slope	R^2
BbF	-0.02 ± 0.01	1.04 ± 0.03	0.98	-0.07 ± 0.02	1.04 ± 0.02	0.98
BkF	-0.03 ± 0.05	1.08 ± 0.05	0.92	-0.02 ± 0.03	1.11 ± 0.08	0.95

of (0.97 ± 0.02) with a regression coefficient of 0.995. On the other hand, the intercept value of the regression line for BkF was (-0.01 ± 0.01) and the slope value was (1.03 ± 0.03) with a regression coefficient R^2 of 0.990. In both cases, the intercept and slope values are statistically equal to 0 and 1, respectively, for a probability level of 95%, showing the accuracy of the method.

Moreover, to test the usefulness of the method, PAH concentrations were calculated using peak area and height measurements in the zero-order GC–MS chromatograms. Table 3 shows the calculated regression lines between the measured values and the real concentrations of BbF and BkF. Although as previously reported, peak height measurements provide better correlation equations to the correct values [23,24] than peak area values, the values of the slopes and R^2 coefficients evidence the presence of systematic errors and a lack of linearity, respectively.

In order to confirm the results obtained peak areas from the FDC of the 248 and 250 *m/z* ions were measured as previously described and then the values were interpolated in the 252 *m/z* regression line. The relative intensity of the characteristic ions was then calculated.

In every sample, the concentration ratio between ions for both BbF and BkF, were within the 15% of the documented ratios. So, it can be concluded that results obtained for the FDC measurements were more accurate and precise than those provided by zero-order chromatography.

It must be noted that the sensitivity of the procedure is limited by the need of confirmation of the relative intensities of ions. In the analysis of BbF and BkF, the less intense ion is *m/z* 248 (77% relative intensity), and so, the LOD calculated using the *m/z* 252 (100% relative intensity) must be divided by 0.77 in order to be able to carry out the calculation of the relative intensities of the three ions of the same molecule to confirm the results.

4. Conclusions

The differentiation of the GC–MS signals proposed can improve the quantification of overlapped analytes. The method also allows the confirmation of the identity of the analytes by measuring the ratio between different ions. The suitability of the developed procedure and its robustness has been evidenced by the accuracy and precision of data provided by this approach. The use of the proposed procedure avoids complex data pretreatment and the use of additional chemometrics software, increasing the sample throughput as compared with multivariate procedures.

Acknowledgements

G.Q. acknowledges the Ministerio de Educación y Ciencia, Secretaría de Estado de Universidades e Investigación (Spain) (EX2004-1245) post-doctoral grant.

References

[1] H.J.G. Debets, A.W. Wijnsma, D.A. Doornbos, H.C. Smit, Anal. Chim. Acta (1985) 17133.
[2] R.G. Brereton, S. Dunkerley, Analyst 124 (1999) 705.
[3] H.R. Keller, D.L. Massart, Anal. Chim. Acta 246 (1991) 379.
[4] C.Y. Airiau, R.G. Brereton, S. Dunkerley, Analyst 125 (2000) 833.
[5] F. Guo, Y. Liang, C. Xu, Huang L, J. Chromatogr. A 1016 (1) (2003) 99.
[6] S.A. Mjos, Anal. Chim. Acta 488 (2) (2003) 231.
[7] H. Shen, B. Grung, O.M. Kvalheim, I. Eide, Anal. Chim. Acta 446 (1–2) (2001) 313.
[8] B.J. Prazen, C.A. Bruckner, R.E. Synovec, B.R. Kowalski, Anal. Chem. 71 (6) (1999) 1093.
[9] X. Hao, W. Cai, Z. Pan, Chemom. Intell. Lab. Syst. 45 (1999) 249.
[10] A. Garrido Frenich, F.J. Arrebola Liébanas, M. Mateu-Sánchez, J.L. Martínez Vidal, Talanta 60 (2003) 765.
[11] E. Pere-Trepat, S. Lacorte, R. Tauler, J. Chromatogr. A 1096 (2005) 111.
[12] E. Bezemer, S. Rutan, Anal. Chem. 73 (2001) 4403.
[13] J.S. Salaua, M. Honinga, R. Taulerb, D. Barcelo, J. Chromatogr. A 795 (1998) 3.
[14] P. Jonsson, A.I. Johansson, J. Gullberg, J. Trygg, A. Jiye, B. Grung, S. Marklund, M. Sjostrom, H. Antti, T. Moritz, Anal. Chem. 77 (2005) 5635.
[15] European Comission, SCF/CS/CNTMP/PAH/29 ADD1 Final, December 4 2002.
[16] IARC, Monographs on the Evaluation of Carcinogenic Risk to Humans, International Agency for Reseach on Cancer, Lyon, 1991, pp. 43–53.
[17] European Comission Council Directive 2004/107/CE, OJ No. L23, January 26, 2005.
[18] E. Manoli, A. Kouras, C. Samara, Chemosphere 56 (2004) 867.
[19] J. Moreira Vaz, Talanta 60 (2003) 687.
[20] V. Yusà, G. Quintás, O. Pardo, A. Pastor, M. de la Guardia, Talanta 69 (4) (2005) 807.
[21] V. Curtis, Environ. Toxicol. Chem. 22 (2003) 50.
[22] P. Parrilla, M. Martínez Galera, J.L. Martínez Vidal, A. Garrido Frenich, Analyst 119 (1994) 2231.
[23] V.R. Meyer, Chromatographia 40 (1995) 15.
[24] J.P. Foley, J. Chromatogr. 384 (1987) 301.
[25] R.E. March, J. Mass Spectrom. 32 (1997) 351.

Available online at www.sciencedirect.com
ScienceDirect
Talanta 74 (2008) 730–735
Talanta
www.elsevier.com/locate/talanta

New hydrazine sensors based on electropolymerized *meso*-tetra (4-sulphonatephenyl)porphyrinate manganese (III)/silver nanomaterial

Maria S.M. Quintino, Koiti Araki *, Henrique E. Toma, Lúcio Angnes *

Departamento de Química Fundamental, Instituto de Química, Universidade de São Paulo, Av. Prof. Lineu Prestes 748, 05508-900 São Paulo, SP, Brazil

Received 19 April 2007; received in revised form 29 June 2007; accepted 2 July 2007
Available online 7 July 2007

Abstract

A new electrocatalytic active porphyrin nanocomposite material was obtained by electropolymerization of *meso*-tetra(4-sulphonatephenyl) porphyrinate manganese(III) complex (MnTPPS) in alkaline solutions containing sub-micromolar concentrations of silver chloride. The modified glassy carbon electrodes efficiently oxidize hydrazine at 10 mV *versus* Ag/AgCl, dramatically decreasing the overpotential of conventional carbon electrodes. The analytical characteristics of this amperometric sensor coupled with batch injection analysis (BIA) technique were explored. Wide linear dynamic range (2.5×10^{-7} to 2.5×10^{-4} mol L^{-1}), good repeatability (R.S.D. = 0.84%, $n = 30$) and low detection (3.1×10^{-8} mol L^{-1}) and quantification (1.0×10^{-7} mol L^{-1}) limits, as well as very fast sampling frequency (60 determinations per hour) were achieved.
© 2007 Elsevier B.V. All rights reserved.

Keywords: Tetrasulphonated-manganese porphyrin; Modified electrode; Electrocatalysis; Hydrazine; Batch injection analysis; Amperometry

1. Introduction

Hydrazine, a liquid colorless compound, is expected to be a human carcinogen [1,2]. This substance is a powerful reducing agent and is widely employed in many industrial applications as reagent, catalyst and corrosion inhibitor. Hydrazine and its derivatives have been used as rocket fuel and as oxygen scavenger in boilers. Other applications include the manufacture of metal films, blowing agents for plastic, photographic chemicals, insecticides, explosives and pharmaceutics. Because this substance (and its derivatives) is applied in such a variety of different fields and has been recognized as carcinogenic and hepatotoxic agent, its quantitative determination is of great analytical importance attracting the interest of many researchers.

Different methods for the determination of hydrazine and its compounds such as flow injection analysis with fluorimetric [3] and chemiluminescence [4,5] detection, optical chemical sensors [6], potentiometric [7], spectrophotometric [8–11] and capillary electrophoresis [12] methods have been described in the literature.

Electroanalytical techniques seem to provide direct and efficient methods for the detection of hydrazine and its derivatives. Nevertheless, a drawback associated with the oxidation of hydrazine at conventional carbon electrodes is the necessity of employing large overpotentials. Elegant solutions for minimizing overvoltage effects have been described using electrocatalytic processes at chemically modified electrodes (CMEs). Electrodes modified with hexacyanoferrates with nickel [13], cobalt [14], palladium [15], copper and cobalt hybrid [16] or phtalocyanines coordinated to iron [17] and cobalt [18] are typical examples. Other CMEs include caffeic [19] and chlorogenic [20] acids, nafion/ruthenium(III) [21] hydroquinone salophen derivatives [22], cobalt porphyrin immobilized on a niobium(V) oxide grafted-silica gel surface [23], carbon fiber microelectrodes modified with rhodium [24], copper–palladium alloy nanoparticle plated electrodes [25] and carbon electrode modified with a thin film of oxymanganese species [26].

In recent years we have described many applications of modified electrodes with molecular films obtained by drop casting

* Corresponding authors.
E-mail address: luangnes@iq.usp.br (L. Angnes).

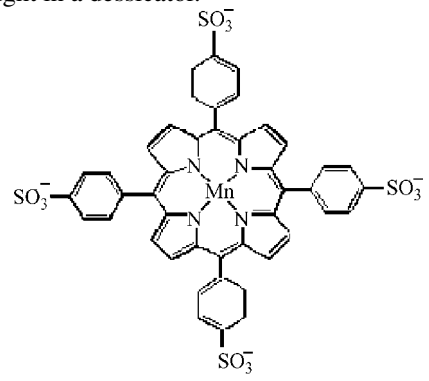
0039-9140/$ – see front matter © 2007 Elsevier B.V. All rights reserved.
doi:10.1016/j.talanta.2007.07.001

or electropolymerization of tetraruthenated cobalt [27–29] and nickel [30] porphyrins. Now we report the use of MnTPPS (*meso*-tetra(4-sulphonatephenyl)porphyrinate manganese(III)) complex for the preparation of nanostructured films exhibiting enhanced electrocatalytic activity for hydrazine oxidation under a very low overpotential (close to 0 V *versus* Ag/AgCl). The possibility of using this electrode as hydrazine sensor is also demonstrated in a batch injection analysis (BIA) [31] arrangement coupled with amperometry. This technique has been employed in our group as an alternative to flow injection analysis (FIA) with excellent results when combined with amperometric sensors presenting good electrocatalytic activity towards the substances to be analyzed [27–30,32–34].

2. Experimental

2.1. Reagents and solutions

$Na_4[(Oac)MnTPPS]{\cdot}5H_2O$ was prepared by reacting the free-base (Aldrich) with 1.3 times stoichiometric excess of manganese(II) acetate in refluxing methanol for 30 min, in a N_2 atmosphere. The procedure was identical to the one utilized for ZnTPPS preparation, described before [35]. The solvent was removed and acetone was added into the concentrated solution, filtered and the solid washed with acetone/methanol 20:1 v/v mixture to remove the unreacted $Mn(CH_3COO)_2$. The solid was kept overnight in a dessicator.



Structure of MnTPPS.

Ultrapure water (Millipore Milli-Q) was used to prepare the solutions. All reagents (Merck, Sigma or Aldrich) were of analytical grade and employed as received. Stock solution of hydrazine sulphate (10^{-2} mol L^{-1}) was daily prepared by dissolving the solid in water. The following dilutions were done with supporting electrolyte (0.1 mol L^{-1} NaOH) just before the batch injection analysis experiments. For the film electrodeposition procedure, 1.0 mg/mL MnTPPS was prepared with 0.1 mol L^{-1} NaOH containing 3.5×10^{-7} mol L^{-1} AgCl.

2.2. Instruments and apparatus

Amperometric and voltammetric measurements were carried out using an EG&G Princeton Applied Research (PAR) potentiostat, Model 263-A, interfaced with a microcomputer. A conventional three-electrodes cell, consisting of a glassy carbon working electrode (Model TL-5, Bioanalytical System, 0.071 cm^2 apparent area), a platinum wire auxiliary electrode and a miniaturized reference electrode, was employed in the voltammetric experiments. The same electrodes were also used in the batch injection analysis (BIA) system for amperometric measurements, as previously described [29]. The injections of the analyte solutions were performed utilizing a motorized electronic micropipette EDP Plus EP-100, from Rainin Instruments. All the potentials cited in this work are referred to the $Ag/AgCl_{sat}$ reference electrode. All the experiments were carried out at room temperature (25 ± 2 °C). The images and composition analysis of the material electrodeposited on carbon paper were obtained in a field emission scanning electron microscope from JEOL model JSM-7410, equipped with EDS accessory.

2.3. Electrode surface modification

The glassy carbon electrodes were mechanically polished with 0.3 and 0.02 μm alumina slurry on a felt cloth, rinsed with deionized water and dried at room temperature. The film electrodeposition was performed by successively scanning the potentials in a suitable range (initial and final potentials: 0 V; upper limit potential: 1.0 V; lower limit potential: −1.6 V) at sweep rate of 100 mV s^{-1}.

3. Results and discussion

3.1. The modified electrode

A typical set of 15 cyclic voltammograms recorded during the film deposition on a glassy carbon electrode immersed in 1.0 mg/mL MnTPPS (0.1 mol L^{-1} NaOH + 3.5×10^{-7} mol L^{-1} AgCl) is illustrated in Fig. 1. The curves show characteristic oxidation and reduction waves with maximum at +200 mV (A1) and −200 mV (C1), respectively, that increase continuously after each potential scan, indicating a progressive deposition of the

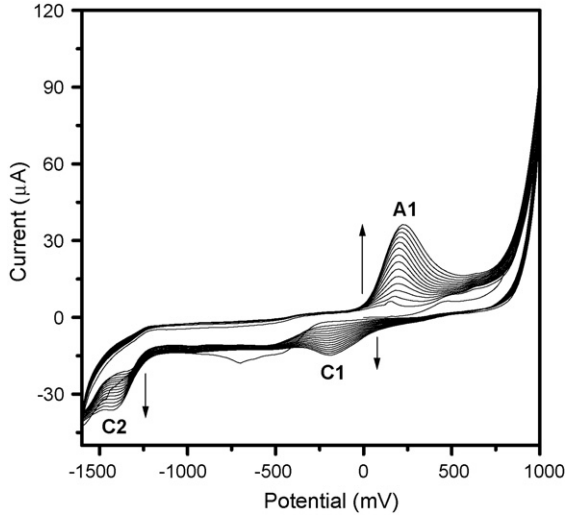


Fig. 1. Cyclic voltammograms registered during the film electrodeposition at a glassy carbon electrode in 1.0 mg/mL MnTPPS alkaline solution (0.1 mol L^{-1} NaOH) containing 3.5×10^{-7} mol L^{-1} AgCl. Scan rate: 100 mV s^{-1}; electrode area: 0.071 cm^2.

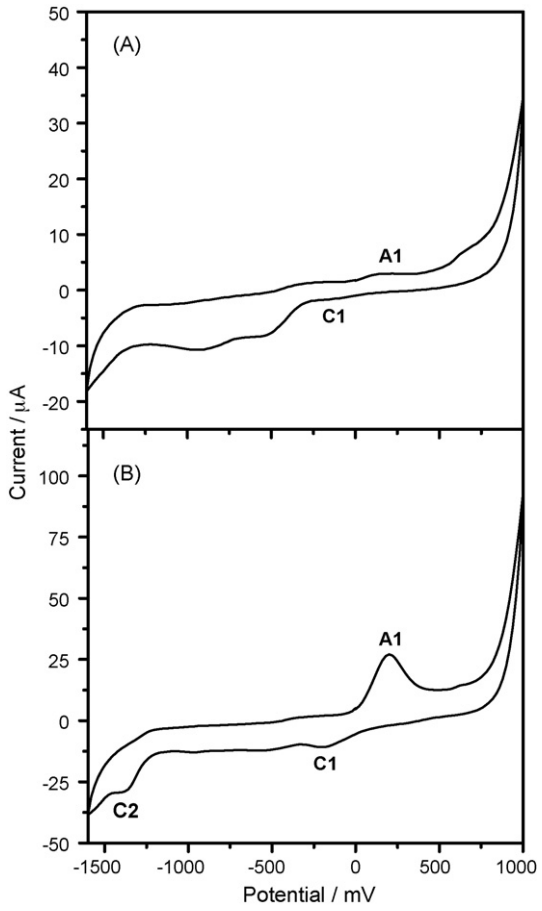


Fig. 2. Cyclic voltammograms obtained for a glassy carbon electrode in 1.0 mg/mL MnTPPS alkaline solution (0.1 mol L^{-1} NaOH) in the absence (A) and in the presence (B) of 3.5×10^{-7} mol L^{-1} AgCl. Each curve represents the latest of 10 cyclic voltamograms registered. Scan rate: 100 mV s^{-1}; electrode area: 0.071 cm^2.

electroactive material on the electrode surface. Another cathodic wave (C2) with peak current at −1.4 V is also observed.

The last event is verified only when the MnTPPS alkaline solution contains silver chloride. The presence of AgCl also seems to influence the film growth process, leading to a higher amount of electrodeposited material. Such experimental facts can be confirmed by comparing the cyclic voltammograms of Fig. 2 where the results for the electrode immersed in alkaline MnTPPS solutions in the absence (Fig. 2A) and presence (Fig. 2B) of silver chloride are shown. If the solution does not contain AgCl, the peak currents A1 and C1 in Fig. 2A are smaller than those ones in Fig. 2B (solution containing AgCl). Another interesting fact is that the peak C2 is not observed in the voltammogram obtained for the electrode in the absence of AgCl.

The presence of silver chloride plays a crucial role in the film formation process. It was observed that when higher concentrations of AgCl were utilized (ranging between 5.0×10^{-7} and 1.5×10^{-6} mol L^{-1}), the cyclic voltammograms obtained in 0.1 mol L^{-1} NaOH showed anodic (E_{pa}) and cathodic (E_{pc}) peak potentials shifting to more positive and negatives values, respectively. In consequence of this dislocation, increase of ΔE_p was observed, suggesting a slower heterogeneous electron transfer process. When lower concentrations were utilized, the peak currents A1 and C1 were smaller but sharper as expected for thinner films.

Scanning electron microscopy images of the samples were obtained in order to shed light on what kind of material is being formed and its morphology as a function of added AgCl concentration. When no silver is present, there are no observable changes on the carbon electrode surface, which remained without any additional structure except those already present in the clean substrate. However, at silver concentrations as low as 1.75×10^{-7} mol L^{-1}, a huge amount of flat islands, 50–150 nm in size appear on the surface. When the concentration of silver is increased to 3.5×10^{-7} and 7.0×10^{-7} mol L^{-1}, the size and thickness seems to increase, as well as the amount of big clusters and brighter spots. But, when the concentration is further increased to 1.4×10^{-6} mol L^{-1}, the number and size of the islands seems to decrease in spite of the bigger amount of deposited material detected by cyclic voltammetry. In fact, at this silver concentration, the growth of bigger three-dimensional clusters is observed and the small islands give place to larger bright clusters in the SEM images. The analysis of such clusters by EDS microanalysis indicates that the majority of such structures are essentially constituted by silver, with trace amounts of manganese. Even the brighter clusters formed in the presence of much lower AgCl concentrations were mainly constituted by silver, but with relatively much higher manganese content than the former ones, as expected. Many attempts were carried out in order to obtain the EDS spectra of the much darker (50–150 nm) structures covering the electrode surface, but high charging effects and low signal precluded the analysis. This is a clear indication that the electrical conductivity and composition of that material is different. Fig. 3A–D was obtained at low acceleration voltage of 1.0 kV in order to enhance the surface features. By increasing the acceleration voltage to 2.0 or more kV the kinetic energy of the incident electrons increases by becoming more penetrating, making possible the visualization of the structures more deeply inside the material. In fact, a close-up at higher acceleration voltage allowed the visualization of small bright round nanoparticles that were not visible at 1.0 kV, showing that the nanofilm is constituted by at least two distinct components: silver nanoparticles and the electropolimerized MnTPPS. Presumably, the silver nanoparticles should be acting as nucleating sites for the formation and growth of the MnTPPS/MnO_2 composite nanoflakes. This explains why low concentrations of AgCl are needed for the electropolimerization of MnTPPS in alkaline media, whose presence was confirmed by UV–vis spectra and EDS analysis of the silver and manganese content.

The above-described behavior also explains the worse electrochemical response of the chemically modified electrodes prepared in such higher silver concentrations. Because of the much higher thickness and size and lower surface area, the electrolyte diffusion become slower particularly for those sites that are deep inside the clusters. Therefore, we found out that the most favorable AgCl concentration for electrode preparation is 3.5×10^{-7} mol L^{-1}, where a suitable coverage and fast electrochemical response are achieved. Accordingly, this condition

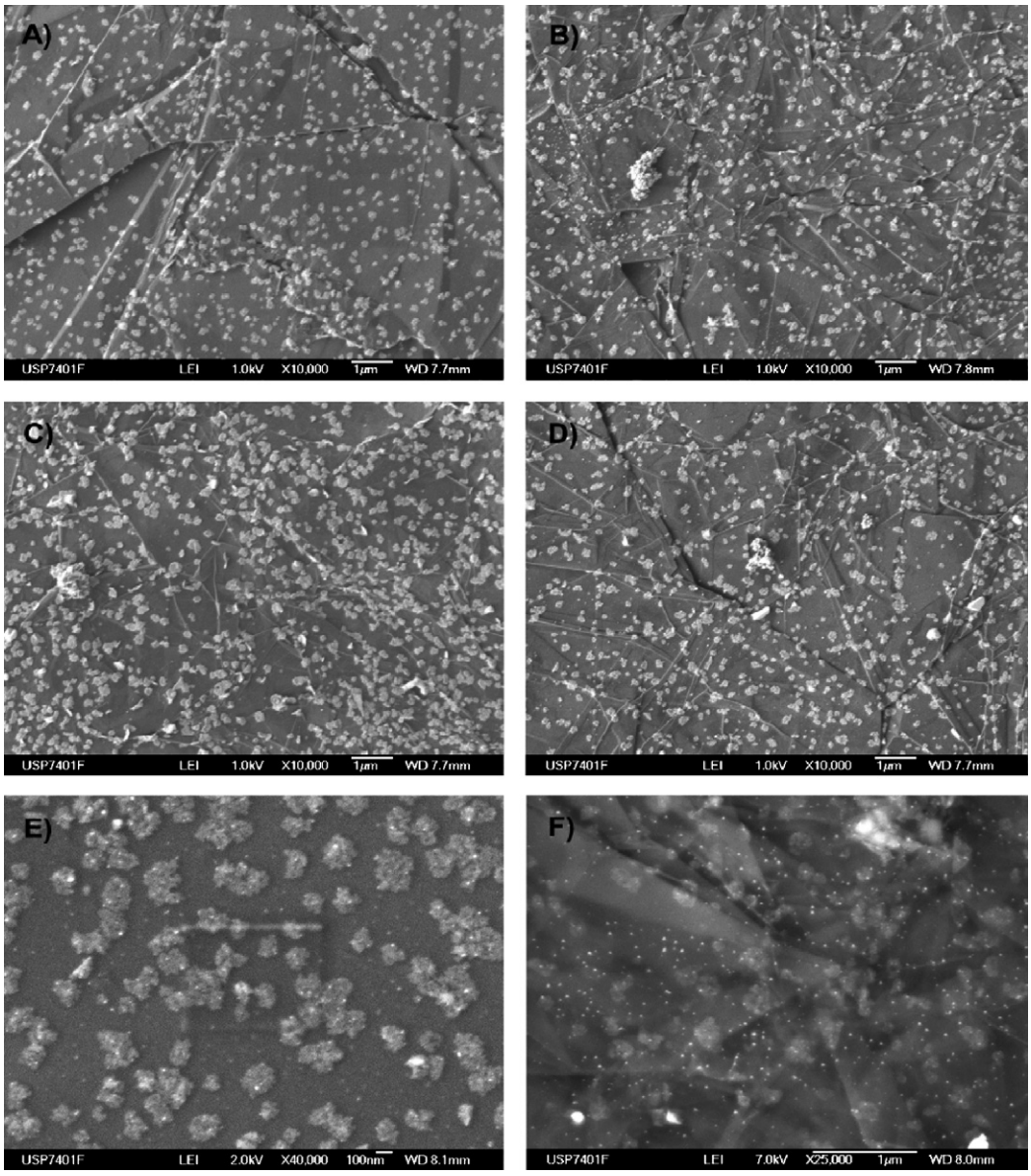


Fig. 3. SEM micrographies showing the carbon electrodes surface after deposition of the nanomaterial of 0.1 mol L^{-1} NaOH + 1.0 mg/mL of MnTPPS solution containing (A) 1.75×10^{-7}; (B) 3.50×10^{-7}; (C) 7.00×10^{-7}; (D) 1.40×10^{-6} mol L^{-1} of AgCl. Images obtained at higher resolution and acceleration voltages are shown in (E) 1.75×10^{-7} and (F) 1.40×10^{-6} mol L^{-1} of AgCl.

was chosen for the electrodeposition of all chemically modified electrodes used in our experiments.

After electrodepositing the nanomaterial film, the electrodes were transferred to a 0.1 mol L^{-1} NaOH solution. The voltammograms of the modified electrode showed an anodic and a cathodic wave with maximum of current at 45 mV and −320 mV, respectively (not shown). This behavior is similar to that observed for electrodeposited manganese oxides [36], in which the main redox couple corresponds to Mn(III)/Mn(IV) process occurring in solid state.

3.2. Electrocatalytic oxidation of hydrazine

The electrodes whose surface was modified with the above described nanomaterial film exhibited an intense electrocatalytic activity for hydrazine oxidation. The oxidation of hydrazine requires very high positive overpotentials at bare glassy carbon electrode, as can be seen in Fig. 4A, leading to a poorly defined anodic wave characteristic of very slow electrode kinetics. In contrast, the catalytic oxidation at the modified electrodes (Fig. 4B) are much sharper and occurs at about 400 mV less positive potentials, increasing the anodic peak current associated with the Mn(III)/Mn(IV) redox pair. The oxidation of the analyte is associated with the electrochemical generation of the Mn(IV) species, as can be inferred from the enhancement of the wave associated with the Mn(III/IV) process and decrease of the associated cathodic wave Mn(IV/III) in the reverse sweep.

3.3. Batch injection analysis

The above described electrocatalytic behavior of the modified electrodes clearly indicates that the heterogeneous electron

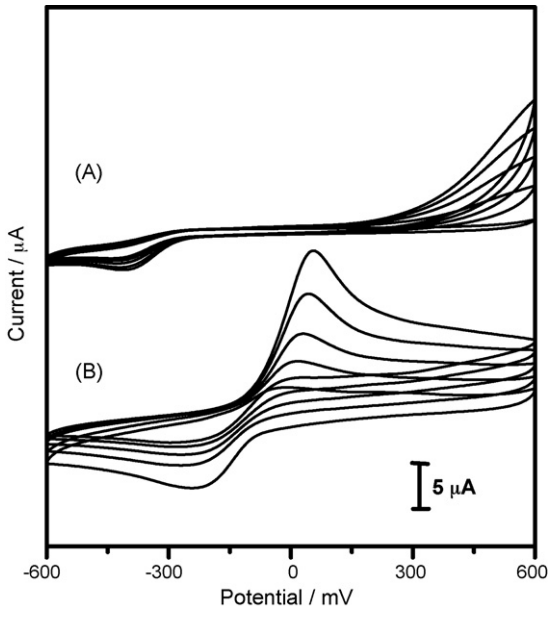


Fig. 4. Cyclic voltammograms obtained for a bare (A) and a modified (B) glassy carbon electrode, immersed in 0.1 mol L^{-1} NaOH containing hydrazine sulphate at different concentrations (0 to 8.0×10^{-4} mol L^{-1}). Scan rate: 20 mV s^{-1}; electrode area: 0.071 cm^2.

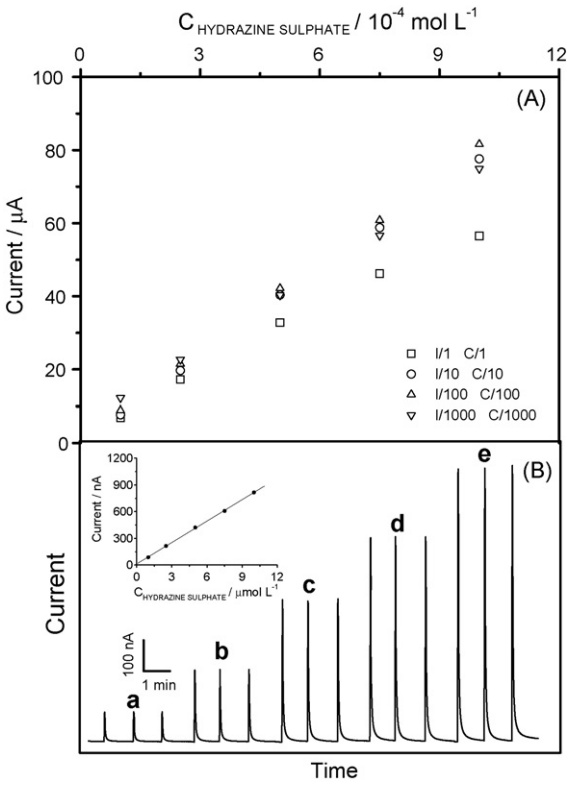


Fig. 5. (A) Calibration plots for BIA amperometric responses utilizing standard solutions of hydrazine sulphate with concentrations changing between: (▽) 1.0×10^{-7} and 10.0×10^{-7} mol L^{-1}, (△) 1.0×10^{-6} and 10.0×10^{-6} mol L^{-1}, (◯) 1.0×10^{-5} and 10.0×10^{-5} mol L^{-1}, (□) 1.0×10^{-4} and 10.0×10^{-4} mol L^{-1}. (B) BIA amperometric responses after injections of (a) 1.0×10^{-6}, (b) 2.5×10^{-6}, (c) 5.0×10^{-6}, (d) 7.5×10^{-6} and (e) 10.0×10^{-6} mol L^{-1} hydrazine sulphate solutions. Inset: correspondent calibration plot; supporting electrolyte: 0.1 mol L^{-1} NaOH; working potential: 10 mV; injected volume: 100 μL; injection speed: 75.3 μL s^{-1}; electrode area: 0.071 cm^2.

transfer process is sufficiently fast and the films are robust enough to be used in a more demanding condition. Accordingly, the modified electrode was used for amperometric detection of hydrazine using batch injection analysis technique. Many parameters were explored in order to find the most suitable conditions for detection of that important analyte. The best distance between electrode and pipette tip was found to be 2 mm. The best injection speed of the programmable pipette was the faster one (dispensing rate = 75.3 μL s^{-1}) and the most favorable volume was 100 μL. Next the potential for analysis was optimized by testing the response of the sensor in a suitable range of potentials. To evaluate the best working potential, a series of determinations were performed in the interval range of −0.12 to 0.05 V, taking the medium value of three determinations. The current signals displayed a continuous increase as a function of the applied potential until 0 V and then leveled off, showing that 10 mV is the best value for analytical purposes.

To evaluate the reproducibility of response, 30 successive injections of 5.0×10^{-5} mol L^{-1} hydrazine sulphate were done, working on a frequency of 60 determinations per hour. For this series of measurements, the relative standard deviation calculated was only 0.84%. The peak current stayed almost unaffected, revealing quite good long-term stability.

Also, a series of experiments was performed with standard solutions of hydrazine sulphate conveniently diluted in order to find the linear working range. The results are shown in Fig. 5A, where the calibration plots for four decades of analyte concentration are shown. Practically the same result was obtained except for a minimum variation in the slopes, indicating that the sensitivity of the electrode was maintained in spite of the increasing current demand. The calibration plots shows the large linear response range between 2.5×10^{-7} and 2.5×10^{-4} mol L^{-1}, that can be expressed by the equation $I = 1.48 \times 10^{-7}A + 0.07A$ L mol^{-1} (correlation coefficient = 0.999). For concentrations higher than 2.5×10^{-4} mol L^{-1}, the slope decreased significantly, suggesting a saturation behavior.

The system had singular behavior exhibiting BIA current values with very favorable signal-to-noise ratio, demonstrated by a particularly stable base line even at very low concentrations (Fig. 5B).

A limit of detection of 3.1×10^{-8} mol L^{-1} (three times the standard deviation of the blank) and a limit of quantification of 1.0×10^{-7} mol L^{-1} (10 times the standard deviation of the blank [37]) were calculated utilizing a calibration plot in the range of 2.5×10^{-7} to 1.0×10^{-6} mol L^{-1}. A comparison between the results here obtained and the one presented by other author [13–24] shows many advantages for the sensor here proposed. The detection limit obtained in present study (3.1×10^{-8} mol L^{-1}) is lower than all values previously presented. The working region (2.5×10^{-7} to 2.5×10^{-4} mol L^{-1}) is also remarkable wide, compared with the majority of the studies.

4. Conclusions

The preparation of electrodes chemically modified with a new nanocomposite material obtained by electrodeposition from a MnTPPS alkaline solution containing trace amounts of AgCl was described. The films constituted by MnTPPS/MnO_2 nanoflakes with embedded silver nanoparticles exhibited excellent electrocatalytic behavior toward hydrazine oxidation in alkaline solution, diminishing significantly the overpotential (∼400 mV) in comparison with a bare glassy carbon electrode. Additionally, the modified electrodes tested as amperometric sensor for hydrazine utilizing batch injection analysis technique showed high precision and repeatability, wide linear working range, low detection and quantification limits, as well as high sampling frequency were achieved, all desirable characteristics for an amperometric sensor.

Acknowledgements

The authors gratefully acknowledge the fellowships from Fundação de Amparo à Pesquisa do Estado de São Paulo and Conselho Nacional de Desenvolvimento Científico e Tecnológico. This work was also supported by Millenium Institute of Complex Materials (IM^2C).

References

[1] H. Zheng, R.C. Shank, Carcinogenesis 17 (1996) 2711.
[2] T. Leakakos, R.C. Shank, Toxicol. Appl. Pharmacol. 126 (1994) 295.
[3] A.L. Ensafi, B. Rezaei, Talanta 47 (1998) 645.
[4] J. Huang, C. Zhang, Z. Zhang, Fresenius J. Anal. Chem. 363 (1999) 126.
[5] A. Safavi, M.R. Baezzat, Anal. Chim. Acta 358 (1998) 121.
[6] C. Gojon, B. Dureault, N. Hovnanian, C. Guizard, J. Sol-Gel Sci. Technol. 14 (1999) 163.
[7] J.-W. Mo, B. Ogorevc, X. Zhang, B. Pihlar, Electroanalysis 12 (2000) 48.
[8] S. Amlathe, V.K. Gupta, Analyst 113 (1988) 1481.
[9] M.I. Evgen'ev, S.Yu. Garmonov, I.I. Evgen'eva, V.V. Ugrichich-Trebinskii, J. Anal. Chem. 53 (1998) 240.
[10] P. Ortega-Barrales, A. Molina-Díaz, M.I. Pascual-Reguera, L.F. Capitán-Vallvey, Anal. Chim. Acta 353 (1997) 115.
[11] A.A. Ensafi, B. Naderi, Microchem. J. 56 (1997) 269.
[12] W. Siangproh, O. Chailapakul, R. Laocharoensuk, J. Wang, Talanta 67 (2005) 903.
[13] D.R. Shankaran, S.S. Narayanan, Russ. J. Electrochem. 37 (2001) 1149.
[14] D.R. Shankaran, S.S. Narayanan, Russ. J. Electrochem. 38 (2002) 987.
[15] H. Razmi, A. Azadbakht, M.H. Sadr, Anal. Sci. 21 (2005) 1317.
[16] A. Abbaspour, M.A. Kamyabi, J. Electroanal. Chem. 576 (2005) 73.
[17] K.I. Ozoemena, T. Nyokong, Talanta 67 (2005) 162.
[18] X. Li, S. Zhang, C. Sun, J. Electroanal. Chem. 553 (2003) 139.
[19] S.M. Golabi, H.R. Zare, Electroanalysis 11 (1999) 1293.
[20] S.M. Golabi, H.R. Zare, J. Electroanal. Chem. 465 (1999) 168.
[21] I.G. Casella, M.R. Guascito, A.M. Salvi, E. Desimoni, Anal. Chim. Acta 354 (1997) 333.
[22] M. Revenga-Parra, E. Lorenzo, F. Pariente, Sens. Actuator B 107 (2005) 678.
[23] C.A. Pessoa, Y. Gushiken, S. Nakagaki, Electroanalysis 14 (2002) 1072.
[24] J.M. Pingarrón, I.O. Hernandéz, A. González-Cortés, P. Yáñez-Sedeño, Anal. Chim. Acta 439 (2001) 281.
[25] C.C. Yang, A.S. Kumar, M.C. Kuo, S.H. Chien, J.M. Zen, Anal. Chim. Acta 554 (2005) 66.
[26] Z. Taha, J. Wang, Electroanalysis 3 (1991) 215.
[27] M.S.M. Quintino, K. Araki, H.E. Toma, L. Angnes, Talanta 68 (2006) 1281.
[28] M.S.M. Quintino, H. Winnischofer, K. Araki, H.E. Toma, L. Angnes, Analyst 130 (2005) 221.
[29] M.S.M. Quintino, K. Araki, H.E. Toma, L. Angnes, Electroanalysis 14 (2002) 1629.
[30] M.S.M. Quintino, H. Winnischofer, M. Nakamura, K. Araki, H.E. Toma, L. Angnes, Anal. Chim. Acta 539 (2005) 215.
[31] M.S.M. Quintino, L. Angnes, Electroanalysis 16 (2004) 513.
[32] M.S.M. Quintino, L. Angnes, Talanta 62 (2004) 231.
[33] M.S.M. Quintino, D. Corbo, M. Bertotti, L. Angnes, Talanta 58 (2002) 943.
[34] M.S.M. Quintino, L. Angnes, J. Pharm. Biomed. Anal. 42 (2006) 400.
[35] C.M.N. Azevedo, K. Araki, L. Angnes, H.E. Toma, Electroanalysis 10 (1998) 467.
[36] M. Hernadéz Ubeda, H. Herrera, H.T. Mishima, B.A. López de Mishima, H.M. Villullas, M. López Teijelo, Electrochim. Acta 44 (1998) 513.
[37] J.C. Miller, J.N. Miller, Statistics for Analytical Chemistry, Harwood, Chichester, 1992.

Available online at www.sciencedirect.com
ScienceDirect
Talanta 74 (2008) 562–569
Talanta
www.elsevier.com/locate/talanta

Determination of volatile organic sulfur compounds in the air at sewage management areas by thermal desorption and gas chromatography–mass spectrometry

Maria Rosa Ras, Francesc Borrull *, Rosa Maria Marcé

Departament de Química Analítica i Química Orgànica, Universitat Rovira i Virgili, Campus Sescelades, Marcel lí Domingo, s/n, 43007 Tarragona, Spain

Received 30 March 2007; received in revised form 8 June 2007; accepted 15 June 2007
Available online 19 June 2007

Abstract

The concentrations of seven volatile organic sulfur compounds (VOSCs) in air samples were determined by active collection on multisorbent tubes followed by two-stage thermal desorption and gas chromatography–mass spectrometry. The compounds studied were ethyl mercaptan (CH_3CH_2SH), dimethyl sulfide ($(CH_3)_2S$), carbon disulfide (CS_2), propyl mercaptan (C_3H_8S), butyl mercaptan ($C_4H_{10}S$), dimethyl disulfide ($(CH_3)_2S_2$) and 1-pentanethiol ($C_5H_{12}S$). Active collection on SilcoSteel multisorbent tubes enabled an air volume of 3000 ml to be sampled without observing breakthrough. This study focused on an exhaustive sampling of several process steps or sections from sewage management plants. A wide range of concentrations was observed. Dimethyl sulfide, carbon disulfide and dimethyl disulfide were the most abundant compounds in all samples, the highest concentrations being 608.5 $\mu g\,m^{-3}$, 658.5 $\mu g\,m^{-3}$ and 857.8 $\mu g\,m^{-3}$, respectively. The less appearing compound was ethyl mercaptan, which was only detected in the sludge digestion process at a maximum concentration of 14.8 $\mu g\,m^{-3}$. The remaining compounds were detected and measured in about half the samples. The sections with the maximum values of VOSCs involved sludge processes such as mixing, thickening and digestion. The results were also strongly influenced by the design characteristics of the sampling point, e.g. whether the sample was taken at a confined site or in the open air.
© 2007 Elsevier B.V. All rights reserved.

Keywords: Volatile organic sulfur compounds; Thermal desorption; Sewage management plant; Odour nuisance

1. Introduction

In the last two decades interest in the determination of volatile sulfur compounds in the atmosphere has increased. This is mainly due to their effects on the environment (they are responsible for acid deposition and the corrosion of metal structures, etc.), to their toxicity even at very low levels, and to the frequent unpleasant smells associated with them [1]. Volatile sulfur compounds are sent into the atmosphere from several natural and anthropogenic sources. Natural sulfur compounds such as hydrogen sulfide, dimethyl sulfide and dimethyl disulfide are released from oceans, marshes, soils, vegetation, and geothermal and volcanic activity [2]. However, the primary emission sources of VOSCs into the atmosphere are anthropogenic [3] and, according to several sources [2], natural emissions constitute roughly 24% of total sulfur emissions, while anthropogenic sulfur emissions, mainly sulfide dioxide, contribute the rest. Volatile sulfur compounds are commonly given off during industrial processes that involve the handling or degradation of organic material. These processes include biogas production, sewage treatment, landfilling, pulp milling and slaughtering [4,5]. Dimethyl disulfide, for example, is produced by many bacteria and fungi found in wastewater, and carbon disulfide and dimethyl sulfide are formed when the amino acids cysteine and methionine decompose [6].

Volatile sulfur compounds have also been identified as the predominant odorants from bioindustry emissions [7] because of their very low odour threshold and extremely negative hedonic value. They therefore contribute to odour pollution even when very small amounts are emitted, which annoys many people,

* Corresponding author. Tel.: +34 977 55 95 60; fax: +34 977 55 84 46.
E-mail address: francesc.borrull@urv.cat (F. Borrull).

0039-9140/$ – see front matter © 2007 Elsevier B.V. All rights reserved.
doi:10.1016/j.talanta.2007.06.017

especially workers and local residents [2,3,7]. Their high toxicity is also well known. The International Labour Organization of the United Nations reports that some sulfur compounds can cause health problems including damage to the human respiratory system even at low concentrations, and that exposure to high levels of VOSCs can be extremely harmful, causing unconsciousness and death [2,4,5].

Previous determinations of sulfur compounds have been conducted in the atmosphere with solid adsorbents or cryogenic trapping to concentrate the sulfur compounds, and gas chromatography to determining them [2]. Kim et al. [8] measured the concentrations of several reduced sulfur compounds (hydrogen sulfide, methyl mercaptan, dimethyl sulfide, carbon disulfide and dimethyl disulfide) from municipal landfill gas samples in Korea. Li and Shooter [2] identified carbonyl sulfide, hydrogen sulfide, sulfur dioxide, carbon disulfide, methyl mercaptan, dimethyl sulfide, dimethyl disulfide and butyl mercaptan in samples from a sewage treatment plant and geothermal areas in Rotorua City (New Zealand). Muezzinoglu [9] also studied the levels of hydrogen sulfide, methyl mercaptan, ethyl mercaptan, 2-propanethiol, dimethylsulfide, dimethyldisulfide and other organic sulfur compounds in the air at polluted creeks from Izmir, Turkey, and nine volatile sulfur compounds were observed in samples from Swedish biogas production and sewage treatment plants by Nielsen and Jonsson [5,10]. In a monitoring campaign in a suburban area near an industrial zone in Greece, Vassilakos et al. [3] found hydrogen sulfide, methyl mercaptan, carbonyl sulfide and carbon disulfide in a concentration range of 0.33–10,700 ppb(v). Devai and DeLaune also identified hydrogen sulfide, carbonyl sulfide, methanethiol, dimethyl sulfide and carbon disulfide in emissions from wastewater treatment plants [11].

The determination of volatile sulfur compounds has several difficulties, including their broad range of concentrations, their highly reactive nature, and the complexity of matrices. Therefore, besides the selection of appropriate sorbent material, some special precautions need to be taken in all steps in the analysis of these compounds. The most practical technique for measuring these compounds is a combination of thermal desorption (TD) and gas chromatography (GC), which has been extensively investigated and used in monitoring campaigns [8,12–17], although many other techniques have also been applied for monitoring VOSCs, such as SPME [2,4,5,18,19].

The present study attempts to characterise the contribution of VOSCs to odour nuisance in particularly affected areas such as sewage management facilities and their surrounding areas. To do so we developed a method for determining ethyl mercaptan, dimethyl sulfide, carbon disulfide, propyl mercaptan, butyl mercaptan, dimethyl disulfide and 1-pentantehiol by dynamic adsorption in multibed sorbent tubes, thermal desorption with cryofocusing in a cold trap, and analysis by gas chromatography and mass spectrometry. Then, in order to study sewage management plant emissions, we conducted an exhaustive sampling campaign of several process points from two sewage treatment areas. Air from several external points close to these kinds of installations was analysed in order to determine how these sulfur emissions affect the surrounding areas.

2. Experimental

2.1. Sorbent tubes

Stainless steel tubes (3.5-in. (89 mm) × 1/4-inch (6.4 mm) O.D.), SilcoSteel coated (which make them suitable for sampling reactive species) and containing about 400 mg of a multisorbent bed of Tenax TA and Unicarb (Markes International Limited, Llantrisant, UK), were first activated by passing 99.999% pure nitrogen gas at a flow rate of 100 ml min^{-1} and at temperatures of 100, 200, 300 and 335 °C each for 1 h, in accordance with the supplier's recommendations, who also warns not to exceed their maximum temperature of 350 °C.

After each use, the tubes were reconditioned by cleaning in the same way but for 15 min at each temperature, as also recommended by the suppliers. The clean tubes were capped with 1/4 in. brass long-term storage caps with 1/4 in. combined PTFE ferrules, coated with aluminium film, stored in hermetically sealable glass jars to prevent any ambient contamination of the sorbents, and used for new analyses within 1 week. Cleaned tubes were tested and, although some artifacts appeared in blank chromatograms, any of them interfered with the target compounds.

2.2. Chemical standards and calibration

Ethyl mercaptan, dimethyl sulfide, carbon disulfide, propyl mercaptan, butyl mercaptan, dimethyl disulfide and 1-pentantehiol were supplied by Aldrich (St. Louis, USA). External calibration was carried out with standards prepared by dilution in methanol for gas chromatography (Merck KGaA, Darmstadt, Germany), ranging between 0.1 and 500 mg l^{-1}. These were freshly prepared at the time of calibration.

External liquid standards were loaded into sorbent tubes by a Calibration Solution Loading Ring (Agilent Technologies, Palo Alto, USA). This was equipped with a tube insert and a gas valve system that allows a 99.999% pure helium flow to pass through the tube at a fixed flow rate of 100 ml min^{-1}. A conventional GC syringe was used to inject 1 μl of each standard dilution into the tube through a septum and this was deposited in the sampling end of the tube. As recommended by the manufacturer, a short time (roughly 20 s) elapsed after the injection and before the needle was withdrawn from the septum to allow the VOSCs to fully evaporate and be retained on the sorbent bed while the solvent was purged from the tube. The tube was then immediately desorbed and the analysis performed, under the same conditions as followed in the samples.

2.3. Sampling

Volatile sulfur compounds were collected using an air sampling pump (SKC, Eighty Four, USA) to pump air samples through preconditioned tubes at a flow rate of 50 ml min^{-1} for 60 min. The pumped air volume was therefore 3000 ml. The pump was calibrated using a DFC-HR digital flow meter (Alltech, Deerfield, USA) before and after each sampling, and the flow rate average was used to determine the volume of air sampled.

Table 1
Target compounds in chromatographic elution order, and their quantifier and qualifier ions

No.	Compound	Quantifier ion[a]	Qualifier ion[a]			t_R (min)	R.S.D. (%), 100 ng ($n=3$)	R.S.D. (%), 1 ng ($n=3$)	MDL ($\mu g\,m^{-3}$)	MQL ($\mu g\,m^{-3}$)
1	Ethyl mercaptan	62 (*100*)	47 (*58*)	45 (*20*)	–	4.09	0.8	1.5	0.04	0.07
2	Dimethyl sulfide	62 (*100*)	47 (*83*)	45 (*50*)	–	4.38	0.6	1.2	0.03	0.07
3	Carbon disulfide	76 (*100*)	44 (*11*)	–	–	4.79	1.2	1.9	0.01	0.03
4	Propyl mercaptan	76 (*100*)	61 (*11*)	47 (*68*)	43 (*57*)	6.83	1.2	2.1	0.04	0.07
5	Butyl mercaptan	90 (*70*)	56 (*100*)	61 (*20*)	47 (*31*)	9.29	1.3	2.4	0.03	0.07
6	Dimethyl disulfide	94 (*100*)	79 (*50*)	61 (*12*)	64 (*10*)	9.91	0.8	2.7	0.02	0.07
7	1-Pentanethiol	104 (*68*)	55 (*100*)	70 (*79*)	61 (*30*)	10.98	0.8	3.3	0.04	0.07

Retention times (t_R), repeatability, expressed as relative standard deviation (R.S.D.%) for the analysis intra-day of 100 ng and 1 ng of VOSCs standard ($n=3$), method's detection limit (MDL) and method's quantification limit (MQL).

[a] The value in italics next to qualifier ions are percent abundances of each ion.

For field sampling, the tubes were transported in a glass jar inside a refrigerated box at 4 °C, and re-placed there immediately after sampling. Samples were analysed as soon as possible, or kept at a 4 °C in the refrigerator during storage and analysed the day after sampling.

2.4. Desorption and analysis

Desorption was carried out on a UNITY thermal desorber coupled to an ULTRA automatic sampler (both from Markes International Limited, Llantrisant, UK). The sorbent tube was heated to 200 °C and to 300 °C, each for 5 min, while 99.999% pure helium gas passed through the tube at a rate of 30 ml min^{-1} to desorb the analytes and focus them into an inert sulfur trap, packed with Tenax TA and Unicarb and designed for sampling volatile sulfur compounds, kept at −10 °C by a Peltier cooler. The trap was then heated to 200 °C at 40 °C s^{-1} for 3 min. The VOSCs were quickly desorbed from the trap and injected into the chromatographic column. A split flow of 10 ml min^{-1} was applied in both tube and trap desorption [20]. Separation and detection were performed in a 6890N gas chromatograph and a 5973 *inert* mass spectrometer (Agilent Technologies), using a TRACSIL Meta.X5 capillary column (60 m, 0.32 mm, 1.0 μm) (TEKNOKROMA, Barcelona, Spain). Helium gas with a purity of 99.999% was used as the carrier at a flow rate of 2 ml min^{-1}. The oven temperature of GC was initially held at 36 °C for 6 min, then raised to 220 °C at a rate of 30 °C min^{-1} and held for 3 min.

The mass spectrometer acquired data in scan mode with an *m/z* interval from 35 to 280. The compounds were quantified by a target ion and identified by qualifier ions and retention time. Table 1 shows the target compounds with their retention times, quantifier ions and qualifier ions.

2.5. Real samples

This study focused on an exhaustive sampling of sewage management plants in Tarragona and Reus. Tarragona and Reus are two close cities (separated by 15 km), on the Mediterranean coast in the south of Catalonia, both with populations of roughly 120,000 habitants. The distance between each sewage management plant and its correspondent urban centre is of about 2 km in both Reus and Tarragona. In this study, special care was taken to compare the concentrations of sulfur compounds in similar areas and at similar processes in the sewage treatment plants, i.e. the sampling points were as similar as possible in each plant. All samples were taken from October to December of 2006, during the day. Moreover, all samples were taken during days when

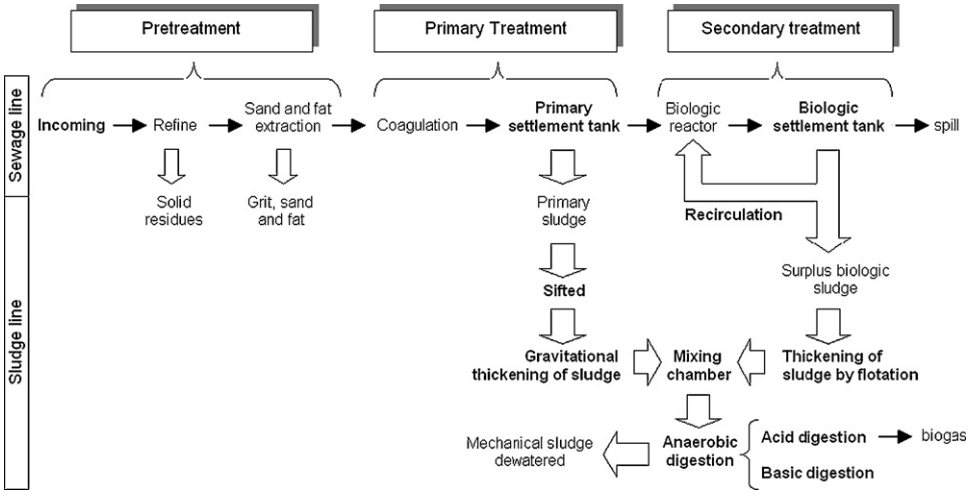


Fig. 1. General scheme of a sewage management plant. Sampled sections are in bold.

wind speed was lower than 5 m s^{-1}, so that it would interfere in sampling as little as possible.

The structures of the two plants are slightly different, though the basic structure (see Fig. 1) is common to both. For example, the Tarragona plant has a sewage sifting system comprising a primary settlement tank, a primary and biological sludge mixing chamber and a digested sludge buffer tank, but the Reus plant does not. On the other hand, the Reus plant has two primary digestion tanks and one secondary digestion tank but the Tarragona plant has only one digestion tank. These differences enabled us to sample the same sewage processing sections in parallel and compare the two sewage management plants.

However, there are also differences in the design of each plant, so several common treatment sections had to be sampled at points with different characteristics. The differences between samples taken in confined spaces and samples taken in open spaces have therefore been considered since, in open spaces, the dispersion of emission gases into the atmosphere will obviously greatly condition the levels of compounds in the air samples. Table 2 shows the treatment sections sampled at both plants and descriptions of each sampling point.

Furthermore, several sites outside these kinds of facilities were sampled, e.g. an external point near a solid waste management plant and an external point near the sewage management plant, where the stink produced by these installations is usually easy to detect. The distance from the plants to these sampled points was of about 50 m. Air from four urban points in Tarragona city was also analysed.

3. Results and discussion

3.1. Method development

3.1.1. Optimisation of thermal desorption parameters

All method conditions were optimised, so that the desorption of the target compounds would be optimum (see Section 2). An exhaustive explanation of the optimisation process is not given in this paper, but some criteria and aspects about thermal desorption optimisation are explained in this section.

In the first thermal desorption step, the tube desorption temperature and time were chosen to allow the maximum desorption efficiency of the analytes from the sorbent tube, thus avoiding their thermal degradation. In the second step, the trap desorption temperature and time were optimised to achieve the rapid and total desorption of the analytes from the trap, thus avoiding memory effects.

The desorption and split flows were also optimised in both steps. In the tube desorption step, the desorption flow, which corresponds to the sum of the trap flow and the split flow, was chosen in order to allow a quantitative desorption of analytes into the cool trap. In the trap desorption step, the desorption flow is the sum of the column flow and the split flow, and this must be enough to desorb all the analytes into the chromatographic column. In this step the split flow strongly influences the shape of the chromatographic peaks. The higher split flows help the analytes to focus into the column more quickly, thus avoiding peak tails and improving their resolution, mainly in most volatile compounds. However, in both steps the split flow obviously determines the response level and, therefore, the method detection limits. We therefore needed to reach a compromise between a good peak shape and a high response level.

With regard to sampling optimisation, the sample volume had to be determined in order to ensure that no breakthrough volume of each analyte was exceeded during sampling. Two identical sorbent tubes connected in series were used to sample different volumes of a highly contaminated atmosphere at a fixed flow rate. Each tube was then analysed to check for target compounds in the back tube. To obtain the lowest possible method detection limits (MDL), we chose the maximum sample volume.

3.1.2. Instrumental calibration

Instrumental repeatability was determined by triplicate thermal desorption analysis, conducted on the same day and at high and low levels, of 100 ng and 1 ng of target compounds, respectively. For all compounds, repeatability, expressed as relative standard deviation (R.S.D.), was good (less than 3.4%). All repeatability values are shown in Table 1.

External calibration was performed by analysing diluted standards. Ten calibration levels were used at amounts between 0.1 ng and 500 ng. Calibration curves showed good linearity and their determination coefficients (r^2) were above 0.999 for all compounds. The lowest calibration level for each compound was taken as the instrumental quantification limit (LOQ) for that compound. LOQ was 0.1 ng for carbon disulfide, and 0.2 ng for the rest.

The instrumental detection limit (LOD) for each compound was defined as the concentration corresponding to three times the noise of the quantifier ion. The lowest was 0.03 ng for carbon disulfide and the highest was 0.13 ng for ethyl and propyl mercaptan.

In the optimisation of sampling volume, sampling was performed by pumping contaminated air through tubes connected in series (see Section 3.1.1.) at a flow rate of 50 ml min^{-1} and for several times. In this way, air volumes were sampled between 500 ml and 3000 ml. It was found that, for all volumes of sampled air, all target compounds were quantitatively retained in the front tube and that none of them appeared in the back tube. To obtain the best possible method detection limits, a sampling volume of 3000 ml was chosen. Method detection limits (MDL) and method quantification limits (MQL) for this sample volume are shown in Table 1.

Recovery was determined by thermal desorption analysis of 1 μl of 100 mg l^{-1} of standard dilution of target compounds and analysis of the same tube in order to check for carryover. Recovery was above 98% for all compounds. Precision in real samples was determined by sampling several sorbent tubes connected in parallel that underwent identical sampling, transport and analytical processes. Precision values ranged between 1.2% and 11.6% ($n = 3$).

Table 2
Sampled sections in sewage management plants from Tarragona and Reus, and description of each sampling site

Tarragona plant sections sampled		Reus plant sections sampled	
Section sampled[a]	Sampling point description	Section sampled[a]	Sampling point description
Raw incoming sewage (a)	Opened chamber	Raw incoming sewage (a)	Opened chamber
Primary settlement tank (b)	Open site upon sewage from the primary treatment	Primary settlement tank (b)	Open site upon sewage from the primary treatment
Primary treated sewage sifted (c)	Closed site where sewage from primary settlement tank is sifted	–	–
Gravitational thickening of sludge (d)	Open site upon the primary sludge	Gravitational thickening of sludge (d)	Open site upon the primary sludge
Biological settlement tank (e)	Open site upon the bio-sewage	Biological settlement tank (e)	Open site upon the bio-sewage
Activated sludge re-circulation (f)	Semi-opened site	Activated sludge re-circulation (f)	Confined site
Thickening of surplus bio-sludge by flotation (g)	Open site upon the bio-sludge	Thickening of surplus bio-sludge by flotation (g)	Confined site
Mixing sludge chamber (h)	Confined site	–	–
Primary or acid digestion tank (i)	Confined site	Two primary or acid digestion tanks (i)	Confined sites
–	–	Secondary or basic digestion tank (j)	Confined site
Sludge buffer tank (k)	Confined site	–	–

[a] Blank boxes corresponds to treatment points that does not exist in that plant, and that are present in the other one (same line).

3.2. Analysis of samples

In the sewage management plants of Tarragona and Reus, preliminary sampling was done by sampling all sections numbered a to k in Table 2. The most abundant compounds measured in all sections were dimethyl sulfide, carbon disulfide and dimethyl disulfide, which were present in almost all samples. This is in agreement with the study made by Li and Shooter, where dimethyl sulfide and carbon disulfide were also present in all samples taken in a wastewater treatment plant, except for dimethyl disulfide, which the authors only found in two of seven locations sampled [2]. Also, Muezzinoglu found dimethyl sulfide to be one of the major components in emissions from a sewage treatment plant [9]. Propyl mercaptan, butyl mercaptan and pentane thiol were detected in roughly half the sampling points, and the least detected compound was ethyl mercaptan, which was identified only in the primary digestion tank of each plant. Table 3 shows the compounds detected in all sections sampled from these plants.

The VOSCs levels were in a wide range of concentrations, depending on the section of treatment sampled and the characteristics of the sampling site. For example, similar low VOSC levels were measured in the raw incoming sewage in (a) the primary settlement tank (b), and the biological settlement tank (e) at both the Tarragona and Reus plants. All measurements were taken in the open air and the concentrations of carbon disulfide, dimethyl sulfide and dimethyl disulfide were below 5 $\mu g\,m^{-3}$. Fig. 2 shows the sum of total target compounds in all sampled sections from both plants. Levels were similar at both plants for the gravitational thickening of sludge processes (d), which have similar design characteristics. These measurements were also taken in the open air.

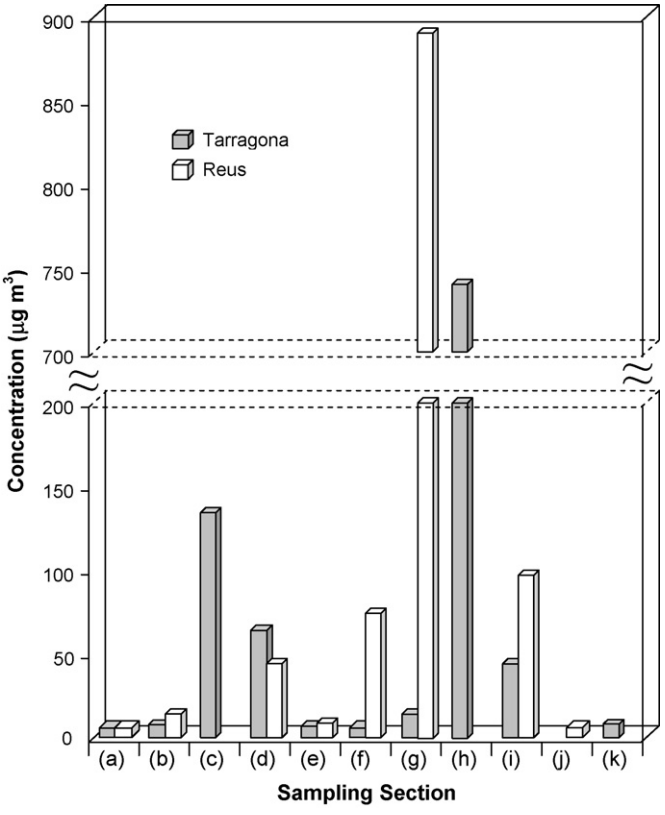


Fig. 2. Sum of target compounds concentrations found in all sampled sections, at both Tarragona and Reus plant.

Table 3
Target compounds identified in both of sewage management plants from Tarragona and Reus, at each sampling point

Sampled sections[a]		Volatile organic sulfur compounds identified[b]						
Sampling point	Plant[c]	Ethyl mercaptan	Dimethyl sulfide	Carbon disulfide	Propyl mercaptan	Butyl mercaptan	Dimethyl disulfide	Pentane thiol
Raw incoming sewage (a)	T			X			X	X
	R		X	X			X	
Primary settlement tank (b)	T		X	X			X	
	R		X	X	X	X	X	
Primary treated sewage sifted (c)	T		X	X	X	X	X	X
	R	–	–	–	–	–	–	–
Gravitational thickening of sludge (d)	T		X	X	X		X	X
	R		X	X			X	X
Biological settlement tank (e)	T		X				X	
	R		X	X			X	
Activated sludge re-circulation (f)	T		X	X			X	
	R		X	X		X	X	
Thickening of surplus bio-sludge by flotation (g)	T		X	X			X	
	R		X	X		X	X	X
Mixing sludge chamber (h)	T		X	X	X	X	X	
	R	–	–	–	–	–	–	–
Primary or acid digestion tank (tank 1) (i)	T	X	X	X	X		X	X
	R	X	X	X	X	X	X	X
Secondary of basic digestion tank (j)	T	–	–	–	–	–	–	–
	R		X	X			X	
Sludge buffer tank (k)	T		X	X		X	X	
	R	–	–	–	–	–	–	–

[a] Sampled sections described in Table 1, which are present in both plants or only in one of them.
[b] T is Tarragona plant and R is Reus plant.
[c] Compounds identified in each sampling point are indicated by X. A dash indicates that the section is not present in that plant.

On the other hand, very different levels of VOSCs were found in the sampling sections with different design characteristics. For example, in the activated sludge re-circulation process (f), which is an open site in the Tarragona plant and a confined site in the Reus plant, the levels of dimethyl disulfide were four times higher in the Reus plant than in the Tarragona plant. Also, the level of dimethyl sulfide was roughly 35 $\mu g\,m^{-3}$ in the Reus plant but this compound was undetected in the Tarragona plant.

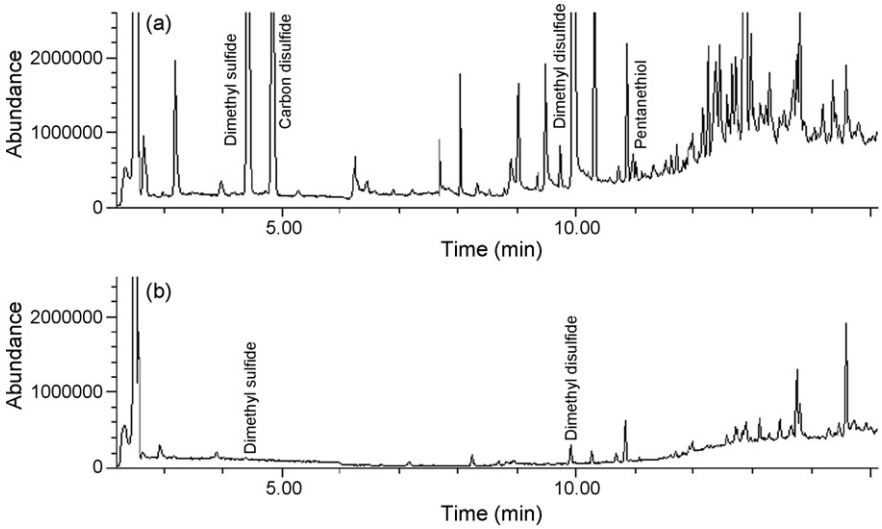


Fig. 3. Chromatograms of samples taken in the thickening of surplus bio-sludge by flotation sampling point from (a) Reus and (b) Tarragona sewage management plants.

However, the greatest difference was found for the thickening of surplus bio-sludge by flotation (g), where the sum of total target compounds was almost 897 $\mu g\,m^{-3}$ in the Reus plant and roughly 13 $\mu g\,m^{-3}$ in the Tarragona plant (see Fig. 2). Fig. 3 shows the chromatogram for these samples.

As it can be seen in Fig. 2, two sampling points, the thickening of bio-sludge by flotation (g) and the mixing sludge chamber (h) from Tarragona plant, presented very high levels of target compounds, with total concentrations of more than 700 $\mu g\,m^{-3}$. Moreover, high levels (>50 $\mu g\,m^{-3}$) were found in three sampling points: the primary treated sewage sifted from Tarragona (c), the gravitational thickening of sludge (d), and the primary digestion tank (i) from both Tarragona and Reus plants. Because of their high levels, these points were chosen for a more extensive sampling in both Tarragona and Reus plants. Ten samples were taken at each point on different days in order to obtain a more representative database for these sections and compare the levels of both plants at some common sampled sections. Table 4 shows the minimum and maximum concentrations of the target compounds and the total target compounds.

In some sampled sections with high levels of VOSCs, a great difference between the maximum and minimum values was observed. This may be due to a wide dispersion between all samples as, for example, in the thickening of surplus by flotation process (g) at the Reus pant, where, in addition to the wide variability in all samples, there was a very poor correlation between the most abundant compounds (dimethyl sulfide, carbon disulfide and dimethyl disulfide). Except for some discrepant samples, which widened the difference between minimum and maximum concentrations, other sections presented more similar values for all samples. For example, the mixing chamber (h) of the Tarragona plant showed high values of carbon disulfide and dimethyl disulfide (over 200 $\mu g\,m^{-3}$) except for one sample for which compounds concentrations were below 10 $\mu g\,m^{-3}$. The levels of carbon disulfide in primary treated sewage sifted (c) from the Tarragona plant also showed poor variability (from 0.3 $\mu g\,m^{-3}$ to 1.9 $\mu g\,m^{-3}$) and the maximum value of 421.1 $\mu g\,m^{-3}$ appeared as a discrepancy. These discrepant samples, which could be caused by different atmospheric conditions from those of the other samples or by different technical aspects of the sewage management process, increase the difficulty in finding normal behaviour in VOSCs emissions.

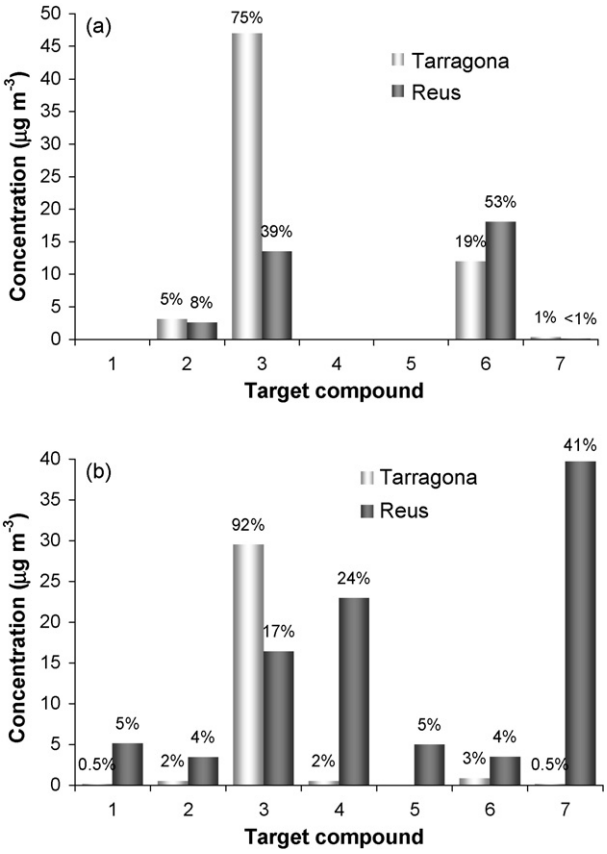


Fig. 4. Values of target compounds, numbered in the *x*-axis as they are presented in Table 1, found in common extensively sampled points from Tarragona and Reus plants: (a) gravitational thickening of sludge and (b) primary or acid digestion tank. Percentage values on each bar indicate the contribution of that compound at the total of target compounds found in that sampling point.

However, the results generally showed good agreement with the preliminary sampling campaign described earlier. For example, if we compare the levels recorded at the common sampled sites, we can see that the results for the gravitational thickening of sludge (d) were similar, but with greater differences in values of carbon disulfide (see Fig. 4a, which shows the contribution made by each detected compound to the total).

Table 4
Range of volatile organic sulfur compounds concentrations in $\mu g\,m^{-3}$ found at sampled sections from Tarragona and Reus ($n = 10$)

Target compound	Primary treated sewage sifted (c)	Gravitational thickening of sludge (d)		Thickening of surplus bio-sludge by flotation (g)		Mixing sludge chamber (h)	Primary or acid digestion tank (i)	
	Tarragona	Tarragona	Reus	Tarragona	Reus	Tarragona	Tarragona	Reus
Ethyl mercaptan	n.d.	n.d.	n.d.	n.d.	n.d.	n.d.	n.d.–0.5	0.3–14.8
Dimethyl sulfide	0.7–7.5	1.1–8.6	0.8–4.6	0.4–11.8	31.9–608.5	7.9–28.5	0.3–0.9	0.4–13.7
Carbon disulfide	0.3–421.1	10.4–104.5	4.8–37.3	n.d.–15.9	16.2–525.2	9.8–658.5	1.8–41.5	6.0–25.2
Propyl mercaptan	n.d.–4.8	n.d.–0.3	n.d.	n.d.	n.d.	n.d.–1.2	n.d.–1.5	n.d.–40.7
Butyl mercaptan	n.d.–1.6	n.d.	n.d.	n.d.	n.d.–2.3	n.d.–1.1	n.d.	2.8–6.7
Dimethyl disulfide	8.7–40.3	2.3–16.2	1.1–34.4	1.5–4.2	81.9–857.8	7.1–496.1	0.2–1.4	1.0–12.0
Pentane thiol	n.d.–11.8	n.d.–1.2	n.d.–0.4	n.d.	n.d.–3.1	n.d.	n.d.–0.4	34.1–49.0
Sum of target compounds	9.8–487.1	26.0–121.1	6.7–60.6	2.0–29.1	314.9–1994.7	26.4–1148.4	3.4–43.8	81.2–106.6

Minimum value–maximum value.

Also found were large differences in VOSCs levels in common sampled sections with different characteristics. For example, in the thickening of surplus bio-sludge by flotation (g), levels at the Reus plant were different from those at the Tarragona plant. Also, the primary or acid digestion tank (i) was the only section in which ethyl mercaptan was detected (in both plants), though the average concentration was higher at the Reus plant. All the other compounds except for carbon disulfide were also present at higher concentrations at the Reus plant (see Fig. 4b). Also, the highest levels for the total sampling campaign of propyl mercaptan, butyl mercaptan, and pentane thiol were observed in the primary digestion tank at the Reus plant.

To determine the influence of emissions on the surrounding areas, we sampled two points affected by emissions from organic matter decomposition processes. Despite the intense odour detected in the open air at both plants, samples taken at these points showed very low levels of VOSCs. In the sample taken near the solid waste management plant, only butyl mercaptan was detected (at a concentration of 0.4 $\mu g\,m^{-3}$). Dimethyl sulfide, dimethyl disulfide and pentanethiol were found in the sampling point external to the sewage management plant (at concentrations of less than 0.2 $\mu g\,m^{-3}$). Moreover, no target compounds were found above the method detection levels at urban points near the sewage plants.

4. Conclusions

An analytical method has been optimised for determining seven volatile organic sulfur compounds in air by TD–GC/MS. The method presents good recoveries for all compounds. The linearity in the responses and the repeatability for all compounds are also good, and it has showed to be suitable for the determination of VOSCs.

The sampling campaign in the sewage management plants of two similar cities enabled comparisons between some of the common sections in the process. Dimethyl sulfide, carbon disulfide and dimethyl disulfide were the most abundant compounds in all samples. On the other hand, ethyl mercaptan was the least detected compound, appearing only in the primary digestion process. The other compounds were detected and measured in about half the samples. The highest concentrations of target compounds were found in processes involving sludge treatment. These were the mixing sludge chamber, the thickening of surplus bio-sludge by flotation and, less intensely, the primary or acid digestion of sludge. The design characteristics of sampled sections were found to be determinant of VOSC concentration.

Acknowledgements

The authors would like to thank the *Dirección General de Investigación* for financial support (CTM2005 01774), the *Agència de Gestió d'Ajuts Universitaris i de Recerca* of the *Generalitat de Catalunya* for M.R. Ras' predoctoral grant (2005FI 00018), and both the Tarragona and the Reus Sewage Management Plants for allowing us to perform the sampling.

References

[1] W. Wardencki, J. Chromatogr. A 793 (1998) 1.
[2] K.-C. Li, D. Shooter, Int. J. Environ. Anal. Chem. 84 (2004) 749.
[3] C. Vassilakos, A. Papadopoulos, M. Lahaniati, T. Maggos, J. Bartzis, P. Papagianakopoulos, Fresenius Environ. Bull. 11 (2002) 516.
[4] F. Lestremau, F.A.T. Andersson, V. Desauziers, J.L. Fanlo, Anal. Chem. 75 (2003) 2626.
[5] A.T. Nielsen, S. Jonsson, J. Chromatogr. A 963 (2002) 57.
[6] S. Rappert, R. Müller, Waste Manage. 25 (2005) 887.
[7] E. Smet, H. Van Langenhove, Biodegradation 9 (1998) 273.
[8] K.-H. Kim, Y.J. Choi, E.C. Jeon, Y. Sunwoo, Atmos. Environ. 39 (2005) 1103.
[9] A. Muezzinoglu, Chemosphere 51 (2003) 245.
[10] A.T. Nielsen, S. Jonsson, Analyst 127 (2002) 045.
[11] I. Devai, R.D. DeLaune, Water Environ. Res. 71 (1999) 203.
[12] K.-H. Kim, Environ. Sci. Technol. 39 (2005) 6765.
[13] K.-H. Kim, D.-W. Ju, S.-W. Joo, Talanta 67 (2005) 955.
[14] K.-H. Kim, Int. J. Environ. Anal. Chem. 86 (2006) 805.
[15] K.-H. Kim, G.-H. Choi, Y.-J. Choi, H.-N. Song, H.-S. Yang, J.-M. Oh, Talanta 68 (2005) 1713.
[16] K.-H. Kim, Atmos. Environ. 39 (2004) 2235.
[17] K.-H. Kim, H. Swan, Z.-H. Shon, G. Lee, J. Kim, C.-H. Kang, Chemosphere 54 (2004) 515.
[18] C. Haberhauer-Troyer, E. Rosenberg, M. Grasserbauer, J. Chromatogr. A. 848 (1999) 305.
[19] E. Davoli, M.L. Gangai, L. Morselli, D. Tonelli, Chemosphere 51 (2003) 357.
[20] M.R. Ras-Mallorquí, R.M. Marcé-Recasens, F. Borrull-Ballarín, Talanta 72 (2007) 941.

Available online at www.sciencedirect.com
ScienceDirect
Talanta 74 (2008) 555–561
Talanta
www.elsevier.com/locate/talanta

An integrated analytical approach for characterizing an organic residue from an archaeological glass bottle recovered in Pompeii (Naples, Italy)

Erika Ribechini [a,*], Francesca Modugno [a], Cecilia Baraldi [b], Pietro Baraldi [c], Maria Perla Colombini [a]

[a] *Dipartimento di Chimica e Chimica Industriale, Università di Pisa, via Risorgimento 35, 56126 Pisa, Italy*
[b] *Dipartimento di Scienze Farmaceutiche, Università di Modena e Reggio Emilia, via G. Campi 183, 41100 Modena, Italy*
[c] *Dipartimento di Chimica, Università di Modena e Reggio Emilia, via G. Campi 183, 41100 Modena, Italy*

Received 30 March 2007; received in revised form 4 June 2007; accepted 15 June 2007
Available online 28 June 2007

Abstract

Within the framework of an Italian research project aimed at studying organic residues found in archaeological objects from the Roman period, the chemical composition of the contents of several glass vessels recovered from archaeological sites from the Vesuvian area (Naples, Italy) was investigated.

In particular, this paper deals with the study of an organic material found in a glass bottle from the archaeological site of Pompeii using a multi-analytical approach, including FT-IR, direct exposure mass spectrometry (DE-MS) and GC–MS techniques.

The overall results suggest the occurrence of a lipid material of vegetable origin. The hypothesis that the native lipid material had been subjected to a chemical transformation procedure before being used is presented and discussed.
© 2007 Elsevier B.V. All rights reserved.

Keywords: FT-IR; DE-MS; GC–MS; Organic remains; Archaeological glass bottle; Pompeii; Free fatty acids; Vegetable lipid material

1. Introduction

In the field of archaeology, knowledge of the chemical composition of amorphous organic residues helps us to clarify several aspects of daily life related to religious customs and rites, diet, medical practices and cosmetics, and a number of artisan activities. In this respect, the archaeological site of Pompeii is unique due to the amount and the quality of its preserved organic materials. Pompeii is a ruined Roman city near modern Naples (Italy) and was destroyed during a catastrophic eruption of the volcano Vesuvius in 79 a.d. The volcano buried the city under many feet of ash and the city was lost for about 1600 years before being discovered. Since then, its excavation has provided an extraordinarily detailed insight into life in the Roman Empire.

The complexity of the composition of organic archaeological remains and the chemical changes undergone by original materials due to human intervention in order to modify the properties of the organic matter, represent the biggest difficulties in terms of their characterization. Moreover, degradation from ageing under the influence of specific burial conditions can induce further changes in the composition of the original materials. Because of all these aspects, the analytical procedures usually used to characterize organic residues from archaeological finds are based on chromatographic techniques coupled with mass spectrometry [1–10]. However, preliminary analyses by Fourier transformed infrared spectroscopy (FT-IR), GC or direct mass spectrometric techniques (DE-MS, direct inlet mass spectrometry) provide a fingerprint and general information on the nature of organic material and may be useful for providing initial hypotheses about the substances present [11–16].

Within the framework of a collaboration between Italian researchers to study residues from archaeological vessels from the Roman period, the chemical composition of the content of several glass vessels recovered in the archaeological sites from the Vesuvian area (Naples, Italy) was investigated. In particular, this paper deals with the study of an organic material found in

* Corresponding author. Tel.: +39 0502219312; fax: +39 0502218260.
E-mail address: erika@dcci.unipi.it (E. Ribechini).

0039-9140/$ – see front matter © 2007 Elsevier B.V. All rights reserved.
doi:10.1016/j.talanta.2007.06.026

a glass bottle from the archaeological site of Pompeii using a multi-analytical approach, including the use of FT-IR, DE-MS (direct exposure mass spectrometry) and GC–MS techniques. FT-IR and DE-MS give an excellent fingerprint of the sample, while GC–MS gives detailed compositional information at a molecular level and can highlight a wide range of classes of natural organic compounds. Complementary information can be obtained using this multi-analytical approach thus enabling us to recognize the organic materials originally present in the object.

2. Experimental

2.1. Reagents

All solvents were Carlo Erba (Milan, Italy) pesticide analysis grade and were used without further purification. Hexadecane (internal standard, IS_1), and *N*,*O*-bis(trimethyl) silyltrifluoroacetamide (BSTFA) containing 1% trimethylchlorosilane were purchased from Sigma–Aldrich (Milan, Italy).

Tridecanoic (internal standard, IS_2), dodecanoic (lauric), tetradecanoic (myristic), hexadecanoic (palmitic), octadecanoic (stearic), (*Z*)-9-octadecenoic (oleic), (*Z*)-11-eicosenoic (gondoic), (*Z*)-13-docosenoic (erucic), (*Z*,*Z*)-9,12-octadecadienoic (linoleic), (*Z*,*Z*,*Z*)-9,12,15-octadecatrienoic (linolenic), octanedioic (suberic), nonanedioic (azelaic), decanedioic (sebacic) acids, trimyristin (trimyristoyl glycerol), tripalmitin (tripalmitoyl glycerol) and tristearin (tristearoyl glycerol) were supplied by Sigma (St. Louis, MO, USA), all with a purity >99%.

2.2. Archaeological samples

The investigated glass bottle from Pompeii was preserved in the National Archaeological Museum of Naples (Italy). The glass bottle contained a homogeneous, pale yellow, soft solid matter, called man1-A in the text.

2.3. Analytical procedures and instrumentation

2.3.1. FT-IR

A Perkin-Elmer FT-IR 1700 spectrometer as used with 32 scans, spectral resolution 2 cm^{-1}, a TGS detector and equipment for purging the gasses inside the cell compartment. Potassium bromide pellets were prepared with a concentration of 1% by grinding the mixed powders in an agate mortar and then pressing them in a die for 1 min at a pressure of 1 MPa. The spectra were linearised in terms of the changing background and compared with a built up database. The recorded FT-IR spectra were also compared with the online SDBS spectra (www.ais.go.jp/RIODB/SDBS).

2.3.2. Direct exposure electron ionisation mass spectrometry

The instrumentation consisted of a direct probe controller (DPC) and a direct exposure probe (DEP), coupled with a Polaris Q ion trap external ionisation mass spectrometer (Thermo Electron Corporation, USA). The analytical procedure based on direct mass spectrometry, already described in the literature [15], can be summarised as follows: the samples (1–3 mg) were analysed after dissolution in dichloromethane (1 mg/ml). Aliquots of 1 μl of the dissolved samples were deposited on the rhenium filament wire of the DEP, and, after the evaporation of the solvent, analysed by mass spectrometry. The source temperature was 230 °C. For the first examination of each sample, the mass spectrometer was scanned over an *m*/*z* range of 50–1000 by programming the probe current as follows: 0 mA for 30 s, from 0 to 1000 mA in 50 s, then 1000 mA for 60 s. Subsequently, once the presence of high molecular and/or polymeric components had been excluded, the mass spectrometer was scanned over an *m*/*z* range of 50–650 and in this case, the probe current was programmed as follows: 0 mA for 20 s, from 0 to 1000 mA in 2 s, then 1000 mA for 60 s. A mass spectral fingerprint was obtained by averaging the mass spectra in the desired time range, corresponding to the peak of the TIC.

2.3.3. Gas chromatography–mass spectrometry

The instrumentation was made up of a trace GC gas chromatograph (ThermoFinnigan, USA) equipped with a programmable temperature vaporizers (PTV) injection port ("constant temperature splitless with surge" mode at 280 °C with a surge pressure of 100 kPa) and a mass spectrometric detector with an ion trap analyser ThermoFinnigan Polaris Q (electronic impact 70 eV, ion source temperature 230 °C, analysed mass interval 50–650μ, interface temperature 280 °C). Chromatographic separation was performed on a chemically bonded fused silica capillary column HP-5MS (Hewlett-Packard), stationary phase 5%phenyl–95%methylpolysiloxane, 30 m × 0.25 mm i.d., 0.25 μm film thickness, connected to a 2 m long deactivated fused silica capillary pre-column, internal diameter 0.32 mm. The gas chromatographic conditions were as follows: initial temperature 80 °C, 2 min isothermal, 10 °C/min up to 200 °C, 4 min isothermal, 6 °C/min up to 280 °C, 40 min isothermal. Carrier gas: He (purity 99.9995%), constant flow 1.2 ml/min.

The analytical procedure used, already described in the literature [3], can be summarised as follows: the sample (1–3 mg) was subjected to alkaline hydrolysis under sonication adding 1 ml of hydroalcoholic KOH solution, at 60 °C for 3 h. After hydrolysis, neutral organic components were extracted with *n*-hexane. After acidification with hydrochloric acid (10 M) of the residual solution, the acidic organic components were extracted with diethyl ether. Aliquots of both fractions were evaporated to dryness under a gentle nitrogen stream and subjected to a derivatisation reaction: the dried extracts were admixed with a solution of internal standard (5 μl of tridecanoic acid solution, 140 μg/g) and derivatised with 20 μl of *N*,*O*-bis(trimethyl)silyltrifluoroacetamide (BSTFA) containing 1% trimethylchlorosilane (at a temperature of 60 °C for 30 min) using 150 μl isooctane as the solvent. After adding 10 μl of hexadecane solution (80 μg/g) as an injection internal standard, 2 μl of the solution were anal-

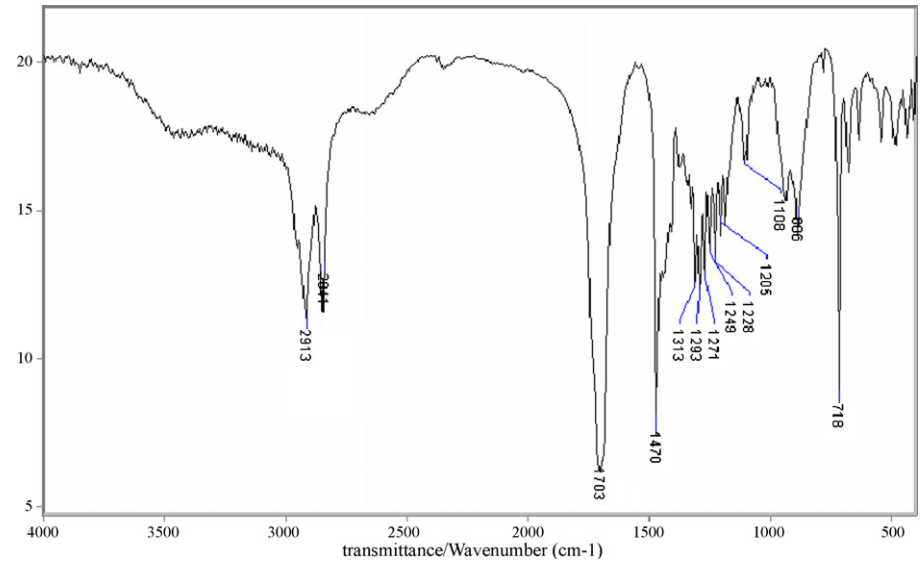


Fig. 1. FT-IR spectrum of sample man1-A.

ysed by GC–MS. Peak assignation was based on comparisons with analysed reference compounds and materials, with library mass spectra (NIST 1.7) and on the interpretation of mass spectra.

3. Results and discussion

3.1. FT-IR analysis

Fig. 1 shows the FT-IR spectrum of sample man1-A, and Table 1 summarises the main vibrational group frequencies with the relative assignment.

The FT-IR spectrum looks like to that of a mixture of mid-long chain fatty acids, such as palmitic and stearic acids, and mid-long chain hydroxy fatty acids. In actual fact, the FT-IR spectra of free fatty acids and free hydroxy fatty acids show several bands with identical or very similar wavenumbers, thus they can be attributed to both classes of compounds. In any case, the weak absorption at around 3500 cm^{-1}, due to OH stretching, would seem to indicate that hydroxy fatty acids are present at a low abundance in the mixture.

Table 1
Assignment of the main vibrational group frequencies in the FT-IR spectrum of sample man1-A, shown in Fig. 1

Wavenumbers (cm^{-1})	Attribution
2913, 2841	CH_3 and CH_2 stretching
1703	C═O free carboxyl stretching
1470, 1443	CH asymm. bending
1375, 1344	CH symm. bending
1313, 1293,1271, 1249, 1228, 1205	CH_2 bending
1108	C—O stretching
945	COOH out of plane bending
728, 718	CH rocking

3.2. DE-MS analysis

The analysis by DE-MS of archaeological samples gives complex mass spectra which need to be carefully interpreted. With this in mind, mass spectra of standard compounds were acquired and used for identification purposes. On the basis of the literature [17–21] and considering the use of an ion trap analyser in our study, the fragmentation patterns observed for some standard molecules and for archaeological materials can be explained as follows.

Palmitic acid (Fig. 2). The molecular ion at *m/z* 256 is clearly visible, together with acylium ion at *m/z* 239 ([*M*−17]). Fragment ions formed by the cleavage of the carbon backbone are

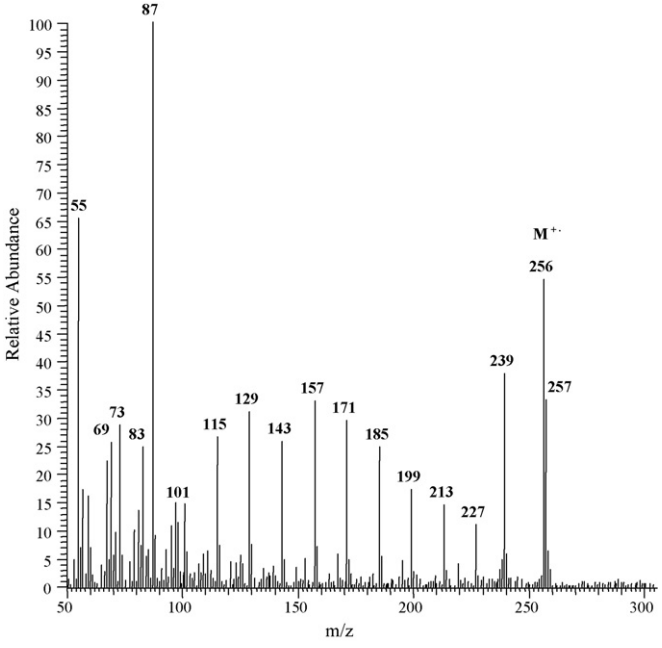


Fig. 2. Mass spectrum of palmitic acid obtained by DE-MS.

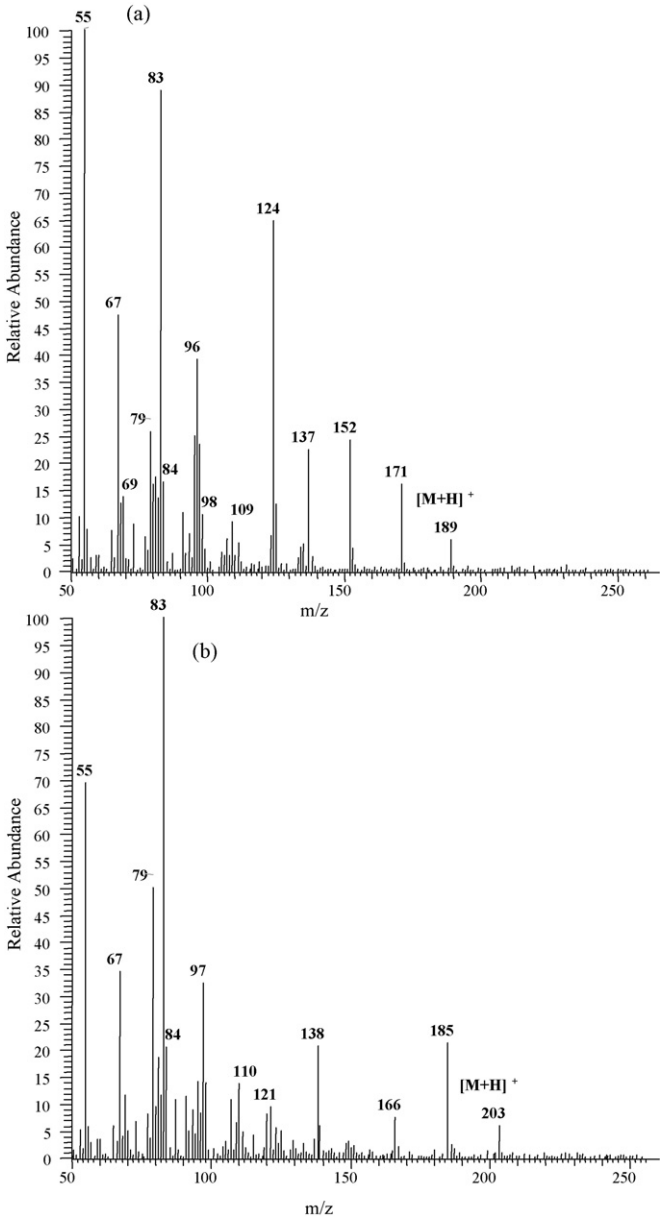


Fig. 3. Mass spectrum of (a) azelaic acid and (b) sebacic acid obtained by DE-MS.

observed at *m/z* 213, 227, 199, 185, 171, 157, 143, 129, 115, 101, 87 and 73 ($[C_nH_{2n}COOH]^+$). Moreover, a peak at *m/z* 257 relative to $[M+H]^+$ ion, probably due to a rearrangement involving the capture of a hydrogen radical in the ion trap, is also visible.

Azelaic and sebacic acids (Fig. 3). Peaks can be seen at *m/z* 189 and 203 relative to $[M+H]^+$ ions, probably due to a rearrangement involving the capture of a hydrogen radical in the ion trap. Peaks at *m/z* 171 and 185 formed by the loss of a water molecule from $[M+H]^+$ were also identified along with those formed by the loss of two water molecules, observed at *m/z* 152 and 166, respectively for azelaic and sebacic acid. Molecular ions (*m/z* 188 and 202) were not detected.

Tristearin, trimyristin and tripalmitin. In the mass spectrum of tristearin, shown in Fig. 4, the fragment ions, formed by the loss of an acylium group ($[M–RCOO]^+$, base peak) at *m/z* 607 and of an acylium group plus an additional hydrogen ($[M–RCOOH]^+$) at *m/z* 606 are very intense. The peak relative to the acylium ion ($[RCO]^+$) is present at *m/z* 267 and another important fragment ion is at *m/z* 341. This last peak corresponds to an ion ($[RCO+74]^+$) containing the glycerol backbone, minus one hydroxy group. Probably, since the ionisation energy of 70 eV produces an extensive fragmentation, the molecular ion (at *m/z* 890) is not detected. The same type of fragment ions were also observed for trimyristin and tripalmitin: in the former with 112 or 56 amu lower (*m/z* at 564, 536, 494, 495, 285 and 211) than the tristearin fragment ions, and, in the latter, with 56 or 28 amu lower (*m/z* at 620, 592, 550, 551, 313 and 239) than the tristearin fragment ions.

Oleic and erucic acids. Under 70 eV electron ionisation, oleic and erucic acids show a similar behaviour, with very low intense molecular peaks at *m/z* 282 and *m/z* 338, respectively, present at very low abundance levels. The peaks at *m/z* 264 and at *m/z* 320, relative to the loss of a water molecule, and at *m/z* 265 and 321, relative to the loss of an OH radical, are present in high abundance. Moreover, peaks due to the cleavage of the carbon backbone (at *m/z* 235, 221, 207, 193, 179 for oleic acid and at *m/z* 291, 277, 263, 249, 235, 221, 207, 193, 179 for erucic acid) are also present.

Following the analysis of standard compounds by DE-MS, we went on to study the archaeological sample man1-A, whose DE-mass spectrum is reported in Fig. 5. Monocarboxylic fatty acids were identified in the DE-mass spectrum by the presence of peaks at *m/z* 143, 157, 171, 185, 199, 213, 227, 256 and 284. All these peaks suggest the occurrence of a lipid material. In particular, the high abundance of peak at *m/z* 256, which is characteristic of the fragmentation of palmitic acid, suggests a predominance of this acid in the sample, and the presence of the peak at *m/z* 284 indicates the occurrence of stearic acid. Moreover, the occurrence of dicarboxylic fatty acids could not be excluded due to the fact that their mass spectra present some peaks that are also present in the mass spectra of monocarboxylic fatty acids.

Table 2
Peak assignment in the chromatogram of acidic fraction of sample man1-A, shown in Fig. 6

No.	Compounds (TMS derivative)	Retention time
1	Dodecanoic acid (lauric acid)	11.0
2	α,ω-Octanedioic acid (suberic acid)	11.6
3	α,ω-Nonanedioic acid (azelaic acid)	12.6
4	Tetradecanoic acid (myristic acid)	13.1
5	α,ω-Decanedioic acid (sebacic acid)	13.6
6	Hexadecanoic acid (palmitic acid)	15.2
7	(*Z*)-9-Octadecenoic acid (oleic acid)	17.9
8	(*E*)-9-Octadecenoic acid	18.0
9	Octadecanoic acid (stearic acid)	18.0
10	10-Hydroxyoctadecenoic acid	21.4
11	10-Hydroxyoctadecanoic acid	21.8
12	9-Hydroxyoctadecanoic acid	22.0
13	9,10-Dihydroxyoctadecanoic acid	23.9
14	9,10-Dihydroxyoctadecanoic acid	24.1
15	Docosanoic acid (behenic acid)	24.9

No. = peak number in the chromatogram. Retention times in minutes.

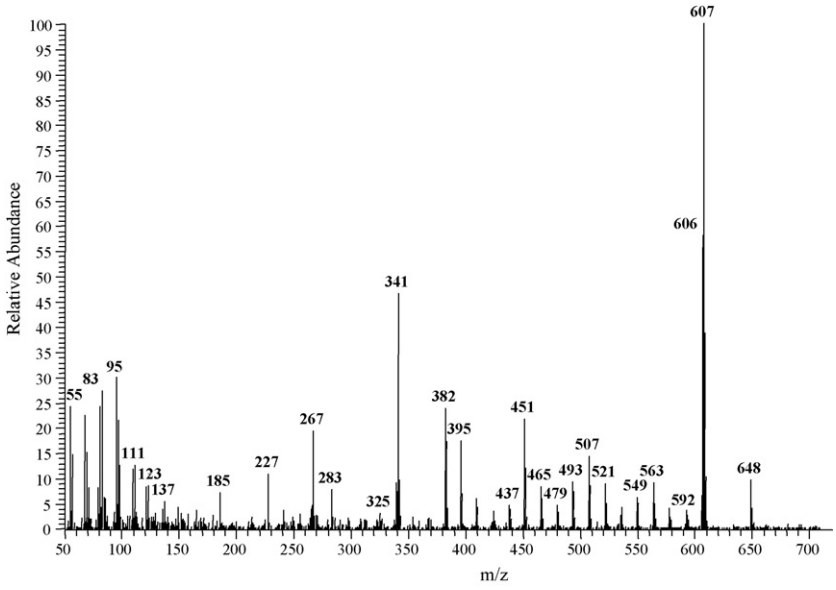


Fig. 4. Mass spectrum of tristearoyl glycerol obtained by DE-MS.

3.3. GC–MS analysis

The GC–MS chromatogram of the acidic fraction is shown in Fig. 6, and Table 2 reports the peak assignment. The neutral fraction did not contain any significant compound. The acidic extracts consisted of a series of linear monocarboxylic even numbered saturated fatty acids ranging from 12 to 22 carbon atoms except the presence of eicosanoic acid (C20) and with palmitic acid being the most prominent. In addition, they consisted of a series of α,ω-dicarboxylic acids, with 8–10 carbon atoms and a series of hydroxycarboxylic fatty acids all formed by 18 carbon atoms, namely, 10-hydroxyoctadecenoic acid, 10-hydroxyoctadecanoic acid, 9-hydroxyoctadecanoic acid, 9,10-dihydroxyoctadecanoic acid (present as a pair of threo-erythro isomers) with 10-hydroxyoctadecanoic acid and 9-hydroxyoctadecanoic acid as the most prominent in this series. Finally, the occurrence of oleic acid and its trans isomer was also ascertained.

The observed hydroxy acids have been previously reported in archaeological organic residues such as mummies [22,23] and pottery vessels [24], and their presence has been associated with radical oxidation pathways of unsaturated fatty acids via hydroxylation/dehydration of double bonds. In particular, these hydroxy acids are generally considered as the intermediates of the oxidation reaction which transforms oleic acid into azelaic acid [24]. Thus, their occurrence suggests that the organic material present in the glass bottle found in Pompeii, originally contained quite high amounts of compounds with unsaturation mainly at position 9, such as oleic acid.

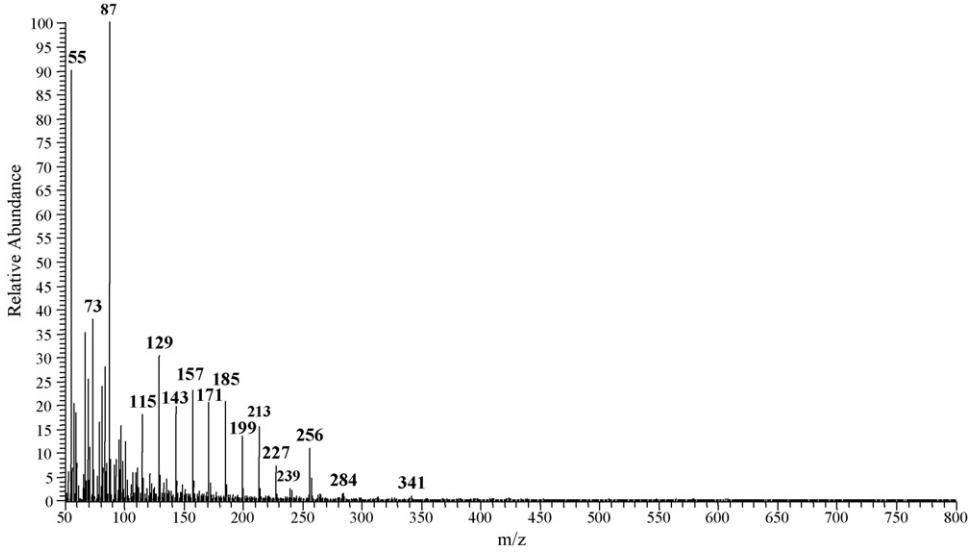


Fig. 5. Mass spectrum of sample man1-A obtained by DE-MS.

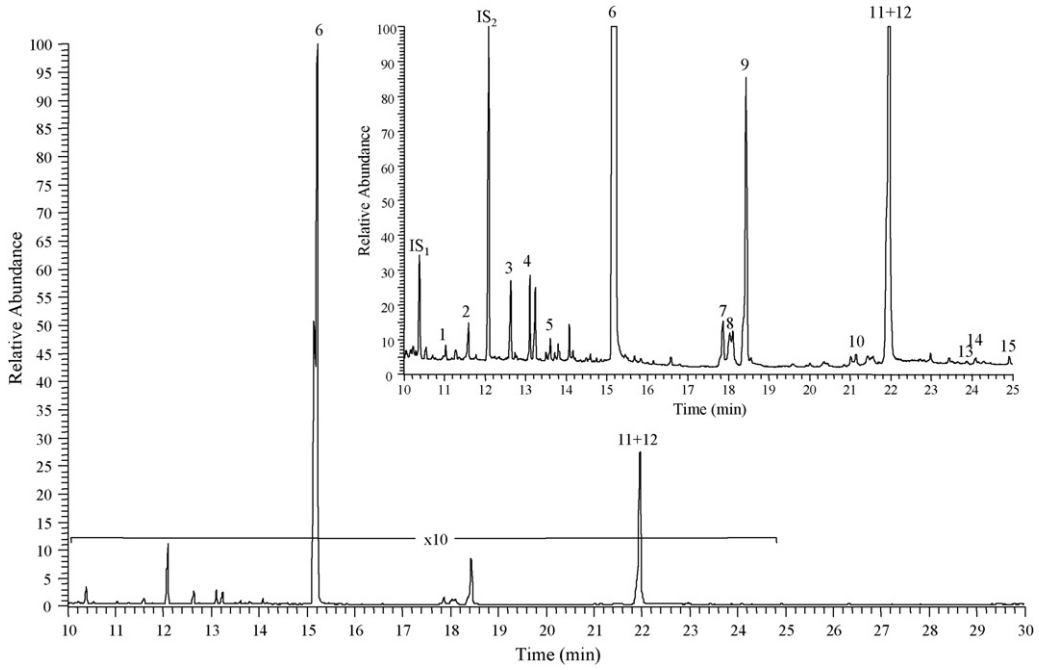


Fig. 6. Total ion current chromatograms of acidic fraction of sample man1-A (the acidic species are present as TMS derivatives).

4. Conclusions

The general chromatographic pattern and the fatty acid profile suggest the occurrence of a lipid material of vegetable origin. The fact that the sample man1-A contains low levels of azelaic acid and the simultaneous presence of quite high levels of the series of hydroxycarboxylic acids with 18 carbon atoms, seems to indicate that the oxidation of the organic material has not yet been completed, highlighting a low degree of oxidation. This phenomenon may be related to the sealing of the glass bottle: as the access of oxygen was prevented, the oxidation process was slowed down.

Since in the FT-IR spectrum there were no bands normally attributed to glycerol, as assessed by comparison with FT-IR spectra database and fatty acid salts [25], and DE-MS analysis ruled out the presence of tri-, di- and mono-acylglycerols, it seems quite probable that the native lipid material had been subjected to a chemical transformation procedure before being used. For instance, according to a recipe described by Pliny the Elder (Naturalis Historia, Book 32), olive oil was warmed together with lead oxide (litargirium) and water to form insoluble lead soaps and an aqueous phase containing glycerol. In Greco-Roman times, glycerol was widely used as an ingredient in moisturizing, emollient or detergent cosmetics due to its emulsifying and lubricating properties, and in pharmaceutical preparations. Moreover, in some ancient Egyptian cosmetics the presence of free fatty acids, lead salts, and lead soaps has been identified, leading to the hypothesis that these metal soaps were used in ancient times for cosmetic production [25].

In this way, the free fatty acids found in the glass bottle man1-A may be interpreted as secondary products of the saponification reaction of olive oil for the production of glycerol. These secondary products may have been recovered after some kind of acidification of lead soap. Interestingly, the results of the analysis of another Pompeii bottle recovered in the same villa showed the presence of glycerol together with traces of fatty acid salts which were probably entrapped in the glycerine-aqueous phase [26].

Moreover, in the glass bottle from Pompeii the occurrence of the trans isomer of the oleic acid seems to indicate that the sample had been heated, since this acid is not common in lipid materials of vegetable origin [27], and is mainly formed during the warming of vegetable lipids containing oleic acid [28].

Acknowledgements

The authors would like to thank Prof. Pietro Giovanni Guzzo for involving them in the Pompeiian artefacts research project and for very useful discussions.

References

[1] R.P. Evershed, S.N. Dudd, M.S. Copley, R. Berstan, A.W. Stott, H. Mottram, S.A. Buckley, Z. Crossman, Acc. Chem. Res. 35 (2002) 660.
[2] R.P. Evershed, C. Heron, J. Goad, Analyst 115 (1990) 1339.
[3] M.P. Colombini, G. Giachi, F. Modugno, P. Pallecchi, E. Ribechini, Archaeometry 45 (2003) 649.
[4] R.P. Evershed, S.N. Dudd, V.A. Anderson-Stojanovic, E.R. Gebhard, J. Archaeol. Sci. 30 (2003) 1.
[5] H.R. Mottram, S.N. Dudd, G.J. Lawrence, A.W. Stott, R.P. Evershed, J. Chromatogr.A 833 (1999) 209.
[6] T.F.M. Oudemans, J.J. Boon, J. Anal. Appl. Pyrol. 20 (1991) 197.
[7] K. Kimpe, P.A. Jacobs, M. Waelkens, J. Chromatogr. A 968 (2002) 151.
[8] A.M. Pollard, C. Heron, Archaeological Chemistry, RCS Paperbacks, Royal Society of Chemistry, Cambridge, 1996, pp. 239–270.
[9] M. Regert, S. Colinart, L. Degrand, O. Decavallas, Archaeometry 43 (2001) 549.
[10] B. Stern, C. Heron, L. Corr, M. Serpico, J. Bourriau, Archaeometry 45 (2003) 457.

[11] H.G.M. Edwards, M.J. Falk, J. Raman Spectrosc. 28 (1997) 211.
[12] M. Regert, C. Rolando, Anal. Chem. 74 (2002) 965.
[13] P.E. McGovern, D.L. Glusker, L.J. Exner, M.M. Voigt, Nature 381 (1996) 480.
[14] N. Garnier, C. Cren-Olivé, C. Rolando, M. Regert, Anal. Chem. 74 (2002) 4868.
[15] F. Modugno, E. Ribechini, M.P. Colombini, Rapid Commun. Mass Spectrom. 20 (2006) 1787.
[16] M.P. Colombini, F. Modugno, E. Ribechini, J. Mass Spectrom. 40 (2005) 675.
[17] R. Ryhage, E. Stenhagen, J. Lipid Res. 1 (1960) 361.
[18] M. Barber, T.O. Merren, W. Kelly, Tetrahedron Lett. 18 (1964) 1063.
[19] A.J. Aasen, W.M. Lauer, R.T. Holman, Lipids 5 (1973) 869.
[20] P. Laakso, Eur. J. Lipid Sci. Technol. 104 (2002) 43.
[21] P. Laakso, P. Manninen, Spectral Prop. Lipids 1 (1999) 141.
[22] F.O. Gülaçar, A. Buchs, A. Susini, J. Chromatogr. 479 (1989) 61.
[23] S.A. Buckley, A.W. Stott, R.P. Evershed, Analyst 124 (1999) 443.
[24] M. Regert, H.A. Bland, S.N. Dudd, P.F. van Bergen, R.P. Evershed, Proc. Roy. Soc. London, Ser. B 265 (1998) 2027–2032.
[25] M. Cotte, P. Dumas, G. Richard, R. Breniaux, Ph. Walter, Anal. Chim. Acta 553 (2005) 105.
[26] P. Baraldi, M.P. Colombini, A. Ciarallo, S. Francesconi, F. Modugno, E. Ribechini, Proceedings of 8th International Conference on Non-Destructive Investigations and Microanalysis for the Diagnostics and Conservation of the Cultural and Environmental Heritage, Lecce, Italy, May 15–19, 2005.
[27] W.W. Christie, Lipid Analysis, 3rd ed., The Oily Press, Bridgwater, England, 2003.
[28] R. Biffoli, Chimica degli alimenti, Edizioni Uses, Firenze, Italy, 1990.

Available online at www.sciencedirect.com
ScienceDirect
Talanta 74 (2008) 648–654
Talanta
www.elsevier.com/locate/talanta

Determination of N-species in soil extracts using microplate techniques

Charles A. Shand *, Berwyn L. Williams, Grace Coutts

Macaulay Institute, Craigiebuckler, Aberdeen AB15 8QH, UK

Received 22 March 2007; received in revised form 14 June 2007; accepted 25 June 2007
Available online 3 July 2007

Abstract

Colourimetric methods for the determination of NO_3^-, NH_4^+ and total N in water extracts of soils using 96-well microplate techniques are described. Nitrate was determined by azo dye formation after reduction to NO_2^- using a solution of hydrazine sulphate. Ammonium in the soil extracts was purified and concentrated by diffusion as NH_3 from small volumes (750 μL) of extract treated with MgO into a H_2SO_4 collector using a double-plate, MicroResp™ method and subsequently determined by the Berthelot reaction. For the determination of total N, samples were oxidised with $K_2S_2O_8$ at 110 °C in a 96 × 1.1 mL polytetrafluoroethylene block with a lid that closed individual wells. The oxidised solutions were transferred to standard plates for colourimetric analysis of NO_3^-. The recovery of N, measured as NO_3^-, from NH_4NO_3 and a range of organic-N compounds was >95%. The limits of quantitation of the colourimetic assays were 0.020 mg N L^{-1} for NO_3^- and 0.051 mg N L^{-1} for NH_4^+. The methods were tested on water extracts derived from a range of 10 nutrient poor soils from Scotland. There were acceptable linear correlations between the results obtained by established methods. For soil extracts analysed by the microplate method, the relationship for NO_3^- was 1.03× result from ion chromatography + 0.0055 ($R^2 = 0.9961$); for NH_4^+ determined by the microplate method, the relationship was 0.9696 × result from a discrete analyser − 0.0169 ($R^2 = 0.9757$) and for total N determined by oxidation in the PTFE microplate the relationship was 0.9435 × result obtained by combustion + 0.0489 ($R^2 = 0.9743$). Purification of the NH_4^+ in water extracts from the 10 different soils by the diffusion method did not result in any systematic difference (paired *t*-test, $p = 0.05$) between measured concentration values determined before and after diffusion.
© 2007 Elsevier B.V. All rights reserved.

Keywords: Colourimetric analysis; Ammonium; Nitrate; Organic nitrogen; Diffusion of ammonia

1. Introduction

The 96-well microplate, developed principally for use as a disposable bioreactor, offers the possibility of N-analysis (NO_2^-, NO_3^-, NH_4^+ and total dissolved N) of soil extracts by adaptation of existing chemistries previously carried out at larger scales, resulting in savings in the amounts of reagents and wastes. Of particular importance among existing methods are those for the determination NO_2^- and NO_3^- involving azo dye formation [1] and those for NH_4^+ involving the Berthelot (or indophenol) reaction [2]. The determination of NO_3^- by azo dye formation requires prior reduction of NO_3^- to NO_2^- and this has often been achieved in flow analysis systems with copperised Cd. The use of copperised Cd in microplates poses constraints because the microplate system involves vertically transmitted light for absorbance measurements. Hydrazine can reduce NO_3^- to NO_2^- and solutions of hydrazine sulphate containing Cu^{2+} as catalyst have been used in automated air-segmented flow systems [3,4]. A disadvantage of hydrazine in such analysis is that it may partially decompose NO_2^- so that simple subtraction of analytical data with and without hydrazine cannot easily be applied to determine NO_3^- in the presence of NO_2^-. However, using an air-segmented flow system under specific conditions of reagent concentration, pH, temperature and time, it is possible to have quantitative recovery of NO_2^- and quantitative conversion of NO_3^- to NO_2^-. Kamphake et al. [3] used hydrazine sulphate at a concentration of 190 mg L^{-1} at 38 °C for approximately 10 min, whereas, Downes [4] used the same concentration of hydrazine sulphate at 33 °C for 7.5 min.

The procedure for the determination of NH_4^+ in soil extracts using the Berthelot reaction is well suited to adaptation in microplates as the method involves the addition of only two solutions to the sample. However, the reaction is prone to interferences from organic-N compounds and from divalent cations which may exist in soil extracts or natural waters [5–9]. These interferences can be overcome by separation of the NH_4^+ by

* Corresponding author. Tel.: +44 1224 498200; fax: +44 1224 311556.
E-mail address: c.shand@macaulay.ac.uk (C.A. Shand).

0039-9140/$ – see front matter © 2007 Elsevier B.V. All rights reserved.
doi:10.1016/j.talanta.2007.06.039

diffusion in the form of NH_3 [10] but microplate methods for this have not been reported. Several methods for the separation of N by diffusion of NH_3 for isotopic analysis exist, such as those involving suspended paper discs soaked in acid [11] and acid traps wrapped in polytetrafluoroethylene membranes [12].

Microplate based methods for the determination of NO_2^-, NO_3^- and NH_4^+ in soil extracts and water using the Berthelot reaction have been reported but involve reduction of the oxidised forms to NH_4^+ with Devarda's alloy, transfer of the reduced solution to a fresh well and the use of sulphamic acid to decompose NO_2^- [13]. The performance of a number of substituted phenols as alternative to phenol or salicylate in the determination of NH_4^+ has been studied; 2-phenylphenol proved to be the most promising with regard to freedom from interferences and a method using this reagent has been described for the determination of NH_4^+ in KCl extracts of soil [8].

A knowledge of the total dissolved N (TDN) in soil extracts and waters is important not only in its own right but also because the difference between TDN and the sum of the inorganic N components (NO_2^--N, NO_3^--N and NH_4^+-N) allows estimation of the amount of organic N. The quantitation of TDN (simultaneously with total dissolved P) in soil extracts has been achieved by oxidation of the extract with $S_2O_8^{2-}$ in closed tubes heated in an autoclave followed by determination of the NO_3^- produced but on-plate oxidation techniques have not been reported [14]. Microplate methods for the direct determination of urea in soil extracts have been reported [15,16]. Other reported microplate procedures for the determination of N in environmental samples are the determination of NO_3^- in waters using brucine [17] and the determination of NO_2^- or NO_3^- in waters by fluorimetry [18,19]. Assessments of the capability of microplate methods for the analysis of NO_3^-, NO_2^- and NH_4^+ in seawater have been made [20,21] and used for monitoring NO_2^-, NO_3^- and NH_4^+ in seawater from aquaculture facilities, although, the determination of NO_3^- involved off-plate Cd reduction of NO_3^- to NO_2^- [22].

Our aims were to: (1) optimise conditions for the determination of NO_3^- by azo dye formation employing hydrazine sulphate solution as the reducing agent; (2) devise an NH_3 diffusion method for the separation and determination of NH_4^+ using microplates; (3) devise an oxidation procedure for the determination of TDN in water extracts of soil by a technique compatible with microplate procedures; (4) establish the limit of quantitation (LOQ) for NO_2^-, NO_3^- and NH_4^+; (5) to test the procedures on water extracts from a range of nutrient-poor Scottish soils.

2. Experimental

2.1. Microplate spectrophotometer

Colourimetric measurements were made using a SPECTRAmax® 190-microplate spectrophotometer (Molecular Devices Corporation, Sunnyvale, California) with a scanning monochromator. The spectrophotometer was controlled using SOFTmax® PRO (Molecular Devices Corporation). Absorbance measurements were made using flat-bottomed, 96 μL × 350 μL well microplates (Thermo Life Sciences, Hampshire, UK).

2.2. Dispensing of solutions

An EDP-Plus™ micropipette (Rainin Instruments, Oakland, CA, USA) with a 25, 250 or 1000 μL liquid end was used to dispense solutions into the microplates. For these volumes the pipette has an accuracy of 1% or better and a precision of 0.3% or better.

2.3. Determination of N components

2.3.1. Nitrate

The method used the following reagents [3,4]. Catalyst solution: dissolve 35.4 mg of $CuSO_4{\cdot}5H_2O$ and 900 mg of $ZnSO_4{\cdot}7H_2O$ together in 900 mL of water and dilute to 1 L. Sodium hydroxide: 40 g L^{-1}, hydrazine sulphate: 1.71 g L^{-1}, sulphanilamide: 10 g L^{-1} in 3.5 M HCl, *N*-(1-naphthyl)ethylenediamine dihydrochloride (NEDD): 1 g L^{-1}. The solution for analysis (135 μL) was pipetted into the microplate followed by 20 μL each of the catalyst, sodium hydroxide and hydrazine sulphate solutions. The mixture was incubated for 15 min at room temperature (23 °C) and 75 μL of sulphanilamide solution added followed by 20 μL of the NEDD solution. The optical density was measured at 540 nm and the NO_3^- concentration determined against a range of aqueous standards (0–1 mg NO_3^--N L^{-1}) prepared from NH_4NO_3.

The conditions for reduction of NO_3^- to NO_2^- using hydrazine were developed from optimisation experiments with a standard solution containing 0.5 mg L^{-1} NO_3^--N prepared from KNO_3. The hydrazine sulphate reagent concentrations investigated were 0, 0.427, 0.855, 1.28, 1.71, 2.14 and 2.99 g L^{-1}. The reaction temperature was 23, 28, 33 or 38 °C and the reaction period was 5 or 15 min. For the reactions at temperatures > ambient (23 °C) the reagents, sample and microplate were preheated in a thermostatically controlled incubator, and returned immediately after adding the reagents.

2.3.2. Nitrite

The concentration of NO_2^- was determined by the same procedure used for NO_3^- but omitting the hydrazine solution and substituting an equal volume of water. Calibration was achieved using a range of standards (0–1 mg N L^{-1}) prepared from KNO_2.

2.3.3. Ammonium

A solution of Gelrite™ (a polysaccharide gum, Duchefa Boichemie B.V., Haarlem, The Netherlands) was prepared by dissolving the solid (1 g L^{-1}) in hot water (about 90 °C). An NH_3 collecting solution was prepared by mixing equal volumes of the hot solution with 0.5 M H_2SO_4. The mixture, which does not set on cooling, was kept in a closed container to minimise uptake of NH_3 from the atmosphere.

We used an adaptation of the 96-well MicroResp™ plate system [23] for the separation of NH_3 in the sample by diffusion. The system (Fig. 1) comprised a flat-bottomed, 96-well

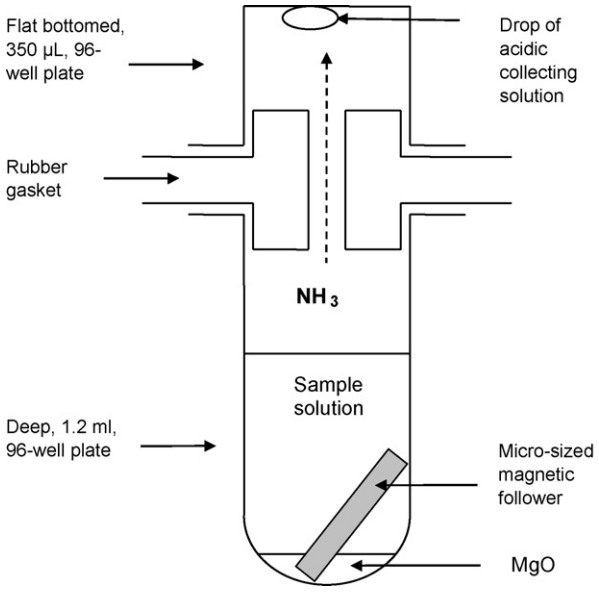


Fig. 1. Apparatus for the diffusion of NH_3.

plate and a round-bottomed 96-well deep well plate connected by a perforated, silicon/PTFE-coated, elastomer gasket. Each of the deep wells contained a magnetic follower (8 mm × 1.5 mm, Fischer Scientific, Loughborough, UK). The NH_3 collecting solution was warmed to aid flow and 10 μL pipetted into the well of the collecting microplate. The gum acts as a thickening agent and prevents the drop from flowing out when the plate is inverted.

The solution for analysis (750 μL), containing <1 mg NH_4^+-N L^{-1}, was pipetted into the deep-well plate. Heavy MgO (10 mg) was added using a drawer device [23] that allowed simultaneous addition to selected wells. The plates were clamped together without delay to prevent loss of NH_3 and the contents of the deep well plate mixed for 5 min using a magnetic stirrer (model B212, Bibby Science Products, Staffordshire, UK). The microplate assembly was left for 9 days in an incubator at 30 °C during which time it was temporarily removed, twice daily at periods 8 h apart, for additional stirring. After incubation the top plate was removed and 140 μL of water added to the well with the collecting drop. Experiments were also conducted for different periods of incubation.

The conditions for diffusion were developed from optimisation experiments with a standard solution containing 1 mg NH_4^+-N L^{-1}. The diffusion periods studied were 2, 7 and 9 days and the amounts of MgO were 10, 25 and 75 mg/well.

The NH_4^+ in solution, derived from the reaction of the diffused NH_3 with the acidic collecting solution, was analysed colourimetrically using the following reagents [24]. Salicylate reagent: dissolve 8.5 g of sodium salicylate in 85 mL of water, add 60 mg of sodium nitroprusside and dilute to 100 mL. Cyanurate reagent: dissolve 2.4 g of NaOH in 90 mL of water; when cool add 0.5 g of sodium dichlorocyanurate and dilute to 100 mL. The reagents were kept in light-proof bottles. The sample in the microplate (150 μL) was treated with 60 μL of the salicylate reagent followed by 60 μL of the cyanurate reagent, and 30 μL of water according to the flow system of Crooke and Simpson [24]. After 30 min the optical density was measured at 660 nm. The NH_4^+ concentration of the sample was determined against a range of matrix-matched standards (0–1 mg NH_4^+-N L^{-1}) prepared from NH_4NO_3. During diffusion there is a volumetric concentration of NH_4^+ (×5) and it is necessary to dilute the solution in the collecting well prior to NH_4^+ colourimetric analysis.

The effect of H_2SO_4 on the colourimetric assay for NH_4^+ was assessed by analysing a 1 mg L^{-1} NH_4^+-N solutions in 1, 10, 50 or 100 mM H_2SO_4 against standards in water. Similarly, the effect of Gelrite™ on the assay was tested by adding 10, 20 or 30 μL of the Gelrite™ solution in 50 mM H_2SO_4 to the microplate well.

2.3.4. Total dissolved N

The method was based on an alkaline $K_2S_2O_8$ oxidation procedure for the simultaneous oxidation of organic N and organic P compounds [14]. Oxidant solution: sodium hydroxide (3 g) was dissolved in 900 mL of water followed by $K_2S_2O_8$ (13.4 g) and the solution diluted to 1 L. Oxidation was performed in a 96 mL × 1.1 mL polytetrafluoroethylene (PTFE) block with a PTFE lid that closed individual wells (Thermo Life Sciences, Hampshire, UK). The sample (300 μL) was pipetted into the well followed by 450 μL of the oxidant solution. The lid was clamped in place using two aluminium plates (10 mm × 108 mm × 172 mm) that bolted together. The assembly was heated in an autoclave at 110 °C for 2 h. After cooling, aliquots of the oxidised solution were transferred to microplates for NO_3^- determination. The TDN concentration of the samples was determined against a range of standards (0–1 mg N L^{-1}) prepared from NH_4NO_3 carried through the procedure.

Tests of complete oxidation were made using solutions (each 3 mg N L^{-1}) of NH_4NO_3, glycine, urea or tris(hydroxymethyl)methylamine (Tris) in water. Recovery was measured against standards (0–0.5 mg N L^{-1}) prepared from KNO_3 carried through the oxidation procedure.

2.4. Soil extracts

Soils with a range of organic matter contents were collected to a depth of 15 cm from sites in Scotland (Table 1). The soils were sieved (6 mm) and 20 g of the fresh soil was extracted with 200 mL of water by shaking for 2 h. The extract was filtered (Whatman, no. 1) and diluted with deionised water for analysis, up to 10× for NH_4^+, up to 20× for NO_3^- and up to 50× for TDN. The soils and extracts were stored at 4 °C. The pH of the field-moist soil was determined in 0.01 M $CaCl_2$ at a soil:solution ratio of 1:3 (v/v). Loss on ignition was determined by heating the oven-dried soil at 700 °C.

2.5. Comparison of results

The results for analysis of NH_4^+-N in the soil extracts were compared with those obtained using an established method with similar chemistry [25] implemented on a Konelab Discrete Analyser, Aqua 20 (Thermo Electron Corporation, Finland). For

Table 1
Soils used to test the microplate based analytical methods

Soil type	Location[a]	LOI[b] (%)	pH	Water extractable		
				NO_3^- (mg N kg^{-1})	NH_4^+	TDN
1. Brown forest soil	Glensaugh (NO 665 798)	12.2	3.72	19.6	2.19	26.5
2. Brown ranker	Sourhope (NT 852 207)	13.1	3.66	4.06	7.06	13.3
3. Hill peat	Cairn O'Mount (NO 651 811)	58.6	4.12	14.4	12.5	31.0
4. Humus	Fetteresso (NO 820 673)	93.0	4.52	0.03	7.43	10.1
5. Humus	Culbin Forest (NH 986 618)	26.1	4.36	15.2	3.77	21.8
6. Humus iron podzol	Strathfinella (NO 679 790)	21.6	3.99	17.4	1.81	22.5
7. Humus iron podzol	Glensaugh (NO 663 787)	9.8	4.60	15.9	1.37	19.8
8. Peaty podzol	Cairn O'Mount (NO 653 805)	37.6	4.04	13.2	0.17	16.0
9. Peaty podzol	Glen Tanar (NO 460 933)	91.3	3.86	0.03	1.47	2.45
10. Stony sandy loam	Glensaugh (NO 666 784)	9.1	4.14	0.05	1.18	2.05

[a] Value in parenthesis is the national grid reference.
[b] Loss on ignition.

NO_3^--N the results were compared with those obtained by ion chromatography using a Dionex DX600 instrument with an AS4-SC column (Dionex Corporation, Sunnyvale, CA, USA) following the manufacture's procedures. For TDN the results were compared with those obtained by an oxidative technique involving conversion of nitrogen compounds to NO and detection by chemiluminescence using a Shmadzu TOC-$V_{CPH/CPN}$ analyser (Shimadzu UK Ltd., Milton Keynes) following the manufacturer's procedure. The Shimadzu analyser was calibrated using KNO_3 and the quality control substances were urea and NH_4NO_3.

2.6. Statistical analysis

Microplate analysis were conducted with a minimum of three replicates. The LOQ of the microplate methods for the determination of NO_3^--N and NH_4^+-N were defined as 10σ, corresponding to an uncertainty of ±30% in the measured values ($10\sigma \pm 3\sigma$) at the 99% confidence level [26]. In the experiments studying the effects of diffusion, the paired *t*-test was used to determine if the mean differences of the measured NH_4^+-N concentrations between methods (*viz* diffused and non-diffused samples) was significantly different from zero [27].

3. Results and discussion

3.1. Reduction of $N0_3^-$ and $N0_2^-$ by hydrazine

The effect of changing the incubation time, temperature and hydrazine concentration in the reagent on the determination of NO_3^- and NO_2^- is shown in Fig. 2. For the reduction of NO_3^-, increasing the concentration of hydrazine increased the initial

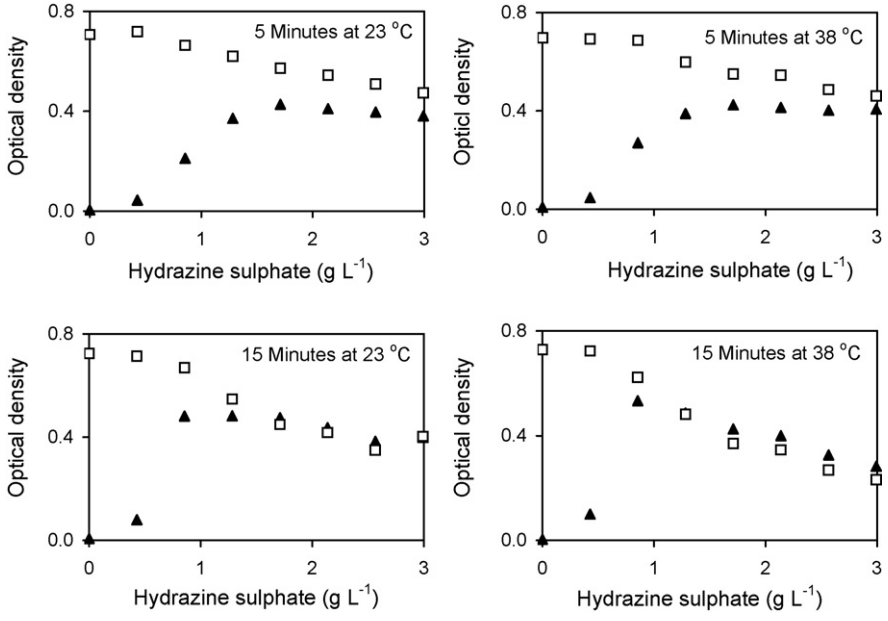


Fig. 2. Effect of the concentration of hydrazine sulphate, reaction time and temperature on the colourimetric response of 0.5 mg L^{-1} of NO_2^--N (□) or 0.5 mg L^{-1} NO_3^--N (▲).

response followed by a plateau region or decline, whereas, for NO_2^- there was a short plateau followed by a general decline. We did not find ideal conditions, where there was no reduction of NO_2^- and quantitative conversion of NO_3^- to NO_2^-. Nitrite is a reactive species and in soil that combines with metallic cations and organic matter, and with notable exceptions, such as urine patches, where nitrification is retarded by high pH and high salt content, most soil extracts do not contain much extractable NO_2^- [28,29]. The absence of NO_2^- in extracts can be confirmed by performing the reaction without hydrazine. The optical density of the azo dye in the microplate method was stable and after adding the NEDD solution the relative standard deviation of the optical density measured at 30 min intervals over 3 h changed by <0.6%.

Our microplate method uses small amounts of hydrazine but there is a need to consider replacing this reagent with one that is environmentally benign. Corn leaf nitrate reductase (EC 1.6.6.1) has been developed [30] as an alternative to hydrazine or Cd for the reduction of NO_3^- to NO_2^- and commercially available test kits have been used in conjunction with microplate colourimetric assay to determine NO_3^- in plant tissue [31]. The working solution of the enzyme is relatively unstable [30] and has a useful lifetime of 8 h at 4 °C. More recently, recombitant forms of yeast or plant derived nitrate reductase, which are much more stable, have become available [32,33]. These recombitant enzymes have useful working solution lifetimes of 2 weeks at 4 °C and in future may substitute for hydrazine in standard methods but consideration of systematic changes that may occur must be made, especially in relation to data related to long-tem field studies.

3.2. Diffusion of NH_3

A period of 9 days at 30 °C was required for the quantitative diffusion of NH_3 from the sample solution in the deep-well plate to the collecting drop. The amount of MgO used had little effect on the collection of NH_3 (Fig. 3). Therefore, the minimum amount of MgO tested (10 mg/well) and a diffusion period of 9 days was adopted for routine use. The blank value for the acid collecting drop over empty deep-wells increased slightly (approximately ×2) during incubation. We attributed this to NH_3 from the gasket.

The microplate diffusion procedure for the separation of NH_4^+ reduces the manual manipulations involved in opening and closing individual diffusion devices and placing collecting devices such as paper soaked with acidic collecting solutions onto hooks. The inevitable delay between adding MgO and closing the bottom and top plates together, or the atmospheric contamination of the collecting drop were not factors which had any noticeable effect on the results. For the soil extracts we analysed, the mean of the differences between the data for samples that had been diffused compared to those that had not was not significantly different (paired t-test, $p = 0.05$) from zero. However, for general use with unknown matrices it is appropriate to adopt the diffusion step. The period of time required for quantitative diffusion of NH_3 by our microplate method (9 days) is similar to that used in our laboratory employing larger-scale apparatus, comprising of a 100 mL diffusion chamber holding 10 mL of sample, and a 10 mL collecting chamber holding 2 mL of acidic collecting solution, for which a period of 7 days is allowed for quantitative diffusion (B.L. Williams, unpublished data).

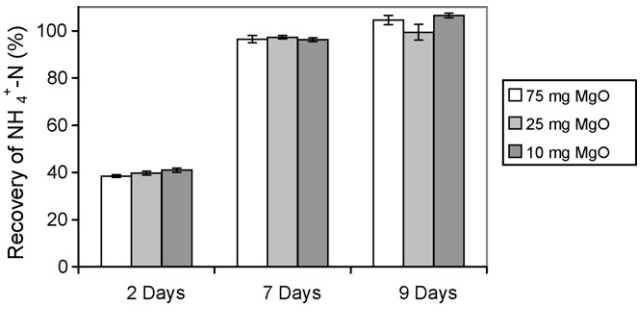


Fig. 3. Effect of the reaction time and the amount of MgO on the diffusion of NH_3. The error bars represent the standard error ($n = 6$).

3.3. Recovery of N from model compounds

The recovery of N as NO_3^- from NH_4NO_3 and the organic N compounds that were oxidised with alkaline $K_2S_2O_8$ in the PTFE block was quantitative. The recoveries (±the standard deviation) were: 100 ± 2.0% for NH_4NO_3, 102 ± 3.7% for glycine, 99 ± 5.1% for Tris and 98 ± 5.4% for urea. The method with alkaline $K_2S_2O_8$ [14,34] is designed to simultaneously oxidise N- and P-compounds. In the course of the reaction the medium becomes acidic through the production of bisulphate, $S_2O_8^{2} + H_20 \rightarrow 2HSO_4^{2-}$ [35] and is convenient when both N and P analysis are required. Although not presented in detail here we found quantitative recovery (>95%) of inorganic orthophosphate from 0.3 mg L^{-1} solutions of glucose phosphate, glycerophosphate, inositol hexaphosphate and nucleic acid but poor recovery (<50%) from trimeta- and tripolyphosphates.

3.4. N Components in soil extracts

The correlations between the results for NO_3^--N, NH_4^+-N and TDN in soil extracts determined by the microplate methods and established methods are shown in Fig. 4. The data shown relates to the extracts which were diluted and the values in the initial extracts are greater for most samples. The NH_4^+ content of the soil extracts measured directly by the colourimetric assay and after separation by diffusion over a 9-day period is shown in Table 2. The data for the diffused samples are based on calibration using a range of internal standards (0–1 mg NH_4^+-N L^{-1}) carried though the procedure. The soil extracts used to test the NH_4^+ diffusion procedure were derived from a separate extraction of the soils that had been stored at 4 °C and had different NH_4^+-N concentrations from those used earlier shown in Fig. 4, although the differences were small. Statistical analysis of the data shown in Table 2 by the paired t-test led to the acceptance of the null hypothesis (at $p = 0.05$) that the mean difference between the two methods was not significantly different from zero.

Although, the model N compounds showed quantitative recovery when oxidised with persulphate there was some indica-

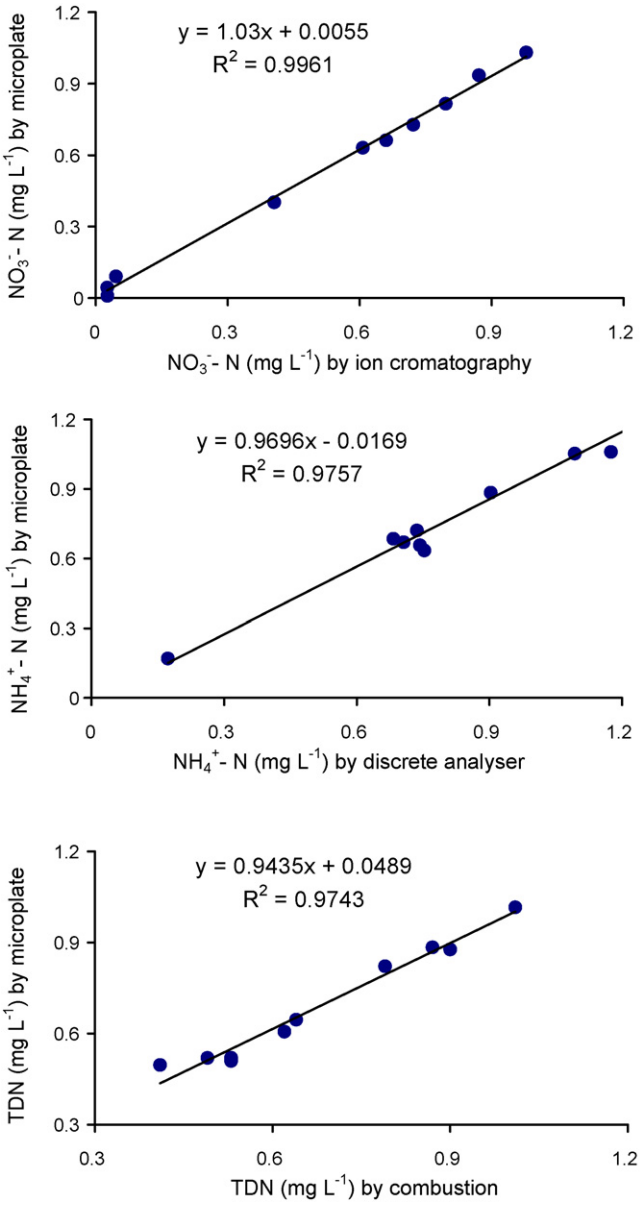


Fig. 4. Relationships between the data for analysis of N components in soil extracts by alternative methods.

Table 2
Apparent NH_4^+-N contents of soil extracts measured before and after separation of NH_3 by diffusion

Soil No.[a]	Apparent NH_4^+-N in diluted soil extract (mg L^{-1})		Volumetric dilution of soil extract
	Before diffusion	After diffusion	
1	0.76	0.66	2×
2	0.82	0.77	10×
3	0.76	0.73	10×
4	0.68	0.69	10×
5	0.95	0.91	5×
6	0.65	0.62	2×
7	0.91	0.90	2×
8	0.42	0.43	None
9	0.93	0.99	2×
10	0.74	0.71	None

[a] See Table 1.

tion of incomplete oxidation or loss of N from the system using the PTFE block when the data was compared with that from the Shimadzu analyser. From the difference between the sum of concentrations of the inorganic N-fractions (NO_3^--N + NH_4^+-N) and the TDN the water extracts were estimated to have between 12 and 40% of the TDN in organic form.

3.5. Limits of quantitation

The LOQ based on repeated measurements of the blank (20 replicates) was 0.003 mg N L^{-1} for NO_2^--N, 0.020 mg N L^{-1} for NO_3^--N and 0.051 mg N L^{-1} for NH_4^+-N.

4. Conclusion

We have developed 96-well microplate procedures for the colourimetric analysis of NH_4^+ and NO_3^- in small volumes of water extracts of nutrient poor soils. To remove substances which may interfere with the colourimetric assay of NH_4^+ we also developed a microplate NH_3 diffusion technique. The determination of total N in soil extracts was achieved by $S_2O_8^{2-}$ oxidation at 110 °C in a closed, 96-well, PTFE microplate followed by NO_3^- analysis. The limits of determination for NO_3^- and NH_4^+ are adequate for the analysis of water extracts of nutrient poor soils as most of the soil extracts required dilution for their NO_3^--N and NH_4^+-N concentrations to be within the range of the standards (0–1 mg N L^{-1}). The methods also appear suited to the determination of N species in water samples with similar or simpler matrix composition to soil solution. The diffusion system also has potential for the purification of samples for $^{15}N/^{14}N$ isotopic ratio studies, and to the direct study of NH_3 loss from soils.

Acknowledgements

The Scottish Executive, Environment and Rural Affairs Department (SEERAD) funded the work. We thank Dr. Renate Wendler for her contribution to the development of the diffusion method and Ms. Miriam Young for technical support.

References

[1] R.N. Sah, Commun. Soil Sci. Plant Anal. 25 (1994) 2841.
[2] P.L. Searle, Analyst 109 (1984) 549.
[3] L.J. Kamphake, S.A. Hannah, J.M. Cohen, Water Res. 1 (1967) 205.
[4] M.T. Downes, Water Res. 12 (1978) 673.
[5] C.S. White, J.R. Gosz, Can. J. Forest Res. 11 (1981) 739.
[6] S. Husted, C.A. Hebbern, M. Mattsson, J.K. Schjoerring, Physiol. Plant. 109 (2000) 167.
[7] D.W. Nelson, Commun. Soil Sci. Plant Anal. 14 (1983) 1051.
[8] E.D. Rhine, G.K. Sims, R.L. Mulvaney, E.J. Pratt, Soil Sci. Soc. Am. J. 62 (1998) 473.
[9] A. Herrmann, V.B. Willett, E.A. Stockdale, D.L. Jones, Soil Biol. Biochem. 37 (2005) 1747.
[10] J.M. Bremner, Inorganic forms of nitrogen, in: C.A. Black, D.D. Evans, J.L. White, L.E. Ensminger, F.E. Clark (Eds.), Methods of Soil Analysis, Agronomy, vol. 9. Part 2. Chemical and Microbiological Properties, American Society of Agronomy, Madison, Wis, 1965, pp. 1179–1237.
[11] P.D. Brooks, J.M. Stark, B.B. McInteer, T. Preston, Soil Sci. Soc. Am. J. 53 (1989) 1707.

[12] P. Sørensen, E.S. Jensen, Anal. Chim. Acta 252 (1991) 201.
[13] G.K. Sims, T.R. Ellsworth, R.L. Mulvaney, Commun. Soil Sci. Plant Anal. 26 (1995) 303.
[14] B.L. Williams, C.A. Shand, M. Hill, C. O'Hara, S. Smith, M.E. Young, Commun. Soil Sci. Plant Anal. 26 (1995) 91.
[15] N.S. Greenan, R.L. Mulvaney, G.K. Sims, Commun. Soil Sci. Plant Anal. 26 (1995) 2519.
[16] W.R. Carlile, K. Dickinson, Acta Hortic. 450 (1997) 71.
[17] C.D. Stanley, J.B. Jones, Soil Crop Sci. Soc. Fl. 51 (1992) 56.
[18] A. Buldt, U. Karst, Anal. Chem. 71 (1999) 3003.
[19] P. Poulin, É. Pelletier, Talanta 71 (2007) 1500.
[20] D. Baudinet, F. Galgani, Estuar. Coast. Shelf Sci. 33 (1991) 459.
[21] A. Aminot, Estuar. Coast. Shelf Sci. 43 (1996) 327.
[22] J. Hernández-López, F. Vargas-Albores, Aquac. Res. 34 (2003) 1201.
[23] C.D. Campbell, S.J. Chapman, C.M. Cameron, M.S. Davidson, J.M. Potts, Appl. Environ. Microbiol. 69 (2003) 3593.
[24] W.M. Crooke, W.E. Simpson, J. Sci. Food Agric. 22 (1971) 9.
[25] Department of the Environment/National Water Council. Method for the spectrophotomertic determination of ammonia in water. In Ammonia in Waters 1981. Methods for the Examination of Waters and Associated Materials. Her Majesty's Stationery Office, London, 1982, pp. 21-24.
[26] L.H. Keith, W. Crummett, J. Deegan Jr., R.A. Libby, J.K. Taylor, G. Wentler, Anal. Chem. 55 (1983) 2210.
[27] D.G. Altman, J.M. Bland, Statistician 32 (1983) 307.
[28] O. Van Cleemput, A.H. Samater, Fert. Res. 45 (1996) 81.
[29] D.C. Whitehead, Grassland Nitrogen, CAB International, Wallingford, Oxon, UK, 1995.
[30] C.J. Patton, A.E. Fischer, W.H. Campbell, E.R. Campbell, Environ. Sci. Technol. 36 (2002) 729.
[31] C.T. MacKown, J.C. Weik, Crop Sci. 44 (2004) 218.
[32] W.H. Campbell, T. Kinnunen-Skidmore, M.J. Brodeur-Canpbell, E.R. Campbell, Am. Lab. News 22 (2004) 12.
[33] W.H. Campbell, P. Song, G.G. Barbier, Environ. Chem. Lett. 4 (2006) 69.
[34] J. Ebina, T. Tsutsui, T. Shirai, Water Res. 17 (1983) 1721.
[35] P.D. Goulden, D.H.J. Anthony, Anal. Chem. 50 (1978) 953.

Available online at www.sciencedirect.com
ScienceDirect
Talanta 74 (2008) 806–814
Talanta
www.elsevier.com/locate/talanta

Polymeric membrane sensors based on Cd(II) Schiff base complexes for selective iodide determination in environmental and medicinal samples

Ashok Kumar Singh *, Sameena Mehtab

Department of Chemistry, Indian Institute of Technology Roorkee, Roorkee 247667, India

Received 9 June 2007; received in revised form 12 July 2007; accepted 13 July 2007
Available online 25 July 2007

Abstract

The two cadmium chelates of schiff bases, *N*,*N*′-bis(salicylidene)-1,4-diaminobutane, (Cd-S_1) and *N*,*N*′-bis(salicylidene)-3,4-diaminotoluene (Cd-S_2), have been synthesized and explored as ionophores for preparing PVC-based membrane sensors selective to iodide(I) ion. Potentiometric investigations indicate high affinity of these receptors for iodide ion. Polyvinyl chloride (PVC)-based membranes of Cd-S_1 and Cd-S_2 using as hexadecyltrimethylammonium bromide (HTAB) cation discriminator and *o*-nitrophenyloctyl ether (*o*-NPOE), dibutylphthalate (DBP), acetophenone (AP) and tributylphosphate (TBP) as plasticizing solvent mediators were prepared and investigated as iodide-selective sensors. The best performance was shown by the membrane of composition (w/w) of (Cd-S_1) (7%):PVC (31%):DBP (60%):HTAB (2%). The sensor works well over a wide concentration range 5.3×10^{-7} to 1.0×10^{-2} M with Nernstian compliance (59.2 mV decade^{-1} of activity) within pH range 2.5–9.0 with a response time of 11 s and showed good selectivity for iodide ion over a number of anions. The sensor exhibits adequate life (3 months) with good reproducibility (S.D. ± 0.24 mV) and could be used successfully for the determination of iodide content in environmental water samples and mouth wash samples.
© 2007 Published by Elsevier B.V.

Keywords: Iodide-selective electrode; Poly(vinyl chloride) membranes; Schiff bases; Potentiometric sensors

1. Introduction

Iodine is an indispensable microelement to humans. Iodine is toxic and its vapors irritate the eyes and lungs. The maximum allowable concentration in air when working with iodine is just 1 mg m^{-3} [1]. Iodine-131 is one of the radionuclides involved in atmospheric testing of nuclear weapons. Iodine plays a key role in many biological activities such as brain functions, cell growth, neurological activities, metabolism and thyroid functions [2]. Iodide ions also present in the composition of various drugs. I^-/I_3^- redox couple contributes to the high performance of dye-sensitized solar cells. Due to vital importance of iodide in environment, medicines and industry, determination of iodide ion is very important in clinical and chemical analysis [3,4].

Numerous analytical methods have been reported for its determination at low concentration levels. These include gas chromatography with mass spectrometry detection [5]; inductively coupled plasma atomic emission mass spectrometry [6]; neutron activation analysis [7]; chemiluminescence [8]; polarography [9]; pulse stripping analysis [10] and flow injection analysis [11]. These methods are time consuming, require large infrastructure backup, high operational cost and not very appropriate for analysis of large number of samples. On the other hand potentiometric sensors offer an inexpensive and convenient method for fast analysis with high sensitivity and selectivity. Ion elective electrodes have emerged as one of the most promising tools for direct determination of various species in biological and industrial analysis. In view of such advantages, efforts have been made to make selective sensors for different anions.

Anion sensing and recognition remains a challenging task because of the limited availability of suitable molecular hosts for anions. In order to have selective sensor for iodide, the most important requirement is to have an ionophore in the sensor which show high affinity towards iodide ion and poor for other anions. Thus, quest for new materials capable of specific and effective recognition of iodide is a topic of current interest. It has been shown that the anion selectivity of the membrane electrodes that are based on metal complexes

* Corresponding author.
E-mail address: akscyfcy@iitr.ernet.in (A.K. Singh).

0039-9140/$ – see front matter © 2007 Published by Elsevier B.V.
doi:10.1016/j.talanta.2007.07.016

is influenced by both the structure of the ligands and the properties of the metal ions [12]. Many sensing agents have been described for the preparation of iodide sensors including Mn(II)porphyrinato [13], Iodide-miconazole ion pair [14], urea derivative [15], silver wire [16], Co(II) and Ni(II) cyclam derivatives [17], Hg(II) bis(benzoin)-semiethylenediamine complex [18], Salophen complex of Co(II) [19]. However, most of these efforts have not been very fruitful. The developed sensors posses narrow working concentration range [14,15,17] and suffer serious interference from lipophilic anions like SCN^-, CN^-, ClO_4^- and Sal^-. Recently, *N*,*N*′-bis(salicylaldehyde-*n*-octyl) diimine cobalt(II) [20] and copper(II) of *N*,*N*″-bis(salicylidene)-1,2-bis(*p*-aminophenoxy)ethane tetradentate complex [21] have also been explored as ionophores in the construction of ion-selective electrodes for iodide. In this manuscript, we have synthesized cadmium complexes of two schiff bases *N*,*N*′-bis(salicylidene)-1,4-diaminobutane (Cd-S_1) and *N*,*N*′-bis(salicylidene)-3,4-diaminotoluene (Cd-S_2) and studied these as ionophores in the preparation of polymeric membrane sensors for low level determination of iodide ion.

2. Experimental

2.1. Reagents

Salicylaldehyde, 1,4-diaminobutane, 3,4-diaminotoluene, triethyleneamine and cadmium(II) perchlorate were purchased from Aldrich and used as received. For membrane preparation, high molecular weight polyvinyl chloride (PVC), *o*-nitrophenyloctyl ether (*o*-NPOE), dibutylphthalate (DBP), acetophenone (AP), tributylphosphate (TBP), hexadecyltrimethylammonium bromide (HTAB) and tetrahydrofuran (THF) were used as received from Fluka. Reagent grade sodium salts of all anions used were of highest purity available from SRL (Mumbai, India) and used without any further purification except for vacuum drying over P_2O_5. Anionic salt solutions were prepared in doubly distilled water and standardized whenever necessary.

2.2. Conditioning of membranes and potential measurements

The membranes were equilibrated for 2 days in 0.01 M NaI solutions. The potentials have been measured by varying the concentration of NaI in test solution in the range 1.0×10^{-8} to 1.0×10^{-2} M. The standard NaI solutions had been obtained by gradual dilution of 0.01 M NaI solution. The potential measurements were carried out at 25 ± 1 °C using saturated calomel electrodes (SCE) as reference electrodes with the following cell assembly:

$$Hg/Hg_2Cl_2|KCl(satd.)|testsolution||PVCmembrane||$$
$$0.001\,MNaI|Hg/Hg_2Cl_2|KCl(satd.)$$

2.3. Fabrication of PVC membranes

PVC membranes have been fabricated as suggested by Craggs et al. [22]. Membranes have been prepared by dissolving appropriate amounts of ionophores (Cd-S_1 or Cd-S_2), cationic additives (HTAB), plasticizers (DBP, *o*-NPOE, AP or TBP) and PVC in THF (5 mL). The components were added in terms of weight percentages. The homogeneous mixture obtained after complete dissolution of all the components, was concentrated by evaporating THF at room temperature and then poured into polyacrylate rings placed on a smooth glass plate. Membranes of ∼0.4 mm thickness were removed carefully from the glass plate and glued to one end of a "Pyrex" glass tube. It is known that the sensitivity, linearity and selectivity obtained for a given ionophore depends significantly on the membrane composition and nature of plasticizer used [23]. Thus, the ratio of membrane ingredients, time of contact and concentration of equilibrating solution were optimized after a good deal of experimentation. Membranes which generate reproducible and stable potentials have been studied. The blank membranes having only PVC as membrane ingredients was also prepared and studied. While membrane having PVC with plasticizer small potentials with slope of ∼5 mV were generated. The activities of ions were calculated from the modified form of the Debye–Hückel equation [24].

3. Results and discussion

3.1. Synthesis of Cd-S_1 and Cd-S_2 complexes

The ionophore ligands *N*,*N*′-bis(salicylidene)-1,4-diaminobutane (S_1) *N*,*N*′-bis(salicylidene)-3,4-diaminotoluene (S_2) were synthesized by the previously described methods [25,26].

3.1.1. Preparation of ligands S_1 and S_2

To a solution of 1.0 g (7.2 mmol) of salicylaldehyde in 50 mL of ethanol, 3.6 mmol of the appropriate amine (1,4-diaminobutane or 3,4-diaminotoluene) was added. The contents were refluxed for 12 h. The products were precipitated after cooling. The precipitates were filtered, washed with cold diethyl ether and dried in vacuum. The ligand products were purified by re-crystallization from ethanol.

3.1.1.1. N,N′-bis(salicylidene)-1,4-diaminobutane (S_1). Yield: 93%. m.p.: 125 °C. Anal. Calc. for (%) $C_{18}H_{20}N_2O_2$: C, 72.95; H, 6.80; N, 9.45. Found (%): C, 72.82; H, 6.72; N, 9.50. Maas (*m*/*z*): 296 (M^+). FT-IR (KBr): $\upsilon_{(O-H)}$ 3417 (b), $\upsilon_{(C=N)}$ 1629 (s), $\upsilon_{(C-H)}$ 1458 (vs), $\upsilon_{(C-O)}$ 1285 (m). ^{1}H NMR (MeOD, 500 MHz) δppm = 12.68 (2H, s, HO–C), 8.57 (2H, s, HC=N), 6.85-7.89 (8H, m, H–Ar), 3.29 (4H, t, H_2C–N), 1.71 (4H, m, C–CH_2–C).

3.1.1.2. N,N′-bis(salicylidene)-3,4-diaminotoluene (S_2). Yield: 78%. m.p.: 112 °C. Anal. Calc. for (%) $C_{21}H_{18}N_2O_2$: C, 76.36; H, 5.45; N, 8.48. Found (%): C, 76.33; H, 5.42; N, 8.44. Mass (*m*/*z*): 330 (M^+). FT-IR (KBr): $\upsilon_{(O-H)}$ 3415 (b), $\upsilon_{(C=N)}$ 1627 (s), $\upsilon_{(C-H)}$ 1465 (vs), $\upsilon_{(C-O)}$ 1289 (m). ^{1}H NMR (CD_3CN, 500 MHz) δppm = 6.96–7.55 (11H, m, H–Ar), 8.7 (2H, s, HC=N), 13.18 (2H, s, HO–C), 2.43 (3H, s, –CH_3).

3.1.2. Synthesis of prepared salanes complexes

To a solution of 1 mmol of the *salane* (S_1 or S_2) in 15 mL of freshly distilled acetonitrile solution, 0.351 g (1 mmol) of cadmium(II) perchlorate salt was added. After 15 min. of stirring 1 mL of triethyleneamine was added to the reaction mixture and these contents were further stirred for 5 h at room temperature. The precipitated product were filtered, washed with cold acetonitrile and dried under vacuum.

3.1.2.1. Cd(II)-S_1 complex. Yield: 65%. m.p.: 152 °C. Anal. Calc. for (%) $C_{18}H_{20}CdClN_2O_6$: C, 42.71; H, 3.58; N, 5.53. Found (%): C, 42.62; H, 3.47; N, 5.84. FAB + Mass (*m*/*z*): 506 (M^+). FT-IR (KBr) cm^{-1}: $\upsilon_{(C=N)}$ 1617 (vs), $\upsilon_{(C-H)}$ 1452 (vs), $\upsilon_{(C-O)}$ 1312 (vs) cm^{-1} (Fig. 1a).

3.1.2.2. Cd(II)-S_2 complex. Yield: 62%. m.p.: 166 °C. Anal. Calc. for (%) $C_{21}H_{16}CdClN_2O_6$: C, 46.69; H, 2.99; N, 5.19. Found (%): C, 46.25; H, 2.82; N, 5.43. FAB + Mass (*m*/*z*): 540 (M^+). FT-IR (KBr) cm^{-1}: $\upsilon_{(C=N)}$ 1613 (vs), $\upsilon_{(C-H)}$ 1459 (vs), $\upsilon_{(C-O)}$ 1319 (vs) cm^{-1} (Fig. 1b).

3.2. Response of different anions

In preliminary experiments, various PVC-membrane ion-selective electrodes with the synthesized schiff base metal complexes were prepared and tested for different anions. The potential response of the electrodes based on Cd-S_1 and Cd-S_2 for different anions are shown in Figs. 2 and 3, respectively. The

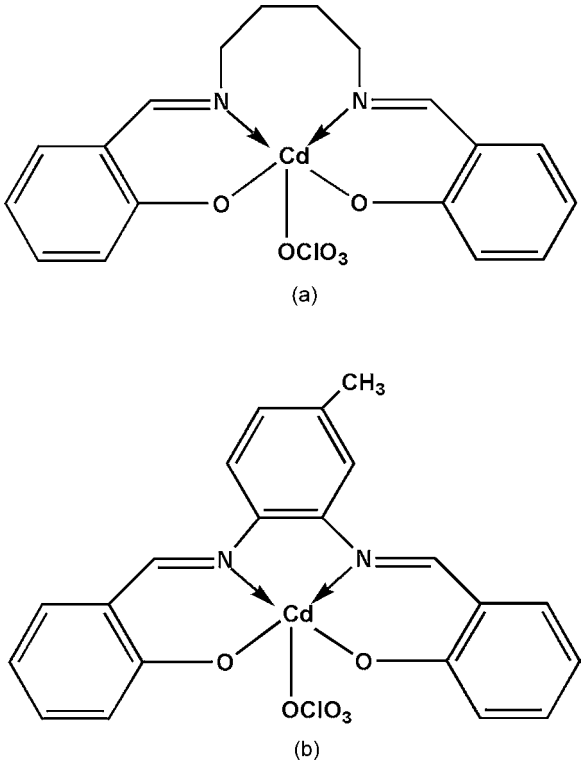


Fig. 1. Structure of *N*,*N*′-bis(salicylidene)-1,4-diaminobutane cadmium complex (Cd-S_1) (a), Structure of *N*,*N*′-bis(salicylidene)-3,4-diaminotoluene cadmium complex (Cd-S_2) (b).

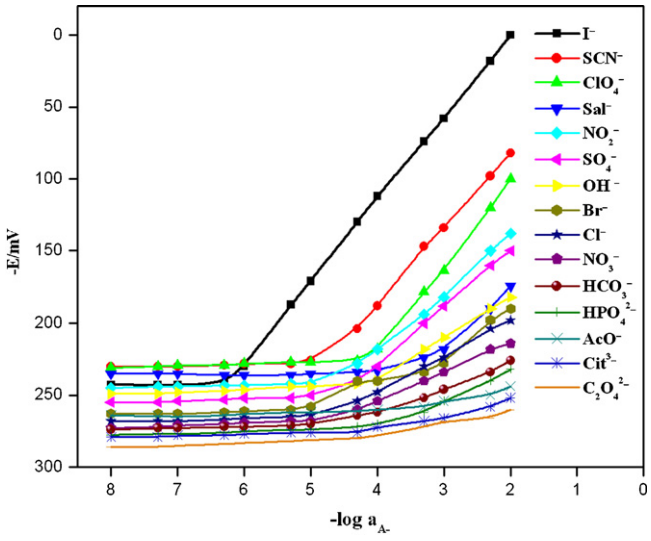


Fig. 2. Potential responses of ion-selective membrane sensor based on Cd-S_1 for various anions.

results exhibited significantly high selectivity to iodide ion over other anions. Hence, the complexes were selected as a carrier for preparation of iodide-selective electrodes.

3.3. The effect of membrane composition on potential response of the iodide sensor

Potential of the membranes of (Cd-S_1) and (Cd-S_2) were investigated as a function of iodide ion activity in the range 1.0×10^{-8} to 1.0×10^{-2} M and the results obtained are compiled in Tables 1 and 2. The electrodes with no carrier (containing PVC, plasticizer and HTAB) displayed insignificant sensitivity towards iodide. The influence of plasticizer on the response characteristics of the iodide electrodes was investigated by using four plasticizers of different polarities including DBP, *o*-NPOE, AP and TBP. The sensor nos. 3 and 16 having membranes with-

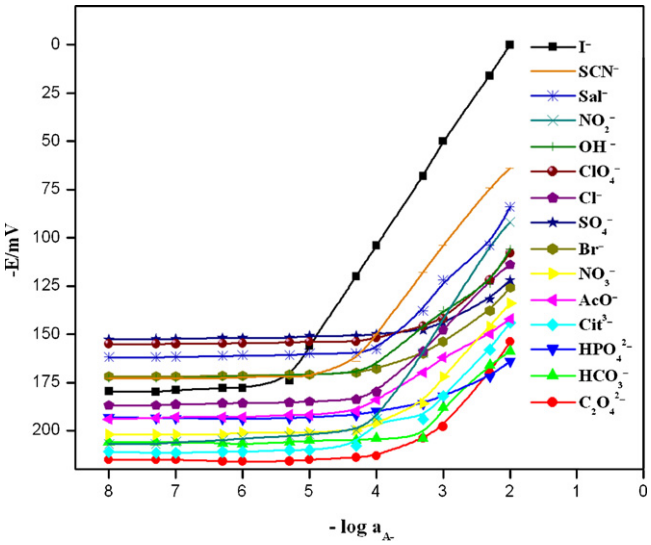


Fig. 3. Potential responses of ion-selective membrane sensor based on Cd-S_2 for various anions.

Table 1
Optimized membrane compositions and their potentiometric response as in iodide sensor (based on Cd-S_1)

Sensor no.	Composition (w/w, %)				Slope (mV decade^{-1} of activity)	Linear range (M)
	Ionophore (Cd-S_1)	HTAB	Plasticizer	PVC		
1	0	3	64, DBP	33	N.M.	N.M.
2	6	0	62, DBP	32	52.8	7.5×10^{-5} to 1.0×10^{-2}
3	6	3	0	91	47.5	6.3×10^{-4} to 1.0×10^{-2}
4	6	3	60, *o*-NPOE	31	65.3	7.8×10^{-5} to 1.0×10^{-2}
5	6	3	60, AP	31	62.0	5.6×10^{-5} to 1.0×10^{-2}
6	6	3	60, TBP	31	61.4	1.2×10^{-5} to 1.0×10^{-2}
7	6	3	60, DBP	31	60.2	7.9×10^{-7} to 1.0×10^{-2}
8	6	2	60, DBP	32	59.6	7.4×10^{-7} to 1.0×10^{-2}
9	6	1	61, DBP	32	57.8	8.4×10^{-6} to 1.0×10^{-2}
10	6	4	59, DBP	31	62.3	5.7×10^{-6} to 1.0×10^{-2}
11	5	2	61, DBP	32	58.4	3.5×10^{-6} to 1.0×10^{-2}
12	7	2	60, DBP	31	59.2	5.3×10^{-7} to 1.0×10^{-2}
13	8	2	59, DBP	31	59.8	8.2×10^{-7} to 1.0×10^{-2}

out plasticizer exhibits a narrow working concentration range of 10^{-4} to 10^{-2} M with a sub Nernstian slope. Improvement in sensors performance was observed by the addition of plasticizer. Among the several membranes tested for each of the carriers, the membranes incorporating DBP showed better potentiometric responses, i.e. higher sensitivity and wider linearity of the calibration plots (sensor nos. 12 and 23). It seems that DBP, as a low polarity and a relatively high mobility, with respect to other plasticizers examined, provides appropriate conditions for incorporation of highly lipophilic iodide ion into the membranes prior to its coordination with the cadmium atom in the complexes [27].

The addition of lipophilic cationic additive in anion selective membranes is necessary to introduce permselectivity [28]. The influence and concentration of the membrane additives was also investigated by incorporating HTAB into the membranes. The potentiometric sensitivity of the membranes based on both carriers was greatly improved in the presence of HTAB as a lipophilic cationic additive, compared to the membranes with no additive at all. Previous studies have shown that there is an optimal concentration of lipophilic ionic additives in the membranes and that gives the best electrode performance. The effect of HTAB concentration in the membrane was investigated at several additive/ionophore mole ratios. The sensors with HTAB/ionophore mole ratios of ~0.55 for both of the carriers exhibited maximum sensitivity over a wide range of iodide concentration.

3.4. Calibration characteristics

Among the different membrane compositions, membranes with ionophore/HTAB/PVC/DBP in (w/w, %) 7(Cd-S_1)/2/31/60 and 6(Cd-S_2)/4/31/59 showed highest sensitivity and widest linear range and were selected as the optimum composition for further studies (Fig. 4). These sensors exhibit the maximum working concentration range of 5.3×10^{-7} to 1.0×10^{-2} M with a slope of 59.2 mV decade^{-1} of activity (sensor no. 12, Table 1) and working concentration range 8.1×10^{-6} to 1.0×10^{-2} M with Nernstian slope of 59.3 mV decade^{-1} of activity (sensor no. 23, Table 2).

3.5. Effect of internal solution

The influence of the concentration of internal solution on the potential response of the polymeric membrane electrodes for

Table 2
Optimized membrane compositions and their potentiometric response as in iodide sensor (based on Cd-S_2)

Sensor no.	Composition (w/w, %)				Slope (mV decade^{-1} of activity)	Linear range (M)
	Ionophore (Cd-S_2)	HTAB	Plasticizer	PVC		
14	0	3	64, DBP	33	N.M.	N.M.
15	6	0	62, DBP	32	62.4	2.4×10^{-4} to 1.0×10^{-2}
16	6	3	0	91	47.8	7.7×10^{-4} to 1.0×10^{-2}
17	6	3	60, *o*-NPOE	31	69.2	6.7×10^{-5} to 1.0×10^{-2}
18	6	3	60, AP	31	67.5	2.8×10^{-5} to 1.0×10^{-2}
19	6	3	60, TBP	31	58.0	9.4×10^{-5} to 1.0×10^{-2}
20	6	3	60, DBP	31	59.0	1.1×10^{-5} to 1.0×10^{-2}
21	6	2	60, DBP	32	57.2	5.2×10^{-5} to 1.0×10^{-2}
22	6	1	61, DBP	32	55.3	5.5×10^{-5} to 1.0×10^{-2}
23	6	4	59, DBP	31	59.3	8.1×10^{-6} to 1.0×10^{-2}
24	5	2	61, DBP	32	58.4	9.8×10^{-6} to 1.0×10^{-2}
25	7	2	60, DBP	31	58.8	8.4×10^{-5} to 1.0×10^{-2}
26	8	2	59, DBP	31	58.9	2.8×10^{-5} to 1.0×10^{-2}

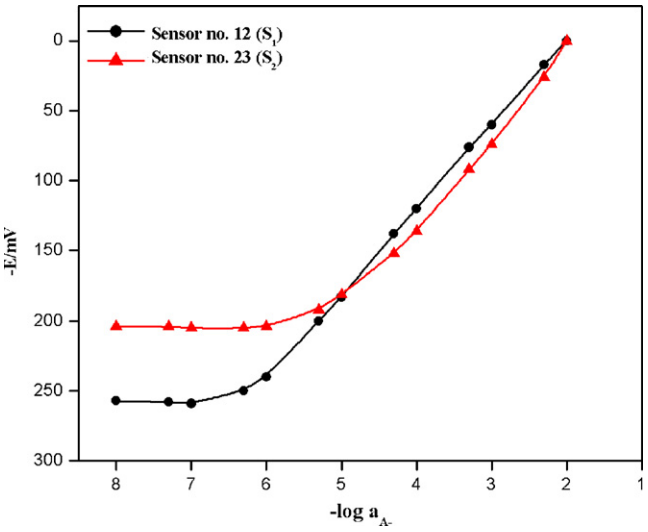


Fig. 4. Calibration plots of iodide-selective sensors based on Cd-S_1 and Cd-S_2 ionophores.

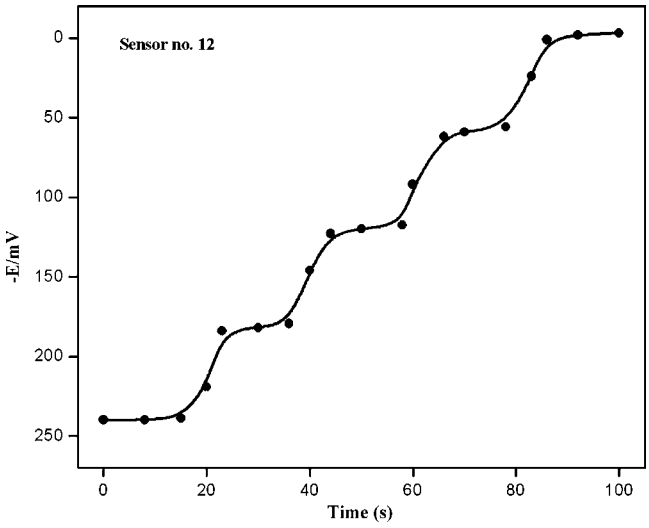


Fig. 6. Dynamic response of the membrane sensor based on Cd-S_1.

iodide ion based on Cd-S_1 and Cd-S_2 ionophores were studied. The concentration was varied from 1.0×10^{-1} to 1.0×10^{-5} M and the potential response of the sensors has been observed. It was found that the best results in terms of slope and working concentration range have been obtained with internal solution of activity 1.0×10^{-3} M. Thus, 1.0×10^{-3} M concentration of the reference solution was quite appropriate for the smooth functioning of the proposed sensors.

3.6. Influence of pH on the on sensors performance

The influence of pH on the response of the potential was examined by use of 10^{-3} M and 10^{-4} M potassium iodide solutions over the pH range 1.0–12.0. To adjust the pH, very small volumes of HNO_3 and NaOH were used. The results for ionophores Cd-S_1 and Cd-S_2 are shown in Fig. 5, which indicated that the sensors exhibits a better response and extended linearity at lower pH values. In alkaline media, the potentiometric response properties of the electrode slightly deteriorated due to hydroxide-coordinated central metal interference. The working pH range for ionophore Cd-S_1 (sensor no. 12) is 2.5–9.0 and Cd-S_2 (sensor no. 23) is 3.0–8.5.

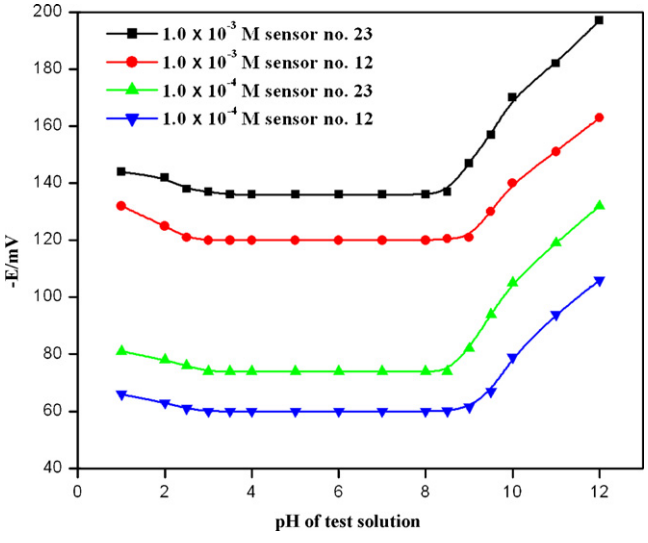


Fig. 5. Effect of pH on potential response of the iodide ion-selective sensors.

3.7. The dynamic response time behavior of the proposed electrode

Dynamic response time is an important factor for iodide sensitive sensor. In this study, the practical response time has been recorded (for sensor no. 12) by changing solutions with different I^- concentrations. The measurement sequence was from the lower (1.0×10^{-6} M) to the higher (1.0×10^{-2} M) concentration. The actual potential versus time traces is shown in Fig. 6. As it is seen, the electrode reached the equilibrium response in a very short time of about 11 s.

To evaluate the reversibility of the electrode, a similar procedure in the opposite direction was adopted. The measurements have been performed in the sequence of high-to-low from (1.0×10^{-2} to 1.0×10^{-3} M) sample concentrations. The results showed that, the potentiometric response of the electrodes was reversible; although the time needed to reach equilibrium values (42 s) were longer than that of low-to high sample concentrations.

3.8. Lifetime of proposed sensor

The lifetime of the sensor (no. 12), which is a measure of sensors durability, was studied over a 4 months period. During this period, the electrode was daily used over extended period (2 h per day), and its slopes and detection limits have been measured. After 3 months changes were observed in the slope (from 59.2 to 58.6 mV decade^{-1} of activity) and detection limit (1.9×10^{-7} to 2.5×10^{-6} M). The reproducibility of the proposed iodide sensor was also investigated. The standard deviations of 10 replicate measurements at 1.0×10^{-3} and 1.0×10^{-4} M were ± 0.24 and ± 0.38 mV decade^{-1}, respectively. Cd-S_1 complex is suffi-

ciently lipophilic, i.e. has very low solubility in aqueous solution. This factor imparts minimizes leaching (loss of components) from the membrane and produces a long and stable response. After life time period swelling in membrane was too high that the membrane became mechanically weak and leaching of ionophore and plasticizer from membrane to aqueous solution took place. Therefore, deviation in potential occurs and slight gradual decrease in slope. It is important to emphasize that sensors were stored in 0.01 M NaI solutions when not in use.

3.9. Selectivity of ion sensing membranes

Selectivity is an important characteristic of a sensor that delineates the extent to which the device may be used in the estimation of analyte ion in the presence of other ions and extent of utility of any sensor in real sample measurement. In this work, the selectivity coefficients of the sensors toward different anionic species (A^{n-}) were evaluated by using both the matched potential method (MPM) [29,30] and the fixed interference method (FIM) [31].

In the MPM, the selectivity coefficient ($K^{Pot}_{I,B}$) was determined by measuring the change in potential upon increasing the primary ion (I^-) activity from an initial value of a_I to a'_I and a_B represents the activity of interfering ion added to the reference solution of primary ion of activity a_I which also brings about same potential change. It is given by expression:

$$K^{Pot}_{I,B} = \frac{\Delta a_I}{a_B} = \frac{a'_I - a_I}{a_B} \quad (1)$$

In the present studies a_I and a'_I were kept at 1.0×10^{-4} and 5.0×10^{-4} M I^- and a_B was experimentally determined. FIM is the most widely used procedure as per IUPAC recommendation for determining selectivity coefficients [32]. In the FIM, the selectivity coefficient was evaluated from potential measurement on solutions containing a fixed concentration of interfering ion (1.0×10^{-2} M) and varying amount of I^- ions. The values of selectivity coefficient so determined are compiled in Table 3. A value of selectivity coefficient equal to 1.0 indicates equal response to both primary ion and interfering ions. A value smaller than 1.0 shows that the sensor is selective to the primary ion over the interfering ion. It is seen from the Table 3, that the selectivity coefficients determined by both the methods are sufficiently smaller than 1.0 indicating that the present sensors are significantly selective to iodide ion over all the interfering ions. Of the two sensors, selectivity of the sensor no. 12 (based on Cd-S_1) was found better than sensor no. 23 (based on Cd-S_2).

Table 3
Selectivity coefficients of iodide-selective sensor nos. 12 and 23 based on the membranes of (Cd-S_1) and (Cd-S_2), respectively

Interfering ion (B)	Selectivity coefficient ($-\log k^{Pot}_{I^-,B}$)			
	(MPM)		(FIM)	
	Sensor no. 12	Sensor no. 23	Sensor no. 12	Sensor no. 23
SCN^-	2.20	2.06	2.27	2.19
CN^-	2.64	2.35	2.78	2.56
Sal^-	2.94	2.32	3.07	2.93
ClO_4^-	3.15	3.06	3.61	2.94
F^-	3.28	3.12	3.83	3.15
NO_2^-	3.80	3.63	3.81	3.62
OH^-	3.3 1	3.18	3.68	3.42
Br^-	3.48	3.40	3.72	3.55
SO_4^{2-}	4.24	4.19	4.41	4.22
Cl^-	4.62	4.38	4.98	4.70
NO_3^-	4.50	4.21	4.81	4.50
HPO_4^{2-}	4.52	4.22	4.80	4.57
CH_3COO^-	4.51	4.32	4.82	4.63
Cit^{3-}	4.56	4.21	4.87	4.71
HCO_3^-	5.13	5.02	5.22	5.13
$C_2O_4^{2-}$	5.56	5.28	5.78	5.56

Thus, sensor no. 12 was compared with some reported iodide-selective sensors (Table 4). It is seen that the selectivity, working concentration range and pH range of the proposed sensor toward iodide is better as compared to reported sensors.

3.10. Response mechanism of the sensor

Fig. 7 demonstrates the suggested the coordination scheme of I^- with cadmium centre in schiff base complexes. The selectivities were mainly controlled by specific interactions between metal centre and anions in the structure of ionophore. The nature of spacer that joins the two imines groups in the schiff base structure has an influence upon the interaction of metal centre with anions. The higher selectivity of iodide towards sensor no. 12 could be explained by the presence of four carbon containing alkyl carbon chain instead of the phenyl moiety in the structure of Cd-schiff base ionophore. An alkyl chain has fewer electrons donating property than a phenyl group, and increases the acidity

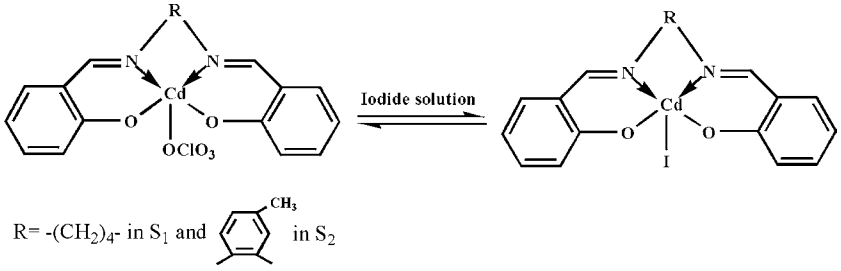


Fig. 7. Response mechanism of ionophores towards iodide ion.

Table 4
Comparison of the potentiometric parameters of the proposed iodide-sensor with the literature reported iodide sensors

Ref. no.	Ionophore name	Linear range (M)	Slope (mV decade^{-1} of activity)	pH range	Selectivity coefficients ($-\log k^{Pot}_{I^-,B}$)	Response time (s)
[13]	Mn(II) porphyrinato	1.0×10^{-6} to 1.0×10^{-2}	59.4	2.0–8.0	Cl^- (3.95), Br^- (3.75), NO_2^- (4.62), NO_3^- (5.0), Sal^- (1.05), SCN^- (1.95), ClO_4^- (2.05), AcO^- (5), SO_4^{2-} (5); *by MPM Method*	8
[14]	Iodide-miconazole ion pair	1.0×10^{-5} to 1.0×10^{-2}	59.8	2.5–8.0	SCN^- (2.2), ClO_4^- (3.0), NO_3^- (2.3) Br^- (2.5), SO_4^{2-} (4.52), Cl^- (2.9), F^- (2.13), AcO (2.42), Cit_3^- (2.24); *by FIM method*	20
[15]	Urea derivative	1.0×10^{-5} to 1.0×10^{-2}	57.7	0.8–7.0	F^- (3.46), Cl^- (3.4), Br^- (2.75), NO_2^- (3.13), NO_3^- (2.27), Sal^- (1.05), SCN^- (1.05), ClO_4^- (1.42); *by SSM Method*	10
[17]	Ni(II) cyclam derivatives	1.0×10^{-5} to 1.0×10^{-1}	58.6	At pH 7.0	NO_2^- (2.5), $H_2PO_4^-$ (1.6), NO_3^- (1.6), SO_4^{2-} (3.9), Br^- (1.9), Cl^- (2.8), $C_2O_4^{2-}$ (3.7), HCO_3^- (2.6); *by MSM method*	3
[18]	Hg(II)bis(benzoin) semiethylenediamine complex	5.0×10^{-7} to 5.0×10^{-4}	58	8.0–10.0	Cl^- (2.40), Br^- (1.9), NO_2^- (2.5), NO_3^- (4.5), SCN^- (1.9), ClO_4^- (2.3); *by SSM method*	N.M
[19]	Salophen complex of Co(III)	5.0×10^{-7} to 1.0×10^{-1}	58.9	3.1–9.8.	SCN^- (3.3), CN^- (3.0), ClO_4^- (3.6), NO_3^- (4.2), Br^- (4.12), SO_4^{2-} (4.52), Cl^- (3.96), NO_2^- (4.68), AcO^- (4.82), Cit_3^- (4.12), HCO_3^- (3.73), $C_2O_4^{2-}$ (3.92); *by MPM method*	15
[21]	Cu(II) Salicylidene complex derivative	8.2×10^{-7} to 1.0×10^{-1}	58.8	2.0–5.0	SCN^- (0.73), ClO_4^- (1.04), NO_2^- (1.29), $H_2PO_4^-$ (2.09), NO_3^- (2.26), SO_4^{2-} (2.28), Br^- (2.52), Cl^- (2.94); *by SSM method*	3
[This work]	Cd(II)Salen (Cd-S_1)	5.3×10^{-7} to 1.0×10^{-2}	59.2	2.5–9.0	SCN^- (2.20), CN^- (2.64), Sal^- (2.94), ClO_4^- (3.15), F^- (3.28), NO_2^- (3.80), OH^- (3.3 1), Br^- (3.48), SO_4^{2-} (4.24), Cl^- (4.62), NO_3^- (4.5), HPO_4^{2-} (4.52), CH_3COO^- (4.51), Cit^{3-} (4.56), HCO_3^- (5.13), $C_2O_4^{2-}$ (5.56); *by MPM method*	11

of the metal ion, so as to improve the interaction of iodide ions and metal centre.

3.11. Effect of non-aqueous content

The sample may contain the non-aqueous content so the performance of the proposed sensor (no. 12) was also assessed in partially non-aqueous media using methanol–water, ethanol–water and acetonitrile–water mixtures. The membrane does not show any appreciable change in working concentration range or slope in mixtures up to 20% (v/v) non-aqueous content (Table 5). Above this, the potentials show an erratic behavior.

4. Analytical performance

4.1. Titration of iodide solution with a standard silver nitrate solution

The proposed iodide membrane sensor (no. 12) was found to work well under laboratory conditions. It was applied successfully as an indicator electrode in the potentiometric titration of 20 mL of 1.0×10^{-4} M KI with 1.0×10^{-3} M $AgNO_3$ and the resulting titration curve are shown in Fig. 8. As can be seen, the amount of iodide can be determined with sensor.

4.2. Determination of iodide containing mouth wash samples

In order to test the analytical utility of sensor it was used to determine iodide in KEXIDONE (Cadex India Ltd.), ALPHA-

Table 5
Performance of sensor no. 12 in partially non-aqueous media

Non-aqueous content (%v/v)	Working concentration range (M)	Slope (mV decade^{-1} activity)
0	5.3×10^{-7} to 1.0×10^{-2}	59.2
Methanol		
10	5.3×10^{-7} to 1.0×10^{-2}	59.2
20	6.8×10^{-7} to 1.0×10^{-2}	59.2
30	4.2×10^{-6} to 1.0×10^{-2}	58.4
35	1.5×10^{-5} to 1.0×10^{-2}	56.5
Ethanol		
10	5.3×10^{-7} to 1.0×10^{-2}	59.2
20	6.1×10^{-7} to 1.0×10^{-2}	59.0
30	3.8×10^{-6} to 1.0×10^{-2}	58.2
35	5.2×10^{-5} to 1.0×10^{-2}	55.9
Acetonitrile		
10	5.3×10^{-7} to 1.0×10^{-2}	59.2
20	5.3×10^{-7} to 1.0×10^{-2}	59.2
30	5.3×10^{-7} to 1.0×10^{-2}	57.6
35	5.3×10^{-7} to 1.0×10^{-2}	57.0

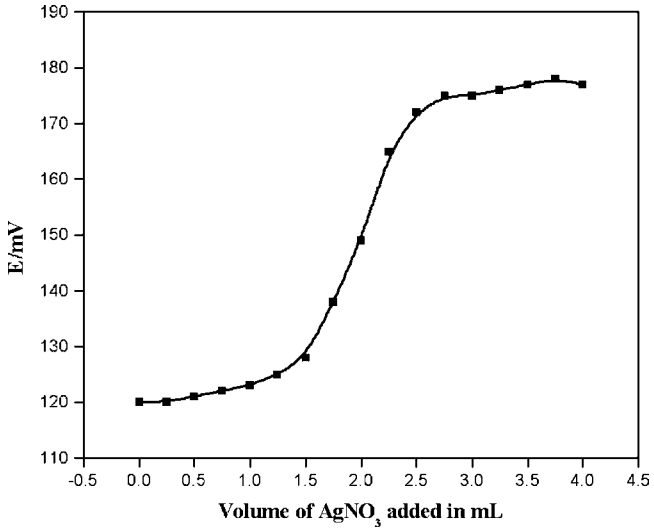


Fig. 8. Potentiometric titration curve for 20 mL of 1.0×10^{-4} M KI with 1.0×10^{-3} M $AgNO_3$ using the proposed sensor (no. 12).

Table 6
Results of determination of iodide ion in mouthwash samples

Sample no.	Sample	Found, % (w/v)	Labelled, % (w/v)
1	KEXIDONE	4.99 ± 0.01	5.0
2	ALPHADINE	0.99 ± 0.02	1.0
3	POVIDINE	4.92 ± 0.01	5.0

DINE (Nicholas Piramal India Ltd.) and POVIDINE (Stadmed Private India Ltd.) mouth wash samples. A sample of 10 mL of sample was burned with 10 mL of 5% H_2O_2 and 4.0 mL of 0.5 M NaOH. The mixture was heated, acidified with H_2SO_4 and diluted with water. The sample solution obtained were analysed by proposed membrane sensor and the results obtained by triplicate measurement are compiled in Table 6. One can see from the table that there is a satisfactory agreement between the determined value and the labeled iodide content.

4.3. Determination of iodide in sea water and river water samples

To demonstrate the usefulness of the proposed sensor for the environmental analysis, its potentiometric response to sea and river water samples were investigated. River water sample from Ganga river (Roorkee, India) and sea water samples from sea coast (Bombay, India). The sample solutions were filtered through 0.45 μm membrane filter (Millipore) within 24 h of collection. Filtrates were stored in polyethylene bottles at 4 °C in the dark. Water samples were used directly by adjusting pH 5.5 by dilute HCl solution. The results of analysis of water samples are compiled in Table 7.

Table 7
Analytical results (mean ± S.D., $n = 3$) for iodide in water samples by proposed sensor

Sample	Added ($\mu g\,L^{-1}$)	Found ($\mu g\,L^{-1}$)	Recovery (%)
Sea water	0	61	
	10	70	98.5
	20	88	97.8
River water	0	46	
	10	55	98.2
	20	73	97.3

5. Conclusion

Among the synthesized cadmium complexes of salens *viz.*, *N*,*N*′-bis(salicylidene)-1,4-diaminobutane (Cd-S_1) and *N*,*N*′-bis(salicylidene)-3,4-diaminotoluene (Cd-S_2) the Cd-S_1 shown high affinity for iodide ion. The sensor no. 12 based on Cd-S_1 with membrane composition 7:2:60:31 (w/w, %) (Cd-S_1:HTAB:DBP:PVC) best. It exhibits widest working concentration range (5.3×10^{-7} to 1.0×10^{-2} M), Nernstian compliance (59.2 mV decade^{-1} of activity), fast response time (11 s), and high selectivity for iodide. Its performance was compared with reported sensors, where it is seen that reported sensors shows significant superiority over them in many aspects like wide concentration range and high selectivity for I^- even over lipophilic anions Sal^-, ClO_4^- and SCN^-. Thus, the sensor prepared is advancement over the reported systems. It also offers a possibility for practical sensing and the determination of iodide ion in real sample solutions.

Acknowledgement

Ms. Sameena Mehtab is grateful to Council of Scientific and Industrial Research, New Delhi, India for providing financial assistance for this work.

References

[1] N.N. Greenwood, A. Earnsltaw, Chem. Elem. (1984) 933.
[2] R.M. Calligaris, in: G. Wilkinson, R.D. Gillard (Eds.), Comprehensive Coordination Chemistry, Oxford, 1987.
[3] Y. Yabu, K. Miyai, S. Hayashizaki, Y. Endo, N. Hata, Y. Tijima, R. Fushimi, Endocrinol. Jpn. 33 (1986) 905.
[4] A.S. Buinovskii, S.A. Bezrukova, N.A. Kolpakova, A.I. Maslyuk, Diagnostika Materialov 70 (2004) 3.
[5] Y. Bichsel, U. Von-Gunten, Anal. Chem. 77 (1999) 34.
[6] E.H. Larsen, M.B. Ludwigsen, J. Anal. Atom. Spectom. 72 (1997) 435.
[7] X. Hou, H. Dahlgaard, B. Rietz, U. Jacobsen, S.P. Nielsen, A. Aarkrog, Anal. Chem. 71 (1999) 2745.
[8] T. Fujiwara, H. Mohammadzai, H. Inoue, T. Kumamaru, Analyst 125 (2000) 759.
[9] J.A. Turner, R.H. Abel, R.A. Osteryoung, Anal. Chem. 47 (1975) 1343.
[10] R.C. Prost, Anal. Chem. 49 (1977) 1199.
[11] J.T. Hakedal, P.K. Egeberg, Analyst 122 (1997) 1235.
[12] E. Bakker, E. Malinowaska, R.D. Schiller, M.E. Meyerhoff, Talanta 41 (1994) 881.
[13] K. Farhadi, R. Maleki, R.H. Yamchi, H. Sharghi, M. Shamsipur, Anal. Sci. 20 (2004) 805.
[14] F. Jalali, M.J. Rajabi, G. Bahrami, M. Shamsipur, Anal. Sci. 21 (2005) 1533.
[15] D.-C. Jeong, H.K. Lee, S. Jeon, Bull. Korean Chem. Soc. 27 (2006) 1985.
[16] D. Dobenik, J. Stergulec, S. Gomi1eek, Fresenius J. Anal. Chem. 354 (1996) 494.
[17] J. Lizondo-Sabater, R. Martynez-Manez, F. Sancenon, M.-J. Seguy, J. Soto, Anal. Chim. Acta 459 (2002) 229.

[18] Y.-Q. Song, R. Yuan, M. Ying, L. Zhi-Qiang, Y.-Q. Chai, H. Cui, G.L. Shen, R.-Q. Yu, Fresenius J. Anal. Chem. 360 (1998) 47.
[19] H.R. Zare, F. Memarzadeh, A. Gorji, M.M. Ardakani, J. Braz. Chem. Soc. 16 (2005) 571.
[20] R. Yuan, Y.-Q. Song, Y.-Q. Chai, S.-X. Xia, Q.-Y. Zhong, B. Yi, M. Ying, G.-L. Shen, R.-Q. Yu, Talanta 48 (1999) 649.
[21] W.-J. Xu, Y.-Q. Chai, R. Yuan, L. Xu, S.-L. Liu, Anal. Sci. 22 (2006) 1345.
[22] A. Craggs, L. Keil, G.J. Moody, J.D.R. Thomas, Talanta 22 (1975) 907.
[23] E. Bakker, P. Buhlmann, E. Pretsch, Chem. Rev. 97 (1997) 3083.
[24] P.C. Meier, Anal. Chim. Acta 136 (1982) 363.
[25] J. Sanmartin, A.M. Garcia-Deibe, M. Fondo, D. Navarro, M.R. Bermejo, Polyhedron 23 (2004) 963–967.
[26] D.N. Kumar, B.S. Garg, J. Therm. Anal. Calorim. 69 (2002) 607.
[27] M.A. Perez, L.P. Marin, J.C. Quintana, M.Y. Pedram, Sens. Actuators B 89 (2003) 262.
[28] U. Schaller, E. Bakker, U.E. Spichiger, E. Pretsch, Anal. Chem. 66 (1994) 391.
[29] Y. Umezawa, K. Umezawa, H. Sato, Pure Appl. Chem. 67 (1995) 507.
[30] V.P.Y. Gadzekpo, G.D. Christian, Anal. Chim. Acta 164 (1984) 279.
[31] E. Bakker, E. Pretsch, P. Bühlmann, Anal. Chem. 72 (2000) 1127.
[32] F.J. Sa'ez de Viteri, D. Diamond, Analyst 119 (1994) 749.

Available online at www.sciencedirect.com
ScienceDirect
Talanta 74 (2008) 1066–1070
Talanta
www.elsevier.com/locate/talanta

Short communication

Identification and quantitative determination of atorvastatin calcium polymorph in tablets using FT-Raman spectroscopy

Dimitra Skorda [a,b], Christos G. Kontoyannis [a,b,*]

[a] *Department of Pharmacy, University of Patras, 26500 Patras, Greece*
[b] *Institute of Chemical Engineering and High Temperature Chemical Proccesses, FORTH, Patras, Greece*

Received 14 April 2007; received in revised form 25 July 2007; accepted 30 July 2007
Available online 3 August 2007

Abstract

Atorvastatin calcium (ATC) is the active pharmaceutical ingredient (API) of the best selling lipid-lowering formulation Lipitor®. Twelve ATC crystal forms are known and several pharmaceutical companies are developing or have developed generic drug formulations based on different ATC polymorphs. The strong overlap of the X-ray diffraction patterns (XRD) of the polymorphs with the respective patterns of the excipients, the presence of small API quantities in the tablet and the similarity of the crystal phase VIII XRD pattern used in the tablet examined in this work to that of phases IV and IX made identification difficult. Quantitative determination of ATC was attempted using Raman spectroscopy (RS), IR spectroscopy and X-ray powder diffraction. It was found that RS exhibited lower detection limit and a calibration model was constructed. Its application on commercial ATC tablets with 40 mg strength yielded an error of 1.25%.
© 2007 Elsevier B.V. All rights reserved.

Keywords: Atorvastatin calcium; X-ray powder diffraction; Polymorphs; Raman; IR; Identification; Quantitative analysis

1. Introduction

The majority of drug compounds and excipients are known to exist in different solid-state forms (i.e. polymorphs, solvates, amorphous state), each form having different physical properties (e.g. melting point, solubility, density and hardness). Polymorphism, can have a profound effect on shelf life, solubility, formulation properties and processing properties of a drug [1]. Furthermore, when medicine is administered orally as a crystalline solid, dissolution rate depends on the exact crystal form of the API, leading to lower or higher biological activity than desired. Moreover, many drugs receive regulatory approval for only a single crystal form or polymorph.

Atorvastatin calcium (ATC) is a synthetic lipid-lowering agent. Atorvastatin is an inhibitor of 3-hydroxy-3-methylglutaryl-coenzyme A (HMG-CoA) reductase. This enzyme catalyzes the conversion of HMG-CoA to mevalonate, an early and rate-limiting step in cholesterol biosynthesis. ATC crystallizes in 12 crystal forms [2–5] and the Form I [2] was initially marketed by Pfizer under the name Lipitor®. Lipitor became the world's first US$ 10-billion-a-year drug and competitors develop or have developed new formulations using different crystal forms, despite the potential patent infringement lawsuits. Therefore, identification of the crystal phase of an active pharmaceutical ingredient (API) in a tablet is of outmost importance.

In the above mentioned patents [2–5], characterization of ATC crystal forms relied solely on the XRD patterns and no other spectroscopic techniques such as IR, Raman and NMR were used and/or reported. Thus identification of an ATC polymorph is difficult to be accomplished with techniques other than XRD since preparation and/or acquisition of the 12 reported ATC forms, in order to record additional spectral information, is impractical.

In the recent bibliography the methods used for the quantitative determination of ATC in formulations were HPLC [6,7], electrophoresis [8] and spectrophotometric determination based on the reaction between the API and bromocresol green, alizarin red, or bromophenol blue producing ion-pair complexes [9]. These methods although sensitive are usually time-consuming and cumbersome thus simpler alternative methods are needed.

* Corresponding author at: Institute of Chemical Engineering and High Temperature Chemical Proccesses, P.O. Box 1414, GR-26500 Patras, Greece. Tel.: +30 2610 997727/969328; fax: +30 2610 997658.
E-mail address: cgk@iceht.forth.gr (C.G. Kontoyannis).

0039-9140/$ – see front matter © 2007 Elsevier B.V. All rights reserved.
doi:10.1016/j.talanta.2007.07.030

The present work was focus in: (a) developing a methodology for identification of the ATC polymorph in a commercial formulation using phase VIII, (b) examining the suitability of XRD, IR and Raman techniques for the quantitative determination of the API in commercial tablets as alternative analytical methods. In this respect the proposed techniques were applied on the ATC tablets, their respective detection limits were determined and a calibration line using the method with the lower detection limit was constructed.

2. Experimental

2.1. Materials used

Atorvastatin calcium form VIII as API having purity as ATC 99.9%, according to the provided certificate of analysis, placebo tablets and 40 mg strength ATC tablets were kindly provided by Specifar SA, Athens, Greece. Each tablet weighted 600 mg yielding a 6.66 wt% API presence. For quantitative analysis purposes labscale batches with 1.00, 3.33, 6.66, 10.00, 13.33, 16.66 and 20.00 wt% atorvastatin calcium were manufactured.

2.2. Characterization of the samples

The X-ray powder diffraction analysis was performed (Philips 1830/40) on finely powdered samples using the Cu Kα (40 kV and 30 mA) radiation and Ni filter with a scanning speed of 0.005° $2\theta\ s^{-1}$. Time constant was set at 2 s. The XRPD pattern of the pure ATC form VIII polymorph is shown in Fig. 1.

The Raman spectra were recorded using a FRA-106/S FT-Raman (Bruker) with the following characteristics: The laser excitation line used, was the 1064 nm of a Nd:YAG laser. A secondary filter was used to remove the Rayleigh line. The scattered light was collected at an angle of 180°. The system was equipped with a liquid N_2 cooled Ge detector (D 418). The power of the incident laser beam was about 370 mW on sample's surface. Typical spectral line width was 0.5 cm^{-1} while the recorded spectra were the average of 300 scans.

All infrared spectra were recorded from 4000 to 400 cm^{-1}, using the EQUINOX 55 (Brucker) FT-IR spectrometer. Each spectrum was the average of 200 scans using a spectral resolution of 4 cm^{-1}. The IR spectra were recorded and stored using a spectroscopic software (OPUS, Version 2.0). FT-IR spectra were obtained from KBr pellets compressed at 8 MPa for 5 min.

For comparison purposes the XRD patterns from literature were digitized using the UN-Scan-IT v.6.0 software from Silk Scientific Inc.

ATC powder was sized using laser diffraction (Mastersizer/S Malvern Instruments, UK) yielding a D [4,3] (diameter of a sphere of equivalent volume to the particle under investigation) equal to 4 μm.

2.3. Stability of the API

The stability of the API through the applied analytical processes was tested by: (a) pelleting pure API under the same conditions as the ATC-KBr tablets prepared for the FT-IR characterization, (b) mixing pure API with itself in the same manner as the excipient–ATC mixtures used during the construction of the calibration line. The XRD pattern and the Raman spectrum of the stressed API were recorded and compared to the pattern and the spectrum recorded before the application of the stressing factor. No differences were observed.

3. Results and discussion

3.1. Identification of atorvastatin calcium polymorph in a tablet

The XRD patterns of the pure API, two placebo formulations, the digitized pattern of form VIII [5] and the 40 mg strength tablet can be seen in Fig. 1. In Fig. 2 the 12 digitized XRPD patterns from references [2–5] can be seen. The pattern of the

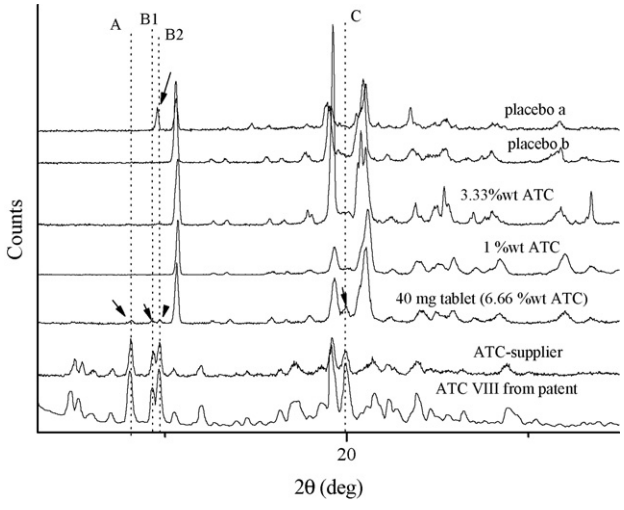


Fig. 1. XRD patterns of (bottom to top): form VIII of ATC from ref. [5]; pure ATC from supplier; tablets of 40 mg strength ATC (6.66 wt% ATC); mixture of 1 wt% ATC; mixture of 3.33 wt% ATC; placebo formulation b; placebo formulation a.

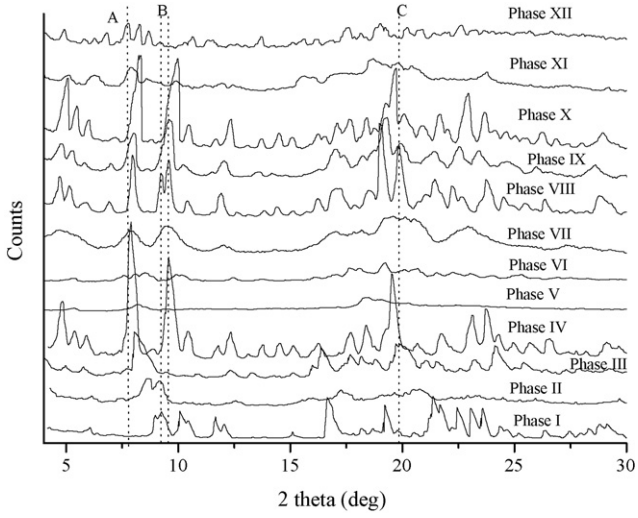


Fig. 2. Digitized powder X-ray diffraction patterns of ATC (forms I, II, IV from ref. [2]; form III from ref. [3]; form V from ref. [4]; forms VI–XII from ref. [5]).

pure atorvastatin calcium found to match the XRD of polymorph crystal phase VIII.

During the development stage, two different placebo formulations (a and b) were examined. The differences between the respective patterns and the pattern of the 40 mg tabs prepared using placebo b were observed in the 2θ regions marked with arrows in Fig. 1 and the dotted lines A, B1, B2 and C and should be attributed to the presence of the API. It can be seen in Fig. 2, that several phases exhibit reflections in the 2θ regions where these differences exist (arrows in Fig. 1). Besides the crystal phase VIII, crystal phases IV, IX, XI and XII are plausible candidates. Phase XI and XII can be ruled-out due to the rather low intensity of their respective reflections. The peaks of XI and XII are also expected to be wide as opposed to the recorded reflections. That leaves out phase IX, which according to the literature [5] may be prepared by maintaining VIII under a humid atmosphere, and phase IV. Phase VIII can be easily distinguished from IV and IX since VIII exhibits a double reflection at 9.4 and 9.6 2θ as opposed to a single strong reflection for crystal phases IV and IX at 9.7 and 9.4 2θ, respectively. It is worth noting at this point that placebo a exhibits also a strong reflection at 9.6 2θ. This reflection, attributed to the presence of 0.8% talc in formulation, masks completely the 2θ region where the double reflection peak is expected to rise making the identification of the presence of phase VIII in the tablet impossible since this doublet reflection differentiates VIII from IV and IX.

The exact reflections, according to the above mentioned patents, of all phases in the 2θ degree regions of interest as well as the corresponding reflections of ATC tabs, prepared with placebo b, can be found in Table 1 where the findings described in the previous paragraph are summarized. From Table 1 it is apparent that only the reflections of phase VIII match satisfactorily (within the experimental error) the API reflections in ATC 40 mg tabs. Furthermore no additional reflections assigned to other polymorphs were detected. It can, thus, be concluded that polymorph VIII was the only atorvastatin calcium polymorph included in ATC 40 mg tablets and no transformation took place during the manufacturing process of the tablets.

Table 1
Characteristic reflections in the 2θ degree region of A, B and C of Fig. 1

Form	A (2θ)	B (2θ)	C (2θ)
I	8.6	9.2, 9.5	21.6
II	8.5	9.0	20.5
III	8.5	–	20.0, 20.3
IV	8.0	9.7	19.6
V	8.0	–	18.4
VI	8.7	10.0	19.5
VII	7.8 (broad)	9.3 (broad)	18.5–21.8 (broad)
VIII	**8.0**	**9.3**, **9.6**	**20.0**
IX	7.9	9.4	19.9
X	8.0	9.6, 10.3	19.4
XI	7.8	8.6, 9.8	19.9 (broad)
XII	8.0	9.4 (small-broad)	19.8 (small-broad-amorphous)
API reflections in tab	**8.1**	**9.3**, **9.7**	**20.1**

As mentioned in the introduction section, application of FT-IR and FT-Raman for identification of an ATC polymorph was not possible since the respective spectra were not available in literature and their acquisition by preparing all 12 polymorphs was difficult if possible at all. On the other hand the finding that ATC VIII remained unchanged facilitates the application of FT-IR and FT-Raman for solid-state quantitative analysis of ATC in a tablet. At this point it should be noted that phase VIII transformation cannot be monitored when it occurs at percentages below the XRD detection limits for the other ATC phases.

3.2. Determination of ATC detection limits of XRD, IR and Raman techniques in tablets

3.2.1. XRD detection limit

In Fig. 1 the XRD patterns of the 40 mg tablet having 6.66 wt% ATC along with the patterns of placebo b–API mixtures with 1 and 3.33 wt% ATC can be seen. It is apparent that the characteristic reflections of VIII at A, B and C 2θ regions can be barely seen in the 3.33 wt% mixture indicating that this can been set as the XRD detection limit for ATC VIII according to Q2B ICH guidelines [10] for visual evaluation of the detection limit.

3.2.2. IR detection limit

In Fig. 3 the FT-IR spectra of placebo b formulation powder, tablets of 40 mg strength ATC form VIII (6.66 wt%), pure ATC VIII (API), mixture of 1 wt% ATC with placebo b and mixture of 3.33 wt% ATC with placebo b. Only the strongest vibrations of ATC at 1509 and 1652 cm^{-1} (marked with arrows in Fig. 3) are barely visible in the tablet spectrum. None of these can be seen in the spectra of 3.33 and 1 wt% mixture. Thus, using the same guidelines as above the detection limit of FT-IR for VIII ATC can be set at 6.66 wt%. At this point it should be noted that the FT-IR results are not to be trusted completely and are reported here only as an indication of the order of magnitude

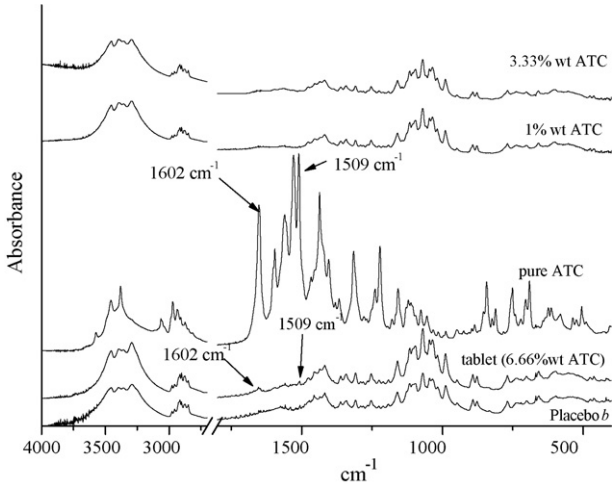


Fig. 3. FT-IR spectra of (bottom to top): placebo powder of ATC tablets; tablets of 40 mg strength ATC; pure ATC VIII (API); mixture of 1 wt% ATC with placebo b; mixture of 3.33 wt% ATC with placebo b.

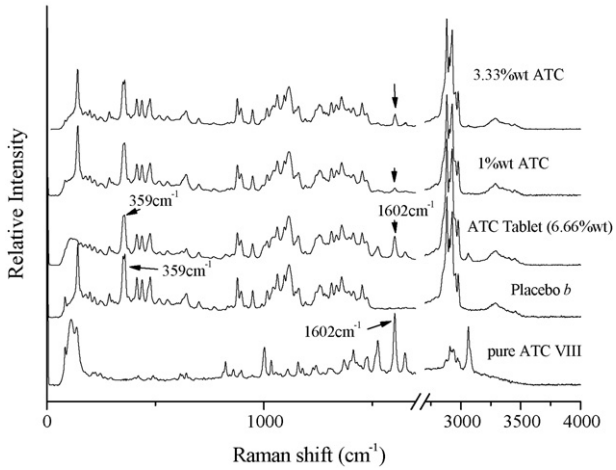


Fig. 4. FT-Raman spectra of (bottom to top): ATC VIII; placebo powder of ATC tablets; tablets of 40 mg strength ATC; mixture of 1 wt% ATC; mixture of 3.33 wt% ATC.

of the detection limit since the particle size of the excipients is unknown and thus Beer's law may not be applicable.

3.2.3. Raman detection limit

In Fig. 4 the FT-Raman spectra of ATC VIII, placebo powder of ATC tablets, tablets with 40 mg strength ATC, mixture of 1 wt% ATC with placebo and mixture of 3.33 wt% ATC with placebo can be seen. The strongest vibration of ATC VIII is at 1602 cm^{-1}, marked with arrows in Fig. 4, and does not overlap with any placebo vibration. This vibration is also clearly visible in the spectrum of 1 wt% mixture of ATC with excipients. Thus the detection limit for Raman spectroscopy is at or slightly below 1 wt% and although Raman spectroscopy cannot be used for the identification of ATC crystal phase, since the spectra of the other crystal phases are unknown, it can be used for the quantitative determination of the API taking also into account that no transformation of phase VIII is expected to take place during the manufacturing process.

3.3. Quantitative determination of ATC in tablets

3.3.1. Calibration model

As mentioned previously, Raman spectroscopy exhibits the lower detection limit and based on this technique a calibration line will be constructed for the quantitative determination of ATC in tablets. The intensity of a Raman line depends on a number of factors including the incident laser power, the frequency of the scattered radiation, the absorptivity of the materials involved in the scattering and the response of the detection system. In addition, the area under a Raman peak is analogous to the concentration of the Raman active species [11].

On solid formulations a plethora of methodologies have been applied in an effort to overcome the problems related to the quantitative analysis. These are stemming from both the technique and the sample. A laser excites a very small portion (usual 1 mm in diameter) of a very difficult to homogenize sample. The presence of numerous excipients with very different and sometimes rather large particle sizes, e.g. 50–100 μm complicates the problem. Since the Raman intensity is proportional to the number of molecules in the sample volume probed, the packing of the sample is an equally important factor. The methods that have been used for normalizing the intensity of Raman signal include the ratio of two analytes in the same spectrum, setting the area of the spectral segment to 1, multiplicative scatter correction, standard normal variate transformation and the use of internal or external standard [12]. In very few cases no normalization was introduced [13,14], but the commercial samples were powdered and a more sophisticated technique based on chemometrics, e.g. PLS, was used. Recently, Markov-transformations have been also applied [15] in extracting quantitative information from FT-Raman data.

In this case for simplicity the ratio of band intensities characteristic for each component was used. In this way differences in the measured intensities of the various spectra obtained from the same tablet which are attributed to factors such as the packing of the powder or the positioning of the sample are taken into account. Possible inhomogeneity problems were dealt by recording five spectra from each specimen from different spots on sample's surface.

In ATC tablets the 1602 cm^{-1} was chosen as the appropriate ATC peak. For the excipients the 359 cm^{-1} band was used. The ratio of the intensities of the two peaks attributed to ATC and to placebo should be equal to:

$$\frac{A^{359}}{A^{1602}} = \frac{I_0 K^{359}_{\text{placebo}} W_{\text{placebo}}}{I_0 K^{1602}_{\text{ATC}} W_{\text{ATC}}} \quad (1)$$

where A is the area under the placebo and the ATC peak, K a factor which includes the frequency and compound dependent terms, I_o the intensity of the incident laser line and W_{placebo} and W_{ATC} represent the weight percentage of placebo and ATC, respectively. Eq. (1) is valid only in the case that there is no chemical interaction between the substances of the sample or band overlapping. Since $W_{\text{ATC}} + W_{\text{placebo}} = 100$ Eq. (1) can be rewritten as:

$$\frac{A^{359}}{A^{1602}} = \frac{K^{359}_{\text{placebo}} \times 100}{K^{1602}_{\text{ATC}}} \frac{1}{W_{\text{ATC}}} - \frac{K^{359}_{\text{placebo}}}{K^{1602}_{\text{ATC}}} \quad (2)$$

For the calibration model of Eq. (2) five Raman spectra from each of the 1.00, 3.33, 6.66, 10.00, 13.33, 16.66 and 20 wt% ATC mixtures with placebo were recorded and the averaged area ratio was used. A plot of the ratios A^{359}/A^{1602} versus $1/W_{\text{ATC}}$, as expected, yielded a straight line:

$$\frac{A^{359}}{A^{1602}} = -0.17 + 16.8 \frac{1}{W_{\text{ATC}}} \quad (3)$$

$n = 7$, correlation coefficient, r, was equal to 0.995 while the standard deviations for the slope and the intercept were found to be 0.097 and 0.037, respectively.

3.3.2. Determination of API in tablets

Tablets with other than 40 mg ATC strength are also available but the API to excipients ratio was the same. Thus, the proposed procedure described in this section can be also applied

Table 2
FT-Raman results obtained from three commercial tablets with 40 mg atorvastatin calcium

Formulation	FT-Raman; mean ± confidence limit[a] (mg/tablet)
T1	39.3 ± 0.6
T2	39.6 ± 0.8
T3	39.7 ± 0.9
Average	39.5 ± 0.8

[a] At 95% confidence limit.

in these tablets too. Five Raman spectra from three different 40 mg strength ATC tablets T1, T2 and T3 were recorded. The average area ratios A^{359}/A^{1602} were entered in Eq. (3) and the calculated W_{ATC} in wt% was transformed to mg of API/tablet and can be seen in Table 2. An average difference of 0.5 mg/tablet or an error of 1.25% was found. An additional advantage of using Raman spectroscopy over the other two techniques is that its application is non-destructive for the tablet.

4. Conclusions

No apparent transformation of atorvastatin calcium VIII to other crystal phases during the manufacturing process of the examined tablets was observed. This statement is true with the assumption that the XRD detection limits for all other ATC phases are similar or preferably lower to that of phase VIII. The identification of phase VIII was facilitated by the modification of the excipients during the development stage of the tablet. A 1 wt% detection limit was calculated from the application of Raman spectroscopy for the quantitative determination of ATC as opposed to 3.33 wt% for XRD 6.66 wt% for IR spectroscopy. A calibration model for Raman spectroscopy was also obtained and its application on 40 mg strength commercial tablets yielded a 1.25% error in the calculation of the ATC concentration.

Acknowledgements

Authors would like to thank Specifar SA for its help and in particular Mr. G. Chalkias from the Department of Product Development.

References

[1] D.J. Grant, in: H.G. Brittain (Ed.), Polymorphism in Pharmaceutical Solids. Chapter 1. Theory and Origin of Polymorphism, Marcel Dekker Inc., New York, 1999, pp. 1–31.
[2] C. Briggs, R. Jennings, R. Wade, K. Harasawa, S. Ichikawa, K. Minohara, S. Nakagawa, US 5,969,156 (1999).
[3] A.T. McKenzie, US 6,121,461 (2000).
[4] A. Ayalon, M. Levinger, S. Roytblat, V. Niddam, R. Lifshitz, J. Aronhime, WO01/36384.
[5] J. Aronhime, R. Lidor-Hadas, V. Niddam-Hildesheim, R. Lifshitz-Liron, E. Kovalevski-Ishai, G. Samburski, WO02/43732.
[6] T.G. Altuntas, N. Erk, J. Liquid Chromatogr. Relat. Technol. 27 (2004) 83–93.
[7] M.K. Pasha, S. Muzeeb, S.J.S. Basha, D. Shashikumar, R. Mullangi, N.R. Srinivas, Biomed. Chromatogr. 20 (2006) 282–293.
[8] E. Guihen, G.D. Sisk, N.M. Scully, J.D. Glennon, Electrophoresis 27 (2006) 2338–2347.
[9] N. Erk, Anal. Lett. 36 (2003) 2699–2711.
[10] The European Agency for the Evaluation of Medical Products. ICH Topc Q2B Note for Guidance on Validation of Analytical Procedures: Methodology GPMP/ICH/281/95, 1996.
[11] D. Strommen, K. Nakamoto, Laboratory Raman Spectroscopy, J. Wiley, New York, 1984, p. 71.
[12] M.J. Pelletier, Appl. Spectrosc. 57 (2003) 20A–42A (and references therein).
[13] R. Szostak, S. Mazurek, Analyst 127 (2002) 144.
[14] S. Mazurek, R. Szostak, J. Pharm. Biomed. Anal. 40 (2006) 1225.
[15] B. De Spiegeleer, B. Baert, N. Diericx, D. Seghers, F. Verpoort, L. Van Vooren, C. Burvenich, G. Slegers, J. Pharm. Biomed. Anal. 44 (2007) 254.

Available online at www.sciencedirect.com
ScienceDirect
Talanta 74 (2008) 1071–1074
Talanta
www.elsevier.com/locate/talanta

Short communication

An effective method for enhancing metal-ions' selectivity of ionic liquid-based extraction system: Adding water-soluble complexing agent

Xiao Qi Sun [a], Bo Peng [a], Ji Chen [a,*], De Qian Li [a], Fang Luo [b]

[a] *Key Laboratory of Rare Earth Chemistry and Physics, Changchun Institute of Applied Chemistry, Chinese Academy of Sciences, Changchun 130022, PR China*
[b] *Key Laboratory of Polyoxometalates Science of Ministry of Education, College of Northeast Normal University, Changchun 130024, PR China*

Received 22 April 2007; received in revised form 25 July 2007; accepted 30 July 2007
Available online 6 August 2007

Abstract

Selective extraction–separation of yttrium(III) from heavy lanthanides into 1-octyl-3-methylimidazolium hexafluorophosphate ($[C_8mim][PF_6]$) containing Cyanex 923 was achieved by adding a water-soluble complexing agent (EDTA) to aqueous phase. The simple and environmentally benign complexing method was proved to be an effective strategy for enhancing the selectivity of $[C_nmim][PF_6]/[Tf_2N]$-based extraction system without increasing the loss of $[C_nmim]^+$.
© 2007 Elsevier B.V. All rights reserved.

Keywords: IL-based extraction; Complexing method; Heavy lanthanides

1. Introduction

Ionic liquids (ILs) have emerged as tunable and potentially "green" solvents for some kinds of applications [1]. Among their unique properities, non-volatility and non-flammability are important advantages over volatile organic compounds (VOCs) for liquid–liquid extraction. Currently, more and more attention [2–5] has been paid to IL-based extraction since the pioneering work by Rogers et al. [6]. In some IL-based systems, the distribution coefficients for metal ions were found to be enhanced obviously, even by several orders higher than those in VOCs [7–9]. As a further investigation indicated, polar ligands and complexes were inclined towards be better solvated by IL and poorly attracted at the IL's interface since the higher polarity of IL than that of VOC [10], which can be used to explain the higher extraction efficiency of metal ions in some IL-based extraction system. In view of the above-mentioned advantages, IL-based extraction could be regarded as a promising green and high-efficiency separation technology. However, recent investigations also revealed that there were some drawbacks in IL-based extraction, such as the lower selectivity for metal ions and ILs' loss to aqueous phase [2]. Hence, several methods have been developed for overcoming the problems. Rogers et al. [11], for instance, tried to control the loss of imidazolium cation to aqueous solutions by using a sacrificial cation-exchanger ($NaBPh_4$). Recent work by Dietz et al. [12] indicated that the synergistic extraction of Sr^{2+} using DCH18C6 and TBP in $[C_nmim][Tf_2N]$ ($n = 2, 5, 6, 8, 10$) depended on the alkyl chain length of $[C_nmim]^+$, and synergistic effect only happened to the ILs with shorter alkyl chain. Unfortunately, the hydrophobicity of IL with shorter alkyl chain was obviously lower than that with longer chain. Accordingly, the means cannot bring higher extraction efficiency, selectivity and lower IL's loss. In additional, Luo et al. [13] synthesized macrocycle ligands to overcome the co-extraction of K^+ during the extraction of Sr^{2+}, and *N*-octyl-aza-18-crown-6 was found to have better selectivity toward Sr^{2+} in the IL-based fission products extraction processes. Another representative work was achieved by Cocalia et al. [14], and they found the extraction of Am^{3+}, Nd^{3+}, Eu^{3+}, UO_2^{2+} by Cyanex 272 (HDEHP) in $[C_{10}mim][NTf_2]$ and dodecane from $[HNO_3]$ solution had the

* Corresponding author. Tel.: +86 431 85262646; fax: +86 431 85262646.
E-mail address: jchen@ciac.jl.cn (J. Chen).

0039-9140/$ – see front matter © 2007 Elsevier B.V. All rights reserved.
doi:10.1016/j.talanta.2007.07.031

identical partitioning equilibria and coordination environment. Obviously, it showed the loss of IL during extraction could be overcome by selecting appropriate extraction system. However, limitation of the method was that the similar IL-based system was not ubiquitous.

As for the rare earth (RE) separation, selectivity is a more important factor than extraction efficiency. Consequently, looking for an appropriate separation method for IL-based extraction is crucial for its potential application in this field. In generally, the controlling aqueous acidity was a common method for achieving RE separation in traditional VOCs-based extraction system. However, quite different from VOCs, the high aqueous acidity will result in not only a gradual decomposition of the imidazolium-type IL [2,9], but also an obvious decrease of metal ions' extraction effciency in the IL-based extraction [15,16]. Thus, to obtain a more green and efficient IL-based extraction separation process, we therefore developed a strategy to improve the separation process. As well known, it is difficult to separate Y(III) from heavy rare earth (HRE) since their similar physical and chemical properities, which is a representative hard problem in the rare earth hydrometallurgy. In this laboratory, the selective extraction by adding EDTA, HEDTA and DTPA to aqueous phase was indicated to be an effective method for separating Y(III) from HRE [17,18]. Besides applied in solvent extraction [19,20], the complexing method was also indicated to be a mature and effective technique to enhance selectivity in some other metal ions separation techniques, such as cation-exchange membrane dialysis [21], electrodialysis [22], ion exchange resin [23] and liquid membranes [24], Therefore, here we report the first study of selective extraction of metal ions into IL phase with adding complexing agent to aqueous phase.

2. Experimental

2.1. Materials

The IL used in this study was 1-octyl-3-methylimidazolium hexafluorophosphate ([C_8mim][PF_6]), which was prepared and purified as described previously [25]. Although the stability of the IL is inferior to that of [$C_n$mim][Tf_2N] [25], however, from the view of evaluating the validity of the separation method, the inferior IL could be considered as an appropriate choice. Cyanex 923 is a mixture of straight-chain alkylated phosphine oxides. As a commercially available extractant, its extraction behaviors of RE in VOCs have been systematically studied in this laboratory [26,27]. The complexing agent solution was prepared by dissolving EDTA into distilled water, which was determined by titration using Zn standard solution and xylenol orange as indicator. The aqueous phase used in the extraction were prepared by mixing the RE(III) solutions with EDTA solution.

2.2. Methods

Five millilitres of aqueous phase and [C_8mim][PF_6] containing Cyanex 923 were mixed and shaken in equilibrium tubes using a mechanical shaker for 60 min at 298 K. The concentrations of RE ions in aqueous phase were determined by inductively coupled plasma mass spectroscopy (ICP-MS, Agilent 7500). The absorbance of $[C_8mim]^+$ were determined using UV–visible spectrophotometer (Shimadzu UVmini-1240) at 211 nm [13], and their corresponding concentrations were calculated with Beer's law plots plotted with standard concentrations of [C_8mim][Cl]. The concentrations of $[PF_6]^-$ were determined with ion chromatograph (Dionex ICS-1500), and calculated with the Beer's law plots formed from series of standard $NaPF_6$ solutions. It should be noticed that the lower $[PF_6]^-$ concentrations of aqueous phase in this study were too little to be responded by ion chromatograph (IC). Thus, to increase their concentrations, the volumes of aqueous phase need to be slowly volatilized into halves at the room temperature to avoid the hydrolysis of PF_6^- [9], as a result, there is only one chromatographic peak corresponding to PF_6^- from $NaPF_6$.

3. Results and discussion

To investigate pH effect on the IL-based extraction process, extraction efficiency of Y^{3+} and aqueous $[C_8mim]^+$ concentration were determined as aqueous phase acidity increased. As can be seen in Fig. 1, quite different from the extraction of RE(III) by Cyanex 923 in hexane [28,29], the extraction efficiency in this Y(III)/Cyanex923/[C_8mim][PF_6] system was found to decrease rapidly with aqueous acidity increased as some other papers described [2,15,16]. Moreover, the higher acidity will cause a gradual increase of $[C_8mim]^+$ in aqueous phase, and the decomposition of [C_8mim][PF_6] is a result of ion exchange of PF_6^- with NO_3^- and acid-catalyzed hydrolysis of PF_6^- to PO_4^{3-} [9,16]. Actually, even the more stable [$C_n$mim][Tf_2N] applied in IL-based extraction were also indicated to have the tendency of decompose at higher acidity since the replacement of Tf_2N^- by NO_3^- [2]. The problems of [$C_n$mim][PF_6]/[Tf_2N] may have important effect on their application for extraction as the traditional mode, and the decomposition will also result in the pollution to aqueous phase, obviously, which is a negative implication for the target "green" process.

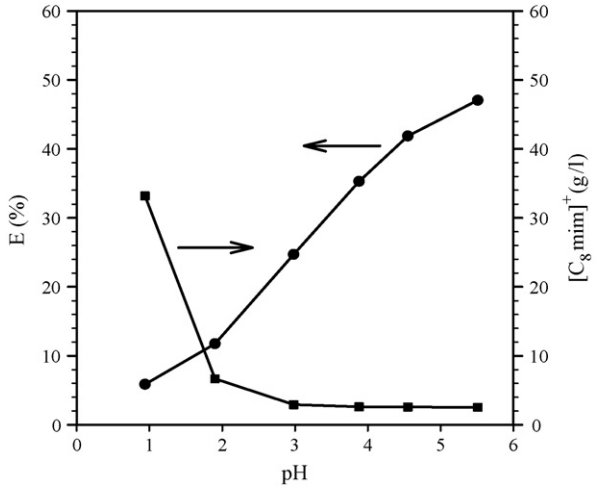


Fig. 1. The pH effects on extraction efficiency of Y(III) (●) and change of $[C_8mim]^+$ concentration (■): $[Y^{3+}] = 4.711 \times 10^{-4}$M; $[Cyanex923]_{(IL)} = 3.5 \times 10^{-2}$M.

As a key property of IL, its concentration's change in aqueous phase during extraction is crucial for evaluating its potential application in the process, moreover, the detailed investigation on concentration's change is also very important to elucidate the extraction mechanism. Nevertheless, there are still some disagreements on this question.

Wei et al. [30] reported that addition of Cu^{2+} in aqueous phase decreased the solubility of $[C_4mim][PF_6]$ at all pH values, the investigation indicated that the contribution of ion exchange between metal ions and $[C_4mim]^+$ for the extraction of metal ions seems insignificant. In contrast to this opinion, Dietz et al. [2] argued that cation-exchange constitute the predominant mode in extraction of Sr^{2+} from acidic nitrate into $C_nmim^+Tf_2N^-$ by DCH18C6, and a obvious increase of $[C_5mim]^+$ in aqueous phase during the extraction was reported. To investigate the concentration change of $[C_8mim][PF_6]$ in aqueous phase, the concentrations of $[C_8mim]^+$ and $[PF_6]^-$ were measured precisely at the same condition before and after extraction.

As shown in Fig. 2, the concentrations of $[C_8mim]^+$ increase as Y^{3+} extracted into the IL phase, contrarily, the concentration of $[PF_6]^-$ was almost invariable. Consequently, the phenomenon indicated that the extraction mechanism of Y^{3+} into $[C_8mim][PF_6]$ containing Cyanex 923 was concerned more $[C_8mim]^+$ but $[PF_6]^-$, and cation-exchange mechanism is a creditable consequence for the IL-based extraction process as most of the cases reported [2,16,31,32]. As can be seen from Fig. 2, the concentrations of $[C_8mim]^+$ in aqueous phase were obviously higher than those of $[PF_6]^-$, and the difference was attributed to the exchange of the cationic complex with $[C_8mim]^+$ between IL phase and aqueous phase, the extracted complex became a part of the IL with its positive charge being balanced by the remaining $[PF_6]^-$ anions [33]. Accordingly, the loss of $[C_8mim]^+$ to aqueous phase during extraction should be an important factor to evaluate "green" quality of the IL-based extraction. To assess influence of complexing agent on the IL-based extraction, the extraction of mixed RE ions into $[C_8mim][PF_6]$ containing Cyanex 923 with different concentrations of EDTA in aqueous phase were conducted. Selection of the extraction system in this study lied in two reasons. Firstly, the separation of Y(III) from HRE(III) is difficult than that of other lanthanides since their similar physical and chemical properities. Secondly, the stability constant of Y(III) and HRE(III) with EDTA is also very similar. In view of the reasons mentioned above, the representative complexing method used to separate Y(III) from HRE(III) will be applied in some other IL-based extraction systems if its validity in this system was verified.

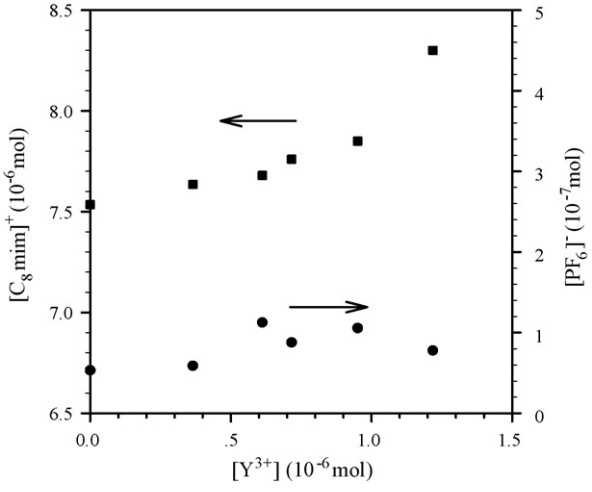


Fig. 2. $[C_8mim]^+$ (■) and $[PF_6]^-$ (●) in aqueous phase vs. $[Y]^{3+}$ extracted to IL phase.

Table 1
Separation factors (β) of Y^{3+} to HRE with increasing EDTA concentration

[EDTA]:[HRE]	$\beta_{Y/Er}$	$\beta_{Y/Tm}$	$\beta_{Y/Yb}$
Without EDTA	1.36	0.43	0.12
1:8	1.42	0.74	0.48
1:6	1.51	0.84	0.7
1:4	1.57	0.95	0.82
1:2	4.29	4.24	4.41

As shown in Fig. 3, the extraction sequences of RE(III) were changed from Er<Y<Tm<Yb to Er<Tm<Yb<Y after EDTA was added. The phenomena could be attributed to the different stability constant between EDTA and RE(III) [34] ($K_{Y–EDTA}$ = 17.38, $K_{Er–EDTA}$ = 17.98, $K_{Tm–EDTA}$ = 18.59, $K_{Yb–EDTA}$ = 18.68). Obviously, order of the stability constant is Y<Er<Tm<Yb. In fact, the added EDTA always complexes with the metal ions possessing higher stability constants firstly, then it can influence on the metal ions with lowers stability constants. The resulting complex is insensitive for extraction, and only free RE(III) (not complexed with EDTA) can take part in the extraction [17,19]. Just because the masking effect in this system, extractabilities for Yb(III), Tm(III) and Er(III) were more suppressed than that of Y(III). Consequently, Y(III) could be selectively extracted from Y/Er/Tm/Yb mixtures. As can be seen from Table 1, the

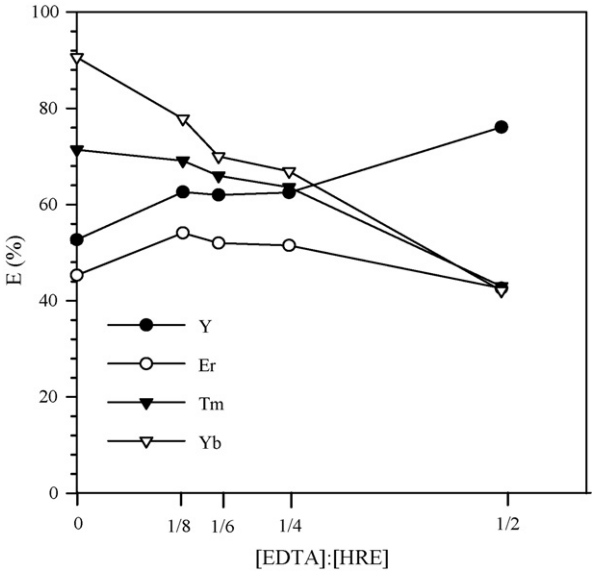


Fig. 3. Influence of EDTA concentration variation on the extraction efficiency of HRE by Cyanex923: $[Y^{3+}] = 1.349 \times 10^{-4}$M; $[Er^{3+}] = 1.024 \times 10^{-4}$M; $[Tm^{3+}] = 1.032 \times 10^{-4}$M; $[Yb^{3+}] = 0.69 \times 10^{-4}$M; $[Cyanex923]_{(IL)} = 3.5 \times 10^{-2}$M.

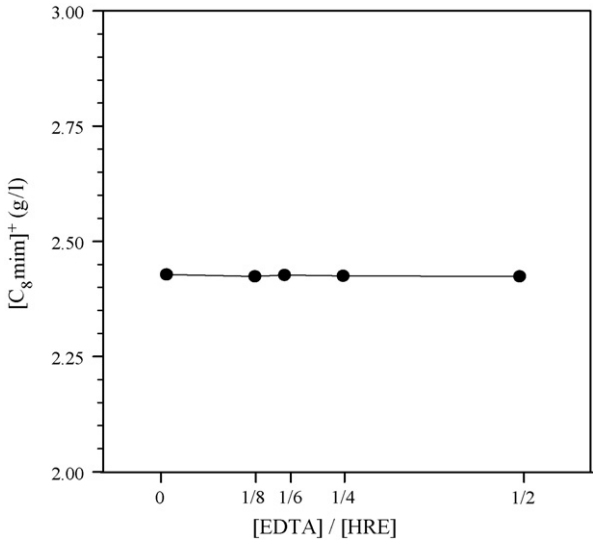


Fig. 4. Concentration of $[C_8mim]^+$ in aqueous phases during the IL-based extraction system using complexing agent.

separation factors of Y(III) to HRE(III) with EDTA were obviously larger than those without the complexing agent, and the separation factors increased with the concentrations of EDTA were enhanced. In this study, when the concentration ratio of EDTA to HRE was 1:2, the separation factors approached to the maximum.

As mentioned above, cation-exchange was a credible mechanism for the extraction process, and the loss of $[C_8mim]^+$ was at least one order higher than that of $[PF_6]^-$ as described in Fig. 2. Accordingly, the loss of $[C_8mim]^+$ to aqueous phase during extraction should be an important factor for evaluating the complexing method in this study. As can be seen from Fig. 4 $[C_8mim]^+$ concentration did not have obvious change during the extraction process, and $[C_8mim]^+$ in aqueous phase was not affected by the added EDTA. The complexing extraction method could be regarded as an effective strategy for selective $[C_8mim][PF_6]$-based extraction of Y(III) from HRE(III).

4. Conclusions

The work in this context focused on developing an appropriate strategy for IL-based extraction system to enhance its separation factors. As mentioned above, the complexing method has been applied effectively in separating Y(III) from HRE(III). The strategy is simple, maneuverable, inexpensive and effective in contrast to some other improved IL-based extraction methods. Its characters lie in higher extraction efficiency, higher selectivity and lower loss of IL phase. In additional, it could also be considered as a potential separation and purification method for the other $[C_nmim][PF_6]/[Tf_2N]$-based extraction system for metal ions on neutral condition without increasing the loss of IL.

Acknowledgements

This project was supported by 'Hundreds Talents Program' from Chinese Academy of Sciences, National Natural Science Foundation of China (50574080) and Distinguished Young Scholar Foundation of Jilin Province (20060114). The authors also wish to thank Cytec Canada, for the sample of Cyanex923.

References

[1] R.D. Rogers, K.R. Seddon, ACS Symposium Series 818, American Chemical Society, Washington, DC, 2002.
[2] M.L. Dietz, J.A. Dzielawa, Chem. Commun. (2001) 2124.
[3] J.F. Liu, G.B. Jiang, Y.G. Chi, Y.Q. Cai, Q.X. Zhou, J.T. Hu, Anal. Chem. 75 (2003) 5870.
[4] M.P. Jensen, J. Neuefeind, J.V. Beitz, S. Skanthakumar, L. Soderholm, J. Am. Chem. Soc. 125 (2003) 15466.
[5] H. Heitzman, B.A. Young, D.J. Rausch, P. Rickert, D.C. Stepinski, M.L. Dietz, Talanta 69 (2006) 527.
[6] J.G. Huddleston, H.D. Willauer, R.P. Swatloski, A.E. Visser, R.D. Rogers, Chem. Commun. (1998) 765.
[7] S. Dai, Y.H. Ju, C.E. Barnes, J. Chem. Soc. Dalton Trans. 8 (1999) 1201.
[8] K. Shimojo, M. Goto, Chem. Lett. 33 (2004) 320.
[9] A.E. Visser, R.D. Rogers, J. Solid State Chem. 171 (2003) 109.
[10] N. Sieffert, G.J. Wipff, J. Phys. Chem. B 110 (2006) 19497.
[11] H. Luo, S. Dai, P.V. Bonnesen, A.C. Buchanan, J.D. Holbrey, N.J. Bridges, R.D. Rogers, Anal. Chem. 76 (2004) 3078.
[12] D.C. Stepinski, M.P. Jensen, J.A. Dzielawa, M.L. Dietz, Green Chem. 7 (2005) 151.
[13] H. Luo, S. Dai, P.V. Bonnesen, Anal. Chem. 76 (2004) 2773.
[14] V.A. Cocalia, M.P. Jensen, J.D. Holbrey, S.K. Spear, D.C. Stepinski, R.D. Rogers, Dalton Trans. (2005) 1966.
[15] K. Shimojo, M. Goto, Anal. Chem. 76 (2004) 5039.
[16] A.E. Visser, R.P. Swatloski, W.M. Reichert, S.T. Griffin, R.D. Rogers, Ind. Eng. Chem. Res. 39 (2000) 3596.
[17] Y.G. Wang, Y. Xiong, S.L. Meng, D.Q. Li, Talanta 63 (2004) 239.
[18] X.B. Sun, Y.G. Wang, D.Q. Li, J. Alloy Compd. 6 (2005) 125.
[19] H. Matsuyama, Y. Miyamoto, M. Teramoto, M. Goto, F. Nakashio, Sep. Sci. Technol. 31 (1996) 799.
[20] S. Nishihama, T. Hirai, I. Komasawa, Ind. Eng. Chem. Res. 39 (2000) 3907.
[21] T.C. Huang, J.K. Wang, Ind. Eng. Chem. Res. 32 (1993) 133.
[22] M. Kubal, T. Machula, N. Strnadova, Sep. Sci. Technol. 33 (1998) 1969.
[23] R.S. Juang, Y.C. Wang, Water Res. 37 (2003) 845.
[24] L.Q. Li, C. Wang, Y.D. Li, J. Membr. Sci. 135 (1997) 173.
[25] J.G. Huddleston, A.E. Visser, W.M. Reichert, H.D. Willauer, G.A. Broker, R.D. Rogers, Green Chem. 3 (2001) 156.
[26] W.P. Liao, G.H. Yu, S.T. Yue, D.Q. Li, Talanta 56 (2002) 613.
[27] W.P. Liao, Q.K. Shang, G.H. Yu, D.Q. Li, Talanta 57 (2002) 1085.
[28] D.Q. Li, C. Wang, Hydrometallurgy 48 (1998) 301.
[29] J. Lu, Z.G. Wei, D.Q. Li, G.X. Ma, Z.C. Jiang, Hydrometallurgy 50 (1998) 77.
[30] G.T. Wei, Z.S. Yang, C.J. Chen, Anal. Chim. Acta 488 (2003) 183.
[31] K. Shimojo, F. Kubota, T. Maruyama, M. Goto, Ind. Eng. Chem. Res. 44 (2005) 4368.
[32] M.P. Jensen, J.A. Dzielawa, P. Rickert, M.L. Dietz, J. Am. Chem. Soc. 124 (2002) 10664.
[33] X.Q. Sun, D.B. Wu, J. Chen, D.Q. Li, J. Chem. Technol. Biotechnol. 82 (2007) 267.
[34] L.G. Sillen, A.E. Martell, Stability Constants of Metal-Ion Complexes, The Chemical Society, Burlington House, London, 1964, pp. 107–113.

Available online at www.sciencedirect.com
ScienceDirect
Talanta 74 (2008) 666–674
Talanta
www.elsevier.com/locate/talanta

Resolution of carboxylate protonation microequilibria of NTA, EDTA and related complexones

Zoltán Szakács [a], Szabolcs Béni [b], Béla Noszál [b,*]

[a] *Laboratory for Speciation, Drug and Trace Analysis, Institute of Chemistry, Eötvös Loránd University, Pázmány Péter sétány 1/a, H-1117 Budapest, Hungary*
[b] *Department of Pharmaceutical Chemistry, Semmelweis University, Hőgyes Endre u. 9, H-1092 Budapest, Hungary*

Received 13 April 2007; received in revised form 19 June 2007; accepted 25 June 2007
Available online 1 July 2007

Abstract

Potentiometric and NMR–pH titrations were carried out on four classical complexones to elucidate their overall and site-specific basicities. NMR–pH profiles and Bjerrum's functions were adjusted to compound-specific symmetries and appropriate evaluation methods were developed. Symmetry-modulated relationships between the macro- and microconstants were deduced and self-consistent sets of microconstants were determined. The inherent basicity of carboxylates surrounded by adjacent, intramolecular ammonium and carboxylate sites have been found to be in the range of 1.83–2.02 log *k* units, which are reduced by 0.05–0.12 log *k* units upon a nearby carboxylate protonation.
© 2007 Published by Elsevier B.V.

Keywords: Protonation; pK_a determination; Strong acidic solution; ^{1}H NMR titration; *In situ* pH monitoring

1. Introduction

Amino-polycarboxylates (complexonates) are versatile polyfunctional ligands of excellent metal complexing capability. These ligands have extensively been used for more than half a century in analytical and applied chemistry, medicine [1,2], agriculture and industry. The large-volume use of EDTA, however, poses environmental problems, since the classical complexones and their metal complexes are hardly biodegradable in the aquatic ecosystem, so extensive research is currently conducted to replace EDTA with its green-chemistry analogues.

All applications of complexones are based on the outstanding stability of their metal complexes. The conditional stability constant is governed by the pH of the solution: in acidic milieu, donor atoms protonate and the bound metal ion is liberated. In order to establish the sound thermodynamic bases of complexone–metal association, tremendous efforts have been invested to characterize the acid–base chemistry of EDTA and related compounds. Following the pioneer works of Schwarzenbach, a vast number of acid dissociation and metal complex stability constants have been determined. Databases have been compiled by critical selection of equilibrium constants for NTA and EDTA [3–5]. In general, the NTA and EDTA macroconstants covering acid–base equilibria in the $10 > pH > 4$ range are considered to be reliable (see Table 1). On the other hand, constants for the most acidic range are scarce and typically erroneous, since the primary experimental method, potentiometric titration cannot be applied at extremal values of pH, due to its known limitations [6–8].

A careful look at Table 1 reveals that some literature protonation constants for carboxylates fall too close. Namely, the site-specific theory of overlapping protonation equilibria defines $\Delta \log K_{min}$, a minimum value for differences between protonation constants, also named as "statistical case" [9–11], corresponding to the fully independent protonation of equivalent groups. Since even covalently distant moieties exhibit a residual basicity-modifying interaction through space [10], any measured $\Delta \log K$ difference should exceed a minimum value set by the statistical case for small molecules [12]. Although this "statistical case" criterion is known since the fundamental work of Bjerrum [9], it seems that even the critical stability constants [3] has overlooked this fact. Hence, the most widely cited acidity constants of EDTA are partly principally erroneous.

* Corresponding author. Tel.: +36 1 217 0891; fax: +36 1 217 0891.
E-mail address: nosbel@hogyes.sote.hu (B. Noszál).

0039-9140/$ – see front matter © 2007 Published by Elsevier B.V.
doi:10.1016/j.talanta.2007.06.035

Table 1
Macroscopic protonation constants for complexonates at $I = 1$ M (KCl) and the differences of their successive carboxylate macroconstants

Ligand	Method	Temperature (°C)	log K_1	log K_2	log K_3	log K_4	log K_5	log K_6	$\Delta_1 \log K$	$\Delta_2 \log K$	$\Delta_3 \log K$	Reference
NTA	Pot. titration	22	9.40 (2[a])	2.32 (2)	1.72 (4)	1.1 (2)	–	–	0.60	0.62	–	This work
	^{1}H NMR	22	9.44 (2)	2.34 (3)	1.75 (5)	1.14 (5)	–	–	0.59	0.61	–	This work
	Pot. titration	25	9.34	2.31	1.75	1.03	–	–	–	–	–	[18]
	Crit. selected	20	8.96	2.27	1.98	0.96	–	–	0.29[b]	0.88	–	[3]
	Crit. selected	25	9.47[c]	2.33[c]	1.78[c]	0.8[c]	–	–	0.55	1.0	–	[5]
	Statist. case	–	–	–	–	–	–	–	0.48	0.48	–	–
HIDA	Pot. titration	22	8.74 (1)	2.20 (2)	1.43 (6)	–	–	–	0.77	–	–	This work
	^{1}H NMR	22	–	2.18 (2)	1.51 (1)	–	–	–	0.74	–	–	This work
	Crit. selected	25	8.67	2.22	–	—	–	–	–	–	–	[3]
	Pot. titration[d]	25	8.59	2.24	1.46	–	–	–	0.78	–	–	[14]
EDDA	Pot. titration	22	9.65 (1)	6.69 (1)	2.32 (1)	1.65 (2)	–	–	0.67	–	–	This work
	^{1}H NMR	22	9.75 (1)	6.57 (2)	–	–	–	–	–	–	–	This work
	Pot. titration[d]	25	9.69	6.72	2.37	1.66	–	–	0.71	–	–	[19]
EDTA	Pot. titration	22	9.86 (2)	6.19 (3)	2.43 (2)	1.94 (3)	1.41 (7)	–	0.49	0.53	–	This work
	^{1}H NMR	22	9.92 (1)	6.26 (1)	–	–	–	0.22 (9)	–	–	–	This work
	Pot. titration	25	9.79	6.21	2.45	1.95	1.50	–	0.50	0.45	–	[18]
	Solubility[d]	20	–	–	–	–	1.62	0.92	–	–	0.70	[20]
	Solubility[d]	21	–	–	2.50	1.95	1.45	−0.10	0.55	0.50	1.55	[21]
	Crit. selected	20	9.95	6.27	2.3	2.2	1.4	−0.1	0.1[b]	0.8	1.5	[3]
	Statist. case	–	–	–	–	–	–	–	0.43	0.35	0.43	–

[a] Uncertainties in parenthesis are the least-squares estimates of standard deviation (1σ) on the last significant digit.
[b] $\Delta \log K$ does not exceed the minimum value defined by the statistical case, therefore one of the corresponding macroconstants is incorrect (biased).
[c] The critically selected constants at $I = 0.1$ M from [5] were converted to $I = 1$ M by the Davies equation.
[d] In $NaClO_4$ medium.

The objectives of this work were to determine the most acidic protonation constants of EDTA, NTA and some related compounds with improved accuracy and precision, and also to decompose the highly composite carboxylate macroconstants into site-specific ones, a task not attempted in previous studies. For these purposes, we used combination of potentiometric and ^{1}H NMR–pH titrations under identical experimental conditions. ^{1}H NMR titration, an effective tool to study overlapping protonation equilibria at the level of individual functional groups [12], has long been recognized to follow the ionization of complexones [13,14]. While the early studies on EDTA protonation covered the pH > 3.5 region [13,14], even the latest site-specific investigations on complexones were confined to the basicity of the amine groups [15,16]. In our work, the ^{1}H NMR titration was extended to the pH < 2 interval, where *in situ* pH values were calculated from the chemical shift of dichloroacetic acid [7,8], the co-titrated indicator molecule. Owing to the high symmetry of COO^- groups, the microscopic protonation constants could either be calculated directly from the macroscopic ones (in NTA, HIDA and EDDA) or with minimal *a priori* assumptions (EDTA) that are based on concepts and evaluation strategies discussed in our previous publications [11,12,17].

2. Experimental

2.1. Chemicals

N-(2-Hydroxyethyl)iminodiacetic acid (HIDA, 98%, Fluka), ethylenediamine-*N*,*N*′-diacetic acid (EDDA, ≥98%, Fluka), EDTA free acid (99.5%, Aldrich), chloroacetic acid (99%, Lancester) were used without further purification. Nitrilotriacetic acid (NTA) and iminodiacetic acid (IDA) were gifts of Sanofi-Aventis Pharmaceutical Works Ltd. (Budapest). The purity of all compounds was confirmed by ^{1}H NMR spectra and pH-metric titration curves. Other base chemicals, like cc. HCl, KOH, KCl, D_2O (≥99.8%), all from Sigma and sodium 3-(trimethylsilyl)-1-propanesulfonate (DSS, ≥99%, Fluka) were also used as received. Bidistilled Millipore water (specific resistance: 18.2 MΩ cm) was used throughout this study.

2.2. Potentiometric titrations

The pH-metric titrations were performed at 22.0 ± 0.1 °C, controlled by a liquid ultrathermostat. A Metrohm 716 DMS Titrino autoburette (Metrohm), equipped with a Metrohm 6.0234.110 combined glass electrode was used. The electrode system was calibrated in terms of hydrogen ion concentration [22–24], p[H] = −log[H$^+$] at constant 1 M ionic strength set by KCl to minimize alkali ion complexation.

The free acid form of the complexone under study was dissolved at a concentration varying between 10 and 50 mM in 20 mL of a stock solution containing 0.3 M KOH and 0.6 M KCl, then titrated with 4 M HCl. Alkalimetric titrations were also performed: a KOH solution of ca. p[H] 9, containing 10–40 mM complexone was brought to p[H] ca. 1 by adding calculated amounts of KCl and HCl. Solubility problems upon acidification were observed only for EDTA above 40 mM. 10 mL of the acidic samples were titrated by the titrant containing 0.1 M KOH and 0.9 M KCl. The titration curves (each with 60–120 point) were evaluated by the OPIUM software [25].

2.3. ^{1}H NMR spectroscopy

^{1}H NMR spectra were recorded at 22 ± 1 °C on 600 MHz Varian Inova, 200 MHz Bruker AMX and 250 MHz Bruker Avance DRX spectrometers (spectral width: 2.4 kHz; digital resolution: 0.07 Hz/point), all equipped with standard 5-mm probeheads. The solvent was H_2O/D_2O 9/1 by volume and the H_2O resonance was diminished by water suppression (presaturation). Chemical shifts were referenced to internal 0.1 mM DSS. This compound is known to be a pH indepedent NMR standard between pH 12 and 2 [26] and was successfully applied in strong acidic solutions as well [7,8].

2.3.1. ^{1}H NMR titrations

The protonation constant and δ_{HInd} parameter of the dichloroacetate indicator were determined at 200 MHz by a recently developed method [7], see Supplementary Information for details and results.

Individual complexone samples of p[H] varying from 11 to 0 were prepared with the following composition: 5 mM complexone, 5 mM dichloroacetic acid, 0.1 mM DSS as internal chemical shift reference, 10% (v/v) D_2O for NMR spectrometer lock, calculated amount of KOH or HCl to attain the predefined p[H] value and KCl to adjust the total ionic strength to 1 M (see Supplementary Information for details).

The same electrode was used to determine the p[H] of each sample at 22.0 ± 0.1 °C as for pH-metry. No correction was applied to allow for the solvent deuterium content. p[H] < 2 values were calculated from the measured chemical shift of dichloroacetate [8], although pH meter readings were also taken for comparison purposes (see Supplementary Information for a detailed comparison).

The chemical shift versus p[H] datasets of the complexones were evaluated by home-written least squares C++ programs based on the standard Levenberg–Marquardt algorithm.

2.3.2. ^{13}C NMR titration of EDTA

Samples of p[H] ranging from −0.7 to 12.0, a constant 30 mM EDTA concentration and 1 M ionic strength were prepared in H_2O/D_2O 9/1. Saturated EDTA solutions were used at 0.3 < p[H] < 2.8 values. $^{13}C\{^1H\}$ NMR spectra were recorded at 150 MHz spectrometer frequency at 25.0 °C and referenced to the ^{13}C signal of internal DSS.

3. Results and discussion

3.1. Protonation equilibria of NTA and related complexonates

3.1.1. NTA

Fig. 1 shows the protonation scheme of the monoprotonated nitrilotriacetate ion. The basicity of the tertiary amine site is characterized by the K_1 macroconstant. Below p[H] 4, overlapping

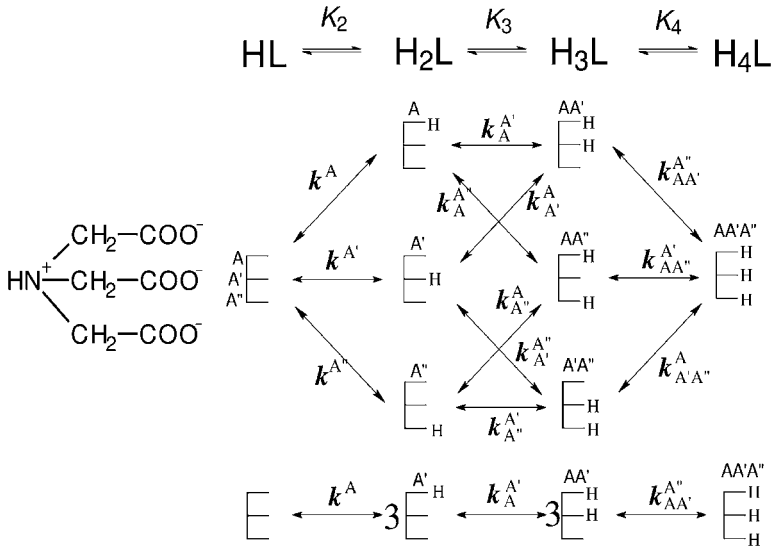


Fig. 1. Macroscopic (top), microscopic (middle) and reduced microscopic (bottom) protonation schemes of nitrilotriacetate.

protonation equilibria of A, A′ and A″, the equivalent carboxylate groups take place and the microscopic protonation constants are measures of their intrinsic basicity. For instance, $k^{A'}_{AA''}$ quantitates the proton affinity of carboxylate A′ in the microspecies denoted by AA″ (ionic charges are omitted), which holds already protons at its A and A″ carboxylate (and of course, amine) sites:

$$AA'' + H^+ \rightleftharpoons AA'A''k^{A'}_{A''} = \frac{[AA'A'']}{[AA''][H^+]} \quad (1)$$

The microscopic protonation scheme in Fig. 1 contains $2^3 = 8$ microspecies. Owing to symmetry, the microspecies with one –COOH group (A, A′ and A″) are indistinguishable and the same holds for AA′, AA″ and A′A″. It suffices therefore to consider the *reduced microequilibrium scheme* (Fig. 1), where degeneracy of certain microspecies is indicated by statistical weights. Since the basicity of equivalent groups is identical, the 12 carboxylate microconstants form a redundant set, there are only three independent equilibrium parameters [11]. The following equations relate the macroscopic and microscopic protonation constants of the NTA carboxylates [9,11]:

$$\log K_2 = \log(3k^A) = \log 3 + \log k^A \quad (2)$$

$$\log K_3 = \log k^{A'}_A \quad (3)$$

$$\log K_4 = \log k^{A''}_{AA'} - \log 3 \quad (4)$$

Eqs. (2)–(4) indicate that all NTA microconstants can be calculated from the stepwise macroconstants. However, reliable values are available only for $\log K_2$ and $\log K_3$ by pH-metry.

In order to obtain $\log K_4$ with a higher accuracy and precision, a ^{1}H NMR titration was carried out. Fig. 2 shows the titration profile of the methylene protons. The observed chemical shift (δ^{obs}) is the weighted average of those of the distinct protonation forms δ_L, δ_{HL}, δ_{H_2L}, δ_{H_3L} and δ_{H_4L}, where the weighting factors are products of $[H^+]$ and the macroconstants [12]:

$$\delta^{obs} = \frac{\delta_L + \delta_{HL}K_1[H^+] + \delta_{H_2L}K_1K_2[H^+]^2 + \delta_{H_3L}K_1K_2K_3[H^+]^3 + \delta_{H_4L}K_1K_2K_3K_4[H^+]^4}{1 + K_1[H^+] + K_1K_2[H^+]^2 + K_1K_2K_3[H^+]^3 + K_1K_2K_3K_4[H^+]^4} \quad (5)$$

Determination of the nine unknown parameters, $\log K_1$ to $\log K_4$ and δ_L to δ_{H_4L} can be attempted by nonlinear regression. For the parameters pertaining to amine protonation and the fully protonated state, accurate values are obtained (±standard deviations): $\log K_1 = 9.40 \pm 0.02$, $\delta_L = 3.179 \pm 0.006$, $\delta_{HL} = 3.805 \pm 0.004$ and $\delta_{H_4L} = 4.45 \pm 0.01$. The remaining parameter estimates, however, are necessarily insignificant (large standard deviations, while the correlation coefficients are near one). The underlying reason is the strong overlap in carboxylate protonations, leading to a joint inflection below pH 4 in the NMR titration curve (Fig. 2). The positions of the δ_{H_2L} and δ_{H_3L} individual chemical shifts of intermediate protonation stages are poorly defined, in

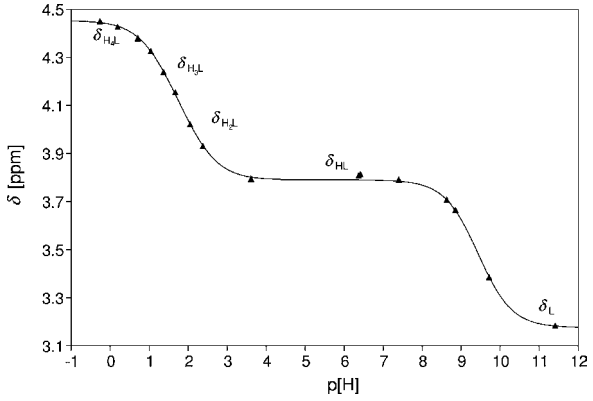


Fig. 2. ^{1}H NMR titration curve of the methylene protons of NTA, as function of p[H]. The computer fit is shown in solid line. About the positions of δ_{H_iL}, the ion-specific chemical shifts, see text.

comparison to the near-horizontal plateaus belonging to the L, HL and H_4L species.

In order to extract the remaining four constants, constraints have been set on the δ_{H_2L} and δ_{H_3L} parameters. Applying the Sudmeier–Reilley relationship [13] to NTA, the CH_2 chemical shift below pH 6 is proportional to the protonation degrees (f) of A, A′ and A″ carboxylates:

$$\delta^{obs} = \delta_{HL} + C_A f_A + C_{A'} f_{A'} + C_{A''} f_{A''} \quad (6)$$

where the C coefficients are pH-independent parameters. Taking δ^{obs} of CH_2 adjacent to carboxylate A as example, the impact of protonation of the closer site (A) is greater than those of the remote ones (A′ and A″): $C_A > C_{A'} = C_{A''}$ [12,13]. Similar relationships hold for the other methylenes with the necessary permutations of carboxylate label indices. Although the C coefficients are not available individually, their sum, the total protonation shift is a well-defined experimental quantity:

$$\Delta\delta^{obs}_{max} = \delta_{H_4L} - \delta_{HL} = C_A + C_{A'} + C_{A''} \quad (7)$$

The protonation degree functions of equivalent sites are identical [13]: $f_A = f_{A'} = f_{A''}$ and their sum equals to the protonation degree of the whole molecule (Bjerrum's classical function):

$$f_A + f_{A'} + f_{A''} = 3f_A = \bar{n}_{(pH)} = \frac{K_2[H^+] + 2K_2K_3[H^+]^2 + 3K_2K_3K_4[H^+]^3}{1 + K_2[H^+] + K_2K_3[H^+]^2 + K_2K_3K_4[H^+]^3} \quad (8)$$

Its value at a particular acidic pH, obtained from the NMR data of NTA, combining Eqs. (6)–(8) is

$$\bar{n}_{(pH)} = 3\frac{\delta^{obs} - \delta_{HL}}{C_A + C_{A'} + C_{A''}} = 3\frac{\delta^{obs} - \delta_{HL}}{\delta_{H_4L} - \delta_{HL}} \quad (9)$$

To put the meaning of Eq. (9) in a different way, evaluation of the NMR–p[H] titration profile of a fully symmetric polybasic molecule can be transformed into the fitting of its Bjerrum function. Though $\bar{n}_{(pH)}$ is accessible also by pH-metric titration, our indicator-based ^{1}H NMR titration technique does not suffer from the shortcomings of potentiometry at pH extremes (compare the scatter of data points at p[H] < 1.5 in Fig. 2 and Fig. S3).

The fitting of Eq. (9) to the measured NMR–pH dataset posed no numerical difficulties and lead to the following macroconstants: $\log K_2 = 2.25 \pm 0.04$, $\log K_3 = 1.83 \pm 0.04$ and $\log K_4 = 1.05 \pm 0.04$. Although these values are identical within 0.1 log units with their pH-metrically measured counterparts, $\log K_2 - \log K_3 = 0.42$ is slightly below the minimum difference of $\log 3 = 0.48$, dictated by the statistical case. Consequently, the first two microconstants calculated by Eqs. (2)–(4), $\log k^A = 1.77$ and $\log k^{A'}_A = 1.83$ would imply that the proton affinity of one carboxylate increases by 0.06 log units as its twin of symmetry gets protonated. Positive cooperativity of H^+-binding sites is chemically unrealistic in small molecules (see [12] and refs. therein).

The intrinsic basicity of one selected carboxylate decreases upon protonation of the remaining ones. This gradual drop in basicity is expressed in terms of pE, the interactivity parameter [12]:

$$pE = \log k^A - \log k^{A'}_A = \log k^{A'}_A - \log k^{A''}_{AA'} \quad (10)$$

Eq. (10) sets the basicity-modifying interaction of two carboxylates independent of the protonation state of the third one. Introducing this constraint into Eqs. (2)–(4) the following function is obtained:

$$\delta^{obs} = \delta_{HL} + \Delta\delta^{max}\frac{k^A[H^+] + 2(k^A)^2E[H^+]^2 + (k^AE)^3[H^+]^3}{1 + 3k^A[H^+] + 3(k^A)^2E[H^+]^2 + (k^AE)^3[H^+]^3} \quad (11)$$

The three-parameter fitting resulted in both statistically and chemically sound values: $\Delta\delta^{max} = 0.664 \pm 0.005$ ppm, $\log k^A = 1.87 \pm 0.03$ and $pE = 0.12 \pm 0.03$. The latter constants and Eq. (10) allow the calculation of all NTA microconstants (see Table 2) and macroconstants (Table 1) that agree well with both our potentiometrically determined values and those converted from the critical selection by Anderegg [5] to the 1 M ionic strength used in this study.

3.1.2. HIDA

To check the accuracy and improve the precision of $\log K_2$ and $\log K_3$ by pH-metric titration (see Table 1), ^{1}H NMR titration was performed. Fig. S4 shows that all NMR resonances of HIDA exhibit downfield shifts upon protonation. Since the adjacent H^a methylenes are the most sensitive sensors of carboxylate protonation, their NMR–p[H] profile was used in the evaluation.

Numerator of the triprotic analogue of Eq. (5) shows that K_2 and δ_{H_2L} are co-dependent parameters. To eliminate their correlation in the evaluation process, δ_{H_2L} was fixed at the arithmetic mean of δ_{HL} and δ_{H_3L}, as it follows from the Sudmeier–Reilley equation for biprotic acids. This approach resulted in chemically reasonable macroconstants, in good agreement with their potentiometric counterparts (see Table 1).

The carboxylate microconstants and the interactivity parameter were calculated from the NMR-based macroconstants listed in Table 1, by well-known relationships [9,11]:

$$\log k^A = \log K_2 - \log 2 = 1.88 \pm 0.02 \quad (12)$$

$$\log k^{A'}_A = \log K_3 + \log 2 = 1.81 \pm 0.01 \quad (13)$$

$$pE = \log k^A - \log k^{A'}_A = 0.07 \pm 0.02 \quad (14)$$

3.1.3. Comparison of carboxylate basicities in NTA and its derivatives

Table 2 summarizes our site-specific basicity data of NTA and HIDA, along with corresponding literature data for analogues containing fewer carboxylate groups. In N-alkylated derivatives of glycine, the basicity of secondary, tertiary and primary amine ($\log k^N$) gradually decreases as expected [29]. Comparison of $\log k^N$ for N,N-dimethyl glycine, MIDA, NTA and HIDA indicates that the CH_2COO^- substituent slightly decreases the

Table 2
Comparison of amine basicity, protonation microconstants and interactivity parameter of COO^- groups and protonation shift of the adjacent methylene hydrogens ($\Delta\delta^{max}$, ppm) in NTA and derivatives at 22 °C and 1 M ionic strength

	Glycine	*N*-Methyl-glicine	*N*,*N*-Dimethyl-glycine	Imino-diacetate (IDA)	*N*-Methyl-imino-diacetate (MIDA)	HIDA	NTA
$\log k^N$	9.75[a]	10.02	9.80[b]	9.29 (2)[c]	9.48[d]	8.74 (1)	9.44 (2)
$\log k^A$	2.35[a]	2.18	2.14[b]	2.24 (2)[c]	2.06[d]	1.88 (2)	1.87 (3)
$\log k^{A'}_A$				2.11 (2)[c]	1.87[d]	1.81 (2)	1.75 (4)
$\log k^{A''}_{AA'}$	–	–	–	–	–	–	1.63 (4)
p*E*	–	–	–	0.13 (3)[c]	0.19[d]	0.07 (2)	0.12 (3)
$\Delta\delta^{max,\,amine}$	0.386[e]	0.51[e]	0.72[e]	0.498[e]	0.70[f]	0.610 (2)	0.613 (6)
$\Delta\delta^{max,\,COO-}$	0.351[e]	0.31[e]	0.35[e]	0.439[e]	0.52[f]	0.512 (2)	0.664 (6)

[a] Ref. [3].
[b] Converted from 0.5 M ionic strength.
[c] Calculated similarly to HIDA from our pH-metric macroconstants.
[d] Ref. [28].
[e] Ref. [13].
[f] Ref. [27].

proton affinity of the nitrogen, while the inductive effect of the 2-hydroxyethyl moiety is more substantial [29].

The intrinsic basicity of the first protonating carboxylate, $\log k^A$ gradually decreases with the number of attached CH_2COO^- groups. The carboxylate pair interactivity parameters coincide in NTA and IDA, and the magnitude of all p*E* values indicates weak interaction of carboxylates, presumably of through space, electrostatic nature rather than $COOH\cdots{}^-OOC$ hydrogen bonds. Virtually the same intermoiety interactions were observed for covalently more remote carboxylate groups of oxidized glutathione [17].

3.2. Protonation equilibria of EDDA and EDTA

It is generally recognized that the two nitrogens in ethylenediamine-based complexones protonate in well-separated steps, near pH 10 and 7 (for a review, see [30]). The H^+ coordination to the carboxylates starts below pH 4 and completes only in the highly acidic range.

3.2.1. EDDA

The potentiometric titration curves of EDDA yielded the macroconstants listed in Table 1. While the amine macroconstants could be verified by processing the ^{1}H NMR–p[H] titration dataset shown in Fig. S5, the biprotic evaluation approach outlined in Section 3.1.2 was incapable to yield $\log K_3$ and $\log K_4$ constants differing beyond the statistical value of $\log 4 = 0.60$. Presumably, the chemical shifts are modulated in this pH interval by effects not directly linked to protonation state, e.g. conformation change(s). Thus, the last two macroconstants by potentiometry were held constants during the NMR evaluation. The optimized $\delta_{H,L}$ values are listed in Table S1.

The microscopic protonation scheme of EDDA consists of two isolated, biprotic subsystems. In the alkaline region, the microequilibria of symmetric N and N′ amine groups are fully characterized by the microconstants k^N and $k^{N'}_N$, while the more overlapping protonations of symmetric A and A′ carboxylates are described in terms of microconstants k^A and $k^{A'}_A$ in the acidic range. Application of Eqs. (12)–(14) to the pH-metric macroconstants of EDDA leads to the following microconstants and pair interactivity parameters: $\log k^N = 9.35 \pm 0.01$, $\log k^{N'}_N = 6.99 \pm 0.01$, $pE_{NN'} = 2.36 \pm 0.01$, $\log k^A = 2.02 \pm 0.01$, $\log k^{A'}_A = 1.95 \pm 0.02$ and $pE_{AA'} = 0.07 \pm 0.02$. The carboxylate interactivity parameter reflects their nearly independent protonation and slight electrostatic interaction through space.

3.2.2. EDTA

The protonation of EDTA carboxylates (denoted by A, A′, B and B′) is of three peculiarities:

(a) the 16 microspecies can be sorted into six types (Fig. 3),
(b) the ^{1}H NMR–pH profile runs partly upfield ("wrong way") upon acidifying (Fig. 4),
(c) the last protonation is even less accessible than that of NTA, HIDA or EDDA.

Thus, the pertinent macro- and microconstants for EDTA are related as follows:

$$K_3 = 4k^A \quad (15)$$

$$K_3K_4 = 2k^Ak^{A'}_A + 4k^Ak^B_A \quad (16)$$

$$K_3K_4K_5 = 4k^Ak^{A'}_Ak^B_{AA'} \quad (17)$$

$$K_3K_4K_5K_6 = k^Ak^{A'}_Ak^B_{AA'}k^{B'}_{AA'B} \quad (18)$$

The potentiometric titrations of EDTA resulted in reproducible Bjerrum's function up to the coordination of nearly five protons (see Fig. S6). Our five macroconstants given in Table 1 satisfy the criteria of minimal difference dictated by the statistical case.

The application of low (5 mM) EDTA concentration and dichloroacetate as an NMR–p[H] indicator allowed the registration of the NMR titration curves of EDTA methylene hydrogens down to "p[H]" −0.7, thus extending the observation range of previous studies [13,14]. However, no macroconstants of chemical sense could be evaluated for the carboxylates, owing to

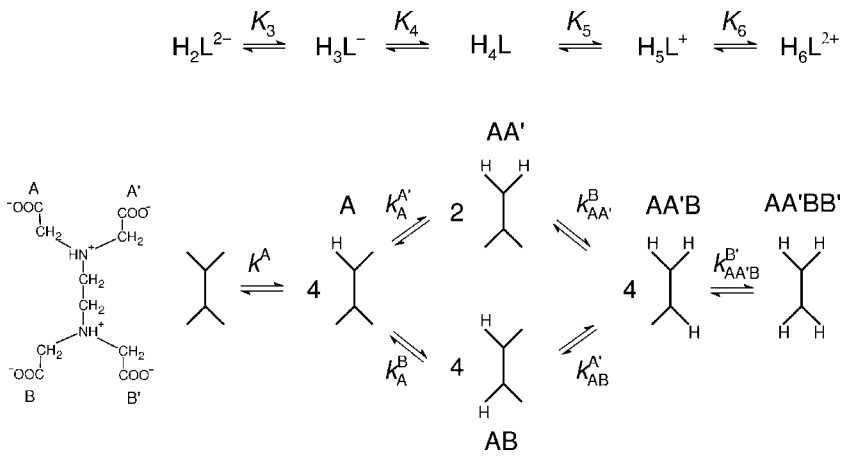


Fig. 3. Macroscopic (top) and reduced microscopic (bottom) protonation schemes of *N*,*N*′ diprotonated EDTA.

reasons similar to those in Section 3.1.1. An attempt to obtain $\log K_5$ more accurately from the p[H] > 1.3 data points when holding the potentiometrically obtained $\log K_3$ and $\log K_4$ values was also unsuccessful. We fitted therefore the hexaprotic extension of Eq. (5) simultaneously to both NMR datasets, keeping the pH-metric $\log K_3$ to $\log K_5$ values constant. The δ_{H_iL} chemical shifts listed in Table S2 and $\log K_6 = -0.37 \pm 0.03$ were obtained from this evaluation. Although the goodness-of-fit of the model to both datasets is excellent (see Fig. 4), the value of $\log K_6$ is unreasonably low and contradicts the microconstants derived below. The altering solvation in highly acidic milieu makes presumably a larger impact than protonation on the ^{1}H chemical shifts [7,31].

The pH-dependent ^{13}C chemical shifts do not provide a sufficient basis for macroconstant calculation either: both methylene carbons exhibit upfield shifts only at p[H] < 2. Interestingly, the COO^- protonation is practically not reflected by the carbonyl resonance ($\Delta\delta_{max} < 0.1$ ppm), whereas protonation of the distant amine groups is accompanied by its 9 ppm upfield shift.

The symmetry-adopted *microequilibrium* scheme of EDTA carboxylates in Fig. 3 shows that all COO^- groups are equivalent with respect to the first coordinating H^+. The corresponding microconstant is obtained by applying the statistical correction

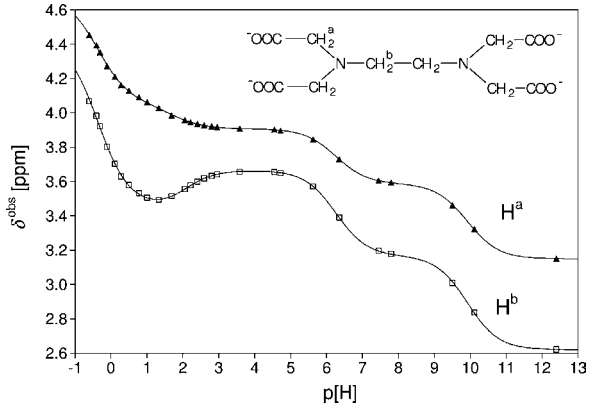


Fig. 4. ^{1}H NMR titration curves of the methylene protons of EDTA, as functions of p[H] with computer fits as solid lines.

to $\log K_3$:

$$\log k^A \equiv \log k^B = \log K_3 - \log 4 = 1.83 \pm 0.02 \quad (19)$$

A distinction between A and B type carboxylates becomes necessary on coordination of the second proton that can attach either to the "geminal" acetate arm, yielding microspecies AA′ or to one of the more distant "vicinal" acetate arms, producing microspecies AB. The multiplicity of AA′ microspecies is two, while that of microspecies AB is four, assuming free rotation about the ethylenediamine backbone.

Combining Eqs. (15) and (16) yields:

$$2K_4 = k_A^{A'} + 2k_A^B \quad (20)$$

Unambiguous calculation of $k_A^{A'}$ and k_A^B from Eq. (20) requires one additional piece of information [11,12]. Even if the ^{1}H or ^{13}C NMR–p[H] profiles would clearly reflect the protonation state of the molecule, only one single f_A function could be derived owing to molecular symmetry. This f_A function would allow the unequivocal calculation of the parameter combination ($k_A^{A'} + 2k_A^B$) only, as shown previously in our case study on oxidized glutathione [11,12]. An NMR spectroscopic distinction between protonation isomers AA′ and AB would require selective spin-labeling of one CH_2COO^- moiety, a cost- and labour-intensive approach indeed. Instead, a deductive method was elaborated to calculate the missing microconstants of EDTA.

First, Eq. (20) can be rewritten in terms of pair interactivity parameters [11,12,17] for the basicity-modifying interactions between A–A′ and A–B carboxylates:

$$k^A(E_{AA'} + 2E_{AB}) = 2K_4 \quad (21)$$

In Section 3.1.1, the carboxylate interactivity parameters within the $-N(CH_2COO^-)_2$ unit have been found identical for IDA and NTA (see Table 2). Since the interactivity parameter of a certain molecular fragment can be transplanted into the analogous fragment of another molecule [11,12,32], the $pE_{AA'} = 0.12$ value of NTA and $pE_{AB} = 0.07$ of EDDA are introduced into the EDTA microspeciation as additional pieces of information. Applying these interactivity parameters, the value of $\log k^A = 1.83$ and

Table 3
Protonation microconstants and interactivity parameters for EDTA carboxylates at 22 °C and 1 M ionic strength

Calculated from our macroconstants		Calculated from macroconstants by Gatez et al. [18]	
Microconstants	Interactivity parameters	Microconstants	Interactivity parameters
$\log k^{A} = 1.83$	$pE_{AA'} = 0.12$	$\log k^{A} = 1.85$	$pE_{AA'} = 0.12$
$\log k_{A}^{A'} = 1.71$	$pE_{AB} = 0.07$	$\log k_{A}^{A'} = 1.73$	$pE_{AB} = 0.07$
$\log k_{A}^{B} = 1.76$		$\log k_{A}^{B} = 1.78$	
$\log k_{AB}^{A'} = 1.64$		$\log k_{AB}^{A'} = 1.66$	
$\log k_{AA'}^{B} = 1.69$		$\log k_{AA'}^{B} = 1.71$	
$\log k_{AA'B}^{B'} = 1.57$		$\log k_{AA'B}^{B'} = 1.59$	

Eq. (21), the calculated $\log K_4 = 1.92$ is obtained, in excellent agreement with the experimental $\log K_4 = 1.94$.

Combining Eqs. (16) and (17), K_5 can be expressed in terms of microconstants:

$$K_5 = \frac{2k^{A}k_{A}^{A'}k_{AA'}^{B}}{k^{A}k_{A}^{A'} + 2k^{A}k_{A}^{B}} \quad (22)$$

Introducing $k_{A}^{A'} = k^{A}E_{AA'}$, $k_{A}^{B} = k^{A}E_{AB}$, and $k_{AA'}^{B} = k^{A}(E_{AB})^2$, K_5 is given as

$$K_5 = \frac{2k^{A}E_{AA'}(E_{AB})^2}{E_{AA'} + 2E_{AB}} \quad (23)$$

which allows the calculation of K_5 from above three basicity parameters (k^{A}, $pE_{AA'}$ and pE_{AB}). The calculated $\log K_5$ value is 1.48. The agreement with our potentiometric value (1.41), and also, with the respective values of Gatez (1.50 [18]), Beck (1.62 [20]) and Kragten (1.45 [21]) certainly justifies the method, and shows that no triple interactivity parameter has to be used.

Applying analogously Eqs. (17) and (18), the expression for K_6 reads:

$$K_6 = \frac{k^{A}E_{AA'}(E_{AB})^2}{4} \quad (24)$$

The calculated value $\log K_6 = 0.97$ is in good agreement with the only value of chemical sense (0.92 [20]). Taking into account the difficulties of the determination, $\log K_6$ can be assessed realistically a value in the range of 0.9 and 1.0.

Concerning the non-monotonous shape of the NMR titration curve, it cannot be explained by the proton migration from NH^{+} to carboxylic group(s) either, as it was found to be the case for backbone nitrogens of DTPA [15] and derivatives [16]. A possible explanation for the "wrong-way" (diamagnetic) protonation shift of H^{b} below p[H] 4 might be the hypothesis of Letkeman and Martell [14]: while the carboxylate group is hydrogen-bonded to the adjacent ammonium site, the rotational freedom of the magnetically anisotropic COOH group increases, thus affecting the backbone methylene chemical shift.

The carboxylate microconstants of EDTA are listed in Table 3. Since our pH-metric $\log K_3$ and $\log K_4$ values show excellent agreement with those measured previously using hydrogen electrode by Gatez et al. [18], the whole microconstant calculation procedure was also carried out using their macroconstants as input, resulting in essentially the same values. In our opinion, these latter values can be regarded as the most accurate site-specific basicity parameters of EDTA to date. From this final set of microconstants, a pH-dependent distribution diagram (Fig. 5) was constructed to quantitate all possible microspecies of EDTA. The microconstants also imply that in species H_3L, the basicity of one carboxylate "remote" from the COOH is 1.17 times greater than that of the adjacent COO^{-}. This value equals to the pH-independent concentration ratio [AB]/[AA′]. Considering the multiplicity of these protonation isomers, a purely statistical protonation pattern would yield a concentration ratio of 2.

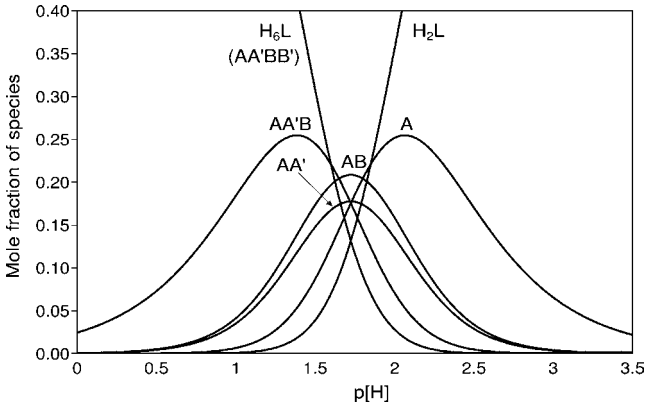


Fig. 5. Distribution of EDTA microspecies in the carboxylate protonatifigon range. See Fig. 4 for abbreviations.

4. Conclusions

Combination of pH-metric and ^{1}H NMR titrations yielded a full set of carboxylate protonation macro- and microconstants for NTA, HIDA, EDDA and EDTA. Our results are in good agreement with authoritative literature values. The hitherto not achieved accuracy and precision of the lowest $\log K$ values for NTA, HIDA and EDDA is warranted by enhanced precision of pH measurements: unbiased $0 < p[H] < 1.5$ values are monitored by the co-titrated NMR indicator dichloroacetate. Special evaluation functions have been developed to alleviate the problems stemming from the high symmetry and low information content of the NMR–p[H] profiles of complexones. NMR–pH titration of EDTA failed to provide directly processable information on the states of carboxylate protonation, presumably due to rup-

ture of intramolecular hydrogen bonding. Potentiometric data, however, yielded macroconstants in agreement with competent literature values, and, using imported interactivity parameters in a deductive approach, also complete sets of self-consistent microconstants.

The methodological improvements and evaluation techniques presented in this work can be of value to assess the intrinsic carboxylate basicities of MRI contrast agents.

Acknowledgements

This work was supported by Grants OTKA T43579 and T48554. The authors are grateful to János Rohonczy (Eötvös Loránd University) and Péter Mátyus (Semmelweis University) for access to the 250 MHz and 200 MHz NMR spectrometers, respectively.

Appendix A. Supplementary data

Supplementary data associated with this article can be found, in the online version, at doi:10.1016/j.talanta.2007.06.035.

References

[1] O. Andersen, Chem. Rev. 9 (1999) 2683.
[2] E. Ernst, Am. Heart. J. 140 (2000) 139.
[3] A.E. Martell, R.M. Smith (Eds.), Critical Stability Constants, Plenum Press, New York, 1974.
[4] G. Anderegg, Critical Survey of Stability Constants of EDTA Complexes, Pergamon, Oxford, 1972.
[5] G. Anderegg, Pure Appl. Chem. 54 (1982) 2693.
[6] M.T. Beck, I. Nagypál, Chemistry of Complex Equilibria, Ellis Horwood Ltd., Chichester, 1990.
[7] Z. Szakács, G. Hägele, Talanta 62 (2004) 819.
[8] Z. Szakács, G. Hägele, R. Tyka, Anal. Chim. Acta 522 (2004) 247.
[9] N. Bjerrum, Z. Phys. Chem. 56 (1923) 219.
[10] B. Noszál, J. Phys. Chem. 90 (1986) 4104.
[11] Z. Szakács, B. Noszál, J. Math. Chem. 26 (1999) 139.
[12] Z. Szakács, M. Kraszni, B. Noszál, Anal. Bioanal. Chem. 378 (2004) 1428.
[13] J.L. Sudmeier, C.N. Reilley, Anal. Chem. 36 (1964) 1698.
[14] P. Letkeman, A.E. Martell, Inorg. Chem. 18 (1979) 1284.
[15] G.M. Ullmann, J. Phys. Chem. B 107 (2003) 1263.
[16] H. Lammers, A.M. van der Heijden, H. van Bekkum, C.F.G.C. Geraldes, J.A. Peters, Inorg. Chim. Acta 277 (1998) 193.
[17] B. Noszál, Z. Szakács, J. Phys. Chem. B 107 (2003) 5074.
[18] J.M. Gatez, E. Merciny, G. Duyckaerts, Anal. Chim. Acta 84 (1976) 383.
[19] I. Grenthe, G. Gardhammar, Acta Chem. Scand. A 28 (1974) 125.
[20] M. Beck, S. Görög, MTA Kémiai Tud, Oszt. Közl. 12 (1959) 265.
[21] J. Kragten, L.G. Decnop-Weever, Talanta 30 (1983) 623.
[22] H.M. Irving, M.G. Miles, L.D. Pettit, Anal. Chim. Acta 38 (1967) 475.
[23] H. Sigel, A.D. Zuberbühler, O. Yamauchi, Anal. Chim. Acta 255 (1991) 63.
[24] P. Gans, Talanta 51 (2000) 33.
[25] M. Kyvala, I. Lukes, Chemometrics '95, Pardubice, Book of Abstracts, 1995, p. 63. http://www.natur.cuni.cz/~kyvala/opium.html.
[26] A. De Marco, J. Magn. Reson. 26 (1977) 527.
[27] D. Chapman, D.R. Lloyd, R.H. Prince, J. Chem. Soc. (1963) 3645.
[28] S. Yamada, J. Nagase, S. Funahashi, M. Tanaka, J. Inorg. Nucl. Chem. 38 (1976) 617.
[29] D.D. Perrin, B. Dempsey, E.P. Serjeant, pK_a Prediction for Organic Acids and Bases, Chapman and Hall, London, 1981.
[30] A. Bencini, A. Bianchi, E. Garcia-Espana, M. Micheloni, J.A. Ramirez, Coord. Chem. Rev. 188 (1999) 97.
[31] E. Grunwald, A. Loewenstein, S. Meiboom, J. Chem. Phys. 27 (1957) 641.
[32] M.A. Santos, M.A. Esteves, M.C. Vaz, J.J.R. Fraústo da Silva, B. Noszál, E. Farkas, J. Chem. Soc., Perkin Trans. 2 (1997) 1977.

Available online at www.sciencedirect.com
ScienceDirect
Talanta 74 (2008) 661–665
Talanta
www.elsevier.com/locate/talanta

A bio-imprinted urease biosensor: Improved thermal and operational stabilities

Mustafa Teke [b], Mustafa Kemal Sezgintürk [a,*], Erhan Dinçkaya [a], Azmi Telefoncu [a]

[a] *Ege University, Faculty of Science, Biochemistry Department, 35100 Bornova-Izmir, Turkiye*
[b] *Muğla University, Science and Art Faculty, Chemistry Department, 48000 Muğla, Turkiye*

Received 29 March 2007; received in revised form 19 June 2007; accepted 25 June 2007
Available online 1 July 2007

Abstract

Despite the increasing number of applications of biosensors in many fields, the construction of a steady biosensor remains still challenging. The high stability of molecularly bio-imprinted enzymes for its substrate can make them ideal alternatives as recognition elements for sensors. Urease (urea aminohydrolase, EC 3.5.1.5), which catalysis the hydrolysis of urea to ammonia and carbon dioxide, has been used in immobilized form in artificial kidney for blood detoxification. According to one report approximately half a million patients worldwide are being supported by haemodialysis.

In this study, the enzyme of urease was first complexed by using a substrate analogue, thiourea, in aqueous medium and then this enzyme was immobilized on gelatin by crosslinking with glutaraldehyde on a glass electrode surface. Similarly, urease noncomplexed with thiourea was also immobilized on a glass electrode in the same conditions. The aim of the study was to compare the two biosensors in terms of their repeatability, pH stability and thermal stability, and also, linear ranges of two biosensors were compared with each other.
© 2007 Published by Elsevier B.V.

Keywords: Bio-imprinted biosensors; Urease biosensor; Biosensor stability; Molecular imprinting technology

1. Introduction

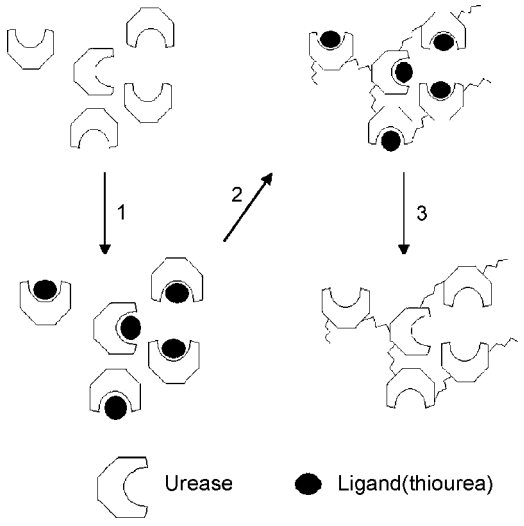
In the past "Molecular Imprinting" was mainly confined to the separation of organic molecules and to nonenzymatic catalysis. With advancement in this technology, its potential and utility in field of biotechnology was also realized [1]. In order to improve it applicability, new variations in the conventional imprinting technique have emerged, such as "bioimprinting", metal chelation imprinting, affinity imprinting and a combination of immobilization and "bioimprinting" [2–8]. Several application areas have been envisaged for imprinted matrices the use of molecularly imprinted polymers in separation and isolation, the use of molecularly imprinted polymers as antibody and receptor mimics in immunoassay-type analyses, the use of molecularly imprinted polymers as enzyme mimics in catalytic applications, and the use of molecularly imprinted polymers in biosensor-like devices [9–13]. The memory of effect of enzymes caused by bio-imprinting without a further immobilization step was found to depend on the water content of medium and was completely lost when the reaction was carried out in the presence of a certain amount of water [14–18]. However, water is an indispensable milieu for most enzymatic reactions. Here we demonstrate that the combinatorial crosslinked imprinting approach. Keyes et al. employed a different kind of methodology to alter the catalytic properties of enzymes [19,20]. In their strategy, the enzyme complexed with ligands was crosslinked by using glutaraldehyde. This whole process was carried out in aqueous buffer, probably because the present imprinting concept in organic solvents was not known to that time.

In our contribution, we discussed potential application of the technique of molecular imprinting with emphasis on an enzyme with its competitive inhibitor and its using for the construction of a biosensor.

Below, schematic illustration of imprinting methodology is showed. The enzyme of urease was first complexed by using thiourea (Scheme 1).

* Corresponding author. Tel.: +90 232 343 86 24; fax: +90 232 343 86 24.
E-mail addresses: msezginturk@hotmail.com, mustafa.kemal.sezginturk@ege.edu.tr (M.K. Sezgintürk).

0039-9140/$ – see front matter © 2007 Published by Elsevier B.V.
doi:10.1016/j.talanta.2007.06.031



Scheme 1. Schematic diagram of the imprinted process (1, modification of the enzyme with thiourea; 2, immobilization and crosslinking with glutaraldehyde; 3, removal of thiourea from the active sites of the enzymes).

And then the enzyme–thiourea complex was immobilized with gelatin by the help of glutaraldehyde on a pH electrode tip. The influence of the imprinting of urease by its competitive inhibitor on the analytical performance such as pH and temperature and operational stabilities, of the resulting biosensor is discussed in this paper.

2. Experimental

2.1. Chemicals

Urease (E.C. 3.5.1.5, Type III: from Jack Beans 29,500 units/g solid), gelatin (Type 3, 225 Bloom), glutaraldehyde (Grade II, 25% aqueous solution) were purchased from Sigma (USA), Tris–HCl, urea, thiourea, were purchased from Merck (Germany).

2.2. Apparatus

pH electrode and pH meter were used for the potentiometric pH measurements (Hanna Instruments, Portugal). A water bath was used for preparation of bioactive material (Stuart scientific Linear Shaker bath SBS 35)(UK). All the measurements were carried out of constant temperature using a thermostat (Haake JF, Germany) Magnetic stirrer (IKA-Combimag, RCO) and pH meter with electrode (WTW pH 538, Germany) for preparing buffer solutions were used. The temperature was maintained at constant in the reaction cell by circulating water at appropriate temperature around the cell compartment during the experiment.

2.3. Procedure

2.3.1. Bio-imprinting of urease with thiourea

In the preparation of bio-imprinting biosensor, firstly, the enzyme urease (30 U/50 μL) and its competitive inhibitor thiourea (1.5 mg/50 μL) were incubated together for 1 h. If urease is added to a mixture of urea and thiourea the activity of the enzyme is strongly diminished. Like urea thiourea is bound to the active centre of the enzyme. Thus the active site of the enzyme is temporarily blocked by the 'false substrate'. The inhibition is called competitive because urea and thiourea compete on equal terms for the binding site of urease. Characteristically increasing the concentration of substrate reduces the effect of the inhibitor. Inhibition can be overcome. Consequently, in our system, by the help of thiourea, the active site of urease can be protected from the negative effects of the immobilization procedure during this process.

2.3.2. Preparation of the imprinted biosensor

Two milligrams per 50 μL of gelatin was added to urease–thiourea mixture mentioned above. This mixture was spread over the glass pH electrode. The electrode was allowed to wait for 30 min for drying. At the end of the preparation step, the bioactive layer of the biosensor was crosslinked by glutaraldehyde (2.5%). Finally, thiourea in the bioactive layer was removed for 1 h by waiting in the distilled water. The other biosensor was prepared in the same way. But there was no pretreatment with thiourea before the immobilization process. The enzyme and gelatin amount, and glutaraldehyde percentage were same as the bio-imprinted biosensor.

2.3.3. Measurement procedure

The bio-imprinted biosensor based on urease was put in to the thermostatic reaction cell containing working buffer (pH 6, 50 mM Tris–HCl buffer) and the magnetic stirrer was fixed at a constant speed. A few minutes later, the pH was equilibrated because of the diffusion between working buffer and pH probe. At this time, urea was injected into the thermostatic reaction cell. pH started to increase and a few minutes later it reached constant value due to the enzymatic reaction equilibration below:

$$\text{urea} + H_2O \xrightarrow{\text{urease}} CO_2 + 2NH_3$$

Measurements were carried out by the change of pH related to urea concentration added to the reaction cell. For all urea concentrations 10 min reaction period was chosen. The enzymatic reaction above was equilibrated within 10 min at all urea concentrations. So, response time was kept constant as 10 min.

3. Results and discussion

The bio-imprinted urease biosensor was compared with urease biosensor in their stability characteristics because the aim of this work was to improve the stabilities of urease biosensor by imprinting technique. For this purpose, for both biosensors optimum temperature and pH, thermal, pH and operational stability investigations were carried out. And all data were compared with each other for each parameter tested.

3.1. Optimum temperatures of the biosensors

The results obtained with two biosensors showed that the best activities were monitored at the same temperature, 30 °C. So,

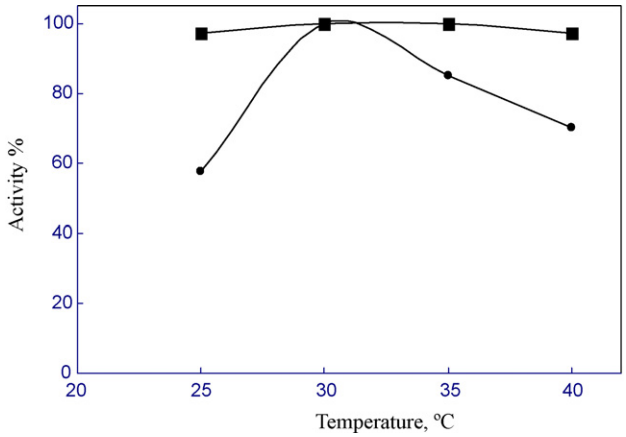


Fig. 1. Temperature dependence of the biosensors ((■) imprinted urease biosensor; (●) urease biosensor. Working conditions: the substrate urea concentration was injected to a final concentration of 1 mM. Tris–HCl buffer, 50 mM and pH 6.0).

there was no shifting on the optimum temperature of the biosensor by complexation with thiourea. Beside, by the biosensor complexed with thiourea before immobilization, it was possible to work in the range of 25–40 °C without activity decrease.

As seen in Fig. 1, bio-imprinted biosensor showed better temperature range for working than the other biosensor. Of course working temperature of a biosensor is determined after its thermal stability studies. These results are discussed below.

3.2. Thermal stabilities of the biosensors

Thermal stability was studied by incubation of the biosensors at 30 °C before the measurements for 3 h. The biosensor unmodified lost 61.4% of its initial activity. However, the biosensor modified with thiourea saved 65% of its original activity. This result is summarized in Table 1.

It should be concluded that, temporary blocked active site of urease by thiourea decreased the possibility of deactivation of the enzyme in the step of crosslinking by glutaraldehyde. Consequently, because of the resistant to immobilization conditions, the modified biosensor was more stabile than unmodified one.

3.3. Optimum pHs of the biosensors

In order to compare optimum pHs of two biosensors buffer solutions with different pH values were used in the experiments. The results showed that optimum pHs of both biosensors were same as 6 (Fig. 2). However, at more acidic pHs than 6, there was a dramatical decrease in the activity of the modified biosensor.

Table 1
Thermal stabilities of the biosensors

	Initial activity	Incubation period (h)	Residual activity (%)
Biosensor 1[a]	100	3	38.6
Biosensor 2[b]	100	3	65

[a] The biosensor with unmodified.
[b] The biosensor modified with thiourea.

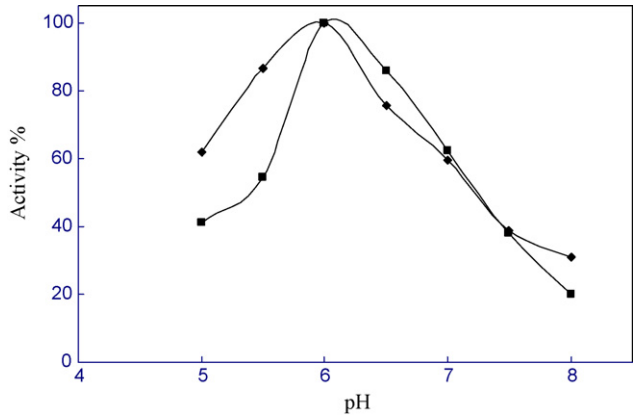


Fig. 2. pH dependence of the biosensors ((■) imprinted urease biosensor; (●) urease biosensor. Working conditions: urea concentration was injected to a final concentration of 1 mM. Tris–HCl buffer with different pH values, 50 mM and 30 °C).

This effect may be caused from the blockage of –COOH groups by hydrogen bond forming between the $–NH_2$ groups of the thiourea and –COOH groups of the enzyme. Besides, as can be seen in the figure, imprinted biosensor was more sensitive to change in the pH value than the other biosensor. The studies in the next step pH stability of the imprinted biosensor supported these results.

3.4. pH stabilities of the biosensors

The pH stability is one of the most important properties of any immobilized enzyme in biosensors. For investigation of pH stabilities of the biosensors both of them were incubated in pH 6, 50 mM Tris–HCl buffer for 3 h.

According to the optimum pH study, the biosensor activity is optimum at pH 6. The stability of the bio-imprinted biosensor was agreed with the results obtained thermal stabilities studies. The results showed that bio-imprinting of the urease increased the pH stability of it. As seen from Table 2 the initial activity of bio-imprinted biosensor decreases at the end of the 3 h incubation period at pH 6 Tris–HCl buffer. The residual activity of the bio-imprinted biosensor was 75.4%. However, the urease biosensor unmodified with thiourea was kept 64.1% of its initial activity.

3.5. Calibration graphs for the biosensors

In this study, the calibration graphs of two biosensors were also investigated. As shown from the figure, calibration graphs

Table 2
pH stabilities of the biosensors

	Initial activity	Incubation period (h)	Residual activity (%)
Biosensor 1[a]	100	3	64.1
Biosensor 2[b]	100	3	75.4

pH stabilities of the biosensors were carried out at pH 6 Tris–HCl buffer.
[a] The biosensor with unmodified.
[b] The biosensor modified with thiourea.

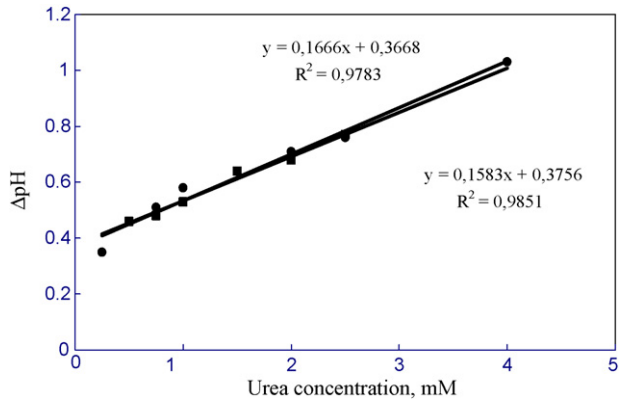


Fig. 3. Calibration graphs for the biosensors ((■) imprinted urease biosensor; (●) urease biosensor. Working conditions: Tris–HCl buffer pH 6.0, 50 mM and 30 °C).

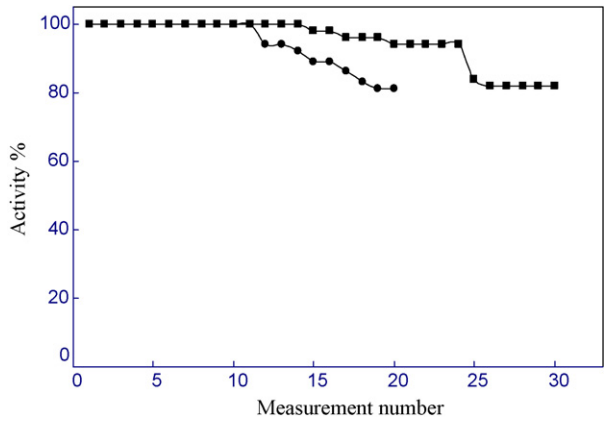


Fig. 4. Operational stabilities ((■) imprinted urease biosensor; (●) urease biosensor. Working conditions: the substrate urea concentration was injected to a final concentration of 1 mM. Tris–HCl buffer, 50 mM and pH 6.0, 30 °C).

were almost same. Moreover, linear ranges of both ones were identical, in the linear concentration range from 0.25 mM to 4 mM urea (Fig. 3).

The results showed that bio-imprinting of urease by its competitive inhibitor, thiourea, did not alter the linear range and detection limits of the biosensor.

K_m values for the bio-imprinted urease and urease biosensors were also calculated. According to the results the K_m values were 1.6 mM and 2.1 mM, respectively. As seen, K_m values supported the idea of bio-imprinting of urease could be advantageous for the biosensor applications.

3.6. Repeatability

The repeatabilities of the biosensors were also studied for 1 mM urea concentration ($n = 15$). The average value (x), the standard deviation (S.D.) and variation coefficient (CV) were 1.1, ±0.12 mM, and 11% for the biosensor unmodified with thiourea, 1.1, ±0.1 mM, and 9% for the bio-imprinted biosensor, respectively. It can be said that there was no effect of complexation with thiourea of the urease on the biosensors repeatabilities and analytical characteristics such as S.D., CV, etc.

3.7. Operational stabilities

The final studies of this investigation were operational studies. In these studies several measurements were carried out by two biosensors. And results showed that, modified biosensor was more stable than the other one in terms of the operational period (Fig. 4).

There was no activity decrease at the end of the 14th measurement with the modified biosensor. And, at the 15th measurement, it was just lost 2% of its initial activity, however, the biosensor unmodified was lost about 11% of its initial activity. This result should support the effect explained in the thermal stability section.

Moreover, the self-life of the biosensors were also determined and compared. Both biosensors were incubated at the working conditions for 5 h. pH measurements before and after incubation were very similar with each other. These results showed that 5 h incubation period was not affected the self of the bioactive layer and its components.

4. Conclusion

In this study, the molecular bio-imprinting technology has been used for the biosensor development. We have developed a novel biosensor for urea determination based on molecularly imprinted of urease. Moreover, this application of bio-imprinting technology was one of the first samples in literature. The sensor exhibits good sensitivity, selectivity and repeatability for urea. Moreover, stability studies showed that molecular bio-imprinted urease biosensor more stable than the other biosensor. Consequently, this way to improve the stabilities of the biosensors should be used by the other enzymes and biosensor. This bio-imprinting method is more convenient and inexpensive and of course simplier than the other imprinting methods. On this basis, the technique should provide a significant easy procedure for the preparation of biosensor system with the desired stabilities for many classes of biologic substance.

References

[1] R.A. Bartsch, M. Maeda, Molecular and Ionic Recognition with Imprinted Polymers, Oxford University Press, Washington, DC, 1998, ACS Symp. Ser. 703.
[2] S.H. Cheong, S. McNiven, A. Rachkov, R. Levi, K. Yano, I. Karube, Macromolecules 30 (1997) 1317.
[3] L. Fischer, R. Miller, B. Ekberg, K. Mosbach, J. Am. Chem. Soc. 113 (1991) 9358.
[4] M. Kempe, L. Fischer, K. Mosbach, J. Mol. Recognit. 6 (1993) 25.
[5] J. Matsui, Y. Miyoshi, O. Doblhoff-Dier, T. Takeuchi, Anal. Chem. 67 (1995) 4404.
[6] D.A. Spivak, K.J. Shea, Macromolecules 31 (1998) 2160.
[7] M.J. Whitcombe, M.E. Rodriguez, P. Villar, E.N. Vulfson, J. Am. Chem. Soc. 117 (1995) 7105.
[8] E. Yilmaz, K. Haupt, K. Mosbach, Angew. Chem. 112 (2000) 2178.
[9] A.G. Mayes, K. Mosbach, Trends Anal. Chem. 16 (1997) 321.
[10] K. Mosbach, O. Ramström, Bio/Technology 14 (1996) 163.
[11] O. Ramström, R.J. Ansell, Chirality 10 (1998) 195.
[12] J. Steinke, D.C. Sherrington, I.R. Dunkin, Adv. Polym. Sci. 123 (1995) 81.
[13] G. Wulff, Angew. Chem. Int. Ed. Engl. 34 (1995) 1812.

[14] J.U. Klein, M.J. Whitcombe, F. Mulholland, E.N. Vulfson, Angew. Chem. 111 (1999) 2100.
[15] F. Peißker, L. Fischer, Bioorg. Med. Chem. 7 (1999) 2231.
[16] B. Sellergren, Angew. Chem. 112 (2000) 1071.
[17] A.A. Vaidya, B.S. Lele, M.G. Kulkarni, R.A. Mashelkar, J. Appl. Polym. Sci. 81 (2001) 1075.
[18] A.A. Vaidya, B.S. Lele, M.G. Kulkarni, R.A. Mashelkar, US Patent 6,379,599 B1 (2002).
[19] S. Saraswathi, M.H. Keyes, Enzyme Microb. Technol. 6 (1984) 98.
[20] T. Takeuchi, J. Haginaka, J. Chromatogr. B 728 (1999) 1.

Available online at www.sciencedirect.com
ScienceDirect
Talanta 74 (2008) 489–497
Talanta
www.elsevier.com/locate/talanta

Sorption of methylene blue on an organoclay bearing thiol groups and application to electrochemical sensing of the dye

Ignas K. Tonlé [a,b,1,2], Emmanuel Ngameni [a,*], Hervé L. Tcheumi [a,1], Victor Tchiéda [a,1], Cédric Carteret [c,3], Alain Walcarius [c,3]

[a] *Laboratoire de Chimie Analytique, Faculté des Sciences, Université de Yaoundé I, B.P. 812 Yaoundé, Cameroun*
[b] *Département de Chimie, Faculté des Sciences, Université de Dschang, B.P. 67 Dschang, Cameroun*
[c] *Laboratoire de Chimie Physique et Microbiologie pour l'Environnement, UMR 7564, CNRS-UHP, Nancy 1; 405, rue de Vandoeuvre, F-54600 Villers-lès-Nancy, France*

Received 1 June 2007; received in revised form 6 June 2007; accepted 7 June 2007
Available online 14 June 2007

Abstract

In this work, a thiol functionalized-clay was prepared by the covalent grafting of 3-mercaptopropyltrimethoxysilane (MPTMS) onto the surface of a natural smectite clay mineral originating from Cameroon. Effectiveness of the grafting process and properties of the resulting hybrid material were studied by various physico-chemical techniques, such as Fourier transform infrared (FTIR) spectroscopy, N_2 adsorption–desorption experiments (surface area measurements by the BET method) and thermal gravimetric analysis (TGA) coupled with mass spectrometry (MS). Sorption of methylene blue (MB), an electroactive cationic dye, was investigated for both the raw clay and its modified counterpart, as a function of shaking time, adsorbate concentration and pH, through batch experiments. A significant enhancement of the adsorption capacity towards MB was observed with the clay bearing thiol groups in comparison with the pristine one. The obtained sorption data matched the Langmuir isotherm model, from which it appeared that the organoclay adsorbed MB at a maximal loading of 1.04 mmol g^{-1}, while the natural clay displayed a significantly poorer performance (0.31 mmol g^{-1}). The uptake of MB by the modified clay was found to be highly affected by pH, the cationic dye being more effectively adsorbed in alkaline medium. The possible use of the thiol functionalized-clay as electrode modifier for MB sensing purposes was then evaluated by means of carbon paste electrodes, using cyclic voltammetry. A calibration curve was obtained in the concentration range from 1×10^{-6} to 1.4×10^{-5} mol L^{-1}, with a detection limit of 4×10^{-7} mol L^{-1} (signal/noise = 3).
© 2007 Elsevier B.V. All rights reserved.

Keywords: Organoclay; Methylene blue; Adsorption; Isotherms; Clay-modified electrode; Carbon paste; Cyclic voltammetry

1. Introduction

In the recent years, growing concern about environmental issues have brought researchers of both analytical and materials science to investigate appropriate processes for the removal and/or monitoring of various pollutants. Among the pollutants, dyes are particularly pointed out, since their presence in water and waste aqueous effluents can cause serious environmental and human health damages [1,2]. For example, inhalation or ingestion of methylene blue (MB) can provoke various harmful effects such as nausea, diarrhea, gastritis, severe headache or mental confusion [3]. In spite of these drawbacks, the use of dyes is still growing in numerous countries, via dyestuff manufacturing, textile industry and others dyeing processes. In 2001, more than 100 000 commercially available dyes were reported, with over 700 000 t produced annually [4]. Recently, on evaluating different materials useful for dyes adsorption, some authors came to the conclusion that about 9% of the 450 000 t of dyestuffs produced in the world are discharged in textile wastewaters [2]. So, many studies have been devoted to the treatment of these wastewaters, aiming at removing dyes, pigments and some other coloring agents. In this respect, inorganic oxides and especially activated carbon have been extensively used as adsorbents [5,6]; however, the activated carbons suffer

* Corresponding author. Tel.: +237 531 19 30; fax: +237 223 98 02.
E-mail addresses: itonle@yahoo.com (I.K. Tonlé), engameni@yahoo.fr (E. Ngameni), walcarius@lcpme.cnrs-nancy.fr (A. Walcarius).
[1] Tel.: +237 531 19 30; fax: +237 223 98 02.
[2] Tel.: +237 754 47 67; fax: +237 345 12 02.
[3] Tel.: +33 3 83 68 52 59; fax: +33 3 83 27 54 44.

0039-9140/$ – see front matter © 2007 Elsevier B.V. All rights reserved.
doi:10.1016/j.talanta.2007.06.006

from their expensive cost and the need for them to be regenerated; consequently, biodegradable and low cost alternatives, such as charred sawdust, carbonized wool waste [2,7], charred plant material [8], chitin and chitosan [9–12], silica [13] and clays [3,14–16] have emerged progressively. Some other treatment processes including ultracentrifugation [17], the use of coagulants [18] or oxidizing agents [19] have been reported, but adsorption remains by far the most efficient and the cheapest method.

Although natural sorbents such as silica and clays are largely used in the elimination of pollutants, they remain subject to some inherent limitations, e.g., low removal capacity, relatively weak binding strength and poor selectivity. Thus, there has been an increasing need to develop more efficient adsorbents during the last few years, and among these researches the elaboration of inorganic–organic hybrid materials that could exhibit high sorption properties, selectivity and sensitivity for a target pollutant has merged as a challenging question [20]. To this end, chemical modification that consists to immobilize on the inorganic support a suitable organic reagent likely to accumulate given species (e.g., heavy metals) has proved to be a promising way to functionalize aluminosilicates [21–24]. In fact, the resulting composite materials were found to enable appreciable enhancement, in either sensitivity or selectivity, compared to their raw counterparts. So, numerous investigations have been carried out on heavy metals uptake by silica-based hybrid materials [21,25–27] or on grafted clays bearing chelating groups [20,22,24,28]. However, investigations dealing with adsorption of dyes by organically modified aluminosilicates are not widespread. The very few examples along these lines deal with the batch and fixed bed sorption of MB by montmorillonite modified by the incorporation into its interlayer space of quaternary ammonium cations [29] or hydroxylaluminic polycation [30], or by the replacement of its inherent interlamellar ions (Na^+, K^+, or Mg^{2+}, Ca^{2+}, etc.) by Cu^{2+} ions [31,32].

On the other hand, the development of electrochemical sensors for the detection and/or quantification of various pollutants at trace levels has attracted an increasing interest in the last decade [33–35]. These devices were often based on carbon paste electrodes (CPEs). Indeed, CPEs display several advantages such as low background currents, reproducible results, simple surface renewability, easy fabrication and modification with a wide range of compounds [36,37]. Among them, clay modified CPEs have been described and mostly applied for electroanalytical purposes [38,39]. For example, MB was immobilized into mordenite zeolithe and the resulting matrix incorporated to a CPE for the electroanalysis of ascorbic acid [40]. Some other works dealing with redox properties of MB were reported but MB was usually applied as an electron mediator system in biosensing analysis [40–43]. The electrochemical behavior of MB has been otherwise investigated at solid electrodes coated with clay films [44–46]. However, to the best of our knowledge, the use of an organically grafted clay material in connection to the electrochemical analysis of MB has not yet been reported.

The purpose of the present work was to evaluate the adsorption properties of a cameroonian smectite-type clay grafted with mercaptopropyl groups, towards the fixation of MB. To this extend, comparison was made between the performance of the raw clay and the organoclay. Particular attention was paid to the effect of pH on the adsorption process, and an attempt was made to establish the sorption mechanism of cationic dyes on the thiol-grafted clay. The possibility of using a CPE modified by the organoclay as electrochemical sensor for the same analyte (i.e., MB which is a cationic electroactive dye) was briefly evaluated.

2. Experimental

2.1. Materials, chemicals and reagents

The starting clay used in this study (*namely "Ba"*) was collected from Baba in the district of Ndop, in Cameroon (Central Africa). After collection, it was crushed, ground and sieved through a 100 μm sieve to remove the larger non-clay fractions. Its chemical composition (given in Table 1) was determined by Inductively Coupled Plasma-Atomic Emission Spectrometry (ICP-AES), on a Jobin-Yvon JY 70 spectrometer (CRPG, Nancy-France) after solubilisation by fusion with lithium metaborate. X-ray diffraction (XDR) measurements performed at the "Laboratoire Environnement et Minéralurgie" (LEM, Nancy-France) on a D8 Bruker diffractometer operating by reflection and using a Co anticathode showed that the clay mineral was formed mainly by montmorillonite, associated to some impurities: quartz (7%), feldspar (4%), hematite (2.2%) and ilmenite (0.3%).

From Table 1, the structural formula of the clay can be expressed as $Ca_{0.06}K_{0.380}Na_{0.450}(Si_{7.025}Al_{0.975})(Al_{3.665}Fe_{0.173}Mg_{0.130}Ti_{0.06})O_{20}(OH)_4$, as calculated after correction for impurities and normalization according to the method proposed by Bain and Smith [47]. It is characterized by a cation exchange capacity of 89 mequiv./100 g, and a specific surface area (N_2 adsorption/desorption, BET) of 155 $m^2\,g^{-1}$ [24].

The study was carried out on the fine fraction of the clay (particles size lower than 12 μm) collected by sedimentation. To this end, 5 g of the raw clay was suspended in 200 mL of water, vigorously stirred, ultrasonicated for about 15 min, and allowed to settle in a sedimentation tube. The suspended solution was decanted and the clay particles recovered by centrifugation. More water was added in the sedimentation tube and the mix-

Table 1
Chemical composition of raw "Ba" clay sample

Constituent	Percentage present
SiO_2	53.65
Al_2O_3	23.89
Al_2O_3	3.60
Fe_2O_3	<0.03
MgO	0.54
CaO	0.35
Na_2O	1.42
K_2O	1.77
TiO_2	0.78
P_2O_5	0.13
L.I.[a]	13.82

[a] L.I.: lost at ignition.

ture shaken again and then allowed to settle once more. The procedure was repeated until a clear liquid was obtained at the top of the tube. The collected material was then dried at room temperature for 24 h.

All chemicals used in adsorption and electrochemical experiments were of analytical grade, and double distilled water was used to prepare the solutions. Methylene Blue (MB), supplied by Riedel-de-Häen, was used as the adsorbate, without any further purification.

2.2. Preparation of the organoclay, instrumentation and analytical procedures

The procedure used for the synthesis of the organoclay is described as follows: 2 mL of 3-mercaptopropyltriethoxysilane (95%, Lancaster) were slowly added to a suspension made of 1 g of the purified raw clay and 25 mL of dry toluene (99.8%, Merck). The mixture was refluxed under argon atmosphere for 24 h, under stirring. The product was then recovered by filtration and washed three times each with about 20 mL of fresh toluene and dried in vacuum at 105 °C for 1 day. The amount of thiol groups (–SH) in the resulting organoclay (denoted MPTMS-Ba throughout the text), determined by elemental analysis at the "Service Central d'Analyses" (CNRS-Lyon, France) was found to be equal to 2.5 mmol/g of clay.

In addition, MPTMS-Ba was characterized by Fourier transform infrared (FTIR) spectrometry, specific surface area measurements and thermogravimetric analysis.

FTIR spectra were obtained on a Perkin-Elmer 2000 spectrometer equipped with a DTGS detector. The spectra resolution was 4 cm^{-1} and the accumulation time was 5 min. Mid-IR (MIR) spectra of the samples were measured using KBr pellets (sample mass fraction of 0.05 in KBr) without any pressure, while near infrared (NIR) spectra needed neither sample preparation nor sample dilution. All the displayed spectra were recorded at room temperature after thermal pretreatment at 90 °C during several hours to evacuate most of physisorbed water. The spectra are presented in a pseudo-absorbance ($\log R$) scale.

In order to determine the specific surface area and the pore volume of the materials, N_2 adsorption–desorption isotherms were recorded at 77 K on a Coulter instrument (model SA 3100). Prior to the analysis, the samples were degassed overnight. The surface area was calculated using the BET equation [48] whereas the pore volume was obtained from the *t*-plot [49].

A simultaneous thermal analysis (STA) device (model SDT 2960, TA Instruments) linked to a Quadrupole Mass Spectrometer QMS 422 allowed simultaneous collection of signals relative to mass loss, heat flow and evolved gases during heating. About 20 mg of clay material was placed on the thermobalance of the STA analyzer, which was purged with helium gas. The measurements were recorded between 30 and 1000 °C with a temperature ramp of 10 °C min^{-1}, and data analysis was performed using Universal Analysis 2000 software package. On each plot, the results were presented by the thermal gravimetric (TG) weight loss curve, and by the first derivative of this curve, known as the differential thermal gravimetric (DTG) curve.

2.3. Batch adsorption studies

Adsorption of MB was performed in the batch mode: to this extend a given mass of adsorbent (raw clay or organoclay) was suspended in a given volume of the dye aqueous solution at a given concentration. The pH of the solution was adjusted using diluted HCl or NaOH and the mixture was shaken at room temperature for a predetermined time. The efficiency of MB adsorption was evaluated from the concentration change of the dye in solution after adsorption, by a UV/vis spectrophotometer (Hitachi, model U 2000) at $\lambda_{max} = 663.5$ nm. A calibration curve previously established for the dye at concentrations lying between 2×10^{-6} and 8×10^{-5} mol L^{-1} was used for the determination of the initial (C_i) and final (C_f) concentrations. The adsorbed amount (Q_{ads}) was calculated using the following relationship (Eq. (1)), where *m* represents the mass of solid added to a solution volume, *v*.

$$Q_{ads}\ (\text{mol g}^{-1}) = \frac{C_i - C_f}{m} \times v \quad (1)$$

2.4. Preparation of the working electrode and electrochemical equipment

The procedure used for the preparation of (organo)clay-modified carbon paste electrodes (namely Ba/CPE or MPTMS-Ba/CPE) was similar as previously described [50]. Briefly, CPEs were obtained by intimately mixing a carbon powder from Alfa (particle size < 325 mesh), a pasting liquid (nujol, Aldrich) and the clay particles (60–30–10%, w/w). A part of the resulting paste material was packed using a spatula into a cylindrical teflon tube (6 mm internal diameter), equipped with a stainless steel screw and piston acting as the electrical contact. The active surface of the electrode was then polished on a sheet of clean paper. When necessary, a fresh surface of the electrode was obtained by pushing slowly a portion of the paste out of the electrode body with the stainless steel piston, and by repeating again the polishing procedure. Ba/CPE and MPTMS-Ba/CPE were used as working electrode in a three-electrode cell configuration, comprised of a Pt wire counter electrode and a saturated calomel electrode (SCE) serving as reference electrode.

Cyclic voltammetry (CV) experiments were conducted using a TIPOL type potentiostat from SOLEA TACUSSEL (France) coupled to EPL2 recorder. Throughout the study, a 0.01 mol L^{-1} phosphate buffer was used as the supporting electrolyte, and pH values were adjusted using diluted solutions of HCl or NaOH. All experiments were carried out at room temperature, the potential ranging from −0.2 to −0.45 V at 50 mV s^{-1}.

3. Results and discussions

3.1. Characterization of the organoclay sorbent

FTIR spectra of the pristine clay (Ba) and the organoclay (MPTMS-Ba) are compared in Fig. 1. Two main features can be noticed, indicating that the starting material undergoes significant change upon interacting with MPTMS:

(i) The decrease in intensity of the OH stretching bands at 3620 cm^{-1} (Fig. 1A), 4560 and 7075 cm^{-1} (Fig. 1B) of the clay after grafting with the organosilane molecules. This fact suggests the participation of the hydroxyl groups in the interaction of MPTMS with the clay surface.

(ii) The appearance of new bands in the spectra of the modified clay, centered at 2930, 2562 and 1451 cm^{-1} (Fig. 1A) which correspond respectively to C–H and S–H stretching vibrations, and C–H scissoring bands of MPTMS-Ba. A group of bands was also observed between 1022 and 1400 cm^{-1}, which were assigned to C–H wagging mode. The bands at 5750 and 4375 cm^{-1} in the NIR spectrum of MPTMS-Ba (Fig. 1B) were attributed to CH_2 groups in the thiol-functionalized clay.

The features (i) and (ii) provide strong evidence for the presence of the organic moieties in the organoclay, in agreement with what was reported by previous works [22,23,51].

N_2 adsorption–desorption curves recorded for the unmodified clay and the organoclay are compared in Fig. 2. The main difference between these isotherms is the presence of a large hysteresis loop on the raw clay curve. This observation is indicative of the presence of a framework mesopores, with a contribution from micropores [52,53]. Upon grafting with MPTMS, a significant change is obtained in the surface area and the total pore volume of the clay, which decreases from 155 to 4 $m^2\ g^{-1}$ and from 0.17 to 0.02 $cm^3\ g^{-1}$, respectively.

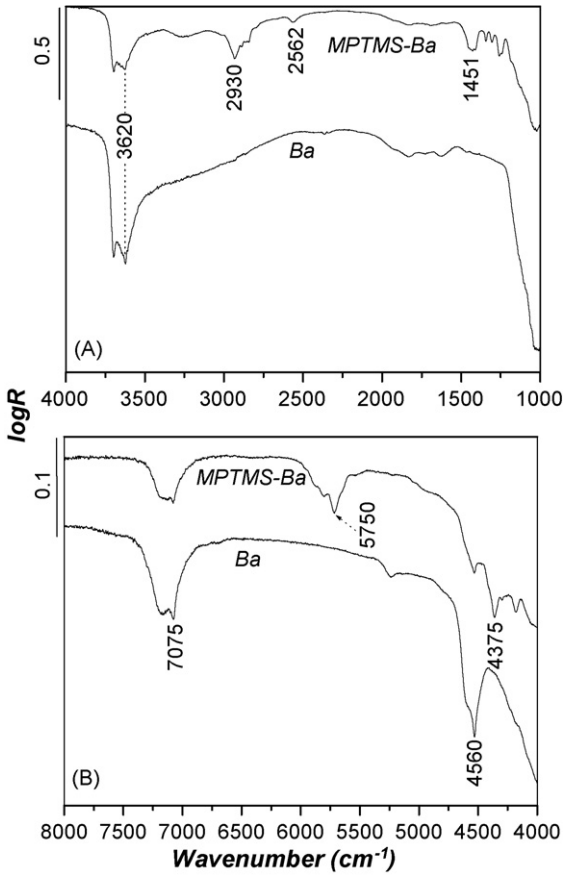


Fig. 1. FTIR spectra of "Ba" clay and "MPTMS-Ba" organoclay: MIR (A) and NIR (B).

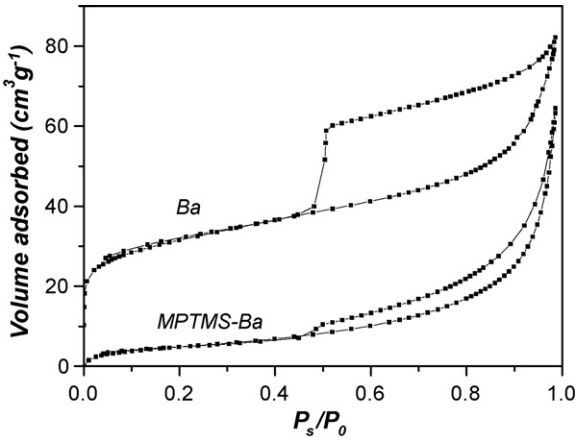


Fig. 2. Nitrogen adsorption–desorption isotherms obtained at 77 K for "Ba" and "MPTMS-Ba" materials.

The *t*-plot curve (not represented here) also showed a complete missing of microporosity concomitant to the grafting process, whereas the average pore diameters for the pristine clay and its modified counterpart remained around 4 nm. These observations support the idea that the access of nitrogen to the surface is blocked by the organic moieties covalently linked at the edge –OH groups of individual clay platelets [23,54].

A typical behavior upon thermal treatment of the "Ba" clay before and after its functionalization by MPTMS grafting is presented in Fig. 3. The DTG curve of the pristine clay showed a weight loss of 6.4% between 30 and 200 °C which is due to the loss of physisorbed and interlayer water; the corresponding peak maximun is centered at 92 °C on the DTG curve. Another weight

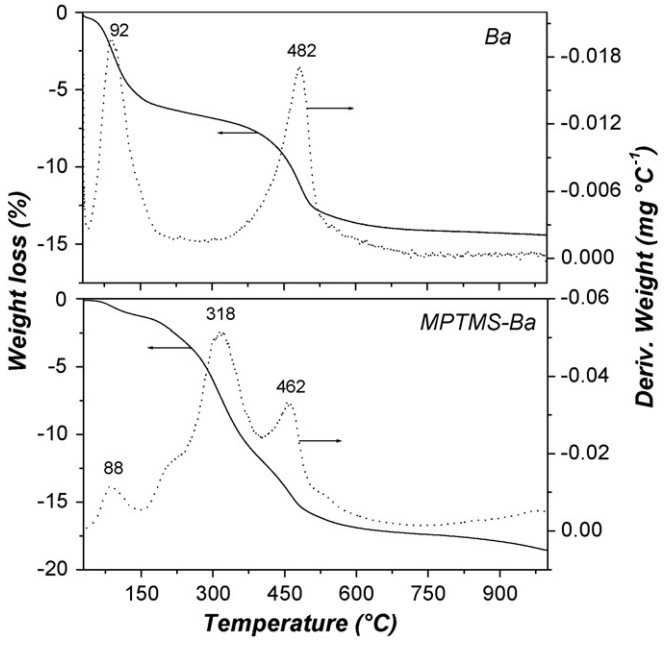


Fig. 3. TG (solid line) and DTG (dotted line) curves obtained under helium streaming) for "Ba" and "MPTMS-Ba" materials.

loss of 7.6% was observed between 200 and 650 °C, with a peak maximum at 482 °C on the DTG curve; this is attributed to the decomposition, that is the dehydroxylation of the clay sheets, including condensation of structural and intra lamellar AlOH or SiOH groups [22].

Three weight losses were observed on the TGA spectrum of the modified clay sample. The first one arises at temperature below 100 °C, with a small peak at 88 °C on the DTG curve. This peak is less intense compared with the corresponding one on the unmodified clay, indicating a lower water content that can be explained by the more hydrophobic character of the grafted clay. The main weight loss (9.8%) was obtained from 150 to 420 °C, with a peak at 318 °C which was absent on the curve of the pristine clay. This fact can be assigned to the decomposition of the grafted organic moieties on the clay surface. The weight loss occurring at 462 °C is attributed to the dehydroxylation process. The total weight loss resulting from the decomposition process was 19.6%, comprising 9.8% change for the dehydration and the dehydroxylation of the clay, and 9.8% for the degradation of MPTMS.

The thermal decomposition of MPTMS-Ba followed by MS analysis revealed the presence of several molecular species the characteristics of which are given in Table 2. The release of H_2O^+ ion (18 g mol^{-1}) was observed at three temperatures between 90 and 450 °C, as the result of the loss of physically adsorbed water and the dehydroxylation of the clay sheets as revealed by TGA. This hypothesis was afforded by MS spectra of the raw clay (data not presented) that showed only water as detected species. The decomposition of the grafted clay was observed via simultaneous release of molecular fragments containing carbon. The presence of specific ions H_2S^+ (34 g mol^{-1}), CH_2SH^+ (47 g mol^{-1}) and $CH_3SCH_2^+$ (61 g mol^{-1}) clearly indicated the fragmentation of the organic molecule MPTMS arising with heating. These observations demonstrated quite conclusively the effectiveness of the grafting process.

3.2. Batch adsorption studies

3.2.1. Kinetics and capacities

The shaking time is a factor of primary importance in adsorption process experiments. The examination of MB adsorption onto Ba and MPTMS-Ba as a function of shaking time is presented in Fig. 4, from which it can be seen that the adsorbed amount of this dye increases with time between 0 and 30 min, the equilibrium being reached within 40–50 min.

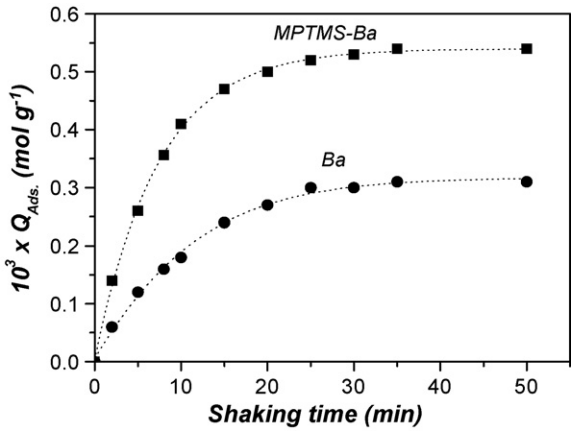


Fig. 4. Variation of the amount of adsorbed MB on "Ba" and "MPTMS-Ba" materials as a function of shaking time. Experimental conditions: 2 mg of adsorbent in 60 mL aqueous solution containing 5×10^{-5} mol L^{-1} of MB (pH 6.6).

The adsorption process was found to be very fast at the early beginning of the experiments, especially for the organoclay, so that a large fraction of the dye was fixed during the first 20 min. At an initial dye concentration of 5×10^{-5} mol L^{-1}, the adsorption capacities for MB were found to be 0.30 mmol g^{-1} on Ba and 0.55 mmol g^{-1} on MPTMS-Ba. These values correspond respectively to 34% of the CEC of the raw clay and to an occupation of 23% of the thiol groups on the organoclay, but it should be mentioned that these data have been obtained at natural pH (6.6) and at a solid-to-solution ratio of 33.3 mg L^{-1} (i.e., MB not in excess). Both of these parameters are likely to affect the binding process.

For the same solid-to-solution ratio as in Fig. 4, Fig. 5 reveals that pH had a dramatic influence on the accumulation of MB on the thiol-functionalized clay. Being rather low in acidic medium (below 0.3 mmol g^{-1} at pH values up to 5), the sorption capacity then increased rapidly in the 6–8 pH range to reach a constant maximal value (about 0.9 mmol g^{-1}) at pH values

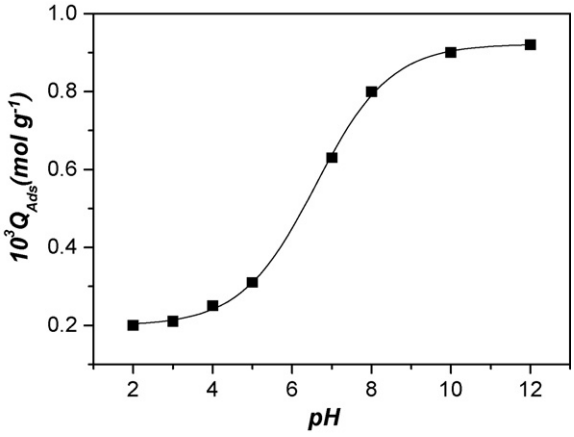


Fig. 5. Influence of pH on the adsorption of MB on "MPTMS-Ba", from a solution containing initially 1.5 mmol of MB per gram of adsorbent. Shaking time: 60 min.

Table 2
Species detected by MS analysis for MPTMS-Ba

Molecular mass (g mol^{-1})	Peak temperature (°C)	Corresponding fragment
18	98–265–456	H_2O^+
34	328	H_2S^+- or/and $H_2O_2^+$
41	308	C_2HO^+ or/and $C_3H_5^+$
42	301	$C_3H_6^+$
47	230	CH_2SH^+
48	320	$CH_4O_2^+$
61	244	$CH_3SCH_2^+$
62	322	$C_2H_6O_2^+$

Table 3
Some adsorption capacities for MB on various adsorbents

Materials	Maximum capacity adsorption (mmol g^{-1})	[MB] (mol L^{-1})	Reference
Pure kaolinite	3.80	7.80×10^{-5}	[3]
Calcined raw kaolin	1.50		
Calcined pure kaolin	2.20		
NaOH-treated pure kaolin	5.50		
Commercial activated carbon	0.90	1.00×10^{-5}	[5]
Charcoal (calcined 2 h at 700 °C)	0.18		
Charcoal (calcined 5.5 h at 700 °C)	0.30		
Rosewood sawdust (treated with H_2SO_4)	0.13	1.56×10^{-4}	[7]
Rosewood sawdust (treated with formaldehyde)	0.14		
Activated carbon	0.16		
Clay	0.19	1.00×10^{-4}	[15]
Clay (montmorillonite + nontronite)	0.06	6.00×10^{-5}	[16]
Diatomaceaous clay (diatomite)	0.45	6.30×10^{-7}	[57]
Polyacrylic acid-bound iron oxide	0.62	1.25×10^{-2}	[58]
Red mud	0.08	3.00×10^{-5}	[59]
Fly ash	0.01		
Sludge ash	0.01	3.50×10^{-5}	[60]
Zeolite (MCM-22)	0.17	2.00×10^{-6}	[61]
Clay (montmorillonite)	0.31	2.00×10^{-5}	This work
Clay (smectite grafted with thiol groups)	1.04		

higher than 9. On the contrary, MB sorption on the pristine clay did not vary significantly in the 3–12 pH range (i.e. capacity around 0.3 mmol g^{-1}), in agreement with previous observations on other clays [16].

These results can be rationalized by considering distinct accumulation mechanisms. On the raw clay, independently on the pH and on the organoclay in acidic medium, the interaction of the dye with the adsorbent is governed by electrostatic interactions. The uptake of its positively-charged form (MB^+) occurs via an ion exchange mechanism. Such a process which is not quantitative, results from an ion exchange equilibrium between MB^+ and the charge-compensating cations of the clay (which are released in solution upon MB^+ uptake) [55]. Apparently, the presence of mercaptopropyl groups grafted on the clay did not affect significantly this ion exchange process as capacities of the same order of magnitude (around 0.3 mmol g^{-1}) were observed for both the raw material and the organoclay. On the other hand, increasing the pH of the medium led to the dramatic enhancement in the sorption capacity of the organoclay. Such an improvement is due to favorable interactions between the thiol groups and dye species, which could involve hydrogen bonding and/or electrostatic effects. In fact, in an alkaline medium the thiol groups on the organoclay, the pK_a of which is around 10.8, are expected to turn negatively charged as a result of their deprotonation [56], whereas the pH had no effect on the ion exchange properties of non-functionalized clay. This pointed out the interest of clay functionalization to improve its sorption properties towards MB^+ species.

To measure the maximal sorption capacities, it was necessary to work in conditions where MB^+ was in large excess over the adsorbent (amount of active ion-exchange centers). For the raw Ba-clay sample, the adsorption capacity (0.31 mmol g^{-1}) was of the same order of magnitude as for other commonly used adsorbents (see some representative data for clays, zeolites, activated carbons, charcoals, sawdusts, or ashes, in Table 3). It should be however mentioned that comparison of the data is not straightforward as the experimental conditions used in these early studies were most often not the same (various particles sizes, various solid-to-solution ratios, different pH, etc.).

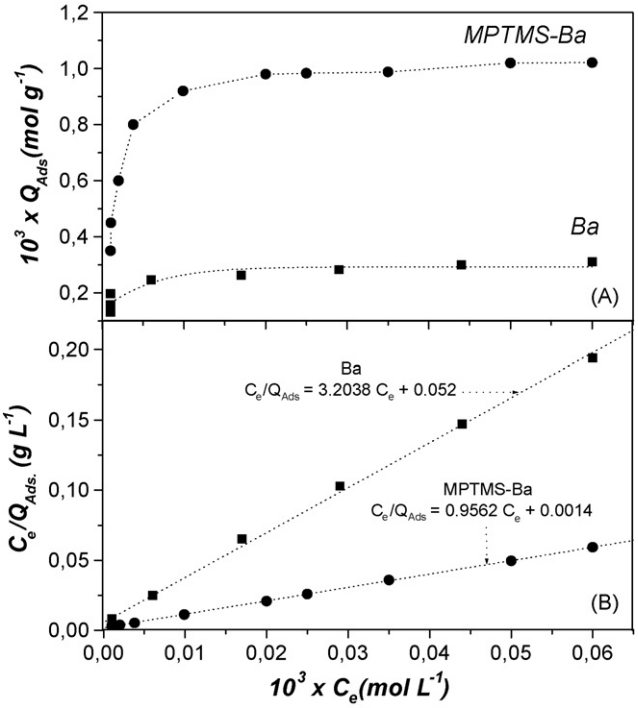


Fig. 6. Sorption isotherms for MB on "Ba" and "MPTMS-Ba" materials (A), and the corresponding Langmuir plots (B). Experimental conditions are the same as in Fig. 6.

By contrast, the adsorption capacity of MPTMS-Ba for MB^+ (1.04 mmol g^{-1}) was by far larger than that of the raw clay (0.31 mmol g^{-1}): this again confirms that clay modification contributes to generate a new material with a better performance regarding the efficiency to immobilize MB^+ species.

3.2.2. *Effect of the dye concentration–sorption isotherms*

Fig. 6(A) displays the variations observed in the amounts of dye immobilized on Ba and MPTMS-Ba sorbents, as a function of the equilibrium MB^+ concentration in solution. These isotherms, which are characterized by sharp increases in sorbed species at low solution concentrations, indicate a good affinity of the adsorbents for MB^+.

As aforementioned, the maximum amount of MB^+ adsorbed by the native clay (Ba) was noticeably lower than that observed for its organically modified form (MPTMS-Ba). Since the amount of adsorbed species, Q_{ads}, reached limiting values for both Ba and MPTMS-Ba when the equilibrium dye concentration in the aqueous phase, C_e, tended to infinity, the experimental isotherms were mathematically treated by the well known Langmuir equation:

$$Q_{ads} = Q_0 \frac{KC_e}{1 + KC_e} \quad (2)$$

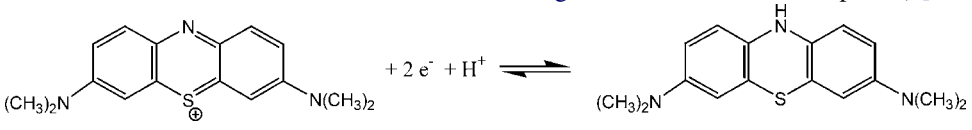
where Q_0 (mol g^{-1}) is the amount of dye adsorbed when saturation is attained and K (L mol^{-1}) is the Langmuir constant.

Eq. (2) can be written in its linearized form as

$$\frac{C_e}{Q_{ads}} = \frac{C_e}{Q_0} + \frac{1}{KQ_0} \quad (3)$$

Hence, by plotting C_e/Q_{ads} as a function of C_e, a straight line will be obtained for the isotherm if the Langmuir model is fitted, and consequently, Q_0 could then be deduced from the slope of the linear curve.

Fig. 6(B) presents the results obtained for Ba and MPTMS-Ba, the experimental conditions being the same as in Fig. 6(A). Linear fittings of the data with high R^2 correlation values (>0.99) indicate that sorption data are satisfactorily described by the Langmuir model. This suggests that MB^+ adsorption is restricted to a monolayer coverage and that the surface of the adsorbent is relatively homogeneous regarding the adsorption sites [15,62], a fact which again is consistent with the binding mechanisms suggested above. The maximal adsorption capacities values calculated from the slopes of the Langmuir plots are 0.31 and 1.08 mmol g^{-1} for Ba and MPTMS-Ba, respectively, which almost match the maximal capacities measured experimentally in conditions of large excess in MB^+ (0.31 and 1.04 mmol g^{-1}, respectively).



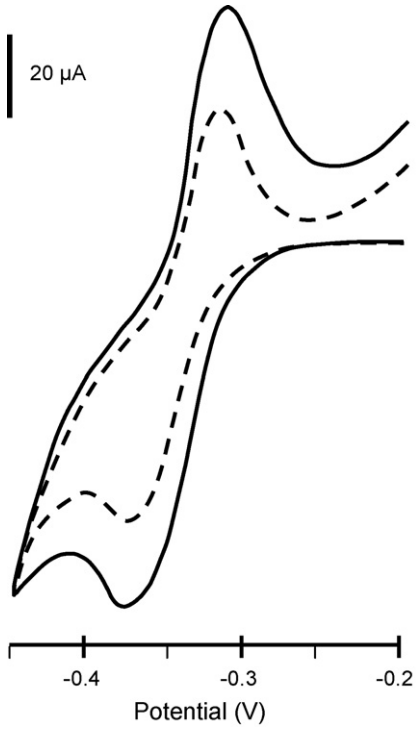


Fig. 7. Cyclic voltammograms recorded at 50 mV s^{-1} using (a) Ba/CPE (dotted line) and (b) MPTMS-Ba/CPE (solid line), after 20 h immersion of the electrode in 10^{-2} mol L^{-1} Na_3PO_4 (at pH 10.0) containing 3×10^{-5} mol L^{-1} of MB.

3.3. *Voltammetric detection of MB subsequent to its accumulation by MPTMS-Ba*

Taking advantage of the above results, we have explored the possibility to exploit the binding properties of the organoclay towards MB^+ to detect the dye voltammetrically. To this end, the materials were inserted into carbon paste electrodes and cyclic voltammetry (CV) was first used to characterize the electrochemical behavior of MB^+ at such modified electrodes.

As shown in Fig. 7, CV curves featured a pair of reversible cathodic and anodic peaks whose potential are not dependent of the nature of the clay (raw or organically modified). These peaks are attributed to the following two-electron, one proton, oxido-reduction processes, in agreement with what was reported for methylene blue in alkaline medium (CV curves depicted in Fig. 7 have been recorded at pH 10) [63–65].

Interestingly, these CV curves were obtained after the electrode has been dipped for a rather long time (20 h) in a diluted solution of MB^+. For a matter of comparison, in the same condition, a bare electrode did not give rise to any measurable signal. The fact that CV peaks were well defined on the clay and organoclay modified electrodes is clearly due to the accumulation of the dye into the materials particles located on the electrode surface. It also appears that peak currents are significantly enhanced at the electrode containing the organoclay as modifier, compared

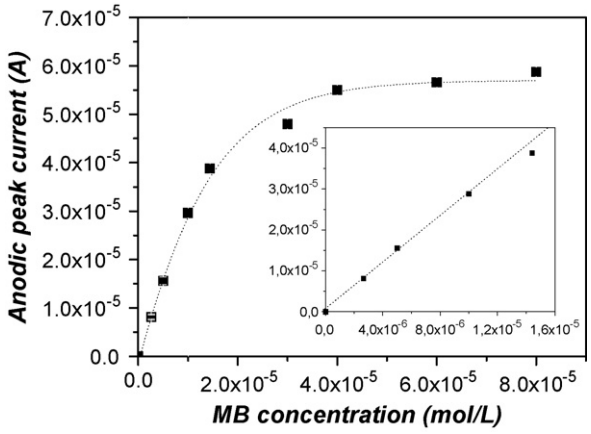


Fig. 8. Dependence of the voltammetric peak currents sampled at MPTMS-Ba/CPE on the MB concentration (after 45 min accumulation in phosphate buffer at pH 10.0). Inset: enlargement of the 0.1–1.4 × 10^{-5} mol L^{-1} concentration range.

to its non-functionalized counterpart, indicating thus that more MB^+ took part in the electrochemical reaction in the former case. This behavior is attributed to the enhancing action of the thiol moieties to which MB^+ is accumulated more effectively than in the pristine clay.

These results suggest that MPTMS-Ba/CPE can be used as an electrochemical sensor for MB^+. We then explored this possibility and Fig. 8 depicts a typical variation in the voltammetric peak currents obtained after 45 min accumulation from solutions containing the dye at concentrations ranging from 1×10^{-6} to 8×10^{-5} mol L^{-1}. The response first increased linearly with MB^+ concentration from 1×10^{-6} mol L^{-1} up to 1.4×10^{-5} mol L^{-1} and then tended to a constant value at concentrations higher than 4×10^{-5} mol L^{-1}, when the adsorption equilibrium was reached. A detection limit of 4×10^{-7} mol L^{-1} was evaluated from a signal-to-noise ratio of 3. These results were obtained by adjusting the pH of the accumulation medium at a value of 10.0, which corresponds to the optimal conditions for effective MB^+ uptake (Fig. 5).

It is relevant to mention that this is the first example of an electrochemical sensor involving a carbon paste electrode modified with an organoclay and applied to the electroanalysis of a dye, although (non-functionalized) clay-modified electrodes have already been reported using MB^+ as the redox probe [44–46]. Most works dealing with the uptake of dyes by various adsorbents were traditionally focussed on the establishment of adsorption isotherms [15,16,29]. To the best of our knowledge, data relative to the use of modified electrodes in connection to the electrochemical analysis of dyes are not available in literature. This work thus points out the interest of such electrodes as a low-cost alternative that might be useful for the determination of dyes in colored effluents.

4. Conclusion

This work has reported the successful preparation of an organic–inorganic hybrid material, which was obtained by grafting an organosilane bearing mercaptopropyl groups onto the surface of a smectite-type natural clay. The effectiveness of the grafting process was clearly demonstrated by several techniques including FTIR, N_2 adsorption/desorption experiments (BET method) and TGA–MS. The adsorption capacity of the organoclay was more than three times higher than that of the raw clay, especially in alkaline medium. This fact was attributed to the enhancing action of thiol groups that accumulate via their unprotonated form the positively charged clay through electrostatic interactions. The uptake of MB^+ is consistent with the Langmuir sorption isotherm. Taking advantage of such improved binding properties, we have successfully demonstrated that a CPE comprising the modified clay allowed the detection of the dye in the micromolar concentration range and down to a limit of 4×10^{-7} mol L^{-1}. This approach can be viewed as an attractive and promising way for the voltammetric analysis of MB^+, which could be readily extended to other electroactive dyes.

Acknowledgements

The authors wish to express their gratitude to the French Ministry of Foreign Affairs for its financial support (Project CORUS no. 02 412 043). Financial support as a part of IFS research project (W 3908-1) granted to IKT is also acknowledged.

References

[1] N. Kannan, M.M. Sundaram, Dyes Pigments 51 (2001) 25.
[2] S.J. Allen, B. Koumanova, J. Univ. Chem. Technol. Met. 40 (2005) 175.
[3] D. Ghosh, K.G. Gbhattacharyya, Appl. Clay Sci. 20 (2002) 295.
[4] T. Robinson, G.M. Mullan, R. Marchant, P. Nigam, Bioresour. Technol. 77 (2001) 247.
[5] J. Avom, J.K. Mbadcam, C. Noubactep, P. Germain, Carbon 35 (1997) 365.
[6] A. Houas, I. Bakir, M. Ksibi, E. Elaloui, J. Chim. Phys. 96 (1999) 479.
[7] V.K. Garg, M. Amita, R. Kumar, R. Gupta, Dyes Pigments 63 (2004) 243.
[8] G. Malmary, F. Perineau, J. Molinier, A. Gaset, J. Chem. Technol. Biotechnol. 35 (1985) 431.
[9] G. McKay, H.S. Blair, J.R. Gardner, J. Colloid Interf. Sci. 95 (1983) 108.
[10] R.S. Juang, R.L. Tseng, F.C. Wu, S.H. Lee, J. Chem. Technol. Biotechnol. 70 (1997) 391.
[11] M.S. Chiou, H.Y. Li, J. Hazard. Mater. 93 (2002) 233.
[12] Q. Fan, S. Hoskote, Y. Hou, J. Hazard. Mater. 112 (2004) 123.
[13] G. McKay, M.S. Otterburn, A.G. Sweeney, Water Res. 14 (1980) 21.
[14] S. Kacha, Z. Derriche, S. Elmaleh, Water Environ. Res. 75 (2003) 15.
[15] A. Gürses, S. Karaca, C. Dogar, R. Bayrak, M. Açilyildiz, M. Yalçin, J. Colloid Interf. Sci. 269 (2004) 310.
[16] A. Gürses, C. Dogar, M. Açilyildiz, R. Bayrak, S. Karaca, J. Hazard. Mater. 131 (2006) 217.
[17] K.N. Majewska, Desalination 71 (1989) 127.
[18] A. Bozdogan, H. Goknil, Marmara Universitesi Fen Bilimleri Dergisi 4 (1987) 83.
[19] G.R. Brower, G.D. Reed, Proceedings of the 41st Industrial Waste Conference, Purdue University, West Lafayette, Indiana, 1985, p. 612.
[20] S. Brandes, F. Denat, M. Meyer, R. Guilard, Actual. Chim. 290 (2005) 108.
[21] A.R. Cestari, C. Airoldi, J. Colloid Interf. Sci. 195 (1997) 338.
[22] L. Mercier, T.J. Pinnavaia, Environ. Sci. Technol. 32 (1998) 2749.
[23] R. Celis, M.C. Hermosin, J. Cornejo, Environ. Sci. Technol. 34 (2000) 4593.
[24] I.K. Tonle, E. Ngameni, D. Njopwouo, C. Carteret, A. Walcarius, Phys. Chem. Chem. Phys. 5 (2003) 4951.
[25] A.M. Klonkowski, B. Grobelna, T. Widernik, A.J. Frydel, W. Mozgawa, Langmuir 15 (1999) 5814.
[26] N. Chiron, R. Guilet, E. Deydier, Water Res. 37 (2003) 3079.
[27] A. Walcarius, M. Etienne, C. Delacote, Anal. Chim. Acta 509 (2004) 87.

[28] M.G. da Fonseca, J.S. Barone, C. Airoldi, Clays Clay Miner. 48 (2000) 638.
[29] R. Wibulswas, Sep. Purif. Technol. 39 (2004) 3.
[30] Z. Bouberka, S. Kacha, M. Kameche, S. Elmaleh, Z. Derriche, J. Hazard. Mater. 119 (2005) 117.
[31] G.R. de Souza, F.L. Fertonani, I.A. Pastre, Eclet. Quim. 28 (2003) 77.
[32] Y.L. Ma, Z.R. Xu, T. Guo, P. You, J. Colloid Interf. Sci. 280 (2004) 283.
[33] G. Lefevre, A. Walcarius, J. Bessière, Electrochim. Acta 44 (1999) 1817.
[34] Z. Navratilova, P. Kula, Fres. J. Anal. Chem. 367 (2000) 369.
[35] H. Guo, Y. Li, X. Cheng, L. Nie, N. He, Sensors 5 (2005) 284.
[36] K. Kalcher, J.M. Kauffmann, J. Wang, I. Svancara, K. Vytras, C. Neuhold, Z. Yang, Electroanalysis 7 (1995) 5.
[37] K. Kalcher, I. Svancara, R. Metelka, K. Vytras, A. Walcarius, in: C.A. Grimes, E.C. Dickey, M.V. Pishko (Eds.), Encyclopedia of Sensors, vol. 4, American Scientific Publishers, Stevenson Ranch, CA, 2006, pp. 283–430.
[38] P. Kula, Z. Navratilova, P. Kulova, M. Kotoucek, Anal. Chim. Acta 385 (1999) 91.
[39] Z. Navratilova, P. Kula, Electroanalysis 15 (2003) 837.
[40] M. Arvand, S. Sohrabnezhad, M.F. Mousavi, M. Shamsipur, M.A. Zanjanchi, Anal. Chim. Acta 491 (2003) 193.
[41] H. Shubo, Z. Min, Y. Zhuobin, L. Xin, Biosens. Bioelectron. 16 (2001) 9.
[42] Y. Hui, L. Nan, X. Shu, X. Jin-Zhong, Z. Jun-Jie, C. Hong-Yuan, Biosens. Bioelectron. 21 (2005) 372.
[43] H. Jun, G. Hedayatollah, R.Z. Saeed, A.M.M. Akbar, A. Shahin, A.S. Akbar, Anal. Lett. 40 (2007) 483.
[44] P. Joo, Colloids Surf. A 49 (1990) 29.
[45] B. Shen, T. Peng, H. Wang, Electrochim. Acta 39 (1994) 527.
[46] V. Ganesan, R. Ramaraj, J. Electroanal. Chem. 490 (2000) 54.
[47] D.C. Bain, B.F.L. Smith, in: M.J. Wilson (Ed.), Clay Mineralogy: Spectroscopic and Chemical Determinative Methods, Chapman & Hall, London, UK, 1994, pp. 301–357.
[48] S.J. Gregg, K.S.W. Sing, Adsorption, Surface Area and Porosity, Academic Press, London, UK, 1988.
[49] B.C. Lippens, J.H. de Boer, J. Catal. 4 (1965) 319.
[50] I.K. Tonle, E. Ngameni, A. Walcarius, Sens. Actuators B 110 (2005) 195.
[51] M. Erdemoglu, S. Erdemoglu, F. Sayilkan, M. Akursu, S. Sener, H. Sayilkan, Appl. Clay Sci. 27 (2004) 41.
[52] Y.H. Su, S. Yamanaka, J. Porous Mater. 5 (1998) 111.
[53] A. Szabo, D. Gournis, M.A. Karakassides, D. Petridis, Chem. Mater. 10 (1998) 639.
[54] K. Song, G. Sandi, Clays Clay Miner. 49 (2001) 119.
[55] F. Helfferich, Ion exchange, Dover Publications, Inc., New York, 1995.
[56] J.P. Danehy, K.N. Parameswaran, J. Chem. Eng. Data 13 (1968) 386.
[57] R.A. Shawabkeh, M.F. Tutunji, Appl. Clay Sci. 24 (2003) 111.
[58] S.Y. Mak, D.H. Chen, Dyes Pigments 61 (2004) 93–98.
[59] S. Wang, Y. Boyjoo, A. Choueib, Z.H. Zhu, Water Res. 39 (2005) 129.
[60] W.C. Huang, P.Y. Fong, Colloids Surf. A 274 (2006) 154.
[61] W. Shaobin, L. Huiting, X. Longya, J. Colloid Interf. Sci. 295 (2006) 71.
[62] M. Hajjaji, M. Alami, A. El Bouadili, J. Hazard. Mater. 135 (2006) 188.
[63] H. Ju, J. Zhou, C. Cai, H. Chen, Electroanalysis 7 (1995) 1165.
[64] S.B. Khoo, F. Chen, Anal. Chem. 74 (2002) 5734.
[65] J. Li, F. Zhao, J. Zhao, B. Zeng, Electrochim. Acta 51 (2005) 297.

Available online at www.sciencedirect.com
ScienceDirect
Talanta 74 (2008) 971–976
Talanta
www.elsevier.com/locate/talanta

Evolving factor analysis-based method for correcting monitoring delay in different batch runs for use with PLS: On-line monitoring of a transesterification reaction by ATR-FTIR

Marcello G. Trevisan [1], Camila M. Garcia, Ulf Schuchardt, Ronei J. Poppi *

Institute of Chemistry, State University of Campinas, P.O. Box 6154, 13084-971, Campinas, SP, Brazil

Received 15 May 2007; received in revised form 2 August 2007; accepted 3 August 2007
Available online 15 August 2007

Abstract

In this work, the base-catalyzed transesterification of soybean oil with ethanol was monitored on-line using mid-infrared spectroscopy (MIRS) and the yield of fatty acid ethyl esters (biodiesel) was obtained by ^{1}H NMR spectroscopy. The MIRS monitoring carried out for 12 min, was performed using a cylindrical internal reflectance cell of PbSe in the range of 3707–814 cm^{-1} with eight co-added scans. Two different data treatment strategies were used: in the first, the models were built using the raw data and in the other, evolving factor analysis (EFA) was used to overcome the sensor time delay due to the on-line analysis, producing significantly better results. In addition, models based on partial least squares (PLS) using three batches for calibration and another for validation were compared with models with just one batch for calibration and three for validation. The models were compared between each other using root mean square error of prediction (RMSEP) and root mean square prediction difference (RMSPD), obtaining relative errors under 3%.
© 2007 Elsevier B.V. All rights reserved.

Keywords: Biodiesel fuel; Middle infrared spectroscopy; Reaction monitoring; Process control; Robustness of models

1. Introduction

In an attempt to reduce global warming and economic dependence on the fossil fuels, governmental and scientific agencies are taking various initiatives in the direction of alternative sources of energy that pollute less and are renewable. In contrast to the recent U.S. '*Biofuels Initiative*' [1], Brazil already has a well-established network for production of ethanol from sugar cane, with high productivity and lower prices on the international market, establish during the first petroleum crisis of the 1970s [2]. Recently, the Brazilian government started another biofuel program, based on the production of biodiesel, with planned progressive additions to the petroleum diesel [3,4].

Although many Brazilian vegetable oils, such as sunflower, cotton, palm, babassu, castor and jatropha, are available to produce biodiesel, only soybean oil has a large enough production to allow the mandatory demand of 2% of biodiesel blend in 2008, called B2. In contradiction to other countries, in Brazil the alcohol most used for transesterification is bioethanol, rather than imported methanol. However, methanol enables a well-defined and stable separation of the subproducts found in biodiesel.

The transesterification or alcoholysis of the triacylglycerols of vegetable oils or animal fats, in the presence of a catalyst, commonly bases such as NaOH or KOH, yields fatty acid monoalkyl esters (biodiesel) with glycerol as a side product. Partial transesterification products (mono- and di-acylglycerols formed during the transesterification process), unreacted triacylglycerols, unseparated glycerol, free fatty acids, residual alcohol and remaining catalyst can contaminate the final products [5]. In this way, the determination of the biodiesel quality is an issue of great importance to the successful commercialization of this fuel. Continuous high fuel quality with no operational problems is a prerequisite for market acceptance of biodiesel. The most commonly employed techniques

* Corresponding author. Tel.: +55 19 3521 3126; fax: +55 19 3521 3023.
E-mail addresses: trevisan@uniararas.br (M.G. Trevisan), ronei@iqm.unicamp.br (R.J. Poppi).
[1] Present address: Faculty of Pharmacy, Hermínio Ometto University Center (UNIARARAS), Av. Dr. Maximiliano Baruto 500, Jardim Universitário, 13607-339 Araras, SP, Brazil.

0039-9140/$ – see front matter © 2007 Elsevier B.V. All rights reserved.
doi:10.1016/j.talanta.2007.08.004

to monitor the transesterification reactions and analyze the biodiesel are gas chromatography (GC) and high-performance liquid chromatography (HPLC). Both GC [6–8] and HPLC [9] analyses and their combination [10] have been reported for biodiesel analysis while gel permeation chromatography (GPC) [11] completes the group of separation techniques. However, despite their high accuracy, these methods are time-consuming and cannot be easily used for the on-line evaluation of fast reversible reactions such as the transesterification. Thus, alternative methods, like the refractive index of the product [12], are in constant development to monitor transesterification reactions.

However spectroscopic techniques like nuclear magnetic resonance (NMR), usually ^{1}H NMR [13–15], and vibrational techniques such as near/mid-infrared [15,16] and Raman spectroscopy [17] are also suitable for monitoring the transesterification reaction and/or controlling the quality of biodiesel only vibrational techniques enable probes for on-line and real-time monitoring [15,18,19]. Vibrational spectroscopic techniques have some attractive characteristics, such as speed, no-sampling requirements, holistic measurements and no need for added reagents [20,21] with great advantages for process monitoring and control [22]. The use of spectroscopic variables, rich in chemical information, combined with traditional physical variables, such as viscosity, temperature, pressure and flow rate, enables improving the overall information about chemical processes [22], contributing to more reliable control systems and high quality products. Although mid-infrared spectroscopy provides much chemical information, intense absorption overlapping requires multivariate calibration techniques, such as partial least squares (PLS) [23] to perform the calibration models.

The aim of the present work is the development of a simple and rapid analytical method for on-line monitoring of the base-catalyzed transesterification kinetics of soybean oil with ethanol using FTIR with a multivariate approach. The reactions were monitored using an ATR CIRCLE (cylindrical internal reflectance cell for liquid evaluation) where continuous sampling of a semi-microreactor was accomplished while ^{1}H NMR spectroscopy was used to determine the fatty acid ethyl ester (FAEE) yields during the reaction.

Infrared spectroscopy has previously been used to monitor the alcoholysis of soybean oil [15,16]. In the present work, on-line monitoring, performed on several batch runs, and the validation set, characterized by a different batch run, showed for the first time the robustness of this new method [24]. A common procedure to monitor on-line reactions is the use of a by-pass system with a continuous sampling of the reactor [20]. In these systems, the principal drawback is correlation of the different sampling times in relation to the direct withdrawal of reactor samples [25,26], producing a time-delay between the real and the measured variations. To get around this situation, evolving factor analysis (EFA) [27] was used to identify the changes in the infrared data during monitoring, enabling correction of the time delay with the ^{1}H NMR kinetics and considerably reducing the prediction errors.

2. Experimental

2.1. Reagents and solutions

Refined soybean oil, edible-grade, exhibiting an iodine number of 131.9 (Wijs solution), a free fatty acid (FFA) content of 0.04% and water content of 0.1% (Cargill, Brazil) was used in all reactions involved in this work. Anhydrous ethanol (Chemco, Brazil) exhibiting water content of 0.44% was used without any further purification. Reagent-grade sodium hydroxide (Vetec, Brazil) was used as catalyst; $CDCl_3$ (Acros, Brazil); acetic acid (Ecibra, Brazil); anhydrous magnesium sulfate (Synth, Brazil) were also used. The Karl–Fischer method was used to determine the water content of the oil and ethanol.

2.2. Apparatus and software

The reactions were carried out in a 500 ml glass flask kept under constant stirring and at a temperature of $27 \pm 1\,^{\circ}C$. The IR measurements were done with an on-line system using silicon tubing (inner diameter of 1 mm) connected to the reactor and a model 78001-22 peristaltic pump (Ismatec IPC, Switzerland) using a flow of 3 ml min^{-1}. A SpectraTech (England) micro CIRCLE (cylindrical internal reflectance cell for liquid evaluation) with a PbSe rod crystal was used to obtain the IR spectra. The reflection angle was 45° with 7.5 reflections and with a cell volume of 0.5 ml [28]. A typical CIRCLE system is represented in Fig. 1. A Bomem (Asea Brown Boveri Ltd. (ABB)) MB-100 Series FTIR spectrometer equipped with a DTGS mid-range detector in the maximum gain level was employed to carry out the IR-measurements. The ^{1}H NMR spectra were obtained under ambient conditions with a GEMINI 2000, operating at 300 MHz and using $CDCl_3$ as solvent (chemical shift of residual protons at 7.26 ppm).

Data analyses were carried out using Matlab 6.5 (The MathWorks) with PLS toolbox (Eigenvector Technologies) version 3.5 in an AMD Athlon 1.3 GHz microcomputer with 256 Mb of RAM, using a Fedora core 3 Linux system. The iPLS toolbox for Matlab is freeware and it was obtained on the web (www.models.kvl.dk).

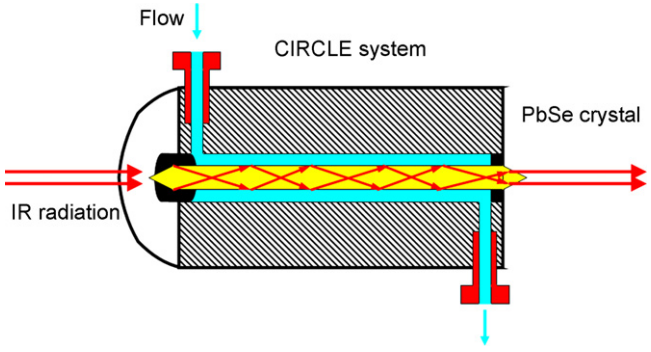


Fig. 1. A typical CIRCLE system used in MIR analysis.

2.3. Monitoring and data analysis

Four batches were carried out with the same procedure according to a general method for the transesterification: 1.00 g of NaOH was dissolved in 31.60 g of ethanol and added in one step to 100.00 g of soybean oil in the glass reaction flask. The reaction mixture was vigorously stirred at $27 \pm 1\,^{\circ}C$. Simultaneous with the addition of the ethanolic solution of the catalyst, the peristaltic pump and spectral monitoring were started.

Infrared on-line monitoring was performed through sequential scans of the reaction medium in a CIRCLE system. The spectral range was from 3707 to 814 cm^{-1} and eight co-added scans with a resolution of 8 cm^{-1} were used for enabling a fast spectrum recorded. In this way, each spectrum was obtained in 15 s and the monitoring was carried out for 12 min. A spectrum of air, obtained before each batch run, was used as background. For each monitored batch, a data matrix with dimensions of 48 sampling times by 751 spectral points was obtained. The data were exported using the GRAMS/32 software and the Matlab software was used to import and analyze the data, by help of the PLS-toolbox.

Seven off-line samples were taken from the reactor during 0.3–12.0 min for each batch. The samples (3 ml) were collected from the reactor using a pipette and then quenched in a test tube that contained 0.3 ml of glacial acetic acid. The samples were washed twice with water, the residual ethanol was removed from the liquid phase via rotatory evaporation and the residues were submitted to ^{1}H NMR analysis to obtain the yields of fatty acid ethyl ester (FAEE). Then a curve was adjusted for each batch, obtaining the kinetic profiles. Thus, from the kinetic equation, a continuous estimated concentration of FAEE at 48 different times between 0.0 and 12.0 min was obtained. These values were used to establish a multivariate model together with the continuously obtained infrared spectra.

3. Results and discussion

The yields of fatty acid ethyl ester (FAEE) were determined by ^{1}H NMR and the kinetic profiles of the batch reactions were adjusted using non-linear fitting from Origin® version 6.0 software. The kinetic profile obtained from the batches can be seen in Fig. 2 and it is governed by the following generic asymptotic equation:

$$\%\text{FAEE}\,(t_{\text{min}}) = A_0 - k_1 a^t \quad (1)$$

Few differences in the calculated kinetic parameters between the batch runs were observed, as shown in Table 1. These differences were, probably, due random errors from the experimental procedure and errors from the ^{1}H NMR determination, as suggests by Schuchardt and co-workers [13]. In this way, all the batches were considered as obtained under normal operation condition (NOC).

Table 1
The kinetic parameters used to fit the NMR experimental points

Parameters	Batch 1	Batch 2	Batch 3	Batch 4
A_0	97.29	95.55	95.10	96.44
k_1	83.72	69.53	64.88	88.87
a	0.48	0.50	0.57	0.50
R^2	0.9791	0.9893	0.9987	0.9643

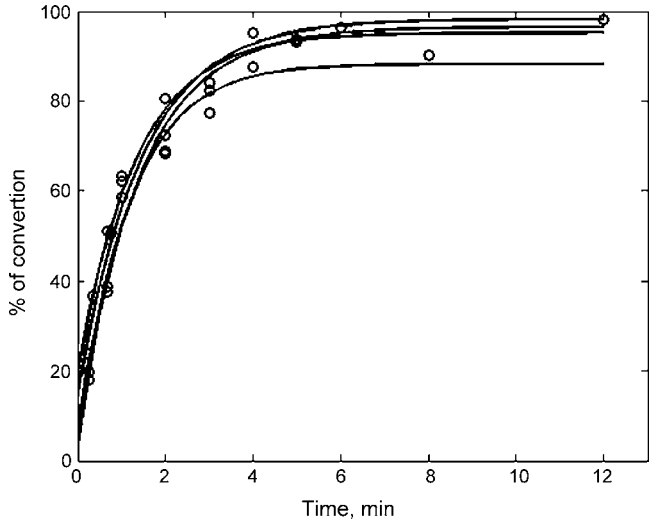


Fig. 2. Kinetic fitting for the transesterification reactions obtained by ^{1}H NMR analysis.

Using the fitted kinetic equation, the estimated concentrations as a function of time were obtained for 48 time points, between 0.0 and 12 min, corresponding to the exact times when the IR spectra were acquired. These estimated FAEE yields were used to construct a multivariate calibration model with the spectral data based on partial least squares regression. The calculated errors were expressed in relation to the estimated concentrations from the fitting model and the true real concentrations obtained by ^{1}H NMR.

Four batch runs were monitored from 0.3 to 12 min, resulting in 751 spectral points for each time interval. Thus, a cuboid of data was formed with dimensions of $4 \times 48 \times 751$. Two strategies were adopted using a cross-validation step, one using leave-one-out batch for validation and in the other using one batch for calibration and the other three for validation. In both cases, the errors were estimated as an average estimated error for each batch run in the cross-validation process.

First of all, several preprocessing were tested, such as derivative, baseline correction, Savitzky–Golay smoothing, mean centering, autoscaling and variables selection using interval PLS [29]. The methodology used for choosing the optimum preprocessing and the number of latent variables were the minimum value of the root mean square prediction difference (RMSPD) [30,31], shown in Eq. (2), a normally distributed absolute error around the time points, expressed as root mean square error of prediction (RMSEP) (Eq. (3)) and the absence of systematic errors:

$$\text{RMSPD}\% = 100\sqrt{\frac{1}{n}\sum_{i=1}^{n}\left(\frac{(\hat{y}_i - y_i)}{y_i}\right)^2} \quad (2)$$

$$\text{RMSEP} = \sqrt{\frac{1}{n}\sum_{i=1}^{n}(\hat{y}_i - y_i)^2} \quad (3)$$

where n is the number of samples and $\hat{y}_i$ and y_i are the estimated and the real concentrations at time i, respectively.

In the first step, the strategy of using only one batch to predict the others was evaluated. In this procedure and in the others, the data were always mean centered and the number of latent variables was determined by root mean square errors of cross-validation (RMSECV). For preprocessing, the data of the first derivative intensity measurements were used, because it was observed that this procedure improves the accuracy of the method, reducing the average relative errors around 10%. All models constructed with different batches used two latent variables. The obtained models were used to predict the other batches, obtaining relative errors in relation to the concentrations estimated by NMR. The results were expressed as averages of all relative errors obtained in each batch, which was 55%.

The other analyses were performed using the data from three batches for calibration and the other one for prediction. The models were constructed in the same way as in the previous analysis, using derivative and average centering and the number of latent variables was determined in the same way. A considerable reduction in the relative errors of prediction was observed, obtaining errors around 30%. This result shows the necessity of introduction of several batch runs in the calibration model, incorporating the intrinsic variability of the batches. Otherwise, higher values of RMSPD can be observed at initial times of the monitoring, as shown in Fig. 3. As the batch runs were analysed using an ATR flow-cell with a continuous sampling of the reactor by a peristaltic pump and the ^{1}H NMR analyses were done employing samples collected directly from the reactor, a considerable time delay between the NMR results and the IR monitoring was observed, prejudicing the prediction in the initial times. Although all the batches were done using the same conditions, the spectral changes in relation to time are different for each batch. For example, significant spectral variations, especially for the wavelengths 1050 and 3300 cm^{-1}, are only observed in the third batch for the 2–3 min interval, as plotted in Fig. 4. Subtracting the first spectrum for each batch, a better visualization of the intrinsic variation of the data can be obtained, as shown in Fig. 5.

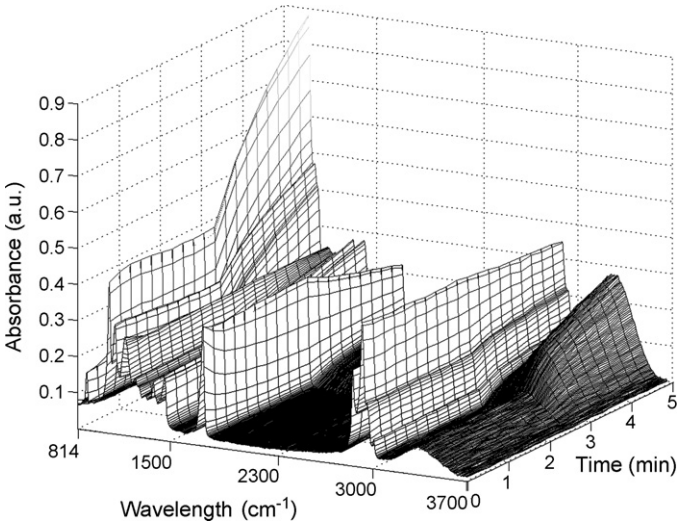


Fig. 4. IR spectra for the third batch in the first 5 min of monitoring.

In an attempt to adjust the sensor responses to the modelled kinetic profile obtained by NMR, evolving factor analysis (EFA) [27] was used to determine the start of spectrum variations of the monitoring and to perform a time-response correction. EFA [32,33] and other chemometric techniques [25,34] can be also employed to monitor any sudden change in the whole reaction system, to visualize the variation of the components and to detect the endpoint of reactions.

Evolving factor analysis consists in following the singular values of the spectral matrix for the first two times; then the first three times, and so on, determining how many factors is present in the data. In our case, as the methodology suggests the possibility for process control, the EFA was performed on

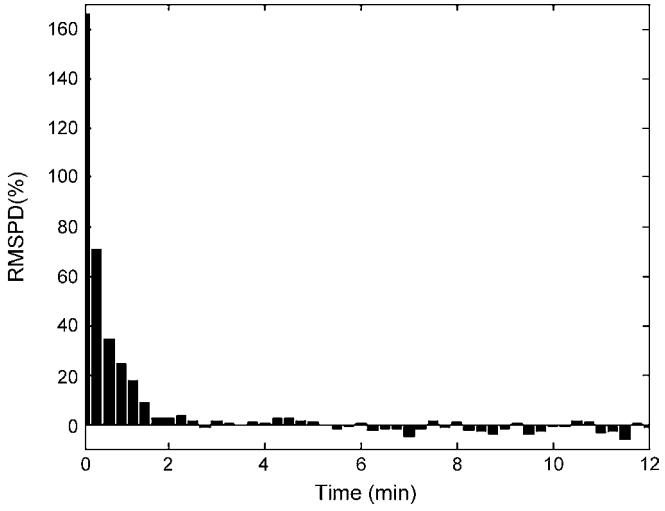


Fig. 3. A relative error of the prediction using three other batches for calibration.

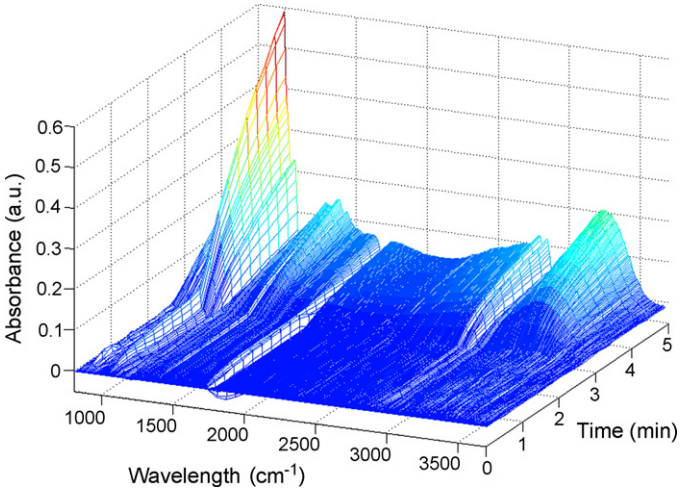


Fig. 5. Monitoring IR data subtracted from the first spectrum, in the first 5 min of monitoring.

Table 2
The obtained threshold values in the different batches by EFA

	Batch 1	Batch 2	Batch 3	Batch 4
Threshold value	−1.7	−1.6	−2.0	−1.5
Cutoff time (min)	2.1	2.8	2.0	2.5

the calibration batches and a threshold from the log of singular values was chosen when the first significant variation from the instrumental noise appears. This strategy was applied to remove the part in the IR monitoring data that has not significant spectrum variation and so, low chemical information. For the calibration batches, the chosen threshold value and its respective times were established comparing with the spectra variations without the first spectrum (Fig. 5). As the significance variation in the IR absorbance is probably related to the start of the reaction (2.1 min) inside of the CIRCLE system, the obtained spectra before these cutoff points were removed from the data, in each batch. The entire obtained threshold and its respective cutoff times for each batch were shown in Table 2.

In Fig. 6, the singular values variation with time and the chosen threshold value for a calibration batch (batch 1) are shown. It is possible to see a higher variation of the first 'factor' close to time of 2 min. In this batch, the selected threshold of the log of the singular values was −1.7 with a corresponding time of 2.1 min. After obtaining a threshold from the calibration batch, EFA was performed again on the validation set taking only the times after the selected threshold. This procedure produce a correction in the times from the different batches, removing the not variation data in the initial times of monitoring. However we can obtain the same information with a visual analysis of Fig. 5, EFA enables the same result with a computational step and with robustness performance. After obtaining a threshold value from

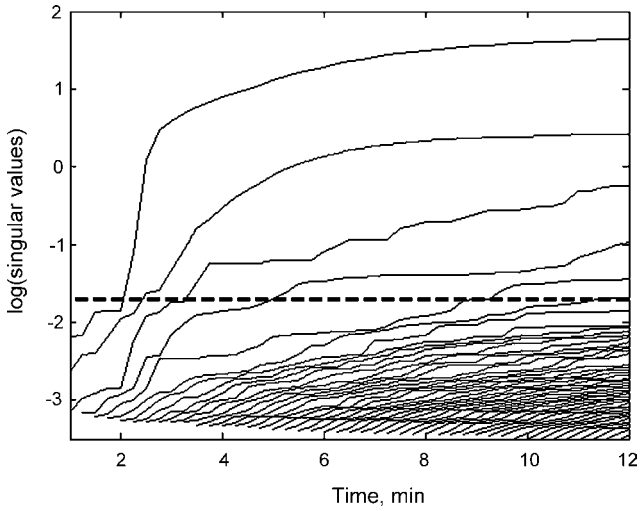


Fig. 6. Evolving factor analysis performed in a calibration batch. The chosen threshold (dashed line) turn the times lower than 2 min of monitoring to be removed.

calibration set, it can be used for estimated and correct the cutoff time and the concentration profile, respectively.

Calibration models were constructed using the two strategies described before, one with one batch for calibration and three for validation and another using three for calibration and only one for validation. After the EFA correction, the already evaluated preprocessing methods were used and the obtained results are show in Table 3. The correction of the times obtained by EFA enables a considerable reduction of the errors of prediction, as shown in Table 4 with errors below 5%. The results in Table 4 also show the necessity to use various batches for calibration, inserting large amounts of variation and reducing the errors of prediction for other batches. The errors were normally distributed in all the batches and the predicted values by the

Table 3
Cross-validation and external validation results for prediction of the yields of the batches using different preprocessing methods

Parameter	Derivative[a]	Baseline correction[b]	SG smoothing[c]	Mean-centering	Autoscaling	iPLS[d]
LV[e]	4	4	5	6	4	4
RMSEC	4.6	4.5	4.4	2.7	3.4	3.3
RMSECv	5.0	4.9	4.8	3.8	3.8	3.6
RMSEP	3.3	2.6	3.1	1.9	2.3	2.0
RMSPD (%)	7.08	4.93	6.92	4.53	6.67	4.74

[a] First derivative obtained by 13 points window.
[b] Obtained using as reference the region between the wavelengths of 1900–2400 cm^{-1}.
[c] Savitzky–Golay smoothing obtained using a 21 points window.
[d] Obtained using 20 intervals, meancenter and the chosen interval was 1693–1839 cm^{-1}.
[e] Latent variables.

Table 4
Comparison of the obtained results for different strategies applied to the reaction evaluation[a]

	Strategy 1 (PLS)	Strategy 2 (PLS)	Strategy 1 (EFA/PLS)	Strategy 2 (EFA/PLS)
RMSEP (%)	55.5	26.5	5.8	3.5
RMSDP max. (%)	65.9	47.4	6.8	4.7
RMSDP min. (%)	33.6	14.3	4.0	2.4
RMSDP average (%)	55.5	26.5	5.8	3.5

[a] Two latent variables.

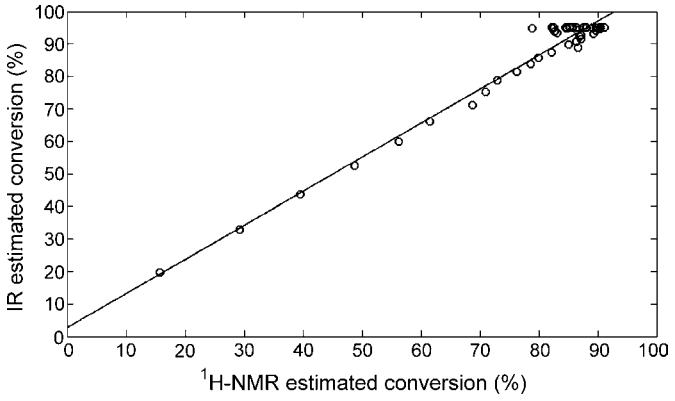


Fig. 7. Relative errors of the prediction using three other batches for calibration, after the time-delay correction by EFA.

model have a good correlation with the real ones (kinetic profile estimated by NMR), as indicated a correlation plot shown in Fig. 7.

4. Conclusion

The proposed method provides an on-line IR determination of FAEE yield in transesterification using ethanol and degummed soybean oil, as an alternative method to ^{1}H NMR analysis. The proposed method suggests a rapid and low cost method with potential to be used in industrial applications, such as process control or monitoring and for reaction optimization.

The EFA strategy to identify the significant changes and to correct the times between the IR sensor (CIRCLE system) and the reactor monitoring was efficient to cause a considerable reduction in the errors of prediction and improve the overall results.

Acknowledgments

MGT and CMG were supported by CNPq, process no. 142111/2003-1 and Capes, respectively. The authors would like to acknowledge Prof. Dr. Carol H. Collins for significant suggestions.

References

[1] S. Herrera, Nat. Biotechnol. 24 (2006) 755.
[2] F. Rosillo-Calle, L.A.B. Cortez, Biomass Bioenergy 14 (1998) 115.
[3] A.C. Pinto, L.L.N. Guarieiro, M.J.C. Rezende, N.M. Ribeiro, E.A. Torres, W.A. Lopes, P.A.D. Pereira, J.B. de Andrade, J. Braz. Chem. Soc. 16 (2005) 1313.
[4] M.F. Pimentel, G. Ribeiro, R.S. da Cruz, L. Stragevitch, J.G.A. Pacheco, L.S.G. Teixeira, Microchem. J. 82 (2006) 201.
[5] G. Knothe, Trans. ASAE 44 (2001) 193.
[6] B. Freedman, W.F. Kwolek, E.H. Pryde, J. Am. Oil Chem. Soc. 63 (1986) 1370.
[7] C. Plank, E. Lorbeer, J. Chromatogr. A 697 (1995) 461.
[8] J. Cvengros, Z. Cvengrosova, J. Am. Oil Chem. Soc. 71 (1994) 1349.
[9] M. Holcapek, P. Jandera, J. Fischer, B. Prokes, J. Chromatogr. A 858 (1999) 13.
[10] M. Lechner, C. BauerPlank, E. Lorbeer, HRC J. High Resolut. Chromatogr. 20 (1997) 581.
[11] G. Arzamendi, E. Arguinarena, I. Campo, L.M. Gandia, Chem. Eng. J. 122 (2006) 31.
[12] W.L. Xie, H.T. Li, J. Am. Oil Chem. Soc. 83 (2006) 869.
[13] G. Gelbard, O. Bres, R.M. Vargas, F. Vielfaure, U.F. Schuchardt, J. Am. Oil Chem. Soc. 72 (1995) 1239.
[14] P.R.C. Neto, M.S.B. Caro, L.M. Mazzuco, M. Nascimento, J. Am. Oil Chem. Soc. 81 (2004) 1111.
[15] G. Knothe, J. Am. Oil Chem. Soc. 77 (2000) 489.
[16] G.F. Zagonel, P. Peralta-Zamora, L.P. Ramos, Talanta 63 (2004) 1021.
[17] G.F. Ghesti, J.L. de Macedo, V.S. Braga, A. de Souza, V.C.I. Parente, E.S. Figueredo, I.S. Resck, J.A. Dias, S.C.L. Dias, J. Am. Oil Chem. Soc. 83 (2006) 597.
[18] P. Felizardo, P. Baptista, M.S. Uva, J.C. Menezes, M.J.N. Correia, J. Near Infrared Spectrosc. 15 (2007) 97.
[19] C.A. McGill, A. Nordon, D. Littlejohn, Analyst 127 (2002) 287.
[20] D.C. Hassell, E.M. Bowman, Appl. Spectrosc. 52 (1998) 18A.
[21] M.G. Trevisan, R.J. Poppi, Quim. Nova 29 (2006) 1065.
[22] S.P. Gurden, J.A. Westerhuis, A.K. Smilde, AIChE J. 48 (2002) 2283.
[23] H. Martens, T. Naes, Multivariate Calibration, John Wiley & Sons, New York, 1989.
[24] M. Zeaiter, J.-M. Roger, V. Bellon-Maurel, D.N. Rutledge, TrAC Trends Anal. Chem. 23 (2004) 157.
[25] M. Garrido, M.S. Larrechi, F.X. Rius, Anal. Chim. Acta 585 (2007) 277.
[26] V. Vojinovic, J.M.S. Cabral, L.P. Fonseca, Sens. Actuators B 114 (2006) 1083.
[27] M. Maeder, Anal. Chem. 59 (1987) 527.
[28] R.P. Sperline, S. Muralidharan, H. Freiser, Appl. Spectrosc. 40 (1986) 1019.
[29] L. Norgaard, A. Saudland, J. Wagner, J.P. Nielsen, L. Munck, S.B. Engelsen, Appl. Spectrosc. 54 (2000) 413.
[30] N.J. Millerihli, T.C. Ohaver, J.M. Harnly, Spectrochim. Acta B 39 (1984) 1603.
[31] A.P. Nascimento, M.G. Trevisan, E.R.M. Kedor-Hackmann, R.J. Poppi, Anal. Lett. 40 (2007) 975.
[32] S.K. Setarehdan, J. Chemom. 18 (2004) 414.
[33] K. De Braekeleer, A. de Juan, F.C. Sanchez, P.A. Hailey, D.C.A. Sharp, P. Dunn, D.L. Massart, Appl. Spectrosc. 54 (2000) 601.
[34] A. Martinez, J. Riu, O. Busto, J. Guasch, F.X. Rius, Anal. Chim. Acta 406 (2000) 257.

Available online at www.sciencedirect.com
ScienceDirect
Talanta 74 (2008) 741–746
Talanta
www.elsevier.com/locate/talanta

Sensitive amperometric biosensor for dichlorovos quantification: Application to detection of residues on apple skin

Gabriela Valdés-Ramírez [a,c], Didier Fournier [b], Maria Teresa Ramírez-Silva [a], J.-L. Marty [c,*]

[a] *Departamento de Química, Universidad Autónoma Metropolitana-Iztapalapa, Área de Química Analítica, San Rafael Atlixco 186, Col. Vicentina, C.P. 09340, Mexico D.F., Mexico*
[b] *IPBS, 117 Route de Narbonne, 31077 Toulouse, France*
[c] *BIOMEM, Centre de Phytopharmacie, UPVD, 52 Avenue Paul Alduy, 66860 Perpignan Cedex, France*

Received 29 March 2007; received in revised form 26 June 2007; accepted 5 July 2007
Available online 10 July 2007

Abstract

This paper presents the construction of an amperometric biosensor for the highly sensitive detection of the organophosphorus insecticide dichlorvos, based on the inhibition of acetylcholinesterase (AChE). The sensitivity of three AChEs from different sources were tested and compared: AChEs from Electric eel (Ee) and genetically engineered (B394) and wild type (B1) from *Drosophila melanogaster* (*Dm*). The enzymes were immobilized by entrapment in a photocrosslinkable PVA-SbQ polymer on a screen printed graphite electrode. The enzyme activity was estimated amperometrically at 100 mV versus Ag/AgCl by measuring the thiocholine produced by the enzymatic hydrolysis of the acetylthiocholine substrate using cobalt phthalocyanine as electron mediator. The pesticide was measured in the presence of 5% acetonitrile without loss of enzyme activity. The best sensitivity was achieved with the *Dm* mutant B394 with a detection limit of 7×10^{-11} M as compared to 1×10^{-8} M with the B1 *Dm* and 6×10^{-7} M with the Ee. The B394 biosensor was used to quantify dichlorvos in a sample of skin apple after extraction with acetonitrile.
© 2007 Published by Elsevier B.V.

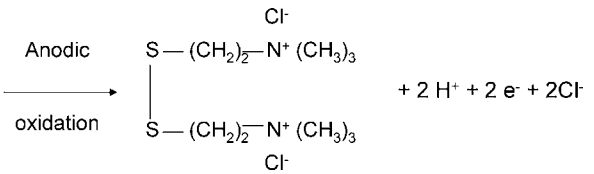
Keywords: Biosensor; Acetylcholinesterase; Dichlorvos; Acetonitrile; Apple

1. Introduction

Organophosphorous pesticides (OPs) are toxic/hazardous compounds that have been used for decades in agriculture, industry and as chemical warfare agents in military applications. The toxic action of OPs is based on their ability to irreversibly modify the catalytic serine residue in acetylcholinesterase (AChE), by phosphorylation the serine of the active site [1,2]. Thus the presence of such pesticides in natural waters and in foodstuffs is a major concern for public health [3,4]. Therefore rapid, simple and sensitive field methods are required to quantify the presence of these compounds [3,5–9]. Traditional analytical technologies used for pesticides quantification are gas chromatography (GC) with different detectors [6] and high performance liquid chromatography with UV detection (HPLC-UV) [6,7]. Nevertheless these methods are known to be expensive and quite laborious.

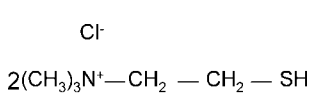
Biosensors are considered an alternative analytical tool for pesticides quantification, due their good selectivity, fast response, miniature size, and reproducible results [9–20].

Amperometric AChE biosensors based on the inhibition of the AChE enzyme by pesticides using screen-printing electrodes have been shown satisfactory results for water samples analysis [9–11]. The activity of the enzyme sensor is measured through the anodic oxidation of the thiocholine (TCh) produced by hydrolysis of the acetylthiocholine (ATCh) substrate (Eq (1)).



(1)

The decrease of the biosensor response is then correlated to the amount of pesticide in the sample following a given incu-

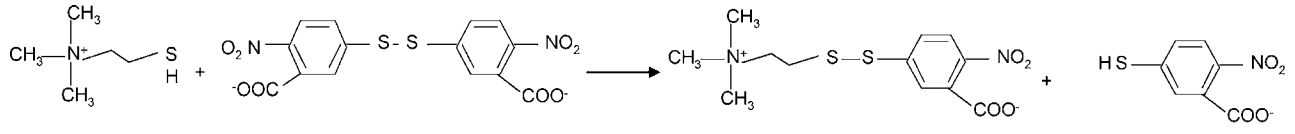


* Corresponding author.
E-mail address: jlmarty@univ-perp.fr (J.-L. Marty).

0039-9140/$ – see front matter © 2007 Published by Elsevier B.V.
doi:10.1016/j.talanta.2007.07.004

bation time [9–16]. In a biosensor design, electronic mediators such as tetracyanoquinodimetane (TCNQ) and cobalt phthalocyanine (CoPC) have been used to decrease the applied potential from 410 to 100 mV versus Ag/AgCl, hindering the oxidation of other compounds thus reducing the interferences [11–14]. Most biosensors have been developed using commercial Ee AChE. Some research groups, including ours have reported the use of genetically modified AChE from *Dm* [9,15–18]. The majority of AChE biosensors reported to date have been designed for detection of pesticides in water samples [17,19]. Application to other matrices such as food samples (fruits and vegetates) has been restricted due to the problems related to the use of these devices in the presence of organic solvents extracts. Several works reported that enzyme biosensors can function in a mixed aqueous–organic phase in low amounts of organic solvents [20,21]. However, these devices suffered from a low sensitivity and have not been used for the quantification of pesticides in solid sample.

The aim of this work was to develop a fast, simple and sensitive amperometric AChE biosensor for direct measurement of dichlorvos in an aqueous–organic solvent mixture and then, to apply the resulting biosensor for dichlorvos quantification in a fruit sample after a direct sample extraction. The strategy is based on the use of a genetically modified AChE enzyme from *Dm* which was engineered both to exhibit a high sensitivity towards dichlorvos and to increase resistance to denaturation by organic solvents. The performance of this biosensor was compared to those based on wild type *Dm* and commercial Ee AChEs. These enzymes are immobilized on screen-printing electrodes using a PVA-SbQ polymeric membrane. The aqueous–organic solvent ratio was chosen in order to use the highest concentration of organic solvent that has no effect on the enzyme activity.



(2)

2. Experimental

2.1. Chemicals and reagents

The wild (B1) and the genetically modified AChE (B 394) form from *Dm* were supplied from IPBS (Toulouse, France). AChE from Ee (EC 3.1.1.7 type V-S), acetylthiocholine iodide and chloride (ATChI, ATChCl), 5,5′-dithiobis(2-nitro-benzoic acid, DTNB) and albumin bovine (BSA), were supplied from Sigma–Aldrich. Acetonitrile HPLC grade was supplied from Carlo Erba. PVA-SbQ was from Toyo Gosei Company (Tokyo, Japan). Dichlorovos was obtained from Chem Service.

Electrodag (PE-410, 423SS, 6037SS) printing pastes obtained from Acheson (UK) and T15 graphite supplied by Lonza (Switzerland) were deposited on transparent PVC sheets (200 mm × 100 mm × 0.5 mm). Screen printed electrodes were prepared in our laboratory (BIOMEM) according to a published procedure [9].

Other chemical reagents used were analytical grade.

2.2. Apparatus

Spectrometric measurements were performed using a Hewlett Packard diode array 8452 A Spectrophotometer. Amperometric measurements were carried out with a 641 VA potentiostat (Metrohm) connected to a Kipped Zonen Flatbed X-t recorder. Screen-printing electrodes were produced using a Micro-Dek 248 printing machine.

3. Methods

3.1. Screen-printing electrodes manufactured

The screen-printing electrodes (SPEs) were fabricated according to a procedure used in the BIOMEM laboratory and published previously [9]. In this work, the working electrode layer was made using a Co-phthalocyanine carbon based paste.

3.2. Spectrometric measurements

The enzymatic activity of AChE was determined using the Ellman method [22]. The method is based on the quantitative and irreversible reaction of thiocholine, the product of the enzyme catalyzed reaction with DTNB, producing a yellow product 5-thio-2-nitrobenzoato that can be detected spectrophotometrically at 412 nm. The reaction is represented in (Eq. (2)).

The assay was performed by adding 0.700 mL of phosphate buffer (0.1 M at pH 7), 0.09 mL H_2O, 0.1 mL DTNB (3 mg/mL), 0.10 mL substrate (ATChI, 10 mM) and 0.01 mL enzyme. The DTNB solution was prepared in phosphate buffer 0.1 M pH 7.0 solution, and ATChI was prepared in 0.9% NaCl solution. The enzymatic activity calculated from the kinetic data (absorbance versus time) was expressed in U/mL. A blank without enzyme was considered as a control.

3.3. Enzyme immobilization

An enzymatic solution (3 μL) containing 30% enzyme solution (1.12 UI/mL) and 70% PVA-SbQ were deposited manually over the surface of the SPE working electrode. The amount of immobilized enzyme per electrode was calculated to be 1 mIU (apparent activity). The electrodes were dry a room temperature and then, exposed for 3 h under neon light at 4 °C degrees

to allow photopolymerization. Finally, the electrodes were conserved for about three days at 10 °C degrees before use.

3.4. Amperometric measurement

The amperometric measurements were carried out in a cell containing 10 mL PBS, at constant 30 °C under continuous magnetic stirring. A potential of 100 mV versus Ag/AgCl SPE pseudo-reference electrode was applied to the working electrode. After the stabilization of the current, 1 mM ATCh (final concentration in the cell) was injected in the reaction cell and the increase in the current intensity was measured. The stabilization time necessary to reach a plateau was 3 min. This current intensity corresponds to the oxidation of the thiocholine, the product of the enzymatic hydrolysis of the ATCh, and it is proportional to the AChE activity. The procedure was repeated three times to test the operational stability of the sensor; between each measurement the cell was washed with phosphate buffer solution (0.1 M at pH 7).

The determination of pesticide and study of the effect of the organic solvent on the activity of the immobilized enzyme was carried out using a three-step procedure. First, the initial response (I_0) of the biosensor was measured in PBS. Then, the biosensor was incubated for 10 min in a 10 mL mixture of acetonitrile-PBS with or without different concentrations of dichlorvos. After 10 min incubation, the biosensor was washed with PBS and the residual response (I_1) was measured again in PBS. The remaining activity (I%) was determined according to the following formula: $\%I = ((I_0 - I_1)/I_0) \times 100$. I% was then related to the inhibitor concentration. To evaluate the effect of the organic solvent on the enzyme activity, identical tests were carried out in different concentration of acetonitrile, in the absence of dichlorvos.

3.5. Pesticide quantification in apple sample

In order to eliminated pesticides residues over a sample, a middle size apple was washed, dry, and kept under refrigeration 1 week. The apple was cut in two parts. One half was treated with a known amount of dichlorvos. The skin was removed and spiked with a known amount of dichlorvos. After the skin was stirred with 5 mL acetonitrile for 10 min to allow extraction. The solvent was removed and evaporated. Finally, 1 mL acetonitrile was added to the dichlorvos residue, an aliquot of this solution was measured with the AChE biosensor to determine the inhibition percentage. The concentration of dichlorvos is determined using the calibration curve. The concentration of pesticide determined was compared with the results obtained for a blank which was made with the same procedure without apple skin. We have verified that the skin without addition of insecticides did not inhibit the enzyme.

4. Results and discussion

4.1. Selection of solvent concentration

The influence of three different concentrations of acetonitrile on the response of the immobilized AChEs was studied. For the three enzymes, the residual activity of the biosensor was determined (Fig. 1). No significant difference in the biosensor response was observed with 1 and 5% acetonitrile (Fig. 1). In the presence of 10% acetonitrile, the percentage of residual activity decreases 30%. As our goal is to use the highest concentration of acetonitrile which has no effect on the biosensor response, a concentration of 5% (v/v) acetonitrile was selected for further inhibition tests with dichlorvos.

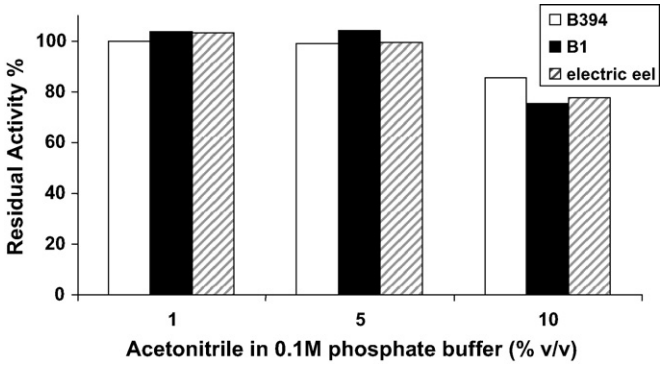


Fig. 1. The effect of acetonitrile on the biosensor responses: B394 *Dm*, B1 *Dm* and Ee. Percentage of relative response after 10 min of incubation in acetonitrile 1, 5 and 10% (v/v). The applied potential was 100 mV vs. the pseudo-reference Ag/AgCl SPE.

4.2. Substrate calibration curves of the biosensor

The substrate calibration curves for ATCh with and without 5% acetonitrile are presented in Fig. 2. The results show that the presence of acetonitrile in the reaction medium has no effect on the biosensor response. The apparent Michaelis-Menten constants for the three enzymes are shown in Table 1.These values have the same order of magnitude in the presence/absence of acetonitrile, showing that 5% solvent does not affect the activity of the enzyme. The same saturation concentration of the substrate (1 mM) was found for all the biosensors tested.

4.3. Dichlorvos detection

The majority of acetylcholinesterse sensors are developed using AChE from electric eel. This enzyme has demonstrated good characteristics in term of stability but lacks of sensitivity for the detection of some organophosphorus compounds and carbamates. We obtained engineered cholinesterases with exceptional qualities [23] and we used these enzymes to develop biosensors for the detection of organophosphorus compounds such as metamediphos [18] and carbamates [24]. The detection of chlorpyriphos is a good example of the quality of those enzymes. The

Table 1
Apparent Michaelis-Menten constants (K_m) for the B394 and B1 *Dm* AChE and for the Ee AChE in the presence/absence of 5% acetonitrile

Enzyme	B394	B1	Electric eel
K_m in buffer (mM)	0.21 ± 0.01	0.18 ± 0.02	0.16 ± 0.01
K_m in 5% acetonitrile (mM)	0.20 ± 0.02	0.12 ± 0.01	0.09 ± 0.01

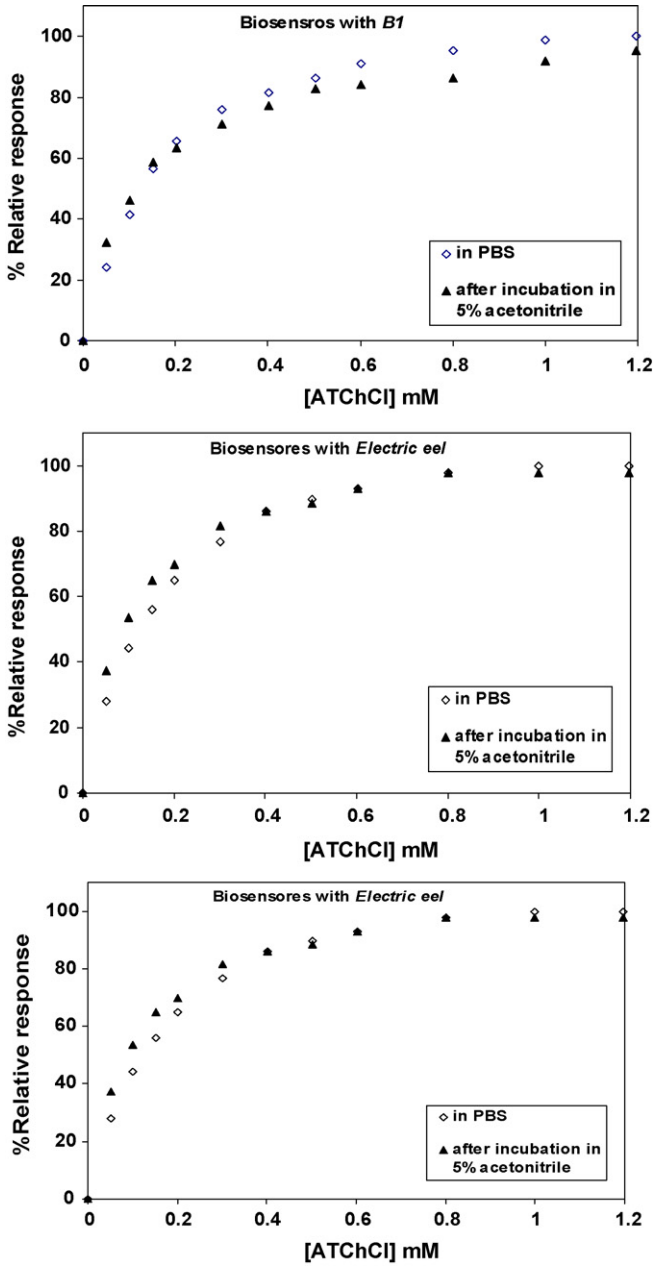


Fig. 2. Substrate calibration curves before and after 10 min incubation in 5% acetonitrile: B394 *Dm* (a), B1 *Dm* (b) and Ee (c) AChE.

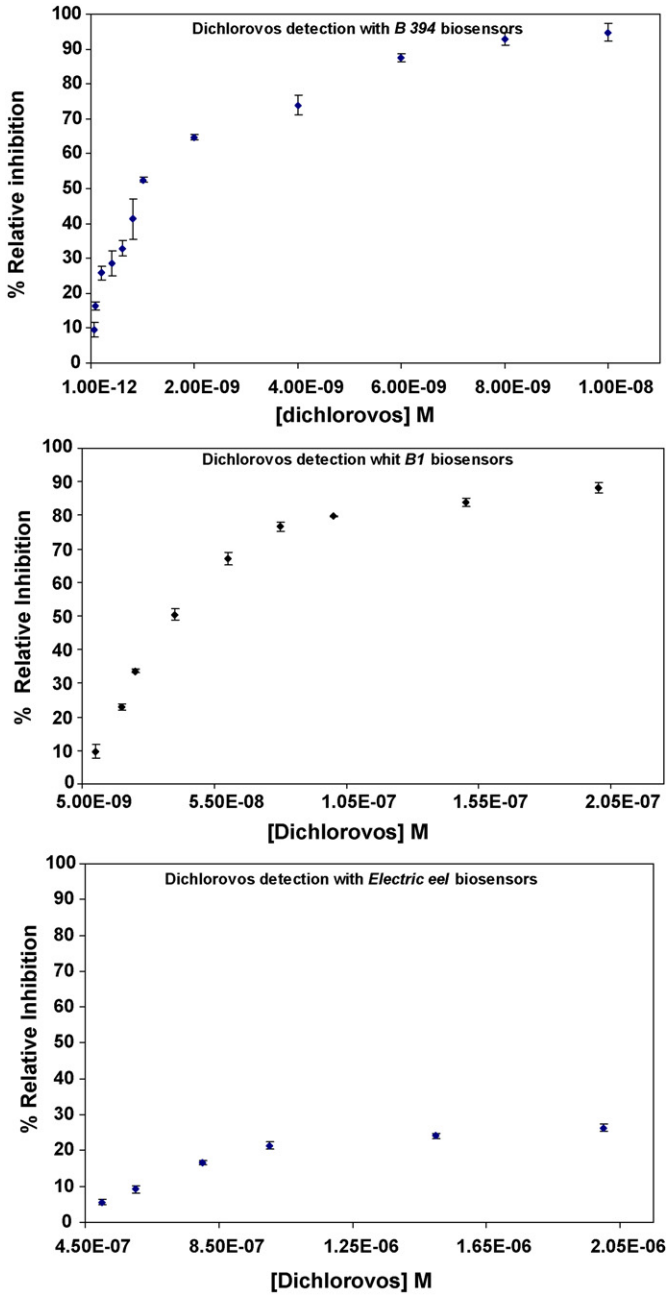


Fig. 3. Inhibition curves of AChE biosensors by dichlorovos. Experimental conditions: 5% acetonitrile, 10 min incubation time, 100 mV applied potential; B394 *Dm* (a), B1 *Dm* (b) and Ee (c) AChE.

inhibition curves of the immobilized AChEs by dichlorvos in the presence of 5% acetonitrile are shown in Fig. 3. Each value represents the average response of measurements obtained with three different electrodes prepared in the same experimental conditions. The detection limit was calculated as 10% inhibition (I_{10}).

Table 2
Inhibition constants K_i for dichlorovos determined by spectrometric analysis with AChE from electric eel, wild type (B1) and recombinant (B394) from *Drosophila melanogaster*

Enzyme	B394	B1	Electric eel
K_i ($\mu M^{-1}\,min^{-1}$)	224	1.9	0.036
LOD (M)	7×10^{-11}	10^{-8}	7×10^{-7}

The K_i of the engineered enzyme (B394) is 117- and 62 222-fold lower than wild type (B1) and electric eel source, respectively (Table 2). The very high sensitivity is confirmed by the results obtained using the same SPE, with the same method of immobilization for the detection of dichlorvos. Table 2 shows a good correlation between K_i and LOD for the detection of dichlorvos. Using biosensor with B394, the LOD obtained is, respectively, 142- and 8570-fold lower than with B1 and electric eel cholinesterase.

Table 3 is a compilation of the results obtained by different researchers for the detection of dichlorvos. Some laboratories developed biosensors using tyrosinase or acetylcholinesterase,

Table 3
Detection limits for dichlorvos using the AChE biosensors in our research and detection limits obtained in other researches

Source	LOD (M)	Origin	Transducer	Detection	Year	Ref.
AChE Ee	23×10^{-6}	SIGMA	Single bead reactor	Electro.	1992	[25]
AChE Ee	0.5×10^{-6}	SIGMA	Graphite	Electro.	2002	[26]
AChE Ee	0.5×10^{-6}	SIGMA	SPE	Electro.	2002	[27]
AChE *Dm*	3.6×10^{-8}	SIGMA	Cho Ox SPE	Electro.	2006	[28]
AChE Ee	1.8×10^{-10}	IPBS				
AChE *Dm*	1.5×10^{-9}	IPBS	SPE	Electro.	2006	[29]
AChE *Dm*	4×10^{-9}	IPBS	SPE	Electro.	2004	[10]
AChE Ee	10×10^{-13}	SIGMA	Nanoporous carbon FIA	Electro.	2005	[30]
AChE *Dm*	10×10^{-18}	IPBS	SPE (FIA)	Electro.	2005	[31]
AChE Ee	10×10^{-13}	SIGMA				
AChE *Dm*	10×10^{-18}	IPBS	SPE	Electro.	2005	[11]
Tyrosinase	0.08×10^{-6}	SIGMA	Coupled with HRP	Electro.	2005	[32]
Tyrosinase	0.06×10^{-6}	SIGMA	Glassy carbon/composite	Electro.	2006	[33]
OPH	50×10^{-6}	Unknown	Lithography FIA	Electro.	2003	[34]
AChE Ee	2.2×10^{-6}	SIGMA	Membrane	Optical	2006	[35]
AChE Ee	0.2×10^{-9}	SIGMA	Membrane	Optical	2007	[36]
AChE Ee	0.6×10^{-6}	SIGMA	SPE	Electro.	This work	
AChE *Dm*	70×10^{-12}	IPBS				

electric eel or genetically engineered enzymes. Usually genetic engineered enzymes show better sensitivity than enzyme from natural sources, varying from two [28] to five [31] order of magnitude. Some authors reported exceptional results with LODs as low as 10^{-17} M [11,31], This high performance is due to the association of a good transducer and the genetically engineered enzyme used in this study. However, such a high sensitivity has its drawback, it was found to be associated with a low repeatability.

4.4. Apple sample analysis

Analysis of dichlorvos in the apple sample was carried out using the B394 biosensor. For inhibition measurements, the biosensor was incubated for 10 min in a solution containing the dichlorvos extract in acetonitrile. This solution was prepared 5% (v/v) of organic sample extract and PBS solution. After incubation, the residual response of the biosensor was measured and compared with the initial response. The concentration of dichlorvos was calculated by interpolation of the inhibition percentage (*I*%) to the calibration curve obtained with standard solution of dichlorvos, the reference was tested following the same procedure (Fig. 3).

The results obtained with the apple sample show a 63% inhibition which is in good agreement with the 65% inhibition percentage obtained with the reference sample (without apple). These results are shown in Table 4.

Table 4
Dichlorovos quantification in apple sample

	Apple simple spiked with dichlorovos	Dichlorovos blank
%Inhibition	63	65
Dichlorovos concentration	2.3×10^{-9} M	2.6×10^{-9} M

5. Conclusions

This work shows the possibility to quantify dichlorvos in solid matrices using biosensors based on genetically modified *Dm* AChEs. The results demonstrate that the use of genetically modified AChE decreased considerably the detection limit (with four orders of magnitude) as compared to biosensors based on wild type *Dm* and Ee AChEs. In addition, the biosensor was able to work in the presence of 5% acetonitrile, which was necessary for the extraction of pesticide from the sample. The use of a disposable biosensor offers some additional advantages such as mass production, possibility for miniaturization and low cost.

Acknowledgements

The authors would like to thank the Red ALFA II for the B***ioSenIntg*** Clave: II-0486-FCFA-FCD-FI project. G.V.R. acknowledges CONACYT for a studentship.

References

[1] M. Eto, Organophosphorous Pesticides, third ed., CRC Press, Cleveland, OH, 1977.
[2] J.J. Kang, H.W. Fang, Biochem. Biophys. Res. Commun. 238 (1997) 367–369.
[3] CICOPLAFEST Catálogo Oficial de Plaguicidas, Secretaria de Agricultura Ganadería y Desarrollo Rural, Secretaria del Medio Ambiente, Recursos Naturales y Pesca, Secretaria de Salud y Secretaria de Comercio y Fomento Industrial, México D.F., 2004.
[4] W.H.O. (World Health Organization), vol. 63, Environmental Health Criteria, Geneva, 1986.
[5] D. Barcelo, Environmental Analysis, Techniques, Applications and Quality Assurance, Elsevier, 1993.
[6] S. Lacorte, D. Barcelo, Environ. Sci. Technol. 28 (1994) 1159–1163.
[7] S. Lacorte, D. Barcelo, J. Chromatogr. A 712 (1995) 103–112.
[8] S. Lacorte, D. Barcelo, Anal. Chim. Acta 296 (1994) 223–234.

[9] B. Bucur, D. Fournier, A. Danet, J.L. Marty, Anal. Chim. Acta 562 (2006) 115–121.
[10] A. Vakurov, C.E. Simpson, C.L. Daly, T.D. Gibson, P.A. Millner, Biosens. Bioelectron. 20 (2004) 1118–1125.
[11] K.A. Law, S.P.J. Higson, Biosens. Bioelectron. 20 (2005) 1914–1924.
[12] S. Andreescu, J.L. Marty, Biomol. Eng. 23 (2006) 1–15.
[13] A.L. Hart, W.A. Collier, D. Janssen, Biosens. Bioelectron. 7 (1997) 645–654.
[14] G.S. Nunes, G. Jeanty, J.L. Marty, Anal. Chim. Acta 5232 (2004) 107–115.
[15] H. Schulze, S. Vorlová, F. Villate, T.T. Bachmann, R.D. Schmid, Biosens. Bioelectron. 18 (2003) 201–209.
[16] S. Andreescu, T. Noguer, V. Magearu, J.-L. Marty, Talanta 57 (2002) 169–176.
[17] G.S. Nunes, T. Montesinos, P.B.O. Marques, D. Fournier, J.L. Marty, Anal. Chim. Acta 343 (2001) 1–8.
[18] P.B.O. Marques, G.S. Nunes, T.C.R. dos Santos, S. Andreescu, J.L. Marty, Biosens. Bioelectron. 20 (2004) 825–832.
[19] A.A. Karyakin, E.E. Kariakina, L. Gorton, Anal. Chem. 68 (1996) 4335–4341.
[20] T. Montesinos, S. Pérez-Munguia, F. Valdez, J.L. Marty, Anal. Chim. Acta 431 (2001) 231–237.
[21] E. Wilkins, M. Carter, J. Voss, D. Ivnitski, Electrochem. Commun. 2 (2002) 786–790.
[22] G.L. Ellman, K.P. Courtney, V. Andres, R.M. Fearstherstone, Biochem. Pharmacol. 7 (1961) 88–90.
[23] Y. Boublik, P. Saint-Aguet, A. Lougarre, M. Arnaud, F. Vilatte, S. Escada-Moncada, D. Fournier, Prot. Eng. 15 (2002) 43–50.
[24] B. Bucur, A. Danet, D. Fournier, J.-L. Marty, Anal. Chim. Acta 562 (2002) 115–121.
[25] S. Kumaran, C. Tran-Minh, Anal. Biochem. 200 (1992) 187–194.
[26] S. Andreescu, L. Barthelmebs, J.-L. Marty, Anal. Chim. Acta 464 (2002) 171–180.
[27] A. Ciucu, C. Ciucu, Roum. Biotechnol. Lett. 7 (2002) 667–676.
[28] M. Del Carlo, A. Pepe, M. Gregorio, M. Mascini, J.-L. Marty, J. Food Protect. 69 (2006) 1406–1411.
[29] M. Shi, J. Xu, S. Zangh, B. Liu, J. Kong, Talanta 68 (2006) 1089–1095.
[30] S. Sotiropoulo, N.A. Chaniotakis, Anal. Chim. Acta 530 (2005) 199–204.
[31] S. Sotiropoulo, D. Fournier, N.A. Chaniotakis, Biosens. Bioelectron. 20 (2005) 2347–2352.
[32] R. Solná, E. Dock, A. Christenson, J. Emnéus, P. Skládal, Anal. Chim. Acta 528 (2005) 9–19.
[33] J.C. Vidal, S. Esteban, J. Gil, J.R. Castillo, Talanta 68 (2006) 791–799.
[34] M.J. Shöning, R. Krause, K. Block, M. Musahmeh, A. Mulchandani, J. Wang, Sens. Actuators B 95 (2003) 291–296.
[35] F.C.M. Wong, M. Ahmad, L.Y. Heng, L.B. Peng, Talanta 69 (2006) 888–893.
[36] V. Vamvakaki, N.A. Chaniotakis, Biosens. Bioelectron. 22 (2007) 2848–2853.

Available online at www.sciencedirect.com
ScienceDirect
Talanta 74 (2008) 518–525
Talanta
www.elsevier.com/locate/talanta

Double interdigitated array microelectrode-based impedance biosensor for detection of viable *Escherichia coli* O157:H7 in growth medium

Madhukar Varshney [a], Yanbin Li [a,b,*]

[a] *Department of Biological and Agricultural Engineering, University of Arkansas, Fayetteville, AR 72701, United States*
[b] *Center of Excellence for Poultry Science, University of Arkansas, Fayetteville, AR 72701, United States*

Received 12 March 2007; received in revised form 13 June 2007; accepted 13 June 2007
Available online 30 June 2007

Abstract

Double interdigitated array microelectrodes (IAM)-based flow cell was developed for an impedance biosensor to detect viable *Escherichia coli* O157:H7 cells after enrichment in a growth medium. This study was aimed at the design of a simple flow cell with embedded IAM which does not require complex microfabrication techniques and can be used repeatedly with a simple assembly/disassembly step. The flow cell was also unique in having two IAM chips on both top and bottom surfaces of the flow cell, which enhances the sensitivity of the impedance measurement. *E. coli* O157:H7 cells were grown in a low conductivity yeast–peptone–lactose–TMAO (YPLT) medium outside the flow cell. After bacterial growth, impedance was measured inside the flow cell. Equivalent circuit analysis indicated that the impedance change caused by bacterial growth was due to double layer capacitance and bulk medium resistance. Both parameters were a function of ionic concentration in the medium, which increased during bacterial growth due to the conversion of weakly charged substances present in the medium into highly charged ions. The impedance biosensor successfully detected *E. coli* O157:H7 in a range from 8.0 to 8.2×10^8 CFU mL^{-1} after an enrichment growth of 14.7 and 0.8 h, respectively. A logarithmic linear relationship between detection time (T_D) in h and initial cell concentration (N_0) in CFU mL^{-1} was $T_D = -1.73 \log N_0 + 14.62$, with $R^2 = 0.93$. Double IAM-based flow cell was more sensitive than single IAM-based flow cell in the detection of *E. coli* O157:H7 with 37–61% more impedance change for the frequency from 10 Hz to 1 MHz. The double IAM-based flow cell can be used to design a simple impedance biosensor for the sensitive detection of bacterial growth and their metabolites.
© 2007 Elsevier B.V. All rights reserved.

Keywords: Impedance detection; Impedance microbiology; *E. coli* O157:H7; Interdigitated array microelectrodes; Flow cell

1. Introduction

Impedance microbiology is applied in a variety of fields ranging from detection and monitoring of microorganisms, detection of antibiotics, analysis of food preservatives, food hygiene, and clinical and pharmaceutical microbiology to environmental sampling [1–6]. This indirect approach to quantitative microbiology quantifies microorganisms by measuring the change in the electrical conductivity of the medium during growth of microorganism [2]. It was first introduced by Stewart [7], however, this technique received the attention to merit only in mid seventies during last century. Growth of microorganisms increases the conductivity of the medium by converting uncharged or weakly charged substances present in the growth medium, such as yeast, peptone, and sugar into highly charged substances such as amino acids, aldehydes, ketones, acids, and other metabolic products [5]. Change in the conductivity of the solution during bacterial growth is recorded by impedance and conductance techniques. Detection time is inversely proportional to the initial numbers of cells present in the medium before growth. Therefore, a high number of cells result in a low detection time and vice versa. Edmiston [8] reported a detection time ranging from 1 to 7 h for the detection of a range of initial bacterial concentrations from 10^7 to 10^1 CFU mL^{-1}. Impedance measurement is commonly preferred over conductance measurement as it accounts for double layer capacitance and dielectric capacitance of the system in addition to the resistance (inverse of conductance) of the solution, while conductance measurement accounts for conductance of the solution only. It has been estimated that a minimum of 10^3 to 10^7 CFU mL^{-1} of bacterial cells are required to produce a detectable change in the impedance signal [9].

* Corresponding author at: Department of Biological and Agricultural Engineering, University of Arkansas, 230 Engineering Hall, Fayetteville, AR 72701, United States. Tel.: +1 479 575 2424; fax: +1 479 575 7139.
E-mail address: yanbinli@uark.edu (Y. Li).

0039-9140/$ – see front matter © 2007 Elsevier B.V. All rights reserved.
doi:10.1016/j.talanta.2007.06.027

Traditionally, thin metal rods or wires immersed in a medium were used as electrodes in the impedance measurement techniques [10–12]. In an attempt to improve sensitivities, add functionalities, and lower the detection limits of impedance techniques, several shapes of electrodes have been developed in last few decades. Of these, microelectrodes fabricated using lithographic techniques have been of great interest because they typically have higher sensitivities than macroelectrodes. The macroelectrodes have a semi-infinite linear diffusion profile resulting in a greater depletion of reactants in contrast to the microelectrodes which has a spherical diffusion profile favoring greater rate of reactant supply to the electrodes [13]. Among microelectrodes, IAM presents promising advantages in terms of low ohmic drop, fast establishment of steady state, rapid kinetics of reaction, and increased signal-to-noise ratio [14,15]. IAM are successfully employed for impedance measurement of bacterial cells during enrichment growth (impedance microbiology) [6,16–19], by capturing bacterial cells to the antibodies immobilized on the surface of electrodes (faradic impedance method) [20–24], or by using dielectrophoresis (DEP) for the capture of cells on the surface of electrodes (dielectrophoretic impedance) [25–29]. To enhance the capability of IAM in impedance sensing, microfluidic flow cells can be added to the IAM to achieve a fully integrated microchip for a broad range of applications including dielectrophoresis and impedance detection [30,31]. The advantages of microfluidic flow cells in combination with embedded IAM are: high detection sensitivity, small volume handling, low contamination during bacterial growth, ability to concentrate cells, and rapid detection of small number of cells. As the surface to volume ratio increases in the microfluidic flow cells with embedded IAM, the distance that conductive ions must diffuse to reach the sensor surface also decreases, thus resulting in rapid reaction kinetics [32]. Current impedance sensing techniques either employ an open IAM chip [16,17,20–24] or are based on the complex multi-step design of a flow cell with an embedded IAM [18,19,29–31], which have limited applications due to clogging and insufficient cleaning.

Selective medium is commonly used to give specificity to impedance detection system for the target bacteria. Yang et al. [16] used IAM-based impedance biosensor for rapid detection of viable *Salmonella* Typhimurium in a selective medium. selenite cystein (SC) broth supplemented with trimethylamine oxide (TMAO·HCl) and mannitol (SC/T/M) was used for the selective growth of *S*. Typhimurium. During the growth of three non-target bacteria (*Listeria monocytogenes*, *Escherichia coli* O157:H7, and *Pseudomonas aeruginosa*) in SC/T/M medium for 16 h, no significant change in the impedance response of the system was observed. The IAM-based biosensor was successfully used to detect a range of *S*. Typhimurium from 4.8 to 5.4×10^5 CFU mL^{-1} after an enrichment growth of 9.3 and 2.2 h, respectively. Non-selective medium can also be used for the impedance detection of bacterial cell growth. In this case, target bacteria from the sample can be separated and concentrated by immunoseparation with conjugated immunomagnetic microbeads. Yang and Li [17] demonstrated the use of general medium—brain heart infusion (BHI) broth, for the detection of *S*. Typhimurium using impedance technique. Anti-*Salmonella* antibodies coated magnetic microbeads were used to separate and concentrate *S*. Typhimurium from the samples followed by the growth of bacterial cells in BHI broth. The impedance measurement was most sensitive at 10 Hz and the IAM-based biosensor was able to detect initial concentrations of 10^1 and 10^6 CFU mL^{-1} of *S*. Typhimurium in a growth time of 8 and 1.5 h, respectively. Gomez-Sjöberg et al. [6] combined immunomagnetic separation and dielectrophoresis with impedance microbiology to design an on-site incubation microfluidic biochip with IAM to detect *Listeria* in a non-selective medium. IAM were used to concentrate bacterial cells by a factor of 10^4 to 10^5 in a detection chamber of volume 400 pL followed by an enrichment growth in a non-selective growth medium (Luria Bertani broth). The detection time for 8.4×10^4 CFU mL^{-1} of *L. monocytogenes* was less than 2 h.

In this study, we designed and tested a simple double IAM-based flow cell for an impedance biosensor to detect viable *E. coli* O157:H7 cells from the samples after an enrichment growth in a low conductivity growth medium. This flow cell with embedded IAM could be easily assembled without the need of complicated microfabrication techniques. The flow cell could also be easily disassembled to clean the electrode for repeated use. The flow cell was also unique by using double IAM on its top and bottom surfaces to enhance the sensitivity in the detection of *E. coli* O157:H7. The impedance change was due to the growth of *E. coli* O157:H7 cells that was analyzed as a function of frequency. An equivalent circuit was designed to curve fit experimental results and to determine parameters of the electrical circuit responsible for impedance change caused by the growth of *E. coli* O157:H7 cells.

2. Experimental

2.1. Bacterial culture and chemicals

Frozen stock of *E. coli* O157:H7 (ATCC 43888) was maintained in brain heart infusion (with 12% glycerol) broth (Remel Inc., Lenexa, KS) at −70 °C. Culture was harvested in brain heart infusion broth maintained at 37 °C for 18–22 h. For enumeration, pure cultures were serially diluted in 0.01 M, pH 7.4 phosphate-buffered saline and surface plated on sorbitol MacConkey agar (Remel Inc., Lenexa, KS), which was incubated at 37 °C for 20–22 h. Yeast extract (BD Inc., Franklin Lakes, NJ), peptone (BD Inc., Franklin Lakes, NJ), lactose (Sigma–Aldrich, St. Louis, MI), and trimethylamine oxide (TMAO, Sigma–Aldrich, St. Louis, MI) were used for the low conductivity growth medium for the enrichment growth of bacterial cells.

2.2. Enrichment growth medium and bacterial growth

Specially designed low conductivity yeast–peptone–lactose–TMAO (YPLT) medium was prepared by mixing yeast extract (10 g/L), peptone (5 g/L), lactose (3.3 g/L), and TMAO (5.0 g/L) in deionized water. The medium was autoclaved at 121 °C for 15 min. Salts such as sodium chloride and disodium phosphate were not added in order to minimize the conductivity of the medium. Growth medium was optimized for the growth of

E. coli O157:H7 cells. Lactose was preferred over the use of glucose, as *E. coli* O157:H7 cells cannot metabolize glucose. TMAO was used for the optimum growth of *E. coli* O157:H7 cells, as it acts as a demetallation and decarbonylation agent that mediates the conversion of thiols to disulfides. Pure culture of *E. coli* O157:H7 was decimally diluted in YPLT medium from 8.0×10^0 to 8.0×10^8 CFU mL^{-1}. Diluted cultures were incubated in a continuous rotation incubator (VWR International, West Chester, PA) and the samples were taken out for impedance measurement at an interval of 2 h from each enriched sample. Samples were immersed in a boiling water bath for 20 min to kill bacterial cells and then were stored at 4 °C until impedance measurement was performed. For the samples with initial concentrations of 8×10^6 and 8×10^8 CFU mL^{-1} of *E. coli* O157:H7, additional samples were taken out at an interval of 30 min from the start till 2 h of enrichment growth to measure the impedance response of the system over a short period of bacterial growth.

2.3. Design of double IAM-based impedance biosensor

IAM chips were obtained from ABtech Scientific Inc. (Richmond, VA), which contained a gold layer (1000 Å) sputtered on borosilicate glass substrate with an adhesion promotion layer of 100 Å titanium–tungsten alloy residing between the glass and gold layer. A topcoat layer of silicon nitride was used to passivate the busses and provide a window through which the active area of electrodes was exposed. The total size of an IAM chip was 2 cm × 1 cm × 0.05 cm with 50 pairs of fingers each of 15 μm width and 4.96 mm length. The space between the fingers was 15 μm. Before assembly, IAM chips were cleaned with 0.1 M sodium hydroxide, 0.1 M hydrochloric acid, acetone, and deionized water, and then dried in a stream of nitrogen. Two IAM chips facing each other were put together with a silicon rubber gasket (thickness 250 μm) between them to assemble a flow cell as shown in Fig. 1a. The gasket was cut in the center (5 mm × 5 mm), to expose the electrode surfaces to detection medium. Both IAM chips were tied together using an elastic band. Holes (diameter 1 mm) were drilled in each of the IAM chips to make inlet and outlet for the fluid flow. Nanoport connectors (Upchurch Scientific, Oak Harbor, WA) were bonded to the inlet and outlet in order to connect tubing for fluid flow. The assembly of the flow cell is shown in Fig. 1b.

2.4. Impedance measurement

Impedance measurement was performed using an IM-6 impedance analyzer (BAS, West Lafayette, IN) with IM-6/THALES software. For all impedance measurements, a sine-modulated ac potential of 100 mV was applied across the flow cell and a Bode plot for the magnitude of impedance and phase angle was plotted for a range of frequency from 10 Hz to 1 MHz. Samples were injected into the flow cell with the help of a syringe pump at a flow rate of 33 μL/min. To observe the effect of the presence of bacterial cells on the impedance measurement, a sample with 5.4×10^4 CFU mL^{-1} of *E. coli* O157:H7 cells after 16 h of growth was centrifuged at 250 × *g* for 15 min (supernatant was separated for impedance measurement) and was compared with a similar sample without centrifugation. The effect of live and dead bacterial cells on impedance measurement was also tested. Bacterial cells were inactivated by immersing in a boiling water bath for 30 min.

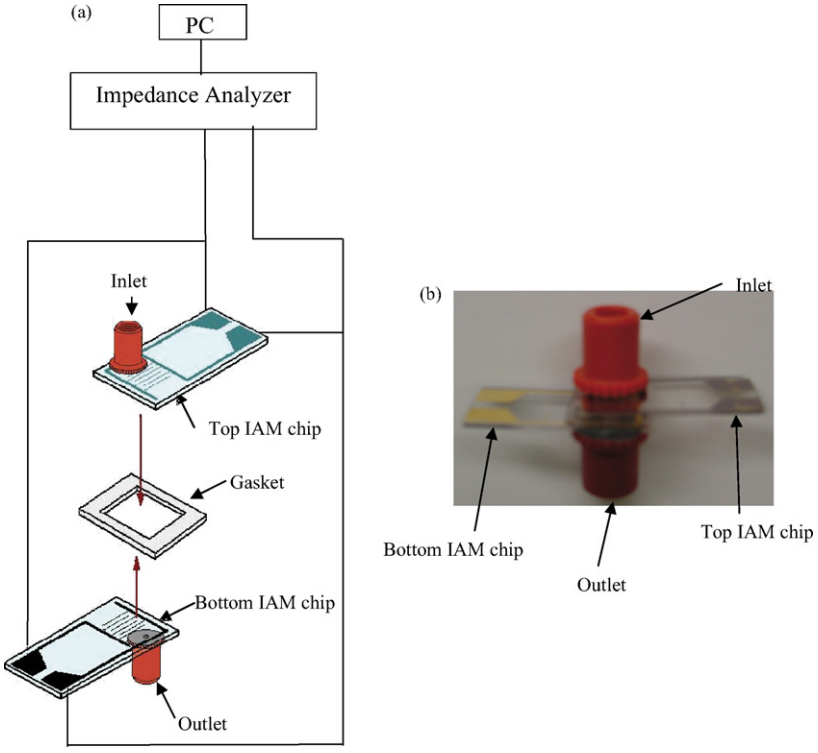


Fig. 1. (a) Schematic diagram of the assembly of double interdigitated array microelectrode-based flow cell and (b) an assembled flow cell.

To monitor the effect of frequency on impedance measurement, the normalized impedance change (NIC) was plotted against growth time for five different frequencies (10 Hz, 270 Hz, 4.18 kHz, 64.6 kHz, and 1 MHz). To plot the growth curves, NIC was plotted against growth time for different concentrations of *E. coli* O157:H7 ranging from 8.0×10^0 to 8.2×10^8 CFU mL^{-1}. NIC was calculated as follows

$$\text{NIC} = \frac{Z_{\text{sample}} - Z_{\text{control}}}{Z_{\text{control}}} \times 100 \quad (1)$$

where Z_{control} is the magnitude of impedance for control sample before growth and Z_{sample} is the magnitude of impedance for a sample containing *E. coli* O157:H7 after an enrichment growth.

3. Results and discussion

3.1. Double IAM-based versus single IAM-based flow cells

Fig. 2a shows the comparison of impedance responses of double and single IAM-based flow cells for the impedance measurement of 8.2×10^4 CFU mL^{-1} of *E. coli* O157:H7 after an enrichment growth of 16 h. The magnitude of impedance measured with double IAM decreased in the range of 61–37% for the range of frequencies from 10 Hz to 1 MHz as compared to single IAM. Since resistance is inversely proportional to the surface area, the resistive impedance for double IAM was lower than single IAM due to the availability of more surface area for impedance measurement. The microelectrodes scan a region called "active region", which has a maximum strength of an electric field and a few microns above the surface. IAM usually results in a sensitive impedance change, if bacterial cells are present in the active region [33]. Radke and Alocilja [20] calculated the range of active region for an electrode with width and space measuring 3 and 4 μm, respectively. IAM is best to detect impedance change when bacterial cells are present in the active region which is 10 μm above the surface of electrodes. When cells are present outside the active region, impedance change is minimized. The presence of IAM on both inside walls (top and bottom) of the detection chamber increases the amount of ions detected due to presence of two active regions of IAM as compared to one active region with single IAM configuration as shown in Fig. 2b. Thus, double IAM-based flow cell was more effective in improving the sensitivity of impedance measurement as compared to single IAM-based flow cell.

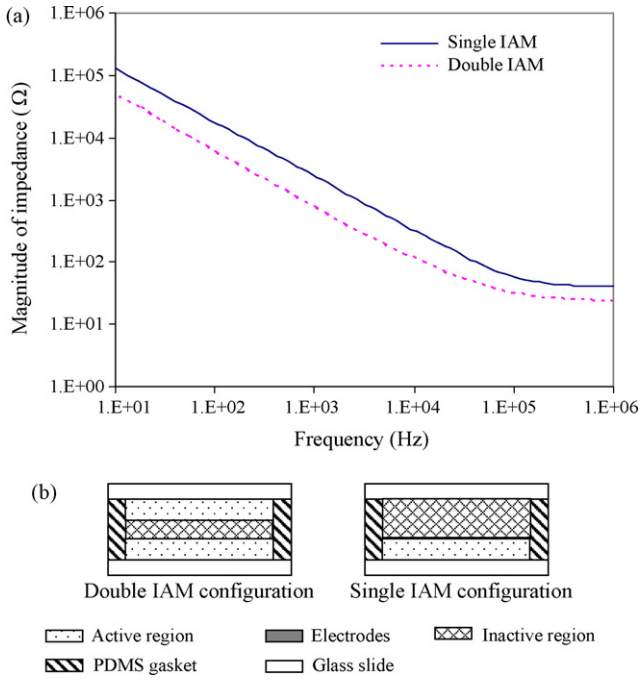


Fig. 2. (a) The magnitude of impedance measured for 8.2×10^4 CFU mL^{-1} of *Escherichia coli* O157:H7 after an enrichment growth of 16 h using double and single interdigitated array microelectrode-based flow cells and (b) schematic diagram of cross section of flow cells with double and single IAM. Double interdigitated array microelectrodes detected more ions in the detection chamber as compared to single interdigitated array microelectrode within the same detection chamber.

3.2. Equivalent circuit analysis for impedance measurement system

The experimental data of impedance biosensor in aqueous solution was represented by an equivalent circuit as shown in Fig. 3a. The equivalent circuit consisted of two double layer capacitor (C_{dl}) (one for each set of electrodes) connected in series with bulk medium resistor (R_{s}). Constant phase element was used to model double layer capacitance of the electrodes. This is commonly favored over the use of a simple capacitor [34]. C_{dl} accounted for the effect of ionic species on the capacitance near the surface of an electrode. R_{s} represented bulk resistance of the solution, accounting for the change in conductivity and charge transport across the bulk solution.

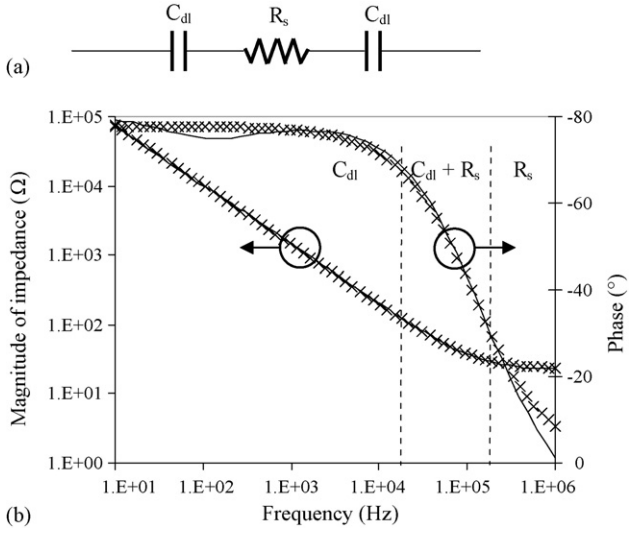


Fig. 3. (a) Equivalent circuit for the impedance measurement of growth of *E. coli* O157:H7 cells in YPLT medium using a double interdigitated array microelectrode-based flow cell and (b) experimental and curve-fitted Bode plots for the impedance measurement of 5.4×10^4 CFU mL^{-1} of *E. coli* O157:H7 after the growth of 16 h. Solid lines show the experimental data, while cross marks show curve-fitted data.

Fig. 3b shows the experimental and simulated data for impedance measurement (both magnitude and phase) of 5.6×10^4 CFU mL^{-1} of *E. coli* O157:H7 after an enrichment growth of 16 h in YPLT medium using double IAM-based flow cell. To validate equivalent circuit, 50 points of the measured data on the impedance spectrum were automatically selected by the IM-6/THALES software and were used as an input to the equivalent circuit, generating a fitting impedance spectrum. Fitting was done by the IM-6/THALES software, using a complex non-linear least-square method. The close agreement between the measured data and fitted spectra indicated that the proposed equivalent circuit provided a feasible, if not unique, model to represent the impedance measurement system. There are three regions in the impedance spectrum. These are represented by two components in the equivalent circuit individually, and their combination. The double layer region dominated by C_{dl} was in the frequency range of 10 Hz to 20 kHz. Resistive region dominated by R_s was in the frequency range of 202 kHz to 1 MHz. The region dominated by both C_{dl} and R_s was in the frequency range of 20–202 kHz.

The frequency dependent characteristics of the three regions can be explained using mathematical relationships between resistance, capacitance, frequency, and impedance. In an electric circuit, the mathematical relationships of resistance, capacitance, and their contribution to the total impedance value are given by

$$\text{resistive impedance}: \quad Z_R = R_s \tag{2}$$

$$\text{capacitive impedance}: \quad Z_c = \frac{1}{2\pi f C_{dl}} \tag{3}$$

Magnitude of total impedance due to a resistor and a capacitor:

$$|Z| = \sqrt{R_s^2 + \frac{1}{(\pi f C_{dl})^2}} \quad \text{(serial connection of } C_{dl} \text{ and } R_s\text{)} \tag{4}$$

The calculations of total impedance based on above equations clearly showed that the values of total impedance at a frequency less than 20 kHz were dominated (≥90%) by double layer capacitance (Eqs. (3) and (4)); while in between 202 kHz and 1 MHz the values of total impedance were dominated (≥90%) by bulk medium resistance (Eqs. (2) and (4)). Contributions of double layer capacitance and bulk medium resistance can also be interpreted by looking at the phase angle values shown in the impedance spectrum (Fig. 2b). The effect of the double layer capacitance at a frequency less than 20 kHz was evident by the phase angle values close to −90° as shown in the Bode plot. In this frequency range, the magnitude of impedance decreased with increase in frequency, as capacitive impedance is inversely proportional to the frequency of the applied potential (Eq. (3)). In the high frequency range from 202 kHz to 1 MHz, resistive region was evident by the phase angle values close to 0° and the magnitude of the impedance was constant for this frequency range, as resistive impedance is independent of frequency (Eq. (2)). For the frequency range of 20–202 kHz, the impedance was controlled both by capacitance and resistance, as the phase angle was in between 0° and −90°.

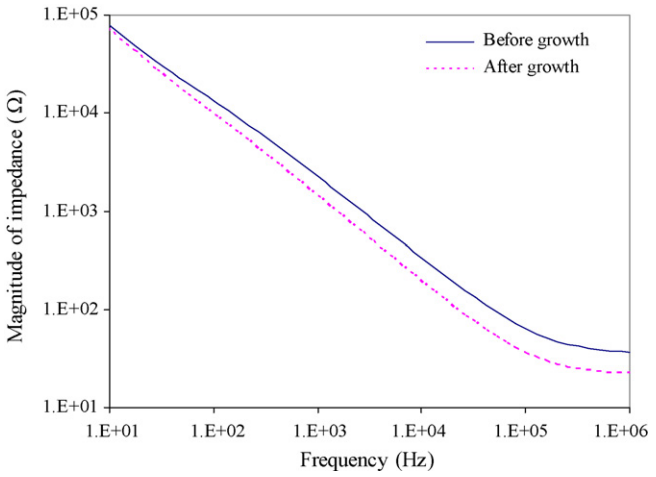


Fig. 4. Bode plot for the magnitude of impedance measured before and after an enrichment growth of 5.4×10^4 CFU mL^{-1} of *E. coli* O157:H7 cells for 16 h in YPLT medium. The impedance was measured for the range of frequencies from 10 Hz to 1 MHz.

3.3. Effect of the growth of E. coli O157:H7 cells on impedance measurement

Fig. 4 shows the impedance measurement of 5.6×10^4 CFU mL^{-1} of *E. coli* O157:H7 before and after an enrichment growth of 16 h in YPLT medium. After growth, the magnitude of impedance decreased for the entire range of frequency, especially for frequency greater than 100 kHz. In order to understand this change in the impedance, the experimental data before and after growth were curve fitted using an equivalent circuit shown in Fig. 3a. Table 1 shows the simulated values of R_s and C_{dl} for the impedance spectrum before and after the growth of *E. coli* O157:H7. Due to *E. coli* O157:H7 growth, the values of double layer capacitance increased and the bulk medium resistance decreased. Thus, change in the impedance values due to bacterial growth was due to double layer capacitance and bulk resistance of the medium, implying that the growth of *E. coli* O15:H7 cells in growth medium can be monitored by measuring the change in the double layer capacitance or the change in the bulk medium resistance in the range of frequencies from 10 Hz to 20 kHz and 202 kHz to 1 MHz, respectively.

Table 1
Simulated values of R_s and C_{dl} in the equivalent circuit for 5.4×10^4 CFU mL^{-1} of *E. coli* O157:H7 cells before and after an enrichment growth of 16 h and their respective percentage change[a] with respect to the samples before growth

	R_s (Ω)	C_{dl} (nF)
Before growth	33.96 ± 3.1	155.0 ± 11.2
After growth	22.59 ± 1.8	227.2 ± 10.1
Change (%)[a]	−33.4	+46.5

[a] Negative change indicates a decrease in parameter value and positive change indicates an increase in parameter value.

The double layer capacitance depends on many factors including electrode potential, temperature, ionic concentrations, type of ions, and electrode surface properties. The values of electrode potential and temperature were constant and hence their effect can be ignored. The value of the double layer capacitance can be expressed as [16]:

$$C_{dl} = \frac{\varepsilon_{dl} A}{d} \quad (5)$$

where ε_{dl} is the dielectric permittivity of the double layer, $\varepsilon_{dl} = \varepsilon_0 \varepsilon_r$, ε_0 the permittivity of the free space and ε_r the relative permittivity of the layer separating ionic charges and the electrode, A the area of the electrode, and d is the thickness of double layer. Substrates present in the microbiological growth medium are generally uncharged or weakly charged but are transformed into highly charged end products as microorganisms to follow metabolic pathways. This results in an increase in the conductivity of the test medium and a decrease in impedance [5]. Metabolic activities during bacterial growth of *E. coli* O157:H7 cells converted uncharged or weakly charged substrates (lactose, yeast extract, peptone, and TMAO) present in YPLT medium into highly charged ions. For example, TMAO was reduced into trimethylamine cations and lactose was metabolized into acid. All these highly charged ions formed in the medium caused an increase in the permittivity of the medium and a decrease in the thickness of the double layer at the same time. These changes together resulted in an increase in the values of C_{dl} and consequently a decrease in the impedance. The decrease in the bulk medium resistance after growth of bacterial cells was also caused by an increase in the concentration of highly charged ions in the medium.

Previous researches related to IAM-based impedance detection systems have shown that during impedance measurement, cells attached to the electrodes do not contribute directly to the double layer capacitance [16,35]. Our results clearly showed that the presence of bacterial cells in the detection sample did not affect the impedance response of the sensor (data not shown). Impedance response of the sensor for bacterial cells was measured for the sample with initial concentration of 5.4×10^4 CFU mL^{-1} of *E. coli* O157:H7 after 16 h of growth. This was compared with the impedance response of the sensor after centrifuging the same sample to remove bacterial cells (supernatant was used for impedance measurement). Previous research had reported that the cell membrane (thickness 5–10 nm) has a capacitance of 0.5–2.5 μF/cm^2 and a resistance of 10^2 to 10^5 Ω cm^2 [34]. The double layer capacitance will only be affected by the presence of cells, if they lie within its thickness, which is typically of the order of several angstroms [36]. Cells attached either specifically or non-specifically to electrodes do not lie within this thickness, hence, they do not directly affect double layer capacitance [37]. In addition to this, the aqueous gap between cells and the electrode surface prevents direct effect of the cell membrane on the interfacial impedance of the electrodes [38]. Therefore, in our research the increase in double layer capacitance was not due to bacterial attachment, but was caused by the change in ionic composition of the double layer. Thus, this change can directly be related to the presence of highly charged by-products produced during bacterial metabolism.

3.4. Effect of frequency on impedance measurement

To monitor the effect of frequency on impedance measurement, the values of NIC were calculated at different frequencies (Eq. (1)), and plotted against growth time. Fig. 5 shows the NIC *versus* growth time for the impedance measurement of the sample with initial concentration of 5.4×10^4 CFU mL^{-1} of *E. coli* O157:H7 at five different frequencies. The values of NIC for all five frequencies decreased with an increase in growth time. The decrease in the values of NIC was more at higher frequencies. Maximum change in the values of NIC with respect to the growth time was observed in the initial 6–8 h growth of bacterial cells. Between 8 and 16 h of growth, the change in the values of NIC was not significantly different ($P > 0.05$). After 6–8 h of growth, maximum changes in the values of NIC were 7.8%, 10.9%, 17.6%, 25.5%, and 30.5% for impedance measurements at frequencies of 10 Hz, 270 Hz, 4.18 kHz, 64.6 kHz, and 1 MHz, respectively. Based on this observation, 1 MHz was chosen to monitor the change in the impedance values corresponding to the growth of *E. coli* O157:H7 cells using double IAM-based flow cell. Bacterial cells were in the "log phase" of growth after a short "lag phase", during which they grow exponentially and produce a huge amount of by-products and thus maximum decrease in the values of NIC was observed during initial 6–8 h of growth of bacterial cells. The food and nutrients available for the bacteria get exhausted as bacterial growth progresses and thus, bacteria tend to shift to "stationary phase" of growth, where the production of by-products is limited and hence, no significant change in the values of NIC was observed between 8 and 16 h of growth of bacterial cells.

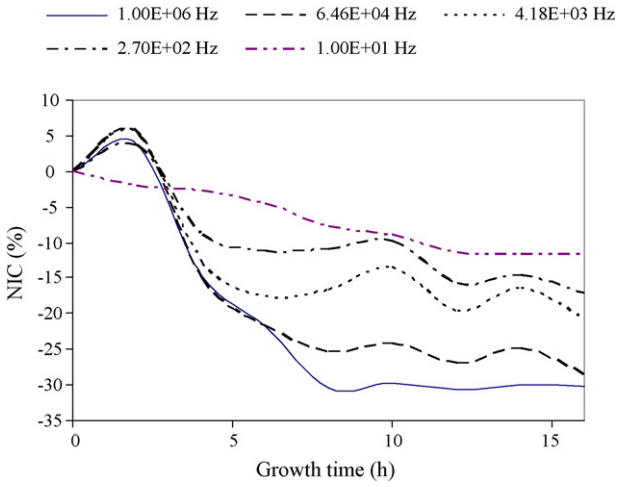


Fig. 5. Normalized impedance change (NIC) *vs*. growth time for the impedance measurement of 5.4×10^4 CFU mL^{-1} of *E. coli* O157:H7 at frequencies of 10 Hz, 270 Hz, 4.18 kHz, 64.6 kHz, and 1 MHz.

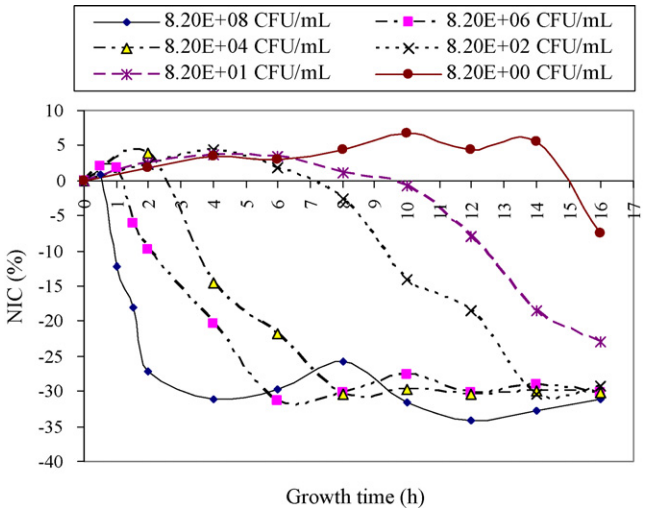


Fig. 6. Growth curves (NIC *vs.* growth time) for a range of 8.0×10^0 to 8.2×10^8 CFU mL^{-1} of *E. coli* O157:H7 cells after an enrichment growth in YPLT medium.

3.5. Detection of E. coli O157:H7 inside the double IAM-based flow cell

The values of NIC calculated at 1 MHz were used to quantify the initial numbers of bacterial cells present in the original samples after an enrichment growth in YPLT medium. Fig. 6 shows the growth curves (NIC *versus* growth time) for a range of initial concentrations of *E. coli* O157:H7 cells from 8.0×10^8 to 8.2×10^8 CFU mL^{-1} present in the sample. The values of NIC were positive at the beginning and then started to decrease. The time when impedance values start to decrease as compared to the NIC values at $t = 0$ h is taken as the detection time. The detection time decreased with increase in the initial numbers of *E. coli* O157:H7 cells present in the sample before growth. High number of cells in the sample at time $t = 0$ h resulted in a rapid change in the conductivity of the solution due to fast bacterial metabolism. As a result of this, high initial number of *E. coli* O157:H7 present in the samples were detected in low detection time and vice versa. Fig. 7 shows the detection time for different concentrations of *E. coli* O157:H7 ranging from 8.0

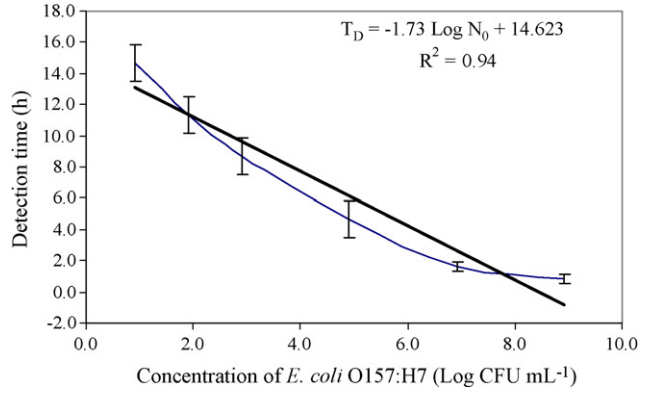


Fig. 7. The linear relationship between the logarithmic values of *E. coli* O157:H7 concentrations and detection times obtained from the impedance measurement of samples at different sampling times after the growth of bacterial cells.

to 8.2×10^8 CFU mL^{-1}. The detection times for 8.0, 8.2×10^1, 8.2×10^2, 8.2×10^4, 8.2×10^6, and 8.2×10^8 CFU mL^{-1} were 14.7, 11.3, 8.7, 4.7, 1.7, and 0.8 h, respectively. The detection time was calculated based on the average of three readings. In this study, an indirect impedance detection method has been used for quantifying initial number of *E. coli* O157:H7 cells present in the sample.

Some researchers have reported that the direct detection of *E. coli* O157:H7 cells in the samples. Suehiro et al. [27] used dielectrophoresis to align 10^5 CFU mL^{-1} of *E. coli* O157:H7 in between the electrodes and the impedance, measurement was conducted in the presence of a low conductivity medium (0.1 M mannitol solution and conductivity 0.2 mS/m) without any enrichment growth. The "pearl bead" formation of cells in between the electrodes acted as conductor. *E. coli* O157:H7 cells behaved as conductor in the presence of mannitol solution as some components of bacterial cells (i.e., cell wall and cytoplasm) were more conductive than the mannitol solution (conductivities of cell wall and cytoplasm are 500 mS/m and 100 mS/m, respectively) [29]. In other studies, the *E. coli* O157:H7 cells were attached to antibodies present on the surface of electrodes and impedance measurement was performed in the presence of a highly conductive redox probes [20,23].

4. Conclusions

Double IAM-based flow cell was successfully used in an impedance biosensor for the detection of *E. coli* O157:H7 in a range from 8.0 to 8.2×10^8 CFU mL^{-1} after an enrichment growth of 14.7 and 0.8 h, respectively. Double IAM-based flow cell was effective in improving the sensitivity of impedance detection by providing more surface area as compared to the single IAM-based flow cell. The equivalent circuit analysis indicated that the change in impedance values due to bacterial growth was caused by both double layer capacitance and bulk medium resistance, and these parameters in turn were the function of the amount of charged ions present in the medium. Specificity of this impedance biosensor could be ensured by the use of selective growth medium or immunoseparation based on magnetic microbeads conjugated with antibodies specific to target bacteria. Impedance measurement in a flow cell can be useful to design a portable instrument for monitoring bacterial cell growth and their metabolites.

Acknowledgments

This project was supported in part by USDA/FAS and the Food Safety Consortium.

References

[1] O.N. Okigbo, G.H. Richardson, J. Food Prot. 48 (1985) 978.
[2] J. Strassburger, J. Hossbach, R. Seidel, Int. J. Med. Microbiol. 274 (1991) 481.
[3] G. Kroyer, K. Futschik, A. Gschwandtner, Proceedings of the 8th European Conference on Food Chemistry, Austrian Chemical Society, Vienna, Austria, September 18–20, 1995, pp. 555–561.
[4] P. Silley, S. Forsythe, J. Appl. Bacteriol. 80 (1996) 233.

[5] M. Wawerla, A. Stolle, B. Schalch, H. Eisgruber, J. Food Prot. 62 (1999) 1488.
[6] R. Gomez-Sjöberg, T. Morisette, R. Bashir, J. Microelectromech. Syst. 14 (2005) 829.
[7] G.N. Stewart, J. Exp. Med. 4 (1899) 235.
[8] A. Edmiston, A. Russell, J. Food Prot. 61 (1998) 1375.
[9] C.J. Felice, M.E. Valentinuzzi, IEEE Trans. Biomed. Eng. 46 (1999) 1483.
[10] B.C. Towe, V.B. Pizziconi, Biosens. Bioeletron. 12 (1997) 893.
[11] C. Berggren, B. Bjarnason, G. Johansson, Biosens. Bioelectron. 13 (1998) 1061.
[12] V.M. Mirsky, M. Mass, C. Krause, O.S. Wolfbeis, Anal. Chem. 7 (1998) 3674.
[13] J. Min, A. Baeumner, Electroanalysis 16 (2004) 724.
[14] C. Amatore, B. Fosset, J. Bartelt, M.R. Deakin, R.M. Wighman, J. Electroanal. Chem. 256 (1988) 255.
[15] M. Ciszkowska, Z. Stojek, J. Electroanal. Chem. 466 (1999) 129.
[16] L. Yang, Y. Li, C.L. Griffis, M.G. Johnson, Biosens. Bioelectron. 19 (2004) 1139.
[17] L. Yang, Y. Li, J. Microbiol. Methods 64 (2006) 9.
[18] R. Gomez, R. Bashir, A. Sarikaya, M.R. Ladisch, J. Sturgis, J.P. Robinson, T. Geng, A.K. Bhunia, H.A. Apple, S. Wereley, Biomed. Microdev. 3 (2001) 201.
[19] R. Gomez, R. Bashir, A.K. Bhunia, Sens. Actuator B 86 (2002) 198.
[20] S.M. Radke, E.C. Alocilja, IEEE Sens. J. 4 (2004) 434.
[21] S.M. Radke, E.C. Alocilja, Biosens. Bioelectron. 20 (2005) 1662.
[22] S.M. Radke, E.C. Alocilja, IEEE Sens. J. 5 (2005) 744.
[23] L. Yang, Y. Li, G.F. Erf, Anal. Chem. 76 (2004) 1107.
[24] L. Yang, Y. Li, Biosens. Bioelectron. 20 (2005) 1407.
[25] F. Aldaeus, Y. Lin, J. Roeraade, G. Amberg, Electrophoresis 26 (2005) 4252.
[26] H. Li, R. Bashir, Sens. Actuator B 86 (2002) 215.
[27] J. Suehiro, R. Yatsunami, R. Hamada, M. Hara, J. Appl. Phys. 32 (1999) 2814.
[28] J. Suehiro, D. Noutomi, R. Hamada, M. Hara, IEEE (2001) 1950.
[29] J. Suehiro, R. Hamda, D. Noutomi, M. Shutou, M. Hara, J. Electrostat. 57 (2003) 157.
[30] B. Chang, C. Chen, S. Ding, D.C. Chen, H. Chang, Sens. Actuator B 105 (2005) 159.
[31] R. Zhou, P. Wang, H. Chang, Electrophoresis 27 (2006) 1376.
[32] S.K. Kim, P.J. Hesketh, C. Li, J.H. Thomas, H.B. Halshall, W.R. Heineman, Biosens. Bioeletron. 20 (2004) 887.
[33] P.V. Gerwen, W. Laureyn, W. Laureys, G. Huyberechts, M. Beeks, K. Baert, J. Suls, W. Sansen, P. Jacobs, L. Hermans, R. Mertens, Sens. Actuator B 49 (1998) 73–80.
[34] S. Gawad, K. Xheung, U. Seger, A. Bertsch, P. Renaud, Lab Chip 4 (2004) 241.
[35] J. Weigener, C.R. Keese, I. Giaever, Exp. Cell Res. 259 (2000) 158.
[36] A.J. Bard, L.R. Faulkner, Electrochemical Methods: Fundamentals and Applications, 2nd ed., John Wiley and Sons, New York, 2000, pp. 368–416.
[37] D. Gingell, Cell contact with solid surfaces, in: R. Galser, D. Gingell (Eds.), Biophysics of the Cell Surface, Springer, New York, 1990, pp. 263–268.
[38] I. Giaever, C.R. Keese, Proc. Natl. Acad. Sci. 88 (1991) 7896.

Available online at www.sciencedirect.com
ScienceDirect
Talanta 74 (2008) 1038–1042
Talanta
www.elsevier.com/locate/talanta

Short communication

Detection of Alzheimer's tau protein using localised surface plasmon resonance-based immunochip

Mun'delanji Vestergaard [a,*], Kagan Kerman [b], Do-Kyun Kim [c], Ha Minh Hiep [a], Eiichi Tamiya [c]

[a] *School of Materials Science, Japan Advanced Institute of Science and Technology, 1-1 Asahidai, Nomi City, Ishikawa 923-1292, Japan*
[b] *Department of Chemistry, University of Saskatchewan, 110 Science Place, Saskatoon, S7N 5C9 Saskatchewan, Canada*
[c] *Department of Applied Physics, Osaka University, 8-1 Mihogaoka, Ibaraki, Osaka 567-0047, Japan*

Received 18 April 2007; received in revised form 6 June 2007; accepted 7 June 2007
Available online 17 June 2007

Abstract

In this study, we present the detection of tau protein, at room temperature, using a multi-spot localised surface plasmon resonance (LSPR)-based immunochip. To the best of our knowledge, this is the first report of an immunochip for tau protein. The detection method includes fabrication of a gold-capped nanoparticle LSPR chip, formation and functionalisation of a self-assembled monolayer (SAM), immobilisation of a suitable linker, effective blocking of non-specific adsorption, immobilisation of a monoclonal anti-tau antibody (tau-mAb), and finally, the optimum conditions for the immuno-reaction between tau-mAb and the antigen were determined. The method has a high performance, enables detection of tau at 10 pg/mL, lower than the cut-off value of 195 pg/mL (for AD) for tau protein in cerebral spinal fluid (CSF). Further, we demonstrated selectivity of the technique by showing that the introduction of bovine serum albumin (BSA), perhaps the most abundant protein component in serum and CSF, does not interfere with the detection of tau. This method also offers a potential platform for studying tau interactions with other proteins and/or potential drug candidates and could also be easily adapted for detecting phosphorylated tau and other AD biomarkers.
© 2007 Elsevier B.V. All rights reserved.

Keywords: Tau; Alzheimer's disease (AD); Localised surface plasmon resonance (LSPR); Immunochip; Immobilisation; Nanoparticles

1. Introduction

Diagnosis of Alzheimer's disease (AD) remains in the hands of medical doctors, who can only at best propose 'probable Alzheimer's or dementia of the Alzheimer type' since there is no current test or procedure that is diagnostic. Diagnosis can only be confirmed on autopsy by histopathological features; such as amyloid plaques, neurofibrillary tangles (NFTs), neuronal thread, neuronal and synaptic loss, and brain atrophy in certain regions of the brain [1,2]. Several biomarkers have been reported [3–5]. To date, the most extensively studied are amyloid beta (Aβ42), tau and, to a lesser extent, phosphorylated tau in cerebral spinal fluid (CSF) samples, typically using enzyme-linked immunosorbent assay (ELISA) techniques, which are less flexible, costly and labour-intensive [6–11]. Chip-based technologies have several advantages over the conventional bioanalysis systems because (i) they enable rapid analysis of a large number of samples in a single experiment, (ii) there is reagent economy, and (iii) the signal-to-noise ratio exhibited by micro- or nano-fabricated biochips is much better than that observed for conventional microtiter plate assay systems [12,13].

Tau is a 50–65 kDa protein. It was first isolated in 1975 as a heat stable protein that promotes assembly, and maintains the structural integrity of microtubules, supports the out-growth of axons and regulates the transport of vesicles and organelles [14,15]. In the brains of AD individuals, tau proteins become abnormally hyperphosphorylated. It is phosphorylated at more than 20 residues, many (but not all) of which are serine/threonine–proline sites. In healthy individuals, 8–10 of these residues are heterogeneously phosphorylated, and lose the

* Corresponding author. Fax: +81 761 51 1665.
E-mail address: munde@jaist.ac.jp (M. Vestergaard).

0039-9140/$ – see front matter © 2007 Elsevier B.V. All rights reserved.
doi:10.1016/j.talanta.2007.06.009

capacity to bind to microtubules. Instead, the phosphorylated tau proteins bind to each other inside nerve cells, tying themselves in "knots" known as NFTs [6,11]. The first report of CSF tau as a biomarker was published in 1993 [16]. Levels of tau are increased in CSF of AD individuals compared to age-matched controls [6–9], probably due to neuronal and axonal degeneration or accumulation of NFTs [10]. A cut-off value of 195 pg/mL tau in CSF can accurately differentiate clinically diagnosed AD cases from controls with 89% specificity [8]. Detection of tau, in vitro, is also studied using microscopy, laser light scattering and fluorescence in conjunction with thioflavins (ThS) as the molecular label [17]. Chromatography and SPR have been used in the study of tau–amyloid β interaction [18]. LSPR-based detection techniques are becoming increasingly popular. Several biomolecules have been detected using LSPR immunosensors [19–21].

In this work, a method based on the immuno-affinity of tau protein towards a monoclonal anti-tau antibody (tau-mAb) immobilised on an LSPR multi-spot nanoparticle chip was employed for the detection of tau protein at room temperature (RT). The approach for LSPR chip fabrication was based on Endo et al.'s [19,20], with some changes for increased detection sensitivity. Optimisation of each analytical procedure and performance (detection limits, reproducibility, stability of chip and reagents) were examined. Further, the selectivity of the technique by introducing bovine serum albumin (BSA), perhaps the most abundant protein component in serum and CSF [22], was assessed.

2. Experimental

2.1. Instrumentation

A thermal evaporator (SVC-700TM/700-2), purchased from Sanyu Electron Co. Ltd., Tokyo, Japan, was used for the deposition of chromium and gold layers. An analogue ionisation vacuum gauge (GI-TL3, ULVAC, Kanagawa, Japan) was used to monitor base pressure and the growth rate in thickness was monitored with a quartz crystal microbalance (QCM, model TM-200R, Maxtek Inc., CA, USA). For evaluation of the optical characteristics of nanoparticle layer substrates, an USB-2000 UV–vis spectrophotometer (wavelength 200–1100 nm); a tungsten halogen light source (LS-1, wavelength range 360–2000 nm); and optical fiber probe bundle (R-400-7 UV–vis fiber core diameter 200 μm, wavelength 250–800 nm) were all purchased from Ocean Optics (Dunedin, USA).

2.2. Reagents

A covalent binding agent (1-Ethyl-3-(3-dimethylaminopropyl) carbodiimide, EDC) was purchased from Dojindo Laboratories (Kumamoto, Japan); 4,4′-Dithiodibutyric acid (DDA) from Aldrich (USA); 3-Aminopropyltriethoxysilane (γ-APTES) from Shin-Etsu Chemical Co. Ltd. (Tokyo, Japan); silica nanoparticles (100 nm i.d.) from Polysciences Inc. (Warrington, PA, USA); gold and chromium (99.9% purity) from Furuya Metal (Tokyo, Japan). Electronic grade of sulfonic acid and hydrogen peroxide (piranha solution) from Kanto Kagaku (Tokyo, Japan); slide glass substrates (S-1111, 76 mm × 26 mm thickness: 0.8–1.0 mm) from Matsunani Glass Ind. Ltd. (Osaka, Japan); protein G and monoclonal anti-tau (anti-mouse IgG) antibody (tau-mAb) from Sigma (St Louis, USA); tau protein (60 kDa) from Calbiochem (USA); *N*-hydroxysuccinimide (NHS), ethanolamine hydrochloride and all other chemicals were purchased from Wako Pure Chemical Industries Ltd. (Osaka, Japan). Ultrapure water (18.3 M Ωcm) from Millipore was used for preparation of all reagents, unless otherwise stated.

2.3. Fabrication of LSPR multi-spot nanoparticle chip

The approach for LSPR chip fabrication was based on Endo et al. [19,20], with some changes. Glass slides were cleaned thoroughly by ultrasonication for 30 min in ethanol, soaked in piranha solution for 30 min, rinsed thoroughly with ultrapure water and finally, dried under a stream of nitrogen gas. For deposition of chromium and gold on the glass slide substrate, a thermal evaporator was used at 2×10^{-5} Torr base pressure and QCM was manually adjusted to deposit the metal elements at approximately 0.5 Å/s and thickness growth was monitored and manually stopped at 5 nm for chromium and 40 nm for gold. (**Warning:** *Piranha solution is hazardous and highly reactive. It may explode on contact with organic solvents. Extreme care and precaution must be taken at all times*.) Silica nanoparticles were surface modified using 1% (v/v) γ-APTES solution in ethanol by continual stirring at RT. After, the suspension was centrifuged at 3500 rpm for 10 min and the supernatant decanted to waste. Ultrapure water was used to wash the amino-surface-modified silica nanoparticles, centrifuged and the supernatant discarded as above. This process was carried out three times. The nanoparticles were then dried at 120 °C for 15 min and stored in a desiccator. Just before use, the silica nanoparticle colloidal solution was prepared at 1% (w/v) by dispersing in ultrapure water. For fabrication of LSPR chip on chromium/gold-deposited glass substrates, first, a 15 multi-spot (3 mm i.d.) silicon sheet was carefully placed on the chip surface. Then, 1 mM DDA solution was introduced to the gold-layered surface and left for 1 h to allow formation of self-assembled monolayer (SAM) of the DDA. EDC (400 mM) and the previously surface activated silica nanoparticles (10 mg/ml) were mixed 1:1 and introduced to the activated SAM for 1 h. The EDC served to activate carboxyl groups of the DDA SAM, which in turn, formed esters between the nanoparticle's amino groups and the SAM's carboxyl groups. After addition of each solution, the slides were washed with 50 mM phosphate buffer solution, pH 7.4 (PBS) to remove excess molecular species and subsequently dried at RT. Deposition of a gold layer (30 nm) to cap the silica nanoparticles (procedure as reported above) completed the fabrication process. Unless, otherwise stated, all analyses were carried out at RT.

2.4. Immobilisation of tau-mAb onto LSPR multi-spot nanoparticle chip

First, the LSPR chip was chemically modified using 1 mM DDA, then EDC (400 mM) and NHS; 100 mM) (1:1, v/v) for

SAM formation and functionalisation of SAM, respectively, following the procedure discussed above. After, we immobilised protein G for 1 h at concentrations between 0 and 200 μg/mL. Then, we blocked unreacted ester groups by immobilising 0.1 M ethanolamine HCl solution, pH 8.5 for 30 min. Tau-mAb was subsequently immobilised and optimised accordingly. Each immobilisation step was followed by stringent washing of the chip surface using PBS and drying.

2.5. Label-free detection of tau protein using LSPR multi-spot nanoparticle chip

Different concentrations of tau protein (~0 to 100 ng/mL) were introduced onto the antibody immobilised LSPR chip for a duration of 1 h followed by thorough rinsing with PBS and 1% (v/v) Tween-20 to block the non-specific adsorption.

2.6. Experimental setup for optical characteristics evaluation

The basis of the detection technique is as follows: upon introducing a ligand and, after, its target molecule, there are changes in the thickness of the gold-capped silica nanoparticle layer surface and this is reflected in an increase in absorbance, enabling detection of the molecular species of interest [23]. Basically, white light (tungsten-halogen light source), emerging from an optical fiber bundle (probe) provided incident light and this light was reflected upon hitting the substrate surface and coupled into the detection probe of the optical fiber bundle and analysed by UV–vis spectrometer in the wavelength range 400–800 nm (Fig. 1).

3. Results and discussion

LSPR phenomenon has previously been utilized to monitor biomolecular interactions on monolayer of Au nanoparticles by several groups [24–26]. Recently, Ruch-Nir et al. prepared silica-stabilized gold island films for transmission LSPR-based sensing [27]. Here, we demonstrate the biosensing capability of silica nanoparticles coated with a thin Au layer for the detection of tau protein. Recently, we employed this device for the detection of DNA hybridization and antibody–antigen interactions [19,20,28]. Gold deposition on the surface of silica nanoparticles enables easy fabrication of a uniform surface with minimum defects. One of the major drawbacks of LSPR chips utilizing the monolayer of Au nanoparticles is the complicated chemistry required to form a self-assembled monolayer (SAM) of Au nanoparticles on a solid surface. During mass-fabrication of numerous chips, small defects in the uniformity of SAMs can cause significant problems in the reproducibility and reliability of the results. Thus, our robust and highly reproducible fabrication technique circumvented these problems that are commonly

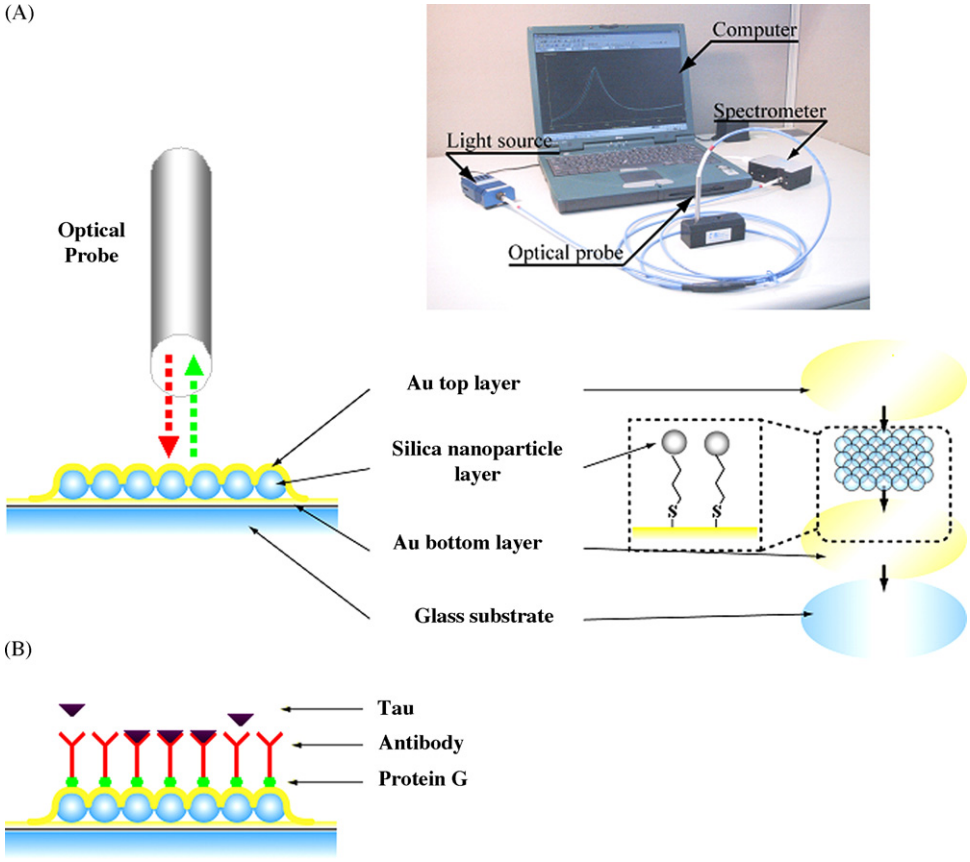


Fig. 1. (A) Localised surface plasmon resonance (LSPR) experimental setup; (B) immobilisation procedure for the immuno-reaction between antibody and antigens onto an LSPR chip surface.

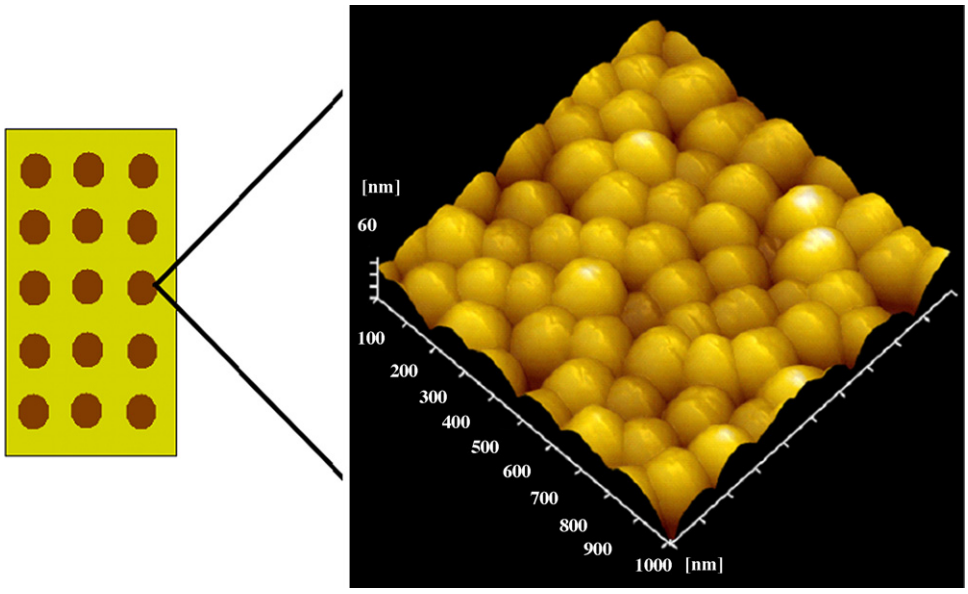


Fig. 2. Atomic force microscopic image of gold-capped nanoparticle LSPR chip, taken in tapping mode with a force constant of 42 N/m, scan rate 0.01 μm/s, resonance frequency 330 Hz and tip curvature radius of 10 nm.

faced during the preparation of Au nanoparticle monolayers on solid surfaces.

We analysed the surface characteristics of the fabricated chip, using atomic force microscopy (AFM, Fig. 2) in tapping mode with a force constant of 42 N/m, scan rate 0.01 μm/s, resonance frequency 330 Hz and tip curvature radius of 10 nm. The chip was stable for a period of 1 week, in agreement with a previous report [28].

The principle behind the detection technique is a characteristic change in wavelength of maximum absorbance (λ_{max}) and/or an increase in absorbance values upon introduction of a molecular species onto the LSPR chip surface [23]. Our detection method exploited changes in the thickness of the gold-capped silica nanoparticles chip surface. After successful fabrication, the optical characteristics of the chip were examined. The mean absorbance at wavelength of maximum absorbance (λ_{max} ~522 nm) was 1.240 a.u. (Fig. 3).

A few carefully conducted steps are of vital importance in order to selectively and sensitively detect the target molecule: (i) effective immobilisation of an antibody, (ii) blocking of non-specific adsorption, and (iii) environment for antibody–antigen interaction. Following the LSPR chip fabrication and SAM functionalisation described in the previous section, we immobilised protein G as our antibody-binding substrate, exploiting the high affinity between the Fc region of antibodies (in our case, anti-mouse IgG) and protein G [29] resulting in 'upright' orientation of the antibody for better interaction with the antigen. For optimal coverage of the chip surface, we conducted a protein G concentration dependence study, which gave 100 μg/mL protein G as the optimum concentration after 1 h immobilisation period (see Supplementary data), in other words, an increase in absorbance values were highest (0.123 a.u.), when the aforementioned protein G concentration was immobilised on the chip surface (Fig. 2). Active ester groups, unreacted with protein G, were passivated using ethanolamine [30].

A tau immunochip was developed by introducing tau-mAb onto the protein G-immobilised chip. The antibody was immobilised at 100 μg/mL for periods between 0 and 2 h. Optimal chip surface coverage was achieved after 1 h immobilisation (see Supplementary data) with a mean absorbance increase of 0.153 a.u (Figs. 3 and 4). We, then, evaluated selectivity/specificity of the sensor by introducing BSA (1 mg/mL) onto the chip surface for 1 h. There was

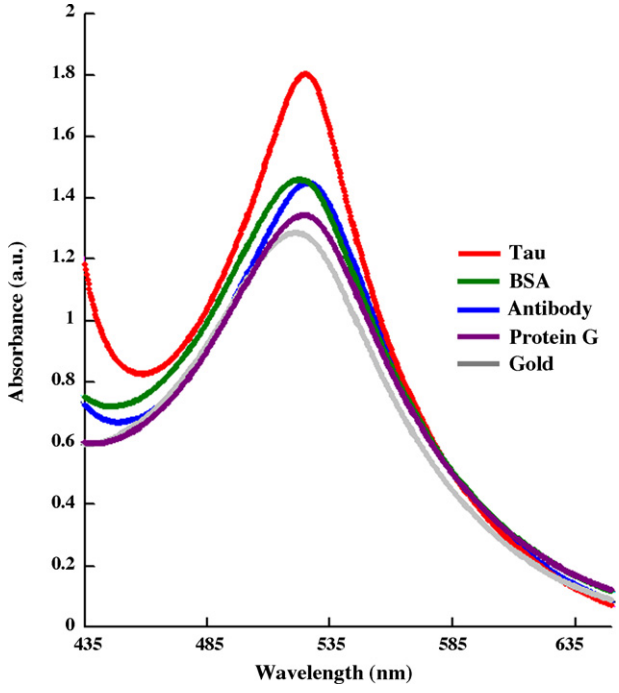


Fig. 3. LSPR spectral studies showing absorbance values of the LSPR gold-capped nanoparticle chip (gold); after subsequent immobilisation of protein G (100 μg/mL,) then tau-mAb (100 μg/mL), BSA (1 mg/mL, and tau protein (100 ng/mL,) each for a period of 1 h at room temperature (RT).

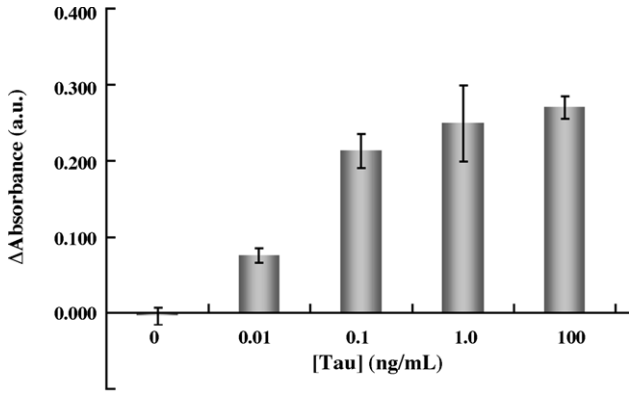


Fig. 4. Detection of tau protein using LSPR immunochip showing an increase in absorbance values after the introduction of the protein, at different concentrations, onto a tau-mAb-immobilised LSPR chip. Immuno-reaction was carried out at RT, for a period of 1 h. The data presented is a mean of three replicates and the error bars represent standard deviation.

hardly any change in the peak absorbance values (Fig. 3) indicating that BSA did not interfere with the sensor performance. BSA was chosen, because it is the most abundant protein component in blood plasma and has been heralded as the potential interfering biomolecule, especially when it comes to detection of low-abundant proteins/biomarkers in biological fluids [22,31]. Moreover, the molecular weights of tau (60 kDa) and BSA (66 kDa) proteins are comparable.

Using the immunochip, tau protein was introduced to the surface and incubated for a period of 1 h. We detected down to 10 pg/mL tau protein (Fig. 4). The results strongly suggest that the presented immunochip has the specificity and sensitivity required for the detection of tau protein in clinical samples since the cut-off value of tau in CSF for accurate differentiation between clinically diagnosed AD cases from controls is 195 pg/mL (for 89% specificity) [11]. Of course, challenges remain. Here we have considered and substantiated that the presence of BSA, the most abundant protein component in plasma and CSF, does not interfere with tau detection using the described immunochip. Other biomolecules such as immunoglobulins are a potential challenge and so are some low-abundant biomolecules. Further studies are under way in our laboratory to apply this sensor to detecting tau protein in clinical samples.

4. Conclusion

We report the first LSPR-based immunochip for tau protein. The detection of 10 pg/mL tau, lower than the cut-off value of 195 pg/mL (for AD) for tau protein in CSF, suggests that the method could be used for tau detection in the aforementioned clinical sample. In addition, this sensitivity puts our method in contention as a viable alternative to ELISA techniques. It has some advantages over ELISA-based assays in that it is direct (label-free), utilizes only one antibody, can detect one sample at a time and has the potential for multiplexed detection for up to 300 samples per chip [20], providing flexibility and a better reagent economy than ELISA systems. The method also offers a potential cost-effective and high-throughput platform for studying tau interactions with other proteins and/or potential drug candidates.

Appendix A. Supplementary data

Supplementary data associated with this article can be found, in the online version, at doi:10.1016/j.talanta.2007.06.009.

References

[1] Lahiri, K. Debomoy, LaFerla, M. Frank, Curr. Alzheimer Res. 3 (2006) 409.
[2] M.G. Spillantini, R.A. Crowther, M. Goedert, Acta Neuropathol. 92 (1996) 42.
[3] T. Sunderland, H. Hampel, M. Takeda, K.T. Putnam, R.M. Cohen, J. Geriatr. Psychiatry Neurol. 19 (2006) 172.
[4] G.L. Milne, E.S. Musiek, J.D. Morrow, Biomarkers 10 (2005) 10.
[5] D.G. Georganopoulou, L. Chang, C.S. Thanxton, E.J. Mufson, W.L. Klein, C.A. Mirkin, Proc. Natl. Acad. Sci. U.S.A. 102 (2005) 2273.
[6] T. Sobow, M. Flirski, P.P. Liberski, Acta Neurobiol. Exp. 64 (2004) 53.
[7] M. Vandermeeren, M. Mercken, E. Vanmechelen, S. Jan, A. Van de Voorde, J.-J. Martin, P. Cras, Neurochemistry 61 (1993) 1828.
[8] T. Sunderland, G. Linker, M. Nadeem, K.T. Putnam, D.L. Friedman, L.H. Kimmel, J. Bergeson, G.J. Manetti, M. Zimmermann, B. Tang, J.J. Bartko, R.M. Cohen, J. Am. Med. Soc. 289 (2003) 2094.
[9] K. Blennow, J. Int. Med. 256 (2004) 224.
[10] M. Sjogren, H. Vanderstichele, H. Agren, O. Zachrisson, M. Edsbagge, Wikkelson, C.K. Nagga, N. Andreasen, P. Davidsson, E. Vanmechelen, K. Blennow, Clin. Chem. 47 (2001) 776.
[11] Y.Y. Hu, S.S. He, X. Wang, Q.H. Duan, I. Grundke-Iqbal, K. Iqbal, J. Wang, Am. J. Pathol. 160 (2002) 1269.
[12] J. Workman Jr., M. Koch, D. Veltkamp, Anal. Chem. 77 (2005) 3789.
[13] A. Talapatra, R. Rouse, G. Hardiman, Pharmacogenomics 3 (2002) 527.
[14] M.D. Eweingarten, A.H. Lockwood, S.-Y. Hwo, M.W. Kirschner, Proc. Natl. Acad. Sci. U.S.A. 72 (1975) 1858.
[15] E. Mandelkow, Nature 402 (1999) 588.
[16] A. Watanabe, M. Hasegawa, M. Suzuki, K. Takio, M. Morishima-Kawashima, K. Titani, T. Arai, K.S. Kosiki, Y. Ihara, J. Biol. Chem. 268 (1993) 25712.
[17] T.C. Gamlin, R.W. Berry, L.I. Binder, Biochemistry 42 (2003) 15009.
[18] M. Perez, R. Cuadros, M.J. Benitez, J.S. Jimenez, J. Alzheimers Dis. 6 (2004) 461.
[19] T. Endo, Y. Yamamura, N. Nagatani, Y. Morita, Y. Takamura, E. Tamiya, Sci. Tech. Adv. Mater. 6 (2005) 491.
[20] T. Endo, K. Kerman, N. Nagatani, H.M. Hiep, D.-K. Kim, Y. Yonezawa, K. Nakano, E. Tamiya, Anal. Chem. 78 (2006) 6465.
[21] A. Haes, W.P. Hall, L. Chang, W.L. Klein, R.P. Van Duyne, Nano Letters 4 (2004) 1029.
[22] N.L. Anderson, N.G. Anderson, Mol. Cell. Proteomics 1 (2002) 845.
[23] A.J. Haes, R.P. Van Duyne, Anal. Bioanal. Chem. 379 (2004) 920.
[24] N. Nath, A. Chilkoti, Anal. Chem. 74 (2002) 504.
[25] N. Nath, A. Chilkoti, Anal. Chem. 76 (2004) 5370.
[26] K. Fujiwara, H. Watarai, H. Itoh, E. Nakahama, N. Ogawa, Anal. Bioanal. Chem. 386 (2006) 639.
[27] I. Ruach-Nir, T.A. Bendikov, I. Doron-Mor, Z. Barkay, A. Vaskevich, I. Rubinstein, J. Am. Chem. Soc. 129 (2007) 84.
[28] T. Endo, K. Kerman, N. Nagatani, Y. Takamura, E. Tamiya, Anal. Chem. 77 (2005) 6976.
[29] K. Kato, L.Y. Barsukov, J.P. Derrick, H. Kim, R. Tanaka, A. Yoshimo, M. Shiraishi, I. Shimada, Y. Arata, G.C.K. Roberts, Structure 3 (1995) 79.
[30] W. Knoll, F.Y. Neumann, S. Schiller, R. Naumann, Phys. Chem. Chem. Phys. 5 (2003) 5169.
[31] S. Roche, L. Tiers, M. Provansal, M.-T. Piva, S. Lehmann, Proteome Sci. 4 (2006) 20.

Available online at www.sciencedirect.com
ScienceDirect
Talanta 74 (2008) 724–729
Talanta
www.elsevier.com/locate/talanta

Modification of CdTe quantum dots as temperature-insensitive bioprobes

Jian-Hao Wang, Hai-Qiao Wang, Yong-Qiang Li, Hai-Li Zhang, Xiu-Qing Li, Xiao-Feng Hua, Yuan-Cheng Cao, Zhen-Li Huang, Yuan-Di Zhao *

Key Laboratory of Biomedical Photonics of Ministry of Education - Wuhan National Laboratory for Optoelectronics - Hubei Bioinformatics and Molecular Imaging Key Laboratory - Key Laboratory of Molecular Biophysics of the Ministry of Education, College of Life Science and Technology, Huazhong University of Science and Technology, Wuhan, HuBei, PR China, 430074

Received 7 March 2007; received in revised form 27 June 2007; accepted 30 June 2007
Available online 7 July 2007

Abstract

CdTe quantum dots (QDs) were synthesized in aqueous solution with 3-mercaptopropionic acid (MPA) as the stabilizer. The photoluminescence (PL) of CdTe QDs (3.5 nm) is found to be temperature-dependent: as the temperature arising from 278 K to 323 K, the PL intensity declines to 50.2% of its original and PL emission peak shows obvious red-shift (∼7 nm). After modification of the QDs surface with denatured ovalbumin, the PL is more temperature-insensitive than before. The PL intensity retains more than 70% of its original and the emission peak shows less red-shift (∼2 nm). Moreover, it is found that the PL intensity and wavelength of denatured ovalbumin coated CdTe QDs are reversible during heating (323 K)–cooling (278 K) cycles. All the studies provide an important theoretical basis for searching temperature-insensitive bioprobes.
© 2007 Elsevier B.V. All rights reserved.

Keywords: Quantum dots; Temperature-insensitive; Photoluminescence; Bioprobe

1. Introduction

With the help of fluorescent probes, the fluorescent microscopy made people deeply understand the cell structure, cell interactions and protein interactions, which accelerated the understanding of the life process [1]. However, traditional organic dyes tend to have bad photostability and easy photobleaching, which confine their further application in biological labeling. As new type of biological labels, QDs offer a number of attractive features, including high photobleaching threshold, good chemical stability, relatively broad and symmetric luminescence bands [2], which was wished to remedy the deficiencies of the fluorescent dyes.

At present, the most available QDs for biological labeling are CdSe/ZnS core/shell ones. However, they are usually synthesized under high-cost and rigorous experiment conditions. Though they have high photoluminescence quantum yield (PL QY), water-soluble process results in a great decrease of PL QY [2]. This affects their further application in biological labeling. While CdTe QDs can be synthesized in a water-phase system and the synthesis is more reproducible and less expensive. Since they have enough PL QY after synthesized in a water-phase system with different stabilizers [3,4], they have the potential of another important labeling materials for biological applications. For example, Gao et al. [5] and Wang et al. [6] used denatured bovine serum albumin (BSA) to modify the QDs surface and facilitated the proper choice of covalent coupling reagents for subsequent bioconjugation.

Hitherto, QDs obtained important achievements in biological labeling [6–14]. For biological labeling, it is desirable to have water-soluble QDs with stable properties that are not affected by environmental factors. But some researches presented the effects of pH [5,15], ligands [16], ionic strength [17] and excitation wavelength [18] on the optical properties of water-soluble QDs for bioprobes. However, few studies concerned the effects of the temperature to the photoluminescence (PL) of the QDs, and most of them were based on chemcophsics [19–21]. What's more, most of studies in life science are carried out in water solution above 273 K. Therefore, it is important to investigate the temperature-dependent PL of CdTe QDs in the 278–323 K scale. Previously, our group found mercaptoacetic acid (MAA) coated CdSe/ZnS QDs are temperature-dependent in the 280–351 K scale [22]. In other words, the PL greatly changed relative to the changes of the ambient temperature. It was also found that

* Corresponding author. Tel.: +86 27 87792235; fax: +86 27 87792202.
E-mail address: zydi@mail.hust.edu.cn (Y.-D. Zhao).

0039-9140/$ – see front matter © 2007 Elsevier B.V. All rights reserved.
doi:10.1016/j.talanta.2007.06.044

the QDs PL spectra were irreversible for their low stability. Therefore, they will bring disadvantageous effects on some PL experiments involved temperature. So studying of temperature-insensitive QDs bioprobes is of great significance for promoting QDs applications in life science.

In this paper, CdTe QDs were synthesized in water-phase system. The PL greatly changed relative to the changes of temperature. And their temperature-insensitivity was greatly increased after modification the QDs surface with denatured ovalbumin. The PL intensity and emission wavelength are both reversible after repeated heating and cooling cycles. The results provide a new approach for seeking temperature-insensitive bioprobes. Therefore, it is of great significance for promoting QDs applications in biology.

2. Experimental

2.1. Materials and reagents

Tellurium power (99.999%), $CdCl_2{\cdot}2.5H_2O$ and $NaBH_4$ (96%) were purchased from Sinopharm Chemical Reagent Co., Ltd., Sephadex G-100 was purchased from Pharmacia. Bovine serum albumin (BSA) was ordered from Roche Biotech (Basel, Switzerland). Human IgG was purchased from Beijing biosynthesis biotechnology Ltd., China, and used without further purification. 3-Mercaptopropionic acid (MPA, 99%) was purchased from Sigma-Aldrich Fine Chemicals. All other chemicals used were of analytical reagent grade. Doubly deionized water was used throughout the experiment.

2.2. Instrumentation and spectrometry

The UV–vis spectrophotometer (UV-2550) was purchased from Shimadzu (Tokyo, Japan). The luminescence spectrometer (LS-55) was purchased from Perkin-Elmer (Wellesley, MA, USA). The column purification system (MD99-2) was purchased from Shanghai Huxi Co. (Shanghai, China). Efforts were made to keep the samples dilute, so that their optical densities (O.D.) were less than 0.2 at the first absorption peak. The PL measurements were treated qualitatively and the heater (DC-0506, Shanghai Hengping Scientific Instrument Co., Ltd., China) was used.

2.3. Preparation of CdTe QDs

CdTe QDs capped with MPA were prepared in previous papers [23,24]. In brief, freshly prepared oxygen-free NaHTe solution was added to nitrogen-saturated $CdCl_2$ aqueous solution, pH 11.5, in the presence of MPA as a stabilizing agent. NaHTe was generated by the reaction of tellurium powder with $NaBH_4$ [25]. The resulting mixture was then subjected to refluxing to control the size of the CdTe QDs. The MPA-coated CdTe QDs were precipitated with acetone and then isolated by centrifugation and decantation to remove free MPA molecules.

The particle size was determined from the first absorption maximum according to the literature [26]. The results showed that the particle diameters of the as-prepared CdTe QDs were around 2.8 nm, 3.1 nm and 3.5 nm, corresponding with the PL peaks of 550 nm, 585 nm and 620 nm, respectively.

2.4. Preparation of denatured proteins coated QDs

Denatured ovalbumin was prepared by chemically treating ovalbumin with $NaBH_4$ [6]. And the main steps are: 0.22 g ovalbumin was dissolved in 100 mL of deionized water, then 0.008 g of $NaBH_4$ was added under stirring. The reaction proceeded at room temperature for 1 h and then at 70 °C until no more gas (H_2) was generated. The MPA-coated CdTe QDs were precipitated with acetone and redissolved into a measured amount of denatured ovalbumin solution. The resulting solution was incubated at 70 °C for 30 min.

Denatured BSA and IgG were used to modify CdTe QDs surface with similar method.

2.5. Column purification

A Sephadex G-100 column (35 cm long and 1 cm diameter) was pre-equilibrated with PBS (0.01 M, pH 7.4); the flow velocity used was 300 μL/min. Different samples with a total volume of 800 μL were loaded onto the column, respectively. A UV source of 280 nm was set up to check the flow from the column, and if necessary the eluted solution was collected for further analysis.

3. Results and discussion

3.1. Temperature-dependent of CdTe QDs

CdTe QDs synthesized in aqueous solution are widely used for biolabeling [3,17]. MPA coated CdTe QDs (3.5 nm) were prepared based on a previous literature report [23,24]. As shown in Fig. 1, with temperature increasing (278 K → 323 K), the PL intensity remained 50.2% of its original accompany with obvi-

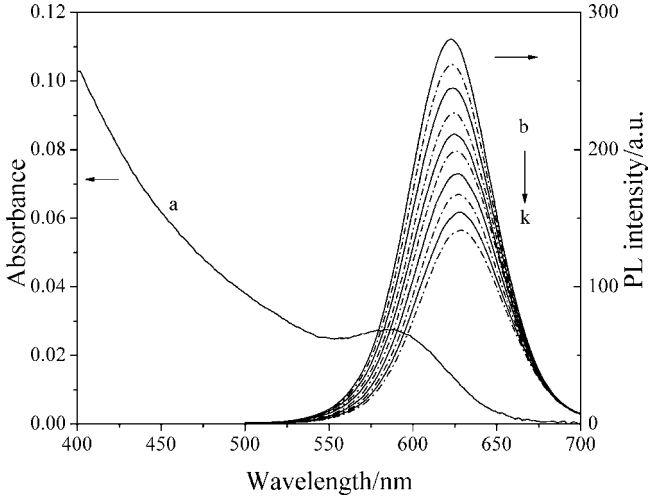


Fig. 1. Spectra of temperature-dependent CdTe quantum dots (3.5 nm). (a) Absorption spectrum at 280 K and photoluminescence spectra (b → k) at: 278 K, 283 K, 288 K, 293 K, 298 K, 303 K, 308 K, 313 K, 318 K, 323 K. (λ_{ex} = 400 nm).

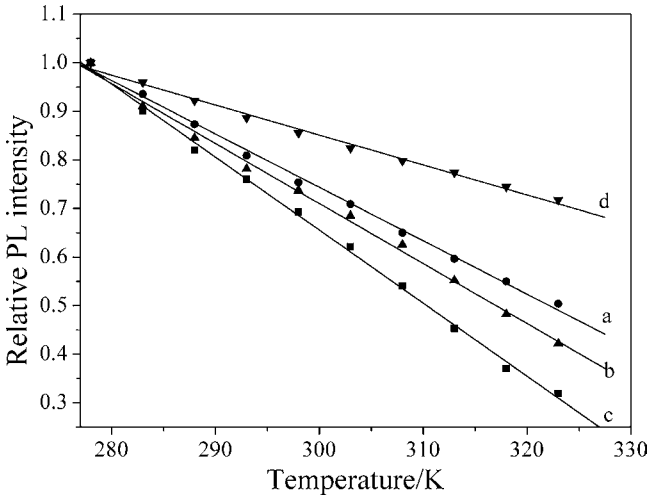


Fig. 2. The effects of increasing temperature on the relative PL intensity of different sized CdTe quantum dots: (a) 3.5 nm, (b) 3.1 nm, (c) 2.8 nm, and (d) denatured ovalbumin-QDs (3.5 nm).

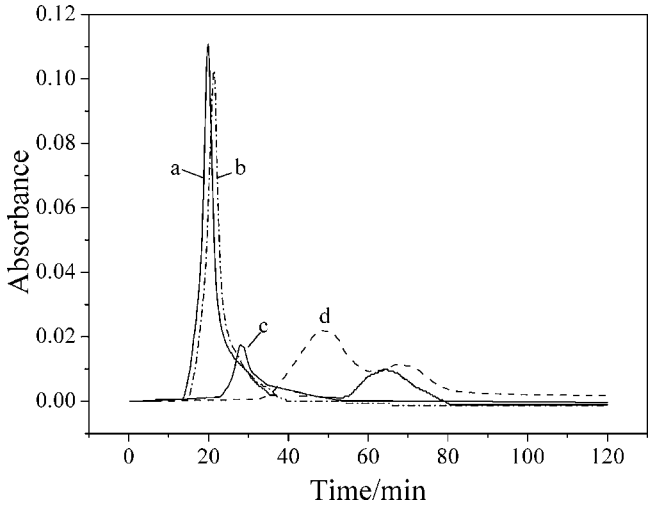


Fig. 3. Sephadex G-100 gel filtration chromatography of the conjugates (a), the conjugates after ultra-centrifugation (b), pure denatured ovalbumin (c) and pure CdTe QDs (d). (For the conjugates, QDs concentration is the same as d, and denatured ovalbumin concentration is the same as c.)

ous red-shift of 7 nm (Fig. 1, b → k), while the absorption spectra without any change (Fig. 1, curve a). Biju et al. [21] thought the decline of PL intensity was caused by the thermal activation of surface traps leading to non-radiative recombination of excitons. And the red-shift of PL wavelength was thought to be the result of increased exciton carrier transfer between the quantum dots at higher temperatures and the thermal activation of emission from lower energy trap states [27].

On the other hand, the temperature-dependent of two other typical kinds of CdTe QDs (3.1 nm, 2.8 nm) was also studied. With the temperature increasing (278 K → 323 K), the results suggested that the PL intensity of these two kinds of CdTe QDs remained 42.2% and 31.3% of their original (Fig. 2, curves b and c), respectively. And the PL emission wavelength shifted towards the red at different rate. Therefore, different sized CdTe QDs possessed different sensitivity to the temperature. Smaller sized CdTe QDs showed more sensitive to temperature. It is speculated that with increasing reflux time, the surface-to-volume ratio of QDs decreased and made the surface defects different [28]. So this results to the different sensitivity to temperature.

The above experimental results showed that the PL of MPA coated CdTe QDs were sensitive to temperature, so they were not ideal temperature-insensitive nanoparticles. Previously, our group confirmed that the CdSe core coated with thinner shells were more sensitive to temperature than that of the ones coated with thicker shells [22]. In other words, modification of QDs surface is important for the PL sensitivity to the temperature. Therefore, denatured ovalbumin was used to modify the QDs surface in this paper. And it is hoped that this method can improve the temperature-insensitivity of CdTe QDs.

3.2. Prove of the conjugation of denatured ovalbumin to CdTe QDs

Firstly, column separation was applied to characterize the coupling process between CdTe QDs (3.5 nm) and denatured ovalbumin. It was found that a big absorbance peak of pure CdTe QDs appeared at 50 min and a smaller one at 70 min (Fig. 3, curve d), while the peak of denatured ovalbumin appeared at 28 min (Fig. 3, curve c), indicating obviously different elution times of these two materials. When denatured ovalbumin combined to QDs, a strong absorption peak in shorter elution time appeared about 21 min (Fig. 3, curve a). By the location of the absorption peaks of QDs and denatured ovalbumin, it was confirmed that the first absorption peak in Fig. 3a was caused by the denatured ovalbumin-QDs. For denatured ovalbumin combined to QDs leads to increasing molecular weight. Another small absorbance peak appeared at 70 min, which was in accordance with the smaller peak of the QDs (Fig. 3, curve d). For curve a and curve d they had the same concentration of QDs, but the absorbance peak area of QDs in curve a was obviously less than that of pure QDs. That is to say, most of QDs had conjugated to denatured ovalbumin. It is proved that the simple mixture of QDs and proteins (for example, electrostatic adsorption) can be separated by ultra-centrifugation [30]. So the conjugates after ultra-centrifugation (Millipore, YM-50) were also loaded onto the column (Fig. 3, curve b). It was found that the small peak caused by QDs disappeared but the bigger one kept constant. This experiment proved that this modification was stable. It was speculated that this was similar to the modification of QDs by denatured BSA. The disulfide bonds were converted to sulfhydryl groups and formed $CdTe_x$(denatured ovalbumin)$_{1-x}$ complex [6].

To choose the optimal ratio of denatured ovalbumin to QDs, different amounts of denatured ovalbumin were used to modify QDs. The QDs (3.1 nm) concentration is 1 μM. It was found that the first absorbance peak of denatured ovalbumin-QDs increased gradually relative to the amount of denatured ovalbumin and reached a certain value when the denatured ovalbumin concentration is higher than 4 μM, which meant that most QDs had been modified by denatured ovalbumin.

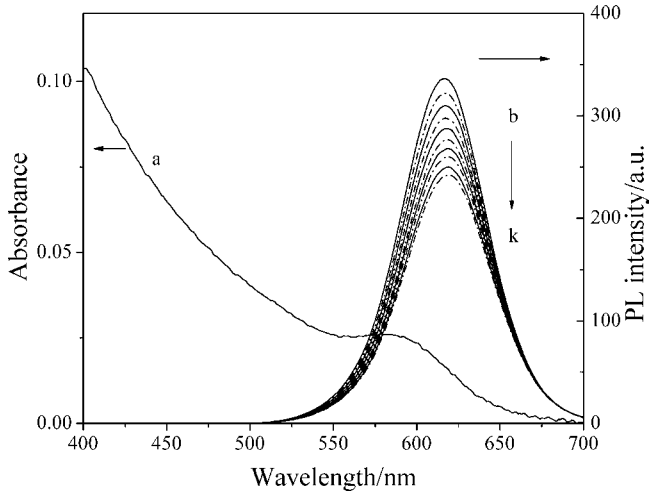


Fig. 4. Spectra of temperature-dependent denatured ovalbumin-QDs (3.5 nm). (a) Absorption spectrum at 280 K and PL spectra (b → k) at: 278 K, 283 K, 288 K, 293 K, 298 K, 303 K, 308 K, 313 K, 318 K, 323 K. (λ_{ex} = 400 nm).

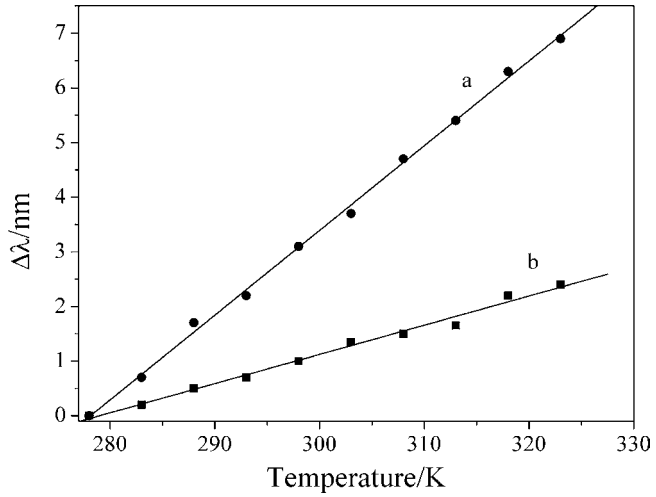


Fig. 5. The effects of increasing temperature on the PL spectral shifts (Δλ) of CdTe QDs (a) and denatured ovalbumin-QDs (b).

3.3. Temperature-dependent of denatured ovalbumin-QDs

Since it was difficult to separate the conjugates and the ovalbumin by Sephadex G-100, higher concentration of QDs was adopted to make most of the denatured ovalbumin conjugate to the QDs. The pure denatured ovalbumin-QDs were acquired by collecting the first absorption peak of the conjugates. After that, the sensitivity of the denatured ovalbumin-QDs to the temperature was measured. Similar to the pure CdTe QDs, it was also found that the absorption spectra remained constant (Fig. 4, curve a). But the PL intensity decreased gradually (Fig. 4, b → k) accompany with micro red-shift.

Further compared PL temperature-sensitivity of CdTe QDs and denatured ovalbumin-QDs, it was found that the PL intensity decreased linearly relative to increase of temperature. As the temperature increased from 278 K to 323 K, for CdTe QDs, the PL intensity decreased to 50.2% of its original, with a rate of ~1.1% K^{-1} (Fig. 2, curve a; $R^2 = 0.997$). While for denatured ovalbumin-QDs, the decreasing rate was much lower. The PL intensity decreased to 71.3% of its original, with a rate of ~0.63% K^{-1} (Fig. 2, curve d; $R^2 = 0.997$). It can also be observed, in both samples, that the PL emission wavelength, λ_{peak}, increased in a linear fashion as temperature arising. Comparing the behaviour of this parameter in different samples, it was concluded that the change of λ_{peak}, towards longer wavelengths, approximately 0.15 nm K^{-1} for QDs (Fig. 5, curve a; $R^2 = 0.999$) and 0.05 nm K^{-1} for denatured ovalbumin-QDs (Fig. 5, curve b; $R^2 = 0.999$). Therefore, the temperature-insensitivity of CdTe QDs was highly improved after modification of denatured ovalbumin. The surface trap states are important factors for the PL changing. It was speculated that the passivation of QDs surface with denatured ovalbumin led to the PL temperature-insensitivity. The increased temperature disturbed the repopulation of mobile electrons and holes on the surface of denatured ovalbumin-QDs. Therefore, some reactions such as oxidation would occur, which cause the decrease of PL intensity of denatured ovalbumin-QDs [22].

Besides, the effect of the quantity of denatured ovalbumin on the temperature-insensitivity was studied, and the results were shown in Fig. 6. As the temperature increased from 278 K to 323 K, the relative fluorescence intensity (F/F_0) rose gradually, and reached a plateau finally. That is to say, the temperature-insensitivity of the QDs increased with the increasing of the quantity of denatured ovalbumin and reached stable. This indicated that the temperature-insensitivity of QDs was decided by the quantity of denatured ovalbumin. The effect of pH on the temperature-insensitivity was also studied, the results showed that the pH value of the solution could change the PL intensity, but it could not influence the temperature-insensitivity.

The above experimental results indicated that the PL intensity and peak wavelength both tend to insensitive to temperature after modification. This property is beneficial to biolabeling. Furthermore, the PL reversibility is another important prop-

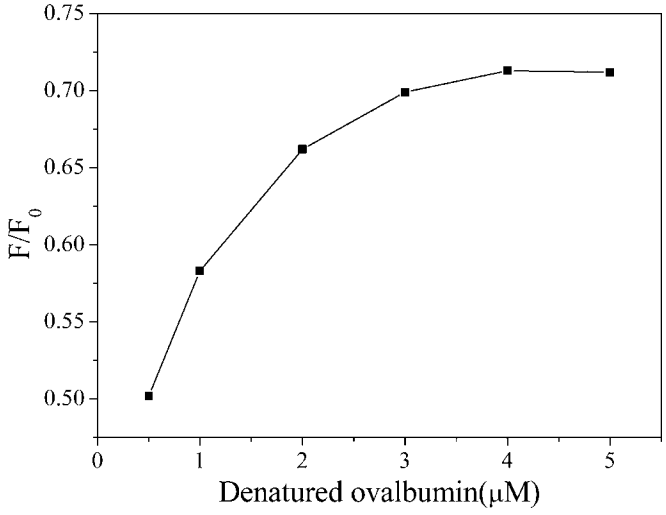


Fig. 6. The relationship between the relative fluorescence intensity (F/F_0) and the quantity of denatured ovalbumin. F: fluorescence intensity at 323 K; F_0: fluorescence intensity at 278 K.

erty for biolabeling. It had been reported that the temperature response of CdSe QDs was reversible in a temperature range from 100 K to 315 K [29]. Biju et al. [21] also found that after four to five heating-cooling cycles, the PL intensity changes were reversible. Gardner et al. [27] found the reversible changes in PL emission characteristics of both suspension and thin film samples. While previously, our group found that the PL of MAA coated CdSe/ZnS QDs was irreversible [22], their PL intensity recovered less than 50% of the original. This property is not suitable for biolabeling. Therefore, the PL reversibility of denatured ovalbumin-QDs was measured. It was repeatedly heated and cooled, the PL intensity (Fig. 7A) and emission wavelength (Fig. 7B) were both reversible satisfactorily. This can be ascribed to thermally activated deep trap states [27].

In addition, the calculation results showed this modification also improved the PL YQ (from 15% to 26%, 293 K). Furthermore, the denatured ovalbumin layer contains functional groups (carboxylic acids, amines, and cysteine residuals) for covalent conjugation to other biomolecules. This study provides CdTe QDs with more opportunities for biolabeling.

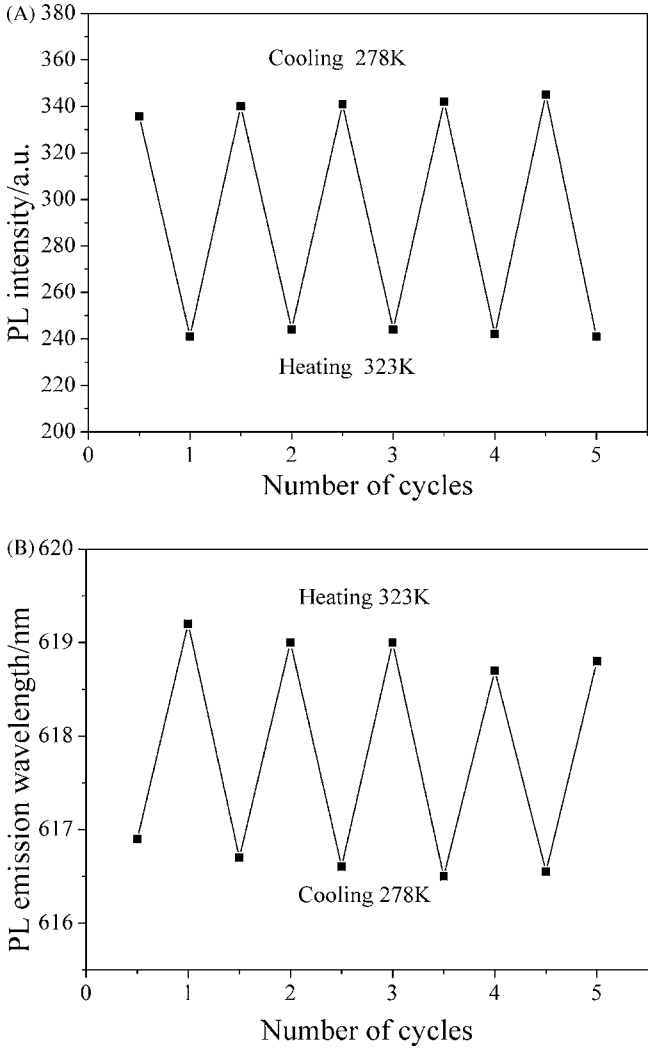


Fig. 7. PL intensity (A) and emission wavelength (B) variations of the denatured ovalbumin-QDs solution during heating (323 K)–cooling (278 K) cycles.

Besides, other denatured proteins (BSA and IgG) with different molecular weight were used to modify the QDs surface. With temperature arising from 278 K to 323 K, the formed multi-thiol-group biomacromolecules had a similar effect on the PL temperature-insensitivity. Their PL intensity remained 77% (BSA) and 73% (IgG) of their original, respectively. Such method by modification of QDs with denatured proteins greatly improved the temperature-insensitivity of CdTe QDs.

Furthermore, the temperature-insensitivity of other two different sized CdTe QDs (2.8 nm, 3.1 nm) modified by denatured ovalbumin was also studied. With temperature arising from 278 K to 323 K, the PL intensity remained 53.1% (2.8 nm) and 65.2% (3.1 nm) of their original, respectively. The denatured ovalbumin coated CdTe QDs had higher PL temperature-insensitivity. This indicated that the differences in PL temperature-insensitivity could be due to different surface-to-volume ratio. The small-sized QDs had higher defect density and more Te atoms with dangling bonds on their surface due to higher surface-to-volume ratio [28]. And at the same time, their emission peaks show less red-shift compared with pure CdTe QDs. This led to less disturb for multiplex imaging. Since QDs have broad excitation spectra and narrow emission bandwidths, which allow simultaneous excitation of particles of different sizes at a single wavelength. These properties pave road for multiplex imaging of biolabeling with CdTe QDs.

3.4. Detection of silver(I) ions by denatured ovalbumin-QDs probes

Another important application of CdTe QDs is that it can be used as selective ion probes [31,32]. It will cause big errors if the CdTe QDs are sensitive to the temperature. Based on this, the temperature-insensitivity of pure CdTe QDs and denatured ovalbumin coated CdTe QDs were tested as silver(I) ion probe (Fig. 8). As the temperature arising, it was found that the change of fluorescence intensity of denatured ovalbumin-QDs (Fig. 8, curve b) was obviously less than that of the pure CdTe QDs

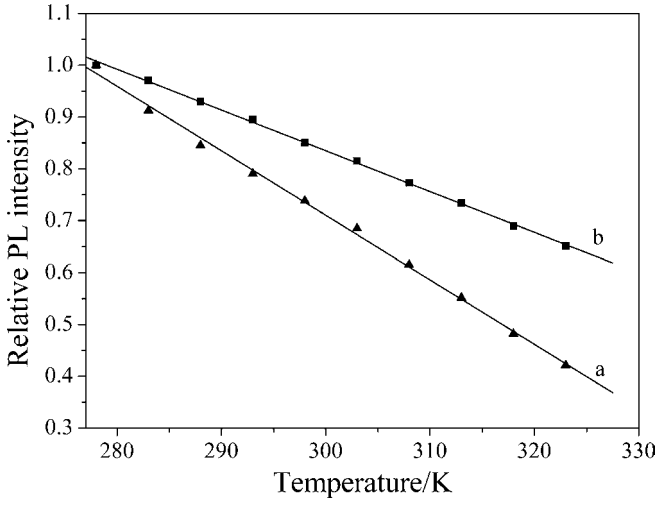


Fig. 8. The comparison of the temperature-insensitivity of pure CdTe QDs (a) and denatured ovalbumin coated CdTe QDs (b) as silver ions probe. [Ag^+]: 2 μM.

(Fig. 8, curve a). This indicated that the denatured ovalbumin improved the temperature-insensitivity of CdTe QDs. It was of great benefit to the application as fluorescence probes.

4. Conclusions

In summary, denatured ovalbumin had been used as capping agents to modify the surface of water-soluble CdTe QDs and render CdTe QDs more temperature-insensitive. Compared with MPA coated CdTe QDs, the PL intensity and emission wavelength of denatured ovalbumin-QDs are more temperature-insensitive. And the PL intensity and emission wavelength are reversible during repeatedly heating and cooling. All of the studies about PL temperature-dependence of denatured ovalbumin-QDs will push broad applications in life science.

Acknowledgements

This work was supported by the National High Technology Research and Development Program of China (863 Program: 2003AA234010), the National Natural Science Foundation of China (Grant Nos. 30670553, 30370387), the Program for Distinguish Young Scientist of Hubei Province (2006ABB020). This work was also supported by the Graduate Innovation Fund of Huazhong University of Science and Technology. Dr. Huang also gratefully appreciated the financial support from the National Natural Science Foundation of China (Grant No. 30400117).

References

[1] M.M. Yang, P. Yang, L.W. Zhang, Chin. Sci. Bull. 39 (1994) 31.
[2] B.J. Marcel, M. Mario, G. Peter, W. Shimon, A.P. Alivisatos, Science 281 (1998) 2013.
[3] S.P. Wang, N. Mamedova, N.A. Kotov, W. Chen, J. Studer, Nano Lett. 2 (2002) 817.
[4] N.N. Mamedova, N.A. Kotov, A.L. Rogach, J. Studer, Nano Lett. 1 (2001) 281.
[5] X.H. Gao, W.C.W. Chan, S.M. Nie, J. Biomed. Opt. 7 (2002) 532.
[6] Q. Wang, Y. Kuo, Y. Wang, G. Shin, C. Ruengruglikit, Q. Huang, J. Phys. Chem. B 110 (2006) 16860.
[7] F.Q. Chen, D. Gerion, Nano Lett. 4 (2004) 1827.
[8] H.J. Tanke, R.W. Dirks, T. Raap, Curr. Opin. Biotech. 16 (2005) 1.
[9] M. Howarth, K. Takao, Y. Hayashi, A.Y. Ting, Proc. Natl. Acad. Sci. U.S.A. 102 (2005) 7583.
[10] U. Hasegawa, S.I.M. Nomura, S.C. Kaul, T. Hirano, K. Akiyoshi, Biochem. Biophys. Res. Commun. 331 (2005) 917.
[11] I.D. Tomlinson, J.N. Mason, R.D. Blakely, S.J. Rosenthal, Method Mol. Biol. 303 (2005) 51.
[12] D.J. Bharali, D.W. Lucey, H. Jaykumar, H.E. Pudavar, P.N. Prasad, J. Am. Chem. Soc. 127 (2005) 11364.
[13] J.F. Weng, X.T. Song, L. Li, H.F. Qian, K.Y. Chen, X.M. Xu, C.X. Cao, J.C. Ren, Talanta 70 (2006) 397.
[14] M.Y. Li, Y.X. Ge, Q.F. Chen, S.K. Xu, N.Z. Wang, X.J. Zhang, Talanta 72 (2007) 89.
[15] J. Aldana, N. Lavelle, Y. Wang, X. Peng, J. Am. Chem. Soc. 127 (2005) 2496.
[16] G. Kalyuzhny, R.W. Murray, J. Phys. Chem. B 109 (2005) 7012.
[17] Q. Ma, X.G. Su, X.Y. Wang, Y. Wan, C.L. Wang, B. Yang, Q.H. Jin, Talanta 67 (2005) 1029.
[18] P.K. Mandal, M. Sarkar, A. Samanta, J. Phys. Chem. A 108 (2004) 9048.
[19] S.F. Wuister, A. Houselt, C.D.M. Doneg, D. Vanmaekelbergh, A. Meijerink, Angew. Chem. Int. Ed. 43 (2004) 3029.
[20] S.F. Wuister, C.D.M. Donega, A.J. Meijerink, J. Am. Chem. Soc. 126 (2004) 10397.
[21] V. Biju, Y. Makita, A. Sonoda, H. Yokoyama, Y. Baba, M. Ishikawa, J. Phys. Chem. B 109 (2005) 13899.
[22] T.C. Liu, Z.L. Huang, H.Q. Wang, J.H. Wang, X.Q. Li, Y.D. Zhao, Q.M. Luo, Anal. Chim. Acta 559 (2006) 120.
[23] J.H. Wang, H.Q. Wang, H.L. Zhang, X.Q. Li, X.F. Hua, Y.C. Cao, Z.L. Huang, Y.D. Zhao, Anal. Bioanal. Chem. 388 (2007) 969.
[24] H. Zhang, Z. Zhou, B. Yang, M.Y. Gao, J. Phys. Chem. B 107 (2003) 8.
[25] T. Rajh, O.I. Mićić, A.J. Nozik, J. Phys. Chem. 97 (1993) 11999.
[26] W.W. Yu, L.H. Qu, W.Z. Guo, X.G. Peng, Chem. Mater. 15 (2003) 2854.
[27] H.C. Gardner, D.E. Gallardo, C. Bertoni, S. Dunn, Proc. SPIE 6195 (2006) 61950N1.
[28] A.L. Rogach, Mater. Sci. Eng. B 69–70 (2000) 435.
[29] G.W. Walker, V.C. Sundar, C.M. Rudzinski, A.W. Wun, M.G. Bawendi, D.G. Nocera, Appl. Phys. Lett. 83 (2003) 3555.
[30] X.F. Hua, T.C. Liu, Y.C. Cao, B. Liu, H.Q. Wang, J.H. Wang, Z.L. Huang, Y.D. Zhao, Anal. Bioanal. Chem. 386 (2006) 1665.
[31] C. Bo, Z. Ping, Anal. Bioanal. Chem. 381 (2005) 986.
[32] A.S. Susha, A.M. Javier, W.J. Parak, A.L. Rogach, Colloids Surf. A 281 (2006) 40.

Available online at www.sciencedirect.com
ScienceDirect
Talanta 74 (2008) 1050–1055
Talanta
www.elsevier.com/locate/talanta

Short communication

Rapid and simple determination of adenine and guanine in DNA extract by micellar electrokinetic chromatography with indirect laser-induced fluorescence detection

Weiping Wang [a,b], Lei Zhou [b], Shumin Wang [b], Zhi Luo [b], Zhide Hu [b,c,*]

[a] College of Chemistry and Life Science, Zhejiang Normal University,Jinhua 321004, PR China
[b] Department of Chemistry, Lanzhou University, Lanzhou 730000, PR China
[c] Institute of Dunhuang Studies of Lanzhou University, Lanzhou 730000, PR China

Received 19 March 2007; received in revised form 18 June 2007; accepted 23 June 2007
Available online 5 November 2007

Abstract

This paper describes a micellar electrokinetic chromatography with indirect laser-induced fluorescence detection method for the simultaneous determination of adenine and guanine in DNA extracts from fungus, maize and soybean. The baseline separation was achieved within 2.5 min with running buffer (pH 9.3) composed of 10 mM borate, 20 mM SDS, 3.0×10^{-7} M fluorescein sodium as background reagent, applied voltage of 27.5 kV, cartridge temperature of 25.0 °C. Good linearity relationships (correlation coefficients > 0.9917) between the second-order derivative peak heights (RFU) and concentrations of the analytes (mg ml^{-1}) were obtained. The detection limits in second-order derivative electrophoregrams were 1.16×10^{-3} mg ml^{-1} for adenine and 0.29×10^{-3} mg ml^{-1} for guanine, respectively. The RSD data of intra-day for migration times and second-order derivative peak heights were less than 0.59 and 4.09%, respectively. This developed method was applied to the analysis of the two purines in DNA extracts with recoveries in the range of 85.3–110.2%. In this work, although the detection sensitivity was lower than that of direct LIF, yet the method has the advantages of rapidness and simplicity. And it would also extend the application range of LIF detector.
© 2007 Published by Elsevier B.V.

Keywords: Micellar electrokinetic chromatography; Indirect laser-induced fluorescence detection; Second-order derivative peak height; Adenine; Guanine

1. Introduction

The separation and determination of purine bases is a challenging and important task owing to the importance of these compounds in a variety of biochemical processes. Adenine (A) and guanine (G) are the building blocks of both DNA and RNA that play a crucial role in protein biosynthesis and the storage of genetic information [1]. A variety of analytical methods for the determination of A and/or G are available, among which HPLC and capillary electrophoresis (CE) followed by UV [2–11] and electrochemical [12–16] detection have drawn extensive attention. Kuhr and Yeung [17] reported the separation and detection of nucleotides and nucleosides by CZE with indirect fluorescence detection. However, to our knowledge, the separation and determination of A and G have not been reported by micellar electrokinetic chromatography (MEKC) combined with Indirect laser-induced fluorescence detection (ILIFD).

One of the most sensitive detection techniques in CE is LIF detection [18–21], which was first introduced into CE by Zare et al. [22]. However, the general applicability of this technique is limited because only a few compounds have native fluorescence [21], and the species that could be derivatizated are limited. In indirect LIF, a certain fluorophore is added to the background electrolyte, which is excited when passing through the detection window, yielding a steady fluorescence background signal. If the analyte band passes through the detection region, some displacement occurred due to maintenance of charge neutrality or quenching, resulting in differences in fluorescence intensity. Yeung and co-worker performed some instructive work in this field [17,23–25]. Although the sensitivity of ILIFD is lower than direct LIF and almost the same as UV detection, the method is quite general. Recently the ILIFD method has been extensively used to detect most kinds of compounds, such as VX and its methylphosphonic acid degradation products [26], anions and

* Corresponding author. Tel.: +86 931 8912540; fax: +86 931 8912582.
E-mail addresses: huzd@lzu.edu.cn, http://www.p02@lzu.cn (Z. Hu).

0039-9140/$ – see front matter © 2007 Published by Elsevier B.V.
doi:10.1016/j.talanta.2007.06.047

cations [27], diuretics [28], aliphatic carboxylic acids [29], thiols [30], alcohols [31], amino-substituted polycyclic aromatic hydrocarbons [32], explosives [33,34], mixtures of nitroaromatic and nitramine explosive compounds and their degradation products [35]. In addition, Liu et al. [36] studied the interactions between protein and drug molecules by microfluidic chip affinity CE with ILIFD, and Currie et al. [37] estimated pK_a values using microchip CE with indirect fluorescence detection.

The purpose of this study was to develop an MEKC-ILIFD combined with second-order derivative electropherogram method for the simple, rapid analysis of A and G in DNA extracts from foods. Fluorescein disodium salt was employed as background reagent. Linearity, reproducibility and detection limits were examined. The feasibility of this method for the analysis of real samples was also investigated with satisfactory results.

2. Experimental

2.1. Apparatus

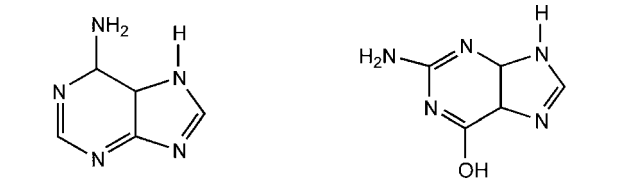
All experiments were performed on a P/ACE MDQ system (Beckman Coulter Instrument, Fullerton, CA, USA) equipped with a LIF detector. The excitation light from an argon ion laser (3 mW) was focused on the capillary window by means of a fiber-optic connection. The excitation was performed at 488 and 520 nm band-pass filter was used for emission. The system was controlled by 32 Karat software (version 7.0). The separation was carried out on a 50.2 cm (40 cm from inlet to the detector) × 75 μm i.d. uncoated fused-silica capillary (Yongnian Photoconductive Fiber Factory, Hebei, China).

The capillary was treated prior to its first use by flushing with methanol for 5 min, distilled water for 2 min, 1.0 M HCl for 5 min, distilled water for 2 min, 0.5 M NaOH for 10 min, distilled water for 2 min, and running buffer for 15 min in sequence, and then the capillary was equilibrated with running buffer under an electric field of 400 V/cm for 20 min. At the beginning of each day, the capillary was rinsed with 1.0 M HCl, 0.5 M NaOH, distilled water and running buffer for 5 min, respectively, and then the capillary was equilibrated with running buffer under an electric field of 400 V/cm for 10 min, finally the capillary was flushed with distilled water for 2 min.

Between runs, a rinse-cycle of 1.0 M HCl for 1 min, 0.5 M NaOH for 1 min, distilled water for 2 min and running buffer for 3 min followed by washing with distilled water for 2 min after each run was used. The capillary was maintained at 25 °C. Sample was injected by applying a pressure of 0.5 psi for 3 s (the injection volume is 12 nl).

2.2. Materials

Standards of adenine (A) and guanine (G) were obtained from the National Institute for Control of Pharmaceutical and Bio-products, China (Chemcial structures and pK_a values for A and G were shown in Fig. 1). Fluorescein disodium salt was of analytical purity and came from Aldrich (France). Samples of



Adenine, pK_1=4.2,pK_2 = 9.8 Guanine, pK_1 = 3.3, pK_2 = 9.2

Fig. 1. Chemcial structures and pK_a values for A and G.

Jew's-ear (Sample 1), maize (Sample 2) and soybean (Sample 3) were obtained from a local supermarket. All other reagents were of analytical reagent grade. Stock solutions (1500 mg ml^{-1} for A, 3000 mg ml^{-1} for G) were prepared with 0.01 M NaOH (stored at 4 °C). Further dilutions were made with triply distilled water to required concentrations. A stock solution of fluorescein disodium salt (1.0×10^{-4} M) was prepared with triply distilled water. All the stock solutions were prepared weekly.

2.3. Preparation of the electrolytes

The running buffers were prepared daily from 100 mM borate, 100 mM SDS (both were dissolved in triply distilled water), and certain amount of fluorescein disodium salt stock solution as background reagent. All the solutions were filtered through a 0.45 μm membrane filter, and the buffers were systematically degassed for 20 min using sonication before CE analysis.

2.4. Sample preparation

DNA extraction procedure after small modifications was based on the method described by ref. [38]. The SDS extraction buffer was composed of 10 mM Tris, 150 mM NaCl, 2 mM Na_2-EDTA, and 1% SDS.

Extraction procedure: All the samples were finely powdered, and then known amount of sample (0.1250 g for Sample 1, 0.1254 g for Sample 2, and 0.1250 g for Sample 3) was thoroughly mixed with 5.00 ml SDS extraction buffer (warmed-up at 65 °C) in a 15 ml centrifugal tube. The sample was incubated at 65 °C for 30 min, during which 2–3 times of thoroughly mix up was necessary, and then centrifugated for 20 min (4000 rpm) at room temperature. The upper layer was withdrawn and extracted twice with 1 volume of chloroform, and then mixed with 0.6 vol of 2-proponal (ice-cooled at −20 °C). After stored at −20 °C for 30 min, the sample was centrifugated as before to deposit DNA. The sedimentation was washed twice with 70% ethanol (ice-cooled at −20 °C), and then evaporated at room temperature. Prior to CE analysis, the dried sample was dissolved with 0.01 M NaOH and stored at −20 °C.

2.5. Recovery study

For recoveries study, appropriate amounts of the analytes (in the range of 75–125% of the original concentration found in samples) were added to the samples containing known amounts of analytes (i.e. previously analyzed samples). The spiked samples

were analyzed in triplicate according to the proposed method. Recovery values of the analyte added to the samples were calculated by interpolating the second-order derivative peak-height (H, RFU) on the calibration curve.

3. Results and discussion

3.1. Separation and detection

In our elementary experiment, only G was detected using CZE mode, as shown in Fig. 2. It can be seen from Fig. 2 that the peak height of G decreased with borate concentration increasing, while the migration time increased with the increasing of the borate concentration. The results showed that A could not be detected within the tested borate concentration range. Therefore, we considered introducing SDS to the running buffer for the purpose of detecting A. Here, 10.0 mM borate sodium was applied in the following experiments.

3.1.1. Effect of SDS concentration on separation

Once appropriate amount of SDS was added to the running buffer, the two compounds could be separated and detected. In order to optimize the effect of SDS concentration on migration time and separation efficiency, 10 mM borate sodium with different SDS concentration ranging from 5 to 40 mM was used to separate compound A and G, as shown in Fig. 3. It can be seen that the two compounds could be baseline separated in the tested range and the resolution was almost not influenced with SDS concentration changing. The migration times of the components increased with increasing SDS concentration due to the decrease of the EOF. Further investigation showed that higher or lower SDS concentration would decrease the peak intensity of compound A. In this work, 20 mM SDS was selected because of its shorter analysis time and higher separation efficiency.

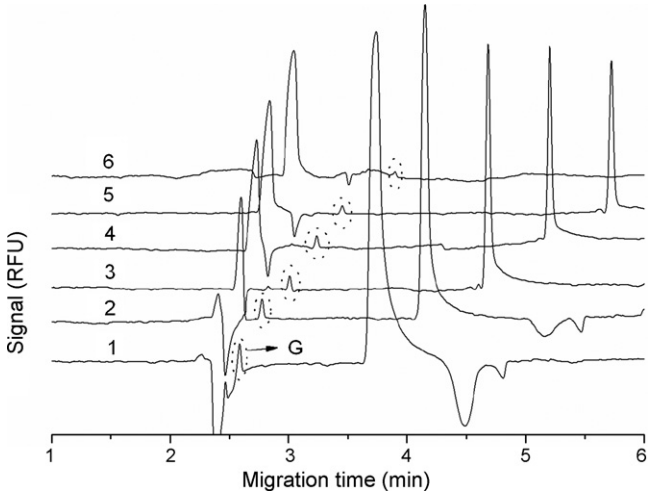


Fig. 2. Effect of borate concentration on separation. (1) 2.5 mM; (2) 5.0 mM; (3) 10.0 mM; (4) 15.0 mM; (5) 20.0 mM; (6) 30.0 mM. Conditions: 2.5–30 mM borate, 10^{-7} M fluorescein sodium; applied voltage: 20.0 kV; cartridge temperature: 25.0 °C; capillary dimension: 50.2 cm (40 cm from inlet to the detector) × 75 μm i.d.; sample injected at 0.5 psi for 3 s.

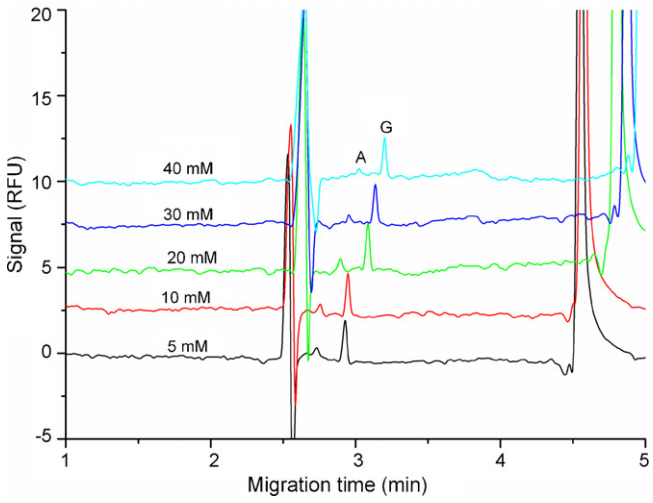


Fig. 3. Effect of SDS concentration on separation. Conditions: 10 mM borate, 5–40 mM SDS, 10^{-7} M fluorescein sodium; other conditions as in Fig. 2.

3.1.2. Effect of pH on separation

pH value of running buffer, which can influence the mobility of analytes by adjusting the velocity of EOF and the charge of analyte molecular, has been acknowledged as one of the most important parameters for CE separation. The effects of buffer pH on the separation of the analytes were shown in Fig. 4. It can be seen from Fig. 4 that A and G could be baseline separated in the tested range of 8.9–9.7, and also the peak elute order was unchanged. At this pH range, G has two negative charges while A is single-charged ion (Adenine: $pK_1 = 4.2$, $pK_2 = 9.8$; Guanine, $pK_1 = 3.3$, $pK_2 = 9.2$). When pH > 9.3 (the measured pH value without adjusting), the migration time of the analytes increased dramatically, while pH < 9.3, migration time changed little with pH changing. In addition, the fluorescence intensity of fluorescein is pH dependent. With increasing pH, fluorescenc intensity increases rapidly and reached a constant level at pH ≥ 8 [39]. At about pH 9.0–10.0, the fluorophore intensity

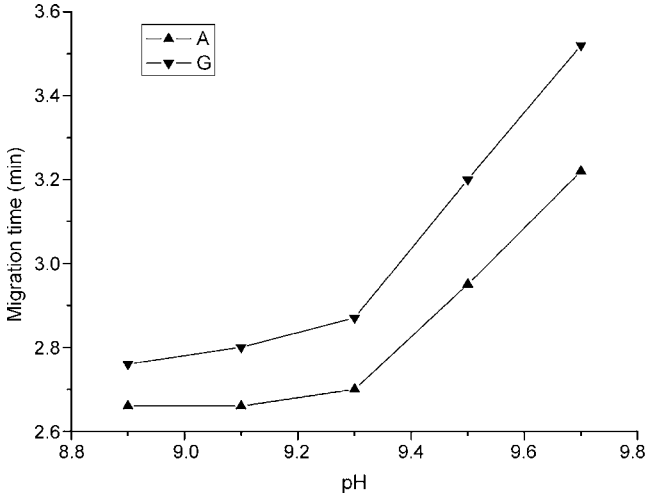


Fig. 4. Effect of buffer pH on separation. Separation conditions: 10 mM borate, 20 mM SDS, 10^{-7} M fluorescein sodium; pH range 8.9–9.7; other conditions as in Fig. 2.

Table 1
Results of linear range, regression data and concentration limits of detection for the analytes

Compound	Linear range* (mg ml^{-1})	a	b	Correlation coefficient	TR (10^{-5})	Detection limits (mg ml^{-1})
A	0.05–1.0	0.032	0.43	0.9922	0.35	1.16×10^{-3}
G	0.025–0.75	0.066	1.92	0.9917	1.6	0.29×10^{-3}

* Calibration curves are expressed as: $H = a + bX$, where H is the second-order derivative peak-height (RFU) and X is the concentration (mg ml^{-1}). a is intercept and b is slope.

was maxium. Therefore, optimum pH 9.3 was selected for the following experiments.

3.1.3. Selection of fluorophore concentration

The influence of fluorescein concentration on fluorescence intensity of the analytes was studied with its concentration ranging from 0.05×10^{-7} to 4.0×10^{-7} M. The signal-to-noise ratios of the studied analytes were used to estimate the sensitivity of this method when using buffers containing different concentrations of fluorescein. The results indicated that the peak heights of the analytes showed little improvement when fluorescein concentration was higher than 3.0×10^{-7} M. In addition,

Table 2
Reproducibility data for the analytes

Compound	Migration time (%)		Second-order derivative peak height (%)	
	Intra-day ($n = 6$)	Inter-day ($n = 3$)	Intra-day ($n = 6$)	Inter-day ($n = 3$)
A	0.59	2.56	4.09	4.94
G	0.50	2.70	0.50	1.68

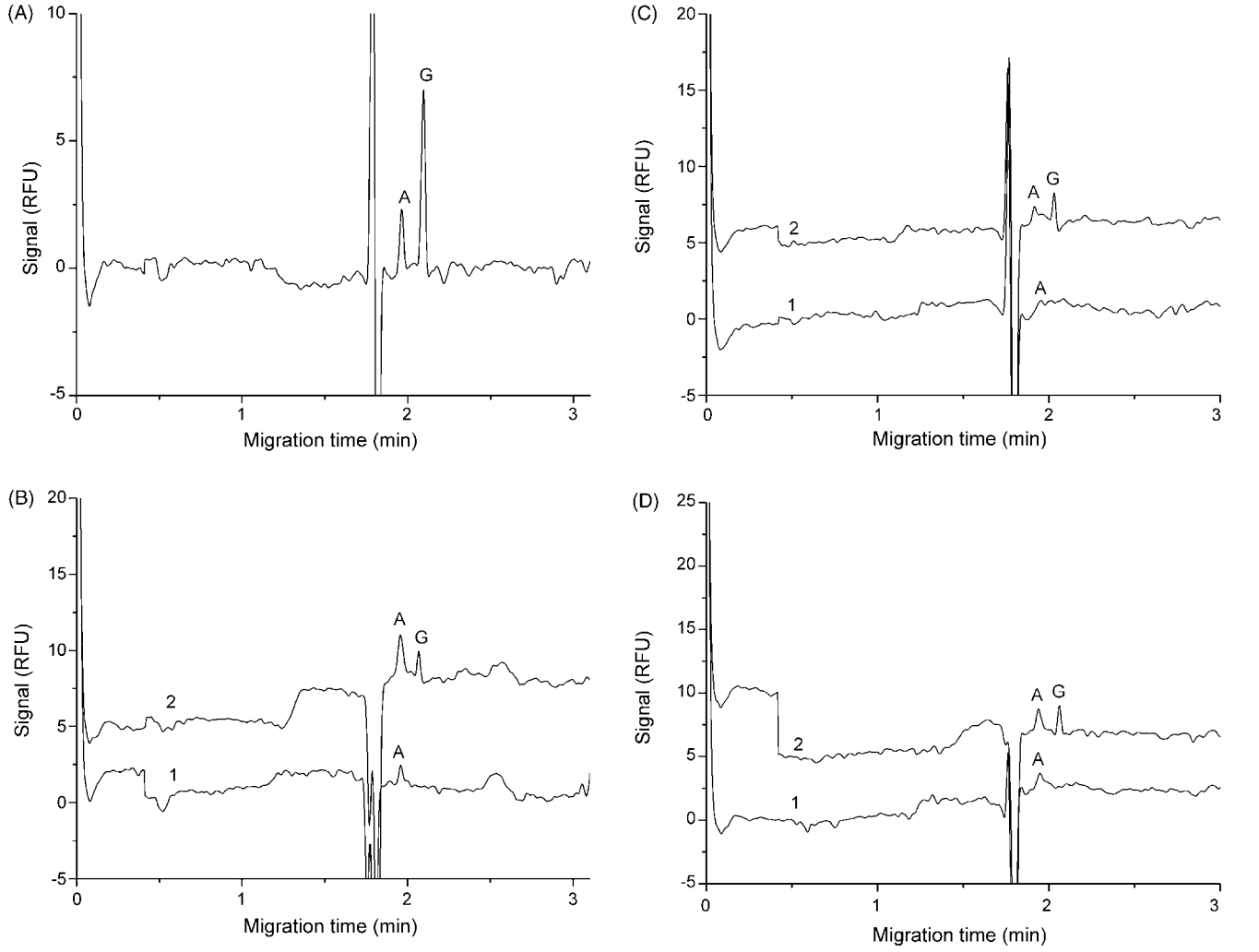


Fig. 5. Typical electropherograms for standard mixtures and samples. (A) Standard mixtures of A and G; (B) Sample 1; (C) Sample 2; (D) Sample 3. 1 stands for unspiked sample and 2 for spiked sample (the three samples were all spiked with 0.1875 mg ml^{-1} A and 0.1250 mg ml^{-1} G). Separation conditions: 10 mM borate, 20 mM SDS, 3.0×10^{-7} M fluorescein sodium, pH 9.3, applied voltage: 27.5 kV; other conditions as in Fig. 2.

the response of fluorescein was a plateau, which made it difficult to measure the changes of fluorescence signal when analytes ions passed through the detection window. A concentration of less than 0.5×10^{-7} M was also unsuitable because of low signal intensity. With respect to the signal-to-noise ratio of the system and peak height of the analytes, 3.0×10^{-7} M fluorescein sodium was chosen as the optimum fluorophore concentration.

3.1.4. Effect of applied voltage and temperature on separation

The effects of applied voltage and cartridge temperature on separation were investigated in the range of 15.0–30.0 kV and 20.0–40.0 °C. The results showed that baseline separation could be obtained in the tested voltage range. In addition, higher separation voltage causes detrimental Joule effect, thus leads to lower separation efficiency. With temperature increasing, the resolution efficiency was decreasing accompanied by shorter analysis time. To obtain better peak shape, and also with respect to other factors, a voltage of 27.5 kV and temperature of 25.0 °C were applied.

According to the results above, the optimum separation conditions were as follows: 10.0 mM borate, 20 mM SDS, 3.0×10^{-7} M fluorescein sodium salt, pH 9.3, applied voltage of 27.5 kV, cartridge temperature of 25 °C.

3.2. Transfer ratio and detection limit

In indirect detection techniques the concentration limit of detection (C_{LOD}) is given by [25]

$$C_{LOD} = \frac{C_M}{TR \times DR} \quad (1)$$

where C_M is the concentration of the background fluorophore, TR is the transfer ratio (the number of fluorescent molecules displaced or quenched per molecule of analyte), and DR is the dynamic reserve. DR is a measure of the stability of the background signal and is defined as the ratio of the background signal to the background noise.

In the present study, the background fluorescence intensity was 20 RFU and the peak-to-peak noise level of the background was 0.002 RFU. DR was calculated to be 10^4. The transfer ratio (TR) was determined by a method similar to that described in the literature [40] except that the second-order derivative peak-height was used instead of the corrected peak area. Table 1

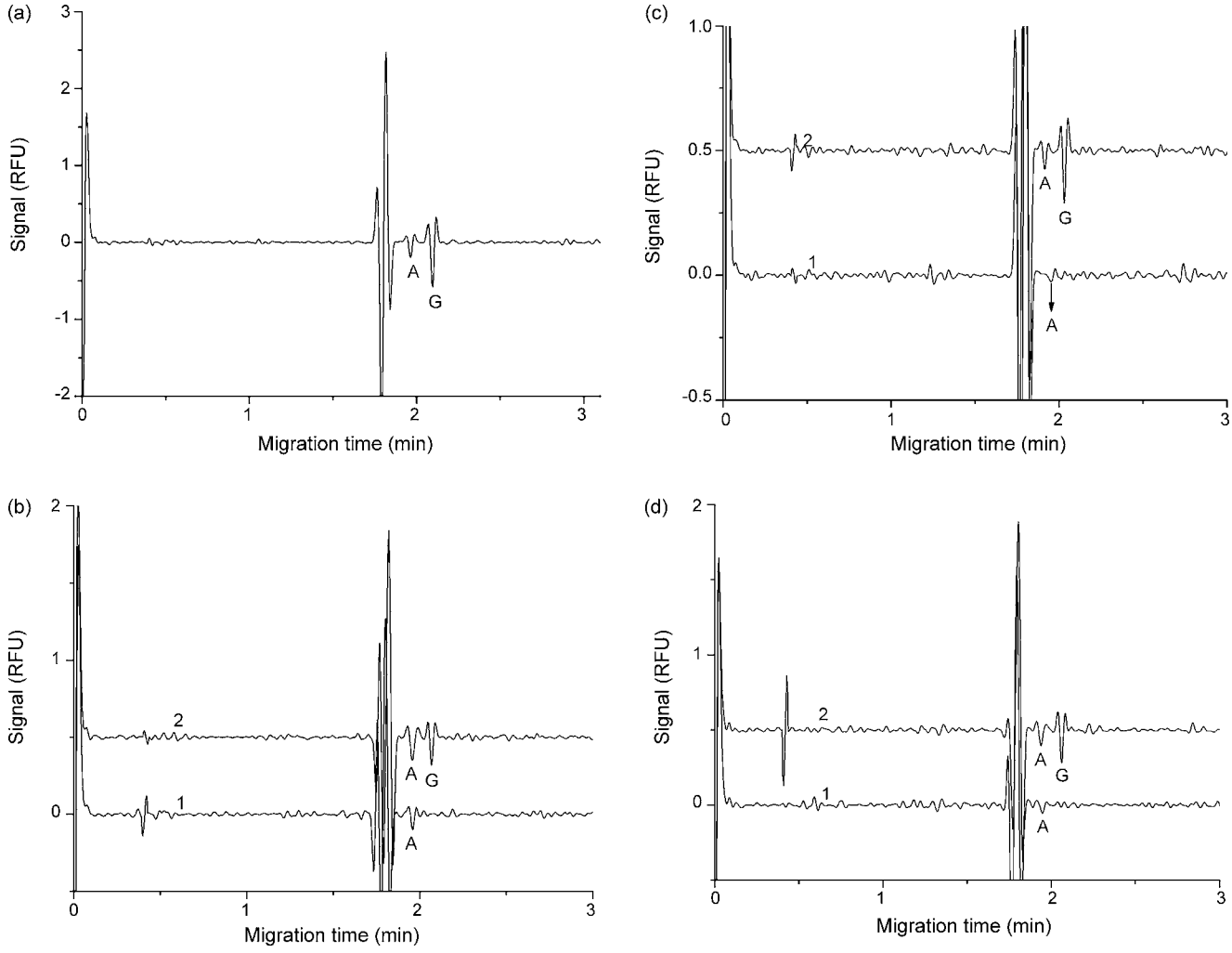


Fig. 6. Second-order derivative electropherograms corresponding to Fig. 5.

Table 3
Determination results of the analytes in the samples ($n = 3$)

Sample	Compound	Content (mg g^{-1})	Recovery (%)
Sample 1	A	11.04	96.9
	G	ND[a]	99.2
Sample 2	A	0.16	110.2
	G	ND[a]	105.3
Sample 3	A	0.96	85.3
	G	ND[a]	108.0

[a] ND, not detected.

summarizes the results for TR, the C_{LOD} calculated from Eq. (1).

3.3. Applications

To evaluate the quantitative applicability of the method, eight standard solutions of the analytes in different concentration range were analyzed under optimum separation conditions. When making standard working curve, we found it difficult to integrate the target peaks due to the baseline drift. Therefore, quantitative analysis was obtained by employing the second-order derivative electropherogram. It has been proved that the second-order derivative was a good determination method when the components partially separated [41–43]. However, satisfactory results were also obtained using second-order derivative in indirect detection. The linearity between the second-order derivative peak-height (H, RFU) and the concentration (X, mg ml^{-1}) was investigated. The peak height (H) was calculated based on: $H = 0.5(H_l + H_r)$, please see Fig. 6(a) for H_l and H_r. The linear regression equations and the detection limits are listed in Table 1. Table 2 provides a summary of the reproducibility data relating to the current system. The listed reproducibility data includes the repeatability of the whole analytical method. Table 2 shows that inter-day deviations are slightly higher due to the experimental differences in solutions makeup, and variations in EOF on a day-to-day basis. The developed method was applied to the analysis of DNA extracts from different foods. However, only A was detectable, and G was not detected in the samples. Probably the presence of G was at a concentration below the detection limit. Therefore, the sample was then spiked with 0.1875 mg ml^{-1} A and 0.1250 mg ml^{-1} G. The electropherograms of the standard mixtures, the unspiked and spiked samples are shown in Figs. 5 and 6 is the corresponding second-order derivative electropherograms to Fig. 5. The determination results of the samples are listed in Table 3.

4. Conclusions

In this work, fluorescein disodium salt was employed as background reagent in MEKC to analyze A and G in DNA extracts from fungus, maize and soybean. Quantitive analysis was successfully obtained by employing second-order derivate electropherogram. This proposed method was rapid and simple, showing important applying tendency for the analysis of purine derivatives in real samples.

References

[1] W.H. Brown, Introduction to Organic and Biochemistry, fourth ed., Brooks/Cole Publication, Monterey, 1987, 418 pp.
[2] T. Wessel, C. Lanvers, S. Fruend, G. Hempel, J. Chromatogr. A 894 (2000) 157.
[3] P.G. Moral, M.J. Arín, J.A. Resines, M.T. Díez, J. Chromatogr. B 826 (2005) 257.
[4] X. Xiong, O.Y. Jin, W.R.G. Baeyens, J.R. Delanghe, X.M. Shen, Y.P. Yang, Electrophoresis 27 (2006) 3243.
[5] Y.C. Huang, C.C. Lin, C.Y. Liu, Electrophoresis 25 (2004) 554.
[6] C.S. Robb, S.C. Yang, P.R. Brown, Electrophoresis 23 (2002) 1900.
[7] D. Friedecký, T. Adam, P. Barták, Electrophoresis 23 (2002) 565.
[8] P. Wang, J.C. Ren, J. Pharm. Biomed. Anal. 34 (2004) 277.
[9] C.W. Klampfl, M. Himmelsbach, W. Buchberger, H. Klein, Anal. Chim. Acta 454 (2002) 185.
[10] S.E. Geldart, P.R. Brown, J. Chromatogr. A 831 (1999) 123.
[11] P. Kießling, G.K.E. Scriba, S. Falco, G. Werner, H. Knoth, M. Hartmann, J. Pharm. Biomed. Anal. 36 (2004) 535.
[12] D.K. Xu, L. Hua, H.Y. Chen, Anal. Chim. Acta 335 (1996) 95.
[13] G. Chen, Q.C. Chu, L.Y. Zhang, J.N. Ye, Anal. Chim. Acta 457 (2002) 225.
[14] G. Chen, X.H. Han, L.Y. Zhang, J.N. Ye, J. Chromatogr. A 954 (2002) 267.
[15] H. Lin, D.K. Xu, H.Y. Chen, J. Chromatogr. A 760 (1997) 227.
[16] J. Wang, G. Chen, A. Muck Jr., Shin Dongchan, A. Fujishima, J. Chromatogr. A 1022 (2004) 207.
[17] W.G. Kuhr, E.S. Yeung, Anal. Chem. 60 (1988) 2642.
[18] J. Jiang, C.A. Lucy, Talanta 72 (2007) 113.
[19] S. Chen, Y.Z. Xu, Y.H. Bi, W. Du, B.F. Liu, Talanta 70 (2006) 63.
[20] J.M. Song, A. Asthana, D.P. Kim, Talanta 68 (2006) 940.
[21] Q. Liu, Y.J. Liu, M.L. Guo, X.B. Luo, S.Z. Yao, Talanta 70 (2006) 202.
[22] E. Gassmann, J.E. Kuo, R.N. Zare, Science 230 (1985) 813.
[23] L. Gross, E.S. Yeung, J. Chromatogr. 480 (1989) 169.
[24] L. Gross, E.S. Yeung, Anal. Chem. 62 (1990) 427.
[25] W.G. Kuhr, E.S. Yeung, Anal. Chem. 63 (1991) 275A.
[26] V.H. Shabtai, N. Gratziany, Z. Liron, Electrophoresis 27 (2006) 1996.
[27] S.J. Chen, M.J. Chen, H.T. Chang, J. Chromatogr. A 1017 (2003) 215.
[28] X.H. Yang, X.C. Wang, X.M. Zhang, J. Sep. Sci. 29 (2006) 677.
[29] T.C. Chiu, M.F. Huang, C.C. Huang, M.M. Hsieh, H.T. Chang, Electrophoresis 23 (2002) 449.
[30] S. Pelletier, C.A. Lucy, J. Chromatogr. A 972 (2002) 221.
[31] C.J. Morin, N.L. Mofaddel, A.M. Desbène, P.L. Desbène, J. Chromatogr. A 872 (2000) 247.
[32] T. Kaneta, Y. Saito, T. Imasaka, J. Chromatogr. A 831 (1999) 285.
[33] S.R. Wallenborg, C.G. Bailey, Anal. Chem. 72 (2000) 1872.
[34] S. Kennedy, B. Caddy, J.M.F. Douse, J. Chromatogr. A 726 (1996) 211.
[35] C.G. Bailey, S.R. Wallenborg, Electrophoresis 21 (2000) 3081.
[36] X.J. Liu, X. Liu, A.Y. Liang, Z. Shen, Y. Zhang, Z.P. Dai, B.H. Xiong, B.C. Lin, Electrophoresis 27 (2006) 3125.
[37] C.A. Currie, W.R. Heineman, H.B. Halsall, C.J. Seliskar, P.A. Limbach, F. Arias, K.R. Wehmeyer, J. Chromagotr. B 824 (2005) 201.
[38] J.C. Zhou, M.J. Yang, X.F. Yang, J.M. Huang, W.H. Ling, Q. Huang, W.L. Li, Food Sci. 26 (2005) 29.
[39] P.L. Desbène, C.J. Morin, A.M. Desbène-Monvernay, R.S. Groult, J. Chromagogr. A 689 (1995) 135.
[40] S.M. Cousins, P.R. Haddad, W. Buchberger, Chromagogr. 671 (1994) 397.
[41] J.Y. Zhang, Z.D. Hu, X.G. Chen, Talanta 65 (2005) 986.
[42] J.P. Xie, X.F. Chen, J.Y. Zhang, J.Q. Liu, J.N. Tian, X.G. Chen, Z.D. Hu, J. Pharm. Biomed. Anal. 36 (2004) 1.
[43] A.J. Chen, J.Y. Zhang, C.H. Li, X.F. Chen, X.G. Chen, Z.D. Hu, J. Sep. Sci. 27 (2004) 569.

Available online at www.sciencedirect.com
ScienceDirect
Talanta 74 (2008) 619–624
Talanta
www.elsevier.com/locate/talanta

Rapid determination of aristolochic acid I and II in medicinal plants with high sensitivity by cucurbit[7]uril-modifier capillary zone electrophoresis

Fang Wei, Yu-Qi Feng *

Department of Chemistry, Wuhan University, Wuhan 430072, PR China

Received 26 March 2007; received in revised form 16 June 2007; accepted 23 June 2007
Available online 1 July 2007

Abstract

Aristolochic acids (AAs) are commonly found in medicinal plants such as *Radix aristolochiae* and have been reported to cause acute hepatitis and end-stage renal failure. Hence, quantitative analysis and quality control for the plants containing AAs is of great importance. In this study, a novel macrocylcic molecule, cucurbit[7]uril (CB[7]) was employed as a modifier in capillary zone electrophoresis (CZE) for rapid determination of aristolochic acid I and II in medicinal plants. In similarity to other macrocyclic molecules, such as cyclodextrins (CDs), CB[7] can be used to manipulate selectivity in CE because it can form inclusion complexes with a variety of guest molecules. During the running process, CB[7] bears a positive charge in the pH range of 2.5–7.5 and can be adsorbed onto the inner wall of a fused-capillary, leading to a reversal of the electroosmotic flow (EOF). By applying a negative polarity, a rapid separation of AA-I and AA-II was achieved within 7 min using 100 mM phosphate buffer (pH 7.5) containing 3 mM CB[7] and 10% acetonitrile (v/v) as modifiers, due to the same directions of the EOF and the electrophoretic mobilities of the analytes. By applying electrokinetic injection with field-enhanced sample stacking, two kinds of aristolochic acids in four medicinal plants were successfully determined with high sensitivity, high separation efficiency, repeatability and recovery. The proposed method was also used to determine AA-I and AA-II in two slimming pills with complex matrix.
© 2007 Elsevier B.V. All rights reserved.

Keywords: Capillary zone electrophoresis; Cucurbit[7]uril; Aristolochic acids I and II; Medicinal plants

1. Introduction

Aristolochic acids (AAs) are structurally related to nitrophenanthrene carboxylic acids found in medicinal plants such as *Radix aristolochiae* [1]. AA-I and AA-II (Fig. 1) are the major toxic components. There are reports indicating that some of these compounds are nephrotoxic and carcinogenic [2–6]. Many countries have banned the use of medicinal plants containing AA-I and AA-II [7]. Therefore, it is important to quantify the AAs content in medicinal plants and related products.

The analysis of AA-I and AA-II is difficult because of their extremely similar structures and identical medicinal activities. Thin layer chromatography (TLC) [8,9], ultraviolet spectrophotometry [10] and high performance liquid chromatography [11–16] have been applied to the analyses of AA-I and/or AA-II in medicinal plants. Recently, capillary electrophoresis (CE) has been proved to be an effective and convenient technique in the analysis of medicinal plants due to its excellent separation efficiency, short analysis time, minimal need of samples and solvents and high versatility in terms of separation modes [17,18]. Successful separation and determination of AA-I and AA-II by CE method were achieved not only for medicinal plants, but also for Chinese prepared medicines (CPMs) [19–23], in which β-cyclodextrin (β-CD) or SDS as modifier and laser-induced fluorescence (LIF) detection or electrochemical detection have been used to improve the selectivity and sensitivity of CE, respectively.

In order to improve the separation selectivity in CE analysis, it is common to use additives. For example, macrocyclic molecules including cyclodextrins (CDs), crown ethers and calixarenes have been widely used for this purpose because their cavities can selectively form inclusion complexes with the analytes through host–guest interactions [24–26]. As a class of potential macrocyclic additives, the cucurbit[*n*]urils (CB[*n*], *n* = 5–8,

* Corresponding author. Tel.: +86 27 87867564; fax: +86 27 68754067.
E-mail address: yqfeng@public.wh.hb.cn (Y.-Q. Feng).

0039-9140/$ – see front matter © 2007 Elsevier B.V. All rights reserved.
doi:10.1016/j.talanta.2007.06.030

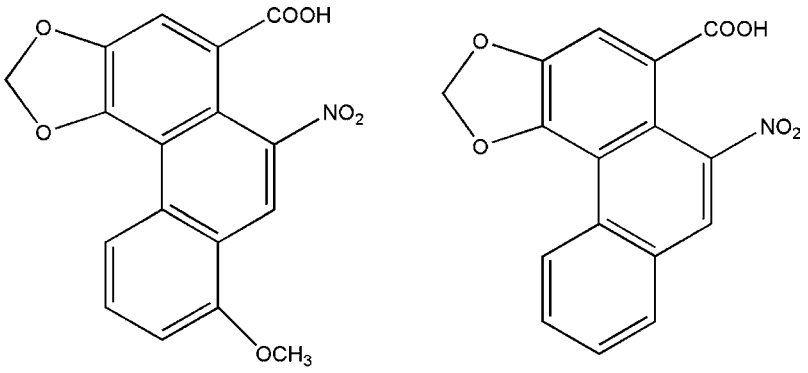


Fig. 1. Structures of aristolochic acids I and II.

10) are a kind of cyclic methylene-linked glycoluril oligomers. They possess a characteristic annular shape with two identical carbonyl-fringed portals, which are also capable of forming inclusion complexes with various molecules by hydrophobic interaction or ion–dipole interaction [27–31]. However, compared to CDs, few applications of CB[*n*]s in separation science have been reported [32–34] mainly due to their poor solubility in common solvents and the difficulty to functionalize these molecules. Among CB[*n*], CB[7] (Fig. 2) has a moderate solubility in water (~20 mM) and contains a cavity size similar to that of β-CD [35–40], making it very potentially useful as a modifier for improving the selectivity of CE. The preliminary results on the use of CB[7] as additive reported in our previous work [32] showed that CB[7] bears positive charge in the pH range of 2.5–7.5 and can be adsorbed onto the inner wall of a fused-capillary, leading to a reversal of the electroosmotic flow (EOF). The reversed EOF may be beneficial for fast separation of strong organic acids, since in this way, the analysis of organic acids can be obtained in a coelectroosmotic mode [41,42].

The poor concentration sensitivity is the main drawbacks of CE, which is due to the limited optical path length for on-line UV detection and the limited volume of sample solution that can be injected, and hinders the applications of CE in the analysis of real samples. Sample stacking is an inherent and exclusive feature of CE and several modes have been developed [43–46], which have shown their usefulness for improving the sensitivity of CE. The simplest stacking modes consist of the hydrodynamic injection (normal stacking mode, NSM) and electrokinetic injection (field-enhanced sample injection, FESI) of sample with electrical conductivity lower than that of the separation buffer. And it has been shown that, electrokinetic injection provides larger sensitivity enhancements compared with hydrodynamic injection [47]. Strong organic acids, which are negative ions in neutral or alkaline conditions due to ionization, can only be electrokinetic injected and concentrated by applying a negative polarity. The reversed EOF (e.g. caused by CB[7] as modifier) is convenient for negative ions stacking by FESI, for no polarity switching is necessary due to the same directions (toward anodic end) of the EOF and the electrophoretic velocity of the analytes.

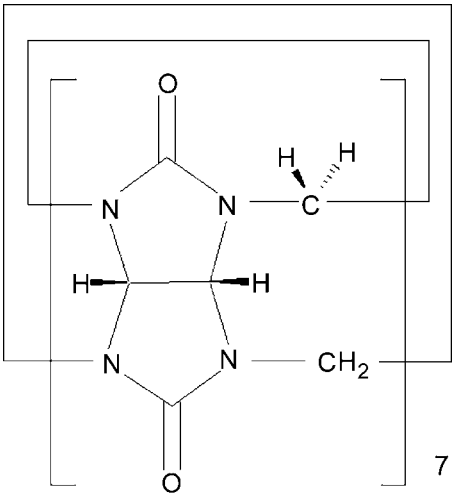


Fig. 2. The structure of CB[7].

This work was to demonstrate that CB[7] can potentially be used as modifier for real sample analysis. A CZE method using CB[7] as modifier was developed for the separation of AA-I and AA-II, with improved resolution and high sensitivity by combining FESI. The separation conditions were systematically optimized by investigating the effects of pH and ionic strength of the buffer, CB[7] concentrations and organic modifier with different compositions. The developed method was then applied for the determination of AA-I and AA-II in four medicinal plants samples with high separation efficiency, high sensitivity, repeatability and recovery. Two slimming pills with complex matrix have also been analyzed.

2. Experimental

2.1. Chemicals and materials

CB[7] was synthesized, purified and characterized as described in the literature [29,34]. The standard mixture sample containing AA-I (29%) and AA-II (66%) was obtained from Sigma (Missouri, United States), and the standard AA-I was obtained from Acros (Geel, Belgium). Sodium hydroxide (NaOH), hydrochloric acid (HCl), disodium hydrogen phosphate (Na_2HPO_4), phosphate acid (H_3PO_4), methanol (MeOH) and acetonitrile (MeCN) and thiourea were obtained from Bei-

jing Chemical Factory (Beijing, China) and were of analytical reagent grade. Four kinds of medicinal plant samples were obtained from local hospital of Chinese traditional medicine. Two slimming pills were purchased from local drug store. Double distilled water was obtained from a quartz apparatus and used for all experiments. The mixed stock solution was prepared by dissolving 5 mg standard mixture of AA-I (29%) and AA-II (66%) in methanol into a 5 mL volumetric flask, and a stock solution of 1 mg/mL AA-I was also prepared. The tested standard solutions for calibration were diluted in methanol prior to use.

Disodium hydrogen phosphate (Na_2HPO_4) buffer with different concentrations were adjusted to the desired pH with 1 M H_3PO_4. The phosphate buffer was then mixed with MeCN by volume ratio, in which CB[7] with different concentrations was dissolved directly by stirring. Before use, the running buffer was generally filtered through a G-4 fritted glass funnel and degassed in an ultrasonic bath for about 5 min.

2.2. Instrument and analytical conditions

The CE analysis was performed on a CAPEL 105 CE system (LUMEX, Russia) equipped with a UV–vis detector. Separations were carried out in an uncoated fused-silica capillary (Yongnian Fiber Plant, Hebei, China) of 50 μm i.d. and an effective length of 51 cm (total length 60 cm). Data collection and manipulation were carried out on Chrom & Spec software for chromatography, Version 1.56. Before use, the capillary was rinsed sequentially with 1 mol/L NaOH (15 min), water (15 min), 1 mol/L HCl (15 min), and water (15 min), followed by conditioning with buffer for 15 min. After each run, the capillary was rinsed with running buffer for 2 min. The inlet/outlet vials were renewed for every run. The UV absorbance detection was performed at 254 nm. The CZE system was operated using "negative" polarity (the anode was located on the detector side). The electrokinetic injection was made by placing the capillary and the cathode into the sample vial and applying a voltage (−6 kV) for 10 s. After the sample was introduced, the cathode and capillary were placed back into the buffer vial, and then an electric field was applied. This system was run at 25 °C at a constant voltage of −25 kV. Under optimized electrophoretic conditions, separations were carried out using a running buffer composed of 0.1 M Na_2HPO_4 (adjusted to pH 7.5 with 1 M H_3PO_4), 3 mM CB[7] and 10% MeCN (v/v). Thiourea was used as EOF marker.

2.3. Sample preparation

For sample preparation, each dried plant was ground into powder. After that, each sample (0.2 g) was firstly marinated in 5 mL methanol for 16 h. Then it was extracted by ultrasonication for 30 min and centrifuged at 3000 rpm for 5 min. The extraction process was conducted thrice, and the extracts were combined and diluted to 20 mL with methanol. The solutions of extracts were then passed through a 0.45 μm membrane filter. Finally, 150 μL of the sample extractions were pipetted into a vial followed by addition of a constant amount of 5 mg/L phthalic acid as IS before sample injection. The internal standard (IS) was introduced to minimize the variation results from the electrokinetic injection and the fluctuation of the electroosmotic flow. The preparation procedures for slimming pills are the same as above.

2.4. Recovery test for AA-I and AA-II

0.1 mg of standard mixture of AA-I and AA-II (AA-I: AA-II = 29:66) was added to the sample of *Caulis aristolochiae manshuriensis*. The mixture was extracted and analyzed by the procedures described earlier, thus the recovery was calculated.

3. Results and discussion

3.1. Optimization of CZE conditions

3.1.1. Effect of pH

The influence of pH on electroosmotic flow has been reported in our previous work [32], and the results showed that CB[7] bears positive charge in the pH range of 2.5–7.5 and can be dynamically adsorbed onto the inner wall of a fused-capillary, leading to a reversal of the electroosmotic flow.

The influence of pH on separation was not significant because of little difference in pK_a values between AA-I and AA-II. And it was found that separation of them can be achieved under all the studied pH range (pH 2.5–7.5) with 2 mM CB[7]. However, rapid separation can be achieved with a running buffer at higher pH because the full ionization of AAs at high pH may lead to the same direction of electrophoretic mobilities of AAs and EOF. Therefore, taking the stability and migration time of AAs into account, pH 7.5 was considered to be the best value for the running buffer.

3.1.2. Effect of buffer concentration

Disodium hydrogen phosphate concentration was changed in the range of 40–120 mM in the buffer containing 2 mM CB[7] (pH 7.5). It was demonstrated that the anodic EOF slightly decreased with the increase of buffer concentration, which may be ascribed to the decreased amount of CB[7] that will interact with the silanol groups of the inner wall of the fused-capillary.

The resolution (R_s) of AA-I and AA-II was obviously improved as buffer concentration increased. However, the migration times of AAs and Joule heat also increased with increasing buffer concentration. Therefore, disodium hydrogen phosphate buffer at the concentration of 100 mM was chosen as optimum.

3.1.3. Effect of CB[7] modifier

The effect of CB[7] concentration on the EOF has also been reported in our previous work [32], and an increased anodic EOF with the increasing concentration of CB[7] (1–5 mM) was observed.

The analysis of AA-I and AA-II by CZE without any modifiers is difficult because of their extremely similar mobilities [20]. The only difference between the structures of AA-I and AA-II is the methoxy group, which may form stronger inclusion complex with CB[7] due to stronger hydrophobic interaction. And it may be the key reason for improvement of separation by the use of CB[7] as modifier. From Fig. 3, it can be seen that the

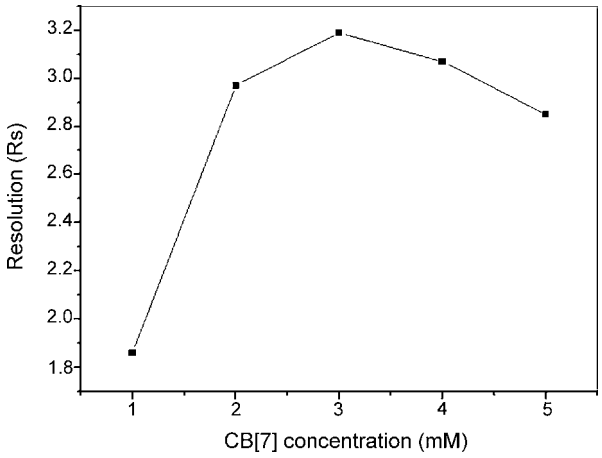


Fig. 3. Effect of CB[7] concentration on resolution for the separation of AA-I and AA-II (10 mg/L). Conditions: Na_2HPO_4 (100 mM, pH 7.5) with different concentrations of CB[7]; −25 kV; 25 °C; 254 nm; sample injection at 30 mbar for 5 s.

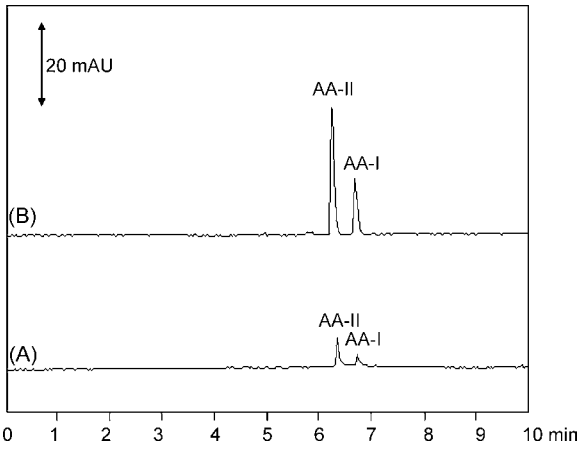


Fig. 4. CE analysis of AA-I and AA-II carried out with: (A) no stacking, (B) FESI stacking. (A) No stacking: 50 mg/L sample in H_2O, hydrodynamic injection for 2 s at 30 mbar. (B) FESI stacking: 0.5 mg/L sample in MeOH, electrokinetic injection for 10 s at −6 kV. Conditions: Na_2HPO_4 (100 mM, pH 7.5): MeCN = 90:10, 3 mM CB[7]; −25 kV; 25 °C; 254 nm.

resolution of AA-I and AA-II generally increased with increasing CB[7] concentration up to a certain point (3 mM) where a maximum was reached.

3.1.4. Effect of organic modifier

The effect of acetonitrile concentration (5–20%, v/v) on the EOF was investigated. It was found that the anodic EOF slowly decreased with increasing of acetonitrile concentration. The decrease in EOF may be ascribed to that increase of organic solvent suppressed protonation of CB[7], leading to the reduction of CB[7] amount adsorbed onto the inner wall of the fused-capillary.

With increasing acetonitrile concentrations of the buffer, obviously improved peak shapes were observed and the resolution of AA-I and AA-II first increased (from 5% to 10%), and then slightly decreased (from 15% to 20%), which was probably due to that the addition of acetonitrile reduced the affinity between the solutes and the cavity of CB[7]. Accordingly, 10% acetonitrile was chosen as optimum.

3.1.5. CB[7] versus β-CD on the separation of AAs

Table 1 summarizes the migration times, efficiency of peaks and resolutions for the separation of AAs in the optimized conditions with CB[7] and β-CD additives. The results suggested that: lower concentration of CB[7] was required for the separation of AAs; the migration times were dramatically shortened by the use of CB[7] because the analysis was carried through a coelectroosmotic mode; high theoretical plate numbers (above 10^5) were obtained both by the use of CB[7] and β-CD; the resolution was slightly lower by the use of CB[7]. Moreover, the use of CB[7] (negative polarity) and β-CD (positive polarity) resulted in opposite migration orders for AA-I and AA-II, which demonstrated that both CB[7] and β-CD are bound strongly with AA-I. Therefore, CB[7] is expected to be complementary to β-CD for separations of negative charged positional isomers.

3.1.6. Optimization of field-enhanced sample injection

In order to improve the sensitivity of the CZE method for determining AAs, field-enhanced sample injection was applied. During the running process, the sample prepared in low-conductivity matrix was injected by applying a negative polarity, and then the sample vial is replaced by the BGS (with CB[7] as modifier) and the separation voltage is applied at negative polarity until all peaks are detected. Methanol and water were examined as low-conductivity matrix, and the results showed that with the solution of methanol, much higher S/N was yielded, which demonstrated that the proposed method using methanol for standard solution and sample extract was a convenient approach as no solvent exchange was required. Samples could be electrokinetically injected up to 10 s at −6 kV under the conditions. A breakdown of the electric current was observed with longer injection time.

The electropherograms obtained after stacking of 0.5 mg/L the mixture of AA-I and AA-II by FESI are shown in Fig. 4B.

Table 1
Effect of CB[7] and β-CD on the separation of AA-I and AA-II

	Concentration (mM)	Separation voltage (kV)	Migration times (min)		Efficiency of peak[a] (10^5)		Resolution[b]
			AA-I	AA-II	AA-I	AA-II	
CB[7]	3	−25	6.8	6.5	1.5	1.5	5.2
β-CD	10[c]	+25	10.1	10.9	1.4	1.2	6.8

[a] Efficiency of peaks was calculated using the equation $N = 16(t_m/w)^2$.
[b] Resolution was calculated using the equation $2(t_{m2} - t_{m1})/(w_1 + w_2)$. Conditions: 100 mM Na_2HPO_4, pH 7.5, 10%MeCN; sample injection at 30m bar for 5 s.
[c] The concentration of β-CD was in accordance with optimized concentration in reference [20].

For comparison, Fig. 4A shows the electropherogram obtained by injecting 50 mg/L the mixture of AA-I and AA-II without stacking. A dramatic sensitivity improvement was found in Fig. 4B, indicating the remarkable stacking ability of FESI under these conditions. The sensitivity enhancement factors [48], calculated by comparing the peak height obtained with FESI to that obtained with usual injection, are 527 for AA-I and 543 for AA-II, respectively.

In a word, by the use of the optimal conditions: 100 mM phosphate buffer (pH 7.5) containing 3 mM CB[7] and 10% acetonitrile (v/v) as modifiers under 25 °C and −25 kV separation voltage with electrokinetic injection by voltage of −6 kV for 10 s, a rapid separation of AA-I and AA-II was achieved within 7 min, and the resolution between two compounds is as high as 5.12, and theoretic plate numbers greater than 170,000 m^{-1} for AA-I and 160,000 m^{-1} for AA-II were obtained.

3.2. Method evaluation

In order to validate the linearity of the method, calibration curves were constructed with a series of standard samples with concentration ranging from 50 ng/mL to 10,000 ng/mL. In all the cases, a constant amount of 5 mg/L phthalic acid was added as IS before sample injection. Linear regression analyses were performed using ratios of peak areas of AAs to that of IS against the respective AAs concentration. The results are listed in Table 2. The regression coefficients (r) were better than 0.999 and the detection and quantification limits were calculated with the S/N set at 3 and 10, respectively. The results showed that this method provided a high sensitivity and a wide linear range for AAs, which is comparable with LC–MS for AAs analysis [15].

The repeatability of the developed method was determined by the intra-day and inter-day precision, as shown in Table 3. Three levels of sample concentration (i.e. 50, 500, 5000 ng/mL) were tested. The intra-day precisions of the relative migration times were below 0.9% and the inter-day precisions below 2.2%. Both were calculate as R.S.D. for five measurements. The intra-day and inter-day precisions of the relative peak areas were calculated in the same way showing values lower than 3.5 and 5.8%, respectively.

3.3. Analysis of real sample

For real samples, extract of *Radix aristolochiae* was experimented for the validation of this method. Fig. 5A shows a typical electropherogram of a real sample, indicating that the contents of AAs could be exactly determined without interference of other components due to great separation performance. The peak identifications of AA-I and AA-II in real sample solutions were assured by standard addition method. The R.S.D. ($n = 5$, intra-day) of relative migration time and peak area were 1.0 and 5.2% for AA-I, and 0.8 and 4.8% for AA-II, respectively. The method precision within 12 h of relative migration time and peak area (as R.S.D., $n = 5$) were 1.2 and 6.1% for AA-I, and 0.8 and 5.3% for AA-II, respectively, which showed that this method has good stability and reproducibility for real sample analysis.

The recovery was determined by standard addition method. The standard spiked extract of *C. a. manshuriensis* was ana-

Table 3
Intra-day and inter-day precisions of relative migration times and peak areas at three different concentrations of the CZE method for detection AAs

Compounds	Concentration (ng/mL)	Precision (R.S.D., %)			
		Intra-day ($n = 5$)		Inter-day ($n = 5$)	
		MT	Area	MT	Area
AA-I	50	0.5	2.5	1.8	5.5
	500	0.4	3.5	2.0	4.5
	5000	0.6	3.2	1.6	5.6
AA-II	50	0.6	2.9	2.2	4.7
	500	0.9	3.1	1.9	4.3
	5000	0.8	3.0	1.7	5.8

The intra-day precisions were calculated by injecting of the standard solution over a day. Inter-day precisions were calculated by injecting the standard solution for continuous 5 days. CE conditions outlined in Section 2.

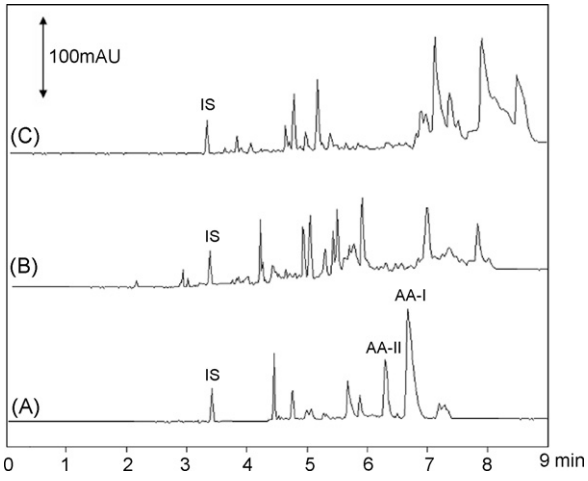


Fig. 5. Electropherograms of medicinal plant sample *Radix aristolochiae* (qingmuxiang) (A); slimming pill sample 1 (B) and slimming pill sample 2 (C). Phthalic acid (IS) was added before sample injection at a concentration of 1.25 mg/L. Conditions: Na_2HPO_4 (100 mM, pH 7.5): MeCN = 90:10, 3 mM CB[7]; −25 kV; 25 °C; 254 nm; sample injection at −6 kV for 10 s.

Table 2
Calibration curves of the CZE method for detection AAs

	Linear range (ng/mL)	Calibration curves			LOD (ng/mL)	LOQ (ng/mL)
		Slope	Intercept	r		
AA-I	50–10000	5.29	0.15	0.9995	11.3	37.5
AA-II	50–10000	6.24	0.19	0.9998	12.5	41.8

Number of data point for calibration curves is eight and three repetition per point. CE conditions outlined in Section 2.

Table 4
Detection results of AA-I and AA-II in medicinal plants by use of this method ($n = 5$, mg/g)

Species	AA-I		AA-II	
	Mean content	R.S.D.	Mean content	R.S.D.
Radix aristolochiae	0.68	5.2	0.23	4.8
Fructus aristolochiae	0.27	4.3	0.053	3.1
Caulis aristolochiae manshuriensis	0.14	4.0	0.017	3.4
Aristolochia fangchi	NF		NF	

NF: not found. CE conditions outlined in Section 2.

lyzed under the optimum conditions. The average recoveries and R.S.D.s were 99% and 4.5% for AA-I, and 90% and 4.0% for AA-II, respectively ($n = 5$).

Four medicinal plants: *Radix aristolochiae* (qingmuxiang), *Fructus aristolochiae*, *C. a. manshuriensis* and *Aristolochia fangchi* have been analyzed by the CZE method, and detection results are summarized in Table 4. From Table 4, it can be seen that the content of AA-I, which has been reported as the major active component to induce renal failure, was much higher than that of AA-II in most cases.

Two slimming pills with complex matrix have also been analyzed, and the AAs were not detected. Typical electropherograms of the two samples are shown in Fig. 5B and Fig. 5C, indicating that this method can be used for analysis of Chinese prepared medicine containing multiple medicinal plants.

4. Conclusions

In this work, a CZE method using CB[7] as modifier was developed for the separation of AA-I and AA-II, with improved resolution and high sensitivity by combining FESI. The developed method has been successfully applied to the determination of AA-I and AA-II in four medicinal plants samples with high separation efficiency, satisfactory sensitivity, repeatability and recovery, which demonstrated that CB[7] as a novel additive can potentially be used for analysis of real samples.

Acknowledgements

This work was partly supported by grants from the Specialized Research Fund for the Doctoral Program of Higher Education (SRFDP), the Program for New Century Excellent Talents in University (NCET-05-0616) and the National Science Fund for Distinguished Young Scholars (No. 20625516).

References

[1] T.T. Jong, M.R. Lee, S.S. Hsiao, J. Pharmaceut. Biomed. 33 (2003) 831.
[2] C.S. Yang, C.H. Lin, S.H. Chang, H.C. Hsu, Am. J. Kidney Dis. 35 (2000) 313.
[3] J.P. Cosyns, M. Jadoul, J.P. Squifflet, F.X. Wese, C. van Ypersele de Strihou, Am. J. Kidney Dis. 33 (1999) 1011.
[4] G.M. Lord, R. Tagore, T. Cook, P. Gower, C.D. Pussey, Lancet 354 (1999) 481.
[5] M. Levi, H.J. Guchelaar, H.J. Woerdenbag, Y.P. Zhu, Pharm. World Sci. 20 (1998) 43.
[6] B. Stengel, E. Jones, Nephrologie 19 (1998) 15.
[7] T.Y. Lee, M.L. Wu, J.F. Deng, D.F. Hwang, J. Chromatogr. B 766 (2001) 169.
[8] J.R. Ioset, G.E. Raoelison, K. Hostettmann, Planta Med. 68 (2002) 856.
[9] J.R. Ioset, G.E. Raoelison, K. Hostettmann, Food Chem. Toxicol. 41 (2003) 29.
[10] T. Seto, T. Hamano, H. Shioda, H. Kamimura, J. Health Sci. 48 (2002) 412.
[11] W. Li, R.K. Li, T. Bo, H.W. Liu, et al., Chromatographia 59 (2004) 233.
[12] A. Blatter, E. Reich, J. Liq. Chromatogr. Rel. Technol. 27 (2004) 2087.
[13] J.H. Jon, S. Chen, T.S. Wu, J. Liq. Chromatogr. Rel. Technol. 26 (2003) 3057.
[14] Y.S. Chang, J.S. Deng, Y.R. Ku, J. Liq. Chromatogr. Rel. Technol. 25 (2002) 961.
[15] S.A. Chan, M.J. Chen, T.Y. Liu, Talanta 60 (2003) 679.
[16] M.C. Lee, C.H. Tsao, S.C. Iou, J. Sep. Sci. 26 (2003) 818.
[17] X.Q. Ma, Q. Shi, J.A. Duan, T.T.X. Dong, K.W.K. Tsim, J. Agric. Food Chem. 50 (2002) 4861.
[18] H.Y. Feng, L.L. Yuan, S.F.Y. Li, J. Chromatogr. A 1014 (2003) 83.
[19] E.S. Ong, E.S.O. Woo, Electrophoresis 22 (2001) 2236.
[20] W. Li, S.X. Gong, D.W. Wen, B.Q. Che, Y.P. Liao, H.W. Liu, X.F. Feng, S.L. Hu, J. Chromatogr. A 1049 (2004) 211.
[21] W. Li, Z. Chen, Y.P. Liao, H.W. Liu, Electrophoresis 27 (2006) 837.
[22] S.C. Hsieh, M.F. Huang, B.S. Lin, H.T. Chang, J. Chromatogr. A 1105 (2006) 127.
[23] X.G. Zhou, C.Y. Zheng, J.Y. Sun, T.Y. You, J. Chromatogr. A 1109 (2006) 152.
[24] R. Kuhn, F. Stoeklin, F. Erni, Chromatographia 33 (1992) 32.
[25] S. Terabe, H. Ozaki, O. Koji, T. Ando, J. Chromatogr. 332 (1985) 211.
[26] D. Shohat, E. Grushka, Anal. Chem. 66 (1994) 747.
[27] W.A. Freeman, W.L. Mock, N.Y. Shih, J. Am. Chem. Soc. 103 (1981) 7367.
[28] J. Kim, I.S. Jung, S.Y. Kim, E. Lee, J.K. Kang, J. Am. Chem. Soc. 122 (2000) 540.
[29] A.I. Day, A.P. Arnold, R.J. Blanch, B. Snushall, J. Org. Chem. 66 (2001) 8094.
[30] A.I. Day, R.J. Blanch, A.P. Arnold, S. Lorenzo, G.R. Lewis, I. Dance, Angew. Chem. Int. Ed. 41 (2002) 275.
[31] J. Lagona, P. Mukhopadhyay, S. Chakrabarti, L. Isaacs, Angew. Chem. Int. Ed. 44 (2005) 4844.
[32] L. Xu, S.M. Liu, C.T. Wu, Y.Q. Feng, Electrophoresis 25 (2004) 3300.
[33] S.M. Liu, L. Xu, C.T. Wu, Y.Q. Feng, Talanta 64 (2004) 929.
[34] F. Wei, S.M. Liu, L. Xu, G.Z. Cheng, C.T. Wu, Y.Q. Feng, Electrophoresis 26 (2005) 2214.
[35] S. Choi, S.H. Park, A.Y. Ziganshina, Y.H. Ko, J.W. Lee, K. Kim, Chem. Commun. 17 (2003) 2176.
[36] B.D. Wagner, N. Stojanovic, A.I. Day, R.J. Blanch, J. Phys. Chem. B 107 (2003) 10741.
[37] O. Winston, G.-K. Marielle, E.K. Angel, Org. Lett. 4 (2002) 1791.
[38] R.J. Blanch, A.J. Sleeman, T.J. White, A.P. Arnold, A.I. Day, Nano Lett. 2 (2002) 147.
[39] H.-J. Kim, W.S. Jeon, Y.H. Ko, K. Kim, Proc. Natl. Acad. Sci. U.S.A. 99 (2002) 5007.
[40] W. Ong, A.E. Kaifer, Organometallics 22 (2003) 4181.
[41] T. Soga, A.G. Ross, J. Chromatogr. A 837 (1999) 231.
[42] M. Chiari, L. Ceriotti, G. Crini, M. Morcellet, J. Chromatogr. A 836 (1999) 81.
[43] J.P. Quirino, S. Terabe, J. Chromatogr. A 902 (2000) 119.
[44] Z.K. Shihabi, J. Chromatogr. A 902 (2000) 107.
[45] J.B. Kim, S. Terabe, J. Pharm. Biomed. Anal. 30 (2003) 1625.
[46] S. Sentellas, E. Moyano, L. Puignou, M.T. Galceran, J. Chromatogr. A 1032 (2004) 193.
[47] J. Hernandez-Borges, A. Cifuentes, F.J. Garcia-Montelongo, M.A. Rodriguez-Delgado, Electrophoresis 26 (2005) 980.
[48] J.B. Kim, K. Otsuka, S. Terabe, J. Chromatogr. A 912 (2001) 343.

Available online at www.sciencedirect.com
ScienceDirect
Talanta 74 (2008) 505–511
Talanta
www.elsevier.com/locate/talanta

Evaluation of tungsten coil electrothermal vaporization-Ar/H_2 flame atomic fluorescence spectrometry for determination of eight traditional hydride-forming elements and cadmium without chemical vapor generation

Peng Wu [a], Xiaodong Wen [b], Liang He [b], Yihua He [b], Minzhu Chen [b], Xiandeng Hou [a,b,*]

[a] *Analytical & Testing Center, Sichuan University, Chengdu, Sichuan 610064, China*
[b] *College of Chemistry, Sichuan University, Chengdu, Sichuan 610064, China*

Received 24 February 2007; received in revised form 12 June 2007; accepted 13 June 2007
Available online 19 June 2007

Abstract

A tungsten coil electrothermal vaporizer (W-coil ETV) was coupled to an Ar/H_2 flame atomic fluorescence spectrometer for the determination of eight traditional hydride-forming elements (i.e., As, Bi, Ge, Pb, Sb, Se, Sn, and Te) as well as cadmium without chemical vapor generation. A small sample volume, typically 20 μL, was manually pipetted onto the W-coil and followed by a fixed electric heating program. During the vaporization step, analyte was vaporized off the coil surface and swept into the quartz tube atomizer of AFS for further atomization and excitation of atomic fluorescence by a flow of Ar/H_2 gas, which was ignited to produce the Ar/H_2 flame. The tungsten coil electrothermal vaporizer and Ar/H_2 flame formed a tandem atomizer to produce reliable atomic fluorescence signals. Under the optimal instrumental conditions, limits of detection (LODs) were found to be better than those by flame atomic absorption spectrometry (FAAS) or inductively coupled plasma optical emission spectrometry (ICP-OES) for all the nine elements investigated. The absolute LODs are better or equivalent to those by hydride generation atomic fluorescence spectrometry (HG-AFS). Possible scattering interferences were studied and preliminary application of the proposed method was also reported.
© 2007 Elsevier B.V. All rights reserved.

Keywords: Tungsten coil; Electrothermal vaporization; Atomic fluorescence spectrometry; Hydride; Flame atomization; Cadmium

1. Introduction

Atomic fluorescence spectrometry (AFS) is a widely used atomic spectrometric technique in trace element analysis, particularly when coupled with hydride generation (HG) for sample introduction. Dědina and Tsalev [1] underlined that atomic fluorescence detection was able to improve the sensitivity by about one order of magnitude over atomic absorption spectrometry (AAS) and optical emission spectrometry (OES) detection, whenever these detection systems are coupled with comparable HG set-ups. In fact, commercialization of HG-AFS instruments has gained a success worldwide [2], especially in China. Using HG, the current AFS instrument shows good sensitivity for hydride-forming elements. The equality or superiority of HG-AFS over other atomic spectrometric techniques for the determination of several hydride-forming elements, for example, arsenic, selenium and mercury, has already been well documented in the literature, especially as an element-selective detector for chromatographic separations [3]. However, the inherent drawbacks of HG, i.e. severe interference from transition metals and limited number of elements capable of forming volatile hydrides, largely hold back the wide applicability of this instrument. Although other elements may be determined by use of various chemical vapor generation techniques coupled to HG-AFS instrument, the number of detectable elements is still limited.

Electrothermal vaporization (ETV) has long been considered as an excellent sample introduction approach for analytical plasma spectrometry; however, this technique has rarely been

* Corresponding author at: Analytical & Testing Center, Sichuan University, Chengdu, Sichuan 610064, China.
E-mail address: houxd@scu.edu.cn (X. Hou).

0039-9140/$ – see front matter © 2007 Elsevier B.V. All rights reserved.
doi:10.1016/j.talanta.2007.06.013

expanded for other atomizers. With electrothermal vaporization, the sample introduction efficiency and absolute detectability, as compared with ICP-OES/MS using pneumatic nebulisation, are considerably increased. Graphite furnaces are the predominant ETV devices in analytical atomic spectrometry [4], but metals such as tungsten, tantalum and molybdenum have also been used [5–7]. Some advantages of tungsten coil vaporizers over graphite furnace vaporizers are obvious, i.e. freedom from carbide forming problems, a lower surface porosity, higher heating rate, much lower power supply, and compactness. A car battery can be employed as the power supply for tungsten coil atomizers [8], and this makes tungsten coil atomizer based portable atomic absorption spectrometer feasible for field use.

Tungsten coil ETV (W-coil ETV) has already been used as electrothermal vaporizers for inductively coupled plasma [9–11] and microwave plasma [12]. Because the sample vaporization occurs in the vaporizer, the plasma energy itself is not required to desolvate the sample so that more energy is available for atomization, ionization and excitation. Jones et al. [13] successfully developed a low-cost, modular W-coil ETV system coupled to ICP-OES for simultaneous determination of 10 elements. Picogram-level LODs were achieved and linear dynamic ranges (LDR) were 3–5 orders of magnitude. A W-coil ETV device has been developed for thermal separation of Pb from matrix elements, which may cause spectral interference, such as aluminium, manganese and iron, by use of a temperature ramp [14]. The W-coil ETV can also be applied to slurry sampling for vaporizing digestion-problematic samples, such as silicon carbide [15], silicon dioxide and silicon nitride powders [16,17], aluminium-based ceramic powders [18], and high purity quartz [19].

Tungsten coil has already been used as an atomizer in AFS [5,20,21]. Winefordner et al. [22] firstly utilized a tungsten wire loop as an atomizer for AFS. Samples containing Ag, Be, Bi, Cu, Mg, Pb, Tl, and Zn were atomized from the tungsten wire loop into an argon stream. Muzgin et al. [23] built a pulsed W-coil electrothermal atomizer for application in AFS and investigated its fundamental analytical characteristics. In all W-coil AFS applications, picogram or sub-picogram instrumental limits of detection for Cd, Pb, Bi and Te were reported [5]. Recently, tungsten coil atomizers have also found promising applications in laser-excited AFS [14,24]. However, W-coil has not been employed as sample introduction device for AFS, therefore, the purpose of this work is to introduce W-coil ETV to AFS to expand the number of detectable elements without chemical vapor generation. Analyte was firstly sputtered off the W-coil ETV and then swept into an argon–hydrogen flame for further atomization and excitation of atomic fluorescence of traditional hydride-forming elements and cadmium.

2. Experimental

2.1. Instrumentation

Fig. 1 shows the schematic diagram of the W-coil ETV-Ar/H_2 flame AFS instrument. A model AFS-2202 non-dispersive atomic fluorescence spectrometer (Beijing Haiguang Instrument Co., Beijing, China) was used in this work. The instrument is equipped with a programmable intermittent reactor and two gas–liquid separators by the manufacturer to facilitate hydride generation and separation, but all these accessories were replaced with a W-coil ETV in this work. Hollow cathode lamps (HCLs, Research Institute of Non-Ferrous Metals, Beijing, China) of conventional hydride-forming elements, namely As, Bi, Ge, Pb, Sb, Se, Sn and Te, plus Cd, were used as the radiation sources for these nine elements, respectively. These modulated high-intensity HCLs are specially designed for AFS. All HCLs were operated at 80 mA except Cd at 70 mA. The emission light beam of the HCL was focused into a quartz tube atomizer (QTA) for the excitation of atomic fluorescence. An electrically heated wire is coiled around the top edge of the QTA to ignite the carrier gas (Ar/H_2) for a stable flame on the top of the QTA for the further atomization and excitation. The resultant atomic fluorescence was detected by a "solar blind" photomultiplier tube (PMT, with its working voltage set at −300 V for all the nine elements), and followed by the amplification of the electric signal and data processing with a personal computer. With a total reading time of 6 s, the peak area of the temporal atomic fluorescence signal was used for quantification because of its good day-to-day repeatability. Other instrumental parameters were summarized in Table 1.

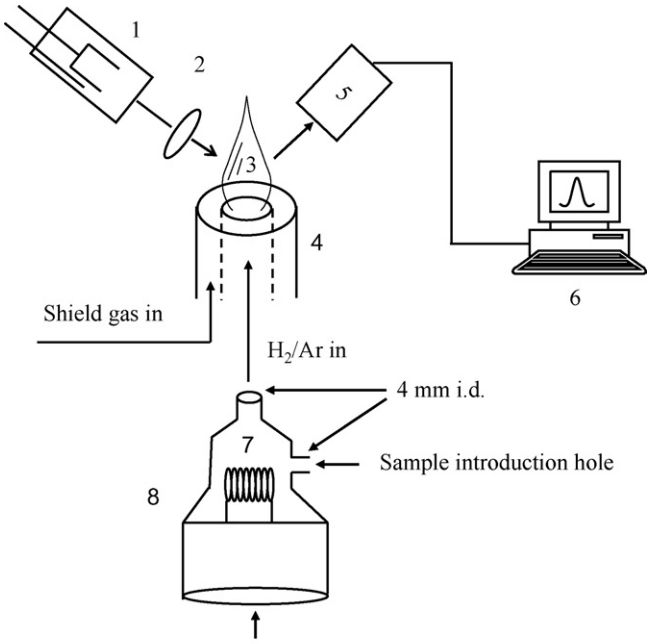


Fig. 1. Schematic diagram of the instrumental arrangement. 1: Hollow cathode lamp; 2: lens; 3: miniaturized Ar/H_2 flame; 4: QTA; 5: PMT and electronics; 6: personal computer; 7: tungsten coil; 8: vaporization cell.

Tungsten coils are obtained from commercially available slide projector bulbs (HLX 64633, OSRAM, Munich, Germany) rated at 15 V and 150 W with a color temperature of 3000 °C at full power. The glass envelope was carefully removed away, and the bulb base was then fitted into a laboratory-constructed mount that connected the power supply and the purge gas tubing. A laboratory-made ETV glass cell was used to protect the

Table 1
Summery of instrumental parameters

Element	Excitation wavelength (nm)	Height of atomizer (mm)	Shield gas flow rate (mL/min)	Argon flow rate (mL/min)	H_2 flow rate (mL/min)	Pyrolysis current (A)	Vaporization temperature (°C)
As	193.7	14	1000	600	160	3.2	1730
Bi	306.8	10	600	400	100	3.4	1900
Cd	228.8	10	500	400	80	3.5	1770
Ge	265.2	6	500	900	80	3.7	1840
Pb	283.3	10	500	400	100	3.9	1850
Sb	217.6	8	500	700	80	3.4	1790
Se	196.0	8	800	500	80	3.4	2130
Sn	286.3	10	900	500	80	3.4	2050
Te	214.3	6	1000	400	160	3.3	1810

tungsten coil from oxidation at high temperature. A reducing gas mixture (Ar/H_2) purged through the cell to sweep the atomic vapor/aerosol to the QTA. The flow rates of H_2 and Ar were controlled by two individual flowmeters and the gases were mixed in a laboratory-constructed mixing chamber. A commercial DC power supply (HY 1791-10S, 0–30 V, Huai'an Yangguang Electronics Ltd. Co., Huai'an, China), which was redesigned and controlled by a Single Chip Micyoco (SCM), was used as a programmable power supply for the W-coil ETV.

A 4 cm silica tube (0.4 cm i.d.) connected the ETV cell to the AFS instrument and served as the interface between the ETV cell and AFS instrument. A typical fluorescence peak profile of cadmium was shown in Fig. 2. As compared with an absorption profile of cadmium from tungsten coil electrothermal atomic absorption [25], the peak width of the fluorescence profile (about 2 s) was broader than that of AAS (about 0.6 s). In tungsten coil AAS, the absorbance is measured just after the analyte atoms sputter from the tungsten coil; while in tungsten coil ETV–AFS, the analyte atoms need to be transported through the silica tube and then reach the atomization cell of AFS, which would definitely cause dispersion of the atom cloud. The transport procedure in W-coil ETV–AFS is similar to the analyte transport in flow injection analysis (FIA). The peak width of the fluorescence profile is associated with the length of the transport tube and the flow rate of the carrier gas.

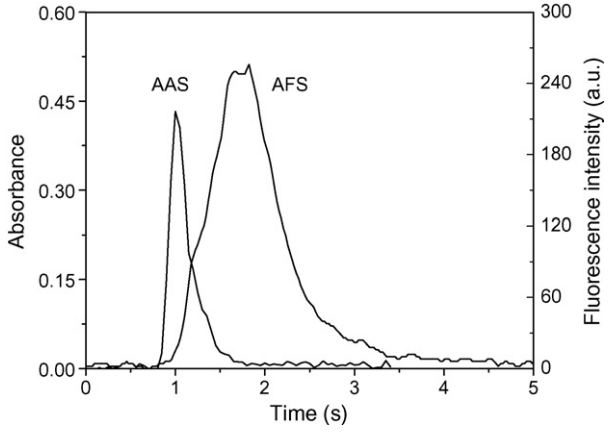


Fig. 2. A comparison of typical signal profiles of equal amount (0.2 ng) of cadmium obtained by W-coil ETV–AFS and W-coil ETAAS. The instrumental conditions for AFS were listed in Table 1; for W-coil ETAAS: 228.8 nm as analytical line, 10 mA HCL current, 800 mL/min argon, 200 mL/min hydrogen, and 1750 °C for atomization.

2.2. Reagents

Standard stock solutions (1000 mg/L) of all nine elements were prepared by dissolving appropriate amounts of at least analytical grade pure metals or metal salts in nitric acid or sub-boiled distilled water. Working standard solutions were obtained by stepwise dilution of the standard stock solutions and stabilized in 0.5% HNO_3 (Analytical grade, Chengdu Kelong Chemical Reagents Co., Chengdu, China). Sodium chloride, ammonium nitrate and hydrochloric acid (Analytical grade, Chengdu Kelong Chemical Reagents Co., Chengdu, China) were used for the investigation or elimination of scattering interference. Five certified reference/standard samples (trace elements in water, GBW (E) 080391 for arsenic, GBW (E) 080401 for cadmium, GBW (E) 080398 for lead, and GBW (E) 080395 for selenium; and GBW08510 for cadmium in rice) were purchased from National Standard Center of China (Beijing, China).

2.3. Operation procedure

For each measurement, 20 μL sample solution was manually pipetted onto the W-coil surface through the sample introduction hole using an AGE micro-syringe (Zhenhai Glass Instrument Co., Ningbo, China). Then, a rubber plug was inserted into the hole before the heating program was administrated. In a typical heating program, firstly 65 s was applied for desolvation, then 20 s for pyrolysis, 4 s for cooling, 5 s for vaporization, 4 s for cleaning, and 10 s for cooling (making ready for next measurement). The heating current and lasting time of every step were programmed via the SCM. The power supply was designed to maintain a constant current at a specific step. Pyrolysis currents and equivalent vaporization temperatures for the nine elements were tabulated in Table 1.

2.4. Coil temperature

The temperature of the W-coil was estimated based on voltamperometric measurement [26], and the relation of resistivity and temperature for W material was referred to Handbook

of Chemistry and Physics [27]. Based on references, approximate equation for calculating the coil surface temperature was obtained as

$$T = 70.113X^{0.8298}$$

$$X = 67.8\left(\frac{V}{I}\right)$$

Here T is the coil temperature in Kelvin; X the resistivity of tungsten; V the applied voltage; I is the applied current.

3. Results and discussion

3.1. Optimization of instrumental parameters

3.1.1. Hydrogen gas flow rate

Vaporization/atomization of analytes from W-coil surface is a complicated physical and chemical process and hydrogen gas affects this process significantly. It is generally believed that the addition of H_2 to a metal atomizer provides a reducing atmosphere for atomization and keeps the tungsten from oxidation. Meanwhile, H_2 also contributes to the buildup of the Ar/H_2 diffusion flame, thus influencing the temperature of the flame. High content of H_2 favors the atomization of volatile elements on a W-coil atomizer, and increases its lifetime significantly. Fig. 3 illustrated the relationship between the H_2 flow rate and the fluorescence intensity for antimony. When H_2 flow rate was higher than 80 mL/min, fluorescence intensity began to decrease, so a flow rate of 80 mL/min was chosen for antimony. Optimized H_2 flow rates for these elements were summarized in Table 1. For the sake of safety, H_2 flow rate higher than 160 mL/min was not investigated.

3.1.2. Argon flow rate

Argon plays a key role in transporting the vaporized analyte aerosol from the W-coil ETV to the QTA: low argon flow rate may lead to analyte loss during the transportation, while high argon flow rate results in short residence time of atoms in the QTA thus short time for excitation and measurements. For all elements investigated, atomic fluorescence peaks generally presented asymmetric, irreproducible, and sometimes double-peaked, at an argon flow rate below 400 mL/min. As an example, the influence of argon flow rate on the atomic fluorescence intensity of antimony is shown in Fig. 4. The intensity of atomic fluorescence for antimony increased sharply when argon flow rate increased from 200 to 700 mL/min and then began to decrease. Hence, an argon flow rate of 700 mL/min was selected for antimony. The results of argon flow rate optimization for the nine elements were listed in Table 1.

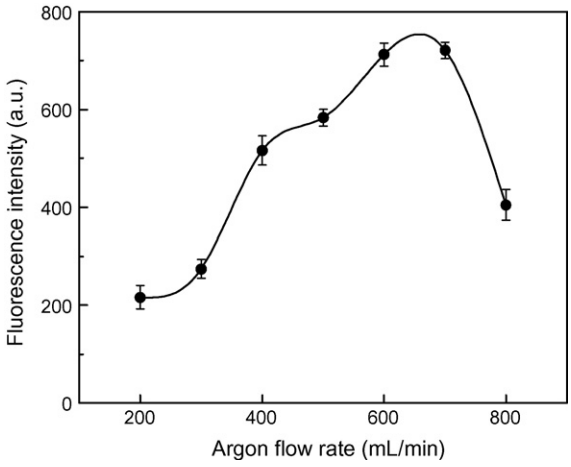


Fig. 4. The influence of argon flow rate on the fluorescence intensity of antimony. Sb: 8 ng, and the error bars represent "± one standard deviation of three trials".

3.1.3. The length of the transporting tube

The transporting tube serves as the interface between the W-coil ETV device and atomic fluorescence spectrometer. It has been shown in graphite furnace ETV that analyte loss occurred due to vapor condensation on the colder ends of the ETV graphite tube, on the graphite cones of the ETV furnace and on the connecting tubing [28]. Similar results were also observed in the current work for the transporting tube, as shown in Fig. 5 for anti-

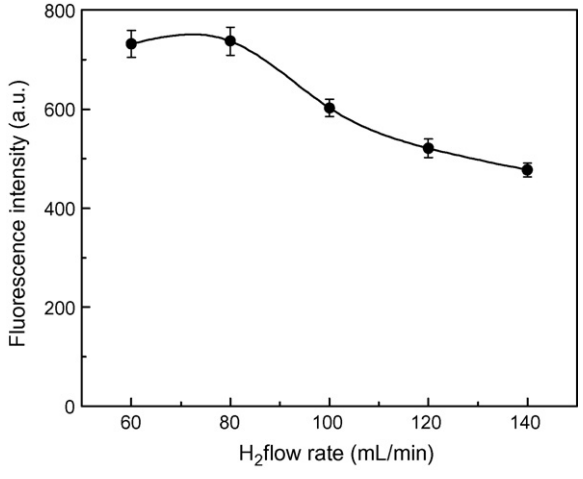


Fig. 3. The influence of H_2 flow rate on the fluorescence intensity of antimony. Sb: 8 ng, and the error bars represent "± one standard deviation of three trials".

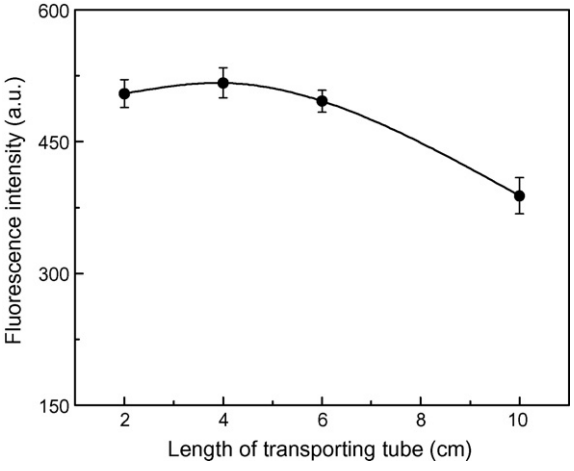


Fig. 5. The effect of the length of transporting tube on the on the fluorescence intensity of antimony. Sb: 4 ng, and the error bars represent "± one standard deviation of three trials".

mony. When it was longer than 6 cm, analyte loss was evident. Meanwhile, when the length of the transporting tube increased, the width of the fluorescence profile also increased. Other tested elements generally showed similar results as antimony. A 4 cm transportation tube was chosen for all elements.

3.1.4. Shield gas flow rate

The role of shield gas is to prevent extraneous air from entering the Ar/H_2 flame to ensure its stability. The miniaturized Ar/H_2 flame in the current work has similarities with the flame-in-gas-shield atomizer employed in hydride atomization developed by Dědina et al. [29–31], but the atomization process in Ar/H_2 flame may not be the same. The same authors also studied the oxygen contamination at trace levels in miniature flame hydride atomizers, and concluded that molecular oxygen resulted in a contraction of the H radical cloud and in consequence decreased the hydride atomization efficiency [32,33]. Although the atomization mechanisms of the current work and theirs may be different, one can still conclude that contamination from oxygen may result in reaction of free atoms with oxygen and hence decrease the free atom population. Optimization of argon shield gas flow rate showed that the setting limit of the current AFS instrument (500 mL/min) was sufficient for most elements studied. Higher flow rate may cause dilution to the atom population in the Ar/H_2 flame. The results for the optimal argon shield gas flow rate were also tabulated in Table 1.

3.1.5. Other instrumental parameters

Other instrumental parameters optimized are the height of atomizer and pyrolysis current and vaporization temperature. The height of atomizer is defined as the distance from the top of the quartz tube atomizer to the point where atomic fluorescence signal is measured. As in the heating program of a typical ETAAS or ETV technique, a pyrolysis step here is used to vaporize sample matrix. The optimal parameters for the best signal-to-noise ratios for the nine elements were summarized in Table 1.

3.1.6. Ar/H_2 flame as a secondary atomizer

In this work, the analyte was first atomized on the W-coil surface, subsequently the analyte atoms/particles were delivered to the atomization cell of AFS by the carrier gas (Ar/H_2). The time needed for the transport of analyte atoms/particles from the W-coil to the Ar/H_2 flame was estimated around 0.2–0.5 s. It is believed that the atoms would congregate quickly and form atom clusters during the transportation. Fig. 6 shows the lead signals obtained with the Ar/H_2 flame on and off, and other elements generally show the same phenomenon. No signals are observed with different concentrations of analyte when the Ar/H_2 flame was off, while calibration curves can be obtained with the Ar/H_2 flame on. Apparently, re-atomization is needed in the Ar/H_2 flame. Considering the temperature of the Ar/H_2 flame, analyte may not be atomized directly, but the energy needed for dissociation of newly formed atom clusters is probably much lower. So the Ar/H_2 flame here worked as a secondary atomizer.

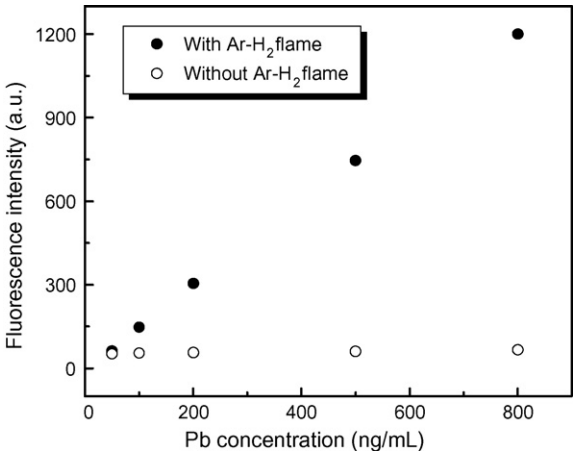


Fig. 6. Lead signals with or without Ar/H_2 flame.

3.2. Analytical figures of merit

Analytical figures of merit of the proposed instrumentation for the nine elements were obtained under the optimized instrumental conditions, and summarized in Table 2. At least 0.99 of R^2 (correlation coefficient) showed good linearity of the calibration curves. The linear dynamic ranges were 2–3 orders of magnitude. LODs (equivalent to 3σ of 11 measurements of a blank solution) were superior to those by FAAS and ICP-OES for all the nine elements but germanium. The LODs of the present work

Table 2
LDR and LODs of this work in comparison with related analytical techniques

Element	This work (ng)	This work (μg/L)	LDR[a] of this work (μg/L)	FAAS (μg/L) [34]	ICP-OES (μg/L) [34]	HG-AFS[b] (ng)	HG-AFS (μg/L)	HG-AFS Ref.
As	0.2	10	2000	150	50	0.2	0.1	[35]
Bi	0.04	2	500	30	30	0.4	0.2	[36]
Cd	0.002	0.08	15	0.8	1	0.02	0.01	[37]
Ge	1	50	10000	300	20	0.8	0.4	[38]
Pb	0.06	3	400	15	10	0.6	0.3	[39]
Sb	0.06	3	1600	45	10	0.6	0.3	[36]
Se	0.6	30	8000	100	50	0.4	0.2	[40]
Sn	0.4	20	4000	150	60	0.8	0.4	[36]
Te	0.06	3	200	30	10	0.6	0.3	[41]

[a] LDR is the upper linear dynamic range, and the rest columns of this table are all LODs.
[b] Sampling volume: 2 mL.

Table 3
Analytical results of certified reference water samples

Element	Sample no.	Certified (mg/L)	Found (mg/L)[a]	Recovery (%)
As	GBW (E) 080391	4.00 ± 0.08	3.89 ± 0.08	97
Cd	GBW (E) 080401	0.100 ± 0.002	0.099 ± 0.002	99
Pb	GBW (E) 080398	0.500 ± 0.020	0.494 ± 0.015	99
Se	GBW (E) 080395	1.00 ± 0.02	0.98 ± 0.06	98

[a] Average ± standard deviation of three replicates.

were compared with those by HG-AFS using the same instrument. Although relative LODs were not comparable, absolute LODs were better or equivalent to those by HG-AFS, which accumulates sensitivity from a large sampling volume.

3.3. Scattering interference

Since the optic system of the AFS is a non-dispersive one, optical scattering interference from matrix particles could be severe and should be considered for this ETV–AFS application. Therefore, five wavelengths were chosen to investigate the scattering interference arising from NaCl matrix, i.e. 196.0 nm (Se), 228.8 nm (Cd), 265.2 nm (Ge), 283.3 nm (Pb), and 306.8 nm (Bi). It was found that up to 10 mg/L NaCl caused no significant scattering interferences. However, when the concentration of NaCl reached 100 mg/L, scattering interferences began to occur and it was wavelength-independent. Moreover, the scattering intensity was almost linear with the increase of NaCl concentration, and this means that the interference is attributed to the scattering of incident light by salt particles that cannot be atomized on tungsten coil.

The use of chemical modifiers has become a common practice in W-coil ET-AAS [42], and this means that chemical modifiers can also be used in W-coil ETV to remove matrix interference. In GF-AAS, NH_4NO_3 was often used to correct NaCl interference [43]. It was proved experimentally that in the presence of 1% NH_4NO_3, no significant scattering interference was observed from 100 mg/L NaCl; when the concentration of NH_4NO_3 increased to 10%, the tolerant limit of NaCl reached 1000 mg/L. The influence of hydrochloric acid or nitric acid at different concentrations (0.1%, 0.5%, 1%, 5% and 10%) on the scattering signal was also investigated. For hydrochloric acid, there was no scattering interference for these elements. However, for nitric acid, scattering interferences occurred when the concentration was higher than 5%. This may be because nitric acid is an oxidative acid, and tungsten oxide may form during the pyrolysis stage with high concentration of nitric acid. The resultant oxide can be flushed into the QTA during the vaporization step and not well atomized in the Ar/H_2 flame, thus causing scattering interferences. Fortunately, a medium of higher than 5% nitric acid is not a choice in most applications.

3.4. Preliminary applications

In order to validate the usefulness of the proposed method, several certified reference water samples (simple matrix) were analyzed with the analytical results shown in Table 3. Besides, a standard reference material GBW08510 (rice, more complicated matrix) for cadmium was also analyzed. Closed-vessel microwave digestion was chosen for decomposing the sample and the digestion procedure was based on a method for corn samples [44]. The analytical result (2.57 ± 0.10 μg/g, $n = 3$) of the rice sample was in good agreement with the certified value (2.60 ± 0.05 μg/g).

4. Conclusion

The proposed W-coil ETV-H_2/Ar flame AFS is sensitive, simple, compact, and cost-effective. Due to the non-dispersive nature of the optical system used in this work, the optical scattering interference can be somewhat severe when the matrix is complex and of high concentration. Fortunately, it can be alleviated by use of chemical modifier or simple dilution of the sample due to the high sensitivity nature of the method. At the present stage, the proposed method would be useful in the analysis of samples of relatively simple matrix such as drinking water, drinks, and vegetables. It is expected that those elements with resonance lines in the sensitive wavelength range of the photomultiplier tube (solar-blind) can be detected with the present method, thus greatly expanding the number of detectable elements with the current AFS instrument by adding only a simple device. With the double-channel capability of the present AFS instrument, two elements can be measured simultaneously. Given modification to the optic design [45], it is possible to explore the multi-element capability of the proposed technique. However, the mechanism of the secondary atomization is still not clear at the present stage.

Acknowledgements

Xiandeng Hou acknowledges the financial support for this project from the National Natural Science Foundation of China (no. 20675053) and the Ministry of Education of China (NCET-04-0869).

References

[1] J. Dědina, D.L. Tsalev, Hydride Generation Atomic Absorption Spectrometry, Wiley, Chichester, 1995.
[2] J. Sherma, J. AOAC Int. 87 (2004) 177A.
[3] J.L. Gómez-Ariza, D. Sánchez-Rodas, I. Giráldez, E. Morales, Talanta 51 (2000) 257.
[4] J.M. Carey, J.A. Caruso, Crit. Rev. Anal. Chem. 23 (1992) 397.
[5] X.D. Hou, B.T. Jones, Spectromchim. Acta Part B 57 (2002) 659.
[6] G.P. Zhong, H. Luo, Z.D. Zhou, X.D. Hou, Appl. Spectrosc. Rev. 39 (2004) 475.

[7] B. Dočekal, S. Gücer, A. Selecká, Spectromchim. Acta Part B 59 (2004) 487.
[8] C.L. Sanford, S.E. Thomas, B.T. Jones, Appl. Spectrosc. 50 (1996) 174.
[9] K. Dittrich, H. Berndt, J.A.C. Broekaert, G. Schaldach, G. Tlög, J. Anal. Atom. Spectrom. 3 (1988) 1105.
[10] P.J. Parsons, Y. Zhou, C.D. Palmer, K.M. Aldous, P. Brockman, J. Anal. Atom. Spectrom. 18 (2003) 4.
[11] A.C. Davis, B.W. Alligood, C.P. Calloway Jr., B.T. Jones, Appl. Spectrosc. 59 (2005) 1300.
[12] Y. Oki, H. Uda, C. Honda, M. Maeda, J. Izumi, T. Morimoto, M. Tanoura, Anal. Chem. 62 (1990) 680.
[13] K. Levine, K.A. Wagner, B.T. Jones, Appl. Spectrosc. 52 (1998) 1165.
[14] X.D. Hou, K.E. Levine, A. Salido, B.T. Jones, M. Ezer, S. Elwood, J.B. Simeonsson, Anal. Sci. 17 (2001) 175.
[15] P. Barth, V. Krivan, J. Anal. Atom. Spectrom. 9 (1994) 773.
[16] P. Barth, S. Hauptkorn, V. Krivan, J. Anal. Atom. Spectrom. 12 (1997) 1351.
[17] P. Barth, S. Hauptkorn, V. Krivan, J. Anal. Atom. Spectrom. 12 (1997) 1359.
[18] M. Lucic, V. Krivan, Fresenius J. Anal. Chem. 363 (1999) 64.
[19] S. Hauptkorn, V. Krivan, B. Gercken, J. Pavel, J. Anal. Atom. Spectrom. 12 (1997) 421.
[20] D.J. Butcher, Appl. Spectrosc. Rev. 37 (2002) 305.
[21] D.J. Butcher, Appl. Spectrosc. Rev. 40 (2005) 147.
[22] M.P. Bratzel, R.M. Dagnall, J.D. Winefordner, Appl. Spectrosc. 24 (1970) 518.
[23] V.N. Muzgin, Yu.B. Atnashev, V.E. Korepanov, A.A. Pupyshev, Talanta 34 (1987) 197.
[24] M. Ezer, S.A. Elwood, B.T. Jones, J.B. Simensson, Anal. Chim. Acta 571 (2006) 136.
[25] X.D. Hou, Y.H. He, P. Wu, M.Z. Chen, B.T. Jones, Asia-Pacific Winter Conference on Plasma Spectrochemistry, Chiang Mai, Thailand, 2005, p. 55.
[26] Z.F. Queiroz, P.V. Oliveira, J.A. Nóbrega, S.S. Silva, I.A. Rufini, S.S. de Sousa, F.J. Krug, Spectrochim. Acta Part B 57 (2002) 1789.
[27] R.C. Weast, Handbook of Chemistry and Physics, 66th ed., CRC Press, Boca Raton, 1985.
[28] J. Bernhardt, T. Buchkamp, G. Hermann, G. Lasnitschka, Spectrochim. Acta Part B 54 (1999) 1821.
[29] A. D'Ulivo, J. Dědina, Spectrochim. Acta Part B 51 (1996) 481.
[30] J. Dědina, A. D'Ulivo, L. Lampugnani, T. Matoušek, R. Zamboni, Spectromchim. Acta Part B 53 (1998) 1777.
[31] A. D'Ulivo, J. Dědina, L. Lampugnani, T. Matoušek, J. Anal. Atom. Spectrom. 17 (2002) 253.
[32] A. D'Ulivo, J. Dědina, L. Lampugnani, J. Anal. Atom. Spectrom. 20 (2005) 40.
[33] A. D'Ulivo, J. Dědina, L. Lampugnani, A. Selecká, Spectrochim. Acta Part B 60 (2005) 1270.
[34] Perkin-Elmer, The Guide to Techniques and Applications of Atomic Spectroscopy, Perkin-Elmer, Norwalk, 1997, p. 5.
[35] Z. Long, J.J. Xin, X.D. Hou, Spectrosc. Lett. 37 (2004) 263.
[36] Y. Li, Chin. J. Anal. Chem. 32 (2004) 205.
[37] G. Li, L. Wu, J.J. Xin, X.D. Hou, J. Anal. Atom. Spectrom. 19 (2004) 1010.
[38] G. Li, W. Li, G.P. Zhong, X.D. Hou, Spectrosc. Lett. 36 (2003) 275.
[39] J. Sun, Spectrosc. Spectr. Anal. 23 (2003) 793.
[40] X. Liu, H. Yu, Z. Zhao, Z. Li, Z. Xu, P. Li, Spectrosc. Spectr. Anal. 25 (2005) 964.
[41] D. Guo, L. Li, G. Wang, Spectrosc. Spectr. Anal. 18 (1998) 719.
[42] J.A. Nóbrega, J. Rust, C.P. Calloway, B.T. Jones, Spectromchim. Acta Part B 59 (2004) 1337.
[43] X. Yin, G. Schlemmer, B. Welz, Anal. Chem. 59 (1987) 1462.
[44] Y.P. Ke, Q. Sun, Z.R. Yang, J.J. Xin, L. Chen, X.D. Hou, Spectrosc. Lett. 39 (2006) 29.
[45] Z.X. Li, Y.A. Guo, Talanta 65 (2005) 1318.

Available online at www.sciencedirect.com
ScienceDirect
Talanta 74 (2008) 470–477
Talanta
www.elsevier.com/locate/talanta

Headspace single drop microextraction combined with HPLC for the determination of trace polycyclic aromatic hydrocarbons in environmental samples

Yunli Wu, Linbo Xia, Rui Chen, Bin Hu *

Department of Chemistry, Wuhan University, Wuhan 430072, China

Received 27 March 2007; received in revised form 31 May 2007; accepted 31 May 2007
Available online 23 June 2007

Abstract

A new method by combining headspace single drop microextraction (HS-SDME) with HPLC fluorescence detection for the determination of trace polycyclic aromatic hydrocarbons (PAHs) in environmental samples was developed. Aqueous solution of saturated β-cyclodextrin was used as extraction solvent and five PAHs were employed as target analytes. The factors affecting the extraction efficiency were studied in detail and the optimal extraction conditions were established. β-cyclodextrin was found to play two important roles, one is the improvement of extraction efficiency of target analytes and the other is the enhancement of their fluorescence intensities in HPLC fluorescence detection. The detection limits for the target analytes were found to be in the range of 0.004–0.247 ng/ml and the relative standard deviations (R.S.D.s) of 5.1–7.1% were obtained. The proposed method was applied to the analysis of trace PAHs in environmental samples with satisfactory results.
© 2007 Elsevier B.V. All rights reserved.

Keywords: Headspace single drop microextraction; HPLC; PAHs; β-cyclodextrin; Environmental samples

1. Introduction

Polycyclic aromatic hydrocarbons (PAHs) are a class of well-known persistent organic pollutants which are commonly found in the environment. The US Environmental Protection Agency (EPA) has identified 16 PAHs as priority pollutants due to their mutagenic and carcinogenic properties [1,2]. PAHs have mainly been found in the process of incomplete combustion of oil spill, fossil fuels, wood and so on. PAHs are so widely spread that they can enter bodies through atmosphere, drinking water, food, and smoking, so it is dangerous to human health. Therefore, great attention was paid to the research on PAHs [1,3–5]. Although, the identification and quantitation of PAHs in environmental samples are important, great problems were encountered due to their low concentration and complex matrices. Thus, sample cleanup and preconcentration are necessary for the analysis of PAHs in environmental samples. Hence, the search for a simple, fast, and effective sample pretreatment method has become an important issue in analytical chemistry [1,2,4,6–8].

Nowadays, there are many sample pretreatment methods for the determination of PAHs in environmental samples. Several techniques have been reported, including Soxhlet extraction (SE), liquid–liquid extraction (LLE), ultrasonic extraction (UE), accelerated solvent extraction (ASE), microwave assisted extraction (MAE), supercritical fluid extraction (SFE), and solid phase extraction (SPE), solid phase microextraction (SPME) [4–7,9–12]. These methods require neither large amount of toxic organic solvents nor expensive equipments.

Single drop microextraction (SDME), as a new technique for sample preparation, was first developed by Liu and Dasgupta [13] in 1996. Subsequently, Jeannot et al. [14] studied its kinetics and mass transfer model. SDME is a simple, fast and inexpensive method for sample preparation. This technique can be divided into two operation modes: direct-SDME and headspace-SDME (HS-SDME). HS-SDME is suitable for the extraction of volatile and semi-volatile organic compounds. Compared with direct-SDME, HS-SDME can avoid the influence of complex matrices. Therefore, HS-SDME is widely used in the analysis of trace volatile and semi-volatile organic compounds [8,15–18].

Cyclodextrins (CDs) are a group of macrocyclic compounds comprising a torus of α-1,4-linked glucose units. The most com-

* Corresponding author. Tel.: +86 27 87218764; fax: +86 27 68754067.
E-mail address: binhu@whu.edu.cn (B. Hu).

0039-9140/$ – see front matter © 2007 Elsevier B.V. All rights reserved.
doi:10.1016/j.talanta.2007.05.057

monly used oligosaccharides are α-, β-, γ-cyclodextrins with six, seven, eight glucopyranose units, respectively [19]. These molecules have high aqueous solubility for the array of hydroxyl functional groups on the exterior of the torus, and they also have a hydrophobic organic cavity in the interior of the torus. These properties enable CDs to form inclusion complex with guest molecules on the basis of size and hydrophobicity [19,20]. Based on the size relationship between the PAHs and the γ-cyclodextrin cavity, Warner et al. [21] developed a γ-cyclodextrin modified solvent extraction method for selective extraction of PAHs in 1988. Butterfield et al. [20] reported that fluorescence intensity of the extracted PAH maybe enhanced by increasing the amount of solid cyclodextrin.

The aim of this work was to develop a new method of HS-SDME for the analysis of five PAHs in environmental samples. Aqueous solution β-cyclodextrin was used in this work, not only as the extraction solvent for HS-SDME, but also as a solvent to enhance the fluorescence intensities of PAHs in HPLC fluorescence detection. The factors that influenced on the extraction efficiency of five PAHs including sample temperature, microdrop volume, stirring rate, extraction time and ionic strength were investigated and optimized. Finally, the proposed method was successfully applied to the analysis of trace PAHs in environmental samples.

2. Experimental

2.1. Standards and reagents

Naphthalene (NAP) was bought from Hengxing Chemical Co. Ltd. (Tianjin, China). Anthracene (ANT) was purchased from Guangfu Fine Chemical Rearch Institute (Tianjin, China). Phenanthrene (PHE), fluoranthene (FLU) and pyrene (PYR) were obtained from Anshan Tianchang Chemical Co. Ltd. (Liaoning, China). The stock standard solutions were prepared by dissolving PAHs in methanol (NAP, PHE, FLU, and PYR: 1 mg/ml; ANT: 0.25 mg/ml). All stock solutions were stored in dark glass bottles at 4 °C. Working standard solutions were prepared daily from their stock standard solutions.

β-cyclodextrin was purchased from Aldrich (Aldrich Chemical Company, USA). The solvent used for the preparation of the mobile phase was methanol (Shanghai Reagent Factory, Shanghai, China). The mobile phase was filtered through 0.45 μm filter prior to use.

All reagents used were of analytical-reagent grade and all aqueous solutions were prepared with high-purity water (Millipore, Milford, MA, USA).

2.2. Sample preparation

2.2.1. Real water sample

Lake water (pH 7.7, East Lake, Wuhan, China) was collected in a 50 ml polyethylene container. The water was filtered through 0.45-μm filter membrane immediately after sampling. Before the extraction step, NaCl was added and the final concentration was 0.2 g/ml.

2.2.2. Leaf samples

Three kinds of leaves including the leaves of *Cinnamomum camphora*, *Populus euramevicana cv*., and *Pine* were collected around coking chemical plant, which were exposed to similar environment. The petioles of the leaves were cut off and the small spider webs, dust particles were wiped off from the surface. In accordance with the literature cited [22], none of the leaves were washed for evaluating total deposition of PAHs. Using *P. euramevicana cv*. leaves as the model analyte, three pretreatment methods were compared.

2.2.2.1. Method 1 [23]. The leaves were powdered, and sieved (0.425 mm). Then, 2.0 g powdered leaves was placed in 100 ml boiling water for 5 min, filtered and allowed to cool down to room temperature. Before HS-SDME, the filtrate was diluted twice, then NaCl was added and the final concentration was 0.2 g/ml.

2.2.2.2. Method 2. A 2.0 g powdered leaves was placed in 100 ml water for 24 h, and then filtered. Before HS-SDME, the filtrate was also diluted twice, then NaCl was added and the final concentration was 0.2 g/ml.

2.2.2.3. Method 3 [24]. The leaves were cut into small pieces. A 2.0 g weighed leaves were placed in a closed jar with 20 ml of 2 mol/l KOH in methanoic solution (methanol:water = 9:1) for 3 h, and then filtered. Due to the high content of methanol in sample solution, the droplet was not stable, so the filtrate was diluted ten times, then NaCl was added before HS-SDME.

2.3. HS-SDME procedure

Extractions were performed according to the following procedure: 10 ml sample solution was added to a 20 ml vial, and a magnetic bar was placed into the solution to ensure efficient stirring during the extraction process. The vial was tightly capped with a PTFE-faced silicone septum and placed on a 85-2A constant temperature magnetic stirrer (Ronghua, Jiangsu, China). Water bath was used to keep the sample temperature. Fig. 1 shows the experimental setup used in this work. A HPLC syringe (Agilent) was washed with acetone and water. Subsequently, it was rinsed at least five times with the extraction solvent. Then, aqueous solution of β-cyclodextrin was withdrawn into the microsyringe. In order to obtain a larger microdrop, a portion of the pipette tip was pulled into the HPLC microsyringe tip, so that it could support a 10-μl-microdrop stably. The insertion and subsequent withdraw of the syringe needle with the pulled pipette tip directly through silicone septum can be described as follows: the silicone septum was firstly pierced by a needle. The pore was enlarged with a pipette tip so that the HPLC microsyringe with a portion of the pipette tip on the needle could be easily insert through silicone septum. The extraction solvent drop was located about 1 cm above the surface of the stirred solution [15]. After extraction, the drop was retracted; the microsyringe was pulled out directly, leaving the pipette tip in the vial; and the microliters extracts were injected into HPLC directly for analysis. The operation is simpler than using organic

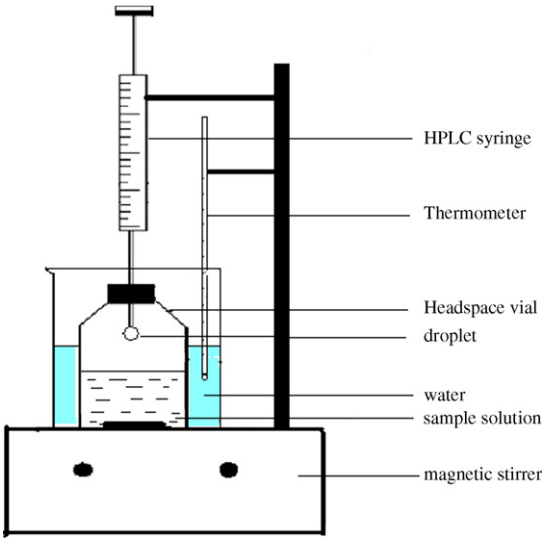


Fig. 1. Schematic setup of HS-SDME.

Table 1
Programme of excitation and emission wavelengths

PAHs	Time (min)	λ_{ex} (nm)	λ_{em} (nm)
NAP	4.3	275	325
PHE	6.9	250	375
ANT	7.6	250	375
FLU	9.1	285	465
PYR	10.2	270	390

solvent as the extraction solvent combined with HPLC, which requires drying of the organic solvent drop by slow nitrogen flow and redissolving in methanol [25].

2.4. Chromatographic system

The HPLC system consisted of Hewlett-Packard (Agilent) 1100 Series components, pump, degasser, and FLD. A C_{18} column (Lichrospher-ODS, 200 mm × 4.6 mm from Hanbon, China, 5-μm particle size) was used. Methanol-water (90:10) was employed as the mobile phase. The flow rate was fixed at 1 ml/min. The excitation and emission wavelengths were shown in Table 1.

3. Results and discussion

3.1. Optimization of the HS-SDME apparatus

In this paper, the factors influencing the extraction efficiency including sample temperature, microdrop volume, stirring rate, extraction time, ionic strength, pH value and the concentration of β-cyclodextrin have been investigated and the optimized experimental conditions are established.

3.1.1. Effect of sample temperature

For HS-SDME, the effect of sample temperature is a very important factor. In this study, temperature in the range of 30–80 °C was investigated. As shown in Fig. 2, the signal intensities of all five PAHs have been elevated by increasing the temperature from 30 to 40 °C. However, the signal intensities of NAP, PHE, and ANT decreased at different slopes when the temperature was above 40 °C, and the analytical signal intensity of FLU and PYR began to decrease at 60 °C. Generally, increasing the temperature could enhance the Henry's constants and diffusion coefficients, so the vapor pressure and the concentration of the analytes in the headspace were consequently increased [25]. As a result, the mass transfer of the analytes into the microdrop was also improved, and the equilibrium time would be shorter [2]. On the other hand, the process in which β-cyclodextrin complexed with PAHs was exothermic reaction, so the amount of the extracted analytes decreased at higher temperature. Thus, based on the experimental results, 40 °C was selected as extraction temperature in the subsequent experiments.

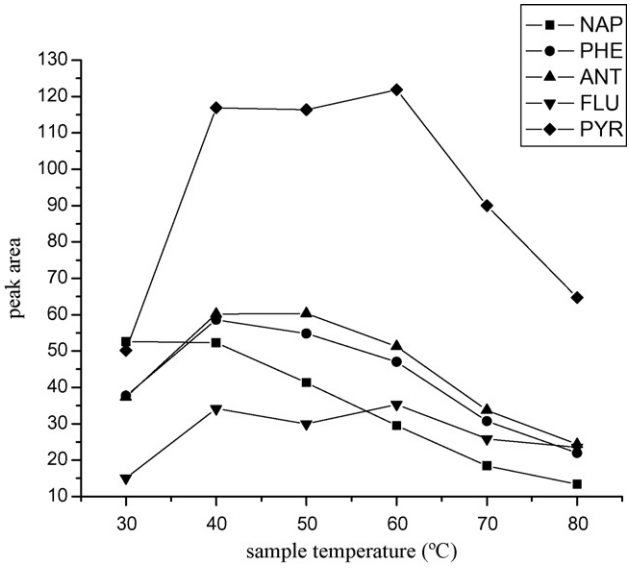


Fig. 2. Effect of sample temperature. Conditions: concentrations of NAP, PHE, ANT, FLU, PYR are 10, 1, 0.25, 10, 10 ng/ml, respectively; extraction time: 10 min; stirring rate: 1000 rpm; NaCl: 0.2 g/ml; microdrop volume: 10 μl.

3.1.2. Effect of microdrop volume

In this work, aqueous solution of β-cyclodextrin was used as extraction solvent instead of organic solvent. The procedure was completely organic solvent-free. As another important factor in HS-SDME, the effect of microdrop volume in the range of 2–12 μl was investigated. As could be seen from Fig. 3, the peak area of PAHs increased significantly with the increase in the drop volume. When the microdrop volume increased further, the drop became unstable due to its gravity. Therefore, a droplet of 10 μl was selected in this work.

3.1.3. Effect of stirring rate

The stirring rate would affect the extraction dynamics remarkably since it could improve the mass transfer. Therefore, increasing the stirring rate could reduce the time required to reach the equilibrium. The effect of stirring rate was evaluated from 300 to 1200 rpm and the results are shown in Fig. 4. It can be seen that the peak area increased with increase in stirring rate. When the stirring rate was above 1000 rpm, the

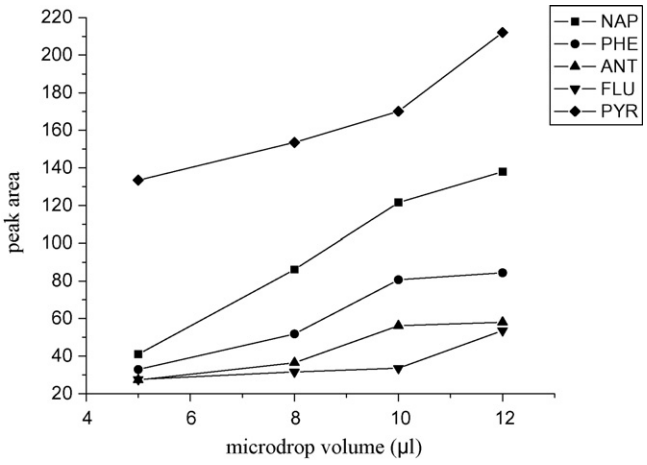


Fig. 3. Effect of microdrop volume. Conditions: concentrations of NAP, PHE, ANT, FLU, PYR are 10, 1, 0.25, 10, 10 ng/ml, respectively; sample temperature: 40 °C; extraction time: 10 min; stirring rate: 1000 rpm; NaCl: 0.2 g/ml.

droplet was usually destroyed by the spattering of solution. Thus, 1000 rpm was chosen as the optimum stirring rate in the present work.

3.1.4. Effect of extraction time

Aqueous solution of β-cyclodextrin was used as the extraction solvent, and the extraction efficiency mainly depended on the formation constant of cyclodextrins inclusion complexes. To investigate the influence of extraction time on the microextraction, extractions were performed in the time range of 2–20 min. As shown in Fig. 5, extraction efficiency increased with increase in time at the beginning, and reached a plateau after 10 min. For NAP, the signal intensity didn't increase after 5 min. This could be explained on the basis of the fact that, the boiling point of NAP is the lowest among five PAHs, and the character of volatility is better than the others. Hence, 10 min was selected as the extraction time for the further experiments.

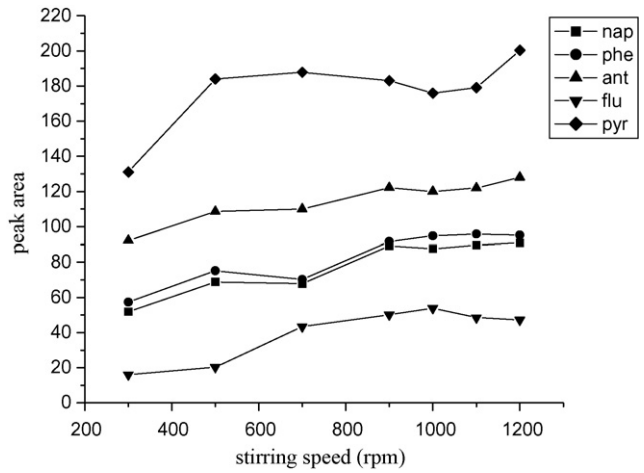


Fig. 4. Effect of stirring rate. Conditions: concentrations of NAP, PHE, ANT, FLU, PYR are 10, 1, 0.25, 10, 10 ng/ml, respectively; sample temperature: 40 °C; extraction time: 10 min; NaCl: 0.2 g/ml; microdrop volume: 10 μl.

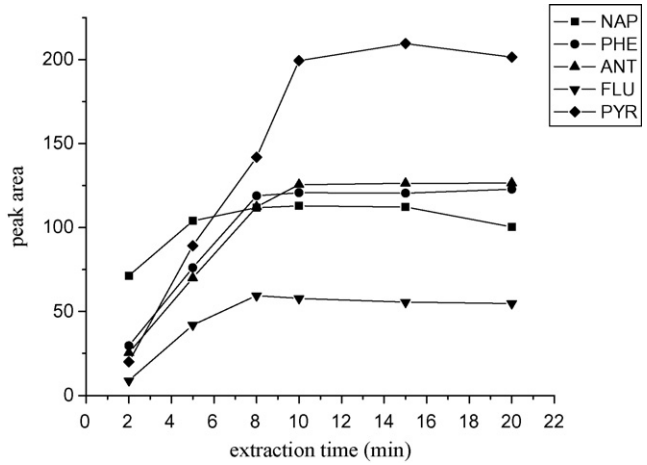


Fig. 5. Effect of extraction time. Conditions: concentrations of NAP, PHE, ANT, FLU, PYR are 10, 1, 0.25, 10, 10 ng/ml, respectively; sample temperature: 40 °C; stirring rate: 1000 rpm; NaCl: 0.2 g/ml; microdrop volume: 10 μl.

3.1.5. Effect of ionic strength

The addition of salt often increased the ionic strength, and thus increased the extraction efficiency due to the salting out effect. For this purpose, different concentrations (0–0.3 g/ml) of NaCl were added to the sample solution to study the effect of NaCl concentration on the extraction efficiency of PAHs, and the results are shown in Fig. 6. As can be seen, the extraction efficiency of PAHs was increased significantly when the amount of NaCl increased. However, the extraction efficiency remained constant when the concentration of NaCl was up 0.2 g/ml. In this study, the concentration of 0.2 g/ml NaCl was used.

3.1.6. Effect of pH value and β-cyclodextrin concentration

The effect of pH on the extraction efficiency of PAHs has been rarely discussed, although two research works [10,26] have been reported previously. The effect of pH on the extraction efficiency of five PAHs was evaluated in this study with potassium dihydrogen phosphate/sodium hydroxide buffer (pH 4–10). The

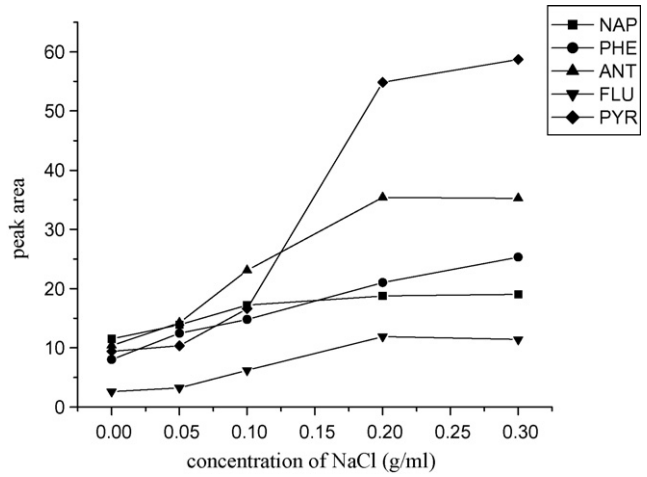


Fig. 6. Effect of ionic strength. Conditions: concentrations of NAP, PHE, ANT, FLU, PYR are 10, 1, 0.25, 10, 10 ng/ml, respectively; sample temperature: 40 °C; extraction time: 10 min; stirring rate: 1000 rpm; microdrop volume: 10 μl.

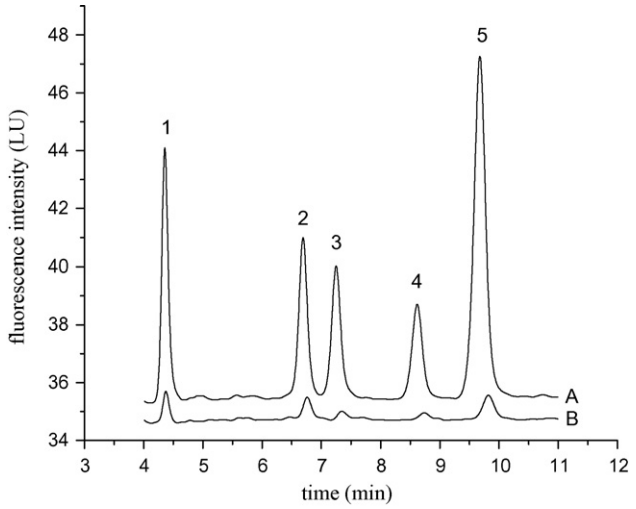


Fig. 7. Comparison of the extraction efficiency by using β-cyclodextrin and water as extraction solvent. (A) Extracted by β-cyclodextrin; (B) extracted by water. (1) NAP; (2) PHE; (3) ANT; (4) FLU; (5) PYR. Conditions: concentrations of NAP, PHE, ANT, FLU, PYR are 10, 1, 0.25, 10, 10 ng/ml, respectively; sample temperature: 40 °C; extraction time: 10 min; stirring rate: 1000 rpm; NaCl: 0.2 g/ml; microdrop volume: 10 μl.

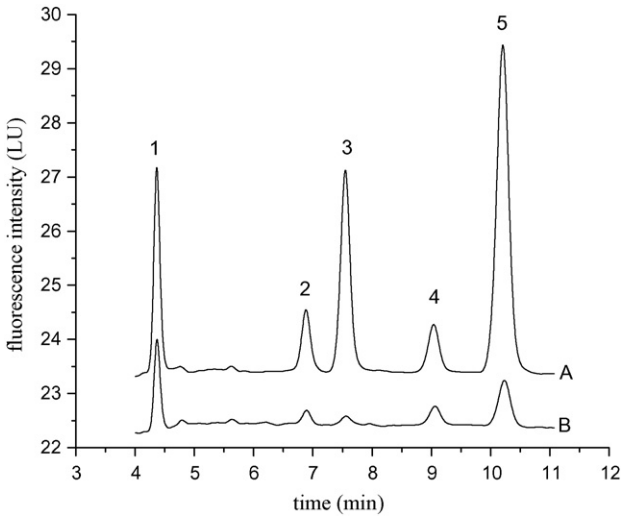


Fig. 8. Comparison of fluorescence intensities in the presence/absence of β-cyclodextrin. (A) Added 0.01 M β-cyclodextrin; (B) without β-cyclodextrin. (1) NAP; (2) PHE; (3) ANT; (4) FLU; (5) PYR. Conditions: concentrations of NAP, PHE, ANT, FLU, PYR are 100, 10, 2.5, 10, 100 ng/ml, respectively; injection: 10 μl.

experimental results indicated that pH has no apparent affecting on the extraction of studied five PAHs.

The effect of β-cyclodextrin on the extraction was also investigated. The different extraction abilities using water and saturated β-cyclodextrin aqueous solution as extraction solvent were comparatively studied, and the experimental results are shown in Fig. 7. After extraction by 8 μl saturated β-cyclodextrin aqueous solution, 8 μl water was mixed to the drop, then the mixture was injected to HPLC, and chromatogram A was obtained. While chromatogram B represented the signal of PAHs extracted by 8 μl water, and then mixed with 8 μl saturated β-cyclodextrin aqueous solution before injecting to HPLC. It is obvious that the signal of five PAHs in chromatogram A is much prominent than that in chromatogram B, which demonstrates a good extraction ability of β-cyclodextrin to extract PAHs. At the same time, the effect of β-cyclodextrin concentration on the extraction of PAHs was studied, and the experimental results indicated that the extraction efficiency of five PAHs was increased obviously with the increase of concentration. Thus, saturated β-cyclodextrin aqueous solution was used as the extraction solvent for HS-SDME extraction of PAHs in this work.

3.2. Effect of β-cyclodextrin on the HPLC-FLD signal

In this study, the effect of β-cyclodextrin on the fluorescence intensities of PAHs in HPLC fluorescence detection was studied. Fig. 8 is the comparison of fluorescence intensities of PAHs in the absence/presence of 0.01 mol/l β-cyclodextrin. As could be seen, the signal intensities of analytes were remarkably stronger in the presence of β-cyclodextrin than its absence. According to the literatures [27,28] the formation constants of the five PAHs/β-cyclodextrin inclusion complexes ranged approximately from 72 to 2753. Since their formation constants are low, the PAHs-β-cyclodextrin inclusion complexes immediately decompose after beginning of the separation process and PAHs reached the detector as pure ones. Under this circumstance, the function of β-cyclodextrin is similar to that by adding β-cyclodextrin to the mobile phase. This is also evident from the Fig. 8 in which the retention times of PAHs are identical in both chromatograms indicating that there are no PAH-β-cyclodextrin interactions during the HPLC separation. From Fig. 8 it can also be seen that much stronger signal of PAHs was obtained by injecting the PAH sample containing β-cyclodextrin than that with no β-cyclodextrin addition.

Table 2
Analytical performance data for five PAHs by HS-SDME-HPLC-FLD

PAHs	LOD (ng/ml)		Actual enrichment factor	R.S.D. (%) (c^*, $n=7$)	Linearity range (ng/ml)	r^2
	Instrument	Method				
NAP	6.0	0.097	30	6.1	0.3–50	0.997
PHE	3.8	0.016	53	7.1	0.05–5	0.993
ANT	1.5	0.004	18	5.6	0.01–1.25	0.996
FLU	28.0	0.247	50	6.7	0.7–50	0.993
PYR	11.6	0.098	20	6.1	0.3–50	0.992

c^*: concentrations of NAP, PHE, ANT, FLU, PYR are 10, 1, 0.25, 10, 10 ng/ml, respectively.

Table 3
Comparison of the LODs (ng/ml) in the literatures for the determination of PAHs with different analytical approaches

Analytical technique[a]	Analytes					References
	NAP	PHE	ANT	FLU	PYR	
HS-SDME-HPLC-FLD	0.097	0.016	0.004	0.247	0.098	This work
Dynamic-LPME-HPLC-UV	–	–	–	0.45	0.60	[25]
MSPME-GC-MS	2.35	1.59	1.82	2.09	1.97	[29]
HF-LPME-GC-MS	0.005	0.010	0.008	0.011	0.006	[30]
in-tube-SPME-HPLC-FLD	0.001	0.006	0.006	–	–	[31]

[a] HS: headspace; SDME: single drop microextraction; HPLC: high performance liquid chromatography; FLD: fluorescence detector; MSPME: micellar solid phase microextraction; GC: gas chromatography; MS: mass spectrometry; LPME: liquid phase microextraction; UV: ultraviolet; HF: hollow fiber; SPME: solid phase microextraction.

3.3. Analytical performance

Under optimal conditions, the analytical performance of this method was investigated and the results are listed in Table 2. Linearity was obtained over the PAHs concentration range of 0.01–50 ng/ml with the correlation coefficient (r^2) ranging from 0.992 to 0.997. The relative standard deviations (R.S.D.s) were all below 10%. The enrichment factors, defined as the ratio of two calibration line slopes after extraction and before extraction, were 18–53-fold. And the limits of detection (LODs, S/N = 3) were in the range of 0.004–0.247 ng/ml. Table 3 also listed the LODs reported in literatures for a comparison. As could been seen, the LODs obtained by this method are lower than the LODs reported in literatures [25,29], but higher than those given in reference [30,31]. The developed method was inexpensive and possesses low detection limits as compared with other literatures shown in Table 3, and could be used for the analysis of trace PAHs in environmental samples.

Table 4
Analytical results (n = 3) for PAHs in real water sample

PAHs	Added (ng/ml)	Determined[a] (ng/ml)	Recovery[b] (%)
NAP	0	0.71 ± 0.05	–
	2	2.88 ± 0.15	108.5 ± 5.1
	5	5.68 ± 0.46	99.4 ± 8.1
	10	10.83 ± 0.23	101.2 ± 2.1
PHE	0	0.38 ± 0.03	–
	0.2	0.57 ± 0.03	95 ± 5.1
	0.5	0.89 ± 0.06	102 ± 6.5
	1	1.35 ± 0.11	97 ± 8.5
ANT	0	0.08 ± 0.01	–
	0.05	0.127 ± 0.01	94 ± 4.7
	0.125	0.217 ± 0.02	109.6 ± 8.0
	0.25	0.332 ± 0.02	100.8 ± 6.9
FLU	0	n.d.[c]	–
	2	2.21 ± 0.14	110.5 ± 6.5
	5	5.23 ± 0.32	104.6 ± 6.1
	10	10.34 ± 0.69	103.4 ± 6.7
PYR	0	0.33 ± 0.02	–
	2	2.48 ± 0.17	107.5 ± 7.0
	5	5.48 ± 0.26	103 ± 4.8
	10	10.35 ± 0.72	100.2 ± 7.0

[a] Mean ± S.D. (n = 3).
[b] Mean ± R.S.D. (n = 3).
[c] n.d.: not determined.

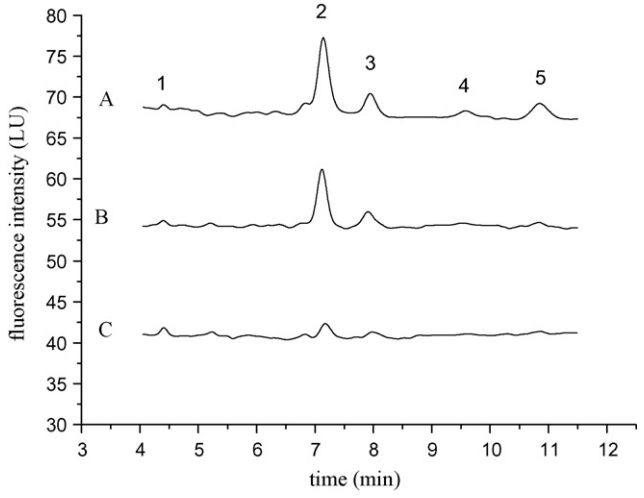


Fig. 9. Chromatogram of HS-LPME from leaves by different pretreatment methods. (A) Distilled by boiling water for 5 min; (B) distilled by water for 24 h; (C) distilled by 2 mol/l KOH in methanoic solution for 3 h. (1) NAP; (2) PHE; (3) ANT; (4) FLU; (5) PYR. Conditions—sample temperature: 40 °C; extraction time: 10 min; stirring rate: 1000 rpm; NaCl: 0.2 g/ml; microdrop volume: 10 μl.

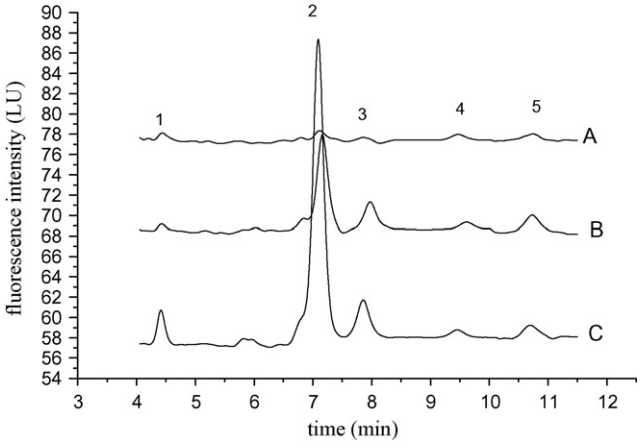


Fig. 10. Chromatograms of PAHs in different leaves around coking chemical plant. (A) *Cinnamomum camphora*; (B) *Populus euramevicana* cv.; (C) *Pine*. (1) NAP; (2) PHE; (3) ANT; (4) FLU; (5) PYR. Conditions—sample temperature: 40 °C; extraction time: 10 min; stirring rate: 1000 rpm; NaCl: 0.2 g/ml; microdrop volume: 10 μl.

3.4. Sample analysis

For real sample analysis, the calibration was obtained by subjecting standard solutions to HS-SDME.

3.4.1. Real water sample

The developed method was applied to the analysis of real water sample collected from East Lake, and the analytical results along with the recoveries for the spiked samples were given in Table 4. As could be seen, the recoveries of five PAHs obtained with the proposed method were ranging from 94.0% to 110.5%.

3.4.2. Leaf samples

Leaves of *P. euramevicana cv*. were employed as the model sample to select the most appropriate sample pretreatment method for different leaf samples. Fig. 9 is the chromatograms obtained with three different sample pretreatment methods described in Section 2.2.2. The results showed that Method 3 had the best extraction efficiency as a whole. Therefore, Method 3 was selected for the following sample analysis.

Method 3 was selected as the pretreatment method, and then followed by HS-SDME, PAHs concentrations of three different type of leaves were determined. The results were shown

Table 5
Analytical results ($n = 3$) for PAHs in leaves around coking chemical plant

Leaves	PAHs	Added (ng g^{-1})	Dertermined[a] (ng g^{-1})	Recovery[b] (%)
Cinnamomum camphora	NAP	0	66 ± 5	–
		200	255 ± 17	94.5 ± 6.7
		500	567 ± 32	100.2 ± 5.7
	PHE	0	19 ± 1.7	–
		20	37 ± 2.6	90 ± 6.9
		50	66 ± 3.6	94 ± 5.5
	ANT	0	n.d.[c]	–
		5	5.1 ± 0.4	102 ± 8.4
		12.5	13 ± 1.0	104 ± 7.8
	FLU	0	78 ± 6	–
		200	268 ± 13	95 ± 5.0
		500	570 ± 26	98.4 ± 4.6
	PYR	0	135 ± 7	–
		200	346 ± 14	105.5 ± 4.0
		500	647 ± 15	102.4 ± 2.3
Populus euramevicana cv.	NAP	0	157 ± 10	–
		200	358 ± 23	100.5 ± 6.4
		500	666 ± 42	101.8 ± 6.3
	PHE	0	334 ± 19	–
		400[d]	688 ± 21	88.5 ± 3.1
	ANT	0	21 ± 1.2	–
		5	26 ± 1.8	100 ± 7.1
		12.5	34 ± 1.9	104 ± 5.7
	FLU	0	257 ± 18	–
		200	461 ± 12	102 ± 2.6
		500	768 ± 58	102.2 ± 7.5
	PYR	0	352 ± 23	–
		200	545 ± 52	96.5 ± 9.6
		500	860 ± 47	101.6 ± 5.5
Pine	NAP	0	989 ± 100	–
		500	1458 ± 144	93.8 ± 9.9
		1000	1919 ± 263	93 ± 8.5
	PHE	0[e]	2484 ± 218	–
		2000[e]	4262 ± 209	88.9 ± 4.9
	ANT	0	31 ± 1.8	–
		12.5	43 ± 1.9	96 ± 4.5
		25	54 ± 2.4	92 ± 4.4
	FLU	0	256 ± 17	–
		200	456 ± 35	100 ± 7.6
		500	757 ± 54	100.2 ± 7.1
	PYR	0	325 ± 23	–
		200	537 ± 35	106 ± 6.6
		500	828 ± 74	100.6 ± 8.9

[a] Mean ± S.D. ($n = 3$).
[b] Mean ± R.S.D. ($n = 3$).
[c] n.d.: not determined.
[d] The extract was diluted 20 times.
[e] The extract was diluted 100 times.

in Fig. 10 and Table 5. It was clear that *Pine* leaves were the most active in PAHs accumulation, especially for NAP, PHE, ANT; while *C. camphora* leaves were inactive. The three different leaves were exposed to the same environment, but they have different capability for the accumulation of PAHs. The reason that led to the above difference may be viewed as follows: the tree's age, species, leaf's size, primary content of PAHs, and so on. Therefore, it maybe meaningful to search for a specific tree for in polluted area. In this work, the leaves spiked with the standard PAHs at different concentrations were analyzed. The results were also shown in Table 5. As can be seen, recovery of about 100% was obtained.

4. Conclusion

In the present study, a new method based on HS-SDME using aqueous solution of β-cyclodextrin as extraction solvent was developed for HPLC-FLD determination of PAHs in environmental samples. The results demonstrated that the spiked recoveries were good. In the proposed work, aqueous solution β-cyclodextrin was used not only as the extraction solvent for HS-SDME, but also as a reagent to enhance the fluorescence intensity of PAHs in HPLC fluorescence detection. The developed HS-SDME method is simple, fast, efficient and organic solvent-free. Moreover, it is suitable for the analysis of trace PAHs in various samples with complex matrices.

Acknowledgements

Financial supports from the Science Fund for Creative Research Groups of NSFC (No. 20621502), National Nature Science Foundation of China (Nos. 20575048 and 20375030), MOE of China (NCET-04-0658) are gratefully acknowledged.

References

[1] R. Doong, S. Chang, Y. Sun, J. Chromatogr. A 879 (2000) 177.
[2] S. Shariati-Feizabadi, Y. Yamini, N. Bahramifar, Anal. Chim. Acta 489 (2003) 21.
[3] S. Waidyanatha, Y. Zheng, S.M. Rappaport, Chem.-Biol. Interact. 145 (2003) 165.
[4] P. Navarro, E. Cortazar, L. Bartolome, M. Deusto, J.C. Raposo, O. Zuloaga, G. Arana, N. Etxebarria, J. Chromatogr. A 1128 (2006) 10.
[5] J.B. Dallarosa, J.G. Monego, E.C. Teixeira, J.L. Stefens, F. Wiegand, Atmos. Environ. 39 (2005) 1609.
[6] O.P. Heemken, N. Theobald, B.W. Wenclawiak, Anal. Chem. 69 (1997) 2171.
[7] P.K. Wong, J. Wang, Environ. Pollut. 112 (2001) 407.
[8] X. Jiang, C. Basheer, J. Zhang, H.K. Lee, J. Chromatogr. A 1087 (2005) 289.
[9] N. Saim, J.R. Dean, M.P. Abdullah, Z. Zakaria, J. Chromatogr. A 791 (1997) 361.
[10] H.W. Chen, Anal. Sci. 24 (2004) 1383.
[11] C.L. Arthur, J. Pawliszyn, Anal. Chem. 62 (1990) 2145.
[12] G. Ouyang, Y. Chen, J. Pawliszyn, Anal. Chem. 77 (2005) 7319.
[13] H. Liu, P.K. Dasgupta, Anal. Chem. 68 (1996) 1817.
[14] M.A. Jeannotand, F.F. Cantwell, Anal. Chem. 68 (1996) 2236.
[15] Q. Xiao, C. Yu, J. Xing, B. Hu, J. Chromatogr. A 1125 (2006) 133.
[16] A. Tankeviciute, R. Kazlauskas, V. Vickackaite, Analyst 126 (2001) 1674.
[17] C.L. Ye, Q.X. Zhoua, X.M. Wang, Anal. Chim. Acta 572 (2006) 165.
[18] S. Sun, Z. Cheng, J. Xie, J. Zhang, Y. Liao, H. Wang, Y. Guo, Rapid Commun. Mass Spectrom. 19 (2005) 1025.
[19] H. Tong, Cyclodextrin Chemistry, Science Press, Beijing, 2001.
[20] M.T. Butterfield, R.A. Agbaria, I.M. Warner, Anal. Chem. 68 (1996) 1187.
[21] L.A. Blyshak, T.M. Rossi, G. Patonay, I.M. Warner, Anal. Chem. 60 (1988) 2127.
[22] A. Alfani, G. Maisto, M.V. Prati, D. Baldantoni, Atmos. Environ. 35 (2001) 3553.
[23] V.G. Zuin, L. Montero, C. Bauer, P. Popp, J. Chromatogr. A 1091 (2005) 2.
[24] V.A. Jouraevaa, D.L. Johnsona, J.P. Hassetta, D.J. Nowak, Environ. Pollut. 120 (2002) 331.
[25] L. Hou, H.K. Lee, J. Chromatogr. A 976 (2002) 377.
[26] C. Basheer, R. Balasubramanian, H.K. Lee, J. Chromatogr. A 1016 (2003) 11.
[27] J.J. Tang, L.J. Cline Love, Anal. Chim. Acta 344 (1997) 137.
[28] L.A. Blyshak, K.Y. Dodson, G. Patonay, I.M. Warner, Anal. Chem. 61 (1989) 955.
[29] V. Pino, J.H. Ayala, A.M. Afonso, V. Gonzalez, Anal. Chim. Acta 477 (2003) 81.
[30] M. Charalabaki, E. Psillakis, D. Mantzavinos, N. Kalogerakis, Chemosphere 60 (2005) 690.
[31] H. Bagheri, A. Salemi, Chromatography 59 (2004) 501.

Available online at www.sciencedirect.com
ScienceDirect
Talanta 74 (2008) 836–843
Talanta
www.elsevier.com/locate/talanta

Solid phase extraction of lead (II), copper (II), cadmium (II) and nickel (II) using gallic acid-modified silica gel prior to determination by flame atomic absorption spectrometry

Fazhi Xie [a,b], Xucong Lin [a], Xiaoping Wu [a], Zenghong Xie [a,*]

[a] *The Department of Chemistry, Fuzhou University, Fuzhou, Fujian 350002, China*
[b] *School of Materials Science and Chemical Engineering, Anhui Institute of Architecture & Industry, Hefei, Anhui 230022, China*

Received 20 April 2007; received in revised form 16 July 2007; accepted 17 July 2007
Available online 26 July 2007

Abstract

The immobilization of gallic acid on the surface of amino group-containing silica gel phases for the formation of a newly chelating matrix (GASG) is described. The newly synthesized extractant, characterized by the diffuse reflectance infrared Fourier transformation spectroscopy and elemental analysis, was used to preconcentrate Pb(II), Cu(II), Cd(II) and Ni(II). The pH ranges for quantitative sorption and the concentrations of HCl for eluting Pb(II), Cd(II), Cu(II) and Ni(II) were opimized, respectively. The sorption capacity of the matrix has been found to be 12.63, 6.09, 15.38, 4.62 mg/g for Pb(II), Cd(II), Cu(II) and Ni(II), respectively, with the preconcentration factor of ∼200 (∼100 for Cd(II)). The effects of flow rates, the eluants, the electrolytes and cations on the metal ions extraction, as well as the chelating matrix stability and reusability, were also studied. The extraction behavior of the matrix was conformed with Langmuir's equation. The present preconcentration and determination method was successfully applied to the analysis of synthetic metal mixture solution and river water samples. The 3σ detection limit and 10σ quantification limit for Pb(II), Cu(II), Cd(II) and Ni(II) were found to be 0.58, 0.86, 0.65, 0.92 μg/L and 1.08, 1.23, 0.87, 1.26 μg/L, respectively.
© 2007 Elsevier B.V. All rights reserved.

Keywords: Solid phase extraction; Silica gel modified with gallic acid (GASG); Heavy metal

1. Introduction

In general, heavy metal ions are toxic, non-biodegradable, and tend to be accumulated in the human vital organs, where they can act progressively over a long period through food chains. The determination of trace heavy metal ions in environmental samples have received increasing attention [1–3]. However, due to the complexity of sample matrix and the frequently low concentrations of metals, there is a crucial need for the extraction and preconcentration of trace elements from matrix before their analysis using atomic absorption spectrometry or other techniques. To obviate these problems, an effective extraction and preconcentration method is necessary. In the last two decades, the solid phase extraction (SPE) approach has gained rapid acceptance. It is considered as alternative to the classical liquid extraction technique, owing to several major advantages in application such as fast, simple, amenability to automation, low disposal costs and extraction time for sample preparation [4,5].

A variety of ligands or functional groups are immobilized onto a solid support matrix as a solid phase extractant for the purpose of extraction and enrichment of trace metal ions from environmental samples. Silica gel as a solid support is of great importance because it possesses some definite advantages [6], such as nondeforming, good mechanical strength and heat-stable. In addition, chelating agents can be easily loaded onto the silica gel with high stability, or be bonded chemically to the support, that affording a higher stability [5]. Recently, some chelating agents have been modified on the silica gel as solid phase extractants for the preconcentration of some metal ions. 8-hydroxyquinoline [7], salicyldoxime [6], 1-(2-thiazolylazo)-2-naphthol [8], dithizone [9], acid red-88 [10], *N*-(3-propyl)-*O*-phenylenediamine [11], thiophene-2-carbaldehyde [12], aminothioamidoanthraquinone [13], formylsalicylicacid [14], thiourea [15], 2-mercaptobenzothiazole[16], dithiocarbamate [17], iminosalicyl- [18], *o*-vanillin [19], 2-hydroxy-5-nonylacetopheneoxime [20], glycerol [21], 2-

* Corresponding author.
E-mail address: zhxie@fzu.edu.cn (Z. Xie).

0039-9140/$ – see front matter © 2007 Elsevier B.V. All rights reserved.
doi:10.1016/j.talanta.2007.07.018

thiophenecarboxaldehyde[22], 1,5-diphenylcarbazide [23], 1,5-bis(di-2-pyridyl) methylene tiocarbohydrazid [24], 2,4,6-trimorpholino-1,3,5-triazin [25], 1,3-diamine propane-3-propyl [26], 3-(1-imidazolyl)propyl [27], thioacetamide [28], methylthiosalicylate [29] are reported as the chelating matrix for metal ions, i.e. Fe(III), Cu(II), Zn(II), Cd(II), Co(II), Ni(II), Pb(II), Hg(II), Ag(I), Au(III) and Pt(II). But most of these immobilized ligands cannot provide more than two coordination sites. Anchoring a multidentate ligand on the surface of silica gel may further enhance the chelating ability of solid phase matrix.

Gallic acid is one kind of natural phenolic compound widely existed in plants and has shown pharmacological properties, e.g. strong antimutagenic, anticarcinogenic, and antioxidant activities [30–32]. As a multidentate ligand with high affinity to metal ions, it was also thought worthwhile to be immobilized on the surface of silica gel after grafting and may fulfill the objective of high chelating ability. This work aims to synthesize a gallic acid functionalized silica gel as chelating matrix through Mannich reaction. It is used as a solid phase extractant for extraction and preconcentration of heavy metal (i.e. lead (II), copper (II), cadmium (II) and nickel (II)) from aqueous sample solution.

2. Experimental

2.1. Apparatus

The diffuse reflectance infrared Fourier transformation (DRIFT) spectra were recorded with the Spectrum 2000 (Perkin-Elmer). A flame atomic absorption spectrometer (WFX-110) of Beijing Rayleigh Analytical Instrumentation Corporation (Beijing, China), equipped with air–acetylene flame was used for metal ion determination. The wavelength used for monitoring Pb, Cu, Cd and Ni is 283.3, 228.8, 324.8 and 232.0 nm, respectively. The elemental analysis of gallic acid modified silica gel was carried out by a Vario EL III elemental analyzer (Elementar, Germany). The pH measurements were conducted by a PHS-3C pH-meter (Dapu instrumentation corp., Ltd. Shanghai, China). A glass tube (200 mm × 10 mm i.d.) was used to study the metal ion sorption on the chelating matrix and washed with 4.0 M HCl, 4.0 M HNO_3, ethanol and deionized water successively. The flow rate of solution through the column was controlled using a peristaltic pump.

2.2. Reagents

Silica gel (60–100 mesh size) and gallic acid were purchased from Shanghai Chemical Reagent corporation, China. 3-aminopropyltriethoxy-silane was procured from Songya Chemical Industry Co., Ltd. It was distilled before use. Stock solutions of lead (II), copper (II), cadmium (II) and nickel (II) (1.0 mg/mL) were prepared from analytical reagent grade $Pb(NO_3)_2$, $3CdSO_4{\cdot}8H_2O$, $CuCl_2$, $NiSO_4{\cdot}7H_2O$ by dissolving the appropriate amount in deionized water, then acidified with 5 mL of concentrated nitric acid. All working solutions were diluted according to requirements. HCl (pH 1.0–2.0), acetate–acetic acid buffer (pH 3.0–5.0), phosphate buffer (pH 6.0–7.0), NH_3–NH_4Cl buffer (pH 8.0–10.0) were used for pH adjustment. All chemicals used were of analytical reagent grade.

2.3. Preparation of GASG

Silica gel was activated by successively immersing it in 6 M HNO_3 and then in 6 M HCl for 24 h. It was filtered and washed with deionized water until free from acid and then dried for 12 h in a furnace at 393 K, and finally degassed at 373 K under vacuum for 10 h.

Immobilization of gallic acid on the surface of silica gel was performed as below: activated silica gel (30 g) was suspended in 200 mL 25% (v/v) 3-aminopropyltriethoxysilane in dry toluene. The mixture was refluxed with stirring for 12 h. The resulting aminopropyl silica gel (APSG) was filtered, washed successively with toluene, ethanol and acetone. It was dried for 12 h at 353 K under vacuum. The nitrogen analysis of APSG suggests that 1.58% of organo silicon has been grafted on silica gel.

The APSG (15 g) was added into a solution of 90 mL formaldehyde (37%) and 1.8 mL glacial acetic acid. The mixture was stirred for 1 h at room temperature. The resulting product was then filtered off and washed with 100 mL ethanol [7]. The silica gel was then stirred for 10 h at 333 K in a solution of 10 g gallic acid in 100 mL deionized water, which was adjusted to pH 8.0 by adding 0.5 M sodium hydroxide solution dropwisely. After completion of the reaction, the mixture was filtered and washed sequentially with 0.05 M HCl, deionized water and ethanol. The residue was heated at 333 K for 6 h and used for heavy metal ion enrichment.

2.4. Batch experiments

GASG (0.1 g) was equilibrated with a buffer solution containing suitable amount of metal ions in a glass stoppered bottle (250 mL) for a fixed period of time. The unextracted heavy metal ion in the solution phase was measured by flame atomic absorption spectrometry (FAAS). This method was used to study the effect of shaking time on the retention of heavy metal ions on present matrix, and also to measure the maximum adsorption capacity, adsorption isotherms, etc.

2.5. Column experiments

In the column experiments, the activated silica gel or GASG (1.0 g) was packed in a glass tube and a solution containing metal ions was adjusted to a suitable pH and percolated at a certain flow rate. The heavy metal retained on the column was eluted with a suitable eluant and determined by FAAS.

2.6. Sample preparation

A certified reference material, river sediment (GBW 08301), was obtained from the National Research Center, Beijing, China. 0.500 g of this certified river sediment was added to a closed polytetrafluoroethylene (PTFE) beaker. Then, 7, 4 and 4 mL of concentrated HNO_3, $HClO_4$ and HF were added, respectively. The mixture was heated at 368 K for 12 h and evaporated nearly

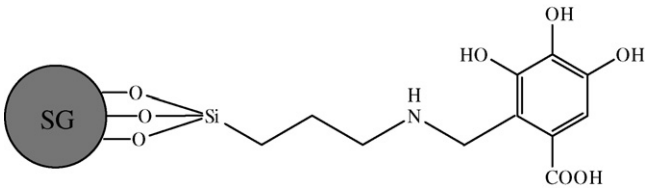


Fig. 1. Proposed chemical structure of GASG.

to dryness. After cooling, the residue was dissolved in 50 mL of 1.0 M HCl, and the solution was filtered.

According to the upper limit of the National Drinking Water Standard (GB 5749-85) [33], 1 L of an artificial water sample, containing 0.3 mg of Fe(III), 0.1 mg of Mn(II), 180 mg of Ca(II), 1.0 mg of Zn(II), 10 mg of Se(IV), and 50 mg of Cr(VI), As(V) and Ag(I), was prepared. Ten microgram of Cu(II), Cd(II), Pb(II) and Ni(II) was added to this artificial water sample.

The surface river water samples were obtained from Ming River (Fuzhou, Fujian, China), and acidified with 2% HNO_3. The samples were then filtered and the filtrates were stored in glass bottles and used for analysis within 3 days.

3. Results and discussion

3.1. Synthesis and characterization of GASG

The proposed chemical structure of the newly synthesized silica gel phase (GASG) is shown in Fig. 1. It has been characterized by elemental analysis and DRIFT spectra analysis. The elemental analysis of GASG suggests that 0.336 mmol/g of functional group has been grafted onto the surface of silica gel. The DRIFT spectrum of GASG exhibits a band at 1688 cm^{-1} which appears to be contributed by C=O stretching vibration and a strong band (707 cm^{-1}) of $–CH_2–NH–CH_2$-bending vibration can be seen [34]. The phenyl vibrations appear at 1618, 1501, 1430, 1318 cm^{-1}. All these observations support the grafted of gallic acid on the surface of silica gel.

3.2. Effect of pH

The heavy metal ion solutions were adjusted to a desired pH (between 1.0 and 10.0) and passed through a column filled with GASG or activated silica gel at optimum conditions (Table 1). The analytes were then eluted using 10 mL HCl from the column and determined by FAAS, which gave the percentage recoveries of the eluted heavy metal ions at various pH. The effect of pH on adsorption was also studied using batch method and the results were found to be consistent with those of column method. The retention experiments were carried out in triplicate to determine the precision of the method. Fig. 2 shows the effect of pH on the retention of heavy metal ions on the modified and activated silica gel. It was found that the heavy metal ions retention on activated silica gel is highly depend on the pH of the sample solution and cannot be quantitatively adsorption. The modified silica gel can quantitatively sorption these ions over a wide range of pH. The optimum pH ranges are 3.0–7.0, 6.0–10.0, 4.0–10.0 and 6.0–10.0 for Pb(II), Cd(II), Cu(II) and Ni(II), respectively. The adsorbed heavy metal ions are not significantly desorbed by distilled water, that indicates the chelating process contributes predominantly to the retention of these heavy metal ions. When pH > 10.0, the silica gel is prone to hydrolysis at high pH.

3.3. Effect of eluant

The elution of Pb(II), Cd(II), Cu(II) and Ni(II) from GASG was examined by using various eluants in the column experiment. Several solutions, such as HCl, H_3PO_4, EDTA and thiourea were tested. The results showed that using thiourea, EDTA and H_3PO_4 does not give reproducible results (recovery < 55%). HCl were found to be the most suitable eluant for stripping off the adsorbed heavy metal ions. At optimum conditions, the effect of concentration of stripping solution on desorption of the analyte from the column was investigated by using 10 mL volumes of various concentration of HCl (0.01–5 M). The results showed that the optimum concentration ranges of HCl for Pb(II), Cd(II), Cu(II) and Ni(II) were 0.05–5.0 M and 0.1–5.0 M, respectively. It was found that 10 mL of volume of eluant was sufficient to obtain the recovery of 96.7–98.9% for all heavy metal ions.

3.4. Effect of flow rate

The degree of metal ion adsorbed on GASG was studied at various flow rates (1.0–15.0 mL/min). The optimum flow rate for Pb(II), Cd(II), Cu(II) and Ni(II) is given in Table 1. To avoid the long time extraction, the flow rate lower than 1.0 mL/min were not employed. However, there was a decrease in the percentage

Table 1
Optimum experimental conditions for the sorption and desorption of metal ions

Experimental parameter	Metal ion			
	Pb	Cu	Cd	Ni
pH range	3.0–7.0	6.0–10.0	4.0–10.0	6.0–10.0
Flow rate (L/min)	1.0–9.0	1.0–8.0	1.0–4.0	1.0–3.5
HCl concentration for desorption (M)	0.05–5.0	0.05–5.0	0.05–5.0	0.1–5.0
Average sorption capacity (mg/g)	12.63	15.38	6.09	4.02
Average recovery (%)	98.2	98.6	96.7	98.9
Standard deviation[a]	0.034	0.043	0.038	0.058
Relative standard deviation (%)	3.44	4.31	3.83	5.80

[a] For five determinations of 1 μg/mL.

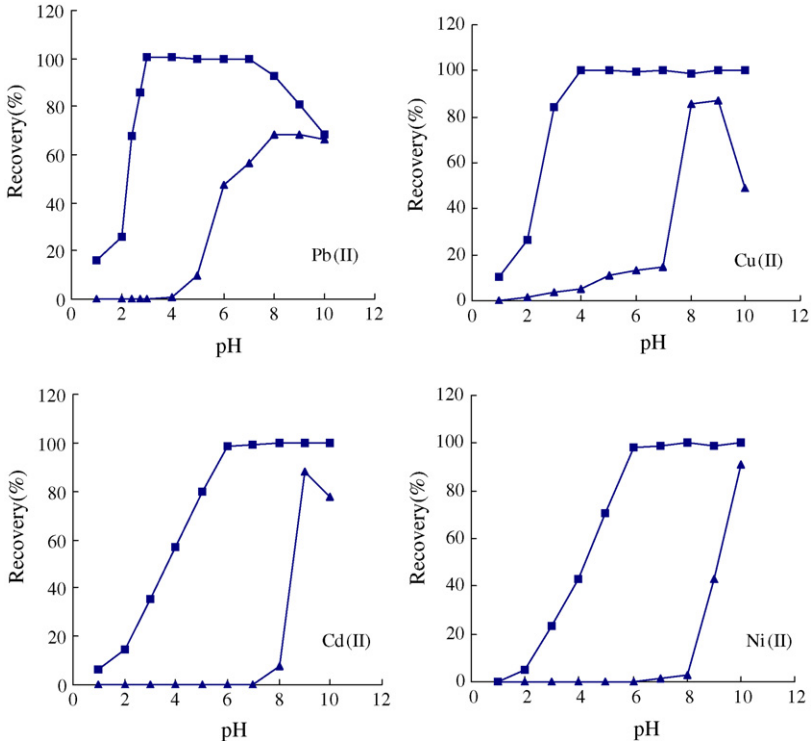


Fig. 2. Effect of pH on the recovery of heavy metal ions from aqueous solution: (■) GASG; (▲) activated silica gel.

of extraction for Pb(II), Cu(II), Cd(II) and Ni(II) at flow rate higher than 9.0, 8.0, 4.0 and 3.5 mL/min, respectively, because of the heavy metal ions cannot be adsorbed sufficiently by the modified silica gel. Therefore, the flow rate was maintained at 2.0 mL/min throughout the column experiment. For desorption, these metal ions can be desorbed quantitatively by the present matrix at a flow rate of 1.0–3.0 mL/min. Above 3.0 mL/min, the recovery for Pb(II), Cu(II), Cd(II) and Ni(II) was <95%.

3.5. Adsorption isotherm

The adsorption isotherms were determined using the batch experiments at room temperature. Solutions of heavy metal ions over the concentration range of 20–180 μg/mL were maintained at the optimum pH (pH 6.0) with 15 mL buffer and shaken for 24 h with the modified silica gel (0.1 g). The metal ions in the supernatant were determined by FAAS and the amount of heavy metal adsorbed was calculated using Eq. (1) as follows:

$$q = \frac{V(C_0 - C)}{m} \tag{1}$$

where C_0 is the initial concentration of heavy metal ions (in μg/mL), C the equilibrium concentration of heavy metal ions (in μg/mL), V the volume of heavy metal ions solutions, m the mass of the modified silica gel (in g) and q is amount of heavy metal ions adsorbed per gram of modified silica gel. Adsorption isotherm is often described by the Langmuir (2) and the Freundlich (3) equations:

$$\frac{C_{eq}}{q} = \frac{C_{eq}}{q_m} + \frac{1}{b \times q_m} \tag{2}$$

where b is a Langmuir constant. q_m a constant representing adsorption capacity, also known as monolayer coverage of the surface, and is a constant related to b. C_{eq} is adsorbate concentration in the solution at equilibrium.

$$\log q = \left(\frac{1}{n}\right) \log C_{eq} + \log K_F \tag{3}$$

In Eq. (3), K_F and n are constants characteristic of the system, where K_F is a measurement of adsorption capacity and $1/n$ of adsorption intensity.

Langmuir constants and Freundlich constants were determined by using the adsorption data through batch experiment. By comparing the correlation coefficients, it can be concluded that the experimental data fit the Langmuir model (R^2: 0.9959, 0.9962, 0.9909, 0.9948 for Pb(II), Cu(II), Cd(II) and Ni(II), respectively) better than the Freundlich model (R^2: 0.9791, 0.9085, 0.4773, 0.8721 for Pb(II), Cu(II), Cd(II) and Ni(II), respectively), because in the former case all the correlation coefficients were higher than 0.990. The metal ion sorption values by GASG at optimum pH is decrease in the following order: Pb(II) >Cu(II) >Cd(II) >Ni(II) indicating that the highest affinity is towards Pb(II) extraction and the lowest for Ni(II).

3.6. Total sorption capacity

The sorption capacity for Pb(II), Cu(II), Cd(II) and Ni(II) was determined by shaking 0.1 g of the GASG with a 100 mL of 100 μg/mL heavy metal ion solution (total amount of metal available for adsorption is much greater than the adsorption capacity) at pH 6.0 for 24 h according to the recommended batch equilibrium procedure at room temperature. The load-

ing capacity of the GASG for each metal ions was calculated form the different batch experiments ($n = 4$). The average values are 12.63 (R.S.D. = 3.34%), 6.09 (R.S.D. = 2.58%), 15.38 (R.S.D. = 1.92%), 4.62 mg/g (R.S.D. = 4.60%) for Pb(II), Cd(II), Cu(II) and Ni(II), respectively.

3.7. Kinetics of metal sorption

The time taken for the extraction of the heavy metal ions and the attainment of the equilibrium condition by the GASG is of considerable importance. The modified silica gel (0.1 g) was equilibrated by shaking with 200 mL of a solution containing 10 mg of heavy metal ion for different time intervals (2, 5, 10, 15, 20, 25, 30, 40, 50 and 60 min), and the recommended batch experiment was applied. The metal ions were four–six times in excess over the sorption capacity. The concentration of heavy metal ions in the supernatant solution was determined and the amount of heavy metal adsorbed was calculated using Eq. (1) and the amount of metal ion loaded on the GASG was calculated by mass balance (in μg/g GASG). The loading half time $t_{1/2}$, defined as the time need to reach 50% of the present matrix total loading capacity, was estimated from the curves (Fig. 3). From the kinetics of Pb(II), Cu(II), Cd(II) and Ni(II) uptake, it was observed that an equilibration time of about 30 min was required for 95–98% sorption. However, the loading half time $t_{1/2}$ was <5 min for Pb(II), Cu(II), Cd(II), and 10 min for Ni(II).

3.8. Effects of electrolytes and cations

The effect of various electrolytes and cations, such as NaCl, $NaNO_3$, KNO_3, Na_2SO_4, Na_3PO_4, Cr(VI), Co(II), Mn(II), Hg(II), Fe(III), Ca(II) and Mg(II) on the retention of heavy metal ions was examined. For this purpose, 50 mL of the test solution containing 30 μg of the studied heavy metal ion and other ions at various concentrations was passed through the column under optimum conditions. The amount of target heavy metal ion extracted was determined after elution. The tolerance limit was taken as the maximum concentration of the foreign substances which caused an approximately ±5% relative error in the determination. The tolerance limits of these substances in enrichment of Pb(II), Cu(II), Cd(II) and Ni(II) on the present matrix are given in Table 2. The results shown that the presence solid phase matrix might be used to enrich all the three heavy metal ions from natural water samples, as their common constituents at normal level do not adversely affect the adsorption efficiency of the matrix for these heavy metal ions.

Table 2
Tolerance limit of electrolytes and cations

Electrolytes/cation	Metal ion			
	Pb(II)	Cd(II)	Cu(II)	Ni(II)
NaCl[a]	0.80	0.50	1.00	0.80
KNO_3[a]	1.20	1.00	1.20	1.20
$NaNO_3$[a]	1.80	1.60	1.80	1.20
Na_2SO_4[a]	0.80	0.60	0.80	0.80
Na_3PO_4[a]	0.02	0.02	0.04	0.02
Ca(II)[a]	0.50	0.05	0.60	0.50
Mg(II)[a]	0.30	0.10	0.20	0.40
Cr(VI)[a]	0.01	0.01	0.02	0.01
Co(II)[b]	0.08	0.06	0.08	0.08
Mn(II)[b]	0.04	0.03	0.04	0.04
Hg(II)[b]	0.01	0.01	0.01	0.01
Fe(III)[b]	0.05	0.04	0.05	0.05

[a] mol/L.
[b] mmol/L.

3.9. Stability and reusability of GASG

Cu(II) was chosen to determine the stability of gallic acid modified silica gel. A 0.1 g of the present matrix was immersed in 15 mL pH 1.0–10.0 buffer solutions for 24 h and then filtered off, washed with deionized water and dried at 333 K. After this treatment, the adsorption capacity of Cu(II) was determined. The result was shown in Fig. 4. It was found that the adsorption capacity is only slightly reduced in the pH range from 1.0 to 10.0. Since the solid support tends to be hydrolysis, the adsorption capacity was not determined at high pH conditions.

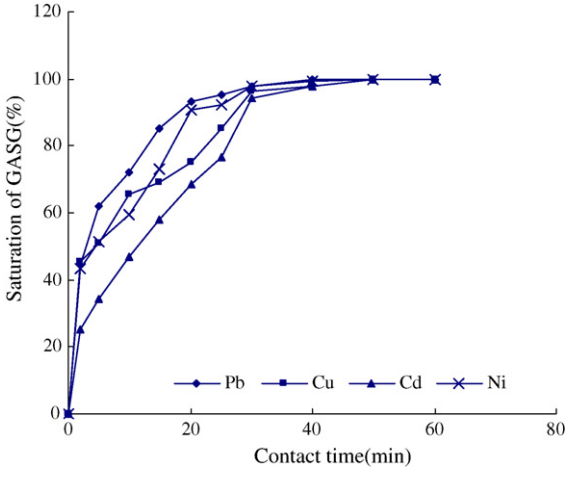


Fig. 3. Kinetics of heavy metal ion sorption on GASG.

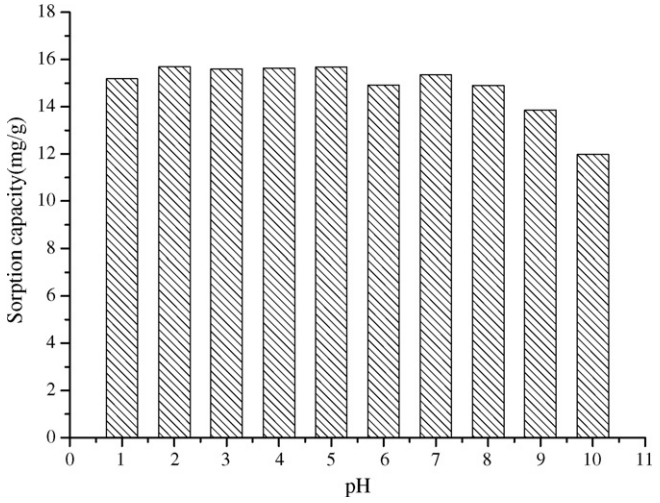


Fig. 4. The stability of GASG (pH 1.0–10.0 buffer solutions).

Table 3
Preconcentration factors and recovery of Pb(II), Cu(II), Cd(II) and Ni(II)

Analyte	Volume of solution passed (mL)	Concentration (ng/mL)	Average recovery[a] (%)	R.S.D[a] (%)	Preconcentration factor
Pb(II)	2000	5.00	96.70	0.96	200
Cu(II)	2000	5.00	99.06	0.41	200
Cd(II)	1000	10.00	97.26	0.92	100
Ni(II)	2000	5.00	96.66	0.81	200

[a] For three determinations.

The reusability of the present matrix was examined after several loading and elution cycles. It was found that the adsorption capacity is slightly decreasing continuously. However, the trace heavy metal ions in natural water samples can also be quantitatively retained after ten repeated uses, and the adsorption capacity can be reach 89.7% compared to the untreated one.

3.10. Preconcentration factor, limits of detection and quantification

Solutions containing 10 μg of the studied heavy metal ion in various volumes were passed through the column packed with 1.0 g of GASG, and the target heavy metal ion preconcentrated on the column was eluted and determined by the above-mentioned procedure. The feed volumes for loading and preconcentration factors are given in Table 3. The preconcentration factor are 200 for Pb(II), Cu(II) and Ni(II), respectively. For Cd(II),the preconcentration factor is 100. The limits of detection and the limits of quantification, as defined by IUPAC [35,36], are 0.58, 0.86, 0.65, 0.92 μg/L and 1.08, 1.23, 0.87, 1.26 μg/L for Pb(II), Cu(II), Cd(II) and Ni(II), respectively.

3.11. Analytical performance

The calibration curves used to determine metal ions with FAAS were made by measuring the absorbance of the working calibration solution (without any enrichment on the present matrix) at optimum operation parameters of the instrument (viz. wavelength, slit width, lamp current, etc.) and the solution conditions (viz. the acid concentration). The linear ranges for measurement have been found to be 1.0–5.0, 0.4–2.6, 0.2–1.0 and 1.0–5.0 μg/mL for Pb, Cu, Cd and Ni, respectively. The linear equation along with regression (R^2) for calibration curve of each metal ion is given in Table 4.

A river sediment reference material (GBW 08301, China) was used for method validation. As seen in Table 5, the results were compared with the certified values using a *t*-test at 95% confidence limits. Good agreement was obtained between the estimated content by the proposed method and the certified values for four metal ions. These results also indicate that the proposed preconcentration method for Pb(II), Cu(II), Cd(II) and Ni(II) is not affected by potential interferences from the major matrix composition of the analyzed river sediment.

Table 4
Linear regression equation and correlation coefficient for Pb(II), Cu(II), Cd(II) and Ni(II) by FAAS[a]

Element	Linear equation[b]	R^2
Pb	$A = 0.025C + 0.002$	0.9999
Cu	$A = 0.156C + 0.005$	0.9994
Cd	$A = 0.203C + 0.005$	0.9997
Ni	$A = 0.051C + 0.006$	0.9978

[a] All the statistical calculations are based on the average of five readings for each standard solution in the given range.
[b] A is the peak height absorbance and C is the concentration in μg/mL.

Table 5
Determination of Pb(II), Cu(II), Cd(II) and Ni(II) in a certified sample

Analyte	Found by present method (μg/g)	Certified value (μg/g)	Relative error (%)
Pb(II)	72 ± 5	79 ± 6	8.9
Cu(II)	47.5 ± 5.0	53 ± 3	10.4
Cd(II)	2.16 ± 0.31	2.45 ± 0.15	11.8
Ni(II)	29.5 ± 3	32[a]	7.8

[a] Reference value.

3.12. Analysis of artificial and natural water samples

At the optimum conditions, water samples (2000 mL) were passed through the column for preconcentration and determination of the target heavy metal ions directly. The data listed in Table 6 shows that the recovery of Pb(II), Cu(II), Cd(II)

Table 6
Determination of Pb(II), Cu(II), Cd(II) and Ni(II) in water samples ($n = 5$)

Samples	Method	Metal ions (μg/L)							
		Pb	R.S.D. (%)	Cu	R.S.D. (%)	Cd	R.S.D. (%)	Ni	R.S.D. (%)
Artificial water	Spiked	10	–	10	–	10	–	10	–
	Direct[a]	9.68 ± 0.36	3.0	9.75 ± 0.30	2.5	9.54 ± 0.38	3.2	9.60 ± 0.26	2.2
River water	APDC/MIBK	8.87 ± 0.26	2.4	5.23 ± 0.21	3.2	ND[b]	–	4.36 ± 0.11	2.1
	Direct	8.56 ± 0.56	5.3	5.10 ± 0.24	3.8	ND	–	4.20 ± 0.24	4.6

[a] Recommended procedure applied directly.
[b] ND: not detected.

Table 7
Comparison of sorption capacities

Matrix	Sorption capacities (mg/g)				Refs.
	Pb	Cu	Cd	Ni	
Gallic acid modified silica gel	12.63	15.38	6.09	4.62	
Support: silica gel					
Resacetophenone	13.80	11.81	6.50	14.89	[37]
o-Dihydroxybenzene	16.99	22.11	3.60	10.45	[38]
Salicyldoxime	–	3.18	6.74	2.35	[6]
1,8-Dihydroxyanthraquinone	15.83	14.40	7.89	6.4	[39,40]
Support: Amberlite XAD-2					
Tiron	12.49	13.98	9.50	12.56	[41]
o-Aminophenol	3.32	3.37	3.42	3.24	[42]
Chromotopic acid	–	8.52	9.37	6.04	[43]
Quinalizarin	5.28	3.15	1.70	–	[44]
Pyrogallol	6.71	4.53	5.22	4.09	[45]
Support: Amberlite XAD-4					
Ammonium pyrrolidine dithiocarbamate	10.25	11.08	9.47	7.21	[46]
Piperidine dithiocarbamate	9.86	10.76	9.18	7.46	[46]
Support: Amberlite XAD-7					
Xylenol orange	–	1.6	2.0	2.6	[47]
Support: cellulous					
Pyrocatechol	21.55	11.83	13.00	8.20	[48]
Pyrogallol	19.14	12.85	11.14	8.70	[49]
Support: polyacrylonitrile					
Aminophosphonic and dithiocarbamate	5.72	2.03	10.45	–	[50]

and Ni(II) from the artificial water and river water samples are satisfactory. In comparison with the method of solvent extraction with APDC/MIBK (ammonium pyrrolidine dithiocarbamate/methyl isobutyl ketone) [33], the sorption of the target heavy metal ions from river water samples are also satisfactory, and the method developed for determination of trace amount of Pb(II), Cu(II), Cd(II) and Ni(II) in water samples has been proved to be reliable.

3.13. Comparison of other solid phase extractant

Based on the results shown in Table 7, the sorption capacity of GASG was better than some known solid phase extractants, such as salicyldoxime [6] modified silica gel and tiron [41], *o*-aminophenol [42], chromotopic acid [43], quinalizarin [44], pyrogallol [45] modified Amberlite XAD-2, etc. The preconcentration factors for those heavy metal ions are also comparable with the values reported for several other chelating resins [6,37–52]. The adsorbed heavy metal ions can readily be desorbed by low concentration acid. The relative short adsorption time ($t_{1/2}$) of GASG for Pb(II), Cu(II), Cd(II) and Ni(II) makes the analytical procedure reasonably fast. As indicated by the results of natural water and river sediment analysis, the matrix effect with the GASG is low. The feasibility of the repeated use of GASG is an additional advantage.

Acknowledgements

This project was financially supported by National Natural Science Foundation (20575012), the National High-Tech R&D Program (the 863 program) (2006AA09z161), the National Key Technologies R&D Program (2006BAK02A21) of China.

References

[1] M. Yang, J.X. Li, J.H. Wang, Talanta 72 (2007) 1710.
[2] Y.L. Yu, Z. Du, J.H. Wang, J. Anal. Atom. Spectrom. 22 (2007) 650.
[3] G. Venkatesh, A.K. Singh, Talanta 71 (2007) 282.
[4] C.F. Poole, Solid-Phase Extraction, Encyclopedia of Separation Science, vol. 3, Academic Press, 2000, p. 1405.
[5] V. Camel, Spectrochim. Acta B 58 (2003) 1177.
[6] A.R. Sarkar, P.K. Datta, M. Sarkar, Talanta 43 (1996) 1857.
[7] U. Pyell, G. Stork, Fresenius J. Anal. Chem. 342 (1992) 281.
[8] O.A. Zaporozhets, O.Y. Nadzhafova, A.I. Zubenko, V.V. Sukhan, Talanta 41 (1994) 2067.
[9] O. Zaporozhets, N. Petruniock, V. Sukhan, Talanta 50 (1999) 865.
[10] R. Kocjan, Mikrochim. Acta 131 (1999) 153.
[11] A.K.L. Magda Ali Abd-ElAziz, I.M. Kenawy, R.R. Lasheen, Anal. Sci. 21 (2005) 923.
[12] M.R. Jamali, Y. Assadi, F. Shemirani, M. Salavati-Niasari, Talanta 71 (2007) 1524.
[13] W. Ngeontae, W. Aeungmaitrepirom, T. Tuntulani, Talanta 71 (2007) 1075.
[14] M.E. Mahmoud, E.M. Soliman, Talanta 44 (1997) 15.
[15] P. Liu, Q. Pu, Z. Su, Analyst 125 (2000) 147.
[16] W.X. Ma, F. Liu, K.A. Li, W. Chen, S.Y. Tong, Anal. Chim. Acta 416 (2000) 191.
[17] M.E. Mahmoud, Anal. Chim. Acta 398 (1999) 297.
[18] L.T. Kubota, J.C. Moreira, Y. Gushikem, Analyst 114 (1989) 1385.
[19] B.S. Garg, R.K. Sharma, J.S. Bist, N. Bhojak, S. Mittal, Talanta 48 (1999) 49.
[20] J.S. Kim, J. Yi, Sep. Sci. Technol. 34 (1999) 2957.
[21] A. Safavi, N. Iranpoor, N. Saghir, S. Momeni, Anal. Chim. Acta 569 (2006) 139.
[22] E.M. Soliman, M.B. Saleh, S.A. Ahmed, Anal. Chim. Acta 523 (2004) 133.

[23] A. Khan, F. Mahmood, M.Y. Khokhar, S. Ahmed, React. Funct. Polym. 66 (2006) 1014.
[24] F. Sánchez Rojas, C. Bosch Ojeda, J.M. Cano Pavón, Talanta 70 (2006) 979.
[25] T. Madrakian, A. Afkhami, M.A. Zolfigol, M. Solgi, J. Hazard. Mater. 128 (2006) 67.
[26] S.V.M. de Moraes, J.L. Brasil, C.D. Milcharek, L.C. Martins, M.T. Laranjo, M.R. Gallas, E.V. Benvenutti, E.C. Lima, Spectrochim. Acta A 62 (2005) 398.
[27] E. Luiz da Silva, MartinsF A.O., A. Valentini, V.T. de Fávere, E. Carasek, Talanta 64 (2004) 181.
[28] Z.H. Xie, F.Z. Xie, L.Q. Guo, X.C. Lin, G.N. Chen, J. Sep. Sci. 28 (5) (2005) 462.
[29] M. Zougagh, A. García de Torres, E. Vereda Alonso, J.M. Cano Pavón, Talanta 62 (2004) 503.
[30] M.N. Peyrat-Maillard, S. Bonnely, C. Berset, Talanta 51 (2000) 709.
[31] S. Shahrzad, I. Bitsch, J. Chromatogr. A 741 (1996) 223.
[32] S. Shahrzad, I. Bitsch, J. Chromatogr. B 705 (1998) 87.
[33] D.L. Xi, Y.S. Sun, X.Y. Liu, Environmental Monitor, High Education Press, Beijing, China, 1994.
[34] Y.K. Ke, H.R. Dong, Handbook of Analytical Chemisty, 2nd ed., Chemical Industry Press, Beijing, China, 2000.
[35] Daniel MacDougall, B. Warren, Crummett, et al., Anal. Chem. 52 (1980) 2242.
[36] G.L. Long, J.D. Winefordner, Anal. Chem. 55 (1983) 712A.
[37] A. Goswami, A.K. Singh, Anal. Chim. Acta 454 (2002) 229.
[38] G. Venkatesh, A.K. Singh, B. Venkataramani, Mikrochim. Acta 144 (2004) 233.
[39] A. Goswami, A.K. Singh, Talanta 58 (2002) 669.
[40] A. Goswami, A.K. Singh, Anal. Bioanal. Chem. 374 (2002) 554.
[41] M. Kumar, D.P.S. Rathore, A.K. Singh, Analyst 125 (2000) 1221.
[42] M. Kumar, D.P.S. Rathore, A.K. Singh, Talanta 51 (2000) 1187.
[43] P.K. Tewari, A.K. Singh, Analyst 124 (1999) 1847.
[44] M. Kumar, D.P.S. Rathore, A.K. Singh, Fresenius J. Anal. Chem. 370 (2001) 377.
[45] M. Kumar, D.P.S. Rathore, A.K. Singh, Mikrochim. Acta 137 (2001) 127.
[46] A. Ramesh, K.R. Mohan, K. Seshaiah, Talanta 57 (2002) 243.
[47] P.K. Tewari, A.K. Singh, Fresenius J. Anal. Chem. 367 (2000) 562.
[48] V. Gurnani, A.K. Singh, B. Venkataramani, Talanta 61 (2003) 889.
[49] V. Gurnani, A.K. Singh, Ind. Eng. Chem. Res. 43 (2004) 2302.
[50] B. Wen, X.Q. Shan, R.X. Liu, H.X. Tang, Fresenius J. Anal. Chem. 363 (1999) 251.
[51] V. Gurnani, A.K. Singh, B. Venkataramani, Anal. Chim. Acta 485 (2003) 221.
[52] V. Gurnani, A.K. Singh, B. Venkataramani, Anal. Bioanal. Chem. 377 (2003) 1079.

Available online at www.sciencedirect.com
ScienceDirect
Talanta 74 (2008) 831–835
Talanta
www.elsevier.com/locate/talanta

In situ chemical reductive growth of platinum nanoparticles on glass slide for the mass fabrication of biosensors

Ming-Hui Yang, Feng-Li Qu, Ya-Shuang Lu, Guo-Li Shen *, Ru-Qin Yu *

Chemistry and Chemical Engineering College, State Key Laboratory of Chemo/Biosensing and Chemometrics, Hunan University, Hunan, Changsha 410082, PR China

Received 6 April 2007; received in revised form 14 July 2007; accepted 17 July 2007
Available online 24 July 2007

Abstract

Platinum nanoparticles (PtNPs) attached to glass slide surface was successfully prepared by using a simple in situ chemical reduction method. In this method, a ~10 nm gold layer was first sputtered uniformly onto the glass slide surface, PtNPs could be grown directly on the gold layer by immersing the glass slide into the grown solution containing H_2PtCl_4 and ascorbic acid. The gold layer sputtered uniformly serves as "seed" for the following growth of PtNPs and high dense of PtNP modified film can be prepared. Control experiment without the gold layer found no obvious formation of PtNPs indicating the importance of the "seed". The electrocatalytic effect of the PtNP film was investigated with the detection of hydrogen peroxide and for the fabrication of biosensors. Glucose oxidase was selected and directly electrodeposited onto the PtNPs modified surface. The resulting biosensor has a fast response time (<10 s) with wide linear range (5×10^{-6} to 2×10^{-2}). The fabrication method is simple, convenient and can be used for the mass fabrication of biosensors. The present preparation method of PtNPs modified film could be used for the preparation of other metal nanoparticle and find electrochemical applications as well as for optical uses.
© 2007 Elsevier B.V. All rights reserved.

Keywords: Biosensor; Enzyme; In situ; Mass fabrication; Platinum nanoparticles

1. Introduction

The interesting optical, electronic, magnetic, and catalytic properties of metal nanoparticles have gained growing interest in recent years and metal nanoparticle modified surfaces are known to be effective for applications in catalysis, electrochemistry, and metal-enhanced spectroscopies [1–7]. Various methods have been explored to attach metal nanoparticles onto different surfaces, including physical, and chemical methods, such as electrochemical process, metal evaporation, and layer-by-layer self-assembly [8–10]. Compared with these strategies, wet chemical approach provides an easier control over nanoparticle size, and density by altering the conditions for chemical preparation [11]. For example, Chang et al. systematically investigated attachment of different metal nanoparticles on indium–tin oxide surface using seed-mediated wet chemical reductive method [12–14].

Although many papers have been devoted to the modification of metal nanoparticles on conductive surfaces such as gold, platinum, and indium–tin oxide, reports of the attachment of nanoparticles on non-conductive surfaces like glass slide, and glass coverslip are rather scarce. If we could attach metal nanoparticles on glass slide or glass coverslip in a simple way, in particular with keeping a moderate dispersion in a monolayer, then it would greatly facilitate the application of metal nanoparticle modified surfaces, for example for electrochemistry, metal-enhanced spectroscopy, and single molecular spectroscopy study.

Metal platinum is one of the mostly researched noble metals as it has been widely used for the fabrication of biosensors, and in fuel cell technology as effective catalyst [15–18]. The PtNPs modified substrates are used increasingly in many electrochemical applications owing to their extraordinary catalytic properties over bulk metal and also found effective for surface-enhanced Raman and IR spectroscopy [19–22]. Gomez et al. deposited platinum nanoparticle ensembles on electrodes and investigated in situ surface-enhanced Raman spectroscopy [21].

In this paper, we reported a simple method to attach platinum nanoparticles onto glass slide surface. First, a ~10 nm gold layer was sputtered uniformly onto the glass slide surface, PtNPs could be grown directly on the gold layer by immersing

* Corresponding authors. Tel.: +86 731 8821355; fax: +86 731 8821355.
E-mail addresses: glshen@hnu.cn (G.-L. Shen), rqyu@hnu.cn (R.-Q. Yu).

0039-9140/$ – see front matter © 2007 Elsevier B.V. All rights reserved.
doi:10.1016/j.talanta.2007.07.013

the glass slide into the grown solution containing H_2PtCl_4 and ascorbic acid. The attachment and structure growth of PtNPs were characterized in detail with scanning electron microscopy (SEM). The ~10 nm gold layer was found indispensable for the growth of nanoparticles as control experiment of bare glass slide without gold layer found very few nanoparticles. The electrocatalytic property of the PtNPs modified surface was investigated with the detection of hydrogen peroxide and for the fabrication of biosensor. For the fabrication of biosensors, glucose oxidase was selected and directly electrodeposited onto the PtNPs attached surface [23,24]. The resulting biosensor displays high sensitivity and wide linear range. The biosensor preparation method can be used for the mass fabrication of biosensors and the method for the attachment of PtNPs may be applicable to other metal nanoparticles and may find wide applications.

2. Experimental

2.1. Apparatus and reagents

Glucose oxidase (GOx, from *Aspergillus niger*; EC 1.1.3.4, type VIII-S; 196,000 unit g^{-1}) was purchased from Sigma. A 1/15 M phosphate buffer (PB, pH 6.98) solution was prepared using Na_2HPO_4 and KH_2PO_4. All other reagents were of analytical grade, and double distilled water was used throughout.

Cyclic voltammetric and amperometric measurements were carried out on CHI 760B electrochemical workstation (Shanghai, China). Scanning electron microscopy (SEM) analysis was performed using a JSM-5600LV microscope (JEOL Ltd., Japan). A three-electrode cell (10 mL) with the modified glass slide as the working electrode, a saturated calomel electrode (SCE) as reference electrode and a platinum foil electrode as counter electrode was used. All potentials were measured and reported versus the SCE and all experiments were carried out at room temperature.

2.2. Attachment of PtNPs on glass slide surface

Typical procedures to attach PtNPs on glass slide are as follows: a piece of glass slide (1 cm^2) was used after washing in acetone, ethanol, and pure water with sonication, and drying with nitrogen gas. First, a ~10 nm gold layer was sputtered onto the slide surface, then, the slide was immersed into solution containing 0.05 mM H_2PtCl_4 and 5 mM ascorbic acid for a constant time at room temperature. After a given time, the slide was removed from the solution, and rinsed with pure water several times, then dried with nitrogen gas.

2.3. Fabrication of biosensors

For the preparation of electrode, an insulated copper wire was connected to the corner of the slide by applying a drop of conductive silver epoxy followed by insulating epoxy. For the fabrication of biosensor, GOx was immobilized onto the PtNPs modified glass slide surface by an electrodeposition method. Electrodeposition was performed using chronoamperometry in PB containing 20 mg/mL GOx and 0.8 mM Triton 100 at a potential of 1.3 V for 30 min.

3. Results and discussion

3.1. Morphological characterization of the PtNP attached surface

The central theme of the present study is to modify the glass slide surface with PtNPs using a simple and reproducible method. A ~10 nm gold layer was uniformly sputtered onto the slide surface and serves as "seed" for the following growth of nanoparticles. Former literature reported using small nanoparticles (size less than 5 nm) as seed and adsorbing the seed onto substrate followed by chemical reduction [12–14]. We assume the sputtered gold layer would be more uniform and stable, and the method would be quite simple. First, the function of the gold layer was investigated. As a control experiment, a bare glass slide was immersed into the growth solution containing H_2PtCl_4 and ascorbic acid. During the chemical reductive process, the colour of the glass slide changed from transparent to darkish brown. It turned out that the PtNPs were just simply falls onto the surface, not grown on the glass slide, as after 12 h of reaction, taking out the slide and rinsing with water for several times, the PtNPs were easily rinsed away. After rinsing, the slide was characterized with SEM as shown in Fig. 1A. It can be seen that very little PtNPs with small size, which were recognized as bright dots, were left on the slide, indicating that without the gold layer, the interaction between glass slide and PtNPs is very weak, because there is no nucleation sites for the growth of nanoparticles. On the contrary, when the slide was sputtered with gold before immersion into the growth solution, the PtNPs are strongly attached onto the slide surface. After washing with water and even sonication, no distinct removal of PtNPs was observed. We expect that this firm binding comes from the initial stable gold layer, and the following PtNPs were grown on this layer.

Fig. 1B shows SEM images recorded after treatment in the growth solution for 2 h. It can be seen PtNPs grew on the glass slide surface with a moderate dispersion. The shape of PtNPs was almost spherical, and the size dispersion was relatively regular, with the diameters of the PtNPs around 50 nm. But there are also small nanoparticles around 10 nm, indicating the particles were grown through a progressive nucleation process, that is, the big nanoparticles were grown from the smaller ones.

The effect of reduction time on the morphology of the nanoparticle film was investigated in detail. Fig. 2 shows SEM images of the glass sample with reduction time of 4 h. It can be seen, increasing the reduction time, the size of the nanoparticles increased, reaching around 80 nm. However, small nanoparticles could be still observed, which shows that during the reduction process, smaller nanoparticles grown into larger ones and at the same time, small nanoparticles are continuously formed. From the lower magnification image (Fig. 2B), one can see that although there are some voids exist, the entire film is relatively intact, dense and has an ordered structure, suitable for further applications. The morphology of the film was further changed

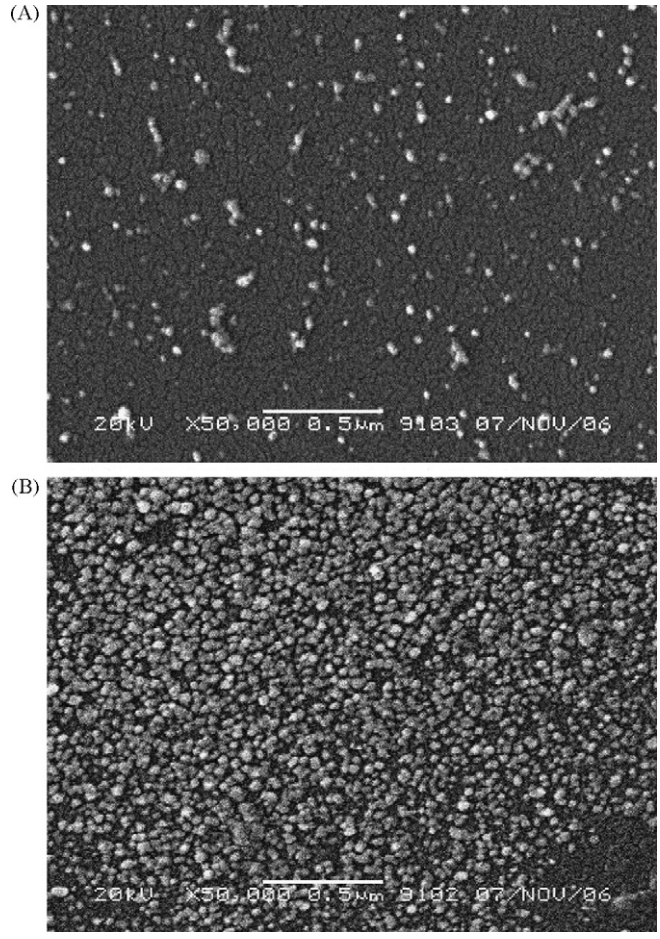


Fig. 1. (A) SEM image of the bare glass slide after immersion into growth solution for 12 h. (B) SEM image of the glass slide sputtered with 10 nm gold and immersion into growth solution for 2 h.

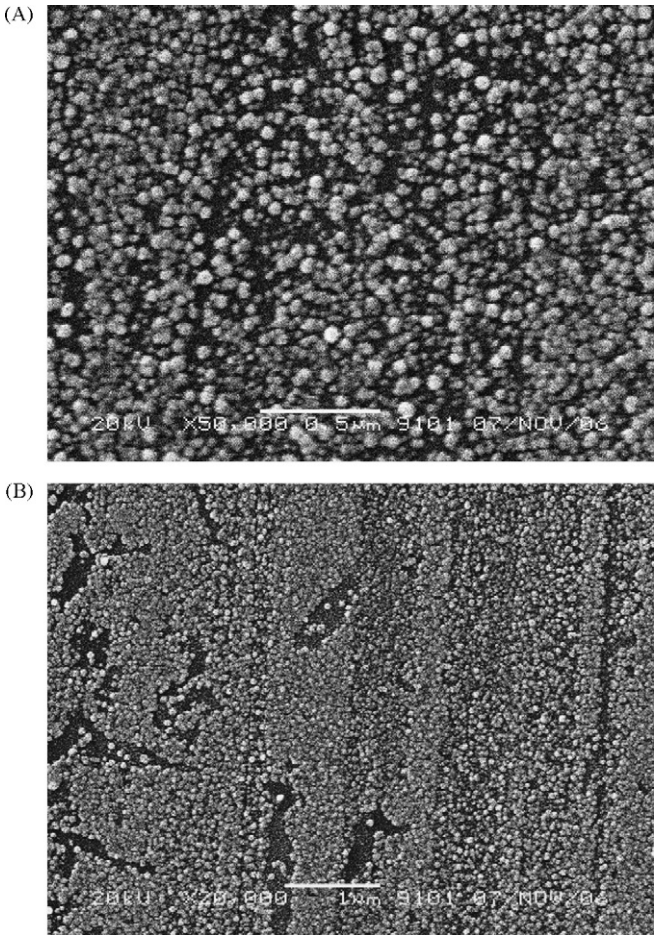


Fig. 2. SEM images of the glass slide sputtered with 10 nm gold and immersed into growth solution for 4 h.

after 12 h of reduction as shown in Fig. 3. At this time, the diameter of the nanoparticles increased to 300 nm, and particles contacted to each other, forming a layered film.

3.2. Electrochemical characterization of the PtNP attached glass slide

From the above SEM characterization, it can be seen that the present method could be used to form PtNP film with different structures, from monolayer to multilayer, and the size of the PtNP can also be altered. At the reduction time of 4 h, the glass slide surface was almost covered with nanoparticles, so this slide could be used as electrode and it would be interesting to investigate the electrochemical performance of the modified glass slide. The glass slide after growth of 4 h was chosen and the following experiments were done using this slide as electrode. First, the conductivity of the electrode was determined and Fig. 4 shows the cyclic voltammograms (CVs) of the glass slide in 20 mM $K_3Fe(CN)_6$ and 0.2 M KCl with different scan rates. The well-defined anodic and cathodic peaks due to the Fe^{3+}/Fe^{2+} redox couple were observed and at 50 mV s^{-1} the peak potentials were 330 and 164 mV with peak separation of 166 mV, which were similar to those observed with the bulk electrode [25,26]. In addition, both of the peak current clearly increase with increasing potential scan rate and are linearly related with the square root of the scan rate in a range from 10 to 200 mV s^{-1}, suggesting a diffusion controlled process. Thus, the conductivity of the electrode is good, indicating the PtNP film is efficient in transferring

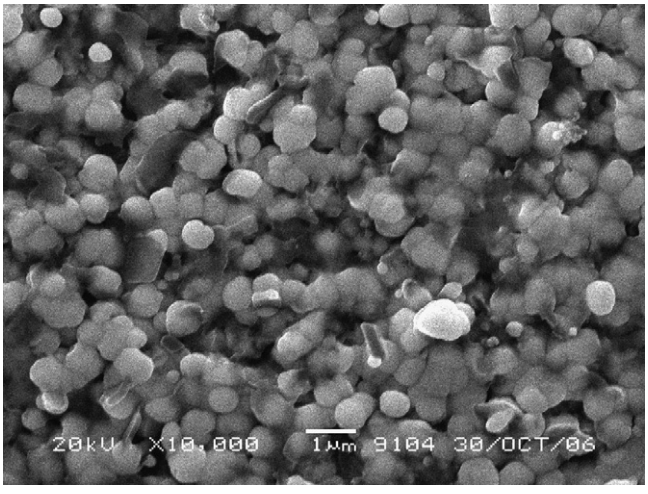


Fig. 3. SEM image of the glass slide sputtered with 10 nm gold and immersed into growth solution for 12 h.

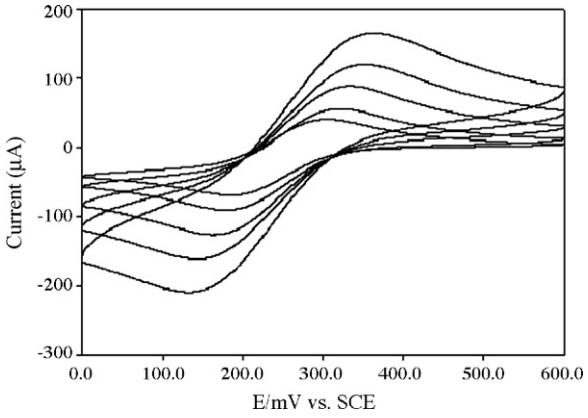


Fig. 4. Cyclic voltammograms (CVs) of the PtNP-modified glass slide in 20 mM $K_3Fe(CN)_6$ containing 0.2 M KCl with different scan rates. From inner to outside: 10, 20,50, 100, and 200 mV s^{-1}.

electrons and forming a diffusion layer. This good conductivity made it possible for further application.

The electrochemical response of the PtNP film toward H_2O_2 was also investigated with potential design of a biosensor. Fig. 5A shows cyclic voltammograms of the film in phosphate buffer in the absence (a) and in presence of 5 mM H_2O_2 (b) between −0.6 and 0.6 V at the scan rate of 100 mV s^{-1}. When H_2O_2 was added to the buffer, an obvious increase of the cathodic and anodic current was observed, indicating the film exhibited excellent electrocatalytic activity toward H_2O_2. Fig. 5B depicts the typical current–time curve at the film modified slide for successive addition of 10 μM H_2O_2 at 0 V. Fast and sensitive response can be observed at the electrode with steady-state current reached within 5 s, showing the reduction of H_2O_2 at the PtNP film is facilely easy.

The stability of the PtNP film in detection of H_2O_2 was investigated. For example, 1 mM H_2O_2 was measured continuously for 10 times, and a relative standard deviation (R.S.D.) of 4.9% was obtained. The satisfactory repeatability indicates the reliability of the film for the determination of H_2O_2 and made it feasible for the further biosensing application.

3.3. Performance of the glucose biosensor

The good performance of the PtNP film toward H_2O_2 and the simple, convenient method for the preparation of the PtNP film made it an ideal biosensing platform for the fabrication of oxidase-based biosensors. In this study, glucose oxidase was selected and directly electrodeposited onto the PtNP film surface. A uniform and biologically active enzyme film could be formed with electrochemically mediated deposition of enzyme on an electrode in the presence of nonionic detergent [23]. The electrodeposition method could produce a much more extensive and compact enzyme film than enzyme film through physical adsorption. After electrodeposition, the biosensor can be used for the detection of glucose. At 0 V, in phosphate buffer with careful magnetic stirring, adding standard glucose solution resulted in an instantaneous current response. Fig. 6 is the calibration curve of the biosensor toward glucose and the insert shows the current plotted versus time for successive addition of

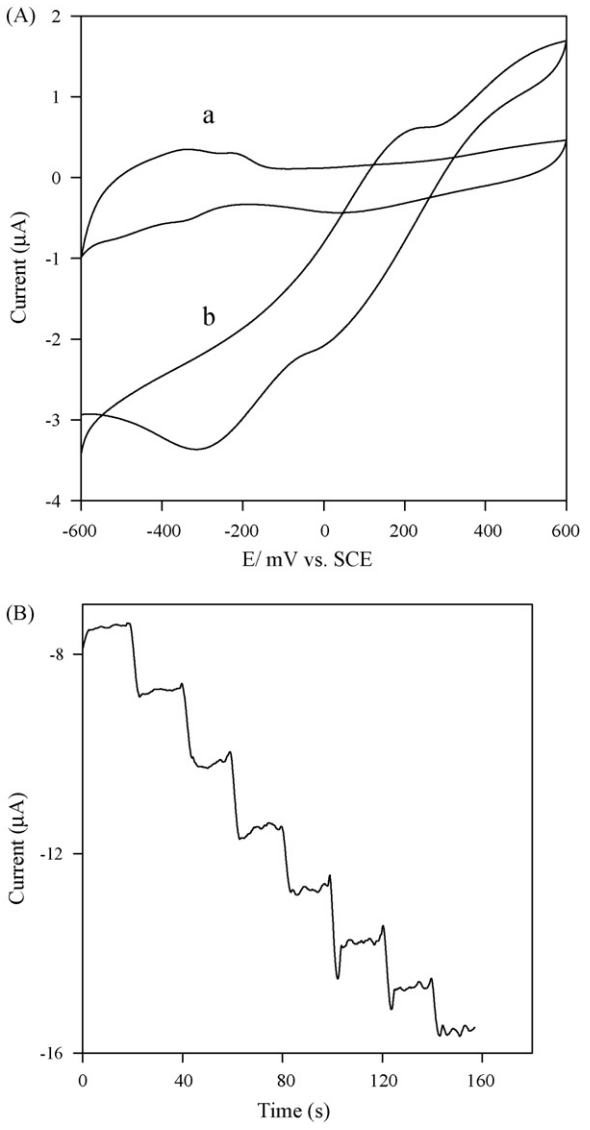


Fig. 5. (A) CVs of the PtNP film in the absence (a) and presence (b) of 5 mM H_2O_2. Scan rate: 100 mV s^{-1}. (B) Current–time curve of the PtNP film to the successive addition of 10 μM H_2O_2 at 0 V.

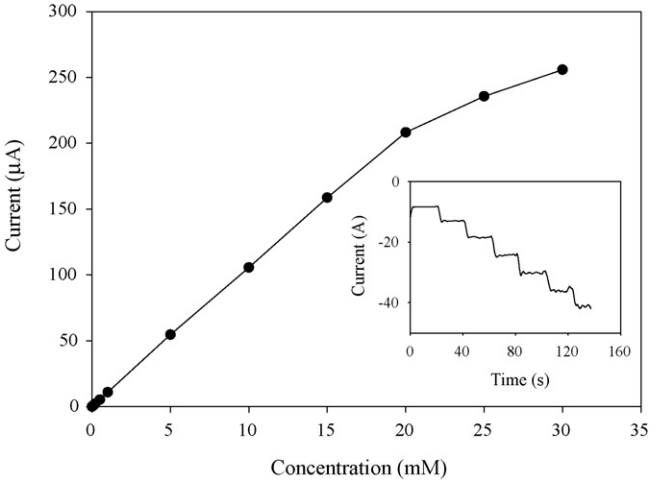


Fig. 6. Calibration curve of the glucose biosensor. Insert: current–time curve of the biosensor to the successive addition of 0.5 mM glucose at 0 V.

Table 1
Comparison of glucose concentration in serum samples determined with the biosensor and the hospital method (values were mean value of three determinations)

Sample	Concentration determined by the biosensor (mM)	Concentration determined by hospital method (mM)
1	7.89	8.01
2	8.65	8.94
3	10.32	10.88
4	11.23	11.78
5	12.67	13.13

0.5 mM glucose. The resulting biosensor has a fast response time (<10 s). The linear calibration range is extended from 5×10^{-6} to 2×10^{-2} M, and the detection limit of 1×10^{-6} M was obtained based on S/N = 3. The wide linear range indicates large amount of enzymes was immobilized onto the electrode surface through electrodeposition. The repeatability of the biosensor was also tested and found satisfactory. The glucose concentration of 0.5 mM was measured continuously for six times, and a R.S.D. of 5.1% was obtained. The low R.S.D. means that both of the enzyme and PtNP film are relatively stable.

For the mass fabrication of biosensors, the reproducibility of the biosensor is very important. To investigate the reproducibility, six different biosensors were prepared carefully, and the current response of the biosensors toward 0.5 mM glucose was detected with R.S.D. of 6.5%. The satisfactory repeatability and reproducibility means the biosensors can be used for practical application.

The selectivity of the biosensor was determined. In this study, the determination of glucose is practically free of interferences. At the low detection potential of 0 V, 0.1 mM ascorbic acid, 0.1 mM uric acid, and 0.1 mM acetaminophen gave slight response current, but compared to the response of 1 mM glucose, the current response are negligible, indicating high selectivity of the biosensor.

The long-term stability of the biosensor was determined. When not in use, the biosensor was stored at 4 °C. The response of the biosensor to 0.5 mM glucose was tested intermittently (every 3 days), and 1 month later, the biosensor still obtained 80% of the initial value, indicating good stability of the sensor.

3.4. Real sample analysis

The applicability of the biosensor was tested by the determination of serum sample glucose concentration. Results were compared with hospital method with glucose kit (Shanghai Kehua-Dongling Diagnostic Products Co. Ltd.). Five samples were analyzed with the results shown in Table 1. Glucose concentrations determined by the two methods agreed rather well, indicating the reliability of the biosensor.

4. Conclusions

In the present work, PtNP film can be grown on glass slide surface by the in situ chemical reduction method. The 10 nm gold layer uniformly sputtered on glass slide surface served as "seed" for the following growth of nanoparticles. The morphology of the PtNP film can be altered by altering the reduction time, that is with increasing reduction time, the size of the nanoparticle increased and the density of the PtNP changed from a monolayer to a multilayer film. The electrochemical application of the PtNP film modified glass slide as working electrode was investigated in detail. In $K_3Fe(CN)_6$ solution, well-defined anodic and cathodic peaks and diffusion controlled process were observed, indicating good conductivity of the film. The electrocatalytic activity of the PtNP film was discussed with hydrogen peroxide detection. Glucose oxidase was selected and directly electrodeposited on the PtNP film. The resulting biosensor has good performance toward glucose. The method for the attachment of PtNPs may be applicable to other metal nanoparticles and may find wide applications.

Acknowledgements

This work was supported by the NNSF of China (Nos. 20675028, 20435010, 20375012, and 20205005).

References

[1] K. Aslan, S.N. Malyn, C.D. Geddes, J. Am. Chem. Soc. 128 (2006) 13372.
[2] D.M. Dotzauer, J.H. Dai, L. Sun, M.L. Bruening, Nano Lett. 6 (2006) 2268.
[3] F.J. Ibanez, F.P. Zamborini, Langmuir 22 (2006) 9789.
[4] S. Shanmukh, L. Jones, J. Driskell, Y.P. Zhao, R. Dluhy, R.A. Tripp, Nano Lett. 6 (2006) 2630.
[5] L. Sun, L.Q. Mao, Talanta 70 (2006) 68.
[6] J. Zhang, J.R. Lakowicz, J. Phys. Chem. B 110 (2006) 2387.
[7] N.F. Zheng, G.D. Stucky, J. Am. Chem. Soc. 128 (2006) 14278.
[8] M.H. Huang, Y. Shao, X.P. Sun, H.J. Chen, B.F. Liu, S.J. Dong, Langmuir 21 (2005) 323.
[9] J.V. Zoval, J. Lee, S. Gorer, R.M. Penner, J. Phys. Chem. B 102 (1998) 1166.
[10] K.J. Klabunde, Y.X. Li, B.J. Tan, Chem. Mater. 3 (1991) 30.
[11] K.C. Grabar, R.G. Freeman, M.B. Hommer, M.J. Natan, Anal. Chem. 67 (1995) 735.
[12] G. Chang, M. Oyama, K. Hirao, J. Phys. Chem. B 110 (2006) 20362.
[13] G. Chang, M. Oyama, K. Hirao, J. Phys. Chem. B 110 (2006) 1860.
[14] G. Chang, J.D. Zhang, M. Oyama, K. Hirao, J. Phys. Chem. B 109 (2005) 1204.
[15] M. Hou, S.J. Sun, Z.L. Jiang, Talanta 72 (2007) 463.
[16] S.B. Zhang, Z.S. Wu, M.M. Guo, G.L. Sheng, R.Q. Yu, Talanta 71 (2007) 1530.
[17] M.A.A. Lomillo, J.G. Ruiz, F.J.M. Pascual, Anal. Chim. Acta 547 (2005) 209.
[18] H.H. Zhou, H. Chen, S.L. Luo, J.H. Chen, W.Z. Wei, Y.F. Kuang, Biosens. Bioelectron. 20 (2005) 1305.
[19] J. Zhang, F.H.B. Lima, M.H. Shao, K. Sasaki, J.X. Wang, J. Hanson, R.R. Adzic, J. Phys. Chem. B 109 (2005) 22701–22704.
[20] V. Komanicky, A. Menzel, K.C. Chang, H. You, J. Phys. Chem. B 109 (2005) 23543.
[21] R. Gomez, J.M. Perez, J. Solla-Gullon, V. Montiel, A. Aldaz, J. Phys. Chem. B 108 (2004) 9943.
[22] A. Miki, S. Ye, M. Osawa, Chem. Commun. 14 (2002) 1500.
[23] N. Matsumoto, X.H. Chen, G.S. Wilson, Anal. Chem. 74 (2002) 362.
[24] S.H. Lim, J. Wei, J.Y. Lin, Q.T. Li, J.K. You, Biosens. Bioelectron. 20 (2005) 2341.
[25] M.H. Yang, F.L. Qu, Y.S. Lu, Y. He, G.L. Shen, R.Q. Yu, Biomaterials 27 (2006) 5944.
[26] M.H. Yang, Y. Yang, H.F. Yang, G.L. Shen, R.Q. Yu, Biomaterials 27 (2006) 246.

Available online at www.sciencedirect.com
ScienceDirect
Talanta 74 (2008) 951–957
Talanta
www.elsevier.com/locate/talanta

A novel sequential injection—Cold vapour atomic absorption spectrometric system for rapid and reliable determination of mercury

Yanlin Zhang, Samuel B. Adeloju *

Sensor and Environmental Technology Research Group, School of Applied Sciences and Engineering, Monash University Gippsland Campus, Churchill, Victoria 3842, Australia

Received 20 April 2007; received in revised form 30 July 2007; accepted 30 July 2007
Available online 19 August 2007

Abstract

A simple and rapid method is described for reliable determination of ultra-trace concentrations of mercury based on a novel combination of a sequential injection (SI) system with cold vapour atomic absorption spectrometry (CVAAS). The SI–CVAAS method achieved a very high sampling frequency of 180 h^{-1}, a detection limit of 0.2–0.3 ng mL^{-1}, a dynamic range of 0–60 ng mL^{-1} and requires only 0.2–0.6 mL of sample. The presence of common metal ions, such as Cu^{2+}, Pb^{2+}, Cd^{2+}, Zn^{2+}, Fe^{3+}, Co^{2+}, Ni^{2+} and Mn^{2+}, did not interfere with the measurement of mercury by this method. Also the interference from organic matter, such as humic substances, was easily reduced or eliminated by appropriate sample dilution. The method was successfully applied to the determination of mercury in lake sediment samples and a river sediment reference material. An average percentage recovery of 101.2% was achieved by the SI–CVAAS method for mercury in the reference material with a R.S.D. of 1.8%.
© 2007 Elsevier B.V. All rights reserved.

Keywords: Sequential injection; Mercury; Cold vapour generation; Atomic absorption spectrometry; Sediment

1. Introduction

Cold vapour atomic absorption spectrometry (CVAAS) is the most widely used technique for the analysis of mercury because of its high sensitivity, resistance to interferences and operational simplicity [1–4]. When used in conjunction with a flow injection analysis (FIA) system, the vapour generation process is improved considerably, particularly in relation to sample and reagent consumption, sample throughput and elimination/minimization of interference [5–8].

An alternate approach to FIA for achieving high sample throughput is sequential injection analysis (SIA) that has gained considerable interest in recent years and has some demonstrated advantages over FIA, such as lower sample/reagent consumption and more compact instrumentation [9–11]. However, SIA also has some limitations, which includes the need to use more than one syringe/peristaltic pumps and a PC controlled multi-port valve for selective and sequential injection of sample solution and reagents into the reaction system. Also, auxiliary valves are often used in such systems and the control of the whole system is also complex because of the need for programming and the involvement of several steps for a single determination. Furthermore, because the sampling rates achieved by SIA are often lower than those of FIA [9–12], it has not attracted as much interest. However, there are inherent limitations with most FIA systems that limit their ability to achieve optimum sensitivity for mercury determination by CVAAS. For this reason, most of the available FI–CVAAS methods do not have adequate sensitivity for the reliable determination of mercury in some environmental samples.

In an attempt to address some of the identified limitations, Doering et al. [8] developed a SI–CVAAS system for mercury determination by using only one pump and one valve, but also required a special control component. However, even with this improvement the system only achieved relatively low sample throughput of 45 h^{-1} compared to up to 90 h^{-1} reported for FIA systems. Evidently, there is still a need for further investigation to improve the design of SI systems used for CVAAS measurement

* Corresponding author. Tel.: +61 3 9902 6450; fax: +61 3 9902 6738.
E-mail address: Sam.Adeloju@sci.monash.edu.au (S.B. Adeloju).

0039-9140/$ – see front matter © 2007 Elsevier B.V. All rights reserved.
doi:10.1016/j.talanta.2007.07.043

to enable similar or better sample throughputs as for FIA systems and, if possible, to achieve better analytical performance.

In the present study, we propose a new design of a SI–CVAAS system for a more rapid and reliable measurement of mercury based on the use of a single channel peristaltic pump together with two 3-way 2-position solenoid valves, controlled by two digital timers with a U-tube as the gas liquid separator (GLS). The optimization of the control system, operation, and performance of the SI/CV–AAS system were investigated, with a particular focus on improvement of sample throughput, accuracy, precision, and reagent consumption. Also the adequacy of the system for quantification of mercury in lake and river sediments was carefully investigated, particularly with respect to the possible interference from other metal ions and organic matter.

2. Experimental

2.1. Reagents and sediment samples

Standard solutions of mercury and other metals were purchased from BDH Chemicals Pty Ltd. (Kilsyth, Victoria, Australia). These solutions were diluted as required for the CVAAS measurements. Analytical reagent grade of potassium dichromate (Sigma–Aldrich Pty Ltd., Castle Hill, NSW, Australia) was used as a stabilizing agent for Hg in solutions. The reagent was heated before use at 300 °C to remove any residual Hg and all mercury standard solutions was stabilized with addition of 0.2% (w/v) potassium dichromate. Sodium borohydride solution was prepared freshly daily by dissolving an appropriate amount of $NaBH_4$ salt (Sigma–Aldrich Pty Ltd.) in 0.01% sodium hydroxide solution. Hydrochloric and nitric acids (BDH Chemicals Pty Ltd.) were of analytical reagent grade. Milli-Q water was used throughout the experiment for dilution and rinsing.

A river sediment reference material AGAL-10, collected from the Hawkesbery River in New South Wales, Australia and provided by Australian Government Analytical Laboratories, was used for the validation of the SI–CVAAS method. Lake sediments were collected from the Gippsland Lakes in Victoria.

2.2. Apparatus

A Perkin-Elmer Model 3030 (Perkin-Elmer Pty Ltd., Rowville, Victoria, Australia) atomic absorption spectrometer was used with a mercury hollow cathode lamp (Varian Australia Pty Ltd., Mulgrave, Victoria, Australia) at a wavelength of 253.7 nm, operating current of 12 mA and a bandwidth of 0.7 nm for the detection of mercury. An absorption cell was assembled in our laboratory with a T-glass tube and cone plastic tips (Axy-Gen Inc., Union City, California, USA) fixed on both ends of the glass tube to give a total length of 16 cm. As shown in Fig. 1 the cell was made in such a way that the middle part of about 6 cm in length was 5 mm in diameter but becomes wider towards the ends so that it follows the shape of the light beam as much as possible. This design achieved the best light density in the cell when used at room temperature.

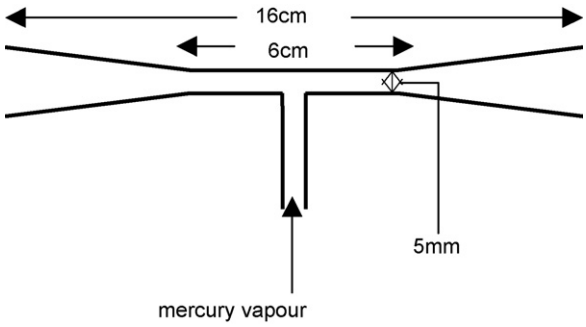


Fig. 1. Configuration of the absorption cell used for the SI–CVAAS measurement of mercury.

The sequential injection system was assembled in our laboratory and composed of a peristaltic pump (Model ISM944, ISMATEC SA, Glattbrugg, Switzerland) and two 3-way 2-position 7425 solenoid valves (Cole-Parmer, Verson Hills, Illinois, USA). Each of the valves was controlled by a Serelic 814 timer (Crouzet Automatismes SA, Valence, France). Tygon pump tubing (Elkay Products Inc., Massachusetts, USA) of 1.6 mm in diameter was used for pumping the liquid. PTFE tubing (Cole-Parmer, Verson Hills, Illinois, USA) was used for the connection of the valves, pump tubing and the gas liquid separator. A U tube was used as the GLS and flexible plastic tubing was used to connect the U tube to the absorption cell. The complete assemblage of the SI system is shown in Fig. 2.

2.3. SI–CVAAS measurement procedure

Prior to initiation of the timer (T1 or T2), both valves (V1 and V2) were switched (Fig. 2) to the off position (left side) and the on position was closed (down side). When T1 was initiated, V1 was switched from water to reductant ($NaBH_4$) so that the reductant coil between the two valves was filled with $NaBH_4$ solution. During this period, V2 was kept open towards the coil direction. When the coil was filled, the status of T1 was automatically changed to "finished" and its output pole initiates the second timer T2 which in turn switched V2 from the off (left) position to the on (down) position to aspirate the sample solution into the tubing connected to the right of the valve. When the sampling period was finished, both valves were switched to

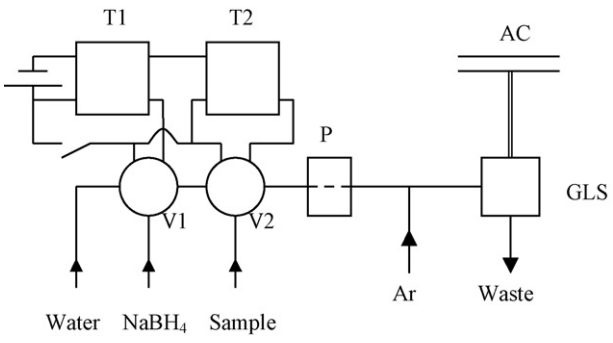


Fig. 2. Diagram of the SI–CVAAS system. T1, T2, timer controller; V1, V2, solenoid valves; P, peristaltic pump; Ar, argon flow; GLS, gas–liquid separator; AC, absorption cell.

the off positions to aspirate water into the tubing to propel the reductant and the sample forward into the gas liquid separator. On the way to the separator, the bands of reductant and sample penetrate each other and mercuric ions were reduced to metallic atoms that were carried into the GLS by the gas carrier downstream of the pump. After phase separation, the mercury atoms were swept into the absorption cell with argon gas and transient absorption signals were recorded. The peak height of the absorption signal was used to calibrate and quantify mercury.

2.4. Pretreatment of sediment samples

The sediment samples were dried at 70 °C in an oven, homogenized and passed through 63 μm Nylon sieve. One gram of the homogenized sample was digested with aqua regia. The sample was heated on a hot plate to near dryness. 5 mL of HCl was added and heated to near dryness. Another 5 mL of HCl was added and heated for 5 min. The sample was filtered through a Whatman filter paper, collected into a 100 mL volumetric flask, and made up to volume with Milli-Q water. The sample was then analysed for mercury by the SI–CVAAS method and quantified by a calibration method.

3. Results and discussion

3.1. System design

The use of SI systems for CVAAS measurement of mercury involves aspiration of adequate sample volumes and reagents through different channels, and subsequent transport to the detector. Typically, these systems comprise of simple manifolds with a single reaction line, functioning as an extension of the holding coil during the reaction/detection sequence. Owing to the penetration of neighbouring sample and reagent zones, both in the reactor and in the holding coil, the reaction between mercuric ions and sodium borohydride is usually initiated as soon as the sample and reagent are aspirated. For this reason, the entire procedure in most SI systems is computer controlled and highly reproducible. This feature is particularly desirable for shortening the reaction time and increasing the sample throughput. However, some studies [9,10] have indicated that such expectations are not valid when the reactions involve evolution of a gas, as in the case of hydride generation. These studies have indicated that partial penetration and mixing of sample and reagent zones result in gas formation during the aspiration stage and inevitably interfere with the precise metering of at least one of the solutions. The subsequent delivery of the contents in the holding coil is also significantly affected due to the compressibility of large gas segments in the conduits. To overcome this problem for the determination of mercury, Ma et al. [9] used air-segmentation to separate the sample and reagent zones, and, hence, to prevent their mixing in the line prior to the gas–liquid separation.

The problem can also be overcome by careful optimization of the analytical parameters for CVAAS measurement of mercury, as vapour generation can readily occur with as low as 0.01% of $NaBH_4$ [5]. Results obtained in the present study have shown that even 1 μg mL^{-1} (0.0001%) of $NaBH_4$ gave 30% of the maximum absorbance; 10 μg mL^{-1} (0.001%) gave over 80% of the maximum absorbance and 100 μg mL^{-1} (0.01%) gave nearly 100% of the expected absorbance. It appears that with such low $NaBH_4$ concentrations, hydrogen gas generated in the reaction coil is too little to cause considerable disturbance to the effective penetration and mixing of the sample and reagent zones. Therefore, no segmentation is required to separate the neighbouring zones of sample and reagent. However, Ma et al. [9] suggested that such segmentation is necessary because the $NaBH_4$ concentration used was much higher (0.2–1%). Such high $NaBH_4$ concentration will definitely cause disturbance to the effective penetration and mixing of the zones. We investigated the effectiveness of using a $NaBH_4$ concentration of 0.2% with our SI–CVAAS method and found that it was not possible to accomplish vapour generation because of the disturbance caused by the large amount of hydrogen gas generated at such high $NaBH_4$ concentration. In addition, by using high $NaBH_4$ concentration, the sample and reagent zones are separated by the hydrogen generated in line. Consequently, this prevented the occurrence of vapour generation in line and, thus, vapour generation can only occur in the GLS when such high $NaBH_4$ concentration is used. This undoubtedly resulted in a significant loss of sensitivity. This observation also suggests that the same consequence may be experienced when the sample and reagent zones are segmented by introduction of an air plug.

Based on the above observations and considerations, the SI–CVAAS system shown in Fig. 2 was adopted for the measurement of mercury to enable substantial improvement in sensitivity. In this system, vapour generation was initiated and completed in the tubular reactor and no additional contribution to the reaction occurs in the GLS.

3.2. Optimization of the SI–CVAAS system

To ensure the achievement of optimum performance of the proposed SI–CVAAS method, the influence of significant parameters, such as pump pressure, flow rate, carrier stream, aspiration sequence of sample and reagent, reagent coil capacity, tubular reactor length, carrier gas flow rate, reductant concentration, and reagent and sample aspiration times, were carefully investigated. The outcomes of these investigations are discussed below.

3.2.1. Influence of pump pressure and flow rate

Preliminary investigations showed that three interactive parameters are fundamental to the optimization of the SI–CVAAS system: (a) the pressure generated by the pump, (b) the flow rate of argon gas, and (c) the volume of the tube connecting the GLS and the absorption cell. The pressure generated by the pump depends on its speed. It is important to emphasize this point because the pressure generated by the pump used in this work is relatively high for FIA and SIA measurements because of its particular pump head parameters and therefore its speed and, hence, the pressure must be carefully regulated. It was found that two extremes existed. At a speed near its maximum (45 rpm) the pressure generated was too high and a high

flow rate of argon gas was needed to balance the pressure and the high gas flow rate in turn increased the dilution of the generated vapour and reduced the sensitivity. In this case, the use of a connection tube (of large diameter and volume) between the GLS and the absorption cell was necessary to moderately disperse the vapour and give good signal. In contrast, a reduction of the pump speed to 60% (27 rpm) resulted in a modest pressure and only a moderate gas flow rate was needed. In this case, a connection tube of small volume between the GLS and the absorption cell was required, and because the dilution of vapour was attenuated, better sensitivity and good signal shape were obtained. The chosen pump speed (27 rpm) and pump tubing (1.6 mm i.d.) gave a liquid flow rate of 7.3 mL min^{-1}, and the connection tube between the GLS and the absorption cell was 4 mm in diameter and 50 cm in length. All further optimization of the SI–CVAAS system was performed with this flow rate.

3.2.2. Carrier stream and aspiration sequence of the sample and the reagent

Acid solutions are usually used as carrier streams in flow injection or sequential injection vapour generation systems. However, because the reductant was not aspirated continuously in our system, the use of an acidic carrier stream is undesirable as this may decompose the aspirated reductant before the vapour generation. In fact, we found that when acid was used as a carrier, no response was obtained for CVAAS measurement of mercury by our SI–CVAAS system. Therefore to prevent the decomposition of the reductant by acid in the carrier stream, we have employed water as the carrier stream. The resulting high sensitivity achieved with water as a carrier stream confirms that the use of an acid as a carrier stream is unnecessary in the proposed SI–CVAAS system.

To determine the possible effect of the sample–reagent aspiration sequence on the sensitivity of SI–CVAAS measurement, we considered two different aspiration sequences, based on the use of 0.2 mL of $NaBH_4$ (0.01%) as reductant and 0.6 mL of 20 μg L^{-1} Hg standard solution. The first involves the aspiration of the sample followed by $NaBH_4$; while the second involves aspiration of $NaBH_4$ followed by the sample. Interestingly, it was found that the first sequence gave a better sensitivity for the SI–CVAAS measurement of mercury than the second one. This appears to be due to the more complete retention and detection of the mercury vapour generated with the use of the first sequence. For this reason, the adopted sequence for all measurement with the SI–CVAAS method involves initial aspiration of the sample, followed by the reductant.

3.2.3. Influence of reagent coil capacity and tubular reactor length

The influence of the use of various sizes of the reagent coil with different volumes on the sensitivity of the mercury measurements with the SI–CVAAS method was investigated. It was found that a reagent volume of 170–200 μL gave the best sensitivity and reproducibility. A reagent coil volume of 170 μL was therefore used in all other investigations.

The effectiveness of the use of pump tubing as the tubular reactor for the vapour generation was also investigated with different lengths of the tubing (1.6 mm i.d.). Only a slight decrease in response was observed when the tubing length was increased from 10 to 50 cm. This observation clearly indicates that the vapour generation process in the SI–CVAAS system is very fast. In order to ensure the lowest sample dispersion and the best sensitivity, a 10 cm tubing length was chosen and used in other investigations.

3.2.4. Influence of carrier gas flow rate

Under the established optimum pump speed of 27 rpm and a liquid flow rate of 7.3 mL min^{-1}, the influence of argon gas flow rate on the mercury response obtained by the SI–CVAAS system was investigated. Fig. 3 shows that the mercury response obtained by this system increased considerably with increasing argon flow rate up to 150 mL min^{-1}. It appears that at the lower flow rates, it was difficult to sweep the mercury vapour quickly enough into the absorption cell and, consequently, significant dispersion occurs prior to reaching the absorption cell, resulting in lower sensitivity. On the other hand, at the higher argon flow rates, dispersion and dilution was also observed and this affected the sensitivity of the mercury measurement. An argon flow rate of 150 mL min^{-1} was therefore chosen as optimum and used in all other measurements.

3.2.5. Reductant concentration

Fig. 4 shows that the sensitivity of the mercury response obtained with the SI–CVAAS system increased considerably with increasing $NaBH_4$ concentration up to 0.01% and no further improvement was observed with the addition of more reductant. However, lower reductant concentration still gave very good sensitivity and reproducibility, especially in the presence of ≥0.001% $NaBH_4$. Even the use of 0.0001% (1 mg L^{-1}) of $NaBH_4$ gave good sensitivity for the mercury response. On the other hand, the use of $NaBH_4$ concentration >0.05% did not result in a better improvement in sensitivity, but instead generated a significant amount of hydrogen gas which disturbed the effective penetration and mixing of the sample and reagent zones, as indicated earlier. The resulting hydrogen gas also caused significant background signal that may result in a large

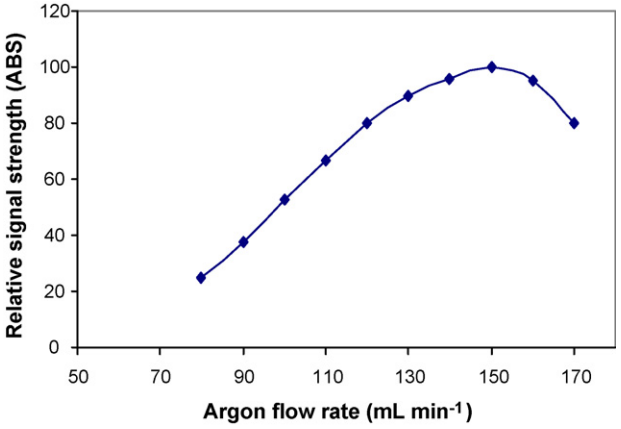


Fig. 3. Influence of argon flow rate on SI–CVAAS measurement of mercury. Other conditions are as described under Section 2.

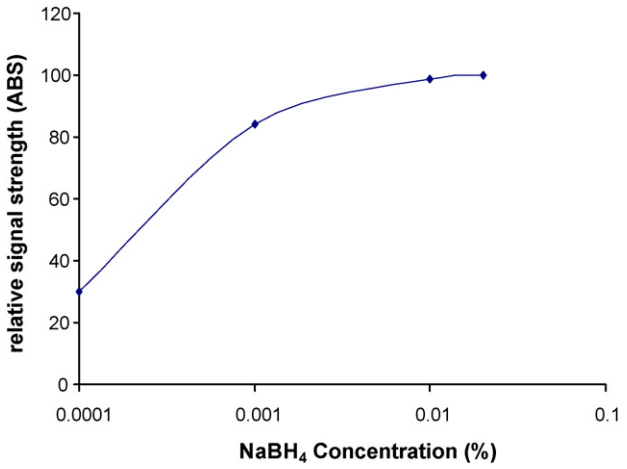


Fig. 4. Influence of $NaBH_4$ concentration on mercury response. Other conditions are as described under Section 2.

error. To avoid such problems, 0.01% of $NaBH_4$ was used in other investigations.

The use of $SnCl_2$ as a reductant was also investigated, but it was found to be a weaker reductant compared to $NaBH_4$, giving only about 50% of the sensitivity obtained with $NaBH_4$.

3.2.6. Reagent and sample aspiration time

The best sensitivity and signal shape obtained with SI–CVAAS measurement of mercury is influenced by the aspiration time and, hence, the quantities of reagent and sample used for the measurements. It was found that the use of a reagent aspiration time between 1.4 and 2.0 s gave similar results. To fill up the reagent coil and to enable enough reagent penetration to the sample zone in the tubular reactor, the minimum aspiration time required was 1.4 s that corresponds to a reagent volume of 170 μL. The use of a reagent volume less than 170 μL, but no more than 200 μL does not affect the sensitivity and signal shape. Therefore, it was not necessary to use an aspiration time over 2 s because it does not improve the sensitivity, and it produced a shoulder peak in front of the main absorption signal. Hence, an aspiration time of 1.6 s was used for the delivery of $NaBH_4$ solution.

An increase in the sample aspiration time from 1 to 7 s resulted in an increase in the sensitivity of the signal. The shape of the signal became distorted when a sample aspiration time of 6 s or longer was employed, resulting in a poor calibration curve. Also, besides the peak distortion, a large tailing of the peak was also observed and this resulted in a reduced sample throughput. A sample aspiration time of 5 s, which corresponds to 0.6 mL sample, was therefore used to overcome these problems, resulting in a good sensitivity and a better calibration curve.

3.2.7. Vapour stripping and gas liquid separator

In metallic form, mercury has a considerable vapour pressure of 0.0016 mbar at 20 °C that corresponds to a concentration of about 14 mg m^{-3} in air [10]. Despite its high vapour pressure, an efficient separation from the liquid phase is still necessary to ensure that all the mercury vapour is transferred to the atomic absorption cell and, hence, to achieve optimum sensitivity. A gas–liquid separator (GLS), of different configurations, is often used to achieve this goal and their performances have been compared [13]. In the present study, enhanced stripping and, hence, better sensitivity was achieved by introduction of the carrier gas prior to reaching the GLS. In contrast, when the carrier gas was introduced into the space above the liquid surface in the GLS, lower sensitivity was obtained. This indicates the difficulty in releasing the mercury atoms out of the liquid without the aid of the carrier gas. Similar observations have been reported for the determination of bismuth, selenium and tellurium by hydride generation AAS [14]. In that study [14], it was found that the residence times for the hydrides were dependent on $NaBH_4$ concentration due to the effectiveness of the resulting hydrogen gas in stripping the hydrides from the reaction solution. Consequently, the hydrides were removed faster when higher $NaBH_4$ concentration was used. Similarly, we found in our study that the separation of the vapour was achieved when the carrier gas was introduced into the liquid below the top surface in the GLS. However, significant amount of aerosols were generated and carried into the absorption cell, causing high background signal. It was also found that the distance between the introduction of the carrier gas and the GLS did not affect the sensitivity, but the tube employed must be over 1.5 mm in diameter. When smaller tube width was used, the sample zone was segmented by the carrier gas, resulting in a peak doublet. For these reasons, a PTFE tube diameter of 1.6 mm and 10 cm in length was used for the delivery of the gas–liquid mixture in all investigations.

3.3. Analytical performance and applications

Table 1 provides the performance data for the SI–CVAAS method for the measurement of mercury with two different sample volumes. Evidently, the sample volume used did not affect the sampling frequency, but influenced the achievable dynamic range, sensitivity and detection limit. The use of a sample volume of 0.24 mL gave a wider dynamic range (0.5–60 ng mL^{-1}), while the use of the larger sample volume enabled the achievement of a lower detection limit of 0.2 ng mL^{-1}. However, it is important to note that the dynamic ranges achieved with both sample volumes were better than the dynamic range of 0–20 ng mL^{-1} reported in some studies [9–11,8]. Also, the sampling frequency of 180 h^{-1} was much better than the 25–90 h^{-1} reported in other studies [9–11,8] and the detection limit is comparable or better than those reported in other studies [9,11,8]. The measurement of mercury with the proposed SI–CVAAS method was also very reproducible with a R.S.D. of 1.8%.

Table 1
Analytical performance of the SI–CVAAS method for mercury measurements

Sample consumption (mL)	0.6	0.24
Sampling frequency (h^{-1})	180	180
Dynamic range (ng mL^{-1})	0.5–40	0.5–60
Regression equation	0.0232[Hg] + 0.0066	0.0092[Hg] + 0.0028
Correlation coefficient	0.9998	0.9999
Detection limit (ng mL^{-1})	0.2	0.31
Precision (%)	1.8	1.9

A major consideration in the successful application of the SI–CVAAS method for the determination of mercury in real samples is the possible interference by metal ions and organic matter. The study of the possible interference of common metal ions on mercury measurements with the system showed that the presence of 100 μg mL^{-1} of Mn^{2+}, Co^{2+}, Ni^{2+}, Cu^{2+}, Zn^{2+}, or Pb^{2+} and 1000 μg mL^{-1} of Fe^{3+} did not cause any interference on the measurement of 10 ng mL^{-1} mercury. It appears that the choice of low $NaBH_4$ concentration may be responsible for the observed lack of interference from the other metal ions because they are less likely to be reduced to metallic form under this condition. It is also important to note that the concentrations of these metal ions in digested sediment samples will be lower than considered and will therefore not cause any interference when used in real samples.

The other possible substances that can interfere with mercury measurement by the SI–CVAAS method are organic matters, such as humic substances. The surface activities of humic substances from sediment have been well documented [15–18] and this property can be affected by a variety of solution parameters, including pH. For example, it has been demonstrated that the surface tension of solution of humic substances from coastal marine sediment exhibited a dependence on the acidity of the solution with a minimum at around pH 4 and this is a consequence of an increase in the amphiphilic character or structure [17,18]. When the SI–CVAAS method was used for sediment samples collected from Lake Wellington (a part of the Gippsland Lakes) in Victoria, Australia, it was found that the organic matter in the sediment, possibly humic substances, caused a significant suppression of the mercury signal if the digested sample solution was not sufficiently diluted. The interference may be caused by the surface-active property of the organic matter that was also extracted during sample preparation. These substances have significant surface activity and the activity was improved when reacted with an alkaline solution of the reductant, resulting in significant foaming above the liquid surface in the U tube during phase separation. In their study on the effect of micellar media on the sensitivity of mercury determination, Gutierrez et al. [19] found that all the anionic surfactants tested caused a significant suppression of the sensitivity of mercury measurement with a FI–CVAAS system. However, no explanation was provided for the observed reduction in sensitivity. It appears therefore that this effect has similar mechanism to that observed in our study with organic matter in sediment. The foaming generated in the gas–liquid separator suggests that the surface-active property may be responsible for observed reduction in the stripping efficiency of mercury atoms from the liquid. It was found that this effect can be eliminated by simply diluting the sample solution to ensure that the organic matter content is low enough in the solution. Table 2 shows the effect of dilution factor on the recovery of mercury in a sediment sample with an organic matter content of 8%. As evident a dilution factor of over 100 was required to eliminate such interference in the lake sediment samples.

Table 3 presents the results obtained with the SI–CVAAS method for mercury determination in the river sediment reference material AGAL-10. Evidently, the results obtained were in a very good agreement with the certified value. Also, the percentage recovery was closed to 100% with a relative standard variation of 1.8%.

Table 2
Effect of sample dilution on the recovery of mercury in lake sediments

Dilution factor	Recovery (%)
25	32.5
50	87.6
100	99.2
250	99.6

Table 3
Mercury concentration found in river sediment reference material and recovery efficiency

Measured value in average ($n=6$, μg g^{-1})	R.S.D. (%, $n=6$)	Certified value (μg g^{-1})	Recovery (%)
11.45 ± 0.32	1.78	11.31 ± 1.17	101.2 ± 2.8

4. Conclusions

The proposed SI–CVAAS method enabled substantial improvement in sensitivity and sample throughput for the detection of mercury by cold vapour-atomic absorption spectrometry. The method also achieved a much wider dynamic range of 0–60 ng mL^{-1}, which was two to three times wider than reported in some studies [9–11,8]. Also, the achievable detection limit of 0.2–0.3 ng mL^{-1} is comparable or better than some of those reported previously [9,11,8]. Common heavy metals such as Cu, Pb, Zn, Co, Ni, Fe and Mn did not interfere with mercury measurements by the SI–CVAAS method, and the method was successfully applied to the determination of mercury in sediment samples.

References

[1] B. Welz, M. Sperling, Atomic Absorption Spectrometry, Wiley-VCH, New York, 1999.
[2] S.B. Adeloju, H.S. Dhindsa, R.K. Tandon, Anal. Chim. Acta 285 (1994) 359.
[3] H. Agemian, A.S.Y. Chau, Anal. Chim. Acta 75 (1975) 297.
[4] K. Matsunaga, S. Takahashi, Anal. Chim. Acta 87 (1976) 487.
[5] S. Río Segade, J.F. Tyson, Spectrochim. Acta Part B: At. Spectrosc. 58 (2003) 797.
[6] T. Guo, J. Baasner, Anal. Chim. Acta 278 (1993) 189.
[7] O. Wurl, O. Elsholz, R. Ebinghaus, Talanta 52 (2000) 51.
[8] W.E. Doering, R.R. James, R.T. Echols, Fresenius J. Anal. Chem. 368 (2000) 475.
[9] H.-B. Ma, Z.-L. Fang, J.-F. Wu, S.-S. Liu, Talanta 49 (1999) 125.
[10] A.N. Anthemidis, G.A. Zachariadis, J.A. Stratis, Talanta 64 (2004) 1053.
[11] F.M. Bauzá de Mirabó, A.Ch. Thomas, E. Rubí, R. Forteza, V. Cerdà, Anal. Chim. Acta 355 (1997) 203.
[12] C. Fernandez, A.C.L. Conceicão, R. Rial-Otero, C. Vaz, J.L. Capelo, Anal. Chem. 78 (2006) 2494.
[13] I.D. Brindle, Sh. Zheng, Spectrochim. Acta Part B: At. Spectrosc. 51 (1996) 1777.

[14] H.-M. Liu, S.-Y. Chen, P.-H. Chang, S-J.J. Tsai, Anal. Chim. Acta 459 (2002) 161.
[15] M. Tschapek, C. Wasowski, Geochim. Cosmochim. Acta 40 (1976) 1343.
[16] K. Yonebayashi, T. Hattori, Sci. Total Environ. 62 (1987) 55.
[17] M. Terashima, S. Fukushima, Colloid. Surf. A: Physicochem. Eng. Aspects 247 (2004) 77.
[18] M.M.D. Sierra, T.G. Rauen, L. Tormen, N.A. Debacher, E.J. Soriano-Sierra, Water Res. 39 (2005) 3811.
[19] J.M. Gutierrez, Y. Madrid, C. Cámara, Spectrochim. Acta Part B: At. Spectrosc. 48 (1993) 1551.

Available online at www.sciencedirect.com
ScienceDirect
Talanta 74 (2008) 599–604
Talanta
www.elsevier.com/locate/talanta

Mixed liquids for single-drop microextraction of organochlorine pesticides in vegetables

Maosheng Zhang [a,c], Jiarong Huang [c], Changlin Wei [c], Binbin Yu [a], Xiaoqing Yang [d], Xi Chen [a,b,*]

[a] *Department of Chemistry and the Key Laboratory of Analytical Sciences of the Ministry of Education, College of Chemistry and Chemical Engineering, Xiamen University, Xiamen 361005, China*
[b] *State Key Laboratory of Marine Environmental Science, Xiamen University, Xiamen 361005, China*
[c] *Zhangzhou Normal University, Department of Chemistry and Environmental Science, Zhangzhou 363000, China*
[d] *College of Foreign Languages and Cultures, Xiamen University, Xiamen 361005, China*

Received 20 April 2007; received in revised form 15 June 2007; accepted 16 June 2007
Available online 6 July 2007

Abstract

A new approach for the extraction of nine kinds of organochlorine pesticides (OCPs) from vegetable samples coupling single-drop microextraction with gas chromatography–mass spectrometry was presented. Experimental parameters, such as organic solvent, exposure time, agitation and organic drop volume were controlled and optimized. An effective extraction was achieved by suspending a 1.00 μL mixed drop of *p*-xylene and acetone (8:2, v/v) to the tip of a microsyringe immersed in a 2 mL donor aqueous solution and stirred at 400 rpm. The approach was applied to the determination of OCPs in vegetable samples with a linearity range of 0.05–20 ng mL^{-1} for α-, β-, γ-, δ-hexachlorobenzene (BHC) and dicofol, 0.5–20 ng mL^{-1} for dieldrin and 2,2-bis(4-chlorophenyl)-1,1-dichloroethane (DDD) or 0.5–50 ng mL^{-1} for 2,2-bis(4-chlorophenyl)-1,1-dichloroethylene (DDE) and 2-(2-chlorophenyl)-2 (4-chlorophenyl)-1,1,1-trichloroethane (*p*,*p*′-DDT). Correspondingly, the determination limit at an S/N of 3 ranged from 0.05 ng mL^{-1} for α-, β-, γ-, δ-BHC to 0.2 ng mL^{-1} for dicofol, dieldrin or *p*,*p*′-DDT. The relative recoveries were from 63.3 to 100%, with repeatability ranging from 8.74 to 18.9% (relative standard deviation, R.S.D.). The single-drop microextraction was proved to be a fast and simple approach for the pre-concentration of organochlorine pesticides in vegetable samples.
© 2007 Elsevier B.V. All rights reserved.

Keywords: Organochlorine pesticides; Single-drop microextraction; GC–MS

1. Introduction

The pesticide usage for food production has provided numerous benefits in terms of increasing production and quality, but it is harmful to the health of human beings if it is inappropriately used. Organochlorines are associated with many chronic diseases. Studies have revealed a correlation between organochlorine exposure and various types of cancer, neurological damage, Parkinson's disease, birth defects, respiratory illness, and abnormal immune system function. Although the use of OCPs has been prohibited in Stockholm Convention on Certain Persistent Organic Pollutants, the monitoring of the trace levels of OCPs in food is still important for health protection and environmental control because OCPs are of difficult degradation, easy accumulation and high toxicity [1].

Recently, researchers pay more attention to the development of OCPs analytical approaches including gas chromatography (GC) [2–4] and gas chromatography–mass spectrometry (GC–MS) [5,6]. Particularly, they have widely accepted/adopted GC–MS owing to its accuracy and sensitivity [7]. In the determination of OCPs in vegetable samples, many preparative processes, such as liquid–liquid extraction (LLE) [8], microwave assistant extraction (MAE) [9], supercritical fluid extraction (SFE) [10,11], solid-phase extraction (SPE) [12,13] and solid-phase microextraction (SPME) [14,15], have been suggested. The frequently used technique, LLE, requiring relatively large volumes of organic solvents, are time-consuming, labor-intensive and hazardous to health. SPE demands a large volume of organic solvents. SPME, a rugged, sensitive and accu-

* Corresponding author. Tel.: +86 592 218 4530; fax: +86 592 218 6401.
E-mail address: xichen@xmu.edu.cn (X. Chen).

0039-9140/$ – see front matter © 2007 Elsevier B.V. All rights reserved.
doi:10.1016/j.talanta.2007.06.041

rate method, has been achieved tremendous success and widely used for testing foods and environmental pollutants, but its application has been hindered by its relatively expensive price and fragile coating layer. Furthermore, MAE and SFE require highly expensive equipments in the practice and are difficult to be popularized.

Single-drop microextraction (SDME), developed in 1996 by Jeannot and Cantwell [16], provides an alternative technique, which integrates sampling, extracting, concentrating and sample introduction into a single step. The advantages of simple processes and less organic solvents in SDME have been attractive. In recent years, SDME has greatly been developed and extensively used for the environmental samples. He and Lee [17] investigated the extraction of 1,2,3-trichlorobenzene using static and dynamic SDME models. de Jager and Andrews [18] reported preliminary work on SDME for the analysis of 11 kinds of organic chlorine pesticides. Liu and Lee [19] introduced continuous-flow microextraction to single-drop microextraction. Xia and Hu [20] developed a method that combined SDME with low-temperature electrothermal vaporization ICP-MS for the determination of trace Be, Co, Pd and Cd in biological samples. Palit and Pardasani [21] described an application of SDME for analysis of chemical warfare agents and related compounds in water by GC–MS in 2005.

Although there have been some reports on SDME, its applications are still limited due to the limited kinds of organic acceptor solvents. Generally, a pure or mixed hydrophobic solvent was selected as an acceptor in SDME. To our knowledge, there is no report on using a hydrophilic solvent as an acceptor solvent in SDME. In this paper, we report a novel mixed liquids of *p*-xylene and acetone (8:2, v/v) as an organic acceptor solvent for the pre-concentration of organochlorine pesticides coupling SDME and GC–MS. Parameters for extraction solvent, solvent volume, drop size, stirring speed and extraction time were selected and optimized. The procedure was then applied to the determination of organochlorine pesticides of vegetable samples.

2. Experimental

2.1. Reagents and materials

α-, β-, γ-, δ-Hexachlorobenzene (BHC), dicofol, dieldrin, 2,2-bis(4-chlorophenyl)-1,1-dichloroethylene (DDE), 2,2-bis(4-chlorophenyl)-1,1-dichloroethane (DDD) and 2-(2-chlorophenyl)-2 (4-chlorophenyl)-1,1,1-trichloroethane (*p*,*p*′-DDT) were obtained from Agro-environmental Protection Institute, Ministry of Agriculture (Tianjin, China). Ultrapure water from a Simplicity Personal Ultrapure Water System (Millipore, USA) was used to prepare all buffers and solutions. Acetone, benzene, dimethylbenzene, chloroform and *n*-hexane were of pesticide-grade. A stock standard solution (200 ng mL^{-1}) of OCPs was prepared in acetone and stored at 0 °C. Working solutions were prepared by dilution of stock standard solution with ultra-pure water and stored at 4 °C.

2.2. Instrumentation

All analysis in this study was carried in an Agilent 6890/5973n GC–MS system (Agilent, USA). The GC was fitted with a HP-5MS capillary column (30 m × 0.32 mm i.d., 0.25 μm film thickness, Hewlett–Packard, Palo Alto, CA, USA). Helium was used as the carrier gas at a flow rate of 1.0 mL min^{-1}. The injector temperature was kept at 280 °C and all injections were made in the splitless mode. The temperature program was arranged with initial temperature of 50 °C, and then increased at 5 °C min^{-1} to 280 °C when it was held for 6 min. The MS was operated in electron impact (EI) mode with an ion source temperature of 230 °C. The target compounds were quantified in the selected ion monitoring (SIM) mode, using characteristic fragment ions for each compound: 219, 181, 111, 147 (α-, β-, γ- and δ-BHC), 253, 331, 279 (dicofol), 79, 263, 279 (dieldrin), 318, 246, 176 (DDE), 235, 178, 165 (DDD), 235, 212, 176, 284 (*p*,*p*′-DDT). The peak areas were calculated based on the respective molecular ions. Selected samples were analyzed in full-scan acquisition for compound confirmation.

2.3. SDME procedure

A 10 μL microsyringe (Shanghai, China) with a bevel tip, used both for extraction and for injecting the extract into the GC–MS containing 1.00 μL organic solvent, was clamped above the vial (3 mL) containing 2 mL of donor aqueous sample and stirred at 400 rpm. The needle of the microsyringe passed through the sample vial septum with the tip immersing in the liquid phase. The plunger was depressed and the 1.00 μL drop of the organic phase was exposed to the sample. The analytes were then allowed to partition between the aqueous solution and the organic phase at room temperature for 30 min. After extraction, the microdrop was retracted into the microsyringe and prepared for the GC–MS analysis. Typical chromatograms of nine kinds of OCPs with a concentration of 200 and 5 ng mL^{-1} by direct injection and SDME modes are shown in Fig. 1a and b.

2.4. Sample preparation

Fresh vegetable (cabbage, cauliflower, Chinese cabbage) was cut into small pieces and an aliquot of 5.00 g was processed. The liquefied juice was extracted by 5 mL of acetone in ultrasonic vibration for 1.5 h from the introducing sample ground by mortar. The extracted juice was diluted at an appropriate concentration using as donor aqueous sample.

To obtain fortified samples, 5.00 g of fresh vegetable was sprayed with 200 μL of stock standard solution of OCPs, and then dried in the room atmosphere.

3. Results and discussion

3.1. Selection of organic solvent

The selection of an appropriate extraction solvent is of major importance for the optimization of the SDME process.

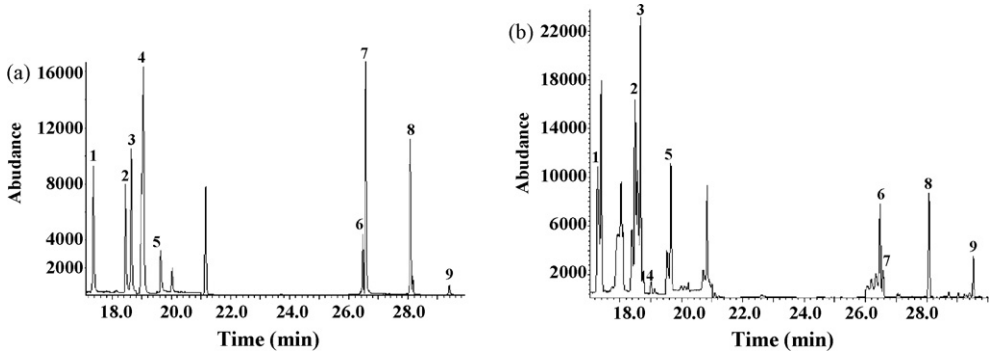


Fig. 1. Chromatograms of GC–MS obtained by direct injection (a) and SDME (b) with nine kinds of organochlorine pesticides, 1, α-BHC; 2, β-BHC; 3, γ-BHC; 4, dicofol; 5, δ-BHC; 6, dieldrin; 7, DDE; 8, DDD and 9, *p,p′*-DDT. (a) Concentration for each pesticide, 200 ng mL^{-1}. (b) Concentration for each pesticide, 5 ng mL^{-1}.

To achieve a good extraction, several solvents with different polarity and water solubility were screened according to their characteristics on the rate of drop dissolution, extraction efficiency, and behavior on gas chromatography. Solvent selection was performed by the extraction of the spiked water sample (2.00 mL at 5 ng mL^{-1}) with the organic solvent drop (1.00 μL) for 30 min at a stirring rate of 400 rpm. The experimental result indicated that *p*-xylene presented the most excellent characteristic as an extraction solvent among the four water-immiscible solvents (chloroform, hexane, benzene and *p*-xylene). Furthermore, the solvent selectivity and stability were evaluated in the experiment that mixed acetone (water-miscible solvents) into *p*-xylene as an extraction solvent. The prepared solvent dissolved well in water when the volume ratio of acetone and *p*-xylene was kept at 4:6. The extraction results of pure *p*-xylene and the mixed solvent of acetone and *p*-xylene (2:8, v/v) are shown in Fig. 2. In terms of analyte peak areas, the mixed solvent with a slighter polarity gave a better extraction result than that of the pure *p*-xylene, which was caused by its better affinity to the slight polarity of analytes. The addition of acetone caused the transferability increase of analytes from the aqueous sample into the extraction solvent. Therefore, acetone was selected and added in the mixed solvent.

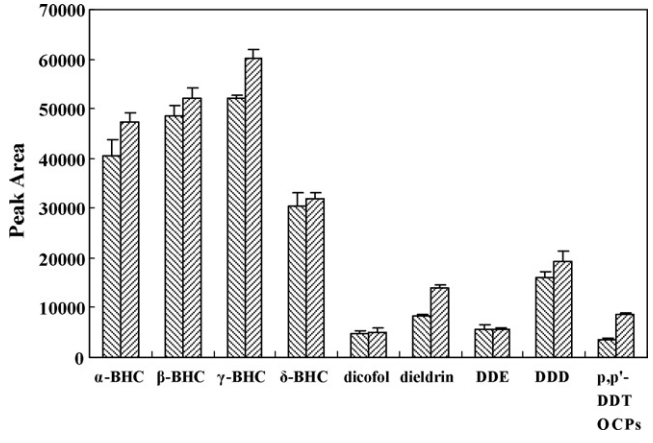


Fig. 2. Comparison of extraction efficiency of pure *p*-xylene (▨) and mixed solvent (▨) experiment conditions: extraction solvent volume: 1.00 μL, extraction time: 30 min, concentration of each pesticide: 5 ng mL^{-1}, stirring rates: 400 rpm, mixed solvent: acetone and *p*-xylene.

3.2. Organic solvent volume

This procedure represents the partitioning of analytes between aqueous and organic solvent. At equilibrium, the distribution ratio for the analytes in the two-phase system is presented as:

$$K = \frac{C_{o,eq}}{C_{a,eq}} \quad (1)$$

where $C_{o,eq}$ is the equilibriumn concentration of analytes in the organic phase and $C_{a,eq}$ the equilibrium concentration of analytes in the aqueous phase.

According to the mass balance relationship:

$$C_t V_a = C_{o,eq} V_o + C_{a,eq} V_a \quad (2)$$

where C_t is the original concentration of analytes, V_o the volume of the organic solvent, and V_a the volume of the aqueous sample.

The amount of the analytes extracted into organic drop is given by

$$N = C_{o,eq} V_o \quad (3)$$

N can be calculated from Eqs. (1)–(3):

$$\frac{1}{N} = \frac{1}{K C_t V_o} + \frac{1}{C_t V_a} \quad (4)$$

In Eq. (4), it shows that the amount of the analytes extracted into organic drop can be increased with the larger organic solvent volume.

Further experiments were carried out to determine the optimum drop volume of the organic solvent. The effect of the organic solvent volume in the range of 0.1–2.5 μL, which were controlled by different grade microsyringes, was tested. Although a better extraction result could be obtained in a larger drop volume, the larger drop tended to be disengaged from the needle of the microsyringe due to the heavier weight and obvious effect of the stir in the extraction. The drop size was kept at 1.00 μL in all the extractions. In addition, the usage of 25 μL microsyringe could hang a larger microdrop, which presented a higher extraction amount than that of the usage of 10 μL microsyringe, but its reproducibility was not so satisfactory. In the experiment, a 10 μL microsyringe was selected.

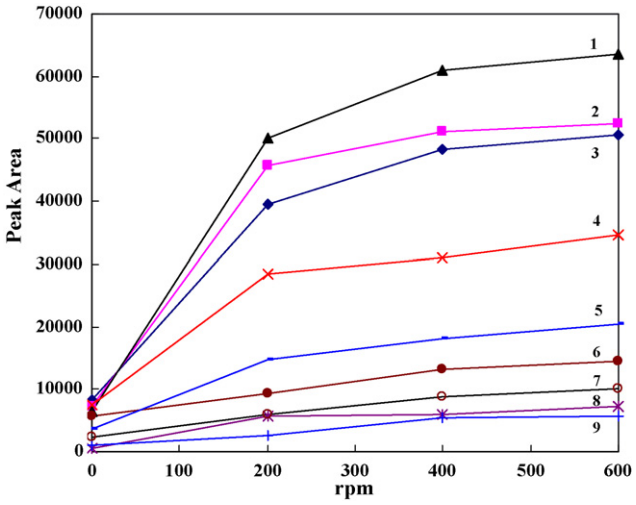


Fig. 3. Relationship between the extraction efficiency and stirring rates. 1, γ-BHC; 2, β-BHC; 3, α-BHC; 4, δ-BHC; 5, DDD; 6, dieldrin; 7, *p*,*p*′-DDT; 8, dicofol and 9, DDE. Other experiment conditions: same as shown in Fig. 2.

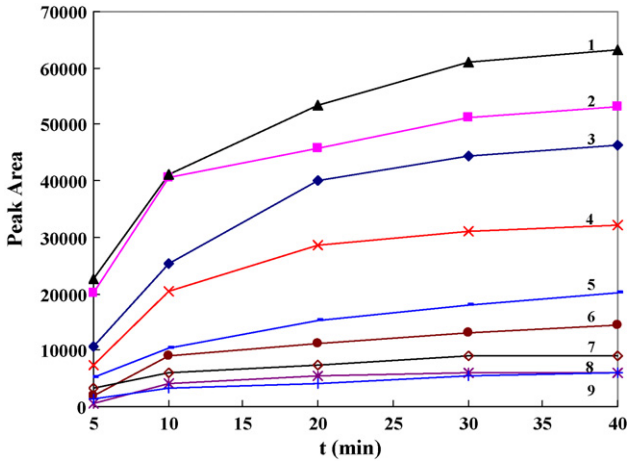


Fig. 4. Relationship between the extraction efficiency and extraction time. 1, γ-BHC; 2, β-BHC; 3, α-BHC; 4, δ-BHC; 5, DDD; 6, dieldrin; 7, *p*,*p*′-DDT; 8, dicofol and 9, DDE. Other experiment conditions: same as shown in Fig. 2.

3.3. Effect of the stirring rate

In the extraction, the increase of the stirring rate reduced the thermodynamic equilibrium time and increases extraction efficiency since a suitable stirring rate makes a continuous exposure of the extraction surface to fresh aqueous sample. For SDME, however, the over stirring rate or sonication would tend to break up the organic drop. To evaluate the effect of sample stirring, donor aqueous sample (spiked at 5 ng mL^{-1} with analytes) were extracted in extraction solvent for 30 min at different stirring rates (0, 200, 400 and 600 rpm) and the result was shown in Fig. 3. It is obvious that the extraction efficiency increased with the increase of the stirring rate, but the microdrops was destabilized or even the air bubble formed at the stirring rate of 600 rpm, which caused a lower precision and worse reproducibility. The results indicated that the stirring speed at 400 rpm was suitable in this work.

3.4. Influence of extraction time

A sufficient extraction time is necessary to attain equilibrium of analytes between the aqueous and organic drop, but a longer extraction time of microextraction to reach complete equilibrium may result in drop dissolution and have a high incidence of drop loss. To investigate the influence of extraction time on the microextraction, donor aqueous sample spiked at 5 ng mL^{-1} with analytes was extracted under a different extraction time at a stirring rate of 400 rpm. As shown in Fig. 4, the extract amount greatly increased with the increase of the extraction time. After 30 min, no dramatic increase was obtained with additional extraction time. To trade off the analytical speed and the highest extraction efficiency, the extraction time of 30 min was employed for further study.

3.5. Performance of the SDME method

Based on the method described above, the following conditions: 2 mL of donor aqueous sample, 1.00 μL of *p*-xylene and acetone mixed organic solvent (8/2: v/v), 400 rpm of stirring rate and the extraction time of 30 min, were chosen for the analytical application of all target compounds in the standard solution. Several experiments were carried out in order to determine analytical characteristics such as linear range, precision, reproducibility and detection limits for the method.

As shown in Table 1, under the optimal conditions, the calibration curves were linear from 0.05 to 20 ng mL^{-1} for α-, β-, γ-, δ-BHC and dicofol, 0.5–20 ng mL^{-1} for dieldrin and DDD or

Table 1
Linear equation, correlation coefficients (r^2), linear range and LOD of the method

Analyte	Linear regression equation[a]	Correlation coefficient	Linear range (ng mL^{-1})	LOD (ng mL^{-1})
α-BHC	$A = 8489\ C - 74.34$	0.9987	0.05–20	0.05
β-BHC	$A = 11006\ C - 94.57$	0.9982	0.05–20	0.05
γ-BHC	$A = 12833\ C - 4379.20$	0.9984	0.05–20	0.05
δ-BHC	$A = 6083\ C - 239.35$	0.9972	0.05–20	0.05
Dicofol	$A = 1431\ C - 791.58$	0.9930	0.05–20	0.2
Dieldrin	$A = 2681\ C + 292.92$	0.9958	0.1–20	0.1
DDE	$A = 1268\ C - 46.15$	0.9994	0.5–50	0.2
DDD	$A = 3649\ C - 374.03$	0.9988	0.1–20	0.1
p,*p*′-DDT	$A = 1811\ C - 643.56$	0.9931	0.5–50	0.2

[a] A, peak area and C, concentration of analytes (ng mL^{-1}).

Table 2
Determination results of organochlorine pesticides in vegetable samples ($n = 6$)

Sample analyte	Cabbage			Cauliflower			Chinese cabbage		
	Detected ($mg\,kg^{-1}$)	Recovery (%)	R.S.D. (%)	Detected ($mg\,kg^{-1}$)	Recovery (%)	R.S.D. (%)	Detected ($mg\,kg^{-1}$)	Recovery (%)	R.S.D. (%)
α-BHC	ND	95.2	15.1	ND	79.9	10.6	ND	98.0	10.4
β-BHC	ND	88.4	18.5	ND	87.0	11.5	ND	86.2	12.9
γ-BHC	ND	89.9	17.0	ND	79.4	17.1	ND	78.4	9.8
δ-BHC	ND	95.4	14.2	ND	83.2	8.7	ND	100.0	13.3
Dicofol	0.032	87.9	10.4	ND	84.7	12.7	ND	80.6	15.4
Dieldrin	ND	90.1	14.8	0.25	63.3	12.8	ND	89.4	8.74
DDE	ND	79.1	17.6	0.17	76.4	13.4	ND	86.1	10.0
DDD	ND	74.2	18.9	ND	80.6	18.1	ND	65.2	16.3
p,*p*′-DDT	ND	94.5	15.4	ND	72.6	12.4	ND	91.4	9.9

0.5–50 $ng\,mL^{-1}$ for DDE and *p*,*p*′-DDT. Correspondingly, the determination limit at an S/N of 3 ranged from 0.05 $ng\,mL^{-1}$ for α-, β-, γ-, δ-BHC to 0.2 $ng\,mL^{-1}$ for dicofol, dieldrin or *p*,*p*′-DDT. All calibration curves were found to have good linearity with correlation coefficients (r^2) ranging from 0.993 to 0.998. The limits of detection (LODs) of all OPs were calculated by comparing the signal-to-noise (S/N) ratio of the lowest detectable concentration at an S/N of 3. The results shown in Table 1 indicate that the obtained LODs were in the range or even better than those of methods such as SPME [14], liquid-phase microextraction [22] and SDME [23] in previous reports.

3.6. Analysis of vegetable samples

The determination of organochlorine pesticides (α-, β-, γ-, δ-BHC, dicofol, dieldrin, DDE, DDD and *p*,*p*′-DDT) in vegetable samples was performed. Vegetable samples including cabbage, cauliflower and Chinese cabbage were purchased from a local free market. 5.00 g of the fresh vegetable was sprayed with 200 μL of stock standard solution of organochlorine pesticides using microsyringe and then dried in the room atmosphere. The SDME was applied under the described optimal conditions. The detection results of organochlorine pesticides in vegetable samples are shown in Table 2. These results indicated that no detectable organochlorine pesticides could be found except for dicofol in the cabbage sample and dieldrin, DDE in the cauliflower sample. The method precision was determined and the relative recovery was found to range from 63.3 to 100%. The R.S.D. was from 8.74 to 18.9%, which indicated that the proposed method is feasible for the determination of organochlorine pesticides in vegetable samples.

4. Conclusions

In this work, we have demonstrated a simple approach for the determination of nine kinds of organochlorine pesticides in vegetable samples by coupling single-drop microextraction with GC–MS, A novel mixed liquids of *p*-xylene and acetone was selected as an organic acceptor solvent. Experimental parameters such as the extraction solvent composition, solvent volume, drop size, stirring speed, and the extraction time were optimized as 2 mL donor aqueous sample, 1.00 μL *p*-xylene and acetone mixed organic solvent (8:2, v/v), 400 rpm of stirring rate and the extraction time of 30 min. The similar recovery and R.S.D. values were obtained for the target compounds. Comparing with the common acceptor solvent, we found that the proposed approach showed better extractions and lower detection limits for organochlorine pesticides. The analytical results confirm that the proposed approach is feasible for the fast determination of organochlorine pesticides in vegetable samples.

Acknowledgements

This research work was financially supported by the Science and Technology Projects of Fujian Province (No. 2005-I-030, 2006Y0026) and Program for New Century Excellent Talents in University of China (NCET), which are gratefully acknowledged.

References

[1] H.Z. Xu, N. Jia, R. Ren, Environ. Sci. Manage. 30 (2005) 83.
[2] M. Gonzalez, K.S.B. Miglioranza, J.E. Aizpun de Moreno, V.J. Moreno, J. Agric. Food Chem. 51 (2003) 1353.
[3] J. Ji, C.H. Deng, H.Q. Zhang, Y.Y. Wu, X.M. Zhang, Talanta 71 (2007) 1068.
[4] R.Q. Yang, A.H. Lv, J.B. Shi, G.B. Jiang, Chemosphere 61 (2005) 347.
[5] E.N. Papadakis, Z. Vryzas, E. Papadopoulou-Mourkidou, J. Chromatogr. A 1127 (2006) 6.
[6] A. Garrido Frenich, J.L. Martínez Vidal, A.D. Cruz Sicilia, M.J. González Rodríguez, P. Plaza Bolaños, Anal. Chim. Acta 558 (2006) 12.
[7] K. Patel, R.J. Fussell, M. Hetmanski, D.M. Goodall, B.J. Keely, J. Chromatogr. A 1068 (2005) 289.
[8] O.S. Fatoki, R.O. Awofolu, J. Chromatogr. A 983 (2003) 225.
[9] Y. Chen, M.Y. Xie, X.F. Gong, J. Food Eng. 81 (2007) 162.
[10] A. Valverde-Garcia, A.R. Fernandez-Alba, M. Contreras, A. Aguera, J. Agric. Food Chem. 44 (1996) 1780.
[11] W. Fiddler, J.W. Pensabene, R.A. Gates, D.J. Donoghue, J. Agric. Food Chem. 47 (1999) 206.
[12] K. Čonka, B. Drobná, A. Kočan, J. Petrík, J. Chromatogr. A 1084 (2005) 33.
[13] M. Barriada-Pereira, M.J. González-Castro, S. Muniategui-Lorenzo, P. López-Mahía, D. Prada-Rodríguez, E. Fernández-Fernández, J. Chromatogr. A 1061 (2004) 133.
[14] F.J. López, E. Pitarch, S. Egea, J. Beltran, F. Hernández, Anal. Chim. Acta 433 (2001) 217.
[15] C.G. Zambonin, M. Quinto, N. De Vietro, F. Palmisano, Food Chem. 86 (2004) 269.

[16] M.A. Jeannot, F.F. Cantwell, Anal. Chem. 68 (1996) 2236.
[17] Y. He, H.K. Lee, Anal. Chem. 69 (1997) 4634.
[18] L.S. de Jager, A.R. Andrews, J. Chromatogr. 50 (1999) 733.
[19] W.P. Liu, H.K. Lee, Anal. Chem. 72 (2000) 4462.
[20] L.B. Xia, B. Hu, Z.C. Jiang, Y.L. Wu, Y. Liang, Anal. Chem. 76 (2004) 2910.
[21] M. Palit, D. Pardasani, A.K. Gupta, D.K. Dubey, Anal. Chem. 77 (2005) 711.
[22] L. Hou, H.K. Lee, J. Chromatogr. A 1038 (2004) 37.
[23] L.J. Jiao, T.Z. Zhang, H.L. Huang, J. Anal. Sci. 21 (2005) 170.

Available online at www.sciencedirect.com
ScienceDirect
Talanta 74 (2008) 526–532
Talanta
www.elsevier.com/locate/talanta

Study on the interaction between silver nanoparticles and nucleic acids in the presence of cetyltrimethylammonium bromide and its analytical application

Jinhua Zheng [a], Xia Wu [a,*], Minqin Wang [b], Dehuan Ran [a], Wei Xu [a], Jinhe Yang [a,*]

[a] *Key Laboratory of Colloid and Interface Chemistry (Shandong University), Ministry of Education, School of Chemistry and Chemical Engineering, Shandong University, Jinan 250100, Shandong, PR China*
[b] *School of Life Science, Shandong University, Jinan 250100, Shandong, PR China*

Received 13 March 2007; received in revised form 13 June 2007; accepted 13 June 2007
Available online 19 June 2007

Abstract

A novel method is proposed in this paper, that is the silver nanoparticle (nanoAg)–cetyltrimethylammonium bromide (CTMAB) is used as the probe of resonance light scattering (RLS) for the determination of nucleic acids. Under optimum conditions, there are linear relationships between the quenching extent of RLS and the concentration of nucleic acids in the range of 4.0×10^{-9}–2.0×10^{-6} g mL^{-1} for fish sperm DNA (fsDNA), 7.0×10^{-9}–1.8×10^{-6} g mL^{-1} for calf thymus DNA (ctDNA) and 6.0×10^{-9}–1.0×10^{-6} g mL^{-1} for yeast RNA (yRNA). The detection limits (S/N = 3) of fsDNA, ctDNA and yRNA are 2.7×10^{-10} g mL^{-1}, 4.8×10^{-10} g mL^{-1} and 7.2×10^{-10} g mL^{-1}, respectively. The studies indicate that there are interactions among nanoAg, CTMAB and fsDNA through electrostatic and chemical affinity, and the nanoAg–CTMAB complex can induce the structural change of base stacking and helicity of fsDNA.
© 2007 Elsevier B.V. All rights reserved.

Keywords: Nucleic acids; Resonance light scattering; Silver nanoparticle

1. Introduction

Silver nanoparticle is widely utilized in material science, physics and chemistry fields because of its particular optical, magnetic, electronic and catalytic properties [1]. It also has important function in anti-inflammation, anti-virus, anti-AIDS and especially anticancer [2,3], and its anticancer activity is associated with its covalent binding with N7 centers of guanine and adenine in DNA [4]. Based on this, the interaction between silver nanoparticles and nucleic acids has aroused abroad interest and attention [5–8]. Previous studies indicate that Ag ions may noncovalently interact with DNA as counter ions to balance the negative charge of the phosphate backbone and/or covalently at a number of different binding sites including the nitrogen centres of nucleobases, sugars and the phosphates. Eichorn et al. [9] proposed that Ag ion binds more strongly with nucleobases than phosphates. Recently, it has been demonstrated that silver nanocluster [10] and nanowires [11] can be formed through a DNA-templated process.

Nucleic acids have an important function in life process, so it is often used as a reference for measurements of other components in biological samples. Up to now, many techniques such as spectrophotometric methods and fluorimetric methods have been developed to determine nucleic acids using some of small molecules as the probe. Since the use of intrinsic fluorescence and ultraviolet absorption of nucleic acid for its determination is limited [12], some methods based on quenching or enhancement of resonance light scattering of various components after their interactions with nucleic acids are proposed [13,14]. Resonance light scattering analysis is attractive because it has several advantages such as: high sensitivity, simplicity and easy performance with an ordinary spectrofluorimeter. The method is widely applied to studies of assembly and aggregation phenomena and the identification of macromolecules [15,16].

In this paper, we synthesized the silver nanoparticles using citrate reduction method and studied the interaction between silver nanoparticles and DNA in the presence of CTMAB. The fresh silver nanoparticles were adopted as RLS probes for the

* Corresponding authors. Tel.: +86 531 88365459; fax: +86 531 88564464.
E-mail addresses: wux@sdu.edu.cn (X. Wu), yjh@sdu.edu.cn (J. Yang).

0039-9140/$ – see front matter © 2007 Elsevier B.V. All rights reserved.
doi:10.1016/j.talanta.2007.06.014

determination of nucleic acids at nanogram levels. The probe showed the high sensitivity and good stability for the determination of nucleic acids. The interaction mechanism of the system was also studied by the transmission electronic microscopy (TEM), circular dichroism spectra (CD), fluorometric method and UV spectrometry.

2. Experimental

2.1. Chemicals

Stock solutions of nucleic acids (100 μg mL^{-1}) were prepared by dissolving commercial fsDNA (Sigma), ctDNA and yRNA (Beijing Baitai Co., China) in 0.05 mol L^{-1} sodium chloride solutions. Silver nanoparticles were prepared: A stock solution of silver nanoparticles (2.0×10^{-4} g mL^{-1}) was prepared by dissolving 0.0158 g of $AgNO_3$ in 40 mL of 0.22-μm filtered doubly distilled water, 2 mL sodium citrate (1%) was added slowly in above $AgNO_3$ solution by heating at 86 °C with stirring for 30 min, the solution color changed gradually from colorless to olivine, diluting to 50 mL finally. Above solutions were stored at 0–4 °C. A 0.05 mol L^{-1} Tris–HCl buffer solution was prepared by dissolving 3.03 g Tris in distilled water and adjusting the pH to 7.6 with HCl. A stock solution of CTMAB (1.00×10^{-2} mol L^{-1}) was prepared by dissolving 1.8222 g CTMAB in 500 mL volumetric flask with water. All the chemicals used were of analytical reagent grade and double-distilled water was used throughout.

2.2. Apparatus

The resonance light scattering spectra and fluorescence spectra were measured using a LS-55 spectrofluorimeter (PE). The surface tension was measured on Processor Tensiometer-K12 (Kr¨uss Corp.). The precise degree of the measurement is 0.01 mN M^{-1} by the Wilhelmy-plate. All absorption spectra were measured on a UV-4100 spectrophotometer (Hitachi). All CD spectra were measured on a J-810S Circular Dichroism Spectrometer (JASCO). TEM images were measured on JEM-100 CXII Transmission Electron Microscope (JEOL). All pH measurements were made with a Delta 320-S acidity meter (Mettler Toledo).

2.3. Procedure

To a 10 mL colorimetric tube, the solutions were added in the following order: nanoAg, DNA (or RNA), CTMAB and Tris–HCl. The mixture was diluted to 5 mL with water and allowed to stand for 20 min. The RLS spectra were obtained by simultaneously scanning the excitation and emission monochromators over the range of 300–500 nm (i.e. $\Delta\lambda = 0$ nm).The intensity of resonance light scattering was measured at the maximum wavelength, with the slit width at 10 nm for the excitation and emission. The quenching extent of RLS of the nanoAg–CTMAB system by nucleic acids was represented as $\Delta I_{RLS} = I^0_{RLS} - I_{RLS}$, where I_{RLS} and I^0_{RLS} are the intensities of the systems with and without nucleic acids.

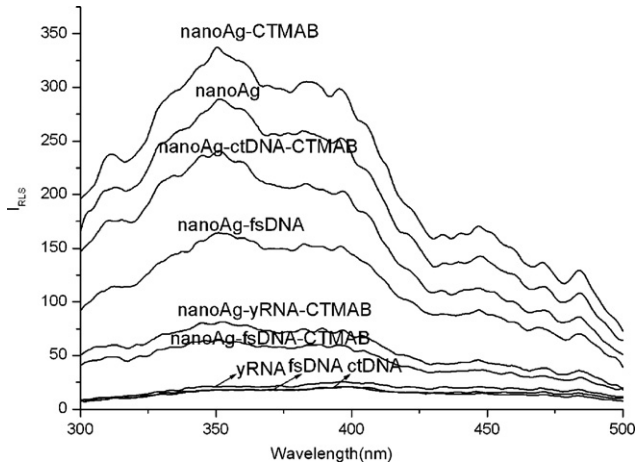


Fig. 1. Resonance light scattering spectra. Conditions: nanoAg: 1.0×10^{-6} g mL^{-1}; fsDNA: 1.0×10^{-6} g mL^{-1}; ctDNA: 1.0×10^{-6} g mL^{-1}; yRNA: 1.0×10^{-6} g mL^{-1}; CTMAB: 8.0×10^{-6} mol L^{-1}; Tris–HCl: 5.0×10^{-3} mol L^{-1} (pH 7.6).

3. Results and discussion

3.1. Resonance light scattering spectra

The resonance light scattering spectra of nanoAg–CTMAB, nanoAg, nanoAg–ctDNA–CTMAB, nanoAg–fsDNA, nanoAg–yRNA–CTMAB and nanoAg–fsDNA–CTMAB are shown in Fig. 1. The maximum scattering peak is located at 351 nm. After adding nucleic acids, the intensity of resonance light scattering is remarkably quenched, which indicates that there are interactions among nanoAg, CTMAB and nucleic acids.

3.2. Effect of pH and buffers

The effects of pH on the ΔI_{RLS} are shown in Fig. 2. It could be seen that the maximum ΔI_{RLS} was obtained at the pH 7.6. The buffer also had a large effect on the intensity of the system. The ΔI_{RLS} (%) for trihydroxymethylaminomethane (Tris)–HCl, hexamethylenetetramine (HMTA)–

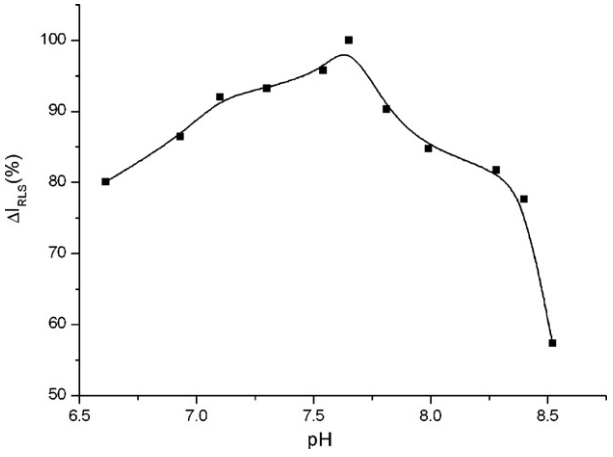


Fig. 2. Effect of pH. Conditions: nanoAg: 1.0×10^{-6} g mL^{-1}; fsDNA: 1.0×10^{-6} g mL^{-1}; CTMAB: 8.0×10^{-6} mol L^{-1}; Tris–HCl: 5.0×10^{-3} mol L^{-1}.

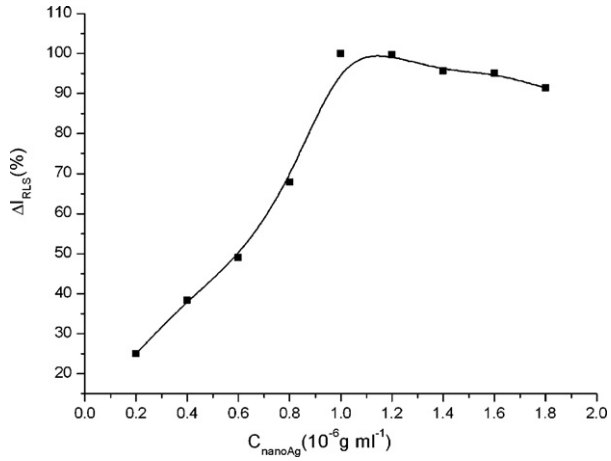


Fig. 3. Effect of the concentration of nanoAg. Conditions: fsDNA: 1.0×10^{-6} g mL^{-1}; CTMAB: 8.0×10^{-6} mol L^{-1}; Tris–HCl: 5.0×10^{-3} mol L^{-1} (pH 7.6).

HCl, $Na_2B_4O_3$–HCl, $NH_3 \cdot H_2O$–NH_4Cl, NaAc–HAc, and NH_4Ac–HCl were 100, 78.8, 89.4, 16.7, 94.3 and 84.8, respectively.

The results indicated that Tris–HCl was the best buffer. Further studies demonstrated that the optimum content of 0.05 mol L^{-1} Tris–HCl was 0.5 mL.

3.3. Effect of nanoAg concentration

From Fig. 3 it can be seen that the ΔI_{RLS} of the system reached a maximum when the concentration of nanoAg is 1.0×10^{-6} g mL^{-1}. So, 1.0×10^{-6} g mL^{-1} is chosen for further experiments.

3.4. Effect of surfactants

The effects of different surfactants on the system were studied (see Table 1). The results showed that DNA could obviously quench the RLS intensity of nanoAg in presence of cationic surfactants, such as cetyltrimethyl ammonium bromide (CTMAB), cetylpyridine bromide (CPB), the quenching extents (ΔI_{RLS} (%)) of them were 100, 82.8, respectively. Whereas anionic surfactants such as sodium dodecyl benzene sulfonate (SDBS) and sodium laurel sulfate (SLS) and nonionic surfactant Triton X-100 had little effect on the system. From above results, it could be seen that the biggest ΔI_{RLS} was obtained in nanoAg–fsDNA–CTMAB system. So, CTMAB was used in the system.

The effect of CTMAB concentration is also tested as shown in Fig. 4a. When the concentration of CTMAB is less than

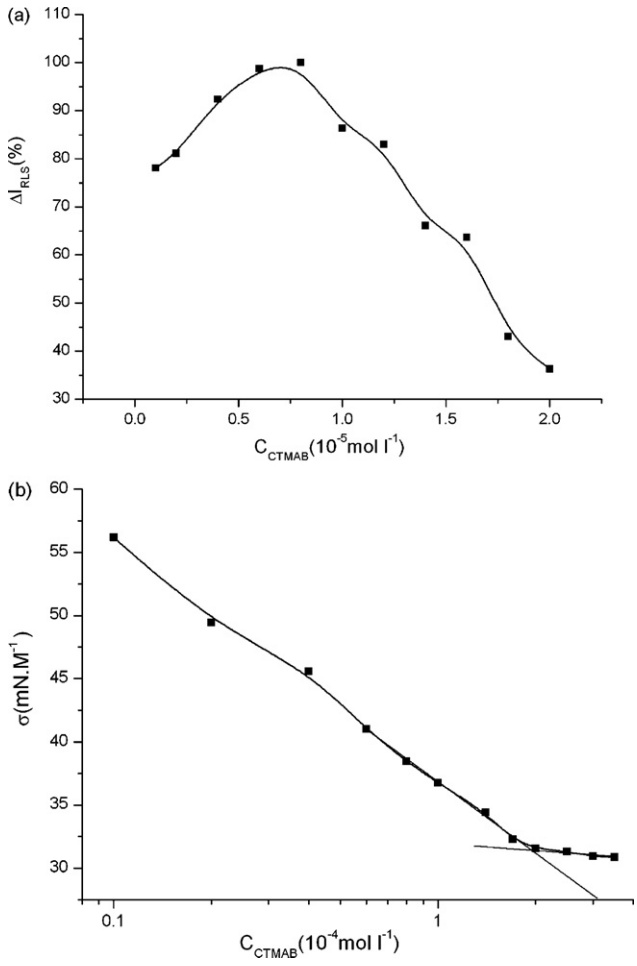


Fig. 4. (a) Effect of CTMAB concentration. Conditions: nanoAg: 1.0×10^{-6} g mL^{-1}; fsDNA: 1.0×10^{-6} g mL^{-1}; Tris–HCl: 5.0×10^{-3} mol L^{-1} (pH 7.6). (b) Surface tension of the system. Conditions: nanoAg: 1.0×10^{-6} g mL^{-1}; fsDNA: 1.0×10^{-6} g mL^{-1}; Tris–HCl: 5.0×10^{-3} mol L^{-1} (pH 7.6).

8.0×10^{-6} mol L^{-1}, the ΔI_{RLS} value increases with the increase of CTMAB concentration. After 8.0×10^{-6} mol L^{-1}, with the gradual addition of CTMAB, the ΔI_{RLS} decreases. The results indicate that the quenching extent of ΔI_{RLS} reaches the maximum when the concentration of CTMAB is 8.0×10^{-6} mol L^{-1}. So, 8.0×10^{-6} mol L^{-1} is chosen in the research.

From Fig. 4b, it can be seen that the surface tension of this system first decreases sharply with the increase of CTMAB concentration, soon gets to a minimum and then remains constant. The concentration 1.9×10^{-4} mol L^{-1} may be regarded as the apparent critical micelle concentration (CMC) of CTMAB in this system. So, it can be seen that the selected concentration of CTMAB is below its CMC, which shows that

Table 1
Effect of surfactants

Surfactants	CTMAB	CPB	TX-100	SDBS	SLS	No surfactants
ΔI_{RLS} (%)	100	82.84	6.17	52.15	55.01	62.14

Note: The concentration of the surfactants is 8.0×10^{-6} mol L^{-1}.

CTMAB exists as the pre-micelle or monomer in the studied system.

3.5. Adding sequence and signal stability

Adding sequence and signal stability are investigated. The experiments indicate that the addition sequence of reagents affects the ΔI_{RLS} intensity of the system, and the order of nanoAg, fsDNA, CTMAB, and Tris–HCl is the best.

Under the optimum condition, the effect of time on the RLS intensity is studied. The results show that the ΔI_{RLS} intensity reaches a maximum at 20 min after all the reagents added, and it remains stable for over 3 h. Therefore, this system exhibits good stability.

3.6. Effect of foreign substances

The interference of foreign substances is shown in Table 2. It was found that most amino acids and protein had not or had little effect on the determination of fsDNA within ±5% relative error.

4. Analytical applications

4.1. Calibration graphs and detection limits

Under the optimum conditions, a linear relationship is obtained between the ΔI_{RLS} and the concentration of nucleic acids. The analytical parameters are given in Table 3. There is good linearity between ΔI_{RLS} and the concentration of nucleic acids in the range of 4.0×10^{-9}–2.0×10^{-6} g mL^{-1} for fsDNA, 7.0×10^{-9}–1.8×10^{-6} g mL^{-1} for ctDNA and 6.0×10^{-9}–1.6×10^{-6} g mL^{-1} for yRNA, their detection limits (S/N = 3) are 2.7×10^{-10} g mL^{-1}, 4.8×10^{-10} g mL^{-1}, 7.2×10^{-10} g mL^{-1}, respectively.

Table 2
Interference from foreign substance

Foreign substance	Concentration coexisting ($\times 10^{-5}$ mol L^{-1})	Change of ΔI_{RLS} (%)
Trp	2.4	3.1
Cys	8.0	5.5
L-His	22	5.0
L-Asp	38	4.8
L-Phe	2.0	−5.15
Pro	1.0	−5.25
DL-Glu	16.9	−4.12
Tyr	4.2	−5.83
GMP	2.0	−4.98
AMP	2.0	−5.25
CMP	4.0	−3.24
UMP	6.4	−3.77
TMP	18.0	−4.25
BSA	0.32 μg mL^{-1}	−5.47
HSA	0.56 μg mL^{-1}	−4.83

Conditions: nanoAg: 1.0×10^{-6} g mL^{-1}; fsDNA: 6.0×10^{-7} g mL^{-1}; CTMAB: 8.0×10^{-6} mol L^{-1}; Tris–HCl: 5.0×10^{-3} mol L^{-1} (pH 7.6).

Table 3
Analytical parameters of this method

Nucleic acid	Linear range (g mL^{-1})	r[a]	LOD[b] (ng mL^{-1})
fsDNA	4.0×10^{-9}–2.0×10^{-6}	0.999	0.27
ctDNA	7.0×10^{-9}–1.8×10^{-6}	0.992	0.48
yRNA	6.0×10^{-9}–1.0×10^{-6}	0.992	0.72

[a] Correlation coefficient.
[b] Limit of detection.

A comparison of this method with other well-known RLS methods is summarized in Table 4. It can be seen that the sensitivity of this method is much higher than that of most other methods. Therefore, this is a rapid, simple and sensitive method which will be a valuable means for studying the biological properties of nucleic acids.

4.2. Determination of actual sample

An actual sample DNA of *Arabidopsis thaliana* was tested by the standard addition method. *Arabidopsis thaliana* was not of major agronomic significance, but it offered important advantages for basic research in genetics and molecular biology fields. The actual sample was isolated from *Arabidopsis thaliana* derived from granular embryogenic calli by using the CTMAB method [23]. The content of DNA in the sample was 5.3×10^{-4} g mL^{-1}, which was obtained by using a Biophotometer (Eppendorf Co.). The sample was diluted 1000 times and determined by this proposed method, the mean value of the five measurements was 5.1×10^{-4} g mL^{-1} and the relative standard deviation was 2.4% ($n = 5$). Hence, the proposed method was suitable for the determination of trace amount of nucleic acids in this sample.

5. The interaction mechanism

5.1. Assembly behavior of nanoAg

The RLS theory [15,24] indicated that the increase of particle aggregation extent was a main reason for the RLS enhancement. From Fig. 1, it can be seen that the resonance light scattering intensity of nanoAg is enhanced in the presence of CTMAB, but the addition of DNA (or RNA) can greatly quench the RLS intensities of both nanoAg and nanoAg–CTMAB, and the latter's RLS intensities have much greater quenching. We presume that the nanoAg and CTMAB can form the lager aggregates, which

Table 4
Comparison of the probe of detection limit of nucleic acids

Probe	Nucleic acids	LOD (ng mL^{-1})	Ref.
CuTSPc	ctDNA/fsDNA	32.4/10.6	[17]
Ferric nanoparticles	ctDNA/ssDNA	3.9/4.4	[18]
Acridine Red	ctDNA/fsDNA/yRNA	0.095/1.3/8.5	[19]
Morin–CTMAB	ctDNA/fsDNA/yRNA	3.4/6.2/4.1	[20]
Pentamethoxyl red	ctDNA/hsDNA	1.1/2.1	[21]
Dequalinium chloride	ctDNA/fsDNA/yRNA	6.2/7.4/7.0	[22]
This probe	ctDNA/fsDNA/yRNA	0.48/0.27/0.72	

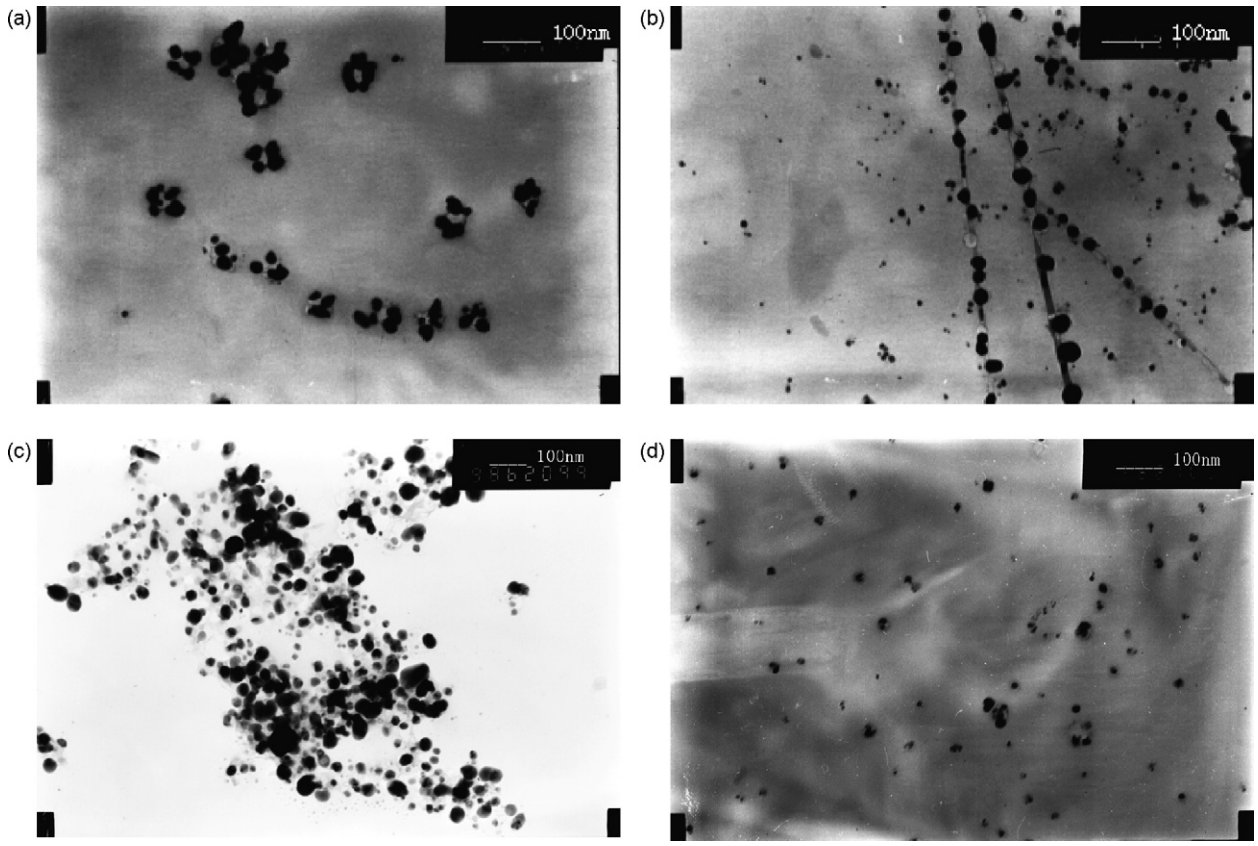


Fig. 5. (a–d) Transmission electronic microscopy. Conditions: nanoAg: 4.0×10^{-6} g mL^{-1}; fsDNA: 4.0×10^{-6} g mL^{-1}; CTMAB: 4.0×10^{-6} mol L^{-1}.

are destroyed by DNA (or RNA) when the Ag nanoparticles are coexistent with CTMAB and nucleic acids.

The TEM data can also support the above conclusion. The TEM images of nanoAg (a), nanoAg–fsDNA (b), nanoAg–CTMAB (c) and nanoAg–CTMAB–fsDNA (d) are shown in Fig. 5. From Fig. 5(a), it can be seen that the diameter of a single silver nanoparticle is about 20 nm, some of them can self-assemble to form silver nanoclusters. When CTMAB is added to the nanoAg system, many particles congregate to form nanoAg–CTMAB aggregates through electrostatic and hydrophobic interactions, resulting in the augment of average particle diameter. However, with the addition of fsDNA to the nanoAg and nanoAg–CTMAB systems, the change of aggregation states of nanoparticles is observed. The image of the former system (Fig. 5(b)) shows that nanoAg follows the strand of DNA template and forms a bead-like string. The image of the latter system (Fig. 5(d)) exhibits that the agglomerated nanoparticles are well dispersed. According to previous study [25], CTMAB and fsDNA can form the ion association complex through electrostatic forces mostly along with hydrophobic forces, this formation of pre-micelle enhances the dissolution of nanoAg in fsDNA–CTMAB complex. In addition, it is well known that DNA has large aspect ratio (length/diameter) and well-defined sequences of base and a variety of superhelix structure, more important, it has a high affinity for metal ions, such as silver, gold, copper, these localized ions can be reduced to form metallic nanoparticles [3,26,27]. And silver nanoparticles strongly favor association with the nucleobases; they can make the rupture and destroy the template function of nucleic acids. The results of TEM indicate that CTMAB can inhibit the interaction between nanoAg and fsDNA, which is attributed to the electrostatic and hydrophobic interaction between CTMAB with positive changes, nanoAg and fsDNA with negative changes. In a word, due to the combination of nucleobases with silver nanoparticles and the interaction between CTMAB and fsDNA, the balance of nanoAg–CTMAB aggregates is destroyed and the particles are dispersed, resulting in the RLS quenching of nanoAg–CTMAB systems.

From the ultraviolet absorption spectra (Fig. 6), it can be seen that nanoAg has weak absorption peak at 410 nm corresponding to its plasmon resonance absorption and another absorption peak at 265 nm corresponding to new, overlapping, electronic bands for small silver nanoclusters. When fsDNA is added to the nanoAg system, the plasmon resonance absorption spectrum of nanoAg–fsDNA (against fsDNA as reference) system decreases in intensity without obvious shift (see insert in Fig. 6), and the absorption peak at 265 nm shifts to shorter wavelength changing to a shoulder at 245 nm with the peak height increasing. Whereas, upon addition of CTMAB to the nanoAg system, the absorption peak at 265 nm has a red-shift to 305 nm, and then adding fsDNA to the nanoAg–CTMAB systems, the absorption intensity of nanoAg–fsDNA–CTMAB (against fsDNA–CTMAB as reference) increases with narrow half-peak width and without any changes in peak position. We

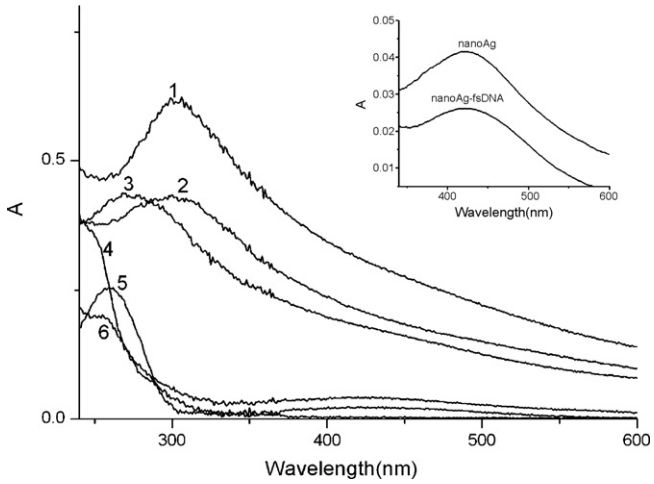


Fig. 6. Absorption spectra of the system. (1) nanoAg–fsDNA–CTMAB vs. fsDNA–CTMAB; (2) nanoAg–CTMAB vs. CTMAB; (3) nanoAg–fsDNA–CTMAB vs. nanoAg–CTMAB; (4) nanoAg–fsDNA vs. fsDNA; (5) fsDNA; (6)nanoAg. Conditions: nanoAg: 2.0×10^{-5} g mL^{-1}; fsDNA: 1.0×10^{-5} g mL^{-1}; CTMAB: 1.0×10^{-5} mol L^{-1}.

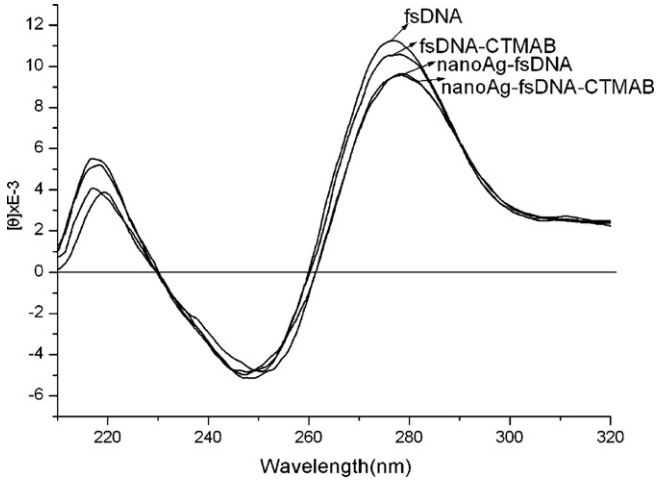


Fig. 7. Far-UV CD spectra. Conditions: nanoAg: 2.0×10^{-6} g mL^{-1}; fsDNA: 5.0×10^{-5} g mL^{-1}; CTMAB: 8.0×10^{-6} mol L^{-1}.

think that the results are attributed to the formation of a bead-like string or well dispersion of nanoAg.

5.2. Structure changes of DNA

In order to study the interaction of system in detail, the effect of four nucleotide acids in nucleic acids (dAMP, dCMP, dGMP and TMP) on the resonance light scattering of nanoAg in the prescence of CTMAB is tested. Under optimum experiment conditions, four nucleotide acids can quench all the resonance light scattering intensity of nanoAg, and dAMP has the biggest quenching among them. Therefore, we speculate that nanoAg is likely to interact mainly with the dAMP part of fsDNA.

The binding modes between nanoAg and nucleic acids are different when their mole ratio is variable [28]. The ultraviolet absorption spectra of nanoAg–fsDNA complex (against nanoAg as reference, data not shown) at various nanoAg concentrations is also investigated, the result indicates that the absorbency of fsDNA changes a little at lower nanoAg concentration. When the nanoAg concentration increases and reaches 4.0×10^{-5} g mL^{-1}, the absorption peak of fsDNA has a gradual blue-shift along with the intensity increasing, which indicates that higher concentration of nanoAg can lead to destabilization of fsDNA. Whereas, in this paper, comparing with fsDNA, the absorbance of nanoAg–fsDNA–CTMAB (against nanoAg–CTMAB as reference) has obvious increase at a fixed nanoAg concetration of 2.0×10^{-5} g mL^{-1}. We deduce that the dipole coupling between the excited electronic states of the fsDNA bases can be altered by its structural changes induced by the silver nanoparticles and CTMAB. A possibility is also suggested by the circular dichroism spectra (Fig. 7) in the wavelength range of 210–300 nm. The CD-spectra can be used to reflect the conformational transition of nucleic acids [29], from Fig. 7 it can be seen that fsDNA has a positive Cotton effect at 275 nm corresponding to base stacking, and a negative Cotton effect at 245 nm corresponding to helicity. The results of CD spectra show that the change of positive peak is bigger than that of negative peak when nanoAg and CTMAB are added into the fsDNA system, it indicates that nanoAg–CTMAB can bind with nucleobases and induce the change of nonplanar and tilted orientations of fsDNA bases, resulting in the much more changes of fsDNA base destacking than helicity. In addition, on addition of nanoAg and CTMAB, the value of ellipticity decreases and the CD spectra has a slight red-shift. We believe that the synergistic action of nanoAg and CTMAB conduce more conformational change of nucleic acids.

5.3. Interaction of nanoAg, CTMAB and fsDNA

ζ of the system at different concentrations of CTMAB is investigated. The results may give direct evidence of the interaction between nanoAg, fsDNA and CTMAB. From Fig. 8, we can find that the ζ of nanoAg–fsDNA is about -33 mV in Tris–HCl buffer. With the addition of CTMAB, ζ of the system increases and reaches 0 when the concentration of CTMAB is up

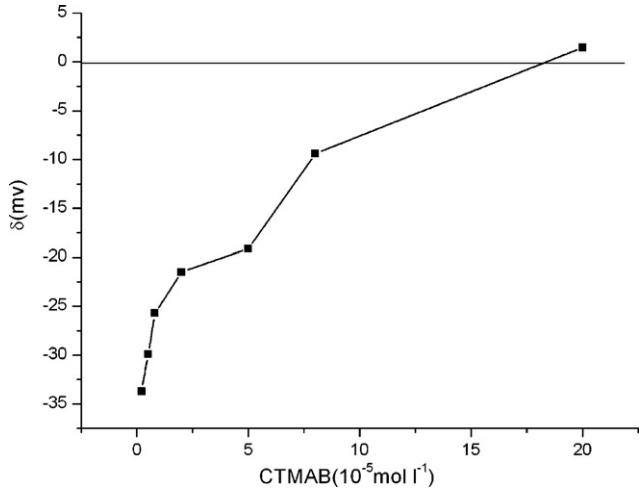


Fig. 8. $\zeta$of nanoAg–fsDNA against concentrations of CTMAB. Conditions: nanoAg: 1.0×10^{-6} g mL^{-1}; fsDNA: 6.0×10^{-7} g mL^{-1}; Tris–HCl: 5.0×10^{-3} mol L^{-1} (pH 7.6).

to 1.8×10^{-4} mol L^{-1}, then increases to a positive ζ, which is attributed to the binding of negatively charged nanoAg–fsDNA with positively charged CTMAB. This indicates that there exist electrostatic interactions among nanoAg, CTMAB and fsDNA.

The ratio of the first to the third fluorescence bands of pyrene monomer (I_1/I_3) is a well-established parameter which reflects the polarity changes of a system experienced by the pyrene probe [30]. A low pyrene monomer value indicates a less polar environment. The results show that the I_1/I_3 of pyrene monomer in system of fsDNA, CTMAB and fsDNA–CTMAB is 1.60, 1.56 and 1.35, respectively, which indicates that the microenvironment of the system has changed after CTMAB and fsDNA are added into the nanoAg. Based on the above facts, it is considered that fsDNA–CTMAB system provides an optimum hydrophobic environment with low polarity for nanoAg.

The apparent binding constant for the nanoAg–fsDNA complex in the presence of CTMAB is also determined using Scatchard analysis [28,31]. The calculated binding constant K is 1.2×10^6 mL g^{-1}, so in the prescence of CTMAB, nanoAg can bind with fsDNA through chemical affinity and exhibit good stability.

6. Conclusions

In this paper, we find that the resonance light scattering of nanoAg–CTMAB decreases with the addition of fsDNA. Based on this, a simple and sensitive method for the determination of nucleic acid has been established. Under optimum conditions, the quenched intensity of RLS is proportional to the concentration of nucleic acids over a wide range (e.g. fsDNA, ctDNA and yRNA), with detection limits at the ng mL^{-1} level. The results for the determination of DNA in actual samples isolated from *Arabidopsis thaliana* are satisfactory. The interaction mechanism investigation indicates that fsDNA can react with silver nanoparticles through chemical affinity in the presence of CTMAB, which resulted in a remarkable RLS quenching of nanoAg–CTMAB. This method is very simple, rapid and effective for determination of nucleic acids, which may be suggested for further uses in biology and nanoscience.

Acknowledgements

This work is supported by Natural Science Foundations of China (20575035) and Shandong Province (Y2003B02).

References

[1] A.G. Wu, W.L. Cheng, Z. Li, J.G. Jiang, E. Wang, Talanta 68 (2006) 693.
[2] J.L. Elechiguerra, J.L. Burt, J.R. Morones, A. Camacho-Bragado, X.X. Gao, H.H. Lara, M.J. Yacaman, J. Nanobiotechnol. 3 (2005) 6.
[3] E. Braun, Y. Eichen, U. Sivan, G. Ben-Yoseph, Nature 391 (1998) 775.
[4] M.J. Bloemink, J. Reedijk, in: A. Sigel, H. Sigel (Eds.), Metal Ions in Biological Systems, vol. 32, Marcel Dekker, New York, 1996, p. 641.
[5] Z. Hossain, F. Huq, J. Inorg. Biochem. 91 (2002) 398.
[6] L.L. Sun, G. Wei, Y.H. Song, Z.G. Liu, L. Wang, Z. Li, Appl. Surf. Sci. 252 (2006) 4969.
[7] V. Bregadze, I. Khutsishvili, J. Chkhaberidze, K. Sologhashvili, Inorg. Chim. Acta 339 (2002) 145.
[8] D.E. DiRico Jr., P.B. Keller, K.A. Hrtman, Nucleic Acids Res. 13 (1985) 251.
[9] G.L. Eichorn, Inorganic Biochemistry, Elsevier/North Holland, New York, 1973 (chapter 34).
[10] J.T. Petty, J. Zheng, N.V. Hud, R.M. Dickson, J. Am. Chem. Soc. 126 (2004) 5207.
[11] S.Q. Cui, Y.C. Liu, Z.S. Yang, X.W. Wei, Mater. Design 28 (2007) 722.
[12] W.E. Schy, M.J. Pleva, Anal. Biochem. 180 (1989) 314.
[13] R.F. Pasternack, P.J. Collings, Science 269 (1995) 935.
[14] Y. Liu, C.Q. Ma, K.A. Li, S.Y. Tong, Anal. Chim. Acta 379 (1999) 39.
[15] C.Z. Huang, K.A. Li, S.Y. Tong, Anal. Chem. 69 (1997) 514.
[16] P.J. Collings, E.J. Gibbs, T.E. Starr, O. Vafek, C. Yee, L.A. Pomerance, R.F. Pasternack, J. Phys. Chem. B 103 (1999) 8474.
[17] Y.X. Li, Y.Q. Wu, J.L. Chen, C.Q. Zhu, L. Wang, S.J. Zhuo, D.H. Zhao, Anal. Bioanal. Chem. 377 (2003) 675.
[18] Y.Q. Cheng, Z.P. Li, Y.Q. Su, Y.S. Fan, Talanta 71 (2007) 1757.
[19] M. Wang, J.H. Yang, X. Wu, F. Huang, Anal. Chim. Acta 422 (2000) 151.
[20] R.T. Liu, J.H. Yang, X. Wu, C.X. Sun, T. Wu, Analyst 126 (2001) 1367.
[21] Q. Wei, H. Zhang, B. Du, Y. Li, X.X. Zhang, Microchim. Acta 151 (2005) 59.
[22] Z.P. Li, K.A. Li, S.Y. Tong, Talanta 55 (2001) 669.
[23] J. Sambrook, E. Fritsch, T. Maintis, Molecular Cloning a Laboratory Manual, 2nd ed., Cold Spring Harbor Laboratory Press, New York, 1989, pp. 9.16–9.19.
[24] Q.-E. Cao, Y.K. Zhao, X.J. Yao, Z.D. Hu, Q.H. Xu, Spectrochim. Acta Part A 56 (2000) 1319.
[25] R.T. Liu, J.H. Yang, X. Wu, C.X. Sun, Anal. Chim. Acta 441 (2001) 303.
[26] K. Keren, M. Krieger, R. Gilad, G.B. Yoseph, U. Sivan, E. Braun, Science 297 (2002) 72.
[27] C.F. Monson, A.T. Woolley, Nano. Lett. 3 (2003) 359.
[28] H. Arakawa, J.F. Neault, H.A. Tajmir-Riahi, Biophys. J. 81 (2001) 1580.
[29] Z.L. Zhang, W.M. Huang, J.L. Tang, E.K. Wang, S.J. Dong, Biophys. Chem. 97 (2002) 7.
[30] A. Nakajima, Spectrochim. Acta A 39 (1983) 913.
[31] M.I. Klotz, Science 217 (1982) 1247.